Delft University of Technology

Slurry Transport

Fundamentals, A Historical Overview & The Delft Head Loss & Limit Deposit Velocity Framework

Miedema, Sape; Ramsdell, R.C.

Important note
To cite this publication, please use the final published version (if applicable).
Please check the document version above.

SLURRY TRANSPORT

Fundamentals, A Historical Overview
& The Delft Head Loss & Limit
Deposit Velocity Framework

2nd Edition

Slurry Transport

Sape a. Miedema

By
Sape A. Miedema
Edited by
Robert C. Ramsdell

TU Delft
open

Slurry Transport (2nd Edition)
Fundamentals, A Historical Overview & The Delft Head Loss & Limit Deposit Velocity Framework

DHLLDV Flow Regime Diagram

Particle diameter (mm)

Undefined

He-Ho

Homogeneous (Ho)

Sliding Flow (SF)

Heterogeneous (He)

SB-SF

Viscous Effects

LDV

SB-He

Sliding Bed (SB)

FB-SB (LSDV)

FB-He

Fixed/Stationary Bed (FB)

Durand Froude number F_L (-)

Line speed (m/s)

Particle diameter d (m)

Dp=0.1524 m, Rsd=1.585, Cvs=0.175, μsf=0.416
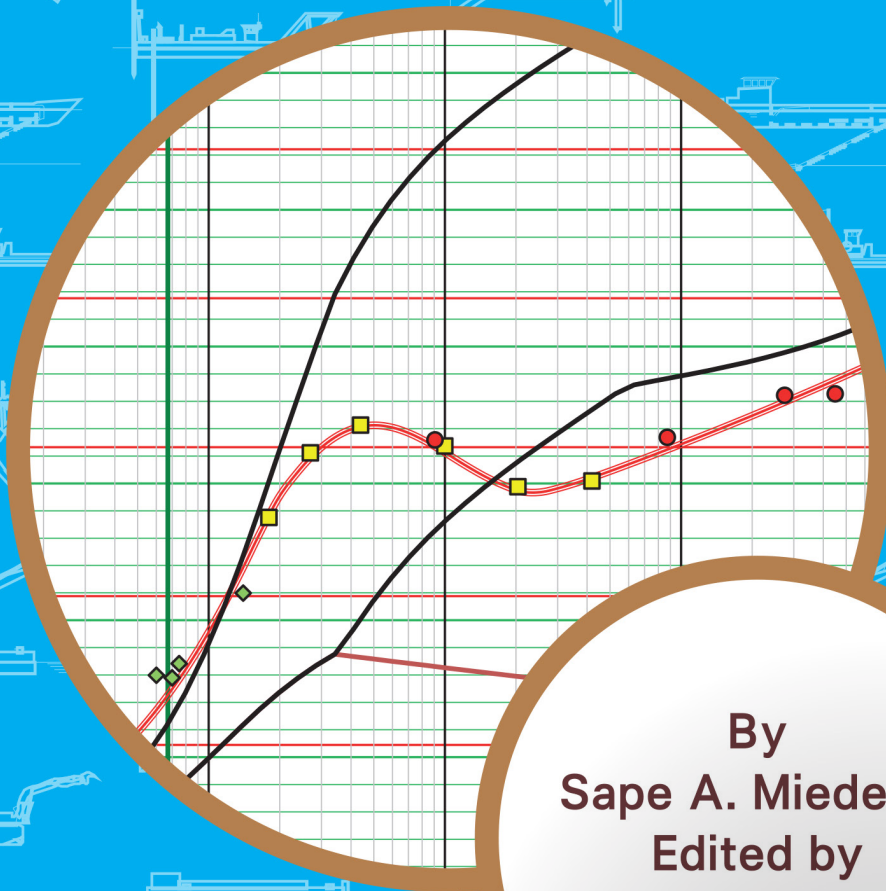
D-HL-LDV

By

Sape A. Miedema

Edited by

Robert C. Ramsdell

Slurry Transport
Fundamentals, A Historical Overview & The Delft Head Loss & Limit Deposit Velocity Framework
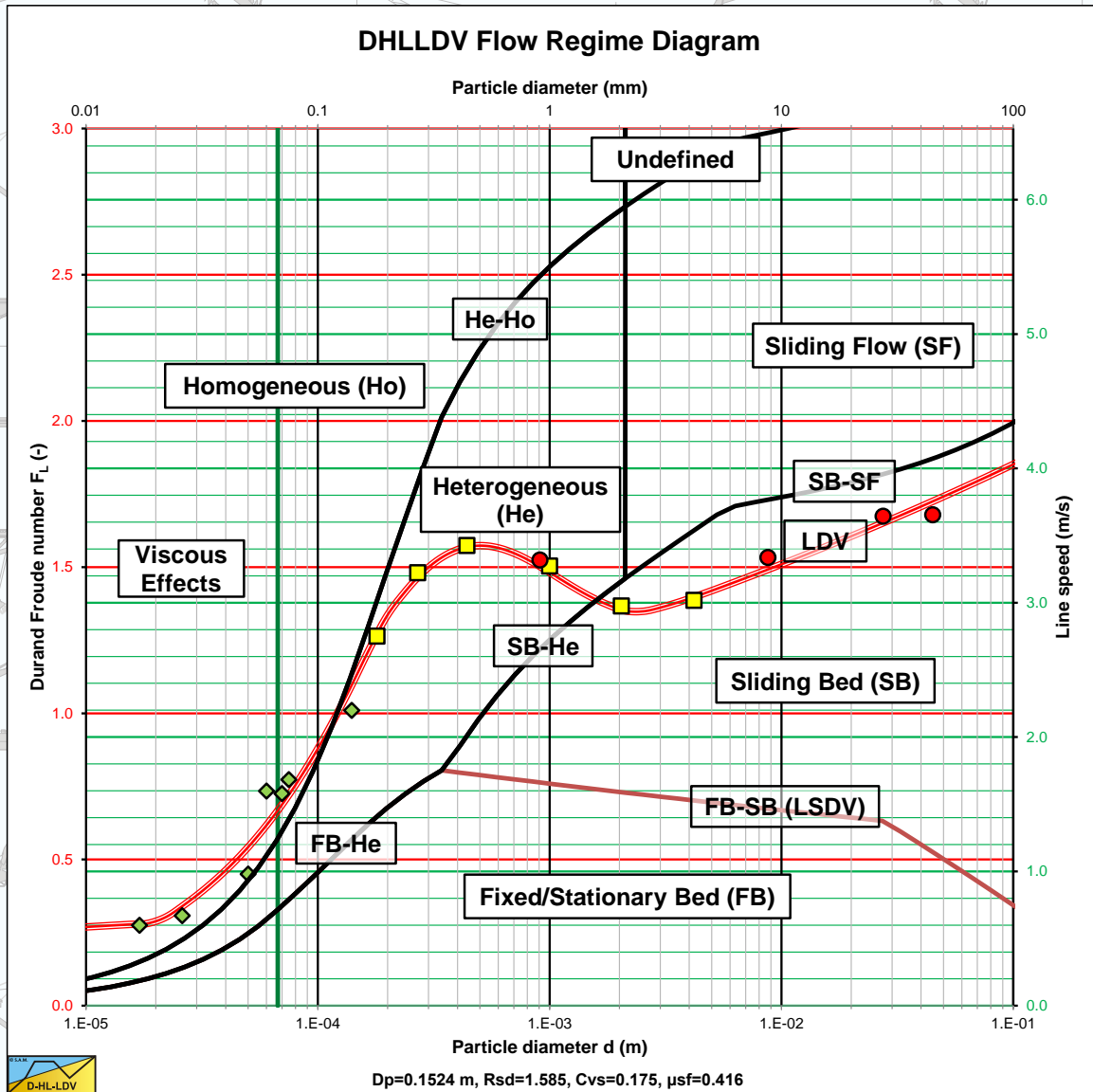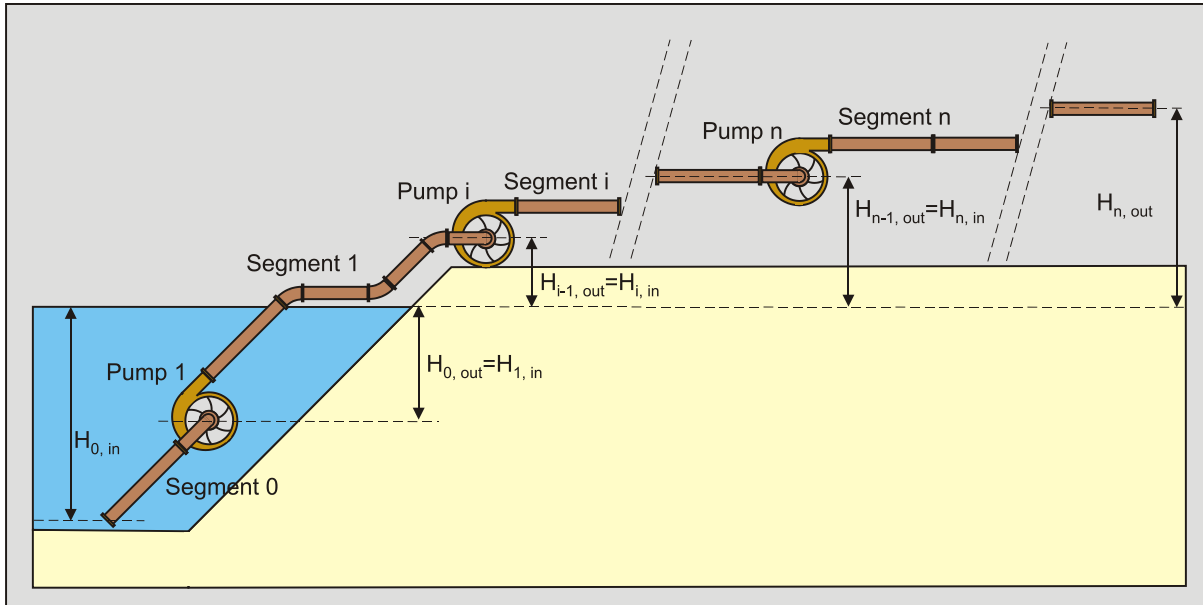## 2nd Edition

By

Sape A. Miedema

Edited by

Robert C. Ramsdell

Version: Monday, September 03, 2018

Design & Production: Dr.ir. S.A. Miedema (SAM-Consult)

Additions & Modifications

Chapter 4.6 Added an alternative equation for hindered settling.
Chapter 6.4.2.1 Added inclined pipes according to Durand & Condolios.
Chapter 6.4.3.1 Added inclined pipes according to Worster & Denny.
Chapter 6.5.6 Added additional experiments of Newitt et al.
Chapter 6.5.7 Added inclined and vertical pipes according to Newitt et al.
Chapter 6.20.2.4 Added an analysis of the Wilson v_{50} method.
Chapter 6.20.3 Modified some equations in the Wilson/Sellgren 4 component model.
Chapter 6.20.3 Added validation & sensitivity analysis to the 4 component model of Wilson/Sellgren.
Chapter 6.20.5 Added inclined pipes according to Wilson et al.
Chapter 6.20.7 Added a new implementation of Wilson et al. stratified flow.
Chapter 6.21.7 Added inclined pipes according to Doron et al.
Chapter 6.22.11 The concentration distribution graphs are modified.
Chapter 6.23 Added a concentration distribution graph.
Chapter 6.24 Modified the Matousek chapter, based on a review by Matousek.
Chapter 6.24 Added the derivation of the solids transport equation.
Chapter 6.24 Added the concentration distribution model of Matousek.
Chapter 6.24 Added 4 concentration profile graphs.
Chapter 6.27.27 Added the Fitton deposit velocity equation.
Chapter 6.27.28 Added the Thomas deposit velocity equation.
Chapter 6.28.9 Added inclined pipes according to Doron et al.
Chapter 6.28.10 Added the Graf & Robinson equation.
Chapter 6.28.11 Added the U Tube as a device to determine the delivered volumetric concentration.
Chapter 7.4 Modified the empirical slip ratio equation for 3LM.
Chapter 7.4 Most graphs modified.
Chapter 7.5 Added figure of angle of attack.
Chapter 7.7.1 Added introduction based on Vlasak experiments.
Chapter 7.7.3 Added the concentration of the bed in the sliding flow regime.
Chapter 7.7.5 Theoretical derivation of particle diameter to pipe diameter ratio.
Chapter 7.8.7 Modified text and equations.
Chapter 7.8.8 Modified text and equations.
Chapter 7.8.9 Modified text and equations.
Chapter 7.9.10 Modified text and equations.
Chapter 7.10.4 Added numerical implementation.
Chapter 7.10.5 Modified the graphs and added 4 graphs.
Chapter 7.10.6 Added numerical implementation hindered settling.
Chapter 7.10.7 Added 8 graphs with hindered settling.
Chapter 7.10.8 Added experimental data of Gillies.
Chapter 7.10.9 Added more conclusions.
Chapter 7.14 Modified the inclined pipes chapter.
Chapter 7.14 Added illustrations of inclined pipes in different flow regimes.
Chapter 7.14 Modified the homogeneous equations for sliding flow.
Chapter 8.2 Modified to match the Excel Workbook.
Chapter 8.3 Added the influence of fines, matching the Excel Workbook.
Chapter 8.5 Added hydraulic gradient and pressure difference.
Chapter 8.6 Added hydraulic gradient and pressure difference.
Chapter 8.7 Added hydraulic gradient and pressure difference.
Chapter 8.8 Added hydraulic gradient and pressure difference.
Chapter 8.9 Added hydraulic gradient and pressure difference.
Chapter 8.9 Added the bed concentration equation.
Chapter 8.10 Modified the text.
Chapter 8.11.7 Added transition fixed bed-sliding bed.
Chapter 8.11.8 Added transition heterogeneous-homogeneous.
Chapter 8.11.9 Added transition slifing bed-heterogeneous.
Chapter 8.12 Modified text and equations.
Chapter 8.13 Added the bed height.
Chapter 8.14 Added the local hindered settling equations to the concentration distribution.

TOC   Page **iii** of **xxvi**

Chapter 9.5 Added comparison of different graded sand & gravel methods.
Chapter 15.4.1-17 Replaced graphs and added graphs.
Chapter 15.5.1 Replaced most graphs and added many more graphs.
Chapter 15.5.2 Added 9 particle diameters.
Chapter 15.5.3 Added 9 concentrations.
Chapter 15.5.4 Added 9 pipe diameters.
Chapter 15.5.5 Added 9 inclination angles.
Chapter 15.5.6 Added 9 solids densities.
Chapter 15.5.7 Added graded solids.
Chapter 15.5.8 Added flow regime transitions 9 concentrations.
Chapter 15.5.9 Added flow regime transitions 9 pipe diameters.
Chapter 15.5.10 Added flow regime transitions 9 solids densities.
Chapter 15.6 Added 3 Layer Model.
Chapter 15.7 Added concentration distribution graphs.

Preface

In dredging, trenching, (deep sea) mining, drilling, tunnel boring and many other applications, sand, clay or rock has to be excavated. The productions (and thus the dimensions) of the excavating equipment range from mm³/sec - cm³/sec to m³/sec. After the soil has been excavated it is usually transported hydraulically as a slurry over a short (TSHD's) or a long distance (CSD's). Estimating the pressure losses and determining whether or not a bed will occur in the pipeline is of great importance. Fundamental processes of sedimentation, initiation of motion and erosion of the soil particles determine the transport process and the flow regimes. In all cases we have to deal with soil and high density soil water mixtures and its fundamental behavior.

The book covers horizontal transport of settling slurries (Newtonian slurries). Non-settling (non-Newtonian) slurries are not covered.

Although some basic knowledge about the subject is required and expected, dimensionless numbers, the terminal settling velocity (including hindered settling), the initiation of motion of particles, erosion and the flow of a liquid through pipelines (Darcy Weisbach and the Moody diagram) are summarized. In the theory derived, the Zanke (1977) equation for the settling velocity is used, the Richardson & Zaki (1954) approach for hindered settling is applied and the Swamee Jain (1976) equation for the Darcy-Weisbach friction factor is used, Moody (1944). The models developed are calibrated using these basic equations and experiments.

An overview is given of experiments and theories found in literature. The results of experiments are considered to be the physical reality. Semi empirical theories based on these experiments are considered to be an attempt to describe the physical reality in a mathematical way. These semi empirical theories in general match the experiments on which they are based, but are also limited to the range of the different parameters as used for these experiments. Some theories have a more fundamental character and may be more generic as long as the starting points on which they are based apply. Observing the results of many experiments gives the reader the possibility to form his/her own impression of the processes involved in slurry transport.

Flow regimes are identified and theoretical models are developed for each main flow regime based on constant volumetric spatial concentration. The 5 main flow regimes are the fixed or stationary bed regime, the sliding bed regime, the heterogeneous regime or the sliding flow regime and the homogeneous regime. It is the opinion of the authors that the basic model should be derived for a situation where the amount of solids in the pipeline is known, the constant volumetric spatial concentration situation.

A new model for the Limit Deposit Velocity is derived, consisting of 5 particle size regions and a lower limit.

Based on the Limit Deposit Velocity a (semi) fundamental relation is derived for the slip velocity. This slip velocity is required to determine constant volumetric transport concentration relations based on the constant volumetric spatial concentration relations. These relations also enable us to determine the bed height as a function of the line speed.

The concentration distribution in the pipe is based on the advection diffusion equation with a diffusivity related to the LDV.

Finally a method is given to determine relations for non-uniform sands based on the superposition principle.

The last chapter is a manual on how to reproduce the Delft Head Loss & Limit Deposit Velocity model.

The DHLLDV Framework is based on numerous experimental data from literature, considered to be the reality.

This book is supported by the website www.dhlldv.com containing many additional graphs and tables with experimental data. The website also has spreadsheets and software implementing the model.

The name Delft in the title of the DHLLDV Framework is chosen because most of the modelling is carried out at the Delft University of Technology and in my home in Delft.

Another book by the author is: The Delft Sand, Clay & Rock Cutting Model
Available on   https://textbooks.open.tudelft.nl/index.php/textbooks

Modeling is an attempt to approach nature without having the presumption to be nature.

This book is dedicated to our wives

Thuy K.T. Miedema
and
Jennifer L. Ramsdell

For their loving support and patience

About the Author

Dr.ir. Sape A. Miedema (November 8th 1955) obtained his M.Sc. degree in Mechanical Engineering with honors at the Delft University of Technology (DUT) in 1983. He obtained his Ph.D. degree on research into the basics of soil cutting in relation with ship motions, in 1987. From 1987 to 1992 he was Assistant Professor at the chair of Dredging Technology. In 1992 and 1993 he was a member of the management board of Mechanical Engineering & Marine Technology of the DUT. In 1992 he became Associate Professor at the DUT with the chair of Dredging Technology. From 1996 to 2001 he was appointed Head of Studies of Mechanical Engineering and Marine Technology at the DUT, but still remaining Associate Professor of Dredging Engineering. In 2005 he was appointed Head of Studies of the MSc program of Offshore & Dredging Engineering and he is also still Associate Professor of Dredging Engineering. In 2013 he was also appointed as Head of Studies of the MSc program Marine Technology of the DUT.

Dr.ir. S.A. Miedema teaches (or has taught) courses on soil mechanics and soil cutting, pumps and slurry transport, hopper sedimentation and erosion, mechatronics, applied thermodynamics related to energy, drive system design principles, mooring systems, hydromechanics and mathematics. He is (or has been) also teaching at Hohai University, Changzhou, China, at Cantho University, Cantho Vietnam, at Petrovietnam University, Baria, Vietnam and different dredging companies in the Netherlands and the USA.

His research focuses on the mathematical modeling of dredging systems like, cutter suction dredges, hopper dredges, clamshell dredges, backhoe dredges and trenchers. The fundamental part of the research focuses on the cutting processes of sand, clay and rock, sedimentation processes in Trailing Suction Hopper Dredges and the associated erosion processes. Lately the research focuses on hyperbaric rock cutting in relation with deep sea mining and on hydraulic transport of solids/liquid settling slurries.

About the Editor

Robert Ramsdell (23rd September 1964) obtained his BA degree in Mathematics at the University of California at Berkeley in 1985. Since 1989 he has worked for Great Lakes Dredge & Dock Company. Robert started as Field Engineer, eventually becoming a Project Engineer then Superintendent, working with Trailing Suction, Cutter Suction and Mechanical dredges on a variety of projects in the United States. From 1995 to 1996 Robert was the Project Engineer on the Øresund Link project in Denmark. In 1996 he joined the Great Lakes Dredge & Dock Production Department as a Production Engineer, becoming Production Engineering Manager in 2005.   In the department Robert's focus has been on developing methods and software for estimating dredge production, recruiting and training Engineers, and developing methods to analyze and improve dredge operations. A particular focus has been in modeling slurry transport for dredging estimating and production optimization.

Acknowledgements

Recommendations

In this book, the author's intention is to introduce the slurry transport in pipelines to the readers by describing the relevant phenomena both physically and mathematically through underlying theories and governing equations. It is a focused work presented by the author to the upcoming generation of researchers and practitioners, in particular. The special feature of the book is that in a chapter, a specific phenomenon is presented starting with a physical description followed by a derivation and ending with discussion and conclusions. All throughout the book, coherence in presentation is maintained.

As a concluding remark, this book can effectively be used as a guide on slurry transport in pipelines.

Professor Subhasish Dey, Indian Institute of Technology Kharagpur, India

Open Access

This book is intentionally published in Open Access with the purpose to distribute it world-wide. In this digital era publishing hard-copies has downsides. Usually it's expensive and new editions take years. Using Open Access creates the possibility of a fast world-wide distribution and the possibility to update the document regularly. This book is published on ResearchGate and the WEDA/CEDA websites, at www.dhlldv.com and others.

On ResearchGate also the publications (conference & journal), Excel Workbooks and Powerpoints are published.

If you have comments, additions or other remarks about this book, please send an email to: s.a.miedema@tudelft.nl.

Table of Contents

Chapter 1:   Introduction.

1.1   Introduction.

In dredging, the hydraulic transport of solids is one of the most important processes. Since the 50's many researchers have tried to create a physical mathematical model in order to predict the head losses in slurry transport. One can think of the models of Durand & Condolios (1952) & Durand (1953), Worster & Denny (1955), Newitt et al. (1955), Gibert (1960), Fuhrboter (1961), Jufin & Lopatin (1966), Zandi & Govatos (1967) & Zandi (1971), Turian & Yuan (1977), Doron et al. (1987) & Doron & Barnea (1993), Wilson et al. (1992) and Matousek (1997). Some models are based on phenomenological relations and thus result in semi empirical relations, other tried to create models based on physics, like the two and three layer models. It is however the question whether slurry transport can be modeled this way at all. Observations in our laboratory show a process which is often non-stationary with respect to time and space. Different physics occur depending on the line speed, particle diameter, concentration and pipe diameter. These physics are often named flow regimes; fixed bed, shearing bed, sliding bed, heterogeneous transport and (pseudo) homogeneous transport. It is also possible that more regimes occur at the same time, like, a fixed bed in the bottom layer with heterogeneous transport in the top layer. It is the observation of the author that researchers often focus on a detail and sub-optimize their model, which results in a model that can only be applied for the parameters used for their experiments.

1.2   Flow Regimes Literature.

Based on the specific gravity of particles with a magnitude of 2.65, Durand (1953) proposed to divide the flows of non-settling slurries in horizontal pipes into four flow regimes based on average particle size as follows:
1.   Homogeneous suspensions for particles smaller than 40 μm (mesh 325)
2.   Suspensions maintained by turbulence for particle sizes from 40 μm (mesh 325) to 0.15 mm (mesh 100)
3.   Suspension with saltation for particle sizes between 0.15 mm (mesh 100) and 1.5 mm (mesh 11)
4.   Saltation for particles greater than 1.5 mm (mesh 11)

Due to the interrelation between particle sizes and terminal and deposition velocities, the original classification proposed by Durand has been modified to four flow regimes based on the actual flow of particles and their size (Abulnaga, 2002).
1.   Flow with a stationary bed
2.   Flow with a moving bed and saltation (with or without suspension)
3.   Heterogeneous
  •   Heterogeneous mixture with saltation and rolling
  •   Heterogeneous mixture with all solids in suspension
4.   Pseudo homogeneous and/or homogeneous mixtures with all solids in suspension

The four regimes of flow can be represented by a plot of the hydraulic gradient versus the average speed of the mixture as in Figure 1.2-1. The 4 transitional velocities are defined as:
• V_1: velocity at or above which the bed in the lower half of the pipe is stationary. In the upper half of the pipe, some solids may move by saltation or suspension. Below V_1 there are no particles above the bed.
• V_2: velocity at or above which the mixture flows as an asymmetric mixture with the coarser particles forming a moving/saltating bed.
• V_3: velocity at or above which all particles move as an asymmetric suspension and below which the solids start to settle and form a moving bed.
• V_4: velocity at or above which all solids move as an almost symmetric suspension.

Wilson (1992) developed a model, which will be discussed in detail later, for the incipient motion of granular solids at V_2, the transition between a stationary bed and a sliding bed. He assumed a hydrostatic pressure exerted by the solids on the wall. Wilson also developed a model for heterogeneous transport with a V_{50}, where 50% of the solids are in a (moving/saltating) bed and 50% in suspension. This percentage is named the stratification ratio. The transitional velocity V_3 is extremely important because it is the speed at which the hydraulic gradient is at a minimum. Although there is evidence that solids start to settle at lower line speeds in complex mixtures, operators and engineers often refer to this transitional velocity as the speed of deposition or critical velocity. Figure 1.2-3 shows the 4 regimes and the velocity and concentration profiles. At very high line speeds the pressure drop will reach an equivalent liquid curve asymptotically. Whether or not this occurs at practical line speeds depends on the particle diameter, pipe diameter and the concentration. For large particle diameters and concentrations it may seem like the pressure drop reaches the water curve asymptotically, but at higher line speeds the pressure drop will increase again up to an equivalent liquid model. Whether or not this equivalent liquid model contains the mixture density instead of the water density, or some value in between is still the question.
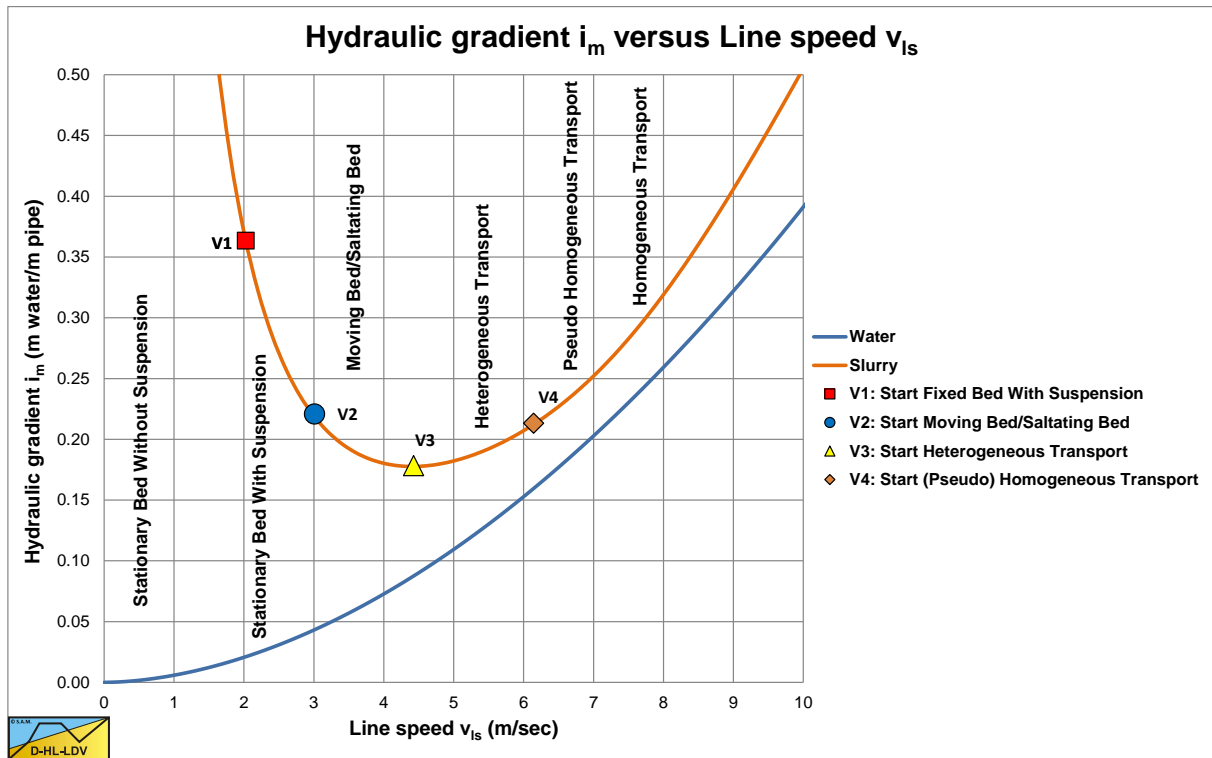
Figure 1.2-1: The 4 regimes and transitional velocities (Abulnaga, 2002), D_p=0.15 m, d_{50}=2 mm, C_{vt}=0.2.

Figure 1.2-1 gives the impression that the 4 flow regimes will always occur sequentially. Starting from a line speed zero and increasing the line speed, first the fixed or stationary bed will occur without suspension, at a line speed V_1 part of the bed starts to erode and particles will be in suspension, at a line speed V_2 the remaining bed will start to slide while the erosion increases with the line speed, at a line speed V_3 the whole bed is eroded and the heterogeneous regime starts and finally at a line speed V_4 the heterogeneous regime transits to the (pseudo) homogeneous regime. In reality not all the regimes have to occur, depending on the particle size, the pipe diameter and other governing parameters.
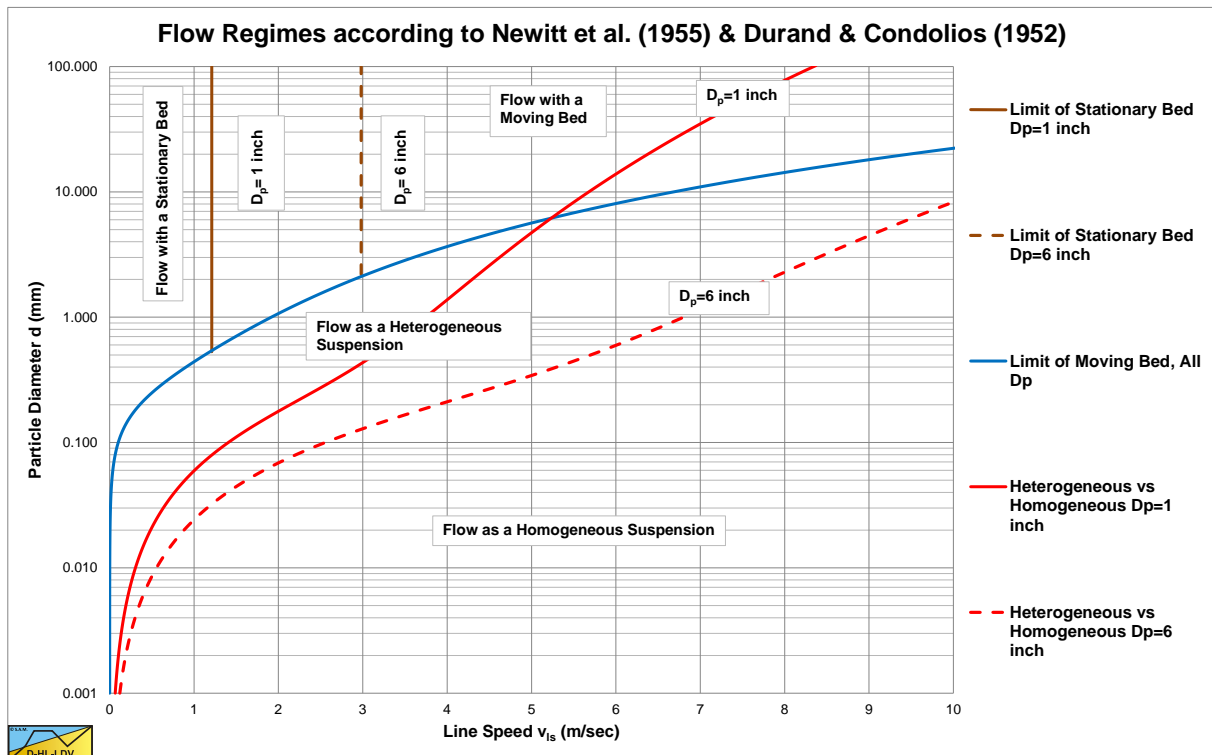
Figure 1.2-2: Flow regimes according to Newitt et al. (1955).

Figure 1.2-2 shows the regimes according to Newitt et al. (1955). From this figure it is clear that not all regimes have to occur and that the transition velocities depend on the particle and the pipe diameter. The influence of the volumetric concentration is not present in this graph. Figure 1.2-3 shows the flow regimes as used by Matousek (2004) also showing velocity and concentration distributions.
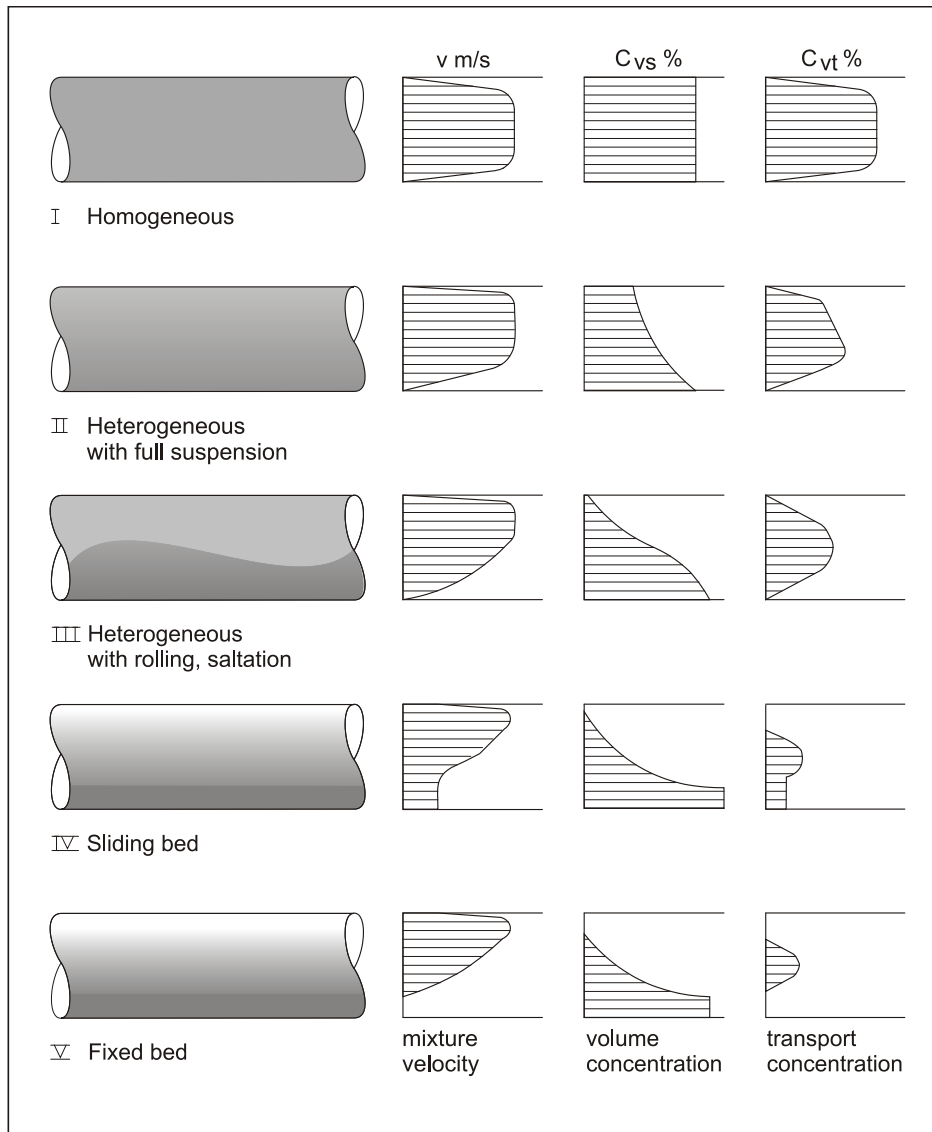
Figure 1.2-3: Different mixture transport regimes.

1.3 The Parable of Blind Men and an Elephant.

Wilson et al. (1992), (1997) and (2006) refer to the old parable of 6 blind men, who always wanted to know what an elephant looks like. Each man could touch a different part of the elephant, but only one part. So one man touched the tusk, others the legs, the belly, the tail, the ear and the trunk. The blind man who feels a leg says the elephant is like a pillar; the one who feels the tail says the elephant is like a rope; the one who feels the trunk says the elephant is like a tree branch; the one who feels the ear says the elephant is like a hand fan; the one who feels the belly says the elephant is like a wall; and the one who feels the tusk says the elephant is like a solid pipe. They then compare notes and learn they are in complete disagreement about what the elephant looks like. When a sighted man walks by and sees the entire elephant all at once, they also learn they are blind. The sighted man explains to them: All of you are right. The reason every one of you is telling a different story is because each one of you touched a different part of the elephant. So actually the elephant has all the features you mentioned.

The story of the blind men and an elephant originated in the Indian subcontinent from where it has widely diffused. It has been used to illustrate a range of truths and fallacies; broadly, the parable implies that one's subjective experience can be true, but that such experience is inherently limited by its failure to account for other truths or a totality of truth. At various times the parable has provided insight into the relativism, opaqueness or inexpressible

nature of truth, the behavior of experts in fields where there is a deficit or inaccessibility of information, the need for communication, and respect for different perspectives (source Wikipedia).
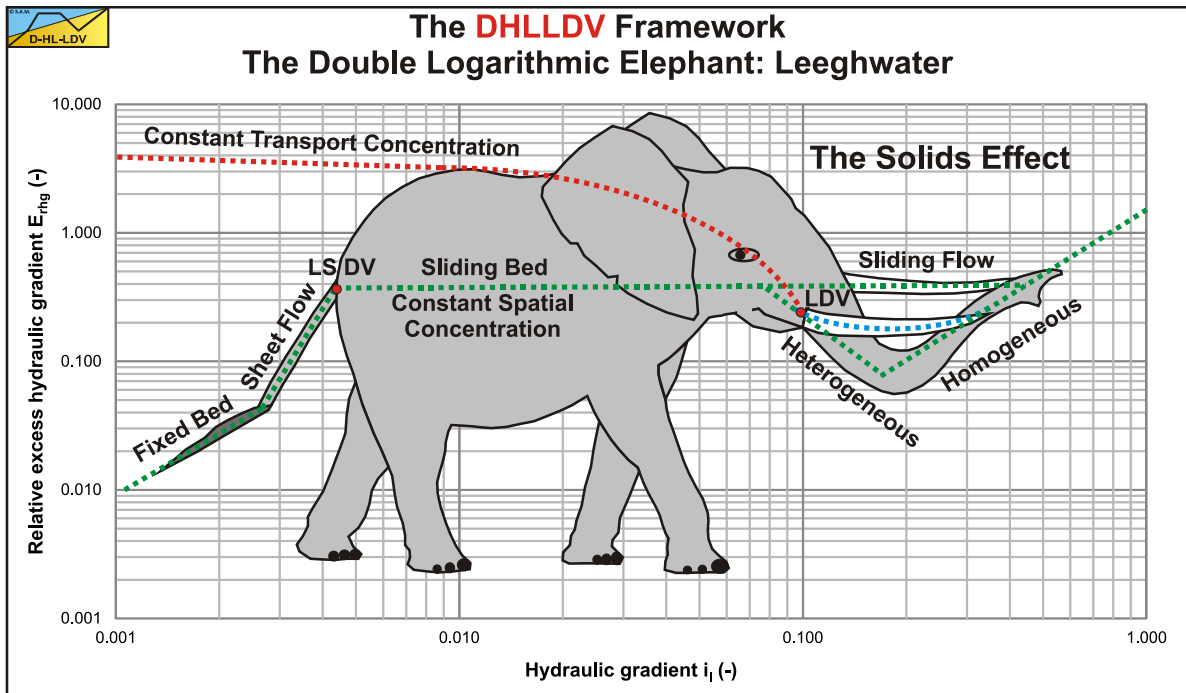
Figure 1.3-1: Flow regimes and the Double Logarithmic Elephant "Leeghwater".

Figure 1.3-1 shows a comparison between the parable of the elephant and slurry flow. Slurry transport also has many truths, points of view. Experiments can be carried out with small versus large pipes, small versus large particles, low versus high concentrations, low versus high line speeds, low versus high particle diameter versus pipe diameter ratios, laminar versus turbulent flow, Newtonian versus non Newtonian liquids, low versus high solid densities, etc. Depending on the parameters used, experiments are carried out in different flow regimes, or maybe at the interface between flow regimes, resulting in different conclusions.

Wilson et al. (1992), (1997) and (2006) show with this parable that the research of slurry flow often focusses on different parts or aspects of the process, but not many times it will give an overview of the whole process. The starting point is that every researcher tells the truth, based on his/her observations. Combining these truths gives an impression of the aggregated truth, which is still not the whole truth. The 6 men for example cannot look inside the elephant, only touch the outside. The internal structure of slurry flow may however be very important to understand the slurry flow behavior. The 6 men cannot access the memory of the elephant, which is supposed to be very good. In long pipelines the overall behavior of the slurry flow does depend on the history, so the memory function is also important. The Double Logarithmic Elephant is named after the student association of Mechanical Engineering of the Delft University of Technology, Leeghwater, using the elephant as their symbol. Leeghwater stands for strength, precision and of course hydraulic transport through the proboscis.

1.4 The Delft Head Loss & Limit Deposit Velocity Framework.

In the following chapters the different models from literature will be analyzed, leading to a new integrated model based on a new classification of the flow regimes. This new model is named the Delft Head Loss & Limit Deposit Velocity Framework (DHLLDV Framework). The Framework is integrated in a way that all flow regimes are described in a consistent way showing the transition velocities. The model is validated by many experiments from literature and experiments carried out in the Delft University Dredging Engineering Laboratory for particles ranging from 0.05 to 45 mm, pipe diameters ranging from 0.0254 to 0.9 m and relative submerged densities ranging from 0.24 to 4 ton/m^3. The model does not just give hydraulic gradient relations, but also Limit Deposit Velocity relations, slip ratio relations (the relation between the volumetric spatial concentration and the volumetric delivered concentration), bed height relations and a concentration distribution model. The Framework also gives a tool to determine the influence of the grading of the sand or gravel. The starting point of the model is a uniform sand or gravel and a constant volumetric spatial concentration. Based on the hydraulic gradient and slip ratio relations, the volumetric delivered concentration hydraulic gradient relations are derived. The latter is very important for practical applications.

Introduction.

1.5 Approach of this book.

The book covers horizontal transport of settling slurries (Newtonian slurries). Pipelines under an angle with the horizontal and non-settling (non-Newtonian) slurries are not covered.

The book has the following approach:
1. Chapter 1 explains the context of slurry flow, based on flow regimes as identified in literature.
2. Chapter 2 gives definitions of the dimensionless numbers and other important parameters as used in the book. Definitions are the language of engineers and scientists and are thus essential for the understanding.
3. Chapter 3 deals with homogeneous Newtonian liquid flow through horizontal circular pipes. Equations and graphs are given to determine the Darcy Weisbach friction factor. The Swamee Jain (1976) equation for the Darcy Weisbach (Moody (1944)) friction factor is used in this book. Also the influence of the concentration of very fine particles on the liquid properties is discussed.
4. Chapter 4 explains the terminal settling velocity of particles, including hindered settling. In the theory derived, the Zanke (1977) equation for the settling velocity is used and the Richardson & Zaki (1954) approach for hindered settling is applied.
5. Chapter 5 shows the basics of the initiation of motion of particles and shells, which is important to understand the behavior of the interface between a bed and the liquid flow above the bed, especially for the stationary and sliding bed regimes. Initiation of motion is the start of sediment motion, but at higher flow velocities also erosion and/or sediment transport will occur. The basics of sediment transport as bed load and suspended load are discussed for open channel flow and pipe flow.
6. Chapter 6 gives an overview of the historical developments of models to predict head losses in slurry flow. The overview starts with the early history, followed by empirical and semi empirical models. The models are given, analyzed and discussed and issues of the models are addressed. The models for the Limit Deposit Velocity (LDV) are discussed, analyzed and compared. Conclusions are drawn regarding the behavior of the LDV related to the solids, liquid and flow parameters. A number of 2 layer models (2LM) and 3 layer models (3LM) based on physics are given and analyzed, as well as other physical models.
7. Chapter 7 describes the new Delft Head Loss & Limit Deposit Velocity (DHLLDV) Framework. The DHLLDV Framework is based on uniform sands or gravels and constant spatial volumetric concentration. This chapter starts with an overview of 8 flow regimes and 6 scenarios. The new models for the main flow regimes, the stationary bed regime without sheet flow and with sheet flow, the sliding bed regime, the heterogeneous regime, the homogeneous regime and the sliding flow regime, are derived and discussed. A new model for the Limit Deposit Velocity is derived, consisting of 5 particle size regions and a lower limit. Based on the LDV a method is shown to construct slip velocity or slip ratio curves from zero line speed to the LDV and above. Based on the slip ratio, the constant delivered volumetric concentration curves can be constructed. Knowing the slip ratio, the bed height for line speeds below the LDV can be determined. New equations are derived for this. The transition from the heterogeneous regime to the homogeneous regime requires special attention. First of all, this transition line speed gives a good indication of the operational line speed and allows to compare the DHLLDV Framework with many models from literature. Secondly the transition is not sharp, but depends on 3 velocities. The line speed where a particle still fits in the viscous sub layer, the transition line speed heterogeneous-homogeneous and the line speed where the lift force on a particle equals the submerged weight of the particle. Finally the grading of the Particle Size Distribution (PSD) is discussed. A method is given to construct resulting head loss, slip velocity and bed height curves for graded sands and gravels.
8. Chapter 8 summarizes the DHLLDV Framework. The essential equations are given, with reference to the original equations, to reproduce the DHLLDV Framework, accompanied with flow charts.
9. In chapter 9 the DHLLDV Framework is compared with other models from literature.
10. Chapter 10 shows how to apply the DHLLDV Framework on the hydraulic transport of a cutter suction dredge.
11. Chapter 11 gives the journal and conference publications of the authors on which this book is based.

The DHLLDV Framework models have been verified and validated with numerous experimental data.

The results of experiments and calculations are shown in standard graphs showing **Hydraulic Gradient** versus **Line Speed i(v_{ls})**, the **Relative Excess Hydraulic Gradient** versus the **Line Speed $E_{rhg}(v_{ls})$** and the **Relative Excess Hydraulic Gradient** versus the **Liquid Hydraulic Gradient** (the clean water resistance) $E_{rhg}(i_l)$. The advantage of the $E_{rhg}(i_l)$ graph is that this type of graph is almost independent of the values of the spatial concentration C_{vs} and relative submerged density R_{sd}. The advantage of the $i_m(v_{ls})$ graph is that is clearly shows head losses versus flow and thus gives an indication of the required power and specific energy, combined with pump graphs. Most experimental data is shown in the **Relative Excess Hydraulic Gradient** versus the **Liquid Hydraulic Gradient** graph, $E_{rhg}(i_l)$.

1.6   Nomenclature.

C_v	Volumetric concentration	-
C_{vs}	Volumetric spatial concentration	-
C_{vt}	Volumetric transport/delivered concentration	-
d	Particle/grain diameter	m
d_{50}	50% passing particle diameter	m
D_p	Pipe diameter	m
E_{rhg}	Relative Excess Hydraulic Gradient	-
i, i_l, i_w	Hydraulic gradient liquid	m.w.c./m
i_m	Hydraulic gradient mixture	m.w.c./m
LSDV	Limit of Stationary Deposit Velocity	m/s
LDV	Limit Deposit Velocity	m/s
m.w.c.	Meters water column, pressure expressed in m.w.c.(10 m.w.c.=100 kPa=1 bar)	m
R_{sd}	Relative submerged density	-
v	Line speed	m/s
v_{ls}	Line speed	m/s
V_1	Transition fixed bed without suspension – fixed bed with suspension	m/s
V_2	Transition fixed bed with suspension – sliding bed with suspension	m/s
V_3	Transition sliding bed with suspension – heterogeneous transport	m/s
V_4	Transition heterogeneous transport – (pseudo) homogeneous transport	m/s
V_{50}	Velocity with 50% stratification according to Wilson	m/s

The default equations (used in the DHLLDV Framework) have a green frame.

Chapter 2:   Dimensionless Numbers & Other Parameters.

A number of dimensionless numbers and other important parameters are be used in this book. This short chapter gives an overview of these dimensionless numbers and parameters.

2.1   Definitions.

2.1.1 The Friction Velocity or Shear Velocity u∗.

The term *friction velocity* comes from the fact that $\sqrt{(\tau_{12}/\rho_l)}$ has the same unit as velocity and it has something to do with the friction force. The bottom shear stress τ_{12} is often represented by friction velocity u_*, defined by:

$$u_* = \sqrt{\frac{\tau_{12}}{\rho_l}} = \sqrt{\frac{\lambda_l}{8}} \cdot v_{ls} \qquad (2.1\text{-}1)$$

2.1.2 The Thickness of the Viscous Sub Layer δv.

Very close to the pipe wall the flow is laminar in the so called viscous sub layer. The thickness of the viscous sub layer is:

$$\delta_v = 11.6 \cdot \frac{v_l}{u_*}$$

$$\qquad (2.1\text{-}2)$$

$$\delta_v^+ = \frac{\delta_v \cdot u_*}{v_l} = 11.6$$

2.2   Dimensionless Numbers.

2.2.1   The Reynolds Number Re.

In fluid mechanics, the **Reynolds number** (**Re**) is a dimensionless number that gives a measure of the ratio of inertial (resistant to change or motion) forces to viscous (heavy and gluey) forces and consequently quantifies the relative importance of these two types of forces for given flow conditions. (The term *inertial forces*, which characterize how much a particular liquid resists any change in motion, are not to be confused with inertial forces defined in the classical way.)
The concept was introduced by George Gabriel Stokes in 1851 but the Reynolds number is named after Osborne Reynolds (1842–1912), who popularized its use in 1883.
Reynolds numbers frequently arise when performing dimensional analysis of liquid dynamics problems, and as such can be used to determine dynamic similitude between different experimental cases.
They are also used to characterize different flow regimes, such as laminar or turbulent flow: laminar flow occurs at low Reynolds numbers, where viscous forces are dominant, and is characterized by smooth, constant liquid motion; turbulent flow occurs at high Reynolds numbers and is dominated by inertial forces, which tend to produce chaotic eddies, vortices and other flow instabilities.

The gradient of the velocity dv/dx is proportional to the velocity v divided by a characteristic length scale L. Similarly, the second derivative of the velocity d^2v/dx^2 is proportional to the velocity v divided by the square of the characteristic length scale L.

$$Re = \frac{\text{Inertial forces}}{\text{Viscous forces}} = \frac{\rho_l \cdot v \cdot \dfrac{dv}{dx}}{\rho_l \cdot v_l \cdot \dfrac{d^2v}{dx^2}} \quad \text{with:} \frac{dv}{dx} \propto \frac{v}{L} \quad \frac{d^2v}{dx^2} \propto \frac{v}{L^2} \quad \Rightarrow \frac{v \cdot L}{v_l} \qquad (2.2\text{-}1)$$

The Reynolds number is a dimensionless number. High values of the parameter (on the order of 10 million) indicate that viscous forces are small and the flow is essentially inviscid. The Euler equations can then be used to model the flow. Low values of the parameter (on the order of 1 hundred) indicate that viscous forces must be considered.

2.2.2   The Froude Number Fr.

The **Froude number (Fr)** is a dimensionless number defined as the ratio of a characteristic velocity to a gravitational wave velocity. It may equivalently be defined as the ratio of a body's inertia to gravitational forces. In fluid mechanics, the **Froude number** is used to determine the resistance of a partially submerged object moving through water, and permits the comparison of objects of different sizes. Named after William Froude (1810-1879), the Froude number is based on the **speed–length ratio** as defined by him.

$$\mathbf{Fr = \frac{Characteristic\ velocity}{Gravitational\ wave\ velocity} = \frac{v}{\sqrt{g \cdot L}}} \tag{2.2-2}$$

Or the ratio between the inertial force and the gravitational force squared according to:

$$\mathbf{\widehat{Fr} = \frac{Inertial\ force}{Gravitational\ force} = \frac{\rho_l \cdot v \cdot \dfrac{dv}{dx}}{\rho_l \cdot g} = \frac{v^2}{g \cdot L}} \tag{2.2-3}$$

The gradient of the velocity **dv/dx** is proportional to the velocity **v** divided by a length scale **L**.

Or the ratio between the centripetal force on an object and the gravitational force, giving the square of the right hand term of equation (2.2-2):

$$\mathbf{\widehat{Fr} = \frac{Centripetal\ force}{Gravitational\ force} = \frac{m \cdot v^2 / L}{m \cdot g} = \frac{v^2}{g \cdot L}} \tag{2.2-4}$$

2.2.3   The Richardson Number Ri.

The Richardson number **Ri** is named after Lewis Fry Richardson (1881-1953). It is the dimensionless number that expresses the ratio of the buoyancy term to the flow gradient term.

$$\mathbf{Ri = \frac{buoyancy\ term}{flow\ gradient\ term} = \left(\frac{g \cdot L \cdot R_{sd}}{v^2} \right)} \tag{2.2-5}$$

The Richardson number, or one of several variants, is of practical importance in weather forecasting and in investigating density and turbidity currents in oceans, lakes and reservoirs.

2.2.4 The Archimedes Number Ar.

The **Archimedes number (Ar)** (not to be confused with Archimedes constant, π), named after the ancient Greek scientist Archimedes is used to determine the motion of liquids due to density differences. It is a dimensionless number defined as the ratio of gravitational forces to viscous forces. When analyzing potentially mixed convection of a liquid, the Archimedes number parameterizes the relative strength of free and forced convection. When Ar >> 1 natural convection dominates, i.e. less dense bodies rise and denser bodies sink, and when **Ar << 1** forced convection dominates.

$$\mathbf{Ar = \frac{Gravitational\ forces}{Viscous\ forces} = \frac{g \cdot L^3 \cdot R_{sd}}{v_l^2}} \tag{2.2-6}$$

The Archimedes number is related to both the Richardson number and the Reynolds number via:

$$Ar = Ri \cdot Re^2 = \left(\frac{g \cdot L \cdot R_{sd}}{v^2} \right) \cdot \left(\frac{v \cdot L}{\nu_l} \right)^2 = \frac{g \cdot L^3 \cdot R_{sd}}{\nu_l^2} \qquad (2.2-7)$$

2.2.5 The Thủy Number Th or Collision Intensity Number.

The new **Thủy number (Th)** is the cube root of the ratio of the viscous forces times the gravitational forces to the inertial forces squared. Thủy is Vietnamese for aquatic, water**.** The gradient of the velocity **v** is proportional to the velocity **v** divided by a length scale **L**. Since slurry transport is complex and inertial forces, viscous forces and gravitational forces play a role, this dimensionless number takes all of these forces into account in one dimensionless number.

$$\widehat{Th} = \frac{\text{Viscous forces}}{\text{Inertial forces}} \cdot \frac{\text{Gravitational forces}}{\text{Inertial forces}} = \frac{1}{Re \cdot \widehat{Fr}} = \frac{\rho_l \cdot \nu_l \cdot \frac{d^2 v}{dx^2}}{\rho_l \cdot v \cdot \frac{dv}{dx}} \cdot \frac{\rho_l \cdot g}{\rho_l \cdot v \cdot \frac{dv}{dx}} = \frac{\nu_l \cdot g}{v^3} \qquad (2.2-8)$$

So:

$$Th = \left(\frac{\nu_l \cdot g}{v^3} \right)^{1/3} \qquad (2.2-9)$$

It is interesting that the length scale does not play a role anymore in this dimensionless number. The different terms compensate for the length scale. The value of this dimensionless parameter is, that the relative excess head losses are proportional with the Thủy number to a certain power. Also the Limit Deposit Velocity in heterogeneous transport has proportionality with this dimensionless number.

2.2.6 The Cát Number Ct or Collision Impact Number.

A special particle Froude number will be introduced here. The Durand & Condolios (1952) particle Froude number **Cát, Ct**, which is Vietnamese for sand grains. This dimensionless number describes the contribution of the solids to the excess head losses.

$$Ct = \left(\frac{v_t}{\sqrt{g \cdot d}} \right)^{5/3} = \left(\frac{1}{\sqrt{C_x}} \right)^{5/3} \qquad (2.2-10)$$

The introduction of this particle Froude number is very convenient in many equations.

2.2.7 The Lắng Number La or Sedimentation Capability Number.

Another new dimensionless number is introduced here. It is the **Lắng** number **La. Lắng** is Vietnamese for sediment and this number represents the capability of the slurry flow to form a bed, either fixed or sliding.

$$La = \frac{v_t \cdot \left(1 - C_{vs} / \kappa_C \right)^\beta}{v_{ls}} \qquad (2.2-11)$$

2.2.8 The Shields Parameter θ.

The Shields parameter, named after Albert Frank Shields (1908-1974), also called the Shields criterion or Shields number, is a non-dimensional number used to calculate the initiation of motion of sediment in a fluid flow. It is a non dimensionalisation of a shear stress. By multiplying both the nominator and denominator by d^2, one can see that it is proportional to the ratio of fluid force on the particle to the submerged weight of the particle.

$$\theta = \frac{F_{shear}}{F_{gravity}} \propto \frac{\rho_l \cdot u_*^2 \cdot d^2}{\rho_l \cdot R_{sd} \cdot g \cdot d^3} = \frac{u_*^2}{R_{sd} \cdot g \cdot d} \tag{2.2-12}$$

The Shields parameter gives an indication of the erodibility of a sediment. If the Shields parameter is below some critical value there will not be erosion, if it's above this critical value there will be erosion. The higher the Shields parameter, the bigger the erosion. The critical Shields parameter depends on the particle diameter, the kinematic viscosity and some other parameters. The boundary Reynolds number as used in Shields graphs.

$$Re_* = \frac{u_* \cdot d}{\nu_l} \tag{2.2-13}$$

The roughness Reynolds number.

$$k_s^+ = \frac{u_* \cdot k_s}{\nu_l} \tag{2.2-14}$$

The distance to the wall Reynolds number:

$$y^+ = \frac{u_* \cdot y}{\nu_l} \tag{2.2-15}$$

2.2.9 The Bonneville Parameter D∗.

The original Shields graph is not convenient to use, because both axes contain the shear velocity u_* and this is usually an unknown, this makes the graph an implicit graph. To make the graph explicit, the graph has to be transformed to another axis system. In literature often the dimensionless grain diameter D_* is used, also called the Bonneville (1963) parameter:

$$D_* = d \cdot \sqrt[3]{\frac{R_{sd} \cdot g}{\nu_l^2}} \tag{2.2-16}$$

The relation between the Shields parameter and the Bonneville parameter is:

$$Re_* = \sqrt{\theta} \cdot D_*^{1.5} \tag{2.2-17}$$

So the Bonneville parameter is a function of the Shields number and the boundary Reynolds number according to:

$$D_* = \left(\frac{Re_*}{\sqrt{\theta}}\right)^{2/3} \tag{2.2-18}$$

2.2.10 The Rouse Number P.

The Rouse number, named after Hunter Rouse (1906-1996), is a non-dimensional number used to define a concentration profile of suspended sediment in sediment transport.

$$P = \frac{v_t}{\kappa \cdot u_*} \quad \text{or} \quad P = \frac{v_t}{\beta \cdot \kappa \cdot u_*} \tag{2.2-19}$$

The factor β is sometimes included to correlate eddy viscosity to eddy diffusivity and is generally taken to be equal to 1 and is therefore usually ignored. The von Karman constant κ is about 0.4.

The value of the Rouse number is an indication of the type of sediment transport and the bed form.

Table 2.2-1: Some interpretations of the value of the Rouse number.

P≥7.5	Little movement.
7.5≥P≥2.5	Bed load (grains rolling and hopping along the bed, bed forms like dunes) to suspension in the lower part.
2.5≥P≥0.8	Incipient suspension (grains spending less and less time in contact with the bed, bed forms increase in wavelength and decrease in amplitude). For P=2.5 there is suspension in the lower part of the channel or pipe, For P=0.8 the suspension reaches the surface.
0.8≥P	Suspension (grains spend very little time in contact with the bed, a plane bed). For P=0.1 the suspension is well developed, for P=0.01 the suspension is homogeneous.

2.2.11 The Stokes Number Stk.

The Stokes number Stk, named after George Gabriel Stokes (1819-1903), is a dimensionless number corresponding to the behavior of particles suspended in a fluid flow. The Stokes number is defined as the ratio of the characteristic time of a particle to a characteristic time of the flow or of an obstacle:

$$\mathbf{Stk} = \frac{\mathbf{t_0 \cdot u_0}}{\mathbf{l_0}} \tag{2.2-20}$$

Where $\mathbf{t_0}$ is the relaxation time of the particle (the time constant in the exponential decay of the particle settling velocity due to drag), $\mathbf{u_0}$ is the velocity of the fluid (liquid) of the flow well away from the particle and $\mathbf{l_0}$ is a characteristic dimension of the flow (typically the pipe diameter). In the case of Stokes flow, which is when the particle Reynolds number is low enough for the drag coefficient to be inversely proportional to the Reynolds number itself, the relaxation time can be defined as:

$$\mathbf{t_0} = \frac{\boldsymbol{\rho_s} \cdot \mathbf{d^2}}{\mathbf{18 \cdot \rho_l \cdot \nu_l}} \tag{2.2-21}$$

In experimental fluid dynamics, the Stokes number is a measure of flow fidelity in particle image velocimetry (PIV) experiments, where very small particles are entrained in turbulent flows and optically observed to determine the speed and direction of fluid movement. For acceptable tracing accuracy, the particle response time should be faster than the smallest time scale of the flow. Smaller Stokes numbers represent better tracing accuracy. For Stk »1, particles will detach from a flow especially where the flow decelerates abruptly. For Stk«0.1, tracing accuracy errors are below 1%. The Stokes number also gives a good indication for small particles being capable of forming a homogeneous mixture with the liquid flow. Assuming, in the case of pipe flow, the line speed as the characteristic velocity $\mathbf{u_0}$ and half the pipe diameter as the characteristic dimension $\mathbf{l_0}$, this gives:

$$\mathbf{Stk} = \frac{\boldsymbol{\rho_s} \cdot \mathbf{d^2}}{\mathbf{18 \cdot \rho_l \cdot \nu_l}} \cdot \frac{\mathbf{2 \cdot v_{ls}}}{\mathbf{D_p}} \quad \text{or} \quad \mathbf{d} = \sqrt{\frac{\mathbf{Stk \cdot 9 \cdot \rho_l \cdot \nu_l \cdot D_p}}{\boldsymbol{\rho_s} \cdot \mathbf{v_{ls}}}} \tag{2.2-22}$$

2.2.12 The Bagnold Number Ba.

The Bagnold number (Ba) is the ratio of grain collision stresses to viscous fluid stresses in a granular flow with interstitial Newtonian fluid, first identified by Ralph Alger Bagnold. The Bagnold number is defined by:

$$\mathbf{Ba} = \frac{\rho_s \cdot d^2 \cdot \lambda^{1/2} \cdot \dot{\gamma}}{\mu_l} = \frac{\rho_s \cdot d^2 \cdot \lambda^{1/2} \cdot \dot{\gamma}}{\rho_l \cdot \nu_l} \quad \mathbf{with:}\ \dot{\gamma} = \frac{dv}{dr}$$

$$\mathbf{With:}\ \lambda = \frac{1}{\left(\left(\frac{C_{vb}}{C_{vs}}\right)^{1/3} - 1\right)} = \frac{1}{\left(\left(\frac{1}{C_{vr}}\right)^{1/3} - 1\right)} = \frac{C_{vr}^{1/3}}{1 - C_{vr}^{1/3}} \tag{2.2-23}$$

$$\mathbf{Boundary\ layer:}\ \dot{\gamma} = \frac{u_*^2}{\nu_l} \quad \Rightarrow \quad \mathbf{Ba} = \frac{\rho_s \cdot d^2 \cdot \lambda^{1/2} \cdot u_*^2}{\rho_l \cdot \nu_l^2}$$

Where C_{vs} is the solids fraction and C_{vb} is the maximum possible concentration, the bed concentration. In flows with small Bagnold numbers (**Ba < 40**), viscous fluid stresses dominate grain collision stresses, and the flow is said to be in the 'macro-viscous' regime. Grain collision stresses dominate at large Bagnold number (**Ba > 450**), which is known as the 'grain-inertia' regime. A transitional regime falls between these two values.

2.3 Applications of Dimensionless Numbers.

2.3.1 The Slurry Flow in the Pipe.

The Reynolds number of the slurry flow in the pipe is:

$$\mathbf{Re_{fl}} = \frac{v_{ls} \cdot D_p}{\nu_l} \tag{2.3-1}$$

The Froude number of the slurry flow in the pipe is:

$$\mathbf{Fr_{fl}} = \frac{v_{ls}}{\sqrt{g \cdot D_p}} \tag{2.3-2}$$

The Froude number is also used in fluid mechanics as:

$$\widehat{\mathbf{Fr}}_{fl} = \frac{v_{ls}^2}{g \cdot D_p} \tag{2.3-3}$$

Where each of the terms on the right has been squared. Here we will use the first definition, according to equation (2.3-2).

The Thủy number of the slurry flow in the pipe in terms of the line speed or the friction velocity is:

$$\mathbf{Th_{ls}} = \left(\frac{\nu_l \cdot g}{v_{ls}^3}\right)^{1/3} \quad \mathbf{or} \quad \mathbf{Th_{fv}} = \left(\frac{\nu_l \cdot g}{u_*^3}\right)^{1/3} \tag{2.3-4}$$

2.3.2 The Terminal Settling Velocity of a Particle.

The Reynolds number of the terminal settling velocity of a particle is:

$$\mathbf{Re_p} = \frac{\mathbf{v_t \cdot d}}{\mathbf{v_l}} \tag{2.3-5}$$

The Froude number of the terminal settling velocity of a particle is:

$$\mathbf{Fr_p} = \frac{\mathbf{v_t}}{\sqrt{\mathbf{g \cdot d}}} = \frac{\mathbf{1}}{\sqrt{\mathbf{C_x}}} \tag{2.3-6}$$

The Froude number is also used in fluid mechanics as:

$$\widehat{\mathbf{Fr}}_{\mathbf{p}} = \frac{\mathbf{v_t^2}}{\mathbf{g \cdot d}} \tag{2.3-7}$$

Where each of the terms on the right has been squared. Here we will use the first definition, according to equation (2.3-6).

The Archimedes number of a particle is:

$$\mathbf{Ar_p} = \frac{\mathbf{g \cdot d^3 \cdot R_{sd}}}{\mathbf{v_l}^2} \tag{2.3-8}$$

The Thủy number of a particle is:

$$\mathbf{Th_p} = \left(\frac{\mathbf{v_l \cdot g}}{\mathbf{v_t^3}} \right)^{1/3} \tag{2.3-9}$$

2.4 Other Important Parameters.

2.4.1 The Slip Velocity and the Slip Ratio.

The slip velocity $\mathbf{v_{sl}}$ is the difference between the velocity of the solids $\mathbf{v_s}$ and the velocity of the liquid $\mathbf{v_l}$ or the velocity of the mixture, the line speed $\mathbf{v_{ls}}$. For small volumetric concentrations the velocity of the liquid almost equals the line speed, but for higher volumetric concentrations there is a difference. It should also be noted that not all particles have the same velocity. Part of the solids may be in a stationary or sliding bed, while another part is suspended in the liquid above the bed. In this book the slip velocity is related to the line speed.

$$\mathbf{v_{sl}} = \mathbf{v_{ls}} - \mathbf{v_s} = \mathbf{v_{ls}} \cdot \left(1 - \frac{\mathbf{v_s}}{\mathbf{v_{ls}}} \right) \tag{2.4-1}$$

The slip ratio ξ is the ratio of the slip velocity $\mathbf{v_{sl}}$ to the line speed $\mathbf{v_{ls}}$. A slip ratio of 0 means that the particles have the same velocity as the liquid. A slip ratio of 1 means that the particles have a velocity of zero.

$$\xi = \frac{\mathbf{v_{sl}}}{\mathbf{v_{ls}}} \tag{2.4-2}$$

2.4.2 The Spatial and Delivered Volumetric Concentration.

The spatial volumetric concentration C_{vs} is the volume occupied by the solids V_s divided by the total mixture volume of a pipe segment V_m.

$$C_{vs} = \frac{V_s}{V_m} \tag{2.4-3}$$

The delivered or transport volumetric concentration C_{vt} is the volume flow of solids Q_s divided by the total mixture volume flow Q_m.

$$C_{vt} = \frac{Q_s}{Q_m} \tag{2.4-4}$$

For a certain control volume the volumetric transport concentration C_{vt} can be determined if the volumetric spatial concentration C_{vs} and the slip velocity v_{sl} are known, given a certain line speed v_{ls}.

$$C_{vt} = \left(1 - \frac{v_{sl}}{v_{ls}}\right) \cdot C_{vs} = (1 - \xi) \cdot C_{vs} \tag{2.4-5}$$

Likewise, for a certain control volume, the volumetric spatial concentration C_{vs} can be determined if the volumetric transport concentration C_{vt} and the slip velocity v_{sl} are known, given a certain line speed v_{ls}.

$$C_{vs} = \left(\frac{v_{ls}}{v_{ls} - v_{sl}}\right) \cdot C_{vt} = \left(\frac{1}{1-\xi}\right) \cdot C_{vt} \tag{2.4-6}$$

A special spatial volumetric concentration is the bed concentration. In soil mechanics the porosity is mostly used, in slurry transport the concentration. Porosities may vary from 40% for very dense sand to 50%. For very loose sand, resulting in bed concentrations C_{vb} of 50% for very loose sand to 60% for very dense sand.

2.4.3 Densities.

When transporting solids mixed with a liquid, the mixture density ρ_m can be determined from the solids density ρ_s and liquid density ρ_l if the spatial volumetric concentration C_{vs} of the solids is known, according to:

$$\rho_m = C_{vs} \cdot \rho_s + (1 - C_{vs}) \cdot \rho_l \tag{2.4-7}$$

If the mixture density ρ_m is known, the spatial volumetric concentration C_{vs} can be determined from the mixture density ρ_m, the solids density ρ_s and the liquid density ρ_l according to:

$$C_{vs} = \frac{\rho_m - \rho_l}{\rho_s - \rho_l} \tag{2.4-8}$$

The specific gravity is the ratio of a solids ρ_s or mixture ρ_m density to the water density, giving:

$$SG = \frac{\rho_s}{\rho_l} \text{ or } \frac{\rho_m}{\rho_l} \quad \text{often referred to as:} \quad S_s = \frac{\rho_s}{\rho_l} \quad \text{and} \quad S_m = \frac{\rho_m}{\rho_l} \tag{2.4-9}$$

The two main densities considered are the density of water and the density of quarts. The density of water is about 1000 kg/m^3 or 1 ton/m^3. The density of water depends on the salinity and the temperature and may vary between 958 kg/m^3 (sweet water at 100 degrees centigrade) and 1030 kg/m^3 (salt water at about 10 degrees centigrade). In this book often a value of 1025 kg/m^3 is used for salt water. The density of quarts (sand and gravel) is about 2650 kg/m^3 or 2.65 ton/m^3.

2.4.4 The Relative Submerged Density R_{sd}.

The relative submerged density R_{sd} is defined as:

$$R_{sd} = \frac{\rho_s - \rho_l}{\rho_l} \tag{2.4-10}$$

2.4.5 Viscosities.

The dynamic (shear) viscosity of a fluid expresses its resistance to shearing flows, where adjacent layers move parallel to each other with different speeds. It can be defined through the idealized situation known as a Couette flow, where a layer of fluid is trapped between two horizontal plates, one fixed and one moving horizontally at constant speed **u**. (The plates are assumed to be very large, so that one need not consider what happens near their edges.)

If the speed of the top plate is small enough, the fluid particles will move parallel to it, and their speed will vary linearly from zero at the bottom to **u** at the top. Each layer of fluid will move faster than the one just below it, and friction between them will give rise to a force resisting their relative motion. In particular, the fluid will apply on the top plate a force in the direction opposite to its motion, and an equal but opposite one to the bottom plate. An external force is therefore required in order to keep the top plate moving at constant speed.

The magnitude **F** of this force is found to be proportional to the speed **u** and the area **A** of each plate, and inversely proportional to their separation **y**:

$$F = \mu_l \cdot A \cdot \frac{u}{y} \tag{2.4-11}$$

The proportionality factor μ_l in this formula is the viscosity (specifically, the dynamic viscosity) of the fluid. The ratio **u/y** is called the rate of shear deformation or shear velocity, and is the derivative of the fluid speed in the direction perpendicular to the plates. Isaac Newton expressed the viscous forces by the differential equation

$$\tau = \mu_l \cdot \frac{\partial u}{\partial y} \tag{2.4-12}$$

Where $\tau = F/A$ and $\partial u/\partial y$ is the local shear velocity. This formula assumes that the flow is moving along parallel lines and the **y** axis, perpendicular to the flow, points in the direction of maximum shear velocity. This equation can be used where the velocity does not vary linearly with **y**, such as in fluid flowing through a pipe.

Use of the Greek letter mu (μ_l) for the dynamic stress viscosity is common among mechanical and chemical engineers, as well as physicists. However, the Greek letter eta (η_l) is also used by chemists, physicists, and the IUPAC.

The kinematic viscosity (also called "momentum diffusivity") is the ratio of the dynamic viscosity μ_l to the density of the fluid (here liquid) ρ_l. It is usually denoted by the Greek letter nu (ν_l).

$$\nu_l = \frac{\mu_l}{\rho_l} \quad \text{or} \quad \mu_l = \nu_l \cdot \rho_l \tag{2.4-13}$$

It is a convenient concept when analyzing the Reynolds number that expresses the ratio of the inertial forces to the viscous forces:

$$Re = \frac{\rho_l \cdot u \cdot L}{\mu_l} = \frac{u \cdot L}{\nu_l} \tag{2.4-14}$$

Where **L** is a typical length scale in the system.

The dimension of dynamic viscosity in SI units is Poiseuille (Pl) and in cgs units Poise (P) or **Pa·s** or **N·s/m²** or **kg/(m·s)**. For example, the dynamic viscosity of water at 20 degrees centigrade is **μ_l=0.0012 Pa·s.**
The dimension of kinematic viscosity in SI units is **m²/s** and in cgs units Stokes (**St**). Typically for water values in the range of **ν_l=0.000001 m²/s** and **ν_l=0.0000013 m²/s** are used.

The dynamic viscosity of water can be estimated by, with the temperature in centigrade:

$$\mu_l = \frac{0.10}{2.1482 \cdot \left((T-8.435) + \sqrt{8078.4 + (T-8.435)^2} \right) - 120} \tag{2.4-15}$$

The kinematic viscosity of the water is temperature dependent. If a temperature of 10° is used as a reference, then the viscosity increases by 27% at 0° and it decreases by 30% at 20° centigrade. For the kinematic viscosity the following equation is often used:

$$\nu_l = \frac{497 \cdot 10^{-6}}{(42.5 + T)^{1.5}} \tag{2.4-16}$$

Table 2.4-1: Dynamic and kinematic viscosity of water.

Temperature	Dynamic Viscosity	Kinematic Viscosity
T	μ_l	ν_l
(ºC)	(Pa·s, N·s/m²) x 10⁻³	(m²/s) x 10⁻⁶
0	1.787	1.787
5	1.519	1.519
10	1.307	1.307
20	1.002	1.004
30	0.798	0.801
40	0.653	0.658
50	0.547	0.553
60	0.467	0.475
70	0.404	0.413
80	0.355	0.365
90	0.315	0.326
100	0.282	0.290

2.4.6 The Particle Size Distribution (PSD).

Soils consist of a mixture of particles of different size, shape and mineralogy. Because the size of the particles obviously has a significant effect on the soil behavior, the grain size and grain size distribution are used to classify soils. The grain size distribution describes the relative proportions of particles of various sizes. The grain size is often visualized in a cumulative distribution graph which, for example, plots the percentage of particles finer than a given size as a function of size. The median grain size, d_{50}, is the size for which 50% of the particle mass consists of finer particles. Soil behavior, especially the hydraulic conductivity, tends to be dominated by the smaller particles; hence, the term "effective size", denoted by d_{10}, is defined as the size for which 10% of the particle mass consists of finer particles.

Sands and gravels that possess a wide range of particle sizes with a smooth distribution of particle sizes are called well graded soils. If the soil particles in a sample are predominantly in a relatively narrow range of sizes, the soil is called uniformly graded soil. If there are distinct gaps in the gradation curve, e.g., a mixture of gravel and fine sand, with no coarse sand, the soils may be called gap graded. Uniformly graded and gap graded soils are both considered to be poorly graded. There are many methods for measuring particle size distribution. The two traditional methods used in geotechnical engineering are sieve analysis and hydrometer analysis.

The size distribution of gravel and sand particles are typically measured using sieve analysis. The formal procedure is described in ASTM D6913-04(2009). A stack of sieves with accurately dimensioned holes between a mesh of wires is used to separate the particles into size bins. A known volume of dried soil, with clods broken down to individual particles, is put into the top of a stack of sieves arranged from coarse to fine. The stack of sieves is shaken for a standard period of time so that the particles are sorted into size bins. This method works reasonably well for particles in the sand and gravel size range. Fine particles tend to stick to each other, and hence the sieving process is not an effective method. If there are a lot of fines (silt and clay) present in the soil it may be necessary to run water through the sieves to wash the coarse particles and clods through.

A variety of sieve sizes are available. The boundary between sand and silt is arbitrary. According to the Unified Soil Classification System, a #4 sieve (4 openings per inch) having 4.75 mm opening size separates sand from gravel and a #200 sieve with an 0.075 mm opening separates sand from silt and clay. According to the British standard, 0.063 mm is the boundary between sand and silt, and 2 mm is the boundary between sand and gravel.

The classification of fine-grained soils, i.e., soils that are finer than sand, is determined primarily by their Atterberg limits, not by their grain size. If it is important to determine the grain size distribution of fine-grained soils, the hydrometer test may be performed. In the hydrometer tests, the soil particles are mixed with water and shaken to produce a dilute suspension in a glass cylinder, and then the cylinder is left to sit. A hydrometer is used to measure the density of the suspension as a function of time. Clay particles may take several hours to settle past the depth of measurement of the hydrometer. Sand particles may take less than a second. Stoke's law provides the theoretical basis to calculate the relationship between sedimentation velocity and particle size. ASTM provides the detailed procedures for performing the Hydrometer test.

Clay particles can be sufficiently small that they never settle because they are kept in suspension by Brownian motion, in which case they may be classified as colloids.

Table 2.4-2: Soil Classification (combined from different sources).

Type of Soil	Particle size (mm)
Clay	< 0.002
Fine Silt	0.002–0.006
Medium Silt	0.006-0.02
Coarse Silt	0.02-0.06
Very Fine Sand	0.06–0.10
Fine Sand	0.10–0.20
Medium Sand	0.20–0.60
Coarse Sand	0.60–1.00
Very Coarse Sand	1.00–2.00
Fine Gravel	2-6
Medium Gravel	6-20
Coarse Gravel	20-60
Cobbles	60-200
Boulders	>200
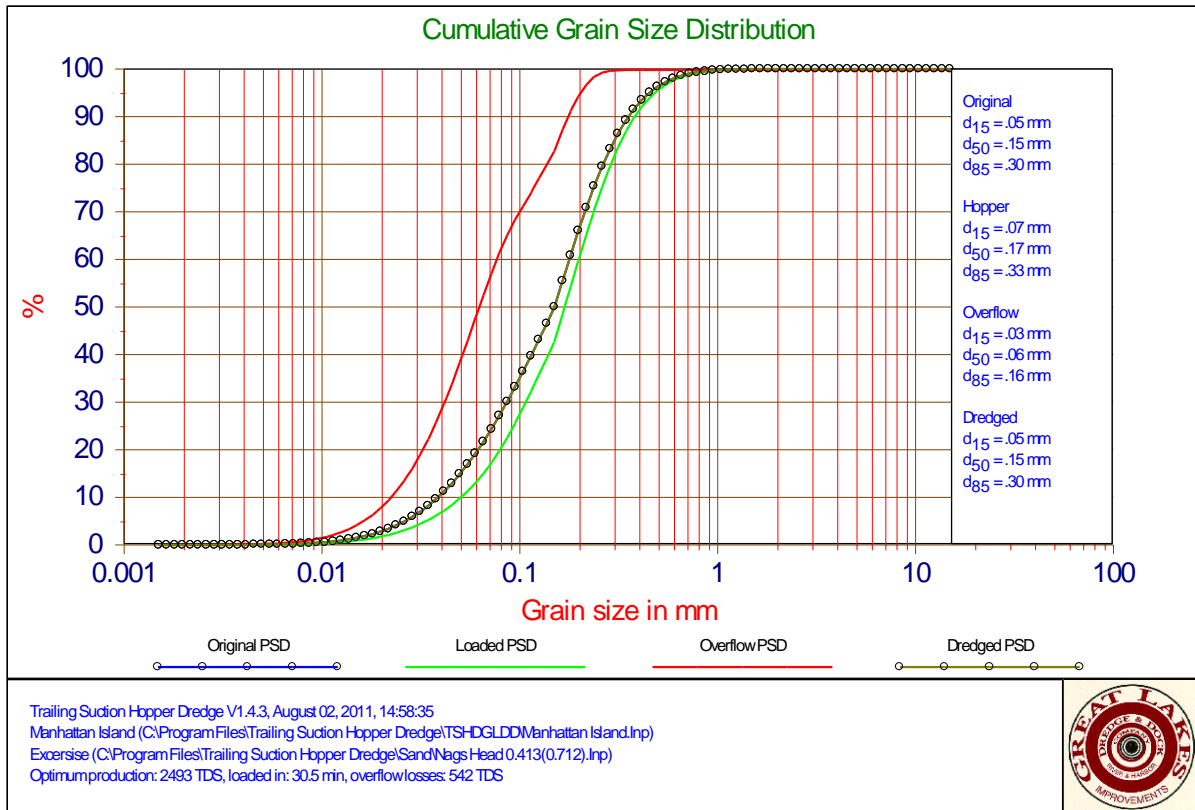
Figure 2.4-1: Some grain distributions of the loading process of a Trailing Suction Hopper Dredge.
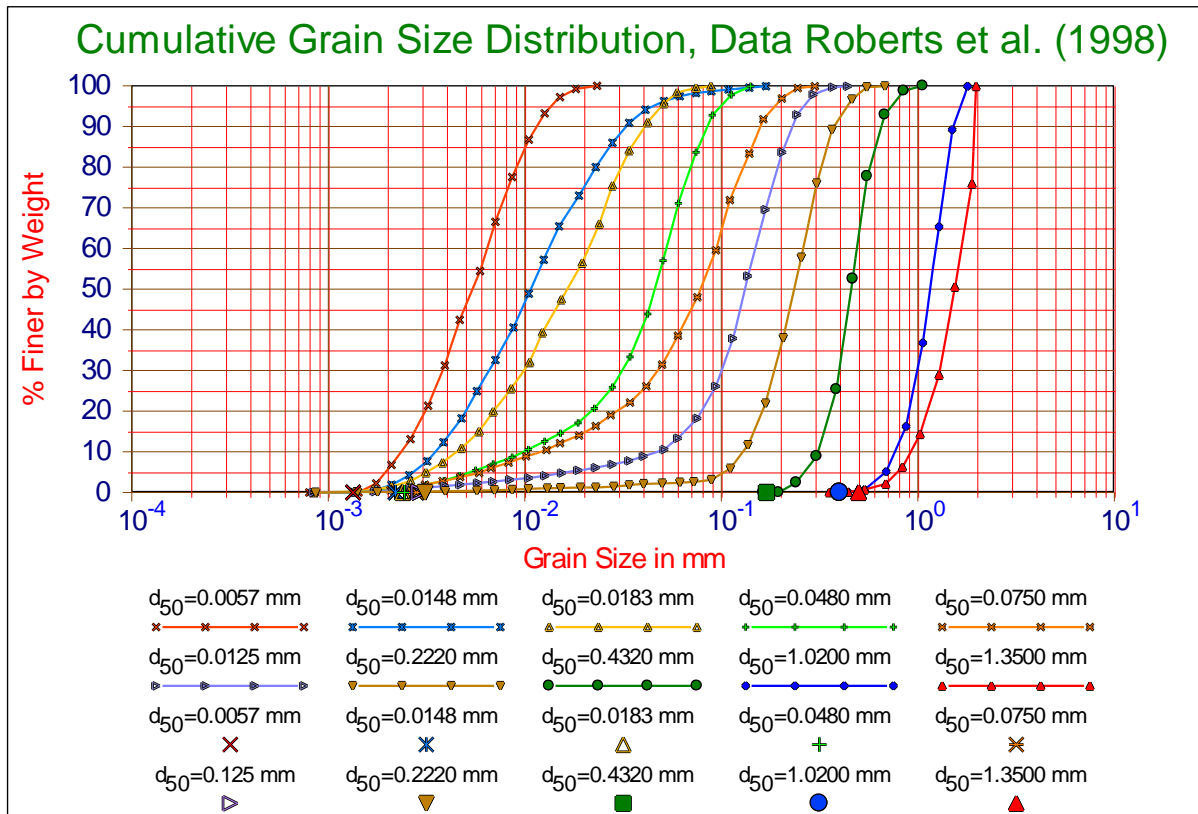
Figure 2.4-2: The particle size distributions of the sands used by Roberts et al. (1998).

Table 2.4-2 gives a classification of sands and gravels. Figure 2.4-1 shows the PSD's of the loading process of a Trailing Suction Hopper Dredger. Three curves are shown, the PSD of the dredged material, the PSD of the material settled in the hopper and the PSD of the material leaving the hopper through the overflow. Figure 2.4-2 shows a number of PSD's of the research of Roberts et al. (1998), investigating the influence of very fine particles on the initiation of motion (see Miedema (2013)). Table 15.3-1 shows commercial sieve mesh dimensions.

2.4.7 The Angle of Internal Friction.

Angle of internal friction for a given soil is the angle on the graph (Mohr's Circle) of the shear stress and normal effective stresses at which shear failure occurs. Angle of Internal Friction, **φ**, can be determined in the laboratory by the Direct Shear Test or the Triaxial Stress Test. Typical relationships for estimating the angle of internal friction, **φ**, are as follows:

Table 2.4-3: Empirical values for φ, of granular soils based on the standard penetration number, (from Bowels, *Foundation Analysis*).

SPT Penetration, N-Value (blows/ foot)	φ (degrees)
0	25 - 30
4	27 - 32
10	30 - 35
30	35 - 40
50	38 - 43

Table 2.4-4: Relationship between φ, and standard penetration number for sands, (from Peck 1974, *Foundation Engineering Handbook*).

SPT Penetration, N-Value (blows/ foot)	Density of Sand	φ (degrees)
<4	Very loose	<29
4 - 10	Loose	29 - 30
10 - 30	Medium	30 - 36
30 - 50	Dense	36 - 41
>50	Very dense	>41

Table 2.4-5: Relationship between φ, and standard penetration number for sands, (from Meyerhof 1956, *Foundation Engineering Handbook*).

SPT Penetration, N-Value (blows/ foot)	Density of Sand	φ (degrees)
<4	Very loose	<30
4 - 10	Loose	30 - 35
10 - 30	Medium	35 - 40
30 - 50	Dense	40 - 45
>50	Very dense	>45

The angle of internal friction is very important when considering a stationary or sliding bed and sheet flow. Since the bed in a pipeline is formed by sedimentation and usually does not have a long history, the bed density or concentration will be relatively low, resulting in very loose to loose sands or gravels. An angle of internal friction of 30º-35º may be expected, resulting in an internal friction coefficient of 0.577-0.700. Of course there may always be exceptions.

Figure 2.4-3 shows the angle of repose of granular materials, which basically is the smallest internal friction angle of a granular material. It is clear from this figure that this angle increases with the particle diameter.
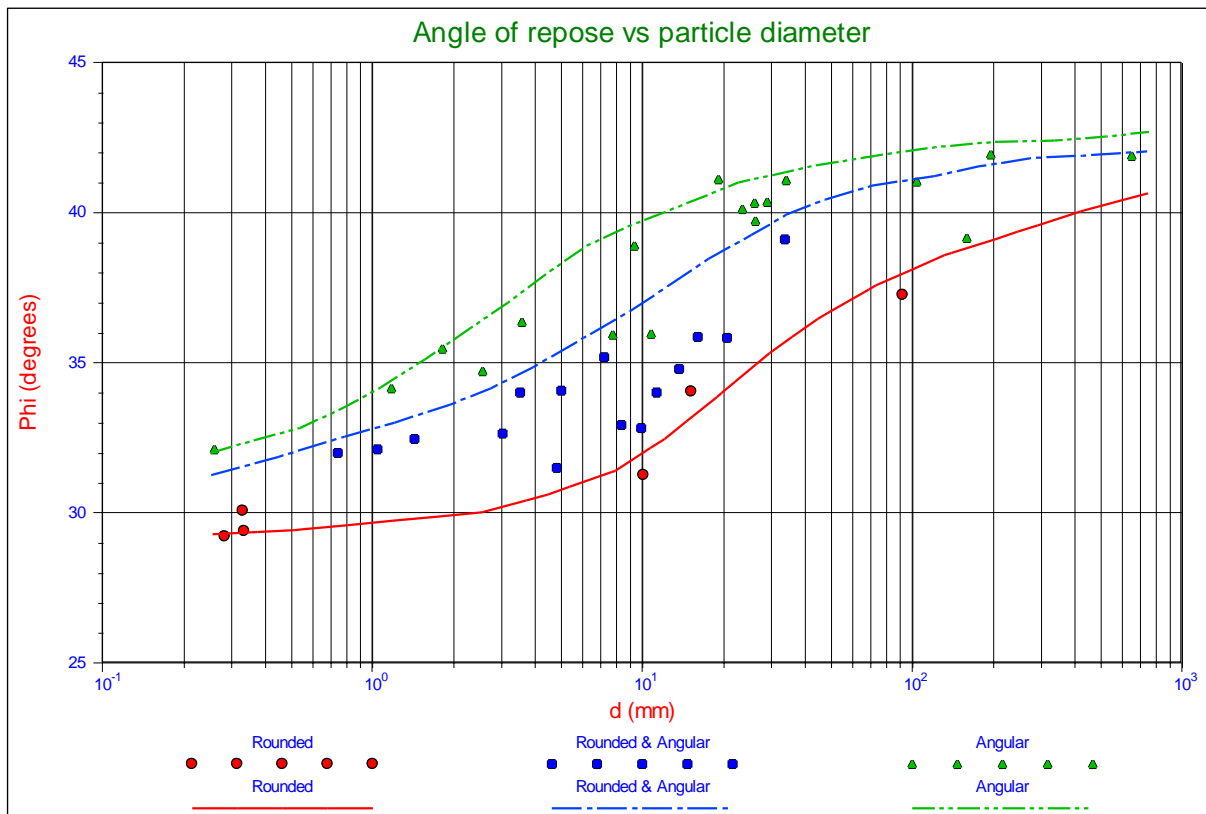
Figure 2.4-3: Angle of repose for granular materials (Simons, 1957).

2.4.8 The Angle of External Friction

The external friction angle, δ, or friction between a soil medium and a material such as the composition from a retaining wall or pile may be expressed in degrees as the following:

Table 2.4-6: External friction angle φ values.

20º	steel piles (NAVFAC)
$0.67 \cdot \varphi - 0.83 \cdot \varphi$	USACE
20º	steel (Broms)
$3/4 \cdot \varphi$	concrete (Broms)
$2/3 \cdot \varphi$	timber (Broms)
$0.67 \cdot \varphi$	Lindeburg
$2/3 \cdot \varphi$	for concrete walls (Coulomb)

The external friction angle can be estimated as **1/3·φ** for smooth retaining walls like sheet piles or concrete surfaces against timber formwork, or as **1/2·φ** to **2/3·φ** for rough surfaces. In the absence of detailed information the assumption of **2/3·φ** is commonly made.

The angle of external friction is very important when considering a stationary or sliding bed. Since the bed in a pipeline is formed by sedimentation and usually does not have a long history, the bed density or concentration will be relatively low, resulting in very loose to loose sands or gravels. An angle of external friction of 20º-24º may be expected, resulting in an external friction coefficient of 0.364-0.445. Of course there may always be exceptions.

Based on Figure 2.4-3 one may expect an increasing external friction angle/coefficient with increasing particle diameter.

2.5 Nomenclature.

	Dimensionless numbers	
Ar	Archimedes number	**-**
Ar$_p$	Archimedes number based on terminal settling velocity	**-**
Ba	Bagnold number	**-**
Ct	Cát number	**-**
D$_*$	The Bonneville parameter or dimensionless particle diameter	**-**
Fr	Froude number	**-**
$\widehat{\mathrm{Fr}}$	Froude number squared	**-**
Fr$_{fl}$	Froude number pipe flow	**-**
$\widehat{\mathrm{Fr}}_{fl}$	Froude number pipe flow squared	**-**
Fr$_p$	Froude number particle based on terminal settling velocity	**-**
$\widehat{\mathrm{Fr}}_p$	Froude number particle based on terminal settling velocity squared	**-**
La	Lắng number	**-**
P	Rouse number	**-**
Re	Reynolds number	**-**
Re$_p$	Particle Reynolds number based on terminal settling velocity	**-**
Re$_*$	Boundary Reynolds number	**-**
Re$_{fl}$	Reynolds number pipe flow	**-**
Ri	Richardson number	**-**
Stk	Stokes number	**-**
Th	Thủy number	**-**
$\widehat{\mathrm{Th}}$	Thủy number cubed	**-**
Th$_{ls}$	Thủy number based on line speed in pipe flow	**-**
Th$_{fv}$	Thủy number based on friction velocity in pipe flow	**-**
Th$_p$	Thủy number based on terminal settling velocity	**-**
θ	Shields parameter	**-**
	Symbols	
C$_{vs}$	Volumetric spatial concentration	**-**
C$_{vt}$	Volumetric transport (delivered) concentration	**-**
C$_{vr}$	Relative volumetric concentration	**-**
C$_{vb}$	Volumetric spatial concentration bed	**-**
C$_x$	Durand drag coefficient	**-**
d	Particle diameter	**m**
d$_{15}$	Particle diameter 15% passing	**m**
d$_{50}$	Particle diameter 50% passing	**m**
d$_{85}$	Particle diameter 85% passing	**m**
D$_p$	Pipe diameter	**m**
F	Force	**N**
F$_{shear}$	Shear force on bed	**N**
F$_{gravity}$	Submerged gravity force on a particle	**N**
g	Gravitational constant, 9.81 m/sec^2	**m/s^2**
k$_s$	The bed roughness (often a function of the particle diameter)	**m**
k$_s^+$	Roughness Reynolds number	**-**
l$_0$	Characteristic dimension of flow	**m**
L	Characteristic length of object or flow	**m**
m	Mass of particle	**kg**
Q$_m$	Volume flow mixture through pipe	**m^3/s**
Q$_s$	Volume flow solids through pipe	**m^3/s**
R$_{sd}$	Relative submerged density	**-**
r	Coordinate perpendicular to the velocity	**m**
SG	Specific gravity	**-**
S$_m$	Specific gravity solids	**-**
S$_m$	Specific gravity mixture	**-**
t$_0$	Relaxation time	**-**
T	Temperature	**C**

u	Velocity of fluid	**m/s**
u$_0$	Velocity of fluid	**m/s**
u$_*$	Friction velocity	**m/s**
v	Characteristic velocity of object	**m/s**
v$_{ls}$	Line speed	**m/s**
v$_{sl}$	Slip velocity	**m/s**
v$_t$	Terminal settling velocity	**m/s**
V$_m$	Volume pipe segment	**m^3**
V$_s$	Volume solids in pipe segment	**m^3**
x	Length direction	**m**
y	Distance to the wall	**m**
y$^+$	Distance to the wall Reynolds number	**-**
β	Hindered settling power (Richardson & Zaki)	**-**
β	Diffusivity factor	**-**
δ$_v$	Thickness of the viscous sub layer	**m**
δ$_v^+$	Dimensionless thickness of viscous sub layer	**-**
γ̇	Velocity gradient	**1/s**
κ	Von Karman constant (about 0.4)	**-**
κ$_C$	Concentration distribution coefficient	**-**
λ$_l$	Darcy-Weisbach friction factor	**-**
λ	Linear concentration according to Bagnold	**-**
τ$_{12}$	Bed shear stress	**kPa**
ν$_l$	Kinematic viscosity	**m^2/s**
ρ$_l$	Density of the liquid	**kg/m^3**
ρ$_s$	Density of solids	**kg/m^3**
ρ$_m$	Density of mixture	**kg/m^3**
ξ	Slip ratio	**-**
μ$_l$	Dynamic viscosity	**N·s/m^2**
η$_l$	Dynamic viscosity	**N·s/m^2**
φ	Angle of internal friction	**rad**
δ	Angle of external friction	**rad**

Chapter 3:   Pressure Losses with Homogeneous Liquid Flow.

3.1 Pipe Wall Shear Stress.

In general objects in a fluid flow experience a resistance proportional to the dynamic pressure of the fluid:

$$\frac{1}{2} \cdot \rho_l \cdot v_{ls}^2 \tag{3.1-1}$$

For an object in a fluid flow (like settling particles) the drag force on the object is the dynamic pressure times a characteristic cross section times a drag coefficient, giving:

$$F_{drag} = C_D \cdot \frac{1}{2} \cdot \rho_l \cdot v_{ls}^2 \cdot A_{obj} \tag{3.1-2}$$

The drag coefficient normally depends on the Reynolds number of the flow. Now with pipe flow, there is no flow around an object, but there is flow inside the pipe. The basic principles however remain the same, giving for the wall shear stress:

$$\tau_w = f \cdot \frac{1}{2} \cdot \rho_l \cdot v_{ls}^2 \tag{3.1-3}$$

The proportionality coefficient **f** is the so called Fanning friction factor, named after John Thomas Fanning (1837-1911). The friction force or drag force on a pipe with diameter D_p and length ΔL is now:

$$F_{drag} = \tau_w \cdot A_{pw} = f \cdot \frac{1}{2} \cdot \rho_l \cdot v_{ls}^2 \cdot \pi \cdot D_p \cdot \Delta L \tag{3.1-4}$$

The pressure difference over the pipe with diameter D_p and length **L** is the drag force divided by the pipe cross section A_p:

$$\Delta p_l = \frac{F_{drag}}{A_p} = \frac{f \cdot \frac{1}{2} \cdot \rho_l \cdot v_{ls}^2 \cdot \pi \cdot D_p \cdot \Delta L}{\frac{\pi}{4} \cdot D_p^2} = 2 \cdot f \cdot \frac{\Delta L}{D_p} \cdot \rho_l \cdot v_{ls}^2 \tag{3.1-5}$$

The notation using the Darcy friction factor also called the Darcy Weisbach friction factor or the Moody friction factor is more convenient here for using the dynamic pressure, giving:

$$\Delta p_l = \lambda_l \cdot \frac{\Delta L}{D_p} \cdot \frac{1}{2} \cdot \rho_l \cdot v_{ls}^2 \tag{3.1-6}$$

Note that the Darcy Weisbach friction factor is 4 times the Fanning friction factor. In terms of the shear stress this gives:

$$\tau_w = \frac{\lambda_l}{4} \cdot \frac{1}{2} \cdot \rho_l \cdot v_{ls}^2 = \frac{\lambda_l}{8} \cdot \rho_l \cdot v_{ls}^2 \tag{3.1-7}$$

The hydraulic gradient i_w (for water) or i_l (for a liquid in general) is:

$$\Delta p_l = \lambda_l \cdot \frac{\Delta L}{D_p} \cdot \frac{1}{2} \cdot \rho_l \cdot v_{ls}^2 \quad \text{and} \quad i_l = i_w = \frac{\Delta p_l}{\rho_l \cdot g \cdot \Delta L} = \frac{\lambda_l \cdot v_{ls}^2}{2 \cdot g \cdot D_p} \tag{3.1-8}$$

In this book the Darcy Weisbach friction factor is used.

3.2   The Darcy-Weisbach Friction Factor.

The value of the wall friction factor λ_l depends on the Reynolds number:

$$\mathbf{Re} = \frac{\mathbf{v_{ls} \cdot D_p}}{\mathbf{\nu_l}} = \frac{\mathbf{\rho_l \cdot v_{ls} \cdot D_p}}{\mathbf{\mu_l}} \tag{3.2-1}$$

For laminar flow (Re<2320) the value of λ_l can be determined according to Poiseuille:

$$\lambda_l = \frac{\mathbf{64}}{\mathbf{Re}} \tag{3.2-2}$$

For turbulent flow (Re>2320) the value of λ_l depends not only on the Reynolds number but also on the relative roughness of the pipe $\mathbf{\varepsilon/D_p}$, which is the absolute roughness $\mathbf{\varepsilon}$ divided by the pipe diameter $\mathbf{D_p}$. A general implicit equation for λ_l is the Colebrook-White (1937) equation:

$$\lambda_l = \frac{1}{\left(2 \cdot \log_{10} \left(\dfrac{2.51}{Re \cdot \sqrt{\lambda_l}} + \dfrac{0.27 \cdot \varepsilon}{D_p} \right) \right)^2} \tag{3.2-3}$$

For very smooth pipes the value of the relative roughness $\mathbf{\varepsilon/D_p}$ is almost zero, resulting in the Prandl & von Karman equation:

$$\lambda_l = \frac{1}{\left(2 \cdot \log_{10} \left(\dfrac{2.51}{Re \cdot \sqrt{\lambda_l}} \right) \right)^2} \tag{3.2-4}$$

At very high Reynolds numbers the value of $\mathbf{2.51/(Re \cdot \sqrt{\lambda_l})}$ is almost zero, resulting in the Nikuradse (1933) equation:

$$\lambda_l = \frac{1}{\left(2 \cdot \log_{10} \left(\dfrac{0.27 \cdot \varepsilon}{D_p} \right) \right)^2} = \frac{5.3}{\left(2 \cdot \ln \left(\dfrac{0.27 \cdot \varepsilon}{D_p} \right) \right)^2} \tag{3.2-5}$$

Because equations (3.2-3) and (3.2-4) are implicit, for smooth pipes approximation equations can be used. For a Reynolds number between 2320 and 10^5 the Blasius equation gives a good approximation:

$$\lambda_l = 0.3164 \cdot \left(\frac{1}{Re} \right)^{0.25} \tag{3.2-6}$$

For a Reynolds number in the range of 10^5 to 10^8 the Nikuradse (1933) equation gives a good approximation:

$$\lambda_l = 0.0032 + \frac{0.221}{Re^{0.237}} \tag{3.2-7}$$

Figure 3.2-1 gives the so called Moody (1944) diagram, in this case based on the Swamee Jain (1976) equation.
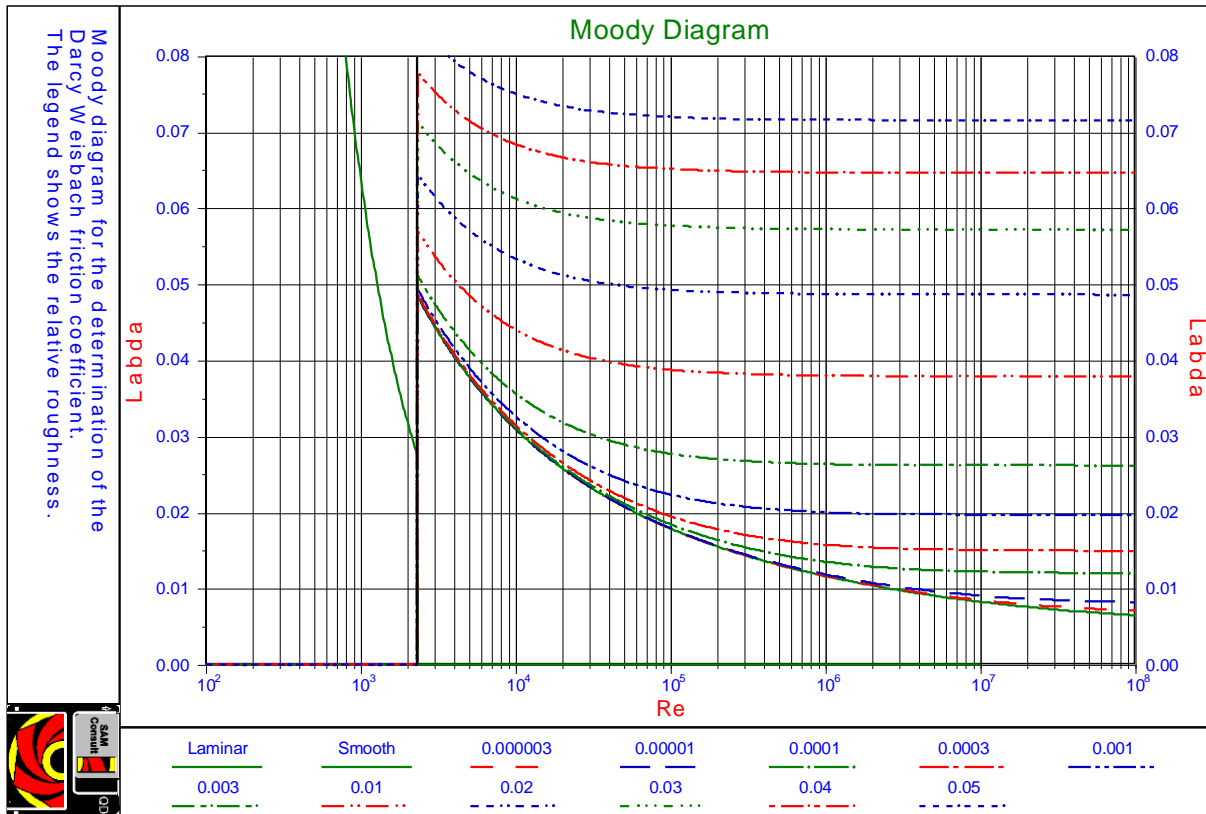
Figure 3.2-1: The Moody diagram determined with the Swamee Jain equation.

Over the whole range of Reynolds numbers above 2320 the Swamee Jain (1976) equation gives a good approximation:

$$\lambda_l = \frac{1.325}{\left(\ln\left(\dfrac{\varepsilon}{3.7 \cdot D_p} + \dfrac{5.75}{Re^{0.9}}\right)\right)^2} = \frac{0.25}{\left(\log_{10}\left(\dfrac{\varepsilon}{3.7 \cdot D_p} + \dfrac{5.75}{Re^{0.9}}\right)\right)^2} \qquad (3.2\text{-}8)$$

3.3 The Equivalent Liquid Model.

Assuming that the pressure losses in a pipe are proportional to the kinetic energy of the eddies and the kinetic energy of the eddies is proportional to the mixture density and the line speed and assuming that there are no losses due to sliding friction or collisions, the pressure losses can be determined by:

$$\Delta p_m = \lambda_l \cdot \frac{\Delta L}{D_p} \cdot \frac{1}{2} \cdot \rho_m \cdot v_{ls}^2 \qquad (3.3\text{-}1)$$

The hydraulic gradient i_m (for mixture) is now:

$$i_m = \frac{\Delta p_m}{\rho_l \cdot g \cdot \Delta L} = \frac{\rho_m}{\rho_l} \cdot \frac{\lambda_l \cdot v_{ls}^2}{2 \cdot g \cdot D_p} = \frac{\rho_m}{\rho_l} \cdot i_l \qquad (3.3\text{-}2)$$

The above assumptions are valid as long as the particles are small enough to be considered part of the eddies. So for larger particles this may not be true anymore.

3.4 Approximation of the Darcy-Weisbach Friction Factor.

It is obvious that the Darcy-Weisbach friction factor λ_l depends on the pipe diameter D_p and the line speed v_{ls}. This may be confused with a direct influence of the pipe diameter D_p and the line speed v_{ls}. So it is interesting to see how the Darcy-Weisbach friction factor λ_l depends on the pipe diameter D_p and the line speed v_{ls}. Figure 3.7-1 shows the Darcy-Weisbach friction factor for smooth pipes as a function of the line speed vls at a number of pipe diameters, while Figure 3.7-2 shows the Darcy-Weisbach friction factor as a function of the pipe diameter D_p at a number of line speeds. In both figures, the Darcy-Weisbach friction factor can be well approximated by a power function

$$\lambda_l = \alpha \cdot \left(v_{ls}\right)^{\alpha_1} \cdot \left(D_p\right)^{\alpha_2} \tag{3.4-1}$$

With:

$$\alpha = 0.01216 \quad \text{and} \quad \alpha_1 = -0.1537 \cdot \left(D_p\right)^{-0.089} \quad \text{and} \quad \alpha_2 = -0.2013 \cdot \left(v_{ls}\right)^{-0.088} \tag{3.4-2}$$

For laboratory conditions both powers are close to **-0.18**, while for real life conditions with higher line speeds and much larger pipe diameters this results in a power for the line speed of about α_1=**-0.155** and for the pipe diameter of about α_2=**-0.168**. This should be considered when analyzing the models for heterogeneous transport, where in real life these adjusted powers should be used.

3.5 The Friction Velocity or Shear Velocity u∗.

The term *friction velocity* comes from the fact that $\sqrt{(\tau_w/\rho_l)}$ has the same unit as velocity and it has something to do with the wall friction force. The wall shear stress τ_w is often represented by friction velocity u_*, defined by:

$$u_* = \sqrt{\frac{\tau_w}{\rho_l}} = \sqrt{\frac{\lambda_l}{8}} \cdot v_{ls} \tag{3.5-1}$$

3.6 The Thickness of the Viscous Sub Layer δv.

Very close to the pipe wall the flow is laminar in the so called viscous sub layer. The thickness of the viscous sub layer is defined as:

$$\delta_v = 11.6 \cdot \frac{v_l}{u_*} \tag{3.6-1}$$

3.7 The Smallest Eddies.

The ratio between the largest eddies and the smallest eddies in turbulent pipe flow is of the magnitude of the Reynolds number to the power of ¾. Assuming that the largest eddies are of the magnitude of the pipe diameter, then this gives for the diameter of the smallest eddies:

$$d_e = \frac{D_p}{Re^{3/4}} = \frac{D_p^{1/4} \cdot v_l^{3/4}}{v_{ls}^{3/4}} \tag{3.7-1}$$

Using the Blasius equation for the Darcy Weisbach friction factor, this gives for the ratio between the diameters of the smallest eddies to the thickness of the viscous sub layer:

$$\frac{d_e}{\delta_v} = 0.017 \cdot Re^{1/8} \tag{3.7-2}$$

For Reynolds numbers ranging from 100,000 for small pipe diameters to 10,000,000 for large pipe diameters this gives a ratio of 0.072 to 0.127, so about 10%.

Darcy-Weisbach friction factor λ vs. Line speed v_{ls}
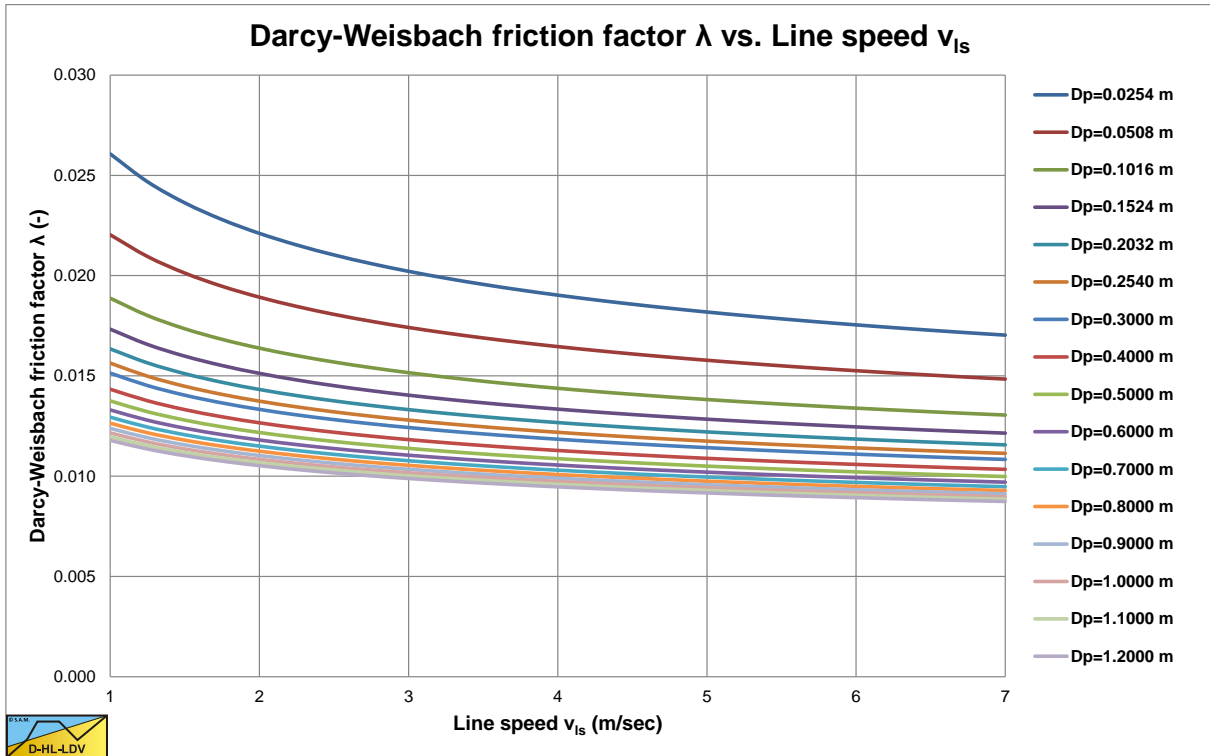
Figure 3.7-1: The Darcy-Weisbach friction factor λ_l for smooth pipes as a function of the line speed v_{ls}.

Darcy-Weisbach friction factor λ vs. Pipe diameter D_p
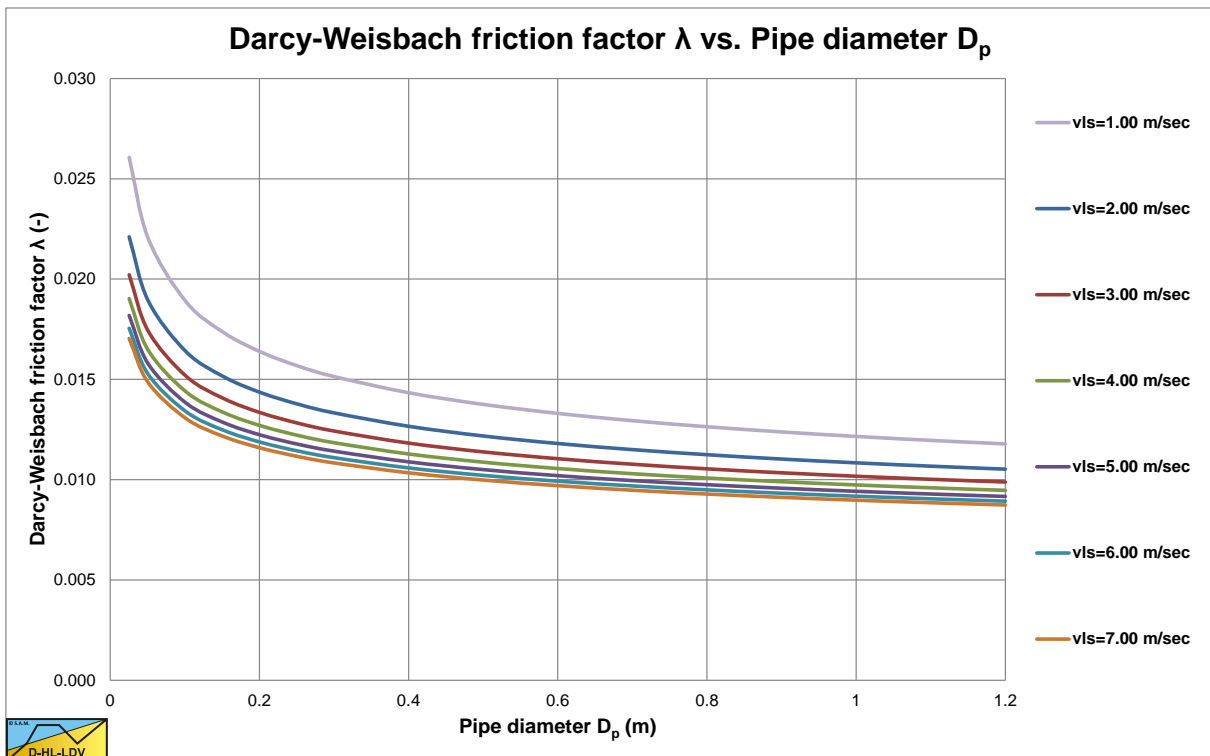
Figure 3.7-2: The Darcy-Weisbach friction factor λ_l for smooth pipes as a function of the pipe diameter D_p.

3.8 The Relative or Apparent Viscosity.

Einstein (1905) published an analysis for the viscosity of dilute suspensions. The result of this analysis is an equation giving the relation between the apparent dynamic viscosity and the volumetric concentration of the solids. The concentrations however are limited to low concentrations.

$$\mu_r = \frac{\mu_m}{\mu_l} = 1 + 2.5 \cdot C_{vs} \qquad \text{(3.8-1)}$$

Thomas (1965) collected data regarding the relative viscosity from 16 sources. The particle materials included polystyrene, rubber latex, glass and methyl methacrylate. The results are shown in Figure 3.8-1. In all studies, either the density of the suspending medium was adjusted or the viscosity of the suspending medium was sufficiently large that settling was unimportant. Examination of the experimental procedure used in these studies shows no basis for eliminating any of the data because of faulty technique; consequently, there must be at least one additional parameter that has not been accounted for. One parameter of importance is the absolute value of the particle diameter. For particles with diameters less than 1 to 10 microns, colloid-chemical forces become important causing non-Newtonian flow behavior. The result is a relative viscosity which increases as particle size is decreased, but which decreases to a limiting value as the shear rate is increased. For particles larger than 1 to 10 microns, the inertial effects due to the restoration of particle rotation after collision result in an additional energy dissipation and consequent increase in relative viscosity with increasing particle diameter.

In flow through capillary tubes, the increase in viscosity observed with large particle size suspensions is opposed by a decrease in viscosity caused by a tendency for particles to migrate toward the center of the tube as the particle diameter is increased. Examination of the data from which Figure 3.8-1 was prepared showed that in several cases the tests covered a sufficient range of shear rates or particle sizes that it was possible to extrapolate to conditions where particle size effects were negligible. For particles less than 1 micron diameter, the limiting value of the relative viscosity was obtained as the intercept of either a linear plot of **1/d** versus **μ_m/μ_l** or a linear plot of **1/(du/dr)** versus **μ_m/μ_l**. For particles larger than 1 to 10 microns, the limiting value of the relative viscosity was obtained as the intercept of a linear plot of **d** versus **μ_m/μ_l**. In the event that large particle size data were also available as a function of shear rate, the reduced particle size data were further corrected by plotting against **1/(du/ dr).** Treatment of the suitable data in this manner gave a unique curve for which the maximum deviation was reduced from three- to six fold over that shown in Figure 3.8-1, that is, to ± 7 % at **$C_{vs}=0.2$** and to ±13 % at **$C_{vs}=0.5$,** as is show in Figure 3.8-2.

Based on this Thomas (1965) derived an equation to determine the relative dynamic viscosity as a function of the concentration **C_{vs}** of the particles in the mixture.

$$\mu_r = \frac{\mu_m}{\mu_l} = 1 + 2.5 \cdot C_{vs} + 10.05 \cdot C_{vs}^2 + 0.00273 \cdot e^{16.6 \cdot C_{vs}} \quad \text{with: } \nu_m = \frac{\mu_m}{\rho_m} \Rightarrow \nu_r = \frac{\nu_m}{\nu_l} = \frac{\mu_m}{\mu_l} \cdot \frac{\rho_l}{\rho_m} \qquad \text{(3.8-2)}$$

The Thomas (1965) equation can be used for pseudo homogeneous flow of small particles.

Figure 3.8-2 shows that the first two terms are valid to a volumetric concentration of about 6%. Adding the 3rd term extends the validity to a volumetric concentration of about 25%. Adding the 4th term extends the validity to a volumetric concentration of 60%, which covers the whole range of concentrations important in dredging applications.

Figure 3.8-3 shows experiments of Boothroyde et al. (1979) with Markham fines (light solids, high concentration) without using the Thomas (1965) viscosity. Figure 3.8-4 shows these experiments using the Thomas (1965) viscosity.

Figure 3.8-5 shows experiments of Thomas (1976) with iron ore (very heavy solids with SG of 4.5-5.3, medium concentration) without using the Thomas (1965) viscosity. Figure 3.8-6 shows these experiments using the Thomas (1965) viscosity.

In both cases the data points are above the ELM curves if the normal liquid viscosity is used. Using the Thomas (1965) viscosity correction places the data points very close to the ELM curves. Applying the Thomas (1965) viscosity gives a good result for the fines, as long as they behave like a Newtonian fluid.
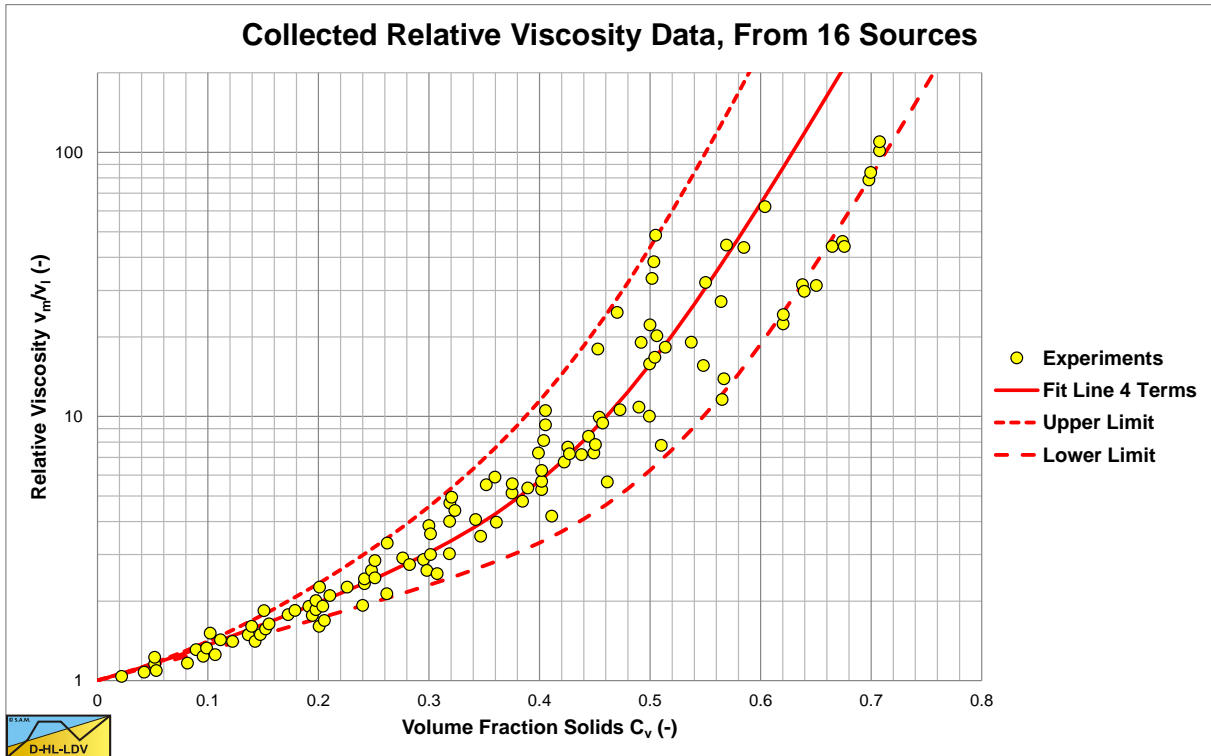
Figure 3.8-1: Collected relative viscosity data from 16 sources by Thomas (1965).
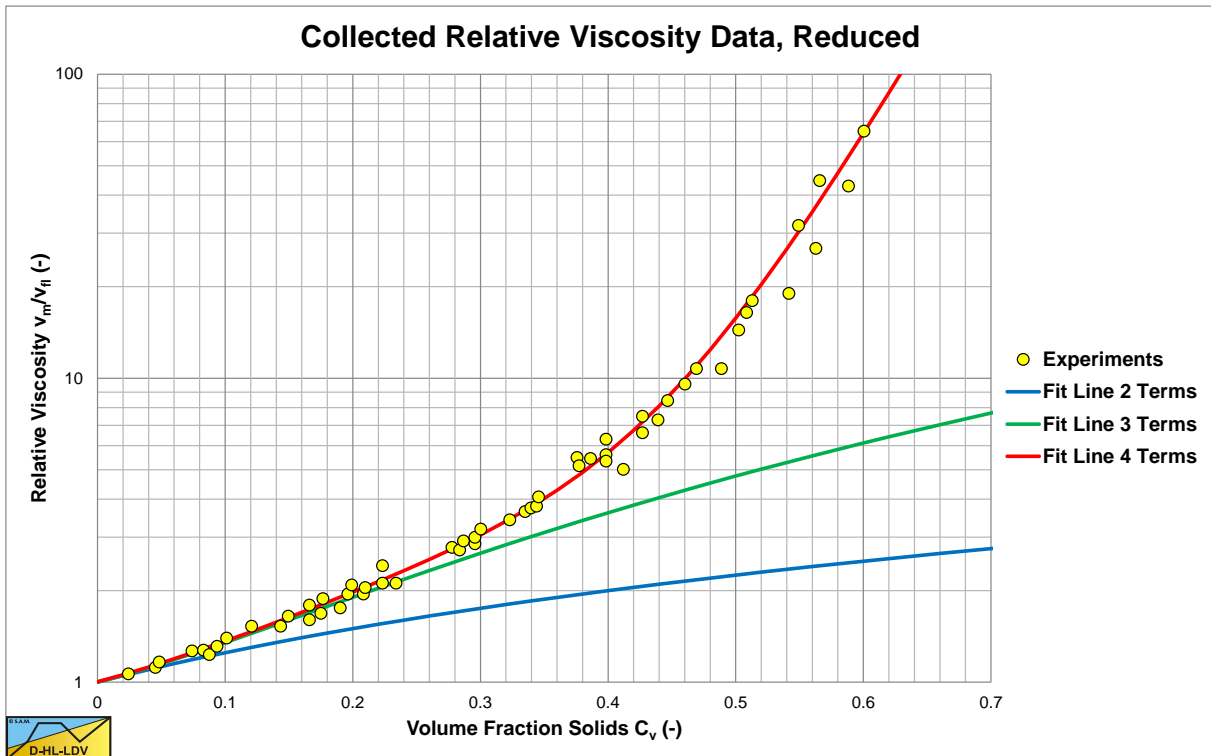
Figure 3.8-2: Collected relative viscosity data from 16 sources by Thomas (1965), reduced.

The limiting particle diameter for particles influencing the viscosity can be determined based on the Stokes number. A Stokes number of **Stk=0.03** gives a good first approximation. The velocity in the denominator can be replaced by **$7.5 \cdot D_p^{0.4}$** as a first estimate of the LDV near operational conditions.

$$d = \sqrt{\frac{Stk \cdot 9 \cdot \rho_l \cdot \nu_l \cdot D_p}{\rho_s \cdot v_{ls}}} \approx \sqrt{\frac{Stk \cdot 9 \cdot \rho_l \cdot \nu_l \cdot D_p}{\rho_s \cdot 7.5 \cdot D_p^{0.4}}} \tag{3.8-3}$$
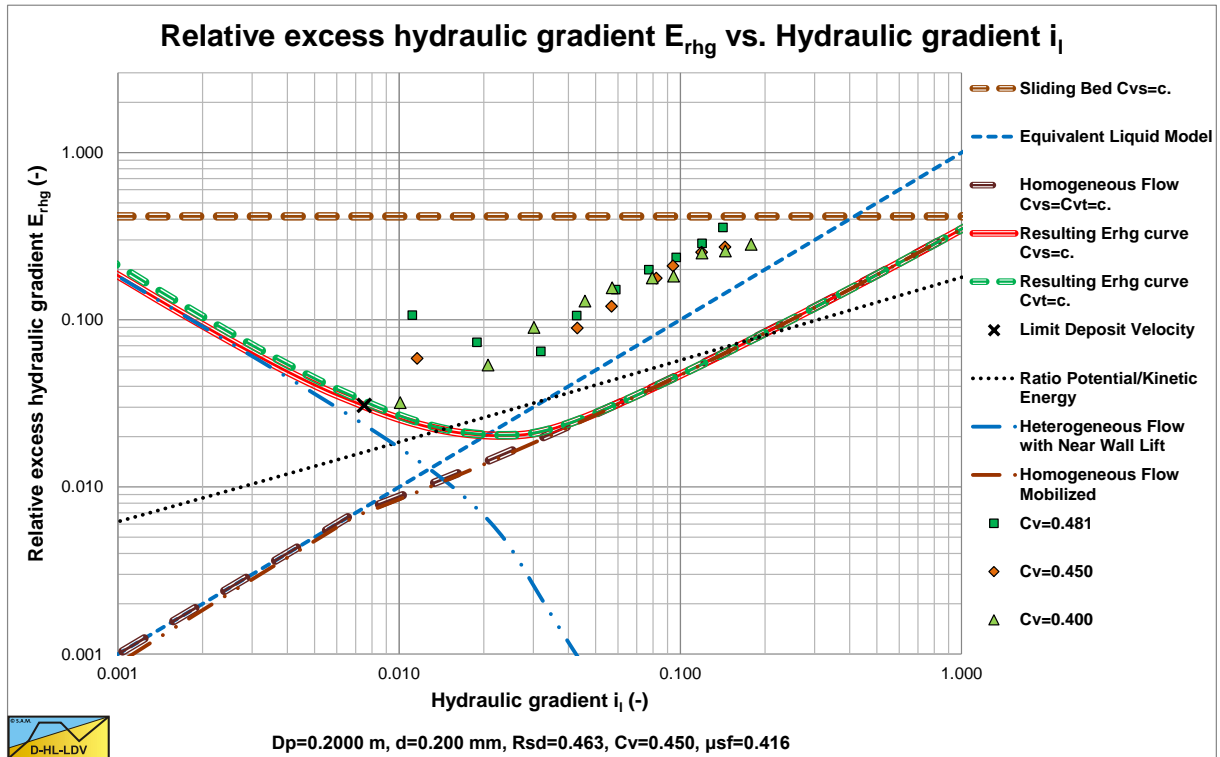
Figure 3.8-3: Markham fines Boothroyde et al. (1979), without Thomas (1965) viscosity.
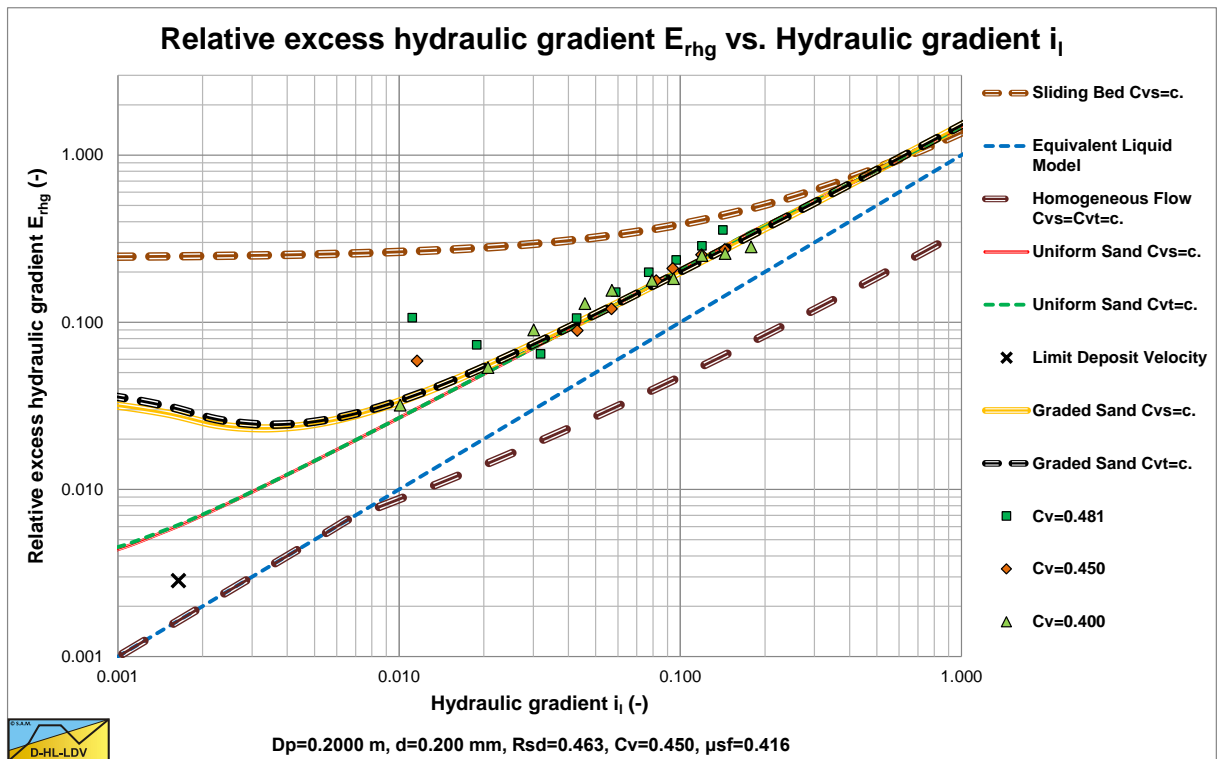
Figure 3.8-4: Markham fines Boothroyde et al. (1979), with Thomas (1965) viscosity.

Figure 3.8-3 shows experimental data versus the DHLLDV Framework for uniform particles with the pure liquid viscosity. The data do not match the curve, but are much higher. Figure 3.8-4. Shows the experimental data versus the DHLLDV Framework for graded particles according to Boothroyde et al. (1979) and full Thomas (1965) viscosity. Now the data match the curve for graded particles.
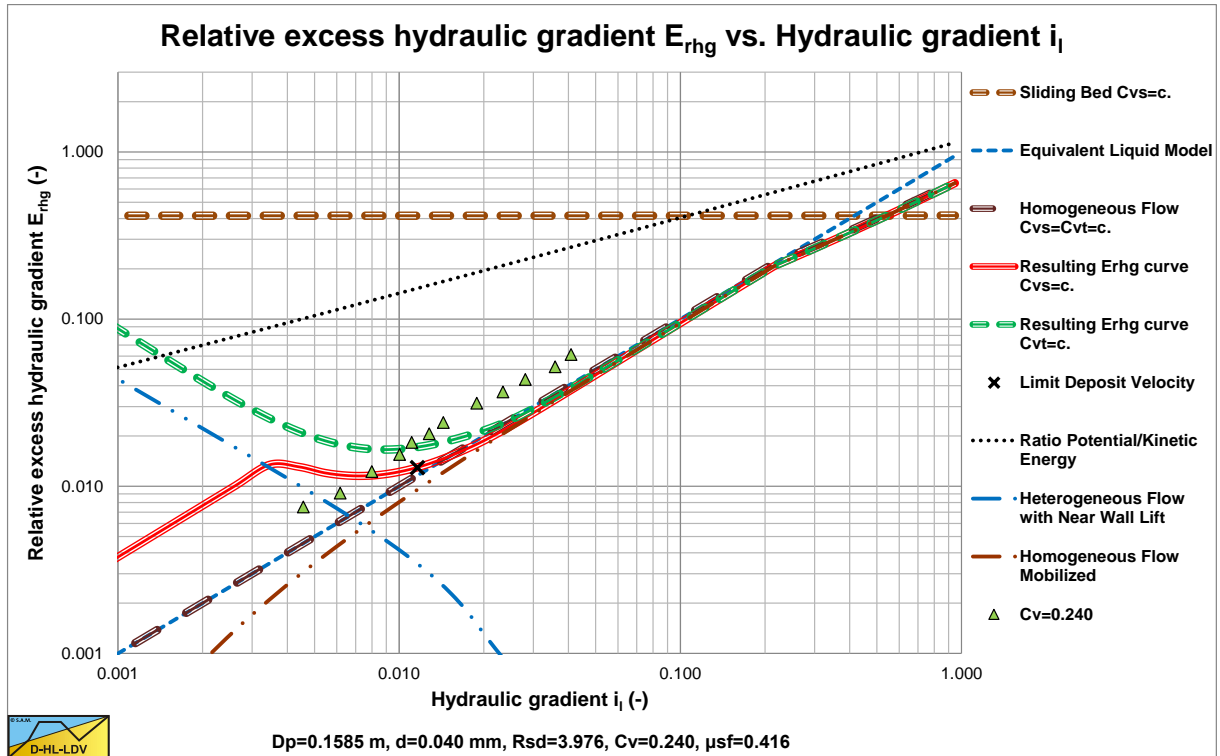
Figure 3.8-5: Iron ore Thomas (1976), without Thomas (1965) viscosity.
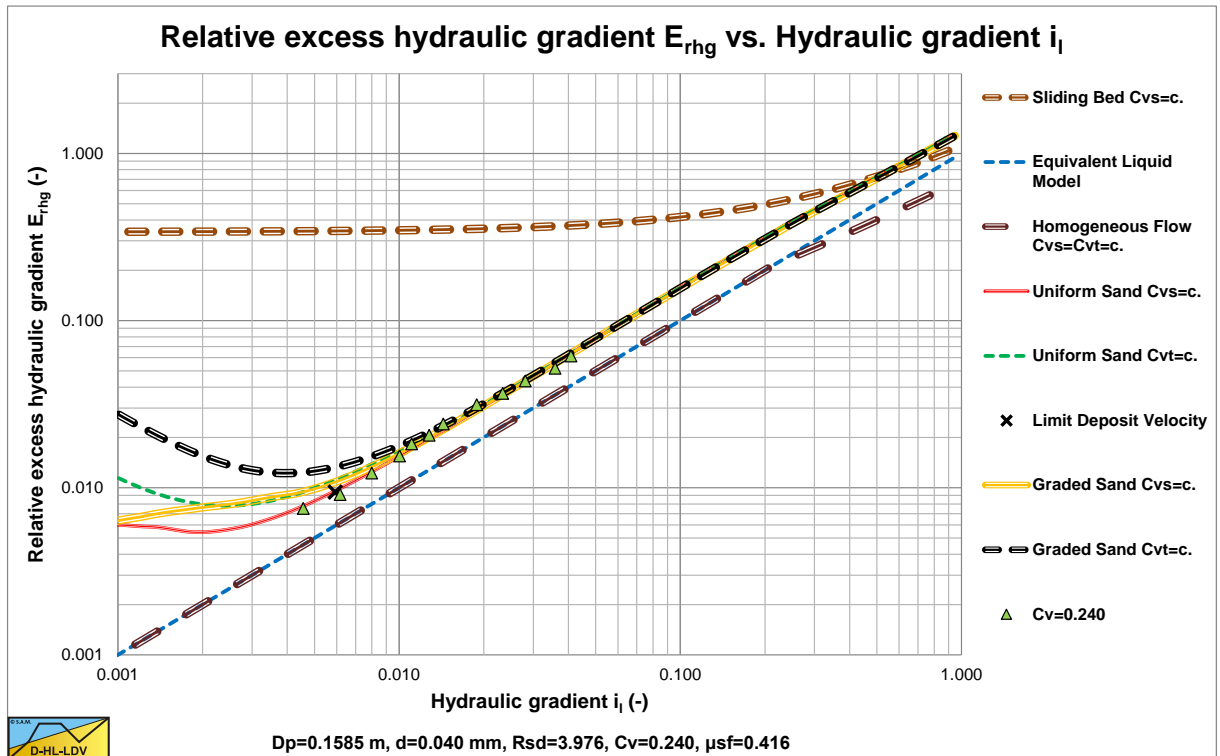
Figure 3.8-6: Iron ore Thomas (1976), with Thomas (1965) viscosity.

Figure 3.8-5 shows the experimental data versus the DHLLDV Framework. Figure 3.8-6 shows these experiments using the Thomas (1965) viscosity based on the particle size distribution mentioned by Thomas (1976). The data points now match the DHLLDV Framework for graded particles and adjusted viscosity

3.9 Nomenclature.

A_{obj}	Cross section of object perpendicular to velocity direction	m^2
A_{pw}	Pipe wall surface	m^2
A_p	Pipe cross section	m^2
C_D	Drag coefficient	-
C_{vs}	Spatial volumetric concentration	-
d	Particle diameter	m
d_e	Diameter smallest eddy	m
D_p	Pipe diameter	m
f	Fanning friction factor	-
F_{drag}	Drag force on object	N
g	Gravitational constant 9.81 m/sec^2	m/s^2
i, i_l, i_w	Hydraulic gradient liquid	m.w.c./m
i_m	Hydraulic gradient mixture	m.w.c./m
ΔL	Length of pipeline	m
Δp_l	Pressure difference over length ΔL liquid	kPa
Δp_m	Pressure difference over length ΔL pseudo homogeneous mixture	kPa
Re	Reynolds number of pipe flow	-
Stk	Stokes number	-
u_*	Friction velocity	m/s
v_{ls}	Line speed	m/s
α	Proportionality constant	-
α_1	Power of line speed	-
α_2	Power of pipe diameter	-
δ_v	Thickness viscous sub-layer	m
ε	Roughness of pipe wall	m
λ_l	Darcy-Weisbach friction factor liquid to wall	-
ρ_l	Liquid density	ton/m^3
ρ_m	Mixture density	ton/m^3
μ_l	Dynamic viscosity liquid	Pa·s
μ_m	Dynamic viscosity pseudo homogeneous mixture	Pa·s
μ_r	Relative dynamic viscosity	-
ν_l	Kinematic viscosity liquid	m^2/s
ν_m	Kinematic viscosity pseudo homogeneous mixture	m^2/s
ν_r	Relative kinematic viscosity	-
τ_w	Wall shear stress	Pa

4.1   Introduction.

Most slurry transport models use the terminal settling velocity, the particle drag coefficient or the particle Froude number. So it is important to have a good understanding of these parameters.

The settling velocity of particles depends on the grain size, shape and specific density. It also depends on the density and the viscosity of the carrier liquid the grains are settling in and upon whether the settling process is laminar or turbulent.

4.2   The Equilibrium of Forces.

The settling velocity of grains depends on the grain size, shape and specific density. Discrete particles do not change their size, shape or weight during the settling process (and thus do not form aggregates). It also depends on the density and the viscosity of the liquid the grains are settling in, and whether the settling process is laminar or turbulent. A discrete particle in a liquid will settle under the influence of gravity. It will accelerate until the frictional drag force of the liquid equals the value of the gravitational force, after which the vertical (settling) velocity of the particle will be constant (Figure 4.2-1), the so called terminal settling velocity.
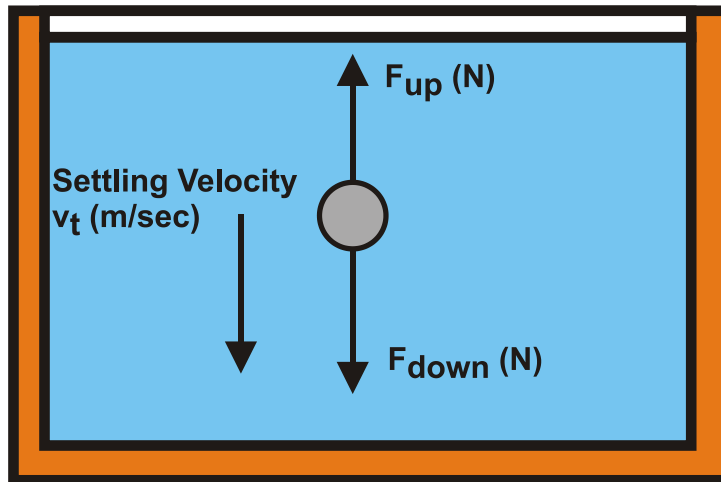
Figure 4.2-1: Forces on a settling particle.

The upward directed force on the particle, caused by the frictional drag of the liquid, can be calculated by:

$$\mathbf{F_{up} = C_D \cdot \frac{1}{2} \cdot \rho_l \cdot v_t^2 \cdot A} \tag{4.2-1}$$

The downward directed force, caused by the difference in density between the particle and the water can be calculated by:

$$\mathbf{F_{down} = (\rho_s - \rho_l) \cdot g \cdot V \cdot \psi} \tag{4.2-2}$$

In this equation a shape factor ψ is introduced to compensate for the shape of real sand grains. This shape factor is 1 for spheres and about 0.7 for real sand particles. The projected surface of the particle is:

$$\mathbf{A = \frac{\pi}{4} \cdot d^2} \tag{4.2-3}$$

The volume of the particle is:

$$V = \frac{\pi}{6} \cdot d^3 \tag{4.2-4}$$

In general, the terminal settling velocity v_t can be determined with the following equation:

$$v_t = \sqrt{\frac{4 \cdot g \cdot (\rho_s - \rho_l) \cdot d \cdot \psi}{3 \cdot \rho_l \cdot C_D}} \tag{4.2-5}$$

The Reynolds number of the settling process determines whether the process is laminar or turbulent. The Reynolds number can be determined by:

$$Re_p = \frac{v_t \cdot d}{\nu_l} \tag{4.2-6}$$

4.3   The Drag Coefficient.

In equation (4.2-5) all parameters are assumed to be known, except for the drag coefficient C_D.
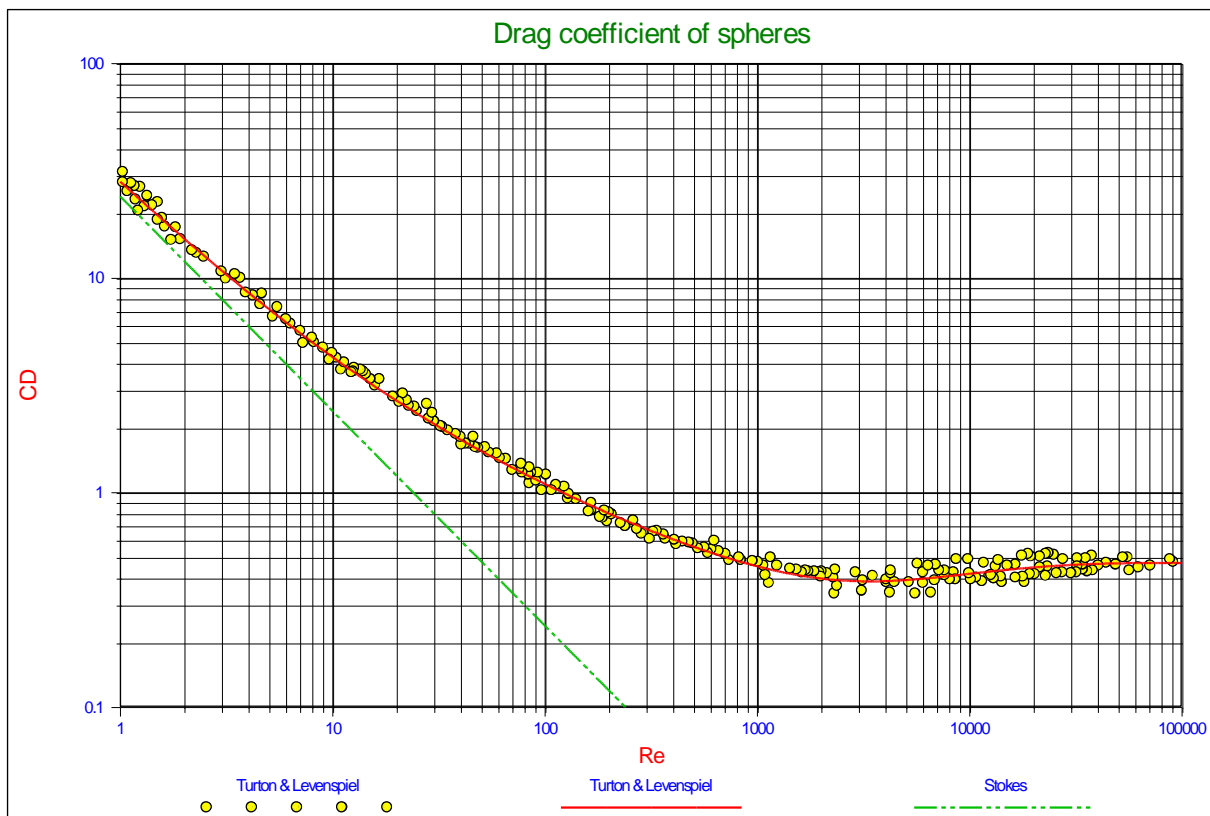
Figure 4.3-1: Experimental data for drag coefficients of spheres as a function of the Reynolds number (Turton & Levenspiel, 1986).

The drag coefficient C_D for spheres depends upon the Reynolds number according to:

The laminar region:

$$Re_p < 1 \qquad \Rightarrow \qquad C_D = \frac{24}{Re_p} \tag{4.3-1}$$

The transitional region:

$$1 < Re_p < 2000 \quad \Rightarrow \quad C_D = \frac{24}{Re_p} + \frac{3}{\sqrt{Re_p}} + 0.34 \tag{4.3-2}$$

The turbulent region:

$$Re_p > 2000 \quad \Rightarrow \quad C_D = 0.445 \tag{4.3-3}$$

As can be seen from the above equations, the drag coefficient C_D is not continuous at the transition points of $Re_p=1$ and $Re_p=2000$. To get a smooth continuous curve the following equations can be applied:

The laminar region:

$$Re_p < 1 \quad \Rightarrow C_D = Re_p \cdot (\frac{24}{Re_p} + \frac{3}{\sqrt{Re_p}} + 0.34) + (1 - Re_p) \cdot \frac{24}{Re_p} \tag{4.3-4}$$

The transitional region:

$$1 < Re_p < 2000 \quad \Rightarrow C_D = \frac{24}{Re_p} + \frac{3}{\sqrt{Re_p}} + 0.34 \tag{4.3-5}$$

The turbulent region:

$$Re_p > 10000 \quad \Rightarrow C_D = \frac{10000}{Re_p} \cdot (\frac{24}{Re_p} + \frac{3}{\sqrt{Re_p}} + 0.34) + (1 - \frac{10000}{Re_p}) \cdot 0.445 \tag{4.3-6}$$
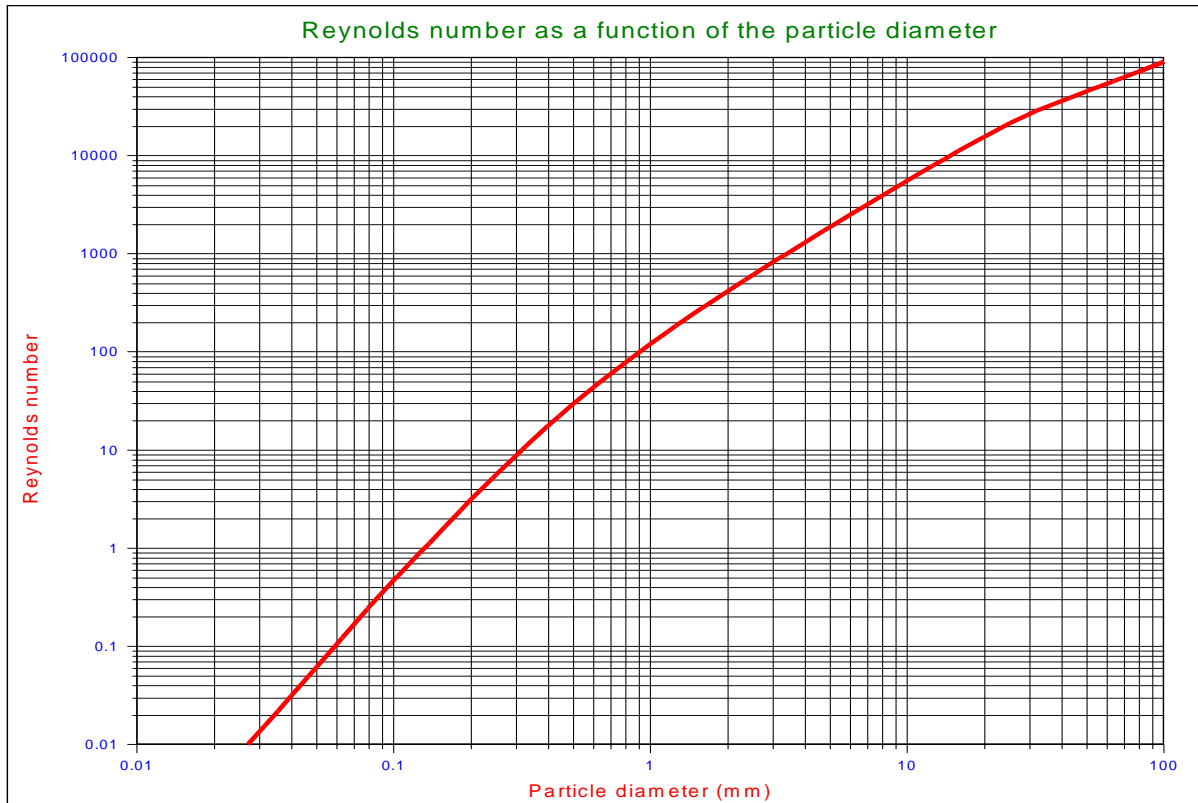
Figure 4.3-2: The particle Reynolds number as a function of the particle diameter.

Figure 4.3-2 shows the particle Reynolds number as a function of the particle diameter for sands and gravels, using the Ruby & Zanke (1977) equation.

Another equation for the transitional region has been derived by Turton & Levenspiel (1986):

$$C_D = \frac{24}{Re_p} \cdot (1 + 0.173 \cdot Re_p^{0.657}) + \frac{0.413}{1 + 16300 \cdot Re_p^{-1.09}}$$

(4.3-7)

It is known that for sands and gravels the drag coefficients, especially at large Reynolds numbers, are larger than the drag coefficient for spheres. Engelund & Hansen (1967) found the following equation based on measurements and found it best suited for natural sands and gravels (Julien, 1995):

$$C_D = \frac{24}{Re_p} + 1.5$$

(4.3-8)

It must be noted here that in general the drag coefficients are determined based on the terminal settling velocity of the particles. Wu & Wang (2006) recently gave an overview of drag coefficients and terminal settling velocities for different particle Corey shape factors. The result of their research is reflected in Figure 4.3-3. Figure 4.3-3 shows the drag coefficients as a function of the Reynolds number and as a function of the Corey shape factor. Figure 4.3-4 shows the drag coefficient for natural sands and gravels. The asymptotic value for large Reynolds numbers is about 1, while equation (4.3-8) shows an asymptotic value of 1.5.

For shells lying flat on the bed, the drag coefficient will be similar to the drag coefficient of a streamlined half body (0.09), which is much much smaller than the drag coefficient for settling (3). So there is a large asymmetry between the settling process and the erosion process of shells, while for more or less spherical sand particles the drag coefficient is considered to be the same in each direction.

Figure 4.4-1 shows the C_D coefficient as a function of the Re_p number. In the transition area the equations are implicit. Iteration 1 shows the resulting C_D values based on equations (4.3-1), (4.3-2) and (4.3-3), while iteration 2 shows the results based on equations (4.3-4), (4.3-5) and (4.3-6). It is clear from this figure that iteration 2 matches the observed data better than iteration 1, but equation (4.3-7) of Turton & Levenspiel (1986) matches the best. This is however for spheres and not for real sand and gravel particles.
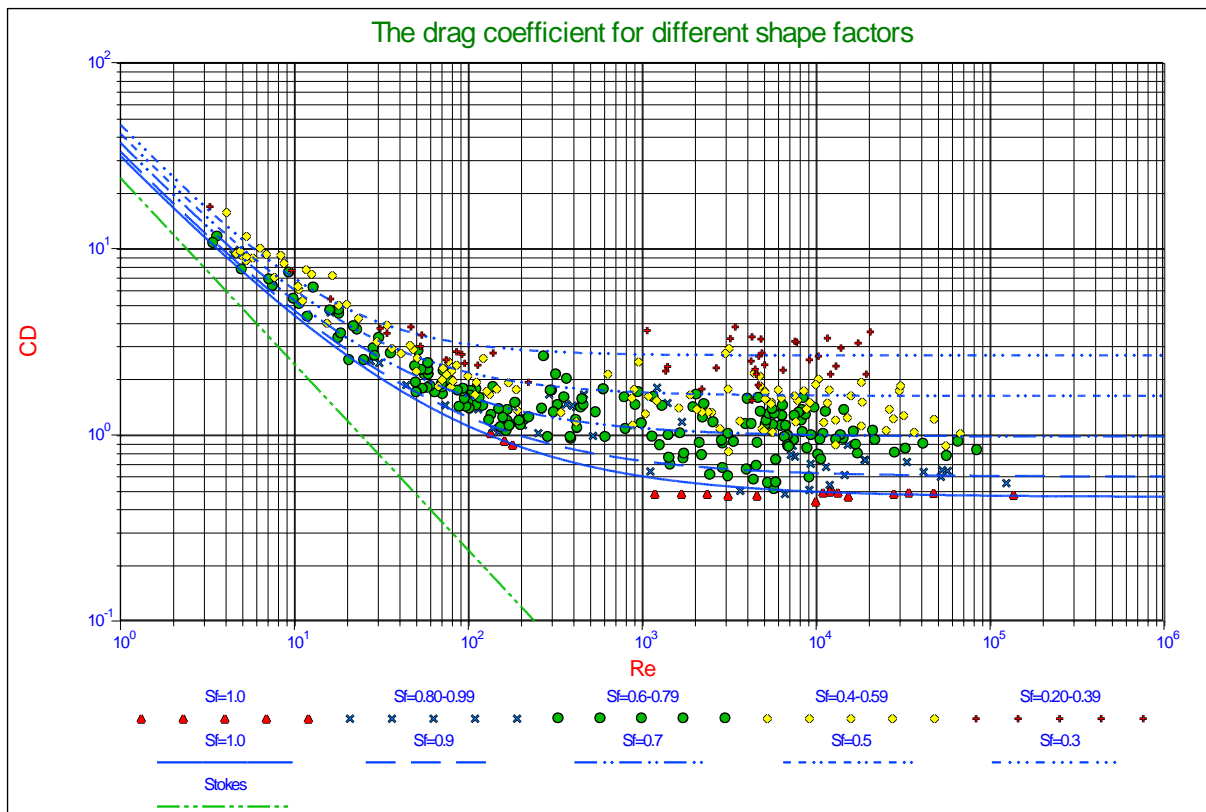
Figure 4.3-3: Drag coefficient as a function of the particle shape (Wu & Wang, 2006).
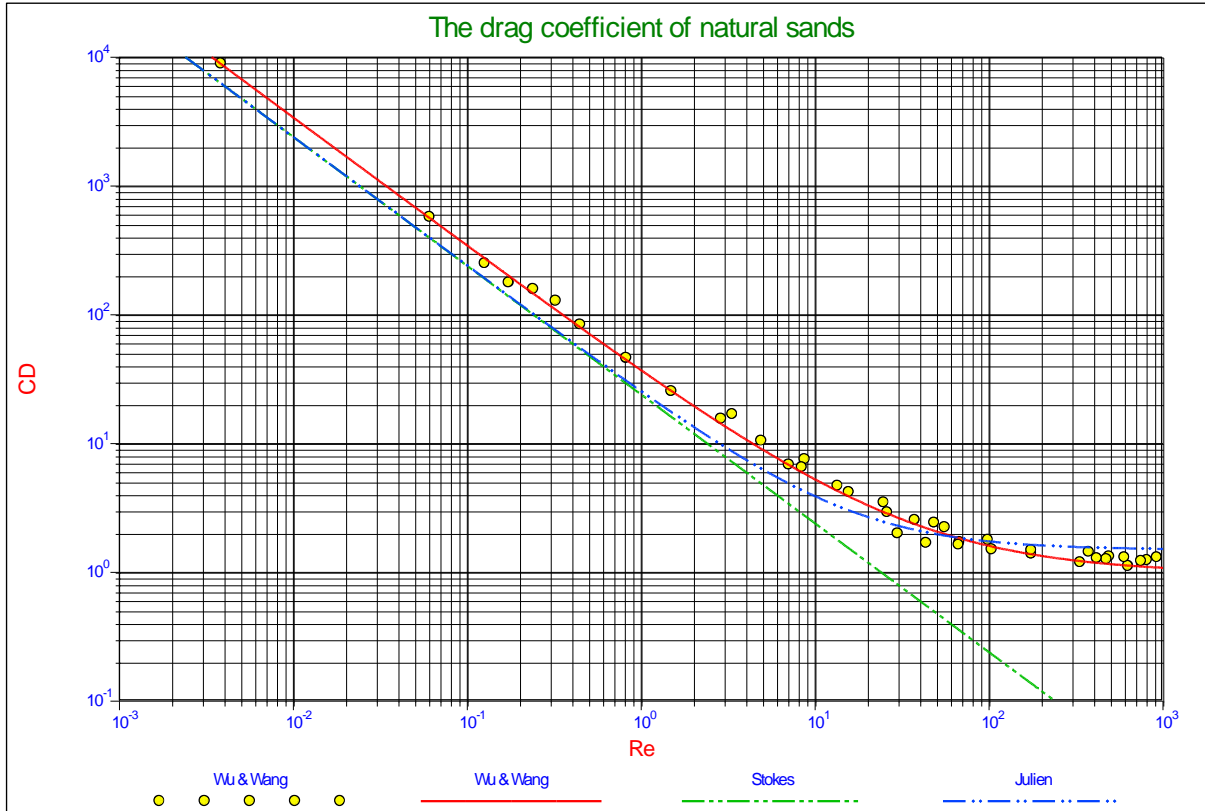
Figure 4.3-4: Drag coefficient for natural sediments ($S_f=\psi=0.7$) (Wu & Wang, 2006).

4.4 Terminal Settling Velocity Equations.

Stokes, Budryck and Rittinger used these drag coefficients to calculate settling velocities for laminar settling (Stokes), a transition zone (Budryck) and turbulent settling (Rittinger) of real sand grains. This gives the following equations for the settling velocity:

Laminar flow, **d<0.1 mm**, according to **Stokes**.

$$\mathbf{v_t = 424 \cdot R_{sd} \cdot d^2}$$ (4.4-1)

Transition zone, **d>0.1 mm** and **d<1 mm**, according to **Budryck**.

$$\mathbf{v_t = 8.925 \cdot \frac{\left(\sqrt{(1 + 95 \cdot R_{sd} \cdot d^3)} - 1\right)}{d}}$$ (4.4-2)

Turbulent flow, **d>1 mm**, according to **Rittinger**.

$$\mathbf{v_t = 87 \cdot \sqrt{R_{sd} \cdot d}}$$ (4.4-3)

With the relative submerged density **R_{sd}** defined as:

$$\mathbf{R_{sd} = \frac{\rho_s - \rho_l}{\rho_l}}$$ (4.4-4)

In these equations the grain diameter is in mm and the settling velocity in mm/sec. Since the equations were derived for sand grains, the shape factor for sand grains is included for determining the constants in these equations.

Another equation for the transitional region (in m and m/sec) has been derived by Ruby & Zanke (1977):

$$v_t = \frac{10 \cdot \nu_l}{d} \cdot \left(\sqrt{1 + \frac{R_{sd} \cdot g \cdot d^3}{100 \cdot \nu_l^2}} - 1 \right) \qquad\qquad \textbf{(4.4-5)}$$

The effective drag coefficient can now be determined by:

$$C_D = \frac{4}{3} \cdot \frac{g \cdot R_{sd} \cdot d \cdot \psi}{v_t^2} \qquad\qquad \textbf{(4.4-6)}$$

Figure 4.4-2 shows the settling velocity as a function of the particle diameter for the Stokes, Budryck, Rittinger & Zanke equations.

Since the equations were derived for sand grains, the shape factor for sand grains is used for determining the constants in the equations. The shape factor can be introduced into the equations for the drag coefficient by dividing the drag coefficient by a shape factor ψ. For normal sands this shape factor has a value of 0.7.

The viscosity of the water is temperature dependent. If a temperature of 10° is used as a reference, then the viscosity increases by 27% at 0° and it decreases by 30% at 20° centigrade. Since the viscosity influences the Reynolds number, the settling velocity for laminar settling is also influenced by the viscosity. For turbulent settling the drag coefficient does not depend on the Reynolds number, so this settling process is not influenced by the viscosity.

Other researchers use slightly different constants in these equations but, these equations suffice to explain the basics of the different slurry transport models.
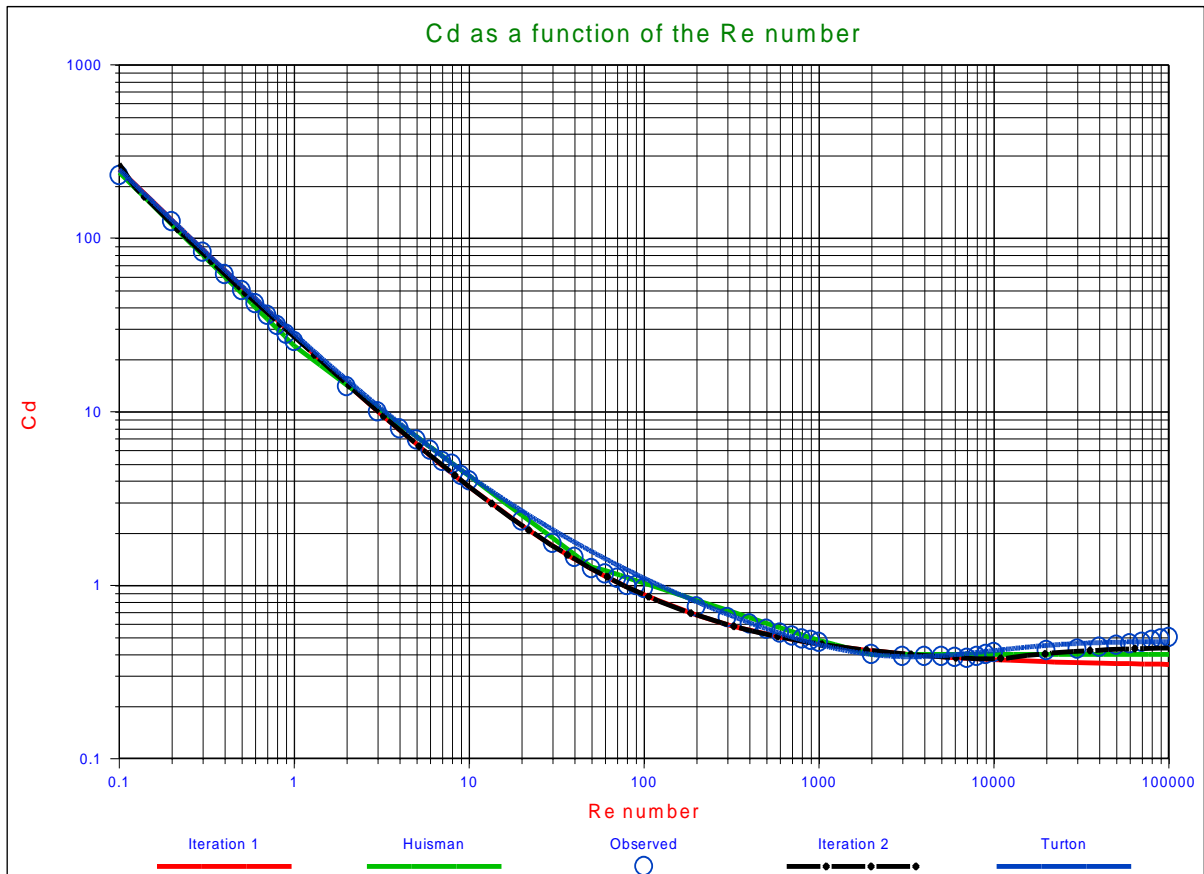
Figure 4.4-1: The drag coefficient as a function of the particle Reynolds number.
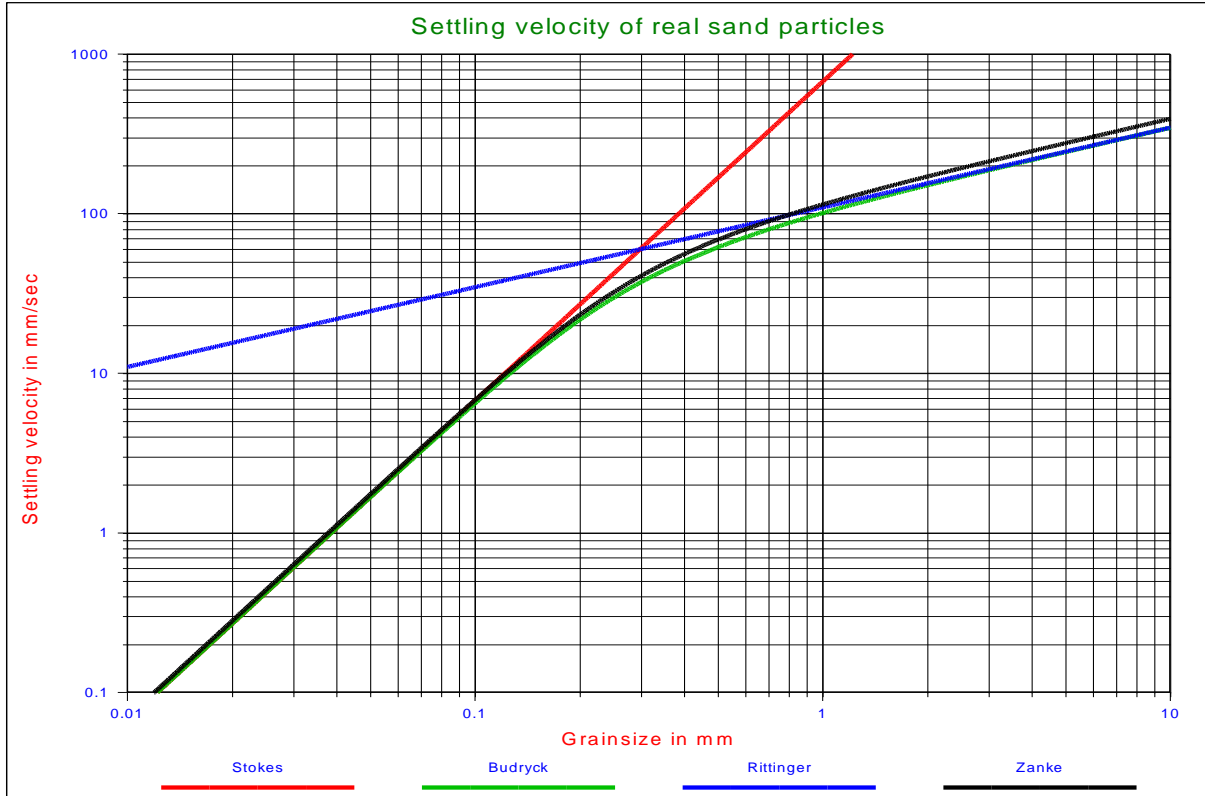
Figure 4.4-2: The settling velocity of individual particles.

The Huisman (1973-1995) Method.

A better approximation and more workable equations for the drag coefficient C_D may be obtained by subdividing the transition region, for instance:

$Re_p < 1$
$$C_D = \frac{24}{Re_p^1}$$
(4.4-7)

$1 < Re_p < 50$
$$C_D = \frac{24}{Re_p^{3/4}}$$
(4.4-8)

$50 < Re_p < 1620$
$$C_D = \frac{4.7}{Re_p^{1/3}}$$
(4.4-9)

$1620 < Re_p$
$$C_D = 0.4$$
(4.4-10)

This power approximation is also shown in Figure 4.4-1. Substitution of these equations in equation (4.2-5) gives:

$Re_p < 1$
$$v_t = \frac{1}{18} \cdot \frac{g^1}{v_l^1} \cdot R_{sd}^1 \cdot d^2$$
(4.4-11)

$1 < Re_p < 50$
$$v_t = \frac{1}{10} \cdot \frac{g^{0.8}}{v_l^{0.6}} \cdot R_{sd}^{0.8} \cdot d^{1.4}$$
(4.4-12)

$50 < Re_p < 1620$

$$v_t = \frac{1}{2.13} \cdot \frac{g^{0.6}}{v_l^{0.2}} \cdot R_{sd}^{0.6} \cdot d^{0.8}$$

(4.4-13)

$1620 < Re_p$

$$v_t = 1.83 \cdot \frac{g^{0.5}}{v_l^0} \cdot R_{sd}^{0.5} \cdot d^{0.5}$$

(4.4-14)

These equations are difficult to use in an actual case because the value of Re_p depends on the terminal settling velocity. The following method gives a more workable solution.

Equation (4.2-5) can be transformed into:

$$C_D \cdot Re_p^2 = \frac{4}{3} \cdot R_{sd} \cdot \frac{g}{v_l^2} \cdot d^3$$

(4.4-15)

This factor can be determined from the equations above:

$Re_p < 1$

$$C_D \cdot Re_p^2 = 24 \cdot Re_p$$

(4.4-16)

$1 < Re_p < 50$

$$C_D \cdot Re_p^2 = 24 \cdot Re_p^{5/4}$$

(4.4-17)

$50 < Re_p < 1620$

$$C_D \cdot Re_p^2 = 4.7 \cdot Re_p^{5/3}$$

(4.4-18)

$1620 < Re_p$

$$C_D \cdot Re_p^2 = 0.4 \cdot Re_p^2$$

(4.4-19)

From these equations the equation to be applied can be picked and the value of Re_p calculated. The settling velocity now follows from:

$$v_t = Re_p \cdot \frac{v_l}{d}$$

(4.4-20)

The Grace Method (1986).

Following the suggestions of Grace (1986), it is found convenient to define a dimensionless particle diameter, which in fact is the Bonneville parameter (d in m and v_t in m/s):

$$D_* = d \cdot \left(\frac{R_{sd} \cdot g}{v_l^2} \right)^{1/3}$$

(4.4-21)

And a dimensionless terminal settling velocity:

$$v_t^* = v_t \cdot \left(\frac{1}{v_l \cdot R_{sd} \cdot g} \right)^{1/3}$$

(4.4-22)

Those are mutually related. Thus using the curve and rearranging gives directly the velocity v_t as a function of particle diameter d. No iteration is required. This described by analytic expressions appropriate for a computational determination of v_t according to Grace Method. Now v_t can be computed according to:

$$v_t = v_t^* \cdot \left(\frac{1}{v_l \cdot R_{sd} \cdot g} \right)^{-1/3}$$

(4.4-23)

$D^* < 3.8$
$$v_t^* = \frac{\left(D^*\right)^2}{18} - 3.1234 \cdot 10^{-4} \cdot \left(D^*\right)^5 + 1.6415 \cdot 10^{-6} \cdot \left(D^*\right)^8$$
$$- 7.278 \cdot 10^{-10} \cdot \left(D^*\right)^{11}$$

(4.4-24)

$3.8 < D^* < 7.58$
$$v_t^* = 10^{-1.5446 + 2.9162 \cdot \log(D^*) - 1.0432 \cdot \log(D^*)^2}$$

(4.4-25)

$7.58 < D^* < 227$
$$v_t^* = 10^{-1.64758 + 2.94786 \cdot \log(D^*) - 1.09703 \cdot \log(D^*)^2 + 0.17129 \cdot \log(D^*)^3}$$

(4.4-26)

$227 < D^* < 3500$
$$v_t^* = 10^{5.1837 - 4.51034 \cdot \log(D^*) + 1.687 \cdot \log(D^*)^2 - 0.189135 \cdot \log(D^*)^3}$$

(4.4-27)

Figure 4.4-3 shows the terminal settling velocity for the iterative method according to equations (4.3-4), (4.3-5) and (4.3-6) and the methods of Huisman (1973-1995) and Grace (1986), using shape factors of 0.5 and 0.7. It can be seen that for small diameters these methods gives smaller velocities while for larger diameters larger velocities are predicted, compared with the other equations as shown in Figure 4.4-2. The iterative method gives larger velocities for the larger diameters, compared with the Huisman and Grace methods, but this is caused by the different way of implementing the shape factor. In the iterative method the shape factor is implemented according to equation 2, while with the Huisman and Grace methods the terminal settling velocity for spheres is multiplied by the shape factor according to equation (4.5-1). For the smaller grain diameters, smaller than 0.5 mm, which are of interest here, the 3 methods give the same results.
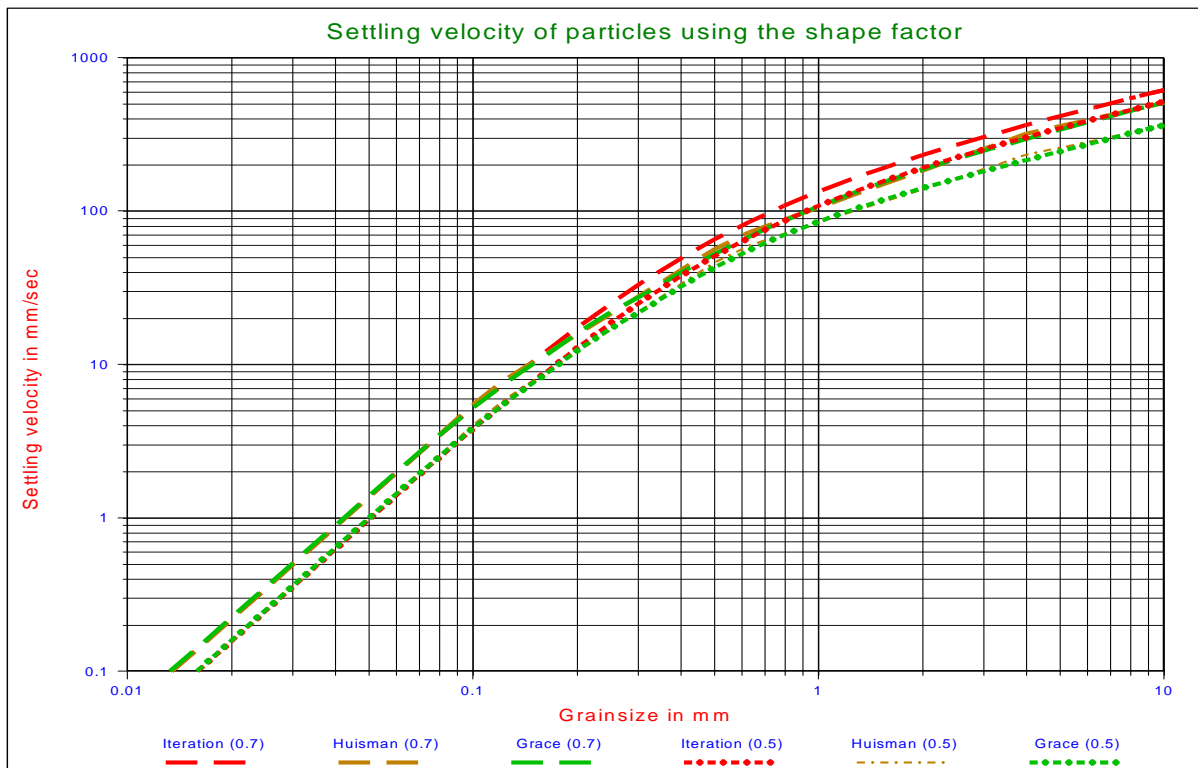
Figure 4.4-3: The settling velocity of individual particles using the shape factor.

4.5   The Shape Factor

In the range of particle Reynolds numbers from roughly unity to about 100, which is the range of interest here, a particle orients itself during settling so as to maximize drag. Generally this means that an oblate or lenticular particle, i.e. a shape with one dimension smaller than the other two, will settle with its maximum area horizontal. The drag of fluid on the particle then depends most critically on this area. This is also the area seen if the particle lies in a stable position on a flat surface. Therefore, for estimation of drag, the non-spherical particle is characterized by the 'area equivalent diameter', i.e. the diameter of the sphere with the same projected area. For particles whose sizes are determined by sieving rather than microscopic analysis, the diameter is slightly smaller than the mesh size. However, unless the particles are needle shaped, the difference between the equivalent diameter and the screen opening is relatively small, generally less than 20%.

Although equation (4.2-5) contains a shape factor, basically all the equations in this chapter are derived for spheres. The shape factor ψ in equation (4.2-5) is one way of introducing the effect of the shape of particles on the terminal settling velocity. In fact equation (4.2-5) uses a shape factor based on the weight ratio between a real sand particle and a sphere with the same diameter. Another way is introducing a factor ξ according to:

$$\xi = \frac{v_t}{v_{ts}}$$

(4.5-1)

Where ξ equals the ratio of the terminal settling velocity of a non-spherical particle v_t and the terminal velocity v_{ts} of a spherical particle with the same diameter. The shape of the particle can be described by the volumetric shape factor K which is defined as the ratio of the volume of a particle and a cube with sides equal to the particle diameter so that $K=0.524$ for a sphere:

$$K = \frac{\text{volume of particle}}{d^3}$$

(4.5-2)

The shape factor ξ is a function of the volumetric form factor K and the dimensionless particle diameter D^* according to equation (4.4-21).

$$\log(\xi) = -0.55 + K - 0.0015 \cdot K^2 + 0.03 \cdot 1000^{K-0.524} + \frac{-0.045 + 0.05 \cdot K^{-0.6} - 0.0287 \cdot 55000^{K-0.524}}{\cosh(2.55 \cdot (\log(D^*) - 1.114))}$$

(4.5-3)

This equation takes a simpler form for sand shaped particles with $K=0.26$:

$$\log(\xi) = -0.3073 + \frac{0.0656}{\cosh(2.55 \cdot (\log(D^*) - 1.114))}$$

(4.5-4)

A value of $K=0.26$ for sand grains would give a volume ratio of 0.26/0.524=0.496 and thus a factor $\psi=0.496$ in equation (4.2-5), while often a factor $\psi=0.7$ is used.

Figure 4.5-1 shows the shape factor ξ as a function of the dimensionless particle diameter D^*, according to equation (4.5-3).

Figure 4.4-3 also shows the terminal settling velocity according to the methods of Huisman (1973-1995) and Grace (1986) using the shape factor according to equation (4.5-4). It can be seen clearly that both methods give the same results. One can see that the choice of the shape factor strongly determines the outcome of the terminal settling velocity.
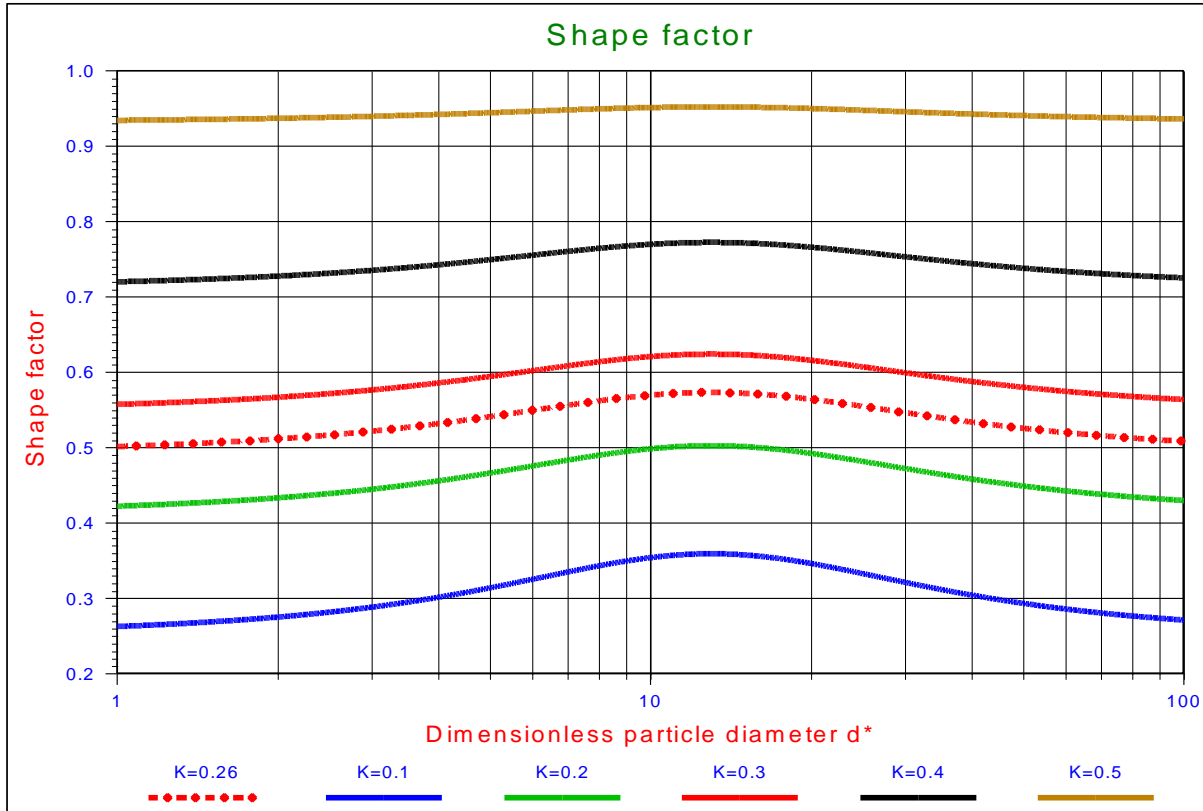
Figure 4.5-1: The shape factor ξ as a function of the dimensionless particle diameter D*.

4.6 Hindered Settling.

The above equations calculate the settling velocities for individual grains. The grain moves downwards and the same volume of water has to move upwards. In a mixture, this means that, when many grains are settling, an average upwards velocity of the water exists. This results in a decrease of the settling velocity, which is often referred to as hindered settling. However, at very low concentrations the settling velocity will increase because the grains settle in each other's shadow. Richardson and Zaki (1954) determined an equation to calculate the influence of hindered settling for volume concentrations C_{vs} between 0 and 0.3. The coefficient in this equation is dependent on the Reynolds number. The general equation yields:

$$\frac{v_{th}}{v_t} = \left(1 - C_{vs}\right)^{\beta} \tag{4.6-1}$$

The following values for β should be used according to Richardson and Zaki (1954):

$Re_p < 0.2$	$\beta = 4.65$
$Re_p > 0.2$ and $Re_p < 1.0$	$\beta = 4.35 \cdot Re_p^{-0.03}$
$Re_p > 1.0$ and $Re_p < 200$	$\beta = 4.45 \cdot Re_p^{-0.1}$
$Re_p > 200$	$\beta = 2.39$

(4.6-2)

However this does not give a smooth continuous curve. Using the following definition does give a continuous curve:

$Re_p < 0.1$	$\beta = 4.65$
$Re_p > 0.1$ and $Re_p < 1.0$	$\beta = 4.35 \cdot Re_p^{-0.03}$
$Re_p > 1.0$ and $Re_p < 400$	$\beta = 4.45 \cdot Re_p^{-0.1}$
$Re_p > 400$	$\beta = 2.39$

(4.6-3)

Other researchers found the same trend but sometimes somewhat different values for the power **β**. These equations are summarized below and shown in Figure 4.6-1.

According to Rowe (1987) this can be approximated by:

$$\beta = \frac{4.7 + 0.41 \cdot Re_p^{0.75}}{1 + 0.175 \cdot Re_p^{0.75}} \tag{4.6-4}$$

Wallis (1969) found an equation which matches Rowe (1987) for small Reynolds numbers and Garside & Al-Dibouni (1977) for the large Reynolds numbers:

$$\beta = \frac{4.7 \cdot (1 + 0.15 \cdot Re_p^{0.687})}{1 + 0.253 \cdot Re_p^{0.687}} \tag{4.6-5}$$

Garside & Al-Dibouni (1977) give the same trend but somewhat higher values for the exponent **β**.

$$\beta = \frac{5.1 + 0.27 \cdot Re_p^{0.9}}{1 + 0.1 \cdot Re_p^{0.9}} \tag{4.6-6}$$

Di Felici (1999) finds very high values for **β** but this relation is only valid for dilute mixtures (very low concentration, less than 5%).

$$\beta = \frac{6.5 + 0.3 \cdot Re_p^{0.74}}{1 + 0.1 \cdot Re_p^{0.74}} \tag{4.6-7}$$
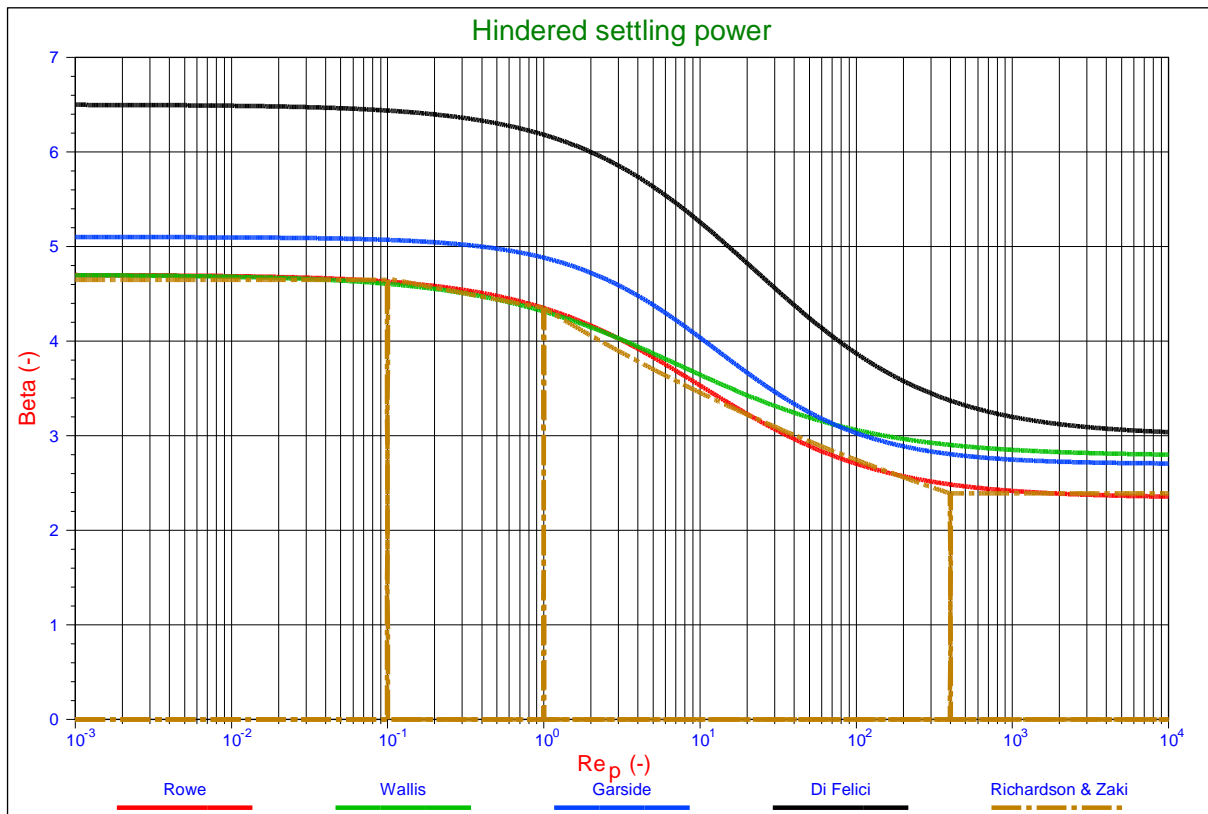
Figure 4.6-1: The hindered settling power according to several researchers.

4.7 Conclusions.

The equation of Ruby & Zanke (1977) will be used to determine the terminal settling velocity for sands and gravels. The equation of Richardson and Zaki (1954) will be used for hindered settling, with the equation of Rowe (1987) for the power **β** in the hindered settling equation. The DHLLDV Framework is calibrated based on these equations.

Using different equations will result in slightly different hydraulic gradients and Limit Deposit Velocities, requiring the constants in the DHLLDV Framework to be adjusted.

Particles with different shapes, like spheres or shells, and particles with different relative submerged densities may require different methods.

One of the main issues is that the Richardson & Zaki (1954) hindered settling equation is based on the spatial volumetric concentration C_{vs} and not on the relative spatial volumetric concentration $C_{vr}=C_{vs}/C_{vb}$.

$$\frac{v_{th}}{v_t} = \left(1-C_{vs}\right)^{\beta} \tag{4.7-1}$$

So even when the spatial volumetric concentration reaches a concentration where a bed with maximum porosity occurs, for sand at about $C_{vs}=50\%$, still a hindered settling velocity is determined, while in reality this hindered settling velocity will be zero. Normal sands will have a porosity of about 40%, so $C_{vb}=60\%$. A fixed bed may have a porosity of 40%, but a sliding bed will have a higher porosity in between 40% and 50%. The porosities mentioned here depend on the type of sand, but are mentioned to give a feeling of the order of magnitude. Since the Richardson & Zaki (1954) equation is based on small concentrations it is better to use a modified equation based on the relative concentration, for example:

$$\frac{v_{th}}{v_t} = \left(1-C_{vr}\right)^{\beta'} \tag{4.7-2}$$

Of course the power of this equation will be different from the original equation. An equation that may even work better is:

$$\frac{v_{th}}{v_t} = e^{-\beta \cdot C_{vr}^{1.25}} \cdot \left(1-C_{vr}^{3}\right) \tag{4.7-3}$$

For small concentrations this equation gives the same result as the original equation, but for concentrations approaching the bed concentration, this equation approaches a zero settling velocity. This would describe the bed behavior much better. So for small concentrations this equation describes hindered settling, while for large relative concentrations approaching 1, the behavior is more close to consolidation. The power **β** in this equation is equal to the original power **β.**

4.8 Nomenclature.

A	Cross section of particle	**m²**
C_D	Drag coefficient	**-**
C_{vs}	Volumetric spatial concentration	**-**
d	Particle diameter	**m**
D_* or d_*	Bonneville parameter or dimensionless particle diameter	**-**
F_{down}	Downwards force on particle	**N**
F_{up}	Upwards force on particle	**N**
g	Gravitational constant 9.81 m/s²	**m/s²**
K	Volumetric form factor	**-**
Re_p	Particle Reynolds number	**-**
R_{sd}	Relative submerged density	**-**
v_t	Terminal settling velocity	**m/s**
v_t^*	Dimensionless terminal settling velocity	**-**
v_{th}	Hindered terminal settling velocity	**m/s**
v_{ts}	Terminal settling velocity sphere	**m/s**
V	Volume of particle	**m³**
β	Hindered settling power	**-**
$ρ_l$	Density of carrier liquid	**ton/m³**
$ρ_s$	Density of solid	**ton/m³**
ψ	Shape factor	**-**
ξ	Shape factor	**-**
$ν_l$	Kinematic viscosity liquid	**m²/s**

Chapter 5:   Initiation of Motion and Sediment Transport.

5.1   Initiation of Motion of Particles.

5.1.1   Introduction.

Entrainment, incipient motion, initiation of motion and threshold velocity are terms often used for the beginning of motion of particles in a bed under the influence of flow. In slurry transport two main flow regimes are the stationary bed regime and the sliding bed regime. In both regimes there is a bed and a fast flowing liquid above the bed. At the interface particles start moving and may become suspended.

Although there may have been others before, Shields (1936) was one of the first who managed to give some physical explanation to the erosion phenomena and to found this with experiments. The results of his research are shown in Figure 5.1-1 together with the resulting theoretical curve from the current research. The original research as carried out by Shields in 1936 was based on a limited number of experiments and should be looked at in the context of the technology in that period. So it was and is a big achievement of Shields to find a relation for the initiation of motion of (spherical) particles that still holds today, although many have carried out additional research and tried to find a physical and mathematical explanation. These explanations usually incorporate phenomena such as gravity, drag, lift and turbulence and are based on sliding, rolling or lifting. Aspects such as, which velocity to use for the drag and the lift, where is the point of action of the drag force, the choice of the angle of repose and the pivoting angle are not always consistent. Especially the definition of incipient motion, is it when one particle starts moving, or many and then how many, is interpreted differently by different researchers. Some use sliding as the main mechanism, others rolling and a few lifting. Almost everybody uses the drag coefficient for spheres because many experiments are carried out for spheres, but real quarts grains have a larger drag coefficient especially at high Reynolds numbers. In general each of these models lacks one of these phenomena and/or aspects. The modeling usually stops, if a model has sufficient correlation with the data of many researchers (Buffington & Montgomery, 1997) and with the original Shields diagram (Shields, 1936).

5.1.1.1 Models on Sediment Threshold.

Since there are many models available, only the most relevant ones, in the context of this book, will be discussed. Shields (1936) introduced the fundamental concepts for initiation of motion and made a set of observations (see Figure 5.1-1) that have become legendary. From dimensional analysis and fluid mechanics considerations he deduced the relation between the ratio of the bed shear stress and the gravitational force on a particle as a function of the boundary Reynolds number $Re_* = u_* \cdot d / v_l$. Based on curve fitting on his observations, the famous Shields curve was born. Later many experiments were carried out by numerous scientists of which Buffington & Montgomery give a nice summary (Buffington & Montgomery, 1997). Buffington also gives a critical analyses of the developments since Shields did his first findings (Buffington, 1999). In fact Shields did not derive a model or an equation, but published his findings as a graph (Figure 5.1-1). It is inconvenient that the Shields diagram is implicit, the friction velocity u_* appears in both the horizontal and the vertical axis. However with modern computers this should not be any problem.

Although less famous, Hjulstrøm also carried out his research in the thirties (Hjulstrøm, 1935) and (Hjulstrøm, 1939). He presented his work in a graph showing the relation between the erosion velocity (average velocity above the bed) and the grain diameter. The graph, although explicit, depends on the water height, standard a height of 100 cm is used. For a certain water height, the Shields diagram can be converted to the Hjulstrøm diagram. A mathematical description of the Hjulstrøm diagram could not be found, but one will be given in the next paragraph. The equilibrium of a single particle resting on a granular bed was studied by White (1940). He obtained an expression for the threshold shear stress, but neglected the lift force. Later Kurihara (1948) extended the model and proposed some empirical equations for the estimation of threshold shear stress. Egiazaroff (1965) found a relation between the threshold shear stress and the particle Reynolds number. He assumed that at the moment of incipient motion the velocity at a height of $0.63 \cdot d$ is equal to the terminal settling velocity of the particle. His results did not match the original Shields data quantitatively, although some relation will exist.
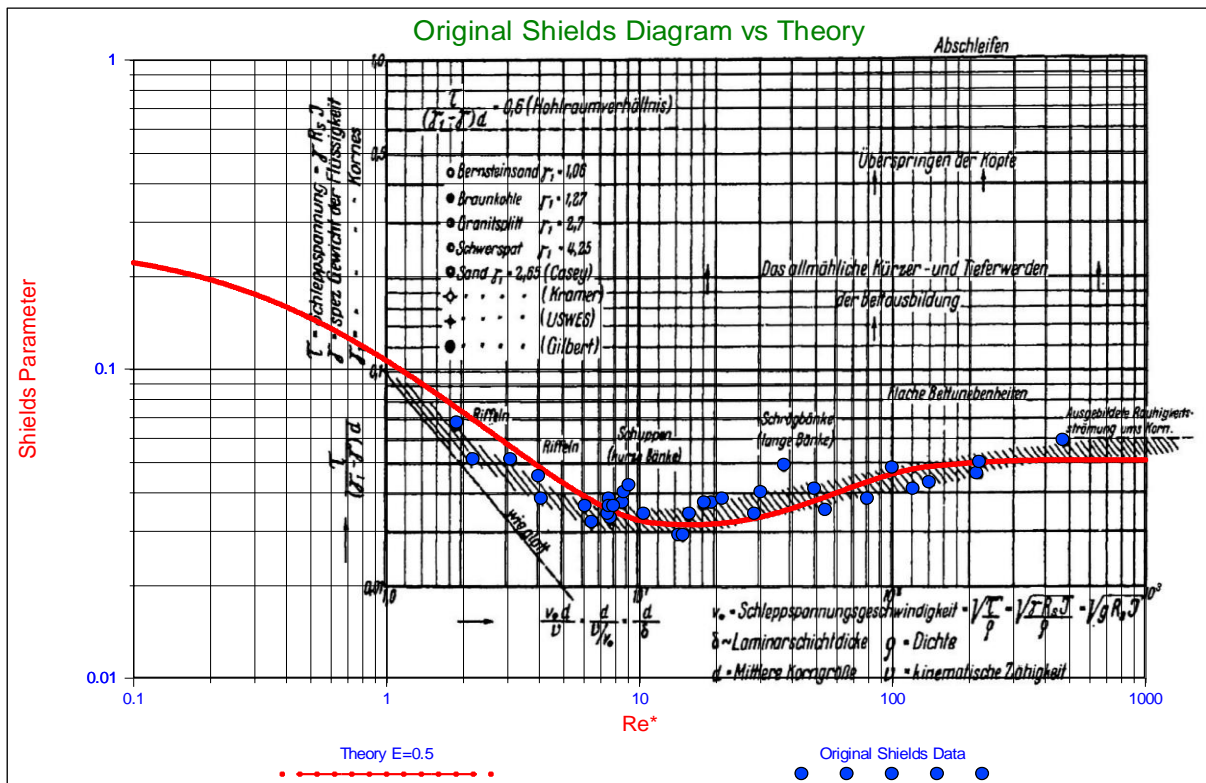
Figure 5.1-1: The original Shields diagram (Shields, 1936) and the resulting theoretical curve from the current research.

An extended Shields diagram was developed by Mantz (1977) followed by a graphical representation of a large volume of data by Yalin & Karahan (1979). The Ikeda-Coleman-Iwagaki model was presented by Ikeda (1982) and is based on the work of Iwagaki (1956) and Coleman (1967). The model is based on the assumption that the initiation of motion mechanism is sliding. Gravity, drag and lift are taken into account, but turbulence and grain placement are neglected. The zero level for the velocity profile is taken at the base of the grain exposed to the flow and the velocity used is at the center of the grain, so at **y=d/2**. This means that the grain is exposed to drag over the full height of the grain. For **d/δ$_v$<0.5** the velocity profile of the viscous sub-layer is applied giving **F(Re∗)=u/u∗=u∗·d/(2·v$_l$)=Re∗/2**, while for **d/δ$_v$>2** the logarithmic velocity profile for rough boundaries is applied giving **F(Re∗)=u/u∗=6.77**. In the transition area, **0.5<d/δ$_v$<2** the fit for the velocity profile proposed by Swamee (1993) or Reichardt (1951) can be used by setting **y=d/2** and **k$_s$=d**. This leads to the following equation for the Shields parameter:

$$\theta = \frac{4}{3} \cdot \frac{\mu_{sf}}{C_D + \mu_{sf} \cdot C_L} \cdot \frac{1}{F(Re_*)^2} \tag{5.1-1}$$

This equation is valid for horizontal beds, but the effect of a slope can easily be incorporated.

Considering two angles of internal friction (repose), **φ=40°**, (**μ$_{sf}$=0.84**) and **φ=60°**, (**μ$_{sf}$=1.73**) and further assuming that **k$_s$=2·d**, **C$_L$=0.85·C$_D$** and using the standard relations for the drag coefficient for spheres, Garcia (2008) shows the resulting curves, compared with the original Shields (1936) data (Figure 5.1-1). The **φ=40°** curve underestimates the values of the Shields parameter compared with the original Shields data, while the **φ=60°** curve gets close, but still gives to small values. A **φ=60°** friction angle however is unreasonably high. The curve predicted follows the trend of Shields data, but is about a factor 1.6 smaller for the **φ=40°** case. A predecessor of this model was advanced by Egiazaroff (1965).
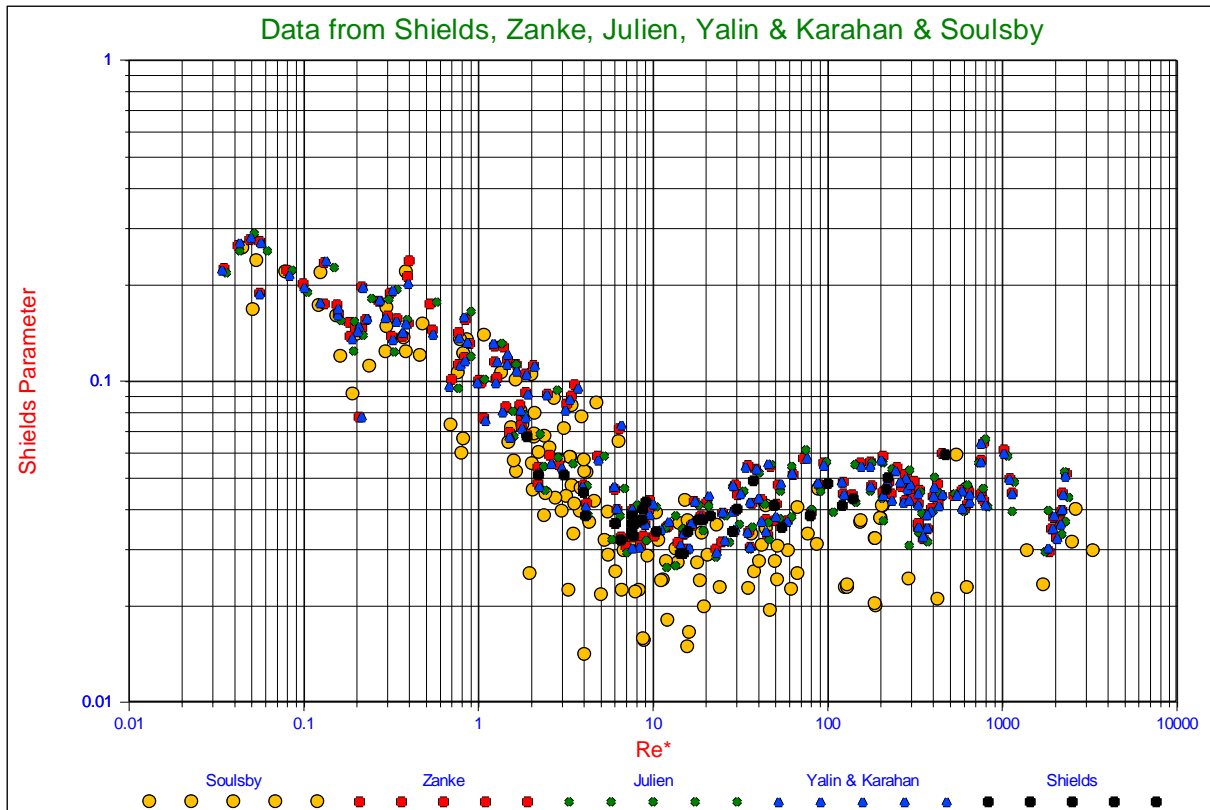
Figure 5.1-2: Data digitized and copied from Zanke (2003), Julien (1995), Yalin & Karahan (1979), Shields (1936) and others.

The Wiberg & Smith (1987A) model is based on the assumption that the initiation of motion mechanism is rolling. Gravity, drag and lift are taken into account and to some extend also turbulence. The equilibrium of moments around a pivot point is taken, where the location of the pivot point is defined as the contact point with an underlying particle under an angle ϕ_0 with the vertical. This angle is named the particle angle of repose or the dilatation angle. This angle differs from the internal friction angle, as used in the Ikeda-Coleman-Iwagaki model, because the internal friction angle (angle of natural repose) is a global soil mechanical parameter, where local variations are averaged out, while the pivot angle is a local angle matching a specific configuration of the grains. The resulting Wiberg-Smith equation is almost equal to the Ikeda-Coleman-Iwagaki equation apart from the difference between the internal friction angle (using the friction coefficient) in equation (5.1-1) and the pivot angle in equation (5.1-2).

$$\theta = \frac{4}{3} \cdot \frac{\tan(\phi_0)}{C_D + \tan(\phi_0) \cdot C_L} \cdot \frac{1}{F(Re_*)^2} \tag{5.1-2}$$

Wiberg & Smith (1987A) use the velocity profile as proposed by Reichardt (1951) providing a smooth transition between the viscous sub layer and the logarithmic profile. A lift coefficient of $C_L=0.2$ is applied in the turbulent region, while it is assumed that particles residing completely in the viscous sub layer are not subject to lift. The calculations are carried out using $\phi_0=50°$ and $\phi_0=60°$ with $k_s=d$. In Wiberg & Smith (1987B) the average velocity on the particle is applied, giving $F(Re_*)=6.0$ for the hydraulic rough region. The model matches the original Shields data well for the turbulent rough region for $\phi_0=60°$, but overestimates the Shields data for the laminar flow in the viscous sub layer. The first conclusion does not come as a surprise, since $\phi_0=60°$ is equal to $\mu_{sf}=1.73$ in the Ikeda-Coleman-Iwagaki model and Wiberg & Smith use a smaller lift coefficient, resulting in a slightly higher curve. For the small Reynolds numbers the resulting curve overestimates the original Shields data. Wiberg & Smith (1987A) solve this by introducing turbulence. They state that periodic intrusions of high momentum liquid erode the viscous sub layer and produce locally higher boundary stresses. When the instantaneous boundary shear stress is sufficiently large, movement is more likely. To implement this the thickness of the viscous sub layer is reduced to 60%, maintaining the momentum of the flow, resulting in higher instantaneous velocities by a factor 1.66. This lowers the curve in the lower Reynolds area and gives a good match with the Shields data. This effect of turbulence however is the same for the whole lower Reynolds area and influences the asymptotic value of the Shields curve going to a Reynolds number of zero.

Dey (1999) developed a detailed model based on rolling as the mechanism for incipient motion. The model includes gravity, drag and lift and even Magnus lift forces, but no turbulence. The Morsi & Alexander (1972) relation for the drag coefficient is used, while the Saffman (1965) approach for the lift force is followed. Additionally the lift due to the Magnus effect is used for large Reynolds numbers. Based on detailed mathematics the lever arms for the equilibrium of moments are derived. The average velocity acting on the sphere is determined by integration of the velocity over the actual surface of the sphere, depending on the virtual bed level. The Reichardt (1951) velocity profile is used. The resulting equation for the Shields parameter is similar to equation (5.1-2), but much more detailed. There is an excellent agreement between the model developed by Dey and the experimental data used for a pivot angle of $\phi_0=32°$. For the particle considered, a particle resting on top of 3 other particles in a dense 3D configuration, the exposure level would be near 1.0 and the protrusion level near 0.8. The protrusion level is the fraction of a particle above the bed. The exposure level is the fraction of a particle exposed to the flow. Since the flow starts at about 20% of the particle diameter below the bed surface, the exposure level is about 0.2 higher than the protrusion level. According to a detailed study of Luckner (2002) this would result in a pivot angle of about $\phi_0=20°$.

Zanke (2001) and (2003) follows an approach different from all other researchers. Starting with a non-dimensional shear stress based on tilting a bed of particles and assuming that the shear stress exerted at the moment the top layer of the particles starts to move, he deducts the influences of turbulence and lift and finds a curve that is in good correlation with experimental data. The base non-dimensional shear stress is set to $\theta=(1-n)\cdot\tan(\varphi/1.5)$, where the porosity n is set to 0.3 and the friction angle to $\phi_0=30°$. This starting point can be disputed since the driving force when tilting a bed until the grains start to move is gravity, while the main influence in initiation of motion is flow. The way turbulence is incorporated, both in drag and in lift is very interesting. The basis of the turbulence influences is the equation formulated by Nezu & Nakagawa (1993) for the turbulence intensity parallel to the wall as a function to the distance to the wall. Close to the wall in the viscous sub layer the turbulence intensity is about $u_{r.m.s.}^+=0.3\cdot y^+$, where the time averaged velocity profile is known to be $u^+=\ell\cdot y^+$. Taking $u_{total}^+=u^++2.2\cdot u_{r.m.s.}^+=1.66\cdot u^+$, should give the same result as Wiberg & Smith (1987A) found by reducing the thickness of the viscous sub layer to 60%. Zanke (2001) uses a factor of 1.8 instead of 2.2, but then his approach is completely different. Zanke (2001) must also have noticed that the asymptotic value of the curve for very low Reynolds numbers decreases when adding the influence of turbulence as stated above. Now it can be discussed whether the virtual bed level for the time averaged velocity and the turbulence intensity are exactly the same. By choosing a lower virtual bed level for the time averaged velocity, the ratio between the turbulence intensity and the time averaged velocity is zero at the virtual bed level for the turbulence intensity, resulting in an asymptotic value that is not influenced by the turbulence. Another interesting addition in the model of Zanke (2001) is the influence of cohesion, although it is the question which fundamental forces are taken into account.

Stevenson, Thorpe & Davidson (2002) and Stevenson, Cabrejos & Thorpe (2002) look at the process of incipient motion from the perspective of chemical engineering and also incorporated the rolling resistance. For small Reynolds numbers (viscous sub layer) the lift force is neglected.

It should be noted that a number of fit equations to the Shields data exist in order to be able to calculate the Shields parameter. A well know equation is the equation of Brownlie (1981) based on the Bonneville (1963) parameter D_*.

$$\theta = \frac{0.22}{D_*^{0.9}} + 0.06 \cdot e^{-17.77 \cdot D_*^{-0.9}} \tag{5.1-3}$$

Soulsby & Whitehouse (1997) defined another fit equation, based on the Bonneville (1963) parameter. The two fit equations differ in the asymptotic values. Brownlie uses 0.06 for very large Reynolds numbers, while Soulsby & Whitehouse use 0.055. As we will see later, this difference is not very relevant. The asymptote for very small Reynolds values for the Brownlie equation is proportional to $D_*^{-0.9}$, while Shields (1936) proposed $0.1\cdot D_*^{-1}$, but Soulsby & Whitehouse found a value of 0.3, matching the mechanistic models as shown in the equations (5.1-1) and (5.1-2).

$$\theta = \frac{0.30}{(1+1.2\cdot D_*)} + 0.055 \cdot \left(1 - e^{-0.02\cdot D_*}\right) \tag{5.1-4}$$

Often it is found that for real sands and gravels the values found for initiation of motion (depending on the definition of course) are smaller than the ones found with the models and with the above equations. For this reason it is proposed to divide these equations by 2 for engineering purposes. Later we will see that this matches using the C_D values for sands and gravels for large Reynolds numbers, but not for small Reynolds numbers.

5.1.1.2 Hjulström (1935), Sundborg (1956) and Postma (1967).

Although the Shields approach is used in this book, the following gives some background information. Hjulström (1935) & (1939) published the famous Hjulström diagram, showing the threshold flow velocity as a function of the particle diameter for a 100 cm water open channel flow. For large particles the threshold flow velocity increases with an increasing particle diameter, but for small particles the threshold flow velocity increases with a decreasing particle diameter. For particles near 0.5 mm a minimum threshold flow velocity is found. Figure 5.1-3 shows the Hjulström diagram. The increase of the threshold flow velocity with a decreasing particle diameter is explained with the phenomenon of cohesion. The research of Shields (1936) which was carried out in the same period of time did not contain such small particle diameters, thus cohesive effects were not included in this research. The Hjulström diagram can be well approximated with the following 2 empirical equations for the threshold flow velocity and the deposition velocity as derived by Miedema (2013).

$$U_c = 1.5 \cdot \left(\frac{\nu_l}{d}\right)^{0.80} + 0.85 \cdot \left(\frac{\nu_l}{d}\right)^{0.35} + 9.5 \cdot \frac{R_{sd} \cdot g \cdot d}{\left(1 + 2.25 \cdot R_{sd} \cdot g \cdot d\right)}$$

(5.1-5)

$$U_d = 77 \cdot \frac{d}{\left(1 + 24 \cdot d\right)}$$

(5.1-6)
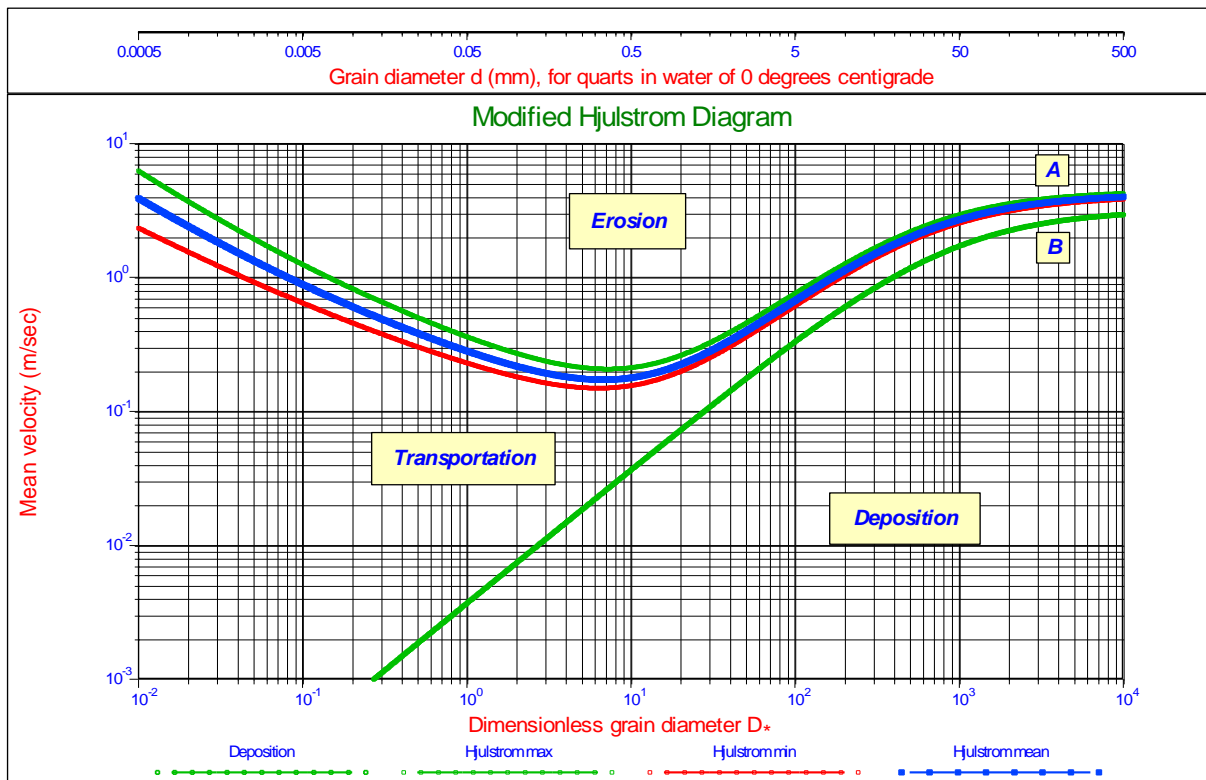
Figure 5.1-3: The modified Hjulström diagram.

Sundborg (1956) modified the Hjulström diagram and included different levels of cohesion, resulting in a more or less constant threshold flow velocity in the absence of cohesive effects for small particle diameters and a similar behavior for cohesive soils. Postma (1967) further improved the diagram and talks about consolidated and unconsolidated soils. Figure 5.1-4 shows a modified Sundborg-Hjulström diagram. Later the research focused more on improving the modeling of the Shields diagram and finding experimental proof for this, resulting in a number of mechanistic models, as summarized by Buffington & Montgomery (1997) and Paphitis (2001), and a number of empirical equations of which the Brownlie (1981) equation and the Soulsby & Whitehouse (1997) equation should be mentioned. The Brownlie (1981) equation results in an increasing Shields value for a decreasing boundary Reynolds number with a power of almost -1. Translated into critical shear stress or shear velocity, this would result in an almost constant critical shear stress and shear velocity for a decreasing particle diameter. The Soulsby & Whitehouse (1997) equation results in an increasing shear stress and shear velocity for an increasing

particle diameter for small particles. The shear stress increases almost linearly with the particle diameter and thus the shear velocity with the square root of the particle diameter. Figure 5.1-4 shows the behavior of both the Brownlie (1981) equation and the Soulsby & Whitehouse (1997) equation in the Sundborg-Hjulström diagram for 4 water depths. The third set of curves in this diagram are curves based on the Miedema (2012A) & (2012B) model, extended with the Zanke (2001) model for cohesion, as will be discussed later. From Figure 5.1-4 it is clear that unconsolidated soils (no cohesion) do not result in a horizontal line, but follow the Soulsby & Whitehouse (1997) equation, resulting in a proportionality between the threshold flow velocity and the particle diameter with a power of 0.5 for very small particles. The Brownlie (1981) equation gives a power of 0 and the Miedema (2010A) & (2010B) & Zanke (2001) model a power of -0.5 for cohesive soils. So the concept of a horizontal curve for unconsolidated/non-cohesive soils according to Sundborg (1956) and Postma (1967) is rejected here, instead the Soulsby & Whitehouse (1997) equation or the Miedema (2012A) & (2012B) model without cohesion should be used.
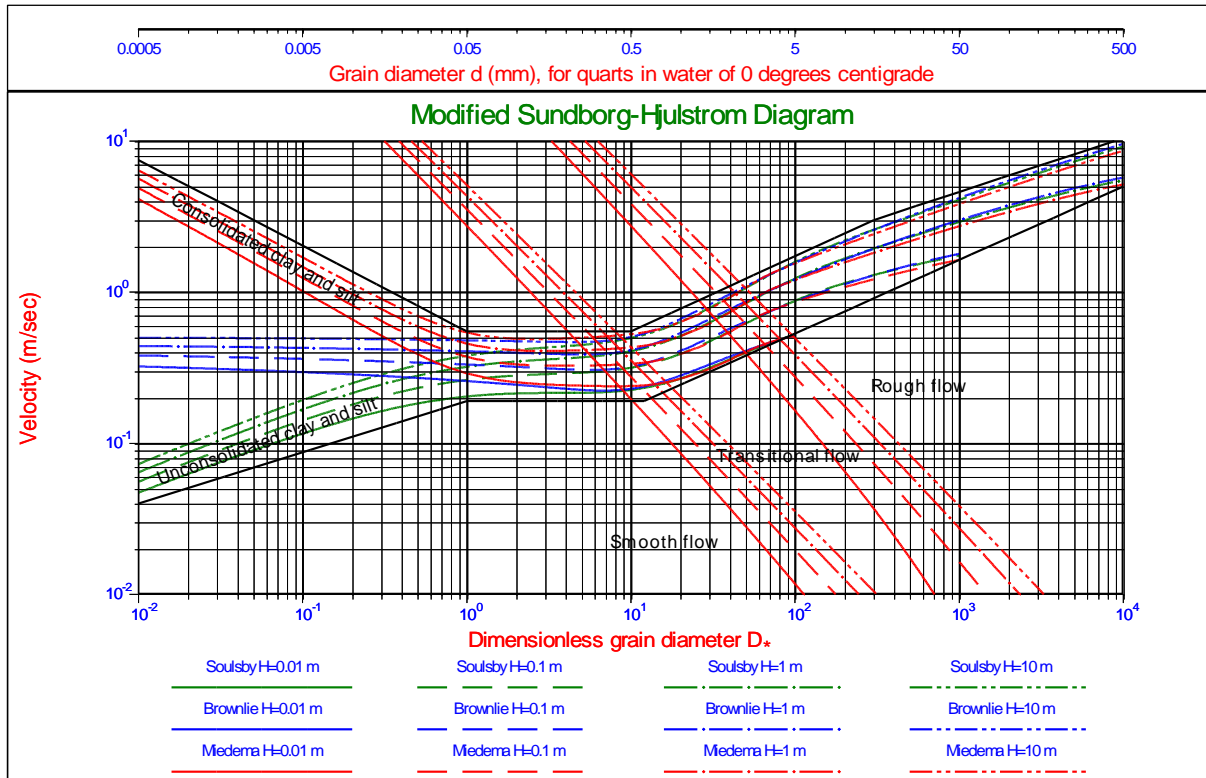
Figure 5.1-4: The modified Sundborg-Hjulström diagram.

5.1.1.3 Shortcomings of the existing models

The existing models have developed during the years and have become more and more detailed. Still some shortcoming have been found and there is space for improvement.

1.   In general the exposure and protrusion levels used have not been well defined.
2.   When rolling is chosen as the mechanism for the initiation of motion, there is a relation between the protrusion level and the pivot angle and this cannot be chosen freely.
3.   The choice of rolling, sliding or lifting as the main mechanism for the initiation of motion has not been motivated well. It is very well possible that at high protrusion levels rolling will occur, while at low protrusion levels the mechanism is sliding and at protrusion levels around zero the mechanism is lifting. Looking at nature this does not sound unreasonable, since nature will choose the mechanism with the least resistance.
4.   All models use the relations for the drag coefficient for spheres, which is reasonable realizing that many experiments are carried out for spheres, but in reality we have to deal with natural sands and gravel, so the drag coefficient for sand should be used.
5.   The models do not incorporate rolling resistance which is reasonable since quarts is very hard and thus the rolling resistance is very low. Still it is interesting to investigate the influence of rolling resistance at very high protrusion levels.
6.   The models are not based on lifting, which is also reasonable, since it can be proven mathematically that initiation of motion by lifting requires a higher shear stress than rolling or sliding, so sliding or rolling will already occur before lifting could occur. Unless the bed is fixed and one single grain is subjected to the flow

at a very low protrusion level.

7. It is difficult to distinguish between the influence of drag and lift, since both are in the denominator of equations (5.1-1) and (5.1-2). Considering full turbulent flow resulting in drag and lift, while turbulence is phased out due to the size of the particles in relation with the size of the small turbulent eddies and considering laminar flow resulting in drag and the influence of small turbulent eddies, enables us to tune the model on the different physical phenomena.

8. The models use the velocity at the center of the sphere, the average velocity on the sphere or the surface averaged velocity on the sphere. Also the lever arms for rolling are sometimes chosen at the center of the sphere or are determined by the surface averaged velocity. Since the forces on the sphere are determined by the square of the velocity in a linear or logarithmic velocity profile, the effective velocity should be determined by the surface averaged square of the velocity. This will give the actual acting point and lever arm.

9. The models are based on velocity profiles and not on the effect of the velocity on the forces on the sphere. Turbulence is a stochastic process and turbulence intensity should not be treated as a velocity profile.

10. The cross section for dragging and lifting is often chosen as the cross section of the sphere and thus chosen equal. The cross section for dragging sand lifting should depend on the protrusion and exposure levels and be different for dragging and lifting.

11. Using a velocity profile in the transition between laminar and turbulent flow is dangerous, since it is not only the velocity that changes, but also the contributions of lift and turbulence and for example the position of the acting point of the drag force.

5.1.1.4 Knowns and Unknowns.

The models identified with equations (5.1-1) and (5.1-2) contain a number of knowns and unknowns. The velocity profile and the drag coefficient can be determined theoretically or with semi-empirical equations. The viscosity (at a fixed temperature) and the Karman constant are known constants. The friction coefficient and the pivot angle can be found from many experiments or calculated geometrically. The main unknowns are the influence of turbulence and the influence of the lift coefficient. It is only useful to have different unknowns in a model if they can be isolated and measured independently. Looking at equations (5.1-1) and (5.1-2) we can see that both drag and lift are in the denominator and both drag and lift can be subject to the influence of turbulence, but then these influences cannot be isolated and measured separately. In general it can be assumed that lift does not occur in a laminar viscous flow, while the influence of small eddies is phased out for larger particles in a turbulent flow. So we will consider drag and turbulence for laminar viscous flow occurring at boundary Reynolds numbers below 5 and we will consider drag and lift for turbulent flow for boundary Reynolds numbers above 70. Since the drag based on the time averaged velocity profile is deterministic, this means that in the laminar viscous flow the only influence to make the model match the measurements is the turbulence, while in the turbulent flow the only influence to make the model match the measurements is the lift force. If there would be some lift force in the laminar viscous flow, the influence will be incorporated in the turbulence modelling, while a possible influence of turbulence in the turbulent region will be incorporated in the lift force modelling.

5.1.2 Velocity Distributions.

In 2D open channel flow, usually a logarithmic velocity profile is assumed, with a very thin viscous sub layer near the bottom. Although the cross section of a pipe does not give a 2D profile, still most researchers use the 2D approach in their models.

5.1.2.1 Scientific Classification.

Figure 5.1-5 shows the classification of flow layers. Starting from the bottom we have:

1. Viscous sub layer: a thin layer just above the bottom. In this layer there is almost no turbulence. Measurement shows that the viscous shear stress in this layer is constant. The flow is laminar. Above this layer the flow is turbulent.

2. Transition layer: also called buffer layer, viscosity and turbulence are equally important.

3. Turbulent logarithmic layer: viscous shear stress can be neglected in this layer. Based on measurement, it is assumed that the turbulent shear stress is constant and equal to bottom shear stress. It is in this layer where Prandtl introduced the mixing length concept and derived the logarithmic velocity profile.

4. Turbulent outer layer: velocities are almost constant because of the presence of large eddies which produce strong mixing of the flow.
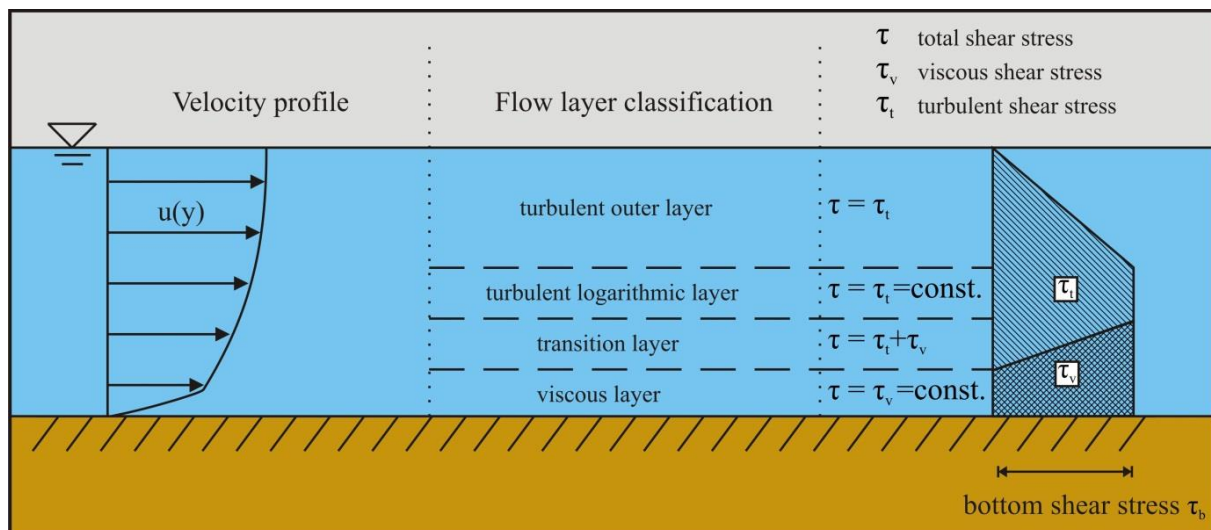
Figure 5.1-5: Scientific classification of flow region
(Layer thickness is not to scale, turbulent outer layer accounts for 80% - 90% of the region).

5.1.2.2 Engineering Classification.

In the turbulent logarithmic layer the measurements show that the turbulent shear stress is constant and equal to the bottom shear stress. By assuming that the mixing length is proportional to the distance to the bottom ($\ell=\kappa \cdot z$), Prandtl obtained the logarithmic velocity profile.

Various expressions have been proposed for the velocity distribution in the transitional layer and the turbulent outer layer. None of them are widely accepted. However, by the modification of the mixing length assumption, see next section, the logarithmic velocity profile applies also to the transitional layer and the turbulent outer layer. Measurement and computed velocities show reasonable agreement. Therefore from the engineering point of view, a turbulent layer with the logarithmic velocity profile covers the transitional layer, the turbulent logarithmic layer and the turbulent outer layer, see Figure 5.1-6.

As to the viscous sub layer, the effect of the bottom (or wall) roughness on the velocity distribution was first investigated for pipe flow by Nikuradse. He introduced the concept of equivalent grain roughness k_s (Nikuradse roughness, bed roughness). Based on experimental data, it was found

1. Hydraulically smooth flow for $u_* \cdot k_s / \nu \leq 5$, bed roughness is much smaller than the thickness of viscous sub layer. Therefore, the bed roughness will not affect the velocity distribution.

2. Hydraulically rough flow for $u_* \cdot k_s / \nu \geq 70$, bed roughness is so large that it produces eddies close to the bottom. A viscous sub layer does not exist and the flow velocity is not dependent on viscosity.

3. Hydraulically transitional flow for **5≤u∗·ks/νl≤70**, the velocity distribution is affected by bed roughness and viscosity.

5.1.2.3 Friction Velocity.

The bottom shear stress is often represented by friction velocity, defined by:

$$\mathbf{u_*} = \sqrt{\frac{\tau_b}{\rho_l}}$$

(5.1-7)

The term *friction velocity* comes from the fact that $\sqrt{\tau_b/\rho_l}$ has the same unit as velocity and it has something to do with friction force.
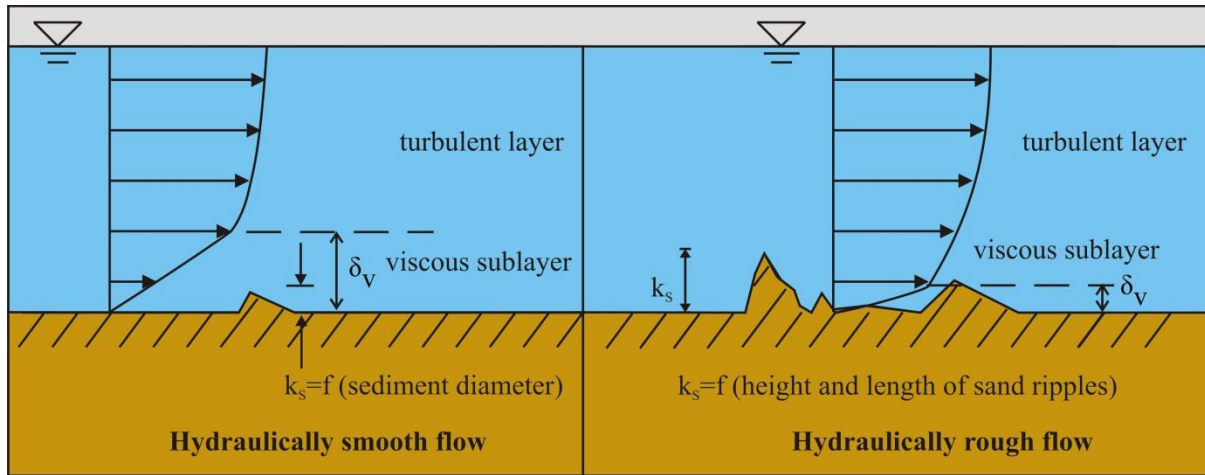
Figure 5.1-6: Engineering classification of flow region (Layer thickness is not to scale).

5.1.2.4 Turbulent Layer.

In the turbulent layer the total shear stress contains only the turbulent shear stress. The total shear stress increases linearly with depth, i.e.

$$\tau_t(\mathbf{y}) = \tau_b \cdot \left(1 - \frac{\mathbf{y}}{\mathbf{h}}\right)$$

(5.1-8)

Expressed using Prandtl's mixing length theory:

$$\tau_t = \rho_l \cdot \ell^2 \left(\frac{d\mathbf{u}}{d\mathbf{y}}\right)^2$$

(5.1-9)

Now assuming the mixing length is:

$$\ell = \kappa \cdot \mathbf{y} \cdot \left(1 - \frac{\mathbf{y}}{\mathbf{h}}\right)^{0.5}$$

(5.1-10)

With **κ** the Von Karman constant (**κ=0.412**) and **h>>y**, we get:

$$\frac{d\mathbf{u}}{d\mathbf{y}} = \frac{1}{\kappa \cdot \mathbf{y}} \cdot \sqrt{\frac{\tau_b}{\rho}} = \frac{\mathbf{u_*}}{\kappa \cdot \mathbf{y}}$$

(5.1-11)

Integration gives the famous logarithmic velocity profile (Law of the Wall):

$$u(y) = \frac{u_*}{\kappa} \cdot \ln\left(\frac{y}{y_0}\right) \tag{5.1-12}$$

Where the integration constant y_0 is the elevation corresponding to zero velocity ($u_{y=y0}=0$), given by Nikuradse in his study of pipe flows.

$$y_0 = 0.11 \cdot \frac{\nu_l}{u_*} \qquad \text{Hydraulically smooth flow} \qquad \frac{u_* \cdot k_s}{\nu_l} \le 5 \tag{5.1-13}$$

$$y_0 = 0.033 \cdot k_s \qquad \text{Hydraulically rough flow} \qquad \frac{u_* \cdot k_s}{\nu_l} \ge 70 \tag{5.1-14}$$

$$\frac{y_0}{k_s} = \frac{1}{9 \cdot k_s^+} + \frac{1}{30} \cdot \left(1 - e^{-\frac{k_s^+}{26}}\right) \qquad \text{Hydraulically transition flow} \qquad 5 < \frac{u_* \cdot k_s}{\nu_l} < 70 \tag{5.1-15}$$
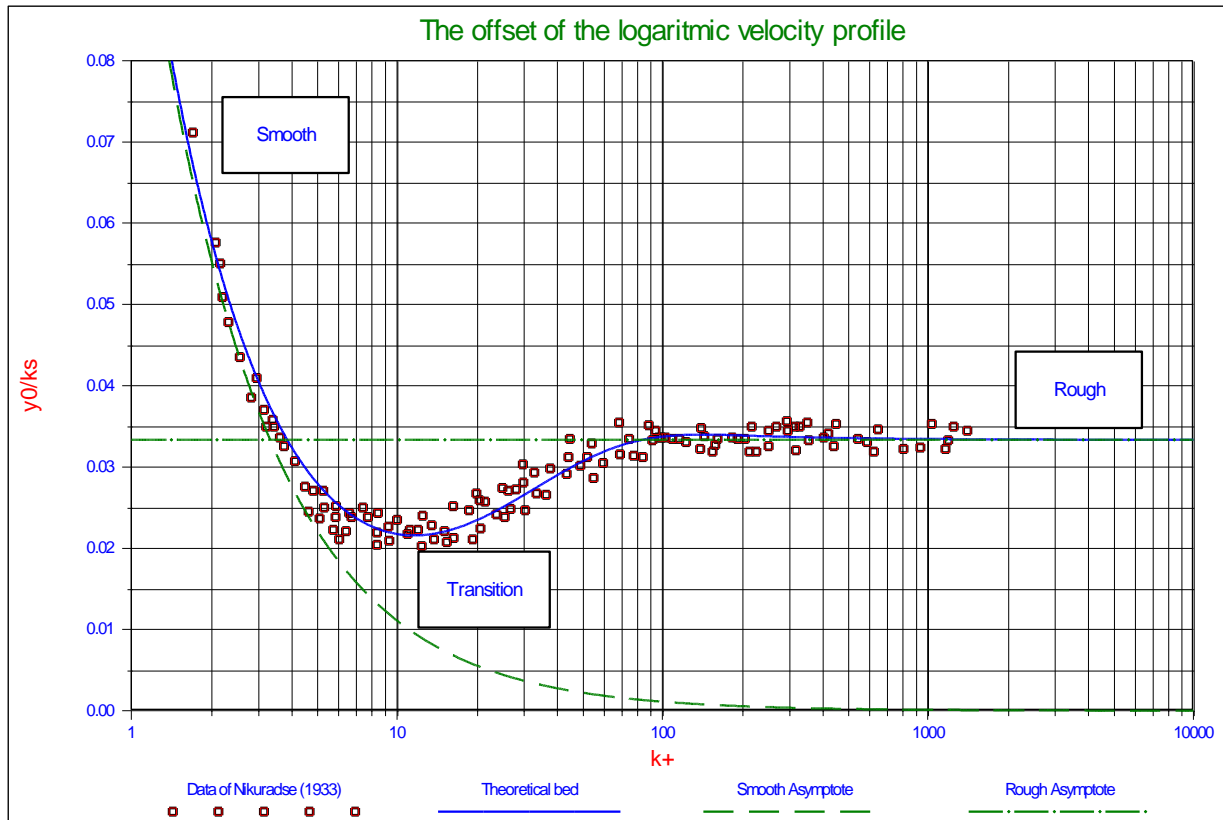
Figure 5.1-7: The transition smooth-rough (Guo & Julien, 2007).

5.1.2.5 Bed roughness

The bed roughness k_s is also called the equivalent Nikuradse grain roughness, because it was originally introduced by Nikuradse in his pipe flow experiments, where grains are glued to the smooth wall of the pipes. The only situation where we can directly obtain the bed roughness is a flat bed consisting of uniform spheres, where $k_s =$ diameter of sphere. But in nature the bed is composed of grains with different size. Moreover, the bed is not flat, various bed forms, e.g. sand ripples or dunes, will appear depending on grain size and current. In that case the bed roughness can be obtained indirectly by the velocity measurement.

5.1.2.6 Viscous Sub-Layer.

In the case of hydraulically smooth flow there is a viscous sub layer. Viscous shear stress is constant in this layer and equal to the bottom shear stress, i.e.

$$\tau_v = \rho_l \cdot \nu_l \cdot \frac{du}{dy} = \tau_b \tag{5.1-16}$$

Integrating and applying $u_{y=0}=0$ gives:

$$u(y) = \frac{\tau_b}{\rho_l} \cdot \frac{y}{\nu_l} = \frac{u_*^2}{\nu_l} \cdot y = y^+ \cdot u_* \tag{5.1-17}$$

Thus, there is a linear velocity distribution in the viscous sub layer. The linear velocity distribution intersects with the logarithmic velocity distribution at the elevation $y=11.6\cdot\nu_l/u_*$, yielding a theoretical viscous sub layer thickness δ_v:

$$\delta_v = 11.6 \cdot \frac{\nu_l}{u_*} \tag{5.1-18}$$

The velocity profile is illustrated in Figure 5.1-8, with the detailed description of the fluid velocity near the bottom.
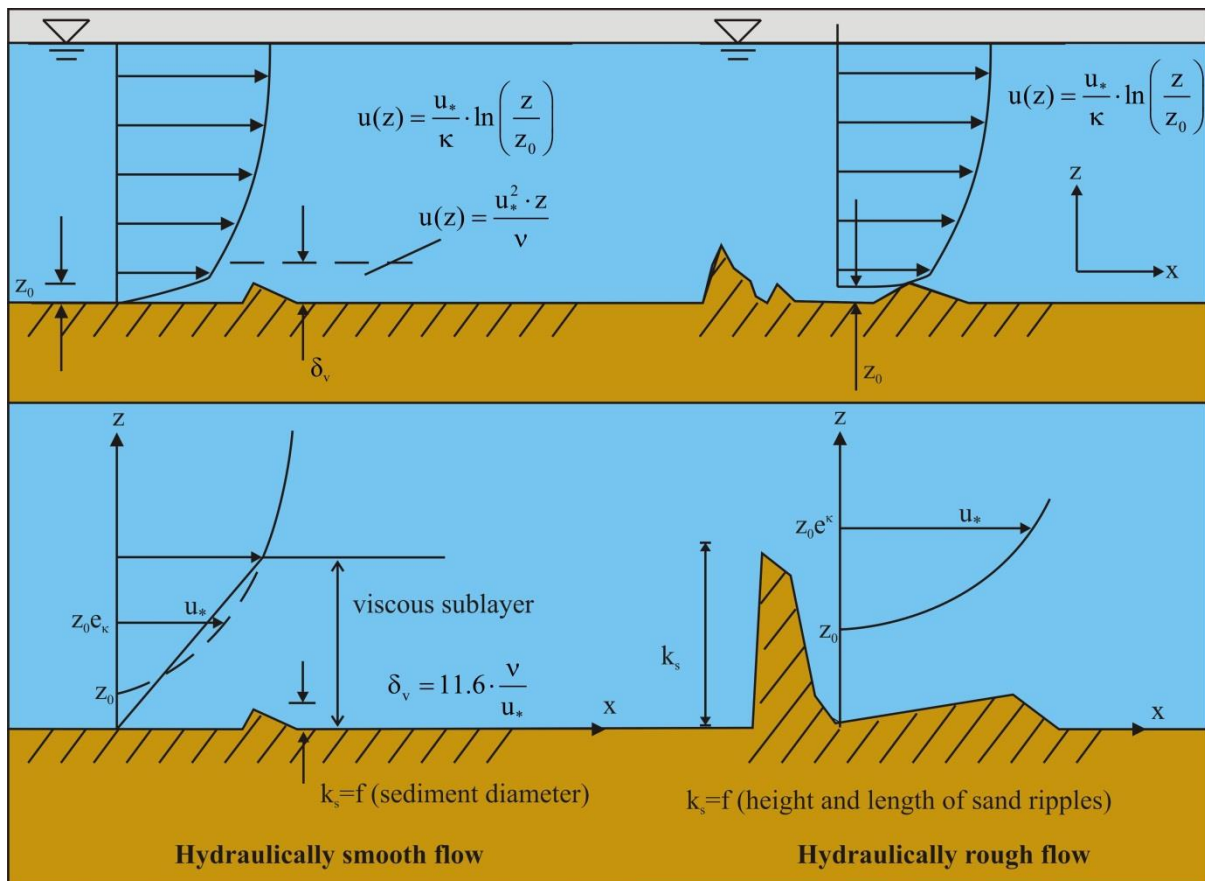
Figure 5.1-8: Illustration of the velocity profile in hydraulically smooth and rough flows (Liu Z. , 2001)

5.1.2.7 The Transition Laminar-Turbulent.

Reichardt (1951) derived an equation for the velocity that describes a laminar linear profile up to an y^+ value of about 5, a turbulent logarithmic profile from an y^+ value of about 40 and a transition velocity profile from 5 to 40 that is in excellent agreement with measurements made in that zone (see Schlichting (1968), p. 601). Equation (5.1-19) and Figure 5.1-9 show this velocity profile. Wiberg & Smith (1987A) and others also use this velocity profile.

$$\frac{u(y)}{u_*} = \frac{\ln(1+\kappa \cdot y^+)}{\kappa} - \frac{\ln(1/9)+\ln(\kappa)}{\kappa} \cdot \left(1 - e^{-\frac{y^+}{11.6}} - \frac{y^+}{11.6} e^{-0.33 \cdot y^+} \right) \tag{5.1-19}$$

5.1.2.8 The Transition Smooth-Rough.

The transition between hydraulic smooth and rough flow can be approximated in many ways, but the resulting equation should match the measurements of Garcia (2008) (Figure 5.1-7). The following equation (derived by the author), give a very good approximation of this transition, where the distance to the wall equals the roughness. Equation (5.1-20) gives the velocity as a function of the non-dimensional distance to the wall y^+.

$$\frac{\bar{u}(y^+)}{u_*} = \frac{1}{\kappa} \cdot \ln\left(\frac{y^+}{0.11}\right) \cdot e^{-0.95 \cdot \frac{k_s^+}{11.6}} + \frac{1}{\kappa} \cdot \ln\left(\frac{y^+}{0.033 \cdot k_s^+}\right) \cdot \left(1 - e^{-0.95 \cdot \frac{k_s^+}{11.6}} \right) \tag{5.1-20}$$

Since $11.6 = \delta_v \cdot u_* / \nu_l = \delta_v^+$ and $0.11 = 0.11 \cdot \delta_v \cdot u_* / \nu_l / 11.6 = 0.0095 \cdot \delta_v^+$ and the influence of the second right hand term (giving 95 instead of 105), equation (5.1-20) can be written as:

$$\frac{\bar{u}(y^+)}{u_*} = \frac{1}{\kappa} \cdot \ln\left(95 \cdot \frac{y^+}{\delta_v^+}\right) \cdot e^{-0.95 \cdot \frac{k_s^+}{\delta_v^+}} + \frac{1}{\kappa} \cdot \ln\left(30 \cdot \frac{y^+}{k_s^+}\right) \cdot \left(1 - e^{-0.95 \cdot \frac{k_s^+}{\delta_v^+}} \right) \tag{5.1-21}$$

In terms of the dimensional parameters for the distance to the wall y, the roughness k_s and thickness of the laminar layer δ_v this gives:

$$\frac{\bar{u}(y)}{u_*} = \frac{1}{\kappa} \cdot \ln\left(95 \cdot \frac{y}{\delta_v}\right) \cdot e^{-0.95 \cdot \frac{k_s}{\delta_v}} + \frac{1}{\kappa} \cdot \ln\left(30 \cdot \frac{y}{k_s}\right) \cdot \left(1 - e^{-0.95 \cdot \frac{k_s}{\delta_v}} \right) \tag{5.1-22}$$

Figure 5.1-10 shows the non-dimensional velocity u^+ at distances $y=k_s$, $y=0.9 \cdot k_s$, $y=0.8 \cdot k_s$, $y=0.7 \cdot k_s$, $y=0.6 \cdot k_s$, $y=0.5 \cdot k_s$ and, $y=0.4 \cdot k_s$ from the wall. Up to a Reynolds number of 20 and above a Reynolds number of 70 equation (5.1-20) matches the measurements very well, between 20 and 70 the equation underestimates the measured values, but overall the resemblance is very good.
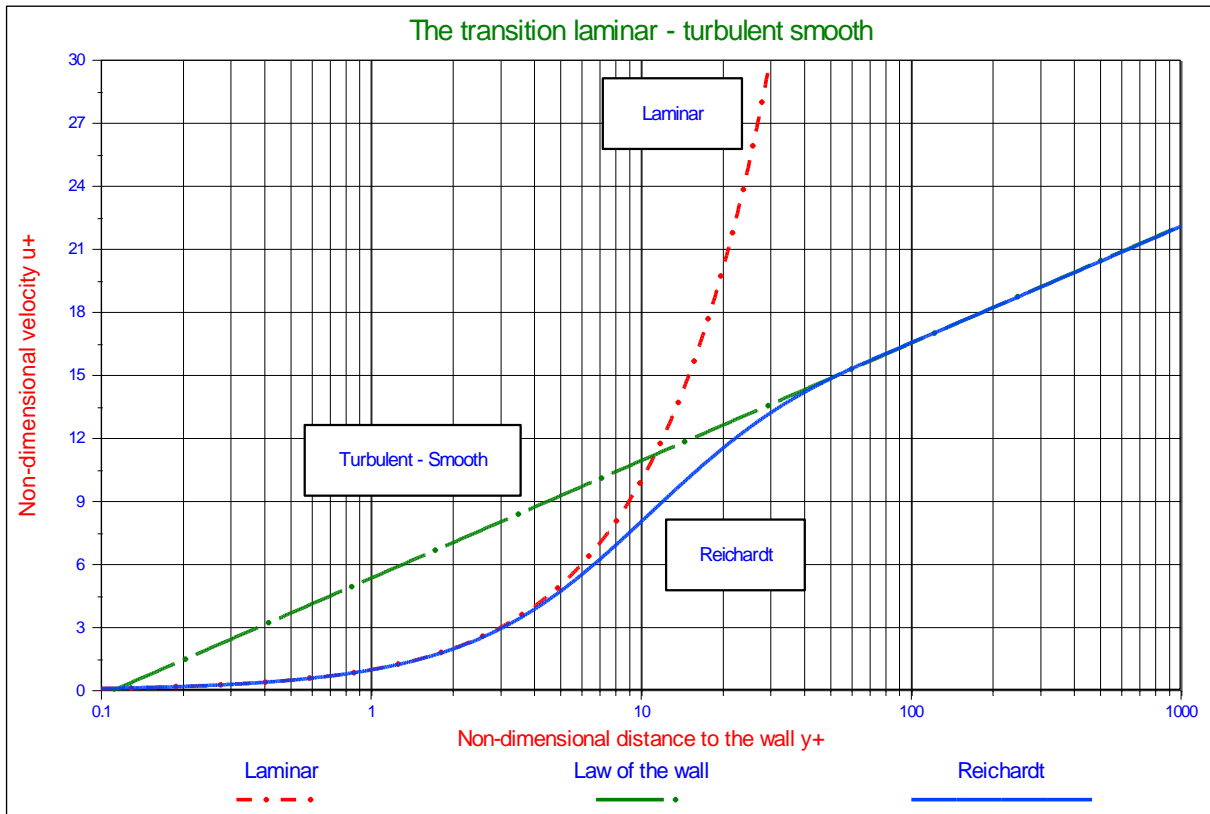
Figure 5.1-9: The velocity profile from laminar to smooth-turbulent.
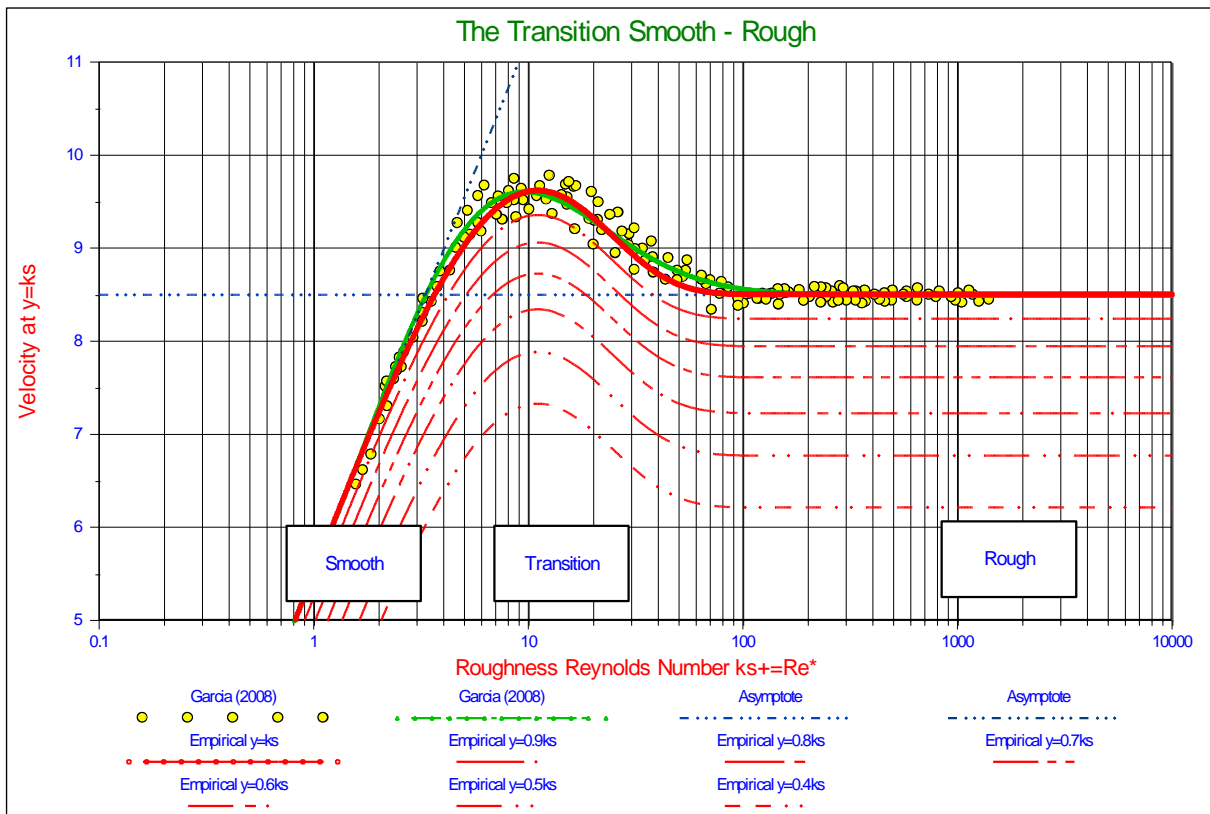
Figure 5.1-10: The transition smooth-rough for a number of distances to the wall.

5.1.3 The Model for Initiation of Motion.

5.1.3.1 The Angle of Internal Friction/the Friction Coefficient.

When the mechanism for the initiation of motion is sliding, friction is involved. The angle of repose of granular material is often referred to as the angle of internal friction of the material in a loose condition. By rotating a bed until the top layer of particles starts to move (slide or roll) the angle of repose is determined, which is the slope angle at that point. Another way of determining this angle is to pour the particles on a surface and measure the slope angle of the cone shaped heap of particles that is formed. In literature a value between **30°-35°** is mentioned for natural sands. Figure 5.1-11 shows the angle of repose for different materials and grain sizes. The relation between the friction coefficient and the angle of repose is:

$$\mu_{sf} = \tan(\phi) \tag{5.1-23}$$

It should be noted that the angle of repose, in this context, is a global soil mechanical parameter, which can be used as an average value when the whole top layer starts to move. Individual particles may encounter a different value. It should also be noted that the angle of repose is related to friction, which always has to do with the dissipation of energy, so it should not be mixed up with the pivot or dilatation angle which is related to resistance but not to the dissipation of energy.
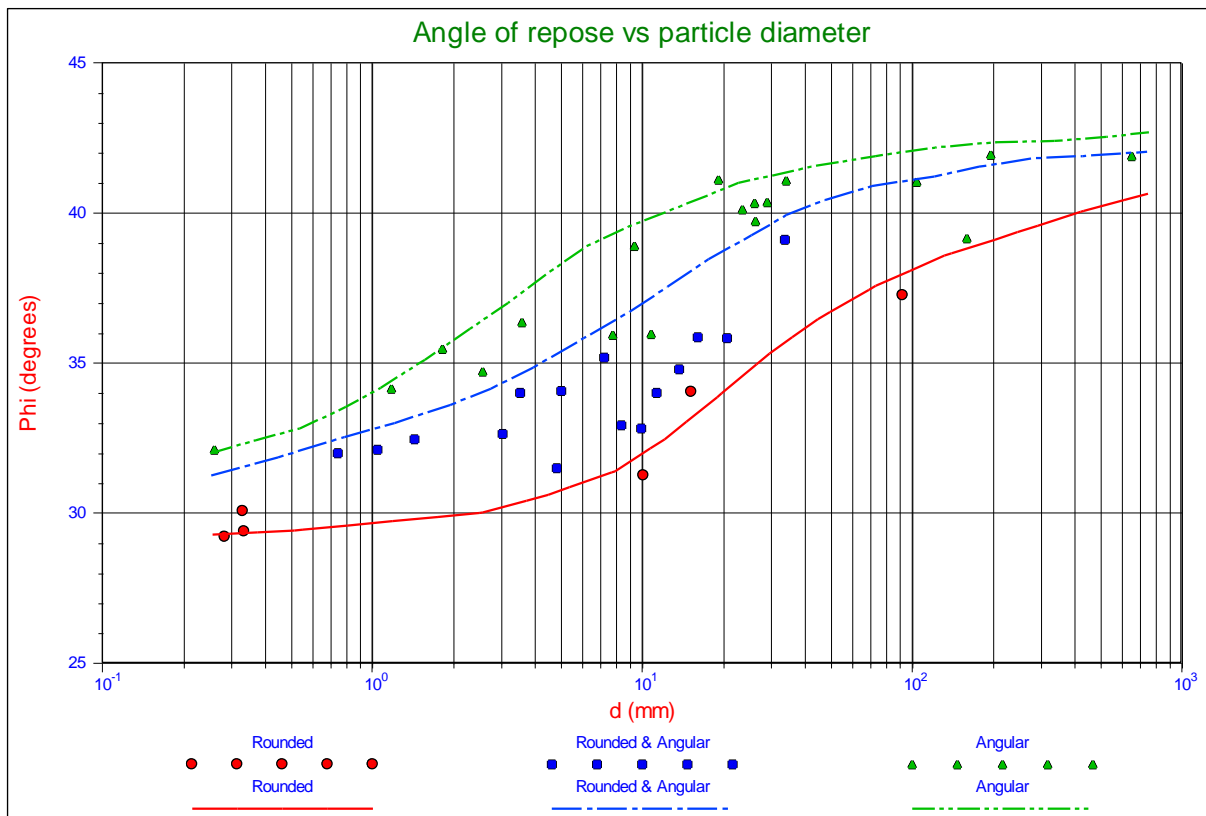
Figure 5.1-11: Angle of repose for granular material (Simons, 1957).

5.1.3.2 The Pivot Angle/the Dilatation Angle.

When the mechanism for the initiation of motion is rolling, a pivot angle is involved. For spheres there is a geometrical relation between the pivot angle and the protrusion level. The pivot angle is sometimes referred to as the dilatation angle, which however is a global soil mechanical parameter and it is preferred not to use it as a local parameter, so we will use the term pivot angle. Luckner (2002) (page 18) determined the pivot angle for **3D** sphere configurations, from protrusion levels ranging from 0% to 82%. In fact the maximum protrusion level of a sphere on top of other spheres in a **3D** configuration is 82%. At a protrusion level of 0%, meaning the sphere is in between and at the same level as the surrounding spheres, the pivot angle is $\psi=90°$ At a protrusion level of 30% the pivot angle is $\psi=59°$, at 80% about $\psi=20°$, at 90% about $\psi=12°$ and of course at 100% $\psi=0°$. In between these values

a linear interpolation can be carried out. It is obvious that one is not free to choose the pivot angle, since it is related to the protrusion level.

Luckner (2002) determined the relation between the protrusion level and the pivot angle by using an ideal tetrahedral arrangement of spheres in a three dimensional approach. With the transformation from protrusion to exposure level and some curve fitting on the calculations of Luckner (2002), the following relation is found between the pivot angle ψ (in degrees) and the exposure level **E**, assuming the pivot angle equals the angle of contact as used here.

$$\psi = -144.12 \cdot E^4 + 342.7 \cdot E^3 - 245.05 \cdot E^2 - 37.184 \cdot E + 104.28 \qquad (5.1\text{-}24)$$

5.1.3.3 The Lift Coefficient

The choice of the lift coefficient is a discussion in many of the models and many different values are found. Sometimes the lift coefficient is expressed as a fraction of the drag coefficient and sometimes as a constant. In most models however lift is present in the turbulent flow, but not in the laminar viscous sub layer. In this model also the choice is made to neglect lift in the laminar region, so for boundary Reynolds numbers below 5. Wiberg & Smith (1987A), Dey (1999), Pilotti & Menduni (2001), Stevenson, Thorpe & Davidson (2002) and others support this assumption. For the turbulent region different values are used for the lift coefficient.
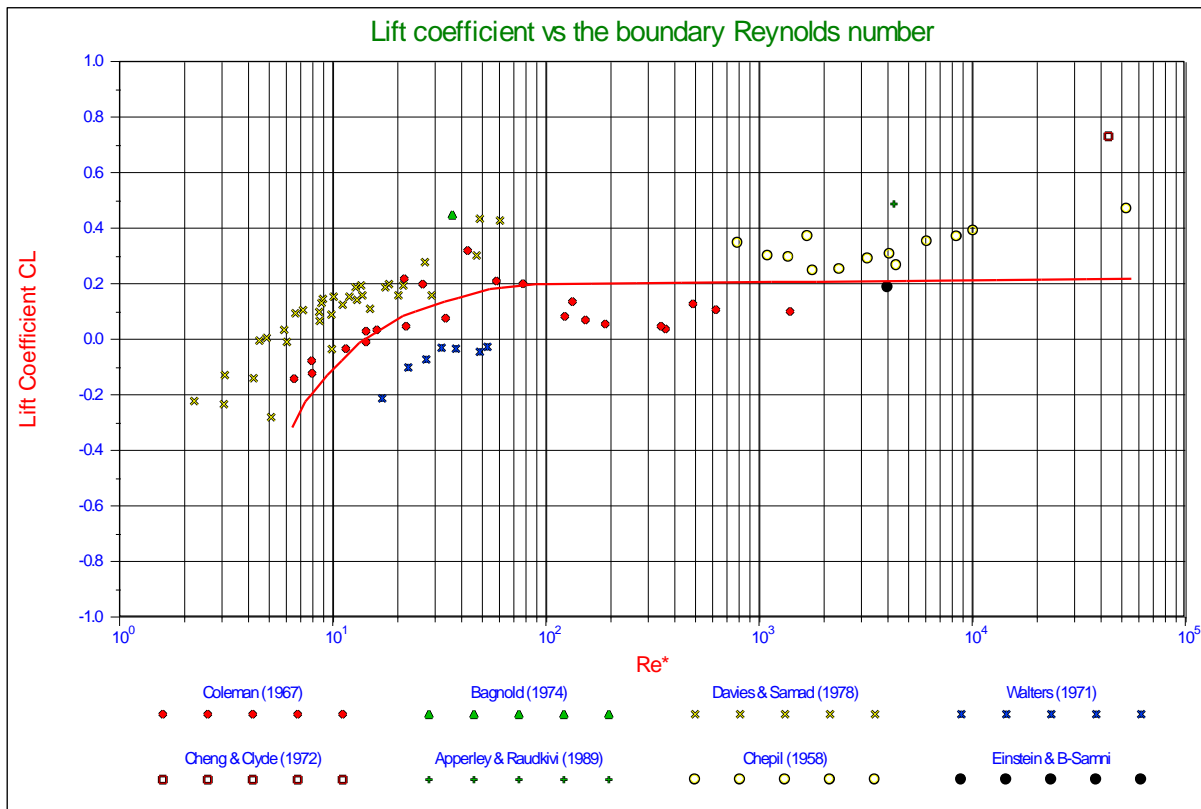
Figure 5.1-12: The lift coefficient as a function of the particle Reynolds number.

Wiberg & Smith (1987A) use a value of 0.2, while using **0.85·C_D** in (Wiberg & Smith, 1987B) inspired by the work of Chepil (1958). Marsh, Western & Grayson (2004) compared 4 models, but also evaluated the lift coefficient as found by a number of researchers as is shown in Figure 5.1-12. For large Reynolds numbers an average value of 0.2 is found, while for small Reynolds numbers the lift coefficient can even become negative. Luckner (2002) found a relation where the lift coefficient is about **1.9·E·C_D** (including the effect of turbulence), which matches the findings of Dittrich, Nestmann & Ergenzinger (1996). For an exposure level of 0.5 this gives **0.95·C_D** which is close to the findings of Chepil (1958). Using a lift coefficient of **0.95·C_D=0.423** for boundary Reynolds numbers above 70, results in Shields curves matching the experimental data.

5.1.3.4 Turbulence

Turbulence describes the stochastic non-deterministic velocity fluctuations in a flow and although coherent structures exist in the occurrence of turbulence, turbulence has no long term memory. The implication of this is that turbulence cannot be described by a velocity profile, but instead it can be described by statistical properties. In general it is described by the turbulence intensity of the horizontal and vertical velocity and the intensity of the Reynolds stress. These intensities reflect the so called r.m.s. (root mean square) values of the velocity fluctuations. Assuming the velocity fluctuations are according to a normal or Gaussian distribution, the time and surface averaged velocity profiles represent the mean value of the distribution, as used in equations (5.1-19) and (5.1-21), while the standard deviation is represented by the r.m.s. value, also called the first moment of the distribution. The second moment and third moment correspond to two times and three times the r.m.s. value. The probability of having an instantaneous velocity higher than the standard deviation in the direction of the mean velocity is 14.9%, for the second moment this is 2.3% and for the third moment 0.13%.

Wiberg & Smith (1987A) reduce the height of the viscous sub layer to 60%, resulting in an increase of 1/0.6=1.66 of the velocity in the viscous sub layer. Assuming a turbulence intensity of $0.3 \cdot y^+ \cdot u_*$ (Nezu & Nakagawa, 1993) and a mean velocity of $y^+ \cdot u_*$, implicitly this means adding 2.2 times the turbulence intensity to the mean velocity. Since Wiberg & Smith only apply this for low boundary Reynolds numbers where the particles are small with regard to the height of the viscous sub layer, implicitly this means adding a turbulence effect to small boundary Reynolds numbers (smooth boundaries) and not to large boundary Reynolds numbers (rough boundaries). Hofland (2005) in his PhD thesis states that fluctuations created by smaller eddies are negligible for larger particles due to phase cancellations when integrated over the surface of a stone. Zanke (2001) and later Luckner (2002) apply turbulent velocity fluctuations both for small and large boundary Reynolds numbers and add 1.8 times the turbulence intensity to the mean velocity. Nezu & Nakagawa (1977) and (1993) and Nezu & Rodi (1986) found the following relation for the turbulence intensity parallel to the wall.

$$\frac{u_{r.m.s.}}{u_*} = 0.3 \cdot y^+ \cdot e^{-\frac{y^+}{10}} + 2.26 \cdot e^{-\frac{y}{h}} \cdot \left(1 - e^{-\frac{y^+}{10}}\right) \tag{5.1-25}$$

The asymptotic value of the ratio between the turbulence intensity and the time and surface averaged velocity is 0.3. Measurements of this ratio, carried out by Eckelman (Hinze, 1975) on smooth walls as a function of the distance to the wall y^+, show a small increase near the wall to a value of 0.38 at $y^+=4$. Approaching the wall further shows a decrease to a value of 0.24, but the measurements do not contradict the assumption of having a ratio at the wall of zero. Kim, Moin and Moser (1987) confirm these findings, but state that additional measurements show a finite value at the wall, although the measurements in their paper do not contradict a value of zero. Zanke (2003) assumes a ratio of zero at the wall and achieves this by shifting the time averaged velocity with respect to the distance to the wall. In fact implicitly this means that the virtual bed level for the time averaged velocity (which is chosen at $0.2 \cdot d$ below the top of the spheres in this paper) is located lower than the virtual bed level for the turbulence intensity.

Considering that the measurements of Eckelman and later Kim, Moin & Moser were carried out on a smooth wall where the wall is the virtual bed level, while here we consider a bed of grains or spheres where a virtual bed level has to be defined, resulting in a correct drag force on the spheres, there is no reason why the two virtual bed levels should be the same. The solution of Zanke, choosing two different virtual bed levels is one way of solving this problem. One can also choose one virtual bed level for both, the time averaged velocity and the turbulence intensity, but consider that below the top of the spheres, the turbulence intensity is decreased, due to the shadow effect of the spheres. Assuming the turbulence intensity to be zero at the virtual bed level and increasing proportional to the square of the distance to the wall, very close to the wall between the grains, and proportional to the distance to the wall above the grains, this can be represented with the following equation:

$$\frac{u'_{r.m.s.}}{u_*} = \frac{u_{r.m.s.}}{u_*} \cdot \left(1 - e^{-y^+}\right) \tag{5.1-26}$$

Another reason for assuming a ratio of zero at the virtual bed level is the fact that the asymptotic value found for the Shields curve for the boundary Reynolds number approaching zero matches the measurements (see Figure 5.1-15). Any ratio larger than zero would lower the curves found. Figure 5.1-13C shows the turbulence intensity according to equation (5.1-25), while Figure 5.1-13A shows the turbulence intensity very close to the wall. Figure 5.1-13B shows the difference between equation (5.1-25) and applying damping on the turbulence intensity very

close to the wall according to equation (5.1-26). The turbulence intensity profile according to equation (5.1-26) does not contradict the findings of Nezu and Nakagawa (1993), Eckelman (Hinze, 1975) and Kim, Moin & Moser (1987) and matches the findings of Zanke (2003). Now it is the question how many times the standard deviation of the turbulence intensity should be used.

Wiberg & Smith (1987A) implicitly used a factor 2.2 and Zanke (2003) used a factor 1.8 explicitly. Since we consider the initiation of motion, particles or spheres will start to entrain if there is one moment when the condition for entrainment is satisfied. On the other hand the Shields curve falls somewhere between critical and general transport, meaning that already many particles at many locations entrain. The factor n in equation (5.1-27), the turbulence intensity factor, is chosen 3. Meaning that the probability of having a higher instantaneous velocity is only 0.13%, so about 1 out of 1000 occurrences of turbulent eddies.

$$\frac{u'_{n \cdot r.m.s.}}{u_*} = n \cdot \frac{u'_{r.m.s.}}{u_*} \qquad\qquad (5.1-27)$$
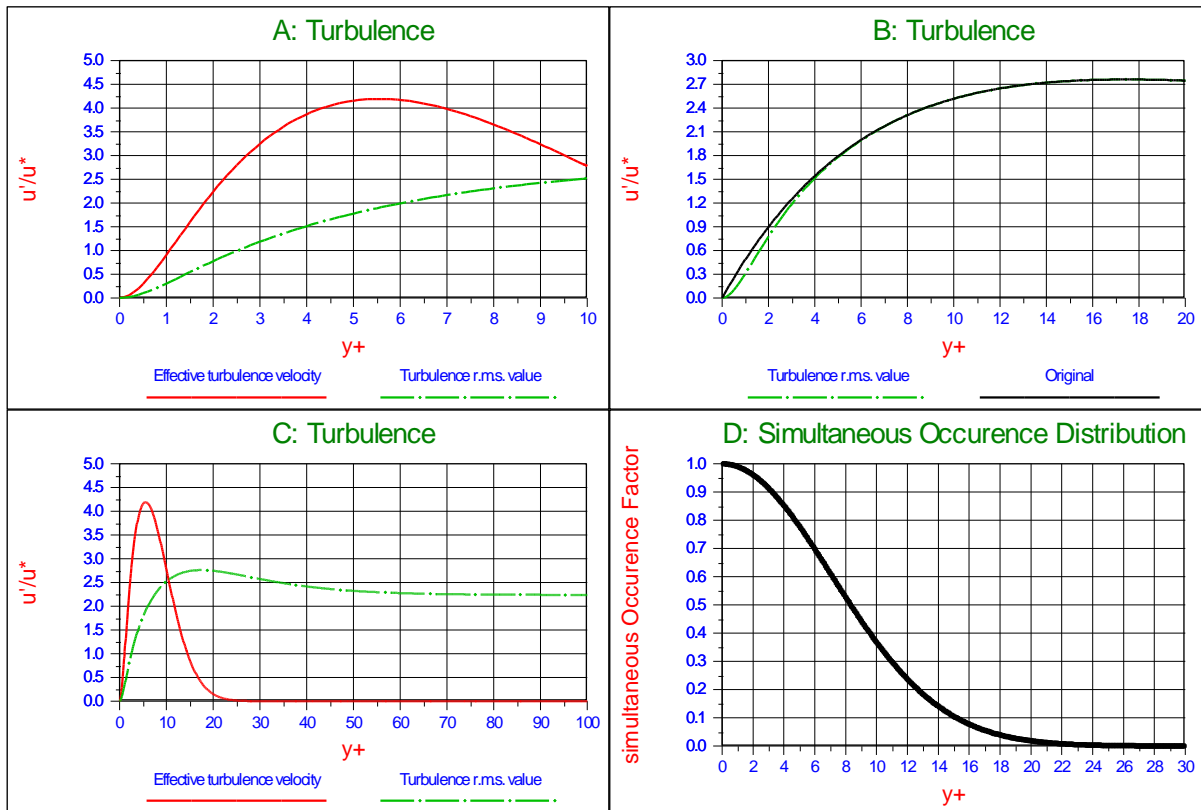
Figure 5.1-13: The contribution of turbulence to the velocity.

The resulting turbulence intensity profile should not be interpreted as a velocity distribution, since it describes the intensity of stochastic turbulent velocity fluctuations. This means that the influence of these fluctuations on the drag force can be derived by integrating the fluctuations over the height of a particle and in fact this should be added to the mean velocity and then the surface averaged value of the square of the total velocity should be determined. Taking the square root of this velocity and deducting the time averaged velocity gives the contribution of the turbulence. Since at one location the turbulent velocity fluctuations will be positive, while at the same time at other locations they will be negative, the probability that at one moment in time the turbulent velocity fluctuations over the height of the particle are unidirectional in the direction of the time averaged velocity is almost zero.

For very small particles having a diameter smaller than or equal to the size of the small turbulent eddies, this may still be the case, but with increasing diameter the influence of the eddies will decrease due to the fact that they cancel each other out. For very large particles the influence of this turbulence will reduce to zero. It is proposed to name this effect the probability of simultaneous occurrence effect and the factor determining the turbulent velocity that should be added to the time averaged velocity, the factor of simultaneous occurrence. The point of action of the resulting surface averaged square of the velocity is assumed not to change, although there is no reason for that.

With the height $\mathbf{y^+}=\mathbf{E \cdot Re_*}$ at the top of a particle with exposure level $\mathbf{E,}$ equation (5.1-28) is proposed for the factor of simultaneous occurrence and this is shown in Figure 5.1-13D. The resulting effective velocity profile is shown in Figure 5.1-13C and Figure 5.1-13A.

$$\frac{\mathbf{u_{eff}}}{\mathbf{u_*}} = \frac{\mathbf{u'_{n \cdot r.m.s.}}}{\mathbf{u_*}} \cdot e^{-\left(\frac{\mathbf{y^+}}{\mathbf{10}}\right)^2} \tag{5.1-28}$$

5.1.3.5 Approach.

Before developing the model a number of assumptions have to be made in order to have starting points for the modeling to match the Shields curve and the measurements from literature. These assumptions have to be reasonable, matching literature and practice. These assumptions are:
1. The bed consists of spheres with one diameter **d**.
2. The virtual bed level is chosen at **0.2·d** below the top of the bed.
3. The criterion for initiation of motion is chosen to be between critical transport and general transport according to Vanoni (1975), Delft Hydraulics (1972) and Graf & Pazis (1977).
4. The exposure level **E** is chosen as **0.5·d**, resulting in a protrusion level of **0.3·d**, meaning that the standard sphere is exposed to the flow for 50% and reaches above the other spheres in the bed for 30%, based on Fenton & Abbot (1977) and Chin & Chiew (1993).
5. For the model an internal friction angle (angle of natural repose) of $\boldsymbol{\varphi}=\mathbf{30°}$ is chosen (for the sliding mechanism), which matches spheres and rounded particles of natural sands and gravel (see Figure 5.1-11).
6. For the model a pivot angle of $\boldsymbol{\psi}=\mathbf{59°}$ is chosen (for the rolling mechanism), which matches a protrusion level of **0.3·d**, based on Luckner (2002).
7. First full laminar flow will be considered up to a boundary/roughness Reynolds number of 11.6 and full turbulent flow above 11.6. The laminar flow is described with equation (5.1-19) and the turbulent flow with equation (5.1-17).
8. Later a transition area is introduced with full laminar flow up to a boundary/roughness Reynolds number of 5, a transition zone from 5 to 70 and a full turbulent flow above 70, with logarithmic interpolation in the transition zone.
9. For the laminar flow, the velocity at the top of the sphere is $0.5 \cdot \mathbf{Re_* \cdot u_*}$, resulting in an acting point at $\boldsymbol{\ell_{Drag}}=\mathbf{0.5}$, meaning at 50% of the flow field (see equation (5.1-19)). This also means the acting point is at **0.25·d** above the center of the sphere (based on a surface averaged square of the velocity).
10. For the turbulent flow, the velocity at the top of the sphere is $\mathbf{ln(0.5/0.033) \cdot u_* / \kappa = 6.6 \cdot u_*}$, resulting in an acting point at $\boldsymbol{\ell_{Drag}}=\mathbf{0.655}$, meaning at 65.5% of the flow field (see equation (5.1-12)). This also means the acting point is at **0.327·d** above the center of the sphere (based on a surface averaged square of the velocity).
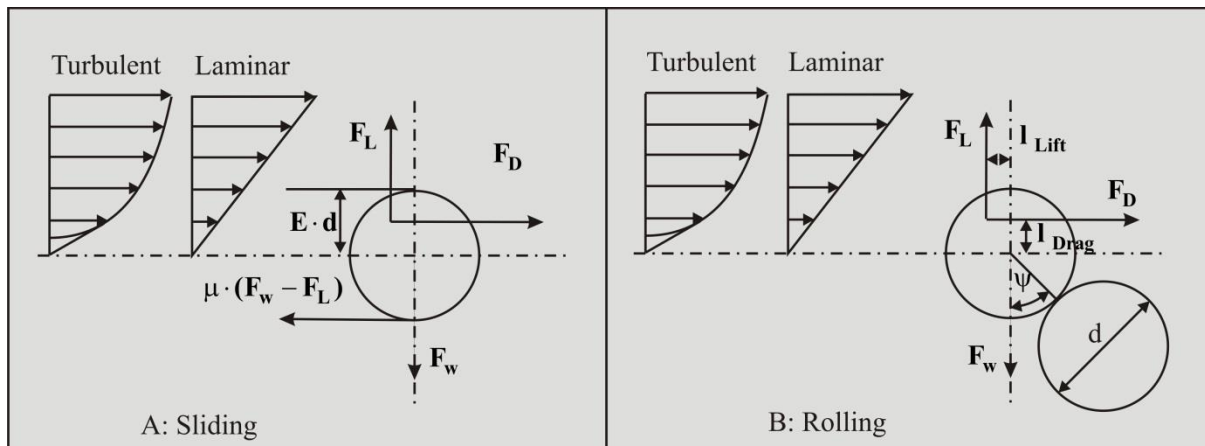
Figure 5.1-14: Drag and lift induced sliding (A) and rolling (B).

In Miedema (2012A) & (2012B), a model for the entrainment of particles as a result of liquid (or air) flow over a bed of particles has been developed based on the above assumptions. The model distinguishes sliding, rolling and lifting as the mechanisms of entrainment. Sliding is a mechanism that occurs when many particles are starting to move and it is based on the global soil mechanical parameter of internal friction. Both rolling and lifting are mechanisms of individual particles and they are based on local parameters such as the pivot angle and the exposure and protrusion rate. Equations (5.1-34), (5.1-38) and (5.1-42) give the Shields parameter for these 3 mechanisms.

5.1.3.6 Drag and Lift Induced Sliding.

Let us consider the steady flow over a bed composed of cohesion less grains. The driving forces are the flow drag and lift forces on the grain, assuming that part of the surface of the particle is hiding behind other particles and only a fraction E (the exposure level) is subject to drag and lift. This gives the following equation for the drag force:

$$F_D = C_D \cdot \frac{1}{2} \cdot \rho_l \cdot \left(\ell_{Drag} \cdot \alpha \cdot u_* \right)^2 \cdot f_D \cdot \frac{\pi \cdot d^2}{4} \tag{5.1-29}$$

The lift force is written in the same way, but it is assumed that the lift force is determined by the velocity difference between the top and the bottom of the particle and the surface that is subject to lift is the projected horizontal cross section subject to the flow, this factor $f_L=1$ for an exposure level $E=0.5$, while the factor for drag $f_D=0.5$ in this case:

$$F_L = C_L \cdot \frac{1}{2} \cdot \rho_l \cdot (\alpha \cdot u_*)^2 \cdot f_L \cdot \frac{\pi \cdot d^2}{4} \tag{5.1-30}$$

The submerged weight of the particle is:

$$F_w = (\rho_q - \rho_l) \cdot g \cdot \frac{\pi \cdot d^3}{6} \tag{5.1-31}$$

At equilibrium the drag force and the friction force are equal (note that the friction force is reduced by the lift):

$$F_D = \mu_{sf} \cdot (F_w - F_L) \tag{5.1-32}$$

Substituting the equations (5.1-29), (5.1-30) and (5.1-31) into (5.1-32) results in the following equation:

$$C_D \cdot \frac{1}{2} \cdot \rho_l \cdot (\ell_{Drag} \cdot \alpha \cdot u_*)^2 \cdot f_D \cdot \frac{\pi \cdot d^2}{4} = \mu_{sf} \cdot \left((\rho_q - \rho_l) \cdot g \cdot \frac{\pi \cdot d^3}{6} - C_L \cdot \frac{1}{2} \cdot \rho_l \cdot (\alpha \cdot u_*)^2 \cdot f_L \cdot \frac{\pi \cdot d^2}{4} \right) \tag{5.1-33}$$

Which can be re-arranged into (showing the Shields parameter):

$$\theta_{sliding} = \frac{u_*^2}{R_{sd} \cdot g \cdot d} = \frac{4}{3} \cdot \frac{1}{\alpha^2} \cdot \frac{\mu_{sf}}{\ell_{Drag}^2 \cdot f_D \cdot C_D + \mu_{sf} \cdot f_L \cdot C_L} \tag{5.1-34}$$

5.1.3.7 Drag and Lift Induced Rolling.

The equilibrium equation for rolling is:

$$F_D \cdot (\ell_{Lever-D} + \cos(\psi + \phi_{Roll})) \cdot R + F_L \cdot (\ell_{Lever-L} + \sin(\psi + \phi_{Roll})) \cdot R = F_w \cdot \sin(\psi + \phi_{Roll}) \cdot R \tag{5.1-35}$$

Substituting the equations (5.1-29), (5.1-30) and (5.1-31) into (5.1-35) gives:

$$C_D \cdot \frac{1}{2} \cdot \rho_l \cdot (\ell_{Drag} \cdot \alpha \cdot u_*)^2 \cdot f_D \cdot \frac{\pi \cdot d^2}{4} \cdot (\ell_{Lever-D} + \cos(\psi + \phi_{Roll})) \cdot R$$

$$+ C_L \cdot \frac{1}{2} \cdot \rho_l \cdot (\alpha \cdot u_*)^2 \cdot f_L \cdot \frac{\pi \cdot d^2}{4} \cdot (\ell_{Lever-L} + \sin(\psi + \phi_{Roll})) \cdot R \tag{5.1-36}$$

$$= (\rho_q - \rho_l) \cdot g \cdot \frac{\pi \cdot d^3}{6} \cdot \sin(\psi + \phi_{Roll}) \cdot R$$

With the additional lever arms for drag and lift:

$$\ell_{\text{Lever-D}} = 1 - 2 \cdot E \cdot (1 - \ell_{\text{Drag}})$$

$$\ell_{\text{Lever-L}} = 0$$

(5.1-37)

Which can be re-arranged into the Shields parameter:

$$\theta_{\text{rolling}} = \frac{u_*^2}{R_{\text{sd}} \cdot g \cdot d} = \frac{4}{3} \cdot \frac{1}{\alpha^2} \cdot \frac{\mu_{\text{rf}}}{\ell_{\text{Drag}}^2 \cdot f_D \cdot C_D + \mu_{\text{rf}} \cdot f_L \cdot C_L}$$

(5.1-38)

With the effective rolling friction coefficient μ_{rf} :

$$\mu_{\text{rf}} = \frac{\sin(\psi + \phi_{\text{Roll}})}{\ell_{\text{Lever-D}} + \cos(\psi + \phi_{\text{Roll}})}$$

(5.1-39)

5.1.3.8 Lift Induced Lifting.

A third possible mechanism for the initiation of motion is pure lifting. This will occur if the lift force is equal to the gravity force according to:

$$F_w = F_L$$

(5.1-40)

Substituting the equations (5.1-29) and (5.1-31) into equation (5.1-40) gives:

$$(\rho_s - \rho_l) \cdot g \cdot \frac{\pi \cdot d^3}{6} = C_L \cdot \frac{1}{2} \cdot \rho_l \cdot (\alpha \cdot u_*)^2 \cdot f_L \cdot \frac{\pi \cdot d^2}{4}$$

(5.1-41)

Which can be re-arranged into the Shields parameter:

$$\theta_{\text{lifting}} = \frac{u_*^2}{R_{\text{sd}} \cdot g \cdot d} = \frac{4}{3} \frac{1}{\alpha^2 \cdot C_L \cdot f_L}$$

(5.1-42)

Since it is assumed that lift only occurs in turbulent flow and not in laminar flow, this mechanism only applies for boundary Reynolds numbers higher than 70. For an exposure level of 0.5, the factor **α=6.6**, the surface coefficient **f$_L$=1** and a lift coefficient of **C$_L$=0.423** is applied, which will be explained in the next paragraph. This results in a Shields parameter of 0.0726 for large boundary Reynolds numbers. How this relates to rolling and sliding will be discussed in the next paragraph.

5.1.3.9 Resulting Graphs.

The resulting graphs are shown in Figure 5.1-15. It is clear from this figure that the Shields curve for the sliding mechanism at an exposure level of 0.5 is lower than the curve for the rolling mechanism, which leads to the main conclusion that the Shields criterion is a criterion based on bulk erosion and not on erosion of individual particles.

The fact that the sliding mechanism gives smaller Shields values than the rolling mechanism for an exposure level of 0.5, does not mean that this will also occur at all other exposure levels. Up to an exposure level of about 0.6 the sliding mechanism gives the smaller Shields values, while the rolling mechanism gives smaller Shields values at greater exposure levels. So the "few" particles with a very high exposure level will be subject to rolling, while the bed as a whole is subject to sliding. The lift mechanism will only occur for individual particles under experimental conditions, since the sliding or rolling mechanisms will always occur before lifting will take place. Figure 5.1-16 shows the Shields curves for different exposure levels, ranging from 0.2 to 1.2, where the curves calculated are for the sliding mechanism up to an exposure level of 0.6 and for the rolling mechanism above that.
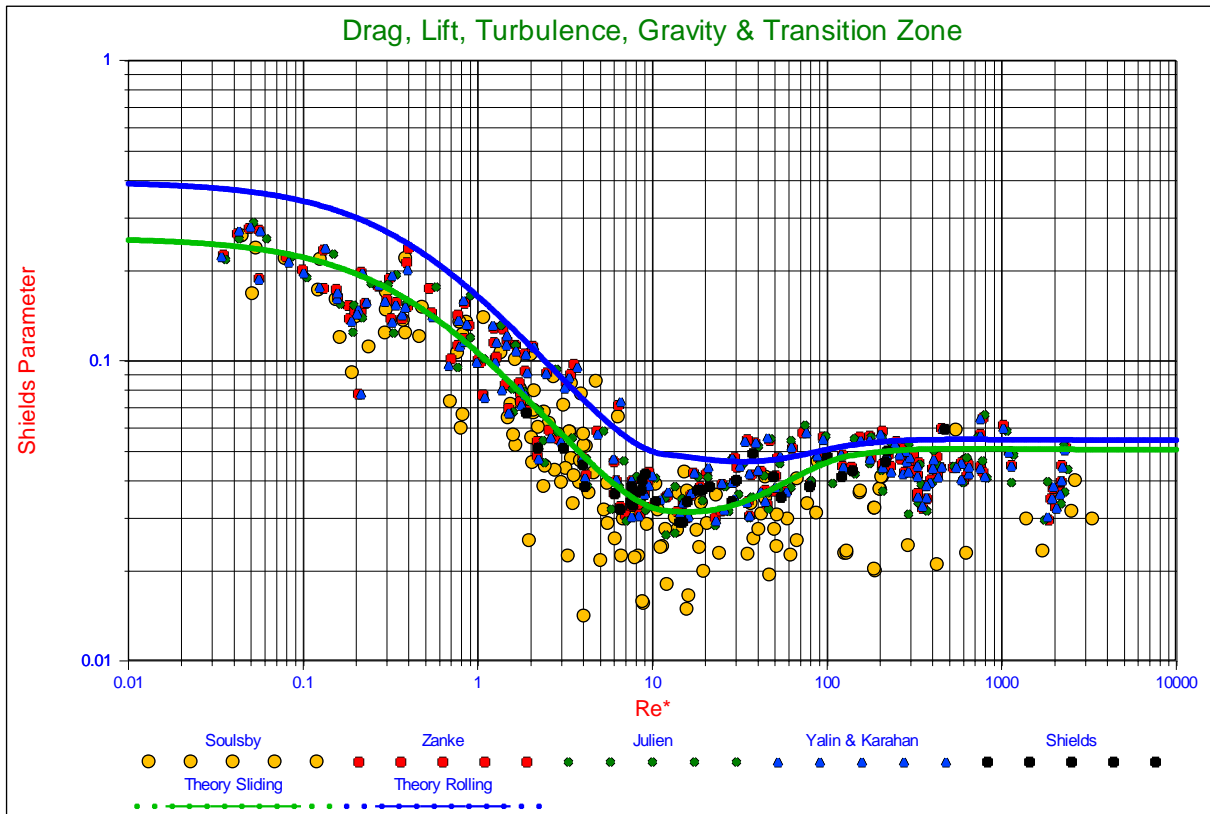
Figure 5.1-15: Drag, lift and turbulence induced initiation of motion with transition interpolation.
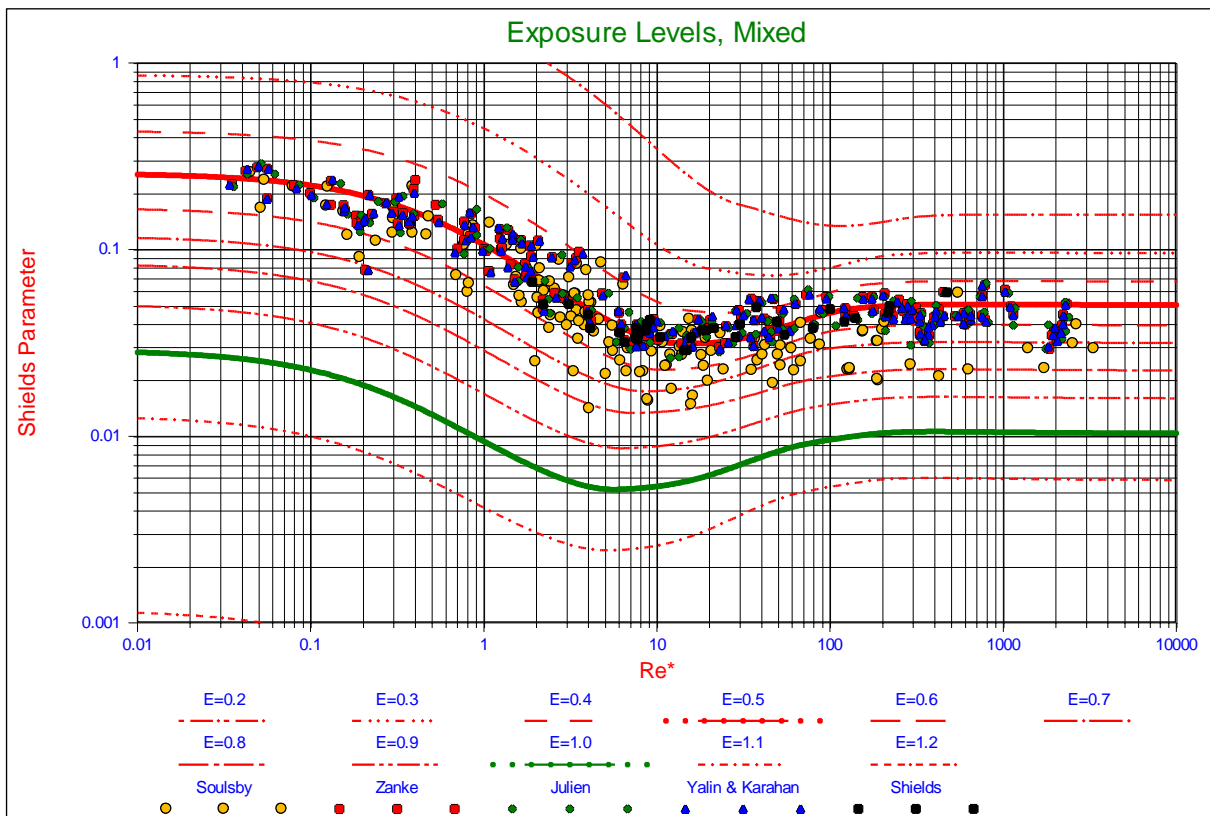
Figure 5.1-16: The Shields curves for sliding and rolling.

5.1.3.10 Natural Sands and Gravels.

As has been described by Miedema (2012A) and (2012B), the drag coefficient of natural sands and gravels differs from the drag coefficient of spheres. For rounded grains this difference is probably not too big, but for angular grains it is. In the laminar region at low Reynolds numbers both spheres and natural particles follow (or almost follow) the Stokes law, giving a drag coefficient of $C_D=24/Re$, while some researchers use $C_D=32/Re$ for natural sands. In the turbulent region however the difference is much larger. At large Reynolds numbers the drag coefficient for spheres is about $C_D=0.445$, while for natural sands and gravels values of $C_D=1\text{-}2$ are used. Using the equation as mentioned in Julien (1995) gives Shields curves as shown in Figure 5.1-17. In the laminar region the curves are almost identical to the curves for spheres, but in the turbulent region the curves gives values of 50% to 60% of the curves for spheres, as mentioned before and as experienced by other researchers. The curves in Figure 5.1-17 are for the sliding mechanism for exposure levels up to 0.6 and the rolling mechanism for larger exposure levels.

$$C_D = \frac{24}{Re_D} + 1.5 \tag{5.1-43}$$
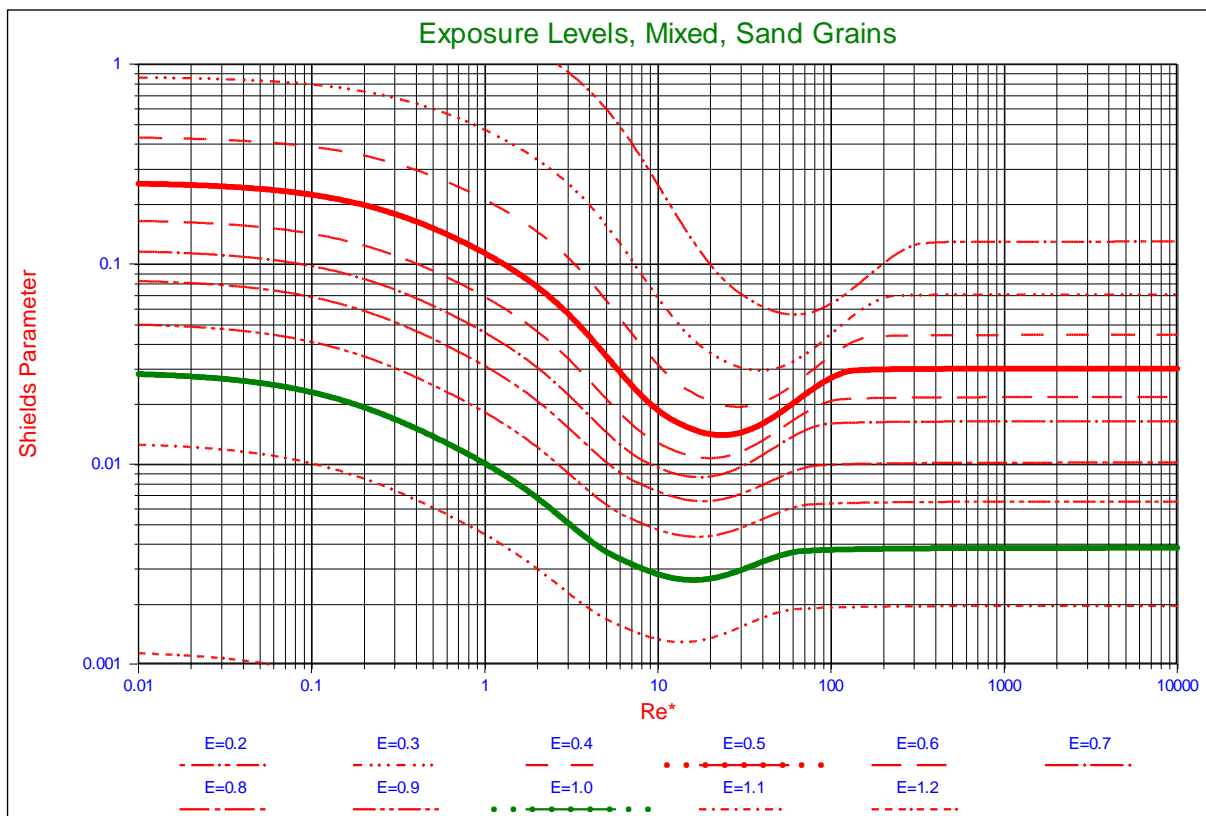
Figure 5.1-17: The Shields curves for natural sands and gravels.

5.1.3.11 The Shields-Parker Diagram.

A well-known application of the Shields curve is the so called Shields-Parker diagram, showing erosion versus no erosion, suspension versus no suspension and ripples versus dunes. This diagram is shown in Figure 5.1-18 with the boundary Reynolds number on the abscissa and Figure 5.1-19 with the particle Reynolds number on the abscissa.
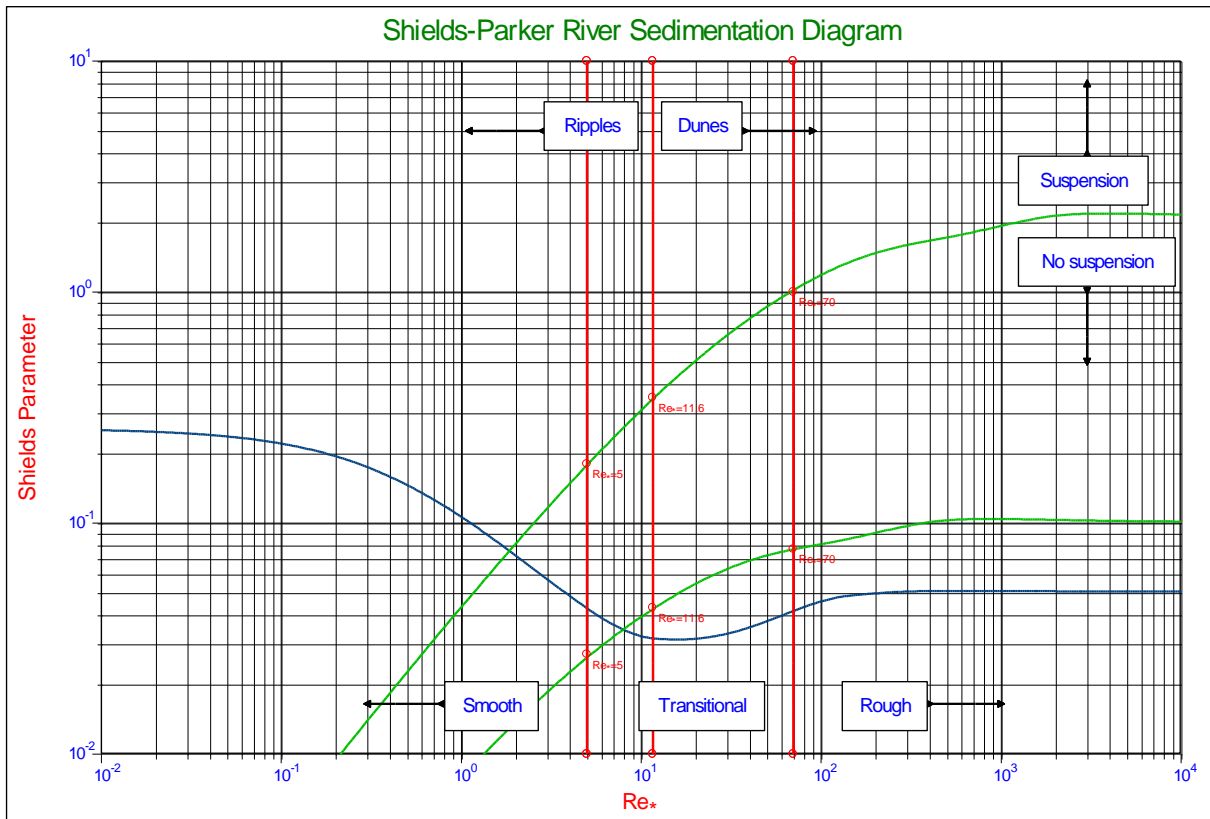
Figure 5.1-18: The Shields-Parker diagram as a function of the roughness Reynolds number.
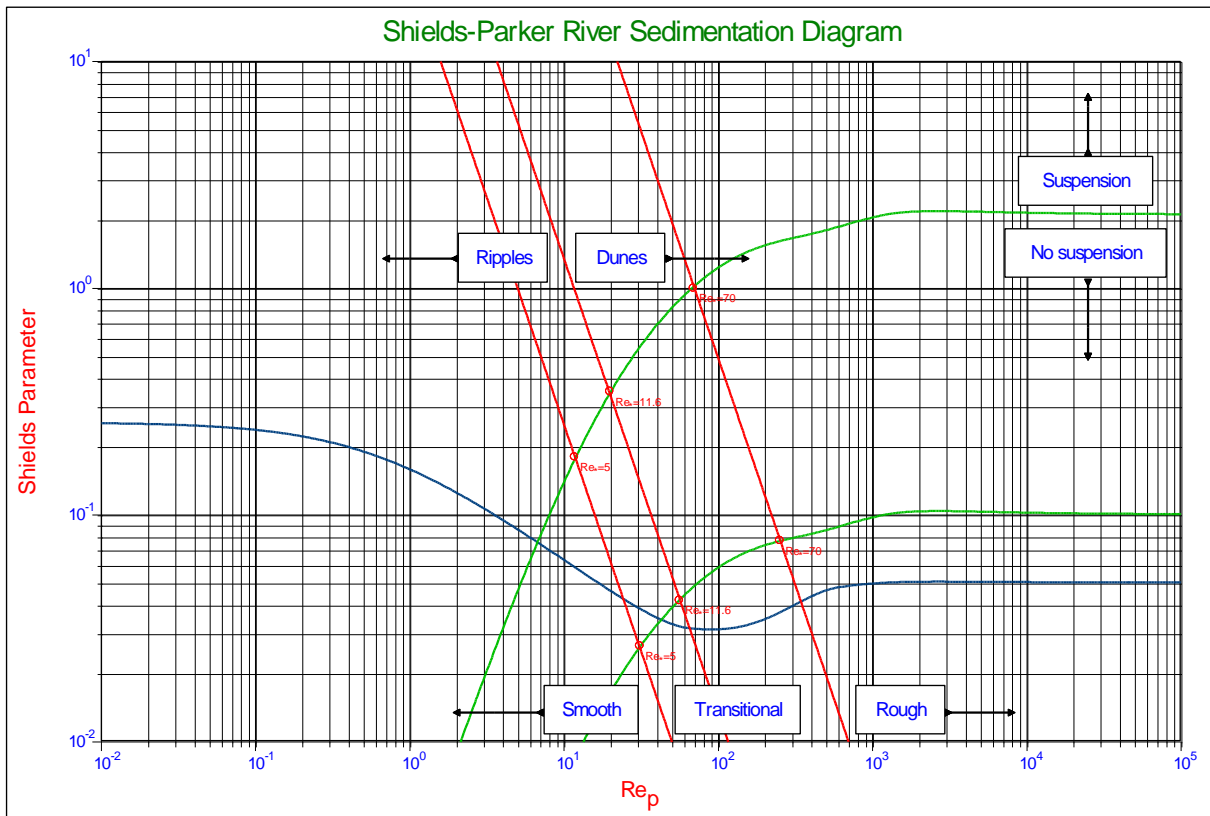
Figure 5.1-19: The Shields-Parker diagram as a function of the particle Reynolds number.

5.1.3.12 Conclusions & Discussion.

A model to explain the Shields curve has been developed, based on realistic values of the properties involved. The model correlates well with the original data of Shields (1936), the data collected by Yalin & Karahan (1979) and the data of others. Sliding, rolling and lifting are considered as the mechanism for entrainment, where sliding correlated the best with the data. Rolling gives higher values than sliding for the Shields parameter, while pure lift only occurs in the turbulent region at even higher values of the Shields parameter than rolling. Since sliding correlates the best and the fact that the original Shields data match critical to general transport, meaning that many particles at many locations are entrained, the main mechanism is sliding. Rolling and lifting are much more mechanisms of individual particles, while sliding may mobilize the whole top layer of the particles. Rolling by pivoting can only occur if a pivot point exists, but when most particles in the top layer start to move, there often is no next particle, creating a pivot point. It can be expected however that particles having a higher exposure level than the 0.5 considered, will start to roll at lower values of the Shields parameter then predicted with the model.

Some new concepts have been introduced, comparing the model developed with already existing models. First of all the definition of the exposure and protrusion level in relation with the flow field and the use of the acting velocity and lever arm. The acting velocity and lever arm are not estimated, but determined based on taking the square root of the surface averaged square of the velocity integrated over the cross section of the particle exposed to the flow. It is surprising that previous researchers choose an average velocity or surface averaged velocity, since we are dealing with forces. To find the acting point of a stress or pressure, the stress or pressure has to be integrated over the cross section exposed to the flow in order to determine the acting point and the effective value.

The introduction of the influence of turbulence is not new, but the introduction of the effective turbulence influence, based on the factor of simultaneous occurrence is. Also here, it is not about a velocity distribution or turbulence intensity distribution, but it is about the probability of the resulting force on a particle taking into account the phase cancellations of the small eddies. The original turbulence intensity profile as proposed by Nezu & Nakagawa (1993) has been modified slightly, so not only the turbulence intensity at the virtual bed is zero, but also the derivative with respect to the distance to the wall. The laminar region is dominated by drag and small eddy turbulence, while the turbulent region is dominated by drag and lift. A transition zone is chosen for non-dimensional particle exposure heights from 5 to 70 and a sophisticated interpolation method is used.

Finally, the virtual bed level is chosen at **0.2·d** below to top of the bed. In literature different values are used for the virtual bed level. Van Rijn (1984) and later Dey (1999) for example used **0.25·d**. To interpret the value of the virtual bed level we have to consider that it is a value used to justify the velocity profile above the bed. Most probably, the velocity profile between the top of the grains will not follow the theoretical velocity profile, but most probably there will already be velocity at lower levels than the assumed virtual bed level. This implies that at very low exposure levels, resulting in negative protrusion levels, the velocity distribution should be corrected with respect to the theoretical profile. This also implies that the virtual bed levels for the time averaged velocities and the turbulence intensity do not necessarily have to be the same, justifying the modified turbulence intensity, but also the assumptions made by Zanke (2003). The fact that the model developed correlates very well with the data for very common values for the different properties, including the virtual bed level, proves that the model gives a good description of reality, without having the presumption of being reality.

5.1.4 Nomenclature Initiation of Motion of Particles.

C_D	Drag coefficient	-
C_L	Lift coefficient	-
d	Sphere, particle or grain diameter	m
D_*	The Bonneville parameter or non-dimensional grain diameter	-
E	Exposure level	-
f_D, f_{Drag}	Fraction of cross section exposed to drag	-
f_L, f_{Lift}	Fraction of top surface exposed to lift	-
F_D	Drag force	N
F_L	Lift force	N
F_W	Weight of a particle	N
g	Gravitational constant	9.81 m/s^2
h	Thickness of the layer of water	m
k_s	Roughness often chosen equal to the particle diameter	m
k_s^+	The non-dimensional roughness or roughness Reynolds number	-

ℓ	The point of action of the drag force	-
ℓ	Mixing length	m
ℓ$_{Drag}$	Drag point of action	-
ℓ$_{Lift}$	Lift point of action	-
ℓ$_{Lever-D}$	Additional lever arm for drag	-
ℓ$_{Lever-L}$	Additional lever arm for lift	-
n	Turbulence intensity factor	-
R	Radius of sphere, particle or grain	m
R$_{sd}$	The relative submerged specific density	-
Re$_D$	The particle drag Reynolds number	-
Re$_*$	Boundary Reynolds number	-
u	Time and surface averaged velocity	m/s
u$_*$	Friction velocity	m/s
u$^+$	Non dimensional time and surface averaged velocity	-
u$_{r.m.s.}$	Turbulence intensity	m/s
u'$_{r.m.s.}$	Modified turbulence intensity	m/s
u'$_{n,r.m.s.}$	The nth moment of the modified turbulence intensity	m/s
u$_{eff.}$	The effective modified turbulence intensity	m/s
u$_{r.m.s.}^+$	Non dimensional turbulence intensity	-
u$_{total}^+$	Non dimensional total velocity	-
U$_c$	Threshold velocity Hjulstrom	m/s
U$_d$	Deposition velocity Hjulstrom	m/s
y	Distance to the wall or virtual bed level	m
y$_0$	Integration constant	m
y$^+$	Non dimensional distance to the wall (Reynolds number)	-
α	The velocity factor at a certain exposure level	-
δ$_v$	Thickness of the viscous sub layer	m
δ$_v^+$	The non-dimensional thickness of the viscous sub layer	11.6
κ	Von Karman constant	0.412
ρ$_l$	Liquid density	kg/m^3
ρ$_s$, ρ$_q$	Solids density, quarts density	kg/m^3
φ,ϕ	Internal friction angle/angle of repose	°
ϕ$_0$	The Coulomb friction angle quarts-quarts	°
ϕ$_{Roll}$	Friction angle for rolling resistance	°
ψ	The dilatation angle	°
ψ	The pivot angle	°
θ	The Shields parameter or non-dimensional shear stress	-
θ$_{sliding}$	The Shields parameter for sliding	-
θ$_{rolling}$	The Shields parameter for rolling	-
θ$_{lifting}$	The Shields parameter for lifting	-
τ	Total shear stress	Pa
τ$_t$	Turbulent shear stress	Pa
τ$_v$	Viscous shear stress	Pa
τ$_b$	Bed shear stress	Pa
ν$_l$	Kinematic viscosity liquid	m^2/sec
μ$_{sf}$	Friction coefficient usually the tangent of the internal friction angle	-
μ$_{rf}$	Equivalent friction coefficient for rolling	-

5.2 Hydraulic Transport of Sand/Shell Mixtures in Relation with the LDV.

5.2.1 Introduction.

This chapter is based on Ramsdell & Miedema (2010), Ramsdell et al. (2011) and Miedema & Ramsdell (2011). When considering pumping shells through a pipeline we have to consider that the shells are not spherical, but more disc shaped. When shells settle they will settle like leaves where the biggest cross section is exposed to the drag. But when they settle, they will settle in the same orientation, flat on the sediment, so the side of the shells is exposed to the horizontal flow in the pipeline. Since the side cross section is much smaller than the horizontal cross section, a much higher velocity is required to make them erode and go back into suspension. The settling velocity is much smaller because of the large area of the cross section.

Now normally pipeline resistance is calculated based on the settling velocity, where the resistance is proportional to the settling velocity of the grains. The Limit Deposit Velocity (LDV) is also proportional to the settling velocity. Since shells have a much lower settling velocity than sand grains with the same weight and much lower than sand grains with the same sieve diameter, one would expect a much lower resistance and a much lower critical velocity, matching the lower settling velocity. Now this is only partly true. As long as the shells are in suspension, on average they want to stay in suspension because of the low settling velocity. But as stated before, settling and erosion are stochastic processes because of the turbulent character of the flow in the pipeline. Since we operate at Reynolds numbers above 1 million the flow is always turbulent, meaning that eddies and vortices occur stochastically making the particles in the flow move up and down, resulting in some particles hitting the bottom of the pipe. Normally these particles will be picked up in the flow because of erosion, so there exists equilibrium between sedimentation and erosion, resulting in not having a bed at the bottom of the pipeline. In fact the capacity of the flow to erode is bigger than the sedimentation. If the line speed decreases, the shear velocity at the bottom of the pipe also decreases and less particles will be eroded, so the erosion capacity is decreasing. Now this does not matter as long as the erosion capacity is bigger than the sedimentation there will not be sediment at the bottom of the pipeline. As soon as the line speed decreases so much that the erosion capacity (erosion flux) is smaller than the sedimentation flux, not all the particles will be eroded, resulting in a bed to be formed at the bottom of the pipe. Having a bed at the bottom of the pipe also means that the cross section of the pipe decreases and the actual flow velocity above the bed increases. This will result in a new equilibrium between sedimentation flux and erosion flux for each bed height.

So from the moment there is a bed, decreasing the flow will result in an almost constant flow velocity above the bed, resulting in equilibrium between erosion and sedimentation. This equilibrium however is sensitive for changes in the line speed and in the mixture density. Increasing the line speed will reduce the bed height; a decrease will increase the bed height. Having a small bed does not really matter, but a thick bed makes the system vulnerable for plugging the pipeline. The LDV in most models is chosen in such a way that a thin bed is allowed. Now for the shells, as said before, there will always be some shells that will reach the bottom of the pipe due to the combination of settling velocity and turbulence. Once these shells are on top of the sediment they are hard to remove by erosion, because they lay flat on the surface and have a small cross section that is exposed to the flow compared with the weight of the shell. So although their settling velocity is much lower than equivalent sand particles, the erosion velocity is much higher. If we look at the beach in an area with many shells, we can always see the shells on top of the sand, covering the sand. In fact the shells are shielding the sand from erosion, because they are hard to erode. The bigger shells will also shield the smaller pieces, because the smaller pieces settle faster.

Compare this with leaves falling from a tree, the bigger leaves, although heavier, will fall slower, because they are exposed to higher drag. The same process will happen in the pipeline. Shells settle slower than sand grains, so they will be on top of the bed (if there is a bed), just like on the beach. Since they are hard to erode, in fact they protect the bed from being eroded, even if the line speed is increased. But there will always be velocities above the bed that will make the shells erode. Now the question is how we can quantify this behavior in order to get control over it. We have to distinguish between sedimentation and erosion. First of all assume shells are disc shaped with a diameter d and a thickness of **α·d** and let's take **α=0.1** this gives a cross section for the terminal settling velocity of **π/4·d²**, a volume of **π/40·d³** and a cross section for erosion of **d²/10**. Two processes have to be analyzed to determine the effect of shells on the critical velocity, the sedimentation process and the erosion process.

5.2.2 The Drag Coefficient.

The drag coefficient C_D depends upon the Reynolds number according to Turton & Levenspiel (1986), which is a 5 parameter fit function to the data:

$$C_D = \frac{24}{Re_p} \cdot (1 + 0.173 \cdot Re_p^{0.657}) + \frac{0.413}{1 + 16300 \cdot Re_p^{-1.09}}$$

(5.2-1)

It must be noted here that in general the drag coefficients are determined based on the terminal settling velocity of the particles. Wu & Wang (2006) recently gave an overview of drag coefficients and terminal settling velocities for different particle Corey shape factors. The result of their research is reflected in Figure 5.2-1. Figure 5.2-1 shows the drag coefficients as a function of the Reynolds number and as a function of the Corey shape factor.
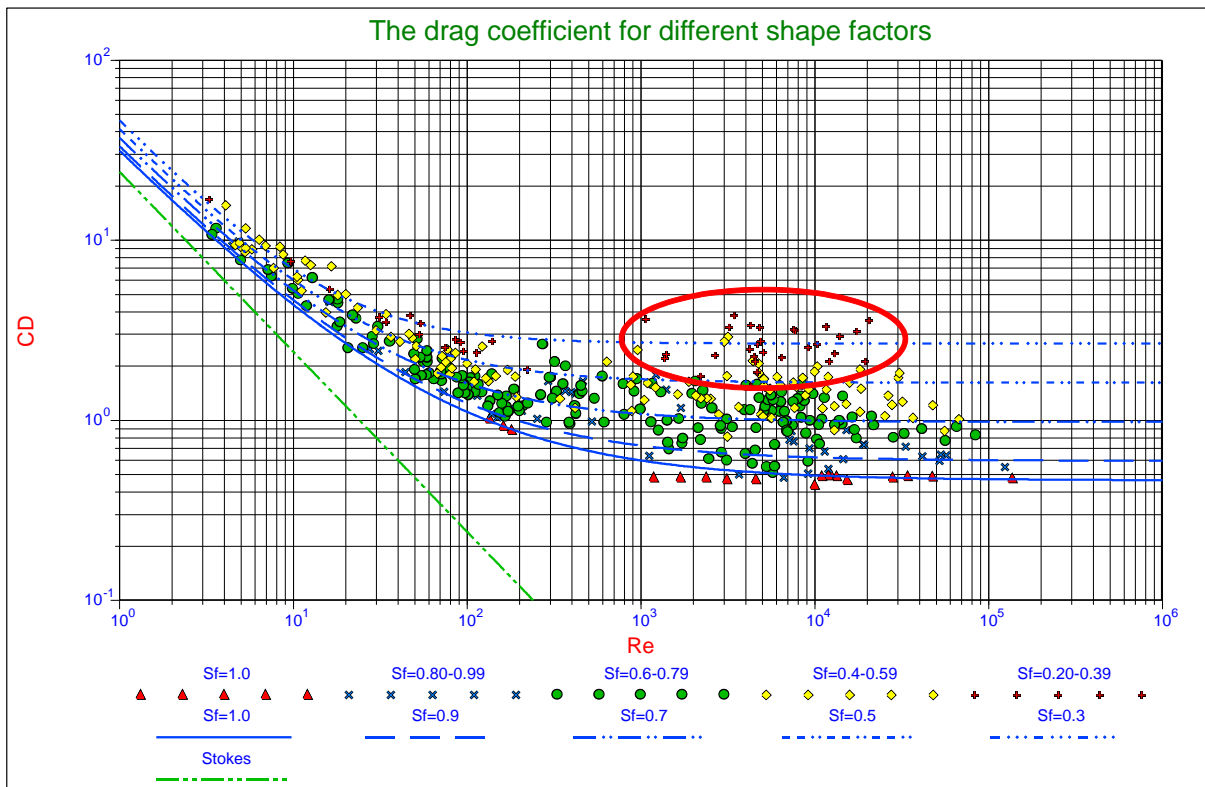
Figure 5.2-1: Drag coefficient as a function of the particle shape (Wu & Wang, 2006).

Figure 5.2-2: Some drag coefficients (source Wikipedia).

For shells settling the Corey shape factor is very small, like 0.1, resulting in high drag coefficients. According to Figure 5.2-1 the drag coefficient should be like:

$$C_D = \frac{32}{Re_p} + 2 \text{ up to } C_D = \frac{36}{Re_p} + 3 \qquad (5.2\text{-}2)$$

For shells lying flat on the bed, the drag coefficient will be similar to the drag coefficient of a streamlined half body (0.09), which is much smaller than the drag coefficient for settling (3). So there is a large asymmetry between the settling process and the erosion process of shells, while for more or less spherical sand particles the drag coefficient is considered to be the same in each direction.

5.2.3 Non-Uniform Particle Size Distributions.

In the model for uniform particle distributions, the roughness k_s was chosen equal to the particle diameter d, but in the case of non-uniform particle distributions, the particle diameter d is a factor d^+ times the roughness k_s, according to:

$$d^+ = \frac{d}{k_s} \qquad (5.2\text{-}3)$$

The roughness k_s should be chosen equal to some characteristic diameter related to the non-uniform particle distribution, for example the d_{50}.

5.2.4 Laminar Region.

For the laminar region (the viscous sub layer) the velocity profile of Reichardt (1951) is chosen. This velocity profile gives a smooth transition going from the viscous sub layer to the smooth turbulent layer.

$$u_{top}^+ = \frac{u(y_{top})}{u_*} = \frac{\ln(1 + \kappa \cdot y_{top}^+)}{\kappa} - \frac{\ln(1/9) + \ln(\kappa)}{\kappa} \cdot \left(1 - e^{-\frac{y_{top}^+}{11.6}} - \frac{y_{top}^+}{11.6} e^{-0.33 \cdot y_{top}^+} \right) \approx y_{top}^+ \qquad (5.2\text{-}4)$$

For small values of the boundary Reynolds number and thus the height of a particle, the velocity profile can be made linear to:

$$u_{top}^+ = y_{top}^+ = d^+ \cdot E \cdot Re_* = d^+ \cdot E \cdot k_s^+ \qquad (5.2\text{-}5)$$

Adding the effective turbulent velocity to the time averaged velocity, gives for the velocity function α_{Lam}:

$$\alpha_{Lam} = y_{top}^+ + u_{eff}^+ (y_{top}^+) \qquad (5.2\text{-}6)$$

5.2.5 Turbulent Region.

Particles that extend much higher into the flow will be subject to the turbulent velocity profile. This turbulent velocity profile can be the result of either a smooth boundary or a rough boundary. Normally it is assumed that for boundary Reynolds numbers less than 5 a smooth boundary exists, while for boundary Reynolds numbers larger than 70 a rough boundary exists. In between in the transition zone the probability of having a smooth boundary is:

$$P = e^{-0.95 \cdot \frac{Re_*}{11.6}} = e^{-0.95 \cdot \frac{k_s^+}{11.6}} \qquad (5.2\text{-}7)$$

This probability is not influenced by the diameter of individual particles, only by the roughness k_s which is determined by the non-uniform particle distribution as a whole. This gives for the velocity function α_{Turb}:

$$\alpha_{Turb} = \frac{1}{\kappa} \cdot \ln\left(95 \cdot \frac{y_{top}^+}{\delta_v^+} + 1\right) \cdot P + \frac{1}{\kappa} \cdot \ln\left(30 \cdot \frac{y_{top}^+}{k_s^+} + 1\right) \cdot (1 - P) \tag{5.2-8}$$

The velocity profile function has been modified slightly by adding 1 to the argument of the logarithm. Effectively this means that the velocity profile starts y_0 lower, meaning that the virtual bed level is chosen y_0 lower for the turbulent region. This does not have much effect on large exposure levels (just a few percent), but it does on exposure levels of 0.1 and 0.2. Not applying this would result in to high (not realistic) shear stresses at very low exposure levels.

5.2.6   The Exposure Level.

Effectively, the exposure level **E** is represented in the equations (5.1-34), (5.1-38) and (5.1-42) for the Shields parameter by means of the velocity distribution according to equations (5.2-6) and (5.2-8) and the sliding friction coefficient μ_{sf} or the pivot angle ψ. A particle with a diameter bigger than the roughness k_s will be exposed to higher velocities, while a smaller particle will be exposed to lower velocities. So it is important to find a relation between the non-dimensional particle diameter d^+ and the exposure level **E**.

5.2.7   The Angle of Repose & the Friction Coefficient.

Miller & Byrne (1966) found the following relation between the pivot angle ψ and the non-dimensional particle diameter d^+, with $c_0 = 61.5°$ for natural sand, $c_0 = 70°$ for crushed quartzite and $c_0 = 50°$ for glass spheres.

$$\psi = c_o \cdot (d^+)^{-0.3} \tag{5.2-9}$$

Wiberg & Smith (1987A) re-analyzed the data of Miller & Byrne (1966) and fitted the following equation:

$$\psi = \cos^{-1}\left(\frac{d^+ + z_*}{d^+ + 1}\right) \tag{5.2-10}$$

The average level of the bottom of the almost moving grain z_* depends on the particle sphericity and roundness. The best agreement is found for natural sand with $z_* = -0.045$, for crushed quartzite with $z_* = -0.320$ and for glass spheres with $z_* = -0.285$. Wiberg & Smith (1987A) used for natural sand with $z_* = -0.020$, for crushed quartzite with $z_* = -0.160$ and for glass spheres with $z_* = 14$. The values found here are roughly 2 times the values as published by Wiberg & Smith (1987A). It is obvious that equation (5.2-10) underestimates the angle of repose for d^+ values smaller than 1.

5.2.8   The Equal Mobility Criterion.

Now two different cases have to be distinguished. Particles with a certain diameter can lie on a bed with a different roughness diameter. The bed roughness diameter may be larger or smaller than the particle diameter. Figure 5.2-3 shows the Shields curves for this case (which are different from the graph as published by Wiberg & Smith (1987A)), combined with the data of Fisher et al. (1983), and based on the velocity distributions for non-uniform particle size distributions. Fisher et al. carried out experiments used to extend the application of the Shields entrainment function to both organic and inorganic sediments over passing a bed composed of particles of different size. Figure 5.2-3 shows a good correlation between the theoretical curves and the data, especially for the cases where the particles considered are bigger than the roughness diameter (**d/k_s>1**). It should be noted that most of the experiments were carried out in the transition zone and in the turbulent regime. Figure 5.2-3 is very important for determining the effect of shells on a bed, because with this figure we can determine the critical Shields parameter of a particle with a certain diameter, lying on a bed with a roughness of a different diameter. In the case of the shells the bed roughness diameter will be much smaller than the shell diameter (dimensions). To interpret Figure 5.2-3 one should first determine the bed roughness diameter and the roughness Reynolds number and take the vertical through this roughness Reynolds number (also called the boundary Reynolds number). Now determine the ratio **d/k_s** and read the Shields parameter from the graph. From this it appears that the bigger this ratio, the smaller the Shields value found. This is caused by the fact that the Shields parameter contains a division by the particle diameter, while the boundary shear stress is only influenced slightly by the changed velocity distribution. Egiazaroff (1965) was one of the first to investigate non-uniform particle size distributions with respect to initiation of motion. He defined a hiding factor or exposure factor as a multiplication factor according to:

$$\theta_{cr,i} = \theta_{cr,d50} \cdot \left(\frac{\log(19)}{\log\left(19 \cdot \dfrac{d_i}{d_{50}}\right)} \right)^2 \qquad\qquad \text{(5.2-11)}$$

The tendency following from this equation is the same as in Figure 5.2-3, the bigger the particle, the smaller the Shields value, while in equation (5.2-11) the d_{50} is taken equation to the roughness diameter k_s. The equal mobility criterion is the criterion stating that all the particles in the top layer of the bed start moving at the same bed shear stress, which matches the conclusion of Miedema (2010) that sliding is the main mechanism of entrainment of particles. Figure 5.2-4 shows that the results of the experiments are close to the equal mobility criterion, although not 100%, and the results from coarse sand from the theory as shown in Figure 5.2-3, matches the equal mobility criterion up to a ratio of around 10. Since shells on sand have a d/k_s ratio bigger than 1, the equal mobility criterion will be used for the interpretation of the shell experiments as also shown in Figure 5.2-3.

5.2.9 Shells.

Dey (2003) has presented a model to determine the critical shear stress for the incipient motion of bivalve shells on a horizontal sand bed, under a unidirectional flow of water. Hydrodynamic forces on a solitary bivalve shell, resting over a sand bed, are analyzed for the condition of incipient motion including the effect of turbulent fluctuations. Three types of bivalve shells, namely Coquina Clam, Cross-barred Chione and Ponderous Ark, were tested experimentally for the condition of incipient motion. The shape parameter of bivalve shells is defined appropriately.

Although the model for determining the Shields parameter of shells is given, the experiments of Dey (2003) were not translated into Shields parameters. It is interesting however to quantify these experiments into Shields parameters and to see how this relates to the corresponding Shields parameters of sand grains. In fact, if the average drag coefficient of the shells is known, the shear stress and thus the friction velocity, required for incipient motion, is known, the flow velocity required to erode the shells can be determined. Figure 5.2-5 and Figure 5.2-6 give an impression of the shells used in the experiments of Dey (2003). From Figure 5.2-5 it is clear that the shape of the shells match the shape of a streamlined half body lying on a surface and thus a drag coefficient is expected of about 0.1, while sand grains have a drag coefficient of about 0.45 at very high Reynolds numbers in a full turbulent flow. The case considered here is the case of a full turbulent flow, since we try to relate the incipient motion of shells to the critical velocity.

Equation (5.1-34) shows the importance of the drag coefficient in the calculation of the incipient motion, while the lift coefficient is often related to the drag coefficient. Whether the latter is true for shells is the question. For sand grains at high Reynolds numbers of then the lift coefficient is chosen to be 0.85 times the drag coefficient or at least a factor between 0.5 and 1, shells are aerodynamically shaped and also asymmetrical. There will be a big difference in the lift coefficient of shells lying on the bed, between convex upwards and convex downwards. A convex upwards shell is like the streamlined half body with a small drag coefficient. A convex downwards shell obviously is easy to catch the flow and start to move, because the drag coefficient is larger and most probably, the lift coefficient is much larger. So it will be the convex upwards shells that armor the bed or the beach.

Now the question is, what the drag coefficient would be, based on the experiments of Dey (2003). Figure 5.2-7 shows the Shields parameters for the three types of shells lying convex upwards on the bed with two types of sand, a d50=0.8 mm and a d50=0.3 mm, also the average values are shown. For the determination of the Shields values, the definition of the Shields parameter has to be used more strictly. Often a definition is used where the Shields parameter equals the ratio between the shear force and the normal force on the grain, resulting in a denominator with the particles diameter.
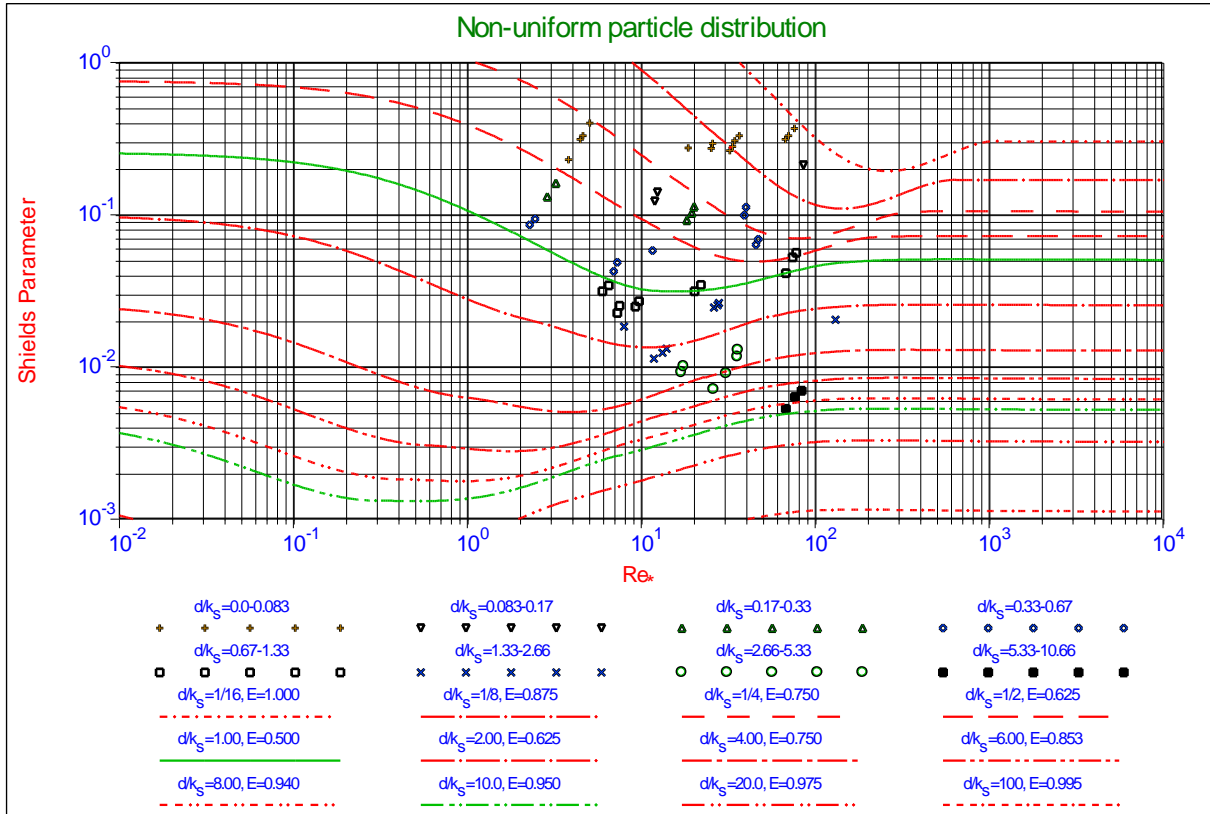
Figure 5.2-3: Non-uniform particle distributions.
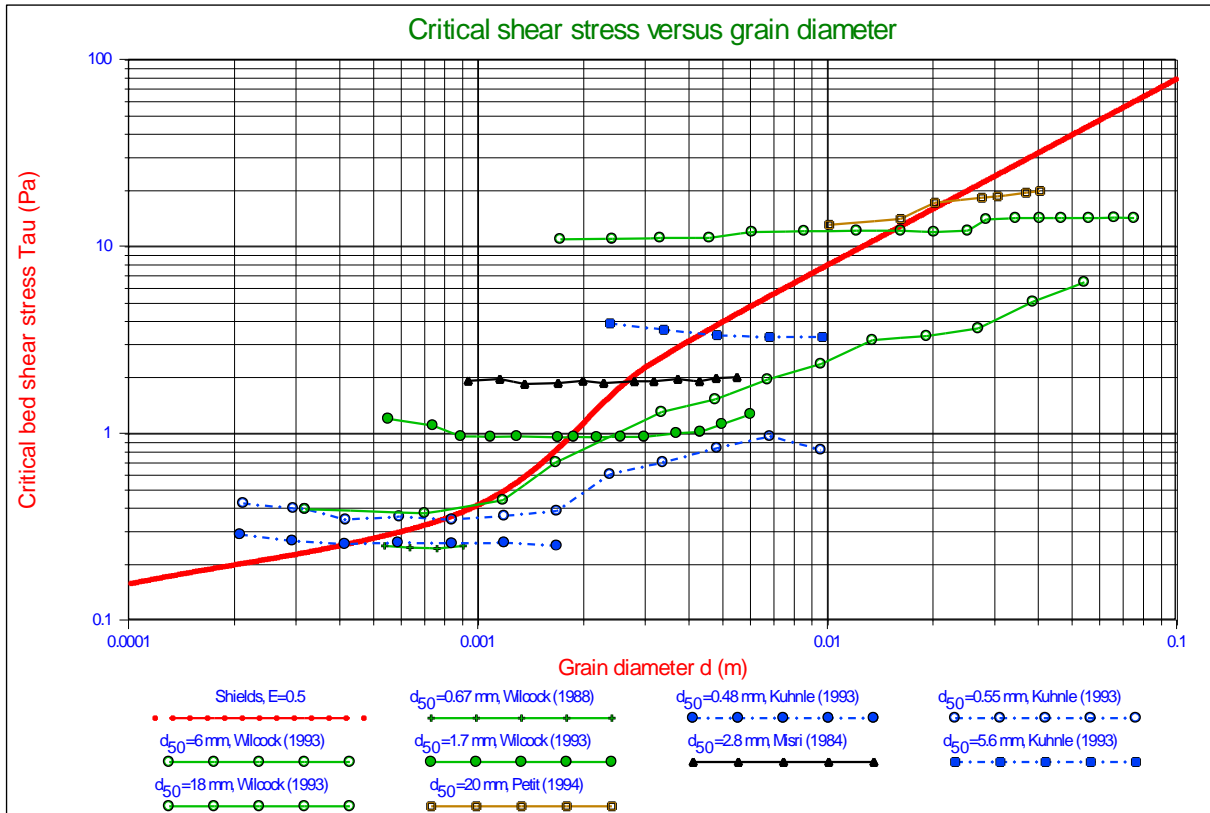
Figure 5.2-4: Critical bed shear stress of individual size fractions in a mixture as a function of grain diameter (modified after van Rijn (2006) and Wilcock (1993)).
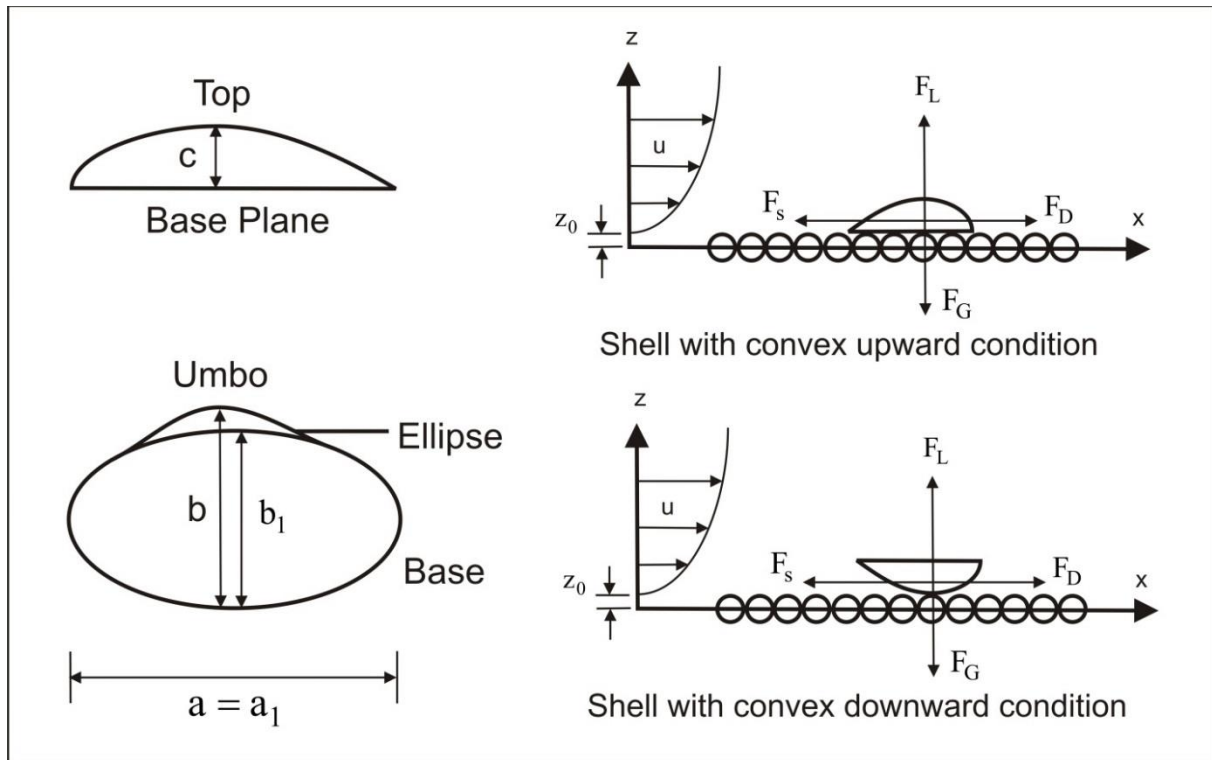
Figure 5.2-5: Shape of bivalve shell (Dey (2003)).

More strictly, the Shields parameter is the shear stress divided by the normal stress and in the case of shells; the normal stress depends on the average thickness of the shell and not the size of the shell. Using this definition, results in useful Shields values. Since convex upwards is important for the critical velocity analysis, this case will be analyzed and discussed. It is clear however from these figures that the convex downwards case results in much smaller Shields values than the convex upwards case as was expected. Smaller Shields values in this respect means smaller shear stresses and thus smaller velocities above the bed causing erosion. In other words, convex downwards shells erode much easier than convex upwards.

Although the resulting Shields values seem to be rather stochastic, it is clear that the mean values of the Chione and the Coquina are close to the Shields curve for $d/k_s=1$. The values for the Ponderous Ark are close to the Shields curve for $d/k_s=3$. In other words, the Ponderous Ark shells are easier to erode than the Chione and the Coquina shells. Looking at the shells in Figure 5.2-6 we can see that the Ponderous Ark shells have ripples on the outside and will thus be subject to a higher drag. On the other hand, the Ponderous Ark shells have an average thickness of 2.69 mm (1.95-3.98 mm) as used in the equation of the Shields parameter, while the Coquina clam has a thickness of 1.6 mm (0.73-3.57 mm) and the Chione 1.13 mm (0.53-2.09 mm). This also explains part of the smaller Shields values of the Ponderous Ark. The average results of the tests are shown in the following table.
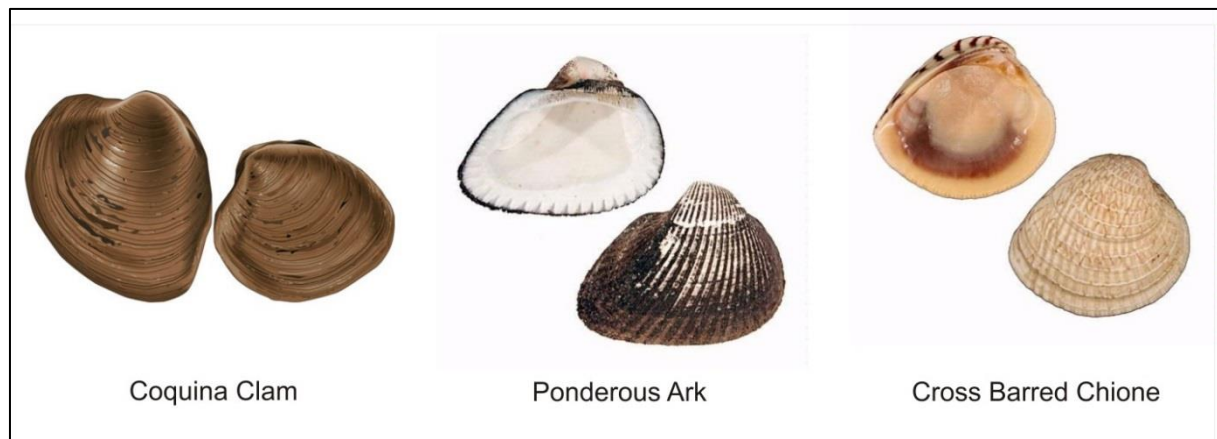
Figure 5.2-6: Selected samples of bivalve shells (Dey (2003)).
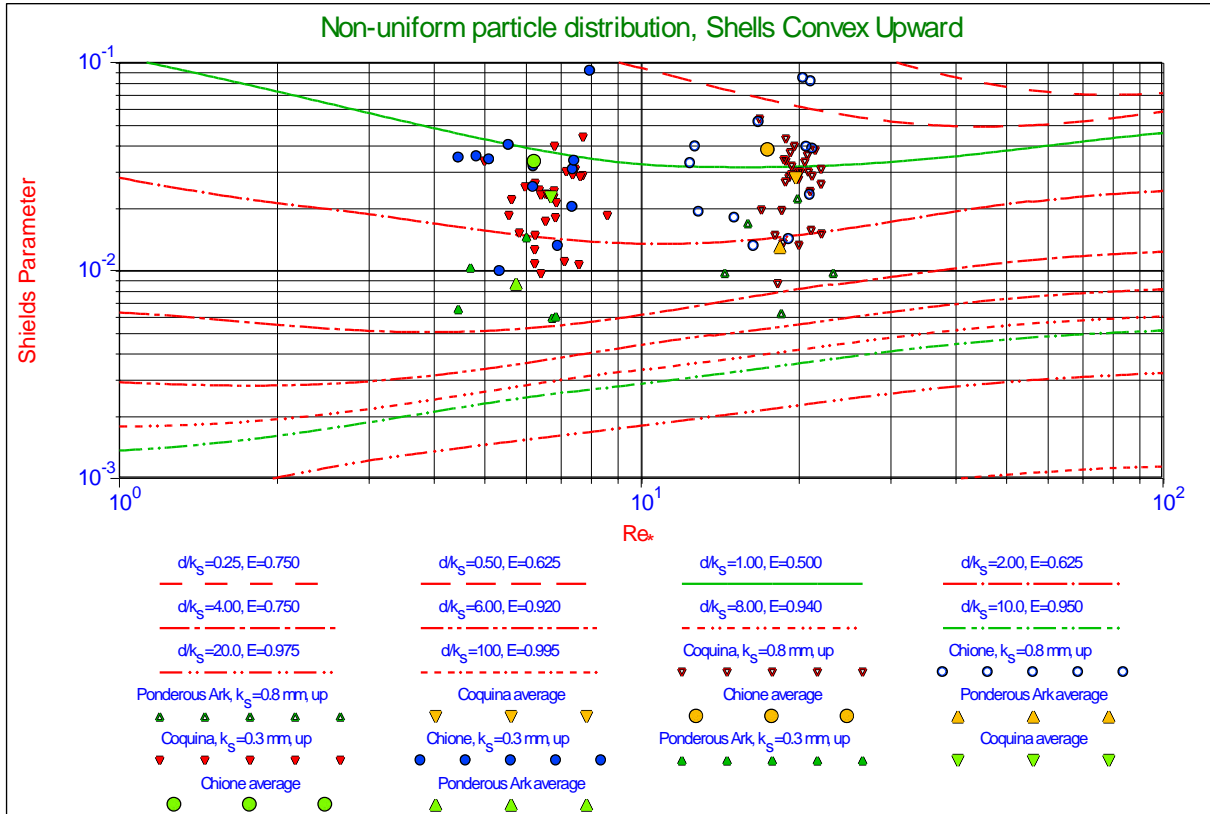
Figure 5.2-7: Shells convex upward.
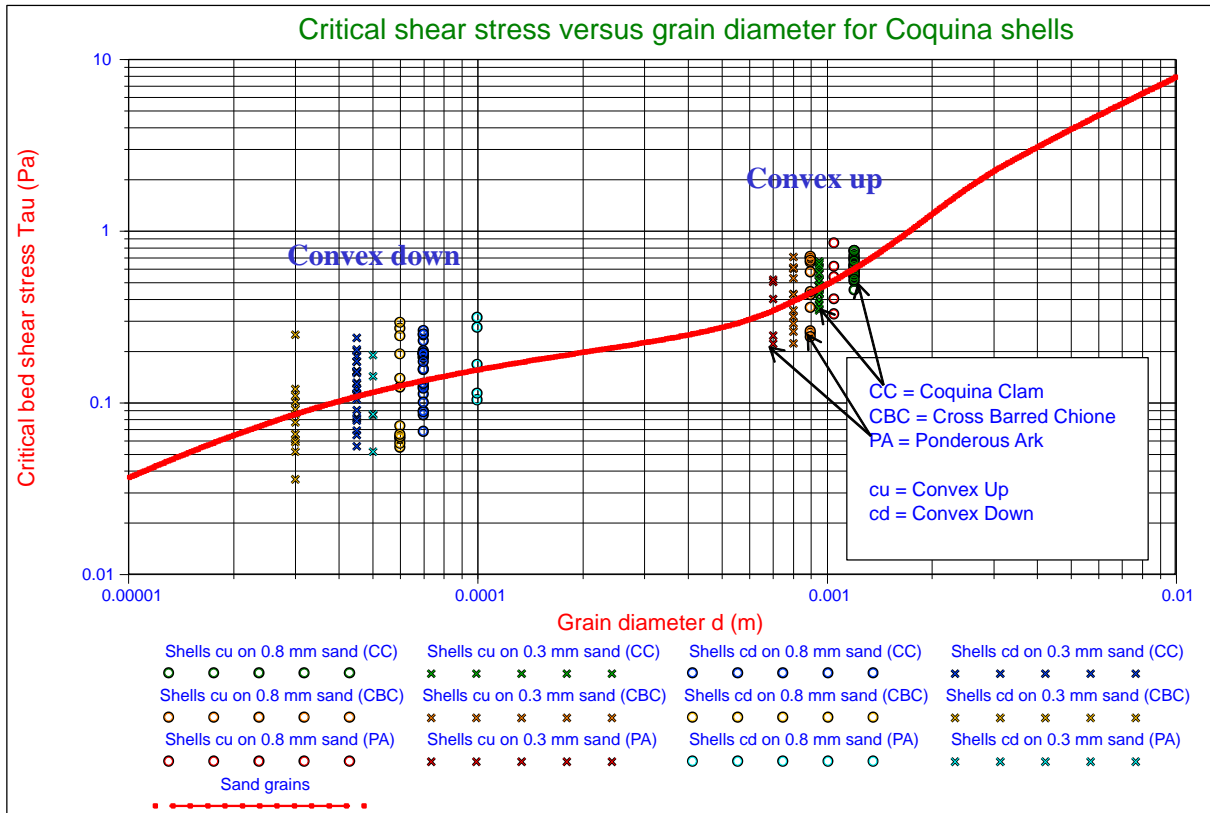
Figure 5.2-8: The critical shear stresses of the shells compared with sand.

Table 5.2-1: Average Shields values.

	d₅₀=0.8 mm		d₅₀=0.3 mm			d₅₀=0.8 mm	d₅₀=0.3 mm
	Re_*	θ	Re_*	θ	d	d/k_s	d/k_s
Coquina Clam	19.78	0.0277	6.71	0.0225	1.60	2.00	5.33
Cross Barred Chione	17.51	0.0378	6.24	0.0333	1.13	1.41	3.76
Ponderous Ark	18.46	0.0129	5.76	0.0086	2.69	3.36	8.97

A closer look at the data, based on this table, shows the following. For the shells on the 0.8 mm sand the **d/kₛ** values vary from 1.41-3.36. The average Shields values found do not match the corresponding curves, but lead to slightly lower **d/kₛ** values. For example, the Cross Barred Chione had a Shields value of 0.0378, but based on the **d/kₛ** value of 1.41, a Shields value of about 0.02 would be expected, a ratio of 1.89. The Coquina Clam had an average Shields value of 0.0277, but based on the **d/kₛ** value of 2.00 a Shields value of about 0.015 would be expected, a ratio of 1.84. The Ponderous Ark had an average Shields value of 0.0129, but based on the **d/kₛ** value of 3.36 a Shields value of about 0.008 would be expected, a ratio of 1.61. For the 0.3 mm sand the average ratio is about 5.5. In other words, the shells require larger Shields values than corresponding sand grains. This effect is larger in the case of shells on a bed with finer sand particles. The exact ratios depend on the type of shells.

5.2.10 The Limit Deposit Velocity.

A familiar phenomenon in the transport of sand slurries is the LSDV (Limit of Stationary Deposit Velocity), the velocity at which the mixture forms a stationary bed in the pipeline. As the velocity increases from the LSDV, the bed starts to slide along the bottom of the pipe. As the velocity increases further the bed begins to erode with the particles either rolling or saltating along the top of the bed, or fully suspended in the fluid, the LDV where all particles are in suspension.

A related concept is that of the minimum friction velocity, **V_imin**, at which the friction in the pipeline is minimized. At low concentrations the **V_imin** may be equal to or just above the LDV, but as concentration increases the LDV starts to decrease while the **V_imin** continues to rise. In operational terms, the **V_imin** represents a point of instability, so we generally try to design our pumping systems to maintain sufficiently high velocities that the system velocity never falls below (or close to) **V_imin** during the operational cycle.

Implicit in most models of slurry transport is the idea that the system can transition smoothly in both directions along the system resistance curves. So if the dredge operator inadvertently feeds too high of a concentration, dropping the velocity close to the minimum friction or even the LDV, he can recover by slowly lowering the mixture concentration, which in turn lowers the density in the pipeline and allows the velocity to recover. Alternatively the operator can increase the pressure by turning up the pumps to raise the velocity. In a sand-sized material this works because the critical and minimum friction velocities are fairly stable, so raising the pumping velocity or lowering the concentration will be enough to start the bed sliding, then erode the bed and return to stable operation.

With a sand-shell mixture, as described above, the LDV and minimum friction velocities become time-dependent parameters. The stochastic nature of the process means that some fraction of the shells will fall to the bottom of the pipe. The asymmetry between deposition and erosion velocity means that these shells will stay on the bottom, forming a bed that grows over time, increasing the critical velocity and minimum friction velocity. Unless the system is operated with very high margins of velocity, the new LDV and **V_imin** eventually fall within the operating range of the system, leading to flow instability and possible plugging.

Now, how to combine this LDV with the erosion behavior of shells. As mentioned above, there are different models in literature for the LDV and there is also a difference between the LDV and the minimum friction velocity. However, whatever model is chosen, the real LDV is the result of an equilibrium of erosion and deposition resulting in a stationary bed. This equilibrium depends on the particle size distribution, the slurry density and the flow velocity. At very low concentrations it is often assumed that the LDV is zero, but based on the theory of incipient motion, there is always a certain minimum velocity required to erode an existing bed.

There are two ways to look at this problem, we can compare the Shields values of the shells with the Shields values of sand particles with a diameter equal to the thickness of the shells, resulting in the factors as mentioned in the previous paragraph or we compare the shear stresses occurring to erode the shells with the shear stresses required for the sand beds used. The latter seems more appropriate because the shear stresses are directly related to the average velocity above the bed with the following relation:

$$\rho_l \cdot u_*^2 = \frac{\lambda_l}{8} \cdot \rho_l \cdot U^2 \tag{5.2-12}$$

Where the left hand side equals the bed shear stress, λ_l the friction coefficient following from the Moody diagram and **U** the average flow velocity above the bed. The average shear stresses are shown in Table 5.2-2.

Table 5.2-2: Average shear stresses.

	d_{50}=0.8 mm				d_{50}=0.3 mm			
	Re$_*$	**θ**	**$\rho_l \cdot u_*^2$**	**ratio**	**Re$_*$**	**θ**	**$\rho_l \cdot u_*^2$**	**ratio**
Coquina Clam	19.78	0.0277	0.72	1.60	6.71	0.0225	0.58	3.41
Cross Barred Chione	17.51	0.0378	0.69	1.53	6.24	0.0333	0.61	3.59
Ponderous Ark	18.46	0.0129	0.56	1.24	5.76	0.0086	0.37	2.18

The Shields values for both sands are about 0.035, resulting in shear stresses of 0.45 Pa for the 0.8 mm sand and 0.17 Pa for the 0.3 mm sand. The ratios between the shear stresses required eroding the shells and the shear stresses required to erode the beds are also shown in Table 5.2-2. For the shells laying convex upwards on the 0.8 mm sand bed these ratio's vary from 1.24-1.60, while this is a range from 2.18-3.41 for the 0.3 mm sand bed. These results make sense, the shear stress required for incipient motion of the shells does not change much because of the sand bed, although there will be some reduction for sand beds of smaller particles due to the influence of the bed roughness on the velocity profile according to equation (5.2-4). Smaller sand particles with a smaller roughness allow a faster development of the velocity profile and thus a bigger drag force on the shells at the same shear stress.

The main influence on the ratios is the size of the sand particles, because smaller particles require a smaller shear stress for the initiation of motion. This is also known from the different models for the LDV, the finer the sand grains, the smaller the critical velocity. In order words, the smaller the velocity to bring the particles in a bed back into suspension. It also makes sense that the ratio between shell erosion shear stress and sand erosion shear stress will approach 1 if the sand particles will have a size matching the thickness of the shells and even may become smaller than 1 if the sand particles are bigger than the shells.

Since the velocities are squared in the shear stress equation, the square root of the ratios has to be taken to get the ratios between velocities. This leads to velocity ratio's from 1.11-1.26 for the 0.8 mm sand and ratio's from 1.48-1.89 for the 0.3 mm sand. Translating this to the LDV, can be carried out under the assumption that the LDV is proportional to the average flow velocity resulting in incipient motion. Although the LDV results from an equilibrium between erosion and deposition of particles and thus is more complicated, the here derived ratios can be used as a first attempt to determine the critical velocities for a sand bed covered with convex upwards shells.

For the coarser sands (around 0.8 mm) this will increase the critical velocity by 11%-26%, while this increase is 48%-89% for the finer 0.3 mm sand. Even finer sands will have a bigger increase, while coarser sands will have a smaller increase. As stated, the shear stress required to erode the shells is almost constant, but decreasing a little bit with decreasing sand particle diameters, an almost constant critical velocity for the shells is expected. From the measurements it is also clear, that very smooth shells (Coquina Clam and Cross Barred Chione) are harder to erode and will have a higher critical velocity than the rough shells (Ponderous Ark).

5.2.11 Conclusions and Discussion.

The LDV for the hydraulic transport of a sand-water mixture depends on a number of physical processes and material properties. The LDV is the result of equilibrium between the deposition of sand particles and the erosion of sand particles. The deposition of sand particles depends on the settling velocity, including the phenomenon of hindered settling as described in this paper. The erosion or incipient motion of particles depends on equilibrium of driving forces, like the drag force, and frictional forces on the particles at the top of the bed. This results in the so called friction velocity and bottom shear stress. Particles are also subject to lift forces and so called Magnus forces, due to the rotation of the particles. So particles that are subject to rotation may stay in suspension due to the Magnus forces and do not contribute to the deposition. From this it is clear that an increasing flow velocity will result in more erosion, finally resulting in hydraulic transport without a bed. A decreasing flow velocity will result in less erosion and an increasing bed thickness, resulting in the danger of plugging the pipeline.

Shells lying convex upwards on the bed in general are more difficult to erode than sand particles, as long as the sand particles are much smaller than the thickness of the shells. The shells used in the research had a thickness varying from 1.13 to 2.69 mm. So the shells armor the bed and require a higher flow velocity than the original sand bed. Now as long as the bed thickness is not increasing, there is no problem, but since hydraulic transport is not a simple stationary process, there will be moments where the flow may decrease and moments where the density may increase, resulting in an increase of the bed thickness. Since the shells are armoring the bed, there will not be a decrease of the bed thickness at moments where the flow is higher or the density is lower, which would be the case if the bed consists of just sand particles. So there is a danger of a bed thickness increasing all the time and finally plugging the pipeline. The question arises, how much we have to increase the flow or flow velocity in order to erode the top layer of the bed where the shells are armoring the bed.

From the research of Dey (2003) it appears that the bottom shear stress to erode the shells varies from 0.56-0.72 Pa for a bed with 0.8 mm sand and from 0.37-0.61 Pa for a bed with 0.3 mm sand. It should be noted that these are shear stresses averaged over a large number of observations and that individual experiments have led to smaller and bigger shear stresses. So the average shear stresses decrease slightly with a decreasing sand particle size due to the change in velocity distribution. These shear stresses require average flow velocities that are 11%-26% higher than the flow velocities required to erode the 0.8 mm sand bed and 48%-89% higher to erode the 0.3 mm sand bed.

From these numbers it can be expected that the shear stresses required to erode the shells, match the shear stresses required to erode a bed with sand grains of 1-1.5 mm and it is thus advised to apply the LDV of 1-1.5 mm sand grains in the case of dredging a sand containing a high percentage of shells, in the case the shells are not too much fragmented.

5.2.12 Nomenclature Hydraulic Transport of Sand/Shell Mixtures.

c_0	Pivot angle at $d^+=1$	°
C_D	Drag coefficient	-
d	Diameter of particle or sphere	m
d^+	Dimensionless particle diameter	-
E	Exposure level	-
k_s	Bed roughness	m
k_s^+	Dimensionless bed roughness	m
LDV	Limit Deposit Velocity	m/s
P	Probability related to transition smooth/rough	-
Re_p	Particle Reynolds number	-
Re_*	Boundary Reynolds number	-
T	Temperature	K
u_*	Friction velocity	m/s
u	Velocity	m/s
u_{top}^+	Dimensionless velocity at top of particle	-
u_{eff}^+	Dimensionless effective turbulent added velocity	-
U	Average velocity above the bed.	m/s
V_{imin}	Minimum friction velocity	m/s
y_{top}	Height of particle	m
y_{top}^+	Dimensionless height of particle	-
z_*	Coefficient	-
α	Shell shape factor	-
α_{Lam}	Laminar velocity function	-
α_{Turb}	Turbulent velocity function	-
δ_v	Thickness of the viscous sub-layer	m
δ_v^+	Dimensionless thickness of the viscous sub-layer	-
κ	Von Karman constant	0.412
λ_l	Friction coefficient (see Moody diagram)	-
ρ_l	Liquid density	ton/m³
ψ	Shape factor particle	-
ψ	Pivot angle	°
θ	Shields parameter	-
θ_{cr}	Critical Shield parameter, initiation of motion	-
μ_{sf}	Sliding friction coefficient	-

5.3 Erosion, Bed Load and Suspended Load.

5.3.1 Introduction.

The initiation of motion deals with the start of movement of particles and may be considered a lower limit for the occurrence of erosion or sediment transport. This is important for the stationary bed regime in slurry transport in order to determine at which line speed erosion will start. Under operational conditions in dredging however the line speeds are much higher resulting in a sliding bed with sheet flow or even heterogeneous flow or homogeneous flow. Models dealing with this are the 2 layer models and the 3 layer models, assuming either a sheet flow layer on top of the bed or a certain velocity and concentration distribution above the bed due to suspended load. To understand these models it is necessary to understand the basics of bed load transport and suspended load and velocity and concentration distributions.

5.3.2 Bed Load Transport in a Sheet Flow Layer.

Of course there are many bed load transport equations. The Meyer-Peter Muller (MPM) equation however is used in some of the 2 layer and 3 layer models and has the advantage of having an almost fundamental derivation as given here, reason to discuss the MPM equation.

The total sediment transport of bed load Q_s can be determined by integrating the volumetric concentration $C_{vs}(z)$ times the velocity $U(z)$ over the height of the flow layer H with a bed width w.

$$Q_s = w \cdot \int_{z=0}^{z=H} C_{vs}(z) \cdot U(z) \cdot dz \tag{5.3-1}$$

Bed load transport q_b is often expressed in the dimensionless form:

$$\Phi_b = \frac{q_b}{d \cdot \sqrt{R_{sd} \cdot g \cdot d}} = \frac{Q_s}{d \cdot \sqrt{R_{sd} \cdot g \cdot d} \cdot w} \tag{5.3-2}$$

The bed load transport parameter q_b is the solids flux per unit width of the bed w. The most famous bed load transport equation is the Meyer-Peter Muller (1948) equation, resulting from the fitting of a large amount of experimental data.

The original MPM equation includes the critical Shields parameter, giving:

$$\Phi_b = \frac{Q_s}{d \cdot \sqrt{R_{sd} \cdot g \cdot d} \cdot w} = \alpha \cdot (\theta - \theta_{cr})^\beta \quad \text{with:} \quad \alpha = 8 \quad \text{and} \quad \beta = 1.5 \tag{5.3-3}$$

The Shields parameter, the dimensionless bed shear stress, is defined as:

$$\theta = \frac{\tau_b}{\rho_l \cdot R_{sd} \cdot g \cdot d} = \frac{u_*^2}{R_{sd} \cdot g \cdot d} \quad \text{or} \quad u_* = \sqrt{\theta \cdot R_{sd} \cdot g \cdot d} \tag{5.3-4}$$

The MPM equation can almost be derived from the velocity and concentration distribution in a sheet flow layer above the bed, assuming a stationary bed. Pugh & Wilson (1999) found a relation for the velocity at the top of the sheet flow layer with a stationary bed. This relation is modified here for a sliding bed, giving:

$$U_H = \gamma \cdot u_* = \gamma \cdot \sqrt{\frac{\lambda_b}{8}} \cdot U_{mean} \quad \text{with:} \quad \gamma = 9.4 \tag{5.3-5}$$

The shear stress on the sheet flow layer has to be transferred to the bed by sliding friction. It is assumed that this sliding friction is related to the internal friction angle, giving for the thickness of the sheet flow layer:

$$H = \frac{\tau_b}{\rho_l \cdot R_{sd} \cdot g \cdot C_{vs,sf} \cdot \tan(\varphi)} \approx \frac{2 \cdot \theta \cdot d}{C_{vb} \cdot \tan(\varphi)}$$

(5.3-6)

With: $C_{vs,sf} \approx 0.5 \cdot C_{vb}$ and $\tan(\varphi)=0.577$

Assuming a linear concentration distribution in the sheet flow layer, starting at the bed concentration C_{vb} at the bottom of the sheet flow layer and ending with a concentration of zero at the top of the sheet flow layer gives:

$$C_{vs}(z) = C_{vb} \cdot \left(\frac{H-z}{H}\right)$$

(5.3-7)

With z the vertical coordinate starting at the bottom of the sheet flow layer and increasing going upwards. The velocity in the sheet flow layer is assumed to start with zero at the bottom and ends with U_H at the top following a power law according to:

$$U(z) = U_H \cdot \left(\frac{z}{H}\right)^n$$

(5.3-8)

The transport of solids in the sheet flow layer can now be determined by integration of the spatial concentration profile times the velocity profile in the sheet flow layer:

$$Q_s = w \cdot \int_0^H C_{vs}(z) \cdot U(z) \cdot dz = w \cdot \int_0^H C_{vb} \cdot \left(\frac{H-z}{H}\right) \cdot U_H \cdot \left(\frac{z}{H}\right)^n \cdot dz$$

$$Q_s = w \cdot C_{vb} \cdot U_H \cdot \int_0^H \left(\frac{H-z}{H}\right) \cdot \left(\frac{z}{H}\right)^n \cdot dz$$

(5.3-9)

This can be rewritten to:

$$Q_s = w \cdot C_{vb} \cdot U_H \cdot \int_0^H \left(\left(\frac{z}{H}\right)^n - \left(\frac{z}{H}\right)^{n+1}\right) \cdot dz$$

(5.3-10)

Integration gives:

$$Q_s = w \cdot C_{vb} \cdot U_H \cdot H \cdot \left(\frac{1}{(n+1)} \cdot \left(\frac{z}{H}\right)^{n+1} - \frac{1}{(n+2)} \cdot \left(\frac{z}{H}\right)^{n+2}\right)_0^H$$

(5.3-11)

With integration from zero to the thickness of the sheet flow layer this gives:

$$Q_s = w \cdot C_{vb} \cdot U_H \cdot H \cdot \left(\frac{1}{(n+1) \cdot (n+2)}\right)$$

(5.3-12)

Substitution of the velocity at the top of the sheet flow layer and the thickness of the sheet flow layer gives:

$$Q_s = w \cdot C_{vb} \cdot \gamma \cdot \sqrt{\theta \cdot R_{sd} \cdot g \cdot d} \cdot \frac{2 \cdot \theta \cdot d}{C_{vb} \cdot \tan(\varphi)} \cdot \left(\frac{1}{(n+1) \cdot (n+2)}\right)$$

(5.3-13)

$$Q_s = \frac{2 \cdot \gamma}{(n+1) \cdot (n+2) \cdot \tan(\varphi)} \cdot \left(w \cdot d \cdot \sqrt{R_{sd} \cdot g \cdot d}\right) \cdot \theta^{3/2}$$

So the dimensionless bed load transport parameter is:

$$\Phi_b = \frac{Q_s}{w \cdot d \cdot \sqrt{R_{sd} \cdot g \cdot d}} = \frac{2 \cdot \gamma}{(n+1) \cdot (n+2) \cdot \tan(\varphi)} \cdot \theta^{3/2}$$

(5.3-14)

This is almost equal to the MPM equation, except for the critical Shields parameter θ_{cr} in the MPM equation. For medium and coarse sands the value of this critical Shields parameter lies between 0.03 and 0.05. The velocities in slurry flow are high, resulting in much higher values of the Shields parameter, so this critical Shields parameter θ_{cr} can be ignored. With an exponent **n=1** for the velocity distribution, an angle of internal friction at the top of the bed giving **tan(φ)=0.577** and a parameter **γ=9.4** for the velocity at the top of the sheet flow layer, a factor **α=5.43** is found, while the original MPM equation uses **α=8**. It is however questionable whether the internal friction angle of 30° at the top of the bed is correct, a smaller angle of internal friction would be expected, resulting in a higher value of **α**. Also the values of **n=1** and **γ=9.4** can be questioned. The equation found can thus easily be matched with the 3 coefficients involved.

5.3.3 Suspended Load Transport in Open Channel Flow.

5.3.3.1 Governing Equations.

Dey (2014) gives a clear description of suspended load transport. A summary is given here. If particles are surrounded by the carrier liquid for a long period of time they are in suspension and the transport mode is named suspended load. Convection of turbulence results in exchange of mass and momentum, including the particles, between layers of liquid flow. Random motion and turbulence results in diffusion, while velocity gradients, due to bulk motion of the liquid, result in advection. When gravity, resulting in the settling of particles, is counterbalanced by turbulence induced diffusion, particles stay in suspension and are transported by the time averaged flow velocity. There is however an active interchange of particles between bed load and suspended load. Suspended load is always accompanied by bed load. The total sediment transport of suspended solids Q_s can be determined by integrating the volumetric concentration $C_{vs}(z)$ times the velocity $U(z)$ over the height of the flow layer H with a bed width w in case of a 2 dimensional geometry.

$$Q_s = w \cdot \int_{z=0}^{z=H} C_{vs}(z) \cdot U(z) \cdot dz$$

(5.3-15)

To solve this equation, both the concentration distribution and the velocity distribution have to be known. Now what is the distribution of the suspended sediment within the liquid (water) layer with height H? The generalised 3 dimensional advection-diffusion equation for a low concentration of suspended sediment motion in an incompressible liquid flow is:

Part I:	$\dfrac{\partial C}{\partial t}$
Part II:	$+\bar{u} \cdot \dfrac{\partial C}{\partial x} + \bar{v} \cdot \dfrac{\partial C}{\partial y} + \bar{w} \cdot \dfrac{\partial C}{\partial z} + C \cdot \left(\dfrac{\partial \bar{u}}{\partial x} + \dfrac{\partial \bar{v}}{\partial y} + \dfrac{\partial \bar{w}}{\partial z} \right)$
Part III:	$= \dot{C}$
Part IV:	$+\dfrac{\partial}{\partial x} \cdot \left((\varepsilon_m + \varepsilon_{sx}) \cdot \dfrac{\partial C}{\partial x} \right) + \dfrac{\partial}{\partial y} \cdot \left((\varepsilon_m + \varepsilon_{sy}) \cdot \dfrac{\partial C}{\partial y} \right) + \dfrac{\partial}{\partial z} \cdot \left((\varepsilon_m + \varepsilon_{sz}) \cdot \dfrac{\partial C}{\partial z} \right)$

(5.3-16)

Part I is the local change of concentration due to time. Part II is the advection of concentration. Part III the rate of change of state of concentration. According to the conservation of mass, this term is the production or dissipation rate per unit volume and is equal to zero. Part IV the diffusion and the mixing of concentration. In viscous flow, the molecular diffusion is prevalent ($\varepsilon_m \neq 0$) and the turbulent diffusion does not exist ($\varepsilon_{sx} = \varepsilon_{sy} = \varepsilon_{sz} = 0$). In contrast, in turbulent flow, molecular diffusion is negligible ($\varepsilon_m \approx 0$) in comparison to turbulent diffusion ($\varepsilon_{sx}, \varepsilon_{sy}, \varepsilon_{sz} \gg 0$). In a stationary 2 dimensional situation, with z the vertical coordinate, the equation reduces to, with on the left hand side the entrainment flux and on the right hand side the depositional flux:

$$\overline{w} \cdot \frac{\partial C}{\partial z} = \frac{\partial}{\partial z} \cdot \left(\varepsilon_{sz} \cdot \frac{\partial C}{\partial z} \right) \tag{5.3-17}$$

Substituting the vertical velocity component by the terminal settling velocity (excluding hindered settling), replacing the notation of the sediment diffusivity in z-direction ε_{sz} by ε_s and integrating the equation, gives:

$$v_t \cdot C + \varepsilon_s \cdot \frac{\partial C}{\partial z} = 0 \tag{5.3-18}$$

Now in a stationary situation, the mean vertical velocity of the particles is zero. One can say however that a fraction of the particles is subjected to the downwards movement by settling, while the remaining fraction is moving upwards by diffusion. This would mean that the concentration in the first term has to be multiplied by a factor smaller than 1. Most probably this factor depends on the particle size, but also on the local concentration. One can also compensate for this by choosing an empirical equation for the diffusivity.

5.3.3.2 A Physical Explanation.

Particles settle through gravity downwards towards the bed with a terminal settling velocity v_t. As the particles settle, a concentration gradient develops, with an increasing concentration downwards. Turbulence however results in an upwards flux of solids maintaining suspended sediment transport. In an equilibrium situation, there is a balance between the downwards settling motion and the upwards diffusion of particles. In a stationary situation it is possible to describe this mathematically.

The downwards flux of solids per unit area of a plane parallel to the bed is (including hindered settling):

$$q_{s,down}(z) = C_{vs}(z) \cdot v_t \cdot \left(1 - C_{vs}(z) \right)^\beta \tag{5.3-19}$$

The exchange of eddies between layers in the turbulent flow results in a flux of solids between these layers, by random turbulent interactions between layers giving mixing at all levels and therefore a transport from areas with a high concentration into areas with a low concentration. This upwards flux of solids per unit area parallel to the bed is:

$$q_{s,up}(z) = -\varepsilon_s \cdot \frac{dC_{vs}(z)}{dz} \tag{5.3-20}$$

The negative sign results from the fact that the sediment flux is upwards, while the concentration gradient is positive downwards. The sediment exchange by turbulence is a diffusion process. This gives for an equilibrium situation:

$$q_{s,up}(z) = q_{s,down}(z)$$

$$-\varepsilon_s \cdot \frac{dC_{vs}(z)}{dz} = C_{vs}(z) \cdot v_t \cdot \left(1 - C_{vs}(z) \right)^\beta \tag{5.3-21}$$

$$C_{vs}(z) \cdot v_t \cdot \left(1 - C_{vs}(z) \right)^\beta + \varepsilon_s \cdot \frac{dC_{vs}(z)}{dz} = 0$$

For the shear stress based on the eddy diffusivity ε_m we can write:

$$\tau(z) = \rho_l \cdot \varepsilon_m \cdot \frac{dU(z)}{dz} \tag{5.3-22}$$

The sediment mass diffusivity ε_s is almost equal to the liquid eddy momentum diffusivity ε_m for small particles. For larger particles β_{sm} is smaller than 1.

$$\varepsilon_s \approx \beta_{sm} \cdot \varepsilon_m \tag{5.3-23}$$

With: $\varepsilon_m = \kappa \cdot u_* \cdot f(z)$ the eddy diffusivity. The models solving this problem found in literature are all for open channel flow. It is the questing whether these solutions are suitable for pipe flow. It is also possible that models not suitable for open channel flow, are suitable for pipe flow. Reason to discuss a number of basic models.

5.3.3.3 Law of the Wall Approach (Rouse (1937)).

In the turbulent layer the total shear stress contains only the turbulent shear stress. Integration gives the famous logarithmic velocity profile (Law of the Wall):

$$U(z) = \frac{u_*}{\kappa} \cdot \ln\left(\frac{z}{z_0}\right) \tag{5.3-24}$$

This gives for the velocity gradient:

$$\frac{d\,U(z)}{dz} = \frac{u_*}{\kappa \cdot z} \tag{5.3-25}$$

The definition of the friction velocity u_* gives:

$$u_* = \sqrt{\frac{\tau_b}{\rho_l}} \quad \Rightarrow \quad \frac{\tau_b}{\rho_l} = u_*{}^2 \tag{5.3-26}$$

Now we can write for the ratio shear stress to liquid density:

$$\frac{\tau(z)}{\rho_l} = \varepsilon_m \cdot \frac{dU(z)}{dz} = \kappa \cdot u_* \cdot z \cdot \frac{dU(z)}{dz} \tag{5.3-27}$$

Based on the Law of the Wall, a linear decrease of the shear stress resulting from eddy viscosity, starting with the bed shear stress at the bed and ending at zero at the free surface, the following can be derived:

$$\frac{\tau(z)}{\rho_l} = \frac{\tau_b}{\rho_l} \cdot \left(\frac{H-z}{H}\right) = u_*{}^2 \cdot \left(\frac{H-z}{H}\right) = \varepsilon_m \cdot \frac{dU(z)}{dz} = \kappa \cdot u_* \cdot z \cdot \frac{dU(z)}{dz} \tag{5.3-28}$$

This gives for the momentum diffusivity and the sediment mass diffusivity:

$$\varepsilon_m = \kappa \cdot u_* \cdot z \cdot \left(\frac{H-z}{H}\right) \quad \text{and} \quad \varepsilon_s = \beta_{sm} \cdot \kappa \cdot u_* \cdot z \cdot \left(\frac{H-z}{H}\right) \tag{5.3-29}$$

This upwards flux of solids per unit area parallel to the bed is now:

$$q_{s,up}(z) = -\beta_{sm} \cdot \kappa \cdot u_* \cdot z \cdot \left(\frac{H-z}{H}\right) \cdot \frac{dC_{vs}(z)}{dz} \tag{5.3-30}$$

Making the upwards flux and downwards flux of solids equal gives:

$$q_{s,up}(z) = q_{s,down}(z)$$
$$-\beta_{sm} \cdot \kappa \cdot u_* \cdot z \cdot \left(\frac{H-z}{H}\right) \cdot \frac{dC_{vs}(z)}{dz} = C_{vs}(z) \cdot v_t \cdot \left(1 - C_{vs}(z)\right)^\beta \tag{5.3-31}$$

Giving the differential equation:

$$C_{vs}(z) \cdot v_t \cdot \left(1 - C_{vs}(z)\right)^\beta + \beta_{sm} \cdot \kappa \cdot u_* \cdot z \cdot \left(\frac{H-z}{H}\right) \cdot \frac{dC_{vs}(z)}{dz} = 0 \tag{5.3-32}$$

This equation can be solved assuming there is no hindered settling, reducing the differential equation to:

$$C_{vs}(z) \cdot v_t + \beta_{sm} \cdot \kappa \cdot u_* \cdot z \cdot \left(\frac{H-z}{H} \right) \cdot \frac{dC_{vs}(z)}{dz} = 0 \tag{5.3-33}$$

Separating the variables gives:

$$\frac{dC_{vs}(z)}{C_{vs}(z)} = -\left(\frac{v_t}{\beta_{sm} \cdot \kappa \cdot u_*} \right) \cdot \left(\frac{1}{z} \right) \cdot \left(\frac{H}{H-z} \right) \cdot dz \tag{5.3-34}$$

The solution of this differential equation is:

$$\ln\left(C_{vs}(z) \right) = \left(\frac{v_t}{\beta_{sm} \cdot \kappa \cdot u_*} \right) \cdot \ln\left(\frac{z-H}{z} \right) + C \tag{5.3-35}$$

If the value of the concentration $C_{vs}(a)$ is known at an elevation a above the bed, the integration constant C can be solved.

$$\ln\left(C_{vs}(a) \right) = \left(\frac{v_t}{\beta_{sm} \cdot \kappa \cdot u_*} \right) \cdot \ln\left(\frac{a-H}{a} \right) + C$$

$$C = \ln\left(C_{vs}(a) \right) - \left(\frac{v_t}{\beta_{sm} \cdot \kappa \cdot u_*} \right) \cdot \ln\left(\frac{a-H}{a} \right) \tag{5.3-36}$$

$$C = \ln\left(C_{vs}(a) \right) + \left(\frac{v_t}{\beta_{sm} \cdot \kappa \cdot u_*} \right) \cdot \ln\left(\frac{a}{a-H} \right)$$

This gives the Rouse (1937) profile:

$$\ln\left(C_{vs}(z) \right) = \ln\left(C_{vs}(a) \right) + \left(\frac{v_t}{\beta_{sm} \cdot \kappa \cdot u_*} \right) \cdot \left(\ln\left(\frac{z-H}{z} \right) + \ln\left(\frac{a}{a-H} \right) \right)$$

$$\ln\left(\frac{C_{vs}(z)}{C_{vs}(a)} \right) = \ln\left(\left(\left(\frac{z-H}{z} \right) \cdot \left(\frac{a}{a-H} \right) \right)^{\left(\frac{v_t}{\beta_{sm} \cdot \kappa \cdot u_*} \right)} \right) \tag{5.3-37}$$

$$\frac{C_{vs}(z)}{C_{vs}(a)} = \left(\left(\frac{H-z}{z} \right) \cdot \left(\frac{a}{H-a} \right) \right)^{\left(\frac{v_t}{\beta_{sm} \cdot \kappa \cdot u_*} \right)}$$

The so called Rouse number is the power in this equation:

$$P = \zeta = \left(\frac{v_t}{\beta_{sm} \cdot \kappa \cdot u_*} \right) \quad \text{with:} \quad \beta_{sm} \approx 1 \quad \Rightarrow \quad P = \left(\frac{v_t}{\kappa \cdot u_*} \right) \tag{5.3-38}$$

The solution found results in the so called Rouse (1937) profiles for the concentration. In literature the elevation a is often chosen to be $0.05 \cdot H$, since at an elevation 0 the solution would give an infinite concentration. This results from the parabolic distribution of the diffusivity as assumed by Rouse. The governing equations are derived for low concentrations, not containing hindered settling. The solution however predicts high concentrations near the bed, requiring hindered settling.
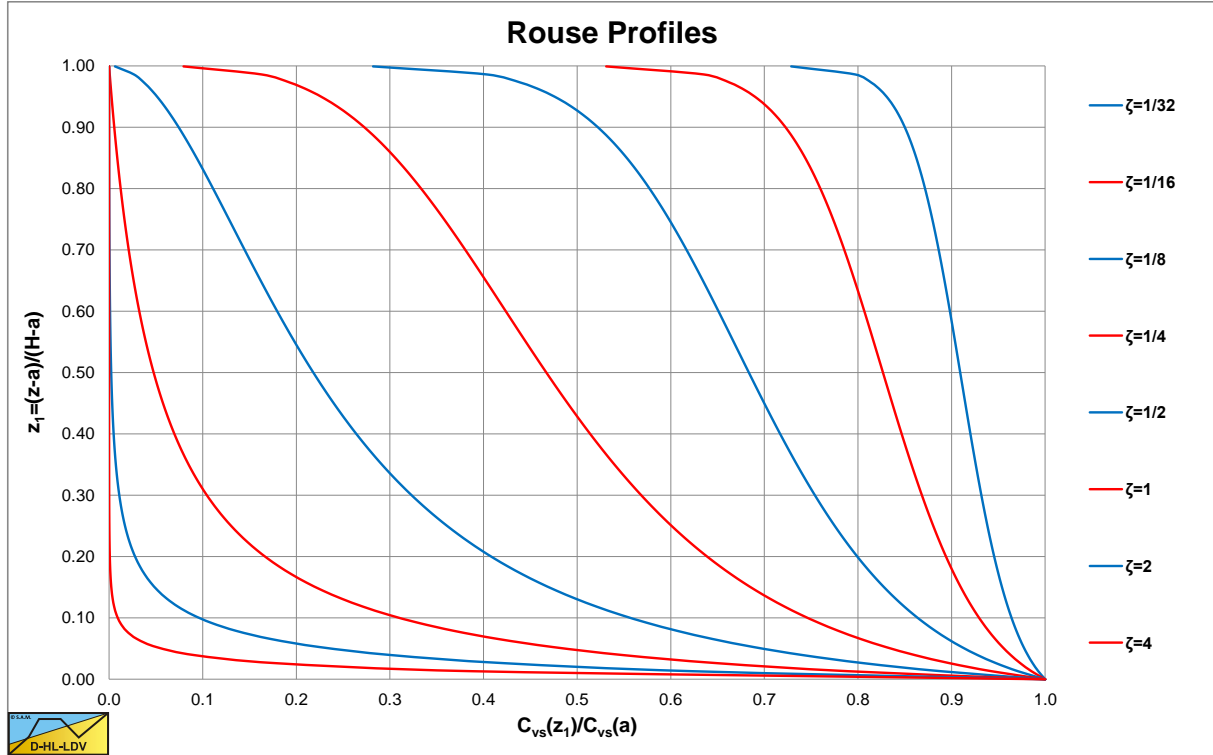
Figure 5.3-1: The Rouse profiles for ζ=1/32 (most right) to ζ=4 (most left).

Figure 5.3-1 shows the Rouse profiles for different values of the Rouse number **P** or ζ, ranging from 1/32 (small particles) to 4 (large particles). The value of **a** is chosen **a=0.05·H**, the abscissa is the concentration ratio **$C_{vs}(z_1)/C_{vs}(a)$** and the ordinate **$z_1=(z-a)/(H-a)$**. **$C_{vs}(a)$** is the concentration at elevation a and often considered the concentration at the bed.

5.3.3.4 The Constant Diffusivity Approach.

If we assume the diffusivity is a constant, the differential equation can be solved. Giving the differential equation in the equilibrium situation:

$$C_{vs}(z) \cdot v_t \cdot \left(1 - C_{vs}(z)\right)^{\beta} + \beta_{sm} \cdot \varepsilon_m \cdot \frac{dC_{vs}(z)}{dz} = 0 \qquad (5.3-39)$$

Ignoring hindered settling (low concentrations) gives:

$$C_{vs}(z) \cdot v_t + \beta_{sm} \cdot \varepsilon_m \cdot \frac{dC_{vs}(z)}{dz} = 0 \qquad (5.3-40)$$

Now the variables have to be separated according to:

$$\frac{dC_{vs}(z)}{C_{vs}(z)} \cdot = -\frac{v_t}{\beta_{sm} \cdot \varepsilon_m} \cdot dz \quad \Rightarrow \quad \ln\left(C_{vs}(z)\right) = -\frac{v_t}{\beta_{sm} \cdot \varepsilon_m} \cdot z + C \qquad (5.3-41)$$

With **$C_{vs}(0)=C_{vB}$**, the concentration at the bottom, the integration constant can be determined giving:

$$C_{vs}(z) = C_{vB} \cdot e^{-\frac{v_t}{\beta_{sm} \cdot \varepsilon_m} \cdot z} \qquad (5.3-42)$$

Although this is just an indicative equation for open channel flow, Doron et al. (1987) and Doron & Barnea (1993) used it in their 2 and 3 layer models.

Assuming the Law of the Wall, one can also determine the average diffusivity by integration (Lane & Kalinske (1941)):

$$\varepsilon_s = \beta_{sm} \cdot \kappa \cdot u_* \cdot z \cdot \left(\frac{H-z}{H}\right) = \beta_{sm} \cdot \kappa \cdot u_* \cdot H \cdot \frac{z}{H} \cdot \left(1 - \frac{z}{H}\right) = \beta_{sm} \cdot \kappa \cdot u_* \cdot H \cdot \tilde{z} \cdot (1 - \tilde{z}) \tag{5.3-43}$$

Integration gives:

$$\bar{\varepsilon}_s = \beta_{sm} \cdot \kappa \cdot u_* \cdot \frac{1}{H} \cdot \int_{z=0}^{z=H} z \cdot \left(\frac{H-z}{H}\right) \cdot dz = \beta_{sm} \cdot \kappa \cdot u_* \cdot \frac{1}{H^2} \cdot \int_{z=0}^{z=H} z \cdot (H-z) \cdot dz$$

$$\bar{\varepsilon}_s = \beta_{sm} \cdot \kappa \cdot u_* \cdot \frac{1}{H^2} \cdot \int_{z=0}^{z=H} \left(z \cdot H - z^2\right) \cdot dz = \beta_{sm} \cdot \kappa \cdot u_* \cdot \frac{1}{H^2} \cdot \left(\frac{1}{2} \cdot z^2 \cdot H - \frac{1}{3} \cdot z^3\right)_{z=0}^{z=H} \tag{5.3-44}$$

$$\bar{\varepsilon}_s = \beta_{sm} \cdot \kappa \cdot u_* \cdot \frac{H}{6}$$

With $C_{vs}(0)=C_{vB}$, the concentration at the bottom, the integration constant can be determined, giving:

$$C_{vs}(z) = C_{vB} \cdot e^{-6 \cdot \frac{v_t}{\beta_{sm} \cdot \kappa \cdot u_*} \cdot \frac{z}{H}} \tag{5.3-45}$$

Wasp (1963) also uses this equation for the concentration distribution in a modified form. He uses the ratio of the concentration at $0.92 \cdot z/D_p$ to $0.50 \cdot z/D_p$. This gives:

$$\frac{C_{vs}(z/D_p = 0.92)}{C_{vs}(z/D_p = 0.50)} = \frac{C_{vB} \cdot e^{-6 \cdot \frac{v_t}{\beta_{sm} \cdot \kappa \cdot u_*} \cdot 0.92}}{C_{vB} \cdot e^{-6 \cdot \frac{v_t}{\beta_{sm} \cdot \kappa \cdot u_*} \cdot 0.50}} = e^{-6 \cdot \frac{v_t}{\beta_{sm} \cdot \kappa \cdot u_*} \cdot (0.92 - 0.50)} = e^{-2.52 \cdot \frac{v_t}{\beta_{sm} \cdot \kappa \cdot u_*}} \tag{5.3-46}$$

Wasp (1963) uses the power of 10 instead of the exponential power, giving:

$$\frac{C_{vs}(z/D_p = 0.92)}{C_{vs}(z/D_p = 0.50)} = e^{-2.52 \cdot \frac{v_t}{\beta_{sm} \cdot \kappa \cdot u_*}} = 10^{-\frac{2.52}{2.30} \cdot \frac{v_t}{\beta_{sm} \cdot \kappa \cdot u_*}} = 10^{-1.096 \cdot \frac{v_t}{\beta_{sm} \cdot \kappa \cdot u_*}} \tag{5.3-47}$$

The factor in the Wasp (1963) equation is not 1.096 but 1.8, resulting in a lower ratio. The Wasp (1963) method will be explained in chapter 6. The difference between the factor 1.096 and 1.8 can be explained by the fact that the theoretical derivation is for open channel flow with a positive velocity gradient to the top. In pipe flow however, the velocity gradient is negative in the top part of the pipe, resulting in downwards lift forces giving a lower concentration at the top of the pipe.

5.3.3.5 The Linear Diffusivity Approach.

Now suppose the diffusivity is linear with the vertical coordinate z, giving:

$$\varepsilon_s = \beta_{sm} \cdot \kappa \cdot u_* \cdot z \tag{5.3-48}$$

The differential equation becomes:

$$\frac{dC_{vs}(z)}{C_{vs}(z)} \cdot = -\frac{v_t}{\beta_{sm} \cdot \kappa \cdot u_*} \cdot \frac{dz}{z} \tag{5.3-49}$$

With the solution, a power law:

$$C_{vs}(z) = C_{vs}(z_0) \cdot \left(\frac{z}{z_0} \right)^{-\frac{v_t}{\beta_{sm} \cdot \kappa \cdot u_*}}$$

(5.3-50)

5.3.3.6 The Hunt (1954) Equation.

Hunt (1954) considered the equilibrium of the solids phase and the liquid phase. For steady uniform flow, he reduced the advection diffusion equation with $\varepsilon_m=0$ and the time averaged concentration being constant and only varying with the vertical distance from the bed. The equation for the solids phase with solids volumetric concentration $C_{vs}(z)$ and solids velocity v_s is now:

$$-v_s \cdot \frac{\partial C_{vs}(z)}{\partial z} - C_{vs}(z) \cdot \frac{\partial v_s}{\partial z} + \frac{\partial}{\partial z} \cdot \left(\varepsilon_{sz} \cdot \frac{\partial C_{vs}(z)}{\partial z} \right) = -\frac{\partial v_s \cdot C_{vs}(z)}{\partial z} + \frac{\partial}{\partial z} \cdot \left(\varepsilon_{sz} \cdot \frac{\partial C_{vs}(z)}{\partial z} \right) = 0$$

(5.3-51)

$$\frac{\partial}{\partial z} \left(-v_s \cdot C_{vs}(z) + \varepsilon_{sz} \cdot \frac{\partial C_{vs}(z)}{\partial z} \right) = 0$$

For the liquid phase with liquid concentration $C_{vl}(z)=(1-C_{vs}(z))$ and liquid velocity v_l the equation is given by:

$$-v_l \cdot \frac{\partial C_{vs}(z)}{\partial z} + \left(1 - C_{vs}(z)\right) \cdot \frac{\partial v_l}{\partial z} + \frac{\partial}{\partial z} \cdot \left(\varepsilon_{lz} \cdot \frac{\partial C_{vs}(z)}{\partial z} \right) =$$

$$\frac{\partial v_l \cdot \left(1 - C_{vs}(z)\right)}{\partial z} - \frac{\partial}{\partial z} \cdot \left(\varepsilon_{lz} \cdot \frac{\partial \left(1 - C_{vs}(z)\right)}{\partial z} \right) = 0$$

(5.3-52)

$$\frac{\partial v_l \cdot C_{vl}(z)}{\partial z} - \frac{\partial}{\partial z} \cdot \left(\varepsilon_{lz} \cdot \frac{\partial C_{vl}(z)}{\partial z} \right) = \frac{\partial}{\partial z} \left(v_l \cdot C_{vl}(z) - \varepsilon_{lz} \cdot \frac{\partial C_{vl}(z)}{\partial z} \right) = 0$$

The time averaged vertical velocity component v_s of the sediment particles (downwards) is equal to the sum of the liquid velocity v_l (upwards) and the terminal settling velocity of the sediment particles in still water $-v_t$. The terminal settling velocity v_t is always a positive number in this derivation and has a minus sign for the downwards direction. The continuity equation shows that the downwards volume flow and the upwards volume flow are equal. Giving:

$$v_s = v_l - v_t \quad \text{and} \quad v_s \cdot C_{vs}(z) + v_l \cdot C_{vl}(z) = 0$$

(5.3-53)

Combining these two equations gives:

$$\left(v_l - v_t \right) \cdot C_{vs}(z) + v_l \cdot C_{vl}(z) = v_l \cdot \left(C_{vs}(z) + C_{vl}(z) \right) - v_t \cdot C_{vs}(z) = 0$$

$$\Rightarrow \quad v_l = v_t \cdot C_{vs}(z)$$

(5.3-54)

$$v_s \cdot C_{vs}(z) + \left(v_s + v_t \right) \cdot C_{vl}(z) = v_s \cdot \left(C_{vs}(z) + C_{vl}(z) \right) + v_t \cdot C_{vl}(z) = 0$$

$$\Rightarrow \quad v_s = -v_t \cdot C_{vl}(z)$$

This gives for the solids phase equation:

$$\frac{\partial}{\partial z}\left(v_t \cdot C_{vl}(z) \cdot C_{vs}(z) + \varepsilon_{sz} \cdot \frac{\partial C_{vs}(z)}{\partial z}\right) = 0 \quad \Rightarrow \quad v_t \cdot C_{vl}(z) \cdot C_{vs}(z) + \varepsilon_{sz} \cdot \frac{\partial C_{vs}(z)}{\partial z} = 0$$

(5.3-55)

$$v_t \cdot \left(1 - C_{vs}(z)\right) \cdot C_{vs}(z) + \varepsilon_{sz} \cdot \frac{\partial C_{vs}(z)}{\partial z} = 0$$

This gives for the liquid phase:

$$\frac{\partial}{\partial z}\left(v_t \cdot C_{vs}(z) \cdot C_{vl}(z) - \varepsilon_{lz} \cdot \frac{\partial C_{vl}(z)}{\partial z}\right) = 0 \quad \Rightarrow \quad v_t \cdot C_{vs}(z) \cdot C_{vl}(z) - \varepsilon_{lz} \cdot \frac{\partial C_{vl}(z)}{\partial z} = 0$$

(5.3-56)

$$v_t \cdot C_{vs}(z) \cdot \left(1 - C_{vs}(z)\right) + \varepsilon_{lz} \cdot \frac{\partial C_{vs}(z)}{\partial z} = 0$$

This gives the well-known Hunt equation, where the diffusivities for the solid and liquid phase are equal.

$$v_t \cdot C_{vs}(z) \cdot \left(1 - C_{vs}(z)\right) + \varepsilon_s \cdot \frac{\partial C_{vs}(z)}{\partial z} = 0$$

(5.3-57)

Including hindered settling according to Richardson & Zaki (1954), the equation looks like:

$$v_t \cdot C_{vs}(z) \cdot \left(1 - C_{vs}(z)\right)^{1+\beta} + \varepsilon_s \cdot \frac{\partial C_{vs}(z)}{\partial z} = 0$$

or

(5.3-58)

$$v_t \cdot C_{vs}(z) \cdot \left(1 - C_{vs}(z)\right)^{\beta} + \varepsilon_s \cdot \frac{\partial C_{vs}(z)}{\partial z} = 0$$

It is however the question whether the power should be **1+β** or **β**, since the Hunt equation already takes the upwards flow of the liquid into account, which is part of hindered settling. Using a power of **β** makes more sense. Hunt assumed a velocity profile according to:

$$\frac{U_{mean} - U(z)}{u_*} = -\frac{1}{\kappa_s} \cdot \left(\left(1 - \frac{z}{H}\right)^{1/2} + B_s \cdot \ln\left(1 - \frac{1}{B_s} \cdot \left(1 - \frac{z}{H}\right)^{1/2}\right)\right)$$

(5.3-59)

This results in a sediment diffusivity ε_s of, with $\beta_{sm} = 1$:

$$\varepsilon_s = 2 \cdot \kappa_s \cdot H \cdot u_* \cdot \left(1 - \frac{z}{H}\right) \cdot \left(B_s - \left(1 - \frac{z}{H}\right)^{1/2}\right)$$

(5.3-60)

With: $\quad \bar{z} = \frac{z}{H} \quad$ **and** $\quad dz = H \cdot d\bar{z}$

The Hunt diffusion advection equation can be written as, without hindered settling:

$$v_t \cdot C_{vs} \cdot \left(1 - C_{vs}\right) + 2 \cdot \kappa_s \cdot u_* \cdot \left(1 - \bar{z}\right) \cdot \left(B_s - \left(1 - \bar{z}\right)^{1/2}\right) \cdot \frac{\partial C_{vs}}{\partial \bar{z}} = 0$$

(5.3-61)

Separation of variables gives:

$$\frac{dC_{vs}}{C_{vs}\cdot\left(1-C_{vs}\right)}=-\frac{v_t}{2\cdot\kappa_s\cdot u_*}\cdot\frac{d\overline{z}}{\left(1-\overline{z}\right)\cdot\left(B_s-\left(1-\overline{z}\right)^{1/2}\right)} \tag{5.3-62}$$

With the solution, knowing the concentration $C_{vs}(a)$ at a distance a from the bed:

$$\frac{C_{vs}(z)}{1-C_{vs}(z)}\cdot\frac{1-C_{vs}(a)}{C_{vs}(a)}=\left(\frac{\sqrt{1-\overline{z}}}{\sqrt{1-\overline{a}}}\cdot\frac{B_s-\sqrt{1-\overline{a}}}{B_s-\sqrt{1-\overline{z}}}\right)^{\frac{v_t}{\kappa_s\cdot B_s\cdot u_*}} \tag{5.3-63}$$

This is known as the Hunt equation. For values of B_s close to 1 and κ_s between 0.31 and 0.44 this equation agrees well with the Rouse equation. The equation is not often used due to its complex nature. One can simplify the equation by assuming a constant diffusivity, for example:

$$\overline{\varepsilon}_s=\beta_{sm}\cdot\kappa\cdot u_*\cdot\frac{H}{6} \tag{5.3-64}$$

According to Lane & Kalinske (1941). The Hunt diffusion advection equation can also be written as, without hindered settling:

$$v_t\cdot C_{vs}(z)\cdot\left(1-C_{vs}(z)\right)+\beta_{sm}\cdot\kappa\cdot u_*\cdot\frac{H}{6}\cdot\frac{\partial C_{vs}(z)}{\partial z}$$

$$=v_t\cdot C_{vs}(\overline{z})\cdot\left(1-C_{vs}(\overline{z})\right)+\beta_{sm}\cdot\kappa\cdot u_*\cdot\frac{1}{6}\cdot\frac{\partial C_{vs}(\overline{z})}{\partial\overline{z}}=0 \tag{5.3-65}$$

Separation of variables gives:

$$\frac{dC_{vs}(\overline{z})}{C_{vs}(\overline{z})\cdot\left(1-C_{vs}(\overline{z})\right)}=-\frac{6\cdot v_t}{\beta_{sm}\cdot\kappa\cdot u_*}\cdot d\overline{z} \tag{5.3-66}$$

With the solution, knowing the concentration $C_{vs}(a)$ at a distance a from the bed:

$$\frac{C_{vs}(z)}{1-C_{vs}(z)}\cdot\frac{1-C_{vs}(a)}{C_{vs}(a)}=e^{-\frac{6\cdot v_t}{\beta_{sm}\cdot\kappa\cdot u_*}\cdot\left(\frac{z-a}{H}\right)} \tag{5.3-67}$$

Taking the distance a from the bed equal to zero and assuming the bottom concentration C_{vB} at that elevation, the equation simplifies to:

$$\frac{C_{vs}(z)}{1-C_{vs}(z)}=\frac{C_{vB}}{1-C_{vB}}\cdot e^{-\frac{6\cdot v_t}{\beta_{sm}\cdot\kappa\cdot u_*}\cdot\frac{z}{H}} \tag{5.3-68}$$

With:

$$C_{vs}(z)=\left(1-C_{vs}(z)\right)\cdot\frac{C_{vB}}{1-C_{vB}}\cdot e^{-\frac{6\cdot v_t}{\beta_{sm}\cdot\kappa\cdot u_*}\cdot\frac{z}{H}} \tag{5.3-69}$$

$$\Rightarrow\quad C_{vs}(z)\cdot\left(1+\frac{C_{vB}}{1-C_{vB}}\cdot e^{-\frac{6\cdot v_t}{\beta_{sm}\cdot\kappa\cdot u_*}\cdot\frac{z}{H}}\right)=\frac{C_{vB}}{1-C_{vB}}\cdot e^{-\frac{6\cdot v_t}{\beta_{sm}\cdot\kappa\cdot u_*}\cdot\frac{z}{H}}$$

Giving:

$$
C_{vs}(z) = \cfrac{\cfrac{C_{vB}}{1-C_{vB}} \cdot e^{-\frac{6 \cdot v_t}{\beta_{sm} \cdot \kappa \cdot u_*} \cdot \frac{z}{H}}}{1+\cfrac{C_{vB}}{1-C_{vB}} \cdot e^{-\frac{6 \cdot v_t}{\beta_{sm} \cdot \kappa \cdot u_*} \cdot \frac{z}{H}}} = \cfrac{e^{-\frac{6 \cdot v_t}{\beta_{sm} \cdot \kappa \cdot u_*} \cdot \frac{z}{H}}}{\cfrac{1-C_{vB}}{C_{vB}} + e^{-\frac{6 \cdot v_t}{\beta_{sm} \cdot \kappa \cdot u_*} \cdot \frac{z}{H}}}
\tag{5.3-70}
$$

If **z=0**, the exponential power equals 1 and the resulting concentration equals the bottom concentration. Integrating the equation over the height of the channel gives for the average concentration:

$$
\bar{C}_{vs} = 1 - \cfrac{\ln\left((1-C_{vB}) \cdot e^{+\frac{6 \cdot v_t}{\beta_{sm} \cdot \kappa \cdot u_*}} + C_{vB}\right)}{\left(\cfrac{6 \cdot v_t}{\beta_{sm} \cdot \kappa \cdot u_*}\right)} = 1 - \cfrac{\ln\left((1-C_{vB}) \cdot e^{+\frac{v_t \cdot H}{\varepsilon_s}} + C_{vB}\right)}{\left(\cfrac{v_t \cdot H}{\varepsilon_s}\right)}
\tag{5.3-71}
$$

In case the argument of the exponential power is close to zero (very small particles), the concentration becomes **C_{vB}**. This follows from Taylor series expansions, first with **C_{vB}** as the variable, second with the argument of the exponential power as the variable, so practically this means homogeneous flow with a uniform concentration equal to the bottom concentration **C_{vB}**. The concentration at the bottom **C_{vB}** can be determined by:

$$
C_{vB} = \cfrac{1-e^{-\bar{C}_{vs} \cdot \frac{v_t \cdot H}{\varepsilon_s}}}{1-e^{-\frac{v_t \cdot H}{\varepsilon_s}}}
\tag{5.3-72}
$$

5.3.4 Conclusions & Discussion Open Channel Flow.

Dey (2014) gives an overview of bed load transport and suspended load transport equations for open channel flow. In open channel flow there is always the assumption of a stationary bed, the assumption of a 2D flow above the bed and a more or less known velocity profile above the bed. The latter results in the Law of the Wall approach for the velocity distribution.

In pipe flow however there may be a stationary or sliding bed, the flow above the bed (if there is a bed) is certainly not 2D, but 3D and the velocity profile is known for a homogeneous flow, but not for the stationary or sliding bed regimes or the heterogeneous flow regime. This velocity profile is not just 3D, but also depends on the height of the bed.

Only if one considers a thin layer above the bed, thin means the layer thickness is small compared to the width of the bed, this may be considered 2D. So the bed load transport process may be considered 2D and can be compared to open channel flow, as long as the sheet flow layer thickness is small compared to the width of the bed. The equation derived may also give good predictions in pipe flow. If the sheet flow layer however becomes too thick, the velocity profile assumed will not match the velocity profile above the bed in a pipe anymore.

Both for bed load and suspended load the velocity profile above a bed in a pipe is 3D and depends on the height of the bed and on the concentration profile. Open channel flow formulations can thus not be applied on the flow in circular pipes. Even in rectangular ducts the influence of the side walls and the velocity distribution is so much different from open channel flow that a different approach has to be applied.

5.3.5 Suspended Load in Pipe Flow.

5.3.5.1 The Constant Diffusivity Approach, Low Concentrations.

If we assume the diffusivity is a constant, the differential equation can be solved. Giving the differential equation in the equilibrium situation without hindered settling:

$$C_{vs}(z) \cdot v_t + \beta_{sm} \cdot \varepsilon_m \cdot \frac{dC_{vs}(z)}{dz} = 0 \qquad (5.3\text{-}73)$$

The coordinate **z** now ranges from 0 to D_p, the pipe diameter. Now the variables have to be separated according to:

$$\frac{dC_{vs}(z)}{C_{vs}(z)} \cdot = - \frac{v_t}{\beta_{sm} \cdot \varepsilon_m} \cdot dz \quad \Rightarrow \quad \ln\left(C_{vs}(z)\right) = - \frac{v_t}{\beta_{sm} \cdot \varepsilon_m} \cdot z + C \qquad (5.3\text{-}74)$$

With $C_{vs}(0)=C_{vb}$ the integration constant can be determined giving:

$$C_{vs}(z) = C_{vb} \cdot e^{- \frac{v_t}{\beta_{sm} \cdot \varepsilon_m} \cdot z} \qquad (5.3\text{-}75)$$

This basic solution is still equal to the solution for open channel flow. Although this is just an indicative equation for open channel flow, Doron et al. (1987) and Doron & Barnea (1993) used it in their 2 and 3 layer models. The difference between pipe flow and open channel flow is in the determination of the diffusivity. Assuming the Law of the Wall, one can also determine the average diffusivity by integration (Lane & Kalinske (1941)):

$$\varepsilon_s = \beta_{sm} \cdot \kappa \cdot u_* \cdot r \cdot \left(\frac{R-r}{R}\right) = \beta_{sm} \cdot \kappa \cdot u_* \cdot R \cdot \frac{r}{R} \cdot \left(1 - \frac{r}{R}\right) = \beta_{sm} \cdot \kappa \cdot u_* \cdot R \cdot \tilde{r} \cdot \left(1 - \tilde{r}\right) \qquad (5.3\text{-}76)$$

Integration over the cross section of the pipe gives:

$$\bar{\varepsilon}_s = \frac{1}{\pi \cdot R^2} \cdot \int_0^{2 \cdot \pi} \int_{r=0}^{r=R} \varepsilon_s \cdot dr \cdot r \cdot d\phi = \beta_{sm} \cdot \kappa \cdot u_* \cdot \frac{R^3}{\pi \cdot R^2} \cdot \int_0^{2 \cdot \pi} \int_{\tilde{r}=0}^{\tilde{r}=1} \tilde{r}^2 \cdot \left(1 - \tilde{r}\right) \cdot d\tilde{r} \cdot d\phi$$

$$= \beta_{sm} \cdot \kappa \cdot u_* \cdot R \cdot \frac{1}{\pi} \cdot \int_0^{2 \cdot \pi} \int_{\tilde{r}=0}^{\tilde{r}=1} \tilde{r}^2 \cdot \left(1 - \tilde{r}\right) \cdot d\tilde{r} \cdot d\phi = \beta_{sm} \cdot \kappa \cdot u_* \cdot R \cdot \frac{1}{\pi} \cdot \int_0^{2 \cdot \pi} \int_{\tilde{r}=0}^{\tilde{r}=1} \left(\tilde{r}^2 - \tilde{r}^3\right) \cdot d\tilde{r} \cdot d\phi \qquad (5.3\text{-}77)$$

$$= \beta_{sm} \cdot \kappa \cdot u_* \cdot R \cdot \frac{2 \cdot \pi}{\pi} \cdot \left(\frac{1}{3} \cdot \tilde{r}^3 - \frac{1}{4} \cdot \tilde{r}^4\right)_0^1 = \frac{\beta_{sm} \cdot \kappa \cdot u_* \cdot R}{6} = \frac{\beta_{sm} \cdot \kappa \cdot u_* \cdot D_p}{12}$$

With $C_{vs}(0)=C_{vB}$, the bottom concentration, the integration constant can be determined, giving:

$$C_{vs}(z) = C_{vB} \cdot e^{-12 \cdot \frac{v_t}{\beta_{sm} \cdot \kappa \cdot u_*} \cdot \frac{r}{D_p}} \qquad (5.3\text{-}78)$$

Wasp (1963) also uses this equation for the concentration distribution in a modified form. He uses the ratio of the concentration at $0.92 \cdot z/D_p$ to $0.50 \cdot z/D_p$. This gives:

$$\frac{C_{vs}(z/D_p = 0.92)}{C_{vs}(z/D_p = 0.50)} = \frac{C_{vB} \cdot e^{-12 \cdot \frac{v_t}{\beta_{sm} \cdot \kappa \cdot u_*} \cdot 0.92}}{C_{vB} \cdot e^{-12 \cdot \frac{v_t}{\beta_{sm} \cdot \kappa \cdot u_*} \cdot 0.50}} = e^{-12 \cdot \frac{v_t}{\beta_{sm} \cdot \kappa \cdot u_*} \cdot (0.92-0.50)} = e^{-5.04 \cdot \frac{v_t}{\beta_{sm} \cdot \kappa \cdot u_*}} \qquad (5.3\text{-}79)$$

Wasp (1963) uses the power of 10 instead of the exponential power, giving:

$$\frac{C_{vs}(z/D_p = 0.92)}{C_{vs}(z/D_p = 0.50)} = e^{-5.04 \cdot \frac{v_t}{\beta_{sm} \cdot \kappa \cdot u_*}} = 10^{-\frac{5.04}{2.30} \cdot \frac{v_t}{\beta_{sm} \cdot \kappa \cdot u_*}} = 10^{-2.19 \cdot \frac{v_t}{\beta_{sm} \cdot \kappa \cdot u_*}} \quad (5.3\text{-}80)$$

The factor in the Wasp (1963) equation is not 2.19 but 1.8, resulting in a slightly higher ratio than the 2.19. The Wasp (1963) method will be explained in chapter 6. The factor 1.8 gives a concentration profile of:

$$C_{vs}(z) = C_{vB} \cdot e^{-9.868 \cdot \frac{v_t}{\beta_{sm} \cdot \kappa \cdot u_*} \cdot \frac{r}{D_p}} \quad (5.3\text{-}81)$$

An approximation for the bottom concentration can be found by integration and acting like it's open channel flow.

$$C_{vs} = C_{vB} \cdot \int_0^1 e^{-9.868 \cdot \frac{v_t}{\beta_{sm} \cdot \kappa \cdot u_*} \cdot \bar{r}} \cdot d\bar{r} = C_{vB} \cdot \left(\frac{\beta_{sm} \cdot \kappa \cdot u_*}{9.868 \cdot v_t} \right) \cdot \left(1 - e^{-9.868 \cdot \frac{v_t}{\beta_{sm} \cdot \kappa \cdot u_*}} \right) \quad (5.3\text{-}82)$$

Giving for the bottom concentration:

$$C_{vB} = C_{vs} \cdot \frac{\left(\dfrac{9.868 \cdot v_t}{\beta_{sm} \cdot \kappa \cdot u_*} \right)}{\left(1 - e^{-9.868 \cdot \frac{v_t}{\beta_{sm} \cdot \kappa \cdot u_*}} \right)} \quad (5.3\text{-}83)$$

5.3.5.2 The Constant Diffusivity Approach, High Concentrations.

The Hunt diffusion advection equation can be written for pipe flow as, without hindered settling:

$$v_t \cdot C_{vs}(r) \cdot \left(1 - C_{vs}(r) \right) + \beta_{sm} \cdot \kappa \cdot u_* \cdot \frac{D_p}{12} \cdot \frac{\partial C_{vs}(r)}{\partial r} = 0 \quad (5.3\text{-}84)$$

The vertical coordinate **r** starts at the bottom of the pipe, **r=0**, and ends at the top of the pipe **r=D_p**. This is with the assumption there is no bed and C_{vB} is the concentration at the bottom of the pipe. With the following solution:

$$C_{vs}(r) = \frac{\dfrac{C_{vB}}{1 - C_{vB}} \cdot e^{-\frac{12 \cdot v_t}{\beta_{sm} \cdot \kappa \cdot u_*} \cdot \frac{r}{D_p}}}{1 + \dfrac{C_{vB}}{1 - C_{vB}} \cdot e^{-\frac{12 \cdot v_t}{\beta_{sm} \cdot \kappa \cdot u_*} \cdot \frac{r}{D_p}}} = \frac{e^{-\frac{12 \cdot v_t}{\beta_{sm} \cdot \kappa \cdot u_*} \cdot \frac{r}{D_p}}}{\dfrac{1 - C_{vB}}{C_{vB}} + e^{-\frac{12 \cdot v_t}{\beta_{sm} \cdot \kappa \cdot u_*} \cdot \frac{r}{D_p}}} \quad (5.3\text{-}85)$$

According to experiments of Matousek (2004) the mean diffusivity divided by the friction velocity and the pipe radius varies between 0.07 and 0.15, with no clear correlation with the mean delivered concentration (0.1-0.4) and the line speed (2-8 m/sec) in fine and medium sands.

$$\bar{\varepsilon}_s = \frac{\beta_{sm} \cdot \kappa \cdot u_* \cdot D_p}{12} = \frac{\beta_{sm} \cdot \kappa \cdot u_* \cdot R}{6}$$

$$\quad (5.3\text{-}86)$$

$$\Rightarrow \quad \frac{\bar{\varepsilon}_s}{u_* \cdot R} = \frac{\beta_{sm} \cdot \kappa}{6} \approx 0.07 \quad \text{for} \quad \beta_{sm} = 1 \quad \text{and} \quad \kappa = 0.4$$

Apparently the factor β_{sm} linking sediment diffusivity to momentum diffusivity is larger than 1 for higher concentrations.

5.3.5.3 The Constant Diffusivity Approach for a Graded Sand.

Karabelas (1977) applied the Hunt (1954) diffusion advection equation to pipe flow for a graded sand, but without hindered settling. Now suppose a graded sand can be divided into **n** fractions with **z** the vertical coordinate. The coordinate **z** is used, including the possibility of a bed. First equation (5.3-84) can be written as:

$$\mathbf{v_t \cdot C_{vs}(z) \cdot \left(1 - C_{vs}(z)\right) + \varepsilon_s \cdot \frac{\partial C_{vs}(z)}{\partial z} = C_{vs}(z) \cdot \left(v_t - v_t \cdot C_{vs}(z)\right) + \varepsilon_s \cdot \frac{\partial C_{vs}(z)}{\partial z}}$$

(5.3-87)

$$\mathbf{= C_{vs}(z) \cdot \left(v_t - v_l\right) + \varepsilon_s \cdot \frac{\partial C_{vs}(z)}{\partial z} = 0}$$

The advection diffusion equation for the **j**th fraction can now be written as:

$$\mathbf{C_{vs,j}(z) \cdot \left(v_{t,j} - v_l\right) + \varepsilon_s \cdot \frac{\partial C_{vs,j}(z)}{\partial z} = 0}$$

(5.3-88)

The upwards liquid velocity $\mathbf{v_l}$ is equal to the sum of the upwards velocities resulting from each fraction:

$$\mathbf{v_l = \sum_{i=1}^{n} v_{t,i} \cdot C_{vs,i}(z)}$$

(5.3-89)

This gives for the advection diffusion equation of the **j**th fraction:

$$\mathbf{C_{vs,j}(z) \cdot \left(v_{t,j} - \sum_{i=1}^{n} v_{t,i} \cdot C_{vs,i}(z)\right) + \varepsilon_s \cdot \frac{\partial C_{vs,j}(z)}{\partial z} = 0}$$

(5.3-90)

This results in a system of **n** coupled differential equations with the general mathematical solution:

$$\mathbf{C_{vs,j}(z) = \frac{G_j \cdot e^{-v_{t,j} \cdot f(z)}}{1 + \sum_{i=1}^{n} G_i \cdot e^{-v_{t,i} \cdot f(z)}}}$$

(5.3-91)

$$\mathbf{With: \quad f(z) = \int_0^z \frac{1}{\varepsilon_s(z)} \cdot dz \quad with: \quad \varepsilon_s(z) = constant \quad \Rightarrow \quad f(z) = \frac{z}{\varepsilon_s}}$$

The variable $\mathbf{G_j}$ is a set of coefficients characteristic of each size fraction, but independent of the space coordinates. The assumption of a constant diffusivity is reasonable, except very close to the wall. For the diffusivity the following is chosen by Karabelas (1977):

$$\mathbf{\varepsilon_s(z) = \zeta \cdot R \cdot u_*}$$

(5.3-92)

Giving for the general solution:

$$\mathbf{C_{vs,j}(z) = \frac{G_j \cdot e^{-\frac{v_{t,j}}{\zeta \cdot u_*} \cdot \frac{z}{R}}}{1 + \sum_{i=1}^{n} G_i \cdot e^{-\frac{v_{t,i}}{\zeta \cdot u_*} \cdot \frac{z}{R}}}}$$

(5.3-93)

For a uniform sand and no bed, using the Lane & Kalinske (1941) approach to determine the mean diffusivity, the solution, equation (5.3-85) is, with **r** starting at the bottom of the pipe:

$$C_{vs}(r) = \frac{\dfrac{C_{vB}}{(1-C_{vB})} \cdot e^{-\frac{6 \cdot v_t}{\beta_{sm} \cdot \kappa \cdot u_*} \cdot \frac{r}{R}}}{1 + \dfrac{C_{vB}}{(1-C_{vB})} \cdot e^{-\frac{6 \cdot v_t}{\beta_{sm} \cdot \kappa \cdot u_*} \cdot \frac{r}{R}}}$$

(5.3-94)

The equation for uniform sands has the same form as the equation for graded sands. The argument of the exponential power differs because a different diffusivity has been chosen using the Lane & Kalinske (1941) approach. Choosing the same mean diffusivity would give the same argument of the exponential power. Apparently one can write:

$$G_j = \frac{C_{vB,j}}{\left(1 - \sum_{i=1}^{n} C_{vB,j}\right)} = \frac{C_{vB,j}}{(1-C_{vB})} \quad \text{with:} \quad \sum_{i=1}^{n} C_{vB,j} = C_{vB}$$

(5.3-95)

So the variable **G_j** is related to the concentration **$C_{vB,j}$** of the **j^{th}** fraction at the bottom of the pipe. With:

$$\sum_{i=1}^{n} C_{vs,i}(z) = \sum_{i=1}^{n} \frac{G_i \cdot e^{-\frac{v_{t,i}}{\zeta \cdot u_*} \cdot \frac{z}{R}}}{1 + \sum_{i=1}^{n} G_i \cdot e^{-\frac{v_{t,i}}{\zeta \cdot u_*} \cdot \frac{z}{R}}} = \frac{\sum_{i=1}^{n} G_i \cdot e^{-\frac{v_{t,i}}{\zeta \cdot u_*} \cdot \frac{z}{R}}}{1 + \sum_{i=1}^{n} G_i \cdot e^{-\frac{v_{t,i}}{\zeta \cdot u_*} \cdot \frac{z}{R}}}$$

(5.3-96)

One can write:

$$\sum_{i=1}^{n} C_{vs,i}(z) \cdot \left(1 + \sum_{i=1}^{n} G_i \cdot e^{-\frac{v_{t,i}}{\zeta \cdot u_*} \cdot \frac{z}{R}}\right) = \sum_{i=1}^{n} G_i \cdot e^{-\frac{v_{t,i}}{\zeta \cdot u_*} \cdot \frac{z}{R}}$$

$$\sum_{i=1}^{n} C_{vs,i}(z) = \sum_{i=1}^{n} G_i \cdot e^{-\frac{v_{t,i}}{\zeta \cdot u_*} \cdot \frac{z}{R}} \cdot \left(1 - \sum_{i=1}^{n} C_{vs,i}(z)\right)$$

(5.3-97)

$$\frac{\sum_{i=1}^{n} C_{vs,i}(z)}{\left(1 - \sum_{i=1}^{n} C_{vs,i}(z)\right)} = \sum_{i=1}^{n} G_i \cdot e^{-\frac{v_{t,i}}{\zeta \cdot u_*} \cdot \frac{z}{R}}$$

Or:

$$\frac{C_{vs,j}(z)}{\left(1 - \sum_{i=1}^{n} C_{vs,i}(z)\right)} = G_j \cdot e^{-\frac{v_{t,j}}{\zeta \cdot u_*} \cdot \frac{z}{R}}$$

(5.3-98)

For the bottom of the pipe where **z=0** this gives:

$$G_j = \frac{C_{vs,j}(0)}{\left(1 - \sum_{i=1}^{n} C_{vs,i}(0)\right)} = \frac{C_{vB,j}}{\left(1 - \sum_{i=1}^{n} C_{vB,i}\right)} = \frac{C_{vB,j}}{\left(1 - C_{vB}\right)} \tag{5.3-99}$$

Proving that equation (5.3-93) can also be written as:

$$C_{vs,j}(z) = \frac{\dfrac{C_{vB,j}}{\left(1 - C_{vB}\right)} \cdot e^{-\frac{v_{t,j}}{\zeta \cdot u_*} \cdot \frac{z}{R}}}{1 + \sum_{i=1}^{n} \dfrac{C_{vB,i}}{\left(1 - C_{vB}\right)} \cdot e^{-\frac{v_{t,i}}{\zeta \cdot u_*} \cdot \frac{z}{R}}} \tag{5.3-100}$$

With **C_vB,j** the concentration of the **j^th** fraction at the bottom of the pipe and **C_vB** the total bottom concentration. Assuming that the mean concentration of each fraction is known a priori and the total mean concentration is known a priori, equation (5.3-98) can be written as:

$$\frac{C_{vs,j}}{\left(1 - C_{vs}\right)} = G_j \cdot \frac{1}{A} \cdot \int_A e^{-\frac{v_{t,j}}{\zeta \cdot u_*} \cdot \frac{z}{R}} \cdot dA \tag{5.3-101}$$

Giving for **G_j** according to Karabelas (1977):

$$G_j = \frac{C_{vs,j}}{\left(1 - C_{vs}\right)} \cdot \frac{1}{\dfrac{1}{A} \cdot \int_A e^{-\frac{v_{t,j}}{\zeta \cdot u_*} \cdot \frac{z}{R}} \cdot dA} = \frac{C_{vs,j}}{\left(1 - C_{vs}\right)} \cdot \frac{1}{E_j}$$

$$\text{With:} \quad E_j \approx 1 + \frac{\left(\dfrac{v_{t,j}}{\zeta \cdot u_*}\right)^2}{8} \cdot \left(1 + \frac{\left(\dfrac{v_{t,j}}{\zeta \cdot u_*}\right)^2}{24}\right) \tag{5.3-102}$$

This solution is valid for a constant diffusivity over the pipe cross section and no hindered settling.

For the case of one dimensional open channel flow with height **H**, Karabelas (1977) gives:

$$G_j = \frac{C_{vs,j}}{\left(1 - C_{vs}\right)} \cdot \frac{1}{\dfrac{1}{H} \cdot \int_0^H e^{-\frac{v_{t,j}}{\zeta \cdot u_*} \cdot \frac{z}{H}} \cdot dz} \tag{5.3-103}$$

Giving for the general solution:

$$C_{vs,j}(z) = \frac{G_j \cdot e^{-\frac{v_{t,j}}{\zeta \cdot u_*} \cdot \frac{z}{H}}}{1 + \sum_{i=1}^{n} G_i \cdot e^{-\frac{v_{t,i}}{\zeta \cdot u_*} \cdot \frac{z}{H}}} \tag{5.3-104}$$
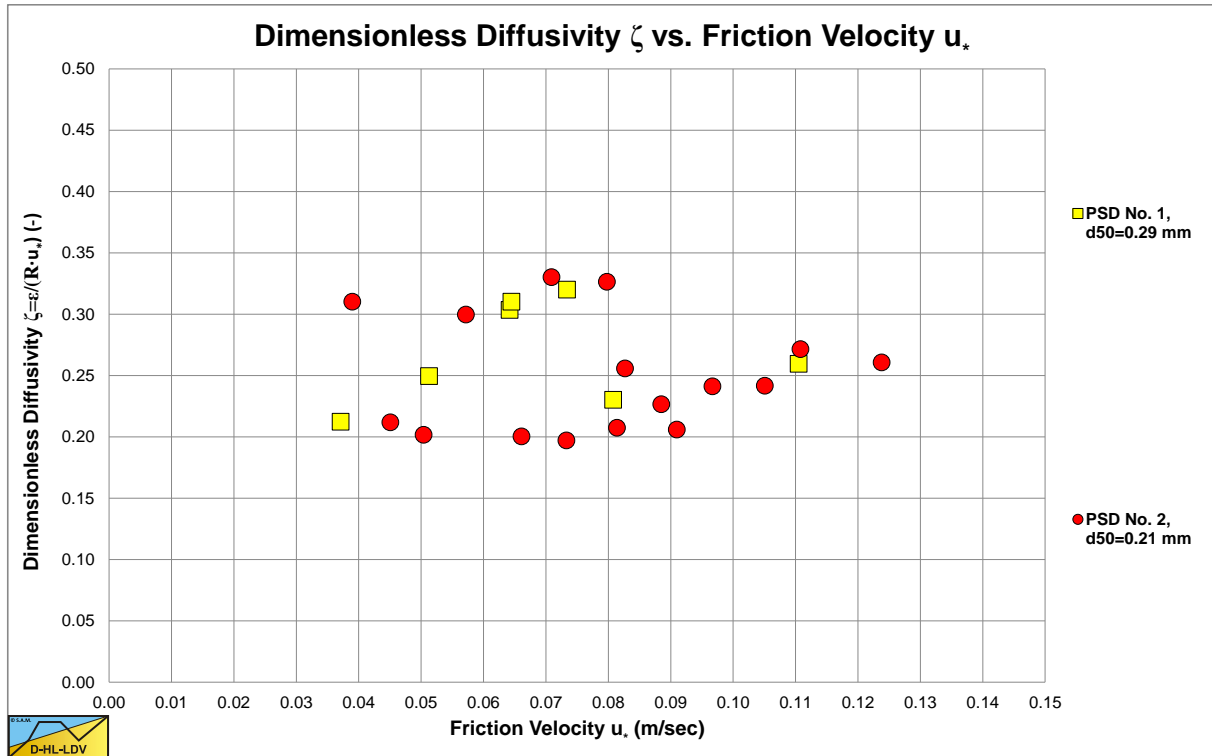
Figure 5.3-2: Measured dimensionless diffusivities in a 0.0504 m pipe, Karabelas (1977).

5.3.6 Conclusions & Discussion Pipe Flow.

For pipe flow the constant lateral diffusivity approach for uniform sands is a good first approximation using the mean diffusivity divided by the friction velocity and the pipe radius ζ with values larger than the theoretical expected values. Karabelas (1977) found an average value of 0.255, which is 3 to 4 times larger than the diffusivity of liquid in the absence of particles. The median particle diameter was nearly equal to the Kolmogorov micro scale of turbulence. Other researchers have used spherical particles with diameters one to two magnitudes larger than the Kolmogorov micro scale of turbulence and found slightly higher diffusivities between 0.3 and 0.4.

The Karabelas (1977) method for graded sands is a good starting point and has been used by several researchers to develop more sophisticated methods, which will be described in chapter 6. The open channel approach of Karabelas (1977) is a good first guess of the parameter G_j. For very small particles this results in an average concentration equal to the concentration at the bottom, meaning homogeneous flow.

$$G_j = \frac{C_{vB,j}}{\left(1 - C_{vB}\right)}$$

(5.3-105)

For a uniform sand this gives:

$$C_{vB,j} = \frac{1 - e^{-\bar{C}_{vs,j} \cdot \frac{v_{t,j} \cdot H}{\varepsilon_s}}}{1 - e^{-\frac{v_t \cdot H}{\varepsilon_s}}}$$

(5.3-106)

Figure 5.3-3 and Figure 5.3-4 show concentration profiles from Karabelas (1977), compared with profiles determined with equation (5.3-70) for open channel flow and uniform sand with $H=D_p$. It should be mentioned that the concentration were very low, 0.3%, so there was no hindered settling. The reason for comparing a graded sand in pipe flow with a uniform sand in open channel flow is, to see if the relatively simple analytical solution gives a good approximation, which it does. The higher the line speed, the better the approximation.
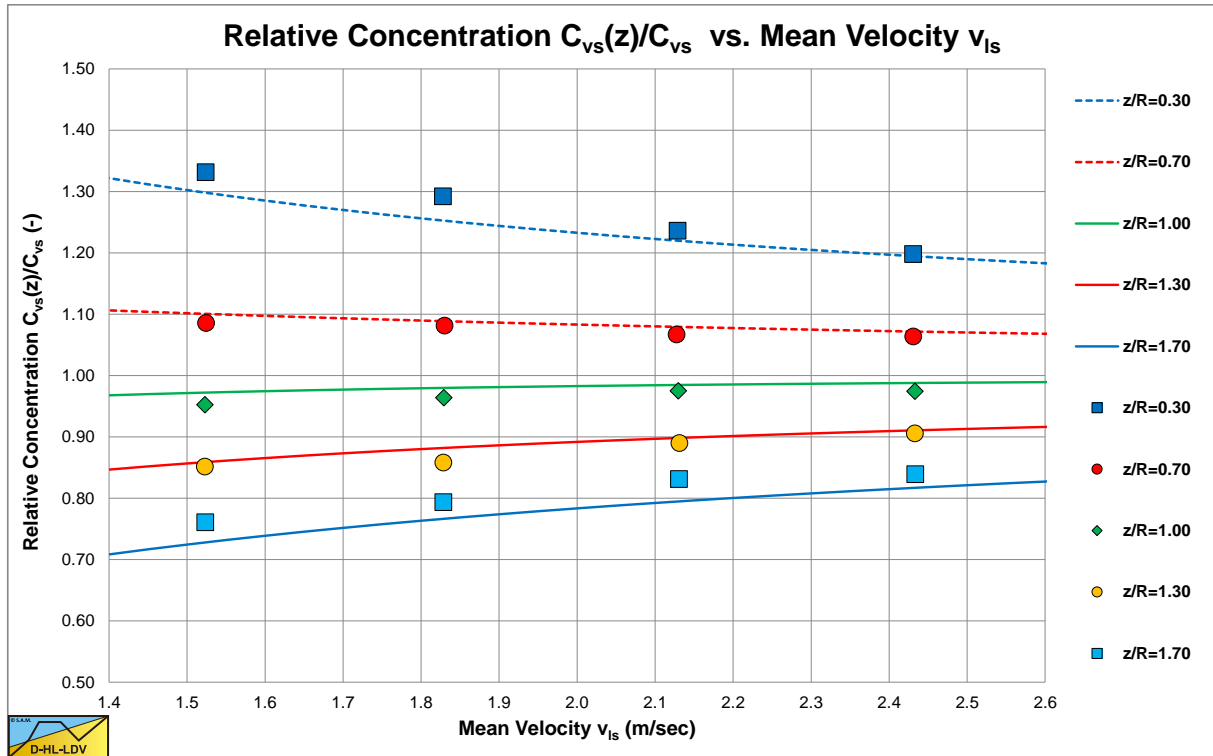
Figure 5.3-3: Concentration profiles in a 0.0504 m pipe, Karabelas (1977).
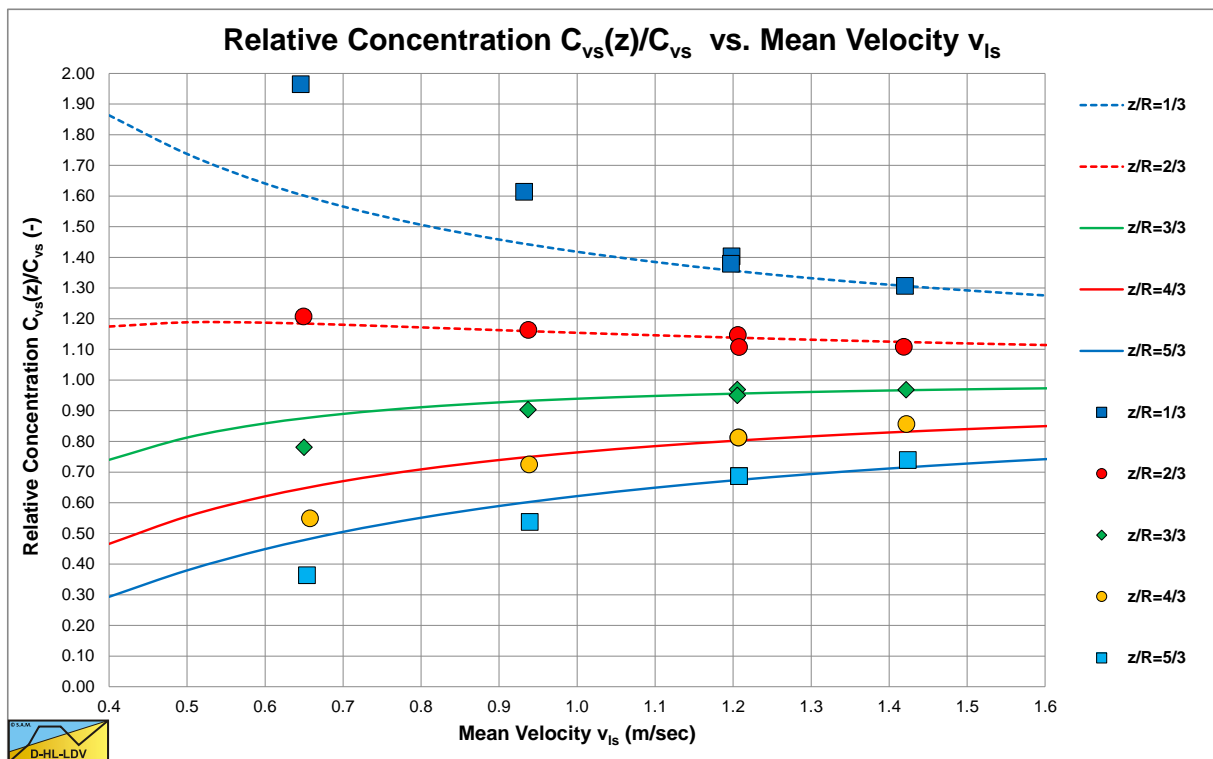
Figure 5.3-4 Concentration profiles in a 0.0753 m pipe, Karabelas (1977).

5.3.7 Nomenclature Erosion, Bed Load and Suspended Load.

a	Elevation above the bed	m
B_s	Factor in Hunt equation	-
C	Volumetric concentration	-
$C_{vs}(z)$	Volumetric concentration	-
$C_{vs,sf}$	Volumetric concentration in sheet flow layer	-
C_{vb}	Volumetric concentration bed	-
C_{vB}	Volumetric concentration bottom of channel or pipe	-
C_{vl}	Volumetric concentration liquid	-
d	Particle diameter	m
D_p	Pipe diameter	m
E	Coefficient in Karabelas approach	-
$f(z)$	Function related to diffusivity integration	s/m
g	Gravitational constant (9.81 m/s^2)	m/s^2
G	Coefficient in Karabelas approach	-
H	Height of the flow layer	m
H	Thickness sheet flow layer	m
i, j	Fraction number	-
n	Number of fractions	-
n	Power used for velocity profile in sheet flow layer	-
P	Rouse number	-
q_b	Bed load transport	m^2/s
$q_{s,down}$	Downwards flow of particles	1/s
$q_{s,up}$	Upwards flow of particles	1/s
Q_s	Total sediment transport or bed load	m^3/s
r	Vertical coordinate in pipe	m
R	Radius of pipe	m
R_{sd}	Relative submerged density (about 1.65 for sand)	-
t	Time	s
u_*	Friction velocity	m/s
$U(z)$	Velocity in the flow layer or in sheet flow layer	m/s
U_H	Velocity at top sheet flow layer	m/s
U_{mean}	Mean velocity in sheet flow layer	m/s
u	Velocity in x direction	m/s
v	Velocity in y direction	m/s
v_l	Vertical velocity liquid upwards	m/s
v_s	Vertical velocity solids or sediment downwards	m/s
v_t	Terminal settling velocity	m/s
w	Velocity in z direction	m/s
w	Bed width	m
x	Coordinate	m
y	Coordinate	m
z	Coordinate	m
z	Vertical position in the flow layer	m
z_0	Starting point logarithmic velocity profile	m
z_1	Ordinate Rouse profile	m
α	Coefficient MPM equation (usually 8)	-
β	Power MPM equation (usually 1.5)	-
β	Richardson & Zaki power hindered settling	-
β_{sm}	Relation sediment mass diffusivity to eddy momentum diffusivity.	-
ε_m	Diffusivity molecular	m/s
ε_m	Eddy momentum diffusivity	m/s
ε_s	Sediment diffusivity	m/s
ε_{sx}	Diffusivity turbulent x direction sediment	m/s
ε_{sy}	Diffusivity turbulent y direction sediment	m/s
ε_{sz}	Diffusivity turbulent z direction sediment	m/s
ε_{lz}	Diffusivity turbulent z direction liquid	m/s

γ	Coefficient velocity top sheet flow layer	**-**
λ$_b$	Bed Darcy Weisbach friction factor	**-**
κ, κ$_s$	von Karman constant	**-**
φ	Internal friction angle bed	**rad**
ρ$_l$	Liquid density	**ton/m^3**
θ	Shields parameter or dimensionless shear stress	**-**
θ$_{cr}$	Critical Shields parameter	**-**
τ(z)	Shear stress as function of vertical coordinate	**Pa**
τ$_b$	Bed shear stress	**Pa**
Φ$_b$	Dimensionless bed load transport	**-**
ζ	Rouse number	**-**
ζ	Relation sediment mass diffusivity to eddy momentum diffusivity in Karabelas approach	**-**

Chapter 6:   Slurry Transport, a Historical Overview.

6.1 Introduction.

In August 2012 the author was approached by a dredging company with the question which head loss model to use for a project with a cutter dredge and a discharge length of 35 km. This raised the following questions:
- What did the company want to know?
- How many booster stations to use?
- What should be the locations of the booster stations?
- What were the real issues?
- What should be the total pump pressure to avoid plugging the line?
- Where to locate the booster stations to avoid cavitation at the entrance of each pump?
- How does this depend on the particle size distribution?

These questions and many others triggered a study in to the existing head loss models. With the knowledge that the main Dutch and Belgium dredging contractors use the Durand & Condolios (1952) and Fuhrboter (1961) models in a modified form, while companies in the USA and Canada often use the Wilson (1992) model in a modified form or the SRC model, the study started with a comparison of these models. Other models that were investigated were the Newitt et al. (1955) model, the Doron & Barnea (1987) model, the Matousek (1997) model and others. Also later models like the 4 component Sellgren & Wilson (2012) model and the 2LM and 3LM models of Wilson (1979-2015), Matousek (1997-2016) and SRC (1991-2016) were investigated.

Usually the models perform well in the neighborhood of the parameters used during the experiments, especially the pipe diameter (small) and the particle diameter, but for real life conditions (large pipe diameters) the models deviate and it's not clear which model matches these conditions. Another issue is that most models are derived for transport (delivered) volumetric concentrations as input and not the spatial volumetric concentrations. The research into the existing models gave some answers but not all.

For the determination of the pressure losses of a solids-water slurry flow many equations, theories and data are available, like Blatch (1906), Howard (1938), Siegfried (Durepaire, 1939), O'Brien & Folsom (1939), Durand & Condolios (1952) and Durand (1953), Gibert (1960), Worster & Denny (1955), Zandi & Govatos (1967), Newitt et al. (1955), Fuhrboter (1961), Jufin & Lopatin (1966), Turian & Yuan (1977), Doron et al. (1987) and Doron & Barnea (1993), Wilson et al. (1997) and Matousek (1997). Some models are based on semi-empirical equations, others on mechanistic or phenomenological models. A number of these models and experimental data will be analyzed and issues found will be addressed. The book shows many graphs with original or reconstructed data and graphs with derived quantities. The author has tried to show as many original experimental data as possible, with the philosophy that the experimental data are based on nature, while most models and equations are local fit results and may thus not be applicable for other sand, gravels or pipe diameters.

This chapter is divided into 4 main sections:
1. Early history up to 1948, describing the phenomena more qualitatively. Blatch (1906), Howard (1938), Siegfried (Durepaire, 1939), O'Brien & Folsom (1939), Wilson (1942) and others. Since the original articles were not available, reproduced graphs were digitized. The graphs shown here only have a qualitative value and should not be used quantitatively.
2. 1948 to present, empirical and semi-empirical models and equations. Soleil & Ballade (1952), Durand & Condolios (1952) and Durand (1953), Gibert (1960), Worster & Denny (1955), Zandi & Govatos (1967), Newitt et al. (1955), Silin, Kobernik & Asaulenko (1958) & (1962), Fuhrboter (1961), Jufin & Lopatin (1966), Charles (1970) and Babcock (1970), Graf et al. (1970) & Robinson (1971), Yagi et al. (1972), A.D. Thomas (1976) & (1979), Turian & Yuan (1977), Kazanskij (1978) and IHC-MTI (1998). In general the original articles were retrieved and the original graphs were digitized. So the graphs shown here both have a qualitative and a quantitative value.
3. 1979 to present, physical 2 layer (2LM) and 3 layer (3LM) models. Wasp et al. (1963), (1970) and (1977), Wilson et al. - GIW (1979), (1992), (1997) and (2006), Doron et al. (1987) and Doron & Barnea (1993), SRC - Shook & Roco (1991) & Gillies (1993), Kaushal & Tomita (2002B), Matousek (1997) and Talmon (2011) & (2013). In general the original articles were retrieved and the original graphs were digitized. So the graphs shown here have both a qualitative and a quantitative value.
4. The Limit Deposit Velocity. The models of Wilson (1942), Durand & Condolios (1952), Newitt et al. (1955), Jufin & Lopatin (1966), Zandi & Govatos (1967), Charles (1970), Graf et al. (1970) & Robinson (1971), Wilson & Judge (1976), Wasp et al. (1977), Thomas (1979), Oroskar & Turian (1980), Parzonka et al. (1981),

Turian et al. (1987), Davies (1987), Schiller & Herbich (1991), Gogus & Kokpinar (1993), Gillies (1993), Van den Berg (1998), Kokpinar & Gogus (2001), Shook et al. (2002), Wasp & Slatter (2004), Sanders et al. (2004), Lahiri (2009), Poloski et al. (2010) and Souza Pinto et al. (2014) are discussed and general trends are identified.

Many graphs are made with the Delft Head Loss & Limit Deposit Velocity Framework (DHLLDV) as a reference system. Additional graphs can be found on the website www.dhlldv.com.

6.1.1 Coordinate Systems.

In literature many different coordinate systems are used. Some coordinate systems are based on measured quantities, like the hydraulic gradient versus the line speed, but many coordinate systems are based on derived quantities. Some of the most used coordinate systems are explained here.

For the ordinate axis often the hydraulic gradient **i** is used, which is defined as:

$$y = i = \frac{\Delta p}{\rho_l \cdot g \cdot \Delta L} \tag{6.1-1}$$

Durand & Condolios (1952) defined the parameter **Φ** for the ordinate axis according to:

$$y = \Phi = \left(\frac{i_m - i_l}{i_l \cdot C_{vt}} \right) \tag{6.1-2}$$

Babcock (1970) used this parameter **Φ** for the ordinate axis, but also this parameter divided by the relative submerged density:

$$y = \left(\frac{i_m - i_l}{i_l \cdot R_{sd} \cdot C_{vt}} \right) \tag{6.1-3}$$

Wilson et al. (1992) defined the stratification ratio, which is used and named in this book as the relative excess hydraulic gradient **E$_{rhg}$**:

$$y = E_{rhg} = \left(\frac{i_m - i_l}{R_{sd} \cdot C_{vt}} \right) \tag{6.1-4}$$

For the abscissa axis often the line speed **v$_{ls}$** is used in combination with the hydraulic gradient **i** on the ordinate axis. To make the abscissa axis dimensionless, the flow Froude number can be used:

$$x = Fr_{fl} = \frac{v_{ls}}{\sqrt{g \cdot D_p}} \tag{6.1-5}$$

Durand & Condolios (1952) defined the parameter **ψ** for the ordinate axis according to:

$$x = \psi = \left(\frac{v_{ls}}{\sqrt{g \cdot D_p}} \right)^2 \cdot \left(\frac{v_t}{\sqrt{g \cdot d_{50}}} \right)^{-1} = \left(\frac{v_{ls}}{\sqrt{g \cdot D_p}} \right)^2 \cdot \sqrt{C_x} \tag{6.1-6}$$

Later the relative submerged density was added to this abscissa axis parameter according to:

$$x = \psi = \left(\frac{v_{ls}}{\sqrt{g \cdot D_p \cdot R_{sd}}} \right)^2 \cdot \left(\frac{v_t}{\sqrt{g \cdot d_{50}}} \right)^{-1} = \left(\frac{v_{ls}}{\sqrt{g \cdot D_p \cdot R_{sd}}} \right)^2 \cdot \sqrt{C_x} \tag{6.1-7}$$

6.2   Early History.

6.2.1   Blatch (1906).

The first experiments discovered were carried out by Nora Stanton Blatch (1906), with a pipeline of 1 inch and sand particles of **d=0.15-0.25 mm** and **d=0.4-0.8 mm**. She used two types of pipes, copper pipes and galvanized steel pipes.

The experiments with the **d=0.15-0.25 mm** sand were carried out using the copper pipe. The results, digitized from a fit line graph (so not the original data points), are shown in Figure 6.2-1. At low line speeds the hydraulic gradient curve is horizontal (small C_{vt}) or decreasing (larger C_{vt}) with increasing line speed. It seems the curves have a minimum near a line speed of 1 m/sec and increase with a further increasing line speed, approaching the liquid curve. It is however not clear whether the curves asymptotically reach the liquid curve or the Equivalent Liquid Model (ELM) curves, or somewhere in between.

The first experiments with the **d=0.4-0.8 mm** sand were also carried out using the copper pipe. The results, digitized from a fit line graph (so not the original data points), are shown in Figure 6.2-2. At low line speeds the hydraulic gradient curve is almost horizontal with increasing line speed. This makes the minimum hard to find. At higher line speeds the curves approach the clean water curves asymptotically.

The second set of experiments with the **d=0.4-0.8 mm** sand were carried out using the galvanized steel pipe. The results, digitized from a fit line graph (so not the original data points), are shown in Figure 6.2-3. At low line speeds the hydraulic gradient curve is almost horizontal with increasing line speed. This makes the minimum hard to find. At higher line speeds the curves approach the clean water curves asymptotically, but less than in the copper pipe. The clean water curve is clearly much steeper than with the copper pipe, due to the wall roughness.

It looks like very small particles (**d=0.2 mm**) tend to have ELM behavior at high line speeds, while medium sized particles (**d=0.55 mm**) approach the clean water curve. The experiments did not contain large particles, so their behavior is not investigated. This behavior depends on many parameters, so one can only draw conclusions for the values of the parameters tested.
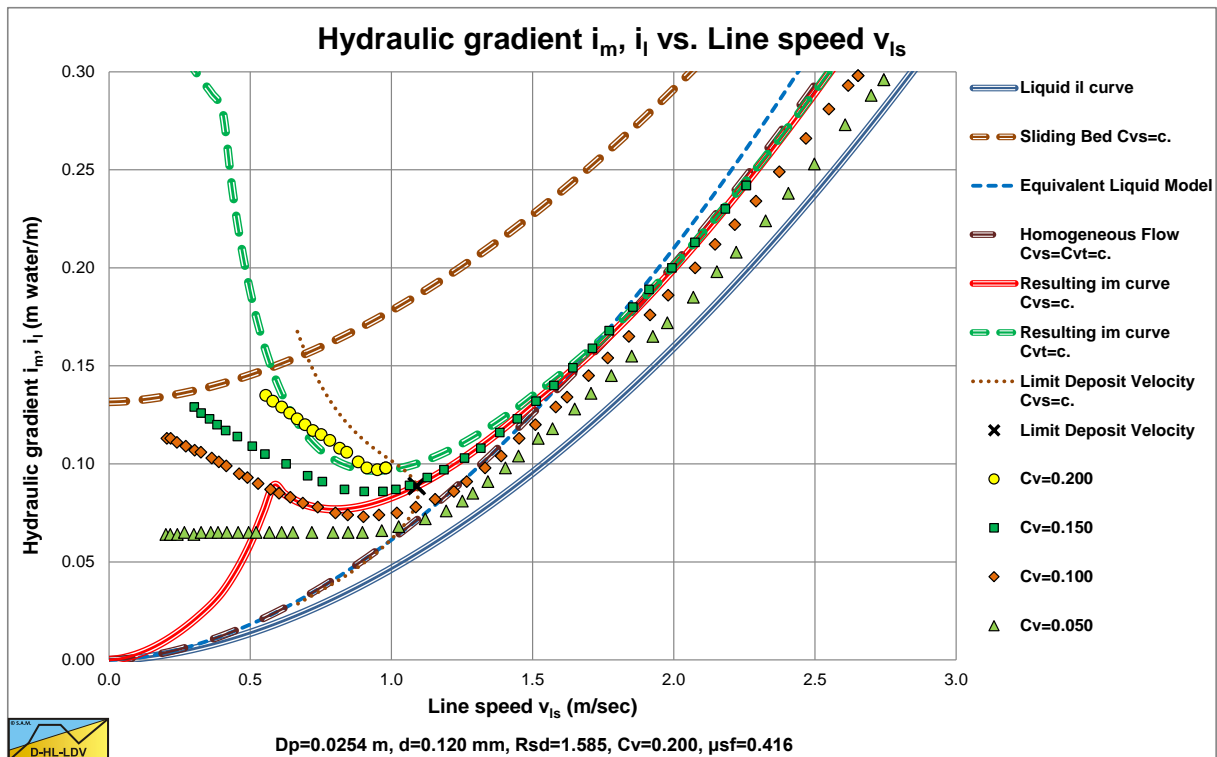
Figure 6.2-1: Sand with d=0.15-0.25 mm in a 1 inch diameter copper pipe.
Data points of Blatch (1906) reconstructed from fit lines (source (Westendorp, 1948)).

In Figure 6.2-1 the data are compared with the DHLLDV Framework for a particle diameter of **d=0.12 mm** and a volumetric concentration of 20%.
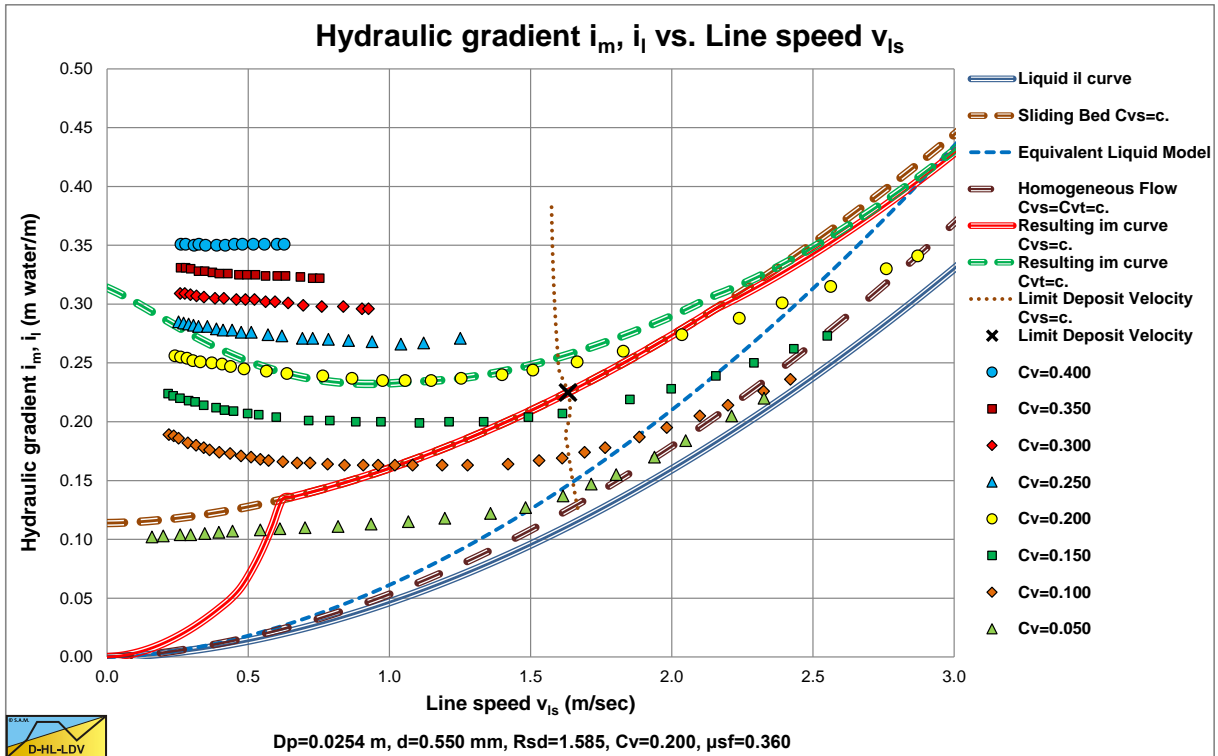
Figure 6.2-2: Sand with d=0.4-0.8 mm in a 1 inch diameter copper pipe.
Data points of Blatch (1906) reconstructed from fit lines (source (Westendorp, 1948)).
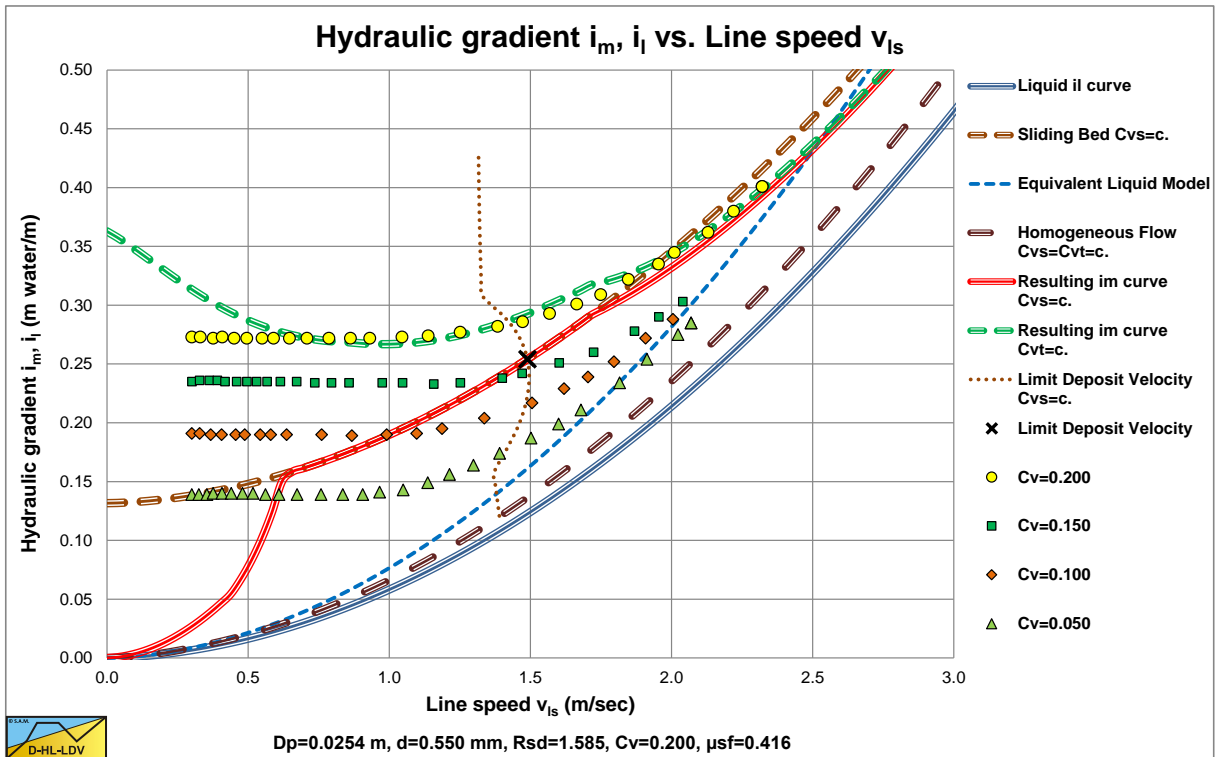
Figure 6.2-3: Sand with d=0.4-0.8 mm in a 1 inch diameter steel pipe.
Data points of Blatch (1906) reconstructed from fit lines (source (Westendorp, 1948)).

6.2.2 Howard (1938).

Howard (1938) carried out experiments with a **d=0.4 mm** graded sand (**d=0.1-2.0 mm**, 80%<0.8 mm) in a 4 inch pipe. The results, digitized from a fit line graph (so not the original data points), are shown in Figure 6.2-4. The hydraulic gradient curves start above a line speed of 2 m/sec and the distance (excess hydraulic gradient) with the liquid hydraulic gradient curve tends to be increasing with increasing line speed. This looks like following the ELM curves for the different concentrations. The curves are however steeper than the ELM curves, which is not observed with any other experiments. An explanation could be that the concentration definition used by Howard (1938) is not the volumetric delivered concentration, but he may have used another definition. The data from the trend lines do not show any resemblance with the DHLLDV Framework.

6.2.3 Siegfried (Durepaire, 1939).

Siegfried (Durepaire, 1939) carried out experiments with a **d=0.3 mm** sand in a 0.072 m diameter pipe. The results, digitized from a fit line graph (so not the original data points), are shown in Figure 6.2-5. The hydraulic gradient curves decrease with an increasing line speed at low line speeds, up to a minimum of the hydraulic gradient curves, after which they increase approaching the liquid hydraulic gradient curve asymptotically.
The magnitude of the hydraulic gradients in the original graph however is too small compared to the experiments of others. An explanation could be that the concentration definition used by Siegfried (Durepaire, 1939) is not the volumetric spatial concentration, but he may have used another definition. Another explanation is that the values on the axis of the graphs, a copy of a copy, were not correct. Figure 6.2-5 is a modified version of the original graph, but the shapes of the hydraulic gradient curves have not changed.

6.2.4 O'Brien & Folsom (1939).

O'Brien & Folsom (1939) carried out experiments with two sands, **d=0.17 mm** and **d=0.27 mm** in a 2 inch and a 3 inch pipe. In their original graphs, the hydraulic gradient is expressed in meters mixture per meter pipe length. The original graph also contains the volumetric concentration of each data point. By recalculating the real hydraulic gradients and grouping the data points in concentration ranges, Figure 6.2-6 and Figure 6.2-7 are constructed. The concentrations in the legends are the average values of the concentration ranges, so some scatter may be expected. Figure 6.2-6 shows a more or less homogeneous behavior. Most data points are in between the ELM curve and the clean water curve. It should be mentioned that the figure only gives the ELM curve for **C$_v$=0.188**. The data points are closer to the ELM curve than to the clean water (liquid) curve. Figure 6.2-7 shows the same behavior, but the data points are closer to the ELM curve.
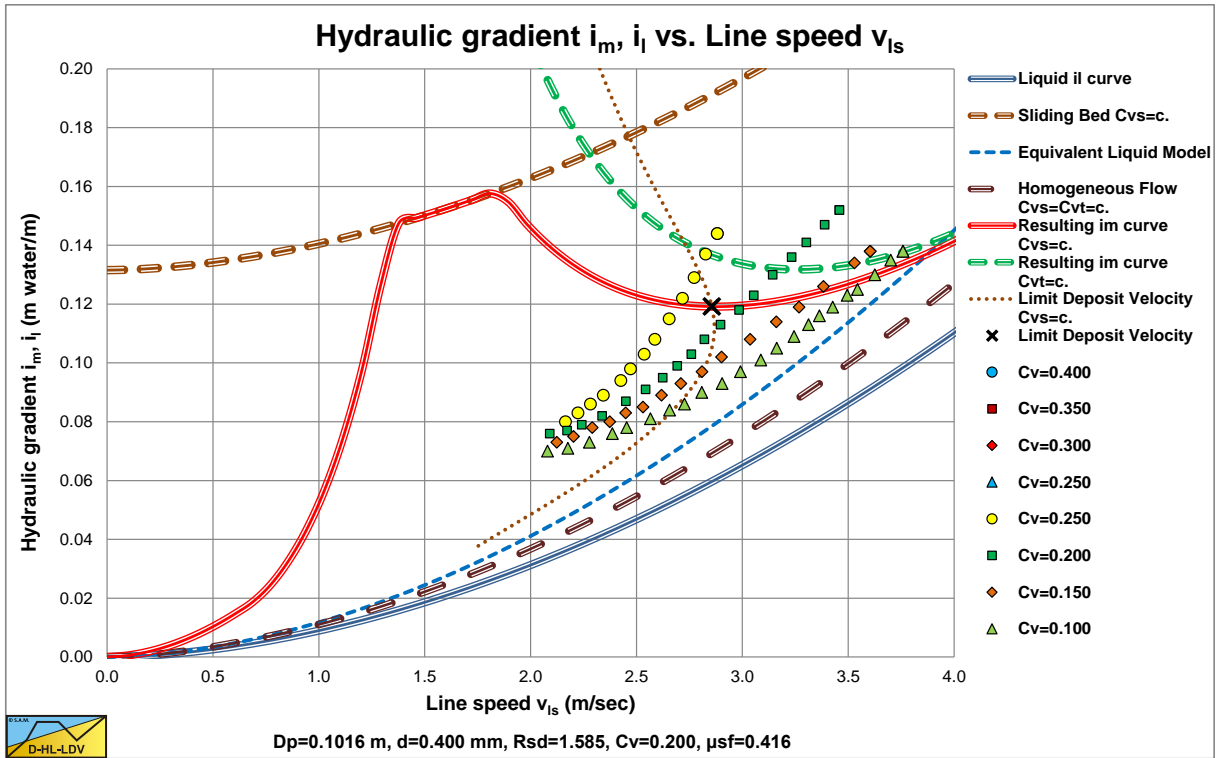
Figure 6.2-4: Sand with d=0.4 mm in a 4 inch diameter pipe.
Data points of Howard (1938) reconstructed from fit lines (source (Westendorp, 1948)).
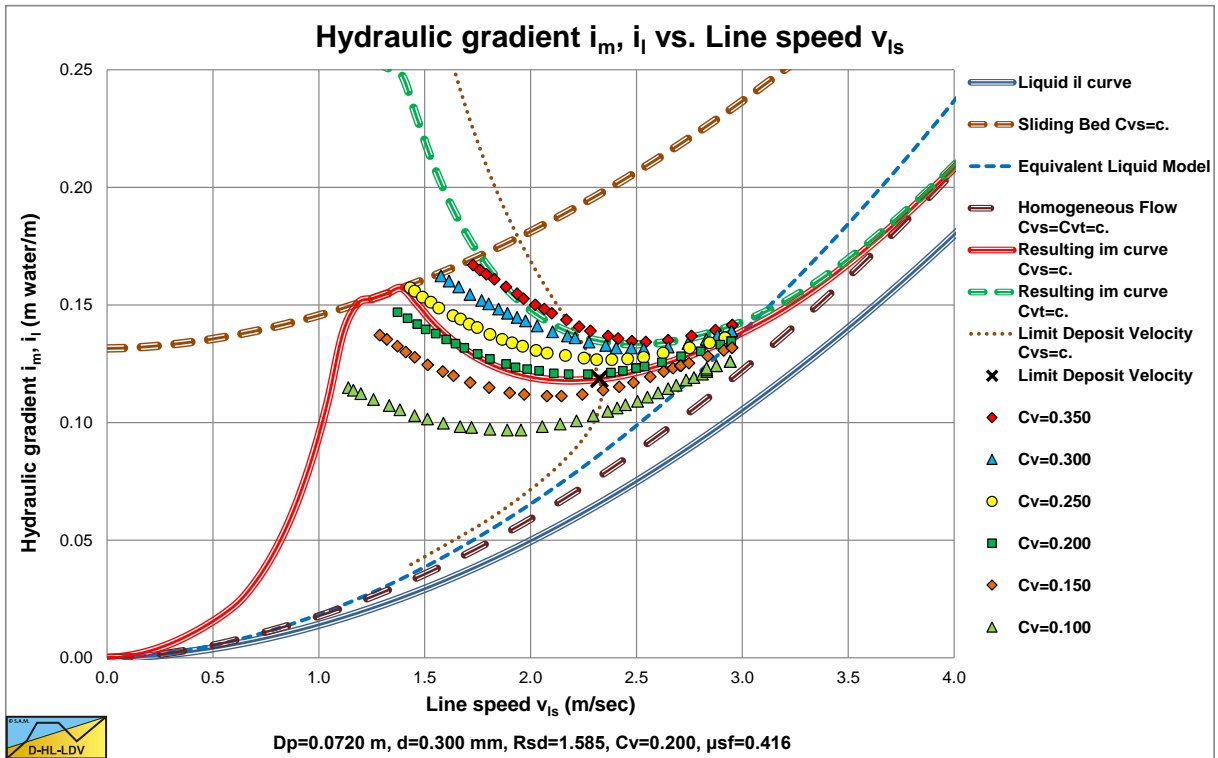
Figure 6.2-5: Sand with d=0.30 mm in a 0.072 m diameter pipe.
Data points of Siegfried (Durepaire, 1939) reconstructed from fit lines (source (Westendorp, 1948)).
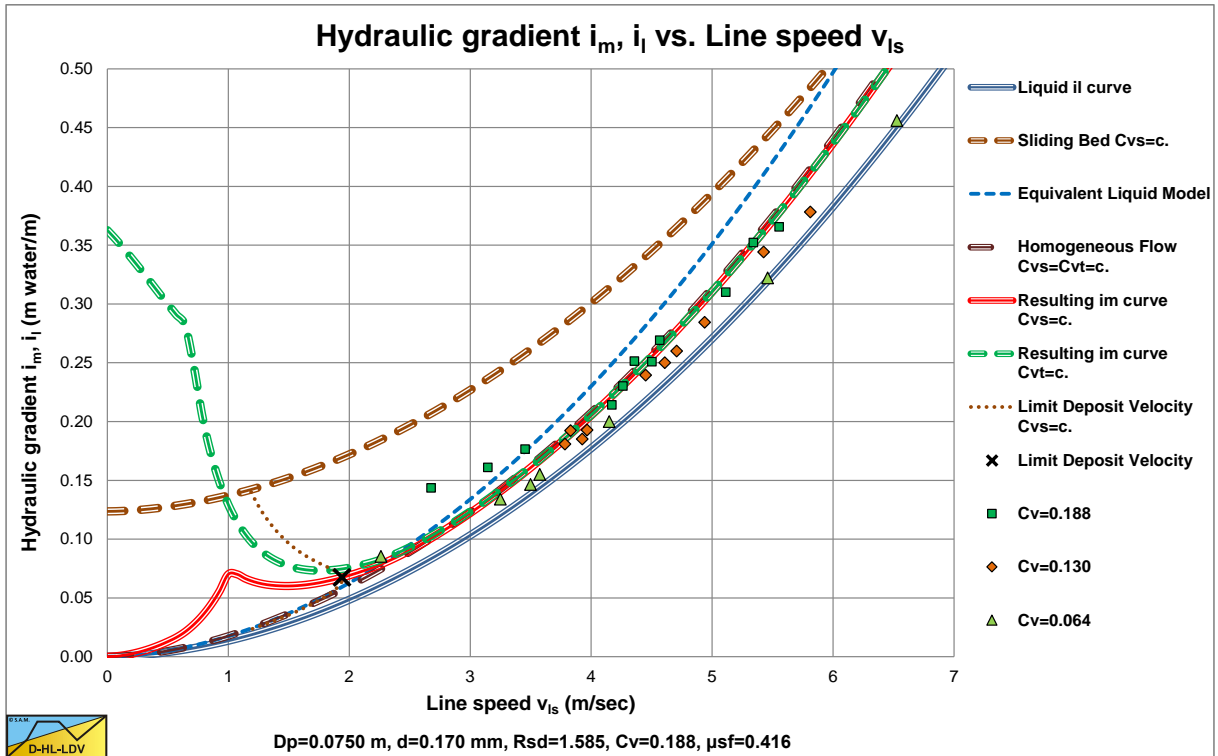
Figure 6.2-6: The data of O'Brien & Folsom (1939) for d=0.17 mm processed.
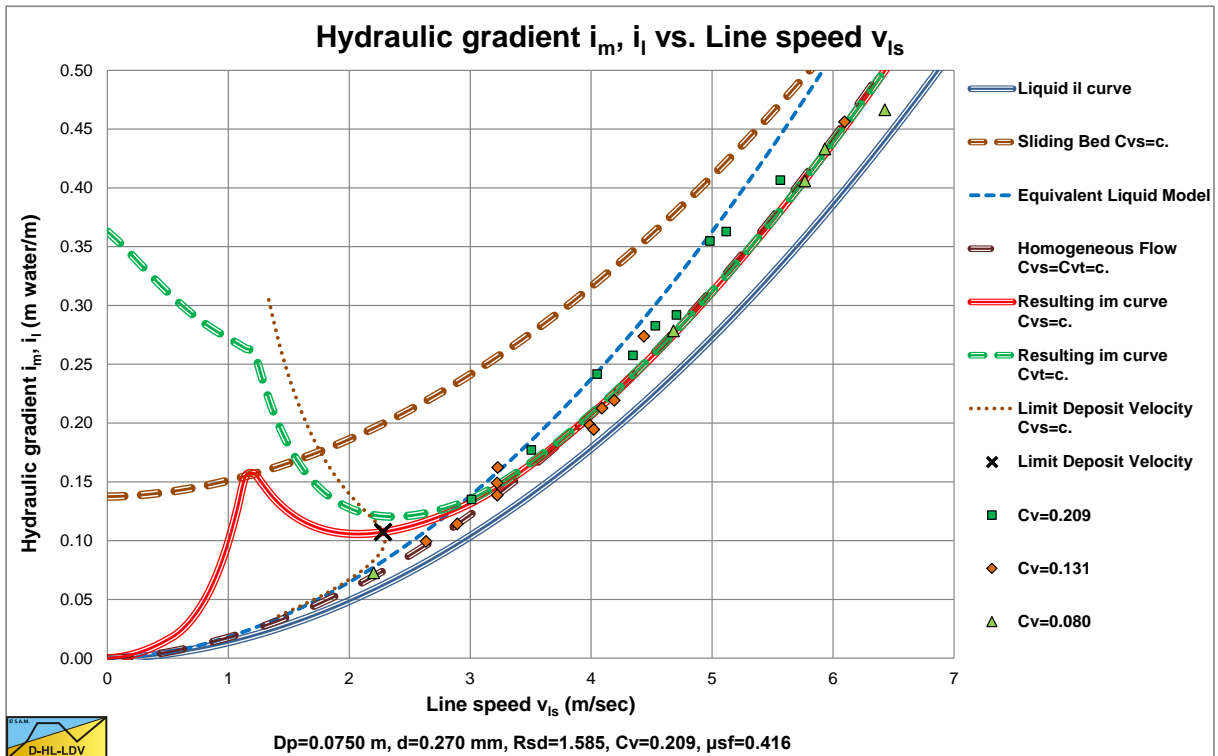
Figure 6.2-7: The data of O'Brien & Folsom (1939) for d=0.27 mm processed.

6.2.5 Conclusions & Discussion Early History.

This chapter is based on an old Dutch report of Westendorp (1948) with additions and modifications of the author and gives the state of the art of slurry transport research up to 1948.

The available experimental data can be divided into two groups, laboratory tests with pipes with a diameter of 2 to 6 inch and full scale tests with pipes with diameters of 0.50 to 0.85 m. The laboratory tests resulted in reasonable data, the full scale tests did not. Reasonable in this case means reproducible data. The data published are limited, meaning that each researcher used one or two pipe diameters and one or two particle diameters. The variation of the line speed was also limited. It is thus not possible to draw quantitative conclusions, but some qualitative conclusions will be discussed.

The flow of water through pipes is influenced by the physical properties of the liquid (viscosity and density) and the geometry of the pipe (diameter and roughness). The flow of sand or gravel with water as the carrier liquid, the physical properties of the solids (density, size, shape, etc.) also play a role. The solids do not have to form a homogeneous mixture with the liquid and may have a behavior that does not follow the hydraulical laws.

Figure 6.2-1, Figure 6.2-2, Figure 6.2-3, Figure 6.2-4, Figure 6.2-5, Figure 6.2-6 and Figure 6.2-7 show a characteristic behavior of the hydraulic gradient versus the line speed. Going from left to right (increasing line speed) the curves are first almost horizontal or decreasing (region I), followed by a transition region (region II), after which the hydraulic gradient will increase and approach the liquid hydraulic gradient (region III). The transition of region II to region III is often named the Limit Deposit Velocity (LDV). In region III almost all solids particles will be in suspension and form a more or less homogeneous liquid. Below the LDV particles will form a bed, fixed or sliding. At higher velocities this particle transport will be a saltating transport. At the lower velocities there will be a bed with particles moving and rolling on top of the bed (sheet flow). The definition of the LDV is very important, since in literature also the transition fixed bed to sliding bed is often used in 2LM and 3LM models. This transition is named here the limit of stationary deposit velocity (LSDV).
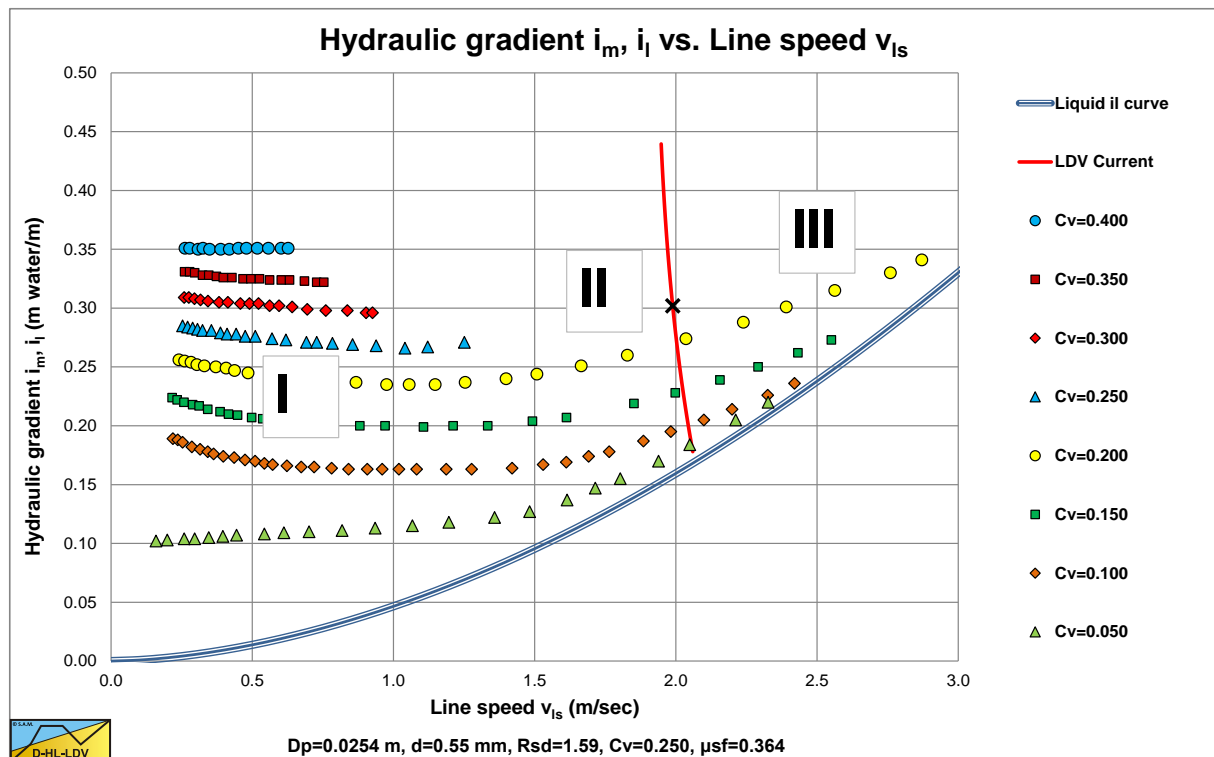
Figure 6.2-8: The regions I, II and III.

So below the LDV there are two types of transport in the pipe:
1. The liquid with the solids in suspension, behaving as a homogeneous liquid.
2. The solids at the bottom of the pipe, not following fluid mechanical laws.
These two types of transport are interrelated. If there is a deposit at the bottom, the real velocity above a bed (deposit) will differ from the cross section averaged line speed. The real velocity above the bed is larger than the line speed.

Region I: The general direction of the hydraulic gradient versus line speed curve is either horizontal or decreasing with increasing line speed, if constant delivered concentration curves are considered. An appropriate physical explanation for this behavior was not yet given in 1948. Some authors suggest that with a decreasing line speed, the bed will occupy part of the pipe cross section in such a way that the velocity above the bed is constant, so equal to the LDV. When the bed height is increasing with decreasing line speed, the bed surface will increase and this the resulting roughness for the flow above the bed, also resulting in a decreasing hydraulic radius, influencing the Darcy-Weisbach friction factor. A further decrease of the line speed may lead to pipe blockage or clogging.

Region II: Is a transition region between region I (fixed or sliding bed) and region III (homogeneous transport). This region is often referred to as heterogeneous transport. For sand suspensions this region is small, however Blatch (1906) stated that this region is small for uniform sands and gets bigger for graded sand, the more graded the bigger. Siegfried (Durepaire, 1939) observed that the curve, given a certain delivered concentration, is higher with increasing line speed than with decreasing line speed. Apparently, removing a fixed or sliding bed (bringing it into suspension) takes more energy than the opposite action, a sort of hysteresis. Region II also contains the point of minimum hydraulic gradient. According to Howard (1938) this happens when the deposit (bed) is completely removed, which is defined as the LDV. The LDV increases with increasing concentration and increasing particle size.

Region III: This region contains the physical situation where the solid-liquid mixture is assumed to be (pseudo) homogeneous. Homogeneous is defined as a transport with a symmetrical velocity distribution with respect to the center of the horizontal pipe and a uniform concentration distribution. Because of gravity, the concentration in the lower half of the pipe will always be higher than in the upper half of the pipe, so real homogeneous transport according to the definition will never occur. With fine sand, the hydraulic gradient curves at high line speeds will approach the clean water curve with increasing line speed. With coarser sand the mixture hydraulic gradient will be larger than the liquid hydraulic gradient. According to O'Brien & Folsom (1939) the larger the particles, the larger the mixture hydraulic gradient. This increase in mixture hydraulic gradient of course depends on the solids concentration.

Vaughn (Howard, 1939) posed that the hydraulic gradient also depends on the viscosity of the mixture and of some characteristic particle size. Dent (Howard, 1939) states that at very high line speeds the hydraulic gradient will deviate from the clean water curve, increase with respect to the liquid hydraulic gradient, but he did not explain this. Wilson (1942) and Danel (Howard, 1939) give an explanation for the observation that with fine sand the mixture hydraulic gradient is lower than the liquid hydraulic gradient. They assume that fine particles influence the occurrence of the small eddies due to turbulence, resulting in less energy dissipation. The particles have to be smaller than the size of the eddies. This will occur for particles with a settling velocity in the Stokes region (d<0.1 mm). Larger particles will not result in such behavior. O'Brien & Folsom (1939) found that at high line speeds and small particles the behavior almost follows the Equivalent Liquid Model.

The Limit Deposit Velocity (LDV): The LDV is not defined clearly. Usually the LDV is defined as the line speed above which all the particles are in suspension or as the line speed above which the mixture hydraulic gradient equals the liquid hydraulic gradient. The LDV increases strongly with an increasing delivered volumetric concentration. The LDV also increases with an increasing particle size, with an increasing pipe diameter and with a decreasing pipe wall roughness. Durepaire (1939) assumes a proportionality between the LDV and the delivered concentration to a power less than 0.5. Franzi (1941) gives a second degree function. The relative submerged density of the solids does not have much influence on the LDV in small diameter pipes (**D_p<0.2 m**), but it does in larger diameter pipes. The LDV will increase with an increasing relative submerged density.

Characteristics of the solids: In 1948 it was not yet clear, which solids characteristics should be used for the determination of the solids effect in slurry flow through pipes. Often the particle size distribution graphs (PSD) are mentioned, but also the relative submerged density, the porosity and the type of material. O'Brien & Folsom (1939) and Wilson (1942) added the terminal settling velocity to this list.

Particle size: Often the PSD is complemented with a mean particle diameter or some other characteristic diameter (for example the d_{10}). Dent (Howard, 1939) does not support the effective particle size as proposed by Howard (1938). The effect of 15% gravel is much larger than the effect of 25% sand. Coarse material has much more influence than fine material. A better characteristic diameter would be the d_{25}. Vaughn (Howard, 1939) states that the ratio of the particle diameter to the pipe diameter is of importance. Franzi (1941) mentions that adding some very fine particles to coarse particles will sometimes reduce the hydraulic gradient. It is thus difficult to find a good characteristic particle diameter.

Terminal settling velocity: From many observations it is clear (Howard, 1938) that the distribution of the particles in a cross section of the pipe is not uniform. On average, the concentration increases towards the bottom of the pipe. O'Brien & Folsom (1939) draw the conclusion that the terminal settling velocity of the particles is the most dominant characteristic the solids. The PSD, relative submerged density, porosity and other parameters are only important in order to quantify the terminal settling velocity. They measure this terminal settling velocity by testing the settling velocity of each fraction in clean water and determining the highest settling velocity of the fraction. Whether or not they take hindered settling into account is not clear. Vaughn (Howard, 1939) remarks that it may be important to determine the settling velocity of a sand-mud mixture, which looks more like reality, probably giving smaller values for the settling velocity.

Modeling: Wilson (1942) assumes that particles in suspension will, on average, keep their vertical position in the flow, also assuming a constant spatial concentration distribution in the pipe cross section. Now suppose particles settle with a terminal settling velocity v_t and are pushed up again by lift forces. This means that the fluid will carry out work to compensate for the loss of potential energy. This work will be larger than the potential energy alone, because there is also a loss of mechanical energy due to viscous friction, both for descending and ascending particles. Wilson (1942) derived the following equation:

$$i_m = i_l + K \cdot \frac{C_{ms} \cdot v_t}{v_{ls}} = \frac{\lambda_l \cdot v_{ls}^2}{2 \cdot g \cdot D_p} + K \cdot \frac{C_{ms} \cdot v_t}{v_{ls}} = \frac{\lambda_l \cdot v_{ls}^2}{2 \cdot g \cdot D_p} \cdot \left(1 + 2 \cdot K \cdot \frac{C_{ms} \cdot v_t \cdot g \cdot D_p}{\lambda_l \cdot v_{ls}^3} \right) \tag{6.2-1}$$

The coefficient K is a proportionality coefficient, C_{ms} is the concentration by weight, v_t the terminal settling velocity and v_{ls} the line speed. With an increasing line speed, the mixture hydraulic gradient will approach the liquid hydraulic gradient asymptotically. For a certain mixture and pipe diameter, there will be a line speed where the mixture hydraulic gradient has a minimum. This minimum is at the line speed:

$$v_{ls,min}^3 = K \cdot \frac{C_{ms} \cdot v_t \cdot g \cdot D_p}{\lambda_l} \tag{6.2-2}$$

Substituting this solution for the minimum hydraulic gradient line speed gives:

$$i_m = 3 \cdot i_l = 3 \cdot \frac{\lambda_l \cdot v_{ls,min}^2}{2 \cdot g \cdot D_p} \tag{6.2-3}$$

In other words, at the minimum hydraulic gradient line speed, the mixture hydraulic gradient is always equal to 3 times the liquid hydraulic gradient, assuming constant values for the other parameters in the equation. Applying this theory on the experiments of Blatch (1906), requires K values between 2 and 10. The maximum K value was found at the minimum hydraulic gradient line speed. A further increasing line speed reduces the K value to a value of 1. It would be interesting to find a fundamental equation for this K value. Lorentz in the discussion on Wilson (1942) disagrees with the above equation. He feels its adding up energy losses, without looking at possible interactions. The two terms in equation (6.2-1) deal with different phases of the problem. The first term deals with the Darcy-Weisbach friction of clean water, the second term with the turbulent energy required to keep the particles in suspension. The energy in the second term could occur in the first term as Darcy-Weisbach friction and in the second term as potential energy. From some measurements of Wilson (1942) this seems to be the case. So equation (6.2-1) does not give a full explanation of the problem, but it's a first reasonable description. Dent (1939) gives a similar equation, which is discussed later.

Blatch (1906) gives for the minimum mixture hydraulic gradient line speed (the economical line speed) some rules of the thumb. For a 1 inch pipe per 1000 m of pipe length the pressure loss is the pressure loss of the liquid at 1 m/s line speed plus 9.6 m.w.c for every 1% of delivered volumetric concentration. For a 32 inch pipe per 1000 m of pipe length the pressure loss is the pressure loss of the liquid at 3 m/sec line speed plus 1.2 m.w.c. for every 1% of delivered volumetric concentration. She also gave the following information:

Table 6.2-1: Some characteristic velocities according to Blatch (1906).

Pipe diameter	Line speed giving blockage	Economical line speed	LDV all particles in suspension
1 inch	0.38 m/sec	1.07 m/sec	2.4-2/7 m/sec
2 inch	0.76 m/sec	1.22 m/sec	-
32 inch	1.8-2.1 m/sec	2.75 m/sec	4.3 m/sec

Table 6.2-2: The LDV values measured by Blatch (1906), source Graf et al.(1970).

Blatch (1906)	D_p=0.0254 m			
d in mm	d in m	Archimedes	LDV in m/sec	F_L
0.20	0.00020	102	0.94	1.04
0.20	0.00020	102	0.92	1.01
0.20	0.00020	102	0.96	1.06
0.55	0.00055	2125	1.26	1.39
0.55	0.00055	2125	1.06	1.17
0.55	0.00055	2125	1.01	1.12
0.55	0.00055	2125	0.96	1.06
0.55	0.00055	2125	1.31	1.44
0.55	0.00055	2125	1.29	1.42

It looks like the LDV values in Table 6.2-2 are in fact the economical line speeds measured by Blatch (1906).

Plugging the line: Decreasing the line speed at a certain delivered concentration will result in an increasing deposit (bed height) until the pipe is blocked completely. If at a low line speed, the delivered concentration is increased, then a certain delivered concentration will also result in pipe blockage. This pipe blockage will occur at higher line speeds if the particles are coarser. Fine particles will result in a smoother bed making rolling transport easier. According to Durepair (1939) this blockage is also determined by the stability of the flow, thus from the interaction between the pump and the mixture flow through the pipeline. According to O'Brien & Folsom (1939) the amount of solids in suspension depend on the amount of turbulence in the pipe. An increase of this turbulence will increase the allowable concentration delivered. A pump will cause more turbulence close behind the pump resulting in a lower probability of blockage than further in the pipeline. If the concentration is suddenly increased, then close behind the pump there will not be blockage, but further in the pipeline this may cause blockage.

The above summary of the state of the art is not the opinion of the author, but it is what was found in literature up to 1948. This is the starting point for the later researchers and puts their findings in a historical perspective.
The concept of Wilson (1942) of using a potential energy approach in order to explain the solids effect of the energy losses is a concept which is also used by Newitt et al. (1955) and more recently by Miedema & Ramsdell (2013), combined with kinetic energy losses. Many researchers developed a hydraulic gradient or pressure loss equation consisting of a Darcy-Weisbach friction term and a second term for the solids effect, usually the latter reversely proportional to the line speed. The equation of Wilson (1942) in this respect is also very similar to the equation of Fuhrboter (1961), assuming that the terminal settling velocity equals about 100 time times the particle diameter for fine and medium sands.
At high line speeds a certain range of particle diameters will result in a curve approaching the liquid curve, while other particle diameters result in a curve approaching the ELM curve.
The concept of the minimum hydraulic gradient velocity (MHGV) gives the basis for a graphical representation of this line speed. In a hydraulic gradient versus line speed graph, 3 curves have to be drawn, the liquid hydraulic gradient curve, 3 times this curve and the mixture hydraulic gradient curve. The intersection point of the mixture hydraulic gradient curve and the 3 times the liquid hydraulic gradient curve is the minimum hydraulic gradient point.

Figure 6.2-9 and Figure 6.2-10 show the MHGV curve for 4 concentrations and 2 pipe diameters. The mixture hydraulic gradient curves are based on the Durand & Condolios (1952) model. The fact that the MHGV curves seem to be a little on the left of the minimum points of the mixture hydraulic gradient curves is the result of a line speed dependent Darcy Weisbach friction factor. In the derivation resulting in 3 times the liquid hydraulic gradient curve, this friction factor is considered a constant.
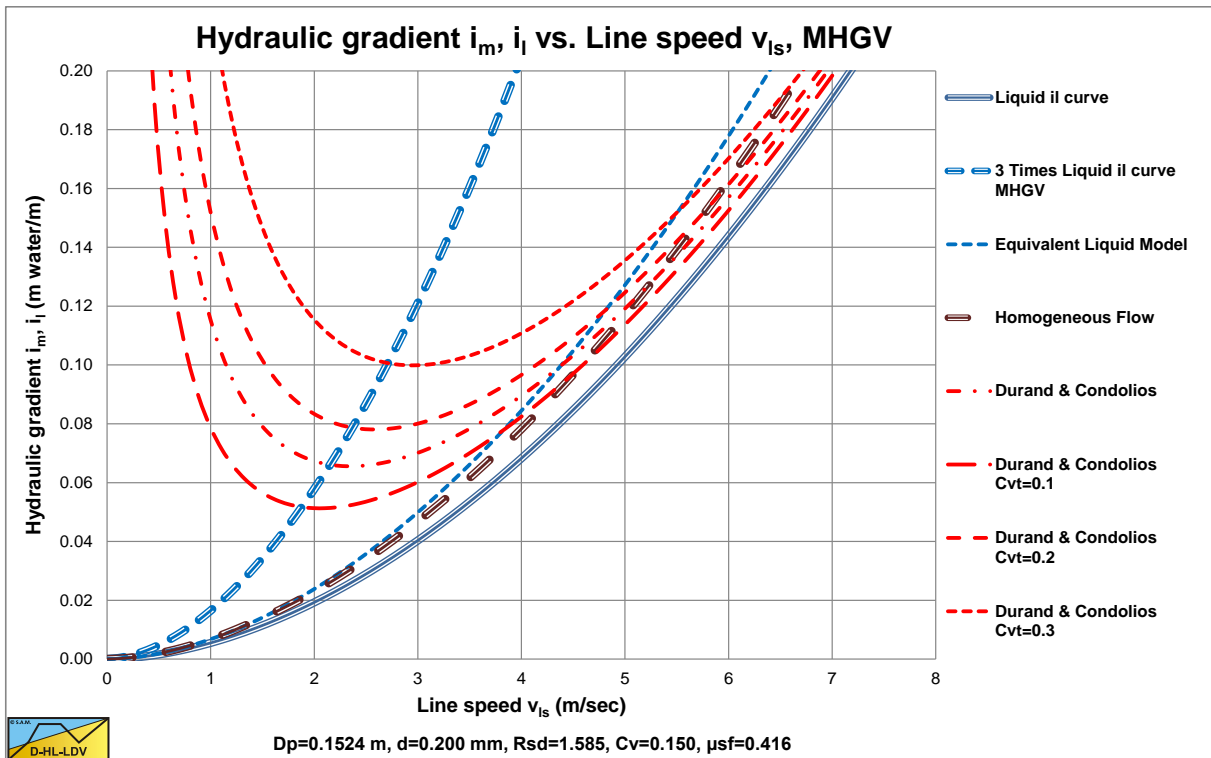
Figure 6.2-9: The MHGV curve for a d=0.2 mm particle in a D_P=0.1524 m (6 inch) pipe.
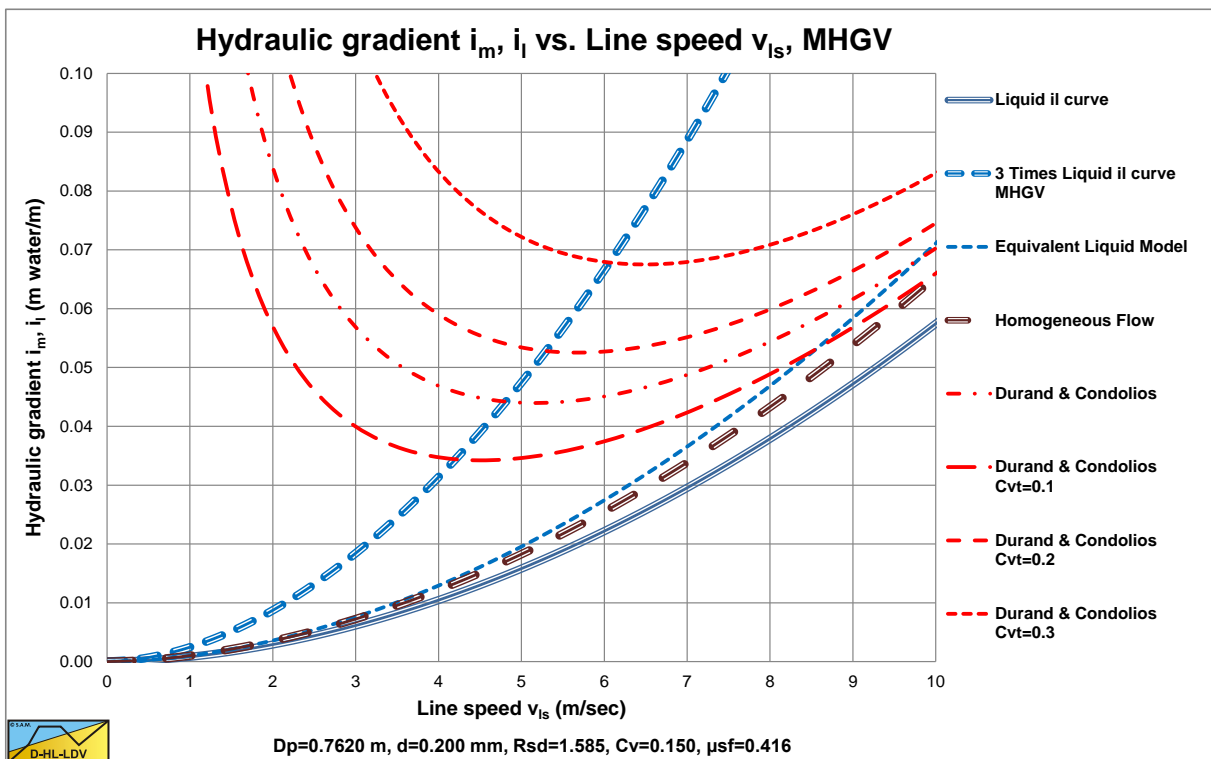
Figure 6.2-10: The MHGV curve for a d=0.2 mm particle in a D_P=0.762 m (30 inch) pipe.

6.3 Empirical and Semi-Empirical Models.

In the period 1949 to present a lot of research has been carried out regarding the head losses of settling slurries. Most researchers developed their equations for the different flow regimes. Models were found for the sliding bed regime, the heterogeneous flow regime and the homogeneous flow regime. Most experiments were carried out measuring the delivered volumetric concentration as a parameter, a few measured the spatial volumetric concentration. Only Yagi et al. (1972) measured both.

Now it is interesting to see with what pipe diameters, particle diameter and relative submerged densities (or solids densities) the different researchers carried out their experiments. It is impossible to produce a complete list, due to the numerous publications. It is also impossible to have a correct number of occurrences, due to the way of counting. The count is per researcher, not per experiment. So the graphs and tables should be used as an indication.

Figure 6.3-1 and Table 6.3-1 show the number of occurrences of different pipe diameters.

Figure 6.3-2 and Table 6.3-2 show the number of occurrences of different particle diameters.

Figure 6.3-3 and Table 6.3-3 show the number of occurrences of different relative submerged densities.

In the following chapters a number of empirical and semi-empirical models are discussed. The list is far from complete. The models chosen all have some contribution to the development of the DHLLDV Framework.
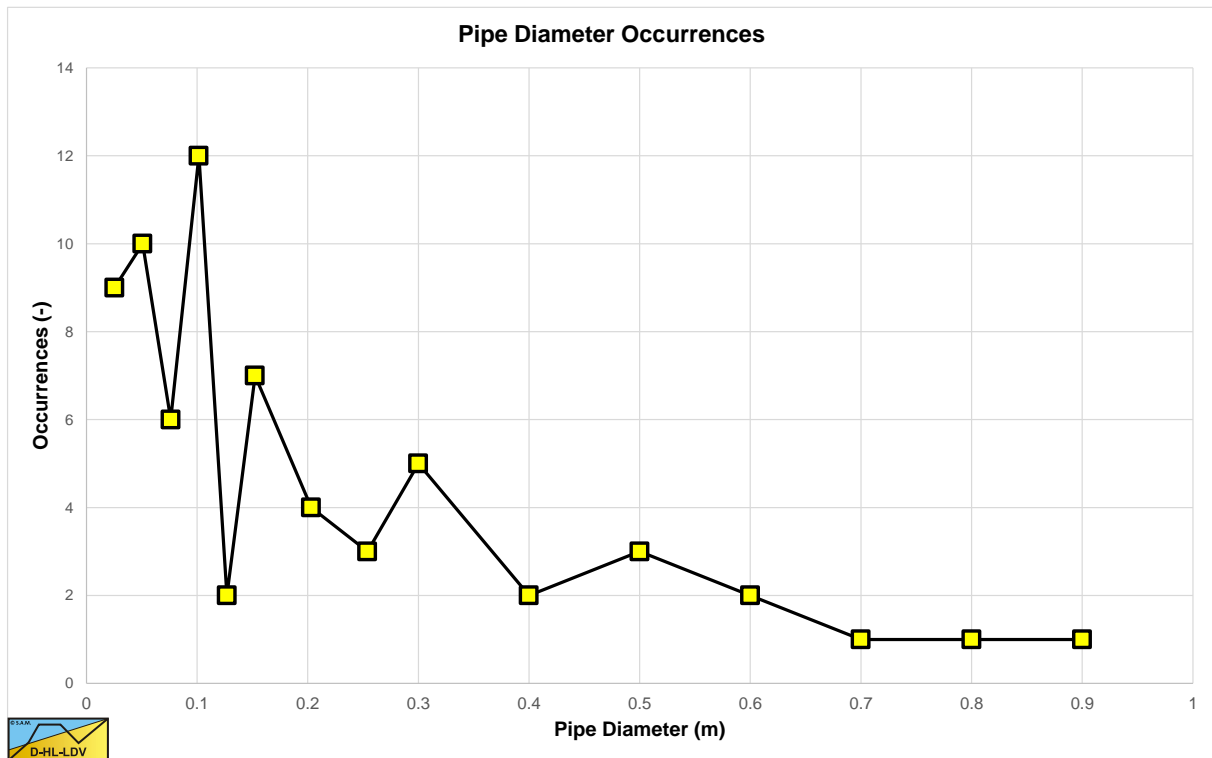
Figure 6.3-1: The number of occurrences of pipe diameters investigated.

About 60% of the researchers used pipe diameters smaller than or equal to 0.1524 m (6 inch). 82% of the researchers used pipe diameters smaller than or equal to 0.3 m (or 12 inch). Only Silin et al. (1958) carried out experiments in the full range of 0.0254 m up to 0.9 m pipe diameters. These experiments form the basis of the Jufin & Lopatin (1966) model.
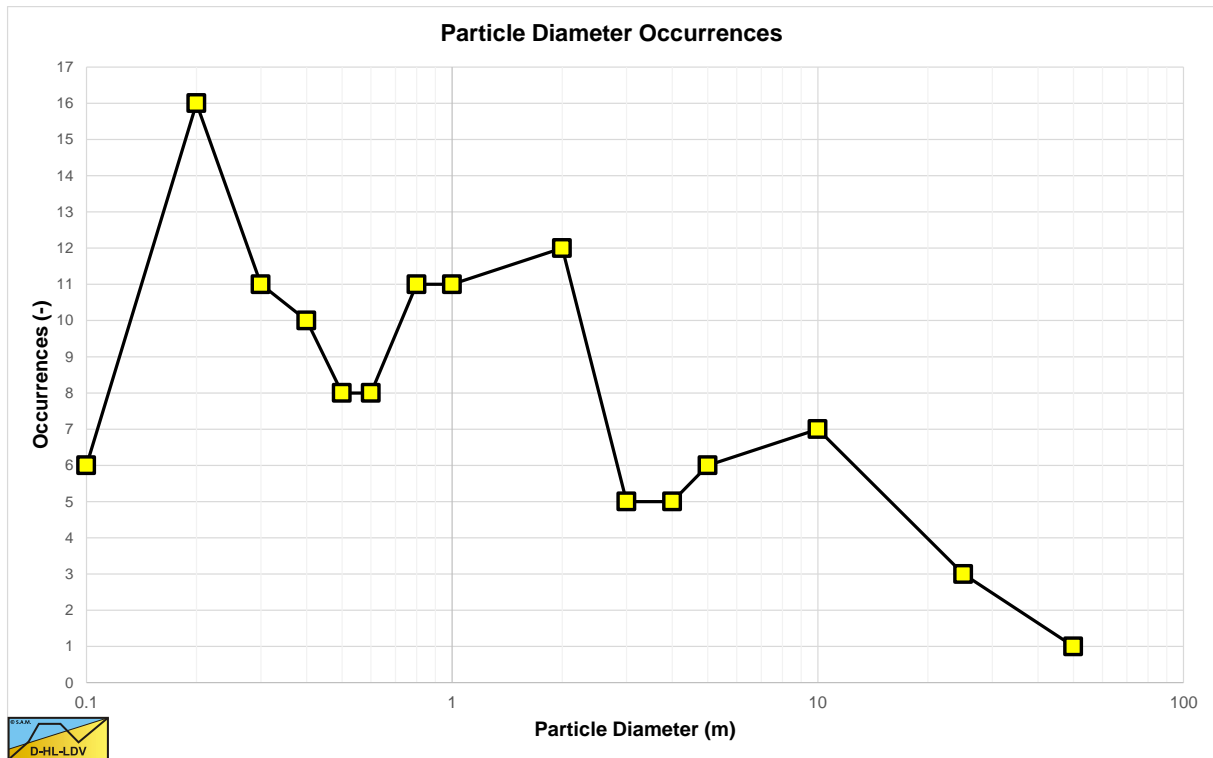
Figure 6.3-2: The number of occurrences of particle diameters investigated.
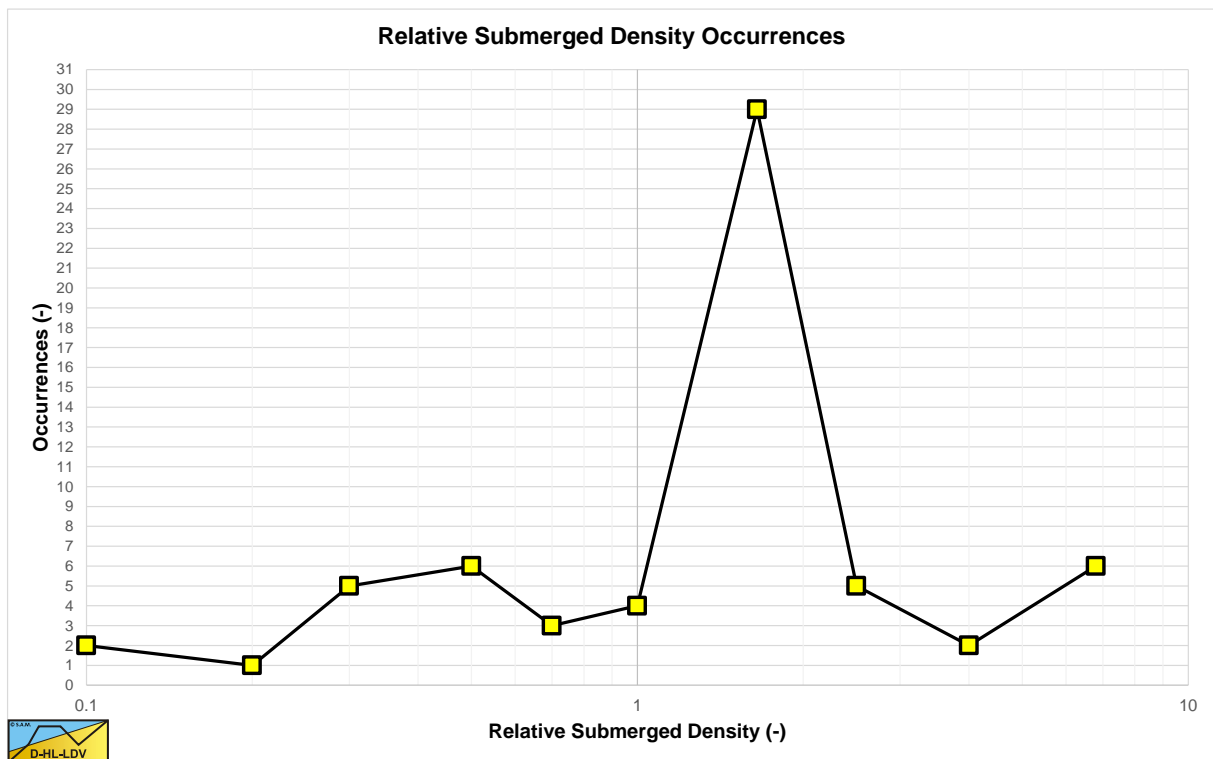
Figure 6.3-3: The number of occurrences of relative submerged densities investigated.

Table 6.3-1: Pipe diameters used by the different researchers investigated.

D_p about	1 inch	2 inch	3 inch	4 inch	5 inch	6 inch	8 inch	10 inch	0.3 m	0.4 m	0.5 m	0.6 m	0.7 m	0.8 m	0.9 m
Babcock	1														
Blatch	1														
Boothroyde							1								
Charles et al.	1	1		1											
Clift							1			1	1				
Doron & Barnea		1													
Durand & Condolios		1		1		1		1	1						
Graf & Robinson				1		1									
Howard				1											
Fuhrboter									1						
Gillies		1				1		1			1				
Karasik									1						
Kazanskij		1									1				
Matousek		1		1		1									
Newitt et al.	1														
Sassoli		1	1												
O'Brien & Folsom		1	1												
Ravelet				1											
Siegfried			1												
Sinclair	1														
Silin et al.	1			1			1		1	1		1		1	1
Soleil & Ballade												1	1		
A.D. Thomas		1		1		1	1	1	1						
Turian et al.	1	1													
Vlasak	1			1											
Wasp et al.	1			1	1										
Wiedenroth					1										
Wilson et al.			1	1											
Worster & Denny			1			1									
Yagi et al.			1	1		1									
Total	9	10	6	12	2	7	4	3	5	2	3	2	1	1	1

Table 6.3-2: Particle diameters used by the different researchers investigated.

d_{50} about	Sand									Gravel					
	≤0.1 mm	0.2 mm	0.3 mm	0.4 mm	0.5 mm	0.6 mm	0.8 mm	1.0 mm	2.0 mm	3.0 mm	4.0 mm	5.0 mm	10 mm	25 mm	50 mm
Babcock	1			1			1	1	1	1					
Blatch		1				1									
Boothroyde		1									1		1		
Charles et al.	1	1			1		1		1						
Clift			1	1		1									
Doron & Barnea										1					
Durand & Condolios		1		1				1	1		1		1	1	
Graf & Robinson				1			1								
Howard					1										
Fuhrboter		1	1		1		1								
Gillies		1	1	1	1		1		1	1					
Karasik		1													
Kazanskij		1							1						
Matousek		1		1	1		1	1	1	1	1	1	1		
Newitt et al.	1	1				1	1	1	1	1		1			
O'Brien & Folsom		1	1												
Ravelet												1	1		
Sassoli		1	1				1								
Siegfried			1												
Sinclair			1	1	1	1	1	1	1						
Silin et al.		1	1	1		1		1	1						
Soleil & Ballade					1	1									
A.D. Thomas	1	1			1										
Turian et al.	1		1	1			1	1	1						
Vlasak												1	1		
Wasp et al.	1	1	1	1		1		1	1						
Wiedenroth		1						1	1				1		
Wilson et al.											1				
Worster & Denny								1			1		1	1	
Yagi et al.			1			1	1	1					1	1	1
Total	6	16	11	10	8	8	11	11	12	5	5	6	7	3	1

Table 6.3-3: Solids relative submerged densities used by the different researchers investigated.

R_{sd} about	0.05-0.15	0.15-0.25	0.25-0.40	0.40-0.60	0.60-0.80	0.80-1.20	1.20-2.00	2.00-3.00	3.00-5.00	>5
Babcock			1			1	1			1
Blatch							1			
Boothroyde				1			1			
Charles et al.	1					1	1	1	1	1
Clift							1			
Doron & Barnea		1								
Durand & Condolios					1		1	1		
Graf & Robinson			1				1			
Howard							1			
Fuhrboter							1			
Gillies			1		1		1			
Karasik							1			
Kazanskij							1			
Matousek			1				1			
Newitt et al.				1			1	1		
O'Brien & Folsom							1			
Ravelet							1	1		
Sassoli							1			
Siegfried							1			
Sinclair				1			1			1
Silin et al.				1		1	1	1		
Soleil & Ballade							1			
A.D. Thomas					1		1		1	1
Turian et al.							1			
Vlasak							1			1
Wasp et al.				1			1			1
Wiedenroth							1			
Wilson et al.	1		1			1	1			
Worster & Denny				1			1			
Yagi et al.							1			
Total	2	1	5	6	3	4	29	5	2	6

SOCIÉTÉ HYDROTECHNIQUE DE FRANCE

TRANSPORT HYDRAULIQUE

ET

DÉCANTATION

DES

MATÉRIAUX SOLIDES

COMPTE RENDU

DES

DEUXIÈMES JOURNÉES DE L'HYDRAULIQUE

GRENOBLE 25-29 JUIN 1952

PUBLIÉ PAR
LA HOUILLE BLANCHE
GRENOBLE · FRANCE

D.A
222 b
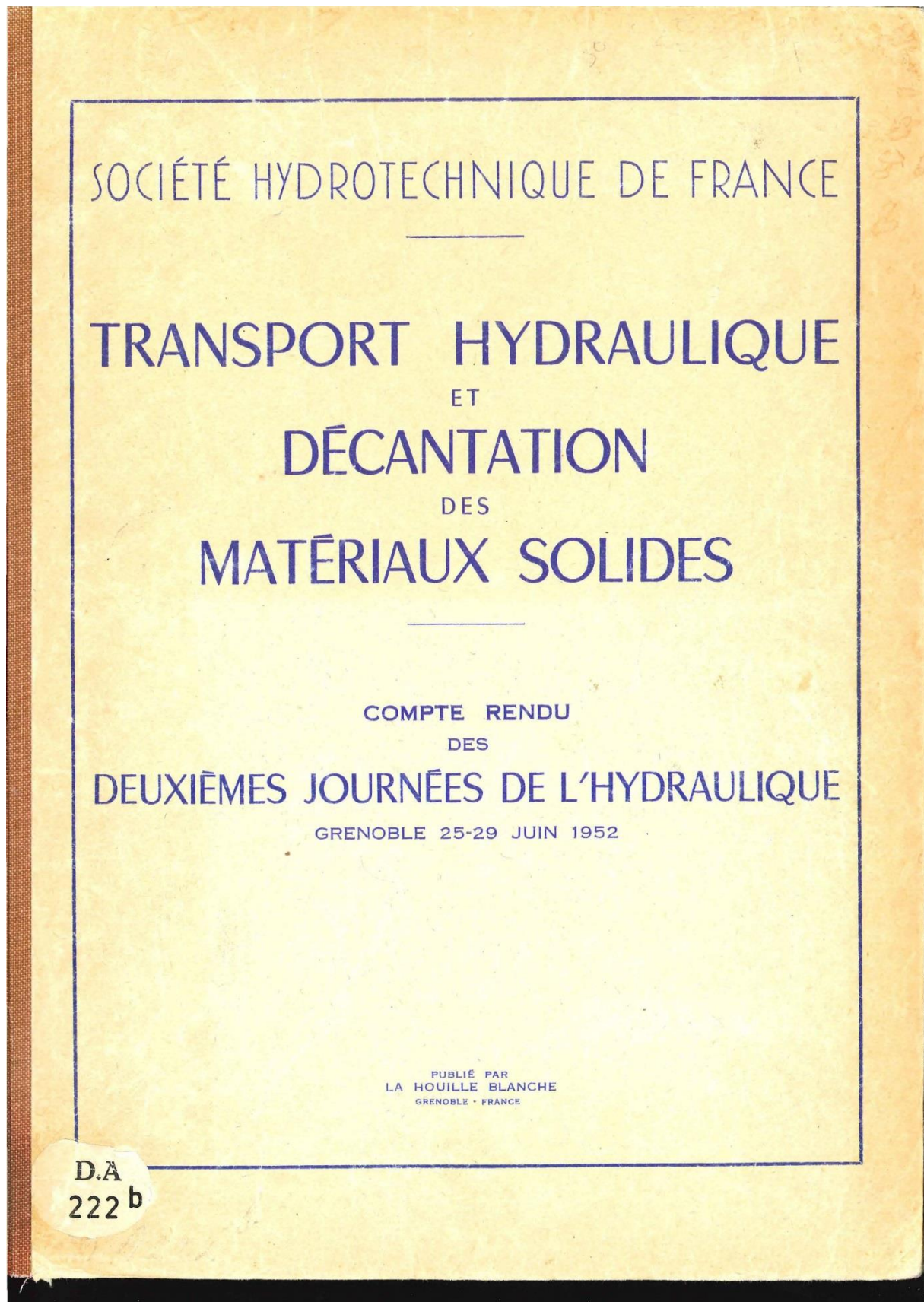
6.4 The Durand & Condolios (1952) School.

6.4.1 Soleil & Ballade (1952).

Soleil & Ballade (1952) carried out experiments on a real dredge with pipe diameters of D_p=0.58 m and D_p=0.70 m. The sands used had diameters of d=0.55 mm, d=0.60 mm and d=0.64 mm. The flows for both pipe diameters were in the same range, resulting in lower line speeds for the larger pipe diameter.

Most probably, the concentrations measured were spatial volumetric concentrations. Most experiments were just above the Limit Deposit Velocity or just below. The experiments below the LDV were in a transition between a stationary bed and the heterogeneous regime. Although there is a lot of scatter, the experiments are shown here, because the number of experimental data with large diameter pipes is very limited. Durand & Condolios (1952) used these experiments in their analysis.

Most experiments in the D_p=0.70 m pipe were carried out in this transition zone, while most experiments in the D_p=0.58 m pipe were carried out in the heterogeneous regime. Again the experiments point to spatial concentration measurements, since the delivered concentrations of the same values at the low line speeds would have given a sliding bed.

Figure 6.4-1, Figure 6.4-2 and Figure 6.4-3 show the experiments in the D_p=0.58 m pipe. Most data points are in the heterogeneous flow regime, but some at low line speeds are in the transition between a fixed bed and the heterogeneous flow regime around the LDV. Both the data points and the DHLLDV Framework prediction do not show a sliding bed.

Figure 6.4-4, Figure 6.4-5 and Figure 6.4-6 show the experiments in the D_p=0.70 m pipe. Most data points are in the transition between a fixed bed and the heterogeneous flow regime below the LDV. Both the data points and the DHLLDV Framework prediction do not show a sliding bed.

Figure 6.4-7 and Figure 6.4-8 show the relative excess hydraulic gradient E_{rhg} in the D_p=0.58 m pipe of all experiments (all particle sizes) for a uniform and a graded prediction of the DHLLDV Framework. For the line speed range considered there is hardly a difference between the uniform and the graded prediction.

Figure 6.4-9 and Figure 6.4-10 show the relative excess hydraulic gradient E_{rhg} in the D_p=0.70 m pipe of all experiments (all particle sizes) for a uniform and a graded prediction of the DHLLDV Framework. For the line speed range considered there is hardly a difference between the uniform and the graded prediction.

In general the experiments match the DHLLDV Framework, however, the transition between the stationary bed regime and the heterogeneous regime seems to be more smooth and does not show the peak. This makes sense, since the DHLLDV Framework does not consider suspension only sheet flow at the top of the bed, while in reality above the bed and above the sheet flow layer there will be suspension.

For practical purposes the line speeds are rather low. In real life line speeds above the LDV would be applied.

Dp=0.5800 m, d=0.550 mm, Rsd=1.585, Cv=0.215, μsf=0.416
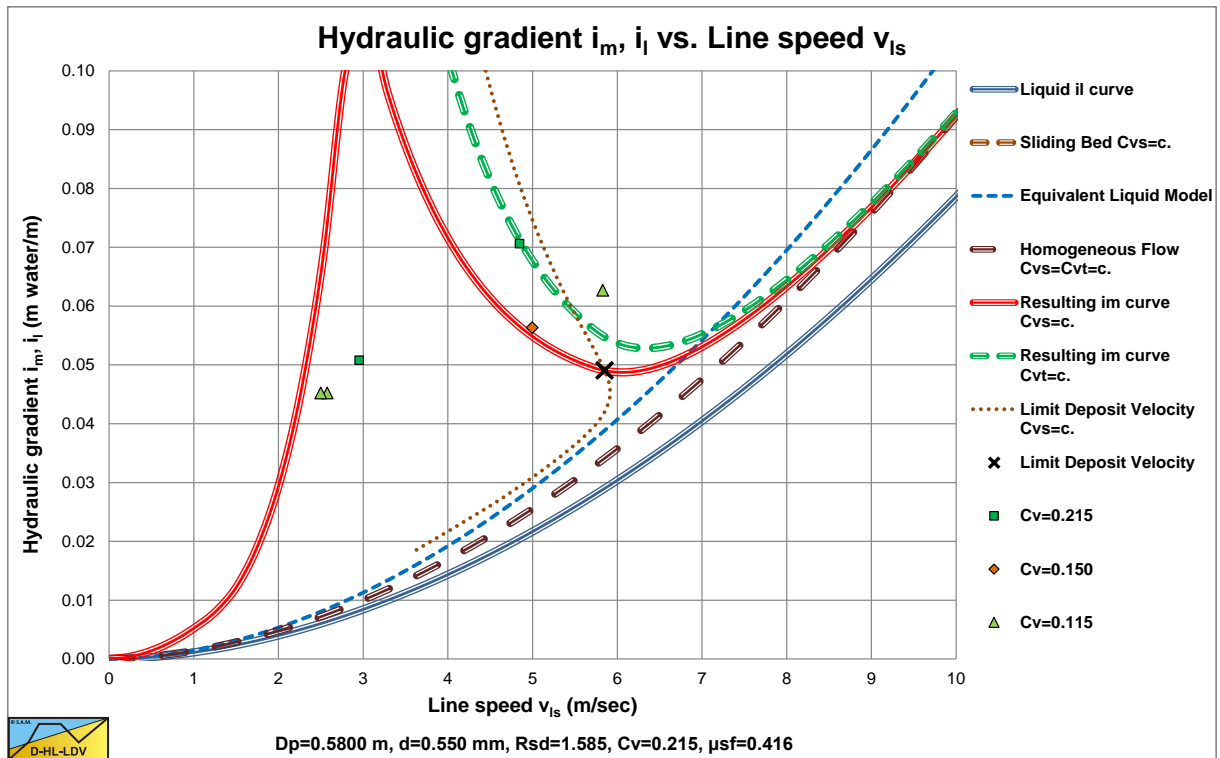
Figure 6.4-1: Experiments with sand d=0.55 mm and a pipe diameter of Dₚ=0.58 m.

Dp=0.5800 m, d=0.600 mm, Rsd=1.585, Cv=0.173, μsf=0.416
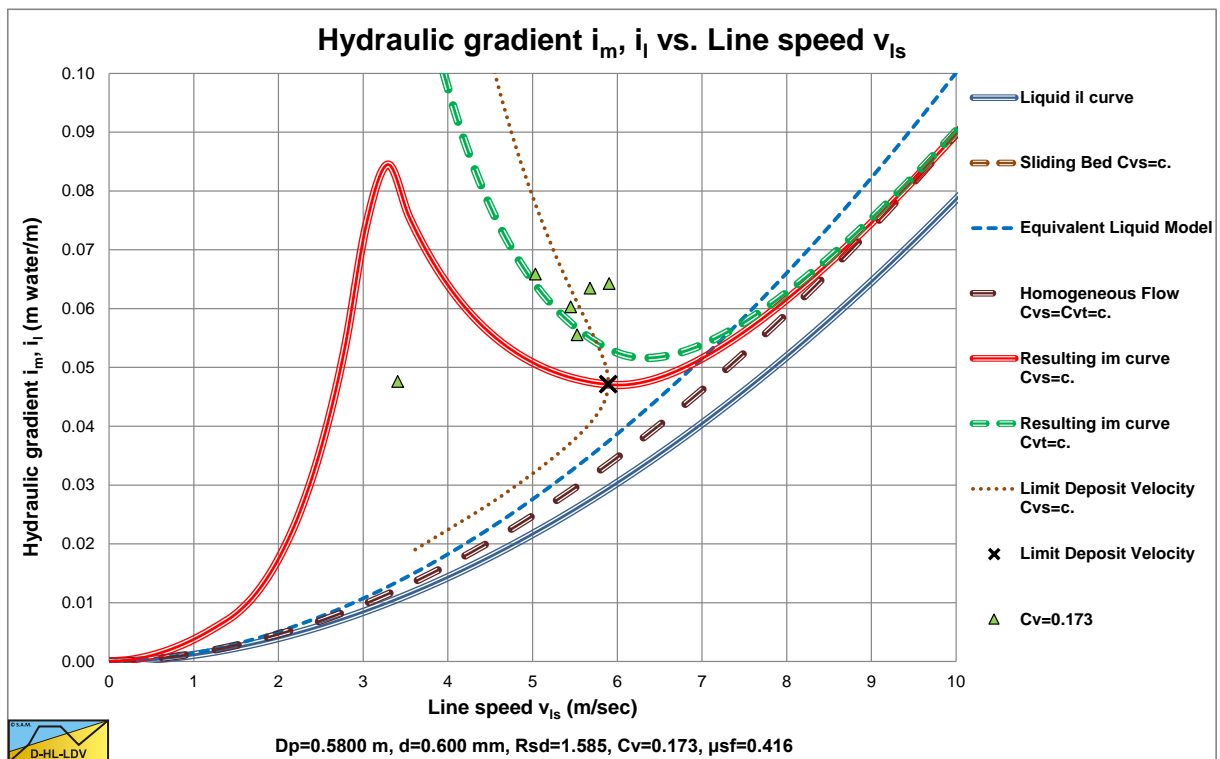
Figure 6.4-2: Experiments with sand d=0.60 mm and a pipe diameter of Dₚ=0.58 m.
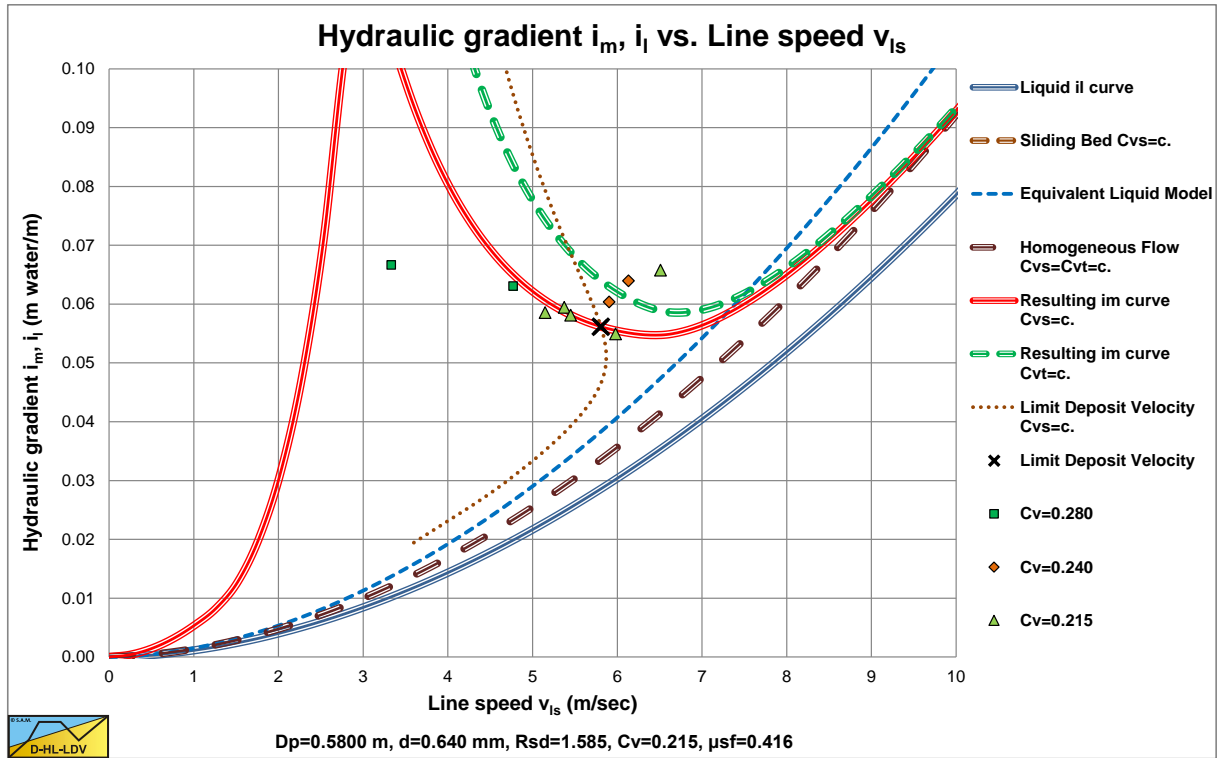
Figure 6.4-3: Experiments with sand d=0.64 mm and a pipe diameter of D_p=0.58 m.
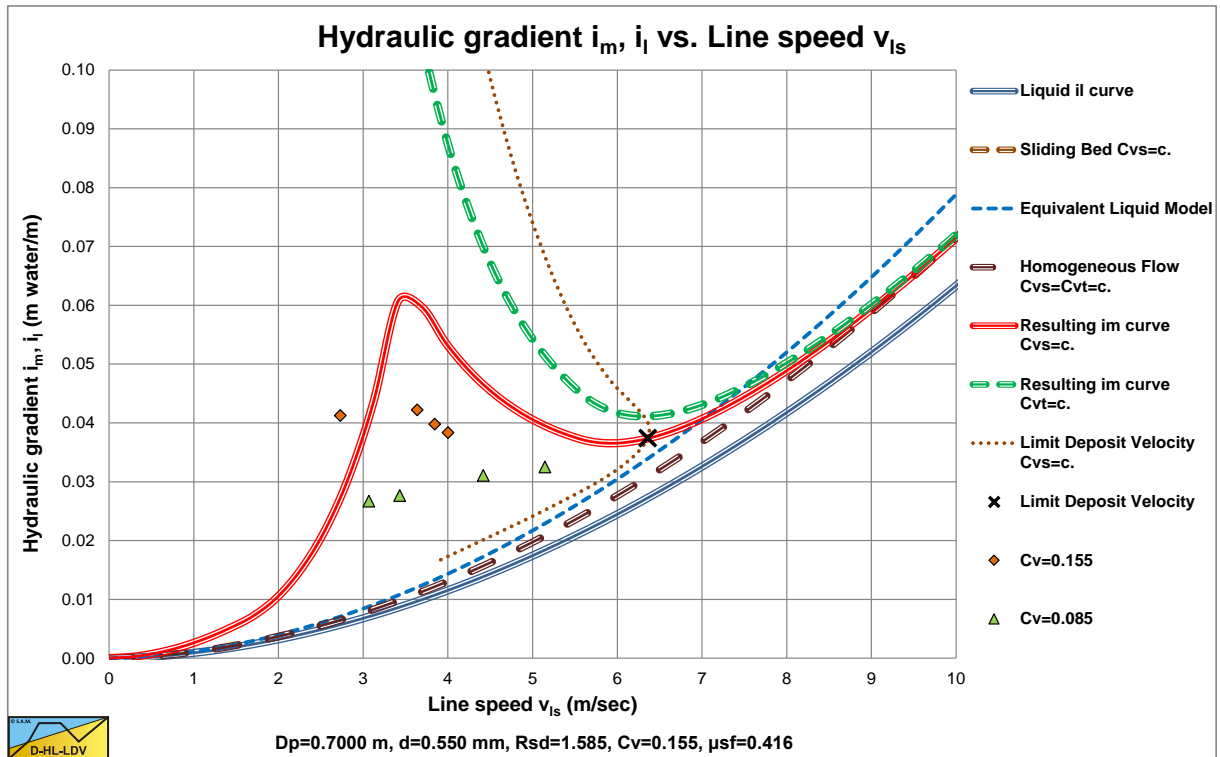
Figure 6.4-4: Experiments with sand d=0.55 mm and a pipe diameter of D_p=0.70 m.

Dp=0.7000 m, d=0.600 mm, Rsd=1.585, Cv=0.180, μsf=0.416
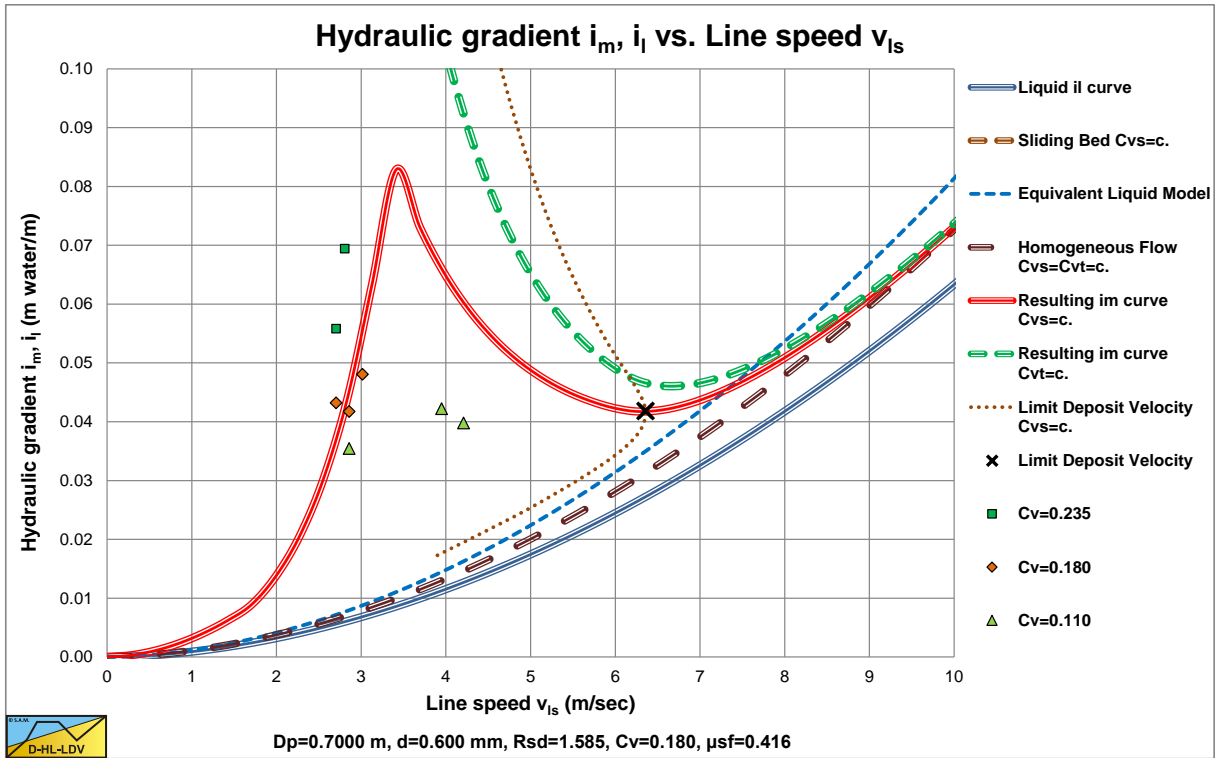
Figure 6.4-5: Experiments with sand d=0.60 mm and a pipe diameter of D$_p$=0.70 m.

Dp=0.7000 m, d=0.640 mm, Rsd=1.585, Cv=0.215, μsf=0.416
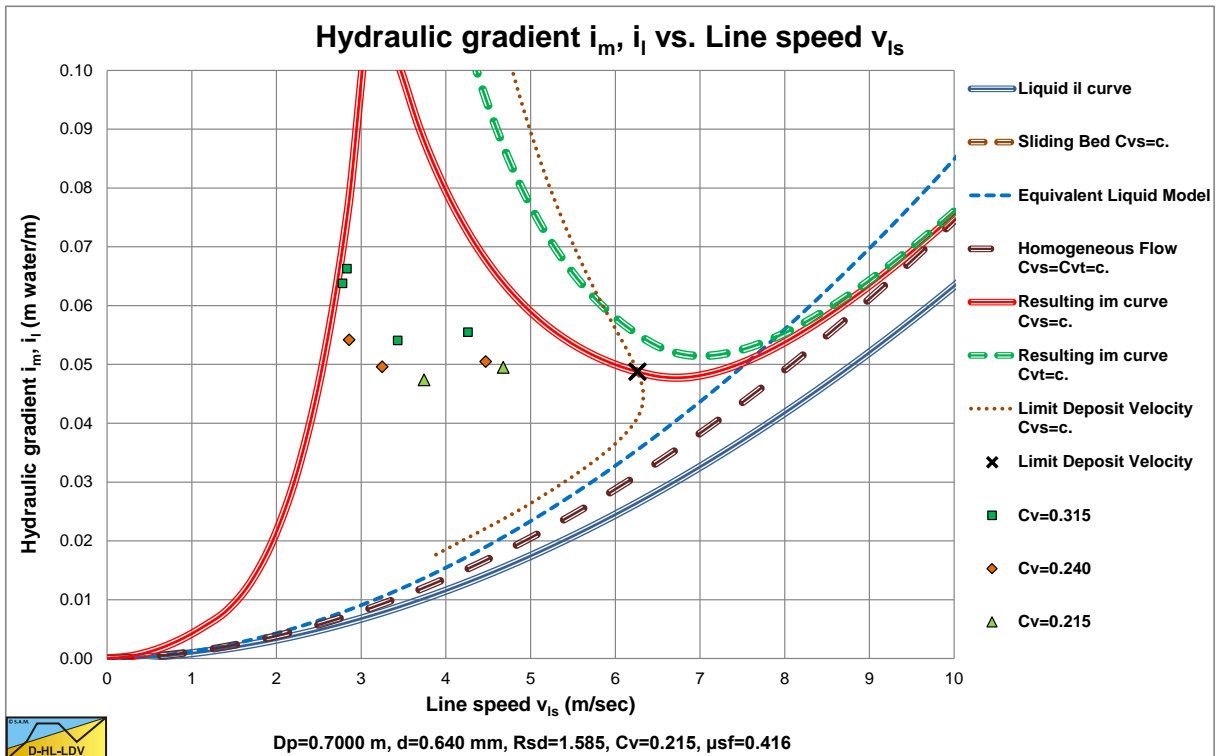
Figure 6.4-6: Experiments with sand d=0.64 mm and a pipe diameter of D$_p$=0.70 m.

Figure 6.4-7: Experiments with sands in a pipe diameter of D_p=0.58 m, uniform.

Figure 6.4-8: Experiments with sands in a pipe diameter of D_p=0.58 m, graded.

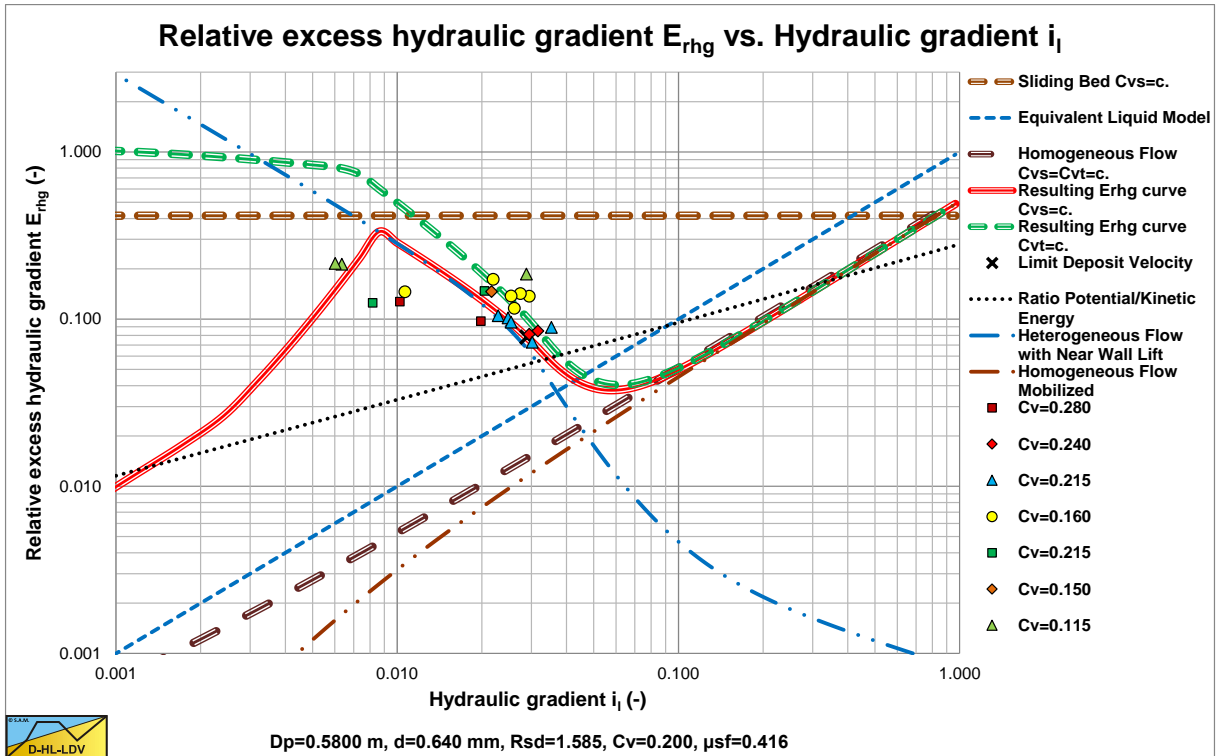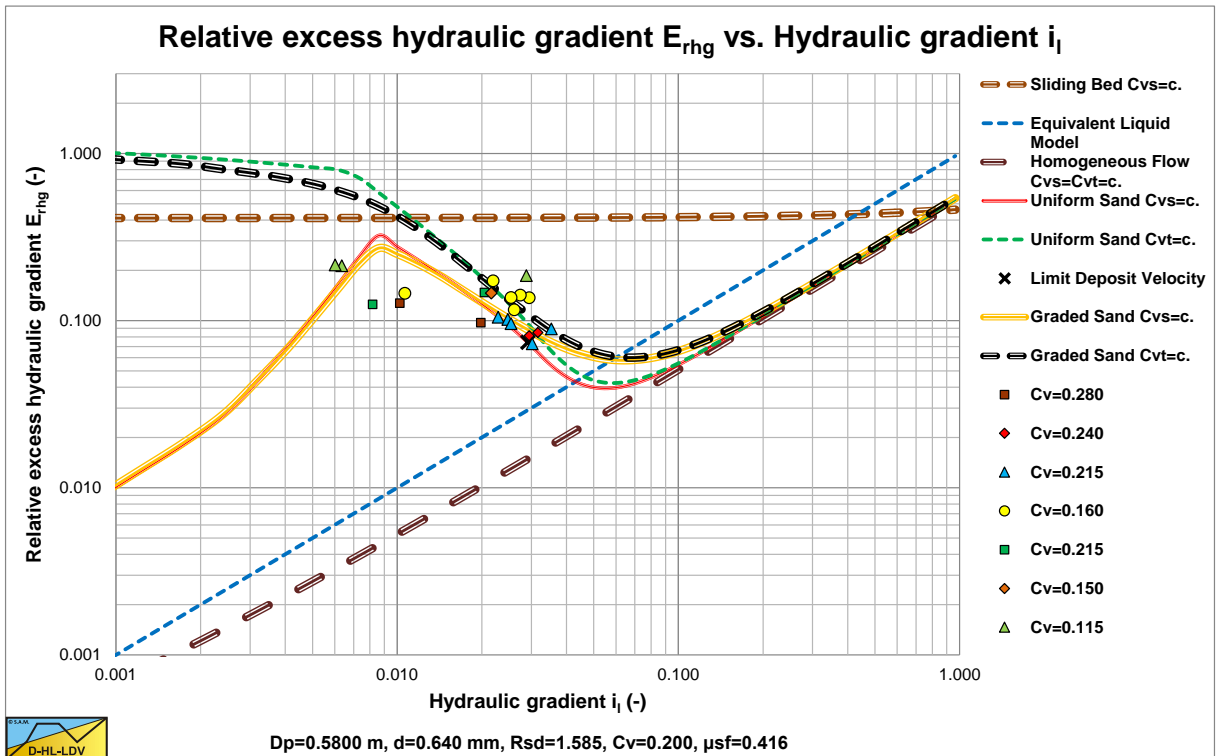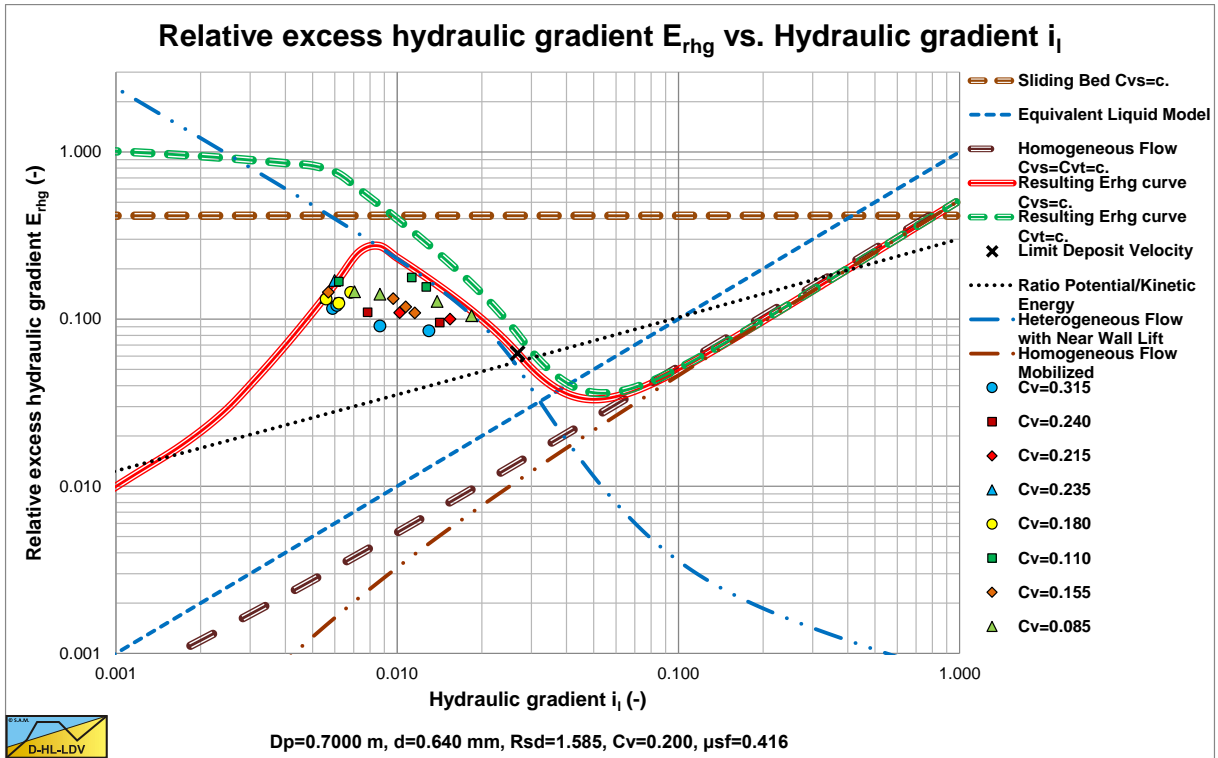**Figure 6.4-9: Experiments with sands in a pipe diameter of D_p=0.70 m, uniform.**
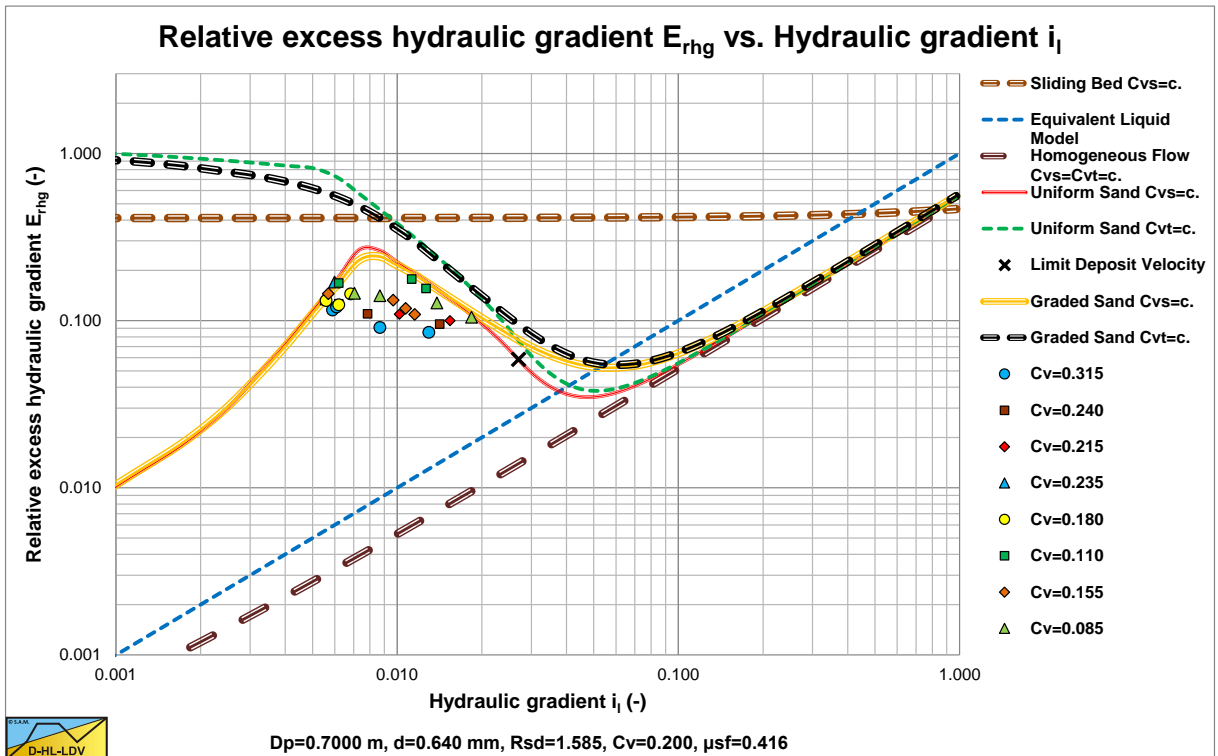

Figure 6.4-10: Experiments with sands in a pipe diameter of D_p=0.70 m, graded.

6.4.2 Durand & Condolios (1952), (1956), Durand (1953) and Gibert (1960).

Durand & Condolios (1952) and Durand (1953) carried out experiments in solids (mostly sand and gravel) with a d_{50} between 0.18 mm and 22.5 mm in pipes with a diameter D_p from 40 to 700 mm and volumetric concentrations C_{vt} from 2% to 22%. The large pipe diameter experiments (D_p=0.58 m and D_p=0.70 m) were carried out by Soleil & Ballade (1952) on a real dredge. Gibert (1960) analyzed the data of Durand & Condolios (1952) and summarized the results. A possible parameter to define the solids effect is the relative excess pressure loss p_{er}:

$$p_{er} = \left(\frac{i_m - i_l}{i_l} \right)$$

(6.4-1)

The first step Durand & Condolios (1952) carried out was to define a parameter Φ, which is the relative excess pressure loss p_{er} divided by the concentration C_{vt} and plot the pressure loss data of two sands with the parameter Φ versus the line speed v_{ls}. The transport regime of the data points is heterogeneous, which means that there will not be much difference between the spatial and the transport concentration. The parameter Φ was defined as:

$$\Phi = \left(\frac{p_{er}}{C_{vt}} \right) = \left(\frac{i_m - i_l}{i_l \cdot C_{vt}} \right)$$

(6.4-2)

With, in general for the hydraulic gradient i:

$$i = \frac{\Delta p}{\rho_l \cdot g \cdot \Delta L}$$

(6.4-3)

The volumetric concentration C_{vt} is the transport concentration, which for high line speeds and heterogeneous transport is considered to be almost equal to the spatial volumetric concentration C_{vs}, assuming that the slip between the particles and the carrying liquid can be neglected. Figure 6.4-11 shows the resulting curves of experiments at different volumetric concentrations in the heterogeneous regime, where the data points of different concentrations apparently converge to one curve. The data points of the two types of sand still result in two different curves. Whether the linear relationship between the relative solids excess pressure is exactly linear with the concentration C_{vt} requires more experiments and especially experiments at much higher concentrations in order to see if hindered settling will have an effect, but for low concentrations the conclusion of Durand & Condolios (1952) seems valid.

The second step Durand & Condolios carried out was to investigate the influence of the pipe diameter D_p. Instead of using the line speed v_{ls} on the horizontal axis, they suggested to use the Froude number of the flow; $Fr_{fl} = v_{ls} / \sqrt{g \cdot D_p}$. Figure 6.4-12 shows how the data points of two sands and 4 pipe diameters converge to two curves, one for each sand. Within the range of the pipe diameters applied and the range of the particle diameters applied, the assumption of Durand & Condolios (1952) that the parameter Φ is proportional to the square root of the pipe diameter and reversely proportional to the flow Froude number, seems very reasonable. Whether this proportionality is linear or to a certain power close to unity is subject to further investigation.

Now that proportionalities have been found between the parameter Φ on one hand and the concentration C_{vt} and the pipe diameter D_p on the other hand, Durand & Condolios (1952) investigated the influence of the particle diameter. Figure 6.4-13 shows the results of experiments in 4 sands and one gravel ranging from a d_{50}=0.20 mm to a d_{50}=4.2 mm in a D_p=0.150 m pipe. Figure 6.4-14 shows the results of 7 gravels.

Figure 6.4-14 shows that in the case of gravels the relation between Φ and Fr_{fl} does not depend on the particle size, but Figure 6.4-13 shows that for smaller particles it does. A parameter that shows such a behavior is the drag coefficient C_D as used to determine the terminal settling velocity v_t of the particles. For small particles the drag coefficient depends strongly on the particle diameter, but for particles larger than about 1 mm, the drag coefficient is a constant with a value of about 0.445 for spheres and up to about 1-1.5 for angular sand grains. Instead of using the drag coefficient directly, Durand & Condolios (1952) choose to use the particle Froude number $Fr_p = v_t / \sqrt{g \cdot d}$. It cannot be emphasized enough that this particle Froude number is different from the reciprocal of the drag coefficient C_D, although it is mixed up in many text books, together with some other errors, resulting in the wrong use and interpretation of the Durand & Condolios (1952) results.
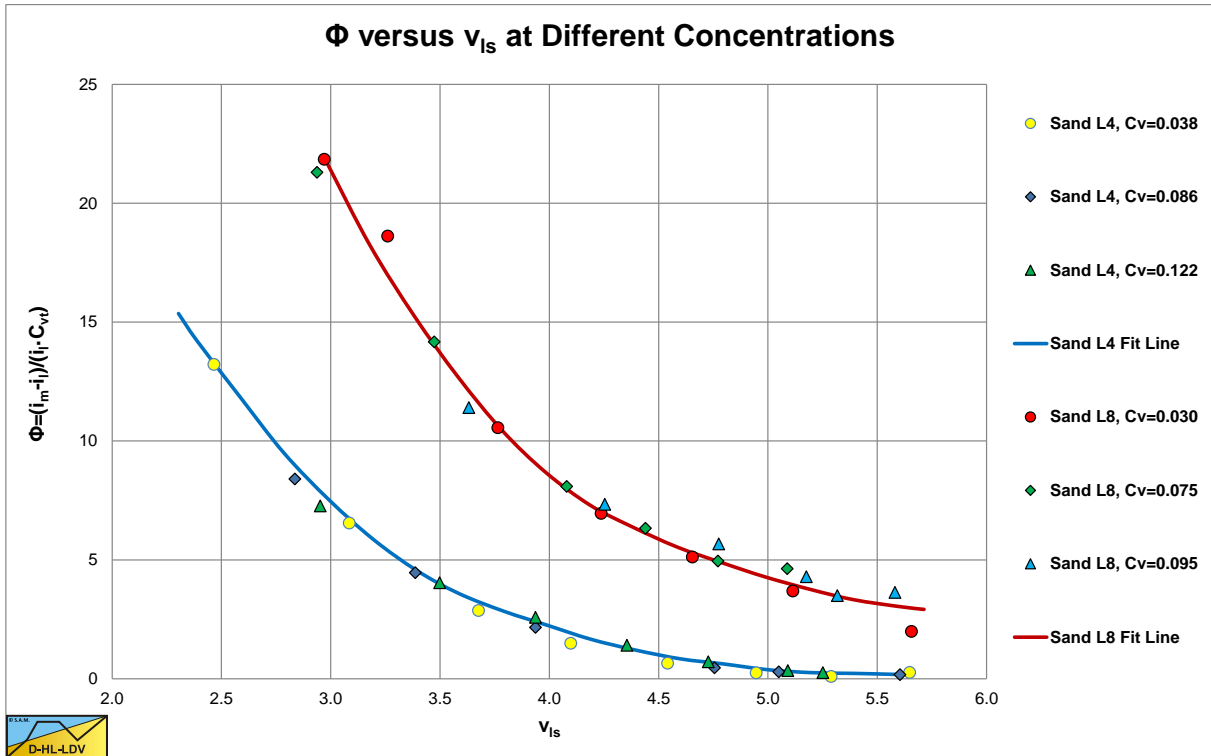
Figure 6.4-11: Φ at different concentrations as a function of the line speed in a D_p=0.150 m pipe.
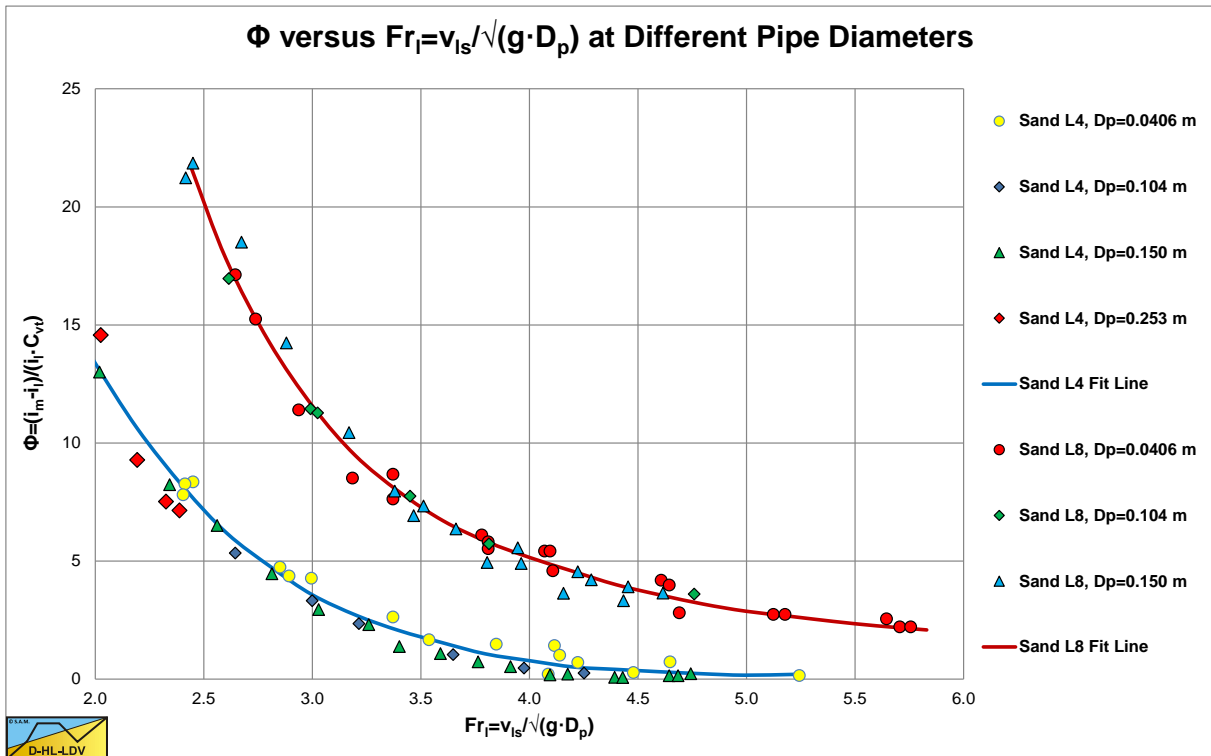
Figure 6.4-12: Φ at different pipe diameters as a function of the flow Froude number Fr_fl.
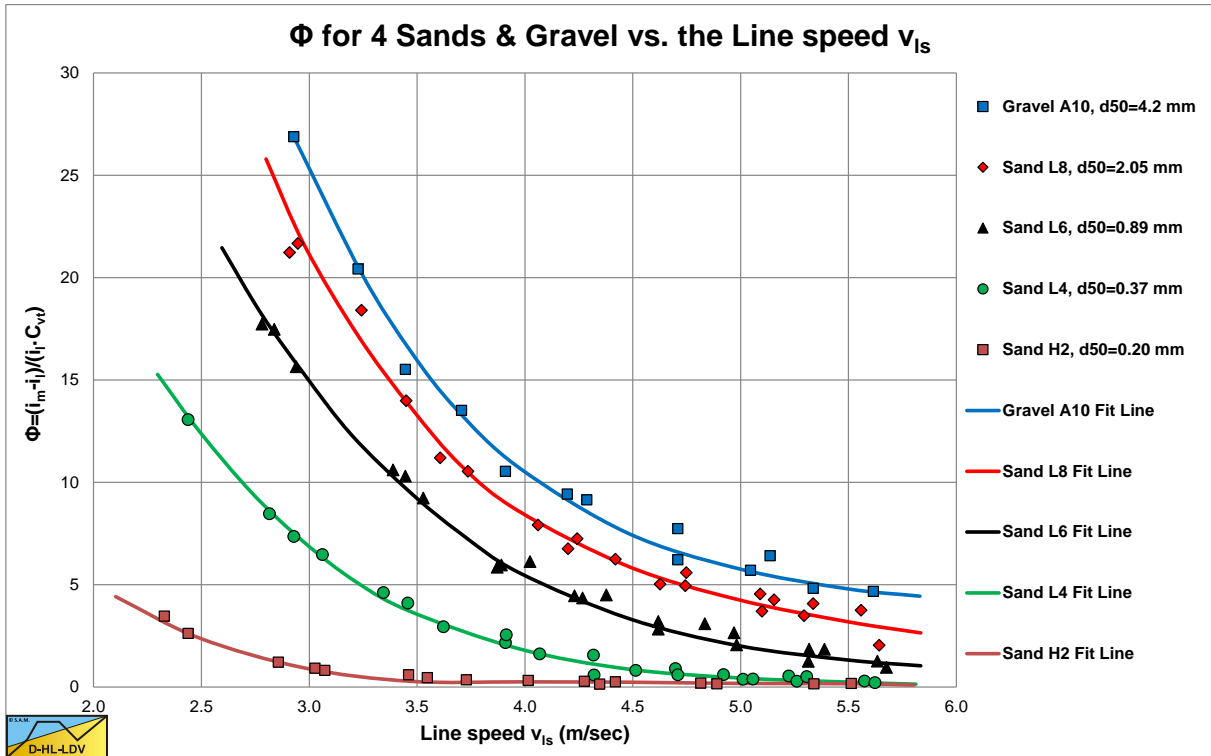
Figure 6.4-13: Φ as a function of v_{ls} for 4 sands and 1 gravel.
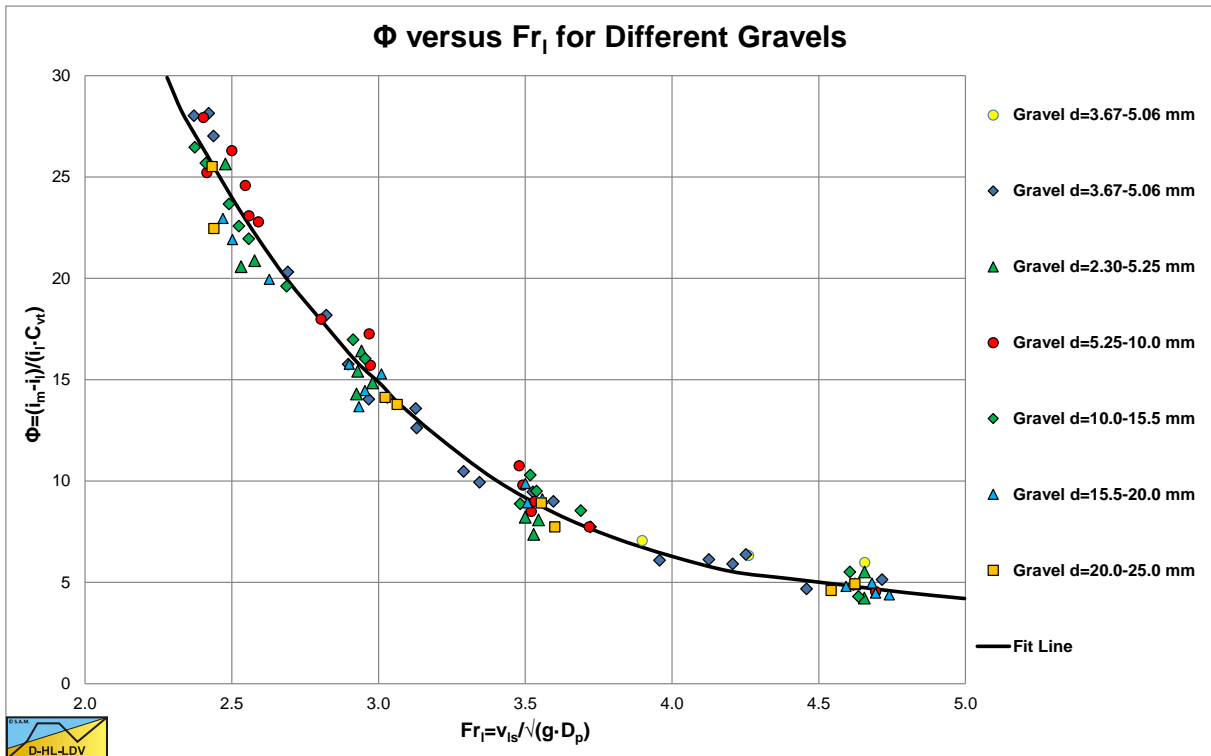
Figure 6.4-14: Φ as a function of Fr_{fl} in 7 gravels.
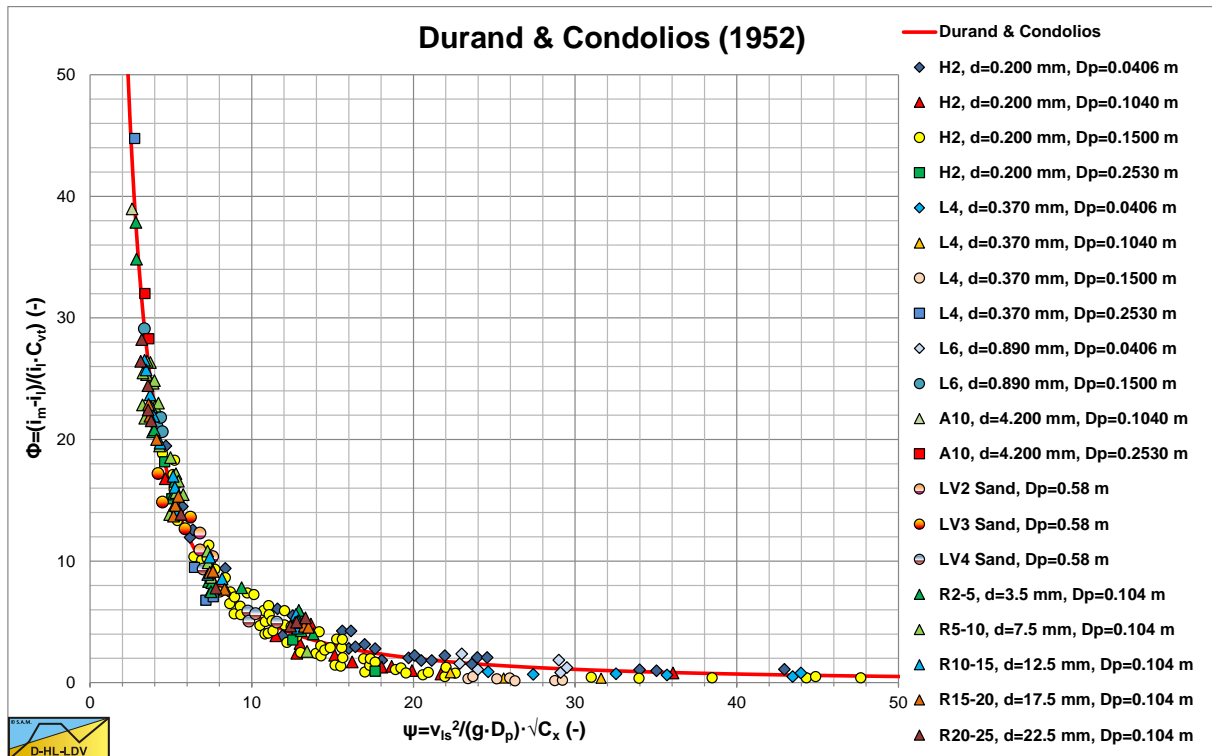
Figure 6.4-15: The relationship of the Durand & Condolios (1952) model, linear.
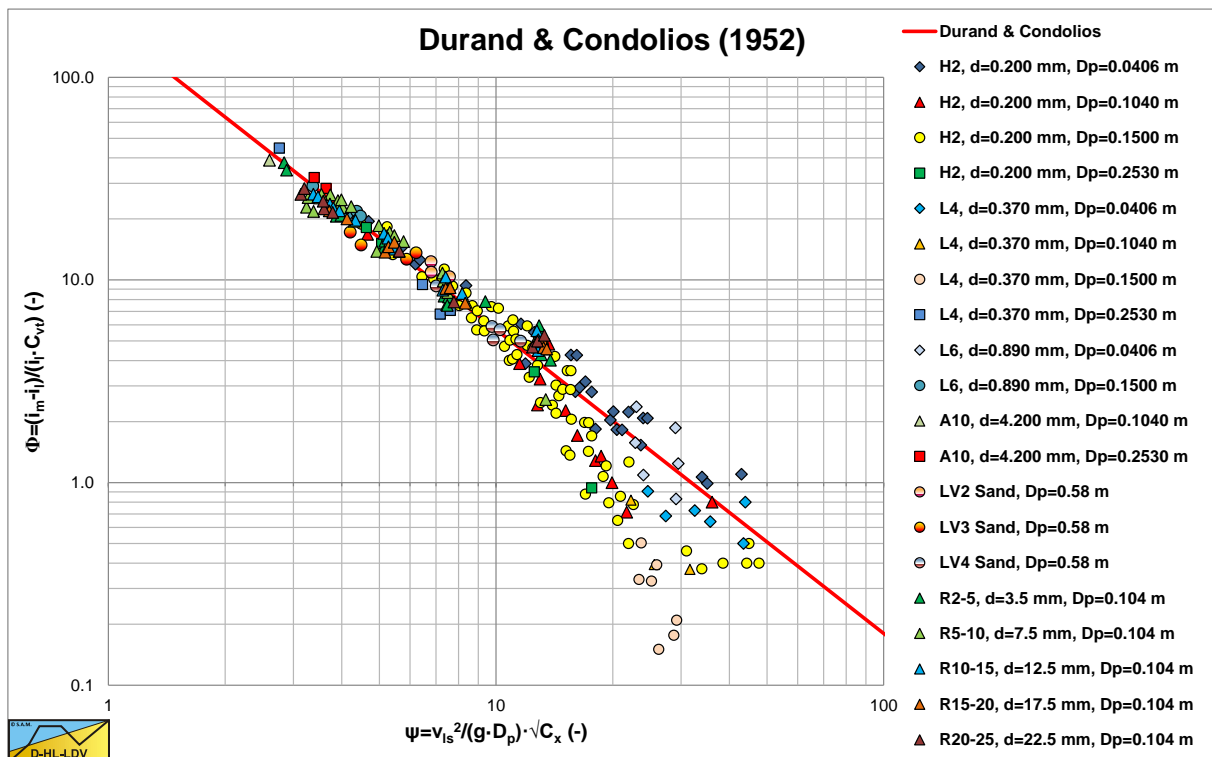
Figure 6.4-16: The relationship of the Durand & Condolios (1952) model, logarithmic.
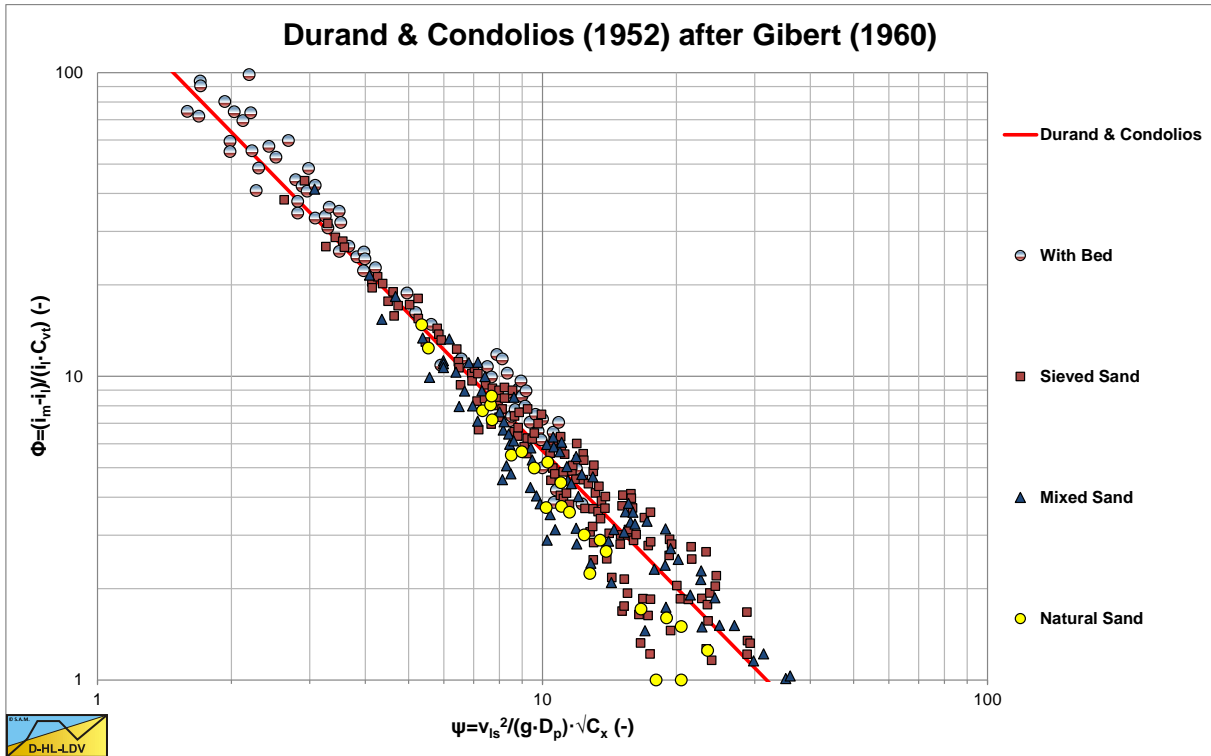
Figure 6.4-17: The relationship of the Durand & Condolios (1952) and Gibert (1960) model, logarithmic. Here distinguished between experiments with a bed, sieved sand, mixed sand and natural sand.
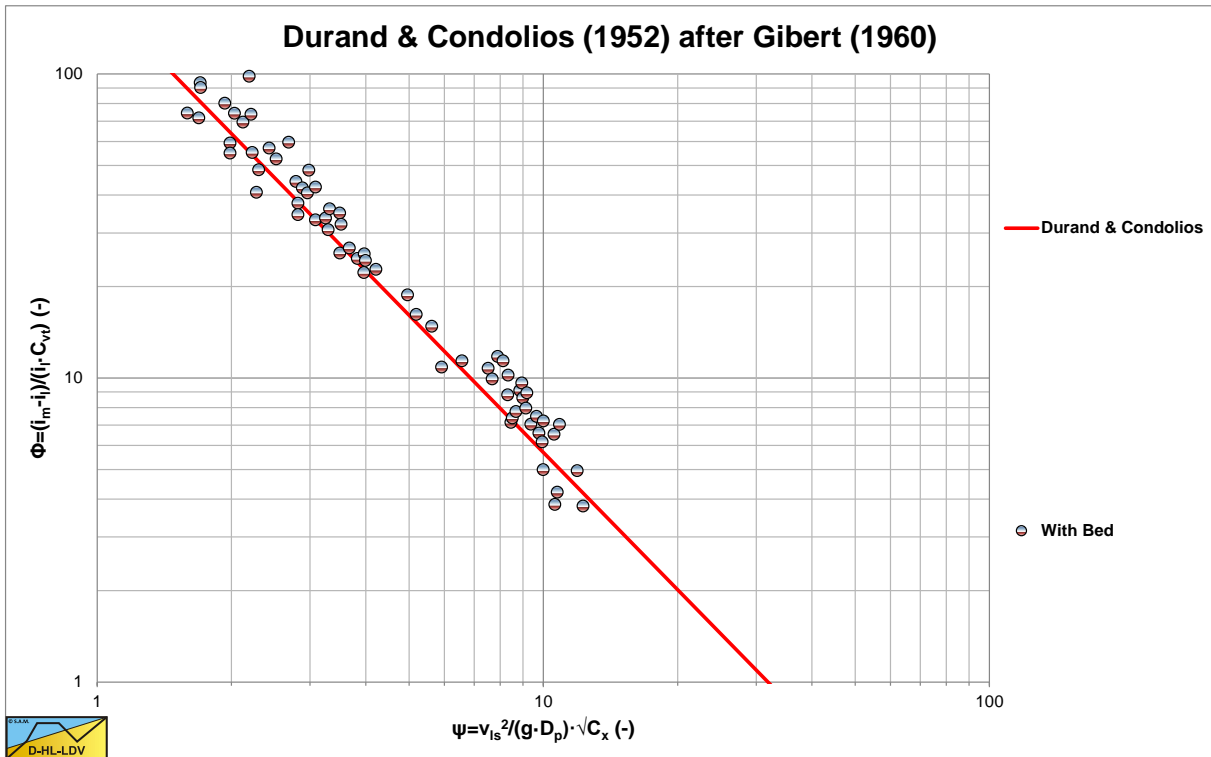
Figure 6.4-18: The relationship of the Durand & Condolios (1952) and Gibert (1960) model, logarithmic. Here experiments with a bed.

In order to make the 5 curves in Figure 6.4-13 converge into one curve, Durand & Condolios (1952) extended the parameter on the horizontal axis with the particle Froude number to:

$$\psi = \left(\frac{v_{ls}}{\sqrt{g \cdot D_p}}\right)^2 \cdot \left(\frac{v_t}{\sqrt{g \cdot d_{50}}}\right)^{-1} \qquad \text{(6.4-4)}$$

With:

$$Fr_{fl} = \left(\frac{v_{ls}}{\sqrt{g \cdot D_p}}\right) \quad \text{and} \quad Fr_p = \frac{1}{\sqrt{C_x}} = \left(\frac{v_t}{\sqrt{g \cdot d_{50}}}\right) \quad \text{and} \quad C_x = \frac{g \cdot d_{50}}{v_t^2} = Fr_p^{-2} \qquad \text{(6.4-5)}$$

Which are the Froude number of the flow Fr_{fl} and the Froude number of the particle Fr_p, which also looks like a sort of reciprocal drag coefficient (but it's not) , which will be explained later. The variable ψ can now also be written in terms of the two Froude numbers as defined above.

$$\psi = Fr_{fl}^2 \cdot Fr_p^{-1} \qquad \text{(6.4-6)}$$

Durand & Condolios (1952) plotted all their data against this new parameter ψ as is shown in Figure 6.4-16 on linear scales and Figure 6.4-15 on logarithmic scales. The assumption of using the particle Froude number Fr_p seemed to be successful. Figure 6.4-17 shows the data points distinguished into 4 groups, experiments where a bed occurred, experiments with sieved sand, experiments with mixed sands and experiments with natural sands. It is obvious from this figure that also the data points from experiments with a bed occurring, follow the same fit curve, see Figure 6.4-18. The curves for different sands, pipe diameters and concentrations converged into one curve with the equation:

$$\Phi = K \cdot \psi^{-3/2} \qquad \text{(6.4-7)}$$

   With : K=176

The constant of 176 is found from the original graph of Durand & Condolios (1952) (source Bain & Bonnington (1970)). The next step was to investigate the influence of the relative submerged density of the particles. Gibert (1960) reported on a set of experiments on plastic, sand and Corundum with 3 different relative densities. Figure 6.4-19 shows the results of these experiments.

By extending the flow Froude number Fr_{fl}, with the relative submerged density R_{sd} the data points converge to one curve for each particle diameter. The liquid flow Froude number Fr_{fl} is modified according to:

$$Fr_{fl} = \frac{v_{ls}}{\sqrt{g \cdot D_p \cdot R_{sd}}} \qquad \text{(6.4-8)}$$

Applying this modified Froude number, nothing changes in the equation for sand with a relative submerged density of about $R_{sd}=1.65$, using in a new constant of 83 instead of 176 for K. The equation for the particle Froude number does not change according to Gibert (1960) because of the relative submerged density R_{sd} and remains:

$$Fr_p = v_t / \sqrt{g \cdot d} \ .$$

The final equation of Durand & Condolios (1952) and later Gibert (1960) now becomes:

$$\Delta p_m = \Delta p_l \cdot \left(1 + \Phi \cdot C_{vt}\right) \qquad \text{(6.4-9)}$$

With:

$$\Phi = \frac{i_m - i_l}{i_l \cdot C_{vt}} = \frac{\Delta p_m - \Delta p_l}{\Delta p_l \cdot C_{vt}} = K \cdot \psi^{-3/2} = K \cdot \left(\frac{v_{ls}^2}{g \cdot D_p \cdot R_{sd}} \cdot \sqrt{C_x} \right)^{-3/2}$$

(6.4-10)

$$K \approx 83$$

Durand & Condolios (1952) and Gibert do not claim that equation (6.4-10) is rigorously exact and believe that a more accurate, although more complex, means of correlating their data is possible. They claim only that their equation brings all their results together quite well, especially if one considers that 310 test points cover a broad range of pipe diameters (D_p=40 to 580 mm), particle diameters (d_{50}=0.2 to 25 mm) and concentrations (C_{vt}=2% to 22.5%).
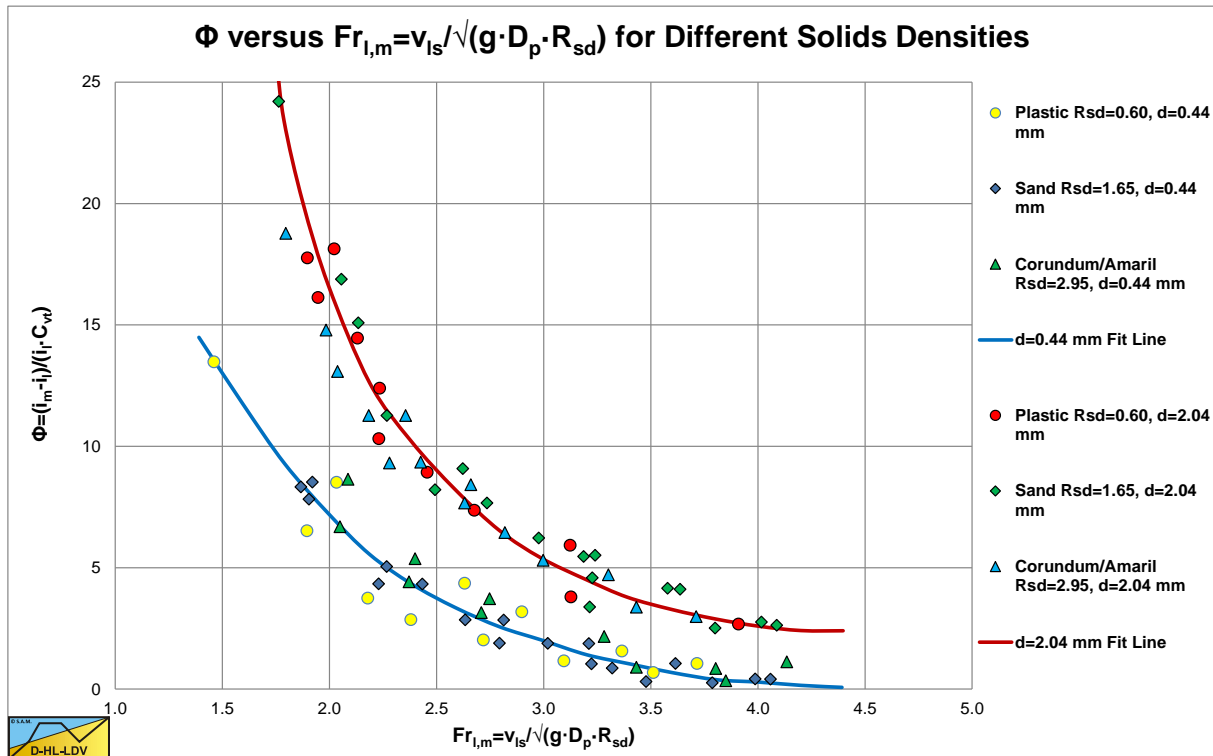
Figure 6.4-19: The influence of the relative submerged density R_{sd}.

In normal sands, there is not only one grain diameter, but a grain size distribution has to be considered. The Froude number for a grain size distribution can be determined by integrating the Froude number as a function of the probability according to:

$$Fr_p = \frac{v_t}{\sqrt{g \cdot d}} = \frac{1}{\sqrt{C_x}} = \frac{1}{\int_0^1 \frac{\sqrt{g \cdot d}}{v_t} dp} = \frac{1}{\sum_{i=1}^n \left(\sqrt{C_x} \right)_i \cdot \Delta p_i}$$

(6.4-11)

It is also possible to split the particle size distribution into **n** fraction and determine the weighted average particle Froude number. Gibert (1960) published a graph with values for the particle Froude number that match the findings of Durand & Condolios (1952). Figure 6.4-20 shows these published values. If one uses the values of Gibert (1960), the whole discussion about whether the C_D or the C_x value should be used can be omitted. Analyzing this table however, shows that a very good approximation of the table values can be achieved by using the particle Froude number to the power 20/9 instead of the power 1, assuming that the terminal settling velocity v_t is determined correctly for the solids considered (Stokes, Budryck, Rittinger or Zanke).

$$\sqrt{C_{x,Gibert}} = \sqrt{C_x}^{-20/9} = C_x^{10/9}$$

(6.4-12)

Figure 6.4-20 shows the original data points, the theoretical reciprocal particle Froude numbers using the Zanke (1977) equation for the terminal settling velocity of sand particles and the curve using a power of 20/9. Only for large particles there is a small difference between the original data and the theoretical curve applying the power of 20/9.
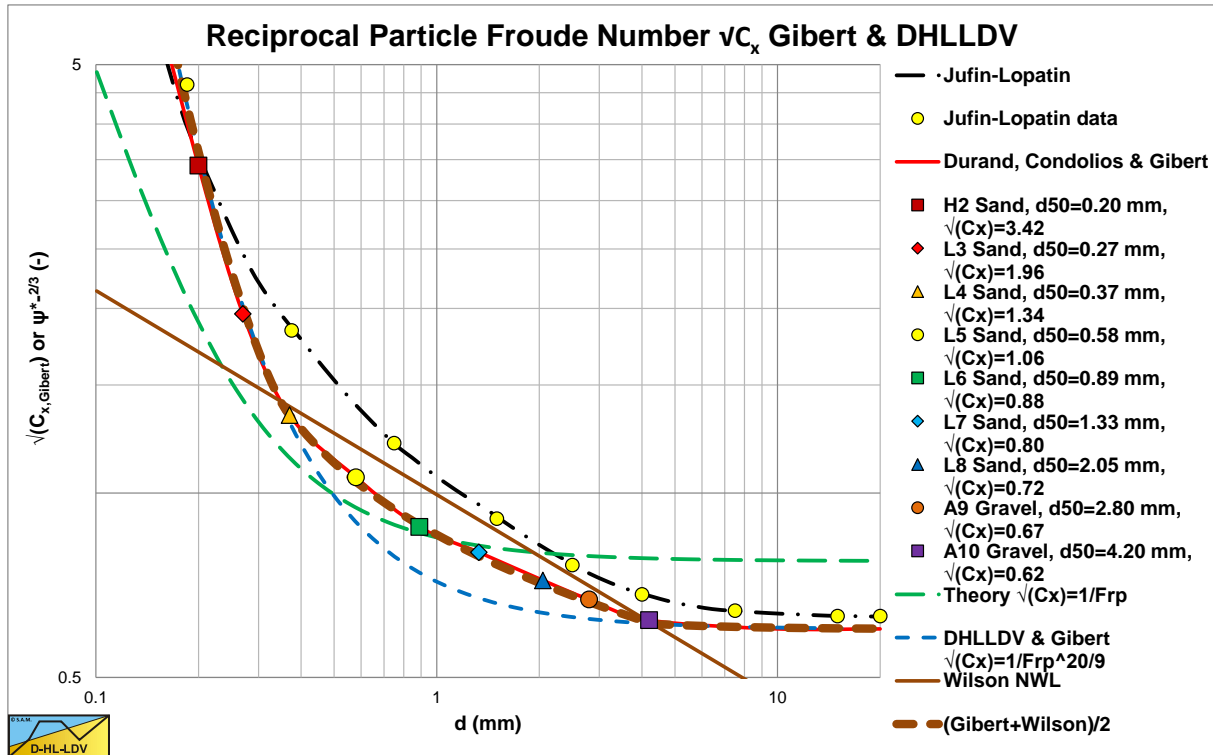
Figure 6.4-20: Modified reciprocal particle Froude number, determined experimentally for various sorts of sand and gravel by Durand & Condolios (1952) and Gibert (1960).

6.4.2.1 Inclined Pipes.

For inclined pipes they modified the solids effect by adding the cosine of the inclination angle according to:

$$\Phi_\theta = \frac{i_{m,\theta} - \sin(\theta) \cdot (1 + R_{sd} \cdot C_{vt}) - i_l}{i_l \cdot C_{vt}} = 81 \cdot \left(\frac{v_{ls}^2 \cdot \sqrt{C_x}}{g \cdot D_p \cdot R_{sd} \cdot \cos(\theta)} \right)^{-3/2}$$

$$i_{m,\theta} = i_l \cdot \left(1 + 81 \cdot \left(\frac{v_{ls}^2 \cdot \sqrt{C_x}}{g \cdot D_p \cdot R_{sd} \cdot \cos(\theta)} \right)^{-3/2} \cdot C_{vt} \right) + \sin(\theta) \cdot (1 + R_{sd} \cdot C_{vt})$$

(6.4-13)

This can be written as:

$$i_{m,\theta} = i_l + \sin(\theta) \cdot (1 + R_{sd} \cdot C_{vt}) + i_l \cdot 81 \cdot \left(\frac{v_{ls}^2 \cdot \sqrt{C_x}}{g \cdot D_p \cdot R_{sd} \cdot \cos(\theta)} \right)^{-3/2} \cdot C_{vt}$$

(6.4-14)

$$i_{m,\theta} = i_{l,\theta} + i_l \cdot 81 \cdot \left(\frac{v_{ls}^2 \cdot \sqrt{C_x}}{g \cdot D_p \cdot R_{sd}} \right)^{-3/2} \cdot C_{vt} \cdot \cos(\theta)^{3/2} + \sin(\theta) \cdot R_{sd} \cdot C_{vt}$$

So the solids effect has to be multiplied with the cosine of the inclination angle to the power of 3/2. This means the solids effect is decreasing with an increasing inclination angle, whether the inclination is upwards or downwards.

6.4.2.2 The Limit Deposit Velocity.

When the flow decreases, there will be a moment where sedimentation of the grains starts to occur. The corresponding line speed is called the Limit Deposit Velocity. Often other terms are used like the critical velocity, critical deposition velocity, deposit velocity, deposition velocity, settling velocity, minimum velocity or suspending velocity. Here we will use the term Limit Deposit Velocity.

Although in literature researchers do not agree on the formulation of the Limit Deposit Velocity, the value of the Limit Deposit Velocity is often derived by differentiating equation (6.4-9) with respect to the line speed v_{ls} and taking the value of v_{ls} where the derivative equals zero. This gives:

$$v_{ls,ldv} = \sqrt{\frac{g \cdot D_p \cdot R_{sd} \cdot \left(\frac{K \cdot C_{vt}}{2}\right)^{2/3}}{\sqrt{C_x}}} \qquad (6.4-15)$$

At line speeds less than the Limit Deposit Velocity sedimentation occurs and part of the cross-section of the pipe is filled with sand, resulting in a higher flow velocity above the sediment. Durand & Condolios (1952) assume equilibrium between sedimentation and scour, resulting in a Froude number equal to the Froude number at the Limit Deposit Velocity.

$$F_L = Fr_{ldv} = \frac{v_{ls,ldv}}{\sqrt{g \cdot D_p \cdot R_{sd}}} = \sqrt{\frac{\left(\frac{K \cdot C_{vt}}{2}\right)^{2/3}}{\sqrt{C_x}}} \qquad (6.4-16)$$

By using the hydraulic diameter concept, at lines speeds less than the Limit Deposit Velocity, the resistance can be determined applying equation (6.4-10) using the hydraulic diameter instead of the pipe diameter. At low flows, resulting in small hydraulic diameters, the hydraulic gradient may be so large that a sliding bed may occur, limiting the hydraulic gradient. But Durand & Condolios (1952) did not perform experiments in that flow region.

Equation (6.4-15) can be written in the form of the Durand Limit Deposit Velocity based on the minimum pressure loss, according to:

$$v_{ls,ldv} = \left(\frac{K \cdot C_{vt}}{2}\right)^{1/3} \cdot \sqrt{\frac{1}{2 \cdot \sqrt{C_x}}} \cdot \sqrt{2 \cdot g \cdot D_{p,H} \cdot R_{sd}} = F_L \cdot \sqrt{2 \cdot g \cdot D_{p,H} \cdot R_{sd}}$$

$$(6.4-17)$$

$$F_L = \left(\frac{K \cdot C_{vt}}{2}\right)^{1/3} \cdot \sqrt{\frac{1}{2 \cdot \sqrt{C_x}}}$$

With minor adjustments for hindered settling and the ratio between the particle size **d** and the pipe diameter D_p according to Wasp et al. (1970), the following equation is derived by Miedema (1995).

$$F_L = \left(\frac{K \cdot C_{vt}}{2}\right)^{1/3} \cdot \sqrt{\frac{(1-C_{vt})^\beta}{2 \cdot \sqrt{C_x}} \cdot \left(\frac{1000 \cdot d}{D_{p,H}}\right)^{1/6}} \qquad (6.4-18)$$

The coefficient **β** is determined with equation (4.6-1). Equation (6.4-18) can be modified to match the original Durand & Condolios (1952) graph according to equation (6.4-19):

$$F_L = 1.9 \cdot \left(\frac{K \cdot C_{vt}}{2}\right)^{1/3} \cdot \sqrt{\frac{(1-C_{vt})^\beta}{2 \cdot \sqrt{C_x}} \cdot \left(\frac{1000 \cdot d}{D_{p,H}}\right)^{1/6}} \cdot e^{-\frac{d}{0.0006}} + 0.6 + 1.3 \cdot \left(1 - e^{-\frac{d}{0.0006}}\right) \qquad (6.4-19)$$

Equation (6.4-19) gives a good approximation of the original F_L graph published by Durand & Condolios (1952). The original graph is shown in Figure 6.4-22, while an approximation for large concentrations is given in Figure 6.4-23. Figure 6.4-24 shows the resulting graph of the modified $F_{L,m}$ equation (6.4-20). Durand & Condolios

(1952) and Gibert used concentrations up to 15% in their graph. Often it is referred to that for higher concentrations the curve of 15% should be used. Figure 6.4-25 shows the curves up to concentrations of 50% according to equation (6.4-20) and shows that for small particle diameters, the value of F_L decreases at the higher concentrations.

$$F_{L,m} = \frac{1.9 \cdot \left(\frac{K \cdot C_{vt}}{2}\right)^{1/3} \cdot \sqrt{\frac{(1-C_{vt})^{\beta}}{2 \cdot \sqrt{C_x}}} \cdot \left(\frac{1000 \cdot d}{D_{p,H}}\right)^{1/6} \cdot e^{-\frac{d}{0.0006}} + 0.6 + 1.3 \cdot \left(1 - e^{-\frac{d}{0.0006}}\right)}{\sqrt{2}} \quad (6.4\text{-}20)$$

It should be noted here that Durand & Condolios (1952) did their experiments in medium pipe diameters. The hydraulic gradients in larger pipes are often not high enough to result in a sliding bed. So it is assumed that the Limit Deposit Velocity of Durand & Condolios (1952) is the velocity below which particles are at rest on the bottom of the pipe, forming a stationary bed and not a sliding bed.

Figure 6.4-26 shows the Limit Deposit Velocity, as a function of the pipe diameter D_p and the particle diameter d according to equation (6.4-18), matching the findings of van den Berg (1998). Figure 6.4-27 shows the Limit Deposit Velocity as a function of the pipe diameter D_p and the particle diameter d, according to equation (6.4-19), matching the findings of Durand & Condolios (1952) and Gibert (1960).

Gibert (1960) analyzed the measurements of Durand & Condolios (1952) and created Figure 6.4-21, showing the Froude number F_L at the Limit Deposit Velocity as a function of the volumetric transport concentration C_{vt} for 5 sands and gravel for pipe diameters D_p of 0.04 m and 0.15 m. He concluded that on average sand H2 has a coefficient F_L=1.7 for higher concentrations, while the other sands and gravel have an F_L=2.1. Tests in a D_p=0.7 m pipeline at concentrations of 15%-20% have resulted in F_L=2.1-2.3. The tendencies found in Figure 6.4-21 confirm the findings of Durand & Condolios (1952), but the asymptotic value of about 1.9 in Figure 6.4-22 and Figure 6.4-23 is a bit low, considering that deposition should be avoided. If we want to predict average behavior, Figure 6.4-24 and Figure 6.4-25 should be used. If we want to prevent deposition at all times, taking into account the scatter, an asymptotic value of about 2.1 should be used, leading to a Limit Deposit Velocity of about 3.3 m/s in a 0.1524 m (6 inch) pipe.
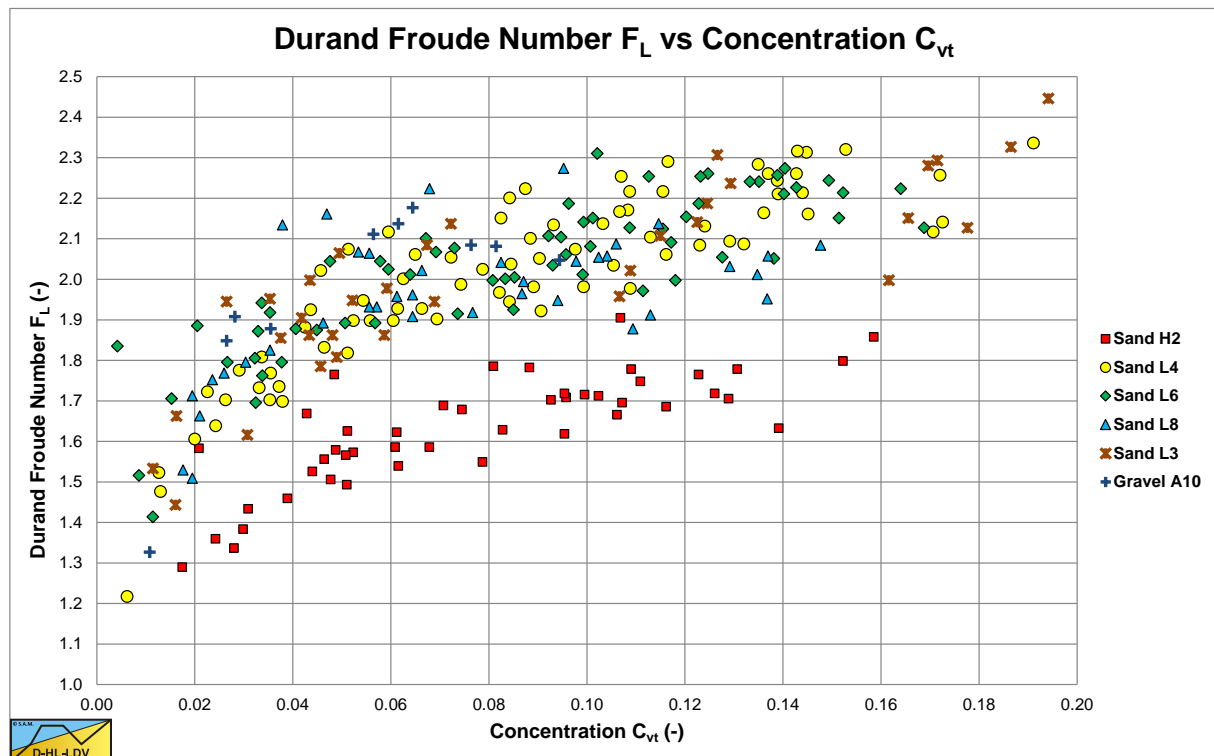
Figure 6.4-21: The Limit Deposit Velocity Froude number F_L as a function of the transport concentration C_{vt} for 5 different sands and gravel.
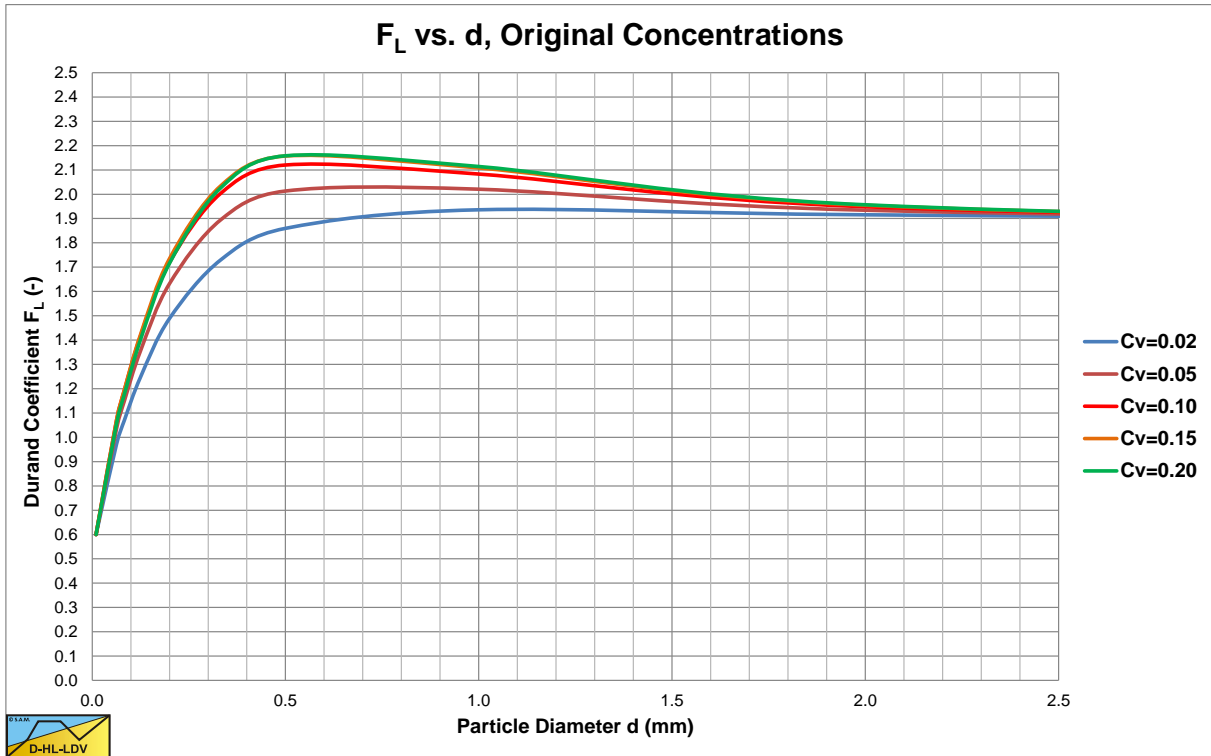
**Figure 6.4-22: Original Durand coefficient approximation according to equation (6.4-19) (D_p=0.5m)
for the original concentrations.**
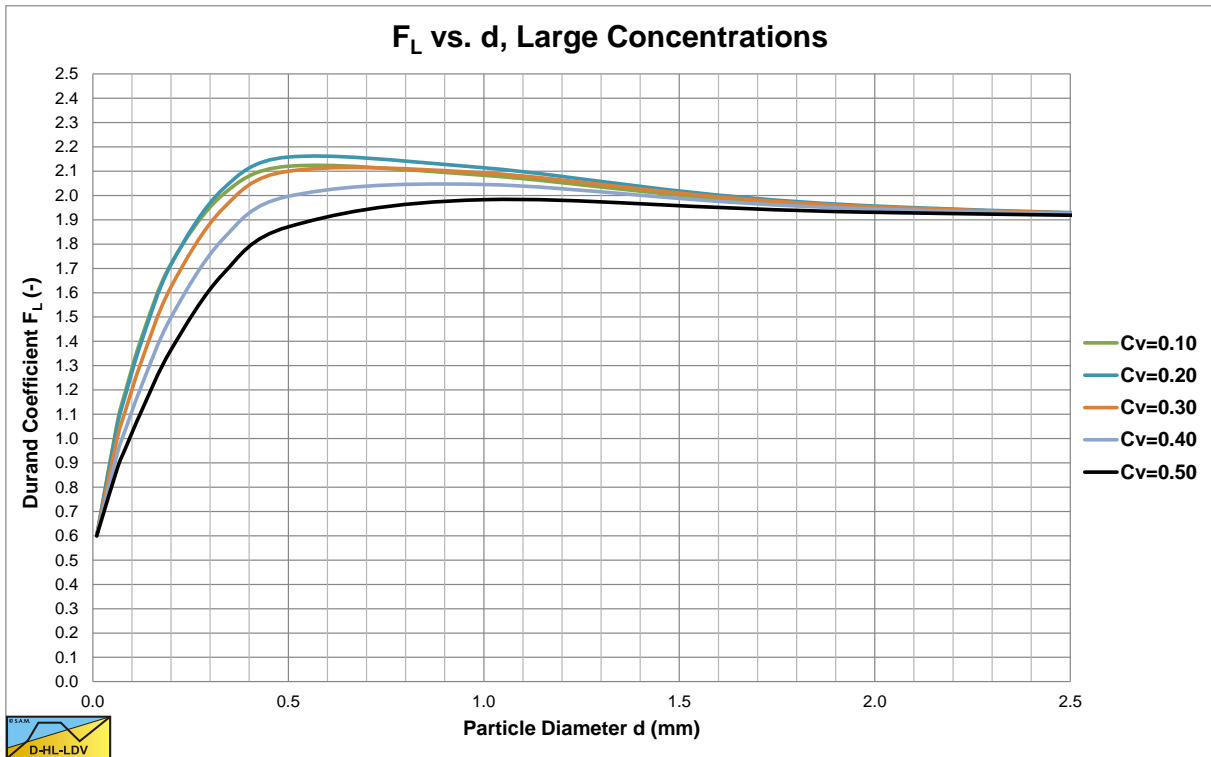
**Figure 6.4-23: Original Durand coefficient approximation according to equation (6.4-19) (D_p=0.5m)
for large concentrations.**
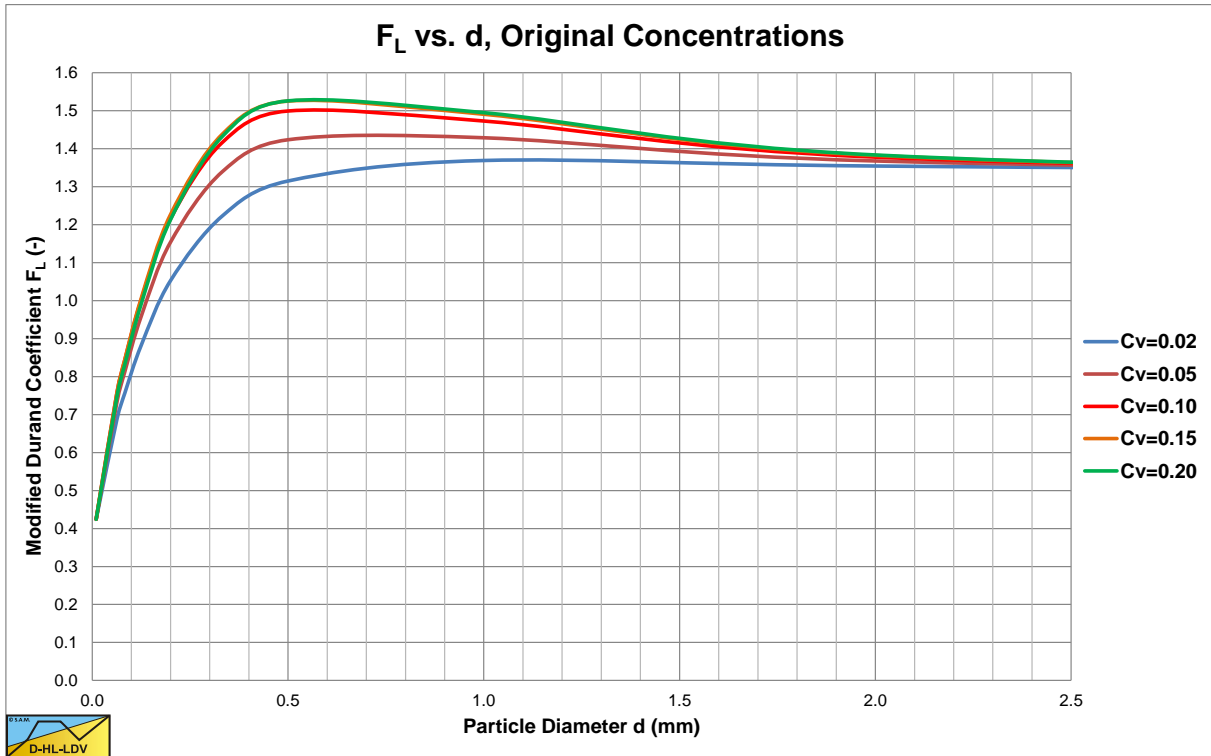
Figure 6.4-24: Modified Durand coefficient approximation according to equation (6.4-20), (D_p=0.5m).
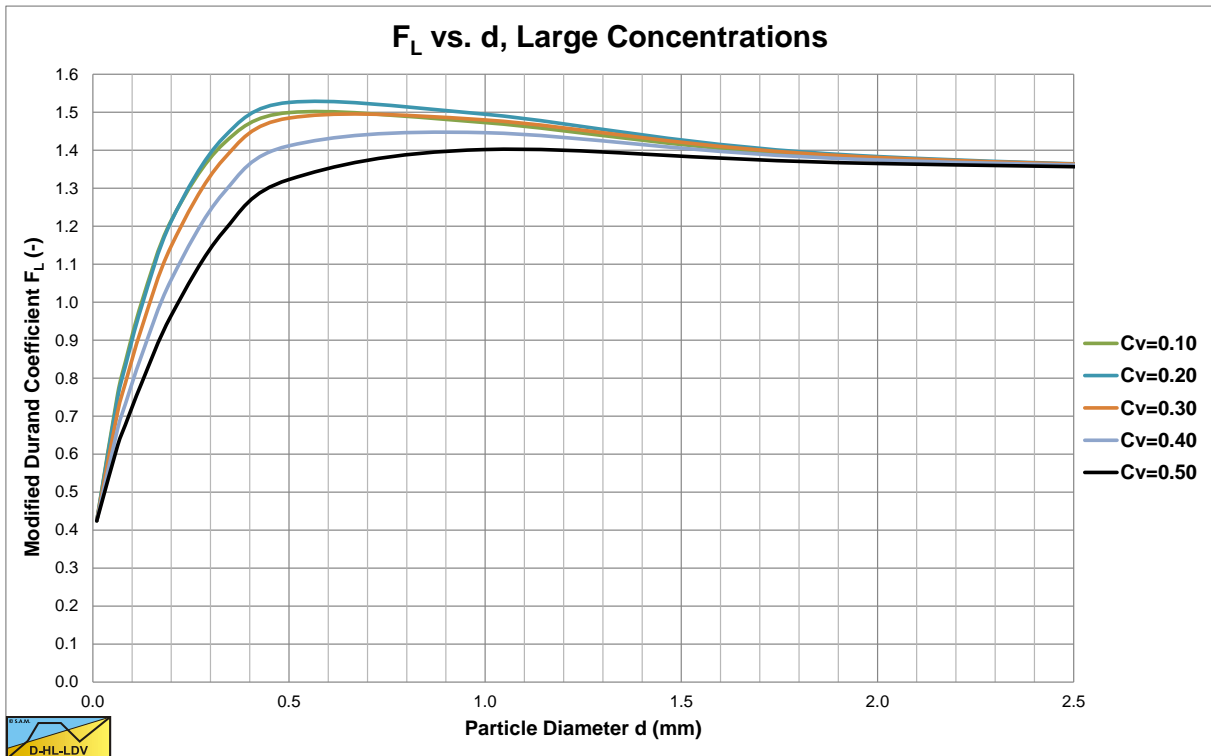
Figure 6.4-25: Modified Durand coefficient approximation according to equation (6.4-20), extrapolated for higher concentrations (D_p=0.5m).
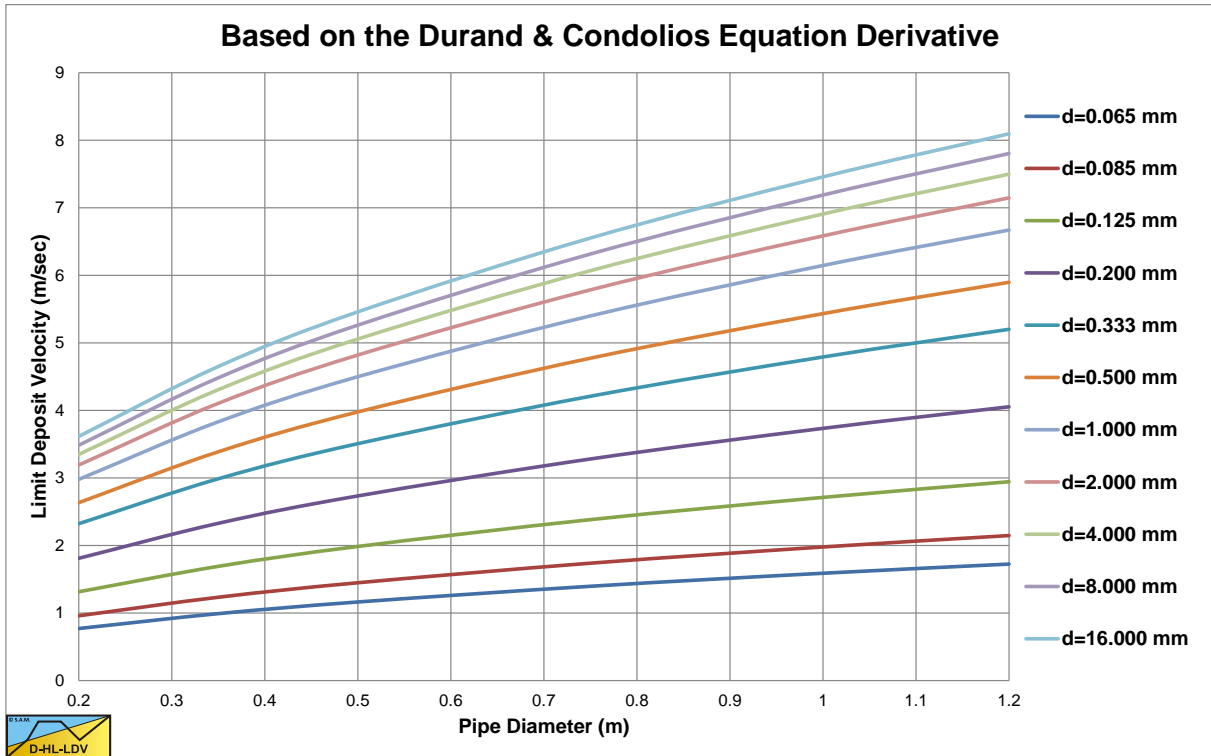
Figure 6.4-26: Limit Deposit Velocity according to equation (6.4-18) at a concentration of 0.1.
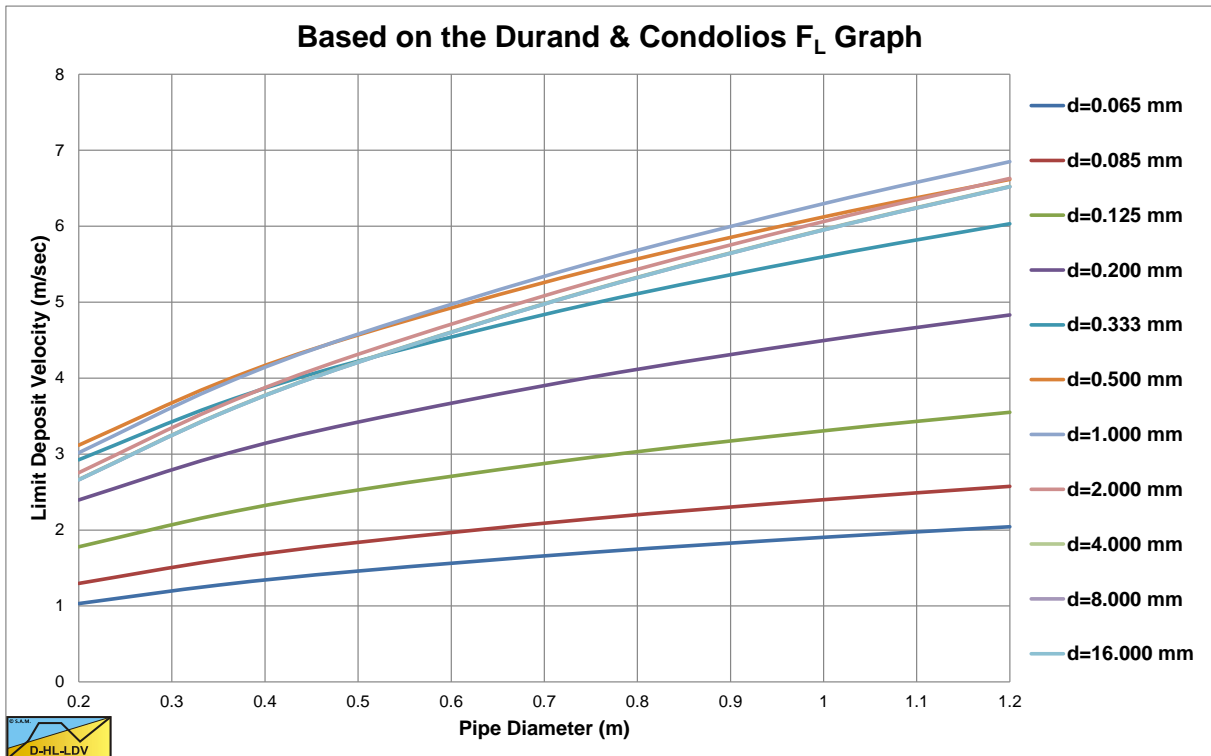
Figure 6.4-27: Limit Deposit Velocity according to equation (6.4-19) at a concentration of 0.1.
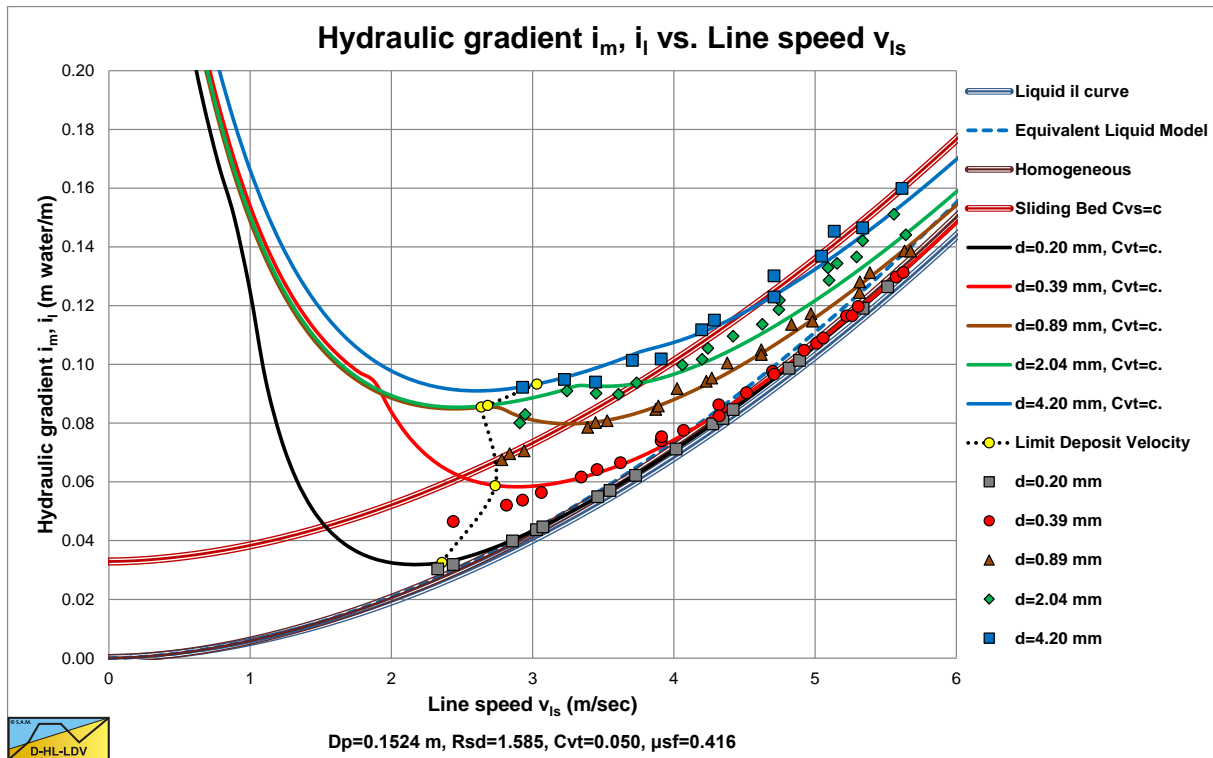
Figure 6.4-28: The data of Figure 6.4-13 as hydraulic gradient versus line speed.
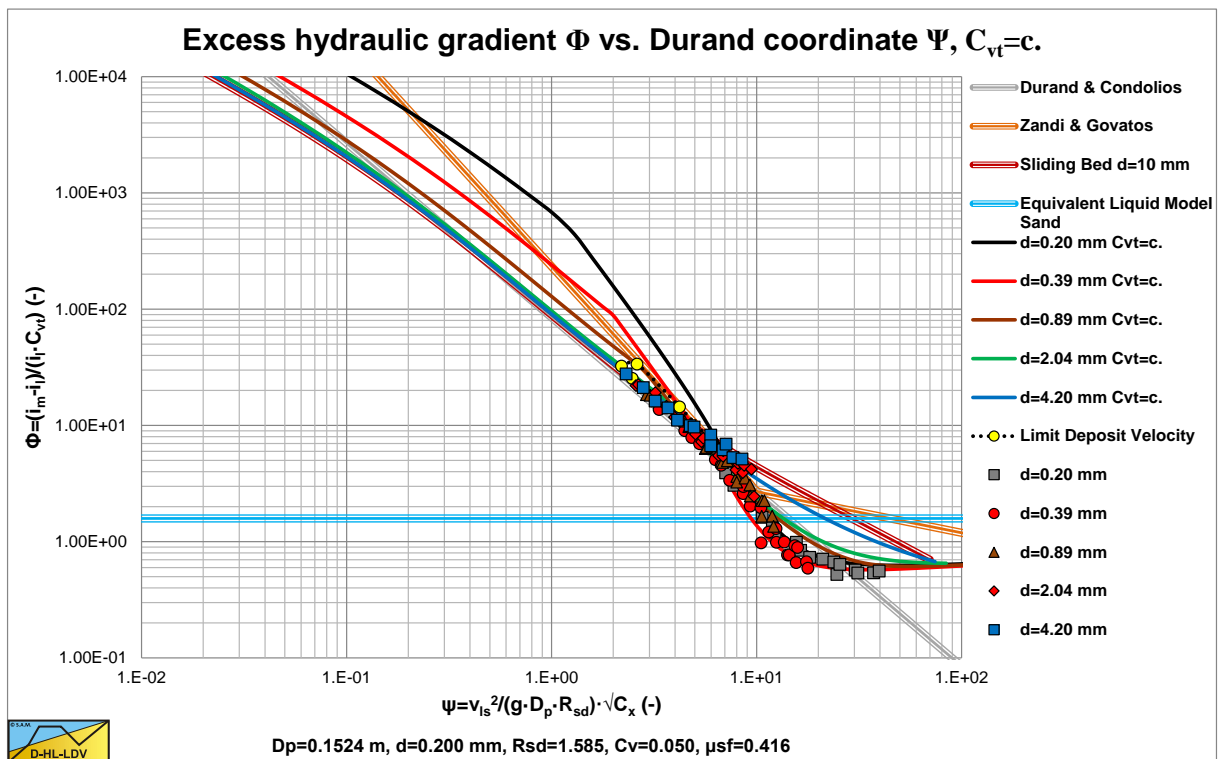
Figure 6.4-29: The data of Figure 6.4-13 in Durand coordinates..

Figure 6.4-28 and Figure 6.4-29 show the data of Figure 6.4-13 in the hydraulic gradient versus line speed graph and in the Durand coordinates graph, normalized for a volumetric concentration of 5%. The solid curves are based on the DHLLDV Framework and match very well.

6.4.3 The Worster & Denny (1955) Model

At about the same time as Durand & Condolios (1952), Worster & Denny (1955) studied flow phenomena of large particles, in particular coal, and produced a similar correlation as Durand & Condolios (1952), except for the inclusion of a term taking into account the specific gravity (relative submerged density) of the solid material and the absence of any parameter of the particle size. In the most general form this equation yields:

$$\Delta p_m = \Delta p_l \cdot \left(1 + \Phi \cdot C_v\right)$$

(6.4-21)

With:

$$\Phi = \frac{i_m - i_l}{i_l \cdot C_v} = \frac{\Delta p_m - \Delta p_l}{\Delta p_l \cdot C_v} = 120 \cdot \left(\frac{v_{ls}^2}{g \cdot D_p \cdot R_{sd}}\right)^{-3/2}$$

(6.4-22)

Figure 6.4-30 shows the data measured by Worster & Denny (1955) as a function of the Worster parameter ψ.

$$\psi = \left(\frac{v_{ls}^2}{g \cdot D_p \cdot R_{sd}}\right)^{1/2}$$

(6.4-23)
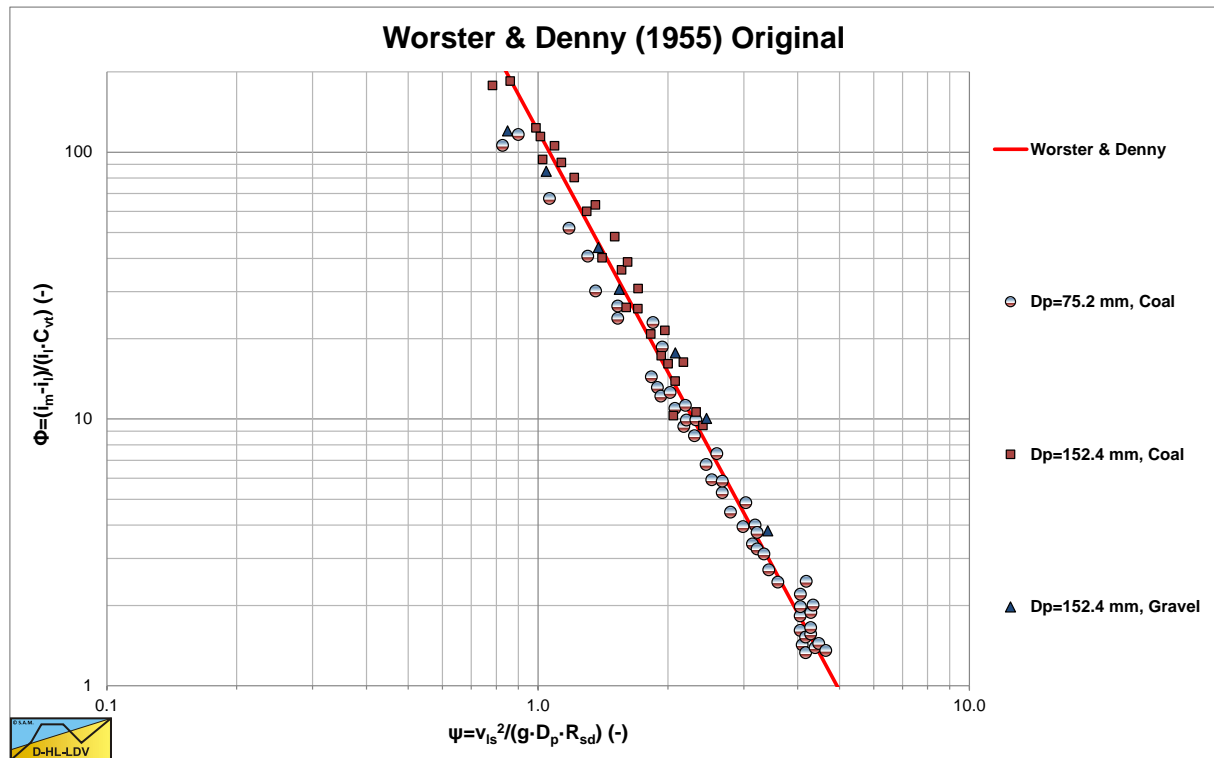
Figure 6.4-30: The data measured by Worster & Denny (1955).

Figure 6.4-31 shows these data as a function of the original Durand parameter **ψ,** not yet containing the relative submerged density, but containing the particle Froude number √C_x. This parameter is:

$$\psi = \left(\frac{v_{ls}^2}{g \cdot D_p}\right) \cdot \sqrt{\frac{g \cdot d}{v_t^2}} = \left(\frac{v_{ls}^2}{g \cdot D_p}\right) \cdot \sqrt{C_x}$$

(6.4-24)

Giving the Worster & Denny (1955) equation:

$$\Phi = \frac{i_m - i_l}{i_l \cdot C_v} = \frac{\Delta p_m - \Delta p_l}{\Delta p_l \cdot C_v} = 172 \cdot \psi^{-3/2} = 172 \cdot \left(\frac{v_{ls}^2 \cdot \sqrt{C_x}}{g \cdot D_p} \right)^{-3/2} \tag{6.4-25}$$
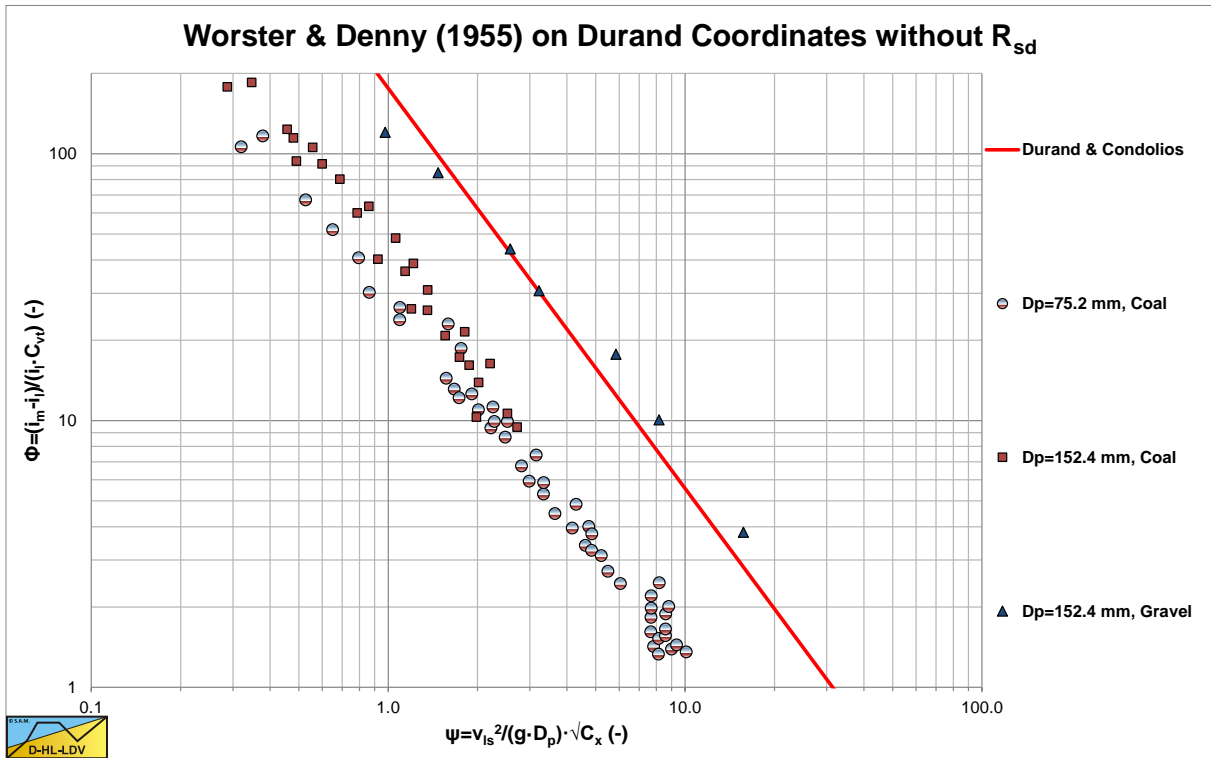
Figure 6.4-31: The data of Worster & Denny (1955) in Durand coordinates, without the correction for the relative submerged density R_{sd}.
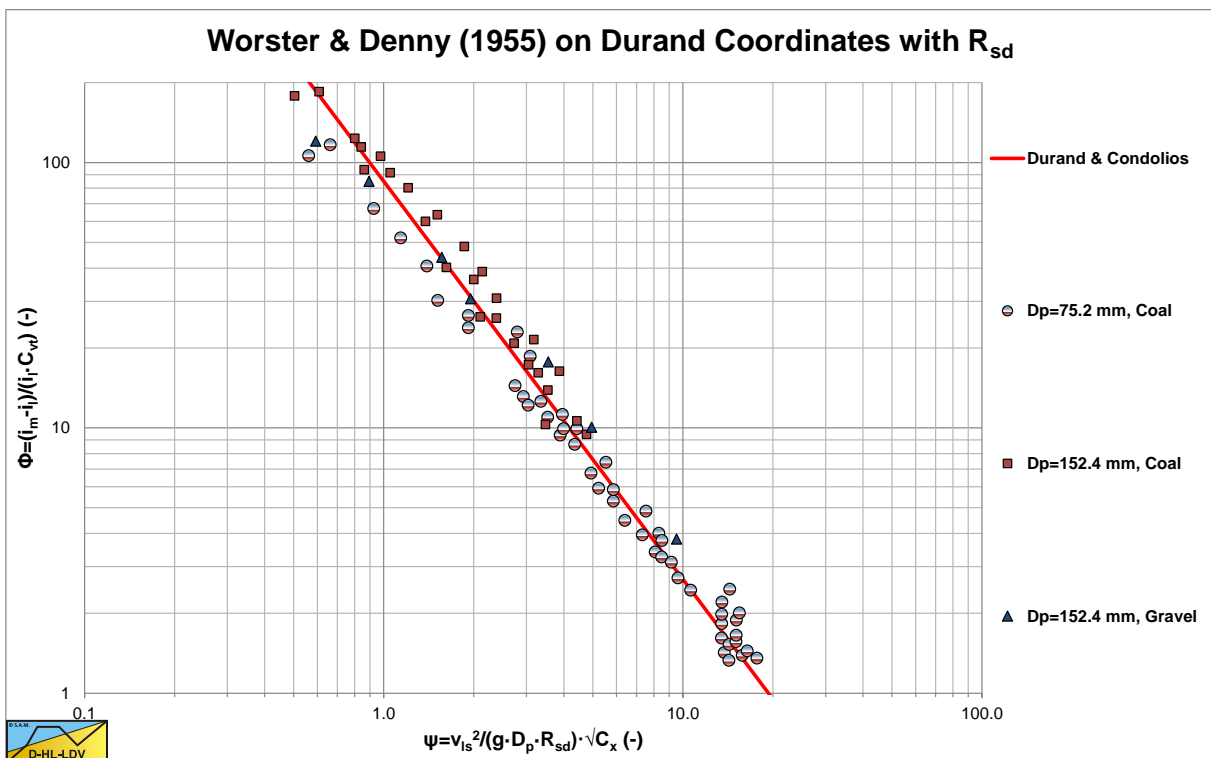
Figure 6.4-32: The data of Worster & Denny (1955) in Durand coordinates and corrected for the relative submerged density R_{sd}.

The data points of coal with a relative submerged density different from sand, deviate from the Durand & Condolios (1952) equation as is obvious from Figure 6.4-31. This equation can be modified to make it applicable to materials having a specific gravity different to that of sand and gravel (R_{sd} =1.65). By taking into account the specific gravity of the solids as Worster & Denny (1955) have done and making the corresponding correction to the constant, using a drag coefficient of 0.4, the following equation is found:

$$\Phi = \frac{i_m - i_l}{i_l \cdot C_v} = \frac{\Delta p_m - \Delta p_l}{\Delta p_l \cdot C_v} = 81 \cdot \left(\frac{v_{ls}^2 \cdot \sqrt{C_x}}{g \cdot D_p \cdot R_{sd}} \right)^{-3/2} \tag{6.4-26}$$

Worster & Denny (1955), estimated the drag coefficient C_D for large coal to be 0.4 and changed the coefficient in the above equation from **176/83** to **172/81** to compensate for the relative submerged density (source Bain & Bonnington (1970)). Figure 6.4-32 shows the data of Worster & Denny (1955), as a function of the modified Durand coordinate taking into account the relative submerged density. The data points match the Durand & Condolios (1952) equation very well after the correction for the relative submerged density. Later Gibert (1960) and Condolios & Chapus (1963A) & (1963B) mention the coefficients to be **180/85** instead of **176/83** (Durand & Condolios (1952)) or **172/81** (Worster & Denny (1955)), based on additional experiments. This difference however is marginal and within the scatter of the observations. It should be mentioned that the numbers 180, 176 and 81 are found in literature, while the numbers 85, 83 and 172 are calculated based on a relative submerged density of 1.65. The value of 180 is found in most publications after 1960.

6.4.3.1 Inclined Pipes.

Worster & Denny (1955) also gave a method for determining the hydraulic gradient for inclined pipes. Basically the method consists of adding up the pure liquid hydraulic gradient, the potential energy term for the mixture and the solids effect times the cosine of the inclination angle.

For pure liquid the hydraulic gradient in an inclined pipe equals the hydraulic gradient in a horizontal pipe of the same length plus the potential energy, giving:

$$i_{l,\theta} = i_l + \sin(\theta) \tag{6.4-27}$$

Including the solids effect this gives:

$$i_{m,\theta} = i_{l,\theta} + (i_m - i_l) \cdot \cos(\theta) + R_{sd} \cdot C_{vs} \cdot \sin(\theta) \tag{6.4-28}$$

Using the relative solids effect, the relative excess hydraulic gradient, this can be written as:

$$i_{m,\theta} = i_{l,\theta} + E_{rhg} \cdot R_{sd} \cdot C_{vs} \cdot \cos(\theta) + R_{sd} \cdot C_{vs} \cdot \sin(\theta) \tag{6.4-29}$$

This can also be written as:

$$i_{m,\theta} = i_l + E_{rhg} \cdot R_{sd} \cdot C_{vs} \cdot \cos(\theta) + (1 + R_{sd} \cdot C_{vs}) \cdot \sin(\theta) \tag{6.4-30}$$

The relative excess hydraulic gradient of an inclined pipe is now:

$$E_{rhg,\theta} = \frac{i_{m,\theta} - i_{l,\theta}}{R_{sd} \cdot C_{vs}} = E_{rhg} \cdot \cos(\theta) + \sin(\theta) \tag{6.4-31}$$

This means that the hydraulic gradient of the mixture, excluding the potential energy term, decreases with the cosine of the inclination angle. Both for ascending and descending pipes. It is the question whether this is true for all flow regimes. Different flow regimes may respond differently to the pipe inclination angle. For a vertical pipe this would mean that the solids effect becomes zero, which is questionable. At least for very small particles, following the equivalent liquid model, it is expected that this will not change because of an inclination angle.

Durand & Condolios (1952) found a power of 3/2 for the cosine of the inclination angle.

6.4.4 The Zandi & Govatos (1967) Model.

Zandi and Govatos (1967) and later Zandi (1971) extended the work of Durand & Condolios (1952) and later Gibert (1960) to other solids and different mixtures. They used a computer and attempted to assess the validity of the Durand & Condolios (1952) correlation in respect of over 2500 data points from a number of sources, covering a wide range of values of all relevant parameters. They conclude that the Durand & Condolios (1952) expression is totally invalid for solids transported by saltation or sliding bed, although their published evidence (Figure 6.4-33) points in another direction. For heterogeneous transport they claim that the available data are more accurately correlated by two expressions (equations (6.4-34) and (6.4-35)).

They defined a non-dimensionless number to characterize the separation of the flow regime, from saltating/sliding bed to heterogeneous suspension:

$$N_{cr} = \frac{v_{ls}^2 \cdot \sqrt{C_D}}{g \cdot R_{sd} \cdot D_p \cdot C_{vt}} \tag{6.4-32}$$

They state that at a critical value of $N_{cr}=40$ the transition between a saltating and a heterogeneous regime occurs. This means that at values below 40 a saltating regime occurs and at values equal to or larger than 40 a heterogeneous flow develops. Babcock (1970) analyzed the work of Zandi & Govatos (1967) and concluded that for graded fine particles the transition already may occur at an index number of 10 instead of 40. Complex mixtures with particles of different sizes may increase the index number. No suggestions are offered for an improved correlation for the saltating/sliding bed flow regime.

Zandi & Govatos (1967) based their results on experiments (2500 data points) on sand with particles up to 25 mm, pipe diameters ranging from 0.0375 m to 0.55 m and volumetric concentrations up to 22%. They introduced a second index, which in fact is the Durand abscissa:

$$\psi = C_{vt} \cdot N_{cr} = \frac{v_{ls}^2 \cdot \sqrt{C_D}}{g \cdot R_{sd} \cdot D_p} :: \left(\frac{v_{ls}^2}{g \cdot D_p \cdot R_{sd}} \right) \cdot \sqrt{\frac{g \cdot d}{v_t^2}} = \left(\frac{v_{ls}^2}{g \cdot D_p \cdot R_{sd}} \right) \cdot \sqrt{C_x} \tag{6.4-33}$$

Zandi & Govatos (1967) use a modified Durand parameter with C_D instead of C_x. At a value of $\psi=10$ they found a dramatic change in behavior of the pressure losses. Below the value of $\psi=10$ for real heterogeneous transport they found:

$$\Delta p_m = \Delta p_l \cdot \left(1 + 280 \cdot \psi^{-1.93} \cdot C_{vt} \right) \tag{6.4-34}$$

Above the value of $\psi=10$ as a transition between heterogeneous and homogeneous transport they found:

$$\Delta p_m = \Delta p_l \cdot \left(1 + 6.3 \cdot \psi^{-0.354} \cdot C_{vt} \right) \tag{6.4-35}$$

Based on equation (6.4-33) $N_{cr}=40$, a Limit Deposit Velocity can be defined:

$$v_{ls,ldv} = \sqrt{\frac{40 \cdot g \cdot R_{sd} \cdot D_p \cdot C_{vt}}{\sqrt{C_D}}} \tag{6.4-36}$$

Figure 6.4-33 shows the Zandi & Govatos (1967) fit relations together with the Durand & Condolios (1952) and Gibert relation. From the measurements as shown in this figure it is not obvious which relation is the best and whether it should be straight lines. The intersection point where the equations (6.4-34) and (6.4-35) intersect is not exactly 10 but 11.1. This intersection point may be considered the transition between heterogeneous and pseudo homogeneous transport. The critical value of $N_{cr}=40$, above which the transport is supposed to be heterogeneous, is difficult to apply and does not match the 2 equations of Zandi & Govatos (1967).
The main value of the work of Zandi & Govatos (1967) lies in recognizing a criterion to differentiate between the saltating/sliding bed regime and the heterogeneous regime. The assertion that the data correlation of Durand & Condolios (1952) is invalid in the case of saltation/sliding bed transport, cannot be accepted based on the evidence

in Figure 6.4-33, where remarkably close grouping of the data points with N_{cr}<**40** is found, around the mean curve of Durand & Condolios (1952), from which their correlation was deduced.
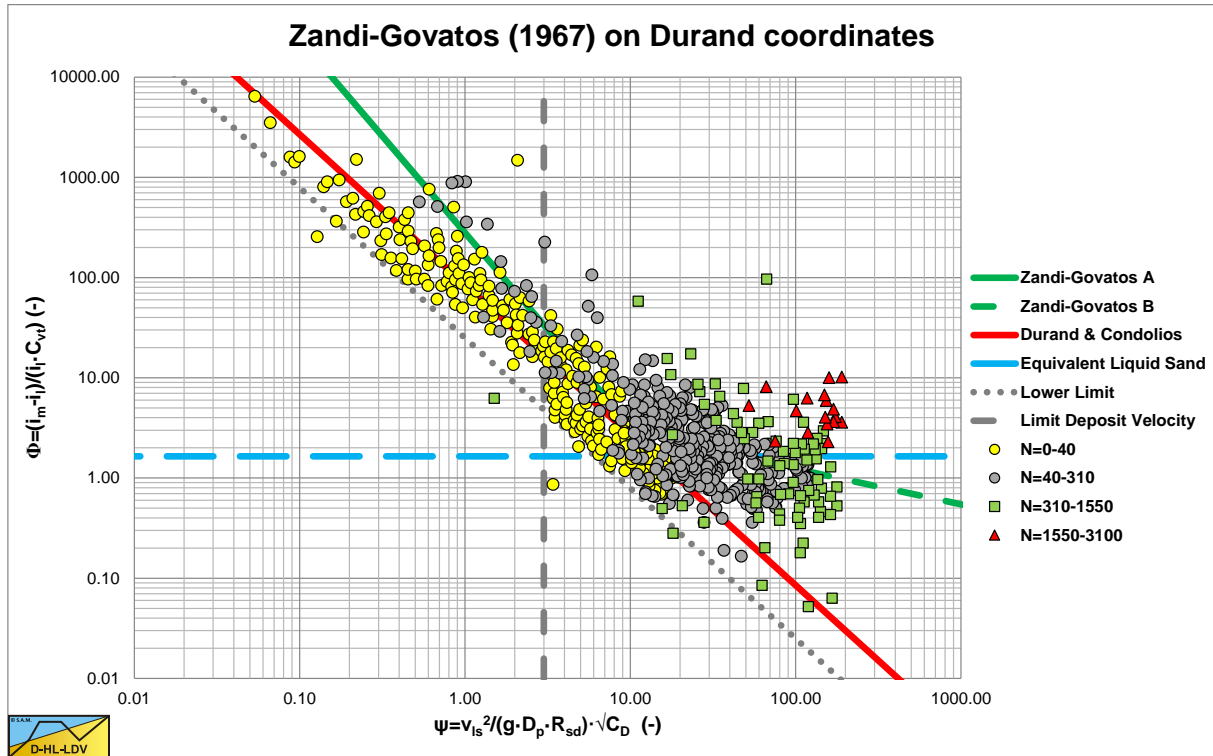
Figure 6.4-33: The Zandi & Govatos (1967) fits for heterogeneous slurry flow.

The data points are digitized from a graph of Wilson (1992) (Fig. 3.2) and are not too accurate. The tendencies however are clear. The horizontal coordinate is the modified Durand coordinate, including the submerged relative density. It should be noted that in the original graph, the Durand and the lower Zandi & Govatos (1967) lines were not drawn correctly. For the drag coefficient in the horizontal coordinate, the particle Froude number is assumed as used by Durand & Condolios (1952) & Gibert (1960). The Durand & Condolios (1952) and Gibert (1960) line is drawn with a constant of 85. The lower limit line has a constant of 25. The critical velocity line is the line for very coarse particles, having a particle Froude number of about 0.8, according to Durand & Condolios (1952) and Gibert (1960). Figure 6.4-33 & Figure 6.4-34 show the solutions of Durand & Condolios (1952) and Gibert (1960), Zandi & Govatos (1967) in a correct way. It seems like Zandi & Govatos (1967) focused on the **ψ** axis when they concluded a **ψ=10** is a transition between two physical processes. However they should have focused on the **Φ** axis where a **Φ= R$_{sd}$** represents the equivalent liquid model or pseudo homogeneous flow. It should also be noted that the power **M=1.7** for very narrow graded sands of Wilson et al. (1997), resulting in a power of **-3.7** of the line speed in the Durand coordinates, matches the power of **-1.93** of Zandi & Govatos (1967), resulting in a power of **-3.86** of the line speed in the Durand coordinates, closely.

Considering a Limit Deposit Velocity of (using the limit **F$_L$=1.34** for large particles):

$$v_{ls,ldv} = F_L \cdot \sqrt{2 \cdot g \cdot D_p \cdot R_{sd}} \approx 1.34 \cdot \sqrt{2 \cdot g \cdot D_p \cdot R_{sd}} \qquad \textbf{(6.4-37)}$$

And:

$$\psi = \frac{v_{ls,ldv}^2}{g \cdot D_p} \cdot \frac{\sqrt{C_x}}{R_{sd}} \qquad \textbf{(6.4-38)}$$

This gives:

$$\psi = \frac{F_L^2 \cdot 2 \cdot g \cdot D_p \cdot R_{sd}}{g \cdot D_p} \cdot \frac{\sqrt{C_x}}{R_{sd}} = 2 \cdot F_L^2 \cdot \sqrt{C_x} = 2 \cdot 1.34^2 \cdot 0.8 = 2.87 \tag{6.4-39}$$

For very fine particles, the particle Froude number may be near a value of 5, resulting in a ψ of almost 18 for sand. For coal with a relative submerged density of 0.4-0.6 the values can be higher.

It is remarkable that at the lower limit of the Limit Deposit Velocity of about 3, there is a sort of limit in the data points.

It should also be mentioned that the Durand & Condolios (1952) and Gibert (1960) line match data points in the heterogeneous regime, but also in the sliding bed/saltation regime. The two lines of Zandi & Govatos (1967) match the heterogeneous regime (upper line) and the transition heterogeneous/pseudo homogeneous (lower line). The fact that many points are below the pseudo homogeneous line for sand, has two reasons. First of all, the location of this line depends on the relative submerged density of the solids, so for coal it will be 0.4-0.6, while for aluminum it will be 2.65. The second reason is that in many cases there is some overshoot; higher velocities are required to reach the pseudo homogeneous regime.
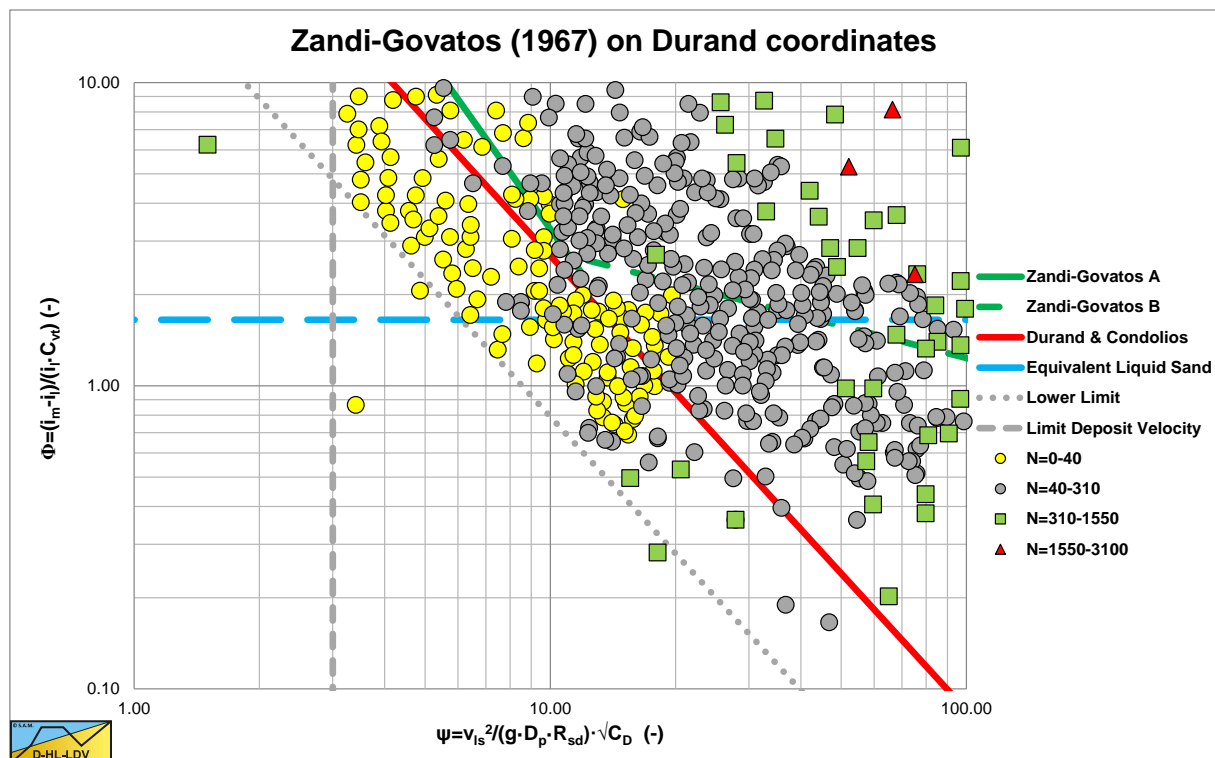
Figure 6.4-34: The Durand & Condolios (1952), Gibert (1960), and Zandi & Govatos (1967) solutions on Durand coordinates, zoomed.

Figure 6.4-35 and Figure 6.4-36 show the results of the DHLLDV Framework for 2 pipe diameters in the same coordinate system as Figure 6.4-33 and Figure 6.4-34 for particles with diameters ranging from 0.1 mm to 10 mm and pipes with diameters of 0.1524 m (6 inch) and 0.762 m 30 inch. The results of the DHLLDV Framework match the data in Figure 6.4-33 very well. It should be noted that Figure 6.4-33 also contains data points with different relative submerged densities, while the DHLLDV Framework here only contains curves for sand and gravel. For the 0.1524 m diameter pipe the curves are around the Durand & Condolios curve, which could be expected. For the 0.762 diameter pipe the curves are in general below the Durand & Condolios curve. Between an abscissa of 1 and 10 the steepness of the curves matches the Zandi & Govatos curve. The behavior of the curves above an abscissa of about 10 explains for the steepness of the Zandi & Govatos curve in that area. At low values of the abscissa the steepness of the curves is less than at values above 1. This is caused by the fact that at low values there is a sliding bed, while at high values the transport is heterogeneous and at values above about 10 the flow is homogeneous.

Excess hydraulic gradient Φ vs. Durand coordinate Ψ, C_{vt}=c.

Dp=0.1524 m, d=0.200 mm, Rsd=1.585, Cv=0.175, μsf=0.416
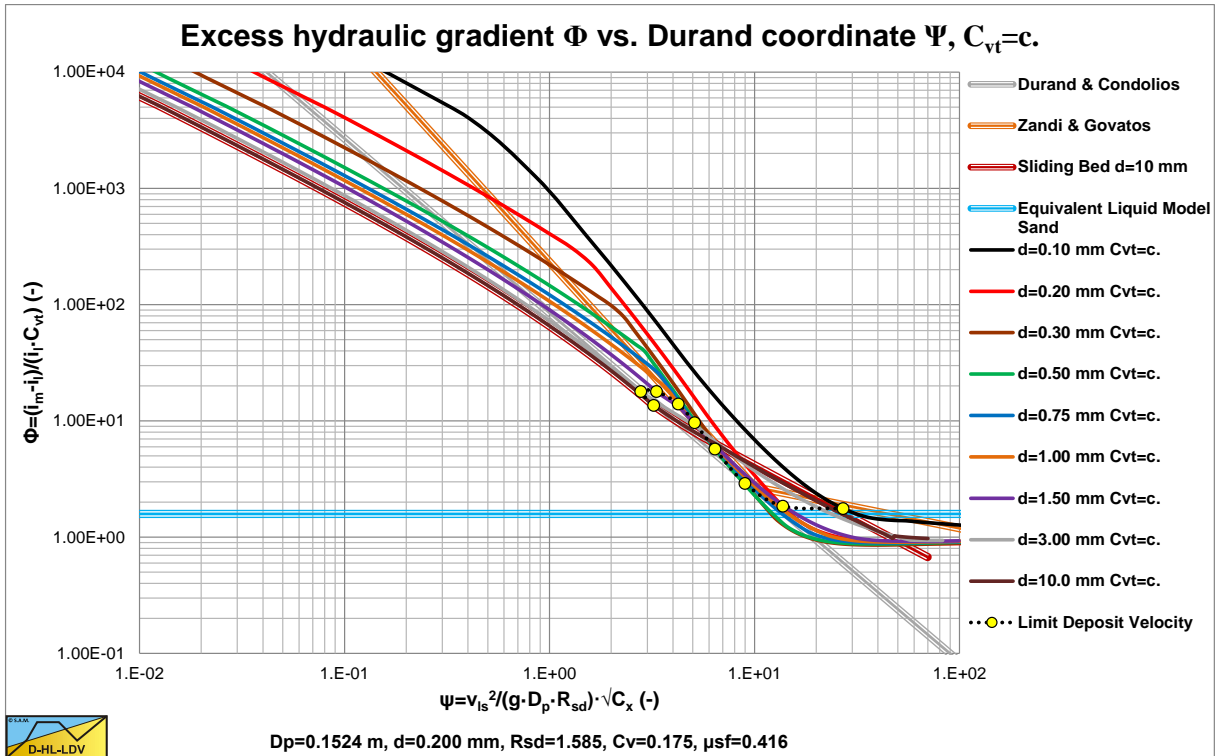
Figure 6.4-35: The DHLLDV Framework for a 0.1524 m diameter pipe.

Excess hydraulic gradient Φ vs. Durand coordinate Ψ, C_{vt}=c.

Dp=0.7620 m, d=0.200 mm, Rsd=1.585, Cv=0.175, μsf=0.416
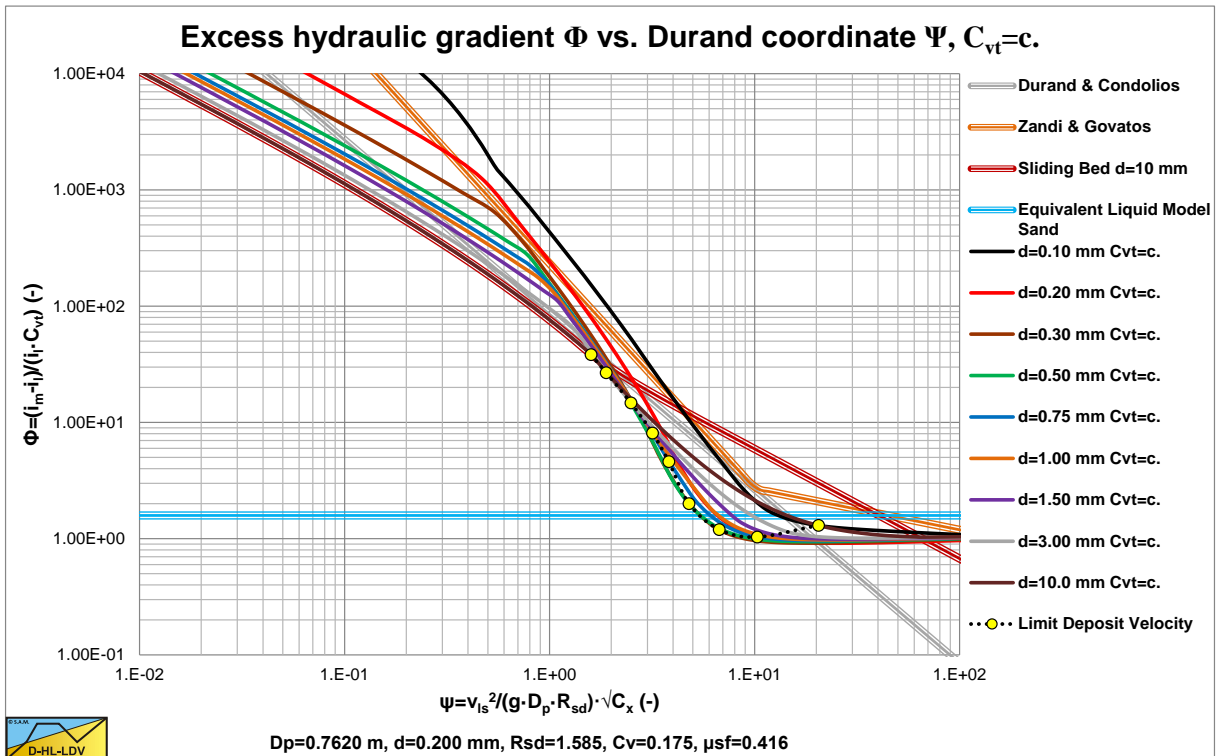
Figure 6.4-36: The DHLLDV Framework for a 0.762 m diameter pipe.

6.4.5 Issues Regarding the Durand & Condolios (1952) and Gibert (1960) Model.

There are 8 issues to be discussed:
1. The drag coefficient of Durand & Condolios (1952) versus the real drag coefficient.
2. The drag coefficient as applied by Worster & Denny (1955),
3. The drag coefficient of Gibert (1960).
4. The relative submerged density as part of the equation.
5. The graph of Zandi & Govatos (1967).
6. The F_L value as published by many authors.
7. The Darcy Weisbach friction coefficient λ_l.
8. The solids effect term in the hydraulic gradient equation.

6.4.5.1 The Drag Coefficient of Durand & Condolios (1952) vs. the Real Drag Coefficient.

It should be noted that Durand & Condolios (1952), Gibert (1960) and Worster & Denny (1955) use the particle Froude number in their equations and not the particle drag coefficient. The particle Froude number Fr_p is:

$$Fr_p = \frac{v_t}{\sqrt{g \cdot d}} \tag{6.4-40}$$

The virtual drag coefficient as used by Durand & Condolios (1952), Gibert (1960) and Worster & Denny (1955), is:

$$C_x = \frac{g \cdot d}{v_t^2} = Fr_p^{-2} \tag{6.4-41}$$

The drag coefficient C_D as used in the equation for the terminal settling velocity is:

$$v_t = \sqrt{\frac{4 \cdot g \cdot (\rho_s - \rho_l) \cdot d \cdot \psi}{3 \cdot \rho_l \cdot C_D}} = \sqrt{\frac{4 \cdot g \cdot R_{sd} \cdot d \cdot \psi}{3 \cdot C_D}} \quad \Rightarrow \quad C_D = \frac{4 \cdot R_{sd} \cdot \psi}{3} \cdot \frac{g \cdot d}{v_t^2} \tag{6.4-42}$$

$$Fr_p^2 = \frac{v_t^2}{g \cdot d} = \frac{4}{3} \cdot \frac{R_{sd} \cdot \psi}{C_D}$$

So the relation between the drag coefficient C_D and the virtual drag coefficient according to Durand and Condolios (1952) C_x is:

$$C_D = \frac{4 \cdot R_{sd} \cdot \psi}{3} \cdot C_x \quad \text{or} \quad \frac{1}{\sqrt{C_x}} = \frac{v_t}{\sqrt{g \cdot d}} = \sqrt{\frac{4 \cdot R_{sd} \cdot \psi}{3}} \cdot \frac{1}{\sqrt{C_D}} \tag{6.4-43}$$

For irregular shaped sand particles with a shape factor of $\psi=0.5$-0.7 and a relative submerged density of $R_{sd}=1.65$ this results in a drag coefficient almost equal to the Durand & Condolios (1952), Gibert (1960) and Worster coefficient. The term $\frac{4 \cdot R_{sd} \cdot \psi}{3} = 2.2 \cdot \psi$ is almost unity for a shape factor of $\psi=0.5$ and since it is used by its square root, the error is just 5%. However for spheres with $\psi=1.0$ this factor is 2.2 which cannot be neglected. For solids with another relative submerged density however, there may be a much bigger difference. Zandi & Govatos (1967) and many others also use the Durand & Condolios (1952), Gibert (1960) and Worster coefficient, although they name it C_D. It is often not clear whether authors used the C_D value or just named it C_D, using the C_x value. Since the error depends on both the shape factor ψ and the relative submerged density R_{sd}, the original particle Froude number Fr_p should be used, because the relation of Durand & Condolios (1952), matching their experiments is based on this particle Froude number.

6.4.5.2 The Drag Coefficient as Applied by Worster & Denny (1955).

Worster & Denny (1955) applied a drag coefficient of 0.4 (source Bain & Bonnington (1970)) to make his data match the Durand & Condolios (1952) equation. Whether this is the C_D or the C_x is not important, because the numerical value is given. A value of 0.4 however is too small for irregular shaped coal. Spheres have a C_D value of 0.445 for turbulent settling. Sand particles may have a value of about 1. So the value used by Worster & Denny is questionable.

6.4.5.3 The Drag Coefficient of Gibert (1960).

Gibert (1960) published a table with numerical values for the virtual drag coefficient or particle Froude number. If one uses the values of Gibert (1960), the whole discussion about whether the C_D or the C_x value should be used can be omitted. Analyzing this table however, shows that a very good approximation of the table values can be achieved by using the particle Froude number to the power 20/9 instead of the power 1, assuming that the terminal settling velocity v_t is determined correctly for the solids considered (Stokes, Budryck, Rittinger or Zanke).

$$\sqrt{C_{x,Gibert}} = \sqrt{C_x}^{-20/9}$$

(6.4-44)

Together with the correction of Gibert (1960), regarding the constant of 85/180, the equation now becomes:

$$\Delta p_m = \Delta p_l \cdot \left(1 + \Phi \cdot C_{vt}\right) \quad \text{with:} \quad \Phi = 85 \cdot \left(\frac{v_{ls}^2 \cdot C_x^{10/9}}{g \cdot D_p \cdot R_{sd}}\right)^{-3/2}$$

(6.4-45)

6.4.5.4 The Relative Submerged Density as Part of the Equation.

In a number of books and publications the relative submerged density R_{sd} is added to both the flow Froude number Fr_{fl} and the particle Froude number Fr_p. This, to enable the use of the equations for different types of solids. Gibert (1960) clearly states that the relative submerged density should only be added to the flow Froude number Fr_{fl} and not to the particle Froude number Fr_p, since it is already part of the terminal settling velocity v_t. Equations (6.4-41) and (6.4-45) are thus the final equations of the Durand & Condolios (1952) and Gibert (1960) model.

6.4.5.5 The Graph of Zandi & Govatos (1967).

The famous graph of Zandi & Govatos (1967) showing many data points on Φ-Ψ coordinates, is often incorrect. The lines of the Durand & Condolios (1952) equation and the line of pseudo homogeneous transport by Zandi & Govatos (1967) are reproduced incorrectly. Only the line of heterogeneous transport by Zandi & Govatos (1967) is correct. Probably this happened by copy paste, but it shows a wrong relation between the data points and the equations. Only in the book of Raudviki (1990) a correct graph is found. Raudviki also gives a good view on the location of the data points and the location of the equivalent liquid model for sand.

6.4.5.6 The F_L Value as Published by Many Authors.

The issue of the Limit Deposit Velocity Froude number F_L is of great importance. In their original publication, Durand & Condolios (1952) published 4 graphs showing the F_L value as a function of the volumetric transport concentration C_{vt} for the sands H2, L4, L6 and L8 (4 different particle diameters), these graphs are summarized in Figure 6.4-37. The Limit Deposit Velocity Froude number is defined as:

$$F_L = Fr_{ldv} = \frac{v_{ls,ldv}}{\sqrt{g \cdot D_p}}$$

(6.4-46)

Based on Figure 6.4-37 the relation between F_L and the particle diameter d can be derived at different concentrations, which is shown in Figure 6.4-38.
With some curve fitting and extrapolation the graph as published by Durand & Condolios (1952) was constructed. The graphs as shown here are directly constructed from the original data points, without curve fitting and/or

extrapolation. The graph as published has an asymptotic value for large particle diameters of about 1.9. Figure 6.4-22 shows a reconstruction of the original Durand & Condolios (1952) graph.
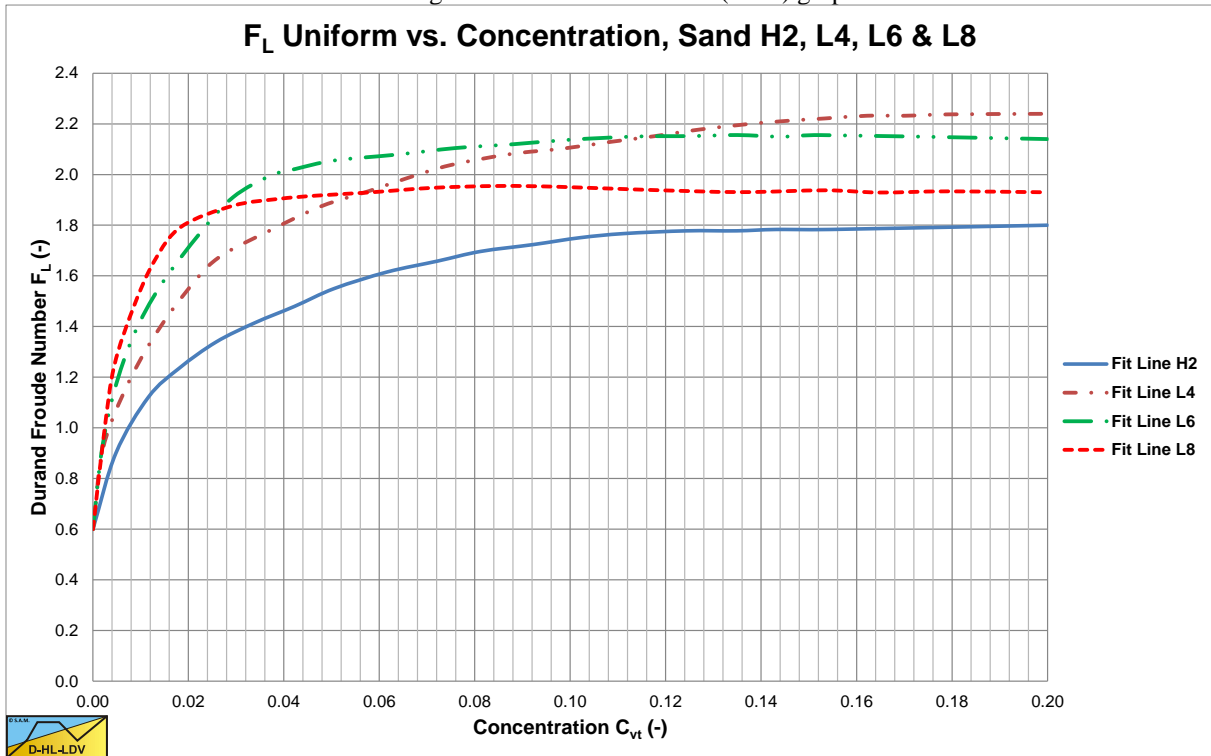
Figure 6.4-37: The trend lines of the F_L value as a function of the concentration.
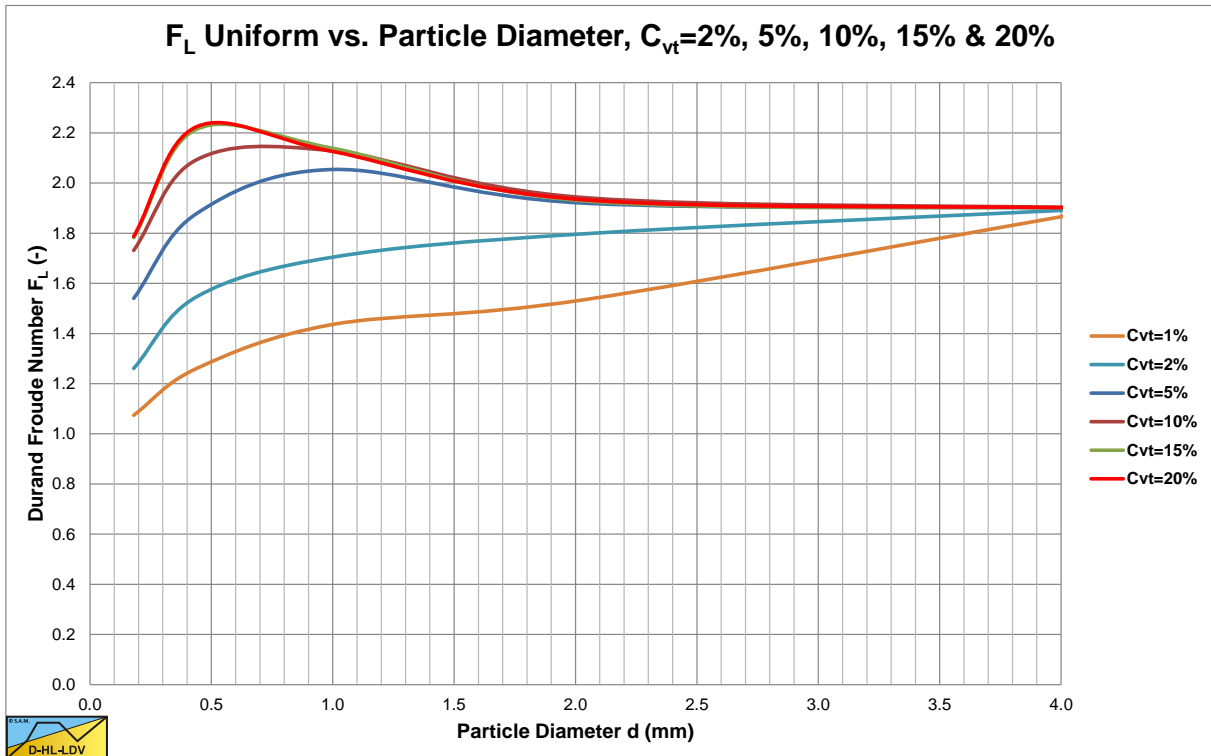
Figure 6.4-38: The trend lines of the F_L value as a function of the particle diameter.

Durand (1953) published his findings in the English language, while the original paper was in the French language. He modified the F_L coefficient, by including the relative submerged density and a factor 2, but he divided the vertical axis only by $\sqrt{2}$, resulting in an asymptotic value of 1.34. Since (probably) most authors of books and publications read the English paper from 1953, this graph was copied and can be found in almost every text book

about slurry transport. The vertical axis should have been divided by $\sqrt{2 \cdot R_{sd}}$ resulting in an asymptotic value of about 1.05, a difference of about 28% or the square root of 1.65.

Now which one of the graphs is correct? Based on LDV's reported by Durand & Condolios (1952) between 2.9 and 3.2 m/s for a 0.1524 diameter pipe, F_L values between 1.34 and 1.48 should be expected. So the conclusion is that the graph of Durand (1953) is the correct graph and in the graph of Durand & Condolios (1952) the data were already divided by the square root of 1.65. The correct graph is shown in Figure 6.4-24.

Later Durand & Condolios (1956) published a graph for non-uniform particle size distributions, where the original Durand & Condolios (1952) graph is considered to be for uniform particle size distributions. Figure 6.4-39 shows the graph of Condolios & Chapus. Figure 6.4-40 gives a comparison of the F_L value for uniform and non-uniform particle size distributions. The trends of uniform and non-uniform particle size distributions are the same, but non-uniform particle size distributions have, in general a much smaller F_L value, at the same d_{50}. This results in much smaller Limit Deposit Velocities. This does not seem to be reasonable. There is no physical explanation for example, why graded coarse particles would have a much lower LDV if they are mixed. The same limiting F_L value of about 1.34 would be expected if all individual particles have this value. An error of the square root of the relative submerged density could be the explanation. So the graph is corrected for the relative submerged density, while it shouldn't. Figure 6.4-41 shows the graph for non-uniform distributed particles corrected for the relative submerged density, while Figure 6.4-42 shows the comparison uniform versus non-uniform distributions. For coarse particles they give similar F_L values for concentrations of 15%-20%. For medium sized particles non-uniform distributed particles give smaller values, but still there is not too much difference. It is assumed in this book that Figure 6.4-42 is the correct graph.

Apparently the original data were determined with:

$$F_{L,original} = \frac{v_{ls,ldv}}{\sqrt{g \cdot D_p \cdot R_{sd}}} \tag{6.4-47}$$

Instead of:

$$F_{L,original} = \frac{v_{ls,ldv}}{\sqrt{g \cdot D_p}} \tag{6.4-48}$$

The final formulation is now:

$$F_L = F_{L,original} \cdot \frac{1}{\sqrt{2}} = \frac{v_{ls,ldv}}{\sqrt{2 \cdot g \cdot D_p \cdot R_{sd}}} \tag{6.4-49}$$

Instead of:

$$F_L = F_{L,original} \cdot \frac{1}{\sqrt{2 \cdot R_{sd}}} = \frac{v_{ls,ldv}}{\sqrt{2 \cdot g \cdot D_p \cdot R_{sd}}} \tag{6.4-50}$$
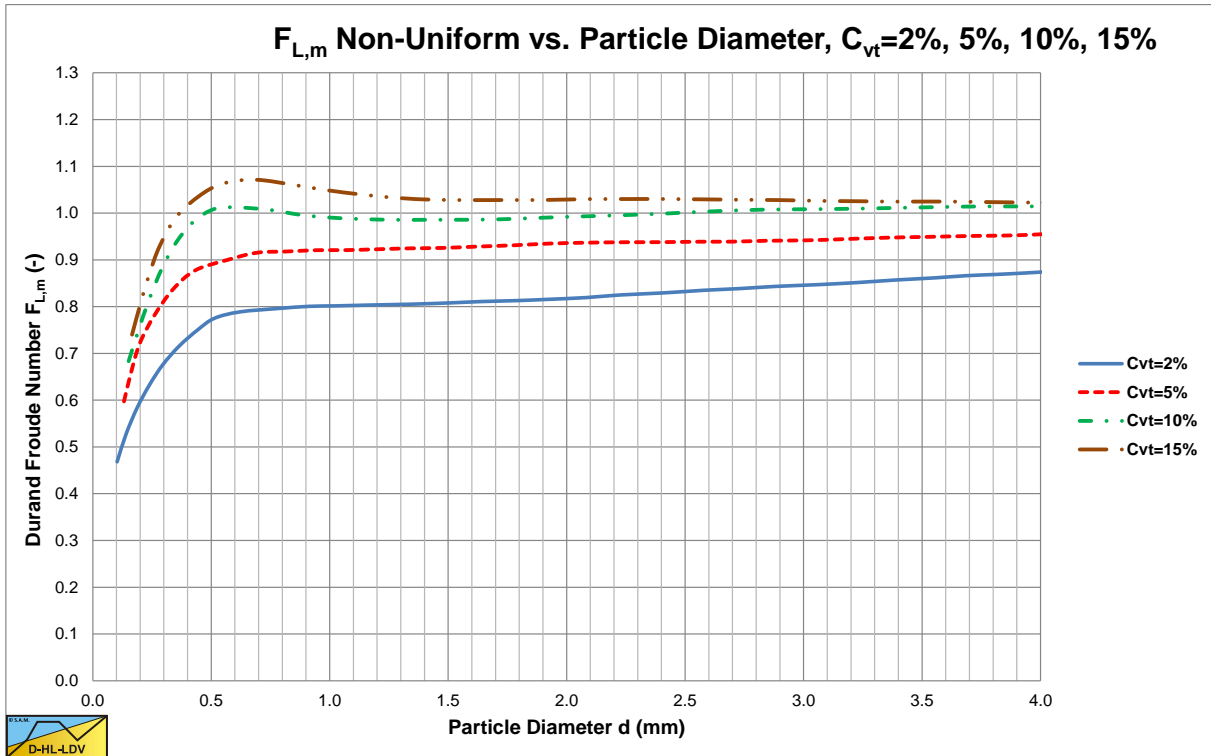
Figure 6.4-39: The trend lines of the F_L value as a function of the particle diameter for non-uniform distributions.
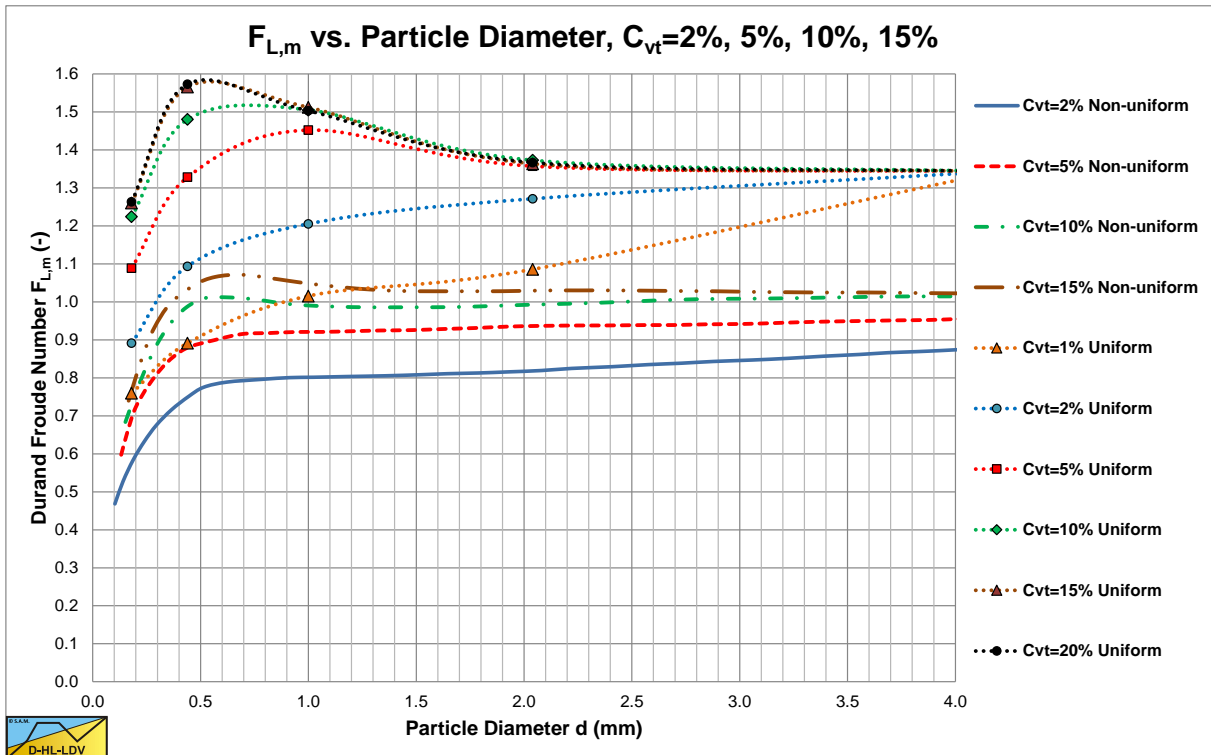
Figure 6.4-40: Comparing uniform and non-uniform distributions.
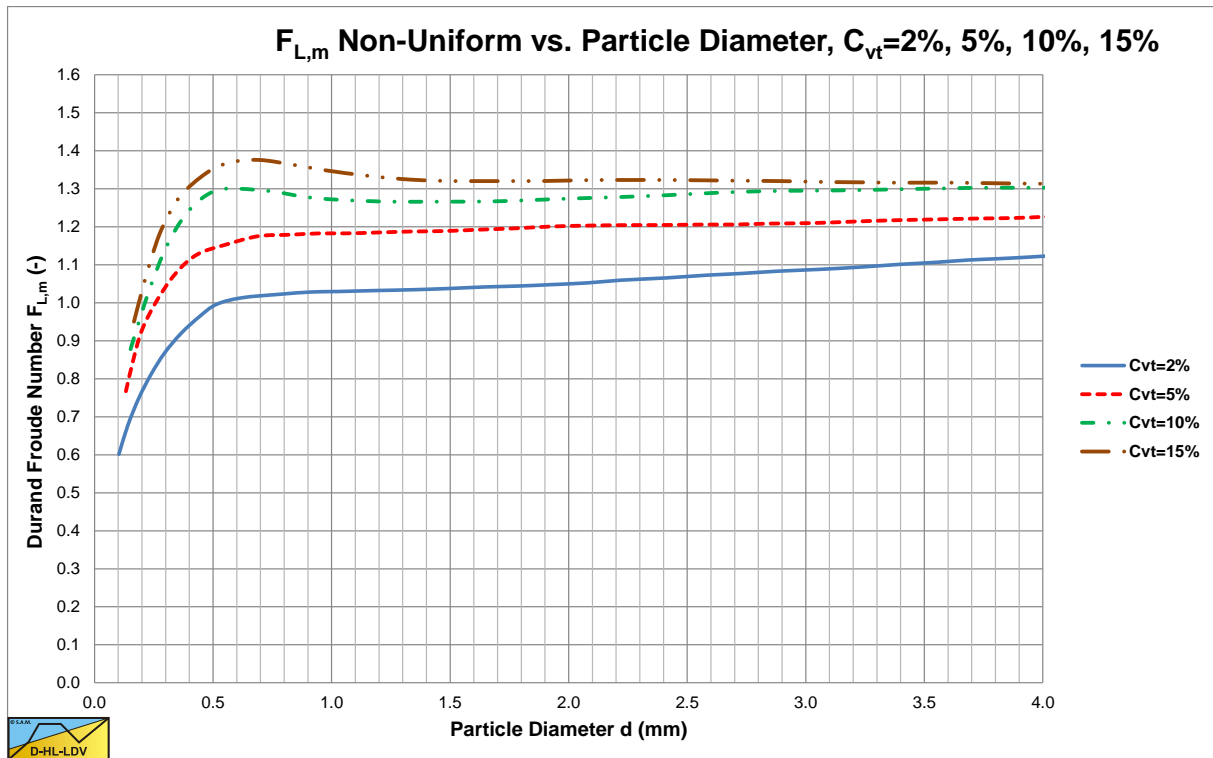
Figure 6.4-41: The trend lines of the F_L value as a function of the particle diameter for non-uniform distributions, modified.
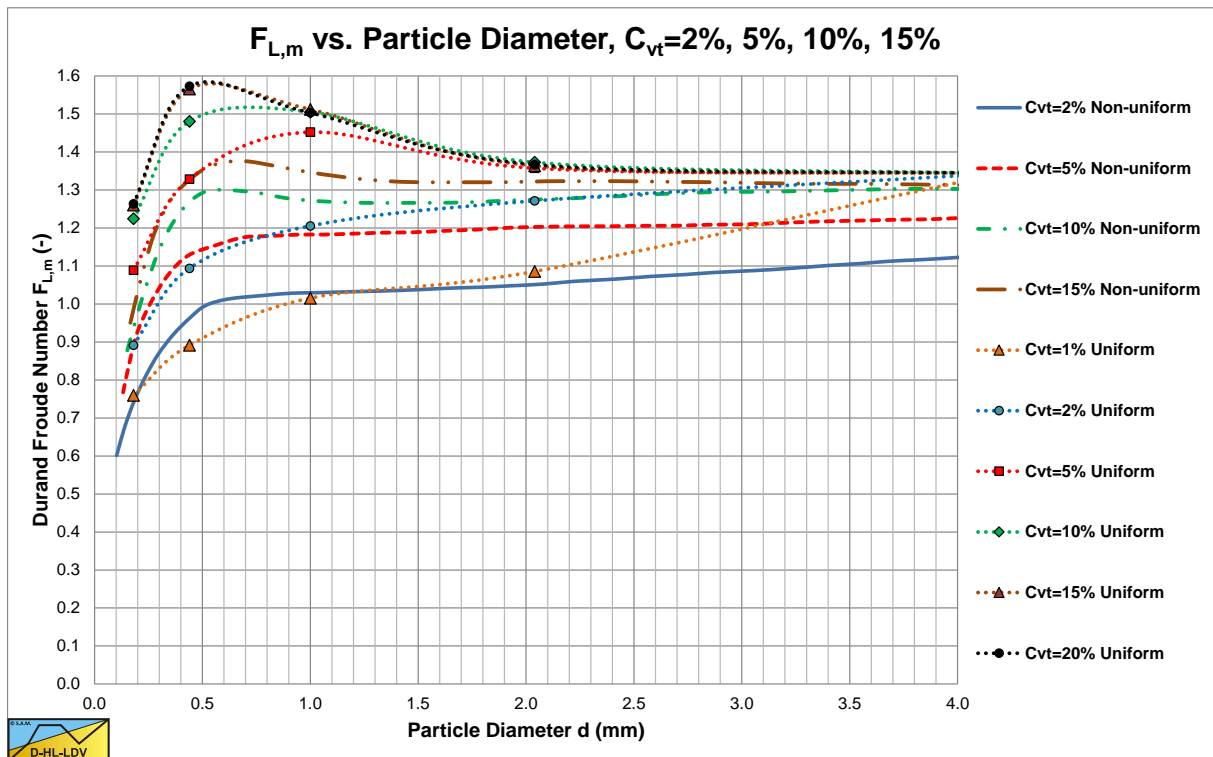
Figure 6.4-42: Comparing uniform and non-uniform distributions, modified.

6.4.5.7 The Darcy-Weisbach Friction Coefficient λ_l.

Many researchers use the following equation for the contribution of the solids to the pressure losses:

$$i_m = i_l \cdot \left(1 + \Phi \cdot C_{vt}\right) \tag{6.4-51}$$

Some other researchers disconnected the solids effect from the hydraulic gradient i_l, implying that the solids effect is independent from the hydraulic gradient, according to:

$$i_m = i_l + \Phi \cdot C_{vt} \tag{6.4-52}$$

Of course the formulation of Φ is different in both equations. Since the hydraulic gradient i_l depends strongly on the value of the friction coefficient λ_l, the formulation of equation (6.4-51) also depends strongly on the friction coefficient λ_l, while the formulation of equation (6.4-52) does not.

Since the friction coefficient λ_l may vary from about 0.01 for large smooth pipes (D_p=1 m) to about 0.04 for small smooth pipes (D_p=0.0254 m), a difference of a factor 4 may occur between both equations when extrapolating from a very small pipe in a laboratory to a large pipe in reality. Since most experiments are carried out in small to medium pipe diameters (D_p=0.0254 m to D_p=0.254 m), this should be taken into consideration. It is thus important to know whether the solids effect depends on the friction coefficient λ_l or not. If it does a formulation like equation (6.4-51) should be used, if it does not a formulation like equation (6.4-52) should be used. The Durand & Condolios (1952) equation in this form will look like:

$$i_m = i_l \cdot \left(1 + 85 \cdot \left(\frac{v_{ls}^2 \cdot C_x}{g \cdot D_p \cdot R_{sd}}\right)^{-3/2} \cdot C_{vt}\right)$$

$$\tag{6.4-53}$$

$$= i_l + 85 \cdot \frac{\lambda_l \cdot R_{sd}}{2} \cdot \left(\frac{v_{ls}^2}{g \cdot D_p \cdot R_{sd}}\right)^{2/2} \cdot \left(\frac{g \cdot D_p \cdot R_{sd}}{v_{ls}^2}\right)^{3/2} \cdot \left(\frac{1}{C_x}\right)^{3/2} \cdot C_{vt}$$

With R_{sd}=1.65 for sands and gravels this gives:

$$i_m = i_l + 70 \cdot \lambda_l \cdot \left(\frac{g \cdot D_p \cdot R_{sd}}{v_{ls}^2}\right)^{1/2} \cdot \left(\frac{1}{C_x}\right)^{3/2} \cdot C_{vt} \tag{6.4-54}$$

This last equation will give the same results as the original equation for sands and gravels. For pipe diameters from D_p=0.0254 m to D_p=1 m, the friction factor λ_l decreases about the same factor as the increase of the square root of the pipe diameter D_p, meaning that the excess pressure losses are almost independent of the pipe diameter D_p.

6.4.5.8 The Solids Effect Term in the Hydraulic Gradient Equation.

In both equations (6.4-51) and (6.4-52), the solids effect is incorporated as one term Φ. This term often consists of a one term equation, often based on Froude numbers. Now the question is whether the solids effect can be described physically by a one term equation. It is very well possible that the solids effect depends on a number of different physical phenomena, each with its own term in the equation. Using just one term may force the curve fit equations, as used by most researchers, into a low correlation equation, just because a one term equation does not describe the processes involved accurately. Using Froude numbers forces the fit equation in a fixed ratio between a number of parameters involved. The flow Froude number forces a fixed ratio between the line speed and the pipe diameter, while the particle Froude number forces a fixed ratio between the terminal settling velocity and the particle diameter. Using an equation for the solids effect with more than one term, without fixing certain ratio's, would probably give a better correlation with the experimental data.

6.5 The Newitt et al. (1955) Model.

Newitt et al. (1955) carried out experiments in a 1 inch pipe with sands of 0.0965 mm, 0.203 mm, 0.762 mm and gravel of 4.5 mm. They also carried out experiments with gravel of 3.2-6.4 mm, coal of 3.2-4.8 mm ($\mathbf{R_{sd}}$ =0.4) and MnO2 of 1.6-3.2 mm ($\mathbf{R_{sd}}$ =3.1). Newitt et al. (1955) distinguished a heterogeneous regime and a sliding bed regime.

6.5.1 The Heterogeneous Regime.

For the heterogeneous regime they assumed that the energy loss due to the solids is based on keeping the particles floating. In other words, due to gravity the particles will move down continuously and the energy required moving them up, the potential energy, results in an excess pressure loss. Based on the conservation of potential energy of the particles the following equation is derived:

$$\Delta p_m = \Delta p_l \cdot \left(1 + K_1 \cdot \left(g \cdot D_p \cdot R_{sd} \right) \cdot v_t \cdot C_{vt} \cdot \left(\frac{1}{v_{ls}} \right)^3 \right)$$

(6.5-1)

$$K_1 = 1100$$

The coefficient $\mathbf{K_1}$**=1100** does not follow from the derivation, but from a best fit of the data points as is shown in Figure 6.5-1. A coefficient based on the potential energy derivation would have a value of around 200. Newitt at al. (1955) state that the process of keeping the particles in suspension is not very efficient, resulting in a much larger coefficient. A factor 5-6 larger would imply an efficiency of 16%-20% which is very low. Newitt et al. (1955) did not take into consideration the loss of kinetic energy due to the collisions during heterogeneous transport. This would give a second term for the excess pressure losses. The data points follow the Newitt et al. (1955) curve reasonably in Figure 6.5-1, although a power of the line speed of less than -3 would give a better fit. For sand, 3 Durand & Condolios (1952) curves are drawn. It is clear that the data points of Newitt et al. (1955) are all above the Durand & Condolios (1952) curves. It is very well possible that the sheet flow has occurred, due to the high hydraulic gradients in such a small pipe (1 inch). For all 3 materials some data points are below the equivalent liquid lines, meaning that the hydraulic gradient is in between the water line and the equivalent liquid line. Now Newitt et al. (1955) carried out their experiments using a 1 inch pipe. In a 1 inch pipe, normally, higher friction coefficients are encountered compared to large pipes as applied in dredging. In a $\mathbf{D_p}$**=1 inch** pipe a friction coefficient of $\mathbf{\lambda_l}$**=0.02** is common, while in a $\mathbf{D_p}$**=1 m** pipe a $\mathbf{\lambda_l}$**=0.01** would be expected. The difference is a factor 2. Since the Newitt et al. (1955) is based on supplying enough potential energy to keep the particles in suspension, the solids effect should not depend on the viscous liquid friction. In a large diameter pipe with much less liquid friction, the solids effect should be the same as in a small diameter pipe. In order to achieve this, equation (6.5-1) will be written in a more general form.

Equation (6.5-1) in a more general form:

$$\Delta p_m = \Delta p_l \cdot \left(1 + \left(\frac{\lambda_l \cdot K_1}{2} \right) \cdot \frac{2 \cdot \left(g \cdot D_p \cdot R_{sd} \right) \cdot v_t}{\lambda_l} \cdot C_{vl} \cdot \left(\frac{1}{v_{ls}} \right)^3 \right)$$

With : λ_l **=0.02** and $K_1 = 1100$ this gives:

(6.5-2)

$$\Delta p_m = \Delta p_l \cdot \left(1 + 11 \cdot \frac{2 \cdot \left(g \cdot D_p \cdot R_{sd} \right) \cdot v_t}{\lambda_l} \cdot C_{vt} \cdot \left(\frac{1}{v_{ls}} \right)^3 \right)$$

$$= \Delta p_l \cdot 1 + \Delta p_l \cdot 11 \cdot \frac{2 \cdot \left(g \cdot D_p \cdot R_{sd} \right) \cdot v_t}{\lambda_l} \cdot C_{vt} \cdot \left(\frac{1}{v_{ls}} \right)^3 = \Delta p_l + 11 \cdot \frac{g \cdot \rho_l \cdot R_{sd} \cdot v_t}{v_{ls}} \cdot C_{vt}$$
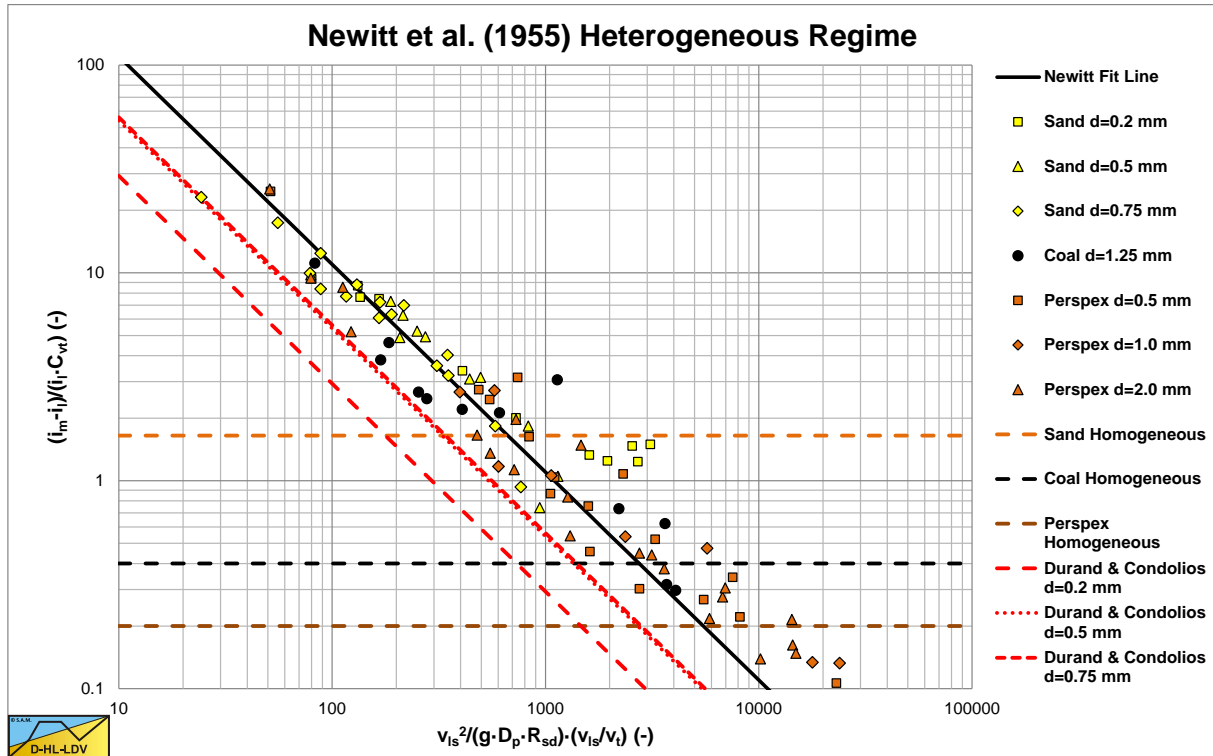
Figure 6.5-1: Correlation for particles travelling as a heterogeneous suspension.

It should be noted that, although the derivation of Newitt et al. (1955) is based on the settling velocity of the particles, hindered settling is not considered. It should also be noted that very small pipe diameters give very high hydraulic gradients, often leading to a sliding bed regime or heterogeneous and (pseudo) homogeneous transport. The Limit Deposit Velocity in such a case is based on the transition between a sliding bed and heterogeneous transport. At much larger pipe diameter, with much smaller hydraulic gradients, the Limit Deposit Velocity is based on the transition between a stationary bed and heterogeneous transport.

6.5.2 The Sliding Bed Regime.

For the sliding bed regime Newitt et al. (1955) assumed that the weight of all the solids is transferred to the pipe bottom, resulting in a friction force, which is equal to the weight of the solids $\rho_l \cdot g \cdot R_{sd} \cdot C_{vt}$ times a friction coefficient μ. They carried out experiments with gravel of 3.2-6.4 mm, coal of 3.2-4.8 mm ($R_{sd} = 0.4$) and MnO2 of 1.6-3.2 mm ($R_{sd} = 3.1$). Figure 6.5-2 and Figure 6.5-3 show the results of these experiments, Figure 6.5-3 with a new coordinate on the vertical axis $(i_m - i_l)/(R_{sd} \cdot C_{vt})$. The advantage of this parameter is that for a sliding bed it gives the friction coefficient μ_{sf} directly.

Below the Limit Deposit Velocity Newitt et al. (1955) found for a sliding bed:

$$\Delta p_m = \Delta p_l \cdot \left(1 + K_2 \cdot \left(g \cdot D_p \cdot R_{sd} \right) \cdot C_{vt} \cdot \left(\frac{1}{v_{ls}} \right)^2 \right)$$

(6.5-3)

$$K_2 = 66$$

Newitt et al. (1955) considered a sliding bed with a friction coefficient of $\mu_{sf} = 0.8$, but an analysis of the data points shows a decreasing tendency with increasing line speed. This matches the constant volumetric transport concentration model, which seems to be applied by Newitt et al. (1955). Friction coefficients of 0.35-0.7 have to be used to make the data points match the theory. The different materials have different friction coefficients. A better average of the friction coefficient would be $\mu_{sf} = 0.66$, matching a friction factor $\lambda_l = 0.02$ and $K_2 = 66$.

Since Newitt et al. (1955) considered the solids effect to be the result of sliding friction, this solids effect should not depend on the viscous friction, although equation (6.5-3) implies this. In a $D_p = 1$ inch pipe a friction coefficient of $\lambda_l = 0.02$ is common, while in a $D_p = 1$ m pipe a $\lambda_l = 0.01$ would be expected. The difference is at least a factor 2.

In a large diameter pipe with much less liquid friction, the solids effect should be the same as in a small diameter pipe. In order to achieve this, equation (6.5-3) will be written in a more general form.
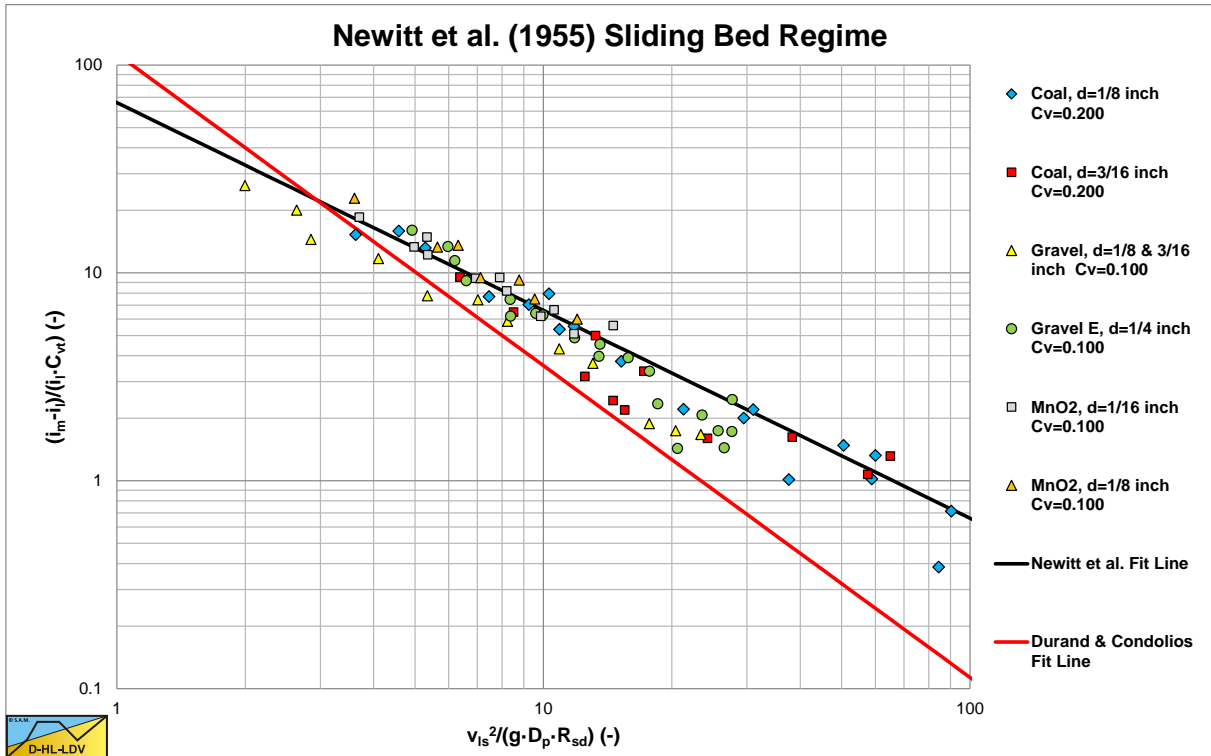
Figure 6.5-2: Correlation for large particles travelling as a sliding bed.
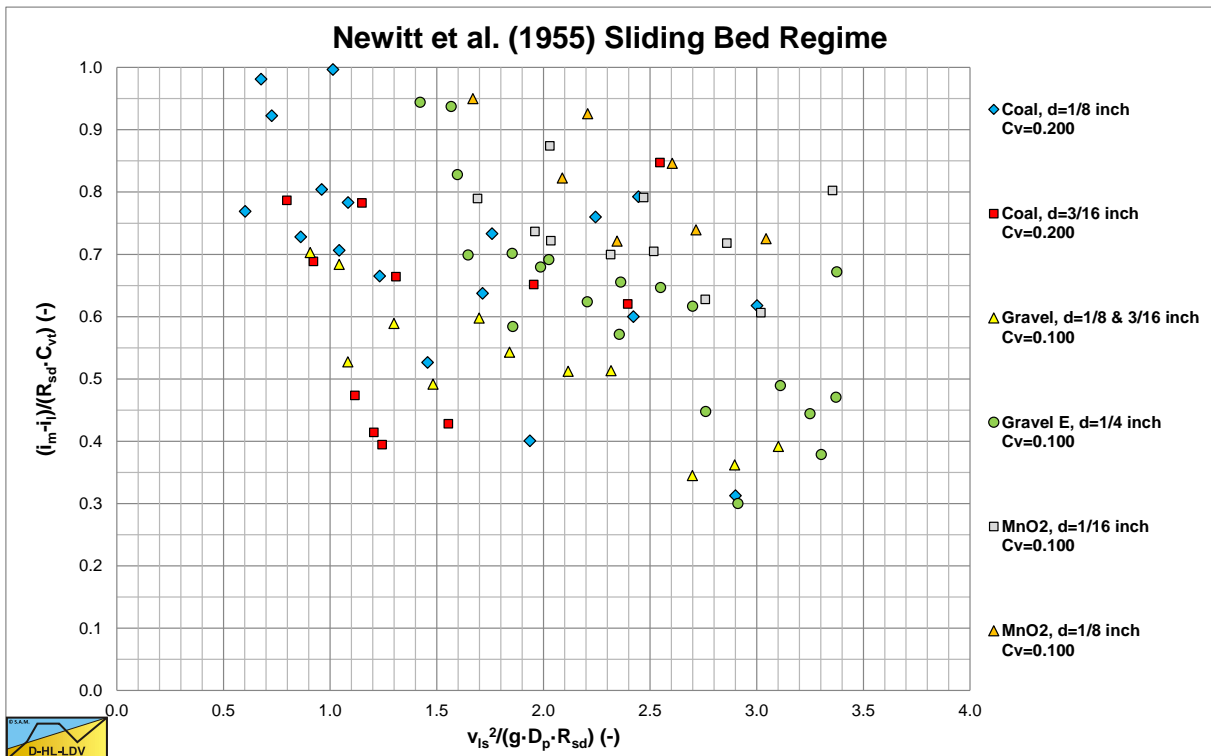
Figure 6.5-3: Large particles travelling in saltation or as a sliding bed.

Equation (6.5-3) in a more general form:

$$\Delta p_m = \Delta p_l \cdot \left(1 + \left(\frac{\lambda_l \cdot K_2}{2} \right) \cdot \frac{2 \cdot \left(g \cdot D_p \cdot R_{sd} \right)}{\lambda_l} \cdot C_{vt} \cdot \left(\frac{1}{v_{ls}} \right)^2 \right)$$

With : $\lambda_l = 0.02$ **and** $K_2 = 66$ **this gives:**

(6.5-4)

$$\Delta p_m = \Delta p_l \cdot \left(1 + 0.66 \cdot \frac{2 \cdot \left(g \cdot D_p \cdot R_{sd} \right)}{\lambda_l} \cdot C_{vt} \cdot \left(\frac{1}{v_{ls}} \right)^2 \right)$$

$$\Delta p_m = \Delta p_l + 0.66 \cdot g \cdot \rho_l \cdot R_{sd} \cdot C_{vt}$$

Note that the 2nd term between the brackets leads to a constant pressure loss independent of the line speed. The friction coefficient of 0.66 of course depends on the type of solids transported.

In the original graph of Newitt et al. (1955), Figure 6.5-2, the Durand & Condolios (1952) curve is incorrect, having the wrong slope (power). Most data points are below the Newitt et al. (1955) approximation for a sliding bed. A line with a steeper slope, so a higher power of the ($1/v_{ls}$) term would give a better fit. This matches the constant volumetric transport concentration behavior.

6.5.3 The Limit Deposit Velocity.

The Limit Deposit Velocity is often defined as the velocity below which the first particles start to settle and a bed will be formed at the bottom of the pipe. Often this Limit Deposit Velocity is a bit smaller than the minimum velocity, which is at a pressure of 3 times the water resistance.

In Hydraulic Engineering it is assumed that particles stay in suspension when the so called friction velocity equals the settling velocity of the particles, giving:

$$u_* \geq v_t \tag{6.5-5}$$

At the minimum resistance velocity this gives:

$$u_*^2 = 3 \cdot \frac{\lambda_l}{8} \cdot v_{ls,ldv}^2 \tag{6.5-6}$$

Or (with $\lambda = 0.01$):

$$v_{ls,ldv} = \sqrt{\frac{8}{3 \cdot \lambda_l}} \cdot v_t \approx 16.33 \cdot v_t \tag{6.5-7}$$

The Limit Deposit Velocity found matches the findings of Newitt et al. (1955). Including the effect of hindered settling, this would result in a decreasing Limit Deposit Velocity with an increasing concentration, according to:

$$v_{ls,ldv} = \sqrt{\frac{8}{3 \cdot \lambda_l}} \cdot v_t \cdot \left(1 - C_{vt} \right)^\beta \approx 16.33 \cdot v_t \cdot \left(1 - C_{vt} \right)^\beta \tag{6.5-8}$$

Newitt et al. (1955) used the following simple equation for the Limit Deposit Velocity:

$$\frac{i_m - i_l}{i_l \cdot C_{vt}} = 1100 \cdot \frac{g \cdot R_{sd} \cdot D_p}{v_{ls,ldv}^2} \cdot \frac{v_t}{v_{ls,ldv}} = 66 \cdot \frac{g \cdot R_{sd} \cdot D_p}{v_{ls,ldv}^2}$$

(6.5-9)

$$\Rightarrow v_{ls,ldv} = 16.67 \cdot v_t$$

Newitt et al. (1955) assume that the transition between a sliding bed/saltation on one hand and a stationary bed on the other hand follow the well-known Durand & Condolios (1952) equation:

$$v_{ls,ldv} = F_L \cdot \sqrt{2 \cdot g \cdot D_p \cdot R_{sd}}$$

(6.5-10)

The factor F_L can be found in the graph published by Durand & Condolios (1952) or by using equation (6.4-20). Newitt et al. (1955) used the graph of Durand (1953) with the factor F_L=1.34 for large particles.

6.5.4 The Transition Heterogeneous vs. (Pseudo) Homogeneous Transport.

Newitt et al. (1955) found that the relative excess hydraulic gradient for (pseudo) homogeneous transport is not exactly the water resistance with the mixture density substituted for the water (liquid) density, but about 60% of the extra resistance, giving:

$$\frac{i_m - i_l}{i_l \cdot C_{vt}} = 0.6 \cdot R_{sd}$$

$$\frac{i_m - i_l}{i_l \cdot C_{vt}} = 1100 \cdot \frac{g \cdot R_{sd} \cdot D_p}{v_{ls,ldv}^2} \cdot \frac{v_t}{v_{ls,ldv}} = 0.6 \cdot R_{sd}$$

(6.5-11)

$$\Rightarrow v_{ls,h=h} = \sqrt[3]{1833 \cdot g \cdot D_p \cdot v_t}$$

6.5.5 Regime Diagrams.

Based on the different transition velocities of Newitt et al. (1955) and the equation for the terminal settling velocity of Zanke (1977), the regime diagram of Newitt et al. (1955) has been reconstructed, see Figure 6.5-4. Now there are 3 issues regarding the equations of Newitt et al. (1955). The first issue is the issue of the error with the F_L graph of Durand & Condolios (1952). The value for large particles should not be 1.34, but about 1.05 and corrected by a factor of 1.1 according to Gibert (1960). The second issue is that it is the question whether for homogeneous transport 60% of the solids weight should be applied, or the full 100%. Here 100% is applied. The third issue is the construction of the regime graph. The curves found by applying the equations, do not exactly match the curves of Newitt et al. (1955), but then in 1955 computers were not yet available. It should be noted that these regime diagrams do not incorporate the influence of the volumetric concentration. The regime diagrams of Newitt et al. (1955) however give a good impression of the different regimes and the transitions between the different regimes.

- For very small particles there will be a transition from a stationary bed to homogeneous flow directly.
- For small particles there will be a transition from a stationary bed to heterogeneous flow to homogeneous flow. For medium sized particles there will be a transition from a stationary bed to a moving bed to heterogeneous flow to homogeneous flow.
- For very large particles there will be a transition from a stationary bed to a moving bed to homogeneous flow directly.

Of course, this depends on the pipe diameter and the concentration. Especially the pipe diameter is playing a very big role in the location of the different transition lines. Figure 6.5-5 shows the regime diagram based on the equations derived here.
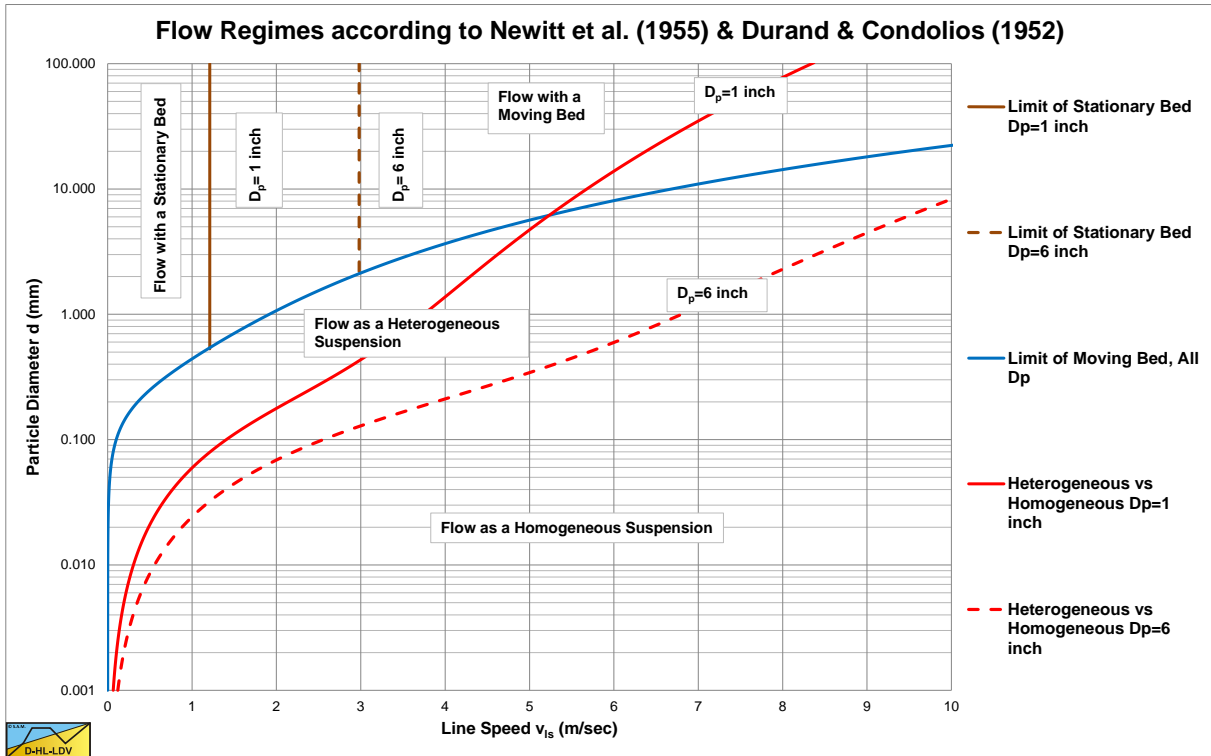
Figure 6.5-4: Flow regimes according to Newitt et al. (1955).
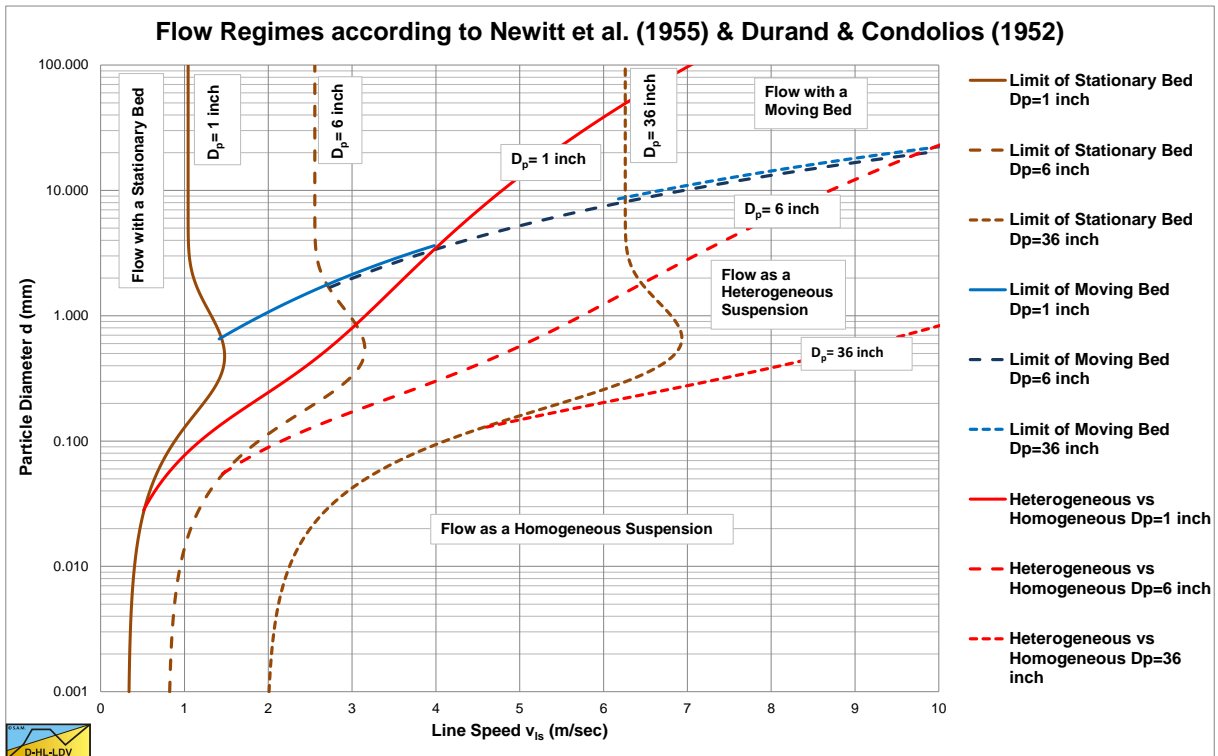
Figure 6.5-5: Flow regimes according to Durand & Condolios (1952) and Newitt et al. (1955), modified.
(Captions for the 36 inch pipe diameter, C$_v$=0.15).

6.5.6 Experiments.
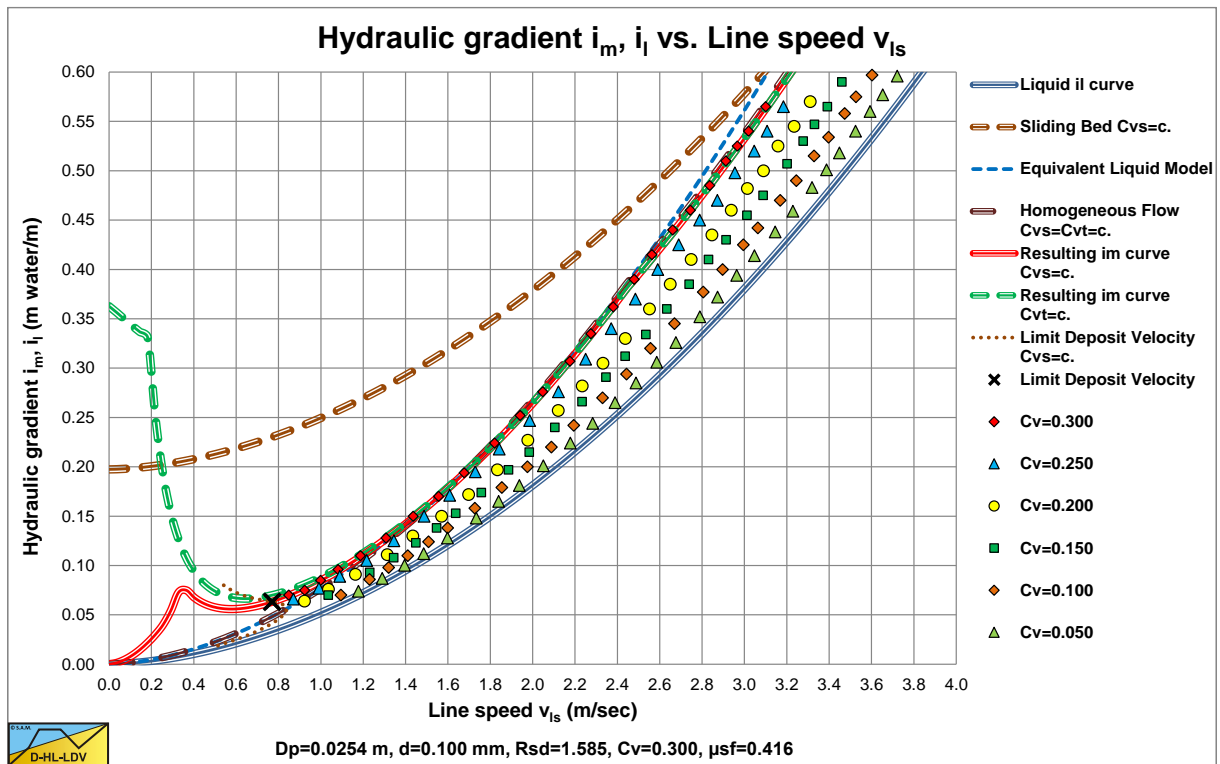
Figure 6.5-6: The hydraulic gradient sand B.
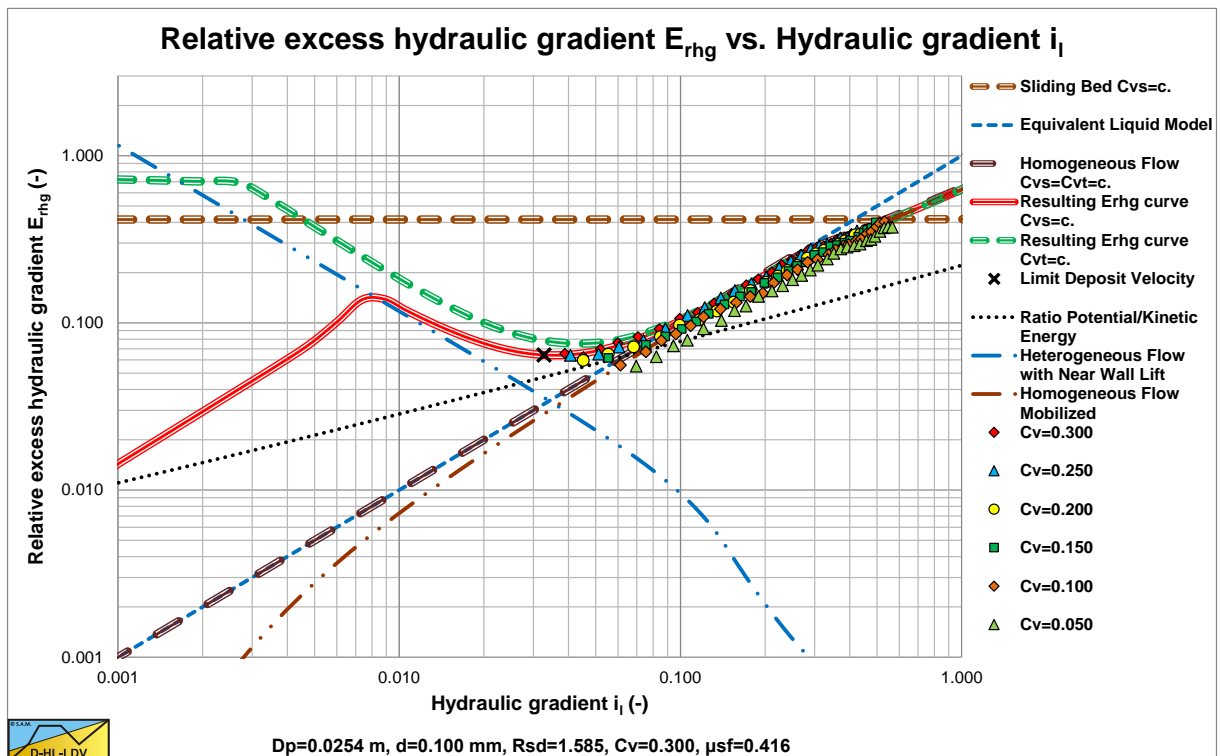
Figure 6.5-7: The relative excess hydraulic gradient Sand B.

Figure 6.5-6 and Figure 6.5-7 show the digitized fit lines for sand B in the hydraulic gradient versus line speed graph and the relative excess hydraulic gradient versus liquid hydraulic gradient graph. Sand B behaves according to the Equivalent Liquid Model.
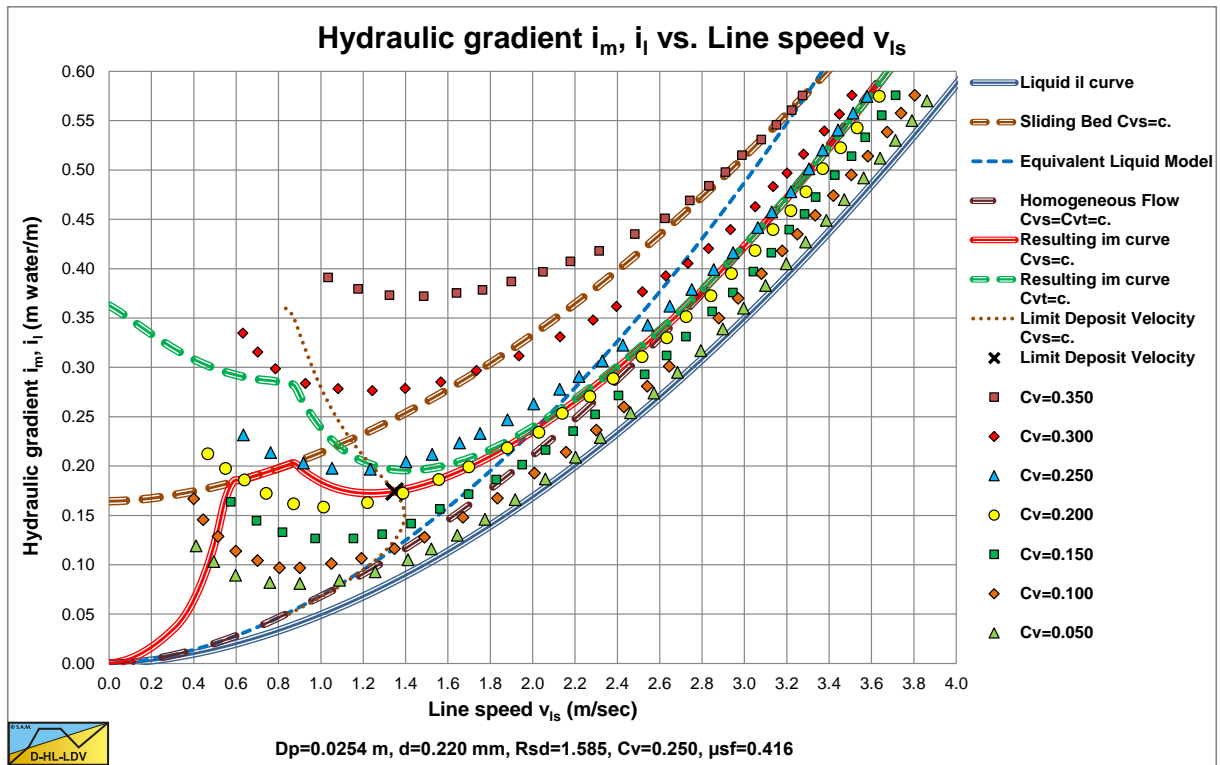
Figure 6.5-8: The hydraulic gradient sand C.
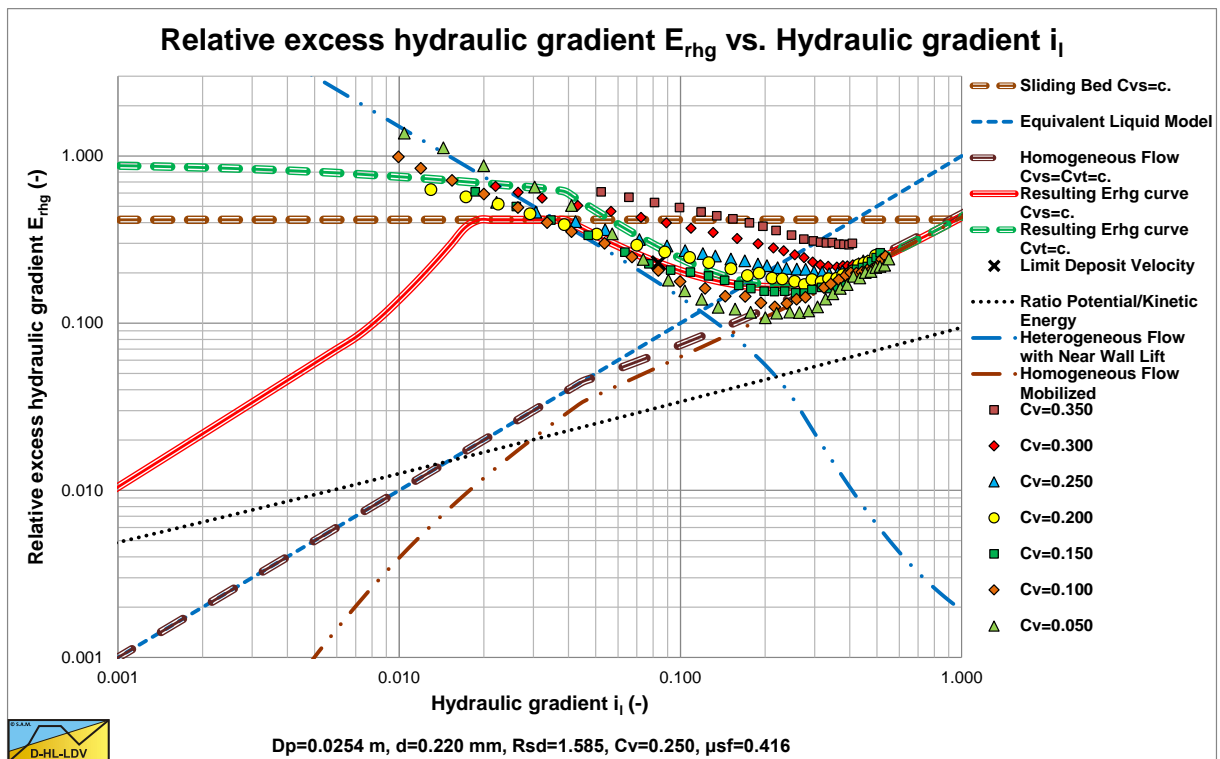
Figure 6.5-9: The relative excess hydraulic gradient Sand C.

Figure 6.5-8 and Figure 6.5-9 show the digitized fit lines for sand B in the hydraulic gradient versus line speed graph and the relative excess hydraulic gradient versus liquid hydraulic gradient graph. Sand C behaves according to the sliding bed regimes at low lines speeds, the heterogeneous flow regime at medium line speeds and the homogeneous flow regime at high line speeds. Up to concentrations of 25% it matches the heterogeneous-homogeneous behavior. The concentrations of 30% and 35% give higher values, possibly due to sliding flow behavior.
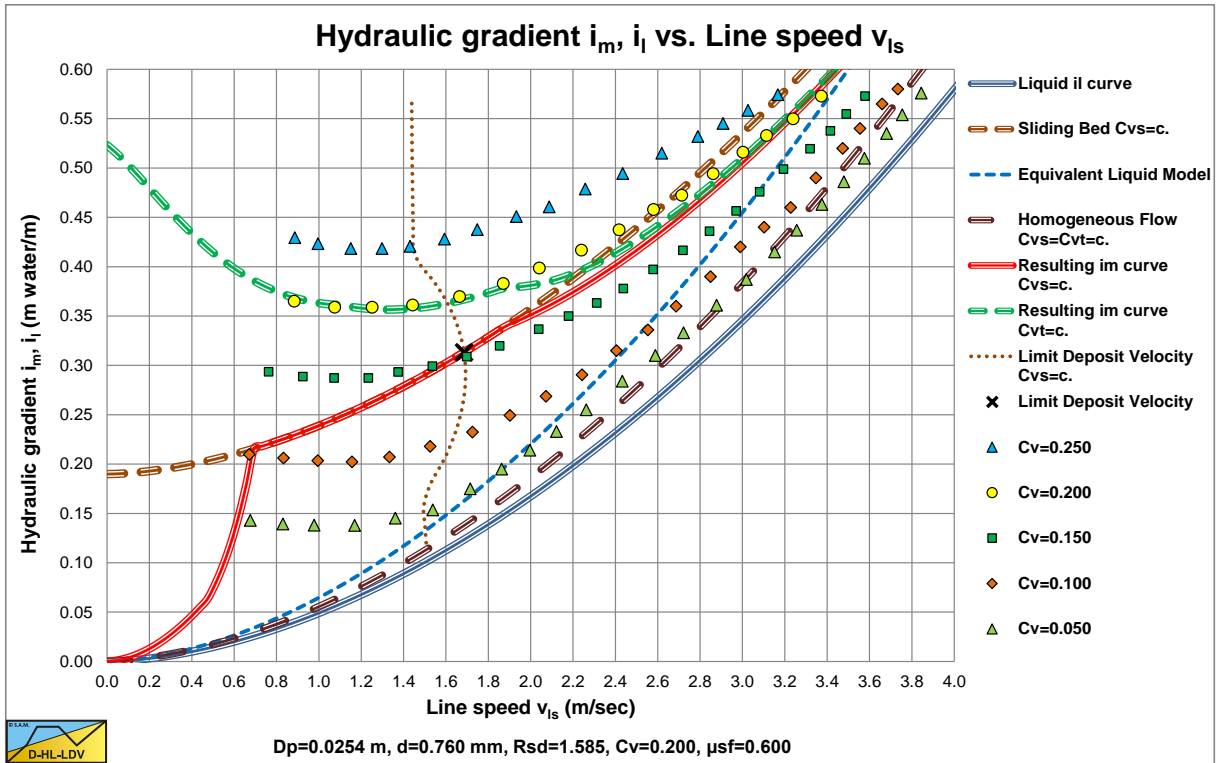
Figure 6.5-10: The hydraulic gradient sand D.
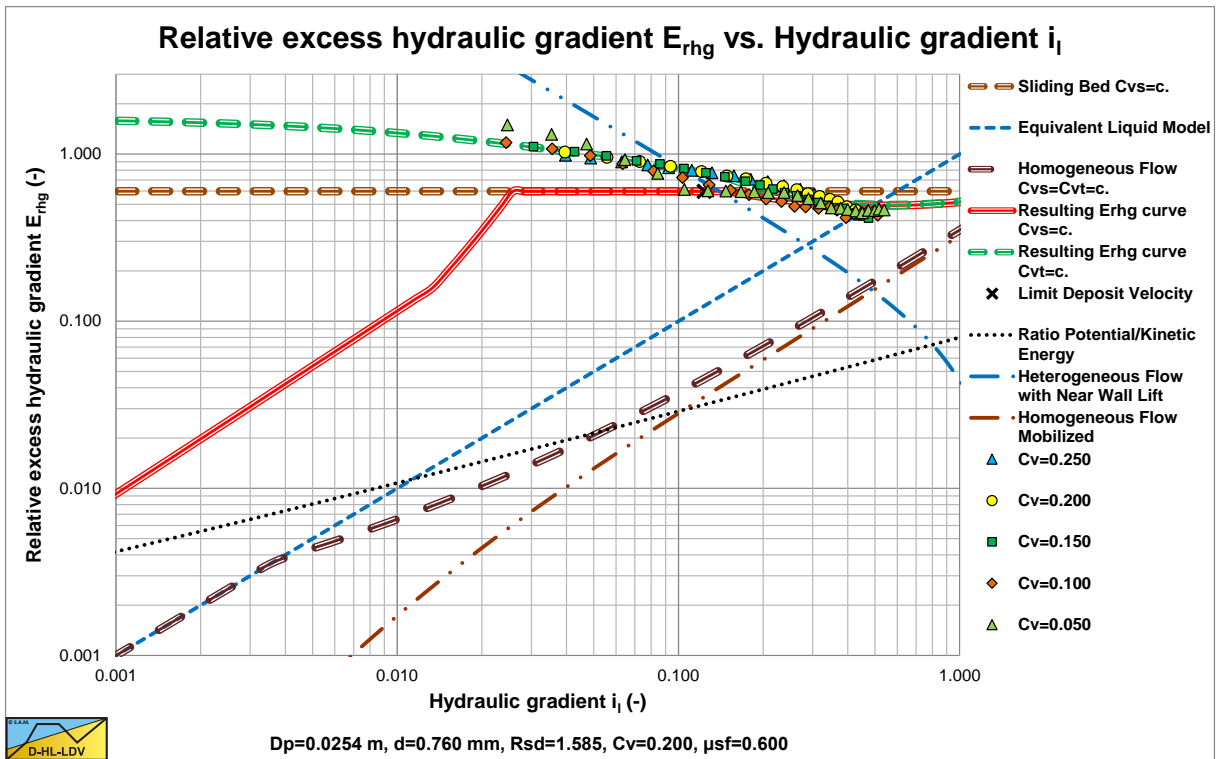
Figure 6.5-11: The relative excess hydraulic gradient Sand D.

Figure 6.5-10 and Figure 6.5-11 show the digitized fit lines for sand B in the hydraulic gradient versus line speed graph and the relative excess hydraulic gradient versus liquid hydraulic gradient graph. Sand D behaves according to the sliding flow regime, a mix of heterogeneous and sliding bed behavior.
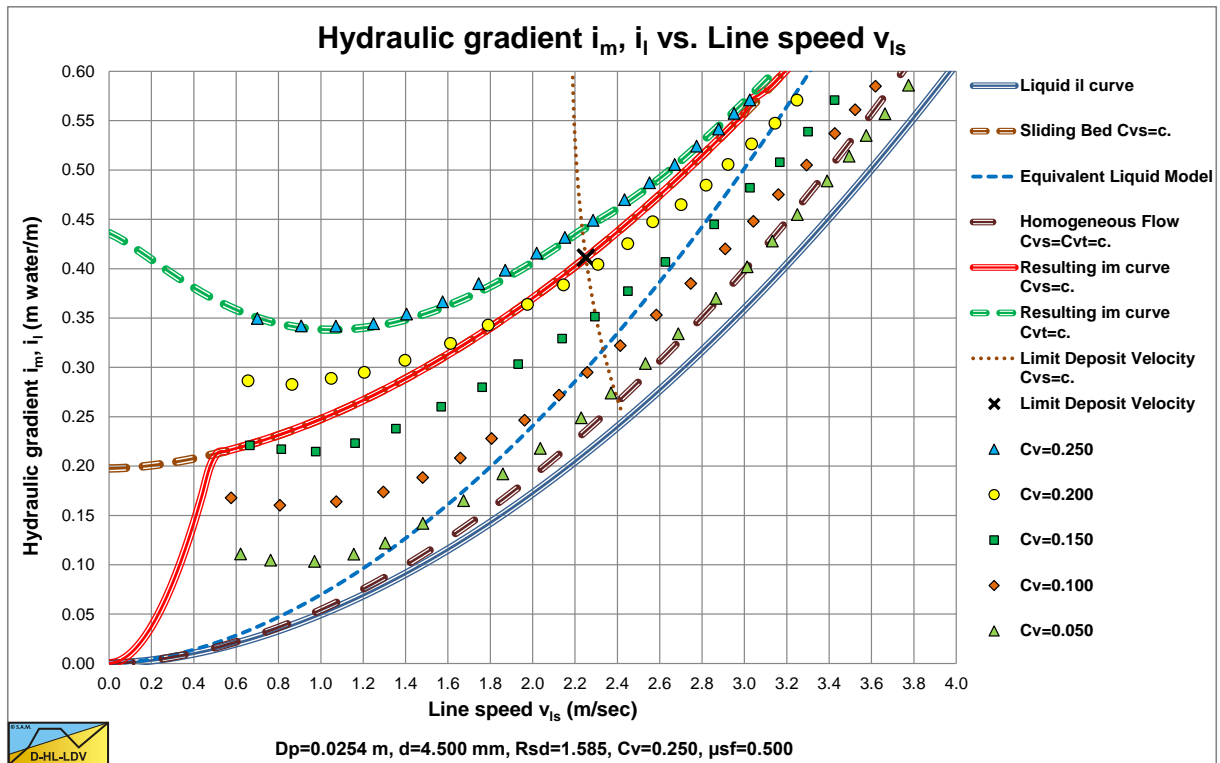
Figure 6.5-12: The hydraulic gradient sand E.
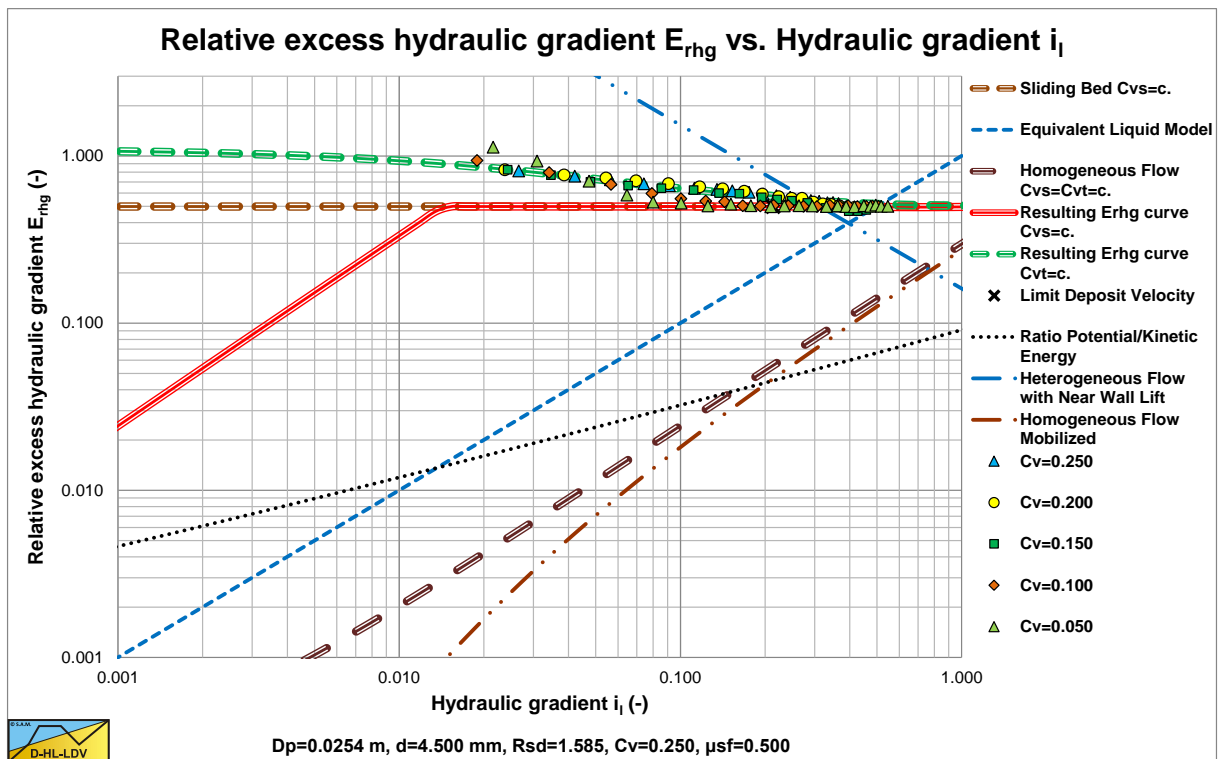
Figure 6.5-13: The relative excess hydraulic gradient Sand E.

Figure 6.5-12 and Figure 6.5-13 show the digitized fit lines for sand B in the hydraulic gradient versus line speed graph and the relative excess hydraulic gradient versus liquid hydraulic gradient graph. Sand E (fine gravel) behaves according to the sliding bed flow regime.

6.5.7 Vertical Pipes.

Newitt et al. (1961) investigated the hydraulic gradient of different solids in vertical pipes of 0.0254 and 0.0508 m diameter (1 and 2 inch pipes). They used sands (density 2.59-2.64 ton/m^3) with diameters of 0.1, 0.19, 0.71 and 1.27 mm, pebbles (density 2.59 ton/m^3) of 3.8 mm, Zircon (density 4.56 ton/m^3) of 0.109 mm, Manganese dioxide (density 4.2 ton/m^3) of 1.37 mm and Perspex (density 1.19 ton/m^3) of 1.2 mm.

3 cases were considered:
1. Very small particles.
2. Medium sized particles.
3. Large particles.

Where the definitions of small, medium and large depend on the pipe diameter and the solids density.

6.5.7.1 Some Theoretical Considerations.

The mass balance of the solids flow gives:

$$A_p \cdot C_{vt} \cdot v_{ls} \cdot \rho_s = A_p \cdot C_{vs} \cdot v_s \cdot \rho_s = A_p \cdot C_{vs} \cdot \left(v_l - v_{th} \right) \cdot \rho_s \tag{6.5-12}$$

Or:

$$C_{vt} \cdot v_{ls} = C_{vs} \cdot v_s = C_{vs} \cdot \left(v_l - v_{th} \right) \tag{6.5-13}$$

In this mass balance it is assumed that the particles (solids) have a velocity v_s smaller than the cross sectional averaged line speed v_{ls} and the liquid (water) has a larger velocity v_l. In the original publication transport concentration is used for spatial concentration. Here spatial volumetric concentration C_{vs} and delivered or transport volumetric concentration C_{vt} are used.

The mass balance of the liquid (water) gives:

$$A_p \cdot \left(1 - C_{vt} \right) \cdot v_{ls} \cdot \rho_l = A_p \cdot \left(1 - C_{vs} \right) \cdot v_l \cdot \rho_l \tag{6.5-14}$$

Or:

$$\left(1 - C_{vt} \right) \cdot v_{ls} = \left(1 - C_{vs} \right) \cdot v_l \tag{6.5-15}$$

This gives for the liquid velocity v_l, assuming the terminal hindered settling velocity v_{th} is known (ascending pipe: a positive terminal hindered settling velocity, descending pipe: a negative terminal hindered settling velocity):

$$v_l = v_{ls} + C_{vs} \cdot v_{th} \tag{6.5-16}$$

If the spatial volumetric concentration is known, the delivered or transport volumetric concentration can be determined according to:

$$C_{vt} = C_{vs} \cdot \left(1 - \frac{v_{th}}{v_{ls}} \right) + C_{vs}^2 \cdot \frac{v_{th}}{v_{ls}} \tag{6.5-17}$$

If the delivered volumetric concentration is known, the spatial volumetric concentration can be determined according to:

$$C_{vs} = -\frac{1}{2} \cdot \left(\frac{v_{ls}}{v_{th}} - 1 \right) + \frac{1}{2} \cdot \sqrt{ \left(\frac{v_{ls}}{v_{th}} - 1 \right)^2 + 4 \cdot C_{vt} \cdot \frac{v_{ls}}{v_{th}} } \tag{6.5-18}$$

6.5.7.2 Additions to Newitt et al. (1961).

Now considering the vertical transport over a period of time Δt. The mixture as a whole has travelled a vertical distance $\Delta H = v_{ls} \cdot \Delta t$. The mass flux $Q_{m,t}$ and the mass transport ΔM_t are now:

$$Q_{m,t} = A_p \cdot C_{vt} \cdot v_{ls} \cdot \rho_s + A_p \cdot (1 - C_{vt}) \cdot v_{ls} \cdot \rho_l$$

$$\Delta M_t = Q_{m,t} \cdot \Delta t = A_p \cdot C_{vt} \cdot v_{ls} \cdot \rho_s \cdot \Delta t + A_p \cdot (1 - C_{vt}) \cdot v_{ls} \cdot \rho_l \cdot \Delta t \tag{6.5-19}$$

$$\Delta M_t = A_p \cdot v_{ls} \cdot \Delta t \cdot \left(C_{vt} \cdot \rho_s + (1 - C_{vt}) \cdot \rho_l \right) = \Delta V \cdot \rho_{m,t}$$

The potential energy $\Delta E_{p,t}$ gained by the transported mixture is now:

$$\Delta E_{p,t} = \Delta M_t \cdot g \cdot \Delta H = A_p \cdot v_{ls} \cdot \Delta t \cdot \left(C_{vt} \cdot \rho_s + (1 - C_{vt}) \cdot \rho_l \right) \cdot g \cdot \Delta H = \Delta V \cdot \rho_{m,t} \cdot g \cdot \Delta H \tag{6.5-20}$$

The work carried out however is based on the spatial concentration in the pipe, giving:

$$\Delta E_{p,s} = \Delta M_s \cdot g \cdot \Delta H = A_p \cdot v_{ls} \cdot \Delta t \cdot \left(C_{vs} \cdot \rho_s + (1 - C_{vs}) \cdot \rho_l \right) \cdot g \cdot \Delta H = \Delta V \cdot \rho_{m,s} \cdot g \cdot \Delta H \tag{6.5-21}$$

This follows from the fact that this work equals the required pressure Δp times the mixture flow Q_v times the period of time Δt. The required pressure is the weight $\Delta M_s \cdot g$ of the column of mixture in the pipe with height ΔH divided by the cross section of the pipe A_p.

$$\Delta p = \frac{\Delta M_s \cdot g}{A_p} = \frac{A_p \cdot v_{ls} \cdot \Delta t \cdot \left(C_{vs} \cdot \rho_s + (1 - C_{vs}) \cdot \rho_l \right) \cdot g}{A_p} = \frac{\Delta V \cdot \rho_{m,s} \cdot g}{A_p} \tag{6.5-22}$$

So the work required is now:

$$\Delta E_{p,s} = \Delta p \cdot Q_v \cdot \Delta t = \Delta p \cdot v_{ls} \cdot A_p \cdot \Delta t = \Delta p \cdot A_p \cdot \Delta H$$

$$= \frac{A_p \cdot v_{ls} \cdot \Delta t \cdot \left(C_{vs} \cdot \rho_s + (1 - C_{vs}) \cdot \rho_l \right) \cdot g}{A_p} = A_p \cdot v_{ls} \cdot \Delta t \cdot \left(C_{vs} \cdot \rho_s + (1 - C_{vs}) \cdot \rho_l \right) \cdot g \cdot \Delta H \tag{6.5-23}$$

The difference between the work carried out and the potential energy gained by the mixture is:

$$\Delta E_{p,s} - \Delta E_{p,t} = A_p \cdot v_{ls} \cdot \Delta t \cdot \left(C_{vs} \cdot \rho_s + (1 - C_{vs}) \cdot \rho_l \right) \cdot g \cdot \Delta H$$

$$- A_p \cdot v_{ls} \cdot \Delta t \cdot \left(C_{vt} \cdot \rho_s + (1 - C_{vt}) \cdot \rho_l \right) \cdot g \cdot \Delta H \tag{6.5-24}$$

$$= A_p \cdot v_{ls} \cdot \Delta t \cdot g \cdot \Delta H \cdot \left(C_{vs} - C_{vt} \right) \cdot \left(\rho_s - \rho_l \right)$$

Substituting the relation between spatial and delivered concentration gives for this difference:

$$\Delta E_{p,s} - \Delta E_{p,t} = A_p \cdot v_{th} \cdot \Delta t \cdot g \cdot \Delta H \cdot \left(C_{vs} - C_{vs}^2 \right) \cdot \left(\rho_s - \rho_l \right) \tag{6.5-25}$$

This is the energy dissipated due to the viscous friction around the particles. This dissipated energy depends on the terminal hindered settling velocity and on the spatial concentration. The pressure required depends on the spatial concentration. For small particles with a small value of the terminal hindered settling velocity, the dissipated energy will also be small, however for large particles like gravel this will not be the case.

6.5.7.3 Correction on the Darcy Weisbach Friction Factor.

The hydraulic gradient for pure liquid flow is:

$$
i_l = \frac{\lambda_l \cdot v_{ls}^2}{2 \cdot g \cdot D_p}
\tag{6.5-26}
$$

Since the liquid velocity is higher, depending on the spatial concentration and the terminal hindered settling velocity, the velocity in this equation should be replaced by the liquid velocity, assuming that the Darcy Weisbach friction factor hardly changes at high Reynolds numbers. This gives for the hydraulic gradient of a mixture in a vertical pipe, assuming the equivalent liquid model is valid:

$$
i_m = \frac{\rho_m}{\rho_l} \cdot \frac{\lambda_l \cdot \left(v_{ls} + C_{vs} \cdot v_{th} \right)^2}{2 \cdot g \cdot D_p} = \frac{\rho_m}{\rho_l} \cdot \frac{\lambda_l \cdot \left(v_{ls}^2 + 2 \cdot C_{vs} \cdot v_{th} \cdot v_{ls} + C_{vs}^2 \cdot v_{th}^2 \right)}{2 \cdot g \cdot D_p}
$$

$$
\tag{6.5-27}
$$

$$
i_m \approx \frac{\rho_m}{\rho_l} \cdot \frac{\lambda_l \cdot \left(v_{ls}^2 + 2 \cdot C_{vs} \cdot v_{th} \cdot v_{ls} \right)}{2 \cdot g \cdot D_p} = \frac{\rho_m}{\rho_l} \cdot \frac{\lambda_l \cdot v_{ls}^2}{2 \cdot g \cdot D_p} + \frac{\rho_m}{\rho_l} \cdot \frac{2 \cdot \lambda_l \cdot C_{vs} \cdot v_{th} \cdot v_{ls}}{2 \cdot g \cdot D_p}
$$

Since normally the spatial concentration will have a value from 0-0.4, the terminal settling velocity has a value of 0.4 m/s for a 10 mm particle and the terminal hindered settling velocity is always smaller, the quadratic term of spatial concentration times terminal hindered settling velocity is negligible for line speeds above 1 m/s. With a line speed of 1 m/s, a spatial concentration of 0.4 and a terminal settling velocity of 0.4 m/s, the second term on the right hand side 30% of the first term, which is significant. Using the terminal hindered settling velocity in this case of 0.11 m/s gives about 8%, which is still significant. For small particles the second term on the right hand side can be neglected.

6.5.7.4 The Magnus Effect.

If a particle is situated near the wall of a vertical conveying pipe in which the velocity gradient is steep, the particle will be subjected to forces which tend to cause it to rotate and to move towards the axis of the pipe. Both turbulent lift caused by a velocity different over the particle in a pipe radial direction and Magnus lift due to the rotation of the particle will cause such a lift force and push particles away from the pipe wall. This way a particle poor or particles free viscous sub layer is created.

6.5.7.5 Experimental Results.

Newitt et al. (1961) found that for small particles the hydraulic gradient follows the equivalent liquid model.

$$
i_m = \frac{\rho_m}{\rho_l} \cdot \frac{\lambda_l \cdot v_{ls}^2}{2 \cdot g \cdot D_p}
\tag{6.5-28}
$$

The experiments were carried out with sand with **d=0.1 mm**, sand with **d=0.19 mm** and Zircon sand with **d=0.109 mm**.
Sand with **d=0.71 mm** and Perspex with **d=1.2 mm** show hydraulic gradients identical to pure liquid with the same average line speeds.
Pebbles with **d=4.2 mm** and Manganese dioxide with **d=1.37 mm** show an excess hydraulic gradient (solids effect) at low line speeds, decreasing to almost zero at high line speeds.

Newitt et al. (1961) found an empirical relation for this behavior, giving:

$$
\frac{i_m - i_l}{C_{vt} \cdot i_l} = 0.0037 \cdot \left(\frac{g \cdot D_p}{v_{ls}^2} \right)^{1/2} \cdot \left(\frac{D_p}{d} \right) \cdot \left(\frac{\rho_s}{\rho_l} \right)^2
\tag{6.5-29}
$$

6.5.7.6 Discussion & Conclusions.

Based on the equivalent liquid model this would give:

$$\frac{i_m - i_l}{C_{vt} \cdot i_l} = \frac{\dfrac{\rho_m}{\rho_l} \cdot \dfrac{\lambda_l \cdot v_{ls}^2}{2 \cdot g \cdot D_p} - \dfrac{\lambda_l \cdot v_{ls}^2}{2 \cdot g \cdot D_p}}{C_{vt} \cdot \dfrac{\lambda_l \cdot v_{ls}^2}{2 \cdot g \cdot D_p}} = \frac{\dfrac{\rho_m}{\rho_l} - 1}{C_{vt}} = \frac{R_{sd} \cdot C_{vs}}{C_{vt}} \approx R_{sd} \tag{6.5-30}$$

So for small particles, where the spatial and delivered concentration do not differ too much, this is equal to the relative submerged density R_{sd}. This means that the maximum value of the Newitt et al. (1961) equation is the relative submerged density or a slightly higher value in case of medium to large particles. Newitt et al. (1961) do not mention this limitation.

The use of dimensionless numbers containing the pipe diameter is questionable, since only 0.0254 m (1 inch) and 0.0508 m (2 inch) pipes are used in the research and only results with the 0.0254 m (1 inch) pipe are shown in the publication. Since the purpose of the equation is to quantify the effect of a particle free or poor viscous sub-layer due to near wall lift, the equation should be based on near wall phenomena. If the particle diameter is larger than the thickness of the viscous sub-layer, the concentration in the viscous sub-layer will be smaller than the cross sectional averaged concentration. Although this concentration effect is not linear with the particle diameter, as a first attempt a linear relation is used. The ratio of the thickness of the viscous sub-layer to the particle diameter is:

$$\frac{\delta_v}{d} = \frac{11.6 \cdot \dfrac{\nu_l}{u_*}}{d} = \frac{11.6 \cdot \nu_l}{\sqrt{\lambda_l / 8} \cdot v_{ls} \cdot d} = \frac{32.81 \cdot \nu_l}{\sqrt{\lambda_l} \cdot v_{ls} \cdot d} \tag{6.5-31}$$

Using this as a reduction of the equivalent liquid model solids effect gives (with a maximum of R_{sd}):

$$\frac{i_m - i_l}{C_{vt} \cdot i_l} = R_{sd} \cdot \frac{\delta_v}{d} = R_{sd} \cdot \frac{32.81 \cdot \nu_l}{\sqrt{\lambda_l} \cdot v_{ls} \cdot d} \tag{6.5-32}$$

For a 0.0254 m (1 inch) pipe and sand or gravel, this equation gives almost the same results as the equation found by Newitt et al. (1961).

The relative submerged density R_{sd} behaves similar to the solids density to a power just below 2, taking into account the solids density to liquid density ratio squared $(\rho_s/\rho_l)^2$ term. The line speed and particle diameter are in the denominator in both equations to the first power, so the behavior is the same. Only the pipe diameter is absent in equation (6.5-32), while it is present in equation (6.5-29) to a power of 1.5. Now whether Newitt et al. (1961) found this relation for the pipe diameter because of the need for dimensionless numbers, or based on experimental data is not clear. Fact is that most of the experiments were carried out with a pipe diameter of 0.0254 m (1 inch), while data of experiments with a 0.0508 m (2 inch) pipe are hardly mentioned. Based on physics there is no reason to assume such a strong dependency on the pipe diameter. The influence of the pipe diameter on the Darcy Weisbach friction factor is taken into account by the Darcy Weisbach friction factor in equation (6.5-32), while the influence of higher line speeds in a larger pipe is taken into account by the line speed itself. The power of 1.5 of the pipe diameter in fact implies that the reduction of the solids effect is much less in larger diameter pipes. The Darcy Weisbach friction factor in the denominator of equation (6.5-32) shows this behavior weakly (a power of 0.1-0.15 of the pipe diameter).

Based on a particle poor viscous sub-layer an alternative equation is derived for the reduction of the solids effect. Whether this reduction reduces the solids effect to zero is the question, since in the core of the flow the small particles will follow the eddies and participate in the energy dissipation. For larger particles and flow with high Bagnold numbers grain collision stresses will dominate over the viscous fluid stresses resulting in a different behavior. This does however not mean that the solids effect reduces to zero. Grain collision stresses also result in energy dissipation and thus a solids effect.

6.6 Silin, Kobernik & Asaulenko (1958) & (1962).

Silin, Kobernik & Asaulenko (1958) & (1962) carried out experiment in pipes with diameters of 0.024 m, 0.103 m, 0.206 m, 0.308 m, 0.410 m, 0.614 m, 0.800 m and 0.900 m. They used particles with diameters of 0.16 mm, 0.23 mm, 0.25 mm, 0.29 mm, 0.33 mm, 0.41 mm, 0.65 mm, 1 mm and 2 mm. The relative submerged densities used were 0.59, 0.85, 1.59 and 2.28. Most probably they used more pipe diameters, particle diameters and relative submerged densities, since most of the original reports are in Russian and difficult to find. The experiments are however very valuable, since a broad range of pipe diameters is covered.

Figure 6.6-1 shows the Durand Froude F_L numbers found for pipe diameters of 0.1 m, 0.2 m and 0.3 m. The graph also shows the Jufin & Lopatin F_L curve and the DHLLDV F_L curve. If only sand particles are considered, it looks like the F_L value decreases slightly with the pipe diameter. This is also part of the Jufin & Lopatin (1966) equation for the LDV, which is based on these experiments. If also other relative submerged densities are considered, it looks like the F_L value increases with decreasing relative submerged density. One should however also consider the volumetric concentrations that may influence the F_L values. The Jufin & Lopatin (1966) curve in the graph is for an 0.3 m pipe, for the smaller pipe diameters the curve is slightly higher.
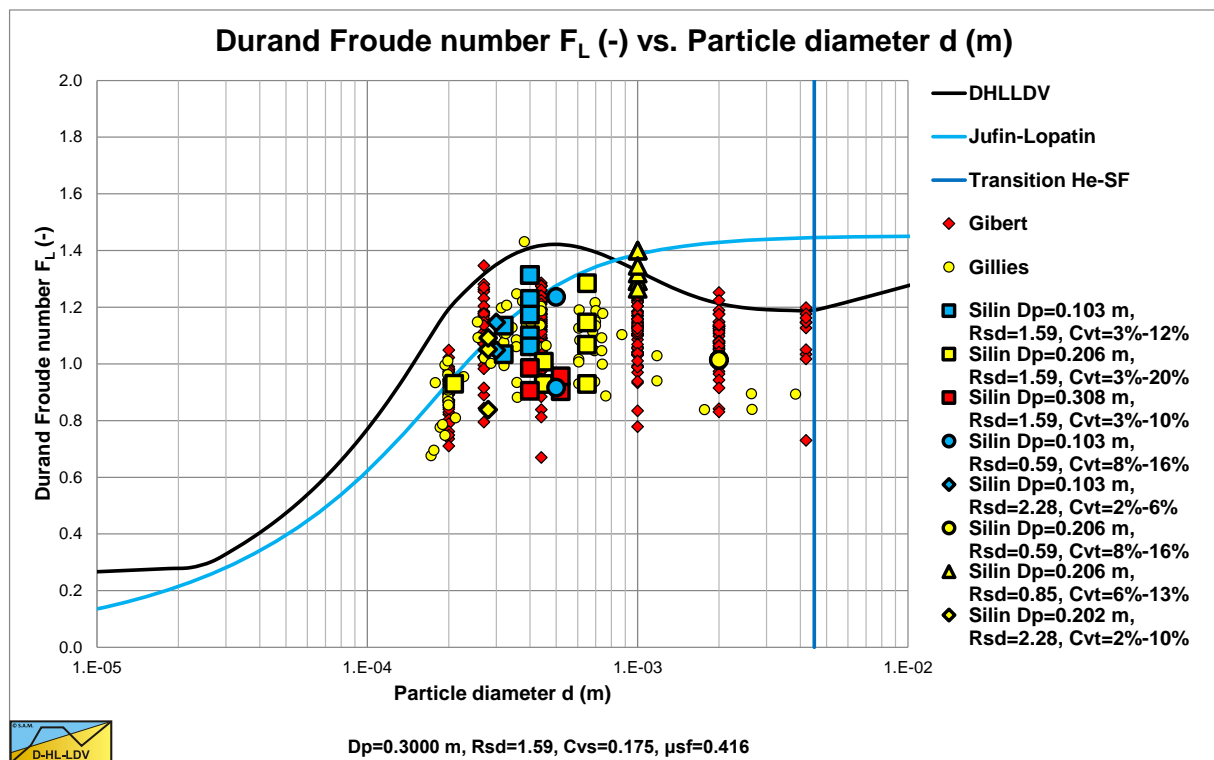
Figure 6.6-1: Durand Froude numbers obtained by Silin et al. (1958).

Figure 6.6-2, Figure 6.6-3, Figure 6.6-4, Figure 6.6-5, Figure 6.6-6 and Figure 6.6-7 show results of experiments carried out by Silin et al. (1958) and used by Jufin & Lopatin (1966) for their model. Figure 6.6-2, Figure 6.6-4 and Figure 6.6-6 show the original data in i_m vs. v_{ls} graphs, while Figure 6.6-3, Figure 6.6-5, and Figure 6.6-7 show processed data in E_{rhg} vs. i_l graphs. These experiments are very valuable, since they were carried out in large diameter pipes. The experiments show a lot of scatter, especially in the E_{rhg} vs. i_l graphs. A general conclusion of these experiments is, that the hydraulic gradient is best estimated with the ELM model.

The Jufin & Lopatin (1966) model, based on these experiments, assumes that the excess head losses are proportional to the square root of the concentration and not linear with the concentration. Analyzing the data shows that part of the data points is in the heterogeneous flow regime and part is in the (pseudo) homogeneous flow regime. For the homogeneous flow regime other researchers have already observed that the excess hydraulic gradient is between 0 and the excess hydraulic gradient of the ELM. This would match the Jufin & Lopatin (1966) observations. Whether this is also true in the heterogeneous flow regime is however contradictory with the observations of most other researchers. Mixing two flow regimes into 1 equation/model is not a good idea, since the physics of both flow regimes differ.
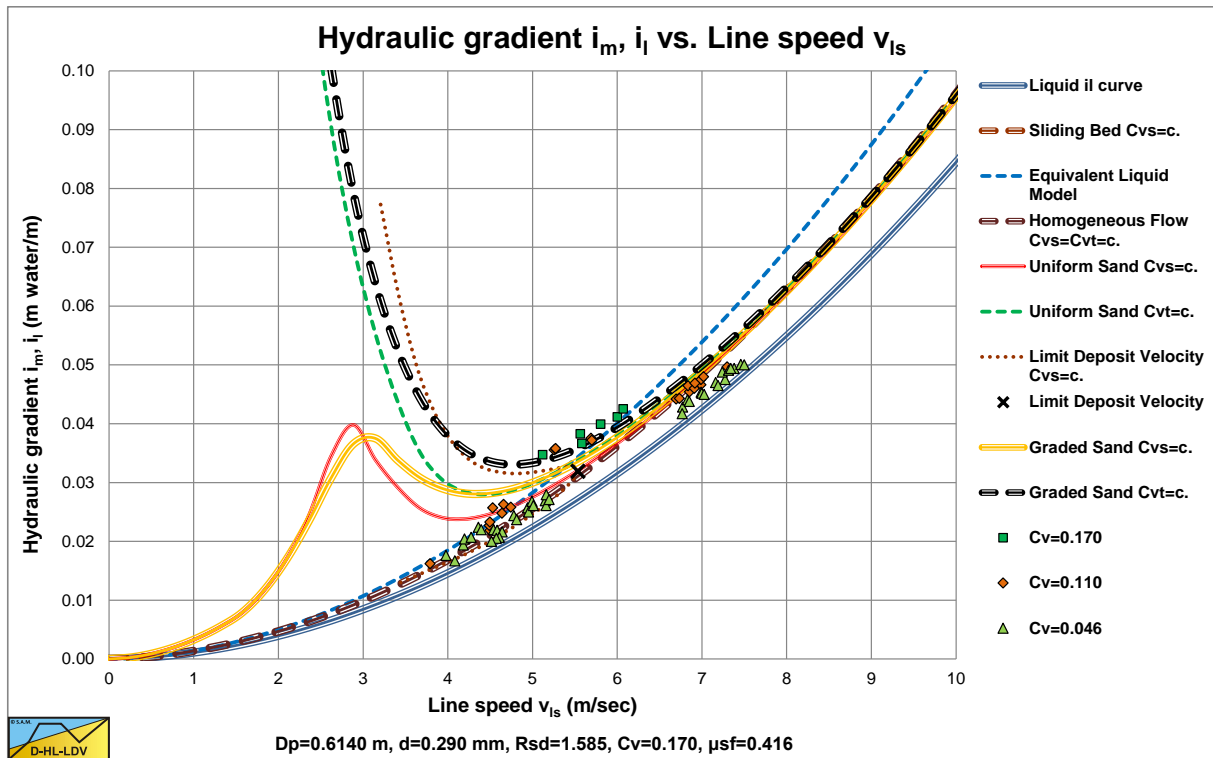
Figure 6.6-2: Experiments of Silin et al. (1958) in an 0.614 m diameter pipe, A.
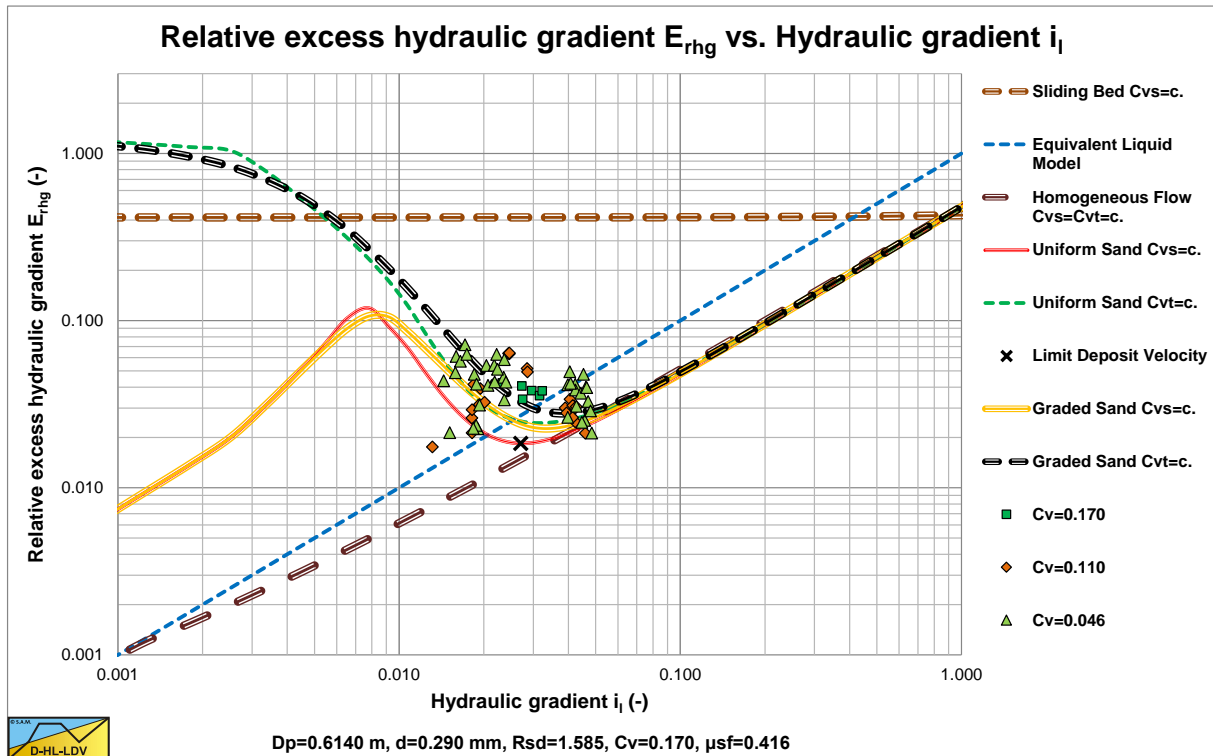
Figure 6.6-3: Experiments of Silin et al. (1958) in an 0.614 m diameter pipe, B.

Figure 6.6-2 and Figure 6.6-3 show the data versus the DHLLDV Framework for uniform and graded sands (more realistic). The data points match the graded curve reasonably. Figure 6.6-2 is for a concentration of 17%. These data points match. Figure 6.6-3 is almost dimensionless and shows the match of all data points. The data points can be divided into two groups. The group on the left is in the heterogeneous flow regime, while the group on the right is more at the transition of the heterogeneous flow regime to the homogeneous flow regime.
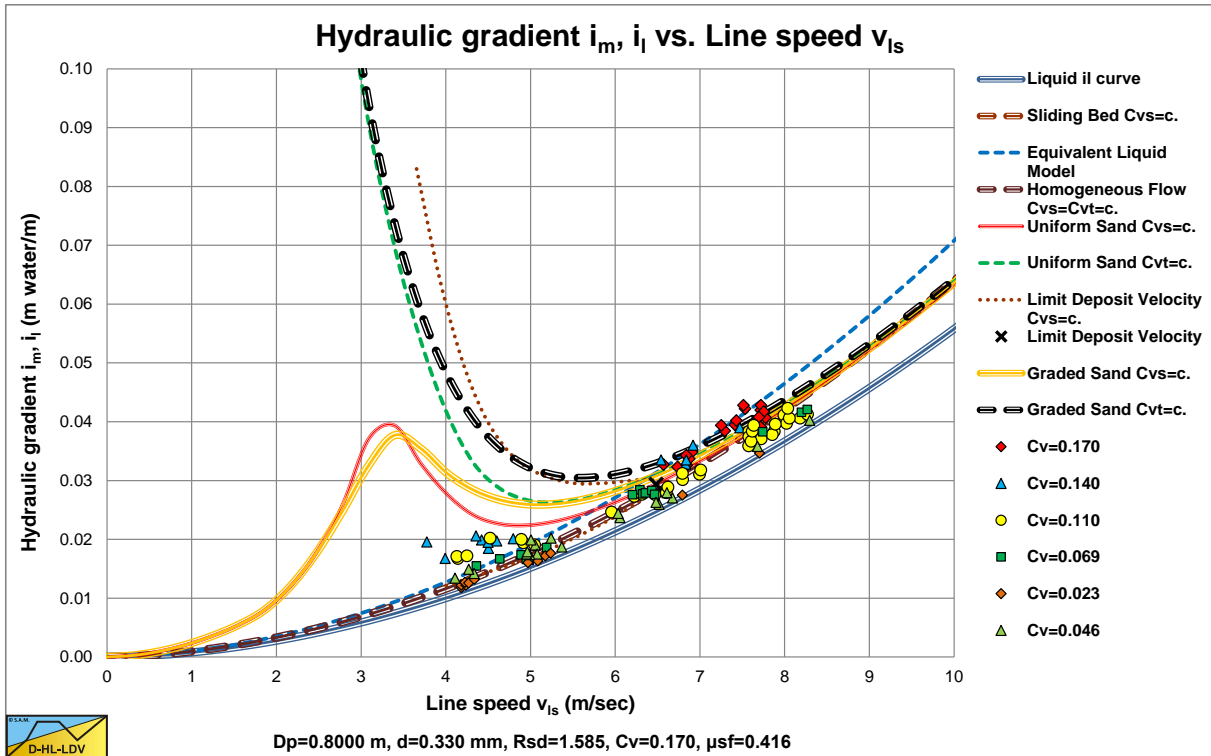
Figure 6.6-4: Experiments of Silin et al. (1958) in an 0.800 m diameter pipe, A.
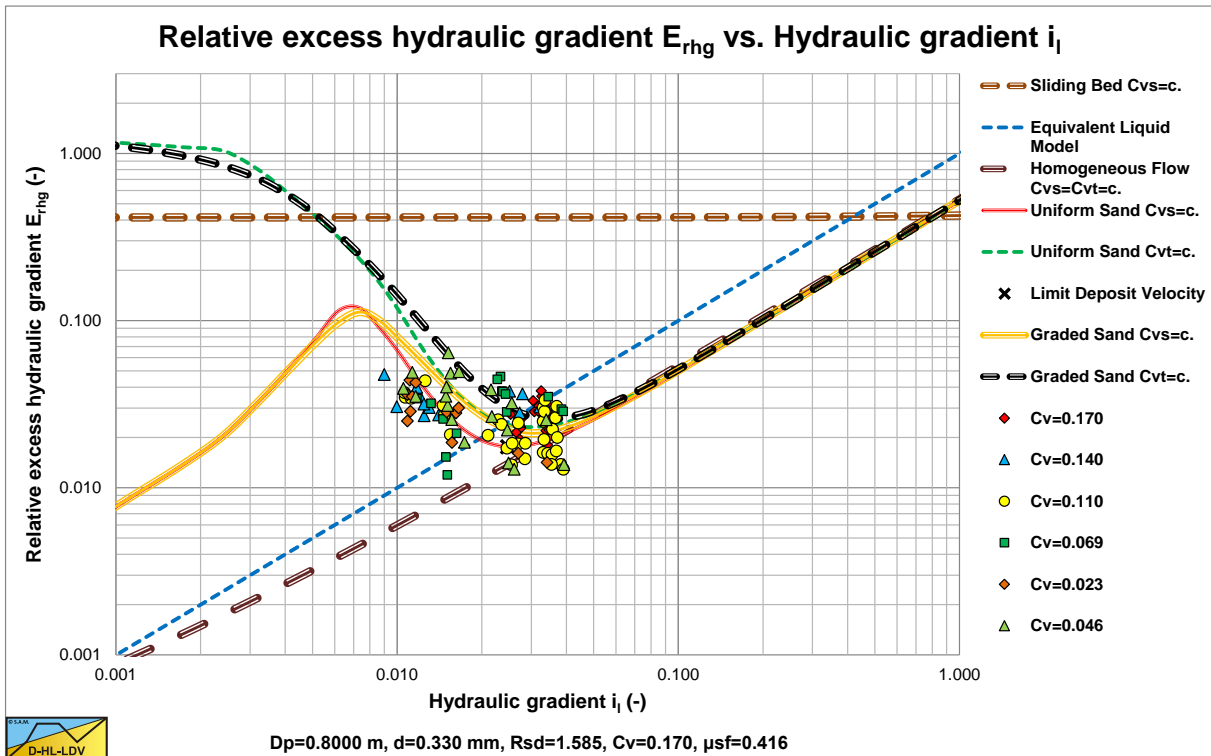
Figure 6.6-5: Experiments of Silin et al. (1958) in an 0.800 m diameter pipe, B.

Figure 6.6-4 and Figure 6.6-5 show the data versus the DHLLDV Framework for uniform and graded sands (more realistic). The data points match the graded curve reasonably. Figure 6.6-4 is for a concentration of 17%. These data points match. Figure 6.6-5 is almost dimensionless and shows the match of all data points. The data points can be divided into two groups. The group on the left is in the heterogeneous flow regime, while the group on the right is more at the transition of the heterogeneous flow regime to the homogeneous flow regime.
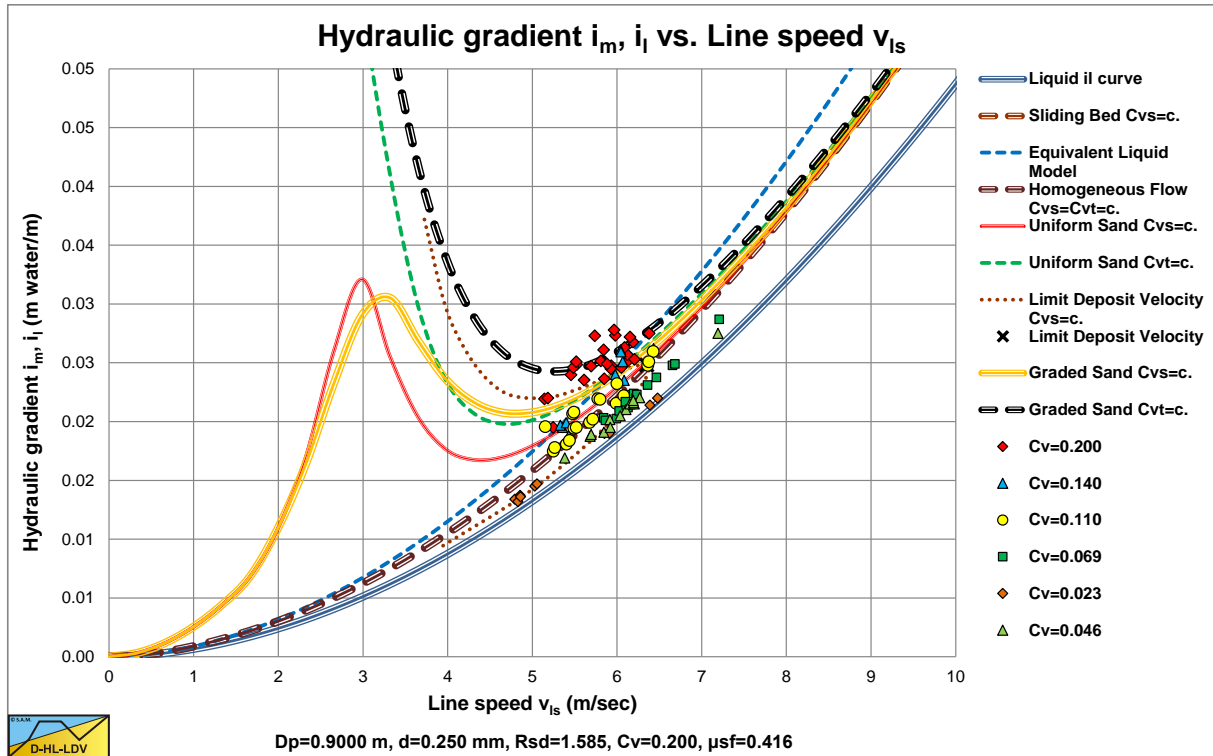
Figure 6.6-6: Experiments of Silin et al. (1958) in an 0.900 m diameter pipe, A.
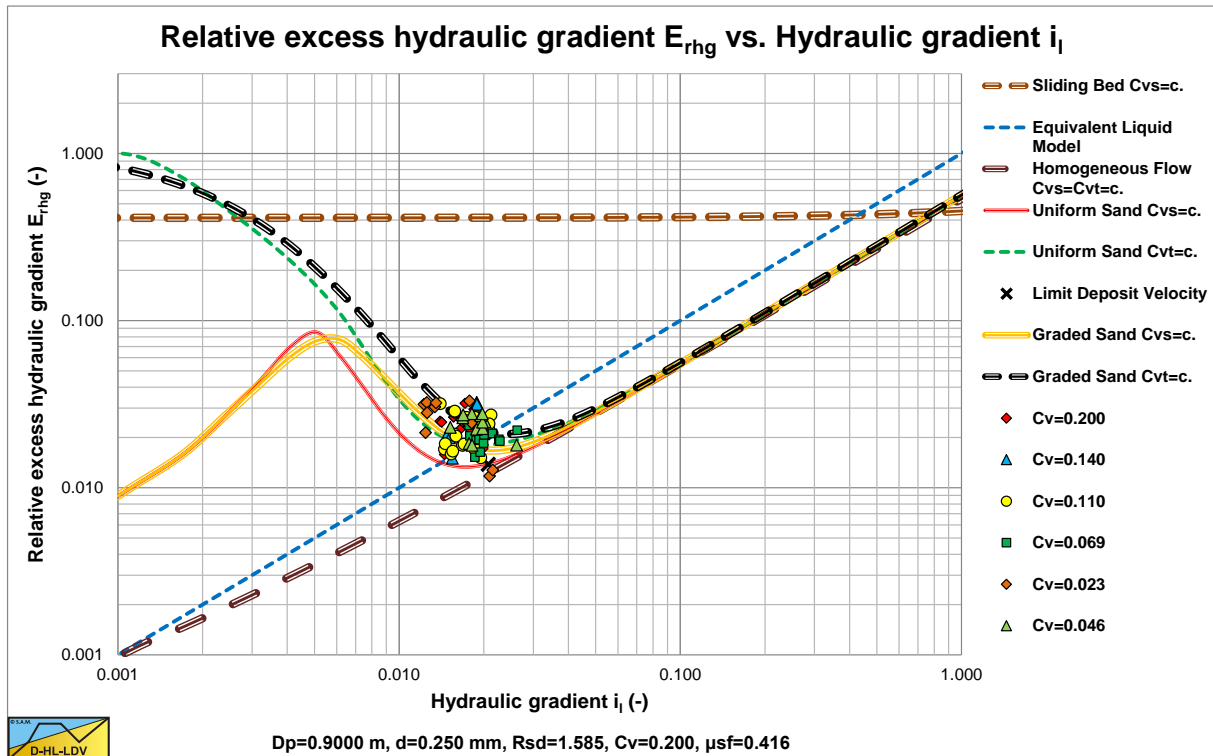
Figure 6.6-7: Experiments of Silin et al. (1958) in an 0.900 m diameter pipe, B.

Figure 6.6-6 and Figure 6.6-7 show the data versus the DHLLDV Framework for uniform and graded sands (more realistic). The data points match the graded curve reasonably. Figure 6.6-6 is for a concentration of 20%. These data points match. Figure 6.6-5 is almost dimensionless and shows the match of all data points. The data points can be divided into two groups. The group on the left is in the heterogeneous flow regime, while the group on the right is more at the transition of the heterogeneous flow regime to the homogeneous flow regime.

6.7 The Fuhrboter (1961) Model.

Fuhrboter (1961) in his PhD thesis, collected data on frictional head loss for slurry flow conditions in a D_p=300 mm laboratory pipeline with sand and gravel with particle diameters ranging from d_{50}=0.18 mm to d_{50}=4.6 mm. His starting points were the research of Durand & Condolios (1952) and Silin et al. (1958) and the assumption that the pressure losses depend on the spatial volumetric concentration. A relation between pressure losses and delivered volumetric concentration depends on the relation between the spatial and the delivered volumetric concentrations. Fuhrboter (1961) defined the Limit Deposit Velocity or often called critical velocity as the velocity above which no stationary or sliding bed will occur. This is the same definition as used by Durand & Condolios (1952), but different from Wilson et al. (1992) who uses the transition velocity between a fixed or stationary bed and a sliding bed as the critical velocity. Fuhrboter (1961) reports in detail about the experiments regarding the Limit Deposit Velocity for sands with d_{50} of 0.18 mm, 0.26 mm, 0.44 mm and 0.83 mm and regarding the pressure losses for sands with d_{50} of 0.26 mm, 0.44 mm and 0.83 mm, based on spatial volumetric concentrations.
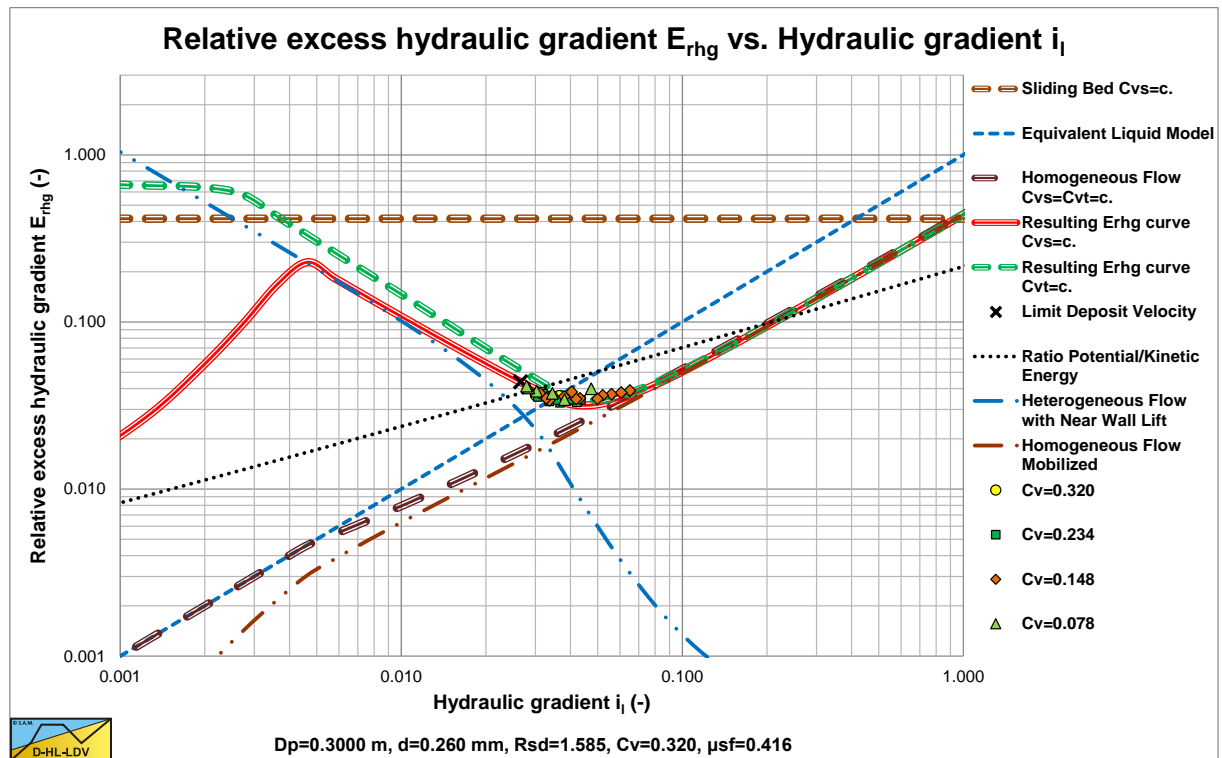
Figure 6.7-1: The data of Fuhrboter with a d_{50}=0.26 mm sand.

Figure 6.7-1, Figure 6.7-2 and Figure 6.7-3 show the E_{rhg} values of Fuhrboter for the d_{50}=0.26 mm, d_{50}=0.44 mm and d_{50}=0.83 mm sands, with:

$$E_{rhg} = \frac{i_m - i_l}{R_{sd} \cdot C_{vs}}$$

(6.7-1)

The figures show clearly that the experiments were carried out in the heterogeneous flow regime, or at the transition between the heterogeneous and the homogeneous flow regimes for small particles. The data in these figures are only the data points above the Limit Deposit Velocity, giving heterogeneous transport. The heterogeneous curves are based on the original Miedema & Ramsdell (2013) equation. The figures also show the ratio between the potential energy losses and the kinetic energy losses, which is small (<10%) for medium and coarse sands.

Figure 6.7-4 shows the Durand F_L values for the Limit Deposit Velocity as measured by Fuhrboter, with:

$$F_L = \frac{v_{ls,ldv}}{\sqrt{2 \cdot g \cdot R_{sd} \cdot D_p}}$$

(6.7-2)

The data in these figures are only the data points above the Limit Deposit Velocity, giving heterogeneous transport. Based on his findings with heterogeneous transport he proposed the following equation for the frictional head loss:

$$\Delta p_m = \Delta p_l + \rho_l \cdot g \cdot \Delta L \cdot \frac{S_k}{v_{ls}} \cdot C_{vs} \qquad (6.7\text{-}3)$$

Fuhrboter (1961) separated the excess pressure losses resulting from the solids from the liquid pressure losses, just like Wilson et al. (1992), but different from Durand & Condolios (1952), Jufin & Lopatin (1966) and Newitt et al. (1955) who used:

$$\Delta p_m = \Delta p_l \cdot \left(1 + \phi \cdot C_v\right) \qquad (6.7\text{-}4)$$

This results in liquid hydraulic gradients independent excess pressure losses in the Fuhrboter (1961) equation.
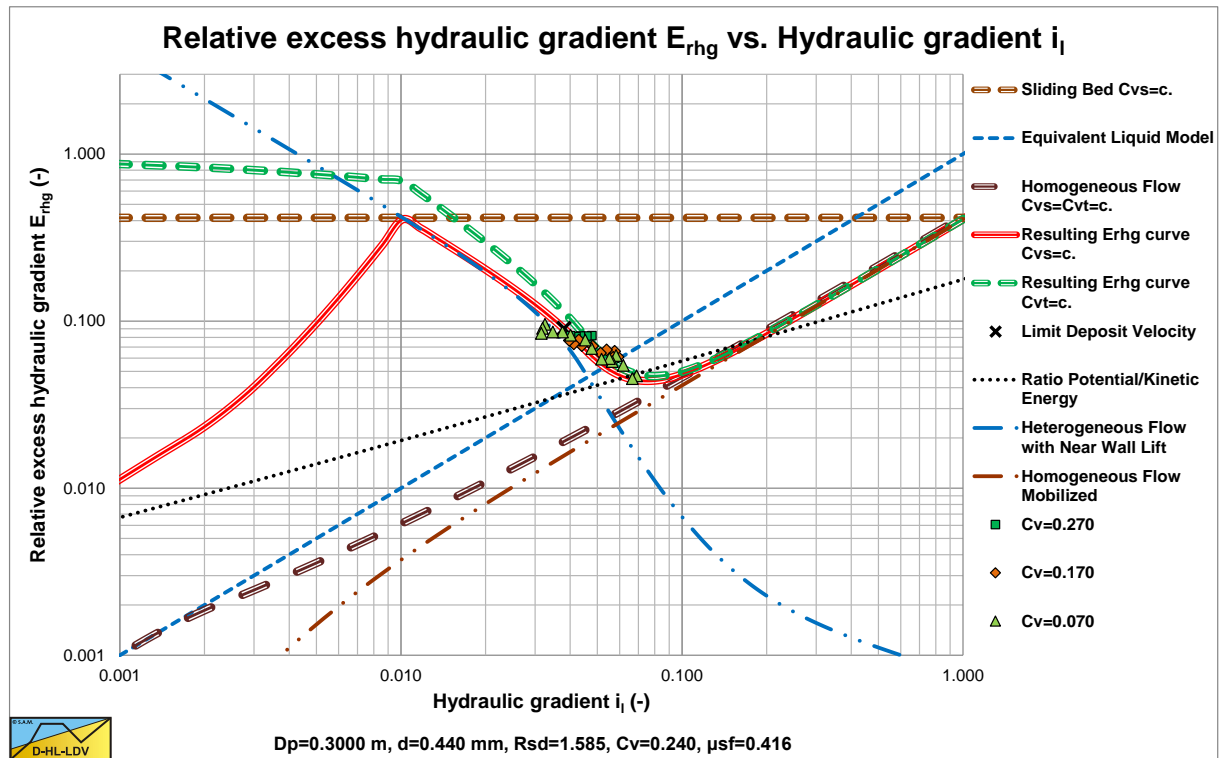
Figure 6.7-2: The data of Fuhrboter with a $d_{50}=0.44$ mm sand.

Fuhrboter (1961) did not give an equation for the S_k factor, but showed a graph, which is reproduced in Figure 6.7-5. The concentration C_{vs} in his equation is the spatial sand concentration and not the delivered volumetric solids concentration C_{vt} (solely the quarts).

In practice the delivered volumetric solids concentration C_{vt} is often used. Based on the propagation velocity of density waves/fluctuations, Fuhrboter (1961) concluded that the velocity of the solids was about 65% (+/- 5%) of the flow velocity of the mixture. The factor 0.65 in fact means a slip factor of 0.65 according to Fuhrboter. Fuhrboter modified equation (6.7-3) to equation (6.7-6), applying the fixed slip of 35%, which of course is questionable.

$$C_{vt} = 0.65 \cdot C_{vs} \quad \Rightarrow \quad S_{kt} = \frac{C_{vs}}{C_{vt}} \cdot S_k \quad \Rightarrow \quad S_{kt} = \frac{1}{0.65} \cdot S_k \qquad (6.7\text{-}5)$$

$$\Delta p_m = \Delta p_l + \rho_l \cdot g \cdot \Delta L \cdot \frac{S_{kt}}{v_{ls}} \cdot C_{vt} \quad \text{or} \quad i_m = i_l + \frac{S_{kt}}{v_{ls}} \cdot C_{vt} \qquad (6.7\text{-}6)$$
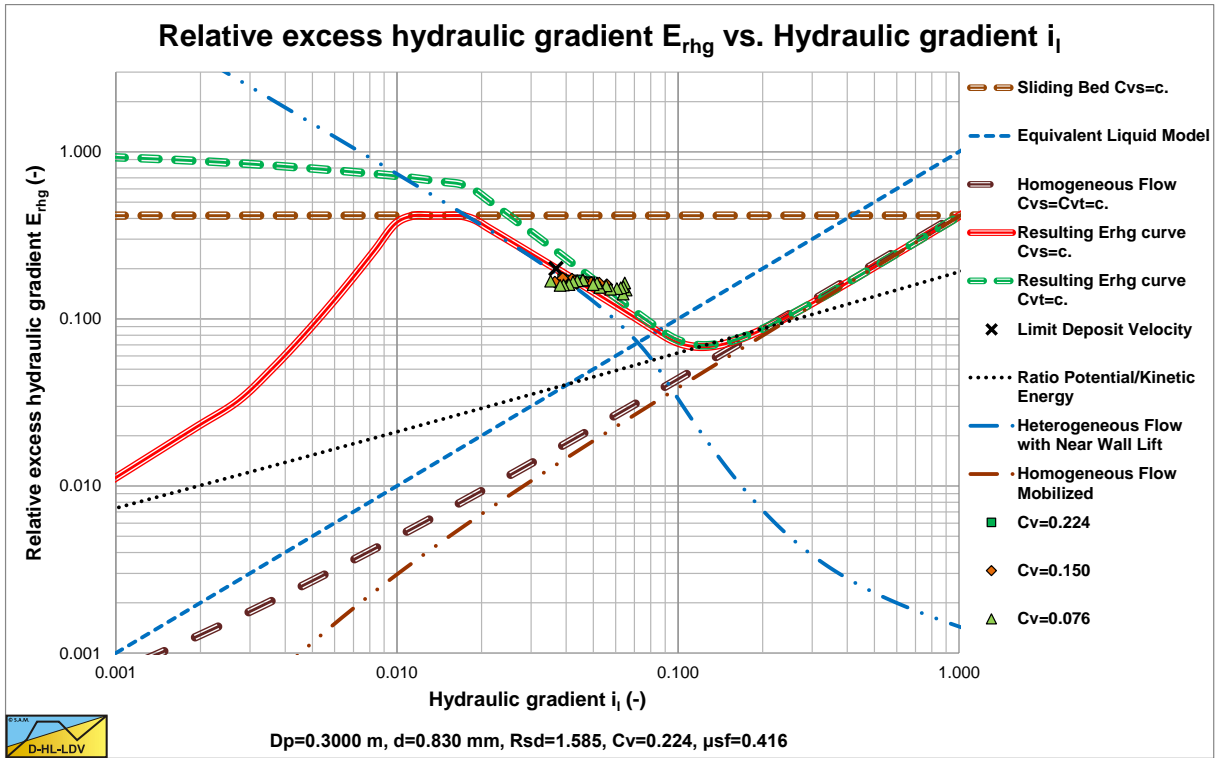
Figure 6.7-3: The data of Fuhrboter with a d_{50}=0.83 mm sand.
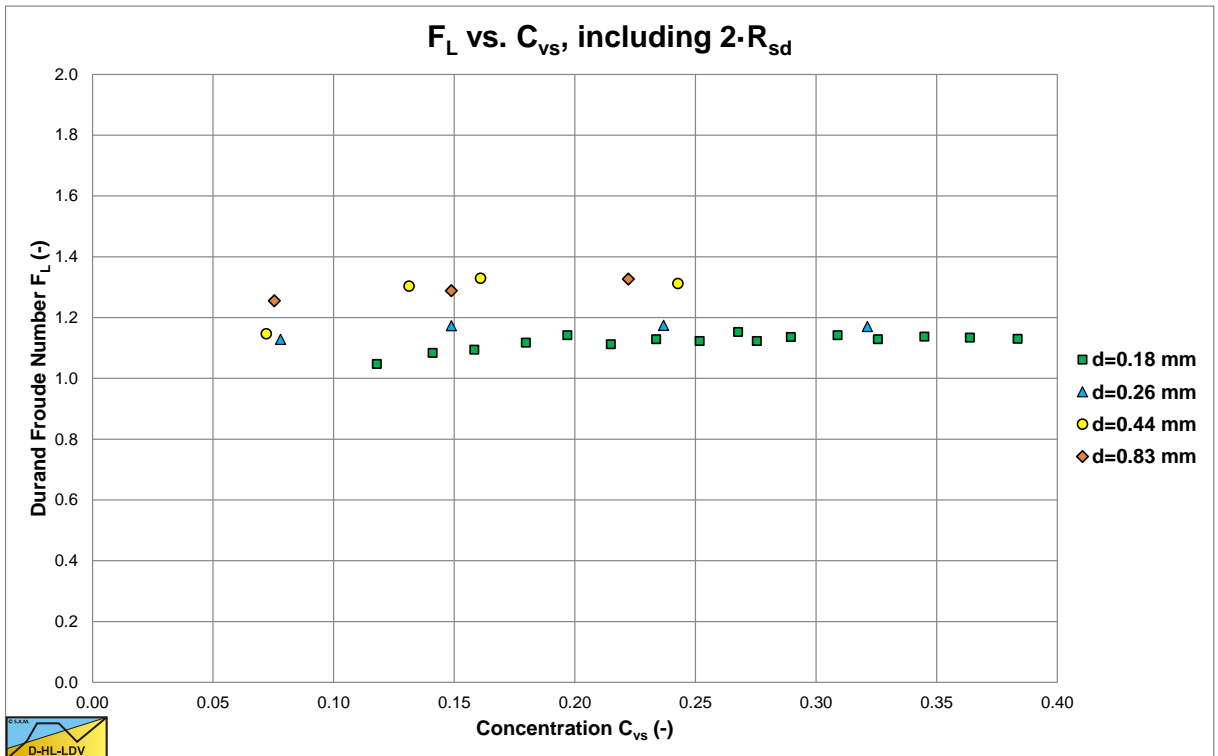
Figure 6.7-4: The Durand F_L factor measured by Fuhrboter.
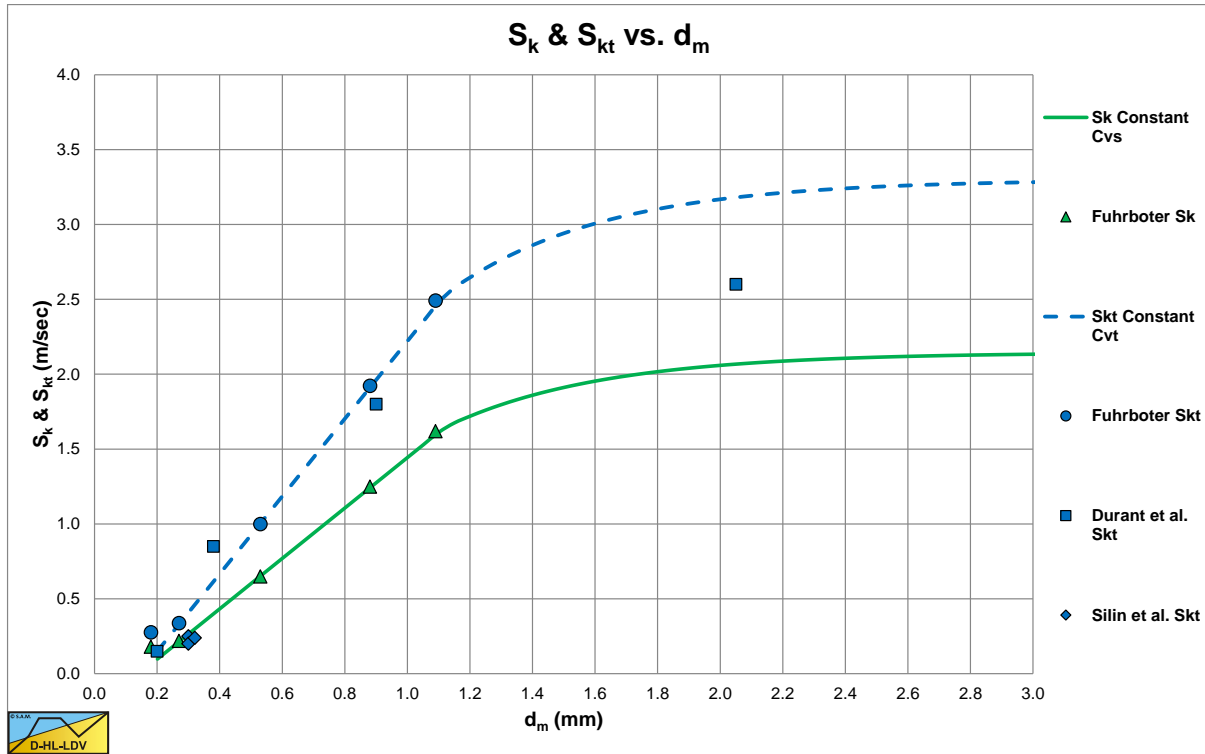
Figure 6.7-5: The transport factor S_k and S_{kt} for the Fuhrboter equation.

The coefficient S_{kt} is an emperical coefficient depending on the solids properties according to Figure 6.7-5 and equation (6.7-7) as found in many textbooks, but not in Fuhrboter (1961).

$$
\begin{aligned}
S_{kt} &= \text{not defined} & d_m &< 0.2 \text{ mm} \\
S_{kt} &= 2.59 \cdot d_m - 0.37 & 0.2 \text{ mm} &\leq d_m < 1.1 \text{ mm} \\
S_{kt} &= \text{according to graph} & 1.1 \text{ mm} &\leq d_m < 3.0 \text{ mm} \\
S_{kt} &\approx 3.3 & 3.0 \text{ mm} &\leq d_m
\end{aligned}
\tag{6.7-7}
$$

Note that the particle diameter is in mm not in m and the graph is for sand. The model of Fuhrboter is very easy to use and to calibrate with own data. The transport factor S_{kt} however has to cover all the effects of the frictional head loss, like the soil properties, the settling process and the liquid properties. Furthermore, the assumption of a constant slip factor is unacceptable for different soils and flow conditions. The conclusion is that the model is only applicable for the conditions in which the experiments of Fuhrboter were carried out.

Equation (6.7-6) can be written in a more general form as:

$$
\Delta p_m = \Delta p_l \cdot \left(1 + 2 \cdot \left(g \cdot D_p \cdot R_{sd} \right) \cdot \left(\frac{S_{kt}}{\lambda_l \cdot R_{sd}} \right) \cdot C_{vt} \cdot \left(\frac{1}{v_{ls}} \right)^3 \right)
\tag{6.7-8}
$$

$$
i_m = i_l + S_{kt} \cdot C_{vt} \cdot \frac{1}{v_{ls}}
$$

Substituting equation (6.7-7) gives for **$0.2 \text{ mm} \leq d_m < 1.1 \text{ mm}$** :

$$
\Delta p_m = \Delta p_l \cdot \left(1 + \left(3140 \cdot d_m - 448 \right) \cdot \frac{g \cdot D_p \cdot R_{sd}}{\lambda_l} \cdot C_{vt} \cdot \left(\frac{1}{v_{ls}} \right)^3 \right)
\tag{6.7-9}
$$

With $\lambda_l=0.015$ and $R_{sd}=1.65$ this would give:

$$\Delta p_m = \Delta p_l \cdot \left(1 + 2 \cdot \left(g \cdot D_p \cdot R_{sd} \right) \cdot \left(40 \cdot S_{kt} \right) \cdot C_{vt} \cdot \left(\frac{1}{v_{ls}} \right)^3 \right) \tag{6.7-10}$$

As stated above, the fixed slip factor of 0.65 was based on the propagation velocity of density waves. The question is whether or not this propagation velocity is a good measure for the slip factor or slip velocity. According to Matousek (1997) the propagation of density waves is a very complex process which is not directly related to the slip velocity of the solids. Yagi et al. (1972), Matousek (1996), Grunsven (2012) and others found that the slip velocity in the heterogeneous regime is just a few percent near the Limit Deposit Velocity and less than 1 percent near the homogeneous regime. In general, the slip can be neglected in the heterogeneous regime. The assumption of a slip factor of 0.65 as used by Fuhrboter (1961) is thus rejected and the conclusion is that the S_k value should be applied and not the S_{kt} value, giving:

$$
\begin{array}{ll}
S_k = \text{not defined} & d_m < 0.2\,\text{mm} \\
S_k = 1.68 \cdot d_m - 0.24 & 0.2\,\text{mm} \le d_m < 1.1\,\text{mm} \\
S_k = \text{according to graph} & 1.1\,\text{mm} \le d_m < 3.0\,\text{mm} \\
S_k \approx 2.15 & 3.0\,\text{mm} \le d_m
\end{array} \tag{6.7-11}
$$

Equation (6.7-3) can be written in a more general form as:

$$\Delta p_m = \Delta p_l \cdot \left(1 + 2 \cdot \left(g \cdot D_p \cdot R_{sd} \right) \cdot \left(\frac{S_k}{\lambda_l \cdot R_{sd}} \right) \cdot C_{vs} \cdot \left(\frac{1}{v_{ls}} \right)^3 \right) \tag{6.7-12}$$

$$i_m = i_l + S_k \cdot C_{vs} \cdot \frac{1}{v_{ls}}$$

Substituting equation (6.7-11) gives for $0.2\,\text{mm} \le d_m < 1.1\,\text{mm}$:

$$\Delta p_m = \Delta p_l \cdot \left(1 + \left(2041 \cdot d_m - 291 \right) \cdot \frac{g \cdot D_p \cdot R_{sd}}{\lambda_l} \cdot C_{vs} \cdot \left(\frac{1}{v_{ls}} \right)^3 \right) \tag{6.7-13}$$

With $\lambda_l=0.015$ and $R_{sd}=1.65$ this would give:

$$\Delta p_m = \Delta p_l \cdot \left(1 + 2 \cdot \left(g \cdot D_p \cdot R_{sd} \right) \cdot \left(40 \cdot S_k \right) \cdot C_{vs} \cdot \left(\frac{1}{v_{ls}} \right)^3 \right) \tag{6.7-14}$$

It should be mentioned that Fuhrboter (1961) found excess pressure losses that decreased with the line speed, but with a power a bit higher than -1 in equation (6.7-3), like -1.2, which would result in a power of about 3.2 in the above equations. This matches the findings of Wilson et al. (1992), who found a power of -1.7 for uniform sands, decreasing to -0.25 for very graded sands. Fuhrboter (1961) also used the mean particle diameter d_m instead of the d_{50}. Although there are small differences for the sands used, this will not lead to a significant change in the S_k graph, so the graph can also be used with the d_{50}.

Figure 6.7-6 shows that the DHLLDV Framework for graded sands may explain the steepness of the data points, which is less steep than for uniform sands.

Finally Figure 6.7-7 shows a lower and upper limit to the S_k value based on the DHLLDV Framework at 20° C. At other temperatures the curves may be slightly different. A lower temperature gives higher curves.
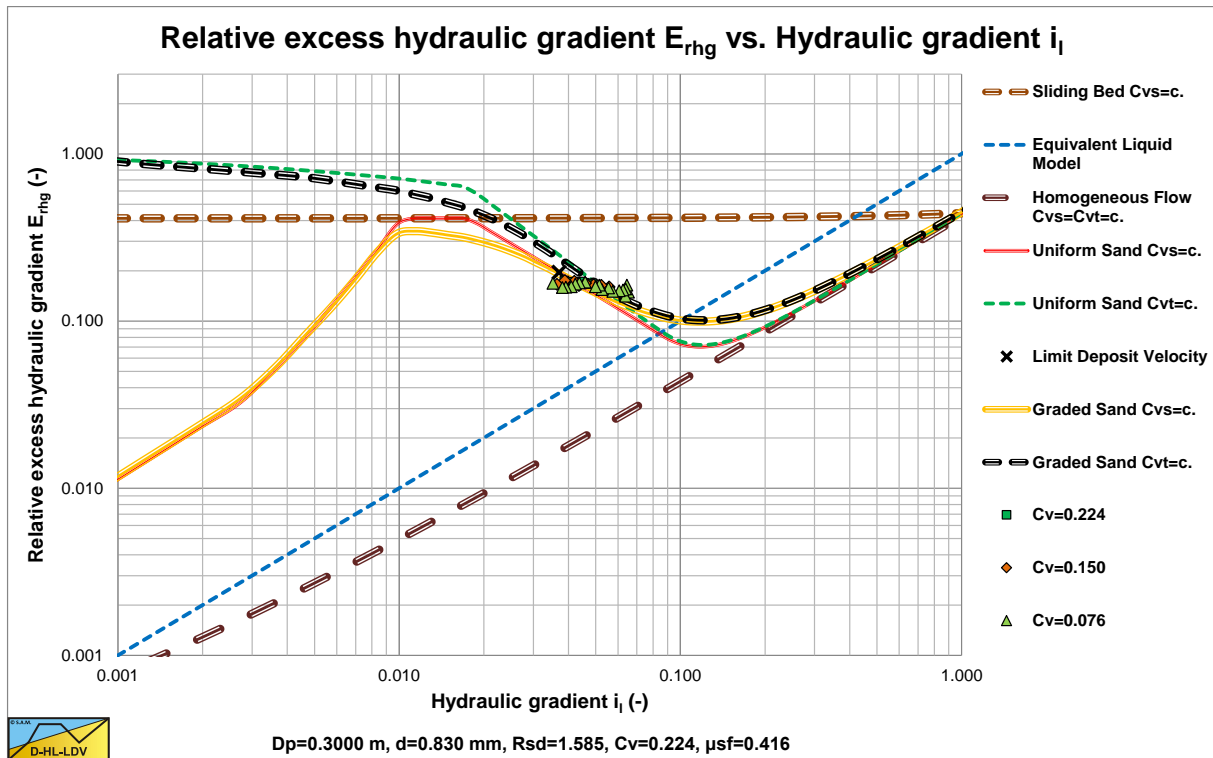
Figure 6.7-6: The data of Fuhrboter with a d_{50}=0.83 mm sand compared with the DHLLDV Framework for a graded sand..
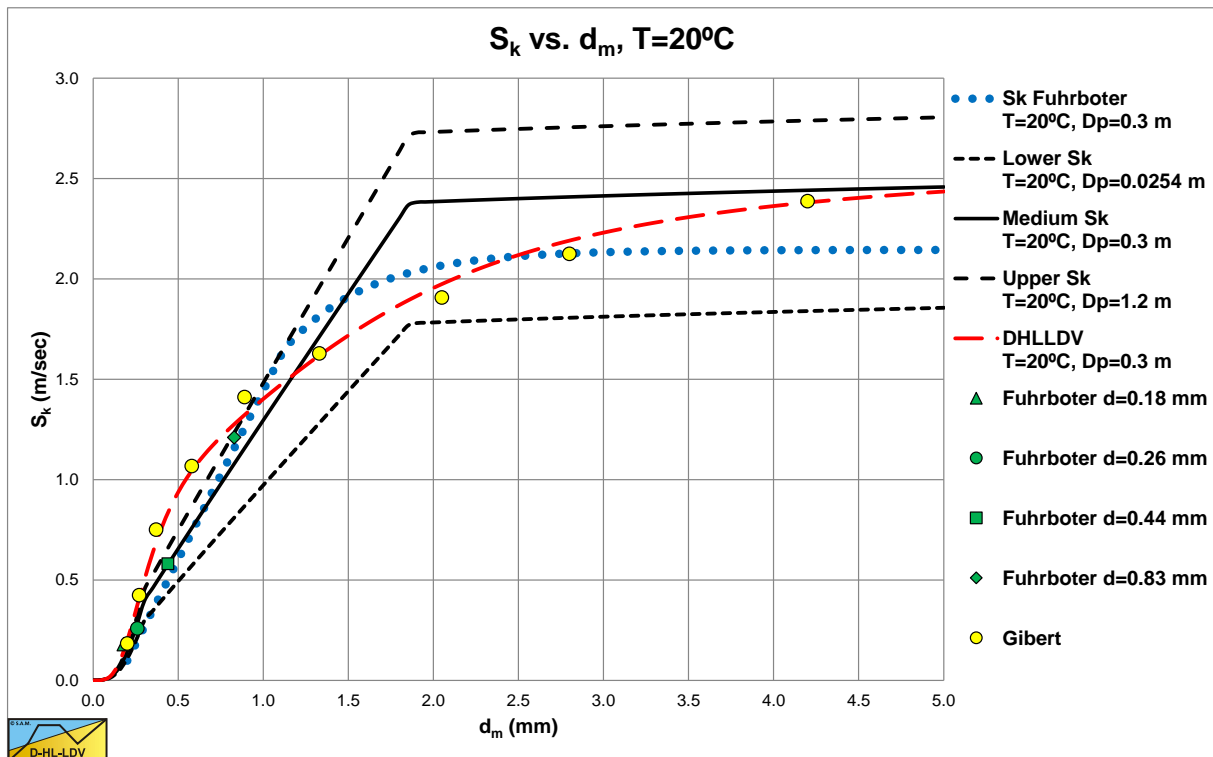
Figure 6.7-7: S_k lower and upper limit based on the DHLLDV Framework.

6.8 The Jufin & Lopatin (1966) Model.

6.8.1 Introduction.

The Jufin & Lopatin (1966) model was constructed as a proposal for the Soviet technical norm in 1966. The authors did not submit a new model but selected the best combination of correlations for the frictional head loss and the critical velocity from four models submitted by different Soviet research institutes. The four models submitted were tested by a large experimental database collected by a number of researchers. The database contained data from both laboratory and field measurements (including data from dredging installations). The data covered a wide range of pipeline sizes (24 – 900 mm) and particle sizes (sand and gravel, 0.25 - 11 mm). Some of the data on which the model is based can be found in the chapters about Silin, Kobernik & Asaulenko (1958), Kazanskij (1978) and on the website www.dhlldv.com.

Kazanskij (1972) gave a summary and sort of manual for the use of the Jufin-Lopatin model. First of all sands and gravels are divided into 4 groups, according to Table 6.8-1. The ψ^* parameter characterizes the particles and is comparable with the Durand & Condolios (1952) $\sqrt{C_x}$ parameter.

$$\psi^* = Fr_p^{3/2} = \left(\frac{v_t}{\sqrt{g \cdot d}} \right)^{3/2} \tag{6.8-1}$$

Table 6.8-1: Group classification of Jufin-Lopatin (1966), source Kazanskij (1972).

Group	Range	ψ^*
A	d<0.06 mm	-
B	d_{60}<10 mm	All
	d_{10}<10 mm<d_{60}	ψ^*<=1.5, d_0<2.5 mm
C	d_{10}<10 mm<d_{60}	ψ^*>1.5, d_0>2.5 mm
D	d_{10}>10 mm	-

The particle diameter d_0 (sometimes named d_{mf}) is the average particle diameter, not a weighted particle diameter, and can be determined by:

$$d_0 = \frac{\sum_{i=1}^{100} d_i}{100} \quad \text{or} \quad d_0 = \frac{\sum_{i=10}^{90} d_i}{9} \tag{6.8-2}$$

So each fraction has the same weight in the determination of the d_0 value. For uniform sands and gravels, the d_0 is equal to the particle diameter.

6.8.2 Group A: Fines.

Group A covers the fines, silt. For silt Jufin & Lopatin (1966) use the ELM without the Thomas (1965) viscosity, so:

$$\Delta p_m = \lambda_l \cdot \frac{\Delta L}{D_p} \cdot \frac{1}{2} \cdot \rho_m \cdot v_{ls}^2 \tag{6.8-3}$$

The hydraulic gradient i_m (for mixture) is now:

$$i_m = \frac{\Delta p_m}{\rho_l \cdot g \cdot \Delta L} = \frac{\rho_m}{\rho_l} \cdot \frac{\lambda_l \cdot v_{ls}^2}{2 \cdot g \cdot D_p} \tag{6.8-4}$$

6.8.3 Group B: Sand.

Group B covers fine and medium sands, with possibly some fine gravel. The equation found by Jufin & Lopatin (1966) was based on the empirical experience, suggesting that the minimum hydraulic gradient at the velocity v_{min} was independent of the mixture flow properties and it was 3 times higher than the hydraulic gradient of water flow at the same velocity in a pipeline. This was also experienced in the American dredging industry (see Turner (1996)). Now most frictional head models follow the equation:

$$\Delta p_m = \Delta p_l \cdot \left(1 + 2 \cdot \Omega \cdot \left(\frac{1}{v_{ls}}\right)^3\right) \quad \text{with:} \quad v_{min} = \Omega^{1/3} \tag{6.8-5}$$

The minimum is found at the cube root of Ω, as is the case with the Durand/Condolios/Gibert, Newitt et al. and Fuhrboter models. The frictional-head-loss correlation by Jufin & Lopatin is:

$$\Delta p_m = \Delta p_l \cdot \left(1 + 2 \cdot \left(\frac{v_{min}}{v_{ls}}\right)^3\right) \tag{6.8-6}$$

With, for quarts particles (sometimes a factor 5.3 is used instead of 5.5) :

$$v_{min} = 5.5 \cdot \left(C_{vt} \cdot \psi^* \cdot D_p\right)^{1/6} = 3.76 \cdot \left(C_{vt} \cdot \psi^* \cdot g \cdot D_p\right)^{1/6} = 3.46 \cdot \left(C_{vt} \cdot \psi^* \cdot g \cdot D_p \cdot R_{sd}\right)^{1/6} \tag{6.8-7}$$

This can be written in a more general form for the hydraulic gradient according to:

$$i_m = i_l \cdot \left(1 + 2 \cdot 41.35 \cdot \left(C_{vt} \cdot \psi^* \cdot g \cdot D_p \cdot R_{sd}\right)^{1/2} \left(\frac{1}{v_{ls}}\right)^3\right) \tag{6.8-8}$$
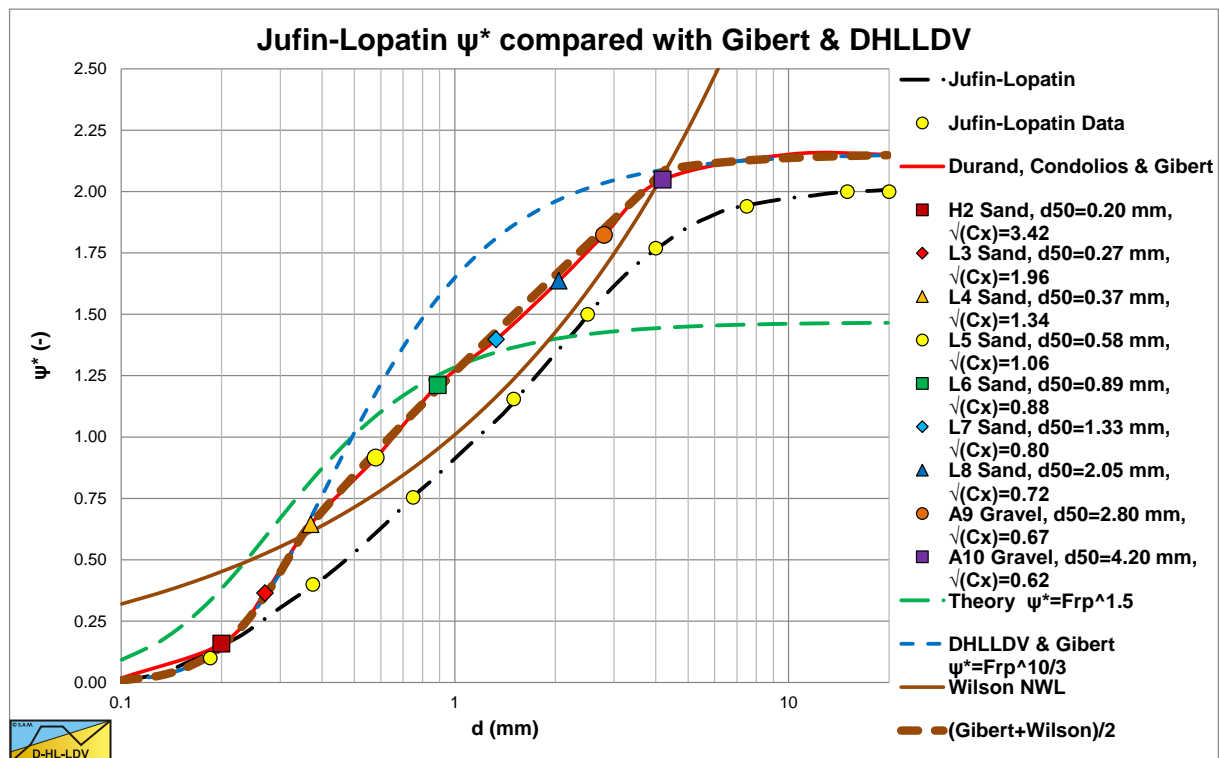
Figure 6.8-1: The Jufin-Lopatin ψ^* compared to Gibert and DHLLDV.

Figure 6.8-1 shows the ψ^* parameter of Jufin & Lopatin (1966) according to Kazanskij (1972). This parameter is compared with the equivalent parameters of Gibert (1960), Fuhrboter (1961) and the DHLLDV Framework (Miedema S. A., 2014). The trends are similar, but especially for medium sands, the values differ. The table of ψ^* values (the black line with yellow circles) does not match equation (6.8-1) (the green line) well. The thick dashed brown line representing the DHLLDV Framework implementation, is closer to the table values. A power of 3 seems more appropriate than a power of 3/2.

Figure 6.8-2 shows a comparison in terms of the Gibert (1960) $\sqrt{C_x}$ value. Of course the trends are similar compared to Figure 6.8-1.
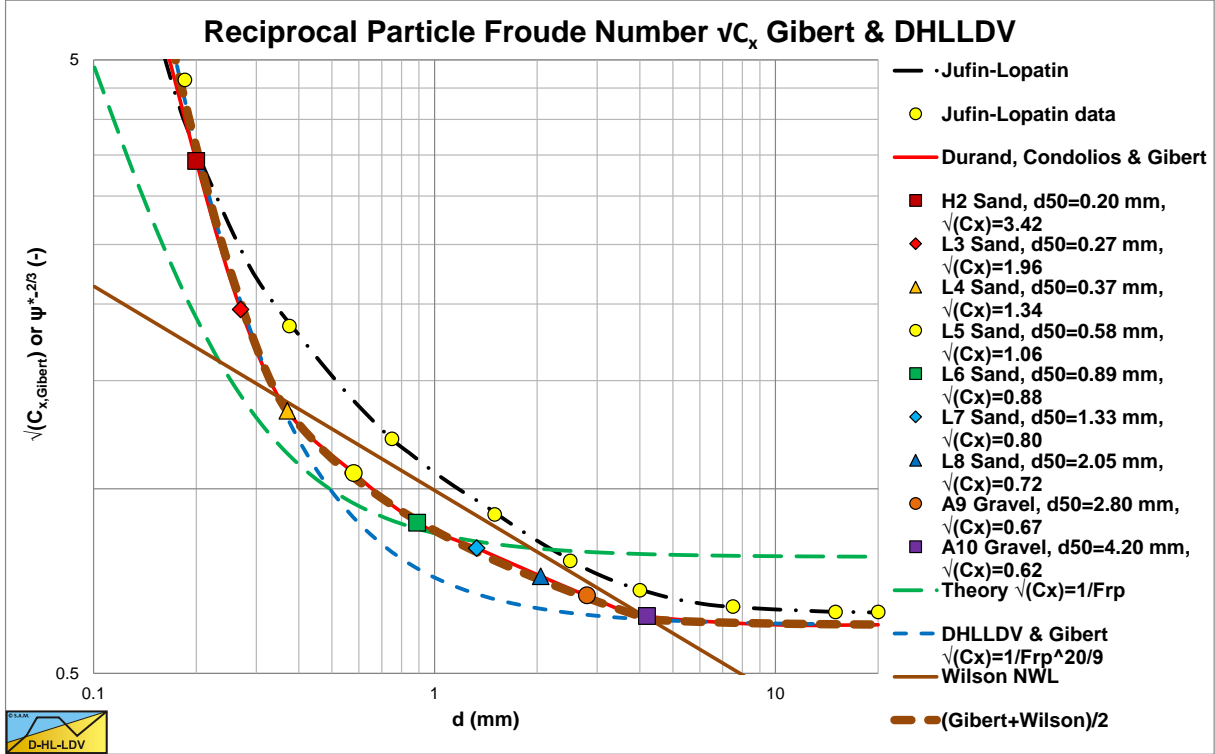
Figure 6.8-2: The reciprocal particle Froude number of Jufin-Lopatin, Gibert and DHLLDV.

Assuming the experiments are carried out with quarts this can be written as:

$$i_m = i_l \cdot \left(1 + 2 \cdot 41.35 \cdot \left(\frac{v_t}{\sqrt{g \cdot d}} \right)^{3/4} \cdot \left(g \cdot D_p \cdot R_{sd} \right)^{1/2} \cdot \left(C_{vt} \right)^{1/2} \left(\frac{1}{v_{ls}} \right)^3 \right) \qquad (6.8\text{-}9)$$

The term v_{min} should have the dimension of velocity, but in equation (6.8-7) it has the dimension of the cube root of velocity. This has to be compensated without violating the model of Jufin Lopatin. Now the product of kinematic viscosity v and the gravitational constant g has the dimension of velocity to the 3rd power. It is not clear whether Jufin & Lopatin carried out experiments in liquids with different viscosities, but for dredging purposes it is neutral using this. This gives for v_{min}, using a kinematic viscosity of 10^{-6} m²/sec and a gravitational constant of 9.81 m/sec²:

$$v_{min} = 44.88 \cdot \left(C_{vt} \cdot \psi^* \cdot g \cdot D_p \cdot R_{sd} \right)^{1/6} \cdot \left(v_l \cdot g \right)^{2/9} \qquad (6.8\text{-}10)$$

Substituting this in equation (6.8-6) gives the equation for the hydraulic gradient.

$$i_m = i_l \cdot \left(1 + 2 \cdot 90389 \cdot \left(\frac{v_t}{\sqrt{g \cdot d}} \right)^{3/4} \cdot \left(g \cdot D_p \cdot R_{sd} \right)^{1/2} \cdot \left(v_l \cdot g \right)^{2/3} \cdot \left(C_{vt} \right)^{1/2} \left(\frac{1}{v_{ls}} \right)^3 \right) \qquad (6.8\text{-}11)$$

6.8.4 The Limit Deposit Velocity.

Jufin & Lopatin (1966) defined the Limit Deposit Velocity as (sometimes a value of 8 is used instead of 8.3):

$$
v_{ls,\,ldv} = 8.3 \cdot \left(C_{vt} \cdot \psi^* \right)^{1/6} \cdot D_p^{1/3}
\tag{6.8-12}
$$

It is clear that this Limit Deposit Velocity also does not have the dimension of velocity, but the cube root of length. To give this Limit Deposit Velocity the dimension of velocity, the equation is modified to (for quarts and water):

$$
v_{ls,\,ldv} = 9.23 \cdot \left(C_{vt} \cdot \psi^* \right)^{1/6} \cdot \left(2 \cdot g \cdot D_p \cdot R_{sd} \right)^{1/3} \cdot \left(v_l \cdot g \right)^{1/9}
\tag{6.8-13}
$$

Which can be written as:

$$
v_{ls,\,ldv} = 9.23 \cdot \left(C_{vt} \right)^{1/6} \cdot \left(\frac{v_t}{\sqrt{g \cdot d}} \right)^{1/4} \cdot \left(2 \cdot g \cdot D_p \cdot R_{sd} \right)^{1/3} \cdot \left(v_l \cdot g \right)^{1/9}
\tag{6.8-14}
$$

Giving:

$$
F_L = \frac{v_{ls,\,ldv}}{\left(2 \cdot g \cdot D_p \cdot R_{sd} \right)^{1/2}} = 9.23 \cdot \frac{\left(C_{vt} \right)^{1/6} \cdot \left(\dfrac{v_t}{\sqrt{g \cdot d}} \right)^{1/4} \cdot \left(v_l \cdot g \right)^{1/9}}{\left(2 \cdot g \cdot D_p \cdot R_{sd} \right)^{1/6}}
\tag{6.8-15}
$$

6.8.5 Broad Graded Sands or Gravels.

The effect of a broad particle size distribution is taken into account by determining an average value of the modified particle Froude number from values of the modified Froude number for soil fraction p_i of different size d_i. The values for ψ^* can also be taken from Table 6.8-1 or Figure 6.8-1.

$$
\psi^* = Fr_{vt}^{1.5} = \sum_{i=1}^{n} Fr_{vt,i}^{1.5} \cdot p_i = \sum_{i=1}^{n} \psi^*(d_i) \cdot p_i
\tag{6.8-16}
$$

Table 6.1: Particle settling parameter for the Jufin-Lopatin (1966) model.

size fraction of solids, d [mm]	particle settling parameter, ψ^* Jufin & Lopatin (1966)	particle settling parameter, ψ^* Jufin (1971)
0.05 - 0.10	0.0204	0.02
0.10 - 0.25	0.0980	0.1
0.25 - 0.50	0.4040	0.4
0.50 - 1.00	0.7550	0.8
1.0 - 2.0	1.1550	1.2
2.0 - 3.0	1.5000	1.5
3.0 - 5.0	1.7700	1.8
5 - 10	1.9400	1.9
10 - 20	1.9700	2.0
>20	2.0000	2.0

6.8.6 Group C: Fine Gravel.

Group C is a transition between medium sized sand and coarse gravel. The equation for v_{min} has to be corrected according to:

$$v_{min} = 5.5 \cdot b \cdot \left(C_{vt} \cdot \psi^* \cdot D_p \right)^{1/6} = 3.76 \cdot b \cdot \left(C_{vt} \cdot \psi^* \cdot g \cdot D_p \right)^{1/6}$$

$$= 3.46 \cdot b \cdot \left(C_{vt} \cdot \psi^* \cdot g \cdot D_p \cdot R_{sd} \right)^{1/6} = 44.88 \cdot b \cdot \left(C_{vt} \cdot \psi^* \cdot g \cdot D_p \cdot R_{sd} \right)^{1/6} \cdot \left(v_l \cdot g \right)^{2/9}$$

(6.8-17)

The correction factor **b** can be determined with:

$$b = 1 + \frac{(\psi - 1.5)}{(2.0 - 1.5)} \cdot (a - 1)$$

(6.8-18)

Where the factor **a** can be found in Table 6.8-2.

Table 6.8-2: Correction factor a, source Kazanskij (1972) .

d_0	10 mm<d_0<20 mm				d_0>20 mm			
ρ_m (ton/m³)	1.02	1.05	1.10	1.20	1.02	1.05	1.10	1.20
D_p<400 mm	1.01	1.18	1.34	1.48	1.11	1.30	1.48	1.68
400 mm<D_p<600 mm	1.14	1.31	1.47	1.64	1.27	1.46	1.62	1.81
600 mm<D_p	1.23	1.41	1.54	1.73	1.38	1.50	1.67	1.86

6.8.7 Group D: Coarse Gravel.

For Group D the correction factor is just **a**, according to Table 6.8-2.

$$v_{min} = 5.5 \cdot a \cdot \left(C_{vt} \cdot 2 \cdot D_p \right)^{1/6} = 3.76 \cdot a \cdot \left(C_{vt} \cdot 2 \cdot g \cdot D_p \right)^{1/6}$$

$$= 3.46 \cdot a \cdot \left(C_{vt} \cdot 2 \cdot g \cdot D_p \cdot R_{sd} \right)^{1/6} = 44.88 \cdot a \cdot \left(C_{vt} \cdot 2 \cdot g \cdot D_p \cdot R_{sd} \right)^{1/6} \cdot \left(v_l \cdot g \right)^{2/9}$$

(6.8-19)

6.8.8 Conclusions & Discussion.

The model of Jufin & Lopatin (1966) for Group A is the ELM model without a viscosity correction.
The models for Groups B, C and D are similar, but Groups C and D have a correction factor. In order to make the Jufin & Lopatin (1966) model comparable with other models, the basic equation is written in terms of the liquid hydraulic gradient plus the solids effect.

$$i_m = i_l + 2 \cdot 90389 \cdot \left(g \cdot D_p \cdot R_{sd} \cdot \psi^* \right)^{1/2} \cdot \left(v_l \cdot g \right)^{2/3} \cdot \left(C_{vt} \right)^{1/2} \left(\frac{1}{v_{ls}} \right)^3 \cdot \frac{\lambda_l \cdot v_{ls}^2}{2 \cdot g \cdot D_p}$$

$$= i_l + 90389 \cdot \frac{\lambda_l \cdot \left(\psi^* \cdot R_{sd} \right)^{1/2} \cdot \left(v_l \cdot g \right)^{2/3}}{\left(g \cdot D_p \right)^{1/2} \cdot \left(C_{vt} \right)^{1/2}} \cdot \frac{C_{vt}}{v_{ls}}$$

(6.8-20)

The Darcy-Weisbach friction factor for a smooth pipe can be approached by:

$$\lambda_l = \alpha \cdot \left(v_{ls} \right)^{\alpha_1} \cdot \left(D_p \right)^{\alpha_2}$$

(6.8-21)

With:

$$\alpha = 0.01216 \quad \text{and} \quad \alpha_1 = -0.1537 \cdot \left(D_p\right)^{-0.089} \quad \text{and} \quad \alpha_2 = -0.2013 \cdot \left(v_{ls}\right)^{-0.088} \tag{6.8-22}$$

For laboratory conditions both powers are close to **-0.18**, while for real life conditions with higher line speeds and much larger pipe diameters this results in a power for the line speed of about **α_1=-0.155** and for the pipe diameter of about **α_2=-0.175**. This should be considered when analyzing the models for heterogeneous transport.

This gives for the Darcy-Weisbach friction factor in a dimensionless form:

$$\lambda_l = 0.01216 \cdot \left(v_{ls}\right)^{-0.155} \cdot \left(D_p\right)^{-0.175} \approx 0.1233 \cdot \left(v_{ls}\right)^{-0.155} \cdot \left(g \cdot D_p\right)^{-0.172} \cdot \left(\nu_l \cdot g\right)^{1/6} \tag{6.8-23}$$

Substitution gives:

$$i_m = i_l + 11145 \cdot \frac{\left(\psi^* \cdot R_{sd}\right)^{1/2} \cdot \left(\nu_l \cdot g\right)^{5/6}}{\left(g \cdot D_p\right)^{0.672} \cdot \left(C_{vs}\right)^{1/2}} \cdot \frac{1}{v_{ls}^{0.155}} \cdot \frac{C_{vs}}{v_{ls}} \tag{6.8-24}$$

With the solids effect factor S_k (to compare with Fuhrboter) defined as:

$$i_m = i_l + S_k \cdot \frac{C_{vs}}{v_{ls}} \quad \text{with:} \quad S_k = 11145 \cdot \frac{\left(\psi^* \cdot R_{sd}\right)^{1/2} \cdot \left(\nu_l \cdot g\right)^{5/6}}{\left(g \cdot D_p\right)^{0.672} \cdot \left(C_{vs}\right)^{1/2}} \cdot \frac{1}{v_{ls}^{0.155}} \tag{6.8-25}$$
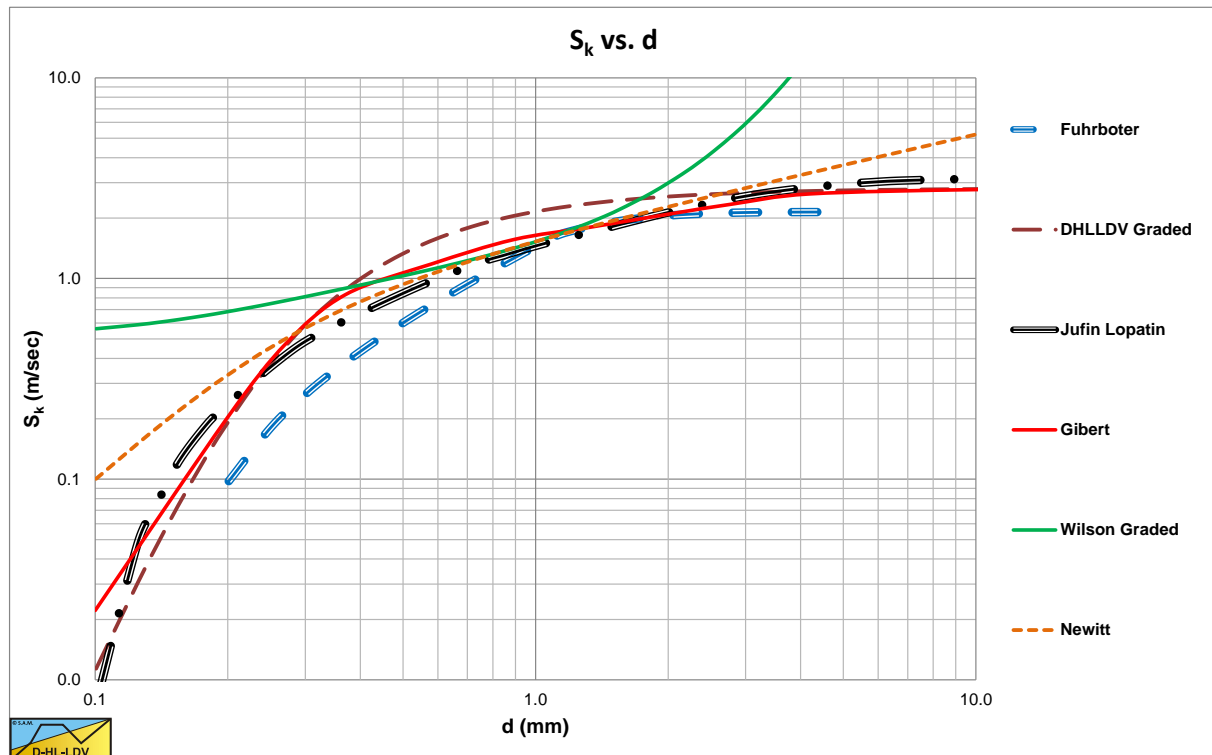
Figure 6.8-3: The S_k of Jufin-Lopatin compared with the original Fuhrboter values for a D_p=0.1016 m (4 inch) pipe and a 25% concentration.

The S_k curve of Jufin-Lopatin matches the original Fuhrboter curve reasonably for a D_p=0.1016 m pipe and 25% spatial volumetric concentration, just as the DHLLDV Framework and the Gibert data. However, the Jufin-Lopatin equation contains the pipe diameter and the concentration and will thus give different results for other pipe diameters and concentrations.

6.9 Charles (1970) and Babcock (1970).

6.9.1 Charles (1970).

The models of Durand & Condolios (1952), Newitt et al. (1955), Worster & Denny (1955), Fuhrboter (1961), Jufin & Lopatin (1966) and Zandi & Govatos (1967) all have in common that the equation for the excess head losses in the heterogeneous regime approaches zero for very high line speeds. Charles (1970) states that this cannot be true, since in general the excess head losses will approach the excess head losses matching the ELM. In other words, for very high line speeds the hydraulic gradient should be determined with the Darcy Weisbach equation, replacing the density of the pure liquid with the mixture density. Most equations have the following form, or can be rewritten to this form:

$$\Phi = \frac{i_m - i_l}{i_l \cdot C_{vt}} = K \cdot \psi^{-\beta} \tag{6.9-1}$$

With:

$$\psi = \left(\frac{v_{ls}^2}{g \cdot D_p \cdot R_{sd}} \right) \cdot \sqrt{C_x} \quad \text{or} \quad \psi = \left(\frac{v_{ls}^2}{g \cdot D_p \cdot R_{sd}} \right) \cdot \sqrt{C_D} \tag{6.9-2}$$

Durand & Condolios (1952) use the first variant, while both Charles (1970) and Babcock (1970) use the second variant. The difference between the two variants is significant and should be taken into account when using this equation. For the factor **K** values in the range of 80-150 have been found. The original Durand & Condolios (1952) equation did not mention a value, however later values in the range of 80-85 are deduced. The value of **β=1.5** for the heterogeneous regime, although values up to 2 are found in literature. In order to get a smooth transition from the heterogeneous regime to the homogeneous regime, Charles (1970) suggested the following equation:

$$\Phi = \frac{i_m - i_l}{i_l \cdot C_{vt}} = K \cdot \psi^{-\beta} + R_{sd} \tag{6.9-3}$$

Or for the relative excess hydraulic gradient:

$$E_{rhg} = \frac{i_m - i_l}{C_{vt} \cdot R_{sd}} = i_l \cdot \left(\frac{K}{R_{sd}} \cdot \psi^{-\beta} + 1 \right) \tag{6.9-4}$$

The disadvantage of this equation is, that the hydraulic gradient can never be smaller than the ELM, which is often observed to be the case. However as an upper limit to the hydraulic gradient the equation is useful. Charles (1970) also suggested to use the Minimum Hydraulic Gradient Velocity (MHGV) as an estimate for the Limit Deposit Velocity (LDV) since these are close. This MHGV can be obtained by differentiating the above equation with respect to the line speed v_{ls}. This gives:

$$i_m = i_l \cdot \left(\frac{K}{R_{sd}} \cdot \psi^{-\beta} + 1 \right) \cdot C_{vt} \cdot R_{sd} + i_l \tag{6.9-5}$$

Or:

$$i_m = \frac{\lambda_l \cdot v_{ls}^2}{2 \cdot g \cdot D_p} \cdot \left(\frac{K}{R_{sd}} \cdot \left(\left(\frac{v_{ls}^2}{g \cdot D_p \cdot R_{sd}} \right) \cdot \sqrt{C_x} \right)^{-1.5} + 1 \right) \cdot C_{vt} \cdot R_{sd} + \frac{\lambda_l \cdot v_{ls}^2}{2 \cdot g \cdot D_p} \tag{6.9-6}$$

$$i_m = \frac{\lambda_l}{2 \cdot g \cdot D_p} \cdot \left(\left(1 + C_{vt} \cdot R_{sd} \right) \cdot v_{ls}^2 + \left(K \cdot \left(\frac{g \cdot D_p \cdot R_{sd}}{\sqrt{C_x}} \right)^{1.5} \cdot C_{vt} \right) \cdot \frac{1}{v_{ls}} \right)$$

This gives for the MHGV:

$$v_{ls,MHGV} = \left(\frac{\left(K \cdot \left(\frac{g \cdot D_p \cdot R_{sd}}{\sqrt{C_x}} \right)^{1.5} \cdot C_{vt} \right)}{2 \cdot \left(1 + C_{vt} \cdot R_{sd} \right)} \right)^{1/3}$$

(6.9-7)

6.9.2 Babcock (1970).

Babcock (1970) adopted the approach of Charles (1970) regarding the transition of the heterogeneous regime to the homogeneous regime. The disadvantage of adding two possible solutions without any correction will probably overestimate the hydraulic gradient near the intersection point of the two regimes. The Wasp et al. (1977) model by means of the vehicle concentration and the Wilson et al (2006) model by means of the stratification ratio, do take this into account.
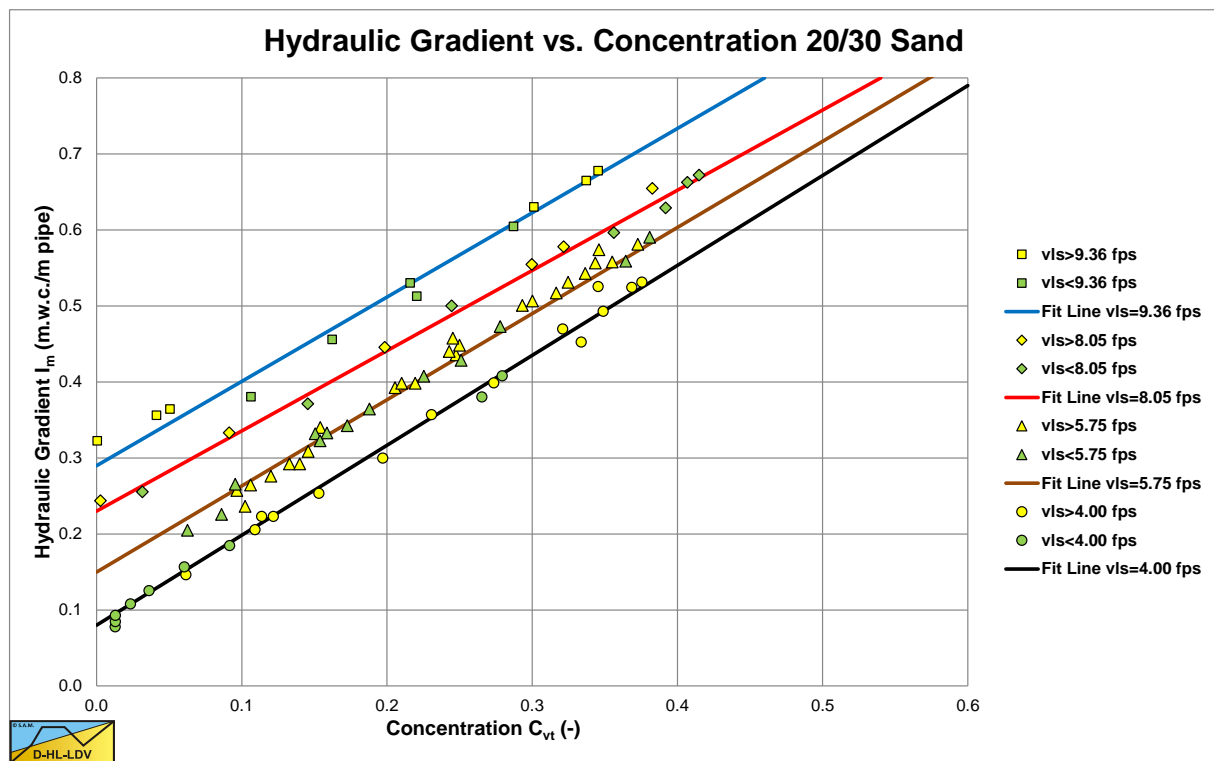

Figure 6.9-1: The dependency of the hydraulic gradient on the concentration, sand mesh 20/30.

The excess hydraulic gradient, the difference between the mixture hydraulic gradient and the pure liquid hydraulic gradient, is supposed to be proportional to the concentration of solids by volume in the mixture, the proportionality assumption. Now it is not always clear what is meant by the concentration of solids by volume in the mixture. The definition points to the spatial concentration, however most researchers have used the delivered concentration. A second assumption as used by Babcock (1970) is adopted from Durand & Condolios (1952), the size independence assumption for coarse particles. Stating that the excess hydraulic gradient is independent of the particle size above a certain particle diameter. The purpose of the research of Babcock (1970) was to verify these assumptions. The research was carried out in a 0.0254 m diameter pipe (1 inch). The first experiments were carried out with a 20/30 mesh quartz sand (coarse). The results are shown in Figure 6.9-1 and show a linear relation between the hydraulic gradient and the volumetric concentration. The equation of these lines is, using equation (6.9-2):

$$\Phi = \frac{i_m - i_l}{i_l \cdot C_{vt}} = 70 \cdot \psi^{-1}$$

(6.9-8)

Inspection of the flow revealed that all of these experiments were in the sliding bed regime. The above equation is very similar to the Newitt et al. (1955) equation.

Next a series of tests were carried out with an 80/100 mesh quartz sand (fine). The results of these experiments are shown in Figure 6.9-2. Up to a volumetric concentration of 20-25% the relation is linear, but above 25% the excess hydraulic gradient starts increasing more than linear. Inspection of the flow showed that at low concentrations most of the material was travelling as suspended load, but at higher concentrations there was a sliding bed and at the highest concentrations even a stationary bed. The following equation was derived from the experiments:

$$\Phi = \frac{i_m - i_l}{i_l \cdot C_{vt}} = 6.3 \cdot \psi^{-0.254} \tag{6.9-9}$$

Note that this equation is very similar to the Zandi & Govatos (1967) equation for pseudo homogeneous flow. The equation correlates well for concentrations up to 20%.

At last a series of experiments were conducted with a 30/45 mesh quartz sand (medium). The results are shown in Figure 6.9-3. Now it seems there is a curvature between 10% and 25% volumetric concentration, while the line straightens for the higher concentrations.

Similar tests were run on 6/8 mesh steel shot, on 10/16 mesh arkosic sand and on 16/30 mesh garnet sand. The results of these experiments are shown in Figure 6.9-4 and Figure 6.9-5, showing the same data points but with a different abscissa and ordinate. These tests clearly showed the occurrence of a sliding bed. The equation following from these experiments is:

$$\frac{i_m - i_l}{i_l \cdot C_{vt} \cdot R_{sd}} = 60.6 \cdot \left(\frac{v_{ls}^2}{g \cdot D_p} \right)^{-1} \quad \text{or} \quad \Phi = \frac{i_m - i_l}{i_l \cdot C_{vt}} = 60.6 \cdot \left(\frac{v_{ls}^2}{g \cdot R_{sd} \cdot D_p} \right)^{-1} = 60.6 \cdot \psi^{-1} \tag{6.9-10}$$

The above equation is very similar to the Newitt et al. (1955) equation. Newitt et al. (1955) found a factor of 66, Babcock (1970) a factor of 70 and a factor of 60.6. These values are very close. With a normal Darcy Weisbach friction factor of about 0.020-0.025 for a 0.0254 m diameter pipe this gives a sliding friction factor of **μ$_{sf}$=0.6-0.875.** This is comparable to Newitt et al. (1955).
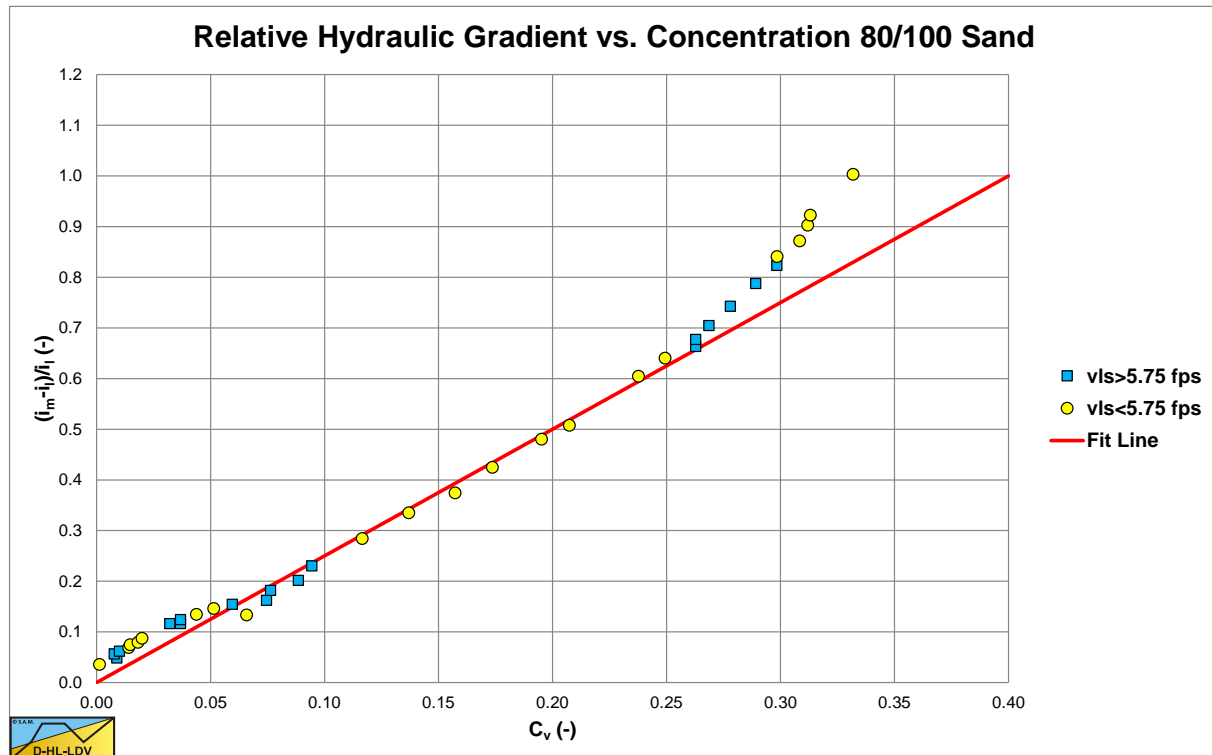
Figure 6.9-2: The dependency of the excess hydraulic gradient on the concentration, sand mesh 80/100.
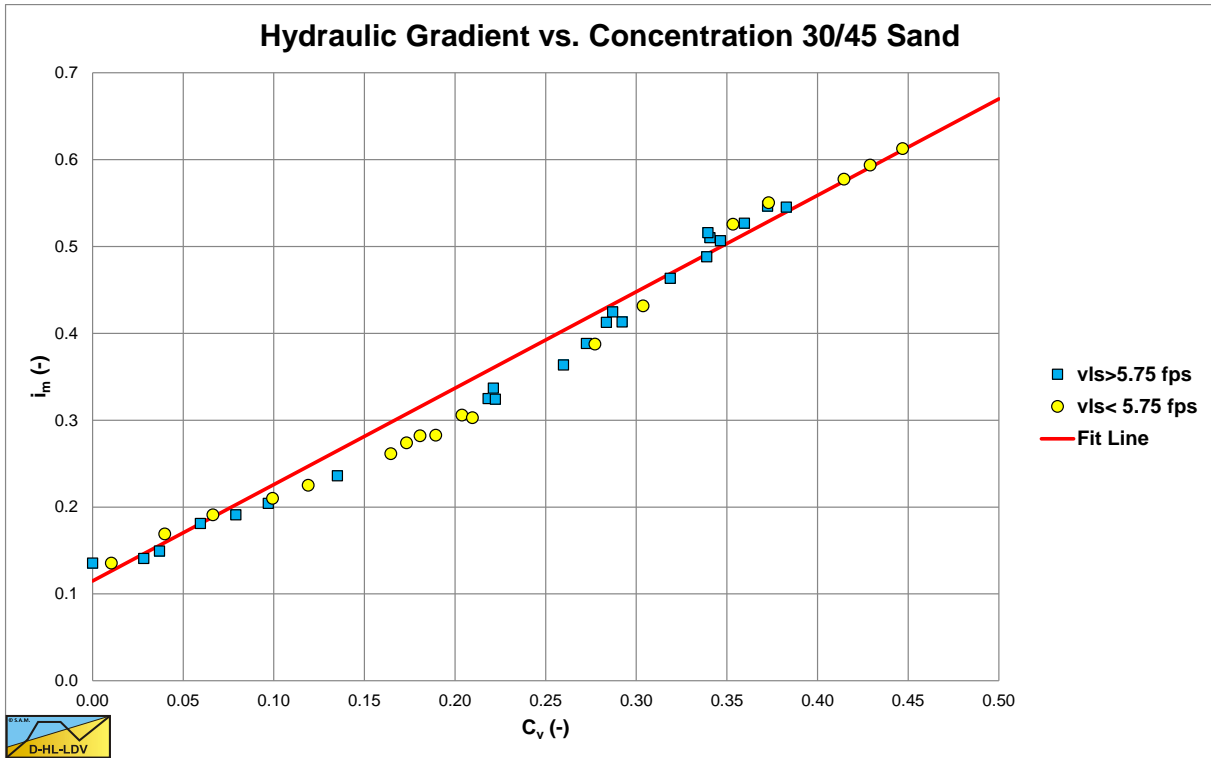
Figure 6.9-3: The dependency of the hydraulic gradient on the concentration, sand mesh 30/45.
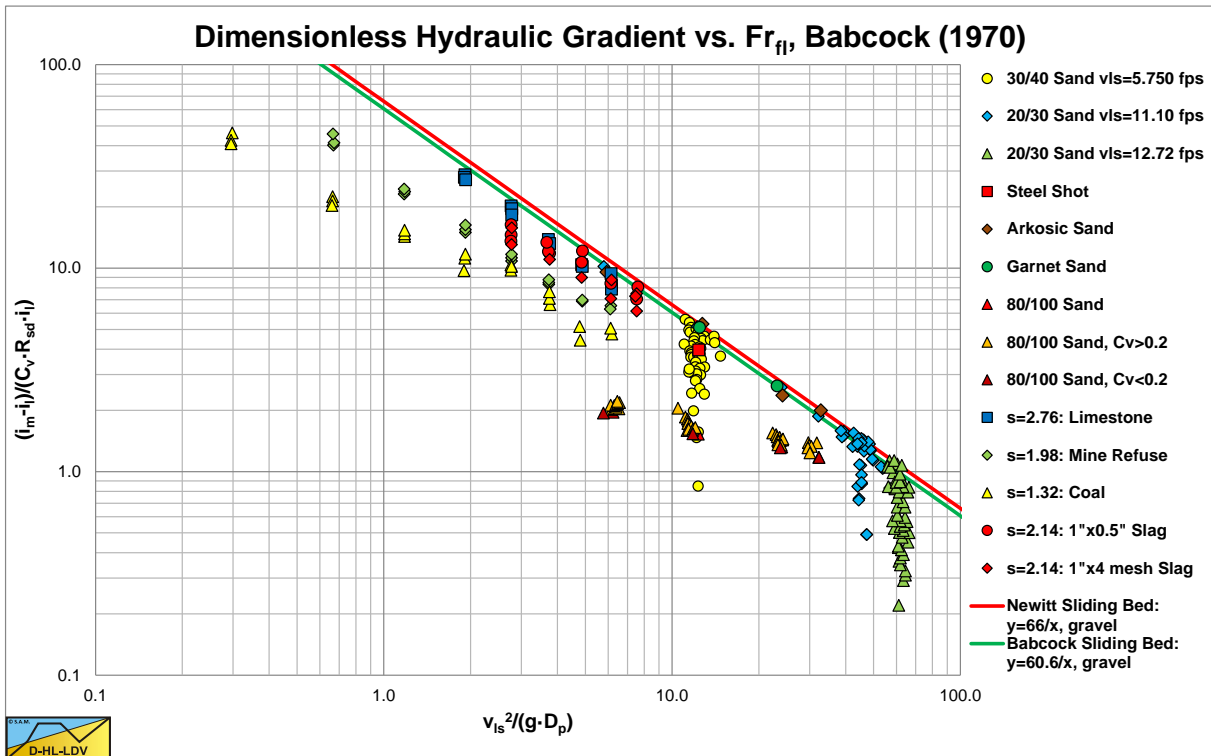
Figure 6.9-4: The dependency of the relative excess hydraulic gradient on the flow Froude number.

Figure 6.9-4 uses the original abscissa and ordinate, Figure 6.9-5 the abscissa and ordinate according to Durand & Condolios (1952).

It is not always clear whether the spatial or the delivered volumetric concentration is used, but for high line speeds there is not much difference.
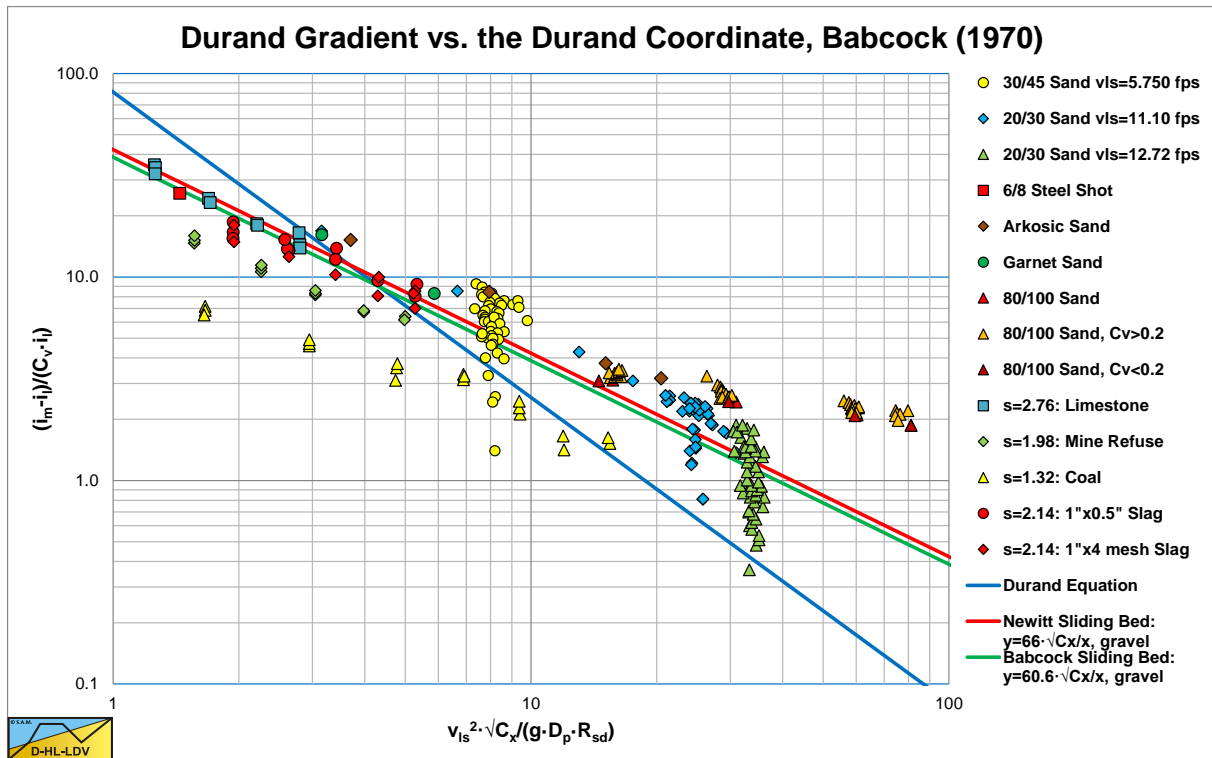
Figure 6.9-5: The dependency of the Durand gradient on the Durand parameter.

Babcock (1970) also compared the experimental data of Nora Stanton Blatch (1906) in similar graphs. The first experiments discovered were carried out by Nora Stanton Blatch (1906), with a pipeline of 1 inch and sand particles of d=0.15-0.25 mm and d=0.4-0.8 mm. At high line speeds, the solids effect is decreasing. Figure 6.9-9 and Figure 6.9-8 show the data points, normalized to a volumetric concentration of 20%.

The data points of Blatch show a considerable scatter, but if one considers the experiments were carried out in 1906, the data points do point in a certain direction. Since the real concentrations are not known, all data points are normalized to a concentration of 10%. In general, the data points follow the sliding bed curves.
Figure 6.9-6 shows the data points in a different coordinate system. For the transformation to Durand coordinates, a relative submerged density of R_{sd} =1.65 and a particle Froude number of $Fr^{-1}=\sqrt{C_x}=1.2/3.42$ are assumed. The tests were carried out in a 1 inch pipe with **d=0.20 mm** and **d=0.55 mm** sand. The $Fr^{-1}=\sqrt{C_x}$ is determined with the Gibert (1960) graph. The data points seem to be parallel to the Newitt et al. (1955) and Babcock sliding bed curves, while the steepness looks a bit smaller than the Durand curve. This could point to a sliding bed and/or sheet flow. Nora Stanton Blatch (1906) however did not give a theoretical explanation of the phenomena she observed.

Figure 6.9-10 and Figure 6.9-11 show the results of the DHLLDV Framework for the range of parameters as used by Babcock (1970). These simulations match the data of Babcock (1970) very well.

The most important observations of Babcock (1970) however are the confirmation of the proportionality of the excess head losses with the volumetric concentration. Although at high concentrations fine particles show some non-linear behavior, for medium and coarse particles in the sliding bed regime the proportionality has been proven. These findings contradict the hydrostatic normal stress approach of Wilson et al. (2006), which would have shown a more than linear increase of the excess head losses with increasing volumetric concentration. These findings confirm the weight approach of Miedema & Ramsdell (2014) assuming a linear relation.
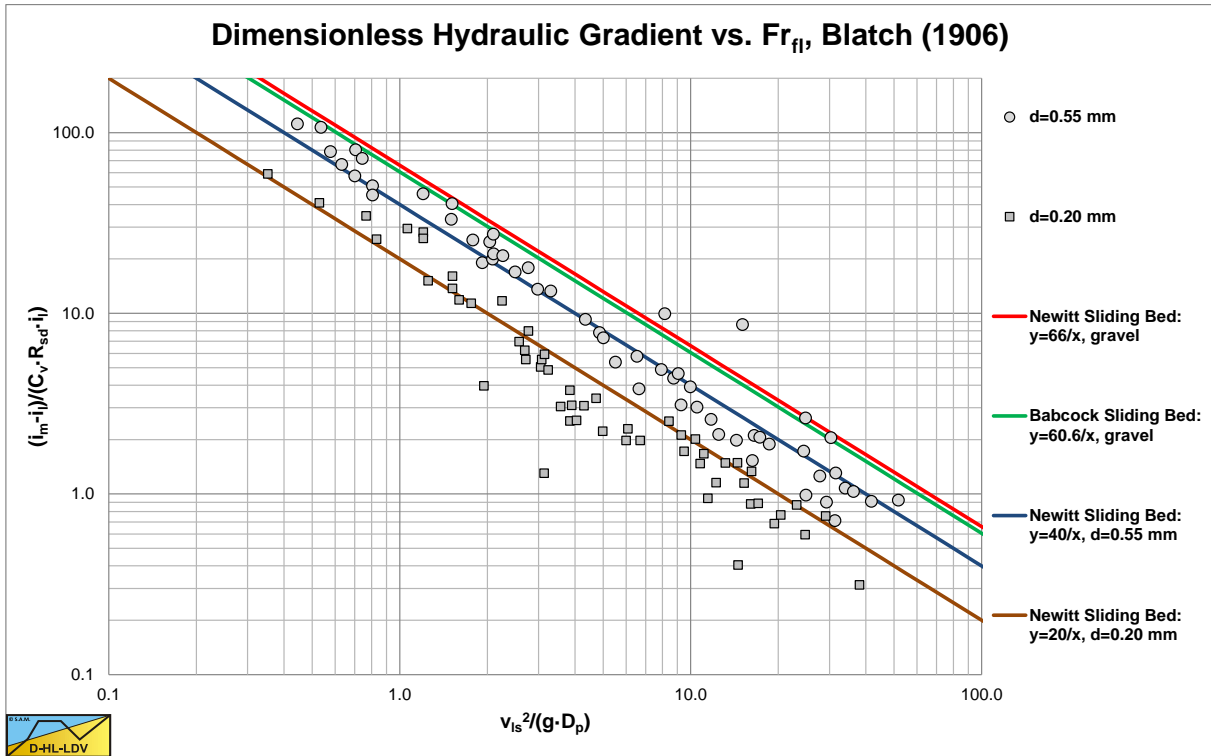
Figure 6.9-6: Original data of Nora Stanton Blatch (1906) on Durand like coordinates, source Babcock (1970).
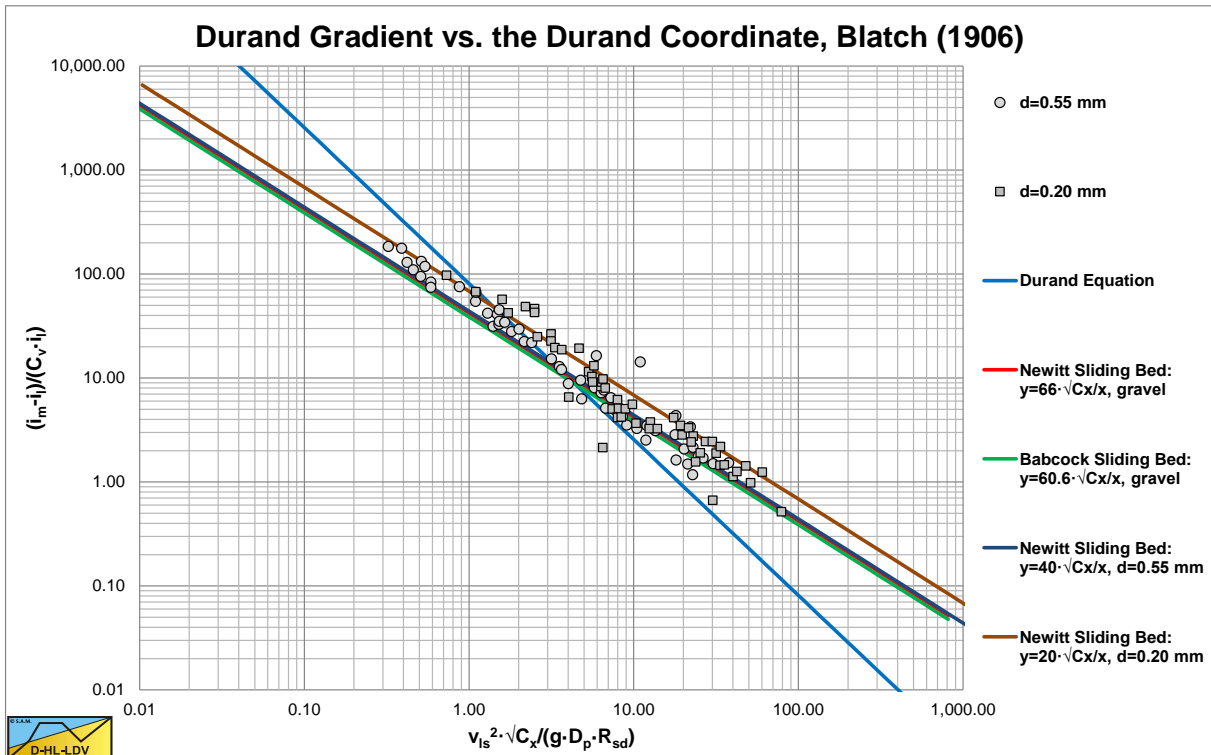
Figure 6.9-7: Original data of Nora Stanton Blatch (1906) on Durand coordinates, source Babcock (1970).
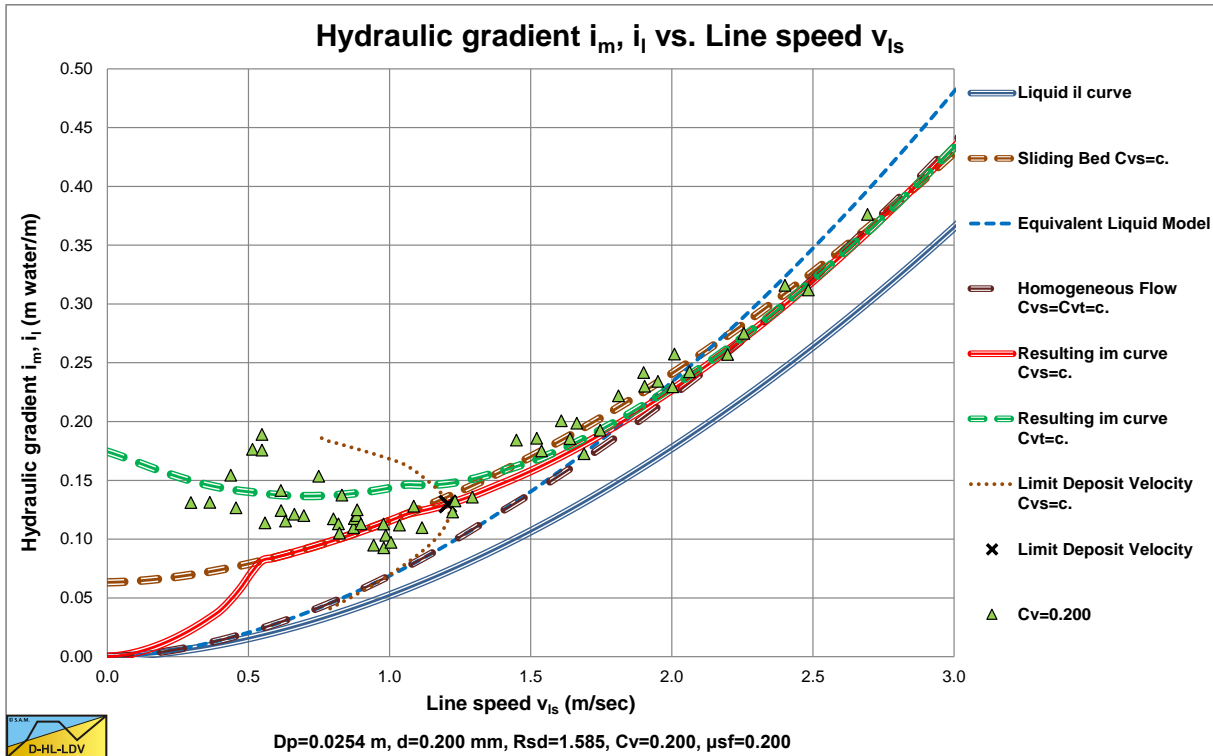
Figure 6.9-8: The hydraulic gradient as a function of the line speed, Blatch (1906), d=0.20 mm.
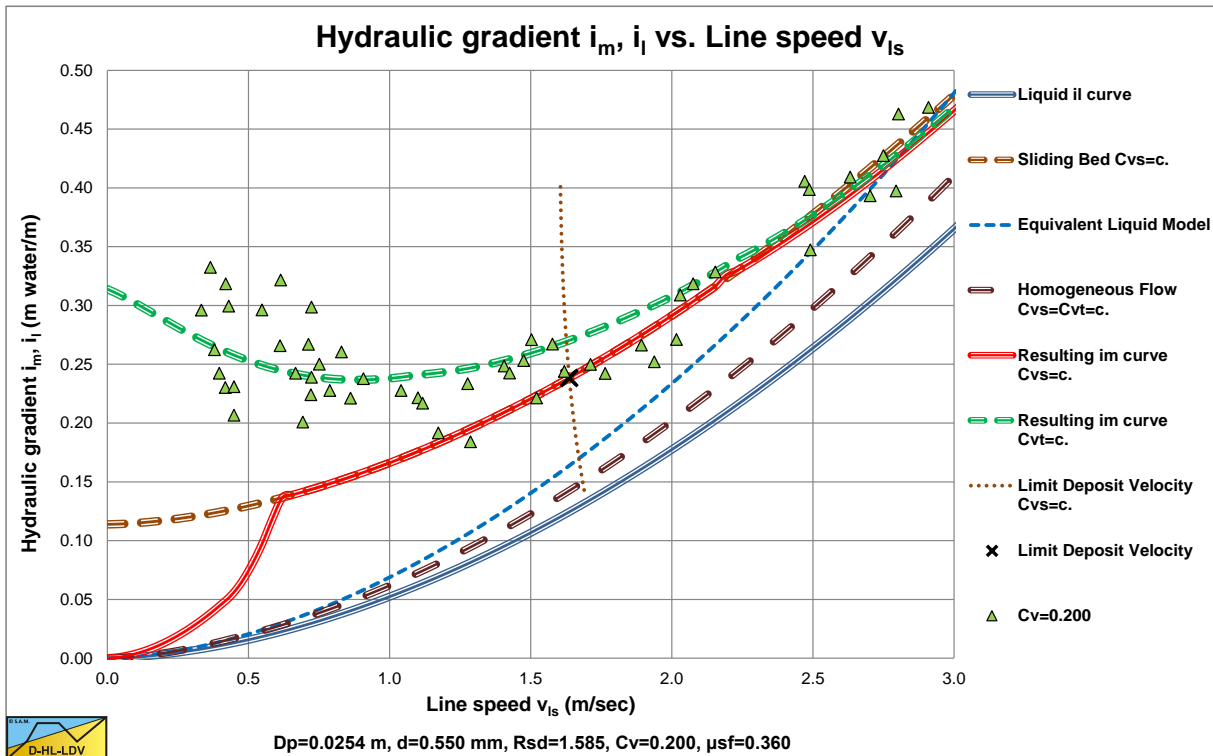
Figure 6.9-9: The hydraulic gradient as a function of the line speed, Blatch (1906), d=0.55 mm.
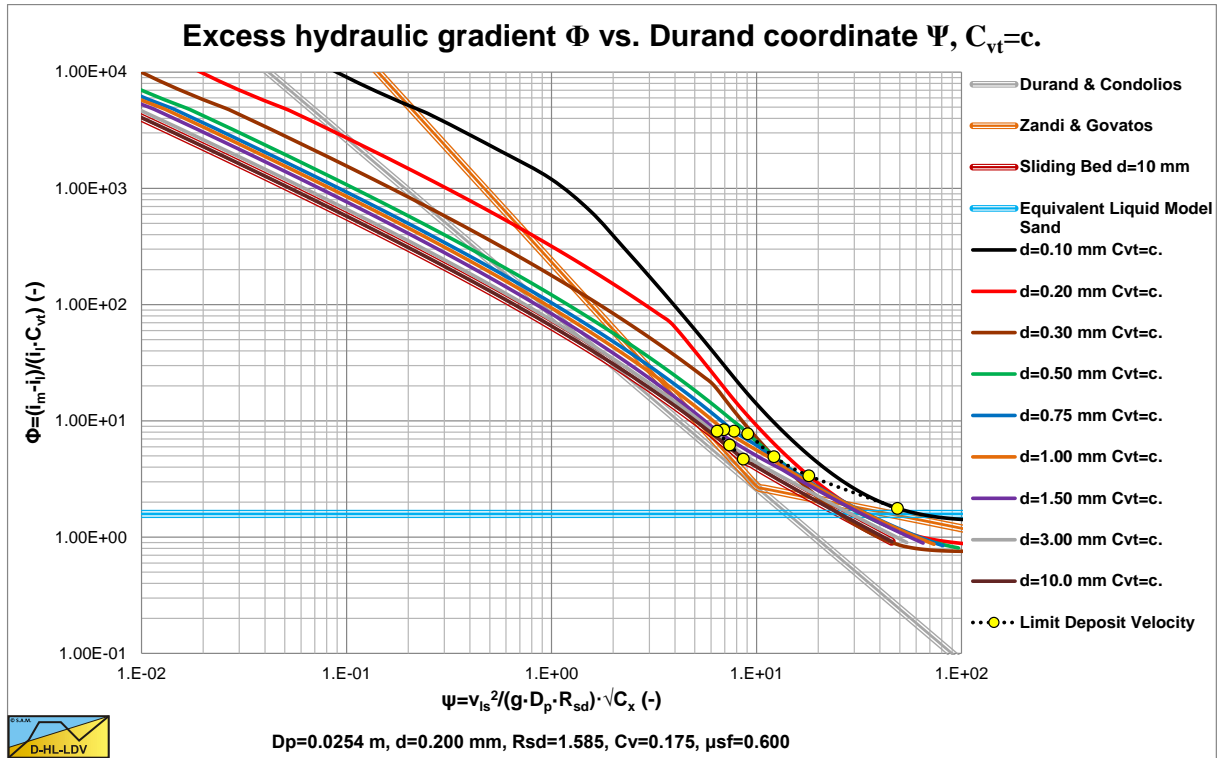
Figure 6.9-10: The DHLLDV results in a 0.0254 m pipe with a sliding friction coefficient of μ_{sf}=0.600.
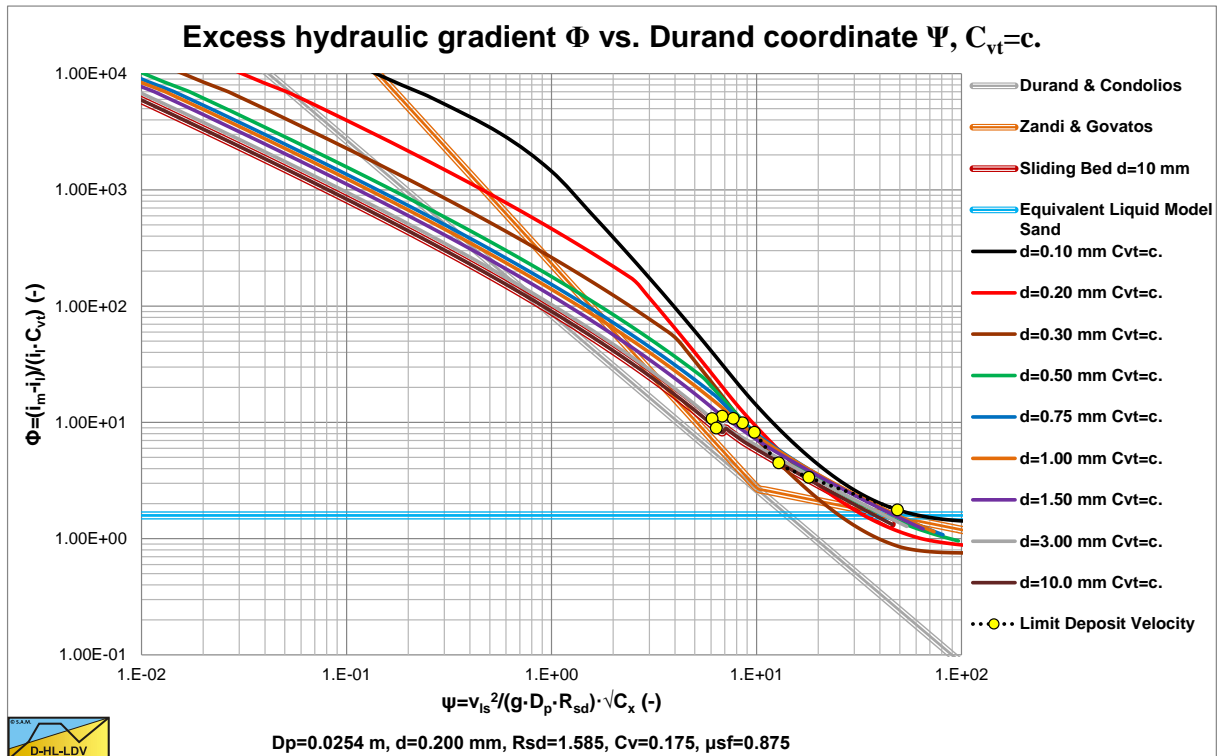
Figure 6.9-11: The DHLLDV results in a 0.0254 m pipe with a sliding friction coefficient of μ_{sf}=0.875.

6.10 Graf et al. (1970) & Robinson (1971).

Graf et al. (1970), Robinson (1971) and Robinson & Graf (1972) conducted experiments on critical deposit velocities for low concentration (**C$_{vs}$<5%**) solid liquid mixtures. The critical deposit velocity is defined here as the velocity at which particles begin to settle from the carrying medium and form a stationary (non-moving) deposit along the invert of the pipe. Since many definitions exist, it is important to keep this definition in mind when interpreting the data. Others defined the critical deposit velocity as the velocity at which particles begin to settle from the carrying medium and form a stationary or sliding deposit along the invert of the pipe, which could give different results, a higher critical deposit velocity. The latter is defined in this book as the LDV, the Graf & Robinson definition as the LSDV. Others use the definition of the minimum hydraulic gradient velocity, referred to in this book as the MHGV. It should be mentioned here that for very fine particles a sliding bed will not occur and the LDV and LSDV are the same. The study was concerned with settling mixtures, which exhibit Newtonian flow characteristics and was analyzed as a two phase flow phenomenon. 4 flow regimes are distinguished, the deposit regime, a separation regime between deposit and no deposit, heterogeneous flow with and without saltation and the pseudo homogeneous regime. The points of division between different flow regimes is somewhat arbitrary. Figure 6.10-2 and Figure 6.10-3 show the different flow regimes for constant spatial and constant delivered volumetric concentration. The simulations are carried out with the DHLLDV Framework and are similar to the graphs shown by Graf & Robinson.
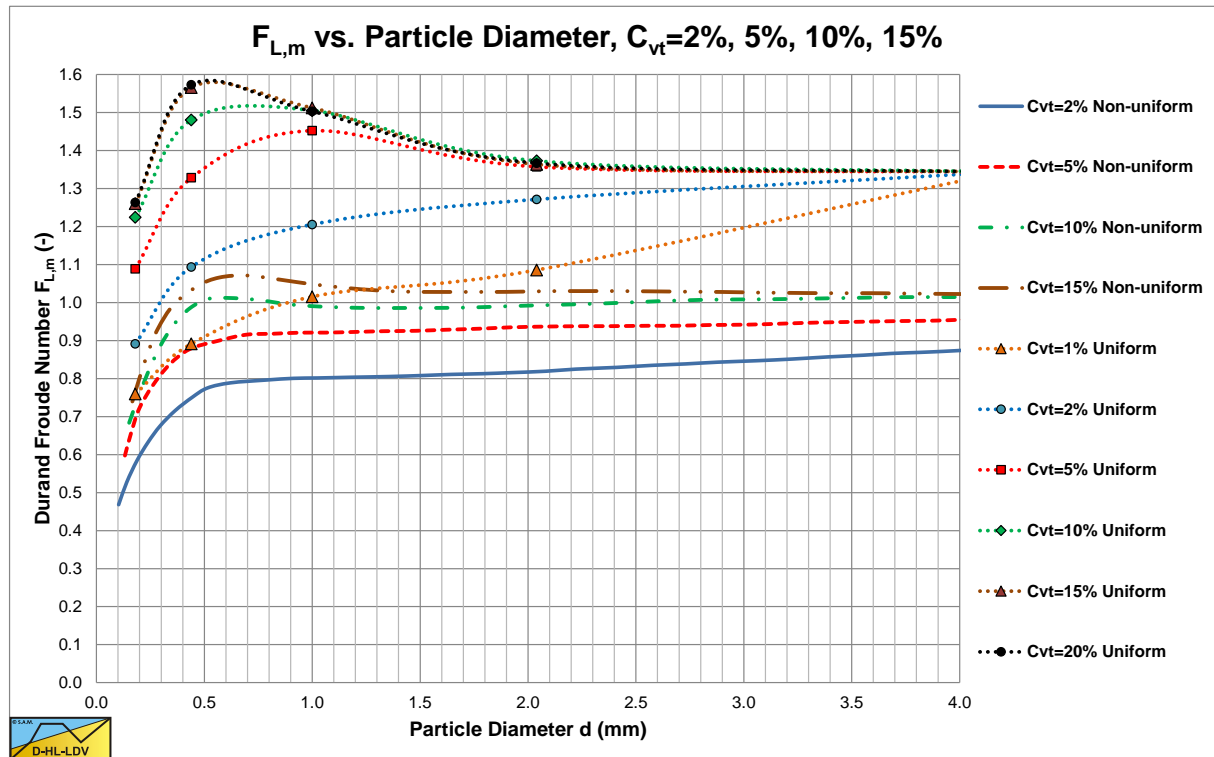
Figure 6.10-1: The Durand & Condolios F$_L$ curves.

$$F_L = \frac{v_{ls,ldv}}{\sqrt{2 \cdot g \cdot D_p \cdot R_{sd}}} \qquad\qquad (6.10-1)$$

Graf & Robinson used the Froude number **F$_L$**, as defined by Durand & Condolios (1952) as a reference. They noted that the curves for uniform sands, as shown in Figure 6.10-1, are too high, while the curves for non-uniform sands seem reasonable. The reason for this is discussed in the chapter about Durand & Condolios, the curves for uniform sands are a factor 1.285 too high. Graf & Robinson then reconstructed the graph based on the Gibert (1960) data, resulting in a graph very similar to the graph of the non-uniform sands, only with slightly higher curves with concentrations up to 10%. Sinclair (1962) found an upper limit of 1.24 for the **F$_L$** value, using:

$$F_{L,max} = \frac{v_{ls,ldv,max}}{\sqrt{2 \cdot g \cdot D_p \cdot R_{sd}}} = 1.3 \cdot \sqrt{R_{sd}^{-0.2}} \qquad\qquad (6.10-2)$$

The upper limit of Durand & Condolios (1952) is about 1.05, while the Gibert (1960) data result in an upper limit of about 1.27. The pipe diameters in all experiments considered here, resulting in the maximum F_L value, are up to 0.1524 m (6 inch).
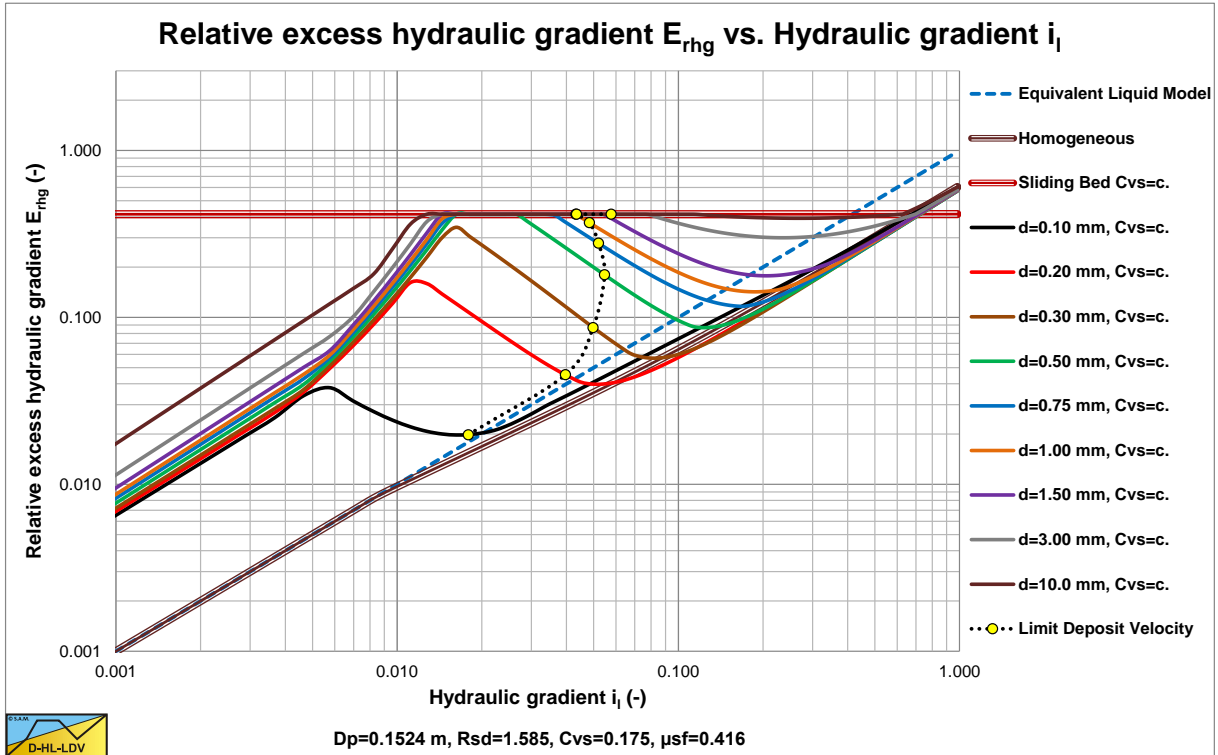
Figure 6.10-2: Flow regimes with constant spatial volumetric concentration.
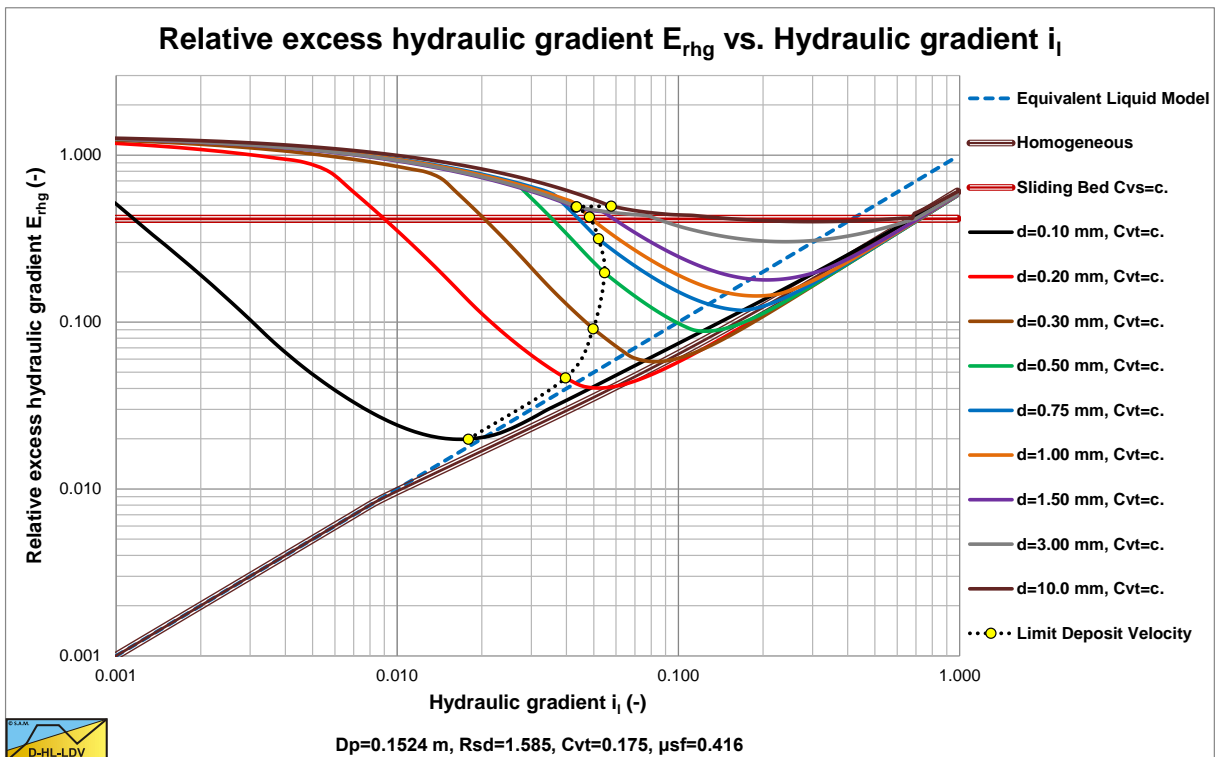
Figure 6.10-3: Flow regimes with constant delivered volumetric concentration.

The experiments of Graf & Robinson were carried out with two pipe diameters, a D_p=**0.1016 m** diameter pipe (4 inch) and a D_p=**0.1524 m** diameter pipe (6 inch). Two sands were used, a sand with **d=0.45 mm** and a sand with **d=0.88 mm**. Also tests with plastic pellets with **d=3.63 mm** were carried out. The experiments were carried out

with constant spatial volumetric concentration, although a lot of scatter was observed. The concentration measured was the delivered volumetric concentration. They also used slightly inclined pipes with positive (θ=1.5º and tan(θ)=0.027) and negative (θ=-3.5º and tan(θ)=-0.06) angles, resulting in a modified F_L number:

$$F_L = \frac{v_{ls,ldv}}{\sqrt{2 \cdot g \cdot D_p \cdot R_{sd}}} \cdot \left(1 - \tan(\theta)\right) \tag{6.10-3}$$

Assuming the concentration was the only important parameter, the following fit function was found:

$$F_L = \frac{v_{ls,ldv}}{\sqrt{2 \cdot g \cdot D_p \cdot R_{sd}}} \cdot \left(1 - \tan(\theta)\right) = 0.901 \cdot C_v^{0.106} \tag{6.10-4}$$

Including the particle diameter in the correlation, the following equation was found:

$$F_L = \frac{v_{ls,ldv}}{\sqrt{2 \cdot g \cdot D_p \cdot R_{sd}}} \cdot \left(1 - \tan(\theta)\right) = 0.928 \cdot C_v^{0.105} \cdot d^{0.058} \tag{6.10-5}$$

It should be mentioned that the concentration was limited to 7% and was most probably based on the spatial volumetric concentration. Meaning a fixed amount of solids in the test loop. Figure 6.10-4 shows the Durand Froude numbers as a function of the concentration, including the above fit line. At a concentration of 15-20%, which is often considered to give the highest LDV, the estimated F_L value is 1.24. The data points of the plastic pellets seem to give higher Durand Froude numbers. The plastic pellets have a relative submerged density R_{sd}=0.34, which is low. Apparently the Durand Froude number increases with decreasing relative submerged density.
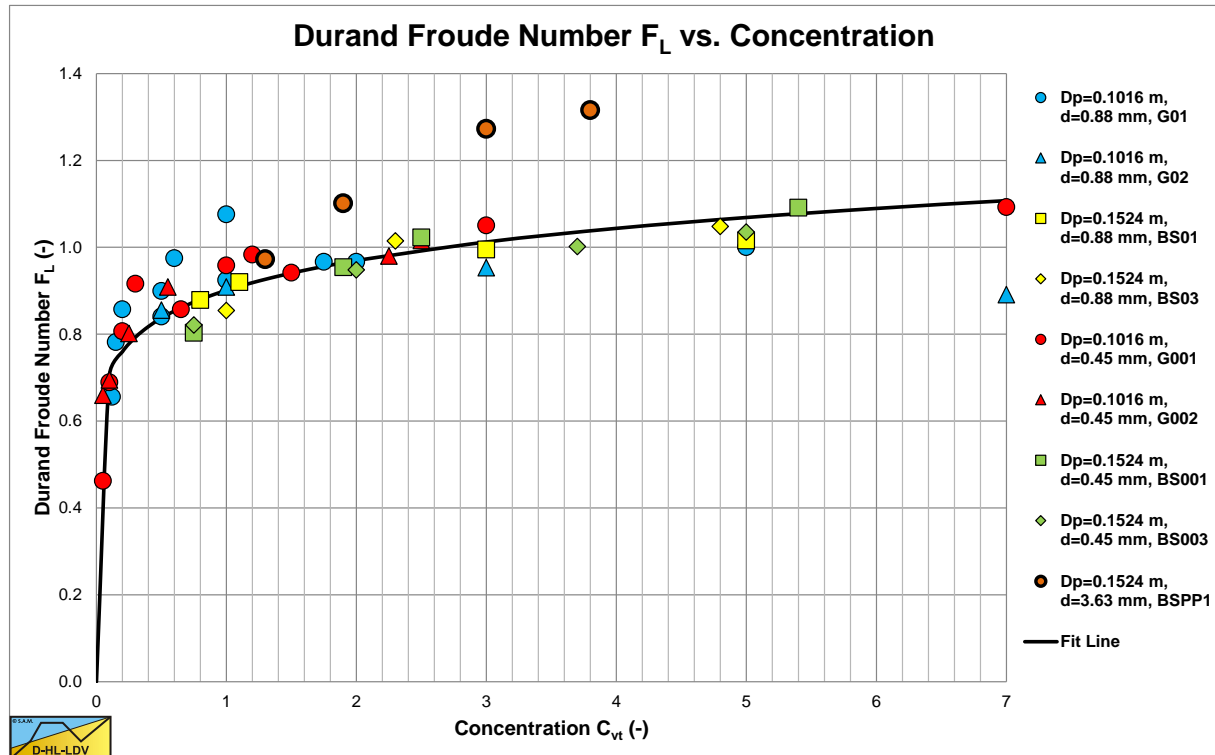

Figure 6.10-4: The Durand Froude numbers as a function of the concentration.

Figure 6.10-5 shows a comparison of the above equation (6.10-5) with the Durand & Condolios (1956) graph for non-uniform sands. It is clear that the above equation (6.10-5) gives considerable higher values for the Durand Froude number F_L.
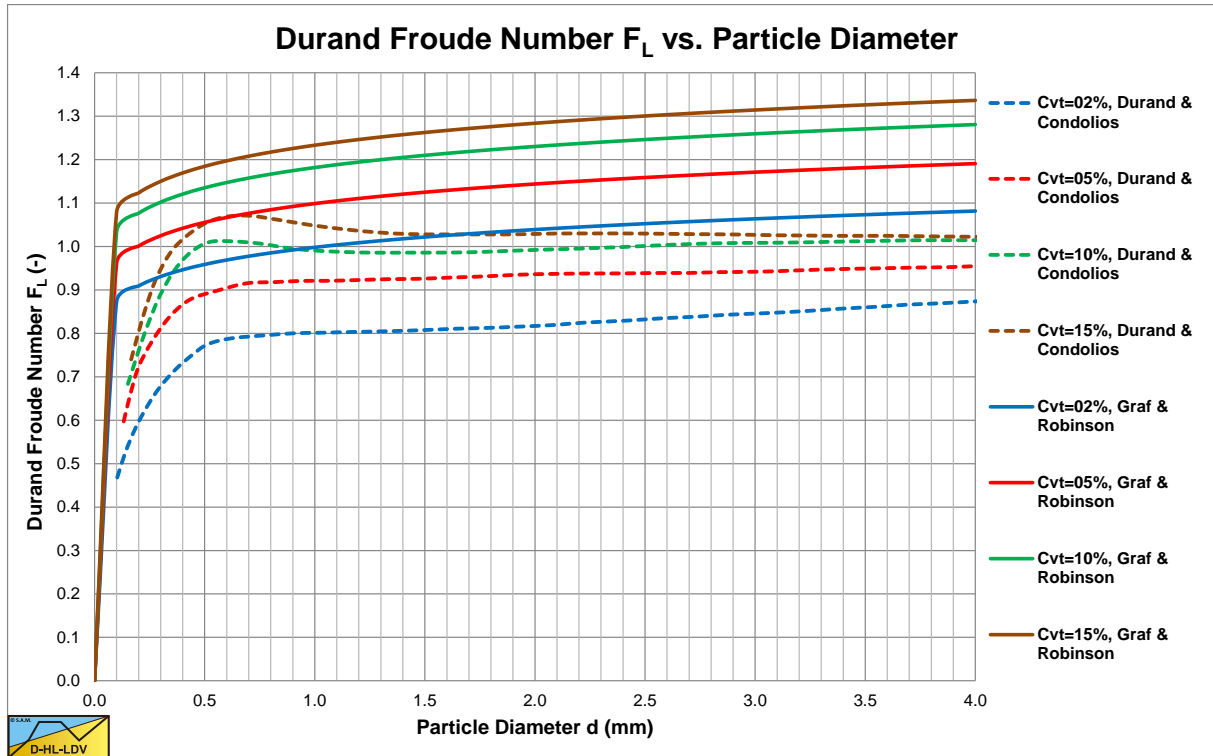
Figure 6.10-5: Comparison of the Durand & Condolios F_L for non-uniform sands with the Graf & Robinson equation.
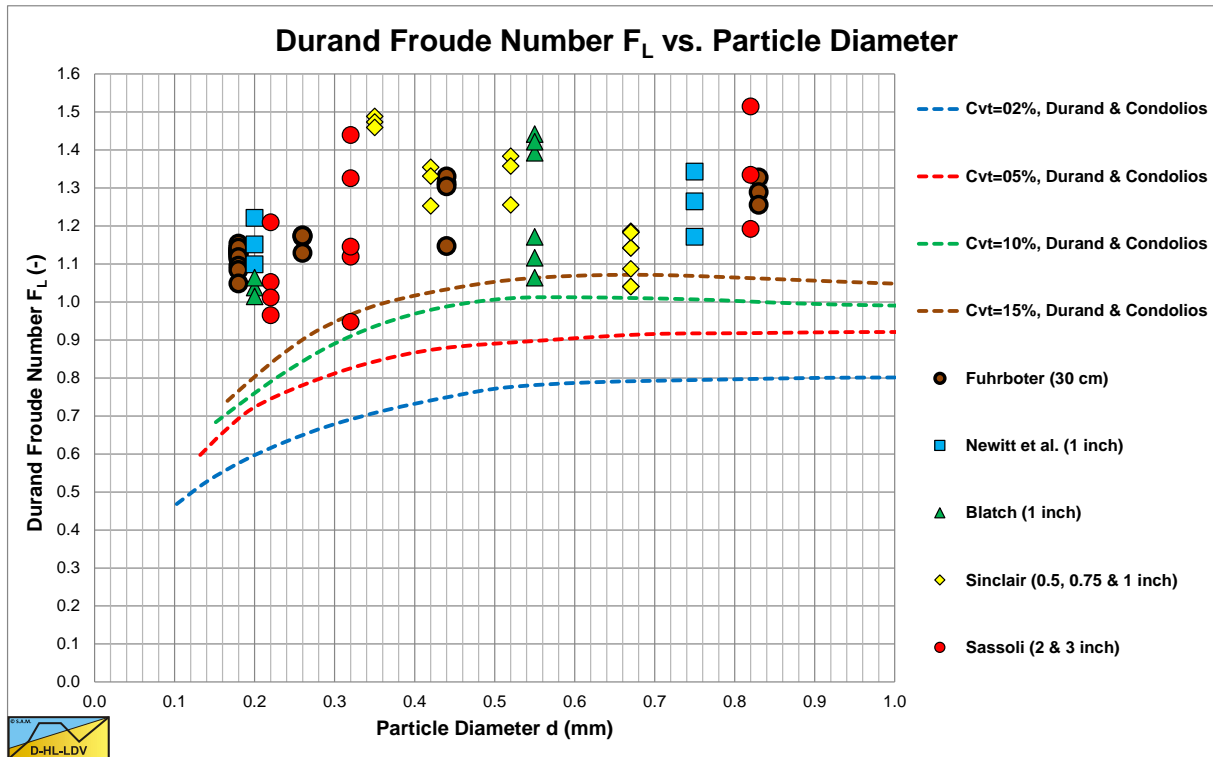
Figure 6.10-6: Durand & Condolios F_L of some other researchers.

Graf et al. (1970) also show Durand FL values of some other researchers as is shown in Figure 6.10-6. The values are much larger than the ones predicted by the Durand & Condolios (1956). It is also noteworthy to mention that apparently the smaller pipe diameters result in larger F_L values. The Fuhrboter (1961) values in a 30 cm (12 inch) pipe are smaller than the other values in much smaller pipes. The maximum values in each column are for concentrations between 15% and 20%. So it looks like the F_L value decreases slightly with increasing pipe diameter.

6.11 Yagi et al. (1972).

6.11.1 Introduction.

Yagi et al. (1972) carried out experiments with sands and gravels in pipes with diameters of 0.087 m, 0.1003 m and 0.1552 m and spatial concentrations up to 40%. In the 0.087 m diameter pipe they used particles with diameters of 0.75 mm and 8.0 mm. In the 0.1003 m diameter pipe they used particles with diameters of 0.25 mm, 0.65 mm, 1.28 mm and 7.0 mm. In the 0.1552 m diameter pipe they used particles with diameters of 0.91 mm, 8.75 mm, 27.5 mm and 45 mm. The ratios of the larger particles to the pipe diameters is very large, up to about 30%. The wide range of particle diameters and particle diameter to pipe diameter ratios and the fact that they measured both the spatial volumetric concentration and the delivered volumetric concentration, makes these experiments very valuable, although almost forgotten in public literature. For the correlation of pressure losses and physical and operational parameters, they use the ϕ and ψ according to Durand & Condolios (1952).

$$\phi = \frac{i_m - i_l}{i_l \cdot C_{vt}} \tag{6.11-1}$$

$$\psi = \frac{v_{ls}^2 \cdot \sqrt{C_x}}{g \cdot R_{sd} \cdot D_p} = \frac{2}{2} \cdot \frac{v_{ls}^2 \cdot \sqrt{C_x}}{g \cdot R_{sd} \cdot D_p} = 2 \cdot F_L^2 \cdot \sqrt{C_x} \tag{6.11-2}$$

Remark: Yagi et al. (1972) use the symbol $\sqrt{C_d}$ or $\sqrt{C_D}$, which normally is the square root of the drag coefficient, but according to their paper they use the $\sqrt{C_x}$ of Durand & Condolios (1952), which is the square root of the particle Froude number.

6.11.2 Pressure Losses.

Yagi et al. (1972) give different equations for constant transport (delivered) volumetric concentration and constant spatial volumetric concentration. However all equations have the following form:

$$\frac{i_m - i_l}{i_l \cdot C_{vt}} = \phi = K \cdot \psi^{-\alpha} \tag{6.11-3}$$

Based on the Durand & Condolios (1952) F_L value for large particles of 1.34 and $\sqrt{C_x}$ of 0.84, Yagi et al. (1972) use a value of $\psi=3$ for the LDV. For very large particles this should be smaller than 3, about 2.22. For the smallest particles used here this should be larger than 3, about 7.5. Based on Durand & Condolios (1952) and others, the value of α is expected to have a value between 1.5 and 2 for heterogeneous flow (spatial concentration), so around and above the LDV. For large particles below the LDV and small particles far below the LDV a value of 1 is expected, based on the sliding bed regime (spatial concentration). For large particles above the LDV a value between 1 and 1.5 is expected based on the sliding flow regime (spatial concentration). For constant delivered volumetric concentration curves, slightly higher values of this power are expected, due to decreasing slip between particles and carrier liquid with increasing line speed. The values found by Yagi et al. (1972) match these trends well, however it should be mentioned that the value of $\psi=3$ is not always an accurate value to separate the sliding bed regime from the heterogeneous regime, sometimes resulting in slightly higher values than expected.

Figure 6.11-1 and Figure 6.11-2 show the data of Yagi et al. (1972) in the ϕ and ψ coordinate system for delivered (transport) volumetric concentration. The sand curve is steeper than the Durand & Condolios (1952) curve, while the gravel curve has about the same steepness. The gravel curve however has a larger coefficient and is thus higher. The sand curve crosses the Durand & Condolios (1952) curve at about $\psi=4.5$, which is close to the LDV of the smaller particles.

In the ϕ and ψ coordinate system, an ordinate equal to the R_{sd} of the solids gives the ELM curve. Now it is known that medium sized particles may have a resistance comparable to the pure liquid resistance, resulting in a sudden drop in Figure 6.11-1. This sudden drop results in a higher value of α for medium sands. Basically what happens is that the heterogeneous flow regime and the pseudo homogeneous flow regime are combined into one equation, one power. The same can happen when the sliding bed regime and the heterogeneous or sliding flow regime are combined into one power. Figure 6.11-5 gives an example of data points in two flow regimes.
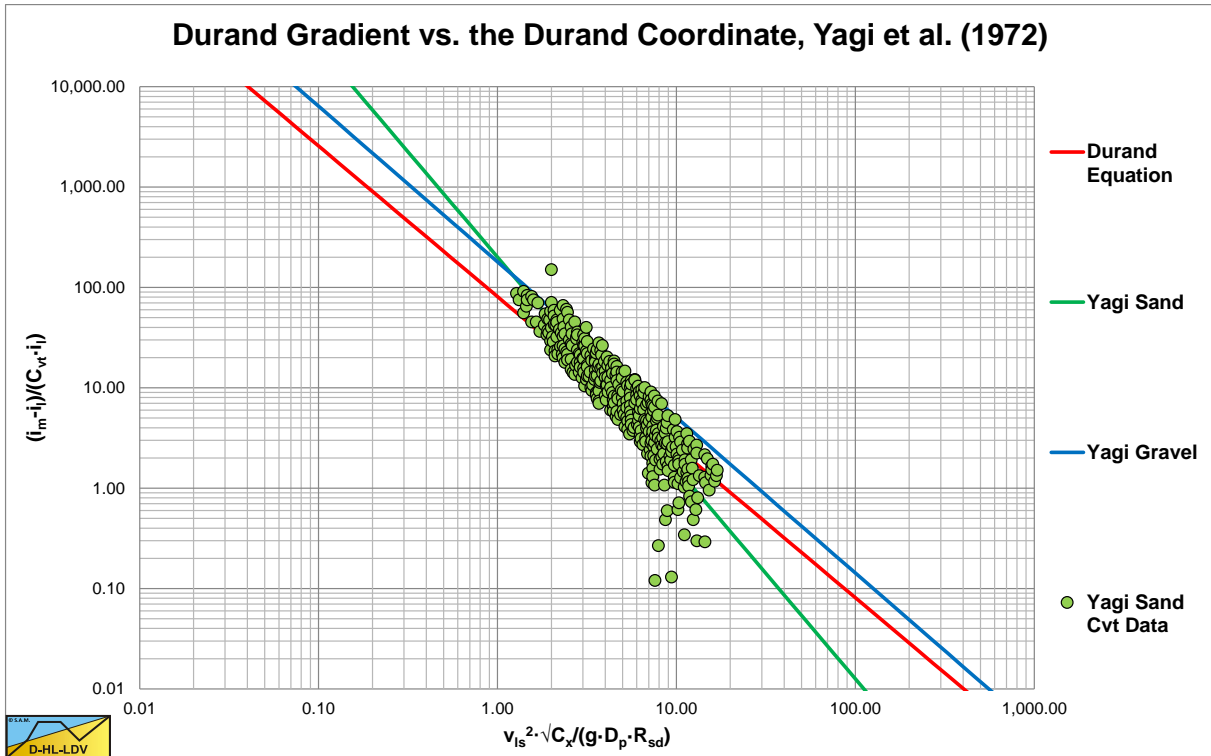
Figure 6.11-1: The data and fit lines of Yagi et al. (1972) for sand, C_{vt}.
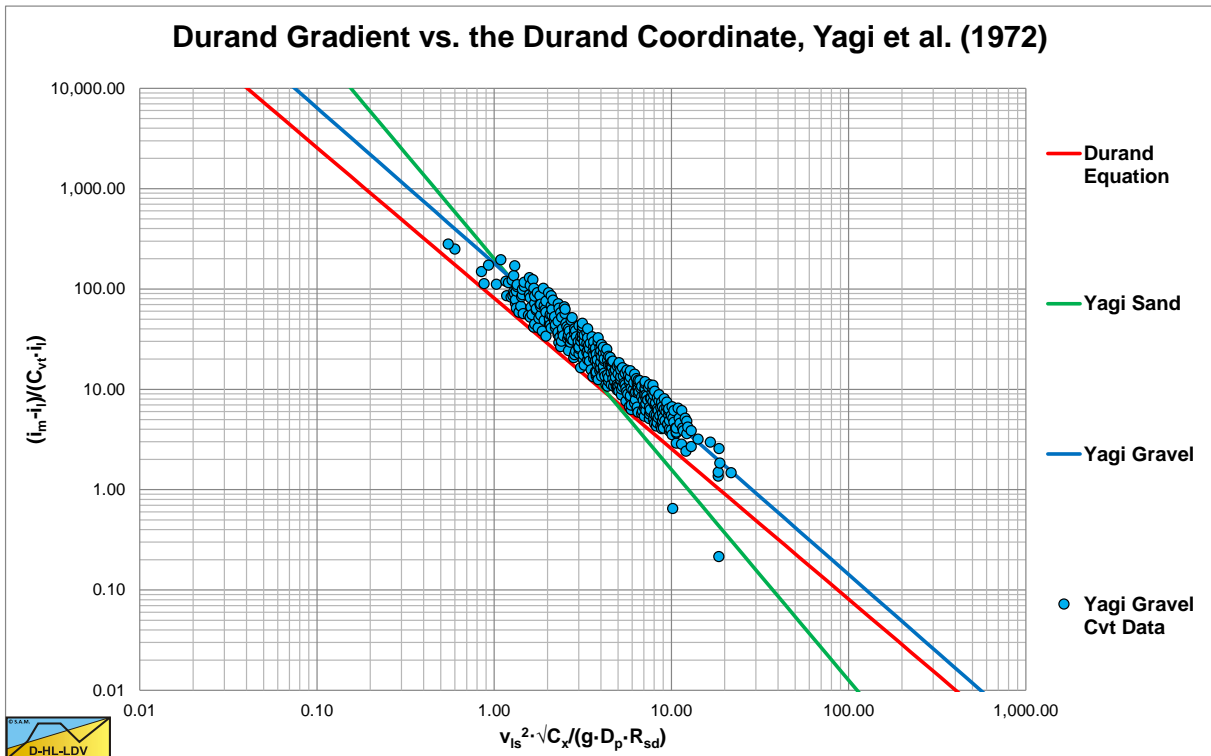
Figure 6.11-2: The data and fit lines of Yagi et al. (1972) for gravel, C_{vt}.

6.11.2.1 Sand.

Only detailed data of the 0.91 mm particles in the 0.1552 m diameter pipe are reported for spatial and delivered volumetric concentrations. Figure 6.11-3 and Figure 6.11-4 show these data in a relative excess hydraulic gradient **E$_{rhg}$** versus liquid hydraulic gradient **i$_l$** graph.

$$E_{rhg} = \frac{i_m - i_l}{R_{sd} \cdot C_{vs}}$$
(6.11-4)

For both cases one cannot distinguish an influence of the concentration. The data points are randomly scattered. The steepness of the delivered concentration data is a bit larger than the steepness of the spatial concentration and the values of the delivered concentration are a bit higher for smaller hydraulic gradient. Near the intersection with the ELM curve (homogeneous flow) the data points are at the same level. One can see in both figures that at the left there is the intersection of the sliding bed regime with the heterogeneous regime, while on the right there is the intersection of the heterogeneous regime with the homogeneous regime. These regime changes will also influence the coefficients found for the equations, which are given below. Above the LDV the powers are equal (**α=2.1**) which means there is hardly any slip between the particles and the carrier liquid. Below the LDV there is a difference of 0.55 in the power, giving an indication of the slip.
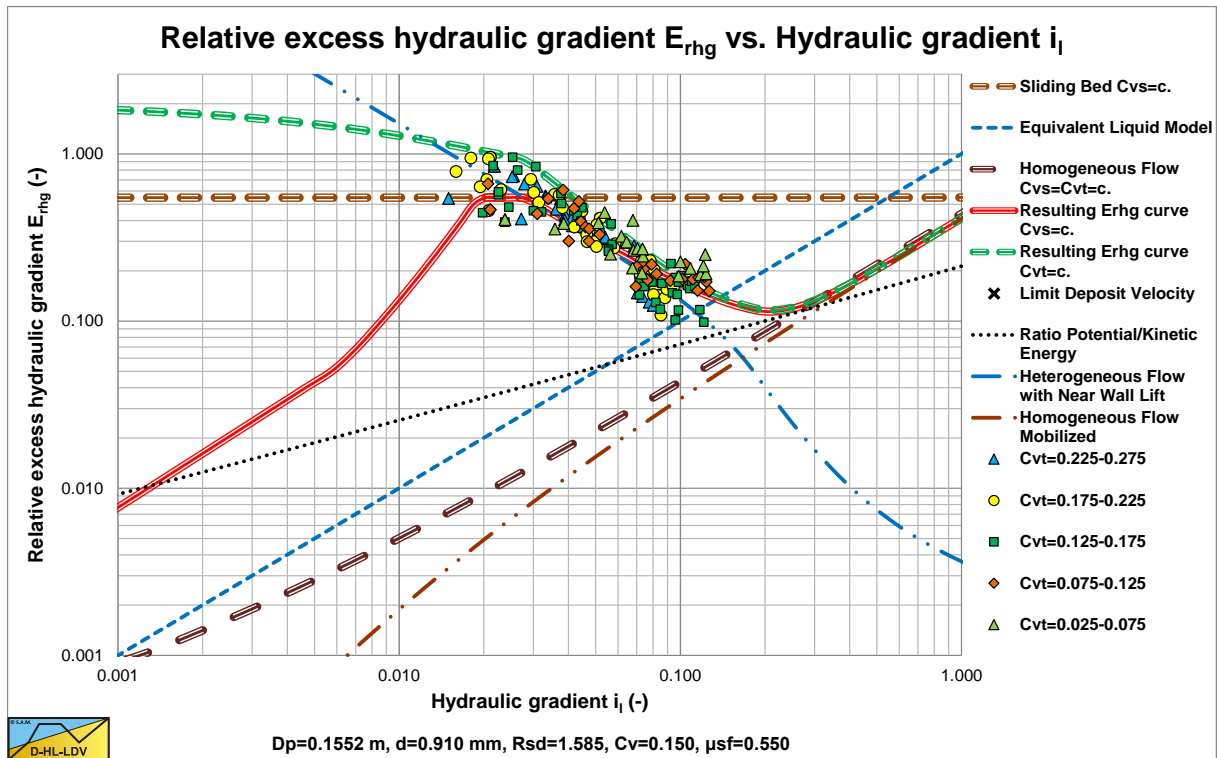
Figure 6.11-3: The Yagi et al. (1972) experiments with coarse sand and spatial concentration.

For sand **ψ<3** (below LDV), spatial volumetric concentration:

$$\frac{i_m - i_l}{i_l \cdot C_{vs}} = \phi = K \cdot \psi^{-1.55} \quad \text{with:} \quad K=100$$
(6.11-5)

For sand **ψ>3** (above LDV), spatial volumetric concentration:

$$\frac{i_m - i_l}{i_l \cdot C_{vs}} = \phi = K \cdot \psi^{-2.1} \quad \text{with:} \quad K=180$$
(6.11-6)

For sand, transport volumetric concentration:

$$\frac{i_m - i_l}{i_l \cdot C_{vt}} = \phi = K \cdot \psi^{-2.1} \quad \text{with:} \quad K=200 \tag{6.11-7}$$
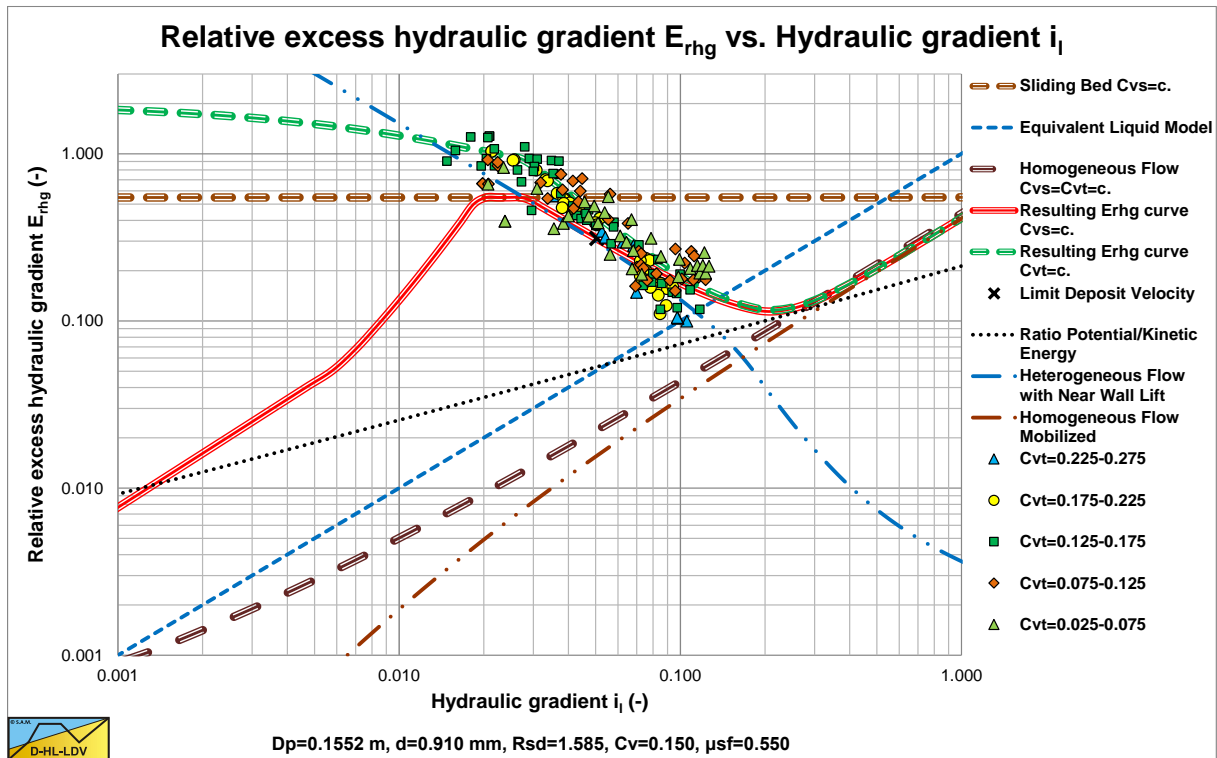
Figure 6.11-4: The Yagi et al. (1972) experiments with coarse sand and transport concentration.

6.11.2.2 Gravel.

In the 0.087 m diameter pipe they used particles with a diameter of 8.0 mm. In the 0.1003 m diameter pipe they used particles with a diameters of 7.0 mm. In the 0.1552 m diameter pipe they used particles with diameters of 8.75 mm, 27.5 mm and 45 mm. Only detailed data of the 8.0 mm particles in the 0.087 m diameter pipe are reported for spatial and delivered volumetric concentrations. Figure 6.11-5 and Figure 6.11-6 show these data in a relative excess hydraulic gradient E_{rhg} versus liquid hydraulic gradient i_l graph. The ratio between the particle diameter and the pipe diameter is about 0.09 which is much larger than the ratio of 0.015-0.018 as mentioned by Wilson et al. (2006) for full stratified flow. Figure 6.11-5 (spatial concentration) shows that the lowest concentrations tend to follow heterogeneous transport, while the higher concentrations tend to follow the sliding bed curve, in between the sliding bed and the heterogeneous curves. One cannot really find an influence of the concentration, as should follow from the Wilson et al. (2006) hydrostatic approach. The data points at lower hydraulic gradients concentrate around $E_{rhg}=0.8$, which is the sliding friction coefficient, but it is rather high. Figure 6.11-6 shows higher E_{rhg} values resulting from slip. At a certain delivered concentration, the spatial concentration is always higher, resulting in a higher E_{rhg} value. The smaller the liquid hydraulic gradient, the higher the slip and the bigger the difference.

For gravel $\psi<3$ (below LDV), spatial volumetric concentration:

$$\frac{i_m - i_l}{i_l \cdot C_{vs}} = \phi = K \cdot \psi^{-1.16} \quad \text{with:} \quad K=98 \tag{6.11-8}$$

For gravel $\psi>3$ (above LDV), spatial volumetric concentration:

$$\frac{i_m - i_l}{i_l \cdot C_{vs}} = \phi = K \cdot \psi^{-1.46} \quad \text{with:} \quad K=138 \tag{6.11-9}$$

For gravel, transport volumetric concentration:

$$\frac{i_m - i_l}{i_l \cdot C_{vt}} = \phi = K \cdot \psi^{-1.55} \quad \text{with:} \quad K = 180$$

(6.11-10)

Below the LDV, the powers differ about 0.4, while above the LDV there is still a difference of 0.1.
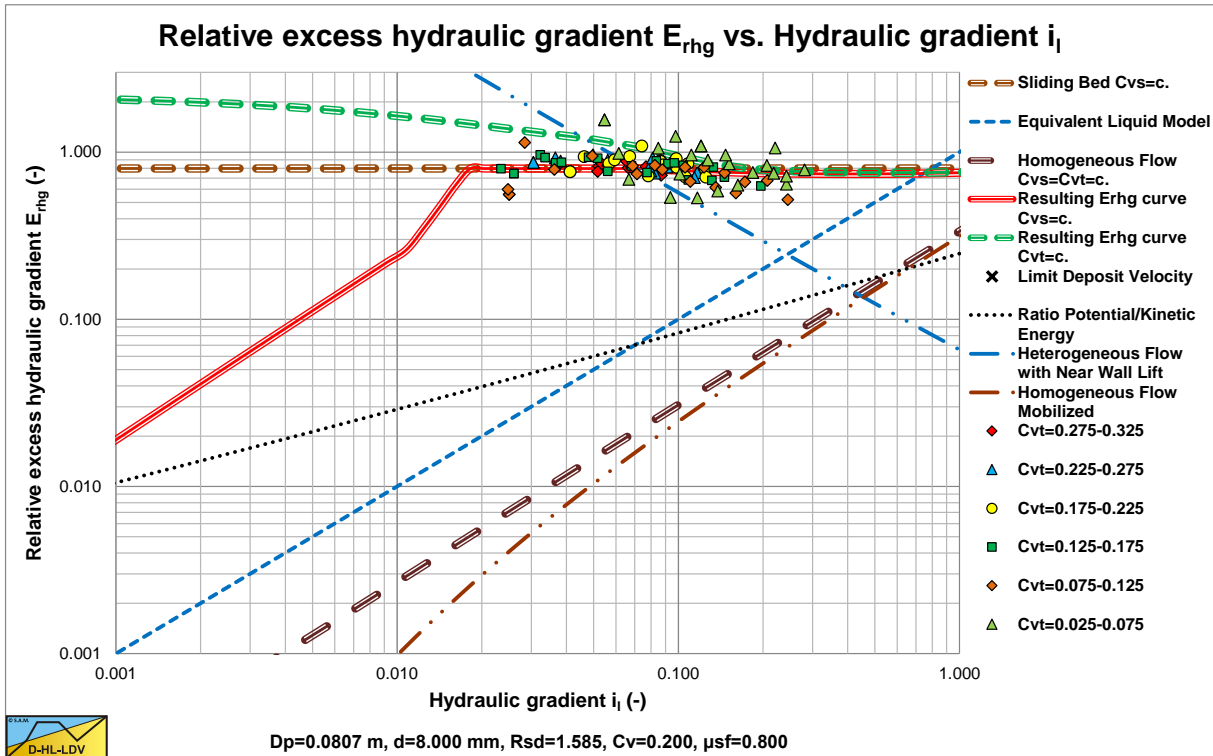

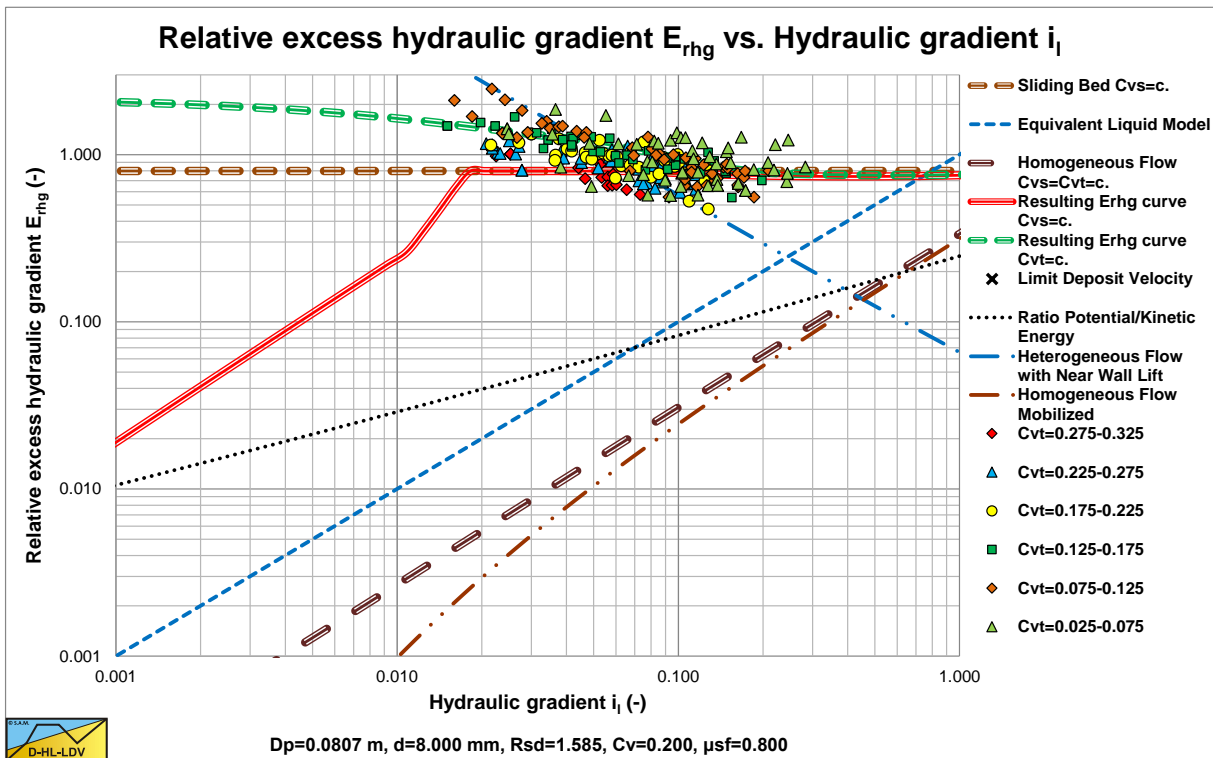**Figure 6.11-5: The Yagi et al. (1972) experiments with gravel and spatial concentration.**

Figure 6.11-6: The Yagi et al. (1972) experiments with gravel and transport concentration.

6.11.3 Limit Deposit Velocity.
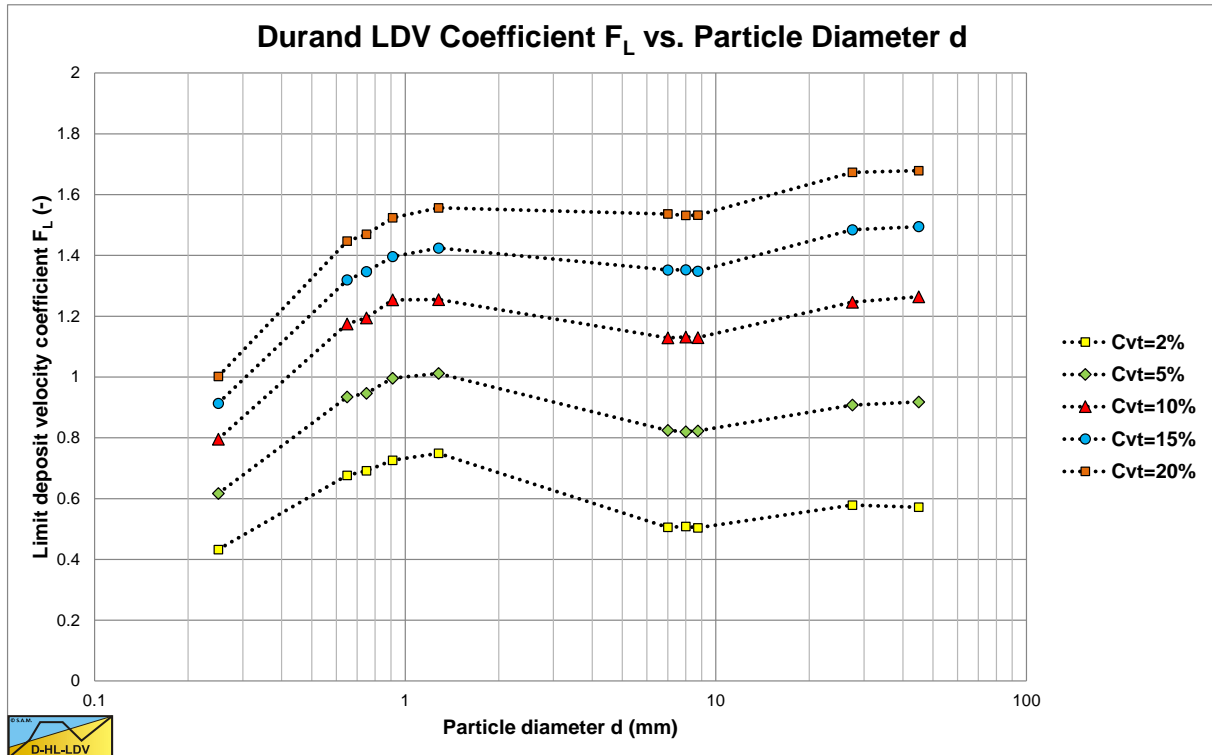
Figure 6.11-7: The Limit Deposit Velocity measured by Yagi et al. (1972).

Figure 6.11-7 shows the LDV **F_L** value, as defined by Durand & Condolios (1952) and measured by Yagi et al. (1972).

Yagi et al. (1972) however did not use the criterion that above the LDV no stationary or sliding bed exists, but they used the criterion of the line speed of minimum hydraulic gradient. For concentrations of about 20%, the line speed of minimum hydraulic gradient matches the LDV closely. However for smaller concentrations this minimum criterion results in much smaller **F_L** values than the ones occurring from the real LDV. This can easily be proven by adding the solids contribution to the carrier liquid hydraulic gradient for a range of concentrations, starting at 1%. The result of this is that only the data points of the 20% concentration can be used to determine the **F_L** value at the LDV.

A second complication is the particle size to pipe diameter ratio. According to Wilson et al. (2006), above a certain ratio there will always be a stratified flow resulting in a sort of bed transport. They use a ratio of 0.015-0.018. Large particles cannot be carried by turbulent eddies anymore because they are too large and the result is a sliding bed or sliding flow, high density flow over the bottom of the pipe. Durand & Condolios (1952) did not do experiments in this range and concluded that the **F_L** value increases with increasing particle diameter to a maximum at a particle diameter of about 0.5 mm, after which it decreases slightly to an asymptotic value of about 1.34 for larger particles (base on the Durand (1953) graph). Here an increase is observed for very large particles. Maybe this is because of the large particle diameter to pipe diameter ratio.

It is also a question whether the LDV still has a meaning in the sliding flow regime, because the definition of the LDV states; the line speed above which there is no stationary or sliding bed. But in the case of high density flow over the bottom of the pipe, how to determine whether it is still a sliding bed with decreasing density with increasing line speed or a high density heterogeneous flow?

Still, also for very large particles an equivalent LDV has to be determined, since i twill be used later to determine the slip. This makes the observations of Yagi et al. (1972) very valuable.

6.11.4 The Slip Velocity.

Yagi et al. (1972) derived an equation for the slip velocity v_{sl}, based on some theoretical considerations and an empirical relation based on experiments. Particles move slower than the cross sectional averaged line speed, while the liquid moves a bit faster, assuming that the line speed equals the average volume flow divided by the total cross section of the pipe. The average velocity of the particles v_p can be derived from the average line speed v_{ls}, the volumetric transport concentration C_{vt} and the volumetric spatial concentration C_{vs}, according to:

$$v_p = v_s = v_{ls} \cdot \frac{C_{vt}}{C_{vs}} \quad \Rightarrow \quad \frac{v_p}{v_{ls}} = \frac{C_{vt}}{C_{vs}} \tag{6.11-11}$$

The average line speed is the weighted average of the velocity of the volume fraction of liquid and the volume fraction of the solids (particles), according to:

$$v_{ls} = v_l \cdot (1 - C_{vs}) + v_p \cdot C_{vs} \quad \Rightarrow \quad v_{ls} = v_l \cdot (1 - C_{vs}) + v_{ls} \cdot C_{vt} \tag{6.11-12}$$

Based on this equation, the average liquid velocity can be derived, which is a bit higher than the average line speed.

$$\frac{v_l}{v_{ls}} = \frac{(1 - C_{vt})}{(1 - C_{vs})} \tag{6.11-13}$$

The slip velocity v_{sl} is the difference between the liquid velocity v_l and the particle (solids) velocity v_p, giving:

$$\xi = \frac{v_{sl}}{v_{ls}} = \frac{v_l}{v_{ls}} - \frac{v_p}{v_{ls}} = \frac{(1 - C_{vt})}{(1 - C_{vs})} - \frac{C_{vt}}{C_{vs}} \tag{6.11-14}$$

The slip ratio ξ is unknown, but Yagi et al. (1972) found an empirical equation based on many experiments for both sands and gravels:

$$\xi = 1.3 \cdot \psi^{-1.4} \quad \text{with:} \quad \psi = \frac{v_{ls}^2}{g \cdot R_{sd} \cdot D_p} \cdot \sqrt{C_D} \tag{6.11-15}$$

Once the slip ratio ξ is known, relations for the volumetric spatial concentration C_{vs} as a function of the volumetric transport concentration C_{vt} on one hand and for the volumetric transport concentration C_{vt} as a function of the volumetric spatial concentration C_{vs} on the other hand can be derived.

$$C_{vs} = \frac{1}{2} \cdot \left(\left(1 - \frac{1}{\xi}\right) + \sqrt{\left(1 - \frac{1}{\xi}\right)^2 + \frac{4 \cdot C_{vt}}{\xi}} \right) \tag{6.11-16}$$

$$C_{vt} = C_{vs} - \xi \cdot \left(C_{vs} - C_{vs}^2 \right) \tag{6.11-17}$$

The validity of this approach completely depends on the correctness of the slip ratio ξ equation (6.11-15). Since this equation has been derived from the experiments of Yagi et al. (1972) the validity should be limited to pipes with diameters of $D_p=0.08$ m up to $D_p=0.155$ m and particles with a diameter $d=0.25$ mm up to $d=45$ mm. It should be noted that there was a lot of scatter in the experimental values of the slip ratio.

Yagi et al. (1972) did not distinguish between different flow regimes, where it is clear from their experiments that at low line speeds there was a sliding or fixed bed regime, while at higher line speeds there was a heterogeneous regime. So the slip ratio ξ equation (6.11-15) is an overall fit function. Analyzing the data of Yagi et al. (1972) shows that there is some curvature in the data points as is shown in Figure 6.11-8.
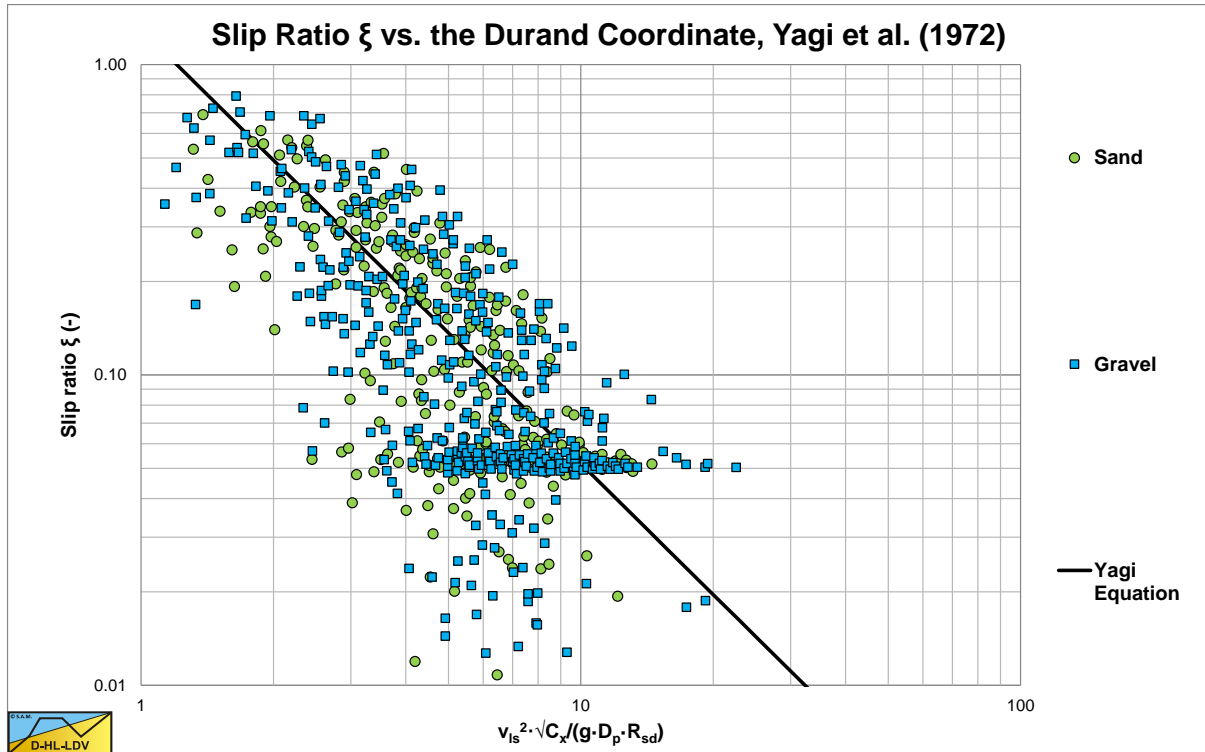
Figure 6.11-8: The slip ratio data points of Yagi et al. (1972).

This curvature results from the fact that there were 2 regimes, the sliding or fixed bed regime and the heterogeneous regime. In other words, at low line speeds the regime was below the Limit Deposit Velocity and at higher line speeds the regime was above the Limit Deposit Velocity. According to Durand & Condolios (1952) the Limit Deposit Velocity of large particles will occur at about **ψ=2.22** for gravel. For sands it may occur at **ψ=3-10**. Since most of the experiments of Yagi et al. (1972) were carried out in gravel and coarse sand, a **ψ=3** is a reasonable transition between the two regimes.

Although the fit equation improves the prediction of the slip velocity to line speed ratio ξ, the enormous scatter as is shown in Figure 6.11-8 can only lead to the conclusion that there is something else governing the slip velocity to line speed ratio ξ. The main problem of many researchers is that they choose **ψ** as their dimensionless number with a fixed ratio between the different parameters. Since **ψ** is dominated by the line speed **v_{ls}** and this line speed is supposed to be reversely proportional to the 3rd power in the relative excess head loss equation, the following equation was proposed by Durand & Condolios (1952):

$$\frac{i_m - i_l}{i_l \cdot C_{vt}} = \phi = K \cdot \psi^{-3/2} \quad \text{with:} \quad K = 85 \tag{6.11-18}$$

This gives a power of 3/2 to the term $g \cdot R_{sd} \cdot D_p$ and a power of -3/2 to the term $\sqrt{C_x}$. This is the result of the choice of choosing Froude numbers. Maybe the behavior of the excess head losses does not just follow the flow Froude number **Fr_{fl}** and the particle Froude number **Fr_p**, but (also) other dimensionless numbers. Note again that Yagi used the drag coefficient and not the particle Froude number.

At small values of the abscissa in Figure 6.11-8, the slip ratio seems to have a maximum value, although the fit curve would give values close to 1 or even exceeding 1. A value higher than 1 is physically impossible, because that means particles are moving in the opposite direction compared to the line speed. The maximum value is 1 for a stationary bed. However it is more likely that a sliding bed will occur at low line speeds and constant delivered concentration.

It should also be mentioned that often the slip velocity is related to the line speed and not to the liquid velocity. For small concentrations there is not much difference between the line speed and the liquid velocity, but for higher concentrations and a high slip ratio there is. So evaluating data one has to consider which definition is used for the slip velocity.

6.12 A.D. Thomas (1976) & (1979).

6.12.1 Head Losses.

A.D. Thomas (1976) investigated scale-up methods for pipeline transport of slurries. To do so he investigated pipes with diameters ranging from 50 mm to 300 mm diameter. The main purpose of this research was to find relations between the excess hydraulic gradient (the solids effect) and the pipe diameter and the line speed. To do so, particles are divided (based on the particle diameter) into 3 flow regimes. Very fine particles are supposed to behave according to the Equivalent Liquid Model (ELM), with or without a correction for the viscosity. Coarse particles are supposed to behave according to heterogeneous models, for which the Durand & Condolios (1952) model was chosen. Medium sized particles behave according to a pseudo heterogeneous flow regime, which is an intermediate between the homogeneous regime and the heterogeneous regime. In all cases this is considered for normal operational line speeds. The hydraulic gradient for pure liquid flow is defined as:

$$i_l = \frac{\lambda_l \cdot v_{ls}^2}{2 \cdot g \cdot D_p} \tag{6.12-1}$$

For rough pipes it is assumed that the Darcy Weisbach friction factor is reversely proportional to the Reynolds number to the power of 0.2. This power depends on the Reynolds number and also on the roughness of the pipe wall. Using this assumption gives for the hydraulic gradient:

$$i_l = \frac{\lambda_l \cdot v_{ls}^2}{2 \cdot g \cdot D_p} = A \cdot v_{ls}^{1.8} \cdot D_p^{-1.2} \tag{6.12-2}$$

Thomas (1976) found from his experiments:

$$i_l = A \cdot v_{ls}^{1.77} \cdot D_p^{-1.18} \tag{6.12-3}$$

Which is close to the theoretical proportionalities. For the ELM the following relation was chosen:

$$i_m = A \cdot v_{ls}^{1.77} \cdot D_p^{-1.18} \cdot \frac{\rho_m}{\rho_l} \tag{6.12-4}$$

Now suppose the Durand & Condolios (1952) equation is used for the heterogeneous regime, this would give the following proportionalities:

$$i_m - i_l = K_1 \cdot v_{ls}^{-3} \cdot D_p^{1.5} \cdot i_l \cdot C_{vt} \tag{6.12-5}$$

Substituting the equation for the pure liquid hydraulic gradient gives:

$$i_m - i_l = K_1 \cdot v_{ls}^{-3} \cdot D_p^{1.5} \cdot i_l \cdot A \cdot v_{ls}^{1.8} \cdot D_p^{-1.2} \cdot C_{vt} = K_2 \cdot v_{ls}^{-1.2} \cdot D_p^{0.3} \cdot C_{vt} \tag{6.12-6}$$

So the excess hydraulic gradient is proportional to the line speed to a power of -1.2 and proportional to the pipe diameter to a power of 0.3. This behavior is generally accepted to describe the heterogeneous behavior of coarse particles. Whether the linear proportionality of the delivered concentration holds is a question. Charles (1970) found that this is the case in the sliding bed regime, but not always in the heterogeneous regime, especially at high concentrations.

It was found that the proportionality with the line speed to a power of -1.2 correlated well with the experimental data up to a certain line speed, after which the power became positive. This certain line speed in fact is the transition (intersection point) between the heterogeneous and the homogeneous regime. The approach of Zandi & Govatos (1967), using two equations, was rejected, because the powers found did not match the experimental data. The Durand & Condolios (1952) approach gives good results for small line speeds, but not for high line speeds, since this approach gives a solids effect that asymptotically reaches zero for high line speeds, while experiments have shown that the asymptotic value should match the ELM behavior. The method of Charles (1970) solves these problems and gives an equation with the following proportionalities:

$$i_m - i_l = K_3 \cdot v_{ls}^{-1.2} \cdot D_p^{0.3} \cdot C_{vt} + K_4 \cdot v_{ls}^{1.8} \cdot D_p^{-1.2} \cdot R_{sd} \cdot C_{vt}$$

Durand & Condolios   **ELM**   **(6.12-7)**

This equation will do well for very small line speeds if the second term is negligible and for very large line speeds when the first term is negligible, but it will give too high values in between and this is the region we are interested in for pseudo heterogeneous flow. Multiplying the second term with a factor 0.7 gives a good match with the experiments of Thomas (1976), giving:

$$i_m - i_l = K_3 \cdot v_{ls}^{-1.2} \cdot D_p^{0.3} \cdot C_{vt} + 0.7 \cdot K_4 \cdot v_{ls}^{1.8} \cdot D_p^{-1.2} \cdot R_{sd} \cdot C_{vt} \tag{6.12-8}$$

This solves the proportionalities of the excess hydraulic gradient with the line speed. However this does not solve the power of the pipe diameter in the first term. The positive power does not correlate the data for different pipe diameters for medium sands. This would require a negative power.

Vocadlo & Charles (1972) proposed the following equation for the transition of the heterogeneous to the homogeneous regime:

$$i_m = K_5 \cdot C_{vt} \cdot R_{sd} \cdot \frac{v_t}{v_{ls}} + i_l \cdot \left(\frac{\mu_m}{\mu_l} \right) \cdot \left(1 + R_{sd} \cdot C_{vt} \right)^{0.8} \tag{6.12-9}$$

The first term, the heterogeneous solids effect, is very similar to the Newitt et al. (1955) equation for heterogeneous transport. The second term is not proportional with the volumetric concentration and follows the same trend as the Talmon (2011) model for homogeneous transport, based on a particle free viscous sub-layer. The second term also follows the model of Jufin & Lopatin (1966), based on experiments in the pseudo heterogeneous and homogeneous regimes. The second term also adjusts for the apparent viscosity due to the solids in the liquid. This equation can be simplified to:

$$i_m - i_l = K_6 \cdot v_{ls}^{-1} + K_7 \cdot v_{ls}^{1.8} \cdot D_p^{-1.2} \tag{6.12-10}$$

Now the excess hydraulic gradient in the first term does not depend on the pipe diameter anymore. For an intermediate particle size of **d=0.48 mm** Thomas (1976) found that this is close, however for the smaller particle size of **d=0.18 mm** he found that the power of the pipe diameter in the first term should be negative to explain for the trends in the experimental data. He proposes the following equation:

$$i_m - i_l = K_8 \cdot v_{ls}^{-1.2} \cdot D_p^b + K_9 \cdot v_{ls}^{1.8} \cdot D_p^{-1.2}$$

or   **(6.12-11)**

$$i_m = K_8 \cdot v_{ls}^{-1.2} \cdot D_p^b + K_{10} \cdot v_{ls}^{1.8} \cdot D_p^{-1.2}$$

The first term now contains the power **b** for the pipe diameter, which is positive for coarse particles, close to zero for intermediate particles and negative for fine particles.

Figure 6.12-1, Figure 6.12-2, Figure 6.12-3 and Figure 6.12-5 show that fine particles at relatively high line speeds result in homogeneous behavior according to the ELM. The graphs for coal slurry are according to the ELM without correction for the viscosity and the slurry density. The graphs for iron ore include a correction for the viscosity and the slurry density.
Figure 6.12-7, Figure 6.12-8, Figure 6.12-9 and Figure 6.12-10 show some data for the **d=0.18 mm** sand and the **d=0.48 mm** sand in different pipe diameters, compared with the DHLLDV Framework. The DHLLDV Framework uses a power of about 0-0.15 for the pipe diameter in the first term of the equations, the power **b**. Still the results of DHLLDV match well with the experimental data of Thomas (1976). How can this be explained?

Thomas (1976) assumes a power of -1.2 for the line speed in the first term of the above equation. When the pipe diameter increases however, also the line speed of the experiments increases, since most experiments are carried out above the LDV. In the pseudo heterogeneous region, the excess hydraulic gradient curves flatten, so the power of -1.2 of the line speed in the first term may be too high, a more negative power is required. Now suppose the power is **a** and the LDV increases with the square root of the pipe diameter. This gives the following equation:

$$v_{ls,ldv} \propto D_p^{1/2} \quad \text{and} \quad D_p \propto v_{ls,ldv}^2$$

<div align="right">

(6.12-12)

</div>

$$i_{m,ldv} \propto v_{ls,ldv}^a \cdot D_p^b \propto v_{ls,ldv}^a \cdot v_{ls,ldv}^{b/2} = v_{ls,ldv}^{a+b/2}$$

Figure 6.12-1: The hydraulic gradient of a coal slurry, d=0.19 mm, in an 0.0522 m diameter pipe.
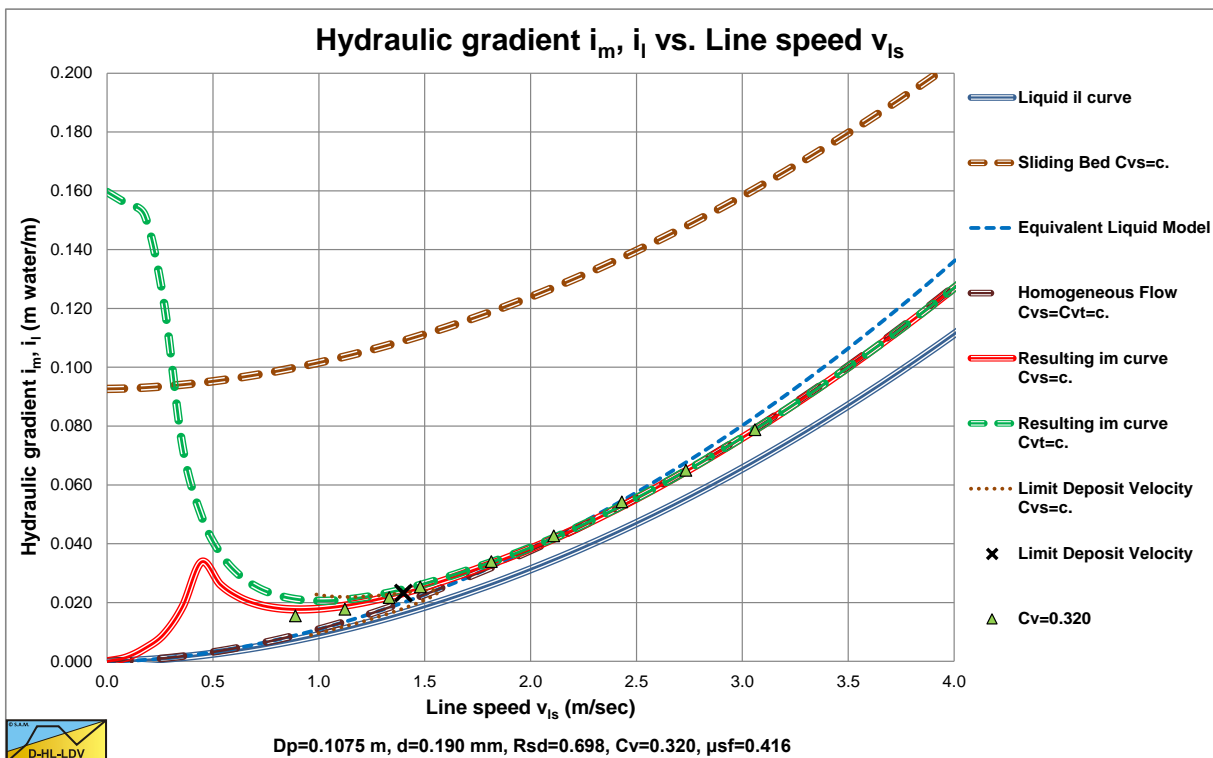
Figure 6.12-2: The hydraulic gradient of a coal slurry, d=0.19 mm, in an 0.1075 m diameter pipe.

Suppose in reality the power **a=-1.7** and the power **b=0**, so **a+b/2=-1.7** or **a=-1.7-b/2** or **b=2·(-1.7-a)**. Using a power of -1.2 would give a power **b=-1**. The Wilson et al. (2006) model uses **a=-1.7** for uniform sands. Zandi & Govatos (1967) use **a=-1.86** and the DHLLDV Framework **a=-1.7**, also for uniform sands. The conclusion is, that different values for the power **a** result in different values for the power **b**. The conclusion of Thomas (1976) regarding the power of the pipe diameter should be interpreted with care.
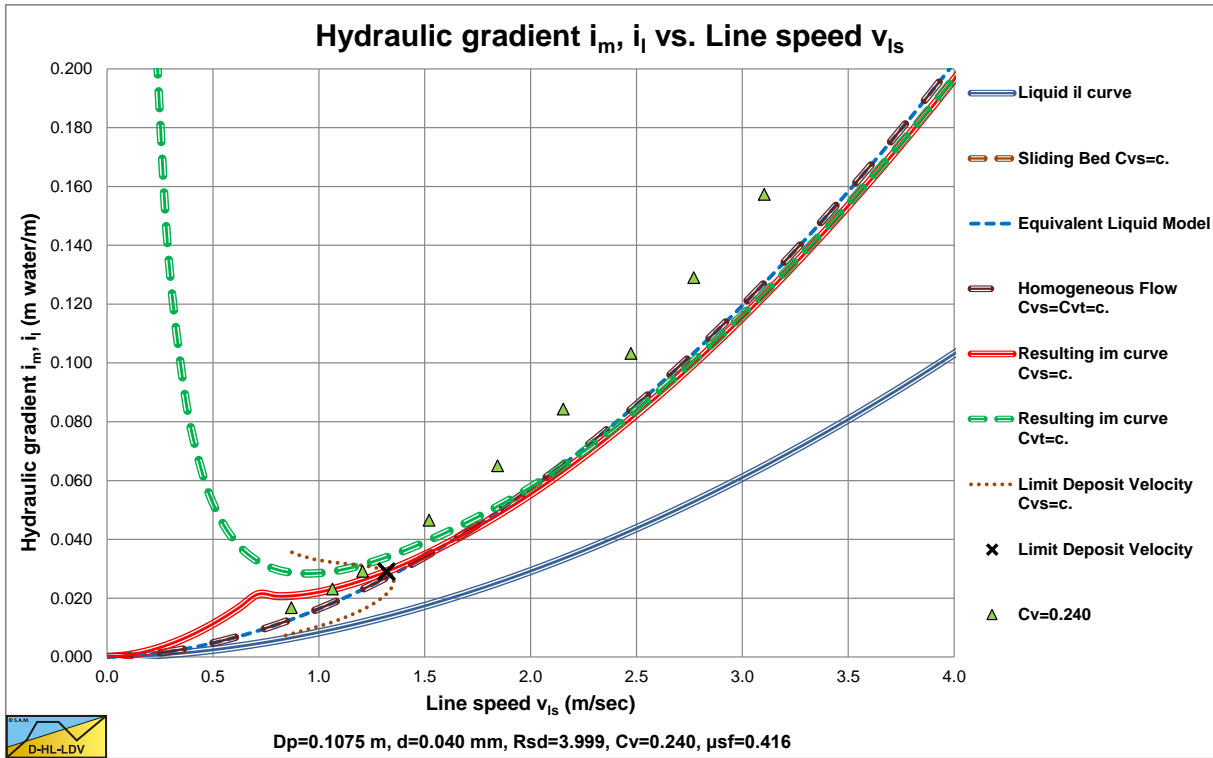
Figure 6.12-3: The hydraulic gradient of an iron ore slurry, d=0.04 mm, in an 0.1075 m diameter pipe, without Thomas (1965) viscosity.
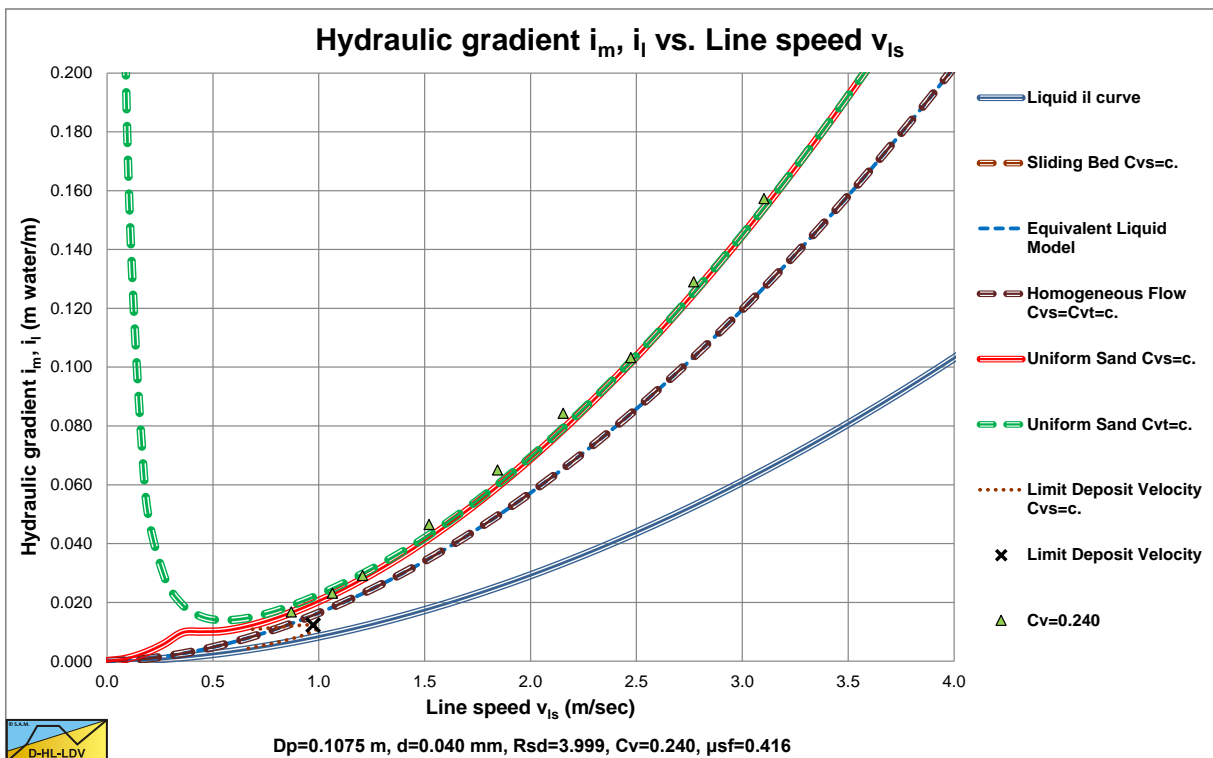
Figure 6.12-4: The hydraulic gradient of an iron ore slurry, d=0.04 mm, in an 0.1075 m diameter pipe, including Thomas (1965) viscosity.
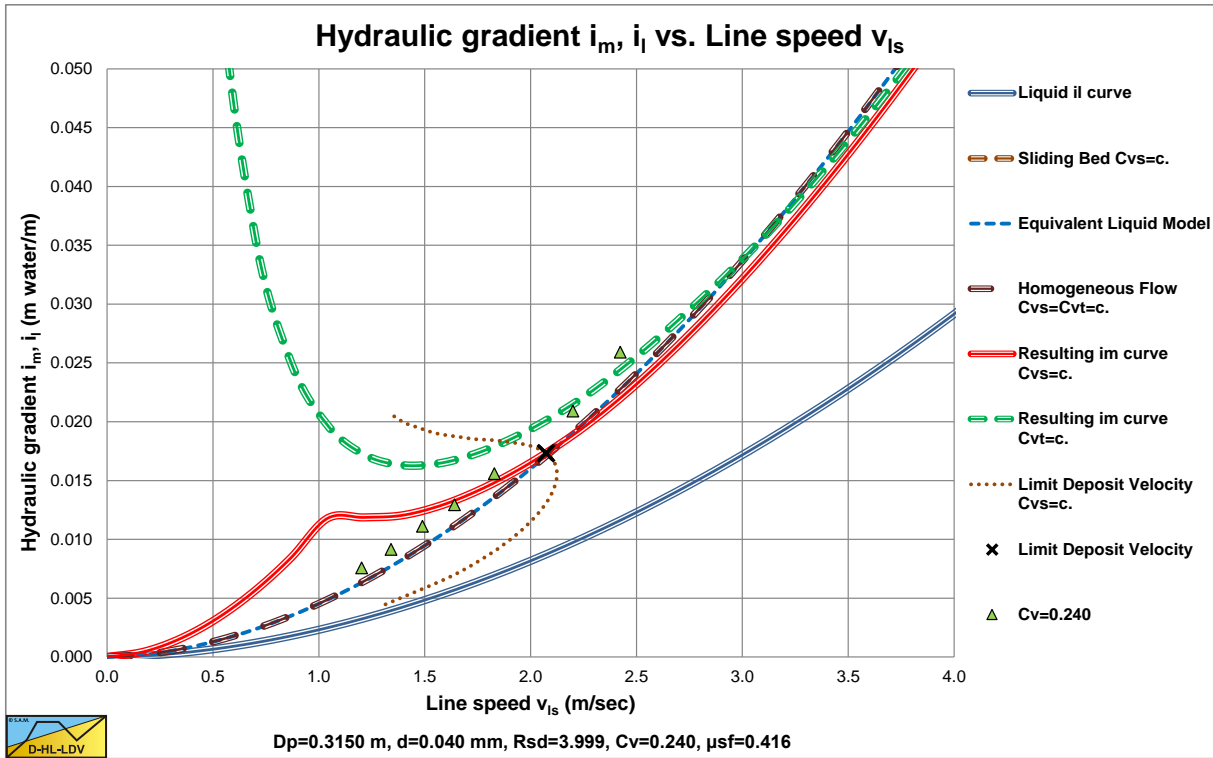
Figure 6.12-5: The hydraulic gradient of an iron ore slurry, d=0.04 mm, in an 0.3150 m diameter pipe, without Thomas (1965) viscosity.
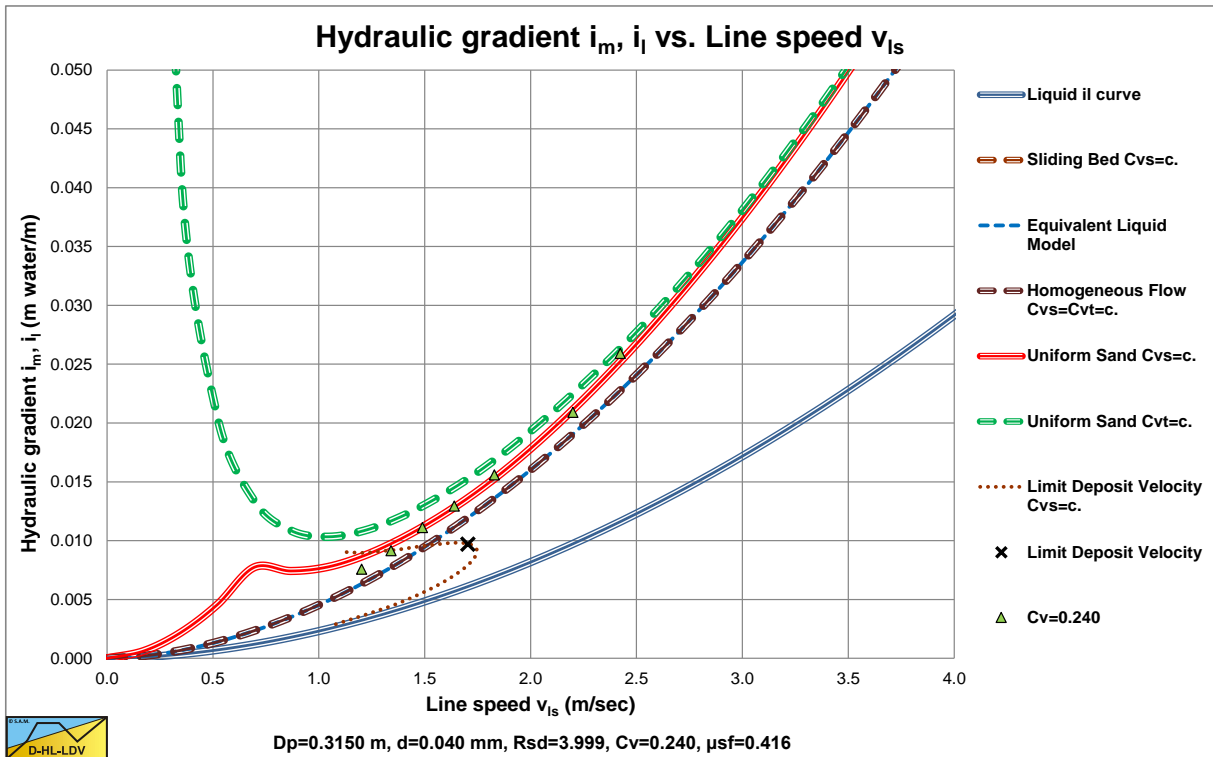
Figure 6.12-6: The hydraulic gradient of an iron ore slurry, d=0.04 mm, in an 0.3150 m diameter pipe, including Thomas (1965) viscosity.
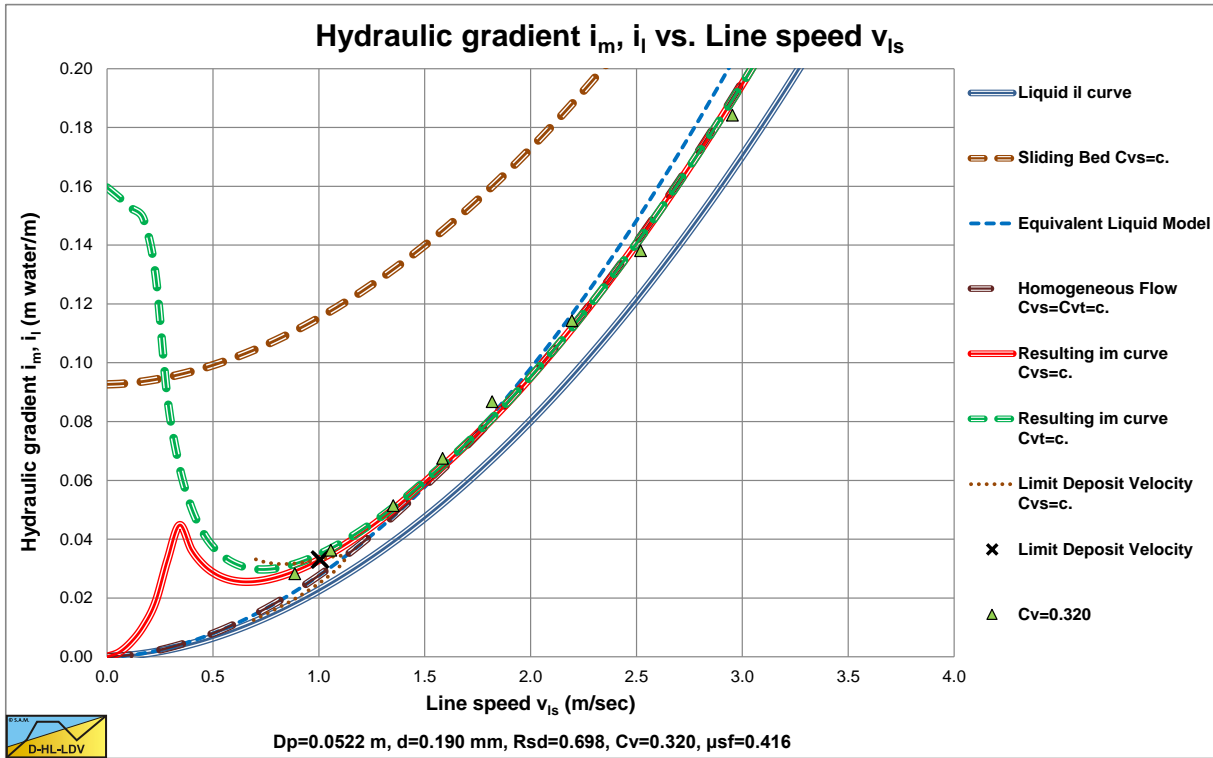
Figure 6.12-7: The hydraulic gradient of a sand slurry, d=0.18 mm, in an 0.0522 m diameter pipe.
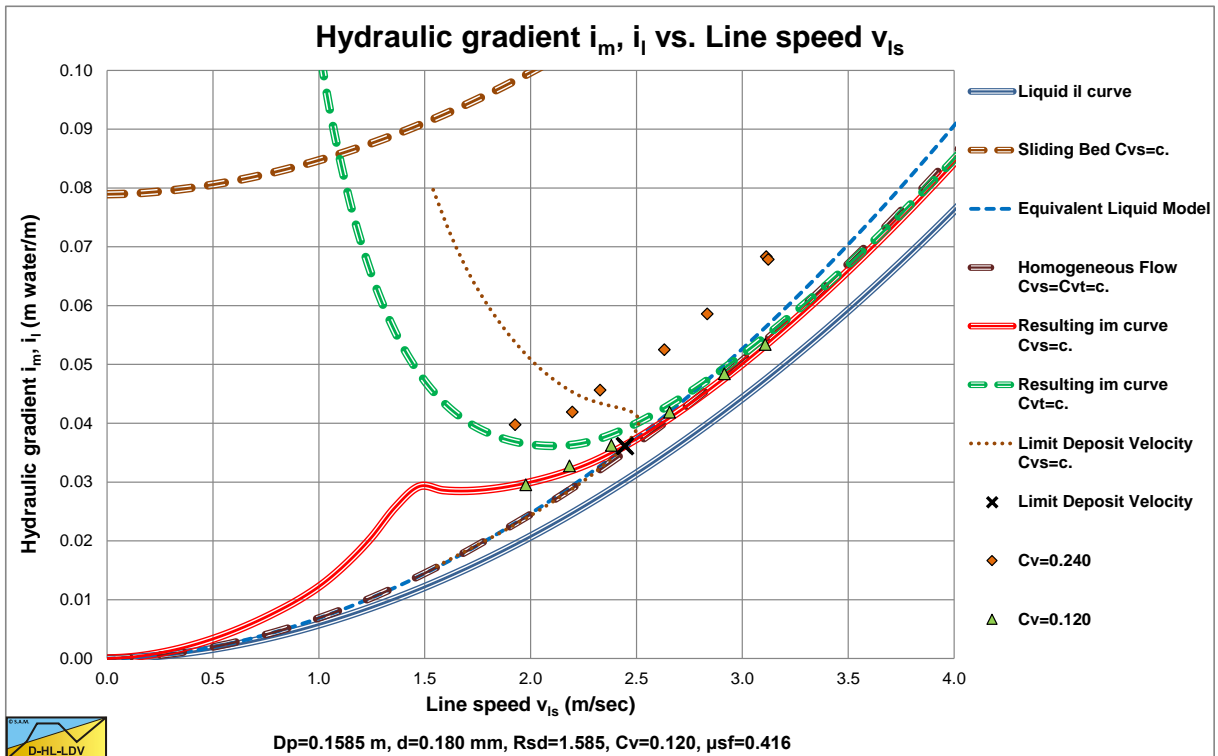
Figure 6.12-8: The hydraulic gradient of a sand slurry, d=0.18 mm, in an 0.1585 m diameter pipe.

Figure 6.12-9: The hydraulic gradient of a sand slurry, d=0.48 mm, in an 0.0522 m diameter pipe.

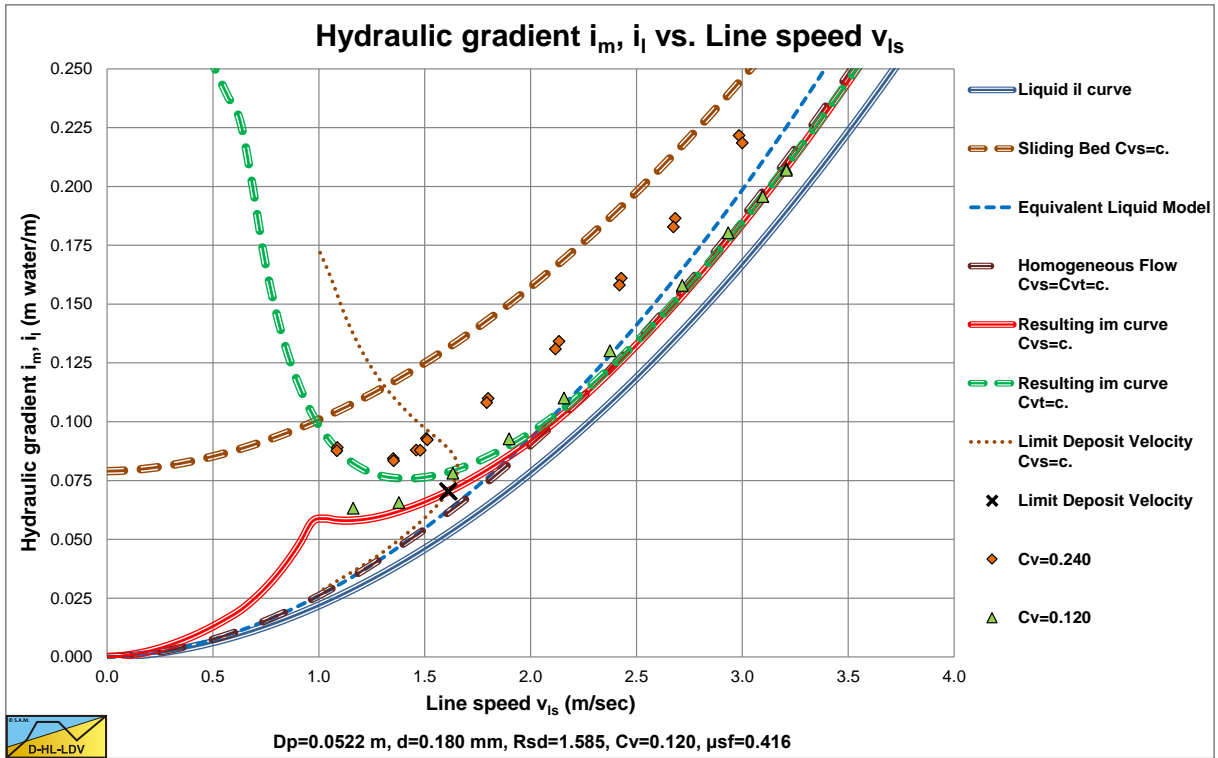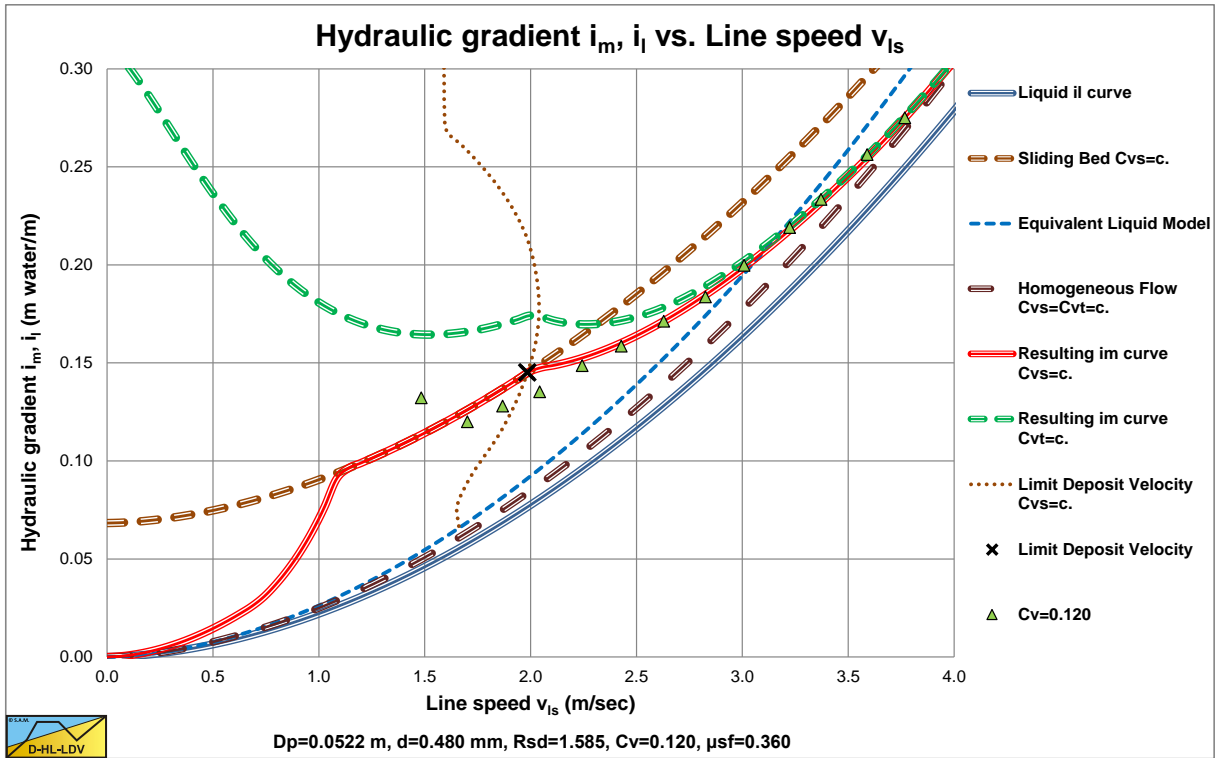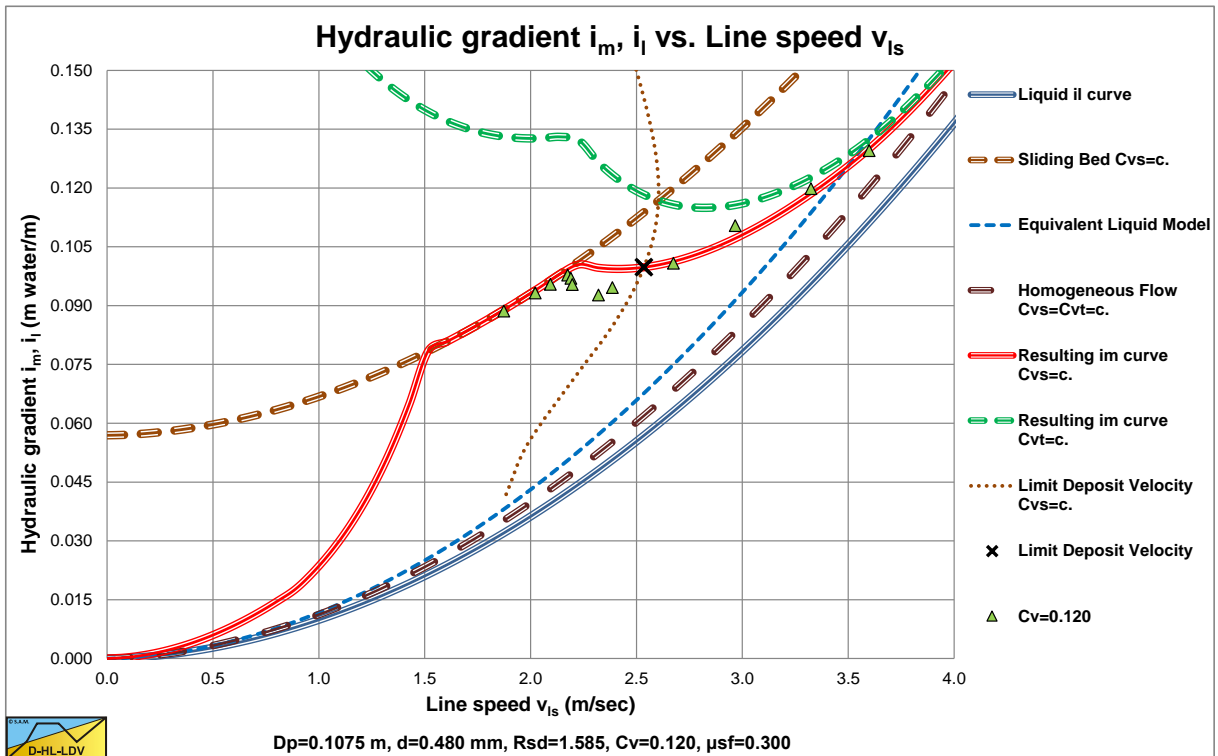**Figure 6.12-10: The hydraulic gradient of a sand slurry, d=0.48 mm, in an 0.1075 m diameter pipe.**

6.12.2 The Limit Deposit Velocity.

Based on the experiments of Thomas (1976) with **d=0.18 mm** sand at volumetric concentrations of 12% and 24%, the following equation was found for the Durand Froude number F_L:

$$F_L = \frac{v_{ls,ldv}}{\sqrt{2 \cdot g \cdot R_{sd} \cdot D_p}} = 0.81 \cdot D_p^{-0.137}$$

(6.12-13)

The derivation is based on the experimental data of Thomas (1976) and may not be very accurate. The main conclusion from this exercise is that the Durand Froude number decreases with increasing pipe diameter, which was also found by Jufin & Lopatin (1966). According to Durand & Condolios (1952) and Gibert (1960) the Durand Froude number F_L is independent from the pipe diameter. Jufin & Lopatin (1966) found a power of -0.167 and here a power of -0.137 was found. This is for fine to coarse particles, but probably not for very fine particles and very coarse particles. Thomas (1979) found that the relation between the LDV and the pipe diameter for fine to coarse particles has a dependency with a power between 0.1 as a lower limit and 0.5 as an upper limit.

Thomas (1979) derived an equation for very small particles, proving that there is a lower limit to the LDV or LSDV. The method is based on the fact that particles smaller than the thickness of the viscous sub layer will be in suspension due to turbulent eddies in the turbulent layer, but may still settle in the laminar viscous sub layer.

The thickness of the thin layer is assumed to be equal to the thickness of the viscous sub layer:

$$\delta_v = 5 \cdot \frac{\nu_l}{u_*}$$

(6.12-14)

By using a force balance on a very thin bed layer in the viscous sub layer, he found the following equation, using a factor 5 for the thickness of the viscous sub-layer instead of the factor 11.6:

$$v_{ls,ldv} = 1.49 \cdot \left(g \cdot R_{sd} \cdot C_{vb} \cdot \nu_l \cdot \mu_{sf} \right)^{1/3} \cdot \sqrt{\frac{8}{\lambda_l}}$$

(6.12-15)

Giving for the Durand Froude number:

$$F_L = \frac{v_{ls,ldv}}{\sqrt{2 \cdot g \cdot D_p \cdot R_{sd}}} = \frac{1.49 \cdot \left(g \cdot R_{sd} \cdot C_{vb} \cdot \nu_l \cdot \mu_{sf} \right)^{1/3} \cdot \sqrt{\frac{8}{\lambda_l}}}{\sqrt{2 \cdot g \cdot D_p \cdot R_{sd}}}$$

(6.12-16)

The Froude number F_L does not depend on the particle size, but on the thickness of the viscous sub layer and so on the Darcy Weisbach friction coefficient. With the parameters C_{vb}=0.6 and μ_{sf}=0.4, the equation reduces to:

$$v_{ls,ldv} = 0.93 \cdot \left(g \cdot R_{sd} \cdot \nu_l \right)^{1/3} \cdot \sqrt{\frac{8}{\lambda_l}}$$

(6.12-17)

The coefficient found from the experiments was 1.1 instead of 0.93. Due to the use of the factor 5 instead of 11.6 for the thickness of the viscous sub-layer this can easily be explained. Using the 11.6 would have given a factor 1.4 instead of 0.93.

The Froude number F_L does depend on the pipe diameter to a power of about -0.4, due to the Darcy Weisbach friction factor included in the equation. The line speed found by Thomas (1979) is however an LSDV and not the LDV, so the LDV may be expected to have a slightly higher value.

The applicability of the equation derived appeared to be **d<0.3·δ_v**. Larger particles will follow different physics.

6.13 The Turian & Yuan (1977) Fit Model.

6.13.1 Introduction.

Turian & Yuan (1977) developed pressure drop correlations for flow of slurries in pipelines for 4 flow regimes. They defined flow with a stationary bed, saltation flow, heterogeneous flow and homogeneous flow. No distinctions have been made for sliding bed flow and sheet flow, so these regimes are part of the 4 regimes defined. A total number of 2848 data points were used to find correlations for each of the 4 regimes. For the stationary bed regime 361 data points were used, for the saltation regime 1230 data points, for the heterogeneous regime 493 data points and for the homogeneous regime 645 data points. The data points are from experiments with a pipe diameter D_p from 0.0126 m to 0.7 m , a relative submerged density R_{sd} from 0.16 to 10.3, a particle size d from 0.03 mm to 38 mm, a solids concentration C_v from 0% to 42% and a mean line speed v_{ls} from 0 m/sec to 6.7 m/sec. It should be mentioned however that most of the experiments were carried out with sand or glass and only 16 data points were found from pipe diameters above 15 cm. Turian & Yuan (1977) correlated the pressure losses to a set of 4 parameters, the volumetric concentration C_v, the Fanning friction factor f, the particle drag coefficient C_D and the flow Froude number Fr. It is not always clear whether the spatial or the transport concentration is used in the equation, but based on an analysis of the resulting equation it is assumed to be the transport concentration. In the original equations of Turian & Yuan (1977), they used the concentration as a percentage. In the equations as found later and as presented here, the concentration is used as a fraction. The result is that all the proportionality coefficients had to be multiplied by 100 to the power of the concentration.

The drag coefficient for the terminal settling velocity C_D is:

$$C_D = \frac{4}{3} \cdot \frac{R_{sd} \cdot g \cdot d}{v_t^2}$$

(6.13-1)

The Froude number Fr of the flow in the Turian & Yuan (1977) equations is:

$$Fr = \frac{v_{ls}^2}{R_{sd} \cdot g \cdot D_p}$$

(6.13-2)

The pressure losses of a liquid can be calculated with:

$$\Delta p_l = 2 \cdot f_l \cdot \rho_l \cdot v_{ls}^2 \cdot \frac{\Delta L}{D_p} = \lambda_l \cdot \frac{1}{2} \cdot \rho_l \cdot v_{ls}^2 \cdot \frac{\Delta L}{D_p}$$

(6.13-3)

The pressure losses of a mixture can be calculated with:

$$\Delta p_m = 2 \cdot f_m \cdot \rho_l \cdot v_{ls}^2 \cdot \frac{\Delta L}{D_p} = \lambda_m \cdot \frac{1}{2} \cdot \rho_l \cdot v_{ls}^2 \cdot \frac{\Delta L}{D_p}$$

(6.13-4)

The general solids excess pressure equation of Turian & Yuan has the following form:

$$f_m - f_l = \frac{\lambda_m}{4} - \frac{\lambda_l}{4} = K \cdot C_v^{\alpha} \cdot f_l^{\beta} \cdot \left(\frac{4}{3} \cdot \frac{R_{sd} \cdot g \cdot d}{v_t^2} \right)^{\gamma} \cdot \left(\frac{v_{ls}^2}{R_{sd} \cdot g \cdot D_p} \right)^{\delta}$$

(6.13-5)

$$f_m - f_l = \frac{\lambda_m}{4} - \frac{\lambda_l}{4} = K \cdot C_v^{\alpha} \cdot f_l^{\beta} \cdot C_D^{\gamma} \cdot Fr^{\delta}$$

The proportionality coefficient K and the powers α, β, γ and δ are determined for each of the 4 flow regimes by correlation techniques. It should be mentioned that the form of this equation limits the possible combinations between the parameters and also the fact that the solids effect is described by one single term limits the physics behind the model.

6.13.2 The Regime Equations.

The friction coefficient **f_m** depends on the regime according to:

Fixed bed/sliding bed, regime 0:

$$f_m - f_l = \frac{\lambda_m}{4} - \frac{\lambda_l}{4} = 12.13 \cdot C_v^{0.7389} \cdot \left(\frac{\lambda_l}{4}\right)^{0.7717} \cdot C_D^{-0.4054} \cdot Fr^{-1.096} \tag{6.13-6}$$

Saltation, regime 1:

$$f_m - f_l = \frac{\lambda_m}{4} - \frac{\lambda_l}{4} = 107.1 \cdot C_v^{1.018} \cdot \left(\frac{\lambda_l}{4}\right)^{1.046} \cdot C_D^{-0.4213} \cdot Fr^{-1.354} \tag{6.13-7}$$

Heterogeneous suspension, regime 2:

$$f_m - f_l = \frac{\lambda_m}{4} - \frac{\lambda_l}{4} = 30.11 \cdot C_v^{0.8687} \cdot \left(\frac{\lambda_l}{4}\right)^{1.200} \cdot C_D^{-0.1677} \cdot Fr^{-0.6938} \tag{6.13-8}$$

Homogeneous suspension, regime 3:

$$f_m - f_l = \frac{\lambda_m}{4} - \frac{\lambda_l}{4} = 8.538 \cdot C_v^{0.5028} \cdot \left(\frac{\lambda_l}{4}\right)^{1.428} \cdot C_D^{0.1516} \cdot Fr^{-0.3531} \tag{6.13-9}$$
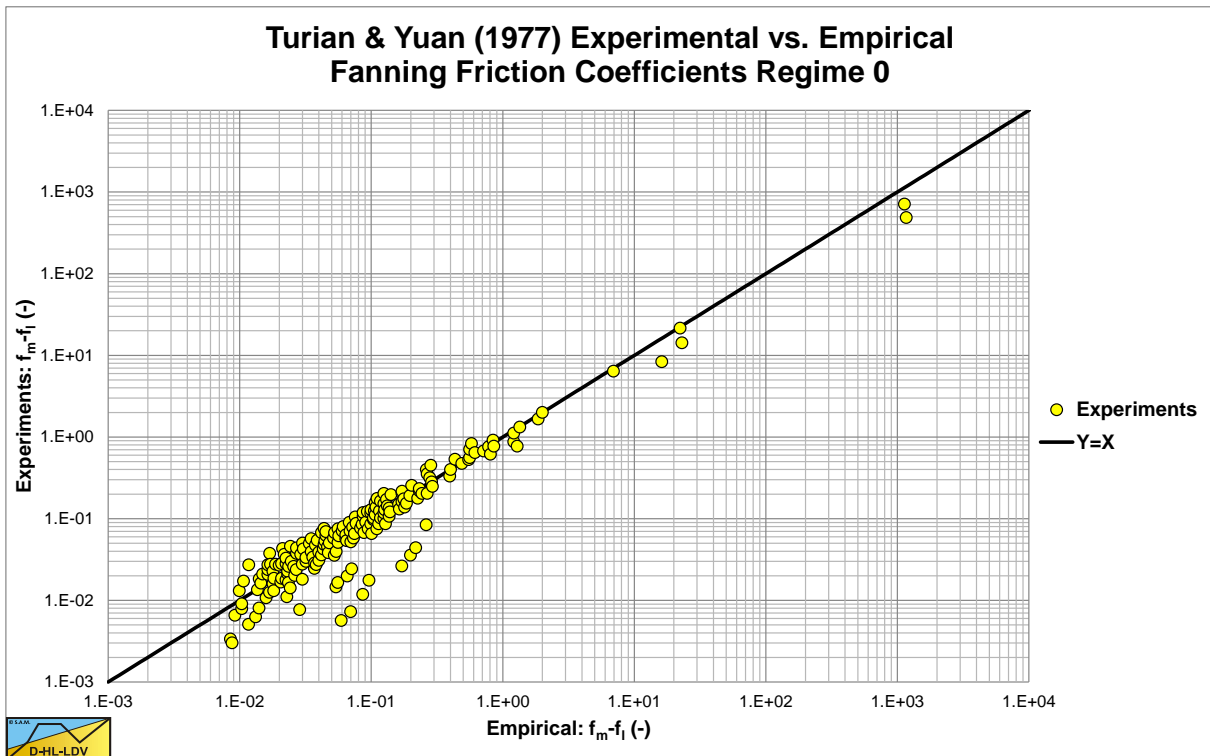
Figure 6.13-1: Correlation regime 0.
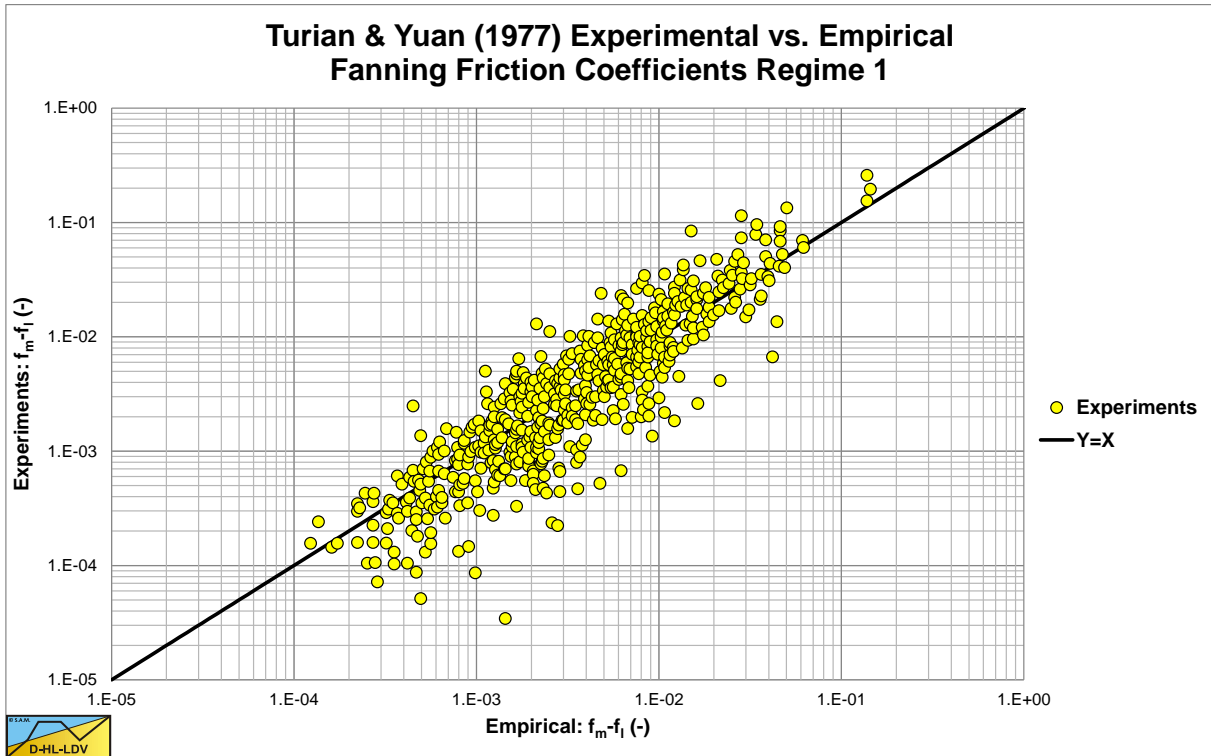
Figure 6.13-2: Correlation regime 1.
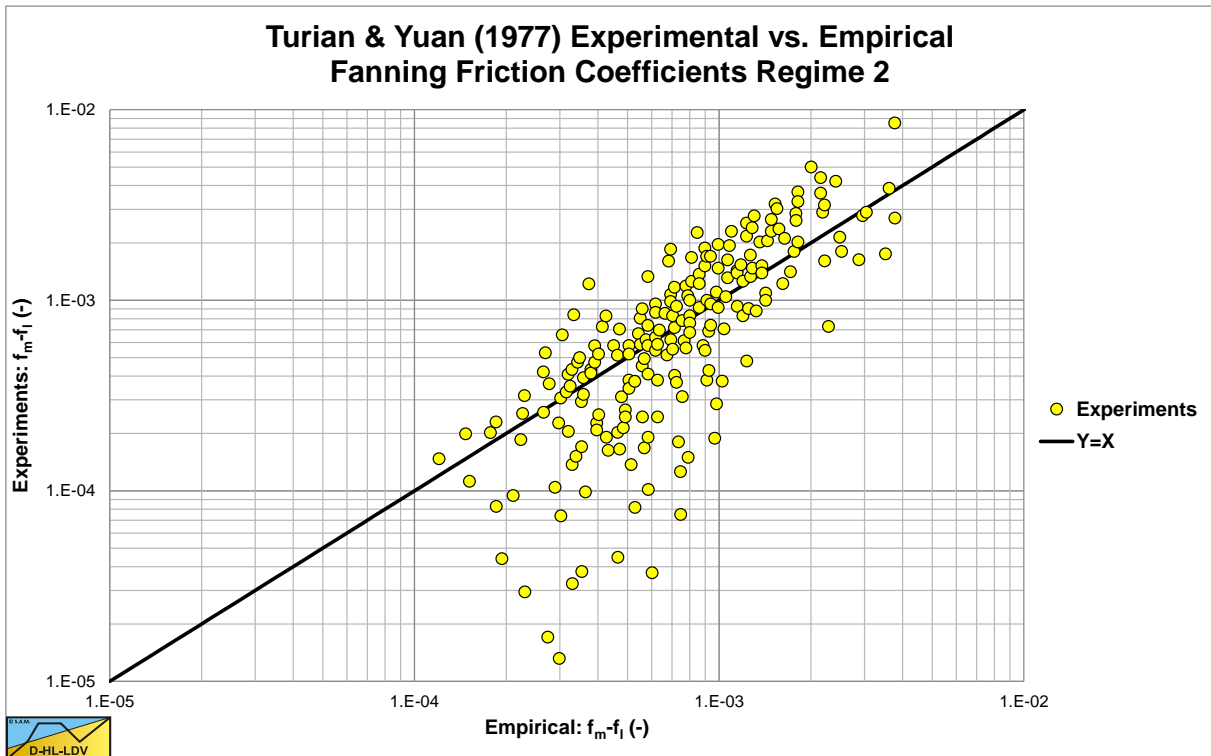
Figure 6.13-3: Correlation regime 2.
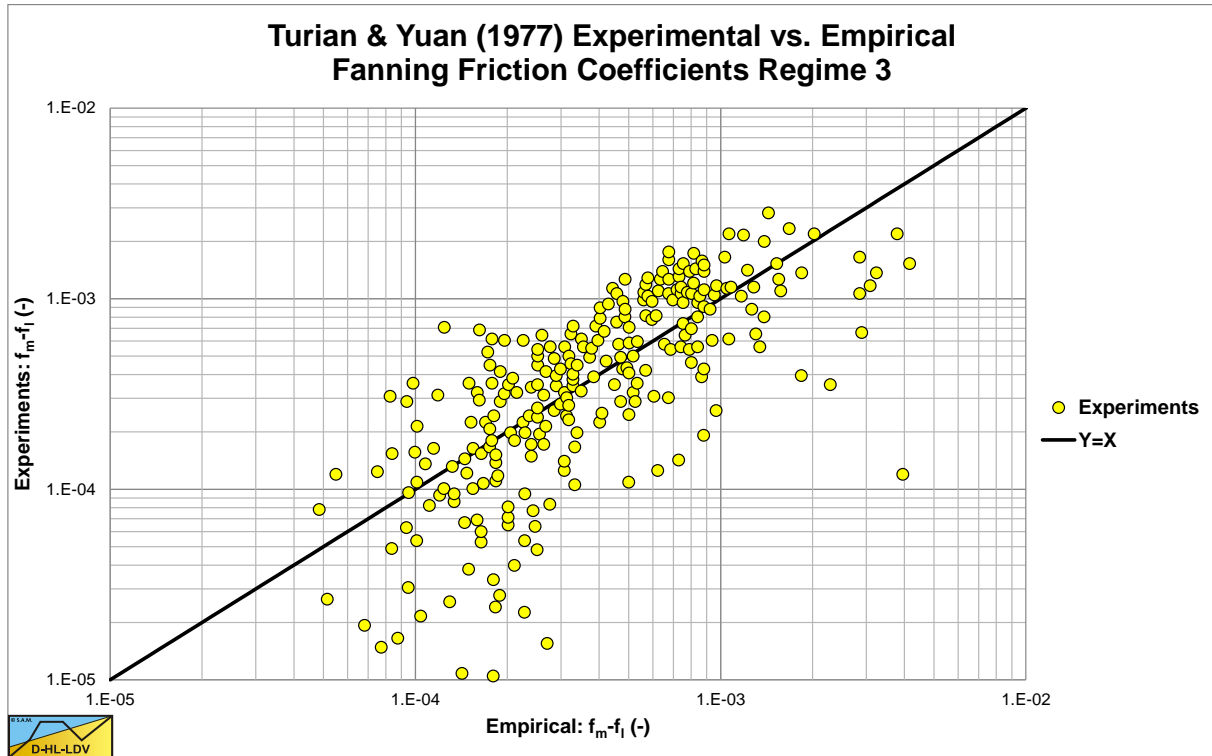
Figure 6.13-4: Correlation regime 3.

6.13.3 Usage of the Equations.

The Fanning friction factor for pure liquid transport can be written as:

$$
f_l = \frac{\Delta p_l}{2 \cdot \rho_l \cdot v_{ls}^2 \cdot \dfrac{\Delta L}{D_p}} = \frac{\lambda_l}{4}
\tag{6.13-10}
$$

The Fanning friction factor for mixture transport can be written as:

$$
f_m = \frac{\Delta p_m}{2 \cdot \rho_l \cdot v_{ls}^2 \cdot \dfrac{\Delta L}{D_p}} = \frac{\lambda_m}{4}
\tag{6.13-11}
$$

Thus:

$$
f_m - f_l = \frac{\lambda_m}{4} - \frac{\lambda_l}{4} = \frac{\Delta p_m - \Delta p_l}{2 \cdot \rho_l \cdot v_{ls}^2 \cdot \dfrac{\Delta L}{D_p}} = \frac{(\Delta p_m - \Delta p_l) \cdot D_p}{2 \cdot \rho_l \cdot v_{ls}^2 \cdot \Delta L}
$$

$$
\tag{6.13-12}
$$

$$
f_m - f_l = \frac{\lambda_m}{4} - \frac{\lambda_l}{4} = \frac{(i_m - i_l) \cdot \rho_l \cdot g \cdot \Delta L}{2 \cdot \rho_l \cdot v_{ls}^2 \cdot \dfrac{\Delta L}{D_p}} = \frac{(i_m - i_l) \cdot g \cdot D_p}{2 \cdot v_{ls}^2}
$$

Or:

$$\Delta p_m - \Delta p_l = \left(f_m - f_l\right) \cdot \frac{2 \cdot \rho_l \cdot v_{ls}^2 \cdot \Delta L}{D_p} = \left(\lambda_m - \lambda_l\right) \cdot \frac{\rho_l \cdot v_{ls}^2 \cdot \Delta L}{2 \cdot D_p}$$

(6.13-13)

$$i_m - i_l = \left(f_m - f_l\right) \cdot \frac{2 \cdot v_{ls}^2}{g \cdot D_p} = \left(\lambda_m - \lambda_l\right) \cdot \frac{v_{ls}^2}{2 \cdot g \cdot D_p}$$

With the Froude number according to equation (6.13-2), the hydraulic gradient can be written as:

$$i_m - i_l = \left(f_m - f_l\right) \cdot \frac{2 \cdot v_{ls}^2}{g \cdot D_p} = \left(f_m - f_l\right) \cdot 2 \cdot R_{sd} \cdot \frac{v_{ls}^2}{R_{sd} \cdot g \cdot D_p} = \left(f_m - f_l\right) \cdot 2 \cdot R_{sd} \cdot Fr$$

(6.13-14)

The relative excess hydraulic gradient E_{rhg} is now:

$$E_{rhg} = \frac{\left(i_m - i_l\right)}{R_{sd} \cdot C_v} = \frac{\left(f_m - f_l\right) \cdot 2 \cdot Fr}{C_v}$$

(6.13-15)

In terms of the hydraulic gradient, the Turian & Yuan (1977) equations can be rewritten as:

Fixed bed/sliding bed, regime 0:

$$\left(i_m - i_l\right) = 8.323 \cdot C_v^{0.7389} \cdot \lambda_l^{0.7717} \cdot C_D^{-0.4054} \cdot Fr^{-0.096} \cdot R_{sd}$$

(6.13-16)

Saltation, regime 1:

$$\left(i_m - i_l\right) = 50.24 \cdot C_v^{1.018} \cdot \lambda_l^{1.046} \cdot C_D^{-0.4213} \cdot Fr^{-0.354} \cdot R_{sd}$$

(6.13-17)

Heterogeneous suspension, regime 2:

$$\left(i_m - i_l\right) = 11.41 \cdot C_v^{0.868} \cdot \lambda_l^{1.200} \cdot C_D^{-0.1677} \cdot Fr^{0.3062} \cdot R_{sd}$$

(6.13-18)

Homogeneous suspension, regime 3:

$$\left(i_m - i_l\right) = 2.358 \cdot C_v^{0.5028} \cdot \lambda_l^{1.428} \cdot C_D^{0.1516} \cdot Fr^{0.6469} \cdot R_{sd}$$

(6.13-19)

In terms of the S_{rs} value, the Turian & Yuan (1977) equations can be rewritten as:

Fixed bed/sliding bed, regime 0:

$$E_{rhg} = \frac{\left(i_m - i_l\right)}{R_{sd} \cdot C_v} = 8.323 \cdot C_v^{-0.2611} \cdot \lambda_l^{0.7717} \cdot C_D^{-0.4054} \cdot Fr^{-0.096}$$

(6.13-20)

Saltation, regime 1:

$$E_{rhg} = \frac{\left(i_m - i_l\right)}{R_{sd} \cdot C_v} = 50.24 \cdot C_v^{0.018} \cdot \lambda_l^{1.046} \cdot C_D^{-0.4213} \cdot Fr^{-0.354}$$

(6.13-21)

Heterogeneous suspension, regime 2:

$$E_{rhg} = \frac{(i_m - i_l)}{R_{sd} \cdot C_v} = 11.41 \cdot C_v^{-0.132} \cdot \lambda_l^{1.200} \cdot C_D^{-0.1677} \cdot Fr^{0.3062}$$

(6.13-22)

Homogeneous suspension, regime 3:

$$E_{rhg} = \frac{(i_m - i_l)}{R_{sd} \cdot C_v} = 2.358 \cdot C_v^{-0.4972} \cdot \lambda_l^{1.428} \cdot C_D^{0.1516} \cdot Fr^{0.6469}$$

(6.13-23)

6.13.4 Analysis of the Turian & Yuan (1977) Equations.

The Turian & Yuan (1977) correlation equations are based on one term for the solids effect of the pressure losses. In their equations they use the drag coefficient C_D and the Froude number Fr, limiting the possible combinations of parameters. The relative submerged density R_{sd}, the particle diameter d and the terminal settling velocity v_t are always present in a prescribed relation of the drag coefficient C_D. The line speed v_{ls}, the relative submerged density R_{sd} and the pipe diameter D_p are presented in a prescribed relation in the Froude number. This limits the number of possible parameter combinations and also the absence of the sliding friction coefficient limits the explanation by real physics of the equations. For the analysis, the equations of Turian & Yuan (1977) are compared with the model of Miedema (2013S) as described in this book. This is illustrated in Figure 6.13-5 and Figure 6.13-6 for an 0.15 m pipe and a 0.2 mm particle.

Regime 0: Fixed bed or sliding bed, equation (6.13-20).

$$E_{rhg} = \frac{(i_m - i_l)}{R_{sd} \cdot C_v} = 8.323 \cdot C_v^{-0.2611} \cdot \lambda_l^{0.7717} \cdot C_D^{-0.4054} \cdot Fr^{-0.096}$$

For the E_{rhg} value, the fixed bed or sliding bed equation is almost independent of the Froude number, which points to a constant E_{rhg} value as a function of the hydraulic gradient or of the line speed. A sliding bed however would require a sliding friction coefficient in the equation, which is absent. This may be compensated partly by the negative power of the drag coefficient, since smaller particles often have a smaller sliding friction coefficient. The negative power of the volumetric concentration can be explained. A power of 0 would be expected for a constant spatial volumetric concentration. A constant transport volumetric concentration would however result in a negative power. The positive power of the friction coefficient and the negative power of the drag coefficient can be explained by the liquid friction in the cross section above the bed. This liquid friction is the sum of the friction on the pipe wall and the friction on the bed. The drag coefficient is to some extent reversely proportional with the size of the bed particles, while the shear stress on the bed is proportional with the particle size. Figure 6.13-5 shows that the constant transport concentration model of Miedema (2013S) in the sliding bed region does not match the Turian & Yuan (1977) model exactly for a 5% concentration, but Figure 6.13-6 shows an almost perfect match if a sliding friction coefficient of 0.416 is applied. Since in both figures the Turian & Yuan (1977) curves decrease with an increasing hydraulic gradient, compared with horizontal curves according to Miedema (2013S) , the Turian & Yuan (1977) equations must be based on a constant volumetric transport (delivered) concentration.

Regime 1: Saltating transport, equation (6.13-21).

$$E_{rhg} = \frac{(i_m - i_l)}{R_{sd} \cdot C_v} = 50.24 \cdot C_v^{0.018} \cdot \lambda_l^{1.046} \cdot C_D^{-0.4213} \cdot Fr^{-0.354}$$

For the E_{rhg} value, the saltating transport equation is almost independent of the volumetric concentration, just like the heterogeneous equation of Miedema (2013S). The saltating transport equation is almost proportional with the wall friction coefficient, giving a slight decrease of the E_{rhg} value with increasing line speed. The proportionality with the C_D value has a negative power of 0.4213, which means that smaller particles have less resistance. This proportionality is however much smaller than estimated by Durand & Condolios (1952), who found a power of 1.275. This power of 1.275 is also applied by Miedema (2013S) . The proportionality with the Froude number has a negative power of 0.354, which is small. This power results in a negative power for the line speed of 0.708, while most models use a negative power between 1 and 2 for the line speed. This small power may be the result of curve fitting over 3 regimes, the sliding bed regime, the heterogeneous regime and the pseudo homogeneous regime. At higher concentrations the heterogeneous regime maybe replaced by the sheet flow regime with a much smaller power

The saltating regime of Turian & Yuan (1977) seems to be more a combination of the heterogeneous regime and the sheet flow regime when it is compared to different other models.
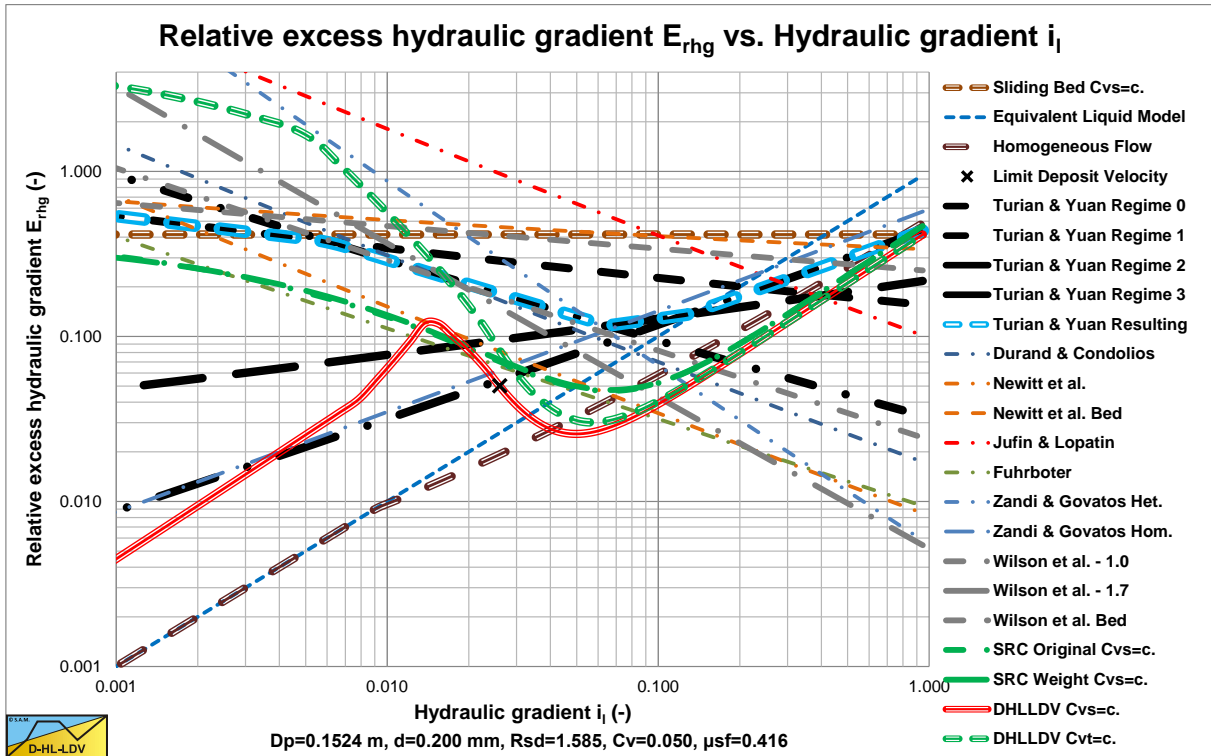
Figure 6.13-5: Turian & Yuan (1977) compared to others for C$_v$=0.05.
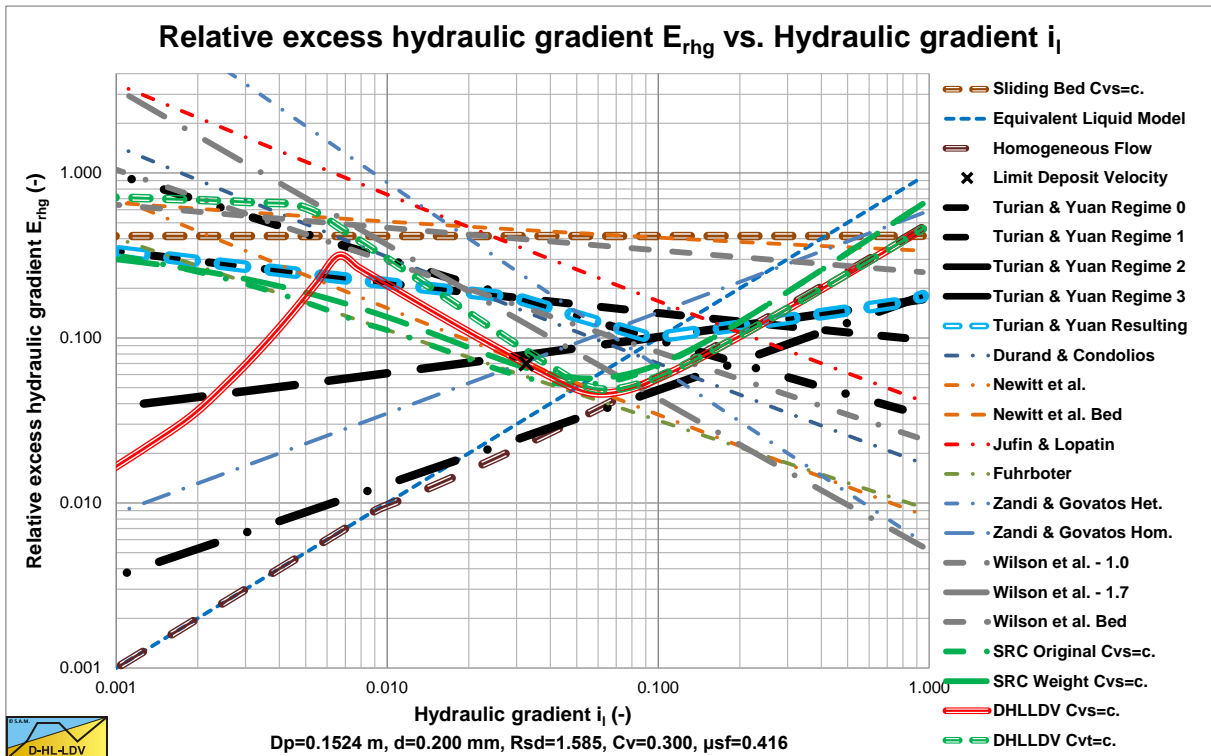
Figure 6.13-6: Turian & Yuan (1977) compared to others for C$_v$=0.30.

The blue dashed lines show the resulting curves of Turian & Yuan (1977). The shape of these curves matches the shape of the DHLLDV Framework, however the values and the steepness do not match. Also a comparison with other models shows that most models show a much steeper curve compared to Turian & Yuan (1977) regime 1, which is supposed to be the heterogeneous regime.

Regime 2: Heterogeneous transport, equation (6.13-22).

$$E_{rhg} = \frac{(i_m - i_l)}{R_{sd} \cdot C_v} = 11.41 \cdot C_v^{-0.132} \cdot \lambda_l^{1.200} \cdot C_D^{-0.1677} \cdot Fr^{0.3062}$$

For the E_{rhg} value, the heterogeneous transport equation is almost independent of the volumetric concentration, just like the heterogeneous equation of Miedema (2013S), although the E_{rhg} will slightly decrease with increasing concentration. The heterogeneous transport equation is almost proportional with the wall friction coefficient, giving a slight decrease of the E_{rhg} value with increasing line speed. The proportionality with the C_D value has a negative power of 0.1677, which means that smaller particles have slightly less resistance, but this is a weak dependency. This proportionality is however much smaller than estimated by Durand & Condolios (1952), who found a power of 1.275 for heterogeneous transport. This power of 1.275 is also applied by Miedema (2013S). The proportionality with the Froude number has a positive power of 0.3062, which is small but this contradicts with all other models for heterogeneous transport which use a negative power between 1 and 2 for the line speed.

The heterogeneous regime of Turian & Yuan (1977) seems to be more a pseudo homogeneous regime or at the transition between heterogeneous and homogeneous regimes when it is compared to different other models.

Regime 3: Homogeneous transport, equation (6.13-23).

$$E_{rhg} = \frac{(i_m - i_l)}{R_{sd} \cdot C_v} = 2.358 \cdot C_v^{-0.4972} \cdot \lambda_l^{1.428} \cdot C_D^{0.1516} \cdot Fr^{0.6469}$$

For the E_{rhg} value, the homogeneous transport equation is reversely proportional to the volumetric concentration, with a power of 0.4972. This contradicts the equivalent liquid model strongly. The homogeneous transport equation is proportional with the wall friction coefficient to a power of 1.428, giving a slight decrease of the E_{rhg} value with increasing line speed. The proportionality with the C_D value has a positive power of 0.1516, which means that smaller particles have slightly higher resistance, but this is a weak dependency. For real homogeneous transport, no dependence is expected. The proportionality with the Froude number has a positive power of 0.6469. A power of 1 would be expected based on the equivalent liquid model.
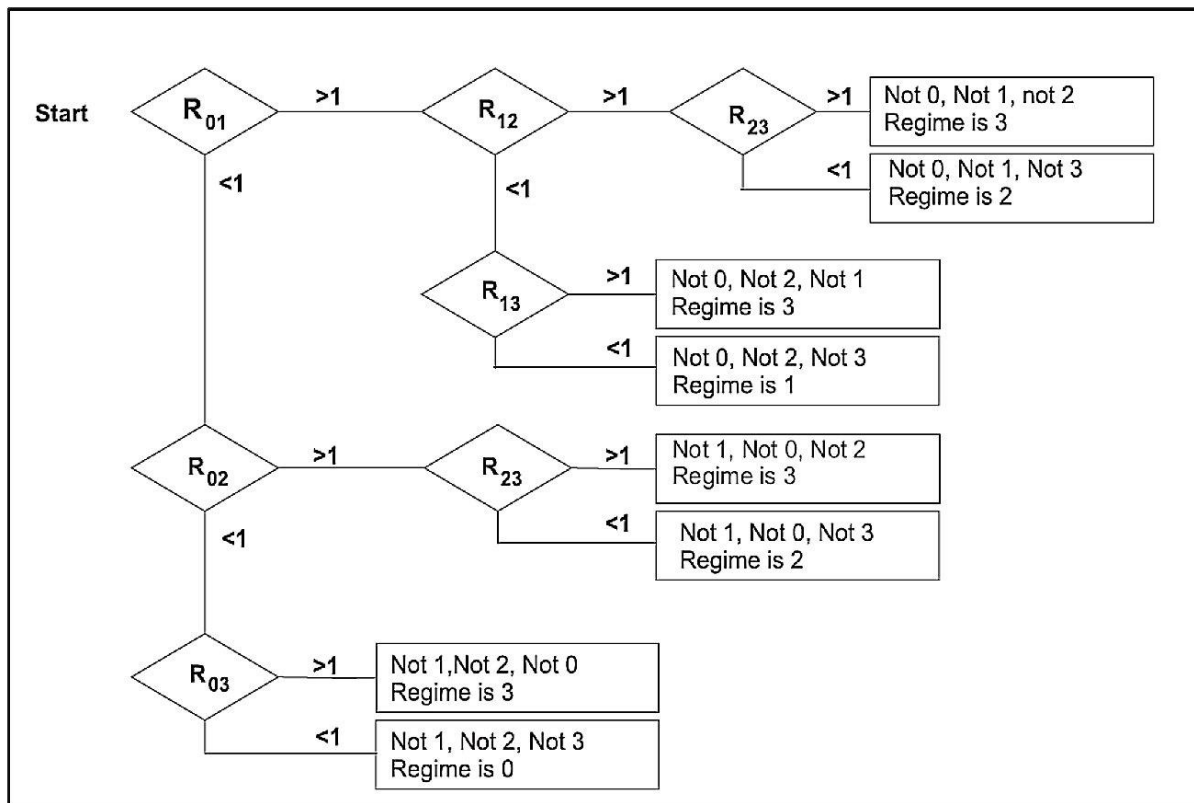
6.13.5 Transition Equations.

Figure 6.13-7: Flow chart for identifying the flow regime.

The transition between two flow regimes can be determined by making the two regime equations equal. The resulting Froude number gives the transition line speed. It is however possible that a regime is skipped, so a sliding

bed could go to a heterogeneous flow directly, without passing the saltation regime. Figure 6.13-7 shows how to identify the regimes.

The transition Froude numbers are:

The transition fixed bed vs. saltating transport:

$$\mathbf{Fr_{01} = 4679 \cdot C_v^{1.083} \cdot f_l^{1.064} \cdot C_D^{-0.0616}} \quad \textbf{with:} \quad \mathbf{R_{01} = \frac{Fr}{Fr_{01}}} \tag{6.13-24}$$

The transition fixed bed vs. heterogeneous transport:

$$\mathbf{Fr_{02} = 0.1044 \cdot C_v^{-0.3225} \cdot f_l^{-1.065} \cdot C_D^{-0.5906}} \quad \textbf{with:} \quad \mathbf{R_{02} = \frac{Fr}{Fr_{02}}} \tag{6.13-25}$$

The transition fixed bed vs. homogeneous transport:

$$\mathbf{Fr_{03} = 1.6038 \cdot C_v^{0.3183} \cdot f_l^{-0.8837} \cdot C_D^{-0.7496}} \quad \textbf{with:} \quad \mathbf{R_{03} = \frac{Fr}{Fr_{03}}} \tag{6.13-26}$$

The transition saltating transport vs. heterogeneous transport:

$$\mathbf{Fr_{12} = 6.8359 \cdot C_v^{0.2263} \cdot f_l^{-0.2334} \cdot C_D^{-0.3840}} \quad \textbf{with:} \quad \mathbf{R_{12} = \frac{Fr}{Fr_{12}}} \tag{6.13-27}$$

The transition saltating transport vs. homogeneous transport:

$$\mathbf{Fr_{13} = 12.522 \cdot C_v^{0.5153} \cdot f_l^{-0.3820} \cdot C_D^{-0.5724}} \quad \textbf{with:} \quad \mathbf{R_{13} = \frac{Fr}{Fr_{13}}} \tag{6.13-28}$$

The transition heterogeneous transport vs. homogeneous transport:

$$\mathbf{Fr_{23} = 40.38 \cdot C_v^{1.075} \cdot f_l^{-0.6700} \cdot C_D^{-0.9375}} \quad \textbf{with:} \quad \mathbf{R_{23} = \frac{Fr}{Fr_{23}}} \tag{6.13-29}$$

6.13.6 Conclusions & Discussion.

Turian & Yuan (1977) developed a set of 4 empirical equations for 4 flow regimes based on a large set of public available experiments and a set of experiments carried out by themselves. Based on these 4 equations a set of 6 possible transition equations were derived. The 4 flow regimes, stationary bed, saltation, heterogeneous transport and homogeneous transport do not cover all possible flow regimes. The sliding bed regime and the sheet flow regime are not covered independently. Often it is very hard to distinguish between the flow regimes based on visual observations, so it is very well possible that in the transition regions the wrong regime has been chosen. Turian & Yuan (1977) choose for a fixed form of their equations.

$$\mathbf{f_m - f_l = \frac{\lambda_m}{4} - \frac{\lambda_l}{4} = K \cdot C_v^{\,\alpha} \cdot f_l^{\,\beta} \cdot \left(\frac{4}{3} \cdot \frac{R_{sd} \cdot g \cdot d}{v_t^2} \right)^{\gamma} \cdot \left(\frac{v_{ls}^2}{R_{sd} \cdot g \cdot D_p} \right)^{\delta}} \tag{6.13-30}$$

Basically all 4 equations have one term for the solids effect and one term for the Darcy Weisbach pressure losses in clean water. This limits the physical meaning of the equations. It is very well possible that the real physics justify 2 or more terms. The fact that Turian & Yuan (1977) use the Froude number and the drag coefficient, implies that the relation between pipe diameter D_p and line speed v_{ls} is fixed and the relation between particle diameter d and terminal settling velocity v_t is fixed. A combination of, for example, the particle diameter d and the thickness of the viscous sub-layer δ, is not possible this way, leaving out other possible physical phenomena.

The difference between spatial and transport concentration is only important for the stationary bed regime, for the other regimes the difference between the two concentrations is negligible and much smaller than the scatter. The stationary bed equation most probably uses the constant transport concentration.
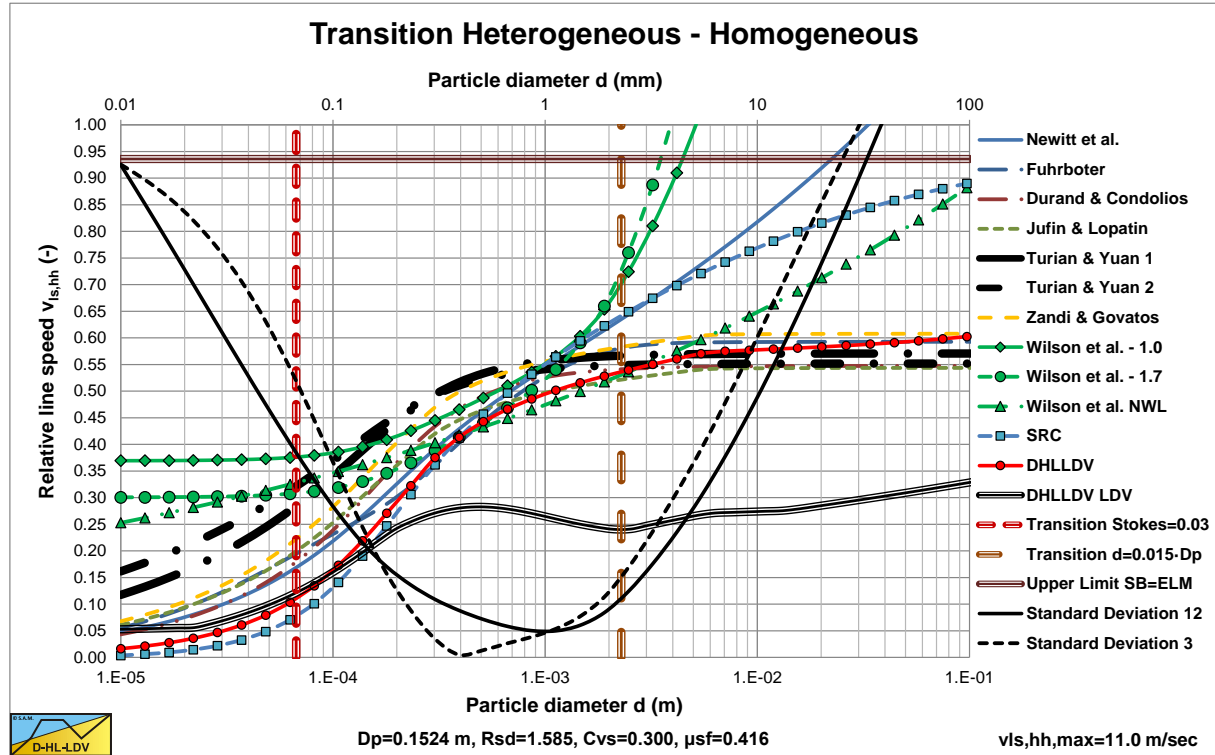

Figure 6.13-8: A comparison of 12 models for heterogeneous transport.

The correlations of the experiments with the empirical equations are shown in Figure 6.13-1, Figure 6.13-2, Figure 6.13-3 and Figure 6.13-4. These graphs show quit some scatter. Most of the experiments were carried out in sand with pipe diameters between 0. 508 m and 0.1524 m (2 and 6 inch). This implies that the resulting equations most probably have value for these conditions.

A comparison of the transition line speed of the heterogeneous and homogeneous regimes, with other models, Figure 6.13-8, shows that the equations give a reasonable prediction for larger particles (d>0.3 mm) at higher concentrations, based on the saltation regime 1 and the heterogeneous regime 2. For very small particles, the saltation and heterogeneous equations overestimate the pressure losses. The velocity on the vertical axis has been made relative by dividing by the line speed in the lower right corner.

Analyzing the 4 flow regimes of Turian & Yuan (1977) and comparing them with other models results in a sort of conversion table.

Table 6.13-1: Regime conversion table.

Turian & Yuan (1977)	**Others, Miedema** (2013S)
Regime 0: Stationary bed.	Stationary bed and sliding bed.
Regime 1: Saltation.	Heterogeneous transport and sheet flow or Fixed/sliding bed (thin layer) with heterogeneous transport above the bed.
Regime 2: Heterogeneous transport.	Heterogeneous transport above the Limit Deposit Velocity and pseudo homogeneous transport.
Regime 3: Homogeneous transport.	Pseudo homogeneous and homogeneous transport.

6.14 Kazanskij (1978) and (1980).

Kazanskij (1978) gave an overview of the state of the art of slurry head loss models up to 1978. He showed the models of Durand & Condolios (1952), Condolios & Chapus (1963A), Bonnington (1961), Chaskelberg & Karlin (1976), Ellis & Round (1963), Kazanskij (1967), Zandi & Govatos (1967), Babcock (1970), Welte (1971), Newitt et al. (1955), Jufin & Lopatin (1966), Silin & Kobernik (1962), Charles (1970), Worster (1955), Fuhrboter (1961), Korzajev (1964), Duckworth & Argyros (1972), Vocadlo (1972), Jufin (1965), Wiedenroth (1967), Brauer (1971), Karasik (1973), Smoldyrev (1970) and Krivenko (1970). Some of the researchers have different models for different flow regimes. Kazanskij (1978) selected 4 models to investigate the scatter of the experimental values of the hydraulic gradient versus the hydraulic gradient determined with the model equations. These 4 models are the model of Durand & Condolios (1952), the model of Fuhrboter (1961), the model of Jufin & Lopatin (1966) and the model of Kazanskij (1978).

Durand & Condolios (1952), Figure 6.14-1:

$$x = 180 \cdot Fr^{-3} \cdot Fr_{xD}^{1.5} = 5531 \cdot \frac{D_p^{1.5} \cdot Fr_{xD}^{1.5}}{v_{ls}^3} \quad \text{and} \quad y = \frac{i_m - i_l}{C_{vt} \cdot i_l} \tag{6.14-1}$$

Fuhrboter (1961), Figure 6.14-2:

$$x = 100 \cdot \frac{S_{kt}}{v_{ls}} = 100 \cdot \frac{2.59 \cdot d - 0.37}{v_{ls}} \quad \text{and} \quad y = \frac{i_m - i_l}{C_{vt}} \tag{6.14-2}$$

Miedema (2014) has shown that the slip ratio of 0.65 as used by Fuhrboter (1961) is not correct. Fuhrboter used the ratio of the propagation velocity of density waves to the line speed as a slip ratio. Since this factor, in the form of 1/0.65, is present in both the abscissa and the ordinate, this does not influence the correlation, but on both the abscissa and the ordinate the values should be multiplied by 0.65. Another minor issue is, that the abscissa and the ordinate are per 100 m of pipe length. This is important for the Fuhrboter graph, since the Fuhrboter equation does not contain a division by the hydraulic gradient, which means the ordinate is not dimensionless. For the other 3 models considered here the ordinates are dimensionless, so this issue does not play a role. From a reconstruction of the data points it also appeared that Kazanskij (1978) used the S_{kt} values of a **d=0.33 mm** particle for the **d=0.30 mm, D_p=0.8 m** and **d=0.275 mm, D_p=0.614 m** particles.

Jufin * Lopatin (1966), Figure 6.14-3:

$$x = 332.75 \cdot \frac{D_p^{0.5} \cdot Fr_{xJ}^{0.75}}{v_{ls}^3} \quad \text{and} \quad y = \frac{i_m - i_l}{\sqrt{C_{vt}} \cdot i_l} \tag{6.14-3}$$

Kazanskij (1978), Figure 6.14-4:

$$x = 180 \cdot \frac{D_p^{0.5} \cdot Fr_{xJ}^{0.75}}{v_{ls}^3} \quad \text{and} \quad y = \frac{i_m - i_l}{C_{vt} \cdot i_l} \tag{6.14-4}$$

Kazanskij (1978) remarks that the accuracy of experiments with concentrations below 8% is not very good. In his paper he shows graphs with and without the experiments below 8%. A general conclusion based on the 4 graphs is that the Jufin & Lopatin model gives the best correlation, especially for the large diameter pipes, which is of interest for the dredging industry. However Jufin & Lopatin also gives a lot of scatter, meaning that the parameters on the axis still do not cover the real slurry transport process.

Based on a reconstruction of the hydraulic gradients versus line speeds, it should be concluded that most data points are in the (pseudo) homogeneous flow regime, except for the very small pipe diameters. The graphs of this reconstruction can be found on www.dhlldv.com.

For all the models 100% means a perfect fit. The other two lines give +/- 80%.
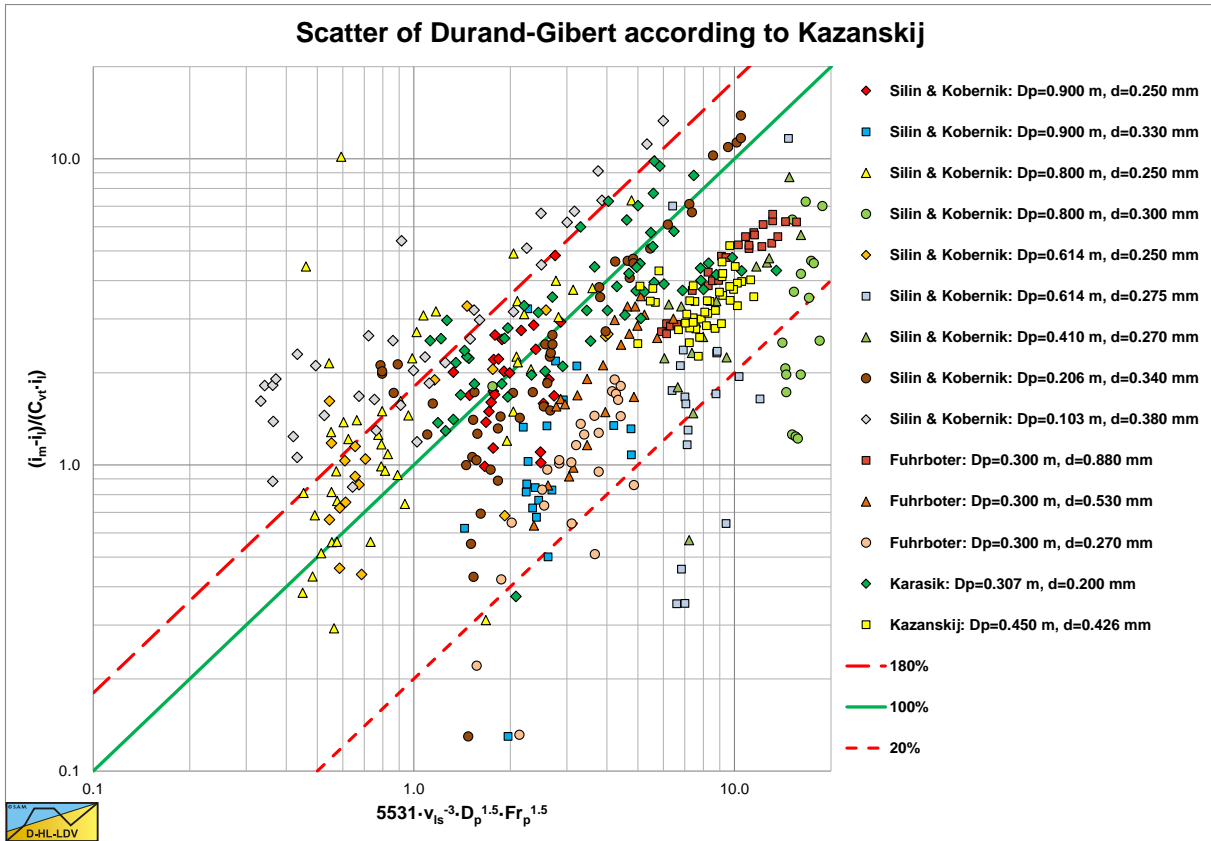
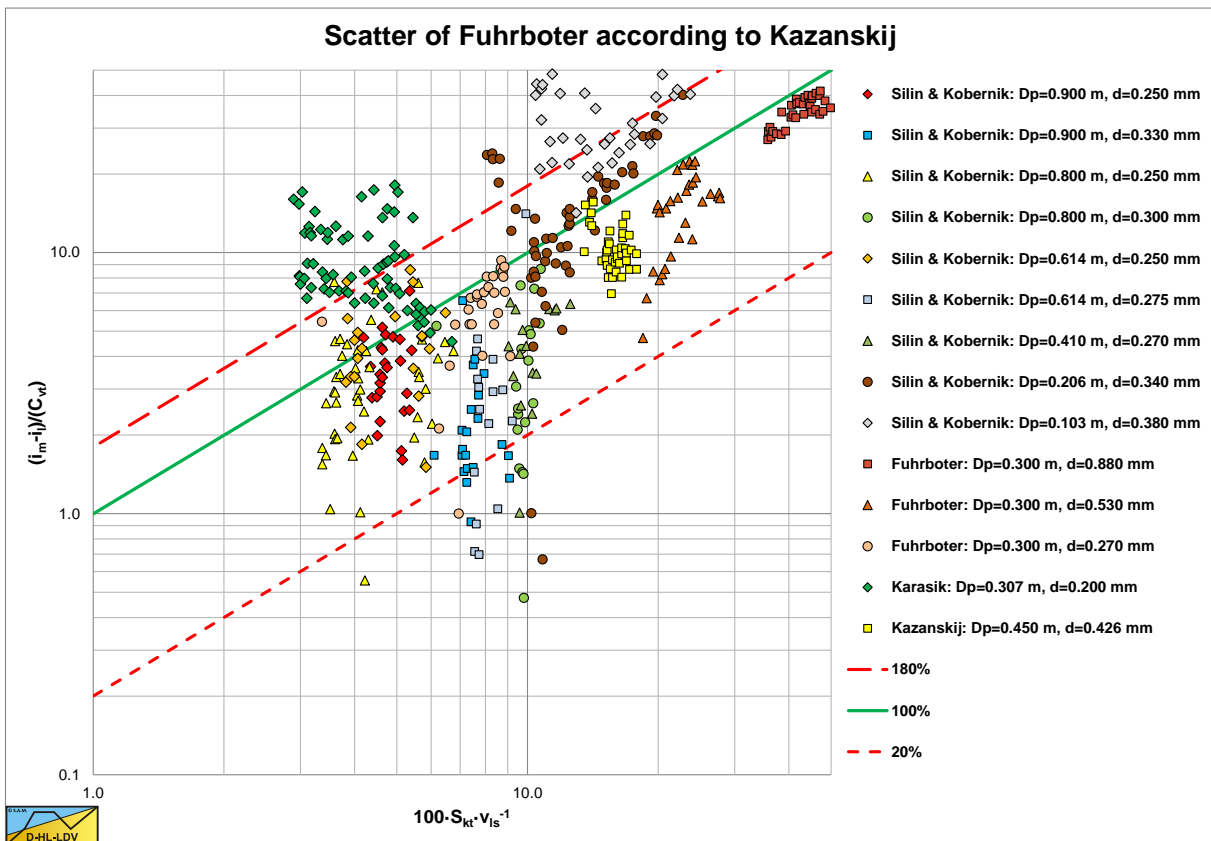**Figure 6.14-1: The fit of the Durand & Condolios model.**

Figure 6.14-2: The fit of the Fuhrboter model.
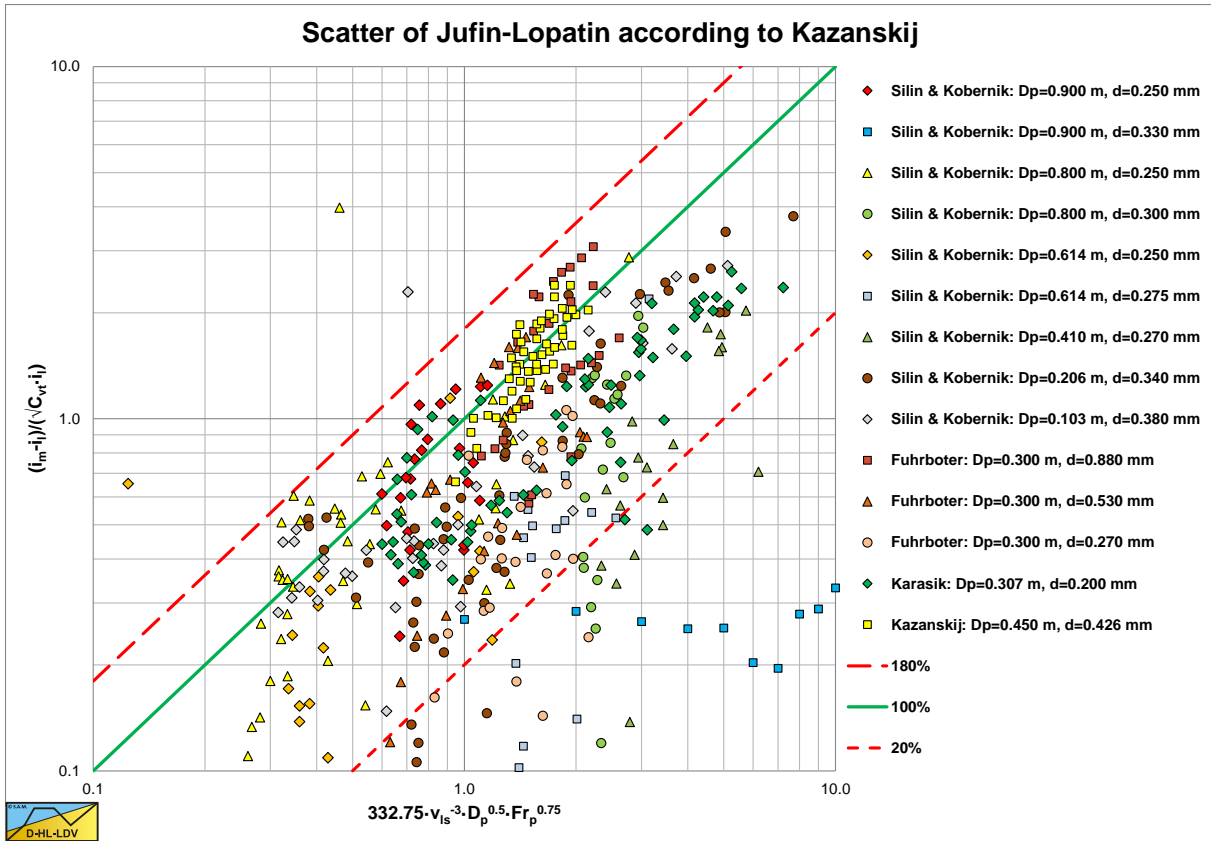
Figure 6.14-3: The fit of the Jufin & Lopatin model.
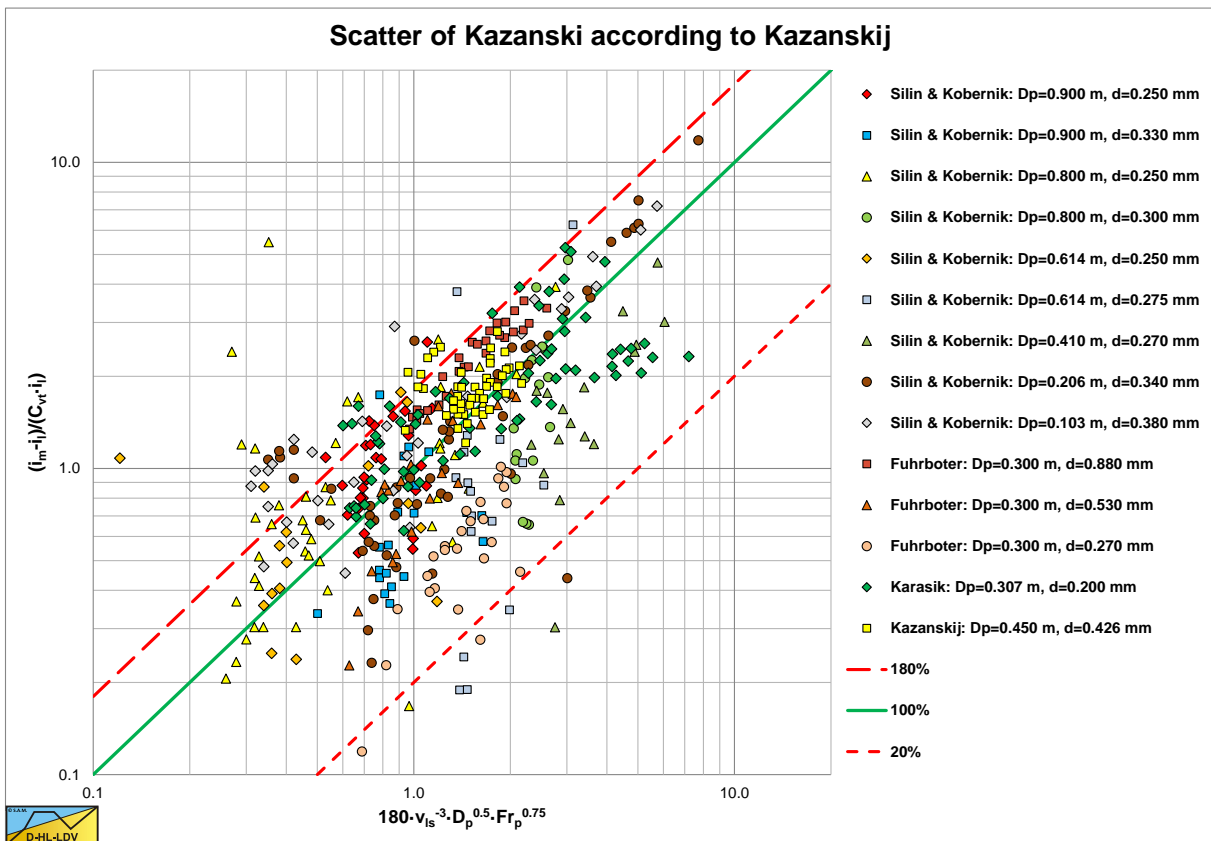
Figure 6.14-4: The fit of the Kazanskij model.

Since many data points are in between the Equivalent Liquid Method (ELM) curve and the liquid curve, it is interesting to create a graph showing the data points compared to the ELM method. The graph with the relative excess hydraulic gradient E_{rhg} versus the liquid hydraulic gradient i_l is suitable for this. Figure 6.14-5 shows this graph. The ELM curve is the curve **y=x**. The graph shows that some experiments were in the heterogeneous region, in which case the heterogeneous curve is also drawn. For the data points below 120% (arbitrary) of the ELM curve, the average ratio is determined, resulting in a factor of 0.624. Below 100% this ratio is 0.55. Below 130% this ratio is 0.67. This means that on average the data points in the homogeneous regime follow 62.4% of the ELM curve. This is close to the 60% as mentioned by Newitt et al. (1955). Miedema (2015) gives a possible explanation for this reduction based on the assumption of a watery viscous sub layer.

From this analysis it is clear that different regimes should not be mixed in one equation. Heterogeneous and homogeneous regimes have a different behavior and require different models.

The relative excess hydraulic gradient E_{rhg} is:

$$E_{rhg} = \left(\frac{i_m - i_l}{R_{sd} \cdot C_{vt}} \right)$$

(6.14-5)

The liquid hydraulic gradient i_l is:

$$i_l = \frac{\Delta p}{\rho_l \cdot g \cdot \Delta L} = \frac{\lambda_l \cdot v_{ls}^2}{2 \cdot g \cdot D_p}$$

(6.14-6)
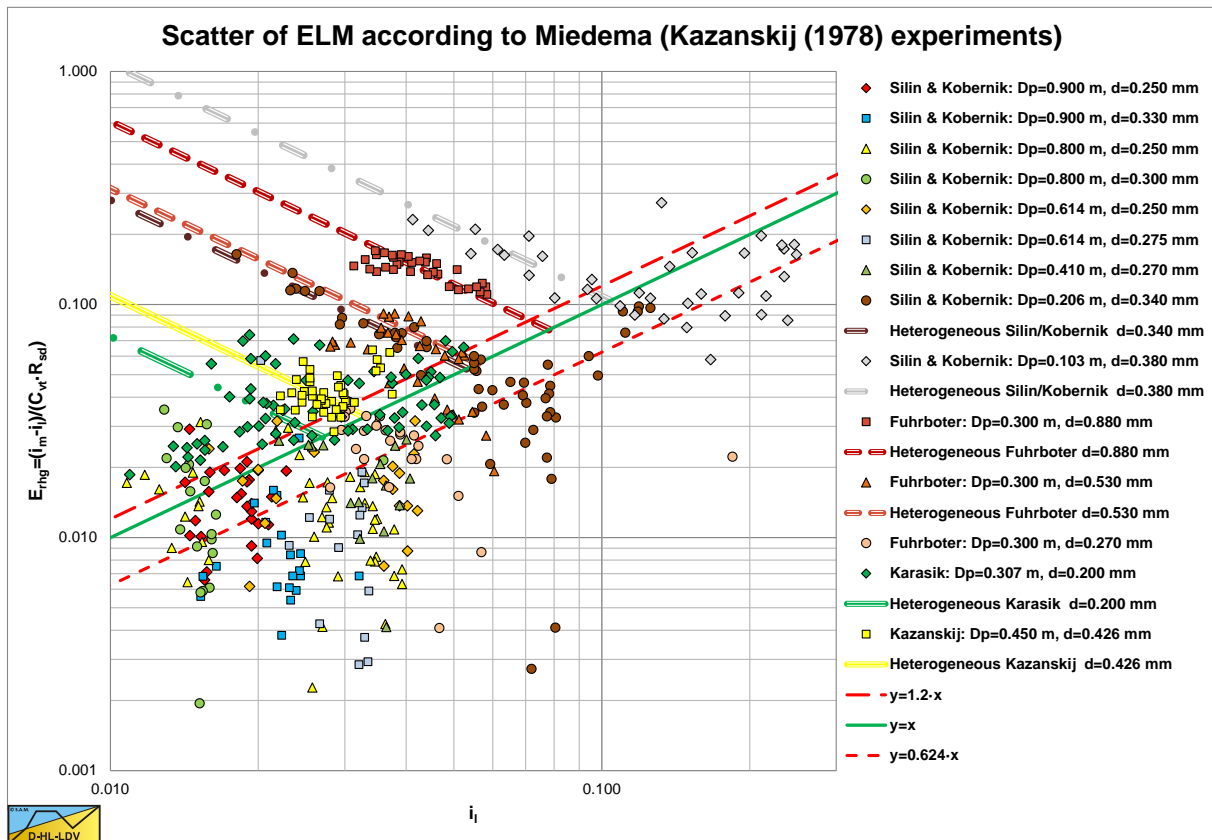
Figure 6.14-5: The fit with the Equivalent Liquid Method.
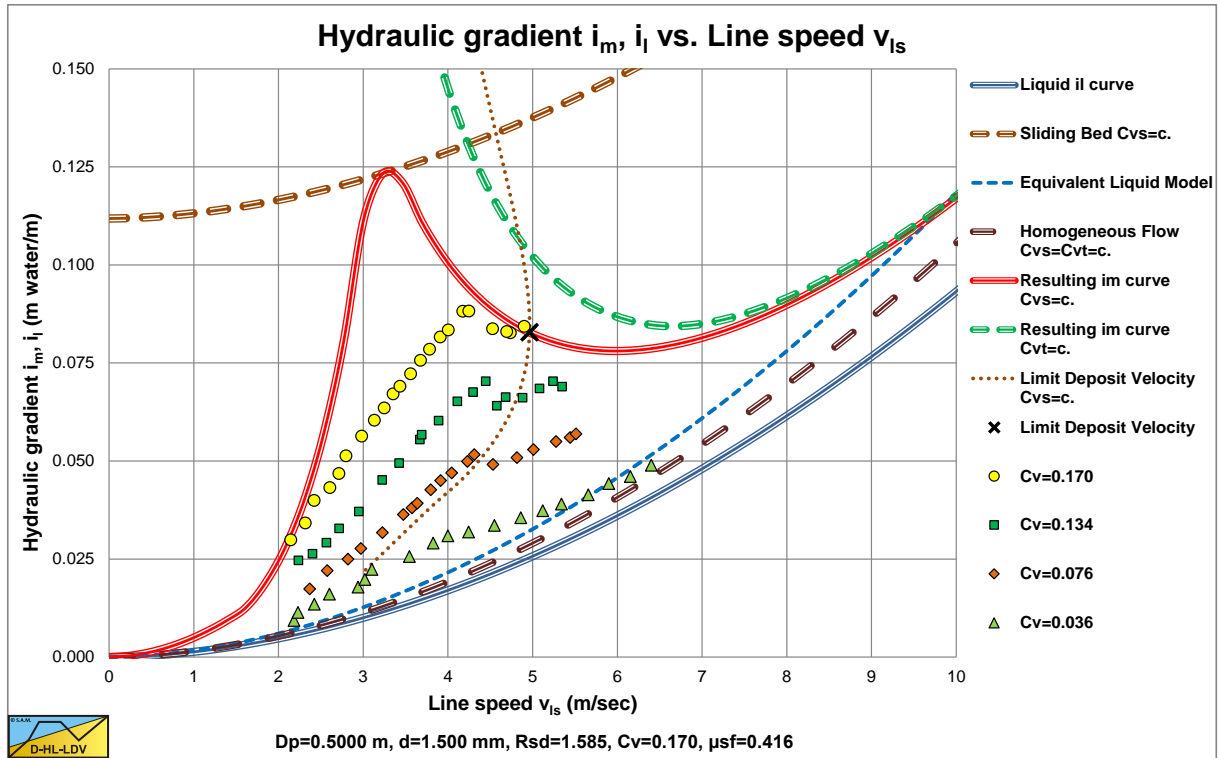
Figure 6.14-6: The hydraulic gradient of the Kazanskij (1980) experiments.
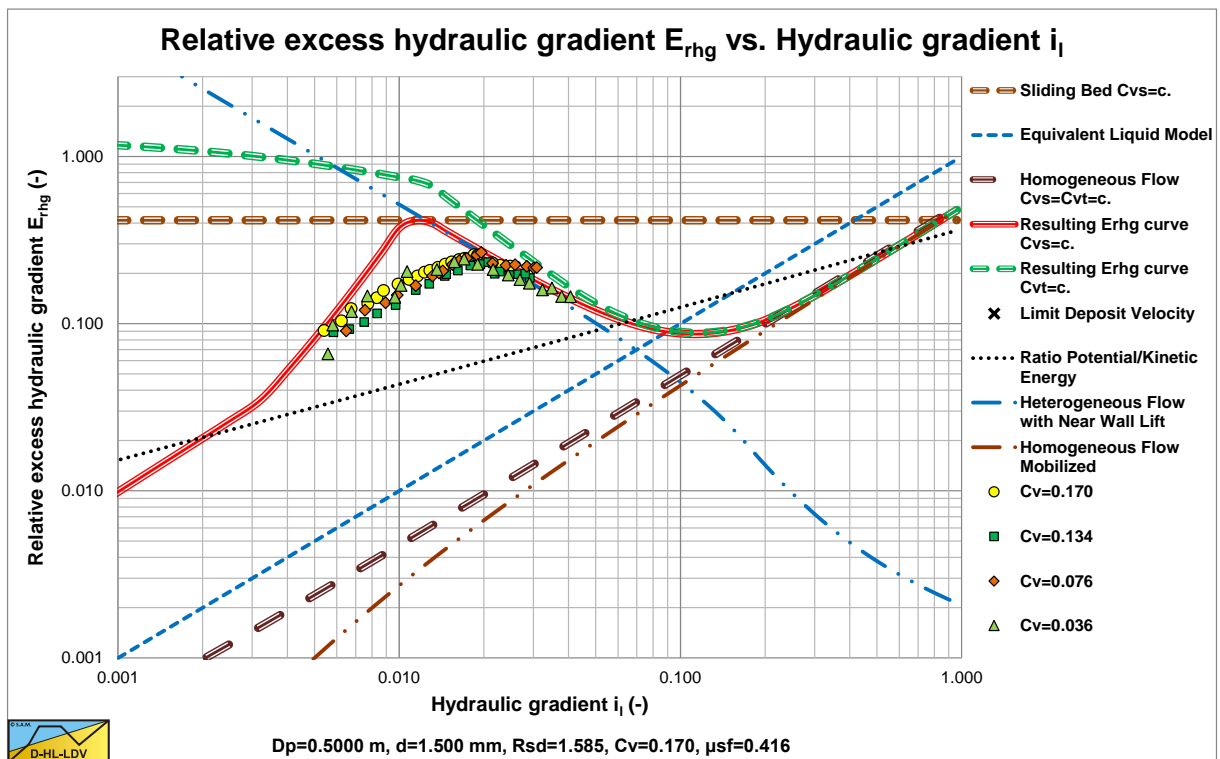
Figure 6.14-7: The relative excess hydraulic gradient of the Kazanskij (1980) experiments.

Kazanskij (1980) carried out experiments in a **D_P=0.5 m** pipe with **d=1.5 mm** particles. The results are shown in Figure 6.14-6 and Figure 6.14-7. The experiments were carried out with constant spatial volumetric concentration, which is also clear from the figures. Most experiments were below the LDV. The value of these experiments is the transition behavior from the fixed bed to the heterogeneous regime, which is more smooth than the DHLLDV Framework prediction. For normal dredging operations this is not very relevant, since most operations are above the LDV, however from a scientific point of view it is.

6.15 The IHC-MTI (1998) Model for the Limit Deposit Velocity.

Van den Berg (1998) published an equation for the LDV as used in IHC-MTI. The background of this equation has not been published and is not clear.

Equation (6.4-18) gives an almost exact match with the equation published by van den Berg (1998), equation (6.15-1). Figure 6.4-26 gives the Limit Deposit Velocity according to equation (6.4-18) at a concentration of 0.1 and Figure 6.15-1 gives the Limit Deposit Velocity according to equation (6.15-1) at a concentration of 0.1. For particle diameters from 0.0850-0.333 mm equation (6.4-18) gives smaller values for the Limit Deposit Velocity.

$$v_{ls,ldv} = 0.298 \cdot \left(5 - \frac{1}{\sqrt{1000 \cdot d}} \right) \cdot \left(\frac{C_v}{C_v + 0.1} \right)^{1/6} \cdot \sqrt{2 \cdot g \cdot D_p \cdot R_{sd}} \qquad (6.15\text{-}1)$$

With the Froude number F_L:

$$F_L = \frac{v_{ls,ldv}}{\sqrt{2 \cdot g \cdot D_p \cdot R_{sd}}} = 0.298 \cdot \left(5 - \frac{1}{\sqrt{1000 \cdot d}} \right) \cdot \left(\frac{C_v}{C_v + 0.1} \right)^{1/6} \qquad (6.15\text{-}2)$$
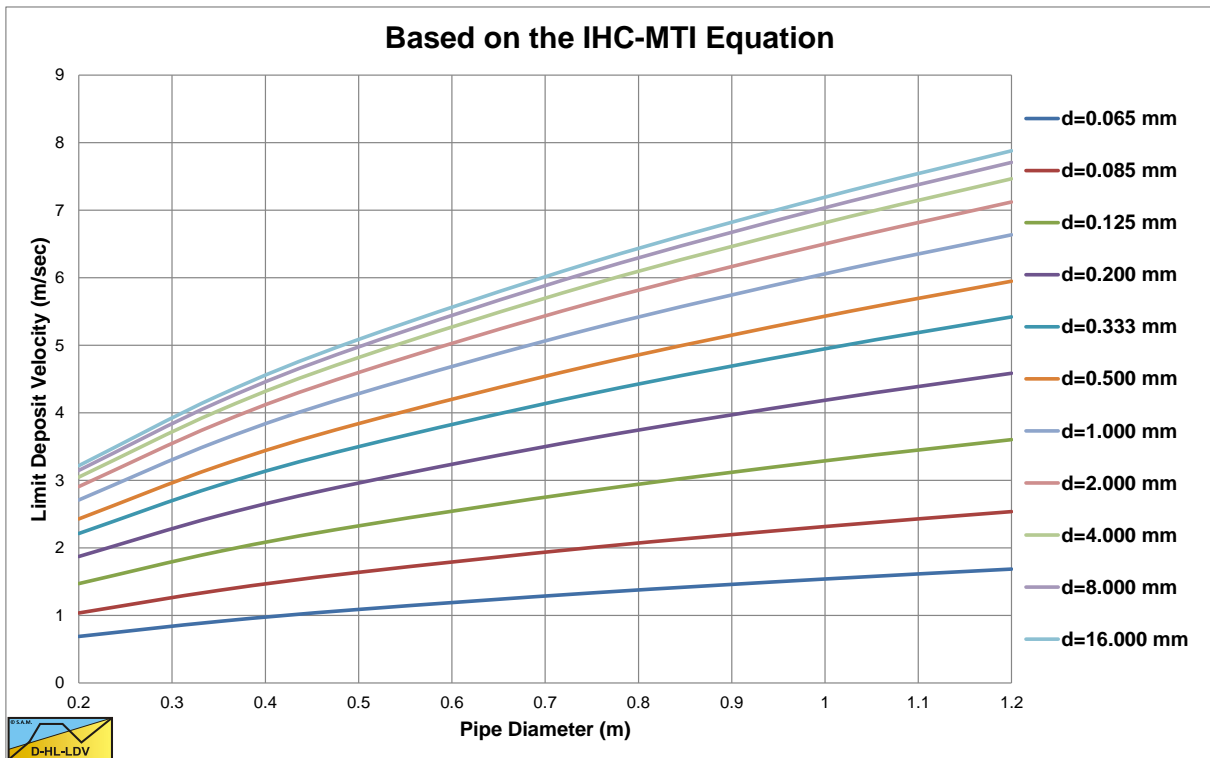

Figure 6.15-1: Limit Deposit Velocity according to equation (6.15-1) at a concentration of 0.1.

6.16 Conclusions & Discussion Empirical and Semi-Empirical Models.

6.16.1 Introduction.

About 60 years after Durand & Condolios (1952) and Newitt et al. (1955) carried out their research, their results are still valid and important. In spite of criticism of Zandi & Govatos (1967), Babcock (Babcock, 1970), Wilson et al. (1992) and others, their equations are still widely used. There are some issues identified, leading to a wrong interpretation of the equations. The main issues are; the wrong use of the particle Froude number $\sqrt{C_x}$ vs. the drag coefficient C_D, the wrong use of the relative submerged density R_{sd} in the particle Froude number $\sqrt{C_x}$, the wrong power of the particle Froude number $\sqrt{C_x}$ and the use of the wrong graph for the Limit Deposit Velocity coefficient F_L in the Durand & Condolios (1952) equations. For the Limit Deposit Velocity coefficient F_L the correction factor of about 1.1 according to Gibert (1960) should be applied. For Newitt et al. (1955) it should be considered that the sliding bed equation is based on an average of some specific materials in a very small pipe (1 inch). Other materials and pipes may lead to sliding friction coefficients in the range of μ_{sf}=**0.35-0.7**. Combining both theories results in a flow regime chart as is shown in Figure 6.5-4 and Figure 6.5-5. In these charts the Newitt et al. (1955) equations are used for the transition moving bed-heterogeneous transport and heterogeneous-homogeneous transport. The Durand & Condolios (1952) approach is used for the stationary bed curve.

Both Durand & Condolios (1952) and Newitt et al. (1955) consider the excess pressure losses for heterogeneous transport to be reversely proportional to the line speed. Zandi & Govatos (1967) found a power of -1.93 and Wilson et al. (1992) a power of -1.7 for uniform particle size distributions and smaller powers up to -0.25 for non-uniform distributions. This leads to relative excess pressure powers of 3, 3.93 and 3.7. Now heterogeneous transport is dominated by the energy losses due to collisions of particles. If we assume that the occurrence of collisions is dominated by the settling velocity of the particles, then the number of collisions per unit of time is almost independent of time and thus of the line speed. This implies that the number of collisions per unit of pipeline length is reversely proportional to the line speed, resulting in a power of -1 of the line speed in the excess pressure losses or -3 in the relative excess pressure losses. If one considers the momentum of the particles in the direction of the line speed, higher powers can be explained.
The final conclusion is, that the 60 year old theories can still be applied if one takes the effort to use them properly.

6.16.2 The Darcy-Weisbach Friction Factor.

The Darcy-Weisbach friction factor of a smooth pipe in a dimensionless form can be determined by:

$$\lambda_l = 0.01216 \cdot \left(v_{ls} \right)^{-0.155} \cdot \left(D_p \right)^{-0.175} \approx 0.1233 \cdot \left(v_{ls} \right)^{-0.155} \cdot \left(g \cdot D_p \right)^{-0.172} \cdot \left(v_l \cdot g \right)^{1/6} \tag{6.16-1}$$

This equation will be substituted in the hydraulic gradient equations in order to get expressions based on the parameters users (dredging companies) know. These are the pipe diameter D_p, the cross section averaged line speed v_{ls} and some characteristic particle diameter d or maybe the PSD. Normally in dredging the solids will be sand or gravel consisting of quarts with a relative submerged density R_{sd} of 1.58-1.65 ton/m³ (depending on the water density, 1.000-1.030 ton/m³). The kinematic viscosity of water depends on the temperature, at 10°C v=0.0000013 m²/sec, at 20°C v=0.0000010 m²/sec.

6.16.3 Heterogeneous Regime.

In order to compare a number of models, the models have to be written in the same form. To do so the form of Fuhrboter (1961) is chosen, the hydraulic gradient of a mixture consists of the liquid hydraulic gradient plus the solids effect. With the solids effect factor S_k (to compare with Fuhrboter) defined as:

$$i_m = i_l + S_k \cdot \frac{C_{vt}}{v_{ls}} \tag{6.16-2}$$

The models chosen for this comparison all have a solids effect reversely proportional to the cross section averaged line speed.

6.16.3.1 Durand & Condolios (1952).

The hydraulic gradient of a mixture according to Durand & Condolios (1952) is:

$$
\begin{aligned}
\mathbf{i_m} &= \mathbf{i_l} + 85 \cdot \left(\frac{\mathbf{v_{ls}^2 \cdot C_x^{10/9}}}{\mathbf{g \cdot D_p \cdot R_{sd}}} \right)^{-3/2} \cdot \mathbf{C_{vt}} \cdot \frac{\lambda_l \cdot \mathbf{v_{ls}^2}}{2 \cdot \mathbf{g \cdot D_p}} \\
&= \mathbf{i_l} + 42.5 \cdot \lambda_l \cdot \left(\mathbf{g \cdot D_p} \right)^{1/2} \cdot \left(\frac{\mathbf{R_{sd}}}{\mathbf{C_x^{10/9}}} \right)^{3/2} \cdot \frac{\mathbf{C_{vt}}}{\mathbf{v_{ls}}}
\end{aligned}
\tag{6.16-3}
$$

The hydraulic gradient can be determined by, after substituting of the Darcy-Weisbach friction factor:

$$
\mathbf{i_m} = \mathbf{i_l} + 5.24 \cdot \left(\nu_l \cdot \mathbf{g} \right)^{1/6} \cdot \left(\mathbf{g \cdot D_p} \right)^{0.328} \cdot \left(\frac{\mathbf{R_{sd}}}{\mathbf{C_x^{10/9}}} \right)^{3/2} \cdot \frac{1}{\mathbf{v_{ls}^{0.155}}} \cdot \frac{\mathbf{C_{vt}}}{\mathbf{v_{ls}}}
\tag{6.16-4}
$$

This gives for the solids effect factor $\mathbf{S_k}$:

$$
\mathbf{S_k} = 5.24 \cdot \left(\nu_l \cdot \mathbf{g} \right)^{1/6} \cdot \left(\mathbf{g \cdot D_p} \right)^{0.328} \cdot \left(\frac{\mathbf{R_{sd}}}{\mathbf{C_x^{10/9}}} \right)^{3/2} \cdot \frac{1}{\mathbf{v_{ls}^{0.155}}}
\tag{6.16-5}
$$

6.16.3.2 Newitt et al. (1955).

The hydraulic gradient of a mixture according to Newitt et al. (1955) is:

$$
\begin{aligned}
\mathbf{i_m} &= \mathbf{i_l} + 1100 \cdot \left(\mathbf{g \cdot D_p \cdot R_{sd}} \right) \cdot \mathbf{v_t} \cdot \mathbf{C_{vt}} \cdot \left(\frac{1}{\mathbf{v_{ls}}} \right)^3 \cdot \frac{\lambda_l \cdot \mathbf{v_{ls}^2}}{2 \cdot \mathbf{g \cdot D_p}} \\
&= \mathbf{i_l} + 550 \cdot \lambda_l \cdot \mathbf{R_{sd}} \cdot \mathbf{v_t} \cdot \frac{\mathbf{C_{vt}}}{\mathbf{v_{ls}}}
\end{aligned}
\tag{6.16-6}
$$

The hydraulic gradient can be determined by, after substituting of the Darcy-Weisbach friction factor:

$$
\mathbf{i_m} = \mathbf{i_l} + 67.8 \cdot \frac{\left(\nu_l \cdot \mathbf{g} \right)^{1/6} \cdot \mathbf{R_{sd}} \cdot \mathbf{v_t}}{\left(\mathbf{g \cdot D_p} \right)^{0.172}} \cdot \frac{1}{\mathbf{v_{ls}^{0.155}}} \cdot \frac{\mathbf{C_{vt}}}{\mathbf{v_{ls}}}
\tag{6.16-7}
$$

This gives for the solids effect factor $\mathbf{S_k}$:

$$
\mathbf{S_k} = 67.8 \cdot \frac{\left(\nu_l \cdot \mathbf{g} \right)^{1/6} \cdot \mathbf{R_{sd}} \cdot \mathbf{v_t}}{\left(\mathbf{g \cdot D_p} \right)^{0.172}} \cdot \frac{1}{\mathbf{v_{ls}^{0.155}}}
\tag{6.16-8}
$$

6.16.3.3 Fuhrboter (1961).

Fuhrboter (1961) already used the notation with solids effect and gave the $\mathbf{S_k}$ value in a graph.

$$
\mathbf{i_m} = \mathbf{i_l} + \mathbf{S_k} \cdot \frac{\mathbf{C_{vt}}}{\mathbf{v_{ls}}}
\tag{6.16-9}
$$

Now Fuhrboter (1961) assumed the $\mathbf{S_k}$ value was proportional with the particle diameter for medium sands and also assumed the terminal setting velocity $\mathbf{v_t} = 100 \cdot \mathbf{d}$. This way the $\mathbf{S_k}$ value is proportional to the terminal setting velocity $\mathbf{v_t}$.

6.16.3.4 Jufin & Lopatin (1966) Group B.

The hydraulic gradient of a mixture according to Jufin & Lopatin (1966) is:

$$
i_m = i_l + 2 \cdot 90389 \cdot \left(g \cdot D_p \cdot R_{sd} \cdot \psi^*\right)^{1/2} \cdot \left(\nu_l \cdot g\right)^{2/3} \cdot \left(C_{vt}\right)^{1/2} \left(\frac{1}{v_{ls}}\right)^3 \cdot \frac{\lambda_l \cdot v_{ls}^2}{2 \cdot g \cdot D_p}
$$

$$
= i_l + 90389 \cdot \frac{\lambda_l \cdot \left(\psi^* \cdot R_{sd}\right)^{1/2} \cdot \left(\nu_l \cdot g\right)^{2/3}}{\left(g \cdot D_p\right)^{1/2} \cdot \left(C_{vt}\right)^{1/2}} \cdot \frac{C_{vt}}{v_{ls}}
$$

(6.16-10)

The hydraulic gradient can be determined by, after substituting of the Darcy-Weisbach friction factor:

$$
i_m = i_l + 11145 \cdot \frac{\left(\psi^* \cdot R_{sd}\right)^{1/2} \cdot \left(\nu_l \cdot g\right)^{5/6}}{\left(g \cdot D_p\right)^{0.672} \cdot \left(C_{vt}\right)^{1/2}} \cdot \frac{1}{v_{ls}^{0.155}} \cdot \frac{C_{vt}}{v_{ls}}
$$

(6.16-11)

This gives for the solids effect factor S_k:

$$
S_k = 11145 \cdot \frac{\left(\psi^* \cdot R_{sd}\right)^{1/2} \cdot \left(\nu_l \cdot g\right)^{5/6}}{\left(g \cdot D_p\right)^{0.672} \cdot \left(C_{vt}\right)^{1/2}} \cdot \frac{1}{v_{ls}^{0.155}}
$$

(6.16-12)

6.16.3.5 Wilson et al. (1992) Heterogeneous.

The hydraulic gradient of a mixture according to Wilson et al. (1992) is:

$$
i_m = i_l + \frac{\mu_{sf}}{2} \cdot C_{vt} \cdot R_{sd} \cdot \left(\frac{v_{50}}{v_{ls}}\right) = i_l + \frac{\mu_{sf}}{2} \cdot R_{sd} \cdot v_{50} \cdot \frac{C_{vt}}{v_{ls}}
$$

(6.16-13)

This gives for the solids effect factor S_k:

$$
S_k = \frac{\mu_{sf}}{2} \cdot R_{sd} \cdot v_{50}
$$

(6.16-14)

For the line speed, where 50% of the particles is in granular contact, v_{50}, Wilson et al. (1992) give the following equation:

$$
v_{50} = w_{50} \cdot \sqrt{\frac{8}{\lambda_l}} \cdot \cosh\left(\frac{60 \cdot d_{50}}{D_p}\right)
$$

(6.16-15)

The terminal settling velocity related parameter w, the particle associated velocity, can be determined by:

$$
w = 0.9 \cdot v_t + 2.7 \cdot \left(R_{sd} \cdot g \cdot \nu_l\right)^{1/3}
$$

(6.16-16)

The terminal settling velocity v_t (strong), the pipe diameter D_p (weak), the particle diameter d_{50} (weak), the line speed v_{ls} (weak) and the kinematic viscosity ν_l (weak) are all present in the characteristic velocity v_{50}. The model of Wilson can be simplified with some fit functions, according to:

$$v_{50} \approx 3.93 \cdot \left(1000 \cdot d_{50}\right)^{0.35} \cdot \left(\frac{R_{sd}}{1.65}\right)^{0.45} \cdot \left(\frac{\nu_{l,actual}}{\nu_{w,20}}\right)^{0.25} \qquad (6.16\text{-}17)$$

This gives for the S_k factor:

$$S_k = 555 \cdot \mu_{sf} \cdot d_{50}^{\,0.35} \cdot R_{sd}^{\,1.45} \cdot \nu_l^{\,0.25} \qquad (6.16\text{-}18)$$

6.16.3.6 DHLLDV Graded, Miedema (2014).

The hydraulic gradient of a mixture according to Miedema (2014) is for graded sands and gravels is:

$$i_m = i_l + \left(\frac{v_t \cdot \left(1 - \dfrac{C_{vs}}{\kappa}\right)^{\beta}}{v_{ls}} + 1.845^2 \cdot \left(\frac{1}{\sqrt{\lambda_l}}\right) \cdot \left(\frac{v_t}{\sqrt{g \cdot d}}\right)^{10/3} \cdot \left(\frac{\left(\nu_l \cdot g\right)^{1/3}}{v_{ls}}\right)^{1}\right) \cdot R_{sd} \cdot C_{vs} \qquad (6.16\text{-}19)$$

Since the potential energy term (first term between brackets) is small compared to the kinetic energy term (second term between brackets) this can be simplified to:

$$i_m = i_l + 1.845^2 \cdot \left(\frac{1}{\lambda_l}\right)^{1/2} \cdot \left(\frac{v_t}{\sqrt{g \cdot d}}\right)^{10/3} \cdot \left(\nu_l \cdot g\right)^{1/3} \cdot R_{sd} \cdot \frac{C_{vs}}{v_{ls}} \qquad (6.16\text{-}20)$$

The hydraulic gradient can be determined by, after substituting of the Darcy-Weisbach friction factor:

$$i_m = i_l + 9.69 \cdot \left(g \cdot D_p\right)^{0.086} \cdot \left(\frac{v_t}{\sqrt{g \cdot d}}\right)^{10/3} \cdot \left(\nu_l \cdot g\right)^{1/4} \cdot \left(v_{ls}\right)^{0.0775} \cdot R_{sd} \cdot \frac{C_{vs}}{v_{ls}} \qquad (6.16\text{-}21)$$

This gives for the solids effect factor S_k:

$$S_k = 9.69 \cdot \left(g \cdot D_p\right)^{0.086} \cdot \left(\frac{v_t}{\sqrt{g \cdot d}}\right)^{10/3} \cdot \left(\nu_l \cdot g\right)^{1/4} \cdot \left(v_{ls}\right)^{0.0775} \cdot R_{sd} \qquad (6.16\text{-}22)$$

6.16.3.7 Comparison.

Table 6.16-1 shows the powers of the different parameters in the S_k equations. Figure 6.16-1, Figure 6.16-2, Figure 6.16-3 and Figure 6.16-4 show the values of S_k for 4 different pipe diameters.

Table 6.16-1: The powers of the different parameters, comparing models.

	R_{sd}	$\nu_l \cdot g$	$g \cdot D_p$	$\sqrt{C_x}$	v_{ls}	C_{vt}	v_t	d_{50}
Durand & Condolios	1.5	0.167	0.328	-2.67	-0.155	0.0	0.0	0.00
Newitt et al.	1.0	0.167	-0.172	0.00	-0.155	0.0	1.0	0.00
Fuhrboter	0.0	0.000	0.000	0.00	0.000	0.0	1.0	0.00
Jufin & Lopatin	0.5	0.833	-0.672	-0.75	-0.155	-0.5	0.0	0.00
Wilson et al.	1.45	0.250	0.000	0.00	0.000	0.0	0.0	0.35
DHLLDV	1.0	0.250	0.086	-2.67	0.078	0.0	0.0	0.00

For a pipe diameter of D_p=0.1016 m (4 inch) the curves are close together for medium and coarse sands. Wilson, Newitt and Jufin-Lopatin give higher values for the fines, while Wilson and Newitt also give higher values for the coarse particles. The latter can be explained by the fact that both have a sliding bed model for coarser particles. Fuhrboter gives relatively small values for medium sands.

For a pipe diameter of D_p=0.2032 m (8 inch) the curves are not too far apart for medium and coarse sands, but further apart compared to the D_p=0.1016 m pipe. The Wilson curve is less steep.

For a pipe diameter of Dp=0.4064 m (16 inch), the curves deviate more. The Wilson curve is less steep again and the Jufin-Lopatin curve is lowering.

For a pipe diameter of Dp=0.8132 m (32 inch), the curves deviate even more. For all pipe diameters the DHLLDV Framework and the Wilson model match very well for particles around d=0.8 mm and the DHLLDV Framework matches well with the Fuhrboter model for particles with d>1 mm.
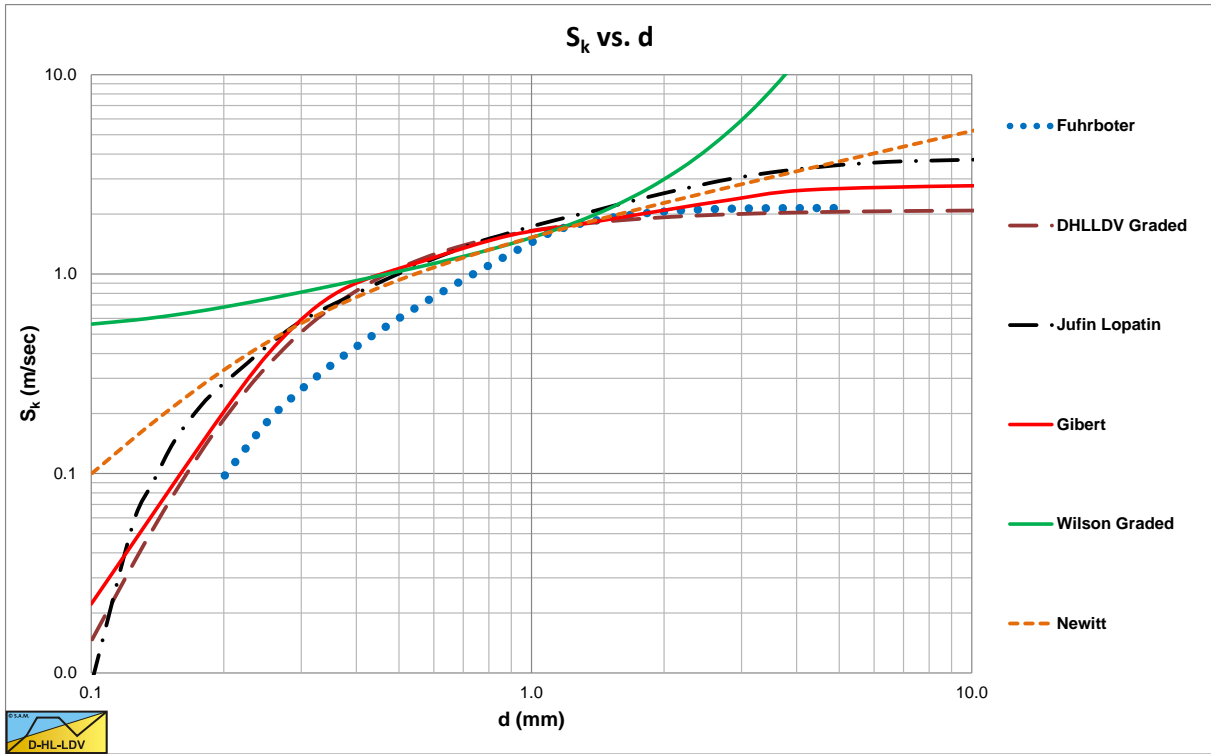

Figure 6.16-1: The Sk value of 6 models for D_p=0.1016 m, v_{ls}=3 m/s and C_{vt}=0.2.
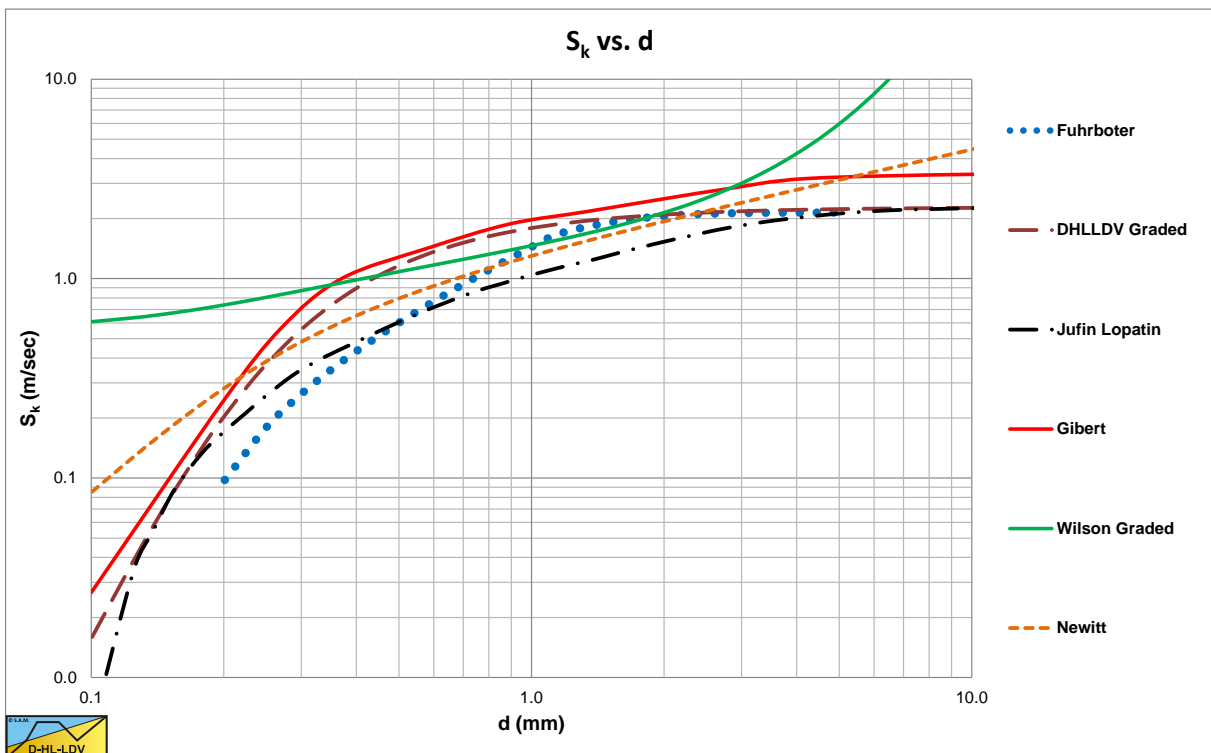
Figure 6.16-2 The Sk value of 6 models for D_p=0.2032 m, v_{ls}=4 m/s and C_{vt}=0.2.

S_k vs. d
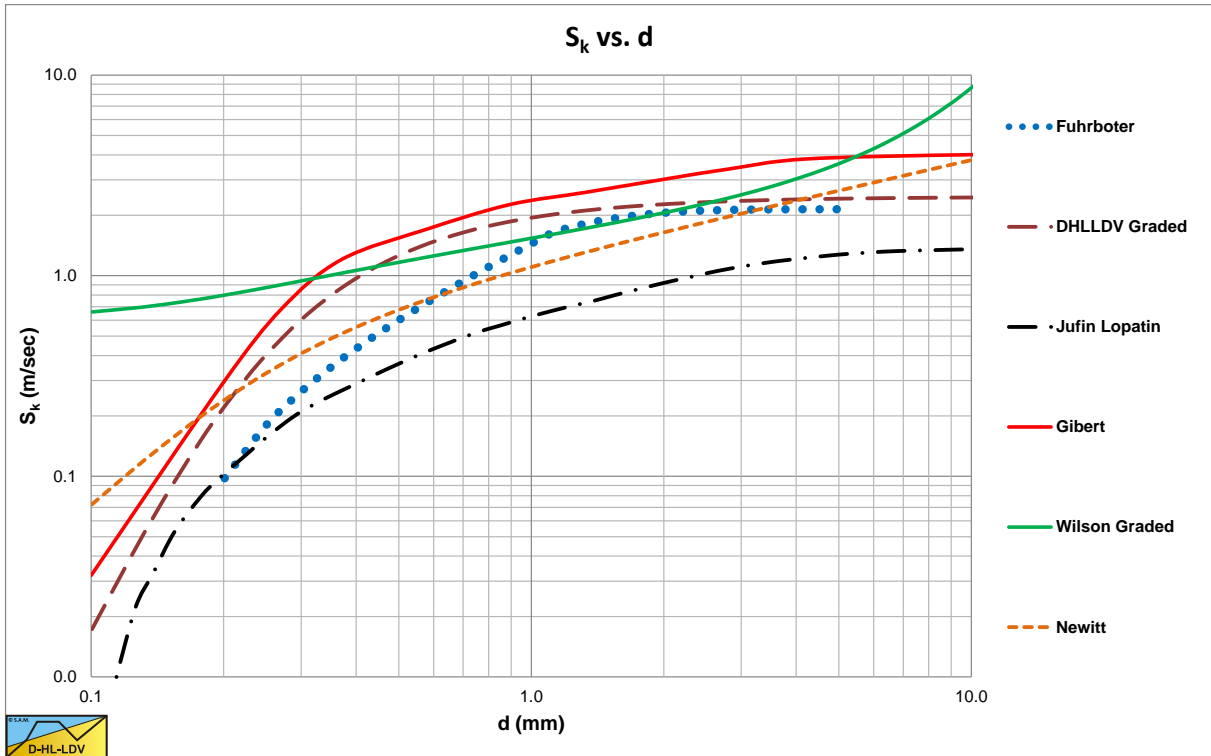
Figure 6.16-3 The Sk value of 6 models for D_p=0.4064 m, v_{ls}=5 m/s and C_{vt}=0.2.
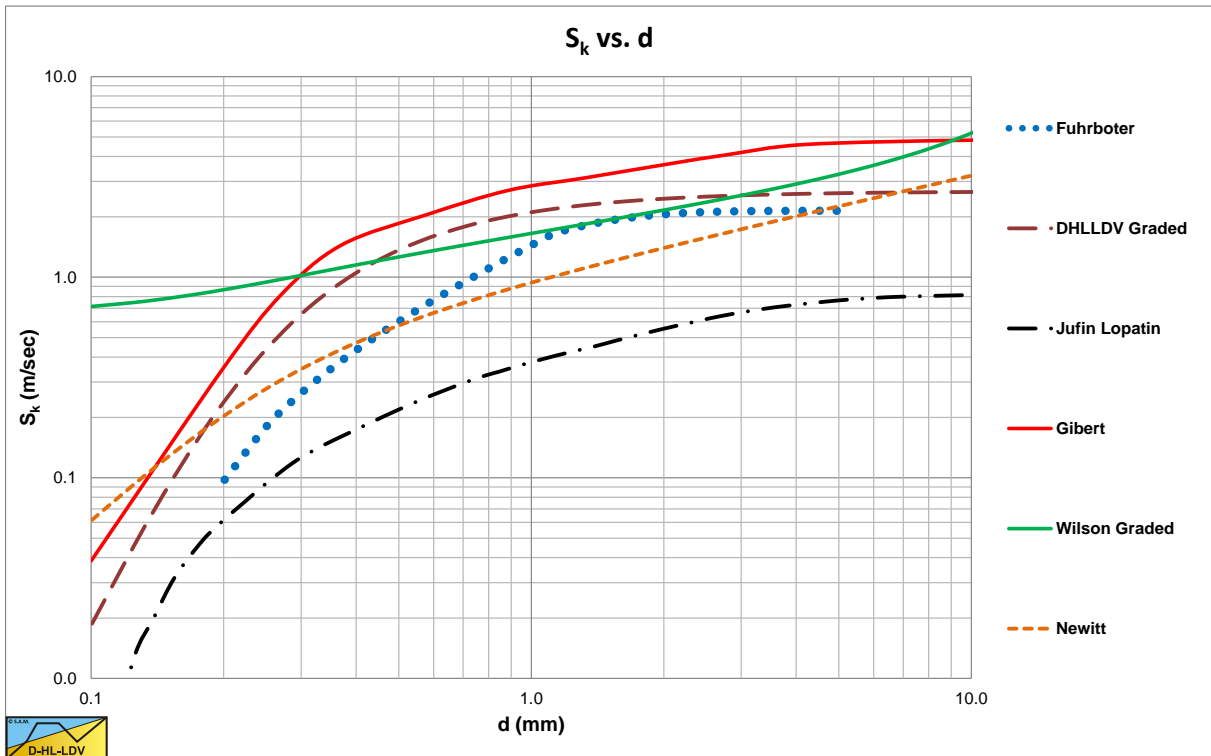
S_k vs. d

Figure 6.16-4 The Sk value of 6 models for D_p=0.8132 m, v_{ls}=6 m/s and C_{vt}=0.2.

It should be mentioned that the Jufin-Lopatin model depends on the concentration, while all other models don't. Since most models are based on experiments with small pipe diameters and medium sands, the tendencies found are no surprise. With small pipe diameters and medium sands the models are very close and the differences will fall within the range of the scatter.

6.16.4 Sliding Bed Regime.

For the sliding bed regime 4 models are chosen for comparison, the Newitt et al. (1955) model, the Babcock (1970) model and the Yagi et al. (1972) models for sand and gravel. The first two models consider delivered volumetric concentration experiments, the last two spatial concentration experiments.

Below the Limit Deposit Velocity Newitt et al. (1955) found for a sliding bed in a 1 inch steel pipe:

$$i_m = i_l \cdot \left(1 + 66 \cdot \left(g \cdot D_p \cdot R_{sd} \right) \cdot C_{vt} \cdot \left(\frac{1}{v_{ls}} \right)^2 \right) \qquad (6.16\text{-}23)$$

Or:

$$i_m = i_l + 33 \cdot \lambda_l \cdot R_{sd} \cdot C_{vt} \qquad (6.16\text{-}24)$$

Substituting the Darcy-Weisbach friction factor equation and a 1 inch pipe diameter, this gives:

$$i_m = i_l + 0.756 \cdot R_{sd} \cdot C_{vt} \cdot \left(v_{ls} \right)^{-0.155} \qquad (6.16\text{-}25)$$

Showing a slight decrease of the solids effect with increasing line speed, as was found by Newitt et al. (1955).

Below the Limit Deposit Velocity Babcock (1970) found for a sliding bed in a 1 inch plastic pipe:

$$i_m = i_l \cdot \left(1 + 60.6 \cdot \left(g \cdot D_p \cdot R_{sd} \right) \cdot C_{vt} \cdot \left(\frac{1}{v_{ls}} \right)^2 \right) \qquad (6.16\text{-}26)$$

Or:

$$i_m = i_l + 30.3 \cdot \lambda_l \cdot R_{sd} \cdot C_{vt} \qquad (6.16\text{-}27)$$

Substituting the Darcy-Weisbach friction factor equation and a 1 inch pipe diameter, this gives:

$$i_m = i_l + 0.694 \cdot R_{sd} \cdot C_{vt} \cdot \left(v_{ls} \right)^{-0.155} \qquad (6.16\text{-}28)$$

In both cases the delivered volumetric concentration was used, meaning that the spatial volumetric concentration was larger, especially with a sliding bed. In both models, the solids effect in the hydraulic gradient depends slightly on the cross section averaged line speed.

Below the Limit Deposit Velocity Yagi et al. (1972) found for a sliding bed in different pipes:

For sand ψ<**3** (below LDV):

$$\frac{i_m - i_l}{i_l \cdot C_{vs}} = \phi = K \cdot \psi^{-1.55} \quad \text{with:} \quad K=100 \qquad (6.16\text{-}29)$$

For gravel ψ<**3** (below LDV):

$$\frac{i_m - i_l}{i_l \cdot C_{vs}} = \phi = K \cdot \psi^{-1.16} \quad \text{with:} \quad K=98 \qquad (6.16\text{-}30)$$

With:

$$\psi = \left(\frac{v_{ls}^2}{g \cdot D_p \cdot R_{sd}} \right) \cdot \sqrt{C_x} \tag{6.16-31}$$

This gives:

For sand $\psi < 3$ (below LDV):

$$i_m = i_l + 50 \cdot \lambda_l \cdot \left(g \cdot D_p \right)^{0.55} \cdot R_{sd}^{1.55} \cdot \left(\frac{1}{\sqrt{C_x}} \right)^{1.55} \cdot \frac{1}{v_{ls}^{1.1}} \cdot C_{vs} \tag{6.16-32}$$

For gravel $\psi < 3$ (below LDV):

$$i_m = i_l + 49 \cdot \lambda_l \cdot \left(g \cdot D_p \right)^{0.16} \cdot \left(\frac{1}{\sqrt{C_x}} \right)^{1.16} \cdot R_{sd}^{1.16} \cdot \frac{1}{v_{ls}^{0.32}} \cdot C_{vs} \tag{6.16-33}$$

Substitution of the Darcy-Weisbach friction factor, a fixed value of 0.6 for $\sqrt{C_x}$ and a fixed value of 1.65 for the relative submerged density, this gives:

$$i_m = i_l + 1.66 \cdot R_{sd} \cdot C_{vs} \cdot \frac{1}{v_{ls}^{0.475}} \tag{6.16-34}$$

With an average line speeds around 5 m/sec, this can be reduced to:

$$i_m = i_l + 0.77 \cdot R_{sd} \cdot C_{vs} \tag{6.16-35}$$

This would imply a high sliding friction factor of 0.83, which was already remarked in the chapter about Yagi et al. (1972). Normally this sliding friction factor has a value in the range 0.35-0.45. The Yagi et al. (1972) equations are based on spatial volumetric concentration, while the Newitt et al. (1955) and Babcock (1970) measurements are based on delivered volumetric concentration. It should be mentioned however that the Newitt et al. (1955) data also show a decreasing solids effect with increasing line speed, but Newitt et al. (1955) just took the average solids effect value. The Yagi et al. (1972) equation for sand is very similar to the Durand & Condolios (1952) equation for heterogeneous transport, which could be expected based on the conclusions of Durand & Condolios (1952).

6.16.5 Homogeneous Regime.

The only scientific equation (and explanation) found for the homogeneous regime was derived by Talmon (2011) & (2013), with $\alpha_h = 6.7$:

$$i_m = i_l \cdot \frac{1 + R_{sd} \cdot C_{vs}}{\left(\alpha_h \cdot \sqrt{\frac{\lambda_l}{8}} \cdot R_{sd} \cdot C_{vs} + 1 \right)^2} \tag{6.16-36}$$

This equation reduces the solids effect compared to the ELM. In some cases it may be necessary to use the Thomas (1965) viscosity to correct for high concentration fines. Others mention a reduction of the solids effect to 60% or even to zero, but no explanation is given.

6.16.6 Validation.

To validate the conclusions, independent experiments are considered. Wiedenroth (1967) carried out experiments in a $D_p = 0.125$ m pipe with fine sand, coarse sand, fine gravel and medium gravel. All experiments were carried out with constant spatial volumetric concentration. Figure 6.16-5 shows the results of fine sand. The heterogeneous

and homogeneous flow regimes can be recognized. The theoretical DHLLDV Framework curve contains the influence of grading and the Thomas (1965) viscosity.
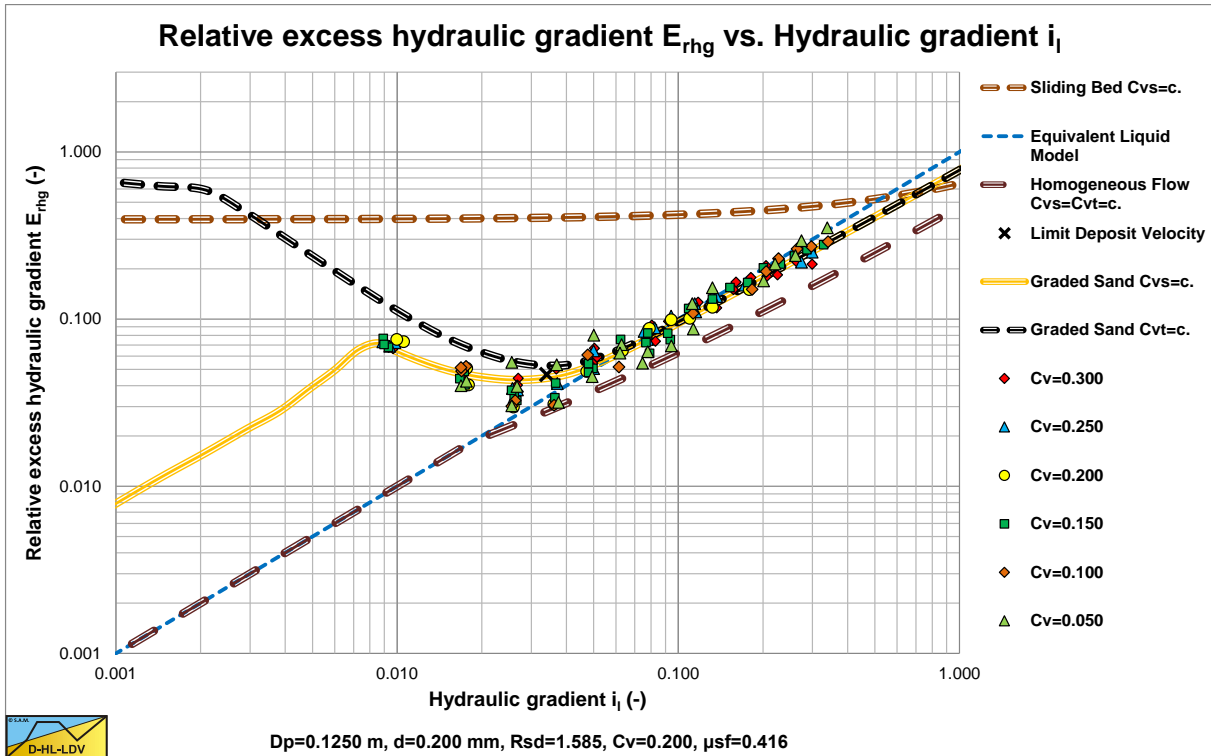

Figure 6.16-5: Experiments of Wiedenroth (1967) with fine sand, C_{vs}.
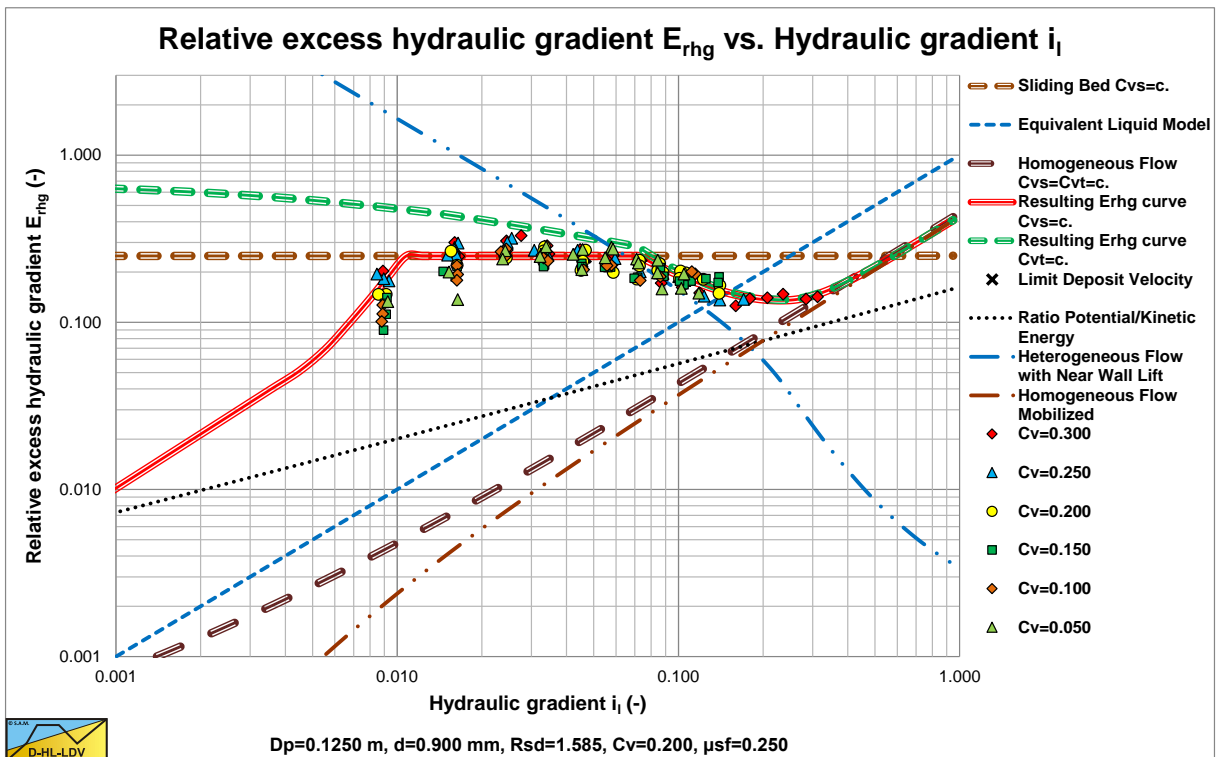**Including the Thomas (1965) viscosity.**

Figure 6.16-6: Experiments of Wiedenroth (1967) with coarse sand, C_{vs}.

Figure 6.16-6 shows the results for coarse sand. The fixed/stationary bed regime, the sliding bed regime and the start of the heterogeneous regime can be recognized. The influence of the volumetric concentration can hardly be identified in the scatter of data points, meaning that the E_{rhg} value is independent of the C_{vs} value.
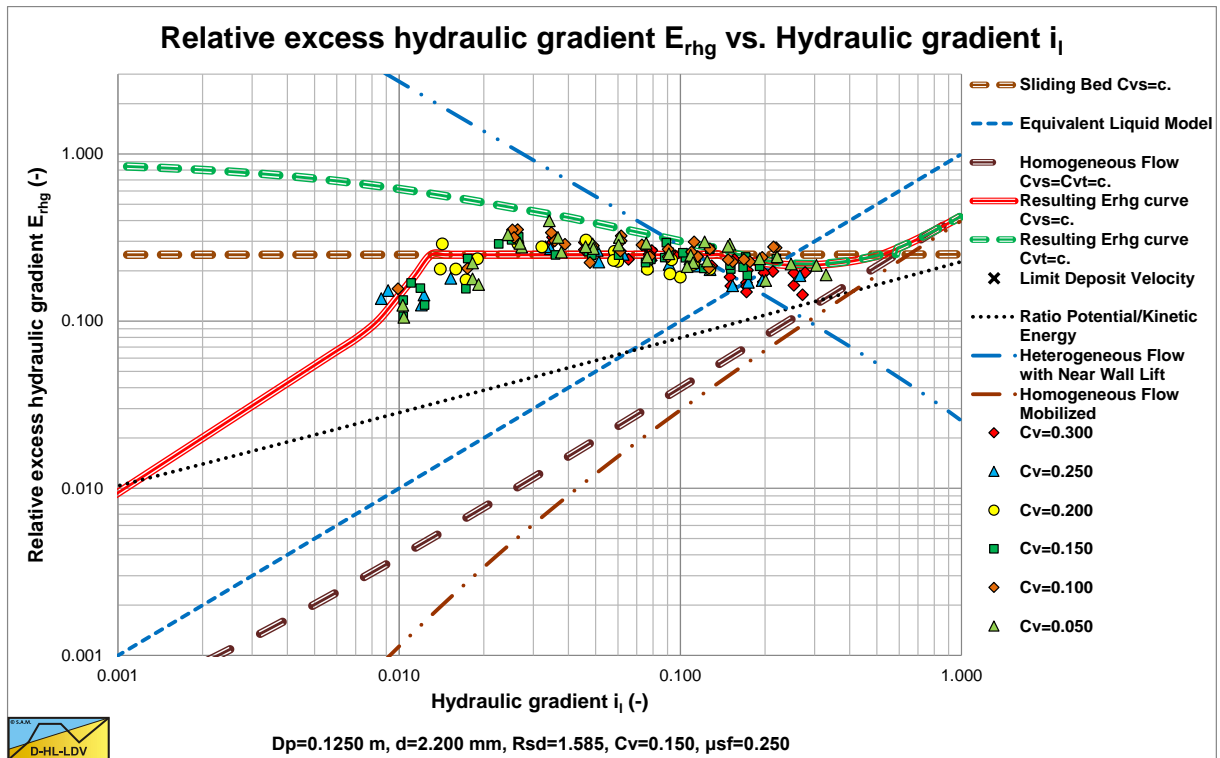
Figure 6.16-7: Experiments of Wiedenroth (1967) with fine gravel, C$_{vs}$.
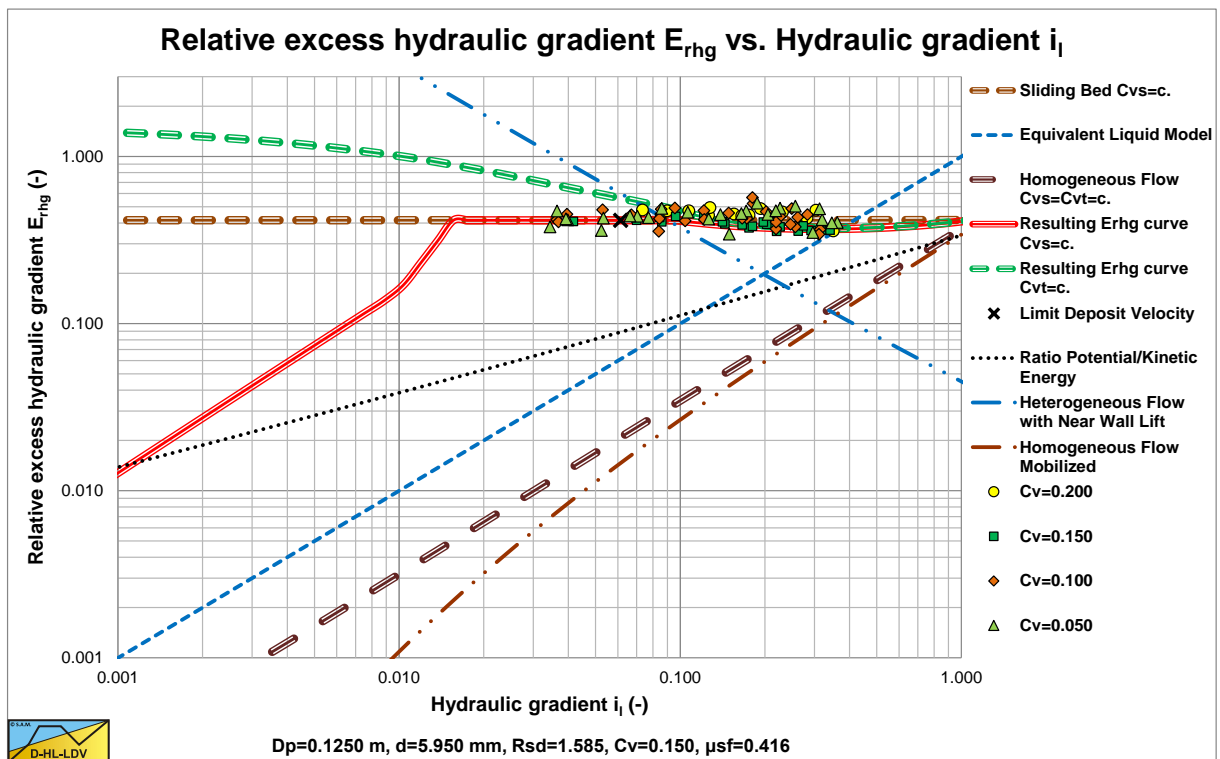
Figure 6.16-8: Experiments of Wiedenroth (1967) with medium gravel, C$_{vs}$.

Figure 6.16-7 shows the results for fine gravel. The fixed/stationary bed, the sliding bed and sliding flow can be distinguished. The data points for high line speeds are in between the heterogeneous and the sliding bed curves. This behavior is identified as sliding flow.

Figure 6.16-8 shows the results for medium gravel. Here the sliding bed and sliding flow regimes can be distinguished. However the particles are so large compared to the pipe diameter, that sliding flow and sliding bed almost have the same behavior.

6.17 Nomenclature Early History & Empirical and Semi-Empirical Models.

a	Correction factor Jufin Lopatin	**-**
A	Proportionality constant	**-**
b	Correction factor Jufin Lopatin	**-**
C_D	Particle drag coefficient	**-**
C_{ms}	Spatial concentration by mass	**-**
C_v	Volumetric concentration	**-**
C_{vs}	Volumetric spatial concentration	**-**
C_{vt}	Volumetric transport/delivered concentration	**-**
C_x	Inverse particle Froude number squared according to Durand & Condolios Fr_p^{-2}	**-**
$C_{x,Gibert}$	Inverse particle Froude number squared according to Gibert	**-**
d	Particle diameter	**m**
d_0	Average particle diameter Jufin Lopatin	**m**
d_{10}	Particle diameter at which 10% by weight is smaller	**m**
d_{25}	Particle diameter at which 25% by weight is smaller	**m**
d_{50}	Particle diameter at which 50% by weight is smaller	**m**
d_{60}	Particle diameter at which 60% by weight is smaller	**m**
d_m	Mean particle diameter	**m**
di	Particle size fraction diameters	**m**
D_p	Pipe diameter	**m**
$D_{p,H}$	Hydraulic diameter pipe cross section above bed	**m**
Du	Durand & Condolios constant (176-181) or (81-85)	**-**
E_{rhg}	Relative excess hydraulic gradient	**-**
f_l	Fanning friction factor liquid	**-**
f_m	Fanning friction factor mixture	
ELM	Equivalent Liquid Model	**-**
$F_L, F_{L,m}$	Durand & Condolios Limit Deposit Velocity coefficient	**-**
Fr_{ldv}	Flow Froude number at the Limit Deposit Velocity/critical velocity	**-**
Fr_{fl}	Flow Froude number	**-**
Fr_p	Particle Froude number $1/\sqrt{C_x}$	**-**
g	Gravitational constant	$9.81 \cdot m/s^2$
i	Hydraulic gradient	**m.w.c./m**
i_m	Hydraulic gradient mixture	**m.w.c./m**
i_w, i_l	Hydraulic gradient water/liquid	**-**
K	Durand & Condolios constant (176-181) or (81-85)	**-**
K	Constant others (Yagi, Babcock, etc.)	**-**
K	Wilson proportionality constant	**-**
K	Turian & Yuan constant	**-**
K_1	Newitt coefficient for heterogeneous transport (1100)	**-**
K_2	Newitt coefficient for sliding/moving bed (66)	**-**
K_1-K_{10}	Proportionality constants Thomas	**-**
$L, \Delta L$	Length of the pipeline	**m**
LDV	Limit Deposit Velocity	**m/s**
LSDV	Limit of Stationary Deposit Velocity	**m/s**
MHGV	Minimum Hydraulic Gradient Velocity	**m/s**
N_{cr}	Zandi & Govatos parameter for Limit Deposit Velocity	**-**
p	Probability	**-**
p_{er}	Relative excess pressure	**-**
Δp	Head loss over a pipeline length ΔL	**kPa**
Δp_m	Head loss of mixture over a pipeline length ΔL	**kPa**
$\Delta p_l, \Delta p_w$	Head loss of liquid/water over a pipeline length ΔL	**kPa**
PSD	Particle Size Diagram/Distribution	**-**
R_{sd}	Relative submerged density	**-**
S_k	Solids effect factor Fuhrboter spatial concentration	**m/s**
S_{kt}	Solids effect factor Fuhrboter transport concentration	**m/s**
u_*	Friction velocity	**m/s**

v_{ls}	Line speed	m/s
$v_{ls,ldv}$	Limit Deposit Velocity (often called critical velocity)	m/s
$v_{ls,h-h}$	Transition velocity heterogeneous vs. homogeneous according to Newitt	m/s
$v_{ls,MHGV}$	Minimum Hydraulic Gradient Velocity	m/s
v_{min}	Minimum gradient velocity	m/s
v_t	Terminal settling velocity of particles	m/s
v_l	Average liquid velocity	m/s
v_p	Average velocity particle	m/s
v_s	Average velocity solids	m/s
v_{50}	50% stratification velocity Wilson	m/s
w	Particle associated velocity	m/s
x	Abscissa	-
y	Ordinate	-
α	Power in Yagi equation	-
α	Darcy Weisbach friction factor constant	-
α	Power of concentration in Turian & Yuan equation	-
$α_1$	Darcy Weisbach friction factor power	-
$α_2$	Darcy Weisbach friction factor power	-
β	Power of Richardson & Zaki equation	-
β	Power of Fanning friction factor liquid in Turian & Yuan equation	-
γ	Power of drag coefficient in Turian & Yuan equation	-
δ	Power of Froude number in Turian & Yuan equation	-
$ρ_l$	Liquid density	ton/m^3
$ρ_w$	Density of water	ton/m^3
$ρ_m$	Mixture density	ton/m^3
$λ_l$	Darcy-Weisbach friction factor liquid to wall	-
$μ_{sf}$	Friction coefficient for sliding bed (see also S_{rs})	-
$μ_l$	Dynamic viscosity liquid	Pa·s
$μ_m$	Dynamic viscosity mixture	Pa·s
Φ	Durand relative excess pressure as ordinate in different graphs	-
ψ	Durand abscissa, equations may differ due to historical development, later the relative submerged density has been added, sometimes the particle Froude number is omitted	-
ψ	Particle shape coefficient, usually near 0.7	-
ψ*	Particle factor Jufin Lopatin	-
v_w, v_l	Kinematic viscosity of water/liquid	m^2/s
v_m	Kinematic viscosity of mixture with Thomas equation	m^2/s
v_r	Relative kinematic viscosity v_m/v_w	-
ξ	Particle shape factor	-
ξ	Slip ratio Yagi	-

6.18 Physical Models.

In the previous chapters empirical and semi empirical models are discussed. These models are either based on a direct curve fit of experimental data or on a curve fit on dimensionless numbers based on assumed physical relations. Direct curve fit of experimental data based on the physical or geometrical parameters varied during the experiments leads to good empirical relations within the ranges the physical and geometrical parameters are varied. Outside these ranges the empirical relations are questionable. Relations based on dimensionless numbers assume physical relations between the parameters of which a dimensionless number consists, however they also pretend validity outside the range experiments were carried out. Another downside is, that the range a dimensionless parameter is varied in, does not imply the parameters the dimensionless parameter consists of can be varied in that range. An example is the Reynolds number consisting of a velocity scale, a length scale and the kinematic viscosity. Often only the velocity scale or the length scale is varied, however varying the Reynolds number also means that the kinematic viscosity can be varied, which is questionable if only 1 liquid is used during the experiments. Another example is the Froude number as used in a number of models. It consists of the velocity scale squared, divided by the length scale. Models based on the Froude number force a relation between the velocity scale and the length scale. This can however be corrected by adding additional dimensionless numbers, but this is often not the case. The advantage of physical models is, that they describe the physics involved. Maybe in the beginning the physics are limited and certain effects are neglected, but the models can be extended in the future. A number of physical models are described here, based on different points of view.

6.18.1 The Newitt et al. (1955) Model.

The Newitt et al. (1955) model distinguishes different flow regimes, enabling the user to determine which flow regime is valid for which situation. Newitt et al. (1955) constructed regime diagrams based on their empirical relations. They distinguished flow with a stationary bed, flow with a moving bed, heterogeneous flow and homogeneous flow. The equations for each flow regime are still empirical, although sometimes based on physical considerations. The moving (sliding) bed regime is based on sliding friction, the heterogeneous regime on potential energy and the homogeneous regime on the Equivalent Liquid Model (ELM). The regime diagrams show that not all regimes occur for each combination of particle and pipe diameter. The Newitt et al. (1955) model however assumes that only one flow regime is present under the circumstances considered. The Newitt et al. (1955) model forms the basis of a number of physical models as discussed in the next chapters.

6.18.2 The Wasp et al. (1963) Model.

The Wasp et al. (1963) model considers a combination of heterogeneous and homogeneous flow at the same time. The PSD is divided into a number of fractions. Based on the concentration profile of each fraction, following from a solution of the advection diffusion equation, the portion of solids in the vehicle is determined. After summation of the portions in the vehicle, viscosity and density of the so called vehicle liquid are adjusted for the concentration of solids in the vehicle liquid. The remainder of the solids is assumed to be in the heterogeneous regime, using the Durand & Condolios (1952) model to determine the hydraulic gradient. Often this remainder is assumed to be in the bed, however the Durand & Condolios (1952) model is developed for heterogeneous flow, which by definition means a combination of suspended and bed flow. So not all suspended flow is in the vehicle.

6.18.3 The Wilson-GIW (1979) Model.

The original Wilson-GIW (1979) model is based on the force balance on a bed with pure liquid above it. After determining all forces (or shear stresses) involved, it follows whether the bed is sliding or not. The line speed where the bed starts sliding depends on the volumetric concentration and is often called the critical velocity. Since there are many definitions of the critical velocity, here this is named the Limit of Stationary Deposit Velocity (LSDV), distinguishing this from the LDV (Limit Deposit Velocity) where there is no stationary or sliding bed. The latter will always occur at a higher line speed. Based on the shear stresses determined, the hydraulic gradient (based on the hydrostatic normal stress approach) and the delivered concentration can be determined.
For the heterogeneous regime the Wilson-GIW (1979) model assumes a diminishing bed with suspension above it. With an empirical relation the portion of solids in the bed can be determined, resulting in a hydraulic gradient. Later the 4 component model of Wilson & Sellgren (2001) was developed. The slurry is divided into 4 components: Homogeneous flow, the fraction **d<0.04 mm**. Pseudo homogeneous flow, the fraction **0.04 mm<d<0.15·μ_r mm**, where **μ_r** is the relative dynamic viscosity. Heterogeneous flow, the fraction **0.15·μ_r mm<d<0.015·D_p**. Stratified flow, **d>0.015·D_p**. Not each component has to be present in the slurry. The hydraulic gradients are determined for each component separately and summed to find the total hydraulic gradient.

6.18.4 The Doron et al. (1987) and Doron & Barnea (1993) Model.

Doron et al. (1987) and Doron & Barnea (1993) 2 layer model, start with solving the advection diffusion equation in order to determine the concentration profile. Based on this concentration profile it is determined whether there is a bed or not. In case of no bed, the bottom concentration is smaller than the bed concentration, the ELM is used. In case of a bed, the model of Wilson-GIW (1979) is used for the determination of the hydraulic gradient of the bed. If there is a bed however, the concentration profile has to be recalculated by solving the advection diffusion equation starting at the bed surface with the bed concentration as a boundary condition. This has to be repeated until the sum of suspended solids and bed solids matches the spatial volumetric concentration that was started with. With a no-slip condition between the solids and the liquid, apart from the hydraulic gradient, also the delivered concentration and the bed height are determined.

6.18.5 The SRC Model.

At the Saskatchewan Research Council (SRC) another 2 layer model was developed. The model starts with the determination of the contact load fraction based on an empirical equation. The contact load fraction is not equal to the bed fraction, but is defined as the fraction contributing to sliding friction. The remainder is the suspended fraction. However before calculating the sliding friction, two adjustments have to be made. First the contact load fraction is submerged in a pseudo liquid consisting of the carrier liquid and the suspended particles, reducing the submerged weight of the contact load fraction and thus the sliding friction, secondly the maximum bed concentration is decreasing with increasing line speed. The latter is of influence, because the SRC model is using the hydrostatic normal stress approach as developed in the Wilson-GIW (1979) model. The hydraulic gradient of the suspended phase is determined based on the ELM.

6.18.6 The Kaushal & Tomita (2002B) Model.

The Kaushal & Tomita (2002B) model is based on the Wasp et al. (1963) model, but with a different approach to determine the suspended load fraction. Where Wasp et al. (1963) determined the suspended load fraction based on a solution of the advection diffusion equation, without interaction between fraction of different particle sizes. Kaushal & Tomita (2002B) based their model on the modified Karabelas (1977) model, including interaction between different particle sizes. The original Karabelas (1977) model is based on the Hunt (1954) equation and not on the Rouse (1937) equation. Kaushal & Tomita (2002B) added the effect of hindered settling and modified the diffusivity, including the effects of particle size and grading and the effect of volumetric concentration. For the heterogeneous portion of the solids (they talk about the bed fraction), the use the Durand & Condolios (1952) model, as is used in the original Wasp et al. (1963) model.

6.18.7 The Matousek (2009) Model.

The Matousek (2009) model is completely different from the other models. The previous models are all based on force equilibria and concentration distributions with the delivered concentration as an output, where the Matousek (2009) model uses the delivered concentration as an input. Based on the Meyer-Peter Muller (1948) equation, the Shields parameter is computed. The Shields parameter results in the bed shear stress. By dividing the suspended layer in a bed associated and a wall associated area, the hydraulic gradient is determined, iterating until both areas give the same hydraulic gradient. Basically, the delivered concentration is the result of the transport in a sheet flow layer and the transport in the sliding bed. The model method is a sort of reversed engineering and gives a completely different concept, although the Wilson-GIW (1979) method is applied for the sliding bed friction.

6.18.8 The Talmon (2011) & (2013) Homogeneous Regime Model.

The Talmon (2011) & (2013) homogeneous regime model has been derived to prove fundamentally that the hydraulic gradient in homogeneous flow can be less than given by the ELM method. By assuming that the viscous sub-layer is particle free and thus having a different viscosity and density, compared to the turbulent layer, an equation is derived, showing the reduction of the hydraulic gradient. The reduction is increasing with an increasing Darcy Weisbach friction factor, an increasing relative submerged density of the solids and an increasing volumetric concentration. The model is developed using equations for open channel flow and requires some adjustment for pipe flow. The concept of the model however is new and proves that the ELM will, most probably, overestimate the hydraulic gradient at high to very high line speeds.

6.19 The Wasp et al. (1963) Model.

6.19.1 Introduction.

Based on coal slurry data accumulated over 13 years of experiments and actual 102 mile pipeline transport, Wasp et al. (1963), (1970) and (1977) proposed to separate the slurry flow into two components: a homogeneous component called the "vehicle" and a heterogeneous component called "Durand" flow. Water and the suspended smaller particles form the so called "two phase carrying liquid" or "vehicle" transporting the heterogeneous coarser particles. According to the model, the total pressure loss is the sum of the losses due to the vehicle and the Durand components, where the rheological properties of the vehicle are influenced by the fine particles it contains. The most important step in the use of the Wasp model is to determine the fraction of the solids which is in the vehicle and the remaining fraction which behaves according to the Durand model. The vehicle fraction can be determined for each particle fraction by assuming a certain concentration distribution in the pipe C_{top}/C_{center}. The vehicle and the Durand concentrations are now:

$$C_{vs,v} = C_{vs} \cdot \frac{C_{top}}{C_{center}}$$

(6.19-1)

$$C_{vs,Du} = C_{vs} - C_{vs,v}$$

Here C_{top} is the solids volume concentration at $r/D_p=0.92$ and C_{center} is the solids volume concentration at $r/D_p=0.5$, where r is the vertical position in the pipe and D_p the pipe diameter. Based on the convection diffusion equation:

$$v_t \cdot C_{vs} + \varepsilon_s \cdot \frac{\partial C_{vs}}{\partial r} = 0$$

(6.19-2)

The following equation is often used to determine the ratio C_{top}/C_{center}.

$$\frac{C_{top}}{C_{center}} = 10^{-1.8 \cdot \frac{v_t}{\beta_{sm} \cdot \kappa \cdot u_*}} = e^{-1.8 \cdot 2.3 \cdot \frac{v_t}{\beta_{sm} \cdot \kappa \cdot u_*}} = e^{-4.14 \cdot \frac{v_t}{\beta_{sm} \cdot \kappa \cdot u_*}}$$

(6.19-3)

Usually β_{sm} is taken as unity ($\beta_{sm}=1$), κ is the von Karman constant ($\kappa=0.35-0.40$). The β_{sm} value varies with particle size, but use of $\beta_{sm}=1$ gives some margin of safety since it lowers the value of C_{top}/C_{center}. Thomas (1965) derived an equation to determine the relative dynamic viscosity as a function of the concentration $C_{vs,v}$ of the particles in the vehicle.

$$\mu_r = \frac{\mu_v}{\mu_l} = 1 + 2.5 \cdot C_{vs,v} + 10.05 \cdot C_{vs,v}^2 + 0.00273 \cdot e^{16.6 \cdot C_{vs,v}}$$

(6.19-4)

$$\rho_v = \rho_l \cdot \left(1 + R_{sd} \cdot C_{vs,v}\right) \quad \text{and} \quad R_{sd,v} = \frac{\rho_s - \rho_v}{\rho_v}$$

Wasp et al. (1970) proposed the following model for the limit deposit velocity to better represent the solid concentrations and the mean particle size for more widely varied particle sizes.

$$v_{ls,ldv} = 3.116 \cdot C_{vs}^{0.186} \cdot \sqrt{2 \cdot g \cdot D_p \cdot R_{sd}} \cdot \left(\frac{d}{D_p}\right)^{1/6} = F_L \cdot \sqrt{2 \cdot g \cdot D_p \cdot R_{sd}}$$

(6.19-5)

$$F_L = 3.116 \cdot C_{vs}^{0.186} \cdot \left(\frac{d}{D_p}\right)^{1/6}$$

Later Azamathulla & Ahmad (2013) mentioned a slightly modified equation, referring to Wasp et al. (1977):

$$v_{ls,ldv} = 3.399 \cdot C_{vs}^{0.2156} \cdot \sqrt{2 \cdot g \cdot D_p \cdot R_{sd}} \cdot \left(\frac{d}{D_p} \right)^{1/6} = F_L \cdot \sqrt{2 \cdot g \cdot D_p \cdot R_{sd}}$$

(6.19-6)

$$F_L = 3.399 \cdot C_{vs}^{0.2156} \cdot \left(\frac{d}{D_p} \right)^{1/6}$$

Others use slightly different coefficients. Souza Pinto et al. (2014) use the following equation. The power of the particle diameter to pipe diameter ratio has changed from 1/6 to 1/16, which must be a mistake because it results in unreasonably high Limit Deposit Velocities.

$$v_{ls,ldv} = 4 \cdot C_{vs}^{1/5} \cdot \sqrt{2 \cdot g \cdot D_p \cdot R_{sd}} \cdot \left(\frac{d}{D_p} \right)^{1/6} = F_L \cdot \sqrt{2 \cdot g \cdot D_p \cdot R_{sd}}$$

(6.19-7)

$$F_L = 4 \cdot C_{vs}^{1/5} \cdot \left(\frac{d}{D_p} \right)^{1/6}$$

The nice thing of the Wasp (1977) model is that heterogeneous and homogeneous regimes are combined in one model, resulting in a smooth transition. However the possible occurrence of heterogeneous transport simultaneously with a sliding bed is not covered. As long as heterogeneous and homogeneous transport are considered, the slip velocity of the particles is very small and can be neglected. The spatial volumetric concentration and the transport or delivered volumetric concentration are almost identical. At velocities near the Limit Deposit Velocity and with graded sands or gravels, this is not the case anymore. Very coarse particles may already form a fixed or sliding bed, while the smaller particles will still be in heterogeneous or homogeneous transport. It is thus questionable how accurate the predictions of this model are for the lower line speeds and graded sands or gravels.

The Wasp model is useful for slurries containing finely divided particles used for long distance transport of solids. For graded sand and gravel, there will not be significant vehicle component and therefore the predictions will be equivalent to the method of Durand. For such materials the estimates based on Wasp model are therefore as good as that based on Durand correlation (Gandhi, 2015).

6.19.2 The WASP Method.

6.19.2.1 Step 1: Prediction Step.

In the first iteration step it is assumed that all the solids form a homogeneous liquid, behaving according to ELM. The apparent viscosity and density of the liquid have to be adjusted, assuming the concentration in the vehicle equals the total concentration, so $C_{vs,v} = C_{vs}$.

$$\mu_r = \frac{\mu_v}{\mu_l} = 1 + 2.5 \cdot C_{vs,v} + 10.05 \cdot C_{vs,v}^2 + 0.00273 \cdot e^{16.6 \cdot C_{vs,v}}$$

(6.19-8)

$$\rho_v = \rho_l \cdot \left(1 + R_{sd} \cdot C_{vs,v} \right) \quad \text{and} \quad R_{sd,v} = \frac{\rho_s - \rho_v}{\rho_v}$$

The Reynolds number can now be determined as, using the apparent dynamic viscosity and density of the vehicle (whenever possible laboratory scale rheology tests should be carried out and these results should be used instead of correlations for slurry viscosity (Gandhi, 2015)):

$$Re_v = \frac{\rho_v \cdot v_{ls} \cdot D_p}{\mu_v} \tag{6.19-9}$$

The Darcy Weisbach friction factor of the vehicle is now:

$$\lambda_v = \frac{1.325}{\left(\ln\left(\dfrac{\varepsilon}{3.7 \cdot D_p} + \dfrac{5.75}{Re_v^{0.9}} \right) \right)^2} \tag{6.19-10}$$

The hydraulic gradient of the vehicle still related to the carrier liquid density is now based on the ELM, following the Abulnaga (2002) examples (note that the $i_{vehicle}$ is expressed as m of water per m of pipe):

$$i_{vehicle} = \lambda_v \cdot \frac{v_{ls}^2}{2 \cdot g \cdot D_p} \cdot \frac{\rho_v}{\rho_l} \tag{6.19-11}$$

The friction velocity used in the first correction step can be determined by:

$$u_* = \sqrt{\frac{\lambda_v}{8}} \cdot v_{ls} = \sqrt{\frac{i_{vehicle} \cdot g \cdot D_p}{4} \cdot \frac{\rho_l}{\rho_v}} \tag{6.19-12}$$

In the second iteration step, the PSD is divided into **n** fractions with index **j** and volumetric concentration $C_{vs,j}$, the number of fractions depending on the grading of the PSD.

A good equation for the required terminal settling velocity has been derived by Ruby & Zanke (1977):

$$v_{tv,j} = \frac{10 \cdot \nu_v}{d_j} \cdot \left(\sqrt{1 + \frac{R_{sd,v} \cdot g \cdot d_j^3}{100 \cdot \nu_v^2}} - 1 \right) \quad \text{with:} \quad \nu_v = \frac{\mu_v}{\rho_v} \tag{6.19-13}$$

The settling velocity depends on the vehicle properties and decreases with an increasing vehicle density and viscosity. The settling velocity of solids is estimated using either vehicle or water properties depending upon the amount of fine particles. The Wasp method is a good correlating tool and therefore estimates using vehicle as well as water properties are calculated for given slurry (Gandhi, 2015).

The Durand & Condolios (1952) particle Froude number is, although Wasp et al. (1977) use the particle drag coefficient in the pure liquid, $C_{D,j}$:

$$Fr_{p,j} = \frac{v_{tv,j}}{\sqrt{g \cdot d_j}} = \frac{1}{\sqrt{C_{x,j}}} \tag{6.19-14}$$

However, in most publications about the Wasp model, the particle drag coefficient C_D is used instead of C_x. For sands and gravels the two coefficients differ a factor 2, but for other solids densities they may differ more or less.

6.19.2.2 Step 2: Correction Steps.

For each fraction the percentage of solids in the vehicle is calculated from:

$$C_{vs,v,j} = C_{vs,j} \cdot \frac{C_{top}}{C_{center}} = 10^{-1.8 \cdot \frac{v_{tv,j}}{\beta_{sm} \cdot \kappa \cdot u_*}} \tag{6.19-15}$$

After computing the vehicle portion for each fraction of the PSD, the total percentage of the solids in the vehicle is determined. The vehicle density and apparent viscosity can be determined, as well as the hydraulic gradient of the vehicle liquid.

$$C_{vs,v} = \sum_{j=1}^{n} C_{vs,v,j}$$ (6.19-16)

And for the apparent dynamic viscosity and vehicle density:

$$\mu_r = \frac{\mu_v}{\mu_l} = 1 + 2.5 \cdot C_{vs,v} + 10.05 \cdot C_{vs,v}^2 + 0.00273 \cdot e^{16.6 \cdot C_{vs,v}}$$ (6.19-17)

$$\rho_v = \rho_l \cdot \left(1 + R_{sd} \cdot C_{vs,v}\right) \quad \text{and} \quad R_{sd,v} = \frac{\rho_s - \rho_v}{\rho_v}$$

The Reynolds number can now be determined as, using the apparent dynamic viscosity of the vehicle and the vehicle density:

$$Re_v = \frac{\rho_v \cdot v_{ls} \cdot D_p}{\mu_v}$$ (6.19-18)

The Darcy Weisbach friction factor of the vehicle is now according to Swamee Jain (1976):

$$\lambda_v = \frac{1.325}{\left(\ln\left(\dfrac{\varepsilon}{3.7 \cdot D_p} + \dfrac{5.75}{Re_v^{0.9}}\right)\right)^2}$$ (6.19-19)

The hydraulic gradient of the vehicle still related to the carrier liquid density is now based on the ELM, assuming Newtonian flow:

$$i_{vehicle} = \lambda_v \cdot \frac{v_{ls}^2}{2 \cdot g \cdot D_p} \cdot \frac{\rho_v}{\rho_l}$$ (6.19-20)

The hydraulic gradient of the remaining solids (not in the vehicle) is determined using the Durand & Condolios (1952) relationship for each fraction. The concentration of each fraction in the heterogeneous regime equals the total concentration of the fraction, minus the concentration present in the homogeneous regime, in the vehicle.

$$C_{vs,Du,j} = C_{vs,j} - C_{vs,v,j}$$ (6.19-21)

The hydraulic gradient for the heterogeneous regime of a fraction is, based on the original Durand & Condolios (1952) relationship:

$$i_{Du,j} = i_l \cdot 82 \cdot C_{vs,Du,j} \cdot \left(\frac{g \cdot D_p \cdot R_{sd}}{v_{ls}^2 \cdot \sqrt{C_{D,j}}}\right)^{3/2} = i_l \cdot Du_j$$ (6.19-22)

If vehicle properties are used for estimating the drag coefficient of the solids then the Durand formula should be based on vehicle properties instead of carrier fluid properties (Gandhi, 2015).

The Reynolds number of the pure liquid can be determined as:

$$Re_l = \frac{\rho_l \cdot v_{ls} \cdot D_p}{\mu_l} = \frac{v_{ls} \cdot D_p}{\nu_l}$$ (6.19-23)

The Darcy Weisbach friction factor of the pure liquid is now according to Swamee Jain (1976):

$$\lambda_l = \frac{1.325}{\left(\ln \left(\dfrac{\varepsilon}{3.7 \cdot D_p} + \dfrac{5.75}{Re_l^{0.9}} \right) \right)^2} \tag{6.19-24}$$

Apparently, the Darcy Weisbach friction factors of the vehicle and the pure liquid differ. For dredging applications with high Reynolds number the difference is small, but for small pipe diameters and lower line speeds it may be significant.

The hydraulic gradient of the pure liquid, assuming Newtonian flow:

$$i_l = \lambda_l \cdot \frac{v_{ls}^2}{2 \cdot g \cdot D_p} \tag{6.19-25}$$

The total hydraulic gradient for the heterogeneous regime is:

$$i_{Du} = \sum_{j=1}^{n} i_{Du,j} = i_l \cdot \sum_{j=1}^{n} Du_j = i_l \cdot Du \tag{6.19-26}$$

The total hydraulic gradient of the vehicle (homogeneous regime) and the heterogeneous regime is now:

$$i_{total} = i_{vehicle} + i_{Du} = \frac{v_{ls}^2}{2 \cdot g \cdot D_p} \cdot \left(\lambda_v \cdot \frac{\rho_v}{\rho_l} + \lambda_l \cdot 82 \cdot \sum_{j=1}^{n} C_{vs,Du,j} \cdot \left(\frac{g \cdot D_p \cdot R_{sd}}{v_{ls}^2 \cdot \sqrt{C_{D,j}}} \right)^{3/2} \right) \tag{6.19-27}$$

This step should be taken with caution. It is not always clear whether the hydraulic gradients are determined with the pure liquid density or with the density computed with equation (6.19-17). It is also not always clear whether the Fanning friction factor or the Darcy Weisbach friction factor is used, which differ by a factor 4. Equation (6.19-27) is the author's interpretation of the Wasp model, matching the example in Wasp et al. (1977).
Both gradients are in terms of the carrier liquid head loss (Gandhi, 2015).

The resulting friction velocity, as used in the next correction step, can be computed by assuming an equivalent Darcy Weisbach friction coefficient according to:

$$\lambda_e = i_{total} \cdot \frac{2 \cdot g \cdot D_p}{v_{ls}^2} \cdot \frac{\rho_l}{\rho_v} \tag{6.19-28}$$

The friction velocity based on the total hydraulic gradient can now be determined by:

$$u_* = \sqrt{\frac{\lambda_e}{8}} \cdot v_{ls} = \sqrt{\frac{i_{total} \cdot g \cdot D_p}{4} \cdot \frac{\rho_l}{\rho_v}} \tag{6.19-29}$$

Using the total hydraulic gradient has an unwanted effect for very low line speeds. The heterogeneous part of the hydraulic gradient will go to infinity if the line speed goes to zero, resulting in 100% suspension for very low line speeds. This is the result of using the Durand & Condolios (1952) equation for the heterogeneous part. Now one can set a lower limit for the line speed in the Wasp model, but this would be dependent on many parameters. Using the vehicle hydraulic gradient gives a better result. The Darcy Weisbach friction factor however should be based on the cross section above the bed and based on a weighted average of the Darcy Weisbach friction factor for the pipe wall and the bed. This approach is described in chapter 7 the DHLLDV Framework. Basically the hydraulic gradient of the DHLLDV Framework is used for the determination of the friction velocity.

Step 2 has to be repeated at least two times. If the difference in hydraulic gradients in two successive iterations (correction steps) is more than for example 5%, another iteration (step 2) is carried out based on the friction velocity resulting from the last iteration. This is repeated until a required accuracy is reached.

Another way to solve the Wasp method is to start with a line speed of zero, assuming all solids are in the bed, so the vehicle is the pure liquid. Now increasing the line speed with small steps and using the friction velocity and the vehicle properties from the previous step, both the vehicle fraction and the hydraulic gradients can be determined. No iterations are required if the line speed steps are small enough. All the graphs at the end of this chapter are determined this way.

6.19.3 Different Versions of the WASP Model.

Is mentioned before, there are different versions of the WASP model used by different authors. The confusion is the result of the use of the hydraulic gradient which describes head loss per unit of pipe length. To convert head loss in terms of pressure in kPa to the hydraulic gradient, the head loss has to be divided by **ρ·g·ΔL**. Some researchers use the pure liquid density, some use the mixture density, some the vehicle density. The hydraulic gradient does not contain density anymore, so it is not clear whether we have head loss per meter of pure liquid or head loss per meter of mixture or vehicle. It is also confusing that many authors use the term pressure drop or loss when they actually talk about the hydraulic gradient.

Design of the pipeline system requires establishment of pressure in the pipe along its length in order to select the pipe wall thickness. The pumping pressure requirements are needed to select the type of pump and pumping power requirements. Therefore both the hydraulic gradient and pressure gradient are important (Gandhi, 2015).

6.19.3.1 Abulnaga (2002).

Just as in the Wasp et al. (1977) book, Abulnaga (2002) is clear about this in his book, by giving numerical examples and giving both the head loss in terms of pressure and the hydraulic gradient. The Darcy Weisbach friction factor is adjusted in the iteration steps for the solids effect and the hydraulic gradient is based on the mixture density.

The Darcy Weisbach friction factor of the vehicle is now according to Swamee Jain (1976):

$$\lambda_v = \frac{1.325}{\left(\ln\left(\frac{\varepsilon}{3.7 \cdot D_p} + \frac{5.75}{Re^{0.9}} \right) \right)^2} \quad \text{and} \quad \rho_m = \rho_l \cdot \left(1 + R_{sd} \cdot C_{vs} \right) \tag{6.19-30}$$

The Darcy Weisbach friction factor is adjusted for the solids effect and the vehicle density:

$$\lambda_{v,new} = \lambda_v \cdot \left(1 + 82 \cdot \sum_{j=1}^{n} C_{vs,Du,j} \cdot \left(\frac{g \cdot D_p \cdot R_{sd}}{v_{ls}^2 \cdot \sqrt{C_{D,j}}} \right)^{3/2} \right) \cdot \frac{\rho_m}{\rho_l} \tag{6.19-31}$$

The head loss and hydraulic gradient can now be determined with:

$$\Delta p_{total} = \lambda_{v,new} \cdot \frac{\Delta L}{D_p} \cdot \frac{1}{2} \cdot \rho_l \cdot v_{ls}^2 \quad \text{and} \quad i_{total} = \frac{\Delta p_{total}}{\rho_l \cdot g \cdot \Delta L} = \lambda_{v,new} \cdot \frac{v_{ls}^2}{2 \cdot g \cdot D_p} \tag{6.19-32}$$

According to the listing in the book of Abulnaga (2002) the mixture density **ρₘ** is not changed during the iterations, which is peculiar. The hydraulic gradient in the book of Abulnaga (2002) is determined by dividing the head loss by the mixture density and will thus give a lower value compared with the above equation. So the head loss equation is correct, but the hydraulic gradient gives head loss per meter mixture and not per meter of pure liquid.

The friction velocity, used to determine the suspended fraction, can now be determined by:

$$u_* = \sqrt{\frac{\lambda_{v,new}}{8}} \cdot v_{ls} = \sqrt{\frac{i_{total} \cdot g \cdot D_p}{4}}$$

(6.19-33)

6.19.3.2 Kaushal & Tomita (2002B).

Kaushal & Tomita (2002B) use the Fanning friction factor based on the modified Wood (1966) equation proposed by Mukhtar (1991), without density correction, giving for the hydraulic gradient of the vehicle:

$$i_{vehicle} = \lambda_m \cdot \frac{v_{ls}^2}{2 \cdot g \cdot D_p} \quad \text{or} \quad i_{vehicle} = 2 \cdot f_m \cdot \frac{v_{ls}^2}{g \cdot D_p}$$

with: $\lambda_m = 4 \cdot f_m$ and $\lambda_m = \frac{\rho_v}{\rho_l} \cdot \lambda_v$ and $\rho_v = \rho_l \cdot \left(1 + R_{sd} \cdot C_{vs,v}\right)$

(6.19-34)

For the solids effect they use (see the Kaushal & Tomita chapter for details) the Durand term, multiplied with the pure liquid hydraulic gradient:

$$i_{bed} = \sum_{j=1}^{n} i_{bed,j} = i_l \cdot 82 \cdot \sum_{j=1}^{n} \left(C_{vs,j} - C_{vs,v,j}\right) \cdot \left(\frac{g \cdot D_p \cdot R_{sd}}{v_{ls}^2 \cdot \sqrt{C_{D,j}}}\right)^{3/2}$$

(6.19-35)

The total hydraulic gradient is the sum of the hydraulic gradient of the vehicle and the hydraulic gradient of the bed, giving:

$$i_{total} = i_{vehicle} + i_{bed} = \lambda_m \cdot \frac{v_{ls}^2}{2 \cdot g \cdot D_p} + i_l \cdot 82 \cdot \sum_{j=1}^{n} \left(C_{vs,j} - C_{vs,v,j}\right) \cdot \left(\frac{g \cdot D_p \cdot R_{sd}}{v_{ls}^2 \cdot \sqrt{C_{D,j}}}\right)^{3/2}$$

(6.19-36)

It is not clear whether both hydraulic gradients are determined with the same liquid/mixture density. The solids effect is determined with the pure liquid density, but the vehicle part may have been determined with the vehicle density. It is assumed that the vehicle density correction is applied, otherwise an asymptotic behavior towards the pure liquid gradient would exist for very high line speeds, which is not shown in their publications. Hydraulic gradients cannot be summated if different densities are applied. Effectively this gives for the total hydraulic gradient:

$$i_{total} = i_{vehicle} + i_{bed} = i_l \cdot \left(\frac{\rho_v}{\rho_l} + 82 \cdot \sum_{j=1}^{n} \left(C_{vs,j} - C_{vs,v,j}\right) \cdot \left(\frac{g \cdot D_p \cdot R_{sd}}{v_{ls}^2 \cdot \sqrt{C_{D,j}}}\right)^{3/2}\right)$$

(6.19-37)

Kaushal & Tomita (2013) used the following diffusivity, see the Kaushal & Tomita chapter for details:

$$\beta_{sm,Kaushal} = 1 + 93.77 \cdot \left(\frac{d_m}{D_p}\right) \cdot \left(\frac{d_j}{d_{mw}}\right) \cdot e^{1.055 \cdot \sigma_g \cdot \frac{C_{vs}}{C_{vb}}}$$

(6.19-38)

6.19.3.3 Lahiri (2009) .

Lahiri (2009) gave an analysis of the shortcomings and proposes a modified WASP model.

- The dimensionless particle diffusivity β_{sm}, does not have to be equal to unity as considered by Wasp et al. (1977). Wasp does not specify beta equal to 1. In the worked out example it was assumed to be 1 (Gandhi, 2015).
- The value of the von Karman constant κ, as assumed to be 0.4 by Wasp et al. (1977) may have a different value at higher line speeds, when the vehicle hydraulic gradient has a major share in the total hydraulic gradient. This was not specified but assumed to be 0.4 for the illustrative example. The variation in von Karman constant with slurry concentration was considered in Chapter 5 of the Wasp book (Gandhi, 2015).

- The terminal settling velocity was used by Wasp (1977) without the effect of hindered settling. However, at higher volumetric concentrations the settling velocity is greatly affected by hindered settling.

Almost the same conclusions were drawn by Kaushal & Tomita (2002B) when they tried to apply the WASP model on their experimental data. But their implementation is different. As noted earlier, the Wasp method is also used assuming vehicle as suspending fluid. Use of vehicle density and viscosity appears to correct for hindered settling effect. However, if hindered settling effect is considered, the problem becomes more complex since there is likely to be a concentration gradient across the vertical axis of the pipeline which would give rise to variation in hindered settling effect (Gandhi, 2015).

Lahiri (2009) modified the WASP method with the following modifications:

- Kaushal and Tomita (2002B) took their experimental data in to consideration for the effect of the solids concentration on the dimensionless particle diffusivity coefficient β_{sm}. Ismael (1952) found that the von Karman constant depends on the solids concentration and decreases with increasing solids concentration. Based on an extensive analysis of the solids concentration profiles and the hydraulic gradients of experiments of coal-water, copper ore-water, sand-water, gypsum-water, glass water and gravel water published in literature (Hsu (1986)) a new relation for $\beta \cdot \kappa$ was developed.

$$\beta_{sm} \cdot \kappa = 430.78 \cdot C_{vs}^{3} - 110.98 \cdot C_{vs}^{2} + 9.5439 \cdot C_{vs}^{1} - 0.1728 \cdot C_{vs}^{0} \qquad \text{(6.19-39)}$$

- Hindered settling was used according to Richardson & Zaki (1954) instead of the terminal settling velocity.

The procedure of the modified WASP model is similar to the original WASP model, but with the above modifications. According to Lahiri (2009) this modified WASP model gives better results. The solids effect is determined using the vehicle hydraulic gradient and not the pure liquid hydraulic gradient. The diffusivity correction only contains the concentration, not the relative concentration or the particle diameter.

Ni et al. (2008) used the same approach as Lahiri (2009) except for the diffusivity modification.

$$i_{total} = i_{vehicle} + i_{bed} = 2 \cdot f_{m} \cdot \frac{v_{ls}^{2}}{g \cdot D_{p}} \cdot \left(1 + 82 \cdot \sum_{j=1}^{n} \left(C_{vs,j} - C_{vs,v,j} \right) \cdot \left(\frac{g \cdot D_{p} \cdot R_{sd}}{v_{ls}^{2} \cdot \sqrt{C_{D,j}}} \right)^{3/2} \right) \qquad \text{(6.19-40)}$$

In the examples, the diffusivity of Lahiri (2009) is not applied, since it gives unrealistic values for low and high concentrations.

6.19.3.4 The DHLLDV Framework.

The DHLLDV Framework, as will be described in detail in chapter 7, uses a different approach for the diffusivity. The diffusivity should have a value in such a way that at the LDV the concentration at the bottom of the pipe equals the bed concentration, similar to Gillies (1993).

$$C_{vB} = C_{vs} \cdot \frac{\left(\dfrac{12 \cdot v_{tv}}{\beta_{sm} \cdot \kappa \cdot u_{*}} \right)}{\left(1 - e^{-12 \cdot \frac{v_{tv}}{\beta_{sm} \cdot \kappa \cdot u_{*}}} \right)} \quad \Rightarrow \quad C_{vb} = C_{vs} \cdot \frac{\left(\dfrac{12 \cdot v_{tv,ldv}}{\beta_{sm,ldv} \cdot \kappa \cdot u_{*,ldv}} \right)}{\left(1 - e^{-12 \cdot \frac{v_{tv,ldv}}{\beta_{sm} \cdot \kappa \cdot u_{*,ldv}}} \right)} \qquad \text{(6.19-41)}$$

Neglecting the denominator, since it's close to unity (say a factor α_{sm}), the diffusivity can be derived. Based on the diffusivity, the portion of the solids in the vehicle can be determined.

$$\beta_{sm,ldv} = 12 \cdot \frac{C_{vs}}{C_{vb}} \cdot \frac{v_{tv,ldv}}{\alpha_{sm} \cdot \kappa \cdot u_{*,LDV}} \quad \text{and} \quad \frac{C_{vs,v}}{C_{vs}} = e^{-(0.92 - 0.5) \cdot \alpha_{sm} \cdot \frac{C_{vb}}{C_{vs}} \cdot \frac{u_{*,LDV}}{u_{*}} \cdot \frac{v_{tv}}{v_{tv,ldv}}} \qquad \text{(6.19-42)}$$

6.19.4 Discussion & Conclusions.

The WASP method was considered state of the art when it was developed in the 70's. It does however lack the influence of a fixed or sliding bed and shear stresses between different layers. This is implemented in the 2LM and 3LM models of Doron et al. (1987), Doron & Barnea (1993), Wilson (1979) and Matousek (2009). The WASP model predicts hydraulic gradients with reasonable accuracy at all volumetric concentrations for all flow velocities.

Basically the WASP model divides each fraction in a homogeneous part (ELM) and a heterogeneous part (Durand & Condolios (1952)). Since the original Durand & Condolios equation already takes the whole hydraulic gradient into account, it is the question whether the WASP model is correct. Because of the division in homogeneous and heterogeneous regimes, the asymptotic value of the hydraulic gradient for very large line speeds will be the ELM, while in the Durand & Condolios equation this asymptotic value will be the liquid hydraulic gradient. Adjusting the apparent viscosity with the Thomas (1965) equation may be valid for very small particles, but not for larger particles, so there should be a limit for this adjustment, for example d=0.06 mm. The adjustment for the liquid density may be correct for all particles, however later research (Talmon (2011) has proven that the hydraulic gradient in the homogeneous phase is less than the ELM. Another issue is the particle drag coefficient. In the description of the WASP model by Lahiri (2009) the particle drag coefficient C_D is used in the Durand & Condolios (1952) equation. The original Durand & Condolios (1952) equation however uses the particle Froude number Fr_p. Whether this makes a big difference or not, depends on how the terminal settling velocity and the drag coefficient are determined. Using the Ruby & Zanke (1977) equation for the terminal settling velocity already includes the shape of the particles and gives a good estimate of the terminal settling velocity for sands and gravels. In this chapter the original Durand & Condolios (1952) approach, based on the particle Froude number is applied.
The Wasp book also considers the effect of shape on settling velocity as explained in Chapter 3 of the Wasp book.

Table 6.19-1 shows 6 possible implementations of the WASP model. Some implementations use the total hydraulic gradient, some the vehicle hydraulic gradient to determine the friction velocity. The Wasp and the DHLLDV implementations correct the hydraulic gradient for the vehicle density in order to get the correct Darcy Weisbach or Fanning friction factor. The argument of the exponential power differs. Wasp is using the settling velocity in the vehicle, based on vehicle viscosity and density. Which is a sort of hindered settling. So for each line speed having different vehicle properties, the particle terminal settling velocity is different. Others use the hindered settling velocity based on the volumetric concentration as a fixed value. The DHLLDV Framework is based on the Limit Deposit Velocity. The hydraulic gradient of the vehicle is usually based on the density of the vehicle and the pure liquid hydraulic gradient. In the Wasp and DHLLDV implementations, the Darcy Weisbach friction factor is based on the vehicle properties, giving a slightly different friction factor compared with the pure liquid properties as used by the other implementations. The solids hydraulic gradient is supposed to be the Durand & Condolios (1952) relation for the heterogeneous fraction. Some implementations however use the vehicle hydraulic gradient or even the mixture hydraulic gradient instead of the pure liquid hydraulic gradient.

The 6 implementations are compared in a set of graphs, showing the implementations with and without hindered settling and modified diffusivities. Without hindered settling and modified diffusivities, 4 implementations are close to the original Wasp model, except for the DHLLDV Framework, which is based on the LDV. With hindered settling and modified diffusivities all models are close for fine particles (d=0.1 mm and d=0.2 mm), but deviate for larger particles. The Kaushal A and DHLLDV Frameworks gives the highest suspended fractions, but in a different way. The Kaushal A implementation is using both hindered settling and a modified diffusivity, the DHLLDV implementation the starting point that at the LDV the bottom concentration equals the bed concentration. The bed concentration can also vary by the particle size distribution as well as particle shape.

Remarks:
- The Kaushal & Tomita (2002B) approach, based on Karabelas (1977), is a more sophisticated approach, considering local hindered settling and diffusivity and numerical integration. Here this is simplified in order to compare the implementation with the other implementations.
- The vehicle hydraulic gradient of the Wasp and DHLLDV implementations is based on the Darcy Weisbach friction factor determined with the Reynolds number based on the vehicle properties, while the other implementations based this on the pure liquid properties.

Both Wasp et al. (1977) and A.D. Thomas (1979) reported LDV values in pipes with diameters ranging from 0.05 m to 0.3 m (2-12 inch) for a d=0.18 mm sand. The resulting Durand Froude numbers are shown in Figure 6.19-1. In both cases the FL value decreases slightly with increasing pipe diameter to a power of about -0.1. The scatter in the graph is mainly due to different volumetric concentrations.

Table 6.19-1: 6 implementations of the WASP model.

Model	Friction Velocity	Argument Suspended Fraction	Vehicle Hydraulic Gradient	Solids Hydraulic Gradient
Wasp	$u_* = \sqrt{\dfrac{i_{total} \cdot g \cdot D_p}{4} \cdot \dfrac{\rho_l}{\rho_v}}$	$\dfrac{v_{tv}}{1 \cdot \kappa \cdot u_*}$	$i_{vehicle} = \dfrac{\rho_v}{\rho_l} \cdot i_{lv}$	$i_{Du} = i_l \cdot Du$
Lahiri & Ni	$u_* = \sqrt{\dfrac{i_{vehicle} \cdot g \cdot D_p}{4}}$	$\dfrac{v_t \cdot \left(1 - C_{vs}\right)^\beta}{1 \cdot \kappa \cdot u_*}$	$i_{vehicle} = \dfrac{\rho_v}{\rho_l} \cdot i_l$	$i_{Du} = \dfrac{\rho_v}{\rho_l} \cdot i_l \cdot Du$
Kaushal A	$u_* = \sqrt{\dfrac{i_{total} \cdot g \cdot D_p}{4}}$	$\dfrac{v_t \cdot \left(1 - C_{vs}\right)^\beta}{\beta_{sm,Kaushal} \cdot \kappa \cdot u_*}$	$i_{vehicle} = \dfrac{\rho_v}{\rho_l} \cdot i_l$	$i_{Du} = i_l \cdot Du$
Kaushal B	$u_* = \sqrt{\dfrac{i_{total} \cdot g \cdot D_p}{4}}$	$\dfrac{v_t \cdot \left(1 - C_{vs}\right)^\beta}{1 \cdot \kappa \cdot u_*}$	$i_{vehicle} = \dfrac{\rho_v}{\rho_l} \cdot i_l$	$i_{Du} = i_l \cdot Du$
Abulnaga	$u_* = \sqrt{\dfrac{i_{total} \cdot g \cdot D_p}{4}}$	$\dfrac{v_t \cdot \left(1 - C_{vs}\right)^\beta}{1 \cdot \kappa \cdot u_*}$	$i_{vehicle} = \dfrac{\rho_m}{\rho_l} \cdot i_l$	$i_{Du} = \dfrac{\rho_m}{\rho_l} \cdot i_l \cdot Du$
DHLLDV	$u_* = \sqrt{\dfrac{i_{vehicle} \cdot g \cdot D_p}{4} \cdot \dfrac{\rho_l}{\rho_v}}$	$\dfrac{\alpha_{sm}}{C_{vr}} \cdot \dfrac{u_{*,ldv}}{u_*} \cdot \dfrac{v_{tv}}{v_{tv,ldv}}$	$i_{vehicle} = \dfrac{\rho_v}{\rho_l} \cdot i_{lv}$	$i_{Du} = i_l \cdot Du$
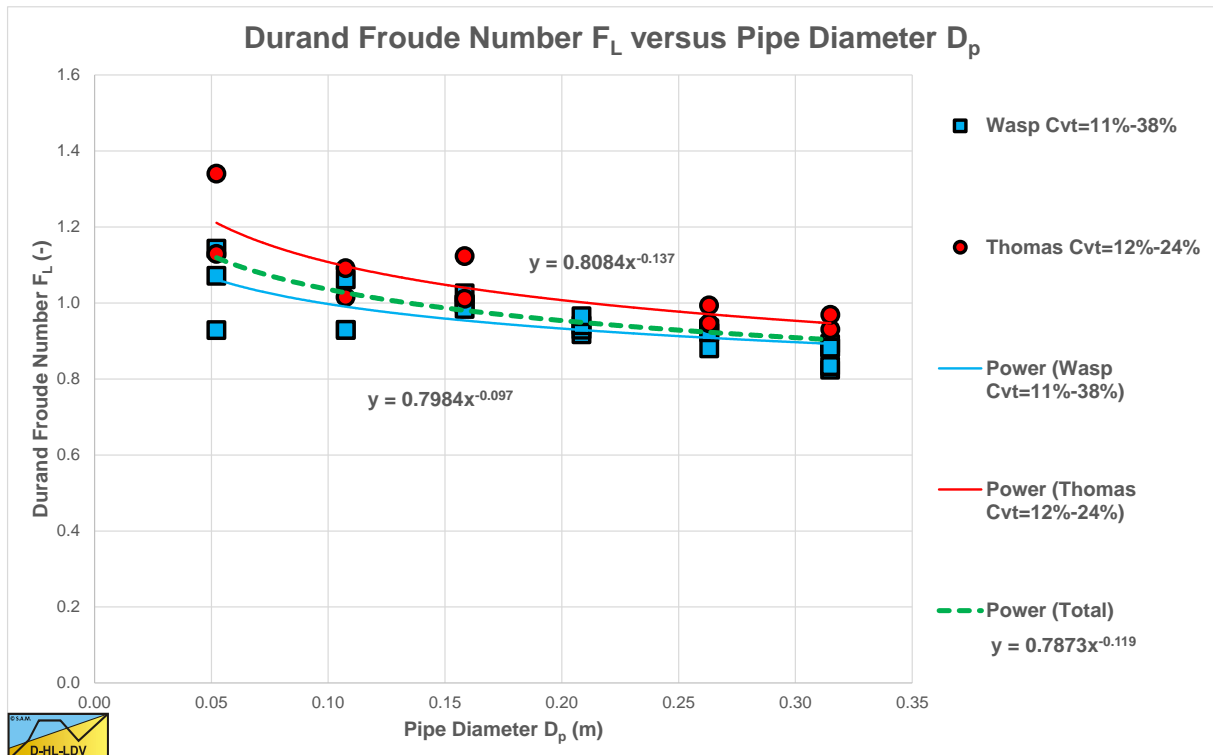
Figure 6.19-1: Durand Froude number F_L versus pipe diameter D_p for a d=0.18 mm sand.

Here the transport concentration is used, because the experimental data was based on the transport concentration.

Figure 6.19-2, Figure 6.19-6, Figure 6.19-10 and Figure 6.19-14 show the results of 6 different approaches of the Wasp model for 4 uniform sands. Here the diffusivities are used as in the original Wasp model and hindered settling is not applied. The Kaushal & Tomita (2002B) and the Lahiri (2009) approach give an almost equal result. Apparently it does not make a lot of difference whether the bed portion is multiplied with the pure liquid or the vehicle hydraulic gradient. The Abulnaga (2002) approach gives a very different result, due to the multiplication with the mixture density. For small particle diameters the results are close to the ELM and the DHLLDV Frameworks.
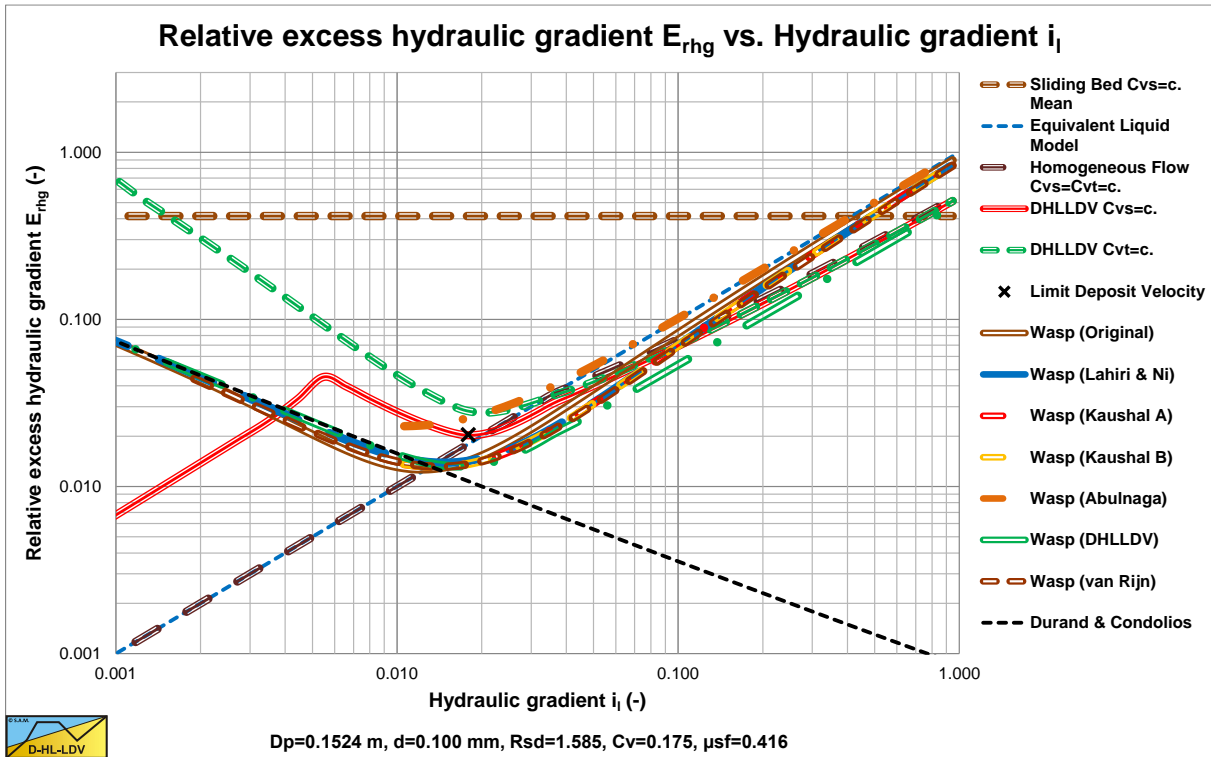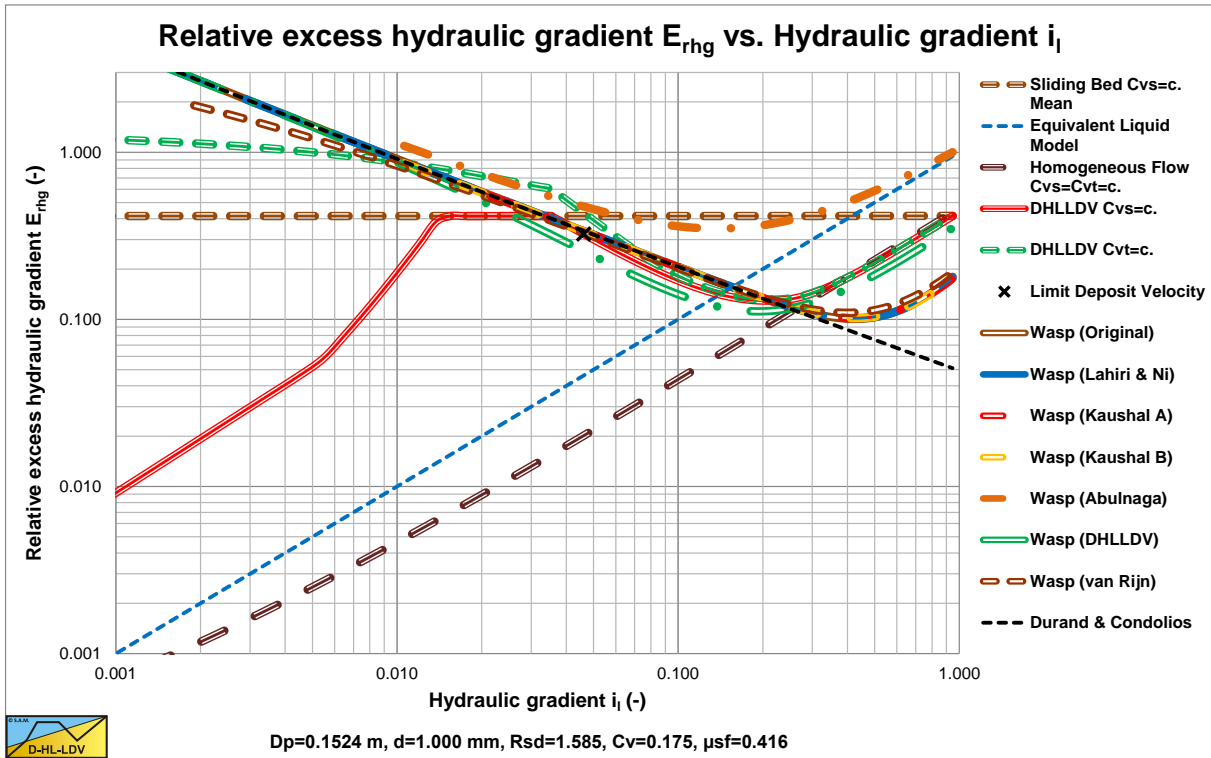

Figure 6.19-2: The Wasp model for a d=0.1 mm sand particle.
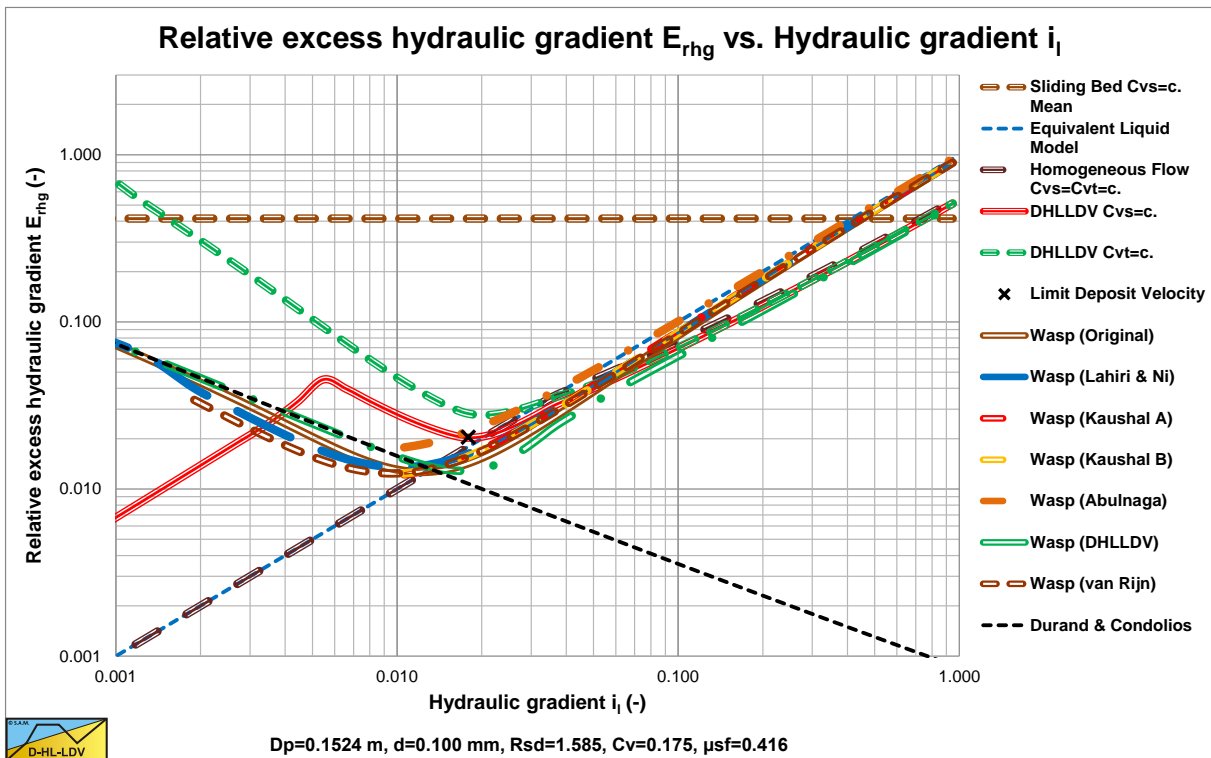
Figure 6.19-3: The Wasp model for a d=0.1 mm sand particle, modified diffusivity and hindered settling.

For the larger particles however the Kaushal & Tomita (2002B) and the Lahiri (2009) approaches (the assumed original Wasp model) underestimate pressure losses compared to the ELM at higher line speeds.
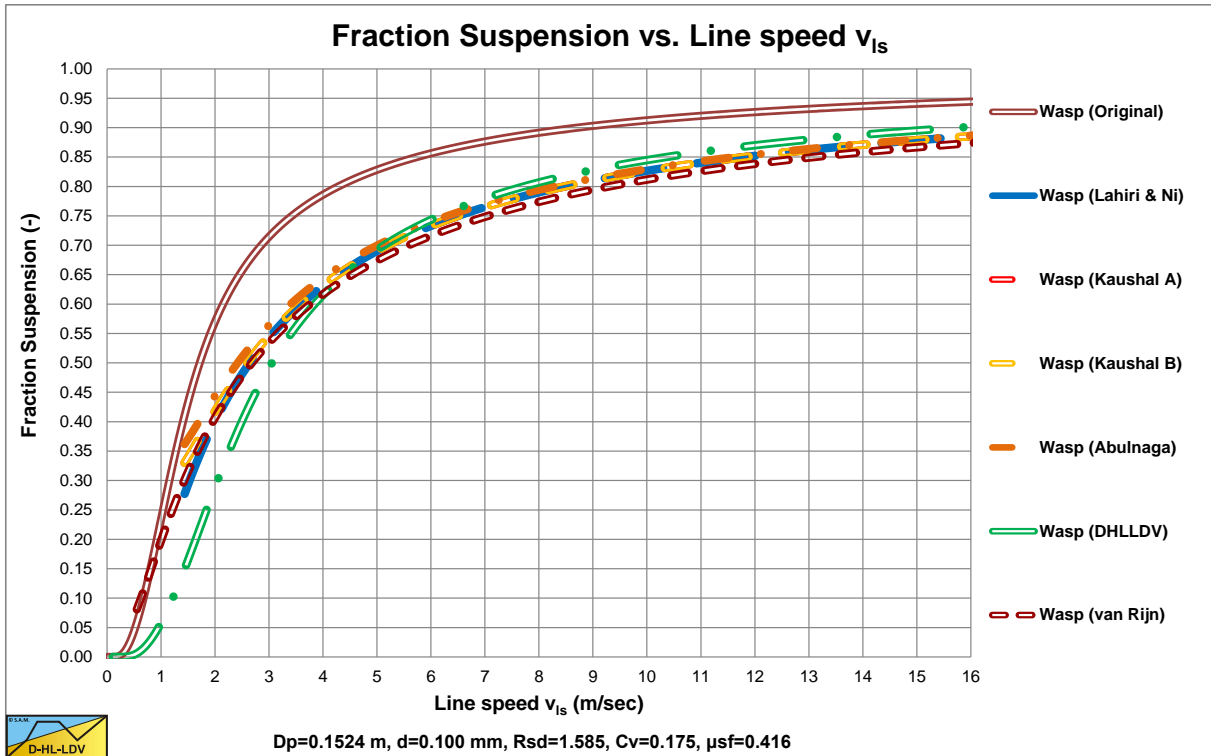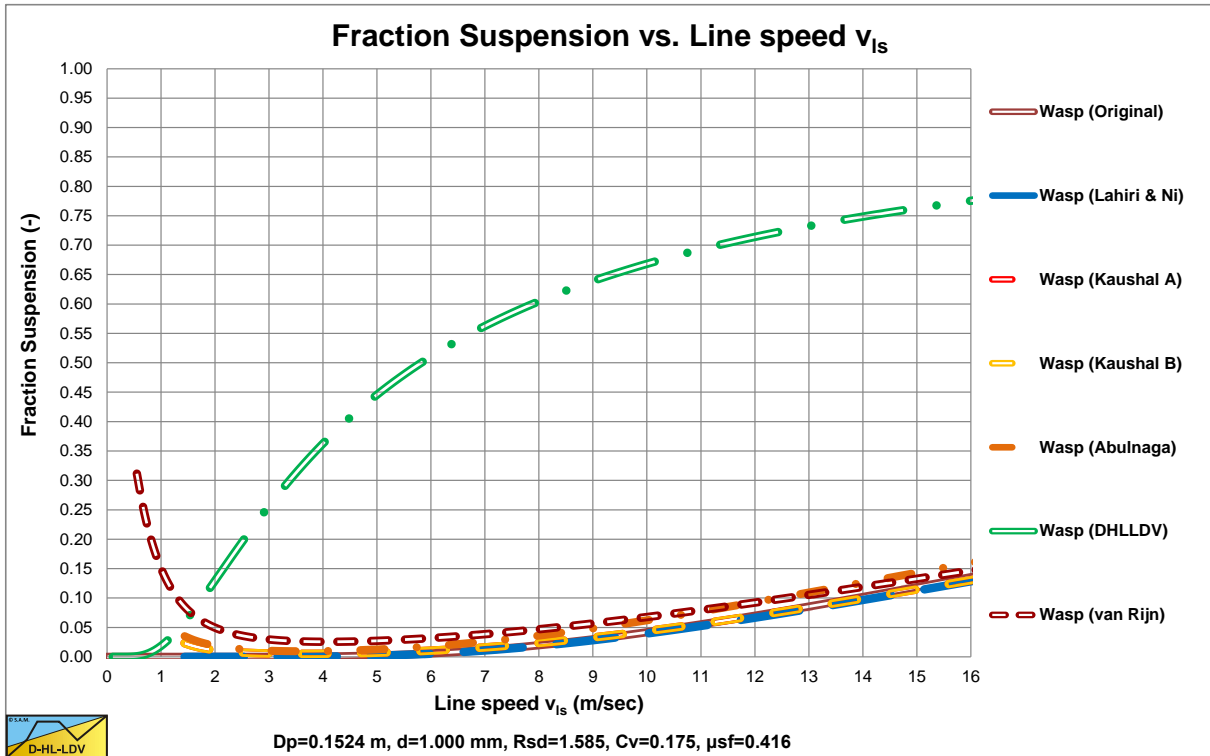

Figure 6.19-4: The suspended fraction for a d=0.1 mm sand particle.
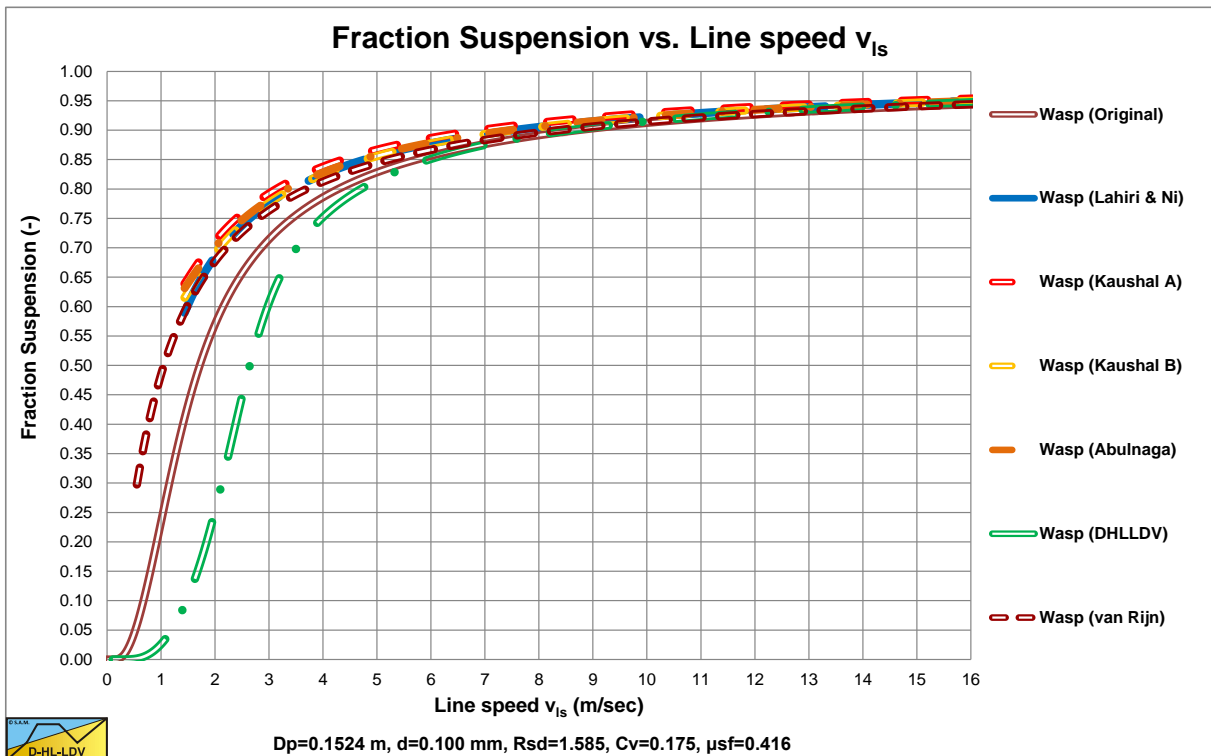
Figure 6.19-5: The suspended fraction for a d=0.1 mm sand particle, modified diffusivity and hindered settling.

Figure 6.19-3, Figure 6.19-7, Figure 6.19-11 and Figure 6.19-15 show the results with hindered settling applied for all 6 approaches. The Kaushal & Tomita (2002B) method also includes their modified diffusivity (Kaushal A). In all cases the curves are closer to the ELM curve, especially for the small particles. Hindered settling and an

increased diffusivity increase the solids fraction in the vehicle and decrease the solids fraction in the bed. The Durand factor, equation (6.19-22) is not affected however. A hydraulic gradient of 0.1 on the abscissa is equivalent to a line speed of 5 m/sec, a line speed of normal operation for the pipe diameter of 0.1524 m.
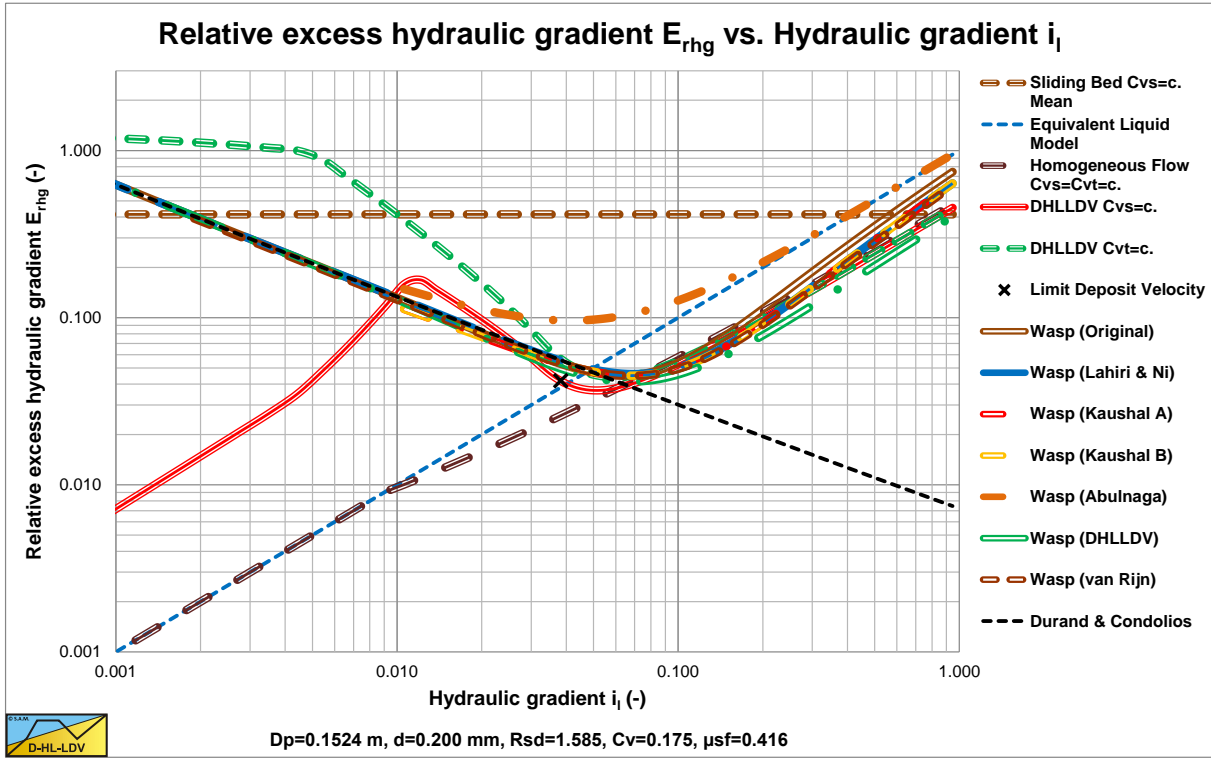
Figure 6.19-6: The Wasp model for a d=0.2 mm sand particle.
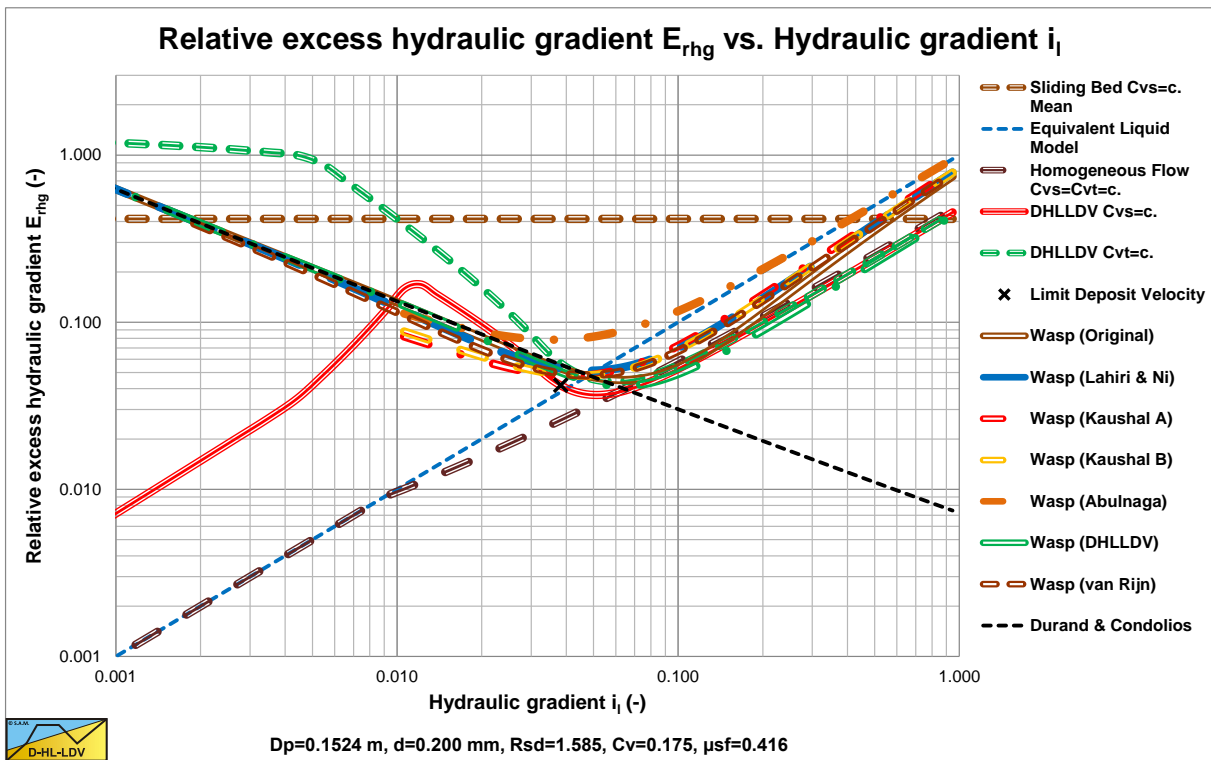
Figure 6.19-7: The Wasp model for a d=0.2 mm sand particle, modified diffusivity and hindered settling.

Adapting the diffusivities and using the hindered settling velocity compensates for the underestimation at higher line speeds, but will underestimate the pressure losses at lower line speeds. Because the Kaushal & Tomita (2002B) (Kaushal A) curves in Figure 6.19-3, Figure 6.19-7, Figure 6.19-11 and Figure 6.19-15 contain the modified

diffusivity, while the Lahiri (2009), the Kaushal & Tomita (2002B) (Kaushal B), the Abulnaga (2002) and the DHLLDV curves do not, the effect of the modified diffusivity is visible. At lower line speeds it reduces the E_{rhg} value, at higher line speeds the E_{rhg} value is increased.

Dp=0.1524 m, d=0.200 mm, Rsd=1.585, Cv=0.175, μsf=0.416
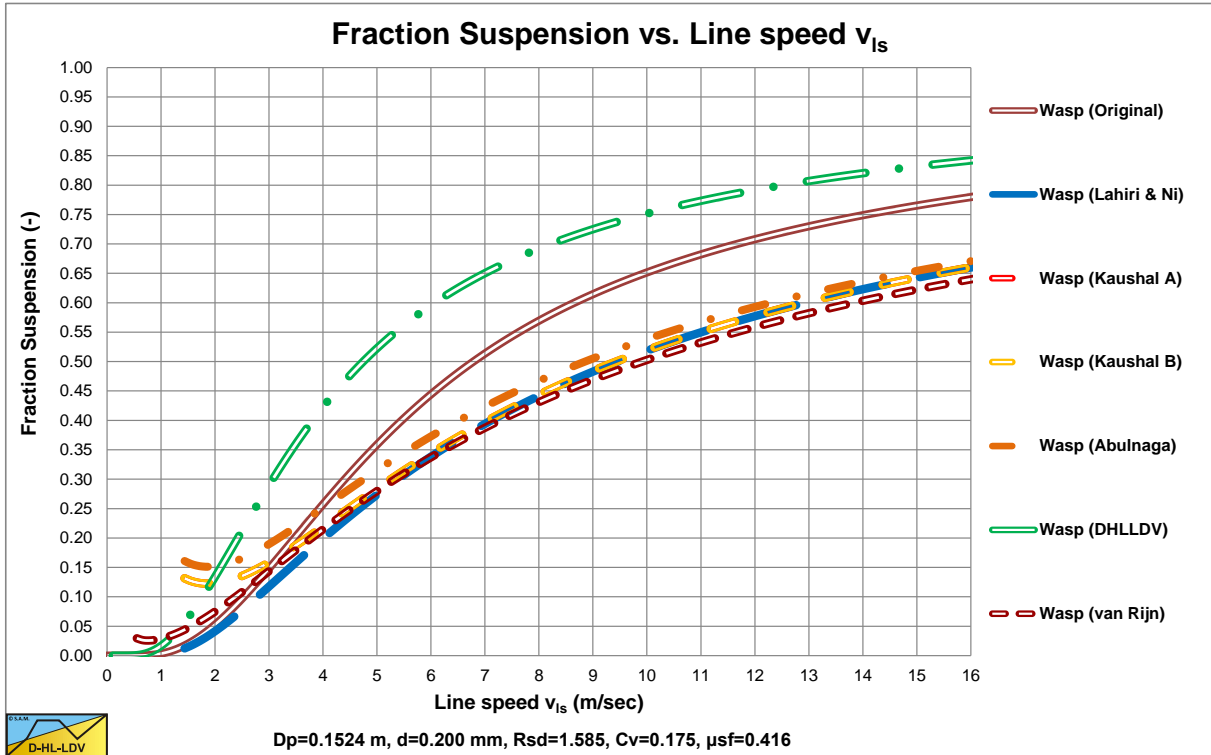
Figure 6.19-8: The suspended fraction for a d=0.2 mm sand particle.

Dp=0.1524 m, d=0.200 mm, Rsd=1.585, Cv=0.175, μsf=0.416
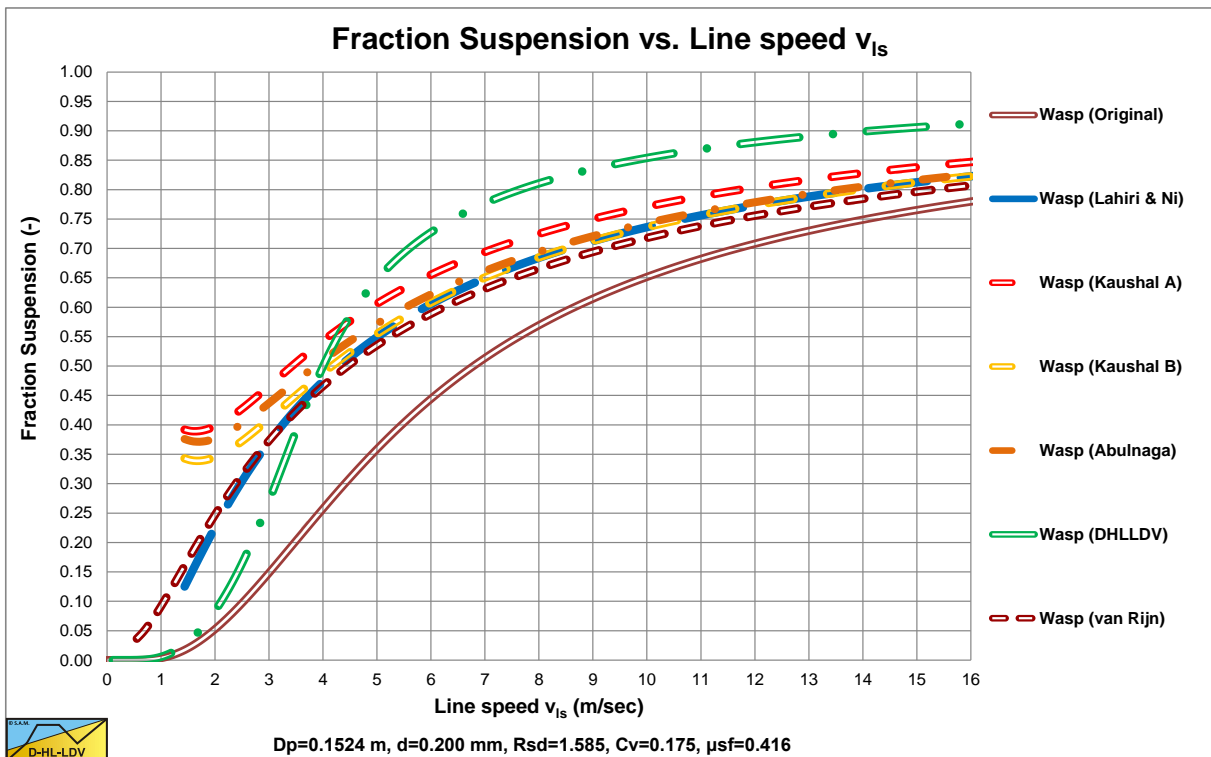
Figure 6.19-9: The suspended fraction for a d=0.2 mm sand particle, modified diffusivity and hindered settling.

Figure 6.19-4, Figure 6.19-8, Figure 6.19-12 and Figure 6.19-16 show the suspended fraction for all 6 implementations, without hindered settling and modified diffusivity. Figure 6.19-5, Figure 6.19-9, Figure 6.19-13

and Figure 6.19-17 show the suspended fraction for all 6 implementations, with hindered settling (all) and modified diffusivity (Kaushal A). It is clear that both hindered settling and the modified diffusivity increase the suspended fraction. The DHLLDV implementation and the Kaushal A implementation with modified diffusivity give about the same suspended fraction for higher line speeds. The DHLLDV implementation gives a higher suspended fraction for larger particles. This is the result of using a diffusivity based on the LDV.
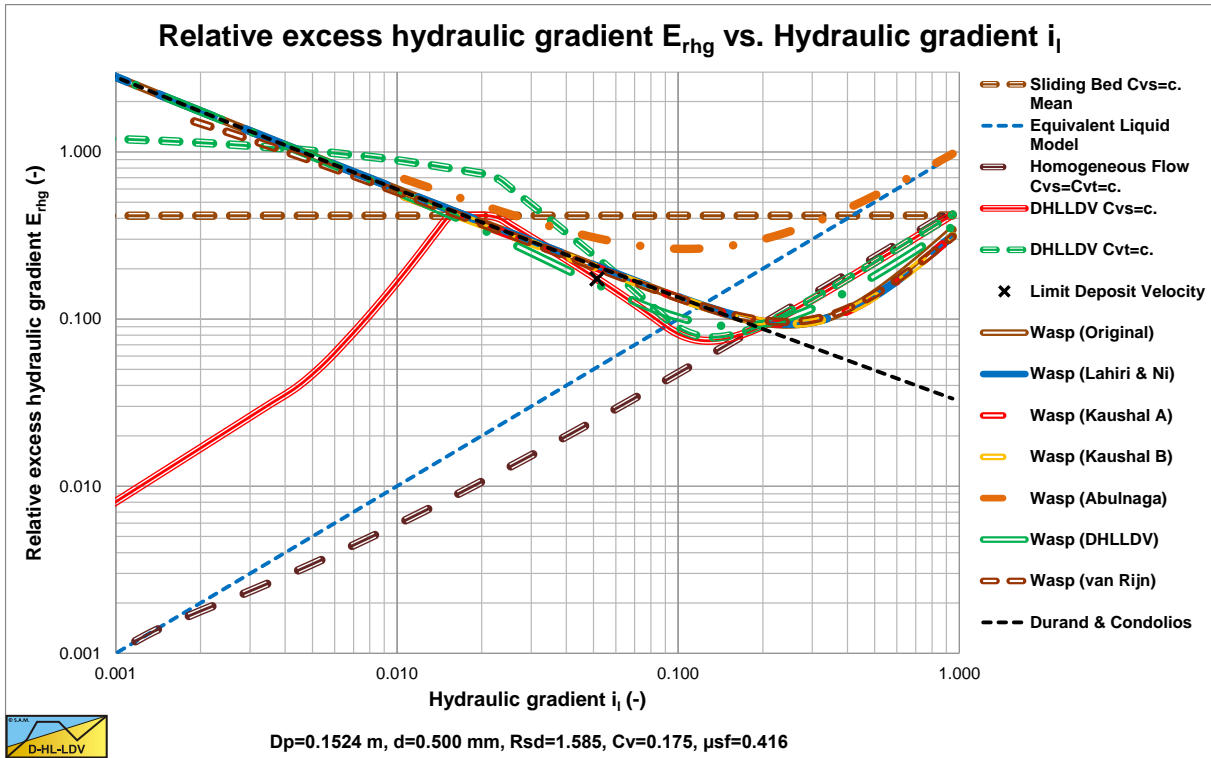
Figure 6.19-10: The Wasp model for a d=0.5 mm sand particle.
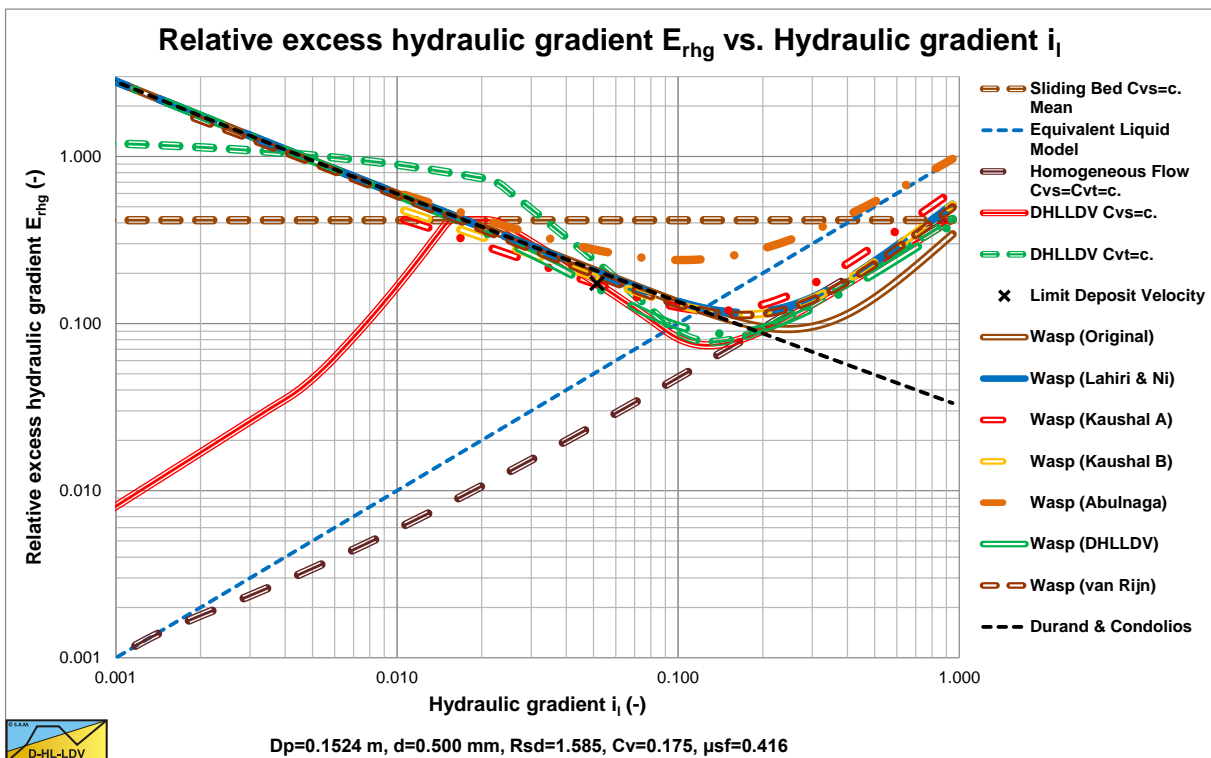
Figure 6.19-11: The Wasp model for a d=0.5 mm sand particle, modified diffusivity and hindered settling.
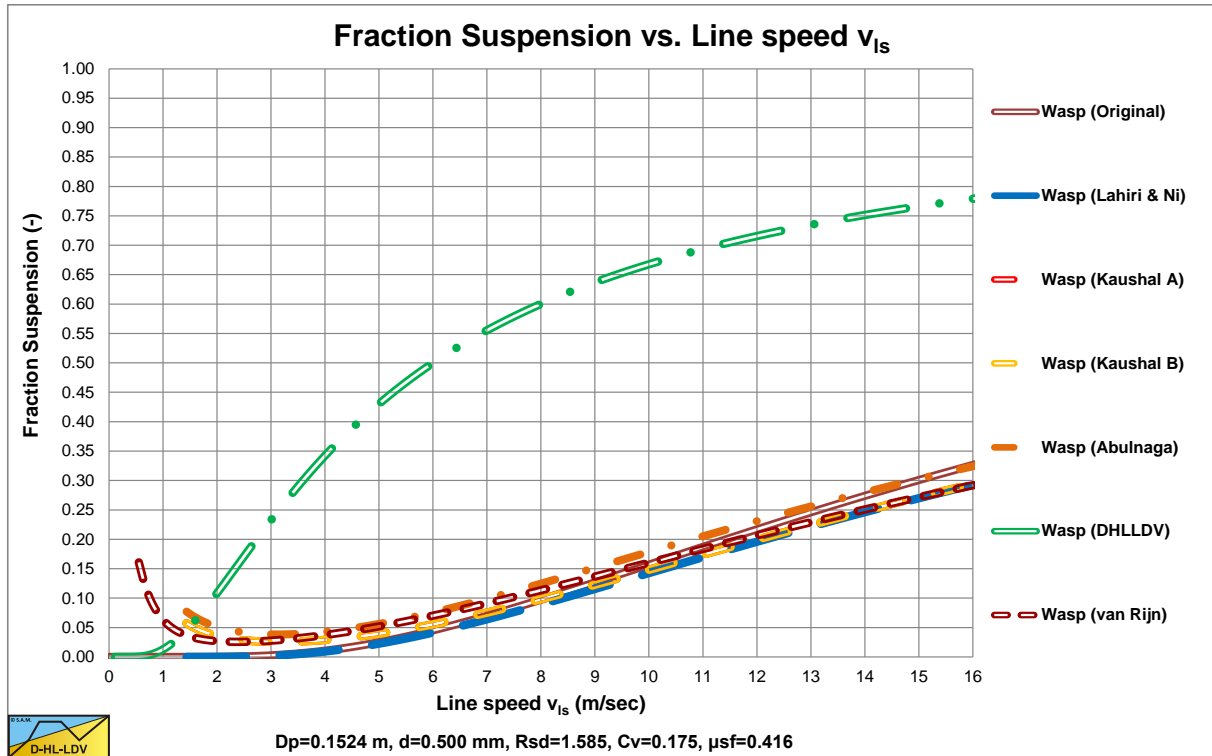
Figure 6.19-12: The suspended fraction for a d=0.5 mm sand particle.
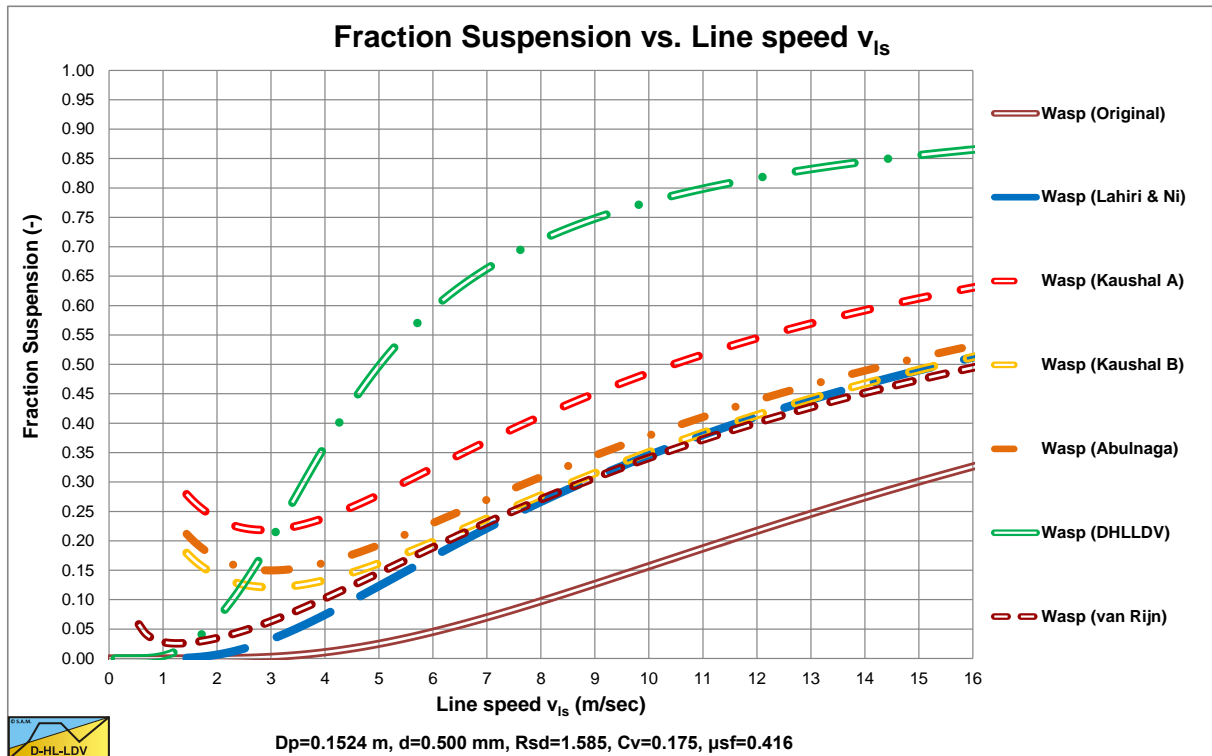
**Figure 6.19-13: The suspended fraction for a d=0.5 mm sand particle,
modified diffusivity and hindered settling.**

The DHLLDV implementation does depend on hindered settling due to its definition of the diffusivity. The model is consistent in itself relating the diffusivity to the LDV in such a way that at the LDV the bottom concentration equals the bed concentration. At higher line speeds the bottom concentration will be lower than the bed concentration. Hindered settling does affect the LDV and the settling velocity, so implicitly the DHLLDV solution depends on hindered settling. Here the DHLLDV implementation is a combination of the Durand & Condolios (1952) model and the ELM. In chapter 7 the combination of DHLLDV and ELM is discussed.

Effectively, both hindered settling and an increased diffusivity, have the effect of reducing the value of the argument in equation (6.19-15), acting like the settling velocity and thus the particle diameter are much smaller. Small particles tend to behave according to the ELM at line speeds high enough. At low line speeds however this effect is limited and the curves behave according to the Durand & Condolios (1952) equation.

Figure 6.19-14: The Wasp model for a d=1.0 mm sand particle.
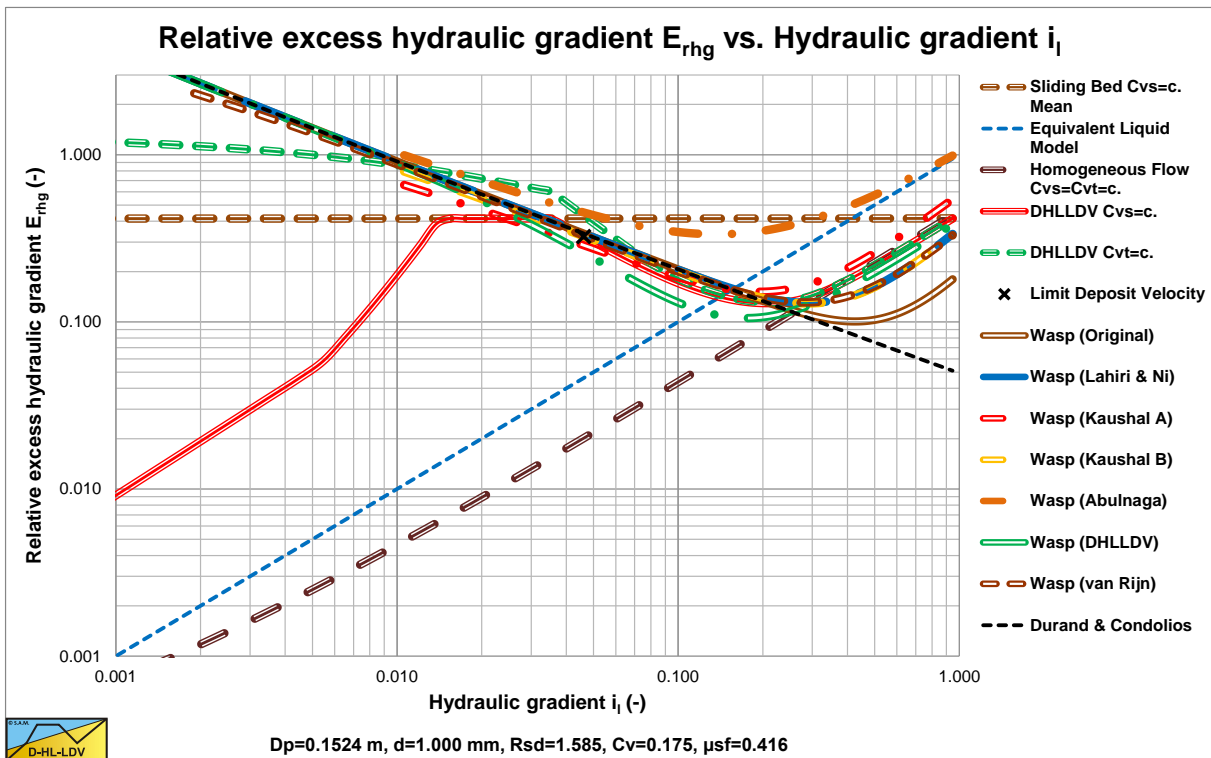
Figure 6.19-15: The Wasp model for a d=1.0 mm sand particle, modified diffusivity and hindered settling.

A combination of the Durand & Condolios (1952) equation (or any equation for the heterogeneous regime) for low line speeds and the ELM model with a reduction factor for line speeds above the intersection point, would

give the same result. However especially the Kaushal & Tomita (2002B) method gives valuable additional information regarding the concentration profile in the pipe. The DHLLDV approach gives almost the same resulting hydraulic gradient as the Kaushal & Tomita (2002B) approach, both with hindered settling and the latter with modified diffusivity. For particles larger than **d>0.015·D_p**, the WASP method underestimates the hydraulic gradient in all cases, except the Abulnaga (2002) approach.

Figure 6.19-16: The suspended fraction for a d=1.0 mm sand particle.
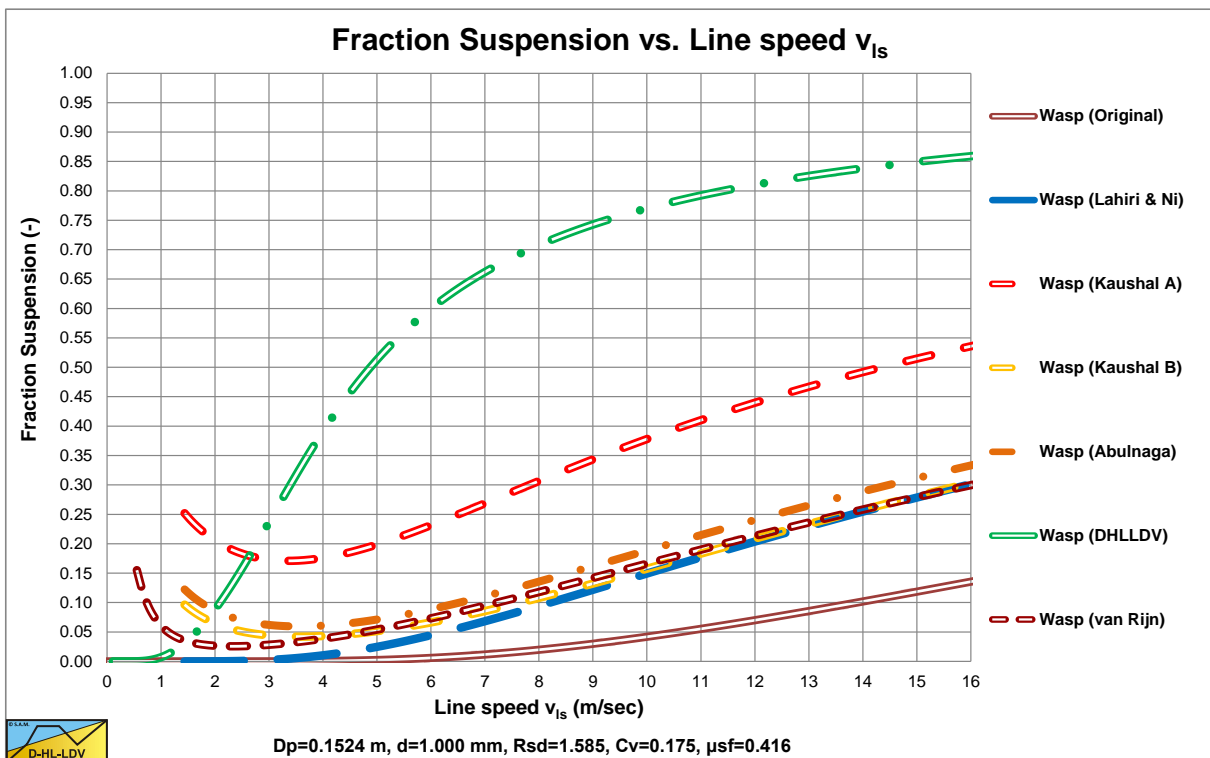
**Figure 6.19-17: The suspended fraction for a d=1.0 mm sand particle,
modified diffusivity and hindered settling.**

6.19.5 Nomenclature Wasp Model.

C_{vt}	Delivered/transport volumetric concentration	-
C_{vs}	Spatial volumetric concentration	-
$C_{vs,j}$	Spatial volumetric concentration, j^{th} fraction	-
$C_{vs,v}$	Spatial volumetric concentration vehicle (homogeneous fraction)	-
$C_{vs,v,j}$	Spatial volumetric concentration vehicle (homogeneous fraction), j^{th} fraction	-
$C_{vs,Du}$	Spatial volumetric concentration Durand fraction (heterogeneous fraction)	-
$C_{vc,Du,j}$	Spatial volumetric concentration Durand fraction (heterogeneous fraction), j^{th} fraction	-
C_{top}	Spatial volumetric concentration at 92% of the pipe diameter, from the bottom of the pipe	-
C_{center}	Spatial volumetric concentration at 50% of the pipe diameter, from the bottom of the pipe	-
C_{vb}	Spatial volumetric concentration bed	-
C_{vB}	Spatial volumetric concentration bottom of pipe	-
C_D	Particle drag coefficient	-
$C_{D,j}$	Particle drag coefficient j^{th} fraction	-
C_x	Durand & Condolios reversed particle Froude number squared	-
$C_{x,j}$	Durand & Condolios reversed particle Froude number squared j^{th} fraction	-
d	Particle diameter	-
d_j	Particle diameter j^{th} fraction	m
d_m	Mean particle diameter, Kaushal & Tomita	m
d_{mw}	Weighed mean particle diameter, Kaushal & Tomita	m
D_p	Pipe diameter	m
Du	Durand & Condolios factor	-
Du_j	Durand & Condolios factor j^{th} fraction	-
E_{rhg}	Relative excess hydraulic gradient	-
f_m	Fanning friction factor mixture, Kaushal & Tomita	-
F_L	Durand & Condolios LDV Froude number	-
Fr_p	Particle Froude number	-
$Fr_{p,j}$	Particle Froude number j^{th} fraction	-
g	Gravitational constant 9.81 m/s^2	m/s^2
i	Hydraulic gradient	-
i_l	Hydraulic gradient pure liquid	-
i_{bed}	Hydraulic gradient bed, Kaushal & Tomita	-
$i_{bed,j}$	Hydraulic gradient bed j^{th} fraction, Kaushal & Tomita	-
$i_{vehicle}$, i_{lv}	Hydraulic gradient vehicle	-
i_{Du}	Hydraulic gradient heterogeneous transport	-
$i_{Du,j}$	Hydraulic gradient heterogeneous transport, contribution j^{th} fraction	-
i_{total}	Total hydraulic gradient, homogeneous plus heterogeneous	-
j	Fraction number	-
ΔL	Length of pipeline	m
LDV	Limit Deposit Velocity	m/s
n	Number of fractions	-
Δp_{total}	Total pressure drop	kPa
r	Position in the pipe, from the bottom of the pipe	m
Re	Reynolds number	-
Re_l	Reynolds number based on pure liquid properties	-
Re_v	Reynolds number based on vehicle properties	-
R_{sd}	Relative submerged density solids in pure liquid	-
$R_{sd,v}$	Relative submerged density solids in vehicle	-
u_*	Friction velocity	m/s
$u_{*,ldv}$	Friction velocity at LDV	m/s
v_{ls}	Line speed	m/s
$v_{ls,ldv}$	Limit Deposit Velocity	m/s
v_t	Terminal settling velocity in pure liquid	m/s
v_{tv}	Terminal settling velocity in the vehicle	m/s

$v_{tv,j}$	Terminal settling velocity in the vehicle of the jth fraction	**m/s**
$v_{tv,ldv}$	Terminal settling velocity in the vehicle at LDV	**m/s**
α_{sm}	Correction factor Relation sediment diffusivity – eddy momentum diffusivity	**-**
β_{sm}	Relation sediment diffusivity – eddy momentum diffusivity	**-**
$\beta_{sm,Kaushal}$	Relation sediment diffusivity – eddy momentum diffusivity, Kaushal & Tomita	**-**
$\beta_{sm,ldv}$	Relation sediment diffusivity – eddy momentum diffusivity, DHLLDV	**-**
ϵ	Pipe wall roughness	**m**
ϵ_s	Sediment diffusivity	**m/s**
κ	Von Karman constant, about 0.4	**-**
λ_l	Darcy Weisbach friction factor based on liquid properties	**-**
λ_m	Darcy Weisbach friction factor mixture, Kaushal & Tomita	**-**
λ_v	Darcy Weisbach friction factor based on vehicle properties	**-**
$\lambda_{v,new}$	Corrected Darcy Weisbach friction factor Abulnaga	**-**
λ_e	Effective Darcy Weisbach friction factor based on total hydraulic gradient	**-**
ρ_l	Density liquid	**ton/m³**
ρ_s	Density solids	**ton/m³**
ρ_m	Density mixture	**ton/m³**
ρ_v	Density vehicle	**ton/m³**
σ_g	PSD grading coefficient, Kaushal & Tomita	**-**
μ_l	Dynamic viscosity liquid	**Pa·s**
μ_v	Dynamic viscosity vehicle	**Pa·s**
μ_r	Relative dynamic viscosity vehicle	**-**
μ_{sf}	Sliding friction factor	**-**
ν_l	Kinematic viscosity pure liquid	**m²/s**
ν_v	Kinematic viscosity vehicle	**m²/s**

6.20 The Wilson-GIW (1979) Models.

6.20.1 The Wilson-GIW (1979) Model for Fully Stratified Flow.

6.20.1.1 Introduction.

The Wilson et al. (1992), (1997) and (2006) model for the hydraulic transport of solids in pipelines is a widely used model for the sliding bed regime. A theoretical background of the model has been published piece by piece in a number of articles over the years. A variety of information provided in these publications makes the model difficult to reconstruct. Wilson (1979) first published his theory in 1979. Riet et al. (1995) & (1996) and Miedema et al. (2002) tried to reproduce the Wilson (1979) model.

A good understanding of the model structure is inevitable for the user who wants to extend or adapt the model to specific slurry flow conditions. The aim of this chapter is to summarize the model theory and submit the results of the numerical analysis carried out on the various model configurations. The numerical results show some differences when compared with the nomographs presented in the literature as the graphical presentations of the generalised model outputs. Model outputs are sensitive on a number of input parameters and on a model configuration used. This chapter contains an overview of a theory of the Wilson et al. (1992) two-layer model (2LM) as it has been published in a number of articles over the years. Results are presented from the model computation. The results provide an insight to the behavior of the mathematical model.

The model is based on an equilibrium of forces acting on the bed. Driving forces and resisting forces can be distinguished. The driving forces on the bed are the shear forces on the top of the bed and the force resulting from the pressure times the bed cross section. The pressure is the result of the sum of the shear force on the pipe wall in the restricted area above the bed and the shear force on the bed, divided by the cross section of this restricted area. The resisting forces are the force as a result of the sliding friction between the bed and the pipe wall and the viscous friction force of the liquid between the particles in the bed and the pipe wall. When the sum of the driving forces equals the sum of the resisting forces, the so called Limit of Stationary Deposit Velocity is reached. At line speeds below the Limit of Stationary Deposit Velocity, the bed is stationary and does not move, because the driving forces are smaller than the maximum resisting forces (maximum if the sliding friction would be fully mobilized, which is not the case at line speeds below the Limit of Stationary Deposit Velocity). At line speeds above the Limit of Stationary Deposit Velocity, the bed is sliding with a speed that is increasing with increasing line speed.

6.20.1.2 The Basic Equations for Flow and Geometry.

In order to understand the model, first all the geometrical parameters are defined. The cross section of the pipe with a particle bed as defined in the Wilson et al. (1992) two layer model has been illustrated by Figure 6.20-1.
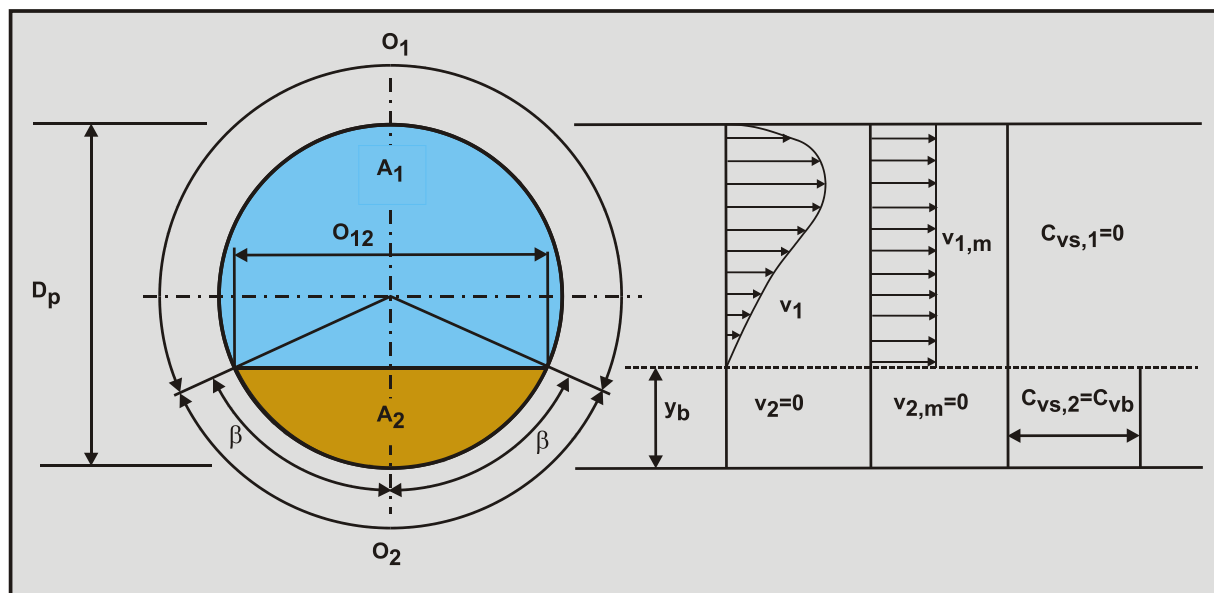
Figure 6.20-1: The definitions for fully stratified flow.

The geometry is defined by the following equations.

The length of the liquid in contact with the whole pipe wall if there is no bed is:

$$\mathbf{O_p = \pi \cdot D_p}$$

(6.20-1)

The length of the liquid or the suspension in contact with the pipe wall:

$$\mathbf{O_1 = D_p \cdot (\pi - \beta)}$$

(6.20-2)

The length of the fixed or sliding bed in contact with the wall:

$$\mathbf{O_2 = D_p \cdot \beta}$$

(6.20-3)

The top surface length of the fixed or sliding bed:

$$\mathbf{O_{12} = D_p \cdot \sin(\beta)}$$

(6.20-4)

The cross sectional area $\mathbf{A_p}$ of the pipe is:

$$\mathbf{A_p = \frac{\pi}{4} \cdot D_p^2}$$

(6.20-5)

The cross sectional area $\mathbf{A_2}$ of the fixed or sliding bed is:

$$\mathbf{A_2 = \frac{\pi}{4} \cdot D_p^2 \cdot \left(\frac{\beta - \sin(\beta) \cdot \cos(\beta)}{\pi} \right)}$$

(6.20-6)

The cross sectional area $\mathbf{A_1}$ above the bed, where the liquid or the suspension is flowing, also named the restricted area:

$$\mathbf{A_1 = A_p - A_2}$$

(6.20-7)

The hydraulic diameter of the cross-section of the pipeline above the bed $\mathbf{D_H}$ as function of the bed height, is equal to four times the cross sectional area divided by the wetted perimeter:

$$\mathbf{D_{H,1} = \frac{4 \cdot A_1}{O_1 + O_{12}}} \quad \text{or simplified:} \quad \mathbf{D_{H,1} = \sqrt{\frac{4 \cdot A_1}{\pi}}}$$

(6.20-8)

The volume balance gives a relation between the line speed $\mathbf{v_{ls}}$, the velocity in the restricted area above the bed $\mathbf{v_r}$ or $\mathbf{v_1}$ and the velocity of the bed $\mathbf{v_b}$ or $\mathbf{v_2}$.

$$\mathbf{v_{ls} \cdot A_p = v_1 \cdot A_1 + v_2 \cdot A_2}$$

(6.20-9)

Thus the velocity in the restricted area above the bed is:

$$\mathbf{v_1 = \frac{v_{ls} \cdot A_p - v_2 \cdot A_2}{A_1}}$$

(6.20-10)

Or the velocity of the bed is:

$$\mathbf{v_2 = \frac{v_{ls} \cdot A_p - v_1 \cdot A_1}{A_2}}$$

(6.20-11)

6.20.1.3 The Shear Stresses Involved.

In order to determine the forces involved, first the shear stresses involved have to be determined. The general equation for the shear stresses is:

$$\tau = \rho_l \cdot u_*^2 = \frac{\lambda_l}{4} \cdot \frac{1}{2} \cdot \rho_l \cdot v^2 \tag{6.20-12}$$

The force **F** on the pipe wall over a length **ΔL** is now:

$$F = \tau \cdot \pi \cdot D_p \cdot \Delta L = \frac{\lambda_l}{4} \cdot \frac{1}{2} \cdot \rho_l \cdot v^2 \cdot \pi \cdot D_p \cdot \Delta L \tag{6.20-13}$$

The pressure **Δp** required to push the solid-liquid mixture through the pipe equals the force divided by the cross-section:

$$\Delta p = \frac{F}{A_p} = \frac{\frac{\lambda_l}{4} \cdot \frac{1}{2} \cdot \rho_l \cdot v^2 \cdot \pi \cdot D_p \cdot \Delta L}{\frac{\pi}{4} \cdot D_p^2} = \lambda_l \cdot \frac{\Delta L}{D_p} \cdot \frac{1}{2} \cdot \rho_l \cdot v^2 \tag{6.20-14}$$

This is the well-known Darcy Weisbach equation. Over the whole range of Reynolds numbers above 2320 (5000<Re<100.000) the Swamee Jain equation gives a good approximation for the friction coefficient:

$$\lambda_l = \frac{1.325}{\left(\ln \left(\frac{0.27 \cdot \varepsilon}{D_p} + \frac{5.75}{Re^{0.9}} \right) \right)^2} \quad \text{with:} \quad Re = \frac{v \cdot D_p}{\nu_l} \tag{6.20-15}$$

This gives for the shear stress on the pipe wall for clean water:

$$. \tau_l = \frac{\lambda_l}{4} \cdot \frac{1}{2} \cdot \rho_l \cdot v_{ls}^2 \quad \text{with:} \quad \lambda_l = \frac{1.325}{\left(\ln \left(\frac{0.27 \cdot \varepsilon}{D_p} + \frac{5.75}{Re^{0.9}} \right) \right)^2} \quad \text{and} \quad Re = \frac{v_{ls} \cdot D_p}{\nu_l} \tag{6.20-16}.$$

For the flow in the restricted area, the shear stress between the liquid and the pipe wall is:

$$\tau_{1,l} = \frac{\lambda_l}{4} \cdot \frac{1}{2} \cdot \rho_l \cdot v_1^2 \quad \text{with:} \quad \lambda_l = \frac{1.325}{\left(\ln \left(\frac{0.27 \cdot \varepsilon}{D_{H,1}} + \frac{5.75}{Re^{0.9}} \right) \right)^2} \quad \text{and} \quad Re = \frac{v_1 \cdot D_{H,1}}{\nu_l} \tag{6.20-17}$$

For the flow in the restricted area, the shear stress between the liquid and the bed is:

$$\tau_{12,l} = \frac{\lambda_{12}}{4} \cdot \frac{1}{2} \cdot \rho_l \cdot (v_1 - v_2)^2 \quad \text{with:} \quad \lambda_{12} = \frac{\alpha \cdot 1.325}{\left(\ln \left(\frac{0.27 \cdot d}{D_{H,1}} + \frac{5.75}{Re^{0.9}} \right) \right)^2} \quad \text{and} \quad Re = \frac{v_1 \cdot D_{H,1}}{\nu_l}$$

$$\tag{6.20-18}$$

The factor **α** as used by Wilson et al. (1992) is 2 or 2.75, depending on the publication and version of his book. Televantos et al. (1979) used a factor of 2.

For the flow between the liquid in the bed and the pipe wall, the shear stress between the liquid and the pipe wall is:

$$\tau_{2,l} = \frac{\lambda_2}{4} \cdot \frac{1}{2} \cdot \rho_l \cdot v_2^2 \quad \text{with:} \quad \lambda_2 = \frac{1.325}{\left(\ln\left(\frac{0.27 \cdot \varepsilon}{d} + \frac{5.75}{Re^{0.9}} \right) \right)^2} \quad \text{and} \quad Re = \frac{v_2 \cdot d}{\nu_l} \tag{6.20-19}$$

Wilson et al. (1992) assume that the sliding friction is the result of a hydrostatic normal force between the bed and the pipe wall multiplied by the sliding friction factor. The average shear stress as a result of the sliding friction between the bed and the pipe wall, according to the Wilson et al. (1992) normal stress approach is:

$$\tau_{2,sf} = \frac{\mu_{sf} \cdot \rho_l \cdot g \cdot R_{sd} \cdot C_{vb} \cdot A_p}{\beta \cdot D_p} \cdot \frac{2 \cdot \left(\sin(\beta) - \beta \cdot \cos(\beta) \right)}{\pi} \tag{6.20-20}$$

It is however also possible that the sliding friction force results from the weight of the bed multiplied by the sliding friction factor. For low volumetric concentrations, there is not much difference between the two methods, but at higher volumetric concentrations there is. The average shear stress as a result of the sliding friction between the bed and the pipe wall, according to the weight normal stress approach is:

$$\tau_{2,sf} = \frac{\mu_{sf} \cdot \rho_l \cdot g \cdot R_{sd} \cdot C_{vb} \cdot A_p}{\beta \cdot D_p} \cdot \frac{\left(\beta - \sin(\beta) \cdot \cos(\beta) \right)}{\pi} \tag{6.20-21}$$

6.20.1.4 The Forces Involved.

First the equilibrium of the forces on the liquid above the bed is determined. This is necessary to find the correct hydraulic gradient. The resisting shear force on the pipe wall O_1 above the bed is:

$$F_{1,l} = \tau_{1,l} \cdot O_1 \cdot \Delta L \tag{6.20-22}$$

The resisting shear force on the bed surface O_{12} betweeen the restricted area and the top of the bed is:

$$F_{12,l} = \tau_{12,l} \cdot O_{12} \cdot \Delta L \tag{6.20-23}$$

The pressure Δp on the liquid above the bed is:

$$\Delta p = \Delta p_2 = \Delta p_1 = \frac{\tau_{1,l} \cdot O_1 \cdot \Delta L + \tau_{12,l} \cdot O_{12} \cdot \Delta L}{A_1} = \frac{F_{1,l} + F_{12,l}}{A_1} \tag{6.20-24}$$

The force equilibrium on the liquid above the bed is shown in Figure 6.20-2.
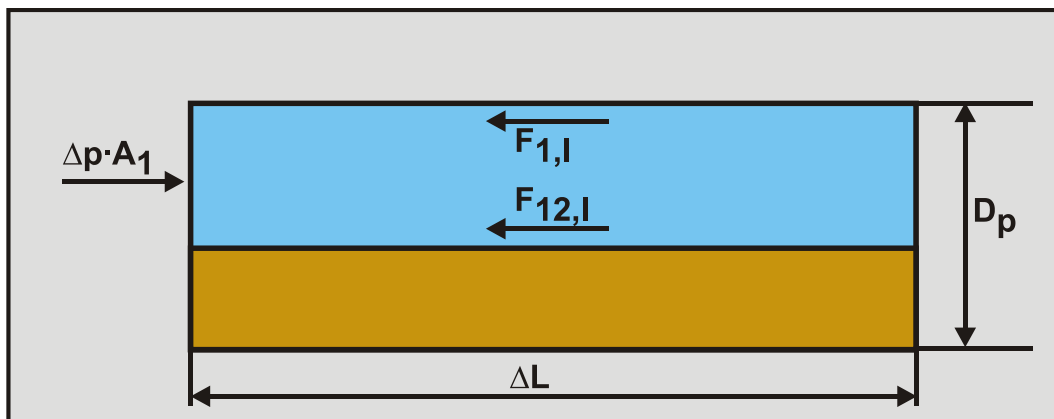
Figure 6.20-2: The forces on the liquid above the bed.

Secondly the equilibrium of forces on the bed is determined as is shown in Figure 6.20-3.
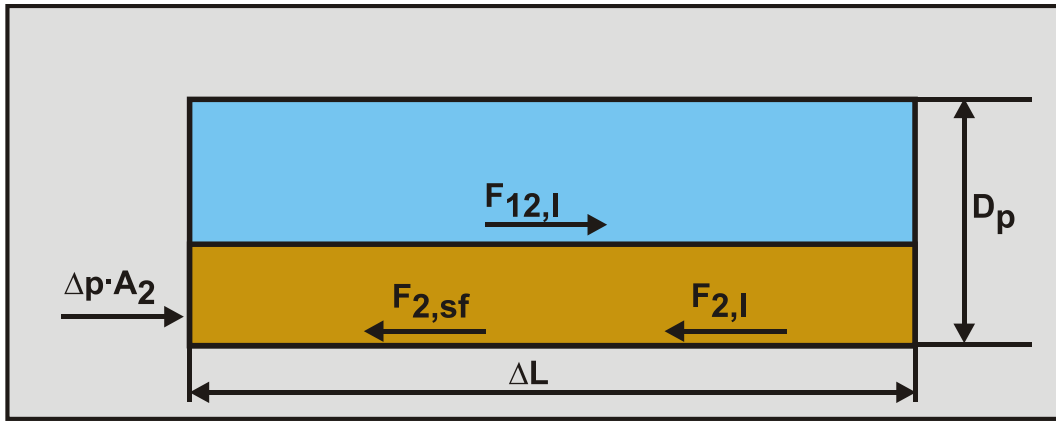
Figure 6.20-3: The forces on the bed.

The driving shear force on the bed surface is:

$$\mathbf{F_{12,l} = \tau_{12,l} \cdot O_{12} \cdot \Delta L} \tag{6.20-25}$$

The driving force resulting from the pressure $\mathbf{\Delta p}$ on the bed is:

$$\mathbf{F_{2,pr} = \Delta p \cdot A_2} \tag{6.20-26}$$

The resisting force between the bed and the pipe wall due to sliding friction is:

$$\mathbf{F_{2,sf} = \tau_{2,sf} \cdot O_2 \cdot \Delta L} \tag{6.20-27}$$

The resisting shear force between the liquid in the bed and the pipe wall is:

$$\mathbf{F_{2,l} = \tau_{2,l} \cdot O_2 \cdot n \cdot \Delta L} \tag{6.20-28}$$

This shear force is multiplied by the porosity n, in order to correct for the fact that the bed consists of a combination of particles and water. There is an equilibrium of forces when:

$$\mathbf{F_{12,l} + F_{2,pr} = F_{2,sf} + F_{2,l}} \tag{6.20-29}$$

Below the Limit of Stationary Deposit Velocity, the bed is not sliding and the force $\mathbf{F_{2,l}}$ equals zero. Since the problem is implicit with respect to the velocities $\mathbf{v_1}$ and $\mathbf{v_2}$, it has to be solved with an iteration process.

In the case when the relative concentration $\mathbf{C_{vr}=C_{vs}/C_{vb}}$ or $\mathbf{C_{vr}=C_{vt}/C_{vb}}$ equals 1, the resistance equals the plug hydraulic gradient, according to:

$$\mathbf{i_{plug} = 2 \cdot \mu_{sf} \cdot R_{sd} \cdot C_{vb}} \tag{6.20-30}$$

Wilson et al. (1992) defined the maximum Limit of Stationary Deposit Velocity as $\mathbf{v_{sm}}$.

The graphs in the following chapter are determined for uniform sands, not taking into account grading. In real life there will almost always be grading, resulting in slightly different curves, depending on the grading.

6.20.1.5 Output with the Wilson et al. (1992) Hydrostatic Stress Approach.
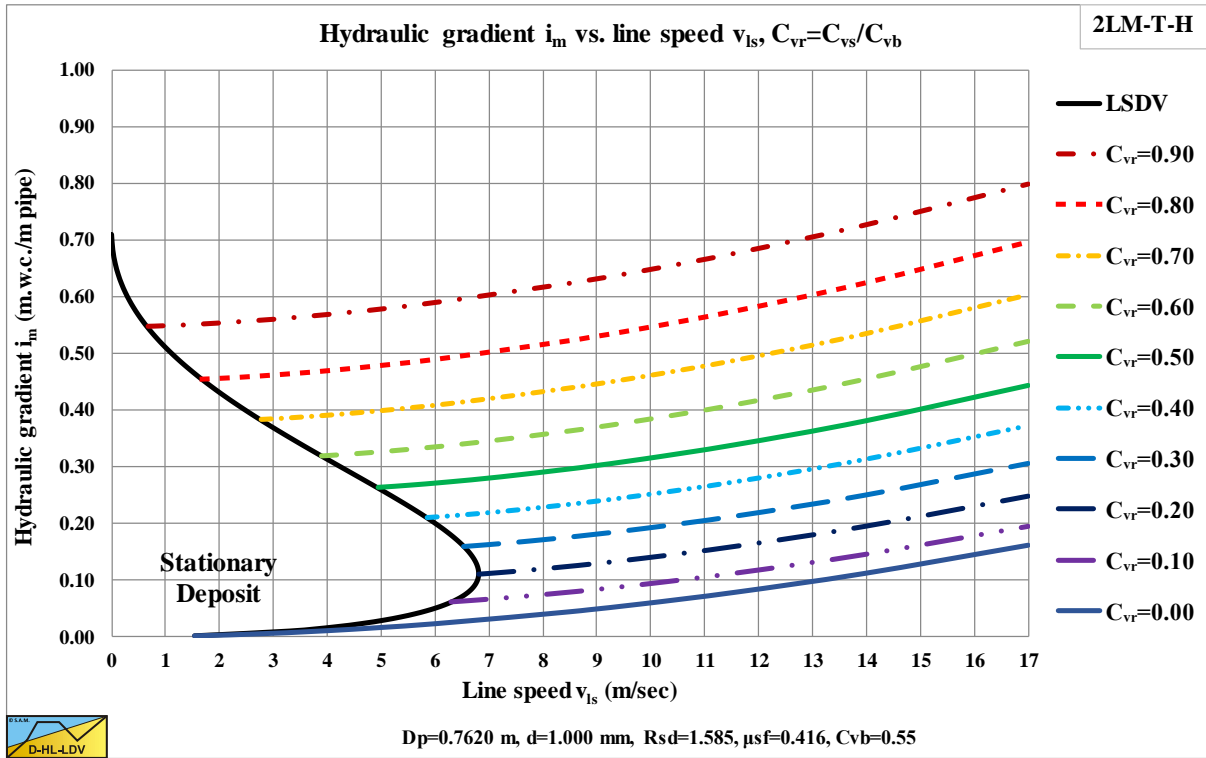
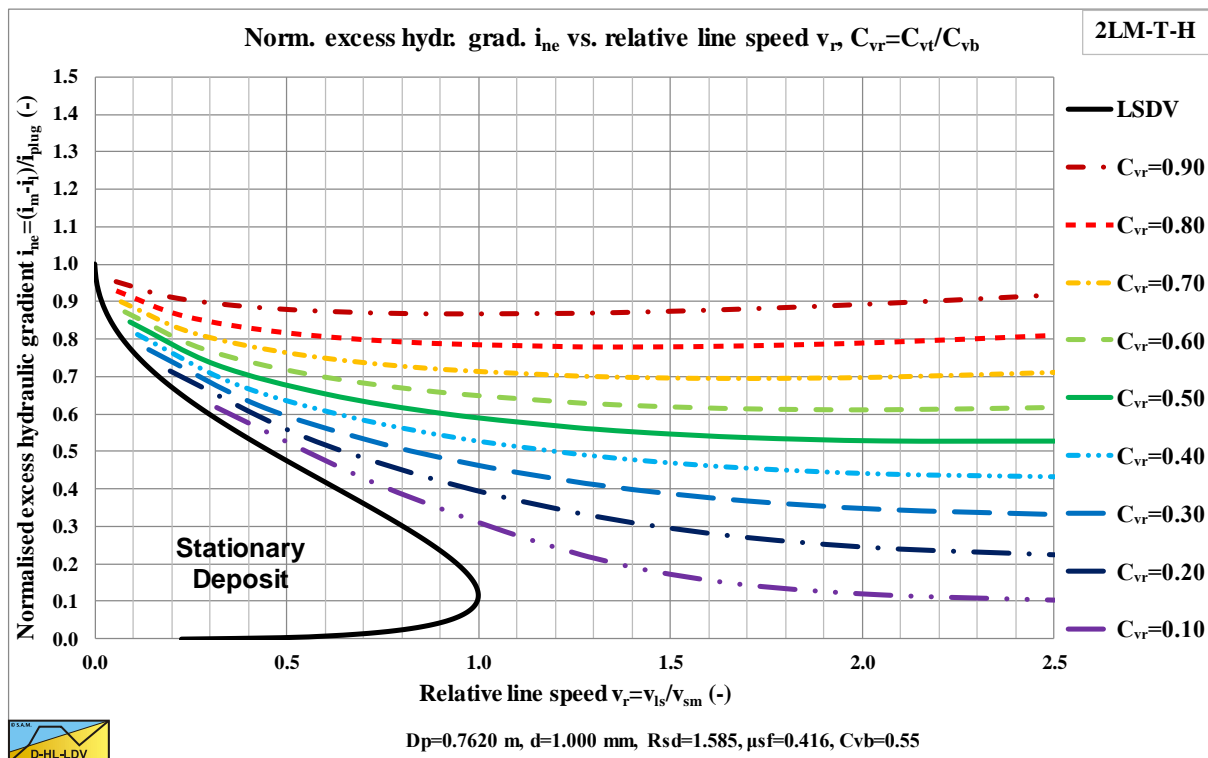**Figure 6.20-4: The hydraulic gradient i_m versus the line speed v_{ls}, $C_{vr}=C_{vs}/C_{vb}$.**
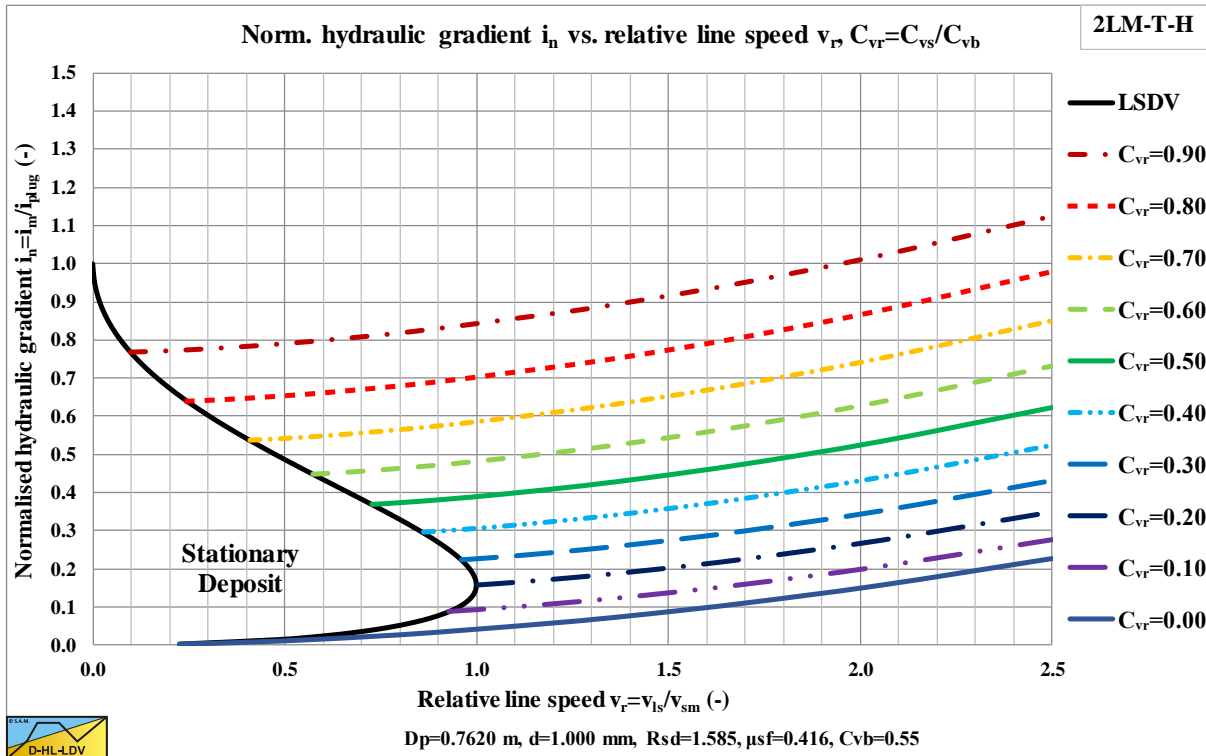
Figure 6.20-5: The normalized hydraulic gradient i_m/i_{plug} versus the relative line speed v_r, $C_{vr}=C_{vs}/C_{vb}$.

The direct outputs of the model are the hydraulic gradient and the bed velocity as shown in Figure 6.20-4, Figure 6.20-5 and Figure 6.20-6. Based on the bed velocity the delivered volumetric concentration C_{vt} and the slip velocity v_{sl} can be determined as is shown in Figure 6.20-7 and Figure 6.20-8. In Figure 6.20-5 the axis are made dimensionless (normalized) by dividing the hydraulic gradient by the plug hydraulic gradient and dividing the line speed v_{ls} by the maximum Limit of Stationary Deposit Velocity v_{sm}. The relative bed velocity increases with

increasing relative spatial volumetric concentration and even becomes 1 for a relative spatial concentration of 1, the bed concentration. The transport or delivered volumetric concentration also increases with increasing relative spatial volumetric concentration, but also with an increasing line speed.
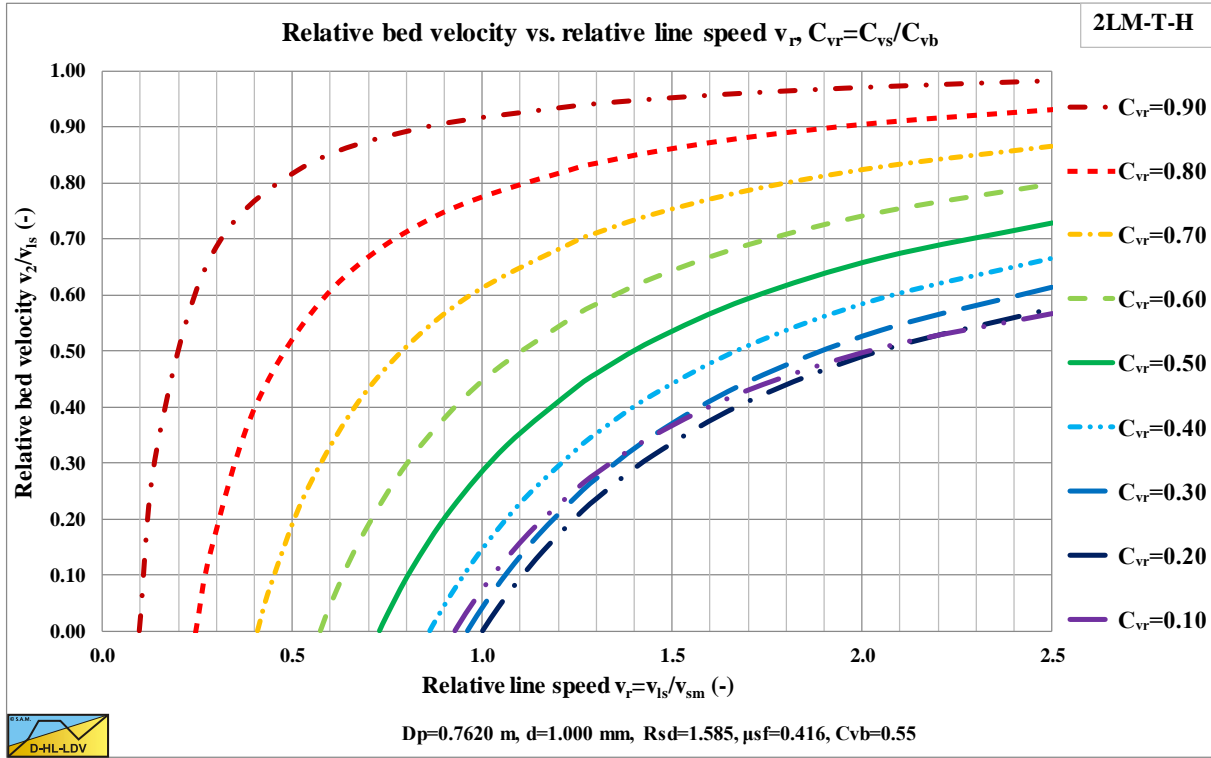
Figure 6.20-6: The relative bed velocity v_2/v_{sl} versus the relative line speed v_r, $C_{vr}=C_{vs}/C_{vb}$.
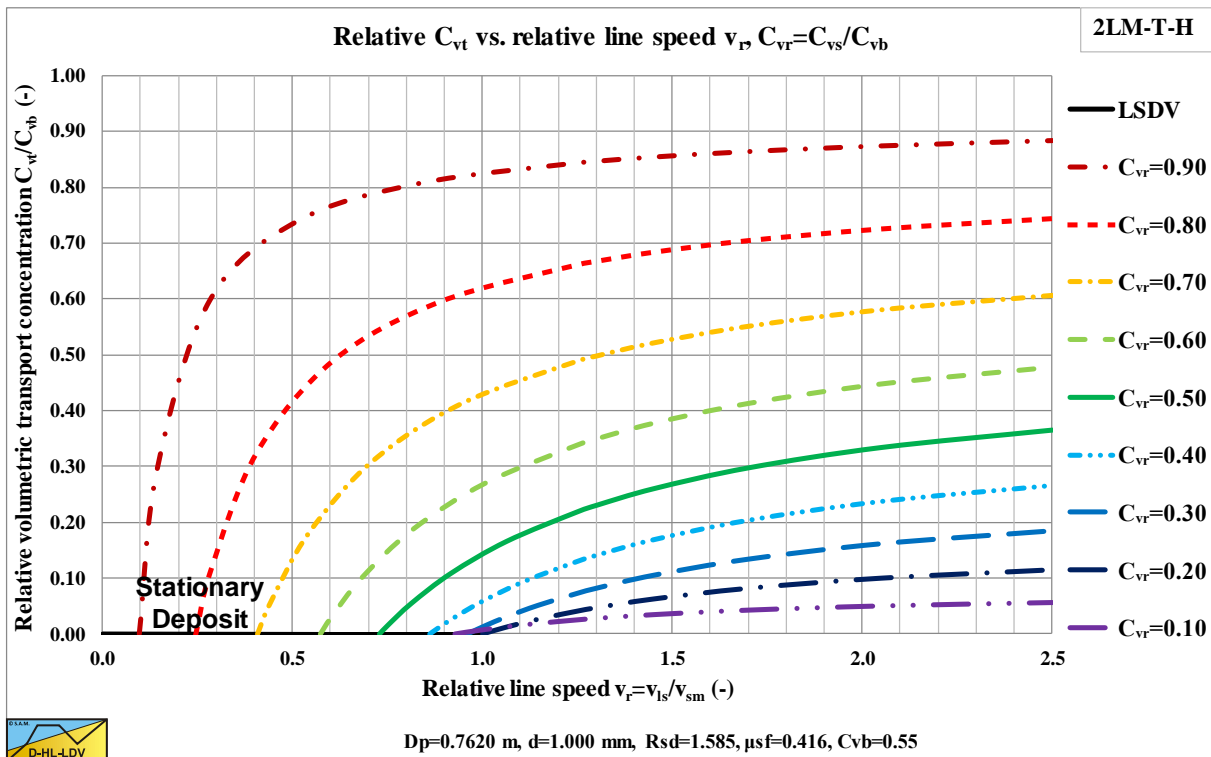
Figure 6.20-7: The relative volumetric transport concentration $C_{vr}=C_{vs}/C_{vb}$ vs. the relative line speed v_r.

Once the delivered volumetric concentration is known, points with equal delivered concentration can be connected and hydraulic gradient curves with constant delivered volumetric concentration can be constructed as is shown in Figure 6.20-9 and Figure 6.20-10. It should be mentioned that these curves do not intersect with the limit of

stationary deposit velocity curve, since there the bed has no velocity, so the delivered concentration is zero. The curves with small delivered concentrations follow the Limit of Stationary Deposit Velocity curve at the upper side. Figure 6.20-8 shows that the slip velocity decreases with an increasing spatial volumetric concentration and even goes to zero if the relative spatial concentration goes to 1, the bed concentration.
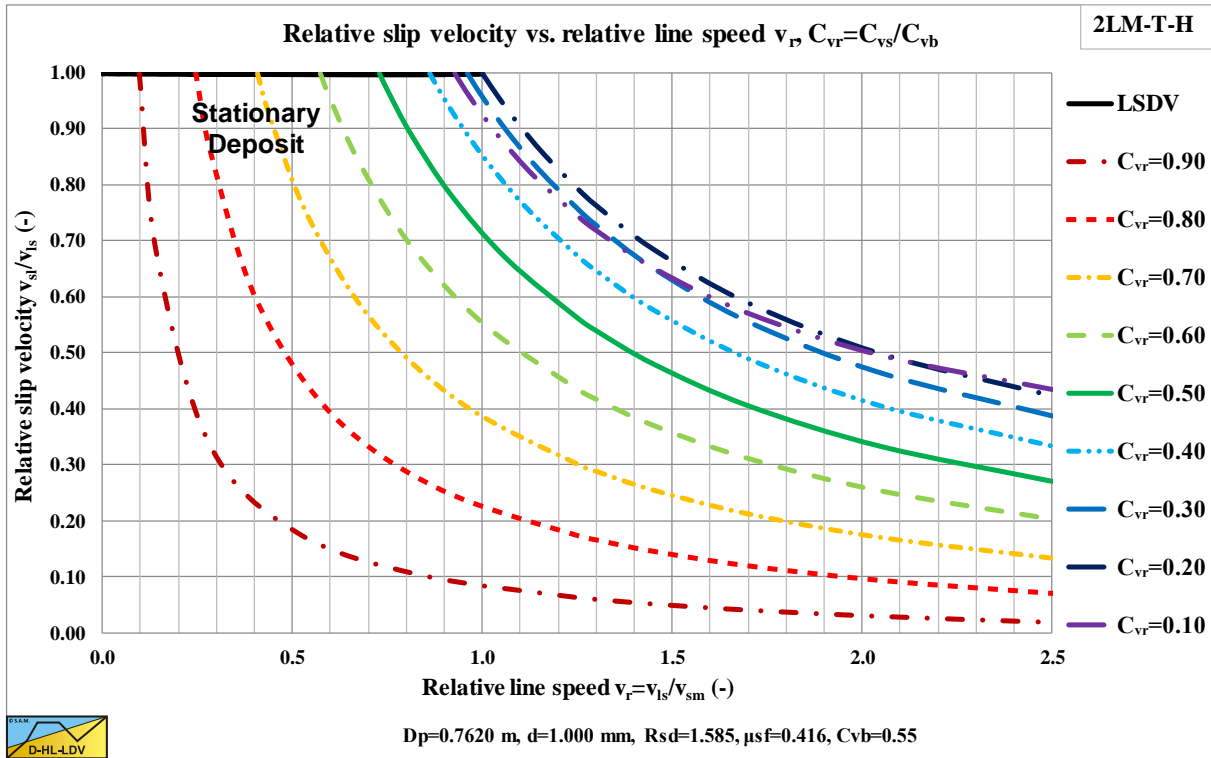
Figure 6.20-8: The relative slip velocity v_{sl}/v_{ls} versus the relative line speed v_r, $C_{vr}=C_{vs}/C_{vb}$.
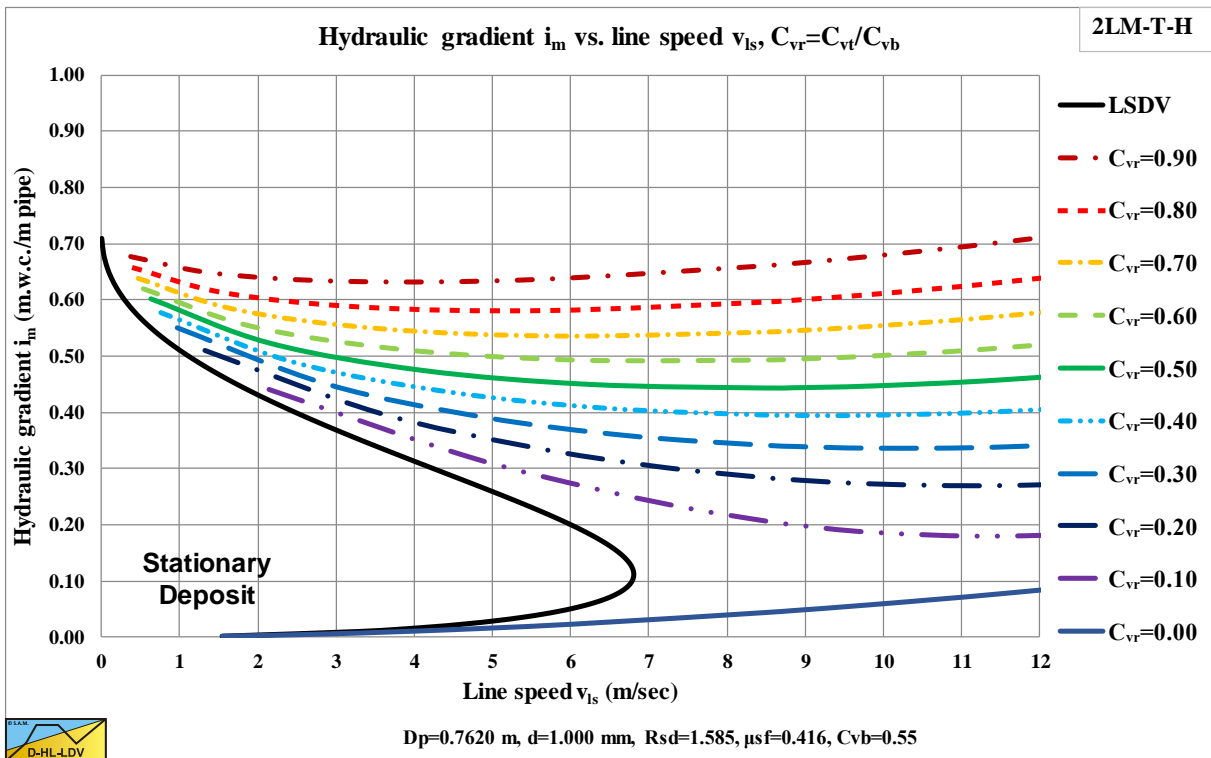
Figure 6.20-9: The hydraulic gradient i_m versus the line speed v_{ls}, $C_{vr}=C_{vt}/C_{vb}$.
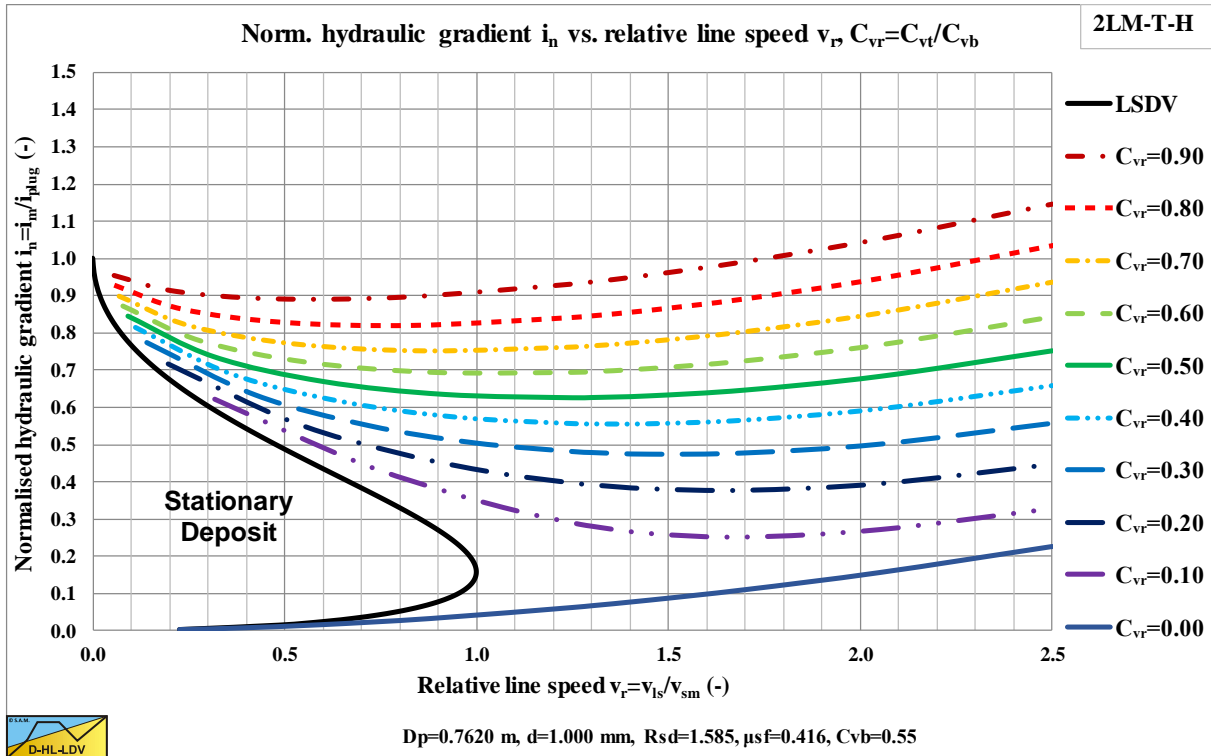
Figure 6.20-10: The normalized hydraulic gradient i_m/i_{plug} versus the relative line speed v_r, $C_{vr}=C_{vt}/C_{vb}$.

Figure 6.20-11 and Figure 6.20-12 show the relative excess hydraulic gradient curves for constant spatial volumetric concentration curves and for constant delivered volumetric concentration curves. The constant spatial volumetric concentration curves are almost horizontal, but have a higher value for a higher relative spatial volumetric concentration, due to the hydrostatic pressure approach for the normal stresses between the bed and the pipe wall. For low relative spatial volumetric concentrations, the relative excess hydraulic gradient has a value close to the sliding friction coefficient μ_{sf}. A relative spatial volumetric concentration of 1 results in a relative excess hydraulic gradient of about 2 times the sliding friction coefficient.
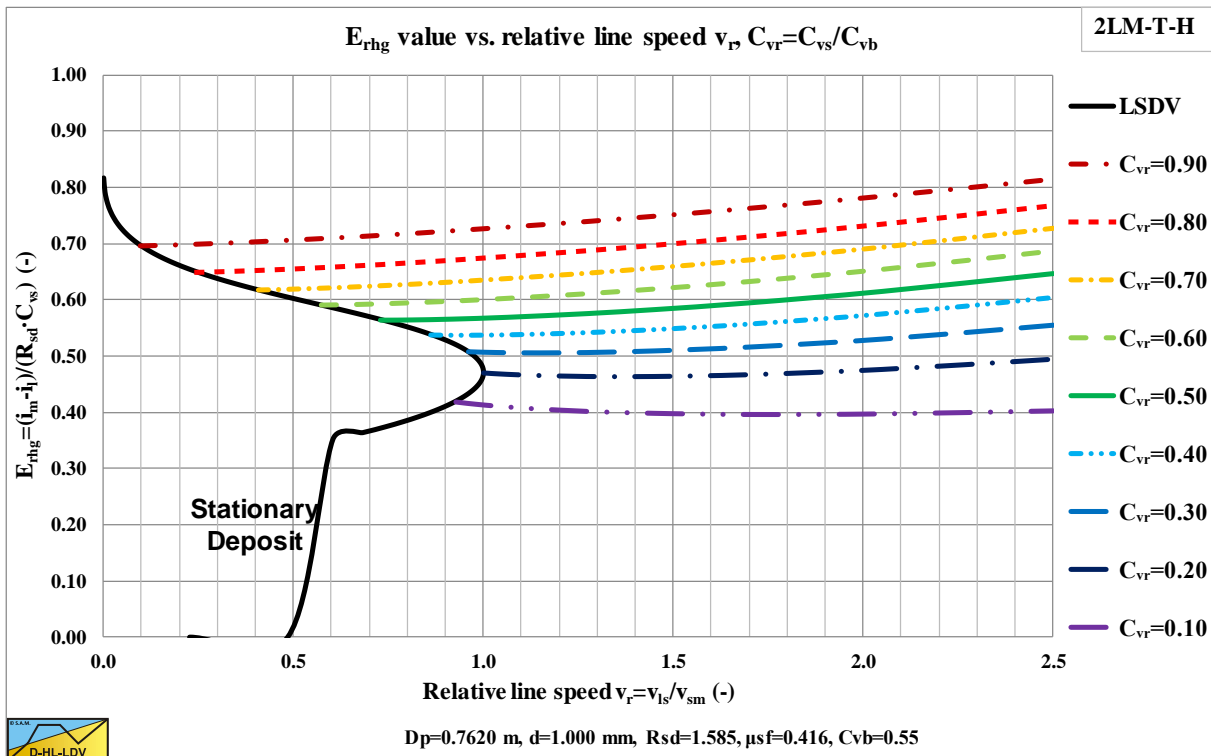
Figure 6.20-11: The relative excess hydraulic gradient E_{rhg} versus the relative line speed v_r, $C_{vr}=C_{vs}/C_{vb}$.
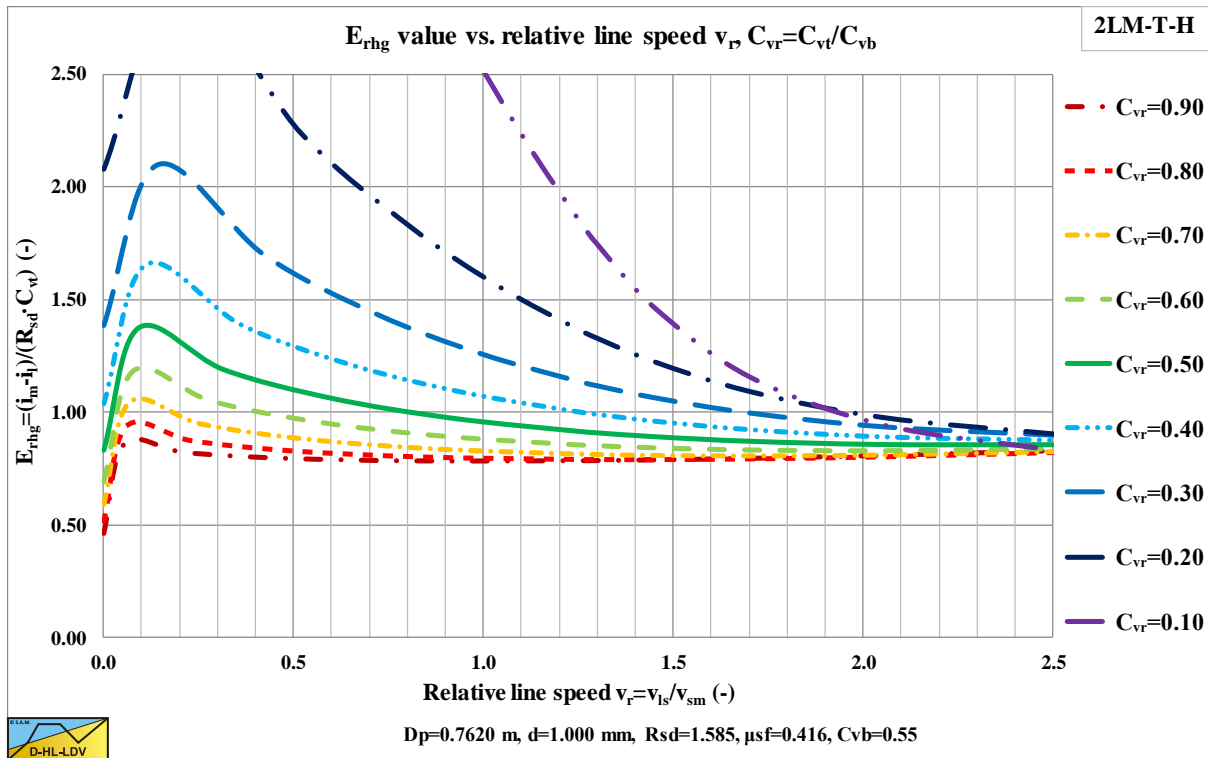
Figure 6.20-12: The relative excess hydraulic gradient E_{rhg} versus the relative line speed v_r, $C_{vr}=C_{vt}/C_{vb}$.

Wilson et al. (1992) often show the excess hydraulic gradient divided (normalized) by the plug hydraulic gradient in their graphs, like in Figure 6.20-13. Their fit functions are also based on this type of graph.

Figure 6.20-13: The normalized excess hydraulic gradient $(i_m-i_l)/i_{plug}$ versus the relative line speed v_r, $C_{vr}=C_{vt}/C_{vb}$.

6.20.1.6 The Fit Functions of Wilson et al. (1992).

Wilson et al. (1992) published the sliding bed model as a nomograph, using a set of parameters ($\mathbf{\mu_{sf}}$=**0.4**, $\mathbf{C_{vb}}$=**0.6** and a factor $\mathbf{\alpha}$=**2.75** for the friction factor on top of the bed). The nomograph and the set of fit function for the normalized excess hydraulic gradient are based on constant volumetric transport concentration curves.

The normalized excess hydraulic gradient is defined as the mixture hydraulic gradient minus the liquid hydraulic gradient divided by the plug hydraulic gradient:

$$\zeta = \frac{i_m - i_l}{i_{plug}} = \frac{i_m - i_l}{2 \cdot \mu_{sf} \cdot R_{sd} \cdot C_{vb}}$$

(6.20-31)

The relative line speed is the ratio between the line speed and the maximum Limit of Stationary Deposit Velocity:

$$v_r = \frac{v_{ls}}{v_{sm}}$$

(6.20-32)

The relative volumetric transport concentration $\mathbf{C_{vr}}$ is:

$$C_{vr} = \frac{C_{vt}}{C_{vb}}$$

(6.20-33)

The maximum Limit of Stationary Deposit Velocity (LSDV) $\mathbf{v_{sm}}$ can be estimated by (Matousek (2004)), with $\mathbf{d}$ in mm and $\mathbf{D_p}$ in m:

$$v_{sm} = \frac{8.8 \cdot \left(\frac{\mu_{sf} \cdot R_{sd}}{0.66} \right)^{0.55} \cdot D_p^{0.7} \cdot d^{1.75}}{d^2 + 0.11 \cdot D_p^{0.7}} \quad \text{and} \quad F_L = \frac{v_{sm}}{\sqrt{2 \cdot g \cdot R_{sd} \cdot D_p}}$$

(6.20-34)
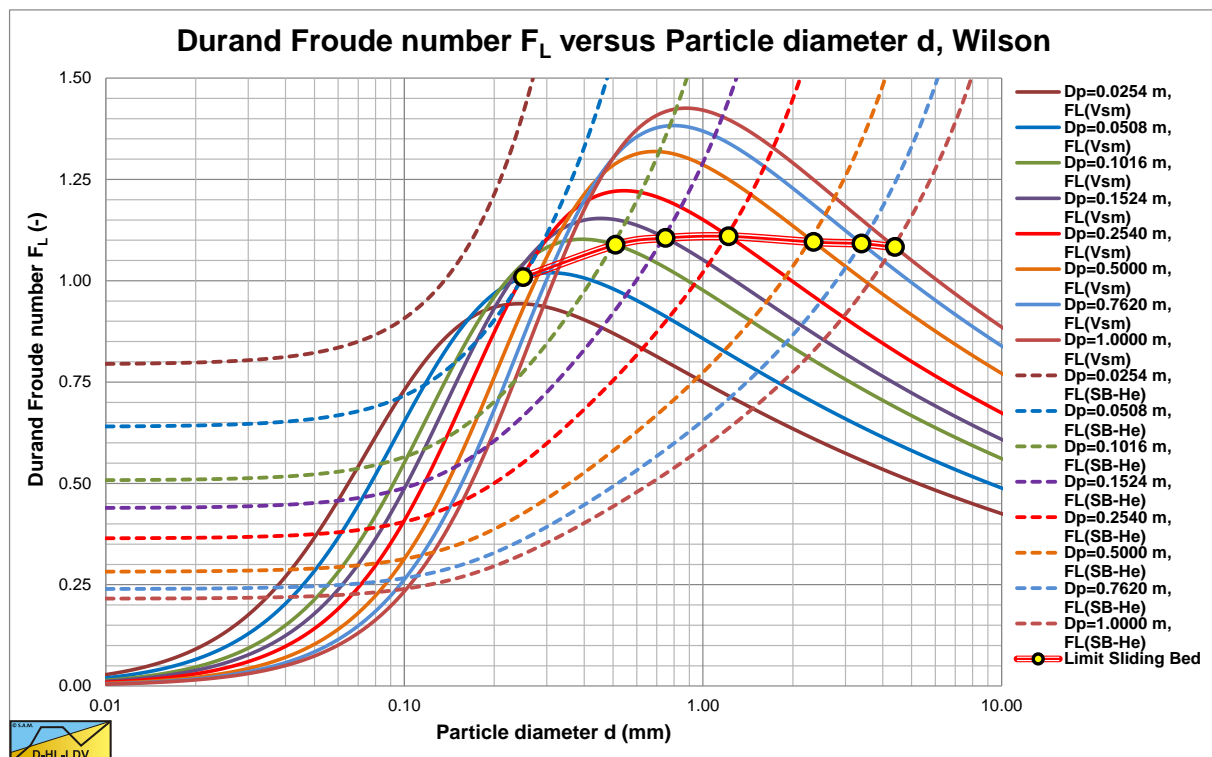
Figure 6.20-14: The Durand Froude number F_L based on v_{sm} for sands and gravels.

Figure 6.20-14 shows the Durand Froude number $\mathbf{F_L}$ for a number of pipe diameters as a function of the particle diameter. The figure also shows the Durand Froude number of the intersection point of the (slightly modified) heterogeneous model with the sliding bed curve (Transition FB-He). If this intersection point is below the LSDV, a sliding bed will never occur, if it is above the LSDV a sliding bed will occur. The figure shows the particle diameter where the sliding bed will occur for each pipe diameter. Other heterogeneous models may give slightly different values.

In the smallest ($\mathbf{D_p=1\ inch}$ and $\mathbf{2\ inch}$) pipe a sliding bed will always occur. A pipe diameter of $\mathbf{D_p=0.1016\ m}$ gives $\mathbf{d=0.49\ mm}$, $\mathbf{D_p=0.1524\ m}$ gives $\mathbf{d=0.78\ mm}$, $\mathbf{D_p=0.254\ m}$ gives $\mathbf{d=1.3\ mm}$, $\mathbf{D_p=0.5\ m}$ gives $\mathbf{d=2.65\ mm}$, $\mathbf{D_p=0.762\ m}$ gives $\mathbf{d=3.8\ mm}$. In the largest ($\mathbf{D_p=1\ m}$) pipe a sliding bed will occur for particles larger than about $\mathbf{d=4.5\ mm}$. The conclusion is, that one cannot just scale head losses, without knowing the flow regimes occurring. The demi-McDonald is shown in Figure 6.20-37 with an example.

The volumetric transport concentration at this maximum Limit of Stationary Deposit Velocity can be estimated by, with $\mathbf{d}$ in mm and $\mathbf{D_p}$ in m (for $\mathbf{C_{rm}}$ in the range 0.05-0.66):

$$\mathbf{C_{rm} = C_{vr,max} = 0.16 \cdot D_p^{0.40} \cdot d^{-0.84} \cdot \left(\frac{R_{sd}}{1.65}\right)^{-0.17}} \tag{6.20-35}$$
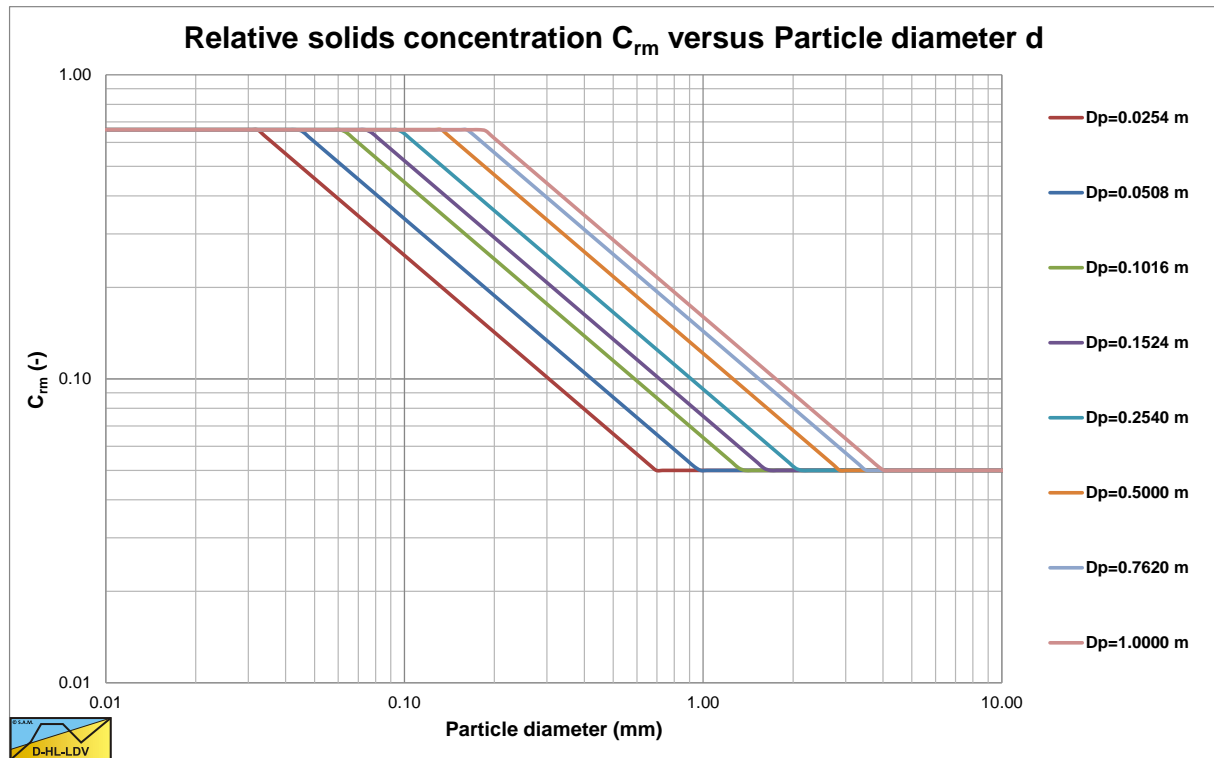
Figure 6.20-15: The maximum relative solids concentration versus the particle diameter.

For other volumetric transport concentrations, the Limit of Stationary Deposit Velocity $\mathbf{v_s}$ can be estimated by:

$$\mathbf{\frac{v_s}{v_{sm}} = 6.75 \cdot C_{vr}^{\alpha} \cdot \left(1 - C_{vr}^{\alpha}\right)^2 \quad if \quad C_{vr,max} \leq 0.33}$$

$$\mathbf{\frac{v_s}{v_{sm}} = 6.75 \cdot \left(1 - C_{vr}\right)^{2 \cdot \beta} \cdot \left(1 - \left(1 - C_{vr}\right)^{\beta}\right) \quad if \quad C_{vr,max} > 0.33} \tag{6.20-36}$$

$$\mathbf{With: \quad \alpha = \frac{\ln(0.333)}{\ln(C_{vr,max})} \quad and \quad \beta = \frac{\ln(0.666)}{\ln(1 - C_{vr,max})}}$$

The asymptotic normalized excess hydraulic gradient for very high line speeds can be determined by:

$$\zeta_\infty = 0.5 \cdot C_{vr} \cdot \left(1 + C_{vr}^{0.66}\right)$$

(6.20-37)

For lower line speeds the normalized excess hydraulic gradient can now be determined by:

$$\zeta = \zeta_\infty + \left(1 - \zeta_\infty\right) \cdot \left(1 + v_r\right)^{-q}$$

(6.20-38)

$$q = 3.6 - 5.2 \cdot C_{vr} \cdot \left(1 - C_{vr}\right) \qquad \text{if} \quad C_{vr} \geq C_{vr,max}$$

or

$$q = \left(3.6 - 5.2 \cdot C_{vr,max} \cdot \left(1 - C_{vr,max}\right)\right) \cdot \frac{C_{vr,max}}{C_{vr}} \qquad \text{if} \quad C_{vr} < C_{vr,max}$$

(6.20-39)
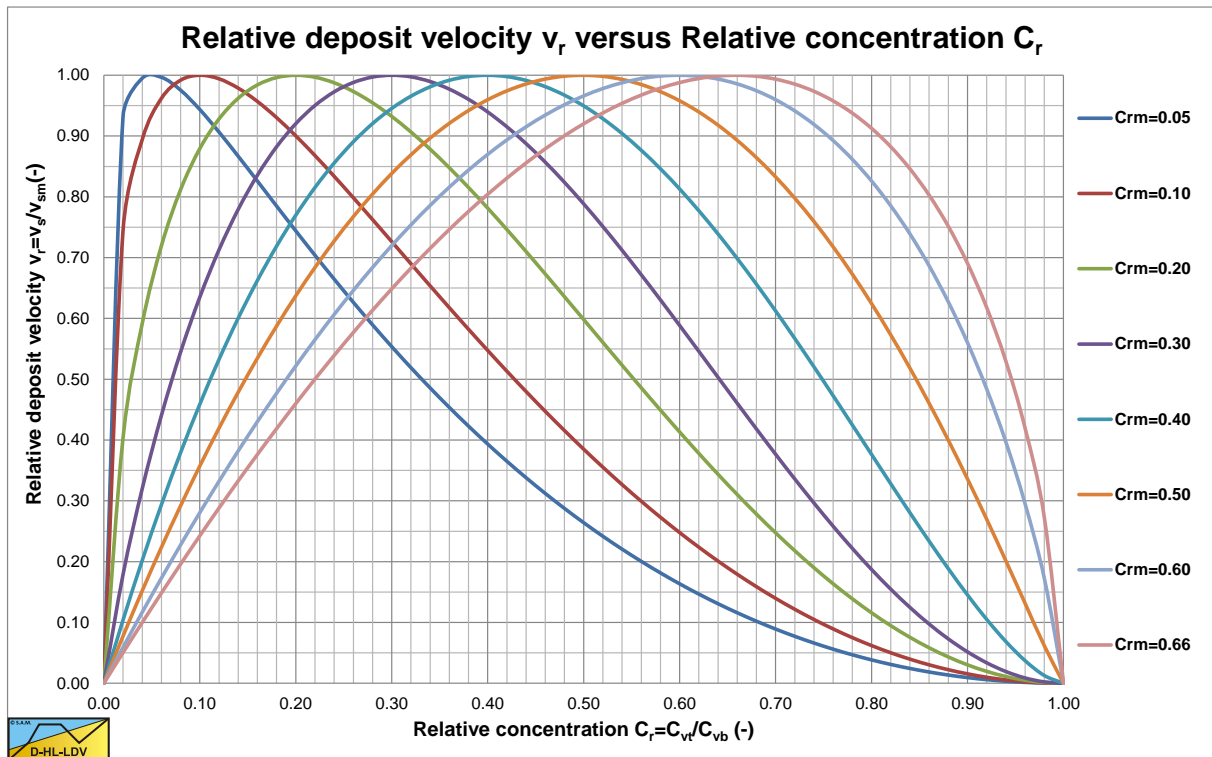
Figure 6.20-16: The relative deposit velocity versus the relative concentration.

Figure 6.20-14 shows the maximum Durand Froude number as a function of the particle diameter (in mm) and the pipe diameter (in m). Figure 6.20-15 shows how the concentration where the maximum LSDV occurs depends on the particle diameter (in mm) and the pipe diameter (in m). Figure 6.20-16 shows how the LSDV depends on the relative concentration and the concentration where the maximum LSDV occurs. Figure 6.20-17 shows a resulting LSDV curve.

Later a shear layer or sheet flow layer was incorporated. If the sharp interface between a bed and the carrier liquid above the bed is replaced by a shear layer, the driving force at the interface is no longer dependent on the roughness of the bed. Therefore the particle size does not influence the maximum LSDV. The Durand Froude number can be determined with the following equation in this case:

$$F_L = \frac{v_{sm}}{\sqrt{2 \cdot g \cdot R_{sd} \cdot D_p}} = \left(\frac{0.018}{\lambda_l}\right)^{0.13}$$

(6.20-40)

The smaller of the two LSDV approximations should be chosen. The above equation is derived for a specific bed concentration and sliding friction coefficient. Other conditions may give a slightly different equation.
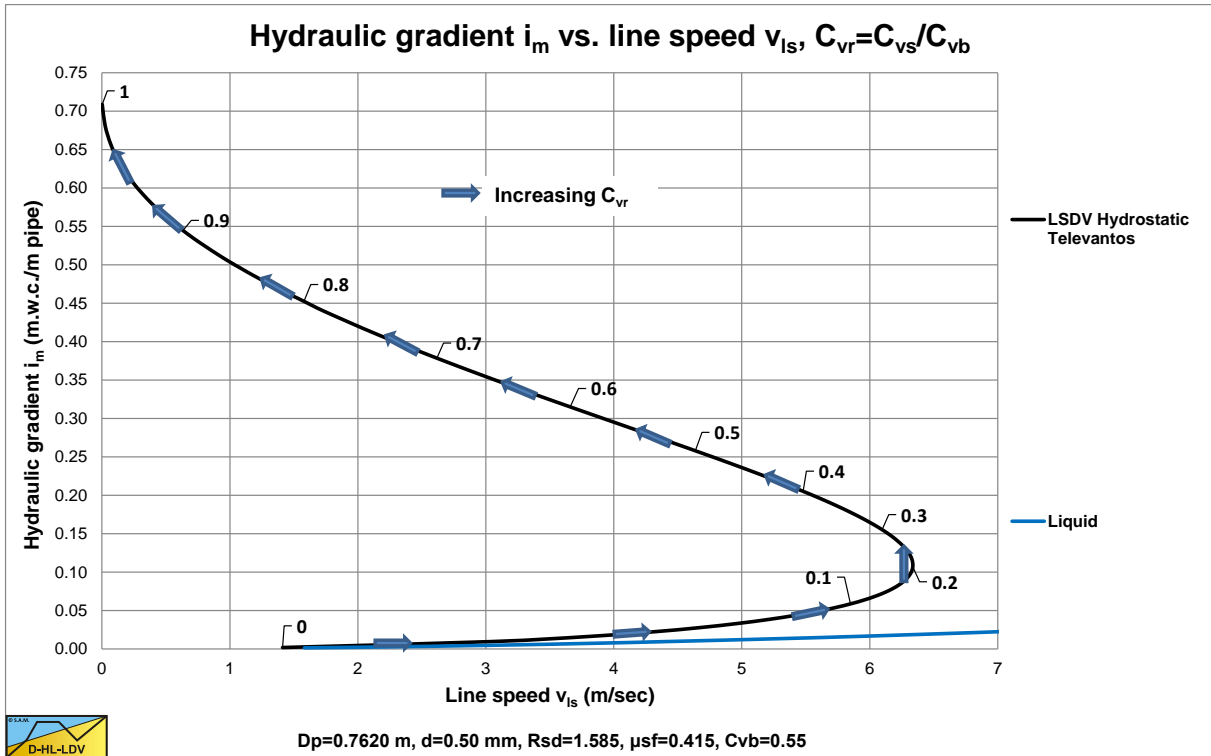
Figure 6.20-17: The LSDV curve.

With these equations, Figure 6.20-18 is reconstructed.
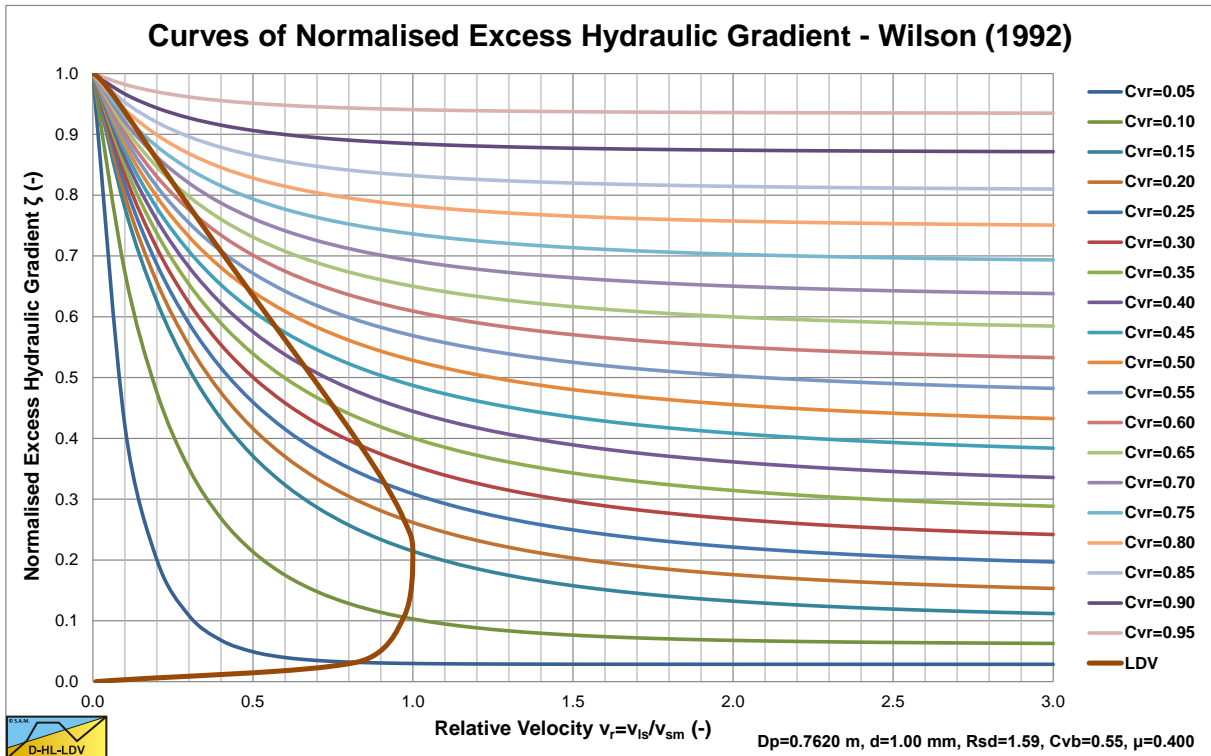
Figure 6.20-18: The fit functions of Wilson et al. (1992).

Of course the curves cannot exist inside the stationary bed region. However here the curves are shown as given by Wilson. This comment is also valid for the next figure.

6.20.1.7 The Fit Functions of Wilson et al. (1997).

The relative excess hydraulic gradient can be approximated by (for a sliding friction coefficient of 0.4 and 0.44):

$$
E_{rhg} = \frac{i_m - i_l}{R_{sd} \cdot C_{vt}} = \left(\frac{0.55 \cdot v_{sm}}{v_{ls}} \right)^{0.25} = 0.861 \cdot \left(\frac{v_{sm}}{v_{ls}} \right)^{0.25} = 2 \cdot \mu_{sf} \cdot \left(\frac{4 \cdot v_{sm}}{3 \cdot v_{ls}} \right)^{0.25} \quad \text{for} \quad \mu_{sf} = 0.40
$$

$$
E_{rhg} = \frac{i_m - i_l}{R_{sd} \cdot C_{vt}} = \left(\frac{0.55 \cdot v_{sm}}{v_{ls}} \right)^{0.25} = 0.861 \cdot \left(\frac{v_{sm}}{v_{ls}} \right)^{0.25} = 2 \cdot \mu_{sf} \cdot \left(\frac{v_{sm}}{v_{ls}} \right)^{0.25} \quad \text{for} \quad \mu_{sf} = 0.44
$$

$$(6.20-41)$$

In the case where the line speed equals the maximum Limit of Stationary Deposit Velocity v_{sm}, this gives:

$$
E_{rhg} = \frac{i_m - i_l}{R_{sd} \cdot C_{vt}} = 2 \cdot \mu_{sf} \cdot \left(\frac{4}{3} \right)^{0.25} \quad \text{or} \quad E_{rhg} = \frac{i_m - i_l}{R_{sd} \cdot C_{vt}} = 2 \cdot \mu_{sf}
$$

$$(6.20-42)$$

This gives for the normalized excess hydraulic gradient at this line speed:

$$
\zeta = \frac{i_m - i_l}{i_{plug}} = \frac{2 \cdot \mu_{sf} \cdot R_{sd} \cdot C_{vt}}{2 \cdot \mu_{sf} \cdot R_{sd} \cdot C_{vb}} = \frac{C_{vt}}{C_{vb}} \cdot \left(\frac{4}{3} \right)^{0.25} \quad \text{or} \quad \zeta = \frac{i_m - i_l}{i_{plug}} = \frac{C_{vt}}{C_{vb}}
$$

$$(6.20-43)$$

Figure 6.20-19 shows the resulting normalized excess hydraulic gradient curves.
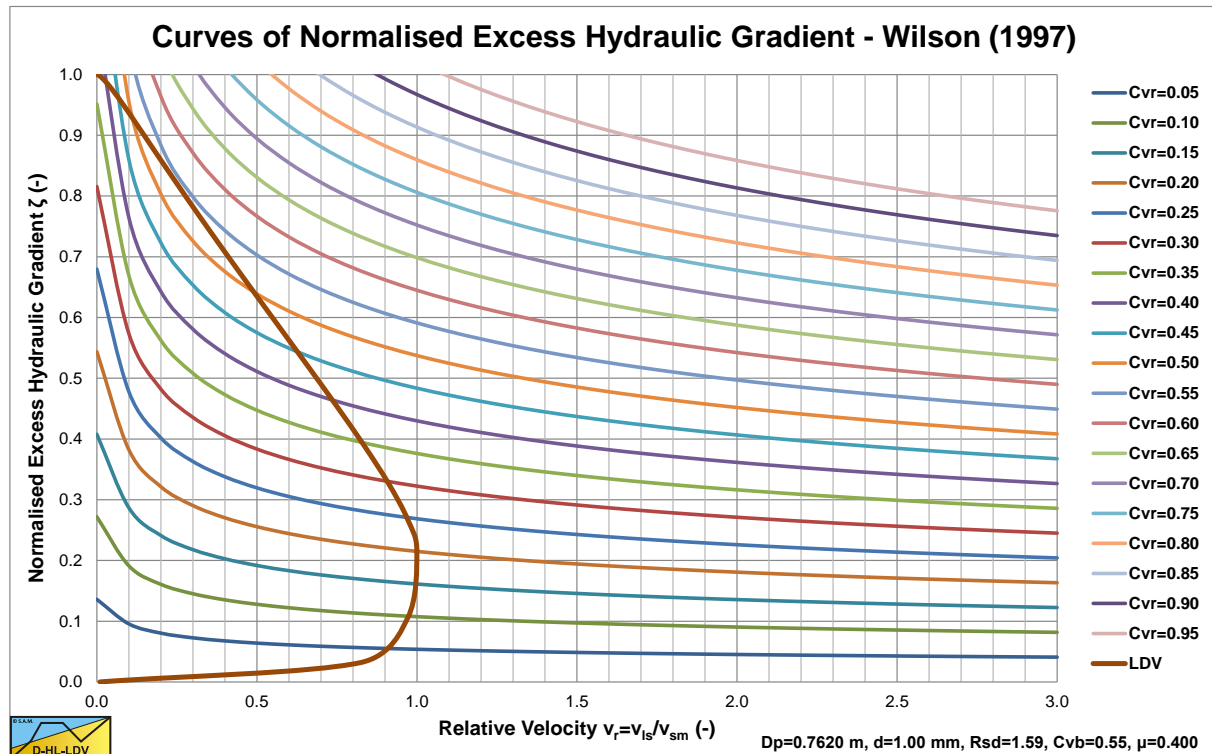
Figure 6.20-19: The fit functions of Wilson et al. (1997).

6.20.1.8 The Stratification Ratio.

The Wilson et al. (1997) model is based on a 100% stationary or sliding bed giving 100% stratification. However at a certain velocity of the liquid above the bed erosion may occur, related to the Shields parameter as described in chapter 5. It is also possible that a shear layer or sheet flow occurs at the top of the bed. Erosion will reduce the bed thickness while a shear layer or sheet flow will influence the Moody friction coefficient at the top of the bed. Whatever the mechanism may be, the bed will dissolve with increasing line speed and transit to (pseudo) homogeneous flow at (very) high line speeds. In order to take this into account, Wilson et al. (1997) defined a stratification ratio, being the amount of particles in the bed (in contact) divided by the total amount of particles in a cross section of the pipe.

$$\mathbf{R = \frac{C_{vc}}{C_{vs}}} \tag{6.20-44}$$

If all the available particles are in the bed the stratification ratio is 1 or 100%. If all the available particles are in suspension the stratification ratio is 0 or 0%. The amount of particles in suspension, being part of the homogeneous, equivalent liquid model, flow equals 1 minus the stratification ratio. To determine the total hydraulic gradient Wilson et al. (1997) adds the stratification ratio times the bed resistance and 1 minus the stratification ratio times the ELM resistance according to:

$$\mathbf{i_m = R \cdot i_{bed} + (1 - R) \cdot i_{hom}} \tag{6.20-45}$$

Basically this means that the superposition principle is applied on a mix of the sliding bed regime and the homogeneous regime. This implies that the behavior of both processes is linear, which does not have to be the case. However, by determining the formulation of the stratification ratio experimentally, resulting in an empirical equation, this will correct itself. This empirical equation is determined based on the hydraulic gradient and not based on the real stratification ratio.

6.20.1.9 Suspension in the Upper Layer.

The basic Wilson et al. (1992) two layer model considers a fixed or sliding bed with water above the bed. So we have a bed layer and a water layer. Wilson et al. (1990) defined a threshold velocity at which particles start suspending. This threshold velocity is defined as:

$$\mathbf{v_u = v_t \cdot \sqrt{\frac{8}{\lambda_l}} \cdot e^{\frac{45 \cdot d}{D_p}}} \quad \text{or} \quad \mathbf{u_* = \sqrt{\frac{\lambda_l}{8}} \cdot v_u = v_t \cdot e^{\frac{45 \cdot d}{D_p}}} \tag{6.20-46}$$

Above this threshold velocity the amount of solids in the bed as a fraction of the total amount of solids has been defined as the stratification ratio **R**. The stratification ratio can now be determined by:

$$\mathbf{R = \left(\frac{v_u}{v_{ls}}\right)^M} \tag{6.20-47}$$

So when the line speed $\mathbf{v_{ls}}$ equals the threshold velocity $\mathbf{v_u}$, the stratification ratio **R** equals 1, meaning that 100% of the particles is in the bed. As the line speed increases, the stratification ratio decreases. The power **M** has a value of 1.7 for very narrow graded sands or gravels, uniform sands or gravels. The more graded a sand or gravel, the smaller the power **M** with a minimum of 0.25. This approach forms the basis of the heterogeneous model of Wilson et al. (1992). The amount of solids in suspension is now 1-$\mathbf{C_{vc}}$/$\mathbf{C_{vs}}$=(1-R).

By determining the amount of solids in suspension and adjusting the fluid density and viscosity and the amount of solids in the bed, the two layer model can be applied for small particles. The Thomas (1965) equation can be used to adjust the viscosity of the liquid/solid mixture. This explains decrease of the LSDV with decreasing particle diameter for particles smaller than about **d=0.7 mm**. It also explains for the increase of the spatial concentration where the maximum LSDV occurs with decreasing particle diameter. The delivered concentration is in this case $\mathbf{C_{vt}}$=(1-R)·$\mathbf{C_{vs}}$. For other solids densities this behavior may be different, since large particles probably have a different influence on the viscosity.

6.20.1.10 Conclusions & Discussion.

The Wilson et al. (1992) model forms a solid base for 2 layer and 3 layer models. The model is based on the force equilibrium on the bed and is capable of determining the Limit of Stationary Deposit Velocity curve for the start of sliding of the bed. The model also gives the bed velocity for line speeds above the Limit of Stationary Deposit Velocity. Although the model is based on constant spatial volumetric concentration curves, based on the bed velocity the delivered volumetric concentration can be determined. Connecting points with constant delivered volumetric concentration, enables to construct constant delivered volumetric concentration curves as used in practice. The model however still has a number of shortcomings. First of all, the Darcy-Weisbach friction factor on the bed is assumed to be constant, not depending on the velocity above the bed (Wilson uses a factor 2 or 2.75). Since above a certain line speed the top layer of the bed will be sheet flow, the Darcy-Weisbach friction factor will increase with increasing line speed. Sheet flow also implies higher velocities of the particles in the sheet flow layer, resulting in higher delivered volumetric concentrations. The model however assumes a solid sliding bed without any particles above the bed, either in suspension or in a sheet flow layer. A second shortcoming is the hydrostatic normal stress between the bed and the wall. This assumption in the model also neglects the presence of particles in suspension or in a sheet flow layer apart from the fact that this assumption is questionable in the first place for beds occupying more than 50% of the pipe. The hydrostatic approach implies an upwards component of the normal stress between the bed and the pipe wall in this case, which normally will not occur.

With regard to the fit functions of Wilson et al. (1992) and (1997), in both cases the fit lines intersect with the Limit of Stationary Deposit Velocity curve, which is not physically possible, since the delivered volumetric concentration is zero on these lines. At line speeds much higher than the Limit of Stationary Deposit Velocity, the fit curves may however be correct.

Since Wilson et al. (1992) and (1997) developed the model in a time period without sophisticated computers and software as we have today, it must have been a tedious job to create his graphs. Nowadays a relatively simple Excel sheet can do the job, resulting in the graphs as shown in this chapter.

Later researchers improved the model, like Doron et al. (1987) a two layer model, Doron & Barnea (1993) a three layer model and Matousek (1997) two and three layer models.

6.20.2 The Wilson-GIW (1992) Model for Heterogeneous Transport.

6.20.2.1 The Full Model.

Assuming that 50% of the solids is moving in the bed by granular contact at a line speed of v_{50}, and assuming a friction coefficient μ_{sf} between the particles and the pipe wall, the friction force in a pipe with length ΔL is:

$$F_{sf} = \frac{\mu_{sf}}{2} \cdot A_p \cdot \Delta L \cdot C_v \cdot (\rho_s - \rho_l) \cdot g \tag{6.20-48}$$

This gives an excess pressure due to the solids of:

$$\Delta p_m - \Delta p_l = \frac{F_{sf}}{A_p} = \frac{\mu_{sf}}{2} \cdot \Delta L \cdot C_v \cdot (\rho_s - \rho_l) \cdot g \tag{6.20-49}$$

In terms of the hydraulic gradient this can be written as:

$$i_m - i_l = \frac{\Delta p_m - \Delta p_l}{\rho_l \cdot g \cdot \Delta L} = \frac{\mu_{sf}}{2} \cdot C_v \cdot \frac{(\rho_s - \rho_l)}{\rho_l} = \frac{\mu_{sf}}{2} \cdot C_v \cdot R_{sd} \tag{6.20-50}$$

Wilson (1997) has defined a stratification ratio or relative solids effect, which tells which fraction of the particles, is in suspension and which part is in the fixed or moving bed, supported by granular contact. Wilson (1997) gives the following general equation for the head losses in hydraulic transport, where μ_{sf} equals the friction factor of a sliding bed, which he has determined to be $\mu_{sf} = 0.44$. For the 50% case this gives:

$$E_{rhg} = R = \frac{i_m - i_l}{R_{sd} \cdot C_v} = \frac{\Delta p_m - \Delta p_l}{\rho_l \cdot g \cdot \Delta L \cdot R_{sd} \cdot C_v} = \frac{\mu_{sf}}{2} \cdot \left(\frac{v_{50}}{v_{ls}} \right)^M \tag{6.20-51}$$

When the line speed v_{ls} equals the v_{50}, the stratification ratio is 0.22 or half the friction coefficient μ_{sf}. This can be written in terms of pressures instead of hydraulic gradient as:

$$\Delta p_m = \Delta p_l + \frac{\mu_{sf}}{2} \cdot \rho_l \cdot g \cdot \Delta L \cdot \left(\frac{v_{50}}{v_{ls}} \right)^M \cdot R_{sd} \cdot C_v \tag{6.20-52}$$

This equation can be written in the more generic form, matching the notations of the other theories:

$$\Delta p_m = \Delta p_l \cdot \left(1 + \frac{\mu_{sf} \cdot g \cdot R_{sd} \cdot D_p}{\lambda_l} \cdot (v_{50})^M \cdot \left(\frac{1}{v_{ls}} \right)^{2+M} \cdot C_v \right) \tag{6.20-53}$$

For the line speed, where 50% of the particles is in granular contact, v_{50}, Wilson gives the following equation:

$$v_{50} = w_{50} \cdot \sqrt{\frac{8}{\lambda_l}} \cdot \cosh\left(\frac{60 \cdot d_{50}}{D_p} \right) \tag{6.20-54}$$

When the power M equals 1, this equation has the same form as the equation of Durand & Condolios, Gibert, Fuhrboter, Jufin Lopatin and Newitt et al. The power M depends on the grading of the sand and can be determined by:

$$M = \left(0.25 + 13 \cdot \sigma^2 \right)^{-1/2} \tag{6.20-55}$$

The variance σ of the PSD (Particle Size Distribution), can be determined by some ratio between the v_{50} and the v_{85}:

$$\sigma = \log\left(\frac{v_{85}}{v_{50}}\right) = \log\left(\frac{w_{85} \cdot \sqrt{\frac{8}{\lambda_l}} \cdot \cosh\left(\frac{60 \cdot d_{85}}{D_p}\right)}{w_{50} \cdot \sqrt{\frac{8}{\lambda_l}} \cdot \cosh\left(\frac{60 \cdot d_{50}}{D_p}\right)}\right) \qquad \text{(6.20-56)}$$

The terminal settling velocity related parameter w, the particle associated velocity, can be determined by:

$$w = 0.9 \cdot v_t + 2.7 \cdot \left(R_{sd} \cdot g \cdot \nu_l\right)^{1/3} \qquad \text{(6.20-57)}$$

It seems this equation mixes the homogeneous and heterogeneous regimes. For very small particles the second term gives a constant particle associated velocity, which matches homogeneous behavior at operational line speeds. Since the homogeneous behavior does not depend on the particle size, this gives a constant or asymptotic particle associated velocity.
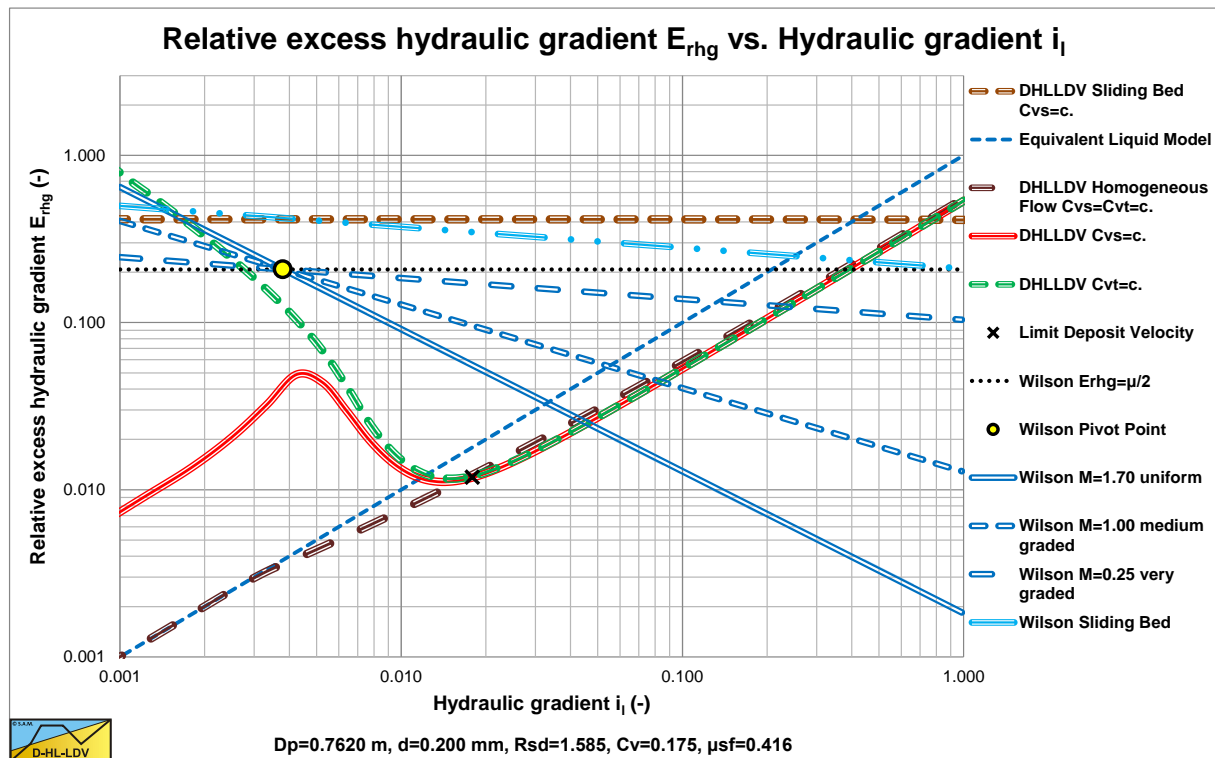
Figure 6.20-20: The power in the Wilson et al. (1992) model, d=0.2 mm.

6.20.2.2 The Simplified Wilson Model.

The model of Wilson can be simplified with some fit functions, according to:

$$v_{50} \approx 3.93 \cdot \left(1000 \cdot d_{50}\right)^{0.35} \cdot \left(\frac{R_{sd}}{1.65}\right)^{0.45} \cdot \left(\frac{\nu_{l,actual}}{\nu_{w,20}}\right)^{-0.25} \qquad \text{(6.20-58)}$$

In which the particle diameter d_{50} is in m and the resulting v_{50} in m/s. The third term on the right had side is the relative viscosity, the actual liquid viscosity divided by the viscosity of water at 20 degrees Centigrade. In normal dredging practice this term is about unity and can be neglected. The factor 1.65 is based on sand in pure water.
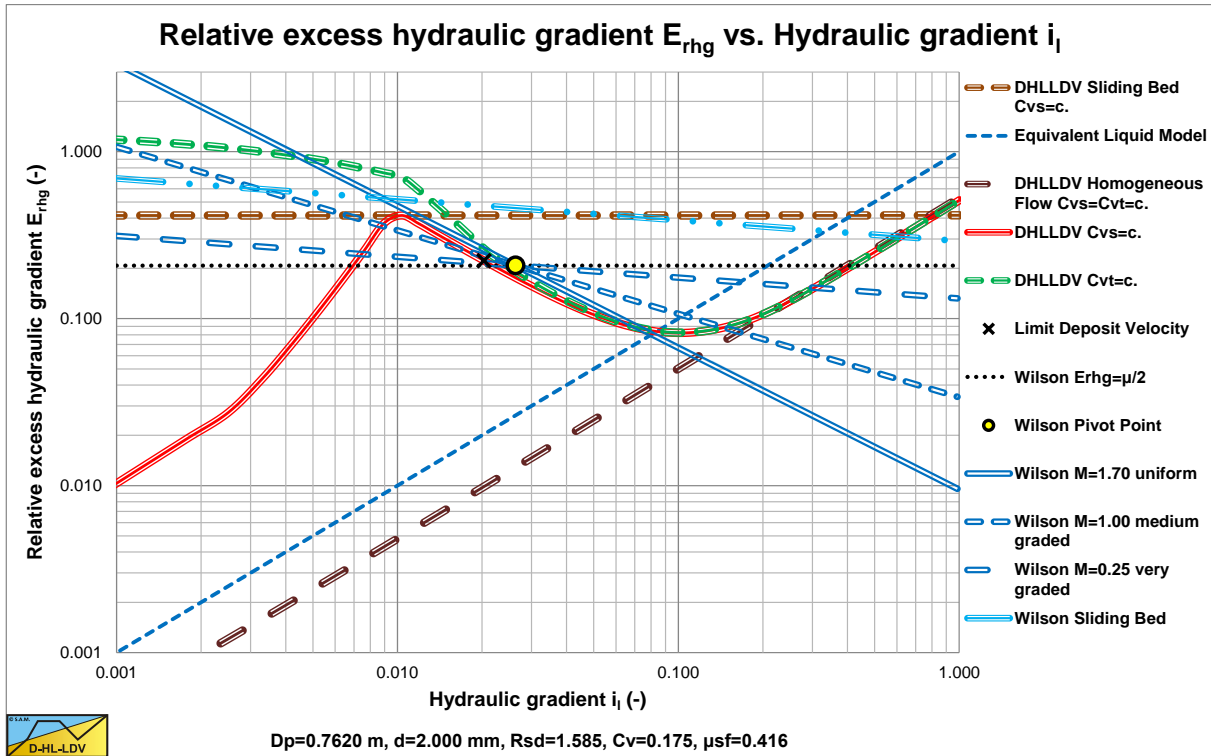
Figure 6.20-21: The power in the Wilson et al. (1992) model, d=2 mm.
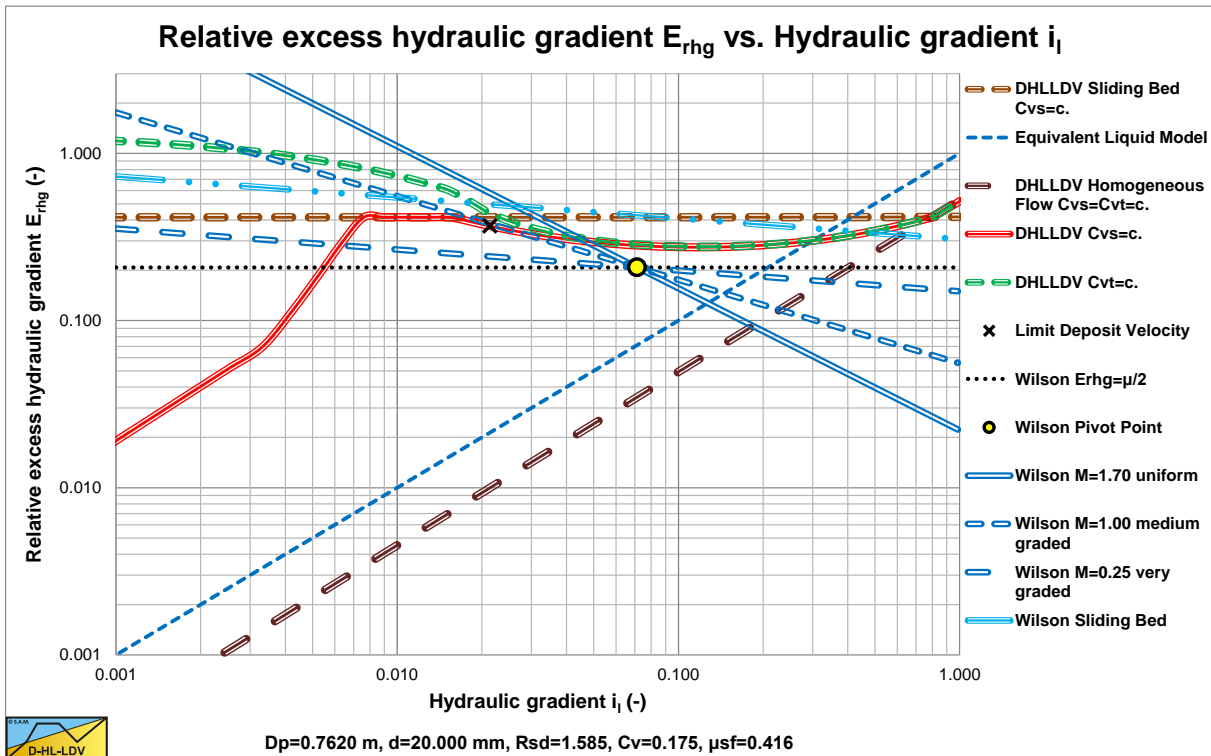
Figure 6.20-22: The power in the Wilson et al. (1992) model, d=20 mm.

In Figure 6.20-20, Figure 6.20-21 and Figure 6.20-22, the DHLLDV Framework is used for comparison.

The exponent **M** is given by the approximation:

$$\mathbf{M} \approx \left(\ln \left(\frac{d_{85}}{d_{50}} \right) \right)^{-1} \tag{6.20-59}$$

Figure 6.20-21 shows the Wilson et al. (1992) model in $E_{rhg}(i_l)$ coordinates. The black dotted line is the $E_{rhg}=\mu_{sf}/2$ line. The yellow circle the point with $v_{ls}=v_{50}$. The heterogeneous Wilson lines have powers of **M=1.7, 1.0 & 0.25**. So heterogeneous lines always cross the yellow circle, the v_{50} point, and are rotated around this point depending on the power **M**. The higher the power **M**, the steeper the line in this graph.

6.20.2.3 Generic Equation.

Based on equation (6.20-53) and equation (6.20-58) and the assumption **M=1** for d_{85}/d_{50}=**2.72** and assuming the liquid is water of 20 degrees Centigrade and the solids are sand (quarts), an equation is derived to compare Wilson with the other theories:

$$i_m = i_l \cdot \left(1 + \frac{\mu_{sf} \cdot g \cdot R_{sd} \cdot D_p}{\lambda_l} \cdot \left(v_{50}\right)^M \cdot \left(\frac{1}{v_{ls}}\right)^{2+M} \cdot C_v\right) \qquad (6.20\text{-}60)$$

For the line speed v_{50}:

$$v_{50} \approx 3.93 \cdot \left(1000 \cdot d_{50}\right)^{0.35} = 44.1 \cdot \left(d_{50}\right)^{0.35} \qquad (6.20\text{-}61)$$

This gives:

$$i_m = i_l \cdot \left(1 + \frac{\mu_{sf} \cdot g \cdot R_{sd} \cdot D_p}{\lambda_l} \cdot \left(44.1 \cdot \left(d_{50}\right)^{0.35}\right)^M \cdot \left(\frac{1}{v_{ls}}\right)^{2+M} \cdot C_v\right) \qquad (6.20\text{-}62)$$

Substituting equation (6.20-61) in equation (6.20-62) gives:

$$i_m = i_l \cdot \left(1 + 44.1^M \cdot \frac{\mu_{sf} \cdot g \cdot R_{sd} \cdot D_p}{\lambda_l} \cdot \left(d_{50}\right)^{0.35 \cdot M} \cdot \left(\frac{1}{v_{ls}}\right)^{2+M} \cdot C_v\right) \qquad (6.20\text{-}63)$$

With the friction coefficient of μ_{sf}=**0.44**, **M=1** and some simplifications, this gives:

$$i_m = i_l \cdot \left(1 + 19.4 \cdot \frac{g \cdot R_{sd} \cdot D_p}{\lambda_l} \cdot \left(d_{50}\right)^{0.35} \cdot \left(\frac{1}{v_{ls}}\right)^3 \cdot C_v\right) \qquad (6.20\text{-}64)$$

Giving each term the dimension of velocity gives:

$$i_m = i_l \cdot \left(1 + 27.64 \cdot \frac{g \cdot R_{sd} \cdot D_p}{\lambda_l} \cdot \left(g \cdot d_{50}\right)^{0.35} \cdot \left(v_l \cdot g\right)^{0.1} \cdot \left(\frac{1}{v_{ls}}\right)^3 \cdot C_v\right) \qquad (6.20\text{-}65)$$

Or:

$$i_m = i_l + 13.82 \cdot \left(g \cdot d_{50}\right)^{0.35} \cdot \left(v_l \cdot g\right)^{0.1} \cdot \frac{1}{v_{ls}} \cdot R_{sd} \cdot C_v \qquad (6.20\text{-}66)$$

The result is an equation where the excess pressure due to the solids is proportional to the pipe diameter D_p and almost proportional to the cube root of the d_{50} of the sand. There is no direct relation with the terminal settling velocity v_t or the particle drag coefficient C_D.

6.20.2.4 Analysis of the v₅₀ Equations.

The analysis in this chapter is based on the personal interpretation of the author of this book.

Figure 6.20-23 shows data of Durand & Condolios (1952) in the relative excess hydraulic gradient versus the line speed graph. The advantage of this graph is that it show the solids effect in a double logarithmic graph, where curved line become straight lines. The graph also contains the horizontal sliding bed curve (dark brown solid line), the 50% sliding bed curve (black dots), the ELM curve (dashed dark blue line) and the minimum **v₅₀** curve (light blue solid line). The intersection line speed of the data series (extrapolated) with the 50% sliding bed curve, the **v₅₀**, increases with increasing particle diameter. The question is how does it increase?

Based on the assumption that Wilson et al. (1992) developed a model for operation conditions, meaning for operational line speeds. Usually this means line speeds above the Limit Deposit Velocity, or slightly below. In the case considered, see Figure 6.20-23, this gives line speeds of about 2.5 m/s up to 5.5 m/s. Now 3 cases can be considered:
1. Fine particles, d<0.0002 mm.
2. Medium particles, 0.0002<d<1 mm.
3. Coarse particles, d>1 mm.

Fine particles are assumed to be transport according to the homogeneous flow regime under operational conditions. So there is a minimum **v₅₀** for particles with a diameter smaller than **d=0.0002 mm**. The resulting minimum curve is shown in Figure 6.20-23 (the solid light blue curve). This curve is close to the data of the **d=0.0002 mm** particles. Since Wilson et al. (1992) used different data to calibrate their model, the match is not exactly. This minimum **v₅₀** can be determined by:

$$ v_{50,min} = 2.7 \cdot \left(R_{sd} \cdot g \cdot v_l\right)^{1/3} \cdot \sqrt{\frac{8}{\lambda_l}} \quad or \quad v_{50,min} = \frac{1}{\mu_{sf}} \cdot \left(R_{sd} \cdot g \cdot v_l\right)^{1/3} \cdot \sqrt{\frac{8}{\lambda_l}} \qquad (6.20-67) $$
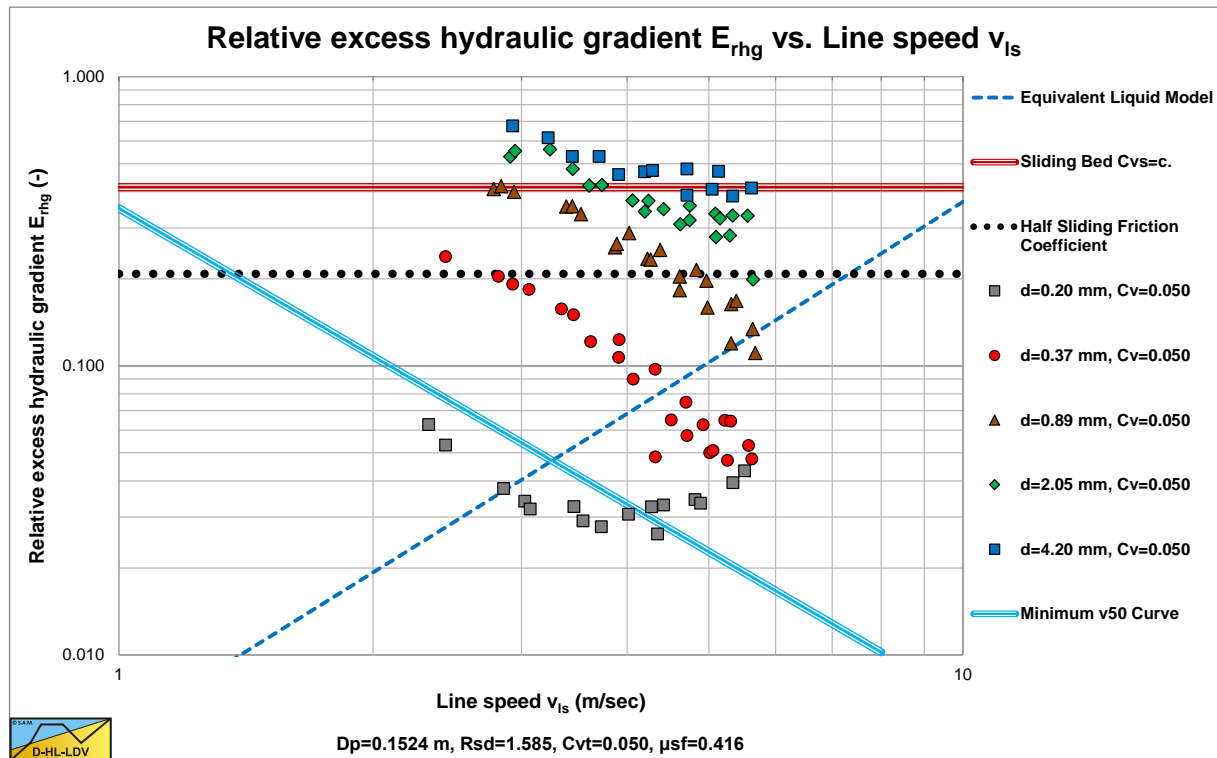
Figure 6.20-23: The data of Durand & Condolios (1952).

For medium sized particles, the **v₅₀** is increasing. Figure 6.20-23 shows this increase for particles with **d=0.37 mm** and **d=0.89 mm**. Wilson et al. (1992) assumed this increase is proportional to the terminal settling velocity **vₜ**. This gives:

$$v_{50} = \left(0.9 \cdot v_t + 2.7 \cdot \left(R_{sd} \cdot g \cdot v_l\right)^{1/3}\right) \cdot \sqrt{\frac{8}{\lambda_l}} \quad \text{or} \quad v_{50} = \left(0.9 \cdot v_t + \frac{1}{\mu_{sf}} \cdot \left(R_{sd} \cdot g \cdot v_l\right)^{1/3}\right) \cdot \sqrt{\frac{8}{\lambda_l}} \qquad \text{(6.20-68)}$$

For coarse particles, the steepness of the decrease of the E_{rhg} parameter with increasing line speed v_{ls} is less than for medium particles. In fact it looks like the larger the particle, the less steep the decrease, where very coarse particles could result in an almost horizontal curve. This also means that the intersection line speed of the extrapolated data points with the 50% sliding bed curve is more far away. A horizontal curve has an intersection v_{50} at infinity. Wilson et al. (1992) took this behavior into account by adding a term with the particle diameter to pipe diameter ratio, according to:

$$v_{50} = \left(0.9 \cdot v_t + 2.7 \cdot \left(R_{sd} \cdot g \cdot v_l\right)^{1/3}\right) \cdot \sqrt{\frac{8}{\lambda_l}} \cdot \cosh\left(\frac{60 \cdot d_{50}}{D_p}\right) \qquad \text{(6.20-69)}$$

The Darcy Weisbach friction coefficient λ_l indirectly gives the influence of the pipe diameter. The cosh term gives the influence of the particle diameter to pipe diameter ratio. Figure 6.20-24 shows the resulting v_{50} curve for a $D_p=0.1524$ m pipe (6 inch) (the thick black solid line).

The v_{50} versus the Particle diameter

Dp=0.1524 m, Rsd=1.585, Cvs=0.300, µsf=0.416
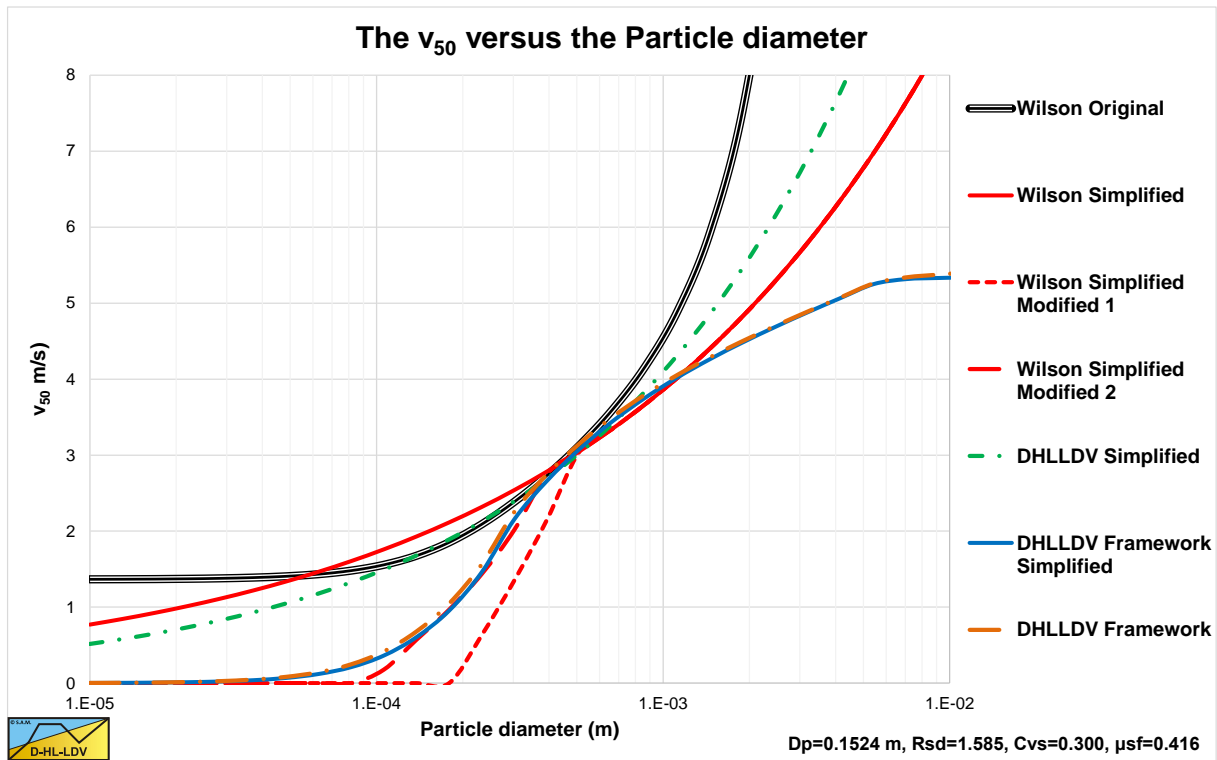
Figure 6.20-24: The v_{50} curves for a $D_p=0.1524$ m pipe.

$$E_{rhg} = R = \frac{i_m - i_l}{R_{sd} \cdot C_v} = \frac{\Delta p_m - \Delta p_l}{\rho_l \cdot g \cdot \Delta L \cdot R_{sd} \cdot C_v} = \frac{\mu_{sf}}{2} \cdot \left(\frac{v_{50}}{v_{ls}}\right)^M \qquad \text{(6.20-70)}$$

For uniform sands Wilson et al. (1992) found a power $M=1.7$ in the above equation, which works well for medium sands, however for the coarser sands the effect of the cosh term in the v_{50} should be accompanied by a decrease of this power as follows from the data in Figure 6.20-23. Durand & Condolios (1952) found that for coarse particles the hydraulic gradient and thus the E_{rhg} parameter does not really increase, based on the particle Froude number. The definition of coarse is related to the pipe diameter by Wilson et al. (1992) being $d=0.015 \cdot D_p$ or $d=D_p/60$. This gives for the v_{50}:

$$v_{50*} = \left(0.9 \cdot v_{t*} + 2.7 \cdot \left(R_{sd} \cdot g \cdot v_l\right)^{1/3}\right) \cdot \sqrt{\frac{8}{\lambda_l}} \cdot \cosh(1) \qquad \text{(6.20-71)}$$

The line speed where the heterogeneous curve intersects with the sliding bed curve is about:

$$
\mathbf{v_{ls*}} = \frac{\mathbf{2}}{\mathbf{3}} \cdot \mathbf{v_{50*}}
\tag{6.20-72}
$$

Now assume this line speed is a constant, given a certain pipe diameter, the power $\mathbf{M}$ for particles of $\mathbf{d > 0.015 \cdot D_p}$ is:

$$
\mathbf{M} = \frac{\ln(\mathbf{2})}{\ln\left(\dfrac{\mathbf{3}}{\mathbf{2}} \cdot \dfrac{\mathbf{v_{50}}}{\mathbf{v_{50*}}}\right)}
\tag{6.20-73}
$$

In these equations the * is used for the particle diameter $\mathbf{d > 0.015 \cdot D_p}$. This approach leads to a continuous behavior of the heterogeneous flow regime.
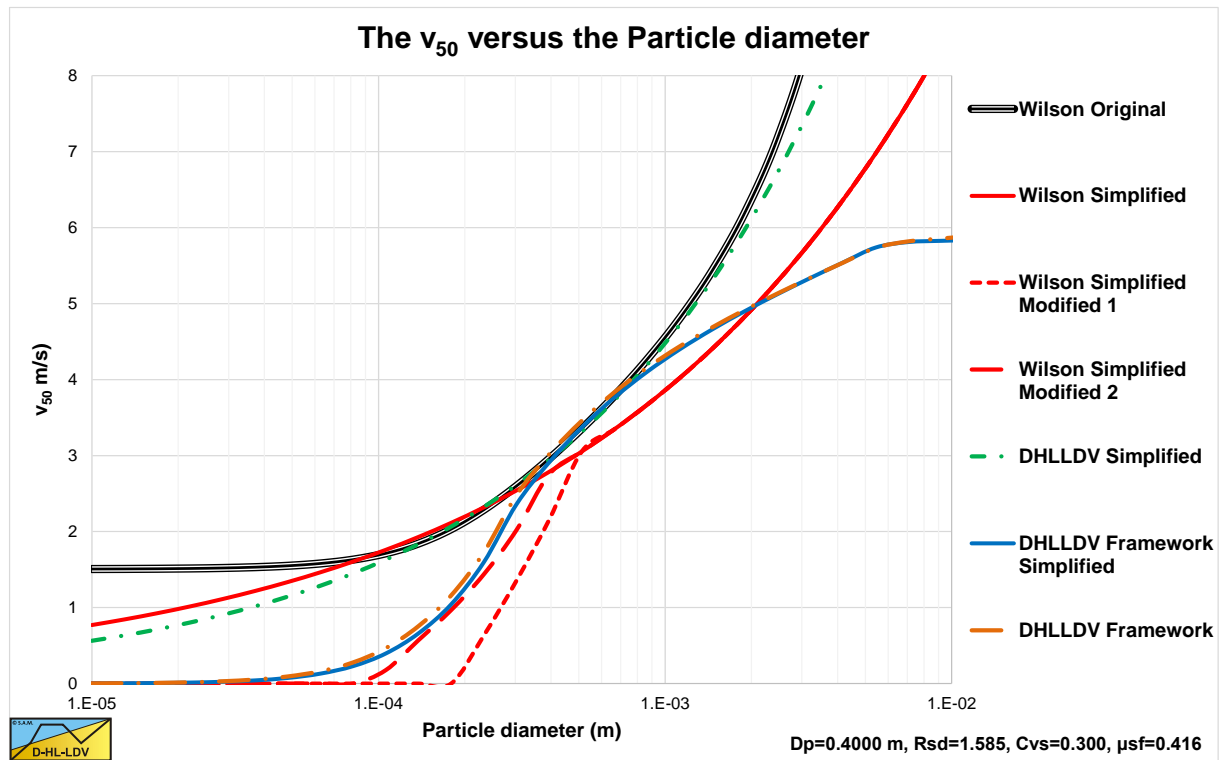
Figure 6.20-25: The v$_{50}$ curves for a D$_p$=0.4 m pipe.

Wilson et al. (1992) simplified the $\mathbf{v_{50}}$ equation to:

$$
\mathbf{v_{50}} \approx \mathbf{3.93} \cdot \left(\frac{\mathbf{d_{50}}}{\mathbf{0.001}}\right)^{\mathbf{0.35}} \cdot \left(\frac{\mathbf{R_{sd}}}{\mathbf{1.65}}\right)^{\mathbf{0.45}} \cdot \left(\frac{\mathbf{v_{l,actual}}}{\mathbf{v_{w,20}}}\right)^{\mathbf{-0.25}}
\tag{6.20-74}
$$

Giving a $\mathbf{v_{50}}$ of 3.93 m/s for a 1 mm sand particle in 20° water. This simplified equation is also shown in Figure 6.20-24 (the solid red line). This equation does not contain the influence of the pipe diameter and only approaches the original equation for medium sands. Later the simplified equation has been adjusted for particles with diameters from 0.2 mm to 0.5 mm with a factor:

$$
\mathbf{f} = \frac{\mathbf{d_h} - \mathbf{0.0002}}{\mathbf{0.0005} - \mathbf{0.0002}}
\tag{6.20-75}
$$

This is also shown in Figure 6.20-24 as the Wilson simplified modified curve (dashed red line). Where the original equation seems to overestimate the solids effect of fine particles, this modification seems to underestimate the solids effect.

Figure 6.20-24, Figure 6.20-25 and Figure 6.20-26 show the original v_{50} method, the simplified and the simplified modified equations. The effect of not having the pipe diameter influence in the simplified and the simplified modified equations results in a deviation of these equations with the original method for large diameter pipes.

The v_{50} versus the Particle diameter

Dp=1.2000 m, Rsd=1.585, Cvs=0.300, μsf=0.416
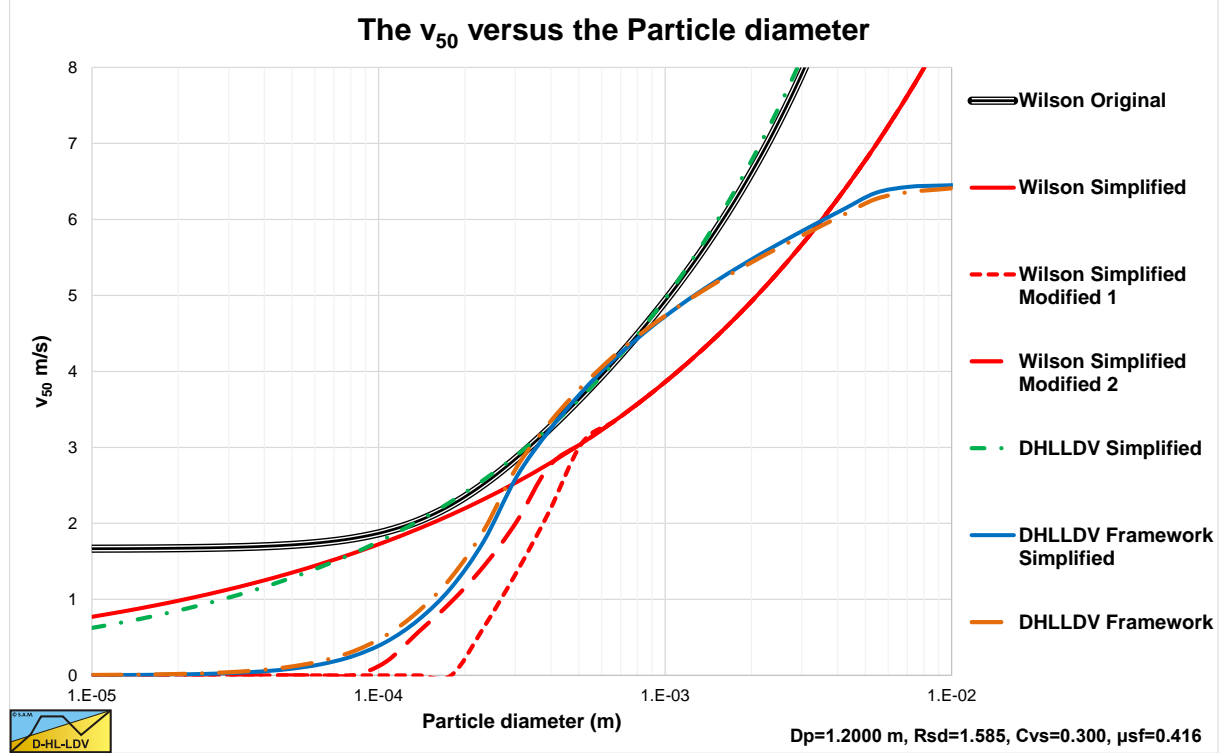
Figure 6.20-26: The v_{50} curves for a D_p=1.2 m pipe.

A better simplification of the v_{50} is achieved with the following equation (DHLLDV simplified, the solid green line):

$$v_{50} \approx 3 \cdot \left(\frac{d_{50}}{0.0005} \right)^{0.45} \cdot \left(\frac{R_{sd}}{1.65} \right)^{0.45} \cdot \left(\frac{\nu_{l,actual}}{\nu_{w,20}} \right)^{-0.25} \cdot \left(\frac{D_p}{0.1524} \right)^{0.092} \tag{6.20-76}$$

Figure 6.20-24, Figure 6.20-25 and Figure 6.20-26 show this equation as well. For a D_p=0.1524 m (6 inch) pipe, this equation gives an almost identical v_{50} compared to the original method for particle diameters in the range of 0.1 to 0.8 mm. For the D_p=0.4 m pipe this range is larger, from 0.1 to 2 mm. For the D_p=1.2 m the range is even larger than for the D_p=0.4 m pipe, the approximation is valid for particles with a diameter from 0.1 mm and above. Still the overestimation of the v_{50} for small particles remains, as a result of the original assumption of Wilson that there is a minimum v_{50}. Figure 6.20-35 shows that also particles with a diameter smaller than 0.1 mm show heterogeneous behavior with a v_{50} much smaller than this minimum v_{50}. The correction with equation (6.20-75) seems too drastic and not at the right location. The following correction factor in the range of particle diameters from 0.1 to 0.3 mm seems more appropriate and approaches the DHLLDV curves closely.

$$f = \frac{d_h - 0.0001}{0.0004 - 0.0001} \tag{6.20-77}$$

A better approach of the v_{50} however is the following equation, based on the DHLLDV Framework:

$$v_{50} \approx 3.4 \cdot \left(\frac{v_t}{\sqrt{g \cdot d}} \right)^{1.96} \cdot \left(\frac{D_p}{0.1524} \right)^{0.092} \cdot \left(\frac{R_{sd}}{1.65} \right)^{-0.092} \cdot \left(\frac{\nu_{l,actual}}{\nu_{w,20}} \right)^{0.27} \tag{6.20-78}$$

Figure 6.20-24, Figure 6.20-25 and Figure 6.20-26 show the results of this equation and also the results of the much more complicated DHLLDV Framework. In the range of particle diameters of 0.3 to 1 mm, this equation matches the original Wilson method very closely. Above 1 mm the original Wilson method goes to infinity (because of the decreasing power **M**), while the DHLLDV simplified equation goes to a constant value (assuming the power **M** does not change) matching the findings of Durand & Condolios (1952). For particles with a diameter smaller than 0.3 mm this equation matches many experimental data and solves the problem of overestimation of the original Wilson method in a more structural way

6.20.2.5 Conclusions & Discussion.

The basic form of the equation for heterogeneous transport, equation (6.20-51), is of the type; hydraulic gradient mixture equals hydraulic gradient carrier liquid + solids effect. This implies that the hydraulic gradient of the carrier liquid and the solids effect are independent like in the Fuhrboter (1961) model. This in contrary with the Durand & Condolios (1952), Newitt et al. (1955) and the Jufin & Lopatin (1966) models. These are of the type; hydraulic gradient mixture equals hydraulic gradient carrier liquid times 1 + solids effect. Equations (6.20-65) and (6.20-66) show the Wilson equation for both types, with correct dimensions.

Basically the model shows straight lines in the $E_{rhg}(i_l)$ graph with the v_{50}, **0.22** point as a pivot point. Depending on the value of the power **M**, the straight line pivots around this point. Figure 6.20-21 shows these straight line for powers of 0.25, 1.0 and 1.7. The power of 1.7 for uniform sands matches very well with the DHLLDV Framework for uniform sands.

The model gives good results if the physics on which it is based occur, medium sized particles. For very fine particles in a large pipe there will never be a sliding bed. The stationary bed will vaporize (erode) with increasing line speed, probably without sheet flow, see Figure 6.20-20. The 50% stratification criterion is not valid here because the sliding friction is not 100% mobilized resulting in a much lower friction. Very large particles will, almost always, be more than 50% stratified, resulting in a sliding bed or sliding flow, so the model is also invalid in this case, see Figure 6.20-22.

The DHLLDV simplified equation gives a much better approximation of the v_{50} parameter and solved a number of shortcomings.

Wilson et al. (2006) suggests the following equation for full stratified flow, based on μ_{sf}=**0.4** (or **0.44**):

$$i_m = i_l + C_{vt} \cdot R_{sd} \cdot 2 \cdot \mu_{sf} \cdot \left(\frac{4 \cdot v_{sm}}{3 \cdot v_{ls}}\right)^{0.25} \quad \text{or} \quad i_m = i_l + C_{vt} \cdot R_{sd} \cdot 2 \cdot \mu_{sf} \cdot \left(\frac{v_{sm}}{v_{ls}}\right)^{0.25} \tag{6.20-79}$$

$$\text{Based on } \mu_{sf} = 0.40 \qquad \qquad \text{Based on } \mu_{sf} = 0.44$$

As is shown in Figure 6.20-22 there will be a discontinuity jumping from the heterogeneous model to the full stratified model, even if the same power of 0.25 is applied. In fact if more than 50% of the solids is stratified, the v_{50} point at E_{rhg}=**0.22** in the 3 graphs will never be reached.

In a number of papers the fully stratified flow term is reduced to 50% or even 25%, so it is not really clear what to use. Assuming a full sliding bed at the Limit of Stationary Deposity Velocity, the equation should be for the constant spatial volumetric case and based on the weight approach:

$$i_m = i_l + C_{vs} \cdot R_{sd} \cdot \mu_{sf} \cdot \left(\frac{v_{sm}}{v_{ls}}\right)^{0.25} \tag{6.20-80}$$

For the constant delivered volumetric case this gives:

$$i_m = i_l + \frac{C_{vs}(v_{sm})}{C_{vt}} \cdot C_{vt} \cdot R_{sd} \cdot \mu_{sf} \cdot \left(\frac{v_{sm}}{v_{ls}}\right)^{0.25} \tag{6.20-81}$$

Where the spatial concentration at the LSDV depends on the line speed and other parameters, but is always larger than 1.

6.20.3 The 4 Component Model of Wilson & Sellgren (2001).

6.20.3.1 Introduction.

Broad particle grading mean that several of the normally considered slurry flow regimes are included. A pipeline slurry friction loss model consisting of three regimes was initially proposed by K.C. Wilson in (2001), then extended to a four components consisting of fluid, pseudo-homogeneous, heterogeneous and fully stratified components, Wilson et al. (2006). It was successively developed and validated for a variety of experimental data covering volumetric solids concentrations of up to nearly 40% and particle sizes of up to 65mm, Sellgren and Wilson (2007).

Four components are distinguished:
1. Homogeneous flow (uses the index **f**), the fraction **d<0.04 mm**.
2. Pseudo homogeneous flow (uses the index **ph**), the fraction **0.04 mm<d<0.2·v_r mm**.
3. Heterogeneous flow (uses the index **h**), the fraction **0.2·v_r mm<d<0.015·D_p**.
4. Stratified flow (uses the index **s**), **d>0.015·D_p**.

The relative kinematic viscosity v_r is the ratio of the kinematic viscosity of the carrier fluid to that of water at 20°C.

The sum of the 4 fractions always has to be equal to unity.

$$X_f + X_{ph} + X_h + X_s = 1 \tag{6.20-82}$$

The total delivered volumetric concentration is the sum of the concentrations of the 4 fractions.

$$C_{vt} = C_{vt,f} + C_{vt,ph} + C_{vt,h} + C_{vt,s} = X_f \cdot C_{vt} + X_{ph} \cdot C_{vt} + X_h \cdot C_{vt} + X_s \cdot C_{vt} \tag{6.20-83}$$

The total hydraulic gradient of the mixture is the sum of the hydraulic (excess) gradients of the 4 fractions.

$$i_m = i_f + \Delta i_{ph} + \Delta i_h + \Delta i_s \quad \text{in} \quad \text{(m carrier liquid/m pipe)} \tag{6.20-84}$$

6.20.3.2 The Homogeneous or Equivalent Fluid Fraction.

In the homogeneous phase, the spatial and transport volumetric concentrations are assumed to be equal.

$$C_{vs,f} = C_{vt,f} \tag{6.20-85}$$

Thomas (1965) derived an equation to determine the effective viscosity μ_f as a function of the concentration $C_{vs,f}$ of the particles in the mixture:

$$\mu_f = \mu_l \cdot \left(1 + 2.5 \cdot C_{vs,f} + 10.05 \cdot C_{vs,f}^2 + 0.00273 \cdot e^{16.6 \cdot C_{vs,f}}\right) \quad \text{with:} \quad \mu_r = \mu_f / \mu_l \tag{6.20-86}$$

The fluid density ρ_f equals the carrier liquid density ρ_l plus the additional density of the homogeneous fraction of the PSD, according to Wilson et al. (2006) the fraction smaller than 0.04 mm.

$$\rho_f = \rho_l \cdot \left(1 + R_{sd} \cdot C_{vs,f}\right) \quad \text{and} \quad v_f = \frac{\mu_f}{\rho_f} \tag{6.20-87}$$

This results in modified fluid properties compared with the carrier liquid, which will be used for all the flow regimes. The hydraulic gradient of the homogeneous flow regime i_f is now:

$$i_l = \frac{\lambda_f \cdot v_{ls}^2}{2 \cdot g \cdot D_p} \quad \Rightarrow \quad i_f = \frac{\Delta p_f}{\rho_l \cdot g \cdot \Delta L} = \frac{\rho_f}{\rho_l} \cdot \frac{\lambda_f \cdot v_{ls}^2}{2 \cdot g \cdot D_p} = \frac{\rho_f}{\rho_l} \cdot i_l \quad \text{with:} \quad \Delta p_f = \lambda_f \cdot \frac{\Delta L}{D_p} \cdot \frac{1}{2} \cdot \rho_f \cdot v_{ls}^2 \tag{6.20-88}$$

The Darcy Weisbach friction factor λ_f is determined based on these fluid properties. The Darcy Weisbach friction factor will not differ much from the Darcy Weisbach friction factor resulting from the carrier liquid properties.

6.20.3.3 The Pseudo Homogeneous Fraction.

In the pseudo homogeneous phase, the spatial and transport volumetric concentrations are also assumed to be equal.

$$\mathbf{C_{vs,ph} = C_{vt,ph}}$$ (6.20-89)

The hydraulic gradient $\Delta\mathbf{i_{ph}}$ is determined with the ELM model without adjusting the effective viscosity according to:

$$\Delta\mathbf{i_{ph} = C_{vs,ph} \cdot \left(\frac{\rho_s - \rho_f}{\rho_f}\right) \cdot i_f = C_{vs,ph} \cdot \left(\frac{\rho_s - \rho_f}{\rho_f}\right) \cdot \frac{\rho_f}{\rho_l} \cdot i_l = C_{vs,ph} \cdot \left(\frac{\rho_s - \rho_f}{\rho_l}\right) \cdot i_l}$$ (6.20-90)

The resulting density $\mathbf{\rho_{fp}}$ for the next flow regime is:

$$\mathbf{\rho_{fp} = \rho_l \cdot \left(1 + R_{sd} \cdot C_{vs,f} + R_{sd} \cdot C_{vs,ph}\right)}$$ (6.20-91)

The fluid viscosity is not adjusted for the density or concentration in this fraction.

6.20.3.4 The Heterogeneous Fraction.

The original Wilson et al. (2006) heterogeneous model is based on a velocity $\mathbf{v_{50}}$, where 50% of the solids are stratified and the other 50% in suspension. The simplified equation to determine this $\mathbf{v_{50}}$ is:

$$\mathbf{v_{50} \approx 3.93 \cdot \left(1000 \cdot d_{50}\right)^{0.35} \cdot \left(\frac{R_{sd}}{1.65}\right)^{0.45} \cdot \left(\frac{\nu_f}{\nu_{l,20}}\right)^{-0.25}}$$ (6.20-92)

The original equation to determine the excess hydraulic gradient is:

$$\Delta\mathbf{i_h = C_{vt} \cdot R_{sd} \cdot \frac{\mu_{sf}}{2} \cdot \left(\frac{v_{50}}{v_{ls}}\right)^M}$$ (6.20-93)

The equation for $\mathbf{v_{50}}$ now has to be adjusted for an average particle diameter of the heterogeneous fraction $\mathbf{d_h}$ and for the relative submerged density according to:

$$\mathbf{v_{50} \approx 3.93 \cdot \left(1000 \cdot d_h\right)^{0.35} \cdot \left(\frac{\rho_s - \rho_{fp}}{\rho_l} \cdot \frac{1}{1.65}\right)^{0.45} \cdot \nu_r^{-0.25}}$$

$$\mathbf{d_h = \frac{\left(0.0002 \cdot \nu_r + \text{Min}\left(0.015 \cdot D_p, d_{max}\right)\right)}{2}}$$ (6.20-94)

The excess hydraulic gradient $\Delta\mathbf{i_h}$ can now be determined according to, where $\mathbf{M}$ is taken as unity:

$$\Delta\mathbf{i_h = \frac{\rho_{fp}}{\rho_l} \cdot C_{vt,h} \cdot \left(\frac{\rho_s - \rho_{fp}}{\rho_{fp}}\right) \cdot \frac{\mu_{sf}}{2} \cdot \left(\frac{v_{50}}{v_{ls}}\right)^M}$$

or (6.20-95)

$$\Delta\mathbf{i_h = \frac{\rho_{fp}}{\rho_l} \cdot C_{vt,h} \cdot \left(\frac{\rho_s - \rho_{fp}}{\rho_{fp}}\right) \cdot \frac{\mu_{sf}}{2} \cdot \left(\frac{v_{50}}{v_{ls}}\right)^M \cdot \frac{d_h - 0.0002}{0.0005 - 0.0002}} \quad \textbf{for} \quad \mathbf{0.0002 < d_h < 0.0005}$$

The resulting density for the next flow regime is:

$$\rho_{fph} = \rho_l \cdot \left(1 + R_{sd} \cdot C_{vs,f} + R_{sd} \cdot C_{vs,ph} + R_{sd} \cdot C_{vs,h}\right) \tag{6.20-96}$$

6.20.3.5 The Fully Stratified Fraction.

In the original model of Wilson et al. (2006) the maximum limit of stationary deposit velocity v_{sm} can be estimated by:

$$v_{sm} = \frac{8.8 \cdot \left(\dfrac{\mu_{sf} \cdot R_{sd}}{0.66}\right)^{0.55} \cdot D_p^{0.7} \cdot d^{1.75}}{d^2 + 0.11 \cdot D_p^{0.7}} \tag{6.20-97}$$

The original excess hydraulic gradient for a fully stratified flow can be approximated by (for a friction coefficient of 0.4):

$$\Delta i_s = C_{vt} \cdot R_{sd} \cdot 2 \cdot \mu_{sf} \cdot \left(\frac{v_{sm}}{v_{ls}}\right)^{0.25} \tag{6.20-98}$$

Wilson et al. (2006) suggest to multiply this equation by 0.5, adjust the relative submerged density, not to adjust v_{sm} and of course use the stratified fraction according to:

$$\Delta i_s = \frac{\rho_{fph}}{\rho_l} \cdot C_{vt,s} \cdot \left(\frac{\rho_s - \rho_{fph}}{\rho_{fph}}\right) \cdot \mu_{sf} \cdot \left(\frac{v_{sm}}{v_{ls}}\right)^{0.25} \tag{6.20-99}$$

The resulting mixture density is now:

$$\rho_m = \rho_l \cdot \left(1 + R_{sd} \cdot C_{vs,f} + R_{sd} \cdot C_{vs,ph} + R_{sd} \cdot C_{vs,h} + R_{sd} \cdot C_{vs,s}\right) = \rho_l \cdot \left(1 + R_{sd} \cdot C_{vs}\right) \tag{6.20-100}$$

6.20.3.6 The Resulting Equation.

The resulting equation of the 4 component model is:

$$i_m = \frac{\rho_f}{\rho_l} \cdot \frac{\lambda_f \cdot v_{ls}^2}{2 \cdot g \cdot D_p} \cdot \left(1 + C_{vt,ph} \cdot \left(\frac{\rho_s - \rho_f}{\rho_f}\right)\right) + \frac{\rho_{fp}}{\rho_l} \cdot C_{vt,h} \cdot \left(\frac{\rho_s - \rho_{fp}}{\rho_{fp}}\right) \cdot \frac{\mu_{sf}}{2} \cdot \left(\frac{v_{50}}{v_{ls}}\right)^M$$

$$\tag{6.20-101}$$

$$+ \frac{\rho_{fph}}{\rho_l} \cdot C_{vt,s} \cdot \left(\frac{\rho_s - \rho_{fph}}{\rho_{fph}}\right) \cdot \mu_{sf} \cdot \left(\frac{v_{sm}}{v_{ls}}\right)^{0.25}$$

The way the different mixture densities are determined is incorrect. For low concentrations the difference is negligible, but for high concentrations it may be significant.

6.20.3.7 Modified 4 Component Model.

Analyzing the 4 component model results in a number of issues, which will be addressed here. The first issue is the way the densities of the carrier liquid with the different fractions is calculated. If a sand or gravel is considered with a volumetric concentration C_{vs} of which a fraction X is in suspension, then the resulting mixture density ρ_x should be determined based on the volume of carrier liquid and the volume of the fraction X and not on the total volume. So the mixture density ρ_x times the volume of the carrier liquid $(1-C_{vs})$ + the volume of the fraction considered $X \cdot C_{vs}$, which is the mass of the mixture, has to be equal to the mass of the carrier liquid $\rho_l \cdot (1-C_{vs})$ + the mass of the solids considered $\rho_s \cdot C_{vs} \cdot X$. This gives the following equation:

$$\rho_x \cdot \left(1 - C_{vs} + C_{vs} \cdot X\right) = \rho_l \cdot \left(1 - C_{vs}\right) + \rho_s \cdot X \cdot C_{vs}$$

$$\frac{\rho_x}{\rho_l} = S_x = \frac{\left(1 - C_{vs}\right) + S_s \cdot X \cdot C_{vs}}{\left(1 - C_{vs} + C_{vs} \cdot X\right)} \quad \text{with:} \quad S_s = \frac{\rho_s}{\rho_l}$$

(6.20-102)

This can be written as, with some reorganization and simplification:

$$\frac{\rho_x}{\rho_l} = S_x = \frac{\left(1 - C_{vs}\right) + S_s \cdot X \cdot C_{vs} + C_{vs} \cdot X - C_{vs} \cdot X}{\left(1 - C_{vs} + C_{vs} \cdot X\right)}$$

$$\frac{\rho_x}{\rho_l} = S_x = \frac{\left(1 - C_{vs}\right) + C_{vs} \cdot X + X \cdot C_{vs} \cdot \left(S_s - 1\right)}{\left(1 - C_{vs} + C_{vs} \cdot X\right)} = 1 + \frac{X \cdot C_{vs} \cdot \left(S_s - 1\right)}{\left(1 - C_{vs} + C_{vs} \cdot X\right)}$$

(6.20-103)

$$\text{If } X = 1 \quad \Rightarrow \quad \frac{\rho_m}{\rho_l} = S_m = 1 + C_{vs} \cdot \left(S_s - 1\right)$$

So if all the particles are considered, **X=1**, the resulting equation reduces to the simple equation also used in the ELM. However if **X<>1** equation (6.20-103) gives a different result compared to equation (6.20-87), (6.20-91) and (6.20-96). Using the relative submerged density R_{sd} this gives:

$$\frac{\rho_x}{\rho_l} = S_x = 1 + \frac{X \cdot C_{vs} \cdot R_{sd}}{\left(1 - C_{vs} + C_{vs} \cdot X\right)}$$

(6.20-104)

This gives for the relative density S_f of the homogeneous mixture of particles with **d<0.000040 m**:

$$S_f = \frac{\rho_f}{\rho_l} = 1 + \frac{X_f \cdot C_{vs} \cdot R_{sd}}{1 - C_{vs} \cdot \left(1 - X_f\right)}$$

(6.20-105)

For the homogeneous and the pseudo homogeneous fraction this gives a relative density of the mixture S_{fp} for particles with **d<0.000200 m** (in water):

$$S_{fp} = \frac{\rho_{fp}}{\rho_l} = 1 + \frac{\left(X_f + X_{ph}\right) \cdot C_{vs} \cdot R_{sd}}{1 - C_{vs} \cdot \left(1 - X_f - X_{ph}\right)}$$

(6.20-106)

Including the heterogeneous fraction, together with the homogeneous and pseudo homogeneous fractions gives a relative density of the mixture S_{fph} for particles with **d<0.015·D$_p$**:

$$S_{fph} = \frac{\rho_{fph}}{\rho_l} = 1 + \frac{\left(X_f + X_{ph} + X_h\right) \cdot C_{vt} \cdot R_{sd}}{1 - C_{vt} \cdot \left(1 - X_f - X_{ph} - X_h\right)}$$

(6.20-107)

Also including the stratified fraction, results in all the particles giving a relative mixture density of $S_{fphs}=S_m$:

$$S_{fphs} = \frac{\rho_{fphs}}{\rho_l} = 1 + \frac{\left(X_f + X_{ph} + X_h + X_s\right) \cdot C_{vt} \cdot R_{sd}}{1 - C_{vt} \cdot \left(1 - X_f - X_{ph} - X_h - X_s\right)} = S_m = \frac{\rho_m}{\rho_l} = 1 + C_{vt} \cdot R_{sd}$$

(6.20-108)

With :

$$X_f + X_{ph} + X_h + X_s = 1$$

Now that all the relative densities are known, the hydraulic gradients will be determined, after adjusting the liquid viscosity according to equations (6.20-86) and (6.20-87).

The relative submerged density of particles in the new homogeneous fluid is:

$$R_{sd,f} = \frac{\rho_s - \rho_f}{\rho_f}$$

(6.20-109)

Now for each fraction the hydraulic gradient, based on the carrier liquid density ρ_l, will be determined as if only that fraction is present in the mixture with a concentration C_{vt}.

Homogeneous regime:

The hydraulic gradient of the homogeneous flow regime i_f is now:

$$i_f = \frac{\rho_f}{\rho_l} \cdot \frac{\lambda_f \cdot v_{ls}^2}{2 \cdot g \cdot D_p} = S_f \cdot \frac{\lambda_f \cdot v_{ls}^2}{2 \cdot g \cdot D_p} = \frac{\rho_f}{\rho_l} \cdot i_l = S_f \cdot i_l$$

(6.20-110)

The difference with pure carrier liquid is the Darcy Weisbach friction factor and the relative density S_f of the resulting homogeneous fluid. For small homogeneous fractions, the Darcy Weisbach friction factor will not differ much from the factor determined for the carrier liquid. So the main difference is the use of the relative density $S_f > 1$ instead of 1.

Pseudo homogeneous regime:

For the pseudo homogeneous regime, the hydraulic gradient i_{ph} is, with a factor A of about 0.6-0.8, also depending on the pipe diameter:

$$i_{ph} = i_f \cdot \left(1 + A \cdot C_{vt} \cdot R_{sd,f}\right) = \frac{\rho_f}{\rho_l} \cdot i_l \cdot \left(1 + A \cdot C_{vt} \cdot R_{sd,f}\right)$$

(6.20-111)

Heterogeneous regime:

The excess hydraulic gradient Δi_h for the heterogeneous regime can now be determined according to:

First consider the v_{50}. If the heterogeneous particles settle in the homogeneous fluid the v_{50} is:

$$v_{50,f} \approx 3.93 \cdot \left(1000 \cdot d_h\right)^{0.35} \cdot \left(\frac{R_{sd,f}}{1.65}\right)^{0.45} \cdot v_r^{-0.25}$$

(6.20-112)

The excess hydraulic gradient Δi_h for the heterogeneous regime is based on the assumption that at a velocity of v_{50}, 50% of the particles are in contact load. If it is considered that these particles are in a heavier fluid formed by the homogeneous particles and the carrier liquid, the weight of these particles has to be corrected, giving:

$$i_h = i_f + C_{vt} \cdot R_{sd,f} \cdot \frac{\mu_{sf}}{2} \cdot \left(\frac{v_{50,f}}{v_{ls}}\right)^M$$

(6.20-113)

Fully stratified regime:

For the fully stratified fraction the same logic applies. If the weight is reduced by the homogeneous fraction and the carrier liquid, the following applies (with β from Figure 6.20-1 for the stratified fraction):

$$i_s = i_f + B \cdot C_{vt} \cdot R_{sd,f} \cdot \mu_{sf} \cdot \left(\frac{v_{sm,f}}{v_{ls}}\right)^{0.25}$$

(6.20-114)

With the factor **B** in the hydrostatic normal stress approach:

$$B = \frac{2 \cdot \left(\sin(\beta) - \beta \cdot \cos(\beta) \right)}{\left(\beta - \sin(\beta) \cdot \cos(\beta) \right)} \tag{6.20-115}$$

The SRC model uses buoyancy for the stratified fraction, based on the density of the suspension above the bed. The stratified fraction however decreases with increasing line speed in this model. The 4 component model does not have such a feature.

The resulting hydraulic gradient of the modified 4 component model is, without buoyancy:

$$
\begin{aligned}
i_{m,f} = &\ X_f \cdot i_f + X_{ph} \cdot \left(i_f \cdot \left(1 + A \cdot C_{vt} \cdot R_{sd,f} \right) \right) + X_h \cdot \left(i_f + C_{vt} \cdot R_{sd,f} \cdot \frac{\mu_{sf}}{2} \cdot \left(\frac{v_{50,f}}{v_{ls}} \right)^M \right) \\
&+ X_s \cdot \left(i_f + B \cdot C_{vt} \cdot R_{sd,f} \cdot \mu_{sf} \cdot \left(\frac{v_{sm,f}}{v_{ls}} \right)^{0.25} \right)
\end{aligned}
\tag{6.20-116}
$$

This can be simplified to:

$$i_m = \frac{\rho_f}{\rho_l} \cdot i_f + \frac{\rho_f}{\rho_l} \cdot C_{vt} \cdot R_{sd,f} \cdot \left(A \cdot X_{ph} \cdot i_f + X_h \cdot \frac{\mu_{sf}}{2} \cdot \left(\frac{v_{50,f}}{v_{ls}} \right)^M + B \cdot \frac{X_s}{1 - \xi_{vsm}} \cdot \mu_{sf} \cdot \left(\frac{v_{sm,f}}{v_{ls}} \right)^{0.25} \right) \tag{6.20-117}$$

The factor **A<1** is included because often the excess hydraulic gradient is smaller than the ELM would give. The factor **B** is included, because with **β=π** the term describes plug flow. For **β<π** the factor **B** decreases with **β, β=π/2** gives **B=1.3** and **β=0** gives **B=1.** So for low concentrations and small fully stratified fractions a value of **B=1** should be chosen, which matches the choice of Wilson for a **B'=0.5**. The weight approach of Miedema & Ramsdell (2014) also uses **B=1**.

The equation derived however has some restrictions. First of all, the heterogeneous term cannot be larger than the fully stratified term, because in that case the heterogeneous fraction would not be heterogeneous but fully stratified, so:

$$\frac{\mu_{sf}}{2} \cdot \left(\frac{v_{50,f}}{v_{ls}} \right)^M > B \cdot \mu_{sf} \cdot \left(\frac{v_{sm,f}}{v_{ls}} \right)^{0.25} \tag{6.20-118}$$

$$\Rightarrow \quad i_m = \frac{\rho_f}{\rho_l} \cdot i_f + \frac{\rho_f}{\rho_l} \cdot C_{vt} \cdot R_{sd,f} \cdot \left(A \cdot X_{ph} \cdot i_f + B \cdot \left(X_h + X_s \right) \cdot \mu_{sf} \cdot \left(\frac{v_{sm,f}}{v_{ls}} \right)^{0.25} \right)$$

Secondly, the heterogeneous term cannot be smaller than the pseudo-homogeneous term, because in that case the heterogeneous fraction would not be heterogeneous but pseudo-homogeneous, so:

$$A \cdot i_f > \frac{\mu_{sf}}{2} \cdot \left(\frac{v_{50,f}}{v_{ls}} \right)^M \tag{6.20-119}$$

$$\Rightarrow \quad i_m = \frac{\rho_f}{\rho_l} \cdot i_f + \frac{\rho_f}{\rho_l} \cdot C_{vt} \cdot R_{sd,f} \cdot \left(A \cdot \left(X_{ph} + X_h \right) \cdot i_f + B \cdot X_s \cdot \mu_{sf} \cdot \left(\frac{v_{sm,f}}{v_{ls}} \right)^{0.25} \right)$$

The third restriction is that the total hydraulic gradient can never be higher than the hydraulic gradient of plug flow, so for the hydrostatic normal stress approach this gives:

$$C_{vt} \cdot \left(A \cdot X_{ph} \cdot i_f + X_h \cdot \frac{\mu_{sf}}{2} \cdot \left(\frac{v_{50,f}}{v_{ls}} \right)^M + B \cdot X_s \cdot \mu_{sf} \cdot \left(\frac{v_{sm,f}}{v_{ls}} \right)^{0.25} \right) > C_{vb} \cdot 2 \cdot \mu_{sf}$$

(6.20-120)

$$i_m = \frac{\rho_f}{\rho_l} \cdot i_f + \frac{\rho_f}{\rho_l} \cdot C_{vb} \cdot R_{sd,f} \cdot 2 \cdot \mu_{sf}$$

The factor 2 is because of the assumption of a hydrostatic normal stress between the particles and the pipe wall according to Wilson. Using a different approach would lead to a different factor. For example the weight approach would lead to a factor 1, giving.

$$i_m = \frac{\rho_f}{\rho_l} \cdot i_f + \frac{\rho_f}{\rho_l} \cdot C_{vb} \cdot R_{sd,f} \cdot \mu_{sf}$$

(6.20-121)

6.20.3.8 Validation & Sensitivity Analysis.

It is interesting to see how the 4 component model behaves compared to the original Wilson et al. (2006) heterogeneous model. To do this the data of Clift et al. (1982) for broad graded granite with a **d_{50}=0.68 mm** in a **D_p=0.2032 m** pipe is used. These experiments are chosen because they were used by Wilson et al. (2006) to calibrate the power of the heterogeneous model. Figure 6.20-27 shows a reconstructed PSD, based on the power **M=1** found by Wilson et al. (2006). The graph also shows the heterogeneous PSD according to the 4 component model and the remaining PSD according to the DHLLDV Framework. This PSD gives a homogeneous fraction (d<0.04 mm) of 0.73%, a pseudo homogeneous fraction (0.04 mm<d<0.20 mm) of 9.96 %, a heterogeneous fraction (0.20 mm<d<3.00 mm) of 82.41% and a stratified fraction (d>3.00 mm) of 6.90%. The **d_h=d_{50}** of the heterogeneous fraction is based on the resulting PSD and not on equation (6.20-94) and is 0.70 mm, slightly larger than the original 0.68 mm. Using equation (6.20-94) gives a **d_h=1.6 mm**. The **d_h** is used to determine the **v_{50}**, which is very important for the magnitude of the hydraulic gradient of the heterogeneous fraction. The **v_{50}** found based on the heterogeneous PSD is 3.40 m/s, while the **v_{50}** found based on equation (6.20-94) equals 4.57 m/s. The latter gives a much higher hydraulic gradient. Since the result of equation (6.20-94) depends on the maximum particle diameter or **0.015·D_p**, this will often give a **d_h** which is pipe diameter dependent. The example here already shows the consequences, so equation (6.20-94) is rejected and the **d_h** has to be based on the heterogeneous PSD.
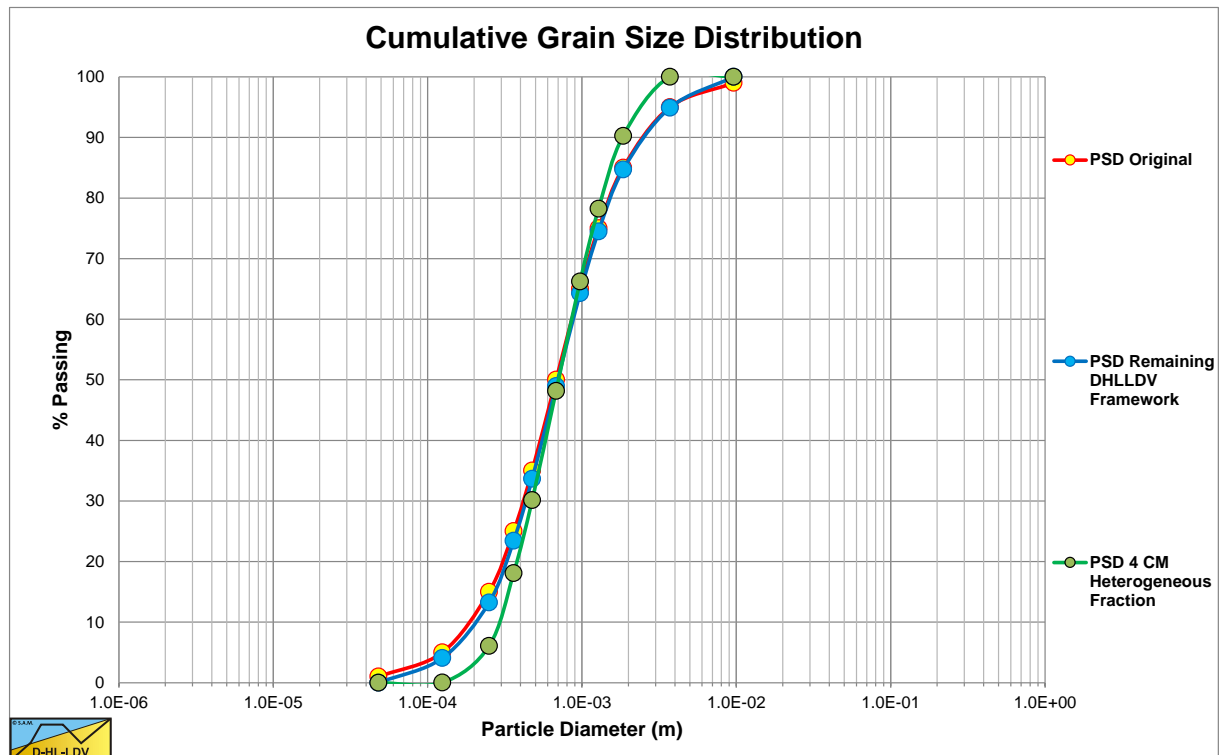
Figure 6.20-27: The PSD of the broad graded granite, reconstructed.

For the original Wilson et al. (2006) model a heterogeneous power **M=0.8** is found, while the simplified method gives a power **M=1.0**. The 4 component model has a power **M=1.0**.
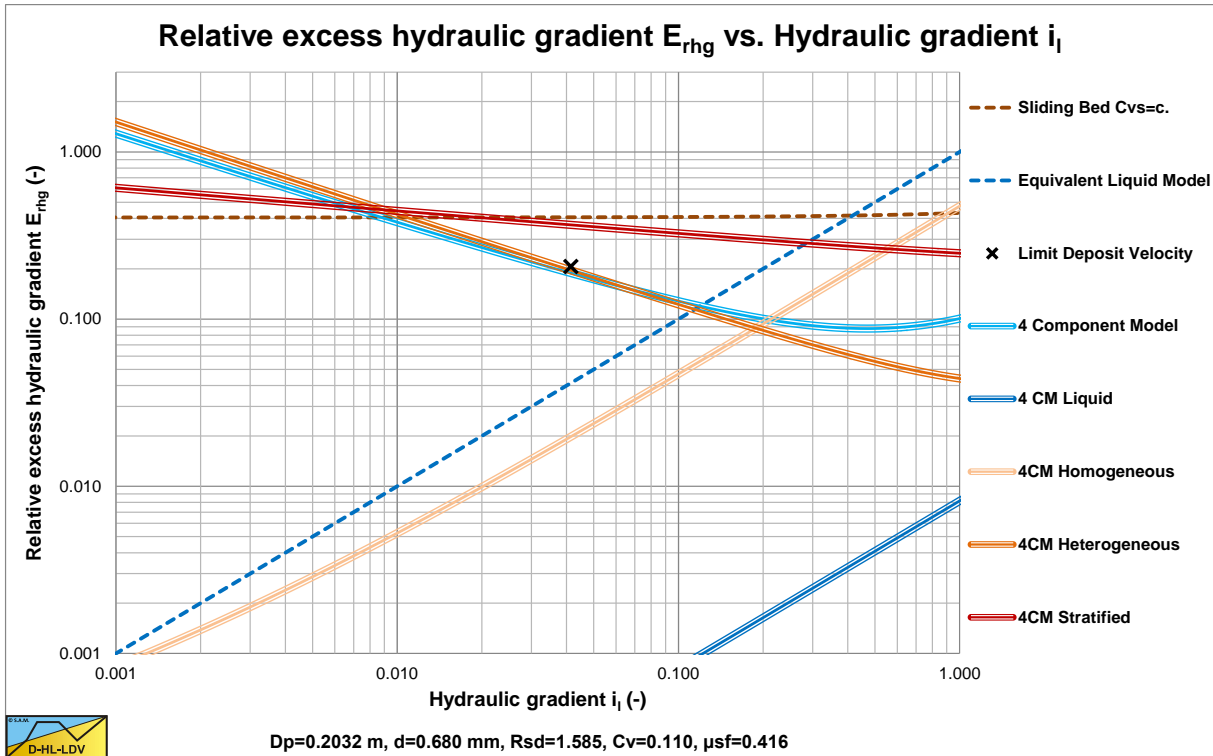
Figure 6.20-28: The 4 components and the resulting curve.
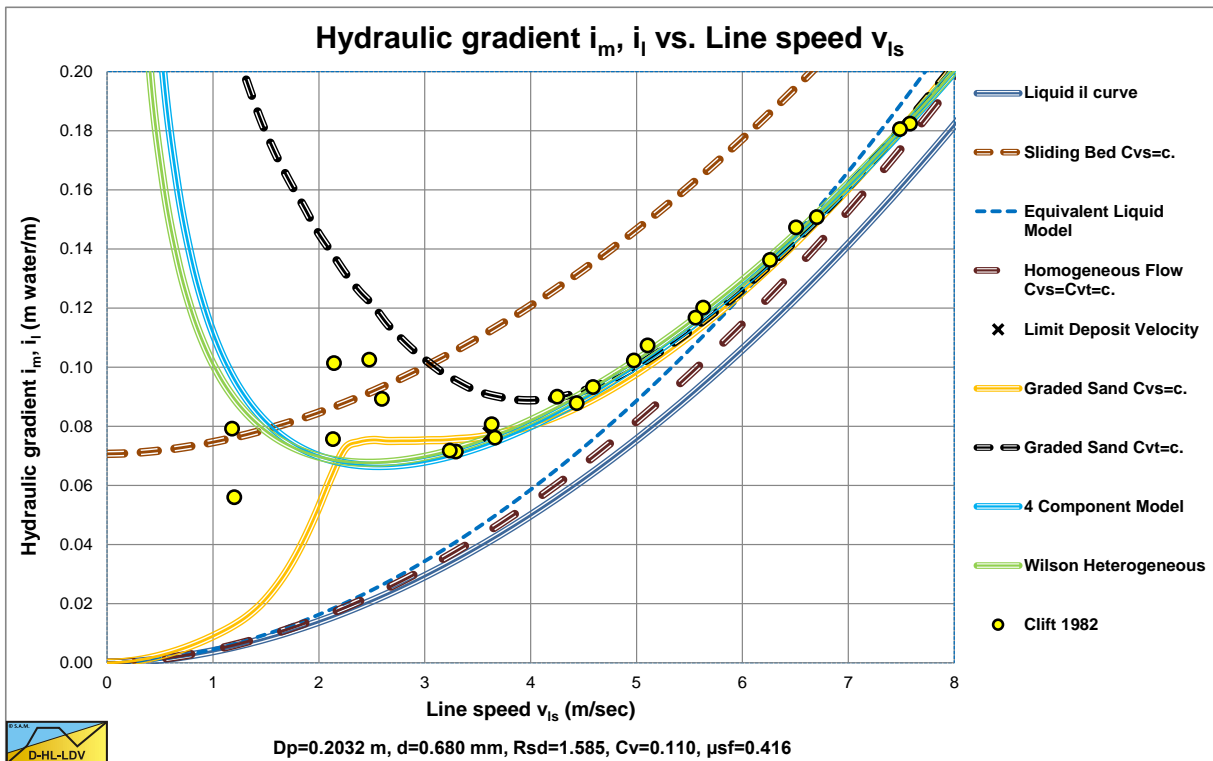
Figure 6.20-29: The experiments of Clift et al. (1982) versus the 4 component model, the heterogeneous model and the DHLLDV Framework, $i_m(v_{ls})$.

Figure 6.20-28 shows the curves for the 4 components as if each component has the concentration of 11%. The resulting curve is also shown based on the fractions of each component. On the left side the resulting 4CM curve is a bit lower than the heterogeneous curve, since the homogeneous, pseudo homogeneous and the stratified

fractions are lower. In the center of the graph the resulting 4CM curve and the heterogeneous curve are almost on top of each other. On the right side the resulting 4CM curve bends upwards because of the increasing values of the homogeneous and pseudo homogeneous curves. Of course this depends on the magnitude of the different fractions.
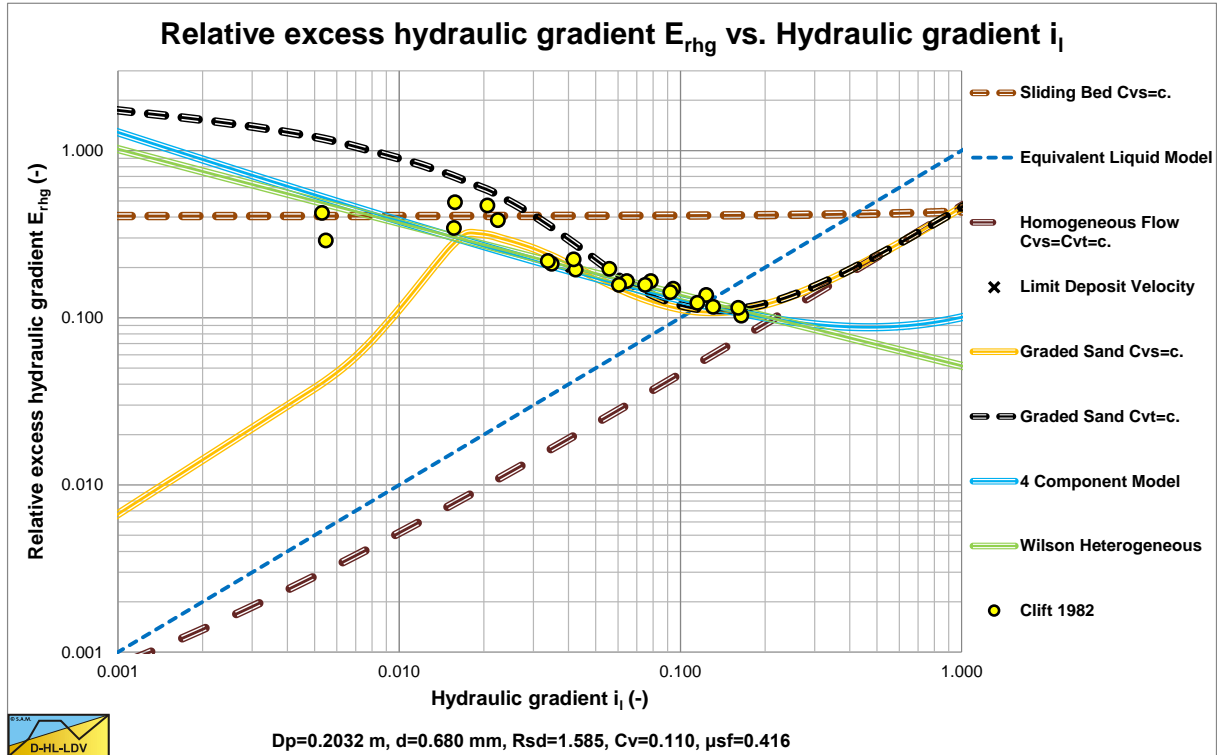
Figure 6.20-30: The experiments of Clift et al. (1982) versus the 4 component model, the heterogeneous model and the DHLLDV Framework, $E_{rhg}(i_l)$.

Figure 6.20-29 and Figure 6.20-30 show the data of Clift et al. (1982) versus the 4 component model, the heterogeneous model and the DHLLDV Framework. From personal communication it is known that both the heterogeneous model and the 4 component model are developed for operational conditions, which is above the LDV. The LDV in the case considered is **$v_{ls,ldv}$=3.63 m/s** or **i_l=0.04**. Above this the models match very well with the experimental data and also with the DHLLDV Framework. It should be mentioned that both the heterogeneous model and the 4 component model do not approach the ELM or the reduced ELM at high line speeds, where the DHLLDV Framework does. The choice of choosing a dh based on the heterogeneous PSD seems to be a good choice, giving a good match with the experimental data.

The grading of the crushed granite is broad, but still the non-heterogeneous fractions are not too large. Reason to investigate a broader graded PSD. Figure 6.20-31 shows the PSD of a very broad graded material with a **d_{50}=0.68 mm**. The ratio **d_{85}/d_{50}=8.154**. Now the homogeneous fraction is 8.77%, the pseudo homogeneous fraction 17.90%, the heterogeneous fraction 50.89% and the stratified fraction 22.44%. The **d_h=d_{50}=0.63 mm**., the **v_{50}=3.22 m/s**. Because of the larger homogeneous fraction, both the fluid viscosity and density are adjusted.

Figure 6.20-32 shows the curves for the 4 individual components and the resulting 4CM. The homogeneous curve is higher because of a larger homogeneous fraction. The pseudo homogeneous, heterogeneous and stratified fraction curves are not influenced by this. On the left side the curves show upwards curvature. This is because of the higher viscosity due to a larger homogeneous fraction. The heterogeneous curve has the same steepness compared to Figure 6.20-28, however the resulting 4CM curve is less steep.

Figure 6.20-33 and Figure 6.20-34 again compare the experimental data of Clift et al. (1982) with the heterogeneous model, the 4 component model and the DHLLDV Framework. Above **$v_{ls,ldv}$=3.63 m/s** or **i_l=0.04** the curves are less steep than the data points, which is expected based on the theory. The 3 models match very well among each other under operational conditions, but deviate both for higher and lower line speeds. At low line speeds the slip (the velocity difference between particles and liquid) increases resulting in plug flow at very low line speeds. This is not covered by the heterogeneous and the 4 component model, since they were derived for operational conditions. Both the heterogeneous and the 4 component model give a hydraulic gradient approaching the pure carrier liquid hydraulic gradient for very high line speeds, and do not follow a reduced ELM model in this

case. The DHLLDV Framework covers both very low and very high line speeds and takes the omissions into consideration.
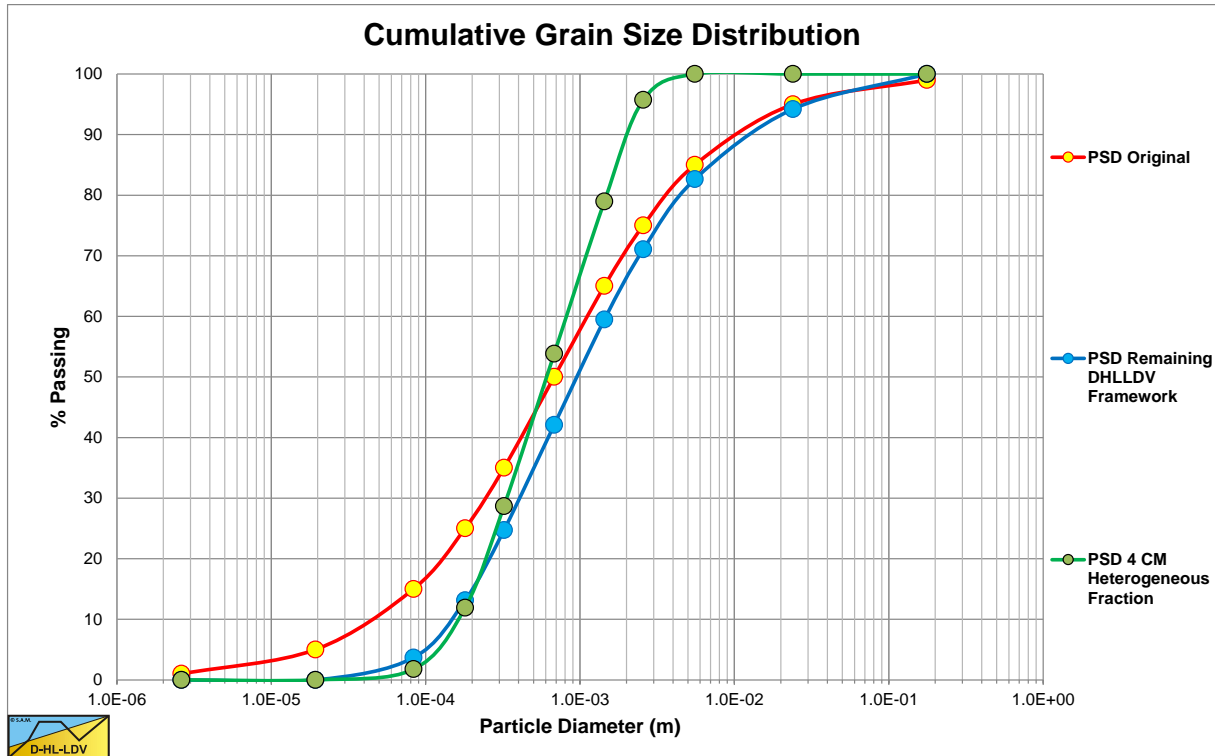
Figure 6.20-31: The PSD of very broad graded granite, reconstructed.
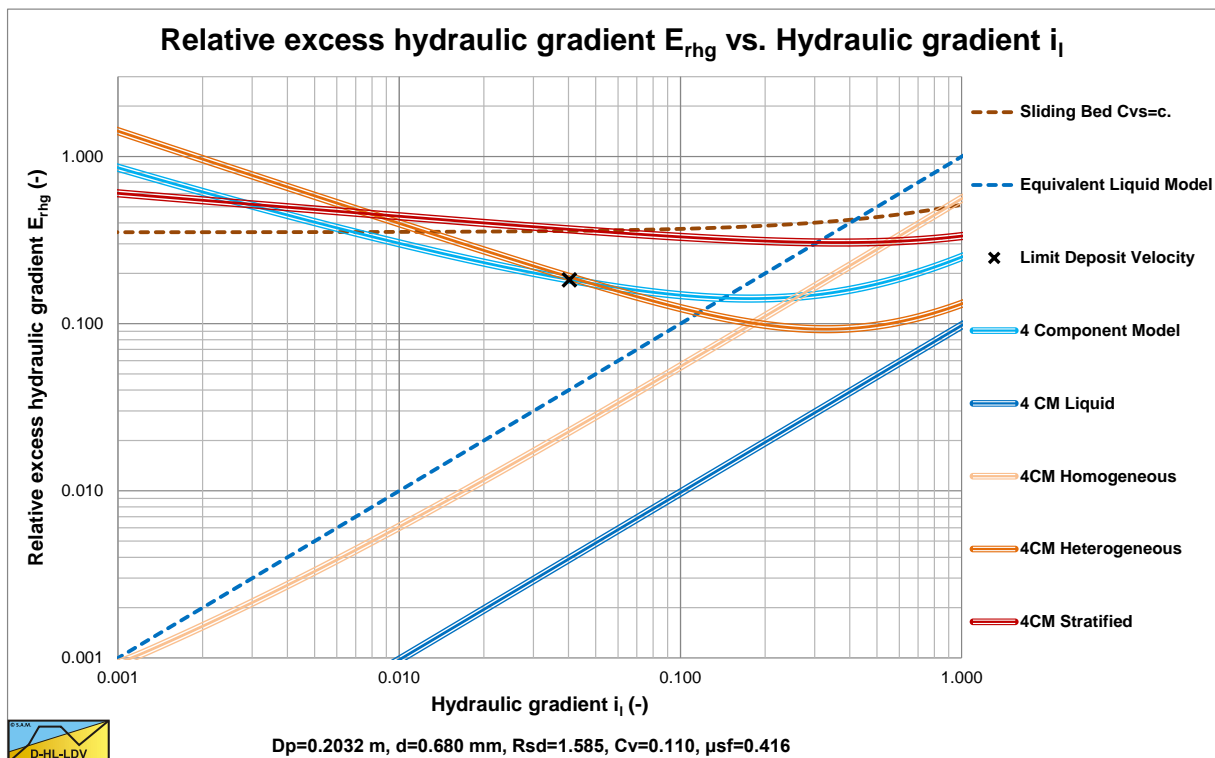
Figure 6.20-32: The 4 components and the resulting curve, very broad graded granite.

Under operational conditions the difference between the heterogeneous model and the 4 component model seems to be marginal and within the scatter of the experimental data. The 4 component model uses fixed boundaries regarding the 4 components, while these boundaries are most probably line speed dependent. Especially the transition heterogeneous-stratified is line speed dependent.

Hydraulic gradient i_m, i_l vs. Line speed v_{ls}

Dp=0.2032 m, d=0.680 mm, Rsd=1.585, Cv=0.110, µsf=0.416
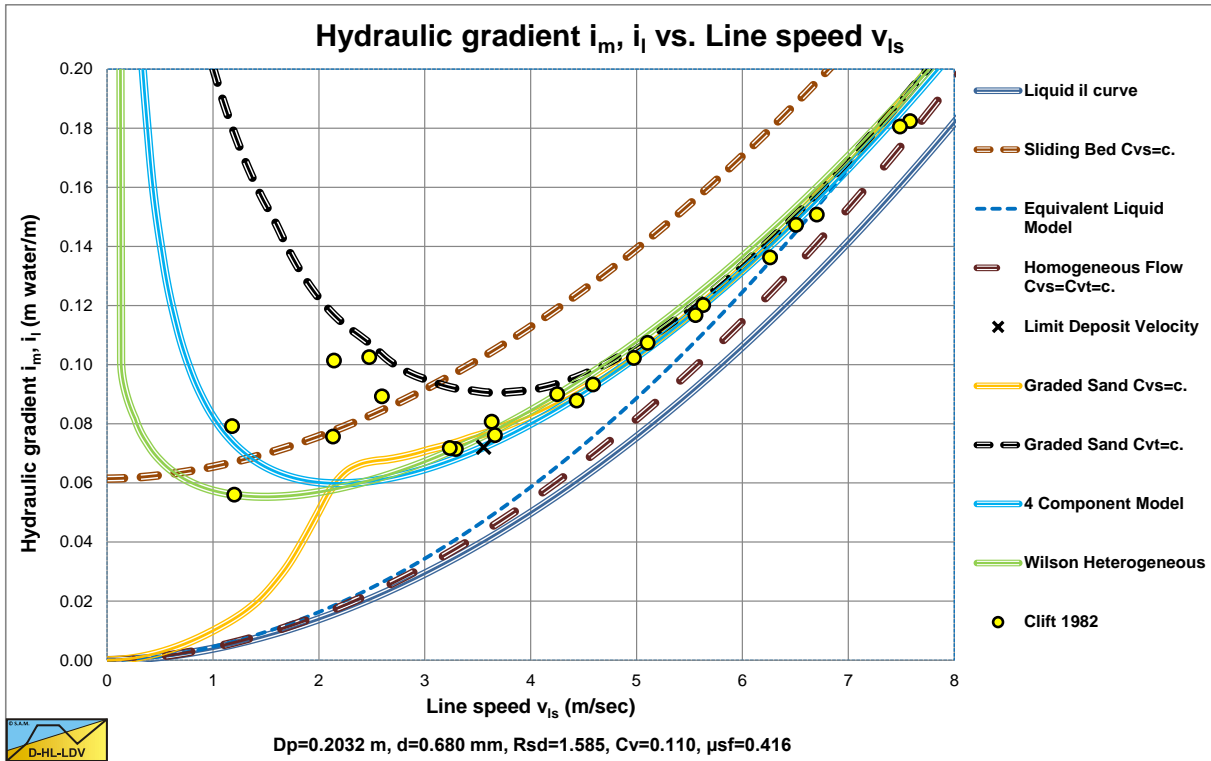
Figure 6.20-33: The experiments of Clift et al. (1982) versus the 4 component model, the heterogeneous model and the DHLLDV Framework, $i_m(v_{ls})$, very broad graded granite.

Relative excess hydraulic gradient E_{rhg} vs. Hydraulic gradient i_l

Dp=0.2032 m, d=0.680 mm, Rsd=1.585, Cv=0.110, µsf=0.416
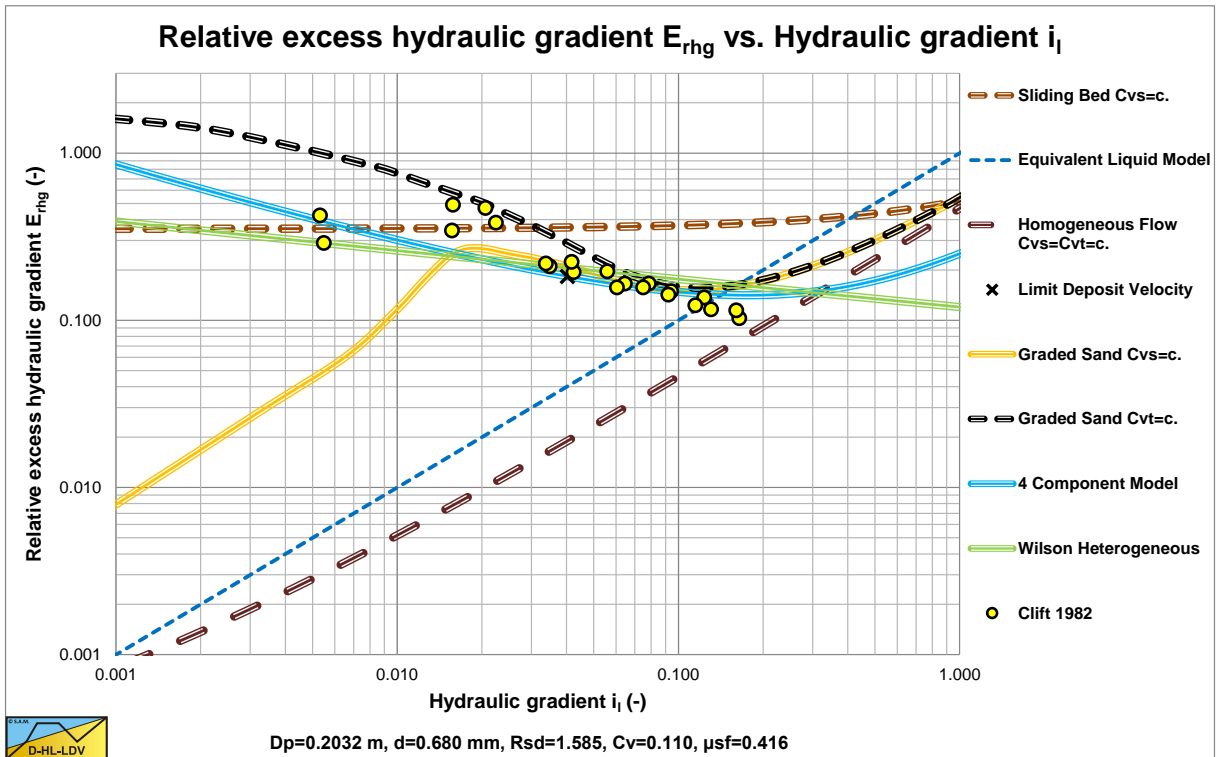
Figure 6.20-34: The experiments of Clift et al. (1982) versus the 4 component model, the heterogeneous model and the DHLLDV Framework, $E_{rhg}(i_l)$, very broad graded granite.

6.20.3.9 Conclusions & Discussion.

The 4 component model of Wilson et al. (2006) divides a PSD into 4 fractions, homogeneous, pseudo homogeneous, heterogeneous and stratified. The method assumes these fractions are fixed and do not depend on the line speed (cross-section averaged velocity in the pipe) of the mixture and hardly on the pipe diameter (only the stratified fraction). The different equations for the 4 flow regimes have been derived for line speeds around the working point of a pump pipeline system based on many experiments. For lower or higher line speeds however, the boundaries of the 4 fractions will differ. If the line speed is much lower, part of the heterogeneous fraction (the coarse part) will be stratified since the heterogeneous hydraulic gradient will not be larger than the stratified hydraulic gradient, decreasing the heterogeneous fraction and increasing the stratified fraction. Also part of the pseudo homogeneous fraction may become heterogeneous, reducing the pseudo homogeneous fraction and increasing the heterogeneous fraction. At much higher line speeds the fine part of the heterogeneous fraction will become pseudo homogeneous, while the fine part of the stratified fraction may become heterogeneous. Whether this is relevant for normal dredging practice is the question, but one should realize this. The equations for the homogeneous and pseudo homogeneous flow are clear, although the way the densities are determined seem incorrect. Apparently Wilson et al. (2006) use the definitions for homogeneous flow both the fluid density and viscosity are influenced by the homogeneous fraction, while for pseudo homogeneous flow only the fluid density is influenced by the pseudo homogeneous fraction. The equation for heterogeneous flow raises some questions. Wilson et al. (2006) state that 50% of the solids are stratified, while the other 50% apparently is in suspension at a line speed v_{50}. They also state that the E_{rhg} parameter at this line speed equals half the friction coefficient, assuming a sliding friction coefficient of μ_{sf}=**0.44**, this gives E_{rhg}=**0.22**. This implies that the 50% solids in suspension do not contribute to the hydraulic gradient, which is awkward. Now, if the 4 component model is used, this is not an issue, since the homogeneous and pseudo homogeneous fractions are taken into account separately, but in case the heterogeneous model is applied individually this is an issue. The following equation would give a correct hydraulic gradient. This equation is in fact already a 2 component model. Adjusting the liquid properties for the real homogeneous fraction would make it a 3 component model.

$$i_m - i_l = C_{vt} \cdot R_{sd} \cdot \left(\mu_{sf} \cdot \frac{1}{2} \cdot \left(\frac{v_{50}}{v_{ls}} \right)^M + A \cdot i_l \cdot \left(1 - \frac{1}{2} \cdot \left(\frac{v_{50}}{v_{ls}} \right)^M \right) \right) \qquad (6.20\text{-}122)$$

It is also strange that the hydrostatic approach to determine the normal force on the pipe wall is not applied here. For small spatial volumetric concentrations the multiplication factor is almost 1, but for large concentrations a value of 1.3 can be reached. Maybe this effect is already included in the factor 0.22 and the power **M**, but this is not clear. If the weight approach of Miedema & Ramsdell (2014) is used, the equation is correct. Another issue is the sliding friction coefficient μ_{sf}. In the equation for the heterogeneous fraction μ_{sf}=**0.44** is used, while the equation for the stratified fraction uses μ_{sf}=**0.4.** The model should be consistent in itself and use one and the same sliding friction coefficient μ_{sf}, unless there is an explicit reason to use different sliding friction coefficients for different flow regimes. In the equations in this chapter, consequently the symbol for the sliding friction factor μ_{sf} is used instead of numerical values. Wilson et al. (2006) use the hydrostatic approach to determine the total normal force between the bed and the pipe wall. The result of this is a normal force larger than the weight of the bed. If the bed fills the pipe for 50%, the weight has to be multiplied by 1.3 and for a full pipe with a factor 2. From 0% to 50% this factor increases from 1 to 1.3. In the original equation of Wilson et al. (2006) for stratified flow, the E_{rhg} value at v_{sm} equals 2 times the sliding friction coefficient, matching the hydrostatic approach for a full pipe, but not for a partially filled pipe. In the 4 component model it is assumed that stratified fraction is only a limited fraction of the PSD, otherwise the stratified model should be applied. If only a limited fraction is stratified, the multiplication factor of the normal force with respect to the weight of the bed is close to 1. This is probably the reason why Wilson et al. (2006) multiplied their original stratified equation with a factor 0.5, resulting in an E_{rhg} value at v_{sm} equal to the sliding friction coefficient μsf. The reason they mention, it's because of the fines, does not make sense, since they already correct the equation for the relative submerged density of the solids, floating in a mixture of the homogeneous, pseudo homogeneous and heterogeneous fractions. Whether the latter is correct is also the question, since the stratified flow is dominated by the weight of the bed as a whole, resulting in sliding friction. The Wilson et al. (2006) model and their 4 component model are not yet internally consistent and still raise some questions. On the other hand the models are based on numerous experiments and are expected to give reasonable predictions in the neighborhood of the working point of normal dredging operations.

Equation (6.20-95) gives a correction for the fact that the v_{50} is overestimated for small particles. The original v_{50} equation gives a constant value for small particles, the simplified equation still overestimates. It would be more convenient to give a better v_{50} equation, instead of correcting a wrong equation.

6.20.4 Near Wall Lift.

Wilson et al. (2000) found that close to the bottom of the pipe the volumetric concentration is lower than just above the bottom of the pipe. They explain this phenomena as the effect of near wall turbulent lift. If there is a strong curvature of the velocity profile, which there is in turbulent flow close to the wall, particles in this flow will be subject to a lift force. This should not be mistaken with Magnus lift in a laminar flow (in the viscous sub-layer). Sellgen and Wilson stated that Matoušek (2006) found from experiments in a vertical 0.15 m-diameter pipeline with narrowly graded sands (Average particle sizes of 0.12, 0.37, 1.84 mm) and concentrations by volume up to about 35% that the medium-sand particles gave less pipe wall friction than both the coarse-sand and fine-sand particles. He discussed various mechanisms and confirmed that the medium-sand particles showed stronger hydrodynamic repelling force off the wall than the others at velocities of practical interest, in accord with theoretical estimations by Wilson & Sellgren (2002).

Wilson et al. (2010) introduced the lift force F_L on a particle as:

$$F_L = C_L \cdot \frac{1}{2} \cdot \rho_l \cdot u_*^2 \cdot \frac{\pi}{4} \cdot d^2 \qquad (6.20\text{-}123)$$

And for the weight of the particle F_W:

$$F_W = (\rho_s - \rho_l) \cdot g \cdot \frac{\pi}{6} \cdot d^3 \qquad (6.20\text{-}124)$$

Giving for the so called lift ratio L_R, the ratio of the lift force on a particle F_L to the weight of a particle F_W:

$$L_R = \frac{F_L}{F_W} = C_L \cdot \frac{3}{4} \cdot \frac{u_*^2}{R_{sd} \cdot g \cdot d} = \frac{3}{4} \cdot C_L \cdot \frac{\rho_l \cdot u_*^2}{\rho_l \cdot R_{sd} \cdot g \cdot d} = \frac{3}{4} \cdot C_L \cdot \theta = C_L \cdot \frac{3}{32} \cdot \frac{\lambda_l \cdot v_{ls}^2}{R_{sd} \cdot g \cdot d} \qquad (6.20\text{-}125)$$

With: θ=Shields parameter.

This ratio will be referred to as the lift force to weight ratio or just the lift ratio. If this ratio is bigger than 1, particles will be lifted, otherwise gravity dominates. Now it is the question whether or not the lift force is completely correct, but it can be used as an indication. In Wilson et al. (2006) a lift coefficient C_L=0.27 is mentioned for spheres and not necessarily for sand and granite.

The line speed where the lift ratio equals 1 can now be determined with:

$$v_{ls,L_R=1}^2 = \frac{32}{3} \cdot \frac{R_{sd} \cdot g \cdot d}{C_L \cdot \lambda_l} \quad \Rightarrow \quad v_{ls,L_R=1} = \left(\frac{32}{3} \cdot \frac{R_{sd} \cdot g \cdot d}{C_L \cdot \lambda_l} \right)^{0.5} \qquad (6.20\text{-}126)$$

Now the idea is that in some circumstances particles will be lifted away from the bottom of the pipe, leaving a particle lean region near the wall, which is in agreement with the concentration profiles found. Medium sized particles show a hydraulic gradient below the ELM curve after passing this curve, see Figure 6.20-35. The asymptotic behavior for very high line speeds cannot be established from the data, since in general experiments are not carried out with very high line speeds, but at line speeds close to operational line speeds or lower. Figure 6.20-36 shows data from Blythe & Czarnotta (1995) also showing crossing the ELM. However these data points seem to return to the ELM at higher line speeds, or at least follow a parallel curve, not approaching the pure liquid behavior.

Based on the so called shear Reynolds number:

$$Re_* = \frac{v_* \cdot d}{\nu_l} \qquad (6.20\text{-}127)$$

A new expression has been derived for the stratification ratio R:

$$E_{rhg} = \frac{i_m - i_l}{R_{sd} \cdot C_{vt}} = R = \frac{0.93}{\theta \cdot \left(Re_*\right)^{1/3}} \tag{6.20-128}$$
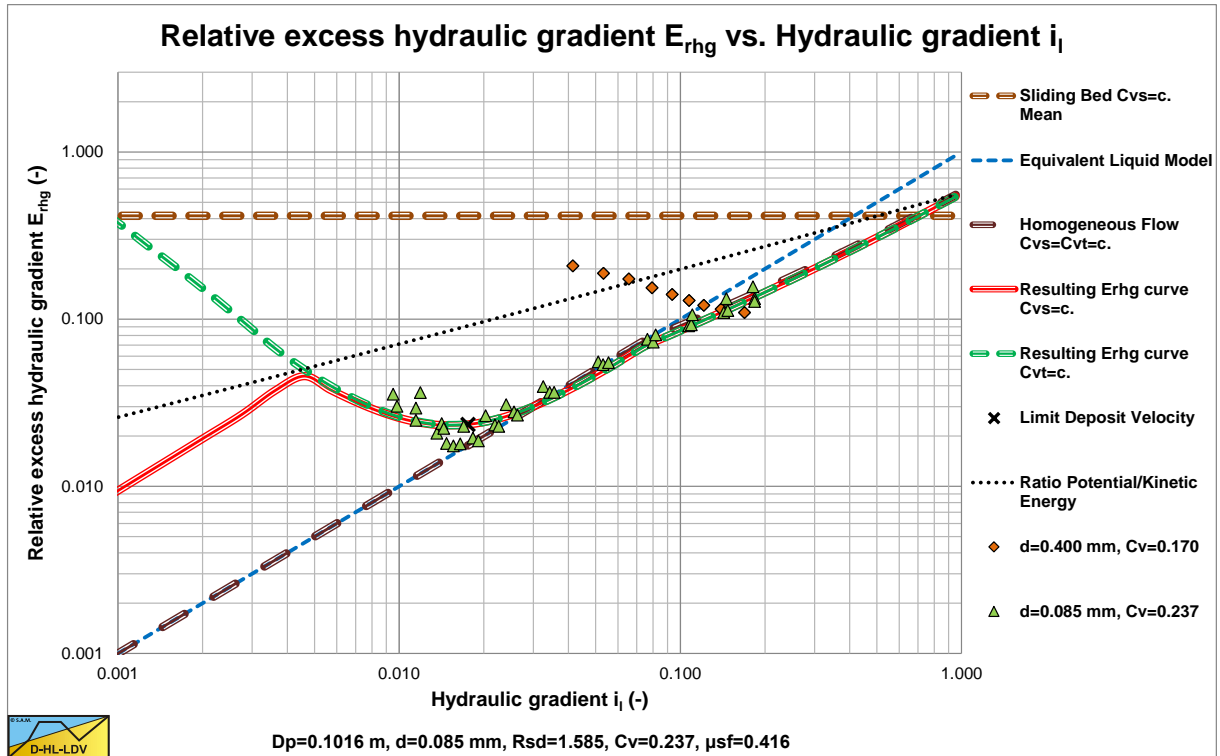
Figure 6.20-35: The data of Whithlock et al. (2004).
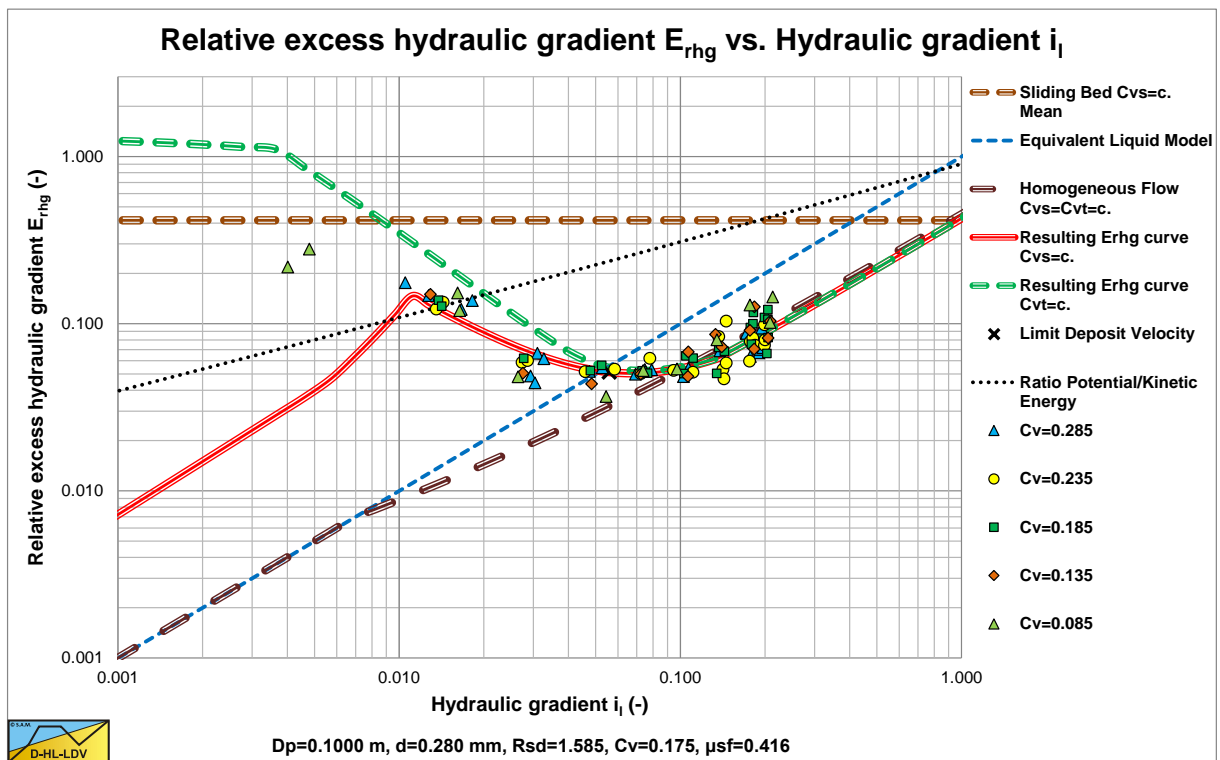
Figure 6.20-36: The data of Blythe & Czarnotta (1995).

The coefficient is slightly different from the original paper (0.93 instead of 0.7) because here the Shields parameter is applied. According to Wilson et al. (2010) the stratification ratio has an upper limit of 0.6. The shear velocity used in this Reynolds number is the shear velocity based on the terminal settling velocity of the particle. Now

assuming a cylinder around the particle with diameter d and height d, the shear stress on the surface of this cylinder follows from the weight of the particle and the surface of this cylinder, so:

$$\tau_c \cdot \pi \cdot d^2 = (\rho_s - \rho_l) \cdot g \cdot \frac{\pi}{6} \cdot d^3$$

$$\tau_c = (\rho_s - \rho_l) \cdot g \cdot \frac{1}{6} \cdot d$$

(6.20-129)

Assuming a similar relation between the shear stress and the shear velocity gives:

$$\tau_c = \rho_l \cdot v_*^2 = (\rho_s - \rho_l) \cdot g \cdot \frac{1}{6} \cdot d$$

$$v_* = \left(\frac{(\rho_s - \rho_l)}{6 \cdot \rho_l} \cdot g \cdot d \right)^{1/2} = \left(\frac{R_{sd} \cdot g \cdot d}{6} \right)^{1/2}$$

(6.20-130)

$$Re_* = \frac{v_* \cdot d}{\nu_l} = \frac{\left(\frac{R_{sd} \cdot g \cdot d}{6} \right)^{1/2} \cdot d}{\nu_l}$$

Now substituting both the Shields parameter and the shear Reynolds number in the stratification ratio equation gives:

$$E_{rhg} = \frac{i_m - i_l}{R_{sd} \cdot C_{vt}} = R = \frac{0.93}{\left(\frac{\lambda_l \cdot v_{ls}^2}{8 \cdot R_{sd} \cdot g \cdot d} \right) \cdot \left(\frac{\left(\frac{R_{sd} \cdot g \cdot d}{6} \right)^{1/2} \cdot d}{\nu_l} \right)^{1/3}}$$

(6.20-131)

$$E_{rhg} = R = \frac{10 \cdot (R_{sd} \cdot g \cdot d)^{1/2} \cdot (R_{sd} \cdot g \cdot \nu_l)^{1/3}}{\lambda_l \cdot v_{ls}^2}$$

With this equation, the proportionality with the line speed is about -1.8. The Shields parameter has a proportionality of 2 because of the line speed squared and about -0.2 because of the Darcy Weisbach friction factor, resulting in a power of -1.8. The shear Reynolds number has a power of 0. So this totals to -1.8, which gives a slightly steeper decrease of the hydraulic gradient or stratification ratio of the original model having a power of -1.7 for uniform PSD's. The simplified heterogeneous model used:

$$E_{rhg} = R = \frac{i_m - i_l}{R_{sd} \cdot C_v} = \frac{\mu_{sf}}{2} \cdot \left(\frac{v_{50}}{v_{ls}} \right)^M$$

(6.20-132)

With:

$$v_{50} \approx 3.93 \cdot (1000 \cdot d_{50})^{0.35} \cdot \left(\frac{R_{sd}}{1.65} \right)^{0.45} \cdot \left(\frac{\nu_{l,actual}}{\nu_{w,20}} \right)^{-0.25}$$

(6.20-133)

$$v_{50} \approx 1.11 \cdot (d_{50})^{0.35} \cdot (R_{sd})^{0.45} \cdot (\nu_l)^{-0.25}$$

For sands and gravels this reduces to:

$$v_{50} \approx 44.1 \cdot (d_{50})^{0.35}$$

(6.20-134)

Giving for the simplified equation (with μ_{sf}=0.44 and M=1.7):

$$E_{rhg} = R = \frac{\mu_{sf}}{2} \cdot \left(\frac{44.1 \cdot (d_{50})^{0.35}}{v_{ls}} \right)^M = 137.4 \cdot \frac{d^{0.6}}{v_{ls}^{1.7}}$$

(6.20-135)

The near wall lift based equation gives:

$$E_{rhg} = R = \frac{d^{1/2}}{\lambda_l \cdot v_{ls}^2}$$

(6.20-136)

For medium sized sand particles in water and large pipe diameters (large flow Reynolds numbers), both equations are close. For example, a 1 mm particle gives a v_{50} of 3.93 m/s, resulting in R=0.22 according to the simplified method. The near wall lift method results in R=0.20, assuming λ_l=0.01 for large diameter pipes.
In both models the stratification ratio increases with increasing particle diameter and relative submerged density. However the relation of the viscosity is different. The simplified model shows a decreasing stratification ratio with increasing viscosity, while the near wall lift shows the opposite. For sands and gravels in water this will not have a significant influence, but for other solids and liquids it might. The appearance of the Darcy Weisbach friction factor in the denominator of the near wall lift equation results in some dependence of the pipe diameter. The dependence on the sliding friction coefficient is not present anymore in the near wall lift equation.

Using the Shields parameter to explain for the stratification ratio seems interesting however.

6.20.5 Inclined Pipes.

Wilson et al. (2006) derived the following equation for heterogeneous transport in horizontal pipes:

$$i_m = i_l + \frac{\mu_{sf}}{2} \cdot \left(\frac{v_{50}}{v_{ls}} \right)^M \cdot R_{sd} \cdot C_{vt}$$

(6.20-137)

For inclined pipes they modified the equation, matching the reasoning of Worster & Denny (1955), but with the use of the power M according to:

$$i_{m,\theta} = i_{l,\theta} + \frac{\mu_{sf}}{2} \cdot \left(\frac{v_{50}}{v_{ls}} \right)^M \cdot R_{sd} \cdot C_{vt} \cdot \cos(\theta)^M + \sin(\theta) \cdot R_{sd} \cdot C_{vt}$$

(6.20-138)

The power M has a value of 1.7 for uniform or narrow graded sands and decreases to 0.25 for very broad graded sands. For narrow graded sands the influence of the inclination angle is similar to the Durand & Condolios (1952) and Gibert (1960) approach with a power of 1.5 versus 1.7 for Wilson et al. (2006). For medium graded sands with a power around 1, the influence is similar to the Worster & Denny (1955) approach.

Wilson et al. (2006) use a graph with experimental data for the Deposition Limit. Their Deposition Limit however is the Limit of Stationary Deposit Velocity (LSDV) and not the Limit Deposit Velocity. The LSDV is the line speed where a bed starts sliding, while the LDV is defined in this book as the line speed above which there is no stationary or sliding bed. The LDV is thus always higher than the LSDV. The LSDV does not always exist. For smaller particles it is very well possible that there is a direct transition between the stationary bed regime and the heterogeneous flow regime. The graph used by Wilson et al. (2006) shows an increasing LSDV with increasing inclination angle up an inclination angle of about 30 degrees above which the LSDV is constant or decreasing. The experimental data stop at an inclination angle of 40 degrees. For negative inclination angles, the LSDV decreases with a decreasing inclination angle. The experimental data stop at an angle of -20 degrees.

6.20.6 The Demi-McDonald of Wilson (1979).

The LSDV of Wilson (1979) based on the 2 layer model was originally given as a nomographic chart, made with the help of Professor F.M. Woods. This nomographic chart is known as the demi-McDonald, because of the shape of the particle diameter curve. Nowadays the fit function equation (6.20-34) is often used.
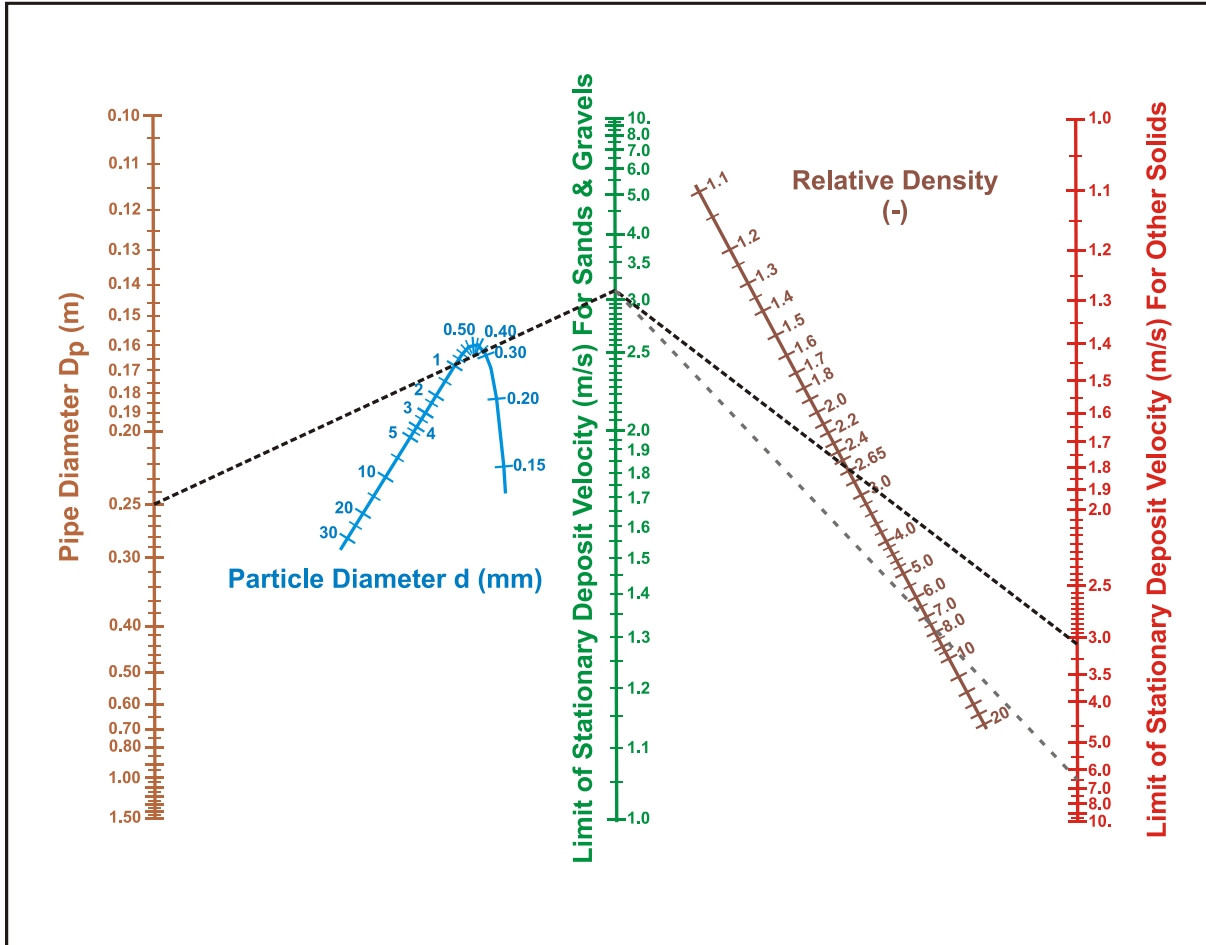
Figure 6.20-37: The demi-McDonald of Wilson (1979).

Figure 6.20-37 shows the demi-McDonald of Wilson (1979). The figure shows an example of the LSDV for a **D_p=0.25 m** diameter pipe and a **d=1 mm** diameter particle. For solids with a density of **ρ_s=2.65 ton/m^3** like sands and gravels, this gives an LSDV of about 3.1 m/s according to the left part of the nomogram. The right part shows that solids with a density of **ρ_s=7.85 ton/m^3** like iron, give an LSDV of about 6.5 m/s.

The maximum Limit of Stationary Deposit Velocity (LSDV) v_{sm} can be estimated by (Matousek (2004)), with **d** in mm and **D_p** in m:

$$v_{sm} = \frac{8.8 \cdot \left(\dfrac{\mu_{sf} \cdot R_{sd}}{0.66} \right)^{0.55} \cdot D_p^{0.7} \cdot d^{1.75}}{d^2 + 0.11 \cdot D_p^{0.7}} \quad \text{and} \quad F_L = \frac{v_{sm}}{\sqrt{2 \cdot g \cdot R_{sd} \cdot D_p}} \tag{6.20-139}$$

6.20.7 The Sliding Bed Regime New Developments.

Based on the developments of the DHLLDV Framework a new equation has been derived for slip ratio in the sliding bed regime. This equation assumes a sliding bed with sheet flow at the top. Suspension is not taken into account. The equation is derived from many fundamental simulations based on the equilibrium equations of the forces on a sliding bed. Based on the results of these simulations an empirical equation is derived. This empirical equation gives the slip ratio as a function of the relative volumetric concentration, the pipe diameter, the sliding

friction coefficient, the LSDV and the line speed. The full equation is equation (7.4-93). Here only the slip ratio at the LSDV is determined.

First of all the relation between the spatial and the delivered concentration can be determined by, based on the slip ratio:

$$C_{vs} = \left(\frac{v_{ls}}{v_{ls} - v_{sl}} \right) \cdot C_{vt} = \left(\frac{1}{1 - \xi} \right) \cdot C_{vt}$$

(6.20-140)

The slip ratio at the LSDV from Figure 7.4-33 can be estimated by the following empirical equation:

$$C_{vr} = \frac{C_{vt}}{C_{vb}}$$

(6.20-141)

$$\xi_{lsdv} = \left(1 - C_{vr} \right) \cdot e^{\left(-\left(0.83 + \frac{\mu_{sf}}{4} + \left(C_{vr} - 0.5 \right)^2 + 0.025 \cdot D_p \right) \cdot D_p^{0.025} \cdot C_{vr}^{0.65} \right)}$$

For the delivered concentration in the above equation, the delivered concentration of all the particles in the heterogeneous and the sliding bed regimes is taken, in case of a very graded sand or gravel. Now knowing the slip ratio, the spatial volumetric concentration can be determined at the LSDV (v_{sm}) and with this the approximation equation for the sliding bed hydraulic gradient according to:

$$i_m = i_l + \frac{C_{vs}(v_{sm})}{C_{vt}} \cdot C_{vt} \cdot R_{sd} \cdot \mu_{sf} \cdot \left(\frac{v_{sm}}{v_{ls}} \right)^{0.25} = i_l + C_{vt} \cdot R_{sd} \cdot \mu_{sf} \cdot \left(\left(\frac{1}{1 - \xi_{lsdv}} \right) \cdot \left(\frac{v_{sm}}{v_{ls}} \right)^{0.25} \right)$$

(6.20-142)

This methodology would also be a good addition to the 4 component model, for the stratified fraction, using $C_{vt,h} + C_{vt,s}$ for the determination of the relative concentration C_{vr}. The homogeneous and pseudo homogeneous fractions are assumed not to have slip. Wilson et al. (2006) do mention that the second term on the right hand side has to be multiplied with some factor, but how to determine this factor is not clear. By using the slip ratio at the LSDV a good quantification of this factor is achieved. The decreasing slip ratio with increasing line speed is quantified with the $(v_{sm}/v_{ls})^{0.25}$ term. This will give good results close to the LSDV. At high line speeds the hydraulic gradient will decrease faster. At very low line speeds the hydraulic gradient is limited to (plug flow):

$$i_m = i_l + C_{vb} \cdot R_{sd} \cdot \mu_{sf}$$

(6.20-143)

6.20.8 Nomenclature Wilson-GIW Models.

A_p	Cross section pipe	m^2
A_1	Cross section above bed	m^2
A_2	Cross section bed	m^2
C_{vb}	Volumetric spatial bed concentration	-
C_{vc}	Spatial volumetric concentration contact load	-
C_{vs}	Spatial volumetric concentration	-
$C_{vs,1}$	Spatial volumetric concentration in cross section 1	-
$C_{vs,2}$	Spatial volumetric concentration in cross section 2	-
$C_{vs,f}$	Spatial volumetric concentration homogeneous fraction	-
C_{vr}	Relative volumetric concentration $C_{vr}=C_{vs}/C_{vb}$	-
$C_{vr,max}$	Relative volumetric concentration at maximum LSDV	-
C_{vt}	Delivered (transport) volumetric concentration	-
$C_{vt,f}$	Delivered (transport) volumetric concentration homogeneous fraction	-
$C_{vt,ph}$	Delivered (transport) volumetric concentration pseudo homogeneous fraction	-
$C_{vt,h}$	Delivered (transport) volumetric concentration heterogeneous fraction	-
$C_{vt,s}$	Delivered (transport) volumetric concentration stratified fraction	-
d	Particle diameter	m

d_{50}	Particle diameter with 50% passing	m
D_H	Hydraulic diameter	m
D_p	Pipe diameter	m
E_{rhg}	Relative excess hydraulic gradient	-
f	Correction factor heterogeneous flow regime	-
F	Force	kN
$F_{1,l}$	Force between liquid and pipe wall	kN
$F_{12,l}$	Force between liquid and bed	kN
$F_{2,pr}$	Force on bed due to pressure	kN
$F_{2,sf}$	Force on bed due to friction	kN
$F_{2,l}$	Force on bed due to pore liquid	kN
F_n	Normal force	kN
F_w	Weight of bed	kN
F_{sf}	Friction force, sliding	kN
Fr	Froude number	-
g	Gravitational constant 9.81 m/s^2	m/s^2
i_{bed}	Hydraulic gradient sliding bed	m/m
i_{hom}	Hydraulic gradient homogeneous flow	m/m
i_l	Hydraulic gradient liquid	m/m
i_m	Hydraulic gradient mixture	m/m
i_{plug}	Hydraulic gradient plug flow	m/m
i_f	Hydraulic gradient homogeneous fraction	m/m
i_{ph}	Hydraulic gradient pseudo homogeneous fraction	m/m
i_h	Hydraulic gradient heterogeneous fraction	m/m
i_s	Hydraulic gradient stratified fraction	m/m
k_s	Bed roughness	m
ΔL	Length of pipe section	m
LDV	Limit Deposit Velocity	m/s
LSDV	Limit of Stationary Deposit Velocity	m/s
M	Power stratification ratio between 0.25 and 1.7	-
n	Porosity bed	-
O_p	Circumference pipe	m
O_1	Circumference pipe above bed	m
O_2	Circumference pipe in bed	m
O_{12}	Width of bed	m
Δp	Pressure difference	kPa
Δp_1	Pressure difference on cross section 1	kPa
Δp_2	Pressure difference on cross section 2	kPa
Δp_l	Pressure difference liquid	kPa
Δp_m	Pressure difference mixture	kPa
Δp_f	Pressure difference homogeneous fluid	kPa
q	Power to determine the normalised excess hydraulic gradient	-
Re	Reynolds number	-
R_{sd}	Relative submerged density	-
R	Stratification ratio	-
R_H	Hydraulic radius	m
S_f	Relative density homogeneous fraction + carrier liquid	-
S_{fp}	Relative density homogeneous & pseudo homogeneous fractions + carrier liquid	-
S_{fph}	Relative density homogeneous & pseudo homogeneous & heterogeneous fractions + carrier liquid	-
S_{fphs}	Relative density homogeneous & pseudo homogeneous & heterogeneous & stratified fractions + carrier liquid	-
S_m	Relative density mixture	-
S_s	Relative density solids	-
u_*	Friction velocity	m/s
v	Velocity	m/s
v_s	Limit of Stationary Deposit Velocity	m/s
v_t	Terminal settling velocity	m/s

v_{t*}	Terminal settling velocity where $d=0.015 \cdot D_p$	m/s
v_u	Threshold velocity	m/s
v_{ls}	Line speed	m/s
v_{ls*}	Line speed of intersection sliding bed-heterogeneous where $d=0.015 \cdot D_p$	m/s
$v_1, v_{1,m}, v_r$	Cross section averaged velocity above bed	m/s
$v_2, v_{2,m}, v_b$	Cross section averaged velocity bed	m/s
v_{sm}	Maximum Limit of Stationary Deposit Velocity (LSDV)	m/s
v_{50}	Line speed with 50% stratification	m/s
$v_{50,min}$	Line speed with 50% stratification for very fine particles	m/s
v_{50*}	Line speed with 50% stratification where $d=0.015 \cdot D_p$	m/s
v_{85}	Line speed with 85% stratification	m/s
v_r	Relative line speed $v_r=v_{ls}/v_{sm}$	-
w_{50}	Particle associated velocity matching the d_{50}	m/s
w_{85}	Particle associated velocity matching the d_{85}	m/s
X	Fraction in general	-
X_f	Homogeneous fraction	-
X_{ph}	Pseudo homogeneous fraction	-
X_h	Heterogeneous fraction	-
X_s	Stratified fraction	-
y_b	Height of bed	m
α	Multiplication factor bed friction	-
α	Power to determine LSDV	-
β	Power to determine LSDV	-
β	Bed angle	rad
ϵ	Pipe wall roughness	m
ρ_l	Density carrier liquid	ton/m^3
ρ_s	Density solids	ton/m^3
ρ_m	Mixture density	ton/m^3
ρ_x	Density mixture with fraction X	ton/m^3
ρ_f	Density homogeneous fluid	ton/m^3
ρ_{fp}	Density homogeneous+pseudo homogeneous fluid	ton/m^3
ρ_{fph}	Density homogeneous+pseudo homogeneous+heterogeneous fluid	ton/m^3
ρ_{fphs}	Density homogeneous+pseudo homogeneous+heterogeneous+stratified fluid	ton/m^3
θ	Shields parameter	-
θ_c	Critical Shields parameter	-
λ	Darcy-Weisbach friction factor	-
λ_l	Darcy-Weisbach friction factor liquid-pipe wall	-
λ_1	Darcy-Weisbach friction factor with pipe wall	-
λ_2	Darcy-Weisbach friction factor with pipe wall, liquid in bed	-
λ_{12}	Darcy-Weisbach friction factor on the bed	-
λ_f	Darcy-Weisbach friction factor based on homogeneous fluid properties	-
ν_l	Kinematic viscosity	m^2/s
$\nu_{l,actual}$	Actual kinematic viscosity liquid	m^2/s
$\nu_{w,20}$	Kinematic viscosity of water at 20 degrees centigrade	m^2/s
ν_f	Kinematic viscosity homogeneous fluid	m^2/s
τ	Shear stress	kPa
τ_l	Shear stress liquid-pipe wall	kPa
$\tau_{1,l}$	Shear stress liquid-pipe wall above bed	kPa
$\tau_{12,l}$	Shear stress bed-liquid	kPa
$\tau_{2,l}$	Shear stress liquid-pipe in bed	kPa
$\tau_{2,sf}$	Shear stress from sliding friction	kPa
μ_{sf}	Sliding friction coefficient	-
μ_l	Dynamic viscosity liquid	Pa·s
μ_f	Dynamic viscosity homogeneous fluid	Pa·s
μ_r	Relative dynamic viscosity	-
σ_n	Normal stress	kPa
ζ	Normalized excess hydraulic gradient	-
ζ_∞	Normalized excess hydraulic gradient at infinite line speed	-

6.21 The Doron et al. (1987) and Doron & Barnea (1993) Model.

6.21.1 The 2 Layer Model (2LM).

Doron et al. (1987) and Doron & Barnea (1993) developed a 2 layer model (2LM) in 1987 and extended it to a 3 layer model (3LM) in 1993. Some elements of the models are similar to the Wilson-GIW (1979) model, other elements are different. In the description of the model the symbols of this book are used.

Now consider a pipe with diameter D_p and cross section A_p, see Figure 6.20-1. Suppose the bottom part of the pipe is filled with a stationary or sliding bed with a bed concentration C_{vb} and above the bed there is heterogeneous transport. 3 indices are used, the index **1** (original **h**) for the heterogeneous transport, the index **2** (original **b**) for the bed and the index **12** (original **i**) for the interface between the bed and the heterogeneous transport. A coordinate system is used starting at the bottom of the pipe with coordinate **y** where the bed height is y_{12} (original y_b). The cross section of the heterogeneous flow is A_1 (original A_h). The cross section of the bed is A_2 (original A_b). The length of the wetted circumference of the heterogeneous flow is O_1 (original S_h). The length of the circumference between the bed and the pipe wall is O_2 (original S_b). The length of the interface between the heterogeneous flow and the bed is O_{12} (original S_i). The angle starting at the vertical and ending at the top of the bed y_{12} is named **β**. The velocity in the heterogeneous cross section is v_1 (original U_h). The velocity of the bed is v_2 (original U_b). The cross section averaged velocity or line speed is v_{ls} (original U_s).
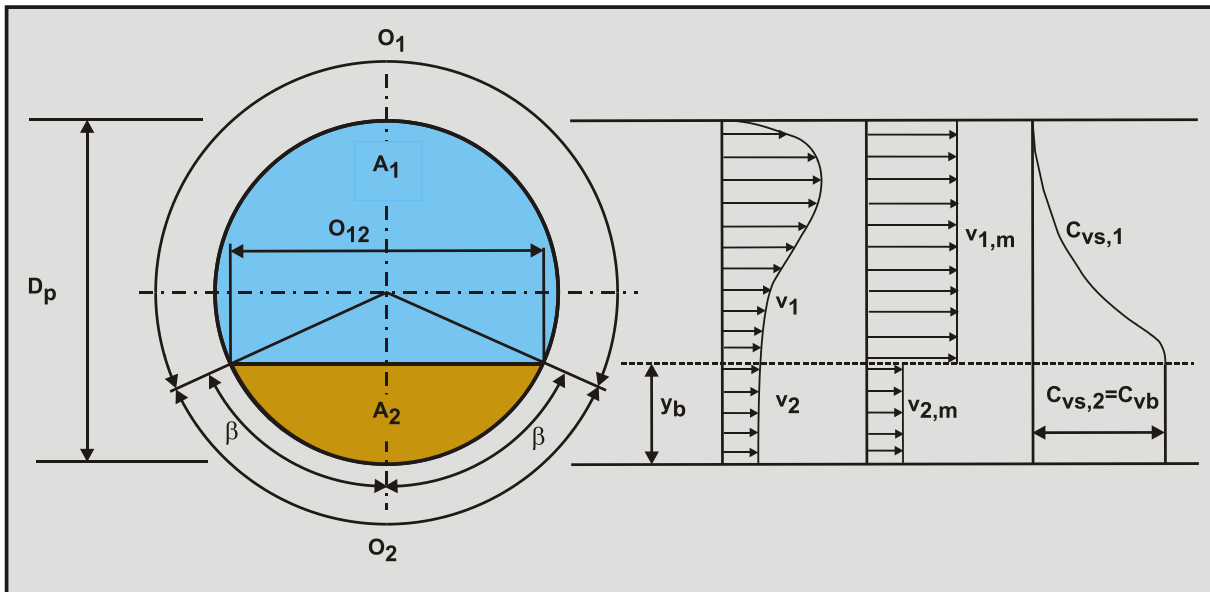
Figure 6.21-1: The 2 layer model with suspension in the upper layer.

For the solids phase the continuity equation yields, neglecting slip between the two phases:

$$v_1 \cdot A_1 \cdot C_{vs,1} + v_2 \cdot A_2 \cdot C_{vb} = v_{ls} \cdot A_p \cdot C_{vt} \qquad (6.21\text{-}1)$$

For the liquid phase the continuity equation yields, neglecting slip between the two phases:

$$v_1 \cdot A_1 \cdot \left(1 - C_{vs,1}\right) + v_2 \cdot A_2 \cdot \left(1 - C_{vb}\right) = v_{ls} \cdot A_p \cdot \left(1 - C_{vt}\right) \qquad (6.21\text{-}2)$$

The force balance on the heterogeneous layer yields:

$$-A_1 \cdot \Delta p = F_{1,l} + F_{12,l} \quad \textbf{and} \quad -A_1 \cdot \frac{\Delta p}{\Delta L} = \tau_{1,l} \cdot O_1 + \tau_{12,l} \cdot O_{12} \qquad (6.21\text{-}3)$$

The first term on the right hand side is the Darcy Weisbach friction between the liquid and the pipe wall, the second term the Darcy Weisbach friction between the liquid and the bed.

The force balance on the bed layer yields:

$$-A_2 \cdot \Delta p + F_{12,l} = F_{2,sf} + F_{2,l} \quad \text{and} \quad -A_2 \cdot \frac{\Delta p}{\Delta L} + \tau_{12,l} \cdot O_{12} = \tau_{2,sf} \cdot O_2 + \tau_{2,l} \cdot O_2 \qquad \text{(6.21-4)}$$

Because the term $\Delta p/\Delta L$, the pressure gradient, is negative, a minus sign is added in front. The first term on the right hand side is the sliding friction between the bed and the pipe wall, the second term is the Darcy Weisbach friction of the pore water with the pipe wall. In the case of a sliding bed, the sliding friction force is a constant, but in case of a fixed bed this force will have a value between zero and the sliding friction force. The normal force between the bed and the pipe wall, necessary to calculate the sliding friction force, consists of two components. The first component is based on the submerged weight of the solid particles in the bed, while the second component is based on the transmission of normal stresses at the heterogeneous-bed interface, resulting in a shear force at the interface. This gives for the normal force F_{N1} resulting from the submerged weight:

$$F_{N1} = \rho_l \cdot g \cdot \Delta L \cdot R_{sd} \cdot C_{vb} \cdot \frac{D_p^2}{2} \cdot \left(\sin(\beta) - \beta \cdot \cos(\beta) \right) \qquad \text{(6.21-5)}$$

This gives for the normal force F_{N1} in the Doron notation:

$$F_{N1} = \rho_l \cdot g \cdot \Delta L \cdot R_{sd} \cdot C_{vb} \cdot \frac{D_p^2}{2} \cdot \left(\left(\frac{2 \cdot y_b}{D_p} - 1 \right) \cdot \beta + \sin(\beta) \right) \qquad \text{(6.21-6)}$$
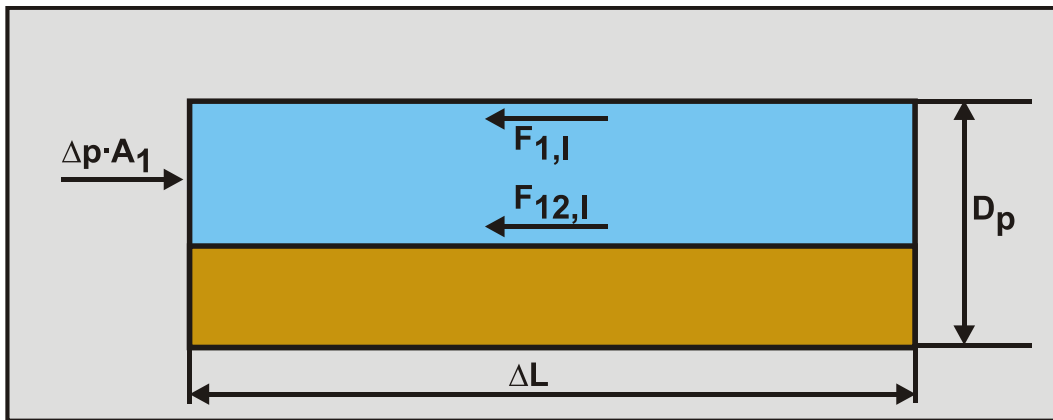
Figure 6.21-2: The forces on the liquid above the bed.
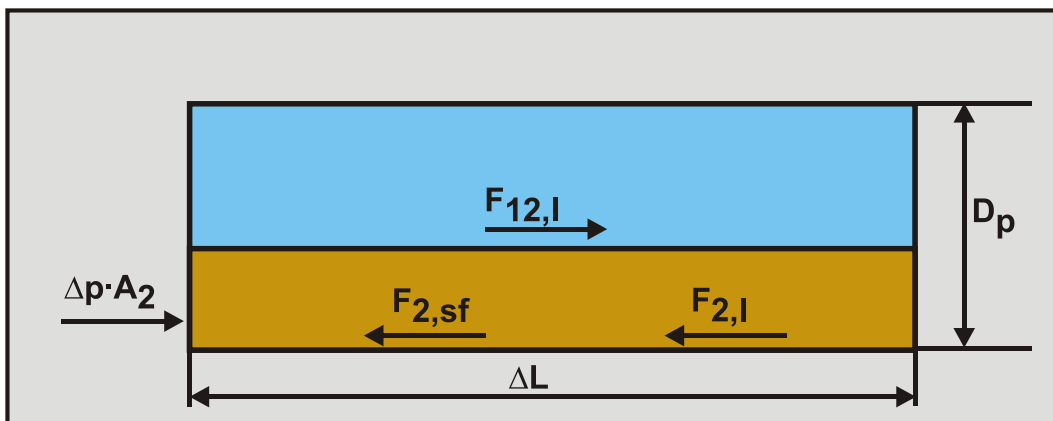
Figure 6.21-3: The forces on the bed.

The normal force is determined using the Wilson (1970) hydrostatic pressure approach. There may be an additional normal force on the bed resulting from the submerged weight of the particles above this bed level. The additional normal force due to transmission of stress from the interface through bed particles is, after Bagnold (1954) and (1957):

$$F_{N2} = \frac{\tau_{12} \cdot O_{12} \cdot \Delta L}{\tan(\varphi)}$$

(6.21-7)

With φ the angle of internal friction at the top of the bed with values of 20° to 40°. The total normal force F_N between the bed and the pipe wall is now:

$$F_N = F_{N1} + F_{N2} = \rho_l \cdot g \cdot \Delta L \cdot R_{sd} \cdot C_{vb} \cdot \frac{D_p^2}{2} \cdot \left(\left(\frac{2 \cdot y_b}{D_p} - 1 \right) \cdot \beta + \sin(\beta) \right) + \frac{\tau_{12} \cdot O_{12} \cdot \Delta L}{\tan(\varphi)}$$

(6.21-8)

Giving for the sliding friction force $F_{2,sf}$ between the bed and the pipe wall in case of a sliding bed:

$$F_{2,sf} = \mu_{sf} \cdot \left(\rho_l \cdot g \cdot \Delta L \cdot R_{sd} \cdot C_{vb} \cdot \frac{D_p^2}{2} \cdot \left(\left(\frac{2 \cdot y_b}{D_p} - 1 \right) \cdot \beta + \sin(\beta) \right) + \frac{\tau_{12} \cdot O_{12} \cdot \Delta L}{\tan(\varphi)} \right)$$

(6.21-9)

The hydrodynamic resistance force $F_{1,l}$ between the liquid in the bed and the pipe wall will only occur if the bed is sliding, this force can be determined by:

$$F_{1,l} = \tau_{1,l} \cdot O_1 \cdot \Delta L \quad \text{and} \quad F_{2,l} = \tau_{2,l} \cdot O_2 \cdot \Delta L$$

(6.21-10)

The hydrodynamic shear stresses may be expressed by:

$$\tau_{1,l} = \frac{F_{1,l}}{O_1 \cdot \Delta L} = \frac{\lambda_1}{8} \cdot \rho_l \cdot v_1^2 \quad \text{and} \quad \tau_{2,l} = \frac{F_{2,l}}{O_2 \cdot \Delta L} = \frac{\lambda_{2,l}}{8} \cdot \rho_2 \cdot v_2^2$$

(6.21-11)

The Darcy Weisbach friction coefficients are evaluated from:

$$\frac{\lambda_1}{4} = \alpha_1 \cdot \left(\frac{v_1 \cdot D_{H1}}{v_1} \right)^{-\beta_1} \quad \text{and} \quad \frac{\lambda_{2,l}}{4} = \alpha_2 \cdot \left(\frac{v_2 \cdot D_{H2}}{v_2} \right)^{-\beta_2}$$

(6.21-12)

The hydraulic diameters of cross sections 1 and 2 can be determined with:

$$D_{H1} = \frac{4 \cdot A_1}{O_1 + O_{12}} \quad \text{and} \quad D_{H2} = \frac{4 \cdot A_2}{O_2 + O_{12}}$$

(6.21-13)

The viscosities v_1 and v_2 are the mean viscosities of the liquid in the two layers and should be taken equal to the liquid viscosity v_l, unless the particles are very small influencing the viscosity. The coefficients α_1 and α_2 were taken 0.046 and the powers β_1 and β_2 both 0.2, for turbulent flow which is normally the case. The interfacial shear stress is expressed in terms of the relative velocity between the two layers.

$$\tau_{12,l} = \frac{\lambda_{12}}{8} \cdot \rho_{12} \cdot (v_1 - v_2)^2 \quad \text{and} \quad F_{12,l} = \tau_{12,l} \cdot O_{12} \cdot \Delta L$$

(6.21-14)

The Darcy Weisbach friction coefficient associated with the interface is evaluated using the Colebrook & White (1937) equation, with the particle diameter for the roughness. According to Televantos et al. (1979) the resulting Darcy Weisbach friction factor should be multiplied by 2, taking into account the effects of particle collisions, as well as entrainment and deposition of particles at the interface, which tend to increase the interfacial friction coefficient.

$$\lambda_{12} = \frac{2 \cdot 1.325}{\left(\ln \left(\frac{d}{3.7 \cdot D_{H1}} + \frac{2.51}{Re_{H1} \cdot \sqrt{\lambda_{12}}} \right) \right)^2} \quad \text{or} \quad \lambda_{12} = \frac{2 \cdot 1.325}{\left(\ln \left(\frac{d}{3.7 \cdot D_{H1}} + \frac{5.75}{Re_{H1}^{0.9}} \right) \right)^2}$$

(6.21-15)

The densities of the two layers are calculated according to:

$$\rho_1 = \rho_s \cdot C_{vs,1} + \rho_l \cdot \left(1 - C_{vs,1}\right)$$

$$\rho_2 = \rho_s \cdot C_{vb} + \rho_l \cdot \left(1 - C_{vb}\right)$$

(6.21-16)

The bed concentration is assumed to be 52%. The viscosity of the mixture is considered equal to the viscosity of the carrier liquid. The particles used are coarse and much larger than the scale of the viscous sub layer, hence they do not affect the apparent viscosity.

The conservation equations deal with the horizontal direction of a horizontal pipe. In the vertical direction of a cross section of the pipe however a dispersion mechanism of the solid particles in the upper layer should be taken into account. This is assumed to be a turbulent diffusion process, which is governed by large scale eddies and tends to make the flow isotropic. It is the cause of a motion of particles from a high concentration zone to a low concentration zone, moving particles upwards. This tendency is balanced at steady state by gravity resulting in the settling of particles on top of the bed. This mechanism is represented by the well-known diffusion equation:

$$\varepsilon' \cdot \frac{\partial^2 C(y)}{\partial y^2} + v_t' \cdot \frac{\partial C(y)}{\partial y}$$

(6.21-17)

Assuming that the concentration only depends on the vertical position and assuming a mean diffusion coefficient and terminal settling velocity, the concentration can be obtained by integrating the above equation twice, giving:

$$C(y) = C_{vb} \cdot e^{\left(-\frac{v_{th}}{\varepsilon} \cdot (y - y_{12})\right)}$$

(6.21-18)

Now assuming a mean cross flow diffusion coefficient of:

$$\varepsilon = 0.052 \cdot u_* \cdot R \quad \text{with:} \quad u_* = \sqrt{\frac{\lambda_1}{8}} \cdot v_1$$

(6.21-19)

Solves the concentration distribution above the bed. The terminal settling velocity can be determined by, for example, the Ruby & Zanke (1977) equation (4.4-5).

$$v_t = \frac{10 \cdot v_l}{d} \cdot \left(\sqrt{1 + \frac{R_{sd} \cdot g \cdot d^3}{100 \cdot v_l^2}} - 1\right)$$

(6.21-20)

For a cluster of particles the Richardson and Zaki (1954) equation (4.6-1) can be applied.

$$\frac{v_{th}}{v_t} = \left(1 - C_{vs}\right)^\beta$$

(6.21-21)

Integration of the above equation gives the mean concentration in the upper dispersed layer:

$$C_{vs,1} = \frac{C_{vb} \cdot D_p^2}{2 \cdot A_1} \cdot \int_{\beta_{12}}^{\pi} e^{\left(-\frac{v_{th}}{\varepsilon} \cdot \frac{D_p}{2} \cdot (\cos(\beta_{12}) - \cos(\beta))\right)} \cdot \sin^2(\beta) \cdot d\beta$$

(6.21-22)

Equations (6.21-1), (6.21-2), (6.21-3), (6.21-4) and the above equation can be solved for any set of operational conditions for the following 5 unknowns: The mean velocity in the dispersed layer, the mean velocity of the bed, the mean concentration in the dispersed layer, the bed height or angle and the pressure gradient.

Three special cases will be considered, fully suspended flow, flow with a stationary bed and flow with a sliding bed.

Flow with a stationary bed:

In this case the bed velocity equals zero, reducing the number of equations. The sliding friction however is no longer defined. This gives:

$$C_{vt,1} = C_{vs,1} = C_{vt} \quad \text{and} \quad v_1 = v_{ls} \cdot \frac{A_p}{A_1} \quad \text{and} \quad v_2 = 0 \tag{6.21-23}$$

Since the average concentration above the bed C_{vt} is known, the bed height y_b or bed angle β can be determined by iteration from:

$$C_{vt} = \frac{C_{vb} \cdot D_p^2}{2 \cdot A_1} \cdot \int_{\beta_{12}}^{\pi} e^{\left(-\frac{v_{th}}{\varepsilon} \cdot \frac{D_p}{2} \cdot \left(\cos(\beta_{12}) - \cos(\beta) \right) \right)} \cdot \sin^2(\beta) \cdot d\beta \tag{6.21-24}$$

Once the bed angle β is determined, all unknowns can be solved, also resulting in the pressure gradient. The static friction force follows from equation (6.21-4). As long as the static friction force is smaller than the sliding friction force, the bed is stationary. As soon as the static friction force found here is larger than the sliding friction force, the bed is sliding and the sliding bed methodology should be used. This was first presented by Wilson (1970)

Flow with a moving bed:

The whole set of equations (6.21-1), (6.21-2), (6.21-3), (6.21-4) and (6.21-22) has to be solved. The concentration profile can be determined with equation (6.21-18).

Fully suspended flow:

When the bed height approaches zero, transition to fully suspended flow occurs. This transition may also occur directly from the stationary bed regime, if the shear stress on the bed is never high enough to make the bed sliding. The pressure gradient can now be determined with:

$$-\frac{\Delta p}{\Delta L} = \lambda_1 \cdot \frac{1}{2} \cdot \rho_m \cdot v_{ls}^2 \tag{6.21-25}$$

$$\rho_m = \rho_l \cdot (1 - C_{vs}) + \rho_s \cdot C_{vs}$$

The no slip condition is still used here, assuming spatial and delivered volumetric concentrations are equal. This is very doubtful at the transition from a bed to full suspended flow. The vertical concentration profile can now be determined with:

$$C(y) = C_{vB} \cdot e^{\left(-\frac{v_{th}}{\varepsilon} \cdot y \right)} \tag{6.21-26}$$

The concentration at the bottom of the pipe C_{vB} is not equal to the bed concentration C_{vb}, but will have a lower value. Since the volumetric concentration of the suspension is known, the concentration at the bottom of the pipe can be determined with:

$$C_{vt} = \frac{C_{vB} \cdot D_p^2}{2 \cdot A_p} \cdot \int_0^{\pi} e^{\left(-\frac{v_{th}}{\varepsilon} \cdot \frac{D_p}{2} \cdot (1 - \cos(\beta)) \right)} \cdot \sin^2(\beta) \cdot d\beta = \frac{2 \cdot C_{vB}}{\pi} \cdot \int_0^{\pi} e^{\left(-\frac{v_{th}}{\varepsilon} \cdot \frac{D_p}{2} \cdot (1 - \cos(\beta)) \right)} \cdot \sin^2(\beta) \cdot d\beta \tag{6.21-27}$$

Or according to Doron et al. (1987):

$$C_{vB} = \frac{\pi}{2} \cdot C_{vt} \cdot \int_0^\pi e^{\left(-\frac{v_{th}}{\epsilon} \cdot \frac{D_p}{2} \cdot (1 - \cos(\beta)) \right)} \cdot \sin^2(\beta) \cdot d\beta \qquad (6.21\text{-}28)$$

Doron et al. (1987) carried out experiments with an 11 m long Plexiglas pipe with an internal diameter of 51 mm (2 inch). They used black Acetal with a density of 1.24 tons/m³, a diameter of 3 mm, a sliding friction coefficient of 0.3 and tan(φ)=0.6. Figure 6.21-8, Figure 6.21-11 and Figure 6.21-14 show some of the hydraulic gradient experimental data in a relative excess hydraulic gradient versus the liquid hydraulic gradient graph, while Figure 6.21-6 shows the observed Limit of Stationary Deposit Velocity (LSDV) and the Minimum Hydraulic Gradient Velocity (MHGV) versus the DHLLDV Framework, giving a good correlation. Figure 6.21-7 shows bed height data of Harada et al. (1989) versus the DHLLDV Framework, also giving a good correlation.

6.21.2 The 3 Layer Model (3LM).

The main limitation of the Doron et al. (1987) 2 layer model is its inability to predict accurately enough the existence of a stationary bed at low line speeds (flow rates). There are cases where a stationary bed was observed, yet the model predicts a moving bed. For dredging practice this is not really important, since dredging practice will not operate in this region of flow rates. However in order to understand the process of slurry flow in all aspects Doron & Barnea (1993) developed a 3 layer model. For high flow rates they still use the 2 layer model, but for low flow rates it is assumed that the bed consists of 2 layers, a stationary layer at the bottom of the pipe and a moving layer above it. The upper portion of the pipe is still occupied with a heterogeneous mixture. The forces on particles at the top of the bed are determined from a moment balance with the drag force giving the driving moment and the submerged weight giving the resisting moment. The derivation is similar to the derivation of the Shields curve in Chapter 5 and will not be discussed here. The 3 layer model gives a lower hydraulic gradient at very low flow rates compared to the 2 layer model, however the experimental data do not confirm the one or the other. Only the observation of a stationary bed at low flow rates would be in favor of the 3 layer model.
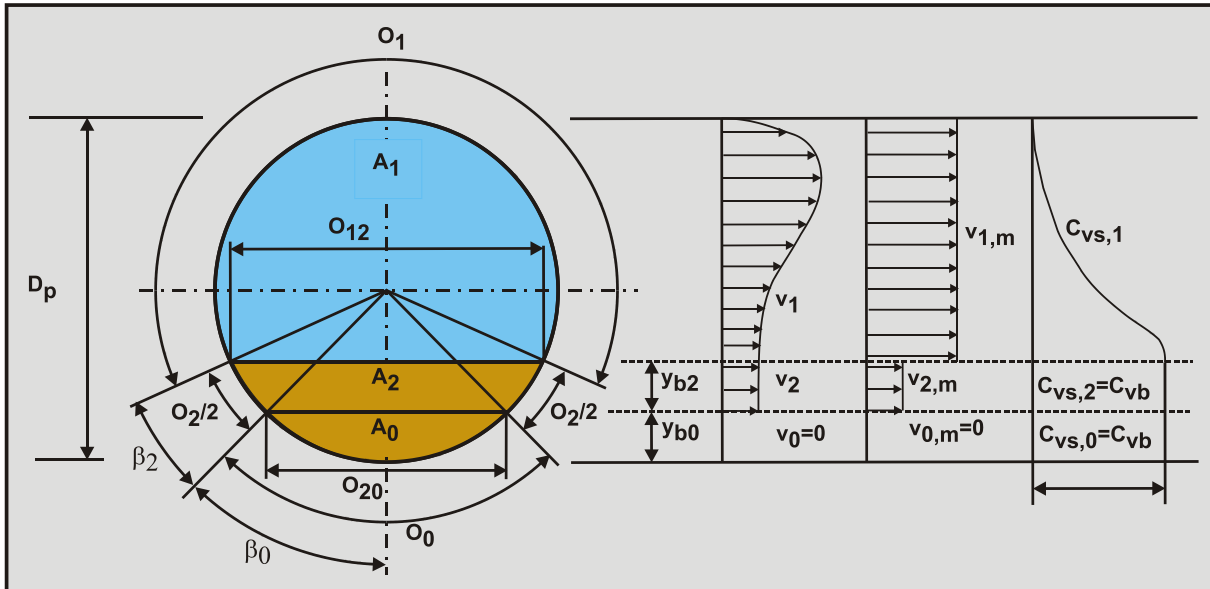
**Figure 6.21-4: The 3 layer model with suspension in the upper layer
and a stationary bed in the lowest layer.**

Figure 6.21-4 shows the heterogeneous upper layer A_1, the moving bed intermediate layer A_2 and the stationary bed lowest layer A_0. The velocity v_2 and the thickness y_{b2} of the moving bed are related based on the equilibrium of moments on a particle, based on cubic packing with $C_{vb}=0.52$. This relation is:

$$v_2 = \sqrt{\frac{0.779 \cdot R_{sd} \cdot g \cdot d}{C_D} \cdot \left(C_{vb} \cdot \frac{y_{b2}}{d} + (1 - C_{vb}) \right)} \qquad (6.21\text{-}29)$$

So the higher the velocity of the moving bed, the thicker the moving bed, until the thickness of the stationary bed is zero and the 2LM has to be applied. Note that it is assumed that the moving bed concentration is assumed to be constant and equal to 0.52 and that the circular shape of the pipe is not taken into account here.

For the solids phase the continuity equation yields, neglecting slip between the two phases:

$$v_1 \cdot A_1 \cdot C_{vs,1} + v_2 \cdot A_2 \cdot C_{vb} = v_{ls} \cdot A_p \cdot C_{vt} \tag{6.21-30}$$

For the liquid phase the continuity equation yields, neglecting slip between the two phases:

$$v_1 \cdot A_1 \cdot \left(1 - C_{vs,1}\right) + v_2 \cdot A_2 \cdot \left(1 - C_{vb}\right) = v_{ls} \cdot A_p \cdot \left(1 - C_{vt}\right) \tag{6.21-31}$$
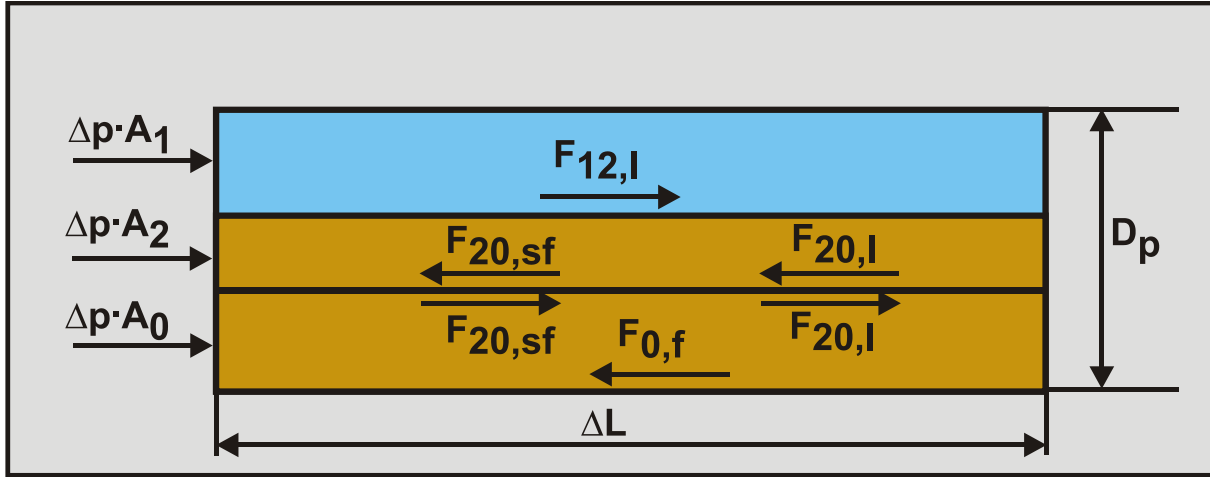
Figure 6.21-5: The forces on the moving bed and the stationary bed.

The force balance on the heterogeneous layer yields, see Figure 6.21-2, similar to the 2LM model:

$$-A_1 \cdot \Delta p = F_{1,l} + F_{12,l} \quad \text{and} \quad -A_1 \cdot \frac{\Delta p}{\Delta L} = \tau_{1,l} \cdot O_1 + \tau_{12,l} \cdot O_{12} \tag{6.21-32}$$

These forces consist of the driving force due to the pressure gradient on the left hand side and the resisting forces due to Darcy Weisbach friction between the liquid with the pipe wall and the liquid with the bed.

The force balance on the moving bed layer yields:

$$-A_2 \cdot \Delta p + F_{12,l} = F_{20,sf} + F_{20,l} + F_{2,sf} + F_{2,l}$$

$$\tag{6.21-33}$$

$$-A_2 \cdot \frac{\Delta p}{\Delta L} + \tau_{12,l} \cdot O_{12} = \tau_{20,sf} \cdot O_{20} + \tau_{20,l} \cdot O_{20} + \tau_{2,sf} \cdot O_2 + \tau_{2,l} \cdot O_2$$

These forces consist of, on the left hand side the driving forces, the force resulting from the pressure gradient and the force resulting from the Darcy Weisbach friction on top of the moving bed. These forces consist of, on the right hand side the resisting forces, the sliding friction force between the moving bed and the stationary bed, the Darcy Weisbach friction force between the moving bed and the stationary bed, the sliding friction force between the moving bed and the pipe wall and the Darcy Weisbach friction force between the moving bed and the pipe wall.

Finally the force balance on the stationary bed layer yields:

$$-A_0 \cdot \Delta p + F_{20,sf} + F_{20,l} = F_{0,f} \quad \text{and} \quad -A_0 \cdot \frac{\Delta p}{\Delta L} + \tau_{20,sf} \cdot O_{20} + \tau_{20,l} \cdot O_{20} = \tau_{0,f} \cdot O_0 \tag{6.21-34}$$

These forces consist of, on the left hand side the driving forces and on the right hand side the resisting force. The driving forces are the force resulting from the pressure gradient, the sliding friction force exerted by the moving bed on top of the stationary bed and the Darcy Weisbach friction force on top of the stationary bed due to a velocity difference between the moving bed and the stationary bed. The resisting force is the friction force between the stationary bed and the pipe wall. Since the stationary bed is not moving, this force is smaller than or equal to the sliding friction force resulting from the sliding friction coefficient. There is no Darcy Weisbach component, because there is no velocity difference between the pipe wall and the liquid in the stationary bed.

The Darcy Weisbach shear stress $\tau_{1,l}$ is calculated with equation (6.21-11), similar to the 2LM model. The Darcy Weisbach shear stress $\tau_{12,l}$ is determined with equation (6.21-14), similar to the 2LM model. The Darcy Weisbach shear stress between the moving bed and the pipe wall $\tau_{2,l}$ is determined with equation (6.21-11), similar to the 2 LM model. The Darcy Weisbach shear stress between the moving bed and the stationary bed $\tau_{20,l}$ is calculated with equation (6.21-14), but of course with the velocities v_2 and v_0, similar to the 2LM model.

Now 3 friction forces are left, the sliding friction between the moving bed and the stationary bed, the sliding friction between the moving bed and the pipe wall and the friction between the stationary bed and the pipe wall. Using the Wilson et al. (2006) hydrostatic normal stress approach, the total normal stress F_N between the bed and the pipe wall is, given a bed angle β:

$$F_N = \rho_l \cdot g \cdot \Delta L \cdot R_{sd} \cdot C_{vb} \cdot A_p \cdot \frac{2 \cdot \left(\sin(\beta) - \beta \cdot \cos(\beta) \right)}{\pi} \tag{6.21-35}$$

This means that the total normal force F_N between the moving + stationary bed and the pipe wall equals, including the Bagnold (1954) and (1957) stresses, matching the 2LM model:

$$\begin{aligned} F_N &= \rho_l \cdot g \cdot \Delta L \cdot R_{sd} \cdot C_{vb} \cdot A_p \cdot \frac{2 \cdot \left(\sin(\beta_0 + \beta_2) - (\beta_0 + \beta_2) \cdot \cos(\beta_0 + \beta_2) \right)}{\pi} \\ &\quad + \frac{\tau_{12,l}}{\tan(\varphi)} \cdot O_{12} \cdot \Delta L \end{aligned} \tag{6.21-36}$$

The normal force F_{N0} between the stationary bed and the pipe wall is, including the Bagnold (1954) and (1957) stresses, according to Doron & Barnea (1993):

$$F_{N0} = \rho_l \cdot g \cdot \Delta L \cdot R_{sd} \cdot C_{vb} \cdot A_p \cdot \frac{2 \cdot \left(\sin(\beta_0) - \beta_0 \cdot \cos(\beta_0) \right)}{\pi} + \frac{\tau_{12,l}}{\tan(\varphi)} \cdot O_0 \cdot \Delta L \tag{6.21-37}$$

This gives for the normal force F_{N2} between the moving bed and the pipe wall, including the Bagnold (1954) and (1957) stresses, according to Doron & Barnea (1993):

$$\begin{aligned} F_{N2} &= F_N - F_{N0} = \rho_l \cdot g \cdot \Delta L \cdot R_{sd} \cdot C_{vb} \cdot A_p \cdot \frac{2 \cdot \left(\sin(\beta_0 + \beta_2) - (\beta_0 + \beta_2) \cdot \cos(\beta_0 + \beta_2) \right)}{\pi} \\ &\quad - \rho_l \cdot g \cdot \Delta L \cdot R_{sd} \cdot C_{vb} \cdot A_p \cdot \frac{2 \cdot \left(\sin(\beta_0) - \beta_0 \cdot \cos(\beta_0) \right)}{\pi} + \frac{\tau_{12,l}}{\tan(\varphi)} \cdot O_2 \cdot \Delta L \end{aligned} \tag{6.21-38}$$

The normal force at the interface between the moving bed and the stationary bed F_{N20} is, including the Bagnold (1954) and (1957) stresses:

$$\begin{aligned} F_{N20} &= \rho_l \cdot g \cdot \Delta L \cdot R_{sd} \cdot C_{vb} \cdot A_p \cdot \frac{\left((\beta_0 + \beta_2) - \sin(\beta_0 + \beta_2) \cdot \cos(\beta_0 + \beta_2) \right)}{\pi} \\ &\quad - \rho_l \cdot g \cdot \Delta L \cdot R_{sd} \cdot C_{vb} \cdot A_p \cdot \frac{\left((\beta_0) - \sin(\beta_0) \cdot \cos(\beta_0) \right)}{\pi} + \frac{\tau_{12,l}}{\tan(\varphi)} \cdot O_{20} \cdot \Delta L \end{aligned} \tag{6.21-39}$$

The maximum shear stress $\tau_{0,f,max}$ between the stationary bed and the pipe wall is, including the Bagnold (1954) and (1957) stresses:

$$\tau_{0,f,max} = \mu_{sf} \cdot \frac{F_{N0}}{\Delta L \cdot O_0} = \mu_{sf} \cdot \frac{F_{N0}}{\Delta L \cdot \beta_0 \cdot D_p}$$

$$= \mu_{sf} \cdot \frac{\rho_l \cdot g \cdot R_{sd} \cdot C_{vb} \cdot A_p}{\beta_0 \cdot D_p} \cdot \frac{2 \cdot \left(\sin(\beta_0) - \beta_0 \cdot \cos(\beta_0) \right)}{\pi} + \mu_{sf} \cdot \frac{\tau_{12,l}}{\tan(\varphi)}$$

(6.21-40)

This gives for the shear stress $\tau_{2,sf}$ between the moving bed and the pipe wall, including the Bagnold (1954) and (1957) stresses:

$$\tau_{2,sf} = \mu_{sf} \cdot \frac{F_{N2}}{\Delta L \cdot O_2} = \mu_{sf} \cdot \frac{F_{N2}}{\Delta L \cdot \beta_2 \cdot D_p}$$

$$= \mu_{sf} \cdot \frac{\rho_l \cdot g \cdot R_{sd} \cdot C_{vb} \cdot A_p}{\beta_2 \cdot D_p} \cdot \left(\begin{array}{c} \frac{2 \cdot \left(\sin(\beta_0 + \beta_2) - (\beta_0 + \beta_2) \cdot \cos(\beta_0 + \beta_2) \right)}{\pi} \\ - \frac{2 \cdot \left(\sin(\beta_0) - \beta_0 \cdot \cos(\beta_0) \right)}{\pi} \end{array} \right) + \mu_{sf} \cdot \frac{\tau_{12,l}}{\tan(\varphi)}$$

(6.21-41)

The shear stress $\tau_{20,sf}$ at the interface between the moving bed and the stationary bed F_{N20} is, including the Bagnold (1954) and (1957) stresses:

$$\tau_{20,sf} = \mu_{sf} \cdot \frac{F_{N20}}{O_{20} \cdot \Delta L} = \mu_{sf} \cdot \frac{\rho_l \cdot g \cdot R_{sd} \cdot C_{vb} \cdot A_p}{O_{20}} \cdot \left(\begin{array}{c} \frac{\left((\beta_0 + \beta_2) - \sin(\beta_0 + \beta_2) \cdot \cos(\beta_0 + \beta_2) \right)}{\pi} \\ - \frac{\left((\beta_0) - \sin(\beta_0) \cdot \cos(\beta_0) \right)}{\pi} \end{array} \right)$$

$$+ \mu_{sf} \cdot \frac{\tau_{12,l}}{\tan(\varphi)}$$

(6.21-42)

The 3 shear forces due to sliding or dynamic friction are now:

$$F_{0,f \le \tau_{0,f,max}} \cdot O_0 \cdot \Delta L = \mu_{sf} \cdot F_{N0}$$

$$F_{2,sf} = \tau_{2,sf} \cdot O_2 \cdot \Delta L = \mu_{sf} \cdot F_{N2}$$

(6.21-43)

$$F_{20,sf} = \tau_{20,sf} \cdot O_{20} \cdot \Delta L = \mu_{sf} \cdot F_{N20}$$

The calculation of the suspended fraction in the upper layer is identical to the procedure of the 2LM model. Now that all the shear stresses are known, the set of equations (6.21-32), (6.21-33) and (6.21-34) can be solved by iteration.

The 3LM model still raises some questions that will be discussed under "Some Issues". Based on the findings of the authors a modified model is proposed under "Modified Doron & Barnea Model".

6.21.3 Conclusions & Discussion.

The Doron et al. (1987) 2 layer model is similar to the Wilson (1979) model regarding the 2 layers and the force balance equations. The model however uses a concentration distribution in the upper layer, where the original Wilson (1979) model assumes pure liquid. The approach of the concentration distribution is based on the concentration distribution in open channel flow and not in a circular closed conduit. The total solids transport in the upper layer is based on the average concentration times the average velocity in the upper layer and not on the concentration distribution times the velocity distribution integrated. The model also ignores the existence of a sheet flow or shear layer influencing both the concentration distribution and the Darcy Weisbach friction factor at the interface. So the applicability of the method used can be questioned, although the concept is very interesting and innovative at the time of the publication.

Doron & Barnea (1995) investigated the Limit of Stationary Deposit Velocity (LSDV), the Minimum Hydraulic Gradient Velocity (MHGV) and the bed height. The LSDV and MHGV, as shown in Figure 6.21-6, are from their own experiments. The 3 layer model overestimates the LSDV, while the DHLLDV Framework is closer to the experimental data. The 3 layer model is close to the MHGV, as is the DHLLDV Framework. Figure 6.21-7 shows bed height experiments of Harada et al. (1989) in a 120 mm x 30 mm conduit with particles with a density of 2.5 ton/m^3. In terms of a hydraulic radius, this would match a circular pipe with a radius of 48 mm. The 3 layer model matches for 0.35 mm and 0.5 mm particles, but overestimates 1 mm particles. The figure shows the bed height according to the DHLLDV Framework, giving a good correlation for the 0.5 mm particle and a concentration of 0.03.

Resuming one can state that the Doron et al. (1987), Doron & Barnea (1993) and Doron & Barnea (1995) model and experiments contain some interesting concepts in addition to the Wilson (1979) 2 layer model. The use of concentration distributions based on open channel flow is however questionable. Not just for this research, but in general for all models discussed in this book.
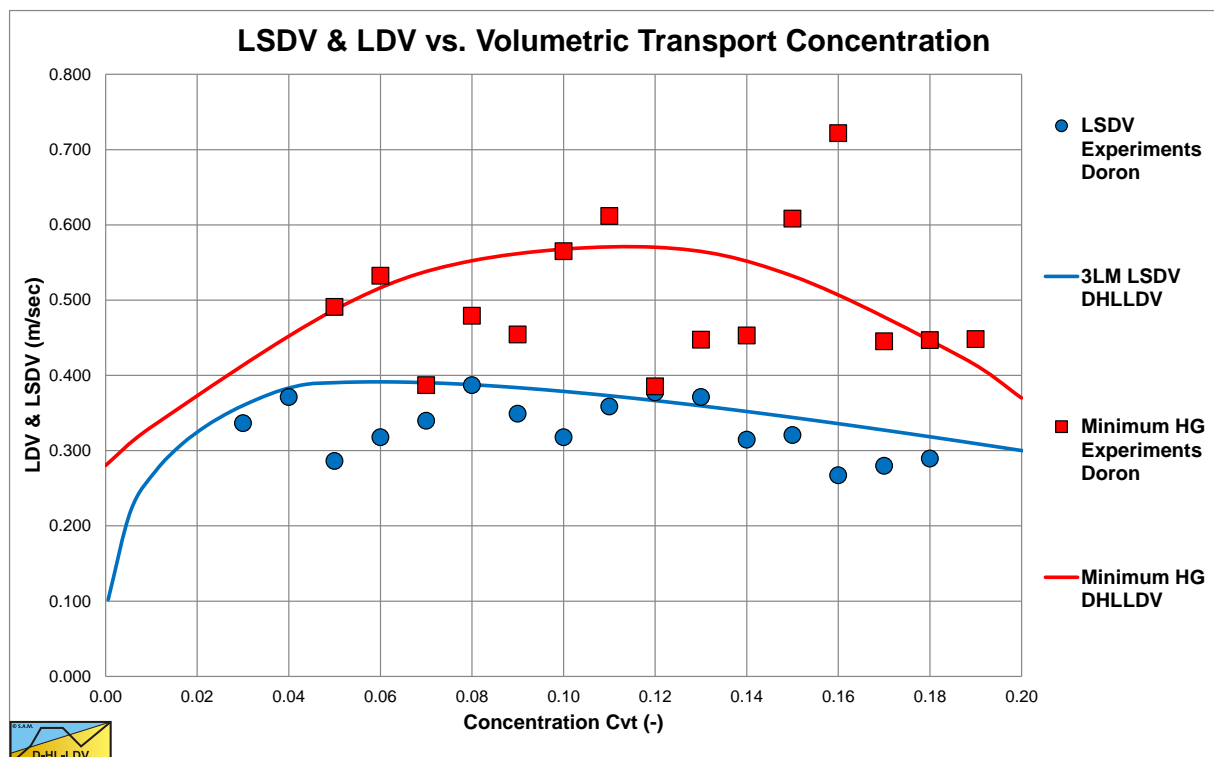
Figure 6.21-6: The LSDV and MHGV according to Doron et al. (1987) and Doron & Barnea (1993).
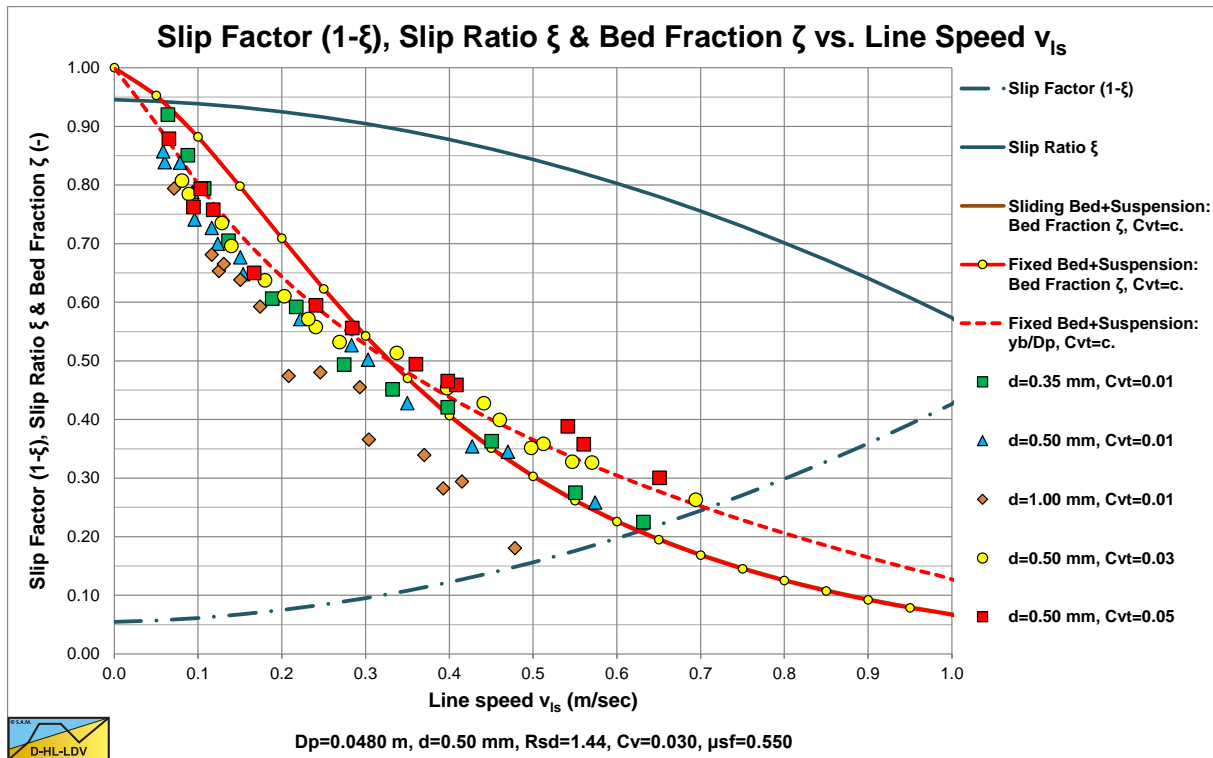
Figure 6.21-7: Bed height measurements of Harada et al. (1989).

6.21.4 Some Issues.

The additional force on top of the bed:

The use of the additional force, resulting from the Bagnold (1954) and (1957) stresses, on top of the bed by Doron et al. (1987), equation (6.21-7), is not so obvious. First of all an extra normal force on the bed requires enough submerged weight of particles on top of the bed, for example in a sheet flow or shear layer, where the shear forces are transferred by inter particle contacts. It is not explained where this force originates from. Secondly, if this force is transferred through the bed, resulting in additional normal stresses on the pipe wall, this force cannot be added to the normal force, but should be treated like the weight in the hydrostatic approach. According to the authors this force should not be present or at least there should be a check if the submerged weight of the particles above the bed justify this force, and thus will probably be compensated by the model later in order to match the experiments. For example by using a smaller sliding friction coefficient. The implementation of the Bagnold (1954) and (1957) stresses in the 3LM model is not correct, a stress balance does not exist, only a force balance. The Bagnold (1954) and (1957) stresses are implemented in a way that they appear on each surface.
This issue is present in both the 2LM and 3LM models.

The Darcy Weisbach friction factor at the interface:

The equation for the Darcy Weisbach friction factor at the interface, as used in the original article of Doron et al. (1987) seems a wrong interpretation of the Televantos et al. (1979) approach. The correct interpretation is given by equation (6.21-15).

The equation for the concentration at the bottom of the pipe:

It seems equation (6.21-28) in the original Doron et al. (1987) paper is incorrect (equation 33). There is no division by the integral. The correct equation is given here:

$$C_{vB} = \frac{\pi}{2} \cdot C_{vt} \cdot \frac{1}{\int_0^\pi e^{\left(-\frac{v_{th}}{\varepsilon} \cdot \frac{D_p}{2} \cdot (1-\cos(\beta))\right)} \cdot \sin^2(\beta) \cdot d\beta} \tag{6.21-44}$$

Now for very small particles or very high velocities, the argument of the e-power gets close to zero, resulting in:

$$C_{vB} = \frac{\pi}{2} \cdot C_{vt} \cdot \frac{1}{\displaystyle\int_0^\pi \sin^2(\beta) \cdot d\beta} = \frac{\pi}{2} \cdot C_{vt} \cdot \frac{1}{\frac{\pi}{2}} = C_{vt} \tag{6.21-45}$$

The concentration at the bottom of the pipe equals the average concentration, also implying that the concentration is equal to the average concentration at any location in the pipe. A true homogeneous flow. With the original equation of Doron et al. (1987) this would give:

$$C_{vB} = \frac{\pi}{2} \cdot C_{vt} \cdot \int_0^\pi \sin^2(\beta) \cdot d\beta = \frac{\pi}{2} \cdot C_{vt} \cdot \frac{\pi}{2} = \left(\frac{\pi}{2}\right)^2 \cdot C_{vt} \approx 2.5 \cdot C_{vt} \tag{6.21-46}$$

Which cannot be true for true homogeneous flow. The correct concentration distribution can be determined by substituting equation (6.21-45) in equation (6.21-26), giving:

$$C(y) = \frac{\pi}{2} \cdot C_{vt} \cdot \frac{e^{\left(-\frac{v_{th}}{\varepsilon} \cdot \frac{D_p}{2} \cdot (1-\cos(\beta))\right)}}{\displaystyle\int_0^\pi e^{\left(-\frac{v_{th}}{\varepsilon} \cdot \frac{D_p}{2} \cdot (1-\cos(\beta))\right)} \cdot \sin^2(\beta) \cdot d\beta} \tag{6.21-47}$$

Use of the concentration distribution to determine the LDV:

Doron et al. (1987) state that the critical velocity can be determined by evaluating the pressure gradient and finding the minimum pressure gradient line speed. This is referred to in this book as the Minimum Hydraulic Gradient Velocity (MHGV). What they did not conclude, a missed opportunity, is the velocity where the concentration at the bottom of the pipe equals the bed concentration. This is referred to in this book as the Limit Deposit Velocity. This occurs when, assuming the hindered terminal settling velocity is zero at bed concentration and the bed angle **β** is zero at the LDV:

$$\int_0^\pi e^{\left(-\frac{v_{th}}{\varepsilon} \cdot \frac{D_p}{2} \cdot (1-\cos(\beta))\right)} \cdot \sin^2(\beta) \cdot d\beta = \frac{\pi}{2} \cdot \frac{C_{vt}}{C_{vb}} \tag{6.21-48}$$

With the diffusion coefficient at the Limit Deposit Velocity:

$$\varepsilon = 0.052 \cdot u_* \cdot R \quad \text{with:} \quad u_* = \sqrt{\frac{\lambda_l}{8}} \cdot v_{ls,ldv} \quad \text{so:} \quad \varepsilon = 0.052 \cdot \sqrt{\frac{\lambda_l}{8}} \cdot R \cdot v_{ls,ldv} \tag{6.21-49}$$

The relation for the Limit Deposit Velocity is defined:

$$\int_0^\pi e^{\left(-\frac{55}{\sqrt{\lambda_l}} \cdot \frac{v_{th}}{v_{ls,ldv}} \cdot (1-\cos(\beta))\right)} \cdot \sin^2(\beta) \cdot d\beta = \frac{\pi}{2} \cdot \frac{C_{vt}}{C_{vb}} \quad \text{with:} \quad \lambda_l = 0.184 \cdot \left(\frac{v_{ls,ldv} \cdot D_p}{\nu_l}\right)^{-0.2} \tag{6.21-50}$$

This method however shows an LDV almost independent of the pipe diameter, continuously increasing with the terminal settling velocity (the particle diameter) and also results in very high LDV values, making it not suitable for the determination of the LDV and raising questions about the concentration distribution approach.

Use of the dynamic and static friction coefficients.

In the 3LM model the dynamic friction coefficient is used for both the friction between the bed and the pipe wall and for the friction between the moving bed and the stationary bed. The latter is sand on sand friction and the

internal friction angle should be used here. The sand on steel friction angle, or external friction angle is usually about 2/3 of the internal friction angle.

6.21.5 Experiments.
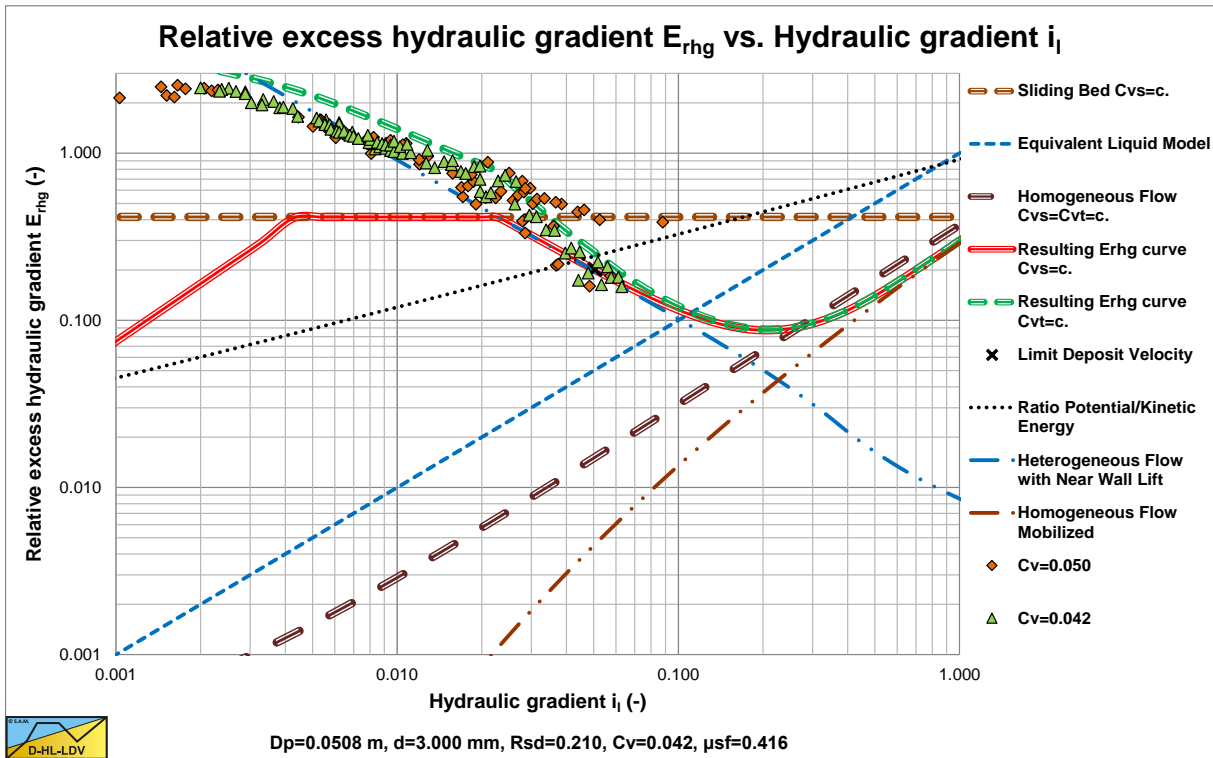
Figure 6.21-8: Data of Doron et al. (1987) and Doron & Barnea (1993) at very low concentrations.
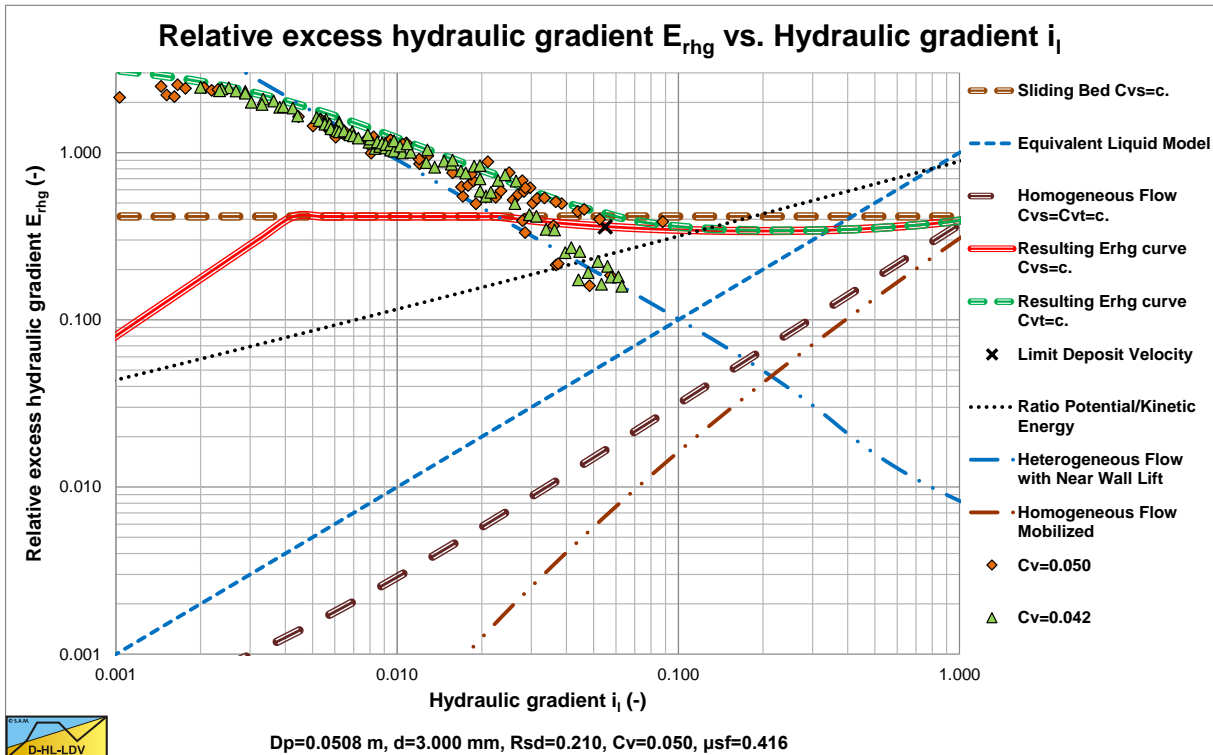
Figure 6.21-9: Data of Doron et al. (1987) and Doron & Barnea (1993) at low concentrations, at the slifding flow criterion.
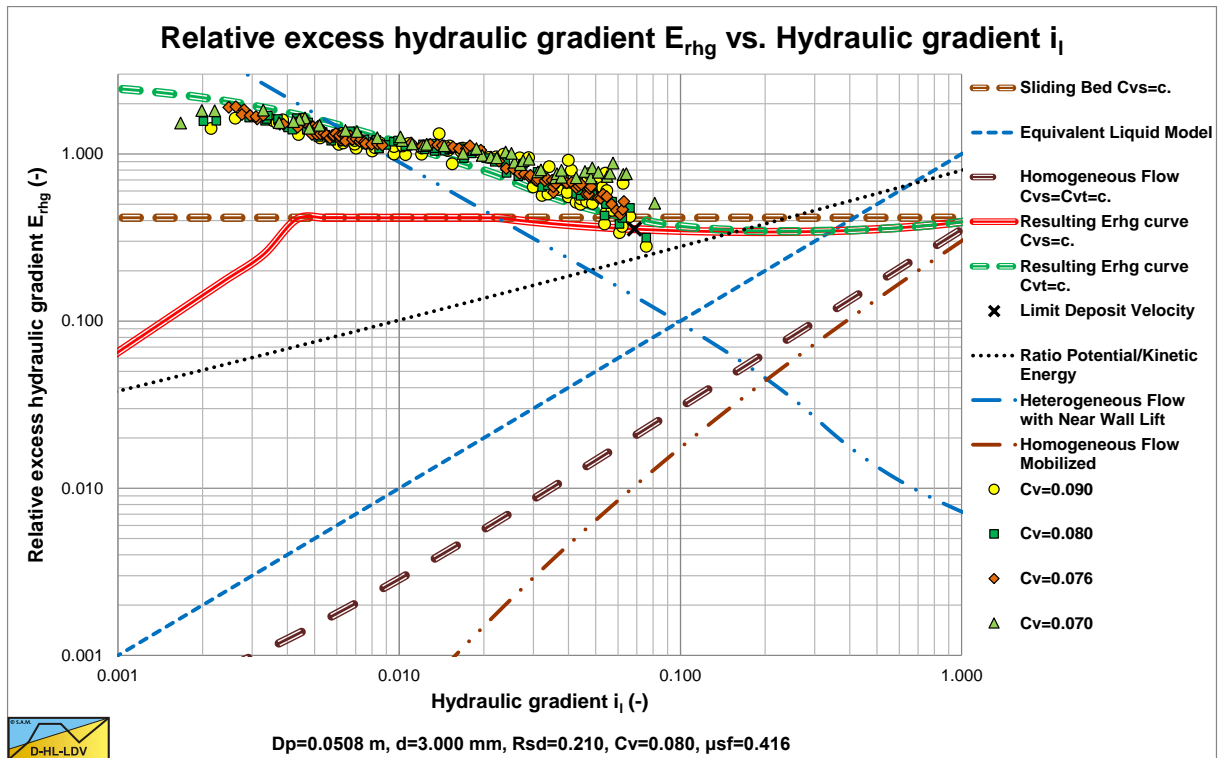
Figure 6.21-10: Data of Doron et al. (1987) and Doron & Barnea (1993) at low/medium concentrations.
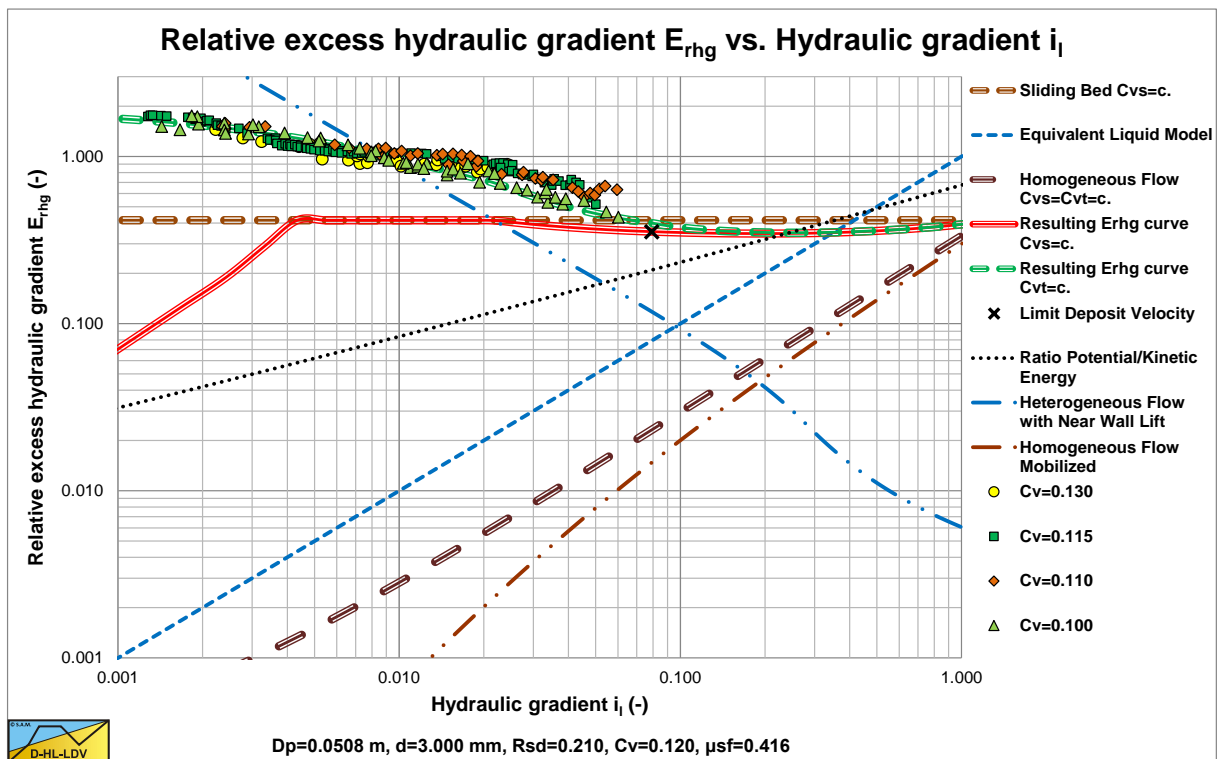
Figure 6.21-11: Data of Doron et al. (1987) and Doron & Barnea (1993) at medium concentrations.

Figure 6.21-8 and Figure 6.21-9 show that for very low concentrations (**C$_{vt}$<5%**) the behavior at higher line speeds is according to the heterogeneous flow regime. At concentrations above 5% the behavior is according to the sliding flow regime. In this case the ratio of the particle diameter to the pipe diameter is 0.059, which is much larger than the ratio 0.015 as proposed by Wilson et al. (1992) as a criterion for full stratified flow.
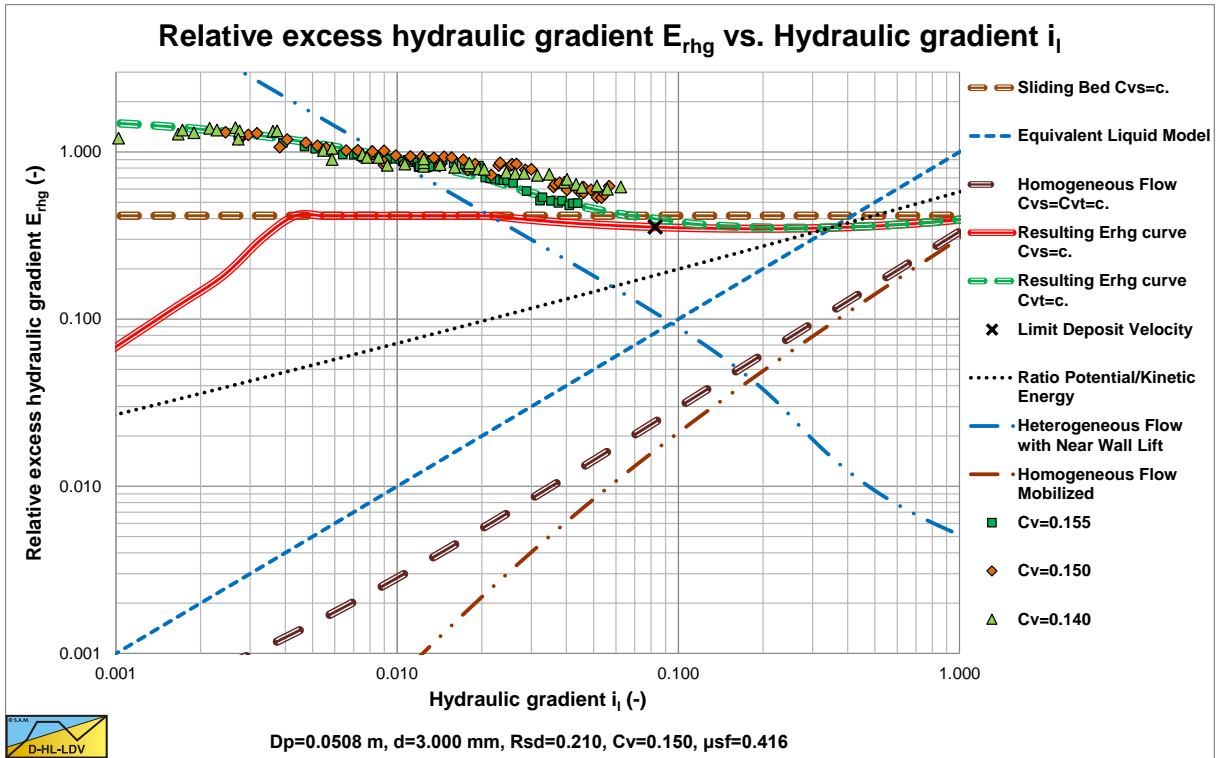
Figure 6.21-12: Data of Doron et al. (1987) and Doron & Barnea (1993) at medium/high concentrations.
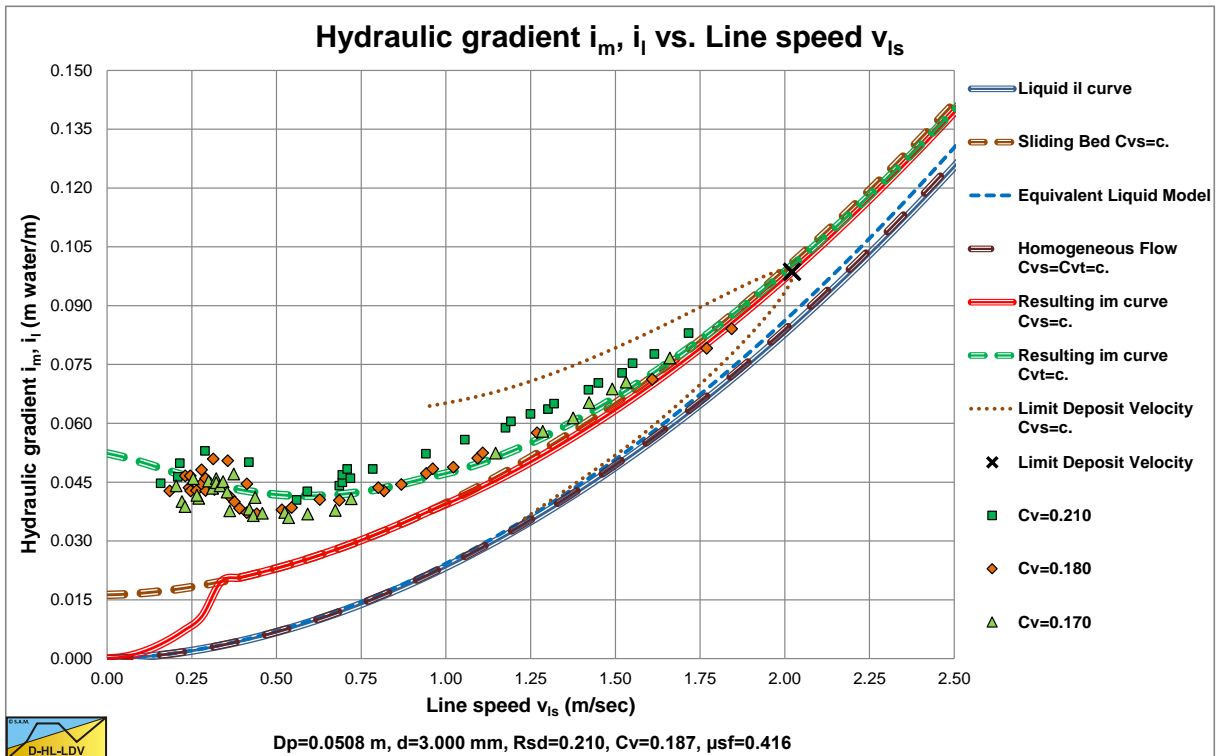
Figure 6.21-13: Data of Doron et al. (1987) and Doron & Barnea (1993) at high concentrations.

Figure 6.21-10, Figure 6.21-11 and Figure 6.21-12 show similar sliding flow behavior. The data of Doron et al. (1987) and Doron & Barnea (1993) are compared with the DHLLDV Framework and give a reasonable good match. Figure 6.21-13 and Figure 6.21-14 show the data as hydraulic gradient and relative excess hydraulic gradient. The comparison with the DHLLDV Framework is satisfactory.

It should be noted that all experiments were carried out below the LDV, so at relatively low line speeds. The concentrations measured were transport concentrations. This implies that at low line speeds there was either fixed bed or sliding bed transport and at the higher line speeds most probably sliding flow transport.
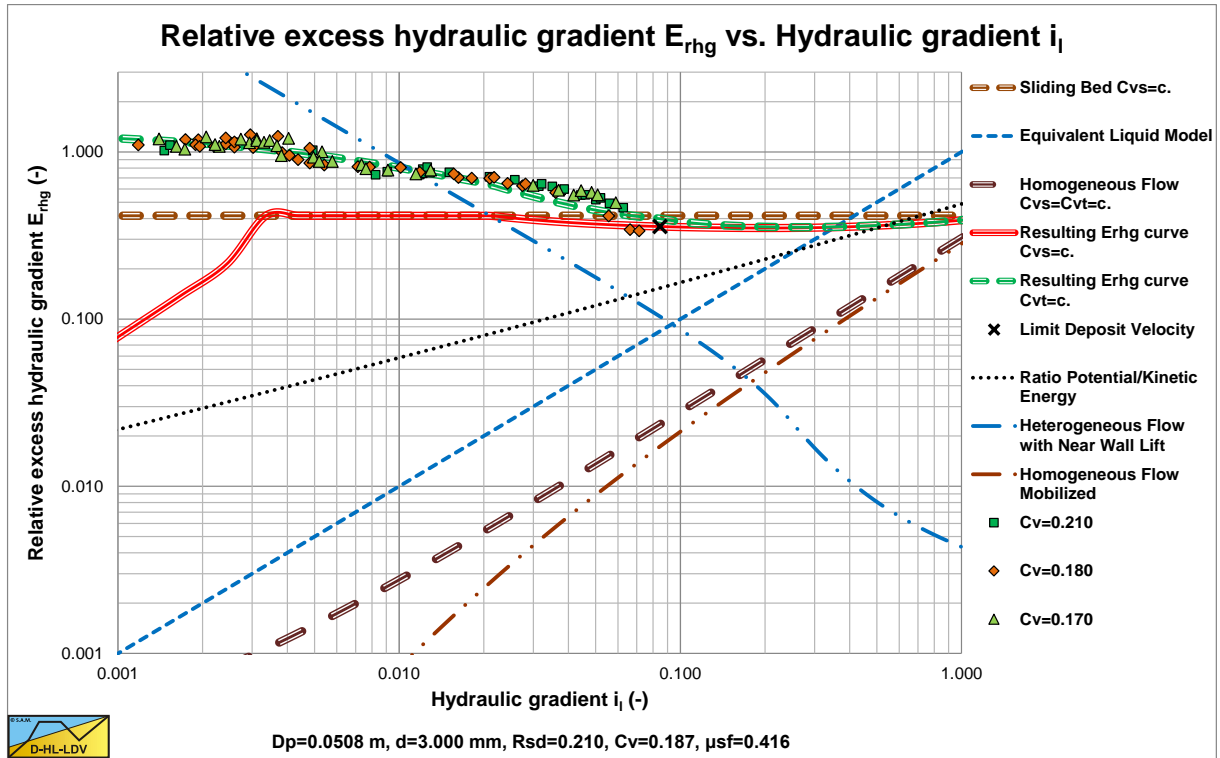
Figure 6.21-14: Data of Doron et al. (1987) and Doron & Barnea (1993) at high concentrations.

6.21.6 Modified Doron & Barnea Model.

Based on the knowledge of today (2015) a number of modifications to the Doron & Barnea models are proposed. First of all, the Bagnold (1954) and (1957) stresses do not act on top of the moving bed, but can still be used to determine the thickness of the moving bed. Secondly the hydrostatic approach of Wilson (1979) to determine the normal force between the bed and the pipe wall is rejected, instead the weight approach of Miedema & Ramsdell (2014) is applied. The last main modification is using two different friction angles for internal friction and external friction. The force balances on the 3 layers do not change because of the modifications, but are given here for completeness of the model.

For the solids phase the continuity equation yields, neglecting slip between the two phases:

$$v_1 \cdot A_1 \cdot C_{vs,1} + v_2 \cdot A_2 \cdot C_{vb} = v_{ls} \cdot A_p \cdot C_{vt} \tag{6.21-51}$$

For the liquid phase the continuity equation yields, neglecting slip between the two phases:

$$v_1 \cdot A_1 \cdot \left(1 - C_{vs,1}\right) + v_2 \cdot A_2 \cdot \left(1 - C_{vb}\right) = v_{ls} \cdot A_p \cdot \left(1 - C_{vt}\right) \tag{6.21-52}$$

The force balance on the heterogeneous layer yields, see Figure 6.21-2, similar to the 2LM model:

$$-A_1 \cdot \Delta p = F_{1,l} + F_{12,l} \quad \text{and} \quad -A_1 \cdot \frac{\Delta p}{\Delta L} = \tau_{1,l} \cdot O_1 + \tau_{12,l} \cdot O_{12} \tag{6.21-53}$$

The force balance on the moving bed layer yields:

$$-A_2 \cdot \Delta p + F_{12,l} = F_{20,sf} + F_{20,l} + F_{2,sf} + F_{2,l}$$

$$-A_2 \cdot \frac{\Delta p}{\Delta L} + \tau_{12,l} \cdot O_{12} = \tau_{20,sf} \cdot O_{20} + \tau_{20,l} \cdot O_{20} + \tau_{2,sf} \cdot O_2 + \tau_{2,l} \cdot O_2 \tag{6.21-54}$$

Finally the force balance on the stationary bed layer yields:

$$-A_0 \cdot \Delta p + F_{20,sf} + F_{20,l} = F_{0,f} \quad \text{and} \quad -A_0 \cdot \frac{\Delta p}{\Delta L} + \tau_{20,sf} \cdot O_{20} + \tau_{20,l} \cdot O_{20} = \tau_{0,f} \cdot O_0 \qquad (6.21\text{-}55)$$

The implementation of the forces resulting from liquid also have not changed (index l). The Darcy Weisbach shear stress $\tau_{1,l}$ is calculated with equation (6.21-11), similar to the 2LM model. The Darcy Weisbach shear stress $\tau_{12,l}$ is determined with equation (6.21-14), similar to the 2LM model. The Darcy Weisbach shear stress between the moving bed and the pipe wall $\tau_{2,l}$ is determined with equation (6.21-11), similar to the 2 LM model. The Darcy Weisbach shear stress between the moving bed and the stationary bed $\tau_{20,l}$ is calculated with equation (6.21-14), but of course with the velocities v_2 and v_0, similar to the 2LM model.

The implementation of the forces due to dynamic or static friction have changed (indices f and sf). In order to determine the friction forces, first the weight of each layer has to be determined.

The weight of the moving bed and the stationary bed F_{W20} is:

$$F_{W20} = \rho_l \cdot g \cdot \Delta L \cdot R_{sd} \cdot C_{vb} \cdot A_p \cdot \frac{\left(\left(\beta_0 + \beta_2\right) - \sin\left(\beta_0 + \beta_2\right) \cdot \cos\left(\beta_0 + \beta_2\right) \right)}{\pi} \qquad (6.21\text{-}56)$$

The weight of the stationary bed F_{W0} is:

$$F_{W0} = \rho_l \cdot g \cdot \Delta L \cdot R_{sd} \cdot C_{vb} \cdot A_p \cdot \frac{\left(\left(\beta_0\right) - \sin\left(\beta_0\right) \cdot \cos\left(\beta_0\right) \right)}{\pi} \qquad (6.21\text{-}57)$$

The weight of the moving bed F_{W2} is:

$$F_{W2} = F_{W20} - F_{W0} = \rho_l \cdot g \cdot \Delta L \cdot R_{sd} \cdot C_{vb} \cdot A_p \cdot \frac{\left(\left(\beta_0 + \beta_2\right) - \sin\left(\beta_0 + \beta_2\right) \cdot \cos\left(\beta_0 + \beta_2\right) \right)}{\pi}$$

$$(6.21\text{-}58)$$

$$-\rho_l \cdot g \cdot \Delta L \cdot R_{sd} \cdot C_{vb} \cdot A_p \cdot \frac{\left(\left(\beta_0\right) - \sin\left(\beta_0\right) \cdot \cos\left(\beta_0\right) \right)}{\pi}$$

Now two cases have to be considered, the interface between the stationary and moving bed layers is below half the pipe diameter, or it is above half the pipe diameter. If it is below half the pipe diameter, part of the weight of the moving bed layer is carried by the pipe wall and the rest is carried by the interface. If it is above half the pipe diameter, the whole weight of the moving bed layer is carried by the interface. In the case it is below half the pipe diameter, again two cases have to be considered, the case where the width of the top of the moving bed layer is smaller than the interface width and the case where it is larger than the interface width. The 3 cases are discussed here:

Case 1a: The interface is below half the pipe diameter and the top width is smaller than the interface width.

Part of the weight of the moving bed layer is carried by the pipe wall. The rest is carried by the interface. The height of the moving bed layer is:

$$y_{b2} = \left(y_{b2} + y_{b0}\right) - y_{b0} = \frac{D_p}{2} \cdot \left(1 - \cos\left(\beta_2 + \beta_0\right)\right) - \frac{D_p}{2} \cdot \left(1 - \cos\left(\beta_0\right)\right)$$

$$(6.21\text{-}59)$$

$$= \frac{D_p}{2} \cdot \left(\cos\left(\beta_0\right) - \cos\left(\beta_2 + \beta_0\right)\right)$$

The part of the moving bed carried by the pipe wall $\mathbf{F_{W2,w}}$ is:

$$F_{W2,w} = \rho_l \cdot g \cdot \Delta L \cdot R_{sd} \cdot C_{vb} \cdot 2 \cdot \left(\begin{array}{l} A_p \cdot \left(\dfrac{\dfrac{\pi}{2} - \left((\beta_0) - \sin(\beta_0) \cdot \cos(\beta_0) \right)}{\pi} \right) \\ \\ O_{20} \cdot \dfrac{D_p}{2} \cdot \left(1 - \cos(\beta_0) \right) \end{array} \right)$$

(6.21-60)

The weight of the moving bed resting on the interface $\mathbf{F_{W2,i}}$ is now:

$$F_{W2,i} = F_{W2} - F_{W2,w}$$

(6.21-61)

The force balance on the moving bed layer yields:

$$-A_2 \cdot \Delta p + F_{12,l} = F_{20,sf} + F_{20,l} + F_{2,sf} + F_{2,l}$$

$$-A_2 \cdot \frac{\Delta p}{\Delta L} + \tau_{12,l} \cdot O_{12} = \tau_{20,sf} \cdot O_{20} + \tau_{20,l} \cdot O_{20} + \tau_{2,sf} \cdot O_2 + \tau_{2,l} \cdot O_2$$

(6.21-62)

$$\text{With}: \quad F_{20,sf} = F_{W2,i} \cdot \tan(\varphi) \quad \text{and} \quad \tau_{20,sf} = \frac{F_{W2,i} \cdot \tan(\varphi)}{\Delta L \cdot O_{20}}$$

$$F_{2,sf} = F_{W2,w} \cdot \tan\left(\frac{2}{3} \cdot \varphi \right) \quad \text{and} \quad \tau_{2,sf} = \frac{F_{W2,w} \cdot \tan\left(\frac{2}{3} \cdot \varphi \right)}{\Delta L \cdot O_{20}}$$

Finally the force balance on the stationary bed layer yields:

$$-A_0 \cdot \Delta p + F_{20,sf} + F_{20,l} = F_{0,f} \quad \text{and} \quad -A_0 \cdot \frac{\Delta p}{\Delta L} + \tau_{20,sf} \cdot O_{20} + \tau_{20,l} \cdot O_{20} = \tau_{0,f} \cdot O_0$$

$$\text{With}: \quad F_{0,f} \le \left(F_{W2,i} + F_{W0} \right) \cdot \tan\left(\frac{2}{3} \cdot \varphi \right) = \left(F_{W2,i} + F_{W0} \right) \cdot \mu_{sf}$$

(6.21-63)

$$\text{and} \quad \tau_{0,f} \le \frac{\left(F_{W2,i} + F_{W0} \right) \cdot \mu_{sf}}{\Delta L \cdot O_0}$$

Case 1b: The interface is below half the pipe diameter and the top width is larger than the interface width.

The part of the weight carried by the interface is the weight of the cross section of the interface width times the thickness of the moving bed layer. The rest of the weight is carried by the pipe wall. The height of the moving bed layer is:

$$y_{b2} = \left(y_{b2} + y_{b0} \right) - y_{b0} = \frac{D_p}{2} \cdot \left(1 - \cos(\beta_2 + \beta_0) \right) - \frac{D_p}{2} \cdot \left(1 - \cos(\beta_0) \right)$$

(6.21-64)

$$= \frac{D_p}{2} \cdot \left(\cos(\beta_0) - \cos(\beta_2 + \beta_0) \right)$$

The weight of the moving bed resting on the interface $\mathbf{F_{W2,i}}$ is:

$$\mathbf{F_{W2,i}} = \rho_l \cdot g \cdot \Delta L \cdot R_{sd} \cdot C_{vb} \cdot y_{b2} \cdot O_{20} \tag{6.21-65}$$

The weight of the moving bed resting on the pipe wall $\mathbf{F_{W2,w}}$ is now:

$$\mathbf{F_{W2,w}} = \mathbf{F_{W2}} - \mathbf{F_{W2,i}} \tag{6.21-66}$$

The force balance on the moving bed layer yields:

$$-\mathbf{A_2} \cdot \Delta p + \mathbf{F_{12,l}} = \mathbf{F_{20,sf}} + \mathbf{F_{20,l}} + \mathbf{F_{2,sf}} + \mathbf{F_{2,l}}$$

$$-\mathbf{A_2} \cdot \frac{\Delta p}{\Delta L} + \tau_{12,l} \cdot O_{12} = \tau_{20,sf} \cdot O_{20} + \tau_{20,l} \cdot O_{20} + \tau_{2,sf} \cdot O_2 + \tau_{2,l} \cdot O_2$$

$$\text{With:} \quad \mathbf{F_{20,sf}} = \mathbf{F_{W2,i}} \cdot \tan(\varphi) \quad \text{and} \quad \tau_{20,sf} = \frac{\mathbf{F_{W2,i}} \cdot \tan(\varphi)}{\Delta L \cdot O_{20}} \tag{6.21-67}$$

$$\mathbf{F_{2,sf}} = \mathbf{F_{W2,w}} \cdot \tan\left(\frac{2}{3} \cdot \varphi\right) \quad \text{and} \quad \tau_{2,sf} = \frac{\mathbf{F_{W2,w}} \cdot \tan\left(\frac{2}{3} \cdot \varphi\right)}{\Delta L \cdot O_{20}}$$

Finally the force balance on the stationary bed layer yields:

$$-\mathbf{A_0} \cdot \Delta p + \mathbf{F_{20,sf}} + \mathbf{F_{20,l}} = \mathbf{F_{0,f}} \quad \text{and} \quad -\mathbf{A_0} \cdot \frac{\Delta p}{\Delta L} + \tau_{20,sf} \cdot O_{20} + \tau_{20,l} \cdot O_{20} = \tau_{0,f} \cdot O_0$$

$$\text{With:} \quad \mathbf{F_{0,f}} \leq \left(\mathbf{F_{W2,i}} + \mathbf{F_{W0}}\right) \cdot \tan\left(\frac{2}{3} \cdot \varphi\right) = \left(\mathbf{F_{W2,i}} + \mathbf{F_{W0}}\right) \cdot \mu_{sf} \tag{6.21-68}$$

$$\text{and} \quad \tau_{0,f} \leq \frac{\left(\mathbf{F_{W2,i}} + \mathbf{F_{W0}}\right) \cdot \mu_{sf}}{\Delta L \cdot O_0}$$

Case 2: The interface is above half the pipe diameter and the top width is always smaller than the interface width.

The full weight of the moving bed layer is resting on the interface. The resisting shear force on the interface due to internal friction $\mathbf{F_{20,sf}}$ + the viscous friction force $\mathbf{F_{20,l}}$ have to be equal to the shear force on top of the moving bed $\mathbf{F_{12,l}}$ + the pressure force $-\mathbf{A_2} \cdot \Delta p$.

The force balance on the moving bed layer reduces to:

$$-\mathbf{A_2} \cdot \Delta p + \mathbf{F_{12,l}} = \mathbf{F_{20,sf}} + \mathbf{F_{20,l}} \quad \text{and} \quad -\mathbf{A_2} \cdot \frac{\Delta p}{\Delta L} + \tau_{12,l} \cdot O_{12} = \tau_{20,sf} \cdot O_{20} + \tau_{20,l} \cdot O_{20}$$

$$\text{With:} \quad \mathbf{F_{20,sf}} = \mathbf{F_{W2}} \cdot \tan(\varphi) \quad \text{and} \quad \tau_{20,sf} = \frac{\mathbf{F_{W2}} \cdot \tan(\varphi)}{\Delta L \cdot O_{20}} \tag{6.21-69}$$

Finally the force balance on the stationary bed layer yields:

$$-A_0 \cdot \Delta p + F_{20,sf} + F_{20,l} = F_{0,f} \quad \text{and} \quad -A_0 \cdot \frac{\Delta p}{\Delta L} + \tau_{20,sf} \cdot O_{20} + \tau_{20,l} \cdot O_{20} = \tau_{0,f} \cdot O_0$$

$$(6.21-70)$$

$$\text{With:} \quad F_{0,f} \leq F_{W20} \cdot \tan\left(\frac{2}{3} \cdot \varphi\right) = F_{W20} \cdot \mu_{sf} \quad \text{and} \quad \tau_{0,f} = \frac{F_{W20} \cdot \mu_{sf}}{\Delta L \cdot O_0}$$

Solution Procedure:

First assume all the solids are in a stationary bed. This results in $\beta_0 + \beta_2$ based on the volumetric concentration given. Based on this total bed angle the velocity above the bed can be determined. Once the velocity is known the concentration distribution above the bed can be determined and the heterogeneous fraction and bed fraction are known. Now the bed height has to be adjusted in order to satisfy the continuity equations.

The Darcy Weisbach friction factors on the pipe wall and the bed interface can be determined, resulting in the pressure gradient in the heterogeneous layer. Once the pressure gradient is known, the force balance on the moving bed layer can be determined assuming a certain β_2. By iteration a force balance on the moving bed layer should be achieved, resulting in a matching β_2 and moving bed velocity v_2.

Now that the forces are known on the stationary bed and the bed angle β_0 is known, the force balance on the stationary bed can be determined. If the resulting friction force between the stationary bed and the pipe wall is smaller than the maximum, the stationary bed is really stationary, but if it's larger, the whole bed is moving/sliding. In the case of a true stationary bed, the Darcy Weisbach friction coefficients have to be adjusted for the moving bed velocity and the procedure has to be repeated.

In the case of a sliding bed (the whole bed is sliding) the 2LM model has to be applied. This can be achieved by taking $\beta_0 = 0$.
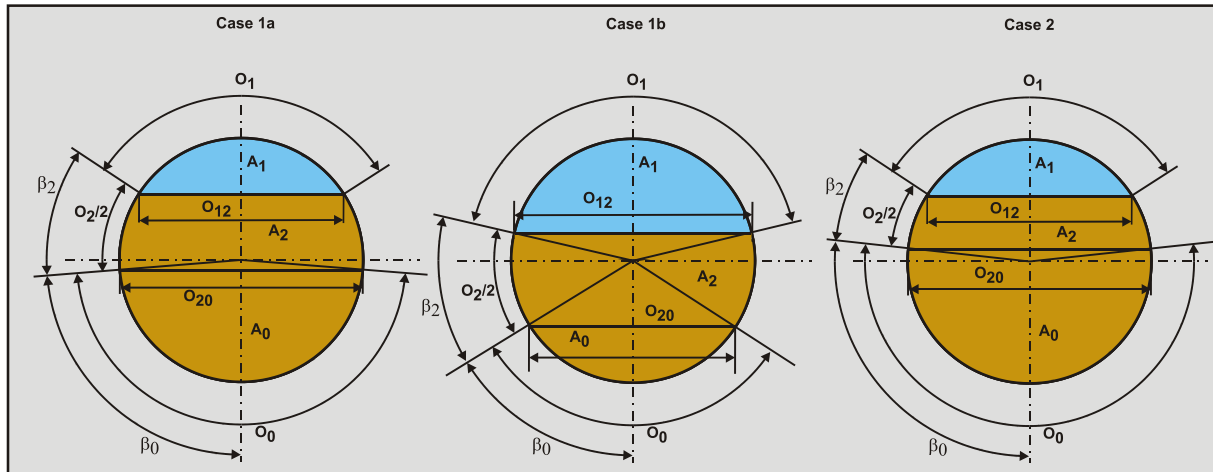
Figure 6.21-15: The 3 cases.

6.21.7 Inclined Pipes.

Doron et al. (1997) investigated the influence of inclined pipes, based on their 2LM and 3LM models. Basically they multiplied the sliding friction with the cosine of the inclination angle and they added the potential energy term, which is proportional with the sine of the inclination angle. They carried out experiments with inclination angles from -7 to +7 degrees. The resulting data however is dominated by the potential energy term.

They also investigated the Limit of Stationary Deposit Velocity (LSDV), the start of a sliding bed. Ascending pipes show an increasing LSDV with a maximum for an inclination angle of about 15 degrees, while descending pipes show a sharp decrease of the LSDV, because gravity becomes the driving force. At a certain negative inclination angle the bed will start sliding downwards because of gravity. It should be mentioned that Doron et al. (1997) use the delivered volumetric concentration, while LSDV models are usually based on spatial volumetric concentration. Especially in the stationary and sliding bed regimes the difference is significant.
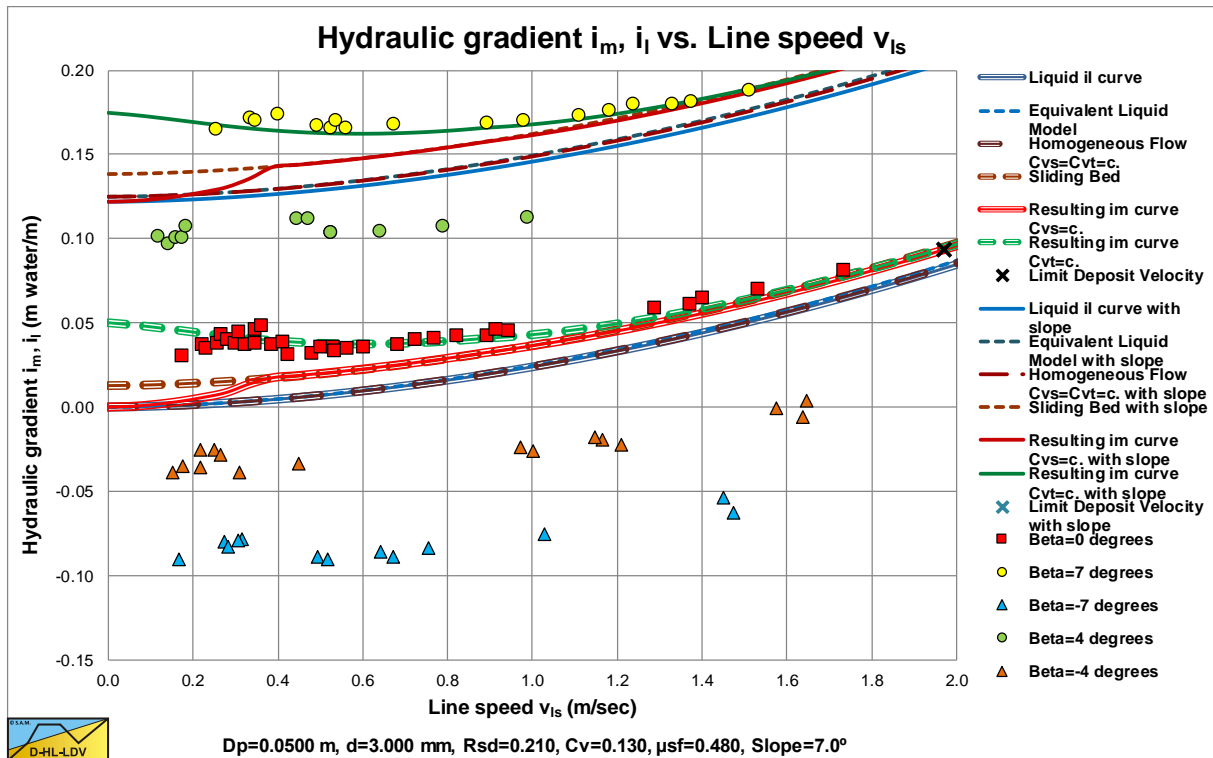
**Figure 6.21-16: The data of Doron et al. (1997) versus
the DHLLDV Framework for a horizontal and a 7º ascending pipe.**
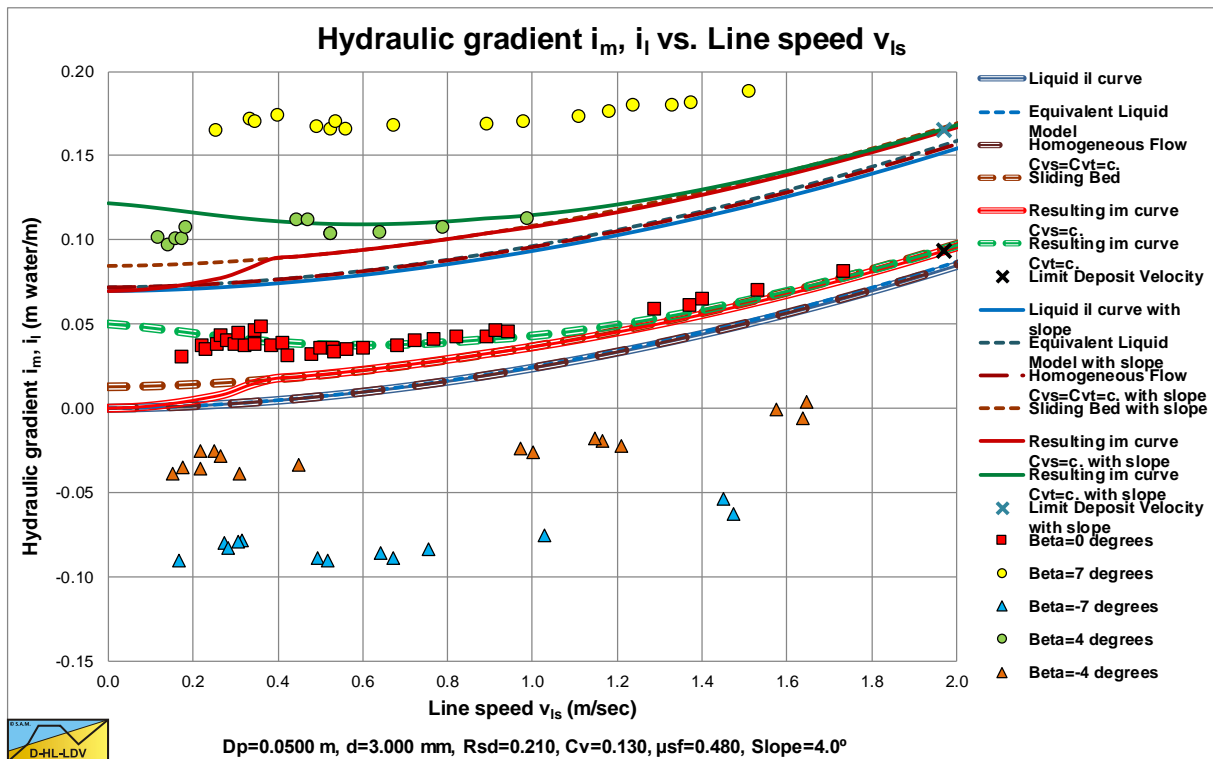
**Figure 6.21-17: The data of Doron et al. (1997) versus
the DHLLDV Framework for a horizontal and a 4º ascending pipe.**

Figure 6.21-16, Figure 6.21-17, Figure 6.21-18 and Figure 6.21-19 show the data of Doron et al. (1997) versus the DHLLDV Framework for a horizontal pipe and a 4º and 7º ascending pipe and a 4º and 7º descending pipe. The solid green lines show the hydraulic gradient for the delivered volumetric concentration. In general the theoretical curves and the experimental data match well, although at very low line speeds the experimental points are lower than the theoretical curves. The theoretical curves are based on a sliding bed and it is possible that at very low line

speeds there is a stationary bed, resulting in smaller hydraulic gradients, since the sliding friction is not fully mobilized. The difference between a horizontal pipe and the inclined pipes is dominated by the potential energy term (the sine), since the cosine is larger than 0.99 for the inclination angles considered, while the sine has a value of 0.12 for a 7° inclination angle. Much larger inclination angles are required to see the influence of the cosine on the sliding friction.
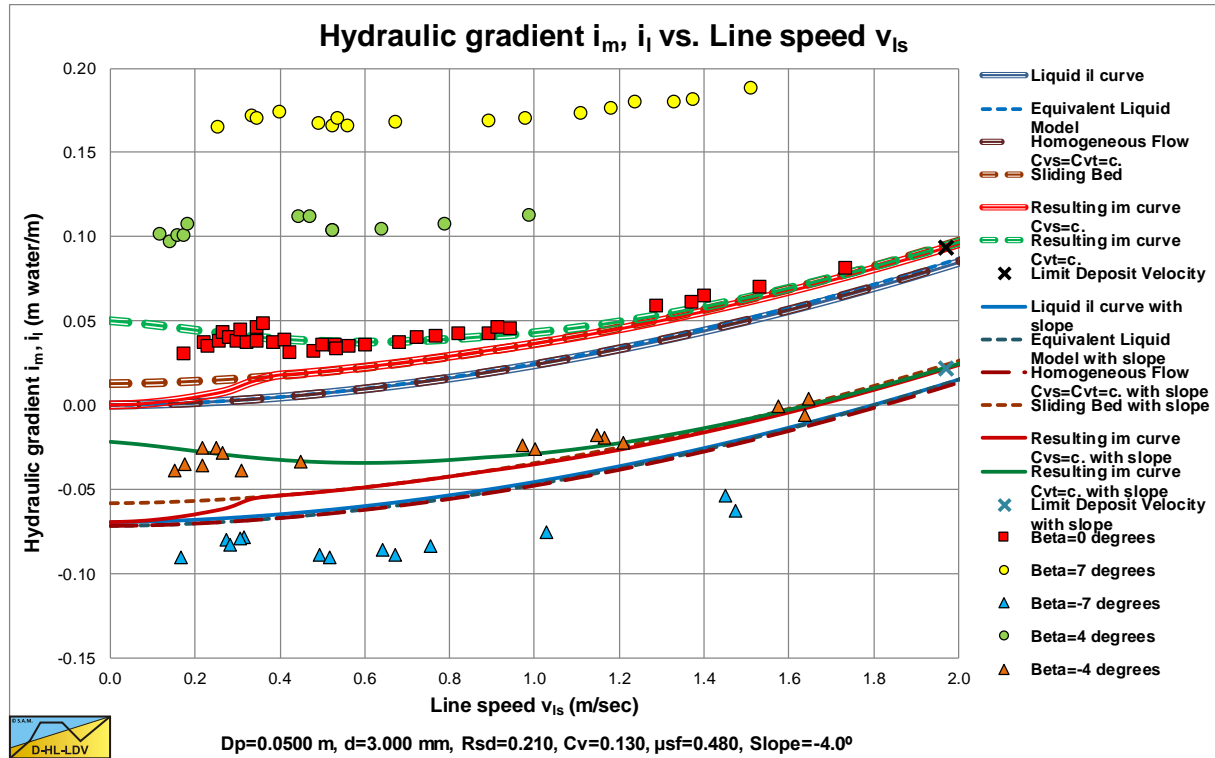
Figure 6.21-18: The data of Doron et al. (1997) versus the DHLLDV Framework for a horizontal and a 4° descending pipe.
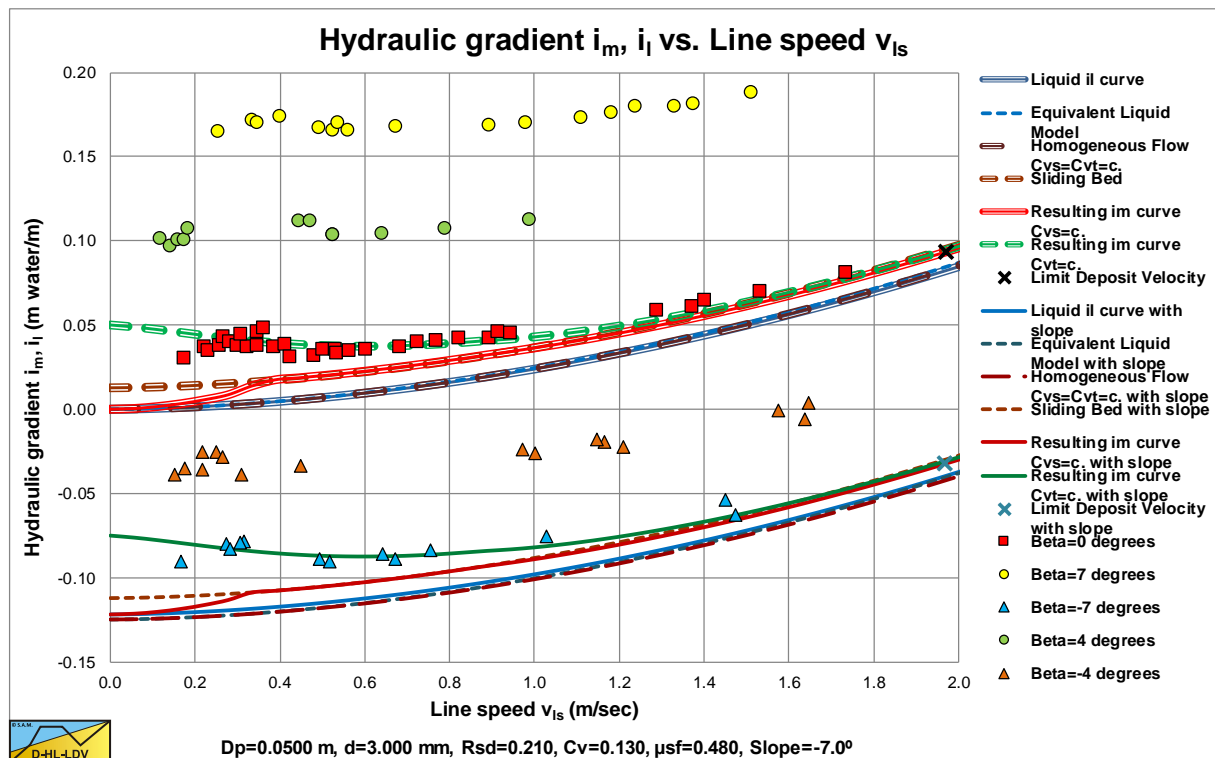
Figure 6.21-19: The data of Doron et al. (1997) versus the DHLLDV Framework for a horizontal and a 7° descending pipe.

6.21.8 Nomenclature Doron & Barnea Models.

A_p	Cross section pipe	m^2
A_0	Cross section stationary bed	m^2
A_1	Cross section above bed, heterogeneous flow	m^2
A_2	Cross section moving/sliding bed	m^2
C	Spatial volumetric concentration	-
C_{vb}	Volumetric spatial bed concentration	-
C_{vB}	Volumetric spatial bottom concentration	-
C_{vs}	Spatial volumetric concentration	-
$C_{vs,0}$	Spatial volumetric concentration in cross section 0	-
$C_{vs,1}$	Spatial volumetric concentration in cross section 1	-
$C_{vs,2}$	Spatial volumetric concentration in cross section 2	-
C_{vt}	Delivered (transport) volumetric concentration	-
d	Particle diameter	m
D_{H1}	Hydraulic diameter cross section 1, heterogeneous flow	m
D_{H2}	Hydraulic diameter cross section 2, moving/sliding bed	m
D_p	Pipe diameter	m
E_{rhg}	Relative excess hydraulic gradient	-
$F_{0,f}$	Static friction force between stationary bed and pipe wall	kN
$F_{1,l}$	Force between liquid and pipe wall	kN
$F_{12,l}$	Force between liquid and moving/sliding bed	kN
$F_{2,sf}$	Force on bed due to friction with the pipe wall	kN
$F_{2,l}$	Force on bed due to pore liquid	kN
$F_{20,sf}$	Force due to friction between moving and stationary bed	kN
$F_{20,l}$	Force on moving bed due to viscous losses at the interface moving – stationary bed	kN
F_N	Normal force	kN
F_{N0}	Normal force stationary bed – pipe wall	kN
F_{N1}	Normal force based on the weight of the bed	kN
F_{N2}	Normal force based on the shear stress on the bed	kN
F_{N2}	Normal force moving bed – pipe wall	kN
F_{N20}	Normal force moving bed – stationary bed	kN
F_{W0}	Weight stationary bed	kN
F_{W2}	Weight moving bed	kN
$F_{W2,i}$	Weight moving bed on interface	kN
$F_{W2,w}$	Weight moving bed on pipe wall	kN
F_{W20}	Weight moving bed + stationary bed	kN
g	Gravitational constant 9.81 m/s^2	m/s^2
i_l	Hydraulic gradient liquid	-
ΔL	Length of pipe section	m
LDV	Limit Deposit Velocity	m/s
$LSDV$	Limit of Stationary Deposit Velocity	m/s
O_p	Circumference pipe	m
O_0	Circumference pipe stationary bed	m
O_1	Circumference pipe above bed, heterogeneous flow	m
O_2	Circumference pipe moving/sliding bed	m
O_{12}	Width of top of bed	m
O_{20}	Width interface moving bed – stationary bed	m
Δp	Pressure difference	kPa
Δp_1	Pressure difference on cross section 1	kPa
Δp_2	Pressure difference on cross section 2	kPa
Re	Reynolds number	-
R_{sd}	Relative submerged density	-
R	Pipe radius	m
u_*	Friction velocity	m/s
v_t	Terminal settling velocity	m/s
v_{th}	Terminal settling velocity hindered	m/s
v_{ls}	Line speed	m/s

v_0	Cross section averaged velocity stationary bed $v_0=0$	m/s
v_1	Cross section averaged velocity above bed, heterogeneous region	m/s
v_2	Cross section averaged velocity moving/sliding bed	m/s
y	Vertical coordinate in pipe	m
y_b	Height of bed	m
y_{b0}	Height of stationary bed	m
y_{b2}	Height of moving/sliding bed	m
α_1	Proportionality factor Darcy Weisbach friction factor cross section 1	-
α_2	Proportionality factor Darcy Weisbach friction factor cross section 2	-
β	Bed angle	rad
β_0	Bed angle stationary bed	rad
β_2	Bed angle moving/sliding bed	rad
β	Richardson & Zaki hindered settling power	-
β_1	Power Darcy Weisbach friction factor cross section 1	-
β_2	Power Darcy Weisbach friction factor cross section 2	-
ϵ	Pipe wall roughness	m
ϵ	Diffusivity	m/s
ρ_l	Density carrier liquid	ton/m^3
ρ_s	Density solids	ton/m^3
ρ_1	Density of fluid in cross section 1	ton/m^3
ρ_2	Density of fluid in cross section 2	ton/m^3
φ	Angle of internal friction bed	^{o}
λ_1	Darcy-Weisbach friction factor with pipe wall	-
λ_2	Darcy-Weisbach friction factor with pipe wall, liquid in bed	-
λ_{12}	Darcy-Weisbach friction factor on the bed	-
ν_l	Kinematic viscosity	m^2/s
$\tau_{0,f,max}$	Maximum shear stress stationary bed – pipe wall	kPa
$\tau_{1,l}$	Shear stress liquid-pipe wall above bed	kPa
$\tau_{12,l}$	Shear stress bed-liquid interface	kPa
$\tau_{2,l}$	Shear stress liquid-pipe in bed, sliding bed – pipe wall	kPa
$\tau_{2,sf}$	Shear stress from sliding friction, sliding bed – pipe wall	kPa
$\tau_{20,sf}$	Shear stress moving bed – stationary bed	kPa
μ_{sf}	Sliding friction coefficient	-
μ_l	Dynamic viscosity liquid	Pa·s

6.22 The SRC Model.

Where the Wilson-GIW (1979) model as discussed in a previous chapter deals with a stationary or sliding bed layer (the lower layer) with a liquid layer above it (the upper layer), the model described here is made to cope with the complexities of industrial slurries. At the Saskatchewan Research Council (SRC) the model has been developed and improved over the years. The SRC model is the result of work carried out by Dr. C.A. Shook (University of Saskatchewan) and his associates at the Saskatchewan Research Council. The SRC model assumes that the suspended solids are distributed uniformly across the entire pipe and that the lower layer also contains the solids that contribute Coulombic friction. One will find an early version of the SRC model in in the Hydrotransport 10 proceedings, Shook et al. (1986). Later the model is discussed in the book of Shook & Roco (1991) and many other publications.
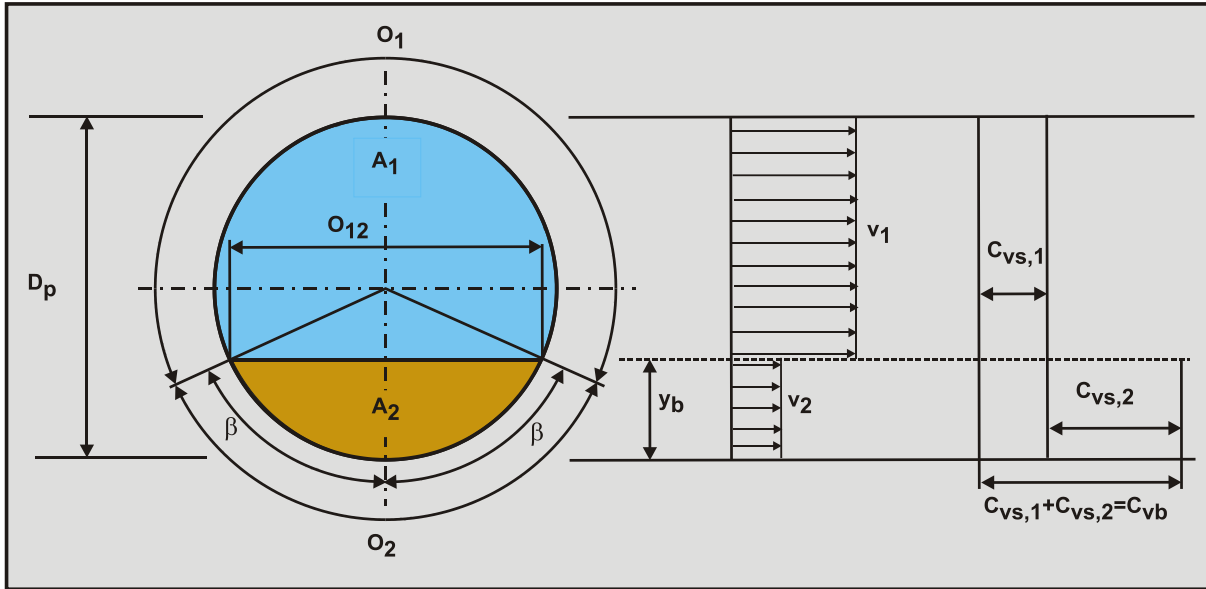
Figure 6.22-1: Definitions of the two layer model, including suspension.

6.22.1 Continuity Equations.

It should be mentioned that the model assumes suspension moving with the cross sectional average line speed v_{ls} over the full pipe cross section. The volumetric flow rate of mixture is:

$$v_{ls} \cdot A_p = v_1 \cdot A_1 + v_2 \cdot A_2$$ (6.22-1)

For the solids, neglecting local slip of the particles relative to the liquid, the flow rate resulting in the delivered concentration is:

$$v_{ls} \cdot A_p \cdot C_{vt} = v_{ls} \cdot A_p \cdot C_{vs,1} + v_2 \cdot A_2 \cdot C_{vs,2}$$ (6.22-2)

In the original model the concentration $C_{vs,1}$ was zero, so now a method must be employed to predict $C_{vs,1}$. In fact the so called contact load $C_{vs,c}$ is determined first and from there the concentration $C_{vs,1}$. Physically $C_{vs,c}$ represents the time averaged volumetric concentration contributing Coulombic friction to the flow. In terms of spatial volumetric concentration, the total spatial volumetric concentration consists of the suspended load concentration and the contact load concentration, so:

$$A_p \cdot C_{vs} = A_p \cdot C_{vs,1} + A_p \cdot C_{vs,c} = A_p \cdot C_{vs,1} + A_2 \cdot C_{vs,2}$$ (6.22-3)

6.22.2 Concentrations.

The SRC model is based on spatial volumetric concentrations. Delivered volumetric concentrations are an output of the model. The total spatial volumetric concentration is according to equation (6.22-3):

$$C_{vs} = C_{vs,1} + C_{vs,c} = C_{vs,1} + \frac{A_2}{A_p} \cdot C_{vs,2} \quad \text{with:} \quad \frac{A_2}{A_p} = \frac{C_{vs,c}}{C_{vs,2}} = \frac{C_{vs,c}}{C_{vb} - C_{vs} + C_{vs,c}} \tag{6.22-4}$$

The spatial contact load concentration is now:

$$C_{vs,c} = \frac{A_2}{A_p} \cdot C_{vs,2} \quad \text{and} \quad C_{vs,2} = \frac{A_p}{A_2} \cdot C_{vs,c} \tag{6.22-5}$$

Shook & Roco (1991) mention two equations to determine the contact load concentration $C_{vc,c}$.

Their first equation:

$$\frac{C_{vs,c}}{C_{vs}} = e^{-0.124 \cdot Ar^{-0.061} \cdot \left(\frac{v_{ls}^2}{g \cdot d}\right)^{-0.028} \cdot \left(\frac{d}{D_p}\right)^{-0.431} \cdot R_{sd}^{-0.272}} \tag{6.22-6}$$

Their second equation:

$$\frac{C_{vs,c}}{C_{vs}} = e^{-0.122 \cdot Ar^{-0.12} \cdot \left(\frac{v_{ls}}{v_{ls,ldv}}\right)^{0.3} \cdot \left(\frac{d}{D_p}\right)^{-0.51} \cdot R_{sd}^{-0.255}} \tag{6.22-7}$$

Shook & Roco (1991), based these equations on the particle Archimedes number:

$$Ar = \frac{4 \cdot g \cdot d^3 \cdot R_{sd}}{3 \cdot v_l^2} \tag{6.22-8}$$

Note that in the first equation only the line speed v_{ls} plays a role. In the second equation the ratio line speed v_{ls} to Limit Deposit Velocity $v_{ls,ldv}$ plays a role.

6.22.3 The Mixture Densities.

Shook & Roco (1991) assume that the particles in contact load are carried by a mixture formed by the carrier liquid and the particles in suspended load. In the upper layer there are only particles in suspended load, giving the mixture in the upper layer a density of:

$$\rho_{m1} = \rho_l \cdot \left(1 - C_{vs,1}\right) + \rho_s \cdot C_{vs,1} = \rho_l + C_{vs,1} \cdot \left(\rho_s - \rho_l\right) \tag{6.22-9}$$

They suppose that the contact load particles are carried by the mixture of the carrier liquid and the suspended load particles. To determine this buoyancy effect, one has to take into account that the available volume for the mixture equals the total bed volume minus the volume occupied by the particles, giving:

$$\rho_{m2} \cdot \left(1 - C_{vs,2}\right) = \rho_l \cdot \left(1 - C_{vs,1} - C_{vs,2}\right) + \rho_s \cdot C_{vs,1} \tag{6.22-10}$$

The mixture density in the lower layer ρ_{m2} is now:

$$\rho_{m2} = \frac{\rho_l \cdot \left(1 - C_{vs,1} - C_{vs,2}\right) + \rho_s \cdot C_{vs,1}}{\left(1 - C_{vs,2}\right)} = \rho_l + \frac{C_{vs,1}}{\left(1 - C_{vs,2}\right)} \cdot \left(\rho_s - \rho_l\right) \tag{6.22-11}$$

6.22.4 Pressure Gradients & Shear Stresses.

The pressure gradient -Δp/ΔL on the liquid above the bed opposes the friction forces due to shear stresses between the liquid and the pipe wall and the liquid and the bed:

$$-\frac{\Delta p}{\Delta L} = \frac{\tau_{1,l} \cdot O_1 + \tau_{12,l} \cdot O_{12}}{A_1} \tag{6.22-12}$$

The pressure gradient -Δp/ΔL on the bed is opposes the friction forces due to shear stresses between the bed and the pipe wall (sliding friction and viscous friction) minus the driving force due to the friction between the liquid in the upper layer and the bed interface:

$$-\frac{\Delta p}{\Delta L} = \frac{\tau_{2,sf} \cdot O_2 + \tau_{2,l} \cdot O_2 - \tau_{12,l} \cdot O_{12}}{A_2} \tag{6.22-13}$$

For the whole pipe cross section this gives the shear forces due to shear stresses between the liquid in the upper layer and the pipe wall and the shear stresses between the bed and the pipe wall. The shear stresses between the upper layer and the lower layer (the bed) are internal and do not play a role here:

$$-\frac{\Delta p}{\Delta L} = \frac{\tau_{2,sf} \cdot O_2 + \tau_{2,l} \cdot O_2 + \tau_{1,l} \cdot O_1}{A_p} \tag{6.22-14}$$

The shear stress $\tau_{1,l}$ on the pipe wall can be evaluated with the well-known Darcy Weisbach equation:

$$\tau_{1,l} = \frac{\lambda_1}{4} \cdot \frac{1}{2} \cdot \rho_{m1} \cdot v_1^2 \quad \text{with:} \quad \lambda_1 = \frac{1.325}{\left(\ln\left(\frac{0.27 \cdot \varepsilon}{D_H} + \frac{5.75}{Re^{0.9}} \right) \right)^2} \quad \text{and} \quad Re = \frac{v_1 \cdot D_H}{v_l} \tag{6.22-15}$$

In their book Shook & Roco (1991) use the cross section average line speed v_{ls} and the pipe diameter D_p in the above equation instead of the velocity in the upper layer v_1 and the hydraulic diameter D_H of the cross section of the upper layer.

For the flow between the liquid in the bed and the pipe wall, the shear stress between the liquid and the pipe wall is:

$$\tau_{2,l} = \frac{\lambda_1}{4} \cdot \frac{1}{2} \cdot \rho_{m2} \cdot v_2^2 \tag{6.22-16}$$

For the flow in the restricted area, the shear stress between the liquid and the bed is:

$$\tau_{12,l} = \frac{\lambda_{12}}{4} \cdot \frac{1}{2} \cdot \rho_l \cdot \left(v_1 - v_2 \right)^2 \quad \text{with:} \quad \lambda_{12} = \frac{\alpha \cdot 1.325}{\left(\ln\left(\frac{0.27 \cdot d}{D_H} + \frac{5.75}{Re^{0.9}} \right) \right)^2} \quad \text{and} \quad Re = \frac{v_1 \cdot D_H}{v_l} \tag{6.22-17}$$

The factor **α** as used by Shook & Roco (1991) is 2.

6.22.5 The Sliding Friction.

In order to use the original liquid density in the sliding friction equation, first the equation of the sliding friction of the bed with the pipe wall has to be written in terms of the new mixture/liquid density ρ_{m2}:

$$\tau_{2,sf} = \frac{\mu_{sf} \cdot g \cdot (\rho_s - \rho_{m2}) \cdot C_{vs,2} \cdot A_p}{\beta \cdot D_p} \cdot \frac{2 \cdot (\sin(\beta) - \beta \cdot \cos(\beta))}{\pi} \tag{6.22-18}$$

The concentration used in this equation is the concentration of the contact load particles in the bed. For the difference between the solids density ρ_s and the mixture density ρ_{m2} we can write:

$$\left(\rho_s - \rho_{m2}\right) = \frac{\rho_s \cdot \left(1 - C_{vs,2}\right)}{\left(1 - C_{vs,2}\right)} - \frac{\rho_l \cdot \left(1 - C_{vs,1} - C_{vs,2}\right) + \rho_s \cdot C_{vs,1}}{\left(1 - C_{vs,2}\right)} \qquad \text{(6.22-19)}$$

Rewriting gives:

$$\left(\rho_s - \rho_{m2}\right) = \frac{\rho_s \cdot \left(1 - C_{vs,1} - C_{vs,2}\right) - \rho_l \cdot \left(1 - C_{vs,1} - C_{vs,2}\right)}{\left(1 - C_{vs,2}\right)}$$

$$\qquad \text{(6.22-20)}$$

$$= \left(\rho_s - \rho_l\right) \cdot \frac{\left(1 - C_{vs,1} - C_{vs,2}\right)}{\left(1 - C_{vs,2}\right)}$$

Shook & Roco (1991) add the effect of the suspended solids reducing the force transmitted to the wall, due to the buoyant effect on the contact load particles and assuming only the concentration $C_{vs,2}$ results in contact with the pipe wall and thus sliding friction, giving:

$$\tau_{2,sf} = \frac{\mu_{sf} \cdot \rho_l \cdot g \cdot R_{sd} \cdot C_{vs,2} \cdot A_p}{\beta \cdot D_p} \cdot \frac{2 \cdot \left(\sin(\beta) - \beta \cdot \cos(\beta)\right)}{\pi} \cdot \frac{\left(1 - C_{vs,1} - C_{vs,2}\right)}{\left(1 - C_{vs,2}\right)} \qquad \text{(6.22-21)}$$

Gillies (1993) also uses this approach. When the suspension concentration $C_{vs,1}$ equals zero, the Wilson et al. (1992) solution is found, with $C_{vs,2}=C_{vb}$. A value of 0.6 is mentioned for C_{vb} and a value of 0.5 is mentioned for μ_{sf}.

$$\tau_{2,sf} = \frac{\mu_{sf} \cdot \rho_l \cdot g \cdot R_{sd} \cdot C_{vb} \cdot A_p}{\beta \cdot D_p} \cdot \frac{2 \cdot \left(\sin(\beta) - \beta \cdot \cos(\beta)\right)}{\pi} \qquad \text{(6.22-22)}$$

The model assumes that the lower layer does contain particles suspended by turbulence. These suspended particles contribute buoyancy helping to reduce the immersed weight of the supported particles. Small particles in the bed become part of the bed and transmit the submerged gravity forces by interparticle contact. Only very small particles are assumed to form a homogeneous carrier liquid with an adjusted viscosity and density. In the case of a uniform particle size distribution (all the particles have the same size), equations (6.22-6), (6.22-7) and (6.22-43) will give a contact load and suspended load fraction $C_{vs,c}$ and $C_{vs,1}$. However, the suspended load particles in the bed are the same sized particles as the contact load particles. So a portion of the same sized particles is carrying part of the submerged weight of the other portion of the same sized particles. In the case of a very graded sand, one may assume that the suspended load particles consist of the fine portion of the PSD and the contact load particles of the coarse part of the PSD. Shook & Roco (1991) use different equations for the determination of the Darcy Weisbach friction factor. Here the Swamee Jain (1976) equation is used. In order to find the equilibrium of forces on the bed (the lower layer) an iterative algorithm has to be used. Outputs are the pressure gradient and the delivered concentration, also resulting in a slip ratio.

The resulting pressure can be determined by:

$$\Delta p = \frac{\Delta F}{A_p} = \frac{\left(\tau_{1,1} \cdot (\pi - \beta) + \tau_{2,1} \cdot \beta + \tau_{2,sf} \cdot \beta\right) \cdot D_p \cdot \Delta L}{A_p} \qquad \text{(6.22-23)}$$

Substituting the shear stresses gives:

$$\Delta p = \frac{\left(\begin{array}{l} \dfrac{\lambda_1}{4}\cdot\dfrac{1}{2}\cdot\rho_{m1}\cdot v_1^2\cdot(\pi-\beta)+\dfrac{\lambda_1}{4}\cdot\dfrac{1}{2}\cdot\rho_{m2}\cdot v_2^2\ \cdot\beta \\[4mm] +\dfrac{\mu_{sf}\cdot\rho_l\cdot g\cdot R_{sd}\cdot C_{vs,2}\cdot A_p}{\beta\cdot D_p}\cdot\dfrac{2\cdot\left(\sin(\beta)-\beta\cdot\cos(\beta)\right)}{\pi}\cdot\dfrac{\left(1-C_{vs,1}-C_{vs,2}\right)}{\left(1-C_{vs,2}\right)}\cdot\beta \end{array}\right)\cdot D_p\cdot\Delta L}{A_p} \tag{6.22-24}$$

This can be simplified to:

$$\Delta p = \lambda_1\cdot\frac{\Delta L}{D_p}\cdot\left(\frac{1}{2}\cdot\rho_{m1}\cdot v_1^2\cdot\frac{(\pi-\beta)}{\pi}+\frac{1}{2}\cdot\rho_{m2}\cdot v_2^2\cdot\frac{\beta}{\pi}\right)$$
$$+\mu_{sf}\cdot\rho_l\cdot g\cdot R_{sd}\cdot C_{vs,2}\cdot\frac{2\cdot\left(\sin(\beta)-\beta\cdot\cos(\beta)\right)}{\pi}\cdot\frac{\left(1-C_{vs,1}-C_{vs,2}\right)}{\left(1-C_{vs,2}\right)}\cdot\Delta L \tag{6.22-25}$$

The hydraulic gradient of the mixture is now:

$$i_m = \frac{\Delta p}{\rho_l\cdot g\cdot\Delta L} = \frac{\lambda_1}{2\cdot g\cdot D_p}\cdot\left(\begin{array}{l} \dfrac{\rho_l+C_{vs,1}\cdot\left(\rho_s-\rho_l\right)}{\rho_l}\cdot v_1^2\cdot\dfrac{(\pi-\beta)}{\pi} \\[5mm] +\dfrac{\rho_l+\dfrac{C_{vs,1}}{\left(1-C_{vs,2}\right)}\cdot\left(\rho_s-\rho_l\right)}{\rho_l}\cdot v_2^2\cdot\dfrac{\beta}{\pi} \end{array}\right)$$
$$+\mu_{sf}\cdot R_{sd}\cdot C_{vs,2}\cdot\frac{2\cdot\left(\sin(\beta)-\beta\cdot\cos(\beta)\right)}{\pi}\cdot\frac{\left(1-C_{vs,1}-C_{vs,2}\right)}{\left(1-C_{vs,2}\right)} \tag{6.22-26}$$

This can be simplified to:

$$i_m = \frac{\lambda_1}{2\cdot g\cdot D_p}\cdot\left(\begin{array}{l} \left(1+C_{vs,1}\cdot R_{sd}\right)\cdot v_1^2\cdot\dfrac{(\pi-\beta)}{\pi} \\[5mm] +\left(1+\dfrac{C_{vs,1}}{\left(1-C_{vs,2}\right)}\cdot R_{sd}\right)\cdot v_2^2\cdot\dfrac{\beta}{\pi} \end{array}\right)$$
$$+\mu_{sf}\cdot R_{sd}\cdot C_{vs,2}\cdot\frac{2\cdot\left(\sin(\beta)-\beta\cdot\cos(\beta)\right)}{\pi}\cdot\frac{\left(1-C_{vs,1}-C_{vs,2}\right)}{\left(1-C_{vs,2}\right)} \tag{6.22-27}$$

Or:

$$i_m = \frac{\lambda_1}{2 \cdot g \cdot D_p} \cdot \left(\begin{array}{c} \left(v_1^2 \cdot \frac{(\pi - \beta)}{\pi} + v_2^2 \cdot \frac{\beta}{\pi} \right) \\ \\ + C_{vs,1} \cdot R_{sd} \cdot v_1^2 \cdot \frac{(\pi - \beta)}{\pi} + \frac{C_{vs,1}}{(1 - C_{vs,2})} \cdot R_{sd} \cdot v_2^2 \cdot \frac{\beta}{\pi} \end{array} \right)$$

$$+ \mu_{sf} \cdot R_{sd} \cdot C_{vs,2} \cdot \frac{2 \cdot (\sin(\beta) - \beta \cdot \cos(\beta))}{\pi} \cdot \frac{(1 - C_{vs,1} - C_{vs,2})}{(1 - C_{vs,2})} \tag{6.22-28}$$

Assuming that the first term between the brackets almost equals the line speed squared, this gives:

$$i_m = \frac{\lambda_1}{2 \cdot g \cdot D_p} \cdot \left(v_{ls}^2 + C_{vs,1} \cdot R_{sd} \cdot v_1^2 \cdot \frac{(\pi - \beta)}{\pi} + \frac{C_{vs,1}}{(1 - C_{vs,2})} \cdot R_{sd} \cdot v_2^2 \cdot \frac{\beta}{\pi} \right)$$

$$+ \mu_{sf} \cdot R_{sd} \cdot C_{vs,2} \cdot \frac{2 \cdot (\sin(\beta) - \beta \cdot \cos(\beta))}{\pi} \cdot \frac{(1 - C_{vs,1} - C_{vs,2})}{(1 - C_{vs,2})} \tag{6.22-29}$$

In terms of the relative excess hydraulic gradient this can be written as:

$$E_{rhg} = \frac{i_m - i_l}{R_{sd} \cdot C_{vs}} = \frac{\lambda_1}{2 \cdot g \cdot D_p} \cdot \left(\frac{C_{vs,1}}{C_{vs}} \cdot v_1^2 \cdot \frac{(\pi - \beta)}{\pi} + \frac{C_{vs,1}}{(1 - C_{vs,2}) \cdot C_{vs}} \cdot v_2^2 \cdot \frac{\beta}{\pi} \right)$$

$$+ \mu_{sf} \cdot \frac{C_{vs,2}}{C_{vs}} \cdot \frac{2 \cdot (\sin(\beta) - \beta \cdot \cos(\beta))}{\pi} \cdot \frac{(1 - C_{vs,1} - C_{vs,2})}{(1 - C_{vs,2})} \tag{6.22-30}$$

6.22.6 The Bed Concentration.

Gillies (1993) used an improved relation for the bed concentration C_{vb}, available at SRC at the time. He presented a mechanistic model for predicting the concentration distribution. A version of that mechanistic model is used to predict the concentration in the lower layer of the SRC model.

$$\frac{C_{vb,max} - C_{vb}}{C_{vb,max} - C_{vs}} = 0.074 \cdot \left(\frac{v_{ls}}{v_t} \right)^{0.44} \cdot (1 - C_{vs})^{0.189} \tag{6.22-31}$$

The maximum bed concentration in this equation depends on particle size and shape and especially the grading of the PSD. Later this is based on the concentration distribution. He also mentioned a relation for the contact load fraction, which was slightly modified later.

$$\frac{C_{vs,c}}{C_{vs}} = e^{-0.0184 \cdot \frac{v_{ls}}{v_t}} \quad \text{or} \quad \text{Matousek} (1997): \frac{C_{vs,c}}{C_{vs}} = e^{-0.024 \cdot \frac{v_{ls}}{v_t}} \tag{6.22-32}$$

In this equation the ratio line speed v_{ls} to terminal settling velocity v_t plays a role.

Kumar et al. (2003) and (2008) used the SRC model for the prediction of the pressure losses as described up to here in combination with the Kaushal & Tomita (2002C) model for the concentration distribution. They did not report implementing later developments.

6.22.7 Discussion & Conclusions Original Model.

First it should be stated that the empirical relations used in this model are only valid for this model and cannot always be applied to other models. An example of this is the contact load ratio.

The model incorporates a number of physical effects. First of all, the higher the line speed, the smaller the contact load fraction, which in the latest version of the model is based on the ratio of the line speed to the terminal setting velocity. Secondly, the suspended fraction is partly carrying the contact load fraction. Whether this is pure buoyancy or based on collisions (interparticle contacts), the macroscopic effect is similar to buoyancy. Thirdly, the porosity of the bed is increasing with increasing line speed. There is a transition of a solid bed to a bed behaving like sheet flow and finally becoming homogeneous flow. At low line speeds the sliding friction is dominant, at high line speeds turbulence.

Analyzing the contact load fraction equations, we find that for very low line speeds the contact load fraction in terms of spatial volumetric concentrations equals the cross section averaged spatial volumetric concentration C_{vs}. With increasing line speeds and/or decreasing terminal settling velocities the contact load fraction decreases. This is what would be expected.

Analyzing the bed concentration equation we find that at very low line speeds, the bed concentration equals the maximum bed concentration, which makes sense. With an increasing line speed or decreasing terminal settling velocity the bed concentration decreases, which is clearer writing the equation as:

$$C_{vb} = C_{vb,max} - 0.074 \cdot \left(\frac{v_{ls}}{v_t} \right)^{0.44} \cdot \left(1 - C_{vs} \right)^{0.189} \cdot \left(C_{vb,max} - C_{vs} \right) \tag{6.22-33}$$

There should be a lower limit to the bed concentration determined this way. The bed or lower layer concentration can never be smaller than the cross section averaged spatial volumetric concentration C_{vs} in the case of very high line speeds, giving homogeneous flow. This happens at a line speed of:

$$v_{ls} = v_t \cdot \left(\frac{1}{0.074 \cdot \left(1 - C_{vs} \right)^{0.189}} \right)^{1/0.44} = \frac{372 \cdot v_t}{\left(1 - C_{vs} \right)^{0.43}} \tag{6.22-34}$$

At very high line speeds the mixture densities ρ_{m1} and ρ_{m2} become equal to the cross section averaged mixture density (the concentration $C_{vs,c}$ for the contact load becomes zero), resulting in the ELM model. The role of the terminal settling velocity in this equation is questionable. This may give good results in certain areas of the different parameters, but not everywhere.

At very low line speeds where the bed velocity is very low, the excess pressure gradient is almost equal to:

$$-\frac{\Delta p_m - \Delta p_l}{\Delta L} \approx \mu_{sf} \cdot \rho_l \cdot g \cdot R_{sd} \cdot C_{vb} \cdot \frac{2 \cdot \left(\sin(\beta) - \beta \cdot \cos(\beta) \right)}{\pi} \tag{6.22-35}$$

For low concentrations and thus small values of β, this can be approximated as:

$$-\frac{\Delta p_m - \Delta p_l}{\Delta L} \approx \mu_{sf} \cdot \rho_l \cdot g \cdot R_{sd} \cdot C_{vs} \quad \Rightarrow \quad i_m - i_l = \mu_{sf} \cdot R_{sd} \cdot C_{vs} \tag{6.22-36}$$

Which is the excess pressure gradient of a sliding bed according to Wilson et al. (1992), assuming the hydrostatic normal stress approach between the bed and the pipe wall is true. However, at the line speeds where this model is verified, the bed concentrations become so low that the hydrostatic approach is almost equal to the weight approach.

Now that the extremes are known, very low line speeds (the sliding bed model) and very high line speeds (the ELM model), it is interesting to investigate what happens for line speeds between the extremes. To make this visible, it is assumed that the excess pressure gradient depends on the sliding bed friction and the difference between the ELM model and the pure liquid model (Darcy Weisbach). The E_{rhg} value is the excess hydraulic gradient $i_m - i_l$ divided by the relative submerged density R_{sd} and the spatial volumetric concentration C_{vs}.

$$E_{rhg} = \cfrac{\left(\begin{array}{l} \mu_{sf} \cdot C_{vs,2} \cdot \dfrac{2 \cdot \left(\sin(\beta) - \beta \cdot \cos(\beta) \right)}{\pi} \cdot \dfrac{\left(1 - C_{vs,1} - C_{vs,2} \right)}{\left(1 - C_{vs,2} \right)} \\[4mm] + \lambda_1 \cdot \dfrac{1}{2 \cdot g \cdot D_p} \cdot \dfrac{C_{vs,1}}{\left(1 - C_{vs,c} \right)} \cdot v_{ls}^2 \end{array} \right)}{C_{vs}}$$

(6.22-37)

In terms of the weight approach the following can be derived:

$$E_{rhg} = \cfrac{\left(\mu_{sf} \cdot C_{vs,c} + \lambda_1 \cdot \dfrac{1}{2 \cdot g \cdot D_p} \cdot \dfrac{\left(C_{vs} - C_{vs,c} \right)}{\left(1 - C_{vs,c} \right)} \cdot v_{ls}^2 \right)}{C_{vs}}$$

(6.22-38)

Comparing the SRC model with the DHLLDV Framework and the Wilson et al. (2006) model (equation (6.20-122) and **A=1**) in a small diameter pipe shows a good resemblance between SRC and DHLLDV for very small particles (Figure 6.22-2) and a good resemblance for coarse particles (Figure 6.22-3) at operational line speeds (**i$_l$=0.03-0.1**). Both models use constant spatial volumetric concentration, but the SRC model as applied here does not have the stationary bed at low line speeds.

The original SRC model does not show the relative excess hydraulic gradient going below the ELM line, which the DHLLDV Framework does. The behavior of the SRC model for coarse sands looks more like graded sand behavior because the curve is less steep, while the DHLLDV Framework is determined for a uniform sand.

The Wilson et al. (2006) is also shown in the figures. For very small particles this model gives very high values, but for coarser particles is matches very well. This results from the way the **v$_{50}$** is determined. Using a **v$_{50}$** proportional to the terminal settling velocity **v$_t$** could solve this.

Figure 6.22-4 and Figure 6.22-5 show a comparison for a large diameter pipe. The results are similar to the small diameter pipe. In the line speed region of normal operations, here 5-6 m/sec, the SRC model and the DHLLDV Framework are close. The Wilson et al. (2006) model overestimates the hydraulic gradient for small particles, but matches very well for medium and coarse particles.

The simplification of the SRC model, by using the weight approach of Miedema & Ramsdell (2014) for the sliding friction, shows a very good resemblance in all cases, fine or coarse particles and small or large pipe diameters, although the hydraulic gradient curves found are a bit higher compared with the original SRC model. Only at very low line speeds and high concentrations the two approaches differ, however this is far outside the line speed region of normal operations. As long as the same equation is used for the determination of the contact load fraction, there is not much difference.

It is remarkable that for the **D$_p$=0.762 m** (30 inch) pipe and the **d=1 mm** particle the 3 models give almost the same hydraulic gradient at the LDV.
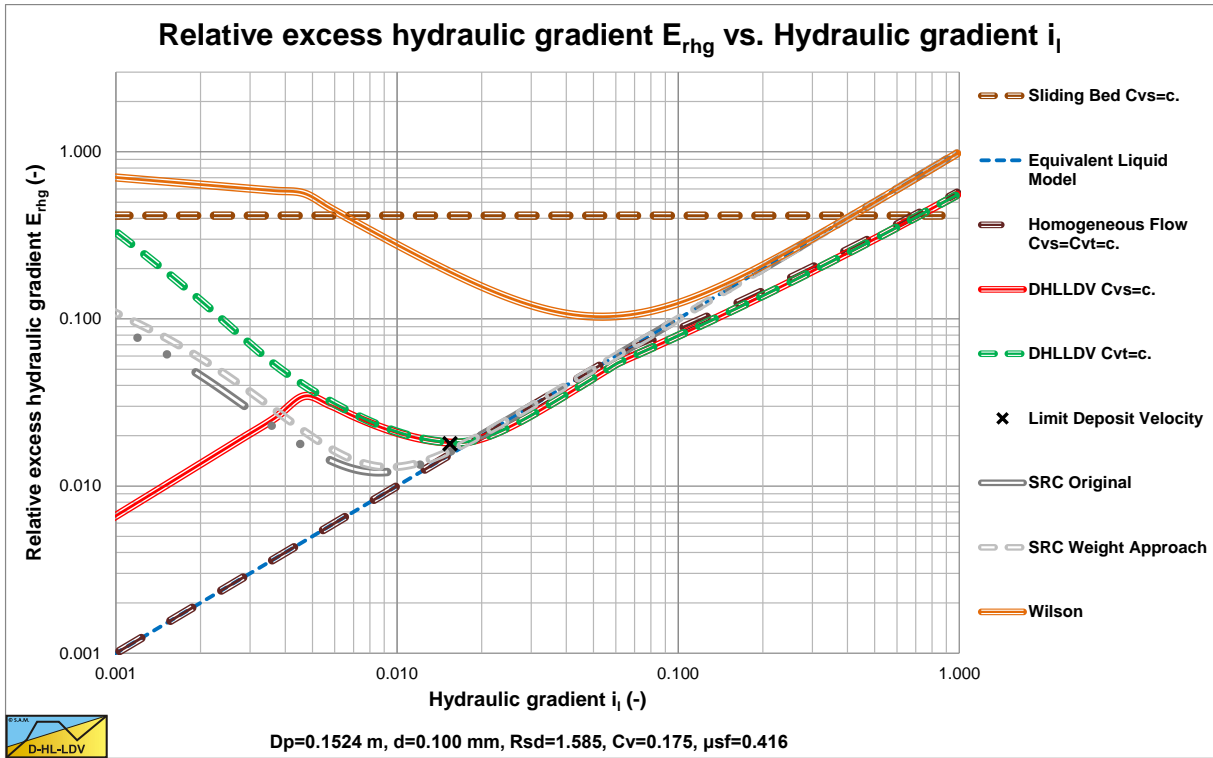
Figure 6.22-2: The SRC model compared to the DHLLDV Framework and the weight approach for d=0.1 mm, original model.
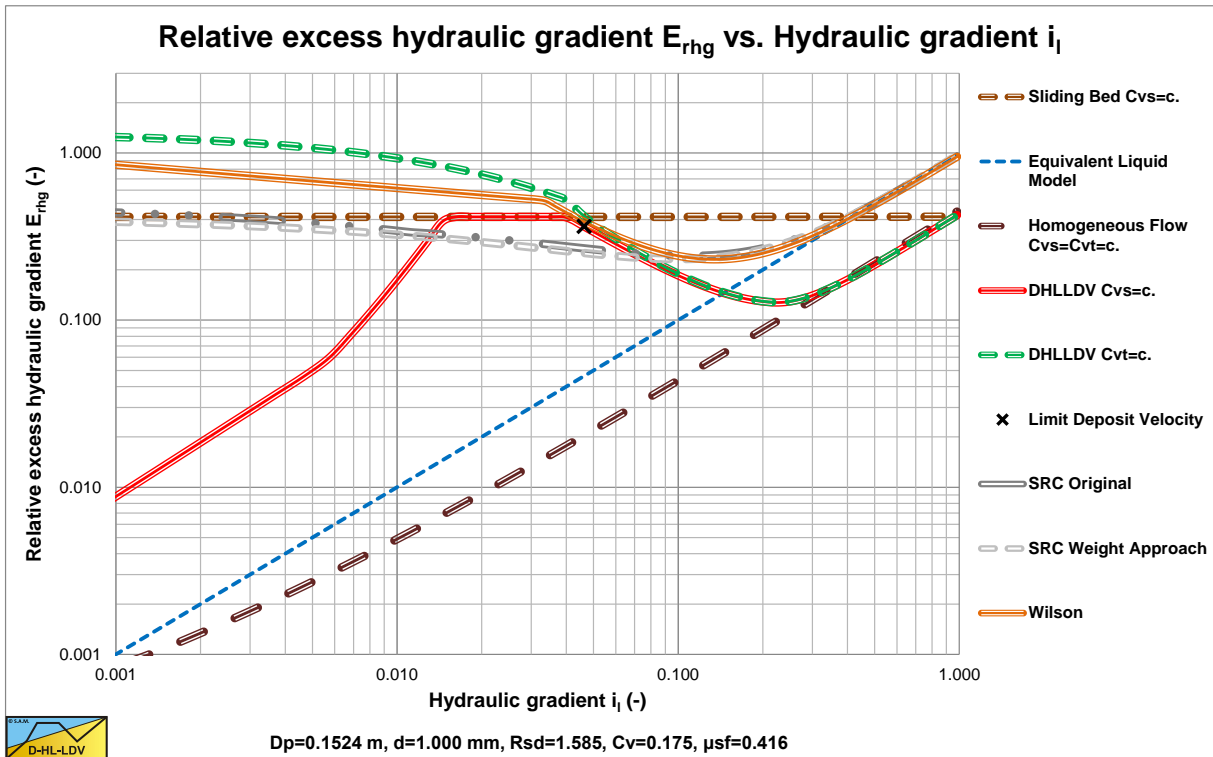
Figure 6.22-3: The SRC model compared to the DHLLDV Framework and the weight approach for d=1.0 mm, original model.
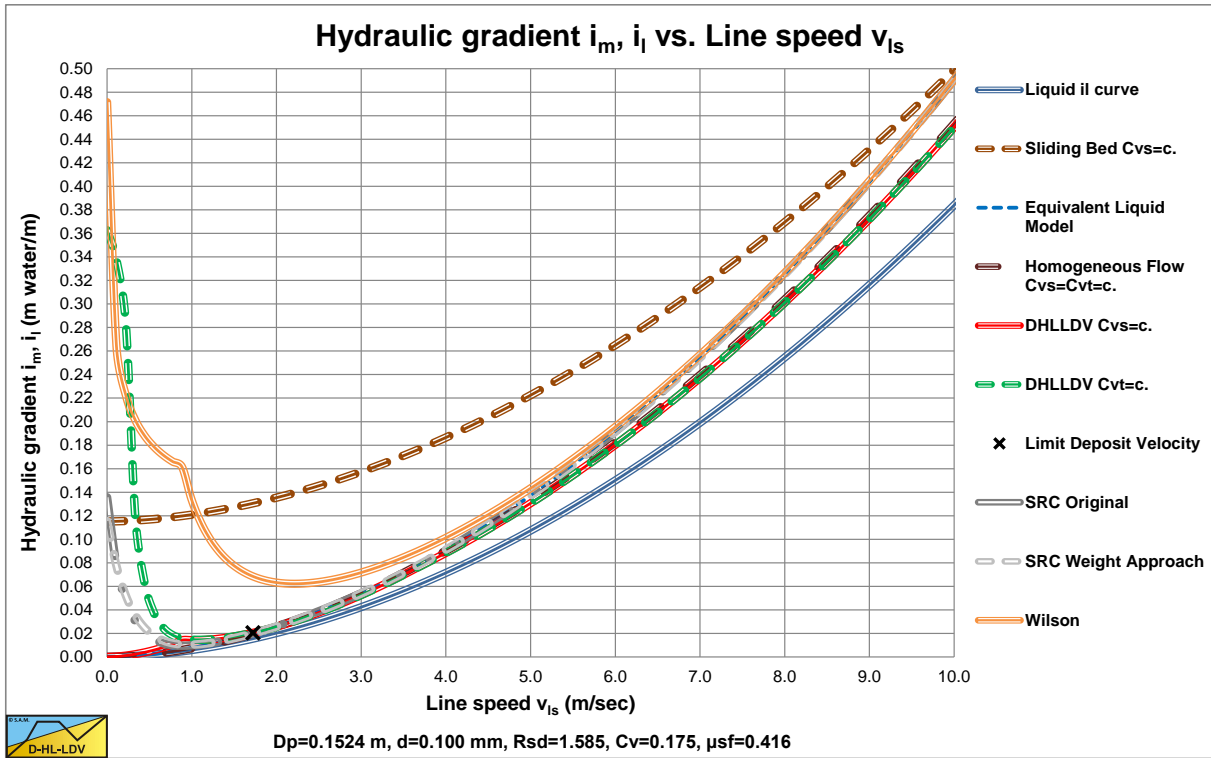
Figure 6.22-4: The SRC model compared to the DHLLDV Framework and the weight approach for d=0.1 mm, original model.
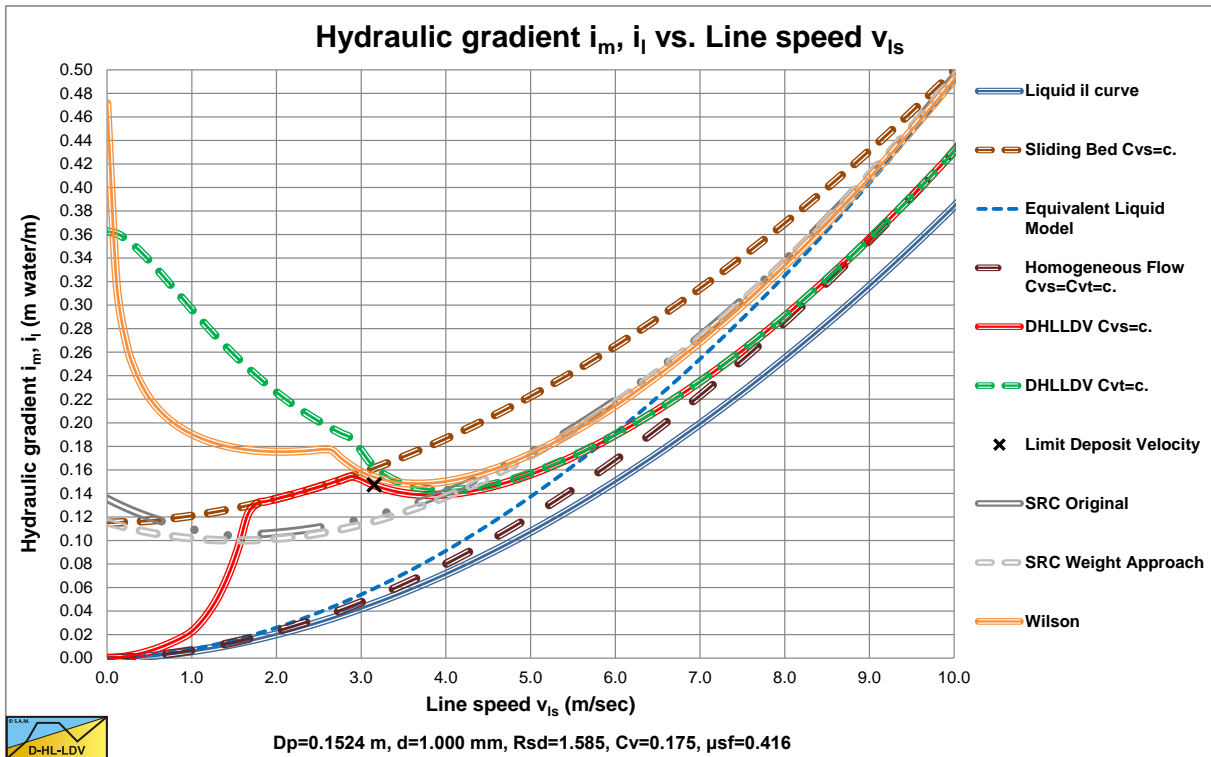
Figure 6.22-5: The SRC model compared to the DHLLDV Framework and the weight approach for d=1.0 mm, original model.

6.22.8 Further Development of the Model.

Experimental evidence of Gillies & Shook (2000A) suggests that an increment in kinetic friction, due to an increase in kinematic particle wall friction, occurs at high concentrations. High means solids concentrations exceeding 30%-35%. A parameter which is useful in quantifying this effect is the linear concentration λ_{lc}, which can be considered to be a measure of the ratio of the particle diameter to the shortest distance between neighboring particles:

$$\lambda_{lc} = \frac{1}{\left(\left(\dfrac{C_{vb,max}}{C_{vs}} \right)^{1/3} - 1 \right)}$$

(6.22-39)

It is peculiar that in some of the SRC related papers, the term in the denominator is reversed, giving a negative linear concentration. Because this is used squared it has no effect. The above equation is the correct equation (Gillies R. G., 2015). If the liquid density is considered to be appropriate to describe the frictional losses, the frictional losses between the liquid and the pipe wall can be determined with:

$$\tau_{1,l} = \frac{(\lambda_1 + \Delta\lambda_1)}{4} \cdot \frac{1}{2} \cdot \rho_l \cdot v_1^2$$

(6.22-40)

With: $\quad \Delta\lambda_1 = (0.0118 \cdot \lambda_{lc})^2$

At high velocities, when the flow is axially symmetric and Coulomb friction is negligible, the total wall shear stress is regarded as the sum of two contributions. The first contribution is based on the Darcy Weisbach friction factor and the liquid density, the second contribution upon the solids density and the linear concentration. If the friction increment is due to particle wall interactions at high solids concentrations, the total frictional losses between the liquid+particles and the pipe wall can be determined with:

$$\tau_{1,l} = \frac{(\lambda_1 \cdot \rho_l + \lambda_s \cdot \rho_s)}{4} \cdot \frac{1}{2} \cdot v_1^2$$

(6.22-41)

With: $\quad \lambda_s = (0.0089 \cdot \lambda_{lc})^2$

And:

$$\tau_{2,l} = \frac{(\lambda_1 \cdot \rho_l + \lambda_s \cdot \rho_s)}{4} \cdot \frac{1}{2} \cdot v_2^2$$

(6.22-42)

Gillies & Shook (2000A) also presented a slightly different equation for the determination of the contact load fraction:

$$\frac{C_{vs,c}}{C_{vs}} = e^{-0.0212 \cdot \frac{v_{ls}}{v_t}}$$

(6.22-43)

For slurry Reynolds numbers less than 192000 they use:

$$\frac{C_{vs,c}}{C_{vs}} = e^{-0.001013 \cdot \frac{v_{ls}}{v_t} \cdot Re^{1/4}}$$

(6.22-44)

This suggests that with highly concentrated slurries of coarse particles, the Coulombic friction increases at low slurry Reynolds numbers.

Later Gillies et al. (2004) give some modifications of the solids term in equation (6.22-41) related to high line speeds. Assuming the Coulombic friction is negligible compared to the kinematic friction, the solids Darcy Weisbach friction coefficient is modified to:

$$\lambda_s = 4 \cdot \lambda_{lc}^{1.25} \cdot \left(0.00005 + 0.00033 \cdot e^{-0.1 \cdot d^+} \right)$$

$$\text{With :} \quad d^+ = \frac{d \cdot u_*}{\nu_l} = \frac{d \cdot \sqrt{\frac{\lambda_l}{8}} \cdot v_{ls}}{\nu_l}$$

(6.22-45)

Although this correlation was obtained at high line speeds, where the effect of Coulombic friction is small, indications show that it is applicable to kinematic friction at all line speeds. A change in the method of predicting the kinematic friction, forces the correlation that is used for predicting the contact load fraction to be modified. Apparently this contact load fraction is a virtual contact load fraction depending on the other parts of the SRC model. The equation for the contact load fraction is now modified to:

$$\frac{C_{vs,c}}{C_{vs}} = e^{-0.0097 \cdot \left(\frac{v_{ls}}{v_t} \right)^{0.864} \cdot Re^{0.193} \cdot Fr^{-0.292}}$$

$$Re = \frac{D_p \cdot v_{ls}}{\nu_l} \cdot \frac{1}{1 + 0.21 \cdot \lambda_m^2} \quad \text{or 120000, whichever is less}$$

(6.22-46)

$$Fr = \frac{v_{ls}}{\left(g \cdot D_p \cdot R_{sd} \right)} \quad \text{or 3.0, whichever is less}$$

The sliding friction factor (Coulombic friction) depends on the ratio of the thickness of the viscous sub layer to the particle diameter, with **μ$_{sf0}$=0.5**, according to:

$$\mu_{sf} = \mu_{sf0} \cdot \left(2 \cdot \left(1 - \frac{\delta_v}{d} \right) \right)$$

$$\text{With :} \quad \delta_v = 5 \cdot \frac{\nu_l}{u_*}$$

(6.22-47)

$$\text{With :} \quad 0.1 \le \left(2 \cdot \left(1 - \frac{\delta_v}{d} \right) \right) \le 1$$

This is of course an adjustment only important for very small particles. SRC found that this adjustment is important for the industrial slurries that were tested at the SRC Pipe Flow Technology Centre. Depending on factors such as the viscosity of the carrier fluid (water and clays), particles with diameters as large as 0.2 mm may contribute significantly to the total kinematic friction (i.e. λ_s is significantly greater than zero). The vast majority of the industrial slurries contain significant concentrations of particles that are 0.2 mm or less (Gillies R. G., 2015). D.P. Gillies (2013) adjusted the equation for the Darcy Weisbach solids contribution friction factor to:

$$\lambda_s = 4 \cdot \lambda_{lc}^{1.25} \cdot \left(A \cdot \ln \left(d^+ \right) + B \right)$$

With : A=-0.000110   and   B=0.00042   for $d^+ \le 19.36$

A=-0.000056   and   B=0.00026   for $d^+ > 19.36$

A=0   and   B=0   for $d^+ > 103.84$

(6.22-48)

6.22.9 Final Conclusions.

The model uses spatial concentration in its inner workings and it predicts delivered concentrations. If the delivered concentration is specified, then iteration is required to come up with the spatial concentration that offers the specified delivered concentration. A model is developed at SRC to predict the concentration distribution. This model's prediction is used to set the concentration in the lower layer of the two-layer model. The latest version of the SRC model can be summarized with the following equations:

The E_{rhg} value is the excess hydraulic gradient i_m-i_l divided by the relative submerged density R_{sd} and the spatial volumetric concentration C_{vs}.

$$E_{rhg} = \frac{i_m - i_l}{C_{vs} \cdot R_{sd}} = \frac{\left(\begin{array}{l} \mu_{sf} \cdot C_{vs,2} \cdot \dfrac{2 \cdot \left(\sin(\beta) - \beta \cdot \cos(\beta) \right)}{\pi} \cdot \dfrac{\left(1 - C_{vs,1} - C_{vs,2} \right)}{\left(1 - C_{vs,2} \right)} \\[3ex] + \lambda_s \cdot \dfrac{\rho_s}{\rho_l} \cdot \dfrac{1}{2 \cdot g \cdot D_p \cdot R_{sd}} \cdot v_{ls}^2 \end{array} \right)}{C_{vs}} \tag{6.22-49}$$

In terms of the weight approach the following can be derived:

$$E_{rhg} = \frac{\left(\mu_{sf} \cdot C_{vs,c} + \lambda_s \cdot \dfrac{\rho_s}{\rho_l} \cdot \dfrac{1}{2 \cdot g \cdot D_p \cdot R_{sd}} \cdot v_{ls}^2 \right)}{C_{vs}} \tag{6.22-50}$$

At very low line speeds, the contact load concentration $C_{vs,c}=C_{vs}$ and the equations reduce to:

$$E_{rhg} = \frac{i_m - i_l}{C_{vs} \cdot R_{sd}} = \mu_{sf} \cdot \frac{2 \cdot \left(\sin(\beta) - \beta \cdot \cos(\beta) \right)}{\pi} \tag{6.22-51}$$

Which is the 2LM solution of Wilson (2006). In terms of the weight approach the following can be derived:

$$E_{rhg} = \mu_{sf} \tag{6.22-52}$$

Which is the sliding bed equation according to Miedema & Ramsdell (2014).
At very high line speeds, the contact load concentration $C_{vs,c}=0$ and the equations reduce to:

$$E_{rhg} = \frac{\lambda_s \cdot \rho_s \cdot \dfrac{1}{2} \cdot v_{ls}^2}{\rho_l \cdot g \cdot D_p \cdot R_{sd} \cdot C_{vs}} = \frac{\lambda_s \cdot \rho_s}{\lambda_l \cdot \rho_l} \cdot \frac{1}{R_{sd} \cdot C_{vs}} \cdot \frac{\lambda_l \cdot v_{ls}^2}{2 \cdot g \cdot D_p} = \frac{\lambda_s \cdot \rho_s}{\lambda_l \cdot \rho_l} \cdot \frac{1}{R_{sd} \cdot C_{vs}} \cdot i_l \tag{6.22-53}$$

The kinetic friction factor contains $\lambda_{lc}^{1.25}$, which depends on the relative concentration $C_{vr}=C_{vs}/C_{vb}$. This gives:

$$\lambda_{lc} = \frac{C_{vr}^{1/3}}{\left(1 - C_{vr}^{1/3} \right)} \tag{6.22-54}$$

This gives:

$$E_{rhg} = 4 \cdot \left(\frac{C_{vr}^{1/3}}{\left(1 - C_{vr}^{1/3} \right)} \right)^{1.25} \cdot \frac{\left(0.00005 + 0.00033 \cdot e^{-0.1 \cdot d^+} \right)}{\lambda_l \cdot R_{sd} \cdot C_{vb} \cdot C_{vr}} \cdot \frac{\rho_s}{\rho_l} \cdot i_l \tag{6.22-55}$$

Or:

$$E_{rhg} = 4 \cdot \left(\frac{C_{vr}^{1/3}}{\left(1 - C_{vr}^{1/3}\right)} \right)^{1.25} \cdot \frac{\left(A \cdot \ln\left(d^+\right) + B\right)}{\lambda_l \cdot R_{sd} \cdot C_{vb} \cdot C_{vr}} \cdot \frac{\rho_s}{\rho_l} \cdot i_l \qquad (6.22\text{-}56)$$

Using the ELM for any line speed gives:

$$E_{rhg} = i_l \qquad (6.22\text{-}57)$$

So the factor in front of the liquid hydraulic gradient is a sort of multiplication factor related to the ELM. Equation (6.22-55) gives a multiplication factor according to Figure 6.22-6 (determined with $\lambda_l=0.015$) for different values of the dimensionless particle diameter. For normal relative concentrations at very high line speeds this factor is about 0.35, meaning that about 35% of the solids effect of the ELM will be taken into account. For very low and high relative concentrations the multiplication factor is greater than 1, which seems too high, since it implies a solids effect greater than the solids effect of the ELM. This also occurs for values of the dimensionless particle diameter at below 100. Equation (6.22-57) gives a multiplication factor of zero for dimensionless particles diameters above 100, meaning that there is no solids effect, just pure liquid resistance.
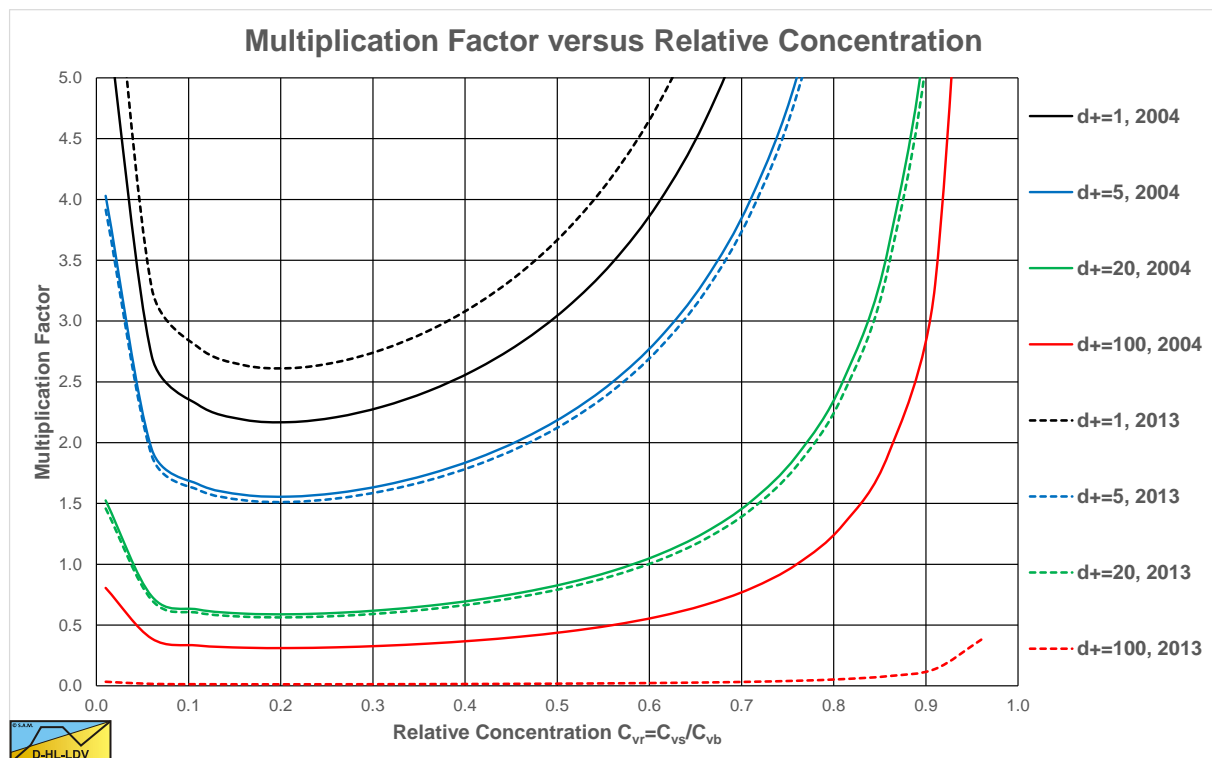
Figure 6.22-6: The multiplication factor.

Equation (6.22-57) gives a multiplication factor of zero for very high line speeds, resulting in a solids effect of zero. This means that at very high line speeds the resistance or hydraulic gradient equals the pure liquid resistance or hydraulic gradient.

Whether the head losses approach the pure liquid head losses it very high line speeds is the question. The concept that solids do not have any effect anymore, even at high concentrations is difficult to defend. Unfortunately there are no experimental data for such high line speeds. The data available show that at high line speeds the head losses are somewhere between the ELM and the pure liquid head losses. A factor of 0.6 or 60% of the solids effect seems reasonable.

Figure 6.22-7 and Figure 6.22-8 show the comparison between the 2004 SRC model, the DHLLDV Framework and the Wilson et al. (2006) model (equation (6.20-122) and **A=0.6**) for a $D_p=0.1524$ m (6 inch) pipe and particles with **d=0.1 mm** and **d=1 mm**. For the **d=0.1 mm** particle, SRC and DHLLDV match again very well for $E_{rhg}=0.03$-**0.1**. Wilson et al. (2006) overestimates as discussed before. For the **d=1 mm** particle the 3 models match very well

for **E_rhg=0.03-0.1**. The SRC model and the Wilson et al. (2006) model curves are a bit lower compared with Figure 6.22-2 and Figure 6.22-3 giving a better correlation with the DHLLDV Framework.
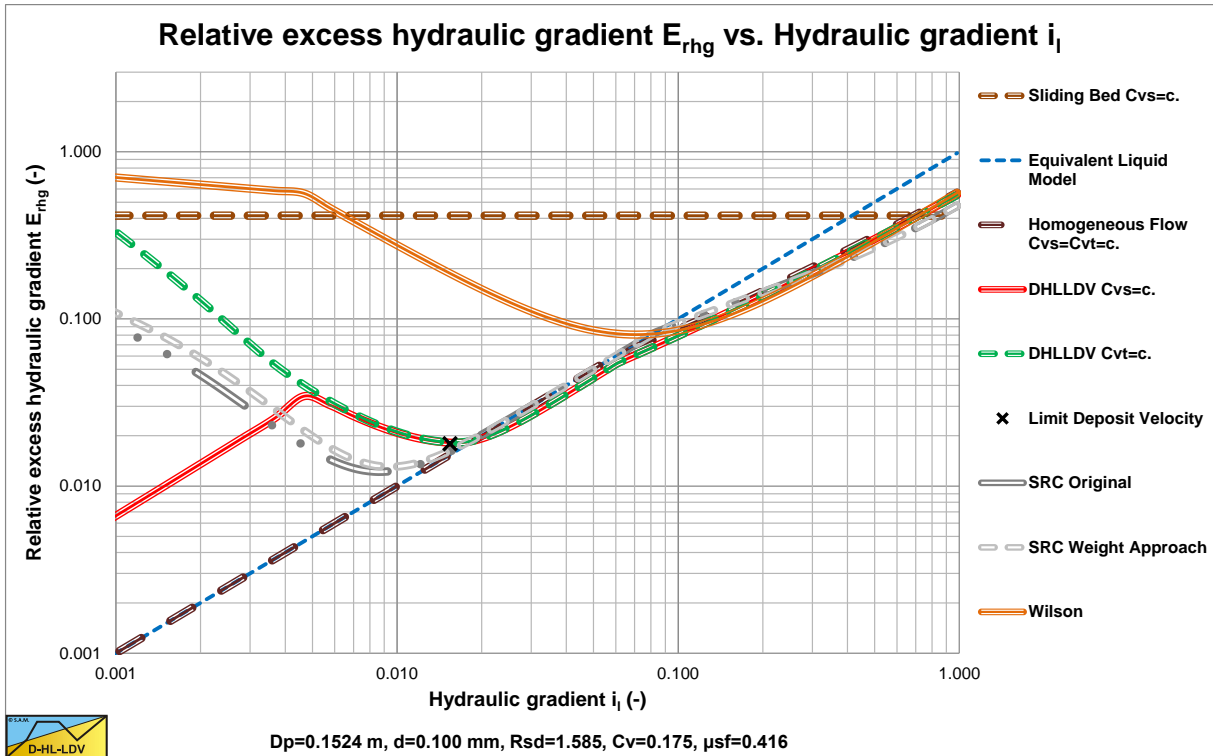
Figure 6.22-7: The SRC model compared to the DHLLDV Framework and the weight approach for d=0.1 mm, 2004 model.
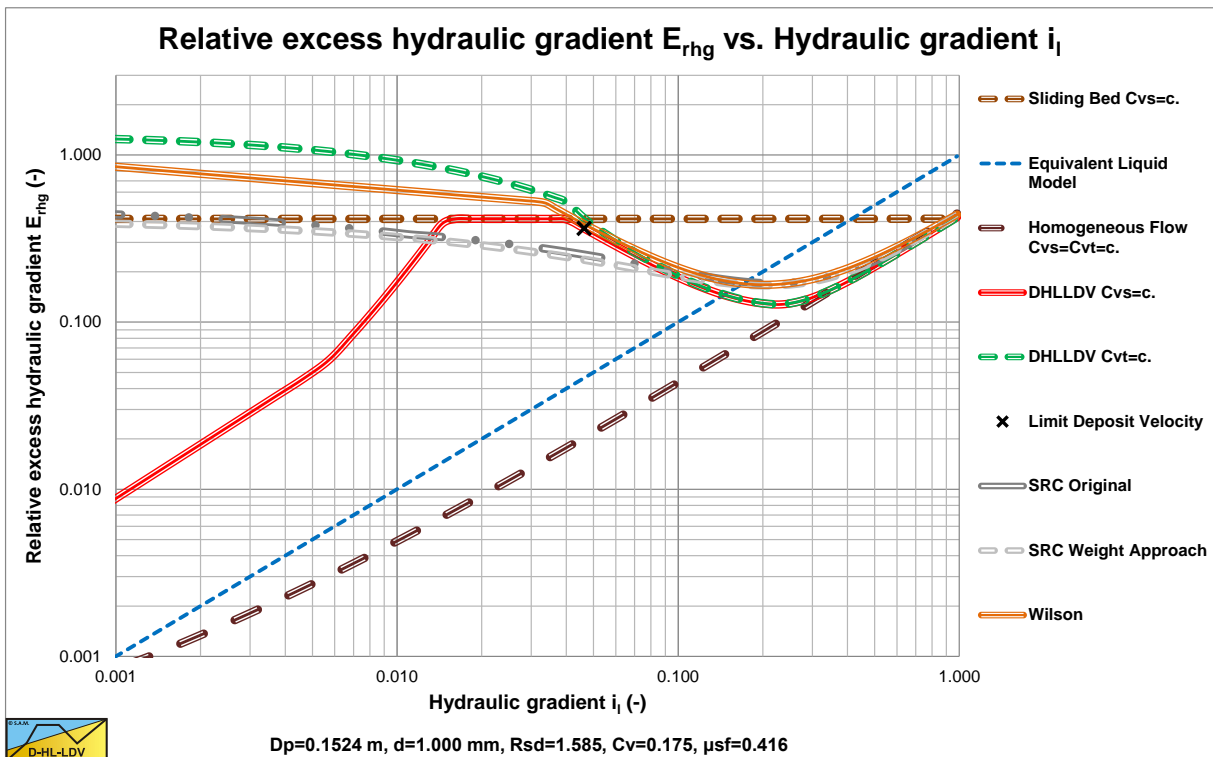
Figure 6.22-8: The SRC model compared to the DHLLDV Framework and the weight approach for d=1.0 mm, 2004 model.

Figure 6.22-9 and Figure 6.22-10 show the comparison between the 2004 SRC model, the DHLLDV Framework and the Wilson et al. (2006) model (equation (6.20-122) and **A=0.6**) for a **D_p=0.762 m** (30 inch) pipe and particles

with **d=0.1 mm** and **d=1 mm**. For the **d=0.1 mm** particle, SRC and DHLLDV match again very well for line speeds between 4 and 7 m/s. Wilson et al. (2006) overestimates as discussed before. For the **d=1 mm** particle the 3 models match very well for line speeds between 4 and 7 m/s.
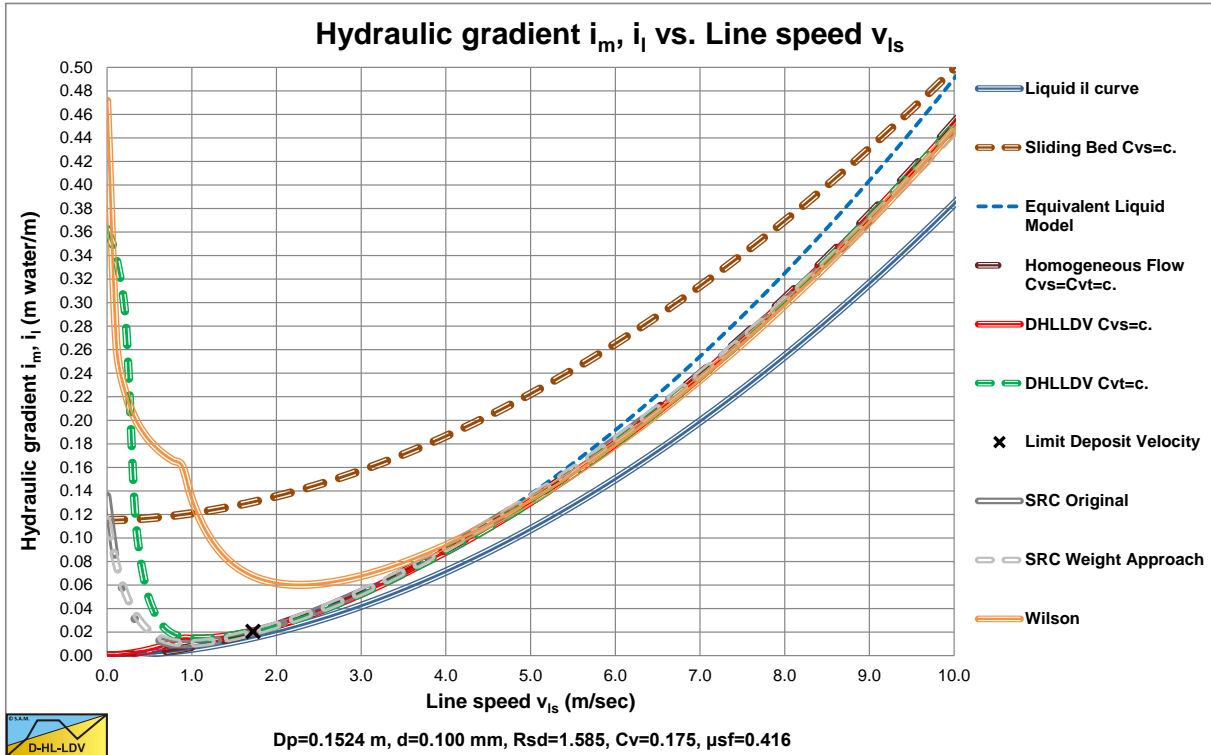
Figure 6.22-9: The SRC model compared to the DHLLDV Framework and the weight approach for d=0.1 mm, 2004 model.
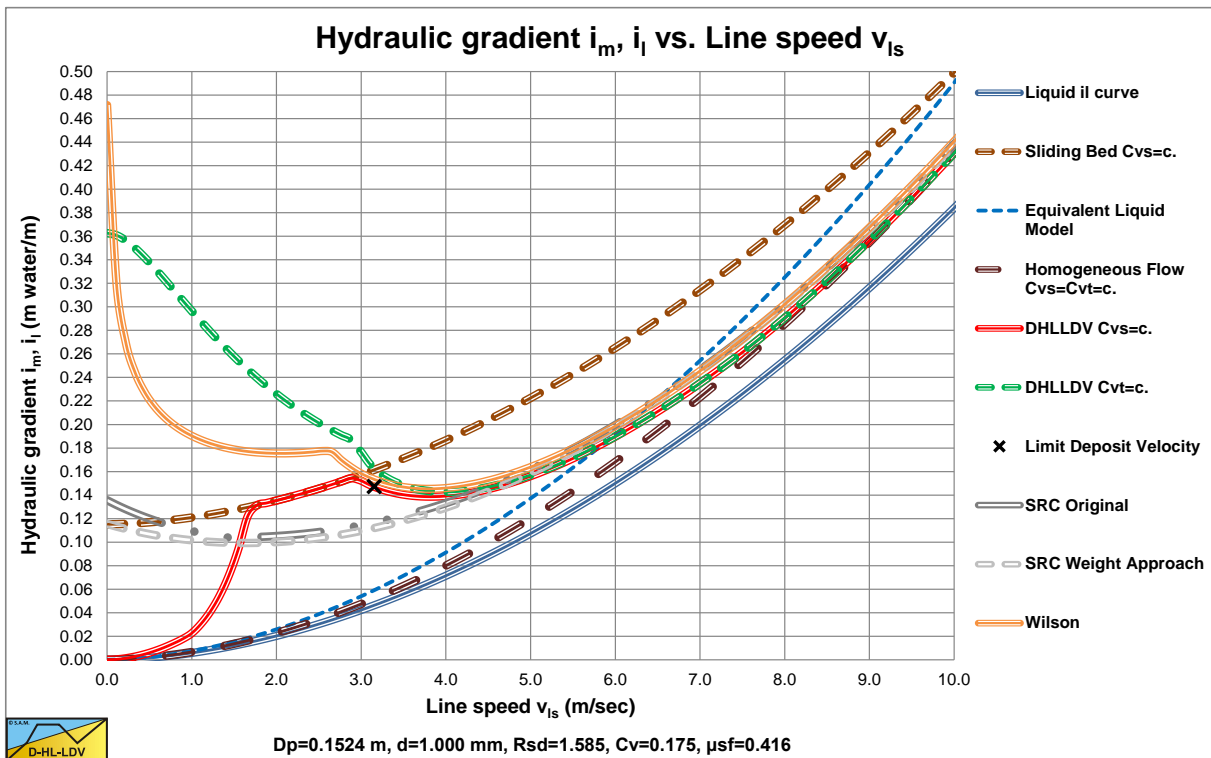
Figure 6.22-10: The SRC model compared to the DHLLDV Framework and the weight approach for d=1.0 mm, 2004 model.

6.22.10 The Limit Deposit Velocity.

Gillies (1993) derived an expression for the Durand & Condolios (1952) Froude number F_L, giving a Limit Deposit Velocity of:

$$v_{ls,ldv} = e^{\left(0.51-0.0073\cdot C_D - 12.5\cdot\left(\frac{(g\cdot v_l)^{2/3}}{g\cdot d}-0.14\right)^2\right)} \cdot \sqrt{2\cdot g\cdot D_p \cdot R_{sd}} \qquad (6.22\text{-}58)$$

With the Froude number F_L:

$$F_L = \frac{v_{ls,ldv}}{\sqrt{2\cdot g\cdot D_p \cdot R_{sd}}} = e^{\left(0.51-0.0073\cdot C_D - 12.5\cdot\left(\frac{(g\cdot v_l)^{2/3}}{g\cdot d}-0.14\right)^2\right)} \qquad (6.22\text{-}59)$$

The Durand & Condolios (1952) Froude number F_L does not depend on the pipe diameter and the volumetric concentration. The Froude number F_L should be considered the maximum F_L at a concentration near 20%. The F_L value increases with the particle diameter to a maximum of 1.64 for **d=0.4 mm** after which it decreases slowly to an asymptotic value of about 1.3 for very large particles. This is consistent with Wilson's (1979) nomogram (which gives the LSDV) and consistent with the F_L graph published by Durand & Condolios (1952). Quantitatively this equation matches the graph of Durand (1953), which differs by a factor 1.28 (to high) from the original graph of Durand & Condolios (1952).

Shook et al. (2002) give the following correlations for the Durand Froude number F_L:

$$F_L = \frac{v_{ls,ldv}}{\sqrt{2\cdot g\cdot D_p \cdot R_{sd}}} = 0.197\cdot Ar^{0.4} = 0.197\cdot\left(\frac{4\cdot g\cdot d^3 \cdot R_{sd}}{3\cdot v_l^2}\right)^{0.4} \qquad \text{for} \quad 80<Ar<160$$

$$F_L = \frac{v_{ls,ldv}}{\sqrt{2\cdot g\cdot D_p \cdot R_{sd}}} = 1.19\cdot Ar^{0.045} = 1.19\cdot\left(\frac{4\cdot g\cdot d^3 \cdot R_{sd}}{3\cdot v_l^2}\right)^{0.045} \qquad \text{for} \quad 160<Ar<540 \qquad (6.22\text{-}60)$$

$$F_L = \frac{v_{ls,ldv}}{\sqrt{2\cdot g\cdot D_p \cdot R_{sd}}} = 1.78\cdot Ar^{-0.019} = 1.78\cdot\left(\frac{4\cdot g\cdot d^3 \cdot R_{sd}}{3\cdot v_l^2}\right)^{-0.019} \qquad \text{for} \quad 540<Ar$$

The Durand & Condolios (1952) Froude number F_L does not depend on the pipe diameter and the volumetric concentration. The Froude number F_L should be considered the maximum F_L at a concentration near 20%.

Figure 6.22-11 and Figure 6.22-12 show the Durand & Condolios (1952) Froude number F_L for small and large pipe diameters in comparison with many other F_L or LDV equations. For small pipe diameters the Gillies (1993) and Shook et al. (2002) equations match well with the DHLLDV Frameworks, but for large pipe diameters they give higher values, since both Gillies (1993) and Shook et al. (2002) have no dependency of the F_L number with respect to the pipe diameter, while the DHLLDV Framework has.

Both models seem to be a fit to the Durand (1953) graph, although based on their own data. As will be concluded more often, the wrong Durand (1953) graph seems to be right based on many data of many researchers. The original Durand & Condolios (1952) graph seems to underestimate the Limit Deposit Velocity.

Figure 6.22-13 shows Durand Froude numbers of Gillies et al. (2000B) and others for a 0.1524 m diameter pipe. The Gillies et al. (2000B) values were originally with the Archimedes number on the abscissa and are transferred to particle diameter for the case all data points were for sand/gravel.
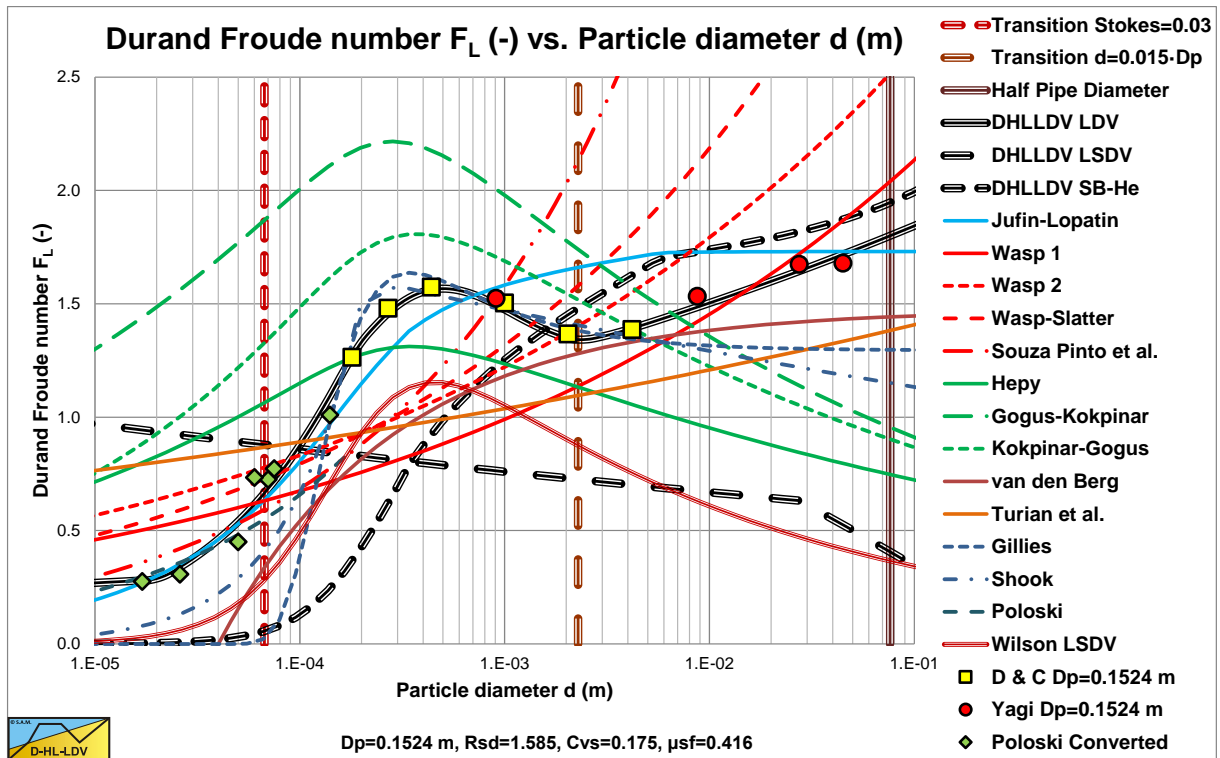
Figure 6.22-11: The different F_L equations compared with Gillies (1993) and Shook et al. (2002), small pipe diameter.
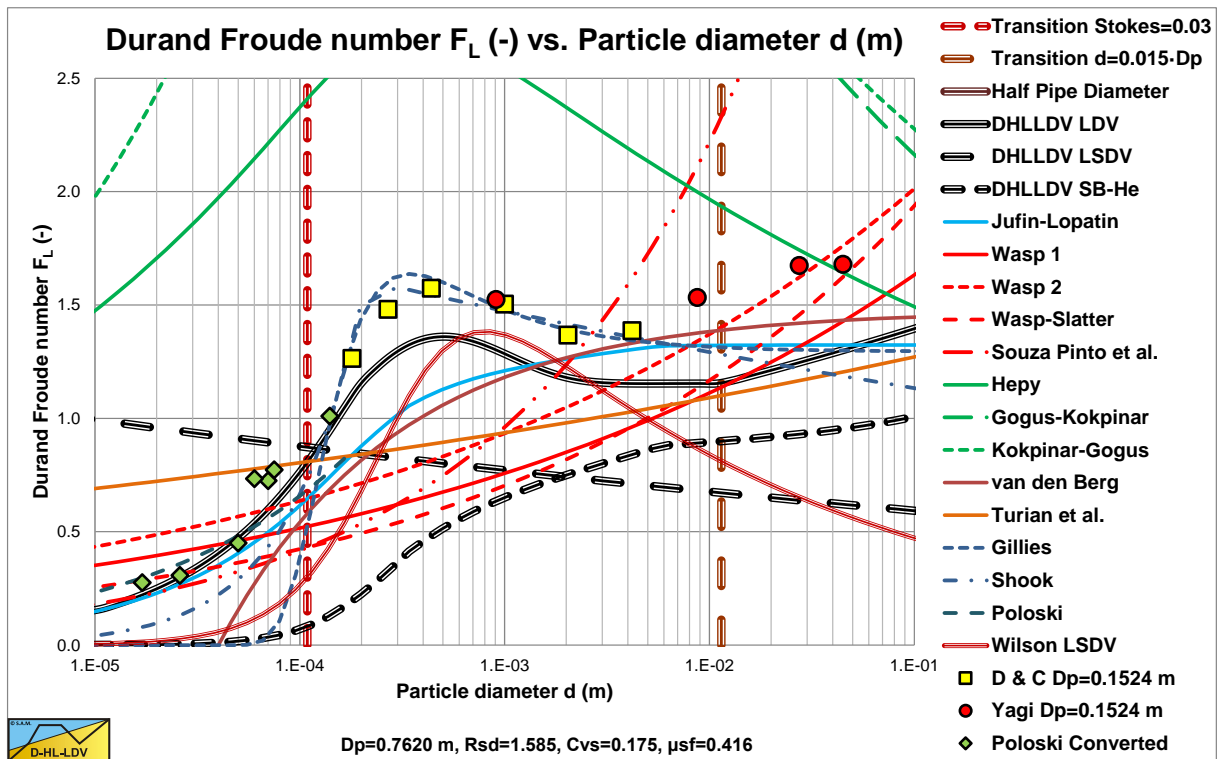
Figure 6.22-12: The different F_L equations compared with Gillies (1993) and Shook et al. (2002), large pipe diameter.
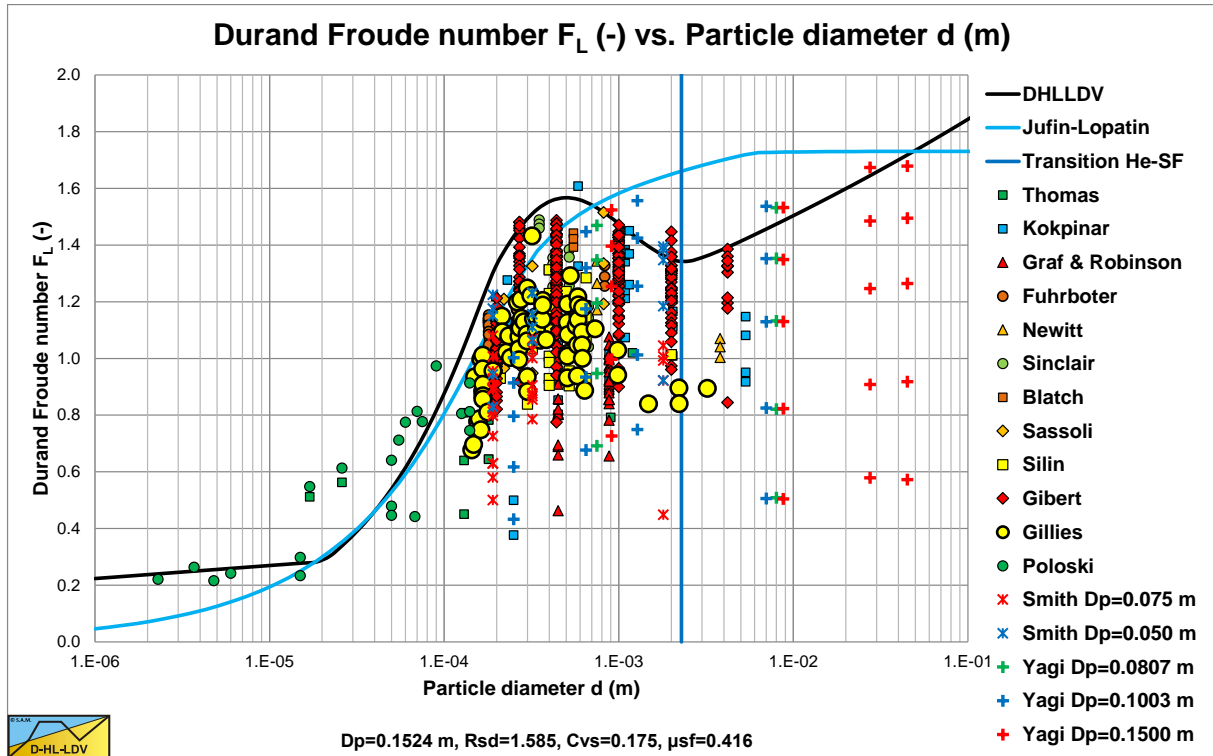
Figure 6.22-13: Durand Froude numbers of Gillies et al. (2000B) and others.
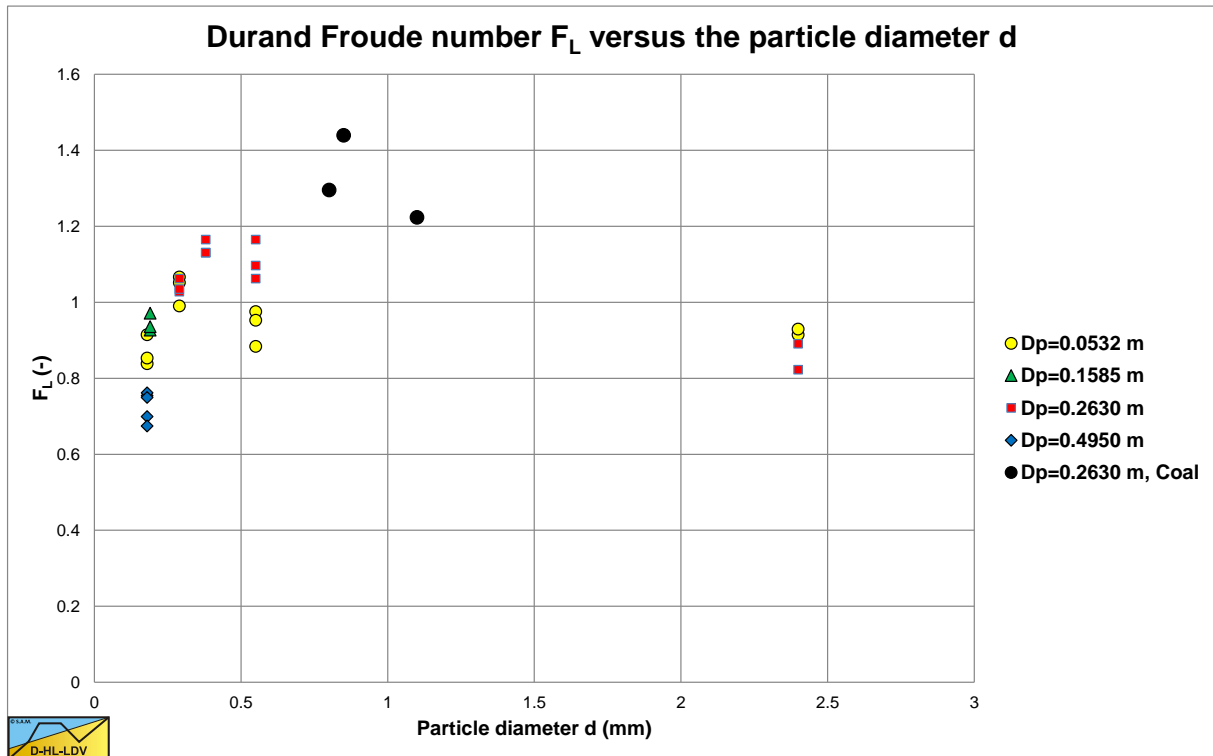
Figure 6.22-14: Durand Froude numbers of Gillies (1993).

6.22.11 Experiments.

Gillies (1993) carries out experiments with small and large pipe diameters and with fine and coarse sand. Some of these experiments with large pipe diameters are shown in the following figures. Figure 6.22-15 shows the data points for a **d=0.18 mm** sand in a **D_p=0.495 m** diameter pipe. The data points do not really match the theoretical curve based on the DHLLDV Framework. Figure 6.22-16 shows the same data points, but here the Thomas (1965)

---

viscosity is included in the DHLLDV Framework, based on about 50% of the concentration. Now there is a good match between experiments and theory.
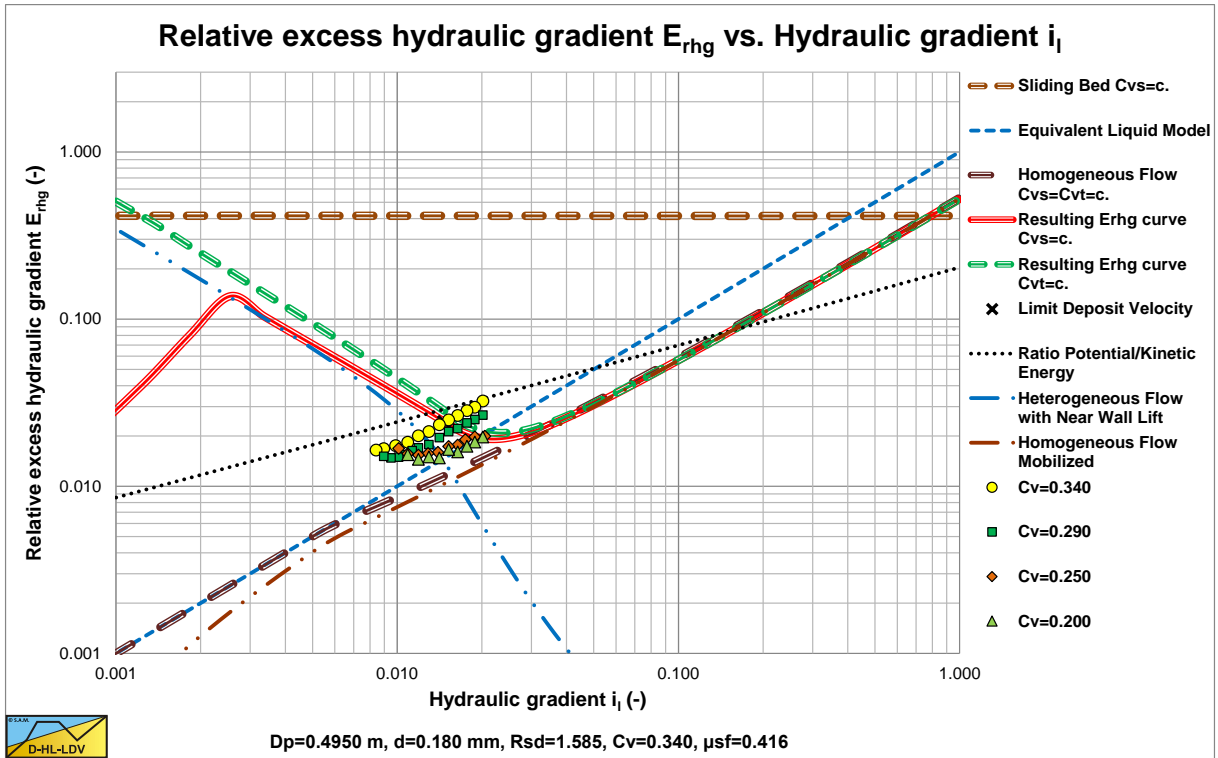
Figure 6.22-15: Data of Gillies (1993) in a large diameter pipe D_P=0.495 m and small particles d=0.18 mm.
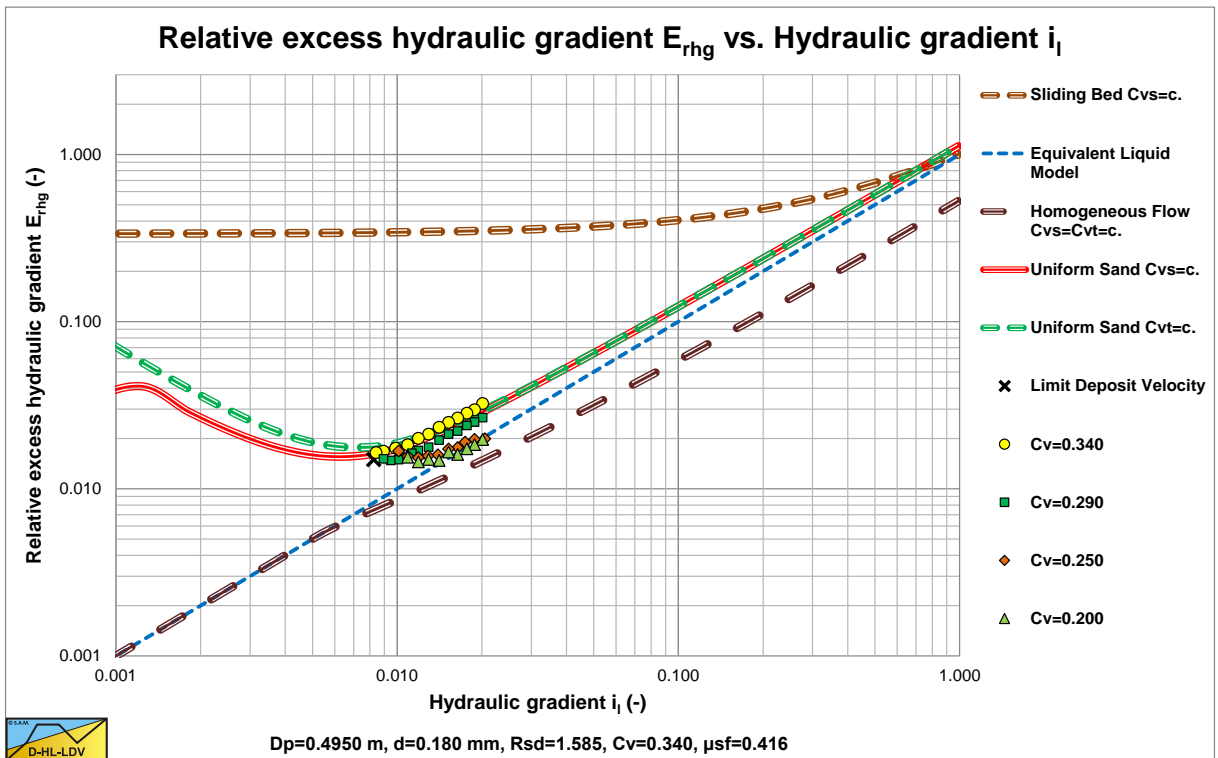
Figure 6.22-16: Data of Gillies (1993) in a large diameter pipe D_P=0.495 m and small particles d=0.18 mm, including Thomas (1965) viscosity.

Figure 6.22-17 shows the data points for a **d=0.29 mm** sand in a **D_P=0.263 m** diameter pipe. The data points match the theoretical curve based on the DHLLDV Framework reasonably.

Figure 6.22-18 shows the same data points, but here the Thomas (1965) viscosity is included in the DHLLDV Framework, based on about 25% of the concentration. Now there is a good match between experiments and theory.
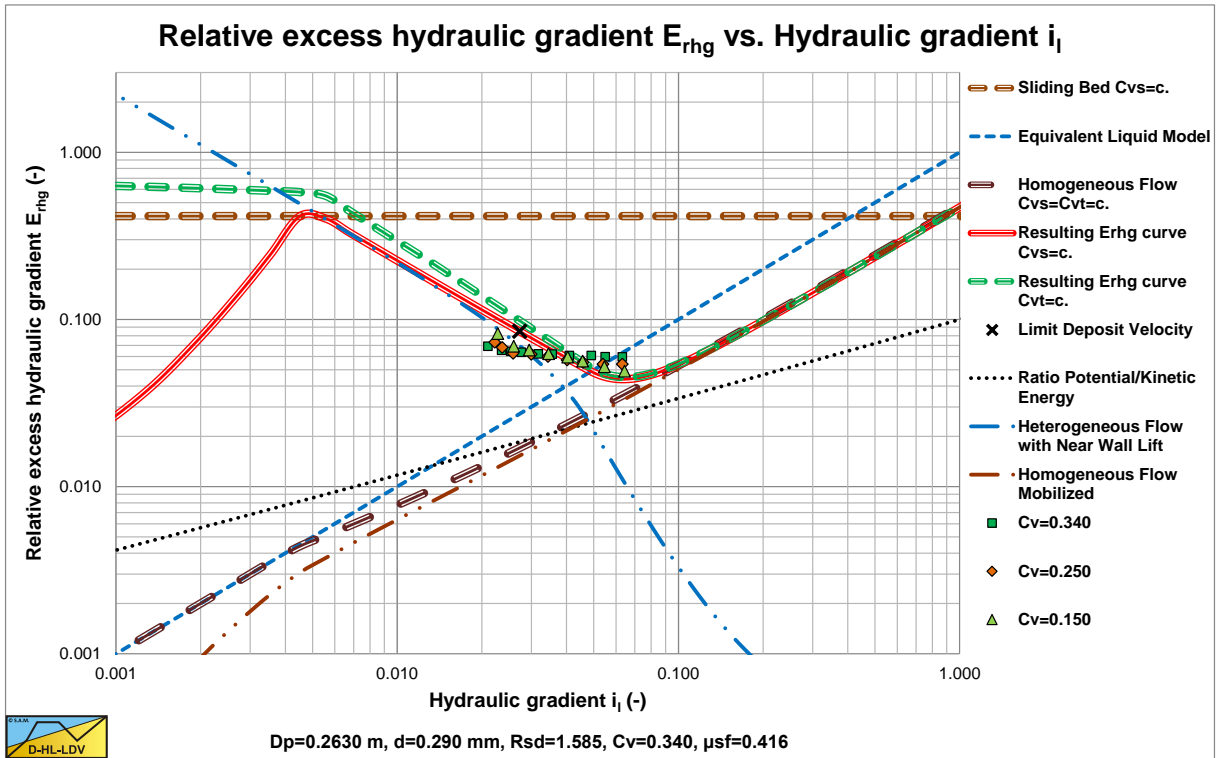
Figure 6.22-17: Data of Gillies (1993) in a large diameter pipe D_P=0.263 m and small particles d=0.29 mm.
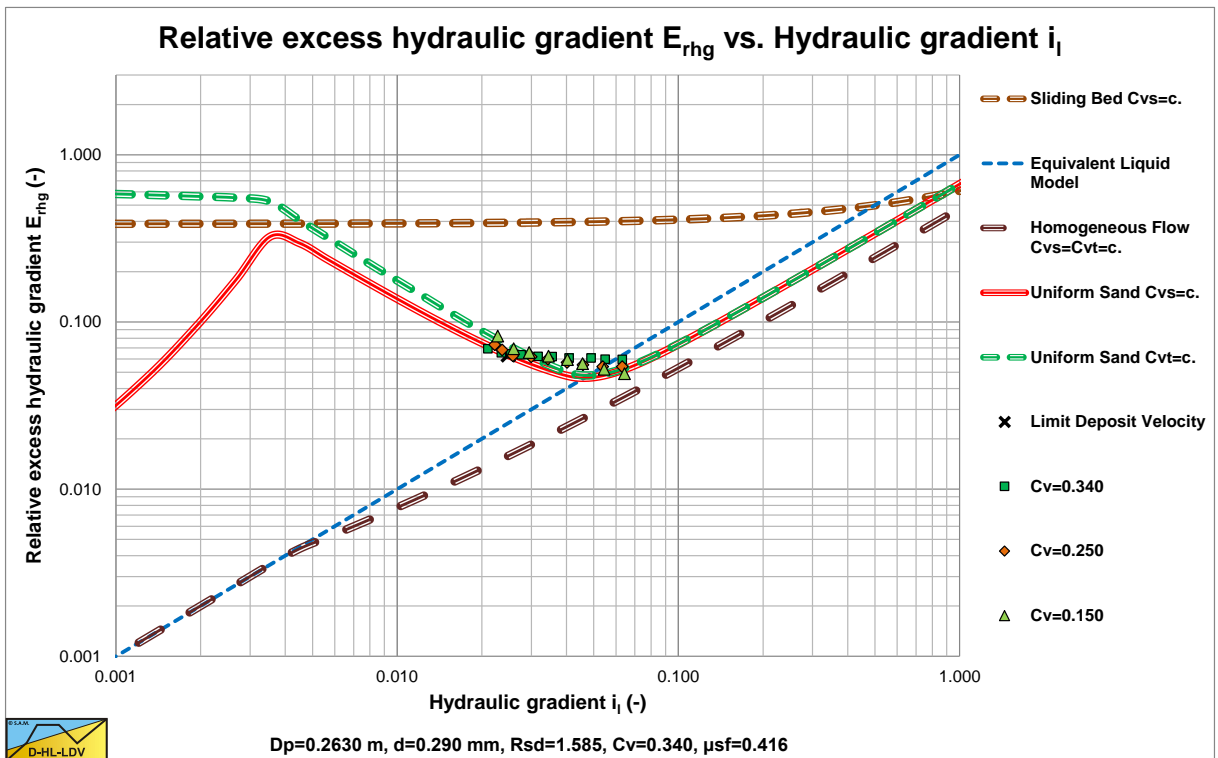
Figure 6.22-18: Data of Gillies (1993) in a large diameter pipe D_P=0.263 m and small particles d=0.29 mm, including Thomas (1965) viscosity.

Figure 6.22-19 shows the data points for a **d=0.38 mm** sand in a **D_P=0.263 m** diameter pipe. The data points match the theoretical curve based on the DHLLDV Framework reasonably. Figure 6.22-20 shows the same data points, but here the Thomas (1965) viscosity is included in the DHLLDV Framework, based on about 25% of the concentration. Now there is a good match between experiments and theory. Apparently the influence of the Thomas (1965) viscosity reduces if the particles size increases. The influence of the Thomas (1965) viscosity is probably smooth. With 100% for very fine particles, reducing to zero for medium sized particles.
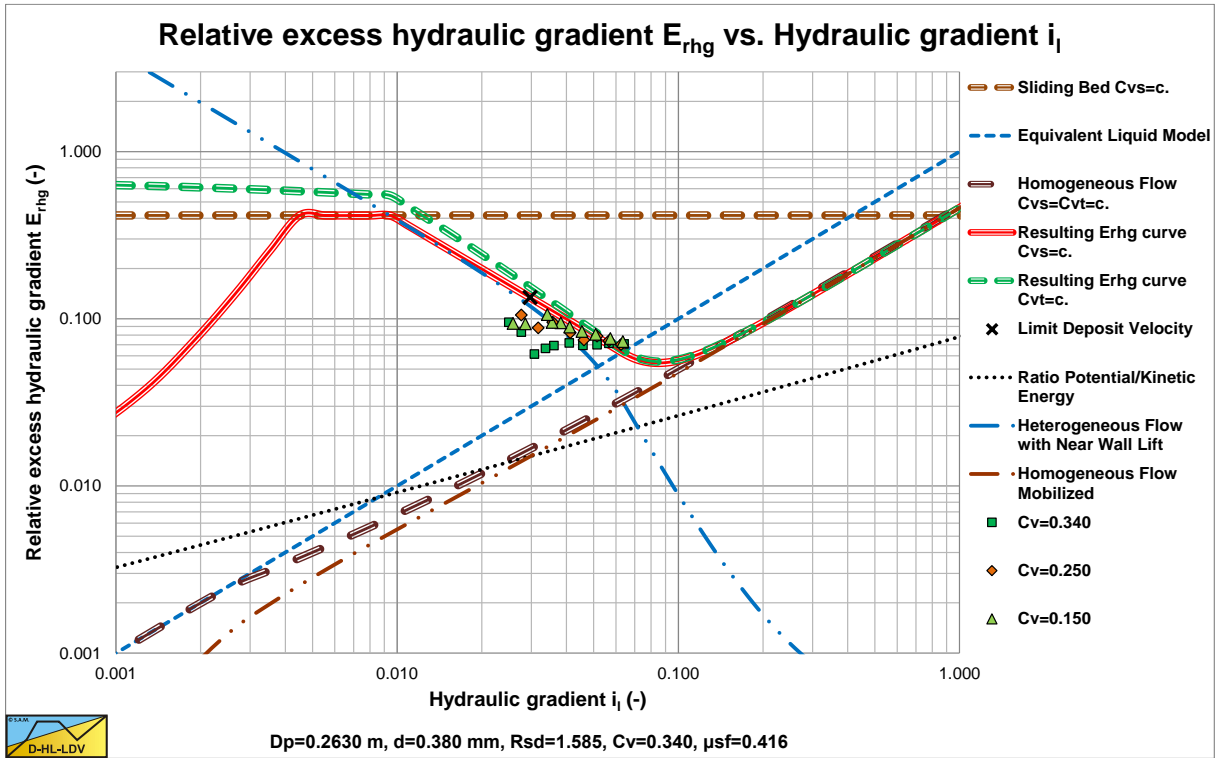
Figure 6.22-19: Data of Gillies (1993) in a large diameter pipe D_P=0.263 m and small particles d=0.38 mm.
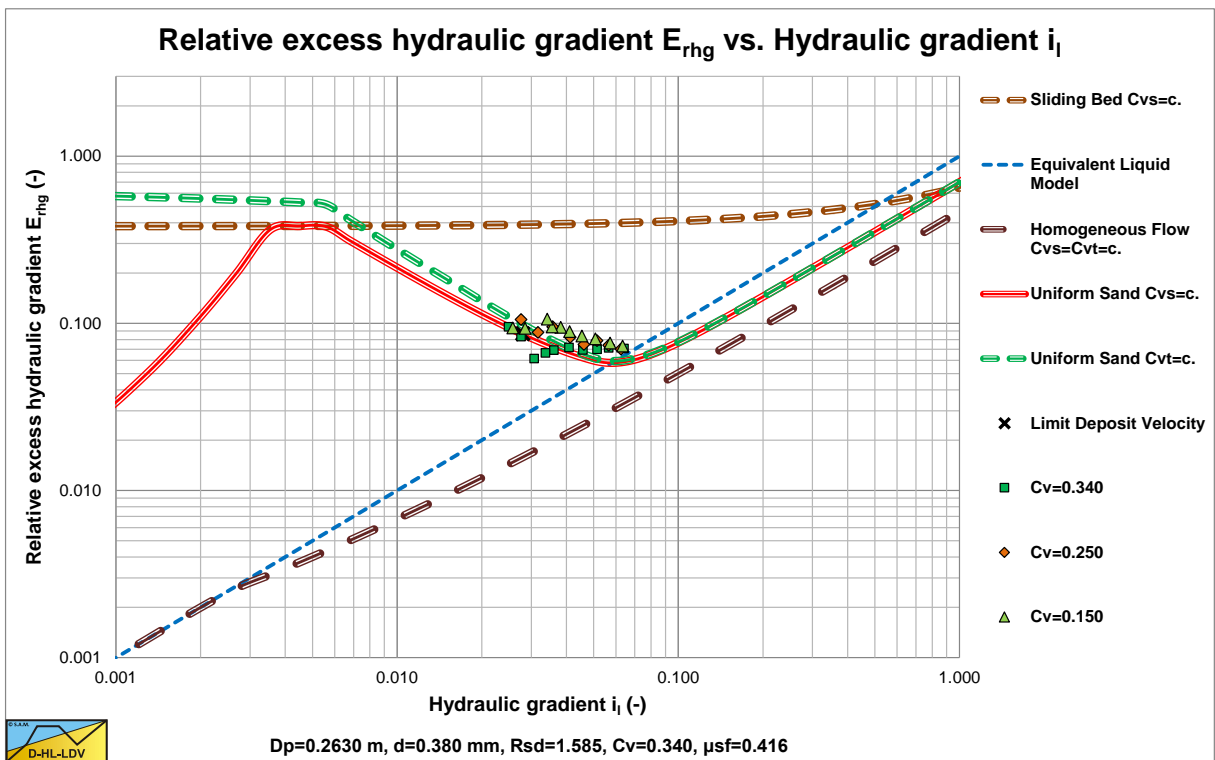
Figure 6.22-20: Data of Gillies (1993) in a large diameter pipe D_P=0.263 m and small particles d=0.38 mm, including Thomas (1965) viscosity.
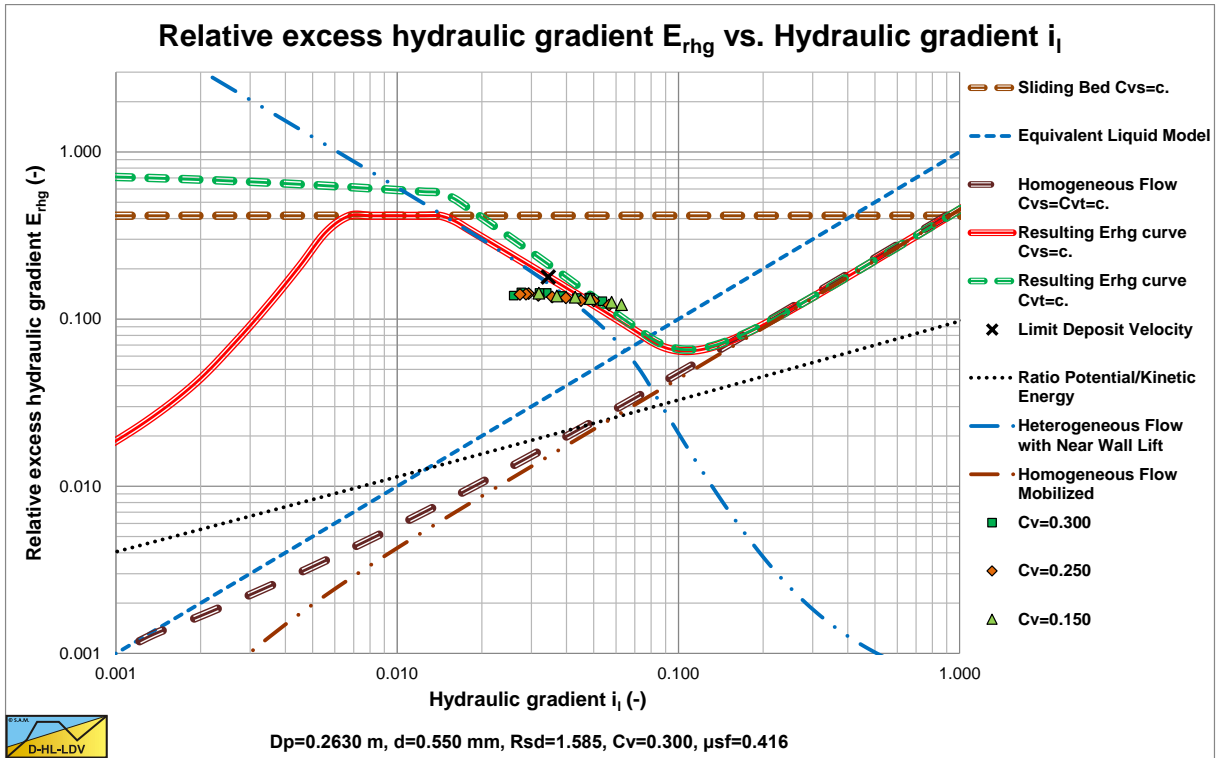
Figure 6.22-21: Data of Gillies (1993) in a large diameter pipe D_p=0.263 m and small particles d=0.55 mm.
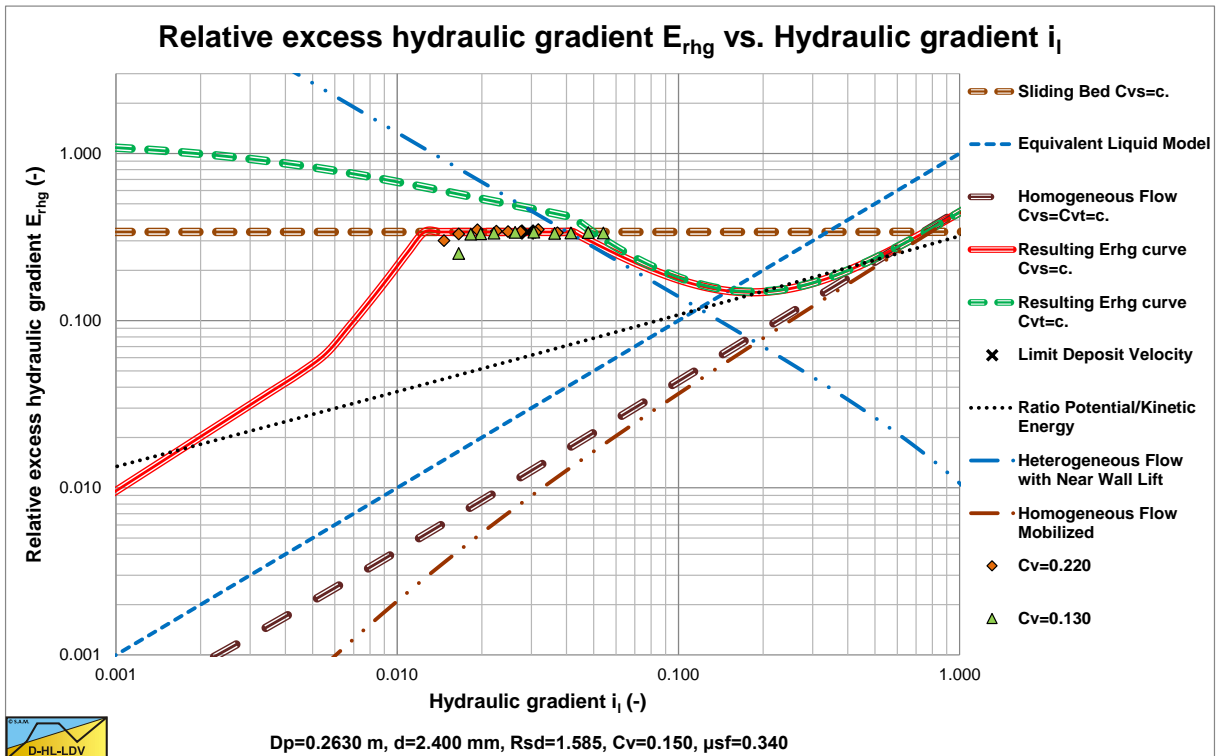
Figure 6.22-22: Data of Gillies (1993) in a large diameter pipe D_p=0.263 m and small particles d=2.4 mm.

Figure 6.22-21 shows the data points for a **d=0.55 mm** sand in a **D_p=0.263 m** diameter pipe. Different concentrations cannot be distinguished, meaning that the hydraulic gradient is proportional to the volumetric concentration. The steepness of the data points is much less than the prediction with the DHLLDV Framework. This may be the result of grading.

Figure 6.22-22 shows the data points for a **d=2.4 mm** sand in a **D_p=0.263 m** diameter pipe. Here the data points confirm the existence of a sliding bed and again different concentrations cannot be distinguished.

Figure 6.22-23: Data of Gillies (1993) in a pipe D_p=0.0532 m and small particles d=0.18 mm, v_{ls}=3.1 m/s.

Figure 6.22-24: Data of Gillies (1993) in a pipe D_p=0.0532 m and small particles d=0.18 mm, v_{ls}=1.8 m/s.
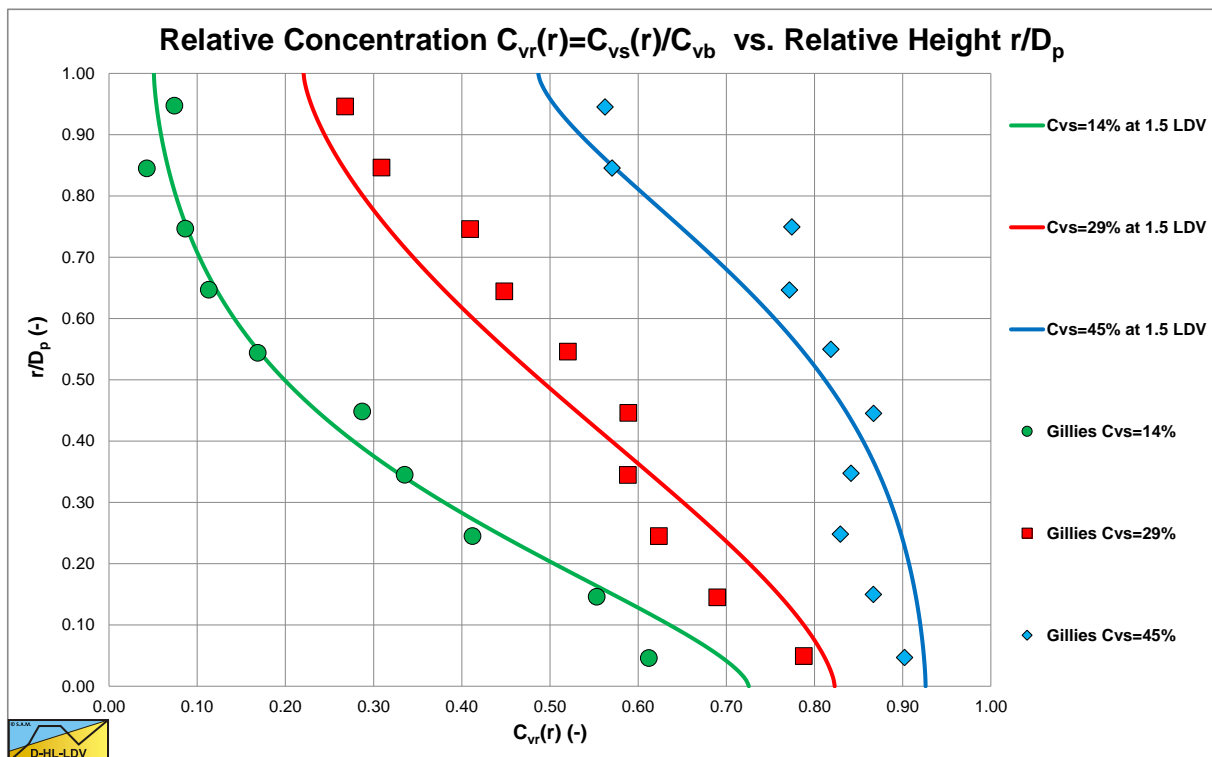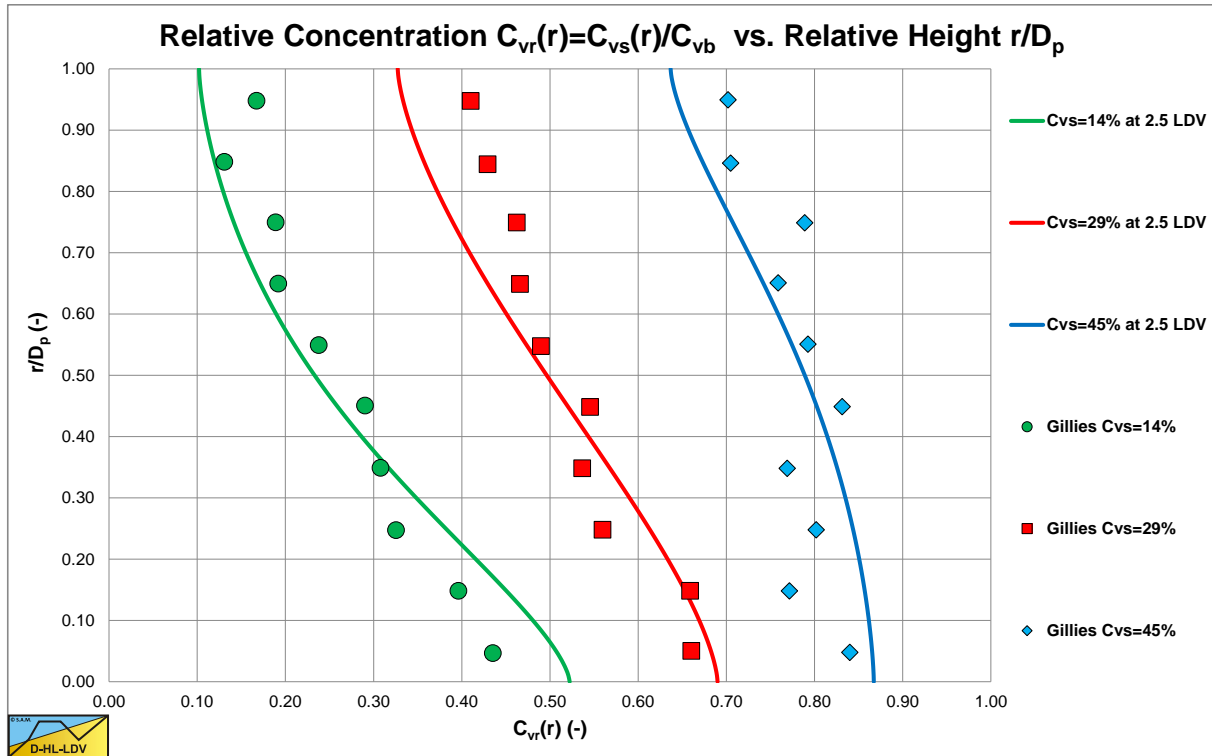
Figure 6.22-23 and Figure 6.22-24 show the concentration distributions for 3 average volumetric concentrations and 2 line speeds for a pipe diameter of D_p=**0.0532 m** and a particle diameter of **d=0.18 m**. The LDV (the line speed where there is no bed anymore) is about 1.2 m/s for a 17.5% volumetric concentration and slightly lower for the higher concentrations. The fit lines are based on the DHLLDV Framework, assuming a bed concentration of 55%. So at a line speed of 1.8 m/s a bottom concentration lower than the bed concentration is expected, but at 3.1 m/s a much lower bottom concentration and a slightly steeper concentration profile is expected.
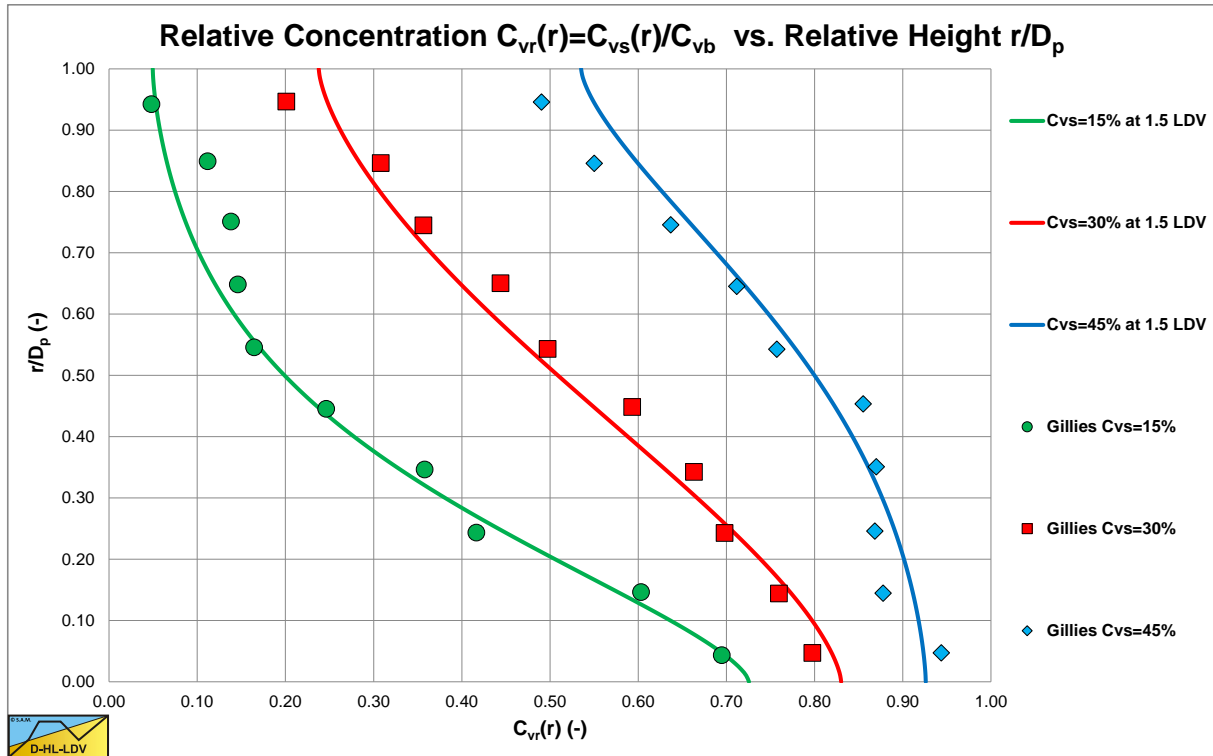
Figure 6.22-25: Data of Gillies (1993) in a pipe D_p=0.0532 m and small particles d=0.29 mm, v_{ls}=3.1 m/s.
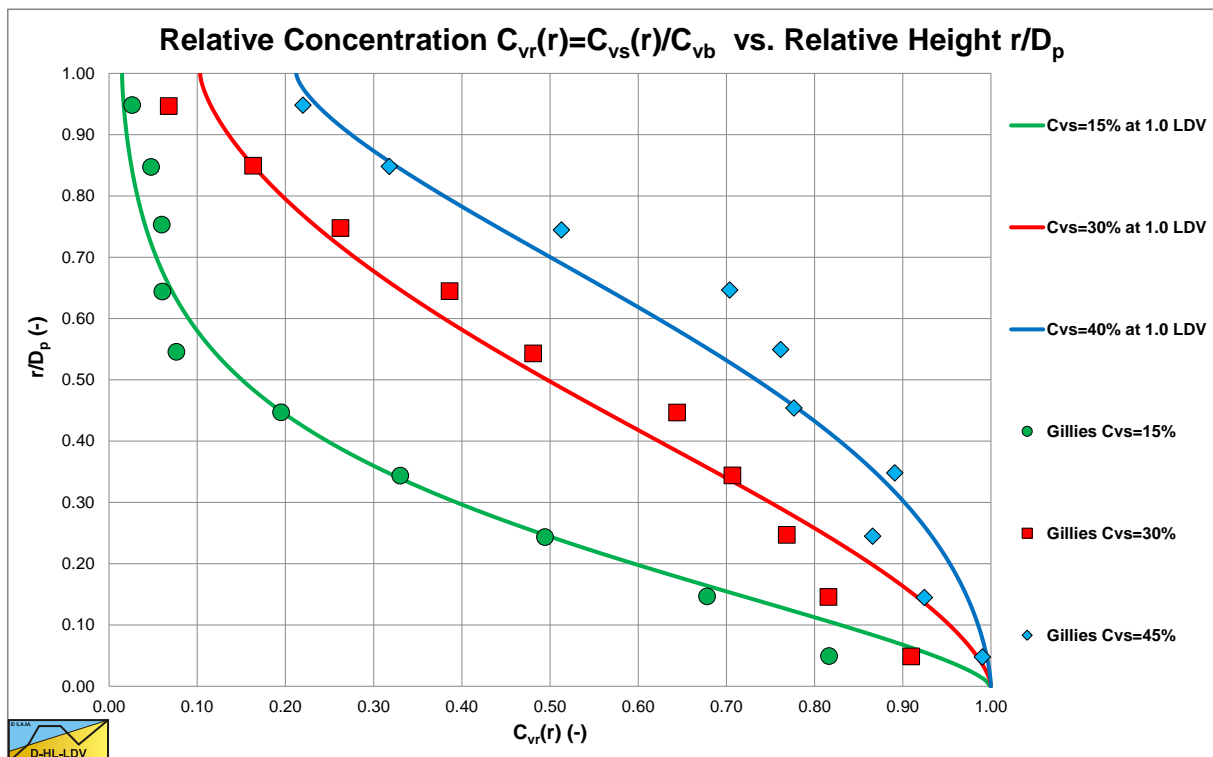
Figure 6.22-26: Data of Gillies (1993) in a pipe D_p=0.0532 m and small particles d=0.29 mm, v_{ls}=1.8 m/s.

Figure 6.22-25 and Figure 6.22-26 show the concentration distributions for 3 average volumetric concentrations and 2 line speeds for a pipe diameter of D_p=**0.0532 m** and a particle diameter of **d=0.29 m**. The LDV (the line speed where there is no bed anymore) is about 1.8 m/s for a 17.5% volumetric concentration and slightly lower for the higher concentrations. The fit lines are based on the DHLLDV Framework, assuming a bed concentration of 55%. So at a line speed of 1.8 m/s a bottom concentration close to the bed concentration is expected, but at 3.1 m/s a lower bottom concentration and a slightly steeper concentration profile is expected.
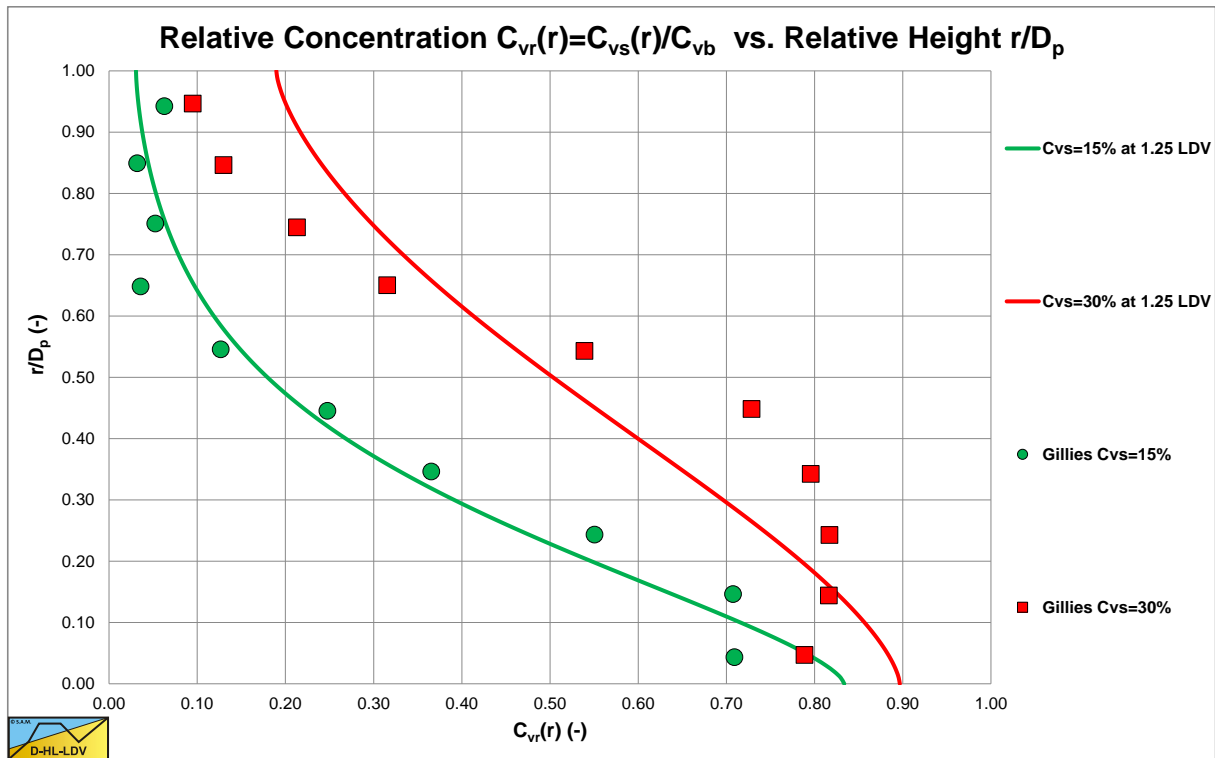
Figure 6.22-27: Data of Gillies (1993) in a pipe D_p=0.0532 m and small particles d=0.55 mm, v_{ls}=3.1 m/s.
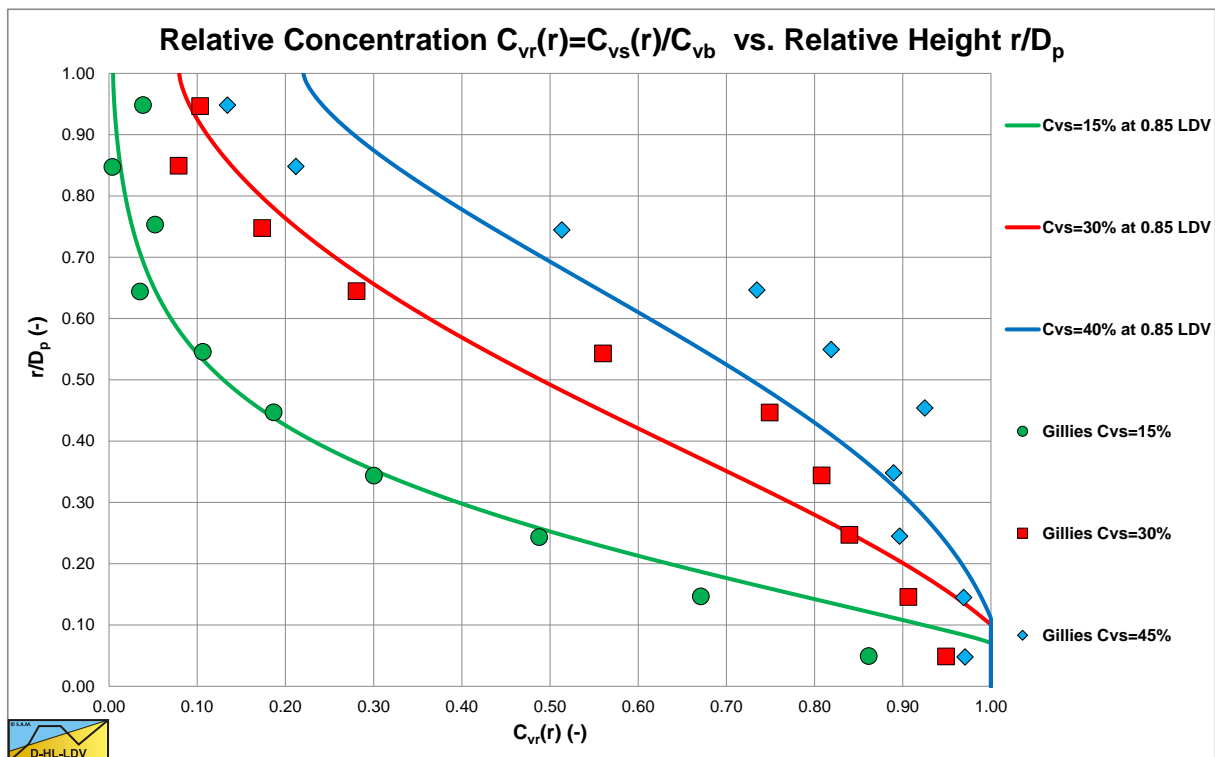
Figure 6.22-28: Data of Gillies (1993) in a pipe D_p=0.0532 m and small particles d=0.55 mm, v_{ls}=2.1 m/s.

Figure 6.22-27 and Figure 6.22-28 show the concentration distributions for 3 average volumetric concentrations and 2 line speeds for a pipe diameter of **D_p=0.0532 m** and a particle diameter of **d=0.55 m**. The LDV (the line speed where there is no bed anymore) is about 2.2 m/s for a 17.5% volumetric concentration and slightly lower for the higher concentrations. The fit lines are based on the DHLLDV Framework, assuming a bed concentration of 55%. So at a line speed of 2.1 m/s a bottom concentration close to the bed concentration is expected. At 3.1 m/s a slightly lower bottom concentration and a slightly steeper concentration profile is expected.
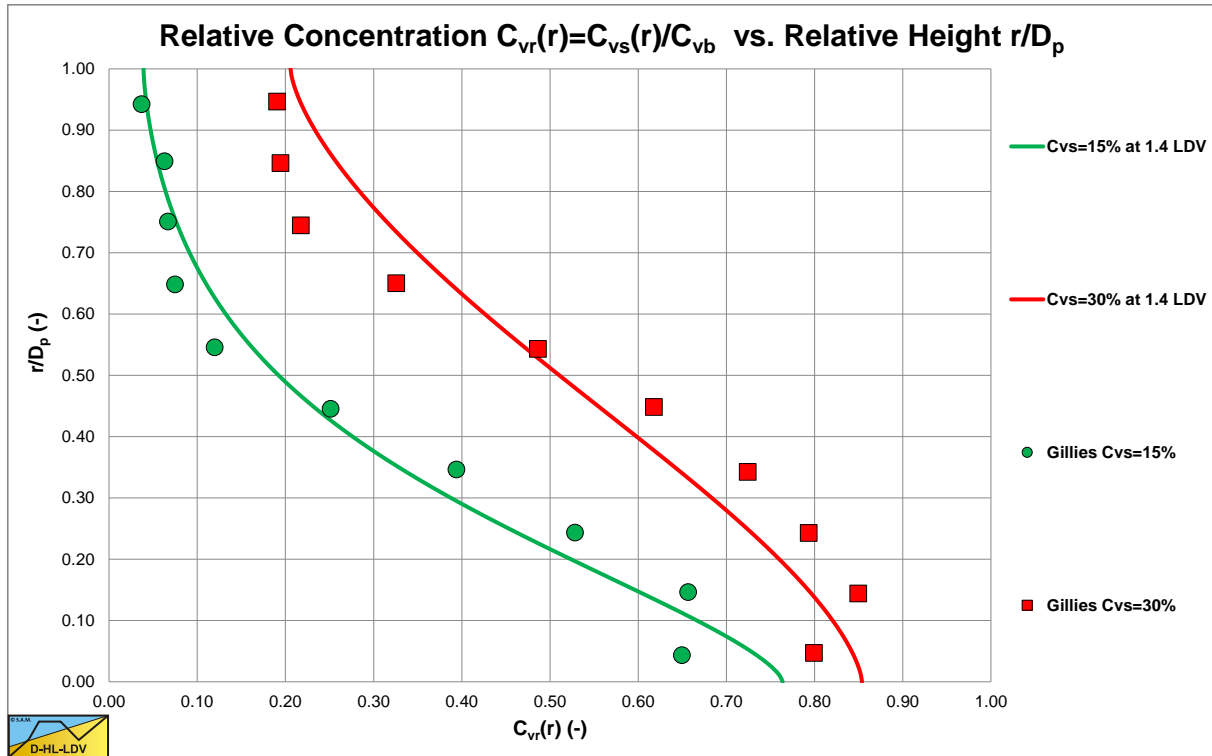
Figure 6.22-29: Data of Gillies (1993) in a pipe D_p=0.0532 m and small particles d=2.4 mm, v_{ls}=3.1 m/s.
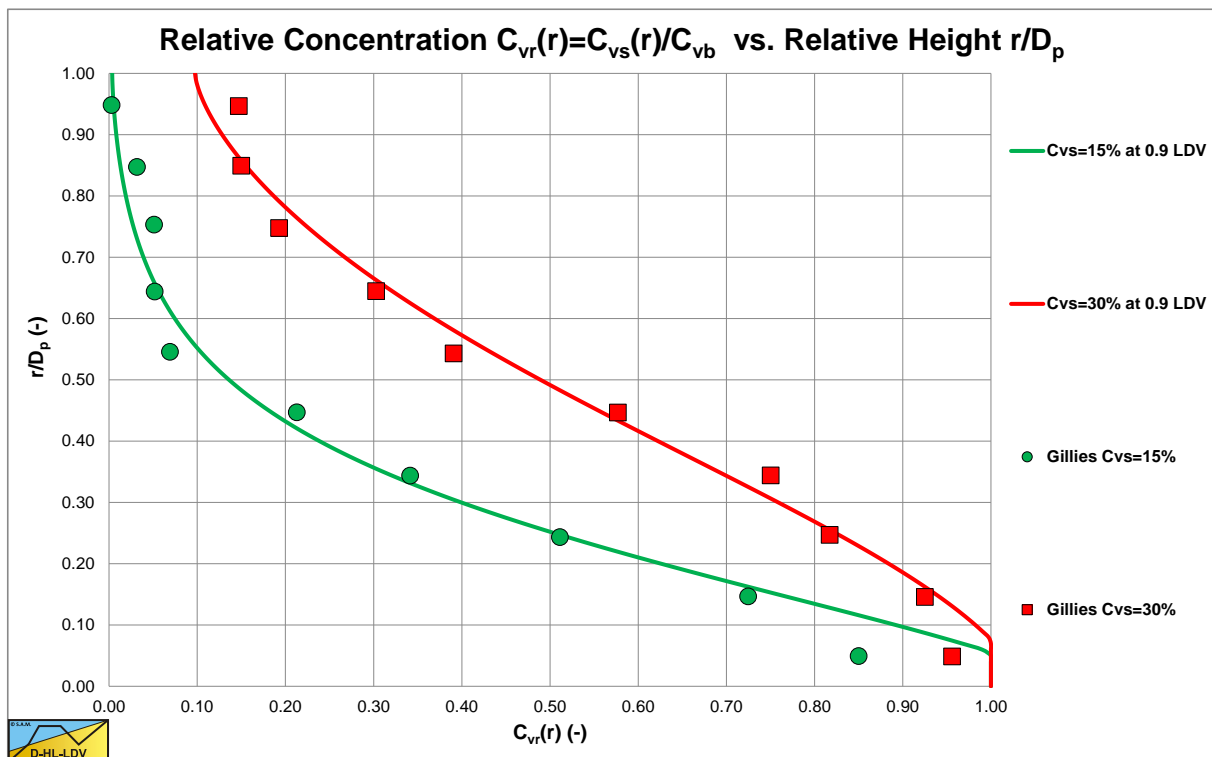
Figure 6.22-30: Data of Gillies (1993) in a pipe D_p=0.0532 m and small particles d=2.4 mm, v_{ls}=1.8 m/s.

Figure 6.22-29 and Figure 6.22-30 show the concentration distributions for 2 average volumetric concentrations and 2 line speeds for a pipe diameter of D_p=0.0532 m and a particle diameter of d=2.4 m. The LDV (the line speed where there is no bed anymore) is about 2.0 m/s for a 17.5% volumetric concentration and slightly lower for the lower and higher concentrations. The fit lines are based on the DHLLDV Framework, assuming a bed concentration of 55%. So at a line speed of 1.8 m/s a bottom concentration close to the bed concentration is expected, but at 3.1 m/s above the LDV a lower bottom concentration and a slightly steeper concentration profile is expected.

In this chapter the concentration profiles in a D_p=0.0532 m pipe are compared with the data of Gillies (1993). In chapter 7.10 the concentration profiles in a D_p=0.263 m pipe are compared with the data of Gillies (1993). In both cases the predictions according to the DHLLDV Framework match well, although not perfect.

It should be mentioned that the LDV values used are an average based on the DHLLDV Framework, while the LDV is concentration dependent. The DHLLDV Framework is a bit conservative giving high values for the LDV.

6.22.12 Nomenclature SRC Model.

Ar	Archimedes number	**-**
A_p	Cross section pipe	m^2
A_1	Cross section above bed	m^2
A_2	Cross section bed	m^2
C_{vb}	Volumetric spatial bed concentration	**-**
$C_{vb,max}$	Maximum volumetric spatial bed concentration	**-**
C_{vs}	Spatial volumetric concentration	**-**
$C_{vs,1}$	Spatial volumetric concentration in cross section 1	**-**
$C_{vs,2}$	Spatial volumetric concentration in cross section 2	**-**
$C_{vs,c}$	Spatial volumetric concentration in contact load	**-**
C_D	Particle drag coefficient	**-**
d	Particle diameter	**m**
d^+	Dimensionless particle diameter	**-**
d_{50}	Particle diameter with 50% passing	**m**
D_H	Hydraulic diameter	**m**
D_p	Pipe diameter	**m**
E_{rhg}	Relative excess hydraulic gradient	**-**
Fr	Froude number	**-**
F_L	Durand & Condolios LDV Froude number	**-**
Fr	Froude number	**-**
g	Gravitational constant 9.81 m/s^2	**m/s^2**
i_l	Hydraulic gradient liquid	**m/m**
i_m	Hydraulic gradient mixture	**m/m**
ΔL	Length of pipe section	**m**
LDV	Limit Deposit Velocity	**m/s**
LSDV	Limit of Stationary Deposit Velocity	**m/s**
O_p	Circumference pipe	**m**
O_1	Circumference pipe above bed	**m**
O_2	Circumference pipe in bed	**m**
O_{12}	Width of bed	**m**
Δp	Pressure difference	**kPa**
Δp_l	Pressure difference liquid	**kPa**
Δp_m	Pressure difference mixture	**kPa**
Re	Reynolds number	**-**
R_{sd}	Relative submerged density	**-**
u_*	Friction velocity	**m/s**
v_t	Terminal settling velocity	**m/s**
v_{ls}	Line speed	**m/s**
$v_{ls,ldv}$	Limit Deposit Velocity	**m/s**
v_1	Cross section averaged velocity above bed	**m/s**
v_2	Cross section averaged velocity bed	**m/s**
y_b	Height of bed	**m**
α	Darcy Weisbach friction factor, multiplication factor	**-**
β	Bed angle	**rad**
ε	Pipe wall roughness	**m**
δ_v	Thickness viscous sub layer	**m**
ρ_l	Density carrier liquid	**ton/m^3**
ρ_s	Density solids	**ton/m^3**
ρ_{m1}	Density in the upper layer	**ton/m^3**
ρ_{m2}	Density in the lower layer	**ton/m^3**
λ_{lc}	Linear concentration	**-**
λ_l	Darcy-Weisbach friction factor liquid-pipe wall	**-**
λ_1	Darcy-Weisbach friction factor with pipe wall	**-**
λ_2	Darcy-Weisbach friction factor with pipe wall, liquid in bed	**-**
λ_{12}	Darcy-Weisbach friction factor on the bed	**-**

λ_s	Solids effect to Darcy-Weisbach friction factor	-
ν_l	Kinematic viscosity	m^2/s
τ_l	Shear stress liquid-pipe wall	kPa
$\tau_{1,l}$	Shear stress liquid-pipe wall above bed	kPa
$\tau_{12,l}$	Shear stress bed-liquid	kPa
$\tau_{2,l}$	Shear stress liquid-pipe in bed	kPa
$\tau_{2,sf}$	Shear stress from sliding friction	kPa
μ_{sf}	Sliding friction coefficient	-
μ_{sf0}	Sliding friction coefficient, basic	-

6.23 The Kaushal & Tomita (2002B) Model.

6.23.1 Introduction.

Kaushal with changing co-authors developed a model for predicting the hydraulic gradient in horizontal pipelines, based on a modified Wasp et al. (1977) model and a modified Karabelas (1977) model. First the different papers are discussed in the right chronological order, after which the model is discussed in detail.

Kaushal et al. (2002A) describe the concentration distribution and the concentration at the pipe bottom at the deposition velocity. The concentration distribution is based on the advection diffusion equation as originally presented by O'Brien (1933) and Rouse (1937) and modified for the upwards flow of the liquid at higher concentrations by Hunt (1954). The original advection diffusion equation gives:

$$
\mathbf{v_t} \cdot \mathbf{C_{vs}(z)} + \varepsilon_s \cdot \frac{\partial \mathbf{C_{vs}(z)}}{\partial \mathbf{z}} = \mathbf{0}
\tag{6.23-1}
$$

The advection diffusion equation as modified by Hunt (1954) gives:

$$
\mathbf{v_t} \cdot \mathbf{C_{vs}(z)} \cdot \left(1 - \mathbf{C_{vs}(z)}\right) + \varepsilon_s \cdot \frac{\partial \mathbf{C_{vs}(z)}}{\partial \mathbf{z}} = \mathbf{0}
\tag{6.23-2}
$$

Giving, in case of constant diffusivity and no hindered settling for uniform sands:

$$
\mathbf{C_{vs}(z)} = \frac{\dfrac{\mathbf{C_{vB}}}{1 - \mathbf{C_{vB}}} \cdot \mathbf{e}^{-\frac{\mathbf{v_t}}{\varepsilon_s} \cdot \frac{\mathbf{z}}{\mathbf{D_p}}}}{1 + \dfrac{\mathbf{C_{vB}}}{1 - \mathbf{C_{vB}}} \cdot \mathbf{e}^{-\frac{\mathbf{v_t}}{\varepsilon_s} \cdot \frac{\mathbf{z}}{\mathbf{D_p}}}} = \frac{\mathbf{e}^{-\frac{\mathbf{v_t}}{\varepsilon_s} \cdot \frac{\mathbf{z}}{\mathbf{D_p}}}}{\dfrac{1 - \mathbf{C_{vB}}}{\mathbf{C_{vB}}} + \mathbf{e}^{-\frac{\mathbf{v_t}}{\varepsilon_s} \cdot \frac{\mathbf{z}}{\mathbf{D_p}}}}
\tag{6.23-3}
$$

At the bottom of the pipe, **z=0**, this gives $\mathbf{C_{vs}(0)=C_{vB}}$, the concentration at the bottom.

The Karabelas (1977) approach for determining the concentration distributions of graded solids is applied with some modifications. The Longwell (1977) approach for the liquid eddy momentum diffusivity is applied instead of a constant diffusivity, making the liquid eddy momentum diffusivity depending on the vertical position in the pipe. Based on Mukhtar (1991) and Kaushal (1995) the factor between the sediment diffusivity and the liquid eddy momentum diffusivity has been modified, by making it dependent on the volumetric concentration, and hindered settling has been added according to Richardson & Zaki (1954).
The new model is compared with experimental data of zinc tailings in a 0.105 m horizontal pipe, with volumetric concentrations of 3.8% to 26% and line speeds of 2 m/s to 3.5 m/s. At very low concentrations the Karabelas (1977) model and the Kaushal et al. (2002A) model give about the same results. At higher concentrations however, the Karabelas (1977) model differs from the experimental data, the higher the concentration, the bigger the difference. The Kaushal et al. (2002A) model gives a very good correlation with the experimental data.

Kaushal & Tomita (2002B) describe the Wasp et al. (1977) and the Gillies et al. (1991) methods for determining hydraulic gradients in slurry flow. The Gillies et al. (1991) method is further referred to as the SRC method and is already described in chapter 6. The Kaushal et al. (2002A) model for determining the concentration profile, the modified Karabelas (1977) model, is applied in order to find the so called Wasp et al. (1977) criterion to determine the solids fraction in suspension. In the Wasp et al. (1977) model, the calculation of the Darcy Weisbach friction factor is determined with the modified Wood (1966) equation and the factor relating the sediment diffusivity to the liquid eddy momentum diffusivity is not 1, but the equation of Kaushal et al. (2002A) is applied.
A comparison between the SRC model, the Wasp et al. (1977) model and the Kaushal & Tomita (2002B) model shows a good agreement for zinc tailings in a 0.105 m pipe at different volumetric concentrations and line speeds. At higher concentrations, up to 26%, the Wasp et al. (1977) model overestimates the experimental data, the Kaushal & Tomita (2002B) modified Wasp et al. (1977) model underestimates slightly, while the Gillies et al. (1991) model overestimates slightly.

Kaushal & Tomita (2002C) used their head loss model based on a modified Wasp et al. (1977) model, but they changed the way the suspended (vehicle) fraction is determined, based on their modified Karabelas (1977) model and not on the modified Wasp et al. (1977) equation. The factor relating the sediment diffusivity to the liquid eddy momentum diffusivity was modified compared to Kaushal et al. (2002A), including the ratio of the particle diameter of a fraction to the weighted mean diameter of the solids. The modified model was compared to the SRC model, the Wasp et al. (1977) model and the Kaushal & Tomita (2002B) model using the experimental data of the zinc tailings in a 0.105 m pipe as they used before. The Wasp et al. (1977) model overestimates the experimental data except for low line speeds, close to the LDV. The SCR model overestimates the data slightly except for low line speeds, close to the LDV. The Kaushal & Tomita (2002B) model underestimates the data for low line speeds, close to the LDV, while the Kaushal & Tomita (2002C) model gives a good match over the full range of line speeds.

Kaushal et al. (2002D) make the model applicable for rectangular ducts. The concept of the model is the same as the Kaushal & Tomita (2002C) model, but the equations for the liquid eddy momentum diffusivity and the factor relating the sediment diffusivity to the liquid eddy momentum diffusivity have been adapted to fit rectangular ducts. The model is compared with data collected by Kaushal (1995) and gives a good correlation for the concentration profiles found for different volumetric concentrations and different line speeds. Kaushal et al. (2003A) show more experimental data of experiments in a rectangular duct of 0.2 m width and 0.05 m height. Again a good correlation was found between the experiments and the model developed. Seshadri et al. (2006) also add equations for the liquid eddy momentum diffusivity.

Kaushal & Tomita (2013) improved their model with a more sophisticated factor for the relation between the sediment diffusivity and the liquid eddy momentum diffusivity, including the influence of mean particle diameter d_m to pipe diameter ratio and the influence of the grading of the PSD. This improvement resulted in a better agreement for both narrow and broad graded PSD's.

6.23.2 The Hydraulic Gradient.

The method to determine the hydraulic gradient is based on the assumption that the total hydraulic gradient in 2 phase flow can be split into two parts, the vehicle hydraulic gradient (homogeneously distributed particles) and the excess hydraulic gradient due to bed formation (heterogeneously distributed particles). An iterative method is suggested. In the prediction step the 2 phase flow is assumed to be completely homogeneous. Based on this assumption the hydraulic gradient is computed using the Darcy Weisbach equation:

$$
i_{vehicle} = \lambda_m \cdot \frac{v_{ls}^2}{2 \cdot g \cdot D_p} \quad \text{or} \quad i_{vehicle} = 2 \cdot f_m \cdot \frac{v_{ls}^2}{g \cdot D_p} \quad \text{with:} \quad \lambda_m = 4 \cdot f_m \tag{6.23-4}
$$

Kaushal & Tomita (2002B) use the Fanning friction factor f_m instead of the Darcy Weisbach friction factor λ_m. The Fanning friction factor has been evaluated using the Wood (1966) equation in the Wasp et al. (1977) model:

$$
f_m = \left(a + b \cdot Re_m^{-c} \right)
$$

$$
a = 0.026 \cdot \left(\frac{\varepsilon}{D_p} \right)^{0.225} + 0.133 \cdot \left(\frac{\varepsilon}{D_p} \right), \quad b = 22 \cdot \left(\frac{\varepsilon}{D_p} \right)^{0.44} \quad \text{and} \quad c = 1.62 \cdot \left(\frac{\varepsilon}{D_p} \right)^{0.134} \tag{6.23-5}
$$

The Fanning friction factor has been evaluated using the modified Wood (1966) equation proposed by Mukhtar (1991):

$$
f_m = \left(a + b \cdot Re_m^{-c} \right) \cdot \left(1 - 0.33 \cdot C_{wf} \right) \quad \text{with } C_{wf} \text{: the concentration by weight}
$$

$$
a = 0.026 \cdot \left(\frac{\varepsilon}{D_p} \right)^{0.225} + 0.133 \cdot \left(\frac{\varepsilon}{D_p} \right), \quad b = 22 \cdot \left(\frac{\varepsilon}{D_p} \right)^{0.44} \quad \text{and} \quad c = 1.62 \cdot \left(\frac{\varepsilon}{D_p} \right)^{0.134} \tag{6.23-6}
$$

The apparent viscosity (Thomas (1965)) and density of the liquid have to be adjusted, assuming the concentration in the vehicle equals the total concentration, so $C_{vs,v} = C_{vs}$.

$$\mu_m = \mu_l \cdot \left(1 + 2.5 \cdot C_{vs,v} + 10.05 \cdot C_{vs,v}^2 + 0.00273 \cdot e^{16.6 \cdot C_{vs,v}} \right)$$

(6.23-7)

$$\rho_m = \rho_l \cdot \left(1 + R_{sd} \cdot C_{vs,v} \right)$$

The Reynolds number can now be determined as, using the apparent viscosity of the vehicle:

$$Re_m = \frac{\rho_m \cdot v_{ls} \cdot D_p}{\mu_m}$$

(6.23-8)

In the first iteration step, for each size fraction of **n** fractions, the ratio of the solids in the vehicle to the solids in the bed is taken as equal to the ratio of the volumetric concentration at $0.92 \cdot D_p$ from the bottom of the pipe to the is based on the friction velocity computed in the prediction step. In next iteration steps this is based on the friction velocity computed in the previous iteration step. Kaushal & Tomita (2002B) use their modified Karabelas (1977) model to determine this (which is described later). The vehicle portion of a size friction is now:

$$C_{vs,v,j} = C_{vs,j} \cdot \frac{C_{top,j}}{C_{center,j}} = C_{vs,j} \cdot \frac{C_{vs,j}(0.92)}{C_{vs,j}(0.50)}$$

(6.23-9)

After computing the vehicle portion for each size fraction, the total percentage of solids in the vehicle is calculated. The total volumetric concentration in the vehicle is the sum of the portions of each size fraction, giving:

$$C_{vs,v} = \sum_{j=1}^{n} C_{vs,v,j}$$

(6.23-10)

The vehicle pressure drop is determined with the Darcy Weisbach equation, but with the viscosity and density based on the total volumetric concentration of solids in the vehicle. The hydraulic gradient of the heterogeneous regime of a fraction is:

$$i_{bed} = \sum_{j=1}^{n} i_{bed,j} = \sum_{j=1}^{n} i_l \cdot 82 \cdot \left(C_{vs,j} - C_{vs,v,j} \right) \cdot \left(\frac{g \cdot D_p \cdot R_{sd}}{v_{ls}^2 \cdot \sqrt{C_{D,j}}} \right)^{3/2}$$

(6.23-11)

For a narrow graded sand this can also be determined without summation by:

$$i_{bed} = i_l \cdot 82 \cdot \left(C_{vs} - C_{vs,v} \right) \cdot \left(\frac{g \cdot D_p \cdot R_{sd}}{v_{ls}^2 \cdot \sqrt{C_D}} \right)^{3/2}$$

(6.23-12)

The total hydraulic gradient of the slurry is the sum of the hydraulic gradient of the vehicle and the hydraulic gradient of the bed, giving:

$$i_m = i_{vehicle} + i_{bed}$$

(6.23-13)

volumetric concentration at the pipe axis, the so called Wasp et al. (1977) criterion. In the first iteration step this If the difference in hydraulic gradients between the prediction step and the first iteration or between two successive iteration steps is greater than, for example, 5%, another iteration step is required. This is repeated until the difference is less than the criterion. This iteration scheme is comparable to the original Wasp et al. (1977) iteration scheme.

6.23.3 The Solids Concentration Distribution.

Wasp et al. (1977) used the advection diffusion equation for uniform sands with constant diffusivity and without hindered setting:

$$
\mathbf{v_t \cdot C_{vs}(z) + \varepsilon_s \cdot \frac{\partial C_{vs}(z)}{\partial z} = 0}
$$
(6.23-14)

Resulting in the following equation to determine the ratio $\mathbf{C_{top}/C_{center}}$.

$$
\frac{\mathbf{C_{top}}}{\mathbf{C_{center}}} = \frac{\mathbf{C_{vs}(z = 0.92 \cdot D_p)}}{\mathbf{C_{vs}(z = 0.50 \cdot D_p)}} = 10^{-1.8 \cdot \frac{\mathbf{v_t}}{\boldsymbol{\beta_{sm} \cdot \kappa \cdot u_*}}} = \mathbf{e}^{-1.8 \cdot 2.3 \cdot \frac{\mathbf{v_t}}{\boldsymbol{\beta_{sm} \cdot \kappa \cdot u_*}}} = \mathbf{e}^{-4.14 \cdot \frac{\mathbf{v_t}}{\boldsymbol{\beta_{sm} \cdot \kappa \cdot u_*}}}
$$
(6.23-15)

Karabelas (1977) used an approach for graded solids as described in chapter 5. The Wasp et al. (1977) model has already been described in chapter 6.

Kaushal et al. (2002A) and Kaushal & Tomita (2002B) used the Karabelas (1977) approach for graded sands to determine the concentration distribution of each fraction, this gives for the advection diffusion equation of the $\mathbf{j^{th}}$ fraction:

$$
\mathbf{C_{vs,j}(z) \cdot \left(v_{t,j} - \sum_{i=1}^{n} v_{t,i} \cdot C_{vs,i}(z) \right) + \varepsilon_s \cdot \frac{\partial C_{vs,j}(z)}{\partial z} = 0}
$$
(6.23-16)

With the general solution:

$$
\mathbf{C_{vs,j}(z) = \frac{G_j \cdot e^{-\frac{v_{t,j}}{\zeta \cdot u_*} \cdot \frac{z}{R}}}{1 + \sum_{i=1}^{n} G_i \cdot e^{-\frac{v_{t,i}}{\zeta \cdot u_*} \cdot \frac{z}{R}}}}
$$
(6.23-17)

Assuming that the mean concentration of each fraction $\mathbf{C_{vs,j}}$ is known a priori and the total mean concentration $\mathbf{C_{vs}}$ is known a priori, equation (6.23-17) can be written as:

$$
\mathbf{\frac{C_{vs,j}}{(1 - C_{vs})} = G_j \cdot \frac{1}{A} \cdot \int_A e^{-\frac{v_{t,j}}{\zeta \cdot u_*} \cdot \frac{z}{R}} \cdot dA}
$$
(6.23-18)

Giving for $\mathbf{G_j}$ according to Karabelas (1977):

$$
\mathbf{G_j = \frac{C_{vs,j}}{(1 - C_{vs})} \cdot \frac{1}{\frac{1}{A} \cdot \int_A e^{-\frac{v_{t,j}}{\zeta \cdot u_*} \cdot \frac{z}{R}} \cdot dA} = \frac{C_{vs,j}}{(1 - C_{vs})} \cdot \frac{1}{E_j}}
$$

(6.23-19)

$$
\mathbf{With: \quad E_j = \frac{1}{A} \cdot \int_A e^{-\frac{v_{t,j}}{\zeta \cdot u_*} \cdot \frac{z}{R}} \cdot dA \approx 1 + \frac{\left(\frac{v_{t,j}}{\zeta \cdot u_*} \right)^2}{8} \cdot \left(1 + \frac{\left(\frac{v_{t,j}}{\zeta \cdot u_*} \right)^2}{24} \right)}
$$

The value for the friction velocity, required in both the Wasp and the Karabelas models is:

$$u_* = \sqrt{g \cdot \frac{D_p}{4} \cdot i_m}$$

(6.23-20)

In the first iteration step this is based on the prediction step. In each next iteration step this is based on the previous iteration step.

The relation between the sediment diffusivity and the liquid eddy momentum diffusivity is, according to Mukhtar (1991) and Kaushal (1995):

$$\varepsilon_s = \beta_{sm} \cdot \varepsilon_m$$

(6.23-21)

$$\beta_{sm} = 1 + 0.12504 \cdot e^{4.22054 \cdot \frac{C_{vs}}{C_{vb}}}$$

Kaushal & Tomita (2002C) modified this equation including the ratio of the particle diameter of a fraction to the weighted mean diameter of the solids.

$$\beta_{sm} = 1 + 0.125 \cdot \left(\frac{d_j}{d_m}\right) \cdot e^{4.22054 \cdot \frac{C_{vs}}{C_{vb}}}$$

(6.23-22)

Kaushal & Tomita (2013) improved the equation again, including the influence of the mean particle diameter d_m to pipe diameter ratio and the influence of the grading of the PSD, giving:

$$\beta_{sm} = 1 + 93.77 \cdot \left(\frac{d_m}{D_p}\right) \cdot \left(\frac{d_j}{d_{mw}}\right) \cdot e^{1.055 \cdot \sigma_g \cdot \frac{C_{vs}}{C_{vb}}}$$

(6.23-23)

With : σ_g in range 1.15-4

With: $93.77 \cdot \left(\dfrac{d_m}{D_p}\right)$ in range 0.125-2.5

The factor σ_g for the PSD grading gives a factor 4 for the broadest grading and a factor 1.15 for the narrowest grading.

For the liquid eddy momentum diffusivity they used the equations suggested by Longwell (1977) :

$$\varepsilon_m = \kappa \cdot u_* \cdot R \cdot \frac{z}{R} \cdot \left(1 - \frac{z}{R}\right) \qquad \text{for} \quad 0 \le \frac{z}{D_p} \le 0.337$$

$$\varepsilon_m = 0.22 \cdot \kappa \cdot u_* \cdot R \qquad \text{for} \quad 0.337 \le \frac{z}{D_p} \le 0.663$$

(6.23-24)

$$\varepsilon_m = \kappa \cdot u_* \cdot R \cdot \left(\frac{z}{R} - 1\right) \cdot \left(2 - \frac{z}{R}\right) \qquad \text{for} \quad 0.663 \le \frac{z}{D_p} \le 1.0$$

With : $\kappa = 0.369$

The data from Kaushal et al. (2005) with **d=0.44 mm** and **D_p=0.0549 m** are compared with the DHLLDV Framework. The maximum LDV for this sand and pipe diameter is about 2.5 m/s. The data points are at 3 m/s, so a bit above the LDV depending on the concentration, resulting in smaller concentrations at the bottom of the pipe.
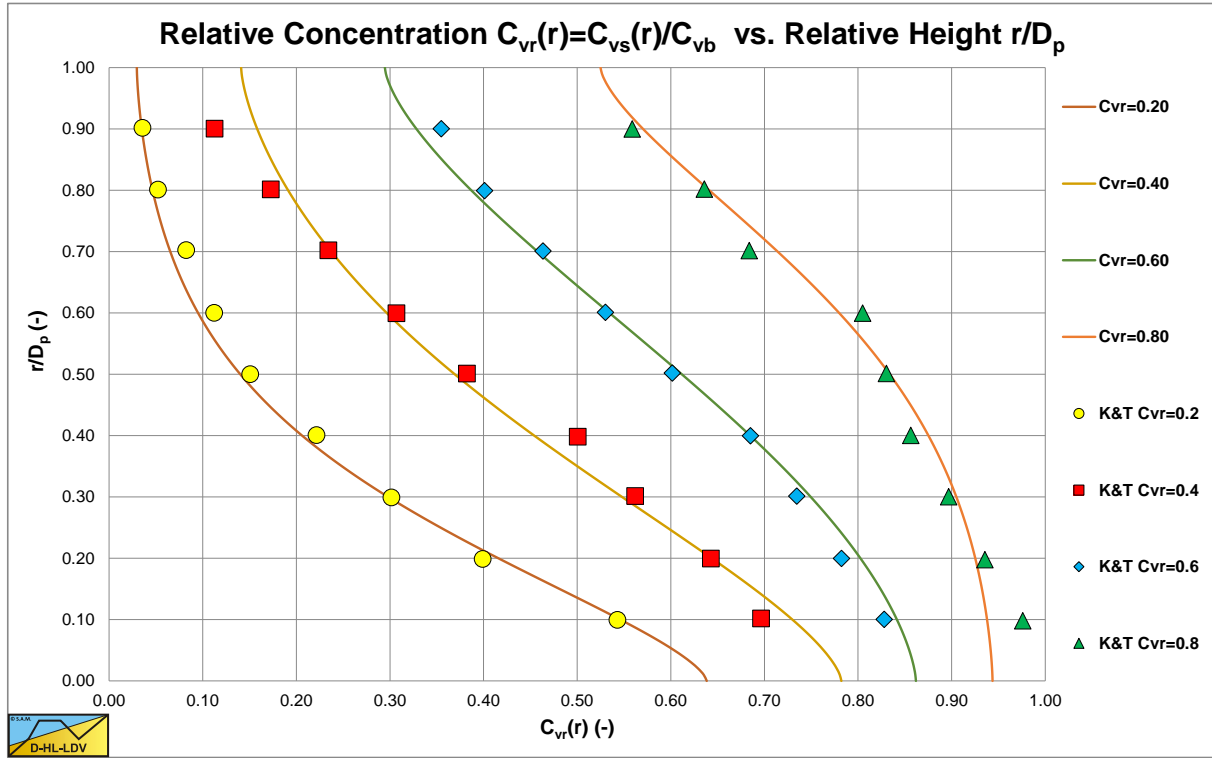
Figure 6.23-1: Data from Kaushal et al. (2005) with local hindered settling.

6.23.3.1 Closed Ducts.

Kaushal et al. (2002D) made the model applicable for a rectangular ducts, giving:

$$\varepsilon_s = \beta_{sm} \cdot \varepsilon_m$$

$$\beta_{sm} = 1 + 0.09322 \cdot e^{5.5423 \cdot \frac{C_{vs}}{C_{vb}}}$$

(6.23-25)

For the liquid eddy momentum diffusivity they used the equations suggested by Brooks & Berggren (1944):

$$\varepsilon_m = \kappa \cdot u_* \cdot H \cdot \frac{z}{H} \cdot \left(1 - \frac{2 \cdot z}{H}\right) \qquad \text{for} \quad 0 \leq \frac{z}{H} \leq 0.337$$

$$\varepsilon_m = 0.11 \cdot \kappa \cdot u_* \cdot H \qquad \text{for} \quad 0.337 \leq \frac{z}{H} \leq 0.663$$

(6.23-26)

$$\varepsilon_m = \kappa \cdot u_* \cdot H \cdot \frac{z}{H} \cdot \left(1 - \frac{2 \cdot z}{H}\right) \qquad \text{for} \quad 0.663 \leq \frac{z}{H} \leq 1.0$$

6.23.3.2 Open Channel Flow.

Seshadri et al. (2006) add equations for the liquid eddy momentum diffusivity for open channel flow:

$$\varepsilon_m = 2.5 \cdot \kappa \cdot u_* \cdot H \cdot \frac{z}{H} \qquad \text{for} \quad 0 \le \frac{z}{H} \le 0.1$$

(6.23-27)

$$\varepsilon_m = 0.25 \cdot \kappa \cdot u_* \cdot H \qquad \text{for} \quad 0.1 \le \frac{z}{H} \le 1.0$$

6.23.4 Discussion & Conclusions.

Up to 2014 the Kaushal & Tomita (2002B) model for the determination of the concentration profile is the most sophisticated model available. The prediction of concentration profiles with experimental data is very good.
However there are some questions about the application of the Wasp et al. (1977) model:

1. The Wasp et al. (1977) criterion for the determination of the suspended load fraction is based on the original Wasp model. Does this criterion still hold if the concentration profile is determined in another way?
2. Kaushal & Tomita (2002B) use the particle drag coefficient C_D in the equation for the heterogeneous regime and not the particle Froude number C_x as used in the original Durand & Condolios (1952) equation. This may give a different result, especially at different solids submerged densities.
3. For very low line speeds, the model behaves like the Durand & Condolios (1952) model, not including sliding bed behavior. The assumption that the Durand & Condolios (1952) model describes bed behavior is incorrect. Durand & Condolios (1952) describe heterogeneous behavior, which is already a combination of bed behavior and suspended flow behavior.
4. For very high line speeds the model behaves like the Darcy Weisbach equation for pure carrier liquid. The model does not have asymptotic behavior towards the ELM model, due to the implementation of the Fanning friction factor.
5. The Hunt equation already takes into account some hindered settling effect because of the upwards liquid velocity. Is it correct to use the full hindered settling equation in the model, or should the power be 1 less?

6.23.5 Nomenclature Kaushal & Tomita Models.

a	Coefficient Fanning friction factor	**-**
b	Coefficient Fanning friction factor	**-**
c	Coefficient Fanning friction factor	**-**
C_{vs}	Spatial volumetric concentration	**-**
$C_{vs,j}$	Spatial volumetric concentration, j^{th} fraction	**-**
$C_{vs,v}$	Spatial volumetric concentration vehicle (homogeneous fraction)	**-**
$C_{vs,v,j}$	Spatial volumetric concentration vehicle (homogeneous fraction), j^{th} fraction	**-**
$C_{vs,Du}$	Spatial volumetric concentration Durand fraction (heterogeneous fraction)	**-**
$C_{vc,Du,j}$	Spatial volumetric concentration Durand fraction (heterogeneous fraction), j^{th} fraction	**-**
C_{top}	Spatial volumetric concentration at 92% of the pipe diameter, from the bottom of the pipe	**-**
$C_{top,j}$	Spatial volumetric concentration at 92% of the pipe diameter, from the bottom of the pipe, j^{th} fraction	**-**
C_{center}	Spatial volumetric concentration at 50% of the pipe diameter, from the bottom of the pipe	**-**
$C_{center,j}$	Spatial volumetric concentration at 50% of the pipe diameter, from the bottom of the pipe, j^{th} fraction	**-**
C_{vb}	Spatial volumetric concentration bed	**-**
C_{vB}	Spatial volumetric concentration bottom of pipe	**-**
C_{vm}	Concentration by weight	**-**
C_D	Particle drag coefficient	**-**
$C_{D,j}$	Particle drag coefficient j^{th} fraction	**-**
C_x	Durand & Condolios reversed particle Froude number squared	**-**
$C_{x,j}$	Durand & Condolios reversed particle Froude number squared j^{th} fraction	**-**
d	Particle diameter	**-**

d_j	Particle diameter j^{th} fraction	**m**
d_m	Mean particle diameter, Kaushal & Tomita	**m**
d_{mw}	Weighed mean particle diameter, Kaushal & Tomita	**m**
D_p	Pipe diameter	**m**
E	Karabelas factor	**-**
E_{rhg}	Relative excess hydraulic gradient	**-**
f_m	Fanning friction factor mixture, Kaushal & Tomita	**-**
g	Gravitational constant 9.81 m/s^2	**m/s^2**
G	Karabelas factor	**-**
i_m	Hydraulic gradient mixture	**-**
i_{bed}	Hydraulic gradient bed, Kaushal & Tomita	**-**
$i_{bed,j}$	Hydraulic gradient bed j^{th} fraction, Kaushal & Tomita	**-**
$i_{vehicle}$, i_{lv}	Hydraulic gradient vehicle	**-**
i_{Du}	Hydraulic gradient heterogeneous transport	**-**
$i_{Du,j}$	Hydraulic gradient heterogeneous transport, contribution j^{th} fraction	**-**
i_{total}	Total hydraulic gradient, homogeneous plus heterogeneous	**-**
j	Fraction number	**-**
ΔL	Length of pipeline	**m**
LDV	Limit Deposit Velocity	**m/s**
n	Number of fractions	**-**
R	Pipe radius	**m**
Re	Reynolds number	**-**
Re_m	Reynolds number	**-**
R_{sd}	Relative submerged density solids in pure liquid	**-**
u_*	Friction velocity	**m/s**
v_{ls}	Line speed	**m/s**
v_t	Terminal settling velocity in pure liquid	**m/s**
$v_{t,j}$	Terminal settling velocity in pure liquid of the jth fraction	
v_{tv}	Terminal settling velocity in the vehicle	**m/s**
$v_{tv,j}$	Terminal settling velocity in the vehicle of the jth fraction	**m/s**
z	Vertical coordinate in pipe	**m**
β_{sm}, ζ	Relation sediment diffusivity – eddy momentum diffusivity	**-**
ε	Pipe wall roughness	**m**
ε_s	Sediment diffusivity	**m/s**
ε_m	Eddy momentum diffusivity	**m/s**
κ	Von Karman constant, about 0.4	**-**
λ_l	Darcy Weisbach friction factor based on liquid properties	**-**
λ_m	Darcy Weisbach friction factor mixture, Kaushal & Tomita	**-**
ρ_l	Density liquid	**ton/m^3**
ρ_s	Density solids	**ton/m^3**
ρ_m	Density mixture	**ton/m^3**
ρ_v	Density vehicle	**ton/m^3**
σ_g	PSD grading coefficient, Kaushal & Tomita	**-**
ν_l	Kinematic viscosity pure liquid	**m^2/s**

6.24 The Matousek (2010), (2011) Model.

6.24.1 Introduction.

The previous model, Wilson-GIW (1979) and Doron et al. (1987), are both based on spatial volumetric concentrations. The original Wilson-GIW (1979) 2 layer model assumes all solids transport takes place in the sliding bed. The Doron et al. (1987) 2 and 3 layer models assume a stationary or sliding bed with a certain concentration and velocity distribution above the bed. So here the solids transport takes place above the bed and if the bed is sliding, also in the bed. Given a certain spatial volumetric concentration, one of the outputs is the delivered volumetric concentration. To find a certain delivered concentration (this is often the operational input), one has to iterate the spatial volumetric concentration until the required delivered concentration is found.

Matousek (2009), (2011) and Matousek & Krupicka (2010), (2011) developed a model where the delivered concentration is an input and the spatial concentration the output. This is achieved by using an erosion equation, relating the erosion rate to the bed shear stress, the so called Meyer-Peter Muller (1948) equation (MPM).

The first version of the model was proposed for settling-slurry flow above stationary deposit (Matousek (2009) and Matousek (2011)). It split the discharge area to the zone associated with a pipe wall and the zone associated with the top of the bed. The challenge was to evaluate bed friction and bed transport correctly in the slurry flow with a transport layer. A semi-empirical formula was suggested for k_s/d (or λ_{12}) and its shape has developed in time as our experience progressed with the flow behavior (experiments) and with the model computational stability. The last suggested version of k_s/d is in Matousek & Krupicka (2014). The solids flow rate and the delivered concentration were determined using a transport formula. The formula was derived theoretically for assumed shapes of a concentration profile (linear) and a velocity profile (power law) across the transport layer (Matousek (2011)). Indeed, the resulting formula gains the form of the MPM equation, but its coefficients differ from the original empirical MPM, they are not constants. The equations for the coefficients were semi-empirically extended (Matousek (2011)) to be applicable also for transport of combined load (not only contact load, i.e. bed load).

In the next step, the model was extended to work not only in the stationary-bed regime but also in the sliding-bed regime (Hydrotransport HT16, 2010). So, contrary to a traditional two-layer model, our model works in both regimes. The model described in this chapter is the HT16-version (2010). In 2011, the model is further modified by generalizing a determination of the bed force F_{sf} using the K-approach and by adding the transport-layer stress contribution to the bed force (Matousek & Krupicka (2011)).

Figure 6.20-1 shows the two layers and the variables used. Many of the geometrical and other equations are similar or equal to the equations discussed with Wilson-GIW (1979) and Doron et al. (1987), but they are repeated here in order to have a self-containing chapter. The model is explained in 14 steps. The inputs of the model are the particle diameter d_{50}, the liquid density ρ_l, the relative submerged density R_{sd}, the liquid viscosity ν_l, the pipe diameter D_p, the roughness of the pipe wall ε, the sliding friction coefficient μ_{sf}, the line speed v_{ls}, the terminal settling velocity v_t, the bed concentration C_{vb} and the delivered volumetric concentration C_{vt}.

The model in fact assumes 3 layers. The bed layer or lower layer and the upper layer above the bed. The upper layer is divided into 2 parts. A bed associated area on top of the bed and a pipe wall associated area, close to the pipe wall.

Starting with some continuity equations, a bed height and a bed velocity, the Shields parameter is determined based on the Meyer-Peter Muller (1948) (MPM) equation, assuming the solids delivered are the result of a sliding bed and an erosion rate above the bed. This should be equal to the solids delivered based on the delivered volumetric concentration times the flow rate. Once the Shields parameter is known, the bed shear stress and the friction velocity can be determined. Based on the friction velocity and an empirical relation for the equivalent bed roughness, the Darcy Weisbach bed friction factor and bed associated radius are determined. The pipe wall associated radius follows from the bed associated radius. Now that all required parameters are known, the hydraulic gradients of the bed associated area and of the pipe wall associated area can be determined. These should be equal, since there can only be one hydraulic gradient. If the difference is significant, the bed height has to be adjusted and the calculation has to be repeated. If the difference is negligible, the equilibrium of forces on the bed is examined. If the driving force is smaller than the maximum resisting force, there is a stationary bed with a bed velocity zero. If the driving force is significantly larger than the resisting force, the bed velocity has to be increased and the calculation has to be repeated until there is an equilibrium. Finally the spatial volumetric concentration and the slip ratio can be determined.

6.24.2 Analytical solution of the solids transport formula for shear-layer flow.

It is assumed that particles are transported exclusively within the shear layer. There is a linear concentration distribution across the shear layer. There is a power law velocity distribution in the shear layer. The velocity at the top of the shear layer is a constant factor times the friction velocity. There is a linear relationship between the bed shear stress and the thickness of the shear layer. In this book the shear layer is often referred to as sheet flow.

A general equation for the solids flow rate in the shear layer with thickness H is:

$$q_s = \int_0^H C_{vs}(y) \cdot u_s(y) \cdot dy \tag{6.24-1}$$

With y the vertical coordinate in the shear layer and u_s the local velocity in the shear layer. For the local concentration in the shear layer a linear distribution is assumed according to:

$$C_{vs}(y) = C_{vb} \cdot \frac{H-y}{H} \tag{6.24-2}$$

So at the bottom of the shear layer ($y=0$) the spatial concentration equals the bed concentration and at the top of the shear layer ($y=H$) the spatial concentration equals zero. For the velocity in the shear layer a power law function is assumed, giving:

$$u_s(y) = u_{sH} \cdot \left(\frac{y}{H}\right)^n \tag{6.24-3}$$

So at the bottom of the shear layer the velocity is zero and at the top of the shear layer the velocity has a maximum u_{sh}. The solids flow rate can now be determined with:

$$q_s = \frac{C_{vb} \cdot u_{sH}}{H^{n+1}} \cdot \int_0^H (H-y) \cdot y^n \cdot dy = \frac{C_{vb} \cdot u_{sH}}{H^{n+1}} \cdot \int_0^H H \cdot y^n - y^{n+1} \cdot dy \tag{6.24-4}$$

Integrating this over the height of the shear layer H gives:

$$q_s = \frac{C_{vb} \cdot u_{sH}}{H^{n+1}} \cdot \int_0^H \left(H \cdot y^n - y^{n+1}\right) \cdot dy = \frac{C_{vb} \cdot u_{sH}}{H^{n+1}} \cdot \left(\frac{H \cdot y^{n+1}}{n+1} - \frac{y^{n+2}}{n+2}\right)_0^H$$

$$\tag{6.24-5}$$

$$= \frac{C_{vb} \cdot u_{sH}}{H^{n+1}} \cdot \frac{H^{n+2}}{(n+1) \cdot (n+2)} = \frac{C_{vb} \cdot u_{sH} \cdot H}{(n+1) \cdot (n+2)}$$

Now assuming that the velocity at the top of the shear layer equals the friction velocity at the bed times a constant, gives:

$$u_{sH} = \gamma \cdot u_{*b} \tag{6.24-6}$$

And:

$$q_s = \frac{C_{vb} \cdot u_{sH} \cdot H}{(n+1) \cdot (n+2)} = \frac{C_{vb} \cdot \gamma \cdot u_{*b} \cdot H}{(n+1) \cdot (n+2)} \tag{6.24-7}$$

It should be mentioned here that this solids flow has the dimension m²/s and not m/s. So multiplied by the width of the bed this gives a volume flow of m³/s.

The Shields parameter by definition is:

$$\theta = \frac{u_{*b}^2}{R_{sd} \cdot g \cdot d} \tag{6.24-8}$$

The shear stress at the top of the shear layer has to be equal to the submerged weight of the shear layer times the iinternal friction coefficient:

$$\rho_l \cdot u_{*b}^2 = H \cdot \frac{C_{vb}}{2} \cdot \rho_l \cdot R_{sd} \cdot g \cdot \tan(\varphi) \tag{6.24-9}$$

This can be written as:

$$H = \frac{2 \cdot u_{*b}^2}{C_{vb} \cdot R_{sd} \cdot g \cdot \tan(\varphi)} = \frac{2 \cdot u_{*b}^2 \cdot d}{C_{vb} \cdot R_{sd} \cdot g \cdot d \cdot \tan(\varphi)} = \frac{2 \cdot \theta \cdot d}{C_{vb} \cdot \tan(\varphi)} \tag{6.24-10}$$

For the solids flow this gives:

$$q_s = \frac{\gamma \cdot u_{*b}}{(n+1) \cdot (n+2)} \cdot \frac{2 \cdot \theta \cdot d}{\tan(\varphi)} = \frac{2 \cdot \gamma}{(n+1) \cdot (n+2) \cdot \tan(\varphi)} \cdot \sqrt{R_{sd} \cdot g \cdot d} \cdot d \cdot \theta^{1.5} \tag{6.24-11}$$

The total solids flow over a bed width O_{12} is:

$$Q_s = q_s \cdot O_{12} = \frac{\gamma \cdot u_{*b}}{(n+1) \cdot (n+2)} \cdot \frac{2 \cdot \theta \cdot d}{\tan(\varphi)} = \frac{2 \cdot \gamma}{(n+1) \cdot (n+2) \cdot \tan(\varphi)} \cdot \sqrt{R_{sd} \cdot g \cdot d} \cdot d \cdot \theta^{1.5} \cdot O_{12} \tag{6.24-12}$$

In a non-dimensional form this can be written as:

$$\Phi = \frac{Q_s}{O_{12} \cdot d \cdot \sqrt{R_{sd} \cdot g \cdot d}} = \frac{2 \cdot \gamma}{(n+1) \cdot (n+2) \cdot \tan(\varphi)} \cdot \theta^{1.5} \tag{6.24-13}$$

This is similar to the Meyer-Peter Muller (1948) (MPM) equation. For high flow velocities giving a large Shields parameter the equations are almost identical.

Before starting the algorithm some parameters have to be determined or defined, that are constant during the iteration process:

The particle Reynolds number Re_p:

$$Re_p = \frac{v_t \cdot d_{50}}{\nu_l} \tag{6.24-14}$$

The internal friction coefficient based on the internal friction angle φ of the bed:

$$\tan(\varphi) = 0.577 \text{ (30° internal friction angle for sands)} \tag{6.24-15}$$

The power of the velocity distribution in the sheet flow layer n:

$$n = 1 \tag{6.24-16}$$

The coefficient of the velocity at the top of the sheet flow layer γ according to Pugh & Wilson (1999):

$$\gamma = 9.4 \tag{6.24-17}$$

The Meyer-Peter Muller (1948) (MPM) equation, based on a stationary bed:

$$\frac{Q_s}{O_{12} \cdot \sqrt{R_{sd} \cdot g \cdot d_{50}^3}} = \alpha \cdot \left(\theta - \theta_{cr}\right)^\beta$$

(6.24-18)

The two coefficients **α** and **β** of the MPM equation can now be determined according to:

$$\alpha = \frac{2 \cdot \gamma}{(n+1) \cdot (n+2) \cdot \tan(\varphi)} + \frac{58}{Re_p^{0.62}}$$

(6.24-19)

$$\beta = 1.2 + \frac{1.3}{Re_p^{0.39}}$$

The critical Shields parameter **θ$_{cr}$** can be determined using a suitable Shields diagram or equation as is discussed in Chapter 5.

6.24.3 The Iteration Process.

Step I: The bed velocity.

The choice of the bed velocity **v$_2$** in between zero and the line speed **v$_{ls}$**.
One can start with for example **v$_2$=0 m/sec**.

Step II: The bed height.

The choice of the bed height **y$_b$** in between zero and the pipe diameter **D$_p$**.
One can start with for example **y$_b$=0.05·D$_p$**.

Step III: Geometry of the discharge area.

The bed angle **β** can be expressed in the bed height **y$_b$** by:

$$\beta = a\cos\left(1 - \left(2 \cdot \frac{y_b}{D_p}\right)\right)$$

(6.24-20)

The bed height **y$_b$** can be expressed in the bed angle **β** by:

$$y_b = \frac{D_p}{2} \cdot \left(1 - \cos(\beta)\right)$$

(6.24-21)

The cross section of the pipe **A$_p$** is:

$$A_p = \frac{\pi}{4} \cdot D_p^2$$

(6.24-22)

The cross section of the bed **A$_2$** is now:

$$A_2 = A_p \cdot \frac{\left(\beta - \sin(\beta) \cdot \cos(\beta)\right)}{\pi}$$

(6.24-23)

The cross section of the restricted area above the bed **A$_1$** is:

$$A_1 = A_p - A_2$$

(6.24-24)

The length of the contact area between the upper layer (1) and the pipe wall **O$_1$** is:

$$O_1 = D_p \cdot (\pi - \beta) \tag{6.24-25}$$

The length of the contact area between the bed (2) and the pipe wall O_2 is:

$$O_2 = D_p \cdot \beta \tag{6.24-26}$$

The length of the interface bed-upper layer (12) O_{12} is:

$$O_{12} = D_p \cdot \sin(\beta) \tag{6.24-27}$$

The hydraulic radius associated with the upper layer R_{h1} is:

$$R_{h1} = \frac{A_1}{O_1 + O_{12}} \tag{6.24-28}$$

Step IV: The velocity in the upper layer.

The velocity in the upper layer above the bed v_1 is:

$$v_1 = \left(\frac{v_{ls} \cdot A_p - v_2 \cdot A_2}{A_1} \right) \tag{6.24-29}$$

Step V: The relative average velocity difference between the upper layer and the bed layer.

The relative average velocity difference between the upper layer and the bed layer v_{12} is:

$$v_{12} = v_1 - v_2 \tag{6.24-30}$$

Step VI: Solids flow rates.

The total solids flow rate, the delivered solids flow rate Q_s is:

$$Q_s = v_{ls} \cdot A_p \cdot C_{vt} \tag{6.24-31}$$

The flow of solids in the upper layer Q_{s1} is:

$$Q_{s1} = v_1 \cdot A_1 \cdot C_{vt,1} \tag{6.24-32}$$

The flow of solids in the bed Q_{s2} is:

$$Q_{s2} = v_2 \cdot A_2 \cdot C_{vb} \tag{6.24-33}$$

The mass continuity equation for the particle transport is:

$$v_{ls} \cdot A_p \cdot C_{vt} = v_1 \cdot A_1 \cdot C_{vt,1} + v_2 \cdot A_2 \cdot C_{vb}$$

$$\tag{6.24-34}$$

$$Q_{s1} = Q_s - Q_{s2} = v_{ls} \cdot A_p \cdot C_{vt} - v_2 \cdot A_2 \cdot C_{vb}$$

Intermezzo 1:

The Shields parameter:

$$\theta = \frac{\tau_{12}}{\rho_l \cdot R_{sd} \cdot g \cdot d_{50}}$$

(6.24-35)

The Meyer-Peter Muller (1948) (MPM) equation, based on a stationary bed:

$$\frac{Q_s}{O_{12} \cdot \sqrt{R_{sd} \cdot g \cdot d_{50}^3}} = \alpha \cdot \left(\theta - \theta_{cr}\right)^{\beta}$$

(6.24-36)

Step VII: Shear stress parameters.

The Shields parameter θ can be determined by the inverse MPM equation:

$$\theta = \left(\frac{Q_s \cdot \dfrac{v_{12}}{v_1}}{\alpha \cdot O_{12} \cdot \sqrt{R_{sd} \cdot g \cdot d_{50}^3}}\right)^{1/\beta} + \theta_{cr}$$

(6.24-37)

The correction of v_{12}/v_1 is applied because the MPM equation gives the erosion rate based on a stationary bed and here is applied for a possible sliding bed. This correction is mathematically not 100% correct, but is a good approach.

The bed shear stress τ_{12} can now be determined by:

$$\tau_{12} = \theta \cdot \rho_l \cdot R_{sd} \cdot g \cdot d_{50}$$

(6.24-38)

The friction velocity u_* is now:

$$u_* = \sqrt{\frac{\tau_{12}}{\rho_l}}$$

(6.24-39)
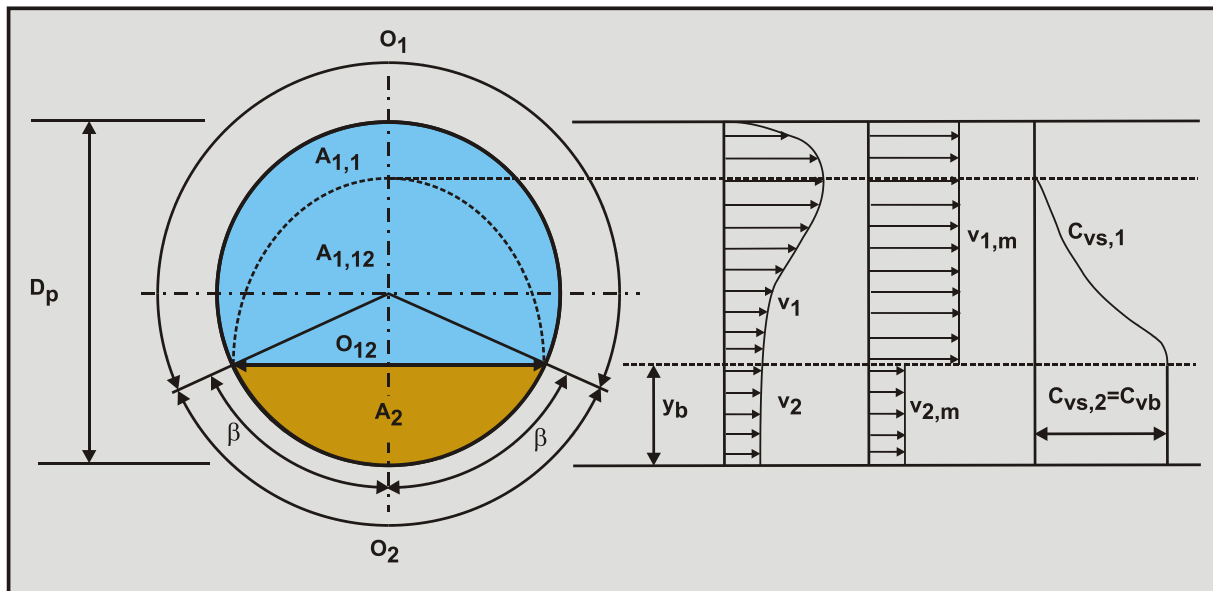
Figure 6.24-1: The bed and wall associated areas.

Intermezzo 2:

The upper layer A_1 can be divided in two parts. A part associated with the pipe wall $A_{1,1}$ and a part associated with the bed interface $A_{1,12}$, see Figure 6.24-1, so.

$$A_1 = A_{1,1} + A_{1,12} \tag{6.24-40}$$

The hydraulic radius associated with the wall $R_{h1,1}$ is now:

$$R_{h1,1} = \frac{A_{1,1}}{O_1} \quad \Rightarrow \quad R_{h1,1} \cdot O_1 = A_{1,1} \tag{6.24-41}$$

The hydraulic radius associated with the bed $R_{h1,12}$ is now:

$$R_{h1,12} = \frac{A_{1,12}}{O_{12}} \quad \Rightarrow \quad R_{h1,12} \cdot O_{12} = A_{1,12} \tag{6.24-42}$$

This gives in terms of the hydraulic gradient i_m:

$$i_m = \lambda_1 \cdot \frac{1}{2 \cdot g \cdot \left(4 \cdot R_{h1,1}\right)} \cdot v_1^2 = \lambda_{12} \cdot \frac{1}{2 \cdot g \cdot \left(4 \cdot R_{h1,12}\right)} \cdot v_{12}^2 \tag{6.24-43}$$

Giving also:

$$\frac{R_{h1,1}}{R_{h1,12}} = \frac{\lambda_1 \cdot v_1^2}{\lambda_{12} \cdot v_{12}^2} \tag{6.24-44}$$

The wall Darcy Weisbach friction factor λ_1 can be determined with any suitable equation, like:

$$\lambda_1 = \frac{1.325}{\left(\ln\left(\frac{\varepsilon}{3.7 \cdot 4 \cdot R_{h1,1}} + \frac{5.75}{Re_1^{0.9}} \right) \right)^2} \tag{6.24-45}$$

The bed Darcy Weisbach friction factor λ_{12} can be determined by:

$$\sqrt{\frac{8}{\lambda_{12}}} = 2.5 \cdot \ln\left(\frac{14.8 \cdot R_{h1,12}}{k_s} \right) \tag{6.24-46}$$

Step VIII: The bed Darcy Weisbach friction factor.

The Darcy Weisbach friction coefficient of the bed interface λ_{12} can now be determined from the friction velocity and the relative velocity between the upper and lower layer:

$$\lambda_{12} = \frac{8 \cdot u_*^2}{v_{12}^2} \tag{6.24-47}$$

Step IX: The hydraulic gradient resulting from the bed friction.

The equivalent bed roughness $\mathbf{k_s}$ can be determined with a number of equations:

$$\frac{k_s}{d_{50}} = 1.35 \cdot \left(\left(\frac{R_{sd}^2}{g \cdot \nu_l}\right)^{1/3} \cdot v_t\right)^{0.5} \cdot \theta^{1.58} \tag{6.24-48}$$

The so called bed associated radius $\mathbf{R_{h1,12}}$ now follows from:

$$R_{h1,12} = \frac{k_s}{B} \cdot e^{\kappa \cdot \sqrt{\frac{8}{\lambda_{12}}}} \tag{6.24-49}$$

With : $\kappa = 0.4$ and $B = 14.8$

The hydraulic gradient resulting from the bed friction $\mathbf{i_{m,12}}$ is now:

$$i_{m,12} = \frac{\lambda_{12}}{R_{h1,12}} \cdot \frac{v_{12}^2}{8 \cdot g} \tag{6.24-50}$$

Step X: The hydraulic gradient resulting from pipe wall friction.

The wall associated radius $\mathbf{R_{h1,1}}$ can be determined once the bed associated radius $\mathbf{R_{h1,12}}$ is known:

$$R_{h1,1} = \frac{A_1 - R_{h1,12} \cdot O_{12}}{O_1} \tag{6.24-51}$$

The Reynolds number associated with the pipe wall is:

$$Re_1 = \frac{v_1 \cdot 4 \cdot R_{h1,1}}{\nu_l} \tag{6.24-52}$$

The hydraulic gradient associated with the pipe wall $\mathbf{i_{m,1}}$ can now be determined with:

$$i_{m,1} = \frac{\lambda_1}{R_{h1,1}} \cdot \frac{v_1^2}{8 \cdot g} \tag{6.24-53}$$

Step XI: Check the hydraulic gradients.

Both hydraulic gradients should be equal within a certain accuracy, so:

$$\left|\frac{i_{m,1} - i_{m,12}}{i_{m,1}}\right| < \text{accuracy} \quad \text{or} \quad \left|\frac{i_{m,1} - i_{m,12}}{i_{m,12}}\right| < \text{accuracy} \tag{6.24-54}$$

If this is not the case, the bed height y_b has to be adjusted and the iteration has to be repeated from **Step II**. If the two hydraulic gradients are equal within a certain accuracy, the hydraulic gradient $\mathbf{i_m}$ equals:

$$i_m = \frac{i_{m,1} + i_{m,12}}{2} \tag{6.24-55}$$

Step XII: Determine the driving and resisting forces on the bed.

The driving force on the bed $\mathbf{F_{dr}}$ with a pipe length $\mathbf{\Delta L}$ equals the pressure gradient on the bed plus the shear stress at the interface times the surface of the bed:

$$\mathbf{F_{dr}} = \Delta p \cdot A_2 + \tau_{12} \cdot O_{12} \cdot \Delta L = i_m \cdot \rho_l \cdot g \cdot \Delta L \cdot A_2 + \tau_{12} \cdot O_{12} \cdot \Delta L \qquad (6.24\text{-}56)$$

The resisting force on the bed $\mathbf{F_{sf}}$ equals the normal force between bed and pipe surface times a sliding friction coefficient, Matousek & Krupicka (2010):

$$\mathbf{F_{sf}} = \mu_{sf} \cdot \rho_l \cdot R_{sd} \cdot g \cdot C_{vb} \cdot A_p \cdot \frac{2 \cdot \left(\sin(\beta) - \beta \cdot \cos(\beta) \right)}{\pi} \cdot \Delta L \qquad (6.24\text{-}57)$$

Later they added the normal force due to the weight of the sheet flow layer, Matousek & Krupicka (2011).

$$\mathbf{F_{sf}} = \mu_{sf} \cdot \rho_l \cdot R_{sd} \cdot g \cdot C_{vb} \cdot A_p \cdot \frac{2}{\pi} \cdot \left(\begin{array}{c} \dfrac{K-1}{3} \cdot \sin^3(\beta) + \sin(\beta) - \dfrac{K+1}{2} \beta \cdot \cos(\beta) \\[2mm] + \dfrac{K-1}{2} \cdot \cos^2(\beta) \cdot \sin(\beta) \end{array} \right) \cdot \Delta L \qquad (6.24\text{-}58)$$

$$+ \frac{\tau_{12} \cdot D_p}{\tan(\varphi)} \cdot \left(\frac{K+1}{2} \cdot \beta - \frac{K-1}{2} \cdot \cos(\beta) \cdot \sin(\beta) \right) \cdot \Delta L$$

With $\mathbf{K=1}$ this gives:

$$\mathbf{F_{sf}} = \mu_{sf} \cdot \rho_l \cdot R_{sd} \cdot g \cdot C_{vb} \cdot A_p \cdot \frac{2 \cdot \left(\sin(\beta) - \beta \cdot \cos(\beta) \right)}{\pi} \cdot \Delta L + \frac{\tau_{12} \cdot D_p \cdot \beta}{\tan(\varphi)} \cdot \Delta L \qquad (6.24\text{-}59)$$

This resisting sliding friction force is based on the hydrostatic normal stress approach of Wilson et al. (1992), which is questioned by Miedema & Ramsdell (2014). They suggest the bed submerged weight approach giving:

$$\mathbf{F_{sf}} = \mu_{sf} \cdot \rho_l \cdot R_{sd} \cdot g \cdot C_{vb} \cdot A_2 = \mu_{sf} \cdot \rho_l \cdot R_{sd} \cdot g \cdot C_{vb} \cdot A_p \cdot \frac{\left(\beta' - \sin(\beta') \cdot \cos(\beta') \right)}{\pi}$$

Now there is a difference in approach between the two methods. Matousek & Krupicka (2010) exclude the sheet flow layer in their calculation of the bed angle $\mathbf{\beta}$, while Miedema & Ramsdell (2014) include the sheet flow layer. This means that the Miedema & Ramsdell (2014) equation gives the weight of all solids in the pipe, while the Matousek & Krupicka (2011) equation adds the contribution of the weight of the sheet flow layer separately, which follows from the bed shear stress and is an essential part of the Matousek & Krupicka (2010) model. The normal stress exerted by the sheet flow layer on the bed has to be corrected for the hydrostatic normal stress approach.

This gives a modified equation according to:

$$\mathbf{F_{sf}} = \mu_{sf} \cdot \left(\rho_l \cdot R_{sd} \cdot g \cdot C_{vb} \cdot A_p + \frac{\tau_{12} \cdot O_{12}}{\tan(\varphi)} \cdot \frac{\pi}{\left(\beta - \sin(\beta) \cdot \cos(\beta) \right)} \right) \cdot \frac{2 \cdot \left(\sin(\beta) - \beta \cdot \cos(\beta) \right)}{\pi} \cdot \Delta L \qquad (6.24\text{-}60)$$

Step XIII: Check the force balance on bed.

In the case of a stationary bed, the resisting force on the bed is bigger than the driving force and the velocity of the bed is zero, a reason to start the iteration with a bed velocity $\mathbf{v_2}$ of zero. If the driving force however is bigger than the resisting force, the bed velocity $\mathbf{v_2}$ should be increased and the iteration should be repeated from step 1 until there is a force equilibrium.

Step XIV: Spatial concentration and slip ratio.

Above the bed a sheet flow layer is assumed with an average concentration of 50% of the bed concentration. The height of this sheet flow layer follows from the shear stress and the weight of the sheet flow layer giving:

$$H = \frac{2 \cdot \tau_{12}}{\rho_l \cdot R_{sd} \cdot g \cdot C_{vb} \cdot \tan(\varphi)} \tag{6.24-61}$$

With the definition of the Shields parameter this can be rewritten to:

$$H = \frac{2 \cdot \theta \cdot d_{50}}{C_{vb} \cdot \tan(\varphi)} \tag{6.24-62}$$

The cross section of the sheet flow layer reduced to the bed concentration is:

$$A_{12,sf} = \frac{H}{2} \cdot O_{12} = \frac{\theta \cdot d_{50}}{C_{vb} \cdot \tan(\varphi)} \cdot O_{12} \tag{6.24-63}$$

The total cross section containing solids with the bed concentration is now, only counting the solids, not the pores:

$$A_s = \left(A_2 + A_{12,sf}\right) \cdot C_{vb} = \left(A_p \cdot \frac{\left(\beta - \sin(\beta) \cdot \cos(\beta)\right)}{\pi} + \frac{\theta \cdot d_{50}}{C_{vb} \cdot \tan(\varphi)} \cdot O_{12}\right) \cdot C_{vb} \tag{6.24-64}$$

This gives a spatial volumetric concentration of:

$$C_{vs} = \frac{A_s}{A_p} = \frac{\left(\beta - \sin(\beta) \cdot \cos(\beta)\right)}{\pi} \cdot C_{vb} + \frac{\theta \cdot d_{50}}{A_p \cdot \tan(\varphi)} \cdot O_{12} \tag{6.24-65}$$

The slip ratio is defined in this book as the ratio of the slip velocity to the line speed $\xi = v_{sl}/v_{ls}$, with:

$$C_{vt} = \left(1 - \frac{v_{sl}}{v_{ls}}\right) \cdot C_{vs} \tag{6.24-66}$$

The slip ratio equals:

$$\xi = \frac{v_{sl}}{v_{ls}} = 1 - \frac{C_{vt}}{C_{vs}} \tag{6.24-67}$$

Matousek & Krupicka (2010) use another formulation for the determination of the spatial volumetric concentration:

$$C_{vs} = \frac{C_{vb} \cdot A_2 + C_{vt,1} \cdot A_1}{A_p} \tag{6.24-68}$$

This formulation is correct in case of a stationary bed, assuming there is hardly slip in the upper layer, so the delivered concentration and the spatial concentration are almost equal. However with a sliding bed or with significant slip in the upper layer, this approach is not very accurate and the concentration in the upper layer does not have to be equal to the initial delivered concentration.

6.24.4 The Concentration Distribution, Including a Sliding Bed.

Matousek & Krupicka (2014) and Matousek et al. (2014) developed the 1-D SDM, 1-Dimensional Stress Distribution based Model, in order to determine the concentration distribution of pipe flow with the possibility of a stationary or sliding bed. The algorithm of this method can be found in these publications.

6.24.4.1 Considerations.

There are three mechanisms that can support particles in a flowing slurry. The first one is the interaction of particles with turbulent eddies of the carrier liquid. The second one is the interaction of particles with other particles sporadic by collisions and the third one permanently in a bed. Particles that do not contribute to the bed, can be dispersed either by diffusive action of turbulent eddies or by particle-particle collisions. The different mechanisms produce different shapes of concentration profiles. It is however very well possible that the mechanisms occur at the same time in a flow, each mechanism supporting a certain fraction of the particles.

Recently attempts have been made to use CFD to model heterogeneous slurry flows in pipes. The advantage is more insight in the internal structure of the flow, the disadvantage is that each simulation is like an experiment, so to find general trends many simulations have to be carried out. Practice still requires engineering models. Reason to develop a one dimensional model predicting the concentration along the vertical axis of a flow cross section, assuming a constant concentration in the transverse direction.

Typical one dimensional models are the open channel models based on turbulent diffusion of the Schmidt-Rouse type. In a general form and a stationary situation, the upwards flow of particles due to diffusion equals the downwards flow due to gravity (hindered settling);

$$q_{s,up}(z) = q_{s,down}(z) \quad \Rightarrow \quad -\varepsilon_s \cdot \frac{dC_{vs}(z)}{dz} = C_{vs}(z) \cdot v_t \cdot \left(1 - C_{vs}(z)\right)^{\beta}$$

$$(6.24\text{-}69)$$

$$C_{vs}(z) \cdot v_t \cdot \left(1 - C_{vs}(z)\right)^{\beta} + \varepsilon_s \cdot \frac{dC_{vs}(z)}{dz} = 0$$

When the power $\beta=1$ the Hunt (1954) equation is found. Some model modifications introduce the effect of a broad PSD of a transported solid fraction (Karabelas (1977)). A key parameter of the turbulent diffusion model is the particle diffusion coefficient ε_s. This is modelled in different ways in different implementations of the model. Kaushal & Tomita (2013) improved their equation, including the influence of the mean particle diameter d_m to pipe diameter ratio, giving for narrow graded sands:

$$\beta_{sm} = 1 + 93.77 \cdot \left(\frac{d_m}{D_p}\right) \cdot e^{1.055 \cdot \sigma_g \cdot \frac{C_{vs}}{C_{vb}}}$$

$$(6.24\text{-}70)$$

$$\text{With :} \quad \sigma_g \text{ in range 1.15-4} \quad \text{and} \quad 93.77 \cdot \left(\frac{d_m}{D_p}\right) \quad \text{in range 0.125-2.5}$$

They stated that their model is appropriate to different flow patterns, including stationary and sliding beds. The question arises however whether coarser grains encounter more intense turbulent support in partially stratified flow. The question also arises whether higher concentrations lead to stronger turbulent support (partially stratified flow). One could ask the question whether the turbulent diffusion equation is valid in partially stratified flow in the first place. Kaushal & Tomita (2013) use the Hunt equation and the Karabelas methodology. To implement the effect of concentration on the terminal settling velocity they use the local concentration to determine the local terminal hindered settling velocity in the solution of the Karabelas method. The Hunt equation however already contains the influence of the upwards liquid flow, because there is a downwards particle flow. Using the hindered settling in the solution of the Karabelas method sort of doubles the effect of hindered settling. At least a factor 1 should be deducted from the hindered settling power to take into account the effect of the upwards liquid velocity as already present in the Hunt equation. The Kaushal & Tomita (2013) models are not capable to simulate the measured sharp change in the concentration gradient at the top of a sliding bed.

Gillies & Shook (1994) modified the general turbulent diffusion equation to make it more suitable for stratified flows. The presence of contact load is represented by the coefficient **κ**:

$$-\varepsilon_s \cdot \frac{dC_{vs}(z)}{dz} = \sqrt{1-\kappa(z)} \cdot C_{vs}(z) \cdot v_t \cdot \left(1-C_{vs}(z)\right)^{\beta} \tag{6.24-71}$$

This coefficient is defined as the ratio of the contact support force to the submerged weight of the particle. If this coefficient equals 1, all particles contribute to contact load, resulting in a bed. If the coefficient equals zero., all particles contribute to suspended load and the model becomes the normal turbulent diffusion model. A value of this coefficient is not proposed however. If the coefficient is z-dependent, like in the above equation, then it could serve as a free empirical parameter taking care of a perfect match between predicted and measured local concentration values, but only if the concentration profile is already known.

Recent analysis of Matousek & Krupicka (2014) and Matousek et al. (2014) has shown that the use of turbulent diffusion models with high values of the particle diffusivity do not seem to be appropriate for stratified flows with concentration gradients of almost zero. Stratified flows with a transport layer (shear layer or sheet flow) require an almost constant concentration gradient in the transport layer and a zero concentration gradient in the sliding or stationary bed below the transport layer. It is difficult to accept that the turbulent diffusion concept with the terminal (hindered) setting velocity of the particle and the particle turbulent diffusivity as key parameters is an appropriate modeling approach to determine concentration profiles in stratified (high concentration) flows. Hybrid modelling taking contact and suspended loads into account separately is a preferred approach. Note of the author: Suspended load may behave according to a turbulent diffusion model, a stationary or sliding bed behaves according to soil mechanics with internal and external friction, which is not included in turbulent diffusion.

6.24.4.2 Summary of the Model.

The abstract of Matousek & Krupicka (2014) gives a good summary of what the model is capable of:

A one-dimensional profile of solids concentration is modeled in a cross section of partially stratified flow of slurry in a pipe. In the flow, a certain proportion of solids is transported as contact load and occupies a sliding bed and a transport layer above the bed. The rest of solid particles is transported as suspended load within and above the transport layer. A model based on a vertical distribution of shear stress is developed to predict a concentration profile in a cross section of such flow. Besides the concentration profile, the model predicts the thickness and velocity of the bed. Furthermore, the model determines a vertical position of the top of the transport layer and a position of the hydrodynamic axis of the flow. Model predictions show a satisfactory match with new experimentally determined profiles collected in slurry flows of four different fractions of glass beads in a 100-mm pipe of their laboratory loop.

Figure 6.24-2, Figure 6.24-3, Figure 6.24-4 and Figure 6.24-5 show experimental concentration profiles as measured by Matousek & Krupicka (2014) in a **D_P=0.1 m** pipe with particles of **d=0.44 mm** and **d=0.53 mm**. The Limit Deposit Velocities are about 2.5 m/s and 2.8 m/s for sand. Since here the particles are spherical glass beads, the LDV values may be a bit smaller. The velocities used in the experiments were about 3.5 m/s and 4 m/s, so above the Limit Deposit Velocities. The experiments are compared with the concentration profiles determined with the DHLLDV Framework as described in chapter 7.10. A bed concentration of 60% is assumed for all cases, based on the maximum bottom concentration measured. The bed concentration should not be changed, it is a fixed value for a certain type of particles. The bottom concentration however will change depending on the spatial concentration and the line speed to LDV ratio. Two settings were used for the coefficient in the hindered settling power. A value of 2.75 for the **d=0.44 mm** particles and the default value of 4 (see chapter 7.10) for the **d=0.53 mm** particles. The **d=0.9 mm** particles (not shown here) also require a factor 4. This factor appears to be constant for a certain type of particle.

From the figures it is clear that a higher line speed gives a steeper concentration profile and a smaller bottom concentration. In general the simulated concentration profiles match the experimental values well.
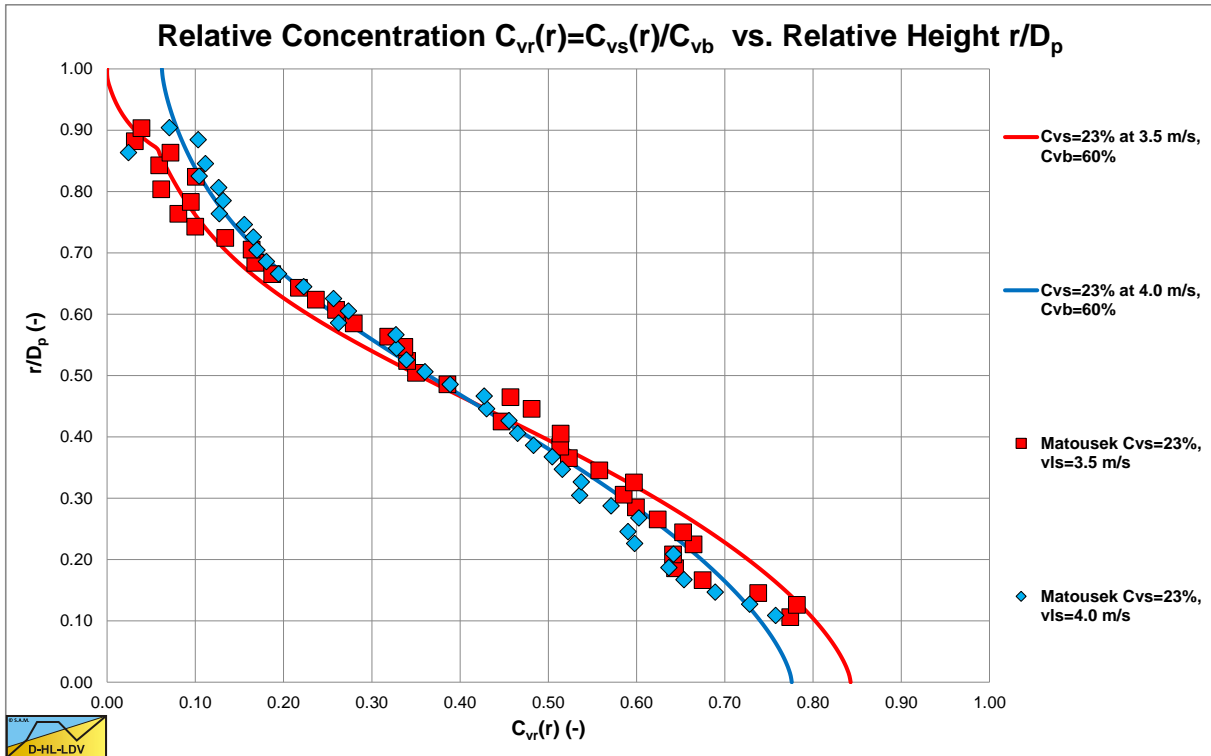
Figure 6.24-2: Experiments of Matousek & Krupicka (2014) in a D_p=0.1 m pipe with d=0.44 mm particles, C_{vs}=0.23.
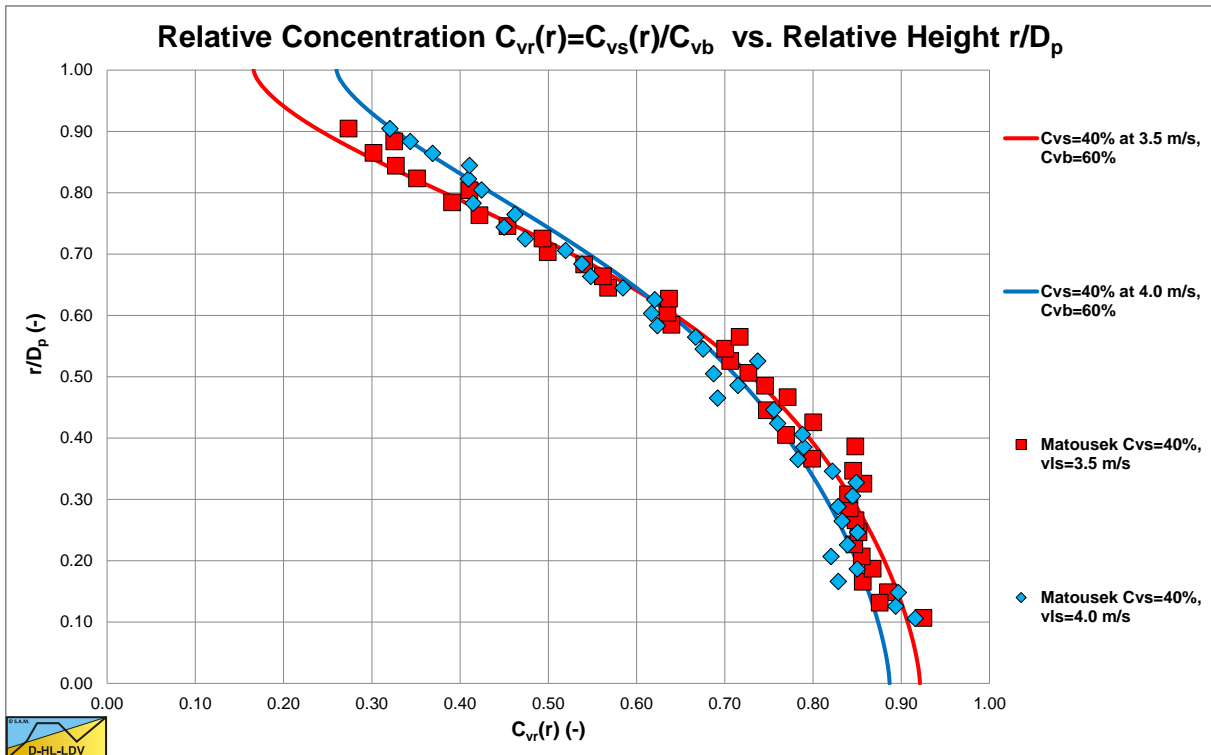
Figure 6.24-3: Experiments of Matousek & Krupicka (2014) in a D_p=0.1 m pipe with d=0.44 mm particles, C_{vs}=0.40.
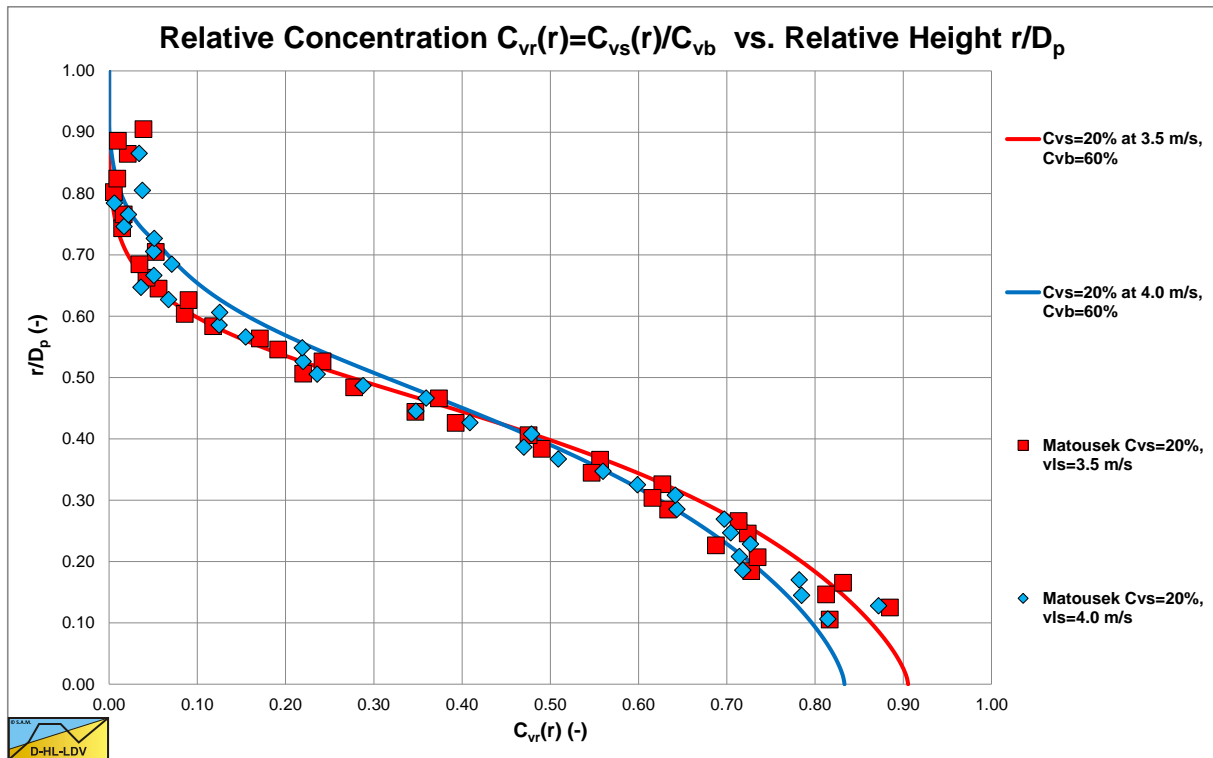
Figure 6.24-4: Experiments of Matousek & Krupicka (2014) in a D_p=0.1 m pipe with d=0.53 mm particles, C_{vs}=0.20.
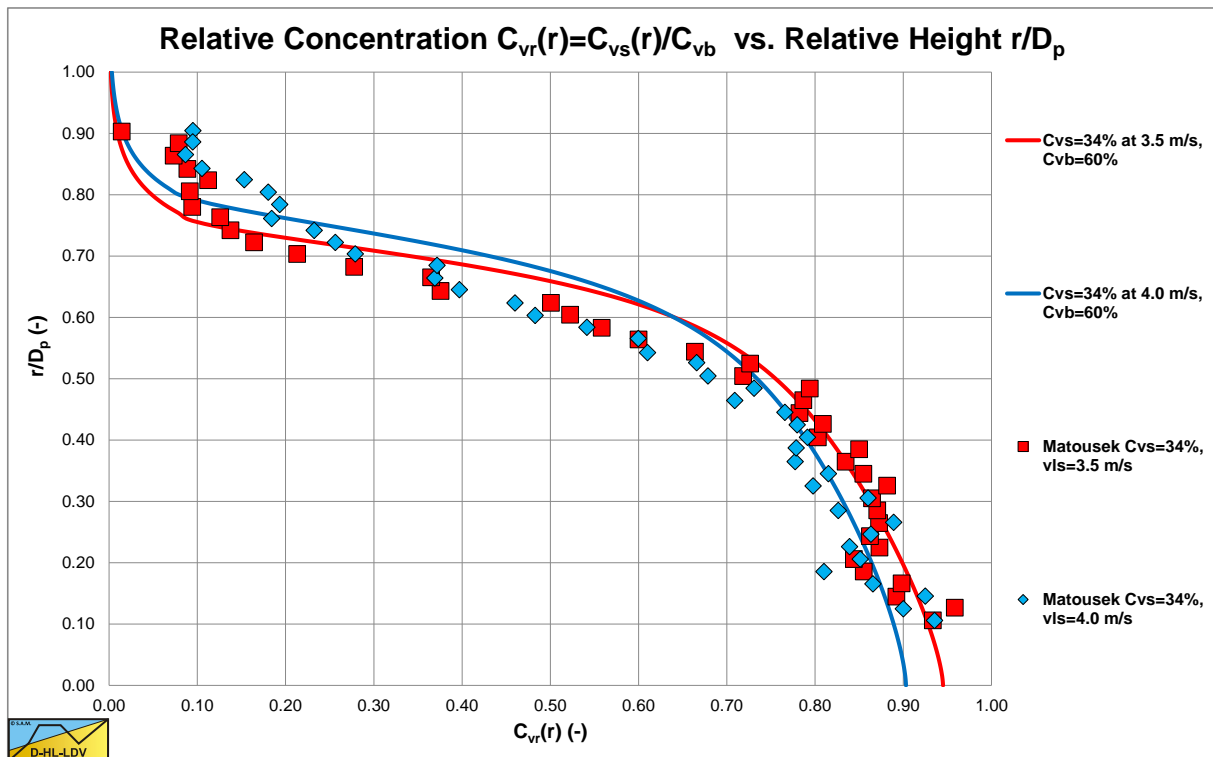
Figure 6.24-5: Experiments of Matousek & Krupicka (2014) in a D_p=0.1 m pipe with d=0.53 mm particles, C_{vs}=0.34.

6.24.5 Conclusions & Discussion.

Matousek (2009), (2011) and Matousek & Krupicka (2010), (2011) developed a new approach for 2LM and 3 LM models. Their approach is in fact a 3LM model with a bed area, a bed associated area and a pipe wall associated area. The model is based on the delivered volumetric concentration as an input and the spatial volumetric concentration, hydraulic gradient, bed height and other parameters as output, after iterations. Wilson-GIW (1979) and Doron et al. (1987) have the spatial volumetric concentration as input and the delivered volumetric concentration as output, after iterations.

The concept of the model is very interesting, however there are still some questions about the implementation. Central in the model are two empirical equations. The Meyer-Peter Muller (1948) equation for the erosion rate and the equation of Matousek & Krupicka (2014) for the equivalent bed roughness. It should be noted, though, that the model transport equation has a theoretical background as shown in the derivation by Matousek (2011). The formula has been validated for C_{vt} up to almost 0.30 and the entire model for even higher C_{vt} values (up to almost 0.40).

The MPM equation is designed for erosion in open channel flow with a free surface, giving the "Law of the Wall" velocity distribution. In pipe flow there will be a completely different velocity profile in the cross section of the pipe. Further it is the question whether MPM can deal with very high erosion rates and volumetric concentrations as present in slurry flow.

The coefficients of the MPM equation are based on integration of the concentration and velocity profile in a sheet flow layer. Based on the Shields parameter found and the width of the bed interface, the cross section of the sheet flow layer can be determined. This cross section however has no relation with the so called bed associated area, which would be expected.

The sliding friction force is determined based on the hydrostatic normal stress approach of Wilson et al. (1992). This approach may give still reasonable values for the sliding friction force up to a bed angle of 90°, but above 90° it strongly overestimates the sliding friction force. Miedema & Ramsdell (2014) investigated this force and came up with the weight approach. A result of the hydrostatic approach may be that at high concentrations the error in the sliding friction force is compensated with a to small sliding friction coefficient.

The sliding friction resisting force misses the weight of the sheet flow layer, corrected for the hydrostatic normal stress approach. The correct equation is given.

The relation for the spatial volumetric concentration may be correct for the case of a stationary bed, but not for the case of a sliding bed. The correct equation is given by the authors.

The wall associated area does not contain any solids in the model, this could be an interesting extension of the model.

There is no check to see if the sheet flow layer either touches the top of the pipe, resulting in a different concentration profile and velocity profile, or occupies the whole bed, resulting in heterogeneous flow. At very high concentrations, resulting in a high value of the bed height, the equations used to determine the concentration and velocity profiles in the sheet flow layer cannot be valid anymore. So the model is limited to a certain spatial volumetric concentration. If theoretically there is a very sliding small bed with a sheet flow layer on top, one can doubt whether such a situation can exist.

The model has been tested with a number of equivalent bed roughness equations, but it would also be interesting to test the model with different erosion rate equations.

Resuming one can say that the Matousek (2009), (2011) and Matousek & Krupicka (2010), (2011) model is based on a new very interesting concept. The user should however be aware of the empirical basis and some limitations of the model.

The new shear stress based concentration profile model is very promising, compared to the traditional turbulent diffusion models for stratified flows. For 100% suspended load one can already discuss whether turbulent diffusion models are appropriate for particles that to not follows the motions of eddies, in stratified flows the particles in contact in a stationary or sliding bed have no relation with turbulence anymore. One has to distinguish here between fluid dynamics (suspended load) and soil mechanics (stratified loads). The new shear stress based model is doing exactly this. Once the mixture hydraulic gradient is known from an appropriate model/method, the height of a stationary or sliding bed and the height of the transport layer (shear layer or sheet flow layer) can be determined, both not following the turbulent diffusion model. Above the transport layer, the concentration profile can be determined with a turbulent diffusion model.

One of the main issues is that the Richardson & Zaki (1954) hindered settling equation is based on the spatial volumetric concentration C_{vs} and not on the relative spatial volumetric concentration $C_{vr}=C_{vs}/C_{vb}$.

$$\frac{v_{th}}{v_t} = \left(1-C_{vs}\right)^{\beta} \tag{6.24-72}$$

So even when the spatial volumetric concentration reaches a concentration where a bed with maximum porosity occurs, for sand at about $C_{vs}=50\%$, still a hindered settling velocity is determined, while in reality this hindered settling velocity will be zero. Normal sands will have a porosity of about 40%, so $C_{vb}=60\%$. A fixed bed may have a porosity of 40%, but a sliding bed will have a higher porosity in between 40% and 50%. The porosities mentioned here depend on the type of sand, but are mentioned to give a feeling of the order of magnitude. Since the Richardson & Zaki (1954) equation is based on small concentrations it is better to use a modified equation based on the relative concentration, for example:

$$\frac{v_{th}}{v_t} = \left(1-C_{vr}\right)^{\beta'} \tag{6.24-73}$$

Of course the power of this equation will be different from the original equation. An equation that may even work better is:

$$\frac{v_{th}}{v_t} = e^{-\beta \cdot C_{vr}^{1.25}} \cdot \left(1-C_{vr}^2\right) \tag{6.24-74}$$

For small concentrations this equation gives the same result as the original equation, but for concentrations approaching the bed concentration, this equation approaches a zero settling velocity. This would describe the bed behavior much better. So for small concentrations this equation describes hindered settling, while for large relative concentrations approaching 1, the behavior is more close to consolidation. The power β in this equation is equal to the original power β.

6.24.6 Nomenclature Matousek Model.

A_p	Cross section pipe	m^2
A_1	Cross section above bed	m^2
$A_{1,1}$	Wall associated cross section upper layer	m^2
$A_{1,12}$	Bed associated cross section upper layer	m^2
A_2	Cross section bed	m^2
$A_{12,sf}$	Cross section sheet flow layer	m^2
C_{vb}	Volumetric spatial bed concentration	-
C_{vs}	Spatial volumetric concentration	-
$C_{vt,1}$	Delivered volumetric concentration in cross section 1, upper layer	-
$C_{vt,2}$	Delivered volumetric concentration in cross section 2, lower layer	-
C_{vt}	Delivered (transport) volumetric concentration	-
d	Particle diameter	m
d_{50}	Particle diameter with 50% passing	m
D_p	Pipe diameter	m
E_{rhg}	Relative excess hydraulic gradient	-
F_{sf}	Force on bed due to sliding friction	kN
F_{dr}	Force on bed due to pressure and shear stress on top of the bed	kN
g	Gravitational constant 9.81 m/s^2	m/s^2
H	Thickness sheet flow layer	m
i_l	Hydraulic gradient liquid	m/m
i_m	Hydraulic gradient mixture	m/m
k_s	Bed roughness	m
ΔL	Length of pipe section	m
LDV	Limit Deposit Velocity	m/s
$LSDV$	Limit of Stationary Deposit Velocity	m/s
n	Power of velocity distribution in sheet flow layer	-
O_p	Circumference pipe	m
O_1	Circumference pipe above bed	m
O_2	Circumference pipe in bed	m
O_{12}	Width of bed	m
Q_s	Total solids flow rate	m^3/s
Q_{s1}	Solids flow rate in the upper layer	m^3/s
Q_{s2}	Solids flow rate in the lower layer, the bed	m^3/s
Re	Reynolds number	-
Re_p	Particle Reynolds number	-
R_{sd}	Relative submerged density	-
R_{h1}	Hydraulic radius upper layer	m
$R_{h1,1}$	Wall associated hydraulic radius upper layer	m
$R_{h1,12}$	Bed associated hydraulic radius upper layer	m
R_{h2}	Hydraulic radius lower layer	m
u_*	Friction velocity	m/s
v_t	Terminal settling velocity	m/s
v_{ls}	Line speed	m/s
v_1	Cross section averaged velocity above bed	m/s
v_2	Cross section averaged velocity bed	m/s
y_b	Height of bed	m
α	MPM coefficient	-
β	MPM coefficient	-
β	Bed angle	rad
ε	Pipe wall roughness	m
φ	Internal friction angle	°
γ	Proportionality constant sheet flow layer	-
ρ_l	Density carrier liquid	ton/m^3
ρ_s	Density solids	ton/m^3
κ	Von Karman constant, about 0.4	-
θ	Shields parameter	-

θ_{cr}	Critical Shields parameter	**-**
λ_l	Darcy-Weisbach friction factor liquid-pipe wall	**-**
λ_1	Darcy-Weisbach friction factor with pipe wall	**-**
λ_2	Darcy-Weisbach friction factor with pipe wall, liquid in bed	**-**
λ_{12}	Darcy-Weisbach friction factor on the bed	**-**
ν_l	Kinematic viscosity	**m^2/s**
τ_l	Shear stress liquid-pipe wall	**kPa**
$\tau_{1,l}$	Shear stress liquid-pipe wall above bed	**kPa**
$\tau_{12,l}$	Shear stress bed-liquid	**kPa**
$\tau_{2,l}$	Shear stress liquid-pipe in bed	**kPa**
$\tau_{2,sf}$	Shear stress from sliding friction	**kPa**
μ_{sf}	Sliding friction coefficient	**-**
ζ	Slip ratio	**-**

6.25 Talmon (2011) & (2013) Homogeneous Regime.

6.25.1 Theory.

Talmon (2013) derived an equation to correct the homogeneous equation (the ELM model) for the slurry density, based on the hypothesis that the viscous sub-layer hardly contains solids at very high line speeds in the homogeneous regime. This theory results in a reduction of the resistance compared with the ELM, but the resistance is still higher than the resistance of clear water. Talmon (2013) used the Prandl approach for the mixing length, which is a 2D approach for open channel flow with a free surface. The Prandl approach was extended with damping near the wall to take into account the viscous effects near the wall, according to von Driest (Schlichting, 1968):

$$\textbf{Pr andl :} \quad \ell = \kappa \cdot z$$

$$\textbf{von Driest :} \quad \ell = \kappa \cdot z \cdot \left(1 - e^{-z^+/A}\right) \quad \textbf{with:} \quad z^+ = \frac{z \cdot u_*}{\nu_l} \quad A=26 \tag{6.25-1}$$

The shear stress between the mixture, the slurry, and the pipe wall is the sum of the viscous shear stress and the turbulent shear stress:

$$\tau = \tau_\nu + \tau_t = \mu_\nu \cdot \frac{\partial u}{\partial z} + \mu_t \cdot \frac{\partial u}{\partial z} = \rho_m \cdot \nu_m \cdot \frac{\partial u}{\partial z} + \rho_m \cdot \nu_t \cdot \frac{\partial u}{\partial z}$$

With for the eddy viscosity : $\tag{6.25-2}$

$$\nu_t = \ell^2 \cdot \left| \frac{\partial u}{\partial z} \right|$$

So the shear stress can be expressed as:

$$\tau = \rho_m \cdot \left(u_*\right)^2 = \rho_m \cdot \left(\nu_m + \ell^2 \cdot \left| \frac{\partial u}{\partial z} \right| \right) \cdot \frac{\partial u}{\partial z} \tag{6.25-3}$$

Solving this with respect to the velocity gradient gives:

$$\frac{\partial u}{\partial z} = \frac{-\frac{\mu_m}{\rho_m} + \sqrt{\left(\frac{\mu_m}{\rho_m}\right)^2 + 4 \cdot \ell^2 \cdot \left(u_*\right)^2}}{2 \cdot \ell^2} = \frac{2 \cdot \left(u^*\right)^2}{\frac{\mu_m}{\rho_m} + \sqrt{\left(\frac{\mu_m}{\rho_m}\right)^2 + 4 \cdot \ell^2 \cdot \left(u_*\right)^2}} \tag{6.25-4}$$

Assuming that the term with the density ratio is relevant only near the pipe wall and not in the center of the pipe, this equation will simulate a mixture with liquid in the viscous sub-layer. In fact, the density ratio reduces the effect of the kinematic viscosity, which mainly affects the viscous sub-layer. The velocity difference u_m-u_{fl} can now be determined with:

$$u_m - u_l = \int_0^{z_{max}} \frac{-\frac{\rho_l}{\rho_m} \cdot \nu_l + \sqrt{\left(\frac{\rho_l}{\rho_m} \cdot \nu_l\right)^2 + 4 \cdot \ell^2 \cdot \left(u_*\right)^2}}{2 \cdot \ell^2} \cdot dz - \int_0^{z_{max}} \frac{-\nu_l + \sqrt{\left(\nu_l\right)^2 + 4 \cdot \ell^2 \cdot \left(u_*\right)^2}}{2 \cdot \ell^2} \cdot dz \tag{6.25-5}$$

This velocity difference, in the center of the pipe is about equal to the difference of the average line speeds. Further it appears that dividing the velocity difference by the friction velocity results in a factor **F**, which only depends on

the volumetric concentration C_{vs}, the relative submerged density R_{sd}, slightly on the line speed v_{ls} in the range 3-10 m/sec and on the pipe diameter D_p, according to:

$$F = \frac{u_m - u_l}{u_*} = \frac{v_{ls,m} - v_{ls,l}}{u_*} = \alpha_h \cdot R_{sd} \cdot C_{vs} = \alpha_h \cdot \left(\frac{\rho_m}{\rho_l} - 1 \right) \tag{6.25-6}$$

The shear stress at the pipe wall of a Newtonian liquid is by definition:

$$\rho_l \cdot \left(u_* \right)^2 = \frac{\lambda_l}{8} \cdot \rho_l \cdot v_{ls,l}^2 \quad \text{and} \quad \rho_m \cdot \left(u_* \right)^2 = \frac{\lambda_m}{8} \cdot \rho_m \cdot v_{ls,m}^2 \tag{6.25-7}$$

From this a relation for the ratio of the Moody friction coefficients of a flow with mixture in the center and carrier liquid in the viscous sub-layer to a flow with 100% liquid can be derived.

$$\frac{\lambda_l}{8} \cdot v_{ls,l}^2 = \frac{\lambda_m}{8} \cdot v_{ls,m}^2 \quad \Rightarrow \quad \frac{\lambda_m}{\lambda_l} = \frac{v_{ls,l}^2}{v_{ls,m}^2} \quad \Rightarrow \quad \frac{\lambda_m}{\lambda_l} = \frac{v_{ls,l}^2}{\left(F \cdot u_* + v_{ls,l} \right)^2} = \frac{1}{\left(F \cdot u_* + 1 \right)^2} \tag{6.25-8}$$

The Talmon (2013) approach resulted in the following equation:

$$\frac{\lambda_m}{\lambda_l} = \frac{1}{\left(F \cdot \dfrac{u_*}{v_{ls,l}} + 1 \right)^2} = \frac{1}{\left(\alpha_h \cdot \sqrt{\dfrac{\lambda_l}{8}} \cdot R_{sd} \cdot C_{vs} + 1 \right)^2} \tag{6.25-9}$$

The resulting equation is:

$$\frac{i_m}{i_l} = \frac{1 + R_{sd} \cdot C_{vs}}{\left(\alpha_h \cdot \sqrt{\dfrac{\lambda_l}{8}} \cdot R_{sd} \cdot C_{vs} + 1 \right)^2} \quad \Rightarrow \quad i_m = i_l \cdot \frac{1 + R_{sd} \cdot C_{vs}}{\left(\alpha_h \cdot \sqrt{\dfrac{\lambda_l}{8}} \cdot R_{sd} \cdot C_{vs} + 1 \right)^2} \tag{6.25-10}$$

In order to find the relative excess hydraulic gradient E_{rhg}, this can be written as:

$$i_m - i_l = i_l \cdot \frac{1 + R_{sd} \cdot C_{vs}}{\left(\alpha_h \cdot \sqrt{\dfrac{\lambda_l}{8}} \cdot R_{sd} \cdot C_{vs} + 1 \right)^2} - i_l \cdot \frac{\left(\alpha_h \cdot \sqrt{\dfrac{\lambda_l}{8}} \cdot R_{sd} \cdot C_{vs} + 1 \right)^2}{\left(\alpha_h \cdot \sqrt{\dfrac{\lambda_l}{8}} \cdot R_{sd} \cdot C_{vs} + 1 \right)^2} \tag{6.25-11}$$

$$= i_l \cdot \frac{R_{sd} \cdot C_{vs} + 1 - \left(\alpha_h \cdot \sqrt{\dfrac{\lambda_l}{8}} \cdot R_{sd} \cdot C_{vs} + 1 \right)^2}{\left(\alpha_h \cdot \sqrt{\dfrac{\lambda_l}{8}} \cdot R_{sd} \cdot C_{vs} + 1 \right)^2}$$

The relative excess hydraulic gradient E_{rhg} is now:

$$E_{rhg} = \frac{i_m - i_l}{R_{sd} \cdot C_{vs}} = i_l \cdot \frac{R_{sd} \cdot C_{vs} + 1 - \left(\alpha_h \cdot \sqrt{\dfrac{\lambda_l}{8}} \cdot R_{sd} \cdot C_{vs} + 1 \right)^2}{R_{sd} \cdot C_{vs} \cdot \left(\alpha_h \cdot \sqrt{\dfrac{\lambda_l}{8}} \cdot R_{sd} \cdot C_{vs} + 1 \right)^2} \tag{6.25-12}$$

The limiting value for the excess hydraulic gradient E_{rhg} for a volumetric spatial concentration C_{vs} approaching zero, becomes irrespective of the relative submerged density R_{sd}:

$$E_{rhg} = \frac{i_m - i_l}{R_{sd} \cdot C_{vs}} = i_l \cdot \left(1 - 2 \cdot \alpha_h \cdot \sqrt{\frac{\lambda_l}{8}}\right) \qquad (6.25\text{-}13)$$

Figure 6.25-1 shows the factor α_h as a function of the term $R_{sd} \cdot C_{vs}$. The value of this coefficient decreases with increasing density according to:

$$\alpha_h = 7.7426 - 1.9302 \cdot \left(R_{sd} \cdot C_{vs}\right) + 0.6187 \cdot \left(R_{sd} \cdot C_{vs}\right)^2$$

$$\qquad (6.25\text{-}14)$$

$$-0.1223 \cdot \left(R_{sd} \cdot C_{vs}\right)^3 + 0.0098 \cdot \left(R_{sd} \cdot C_{vs}\right)^4$$

Talmon (2013) used $\alpha_h = 6.7$ as a fixed value. The model underestimates the hydraulic gradient in a number of cases (small and large particles) as Talmon (2013) proves with the examples shown in his paper. Only for $d_{50}=0.37$ mm and $D_p=0.15$ m (medium particles) there is a good match. The philosophy behind this theory, combining a viscous sub-layer with water with a kernel with mixture, is however very interesting, because it explains fundamentally why the pressure can be lower than the pressure according to the ELM, as has been shown by many researchers. The model has been derived using the standard mixing length equation for 2D flow. Applying the Nikuradse (1933) equation for the mixing length in pipe flow may give different quantitative results.
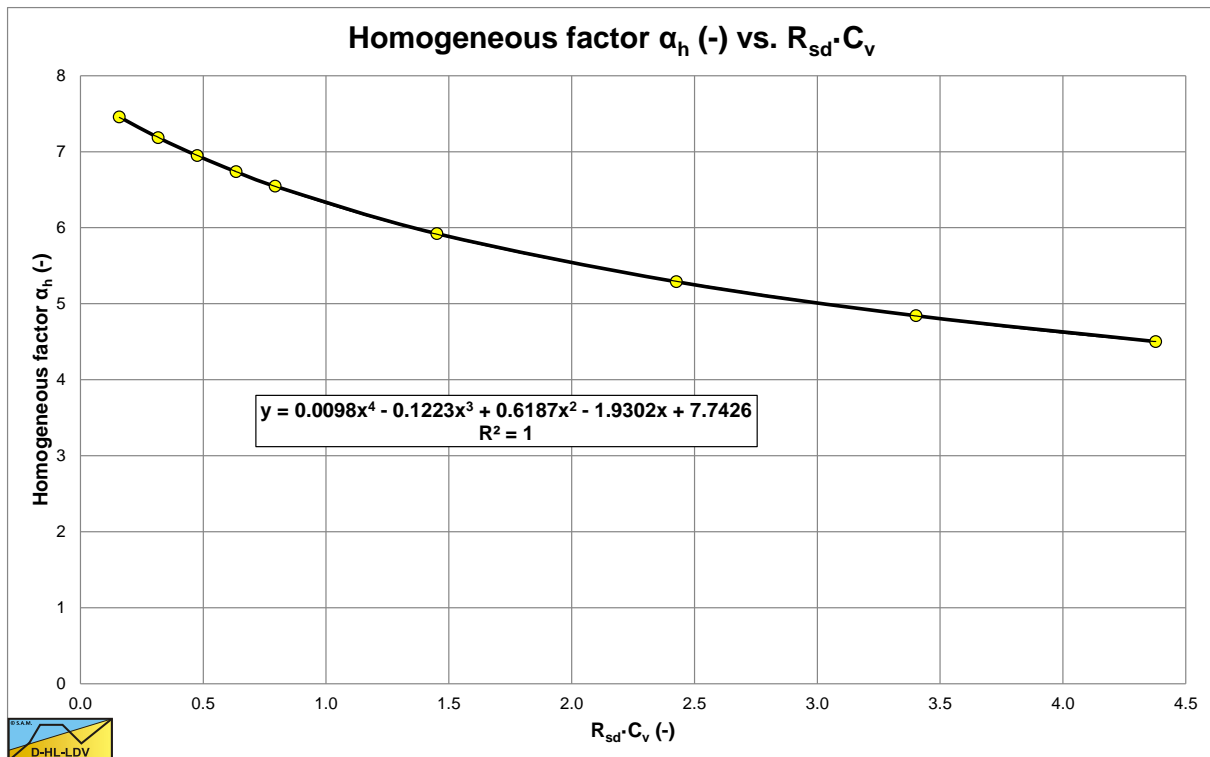
Figure 6.25-1: The coefficient α_h as a function of the mixture density.

6.25.2 Nomenclature Talmon Model.

A	Von Driest damping factor (26)	**-**
D_p	Pipe diameter	**m**
E_rhg	Relative excess hydraulic gradient	**-**
F	Homogeneous reduction factor	**-**
g	Gravitational constant (9.81)	**m/s²**
ΔL	Length of pipe segment considered	**m**
i_m	Mixture hydraulic gradient	**m/m**
i_l	Liquid hydraulic gradient	**m/m**
R_sd	Relative submerged density (sand 1.65)	**-**
u	Velocity	**m/s**
u_l	Velocity liquid	**m/s**
u_m	Velocity mixture	**m/s**
u∗	Friction velocity	**m/s**
v_ls	Line speed	**m/s**
v_ls,l	Line speed liquid	**m/s**
v_ls,m	Line speed mixture	**m/s**
z	Distance to the wall	**m**
α_h	Homogeneous factor	**-**
λ_l	Darcy-Weisbach friction factor liquid	**-**
λ_m	Darcy-Weisbach friction factor mixture	**-**
ρ_l	Density liquid	**ton/m³**
ρ_m	Density mixture	**ton/m³**
κ	Von Karman constant (0.4)	**-**
τ	Shear stress	**kPa**
τ_v	Viscous shear stress	**kPa**
τ_t	Turbulent shear stress	**kPa**
μ_v	Viscous dynamic viscosity	**Pa·s**
μ_t	Turbulent dynamic viscosity	**Pa·s**
μ_l	Dynamic viscosity liquid	**Pa·s**
μ_m	Dynamic viscosity mixture	**Pa·s**
ν_l	Kinematic viscosity liquid	**m²/s**
ν_m	Kinematic viscosity mixture	**m²/s**
ν_t	Turbulence viscosity	**m²/s**
ℓ	Mixing length	**m**

6.26 Conclusions & Discussion Physical Models.

It should be noted that most models are based on constant delivered volumetric concentration experiments. For the high line speed heterogeneous and homogeneous regimes the spatial and delivered volumetric concentrations are close, almost equal. However for the sliding bed regime and the low line speed heterogeneous regimes they differ and the lower the line speed the larger the difference. This often results in a more negative power of the excess pressure gradient related to the line speed.

6.26.1 The Newitt et al. (1955) Model.

The Newitt et al. (1955) models already distinguish 3 main flow regimes. The sliding bed regime, the heterogeneous regime and the homogeneous regime. In the sliding bed regime, the excess hydraulic gradient is independent from the line speed, it mainly depends on the weight of the bed and a sliding friction coefficient. In the heterogeneous regime the excess hydraulic gradient depends reversely on the line speed. In the homogeneous regime the excess hydraulic gradient is proportional to the line speed squared and is similar to the ELM. Based on the formulations of the 3 flow regimes a regime diagram is constructed, but still with sharp transitions between the flow regimes.

6.26.2 The Wasp et al. (1963) Model.

One of the shortcomings of the Newitt et al. (1955) models is the sharp transition between the flow regimes and the inability to deal with graded solids. The Wasp et al. (1963) model deals with the transition of the heterogeneous regime and the homogeneous regime. The graded solids are divided into fractions. For each fraction the portion in suspension is determined, based on the advection diffusion equation. By summation of these portions the total amount of solids in suspension is determined. The amount of solids in suspension behave according to the ELM, while the remaining amount of solids behave heterogeneously according to Durand & Condolios (1952). This way a smooth transition is achieved between the heterogeneous and homogeneous flow regime and the grading of the solids is taken into account. The method works well for solids with a lot of fines, while coarse uniform solids behave according to Durand & Condolios (1952).

6.26.3 The Wilson-GIW (1979) Model.

The Wilson-GIW (1979) model started as a 2 layer model with a sliding or stationary bed and pure liquid above it. Based on an equilibrium of forces acting on the bed, the bed velocity and the hydraulic gradient can be determined. First however it is determined whether the bed is sliding or is stationary, resulting in a LSDV curve. The method is based on the spatial volumetric concentration and outputs the delivered volumetric concentration. By iteration constant delivered concentration curves can be constructed. The main shortcoming of the original model is the inability to deal with suspended particles. This model deals with the sliding bed regime solely. The model uses a hydrostatic approach to determine the normal stress between the bed and the pipe wall. This approach is questionable.

Later a model for the heterogeneous regime is added, based on the so called stratification ratio. A stratification ratio of 1 means that all the solids are in the bed, a stratification ratio of 0 means all particles are suspended. Based on a velocity where the stratification ratio is 50% and a power function for the stratification ratio, the excess hydraulic gradient can be determined. The excess hydraulic gradient is reversely proportion to the line speed to a power between 0.25 for very graded solids up to 1.7 for uniform solids.

Recently a 4 component model was introduced, based on 4 components, particle size regions. Very fine particles behave homogeneously, with or without correction of the liquid properties. Fine to medium particles behave pseudo homogeneously, according to the ELM. Medium to coarse particles behave heterogeneously and very coarse particles behave stratified, according to the sliding bed regime. By splitting a PSD into 4 fractions, determining the excess hydraulic gradient for each fraction and adding up the excess hydraulic gradients, the total excess hydraulic gradient is determined. The downside is, that the division between the 4 fractions depends on the particles size and the pipe diameter and not on the line speed or relative submerged density. So this model is only applicable for sands in a certain line speed region.

6.26.4 The Doron et al. (1987) and Doron & Barnea (1993) Model.

The Doron & Barnea (1993) model started as a 2 layer model, with suspension above a sliding bed. The portion of the solids in suspension is determined with the concentration distribution above the bed, based on the advection diffusion equation for open channel flow. This is an addition compared to the Wilson-GIW (1979) model, which

only has pure liquid above the sliding bed. The 2 layer model gives good predictions, however always predicts a sliding bed for constant delivered volumetric concentrations. To deal with this a 3 layer model was developed containing a stationary bed at the bottom of the pipe, a moving bed on top of it and a heterogeneous layer above the moving bed. Based on a set of continuity and force equilibrium equations, the amount of solids in the heterogeneous layer and the thickness and the velocity of the moving bed layer are determined. If the friction on the stationary layer exceeds the available sliding friction, the whole bed is sliding, if not, the stationary layer is assumed to be real stationary. The 3 layer model predicts a stationary bed at very low line speeds.

6.26.5 The SRC Model.

The SRC model is also developed for graded solids with a lot of fines, comparable to the Wasp et al. (1963) model. The main difference is, that the SRC model uses the sliding bed model, comparable to the Wilson-GIW (1979) model for the bed fraction. The model does not use an advection diffusion equation to determine the suspended fraction, but instead it uses an empirical equation to determine the contact load fraction. The remainder is the solids in suspension. The solids in suspension are also assumed to be present in the bed and increase the liquid density, resulting in a lower relative submerged density of the solids. The maximum bed concentration depends on the line speed and decreases with increasing line speed. At a certain line speed, the bed concentration is so low that one cannot call it a bed anymore. Still it moves over the bottom of the pipe and has a sort of sliding bed behavior. This will be named the sliding flow regime.

6.26.6 The Kaushal & Tomita (2002B) Model.

Kaushal & Tomita (2002B) have modified the Wasp et al. (1963) model. They noticed that the way of determining the suspended fraction, does not always give proper results. Especially for coarser particles, the Wasp model is just the Durand & Condolios (1952) model. By using the Karabelas (1977) approach for graded solids in a circular pipe and modifying the diffusivity, they managed to overcome the shortcomings of the Wasp method. The diffusivity now depends on the size of a particle fraction and on the volumetric concentration. The concentration distribution model now also gives good results for coarse particles. In the heterogeneous regime the model is as good as the Durand & Condolios (1952) model, just as the Wasp model.

6.26.7 The Matousek (2009) Model.

The Matousek (2009) model is a sort of reversed engineering model. The starting point is the delivered volumetric concentration. Based on the Meyer-Peter Muller equation, the Shields parameter is determined. From the Shields parameter the bed shear stress is determined. Based on the continuity and force equilibrium equations, the bed velocity is determined. By iteration an equilibrium situation has to be determined where the total delivered concentration matches the input. The methodology also outputs the bed height. The model is suitable for the sliding bed regime and the stationay bed regime, but not for the heterogeneous or homogeneous regimes.

6.26.8 The Talmon (2011) & (2013) Homogeneous Regime Model.

Many researchers have found that at high line speeds the flow regime is the homogeneous regime, following the ELM. However they also noticed that the hydraulic gradient is often between the pure liquid hydraulic gradient and the ELM. In terms of the excess hydraulic gradient this means that the excess hydraulic gradient is between zero and the excess hydraulic gradient of the ELM. One should keep in mind that measurements in the homogeneous regime are mostly at line speeds just above the heterogeneous regime. For very fine and fine particles almost real homogeneous behavior is observed, but for medium and coarse particles this is more pseudo homogeneous behavior, which is still a transition region from heterogeneous to true homogeneous behavior.
Talmon (2011) & (2013) developed a method to prove that the excess hydraulic gradient is slightly lower than the ELM excess hydraulic gradient. The method is based on the assumption that the viscous sub-layer is particle free, while outside the viscous sub-layer there is a uniform distribution of particles. The method is based on the velocity distribution of open channel flow, but gives promising results.

6.27 The Limit Deposit Velocity (LDV).

6.27.1 Introduction.

The Limit Deposit Velocity is defined here as the line speed where there is no stationary bed or sliding bed. Below the LDV there may be either a stationary or fixed bed or a sliding bed. For the LDV often the Minimum Hydraulic Gradient Velocity (MHGV) is used. For higher concentrations this MHGV may be close to the LDV, but for lower concentrations this is certainly not the case. Yagi et al. (1972) reported using the MHGV, making the data points for the lower concentrations to low. Wilson (1979) derived a method for the transition between the stationary bed and the sliding bed, which is named here the Limit of Stationary Deposit Velocity (LSDV). Since the transition stationary bed versus sliding bed, the LSDV, will always give a smaller value than the moment of full suspension or saltation, the LDV, one should use the LDV, to be sure there is no deposit.

Figure 6.27-1 shows many data points of various authors for sand and gravel in water. Each column of data points shows the results of experiments with different volumetric concentrations, where the highest point were at volumetric concentrations of about 20%. The experimental data also showed that smaller pipe diameters, in general, give higher Durand & Condolios (1952) Froude F_L numbers. The two curves in the graph are for the Jufin & Lopatin (1966) equation, which is only valid for sand and gravel, and the DHLLDV Framework which is described in chapter 7 of this book. Both models give a sort of upper limit to the LDV. The data points of the very small particle diameters, Thomas (1979), were carried out in a 0.0189 m pipe, while the graph is constructed for an 0.1016 (4 inch) pipe, resulting in a slightly lower curve. Based on the upper limit of the data points, the following is observed, from very small particles to very large particles (left to right in the graph):

1. For very small particles, there seems to be a lower limit for the F_L value.
2. For small particles, the F_L value increases to a maximum for a particle size of about **d=0.5 mm**.
3. For medium sized particles with a particle size **d>0.5 mm**, the F_L value decreases to a minimum for a particle size of about **d=2 mm**. Above 2 mm, the F_L value will remain constant according to Durand & Condolios (1952).
4. For particles with **d/D$_p$>0.015**, the Wilson et al. (1992) criterion for real suspension/saltation, the F_L value increases again. This criterion is based on the ratio particle diameter to pipe diameter and will start at a large particle diameter with increasing pipe diameter.

Because there are numerous equations for the LDV, some based on physics, but most based on curve fitting, a selection is made of LDV equations and methods from literature. The results of these equations are discussed in the conclusions and discussion.
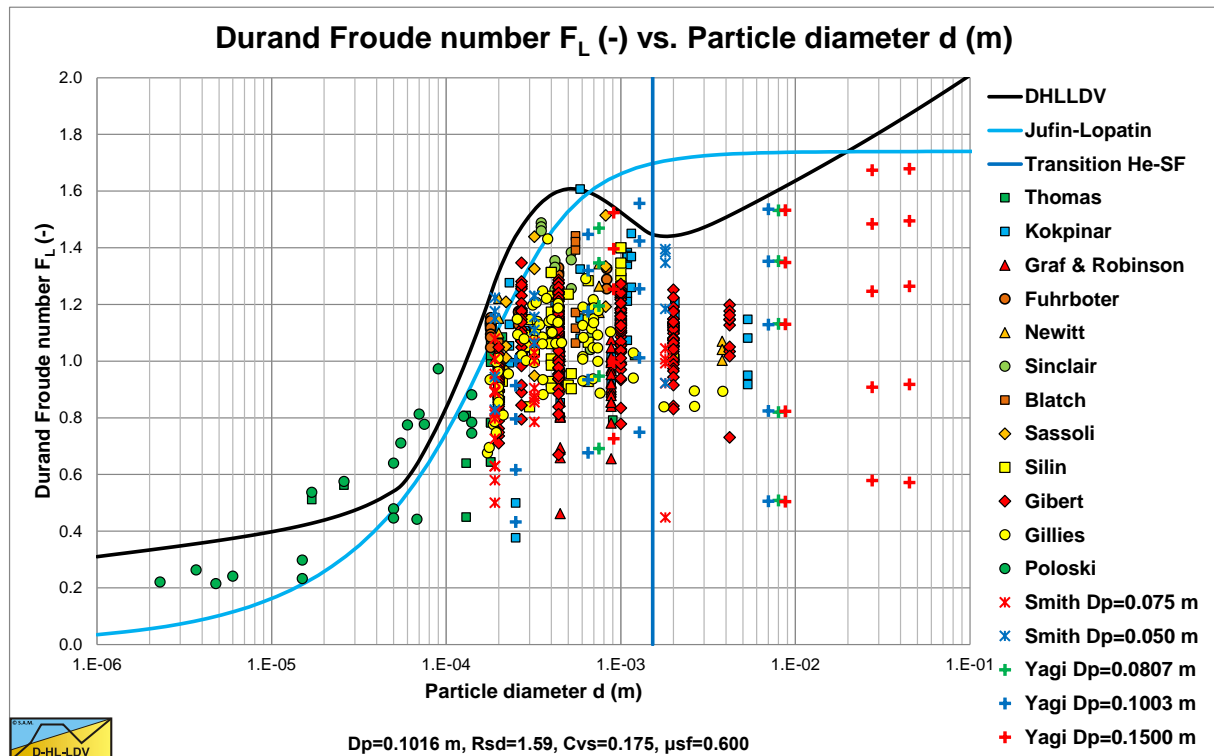
Figure 6.27-1: LDV data of many authors.

6.27.2 Wilson (1942).

Wilson (1942) used the minimum hydraulic gradient velocity (MHGV) for the LDV. This concept has been followed by many others, but has nothing to do with the physical LDV, only with the minimum power requirement. The model is based on the terminal settling velocity.

6.27.3 Durand & Condolios (1952).

Durand & Condolios (1952) derived a relatively simple equation based on the Froude number of the flow.

$$F_L = \frac{v_{ls,ldv}}{\sqrt{2 \cdot g \cdot R_{sd} \cdot D_p}}$$

(6.27-1)

For the value of the Froude number F_L a graph is published, showing an increasing value up to a maximum of about 1.55 at a particle size of d=0.5 mm, after which F_L decreases to an asymptotic value of about 1.34 for very large particles. The graph also shows a dependency of the LDV with respect to the volumetric concentration. The Froude number F_L shows a maximum for volumetric concentrations between 15% and 20%. The F_L value does not depend on the pipe diameter and the relative submerged density, only on the particle diameter and the volumetric concentration. It should be mentioned that there is a discrepancy of a factor $R_{sd}^{1/2}$ between the graph published by Durand & Condolios (1952) and the graph published by Durand (1953), giving a factor of about 1.28. The graph as used by many authors overestimates the Durand Froude number by this factor. Figure 6.27-2, Figure 6.27-3, Figure 6.27-4 and Figure 6.27-5 show the correct and incorrect Durand Froude numbers compared with many other equations. Compared with data from many authors however, the wrong graph seems to be right with respect to the prediction of the LDV, which is probably the reason nobody found this mistake or made comments about it.

6.27.4 Newitt et al. (1955).

Newitt et al. (1955), like Wilson (1942), focused on the terminal settling velocity in their modeling. They did not really give an equation for the LDV, however they gave a relation for the transition between the sliding bed regime and the heterogeneous regime based on the terminal settling velocity, giving $v_{SB-He}=17 \cdot v_t$. This regime transition velocity may however be considered a lower limit to the LDV.

6.27.5 Jufin & Lopatin (1966).

Jufin & Lopatin (1966) defined the Limit Deposit Velocity as (sometimes a value of 8 is used instead of 8.3):

$$v_{ls,\,ldv} = 8.3 \cdot \left(C_{vt} \cdot \psi^* \right)^{1/6} \cdot D_p^{1/3}$$

(6.27-2)

It is clear that this Limit Deposit Velocity also does not have the dimension of velocity, but the cube root of length. In dimensionless for giving:

$$F_L = \frac{v_{ls,\,ldv}}{\left(2 \cdot g \cdot D_p \cdot R_{sd} \right)^{1/2}} = 9.23 \cdot \frac{\left(C_{vt} \right)^{1/6} \cdot \left(\frac{v_t}{\sqrt{g \cdot d}} \right)^{1/4} \cdot \left(\nu_l \cdot g \right)^{1/9}}{\left(2 \cdot g \cdot D_p \cdot R_{sd} \right)^{1/6}}$$

(6.27-3)

The Froude number F_L decreases with increasing pipe diameter (power -1/6) and increases with increasing particle diameter. The F_L value also decreases with increasing relative submerged density (power -1/6).

6.27.6 Zandi & Govatos (1967).

Zandi & Govatos (1967) defined a parameter **N** and stated that **N<40** means saltating flow and **N>40** heterogeneous flow. Apparently in their perception heterogeneous flow cannot contain saltation, which differs from the perception of others. The parameter N is:

$$
N = \frac{v_{ls}^2 \cdot \sqrt{C_D}}{g \cdot R_{sd} \cdot D_p \cdot C_{vt}} < 40
\tag{6.27-4}
$$

This gives for the Limit Deposit Velocity:

$$
v_{ls,ldv} = \sqrt{\frac{40 \cdot g \cdot R_{sd} \cdot D_p \cdot C_{vt}}{\sqrt{C_D}}}
\tag{6.27-5}
$$

In terms of the Durand & Condolios (1952) Froude number **F$_L$** this gives:

$$
F_L = \frac{v_{ls,ldv}}{\sqrt{2 \cdot g \cdot R_{sd} \cdot D_p}} = \sqrt{\frac{20 \cdot C_{vt}}{\sqrt{C_D}}}
\tag{6.27-6}
$$

From literature it is not clear whether Zandi & Govatos (1967) used the particle drag coefficient or the particle Froude number. In the perception of Zandi & Govatos (1967), the Froude number **F$_L$** depends on the volumetric concentration and on the particle drag coefficient, which means a constant value for large particles.

6.27.7 Charles (1970).

Charles (1970) suggested to use the Minimum Hydraulic Gradient Velocity (MHGV) as an estimate for the Limit Deposit Velocity (LDV) since these are close. This MHGV can be obtained by differentiating the above equation with respect to the line speed **v$_{ls}$**. This gives:

$$
i_m = i_l \cdot \left(\frac{K}{R_{sd}} \cdot \psi^{-1.5} + 1 \right) \cdot C_{vt} \cdot R_{sd} + i_l
\tag{6.27-7}
$$

Or:

$$
i_m = \frac{\lambda_l \cdot v_{ls}^2}{2 \cdot g \cdot D_p} \cdot \left(\frac{K}{R_{sd}} \cdot \left(\left(\frac{v_{ls}^2}{g \cdot D_p \cdot R_{sd}} \right) \cdot \sqrt{C_x} \right)^{-1.5} + 1 \right) \cdot C_{vt} \cdot R_{sd} + \frac{\lambda_l \cdot v_{ls}^2}{2 \cdot g \cdot D_p}
$$

$$
\tag{6.27-8}
$$

$$
i_m = \frac{\lambda_l}{2 \cdot g \cdot D_p} \cdot \left(\left(1 + C_{vt} \cdot R_{sd} \right) \cdot v_{ls}^2 + \left(K \cdot \left(\frac{g \cdot D_p \cdot R_{sd}}{\sqrt{C_x}} \right)^{1.5} \cdot C_{vt} \right) \cdot \frac{1}{v_{ls}} \right)
$$

This gives for the MHGV:

$$
v_{ls,MHGV} = \left(\frac{\left(K \cdot \left(\frac{g \cdot D_p \cdot R_{sd}}{\sqrt{C_x}} \right)^{1.5} \cdot C_{vt} \right)}{2 \cdot \left(1 + C_{vt} \cdot R_{sd} \right)} \right)^{1/3}
\tag{6.27-9}
$$

6.27.8 Graf et al. (1970) & Robinson (1971).

Graf et al. (1970) & Robinson (1971) carried out experiments at low concentrations in pipes with small positive and negative inclination angles. They added the inclination angle to the Durand Froude number F_L.

Assuming the concentration was the only important parameter, the following fit function was found:

$$F_L = \frac{v_{ls,ldv}}{\sqrt{2 \cdot g \cdot D_p \cdot R_{sd}}} \cdot \left(1 - \tan(\theta)\right) = 0.901 \cdot C_v^{0.106} \tag{6.27-10}$$

Including the particle diameter in the correlation, the following equation was found:

$$F_L = \frac{v_{ls,ldv}}{\sqrt{2 \cdot g \cdot D_p \cdot R_{sd}}} \cdot \left(1 - \tan(\theta)\right) = 0.928 \cdot C_v^{0.105} \cdot d^{0.058} \tag{6.27-11}$$

6.27.9 Wilson & Judge (1976).

The Wilson & Judge (1976) correlation is used for particles for which the Archimedes number is less than about 80. The correlation is expressed in terms of the Durand Froude number F_L according to:

$$F_L = \frac{v_{ls,ldv}}{\sqrt{2 \cdot g \cdot D_p \cdot R_{sd}}} = \left(2 + 0.3 \cdot \log_{10}\left(\frac{d}{D_p \cdot C_D}\right)\right) \tag{6.27-12}$$

This gives for the Limit Deposit Velocity:

$$v_{ls,ldv} = \left(2 + 0.3 \cdot \log_{10}\left(\frac{d}{D_p \cdot C_D}\right)\right) \cdot \sqrt{2 \cdot g \cdot D_p \cdot R_{sd}} \tag{6.27-13}$$

The applicability is approximately where the dimensionless group in the logarithm is larger than 10^{-5}.

6.27.10 Wasp et al. (1977).

Wasp et al. (1977) derived an equation similar to the Durand & Condolios (1952) equation, but instead of using a graph for the Froude number F_L, they quantified the influence of the concentration and the particle diameter to pipe diameter ratio. It should be noted that there are several almost similar equations found in literature where the powers of the volumetric concentration and the proportionality coefficient may differ slightly.

$$v_{ls,ldv} = 4 \cdot C_{vs}^{1/5} \cdot \sqrt{2 \cdot g \cdot D_p \cdot R_{sd}} \cdot \left(\frac{d}{D_p}\right)^{1/6} = F_L \cdot \sqrt{2 \cdot g \cdot D_p \cdot R_{sd}}$$

$$\tag{6.27-14}$$

$$F_L = \frac{v_{ls,ldv}}{\sqrt{2 \cdot g \cdot D_p \cdot R_{sd}}} = 4 \cdot C_{vs}^{1/5} \cdot \left(\frac{d}{D_p}\right)^{1/6}$$

The Froude number F_L decreases slightly with increasing pipe diameter and increases slightly with increasing particle diameter. The increase of F_L with increasing volumetric concentration, without finding a maximum, is probably due to the fact that the volumetric concentrations were hardly higher than 20%.

The equations are also found in literature with slightly different coefficients for the volumetric concentration and the proportionality constant. The behavior however is the same. With an equation of this type never a maximum LDV for particle diameters close to 0.5 mm can be found, since the equations give a continues increase of the LDV with increasing particle diameter.

$$v_{ls,ldv} = 3.8 \cdot C_{vs}^{0.25} \cdot \sqrt{2 \cdot g \cdot D_p \cdot R_{sd}} \cdot \left(\frac{d}{D_p}\right)^{1/6} = F_L \cdot \sqrt{2 \cdot g \cdot D_p \cdot R_{sd}}$$

(6.27-15)

$$F_L = \frac{v_{ls,ldv}}{\sqrt{2 \cdot g \cdot D_p \cdot R_{sd}}} = 3.8 \cdot C_{vs}^{0.25} \cdot \left(\frac{d}{D_p}\right)^{1/6}$$

6.27.11 Thomas (1979).

Thomas (1979) derived an equation for very small particles, proving that there is a lower limit to the LDV. The method is based on the fact that particles smaller than the thickness of the viscous sub layer will be in suspension due to turbulent eddies in the turbulent layer, but may still settle in the laminar viscous sub layer. By using a force balance on a very thin bed layer in the viscous sub layer, he found the following equation:

$$v_{ls,ldv} = 1.49 \cdot \left(g \cdot R_{sd} \cdot C_{vb} \cdot \nu_l \cdot \mu_{sf}\right)^{1/3} \cdot \sqrt{\frac{8}{\lambda_l}}$$

(6.27-16)

$$F_L = \frac{v_{ls,ldv}}{\sqrt{2 \cdot g \cdot D_p \cdot R_{sd}}} = \frac{1.49 \cdot \left(g \cdot R_{sd} \cdot C_{vb} \cdot \nu_l \cdot \mu_{sf}\right)^{1/3} \cdot \sqrt{\frac{8}{\lambda_l}}}{\sqrt{2 \cdot g \cdot D_p \cdot R_{sd}}}$$

(6.27-17)

The Froude number F_L does not depend on the particle size, but on the thickness of the viscous sub layer and so on the Darcy Weisbach friction coefficient. The Froude number F_L does depend on the pipe diameter to a power of about -0.4, due to the Darcy Weisbach friction factor. The line speed found by Thomas (1979) is however an LSDV and not the LDV, so the LDV may be expected to have a higher value. Thomas (1979) also found that the relation between the LDV and the pipe diameter has a dependency with a power between 0.1 as a lower limit and 0.5 as an upper limit.

6.27.12 Oroskar & Turian (1980).

Oroskar & Turian (1980) derived an equation based on balancing the energy required to suspend the particles with the energy derived from the dissipation of an appropriate fraction of the turbulent eddies.

$$\frac{v_{ls,ldv}}{\sqrt{g \cdot d \cdot R_{sd}}} = \left(5 \cdot C_{vs} \cdot \left(1 - C_{vs}\right)^{2 \cdot \beta - 1} \cdot \left(\frac{D_p}{d}\right) \cdot \left(\frac{D_p \cdot \sqrt{g \cdot d \cdot R_{sd}}}{\nu_l}\right)^{1/8}\right)^{8/15}$$

(6.27-18)

In terms of the Froude number F_L this gives:

$$F_L = \frac{v_{ls,ldv}}{\sqrt{2 \cdot g \cdot R_{sd} \cdot D_p}}$$

$$= \left(5 \cdot C_{vs} \cdot \left(1 - C_{vs}\right)^{2 \cdot \beta - 1} \cdot \left(\frac{D_p}{d}\right) \cdot \left(\frac{D_p \cdot \sqrt{g \cdot d \cdot R_{sd}}}{\nu_l}\right)^{1/8}\right)^{8/15} \cdot \frac{\sqrt{g \cdot d \cdot R_{sd}}}{\sqrt{2 \cdot g \cdot R_{sd} \cdot D_p}}$$

(6.27-19)

The Froude number F_L shows a maximum somewhere near 15%-20% depending on the particle diameter. The F_L value increases slightly with an increasing pipe diameter (power 1/10). The F_L value does not depend directly on the particle diameter. The F_L value depends very slightly on the relative submerged density (power 1/30). Oroskar & Turian (1980) also published an empirical equation based on many experiments.

$$\frac{v_{ls,ldv}}{\sqrt{g \cdot d \cdot R_{sd}}} = 1.85 \cdot C_{vs}^{0.1536} \cdot \left(1 - C_{vs}\right)^{0.3564} \cdot \left(\frac{D_p}{d}\right)^{0.378} \cdot \left(\frac{D_p \cdot \sqrt{g \cdot d \cdot R_{sd}}}{\nu_l}\right)^{0.09} \tag{6.27-20}$$

In terms of the Froude number F_L this gives:

$$
\begin{aligned}
F_L &= \frac{v_{ls,ldv}}{\sqrt{2 \cdot g \cdot R_{sd} \cdot D_p}} \\
&= 1.85 \cdot C_{vs}^{0.1536} \cdot \left(1 - C_{vs}\right)^{0.3564} \cdot \left(\frac{D_p}{d}\right)^{0.378} \cdot \left(\frac{D_p \cdot \sqrt{g \cdot d \cdot R_{sd}}}{\nu_l}\right)^{0.09} \cdot \frac{\sqrt{g \cdot d \cdot R_{sd}}}{\sqrt{2 \cdot g \cdot R_{sd} \cdot D_p}}
\end{aligned}
\tag{6.27-21}
$$

The Froude number F_L shows a maximum somewhere near 15%-20% concentration depending on the particle diameter. The F_L value decreases very slightly with increasing pipe diameter (power -0.032). The FL value increases slightly with increasing particle diameter (power 0.167). The FL value increases slightly with an increasing relative submerged density (power 0.045).

In the comparison of Oroskar & Turian (1980), the empirical equation gives less deviation compared to the theoretical equation. The main difference between the two equations is the dependency of the F_L value on the pipe diameter (+0.1 versus -0.032).

6.27.13 Parzonka et al. (1981).

Parzonka et al. (1981) investigated to influence of the spatial volumetric concentration on the LDV. The data obtained from literature covered a wide range of pipe diameters, from 0.0127 m to 0.8000 m. The particles were divided into 5 categories:
1. Small size sand particles ranging from 0.1 mm to 0.28 mm.
2. Medium and coarse size sand particles ranging from 0.4 mm to 0.85 mm.
3. Coarse size sand and gravel ranging from 1.15 mm to 19 mm.
4. Small size high density materials ranging from 0.005 mm to 0.3 mm.
5. Coal particles ranging from 1 mm to 2.26 mm.

Their conclusion state that the spatial concentration has a large influence on the LDV. The increase of the LDV with increasing concentration was already recognized before, but the occurrence of a maximum LDV at a concentration of about 15% and a decrease of the LDV with further increasing concentration was not commonly noted. Parzonka et al. (1981) also concluded that the presence of very small particles in the PSD reduces the LDV. It should be noted that Parzonka et al. (1981) collected a lot of valuable data.

6.27.14 Turian et al. (1987).

Turian et al. (1987) improves the relation of Oroskar & Turian (1980), based on more experiments, giving:

$$
\begin{aligned}
v_{ls,ldv} &= 1.7951 \cdot C_{vs}^{0.1087} \cdot \left(1 - C_{vs}\right)^{0.2501} \cdot \left(\frac{D_p \cdot \sqrt{g \cdot D_p \cdot R_{sd}}}{\nu_l}\right)^{0.00179} \cdot \left(\frac{d}{D_p}\right)^{0.06623} \\
&\quad \cdot \sqrt{2 \cdot g \cdot R_{sd} \cdot D_p}
\end{aligned}
\tag{6.27-22}
$$

In terms of the Froude number F_L this gives:

$$
\begin{aligned}
F_L &= \frac{v_{ls,ldv}}{\sqrt{2 \cdot g \cdot R_{sd} \cdot D_p}} \\
&= 1.7951 \cdot C_{vs}^{0.1087} \cdot \left(1 - C_{vs}\right)^{0.2501} \cdot \left(\frac{D_p \cdot \sqrt{g \cdot D_p \cdot R_{sd}}}{\nu_l}\right)^{0.00179} \cdot \left(\frac{d}{D_p}\right)^{0.06623}
\end{aligned}
\tag{6.27-23}
$$

The Froude number F_L shows a maximum somewhere near 15%-20% concentration depending on the particle diameter. The Froude number F_L increases slightly with increasing particle diameter. The Froude number F_L decreases slightly with increasing pipe diameter with a power of -0.0635.

6.27.15 Davies (1987).

Davies (1987) based the LDV on the equilibrium between the gravity force and the eddy velocity pressure force. Only eddies with a size close to the particle diameter can lift the particles. Much smaller eddies are not strong enough and will be involved in viscous dissipation, while much larger eddies cannot closely approach the bottom of the pipe where the solids are sedimented. The downward directed force, the sedimentation force, caused by the difference in density between the particle and the water can be calculated by:

$$\mathbf{F_{down}} = (\rho_s - \rho_l) \cdot g \cdot \frac{\pi}{6} \cdot d^3 \cdot \left(1 - C_{vs}\right)^n \tag{6.27-24}$$

Where **n** depends on the Reynolds number related to the terminal settling velocity. The eddy fluctuation force equals the eddy pressure times the area of the particle, giving:

$$\mathbf{F_{up}} = \rho_l \cdot \frac{\pi}{4} \cdot d^2 \cdot v_{ef}^2 \tag{6.27-25}$$

Where v_{ef} is the turbulent fluctuation velocity for the eddies concerned. When no particles are settling on the bottom of the pipe, so all the particles are just being lifted by the eddies, this results in a turbulent fluctuation velocity:

$$\mathbf{v_{ef}} = \sqrt{\frac{2}{3} \cdot g \cdot R_{sd} \cdot d \cdot \left(1 - C_{vs}\right)^n} \tag{6.27-26}$$

The last step is to relate the turbulent fluctuation velocity to the LDV. The turbulent fluctuation velocity is related to the power dissipated per unit mass of fluid by:

$$\mathbf{v_{ef}^3} = \mathbf{P} \cdot \mathbf{d} \quad \text{with:} \quad P = \lambda_l \cdot \frac{v_{ls,ldv}^3}{2 \cdot D_p} \tag{6.27-27}$$

Using an approximation for the Darcy Weisbach friction factor according to Blasius:

$$\lambda_l = \frac{0.3164}{Re^{1/4}} \approx 0.32 \cdot v_l^{0.25} \cdot v_{ls}^{-0.25} \cdot D_p^{-0.25} \tag{6.27-28}$$

Gives:

$$\mathbf{v_{ef}} = \left(0.16 \cdot v_l^{0.25} \cdot v_{ls,ldv}^{2.75} \cdot D_p^{-1.25} \cdot d\right)^{1/3} \quad \text{or} \quad \mathbf{v_{ef}} = \left(\lambda_l \cdot \frac{v_{ls,ldv}^3}{2 \cdot D_p} \cdot d\right)^{1/3} \tag{6.27-29}$$

The eddy velocity is corrected for the presence of particles by:

$$\mathbf{v_{ef}} \cdot \left(1 + \alpha \cdot C_{vs}\right) = \left(0.16 \cdot v_l^{0.25} \cdot v_{ls,ldv}^{2.75} \cdot D_p^{-1.25} \cdot d\right)^{1/3}$$

or

$$\mathbf{v_{ef}} \cdot \left(1 + \alpha \cdot C_{vs}\right) = \left(\lambda_l \cdot \frac{v_{ls,ldv}^3}{2 \cdot D_p} \cdot d\right)^{1/3} \tag{6.27-30}$$

Now equating the sedimentation velocity and the eddy velocity gives:

$$\frac{\left(0.16 \cdot \nu_l^{0.25} \cdot v_{ls,ldv}^{2.75} \cdot D_p^{-1.25} \cdot d\right)^{1/3}}{\left(1 + \alpha \cdot C_{vs}\right)} = \sqrt{\frac{2}{3} \cdot g \cdot R_{sd} \cdot d \cdot \left(1 - C_{vs}\right)^n} \tag{6.27-31}$$

Or:

$$\frac{\left(\lambda_l \cdot \frac{v_{ls,ldv}^3}{2 \cdot D_p} \cdot d\right)^{1/3}}{\left(1 + \alpha \cdot C_{vs}\right)} = \sqrt{\frac{2}{3} \cdot g \cdot R_{sd} \cdot d \cdot \left(1 - C_{vs}\right)^n} \tag{6.27-32}$$

Giving:

$$v_{ls,ldv} = 1.066 \cdot \left(1 + \alpha \cdot C_{vs}\right)^{1.091} \cdot \left(1 - C_{vs}\right)^{0.545 \cdot n} \cdot \nu_l^{-0.091} \cdot d^{0.181} \cdot \left(2 \cdot g \cdot R_{sd}\right)^{0.545} \cdot D_p^{0.455}$$

or :

$$v_{ls,ldv} = 0.727 \cdot \left(\frac{1}{\lambda_l}\right)^{1/3} \cdot \left(\frac{d}{D_p}\right)^{1/6} \cdot \left(1 + \alpha \cdot C_{vs}\right) \cdot \left(1 - C_{vs}\right)^{1/2 \cdot n} \cdot \left(2 \cdot g \cdot R_{sd} \cdot D_p\right)^{1/2} \tag{6.27-33}$$

The Durand Froude number is now:

$$F_L = \frac{v_{ls,ldv}}{\sqrt{2 \cdot g \cdot D_p \cdot R_{sd}}} = 1.066 \cdot \left(1 + \alpha \cdot C_{vs}\right)^{1.091} \cdot \left(1 - C_{vs}\right)^{0.545 \cdot n} \cdot \nu_l^{-0.091} \cdot d^{0.181} \cdot \left(\frac{2 \cdot g \cdot R_{sd}}{D_p}\right)^{0.045}$$

or :

$$F_L = \frac{v_{ls,ldv}}{\sqrt{2 \cdot g \cdot D_p \cdot R_{sd}}} = 0.727 \cdot \left(\frac{1}{\lambda_l}\right)^{1/3} \cdot \left(\frac{d}{D_p}\right)^{1/6} \cdot \left(1 + \alpha \cdot C_{vs}\right) \cdot \left(1 - C_{vs}\right)^{1/2 \cdot n} \tag{6.27-34}$$

The resulting equation gives a maximum Durand Froude number near a concentration of 15%. The factor **α=3.64** according to Davies (1987). The equations containing the Darcy Weisbach friction factors were not reported by Davies (1987), but they give a better understanding. In fact the approximation used by Davies (1987) for the Darcy Weisbach friction factor is appropriate for small Reynolds numbers, but not for large Reynolds numbers as occur in dredging operations. The Durand Froude number decreases with the pipe diameter to a power depending on the Reynolds number, due to the Darcy Weisbach friction factor. Davies (1987) found a power of -0.045, but at larger Reynolds numbers this may approach -0.1.

6.27.16 Schiller & Herbich (1991).

Schiller & Herbich (1991) proposed an equation for the Durand & Condolios (1952) Froude number.

$$F_L = \frac{v_{ls,ldv}}{\sqrt{2 \cdot g \cdot D_p \cdot R_{sd}}} = 1.3 \cdot C_{vs}^{0.125} \cdot \left(1 - e^{-6.9 \cdot d_{50}}\right) \tag{6.27-35}$$

The particle diameter in this equation is in mm. The equation is just a fit function on the Durand & Condolios (1952) data and has no physical meaning.

6.27.17 Gogus & Kokpinar (1993).

Gogus & Kokpinar (1993) proposed the following equation based on curve fitting:

$$v_{ls,ldv} = 0.124 \cdot \left(\frac{D_p}{d}\right)^{0.537} \cdot C_{vs}^{0.322} \cdot R_{sd}^{0.121} \cdot \left(\frac{v_t \cdot d}{\nu_l}\right)^{0.243} \cdot \sqrt{g \cdot D_p} \tag{6.27-36}$$

With the Froude number F_L:

$$F_L = \frac{v_{ls,ldv}}{\sqrt{2 \cdot g \cdot D_p \cdot R_{sd}}} = 0.088 \cdot \left(\frac{D_p}{d}\right)^{0.537} \cdot C_{vs}^{0.322} \cdot R_{sd}^{-0.379} \cdot \left(\frac{v_t \cdot d}{\nu_l}\right)^{0.243} \tag{6.27-37}$$

The Froude number F_L depends strongly on the pipe diameter. An increasing pipe diameter results in an increasing F_L. The F_L value decreases with increasing relative submerged density. The influence of the particle diameter is more complex. First the F_L value increases up to a particle diameter of 0.5 mm, for larger particles the F_L value decreases, so there is a maximum near **d=0.5 mm**.

6.27.18 Gillies (1993).

Gillies (1993) derived an expression for the Durand & Condolios (1952) Froude number F_L, giving a Limit Deposit Velocity of:

$$v_{ls,ldv} = e^{\left(0.51 - 0.0073 \cdot C_D - 12.5 \cdot \left(\frac{(g \cdot \nu_l)^{2/3}}{g \cdot d} - 0.14\right)^2\right)} \cdot \sqrt{2 \cdot g \cdot D_p \cdot R_{sd}} \tag{6.27-38}$$

With the Froude number F_L:

$$F_L = \frac{v_{ls,ldv}}{\sqrt{2 \cdot g \cdot D_p \cdot R_{sd}}} = e^{\left(0.51 - 0.0073 \cdot C_D - 12.5 \cdot \left(\frac{(g \cdot \nu_l)^{2/3}}{g \cdot d} - 0.14\right)^2\right)} \tag{6.27-39}$$

The Durand & Condolios (1952) Froude number F_L does not depend on the pipe diameter and the volumetric concentration. The Froude number F_L should be considered the maximum F_L at a concentration near 20%. The F_L value increases with the particle diameter to a maximum of 1.64 for **d=0.4 mm** after which it decreases slowly to an asymptotic value of about 1.3 for very large particles. This is consistent with Wilson's (1979) nomogram (which gives the LSDV) and consistent with the F_L graph published by Durand & Condolios (1952). Quantitatively this equation matches the graph of Durand (1953), which differs by a factor 1.28 (to high) from the original graph.

6.27.19 Van den Berg (1998).

Van den Berg (1998) and (2013) gave an equation for the Froude number F_L:

$$v_{ls,ldv} = 0.298 \cdot \left(5 - \frac{1}{\sqrt{1000 \cdot d}}\right) \cdot \left(\frac{C_v}{C_v + 0.1}\right)^{1/6} \cdot \sqrt{2 \cdot g \cdot D_p \cdot R_{sd}} \tag{6.27-40}$$

With the Froude number F_L:

$$F_L = \frac{v_{ls,ldv}}{\sqrt{2 \cdot g \cdot D_p \cdot R_{sd}}} = 0.298 \cdot \left(5 - \frac{1}{\sqrt{1000 \cdot d}}\right) \cdot \left(\frac{C_v}{C_v + 0.1}\right)^{1/6} \tag{6.27-41}$$

The Froude number F_L increases with increasing particle diameter. The F_L value does not show a maximum for a concentration around 20%, but continues to increase. The F_L value does not depend on the pipe diameter.

6.27.20 Kokpinar & Gogus (2001).

Kokpinar & Gogus (2001) proposed the following equation based on curve fitting:

$$v_{ls,ldv} = 0.055 \cdot \left(\frac{D_p}{d} \right)^{0.6} \cdot C_{vs}^{0.27} \cdot R_{sd}^{0.07} \cdot \left(\frac{v_t \cdot d}{v_l} \right)^{0.3} \cdot \sqrt{g \cdot D_p} \tag{6.27-42}$$

With the Froude number F_L:

$$F_L = \frac{v_{ls,ldv}}{\sqrt{2 \cdot g \cdot D_p \cdot R_{sd}}} = 0.0389 \cdot \left(\frac{D_p}{d} \right)^{0.6} \cdot C_{vs}^{0.27} \cdot R_{sd}^{-0.43} \cdot \left(\frac{v_t \cdot d}{v_l} \right)^{0.3} \tag{6.27-43}$$

The Froude number F_L depends strongly on the pipe diameter. An increasing pipe diameter results in an increasing F_L. The F_L value decreases with increasing relative submerged density. The influence of the particle diameter is more complex. First the F_L value increases up to a particle diameter of 0.5 mm, for larger particles the F_L value decreases, so there is a maximum near **d=0.5 mm**. The equation behaves similar to the Gogus & Kokpinar (1993) equation.

6.27.21 Shook et al. (2002).

Shook et al. (2002) give the following correlations for the Durand Froude number F_L:

$$F_L = \frac{v_{ls,ldv}}{\sqrt{2 \cdot g \cdot D_p \cdot R_{sd}}} = 0.197 \cdot Ar^{0.4} = 0.197 \cdot \left(\frac{4 \cdot g \cdot d^3 \cdot R_{sd}}{3 \cdot v_l^2} \right)^{0.4} \quad \text{for} \quad 80 < Ar < 160$$

$$F_L = \frac{v_{ls,ldv}}{\sqrt{2 \cdot g \cdot D_p \cdot R_{sd}}} = 1.19 \cdot Ar^{0.045} = 1.19 \cdot \left(\frac{4 \cdot g \cdot d^3 \cdot R_{sd}}{3 \cdot v_l^2} \right)^{0.045} \quad \text{for} \quad 160 < Ar < 540 \tag{6.27-44}$$

$$F_L = \frac{v_{ls,ldv}}{\sqrt{2 \cdot g \cdot D_p \cdot R_{sd}}} = 1.78 \cdot Ar^{-0.019} = 1.78 \cdot \left(\frac{4 \cdot g \cdot d^3 \cdot R_{sd}}{3 \cdot v_l^2} \right)^{-0.019} \quad \text{for} \quad 540 < Ar$$

The Durand & Condolios (1952) Froude number F_L does not depend on the pipe diameter and the volumetric concentration. The Froude number F_L should be considered the maximum F_L at a concentration near 20%. Shook et al. (2002), based these equations on the particle Archimedes number:

$$Ar = \frac{4 \cdot g \cdot d^3 \cdot R_{sd}}{3 \cdot v_l^2} \tag{6.27-45}$$

6.27.22 Wasp & Slatter (2004).

Wasp & Slatter (2004) derived an equation for the LDV of small particles in large pipes, based on the work of Wasp & Slatter.

$$v_{ls,ldv} = 0.18 \cdot R_{sd}^{1/2} \left(\frac{d_{95} \cdot \sqrt{g \cdot D_p}}{v_l} \right)^{0.22} \cdot e^{4.34 \cdot C_{vs}} \tag{6.27-46}$$

With the Froude number F_L:

$$F_L = \frac{v_{ls,ldv}}{\sqrt{2 \cdot g \cdot D_p \cdot R_{sd}}} = \frac{0.18 \cdot \left(\frac{d_{95} \cdot \sqrt{g \cdot D_p}}{\nu_l} \right)^{0.22} \cdot e^{4.34 \cdot C_{vs}}}{\sqrt{2 \cdot g \cdot D_p}} \tag{6.27-47}$$

The Froude number F_L does not depend on the relative submerged density. The F_L value decreases with increasing pipe diameter (power -0.39). The F_L value increases with increasing particle diameter (power +0.22).

6.27.23 Sanders et al. (2004).

Sanders et al. (2004) investigated the deposition velocities for particles of intermediate size in turbulent flows. Their starting points were the models of Wilson & Judge (1976) and Thomas (1979).

Sanders et al. (2004) define a dimensionless particle diameter according to:

$$d^+ = v_{ls,ldv} \cdot \sqrt{\frac{\lambda_l}{8}} \cdot \frac{d}{\nu_l} \tag{6.27-48}$$

Based on this dimensionless particle diameter and equation was derived for the Limit Deposit Velocity, giving:

$$v_{ls,ldv}^* = \frac{v_{ls,ldv} \cdot \sqrt{\frac{\lambda_l}{8}}}{\left(g \cdot \nu_l \cdot R_{sd} \right)^{1/3}} = \frac{0.76 + 0.15 \cdot d^+}{\left(\left(C_{vb} - C_{vs} \right)^{0.88} \right)^{1/3}} \tag{6.27-49}$$

This equation is implicit in the LDV, because the dimensionless particle diameter also contains the LDV. However with some rewriting the equation can be made explicit, giving:

$$v_{ls,ldv} = \sqrt{\frac{8}{\lambda_l}} \cdot \frac{0.76 \cdot \left(g \cdot \nu_l \cdot R_{sd} \right)^{1/3}}{\left(\left(C_{vb} - C_{vs} \right)^{0.88} \right)^{1/3} - 0.15 \cdot \frac{d}{\nu_l} \cdot \left(g \cdot \nu_l \cdot R_{sd} \right)^{1/3}}$$

$$= \sqrt{\frac{8}{\lambda_l}} \cdot \frac{0.76}{\left(\frac{\left(C_{vb} - C_{vs} \right)^{0.88}}{\left(g \cdot \nu_l \cdot R_{sd} \right)} \right)^{1/3} - 0.15 \cdot \frac{d}{\nu_l}} \approx \sqrt{\frac{8}{\lambda_l}} \cdot \frac{0.76}{34 - 150000 \cdot d} \text{ for sand and water} \tag{6.27-50}$$

With the water and sand properties the Thomas (1979) equation would give 0.018, excluding the Darcy Weisbach term, while Sanders et al. (2004) give 0.022 for very small particles. Sanders et al. (2004) however show an increasing LDV with increasing particle diameter, while the Thomas (1979) equation is independent of the particle size. When the denominator becomes zero, the Sanders et al. (2004) relation becomes infinite (at 0.226 mm for sand and water). So somewhere for **d<0.226** mm another mechanism will prevail.

6.27.24 Lahiri (2009).

Lahiri (2009) investigated the relation of the LDV with the solids density to liquid density ratio, with the pipe diameter, with the particle diameter and with the volumetric concentration. He did not give an equation, but he gave the relation with the 4 parameters. The relation between the LDV and the solids density, liquid density ratio gives a power of 0.3666. Translated in to the relation with the relative submerged density the power found is 0.2839. The relation between the LDV and the pipe diameter gives a power of 0.348. Almost matching the power of 1/3 as found by Jufin & Lopatin (1966). The relation between the LDV and the particle diameter is very weak giving a power of 0.042. The relation between the LDV and the volumetric concentration shows a maximum LDV

at a volumetric concentration of about 15%. At very low concentrations and at concentrations near 40%, the LDV is reduced to about 60% of the maximum at 15%. This matches the findings of Durand & Condolios (1952).

6.27.25 Poloski et al. (2010).

Poloski et al. (2010) investigated the Limit Deposit Velocity of small but dense particles. Their concept is based on considering that the sedimentation force (the submerged gravity force on a particle) equals the eddy fluctuation velocity drag force on the particle. Only eddies with a size close to the particle diameter can lift the particles. Much smaller eddies are not strong enough and will be involved in viscous dissipation, while much larger eddies cannot closely approach the bottom of the pipe where the solids are sedimented. The approach is similar to the Davies (1987) approach, but they added a drag coefficient in the eddy fluctuation force, where Davies (1987) used a factor 1. The resulting Durand Froude number is:

$$
F_L = \frac{v_{ls,ldv}}{\sqrt{2 \cdot g \cdot D_p \cdot R_{sd}}} = 0.417 \cdot Ar^{0.15} = 0.417 \cdot \left(\frac{4 \cdot g \cdot d^3 \cdot R_{sd}}{3 \cdot v_l^2} \right)^{0.15} \quad \text{for} \quad 80 > Ar \tag{6.27-51}
$$

Their original equation differs due to the fact that they did not use the 2 in the Durand Froude number, so their original factor was 0.59 instead of 0.417. At higher concentrations there is a deviation according to:

$$
F_L = \frac{v_{ls,ldv}}{\sqrt{2 \cdot g \cdot D_p \cdot R_{sd}}} = 0.417 \cdot Ar^{0.15} \cdot \left(1 - C_{vs}\right)^{n/2} \cdot \left(1 + \alpha \cdot C_{vs}\right) \tag{6.27-52}
$$

This gives a maximum Durand Froude number F_L for:

$$
C_{vs} = \frac{\left(2 \cdot \alpha - n\right)}{\alpha \cdot \left(n + 2\right)} \tag{6.27-53}
$$

With **n=4** and **α=3.64**, the maximum Durand Froude number F_L will occur at a concentration C_{vs}=**0.15**. Different values of **n** and **α** will give a slightly different concentration.

6.27.26 Souza Pinto et al. (2014).

Souza Pinto et al. (2014) also derived an equation for the LDV based on the work of Wasp & Slatter.

$$
v_{ls,ldv} = 0.124 \cdot R_{sd}^{1/2} \left(\frac{d \cdot \sqrt{g \cdot D_p}}{v_l} \right)^{0.37} \cdot \left(\frac{d \cdot \psi}{D_p} \right)^{-0.007} \cdot e^{3.1 \cdot C_{vs}} \tag{6.27-54}
$$

With the Froude number F_L:

$$
F_L = \frac{v_{ls,ldv}}{\sqrt{2 \cdot g \cdot D_p \cdot R_{sd}}} = \frac{0.124 \cdot R_{sd}^{1/2} \left(\dfrac{d \cdot \sqrt{g \cdot D_p}}{v_l} \right)^{0.37} \cdot \left(\dfrac{d \cdot \psi}{D_p} \right)^{-0.007} \cdot e^{3.1 \cdot C_{vs}}}{\sqrt{2 \cdot g \cdot D_p \cdot R_{sd}}} \tag{6.27-55}
$$

The Froude number F_L does not depend on the relative submerged density. The F_L value decreases with increasing pipe diameter (power -0.312). The F_L value increases with increasing particle diameter (power +0.3).

6.27.27 Fitton (2015).

Fitton (2015) gives an improvement to the Wasp (1977) equation and compares it with some other equations. The equation is empirical and is valid for both pipes and open channel flow. The equation adds a viscosity term to the LDV, which for water almost gives the original Wasp (1977) equation.

$$v_{ls,ldv} = 1.48 \cdot C_{vs}^{0.19} \cdot \sqrt{2 \cdot g \cdot D_p \cdot R_{sd}} \cdot \left(\frac{d}{D_p}\right)^{1/6} \cdot \left(\nu_l \cdot \rho_l\right)^{-0.12} = F_L \cdot \sqrt{2 \cdot g \cdot D_p \cdot R_{sd}}$$

(6.27-56)

$$F_L = \frac{v_{ls,ldv}}{\sqrt{2 \cdot g \cdot D_p \cdot R_{sd}}} = 1.48 \cdot C_{vs}^{0.19} \cdot \left(\frac{d}{D_p}\right)^{1/6} \cdot \left(\nu_l \cdot \rho_l\right)^{-0.12}$$

The equation can also be used for non-Newtonian fluids. In that case the Bingham plastic viscosity at a tangent of at least 400 s^{-1} should be used.

6.27.28 Thomas (2015).

Thomas (2015) modified the Wilson & Judge (1976) equation to make it suitable for finer particles and larger pipes. The original correlation is expressed in terms of the Durand Froude number F_L according to:

$$F_L = \frac{v_{ls,ldv}}{\sqrt{2 \cdot g \cdot D_p \cdot R_{sd}}} = \left(2 + 0.3 \cdot \log_{10}\left(\frac{d}{D_p \cdot C_D}\right)\right)$$

(6.27-57)

This gives for the Limit Deposit Velocity:

$$v_{ls,ldv} = \left(2 + 0.3 \cdot \log_{10}\left(\frac{d}{D_p \cdot C_D}\right)\right) \cdot \sqrt{2 \cdot g \cdot D_p \cdot R_{sd}}$$

(6.27-58)

The new correlation gives:

$$F_L = \frac{v_{ls,ldv}}{\sqrt{2 \cdot g \cdot D_p \cdot R_{sd}}}$$

$$= \left(2 + 0.305 \cdot \log_{10}\left(\frac{d}{D_p \cdot C_D}\right) + 0.00011 \cdot \left(\frac{d}{D_p \cdot C_D}\right)^{-0.489} - 0.044 \cdot \left(10^7 \cdot \left(\frac{d}{D_p \cdot C_D}\right)\right)^{-1.06}\right)$$

(6.27-59)

This gives for the Limit Deposit Velocity:

$$v_{ls,ldv} = \left(2 + 0.305 \cdot \log_{10}\left(\frac{d}{D_p \cdot C_D}\right) + 0.00011 \cdot \left(\frac{d}{D_p \cdot C_D}\right)^{-0.489} - 0.044 \cdot \left(10^7 \cdot \left(\frac{d}{D_p \cdot C_D}\right)\right)^{-1.06}\right)$$

$$\cdot \sqrt{2 \cdot g \cdot D_p \cdot R_{sd}}$$

(6.27-60)

Although the publication mentions the deposit limit, most probably it is the Limit of Stationary Deposit Velocity and not the Limit Deposit Velocity.

6.27.29 Conclusions & Discussion.

Figure 6.27-2, Figure 6.27-3, Figure 6.27-4 and Figure 6.27-5 show the Limit Deposit Velocities of DHLLDV (see Chapter 7), Durand & Condolios (1952), Jufin & Lopatin (1966), Wasp et al. (1970), Wasp & Slatter (2004), Souza Pinto et al. (2014), Hepy et al. (2008), Gogus & Kokpinar (1993), Kokpinar & Gogus (2001), van den Berg (1998), Turian et al. (1987) and Gillies (1993) for 4 pipe diameters. The curves of Hepy et al. (2008), Gogus & Kokpinar (1993) and Kokpinar & Gogus (2001) show a maximum F_L value for particles with a diameter near **d=0.5 mm**. However these models show an increasing F_L value with the pipe diameter, which contradicts the numerous experimental data, showing a slight decrease. The models of Turian et al. (1987), Wasp et al. (1970), Wasp & Slatter (2004) and Souza Pinto et al. (2014) show an increasing F_L value with increasing particle diameter and a slight decrease with the pipe diameter. Jufin & Lopatin (1966) show an increase with the particle diameter and a slight decrease with the pipe diameter (power -1/6). The model of van den Berg (1998) shows an increasing F_L with the particle diameter, but no dependency on the pipe diameter. Durand & Condolios (1952) did not give an equation but a graph. The data points as derived from the original publication in (1952) (Low Correct) and from Durand (1953) (High Incorrect) are shown in the graphs. The data points show a maximum for **d=0.5 mm**. They did not report any dependency on the pipe diameter. The model of Gillies (1993) tries to quantify the Durand & Condolios (1952) data points (but the incorrect ones) but does not show any dependency on the pipe diameter for the F_L Froude number. The increase of the FL value with the pipe diameter of the Hepy et al. (2008), Gogus & Kokpinar (1993) and Kokpinar & Gogus (2001) models is probably caused by the forced d/D_p relation. With a strong relation with the particle diameter and a weak relation for the pipe diameter, the pipe diameter will follow the particle diameter. Another reason may be the fact that they used pipe diameters up to 0.1524 m (6 inch) and the smaller the pipe diameter the more probable the occurrence of a sliding bed and other limiting conditions.

The figures show that for small pipe diameters all models are close. The reason is probably that most experiments are carried out with small pipe diameters. Only Jufin & Lopatin (1966) covered a range from 0.02 m to 0.9 m pipe diameters. Recently Thomas (2014) gave an overview and analysis of the LDV (or sometimes the LSDV). He repeated the findings that the LDV depends on the pipe diameter with a power smaller than 0.5 but larger than 0.1. The value of 0.1 is for very small particles, while for normal sand and gravels a power is expected between 1/3 according to Jufin & Lopatin (1966) and 1/2 according to Durand & Condolios (1952). Most equations are one term equations, making it impossible to cover all aspects of the LDV behavior. Only Gillies (1993) managed to construct an equation that gets close. The Gillies (1993) equation would be a good alternative in a modified form, incorporating the pipe diameter and relative submerged density effects, valid for particle with **d>0.2 mm**, like:

$$v_{ls,ldv} = 1.05 \cdot e^{\left(0.51 - 0.0073 \cdot C_D - 12.5 \cdot \left(\frac{(g \cdot \nu_l)^{2/3}}{g \cdot d} - 0.14\right)^2\right)} \cdot \left(2 \cdot g \cdot D_p \cdot R_{sd}\right)^{0.42} \cdot \left(\frac{1.585}{R_{sd}}\right)^{0.12} \tag{6.27-61}$$

With the Froude number F_L:

$$F_L = \frac{v_{ls,ldv}}{\sqrt{2 \cdot g \cdot D_p \cdot R_{sd}}} = 1.05 \cdot \frac{e^{\left(0.51 - 0.0073 \cdot C_D - 12.5 \cdot \left(\frac{(g \cdot \nu_l)^{2/3}}{g \cdot d} - 0.14\right)^2\right)}}{\left(2 \cdot g \cdot D_p \cdot R_{sd}\right)^{0.08}} \cdot \left(\frac{1.585}{R_{sd}}\right)^{0.12} \tag{6.27-62}$$

Lately Lahiri (2009) performed an analysis using artificial neural network and support vector regression. Azamathulla & Ahmad (2013) performed an analysis using adaptive neuro-fuzzy interference system and gene-expression programming. Although these methodologies may give good correlations, they do not explain the physics. Lahiri (2009) however did give relations for the volumetric concentration, the particle diameter, the pipe diameter and the relative submerged density.

Resuming, the following conclusions can be drawn for sand and gravel:
1. The LDV is proportional to the pipe diameter to a power between 1/3 and 1/2 (about 0.4).
2. The LDV has a lower limit for very small particles, after which it increases to a maximum at a particle diameter of about **d=0.5 mm**.
3. For larger particles the LDV decreases to a particle diameter of about 2 mm.
4. For very large particles the LDV remains constant.

5. For particles **d>0.015·D$_p$**, the LDV increases again. This limit is however questionable and requires more research.

The relation between the LDV and the relative submerged density is not very clear, however the data shown by Kokpinar & Gogus (2001) and the conclusions of Lahiri (2009) show that the **F$_L$** value decreases with increasing solids density and thus relative submerged density **R$_{sd}$** to a power of -0.2 to -0.4.

The volumetric concentration leading to the maximum LDV is somewhere between 15% and 25%, depending on the particle diameter. For small concentrations a minimum LDV is observed by Durand & Condolios (1952). This minimum LDV increases with the particle diameter and reaches the LDV of 20% at a particle diameter of 2 mm with a pipe diameter of 0.1524 m (6 inch).

For the dredging industry the Jufin & Lopatin (1966) equation gives a good approximation for sand and gravel, although a bit conservative. The model of van den Berg (1998) is suitable for large diameter pipes as used in dredging sand and/or gravel, but underestimates the LDV for pipe diameters below 0.8 m. Both models tend to underestimate the LDV for particle diameters below 1 mm.

Analyzing the literature, equations and experimental data, the LDV can be divided into a number of regimes for sand and gravel:

1. Very small particles, smaller than about 50% of the thickness of the viscous sub layer, a lower limit of the LDV. This is for particles up to about 0.015 mm in large pipes to 0.04 mm in very small pipes.
2. Small particles up to about 0.15 mm, a smooth bed, show an increasing LDV with increasing particle diameter.
3. Medium particles with a diameter from 0.15 mm up to a diameter of 2 mm, a transition zone from a smooth bed to a rough bed. First the LDV increases to a particle diameter of about 0.5 mm, after which it decreases slowly to an asymptotic value at a diameter of 2mm.
4. Large particles with a diameter larger than 2 mm, a rough bed, giving a constant LDV.
5. Particles with a particle diameter to pipe diameter ratio larger than about 0.015 cannot be carried by turbulent eddies, just because the eddies are not large enough. This will probably result in an increasing LDV with the particle diameter.

The above conclusions are the starting points of the DHLLDV Limit Deposit Velocity Model as derived and described in Chapter 7 and already shown in the figures.
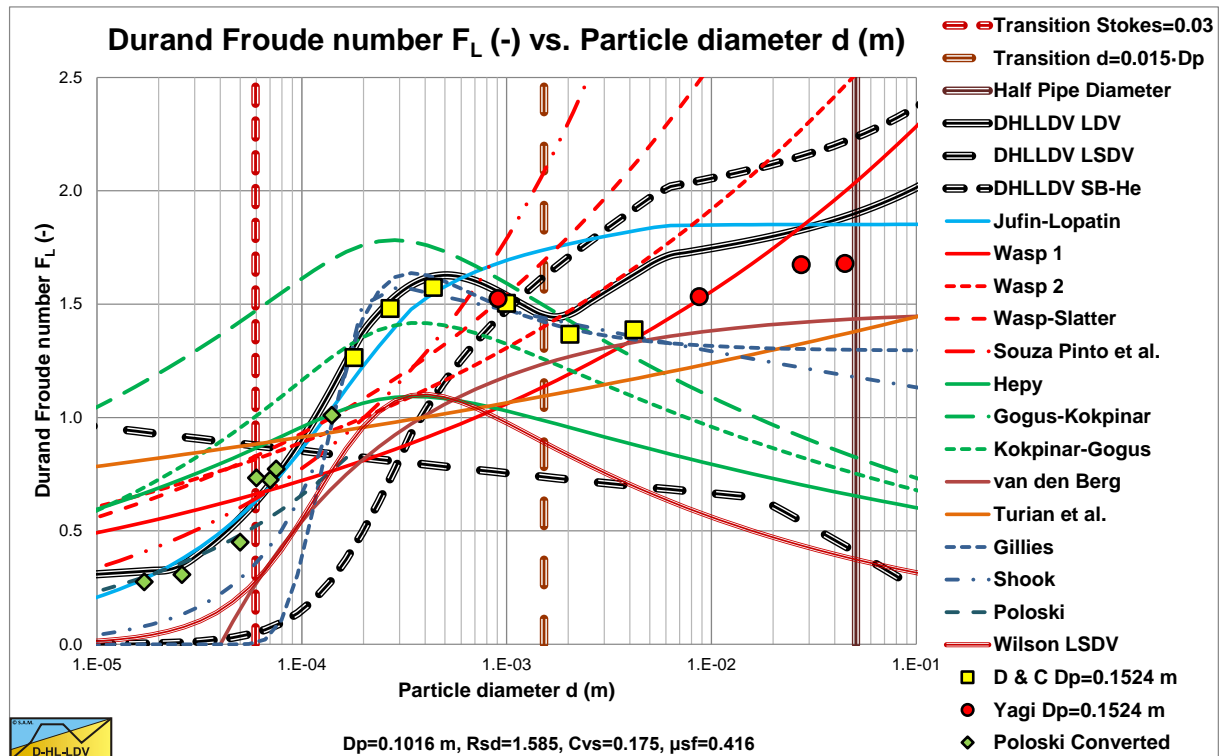
Figure 6.27-2: A number of LDV models for an 0.1016 m (4 inch) pipe and 17.5% concentration.
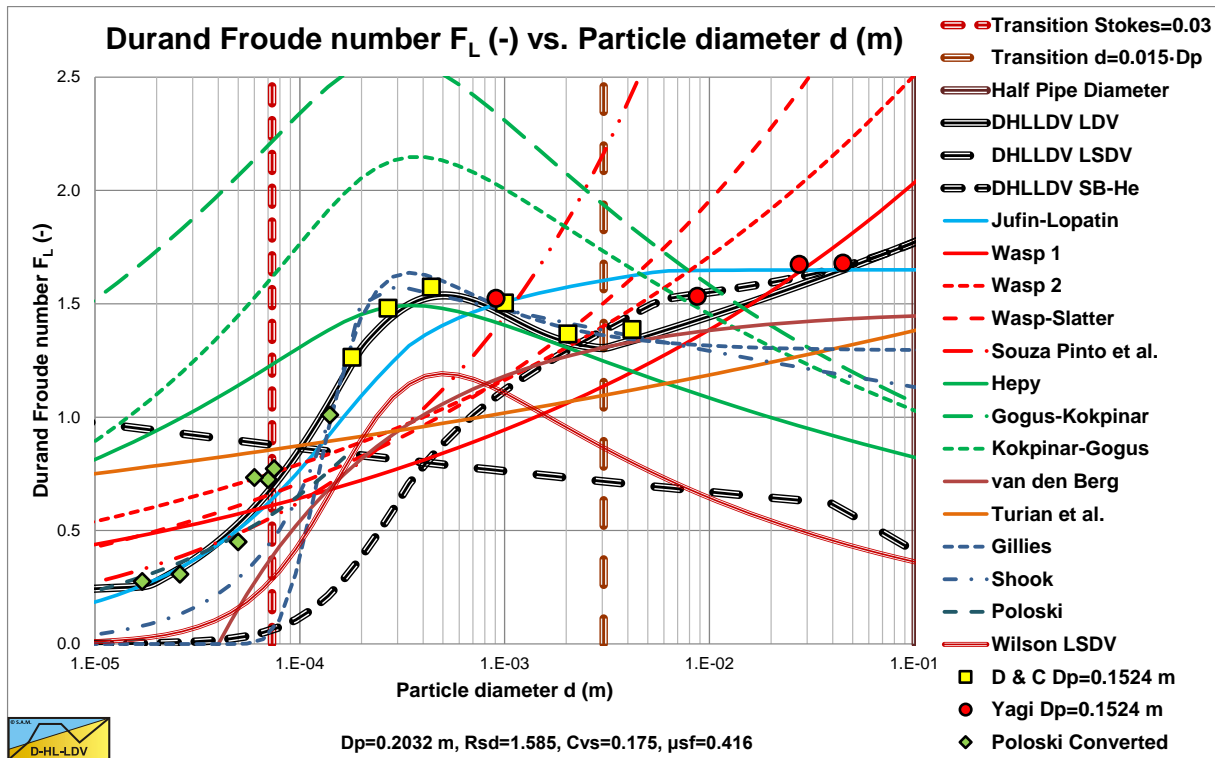
Figure 6.27-3: A number of LDV models for an 0.2032 m (8 inch) pipe and 17.5% concentration.

The LSDV curve in these figures shows the start of a sliding bed. The Sb-He curve shows the transition of a sliding bed to heterogeneous flow. The intersection point of these two curves shows the start of occurrence of a sliding bed. For smaller particles a sliding bed will never occur, because the particles are already suspended before the bed can start sliding. Larger particles will show a sliding bed. It is also clear that the Wilson LSDV curve is considerably lower than the DHLLDV curve, the Durand & Condolios, Yagi et al. and Poloski data for the smaller pipe diameters. It should be mentioned that the Wilson LSDV curve is the maximum curve at a concentration of about 10%. Other concentrations will show lower curves. The DHLLDV curve is also the maximum curve.
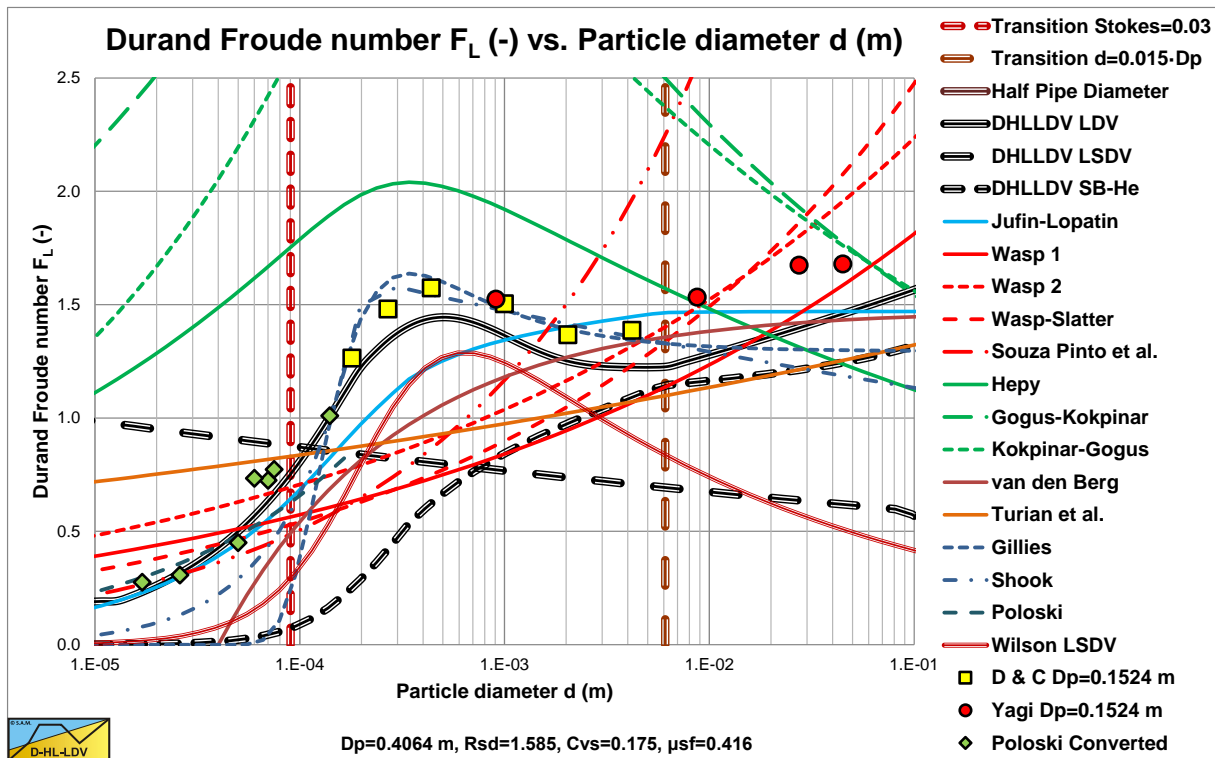
Figure 6.27-4: A number of LDV models for an 0.4064 m (16 inch) pipe and 17.5% concentration.
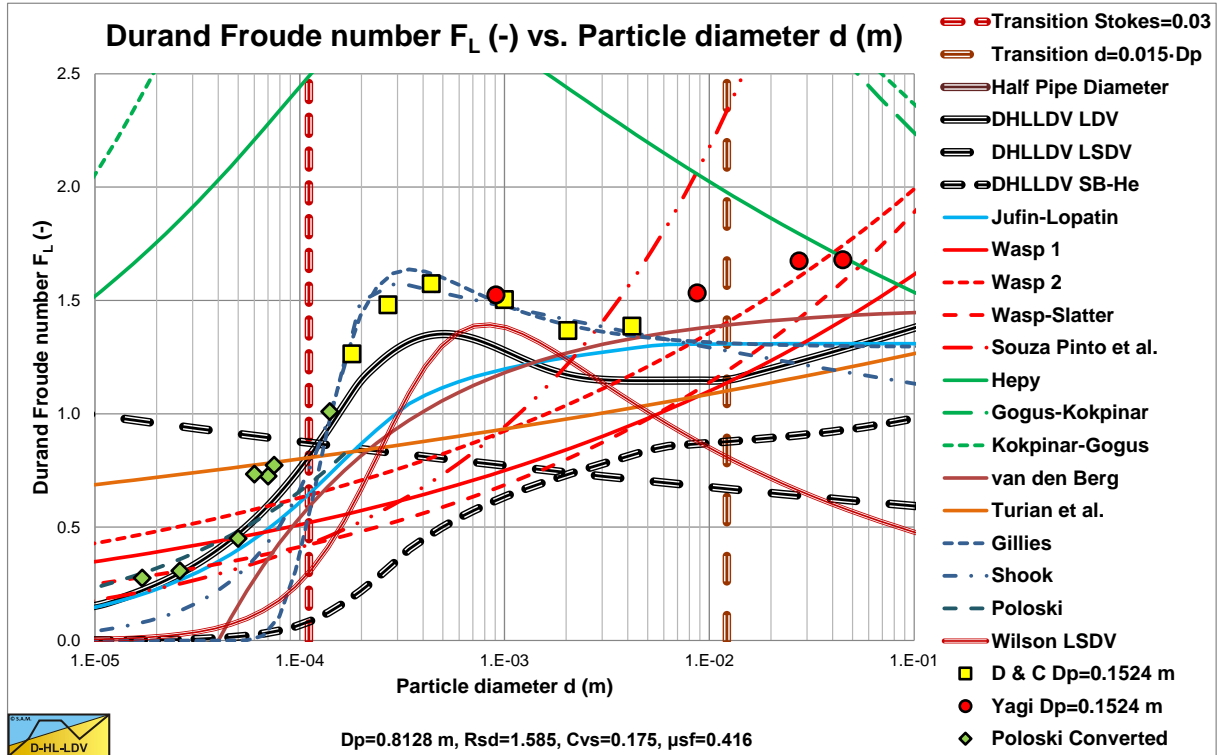
Figure 6.27-5: A number of LDV models for an 0.8128 m (32 inch) pipe and 17.5% concentration.

6.27.30 Nomenclature Limit Deposit Velocity.

$\mathbf{Ar}$	Archimedes number	**-**
$\mathbf{C_D}$	Particle drag coefficient	**-**
$\mathbf{C_{vs}}$	Spatial volumetric concentration	**-**
$\mathbf{C_{vt}}$	Delivered (transport) volumetric concentration	**-**
$\mathbf{d}$	Particle diameter	**m**
$\mathbf{d_{50}}$	Particle diameter 50% passing	**m**
$\mathbf{D_p}$	Pipe diameter	**m**
$\mathbf{E_{rhg}}$	Relative excess hydraulic gradient	**-**
$\mathbf{F_L}$	Durand & Condolios LDV Froude number	**-**
$\mathbf{F_{down}}$	Downwards force on particle, gravity	**kN**
$\mathbf{F_{up}}$	Upwards force on particle, drag	**kN**
$\mathbf{g}$	Gravitational constant (9.81 m/s^2)	**m/s^2**
$\mathbf{i_m}$	Mixture hydraulic gradient	**m/m**
$\mathbf{i_l}$	Liquid hydraulic gradient	**m/m**
$\mathbf{\Delta L}$	Length of pipe segment considered	**m**
$\mathbf{LDV}$	Limit Deposit Velocity	**m/s**
$\mathbf{LSDV}$	Limit of Stationary Deposit Velocity	**m/s**
$\mathbf{MHGV}$	Minimum Hydraulic Gradient Velocity	**m/s**
$\mathbf{n}$	Power hindered settling	**-**
$\mathbf{N}$	Zandi & Govatos parameter	**-**
$\mathbf{P}$	Power dissipated per unit mass of liquid	**kW**
$\mathbf{R_{sd}}$	Relative submerged density (sand 1.65)	**-**
$\mathbf{u_*}$	Friction velocity	**m/s**
$\mathbf{v_{ef}}$	Eddy fluctuation velocity	**m/s**
$\mathbf{v_{ls}}$	Line speed	**m/s**
$\mathbf{v_{ls,ldv}}$	Limit Deposit Velocity	**m/s**
$\mathbf{v_{SB\text{-}He}}$	Transition sliding bed regime with heterogeneous regime	**m/s**
$\mathbf{v_t}$	Terminal settling velocity	**m/s**
$\mathbf{\alpha}$	Correction factor eddy velocity	**-**
$\mathbf{\beta}$	Hindered settling power, Richardson & Zaki	**-**
$\mathbf{\rho_l}$	Density liquid	**ton/m^3**
$\mathbf{\rho_s}$	Density solids	**ton/m^3**
$\mathbf{\rho_m}$	Density mixture	**ton/m^3**
$\mathbf{\psi}$	Shape factor	**-**
$\mathbf{\psi^*}$	Jufin Lopatin particle Froude number	**-**
$\mathbf{\mu_{sf}}$	Sliding friction coefficient	**-**
$\mathbf{\nu_l}$	Kinematic viscosity liquid	**m^2/s**
$\mathbf{\lambda_l}$	Darcy Weisbach friction factor	**-**
$\mathbf{\theta}$	Pipe inclination angle	**rad**

6.28 Inclined Pipes.

In dredging inclined pipes occur in ladders of cutter suction dredgers and suction pipes of trailing suction hopper dredgers. On land inclined pipes occur going up and down slopes. So inclined pipes may have positive and negative inclination angles up to 45°. The question is, what is the influence of the inclination angle on the hydraulic gradient, on the Limit of Stationary Deposit Velocity (LSDV) and on the Limit Deposit Velocity (LDV). The effect of inclined pipes is expressed based on the length of the pipe, not the horizontal distance. A number of cases have to be distinguished.

6.28.1 Pure Carrier Liquid.

First of all, the flow of pure carrier liquid. The equilibrium of forces on the liquid is:

$$-\frac{dp}{dx} \cdot A \cdot L = \tau_l \cdot O \cdot L + \rho_l \cdot A \cdot L \cdot g \cdot \sin(\theta) \tag{6.28-1}$$

The hydraulic gradient can now be determined with:

$$i_{l,\theta} = -\frac{dp}{dx} \cdot \frac{A \cdot L}{\rho_l \cdot A \cdot L \cdot g} = \frac{\tau_l \cdot O \cdot L}{\rho_l \cdot A \cdot L \cdot g} + \frac{\rho_l \cdot A \cdot L \cdot g \cdot \sin(\theta)}{\rho_l \cdot A \cdot L \cdot g} = i_l + \sin(\theta) \tag{6.28-2}$$

So apparently the hydraulic gradient increases with the sine of the inclination angle. Which also means that a downwards slope with a negative inclination angle gives a negative sine and thus a reduction of the hydraulic gradient. In this case the hydraulic gradient may even become negative.

6.28.2 Stationary Bed Regime.

The equilibrium of forces on the layer of liquid above the bed is:

$$-\frac{dp}{dx} \cdot A_1 \cdot L = \tau_1 \cdot O_1 \cdot L + \tau_{12} \cdot O_{12} \cdot L + \rho_l \cdot A_1 \cdot L \cdot g \cdot \sin(\theta) \tag{6.28-3}$$

Since the bed is not moving, the friction between the bed and the pipe wall compensates for the weight component of the bed. The hydraulic gradient can now be determined with:

$$i_{m,\theta} = -\frac{dp}{dx} \cdot \frac{A_1 \cdot L}{\rho_l \cdot A_1 \cdot L \cdot g} = \frac{\tau_1 \cdot O_1 \cdot L + \tau_{12} \cdot O_{12} \cdot L}{\rho_l \cdot A_1 \cdot L \cdot g} + \frac{\rho_l \cdot A_1 \cdot L \cdot g \cdot \sin(\theta)}{\rho_l \cdot A_1 \cdot L \cdot g} = i_m + \sin(\theta) \tag{6.28-4}$$

Which is the hydraulic gradient of a stationary bed in a horizontal pipe plus the sine of the inclination angle. The weight of the solids do not give a contribution to the hydraulic gradient, since it is carried by the pipe wall.

6.28.3 Sliding Bed Regime.

The equilibrium of forces on the layer of liquid above the bed is:

$$-\frac{dp}{dx} \cdot A_1 \cdot L = \tau_1 \cdot O_1 \cdot L + \tau_{12} \cdot O_{12} \cdot L + \rho_l \cdot A_1 \cdot L \cdot g \cdot \sin(\theta) \tag{6.28-5}$$

The cross-section of the bed and the layer of liquid above the bed can be determined with:

$$A_2 = \frac{C_{vs}}{C_{vb}} \cdot A \quad \text{and} \quad A_1 = A - A_2 \tag{6.28-6}$$

The weight of the bed, including pore water is:

$$W_b = \rho_b \cdot A_2 \cdot L \cdot g = \left(\rho_s \cdot C_{vb} + \rho_l \cdot \left(1 - C_{vb} \right) \right) \cdot A_2 \cdot L \cdot g$$

$$= \left(\left(\rho_s - \rho_l \right) \cdot C_{vb} + \rho_l \right) \cdot A_2 \cdot L \cdot g = \rho_l \cdot R_{sd} \cdot C_{vs} \cdot A \cdot L \cdot g + \rho_l \cdot A_2 \cdot L \cdot g \tag{6.28-7}$$

The submerged weight of the bed can be determined with:

$$W_{b,s} = \left(\rho_s - \rho_l \right) \cdot C_{vb} \cdot A_2 \cdot L \cdot g = \rho_l \cdot R_{sd} \cdot C_{vs} \cdot A \cdot L \cdot g \tag{6.28-8}$$

This gives for the equilibrium of forces on the bed:

$$-\frac{dp}{dx} \cdot A_2 \cdot L = \tau_2 \cdot O_2 \cdot L - \tau_{12} \cdot O_{12} \cdot L + W_b \cdot \sin(\theta) + \mu_{sf} \cdot W_{b,s} \cdot \cos(\theta) \tag{6.28-9}$$

$$-\frac{dp}{dx} \cdot A_2 \cdot L = \tau_2 \cdot O_2 \cdot L - \tau_{12} \cdot O_{12} \cdot L + W_{b,s} \cdot \sin(\theta) + \mu_{sf} \cdot W_{b,s} \cdot \cos(\theta) + \rho_l \cdot A_2 \cdot L \cdot g \cdot \sin(\theta)$$

For the whole pipe cross section, the two contributions can be added, giving:

$$-\frac{dp}{dx} \cdot A \cdot L = \tau_1 \cdot O_1 \cdot L + \tau_2 \cdot O_2 \cdot L + \rho_l \cdot A \cdot L \cdot g \cdot \sin(\theta) \tag{6.28-10}$$

$$+ \rho_l \cdot R_{sd} \cdot C_{vs} \cdot A \cdot L \cdot g \cdot \sin(\theta) + \mu_{sf} \cdot \rho_l \cdot R_{sd} \cdot C_{vs} \cdot A \cdot L \cdot g \cdot \cos(\theta)$$

This can also be written as:

$$-\frac{dp}{dx} \cdot A \cdot L = \tau_1 \cdot O_1 \cdot L + \tau_2 \cdot O_2 \cdot L + \rho_m \cdot A \cdot L \cdot g \cdot \sin(\theta) \tag{6.28-11}$$

$$+ \mu_{sf} \cdot \rho_l \cdot R_{sd} \cdot C_{vs} \cdot A \cdot L \cdot g \cdot \cos(\theta)$$

In terms of the hydraulic gradient this gives:

$$i_{m,\theta} = -\frac{dp}{dx} \cdot \frac{A \cdot L}{\rho_l \cdot g \cdot L \cdot A} = \frac{\tau_1 \cdot O_1 \cdot L + \tau_2 \cdot O_2 \cdot L}{\rho_l \cdot g \cdot L \cdot A} + \left(1 + R_{sd} \cdot C_{vs} \right) \cdot \sin(\theta) \tag{6.28-12}$$

$$+ \mu_{sf} \cdot R_{sd} \cdot C_{vs} \cdot \cos(\theta)$$

In chapter 7.4 it will be proven that the first term on the right hand side almost equals the pure liquid hydraulic gradient i_l, without pipe inclination, so:

$$i_{m,\theta} = i_l + \left(1 + R_{sd} \cdot C_{vs} \right) \cdot \sin(\theta) + \mu_{sf} \cdot R_{sd} \cdot C_{vs} \cdot \cos(\theta) \tag{6.28-13}$$

$$i_{m,\theta} = \left(i_l + \sin(\theta) \right) + R_{sd} \cdot C_{vs} \cdot \left(\mu_{sf} \cdot \cos(\theta) + \sin(\theta) \right)$$

Giving for the mixture hydraulic gradient with pipe inclination:

$$i_{m,\theta} = i_{l,\theta} + R_{sd} \cdot C_{vs} \cdot \left(\mu_{sf} \cdot \cos(\theta) + \sin(\theta) \right) \tag{6.28-14}$$

6.28.4 Homogeneous Regime.

In the homogeneous flow regime, the hydraulic gradient is:

$$i_m = i_l + i_l \cdot R_{sd} \cdot C_{vs} = i_l \cdot (1 + R_{sd} \cdot C_{vs})$$ (6.28-15)

For an inclined pipe only the lifting of the mixture has to be added, giving:

$$i_{m,\theta} = i_{l,\theta} + i_{l,\theta} \cdot R_{sd} \cdot C_{vs} = i_l \cdot (1 + R_{sd} \cdot C_{vs}) + \sin(\theta) \cdot (1 + R_{sd} \cdot C_{vs})$$

$$= (i_l + \sin(\theta)) \cdot (1 + R_{sd} \cdot C_{vs})$$

(6.28-16)

or

$$= i_l \cdot (1 + A \cdot R_{sd} \cdot C_{vs}) + \sin(\theta) \cdot (1 + R_{sd} \cdot C_{vs})$$

Some researchers found that the hydraulic gradient does not increase for 100% with the solids effect, but just with about 60% of the solids effect. In this case the factor **A** should be taken 0.6 instead of 1.0. The solids effect in the inclination part of the equation always counts for 100% however, since it's the increase or decrease of the potential energy of the mixture.

6.28.5 Conclusions So Far.

For pure liquid, the fixed bed regime, the sliding bed regime and the homogeneous flow regime, the influence of the inclination angle can be determined fundamentally, based on the spatial volumetric concentration. The latter is very important. For a sliding bed, the force to move the bed upwards depends on the submerged weight of the bed and the inclination angle, but not on the velocity of the bed. For homogeneous flow it is assumed that spatial and transport concentration are almost equal. The question is now, what is the influence of the inclination angle in the heterogeneous flow regime? Different researchers have different methods. These methods are described in the next chapters.

6.28.6 The Heterogeneous Flow Regime, Durand & Condolios and Gibert.

The basic equation of Durand & Condolios (1952) and Gibert (1960) for the solids effect is given by:

$$\Phi = \frac{i_m - i_l}{i_l \cdot C_{vt}} = 81 \cdot \left(\frac{v_{ls}^2 \cdot \sqrt{C_x}}{g \cdot D_p \cdot R_{sd}} \right)^{-3/2}$$

(6.28-17)

$$i_m = i_l \cdot \left(1 + 81 \cdot \left(\frac{v_{ls}^2 \cdot \sqrt{C_x}}{g \cdot D_p \cdot R_{sd}} \right)^{-3/2} \cdot C_{vt} \right)$$

For inclined pipes they modified the solids effect by adding the cosine of the inclination angle according to:

$$\Phi_\theta = \frac{i_{m,\theta} - \sin(\theta) \cdot (1 + R_{sd} \cdot C_{vt}) - i_l}{i_l \cdot C_{vt}} = 81 \cdot \left(\frac{v_{ls}^2 \cdot \sqrt{C_x}}{g \cdot D_p \cdot R_{sd} \cdot \cos(\theta)} \right)^{-3/2}$$

(6.28-18)

$$i_{m,\theta} = i_l \cdot \left(1 + 81 \cdot \left(\frac{v_{ls}^2 \cdot \sqrt{C_x}}{g \cdot D_p \cdot R_{sd} \cdot \cos(\theta)} \right)^{-3/2} \cdot C_{vt} \right) + \sin(\theta) \cdot (1 + R_{sd} \cdot C_{vt})$$

This can be written as:

$$i_{m,\theta} = i_l + \sin(\theta) \cdot (1 + R_{sd} \cdot C_{vt}) + i_l \cdot 81 \cdot \left(\frac{v_{ls}^2 \cdot \sqrt{C_x}}{g \cdot D_p \cdot R_{sd} \cdot \cos(\theta)} \right)^{-3/2} \cdot C_{vt}$$

<div align="right">(6.28-19)</div>

$$i_{m,\theta} = i_{l,\theta} + i_l \cdot 81 \cdot \left(\frac{v_{ls}^2 \cdot \sqrt{C_x}}{g \cdot D_p \cdot R_{sd}} \right)^{-3/2} \cdot C_{vt} \cdot \cos(\theta)^{3/2} + \sin(\theta) \cdot R_{sd} \cdot C_{vt}$$

So the solids effect has to be multiplied with the cosine of the inclination angle to the power of 3/2. This means the solids effect is decreasing with an increasing inclination angle, whether the inclination is upwards or downwards. It should be mentioned that the hydraulic gradient is based on the length of the pipe and not on the horizontal length component.

6.28.7 The Heterogeneous Flow Regime, Worster & Denny.

Worster & Denny (1955) have a slightly different approach. They state that the hydraulic gradient in an inclined pipe equals the sum of the hydraulic gradients of the horizontal component and the vertical component. This gives the following equation:

$$i_{m,\theta} = i_{l,\theta} + i_l \cdot 81 \cdot \left(\frac{v_{ls}^2 \cdot \sqrt{C_x}}{g \cdot D_p \cdot R_{sd}} \right)^{-3/2} \cdot C_{vt} \cdot \cos(\theta) + \sin(\theta) \cdot R_{sd} \cdot C_{vt} \qquad (6.28\text{-}20)$$

The difference with Durand & Condolios (1952) and Gibert (1960) is the power of the cosine. In both cases, the equations match the hydraulic gradient of a horizontal pipe if the inclination angle equals zero and a vertical pipe if the inclination angle equals 90 degrees, whether the inclination is upwards (positive inclination angle) or downwards (negative inclination angle). The homogeneous component for vertical pipes is still missing here.

6.28.8 The Heterogeneous Flow Regime, Wilson et al.

Wilson et al. (2006) derived the following equation for heterogeneous transport in horizontal pipes:

$$i_m = i_l + \frac{\mu_{sf}}{2} \cdot \left(\frac{v_{50}}{v_{ls}} \right)^M \cdot R_{sd} \cdot C_{vt} \qquad (6.28\text{-}21)$$

For inclined pipes they modified the equation, matching the reasoning of Worster & Denny (1955), but with the use of the power **M** according to:

$$i_{m,\theta} = i_{l,\theta} + \frac{\mu_{sf}}{2} \cdot \left(\frac{v_{50}}{v_{ls}} \right)^M \cdot R_{sd} \cdot C_{vt} \cdot \cos(\theta)^M + \sin(\theta) \cdot R_{sd} \cdot C_{vt} \qquad (6.28\text{-}22)$$

The power M has a value of 1.7 for uniform or narrow graded sands and decreases to 0.25 for very broad graded sands. For narrow graded sands the influence of the inclination angle is similar to the Durand & Condolios (1952) and Gibert (1960) approach with a power of 1.5 versus 1.7 for Wilson et al. (2006). For medium graded sands with a power around 1, the influence is similar to the Worster & Denny (1955) approach.

6.28.9 The Sliding Bed Regime, Doron et al.

Doron et al. (1997) investigated the influence of inclined pipes, based on their 2LM and 3LM models. Basically they multiplied the sliding friction with the cosine of the inclination angle and they added the potential energy term, which is proportional with the sine of the inclination angle. They carried out experiments with inclination angles from -7 to +7 degrees. The resulting data however is dominated by the potential energy term, because of the small inclination angles.

6.28.10 The Limit Deposit Velocity.

Wilson et al. (2006) use a graph with experimental data for the Deposition Limit. Their Deposition Limit however is the Limit of Stationary Deposit Velocity (LSDV) and not the Limit Deposit Velocity. The LSDV is the line speed where a bed starts sliding, while the LDV is defined in this book as the line speed above which there is no stationary or sliding bed. The LDV is thus always higher than the LSDV. The LSDV does not always exist. For smaller particles it is very well possible that there is a direct transition between the stationary bed regime and the heterogeneous flow regime. The graph used by Wilson et al. (2006) shows an increasing LSDV with increasing inclination angle up to an inclination angle of about 30 degrees above which the LSDV is constant or decreasing. The experimental data stop at an inclination angle of 40 degrees. For negative inclination angles, the LSDV decreases with a decreasing inclination angle. The experimental data stop at an angle of -20 degrees.
The research of Doron et al. (1997) gives a similar result. They also investigated the LSDV and not the LDV. The maximum LSDV was found at about 15 degrees inclination angle.

The behavior of the LSDV for inclined pipes can be explained assuming that the LSDV is the intersection point of the stationary bed regime and the sliding bed regime. In the stationary bed regime the hydraulic gradient is:

$$i_{m,\theta} = i_m + \sin(\theta)$$

(6.28-23)

In the sliding bed regime the hydraulic gradient is:

$$i_{m,\theta} = i_l + \sin(\theta) + R_{sd} \cdot C_{vs} \cdot \left(\mu_{sf} \cdot \cos(\theta) + \sin(\theta) \right)$$

(6.28-24)

The intersection point (line speed) occurs when both hydraulic gradients are equal, so:

$$i_m + \sin(\theta) = i_l + \sin(\theta) + R_{sd} \cdot C_{vs} \cdot \left(\mu_{sf} \cdot \cos(\theta) + \sin(\theta) \right)$$

(6.28-25)

$$\text{So :} \quad i_m - i_l = R_{sd} \cdot C_{vs} \cdot \left(\mu_{sf} \cdot \cos(\theta) + \sin(\theta) \right)$$

Assuming i_m equals the hydraulic gradient in the restricted area above the bed with a Darcy Weisbach friction coefficient λ_m based on the flow above the bed, this gives:

$$F_L^2 = \frac{v_{ls,lsdv}^2}{2 \cdot g \cdot R_{sd} \cdot D_p} = \frac{\left(\mu_{sf} \cdot \cos(\theta) + \sin(\theta) \right) \cdot C_{vs}}{\left(\dfrac{\lambda_m}{\left(1 - C_{vr}\right)^2} - \lambda_l \right)}$$

(6.28-26)

$$\text{With :} \quad i_m = \lambda_m \cdot \frac{v_{ls}^2}{\left(1 - C_{vr}\right)^2 \cdot 2 \cdot g \cdot D_p} \quad \text{and} \quad i_l = \lambda_l \cdot \frac{v_{ls}^2}{2 \cdot g \cdot D_p}$$

The Darcy Weisbach friction coefficient λ_m may be dependent on the size of the particles in the bed. The above derivation is indicative, because suspension and the particle slip velocity are not taken into account. Using a sliding friction factor of 0.4 does result in a 40% higher LSDV for an inclination angle of 30 degrees, where the Wilson et al. (2006) graph predicts an increase of 25%-30%. The above equation does show a maximum at 66 degrees inclination angle with a 57% increase of the LSDV.

The experiments of Graf & Robinson (1970) resulted in a modified F_L number for the LDV:

$$F_L = \frac{v_{ls,ldv}}{\sqrt{2 \cdot g \cdot D_p \cdot R_{sd}}} \cdot \left(1 - \tan(\theta) \right)$$

(6.28-27)

Apparently the LDV decreases with increasing inclination angle for an ascending pipe. The inclination angles used were however very small.

6.28.11 The U Tube as a Device to Determine the Delivered Volumetric Concentration.

6.28.11.1 The Vertical Ascending Pipe.

The mass balance of the solids flow gives:

$$\mathbf{A_p \cdot C_{vt} \cdot v_{ls} \cdot \rho_s = A_p \cdot C_{vs} \cdot v_s \cdot \rho_s = A_p \cdot C_{vs} \cdot \left(v_l - v_{th}\right) \cdot \rho_s} \tag{6.28-28}$$

Or:

$$\mathbf{C_{vt} \cdot v_{ls} = C_{vs} \cdot v_s = C_{vs} \cdot \left(v_l - v_{th}\right)} \tag{6.28-29}$$

In this mass balance it is assumed that the particles (solids) have a velocity $\mathbf{v_s}$ smaller than the cross sectional averaged line speed $\mathbf{v_{ls}}$ and the liquid (water) has a larger velocity $\mathbf{v_l}$. The mass balance of the liquid (water) gives:

$$\mathbf{A_p \cdot \left(1 - C_{vt}\right) \cdot v_{ls} \cdot \rho_l = A_p \cdot \left(1 - C_{vs}\right) \cdot v_l \cdot \rho_l} \tag{6.28-30}$$

Or:

$$\mathbf{\left(1 - C_{vt}\right) \cdot v_{ls} = \left(1 - C_{vs}\right) \cdot v_l} \tag{6.28-31}$$

This gives for the liquid velocity $\mathbf{v_l}$, assuming the terminal hindered settling velocity $\mathbf{v_{th}}$ is known:

$$\mathbf{v_l = v_{ls} + C_{vs} \cdot v_{th}} \tag{6.28-32}$$

If the spatial volumetric concentration $\mathbf{C_{vs}}$ is known, the delivered or transport volumetric concentration $\mathbf{C_{vt}}$ can be determined according to:

$$\mathbf{C_{vt} = C_{vs} \cdot \left(1 - \frac{v_{th}}{v_{ls}}\right) + C_{vs}^2 \cdot \frac{v_{th}}{v_{ls}}} \tag{6.28-33}$$

If the delivered volumetric concentration $\mathbf{C_{vt}}$ is known, the spatial volumetric concentration $\mathbf{C_{vs}}$ can be determined according to:

$$\mathbf{C_{vs} = -\frac{1}{2} \cdot \left(\frac{v_{ls}}{v_{th}} - 1\right) + \frac{1}{2} \cdot \sqrt{\left(\frac{v_{ls}}{v_{th}} - 1\right)^2 + 4 \cdot C_{vt} \cdot \frac{v_{ls}}{v_{th}}}} \tag{6.28-34}$$

For low concentrations and/or particles with a small terminal settling velocity this can be approximated by:

$$\mathbf{C_{vt} = C_{vs} \cdot \left(1 - \frac{v_{th}}{v_{ls}}\right)} \tag{6.28-35}$$

And:

$$\mathbf{C_{vs} = C_{vt} \cdot \left(\frac{v_{ls}}{v_{ls} - v_{th}}\right)} \tag{6.28-36}$$

In an ascending vertical pipe the spatial volumetric concentration $\mathbf{C_{vs}}$ is larger than the delivered volumetric concentration $\mathbf{C_{vt}}$.

Since the liquid velocity is higher than the line speed, depending on the spatial concentration and the terminal hindered settling velocity, the line speed in the hydraulic gradient equation should be replaced by the liquid velocity, assuming that the Darcy Weisbach friction factor hardly changes at high Reynolds numbers. This gives for the hydraulic gradient of a mixture in a vertical pipe:

$$i_m = \frac{\rho_m}{\rho_l} \cdot \frac{\lambda_l \cdot \left(v_{ls} + C_{vs} \cdot v_{th}\right)^2}{2 \cdot g \cdot D_p} = \frac{\rho_m}{\rho_l} \cdot \frac{\lambda_l \cdot \left(v_{ls}^2 + 2 \cdot C_{vs} \cdot v_{th} \cdot v_{ls} + C_{vs}^2 \cdot v_{th}^2\right)}{2 \cdot g \cdot D_p}$$

(6.28-37)

$$i_m \approx \frac{\rho_m}{\rho_l} \cdot \frac{\lambda_l \cdot \left(v_{ls}^2 + 2 \cdot C_{vs} \cdot v_{th} \cdot v_{ls}\right)}{2 \cdot g \cdot D_p} = \frac{\rho_m}{\rho_l} \cdot \frac{\lambda_l \cdot v_{ls}^2}{2 \cdot g \cdot D_p} + \frac{\rho_m}{\rho_l} \cdot \frac{2 \cdot \lambda_l \cdot C_{vs} \cdot v_{th} \cdot v_{ls}}{2 \cdot g \cdot D_p}$$

So in an ascending vertical pipe the Darcy Weisbach friction losses as larger than the losses found based on the equivalent liquid model.

6.28.11.2 The Vertical Descending Pipe.

The mass balance of the solids flow gives:

$$A_p \cdot C_{vt} \cdot v_{ls} \cdot \rho_s = A_p \cdot C_{vs} \cdot v_s \cdot \rho_s = A_p \cdot C_{vs} \cdot \left(v_l + v_{th}\right) \cdot \rho_s$$

(6.28-38)

Or:

$$C_{vt} \cdot v_{ls} = C_{vs} \cdot v_s = C_{vs} \cdot \left(v_l + v_{th}\right)$$

(6.28-39)

In this mass balance it is assumed that the particles (solids) have a velocity v_s smaller than the cross sectional averaged line speed v_{ls} and the liquid (water) has a larger velocity v_l. The mass balance of the liquid (water) gives:

$$A_p \cdot \left(1 - C_{vt}\right) \cdot v_{ls} \cdot \rho_l = A_p \cdot \left(1 - C_{vs}\right) \cdot v_l \cdot \rho_l$$

(6.28-40)

Or:

$$\left(1 - C_{vt}\right) \cdot v_{ls} = \left(1 - C_{vs}\right) \cdot v_l$$

(6.28-41)

This gives for the liquid velocity v_l, assuming the terminal hindered settling velocity v_{th} is known:

$$v_l = v_{ls} - C_{vs} \cdot v_{th}$$

(6.28-42)

If the spatial volumetric concentration C_{vs} is known, the delivered or transport volumetric concentration C_{vt} can be determined according to:

$$C_{vt} = C_{vs} \cdot \left(1 + \frac{v_{th}}{v_{ls}}\right) - C_{vs}^2 \cdot \frac{v_{th}}{v_{ls}}$$

(6.28-43)

If the delivered volumetric concentration C_{vt} is known, the spatial volumetric concentration C_{vs} can be determined according to:

$$C_{vs} = \frac{1}{2} \cdot \left(\frac{v_{ls}}{v_{th}} + 1\right) + \frac{1}{2} \cdot \sqrt{\left(\frac{v_{ls}}{v_{th}} + 1\right)^2 - 4 \cdot C_{vt} \cdot \frac{v_{ls}}{v_{th}}}$$

(6.28-44)

For low concentrations and/or particles with a small terminal settling velocity this can be approximated by:

$$C_{vt} = C_{vs} \cdot \left(1 + \frac{v_{th}}{v_{ls}}\right)$$

(6.28-45)

And:

$$C_{vs} = C_{vt} \cdot \left(\frac{v_{ls}}{v_{ls} + v_{th}}\right)$$

(6.28-46)

In a descending vertical pipe the delivered volumetric concentration C_{vt} is larger than the spatial volumetric concentration C_{vs}.

Since the liquid velocity is smaller than the line speed, depending on the spatial concentration and the terminal hindered settling velocity, the line speed in the hydraulic gradient equation should be replaced by the liquid velocity, assuming that the Darcy Weisbach friction factor hardly changes at high Reynolds numbers. This gives for the hydraulic gradient of a mixture in a vertical pipe:

$$i_m = \frac{\rho_m}{\rho_l} \cdot \frac{\lambda_l \cdot \left(v_{ls} - C_{vs} \cdot v_{th}\right)^2}{2 \cdot g \cdot D_p} = \frac{\rho_m}{\rho_l} \cdot \frac{\lambda_l \cdot \left(v_{ls}^2 - 2 \cdot C_{vs} \cdot v_{th} \cdot v_{ls} + C_{vs}^2 \cdot v_{th}^2\right)}{2 \cdot g \cdot D_p}$$

(6.28-47)

$$i_m \approx \frac{\rho_m}{\rho_l} \cdot \frac{\lambda_l \cdot \left(v_{ls}^2 - 2 \cdot C_{vs} \cdot v_{th} \cdot v_{ls}\right)}{2 \cdot g \cdot D_p} = \frac{\rho_m}{\rho_l} \cdot \frac{\lambda_l \cdot v_{ls}^2}{2 \cdot g \cdot D_p} - \frac{\rho_m}{\rho_l} \cdot \frac{2 \cdot \lambda_l \cdot C_{vs} \cdot v_{th} \cdot v_{ls}}{2 \cdot g \cdot D_p}$$

So in an ascending vertical pipe the Darcy Weisbach friction losses as larger than the losses found based on the equivalent liquid model.

6.28.11.3 Determination of the Delivered Volumetric Concentration.

Now suppose in both the ascending and the descending pipes the hydraulic gradients are measured with differential pressure transducers. The delivered volumetric concentration C_{vt} is equal in both pipes. Using the index a for the ascending pipe and the index d for the descending pipe, this gives for the ascending pipe:

$$i_{m,a} = \frac{\rho_{m,a}}{\rho_l} \cdot \frac{\lambda_l \cdot v_{ls}^2}{2 \cdot g \cdot D_p} + \frac{\rho_{m,a}}{\rho_l} \cdot \frac{2 \cdot \lambda_l \cdot C_{vs,a} \cdot v_{th} \cdot v_{ls}}{2 \cdot g \cdot D_p} + \frac{\rho_{m,a}}{\rho_l}$$

(6.28-48)

$$C_{vs,a} = C_{vt} \cdot \left(\frac{v_{ls}}{v_{ls} - v_{th}}\right) \quad \Rightarrow \quad \rho_{m,a} = \rho_l \cdot \left(1 + R_{sd} \cdot C_{vs,a}\right)$$

(6.28-49)

For the descending pipe this gives:

$$i_{m,d} = \frac{\rho_{m,d}}{\rho_l} \cdot \frac{\lambda_l \cdot v_{ls}^2}{2 \cdot g \cdot D_p} - \frac{\rho_{m,d}}{\rho_l} \cdot \frac{2 \cdot \lambda_l \cdot C_{vs,d} \cdot v_{th} \cdot v_{ls}}{2 \cdot g \cdot D_p} - \frac{\rho_{m,d}}{\rho_l}$$

(6.28-50)

$$C_{vs,d} = C_{vt} \cdot \left(\frac{v_{ls}}{v_{ls} + v_{th}}\right) \quad \Rightarrow \quad \rho_{m,d} = \rho_l \cdot \left(1 + R_{sd} \cdot C_{vs,d}\right)$$

(6.28-51)

The difference of the two hydraulic gradients is now:

$$i_{m,a} - i_{m,d} = \frac{\rho_{m,a}}{\rho_l} \cdot \frac{\lambda_l \cdot v_{ls}^2}{2 \cdot g \cdot D_p} + \frac{\rho_{m,a}}{\rho_l} \cdot \frac{2 \cdot \lambda_l \cdot C_{vs,a} \cdot v_{th} \cdot v_{ls}}{2 \cdot g \cdot D_p} + \frac{\rho_{m,a}}{\rho_l}$$

(6.28-52)

$$- \left(\frac{\rho_{m,d}}{\rho_l} \cdot \frac{\lambda_l \cdot v_{ls}^2}{2 \cdot g \cdot D_p} - \frac{\rho_{m,d}}{\rho_l} \cdot \frac{2 \cdot \lambda_l \cdot C_{vs,d} \cdot v_{th} \cdot v_{ls}}{2 \cdot g \cdot D_p} - \frac{\rho_{m,d}}{\rho_l}\right)$$

This gives:

$$i_{m,a} - i_{m,d} = \left(\frac{\rho_{m,a}}{\rho_l} - \frac{\rho_{m,d}}{\rho_l} \right) \cdot \frac{\lambda_l \cdot v_{ls}^2}{2 \cdot g \cdot D_p}$$

$$+ \left(\frac{\rho_{m,a}}{\rho_l} \cdot \frac{2 \cdot \lambda_l \cdot C_{vs,a} \cdot v_{th} \cdot v_{ls}}{2 \cdot g \cdot D_p} + \frac{\rho_{m,d}}{\rho_l} \cdot \frac{2 \cdot \lambda_l \cdot C_{vs,d} \cdot v_{th} \cdot v_{ls}}{2 \cdot g \cdot D_p} \right) \qquad \textbf{(6.28-53)}$$

$$+ \left(\frac{\rho_{m,a}}{\rho_l} + \frac{\rho_{m,d}}{\rho_l} \right)$$

If the terminal hindered settling velocity is very small compared to the line speed, giving an average mixture density based on the delivered concentration, this can be simplified to:

$$i_{m,a} - i_{m,d} = 2 \cdot \frac{\rho_m}{\rho_l} \cdot \frac{\lambda_l \cdot C_{vt} \cdot v_{th} \cdot v_{ls}}{g \cdot D_p} + 2 \cdot \frac{\rho_m}{\rho_l} = 2 \cdot \frac{\rho_m}{\rho_l} \cdot \left(\frac{\lambda_l \cdot C_{vt} \cdot v_{th} \cdot v_{ls}}{g \cdot D_p} + 1 \right) \qquad \textbf{(6.28-54)}$$

So the mixture density is:

$$\rho_m = \rho_l \cdot \frac{\left(i_{m,a} - i_{m,d} \right)}{2 \cdot \left(\frac{\lambda_l \cdot C_{vt} \cdot v_{th} \cdot v_{ls}}{g \cdot D_p} + 1 \right)} \qquad \textbf{(6.28-55)}$$

This gives for the delivered volumetric concentration C_{vt}:

$$\rho_l \cdot \left(1 + R_{sd} \cdot C_{vt} \right) = \rho_l \cdot \frac{\left(i_{m,a} - i_{m,d} \right)}{2 \cdot \left(\frac{\lambda_l \cdot C_{vt} \cdot v_{th} \cdot v_{ls}}{g \cdot D_p} + 1 \right)}$$

$$\qquad \textbf{(6.28-56)}$$

$$C_{vt} = \frac{1}{R_{sd}} \cdot \left(\frac{\left(i_{m,a} - i_{m,d} \right)}{2 \cdot \left(\frac{\lambda_l \cdot C_{vt} \cdot v_{th} \cdot v_{ls}}{g \cdot D_p} + 1 \right)} - 1 \right)$$

Again if the terminal hindered settling velocity is very small this can be simplified to:

$$C_{vt} = \frac{1}{R_{sd}} \cdot \left(\frac{\left(i_{m,a} - i_{m,d} \right)}{2} - 1 \right) \qquad \textbf{(6.28-57)}$$

This equation is often used to determine the delivered volumetric concentration C_{vt}. For larger particles with a significant terminal hindered settling velocity however, this equation overestimates the delivered volumetric concentration. The error increases with increasing delivered volumetric concentration, terminal hindered settling velocity and line speed and decreases with increasing pipe diameter. Equation (6.28-56) results in a second degree polynomial and can be solved with the well-known ABC equation.

Now if the spatial volumetric concentration in a horizontal pipe is determined with for example a well calibrated nuclear density meter, the delivered volumetric concentration can be determined with a U Tube. Knowing both concentrations, the so called slip velocity can be determined. Using equation (6.28-56) will give a more accurate estimate of the delivered volumetric concentration and thus of the slip velocity.

6.28.12 Conclusions.

After adding the potential energy terms to the hydraulic gradient in a correct way, the pipe inclination effect can be taken into account by multiplying the solids effect term with the cosine of the inclination angle to a power ranging from 1.0 to 1.7. Different researchers give different powers, most probably because the models are either empirical or have different physical backgrounds. This implies that the solids effect reduces to zero for a vertical pipe, which is doubtful, especially for very small particles giving homogeneous flow (ELM). One would expect an equation of the following form:

$$i_{m,\theta} = i_l \cdot \left(1 + \alpha \cdot R_{sd} \cdot C_{vs} \cdot \sin(\theta)^{\beta_1}\right) + E_{rhg} \cdot R_{sd} \cdot C_{vs} \cdot \cos(\theta)^{\beta_2} + \left(1 + R_{sd} \cdot C_{vs}\right) \cdot \sin(\theta) \qquad (6.28\text{-}58)$$

The first term on the right hand side is the Darcy Weisbach friction, including the mobilized ELM (the homogeneous solids effect) corrected for the inclination angle. The second term is the heterogeneous solids effect corrected for the inclination angle. The third term is the potential energy term. So where the heterogeneous solids effect decreases with the inclination angle, the homogeneous solids effect increases. In this form a vertical pipe shows mobilized/reduced ELM behavior, which is observed by Newitt et al. (1961).

The LSDV increases with increasing inclination angle to a maximum with 25%-30% increase for an inclination angle of 15 to 30 degrees. This probably depends on the spatial volumetric concentration, the particle size, the relative submerged density and the particle slip, but not enough data could be found to quantify this.

6.28.13 Nomenclature Inclined Pipes.

A, A_p	Cross section pipe	m^2
A_1	Cross section restricted area above the bed	m^2
A_2	Cross section bed	m^2
C_{vb}	Bed volumetric concentration	-
C_{vs}	Spatial volumetric concentration	-
C_{vt}	Delivered volumetric concentration	-
C_x	Inverse particle Froude number	-
D_p	Pipe diameter	m
g	Gravitational constant (9.81)	m/s^2
i_l	Hydraulic gradient liquid without pipe inclination	-
$i_{l,\theta}$	Hydraulic gradient liquid with pipe inclination	-
i_m	Hydraulic gradient mixture without pipe inclination	-
$i_{m,\theta}$	Hydraulic gradient mixture with pipe inclination	-
L	Length of pipe	m
M	Wilson heterogeneous power (0.25-1.7)	-
O_1	Circumference restricted area above the bed in contact with pipe wall	m
O_2	Circumference of bed with pipe wall	m
O_{12}	Width of the top of the bed	m
p	Pressure in pipe	kPa
R_{sd}	Relative submerged density of solids	-
v_{ls}	Line speed	m/s
v_{50}	50% stratification velocity	m/s
W_b	Weight of the bed	ton
$W_{b,s}$	Submerged weight of the bed	ton
x	Distance in pipe length direction	m
ρ_b	Density of the bed including pore water	ton/m^3
ρ_s	Density of the solids	ton/m^3
ρ_l	Density of the liquid	ton/m^3
ρ_m	Mixture density	ton/m^3
τ_1	Shear stress between liquid and pipe wall	kPa
τ_{12}	Shear stress on top of the bed	kPa
θ	Inclination angle (positive upwards, negative downwards)	°
μ_{sf}	Sliding friction coefficient	-
Φ	Durand ordinate	-

6.29 Starting Points DHLLDV Framework.

The DHLLDV Framework, as will be described in the next chapter, has starting points based on analysis of all models investigated in this chapter and based on the fundamentals. Most starting points are based on experiments and models for sand and gravel, although also other solids are investigated.

6.29.1 The Liquid Properties.

If the solids contain fines, the liquid properties have to be adjusted. The dynamic viscosity and the liquid density are influence by this. A number of models deal with graded solids with a high fraction of fines. So for these models the adjustment is essential. The definition of fines is not very clear. Often a particle diameter is used, however it also seems to make sense to use a particle diameter to pipe diameter ratio, since the size of eddies also depends on the pipe diameter. In true homogeneous flow both the liquid viscosity and the liquid density have to be adjusted. In pseudo homogeneous flow only the liquid density. Usually the equations of D.G. Thomas (1965) are used for this. The liquid property adjustments have to be carried out before identifying flow regimes.

6.29.2 Possible Flow Regimes.

There are 5 main flow regimes identified, most also identified by other researchers. These are:
1. The stationary bed flow regime, with or without sheet flow or suspension.
2. The sliding bed flow regime, usually with sheet flow or suspension.
3. The heterogeneous flow regime.
4. The homogeneous flow regime.
5. The sliding flow regime or stratified flow regime.
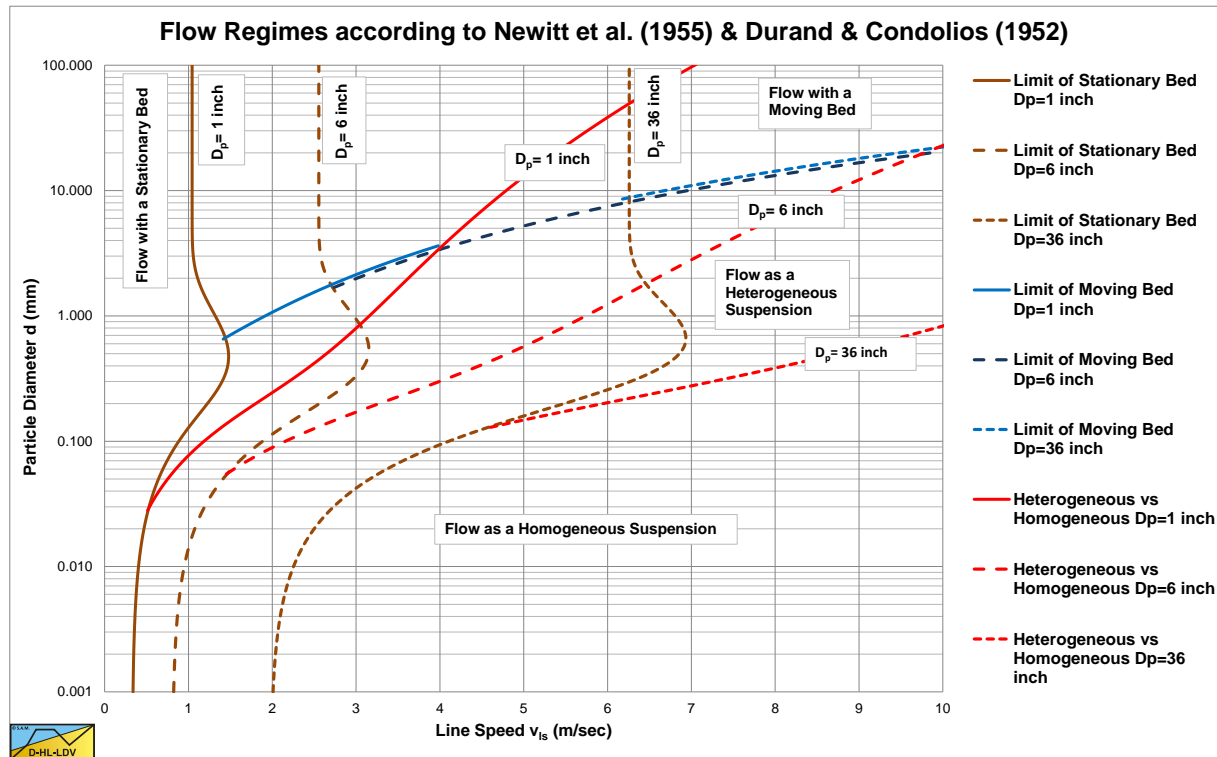
Figure 6.29-1: Flow regimes according to Durand & Condolios (1952) and Newitt et al. (1955), modified. (Captions for the 36 inch pipe diameter, C_v=0.15).

When starting at line speed zero and increasing the line speed, not all flow regimes have to occur, depending on the particle size and the particle size to pipe diameter ratio. It also matters whether a constant spatial volumetric concentration or a constant delivered volumetric concentration is considered.

For a constant spatial volumetric concentration, the following scenarios are possible.

1. Fine particles and a small **d/D$_p$** ratio. A stationary bed without sheet flow or suspension, a stationary bed with sheet flow or suspension, heterogeneous flow and (pseudo) homogeneous flow.

2. Medium/coarse particles and a small/medium **d/D$_p$** ratio. A stationary bed without sheet flow or suspension, a stationary bed with sheet flow or suspension, a sliding bed with sheet flow or suspension, heterogeneous flow and (pseudo) homogeneous flow.

3. Very coarse particles and a large **d/D$_p$** ratio. A stationary bed without sheet flow or suspension, a stationary bed with sheet flow or suspension, a sliding bed with sheet flow or suspension, sliding/stratified flow and (pseudo) homogeneous flow.

For a constant delivered volumetric concentration, the following scenarios are possible.

1. Fine particles and a small **d/D$_p$** ratio. A stationary bed with sheet flow or suspension, a sliding bed with sheet flow or suspension, heterogeneous flow and (pseudo) homogeneous flow.

2. Medium/coarse particles and a small/medium **d/D$_p$** ratio. A stationary bed with sheet flow or suspension, a sliding bed with sheet flow or suspension, heterogeneous flow and (pseudo) homogeneous flow.

3. Very coarse particles and a large **d/D$_p$** ratio. A stationary bed with sheet flow or suspension, a sliding bed with sheet flow or suspension, sliding/stratified flow and (pseudo) homogeneous flow.

6.29.3 Flow Regime Behavior.

For a constant spatial volumetric concentration, the following flow regime behavior is observed:

1. In the stationary bed regime the hydraulic gradient increases with the square of the line speed until sheet flow starts to occur, after which it increases with the line speed to a higher power.

2. In the sliding bed regime the excess hydraulic gradient does not depend on the line speed. It does however depend on the sliding friction factor and the relative submerged density and of course on the spatial concentration. The dependency on the spatial concentration as described by Wilson et al. (2006), the hydrostatic normal stress approach, has not been observed. Instead a linear dependency with the volumetric concentration is observed. The excess hydraulic gradient does not depend on the particle size, but there could be some relation between the particle size and the sliding friction factor. There could also be a relation between the particle size to pipe diameter ratio and the sliding friction factor.

3. In the heterogeneous regime the excess hydraulic gradient is reversely proportional to the line speed with a power varying from -1 to -2. Most researchers found a value close to -1, but some researchers use more negative powers up to -1.86 (Zandi & Govatos (1967)). One can say in general, the more uniform the solids, the more negative the power.

4. In the homogeneous regime everybody agrees that the excess hydraulic gradient is between zero and the ELM excess hydraulic gradient. There are different formulations to quantify this, but no general rule could be found. It does seem however that the higher the concentration, the lower the excess hydraulic gradient, using a scale of 0 to 1 from the pure liquid excess hydraulic gradient (0) to the ELM excess hydraulic gradient (1). The new methodology of Talmon (2011), assuming a particle free viscous sub-layer, seems promising to quantify this effect.

5. The sliding flow regime or fully stratified regime has not been identified as such, but has been observed by many researchers. This flow regime occurs when the concentration of the bed becomes so small that one cannot speak of a bed anymore, but the particles are still stratified and the excess hydraulic gradient behaves like a sliding bed. It has been observed that this occurs above a certain particle diameter to pipe diameter ratio and above some threshold concentration (5%-6%). Wilson et al. (2006) suggests using a power of -0.25 for the relation between the excess hydraulic gradient and the line speed.

For a constant delivered volumetric concentration, the following behavior is observed:

1. At very low line speeds a combination of a stationary bed with a moving bed above and suspension above the moving bed is observed. A 3 layer or multi-layer model is required. The spatial volumetric concentration will increase with decreasing line speed to the bed concentration, resulting in a maximum excess hydraulic gradient based on a pipe filled 100% with bed. This is not in a range of normal operational parameters, so most researchers did not carry out experiments in this range and did not discover this asymptotic behavior.

2. At a still low line speed the whole bed starts moving and a 2 layer model gives a good prediction. The excess hydraulic gradient decreases with the line speed to a small negative power, less negative than -1. The higher the line speed, the higher the bed velocity and the larger the fraction of particles in suspension or in a sheet flow layer.

3. Above a certain line speed the sliding bed behavior has a transition to heterogeneous behavior, where the excess hydraulic gradient is reversely proportional to the line speed with a power slightly more negative than in the constant spatial volumetric concentration situation. Since most experiments are carried out with delivered volumetric concentration measurements, it is not always clear whether the powers observed (-1 to -2) are for delivered or spatial volumetric concentrations.

4. At higher line speeds in the homogeneous or pseudo homogeneous regimes, the spatial and delivered concentrations are almost equal and the same behavior is observed.

5. At higher line speeds in the sliding flow regime, the spatial and delivered concentrations are almost equal and the same behavior is observed.

6.29.4 The LSDV, LDV and MHGV.

Many definitions exist for the line speed above which there is no bed. The Limit of Stationary Deposit Velocity (LSDV) is the velocity above which the bed is sliding and below which the bed is stationary. The Limit Deposit Velocity (LDV) is the velocity above which there is no stationary or sliding bed. The Minimum Hydraulic Gradient Velocity (MHGV) is the line speed where the hydraulic gradient is at a minimum. It is observed that fine particles often do not result in a sliding bed but have a direct transition from a stationary bed to heterogeneous transport. The bed vaporizes by particle suspension. Coarser particle will have a transition from a stationary bed (with sheet flow) to a sliding bed (LSDV) to heterogeneous transport. The occurrence of a sliding bed also depends on the particle diameter to pipe diameter ratio. In very small diameter pipes (1 inch) almost every normal particle diameter in sand will result in a sliding bed. However in large diameter pipes (1 m) as used in dredging, particles have to be very coarse (gravel) to result in a sliding bed. So in this case most sand particles will have a direct transition from a stationary bed to heterogeneous transport. The LSDV does not exist in the latter case, the LDV always exists.

In general the LDV depends on the particle diameter, the pipe diameter and the volumetric concentration. Different researchers found that the maximum LDV occurs at a volumetric concentration between 10% and 20%, probably closer to 20%. They also found that the LDV increases with the pipe diameter to a power between 1/3 and 1/2.

The relation with the particle diameter is more complex.

For very fine particles, fitting in the viscous sub-layer, a lower limit to the LDV is found. This lower limit does not depend on the particle diameter and only weak (power 0.1) on the pipe diameter, since the thickness of the viscous sub-layer depends weak on the pipe diameter.

For fine particles the LDV increases with the particle diameter up to a particle diameter of about 0.5 mm where a maximum is reached.

Medium to coarse particles first show a decrease of the LDV with increasing particle diameter, after which the LDV remains constant.

For a large particle diameter to pipe diameter ratio (>0.015) it looks like the LDV is increasing again with the particle diameter. It is the question however what is the value of the LDV here, since in this case the sliding flow regime will occur and the value of the LDV is more the MHGV, just a number to use in calculations without a real physical meaning.

There also seems to be a lower limit to the LDV over the whole range of particle diameters. It looks like this lower limit is caused by the transition between the sliding bed regime and the heterogeneous regime. This lower limit has hardly any effect on the LDV of fine particles, since the sliding bed regime will not occur there, but it will have a strong effect on medium and coarse particles in small diameter pipes, where the sliding bed regime is most likely to occur.

6.29.5 The Slip Velocity or Slip Ratio.

The slip velocity has two definitions. First the slip velocity is the difference between the solids velocity and the liquid velocity. Second the slip velocity is the difference between the solids velocity and the line speed, the cross sectional averaged mixture velocity. For small concentrations there is not much difference, but for large concentrations there is. Since the line speed is one of the inputs of every model, the second definition is used, but one should consider this is not 100% correct scientifically.

The slip ratio is defined here as the ratio of the slip velocity to the line speed. So a slip ratio of 1 means the particles have no velocity, while a slip ratio of 0 means the particles move with the line speed.

Above the LDV the slip ratio is relatively small, depending on the particle properties. In the homogeneous regime the slip ratio will be close to zero. Below the LDV the slip ratio will increase with decreasing line speed. Not to 1 as many understand, but to a value depending on the delivered concentration.

Suppose the delivered concentration equals the bed concentration at line speeds close to zero, so the whole pipe is filled with a bed, this means the bed will have a velocity equal to the line speed and the slip ratio equals zero.

Now suppose the delivered concentration is almost zero, so almost pure liquid being transported. At line speeds close to zero there will be a stationary of slowly sliding bed, but the bed velocity must be almost zero, otherwise the delivered concentration cannot be close to zero. So a pipe almost fully occupied with bed and hardly any delivered concentration, results in a slip ratio of almost 1. The asymptotic value of the slip ratio for a delivered concentration approaching zero is equal to 1.

Now suppose the delivered concentration is 50% of the bed concentration. At line speeds close to zero there will be a stationary of slowly sliding bed with some space above it transporting the mixture. The spatial concentration in the pipe is almost the bed concentration, since the pipe is almost completely occupied with bed, but the delivered concentration is 50% of the bed concentration. This means that on average the particles move with 50% of the line speed, giving a slip ratio of 0.5.

This means that the maximum slip ratio equals (**1-C$_{vt}$/C$_{vb}$**) at line speed zero, decreasing to a certain value at the LDV. Above the LDV the slip ratio will decrease rapidly. From the observations the conclusion can be drawn that the slip ratio decreases slowly in the sliding bed regime, but rapidly the closer the line speed gets to the LDV.

6.29.6 The Concentration Distribution.

The concentration distribution in a pipe gives information about the internal structure of the flow. Not many researchers report experimental concentration distributions, but some do. In general the concentration distribution is not part of the head loss models or equations, but in the Wasp or Wasp related models it is. The measured concentration distributions are usually predicted with solutions of the advection diffusion equations for open channel flow. Often these equations can be solved analytically, resulting in convenient equations. For pipe flow however the equations have to be solved numerically and also integrated numerically in order to find the correct cross section averaged spatial concentration.

The concentration distribution depends on the terminal settling velocity and the diffusivity. Often the non-hindered terminal settling velocity and some known diffusivity or diffusivity distribution are used. This however does not give satisfying results. Using the hindered settling velocity and a particle diameter and concentration dependent diffusivity gives better results. Kaushal & Tomita (2002B) found relations for this. Using the local hindered terminal settling velocity and concentration gives even better results.

6.29.7 The Dimensionless Numbers used.

The use of dimensionless numbers in the head loss models, especially the models for the heterogeneous regime, and in the LDV models is dangerous and misleading. In a number of models the flow Froude number and the particle Froude number are used. Also the particle diameter to pipe diameter ratio is often used. In these numbers the ratio between different independent parameters is present. For example the velocity divided by the square root of a diameter in the Froude number. When one of these parameters is varied over a wide range, while the other parameter is only varied over a small range, using the dimensionless number may give a good correlation in a regression. However when the parameter with the small range is used outside that range, unexpected results may appear. This is observed with the flow Froude number resulting in a proportionality of the head losses with the pipe diameter which is not correct, but also with the Durand Froude number for the LDV and the particle diameter to pipe diameter ratio, resulting in a relation of the LDV with the pipe diameter which is not correct. It is better to start unbiased with all independent parameters based on physics. If the result is dimensionless numbers in the equations, it may be convenient.

6.29.8 The Type of Graph used.

Usually head loss graphs are shown with the line speed on the abscissa and the hydraulic gradient on the ordinate. This is convenient in combination with pump head curves to determine the working point, by multiplying the hydraulic gradient with **ρ$_l$·g·ΔL**. However if experiments are carried out with different concentrations also giving some scatter, a messy graph is the result. The graph is not non-dimensional and it is difficult to compare different experiments. Using another type of graph mainly solves this problem. Using the relative excess hydraulic gradient on the ordinate and the liquid hydraulic gradient on the abscissa on double logarithmic coordinates, creates an almost dimensionless graph. Almost, because some flow regimes are still more or less concentration dependent. Another advantage is that lines that are (power) curved in the hydraulic gradient versus line speed graph, become straight lines in the double logarithmic relative excess hydraulic gradient versus liquid hydraulic gradient graph. For the LDV a graph is used with the Durand Froude number **F$_L$** on the linear ordinate and the particle diameter on the logarithmic abscissa. In this graph the **F$_L$** value only depends slightly on the pipe diameter, with a power of about -0.1.

Chapter 7:   The Delft Head Loss & Limit Deposit Velocity Framework.

7.1 Introduction.

7.1.1 Considerations.

In the last decades many head loss models for slurry transport have been developed. Not just for the dredging industry but also for coal and phosphate transport and in the chemical industries. Some models are based on the phenomena occurring combined with dimensionless parameters, resulting in semi-empirical equations (Durand & Condolios (1952), Gibert (1960), Worster & Denny (1955), Jufin Lopatin (1966), Zandi & Govatos (1967), Fuhrboter (1961)), while others are based on physics with 2 and 3 layer models (Newitt et al. (1955), Wasp et al. (1977), Doron & Barnea (1987), Wilson (1979), the SRC model (1991) and Matousek (2009)). The physical models are based on stationary transport in time and space, while the semi-empirical models may incorporate non-stationary or dynamical processes. An analysis of these models and of data collected from numerous publications for particles with densities ranging from 1.14 ton/m^3 to 3.65 ton/m^3, particle diameters ranging from 0.005 mm up to 45 mm, concentrations up to 45% and pipe diameters from 0.0254 m up to 0.9 m has led to an overall model of head losses in slurry transport, a sort of Framework. The Framework is based on 5 main flow regimes determining the source of energy losses, the fixed or stationary bed regime, the sliding bed regime, the heterogeneous flow regime, the homogeneous flow regime and the sliding flow regime.. One can distinguish viscous friction losses, dry friction losses, potential energy losses, kinetic energy losses, Magnus lift work, turbulent lift work and turbulent eddy work. The losses do not have to occur at the same time. Usually one or two will be dominant depending on the flow regime.

Although sophisticated 2 and 3 layer models exist for slurry flow (here the flow of sand/gravel water mixtures), the main Dutch and Belgium dredging companies still use modified Durand & Condolios (1952) and Fuhrboter (1961) models, while the main dredging companies in the USA and Canada use a modified Wilson et al. (1992) model for heterogeneous transport and sliding bed transport or the SRC model. When asked why these companies don't use the more sophisticated models, they answer that they require models that match their inputs and they feel that the 2 and 3 layer models are still in an experimental phase, although these models give more insight in the physics. Usually the companies require a model based on the particle size distribution or d_{50}, the pipe diameter D_p, the line speed v_{ls}, the relative submerged density R_{sd} and the temperature (the viscosity of the carrier liquid v_l). Parameters like the bed associated hydraulic radius are not known in advance and thus not suitable. Usually the dredging companies operate at high line speeds above the Limit Deposit Velocity (LDV) in the heterogeneous or homogeneous regime. This implies that the bed has dissolved and 2 and 3 layer models are not applicable anyway.

Still there is a need for improvement, since the existing models give reasonably good predictions for small diameter pipes, but not for large diameter pipes as used in dredging. Recent projects require line lengths up to 35 km with 5 to 6 booster pumps and large diameter pipes. Choosing the number of booster pumps and the location of the booster pumps depends on the head losses. However it should be considered that the slurry transport process is not stationary. Densities may vary from a water density of 1 ton/m^3 to densities of 1.6 ton/m^3 and particle size distributions will change over time. This results in a dynamic process where pumps, pump drives and slurry transport interact. The fundamental 2 and 3 layer models require a stationary approach, while the more empirical equations may take the dynamic effects as time and place averaged effects into account. The question is whether a semi empirical approach is possible, covering the whole range of pipe diameters and giving the empirical equations a more physical background, but still using the parameters available to the dredging industry.

Transporting sand with water through a pipeline, in general, results in an increase of the pressure required compared with pumping water or pure liquid. Since pressure times flow equals power and power times time equals energy, this can also be interpreted as an increase of the energy required to pump the solids. Energy or work also equals force times distance or stress times volume. The fact that more power is required to pump a solid-liquid mixture compared with just pumping the liquid implies that there are additional energy losses and energy dissipation when pumping the solids. In order to go into detail to the model developed, first the different types of energy dissipation due to the solids effect are discussed.

It is clear that the flow regimes and the magnitude of the relative excess hydraulic gradient depends strongly on the pipe diameter and the particle diameter. In the large pipe a sliding bed will never occur in the constant spatial volumetric concentration case. In the small pipe however it will for particles larger than 0.5 mm. In the small pipe, the larger particles exceed the ratio **d/D$_p$>0.015** as set by Wilson et al. (1997), resulting in almost 100% stratified

flow, here considered to be the sliding flow regime. In the large pipe this criterion is never met, except when pumping large gravel, cobbles or boulder sized pieces such as cut rock or clayballs.
.
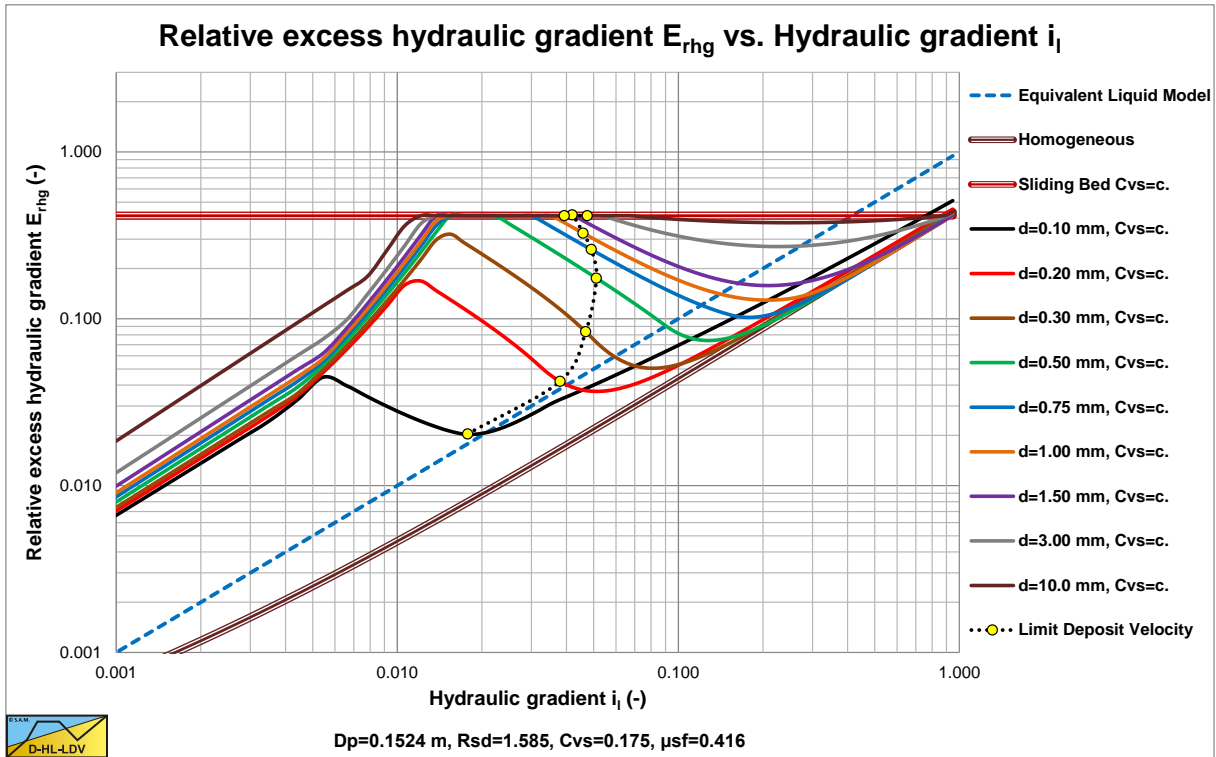
Figure 7.1-1: The relative excess hydraulic gradient as a function of the hydraulic gradient, constant C_{vs} and D_p=0.1524 m.
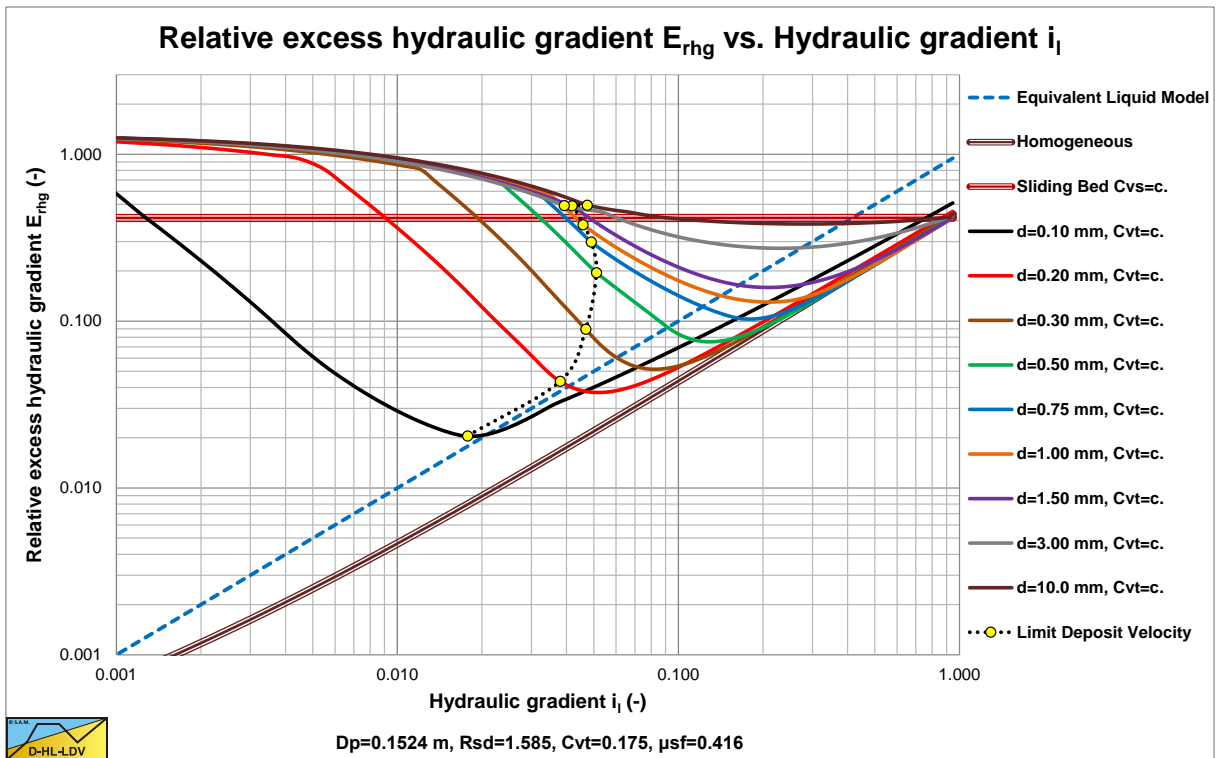
Figure 7.1-2: The relative excess hydraulic gradient as a function of the hydraulic gradient, constant C_{vt} and D_p=0.1524 m.

Relative excess hydraulic gradient E_{rhg} vs. Hydraulic gradient i_l

Dp=1.0000 m, Rsd=1.585, Cvs=0.175, μsf=0.416
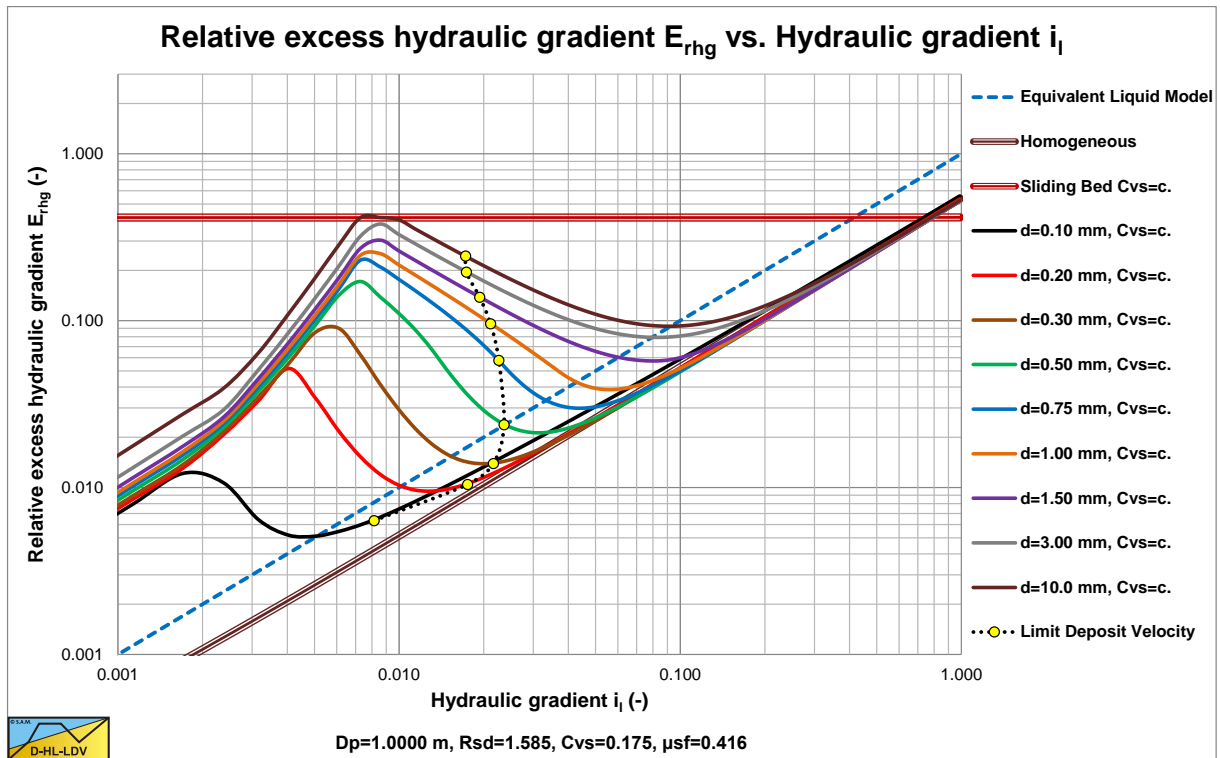
Figure 7.1-3: The relative excess hydraulic gradient as a function of the hydraulic gradient, constant C_{vs} and D_p=1 m.

Relative excess hydraulic gradient E_{rhg} vs. Hydraulic gradient i_l

Dp=1.0000 m, Rsd=1.585, Cvt=0.175, μsf=0.416
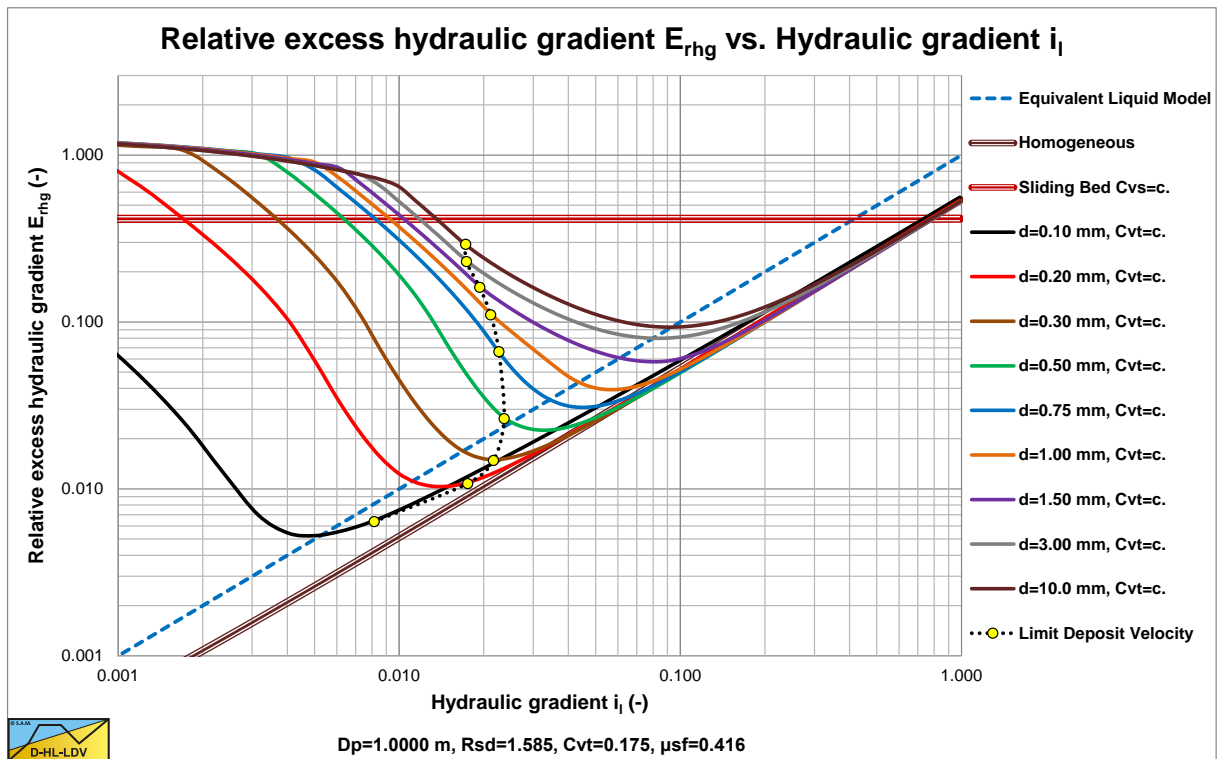
Figure 7.1-4: The relative excess hydraulic gradient as a function of the hydraulic gradient, constant C_{vt} and D_p=1 m.

Figure 7.1-1, Figure 7.1-2, Figure 7.1-3 and Figure 7.1-4 show the results of the energy approach for 9 sands ranging from **d=0.1 mm** up to **d=10 mm** in pipes with diameters of **D_p=0.1524 m** and **D_p=1 m**. For each pipe diameter the constant spatial volumetric concentration curves and the constant delivered volumetric concentration curves are shown.

On the **E_{rhg}** graph the regimes are clearly distinguishable: the fixed bed is an upward-sloping line on the left, the sliding bed regime is the flat (horizontal) line at about 0.4 (the sliding friction factor), the heterogeneous regime is the downward-sloping line in the middle, and the pseudo-homogeneous regime is upward-sloping on the left. For large particles the sliding flow regime is almost flat (similar to sliding bed), in the flow region of the heterogeneous regime. The figures above clearly show how the available regimes change with pipe diameter.

So head losses from experiments in pipes of 0.1524 m can hardly be translated into head losses for a pipe of 1 m as often used in dredging. The physical processes are different. Small pipe sliding bed versus large pipe no sliding bed and small pipe sliding flow versus large pipe no sliding flow. In fact the smaller the pipe diameter, the higher the probability of the occurrence of a sliding bed and sliding flow and the larger the pipe diameter, the lower the probability of the occurrence of a sliding bed and sliding flow. Only if the physical processes involved are similar, is scaling possible.

This explains why many equations and models from literature give good results for small pipe diameters, but deviate for large diameter pipes. The way energy is dissipated in small diameter pipes is often different from the way it is dissipated in large diameter pipes at operational line speeds. It also explains while a lot of research is focused on 2 and 3 layer transport with a sliding bed, which often occurs in small pipes, but much less in large pipes.

7.1.2 Energy Dissipation.

When a liquid is transported through a pipeline, energy is dissipated by viscous friction and by turbulence (assuming high Reynolds numbers). When solids are added, there will also be energy dissipation in the form of potential losses, kinetic losses and possibly friction losses and losses due to Magnus and turbulent lift work and turbulence in general.

- Potential energy losses. In turbulent flow, because the solids are under the influence of gravity and the turbulence has to keep them floating. The potential energy losses will depend on the terminal settling velocity and be influenced by hindered settling. Since the settling process does not depend on the line speed, at a higher line speed the energy dissipation per unit of time will not change. This implies that the energy dissipation per unit of pipeline length is reversely proportional with the line speed. So at high line speeds the influence of the potential energy losses will diminish.
- Kinetic energy losses. During transport, because the particles interact with the wall, with each other and with the turbulent eddies and in all cases they lose part of their kinetic energy. With the kinetic energy losses one may expect that the number of interactions is more or less constant in time, so at higher line speeds the number of interactions per unit of line length will decrease reversely proportional with the line speed, resulting in a decrease of the excess pressure due to the solids. At higher line speeds however the momentum of the particles also increases and it is more difficult to change the direction of the particles. This might decrease the number of interactions with the wall per unit of time. The total losses will be reversely proportional with the line speed to a power higher than 1, let's say a proportionality with a power between -1 and -2. The proportionality depends on the physical properties and the grading of the solids. Although near wall lift will exist at low line speeds, it is negligible until a certain line speed where the lift force is strong enough to keep the solids away from the wall. At this line speed there are no more interactions with the wall and the excess pressure due to interactions collapses. At about the same line speed the lift forces start driving the solids to the center of the pipe resulting in a more homogeneous flow. The pure heterogeneous regime stops abruptly, because there are no more interactions with the wall, and the pseudo homogeneous regime starts, based on the work of lift forces and turbulence. The transition line speed depends on the particle and the pipe diameter. So the sudden regime change as described will only occur in uniform or very narrow graded sands.
- Sliding and rolling friction. Sliding and rolling friction occur if there is a sliding or moving bed. Forces are transmitted directly between particles and the internal and external friction coefficients determine the friction forces. These coefficients are dependent on the type of solids and the particle size distribution.
- Magnus lift work. When the thickness of the viscous sub-layer is bigger than the particle diameter, particles with rotation due to interactions with the wall will be subjected to Magnus lift forces. This will only occur for the combination of a low line speed and small particles. The Magnus lift forces will carry out work if they actually lift the particles, contributing to the energy losses. When the line speed increases, the thickness of the viscous sub-layer decreases and the particles do not fit in the viscous sub-layer anymore. The Magnus lift work will diminish when the size of the particles is bigger than the layer thickness. At a higher line speed, the turbulent lift and turbulent eddies will take over.
- Turbulent lift and eddy work. At high line speeds the turbulent lift and turbulent eddies becomes important. Since lift force times the distance over which it acts equals the work carried out, this will also result in energy losses. Since the lift force increases with the velocity gradient near the wall, the losses due to the lift force

will increase with the line speed. At relatively low line speeds most solids will be transported in the bottom part of the pipeline, resulting in an asymmetrical concentration profile, matching heterogeneous flow. This results in an opposite asymmetrical velocity profile, with the highest flow at the top of the pipeline. Below a certain line speed the lift force on a particle is smaller than the weight of the particle and the lift force will not carry out any work. But above this transition velocity suddenly the particles will be lifted. The lift forces are dependent on the velocity gradient and thus will appear at the full circumference of the pipe, but they will first start pushing the solids upwards from the bottom and thus start to create a more symmetrical concentration and velocity profile. With increasing line speed the concentration and velocity profile will get closer to the symmetrical profiles, matching pseudo homogeneous transport.

Resuming it can be stated that the potential and kinetic losses decrease with an increasing line speed with a power of the line speed between -1 and -2, while the losses due to near wall lift forces increase with an increasing line speed, until the pseudo homogeneous regime is reached. For each combination of particle and pipe diameter, there exists a transition line speed. Below this line speed kinetic losses dominate the excess pressure; above this line speed the work carried out by turbulent lift and eddy forces dominates the excess pressure. For uniform sand, kinetic losses and work carried out by lift forces will not occur at the same line speed. For graded sands a transition region, with respect to the line speed, will occur, the size of which depending on the grading. In the case where the particles are much smaller than the thickness of the viscous sub layer, theoretically there is Magnus lift if the particles are rotating. One may expect that the excess pressure due to the solids will continue decreasing with increasing line speed. In this case the excess pressure will reach zero asymptotically and there is no solids effect at very high line speeds. It is obvious that the collapse of the interactions with the wall, resulting in a collapse of the kinetic losses, due to the lift force, will happen at about the same line speed where the work of the lift forces starts increasing. This is the transition line speed between heterogeneous and pseudo homogeneous transport. It is not possible that the collapse of the kinetic losses appears at a line speed higher than the line speed where the work carried out by the lift forces starts, for uniform sands. It might be possible that this collapse appears at a slightly lower line speed, resulting in a collapse of the excess pressure, but at higher line speeds this will increase again because of the work of the lift forces.

Wilson et al. (1997) introduced the Stratification Ratio **R**, which in fact equals the relative excess hydraulic gradient E_{rhg}. The higher the Stratification Ratio, the more asymmetrical the concentration and the velocity profile in the pipe. With increasing line speed, the Stratification Ratio decreases with power of 0.25-1.7, depending on the grading of the sand. However, once the transition line speed between heterogeneous and homogeneous transport is passed, the relative excess hydraulic gradient will increase again, while the stratification decreases. The term Stratification Ratio corresponds with the heterogeneous transport, with potential and kinetic losses, but not with the pseudo homogeneous transport with losses due to lift work. Therefore a new term is introduced, the **S**lip **R**elative **S**quared or S_{rs}, which is the ratio between the slip velocity and the terminal settling velocity squared. Where the slip velocity is defined as; the contribution of the velocity difference between the line speed and the particle velocity to explain for the head losses. Mathematically the **Stratification Ratio Solids** and the **Slip Relative Squared** are the same, but physically the **Slip Relative Squared** tells more about the physics of the heterogeneous hydraulic transport. So the S_{rs} value explains for the kinetic energy losses in the heterogeneous flow regime. The potential energy losses are taken into account by the **Settling Velocity Hindered Relative**, the S_{hr} value. These potential energy losses are present both in the heterogeneous flow regime and the homogeneous flow regime.

Many graphs in this book and specifically this chapter have the relative excess hydraulic gradient as the ordinate and the hydraulic gradient of pure liquid as the abscissa. Since the relative excess hydraulic gradient equals the mixture hydraulic gradient minus the pure liquid hydraulic gradient, divided by the relative submerged density of the solids and the volumetric concentration, the graph is almost dimensionless. Almost, because there is are still some non-linear effects of the relative submerged density and the volumetric concentration. The mixture hydraulic gradient minus the pure liquid hydraulic gradient is often called the solids effect, so the increase of the hydraulic gradient due to the presence of solids. The volumetric concentration can be either the spatial or the transport concentration, depending on the measurement method. Most researchers, in their models, assume the mixture hydraulic gradient equals the pure liquid hydraulic gradient plus the solids effect. Only the more physical models, the 2LM and 3 LM models, have a different approach.
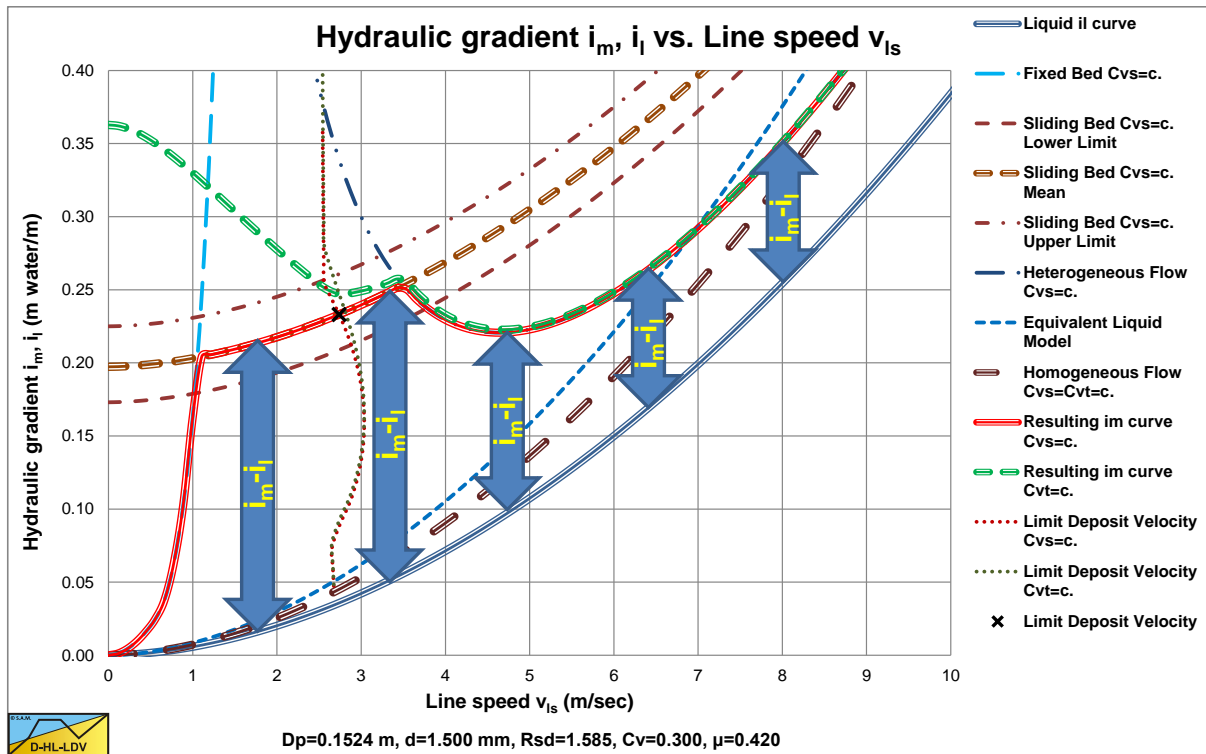
Figure 7.1-5: The hydraulic gradient i_m, i_l and excess hydraulic gradient i_m-i_l.
Constant spatial volumetric concentration.
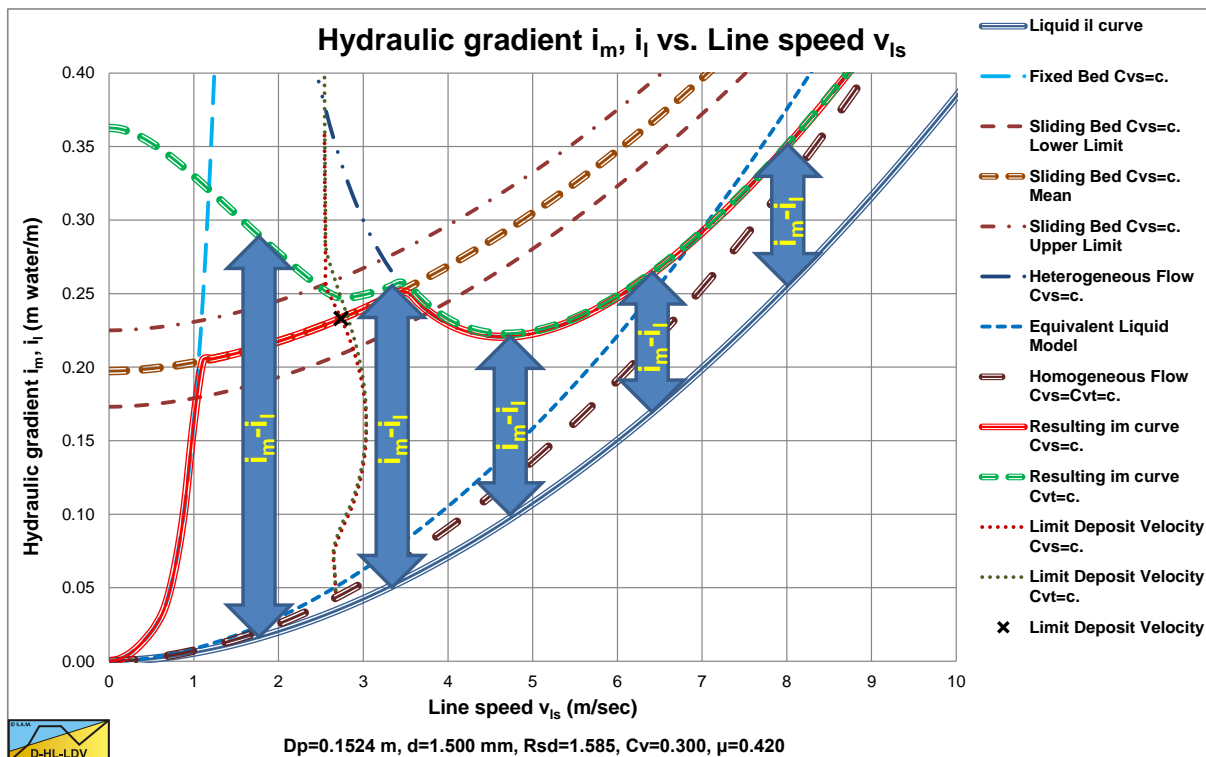
Figure 7.1-6: The hydraulic gradient i_m, i_l and excess hydraulic gradient i_m-i_l.
Constant delivered (transport) volumetric concentration.

Figure 7.1-5 and Figure 7.1-6 show the solids effect for the constant spatial volumetric concentration C_{vs} case and the constant transport volumetric concentration C_{vt} case. The solids effect in general decreases with increasing line speed. For low line speeds the C_{vt} case gives a higher solids effect compared with the C_{vs} case due to increasing slip with decreasing line speed.
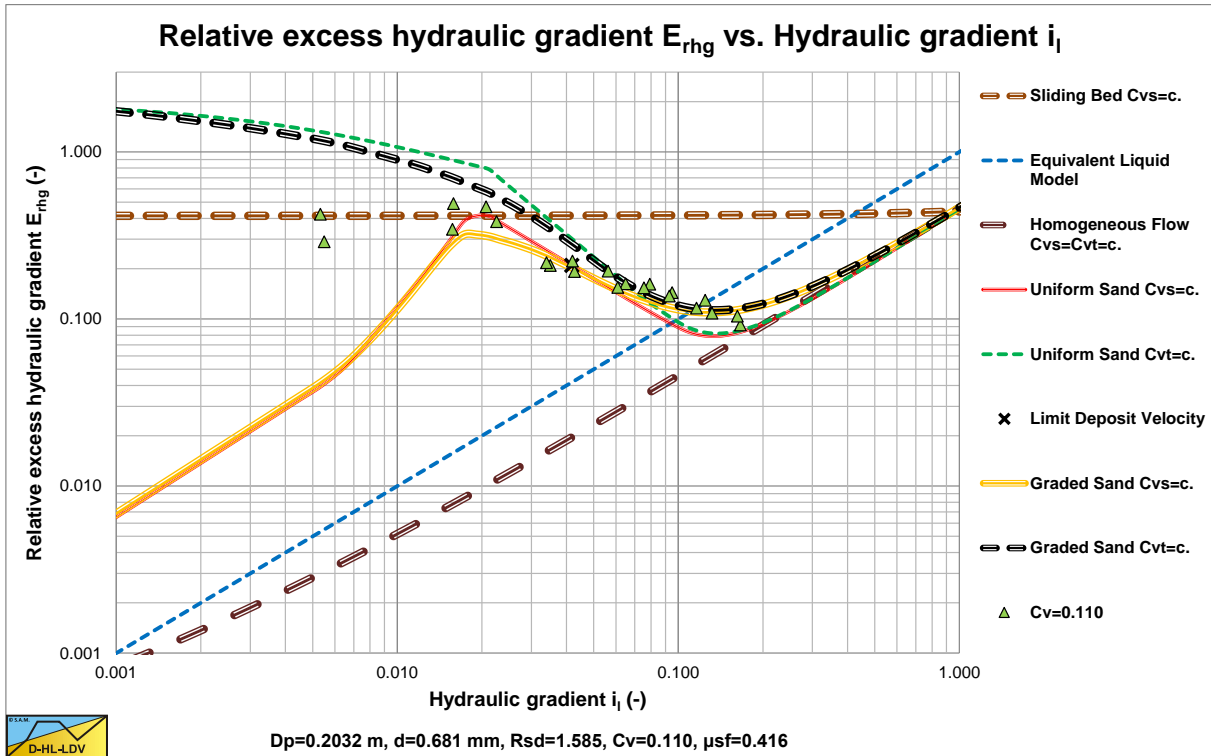
Figure 7.1-7: Behavior of narrow graded crushed granite slurry after Clift et al. (1982).
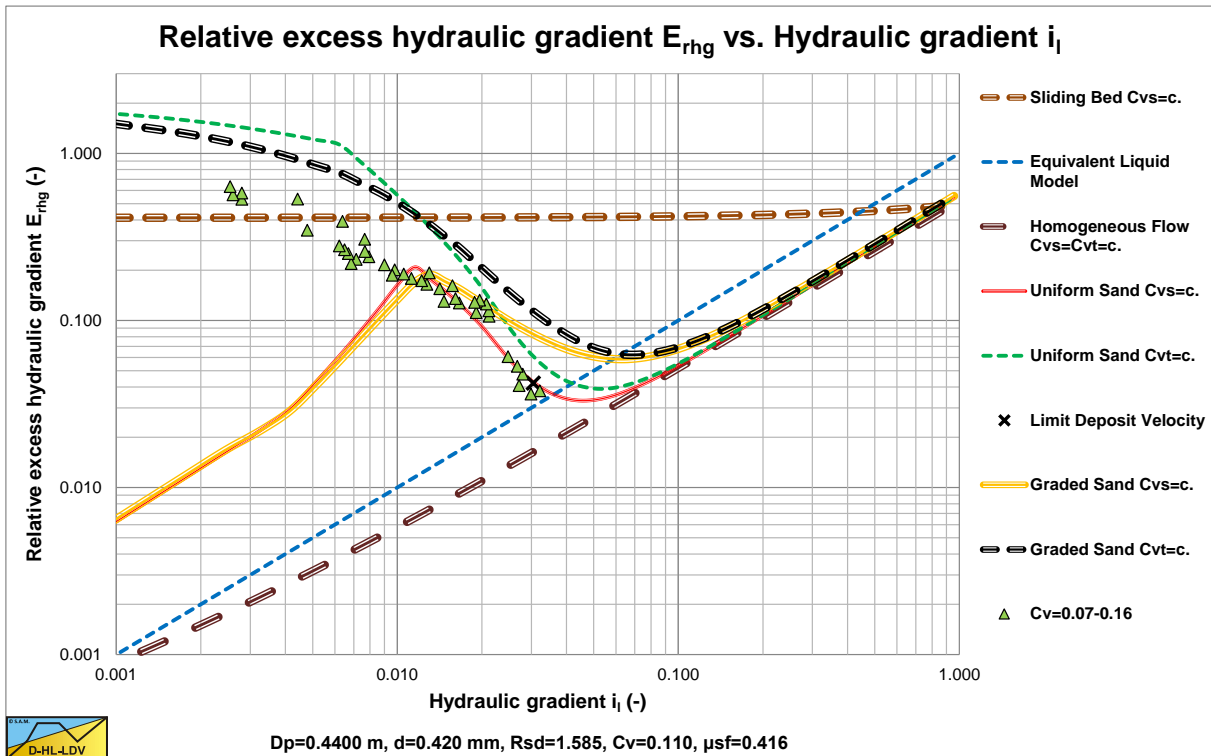
Figure 7.1-8: Behavior of narrow graded crushed granite slurry after Clift et al. (1982).

Figure 7.1-7 shows a case where the transition velocity is the same for the collapse of the kinetic interactions and the start of the lift work. Figure 7.1-8 shows a case where the transition velocity of the lift work is higher than the transition velocity for the collapse of the kinetic interactions. The latter results in a collapse of the relative excess hydraulic gradient. In both examples the same solids are used, but in the latter case the pipe diameter is bigger. Other experiments by Clift et al. (1982) with narrow graded 0.42 mm masonry sand, shows exactly the same phenomena.

7.1.3 Starting Points.

Before discussing the Delft Head Loss & Limit Deposit Velocity (DHLLDV) Framework in detail, some starting points have to be pointed out. First of all, the Framework is based on a set of 5 sub-models for 5 main flow regimes. These sub-models are all based on a constant spatial volumetric concentration C_{vs}. Curves for constant volumetric transport concentration C_{vt} are derived from the 5 sub-models based on the slip velocity v_{sl}. The slip velocity v_{sl} is defined as the difference between the velocity of the mixture v_{ls} and the velocity of the solids v_s:

$$v_{sl} = v_{ls} - v_s = v_{ls} \cdot \left(1 - \frac{v_s}{v_{ls}}\right) = v_{ls} \cdot \left(1 - \frac{C_{vt}}{C_{vs}}\right) \tag{7.1-1}$$

For a certain control volume the volumetric transport concentration C_{vt} can be determined if the volumetric spatial concentration C_{vs} and the slip velocity v_{sl} are known, given a certain line speed v_{ls}.

$$C_{vt} = \left(1 - \frac{v_{sl}}{v_{ls}}\right) \cdot C_{vs} \tag{7.1-2}$$

Likewise, for a certain control volume, the volumetric spatial concentration C_{vs} can be determined if the volumetric transport concentration C_{vt} and the slip velocity v_{sl} are known, given a certain line speed v_{ls}.

$$C_{vs} = \left(\frac{v_{ls}}{v_{ls} - v_{sl}}\right) \cdot C_{vt} \tag{7.1-3}$$

These equations will be used a lot in the following derivations and are considered to be well known. The 5 main flow regimes are:

1. A **Fixed Bed** (FB) regime or restricted pipe regime. The behavior of this main flow regime is, the solids form a bed at the bottom of the pipe. This bed is stationary (fixed), so the liquid has to flow through a restricted area above the bed, resulting in higher pressure losses. At higher line speeds it is probable that part of the solids start eroding and be transported heterogeneously above the bed. At the Limit Deposit Velocity, the bed has been eroded completely. As long as the pressure losses correspond with the behavior of flow through the restricted area above the bed, the flow regime is considered to be a fixed bed regime.
2. A **Sliding Bed (SB)** regime or sliding friction dominated regime. The behavior of this main flow regime is, the solids form a sliding bed at the bottom of the pipe. The pressure losses are the sum of the losses as a result of the sliding friction of the solids and the viscous friction of the liquid. At higher line speeds it is probable that part of the solids start eroding and be transported heterogeneously above the bed. At the Limit Deposit Velocity, the bed has been eroded completely. At higher concentration it is possible that sheet flow occurs and the sliding bed curve is followed right of the intersection with the heterogeneous transport curve. As long as the pressure losses correspond with the behavior of sliding friction, the pressure loss curves are parallel with the clean water resistance curve in the i_m versus v_{ls} plot, the sliding bed regime is considered.
3. **Heterogeneous** (He) transport or collision dominated regime. The behavior of this main flow regime is, the solids interact with the pipe wall through collisions. The solids are distributed non-uniformly over the cross section of the pipe with higher concentrations at the bottom of the pipe. This may be due to saltation or to Brownian motions of the particles in turbulent transport. For very small particles this may follow the fixed bed regime directly, for coarse particles this will follow the sliding bed regime.
4. **Homogeneous** (Ho) transport. The behavior of this main flow regime is, the particles are uniformly distributed over the cross section of the pipe due to the mixing capability of the turbulent flow. The pressure losses behave according to Darcy Weisbach, but with the mixture density as the liquid density. For very fine particles the viscosity has to be adjusted by the apparent viscosity.
5. The **Sliding Flow** (SF) regime. If the ratio between the particle diameter and the pipe diameter is above a certain value and the spatial volumetric concentration is above about 5%, the turbulence is not capable of carrying the particles anymore. This will result in a high speed flow with the characteristics of sliding friction, however the bed concentration decreases with increasing line speed. So it's named **Sliding Flow**.

The hydraulic gradient i_w (for water) or i_l (for a liquid in general) and for a mixture are:

$$i_l = i_w = \frac{\Delta p_l}{\rho_l \cdot g \cdot \Delta L} = \frac{\lambda_l \cdot v_{ls}^2}{2 \cdot g \cdot D_p} \quad \text{and} \quad i_m = \frac{\Delta p_m}{\rho_l \cdot g \cdot \Delta L} = \frac{\lambda_m \cdot v_{ls}^2}{2 \cdot g \cdot D_p}$$

(7.1-4)

The **Relative Excess Hydraulic Gradient E_{rhg}** is the difference between the mixture gradient i_m (in meters of carrier liquid column) and the hydraulic gradient i_l divided by the relative submerged density R_{sd} and the volumetric concentration C_{vs}. This E_{rhg} will also be referred to as the **solids effect**. The **Slip Relative Squared S_{rs}** is the **Slip Velocity** of a particle v_{sl} divided by the **Terminal Settling Velocity** of a particle v_t squared and this S_{rs} value is a good indication of the excess pressure losses due to the solids in the heterogeneous regime. The **Settling Velocity Hindered Relative S_{hr}** is the ratio between the hindered settling velocity $v_t \cdot (1 - C_{vs}/\kappa_C)^\beta$ and the line speed v_{ls}, divided by the relative submerged density R_{sd} and the volumetric concentration C_v. For all regimes the E_{rhg} value is:

$$E_{rhg} = \frac{i_m - i_l}{R_{sd} \cdot C_{vs}}$$

(7.1-5)

In the heterogeneous regime the relation between these parameters is:

$$E_{rhg} = \frac{i_m - i_l}{R_{sd} \cdot C_{vs}} = S_{hr} + S_{rs}$$

(7.1-6)

Figure 7.1-9, Figure 7.1-10, Figure 7.1-11 and Figure 7.1-12 show the 5 main flow regimes for small, medium and large particles in an 0.1524 m (6 inch) pipeline. The abscissa, the horizontal axis, is the line speed v_{ls}. The ordinate, the vertical axis, is the hydraulic gradient of the mixture i_m. The red solid line is the constant volumetric spatial concentration C_{vs} line. The green dashed line the constant volumetric transport concentration C_{vt} line. The light brown dashed lines show the sliding bed curves, where the thick line is based on the sliding friction coefficient and the thin lines give a margin of +/- 12.5% of the sliding friction coefficient. The solid blue line is the pure liquid hydraulic gradient, the dashed blue line the ELM (Equivalent Liquid Model) curve and the dark brown dashed line the theoretical homogeneous regime curve. The dotted lines give the Limit Deposit Velocity curves for spatial and transport concentration.

For very fine particles, the fixed bed regime transits directly to the heterogeneous regime, without the occurrence of the sliding bed regime. This can be seen in Figure 7.1-9 because the intersection point is below the sliding bed curve. The Limit Deposit Velocity is at the transition between the heterogeneous regime and the homogeneous regime. Although there is some slip above the Limit Deposit Velocity, the slip and thus the difference between the constant volumetric spatial concentration C_{vs} lines and the constant volumetric transport concentration C_{vt} lines increases with a decreasing line speed at line speeds below the Limit Deposit Velocity. The intersection point between the fixed bed regime and the heterogeneous regime will be at an increasing E_{rhg} value with an increasing particle diameter.

For medium particles, Figure 7.1-10, the intersection point between the fixed bed regime and the heterogeneous regime lies above the sliding bed regime curve, meaning that the fixed bed regime is followed by the sliding bed regime, followed by the heterogeneous regime, with increasing line speed. The Limit Deposit Velocity is now somewhere between the intersection of the sliding bed regime with heterogeneous regime and the heterogeneous regime with the homogeneous regime. The larger the particle the closer is the Limit Deposit Velocity to the intersection of the sliding bed regime with heterogeneous regime.

The examples given here are for an 0.1524 m pipe. For other pipe diameters, the sliding bed (constant sliding friction coefficient) and the homogeneous regime curves, will stay at the same position and do not depend on the pipe diameter. The fixed bed curve will move to the right with increasing pipe diameter, while the heterogeneous regime curve will move to the left with increasing pipe diameter. One could also say that both curves move downwards with an increasing pipe diameter.

The transitions between the main flow regimes are not instantaneous, but gradually. Special attention will be given to the transition between the heterogeneous regime and the homogeneous regime.
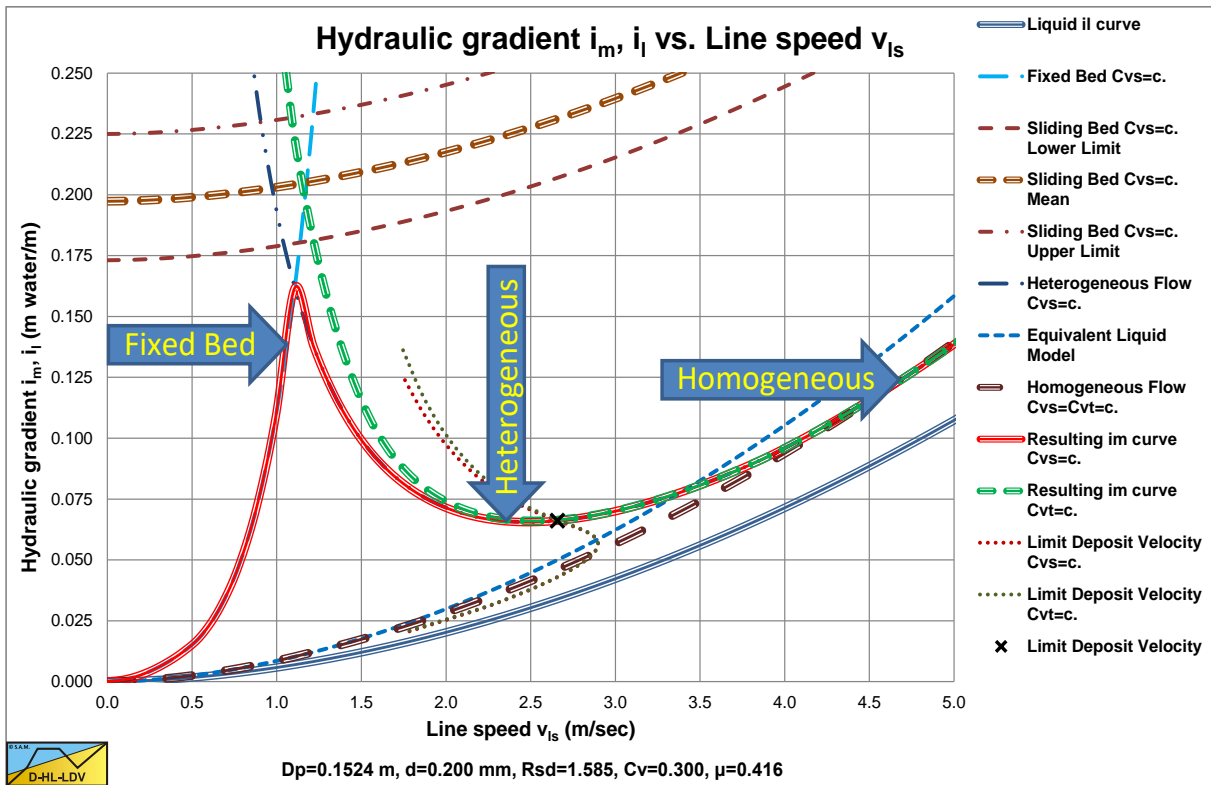
Figure 7.1-9: The 3 main flow regimes for fine particles.
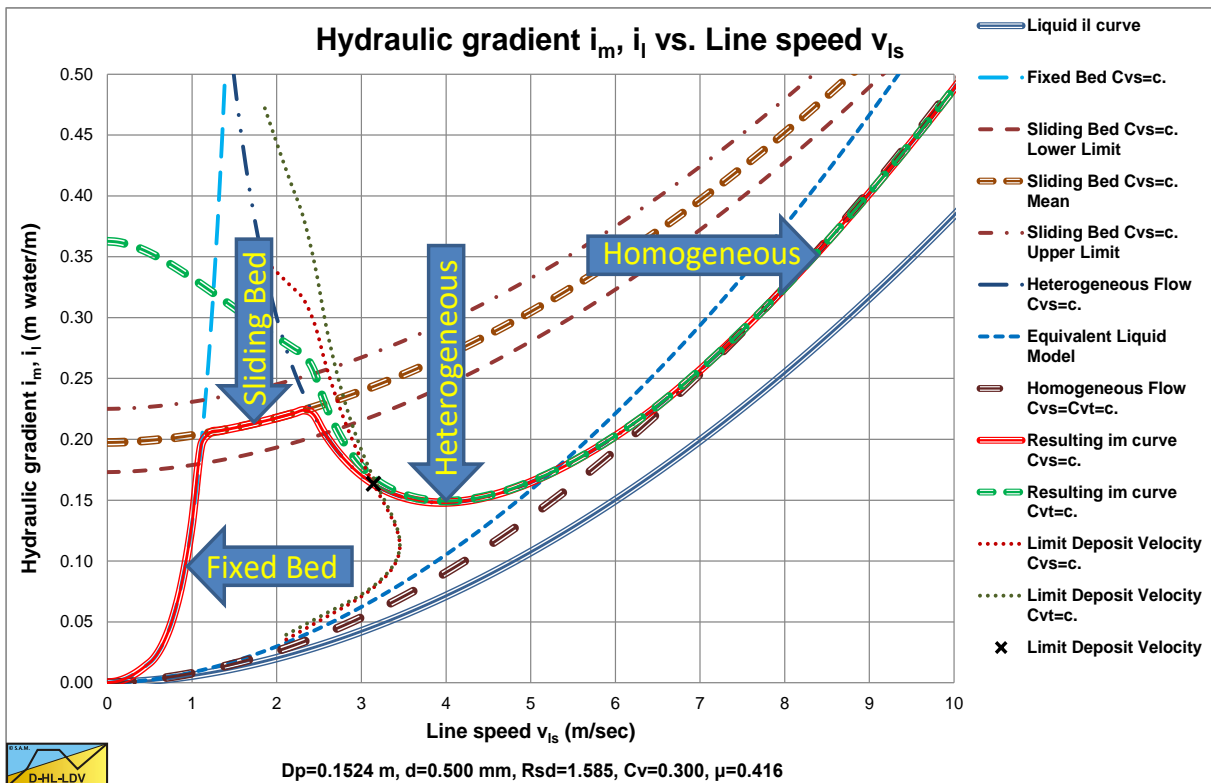
Figure 7.1-10: The 4 main flow regimes for medium particles.

For large particles, Figure 7.1-11, the behavior is similar to the medium particles, except for the fact that the Limit Deposit Velocity is at the sliding bed regime, below the intersection point between the sliding bed regime and the heterogeneous regime. This is possible because in reality this transition is not sharp but gradual.

Very coarse particles, Figure 7.1-12, show sliding flow behavior. Turbulence is not capable anymore to bring the particles in suspension. The behavior is a mix of sliding bed and heterogeneous flow.

Figure 7.1-11: The 4 main flow regimes for coarse particles.

Figure 7.1-12: The 3 main flow regimes for very coarse particles, including sliding flow.
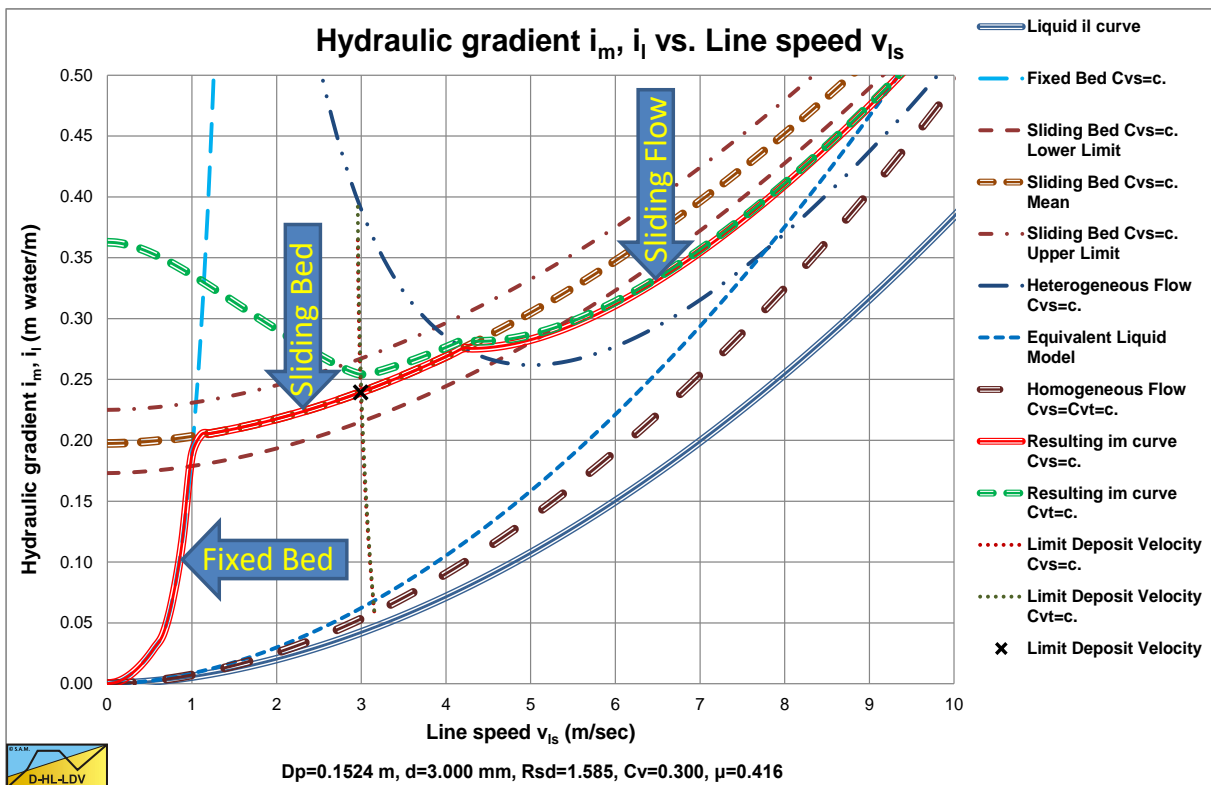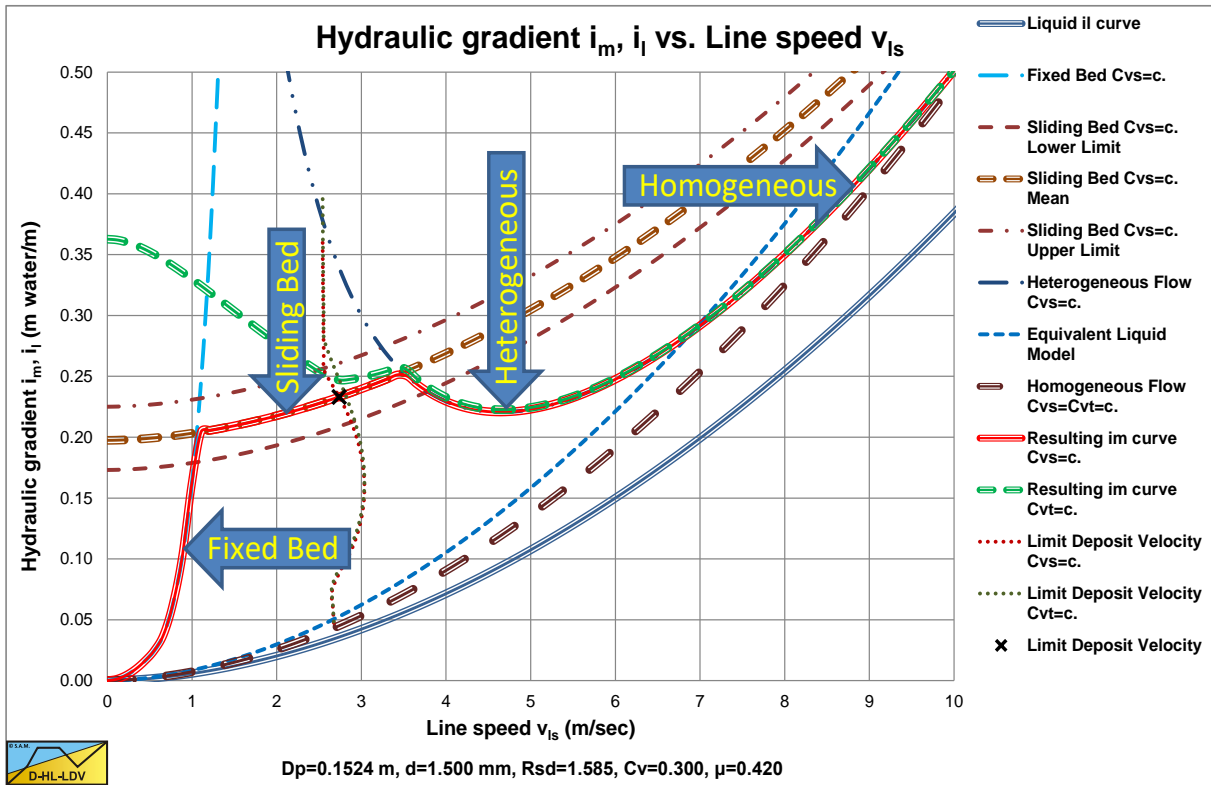
7.1.4 Approach.

Chapter 7 describes the new Delft Head Loss & Limit Deposit Velocity (DHLLDV) Framework. The DHLLDV Framework is based on uniform sands or gravels and constant spatial volumetric concentration.

1. An explanation of the Delft Head Loss & Limit Deposit Velocity Framework.
2. A detailed description of the 8 different flow regimes and 6 scenarios is given. The occurrence of flow regimes depends on the particle to pipe diameter ratio and on the spatial volumetric concentration. Figure 7.1-13 gives an example of the different flow regimes occurring depending on the particle diameter and the line speed. Each pipe diameter and each spatial volumetric concentration requires such a graph.
3. The stationary bed regime without sheet flow and with sheet flow. The stationary bed without sheet flow is based on a 2 layer model for low line speeds and a 3 layer model for higher line speeds. Usually the bed starts sliding when there is sheet flow, however for small particles it is possible that there is a direct transition from the stationary bed regime to the heterogeneous flow regime.
4. The sliding bed regime. The sliding bed is based on a 3 layer model showing an almost constant relative excess hydraulic gradient equal to the sliding friction coefficient. The sliding bed regime does not always occur. The larger the particles and the larger the volumetric concentration, the higher the probability of the occurrence of a sliding bed.
5. The heterogeneous regime. The heterogeneous model is based on energy considerations, resulting in a two component model, potential energy losses and kinetic energy losses.
6. The homogeneous regime. The homogeneous model is based on the equivalent liquid model (ELM) with a correction based on a particle free viscous sub layer.
7. The sliding flow regime. The sliding flow model assumes a high speed flow with the macroscopic behavior of sliding friction and heterogeneous flow. The porosity of the bed increases with the line speed and particles do not necessarily rest on each other.
8. A new model for the Limit Deposit Velocity is derived, consisting of 5 particle size regions and a lower limit. This model is based on the ratio of the potential energy of the particles to the total energy in the liquid flow for small particles and on a limiting small bed for large particles.
9. Based on the LDV a method is shown to construct slip velocity or slip ratio curves from zero line speed to the LDV. Based on the slip ratio, the constant delivered volumetric concentration curves can be constructed. The resulting model is compared with models from literature.
10. The concentration distribution. Also based on the LDV, in this case the assumption that at the LDV the concentration at the bottom of the pipe equals the bed concentration, a new diffusivity approach is developed. The resulting concentration distributions are compared with experiments.
11. The transition heterogeneous versus homogeneous in detail. The transition from the heterogeneous regime to the homogeneous regime requires special attention. First of all, the transition line speed gives a good indication of the operational line speed and allows to compare the DHLLDV Framework with many models from literature. Secondly, at this transition collisions disappear due to near wall lift, while homogeneous transport is mobilized due to turbulence.
12. Knowing the slip ratio, the bed height for line speeds below the LDV can be determined. Since the LDV is defined as the line speed above which a sliding or stationary bed does not exist, below this line speed a bed does exist. New equations are derived for this.
13. Finally the grading of the Particle Size Distribution (PSD) is discussed. A method is given to construct resulting head loss, slip velocity and bed height curves for graded sands and gravels.
14. Inclined pipes. In real life often inclined pipes are used. Whether its in the ladder of a CSD, the suction pipe of a TSHD or an upwards or downwards slope, the hydraulic gradient will differ from a horizontal pipe. The effect of an inclined pipe is derived both for the hydraulic gradient and for the LDV.
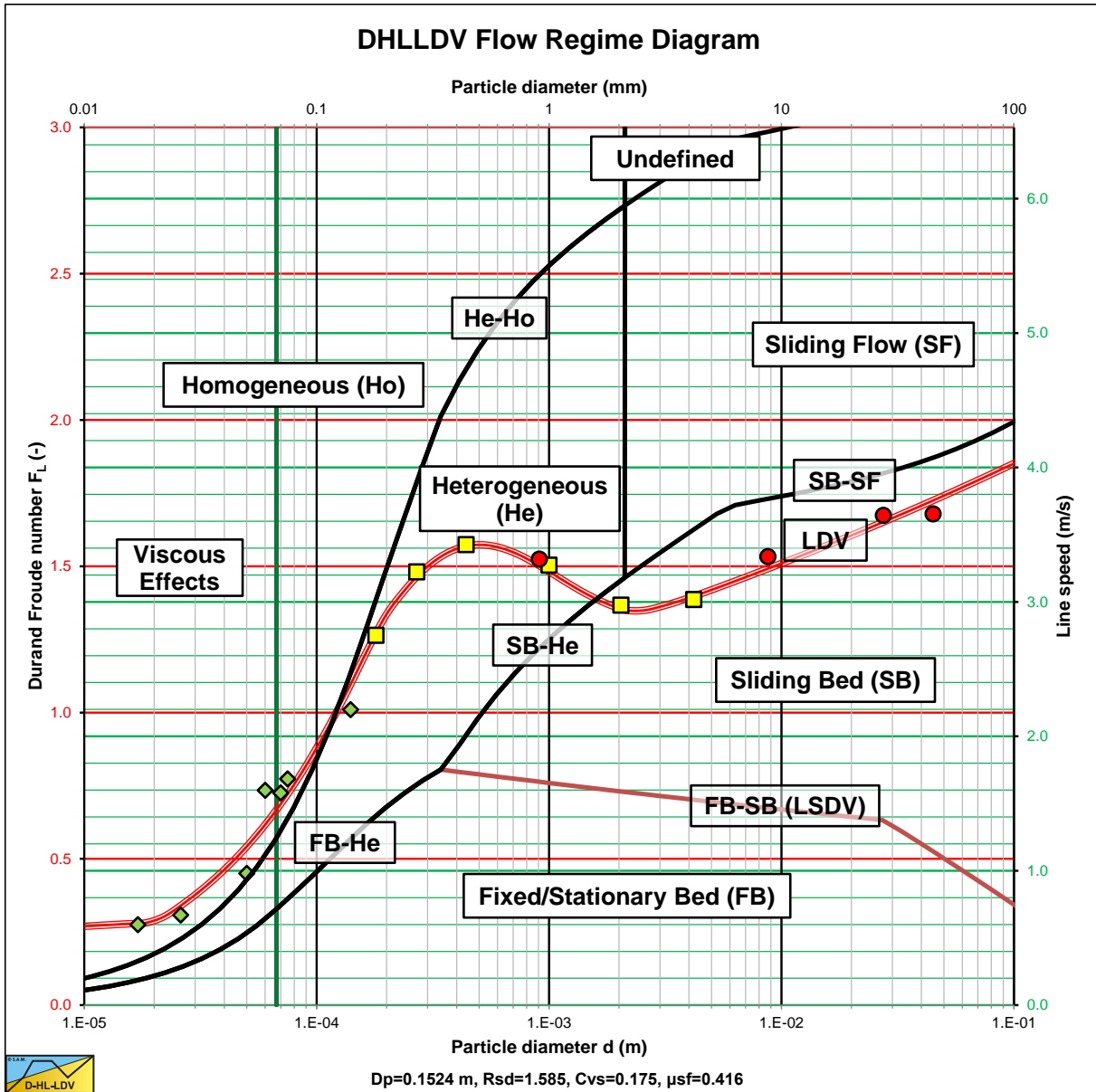
Figure 7.1-13: An example of a flow regime diagram.

7.1.5 Nomenclature Introduction.

C_{vs}	Spatial volumetric concentration	-
C_{vt}	Delivered (transport) volumetric concentration	-
d	Particle diameter	m
d_{50}	50% passing particle diameter	m
D_p	Pipe diameter	m
E_{rhg}	Relative excess hydraulic gradient	-
ELM	Equivalent Liquid Model	-
g	Gravitational constant 9.1 m/s^2	m/s^2
i_l	Liquid hydraulic gradient	m/m
i_w	Water hydraulic gradient	m/m
i_m	Mixture hydraulic gradient	m/m
ΔL	Length of pipe	m
LDV	Limit Deposit Velocity	m/s
Δp_l	Pressure difference liquid	kPa
Δp_m	Pressure difference mixture	kPa
PSD	Particle Size Diagram	-
R	The Wilson stratification ratio	-
R_{sd}	Relative submerged density	-
S_{hr}	Settling velocity Hindered Relative	-
S_{rs}	Slip velocity Relative Squared	-
v_{ls}	Line speed	m/s
v_s	Velocity solids	m/s
v_{sl}	Slip velocity	m/s
v_t	Terminal settling velocity	m/s
ρ_l	Liquid density	ton/m^3
ρ_m	Mixture density	ton/m^3
κ_C	Concentration eccentricity hindered settling	-
λ_l	Darcy Weisbach friction factor	-
μ_{sf}	Sliding friction coefficient	-
ν_l	Kinematic viscosity	m^2/s

7.2 Flow Regimes and Scenario's.

7.2.1 Introduction.

In dredging, the hydraulic transport of solids is one of the most important processes. Since the 50's many researchers have tried to create a physical mathematical model in order to predict the head losses in slurry transport. We can think of the models of Durand, Condolios, Gibert, Worster, Zandi & Govatos, Jufin Lopatin, Fuhrboter, Newitt, Doron, Wilson, Matousek, Turian & Yuan and the SRC model. Some models are based on phenomenological relations and thus result in semi empirical relations, others tried to create models based on physics, like the two and three layer models. It is however the question whether slurry transport can be modeled this way at all. Observations in our laboratory show a process which is often non-stationary with respect to time and space. Different physics occur depending on the line speed, particle diameter, concentration and pipe diameter. These physics are often named flow regimes; fixed bed with and without sheet flow or suspension, sliding bed, heterogeneous transport, (pseudo) homogeneous transport and sliding flow. It is also possible that more regimes occur at the same time, like, a fixed bed in the bottom layer with heterogeneous transport in the top layer.

It is the observation of the authors that researchers often focus on a detail and sub-optimize their model, which results in a model that can only be applied for the parameters used for their experiments. At high line speeds the volumetric spatial concentration (volume based) and the volumetric transport concentration (volume flux based) are almost equal, because all the particles are in suspension with a small slip related to the carrier liquid velocity. The difference of the head loss between the two concentrations will be within the margin of the scatter of the experiments. At low line speeds however, there may be a sliding or fixed bed, resulting in a big difference between the two concentrations and thus between laboratory and real life situations.

This chapter describes 8 flow regimes and 6 possible scenarios.

The flow regimes for constant spatial volumetric concentration C_{vs} are, from line speed zero with increasing line speed:
1: Fixed bed without suspension (fine particles) or sheet flow (coarse particles).
2: Fixed bed with suspension (fine particles) or sheet flow (coarse particles).
3: Fixed bed with suspension (fine particles) or sliding bed with sheet flow (coarse particles).
For fine to coarse particles $d/D_p<0.015$:
5: Heterogeneous transport $C_{vs}\approx C_{vt}$.
5/6: Pseudo homogeneous transport, $C_{vs}\approx C_{vt}$.
6: Homogeneous transport, $C_{vs}\approx C_{vt}$.
For very coarse particles $d/D_p>0.015$:
7: Sliding flow.

The flow regimes for constant delivered volumetric concentration C_{vt} are, from line speed zero with increasing line speed:
8: Fixed bed with suspension (fine particles) or sheet flow (coarse particles).
4: Fixed bed with suspension (fine particles) or sliding bed with sheet flow (coarse particles).
For fine to coarse particles $d/D_p<0.015$:
5: Heterogeneous transport $C_{vs}\approx C_{vt}$.
5/6: Pseudo homogeneous transport, $C_{vs}\approx C_{vt}$.
6: Homogeneous transport, $C_{vs}\approx C_{vt}$.
For very coarse particles $d/D_p>0.015$:
7: Sliding flow.

3 scenarios are based on a constant volumetric spatial concentration (usually in a laboratory) and 3 scenarios are based on a constant volumetric transport concentration (usually in real life). The flow regimes and scenarios are explained and examples of experiments are given. Based on the experimental evidence, one can conclude that the approach followed in this book gives a good resemblance with the reality.

7.2.2 Concentration Considerations.

Based on an analysis of many experiments from literature, 8 flow regimes and 6 scenarios can be distinguished, which will be discussed in the next chapters. In order to understand these 8 flow regimes and 6 scenarios, the difference between the spatial volumetric concentration C_{vs} and the volumetric transport (delivered) concentration C_{vt} will first be discussed. In hydraulic transport, 2 definitions of the concentration are often used. Contractors are interested in the delivered volumetric concentration, also named the volumetric transport concentration C_{vt}. C_{vt} is defined as the ratio between the volume flow of solids and the volume flow of the mixture. In general one can say that the average solids velocity will be smaller than the average mixture velocity. The difference is called the slip velocity. The spatial volumetric concentration C_{vs} is defined as the volume of solids divided by the volume of the mixture containing these solids. So the spatial volumetric concentration is based on a volume ratio, while the delivered volumetric concentration is based on a volume flux ratio. Concentration (C_{vs}) is usually derived from density meter or U-loop readings as:

$$C_{vs} = \frac{\rho_m - \rho_l}{\rho_s - \rho_l} \text{ (density meter)} \quad \text{or} \quad C_{vt} = \frac{\rho_m - \rho_l}{\rho_s - \rho_l} \text{ (U-loop)} \tag{7.2-1}$$

A radioactive density meter reads a density of the entire mass of slurry in the pipe, and thus is best suited to measuring C_{vs}. In addition the placement of the meter in horizontal or vertical pipe, can affect the readings. A U-tube device reads the delivered density and is thus best suited to measuring C_{vt}. In a closed loop system, we will know the volume of the closed loop and amount of material added, and thus can calculate C_{vs} directly, but not necessarily C_{vt}. The volumetric delivered (transport) concentration is:

$$C_{vt} = \frac{\dot{V}_s}{\dot{V}_m} = \frac{Q_s}{Q_m} = \frac{v_s \cdot A_s}{v_m \cdot A_p} = \frac{v_s \cdot C_{vs} \cdot A_p}{v_m \cdot A_p} = C_{vs} \cdot \frac{v_s}{v_m} \tag{7.2-2}$$

With v_s the average velocity of the solids and v_m the average velocity of the mixture, also called the line speed v_{ls}. The volumetric spatial concentration is based on the volume ratio solids/mixture according to:

$$C_{vs} = \frac{V_s}{V_m} \tag{7.2-3}$$

The slip velocity v_{sl} is defined as the difference between the velocity of the mixture v_m and the velocity of the solids v_s:

$$v_{sl} = v_m - v_s = v_m \cdot \left(1 - \frac{v_s}{v_m}\right) = v_m \cdot \left(1 - \frac{C_{vt}}{C_{vs}}\right) \tag{7.2-4}$$

Because of the fact that most experiments are carried out in a closed loop system, the concentration might be determined by the ratio of the volume of solids divided by the volume of the closed loop system.

$$C_{vs} = \frac{V_s}{V_{cl}} \tag{7.2-5}$$

This means that the concentration of solids in the liquid above the bed will be much smaller once a bed is formed. Now assume a bed with a porosity n of about 40% containing 50% of the solids, matching the v_{50} of Wilson (1997). This gives for the total bed volume in the closed loop system:

$$V_b = \frac{V_s}{2} \cdot \frac{1}{1-n} = \frac{C_{vs} \cdot V_{cl}}{2 \cdot (1-n)} \tag{7.2-6}$$

The volume of solids in suspension is the same, so the volume of the solids in the liquid is:

$$V_{s,s} = \frac{V_s}{2} \tag{7.2-7}$$

The volume of the mixture in suspension above the bed equals the closed loop volume minus the bed volume.

$$V_{m,s} = V_{cl} - V_b = V_{cl} - \frac{C_{vs} \cdot V_{cl}}{2 \cdot (1-n)} = V_{cl} \cdot \left(\frac{2 \cdot (1-n) - C_{vs}}{2 \cdot (1-n)} \right) \qquad (7.2-8)$$

The concentration of the solids in suspension is the volume of these solids, divided by the volume of the closed loop system minus the volume of the bed.

$$C_{vs,s} = \frac{V_s}{2 \cdot V_{m,s}} = \frac{C_{vs}}{2 \cdot \left(\frac{2 \cdot (1-n) - C_{vs}}{2 \cdot (1-n)} \right)} = \frac{(1-n) \cdot C_{vs}}{2 \cdot (1-n) - C_{vs}} \approx \frac{0.6 \cdot C_{vs}}{1.2 - C_{vs}} = \frac{C_{vs}}{2 - 1.66 \cdot C_{vs}} \qquad (7.2-9)$$

Of course the closed loop will not consist of just horizontal parts where a bed may occur, but the above example is just meant to give an indication.

This implies that at low spatial volumetric concentrations C_{vs}, the concentration in the suspension phase, the heterogeneous transport phase, is 50% of the total volumetric concentration. At a high concentration of $C_{vs}=0.3$, the concentration of the heterogeneous phase is still reduced to 0.2. At a concentration of $C_{vs}=0.6$, the above equation results in a concentration of 0.6, which makes sense, since this is solid sand and there is no suspension anymore. When experiments are carried out it should be clear which concentration is used. Is it the concentration based on the volume of the closed loop system, giving some constant volumetric spatial concentration? Is it the concentration based on radio active density meters in the pipe section where also the hydraulic gradient is measured, resulting in a spatial volumetric concentration? Or is the concentration measured with a U-tube resulting in a volumetric transport concentration.

Now in a real life production situation there is not a closed loop system, but an open system. There is not a fixed amount of solids in the pipeline, which can be divided in a part in a bed and the rest in suspension. Instead, the supply at the suction mouth can vary from water to twice or more that the delivered concentration. In a stable situation, the production that enters the system is equal to the production that leaves the system. The concentration is determined at the suction mouth and although there may be a bed in part of the pipeline, this does not change the transport concentration, it just increases the line speed and concentration above the bed compared with a pipeline without a bed, due to the conservation of volume in the pipeline. The conclusion of the above considerations is that for a good interpretation of the results of experiments, the method of determining the concentration should be known. It is also important how the results are presented. Graf & Robinson (1970) for example, present their results based on a constant amount of solids in their closed loop system, while Doron & Barnea (1987) connect data points with constant volumetric transport concentration. The presentations of the results are different, while the physics are the same.
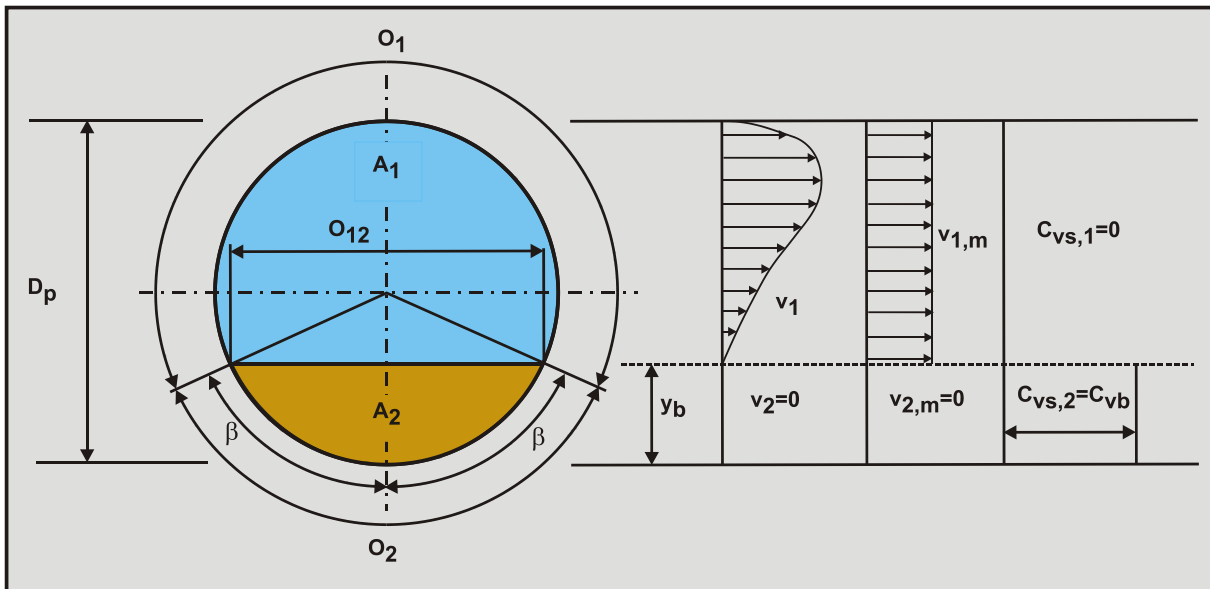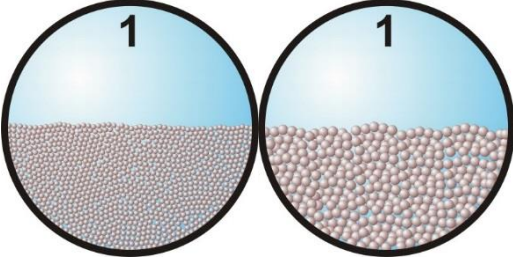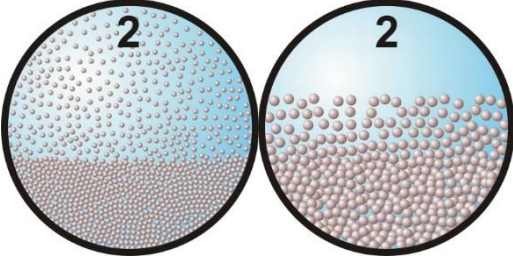
Figure 7.2-1: The definitions for fully stratified flow.

7.2.3   The 8 Flow Regimes Identified.

In literature different flow patterns or flow regimes are distinguished. Durand & Condolios (1952) distinguish 4 regimes, based on the particle size. Abulnaga (2002) also distinguished 4 regimes based on the actual flow of particles and their size. Matousek (2004) in his lecture notes distinguishes 6 flow regimes. Here we will consider 8 flow regimes and 6 scenarios for laboratory and real life conditions. These are (Figure 7.2-1 gives some definitions of fully stratified flow in a pipe):

Table 7.2-1: The 8 possible flow regimes.

1: Fixed bed without suspension or sheet flow, constant C_{vs}.

Under laboratory circumstances with a constant spatial volumetric concentration C_{vs}, at low line speeds all the particles are in a stationary (fixed) bed at the bottom of the pipe. Above the bed the liquid is flowing through a smaller cross-section $A_1=A_p-A_2$. This gives a higher effective line speed $v_{ls,e}=v_{ls} \cdot A_p/A_1$. Since the bottom of this cross–section consists of particles, the resulting Darcy-Weisbach friction factor λ_m has to be determined by taking a weighted average of the friction factor of the liquid-bed interface λ_{12} and the friction factor of the liquid-pipe wall interface λ_l. The method of Miedema & Matousek (2014) can be applied to determine the Darcy-Weisbach friction coefficient λ_{12} on the liquid-bed interface. This method does distinguish between fine and coarse particles. The particle diameter influences the Darcy-Weisbach friction coefficient λ_{12} by using the particle diameter as the bed roughness.

The Shields parameter is below a critical Shields value of about 1 so no sheet flow or suspension occurs.

The total pressure loss is thus determined by viscous friction on the liquid-bed interface and the liquid-pipe wall interface, the spatial volumetric concentration and the particle diameter.

2: Fixed bed with suspension or sheet flow, constant C_{vs}.

Under laboratory circumstances with a constant spatial volumetric concentration C_{vs}, at medium-low line speeds most of the particles are in a stationary (fixed) bed at the bottom of the pipe. Above the bed a suspension (fine particles) or a sheet flow (coarse particles) is flowing through a smaller cross-section $A_1=A_p-A_2$. This gives a higher effective line speed $v_{ls,e}=v_{ls} \cdot A_p/A_1$. Since the bottom of this cross–section consists of particles, the Darcy-Weisbach friction factor λ_m has to be determined by taking a weighted average of the friction factor of the liquid-bed interface λ_{12} and the friction factor of the liquid-pipe wall interface λ_l. The method of Miedema & Matousek (2014) for sheet flow can be applied to determine the friction coefficient λ_{12} on the liquid-bed interface. This method does distinguish between fine and coarse particles and gives an explicit relation for the Darcy-Weisbach friction factor. The particle diameter influences the Darcy-Weisbach friction coefficient λ_{12} slightly.

The Shields parameter is above a critical Shields value of about 1, so sediment transport/erosion occurs in the form of sheet flow or suspension.

The total pressure loss is thus determined by viscous friction, shear stresses in the sheet flow layer, the spatial volumetric concentration and the particle diameter.
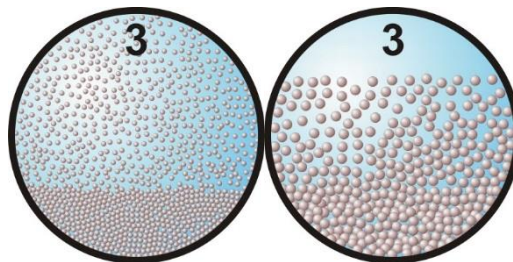
3: Fixed bed with suspension or sliding bed with sheet flow, constant C_{vs}.

Under laboratory circumstances with a constant spatial volumetric concentration C_{vs}, for coarse particles the bed is sliding with sheet flow at the top, where the thickness of the sheet flow layer increases with an increasing velocity difference between the flow above the bed and the bed, while for fine particles the shear stress on the bed is not high enough to make it start sliding, but more and more particles will be in suspension as the line speed increases. For fine particles the behavior starts following the heterogeneous behavior more and more with increasing line speed.

Since coarse particles in sheet flow require an upwards force at least equal to their submerged weight, which results from interparticle forces, an equal downwards force will act on the bed-sheet flow layer interface. The result is a total normal force between the bed and the pipe wall of about the submerged weight of the particles. From experiments it appears that this normal force is almost a constant times the spatial volumetric concentration, according to the Newitt et al. (1955) model. This vertical force times the friction coefficient μ_{sf} determines the sliding friction force. The friction coefficient μ_{sf} will have a value of about 0.416, but should preferably be determined by experiments, since it is a property of the particles depending on the shape of the particles.

The Shields parameter is above a critical Shields value of 1, so sediment transport/erosion occurs.

The total pressure loss is thus determined by sliding friction between the bed and the pipe wall for coarse particles and by energy losses due to collisions for fine particles.
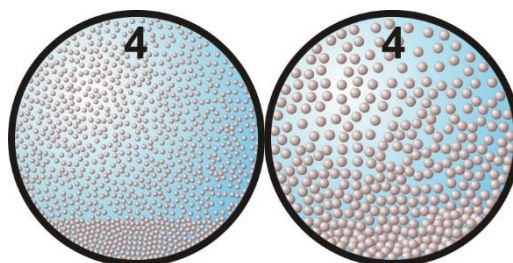
4: Fixed bed with suspension or sliding bed with sheet flow, constant C_{vt}.

Under laboratory circumstances with a constant spatial volumetric concentration C_{vs}, for coarse particles the bed is sliding with sheet flow, where the thickness of the sheet flow layer increases further with an increasing velocity difference between the flow above the bed and the bed, while for fine particles the shear stress on the bed is not high enough to make it start sliding, but almost all particles will be in suspension as the line speed increases. For fine particles the behavior starts following the heterogeneous behavior as the line speed increases.

Since coarse particles in sheet flow require an upwards force at least equal to their submerged weight, which results from interparticle forces, an equal downwards force will act on the bed. The result is a total normal force

between the bed and the pipe wall of about the submerged weight of the particles. From experiments it appears that this normal force is almost a constant times the spatial volumetric concentration, according to the Newitt et al. (1955) model. This vertical force times the friction coefficient μ_{sf} determines the sliding friction force. The friction coefficient μ_{sf} will have a value of about 0.416, but should preferably be determined by experiments, since it is a property of the particles depending on the shape of the particles.

The difference with flow regime 3 is, that here the transport/delivered concentration is known. With decreasing line speed and constant delivered volumetric concentration, the spatial volumetric concentration is increasing. The spatial concentration will be higher than the delivered concentration, resulting in a higher resistance. So the constant C_{vt} curve will always be higher than the constant C_{vs} curve. The difference increases with decreasing line speed.

The Shields parameter is above a critical Shields value of 1, so sediment transport/erosion occurs.

The total pressure loss is thus determined by sliding friction between the bed and the pipe wall for coarse particles and by energy losses due to collisions for fine particles.
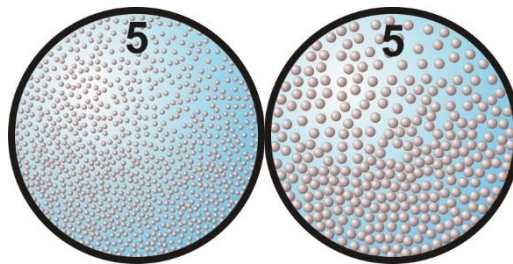
5: Heterogeneous transport, $C_{vt} \approx C_{vs}$.

When the line speed increases further, the difference between spatial and delivered concentration becomes smaller. At a certain line speed the macroscopic behavior changes from stationary or sliding bed behavior to heterogeneous behavior.

The turbulent forces interacting with the particles are not strong enough to create a uniform distribution throughout the cross-section of the pipe. A definite concentration gradient exists along the vertical profile of the pipe with the highest concentration at the bottom. There may still be deposits, but most particles move in suspension or a sort of sheet flow layer. There is however an interaction between the particles and the bottom of the pipe. These interactions, collisions, cause the loss of kinetic energy of the particles and are the main cause of the pressure losses. Since the number of collisions per unit of time depends mainly on the terminal settling velocity of the particles, it will be almost constant, resulting in pressure losses that are reversely proportional with the line speed or the line speed to a higher power. Since the particles move up and down in the pipe, based on the terminal settling velocity and hindered settling, there are also potential energy losses. The pressure losses can be determined according to Durand & Condolios (1952), Jufin & Lopatin (1966), Miedema & Ramsdell (2013) or others. The heterogeneous model is the same for fine and coarse particles, but the line speed range where it occurs depends on the particle size.

The Shields parameter is very high above the Shields curve, resulting in suspension/saltation.

The total pressure loss is determined by potential and kinetic energy losses.
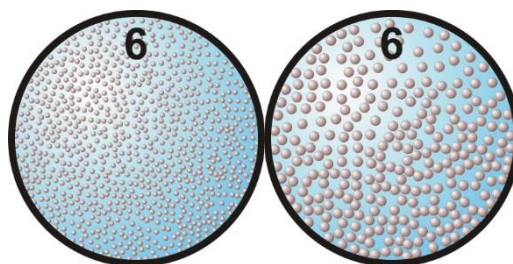
6: Homogeneous transport, $C_{vt} \approx C_{vs}$.

When the line speed increases further, the difference between spatial and delivered concentration becomes smaller and smaller. The turbulent forces interacting with the particles are strong enough to create a uniform distribution throughout the cross-section of the pipe.

The turbulent forces interacting with the particles are so strong that the mixture has an almost uniform distribution throughout the cross-section of the pipe. True homogeneous flows is not possible, since for the turbulent forces to overcome gravity, a concentration gradient has to exist. Pseudo homogeneous regimes usually occur with very fine particles or at very high line speeds. The pressure losses in this regime can be modeled using the adapted/modified equivalent liquid model (ELM). It is assumed that the spatial volumetric concentration C_{vs} and the volumetric transport (delivered) concentration C_{ts} are almost equal.

The Shields parameter is very high above the Shields curve, resulting in a suspension.

The total pressure loss is determined by the work carried out by lift forces and turbulent dispersion.

5/6: Pseudo homogeneous transport, $C_{vt} \approx C_{vs}$.

At the line speed where heterogeneous and homogeneous transport meet, there will be a transition between the two regimes. If the turbulent near wall lift force equals the submerged weight of the particle, this lift force will prevent the particles from hitting the bottom of the pipe, resulting in a sudden drop of the heterogeneous pressure losses. At slightly higher line speeds the lift force is strong enough to push the particles into the turbulent flow, where turbulent dispersion will take care of further mixing. In between there may be a gap resulting in almost no additional pressure losses. This occurs for particles with diameter from 0.1-0.5 mm with bigger pipe diameters. The pressure losses can be determined according to Miedema &Ramsdell (2013).

The Shields parameter is very high above the Shields curve, resulting in a suspension.

The total pressure loss is determined by decreasing potential and kinetic energy losses and by increasing equivalent liquid model (ELM) behavior.
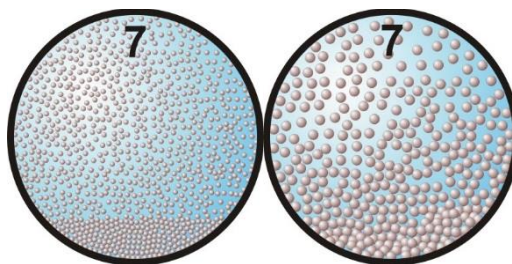
7: Sliding Flow.

At relatively low concentrations and relatively small particle diameters, the sliding bed regime will have a transition to the heterogeneous regime at the intersection of the two regimes. This is the result of lift forces strong enough to lift the particles and turbulent dispersion to mix them into a heterogeneous mixture. However when the weight of the bed is bigger than the total lift forces, this will not occur and the particles stay in the bed in a sort of sheet flow. A second reason may be that at high concentrations the space above the bed is not big enough to fully develop turbulence. The pressure losses in this regime are much higher than the pressure losses with heterogeneous transport at lower concentrations. The pressure losses can be determined according to Miedema &Ramsdell (2013). The term Sliding Flow is chosen, because there is flow but the flow resistance has the character of sliding friction.

The Shields parameter is far above the Shields curve, so sediment transport/erosion occurs.

The total pressure loss is thus determined by a combination of sliding friction between the bed and the pipe wall and kinetic and potential energy losses. The larger the particle diameter to pipe diameter ratio, the more this tends to sliding friction behavior and the smaller the heterogeneous contribution.
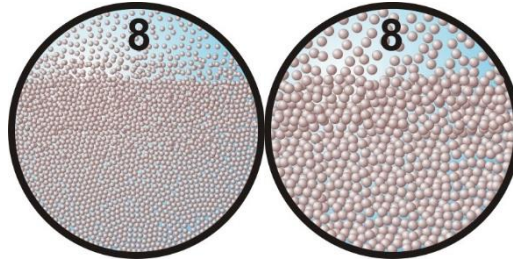
8: Fixed bed with suspension, constant C$_{vt}$.

Under real life conditions, there will be a "constant" volumetric transport concentration with decreasing line speed. There will be equilibrium between erosion and deposition, resulting in a certain bed height. Gibert (1960) has proposed that the Froude number will be equal to the Froude number at the Limit Deposit Velocity. In this case, the Limit Deposit Velocity is defined as the velocity where the sliding bed has vaporized due to erosion. With decreasing line speed, the bed height increases and so do the pressure losses. Once the bed height is known, the pressure losses can be determined according to the Newitt et al. (1955) model. This regime occurs if the relative excess hydraulic gradient is high enough to result in a sliding bed and so this will occur much more with small pipe diameters then with large pipe diameter.

The Shields parameter is above the a critical Shields value, so erosion occurs.

The total pressure loss is thus determined by sliding friction between the bed and the pipe wall, where the spatial concentration is increasing with decreasing line speed, while the transport concentration is a constant.

7.2.4 The 6 Scenario's Identified.

In pipes with small diameters the hydraulic gradient will be relatively high, resulting in relatively high hydraulic gradients when transporting a mixture. This results in hydraulic gradients approaching the hydraulic gradient required to create a sliding bed. In pipes with large diameters the hydraulic gradient will be relatively small, also resulting in relatively small hydraulic gradients when transporting a mixture. This results in hydraulic gradients too small compared with the hydraulic gradient required to create a sliding bed.

From the 8 flow regimes, 6 scenarios can be constructed, where a scenario does not have to contain all 8 flow regimes. A scenario describes the flow regime behavior when the line speed increases from zero to a certain maximum. This maximum is arbitrary but should be related to practical line speeds. So this maximum increases with increasing pipe diameter.

The 8 flow regimes and 6 scenarios are shown in Figure 7.2-2, Figure 7.2-3, Figure 7.2-4, Figure 7.2-5, Figure 7.2-6 and Figure 7.2-7. Figure 7.2-2 and Figure 7.2-3 show the scenario's **L1** for laboratory conditions and **R1** for real life conditions for fine sands. Figure 7.2-4 and Figure 7.2-5 show the scenario's **L2** for laboratory conditions and **R2** for real life conditions for coarse sands. Figure 7.2-6 and Figure 7.2-7 show the scenario's **L3** for laboratory conditions and **R3** for real life conditions for gravels.

The difference between laboratory conditions and real life conditions can be found at low line speeds where the volumetric spatial **C$_{vs}$** and transport **C$_{vt}$** concentrations differ substantially due to slip. At higher line speeds with heterogeneous and (pseudo) homogeneous transport it is assumed that the slip velocity **v$_{sl}$** is small compared to the line speed **v$_{ls}$**.

Most of the graphs are made for sands and gravels with water as the carrier liquid, however the modelling is also valid for other solids and other liquids.

7.2.4.1 Scenarios L1 & R1.
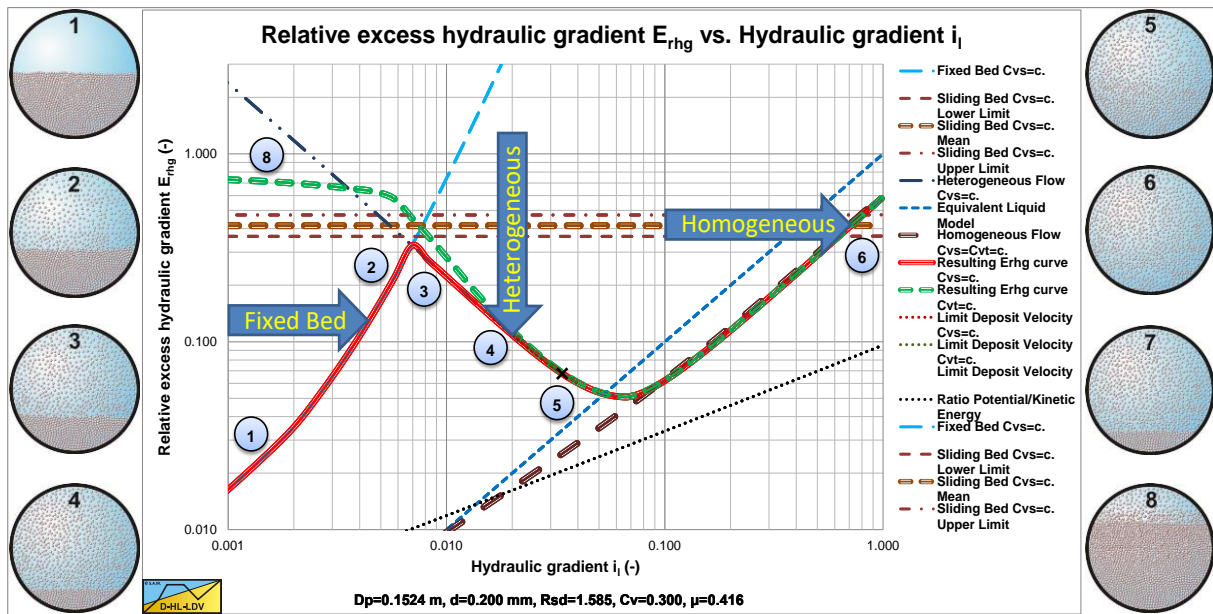
Figure 7.2-2: The definition of the pressure losses, scenario's L1 and R1, $E_{rhg}(i_l)$.

Table 7.2-2: Scenario's L1 and R1.

Scenario L1 (the red solid line)

Table 7.2-3: Indication of occurrence of L1.

D_p	d	C_v
<<	>>	>>
<	>	>
-	-	-
>	<	<
>>	<<	<<

Starting at a line speed $v_{ls}=0$, there will be a stationary (fixed) bed (**1**). When the line speed is increased, there will not be erosion until the Shields parameter is high enough above the Shields curve. Increasing the line speed further will result in erosion and suspension or sheet flow of the particles (**2**). The upwards directed solid red curve becomes steeper.

At a certain line speed, the macroscopic behavior will have a transition from fixed bed to heterogeneous (**3**). This also means that the excess pressure losses go from shear stress dominated to collision dominated. Increasing the line speed further results in heterogeneous transport (**5**). The solid red curve is downwards directed.

The Limit Deposit Velocity is somewhere in the heterogeneous flow regime.

Increasing the line speed further, results in a transition region between heterogeneous transport and (pseudo) homogeneous transport (**5/6**). At very high line speeds, the regime will be the homogeneous regime (**6**). Whether this regime will be reached with practical line speeds depends completely on the combination of the parameters involved. The solid red curve is upwards directed again.

Scenario R1 (the green dashed line)

Table 7.2-4: Indication of occurrence of R1.

D_p	d	C_v
<<	>>	>>
<	>	>
-	-	-
>	<	<
>>	<<	<<

Starting at a line speed v_{ls}=0, there will be equilibrium between erosion and deposition, resulting in a certain bed height. Above the bed there will be heterogeneous transport or suspension. At very low line speeds, the hydraulic gradient is so high that a sliding bed may occur (**8**). At these low line speeds, it is also possible that only part of the bed is siding resulting in sliding friction that is not fully mobilized. The green dashed curve is slightly downwards directed. The height of the green dashed line depends on the C_{vt}. A smaller C_{vt} gives a higher green dashed line, because a smaller C_{vt} will have more slip. The red solid line (constant C_{vs}) is hardly influenced by the spatial concentration.

At higher line speeds, the bed has a higher velocity and starts vaporizing, the hydraulic gradient drops, resulting in a transition towards heterogeneous behavior (**4**) and at higher line speeds full heterogeneous behavior (**5**). The dashed green line is downwards directed.

The Limit Deposit Velocity is somewhere in the heterogeneous flow regime.

Increasing the line speed further, results in a transition region between heterogeneous transport and (pseudo) homogeneous transport (**5/6**). At very high line speeds, the regime will be the homogeneous regime (**6**). Whether this regime will be reached with practical line speeds depends completely on the combination of the parameters involved. The green dashed line is upwards directed again. The solid red line and the dashed green line coincide.
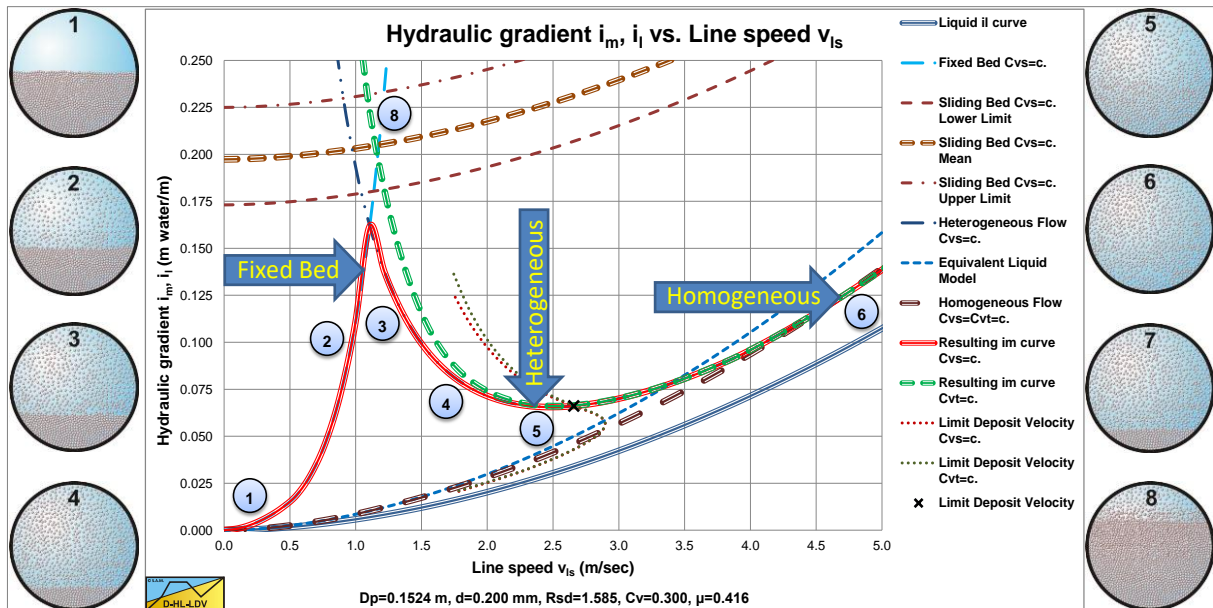
Figure 7.2-3: The definition of the pressure losses, scenario's L1 and R1, $i_m(v_{ls})$.

7.2.4.2 Scenarios L2 & R2.
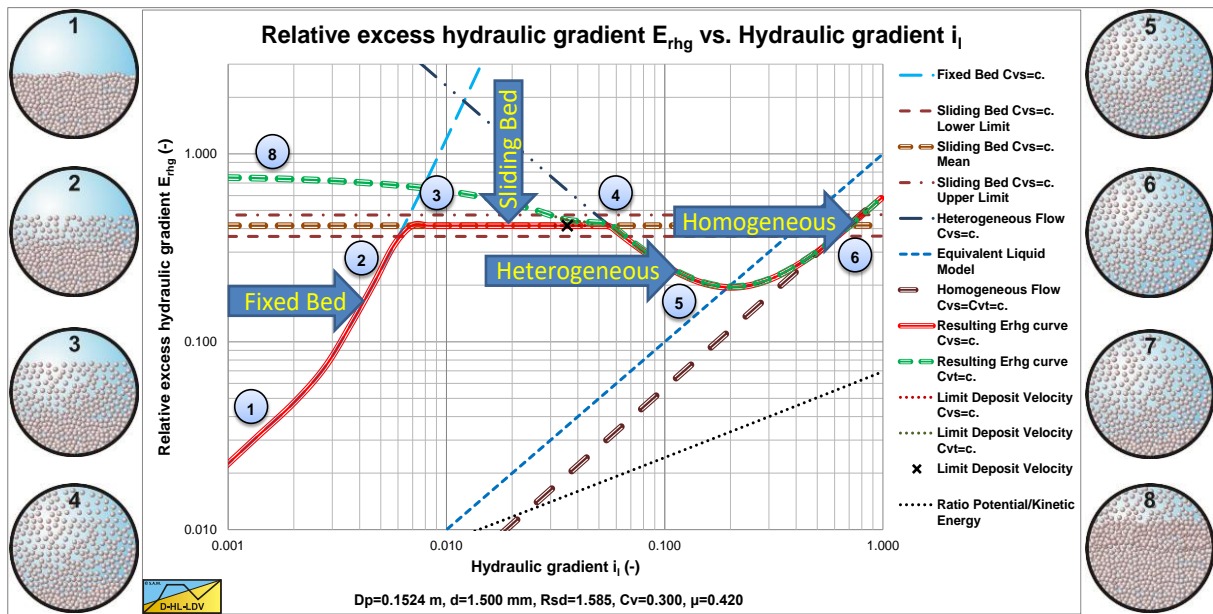
Figure 7.2-4: The definition of the pressure losses, scenario's L2 and R2, $E_{rhg}(i_l)$.

Table 7.2-5: Scenario's L2 and R2.

Scenario L2 (the red solid line)

Table 7.2-6: Indication of occurrence of L2.

D_p	d	C_v
<<	>>	>>
<	>	>
-	-	-
>	<	<
>>	<<	<<

Starting at a line speed $v_{ls}=0$, there will be a stationary (fixed) bed (**1**). When the line speed is increased, there will not be erosion until the Shields parameter is high enough above the Shields curve. Increasing the line speed further will result in erosion and suspension or sheet flow of the particles (**2**). The upwards directed solid red curve becomes steeper.

At a certain line speed, the hydraulic gradient is high enough to make the bed to start sliding (**3**). Increasing the line speed further will result in an increase of the velocity of the bed and an increase of the erosion. The relative excess hydraulic gradient remains constant, because the weight of the suspension and the bed is a constant, resulting in an almost constant friction force. Increasing the line speed further will give a transition to heterogeneous transport (**5**). The solid red line is first horizontal and then downwards directed.

The Limit Deposit Velocity is somewhere at the right of the sliding bed regime.

Increasing the line speed further, results in a transition region between heterogeneous transport and (pseudo) homogeneous transport (**5/6**). At very high line speeds, the regime will be the homogeneous regime (**6**). Whether this regime will be reached with practical line speeds depends completely on the combination of the parameters involved. The solid red curve is upwards directed again.

Scenario R2 (the green dashed line)

Table 7.2-7: Indication of occurrence of R2.

D_p	d	C_v
<<	>>	>>
<	>	>
-	-	-
>	<	<
>>	<<	<<

Starting at a line speed $v_{ls}=0$, there will be equilibrium between erosion and deposition, resulting in a certain bed height. Above the bed there will be heterogeneous transport or suspension. At very low line speeds, the hydraulic gradient is so high that a sliding bed may occur (**8**). At these low line speeds, it is also possible that only part of the bed is siding resulting in sliding friction that is not fully mobilized. The green dashed curve is slightly downwards directed. The height of the green dashed line depends on the C_{vt}. A smaller C_{vt} gives a higher green dashed line, because a smaller C_{vt} will have more slip. The red solid line (constant C_{vs}) is hardly influenced by the spatial concentration.

At higher line speeds, the bed has a higher velocity and starts vaporizing, the hydraulic gradient drops, resulting in a transition towards heterogeneous behavior (**4**) and at higher line speeds full heterogeneous behavior (**5**). The dashed green line is downwards directed.

The Limit Deposit Velocity is somewhere at the right of the sliding bed regime.

Increasing the line speed further, results in a transition region between heterogeneous transport and (pseudo) homogeneous transport (**5/6**). At very high line speeds, the regime will be the homogeneous regime (**6**). Whether this regime will be reached with practical line speeds depends completely on the combination of the parameters involved. The solid red curve is upwards directed again.

Figure 7.2-5: The definition of the pressure losses, scenario's L2 and R2, $i_m(v_{ls})$.

7.2.4.3 Scenarios L3 & R3.
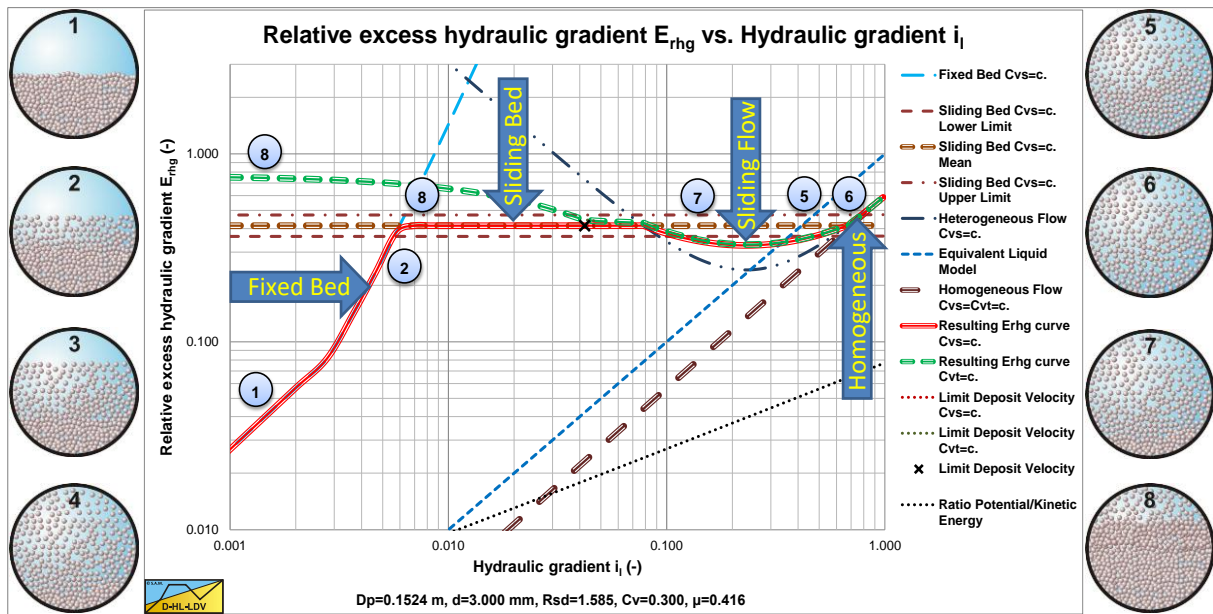
Figure 7.2-6: The definition of the pressure losses, scenario's L3 and R3, $E_{rhg}(i_l)$.

Table 7.2-8: Scenario's L3 and R3.

Scenario L3 (the red solid line)

Table 7.2-9: Indication of occurrence of L3.

D_p	d	C_v
<<	>>	>>
<	>	>
-	-	-
>	<	<
>>	<<	<<

Starting at a line speed $v_{ls}=0$, there will be a stationary (fixed) bed (**1**). When the line speed is increased, there will not be erosion until the Shields parameter is high enough above the Shields curve. Increasing the line speed further will result in erosion and suspension or sheet flow of the particles (**2**). The upwards directed solid red curve becomes steeper.

At a certain line speed, the hydraulic gradient is high enough to make the bed to start sliding (**3**). Increasing the line speed further will result in an increase of the velocity of the bed and an increase of the erosion. The relative excess hydraulic gradient remains constant, because the weight of the suspension and the bed is a constant, resulting in an almost constant friction force. Increasing the line speed further will give a transition to sliding flow (**7**). The solid red line is first horizontal and then slightly downwards directed.

The Limit Deposit Velocity is somewhere at the right of the sliding bed regime or in the sliding flow regime.

Increasing the line speed further, results in a transition region between sliding flow and (pseudo) homogeneous transport (**5/6**). At very high line speeds, the regime will be the homogeneous regime (**6**). Whether this regime will be reached with practical line speeds depends completely on the combination of the parameters involved. The solid red curve is upwards directed again.

Scenario R3 (the green dashed line)

Table 7.2-10: Indication of occurrence of R3.

D_p	d	C_v
<<	>>	>>
<	>	>
-	-	-
>	<	<
>>	<<	<<

Starting at a line speed $v_{ls}=0$, there will be equilibrium between erosion and deposition, resulting in a certain bed height. Above the bed there will be heterogeneous transport or suspension. At very low line speeds, the hydraulic gradient is so high that a sliding bed may occur (**8**). At these low line speeds, it is also possible that only part of the bed is siding resulting in sliding friction that is not fully mobilized. The green dashed curve is slightly downwards directed. The height of the green dashed line depends on the C_{vt}. A smaller C_{vt} gives a higher green dashed line, because a smaller C_{vt} will have more slip. The red solid line (constant C_{vs}) is hardly influenced by the spatial concentration.

At higher line speeds, the bed has a higher velocity and starts vaporizing, the hydraulic gradient drops, resulting in a transition towards sliding flow behavior (**7**) and at higher line speeds full heterogeneous behavior (**5**). The dashed green line is slightly downwards directed.

The Limit Deposit Velocity is somewhere at the right of the sliding bed regime or in the sliding flow regime.

Increasing the line speed further, results in a transition region between heterogeneous transport and (pseudo) homogeneous transport (**5/6**). At very high line speeds, the regime will be the homogeneous regime (**6**). Whether this regime will be reached with practical line speeds depends completely on the combination of the parameters involved. The solid red curve is upwards directed again.
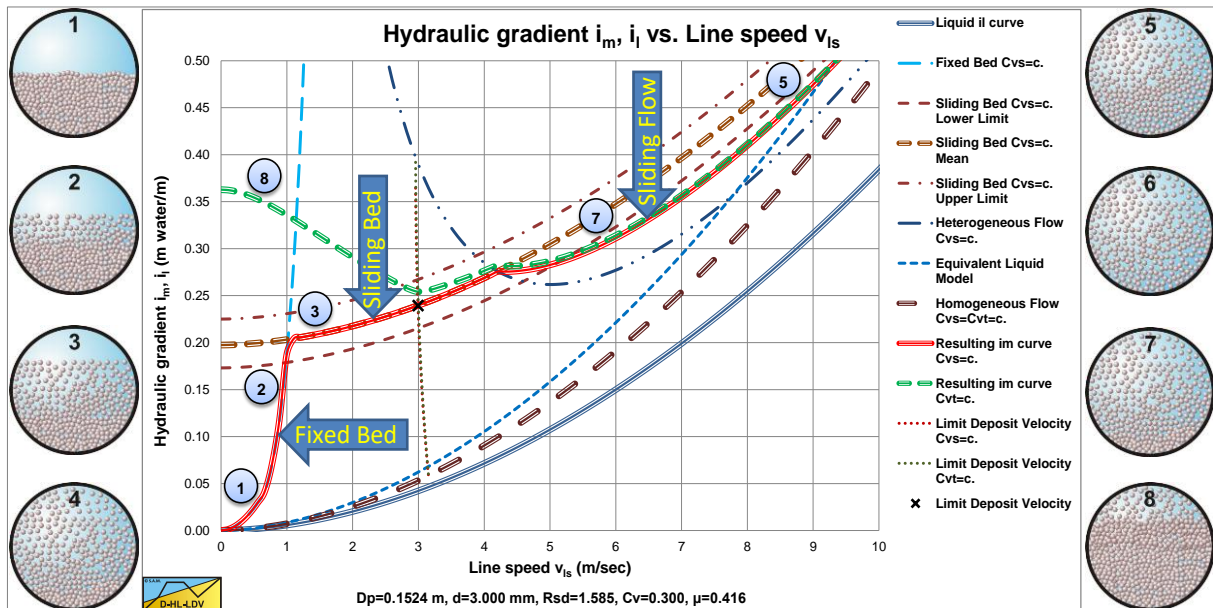
Figure 7.2-7: The definition of the pressure losses, scenario's L3 and R3, $i_m(v_{ls})$.

7.2.4.4 Conclusions & Discussion.

From Figure 7.2-2, Figure 7.2-3, Figure 7.2-4, Figure 7.2-5, Figure 7.2-6 and Figure 7.2-7. it is clear that the characterization of flow regimes of Durand (1952), Abulnaga (2002) or Matousek (2004) is not adequate enough to identify all possible scenarios. Flow regime graphs like the ones published by Newitt (1955) or King (2002) (based on Turian & Yuan (1977)) already give a better understanding. These graphs however do not show the difference between laboratory (C_{vs}) and real life (C_{vt}) conditions and do not take the sliding flow effect into account, probably because the volumetric concentrations were not high enough.

7.2.5 Verification & Validation.

The **Relative Excess Hydraulic Gradient E_{rhg}** is the contribution of the solids to the relative hydraulic gradient. The word relative is used here because the hydraulic gradient is divided by the volumetric concentration C_v and the relative submerged density R_{sd} in order to determine the E_{rhg}. The E_{rhg} can be applied for all flow regimes. The relative submerged density R_{sd} is defined as:

$$R_{sd} = \frac{\rho_s - \rho_l}{\rho_l}$$

(7.2-10)

The **Slip Relative Squared S_{rs}** is the **Slip Velocity** of a particle v_{sl} divided by the **Terminal Settling Velocity** of a particle v_t squared and this S_{rs} value is a good indication of the excess pressure losses due to the kinetic energy losses of the solids. The **Settling Velocity Hindered Relative S_{hr}** is the ratio between the hindered settling velocity $v_t \cdot (1-C_v/\kappa)^\beta$ and the line speed v_{ls}, divided by the relative submerged density R_{sd} and the volumetric concentration C_v. The S_{hr} value gives a good approximation of the potential energy losses of the solids. The S_{hr} and S_{rs} are derived and can be applied for the heterogeneous regime.

$$E_{rhg} = \frac{i_m - i_l}{R_{sd} \cdot C_v} = R_{ss} = S_{hr} + S_{rs} = \left(\frac{v_t \cdot \left(1 - \frac{C_v}{\kappa_C}\right)^\beta}{v_{ls}} \right) + \left(\frac{v_{sl}}{v_t} \right)^2$$

(7.2-11)

The **Stratification Ratio** of the **Solids R** is a measure for the level of stratification of slurry as introduced by Wilson et al. (1997). A high stratification ratio means that the slurry is (almost) fully stratified; the liquid phase and the sediment (bed) phase are almost separated.

Under laboratory conditions with constant volumetric spatial concentration C_{vs}, the E_{rhg} is limited by the value of the sliding friction coefficient μ_{sf}. The lower limit of the E_{rhg} is when the heterogeneous regime transits to the (pseudo) homogeneous regime. Also here the S_{rs} is derived and can be applied for the heterogeneous regime only. Resuming, the E_{rhg} is valid for all flow regimes, the S_{rs} is valid for the heterogeneous regime and the friction factor μ_{sf} is valid for the sliding bed regime. In the following examples the $E_{rhg}(i_l)$ graph will be used. The advantage of the $E_{rhg}(i_l)$ graph is that this type of graph is almost independent of the values of concentration C_{vs} and relative submerged density R_{sd}, but also almost independent of the pipe wall roughness and the temperature (kinematic viscosity). A disadvantage may be that it will take more effort to transform this graph back to real life data, the hydraulic gradient or pressure versus the line speed.

In these graphs always the lines for fixed/stationary bed (constant C_{vs}, thick solid red upwards on the left), ELM (thin dashed dark blue, upwards), homogeneous transport (thick dashed dark brown, upwards), heterogeneous transport (C_{vs} thick solid red downwards, C_{vt} thick dashed green downwards), sliding bed (C_{vs} thick solid red horizontal and constant C_{vt} thick dashed green slightly downwards) are drawn, in order to form a reference system.

The graphs show 3 additional lines. The thin dotted black line shows the ratio of the potential energy to the kinetic energy for heterogeneous transport. The thin blue dash-dot-dot line shows the heterogeneous curve without transitions to other flow regimes. The thin brown dash-dot-dot line shows the mobilization of homogeneous transport. The latter two lines added give the transition from the heterogeneous to the homogeneous flow regime.

All data are compared with the DHLLDV Framework.

7.2.5.1 L1: Fixed Bed & Heterogeneous, Constant C_{vs}.
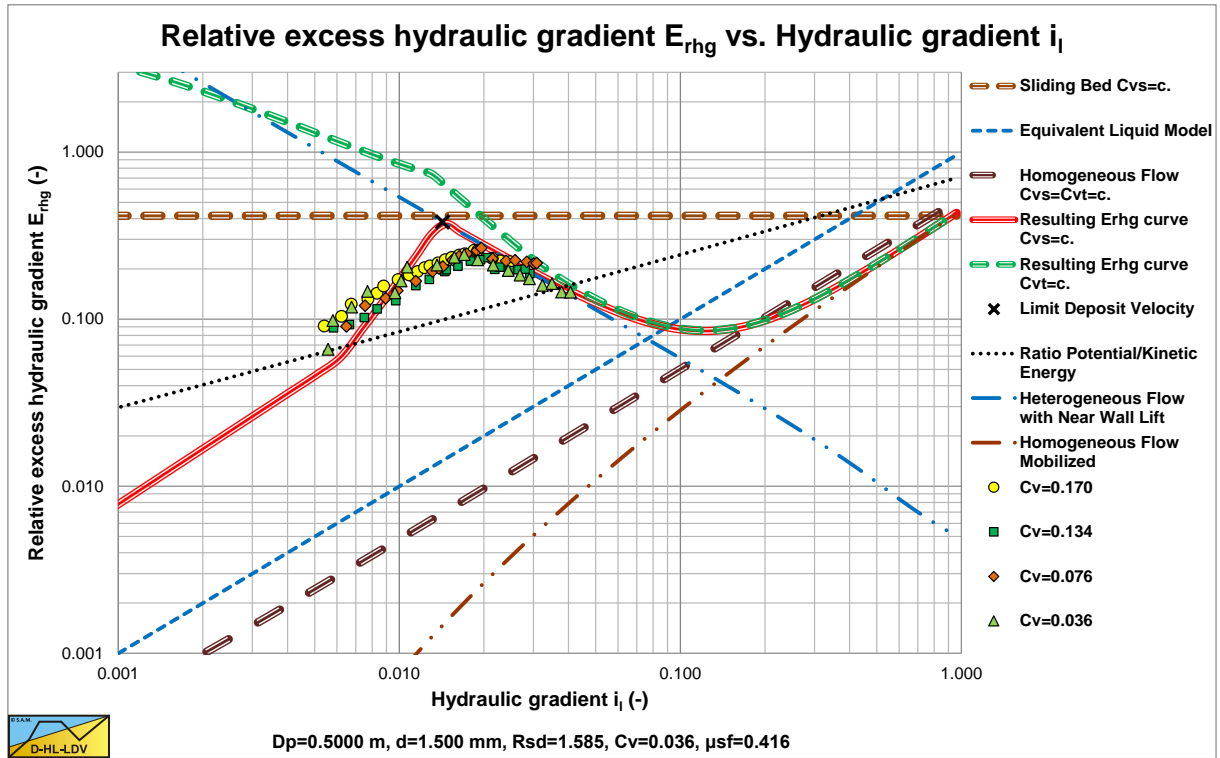
Figure 7.2-8: Kazanskij (1980), sand, low concentration
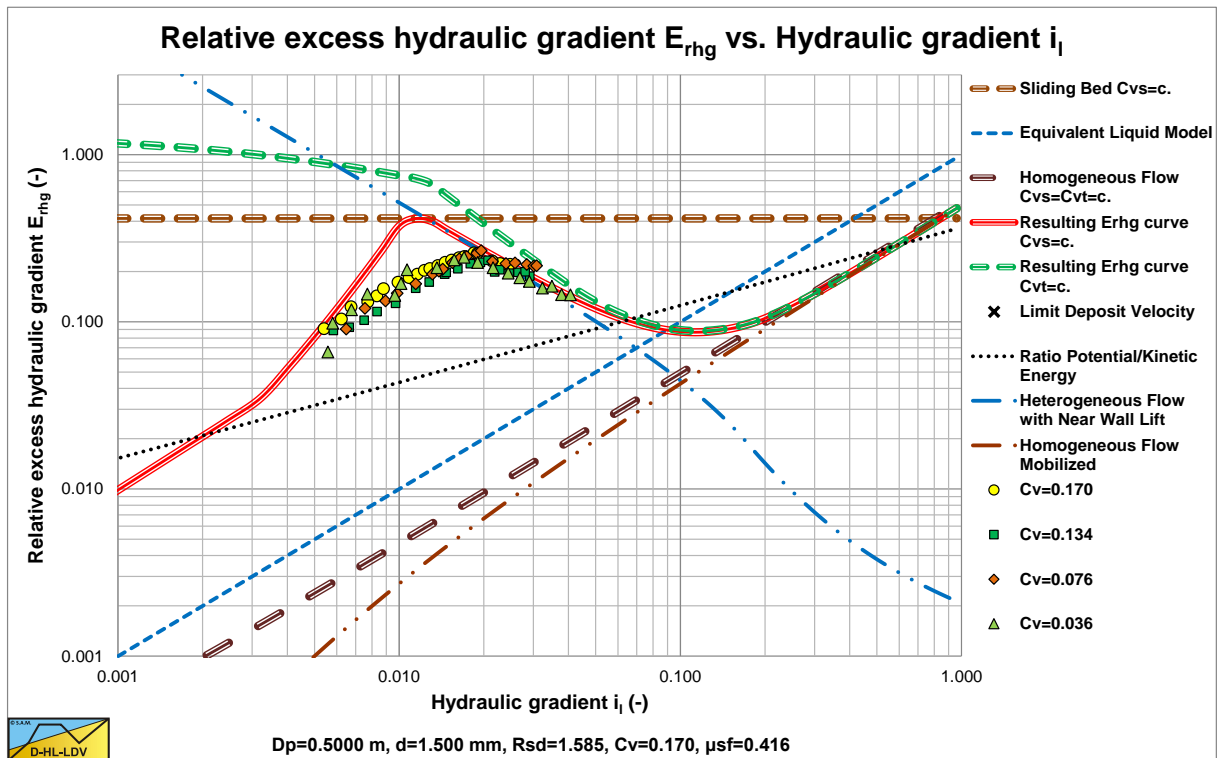
Figure 7.2-9: Kazanskij (1980), sand, high concentration

These experiments clearly show the transition of a fixed bed (flow regimes 1 and 2) to heterogeneous transport (flow regime 5) at a constant volumetric spatial concentration. The solid lines are drawn for a **C_{vs}=0.036 & 0.17** and may differ slightly for other concentrations. The transition is smoother than the DHLLDV Framework predicts.

7.2.5.2 R1: Heterogeneous, Constant C_{vt}.
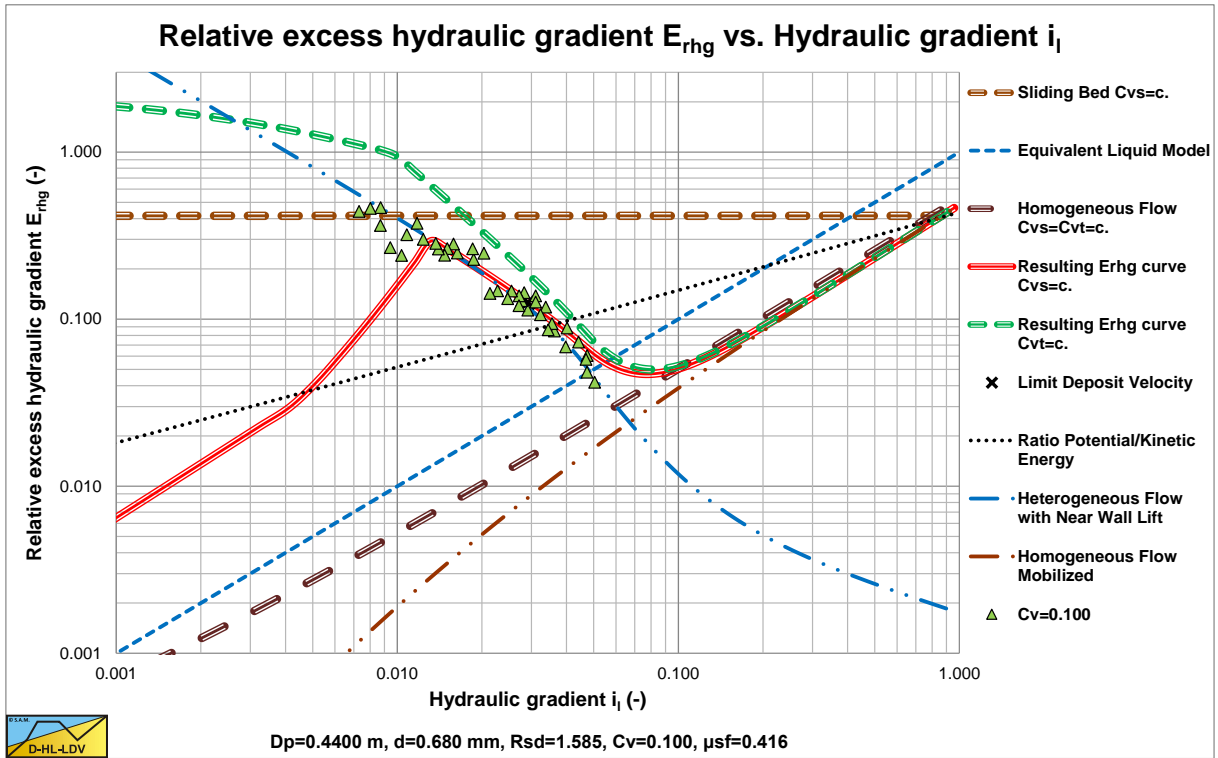
Figure 7.2-10: Clift et al. (1982), narrow graded crushed granite.
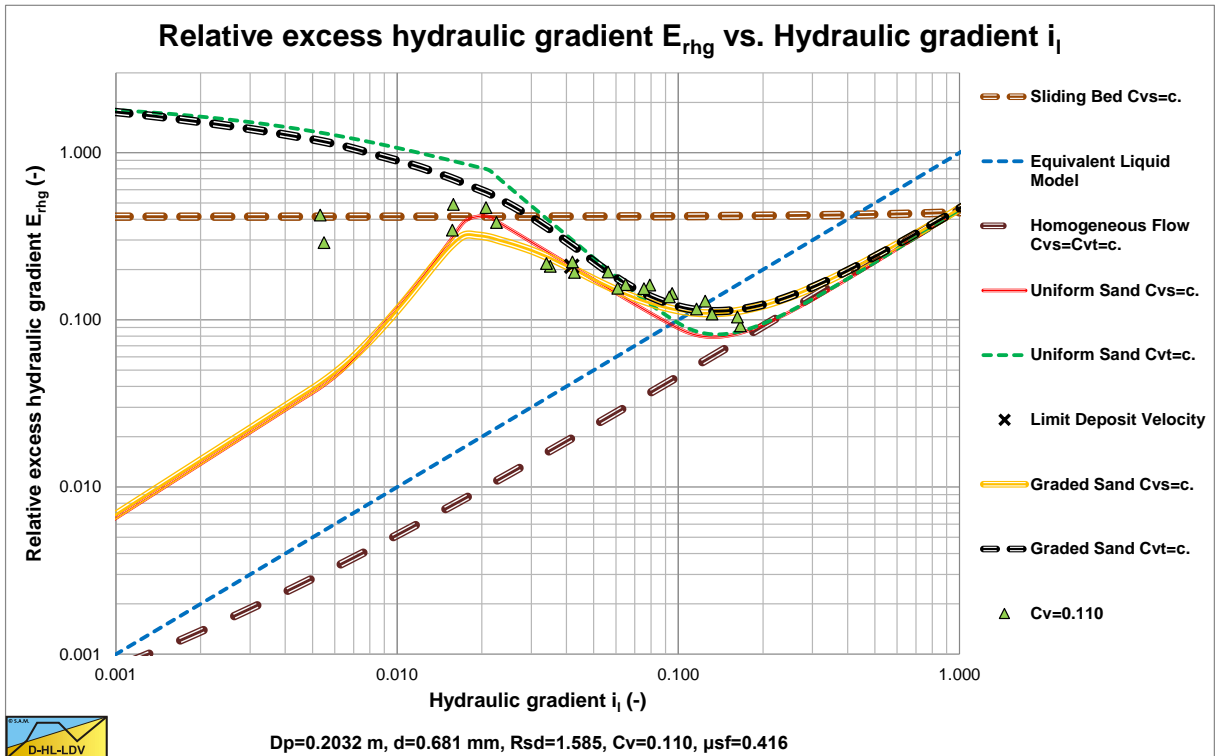
Figure 7.2-11: Clift et al. (1982), broad graded crushed granite.

These experiments show that at line speeds below the Limit Deposit Velocity and constant C_{vt}, the heterogeneous line is still followed. The grading of the sand makes the heterogeneous curve less steep, but this depends on the grading, the particle size and the pipe diameter.

7.2.5.3 L2: Fixed & Sliding Bed – Heterogeneous & Sliding Flow, Constant Cvs.

Figure 7.2-12: Wiedenroth (1967), coarse sand.

Figure 7.2-13: Wiedenroth (1967), medium sand.
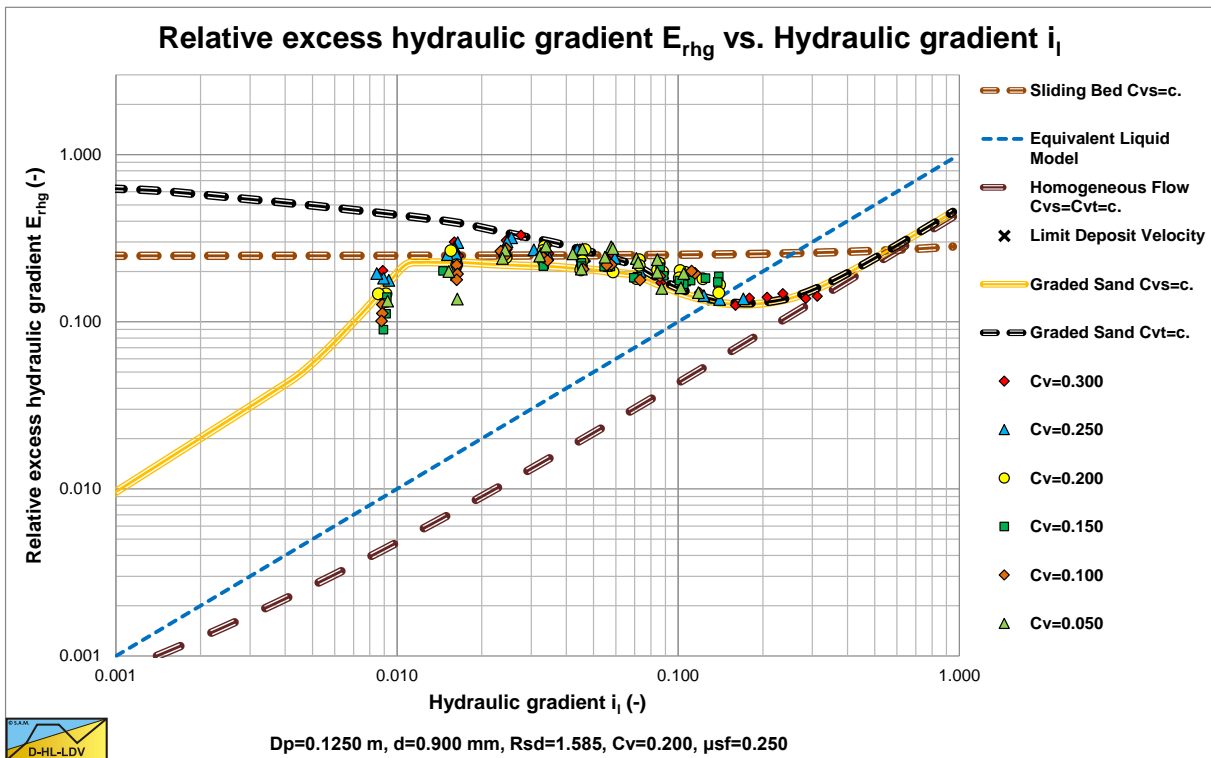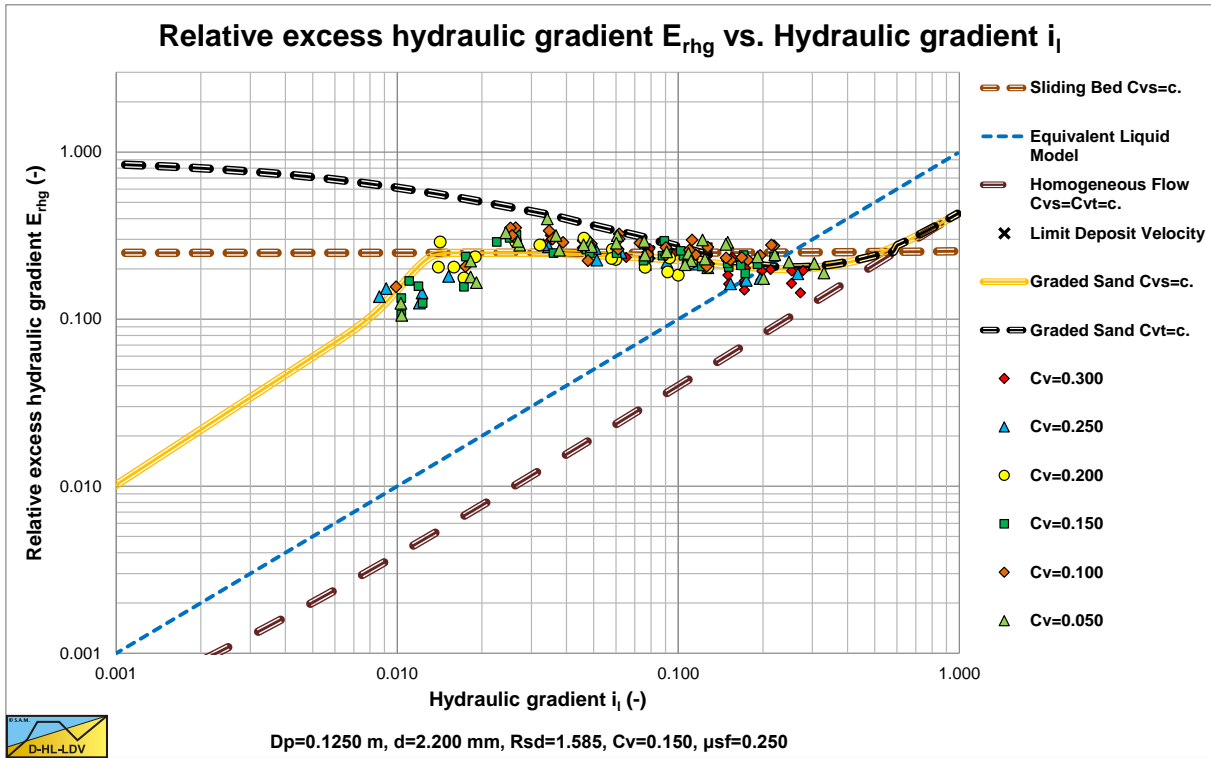
These experiments at constant **Cvs**, show a fixed bed to sliding bed to heterogeneous behavior. In both figures it is clear that the curve for graded sands match the data points better. The effect of the grading is different for different particle sizes.

7.2.5.4 R2, R3: Sliding Bed & Sliding Flow, Constant C$_{vt}$.
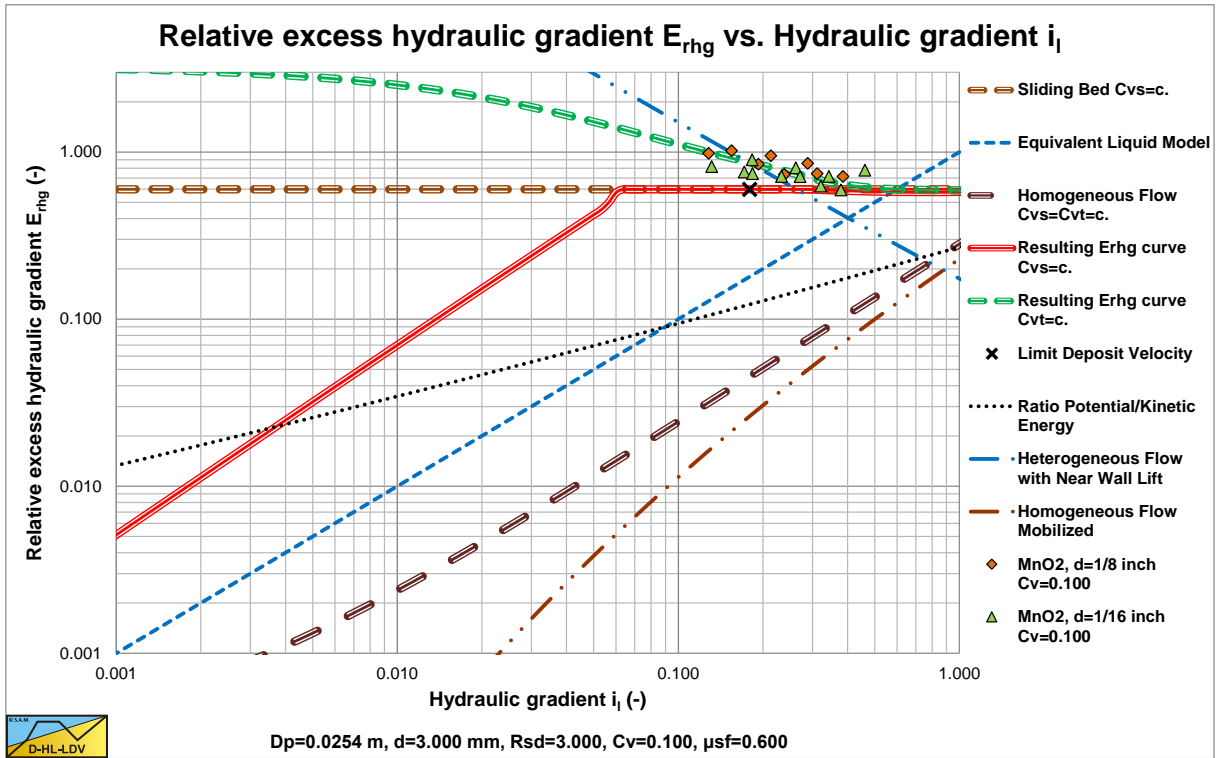
Figure 7.2-14: Newitt et al. (1955), MnO2.
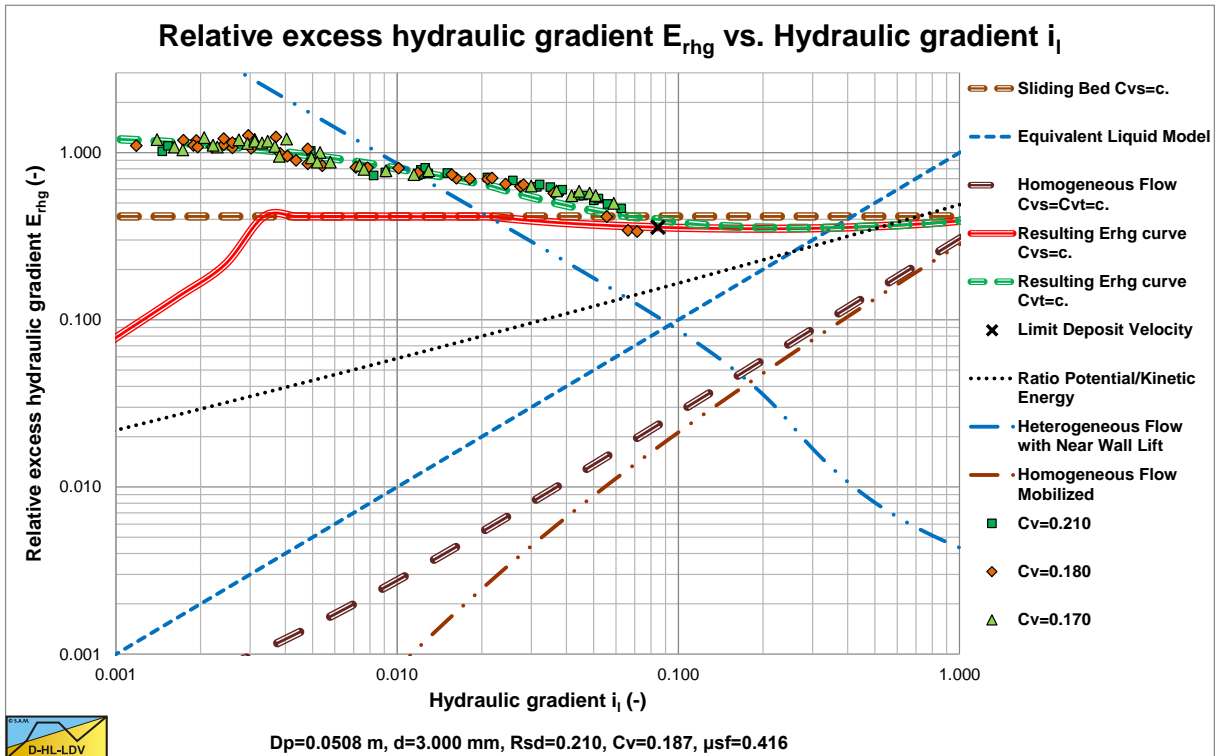
Figure 7.2-15: Doron & Barnea (1993), Acetal.

These experiments show the constant **C$_{vt}$** behavior at small line speeds, with a sliding/fixed bed and sliding flow behavior. The DHLLDV Framework gives a good prediction for both heavy (MnO2) and light (Acetal) solids.

7.2.5.5 L1, R1, L2, R2:, Homogeneous.
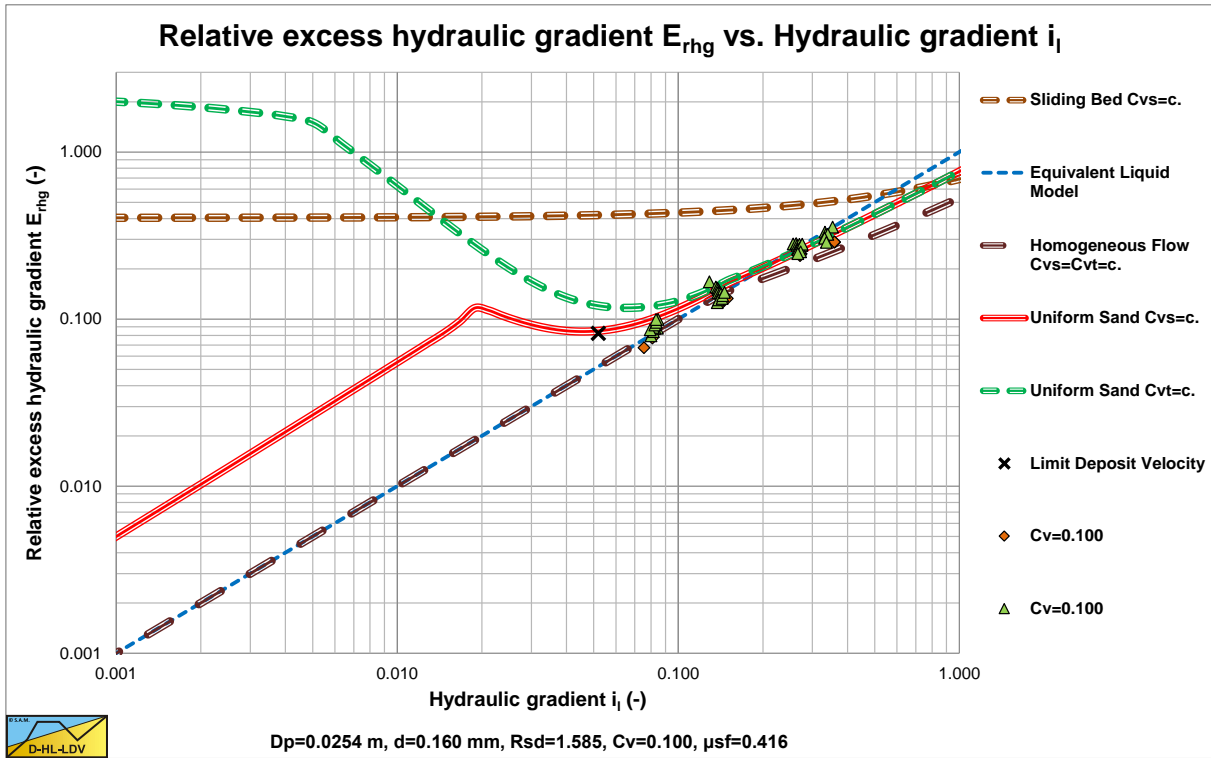
Figure 7.2-16: Babcock (1970), sand.
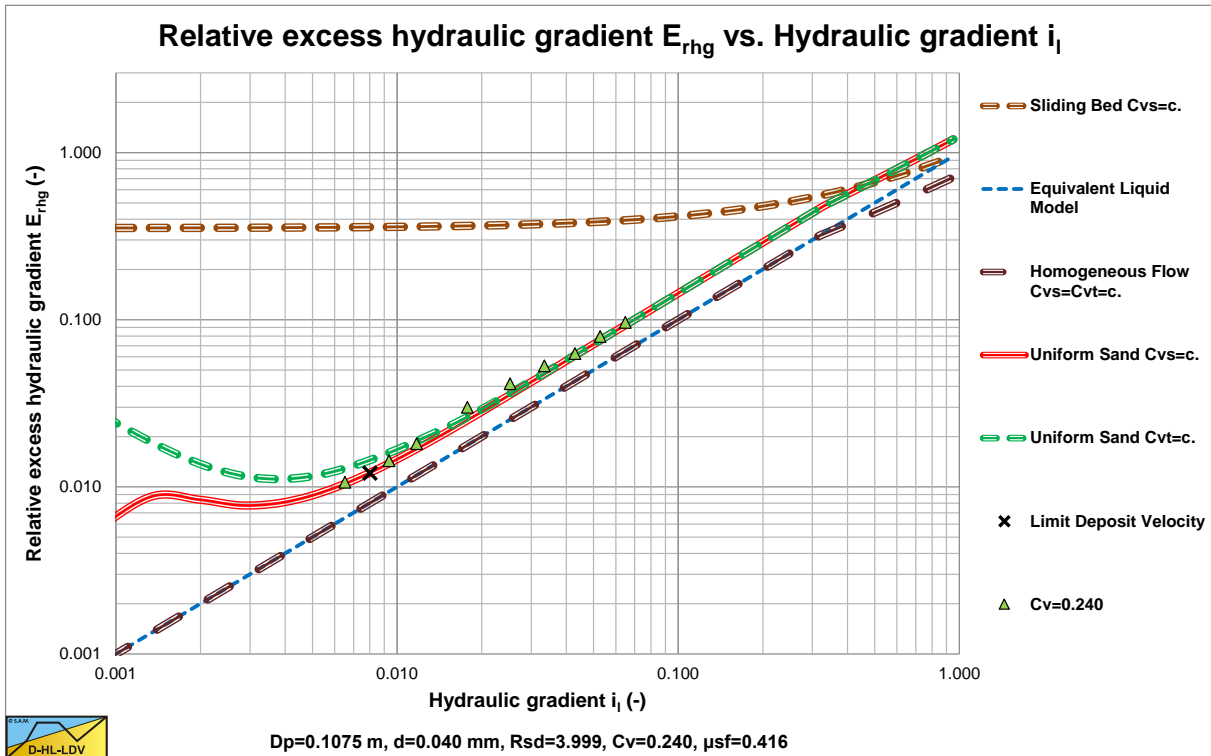
Figure 7.2-17: Thomas (1976), iron ore.

These experiments show homogeneous behavior, which occurs with small particles at relatively high line speeds. The Thomas (1976) graph also includes Thomas (1965) viscosity for very small particles.

7.2.5.6 L3, R3: Sliding Bed & Sliding Flow, Constant C$_{vs}$.
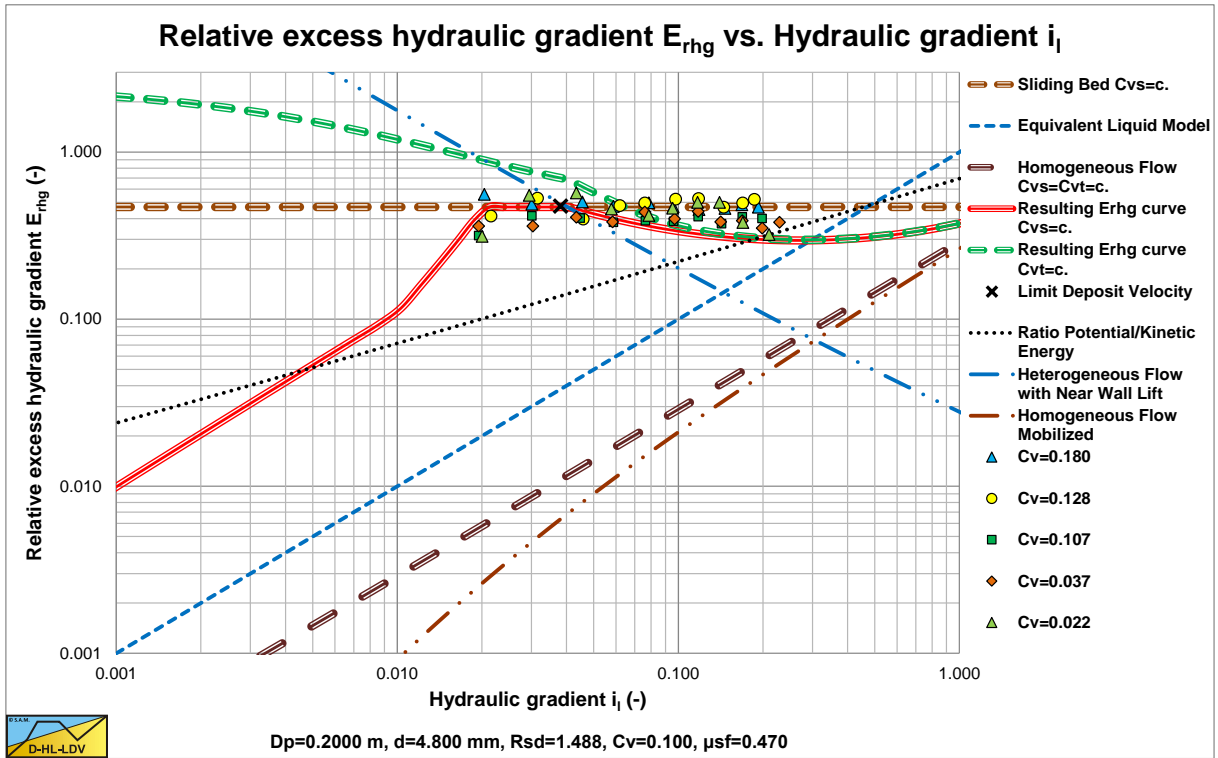
Figure 7.2-18: Boothroyde (1979), gravel.
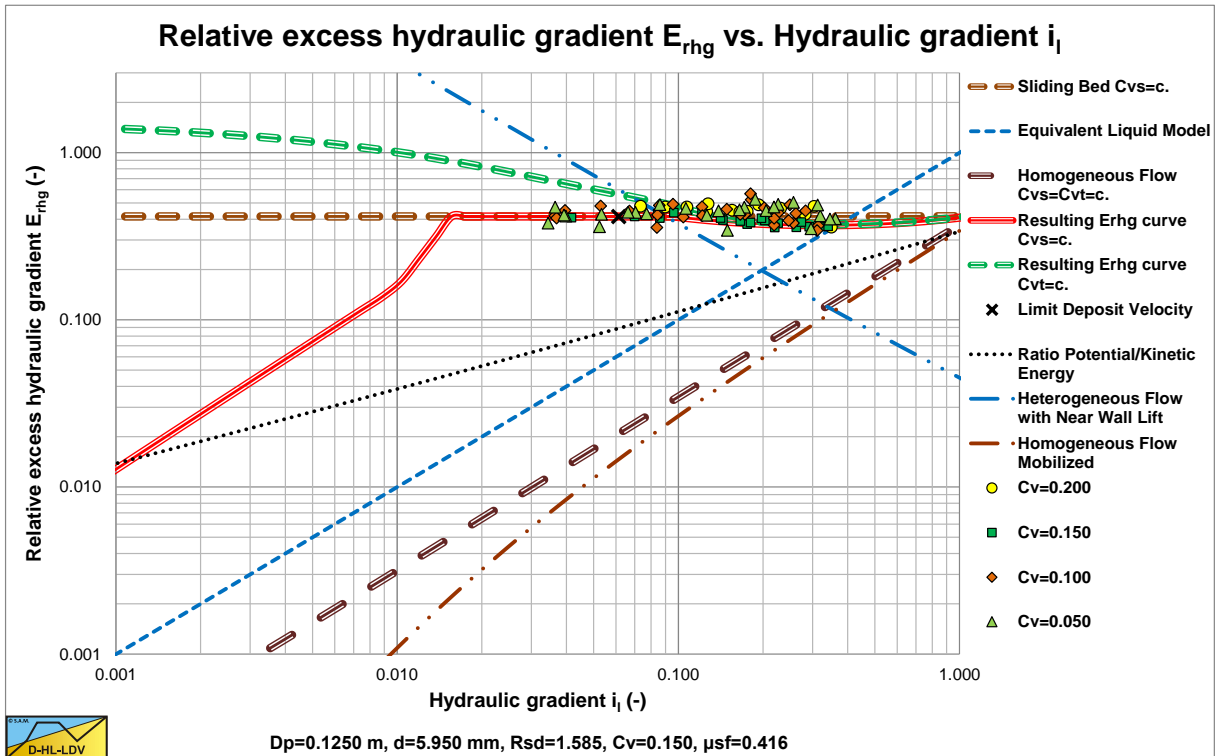
Figure 7.2-19: Wiedenroth (1967), gravel.

These experiments show the sliding bed and sliding flow regimes. Beyond the intersection point between a sliding bed and heterogeneous flow, the sliding flow curve is followed.

7.2.6 Discussion & Conclusions.

The experimental graphs are given without a lot of explanation, because they should speak for themselves. These graphs show the different flow regimes and sometimes more than one flow regime. In general there is a lot of scatter. This is caused by the way experiments were carried out and specifically the accuracy of the concentration measurements. Sometimes concentrations within a certain bandwidth (for example 10-15%) are given with an average mentioned on the graph (for example 12.5%). But in spite of the scatter, the graphs clearly show the different regimes.

From these graphs and the regime and scenario definitions, it should be clear that experiments carried out in very small pipelines, like 1 inch diameter pipelines, can never be compared with experiments in very large pipelines, like 1 m diameter pipelines. In a 1 m diameter pipeline it is difficult to get a sliding bed regime, while in a 1 inch diameter pipeline it is very difficult not to get a sliding bed regime, due to the high hydraulic gradients. It is like comparing laminar and turbulent flow.

Each regime has its own physical and mathematical model. The fixed bed regime can be modeled with flow through a restricted cross section using the Televantos (1979) method for determining the friction factor. The sliding bed regime and partly the sliding flow regime can be modeled using the Newitt et al. (1955) method, with the appropriate friction factor (0.35-0.7). The heterogeneous regime can be modeled with one of the existing equations or with the Miedema et al. (2013) model. The homogeneous regime can be modeled using the equivalent liquid model, using 100% of the solids or for example using 60% of the solids, like some authors do. For the fixed bed/sliding bed regimes below the Limit Deposit Velocity, a 2 layer or 3 layer model can be used, but the Durand & Condolios (1952) approach, considering a flow Froude number which is equal to the flow Froude number at the Limit Deposit Velocity, also gives good results.

Just carrying out some curve fits and drawing conclusions is very dangerous, because the experiments may cover 2 or more regimes. For example, if 50% of the experiments are in the heterogeneous regime and 50% of the experiments are in the homogeneous regime, a curve fit would give a horizontal line in the $E_{rhg}(i_l)$ graph. If we look at experiments where 50% is in the fixed bed regime (constant C_{vs}) and 50% is in the heterogeneous regime (for example Figure 7.2-8 & Figure 7.2-12), the result of a curve fit is also a horizontal line. The cases however are completely different.

Recognizing the different regimes and especially the transitions between the different regimes is crucial in understanding what is physically happening.

The DHLLDV Framework gives a good match with most of the experiments shown here. In this book many more experiments are shown, usually compared to the DHLLDV Framework. The DHLLDV Framework gives good results for fine sands up to fine gravel in small to large pipes, compared to the experiments. For very coarse particles however still more research is required.

7.2.7 Nomenclature Flow Regimes & Scenario's.

A_2	Cross section of the bed in the pipe	m^2
A_1	Cross section of the mixture in suspension above the bed	m^2
A, A_p	Cross section of the pipe	m^2
A_2	Cross section of the solids in the pipe	m^2
C_v	Volumetric concentration	-
C_{vs}	Volumetric spatial concentration	-
$C_{vs,s}$	Volumetric spatial concentration of the mixture in suspension above a fixed or sliding bed	-
C_{vt}	Volumetric transport (delivered) concentration	-
d	Particle diameter	mm
d_{50}	Median particle diameter - 50% by weight is smaller	mm
D_p	Pipe diameter	m
E_{rhg}	Relative Excess Hydraulic Gradient	-
i_m	Mixture head loss	m/m
i_l	Liquid hydraulic gradient	m/m
i_w	Water hydraulic gradient	m/m
n	Porosity	-
O_1	Circumference liquid-pipe wall	m
O_2	Circumference bed-pipe wall	m
O_{12}	Width liquid-bed interface	m
Q_m or $\dot{V}_m$	Flow rate of mixture	m^3/s
Q_s or $\dot{V}_s$	Flow rate of solids	m^3/s
R_{sd}	Relative submerged density	-
R	Stratification ratio Wilson	-
S_{rs}	Slip Relative Squared or Stratification Ratio Solids	-
S_{hr}	Settling velocity Hindered Relative	-
v_{ls}	Velocity of the slurry, line speed	m/s
$v_{ls,e}$	Effective line speed. Line speed above the fixed or moving bed.	m/s
v_m	Velocity of the slurry, line speed (same as v_{ls})	m/s
v_s	Average velocity of the solids	m/s
v_{sl}	Slip velocity of the solids relative to the mixture	m/s
V_b	Volume of the bed	m^3
V_{cl}	Volume of the closed loop	m^3
V_m	Volume of the mixture in a pipe	m^3
$V_{m,s}$	Volume of the mixture in suspension above the bed	m^3
V_s	Volume of the solids in a pipe	m^3
$V_{s,s}$	Volume of the solids in suspension above the bed	m^3
v_t	Terminal settling velocity of the particles	m/s
β	Richardson & Zaki hindered settling power	-
λ_1	Darcy-Weisbach friction factor between liquid and pipe wall	-
λ_2	Darcy-Weisbach friction factor between liquid and pipe wall in bed	-
λ_{22}	Darcy-Weisbach friction factor between liquid and bed	-
κ_C	Concentration eccentricity factor.	-
μ_{sf}	Friction coefficient for a sliding bed	-
ρ_l, ρ_w	Density of the liquid	ton/ m^3
ρ_m	Density of the mixture	ton/ m^3
ρ_s	Density of the solids	ton/ m^3

7.3 A Head Loss Model for Fixed Bed Slurry Transport.

7.3.1 The Basic Equations for Flow and Geometry.

In order to understand the fixed bed model, first all the geometrical parameters are defined. The cross section of the pipe with a particle bed as defined in the Wilson et al. (1992) two layer model has been illustrated by Figure 6.20-1, here Figure 7.3-1.
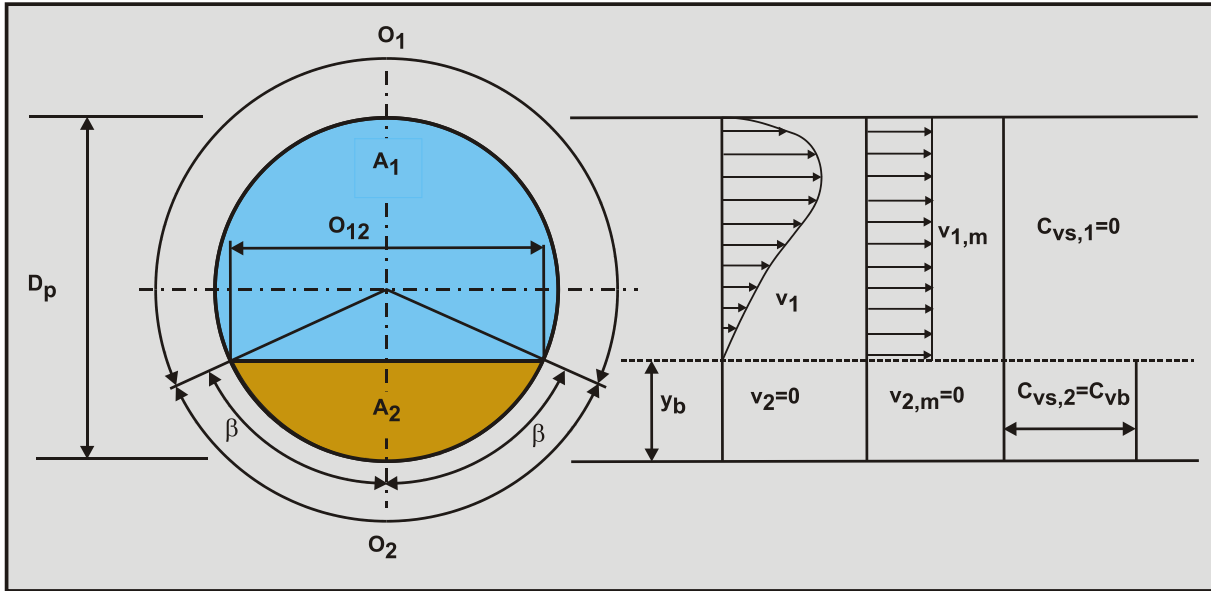
Figure 7.3-1: The definitions for fully stratified flow.

The geometry is defined by the following equations.

The length of the liquid in contact with the whole pipe wall if there is no bed is:

$$O_p = \pi \cdot D_p \tag{7.3-1}$$

The length of the liquid or the suspension in contact with the pipe wall:

$$O_1 = D_p \cdot (\pi - \beta) \tag{7.3-2}$$

The length of the fixed or sliding bed in contact with the wall:

$$O_2 = D_p \cdot \beta \tag{7.3-3}$$

The top surface length of the fixed or sliding bed:

$$O_{12} = D_p \cdot \sin(\beta) \tag{7.3-4}$$

The cross sectional area A_p of the pipe is:

$$A_p = \frac{\pi}{4} \cdot D_p^2 \tag{7.3-5}$$

The cross sectional area A_2 of the fixed or sliding bed is:

$$A_2 = \frac{\pi}{4} \cdot D_p^2 \cdot \left(\frac{\beta - \sin(\beta) \cdot \cos(\beta)}{\pi} \right) \tag{7.3-6}$$

The cross sectional area A_1 above the bed, where the liquid or the suspension is flowing, also named the restricted area:

$$A_1 = A_p - A_2 \tag{7.3-7}$$

The hydraulic diameter $D_{H,1}$ of the cross-sectional area above the bed as function of the bed height, is equal to four times the cross sectional area divided by the wetted perimeter:

$$D_{H,1} = \frac{4 \cdot A_1}{O_1 + O_{12}} \quad \text{or simplified:} \quad D_{H,1} = \sqrt{\frac{4 \cdot A_1}{\pi}} \tag{7.3-8}$$

The volume balance gives a relation between the line speed v_{ls}, the velocity in the restricted area above the bed v_r or v_1 and the velocity of the bed v_b or v_2.

$$v_{ls} \cdot A_p = v_1 \cdot A_1 + v_2 \cdot A_2 \tag{7.3-9}$$

Thus the velocity in the restricted area above the bed is:

$$v_1 = \frac{v_{ls} \cdot A_p - v_2 \cdot A_2}{A_1} \tag{7.3-10}$$

Or the velocity of the bed is (for a fixed bed $v_2=0$):

$$v_2 = \frac{v_{ls} \cdot A_p - v_1 \cdot A_1}{A_2} \tag{7.3-11}$$

7.3.2 The Shear Stresses Involved.

In order to determine the forces involved, first the shear stresses involved have to be determined. The general equation for the shear stresses is:

$$\tau = \rho_l \cdot u_*^2 = \frac{\lambda_l}{4} \cdot \frac{1}{2} \cdot \rho_l \cdot v^2 \tag{7.3-12}$$

The force F on the pipe wall over a length ΔL is now:

$$F = \tau \cdot \pi \cdot D_p \cdot \Delta L = \frac{\lambda_l}{4} \cdot \frac{1}{2} \cdot \rho_l \cdot v^2 \cdot \pi \cdot D_p \cdot \Delta L \tag{7.3-13}$$

The pressure Δp required to push the solid-liquid mixture through the pipe is:

$$\Delta p = \frac{F}{A_p} = \frac{\frac{\lambda_l}{4} \cdot \frac{1}{2} \cdot \rho_l \cdot v^2 \cdot \pi \cdot D_p \cdot \Delta L}{\frac{\pi}{4} \cdot D_p^2} = \lambda_l \cdot \frac{\Delta L}{D_p} \cdot \frac{1}{2} \cdot \rho_l \cdot v^2 \tag{7.3-14}$$

This is the well-known Darcy Weisbach equation. Over the whole range of Reynolds numbers above 2320 the Swamee Jain equation gives a good approximation for the friction coefficient:

$$\lambda_l = \frac{1.325}{\left(\ln\left(\frac{0.27 \cdot \varepsilon}{D_p} + \frac{5.75}{Re^{0.9}}\right)\right)^2} \quad \text{with:} \quad Re = \frac{v \cdot D_p}{\nu_l} \tag{7.3-15}$$

This gives for the shear stress on the pipe wall for clean water:

$$\tau_l = \frac{\lambda_l}{4} \cdot \frac{1}{2} \cdot \rho_l \cdot v_{ls}^2 \quad \text{with:} \quad \lambda_l = \frac{1.325}{\left(\ln\left(\frac{0.27 \cdot \varepsilon}{D_p} + \frac{5.75}{Re^{0.9}}\right)\right)^2} \quad \text{and} \quad Re = \frac{v_{ls} \cdot D_p}{\nu_l} \tag{7.3-16}$$

For the flow in the restricted area, the shear stress between the liquid and the pipe wall is:

$$\tau_{1,l} = \frac{\lambda_1}{4} \cdot \frac{1}{2} \cdot \rho_l \cdot v_1^2 \quad \text{with:} \quad \lambda_1 = \frac{1.325}{\left(\ln\left(\frac{0.27 \cdot \varepsilon}{D_H} + \frac{5.75}{Re^{0.9}}\right)\right)^2} \quad \text{and} \quad Re = \frac{v_1 \cdot D_H}{\nu_l} \tag{7.3-17}$$

For the flow in the restricted area, the shear stress between the liquid and the bed is:

$$\tau_{12,l} = \frac{\lambda_{12}}{4} \cdot \frac{1}{2} \cdot \rho_l \cdot v_1^2 \quad \text{with:} \quad \lambda_{12} = \frac{\alpha \cdot 1.325}{\left(\ln\left(\frac{0.27 \cdot d}{D_H} + \frac{5.75}{Re^{0.9}}\right)\right)^2} \quad \text{and} \quad Re = \frac{v_1 \cdot D_H}{\nu_l} \tag{7.3-18}$$

The factor **α** as used by Wilson et al. (1992) is 2 or 2.75, depending on the publication and version of his book. Televantos et al. (1979) used a factor of 2. For the flow between the liquid in the bed and the pipe wall, the shear stress between the liquid and the pipe wall is:

$$\tau_{2,l} = \frac{\lambda_2}{4} \cdot \frac{1}{2} \cdot \rho_l \cdot v_2^2 \quad \text{with:} \quad \lambda_2 = \frac{1.325}{\left(\ln\left(\frac{0.27 \cdot \varepsilon}{d} + \frac{5.75}{Re^{0.9}}\right)\right)^2} \quad \text{and} \quad Re = \frac{v_2 \cdot d}{\nu_l} \tag{7.3-19}$$

Wilson et al. (1992) assume that the sliding friction is the result of a hydrostatic normal force between the bed and the pipe wall multiplied by the sliding friction factor. The average shear stress as a result of the sliding friction between the bed and the pipe wall, according to the Wilson et al. (1992) normal stress approach is:

$$\tau_{2,sf} = \frac{\mu_{sf} \cdot \rho_l \cdot g \cdot R_{sd} \cdot C_{vb} \cdot A_p}{\beta \cdot D_p} \cdot \frac{2 \cdot (\sin(\beta) - \beta \cdot \cos(\beta))}{\pi} \tag{7.3-20}$$

It is however also possible that the sliding friction force results from the weight of the bed multiplied by the sliding friction factor. For low volumetric concentrations, there is not much difference between the two methods, but at higher volumetric concentrations there is. The average shear stress as a result of the sliding friction between the bed and the pipe wall, according to the weight normal stress approach is:

$$\tau_{2,sf} = \frac{\mu_{sf} \cdot \rho_l \cdot g \cdot R_{sd} \cdot C_{vb} \cdot A_p}{\beta \cdot D_p} \cdot \frac{(\beta - \sin(\beta) \cdot \cos(\beta))}{\pi} \tag{7.3-21}$$

7.3.3 The Forces Involved.

First the equilibrium of the forces on the liquid above the bed is determined. This is necessary to find the correct hydraulic gradient.

The resisting shear force on the pipe wall O_1 above the bed is:

$$\mathbf{F_{1,l} = \tau_{1,l} \cdot O_1 \cdot \Delta L}$$

(7.3-22)

The resisting shear force on the bed surface O_{12} is:

$$\mathbf{F_{12,l} = \tau_{12,l} \cdot O_{12} \cdot \Delta L}$$

(7.3-23)

The pressure $\mathbf{\Delta p}$ on the liquid above the bed is:

$$\mathbf{\Delta p = \Delta p_2 = \Delta p_1 = \frac{\tau_{1,l} \cdot O_1 \cdot \Delta L + \tau_{12,l} \cdot O_{12} \cdot \Delta L}{A_1} = \frac{F_{1,l} + F_{12,l}}{A_1}}$$

(7.3-24)

The force equilibrium on the liquid above the bed is shown in Figure 6.20-2.
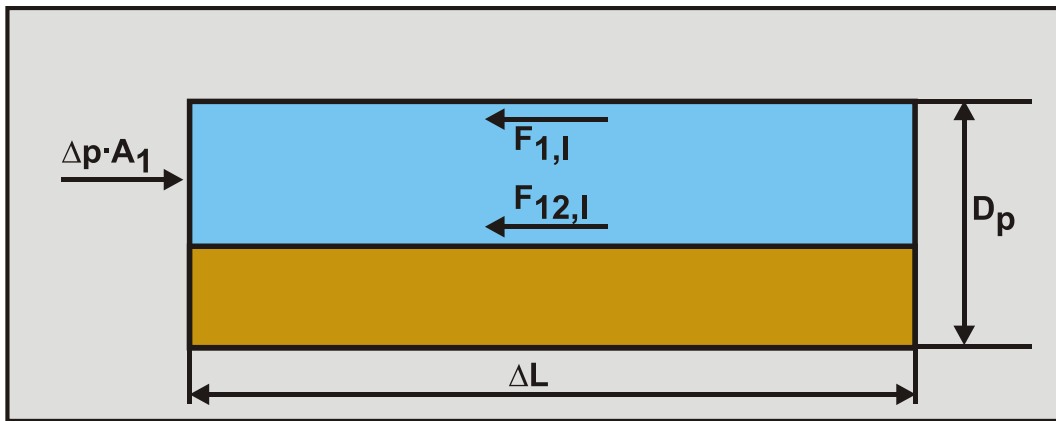
Figure 7.3-2: The forces on the liquid above the bed.

Secondly the equilibrium of forces on the bed is determined as is shown in Figure 6.20-3.
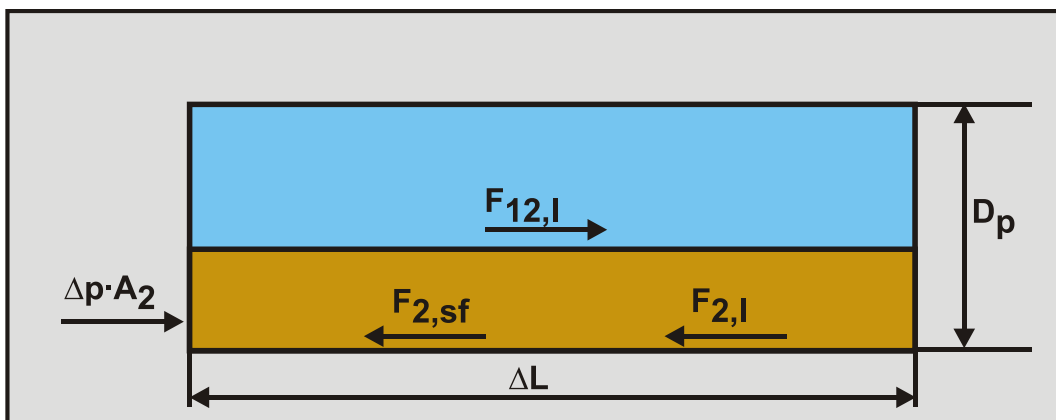
Figure 7.3-3: The forces on the bed.

The driving shear force on the bed surface is:

$$F_{12,l} = \tau_{12,l} \cdot O_{12} \cdot \Delta L \tag{7.3-25}$$

The driving force resulting from the pressure Δp on the bed is:

$$F_{2,pr} = \Delta p \cdot A_2 \tag{7.3-26}$$

The resisting force between the bed and the pipe wall due to sliding friction is:

$$F_{2,sf} = \tau_{2,sf} \cdot O_2 \cdot \Delta L \tag{7.3-27}$$

The resisting shear force between the liquid in the bed and the pipe wall is:

$$F_{2,l} = \tau_{2,l} \cdot O_2 \cdot n \cdot \Delta L \tag{7.3-28}$$

This shear force is multiplied by the porosity n, in order to correct for the fact that the bed consists of a combination of particles and water. There is an equilibrium of forces when:

$$F_{12,l} + F_{2,pr} = F_{2,sf} + F_{2,l} \tag{7.3-29}$$

Below the Limit of Stationary Deposit Velocity, the bed is not sliding and the force $F_{2,l}$ equals zero. Since the problem is implicit with respect to the velocities v_1 and v_2, it has to be solved with an iteration process.

The mixture pressure is now:

$$\Delta p_m = \frac{\lambda_1 \cdot O_1 + \lambda_{12} \cdot O_{12}}{4 \cdot (1 - C_{vr}) \cdot A_p} \cdot \frac{1}{2} \cdot \rho_l \cdot v_1^2 \cdot \Delta L \quad \text{with:} \quad C_{vr} = \frac{C_{vs}}{C_{vb}} \tag{7.3-30}$$

The excess pressure or excess hydraulic gradient can be written as:

$$\Delta p_m - \Delta p_l = \left((\lambda_1 \cdot O_1 + \lambda_{12} \cdot O_{12}) \cdot \left(\frac{1}{1 - C_{vr}} \right)^3 - \lambda_1 \cdot O_p \right) \cdot \frac{1}{2} \cdot \rho_l \cdot v_{ls}^2 \cdot \frac{\Delta L}{4 \cdot A_p}$$

or $\tag{7.3-31}$

$$i_m - i_l = \left((\lambda_1 \cdot O_1 + \lambda_{12} \cdot O_{12}) \cdot \left(\frac{1}{1 - C_{vr}} \right)^3 - \lambda_1 \cdot O_p \right) \cdot \frac{v_{ls}^2}{8 \cdot g \cdot A_p}$$

In terms of the relative excess hydraulic gradient this can be written as:

$$E_{rhg} = \frac{i_m - i_l}{R_{sd} \cdot C_{vs}} = \left((\lambda_1 \cdot O_1 + \lambda_{12} \cdot O_{12}) \cdot \left(\frac{1}{1 - C_{vr}} \right)^3 - \lambda_1 \cdot O_p \right) \cdot \frac{v_{ls}^2}{8 \cdot g \cdot A_p \cdot R_{sd} \cdot C_{vs}} \tag{7.3-32}$$

7.3.4 The Relative Roughness.

In the Wilson (1992) approach the Darcy-Weisbach friction factor between the liquid and the top of the bed is crucial, together with the multiplication factor as applied by Televantos et al. (1979) of 2-2.75. In this approach the particle diameter **d** is used as a bed roughness k_s and the resulting Darcy-Weisbach friction factor multiplied by 2 or 2.75. Another approach found in literature is the approach of making the effective bed roughness a function of the Shields parameter. Many researchers developed equations for this purpose, but the fact that many equations exist usually means that the physics are not understood properly. Following is a list of existing equations in order of time.

Nielsen (1981)

$$\frac{k_s}{d} = 190 \cdot \sqrt{\theta - \theta_c} \tag{7.3-33}$$

Grant & Madsen (1982)

$$\frac{k_s}{d} = 430 \cdot \left(\sqrt{\theta} - 0.7 \cdot \sqrt{\theta_c} \right)^2 \tag{7.3-34}$$

Wilson (1988) based his equation on experiments in closed conduits.

$$\frac{k_s}{d} = 5 \cdot \theta \tag{7.3-35}$$

Wikramanayake & Madsen (1991)

$$\frac{k_s}{d} = 60 \cdot \theta \tag{7.3-36}$$

Wikramanayake & Madsen (1991)

$$\frac{k_s}{d} = 340 \cdot \left(\sqrt{\theta} - 0.7 \cdot \sqrt{\theta_c} \right)^2 \tag{7.3-37}$$

Madsen et al. (1993)

$$\frac{k_s}{d} = 15 \tag{7.3-38}$$

Van Rijn (1993)

$$\frac{k_s}{d} = 3 \cdot \theta \tag{7.3-39}$$

Camenen et al. (2006) collected many data from literature and found a best fit equation. The data however was a combination of experiments in closed and not closed conduits.

$$\frac{k_s}{d} = 0.6 + 1.8 \cdot \left(\frac{v_{t*}^{1.2}}{Fr^{2.4}} \right) \cdot \theta^{1.7} \tag{7.3-40}$$

Or:

$$\frac{k_s}{d} = 0.6 + 2.4 \cdot \left(\frac{\theta}{\theta_{cr,ur}} \right)^{1.7}$$

(7.3-41)

With: $\theta_{cr,ur} = 1.18 \cdot \frac{Fr^{1.4}}{v_{t*}^{0.7}}$

With: $v_{t*} = \left(\frac{R_{sd}^2}{g \cdot v_l} \right)^{1/3} \cdot v_t$ & $Fr = \frac{v_{ls}}{\sqrt{g \cdot R_H}}$

(7.3-42)

Matousek (2007) based his first equation on a limited amount of experiments in a closed conduit.

$$\frac{k_s}{d} = 1.3 \cdot \theta^{1.65}$$

(7.3-43)

Matousek & Krupicka (2009) improved his relation based on more experiments.

$$\frac{k_s}{d} = 260 \cdot \left(\frac{R}{d} \right)^1 \cdot \left(\frac{v_t}{v_r} \right)^{2.5} \cdot \theta^{1.7}$$

(7.3-44)

Krupicka & Matousek (2010) improved their relation again and gave it a form similar to the Camenen et al. (2006) equation.

$$\frac{k_s}{d} = 1.7 \cdot \left(\frac{v_{t*}^{1.1}}{Fr^{2.3}} \right) \cdot \left(\frac{R}{d} \right)^{0.32} \cdot \theta^{1.4}$$

(7.3-45)

Krupicka & Matousek (2010) also gave a more explicit equation to determine the Darcy-Weisbach friction factor λ_b without having to use the bed roughness k_s/d.

$$\lambda_{12} = 0.25 \cdot \left(\frac{v_{t*}^{0.58}}{Fr^{1.3}} \right) \cdot \left(\frac{R}{d} \right)^{-0.36} \cdot \theta^{0.74}$$

(7.3-46)

By using the standard equation for the Shields parameter:

$$\theta = \frac{\frac{\lambda_{12}}{8} \cdot v_{ls}^2}{R_{sd} \cdot g \cdot d}$$

(7.3-47)

This can be written explicitly as:

$$\lambda_{12}^{0.26} = 0.25 \cdot \left(\frac{v_{t*}^{0.58}}{Fr^{1.3}} \right) \cdot \left(\frac{R}{d} \right)^{-0.36} \cdot \left(\frac{\frac{1}{8} \cdot (v_1 - v_2)^2}{R_{sd} \cdot g \cdot d} \right)^{0.74}$$

(7.3-48)

Whether this is the purpose of this equation is not clear, but mathematically it's correct.
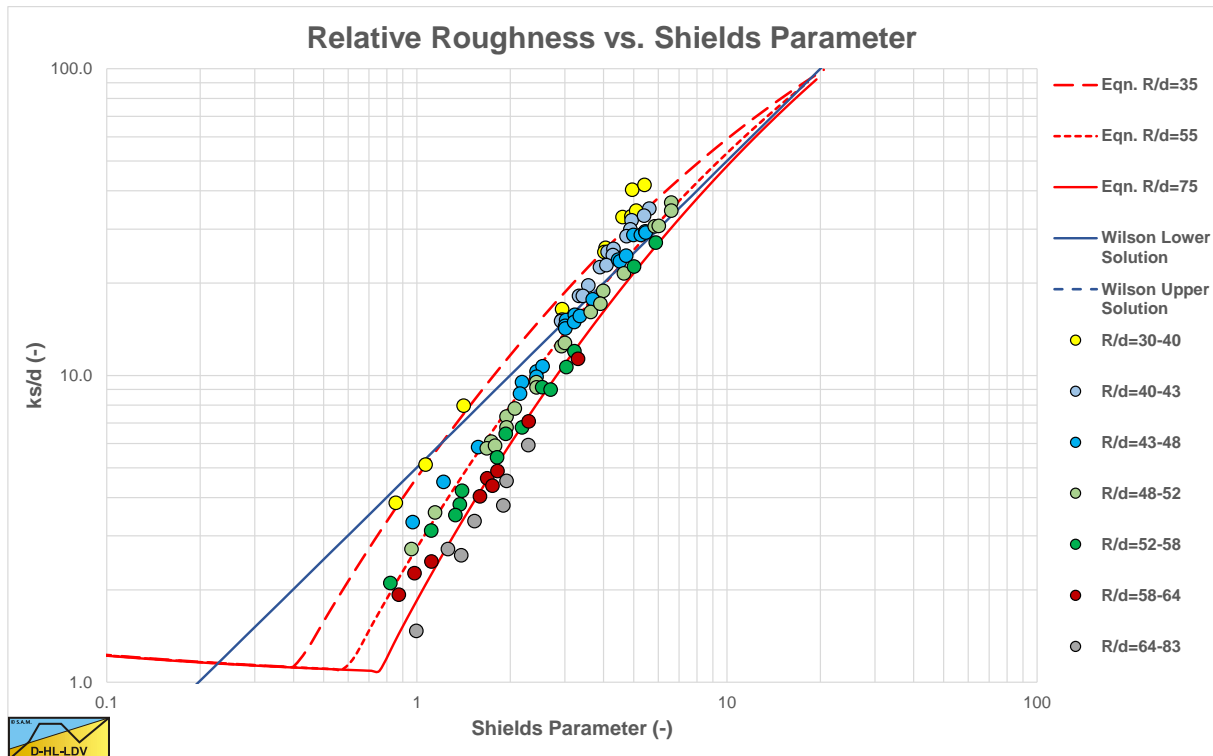
Figure 7.3-4: The original data of Wilson (1988).
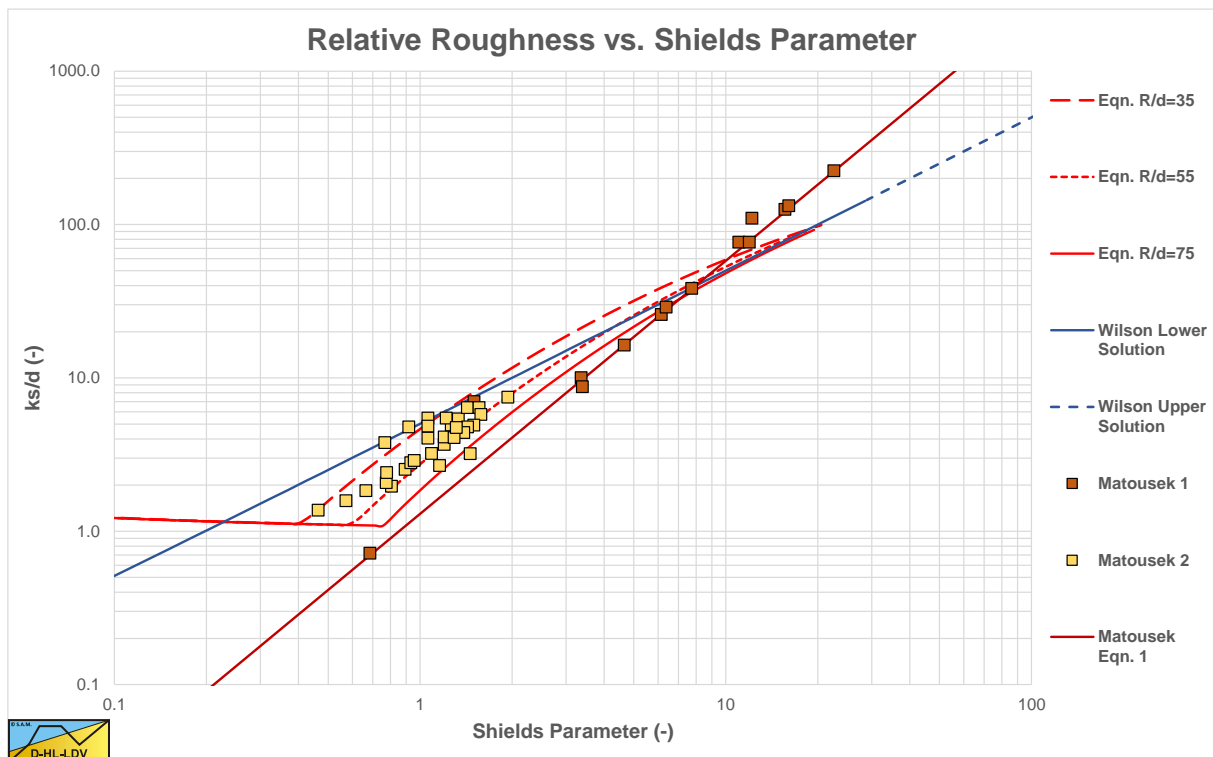
Figure 7.3-5: The data of Matousek & Krupicka as used in a number of their papers.

Camenen & Larson (2013) wrote a technical note on the accuracy of equivalent roughness height formulas in practical applications. They already concluded that most equations are based on a relation between the relative roughness k_s/d and the Shields parameter.

The relative roughness is a parameter that often has nothing to do with the real roughness of the bed, but it is a parameter to use in calculations to estimate an equivalent roughness value in the case of sheet flow. Sheet flow is a layer of particles flowing with a higher speed than the bed and with a velocity gradient, from a maximum velocity at the top to the bed velocity at the solid bed.

Camenen & Larson (2013) also concluded that the equations are implicit and have to be solved by iteration, since the Shields parameter depends on the relative roughness through the Darcy-Weisbach friction factor.

$$
\lambda_{12} = 8 \cdot \left(\frac{\kappa}{\ln\left(\frac{3.7 \cdot D_H}{k_s} \right)} \right)^2 = 8 \cdot \left(\frac{\kappa}{\ln\left(\frac{14.8 \cdot R_H}{k_s} \right)} \right)^2
$$

(7.3-49)
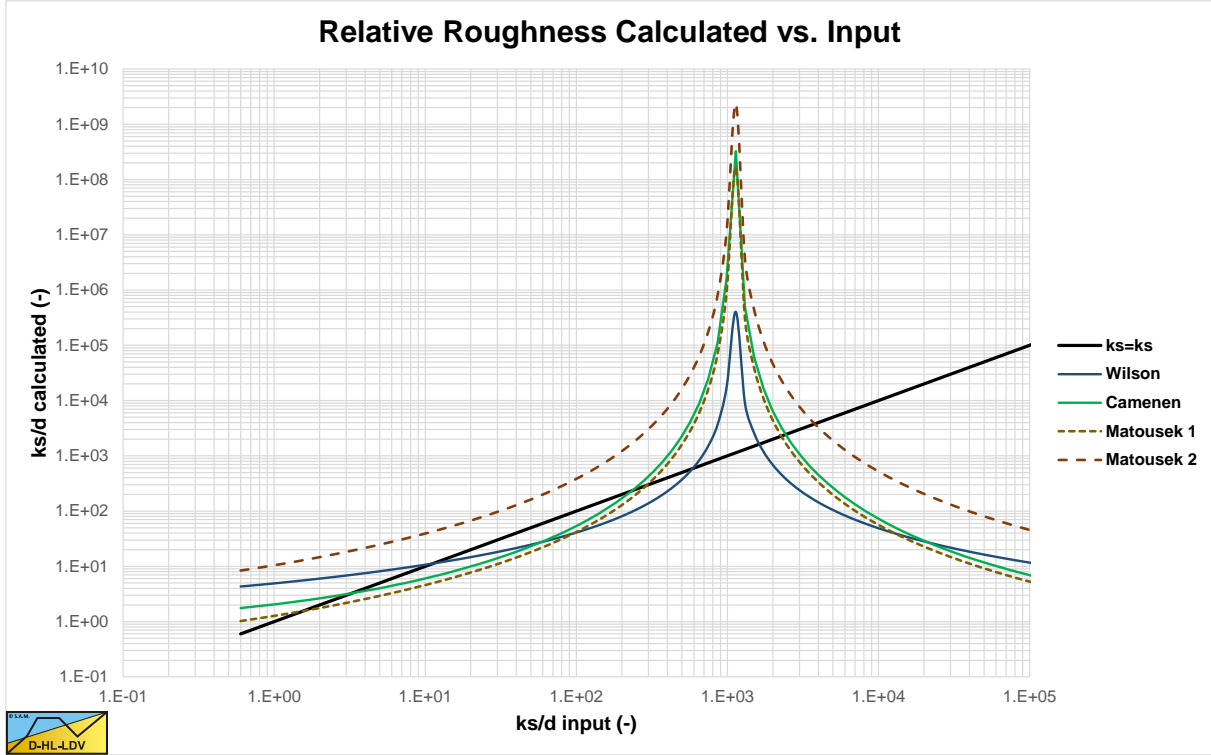
Figure 7.3-6: The relative roughness calculated versus the relative roughness input.

The Darcy-Weisbach friction factor as applied here is for very large Reynolds numbers. Camenen & Larson (2013) stated that this implicit equation is difficult to solve and that it has either two solution or no solution at all. Mathematically this is not correct. There are 3 solutions or there is 1 solution as is shown in Figure 7.3-6. Figure 7.3-6 (v_{ls}=**2 m/sec** & **R=0.0525 m**) shows the calculated k_s/d versus the input k_s/d for the Wilson (1988) equation, the Matousek (2009) equation, the improved Matousek (2010) equation and the Camenen et al. (2006) equation. The Wilson (1988) , Matousek (2009) and Camenen et al. (2006) equations show 3 intersection points with the $k_{s,calculated}=k_{s,input}$ line (y=x). Matousek (2010) only shows 1 intersection point. It is clear that the intersection point right from the peaks is a point for $k_{s,input}$>**14.8·R_h** which is physical nonsense, so this solution should be eliminated. Still in a numerical solver this could be output.

$$
\frac{k_s}{d} = \frac{3.7 \cdot D_H}{d} \cdot e^{-\kappa \cdot \sqrt{\frac{8}{\lambda_b}}} = \frac{14.8 \cdot R_H}{d} \cdot e^{-\kappa \cdot \sqrt{\frac{8}{\lambda_b}}}
$$

(7.3-50)

Now there are either 2 or 0 solutions left, depending on the different parameters and the model chosen. Figure 7.3-7 shows the relative roughness versus the Shields parameter for the 4 models as used above and mathematical solutions for a number of velocities above the bed (assuming the bed has no velocity) using the following equation.

$$
\frac{k_s}{d} = \frac{14.8 \cdot R_H}{d} \cdot e^{-\kappa \cdot \sqrt{\frac{v_{ab}^2}{\theta \cdot R_{sd} \cdot g \cdot d}}}
$$

(7.3-51)
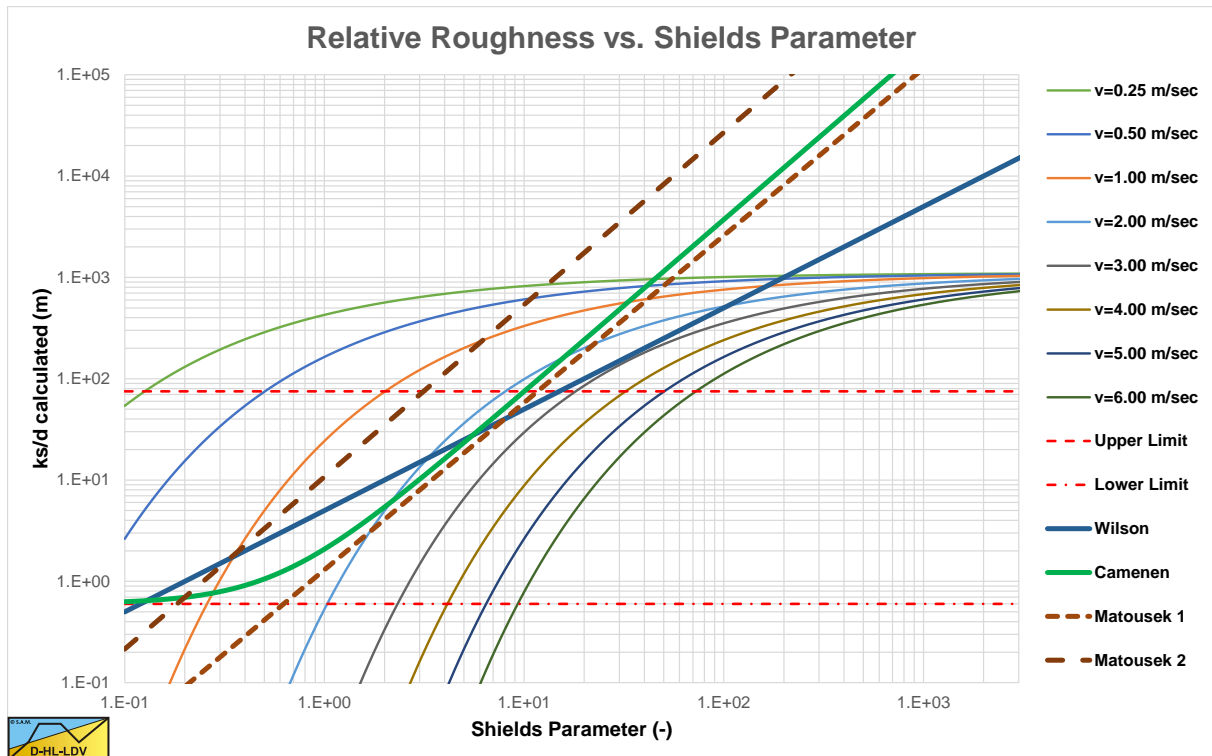
Figure 7.3-7: The relative roughness versus the Shields parameter.

Also this figure shows either two intersection points with a specific velocity, or no intersection point. It also shows that if a model intersects with a constant velocity curve close to the tangent point, the solution is very sensitive to small variations in the parameters or there is no solution at all. From analyzing a number of the models it appeared that each model has solutions up to a maximum velocity above the bed depending on the particle diameter **d** and the bed associated hydraulic radius **R$_H$**. Of course other parameters like the relative submerged density of the particles **R$_{sd}$** and the kinematic viscosity **ν$_l$** of the carrier liquid also play a role. Now suppose one of the models is correct, then above this maximum velocity no solution exists. But since this is true for all models, there exists a velocity above the bed above which no solutions exist at all. Figure 7.3-8 and Figure 7.3-9 clearly show the lower and upper solution for the Wilson (1988) equation in two different coordinate systems. This together with the fact that below this maximum velocity always two solutions exist, leaving us with the question which of the two solutions should be chosen, gives us no other choice than to reject the hypothesis that an equivalent roughness should be used as a function of the Shields parameter. Apparently this does not work. The question is, why all the researchers didn't relate the Darcy-Weisbach friction factor directly to the parameters involved, skipping the relative roughness and the Shields parameter. Most probably because in erosion and sediment transport it's a custom to use these parameters.

7.3.5 The Darcy-Weisbach friction factor first attempt.

Analyzing Figure 7.3-4, Figure 7.3-5 and the latest developments of the relative roughness equations shows that the relative roughness depends on the bed associated hydraulic radius, on the terminal settling velocity of the particles, on the Froude number of the flow and on the ratio between the particle diameter and the bed associated hydraulic radius. In Figure 7.3-4 different hydraulic radii are shown with different colors and this shows that a different hydraulic radius forms a group of data points within a certain band width. The Darcy-Weisbach friction factor increases exponentially with increasing line speed and also increases with decreasing bed associated hydraulic radius.
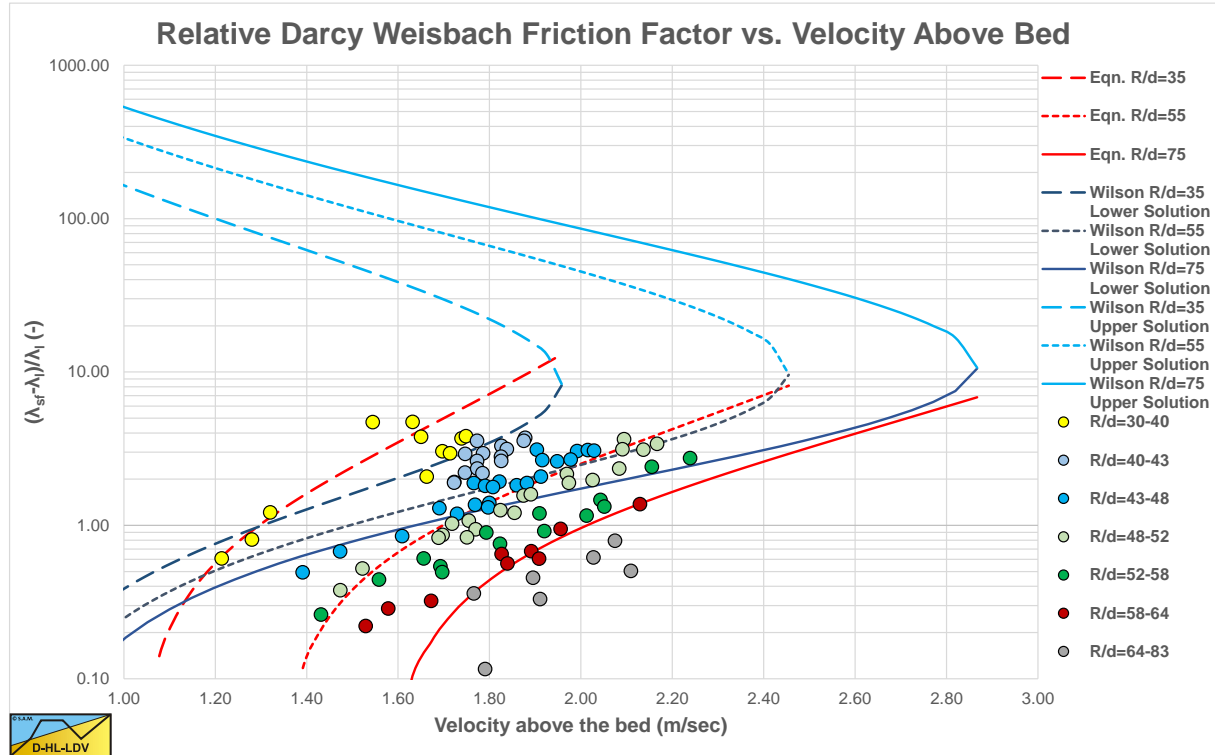
Figure 7.3-8: The Wilson (1988) experiments with the relative Darcy-Weisbach friction factor.

Figure 7.3-8 shows the Wilson (1988) experiments with the relative Darcy-Weisbach friction factor versus the velocity above the bed. Also in this graph the different bed associated hydraulic radii can be distinguished. Wilson (1988) used a multiplication factor of 2.75 and later 2.0, which in this graph equals 1.75 and 1.0 on the vertical axis. From the graph it is clear that this factor can be somewhere between 0.1 and 5.0, giving a multiplication factor from 1.1 to 6.0. It is however important what the value of this factor is at the Limit of Stationary Deposit Velocity, the moment the bed starts sliding. Based on the graph a relative factor of 1-2 or a multiplication factor from 2-3 seems reasonable. The graph however gives more information. Figure 7.3-9 shows the same data points but now with the Darcy-Weisbach friction factor on the vertical axis. Both graphs also show the lower and upper solution of the Wilson (1988) equation. Other equations would give a similar shape of the lower and upper solution.

Based on the Wilson (1988) and the Krupicka & Matousek (2010) experiments, complemented with (still confidential) experiments in the Laboratory of Dredging Engineering an empirical explicit equation has been developed for the relation between the Darcy-Weisbach friction factor and the different parameters involved. This equation is:

$$\lambda_{12} = 0.06 \cdot \sinh\left(48 \cdot \mathrm{Fr}^{2.83} \cdot \mathrm{Re}^{-0.33} \cdot v_{t*}^{-0.5}\right) \tag{7.3-52}$$

$$\text{With}: \ v_{t*} = \left(\frac{R_{sd}^2}{g \cdot v_l}\right)^{1/3} \cdot v_t, \quad \mathrm{Fr} = \frac{v_{ab}}{\sqrt{g \cdot 2 \cdot D_H}}, \quad \mathrm{Re} = \frac{v_{ab} \cdot 2 \cdot D_H}{v_l} \tag{7.3-53}$$
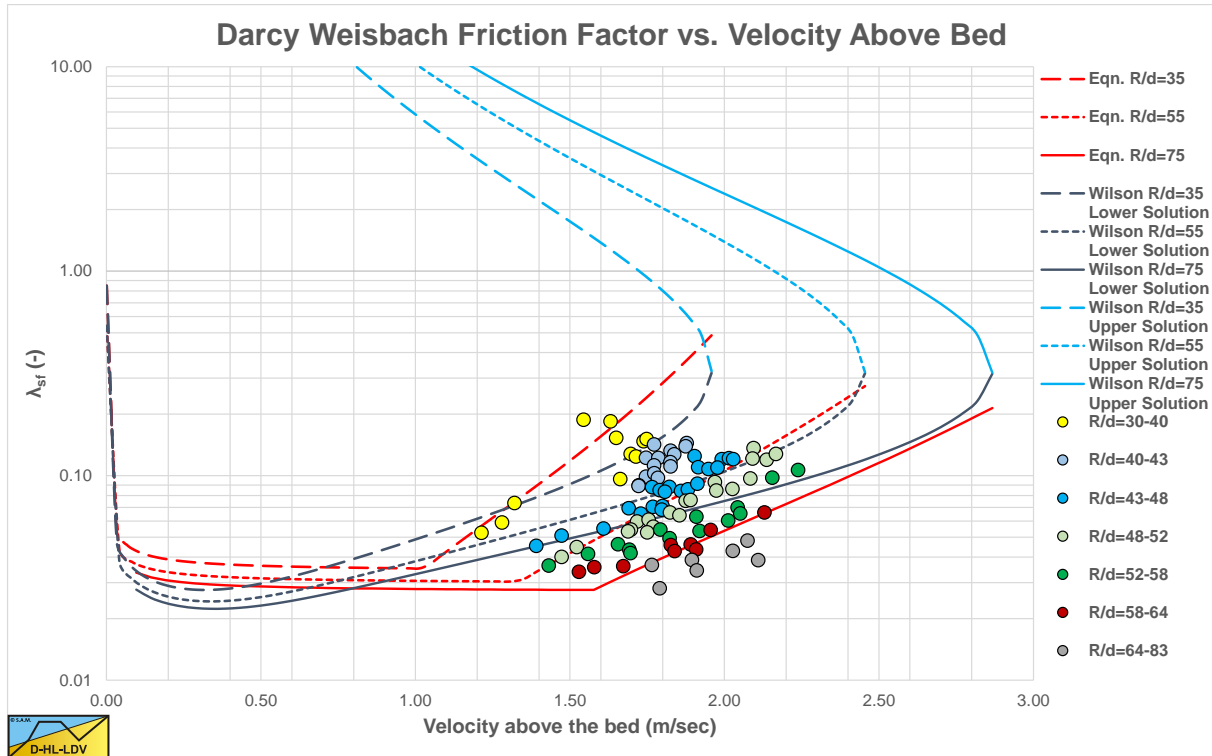
Figure 7.3-9: The Wilson (1988) experiments with the Darcy-Weisbach friction factor.

Figure 7.3-4, Figure 7.3-5, Figure 7.3-8 and Figure 7.3-9 show the resulting curves for $R_H/d=35$, 55 and 75 for the Wilson (1988) experiments. If the resulting Darcy-Weisbach friction factor is smaller than the result of equation (7.3-18), this equation is used. The curves can be extended for higher velocities above the bed, but are limited here to the maximum velocity of the solutions based on the Wilson (1988) equation. One can see that the resulting curves match the data points well and also match the curvature through the data points much better than the Wilson (1988) equation. The factor 2 in both the Froude number and the Reynolds number is to compensate for the fact that in the old equations the bed associated radius is used. The bed associated radius depends not only on the real hydraulic radius, but also on the contribution of the bed friction to the total friction. This bed associated radius can only be determined based on experiments. At high velocities where the bed friction dominates the total friction, the bed associated radius may get a value of 2 times the real hydraulic radius. Since here we are looking for an explicit expression, the real hydraulic radius or hydraulic diameter is used, compensated with this factor 2.
At small line speeds this factor may be near 1, but at line speeds that matter, the factor of 2 gives a good estimation.

7.3.6 Conclusion & Discussion

For the modeling of the Darcy-Weisbach friction factor on a bed with high velocity above the bed, usually relations between the equivalent relative roughness **k_s/d** and the Shields parameter **θ** are used. This approach has some complications. There are either 3 solutions or just 1 solution, where the solution with the highest relative roughness is physically impossible and unreasonable. Leaving either 2 or 0 solutions. Now Camenen & Larson (2013) suggested to use the lower solution, but in literature (Krupicka & Matousek (2010)) also data points are found on the upper branch of the solution.
Probably for relatively small Shields parameters, this method gives satisfactory results, but surely not for larger Shields parameters. Another point of discussion is, that most equations are based on experiments, where the Shields parameter was measured and the relative roughness was determined with an equation similar to equation (7.3-51). In engineering practice however this is not possible since the Shields parameter is not an input but is supposed to be an output. So besides a number of mathematical issues, the method is also not suitable for engineering practice. This is the reason for a first attempt to find an explicit practical equation for the Darcy-Weisbach friction factor directly. As long as the flow over a bed does not cause particles to start moving, the standard Darcy-Weisbach friction factor equation (7.3-18) is used, where the roughness is replaced by the particle diameter. Some use the particle diameter times a factor, but based on the experiments used here, a factor of 1 seems suitable. As soon as the top layer of the bed starts sliding, while the bed itself is still stationary, the Darcy-Weisbach friction factor increases according to equation (7.3-52). The higher the velocity difference between the flow above the bed and the bed, the thicker the layer of sheet flow and the higher the Darcy-Weisbach friction factor. To investigate the

influence of this new approach, two simulations were carried out. The first simulation with a fixed factor of 2 for the Darcy-Weisbach friction factor, as is shown in Figure 7.3-10. A second simulation with the new approach as described here as is shown in Figure 7.3-11.
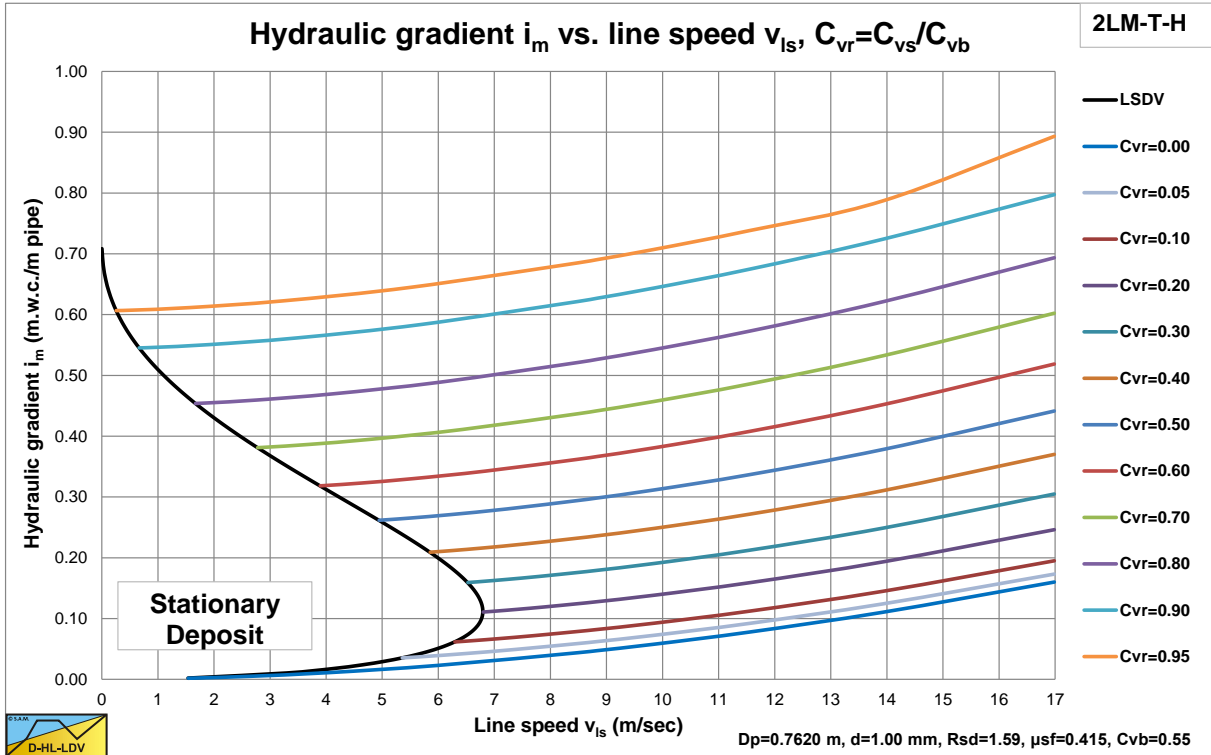
Figure 7.3-10: The resistance curves with a fixed Darcy-Weisbach friction factor.
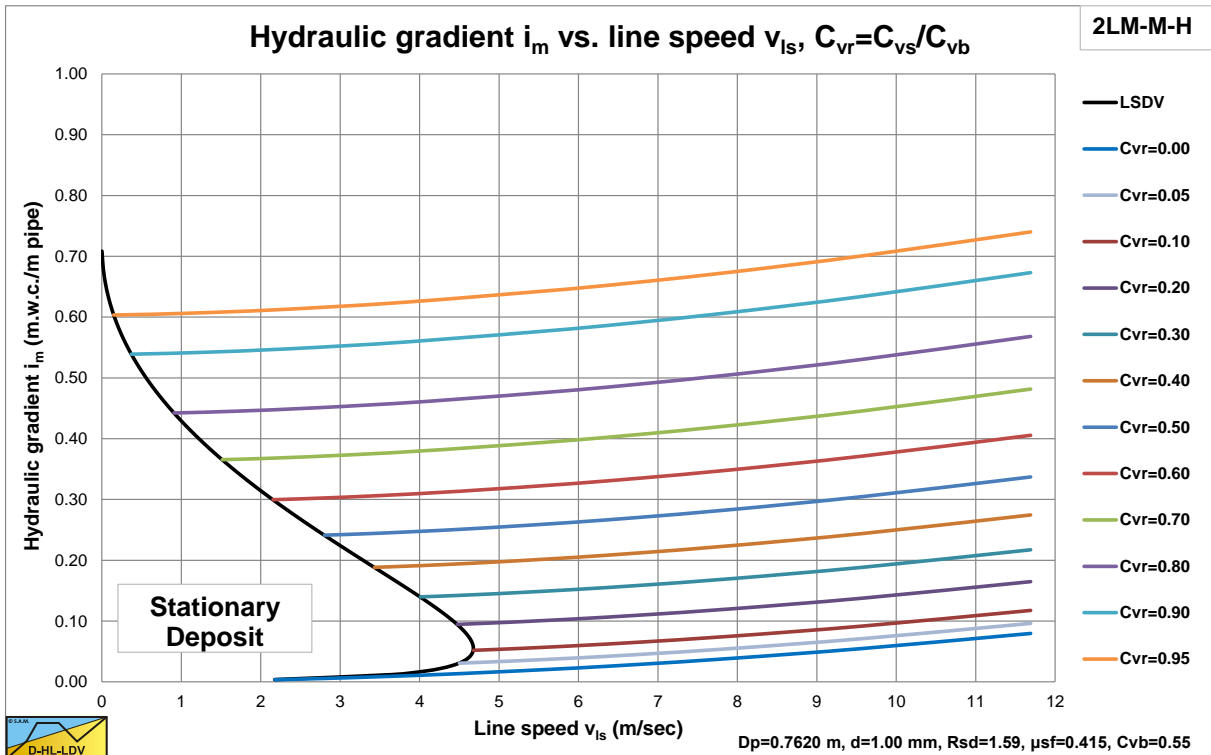
Figure 7.3-11: The resistance curves according to equation (7.3-52).

With the new approach there were some issues with the convergence of the numerical method, resulting in a maximum relative spatial volumetric concentration of 0.95. The difference between the two simulations is significant. The maximum Limit of Stationary Deposit Velocity (the velocity where the bed starts sliding) is about

6.8 m/sec with the fixed Darcy-Weisbach friction factor, while this is about 4.6 m/sec with the new approach. But the shape of the Limit of Stationary Deposit Velocity curves are different, especially at higher concentrations. Also the maximum occurs at a lower concentration. It is thus very important to have a good formulation for the friction on the top of the bed due to sheet flow, in order to have a good prediction of the Limit of Stationary Deposit Velocity. Of course, this is a first attempt to find an explicit formulation for the Darcy-Weisbach friction factor, so improvements are expected in the near future.

7.3.7 The Darcy Weisbach friction factor second attempt.

The most promising equations in terms of the relative roughness as a function of the Shields parameter are the equations of Camenen et al. (2006) and Krupicka & Matousek (2010) because they are based on the extensive experimental databases. Only one relation is available in an explicit form, the Miedema (2014) relation, equation (7.3-52). The results of this equation are shown in Figure 7.3-9. The Krupicka & Matousek (2010) equation (7.3-45) is almost explicit, although it still uses the bed associated hydraulic radius. The two relations differ in the fact that one is concave and the other convex. Still in the region of the data points both may give a good correlation coefficient. The Krupicka & Matousek (2010) equation will give a rapid increase of the Darcy-Weisbach friction factor at low velocities, where the increase decreases with increasing velocity. The Miedema (2014) equation gives a continuous increasing Darcy-Weisbach friction factor with an increasing increase with the velocity. The downside of the Miedema (2014) equation is that it is derived based on the bed associated hydraulic radius and applied for the hydraulic radius by applying a factor 2, which might sometimes be the case, but not always. Looking at the lower solution of the Wilson (1988) equation (7.3-35) in Figure 7.3-9, its shape shows more similarity with the Miedema (2014) equation. The purpose of this research is to find an explicit formulation of the bed friction factor as a function of known variables like the pipe diameter or hydraulic radius (based on the bed height without sheet flow), the relative submerged density of the particles, the velocity difference between the flow above the bed and the bed itself, the Darcy-Weisbach friction factors of clean water with the pipe wall λ_1 and clean water with the bed without sheet flow, the particle diameter and the terminal settling velocity of the particle.

Table 7.3-1: Experimental data used for calibration of friction-factor correlations

solids and size [mm]	solids density [kg/m3]	pipe B x H [mm]	data source
sand - 0.7	2670	93.8 x 93.8	Nnadi & Wilson 1992
nylon - 3.94	1140	93.8 x 93.8	Nnadi & Wilson 1992
bakelite - 0.67	1560	93.8 x 93.8	Nnadi & Wilson 1992
bakelite - 1.05	1560	93.8 x 93.8	Nnadi & Wilson 1992
ballotini - 0.18	2450	50.8 x 51.2	Matousek et al. 2013
sand - 0.125	2650	88 x 288	Bisschop et al. 2014

Based on the experimental data in Table 7.3-1, regressions are carried out on different types of equations. In all cases the input quantities were the measured hydraulic gradient, the velocity above the bed and the dimensions of the restricted area above the bed.

The equations tested are exponential and power equations with the velocity above the bed, the hydraulic radius of the discharge area above the bed, the relative submerged density, the Darcy-Weisbach friction factor for pipe wall in case of flow of water in a pipe, the Darcy-Weisbach friction factor of clean water flow above the bed, the particle diameter and the terminal settling velocity as input parameters. The exponential equation was chosen because at larger values of the argument it has the same behavior as equation (7.3-52). Both types of equations give the same correlation coefficient of about 0.87. An important difference between the exponential and the power approach is that the exponential equation will have an offset bigger than zero for very small velocities, while the power approach has an offset equal to zero. As a first thought the offset should be the Darcy-Weisbach friction factor based on the particle diameter according to equation (7.3-18). However applying this, reduced the correlation coefficient considerably (see Table 7.3-2). Applying the clean water wall Darcy-Weisbach friction factor, did increase the correlation coefficient to a value of 0.91 when it was multiplied by 0.8. The resulting power equation containing all parameters is:

$$\lambda_{12} = 0.8 \cdot \lambda_1 + 0.036 \cdot \frac{(v_1 - v_2)^{2.462} \cdot d^{0.809}}{R_H^{1.12} \cdot R_{sd}^{0.847} \cdot v_t^{0.461}} \quad \text{with:} \quad \lambda_1 = \frac{1.325}{\left(\ln\left(\frac{0.27 \cdot \varepsilon}{D_H} + \frac{5.75}{Re^{0.9}} \right) \right)^2} \quad \text{(7.3-54)}$$

Adding the clean water Darcy-Weisbach friction factor of the pipe wall to the power term in this equation did not increase the correlation coefficient. Wilson (1988) stated that the bed friction factor of sheet flow does not depend on the particle diameter and thus also not on the terminal settling velocity. To investigate this, the regression was also carried out omitting the particle diameter and the terminal settling velocity. The result is the following equation, which gives a correlation coefficient of 0.90, almost the same as the above equation.

$$\lambda_{12} = 0.8 \cdot \lambda_1 + 0.000527 \cdot \frac{(v_1 - v_2)^{2.422}}{R_H^{1.017} \cdot R_{sd}^{1.474}} \quad \text{or} \quad \lambda_{12} = 0.8 \cdot \lambda_1 + 0.004936 \cdot \frac{Fr^{2.292} \cdot Re^{0.129}}{R_{sd}^{1.474}} \tag{7.3-55}$$

The Darcy-Weisbach friction factors found from the experiments, combined with the predicted Darcy-Weisbach friction factors based on the power equation and the exponential equation are shown in Figure 7.3-12. The coverage of the experimental data point by the predicted data points is reasonable, but sufficient for the purpose of this study. The scatter of the experimental data points is much larger than the predicted data points, which makes sense, because normally a curve fit approach narrows the scatter.

One can question whether the Reynolds numbers should contain the average velocity in the cross section above the bed v_1 or the velocity difference between this average velocity and the bed velocity (v_1-v_2). However since the experiments used were carried out with a stationary bed, v_2 was zero, so it does not make a difference here.

Table 7.3-2: Correlation coefficient for friction-factor correlations.

Equation	Value of correlation coefficient	Remarks
Exponential	0.914	With particle parameters
Exponential	0.906	Without particle parameters
Power (equation (7.3-54))	0.911	With particle parameters
Power (equation (7.3-55))	0.893	Without particle parameters
Dimensionless (eqn. (7.3-56))	0.864	Without particle parameters
Dimensionless (eqn. (7.3-57))	0.909	With particle parameters

Figure 7.3-13 shows the predicted versus the measured Darcy-Weisbach bed friction factors. In order to compare the resulting equations with the original equation of Wilson (1988), the relative roughness based on the bed associated hydraulic radius has been determined for the original data and for the power and the exponential equations. The result is shown in Figure 7.3-14. The power fit and exponential fit give the same image as the original data. The data points with very high Shields numbers are from Bisschop et al. (2014) with velocities above the stationary bed up to 6 m/s. Equation (7.3-55) is also shown in dimensionless notation as a function of the Froude number, the Reynolds number and the relative submerged density. The dependency on the Reynolds number is weak and on the relative submerged density a bit more than half the power of the Froude number. To simplify the equation, the Froude number as used by Durand & Condolios (1952) can be used. After re-evaluating (optimizing) the first term in the equation for the highest correlation coefficient leading to a factor 0.7, this gives:

$$\lambda_{12} = 0.7 \cdot \lambda_1 + 0.0476 \cdot \left(\frac{(v_1 - v_2)}{\sqrt{2 \cdot g \cdot D_H \cdot R_{sd}}} \right)^{2.58} = 0.7 \cdot \lambda_1 + 0.0476 \cdot Fr_{DC}^{2.58} \tag{7.3-56}$$

The correlation coefficient for this equation is 0.865, a bit less than the 0.9 of the previous equation, but still acceptable (Miedema & Matousek (2014)).

Finally the idea came up that in a sheet flow layer the energy losses do not only depend on the submerged weight of the particles, but kinetic energy losses will also depend on the mass of the particles. To add a dimensionless term including the particle mass, the mass of the particle m_p is divided by the weight of 1 m³ of the carrier liquid. Miedema & Ramsdell (2014) found the following equation:

$$\lambda_{12} = 0.83 \cdot \lambda_1 + 0.37 \cdot \left(\frac{(v_1 - v_2)}{\sqrt{2 \cdot g \cdot D_H \cdot R_{sd}}} \right)^{2.73} \cdot \left(\frac{\rho_s \cdot \frac{\pi}{6} \cdot d^3}{\rho_l \cdot 1^3} \right)^{0.094} = 0.83 \cdot \lambda_1 + 0.37 \cdot Fr_{DC}^{2.73} \cdot \left(\frac{m_p}{\rho_l} \right)^{0.094} \tag{7.3-57}$$
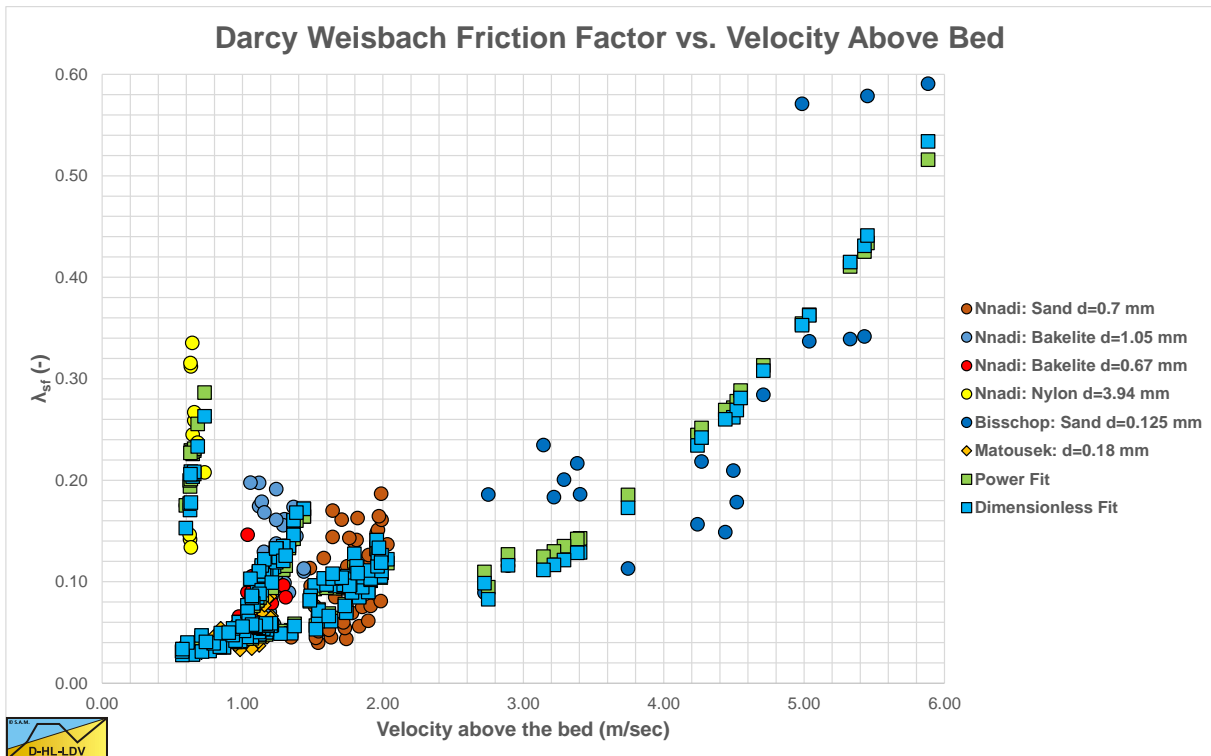
Figure 7.3-12: The measured and predicted Darcy-Weisbach friction factors.
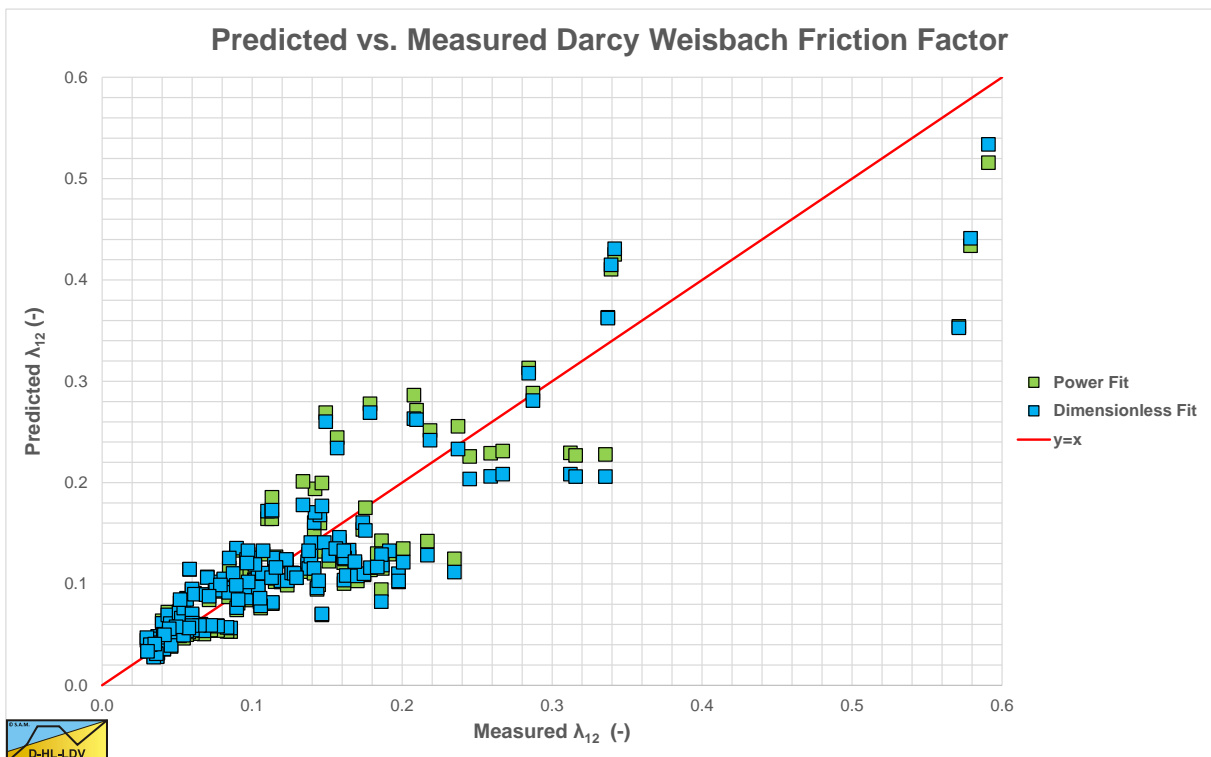
Figure 7.3-13: The measured versus the predicted Darcy-Weisbach bed friction factors.
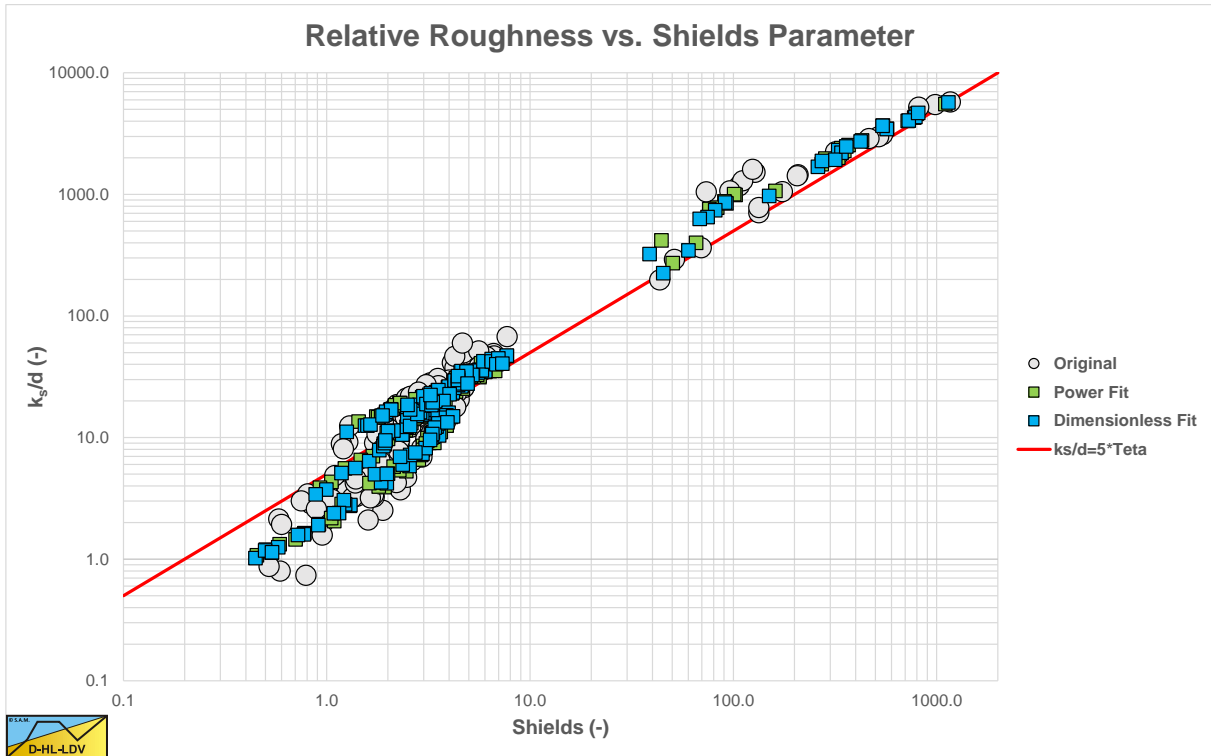
Figure 7.3-14: The apparent relative roughness versus the Shields parameter.
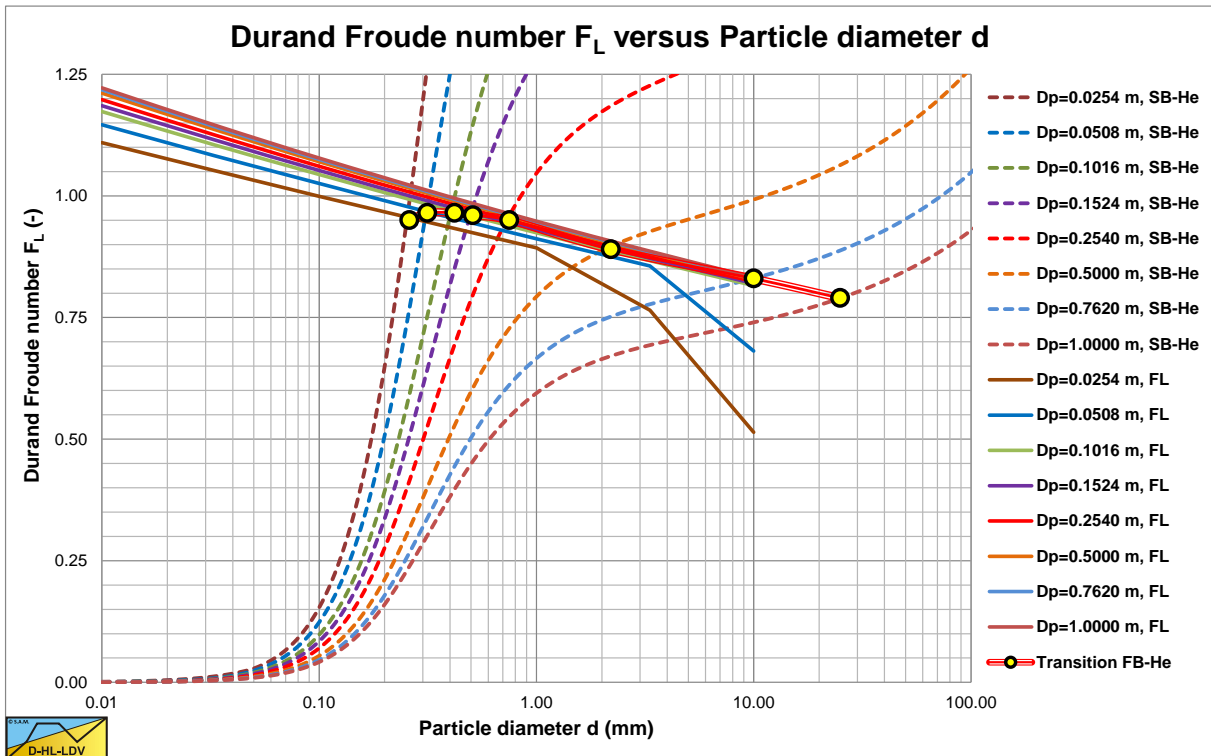
Figure 7.3-15: The resulting Durand Froude number curves and
transition sliding bed-heterogeneous regime curves.

Figure 7.3-15 shows the resulting Durand Froude number maximum LSDV curves, without the effect of suspended particles. Also the curves showing the theoretical transition between the sliding bed regime and the heterogeneous regime are shown. If this curve is below the LSDV curve, the stationary bed will transit directly to the heterogeneous regime. If the curve is above the LSDV curve, there will be a sliding bed. The LSDV curves can be approximated with the following equation:

$$F_L = 0.947 \cdot d^{-0.056 \cdot D_p^{0.05}} \cdot \ln\left(e \cdot D_p^{0.014}\right) = 0.947 \cdot d^{-0.056 \cdot D_p^{0.05}} \cdot \left(1 + 0.014 \cdot \ln\left(D_p\right)\right) \tag{7.3-58}$$

The graph and the equation assume that all particles are in the bed, resulting in decreasing curves. This makes sense, since smaller particles resulting in a smaller bed friction, so the velocity where the bed starts sliding, the LSDV, decreases with increasing particle diameter.

Since both the wall shear stress and the bed interface shear stress depend linear on the liquid density and the velocity above the bed squared, a higher liquid density resulting from a smaller stratification ratio, will result in a smaller LSDV, ignoring viscosity effects. An additional effect is the decrease of the relative submerged density with increasing liquid density. This decrease in relative submerged density results in a decrease of the weight of the bed and thus of the sliding friction force. Resulting in a lower LSDV. Including the viscosity effect reduces the Reynolds number and increases the Darcy Weisbach friction factor, reducing the LSDV even more. All these effects however are not enough to reproduce the strong decrease of the LSDV with decreasing particle diameter of the famous Wilson et al. (2006) demi McDonald.

7.3.8 Conclusions & Discussion.

The goal of this study, finding an explicit relation between the bed Darcy-Weisbach friction factor and the known variables has been reached. Four equations have been found by regression, the first one based on 6 variables, the second and third based on 4 variables and the fourth again based on 6 variables. The 7 variables involved are the velocity difference between the bed and the flow above the bed u, the hydraulic radius of the flow above the bed R_H, the relative submerged density R_{sd}, the particle diameter d, the terminal settling velocity of the particles v_t, the mass of the particle m_p and the wall Darcy-Weisbach friction factor λ_1. The second equation is independent on the particle related variables, the particle diameter d and the terminal settling velocity v_t. Both equations have about the same correlation coefficient, 0.91 and 0.90. This supports the hypothesis of Wilson (1988) that the excess head losses due to sheet flow hardly depend on the particle related variables.

It should be considered however that the bed Darcy-Weisbach friction factor λ_{12} is determined from the hydraulic gradient, keeping the wall Darcy-Weisbach friction factor λ_1 constant based on clean water flow and the pipe wall roughness. So all the additional head losses are considered to be caused by the increasing bed Darcy-Weisbach friction factor. In reality, the sheet flow will also influence the wall Darcy-Weisbach friction factor, especially at high velocities where the sheet flow may reach or almost reach the wall. For the purpose of determining hydraulic gradients this is not to relevant if the sheet flow is considered a black box with inputs (v_1-v_2), R_H, R_{sd}, d, v_t and λ_1 and an output λ_{12}. However if the internal structure of the sheet flow has to be known in order to determine for example the delivered concentration, the equations may not be sufficient.

Matousek (2009) uses the internal structure in his head loss model to determine the delivered concentration. Miedema & Ramsdell (2013) based their model on the spatial concentration, using a holdup function to determine the delivered concentration (not yet published).

At first 4 equations were derived, exponential and power, with and without particle related variables. The correlation coefficients did not differ much. The author has chosen to use the two power equations in this chapter because of the applicability in their models.

Based on the two resulting equations the conclusion can be drawn that the bed Darcy-Weisbach friction factor depends on the wall Darcy-Weisbach friction factor at low velocities, depends weakly on the particle related variables, depends strongly on the velocity difference between bed and flow above the bed with a power of about 2.4-2.5, depends reversely proportional on the hydraulic radius of the discharge area above the bed to a power of about 1 and depends reversely proportional on the relative submerged density of the solids to a power of about 1.5. A further simplification, using the Durand & Condolios (1952) Froude number to the power 2.58 still gives an acceptable correlation coefficient. Adding the mass of the particle m_p to the equation increases the correlation coefficient to about 0.91, which seems to be the maximum achievable with the given dataset. This last equation (7.3-57) is the equation used in the DHLLDV Framework.

Showing the measured and predicted data in the k_s/d versus Shields parameter coordinate system, Figure 7.3-14, leads to the conclusion that the predicted k_s/d values match equation (7.3-35) well. Although at small values (up to about 2) of the Shields parameter equation (7.3-35) overestimates the k_s/d values, while at larger values of the Shields parameter equation (7.3-35) underestimates the k_s/d values. But this was already the case with the original experimental data of Nnadi & Wilson (1992).

The resulting equations are satisfying, but the coefficients and powers will probably change slightly if more experimental data is available. The resulting equations are derived for rectangular cross sections. Circular cross section may also result in different coefficients and powers, however some first tests on limited data show similar tendencies.

7.3.9 Nomenclature Fixed Bed Regime.

A_p	Cross section pipe	m^2
A_1	Cross section above bed	m^2
A_2	Cross section bed	m^2
C_{vb}	Volumetric bed concentration	-
C_{vs}	Spatial volumetric concentration	-
C_{vr}	Relative spatial volumetric concentration	-
d	Particle diameter	m
D_H	Hydraulic diameter	m
D_p	Pipe diameter	m
E_{rhg}	Relative excess hydraulic gradient	-
F	Force	kN
$F_{1,l}$	Force between liquid and pipe wall	kN
$F_{12,l}$	Force between liquid and bed	kN
$F_{2,pr}$	Force on bed due to pressure	kN
$F_{2,sf}$	Force on bed due to friction	kN
$F_{2,l}$	Force on bed due to pore liquid	kN
Fr	Froude number	-
Fr_{DC}	Durand Froude number	-
g	Gravitational constant 9.81	m/s^2
i_l	Hydraulic gradient liquid	-
i_m	Hydraulic gradient mixture	-
i_{plug}	Hydraulic gradient plug flow	-
k_s	Bed roughness (input=measured versus calculated=predicted)	m
ΔL	Length of pipe section	m
n	Porosity	-
O_p	Circumference pipe	m
O_1	Circumference pipe above bed	m
O_2	Circumference pipe in bed	m
O_{12}	Width of bed	m
p	Pressure	kPa
Δp	Pressure difference	kPa
Δp_1	Pressure difference cross-section 1	kPa
Δp_2	Pressure difference cross-section 2	kPa
Δp_m	Pressure difference mixture	kPa
Re	Reynolds number	-
R_{sd}	Relative submerged density	-
R	Bed associated radius	m
R_H	Hydraulic radius	m
u_*	Friction velocity	m/s
v	Velocity	m/s
v_r	Relative velocity	-
$v_{1,m}$	Velocity in cross-section 1	m/s
$v_{2,m}$	Velocity in cross-section 2	m/s
v_t	Terminal settling velocity	m/s
v_{t*}	Dimensionless terminal settling velocity	-
v_{ls}	Line speed	m/s
v_1	Velocity above bed	m/s
v_2	Velocity bed	m/s
α	Multiplication factor	-
β	Bed angle	rad
ε	Pipe wall roughness	m
κ	Von Karman constant (0.4)	-
ρ_l	Density carrier liquid	ton/m^3
ρ_s	Density solids	ton/m^3
θ	Shields parameter	-
θ_{cr}	Critical Shields parameter	-

λ	Darcy-Weisbach friction factor	-
λ_l	Darcy-Weisbach friction factor liquid-pipe wall	-
λ_1	Darcy-Weisbach friction factor with pipe wall	-
λ_2	Darcy-Weisbach friction factor with pipe wall	-
λ_{12}	Darcy-Weisbach friction factor on the bed	-
ν_l	Kinematic viscosity	m^2/s
τ	Shear stress	kPa
τ_l	Shear stress liquid-pipe wall	kPa
$\tau_{1,l}$	Shear stress liquid-pipe above bed	kPa
$\tau_{12,l}$	Shear stress bed-liquid	kPa
$\tau_{2,l}$	Shear stress liquid-pipe in bed	kPa
$\tau_{2,sf}$	Shear stress from sliding friction	kPa
μ_{sf}	Sliding friction coefficient	-

7.4 A Head Loss Model for Sliding Bed Slurry Transport.
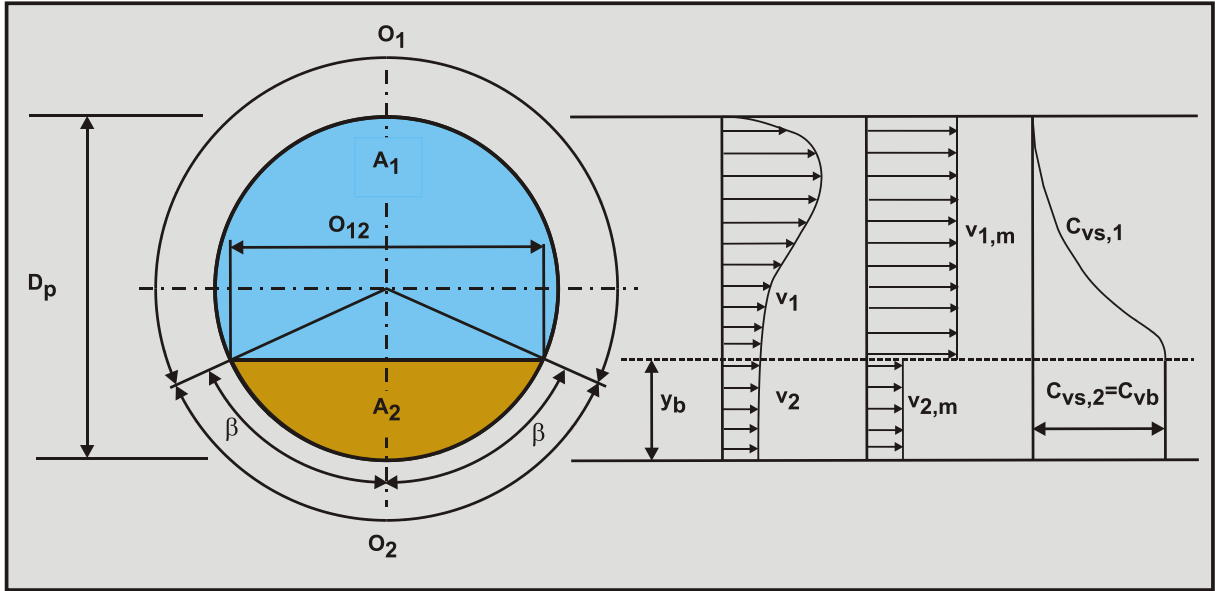
Figure 7.4-1: Definitions of sliding bed transport.

7.4.1 The Friction Force on the Pipe Wall.

The friction force $\mathbf{F_{sf}}$ between the bed and the pipe wall equals the normal force $\mathbf{F_n}$ on the pipe wall times the friction coefficient $\mathbf{\mu_{sf}}$, giving:

$$\mathbf{F_{sf}} = \mathbf{\mu_{sf}} \cdot \mathbf{F_n} \tag{7.4-1}$$

The normal force $\mathbf{F_n}$ on the pipe wall is the normal stress $\mathbf{\sigma_n}$ on the pipe wall, integrated over the contact angle $\mathbf{\beta}$ of the bed with the pipe wall.

$$\mathbf{F_n} = \Delta \mathbf{L} \cdot \int_{-\beta}^{\beta} \mathbf{\sigma_n} \cdot \mathbf{R} \cdot \mathbf{d\alpha} = \Delta \mathbf{L} \cdot \frac{\mathbf{D_p}}{\mathbf{2}} \cdot \int_{-\beta}^{\beta} \mathbf{\sigma_n} \cdot \mathbf{d\alpha} = \Delta \mathbf{L} \cdot \mathbf{D_p} \cdot \int_{0}^{\beta} \mathbf{\sigma_n} \cdot \mathbf{d\alpha} \tag{7.4-2}$$

The vertical stress $\mathbf{\sigma_v}$ at an angle $\mathbf{\alpha}$ with the vertical can be derived from the height of the bed $\mathbf{h_b}$ at that location for $\mathbf{\beta \leq \pi/2}$ according to Figure 7.4-2:

$$\mathbf{h_b} = \mathbf{R} \cdot \left(\cos(\alpha) - \cos(\beta) \right) = \frac{\mathbf{D_p}}{\mathbf{2}} \cdot \left(\cos(\alpha) - \cos(\beta) \right) \tag{7.4-3}$$

The vertical stress $\mathbf{\sigma_v}$ is the submerged weight per unit of area at the specific location at the pipe wall.

$$\mathbf{\sigma_v} = \mathbf{\rho_l} \cdot \mathbf{g} \cdot \mathbf{R_{sd}} \cdot \mathbf{C_{vb}} \cdot \frac{\mathbf{D_p}}{\mathbf{2}} \cdot \left(\cos(\alpha) - \cos(\beta) \right) \tag{7.4-4}$$

It should be mentioned that the height $\mathbf{h_b}$ is different for an angle $\mathbf{\beta > \pi/2}$. For $\mathbf{\beta > \pi/2}$ there are two cases.

For $\mathbf{0 \leq \alpha < \pi - \beta}$ the vertical stress is based on the distance from the pipe wall at angle $\mathbf{\alpha}$ to the free surface of the bed according to Figure 7.4-7, giving for the height of the bed column:

$$\mathbf{h_b} = \mathbf{R} \cdot \left(\cos(\alpha) - \cos(\beta) \right) = \frac{\mathbf{D_p}}{\mathbf{2}} \cdot \left(\cos(\alpha) - \cos(\beta) \right) \tag{7.4-5}$$

And for the vertical normal stress:

$$\sigma_v = \rho_l \cdot g \cdot R_{sd} \cdot C_{vb} \cdot \left(\cos(\alpha) - \cos(\beta)\right) \cdot \frac{D_p}{2} \qquad (7.4\text{-}6)$$
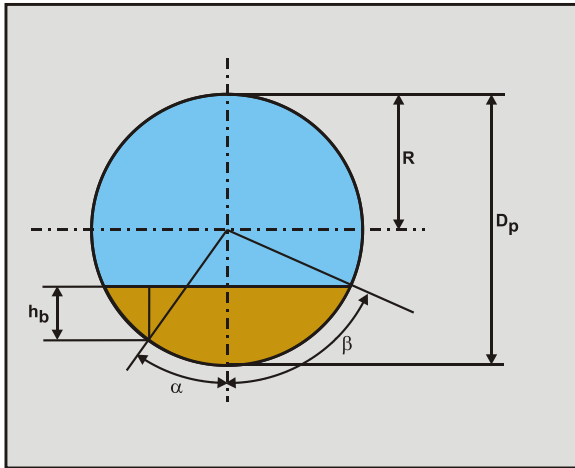
Figure 7.4-2: The location of an element at the pipe wall and the height of the bed column.
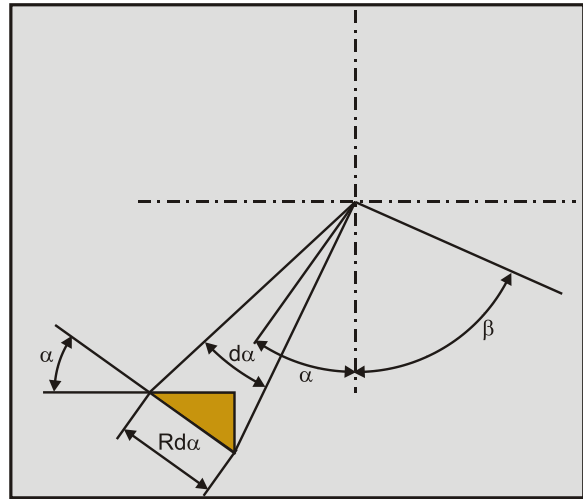
Figure 7.4-3: An element at the pipe wall.
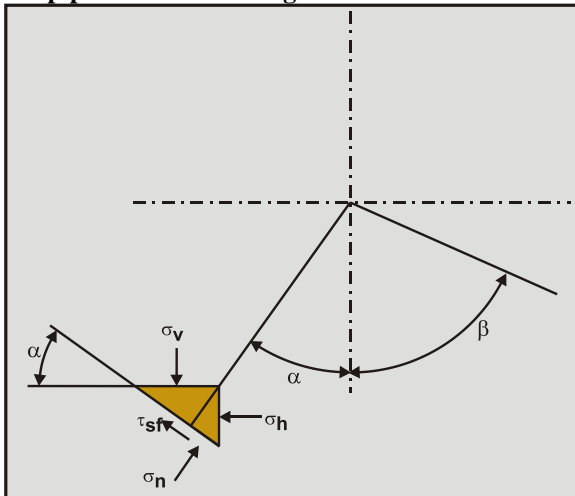
Figure 7.4-4: The stresses at and near the pipe wall.
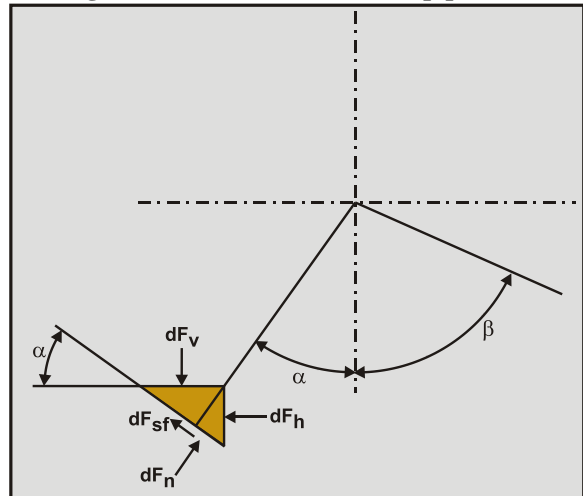
Figure 7.4-5: The forces at and near the pipe wall.

For **π-β<α<π/2** the normal stress is based on the two times distance from the pipe wall at angle **α** to the center line of the pipe according to Figure 7.4-6, giving for the height of the bed column:

$$h_b = 2 \cdot R \cdot \cos(\alpha) = D_p \cdot \cos(\alpha) \qquad (7.4\text{-}7)$$

And for the vertical normal stress:

$$\sigma_v = \rho_l \cdot g \cdot R_{sd} \cdot C_{vb} \cdot 2 \cdot \cos(\alpha) \cdot \frac{D_p}{2} \qquad (7.4\text{-}8)$$

On the bed element at the pipe wall (Figure 7.4-5) there has to be an equilibrium of forces in the horizontal and in the vertical direction, thus for the vertical direction.

$$dF_n \cdot \cos(\alpha) + dF_{sf} \cdot \sin(\alpha) = dF_v \qquad (7.4\text{-}9)$$

For the horizontal direction this gives:

$$\mathbf{dF_n \cdot \sin(\alpha) - dF_{sf} \cdot \cos(\alpha) = dF_h}$$

(7.4-10)

In terms of stresses this gives for the vertical equilibrium:

$$\mathbf{\sigma_n \cdot \cos(\alpha) \cdot R \cdot d\alpha + \tau_{sf} \cdot \sin(\alpha) \cdot R \cdot d\alpha = \sigma_v \cdot R \cdot d\alpha \cdot \cos(\alpha)}$$

(7.4-11)

For the horizontal equilibrium this gives:

$$\mathbf{\sigma_n \cdot \sin(\alpha) \cdot R \cdot d\alpha - \tau_{sf} \cdot \cos(\alpha) \cdot R \cdot d\alpha = \sigma_h \cdot R \cdot d\alpha \cdot \sin(\alpha)}$$

(7.4-12)

With the relation between the normal stress and the shear stress:

$$\mathbf{\tau_{sf} = \mu_{sf,e} \cdot \sigma_n}$$

(7.4-13)

This gives for the vertical equilibrium:

$$\mathbf{\sigma_n \cdot \left(\cos(\alpha) + \mu_{sf,e} \cdot \sin(\alpha)\right) \cdot R \cdot d\alpha = \sigma_v \cdot R \cdot d\alpha \cdot \cos(\alpha)}$$

(7.4-14)

For the horizontal equilibrium this gives:

$$\mathbf{\sigma_n \cdot \left(\sin(\alpha) - \mu_{sf,e} \cdot \cos(\alpha)\right) \cdot R \cdot d\alpha = \sigma_h \cdot R \cdot d\alpha \cdot \sin(\alpha)}$$

(7.4-15)

Since friction is always in the opposite direction of the interface velocity, 3 cases can be distinguished:
1. The bed is stationary and the liquid above the bed is also stationary. Since there is no velocity in any direction, the friction can be mobilized between 0 and a maximum value in any direction, counteracting forces that may occur. Since in this case the only force is the gravitational force, there may be friction between the bed and the pipe wall counteracting gravity with a maximum of $\mathbf{\mu_{sf,e} = \mu_{sf}}$.
2. The bed is stationary, but the liquid above the bed has a certain velocity resulting in a shear stress and thus shear force on the bed. There will be a friction force between the bed and the pipe wall counteracting the shear force on the bed, but this does not mean the friction is fully mobilized. There may still be some friction capacity left counteracting gravity in the cross section of the pipe.
3. The bed is sliding. The friction force on the bed is opposite to the velocity of the bed. There is no friction mobilized in the cross section of the pipe, so $\mathbf{\mu_{sf,e} = 0}$.

When the line speed increases from 0 m/sec to a line speed above the Limit of Stationary Deposit Velocity, the friction undergoes a transition from mobilization in the cross section of the pipe counteracting gravity, to mobilization in the longitudinal direction of the pipe counteracting shear and pressure. Since the effective mobilized friction is only known in the case of a sliding bed, first a generic solution will be derived for the normal force between the bed and the pipe wall, taking into consideration that the integrated vertical components of the normal force and the wall friction force should always be equal to the weight of the bed.

7.4.2 The Active/Passive Soil Failure Approach.

Given a vertical stress $\mathbf{\sigma_v}$ at the pipe wall according to equation (7.4-4) for the case where $\mathbf{\beta \leq \pi/2}$ and equations (7.4-6) and (7.4-8) for the case where $\mathbf{\beta > \pi/2}$ and considering that the vertical stress $\mathbf{\sigma_v}$ is only present in the bottom half of the pipe, it can be assumed that the horizontal stress $\mathbf{\sigma_h}$ is a factor $\mathbf{K}$ times the vertical stress $\mathbf{\sigma_v}$. According to soil mechanics, this factor $\mathbf{K}$ should be in between the factor for active failure $\mathbf{K_a}$ and the factor for passive failure $\mathbf{K_p}$. These two factors depend on the angle of internal friction of the sand bed $\mathbf{\varphi}$, which for a loose packed bed will have a value near 30º. The $\mathbf{K_a}$ value is 1/3 and the $\mathbf{K_p}$ value 3 for an internal friction angle of 30º. The $\mathbf{K}$ value cannot be smaller than $\mathbf{K_a}$ or bigger than $\mathbf{K_p}$.

The coefficients for active $\mathbf{K_a}$ and passive $\mathbf{K_p}$ failure are:

$$K_a = \frac{1-\sin(\varphi)}{1+\sin(\varphi)} \quad \text{and} \quad K_p = \frac{1+\sin(\varphi)}{1-\sin(\varphi)} \tag{7.4-16}$$

This gives for the horizontal stress $\boldsymbol{\sigma_h}$ near the pipe wall:

$$\sigma_h = K \cdot \sigma_v \tag{7.4-17}$$

The forces on an element $\mathbf{R \cdot d\alpha}$ on the pipe wall per unit of pipe length are now:

$$\mathbf{dF_v = \sigma_v \cdot \cos(\alpha) \cdot R \cdot d\alpha \cdot \Delta L} \tag{7.4-18}$$
$$\mathbf{dF_h = \sigma_h \cdot \sin(\alpha) \cdot R \cdot d\alpha \cdot \Delta L} \tag{7.4-19}$$

The components of these forces normal to the pipe wall are:

$$\mathbf{dF_{v,n} = \sigma_v \cdot \cos(\alpha) \cdot R \cdot d\alpha \cdot \cos(\alpha) \cdot \Delta L} \tag{7.4-20}$$
$$\mathbf{dF_{h,n} = \sigma_h \cdot \sin(\alpha) \cdot R \cdot d\alpha \cdot \sin(\alpha) \cdot \Delta L} \tag{7.4-21}$$

This gives for the normal force on an element $\mathbf{R \cdot d\alpha}$ on the pipe wall:

$$\mathbf{dF_n = dF_{v,n} + dF_{h,n} = \sigma_v \cdot \cos^2(\alpha) \cdot R \cdot d\alpha \cdot \Delta L + \sigma_h \cdot \sin^2(\alpha) \cdot R \cdot d\alpha \cdot \Delta L} \tag{7.4-22}$$

Substituting equation (7.4-17) gives:

$$\mathbf{dF_n = dF_{v,n} + dF_{h,n} = \sigma_v \cdot \left(\cos^2(\alpha) + K \cdot \sin^2(\alpha) \right) \cdot R \cdot d\alpha \cdot \Delta L} \tag{7.4-23}$$

The normal stress on the pipe wall is now:

$$\mathbf{\sigma_n = \frac{dF_n}{R \cdot d\alpha \cdot \Delta L} = \frac{dF_{v,n} + dF_{h,n}}{R \cdot d\alpha \cdot \Delta L} = \sigma_v \cdot \left(\cos^2(\alpha) + K \cdot \sin^2(\alpha) \right)} \tag{7.4-24}$$

To determine the total normal force $\mathbf{F_n}$ on the pipe wall, this normal stress has to be integrated. Two cases have to be considered. The first case considers a bed which occupies less than or equal to 50% of the pipe, so $\boldsymbol{\beta \leq \pi/2}$. The second case considers a bed which occupies more than 50% of the pipe, so $\boldsymbol{\beta > \pi/2}$.

Case 1: $\boldsymbol{\beta \leq \pi/2}$

For $\boldsymbol{0 \leq \alpha < \beta}$ the normal stress is based on the distance from the pipe wall at angle $\boldsymbol{\alpha}$ to the free surface of the bed as is shown in Figure 7.4-2, giving:

$$\mathbf{\sigma_n = \rho_l \cdot R_{sd} \cdot g \cdot C_{vb} \cdot R \cdot \left(\cos(\alpha) - \cos(\beta) \right) \cdot \left(K \cdot \sin^2(\alpha) + \cos^2(\alpha) \right)} \tag{7.4-25}$$

Integrating from $\boldsymbol{\alpha=0}$ to $\boldsymbol{\alpha=\beta}$ and multiplying by 2 for the left and right side gives for the normal force:

$$\mathbf{F_n = 2 \cdot \rho_l \cdot R_{sd} \cdot g \cdot C_{vb} \cdot R^2 \cdot \int_0^\beta \left(\cos(\alpha) - \cos(\beta) \right) \cdot \left(K \cdot \sin^2(\alpha) + \cos^2(\alpha) \right) \cdot d\alpha \cdot \Delta L} \tag{7.4-26}$$

Substituting the upper and lower boundary gives:

$$F_n = 2 \cdot \rho_l \cdot R_{sd} \cdot g \cdot C_{vb} \cdot R^2 \cdot \left(\frac{K-1}{3} \cdot \sin^3(\beta) + \sin(\beta) - \frac{K+1}{2} \cdot \beta \cdot \cos(\beta) + \frac{K-1}{2} \cdot \sin(\beta) \cdot \cos^2(\beta) \right) \cdot \Delta L$$

(7.4-27)

Case 2: β>π/2
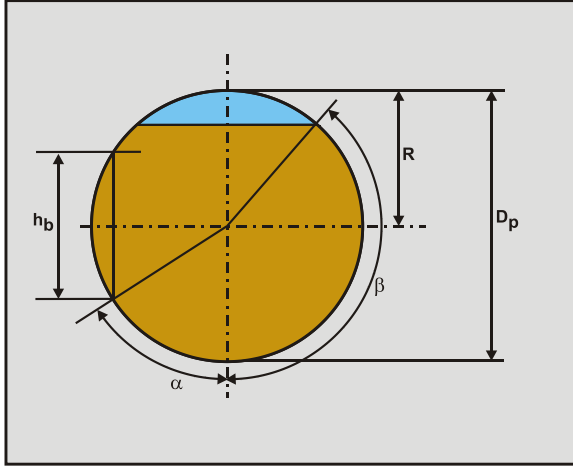
Figure 7.4-6: The height of the bed column for π-β<α<π/2.
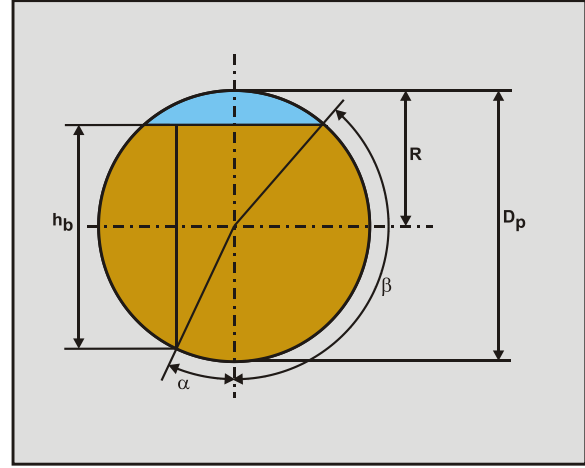
Figure 7.4-7: The height of the bed column for 0≤α<π-β.

For **0≤α<π-β** the normal stress is based on the distance from the pipe wall at angle **α** to the free surface of the bed, giving:

$$\sigma_n = \rho_l \cdot R_{sd} \cdot g \cdot C_{vb} \cdot R \cdot \left(\cos(\alpha) - \cos(\beta) \right) \cdot \left(K \cdot \sin^2(\alpha) + \cos^2(\alpha) \right)$$

(7.4-28)

For **π-β<α<π/2** the normal stress is based on the two times distance from the pipe wall at angle **α** to the center line of the pipe, giving:

$$\sigma_n = \rho_l \cdot R_{sd} \cdot g \cdot C_{vb} \cdot R \cdot 2 \cdot \cos(\alpha) \cdot \left(K \cdot \sin^2(\alpha) + \cos^2(\alpha) \right)$$

(7.4-29)

Integrating from **α=0** to **α= π/2** gives for the normal force:

$$F_n = 2 \cdot \rho_l \cdot R_{sd} \cdot g \cdot C_{vb} \cdot R^2 \cdot \int_0^{\pi-\beta} \left(\cos(\alpha) - \cos(\beta) \right) \cdot \left(K \cdot \sin^2(\alpha) + \cos^2(\alpha) \right) \cdot d\alpha \cdot \Delta L$$

(7.4-30)

$$+ 2 \cdot \rho_l \cdot R_{sd} \cdot g \cdot C_{vb} \cdot R^2 \cdot \int_{\pi-\beta}^{\pi/2} 2 \cdot \cos(\alpha) \cdot \left(K \cdot \sin^2(\alpha) + \cos^2(\alpha) \right) \cdot d\alpha \cdot \Delta L$$

Substituting the upper and lower boundaries gives:

$$F_n = 2 \cdot \rho_l \cdot R_{sd} \cdot g \cdot C_{vb} \cdot R^2 \cdot \Delta L \cdot \left(\begin{array}{c} \frac{K-1}{3} \cdot \sin^3(\beta) + \sin(\beta) - \frac{K+1}{2} \cdot (\pi - \beta) \cdot \cos(\beta) - \frac{K-1}{2} \cdot \sin(\beta) \cdot \cos^2(\beta) \\ \\ + \frac{2}{3} \cdot (K-1) + 2 - \frac{2}{3} \cdot (K-1) \cdot \sin^3(\beta) - 2 \cdot \sin(\beta) \end{array} \right)$$

(7.4-31)

Figure 7.4-8 Shows the results of equations (7.4-27) and (7.4-31) for the cases of active failure $\mathbf{K=K_a}$, passive failure $\mathbf{K=K_p}$ and neutral $\mathbf{K=1}$ for an angle of internal friction of $\boldsymbol{\varphi=27.5^o}$. The figure also shows the weight of the bed and the ratio between the normal force and the weight for all cases.
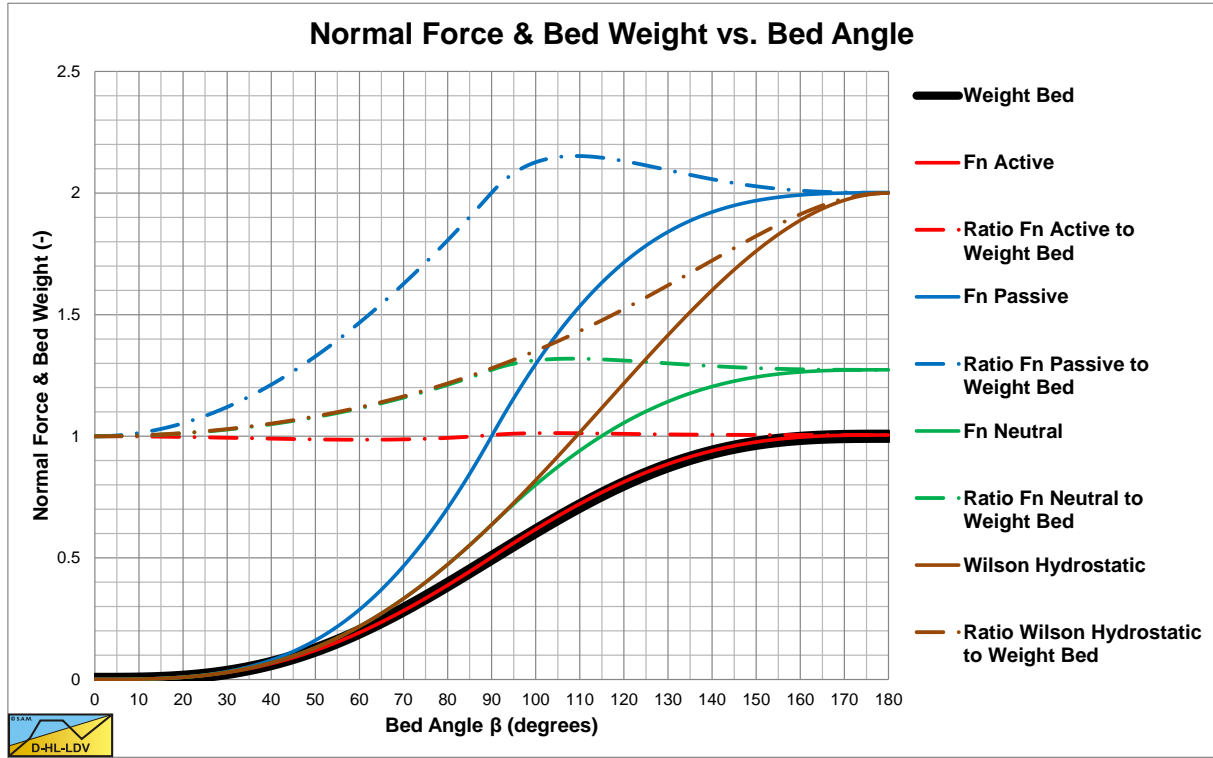
Figure 7.4-8: The normal force in relation to the bed fraction and the bed angle ($\varphi=27.5^o$).

The components of these forces tangent to the pipe wall are:

$$\mathbf{dF_{v,t} = \sigma_v \cdot \cos(\alpha) \cdot R \cdot d\alpha \cdot \sin(\alpha) \cdot \Delta L} \tag{7.4-32}$$

$$\mathbf{dF_{h,t} = -\sigma_h \cdot \sin(\alpha) \cdot R \cdot d\alpha \cdot \cos(\alpha) \cdot \Delta L} \tag{7.4-33}$$

This gives for the tangent force on an element $\mathbf{R \cdot d\alpha}$ on the pipe wall:

$$\mathbf{dF_t = dF_{v,t} + dF_{h,t} = \sigma_v \cdot \sin(\alpha) \cdot \cos(\alpha) \cdot R \cdot d\alpha \cdot \Delta L - \sigma_h \cdot \sin(\alpha) \cdot \cos(\alpha) \cdot R \cdot d\alpha \cdot \Delta L} \tag{7.4-34}$$

Substituting equation (7.4-17) gives:

$$\mathbf{dF_t = dF_{v,t} + dF_{h,t} = \sigma_v \cdot \sin(\alpha) \cdot \cos(\alpha) \cdot (1-K) \cdot R \cdot d\alpha \cdot \Delta L} \tag{7.4-35}$$

The tangential or friction stress on the pipe wall is now:

$$\mathbf{\tau_{sf} = \tau_t = \frac{dF_t}{R \cdot d\alpha \cdot \Delta L} = \frac{dF_{v,t} + dF_{h,t}}{R \cdot d\alpha \cdot \Delta L} = \sigma_v \cdot \sin(\alpha) \cdot \cos(\alpha) \cdot (1-K) = \mu_{sf,e} \cdot \sigma_n} \tag{7.4-36}$$

With:

$$\mathbf{\sigma_n = \frac{dF_n}{R \cdot d\alpha \cdot \Delta L} = \frac{dF_{v,n} + dF_{h,n}}{R \cdot d\alpha \cdot \Delta L} = \sigma_v \cdot \left(\cos^2(\alpha) + K \cdot \sin^2(\alpha)\right)} \tag{7.4-37}$$

Giving:

$$\sin(\alpha) \cdot \cos(\alpha) \cdot (1-K) = \mu_{sf,e} \cdot \left(\cos^2(\alpha) + K \cdot \sin^2(\alpha)\right)$$

(7.4-38)

The **K** factor is related to the wall friction coefficient according to:

$$K = \frac{\sin(\alpha) \cdot \cos(\alpha) - \mu_{sf,e} \cdot \cos^2(\alpha)}{\sin(\alpha) \cdot \cos(\alpha) + \mu_{sf,e} \cdot \sin^2(\alpha)}$$

(7.4-39)

In the case of a sliding bed, there is no friction in the cross section of the pipe (Figure 7.4-4), so the only solution is **K=1**, which is the neutral curve for the normal force **F_n** as a function of the angle **β** in Figure 7.4-8. In the case of a stationary bed, the relation between the factor **K** and the effective sliding friction coefficient **$\mu_{sf,e}$** depends on the angle **α**, no general solution exists. **K=1** will simplify the equations and also appears to be to correct value for **K** to ensure that the vertical component of the normal stress will carry the submerged weight of the bed. The resulting normal force **F_n** is bigger than the weight of the bed, starting with a factor 1 for a **β=0**, increasing to a factor of 1.27 at **β=π/2,** increasing to a maximum of 1.32 at **β=0.6·π** and after that decreasing slowly to 1.27 at **β=π.** So above **β=π/2** the factor is almost constant with an average value of 1.293.

7.4.3   The Hydrostatic Normal Stress Distribution Approach.
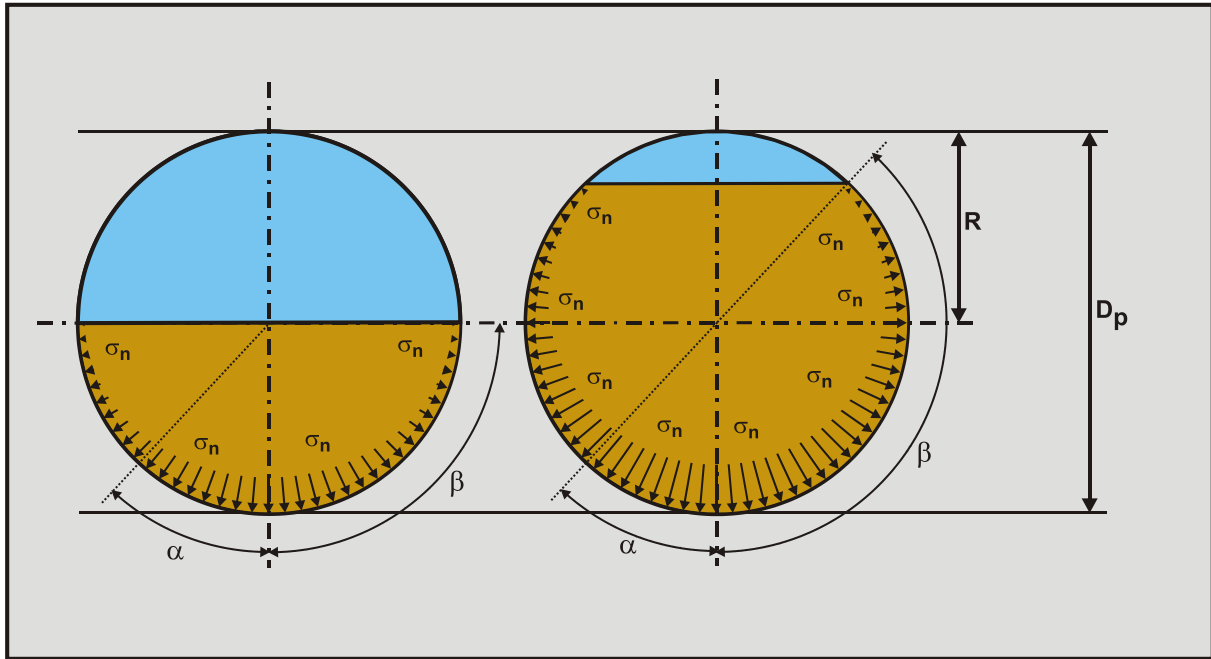
Figure 7.4-9: The hydrostatic normal stress distribution according to Wilson et al. (1992).

Wilson et al. (1992) assume a hydrostatic normal stress distribution on the pipe wall as if the bed was a liquid as is shown in Figure 7.4-9. The left picture shows the normal stress distribution up to a bed angle **β** of **π/2**, the right picture for **β > π/2**. The normal stress as a function of the angle **α**, given a bed angle **β** can be expressed by:

$$\sigma_n = \rho_l \cdot g \cdot R_{sd} \cdot C_{vb} \cdot \frac{D_p}{2} \cdot \left(\cos(\alpha) - \cos(\beta)\right)$$

(7.4-40)

This is different from the assumption that the friction force **F_{sf}** equals the submerged weight **F_W** times the sliding friction coefficient **μ_{sf}**.

The total normal force **F_N** follows from integration of the normal stress:

$$F_n = \Delta L \cdot \int_{-\beta}^{\beta} \sigma_n \cdot R \cdot d\alpha = 2 \cdot \Delta L \cdot \int_{0}^{\beta} \rho_l \cdot g \cdot R_{sd} \cdot C_{vb} \cdot \frac{D_p^2}{4} \cdot \left(\cos(\alpha) - \cos(\beta)\right) \cdot d\alpha$$

$$= \rho_l \cdot g \cdot \Delta L \cdot R_{sd} \cdot C_{vb} \cdot \frac{D_p^2}{2} \cdot \int_{0}^{\beta} \left(\cos(\alpha) - \cos(\beta)\right) \cdot d\alpha$$

(7.4-41)

This gives for the normal force F_N:

$$F_n = \rho_l \cdot g \cdot \Delta L \cdot R_{sd} \cdot C_{vb} \cdot \frac{D_p^2}{2} \cdot \left(\sin(\beta) - \beta \cdot \cos(\beta)\right)$$

(7.4-42)

So the sliding friction force is:

$$F_{sf} = 2 \cdot \mu_{sf} \cdot \rho_l \cdot g \cdot \Delta L \cdot R_{sd} \cdot C_{vb} \cdot A_p \cdot \frac{\left(\sin(\beta) - \beta \cdot \cos(\beta)\right)}{\pi}$$

(7.4-43)

The submerged weight of the bed F_w is given by:

$$F_w = \rho_l \cdot g \cdot \Delta L \cdot R_{sd} \cdot C_{vb} \cdot A_p \cdot \frac{\left(\beta - \sin(\beta) \cdot \cos(\beta)\right)}{\pi}$$

(7.4-44)

So the ratio between the normal force and the submerged weight is:

$$\frac{F_n}{F_w} = \frac{2 \cdot \left(\sin(\beta) - \beta \cdot \cos(\beta)\right)}{\left(\beta - \sin(\beta) \cdot \cos(\beta)\right)}$$

(7.4-45)

For small values of **β**, up to 60 degrees, this ratio is just above 1. But at larger angles (larger concentrations), this ratio is bigger than 1, with a maximum of 2 when the whole pipe is occupied with a bed and **β=π**.
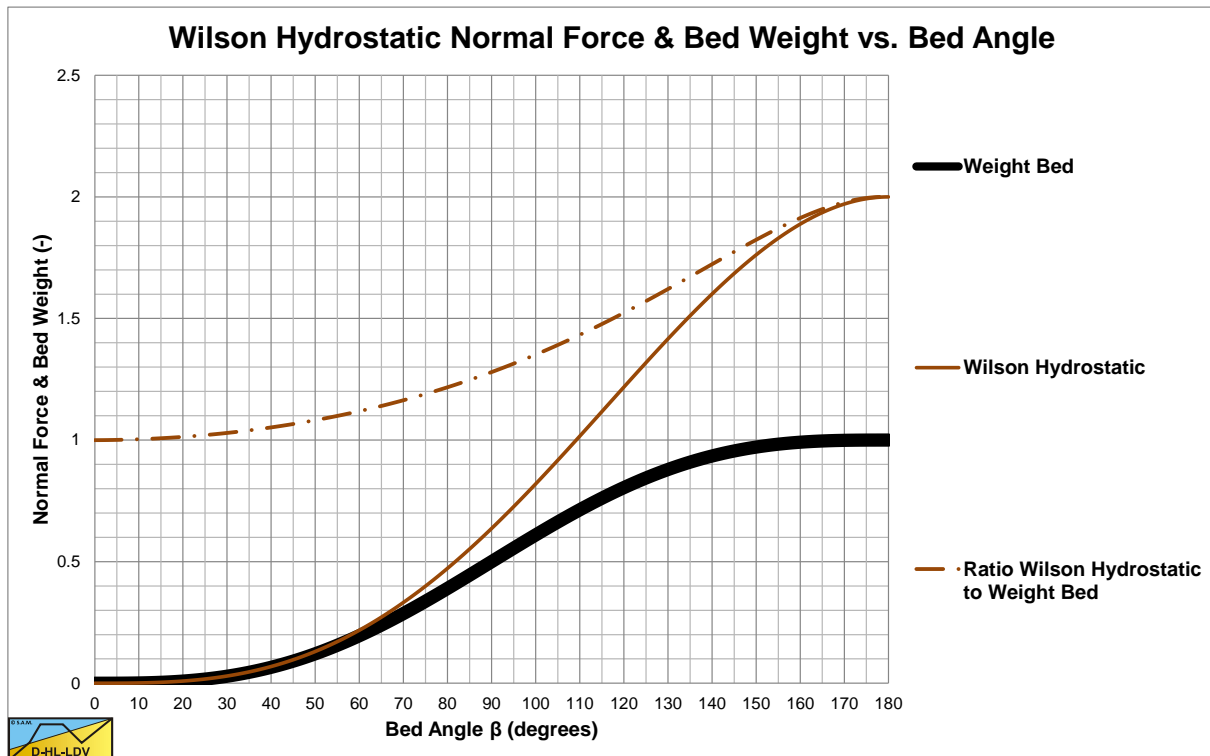
Figure 7.4-10: The normal force F_n, the submerged weight F_w and the ratio F_n/F_w.

The pressure losses due to the sliding friction of the bed based on the hydrostatic normal stress distribution are now:

$$
\Delta p_m - \Delta p_l = \frac{F_{sf}}{A_p} = \frac{\mu_{sf} \cdot F_n}{\frac{\pi}{4} \cdot D_p^2} = 2 \cdot \mu_{sf} \cdot \rho_l \cdot g \cdot \Delta L \cdot R_{sd} \cdot C_{vb} \cdot \frac{\left(\sin(\beta) - \beta \cdot \cos(\beta)\right)}{\pi} \tag{7.4-46}
$$

This gives for the hydraulic gradient:

$$
i_m - i_l = \frac{F_{sf}}{A_p \cdot \rho_l \cdot g \cdot \Delta L} = \frac{\mu_{sf} \cdot F_n}{\frac{\pi}{4} \cdot D_p^2 \cdot \rho_l \cdot g \cdot \Delta L} = 2 \cdot \mu_{sf} \cdot R_{sd} \cdot C_{vb} \cdot \frac{\left(\sin(\beta) - \beta \cdot \cos(\beta)\right)}{\pi} \tag{7.4-47}
$$

In the case where the bed occupies the whole pipe cross section, **β=π**, this gives the so called plug gradient:

$$
i_{plug} = i_m - i_l = 2 \cdot \mu_{sf} \cdot R_{sd} \cdot C_{vb} \cdot \frac{\left(\sin(\pi) - \pi \cdot \cos(\pi)\right)}{\pi} = 2 \cdot \mu_{sf} \cdot R_{sd} \cdot C_{vb} \tag{7.4-48}
$$

This gives for the relative excess hydraulic gradient E_{rhg}:

$$
E_{rhg} = \frac{i_m - i_l}{R_{sd} \cdot C_{vs}} = \mu_{sf} \cdot \frac{2 \cdot \left(\sin(\beta) - \beta \cdot \cos(\beta)\right)}{\left(\beta - \sin(\beta) \cdot \cos(\beta)\right)} \tag{7.4-49}
$$

7.4.4 The Normal Force Carrying the Weight Approach.

With this approach it is assumed that there can only be a normal force between the bed and the pipe wall in the bottom half of the pipe. Bed in the top half of the pipe transfers the submerged weight to the bottom half of the pipe. If the bed occupies less than or equal to half of the pipe cross section, the solution is equal to the Wilson et al. (1992) hydrostatic approach. If the bed occupies more than half of the pipe cross section, the solution differs.
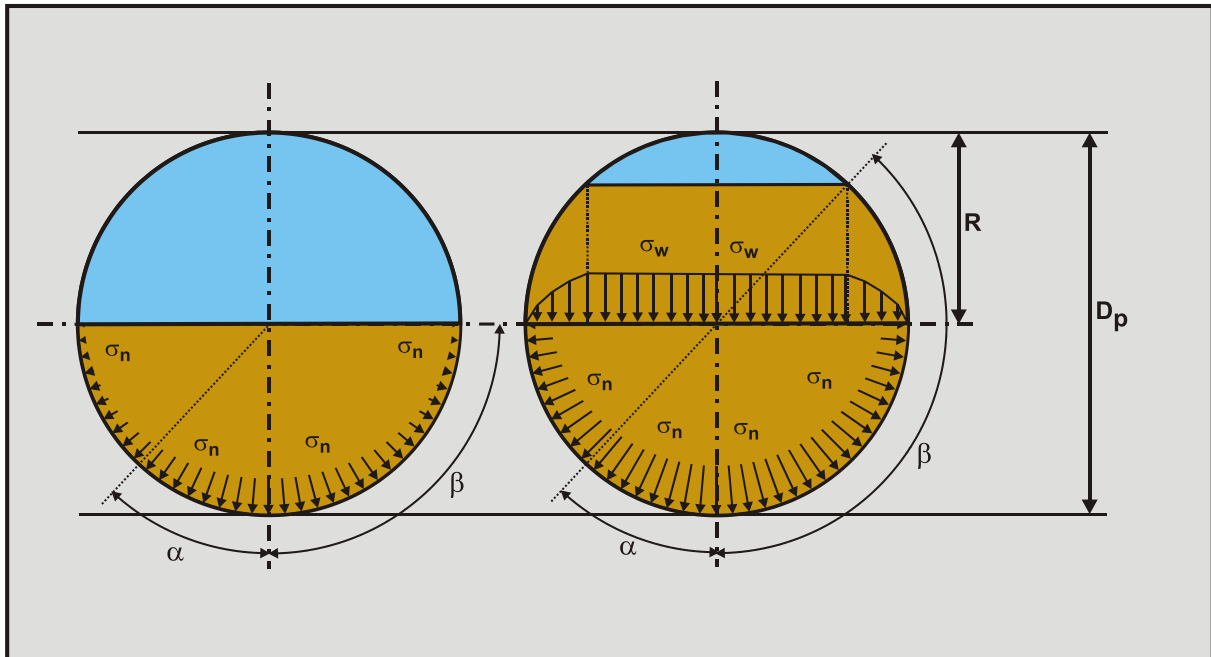
Figure 7.4-11: The normal stress and weight distribution.

Figure 7.4-11 shows these two cases. Figure 7.4-2, Figure 7.4-3, Figure 7.4-4 and Figure 7.4-5 show the stresses on the pipe wall.

It is obvious that the vertical component of the normal stress on the pipe wall has to carry the submerged weight of the bed.

The vertical stress as a result of the submerged weight at a point under an angle $\boldsymbol{\alpha}$ is:

$$\sigma_v = \rho_l \cdot R_{sd} \cdot g \cdot C_{vb} \cdot \left(\cos(\alpha) - \cos(\beta)\right) \cdot R \tag{7.4-50}$$

The vertical force exerted on a strip pipe wall with a length $\boldsymbol{\Delta L}$ is:

$$\Delta F_v = \sigma_v \cdot \cos(\alpha) \cdot R \cdot d\alpha \cdot \Delta L \tag{7.4-51}$$

The normal force exerted on a strip pipe wall with a length $\boldsymbol{\Delta L}$ is:

$$\Delta F_n = \sigma_n \cdot R \cdot d\alpha \cdot \Delta L \tag{7.4-52}$$

The vertical component of the normal force exerted on a strip pipe wall with a length $\boldsymbol{\Delta L}$ is:

$$\Delta F_{n,v} = \sigma_n \cdot \cos(\alpha) \cdot R \cdot d\alpha \cdot \Delta L \tag{7.4-53}$$

The vertical component of the normal force has to be equal to the vertical force resulting from the submerged weight according to:

$$\sigma_n \cdot \cos(\alpha) \cdot R \cdot d\alpha \cdot \Delta L = \rho_l \cdot R_{sd} \cdot g \cdot C_{vb} \cdot \left(\cos(\alpha) - \cos(\beta)\right) \cdot R \cdot \cos(\alpha) \cdot R \cdot d\alpha \cdot \Delta L \tag{7.4-54}$$

This can be simplified to:

$$\sigma_n \cdot R \cdot d\alpha \cdot \Delta L = \rho_l \cdot R_{sd} \cdot g \cdot C_{vb} \cdot \left(\cos(\alpha) - \cos(\beta)\right) \cdot R \cdot R \cdot d\alpha \cdot \Delta L \tag{7.4-55}$$

The total normal force follows from integration of the normal stress:

$$F_n = \int_{-\beta}^{\beta} \sigma_n \cdot R \cdot d\alpha \cdot \Delta L = 2 \cdot \rho_l \cdot R_{sd} \cdot g \cdot C_{vb} \cdot R^2 \cdot \int_0^{\beta} \left(\cos(\alpha) - \cos(\beta)\right) \cdot d\alpha \cdot \Delta L \tag{7.4-56}$$

Per unit of length and for both sides of the bed this gives:

$$F_n = 2 \cdot \rho_l \cdot R_{sd} \cdot g \cdot C_{vb} \cdot R^2 \cdot \left(\sin(\beta) - \beta \cdot \cos(\beta)\right) \cdot \Delta L$$

$$= 2 \cdot \rho_l \cdot R_{sd} \cdot g \cdot C_{vb} \cdot A_p \cdot \frac{\left(\sin(\beta) - \beta \cdot \cos(\beta)\right)}{\pi} \cdot \Delta L \tag{7.4-57}$$

So the sliding friction force is (equal to the Wilson et al. (1992) hydrostatic approach):

$$F_{sf} = 2 \cdot \mu_{sf} \cdot \rho_l \cdot g \cdot R_{sd} \cdot C_{vb} \cdot A_p \cdot \frac{\left(\sin(\beta) - \beta \cdot \cos(\beta)\right)}{\pi} \cdot \Delta L \tag{7.4-58}$$

If the bed occupies more than half the cross section of the pipe, for $\boldsymbol{\beta > \pi/2}$ we get:

For $\boldsymbol{0 \leq \alpha < \pi - \beta}$ the normal stress is based on the distance from the pipe wall at angle $\boldsymbol{\alpha}$ to the free surface of the bed, giving:

$$\sigma_n = \rho_l \cdot R_{sd} \cdot g \cdot C_{vb} \cdot \left(\cos(\alpha) - \cos(\beta)\right) \cdot R \tag{7.4-59}$$

For $\boldsymbol{\pi - \beta < \alpha < \pi/2}$ the normal stress is based on the two times distance from the pipe wall at angle $\boldsymbol{\alpha}$ to the center line of the pipe, giving:

$$\sigma_n = \rho_l \cdot R_{sd} \cdot g \cdot C_{vb} \cdot 2 \cdot \cos(\alpha) \cdot R \tag{7.4-60}$$

Integrating from $\alpha=0$ to $\alpha=\pi/2$ gives for the normal force:

$$F_n = 2 \cdot \rho_l \cdot R_{sd} \cdot g \cdot C_{vb} \cdot R^2 \cdot \Delta L \cdot \int_0^{\pi-\beta} (\cos(\alpha) - \cos(\beta)) \cdot d\alpha$$

$$+2 \cdot \rho_l \cdot R_{sd} \cdot g \cdot C_{vb} \cdot R^2 \cdot \Delta L \cdot \int_{\pi-\beta}^{\pi/2} 2 \cdot \cos(\alpha) \cdot d\alpha \tag{7.4-61}$$

Giving:

$$F_n = 2 \cdot \rho_l \cdot R_{sd} \cdot g \cdot C_{vb} \cdot R^2 \cdot \Delta L \cdot \left(-(\pi-\beta) \cdot \cos(\beta) + 2 - \sin(\beta) \right)$$

$$= 2 \cdot \rho_l \cdot R_{sd} \cdot g \cdot C_{vb} \cdot A_p \cdot \Delta L \cdot \frac{\left(-(\pi-\beta) \cdot \cos(\beta) + 2 - \sin(\beta) \right)}{\pi} \tag{7.4-62}$$

Giving for the sliding friction force:

$$F_{sf} = \mu_{sf} \cdot 2 \cdot \rho_l \cdot R_{sd} \cdot g \cdot C_{vb} \cdot A_p \cdot \frac{\left(-(\pi-\beta) \cdot \cos(\beta) + 2 - \sin(\beta) \right)}{\pi} \cdot \Delta L \tag{7.4-63}$$

The pressure losses due to the sliding friction of the bed based on the normal stress carrying the weight distribution is now:

$$\Delta p_m - \Delta p_l = \frac{F_{sf}}{A_p} = \frac{\mu_{sf} \cdot F_n}{\frac{\pi}{4} \cdot D_p^2} = 2 \cdot \mu_{sf} \cdot \rho_l \cdot g \cdot \Delta L \cdot R_{sd} \cdot C_{vb} \cdot \frac{\left(-(\pi-\beta) \cdot \cos(\beta) + 2 - \sin(\beta) \right)}{\pi} \tag{7.4-64}$$

This gives for the hydraulic excess gradient:

$$i_m - i_l = \frac{F_{sf}}{A_p \cdot \rho_l \cdot g \cdot \Delta L} = \frac{\mu_{sf} \cdot F_n}{\frac{\pi}{4} \cdot D_p^2 \cdot \rho_l \cdot g \cdot \Delta L} = 2 \cdot \mu_{sf} \cdot R_{sd} \cdot C_{vb} \cdot \frac{\left(-(\pi-\beta) \cdot \cos(\beta) + 2 - \sin(\beta) \right)}{\pi} \tag{7.4-65}$$

In the case where the bed occupies the whole pipe cross section, $\beta=\pi$, this gives the so called plug gradient:

$$i_{plug} = i_m - i_l = 2 \cdot \mu_{sf} \cdot R_{sd} \cdot C_{vb} \cdot \frac{\left(-(\pi-\pi) \cdot \cos(\pi) + 2 - \sin(\pi) \right)}{\pi} = \frac{4}{\pi} \cdot \mu_{sf} \cdot R_{sd} \cdot C_{vb} \tag{7.4-66}$$

This gives for the relative excess hydraulic gradient E_{rhg}:

$$E_{rhg} = \frac{i_m - i_l}{R_{sd} \cdot C_{vs}} = \mu_{sf} \cdot \frac{2 \cdot \left(-(\pi-\beta) \cdot \cos(\beta) + 2 - \sin(\beta) \right)}{\left(\beta - \sin(\beta) \cdot \cos(\beta) \right)} \tag{7.4-67}$$

7.4.5 The Submerged Weight Approach.

The submerged weight approach assumes that the sliding friction between the bed and the pipe wall results from the submerged weight and not from normal stress, see Figure 7.4-12. Scientifically this is incorrect, however in reality a sliding bed is not a solid object, but consists of many particles with their own behavior. The submerged weight of the bed $\mathbf{F_w}$ is given by:

$$\mathbf{F_w} = \rho_l \cdot g \cdot \Delta L \cdot R_{sd} \cdot C_{vb} \cdot \frac{D_p^2}{4} \cdot \left(\beta - \sin(\beta) \cdot \cos(\beta)\right) \tag{7.4-68}$$

The pressure losses due to the sliding friction of the bed based on the submerged weight is now:

$$\Delta p_m - \Delta p_l = \frac{F_{sf}}{A_p} = \frac{\mu_{sf} \cdot F_w}{\frac{\pi}{4} \cdot D_p^2} = \mu_{sf} \cdot \rho_l \cdot g \cdot \Delta L \cdot R_{sd} \cdot C_{vb} \cdot \frac{\left(\beta - \sin(\beta) \cdot \cos(\beta)\right)}{\pi} \tag{7.4-69}$$

This gives for the excess hydraulic gradient:

$$i_m - i_l = \frac{F_{sf}}{A_p \cdot \rho_l \cdot g \cdot \Delta L} = \frac{\mu_{sf} \cdot F_w}{\frac{\pi}{4} \cdot D_p^2 \cdot \rho_l \cdot g \cdot \Delta L} = \mu_{sf} \cdot R_{sd} \cdot C_{vb} \cdot \frac{\left(\beta - \sin(\beta) \cdot \cos(\beta)\right)}{\pi} = \mu_{sf} \cdot R_{sd} \cdot C_{vs}$$
$$\tag{7.4-70}$$

In the case where the bed occupies the whole pipe cross section, $\beta=\pi$, this gives the so called plug gradient:

$$i_{plug} = i_m - i_l = \mu_{sf} \cdot R_{sd} \cdot C_{vb} \cdot \frac{\left(\pi - \sin(\pi) \cdot \cos(\pi)\right)}{\pi} = \mu_{sf} \cdot R_{sd} \cdot C_{vb} \tag{7.4-71}$$

This gives for the relative excess hydraulic gradient $\mathbf{E_{rhg}}$:

$$E_{rhg} = \frac{i_m - i_l}{R_{sd} \cdot C_{vs}} = \mu_{sf} \quad \text{and} \quad i_m - i_l = \mu_{sf} \cdot R_{sd} \cdot C_{vs} \tag{7.4-72}$$
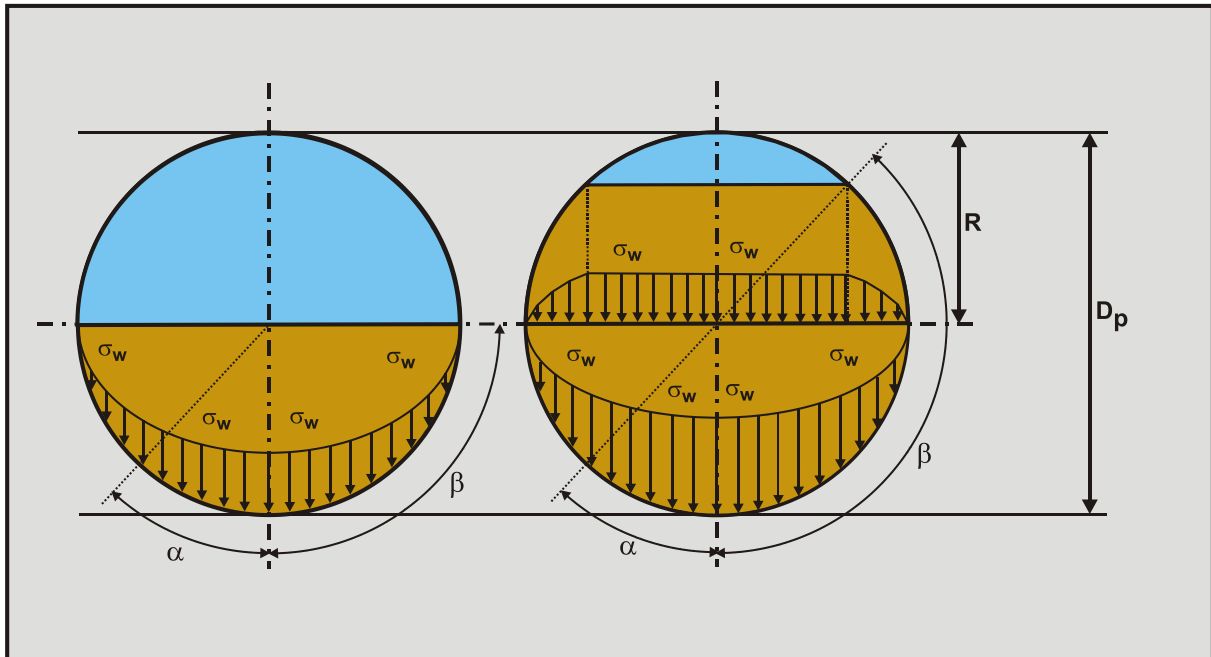
Figure 7.4-12: The submerged weight distribution.

7.4.6 Summary.

In the case when the relative concentration $C_{vr}=C_{vs}/C_{vb}$ or $C_{vr}=C_{vt}/C_{vb}$ equals 1, the hydraulic gradient equals the plug resistance, according to:

Table 7.4-1: Summary of the 3 approaches.

Wilson hydrostatic approach	Normal stress approach	Submerged weight approach
$i_{plug} = 2 \cdot \mu_{sf} \cdot R_{sd} \cdot C_{vb}$	$i_{plug} = \dfrac{4}{\pi} \cdot \mu_{sf} \cdot R_{sd} \cdot C_{vb}$	$i_{plug} = \mu_{sf} \cdot R_{sd} \cdot C_{vb}$

There are a number of approaches to determine the sliding friction force on a moving bed. These approaches are the original Wilson (1992) approach, based on the assumption that there is a hydrostatic pressure between the bed and the pipe wall. This assumes a pressure distribution as if the bed were a fluid, but the pipe wall friction based on the sliding coefficient of friction. The second approach assumes that the vertical component of the normal stress has to carry the weight of the bed. This approach is similar to the Wilson (1992) approach for pipes filled up to 50% with sand. Above 50% there is a significant difference between the two approaches, as the portion of the bed above the centerline of the pipe contributes weight but no friction. Another approach is the active/passive soil resistance approach, but it only gives solutions if the factor **K=1**, making it equivalent to the second approach. The third approach assumes that the sliding friction force is the result of the submerged weight of the bed times a sliding friction coefficient. In all 3 cases, solving the force equilibrium equations result in a Limit of Stationary Deposit Velocity curve (here defined as the velocity at which the bed starts sliding) and resistance curves based on constant spatial volumetric concentration. Figure 7.4-13, Figure 7.4-14 and Figure 7.4-15 give the hydraulic gradients for the 3 approaches for the constant spatial volumetric concentration curves. It is clear from these figures that the Wilson hydrostatic approach gives the highest hydraulic gradients (maximum factor 2 normal force to weight ratio), followed by the normal force carrying the weight approach (maximum factor 1.3 normal force to weight ratio), followed by the submerged weight approach (maximum factor 1 normal force to weight ratio).

Based on the force equilibrium equations, the velocity of the sliding bed is determined and shown in Figure 7.4-16, Figure 7.4-17 and Figure 7.4-18 for the 3 approaches. Once the bed velocity is known, the delivered or transport concentration can be determined as is shown in Figure 7.4-19, Figure 7.4-20 and Figure 7.4-21. Now the transport concentrations are determined, hydraulic gradient curves for constant delivered or transport concentration can be determined by interpolation. Figure 7.4-22, Figure 7.4-23 and Figure 7.4-24 show the hydraulic gradients as a function of the delivered volumetric concentration. The curves never touch the Limit Deposit Velocity curves, since the delivered volumetric concentration is always zero on these curves, due to the assumption that there is only transport of particles if the bed is sliding. Figure 7.4-25, Figure 7.4-26 and Figure 7.4-27 show the relative excess hydraulic gradient (E_{rhg}) as a function of the spatial concentration. In the case of the submerged weight approach, this gives an almost constant E_{rhg} very close to the sliding friction coefficient μ_{sf}.

Now which approach to use? If there is only transport through a sliding bed, the second approach should be applied. The Wilson hydrostatic approach overestimates the total normal force between the bed and the pipe wall if the pipe is filled with more than 50% by the bed, by assuming both horizontal and vertical components of normal stress for the entire perimeter of the pipe filled by the bed. The normal stress carrying the weight of the bed approach gives a correct value for the normal force in this case. In practice however the pipe will never be filled more than 50% (this would cause plugging) so for practical applications the Wilson hydrostatic approach is suitable.

In practice however the sand transport will not only take place through a sliding bed only. If the velocity above the bed is high enough, sheet flow will occur. Sheet flow is a layer of fast moving particles on the top of the bed. The weight of these particles is still transferred to the bed and will contribute to the sliding friction force, but this layer of sheet flow will not result in sliding friction where it is in contact with the pipe wall. Of course, the higher the line speed, the thicker the layer of sheet flow (Miedema (2014)). This thicker layer of sheet flow implies a thinner bed and larger part of the solids that do not contribute to normal stresses on the wall, so the more the submerged weight approach is more valid.

Figure 7.4-13 to Figure 7.4-27 show a comparison between the 3 methods for the wall friction, using the Miedema & Matousek (2014) approach for the bed friction.
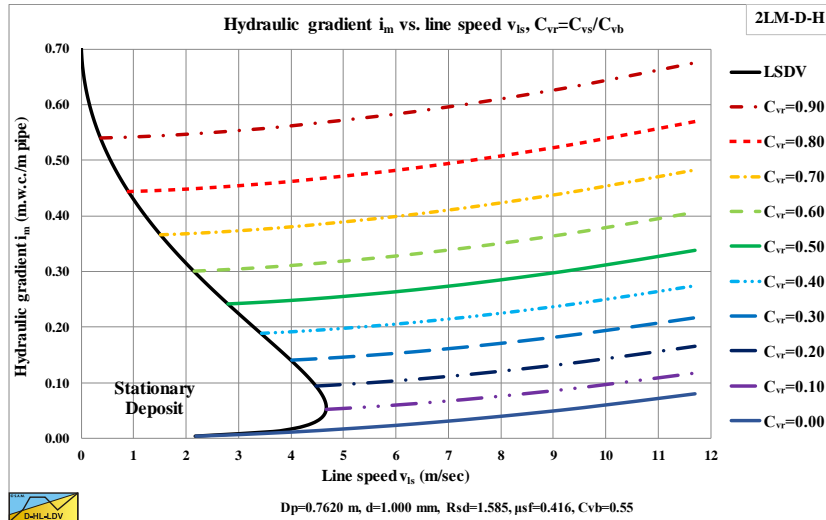
Figure 7.4-13: The hydraulic gradient i_m versus the line speed v_{ls}, $C_{vr}=C_{vs}/C_{vb}$. The hydrostatic Wilson approach.
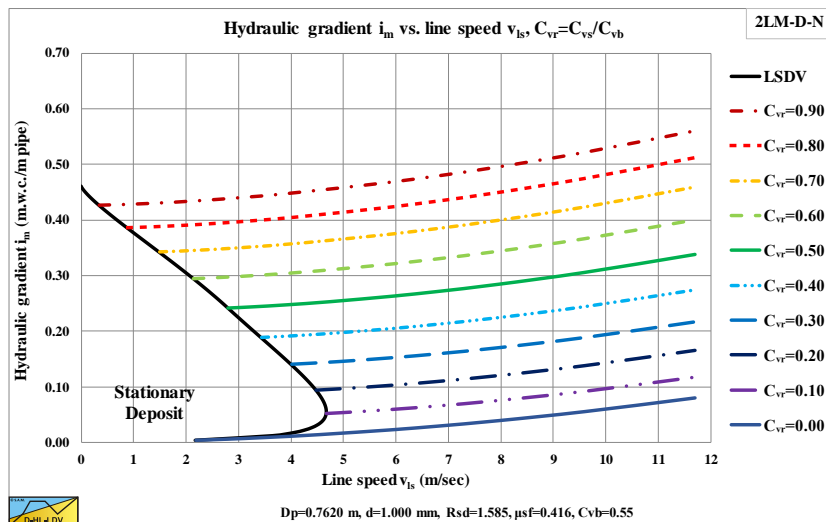
Figure 7.4-14: The hydraulic gradient i_m versus the line speed v_{ls}, $C_{vr}=C_{vs}/C_{vb}$. The normal force carrying the weight approach.
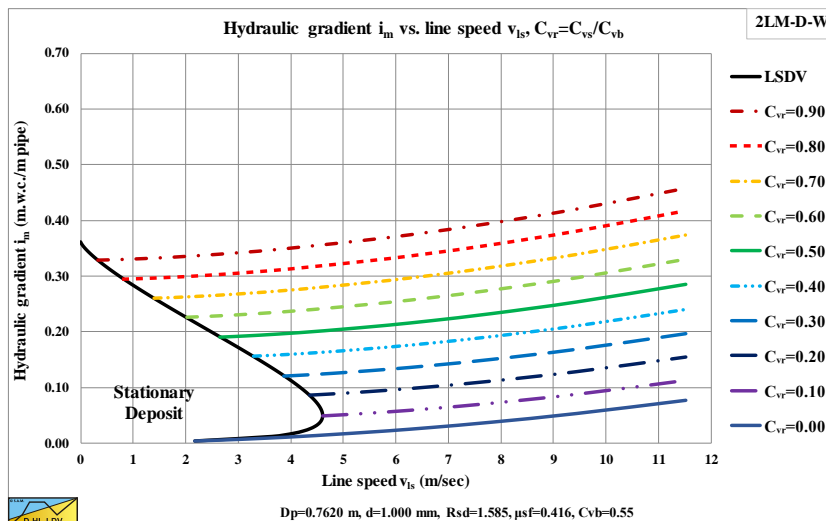
Figure 7.4-15: The hydraulic gradient i_m versus the line speed v_{ls}, $C_{vr}=C_{vs}/C_{vb}$. The submerged weight approach.
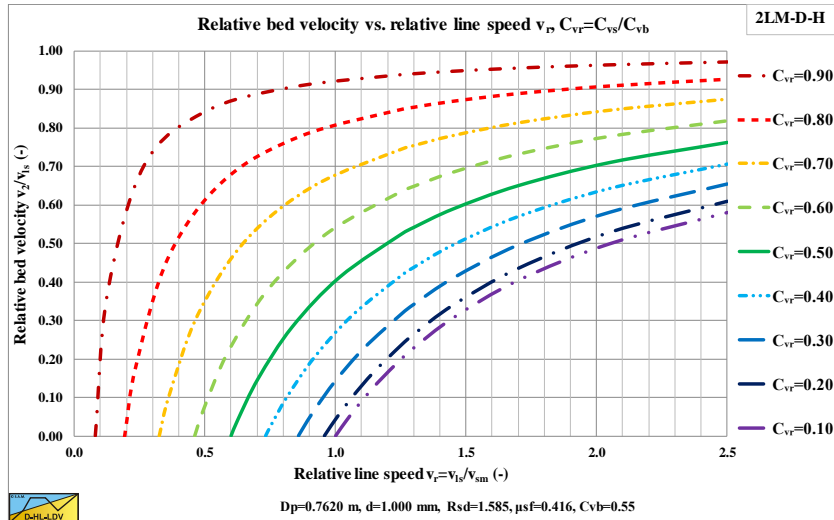
Figure 7.4-16: The relative bed velocity v_2/v_{ls} versus the relative line speed $v_r=v_{ls}/v_{sm}$, $C_{vr}=C_{vs}/C_{vb}$. The hydrostatic Wilson approach.
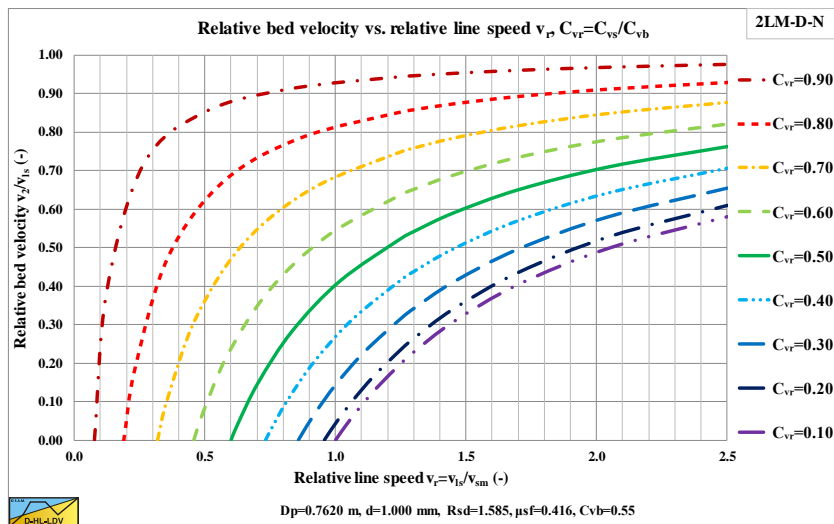
Figure 7.4-17: The relative bed velocity v_2/v_{ls} versus the relative line speed $v_r=v_{ls}/v_{sm}$, $C_{vr}=C_{vs}/C_{vb}$. The normal force carrying the weight approach.
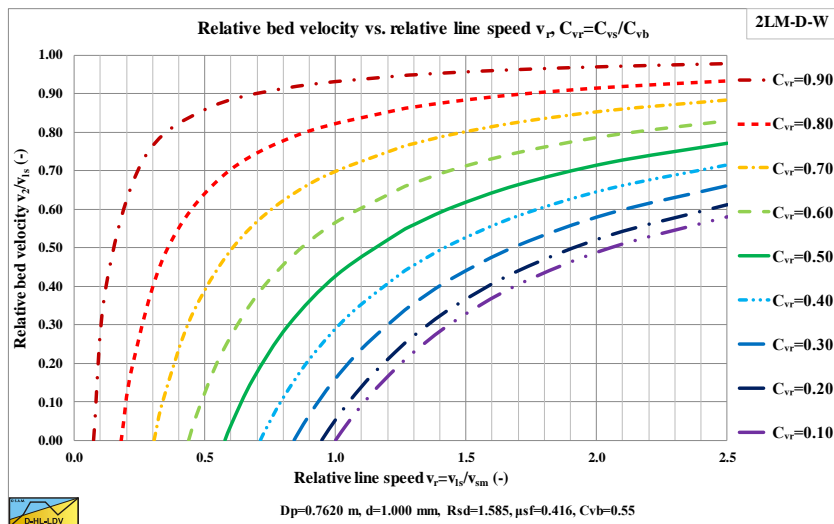
Figure 7.4-18: The relative bed velocity v_2/v_{ls} versus the relative line speed $v_r=v_{ls}/v_{sm}$, $C_{vr}=C_{vs}/C_{vb}$. The submerged weight approach.
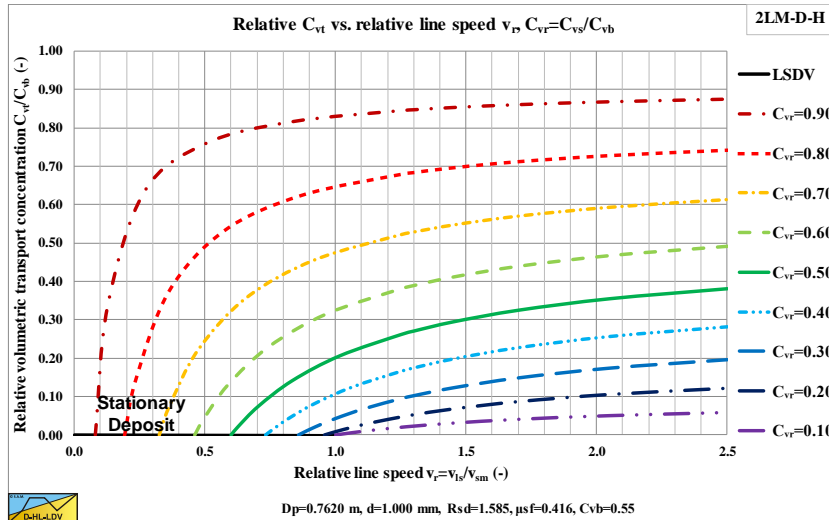
Figure 7.4-19: The relative volumetric transport concentration C_{vt}/C_{vb} versus the relative line speed $v_r=v_{ls}/v_{sm}$, $C_{vr}=C_{vs}/C_{vb}$. The hydrostatic Wilson approach.
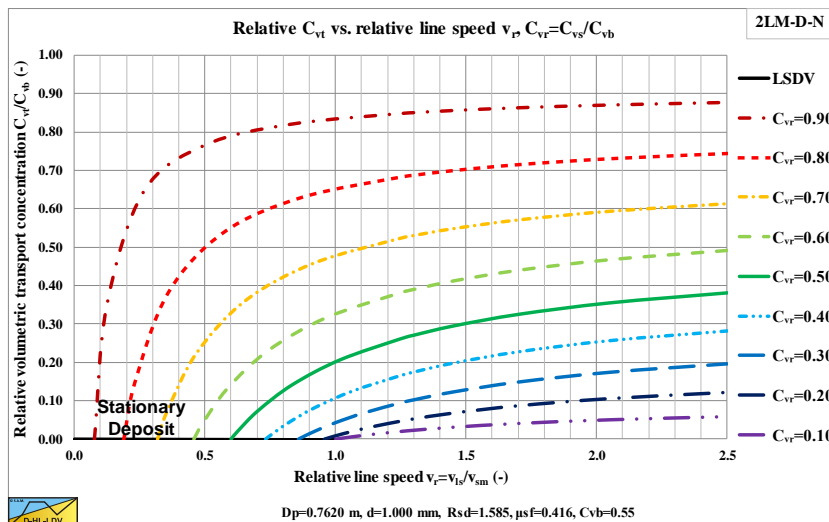
Figure 7.4-20: The relative volumetric transport concentration C_{vt}/C_{vb} versus the relative line speed $v_r=v_{ls}/v_{sm}$, $C_{vr}=C_{vs}/C_{vb}$. The normal force carrying the weight approach.
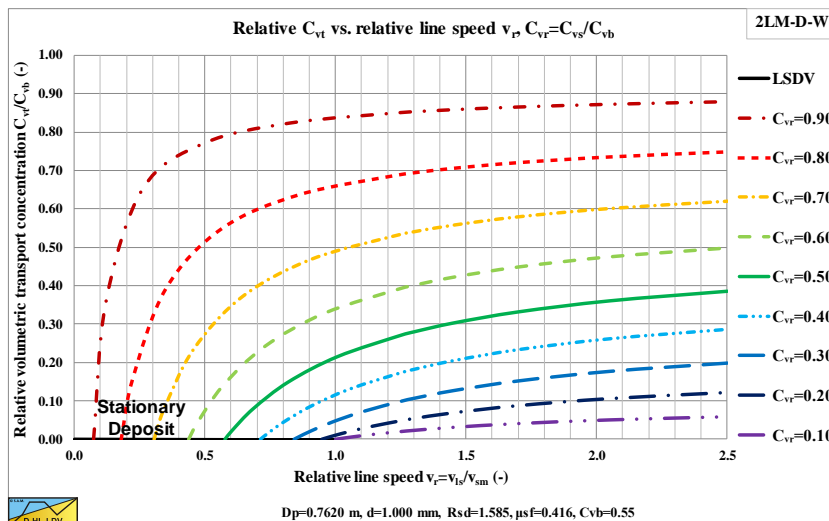
Figure 7.4-21: The relative volumetric transport concentration C_{vt}/C_{vb} versus the relative line speed $v_r=v_{ls}/v_{sm}$, $C_{vr}=C_{vs}/C_{vb}$. The submerged weight approach.
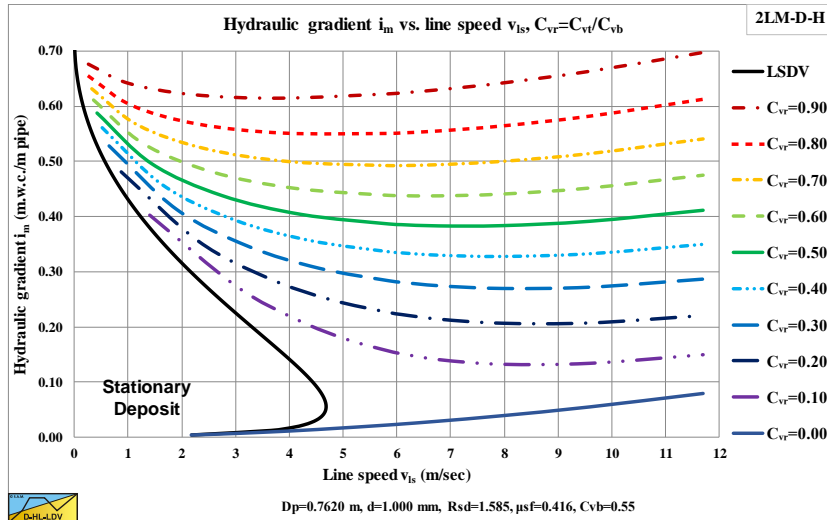
Figure 7.4-22: The hydraulic gradient i_m versus the line speed v_{ls}, $C_{vr}=C_{vt}/C_{vb}$. The hydrostatic Wilson approach.
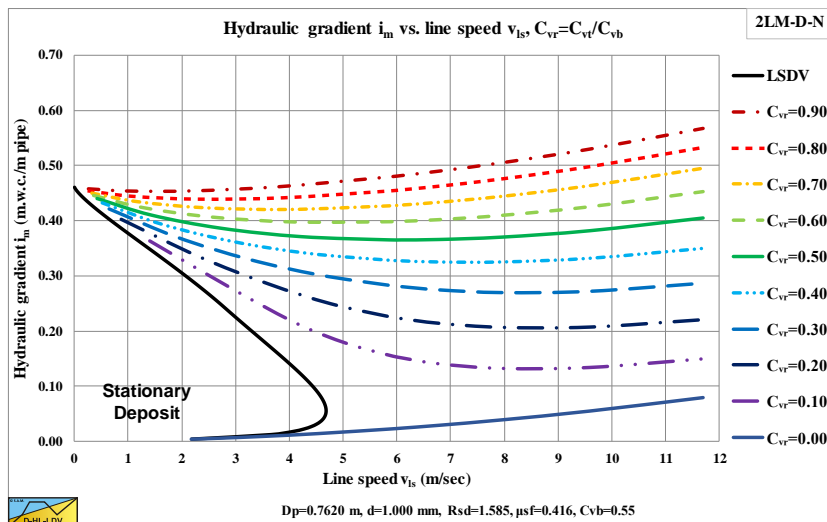
Figure 7.4-23: The hydraulic gradient i_m versus the line speed v_{ls}, $C_{vr}=C_{vt}/C_{vb}$. The normal force carrying the weight approach.
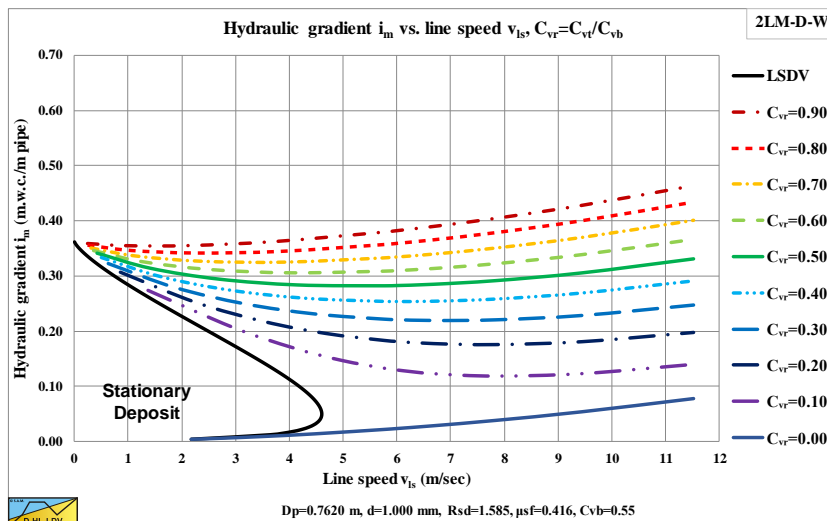
Figure 7.4-24: The hydraulic gradient i_m versus the line speed v_{ls}, $C_{vr}=C_{vt}/C_{vb}$. The submerged weight approach.
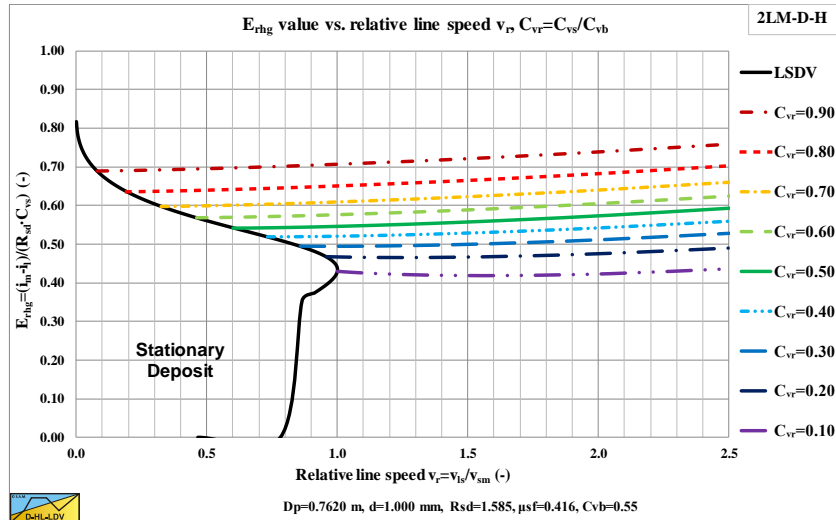
Figure 7.4-25: The relative excess hydraulic gradient E_{rhg} versus the relative line speed $v_r=v_{ls}/v_{sm}$, C_{vs}. The hydrostatic Wilson approach.
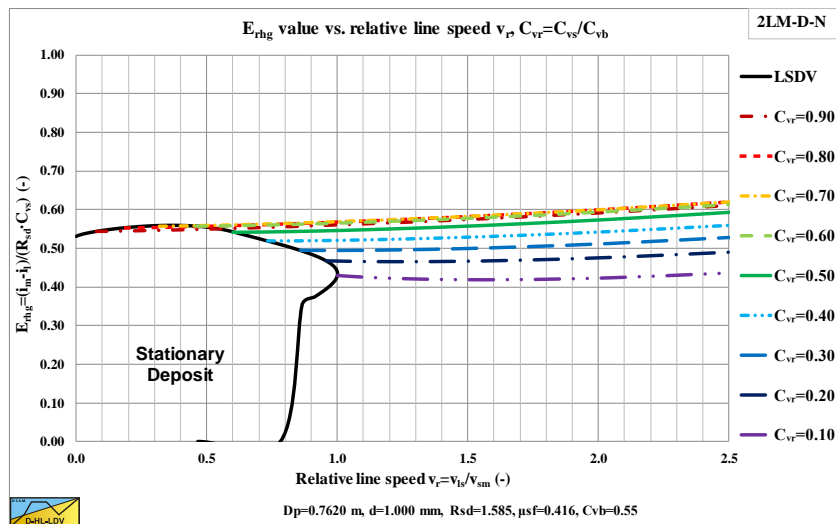
Figure 7.4-26: The relative excess hydraulic gradient E_{rhg} versus the relative line speed $v_r=v_{ls}/v_{sm}$, C_{vs}. The normal force carrying the weight approach.
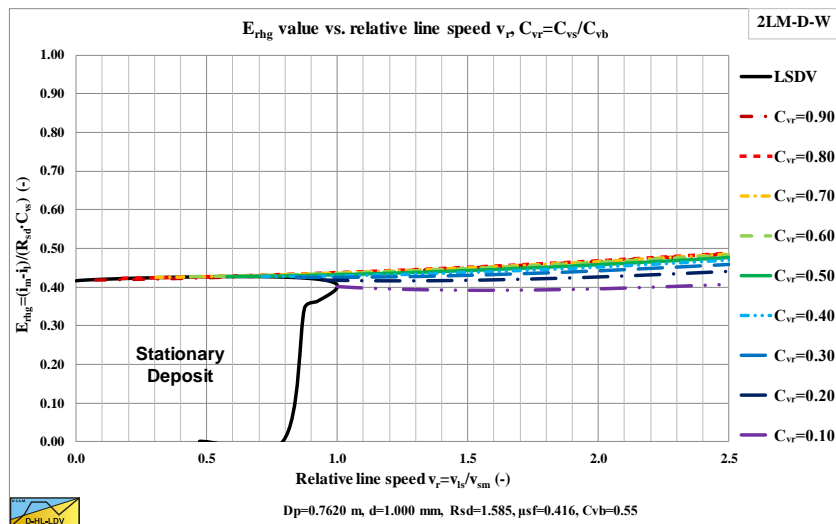
Figure 7.4-27: The relative excess hydraulic gradient E_{rhg} versus the relative line speed $v_r=v_{ls}/v_{sm}$, C_{vs}. The submerged weight approach.

7.4.7 The 3 Layer Model.

In the 2 layer model only the bed is transporting solids with the bed velocity. In the 3 layer model, the top of the bed is moving with a higher velocity as a sheet flow layer, so it is expected that the total transport of solids is larger in the 3LM compared to the 2LM.

Pugh & Wilson (1999) found a relation for the velocity at the top of the sheet flow layer with a stationary bed. This relation is modified here for a sliding bed, giving:

$$
U_H = \gamma \cdot u_* + v_2 = \gamma \cdot \sqrt{\frac{\lambda_{12}}{8}} \cdot (v_1 - v_2) + v_2 = U_{H0} + v_2 \quad \text{with:} \quad \gamma = 9.4 \tag{7.4-73}
$$

The shear stress on the sheet flow layer has to be transferred to the bed by sliding friction. It is assumed that this sliding friction is related to the internal friction angle, giving for the thickness of the sheet flow layer:

$$
H = \frac{\tau_{12}}{\rho_l \cdot R_{sd} \cdot g \cdot C_{vs,sf} \cdot \tan(\varphi)} \approx \frac{2 \cdot \theta \cdot d}{C_{vb} \cdot \tan(\varphi)} \tag{7.4-74}
$$

With: $\quad C_{vs,sf} = 0.4 \cdot C_{vb} - 0.5 \cdot C_{vb} \quad$ and $\quad \tan(\varphi) = 0.577$

Assuming a linear concentration distribution in the sheet flow layer, starting at the bed concentration C_{vb} at the bottom of the sheet flow layer and ending with a concentration of zero at the top of the sheet flow layer gives:

$$
C_{vs}(z) = C_{vb} \cdot \left(\frac{H - z}{H} \right) \tag{7.4-75}
$$

With z the vertical coordinate starting at the bottom of the sheet flow layer and increasing going upwards. The velocity in the sheet flow layer is assumed to start with the bed velocity at the bottom and ends with U_H at the top following a power law according to:

$$
U(z) = U_{H0} \cdot \left(\frac{z}{H} \right)^n + v_2 \tag{7.4-76}
$$

The cross section of the sheet flow layer, reduced to the bed concentration C_{vb} is, assuming the average spatial sheet flow layer concentration is 50% of the bed concentration:

$$
\Delta A_{sf} = H \cdot O_{12} \cdot \frac{C_{vs,sf}}{C_{vb}} \approx \frac{H \cdot O_{12}}{2} \tag{7.4-77}
$$

The total amount of solids transported Q_s is the amount transported in the remaining bed Q_2 + the amount transported in the sheet flow layer Q_{12}. The amount of solids transported in the bed is, corrected for the solids in the sheet flow layer:

$$
Q_2 = v_2 \cdot (A_2 - \Delta A_{sf}) \cdot C_{vb} \tag{7.4-78}
$$

The transport of solids in the sheet flow layer can now be determined by integration of the spatial concentration profile times the velocity profile in the sheet flow layer:

$$
Q_{12} = O_{12} \cdot \int_0^H C_{vs}(z) \cdot U(z) \cdot dz = O_{12} \cdot \int_0^H C_{vb} \cdot \left(\frac{H - z}{H} \right) \cdot \left(U_{H0} \cdot \left(\frac{z}{H} \right)^n + v_2 \right) \cdot dz \tag{7.4-79}
$$

$$
Q_{12} = O_{12} \cdot C_{vb} \cdot \left(v_2 \cdot \int_0^H \left(\frac{H - z}{H} \right) \cdot dz + U_{H0} \cdot \int_0^H \left(\frac{H - z}{H} \right) \cdot \left(\frac{z}{H} \right)^n \cdot dz \right) \tag{7.4-80}
$$

This can be rewritten to:

$$Q_{12} = O_{12} \cdot C_{vb} \cdot \left(v_2 \cdot \int_0^H \left(1 - \frac{z}{H}\right) \cdot dz + U_{H0} \cdot \int_0^H \left(\left(\frac{z}{H}\right)^n - \left(\frac{z}{H}\right)^{n+1} \right) \cdot dz \right) \qquad (7.4\text{-}81)$$

Integration gives:

$$Q_{12} = O_{12} \cdot C_{vb} \cdot \left(v_2 \cdot \left(z - \frac{1}{2} \cdot z^2 \right) + U_{H0} \cdot H \cdot \left(\frac{1}{(n+1)} \cdot \left(\frac{z}{H}\right)^{n+1} - \frac{1}{(n+2)} \cdot \left(\frac{z}{H}\right)^{n+2} \right) \right) \Bigg|_0^H \qquad (7.4\text{-}82)$$

With integration from zero to the thickness of the sheet flow layer this gives:

$$Q_{12} = H \cdot O_{12} \cdot C_{vb} \cdot \left(\frac{v_2}{2} + \frac{U_{H0}}{(n+1) \cdot (n+2)} \right) \qquad (7.4\text{-}83)$$

The total flow of solids equals the bed flow plus the sheet flow, which can be estimated by:

$$Q_s = Q_2 + Q_{12} = v_2 \cdot \left(A_2 - \Delta A_{sf} \right) \cdot C_{vb} + \left(v_2 + \frac{2 \cdot U_{H0}}{(n+1) \cdot (n+2)} \right) \cdot \Delta A_{sf} \cdot C_{vb} \qquad (7.4\text{-}84)$$

The delivered volumetric concentration equals the solids flow divided by the total flow:

$$C_{vt} = \frac{Q_s}{v_{ls} \cdot A_p} \qquad (7.4\text{-}85)$$

The above equations describe a relatively simple method to add sheet flow to the 2LM (2 layer model). This is possible because an explicit relation for the Darcy-Weisbach friction factor has been developed. Analyses of the above equations shows that the sheet flow concentration is not really important. Choosing a smaller sheet flow concentration results in a thicker sheet flow layer, but does not influence the velocity at the top of the sheet flow layer. A smaller sheet flow concentration does also not influence the reduced sheet flow cross-section and thus it does not influence the resulting delivered volumetric concentration.

Figure 7.4-28 to Figure 7.4-35 show a comparison between the 2LM and 3LM approach using the Miedema & Matousek (2014) method for the bed friction and the weight approach of Miedema & Ramsdell (2014) for the wall friction.

This model gives good predictions up to a certain line speed. First of all when the line speed is increasing, a part of the solids will be in suspension above the bed or above the sheet flow layer. This part of the solids is not taken into account in the model. This part will reduce the bed fraction, reduce the slip ratio and reduce the hydraulic gradient. Secondly, if the thickness of the sheet flow layer approaches the bed height, the whole bed will become sheet flow and the assumption of having sliding friction between the bed and the pipe wall will no longer be valid. This will also result in a strong decrease of the slip ratio and the hydraulic gradient. In fact there will no longer be a sliding bed and a heterogeneous model should be used.

Figure 7.4-36 shows a comparison between the 3LM and the DHLLDV Framework regarding the slip ratio. At very low line speeds both models match close, but above a certain line speed, the DHLLDV Framework shows a strong reduction of the slip ratio, due to suspension and a dissolving bed. The conclusion is, that the 3LM model is suitable for very low line speeds, but not for line speeds close to the LDV, the line speed where the bed has been dissolved completely. Extending the 3LM with suspension above the sheet flow layer might improve the model.

The total flow of solids can be related to the Shields parameter, which is:

$$\theta = \frac{\tau_{12}}{\rho_l \cdot R_{sd} \cdot g \cdot d} = \frac{u_*^2}{R_{sd} \cdot g \cdot d} \quad \text{or} \quad u_* = \sqrt{\theta \cdot R_{sd} \cdot g \cdot d} \tag{7.4-86}$$

The velocity on top of the sheet flow layer can now be written as:

$$U_H = \gamma \cdot u_* + v_2 = \gamma \cdot \sqrt{\theta \cdot R_{sd} \cdot g \cdot d} + v_2 \tag{7.4-87}$$

$$\text{With:} \quad U_{H0} = \gamma \cdot \sqrt{\theta \cdot R_{sd} \cdot g \cdot d}$$

The total flow of solids equals the bed flow plus the sheet flow, which can be estimated by after substitution of the sheet flow layer cross section and the velocity on top of the sheet flow layer:

$$Q_s = v_2 \cdot \left(A_2 - \frac{H \cdot O_{12}}{2} \right) \cdot C_{vb} + \left(v_2 + \frac{2 \cdot \gamma \cdot \sqrt{\theta \cdot R_{sd} \cdot g \cdot d}}{(n+1) \cdot (n+2)} \right) \cdot \frac{H \cdot O_{12}}{2} \cdot C_{vb} \tag{7.4-88}$$

Substituting the equation for the sheet flow layer thickness gives:

$$Q_s = v_2 \cdot \left(A_2 - \frac{\theta \cdot d \cdot O_{12}}{C_{vb} \cdot \tan(\varphi)} \right) \cdot C_{vb} + \left(v_2 + \frac{2 \cdot \gamma \cdot \sqrt{\theta \cdot R_{sd} \cdot g \cdot d}}{(n+1) \cdot (n+2)} \right) \cdot \frac{\theta \cdot d \cdot O_{12}}{C_{vb} \cdot \tan(\varphi)} \cdot C_{vb}$$

$$Q_s = v_2 \cdot A_2 \cdot C_{vb} + \frac{2 \cdot \gamma \cdot \sqrt{\theta \cdot R_{sd} \cdot g \cdot d}}{(n+1) \cdot (n+2)} \cdot \frac{\theta \cdot d \cdot O_{12}}{C_{vb} \cdot \tan(\varphi)} \cdot C_{vb} \tag{7.4-89}$$

$$Q_s = v_2 \cdot A_2 \cdot C_{vb} + \frac{2 \cdot \gamma}{(n+1) \cdot (n+2) \cdot \tan(\varphi)} \cdot d \cdot \sqrt{R_{sd} \cdot g \cdot d} \cdot O_{12} \cdot \theta^{3/2}$$

The first term on the right hand side shows the solids transport assuming that all solids in the pipe are transported in the bed with cross section A_2 with a velocity v_2. The second term on the right hand side shows the additional solids transport, because the velocity in the sheet flow layer is higher than the bed velocity. The latter is not the total solids transport in the sheet flow layer, just the additional solids transport compared with the case where there is no sheet flow layer. In the case of a stationary bed, $v_2=0$, this gives:

$$Q_s = \frac{2 \cdot \gamma}{(n+1) \cdot (n+2) \cdot \tan(\varphi)} \cdot d \cdot \sqrt{R_{sd} \cdot g \cdot d} \cdot O_{12} \cdot \theta^{3/2} \tag{7.4-90}$$

This can be written as a transport equation similar to the Meyer-Peter Muller (1948) (MPM) equation, giving the solids transport rate per unit of width of the bed in a dimensionless form:

$$\frac{Q_s}{d \cdot \sqrt{R_{sd} \cdot g \cdot d} \cdot O_{12}} = \frac{2 \cdot \gamma}{(n+1) \cdot (n+2) \cdot \tan(\varphi)} \cdot \theta^{3/2} = \alpha \cdot \theta^\beta \tag{7.4-91}$$

The original MPM equation includes the critical Shields parameter, giving:

$$\frac{Q_s}{d \cdot \sqrt{R_{sd} \cdot g \cdot d} \cdot O_{12}} = \alpha \cdot (\theta - \theta_{cr})^\beta \quad \text{with:} \quad \alpha=8 \quad \text{and} \quad \beta=1.5 \tag{7.4-92}$$

For high values of the Shields parameter, both equations behave the same. With **n=1** and **tan(φ)=0.6**, the theoretical equation gives **α=5.22**. With **n=1** and **tan(φ)=0.4**, the theoretical equation gives **α=8**. With **n=0.537** and **tan(φ)=0.6**, the theoretical equation also gives **α=8.** So both equations give results in the same range.
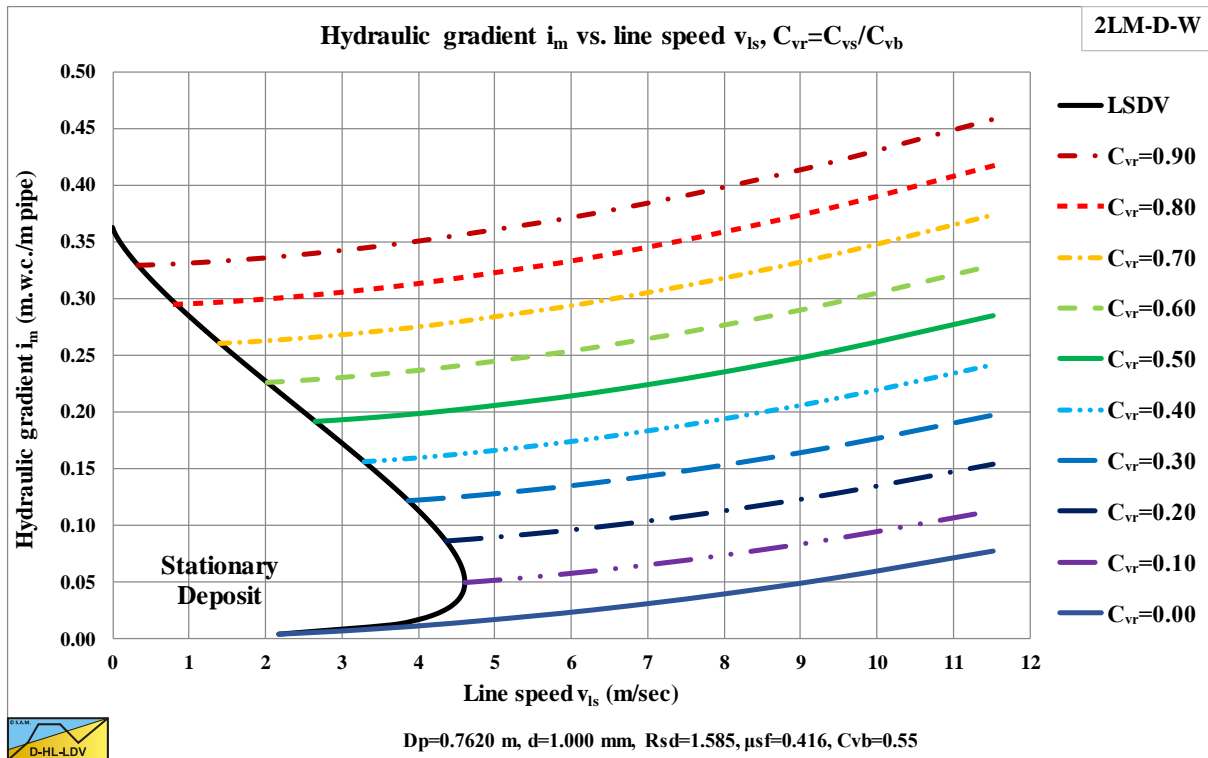
Figure 7.4-28: The hydraulic gradient i_m versus the line speed v_{ls}, $C_{vr}=C_{vs}/C_{vb}$.
The submerged weight approach, without sheet flow.
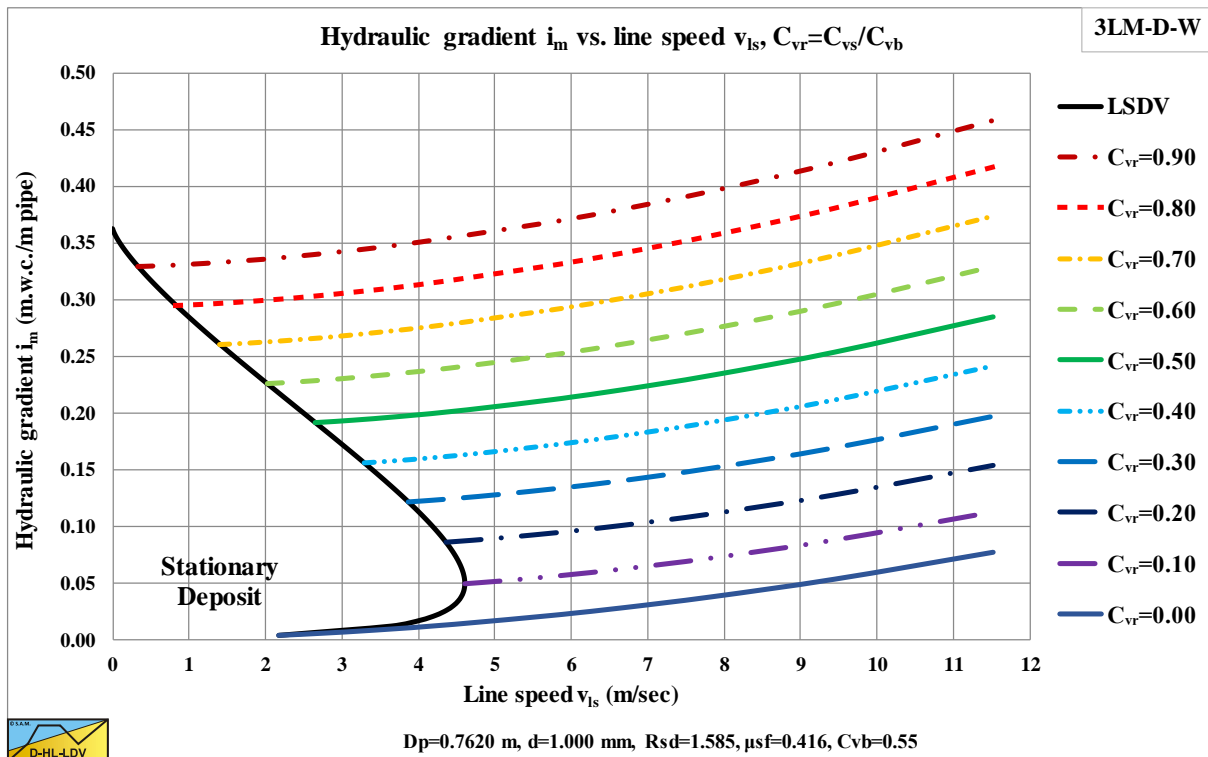
Figure 7.4-29: The hydraulic gradient i_m versus the line speed v_{ls}, $C_{vr}=C_{vs}/C_{vb}$.
The submerged weight approach, with sheet flow.

The sheet flow at the top of the bed does not influence the hydraulic gradient in the constant C_{vs} graphs, since in both the 2LM and the 3LM use the same equation is used for the bed shear stress. In the constant C_{vt} graphs however there is a difference because the transport concentration is influenced by the sheet flow. Also the slip and the bed fraction are influenced by the sheet flow.
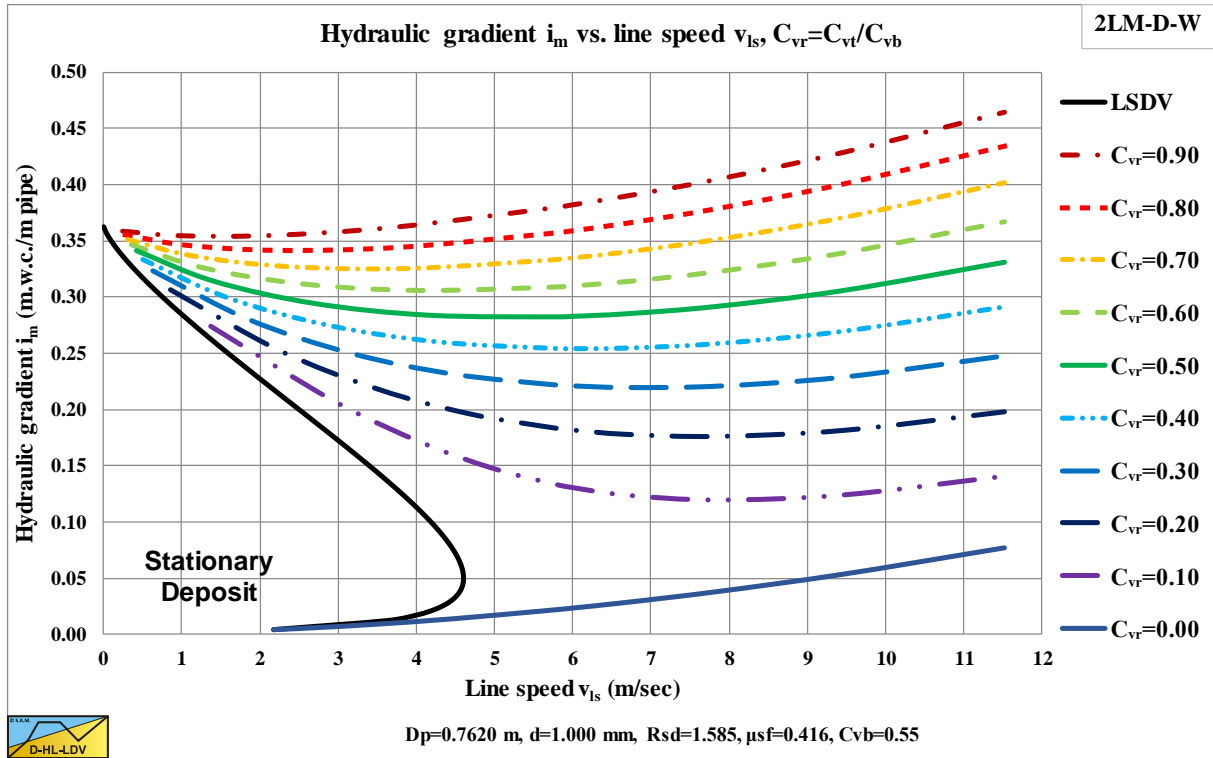
Figure 7.4-30: The hydraulic gradient i_m versus the line speed v_{ls}, $C_{vr}=C_{vt}/C_{vb}$.
The submerged weight approach, without sheet flow.
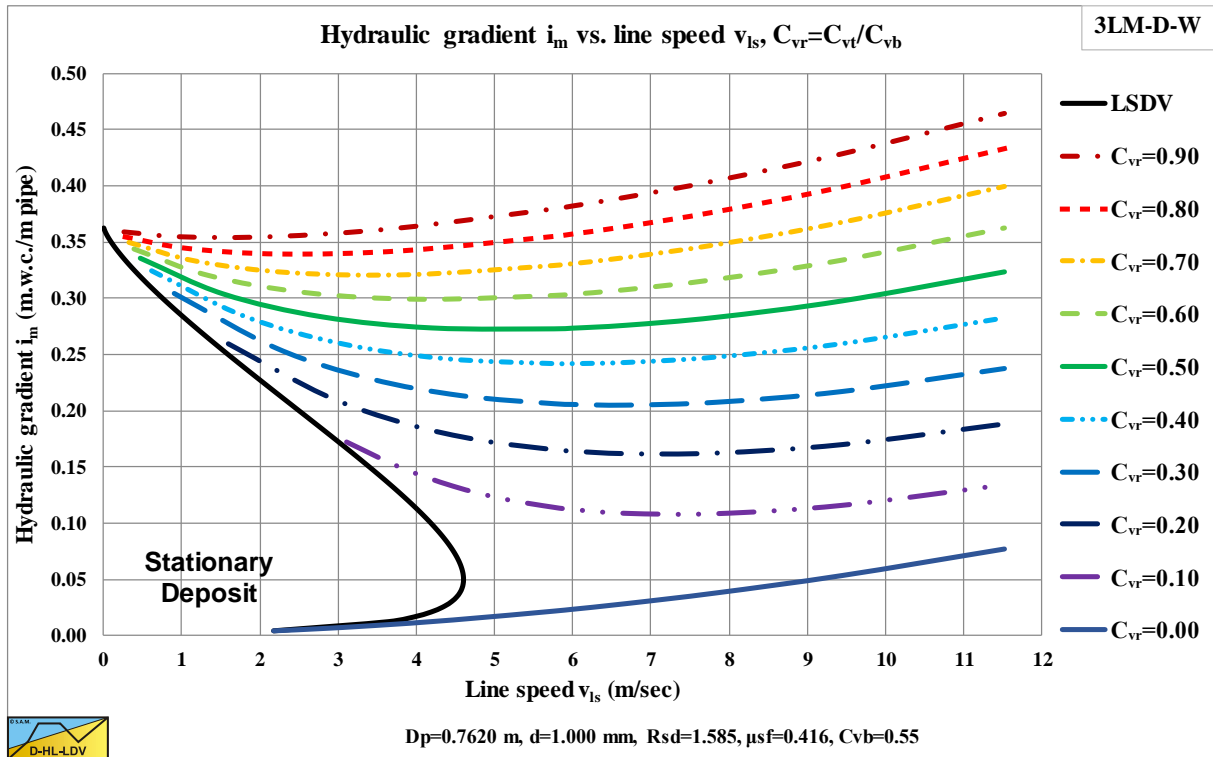
Figure 7.4-31: The hydraulic gradient i_m versus the line speed v_{ls}, $C_{vr}=C_{vt}/C_{vb}$.
The submerged weight approach, with sheet flow.
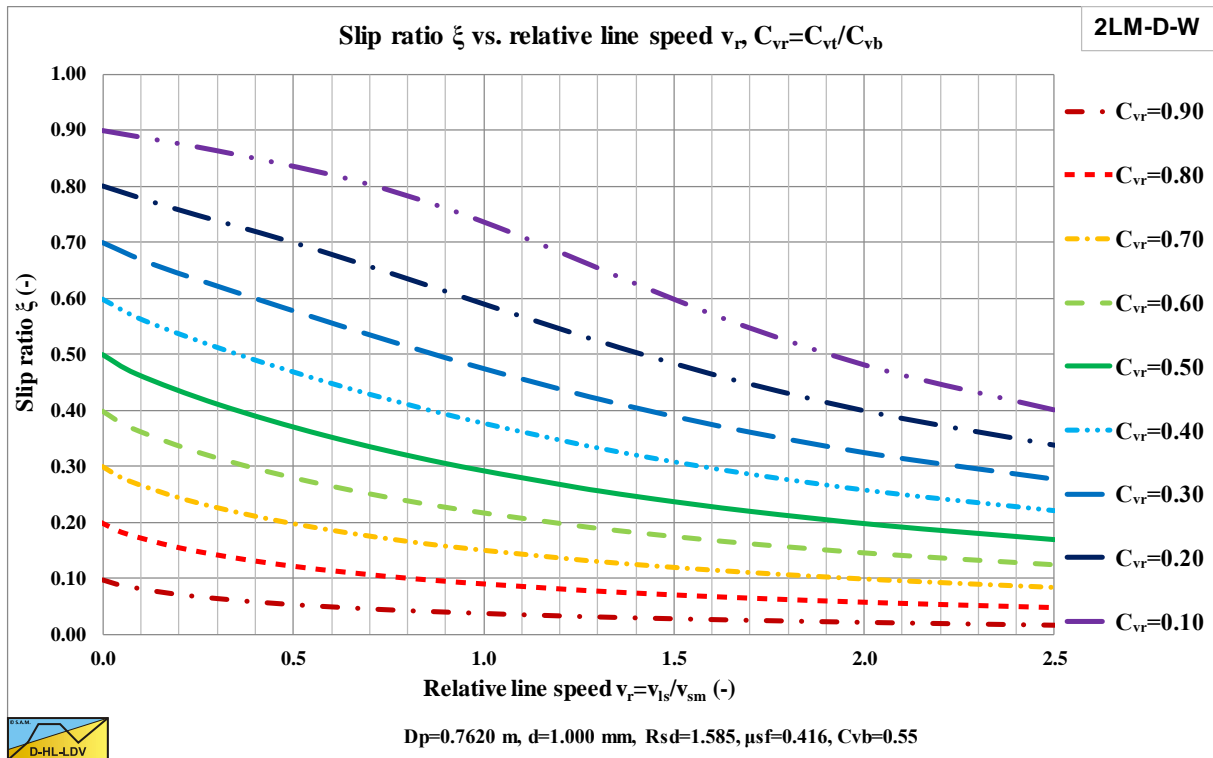
Figure 7.4-32: The slip factor (1-ξ) resulting from the 2 layer model.
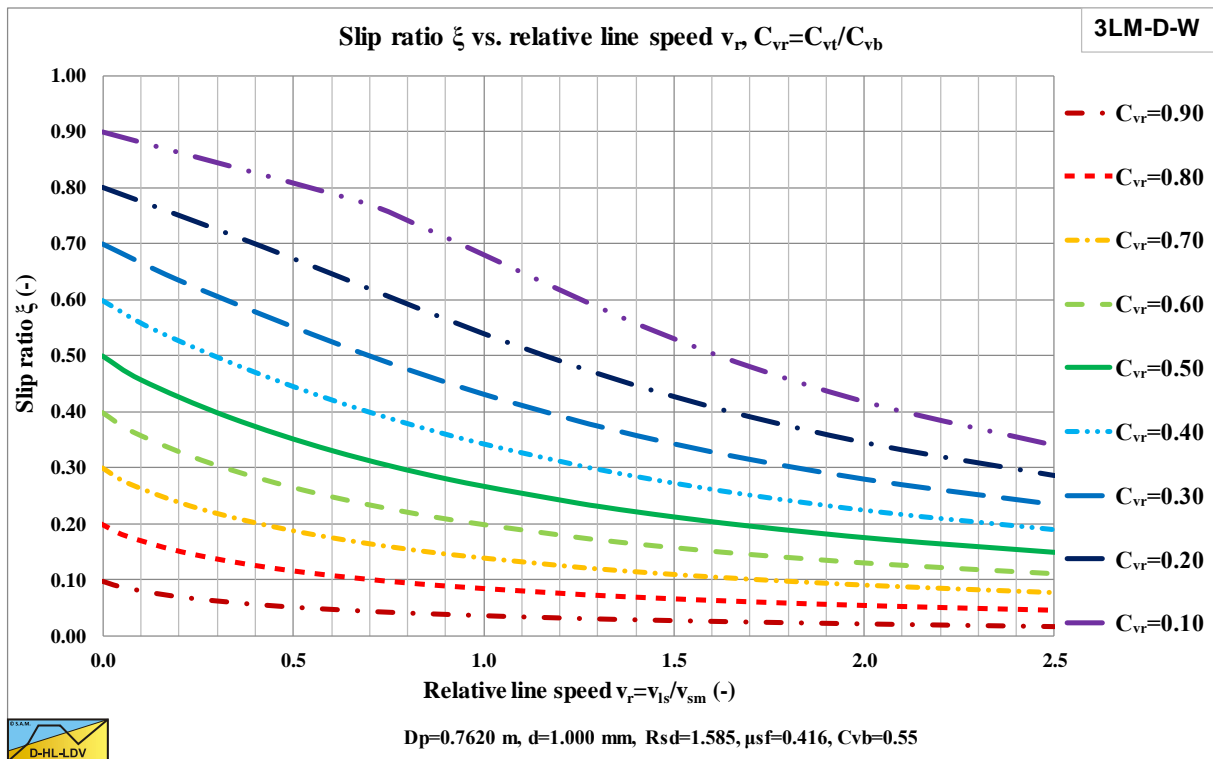
Figure 7.4-33: The slip factor (1-ξ) resulting from the 3 layer model.

The slip ratio of the 3 layer model is smaller than the slip factor of the 2 layer model, which is expected. This means that the 3 layer model results in less slip, which is to be expected.
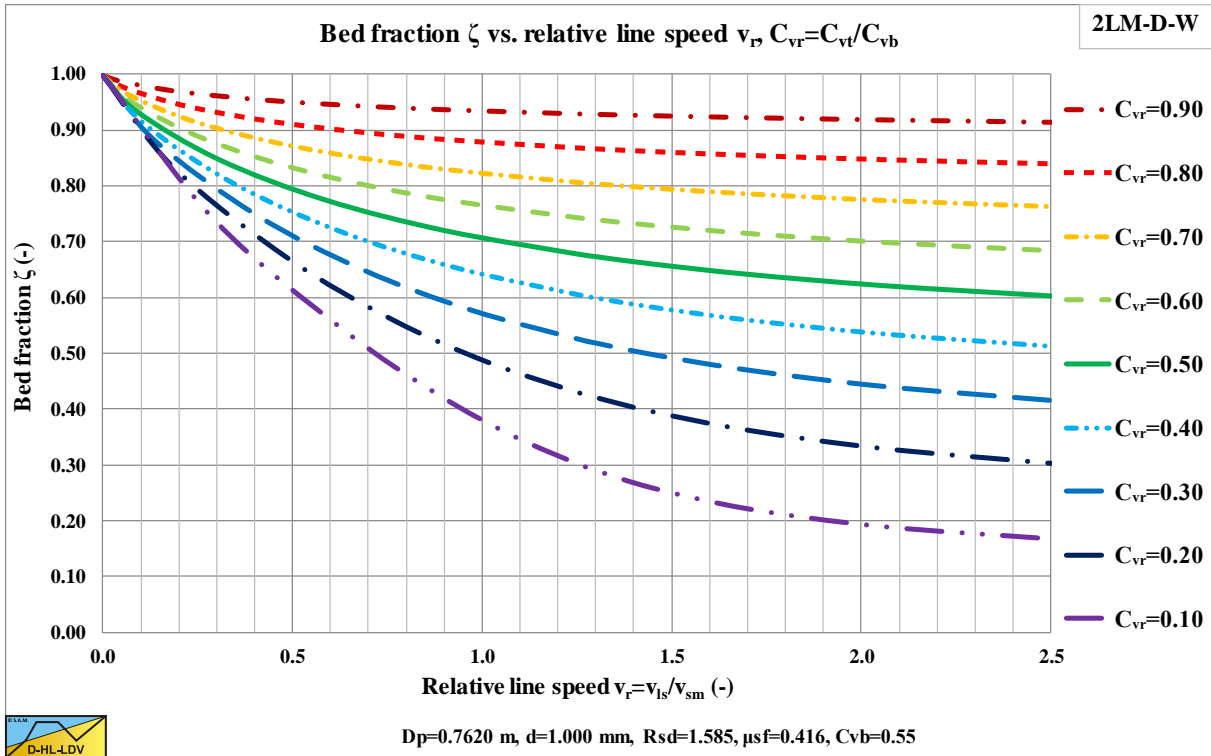
Figure 7.4-34: The bed fraction ζ resulting from the 2 layer model.
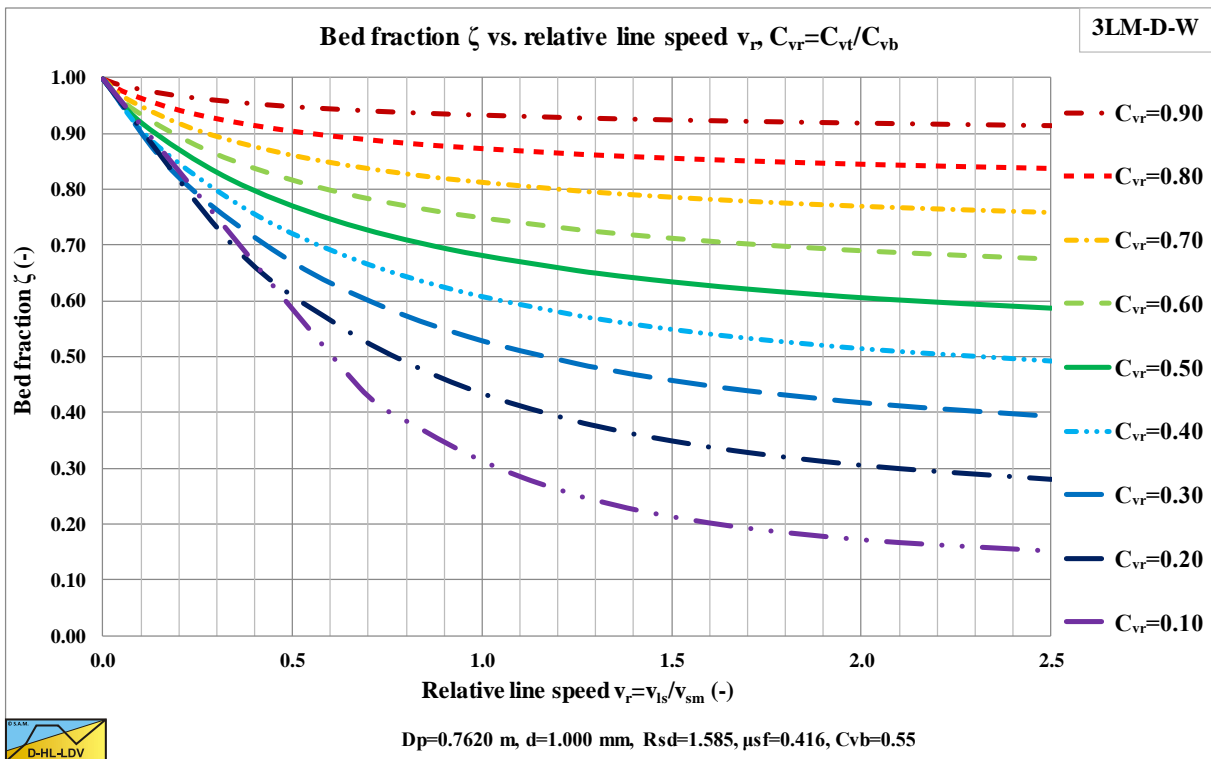
Figure 7.4-35: The bed fraction ζ resulting from the 3 layer model.
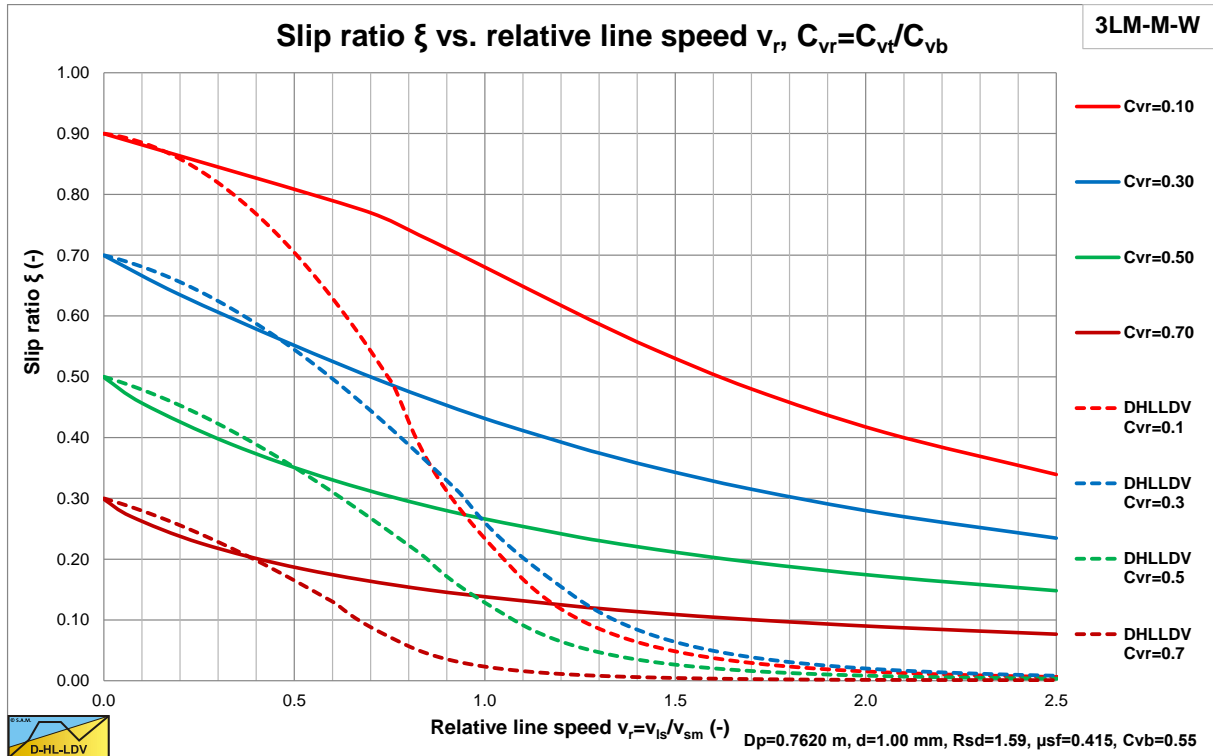
Figure 7.4-36: A comparison of the slip ratio, 3LM versus DHLLDV.

The slip ratio from Figure 7.4-33 can be estimated by the following empirical equation:

$$
C_{vr} = \frac{C_{vt}}{C_{vb}} \quad \text{and} \quad \alpha = 0.58 \cdot C_{vr}^{-0.42}
$$

$$
\frac{1}{1 - \xi_{v_{ls,lsdv}}} = C_{vr}^{-0.5}
$$

$$
\xi = \left(1 - C_{vr}\right) \cdot e^{\left(-\left(0.83 + \frac{\mu_{sf}}{4} + \left(C_{vr} - 0.5 - 0.075 \cdot D_p\right)^2 + 0.025 \cdot D_p \right) \cdot D_p^{0.025} \cdot \left(\frac{v_{ls}}{v_{ls,lsdv}} \right)^{\alpha} \cdot C_{vr}^{0.65} \cdot \left(\frac{R_{sd}}{1.585} \right)^{0.1} \right)}
$$

(7.4-93)

This equation has been developed based on the 3 layer approach, but is considered empirical. With additional simulations or modifications of the fundamental model, this equation may change in the future.

7.4.8 Nomenclature Sliding Bed Regime.

A_p	Cross section pipe	m^2
A_1	Cross section above bed	m^2
A_2	Cross section bed	m^2
A_{sf}	Cross section sheet flow layer	m^2
C_{vb}	Volumetric bed concentration	-
C_{vs}	Spatial volumetric concentration	-
$C_{vs,1}$	Spatial volumetric concentration upper layer	-
$C_{vs,2}$	Spatial volumetric concentration lower layer, bed	-
$C_{vs,sf}$	Average spatial concentration in sheet flow layer	-
C_{vt}	Delivered (transport) volumetric concentration	-
C_{vr}	Relative volumetric concentration	-
d	Particle diameter	m
D_p	Pipe diameter	m
E_{rhg}	Relative excess hydraulic gradient	-
F_n	Normal force	kN
F_t	Tangent force	kN
F_w	Weight of bed	kN
F_{sf}	Sliding friction force	kN
F_h	Horizontal force	kN
$F_{h,n}$	Component horizontal force normal to pipe wall	kN
$F_{h,t}$	Component horizontal force tangent to pipe wall	kN
F_v	Vertical force	kN
$F_{v,n}$	Component vertical force normal to pipe wall	kN
$F_{v,t}$	Component vertical force tangent to pipe wall	kN
h_b	Bed height above point on the pipe wall	m
H	Thickness sheet flow layer	m
g	Gravitational constant 9.81 m/s^2	m/s^2
i_l	Hydraulic gradient pure liquid	m/m
i_m	Hydraulic gradient mixture	m/m
i_{plug}	Hydraulic gradient plug flow	m/m
K	Failure factor, ratio horizontal stress to vertical stress	-
K_a	Factor of active failure	-
K_p	Factor of passive failure	-
ΔL	Length of pipe section	m
n	Power of velocity distribution in sheet flow layer	-
O_p	Circumference pipe	m
O_1	Circumference pipe above bed	m
O_2	Circumference pipe in bed	m
O_{12}	Width of bed	m
Δp_l	Head loss pure liquid	kPa
Δp_m	Head loss mixture	kPa
Q_s	Total amount of solids transported by volume	m^3/s
Q_2	Amount of solids transported in the bed	m^3/s
Q_{12}	Amount of solids transported in the sheet flow layer	m^3/s
R_{sd}	Relative submerged density	-
R	Pipe radius	m
u_*	Friction velocity	m/s
U_H	Velocity at the top of the sheet flow layer	m/s
U_{H0}	Velocity at the top of the sheet flow layer with fixed bed	m/s
v_{ls}	Line speed	m/s
v_r	Relative line speed	-
v_{sm}	Maximum Limit of Stationary Deposit Velocity	m/s
v_1	Velocity above bed	m/s
$v_{1,m}$	Mean velocity above bed, upper layer	m/s
v_2	Velocity bed	m/s
$v_{2,m}$	Mean velocity bed, lower layer	m/s

y_b	Height of bed	m
z	Vertical coordinate in sheet flow layer	m
α	Angle of position in bed	rad
α	Factor MPM equation	-
β	Bed angle	rad
β	Power MPM equation	-
φ	Angle of internal friction	rad
γ	Wilson factor velocity at top of sheet flow layer	-
$ρ_l$	Density carrier liquid	ton/m³
θ	Shields parameter	-
$θ_c$	Critical Shields parameter	-
$λ_{12}$	Darcy-Weisbach friction factor on the bed	-
$τ_{12}$	Shear stress bed-liquid	kPa
$τ_{sf}$	Shear stress due to sliding friction	kPa
$τ_t$	Shear stress in bed tangent to pipe wall	kPa
$μ_{sf}$	Sliding friction coefficient	-
$μ_{sf,e}$	Effective or mobilized sliding friction coefficient	-
$σ_n$	Normal stress	kPa
$σ_h$	Horizontal stress	kPa
$σ_v$	Vertical stress	kPa
ζ	Bed fraction	-
ξ	Slip ratio	-

7.5 A Head Loss Model for Heterogeneous Slurry Transport.

7.5.1 Introduction.

Most well-known head loss equations for heterogeneous transport, Durand & Condolios (1952), Fuhrboter (1961), Newitt et al. (1955), Jufin & Lopatin (1966) and Wilson et al. (1992) are based on a single excess pressure term for the solids effect. This term is usually based on curve fitting, some physics or dimensionless numbers. The main question is, can the excess pressure (the solids effect) accurately be described by just one term and if so, does this term depend on the hydraulic gradient of the carrier liquid or is it independent. The model as derived here is based on the assumption that the excess hydraulic gradient is the result of energy losses. These energy losses are identified as potential energy losses and kinetic energy losses. One could distinguish more types of energy losses and maybe come with a more accurate equation, but the current approach already gives a good correlation with the data of many researchers. The potential energy losses are dominated by the terminal settling velocity of the particles, including hindered settling. The kinetic energy losses are dominated by the ratio between the slip velocity of the particles and the terminal settling velocity of the particles (without hindered settling). The slip velocity cannot be derived fundamentally (yet), but is approximated by a function with the dimension of velocity. The final result is an equation with 3 independent terms. The viscous friction losses according to Darcy Weisbach, using the Moody diagram for the friction coefficient, the potential energy losses, using an approach similar to Newitt et al. (1955) and the kinetic energy losses as derived in this chapter.

7.5.2 Physical Energy Considerations.

To give some direction to the form of the semi-empirical equations, a simple power/energy balance will be derived (see Miedema &Ramsdell (2013)). Assuming that the additional pressure resulting from the solids in the liquid is the result of the energy required to keep the particles in suspension and take the losses of kinetic energy in to account, the following theory can be derived, starting with potential energy losses:

Potential Energy.

The power $\Delta P_{s,\,pot}$ required to pump the solids/liquid mixture over a distance ΔL because of the constant loss of potential energy, is the result of the pressure difference $\Delta p_{s,\,pot}$ times the cross-section of the pipe A_p times the line speed v_{ls}.

$$\Delta P_{s,pot} = \Delta p_{s,pot} \cdot A_p \cdot v_{ls} \tag{7.5-1}$$

The potential energy of 1 particle at a factor κ_C times half the pipe diameter is (the eccentricity factor), assuming that on average particles are located at a distance $\kappa_C \cdot D_p/2$ from the bottom of the pipe, with $\kappa_C < 1$:

$$\Delta E_{s,pot} = m_p \cdot g \cdot \kappa_C \cdot \frac{D_p}{2} = \left(\rho_s - \rho_l\right) \cdot \frac{\pi}{6} \cdot d^3 \cdot g \cdot \left(\kappa_C \cdot \frac{D_p}{2}\right) \tag{7.5-2}$$

The number of particles in a pipeline with length ΔL is:

$$n = \frac{A_p \cdot \Delta L \cdot C_{vs}}{\frac{\pi}{6} \cdot d^3} \tag{7.5-3}$$

The potential energy $\Delta E_{s,pot,tot}$ available in the solid/liquid mixture over a distance ΔL, assuming the particles are at a distance $\kappa_C \cdot D_p/2$ from the bottom of the pipe is now:

$$\Delta E_{s,pot,tot} = n \cdot \Delta E_{s,pot} = A_p \cdot \Delta L \cdot C_{vs} \cdot \left(\rho_s - \rho_l\right) \cdot g \cdot \left(\kappa_C \cdot \frac{D_p}{2}\right) \tag{7.5-4}$$

The time Δt required for the settling of the particles, based on the average location at a distance $\kappa_C \cdot D_p/2$ from the bottom of the pipe is (including the effect of hindered settling, here Richardson & Zaki (1954) is used):

$$\Delta t = \frac{\left(\kappa_C \cdot \dfrac{D_p}{2} \right)}{v_t \cdot \left(1 - \dfrac{C_{vs}}{\kappa_C} \right)^{\beta}} \qquad (7.5\text{-}5)$$

If $\kappa_C < 1$, the concentration C_{vs} is not evenly distributed over the height of the pipe and will be higher in the bottom of the pipe. This is taken into account by dividing the average concentration by κ_C. So the power required to keep the particles in suspension, is equal to the potential energy $\Delta E_{pot, tot}$, divided by the time Δt required to move from the center of the pipe to the bottom is:

$$\frac{\Delta E_{s,pot,tot}}{\Delta t} = A_p \cdot \Delta L \cdot C_{vs} \cdot \left(\rho_s - \rho_l \right) \cdot g \cdot v_t \cdot \left(1 - \frac{C_{vs}}{\kappa_C} \right)^{\beta} \qquad (7.5\text{-}6)$$

Equation (7.5-1) and (7.5-6) should be equal, resulting in a required pressure gradient of:

$$\frac{\Delta p_{s,pot}}{\Delta L} = \frac{C_{vs} \cdot \left(\rho_s - \rho_l \right) \cdot g \cdot v_t \cdot \left(1 - \dfrac{C_{vs}}{\kappa_C} \right)^{\beta}}{v_{ls}} \qquad (7.5\text{-}7)$$

In terms of the solids effect due to potential energy $i_{s,pot}$ on the hydraulic gradient i this gives:

$$i_{s,pot} = \frac{\Delta p_{s,pot}}{\rho_l \cdot g \cdot \Delta L} = \frac{v_t \cdot \left(1 - \dfrac{C_{vs}}{\kappa_C} \right)^{\beta}}{v_{ls}} \cdot R_{sd} \cdot C_{vs} \qquad (7.5\text{-}8)$$

In terms of the relative excess hydraulic gradient component due to potential energy losses S_{hr} (Settling velocity Hindered Relative), this gives the ratio between the hindered settling velocity in the lower part of the pipe to the line speed:

$$S_{hr} = \frac{i_{s,pot}}{R_{sd} \cdot C_{vs}} = \frac{v_t \cdot \left(1 - \dfrac{C_{vs}}{\kappa_C} \right)^{\beta}}{v_{ls}} \qquad (7.5\text{-}9)$$

The factor κ_C will have a value smaller or equal to 1, depending on the asymmetry of the concentration profile over the vertical in the pipe. If this concentration profile is symmetrical, a value of 1 should be used. However in general in heterogeneous transport the concentration in the bottom half of the pipe will be higher than in the top half. If 100% of the particles would be in the lower half of the pipe, a factor of ½ should be used, but this is seldom the case. A factor of 2/3 or 4/5 seems to be more reasonable. The smaller this factor, the smaller the potential energy losses.

Substituting the equation for the liquid resistance Δp_l gives:

$$\Delta p_m = \Delta p_l + \Delta p_{s,pot} = \Delta p_l \cdot \left(1 + \frac{\Delta p_{s,pot}}{\Delta p_l} \right) = \Delta p_l \cdot \left(1 + \Phi \cdot C_{vs} \right) \qquad (7.5\text{-}10)$$

In terms of the hydraulic gradient this can also be written as:

$$i_m = i_l + i_{s,pot} = i_l \cdot \left(1 + \frac{i_{s,pot}}{i_l} \right) = i_l \cdot \left(1 + \Phi \cdot C_{vs} \right) \qquad (7.5\text{-}11)$$

According to equation (7.5-7) the extra pressure losses due to the potential energy losses of the solids is proportional to the volumetric concentration C_{vs}, the submerged density of the solids $(\rho_s-\rho_l)$, the terminal settling velocity of the particles v_t and inversely proportional with the line speed v_{ls}. The terminal settling velocity v_t however is influenced by hindered settling (using Richardson & Zaki (1954)), while the friction factor λ_l is influenced by the Reynolds number **Re** of the flow in the pipe according to Moody diagram. This results in:

$$\Phi = 2 \cdot \frac{\left(g \cdot D_p \cdot R_{sd}\right) \cdot v_t \cdot \left(1 - \dfrac{C_{vs}}{\kappa_C}\right)^{\beta}}{\lambda_l\left(Re\right)} \cdot \left(\frac{1}{v_{ls}}\right)^3 \tag{7.5-12}$$

The power β is a function of the particle Reynolds number $\dfrac{v_t \cdot d}{\nu_l}$, while the friction factor λ_l is a weak function of the Reynolds number of the flow in the pipe $\dfrac{v_{ls} \cdot D_p}{\nu_l}$. Equation (7.5-10) can also be written as:

$$\Delta p_m = \Delta p_l \cdot \left(1 + 2 \cdot \Omega \cdot \left(\frac{1}{v_{ls}}\right)^3\right) \quad \text{with:} \quad \Omega = \frac{\left(g \cdot D_p \cdot R_{sd}\right) \cdot v_t \cdot \left(1 - \dfrac{C_{vs}}{\kappa_C}\right)^{\beta}}{\lambda_l\left(Re\right)} \cdot C_{vs} \tag{7.5-13}$$

Taking the derivative of equation (7.5-13) with respect to the line speed v_{ls} and making the derivative equal to 0 to find the minimum, results in a minimum at a line speed of:

$$v_{ls,min} = \Omega^{1/3} = \left(\frac{\left(g \cdot D_p \cdot R_{sd}\right) \cdot v_t \cdot \left(1 - \dfrac{C_{vs}}{\kappa_C}\right)^{\beta}}{\lambda_l\left(Re\right)} \cdot C_{vs}\right)^{1/3} \tag{7.5-14}$$

$$\Delta p_{m,min} = 3 \cdot \Delta p_l$$

So the minimum resistance equals 3 times the water resistance. Equations (7.5-10) and (7.5-13) are based on some assumptions and give an idea of what resistance equation could look like. In fact these equations are very similar to the Newitt et al. (1955) equation, except for the fact that hindered settling is taken into account. For a λ_l value of 0.02 (high Reynolds number, smooth pipe, small pipe diameter) a factor of 100 is found for $2/\lambda_l$, while Newitt et al. (1955) found a factor of 1100, which is 11 times as much as the theoretical value if hindered settling is not taken into account. Now Newitt et al. (1955) tried to explain all the excess losses being potential energy losses with a low efficiency for the potential energy. A factor of 11 without hindered settling and an even much higher factor if hindered settling is included can hardly be explained by some efficiency factor. Apparently the loss of potential energy only explains part of the pressure losses. The other part of the pressure losses will be explained by the loss of kinetic energy.

Kinetic Energy.

The power $\Delta P_{s, kin}$ required to pump the solids/liquid mixture over a distance ΔL because of the constant loss of kinetic energy due to impact of the particles with the wall and due to acceleration and deceleration in eddies, is the result of the pressure difference $\Delta p_{s, kin}$ times the cross-section of the pipe A_p times the line speed v_{ls}.

$$\Delta P_{s,kin} = \Delta p_{s,kin} \cdot A_p \cdot v_{ls} \tag{7.5-15}$$

The slip velocity v_{sl} is defined as the difference between the average liquid velocity v_l and the average particle velocity v_p resulting in a drag force.

$$v_{sl} = v_l - v_p \tag{7.5-16}$$

The volume flow of mixture Q_m is equal to the volume flow of liquid Q_l plus the volume flow of particles Q_p, thus:

$$Q_m = Q_l + Q_p \quad \Rightarrow \quad A_p \cdot v_{ls} = A_p \cdot (1 - C_{vs}) \cdot v_l + A_p \cdot C_{vs} \cdot v_p \tag{7.5-17}$$

Giving:

$$v_{ls} = v_l + C_{vs} \cdot (v_p - v_l) = v_l - C_{vs} \cdot v_{sl} \tag{7.5-18}$$

The liquid velocity v_l is higher than the line speed v_{ls}. As we will see later, the slip velocity v_{sl} is much smaller than the line speed v_{ls} and in general this effect can be neglected. Only at very small line speeds, at high concentrations and with large particles, the equations derived may need a correction. However this will in general be far below the Limit Deposit Velocity $v_{ls,ldv}$, while here heterogeneous transport is considered.

$$v_l = v_{ls} + C_{vs} \cdot v_{sl} \tag{7.5-19}$$

Suppose particles hit the wall or interact with eddies and loose some of their speed, let's say by a value v_{sl}, the slip velocity. The kinetic energy lost by the particle is now:

$$\Delta E_{s,kin,p} = \frac{1}{2} \cdot m_p \cdot v_l^2 - \frac{1}{2} \cdot m_p \cdot (v_l - v_{sl})^2 = \frac{1}{2} \cdot m_p \cdot \left(2 \cdot v_l \cdot v_{sl} - v_{sl}^2\right) \tag{7.5-20}$$

$$\Delta E_{s,kin,p} = \frac{1}{2} \cdot m_p \cdot \left(2 \cdot (v_{ls} + C_{vs} \cdot v_{sl}) \cdot v_{sl} - v_{sl}^2\right) = \frac{1}{2} \cdot m_p \cdot \left(2 \cdot v_{ls} \cdot v_{sl} + (2 \cdot C_{vs} - 1) \cdot v_{sl}^2\right)$$

Assuming that the slip velocity v_{sl} is much smaller than the line speed v_{ls}, this gives:

$$m_p = \rho_s \cdot \frac{\pi}{6} \cdot d^3 \quad \textbf{giving:} \quad \Delta E_{s,kin,p} = \frac{1}{2} \cdot m_p \cdot 2 \cdot v_{ls} \cdot v_{sl} = m_p \cdot v_{ls} \cdot v_{sl} = \rho_s \cdot \frac{\pi}{6} \cdot d^3 \cdot v_{ls} \cdot v_{sl} \tag{7.5-21}$$

The number of particles in a pipeline with length ΔL and cross-section of the pipe A_p is:

$$n = \frac{A_p \cdot \Delta L \cdot C_{vs}}{\frac{\pi}{6} \cdot d^3} \tag{7.5-22}$$

Giving for the total loss of kinetic energy in a pipe with length ΔL and cross-section of the pipe A_p :

$$\Delta E_{s,kin,tot} = n \cdot \Delta E_{s,kin,p} = A_p \cdot \Delta L \cdot C_{vs} \cdot \rho_s \cdot v_{ls} \cdot v_{sl} \tag{7.5-23}$$

The order of magnitude of the time required to dissipate this energy can be determined assuming that this energy also follows from the drag force on a particle:

$$F_D = C_D \cdot \frac{1}{2} \cdot \rho_l \cdot v_{sl}^2 \cdot A_s \tag{7.5-24}$$

The total drag force on n particles is now:

$$F_{D,tot} = n \cdot C_D \cdot \frac{1}{2} \cdot \rho_l \cdot v_{sl}^2 \cdot A_s = \frac{3 \cdot A_p \cdot \Delta L \cdot C_{vs} \cdot C_D \cdot \rho_l \cdot v_{sl}^2}{4 \cdot d} \tag{7.5-25}$$

Since energy or work equals force $F_{D, tot}$ times a distance s, for the distance we find:

$$s = \frac{\Delta E_{s,kin,tot}}{F_{D,tot}} = \frac{4 \cdot \rho_s \cdot v_{ls} \cdot d}{3 \cdot \rho_l \cdot v_{sl} \cdot C_D} \tag{7.5-26}$$

The time required to travel the distance s equals the distance s divided by the line speed v_{ls}, thus:

$$\Delta t = \frac{4 \cdot \rho_s \cdot d}{3 \cdot \rho_l \cdot v_{sl} \cdot C_D} \tag{7.5-27}$$

In the Stokes region this can be written as the relaxation time used in the Stokes number:

$$\Delta t = \frac{4 \cdot \rho_s \cdot d}{3 \cdot \rho_l \cdot v_{sl} \cdot C_D} = \frac{4 \cdot \rho_s \cdot d \cdot Re_p}{3 \cdot \rho_l \cdot v_{sl} \cdot 24} = \frac{4 \cdot \rho_s \cdot d \cdot v_{sl} \cdot d}{3 \cdot \rho_l \cdot v_{sl} \cdot 24 \cdot \nu} = \frac{d^2 \cdot \rho_s}{18 \cdot \rho_l \cdot \nu} \tag{7.5-28}$$

The power required for constantly adding the dissipated kinetic energy to the mixture equals the energy losses divided by the time in which they take place, thus:

$$\Delta P_{s,kin} = \frac{\Delta E_{s,kin,tot}}{\Delta t} = \frac{3 \cdot A_p \cdot \Delta L \cdot C_{vs} \cdot \rho_l \cdot v_{ls} \cdot v_{sl}^2 \cdot C_D}{4 \cdot d} \tag{7.5-29}$$

This gives the hydraulic gradient required for the compensation of the losses of kinetic energy of:

$$\frac{\Delta p_{s,kin}}{\Delta L} = \frac{\Delta P_{s,kin}}{A_p \cdot \Delta L \cdot v_{ls}} = \frac{3 \cdot \rho_l \cdot v_{sl}^2 \cdot C_D}{4 \cdot d} \cdot C_{vs} \tag{7.5-30}$$

In the Stokes region the drag coefficient C_D is:

$$C_D = \frac{24}{Re_p} = \frac{24 \cdot \nu_l}{v_{sl} \cdot d} \tag{7.5-31}$$

For the laminar Stokes region the hydraulic gradient can now be written as:

$$\frac{\Delta p_{s,kin}}{\Delta L} = \frac{\Delta P_{s,kin}}{A_p \cdot \Delta L \cdot v_{ls}} = 18 \cdot \frac{\rho_l \cdot v_{sl} \cdot \nu_l}{d^2} \cdot C_{vs} \tag{7.5-32}$$

In the turbulent region the drag coefficient C_D is:

$$\begin{aligned} C_D &= 0.445 \quad \text{for spheres} \\ C_D &\approx 1 \quad\quad \text{for sand} \end{aligned} \tag{7.5-33}$$

For the turbulent region the hydraulic gradient can now be written as:

$$\frac{\Delta p_{s,kin}}{\Delta L} = 0.33 \cdot \frac{\rho_l \cdot v_{sl}^2}{d} \cdot C_{vs} \quad \text{for spheres}$$

$$\tag{7.5-34}$$

$$\frac{\Delta p_{s,kin}}{\Delta L} = 0.75 \cdot \frac{\rho_l \cdot v_{sl}^2}{d} \cdot C_{vs} \quad \text{for sand particles}$$

Using the equation for the drag coefficient to replace the drag coefficient in equation (7.5-30) with the terminal settling velocity, gives:

$$C_D = \frac{4 \cdot g \cdot (\rho_s - \rho_l) \cdot d}{3 \cdot \rho_l \cdot v_t^2} = \frac{4 \cdot g \cdot R_{sd} \cdot d}{3 \cdot v_t^2} \tag{7.5-35}$$

This gives for the pressure losses due to kinetic energy:

$$\frac{\Delta p_{s,kin}}{\Delta L} = \rho_l \cdot \left(\frac{v_{sl}}{v_t}\right)^2 \cdot g \cdot R_{sd} \cdot C_{vs} \tag{7.5-36}$$

In terms of the hydraulic gradient this gives:

$$i_{s,kin} = \frac{\Delta p_{s,kin}}{\rho_l \cdot g \cdot \Delta L} = \left(\frac{v_{sl}}{v_t}\right)^2 \cdot R_{sd} \cdot C_{vs} \tag{7.5-37}$$

In terms of the relative excess hydraulic gradient component E_{rhg} due to kinetic energy losses S_{rs} this gives the ratio of the slip velocity to the terminal settling velocity squared:

$$S_{rs} = \frac{i_{s,kin}}{R_{sd} \cdot C_{vs}} = \left(\frac{v_{sl}}{v_t}\right)^2 \tag{7.5-38}$$

Viscous + Potential + Kinetic Energy.

The total pressure required to push the solids/liquid mixture through the pipeline is now:

$$\Delta p_m = \Delta p_l + \Delta p_{s,pot} + \Delta p_{s,kin} = \Delta p_l \cdot \left(1 + \frac{\Delta p_{s,pot}}{\Delta p_l} + \frac{\Delta p_{s,kin}}{\Delta p_l}\right) \tag{7.5-39}$$

Substituting equations (7.5-7) for the potential energy losses and (7.5-36) for the kinetic energy losses gives:

$$\Delta p_m = \Delta p_l \cdot \left(1 + \frac{\rho_l \cdot \left(\frac{v_t \cdot \left(1 - \frac{C_{vs}}{\kappa_C}\right)^\beta}{v_{ls}}\right) \cdot g \cdot R_{sd} \cdot C_{vs}}{\lambda_l \cdot \frac{1}{D_p} \cdot \frac{1}{2} \cdot \rho_l \cdot v_{ls}^2} + \frac{\rho_l \cdot \left(\frac{v_{sl}}{v_t}\right)^2 \cdot g \cdot R_{sd} \cdot C_{vs}}{\lambda_l \cdot \frac{1}{D_p} \cdot \frac{1}{2} \cdot \rho_l \cdot v_{ls}^2}\right) \tag{7.5-40}$$

$$\Delta p_m = \Delta p_l \cdot \left(1 + \frac{\left(2 \cdot g \cdot R_{sd} \cdot D_p\right)}{\lambda_l} \cdot C_{vs} \cdot \frac{1}{v_{ls}^2} \cdot \left(\frac{v_t \cdot \left(1 - \frac{C_{vs}}{\kappa_C}\right)^\beta}{v_{ls}} + \left(\frac{v_{sl}}{v_t}\right)^2\right)\right)$$

In terms of the hydraulic gradient i_m this gives:

$$i_m = i_l \cdot \left(1 + \frac{\left(2 \cdot g \cdot R_{sd} \cdot D_p\right)}{\lambda_l} \cdot C_{vs} \cdot \frac{1}{v_{ls}^2} \cdot \left(\frac{v_t \cdot \left(1 - \frac{C_{vs}}{\kappa_C}\right)^\beta}{v_{ls}} + \left(\frac{v_{sl}}{v_t}\right)^2\right)\right) \tag{7.5-41}$$

In terms of the relative excess hydraulic gradient E_{rhg} this gives:

$$E_{rhg} = \frac{i_m - i_l}{R_{sd} \cdot C_{vs}} = \frac{v_t \cdot \left(1 - \dfrac{C_{vs}}{\kappa_C}\right)^{\beta}}{v_{ls}} + \left(\frac{v_{sl}}{v_t}\right)^2 = S_{hr} + S_{rs} \tag{7.5-42}$$

Note that the term for potential energy losses contains the hindered settling influence, while the kinetic energy term does not, because the drag coefficient is replaced by the terminal settling velocity without hindered settling. The first term is similar to the Newitt et al. (1955) equation (1955), but with a different coefficient. Newitt et al. (1955) uses a factor of 1100, which should be the result of **2/λ_l**. However, applying a **λ_l=0.02** for smooth pipes and high Reynolds numbers results in a factor of 100. Newitt et al. (1955) however did not include the kinetic energy term as such. Equation (7.5-21) shows that the loss of kinetic energy is proportional to the line speed v_{ls} and the slip velocity v_{sl}. The question is, is the slip velocity v_{sl} a constant or does it depend on parameters like the line speed v_{ls}, the terminal settling velocity v_t and the concentration C_{vs}.

7.5.3 Estimating the Slip Velocity.

In order to get some impression regarding the slip velocity, first consider that the kinetic energy losses depend on collisions between particles and the pipe wall. According to equation (7.5-21) the slip velocity can be expressed as:

$$\Delta E_{s,kin,p} = m_p \cdot v_{ls} \cdot v_{sl} \quad \Rightarrow \quad v_{sl} = \frac{\Delta E_{s,kin,p}}{m_p \cdot v_{ls}} \tag{7.5-43}$$

Which is roughly the energy loss per collision or interaction, divided by the momentum of the particle.

Small Particles:
Now suppose the energy loss per collision or interaction equals the kinetic energy of a particle, based on a factor **α_k** times the terminal settling velocity v_t:

$$\Delta E_{s,kin,p} = \frac{1}{2} \cdot m_p \cdot \left(\alpha_k \cdot v_t\right)^2 \quad \Rightarrow \quad v_{sl} = \frac{\frac{1}{2} \cdot m_p \cdot \left(\alpha_k \cdot v_t\right)^2}{m_p \cdot v_{ls}} = \frac{\alpha_k^2}{2} \cdot \frac{v_t^2}{v_{ls}} \tag{7.5-44}$$

The contribution of the kinetic energy losses to the relative excess hydraulic gradient E_{rhg}, the S_{rs} parameter is now:

$$S_{rs} = \left(\frac{v_{sl}}{v_t}\right)^2 = \left(\frac{\alpha_k^2}{2} \cdot \frac{v_t}{v_{ls}}\right)^2 = \frac{\alpha_k^4}{4} \cdot \frac{v_t^2}{v_{ls}^2} \tag{7.5-45}$$

Large Particles:
Another assumption may be that the translational kinetic energy loss per interaction is proportional to the momentum of a particle based on the terminal setting velocity v_t with a factor **α_m**.

$$\Delta E_{s,kin,p} = m_p \cdot \left(\alpha_m \cdot v_t\right) \quad \Rightarrow \quad v_{sl} = \frac{\alpha_m \cdot m_p \cdot v_t}{m_p \cdot v_{ls}} = \alpha_m \cdot \frac{v_t}{v_{ls}} \tag{7.5-46}$$

The contribution of the kinetic energy losses to the relative excess hydraulic gradient E_{rhg}, the S_{rs} parameter is now:

$$S_{rs} = \left(\frac{v_{sl}}{v_t}\right)^2 = \left(\alpha_m \cdot \frac{1}{v_{ls}}\right)^2 = \alpha_m^2 \cdot \frac{1}{v_{ls}^2} \tag{7.5-47}$$

Medium Particles:

The transition between the above two assumptions could be that the translational kinetic energy loss per interaction is proportional to the terminal settling velocity to a power of 1.5, based on the terminal setting velocity v_t with a factor α_t.

$$\Delta E_{s,kin,p} = m_p \cdot \left(\alpha_t \cdot v_t \right)^{3/2} \quad \Rightarrow \quad v_{sl} = \frac{\alpha_t^{3/2} \cdot m_p \cdot v_t^{3/2}}{m_p \cdot v_{ls}} = \alpha_t^{3/2} \cdot \frac{v_t^{3/2}}{v_{ls}} \tag{7.5-48}$$

The contribution of the kinetic energy losses to the relative excess hydraulic gradient E_{rhg}, the S_{rs} parameter is now:

$$S_{rs} = \left(\frac{v_{sl}}{v_t} \right)^2 = \left(\alpha_t^{3/2} \cdot \frac{v_t^{1/2}}{v_{ls}} \right)^2 = \alpha_t^3 \cdot \frac{v_t}{v_{ls}^2} \tag{7.5-49}$$

Although these are reasonable first assumptions, the loss of kinetic energy will most probably depend on more factors. Assuming that the loss of translational kinetic energy is mainly caused by the transition of translational kinetic energy to rotational kinetic energy, whether this is the result of interactions with the viscous sub-layer velocity gradient or by collision to the pipe wall. The rotation of the particles results in a radial inwards lift force (for example the near wall lift force) due to the velocity gradient, especially in the viscous sub-layer and due to the magnitude of the slip velocity. This radial inwards lift force will first decelerate the particle outward radial velocity and then accelerate particles giving them an inward radial velocity. It seems like particles having an outward radial velocity, will bounce back on the viscous sub-layer or for large particles partly on the viscous sub-layer and partly on the pipe wall. Since the velocity gradient in the viscous sub-layer, but also in the buffer layer, increases with the line speed and the inwards radial lift force depends on this velocity gradient, the time and thus the penetration distance required to make a particle bounce back on the viscous sub-layer will be reversely proportional to the line speed. So the increase of the velocity gradient in the viscous sub-layer with the line speed on one hand and the time required to develop enough lift force to make the particle bounce back being reversely proportional to the line speed, neutralize each other. Maybe not completely, but the result will be that the loss of kinetic translational energy, being the gained rotational kinetic energy, will be almost independent of the line speed. Since a slurry in general does not consist of spherical particles, will not be uniform in general and will have a lot of interactions between the particles, a real slurry may deviate from this assumption, resulting in at least a different proportionality constant as is discussed later. Still the starting point will be that the loss of translational kinetic energy is independent of the line speed. Non-spherical particles will have a larger drag coefficient and will be more sensitive for loosing translational energy, resulting in higher losses. The gained rotational energy will be dissipated in the turbulent flow.

A first parameter is the ratio of the thickness of the viscous sub-layer to the particle diameter, since the interaction or collision with the pipe wall will take place in the viscous sub-layer. Due to the interaction or collision, the particle will start rotating and part of the translational kinetic energy will be transferred into rotational kinetic energy, which will be transferred into heat by viscous friction later. This ratio is an indication of the concentration of particles in the viscous sub layer, due to geometry, and is a measure for the lubrication in the viscous sub layer. This ratio can never be larger than 1 (only for very small particles and/or very low line speeds), meaning the concentration in the viscous sub layer equals the average concentration. The ratio of the thickness of the viscous sub-layer to the particle diameter is:

$$\frac{\delta_v}{d} = \frac{11.6 \cdot \dfrac{v_l}{u_*}}{d} = \frac{11.6 \cdot v_l}{\sqrt{\lambda_l / 8} \cdot v_{ls} \cdot d} = \frac{32.81 \cdot v_l}{\sqrt{\lambda_l} \cdot v_{ls} \cdot d} \tag{7.5-50}$$

A second parameter is the ratio between the terminal settling velocity and the maximum velocity in the viscous sub-layer, giving an indication of the angle under which the particle will hit the viscous sub-layer, the angle of attack or the collision impact factor (Figure 7.5-1):

$$\text{angle of attack} = \left(\frac{v_t}{11.6 \cdot u_*} \right) = \left(\frac{v_t}{11.6 \cdot \sqrt{\dfrac{\lambda_l}{8}} \cdot v_{ls}} \right) = \left(\frac{v_t}{4.1 \cdot \sqrt{\lambda_l} \cdot v_{ls}} \right) \tag{7.5-51}$$
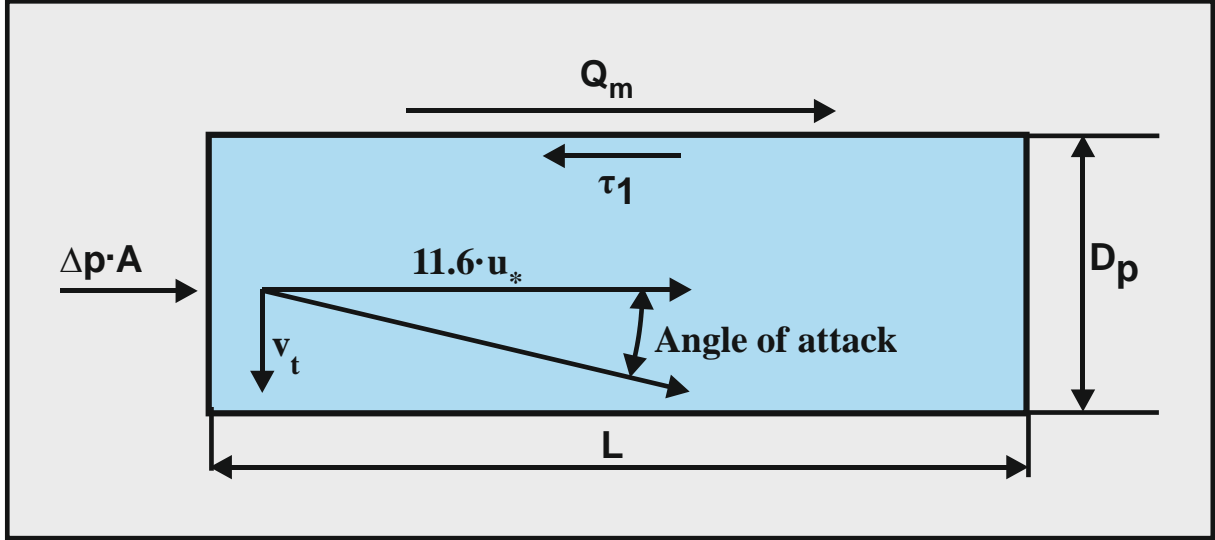
Figure 7.5-1: The angle of attack.

A third parameter is the drag coefficient C_D. Different drag coefficients are involved. On one hand the translational drag coefficient, used to determine the translational drag force. On the other hand the rotational drag force used to determine the rotational acceleration of a particle in a flow with rotation. In its current form, the coefficient as used here describes the drag coefficient of the particle.

A fourth parameter is the relative submerged density R_{sd}.

Since Durand & Condolios (1952) already determined the influence of the particle Froude number on the head losses, this particle Froude number will be used as a measure for the drag coefficients, so resulting equations can be compared.

$$\mathbf{Fr_p} = \left(\frac{v_t}{\sqrt{g \cdot d}}\right) = \left(\frac{4}{3} \cdot \frac{\xi \cdot R_{sd}}{C_D}\right)^{1/2} \approx \left(\frac{R_{sd}}{C_D}\right)^{1/2} \tag{7.5-52}$$

The Froude number on the right side is a modified Froude number, calibrated on experiments and the use of the Zanke settling velocity equation. Last but not least, the terminal settling velocity is chosen as a fifth parameter. This gives for the translational kinetic energy loss per interaction or collision:

$$\Delta E_{s,kin,p} = m_p \cdot v_{sl} \cdot v_{ls} = c \cdot m_p \cdot \left(\frac{\delta_v}{d}\right)^{\alpha_1} \cdot \left(\frac{v_t}{11.6 \cdot u_*}\right)^{\alpha_2} \cdot \left(\left(\frac{R_{sd}}{C_D}\right)^{1/2}\right)^{\alpha_3} \cdot v_t \cdot v_{ls} \tag{7.5-53}$$

This can also be written as:

$$\Delta E_{s,kin,p} = m_p \cdot v_{sl} \cdot v_{ls} = c \cdot m_p \cdot \left(\frac{32.81 \cdot \nu_l}{\sqrt{\lambda_l} \cdot v_{ls} \cdot d}\right)^{\alpha_1} \cdot \left(\frac{v_t}{4.1 \cdot \sqrt{\lambda_l} \cdot v_{ls}}\right)^{\alpha_2} \cdot \left(\left(\frac{R_{sd}}{C_D}\right)^{1/2}\right)^{\alpha_3} \cdot v_t \cdot v_{ls} \tag{7.5-54}$$

Because of the assumption that the loss of translational kinetic energy per interaction is independent of the line speed, the following condition is valid:

$$\alpha_1 + \alpha_2 = 1 \tag{7.5-55}$$

Equation (7.5-54) can also be written as, matching the Durand & Condolios (1952) particle Froude number:

$$\Delta E_{s,kin,p} = c \cdot m_p \cdot \left(\frac{32.81}{\sqrt{\lambda_l}}\right)^{\alpha_1} \cdot \left(\frac{1}{4.1 \cdot \sqrt{\lambda_l}}\right)^{\alpha_2} \cdot \frac{v_t^{\alpha_2 + \alpha_3}}{\sqrt{g \cdot d}^{2 \cdot \alpha_1 + \alpha_3}} \cdot \frac{(\nu_l \cdot g)^{\alpha_1}}{v_{ls}^{\alpha_1 + \alpha_2}} \cdot v_t \cdot v_{ls} \qquad (7.5\text{-}56)$$

Assuming the terms in this equation are dimensionless as well, the following relations are found:

$$\alpha_2 + \alpha_3 = 2 \cdot \alpha_1 + \alpha_3 \quad \Rightarrow \quad \alpha_2 = 2 \cdot \alpha_1 \quad \text{and} \quad \alpha_1 + \alpha_2 = 3 \cdot \alpha_1 \quad \Rightarrow \quad \alpha_2 = 2 \cdot \alpha_1 \qquad (7.5\text{-}57)$$

This gives $\alpha_1 = 1/3$ and $\alpha_2 = 2/3$. In order to find a value for α_3, the data of Gibert (1960) are used. According to Miedema (2013) the total power of the particle Froude number in the Durand & Condolios (1952) equation should not be 1.5, but about 10/3, which is $\alpha_2 + \alpha_3$ squared. This gives: $\alpha_2 + \alpha_3 = 10/6 = 5/3$. Since $\alpha_2 = 2/3$, this gives: $\alpha_3 = 1$:

$$\Delta E_{s,kin,p} = c \cdot m_p \cdot \left(\frac{\delta_v}{d}\right)^{2/6} \cdot \left(\frac{v_t}{11.6 \cdot u_*}\right)^{4/6} \cdot \left(\frac{v_t}{\sqrt{g \cdot d}}\right)^1 \cdot v_t \cdot v_{ls} \qquad (7.5\text{-}58)$$

Or:

$$\Delta E_{s,kin,p} = 1.25 \cdot c \cdot m_p \cdot \left(\frac{1}{\sqrt{\lambda_l}}\right) \left(\frac{v_t}{\sqrt{g \cdot d}}\right)^{5/3} \cdot \left(\frac{(\nu_l \cdot g)^{1/3}}{v_{ls}}\right) \cdot v_t \cdot v_{ls} \quad \text{with:} \quad \left(\frac{32.81}{4.1^2}\right)^{1/3} = 1.25 \qquad (7.5\text{-}59)$$

The above equations give for the slip velocity:

$$v_{sl} = \frac{\Delta E_{s,kin,p}}{m_p \cdot v_{ls}} = c \cdot \left(\frac{\delta_v}{d}\right)^{2/6} \cdot \left(\frac{v_t}{11.6 \cdot u_*}\right)^{4/6} \cdot \left(\frac{v_t}{\sqrt{g \cdot d}}\right)^1 \cdot v_t \qquad (7.5\text{-}60)$$

Or, using other dimensionless relations:

$$v_{sl} = 1.25 \cdot c \cdot \left(\frac{1}{\sqrt{\lambda_l}}\right) \left(\frac{v_t}{\sqrt{g \cdot d}}\right)^{5/3} \cdot \left(\frac{(\nu_l \cdot g)^{1/3}}{v_{ls}}\right) \cdot v_t \qquad (7.5\text{-}61)$$

Also based on Durand & Condolios (1952) and many others, the proportionality coefficient c is determined to be about $c = 6.8$. The powers and the proportionality coefficient match the findings of Miedema & Ramsdell (2013), but with the addition of the friction coefficient λ_l in the equations and a slightly higher power of the line speed term, 1 instead of 0.89. In the slip velocity notation, Durand & Condolios (1952), Newitt at al. (1955), Fuhrboter (1961) and Jufin & Lopatin (1966) would have a power of 0.5, Zandi & Govatos (1967) a power of 0.93 and Wilson et al. (1992) a maximum power of 0.85. Wilson et al. (1992) state that the highest power has to be applied for uniform sands, while this power decreases depending on the sand. An upper limit of a power of 1, matching the assumption that the energy loss per interaction does not depend on the line speed, seems reasonable. The reason for a lower power for non-uniforms sands and gravels may be found in the way the E_{rhg} curves for the different fractions are added to a curve for the whole PSD. For the full range of particle diameters the contribution of the translational kinetic energy losses, the S_{rs} parameter, is:

$$S_{rs} = \left(\frac{v_{sl}}{v_t}\right)^2 = 8.5^2 \cdot \left(\frac{1}{\lambda_l}\right) \left(\frac{v_t}{\sqrt{g \cdot d}}\right)^{10/3} \cdot \left(\frac{(\nu_l \cdot g)^{1/3}}{v_{ls}}\right)^2 = \frac{8.5^2}{8} \cdot \left(\frac{v_t}{\sqrt{g \cdot d}}\right)^{10/3} \cdot \left(\frac{(\nu_l \cdot g)^{1/3}}{\sqrt{\lambda_l / 8} \cdot v_{ls}}\right)^2 \qquad (7.5\text{-}62)$$

Giving for the relative excess hydraulic gradient, the E_{rhg} parameter:

$$E_{rhg} = \frac{i_m - i_l}{R_{sd} \cdot C_{vs}} = S_{hr} + S_{rs} = \frac{v_t \cdot \left(1 - \dfrac{C_{vs}}{0.175 \cdot (1 + \beta)}\right)^\beta}{v_{ls}} + 8.5^2 \cdot \left(\frac{1}{\lambda_l}\right) \left(\frac{v_t}{\sqrt{g \cdot d}}\right)^{10/3} \cdot \left(\frac{(\nu_l \cdot g)^{1/3}}{v_{ls}}\right)^2 \qquad (7.5\text{-}63)$$

The resulting equation, **which is the main finding of this chapter**, can be considered to be the sedimentation capability (potential energy losses) plus the collision intensity times the collision impact (kinetic energy losses). The coefficient of 8.5 is a good first estimate, but may vary around 8.5 depending on the character of the sand or gravel. In this study, most experiments match the equation well using the coefficient of 8.5. This equation is the basis of the DHLLDV heterogeneous regime model and is used for both uniform and graded sands and gravels.
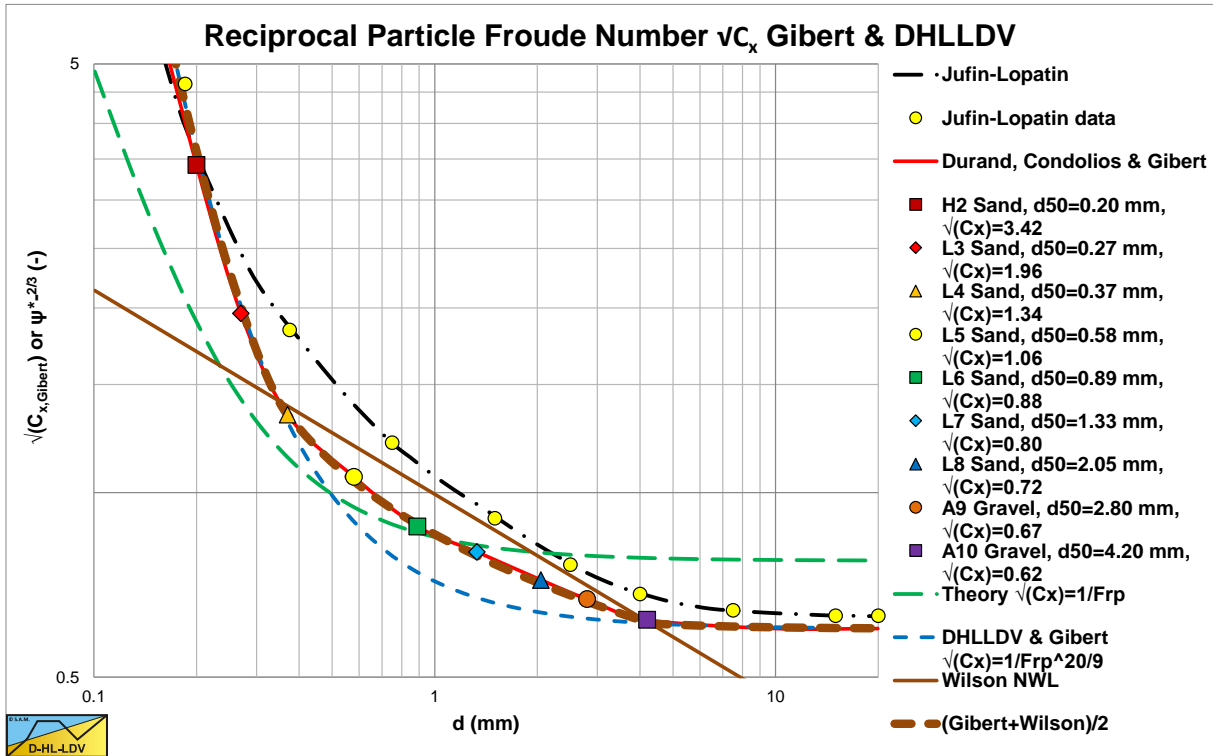
Figure 7.5-2: Reciprocal particle Froude number after Gibert (1960).
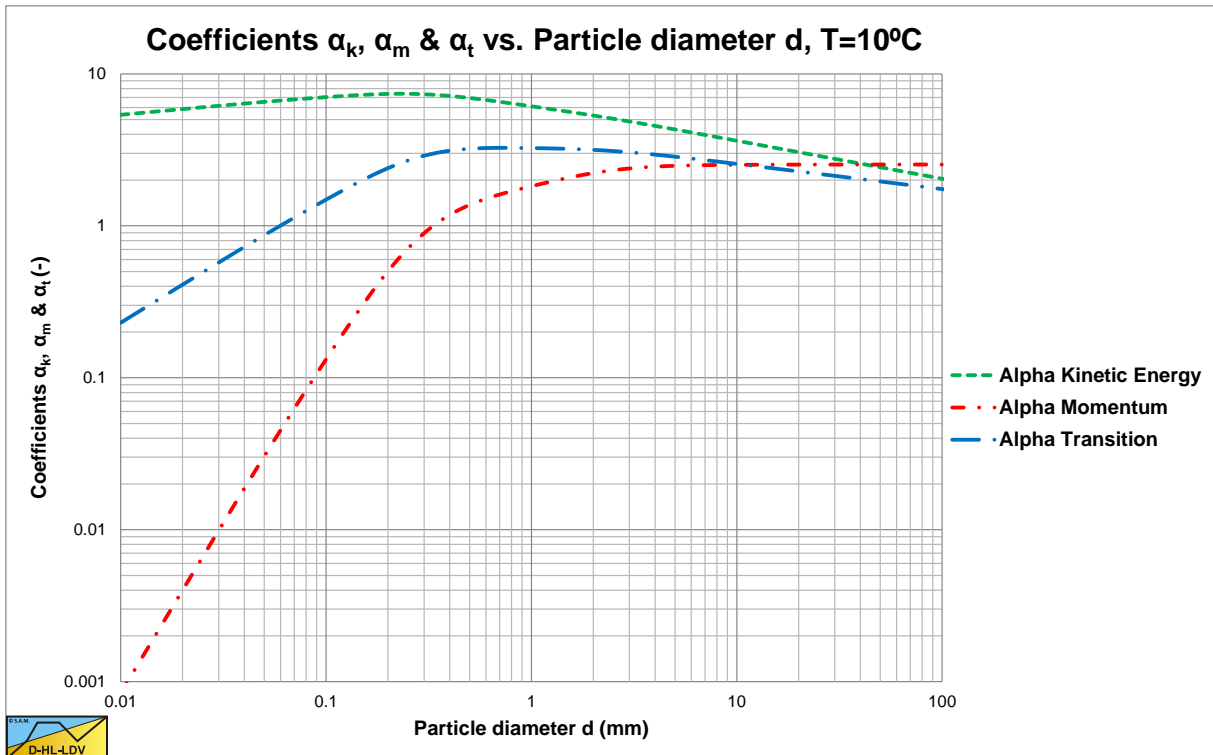
Figure 7.5-3: The factors α_k, α_m and α_t as a function of the particle diameter for a D_p=0.3 m pipe and T=10ºC.

7.5.4 Simplified Models.

It is now interesting to see if the equation derived can be simplified for 6 specific cases. To do this two kinematic viscosities and three pipe diameters are considered for sand and gravel. The two kinematic viscosities match temperatures of 10ºC (reality) and 20ºC (laboratory), the pipe diameters are 0.0254 m (small), 0.3 m (medium) and 1.2 m (large). The relative submerged density is assumed to be 1.585 for salt water.

Figure 7.5 2 shows the 3 coefficients as a function of the particle diameter for a **D_p=0.3 m** pipe and **T=10ºC**, while Table 7.5 1 shows the viscosities and Darcy Weisbach friction factors used here. The simplified models are based on a power of 3 of the particle Froude number instead of 10/3.

Table 7.5-1: The viscosities and Darcy Weisbach friction coefficients.

	Viscosity (m²/s)	D_p=0.0254 m	D_p=0.3 m	D_p=1.2 m
T=10ºC	0.0000013	0.0214	0.0113	0.0085
T=20ºC	0.0000010	0.0202	0.0109	0.0082

7.5.4.1 Simplified Model for Small Particles, d<0.3 mm.

For small particles, **d<0.3 mm**, in terms of the kinetic translational energy of a particle based on the terminal settling velocity, the following expression can now be found:

$$\Delta E_{s,kin,p} = \frac{1}{2} \cdot m_p \cdot \left(\alpha_k \cdot v_t \right)^2 = 2 \cdot 8.5 \cdot \frac{\left(\nu_l \cdot g \right)^{1/3}}{\sqrt{\lambda_l} \cdot \sqrt{g \cdot d}} \cdot \left(\frac{v_t}{\sqrt{g \cdot d}} \right)^{1/2} \cdot \frac{1}{2} \cdot m_p \cdot v_t^2 \tag{7.5-64}$$

The factor **α_k** is now:

$$\alpha_k = \sqrt{2 \cdot 8.5 \cdot \frac{\left(\nu_l \cdot g \right)^{1/3}}{\sqrt{\lambda_l} \cdot \sqrt{g \cdot d}} \cdot \left(\frac{v_t}{\sqrt{g \cdot d}} \right)^{1/2}} \tag{7.5-65}$$

So for small particles, the slip velocity can be determined as:

$$v_{sl} = \frac{\Delta E_{s,kin,p}}{m_p \cdot v_{ls}} = \frac{\left(\alpha_k \cdot v_t \right)^2}{2 \cdot v_{ls}} \tag{7.5-66}$$

This gives for the contribution of the kinetic energy losses to the relative excess hydraulic gradient **E_{rhg}**, the **S_{rs}** parameter, for small particles as a first estimate:

$$S_{rs} = \left(\frac{v_{sl}}{v_t} \right)^2 = \left(\frac{\alpha_k^2}{2} \cdot \frac{v_t}{v_{ls}} \right)^2 = \beta_k \cdot \frac{v_t^2}{v_{ls}^2} \tag{7.5-67}$$

In terms of the excess hydraulic gradient **E_{rhg}** this gives:

$$E_{rhg} = \frac{i_m - i_l}{R_{sd} \cdot C_{vs}} = S_{hr} + S_{rs} = \frac{v_t \cdot \left(1 - \dfrac{C_{vs}}{0.175 \cdot (1+\beta)} \right)^\beta}{v_{ls}} + \beta_k \cdot \frac{v_t^2}{v_{ls}^2} \tag{7.5-68}$$

Table 7.5-2: Values of α_k and β_k.

	D_p=0.0254 m	D_p=0.3 m	D_p=1.2 m
α_k - T=10ºC	5.51	6.47	6.94
β_k - T=10ºC	230.69	436.88	580.80
α_k - T=20ºC	5.72	6.67	7.16
β_k - T=20ºC	266.87	494.58	657.42

7.5.4.2 Simplified Model for Medium Sized Particles, 0.3 mm≤d≤2 mm.

In terms of the transition range of particles, **d=0.3 mm** to about **d=2 mm,** based on the terminal settling velocity to the power 1.5 this gives:

$$\Delta E_{s,kin,p} = \alpha_t^{3/2} \cdot m_p \cdot v_t^{3/2} = 8.5 \cdot \frac{(v_l \cdot g)^{1/3}}{\sqrt{\lambda_l} \cdot \sqrt[4]{g \cdot d}} \cdot \left(\frac{v_t}{\sqrt{g \cdot d}} \right)^1 \cdot m \cdot v_t^{3/2} \tag{7.5-69}$$

The factor α_t is now:

$$\alpha_t = \left(8.5 \cdot \frac{(v_l \cdot g)^{1/3}}{\sqrt{\lambda_l} \cdot \sqrt[4]{g \cdot d}} \cdot \left(\frac{v_t}{\sqrt{g \cdot d}} \right)^1 \right)^{2/3} \tag{7.5-70}$$

So for medium sized particles, the slip velocity can be determined as:

$$v_{sl} = \frac{\Delta E_{s,kin,p}}{m_p \cdot v_{ls}} = \frac{(\alpha_t \cdot v_t)^{3/2}}{v_{ls}} \tag{7.5-71}$$

This gives for the contribution of the kinetic energy losses to the excess hydraulic gradient E_{rhg}, the S_{rs} parameter, for particles from about **d=0.3 mm** to about **d=2 mm** as a first estimate:

$$S_{rs} = \left(\frac{v_{sl}}{v_t} \right)^2 = \left(\frac{\alpha_t^{3/2} \cdot v_t^{1/2}}{v_{ls}} \right)^2 = \beta_t \cdot \frac{v_t}{v_{ls}^2} \tag{7.5-72}$$

Table 7.5-3: Values of α_t and β_t.

	D_p=0.0254 m	D_p=0.3 m	D_p=1.2 m
α_t - T=10ºC	2.42	3.00	3.29
β_t - T=10ºC	14.19	26.87	35.72
α_t - T=20ºC	2.41	2.96	3.25
β_t - T=20ºC	13.95	25.84	34.35

The value of **2.97** is an average in the range **d=0.3 mm** to **d=2 mm.** In terms of the relative excess hydraulic gradient E_{rhg} this gives:

$$E_{rhg} = \frac{i_m - i_l}{R_{sd} \cdot C_{vs}} = S_{hr} + S_{rs} = \frac{v_t \cdot \left(1 - \dfrac{C_{vs}}{0.175 \cdot (1+\beta)}\right)^{\beta}}{v_{ls}} + \beta_t \cdot \frac{v_t}{v_{ls}^2} \tag{7.5-73}$$

7.5.4.3 Simplified Model for Large Particles, d>2 mm.

For large particles, **d>2 mm,** in terms of the momentum of a particle, based on the terminal settling velocity this gives:

$$\Delta E_{s,kin,p} = \alpha_m \cdot m_p \cdot v_t = 8.5 \cdot \left(\frac{\nu_l \cdot g}{\sqrt{\lambda_l}}\right)^{1/3} \cdot \left(\frac{1}{\sqrt{\lambda_l}}\right)^{2/3} \cdot \left(\frac{v_t}{\sqrt{g \cdot d}}\right)^{3/2} \cdot m \cdot v_t \tag{7.5-74}$$

The factor α_m is now:

$$\alpha_m = 8.5 \cdot \left(\frac{\nu_l \cdot g}{\sqrt{\lambda_l}}\right)^{1/3} \cdot \left(\frac{1}{\sqrt{\lambda_l}}\right)^{2/3} \cdot \left(\frac{v_t}{\sqrt{g \cdot d}}\right)^{3/2} \tag{7.5-75}$$

So for large particles, the slip velocity can be determined as:

$$v_{sl} = \frac{\Delta E_{s,kin,p}}{m_p \cdot v_{ls}} = \alpha_m \cdot \frac{v_t}{v_{ls}} \tag{7.5-76}$$

This gives for the contribution of the kinetic energy losses to the excess hydraulic gradient E_{rhg}, the S_{rs} parameter, for large particles as a first estimate:

$$S_{rs} = \left(\frac{v_{sl}}{v_t}\right)^2 = \left(\frac{\alpha_m}{v_{ls}}\right)^2 = \beta_m \cdot \frac{1}{v_{ls}^2} \tag{7.5-77}$$

In terms of the excess hydraulic gradient E_{rhg} this gives:

$$E_{rhg} = \frac{i_m - i_l}{R_{sd} \cdot C_{vs}} = S_{hr} + S_{rs} = \frac{v_t \cdot \left(1 - \dfrac{C_{vs}}{0.175 \cdot (1+\beta)}\right)^{\beta}}{v_{ls}} + \beta_m \cdot \frac{1}{v_{ls}^2} \tag{7.5-78}$$

Table 7.5-4: Values of α_m and β_m.

	D_p=0.0254 m	D_p=0.3 m	D_p=1.2 m
α_m - T=10ºC	1.84	2.53	2.92
β_m - T=10ºC	3.39	6.42	8.54
α_m - T=20ºC	1.74	2.36	2.73
β_m - T=20ºC	3.02	5.59	7.43

7.5.4.4 Summary Approximations.

Figure 7.5-3 shows α_k, α_m and α_t as a function of the particle diameter for a D_p=0.3 m pipe and T=10ºC. From this figure it is obvious that for small particles (d<0.3 mm) the translational kinetic energy loss per interaction about equals a factor times the kinetic energy of the particle based on the terminal settling. For large particles (d>2 mm) the translational kinetic energy loss per interaction equals a factor times the momentum of the particle based on the terminal settling velocity. Apparently the losses of small particles are based on kinetic energy and the losses of large particles are based on momentum. This makes sense, since the small particles are smaller than the thickness of the viscous sub-layer, resulting in an interaction with the viscous sub-layer without any collision with the pipe wall. So the kinetic energy losses result from translational and rotational drag forces, which are proportional to velocity squared. For large particles on the other hand, the interactions will be dominated by collisions with the pipe wall. These particles will be much larger than the thickness of the viscous sub-layer, so there will not be much influence of the viscous sub-layer. Collisions with the pipe wall will also result in rotation of the particle and thus lift forces, but this is much more momentum based. For particles from about d=0.3 mm to about d=2 mm there is a transition area going from kinetic energy based losses to momentum based losses.

Independent of the assumption that the translational kinetic energy losses per interaction are independent from the line speed, it is obvious that for small particles (up to about d=0.3 mm) the excess head losses are proportional to the terminal settling velocity squared. For medium particles (from about d=0.3 mm to about d=2 mm) the excess head losses are proportional to the terminal settling velocity. For large particles (larger than about d=2 mm) the excess head losses are independent of the terminal settling velocity and thus the particle diameter. This also explains why different researchers found different relations based on the size of the particles used. The boundaries of d=0.3 mm and d=2 mm are an indication and depend on the kinematic viscosity ν_l, the relative submerged density R_{sd} and the Darcy-Weisbach friction factor λ_l (so also the pipe diameter D_p). For other powers of the line speed term, the proportionality coefficients will also be different.

7.5.4.5 Comparison with Durand & Condolios (1952).

Equation (7.5-62) is written in terms of known parameters like the line speed v_{ls}, the kinematic viscosity v_l, the gravitational constant g, the terminal settling velocity v_t, the particle diameter d and the Darcy-Weisbach friction factor λ_l, although it is derived from more fundamental parameters like the thickness of the viscous sub-layer δ_v and the velocity at the thickness of the viscous sub-layer $11.6 \cdot u_*$ (angle of attack). Now knowing that the Darcy-Weisbach friction factor λ_l is reversely proportional to the line speed v_{sl} and the pipe diameter D_p, both reversed to a power ranging from 0.15-0.2, this gives an additional proportionality for these parameters to a power of 0.15-0.2. The resulting power of the line speed becomes this way -1.8 and the resulting power of the pipe diameter 0.2. The combination of the potential energy term being reversely proportional to the line speed with a power of -1 and the kinetic energy term being reversely proportional with the line speed to a power of -2, results in an additional increase of the power of the line speed by about 0.1 in the range of relevant line speeds.

The resulting power of the line speed in the kinetic energy term of about -2+0.2+0.1= -1.7 or -2+0.15+0.1=-1.75 is in between the power of -1.7 for uniform sands and gravels as found by Wilson et al. (1992) and the power of -1.93 as found by Zandi & Govatos (1967). Wilson et al. (1992) state that the power of -1.7 in absolute terms is the maximum power, which is explained by the above reasoning. The power of 0.2 of the pipe diameter gives a weak dependency and can easily be overlooked if only experiments are carried out in a narrow range of pipe diameters like most researchers have done. The result of this is that most researchers did not find a correlation between the excess pressure losses and the pipe diameter. Durand & Condolios (1952), however did. Writing their equation in terms of the relative excess hydraulic gradient E_{rhg} gives:

$$E_{rhg} = \frac{i_m - i_l}{R_{sd} \cdot C_{vs}} = 13.08^2 \cdot \lambda_l \cdot D_p^{1/2} \cdot \left(\frac{v_t}{\sqrt{g \cdot d}} \right)^{10/3} \cdot \frac{1}{v_{ls}}$$

(7.5-79)

$$\propto D_p^{-0.15} \cdot v_{ls}^{-0.2} \cdot D_p^{1/2} \cdot \left(\frac{v_t}{\sqrt{g \cdot d}} \right)^{10/3} \cdot \frac{1}{v_{ls}}$$

Applying the proportionalities between the Darcy-Weisbach friction factor λ_l and the line speed v_{ls} (-0.2) and the pipe diameter D_p (-0.15) gives for both equations:

$$E_{rhg} \propto D_p^{0.35} \cdot \left(\frac{v_t}{\sqrt{g \cdot d}} \right)^{10/3} \cdot \left(\frac{1}{v_{ls}} \right)^{1.2} \quad \text{vs.} \quad E_{rhg} \propto D_p^{0.15} \cdot \left(\frac{v_t}{\sqrt{g \cdot d}} \right)^{10/3} \cdot \left(\frac{1}{v_{ls}} \right)^{1.7}$$

(7.5-80)

Durand & Condolios   **DHLLDV**

Of course the potential energy term is not taken into account here separately, because Durand & Condolios (1952) did not take it into account, however it is taken into account by reducing the power of the line speed. Still both equations show a large similarity. It should be mentioned that the power of the particle Froude number is the same in both equations, since this power has been derived from the Gibert (1960) graph. The power of the pipe diameter differs by a power of 0.2, explaining why the Durand & Condolios (1952) equation overestimates the pressure losses in large diameter pipes. The power of the line speed differs, since Durand & Condolios (1952) considered both uniform and non-uniform sands and gravels, while here (DHLLDV) only uniform sands and gravels are considered. For small and medium sized pipes both models are very close in the neighborhood of the intersection of the heterogeneous and homogeneous regimes

7.5.5 The Slip Velocity Applied to the Fuhrboter Equation.

Now suppose the reversed proportionality with the line speed is 0.5 for the slip velocity and 1 for the relative excess hydraulic gradient, like many researchers have found for non-uniform sands and gravels, then what would the equations look like, matching the experiments from literature as good as possible? First the equations for the translational kinetic energy losses are modified, based on keeping the transition of the heterogeneous regime to the homogeneous regime at the same line speed and a power of the particle Froude number of 3:

$$
\Delta E_{s,kin,p} = 1.75 \cdot m_p \cdot \left(\frac{\delta_v}{d} \right)^{1/6} \cdot \left(\frac{v_t}{11.6 \cdot u_*} \right)^{1/3} \cdot \left(\frac{v_t}{\sqrt{g \cdot d}} \right)^{7/6} \cdot v_t \cdot v_{ls}
\tag{7.5-81}
$$

$$
\Delta E_{s,kin,p} = 1.75 \cdot m_p \cdot \left(\frac{32.81}{4.1^2} \right)^{1/6} \cdot \left(\frac{1}{\sqrt{\lambda_l}} \right)^{1/2} \cdot \left(\frac{v_t}{\sqrt{g \cdot d}} \right)^{3/2} \cdot \left(\frac{(v_l \cdot g)^{1/3}}{v_{ls}} \right)^{1/2} \cdot v_t \cdot v_{ls}
\tag{7.5-82}
$$

The above equations give for the slip velocity, Miedema & Ramsdell (2013):

$$
v_{sl} = \frac{\Delta E_{s,kin,p}}{m_p \cdot v_{ls}} = 1.75 \cdot \left(\frac{\delta_v}{d} \right)^{1/6} \cdot \left(\frac{v_t}{11.6 \cdot u_*} \right)^{1/3} \cdot \left(\frac{v_t}{\sqrt{g \cdot d}} \right)^{7/6} \cdot v_t
\tag{7.5-83}
$$

Or:

$$
v_{sl} = 1.75 \cdot \left(\frac{32.81}{4.1^2} \right)^{1/6} \cdot \left(\frac{1}{\sqrt{\lambda_l}} \right)^{1/2} \cdot \left(\frac{v_t}{\sqrt{g \cdot d}} \right)^{3/2} \cdot \left(\frac{(v_l \cdot g)^{1/3}}{v_{ls}} \right)^{1/2} \cdot v_t
\tag{7.5-84}
$$
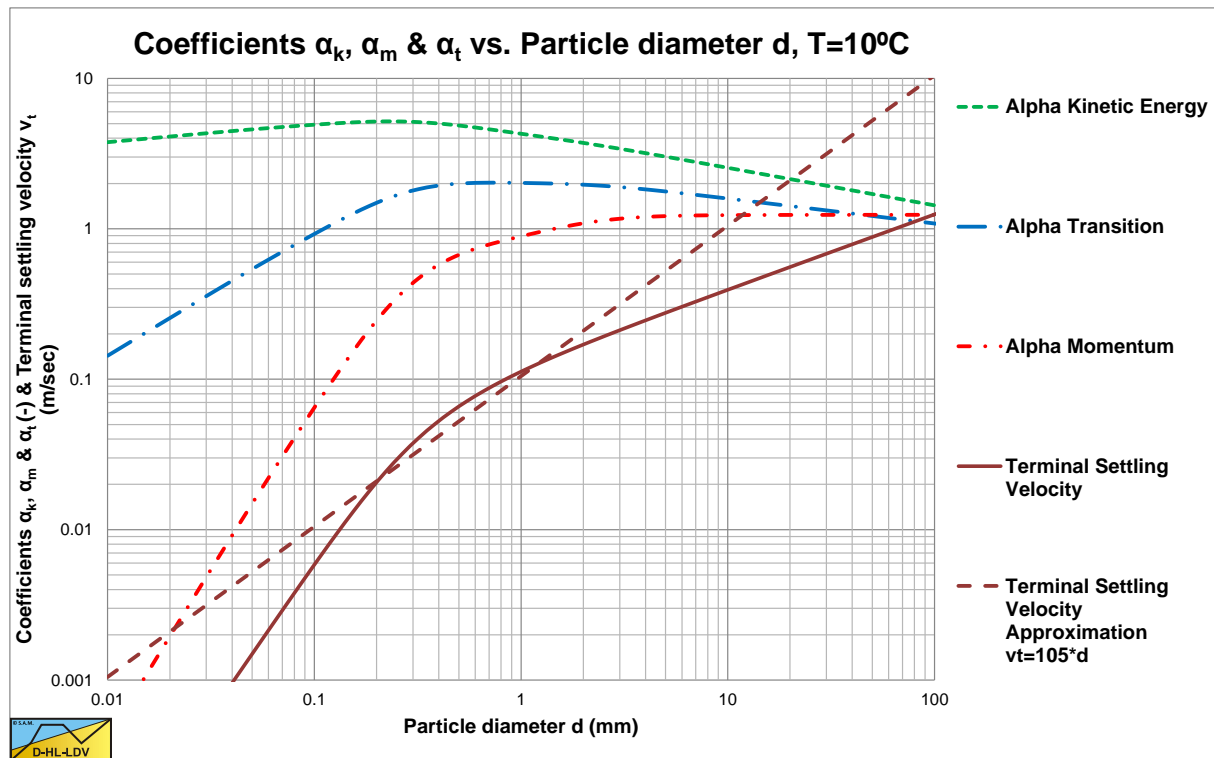
Figure 7.5-4: The factors α_k, α_m and α_t as a function of the particle diameter for a D_P=0.3 m pipe and T=10ºC.

This gives for the relative excess hydraulic gradient:

$$
E_{rhg} = \frac{i_m - i_l}{R_{sd} \cdot C_{vs}} = S_{hr} + S_{rs} = \frac{v_t \cdot \left(1 - \frac{C_{vs}}{\kappa_C}\right)^{\beta}}{v_{ls}} + 2.19^2 \cdot \left(\frac{1}{\sqrt{\lambda_l}}\right) \cdot \left(\frac{v_t}{\sqrt{g \cdot d}}\right)^3 \cdot \left(\frac{(v_l \cdot g)^{1/3}}{v_{ls}}\right)^1
\tag{7.5-85}
$$

Figure 7.5-4 shows the 3 coefficients as a function of the particle diameter for a D_p=0.3 m pipe and T=10ºC, while Table 7.5-5 shows the viscosities and Darcy Weisbach friction factors used here. Fuhrboter (1961) found a Darcy-Weisbach friction factor λ_l=0.014. Since for very small particles (Stokes region) the terminal settling velocity is proportional with the particle diameter squared, the S_{rs} value and thus the S_k value is proportional with the particle diameter to the 4th power. This is the reason of the starting point of the original S_k curve at a particle diameter of 0.2 mm.

Table 7.5-5: The viscosities and Darcy Weisbach friction coefficients.

	Viscosity (m²/s)	D_p=0.0254 m	D_p=0.3 m	D_p=1.2 m
T=10ºC	0.0000013	0.0214	0.0113	0.0085
T=20ºC	0.0000010	0.0202	0.0109	0.0082

7.5.5.1 Simplified Model for Small Particles, d<0.3 mm.

In terms of the kinetic translational energy of a particle based on the terminal settling velocity for small particles, the following expression can be found:

$$
\Delta E_{s,kin,p} = \frac{1}{2} \cdot m_p \cdot \left(\alpha_k \cdot v_t\right)^2 \cdot v_{ls}^{1/2}
$$

$$
= 2 \cdot 1.75 \cdot \left(\frac{32.81 \cdot v_l \cdot g}{4.1^2}\right)^{1/6} \cdot \left(\frac{1}{\sqrt{\lambda_l}}\right)^{1/2} \cdot \left(\frac{v_t}{\sqrt{g \cdot d}}\right)^{1/2} \cdot \left(\frac{1}{\sqrt{g \cdot d}}\right)^1 \cdot v_{ls}^{1/2} \cdot \frac{1}{2} \cdot m_p \cdot v_t^2
\tag{7.5-86}
$$

The factor α_k is now:

$$
\alpha_k = \sqrt{2 \cdot 1.75 \cdot \left(\frac{32.81 \cdot v_l \cdot g}{4.1^2}\right)^{1/6} \cdot \left(\frac{1}{\sqrt{\lambda_l}}\right)^{1/2} \cdot \left(\frac{v_t}{\sqrt{g \cdot d}}\right)^{1/2} \cdot \left(\frac{1}{\sqrt{g \cdot d}}\right)^1}
\tag{7.5-87}
$$

This gives for the contribution of the kinetic energy losses to the relative excess hydraulic gradient E_{rhg}, the S_{rs} parameter, for very small particles as a first estimate:

$$
S_{rs} = \left(\frac{v_{sl}}{v_t}\right)^2 = \left(\frac{\alpha_k^2}{2} \cdot \frac{v_t}{v_{ls}^{1/2}}\right)^2 = \beta_k \cdot \frac{v_t^2}{v_{ls}}
\tag{7.5-88}
$$

In terms of the relative excess hydraulic gradient E_{rhg} this gives:

$$
E_{rhg} = \frac{i_m - i_l}{R_{sd} \cdot C_{vs}} = S_{hr} + S_{rs} = \frac{v_t \cdot \left(1 - \frac{C_{vs}}{\kappa_C}\right)^{\beta}}{v_{ls}} + \beta_k \cdot \frac{v_t^2}{v_{ls}}
\tag{7.5-89}
$$

Table 7.5-6: Values of α_k and β_k.

	D_p=0.0254 m	D_p=0.3 m	D_p=1.2 m
α_k - T=10ºC	4.18	4.53	4.69
β_k - T=10ºC	76.55	105.34	121.46
α_k - T=20ºC	4.40	4.76	4.93
β_k - T=20ºC	93.90	127.83	147.38

7.5.5.2 Simplified Model for Medium Sized Particles, 0.3 mm≤d≤2 mm.

In terms of the transition range of particles based on the terminal settling velocity to the power 1.5 this gives:

$$\Delta E_{s,kin,p} = m_p \cdot \left(\alpha_t \cdot v_t\right)^{3/2} \cdot v_{ls}^{1/2}$$

$$= 1.75 \cdot \left(\frac{32.81 \cdot \nu_l \cdot g}{4.1^2}\right)^{1/6} \cdot \left(\frac{1}{\sqrt{\lambda_l}}\right)^{1/2} \cdot \left(\frac{1}{\sqrt{g \cdot d}}\right)^{1/2} \cdot \left(\frac{v_t}{\sqrt{g \cdot d}}\right)^1 \cdot v_{ls}^{1/2} \cdot m_p \cdot v_t^{3/2} \tag{7.5-90}$$

The factor α_t is now:

$$\alpha_t = \left(1.75 \cdot \left(\frac{32.81 \cdot \nu_l \cdot g}{4.1^2}\right)^{1/6} \cdot \left(\frac{1}{\sqrt{\lambda_l}}\right)^{1/2} \cdot \left(\frac{1}{\sqrt{g \cdot d}}\right)^{1/2} \cdot \left(\frac{v_t}{\sqrt{g \cdot d}}\right)^1\right)^{2/3} \tag{7.5-91}$$

This gives for the contribution of the kinetic energy losses to the relative excess hydraulic gradient E_{rhg}, the S_{rs} parameter, for particles from about **d=0.3 mm** to about **d=2 mm** as a first estimate:

$$S_{rs} = \left(\frac{v_{sl}}{v_t}\right)^2 = \left(\frac{\alpha_t^{3/2} \cdot v_t^{1/2}}{v_{ls}^{1/2}}\right)^2 = \beta_t \cdot \frac{v_t}{v_{ls}} \tag{7.5-92}$$

In terms of the relative excess hydraulic gradient E_{rhg} this gives:

$$E_{rhg} = \frac{i_m - i_l}{R_{sd} \cdot C_{vs}} = S_{hr} + S_{rs} = \frac{v_t \cdot \left(1 - \frac{C_{vs}}{\kappa_C}\right)^\beta}{v_{ls}} + \beta_t \cdot \frac{v_t}{v_{ls}} \tag{7.5-93}$$

Table 7.5-7: Values of α_t and β_t.

	D_p=0.0254 m	D_p=0.3 m	D_p=1.2 m
α_t - T=10ºC	1.68	1.86	1.95
β_t - T=10ºC	4.71	6.48	7.47
α_t - T=20ºC	1.70	1.88	1.97
β_t - T=20ºC	4.91	6.68	7.70

7.5.5.3 Simplified Model for Large Particles, d>2 mm.

In terms of the momentum of a particle based on the terminal settling velocity for large particles this gives:

$$\Delta E_{s,kin,p} = m_p \cdot \left(\alpha_m \cdot v_t \right) \cdot v_{ls}^{1/2} = 1.75 \cdot \left(\frac{32.81 \cdot v_l \cdot g}{4.1^2} \right)^{1/6} \cdot \left(\frac{1}{\sqrt{\lambda_l}} \right)^{1/2} \cdot \left(\frac{v_t}{\sqrt{g \cdot d}} \right)^{3/2} \cdot v_{ls}^{1/2} \cdot m_p \cdot v_t \qquad (7.5\text{-}94)$$

The factor α_m is now:

$$\alpha_m = 1.65 \cdot \left(\frac{32.81 \cdot v_l \cdot g}{4.1^2} \right)^{1/6} \cdot \left(\frac{1}{\sqrt{\lambda_l}} \right)^{1/2} \cdot \left(\frac{v_t}{\sqrt{g \cdot d}} \right)^{4/3} \qquad (7.5\text{-}95)$$

This gives for the contribution of the kinetic energy losses to the relative excess hydraulic gradient E_{rhg}, the S_{rs} parameter, for very large particles as a first estimate:

$$S_{rs} = \left(\frac{v_{sl}}{v_t} \right)^2 = \left(\frac{\alpha_m}{v_{ls}^{1/2}} \right)^2 = \beta_m \cdot \frac{1}{v_{ls}} \qquad (7.5\text{-}96)$$

In terms of the relative excess hydraulic gradient E_{rhg} this gives:

$$E_{rhg} = \frac{i_m - i_l}{R_{sd} \cdot C_{vs}} = S_{hr} + S_{rs} = \frac{v_t \cdot \left(1 - \frac{C_{vs}}{\kappa_C} \right)^{\beta}}{v_{ls}} + \beta_m \cdot \frac{1}{v_{ls}} \qquad (7.5\text{-}97)$$

Table 7.5-8: Values of α_m and β_m.

	D_p=0.0254 m	D_p=0.3 m	D_p=1.2 m
α_m - T=10ºC	1.06	1.24	1.33
β_m - T=10ºC	1.11	1.53	1.77
α_m - T=20ºC	1.03	1.20	1.28
β_m - T=20ºC	1.05	1.44	1.65

7.5.5.4 Summary Approximations.

The above equations are quite similar to the Fuhrboter (1961) approach. If the potential energy term is neglected and taking into consideration that the equations are derived for a constant spatial volumetric concentration, while Fuhrboter (1961) corrected for a ratio of 0.65 between the constant delivered concentration and the constant spatial concentration and further assuming that in the transition region the terminal settling velocity is about 105-115 times the particle diameter, the following relations can be derived for the S_k parameter of Fuhrboter (1961):

$$S_k = E_{rhg} \cdot R_{sd} = \left(S_{hr} + S_{rs}\right) \cdot R_{sd} \tag{7.5-98}$$

It should be mentioned that the particle diameter in these equations is in m, while Fuhrboter (1961) used the particle diameter in mm in his equations. Figure 7.5-5 shows the original S_k curve of Fuhrboter (1961) and the estimated curves, based on the kinetic energy approach, with upper and lower limits. The resemblance of the Fuhrboter curve with the average curve as derived here is remarkable. Only for very small particles the original curve gives smaller S_k values. The data points have been recalculated, based on the original data of Fuhrboter (1961), giving slightly higher values, matching the theoretical and approximation curves, except for the 0.83 mm particles. The latter could be caused by the non-uniform PSD of this sand.

However the difference between the lower and upper limit is large. Fuhrboter (1961) carried out his experiments in a 0.3 m pipe, which is close to the average curve. For the full range of particle diameters the contribution of the translational kinetic energy losses, the S_{rs} parameter, is:

$$S_{rs} = \left(\frac{v_{sl}}{v_t}\right)^2 = 2.19^2 \cdot \left(\frac{1}{\sqrt{\lambda_l}}\right) \cdot \left(\frac{v_t}{\sqrt{g \cdot d}}\right)^{10/3} \cdot \left(\frac{\left(v_l \cdot g\right)^{1/3}}{v_{ls}}\right)^1 \tag{7.5-99}$$

Giving for the relative excess hydraulic gradient, the E_{rhg} parameter:

$$E_{rhg} = \frac{i_m - i_l}{R_{sd} \cdot C_{vs}} = S_{hr} + S_{rs} = \frac{v_t \cdot \left(1 - \frac{C_{vs}}{\kappa_C}\right)^\beta}{v_{ls}} + 2.19^2 \cdot \left(\frac{1}{\sqrt{\lambda_l}}\right) \cdot \left(\frac{v_t}{\sqrt{g \cdot d}}\right)^{10/3} \cdot \left(\frac{\left(v_l \cdot g\right)^{1/3}}{v_{ls}}\right)^1 \tag{7.5-100}$$

Equation (7.5-62) is derived for uniform sands and gravels, while equation (7.5-100) is suitable for non-uniform sands and gravels, matching equations of different researchers. Both equations give about the same intersection point with the homogeneous regime and also give about the same pressure losses at line speeds around that intersection point. The S_k factor can be approached for all particle diameters according to the following equation as is also shown in Figure 7.5-5:

$$S_k = \left(v_t \cdot \left(1 - \frac{C_{vs}}{\kappa_C}\right)^\beta + 2.19^2 \cdot \left(\frac{1}{\sqrt{\lambda_l}}\right) \cdot \left(\frac{v_t}{\sqrt{g \cdot d}}\right)^{10/3} \cdot \left(v_l \cdot g\right)^{1/3}\right) \cdot R_{sd} \tag{7.5-101}$$
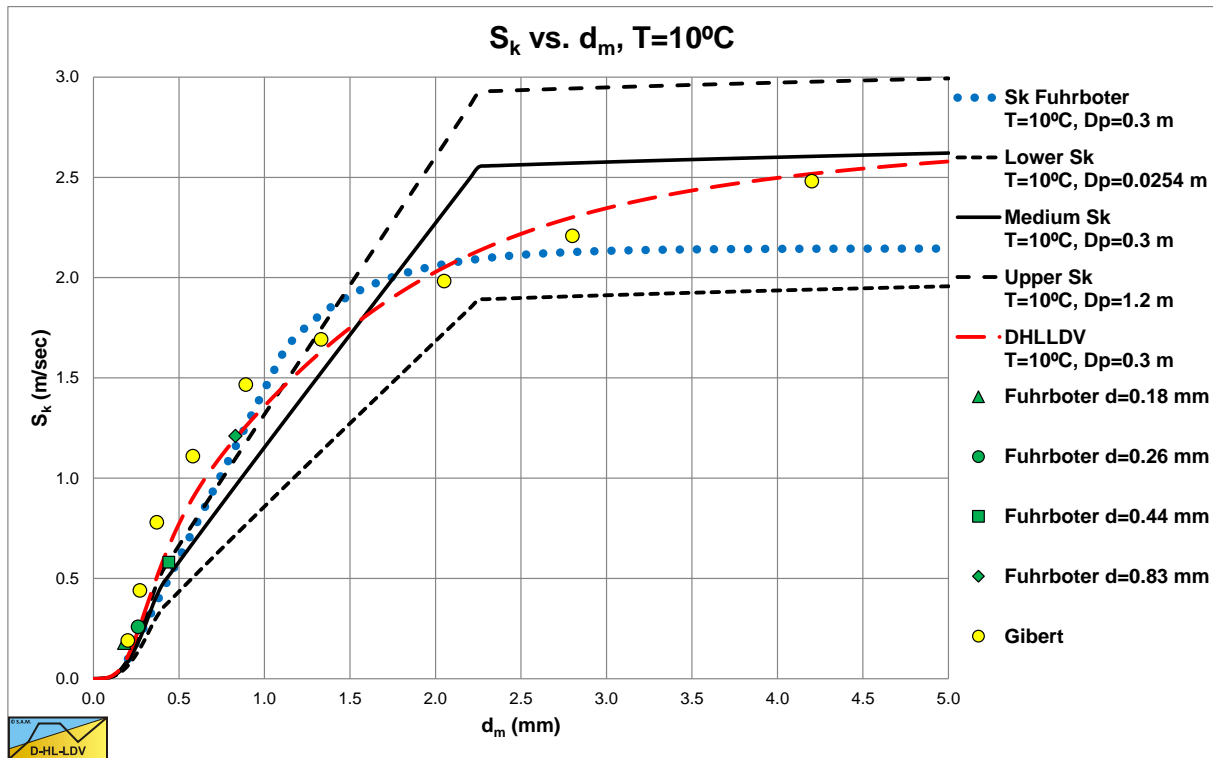
Figure 7.5-5: The S_k value, original and derived, for a D_p=0.3 m pipe and T=10ºC.
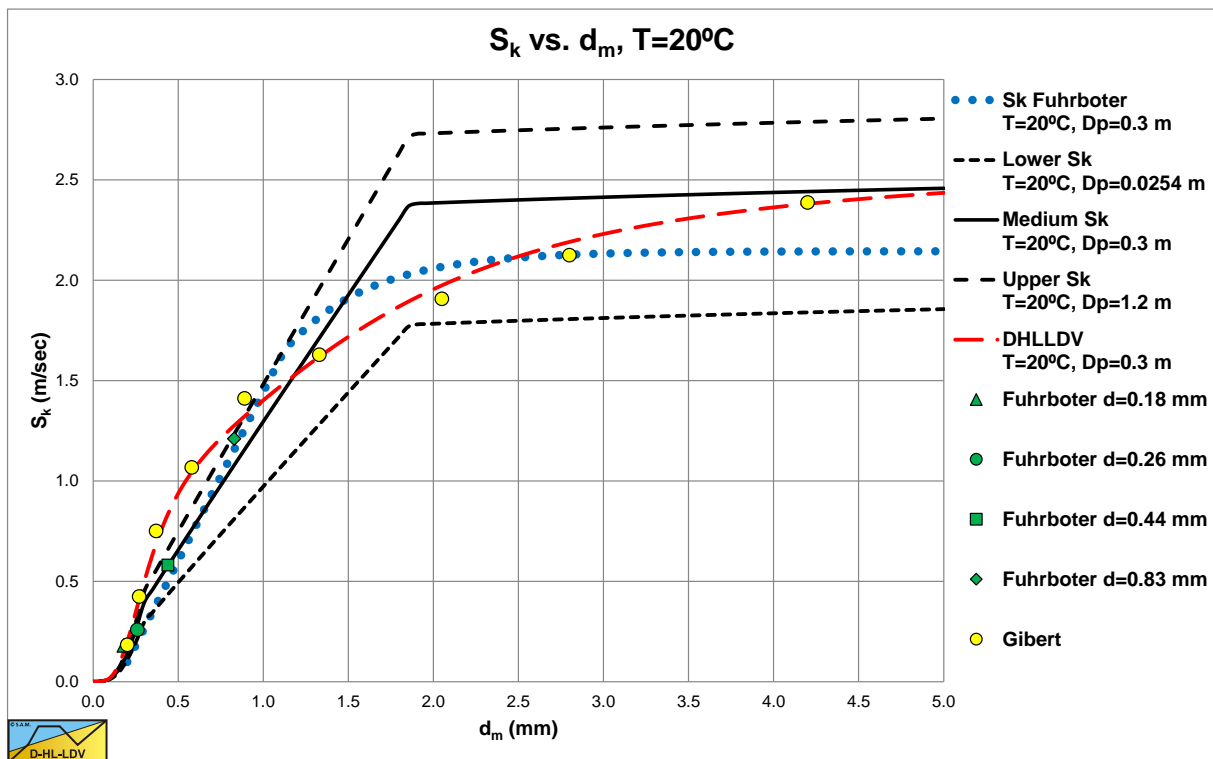
Figure 7.5-6: The S_k value, original and derived, for a D_p=0.3 m pipe and T=20ºC.

7.5.6 The Concentration Eccentricity Coefficient.

The concentration eccentricity coefficient κ_C tells what the concentration profile looks like. If the concentration profile is symmetrical with respect to the center of the pipe the coefficient has a value of 1. This will be the case with very small particles and homogeneous flow. With coarse particles however the mean position of the particles will be below the center of the pipe, so the coefficient will have a value smaller than 1. The potential energy term contains the following term, which is also used in the LDV equations:

$$\left(1 - \frac{C_{vs}}{\kappa_C}\right)^{\beta} \cdot C_{vs} \tag{7.5-102}$$

It is known from literature that the LDV has a maximum for a concentration in the range 15%-20%. This is only possible if this term has a maximum in this range. To find this maximum, the derivative with respect to the concentration is taken:

$$\frac{d}{dC_{vs}}\left(\left(1 - \frac{C_{vs}}{\kappa_C}\right)^{\beta} \cdot C_{vs}\right) = \left(1 - \frac{C_{vs}}{\kappa_C}\right)^{\beta} - \frac{C_{vs} \cdot \beta}{\kappa_C} \cdot \left(1 - \frac{C_{vs}}{\kappa_C}\right)^{\beta-1}$$

$$\left(1 - \frac{C_{vs,max}}{\kappa_C}\right)^{\beta-1} \cdot \left(\left(1 - \frac{C_{vs,max}}{\kappa_C}\right) - \frac{C_{vs,max} \cdot \beta}{\kappa_C}\right) = 0 \quad \Rightarrow \quad 1 - \frac{C_{vs,max}}{\kappa_C} \cdot (1 + \beta) = 0 \tag{7.5-103}$$

$$\kappa_C = C_{vs,max} \cdot (1 + \beta) \quad \text{or} \quad C_{vs,max} = \frac{\kappa_C}{(1 + \beta)}$$

The concentration eccentricity coefficient is a function of the concentration where the maximum occurs and vice versa. Since κ_C can never be larger than 1 for homogeneous flow, the concentration where the maximum occurs only depends on the hindered settling power β. This power has a maximum of 4.7 for very small particles, according to Richardson & Zaki (1954). This results in a concentration where the maximum occurs of 17.5%, exactly in the middle of the range where the maximum LDV is observed. This gives for the concentration eccentricity coefficient κ_C:

$$\kappa_C = 0.175 \cdot (1 + \beta) \tag{7.5-104}$$

For very large particles with a hindered settling power of about 2.4, this gives a concentration eccentricity coefficient of 0.595. This is about 60% of the radius of the pipe measured from the bottom of the pipe, which seems reasonable.

7.5.7 Discussion & Validation.

Until now papers of the following researchers have been used to analyze, verify and validate the new theory regarding the head loss curves: Blatch (1906), O'Brien & Folsom (1939), Soleil & Ballade (1952), Durand & Condolios (1952), Newitt et al. (1955), Worster & Denny. (1955), Gibert (1960), Fuhrboter (1961), Silin & Kobernik (1962), Thomas (1965), Zandi & Govatos (1967), Wiedenroth (1967), Fowkes & Wancheck (1969), Babcock (1970), Graf et al. (1970), Yagi et al. (1972), Karasik (1973), Kazanskij (1978), Boothroyde et al. (1979), Kazanskij (1980), Clift et al. (1982), Scheurel (1985), Doron et al. (1987), Gillies (1993), Blythe & Czarnotta (1995), Doron et al. (1995), Matousek (1997), Schaan et al. (2000), Matousek (2004), Gillies et al. (2004), Whitlock et al. (2004), Ni et al. (2004), Ming et al. (2007), Ni et al. (2008), Vlasak (2008), Ravelet et al. (2012) and Vlasak et al. (2012). Because of the enormous amount of data it is not possible to show everything, so a selection of graphs giving the essence of the verification and validation will be shown.

Figure 7.1-7 & Figure 7.1-8 already show a good correlation between the new heterogeneous regime model and the experiments of Clift et al. (1982) for a medium **d=0.68 mm** sand and medium pipe diameters of **D_P=0.2 m** and **D_P=0.44 m**.

Figure 7.5-7 & Figure 7.5-8 show data of Durand & Condolios (1952) as published by Gibert (1960) with particles ranging from a diameter of **d=0.2 mm** up to **d=4.2 mm** in a pipe with a diameter of **D$_p$=0.15 m**.
Figure 7.5-9 shows data of Whitlock et al. (2004) with particles ranging from a diameter of **d=0.085 mm** up to **d=0.4 mm** in a pipe with a diameter of **D$_p$=0.1 m**.
Figure 7.5-10 shows data of Clift et al. (1982) with particles with a diameter **d=0.6 mm** in a pipe with a diameter of **D$_p$=0.49 m**.
More Graphs can be found in Miedema (2013) and Ramsdell & Miedema (2013) and in other chapters.

For the interpretation of the graphs one should realize that for dredging practice pipe diameters of 0.1 or 0.15 m or even smaller are not really representative for dredging using diameters up to 1.2 m. Although the graphs show a good correlation between the experiments and the theoretical lines, to make the theory appropriate for dredging practice, there should be evidence that there is also a good correlation for the larger pipe diameters. That's the reason why some graphs are added for pipe diameters up to **D$_p$=0.49 m** and even larger. Figure 7.1-8 and Figure 7.5-10 show some of these experiments.

All the graphs show a good correlation between the experiments and the theoretical curves, but they show more. All the graphs show that there is an intersection between heterogeneous and homogeneous transport regimes, but often the experiments continue to excess pressures below the homogeneous curve and at higher line speeds tend to move into the direction of the homogeneous curve. The graphs also show that this specifically occurs for medium sized particles. Very small particles follow the heterogeneous curve and then bend to the homogeneous curve. Large particles will probably follow the sliding bed curve and from there continue with (pseudo) heterogeneous transport at very high line speeds. In dredging practice it is known that very small particles behave homogeneous. For medium sized particles it is assumed that they follow the water resistance curve, while larger particles will have excess pressure. This is explained with the graphs shown here.

Another phenomenon that is shown in Figure 7.5-7 & Figure 7.5-8 is the transition between the sliding bed regime and the heterogeneous regime for the **d=2.05 mm** and the **d=4.20 mm** particles. In both cases the data points lie on or above the theoretical curves at higher line speeds, but below the curves at low line speeds, close to the sliding bed curve. The smaller particles do not show this kind of behavior, but then the hydraulic gradients of the smaller particles are much smaller.

Last but not least Figure 7.5-10 shows clearly that below the Limit Deposit Velocity, the data points continue to follow the theoretical curve for heterogeneous transport (the Limit Deposit Velocity is at about **i$_w$=0.02-0.03**). This has also been observed by Durand & Condolios (1952) and Zandi & Govatos (1967).

The new approach of modeling head losses in slurry transport based on energy considerations, giving 3 terms for the head losses, correlates well with many experiments. In the head loss equation 3 terms can be distinguished, the viscous friction losses, the potential energy losses and the kinetic energy losses. The kinetic energy losses are based on the slip velocity required to explain these losses.

Introducing three new dimensionless numbers, the **Durand & Condolios** (1952) Froude number **Cát, Ct** (Vietnamese for sand grains)**,** the **Lắng** number **La** (**Lắng** is Vietnamese for sediment) and the **Thủy** number **Th** (**Thủy** is Vietnamese for aquatic, water) simplifies the resulting equations.

The Durand & Condolios (1952) particle Froude number **Ct** giving the contribution of the solids to the excess head losses, **the collision impact**, is:

$$
Ct = \left(Fr_p\right)^{5/3} = \left(\frac{1}{\sqrt{C_x}}\right)^{5/3} \tag{7.5-105}
$$

The new **Thủy** number **(Th)** is the cube root of the ratio of the viscous forces times the gravitational forces to the inertial forces squared. The Thủy number gives the contribution of the liquid flow, in dredging applications water, to the excess head losses, **the collision intensity**. Defining the **Thủy** number **(Th)** to:

$$
Th = \left(\frac{\nu_l \cdot g}{v^3}\right)^{1/3} \tag{7.5-106}
$$
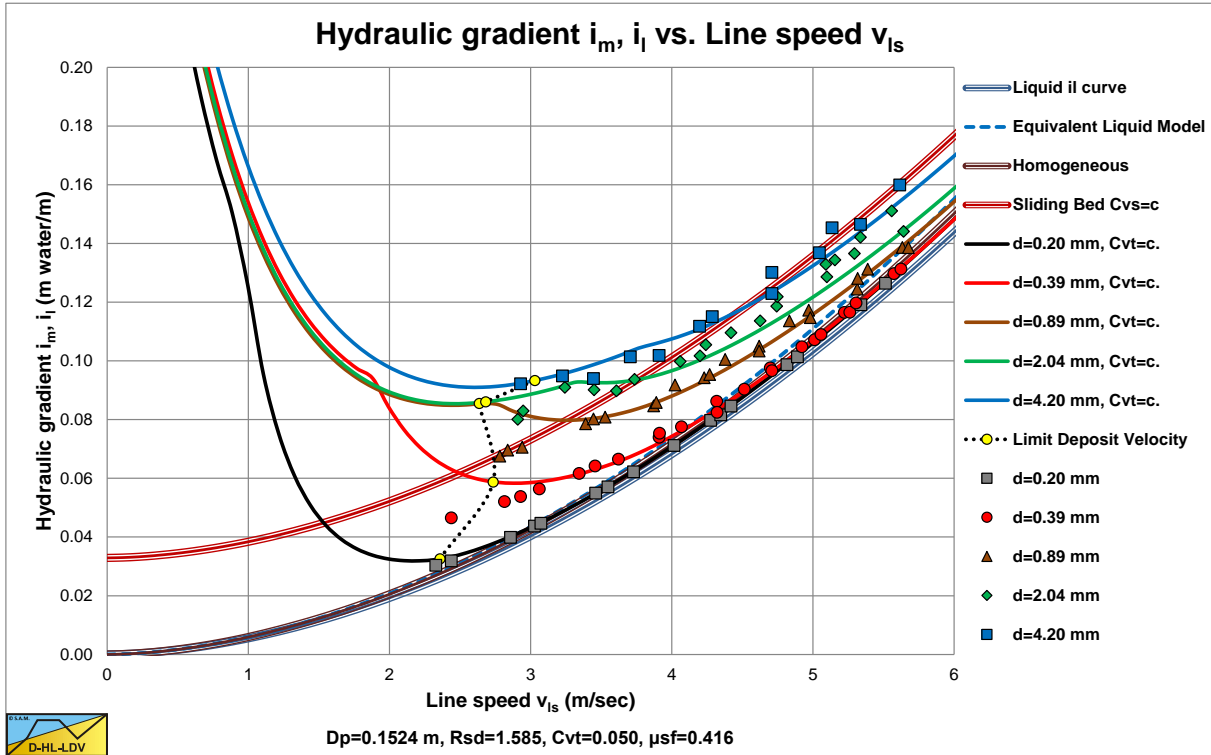
Figure 7.5-7: Data from Gibert (1960) in a i_m-v_{ls} graph.
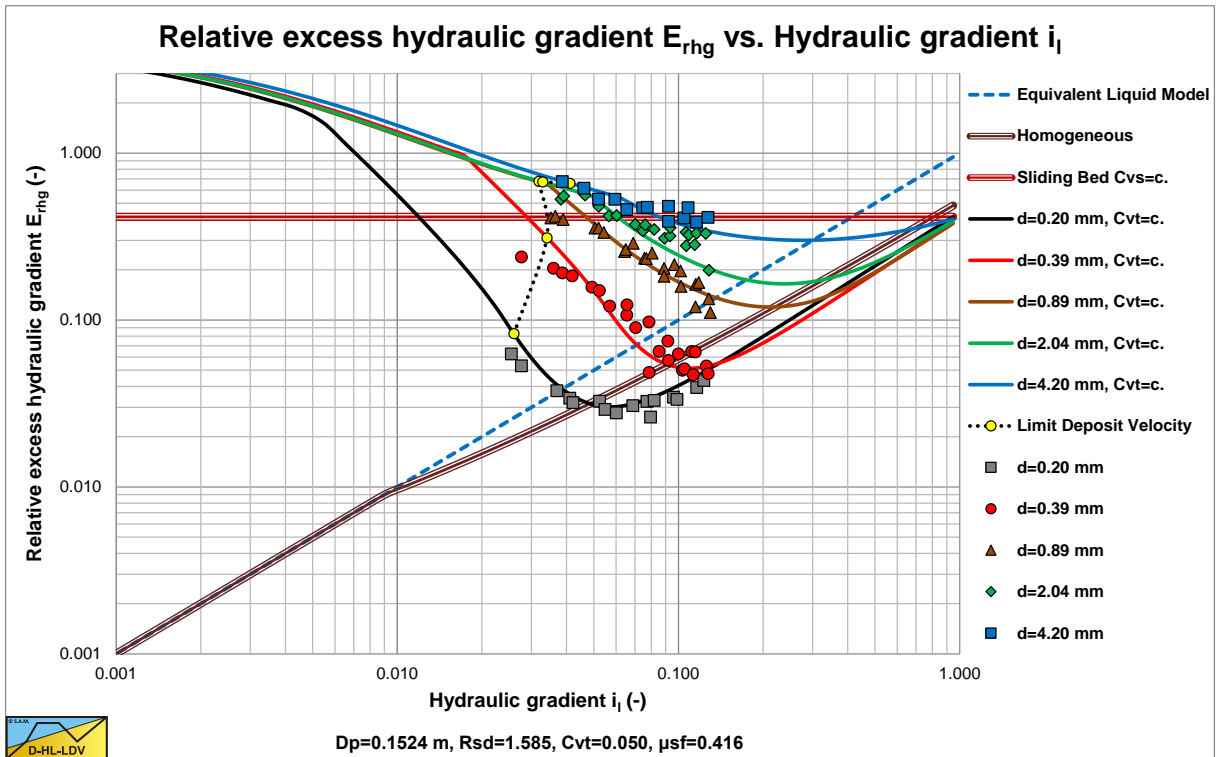
Figure 7.5-8: Data from Gibert (1960) in a $E_{rhg}(i_l)$ graph.

The third new dimensionless number as introduced here. It is the **Lắng** number **La. Lắng** is Vietnamese for sediment and this number represents the capability of the slurry flow to form a bed, **the sedimentation capability**, either fixed or sliding.

$$La = \frac{v_t \cdot \left(1 - C_v / \kappa_C\right)^\beta}{v_{ls}} \tag{7.5-107}$$

This gives for the hydraulic gradient:

$$i_m = i_l \cdot \left(1 + \frac{\left(2 \cdot g \cdot R_{sd} \cdot D_p\right)}{\lambda_l} \cdot C_{vs} \cdot \frac{1}{v_{ls}^2} \cdot \left(La + \frac{8.5^2}{8} \cdot Ct^2 \cdot Th_{fv}^2\right)\right) \tag{7.5-108}$$
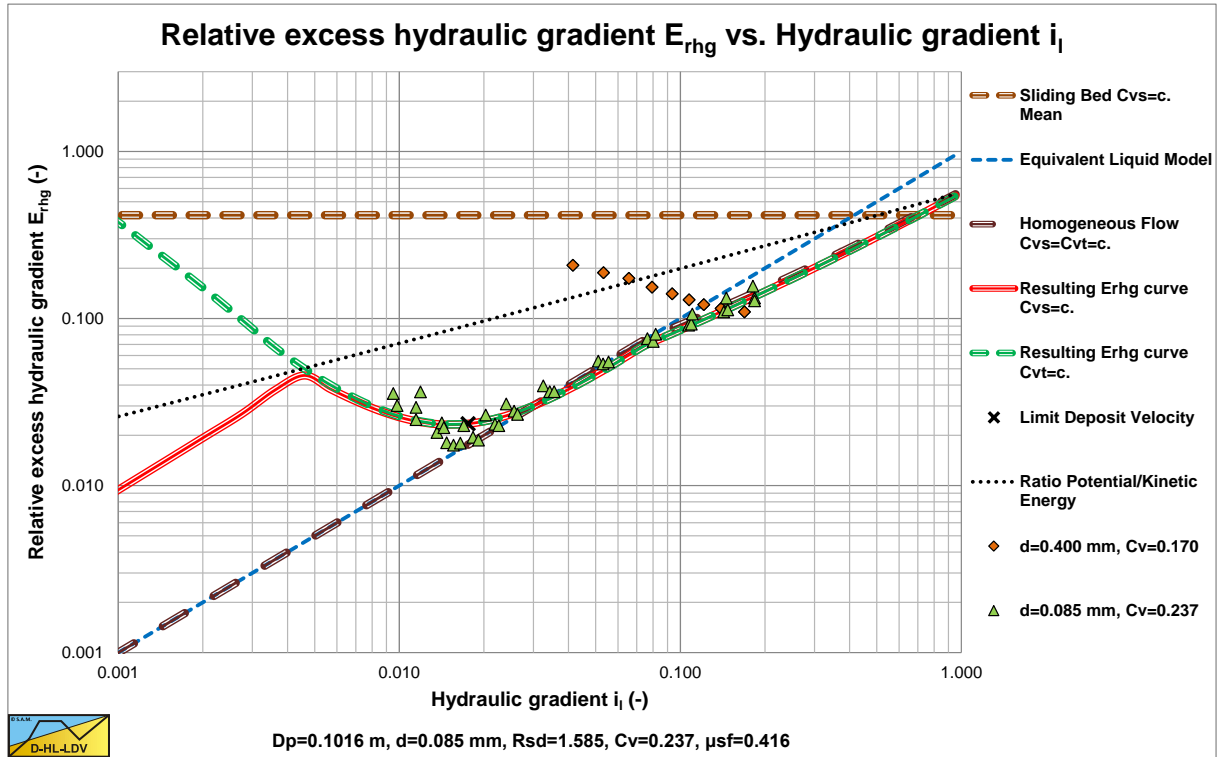
Figure 7.5-9: Data of Whitlock et al. (2004).
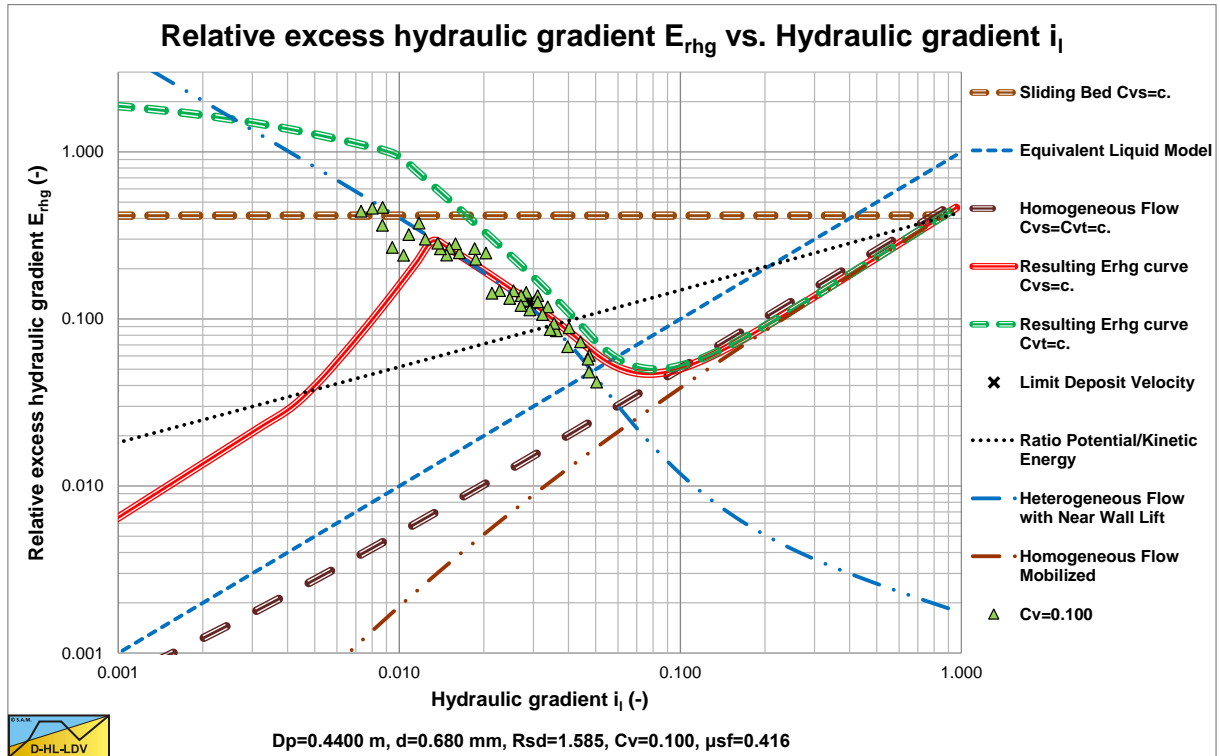
Figure 7.5-10: Data from Clift et al. (1982).

7.5.8 Nomenclature Heterogeneous Regime.

A_p	Cross section of a pipe with diameter D_p	m^2
A_s	Cross section of a solid particle with diameter d	m^2
c	Proportionality constant	-
C_D	Particle drag coefficient	-
C_v	Volumetric concentration	-
C_{vs}	Volumetric spatial concentration	-
$C_{vs,max}$	Volumetric spatial concentration where maximum LDV occurs	-
C_{vt}	Volumetric transport/delivered concentration	-
C_x	Inverse particle Froude number squared according to Durand & Condolios Fr_p^{-2}	-
d	Particle diameter	m
d_{50}	Particle diameter at which 50% by weight is smaller	m
D_p	Pipe diameter	m
E_{rhg}	Relative excess hydraulic gradient	-
$\Delta E_{s,kin,p}$	Energy loss of 1 particle at interaction	N·m
$\Delta E_{s,kin,tot}$	Energy loss of all particles	N·m
$\Delta E_{s,pot}$	Average potential energy of 1 particle	N·m
$\Delta E_{s,pot,tot}$	Total potential energy of **n** particles	N·m
F_D	Drag force on a particle	N
$F_{D,tot}$	Drag force on all particles	N
Fr_p	Particle Froude number	-
g	Gravitational constant 9.81·m/s²	m/s^2
i	Hydraulic gradient	m/m
i_m	Hydraulic gradient mixture	m/m
i_w, i_l	Hydraulic gradient water/liquid	m/m
$i_{s,pot}$	Hydraulic gradient due to potential energy losses of particles	m/m
$i_{s,kin}$	Hydraulic gradient due to kinetic energy losses of particles	m/m
L, ΔL	Length of the pipeline	-
m	Mass of 1 particle	kg
n	Number of particles in a pipe with length ΔL	-
Δp	Head loss over a pipeline length ΔL	kPa

Δp_l	Head loss of liquid over a pipeline length ΔL	kPa
Δp_m	Head loss of mixture over a pipeline length ΔL	kPa
$\Delta p_{m,min}$	Head loss of mixture over a pipeline length ΔL where minimum occurs	kPa
$\Delta p_{s,pot}$	Pressure required to compensate for potential energy losses	kPa
$\Delta P_{s,kin}$	Power required to compensate for kinetic energy losses	kW
$\Delta P_{s,pot}$	Power required to compensate for potential energy losses	kW
Q_l	Volume flow of liquid/water	m³/s
Q_m	Volume flow of mixture	m³/s
Q_p	Volume flow of particles	m³/s
Re	Reynolds number	-
Re_p	Particle Reynolds number	-
R_{sd}	Relative submerged density	-
s	Distance	m
S_{hr}	Settling velocity Hindered Relative	-
S_{rs}	Slip ratio squared/Stratification ratio solids/Friction coefficient (see also μ_{sf})	-
Δt	Time interval	s
v_{ls}	Line speed	m/s
$v_{ls,min}$	Line speed where minimum pressure occurs	m/s
v_p	Particle velocity in direction of average flow	m/s
v_{sl}	Slip velocity	m/s
v_t	Terminal settling velocity of particles	m/s
u_*	Friction velocity	m/s
α_k	Factor for kinetic energy losses (fine particles)	-
α_m	Factor for momentum energy losses (large particles)	-
α_t	Factor for transition energy losses (medium particles)	-
α_1	Power of viscous sub-layer thickness to particle diameter ratio	-
α_2	Power of angle of attack	-
α_3	Power of relative submerged density to drag coefficient ratio	-
β	Power of Richardson & Zaki equation	-
β_k	Factor for kinetic energy losses (fine particles)	-
β_m	Factor for momentum energy losses (large particles)	-
β_t	Factor for transition energy losses (medium particles)	-
δ_v	Thickness viscous sub-layer	m
ρ_l	Liquid density	ton/m³
ρ_w	Density of water	ton/m³
ρ_s	Density of solids	ton/m³
ρ_q	Density of quarts (2.65 ton/m³)	ton/m³
λ_l	Darcy-Weisbach friction factor	-
κ_C	Concentration eccentricity coefficient	-
μ	Friction coefficient for sliding bed (see also S_{rs})	-
Φ	Durand relative excess pressure coefficient	-
Ω	Excess pressure factor	(m/s)³
ψ	Durand abscissa	-
v_w, v_l	Kinematic viscosity of water/liquid	m²/s
v_m	Kinematic viscosity of mixture with Thomas equation	m²/s
v_r	Relative kinematic viscosity v_m/v_l	-
ζ	Shape factor	-
Ct	**Cát** number, collision impact	-
La	**Lắng** number, sedimentation capability	-
Th	**Thủy** number, collision intensity	-

7.6 A Head Loss Model for Homogeneous Slurry Transport.

7.6.1 Homogeneous Transport – The Equivalent Liquid Model (ELM).

Slurry transport in horizontal and vertical pipelines is one of the major means of transport of sands and gravels in the dredging industry. There exist 5 main flow regimes, the fixed or stationary bed regime, the sliding bed regime, the heterogeneous flow regime, the homogeneous flow regime and the sliding flow regime. Of course the transitions between the regimes are not very sharp, depending on parameters like the particle size distribution. In the case of very fine particles and/or very high line speeds, the mixture is often considered to be a liquid with the liquid density ρ_l equal to the mixture density ρ_m, where the liquid density ρ_l can be replaced by the mixture density ρ_m in the hydraulic gradient equations. The velocity profile in a cross section of the pipe is considered to be symmetrical and the slip between the particles and the liquid is considered negligible. The concentration is assumed to be uniform over the cross section. Thus, the transport (or delivered) concentration and the spatial concentration are almost equal and will be named C_v. This is often referred to as the equivalent liquid model (ELM).
Since the pressure losses are often expressed in terms of the hydraulic gradient, first some basic equations for the hydraulic gradient and the relative excess hydraulic gradient (solids effect) are given. The hydraulic gradient according to the equivalent liquid model is:

$$i_m = \frac{\Delta p_m}{\rho_l \cdot g \cdot \Delta L} = \frac{\lambda_m \cdot v_{ls}^2}{2 \cdot g \cdot D_p} \cdot \frac{\rho_m}{\rho_l} \quad \text{with:} \quad \lambda_m = \lambda_l \tag{7.6-1}$$

Where it is assumed that the Darcy-Weisbach friction factors for liquid λ_l and mixture λ_m are equal. This can also be written as:

$$i_m = i_l \cdot (1 + R_{sd} \cdot C_v) \tag{7.6-2}$$

Newitt et al. (1955) found that only 60% of the solids weight should contribute to the mixture density in order to obtain the equivalent liquid model, but this depends on the line speed and possibly on other parameters as well. Many others also found hydraulic gradients below the ELM at high line speeds. Wilson et al. (1992) explain this with the effect of near wall lift resulting in an almost particle free viscous sub layer. However for very small particles values are found giving a higher value of the hydraulic gradient, which is often explained by correcting (increase) the apparent kinematic viscosity, for example with the Thomas (1965) equation. The pressure losses can be shown in an almost dimensionless form in a double logarithmic graph with the relative excess hydraulic gradient E_{rhg} as the ordinate and the hydraulic liquid gradient i_l as the abscissa. In terms of the relative excess hydraulic gradient, E_{rhg}, the above equation can be written as:

$$E_{rhg} = \frac{i_m - i_l}{R_{sd} \cdot C_v} = \frac{\lambda_l \cdot v_{ls}^2}{2 \cdot g \cdot D_p} = i_l \tag{7.6-3}$$

So in the $E_{rhg}(i_l)$ graph the above equation results in a straight line giving $E_{rhg}=i_l$. Figure 7.6-1 shows experimental data of Thomas (1976) of **d=0.04 mm** iron ore in a **D_P=0.1075 m** horizontal pipe versus the Delft Head Loss & Limit Deposit Velocity (DHLLDV) Framework, where the 4 term Thomas (1965) viscosity equation and the homogeneous flow correction equation (7.6-37) with **A_{Cv}=3** are implemented. The match is remarkable.

7.6.2 Approach.

In order to test the Talmon (2011) & (2013) method of incorporating a particle free viscous sub-layer and to check if there are alternative methods the following approach is followed:
1. Method 1: First the Talmon (2011) & (2013) method is discussed briefly.
2. Method 2: Since the Talmon (2011) & (2013) method uses a 2D approach, with von Driest damping (Schlichting, 1968), but without a real concentration profile, in this second method the equations are derived for pipe flow with the Nikuradse (1933) mixing length equation, without von Driest damping (Schlichting, 1968) and without a real concentration profile. The results are corrected for the volume flow.
3. Method 3: Von Driest damping (Schlichting, 1968) is added to method 2, resulting in a velocity profile comparable and very close to the Talmon (2011) & (2013) method 1. So method 1 and method 3 are equivalent.
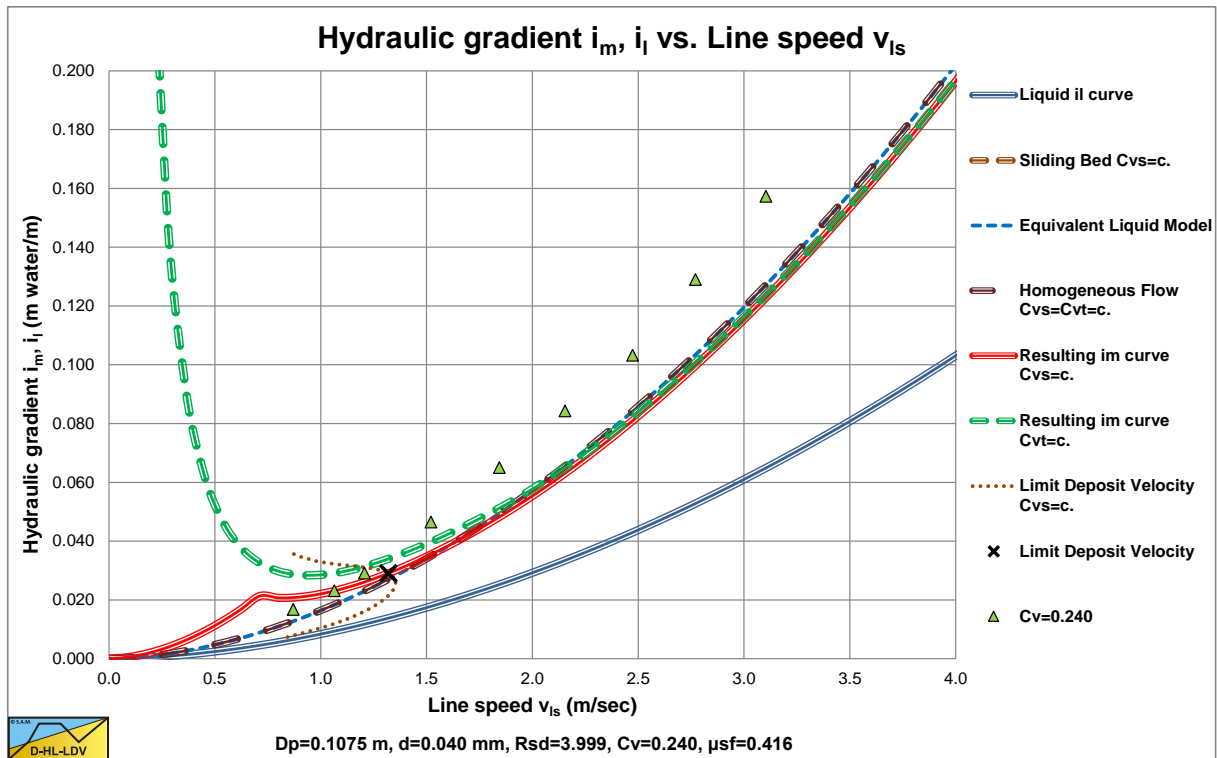
Figure 7.6-1: The Thomas (1976) experimental data in a $i_m(v_{ls})$ graph without Thomas (1965) viscosity.
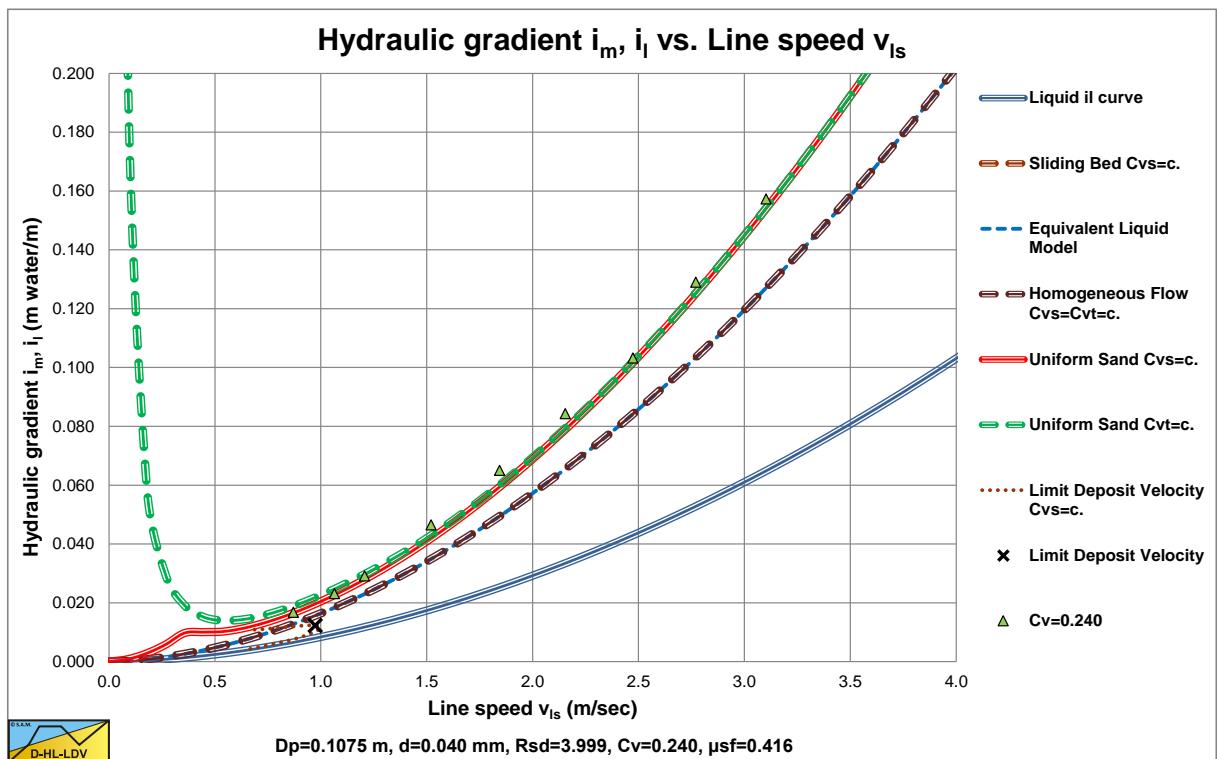
Figure 7.6-27.6-3: The Thomas (1976) experimental data in a $i_m(v_{ls})$ graph with Thomas (1965) viscosity.

4. Method 4: The "Law of the Wall" 2D approach without von Driest damping (Schlichting, 1968).
5. The 4 methods are compared and an equation describing the average behavior is derived.
6. Method 5: Finally a concentration profile is added to method 2. This method can simulate all previous methods, depending on the concentration profile chosen.
7. Based on experiments a value for the parameters of the concentration profile is chosen.

7.6.3 Method 1: The Talmon (2011) & (2013) Homogeneous Regime Equation.

Talmon (2011) & (2013) derived an equation to correct the homogeneous equation (the ELM model) for the slurry density, based on the hypothesis that the viscous sub-layer hardly contains solids at very high line speeds in the homogeneous regime. This theory results in a reduction of the resistance compared with the ELM, but the resistance is still higher than the resistance of clear liquid. Talmon (2011) & (2013) used the Prandtl approach for the mixing length, which is a 2D approach for open channel flow with a free surface.

The Prandtl approach was extended with damping near the wall to take into account the viscous effects near the wall, according to von Driest (Schlichting, 1968). The Talmon (2011) & (2013) approach resulted in the following equation, with **$\alpha_h=6.7$**:

$$
\frac{\lambda_m}{\lambda_l} = \frac{1}{\left(\alpha_h \cdot \sqrt{\dfrac{\lambda_l}{8}} \cdot R_{sd} \cdot C_v + 1 \right)^2} \quad \text{and} \quad E_{rhg} = i_l \cdot \frac{R_{sd} \cdot C_v + 1 - \left(\alpha_h \cdot \sqrt{\dfrac{\lambda_l}{8}} \cdot R_{sd} \cdot C_v + 1 \right)^2}{R_{sd} \cdot C_v \cdot \left(\alpha_h \cdot \sqrt{\dfrac{\lambda_l}{8}} \cdot R_{sd} \cdot C_v + 1 \right)^2} = \alpha_E \cdot i_l
$$

$$
\tag{7.6-4}
$$

This equation underestimates the hydraulic gradient (overestimates the effect of a particle free viscous sub layer) in a number of cases (small and large particles) as Talmon (2011) & (2013) proves with the examples shown in his papers. Only for **$d_{50}=0.37$ mm** and **$D_p=0.15$ m** (medium particles) there is a good match. The philosophy behind this theory, combining a viscous sub-layer with liquid with a kernel with mixture, is however very interesting, because it explains fundamentally why the hydraulic gradient can be lower than the hydraulic gradient according to the ELM, as has been shown by many researchers. The model has been derived using the standard mixing length equation for 2D flow and without a concentration distribution. When reproducing this method it was found that the coefficient **α_h** is not a constant but this coefficient depends on the value of **$R_{sd} \cdot C_v$** according to Figure 6.25-1. The value of 6.7 is found for a value of about 0.6 of the abscissa.
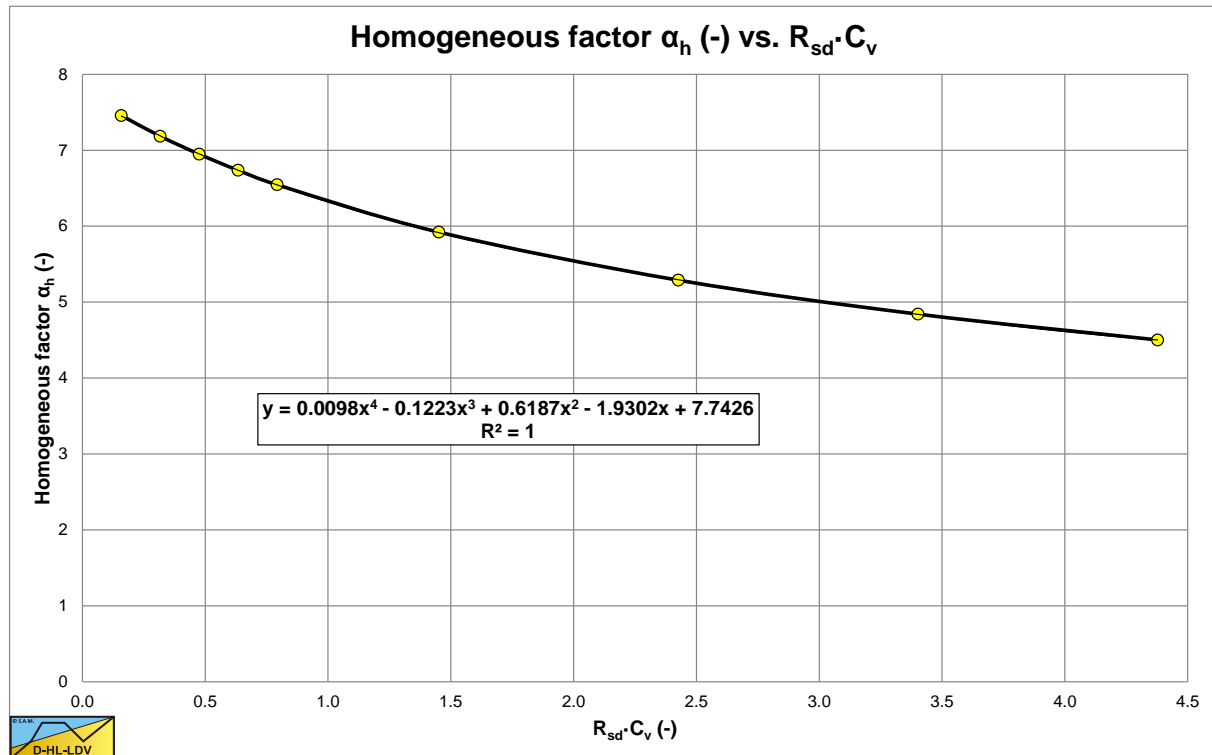
Figure 7.6-4: The coefficient α_h as a function of $R_{sd} \cdot C_v$ for method 1.

7.6.4 Method 2: The Approach using the Nikuradse (1933) Mixing Length.

The concept of Talmon (2011) & (2013) is adopted, but modified by using pipe flow with the Prandtl (1925) and Nikuradse (1933) mixing length equations, a linear shear stress distribution with a maximum at the pipe wall and zero in the center and a concentration distribution, assuming that in the homogeneous regime the mixture can be considered a Newtonian liquid with properties slightly different from those of water. The shear stress between the mixture, the slurry, and the pipe wall is the sum of the viscous shear stress and the turbulent shear stress:

$$\tau = \tau_v + \tau_t = \mu_v \cdot \frac{\partial u}{\partial z} + \mu_t \cdot \frac{\partial u}{\partial z} = \rho_m \cdot \nu_m \cdot \frac{\partial u}{\partial z} + \rho_m \cdot \nu_t \cdot \frac{\partial u}{\partial z} \quad \text{with:} \quad \nu_t = \ell^2 \cdot \left| \frac{\partial u}{\partial z} \right| \qquad (7.6\text{-}5)$$

Now the shear stress can be expressed as (with **z** the distance from the pipe wall):

$$\tau = \rho_m \cdot \left(u_* \right)^2 \cdot \left(\frac{R-z}{R} \right) = \rho_m \cdot \left(\nu_m + \ell^2 \cdot \left| \frac{\partial u}{\partial z} \right| \right) \cdot \frac{\partial u}{\partial z} \quad \text{with:} \quad R = D_p / 2 \qquad (7.6\text{-}6)$$

This is a second degree function of the velocity gradient. Solving this with respect to the velocity gradient gives:

$$\frac{\partial u}{\partial z} = \frac{-\frac{\mu_m}{\rho_m} + \sqrt{\left(\frac{\mu_m}{\rho_m} \right)^2 + 4 \cdot \ell^2 \cdot \left(u_* \right)^2 \cdot \left(\frac{R-z}{R} \right)}}{2 \cdot \ell^2} = \frac{2 \cdot \left(u_* \right)^2 \cdot \left(\frac{R-z}{R} \right)}{\frac{\mu_m}{\rho_m} + \sqrt{\left(\frac{\mu_m}{\rho_m} \right)^2 + 4 \cdot \ell^2 \cdot \left(u_* \right)^2 \cdot \left(\frac{R-z}{R} \right)}} \qquad (7.6\text{-}7)$$

A required condition for pipe flow is, that the integral of the velocity over the pipe cross-section equals the average line speed times the cross-section, so:

$$\int_0^R \frac{\partial u}{\partial z} \cdot 2 \cdot \pi \cdot \left(R - z \right) \cdot dz = v_{ls} \cdot \pi \cdot R^2 \qquad (7.6\text{-}8)$$
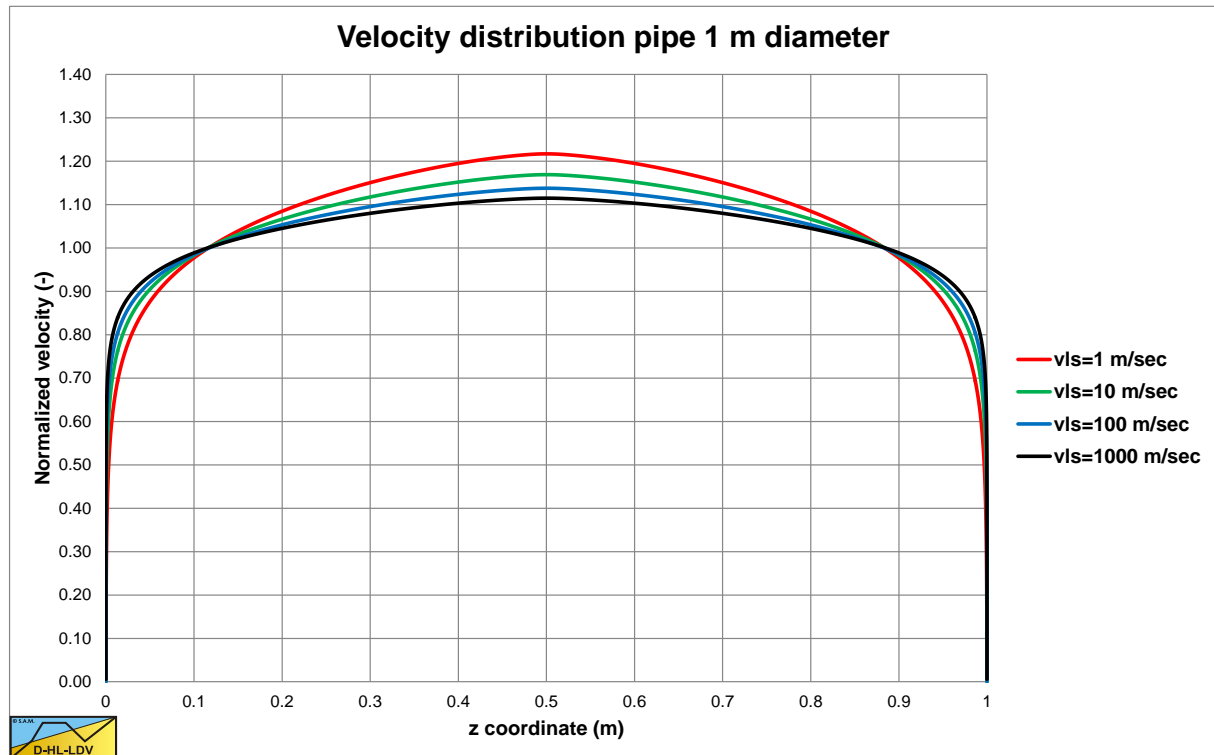
Figure 7.6-5: The resulting velocity distributions in a D_p=1 m pipe, corrected for the flow.

The Nikuradse (1933) equation for the mixing length in pipe flow for large Reynolds numbers is:

$$\frac{\ell}{R} = 0.14 - 0.08 \cdot \left(1 - \frac{z}{R}\right)^2 - 0.06 \cdot \left(1 - \frac{z}{R}\right)^4 = 0.14 \cdot \left(1 - \frac{4}{7} \cdot \left(1 - \frac{z}{R}\right)^2 - \frac{3}{7} \cdot \left(1 - \frac{z}{R}\right)^4\right) \tag{7.6-9}$$

The velocity profile can be determined by numerical integration. This velocity profile however, should result in an average velocity equal to the line speed used to determine the friction velocity. This appeared to be valid for very high line speeds (Reynolds numbers) in the range of 1300-1500 m/sec, which is far above the range dredging companies operate (3-10 m/sec). For line speeds in the range 3-10 m/sec, the velocity profile resulted in an average velocity smaller than the line speed with a factor 0.8-1.0. Introducing a factor **β** and an extra term in the mixing length equation solves this problem. The original Nikuradse (1933) equation is multiplied with a factor **β** and an extra term is added to ensure that **ℓ/R=κ·z** for **z=0**, like is the case in the original equation. The factor **β** is determined for each calculation in such a way, that the flow following from the line speed times the cross section of the pipe, equals the flow from integration of the velocity profile.

$$\frac{\ell}{R} = \beta \cdot \left(0.14 - 0.08 \cdot \left(1 - \frac{z}{R}\right)^2 - 0.06 \cdot \left(1 - \frac{z}{R}\right)^4\right) + (1 - \beta) \cdot \kappa \cdot \frac{z}{R} \cdot e^{-\frac{z}{0.00002 \cdot R}} \tag{7.6-10}$$

Figure 7.6-5 shows the resulting velocity distributions for a 1 m diameter pipe. Now the concept is, that a mixture flow with liquid as a carrier liquid in the viscous sub layer will have a lower resistance than a mixture flow with mixture in the viscous sub-layer. One can also say that in order to get the same pipeline resistance, the velocity in the center of the pipe of mixture with liquid in the viscous sub-layer u_m has to be higher than the case with mixture or liquid in the whole pipe u_l. Assuming that the dynamic viscosity of the mixture is equal to the dynamic viscosity of the carrier liquid, $\mu_m = \mu_l$, in the viscous sub-layer and the boundary layer where no solids are present, gives:

$$\frac{\partial u}{\partial z} = \frac{-\frac{\rho_l}{\rho_m} \cdot \nu_l + \sqrt{\left(\frac{\rho_l}{\rho_m} \cdot \nu_l\right)^2 + 4 \cdot \ell^2 \cdot (u_*)^2 \cdot \left(\frac{R - z}{R}\right)}}{2 \cdot \ell^2} \tag{7.6-11}$$

Now assuming that the term with the density ratio is relevant only near the pipe wall and not in the center of the pipe, this equation will simulate a mixture with liquid in the viscous sub-layer. In fact, the density ratio reduces the effect of the kinematic viscosity, which mainly affects the viscous sub-layer. The velocity difference in the center of the pipe between mixture and liquid, u_m-u_l, can now be determined with:

$$u_m - u_l = \int_0^R \left(\frac{\partial u}{\partial z}\right)_m \cdot dz - \int_0^R \left(\frac{\partial u}{\partial z}\right)_l \cdot dz = \int_0^R \frac{-\frac{\rho_l}{\rho_m} \cdot \nu_l + \sqrt{\left(\frac{\rho_l}{\rho_m} \cdot \nu_l\right)^2 + 4 \cdot \ell^2 \cdot (u_*)^2 \cdot \left(\frac{R - z}{R}\right)}}{2 \cdot \ell^2} \cdot dz$$

$$- \int_0^R \frac{-\nu_l + \sqrt{(\nu_l)^2 + 4 \cdot \ell^2 \cdot (u_*)^2 \cdot \left(\frac{R - z}{R}\right)}}{2 \cdot \ell^2} \cdot dz \tag{7.6-12}$$

This velocity difference, in the center of the pipe, is about equal to the difference of the average line speeds, however both can be determined numerically. Further it appears from the numerical solution of this equation, that dividing the velocity difference by the average liquid velocity u_l or $v_{ls,l}$ results in a factor **F**, which only depends on the volumetric concentration C_v, the relative submerged density R_{sd} and slightly on the line speed v_{ls} in the range 3-10 m/sec and on the pipe diameter D_p through the Darcy-Weisbach friction factor λ_l, according to:

$$F = \frac{u_m - u_l}{u_l} = \frac{v_{ls,m} - v_{ls,l}}{v_{ls,l}} = \alpha_h \cdot \lambda_l \cdot R_{sd} \cdot C_v = \alpha_h \cdot \lambda_l \cdot \left(\frac{\rho_m}{\rho_l} - 1\right) \tag{7.6-13}$$

The shear stress at the pipe wall of a Newtonian liquid is by definition:

$$\rho_l \cdot (u_*)^2 = \frac{\lambda_l}{8} \cdot \rho_l \cdot v_{ls,l}^2 \quad \text{and} \quad \rho_m \cdot (u_*)^2 = \frac{\lambda_m}{8} \cdot \rho_m \cdot v_{ls,m}^2 \tag{7.6-14}$$

From this a relation for the ratio of the Darcy-Weisbach friction coefficients of a flow with mixture in the center and carrier liquid in the viscous sub-layer to a flow with 100% liquid can be derived.

$$\frac{\lambda_l}{8} \cdot v_{ls,l}^2 = \frac{\lambda_m}{8} \cdot v_{ls,m}^2 \quad \Rightarrow \quad \frac{\lambda_m}{\lambda_l} = \frac{v_{ls,l}^2}{v_{ls,m}^2} \quad \Rightarrow \quad \frac{\lambda_m}{\lambda_l} = \frac{v_{ls,l}^2}{\left(F \cdot v_{ls,l} + v_{ls,l}\right)^2} = \frac{1}{\left(F+1\right)^2} \tag{7.6-15}$$

Equation (7.6-15) is independent of the method used, but the factor **F**, the velocity ratio, is. Substituting the factor **F** from equation (7.6-13) gives:

$$\frac{\lambda_m}{\lambda_l} = \frac{1}{\left(F+1\right)^2} = \frac{1}{\left(\alpha_h \cdot \lambda_l \cdot R_{sd} \cdot C_v + 1\right)^2} \tag{7.6-16}$$

This ratio depends on the homogeneous factor α_h, the Darcy-Weisbach friction factor λ_l, the volumetric concentration C_v and the relative submerged density R_{sd}. The ratio of the hydraulic gradients is now:

$$\frac{i_m}{i_l} = \frac{\lambda_m \cdot \rho_m}{\lambda_l \cdot \rho_l} = \frac{1 + R_{sd} \cdot C_v}{\left(\alpha_h \cdot \lambda_l \cdot R_{sd} \cdot C_v + 1\right)^2} \quad \Rightarrow \quad i_m = i_l \cdot \frac{1 + R_{sd} \cdot C_v}{\left(\alpha_h \cdot \lambda_l \cdot R_{sd} \cdot C_v + 1\right)^2} \tag{7.6-17}$$

This gives for the excess hydraulic gradient i_m-i_l (the solids effect):

$$i_m - i_l = i_l \cdot \frac{1 + R_{sd} \cdot C_v}{\left(\alpha_h \cdot \lambda_l \cdot R_{sd} \cdot C_v + 1\right)^2} - i_l \cdot \frac{\left(\alpha_h \cdot \lambda_l \cdot R_{sd} \cdot C_v + 1\right)^2}{\left(\alpha_h \cdot \lambda_l \cdot R_{sd} \cdot C_v + 1\right)^2}$$

$$\tag{7.6-18}$$

$$= i_l \cdot \frac{1 + R_{sd} \cdot C_v - \left(\alpha_h \cdot \lambda_l \cdot R_{sd} \cdot C_v + 1\right)^2}{\left(\alpha_h \cdot \lambda_l \cdot R_{sd} \cdot C_v + 1\right)^2}$$

The relative excess hydraulic gradient E_{rhg} is now:

$$E_{rhg} = \frac{i_m - i_l}{R_{sd} \cdot C_v} = i_l \cdot \frac{1 + R_{sd} \cdot C_v - \left(\alpha_h \cdot \lambda_l \cdot R_{sd} \cdot C_v + 1\right)^2}{R_{sd} \cdot C_v \cdot \left(\alpha_h \cdot \lambda_l \cdot R_{sd} \cdot C_v + 1\right)^2} = \alpha_E \cdot i_l \tag{7.6-19}$$

The limiting value for the relative excess hydraulic gradient E_{rhg} for a volumetric concentration C_v approaching zero, becomes:

$$E_{rhg} = \frac{i_m - i_l}{R_{sd} \cdot C_v} = i_l \cdot \left(1 - 2 \cdot \alpha_h \cdot \lambda_l\right) \tag{7.6-20}$$

For sand and gravel with a density of 2.65 ton/m³, the factor α_h is about 9.3, almost independent of the pipe diameter D_p and the line speed v_{ls} for pipes with diameters of 0.5 m up to 1.2 m and line speeds from 2 m/sec up to 10 m/sec. For very small pipes and very low line speeds, like D_p=0.1 m and v_{ls}=1 m/sec, this factor decreases to about 8.5. The factor α_h is not 100% linear with the term $R_{sd} \cdot C_v$ for sands with a density of 2.65 ton/m³ and volumetric concentrations up to 35-40%. Since the solution depends on $R_{sd} \cdot C_v$ combined, the factor α_h also depends on this and not on R_{sd} and C_v separately. Figure 7.6-6 shows the dependency of the factor α_h on the relative excess density $R_{sd} \cdot C_v$. The factor α_E decreases with increasing concentration and relative submerged density of the solids and increases with increasing line speed. At normal line speeds (3-6 m/sec) and concentrations (0.1-0.3) this factor is about **0.74-0.78** (see Figure 7.6-11). A larger pipe gives less reduction. This is caused by the smaller Darcy-Weisbach friction coefficient λ_l of larger pipes.
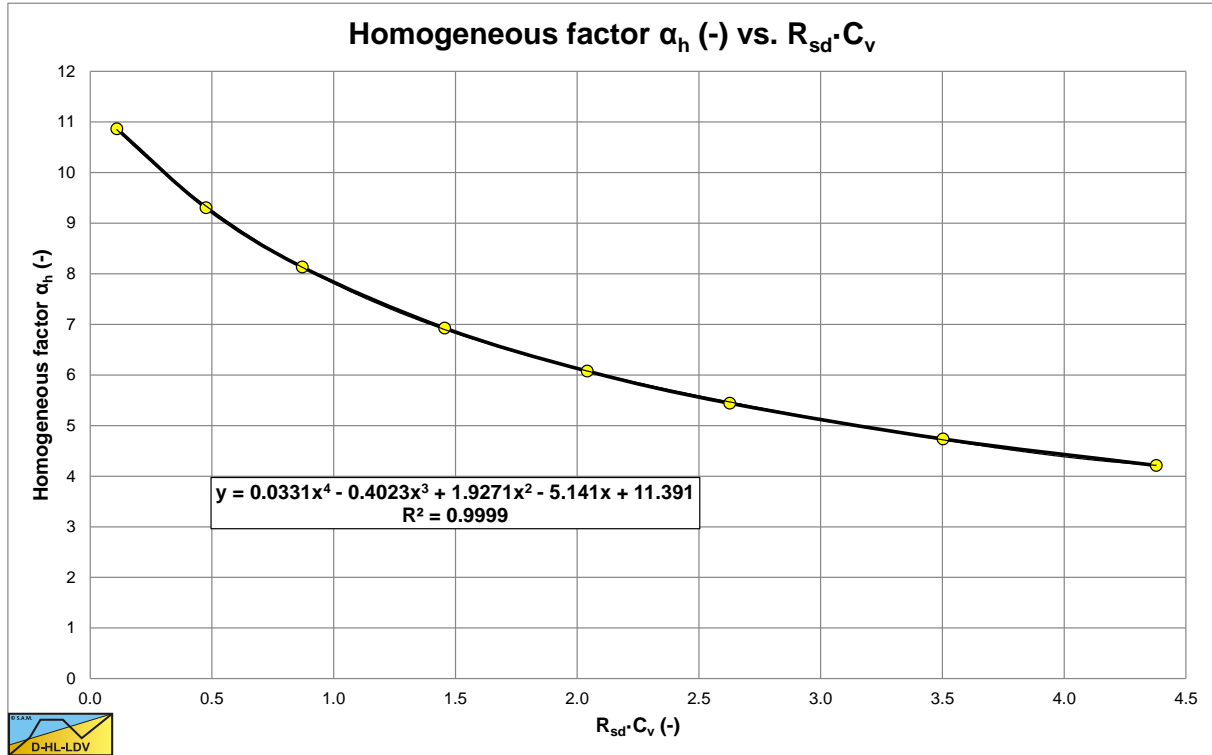
Figure 7.6-6: The homogeneous factor α_h as a function of $R_{sd} \cdot C_v$ for method 2.

7.6.5 Method 3: Adding the von Driest (Schlichting, 1968) Damping to Method 2.

Talmon (2013) used the Prandtl approach for the mixing length, which is a 2D approach for open channel flow with a free surface. The Prandtl approach was extended with damping near the wall to take into account the viscous effects near the wall, according to von Driest (Schlichting, 1968):

$$\textbf{Pr andl :} \qquad \ell = \kappa \cdot z$$

$$\textbf{von Driest :} \; \ell = \kappa \cdot z \cdot \left(1 - e^{-z^+/A}\right) \quad \textbf{with:} \quad z^+ = \frac{z \cdot u_*}{\nu_l} \quad A = 26 \tag{7.6-21}$$

Figure 7.6-9 and Figure 7.6-7 show the velocity profile and the mixing length profile of the Talmon (2013) approach with von Driest (Schlichting, 1968) damping and the Nikuradse (1933) approach without damping. In both cases, the mixing length equations have been corrected in order to get the correct volume flow. There is a clear difference of the velocity profiles. Applying the von Driest (Schlichting, 1968) damping to the Nikuradse (1933) equation (7.6-9) for the mixing length in pipe flow for large Reynolds numbers according to:

$$\frac{\ell}{R} = 0.14 \cdot \left(1 - \frac{4}{7} \cdot \left(1 - \frac{z}{R}\right)^2 - \frac{3}{7} \cdot \left(1 - \frac{z}{R}\right)^4\right) \cdot \left(1 - e^{-z^+/A}\right) \tag{7.6-22}$$

Gives almost exactly the same results as the Talmon (2013) approach, although the mixing length is completely different as is shown in Figure 7.6-8. Only very close to the wall, where the viscous effects dominate, the same mixing lengths are found. Apparently, the von Driest damping, effective close to the pipe wall, dominates the effect of a particle free viscous sub layer, as expected. The results are almost independent of the pipe diameter D_p and the line speed v_{ls}. Figure 7.6-10 shows that the velocity profiles determined with equation (7.6-21) (Talmon) and equation (7.6-22) (Miedema) are almost the same and the behavior with respect to the hydraulic gradient reduction is equivalent.

7.6.6 Method 4: The Law of the Wall Approach.

Often for open channel flow the so called "Law of the Wall" equations are used. Since in dredging the pipe wall is assumed to be smooth due to the continuous sanding of the pipe wall, the smooth wall approach is discussed here. Based on the following assumption for the mixing length by Prandtl (1925) and the assumption that the viscous shear stress is negligible in the turbulent region, the famous logarithmic velocity equation, "Law of the Wall" for the turbulent flow is derived:

$$
\tau = \tau_{wall} \cdot \left(1 - \frac{z}{R}\right) = \rho_l \cdot \ell^2 \cdot \left(\frac{du}{dz}\right)^2 \quad \text{and} \quad \ell = \kappa \cdot z \cdot \left(1 - \frac{z}{R}\right)^{0.5} \tag{7.6-23}
$$

This "Law of the Wall" is also a 2D approach for open channel flow and does not correct for pipe flow. The general equation for the velocity profile as a function of the distance to the smooth wall is:

$$
u(z) = \frac{u_*}{\kappa} \cdot \ln\left(\frac{z}{z_0}\right) \quad \text{with:} \quad z_0 = 0.11 \cdot \frac{\nu_l}{u_*} \tag{7.6-24}
$$

For the 100% liquid (or mixture) the velocity profile is defined as:

$$
u_l(z) = \frac{u_*}{\kappa} \cdot \ln\left(\frac{z}{z_{0,l}}\right) \quad \text{with:} \quad z_{0,l} = 0.11 \cdot \frac{\nu_l}{u_*} \tag{7.6-25}
$$

For the mixture with liquid in the viscous sub-layer the velocity profile can be defined as:

$$
u_m(z) = \frac{u_*}{\kappa} \cdot \ln\left(\frac{z}{z_{0,m}}\right) \quad \text{with:} \quad z_{0,m} = 0.11 \cdot \frac{\nu_l}{u_*} \cdot \frac{\rho_l}{\rho_m} \tag{7.6-26}
$$

The velocity difference at the center of the pipe is now:

$$
u_m(R) - u_l(R) = \frac{u_*}{\kappa} \cdot \ln\left(\frac{R}{z_{0,m}}\right) - \frac{u_*}{\kappa} \cdot \ln\left(\frac{R}{z_{0,l}}\right)
$$

$$
\tag{7.6-27}
$$

$$
= \frac{u_*}{\kappa} \cdot \ln\left(\frac{R \cdot u_*}{0.11 \cdot \nu_l} \cdot \frac{\rho_m}{\rho_l}\right) - \frac{u_*}{\kappa} \cdot \ln\left(\frac{R \cdot u_*}{0.11 \cdot \nu_l}\right) = \frac{u_*}{\kappa} \cdot \ln\left(\frac{\rho_m}{\rho_l}\right)
$$

This gives for the Darcy-Weisbach friction coefficient ratio:

$$
\frac{\lambda_m}{\lambda_l} = \frac{v_{ls,l}^2}{v_{ls,m}^2} = \frac{u_l^2}{u_m^2} = \frac{u_l}{\left(\frac{u_*}{\kappa} \cdot \ln\left(\frac{\rho_m}{\rho_l}\right) + u_l\right)^2} = \frac{1}{\left(\frac{1}{\kappa} \cdot \ln\left(\frac{\rho_m}{\rho_l}\right) \cdot \sqrt{\frac{\lambda_l}{8}} + 1\right)^2} \quad \text{with:} \quad u_* = \sqrt{\frac{\lambda_l}{8}} \cdot u_l \tag{7.6-28}
$$

The relative excess hydraulic gradient E_{rhg} is now:

$$
E_{rhg} = \frac{i_m - i_l}{R_{sd} \cdot C_v} = i_l \cdot \frac{1 + R_{sd} \cdot C_v - \left(\frac{1}{\kappa} \cdot \ln\left(\frac{\rho_m}{\rho_l}\right) \cdot \sqrt{\frac{\lambda_l}{8}} + 1\right)^2}{R_{sd} \cdot C_v \cdot \left(\frac{1}{\kappa} \cdot \ln\left(\frac{\rho_m}{\rho_l}\right) \cdot \sqrt{\frac{\lambda_l}{8}} + 1\right)^2} = \alpha_E \cdot i_l \tag{7.6-29}
$$
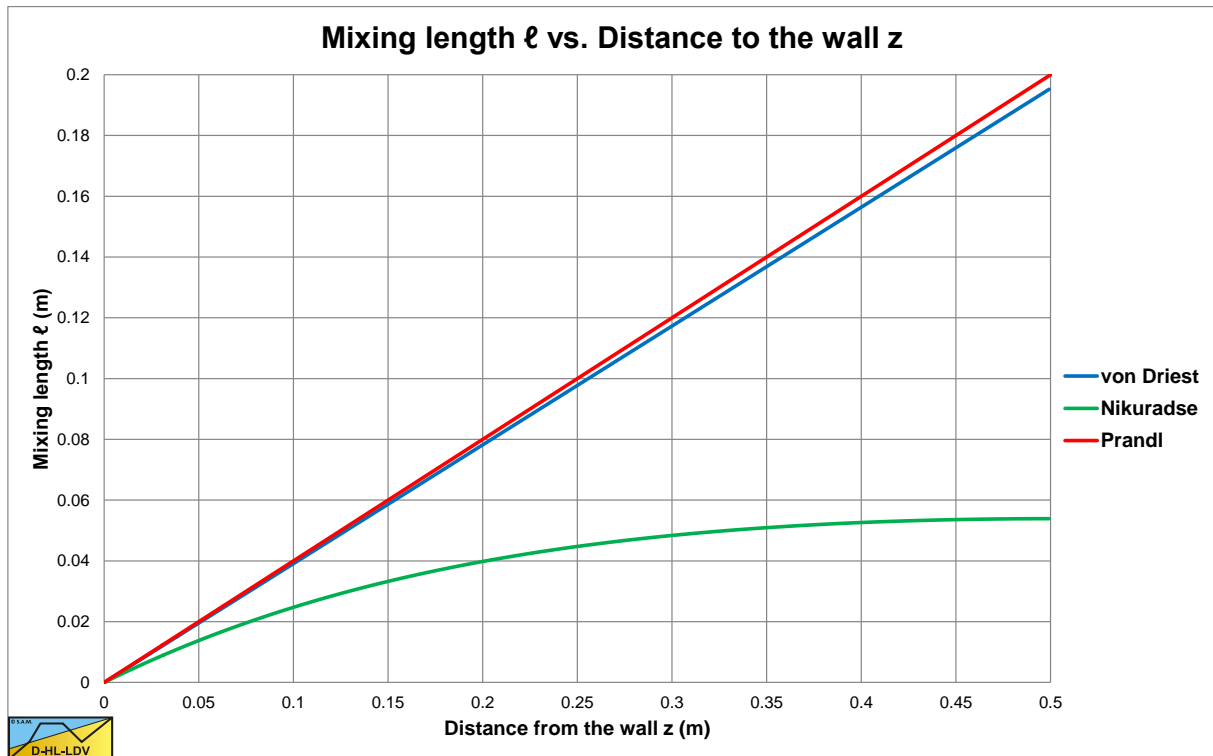
Figure 7.6-7: The mixing length versus the distance to the wall for a D_p=1 m pipe at a line speed v_{ls}=5 m/sec, $\kappa_{Prandtl}$=0.4, $\kappa_{vonDriest}$=0.3915 & $\kappa_{Nikuradse}$=0.4, without von Driest (Schlichting, 1968) damping.
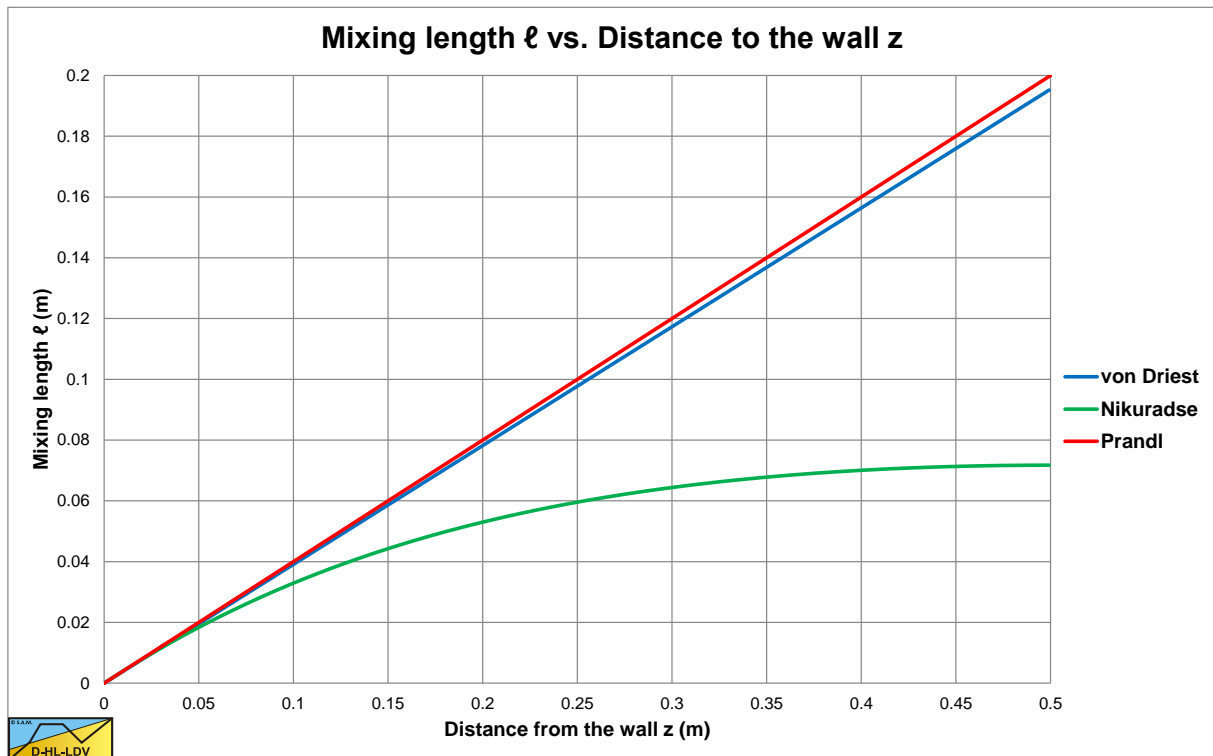
Figure 7.6-8: The mixing length versus the distance to the wall for a D_p=1 m pipe at a line speed v_{ls}=5 m/sec, $\kappa_{Prandtl}$=0.4, $\kappa_{vonDriest}$=0.3915 & $\kappa_{Nikuradse}$=0.4, with von Driest (Schlichting, 1968) damping.
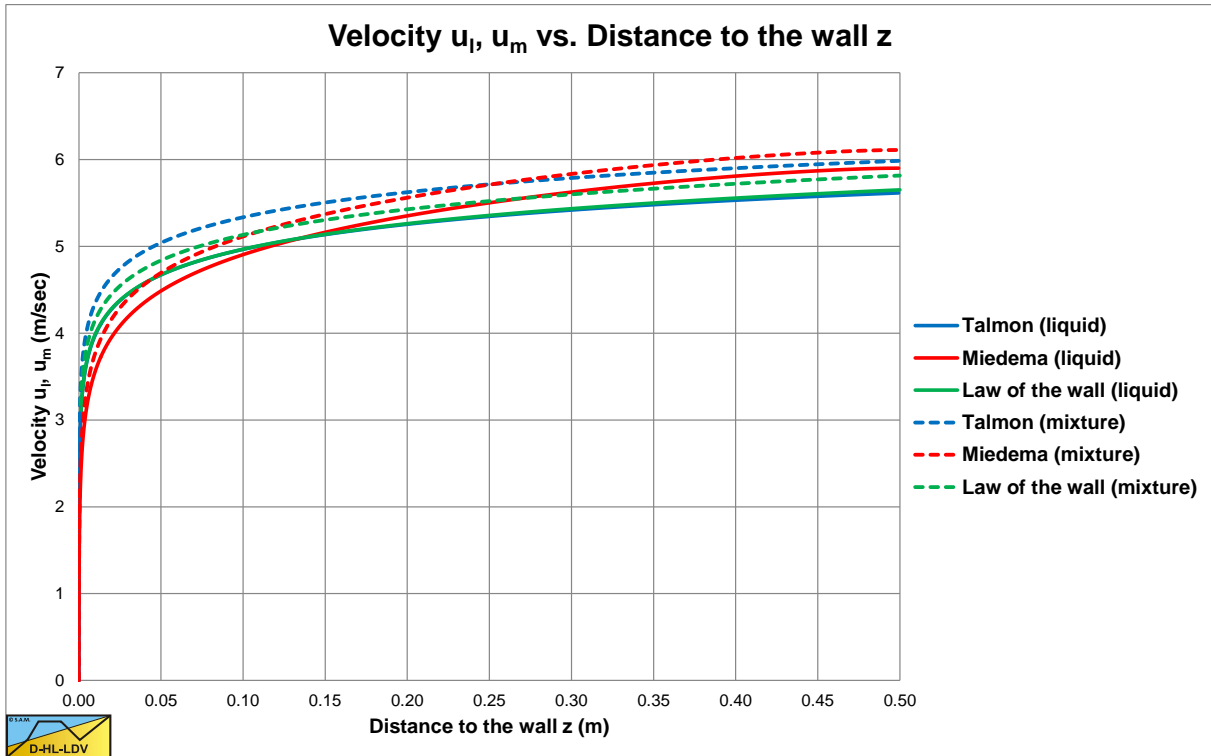
Figure 7.6-9: The velocity versus the distance to the wall for a D_p=1 m pipe at a line speed v_{ls}=5 m/sec, $\kappa_{Prandtl}$=0.4, $\kappa_{vonDriest}$=0.3915 & $\kappa_{Nikuradse}$=0.4, without von Driest (Schlichting, 1968) damping.
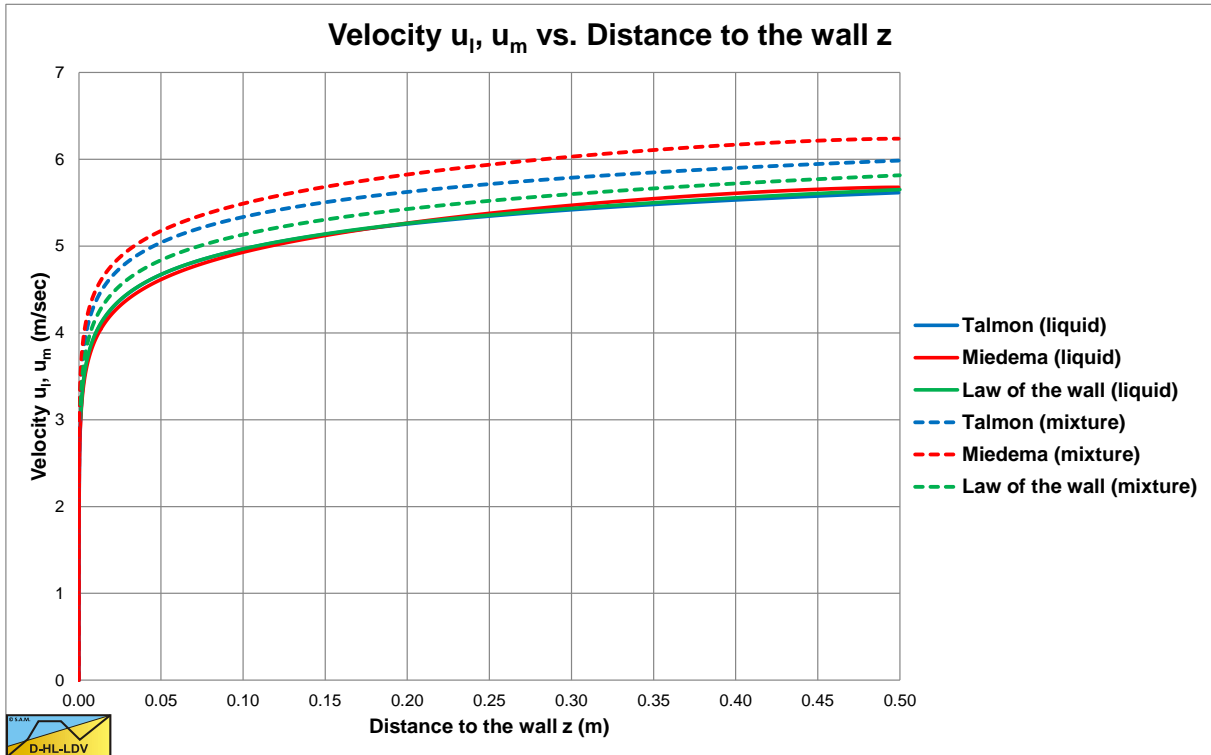
Figure 7.6-10: The velocity versus the distance to the wall for a D_p=1 m pipe at a line speed v_{ls}=5 m/sec, $\kappa_{Prandtl}$=0.4, $\kappa_{vonDriest}$=0.3915 & $\kappa_{Nikuradse}$=0.4, with von Driest (Schlichting, 1968) damping.

7.6.7 Comparison of the Models.

Now 3 formulations are found for the reduction of the Darcy-Weisbach friction factor and the relative excess hydraulic gradient E_{rhg} for slurry transport of a mixture with pure carrier liquid (water) in the viscous sub-layer, these are equations (7.6-4), (7.6-16) & (7.6-19) and (7.6-28) & (7.6-29):

Law of the Wall (no damping)	Nikuradse (no damping)	Prandl – von Driest (damping)

$$\frac{\lambda_m}{\lambda_l} = \frac{1}{\left(\frac{1}{\kappa} \cdot \ln\left(1 + R_{sd} \cdot C_v\right) \cdot \sqrt{\frac{\lambda_l}{8}} + 1 \right)^2} \qquad \frac{\lambda_m}{\lambda_l} = \frac{1}{\left(\alpha_h \cdot \lambda_l \cdot R_{sd} \cdot C_v + 1 \right)^2} \qquad \frac{\lambda_m}{\lambda_l} = \frac{1}{\left(\alpha_h \cdot \sqrt{\frac{\lambda_l}{8}} \cdot R_{sd} \cdot C_v + 1 \right)^2}$$

$\kappa = 0.4$	$\alpha_h = 9.3$	$\alpha_h = 6.7$
Miedema	**Miedema**	**Talmon**

Since the above solutions are not (very) sensitive for changes in the pipe diameter D_p or the line speed v_{ls}, but mainly for changes of the density ratio ρ_m/ρ_l, a comparison is made for a D_p=1 m diameter pipe at a line speed of v_{ls}=5 m/sec in sand with a solids density of 2.65 ton/m^3 and a virtual solid with a density of 10 ton/m^3. Figure 7.6-11 and Figure 7.6-12 show the Darcy-Weisbach friction factor ratios and the relative excess hydraulic gradient coefficient α_E. The methods 2 and 4 without damping do not differ too much, both give a reduction on the solids effect of about 18-26% in sand for medium concentrations. The methods 1 and 3 with damping however give a reduction on the solids effect of about 55-65% in sand, almost 3 times as much. For the virtual solid with a solids density of 10 ton/m^3, the reductions are 18-30% and 65-80%. Based on the data as shown by Talmon (2013), the reduction of the solids effect of 55-65% with method 1 with damping is overestimating the reduction, while the two methods without damping seem to underestimate the reduction, assuming that the reduction measured is caused by the effect of a lubricating viscous sub-layer.

If damping is added to the Nikuradse (1933) mixing length equation, method 3, the same results are obtained as the Prandtl mixing length equation with von Driest (Schlichting, 1968) damping, method 1. Apparently the mixing length damping dominates the difference between the 3 methods. The von Driest modification is an empirical damping function that fits experimental data, and also changes the near-wall asymptotic behavior of the eddy viscosity v_t, from z^2 to z^4. Although neither of them are correct (DNS-data gives v_t proportional to z^3), the von Driest damping generally improves the predictions. It has, since its first appearance, repeatedly been used in turbulence models to introduce viscous effects in the near-wall region. The von Driest damping however has never been developed to deal with the problem of a lubricating viscous sub-layer as is elaborated in this chapter.

Because of the overestimation of methods 1 and 3 and the underestimation of methods 2 and 4, an average between Prandtl without damping, method 3, and Prandtl with damping, method 1, could be used according to (with α_h about 6.7):

$$\frac{\lambda_m}{\lambda_l} = \frac{1}{\left(\frac{\left(\frac{1}{\kappa} \cdot \ln\left(1 + R_{sd} \cdot C_v\right) + \alpha_h \cdot R_{sd} \cdot C_v \right)}{2} \cdot \sqrt{\frac{\lambda_l}{8}} + 1 \right)^2} \qquad (7.6-30)$$

The results of this equation are also shown in Figure 7.6-11 and Figure 7.6-12. For sands with a solids density of 2.65 ton/m^3 this gives a reduction of about 35-45%, on average 40%. The downside of this equation is, that the equation gives a fixed result for a fixed $R_{sd} \cdot C_v$ value and is not adaptable to more experimental data. Reason to investigate the possibility of applying a concentration profile, where the concentration equals zero at the pipe wall and increases, with a sort of von Driest damping function, to a maximum value at the center of the pipe. This concentration profile has to be corrected, based on numerical integration, to ensure that the average concentration matches a given value.
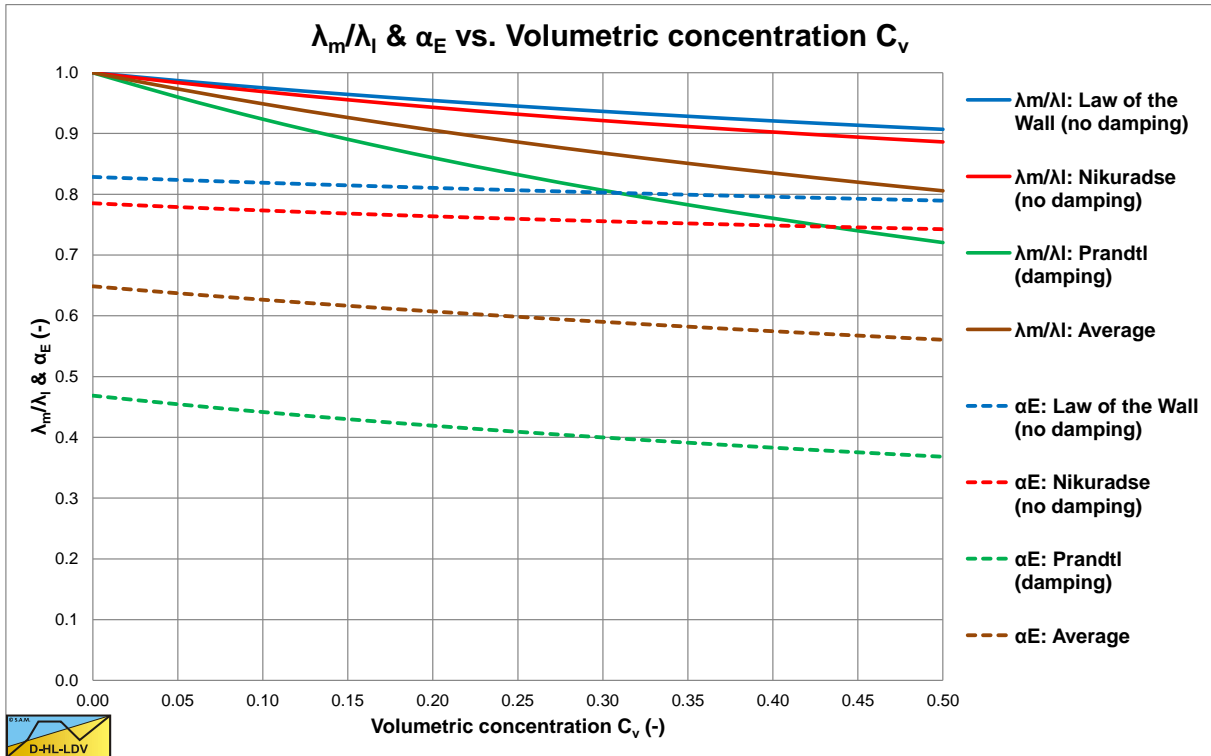
Figure 7.6-11: The Darcy-Weisbach friction coefficient ratio λ_m/λ_l and the factor α_E as a function of the volumetric concentration C_v at D_p=1 m, v_{ls}=5 m/sec and solids density of 2.65 ton/m³.
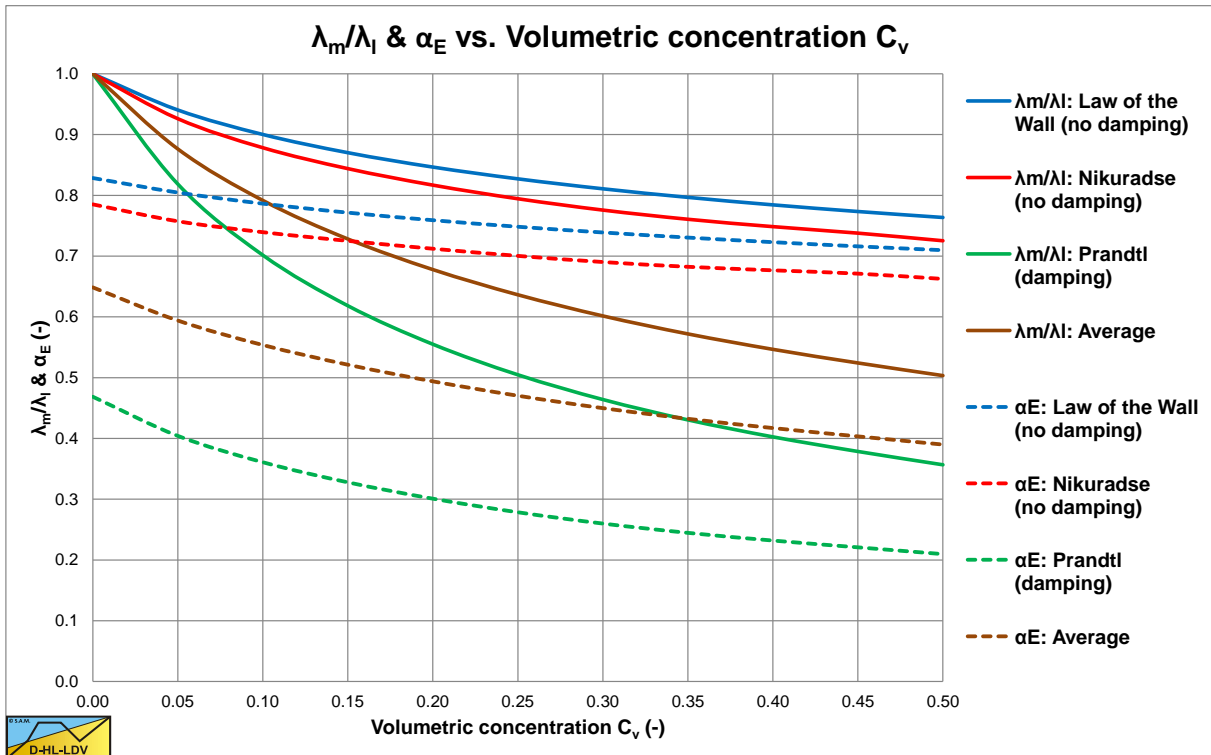
Figure 7.6-12: The Darcy-Weisbach friction coefficient ratio λ_m/λ_l and the factor α_E as a function of the volumetric concentration C_v at D_p=1 m, v_{ls}=5 m/sec and solids density of 10 ton/m³.

7.6.8 Method 5: Applying a Concentration Profile to Method 2.

The original Talmon (2013) concept assumes a constant density ratio for the whole cross section of the pipe. This of course is not in agreement with the physical reality. The concept assumes carrier liquid in the viscous sub-layer and mixture in the remaining part of the cross-section, but uses a constant density ratio. In order to correct this a damping factor for the density ratio α_ρ is proposed. This density ratio damping factor takes care that there is only carrier liquid very close to the wall. The factor A_ρ determines the thickness of this carrier liquid layer. If A_ρ equals zero, the solution obtained with Prandtl or Nikuradse with von Driest damping is found, methods 1 and 3. If A_ρ equals 4.13 the solution of the "Law of the Wall" is found, method 4, and if A_ρ equals 3.02 the solution of the Nikuradse equation without damping is found, method 2. The concentration profile and the density ratio are defined as:

$$
\mathbf{C_{v,z} = C_{v,max} \cdot \left(1 - e^{-A_\rho \cdot \frac{z}{\delta_v}}\right)} \quad \text{and} \quad \mathbf{\alpha_\rho = \frac{1 + R_{sd} \cdot C_{v,z}}{1 + R_{sd} \cdot C_v}}
\tag{7.6-31}
$$

The maximum concentration $\mathbf{C_{v,max}}$ in the concentration profile is found by integrating the concentration profile over the cross-section of the pipe and making it equal to the average concentration multiplied with the cross section of the pipe according to:

$$
\mathbf{\int_0^R C_{v,z} \cdot 2 \cdot \pi \cdot (R - z) \cdot dz = 2 \cdot \pi \cdot C_{v,max} \cdot \int_0^R \left(1 - e^{-A_\rho \cdot \frac{z}{\delta_v}}\right) \cdot (R - z) \cdot dz = C_v \cdot \pi \cdot R^2}
\tag{7.6-32}
$$

The maximum concentration $\mathbf{C_{v,max}}$ is now equal to average concentration $\mathbf{C_v}$ times a correction factor.

$$
\mathbf{C_{v,max} = C_v \cdot \frac{\pi \cdot R^2}{2 \cdot \pi \cdot \left(\frac{R^2}{2} - \frac{R \cdot \delta_v}{A_\rho} + \left(\frac{\delta_v}{A_\rho}\right) \cdot \left(1 - e^{-A_\rho \cdot \frac{R}{\delta_v}}\right)\right)}}
\tag{7.6-33}
$$

The velocity gradient, including the concentration profile, is now:

$$
\mathbf{\frac{\partial u}{\partial z} = \frac{-\alpha_\rho \cdot \nu_l + \sqrt{(\alpha_\rho \cdot \nu_l)^2 + 4 \cdot \ell^2 \cdot (u^*)^2 \cdot \left(\frac{R - z}{R}\right)}}{2 \cdot \ell^2}}
\tag{7.6-34}
$$

The integrated velocity difference $\mathbf{u_m \text{-} u_l}$ is now:

$$
\mathbf{v_{ls,m} - v_{ls,l} \approx u_m - u_l = \int_0^R \frac{-\alpha_\rho \cdot \nu_l + \sqrt{(\alpha_\rho \cdot \nu_l)^2 + 4 \cdot \ell^2 \cdot (u^*)^2 \cdot \left(\frac{R - z}{R}\right)}}{2 \cdot \ell^2} \cdot dz}
$$
$$
\mathbf{- \int_0^R \frac{-\nu_l + \sqrt{(\nu_l)^2 + 4 \cdot \ell^2 \cdot (u^*)^2 \cdot \left(\frac{R - z}{R}\right)}}{2 \cdot \ell^2} \cdot dz}
\tag{7.6-35}
$$

For the resulting Darcy-Weisbach friction factor ratio this can be approximated by:

$$
\mathbf{\frac{\lambda_m}{\lambda_l} = \frac{1}{\left(\frac{A_{C_v}}{\kappa} \cdot \ln\left(\frac{\rho_m}{\rho_l}\right) \cdot \sqrt{\frac{\lambda_l}{8}} + 1\right)^2}}
\tag{7.6-36}
$$

Where A_{Cv} depends on the value of A_ρ. The relative excess hydraulic gradient E_{rhg} is now:

$$E_{rhg} = \frac{i_m - i_l}{R_{sd} \cdot C_v} = i_l \cdot \frac{1 + R_{sd} \cdot C_v - \left(\frac{A_{Cv}}{\kappa} \cdot \ln\left(\frac{\rho_m}{\rho_l}\right) \cdot \sqrt{\frac{\lambda_1}{8}} + 1 \right)^2}{R_{sd} \cdot C_v \cdot \left(\frac{A_{Cv}}{\kappa} \cdot \ln\left(\frac{\rho_m}{\rho_l}\right) \cdot \sqrt{\frac{\lambda_1}{8}} + 1 \right)^2} = \alpha_E \cdot i_l \qquad (7.6\text{-}37)$$

Now, from numerical solutions, it appears that equations (7.6-36) and (7.6-37) give a very good approximation of all 4 methods for the range of parameters as normally used in dredging. The factor $A_{Cv}=1$ for the "Law of the Wall" (method 4), $A_{Cv}=1.25$ for the Nikuradse solution without damping (method 2) and $A_{Cv}=3.4$ for the Prandtl and Nikuradse solutions with von Driest damping (methods 1 and 3). The average equation (7.6-30) has a coefficient of $A_{Cv}=2.2$ and $A_\rho=1.05$. Table 7.6-1 gives an overview of these values.

Figure 7.6-14 shows a lower limit of the data, an upper limit of the data and the curve of Talmon (2013), method 1, compared with experimental data of Talmon (2011) in a vertical pipe. The lower and upper limit are determined for the particles from **d=0.345 mm** to **d=0.750 mm**. The finest particles of **d=0.125 mm** show less or even a reversed influence, probably because of the Thomas (1965) viscosity effect.
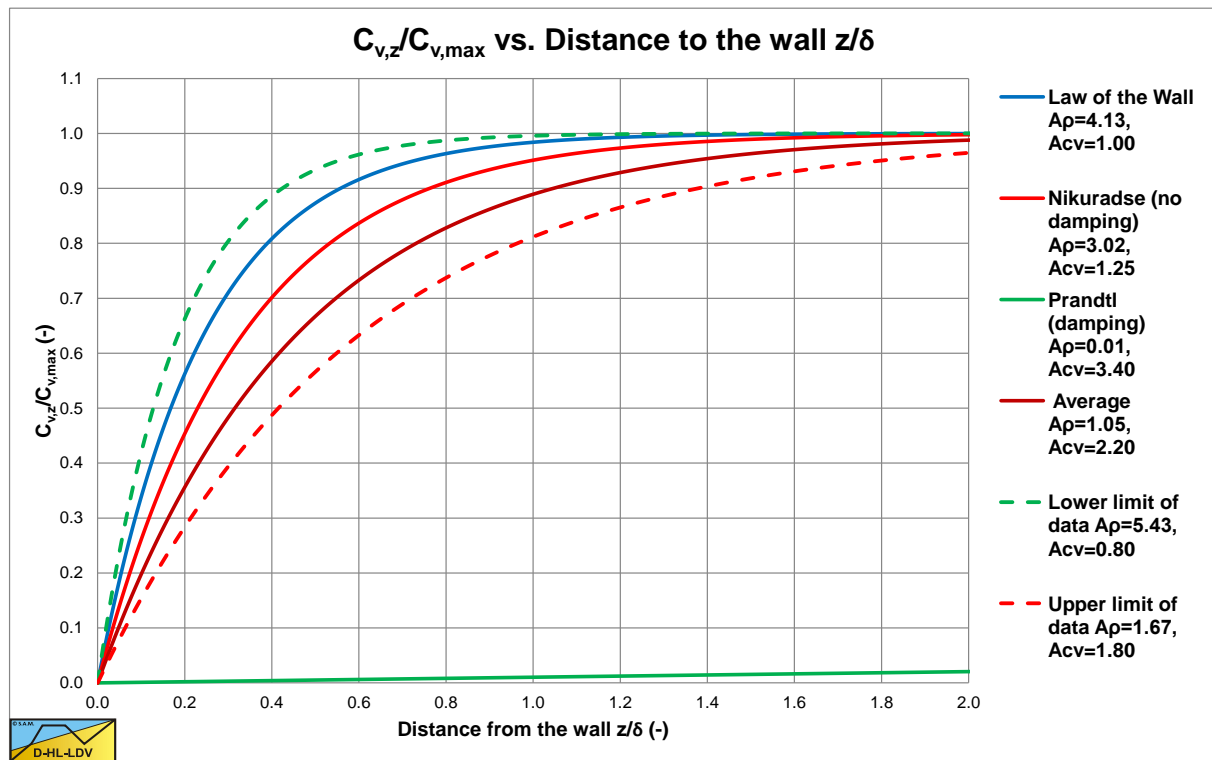
Figure 7.6-13: The concentration distribution for the cases considered from Table 7.6-1.

Table 7.6-1: Some A_ρ and A_{Cv} values.

	A_ρ	A_{Cv}
Law of the Wall	4.13	1.00
Nikuradse (no damping)	3.02	1.25
Prandtl (damping)	0.01	3.40
Average	1.05	2.20
Lower limit of data	5.43	0.80
Upper limit of data	1.67	1.80

Figure 7.6-13 shows the concentration profiles for **D_p=1 m, v_{ls}=5 m/sec, δ=0.088 mm** for the cases considered in.
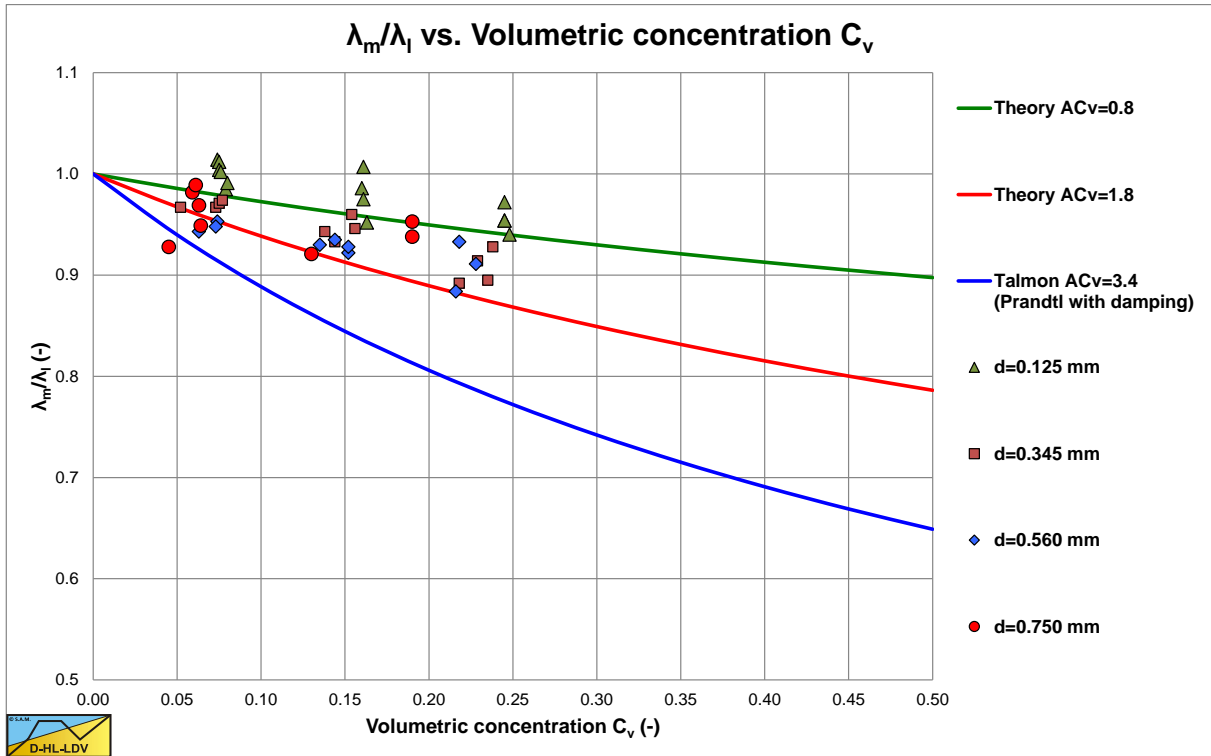
Figure 7.6-14: Talmon (2011) data compared with the theory.

Figure 7.6-1 shows experimental data of Thomas (1976) of iron ore in a horizontal pipe, where the theoretical curve contains both the Thomas (1965) viscosity and equation (7.6-37) with **A$_{Cv}$=1.3**, the average of the lower and upper limit.

7.6.9 Applicability of the Model.

Homogeneous transport is defined as transport where the concentration distribution is close to being uniform and the head losses behave similar to the Darcy Weisbach head losses, but with some correction.

The basis of the homogeneous transport regime model is the equivalent liquid model (ELM). In terms of the relative excess hydraulic gradient, **E$_{rhg}$**, this can be written as:

$$E_{rhg} = \frac{i_m - i_l}{R_{sd} \cdot C_{vs}} = \frac{\lambda_l \cdot v_{ls}^2}{2 \cdot g \cdot D_p} = i_l \tag{7.6-38}$$

Talmon (2013) derived an equation to correct the homogeneous equation (the ELM model) for the slurry density, based on the hypothesis that the viscous sub-layer hardly contains solids at very high line speeds in the homogeneous regime. This theory results in a reduction of the resistance compared with the ELM, but the resistance is still higher than the resistance of clear water. Talmon (2013) used the Prandl approach for the mixing length, which is a 2D approach for open channel flow with a free surface. The Prandl approach was extended with damping near the wall to take into account the viscous effects near the wall, according to von Driest (Schlichting, 1968). Miedema (2015A) improved the equation for pipe flow and a concentration distribution giving for the relative excess hydraulic gradient **E$_{rhg}$**:

$$E_{rhg} = \frac{i_m - i_l}{R_{sd} \cdot C_{vs}} = i_l \cdot \frac{1 + R_{sd} \cdot C_{vs} - \left(\frac{A_{C_v}}{\kappa} \cdot \ln\left(\frac{\rho_m}{\rho_l} \right) \cdot \sqrt{\frac{\lambda_l}{8}} + 1 \right)^2}{R_{sd} \cdot C_{vs} \cdot \left(\frac{A_{C_v}}{\kappa} \cdot \ln\left(\frac{\rho_m}{\rho_l} \right) \cdot \sqrt{\frac{\lambda_l}{8}} + 1 \right)^2} \tag{7.6-39}$$
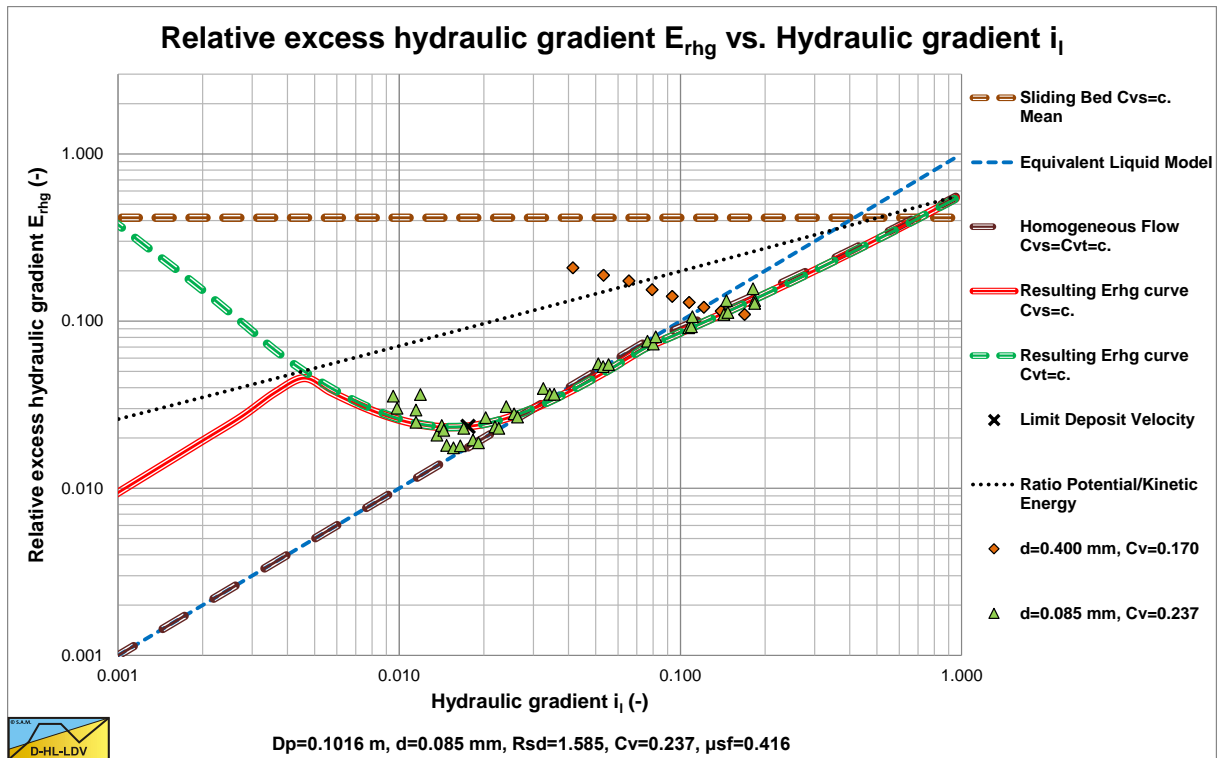
Figure 7.6-15: Experimental data of Whitlock et al. (2004).
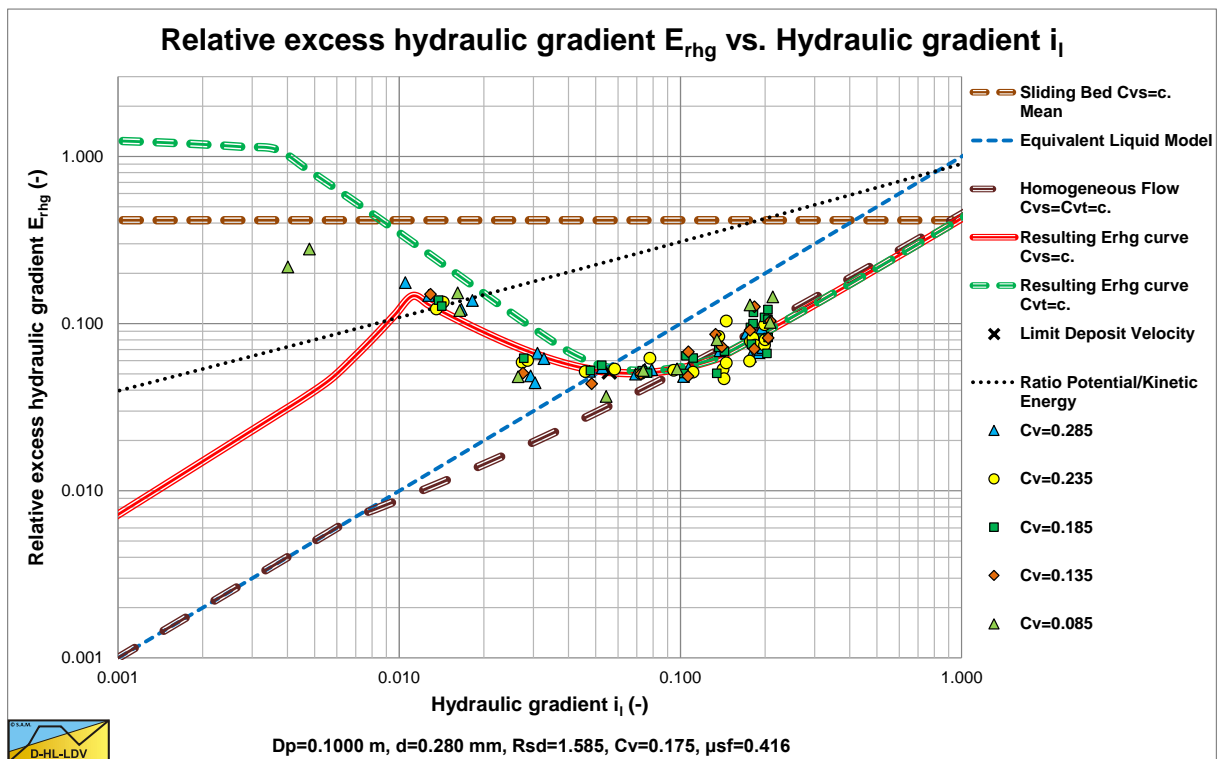
Figure 7.6-16: Experiments of Blythe & Czarnotta (1995).

The resulting equation (7.6-39) with **A$_{Cv}$=3** gives a good average behavior based on the data of Talmon (2011) and Thomas (1976). Since the model is based on a particle free viscous sub-layer and the viscosity of the carrier liquid, it may not give good predictions for very small particles. Very small particles may influence the viscosity and fit completely in the viscous sub layer, especially at low line speeds. It is observed that very small particles behave according to the ELM, if necessary corrected for the viscosity and density. Medium and large particles show the reduction according to equation (7.6-39). The transition of the ELM to the reduced ELM appears to

depend on the ratio of the thickness of the viscous sub layer to the particle diameter with a maximum of 1. This ratio is an indication of the concentration reduction in the viscous sub layer, giving:

$$
E_{rhg} = \frac{i_m - i_l}{R_{sd} \cdot C_{vs}} = i_l \cdot \left(1 - \left(1 - \frac{1 + R_{sd} \cdot C_{vs} - \left(\frac{A_{C_v}}{\kappa} \cdot \ln\left(\frac{\rho_m}{\rho_l} \right) \cdot \sqrt{\frac{\lambda_l}{8}} + 1 \right)^2}{R_{sd} \cdot C_{vs} \cdot \left(\frac{A_{C_v}}{\kappa} \cdot \ln\left(\frac{\rho_m}{\rho_l} \right) \cdot \sqrt{\frac{\lambda_l}{8}} + 1 \right)^2} \right) \left(1 - \left(\frac{\delta_v}{d} \right) \right) \right) \tag{7.6-40}
$$

Figure 7.6-15 shows experimental data of Whitlock et al. (2004) showing that very small particles (**d=0.085 mm**) have a rather sharp transition from the heterogeneous regime to the ELM, while at higher line speeds the reduction due to a lower concentration in the homogeneous regime is mobilized. Larger particles (**d=0.4 mm**) however seem to have some overshoot. Figure 7.6-16 shows experiments of Blythe & Czarnotta (1995). From these experiments it is clear that the relative excess hydraulic gradient crosses the ELM curve, after which it tends to go back to the direction of the homogeneous curve (reduced ELM or RELM) asymptotically.

7.6.10 Conclusions.

The concept of Talmon (2013) is applicable for determining the pressure losses in the homogeneous regime, however this concept has to be modified with respect to the shear stress distribution, the concentration distribution and a check on conservation of volume flow and concentration. The resulting equations (7.6-36) and (7.6-37) with A_{C_v}=**1.3** give a good average behavior based on the data of Talmon (2011) and Thomas (1976). The original factor A_{C_v}=**3.4** of Talmon (2013) seems to overestimate the reduction of the solids effect. It should be mentioned that the experiments as reported by Talmon (2011) were carried out in a vertical pipe ensuring symmetrical flow. For horizontal pipes the results may differ, since the velocity and concentration profiles are not symmetrical at the line speeds common in dredging. Since the model is based on a particle free viscous sub-layer and the viscosity of the carrier liquid, it may not give good predictions for very small or large particles. Very small particles may influence the viscosity, while very large particles are not influenced by the viscous sub-layer.

Using the resulting equations (7.6-36) and (7.6-37), implies using von Driest damping in combination with a concentration profile. The resulting equations (7.6-36) and (7.6-37) are flexible in use.
The error of using A_{C_v}=**1-3** is difficult to define. With respect to the relative excess hydraulic gradient E_{rhg} the accuracy is about +/- 10%. With respect to the hydraulic gradient i_m, which is of interest for the dredging companies, the accuracy is better to much better, since this hydraulic gradient equals i_m=i_l+E_{rhg}·R_{sd}·C_v.

The homogeneous flow regime is modelled as a reduced equivalent liquid model (RELM) with mobilization of the reduction based on the ratio between the thicknesses of the viscous sub layer to the particle diameter. For very small particles there is no reduction at low line speeds. The reduction is in effect at higher line speeds. Medium and large particles encounter this reduction however also at lower line speeds.

Equations **(7.6-39)** and **(7.6-40)** are implemented in the Delft Head Loss & Limit Deposit Velocity (DHLLDV) Framework with a default value of A_{C_v}=**3** (see Miedema & Ramsdell (2014))**.**

The latest calibrations with experiments show that A_{C_v}=**2.5-3**.

7.6.11 Nomenclature Homogeneous Regime.

A	Von Driest damping factor (26)	-
A_{Cv}	Concentration factor	-
A_ρ	Density factor	-
C_v	Concentration averaged over the cross section of the pipe	-
$C_{v,z}$	Concentration at distance z of the pipe wall	-
$C_{v,max}$	Maximum concentration in the center of the pipe	-
d	Particle diameter	m
d_{50}	50% passing particle diameter	M
D_p	Pipe diameter	m
E_{rhg}	Relative excess hydraulic gradient	-
F	Homogeneous reduction factor	-
g	Gravitational constant (9.81)	m/s^2
ΔL	Length of pipe segment considered	m
i_m	Mixture hydraulic gradient	m/m
i_l	Liquid hydraulic gradient	m/m
Δp_m	Pressure loss mixture over a length ΔL	kPa
R	Pipe radius	m
R_{sd}	Relative submerged density (sand 1.65)	-
u	Velocity	m/s
u_l	Velocity liquid	m/s
u_m	Velocity mixture	m/s
u_*	Friction velocity	m/s
v_{ls}	Line speed	m/s
$v_{ls,l}$	Line speed liquid	m/s
$v_{ls,m}$	Line speed mixture	m/s
z	Distance to the wall	m
z^+	Dimensionless distance to the wall	-
z_0	Constant velocity profile liquid	m
$z_{0,m}$	Constant velocity profile mixture	m
α_h	Homogeneous factor	-
α_E	Homogeneous factor E_{rhg} value	-
β	Nikuradse correction factor	-
δ_v	Thickness viscous sub-layer	m
λ_l	Darcy-Weisbach friction factor liquid	-
λ_m	Darcy-Weisbach friction factor mixture	-
ρ_l	Density liquid	ton/m^3
ρ_m	Density mixture	ton/m^3
κ	Von Karman constant (0.4)	-
τ	Shear stress	kPa
τ_{wall}	Shear stress at the wall	kPa
τ_v	Viscous shear stress	kPa
τ_t	Turbulent shear stress	kPa
μ_v	Viscous dynamic viscosity	Pa·s
μ_t	Turbulent dynamic viscosity	Pa·s
μ_l	Dynamic viscosity liquid	Pa·s
μ_m	Dynamic viscosity mixture	Pa·s
ν_l	Kinematic viscosity liquid	m^2/s
ν_m	Kinematic viscosity mixture	m^2/s
ν_t	Turbulence viscosity	m^2/s
ℓ	Mixing length	m

7.7 The Sliding Flow Regime.

7.7.1 Introduction.

Vlasak et al. (2012) and (2014) investigated the transport of coarse particles in a D_p=0.1 m pipe in the Institute of Hydrodynamics in Prague. The particles had a d_{50}=11.0-11.7 mm diameter and were transported with line speeds in the range of 1.5 m/s to 5.5 m/s. The density of the particles is 2.787 ton/m^3 and the carrier liquid was water. Concentrations in the range of 3% to 15% were used. So, the particles had a diameter of about 10-11% of the pipe diameter.

In the horizontal pipe section the flow was significantly stratified. For low line speeds the individual particles were sliding and rolling over the bottom of the pipe. Increasing the line speed resulted in ripples and dunes. In the lower line speed range the sliding bed layer was combined with saltation on top of the bed and dunes appearing and disappearing. With increasing line speed the thickness of the sliding bed decreased and particle saltation became the dominant mode of particle movement. However, most particles remained in contact with the pipe wall. The pressure drops were mainly produced by mechanical friction between the particles and the pipe wall, also resulting in relatively high slip ratio values. The transport was dominated by particle-particle interactions and particle-wall interactions. The horizontal particle velocities increased with the vertical distance from the pipe bottom. Saltating (free) particles had a much higher horizontal velocity compared with the particles in the bed.

The concentration distribution is important to understand the internal structure of the mixture flow. At low line speeds (Figure 7.7-9) the local concentration tends to approach zero at the upper portion of the pipe. This region increased with decreasing concentration and occupied 30%-50% of the pipe. A nearly linear concentration profile was observed in the lower part of the pipe, increasing from a bottom concentration at the bottom of the pipe to almost zero at a height of 50%-70% of the pipe. The bottom concentration decreased with a decreasing cross sectional averaged concentration. Very dense sand or gravel has a concentration up to 66%. Very loose sand or gravel a concentration of about 50%. Below 50% the particles do not rest on top of each other, however in a fast-flowing sliding bed this is possible because of the kinetic particle-particle interactions. Moderate line speeds (Figure 7.7-10) showed the same behavior, but with smaller bottom concentrations. At high line speeds (Figure 7.7-11) the bottom concentrations decreased further, but with the same shape of the concentration profile. In general, the particles tend to occupy the bottom part of the pipe and the concentration profile is symmetrical to the vertical plane of symmetry. The higher concentrations shown at the top of the pipe were detected as errors due to the effect of the pipe material on gamma-ray absorption.

According to the DHLLDV Framework of Miedema (June 2016) the Limit Deposit Velocity (LDV) of the particles used by Vlasak et al. (2012) and (2014) has a value around 3 m/s. For small particles, this LDV is the velocity above which no stationary or sliding bed exists. It is the question however whether for such large particles an LDV still exists since the particles continue to occupy the bottom part of the pipe even at high line speeds. Maybe at low concentrations this may be the case, but at high concentrations there is not enough turbulent energy to completely remove the bed. It seems also at high line speeds there is still a sort of bed, but with decreased concentration as the line speed increases.

Apparently very coarse particles do not follow the heterogeneous and homogeneous flow regimes at high line speeds as has been described by Miedema (June 2016), but follow a different behavior, which is named the sliding flow regime. In the sliding flow regime, the hydraulic gradient is dominated by sliding and/or rolling friction instead of collisions as in the heterogeneous regime. As long as the bed has a high concentration preventing the particles to start rolling, the normal sliding friction coefficient as used in the sliding bed regime can be applied. However, if the bed concentration reduces below 50%, giving particles more freedom to roll, the observed sliding friction coefficient may reduce because the rolling friction coefficient is always smaller than the sliding friction coefficient.

7.7.2 Literature & Theory.

For fine and medium sized particles there is a transition from a sliding bed to heterogeneous transport at a certain line speed. However for large particles the turbulence is not capable of lifting the particles enough resulting in a sort of sliding bed behavior above this transition line speed. One reason for this is that the largest eddies are not large enough with respect to the size of the particles. Sellgren & Wilson (2007) use the criterion d/D_p>0.015 for this to occur. Zandi & Govatos (1967) use a factor N<40 as a criterion, with:

$$N = \frac{v_{ls}^2 \cdot \sqrt{C_x}}{g \cdot R_{sd} \cdot D_p \cdot C_{vt}}$$

(7.7-1)

At the Limit Deposit Velocity $v_{ls,ldv}$ this equation can be simplified for coarse particles by using:

$$F_L = \frac{v_{ls,ldv}}{\sqrt{2 \cdot g \cdot D_p \cdot R_{sd}}} \approx 1.34 \quad \text{and} \quad \sqrt{C_x} \approx 0.6 \text{ for coarse sand}$$

(7.7-2)

Giving:

$$N = \frac{v_{ls}^2 \cdot \sqrt{C_x}}{g \cdot R_{sd} \cdot D_p \cdot C_{vt}} = \left(\frac{v_{ls}^2}{2 \cdot g \cdot R_{sd} \cdot D_p} \right) \cdot \frac{2 \cdot \sqrt{C_x}}{C_{vt}} = 1.34^2 \cdot \frac{2 \cdot 0.6}{C_{vt}} = \frac{2.37}{C_{vt}}$$

(7.7-3)

This gives **N=2.37/C$_{vt}$<40** or **C$_{vt}$>0.059** for sliding flow to occur. This criterion apparently is based on the thickness of sheet flow. If the bed is so thin that the whole bed becomes sheet flow, there will not be sliding flow, but more heterogeneous behavior. The values used in both criteria are a first estimate based on literature and may be changed in the future.

A pragmatic approach to determine the relative excess hydraulic gradient in the sliding flow regime is to use a weighted average between the heterogeneous regime and the sliding bed regime. First the factor between particle size and pipe diameter is determined:

$$f = \frac{4}{3} - \frac{1}{3} \cdot \frac{d}{r_{d/Dp} \cdot D_p} \quad \text{with: } 0 \le f \le 1$$

(7.7-4)

Secondly the weighted average hydraulic gradient or relative excess hydraulic gradient is determined:

$$i_{m,SF} = i_{m,HeHo} \cdot f + i_{m,SB} \cdot (1-f)$$

or

$$E_{rhg,SF} = E_{rhg,HeHo} \cdot f + \mu_{sf} \cdot (1-f)$$

(7.7-5)

Figure 7.7-1 and Figure 7.7-2 show the relative excess hydraulic gradient of 9 particle diameters for a constant delivered volumetric concentration of 17.5%. The graphs also show the horizontal sliding bed curve for constant spatial volumetric concentration, the ELM curve and the homogeneous curve as a reference system. The LDV points for each particle diameter are also shown.

Figure 7.7-1 shows that large particles in a **D$_p$=0.1524 m** pipe have a much less steep curve than the smaller particles due to sliding flow. Sliding flow starts with particles of about **d=2.3 mm**. Figure 7.7-2 shows that this does not occur in a large **D$_p$=1 m** pipe. Here sliding flow starts with particles of about **d=15 mm**, which are not in the graph.

The resulting curves match very well with the SRC model in the range of operational line speeds. Figure 7.7-3 and Figure 7.7-4 show this for a **d=3 mm** particle in a **D$_p$=0.1524 m** (6 inch) pipe.. The SRC model used here is a simplified model as described in chapter 6. The relative hydraulic excess gradient seems to differ, but in the hydraulic gradient graph it is clear that there is not much difference in the range of line speeds of 4-6 m/sec. Both the SRC model and the DHLLDV Framework are based on constant spatial volumetric concentration. The Wilson curve gives a higher curve, but the Wilson model is based on a constant delivered volumetric concentration.
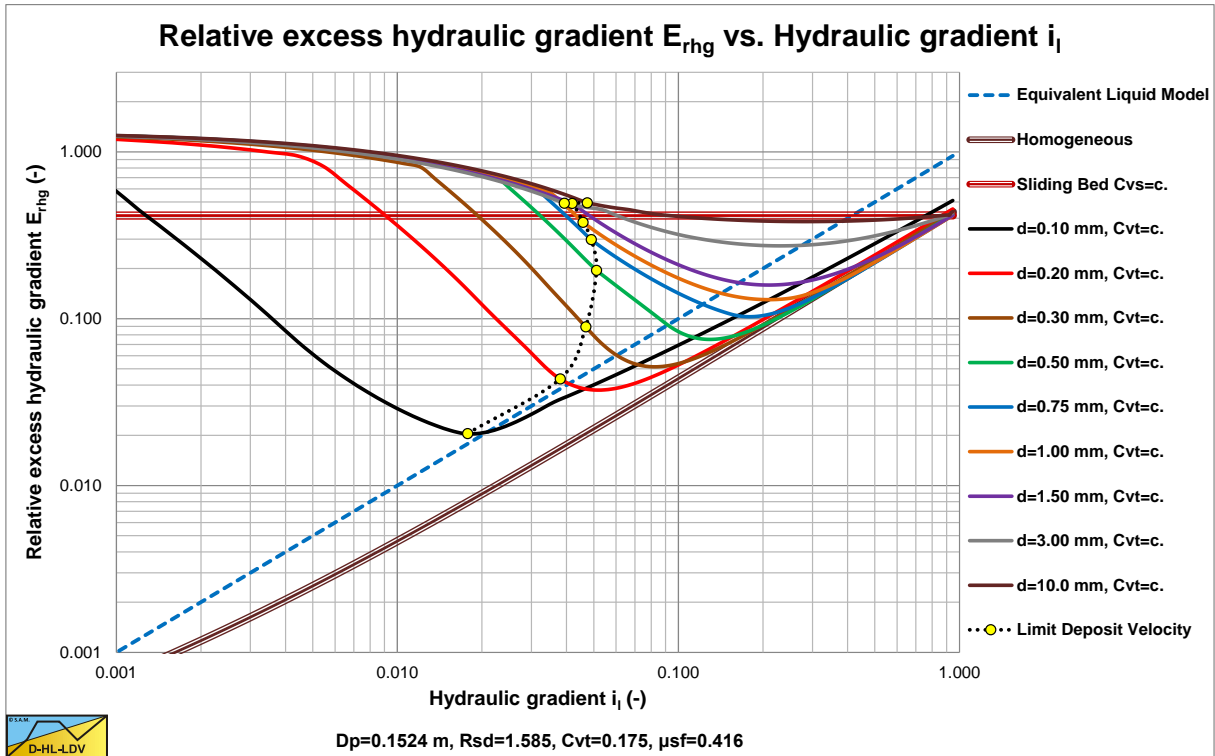
Figure 7.7-1: The relative excess hydraulic gradient as a function of the hydraulic gradient, constant C_{vt} and D_p=0.1524 m.
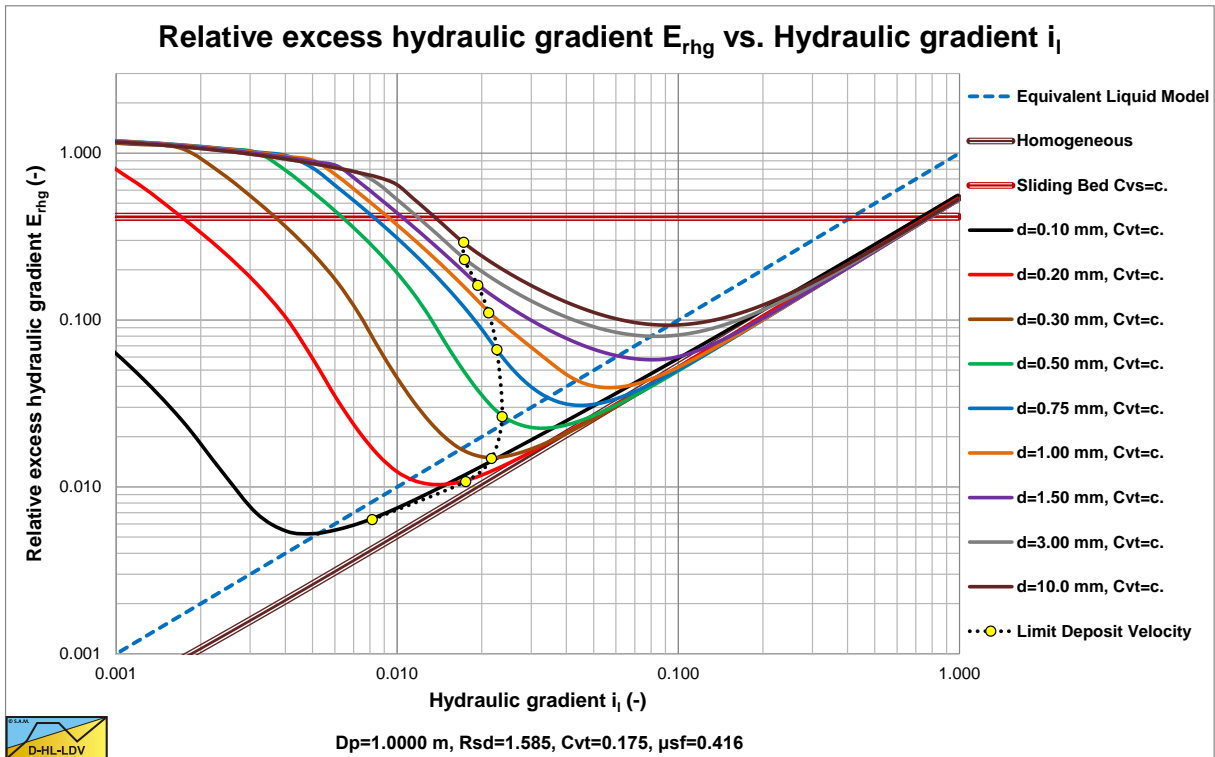
Figure 7.7-2: The relative excess hydraulic gradient as a function of the hydraulic gradient, constant C_{vt} and D_p=1 m.

Dp=0.1524 m, d=3.000 mm, Rsd=1.585, Cv=0.175, μsf=0.416
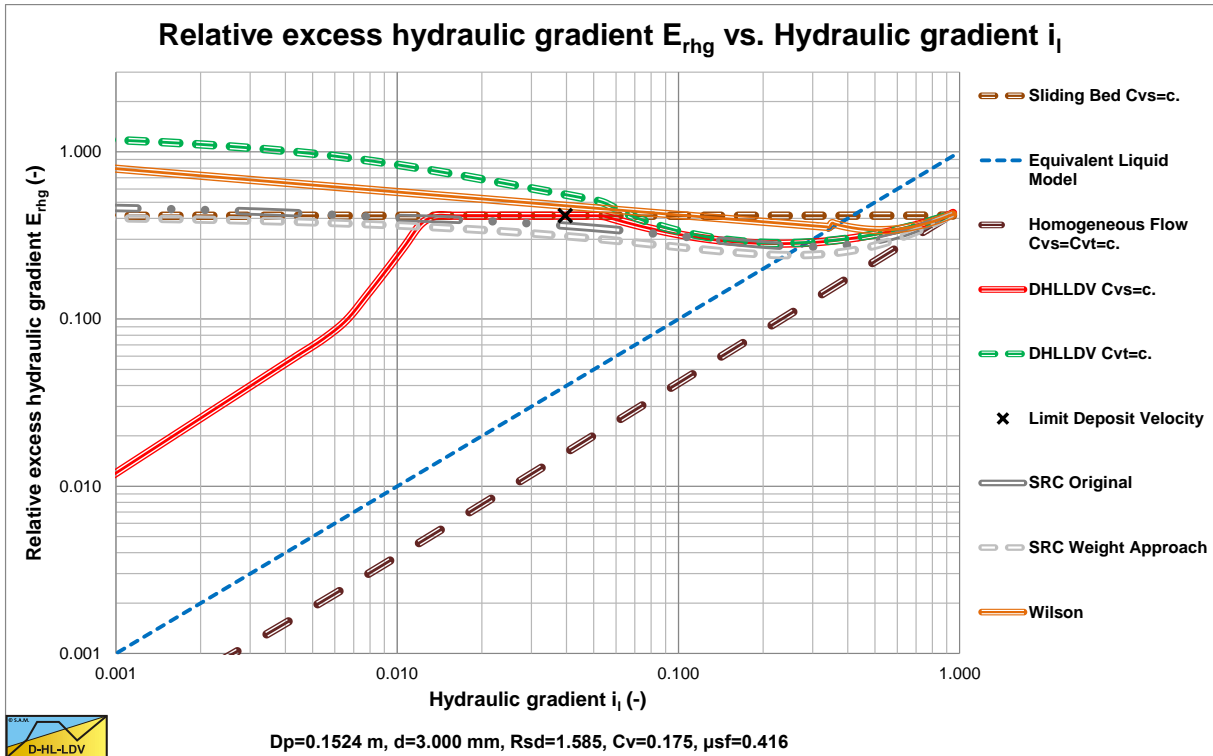
Figure 7.7-3: The sliding flow regime in the E_rhg vs. i_l graph.

Dp=0.1524 m, d=3.000 mm, Rsd=1.585, Cv=0.175, μsf=0.416
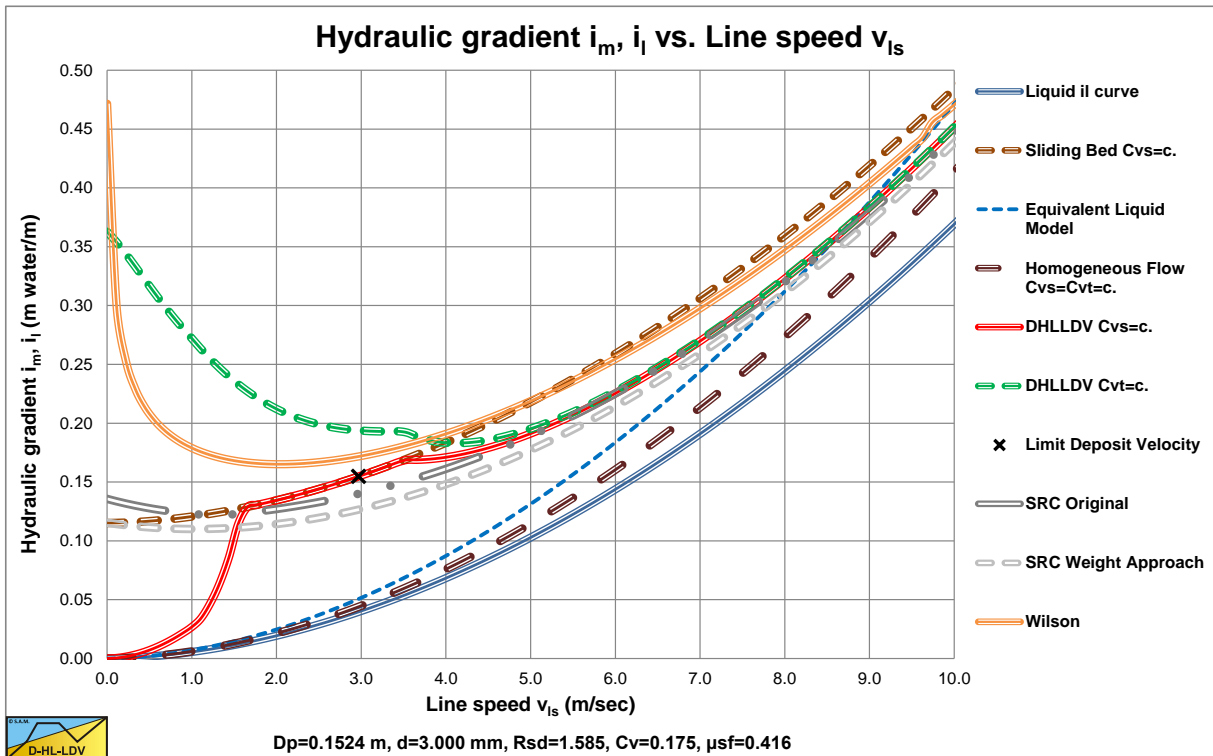
Figure 7.7-4: The sliding flow regime in the i_m vs. v_ls graph.
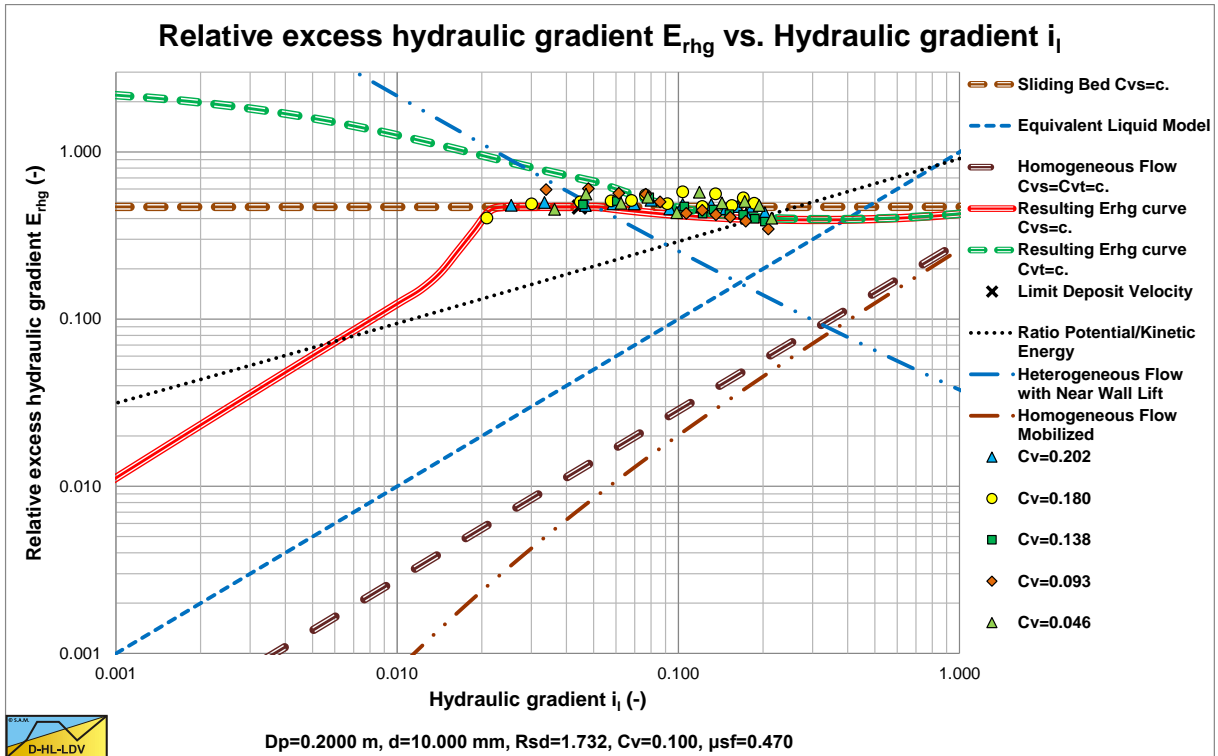
Figure 7.7-5: An example of sliding flow behavior, Boothroyde et al. (1979).
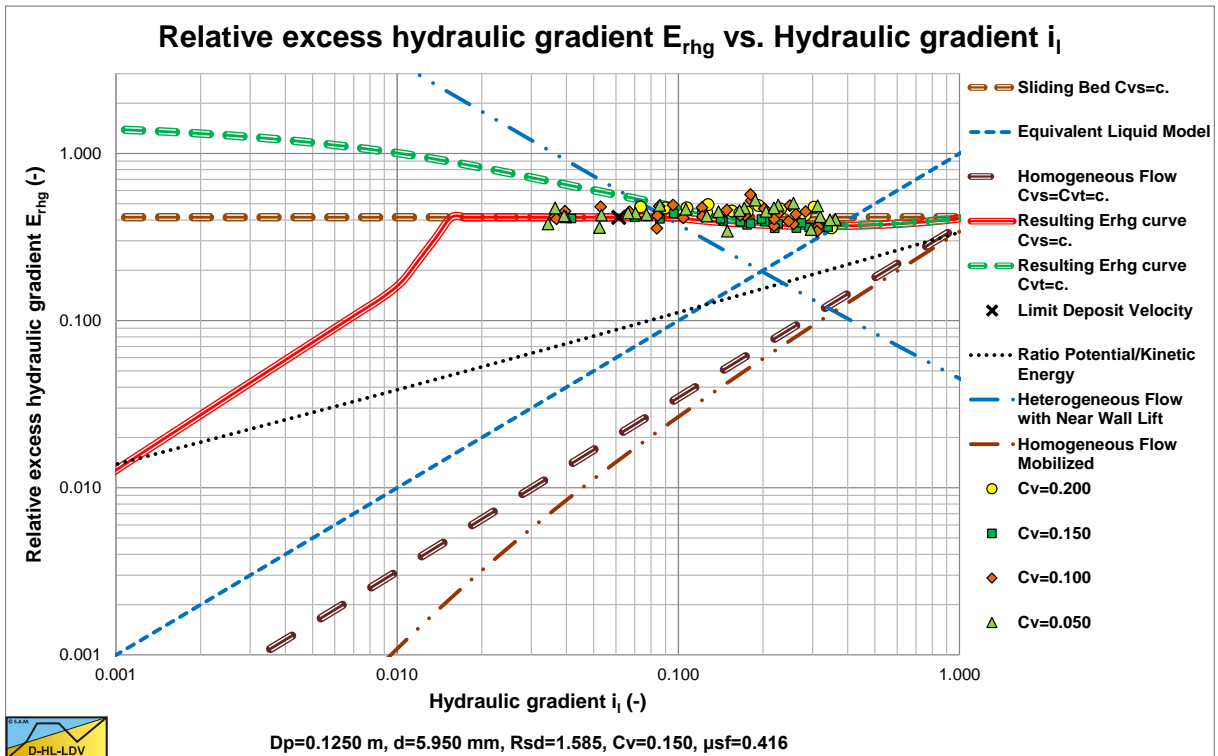
Figure 7.7-6: Another example of sliding flow behavior, Wiedenroth (1967).
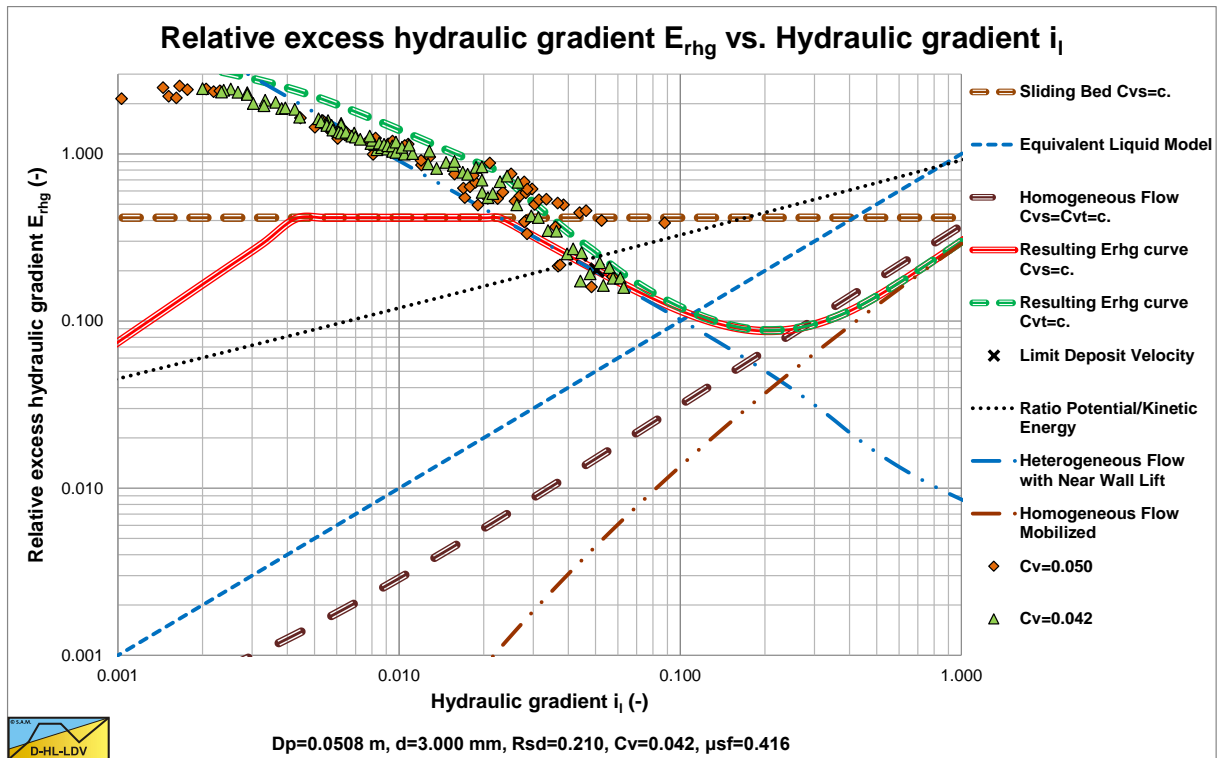
Figure 7.7-7: Heterogeneous behavior at low concentrations, Doron & Barnea (1993).
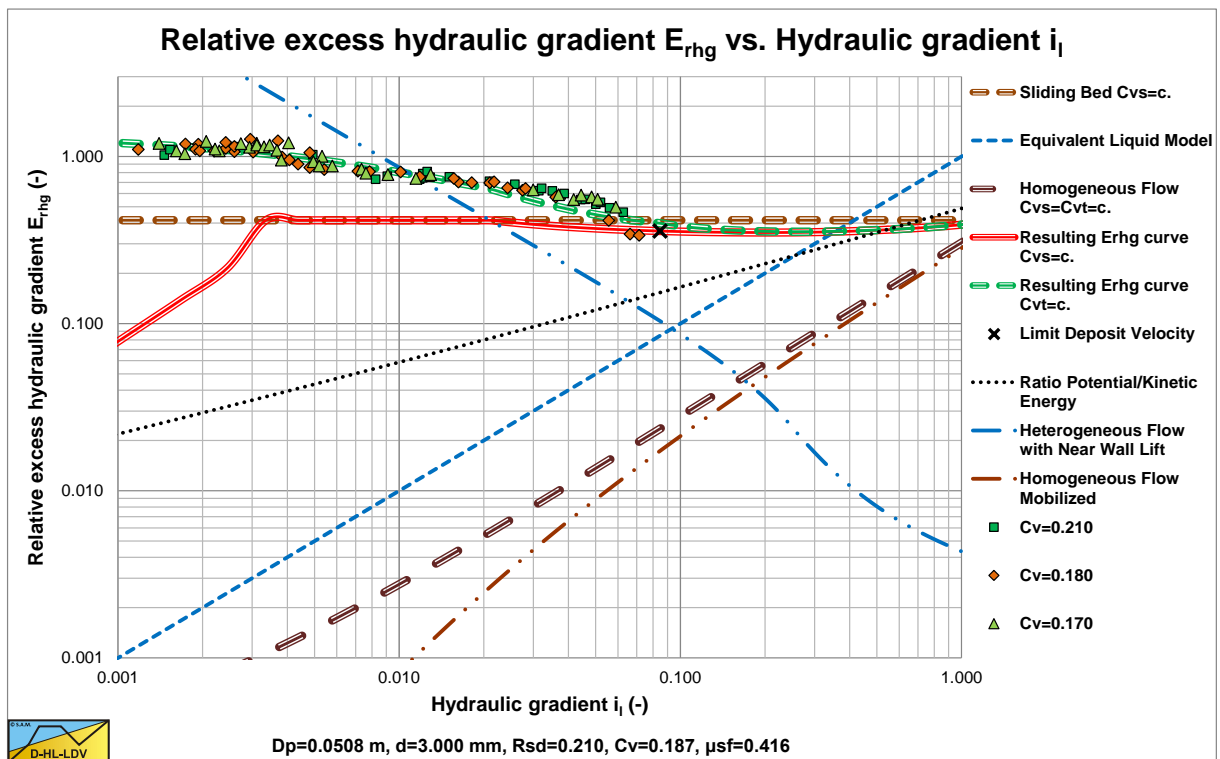
Figure 7.7-8: Sliding flow behavior at higher concentrations, Doron & Barnea (1993).

7.7.3 The Concentration Distribution.

In the case of **Sliding Flow**, the bottom concentration decreases with increasing line speed and with decreasing spatial concentration. The bottom concentration can be determined with the following equation, where the bottom concentration can never be larger than the maximum bed concentration C_{vb} and never smaller than the spatial concentration C_{vs}. The Limit of Stationary Deposit Velocity (LSDV) has to be determined at a concentration of 17.5%, because the equation is calibrated for $C_{vs}=0.175$.

$$C_{vB} = 3.1 \cdot C_{vb} \cdot \left(\frac{v_{ls,lsdv}}{v_{ls}}\right)^{0.4} \cdot \left(\frac{C_{vs}}{C_{vb}}\right)^{0.5} \cdot v_t^{1/6} \cdot e^{D_p} \quad \text{with: } 1.1 \cdot C_{vs} \leq C_{vB} \leq C_{vb} \tag{7.7-6}$$

To determine the concentration distribution, the procedure outlined in chapter 7.10 should be followed with a line speed to Limit Deposit Velocity ratio of 1 and a bottom/bed concentration as determined with the above equation. Physically this means that a sliding bed will transit to sliding flow by increasing the porosity between the particles with increasing line speed. The Limit Deposit Velocity has no physical meaning in the Sliding Flow Regime.

The concentration distribution is now:

$$C_{vs}(f) = C_{vB} \cdot e^{-\frac{\alpha_{sm}}{C_{vr}} \cdot f} \quad \text{with: } C_{vr} = \frac{C_{vs}}{C_{vB}} \tag{7.7-7}$$

$$\alpha_{sm} = 0.9847 + 0.304 \cdot C_{vr} - 1.196 \cdot C_{vr}^2 - 0.5564 \cdot C_{vr}^3 + 0.47 \cdot C_{vr}^4$$
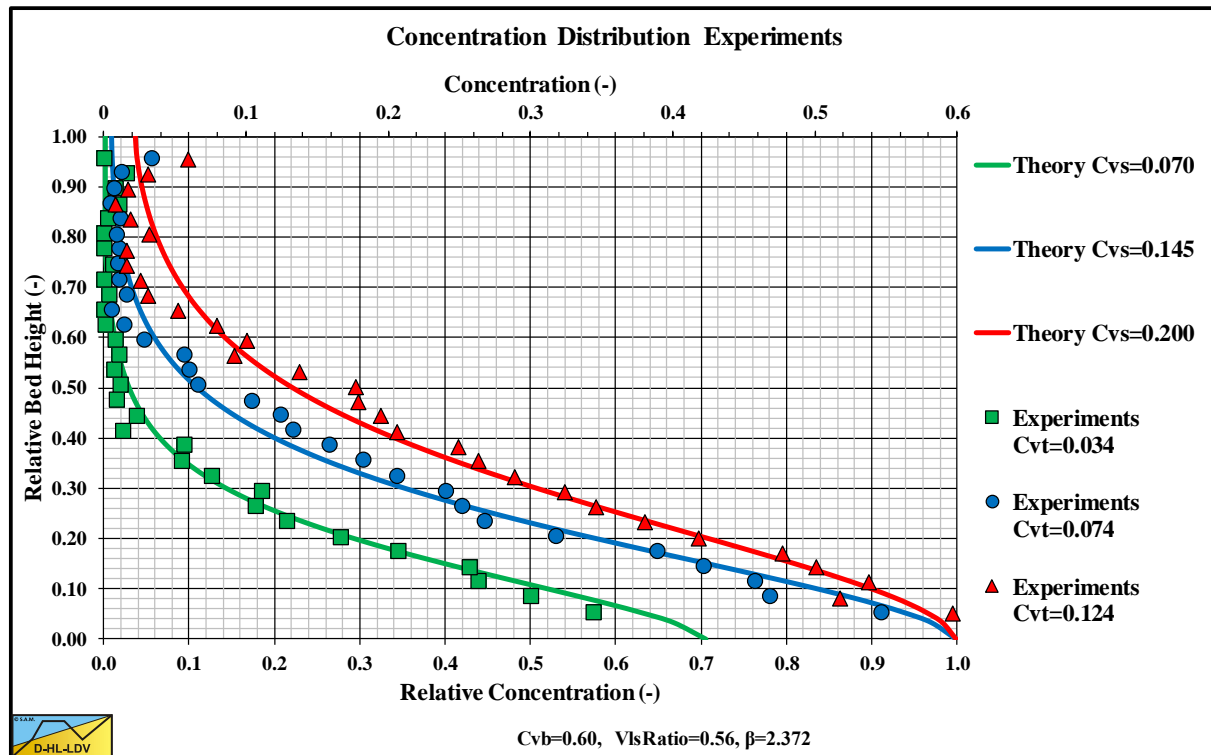
Figure 7.7-9: Experiments of Vlasak et al. (2014) in a D_p=0.1 m pipe and d=11 mm particles at v_{ls}=1.8 m/s.

Figure 7.7-9, Figure 7.7-10 and Figure 7.7-11 show experimental results of Vlasak et al. (2014) in a **D_p=0.1 m** pipe and **d=11 mm** particles at 3 different line speeds. The **d/D_p** ratio equals 0.11, so this is certainly in the **Sliding Flow** regime. The experiments show a decreasing bottom concentration with increasing line speed and a decreasing bottom concentration with decreasing spatial concentration according to the above equation. The volumetric concentrations used to simulate the measured concentration profiles are higher than the volumetric concentrations

mentioned by Vlasak et al. (2014). Most probably Vlasak et al. (2014) measured delivered concentrations, while here spatial concentrations should be used. It should be mentioned that the experiments show some small concentration at the top of the pipe, which is not always predicted. The predictions and the experimental data however match well. These experimental concentration profiles required a factor 2 in the hindered settling power instead of the default value of 4.
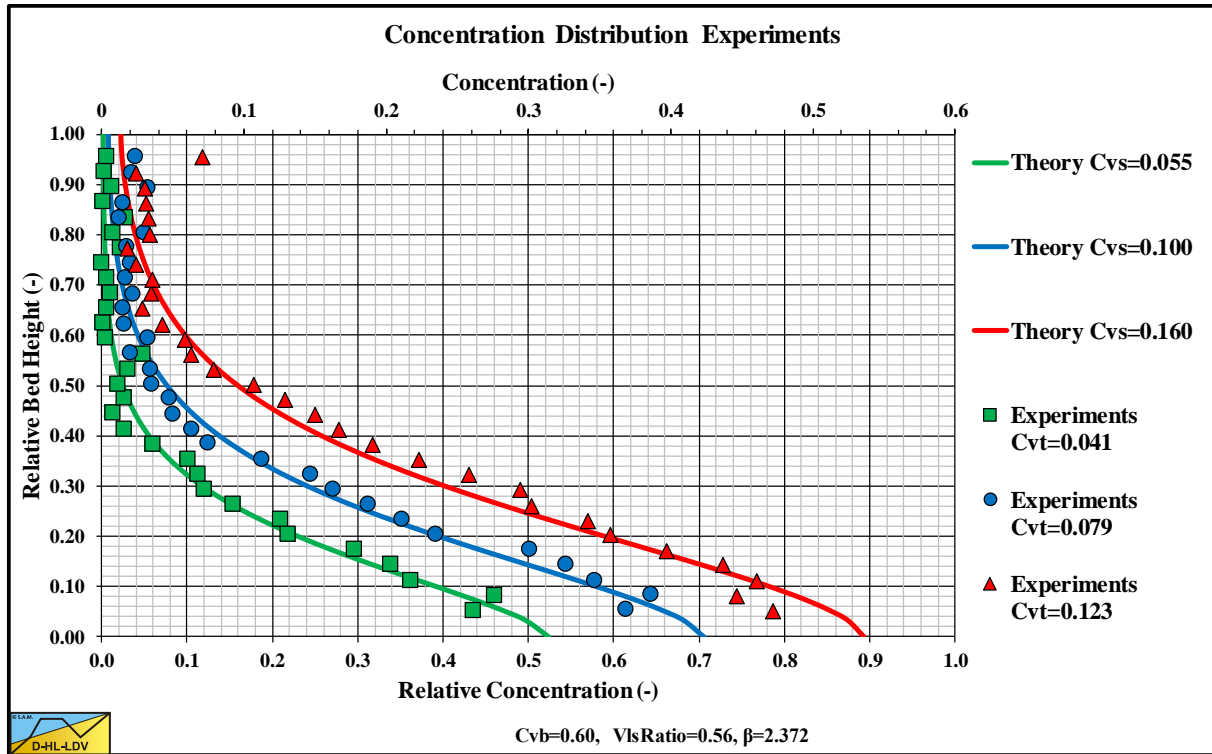
Figure 7.7-10: Experiments of Vlasak et al. (2014) in a D_p=0.1 m pipe and d=11 mm particles at v_{ls}=2.8 m/s.
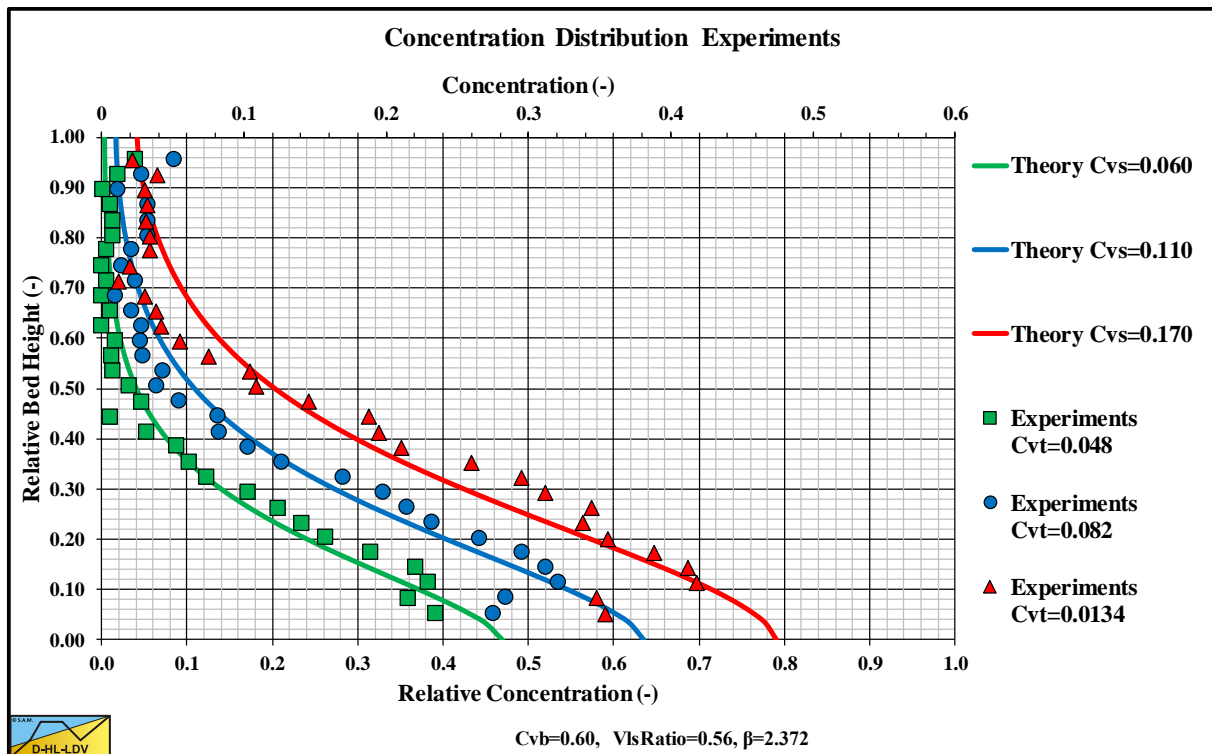
Figure 7.7-11: Experiments of Vlasak et al. (2014) in a D_p=0.1 m pipe and d=11 mm particles at v_{ls}=4.1 m/s.

7.7.4 Verification & Validation.

Figure 7.7-5 and Figure 7.7-6 show sliding flow behavior for two types of gravel, with **d=6 mm** and **d=10 mm** and constant spatial volumetric concentrations. At higher line speeds or liquid hydraulic gradients the relative excess hydraulic gradient of the DHLLDV Framework tends to decrease slightly. This occurs when the liquid hydraulic gradient is close to the intersection point between the sliding bed/sliding flow curve and the ELM curve. In this region however the line speeds are so high that there are hardly any experimental data available. The data here is obtained from Boothroyde et al. (1979) and Wiedenroth (1967).

Figure 7.7-7 and Figure 7.7-8 show heterogeneous behavior at very low concentrations and sliding flow behavior at higher concentrations. These experiments by Doron & Barnea (1993) were carried out with delivered volumetric concentration measurements. They clearly show that at very low concentrations there is still heterogeneous behavior, while the higher concentrations show sliding flow behavior.

The weighted average approach seems to give good results. Still the criterion for sliding flow, **d>0.015·D$_p$**, is too simple and requires more research, which will be explained in the next chapter.

For the concentration distribution, the bottom/bed concentration has to be determined first. Secondly the concentration profile can be determined based on a line speed to Limit Deposit Velocity ratio of 1.

In the sliding flow regime, the LDV doesn't really have a physical meaning. At high line speeds the bed continues to show sliding friction behavior, but the porosity of the bed increases with increasing line speed.

Figure 7.7-12 shows observed heterogeneous and sliding flow (fully stratified) behavior. Heterogeneous behavior means that the heterogeneous curve is followed. Sliding Flow behavior means that the sliding friction curve is followed. The transition between the two flow regimes is close to 0.015 as mentioned by Sellgren & Wilson (2007). However, only experiments in small diameter pipes were found for fully stratified flow. Some experiments close to the 0.015 ratio show transition behavior. The hydraulic gradient curves lie between the heterogeneous and sliding flow curves. Most experiments were carried out with natural particles. Some experiments were carried out with glass and aluminum beads. Since the latter experiments had particles far above the 0.015 ratio, a difference between natural particles and beads could not be distinguished. Also the influence of the volumetric concentration could not be determined, since most experiments were carried out at medium relative volumetric concentrations.
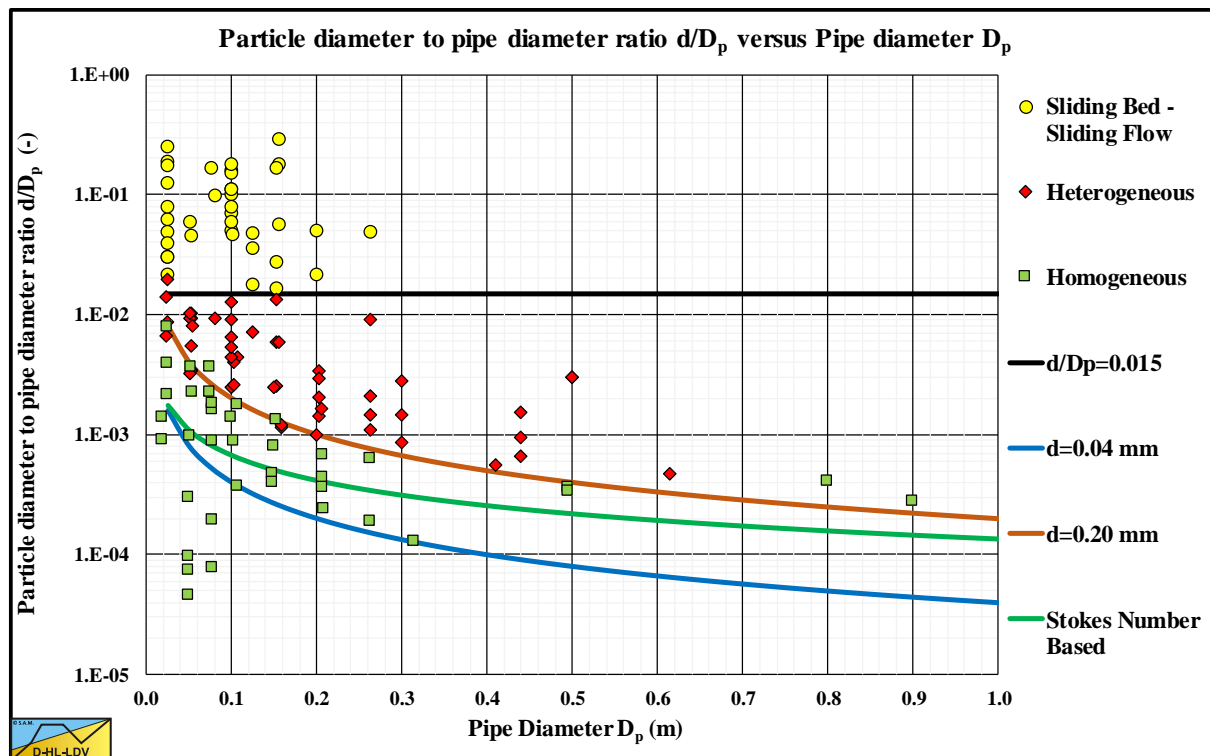
Figure 7.7-12: Observed Heterogeneous and Sliding Flow regimes.

7.7.5 The Particle Diameter to Pipe Diameter Ratio.

The particle diameter to pipe diameter ratio, **d>0.015·D$_p$**, is to simple. Also, no physical background has been found. So here an attempt is described to find a more fundamental background. The question is, does this ratio only depend on the diameter ratio, or are other parameters like the relative submerged density or the viscosity also involved.

The Sliding Flow Regime is described as a high concentrated flow of particles at the bottom of the pipe, behaving like a sliding bed, but with a lower concentration compared to the bed concentration. The top of this sliding flow may show sheet flow, similar to the sliding bed behavior. Sliding flow means that there is no or hardly any suspension above the sliding flow, the low concentrated bed. This implies that there is an equilibrium of deposition and suspension at the top of the sliding flow layer. The amount of particles being suspended are equal to the amount of particles depositioning. Particles being suspended is related to the bed shear stress or the Shields Number (dimensionless bed shear stress). Particles depositioning (settling) is related to the terminal settling velocity. Since sliding flow means, hardly any suspension above the bed, hindered settling does not have to be taken into account. Since the flow results in sliding friction (sliding bed behavior), an indication of the bed shear stress is available. So the criterion for the particle diameter to pipe diameter is:

$$\mathbf{v_t = \alpha_s \cdot u_*}$$
(7.7-8)

The terminal settling velocity is equal to the so called friction velocity. This is often used as a criterion for suspension vs. no suspension (see also Chapter 5 and Chapter 7.8). This criterion can be translated in terms of the Shields parameter by:

$$\mathbf{v_t = \sqrt{\frac{4 \cdot g \cdot R_{sd} \cdot d \cdot \psi}{3 \cdot C_D}} = \alpha_s \cdot u_*}$$
(7.7-9)

Giving:

$$\mathbf{\theta = \frac{u_*^2}{g \cdot R_{sd} \cdot d} = \frac{1}{\alpha_s^2} \cdot \frac{4 \cdot \psi}{3 \cdot C_D}}$$
(7.7-10)

For spheres this gives a Shields parameter of 3 and for real sand particles about 1, with **α$_s$=1**.

For the derivation, first the equilibrium of forces on the layer of liquid above the sliding flow is derived, in order to have an expression for the pressure gradient.

$$\mathbf{\tau_1 \cdot D_p \cdot (\pi - \beta) \cdot \Delta L + \tau_{12} \cdot D_p \cdot \sin(\beta) \cdot \Delta L = \Delta p \cdot A_p \cdot (1 - C_{vr})}$$
(7.7-11)

The bed shear stress equals the carrier liquid density times the friction velocity squared. Now assume the pipe wall shear stress is a factor times the bed shear stress, this gives:

$$\mathbf{\alpha_\tau \cdot \rho_l \cdot u_*^2 \cdot D_p \cdot (\pi - \beta) \cdot \Delta L + \rho_l \cdot u_*^2 \cdot D_p \cdot \sin(\beta) \cdot \Delta L = \Delta p \cdot A_p \cdot (1 - C_{vr})}$$
(7.7-12)

Now we find for the pressure gradient:

$$\mathbf{\Delta p = \frac{\rho_l \cdot u_*^2 \cdot D_p \cdot \Delta L \cdot (\sin(\beta) + \alpha_\tau \cdot (\pi - \beta))}{A_p \cdot (1 - C_{vr})}}$$
(7.7-13)

The equilibrium of forces on the bed is:

$$\mathbf{\rho_l \cdot u_*^2 \cdot D_p \cdot \sin(\beta) \cdot \Delta L + \Delta p \cdot A_p \cdot C_{vr} = \mu_{sf} \cdot (\rho_s - \rho_l) \cdot g \cdot A_p \cdot C_{vs} \cdot \Delta L}$$
(7.7-14)

Substituting the pressure gives:

$$\rho_l \cdot u_*^2 \cdot D_p \cdot \sin(\beta) \cdot \Delta L + \frac{\rho_l \cdot u_*^2 \cdot D_p \cdot \Delta L \cdot \left(\sin(\beta) + \alpha_\tau \cdot (\pi - \beta)\right)}{A_p \cdot (1 - C_{vr})} \cdot A_p \cdot C_{vr}$$

$$= \mu_{sf} \cdot (\rho_s - \rho_l) \cdot g \cdot A_p \cdot C_{vb} \cdot C_{vr} \cdot \Delta L \qquad (7.7-15)$$

This can be simplified to:

$$\frac{\rho_l \cdot u_*^2 \cdot D_p \cdot \left(\sin(\beta) + \alpha_\tau \cdot (\pi - \beta) \cdot C_{vr}\right)}{(1 - C_{vr})} = \mu_{sf} \cdot (\rho_s - \rho_l) \cdot g \cdot A_p \cdot C_{vb} \cdot C_{vr} \qquad (7.7-16)$$

The friction velocity squared is now:

$$u_*^2 = \frac{\pi}{4} \cdot \frac{\mu_{sf} \cdot R_{sd} \cdot g \cdot D_p \cdot C_{vb} \cdot C_{vr} \cdot (1 - C_{vr})}{\left(\sin(\beta) + \alpha_\tau \cdot (\pi - \beta) \cdot C_{vr}\right)} \qquad (7.7-17)$$

The general equation for the terminal settling velocity is:

$$u_*^2 = \frac{\pi}{4} \cdot \frac{\mu_{sf} \cdot R_{sd} \cdot g \cdot D_p \cdot C_{vb} \cdot C_{vr} \cdot (1 - C_{vr})}{\left(\sin(\beta) + \alpha_\tau \cdot (\pi - \beta) \cdot C_{vr}\right)} \qquad (7.7-18)$$

The terminal settling velocity equation is:

$$v_t = \sqrt{\frac{4}{3} \cdot \frac{R_{sd} \cdot g \cdot d \cdot \psi}{C_D}} \quad \Rightarrow \quad v_t^2 = \frac{4}{3} \cdot \frac{R_{sd} \cdot g \cdot d \cdot \psi}{C_D} \qquad (7.7-19)$$

So:

$$\frac{4}{3} \cdot \frac{R_{sd} \cdot g \cdot d \cdot \psi}{C_D} = \alpha_s^2 \cdot \frac{\pi}{4} \cdot \frac{\mu_{sf} \cdot R_{sd} \cdot g \cdot D_p \cdot C_{vb} \cdot C_{vr} \cdot (1 - C_{vr})}{\left(\sin(\beta) + \alpha_\tau \cdot (\pi - \beta) \cdot C_{vr}\right)} \qquad (7.7-20)$$

This gives for the particle diameter to pipe diameter ratio:

$$\frac{d}{D_p} = \alpha_s^2 \cdot \frac{3 \cdot \pi}{16} \cdot \frac{C_D}{\psi} \cdot \frac{\mu_{sf} \cdot C_{vb} \cdot C_{vr} \cdot (1 - C_{vr})}{\left(\sin(\beta) + \alpha_\tau \cdot (\pi - \beta) \cdot C_{vr}\right)} \qquad (7.7-21)$$

In this equation all parameters are known except the α_τ ratio. This ratio depends on the relative concentration, the line speed, the particle diameter and the pipe diameter and maybe also on the relative submerged density. To determine an equation for this ratio, many simulations with the 3 Layer Model are carrier out, resulting in the following empirical equation:

$$\alpha_\tau = (9.6117 \cdot C_{vr}^4 - 14.612 \cdot C_{vr}^3 + 8.8395 \cdot C_{vr}^2 - 2.1079 \cdot C_{vr} + 0.4746)$$

$$\cdot \frac{e^{\left(0.7 * \frac{v_{ls,ldv}}{v_{ls,lsdv}}\right)}}{4} \cdot \left(0.933 \cdot D_p\right)^{-0.296} \cdot \left(0.625 - 0.055 \cdot \ln(d)\right) \qquad (7.7-22)$$

If the wall shear stress is ignored, the following equation is valid:

$$\frac{d}{D_p} = \alpha_s^2 \cdot \frac{3 \cdot \pi}{16} \cdot \frac{C_D}{\psi} \cdot \frac{\mu_{sf} \cdot C_{vb} \cdot C_{vr} \cdot (1 - C_{vr})}{\sin(\beta)} \tag{7.7-23}$$

For spheres, using **α_s=1**, **C_D=0.445**, **ψ=1**, **μ_{sf}=0.44** and **C_{vb}=0.6**, the following graph can be constructed:
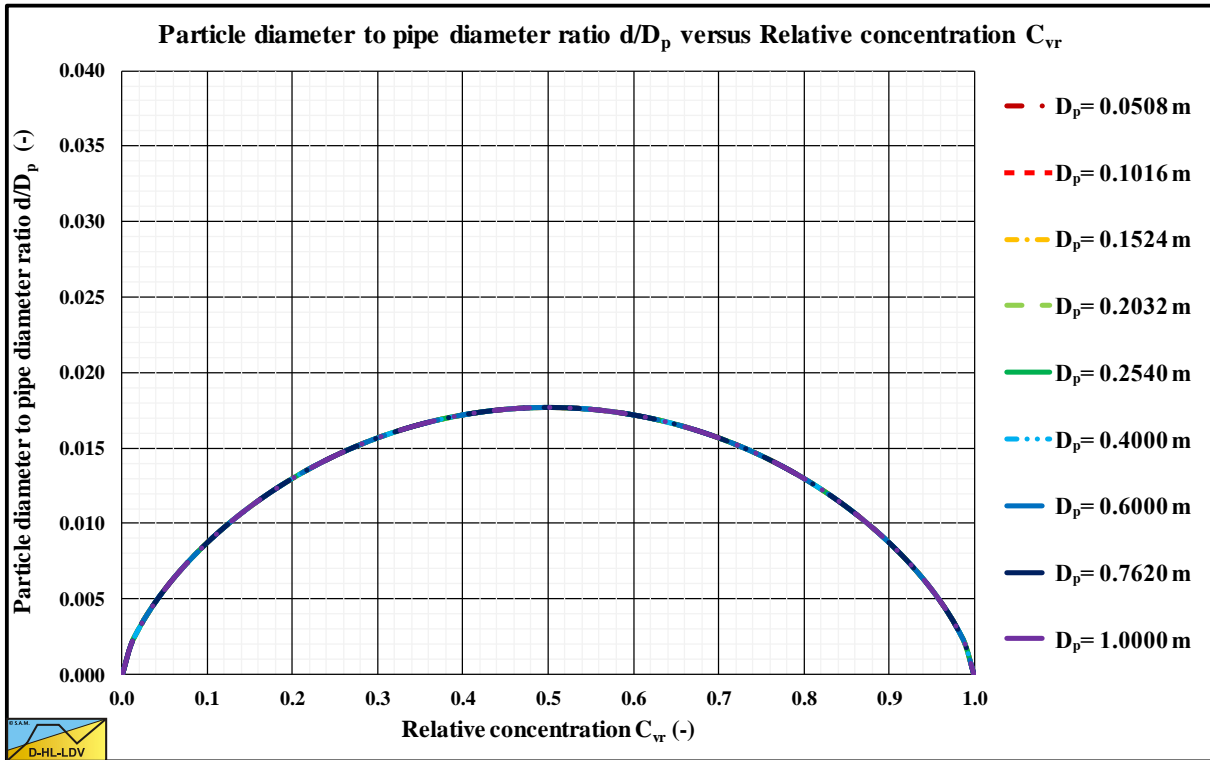
Figure 7.7-13: The particle diameter to pipe diameter ratio for spheres without wall shear stress.

Figure 7.7-13 shows a particle diameter to pipe diameter ratio in the relative concentration range of 0.2-0.8 (operational range) of 0.013-0.018, matching Sellgren & Wilson (2007) mentioning 0.015-0.018 in several publications. A fundamental derivation of Sellgren & Wilson (2007) could not be found, but it is remarkable how close equation (7.7-23) approaches these values. Adding the wall shear stress, equation (7.7-21), gives slightly smaller values for spheres. For sands and gravels larger values are found.

Since the Sliding Flow Regime only occurs for large particles, the drag coefficient is about 1 for sand particles and 0.445 for spheres. The shape coefficient is about 0.77 for sand particles and 1 for spheres.

Figure 7.7-14 shows the shear stress ratio for a specific case, which is used for the derivation of the semi-empirical equation. Figure 7.7-15 shows the resulting particle diameter to pipe diameter ratio. Apparently this ratio is not just a fixed number (0.015), but it depends strongly on the relative concentration. There is also a linear proportionality with the sliding friction coefficient, the bed concentration and the particle dragcoefficient and a reversed proportionality with the particle shape factor. The proportionality with the pipe diameter is weak, while the proportionality with the particle diameter is very weak. The latter 2 proportionalities are because of the influence on the shear stress ratio. The proportionality of the line speed is also because of the presence in the shear stress ratio. Since sliding flow occurs above the Limit Deposit Velocity, the LDV/LSDV ratio is used in the shear stress equation, however instead of the LDV any line speed can be chosen to see the effect.

Since the starting assumption that the terminal settling velocity equals the friction velocity on top of the bed is only indicative for the occurrence of suspension, Figure 7.7-15 is also indicative. For normal relative concentrations the particle diameter to pipe diameter ratio is between 0.03 and 0.04, roughly twice the value as used by Sellgren & Wilson (2007).
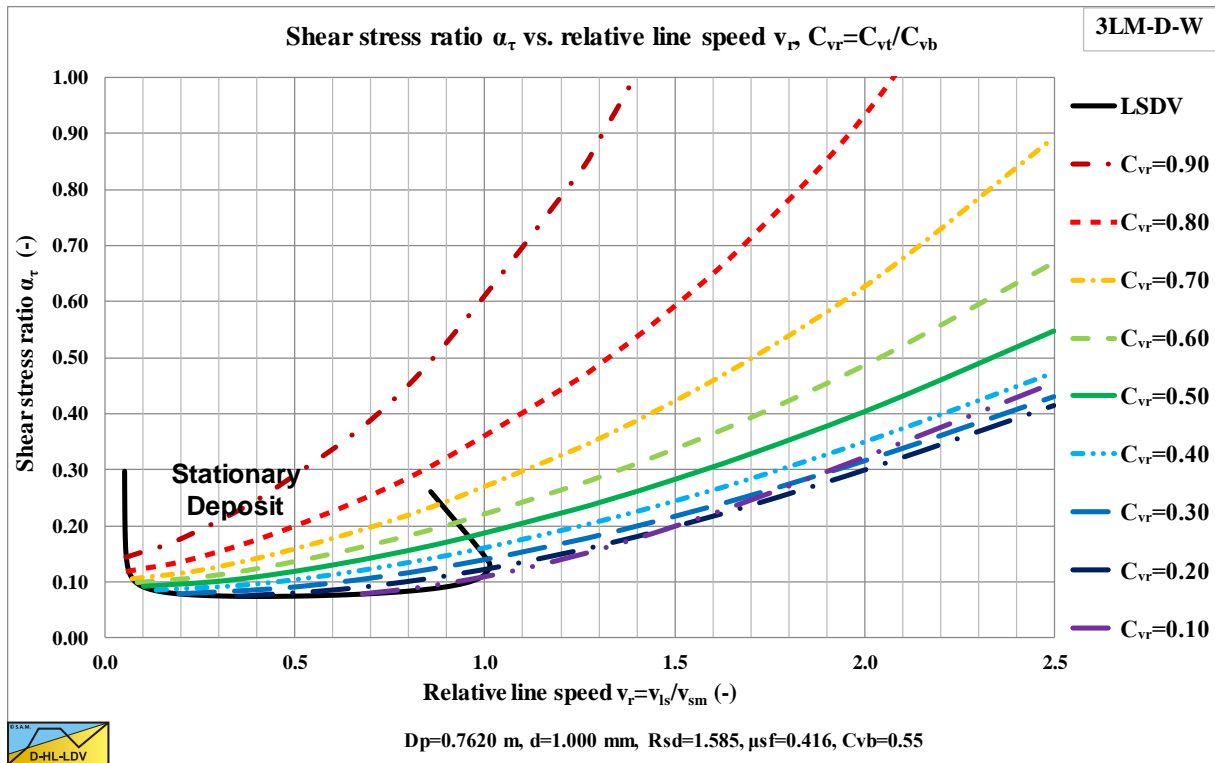
Figure 7.7-14: The shear stress ratio versus the relative line speed.
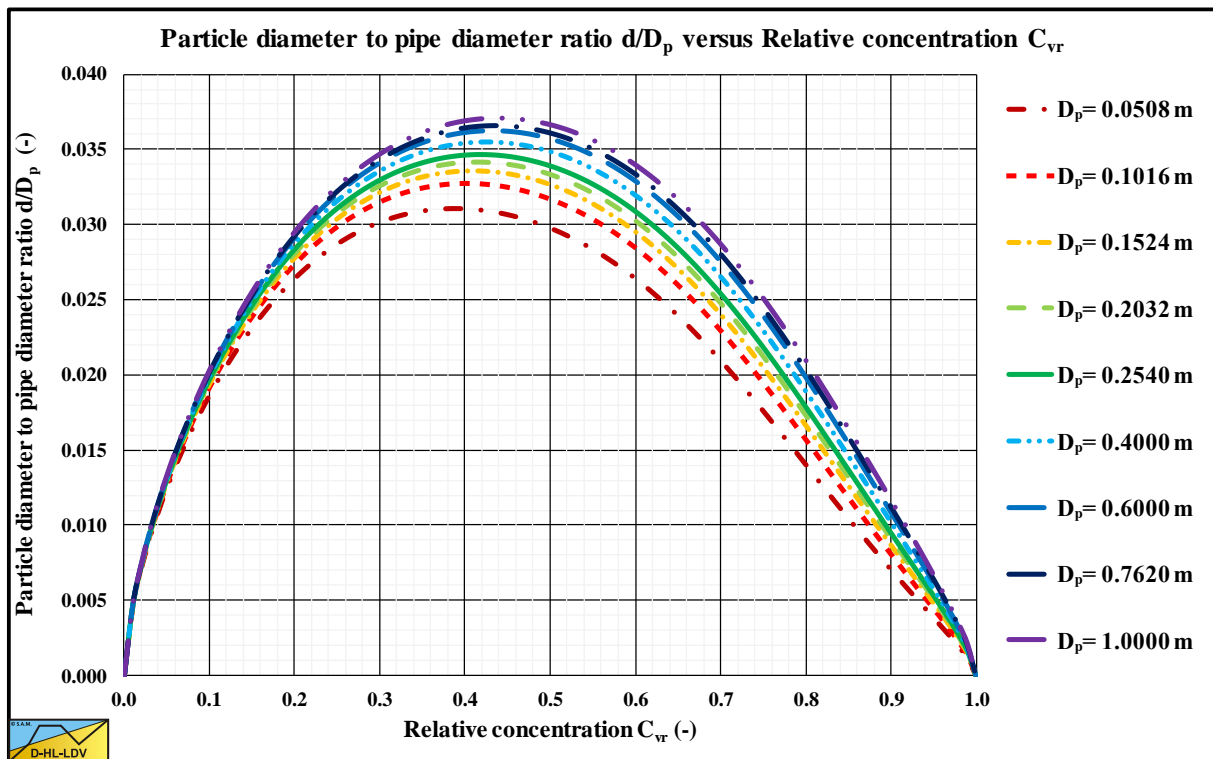
Figure 7.7-15: The particle diameter to pipe diameter ratio for natural sands and gravels.
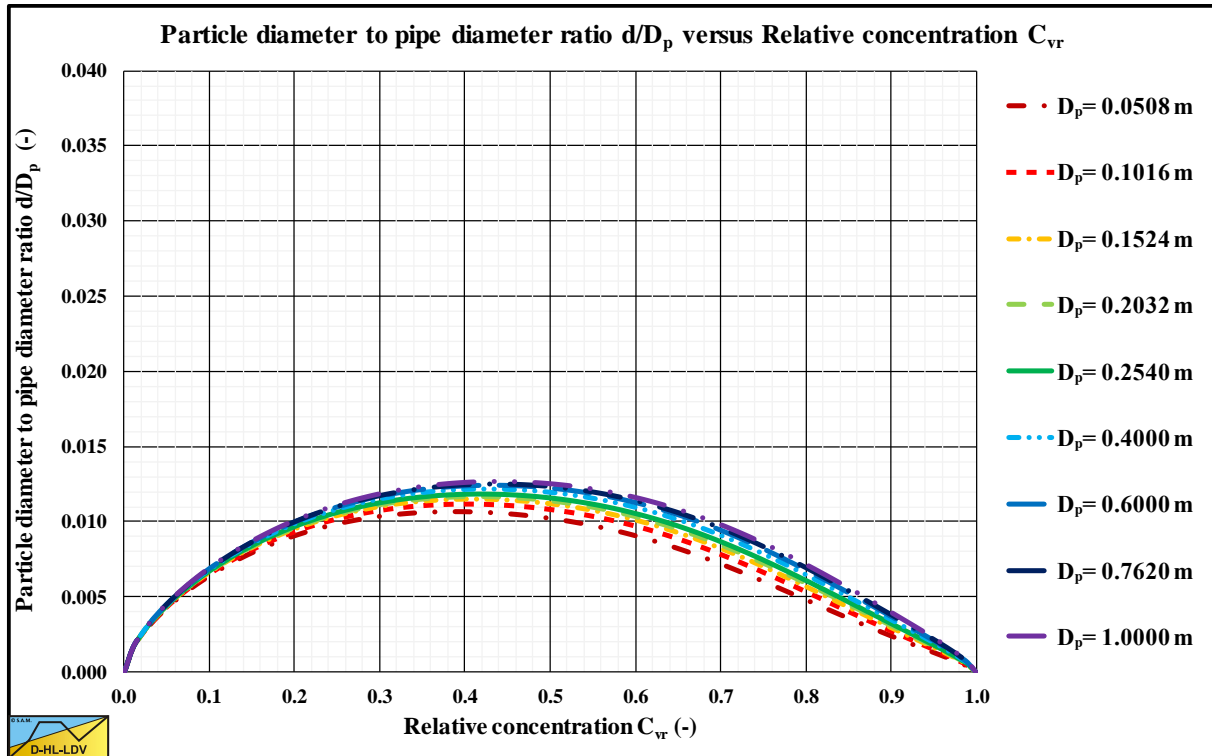
Figure 7.7-16: The particle diameter to pipe diameter ratio for spheres.

Figure 7.7-16 shows the particle diameter to pipe diameter ratio for spheres, which is much smaller than the ratio for natural sands and gravels. The peak value is close to the value of 0.015 as mentioned by Sellgren & Wilson (2007). The main reason for this is the smaller drag coefficient and the shape factor of 1. In equation (7.7-21).

For practical use and continuity half the theoretical diameter ratio is used as a start for sliding flow, while the transition from heterogeneous flow to sliding flow extends to twice the theoretical value found in Figure 7.7-15 and Figure 7.7-16.

For sands and gravels and relative volumetric concentrations close to 0.5, this gives a starting ratio of about $r_{d/Dp}$=**0.019** and full mobilization of sliding flow at $r_{d/Dp}$=**0.076.** For spheres this gives a starting ratio of about $r_{d/Dp}$=**0.007** and full mobilization of sliding flow at $r_{d/Dp}$=**0.028.** In both cases for a D_p=**0.762 m** pipe.

The order of magnitude of the diameter ratio matches the Sellgren & Wilson (2007) value of 0.015-0.018, however here it's not a constant, but it is depending on many parameters.

7.7.6 Conclusions.

The theoretical particle diameter to pipe diameter ratio matches the Sellgren & Wilson (2007) value of 0.015-0.018 for spheres if the pipe wall shear stress is not taken into account for medium relative volumetric concentrations. If the pipe wall shear stress is taken into account, slightly smaller values are found. For sand and gravel particles the values are roughly a factor 3 larger. This is mainly caused by the particle drag coefficient and the particle shape factor. Large spheres (which we consider here) have a drag coefficient of about 0.445 and a shape factor of 1. Sand and gravel particles have a drag coefficient of about 1 and a shape factor of about 0.77. For sands and gravels this of course depends on their shape.

Since spheres have a larger terminal settling velocity, the deposition is larger compared to sands and gravels. This results in a smaller particle diameter to pipe diameter ratio where the particles are not suspended anymore.

At very low (and high) relative concentrations the particle diameter to pipe diameter ratio is very small, implying that it is easy to have a thin layer of small particles at the pipe bottom. On the other hand, the sheet flow will dissolve this thin layer, resulting in a minimum relative concentration for the Sliding Flow Regime.
Since the assumption of terminal settling velocity equals the friction velocity is indicative, a transition from half the calculated ratio to double the calculated ratio is introduced, in order to have a smooth transition from the Heterogeneous Flow Regime to the Sliding Flow Regime.

7.7.7 Nomenclature Sliding Flow Regime.

A_p	Pipe cross section	m^2
C_D	Particle drag coefficient	-
C_x	Durand & Condolios particle Froude number	-
C_{vt}	Delivered (transport) volumetric concentration	-
C_{vs}	Spatial volumetric concentration	-
C_{vb}	Bed concentration low line speeds	-
C_{vB}	Bed/bottom concentration high line speeds, Sliding Flow Regime	-
C_{vr}	Relative spatial concentration C_{vs}/C_{vb}	-
d	Particle diameter	m
D_p	Pipe diameter	m
E_{rhg}	Relative excess hydraulic gradient	-
$E_{rhg,HeHo}$	Relative excess hydraulic gradient heterogeneous & homogeneous regimes	-
$E_{rhg,SF}$	Relative excess hydraulic gradient sliding flow regime	-
f	Sliding Flow mobilization factor	-
F_L	Durand & Condolios LDV Froude number	-
g	Gravitational constant 9.81 m/s^2	m/s^2
i_l	Hydraulic gradient pure liquid	m/m
i_m	Hydraulic gradient mixture	m/m
$i_{m,HeHo}$	Hydraulic gradient heterogeneous & homogeneous regimes	m/m
$i_{m,SB}$	Hydraulic gradient sliding bed regime	m/m
$i_{m,SF}$	Hydraulic gradient sliding flow regime	m/m
L	Length of pipe	m
LDV	Limit Deposit Velocity	m/s
N	Zandi & Govatos parameter	-
p	Pressure	kPa
r	Vertical coordinate in pipe starting at the bottom	m
$r_{d/Dp}$	Minimu particle diameter to pipe diameter ratio	-
R_{sd}	Relative submerged density	-
u_*	Friction velocity	m/s
v_{ls}	Line speed	m/s
$v_{ls,ldv}$	Limit Deposit Velocity	m/s
$v_{ls,lsdv}$	Limit of Stationary Velocity (start sliding bed)	m/s
v_t	Terminal settling velocity particles	m/s
α_τ	Shear stress ratio τ_1/τ_{12}	-
β	Richardson & Zaki hindered settling power	-
β	Bed angle with vertical	rad
ρ_l	Carrier liquid density	ton/m^3
ρ_s	Solids density	ton/m^3
τ_1	Pipe wall shear stress	kPa
τ_{12}	Bed shear stress	kPa
μ_{sf}	Sliding friction factor	-
ψ	Shape factor (volume particle/volume sphere)	-

7.8 The Limit Deposit Velocity.

7.8.1 Introduction.

When the flow velocity decreases, there will be a moment where sedimentation of the particles starts to occur. The corresponding line speed is called the Limit Deposit Velocity. Often other terms are used like the critical velocity, critical deposition velocity, deposit velocity, deposition velocity, settling velocity, minimum velocity or suspending velocity. Here we will use the term Limit Deposit Velocity. This Limit Deposit Velocity may be considered the transition between two different flow regimes, however for most sands it will be somewhere in the heterogeneous regime. The possible transitions are shown in Table 7.8-1. The transitions fixed bed to sliding bed (Limit of Stationary Deposit Velocity) is not considered to be the Limit Deposit Velocity, because it is followed by the transition sliding bed or fixed bed to heterogeneous transport, which is considered to be one of the 3 possible Limit Deposit Velocities. The other 2 are; the LDV close to the transition of heterogeneous transport to homogeneous transport and the LDV somewhere in the heterogeneous regime. The Limit of Sliding Bed Velocity (LSBV), the transition of the sliding bed regime with the homogeneous regime, is always at very high line speeds beyond the operational range.

Table 7.8-1: Possible transitions.

	Fixed Bed	Sliding Bed	Heterogeneous	Homogeneous (ELM)
Fixed Bed		**LSDV**	**LDV (Fine & Medium)**	
Sliding Bed			**LDV (Coarse)**	**LSBV**
Heterogeneous				**LDV (Very Fine)**
Homogeneous				

The 5 transition velocities can be determined knowing the equations for the hydraulic gradient in the different regimes. These equations are:

The homogeneous regime, according to the ELM:

$$
\mathbf{i_m = i_l \cdot \left(1 + R_{sd} \cdot C_{vs}\right)}
\tag{7.8-1}
$$

And for the relative excess hydraulic gradient:

$$
\mathbf{E_{rhg} = \frac{i_m - i_l}{R_{sd} \cdot C_{vs}} = i_l}
\tag{7.8-2}
$$

The heterogeneous regime:

$$
\mathbf{i_m = i_l \cdot \left(1 + \frac{\left(2 \cdot g \cdot R_{sd} \cdot D_p\right)}{\lambda_l} \cdot C_{vs} \cdot \frac{1}{v_{ls}^2} \cdot \left(\frac{v_t}{v_{ls}} \cdot \left(1 - \frac{C_{vs}}{\kappa_C}\right)^\beta + \frac{8.5^2}{\lambda_l} \cdot \left(\frac{v_t}{\sqrt{g \cdot d}}\right)^{10/3} \cdot \left(\frac{\left(v_l \cdot g\right)^{1/3}}{v_{ls}}\right)^2\right)\right)}
\tag{7.8-3}
$$

And for the relative excess hydraulic gradient:

$$
\mathbf{E_{rhg} = \frac{i_m - i_l}{R_{sd} \cdot C_{vs}} = \frac{v_t}{v_{ls}} \cdot \left(1 - \frac{C_{vs}}{\kappa_C}\right)^\beta + \frac{8.5^2}{\lambda_l} \cdot \left(\frac{v_t}{\sqrt{g \cdot d}}\right)^{10/3} \cdot \left(\frac{\left(v_l \cdot g\right)^{1/3}}{v_{ls}}\right)^2}
\tag{7.8-4}
$$

The sliding bed regime:

$$
\mathbf{i_m = i_l \cdot \left(1 + \mu_{sf} \cdot \frac{\left(2 \cdot g \cdot R_{sd} \cdot D_p\right)}{\lambda_l} \cdot C_{vs} \cdot \frac{1}{v_{ls}^2}\right)}
\tag{7.8-5}
$$

And for the relative excess hydraulic gradient:

$$\mathbf{E_{rhg}} = \frac{\mathbf{i_m - i_l}}{\mathbf{R_{sd} \cdot C_{vs}}} = \mu_{sf}$$

(7.8-6)

For the LDV in the heterogeneous regime a different approach has to be applied. This statement is based on the analysis of many public available data. The transition velocities found, always lie in between the transition velocity of a sliding bed to heterogeneous transport and the transition velocity of heterogeneous to homogeneous transport. This will be discussed in a next paragraph.

The Limit Deposit Velocity is defined here as the line speed above which there is no stationary bed or sliding bed, Thomas (1962). Below the LDV there may be either a stationary or fixed bed or a sliding bed. For the critical velocity often the Minimum Hydraulic Gradient Velocity (MHGV) is used, Wilson (1942). For higher concentrations this MHGV may be close to the LDV, but for lower concentrations this is certainly not the case. Yagi et al. (1972) reported using the MHGV, making the data points for the lower concentrations to low, which is clear from Figure 7.8-1.

Another weak point of the MHGV is, that it depends strongly on the model used for the heterogeneous flow regime. Durand and Condolios (1952), Fuhrboter (1961), Jufin and Lopatin (1966) and others will each give a different MHGV. In dredging the process is instationary, meaning a constantly changing PSD and concentration in long pipelines, making it almost impossible to determine the MHGV.

Wilson (1979) derived a method for determining the transition velocity between the stationary bed and the sliding bed, which is named here the Limit of Stationary Deposit Velocity (LSDV). Since the transition stationary bed versus sliding bed, the LSDV, will always give a smaller velocity value than the moment of full suspension or saltation, the LDV, one should use the LDV, to be sure there is no deposit at all. For small particles it is also possible that the bed is already completely suspended before the bed could ever start sliding (theoretically). In that case an LSDV does not even exist. This is the reason for choosing the LDV as the critical velocity and developing a new model for this, independent of the head loss model and always existing.

The Froude number $\mathbf{F_L}$ is often used for the LDV, because it allows comparison of the LDV for different pipe diameters $\mathbf{D_p}$ and relative submerged densities $\mathbf{R_{sd}}$ without having to change the scale of the graph, this is defined as:

$$\mathbf{F_L} = \frac{\mathbf{v_{ls,ldv}}}{\sqrt{\mathbf{2 \cdot g \cdot R_{sd} \cdot D_p}}} = \frac{\mathbf{LDV}}{\sqrt{\mathbf{2 \cdot g \cdot R_{sd} \cdot D_p}}}$$

(7.8-7)

The research consisted of two parts, analyzing the experimental data and analyzing the resulting models based on these data. First the experimental data will be discussed. It should be noted that sometimes the 2 and the relative submerged density $\mathbf{R_{sd}}$ are omitted. Because there are numerous data and equations for the critical velocity (LSDV, LDV or MHGV), some equations based on physics, but most based on curve fitting, a selection is made of the equations and methods from literature. The literature analyzed are from Wilson (1942), Durand and Condolios (1952), Newitt et al. (1955), Jufin and Lopatin (1966), Zandi and Govatos (1967), Charles (1970), Graf et al. (1970), Wilson and Judge (1976), Wasp et al. (1977), Wilson and Judge (1977), Thomas (1979), Oroskar and Turian (1980), Parzonka et al. (1981), Turian et al. (1987), Davies (1987), Schiller and Herbich (1991), Gogus and Kokpinar (1993), Gillies (1993), Berg (1998), Kokpinar and Gogus (2001), Shook et al. (2002), Wasp and Slatter (2004), Sanders et al. (2004), Lahiri (2009), Poloski et al. (2010) and Souza Pinto et al. (2014).

7.8.2 Experimental Data.

Figure 7.8-1 shows many data points of various authors for sand and gravel in water. Each column of data points shows the results of experiments with different volumetric concentrations, where the highest points were at volumetric concentrations of about 15%–20%, higher concentrations gave lower points. The experimental data also shows that smaller pipe diameters, in general, give higher Durand and Condolios (1952) Froude $\mathbf{F_L}$ numbers.

The two curves in the graph are for the Jufin and Lopatin (1966) equation, which is only valid for sand and gravel, and the DHLLDV Framework which is described in this chapter. Both models give a sort of upper limit to the LDV. The data points of the very small particle diameters, Thomas (1979) and Poloski (2010), were carried out in

very small to medium diameter pipes, while the two curves are constructed for a 0.1524 (6 inch) pipe, resulting in slightly lower curves. Data points above the DHLLDV curve are in general for pipe diameters smaller than 0.1524 m. Some special attention is given to the relation between the Durand Froude F_L number and the pipe diameter D_p. Both Thomas (1979) and Wasp et al. (1977) carried out research with a **d = 0.18 mm** particle in 6 pipe diameters, see Figure 7.8-2. These experiments show a slight decrease of the F_L value with increasing pipe diameter with a power close to –0.1.
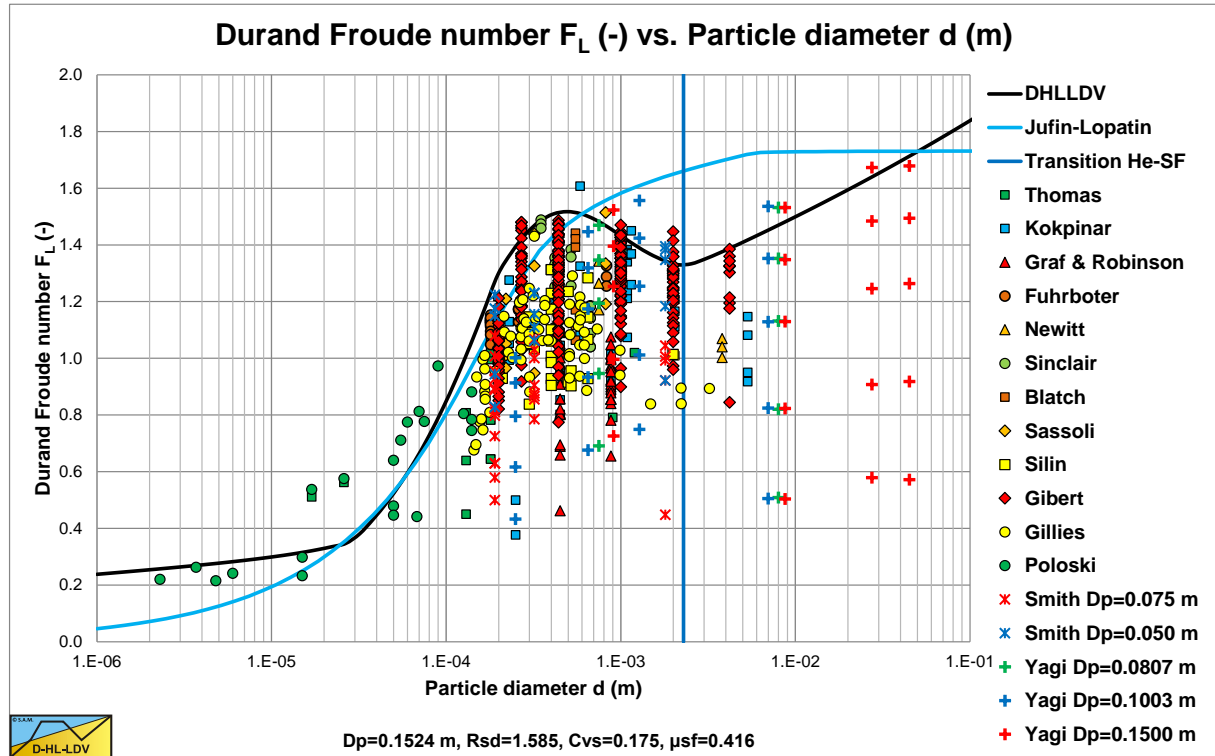
Figure 7.8-1: Experimental data in different pipe diameters.
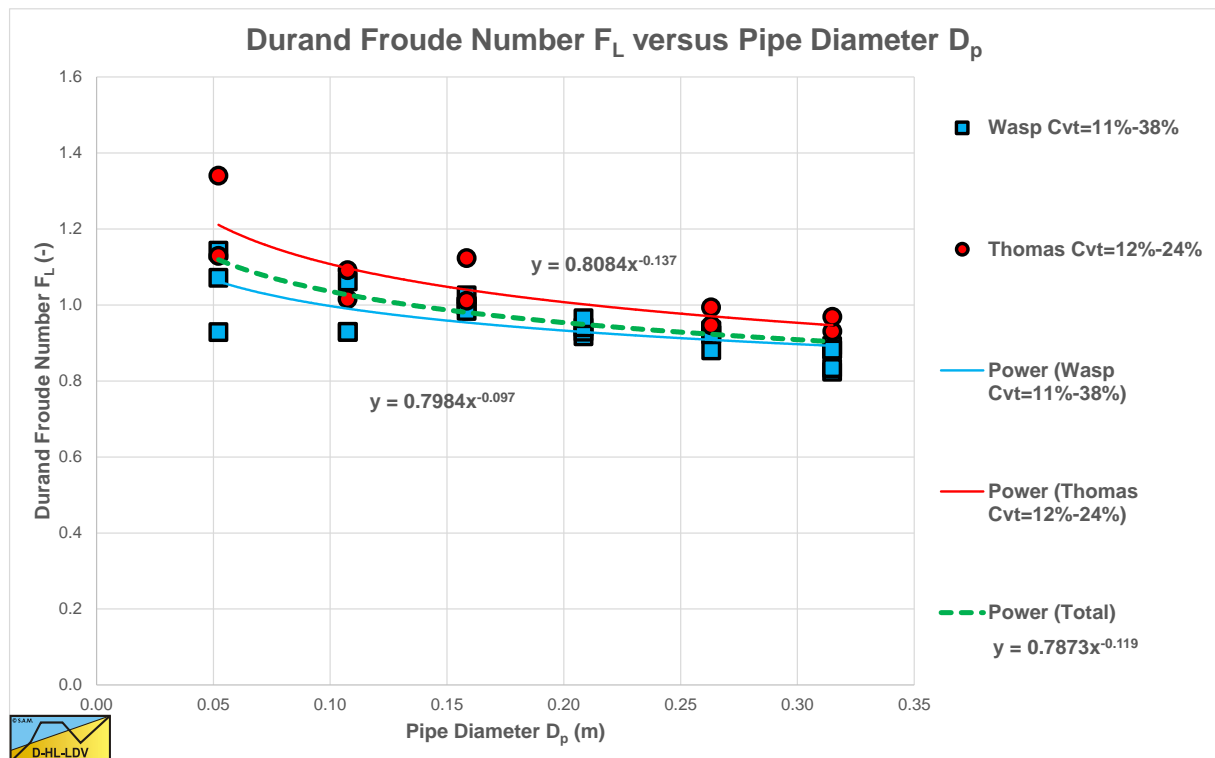
Figure 7.8-2: Data of Thomas (1979) and Wasp et al. (1977) with different pipe diameters.

7.8.3 Equations & Models.

Figure 7.8-3 and Figure 7.8-4 show the Limit Deposit Velocities of DHLLDV, Durand and Condolios (1952), Jufin and Lopatin (1966), Wasp et al. (1970), Wasp and Slatter (2004), Souza Pinto et al. (2014), Hepy et al. (2008), Gogus and Kokpinar (1993), Kokpinar and Gogus (2001), Berg (1998), Turian et al. (1987) and Gillies (1993) for 2 pipe diameters. The curves of Hepy et al. (2008), Gogus and Kokpinar (1993) and Kokpinar and Gogus (2001) show a maximum F_L value for particles with a diameter near $d = 0.5$ **mm**. However these models show an increasing F_L value with the pipe diameter, which contradicts the numerous experimental data, showing a slight decrease. The models of Turian et al. (1987) , Wasp et al. (1970), Wasp and Slatter (2004) and Souza Pinto et al. (2014) show an increasing F_L value with increasing particle diameter and a slight decrease with the pipe diameter.

Jufin and Lopatin (1966) show an increase with the particle diameter and a slight decrease with the pipe diameter (power –1/6). The model of van den Berg (1998) shows an increasing F_L with the particle diameter, but no dependency on the pipe diameter. Durand and Condolios (1952) did not give an equation but a graph. The data points as derived from the original publication in (1952) and from Durand (1953) are shown in the graphs. The data points show a maximum for $d = 0.5$ **mm**. They did not report any dependency on the pipe diameter. The model of Gillies (1993) tries to quantify the Durand and Condolios (1952) data points but does not show any dependency on the pipe diameter for the F_L Froude number. The increase of the F_L value with the pipe diameter of the Hepy et al. (2008), Gogus and Kokpinar (1993) and Kokpinar and Gogus (2001) models is probably caused by the forced d/D_p relation. With a strong relation with the particle diameter and a weak relation for the pipe diameter, the pipe diameter will follow the particle diameter. Another reason may be the fact that they used pipe diameters up to 0.1524 m (6 inch) and the smaller the pipe diameter the more probable the occurrence of a sliding bed and other limiting conditions, due to the larger hydraulic gradient helping the bed to start sliding.

The figures show that for small pipe diameters all models are close. The reason is probably that most experiments are carried out with small pipe diameters. Only Jufin and Lopatin (1966) covered a range from 0.02 m to 0.9 m pipe diameters. Recently Thomas (2014) gave an overview and analysis of the LDV (or sometimes the LSDV). He repeated the findings that the LDV depends on the pipe diameter with a power smaller than 0.5 but larger than 0.1. The value of 0.1 is for very small particles, while for normal sand and gravels a power is expected between 1/3 according to Jufin and Lopatin (1966) and 1/2 according to Durand and Condolios (1952). Most equations are one term equations, making it impossible to cover all aspects of the LDV behavior. Only Gillies (1993) managed to construct an equation that gets close to the original Durand and Condolios (1952) graph.

Figure 7.8-3: A number of LDV models in a 0.1524 m (6 inch) pipe.
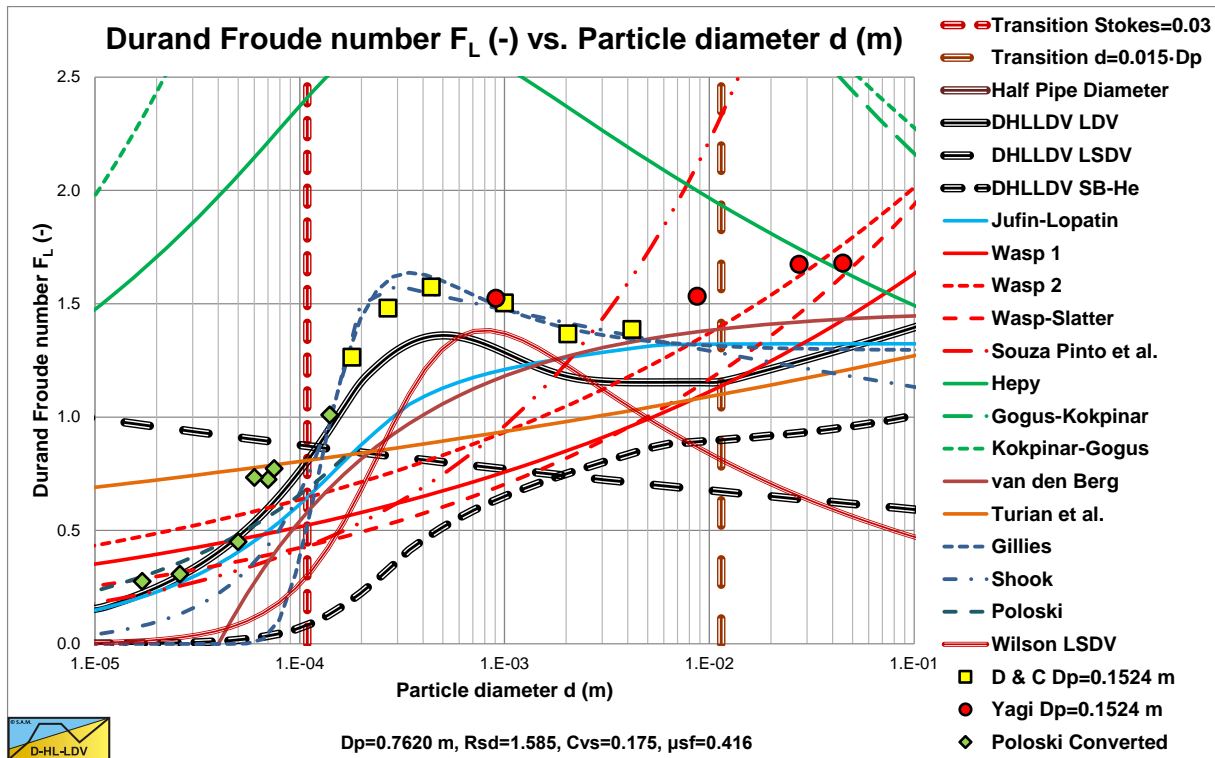
Figure 7.8-4: A number of LDV models in a 0.762 m (30 inch) pipe.

7.8.4 Conclusions Literature.

The models analyzed result in a number of dominating parameters. These are the particle diameter **d**, the pipe diameter **D_p**, the liquid density **ρ_l** and kinematic viscosity **ν_l**, the solids density **ρ_s**, the sliding friction coefficient **μ_{sf}**, the bed concentration **C_{vb}** and the spatial volumetric concentration **C_{vs}**. Derived parameters are the relative submerged density **R_{sd}**, the Darcy Weisbach friction factor for pure liquid flow **λ_l** and the thickness of the viscous sub-layer **δ_v**. Dimensionless numbers are not considered at first, since they may lead to wrong interpretations. Lately Lahiri (2009) performed an analysis using artificial neural network and support vector regression. Azamathulla and Ahmad (2013) performed an analysis using adaptive neuro-fuzzy interference system and gene-expression programming. Although these methodologies may give good correlations, they do not explain the physics. Lahiri (2009) however did give statistical relations for the dependency on the volumetric concentration, the particle diameter, the pipe diameter and the relative submerged density.

Resuming, the following conclusions can be drawn for sand and gravel:
The pipe diameter **D_p**: The LDV is proportional to the pipe diameter **D_p** to a power between 1/3 and 1/2 (about 0.4) for small to large particles (Thomas (1979), Wasp et al. (1977), Lahiri (2009) and Jufin and Lopatin (1966)) and a power of about 0.1 for very small particles (Thomas (1979), Wilson and Judge (1976), Sanders et al. (2004) and Poloski et al. (2010)).
The particle diameter **d**: The LDV has a lower limit for very small particles, after which it increases to a maximum at a particle diameter of about **d = 0.5 mm** (Thomas (1979), Thomas (2014), Durand and Condolios (1952), Gillies (1993) and Poloski et al. (2010)). For medium sized particles with a particle size d > 0.5 mm, the **F_L** value decreases slightly to a minimum for a particle size of about **d = 2 mm** (Durand and Condolios, 1952; Gillies, 1993; Poloski et al., 2010). Above 2 mm, the **F_L** value will remain constant according to Durand and Condolios (1952) and Gillies (1993). For particles with **$d/D_p > 0.015$**, the Wilson et al. (1992) criterion for real suspension/saltation, the **F_L** value increases again. This criterion is based on the ratio particle diameter to pipe diameter and will start at a large particle diameter with increasing pipe diameter. Yagi et al. (1972) reported many data points in this region showing an increasing **F_L** value.
The relative submerged density **R_{sd}**: The relation between the LDV and the relative submerged density is not very clear, however the data shown by Kokpinar and Gogus (2001) and the conclusions of Lahiri (2009) show that the **F_L** value decreases with increasing solids density and thus relative submerged density **R_{sd}** to a power of –0.1 to –0.4.
The spatial volumetric concentration **C_{vs}**: The volumetric concentration leading to the maximum LDV is somewhere between 15% and 20% according to Durand and Condolios (1952). Lahiri (2009) reported a maximum

at about 17.5%, while Poloski et al. (2010) derived 15%. This maximum LDV results from on one hand a linear increase of the sedimentation with the concentration and on the other hand a reduced sedimentation due to the hindered setting. These two counteracting phenomena result in a maximum, which is also present in the equation of the potential energy. For small concentrations a minimum LDV is observed by Durand and Condolios (1952). This minimum LDV increases with the particle diameter and reaches the LDV of 20% at a particle diameter of 2 mm with a pipe diameter of 0.1524 m (6 inch).

For the dredging industry the Jufin and Lopatin (1966) equation gives a good approximation for sand and gravel, although a bit conservative. The model of Berg (1998) is suitable for large diameter pipes as used in dredging for sand and/or gravel, but underestimates the LDV for pipe diameters below 0.8 m. Both models tend to underestimate the LDV for particle diameters below 1 mm.

7.8.5 Starting Points DHLLDV Framework.

Analyzing the literature, equations and experimental data, the LDV can be divided into 5 regions for sand and gravel:
1. Very small particles, smaller than about 50% of the thickness of the viscous sub layer, giving a lower limit of the LDV. This is for particles up to about 0.15 mm in large pipes to 0.04 mm in very small pipes.
2. Small particles up to about 0.2 mm, a smooth bed, show an increasing LDV with increasing particle diameter.
3. Medium particles with a diameter from 0.2 mm up to a diameter of 2 mm, a transition zone from a smooth bed to a rough bed. First the LDV increases to a particle diameter of about 0.5 mm, after which it decreases slowly to an asymptotic value at a diameter of about 2 mm.
4. Large particles with a diameter larger than 2 mm, a rough bed, giving a constant LDV.
5. Particles with a particle diameter to pipe diameter ratio larger than about 0.015 cannot be carried by turbulent eddies, just because eddies are not large enough. This will probably result in an increasing LDV with the particle diameter. Yagi et al. (1972) reported many data points in this region showing this increase.

The above conclusions are the starting points of the DHLLDV Limit Deposit Velocity Model and has been shown in the figures.

7.8.6 The Transition Fixed Bed – Sliding Bed (LSDV).

The transition fixed bed – sliding bed is not considered to be a real Limit Deposit Velocity, but it is a regime change and thus will be discussed here. This transition is named the Limit of Stationary Deposit Velocity (LSDV) resulting from 2LM or 3LM analysis like the Wilson et al. (1992) model. This transition will only occur above a certain particle diameter to pipe diameter ratio. Very small particles will never have a sliding bed. But medium sized particles that will have a sliding bed in small pipe diameters, may not have a sliding bed in large pipe diameters. Mathematically however, the transition line speed can always be determined, even though the transition will not occur in reality. In such a case the bed is already completely suspended before it could start sliding.

The total hydraulic gradient of a sliding bed $i_{m,sl}$ is considered to be equal to the hydraulic gradient required to move clear liquid through the pipe i_l and the sliding friction hydraulic gradient resulting from the friction force between the solids and the pipe i_{sf}, is:

$$i_{m,sb} = i_l + i_{sf} = \lambda_l \cdot \frac{v_{ls}^2}{2 \cdot g \cdot D_p} + \mu_{sf} \cdot C_{vs} \cdot R_{sd} \tag{7.8-8}$$

The hydraulic gradient $i_{m,fb}$ due to the flow through the restricted area A_H above the bed is:

$$i_{m,fb} = \lambda_r \cdot \frac{v_{ls,r}^2}{2 \cdot g \cdot D_H} = \lambda_r \cdot \frac{v_{ls}^2}{2 \cdot g \cdot D_H} \cdot \left(\frac{A_p}{A_H} \right)^2 \tag{7.8-9}$$

This gives for the transition line speed:

$$v_{ls,FBSB}^2 = \frac{2 \cdot \mu_{sf} \cdot g \cdot C_{vs} \cdot R_{sd}}{\dfrac{\lambda_r}{D_H} \cdot \left(\dfrac{A_p}{A_H} \right)^2 - \dfrac{\lambda_l}{D_p}} \tag{7.8-10}$$

7.8.7 The Transition Heterogeneous – Homogeneous (LDV Very Fine Particles).

For very fine particles, the Limit Deposit Velocity is close to the transition between the heterogeneous regime and the homogeneous regime. Values found in literature (Thomas (1976)) are between 80% and 100% of this transition velocity. This transition velocity can be determined by making the relative excess pressure contributions of both regimes equal, according to:

$$
R_{sd} \cdot C_{vs} = \frac{\left(2 \cdot g \cdot R_{sd} \cdot D_p\right)}{\lambda_l} \cdot C_{vs} \cdot \frac{1}{v_{ls}^2} \cdot \left(\frac{v_t}{v_{ls}} \cdot \left(1 - \frac{C_{vs}}{\kappa_C}\right)^{\beta} + \frac{8.5^2}{\lambda_l} \cdot \left(\frac{v_t}{\sqrt{g \cdot d}}\right)^{10/3} \cdot \left(\frac{\left(\nu_l \cdot g\right)^{1/3}}{v_{ls}}\right)^2 \right) \tag{7.8-11}
$$

This gives for the transition velocity between the heterogeneous regime and the homogeneous regime:

$$
v_{ls,HeHo}^4 = \frac{2 \cdot g \cdot D_p}{\lambda_l} \cdot \left(v_t \cdot \left(1 - \frac{C_{vs}}{\kappa_C}\right)^{\beta} \cdot v_{ls,HeHo} + \frac{8.5^2}{\lambda_l} \cdot \left(\frac{v_t}{\sqrt{g \cdot d}}\right)^{10/3} \cdot \left(\nu_l \cdot g\right)^{2/3} \right) \tag{7.8-12}
$$

This equation implies that the transition line speed depends reversely on the Darcy Weisbach viscous friction coefficient λ_l. Since the viscous friction coefficient λ_l depends reversely on the pipe diameter D_p with a power of about **0.2**, the transition line speed will depend on the pipe diameter with a power of about **(1.2/4) =0.3**. It is advised to use the Thomas (1965) viscosity correction for this transition line speed, otherwise to high transition velocities may be found. The equation derived is implicit and has to be solved iteratively.

7.8.8 The Transition Sliding Bed – Heterogeneous (LDV Coarse Particles).

When a sliding bed is present, particles will be in suspension above the sliding bed. The higher the line speed, the more particles will be in suspension. The interaction between the particles in suspension and the particles in the bed will still be by inter particle interactions, reason that the sliding bed is still carrying the weight of all the particles in suspension. Apparently the weight of all the particles is resulting in sliding friction. At a certain line speed all the particles will be in suspension and the sliding bed regime transits to heterogeneous flow. The particles now interact with the pipe wall by collisions and not by sliding friction anymore.

At the transition line speed the excess pressure losses of both regimes should be equal, giving

$$
\mu_{sf} = \frac{v_t}{v_{ls}} \cdot \left(1 - \frac{C_{vs}}{\kappa_C}\right)^{\beta} + \frac{8.5^2}{\lambda_l} \cdot \left(\frac{v_t}{\sqrt{g \cdot d}}\right)^{10/3} \cdot \left(\frac{\left(\nu \cdot g\right)^{1/3}}{v_{ls}}\right)^2 \tag{7.8-13}
$$

Resulting in the transition velocity at:

$$
v_{ls,SBHe}^2 = \frac{v_t \cdot \left(1 - \dfrac{C_{vs}}{\kappa_C}\right)^{\beta} \cdot v_{ls,SBHe} + \dfrac{8.5^2}{\lambda_l} \cdot \left(\dfrac{v_t}{\sqrt{g \cdot d}}\right)^{10/3} \cdot \left(\nu_l \cdot g\right)^{2/3}}{\mu_{sf}} \tag{7.8-14}
$$

This equation shows that the transition between the sliding bed regime and the heterogeneous regime depends on the sliding friction coefficient. Implicitly Newitt et al. (1955) already found this, but didn't explicitly mention this, because they assumed that potential energy is responsible for all the excess head losses in heterogeneous flow. The equation derived is a second degree function and can be written as:

$$
-v_{ls,SBHe}^2 + \frac{v_t \cdot \left(1 - \dfrac{C_{vs}}{\kappa_C}\right)^{\beta}}{\mu_{sf}} \cdot v_{ls,SBHe} + \frac{\dfrac{8.5^2}{\lambda_l} \cdot \left(\dfrac{v_t}{\sqrt{g \cdot d}}\right)^{10/3} \cdot \left(\nu_l \cdot g\right)^{2/3}}{\mu_{sf}} = 0 \tag{7.8-15}
$$

With:

$$A = -1$$

$$B = \frac{v_t \cdot \left(1 - \dfrac{C_{vs}}{\kappa_C}\right)^{\beta}}{\mu_{sf}}$$

(7.8-16)

$$C = \frac{\dfrac{8.5^2}{\lambda_l} \cdot \left(\dfrac{v_t}{\sqrt{g \cdot d}}\right)^{10/3} \cdot (v_l \cdot g)^{2/3}}{\mu_{sf}}$$

$$V_{ls,SBHe} = \frac{-B - \sqrt{B^2 - 4 \cdot A \cdot C}}{2 \cdot A}$$

The lower limit of the LDV is found to be about 80% of this transition line speed. This also implies that the transition of a sliding bed to heterogeneous transport is not sharp, an intersection point, but it's a gradual process starting at about 80% of the transition line speed.

7.8.9 The Transition Sliding Bed – Homogeneous (LSBV).

The transition sliding bed – homogeneous is not considered to be a Limit Deposit Velocity here, because for normal dredging operations this is out of range.
The total hydraulic gradient of a sliding bed $i_{m,sl}$ is considered to be equal to the hydraulic gradient required to move clear liquid through the pipe i_l and the sliding friction hydraulic gradient resulting from the friction force between the solids and the pipe i_{sf}, is:

$$i_{m,sb} = i_l + i_{sf} = \lambda_l \cdot \frac{v_{ls}^2}{2 \cdot g \cdot D_p} + \mu_{sf} \cdot C_{vs} \cdot R_{sd}$$

(7.8-17)

The total hydraulic gradient of homogeneous flow according to the ELM model is:

$$i_{m,ho} = i_l + i_s = \lambda_l \cdot \frac{v_{ls}^2}{2 \cdot g \cdot D_p} \cdot \left(1 + R_{sd} \cdot C_{vs}\right)$$

(7.8-18)

$$= \lambda_l \cdot \frac{v_{ls}^2}{2 \cdot g \cdot D_p} + \lambda_l \cdot \frac{v_{ls}^2}{2 \cdot g \cdot D_p} \cdot R_{sd} \cdot C_{vs}$$

At the transition velocity both are equal giving:

$$\mu_{sf} = \lambda_l \cdot \frac{v_{ls}^2}{2 \cdot g \cdot D_p} \cdot$$

(7.8-19)

So the transition velocity is:

$$v_{ls,sb-ho}^2 = \frac{2 \cdot \mu_{sf} \cdot g \cdot D_p}{\lambda_l}$$

(7.8-20)

7.8.10 The Limit Deposit Velocity (LDV All Particles).

7.8.10.1 Introduction.

Before starting with the derivation of the model two phenomena will be discussed, supporting the philosophy behind the model. First the turbulent velocity distribution above a bed, ranging from a very smooth bed to a very rough bed. Second the suspension criterion from the Shields-Parker diagram.

In the turbulent layer the total shear stress contains only the turbulent shear stress. Integration of the shear stress gives the famous logarithmic velocity profile (Law of the Wall):

$$ u(y) = \frac{u_*}{\kappa} \cdot \ln\left(\frac{y}{y_0}\right) \tag{7.8-21} $$

Where the integration constant y_0 is the elevation corresponding to zero velocity ($u_{y=y0}=0$), given by Nikuradse by the study of the pipe flows.

$$ y_0 = 0.11 \cdot \frac{\nu_l}{u_*} \qquad \text{Hydraulically smooth flow} \qquad \frac{u_* \cdot k_s}{\nu_l} \leq 5 \tag{7.8-22} $$

$$ y_0 = 0.033 \cdot k_s \qquad \text{Hydraulically rough flow} \qquad \frac{u_* \cdot k_s}{\nu_l} \geq 70 \tag{7.8-23} $$

$$ \frac{y_0}{k_s} = \frac{1}{9 \cdot k_s^+} + \frac{1}{30} \cdot \left(1 - e^{-\frac{k_s^+}{26}}\right) \qquad \text{Hydraulically transition flow} \qquad 5 < \frac{u_* \cdot k_s}{\nu_l} < 70 \tag{7.8-24} $$
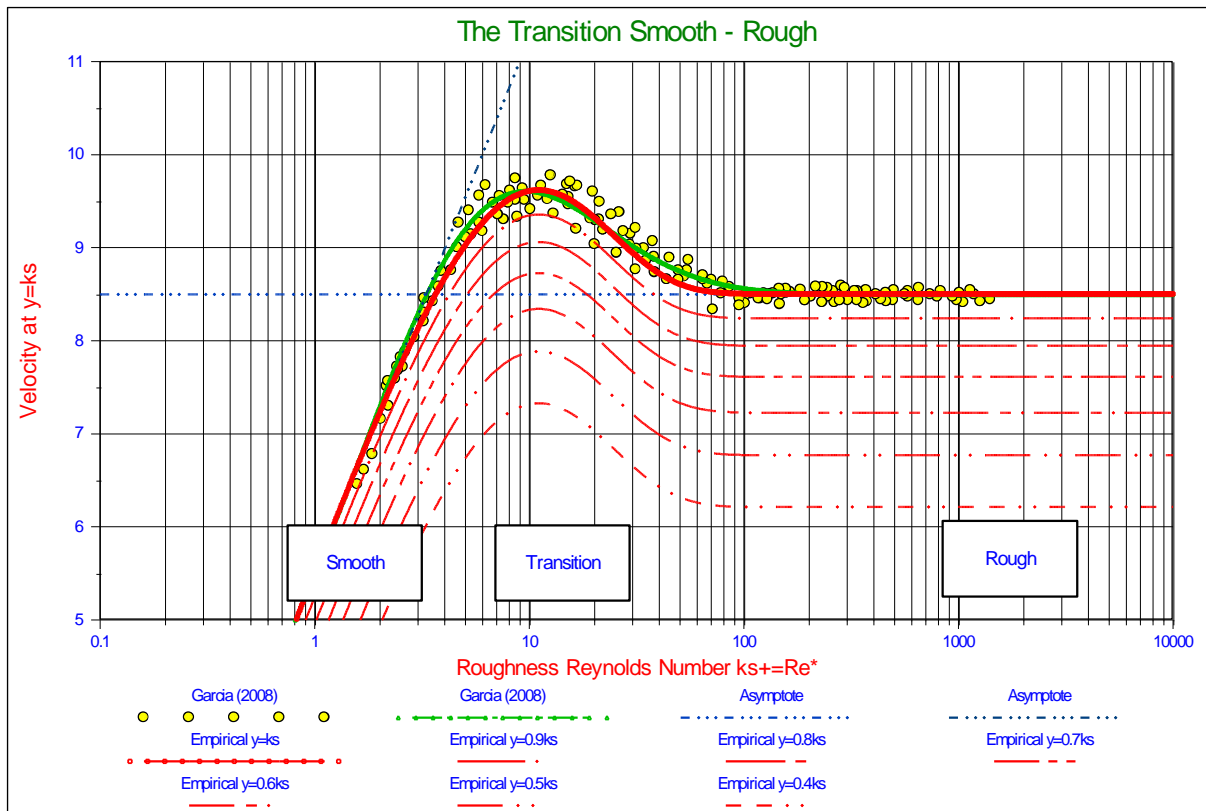
Figure 7.8-5: The transition smooth-rough for a number of distances to the wall.

The transition between hydraulic smooth and rough flow can be approximated in many ways, but the resulting equation should match measurements like shown in Garcia (2008) (fig. 2.3). The following equation (derived by

the Miedema (2012A)), gives a very good approximation of this transition, where the distance to the wall equals the roughness. Equation (7.8-25) gives the velocity as a function of the non-dimensional distance to the wall $\mathbf{y^+}$.

$$\frac{\overline{\mathbf{u}}(\mathbf{y^+})}{\mathbf{u_*}} = \frac{1}{\kappa} \cdot \ln\left(\frac{\mathbf{y^+}}{0.11}\right) \cdot \mathbf{e}^{-0.95 \cdot \frac{\mathbf{k_s^+}}{11.6}} + \frac{1}{\kappa} \cdot \ln\left(\frac{\mathbf{y^+}}{0.033 \cdot \mathbf{k_s^+}}\right) \cdot \left(1 - \mathbf{e}^{-0.95 \cdot \frac{\mathbf{k_s^+}}{11.6}}\right) \tag{7.8-25}$$

Since $\mathbf{11.6 = \delta_v \cdot u_* / \nu = \delta_v^+}$ and $\mathbf{0.11 = 0.11 \cdot \delta_v \cdot u_* / \nu / 11.6 = 0.0095 \cdot \delta_v^+}$ and the influence of the second right hand term (giving 95 instead of 105), equation (5.1-20) can be written as:

$$\frac{\overline{\mathbf{u}}(\mathbf{y^+})}{\mathbf{u_*}} = \frac{1}{\kappa} \cdot \ln\left(95 \cdot \frac{\mathbf{y^+}}{\delta_v^+}\right) \cdot \mathbf{e}^{-0.95 \cdot \frac{\mathbf{k_s^+}}{\delta_v^+}} + \frac{1}{\kappa} \cdot \ln\left(30 \cdot \frac{\mathbf{y^+}}{\mathbf{k_s^+}}\right) \cdot \left(1 - \mathbf{e}^{-0.95 \cdot \frac{\mathbf{k_s^+}}{\delta_v^+}}\right) \tag{7.8-26}$$

In terms of the dimensional parameters for the distance to the wall $\mathbf{y}$, the roughness $\mathbf{k_s}$ and thickness of the laminar layer $\mathbf{\delta_v}$ this gives:

$$\frac{\overline{\mathbf{u}}(\mathbf{y})}{\mathbf{u_*}} = \frac{1}{\kappa} \cdot \ln\left(95 \cdot \frac{\mathbf{y}}{\delta_v}\right) \cdot \mathbf{e}^{-0.95 \cdot \frac{\mathbf{k_s}}{\delta_v}} + \frac{1}{\kappa} \cdot \ln\left(30 \cdot \frac{\mathbf{y}}{\mathbf{k_s}}\right) \cdot \left(1 - \mathbf{e}^{-0.95 \cdot \frac{\mathbf{k_s}}{\delta_v}}\right) \tag{7.8-27}$$

Figure 7.8-5 shows the non-dimensional velocity $\mathbf{u^+}$ at distances $\mathbf{y=k_s}$, $\mathbf{y=0.9k_s}$, $\mathbf{y=0.8k_s}$, $\mathbf{y=0.7k_s}$, $\mathbf{y=0.6k_s}$, $\mathbf{y=0.5k_s}$ and, $\mathbf{y=0.4k_s}$ from the wall. Up to a Reynolds number of 20 and above a Reynolds number of 70 equation (7.8-27) matches the measurements very well, between 20 and 70 the equation underestimates the measured values, but overall the resemblance is very good.

Figure 7.8-5 shows a shape of the curves similar to the shape of the LDV curve as reported by Durand & Condolios (1952).

A well-known application of the Shields curve is the so called Shields-Parker diagram, showing erosion versus no erosion, suspension versus no suspension and ripples versus dunes. This diagram is shown in Figure 7.8-6. The criterion used for the suspension curve is:

$$\mathbf{v_t = u_*} \tag{7.8-28}$$

The terminal settling velocity equals the friction velocity. Now this is not an absolute criterion, much more an indication.

At a point $\mathbf{Re_*=2}$ and $\mathbf{\theta=0.08}$ the suspension curve crosses the Shields curve. At smaller Reynolds numbers the suspension curve is lower than the Shields curve. For sand this intersection point is for particles with $\mathbf{d=0.146\ mm}$. Physically this means that particles smaller than $\mathbf{d=0.146\ mm}$ once in suspension will stay in suspension even if the Shields number is below the Shields curve. However if there is some bed, a much higher line speed is required to erode the bed, because the bed is very smooth. Whether or not a bed will be present depends on the history. If the line speed is gradually increased starting from zero, there will be a bed and a relatively high line speed is required to erode the bed. However, if the line speed is gradually decreased starting with a very high line speed, all particles will be in suspension and remain in suspension until the line speed is low enough.
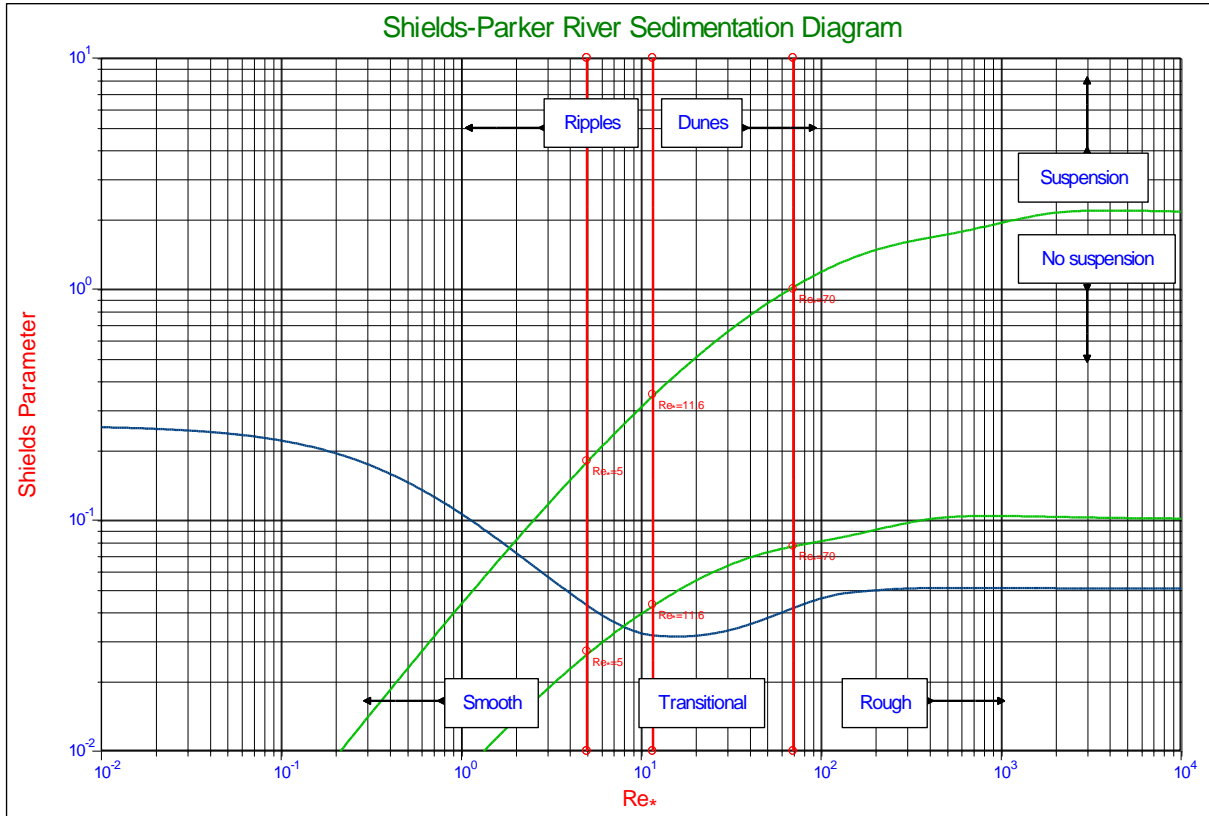
Figure 7.8-6: The Shields-Parker diagram as a function of the roughness Reynolds number Re∗.

7.8.10.2 Very Small Particles, the Lower Limit.

Thomas (1979) investigated the Limit Deposit Velocity for very small particles and found that there is a lower limit to the LDV independent of the particle size. According to Figure 7.8-6 this occurs for particles smaller than **d=0.146 mm**, although this is just an indication. This lower limit is based on the assumption that the very small particles are smaller than the thickness of the viscous sub layer and still settle in this laminar flow, while particles in the turbulent flow are carried by the small eddies. At the moment of sliding the shear stress τ_{12} at the top of the thin layer with thickness **h**, equals the sliding friction force divided by the total sliding surface:

$$\tau_{12} = \frac{F_{sf}}{D_p \cdot \Delta L} = \mu_{sf} \cdot h \cdot \rho_l \cdot R_{sd} \cdot (1-n) \cdot g = \mu_{sf} \cdot h \cdot \rho_l \cdot R_{sd} \cdot C_{vb} \cdot g \tag{7.8-29}$$

The thickness of the thin layer is assumed to be equal to the thickness of the viscous sub layer:

$$h = \delta_v = 11.6 \cdot \frac{\nu_l}{u_*} \tag{7.8-30}$$

Thomas (1979) used a factor 5 instead of 11.6. Substituting this layer thickness gives:

$$\tau_{12} = 11.6 \cdot \mu_{sf} \cdot \frac{\nu_l}{u_*} \cdot \rho_l \cdot R_{sd} \cdot C_{vb} \cdot g = \rho_l \cdot u_*^2 \tag{7.8-31}$$

This gives for the friction velocity:

$$u_*^3 = 11.6 \cdot \mu_{sf} \cdot \nu_l \cdot R_{sd} \cdot C_{vb} \cdot g \quad \text{or} \quad u_* = 2.26 \cdot \left(\mu_{sf} \cdot \nu_l \cdot R_{sd} \cdot C_{vb} \cdot g \right)^{1/3} \tag{7.8-32}$$

With a bed concentration **C$_{vb}$=0.6** and a sliding friction coefficient of **μ$_{sf}$=0.4** this gives:

$$\mathbf{u_* = 1.4 \cdot \left(\nu_l \cdot R_{sd} \cdot g\right)^{1/3}} \quad \text{or} \quad \mathbf{u_* = 0.0387} \tag{7.8-33}$$

For sand with a relative submerged density of $\mathbf{R_{sd}=1.65}$, water with a viscosity of $\mathbf{\nu_l=0.0000013\ m^2/sec}$ this gives a friction velocity of 0.0387 m/sec. In terms of the Limit Deposit Velocity the following is found:

$$\mathbf{u_* = \sqrt{\frac{\lambda_l}{8}} \cdot v_{ls,ldv} = 1.4 \cdot \left(\nu_l \cdot R_{sd} \cdot g\right)^{1/3}} \quad \text{or} \quad \mathbf{u_* = \sqrt{\frac{\lambda_l}{8}} \cdot v_{ls,ldv} = 0.0387}$$

$$\mathbf{v_{ls,ldv} = 1.4 \cdot \left(\nu_l \cdot R_{sd} \cdot g\right)^{1/3} \cdot \sqrt{\frac{8}{\lambda_l}}} \quad \text{or} \quad \mathbf{v_{ls,ldv} = 0.0387 \cdot \sqrt{\frac{8}{\lambda_l}}} \tag{7.8-34}$$

$$\mathbf{v_{ls,ldv} = 3.96 \cdot \frac{\left(\nu_l \cdot R_{sd} \cdot g\right)^{1/3}}{\sqrt{\lambda_l}}} \quad \text{or} \quad \mathbf{v_{ls,ldv} = 0.11 \cdot \sqrt{\frac{1}{\lambda_l}}}$$

For small pipes with $\mathbf{\lambda_l=0.03}$ this gives $\mathbf{v_{ls,ldv}=0.64\ m/sec}$, for medium pipes with $\mathbf{\lambda_l=0.02}$ this gives $\mathbf{v_{ls,ldv}=0.78\ m/sec}$ and for large pipe diameters with $\mathbf{\lambda_l=0.01}$ this gives $\mathbf{v_{ls,ldv}=1.10\ m/sec}$. The LDV increases with the pipe diameter to a power of about 0.1 as already noted by Thomas (1979). Because Thomas (1979) used a factor 5 for the thickness of the viscous sub layer instead of the 11.6 as used here, he found a theoretical coefficient of 0.933 instead of the coefficient 1.4 found here. Based on his experiments he corrected this factor to 1.1. Now the value of the thickness of the viscous sub layer is just a mathematical thickness, so it is very well possible that the thickness as used here is smaller than the one using the coefficient of 11.6 and larger than using the coefficient of 5. Based on the experimental coefficient of 1.1 as found by Thomas (1979) the coefficient for the thickness of the viscous sub layer involved should be 5.62, almost 50% of the thickness of the viscous sub layer. It should be noted that the velocity found this way is in fact the LSDV and not the LDV. The LSDV is the Limit of Stationary Deposit, so the line speed where the bed starts sliding, while the LDV is the Limit Deposit Velocity, the line speed where all particles are in suspension and there is also no sliding bed anymore. The LDV is always higher than the LSDV. However it is the question whether for very small particles residing in the viscous sub layer, the situation of having 100% of the particles in suspension will ever occur. Another issue is the apparent viscosity. As the volumetric concentration increases, so does the apparent viscosity for very small particles, according to Thomas (1965). To include the viscosity effect and to be on the safe side, the factor 1.4 is used in the DHLLDV Framework.

In terms of the Durand & Condolios Froude number this gives:

$$\boxed{\mathbf{F_L = \frac{v_{ls,ldv}}{\sqrt{2 \cdot g \cdot R_{sd} \cdot D_p}} = 3.96 \cdot \frac{\left(\nu_l \cdot R_{sd} \cdot g\right)^{1/3}}{\sqrt{\lambda_l} \cdot \sqrt{2 \cdot g \cdot R_{sd} \cdot D_p}} \approx \frac{0.02}{\sqrt{\lambda_l \cdot D_p}}}} \tag{7.8-35}$$

7.8.10.3 Smooth Bed.

Small particles are kept in suspension by the turbulent eddies if there is enough turbulent energy in the liquid flow. This will of course only be valid for particles small enough to be carried by these eddies. The potential energy losses of the particles are decreasing with increasing line speed, while the energy losses of the liquid flow are increasing with increasing line speed. Now it is assumed that a certain fraction of the energy losses of the liquid flow is available for the suspension of the particles. This fraction is defined as $\mathbf{1/\alpha_p^3}$. So at the line speed where the potential energy losses are equal to $\mathbf{1/\alpha_p^3}$ times the liquid energy losses, all particles will be in suspension. At a lower line speed some particles will form a bed at the bottom of the pipe. The potential energy losses of the particles can be expressed by means of the excess hydraulic gradient due to potential energy. The liquid flow energy losses can be expressed in terms of the liquid hydraulic gradient. This gives:

$$\mathbf{\frac{v_t \cdot \left(1 - \dfrac{C_{vs}}{\kappa_C}\right)^{\beta} \cdot C_{vs} \cdot R_{sd}}{v_{ls,ldv}} = \frac{1}{\alpha_p^3} \cdot \frac{\lambda_l \cdot v_{ls,ldv}^2}{2 \cdot g \cdot D_p}} \tag{7.8-36}$$

This gives for the Limit Deposit Velocity:

$$
v_{ls,ldv}^3 = \alpha_p^3 \cdot \frac{v_t \cdot \left(1 - \frac{C_{vs}}{\kappa_C}\right)^\beta \cdot C_{vs} \cdot \left(2 \cdot g \cdot R_{sd} \cdot D_p\right)}{\lambda_l}
\tag{7.8-37}
$$

This equation shows that the Limit Deposit Velocity of small particles depends on the terminal settling velocity with a correction for hindered settling $v_t \cdot (1-C_{vs}/\kappa_C)^\beta$, the spatial volumetric concentration C_{vs}, the relative submerged density R_{sd}, the pipe diameter D_p and the Darcy Weisbach friction factor λ_l. The term $(1-C_{vs}/\kappa_C)^\beta \cdot C_{vs}$ has a maximum at a spatial concentration of 15% for small particles and at about 20-25% for large particles, depending on the value of the power β and the factor κ_C. In terms of the Durand & Condolios LDV Froude number F_L factor this can be written as:

$$
F_{L,s} = \frac{v_{ls,ldv}}{\left(2 \cdot g \cdot R_{sd} \cdot D_p\right)^{1/2}} = \alpha_p \cdot \left(\frac{v_t \cdot \left(1 - \frac{C_{vs}}{\kappa_C}\right)^\beta \cdot C_{vs}}{\lambda_l \cdot \left(2 \cdot g \cdot R_{sd} \cdot D_p\right)^{1/2}}\right)^{1/3}
\tag{7.8-38}
$$

$$
\text{with :} \quad \alpha_p = 3.4 \cdot \left(\frac{1.65}{R_{sd}}\right)^{2/9}, \quad \kappa_C = 0.175 \cdot (1+\beta)
$$

The values found for $\alpha_p=3.4$ and $\kappa_C=0.175*(1+\beta)$ are based on many experiments from literature. The value of α_p of 3.4 found shows that the LDV occurs when the potential energy losses of the particles are about 2.54% of the energy losses of the liquid flow for small particles. The value of κ_C means that the average particle is at $0.175*(1+\beta)$ of the radius of the pipe, measured from the bottom of the pipe and not at the radius. This is in fact the concentration eccentricity factor. It also appears that the Limit Deposit Velocity found for small particles is close to the transition between the heterogeneous regime and the homogeneous regime, which makes sense, because in the homogeneous regime all particles are supposed to be in suspension.

The value of $\alpha_p=3.4$ is based on the maximum LDV values found in literature and not on a best fit. In fact α_p may vary from 3.0 as a lower limit to 3.4 as an upper limit. So the value of 3.4 is conservative. A best fit would probably give a value of about 3.2. However in dredging the LDV should be a safe LDV, since the particle size, the concentration and the line speed may vary in time.

7.8.10.4 Rough Bed.

When the particles are larger, the small eddies are not strong enough to keep them in suspension. The transport mechanism over the bottom of the pipe will be more saltation or similar to sheet flow. For medium and large particles in sedimentation transport it is often assumed that particles are in suspension or in saltation when the friction velocity is larger than the terminal settling velocity, $u^*>v_t$. Larger particles will be more difficult to keep in suspension, but at a certain bed shear stress saltation will take over. Whether this occurs exactly at $u^*=v_t$ can be questioned, but some proportionality seems reasonable since the friction velocity is proportional to the bed shear stress. The Shields-Parker diagram, Figure 7.8-6, (Garcia, 2008), uses this assumption. Substituting the friction velocity for the terminal settling velocity gives:

$$
\frac{u_* \cdot \left(1 - \frac{C_{vs}}{\kappa_C}\right)^\beta \cdot C_{vs} \cdot R_{sd}}{v_{ls,ldv}} = \frac{1}{\alpha_p^3} \cdot \frac{\lambda_l \cdot v_{ls,ldv}^2}{2 \cdot g \cdot D_p}
\tag{7.8-39}
$$

The question is now, what to use for the friction velocity u^*? In general a limiting volumetric bed concentration can be assumed for a line speed just below the Limit Deposit Velocity $C_{vs,ldv}$. This limiting concentration is the cross section of particles in the bed at the LDV divided by the pipe cross section, and not the total concentration, since most of the particles are in suspension or saltation. The limiting volumetric bed concentration can be divided by the bed concentration C_{vb} giving a relative limiting volumetric bed concentration $C_{vr,ldv}$. This relative limiting

volumetric bed concentration gives the fraction of the bed related to the pipe cross section. In terms of the bed shear stress this gives:

$$
u_* = \sqrt{\frac{\tau_{12}}{\rho_l}} \quad \text{with:} \quad \tau_{12} = \mu_{sf} \cdot g \cdot \rho_l \cdot R_{sd} \cdot \frac{\pi}{4} \cdot D_p \cdot C_{vr,ldv} \cdot C_{vb}
\tag{7.8-40}
$$

The shear stress can be derived by assuming that there is a thin layer of sand covering the bottom of the pipe with a thickness **h** over the full diameter of the pipe. The weight of this thin layer is:

$$
F_W = h \cdot D_p \cdot \Delta L \cdot \rho_l \cdot R_{sd} \cdot (1-n) \cdot g
\tag{7.8-41}
$$

The friction force of this thin layer of sand on the bottom of the pipe is:

$$
F_{sf} = \mu_{sf} \cdot h \cdot D_p \cdot \Delta L \cdot \rho_l \cdot R_{sd} \cdot (1-n) \cdot g
\tag{7.8-42}
$$

At the moment of sliding the shear stress at the top of the thin layer equals the sliding friction force divided by the total sliding surface:

$$
\tau_{12} = \frac{F_{sf}}{D_p \cdot \Delta L} = \mu_{sf} \cdot h \cdot \rho_l \cdot R_{sd} \cdot (1-n) \cdot g
\tag{7.8-43}
$$

The volumetric concentration of the bed with respect to the full cross section of the pipe is:

$$
C_{vs,ldv} = \frac{h \cdot D_p \cdot (1-n)}{\frac{\pi}{4} \cdot D_p^2} = \frac{4}{\pi} \cdot \frac{h \cdot (1-n)}{D_p}
\tag{7.8-44}
$$

This gives for the thickness of the thin layer **h**:

$$
h = C_{vs,ldv} \cdot \frac{\pi}{4} \cdot \frac{D_p}{(1-n)}
\tag{7.8-45}
$$

So now the shear stress equals, in terms of the relative limiting volumetric concentration:

$$
\tau_{12} = \mu_{sf} \cdot C_{vs,ldv} \cdot \frac{\pi}{8} \cdot \rho_l \cdot 2 \cdot g \cdot R_{sd} \cdot D_p = \mu_{sf} \cdot \frac{\pi}{8} \cdot \rho_l \cdot \left(2 \cdot g \cdot R_{sd} \cdot D_p \right) \cdot \frac{C_{vs,ldv}}{C_{vb}} \cdot C_{vb}
$$
$$
\tau_{12} = \mu_{sf} \cdot \frac{\pi}{8} \cdot \rho_l \cdot \left(2 \cdot g \cdot R_{sd} \cdot D_p \right) \cdot C_{vr,ldv} \cdot C_{vb}
\tag{7.8-46}
$$

Substituting the shear stress for the friction velocity gives:

$$
\frac{\sqrt{\frac{\tau_{12}}{\rho_l}} \cdot \left(1 - \frac{C_{vs}}{\kappa_C} \right)^{\beta} \cdot C_{vs} \cdot R_{sd}}{v_{ls,ldv}} = \frac{1}{\alpha_p^3} \cdot \frac{\lambda_l \cdot v_{ls,ldv}^2}{2 \cdot g \cdot D_p}
\tag{7.8-47}
$$

Thus, based on the limiting volumetric concentration:

$$
\frac{\sqrt{\frac{\rho_l \cdot \mu_{sf} \cdot \frac{\pi}{8} \cdot C_{vr,ldv} \cdot C_{vb} \cdot \left(2 \cdot g \cdot R_{sd} \cdot D_p \right)}{\rho_l}} \cdot \left(1 - \frac{C_{vs}}{\kappa_C} \right)^{\beta} \cdot C_{vs} \cdot R_{sd}}{v_{ls,ldv}} = \frac{1}{\alpha_p^3} \cdot \frac{\lambda_l \cdot v_{ls,ldv}^2}{2 \cdot g \cdot D_p}
\tag{7.8-48}
$$

This can be rewritten as:

$$\frac{\left(2\cdot g\cdot R_{sd}\cdot D_p\right)^{1/2}\cdot\left(\mu_{sf}\cdot C_{vb}\cdot\dfrac{\pi}{8}\right)^{1/2}\cdot C_{vr,ldv}^{1/2}\cdot\left(1-\dfrac{C_{vs}}{\kappa_C}\right)^{\beta}\cdot C_{vs}\cdot R_{sd}}{v_{ls,ldv}}=\frac{1}{\alpha_p^3}\cdot\frac{\lambda_l\cdot v_{ls,ldv}^2}{2\cdot g\cdot D_p} \tag{7.8-49}$$

So the limit deposit velocity LDV is now for medium and large particles:

$$v_{ls,ldv}^3=\alpha_p^3\cdot\frac{\left(1-\dfrac{C_{vs}}{\kappa_C}\right)^{\beta}\cdot C_{vs}\cdot\left(\mu_{sf}\cdot C_{vb}\cdot\dfrac{\pi}{8}\right)^{1/2}\cdot C_{vr,ldv}^{1/2}}{\lambda_l}\cdot\left(2\cdot g\cdot R_{sd}\cdot D_p\right)^{3/2} \tag{7.8-50}$$

And the Durand & Condolios LDV Froude number:

$$F_{L,r}=\frac{v_{ls,ldv}}{\left(2\cdot g\cdot R_{sd}\cdot D_p\right)^{1/2}}=\alpha_p\cdot\left(\frac{\left(1-\dfrac{C_{vs}}{\kappa_C}\right)^{\beta}\cdot C_{vs}\cdot\left(\mu_{sf}\cdot C_{vb}\cdot\dfrac{\pi}{8}\right)^{1/2}\cdot C_{vr,ldv}^{1/2}}{\lambda_l}\right)^{1/3} \tag{7.8-51}$$

The limiting relative volumetric concentration $C_{vr,ldv}$ appears to depend on the pipe diameter D_p and the relative submerged density R_{sd}. With a constant thickness of the thin layer h, the amount of solids in this thin layer is proportional to the pipe diameter D_p. The cross section of the pipe however is proportional to the pipe diameter D_p squared. So the limiting relative volumetric concentration $C_{vr,ldv}$ will be reversely proportional to the pipe diameter. The limiting relative volumetric concentration $C_{vr,ldv}$ is decreasing with increasing relative submerged density R_{sd}. This can be explained by assuming that a certain critical bed shear stress τ_{12} requires a decreasing relative volumetric concentration $C_{vr,ldv}$ with an increasing relative submerged density R_{sd}. In the sliding flow regime, the particles are so large that they flow over the bottom of the pipe giving sliding friction behavior, the limiting relative volumetric concentration increases with an increasing particle diameter to pipe diameter ratio. The criterion for sliding flow of Wilson et al. (1992) is applied here. When the particles are large it is also the question whether they still fit in the thin layer with thickness h.

$$d\le 0.015\cdot D_p\qquad C_{vr,ldv}=0.00017\cdot D_p^{-1}\cdot\left(\frac{R_{sd}}{1.65}\right)^{-1}=\frac{0.0055}{2\cdot g\cdot R_{sd}\cdot D_p}$$

$$d>0.015\cdot D_p\qquad C_{vr,ldv}=0.00017\cdot D_p^{-1}\cdot\left(\frac{R_{sd}}{1.65}\right)^{-1}\cdot\left(\frac{d}{0.015\cdot D_p}\right)^{1/2}=\frac{0.045}{2\cdot g\cdot R_{sd}\cdot D_p}\cdot\left(\frac{d}{D_p}\right)^{1/2} \tag{7.8-52}$$

The F_L value can now be determined according to:

$$F_{L,s}\le F_{L,r}\qquad\Rightarrow\qquad F_L=F_{L,s}$$

$$F_{L,s}>F_{L,r}\qquad\Rightarrow\qquad F_L=F_{L,s}\cdot e^{-d/d_0}+F_{L,r}\cdot\left(1-e^{-d/d_0}\right)$$

$$\text{with :}\qquad d_0=0.0005\cdot\left(\frac{1.65}{R_{sd}}\right) \tag{7.8-53}$$

This can be compared with the transition between hydraulic smooth and rough flow, equation (7.8-27) and Figure 7.8-5, which can be approximated in many ways, but the resulting equation should match measurements like shown

in Garcia (2008). The coefficients α_p, κ and d_0 are found by calibrating the equations on as much experimental data as possible. It is not tried to get the best fit, but to be on the safe side, 90-95% of the data points should be below the resulting LDV curve. In general, the maximum LDV curves are found at a concentration of about 15-20%. Above 20% the LDV decreases again.

When the Limit Deposit Velocity found this way is smaller than the transition velocity between the sliding bed regime and the heterogeneous regime, the latter should be chosen for the LDV. Whether this is exactly this transition velocity is a question, but since a LDV smaller than this transition velocity would result in an E_{rhg} value in the heterogeneous regime higher than the sliding bed E_{rhg}, which is impossible, this transition is chosen as a limitation to the LDV curves.
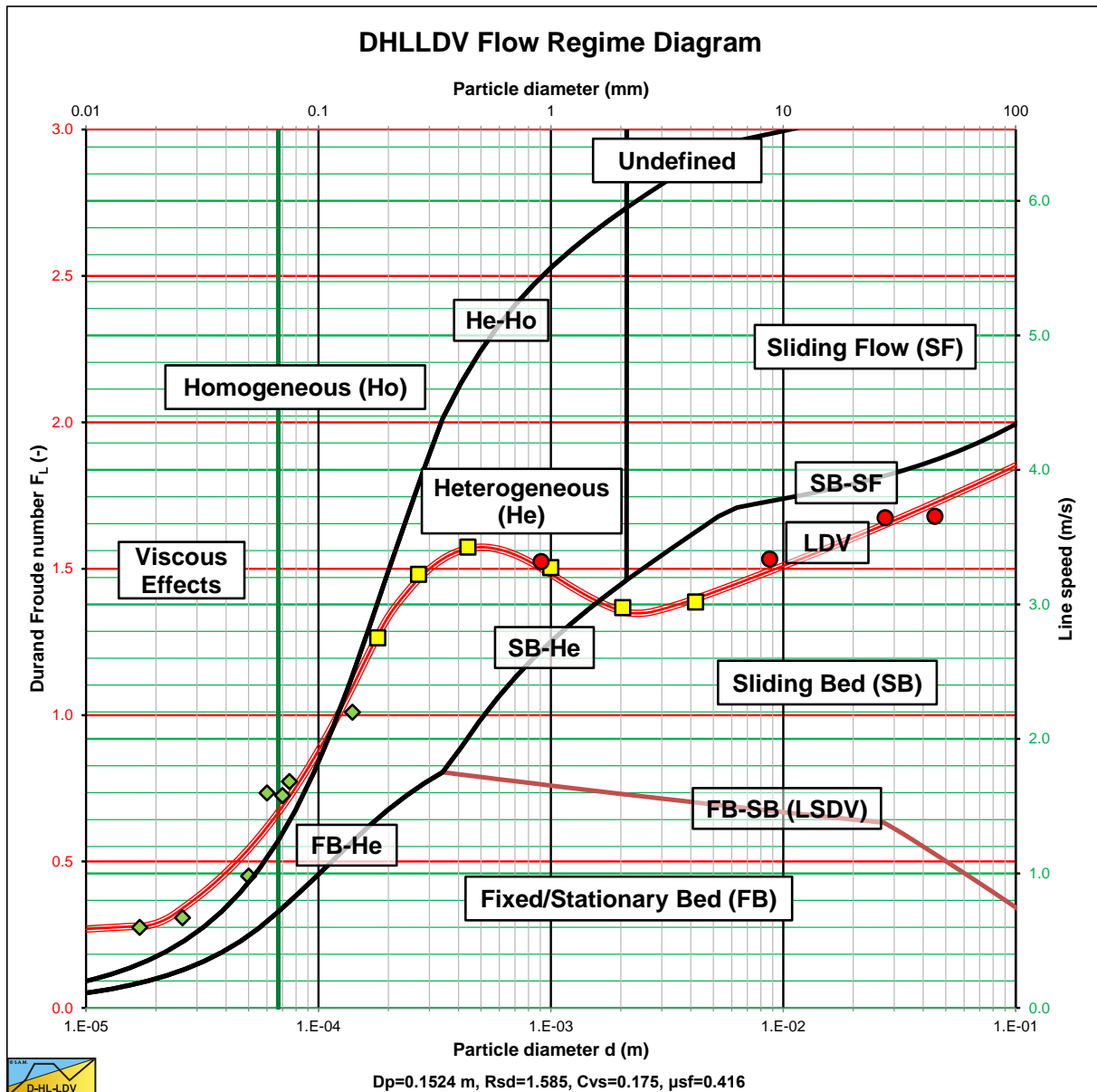
Figure 7.8-7: The resulting flow regime diagram.

Figure 7.8-7 shows a resulting flow regime diagram, based on the transition velocities and the LDV. The transition curves are based on behavior. For example the transition SB-He shows when the flow transits from sliding bed behavior to heterogeneous behavior. This does not mean that at the transition there is still a sliding bed, it means up to the transition the hydraulic gradient is sliding friction dominated. This is the reason why the LDV curve can be below or above the transition curve. The LDV and the LSDV curves however do mean there is a sharp transition. The figure also shows upper limit LDV data from different sources. The green diamonds are from the Poloski et al. (2010) research of very fine particles. The yellow squares from Durand & Condolios (1952) of fine sands to fine gravels. The red circles are from Yagi et al. (1972) of medium sands to coarse gravel.

7.8.11 The Resulting Limit Deposit Velocity Curves.

Now that the 5 transition velocities and the Limit Deposit Velocity have been found, how to apply them?

In slurry transport applications like dredging, the slurry transport process is not steady state, but dynamical. At the entrance of the pipeline the volumetric concentration and the particle size distribution, PSD, will vary in time. Because of this the hydraulic gradient will vary, resulting in a varying line speed. Even with steady state volumetric concentration and PSD, moving dunes and large vortices may occur. So to be safe, the maximum LDV curve should be used, which occurs at a volumetric concentration of about 20%.
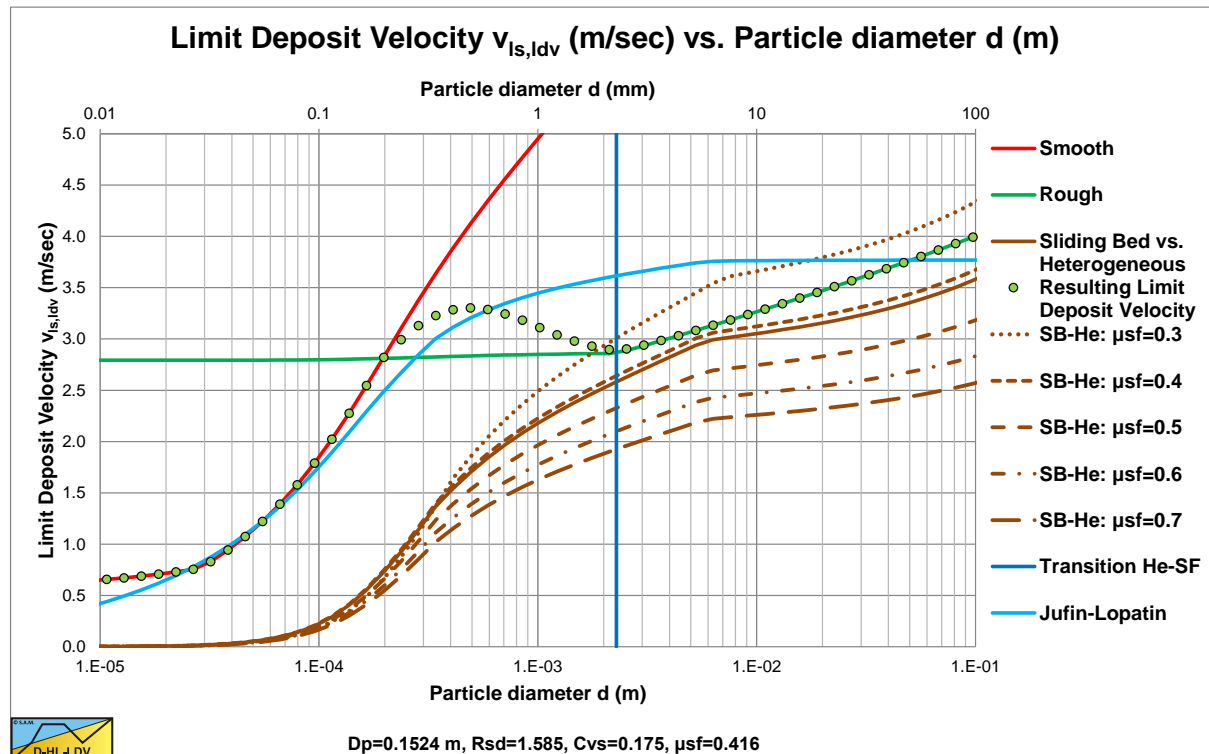
Figure 7.8-8: The construction of the LDV curve.

Figure 7.8-8 shows the construction of the LDV curve for sands and gravels in a 6 inch (0.1524 m) pipe, for a 20% volumetric concentration. Up to a particle diameter of about 0.15 mm the resulting curve follows the smooth curve (red line). From 0.15 mm to about 2 mm the resulting curve follows the transition equation. Above 2mm, in this case the transition velocity between the sliding bed regime and the heterogeneous regime is followed. Finally above about 10 mm the sliding flow criteria is followed. The shape of the curve depends strongly on the pipe diameter. With small diameter pipes, the transition velocity between the sliding bed regime and the heterogeneous regime will be dominant for larger particles. While for large pipe diameters as used in dredging, this will hardly have any influence. The graph also contains the Jufin & Lopatin (1966) LDV curve, which is a one equation curve. This equation is chosen because of the range of pipe diameters, from about 1 inch to 90 cm, investigated. Of course a one equation model can never result in a complex curve based on different criteria as is shown here. However for practical purposes it also gives a good and safe result.

Figure 7.8-9 shows the same LDV curve, but now with experimental data and as the Durand & Condolios LDV Froude number F_L. Each column of data points represents a series of experiments with different volumetric concentrations. The lowest points a concentration of 1-5%, the highest point a concentration of 15-25%.
Most of the data points above the curve are from pipe diameters smaller than 6 inch (0.1524 m). From these experiments it is concluded that the F_L value increases slightly with decreasing pipe diameter. The highest points are from the smallest pipe diameters. The Fuhrboter (1961) experiments were carried out in a 30 cm diameter pipe and it is clear that these points are lower.
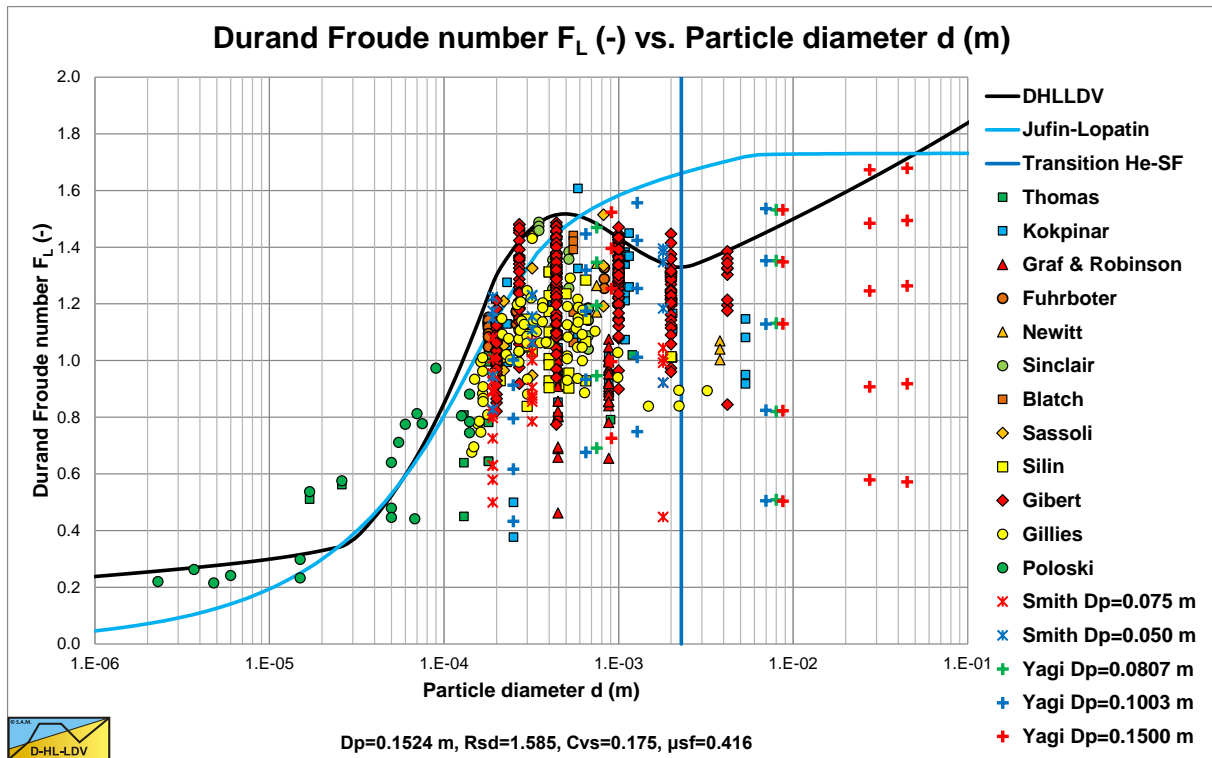
Figure 7.8-9: The resulting LDV curve versus experimental data.
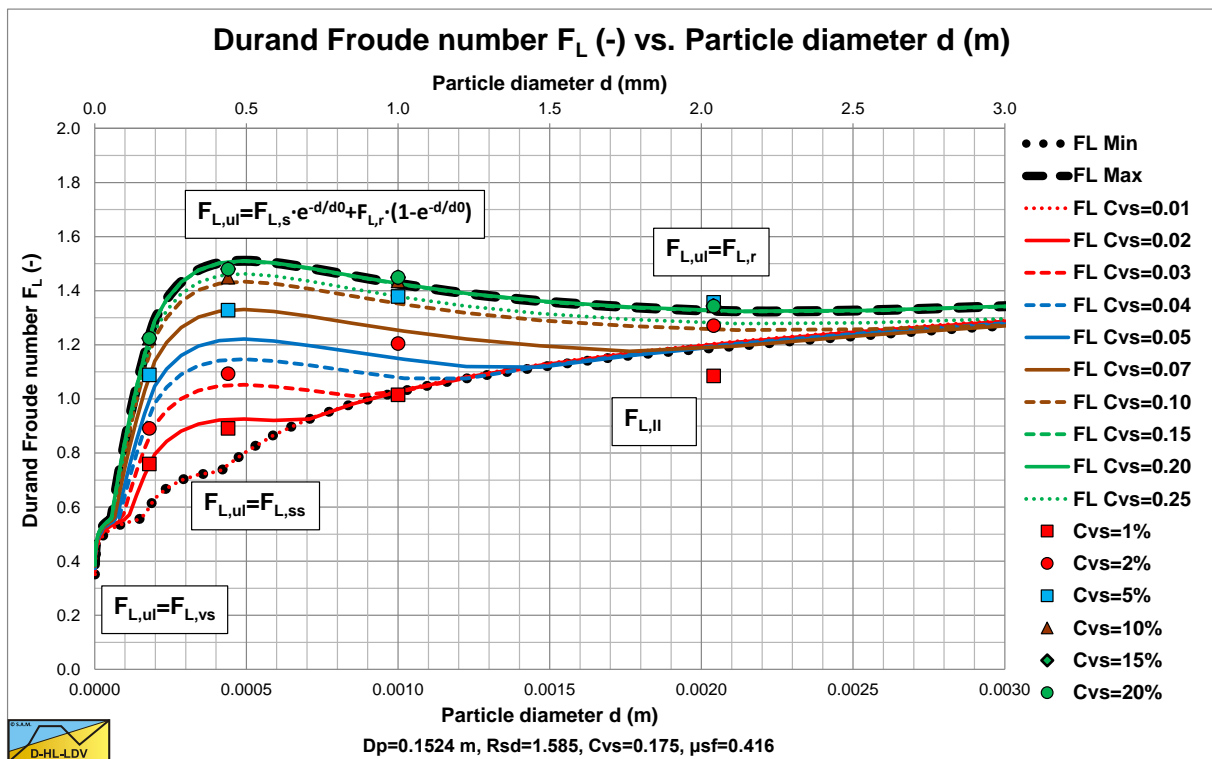
Figure 7.8-10: The resulting LDV curve for different concentrations on a linear axis.

Figure 7.8-10 shows the resulting LDV curves for volumetric concentrations from 1% to 25% on a linear horizontal axis. The horizontal axis is limited to particles of 2.5 mm in order to compare this graph with the famous Durand & Condolios (1952) graph. Although the Durand & Condolios graph as copied by many authors contains an error on the vertical axis by a factor 1.285, giving an asymptotic value of 1.34 for large particles (which should have been 1.05), the resemblance with their graph is remarkable. Based on the experiments published by Gibert (1960) and others, the wrong Durand & Condolios graph seems to be the right graph. It is remarkable however that 1.285^2 equals 1.65, the relative submerged density of the quarts. It seems that in the original Durand & Condolios (1952)

graph the relative submerged density was already taken into account, although not mentioned in their equation. A simple example may show this. The LDV's measured were between 2.95 and 3.2 m/s in a 0.1524 m pipe. This gives an F_L value between 1.35 and 1.47 matching their latest graph very well.
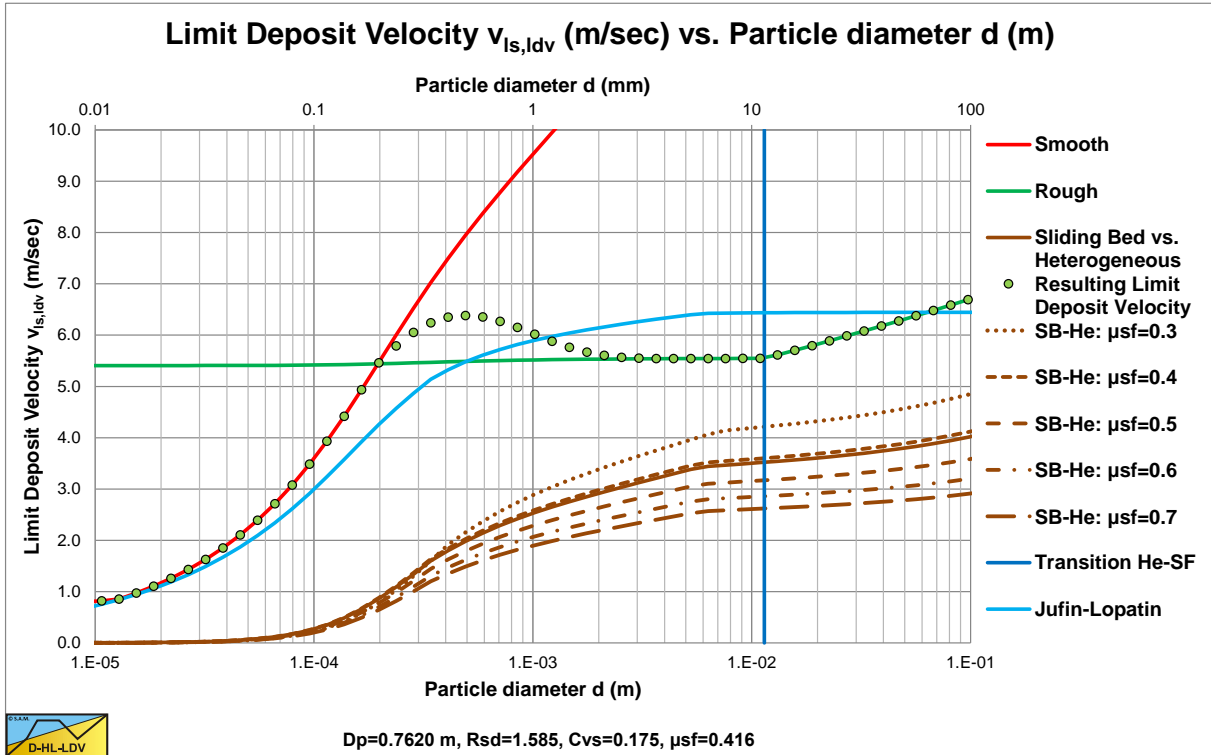
Figure 7.8-11: The construction of the LDV curve for large diameter pipes.
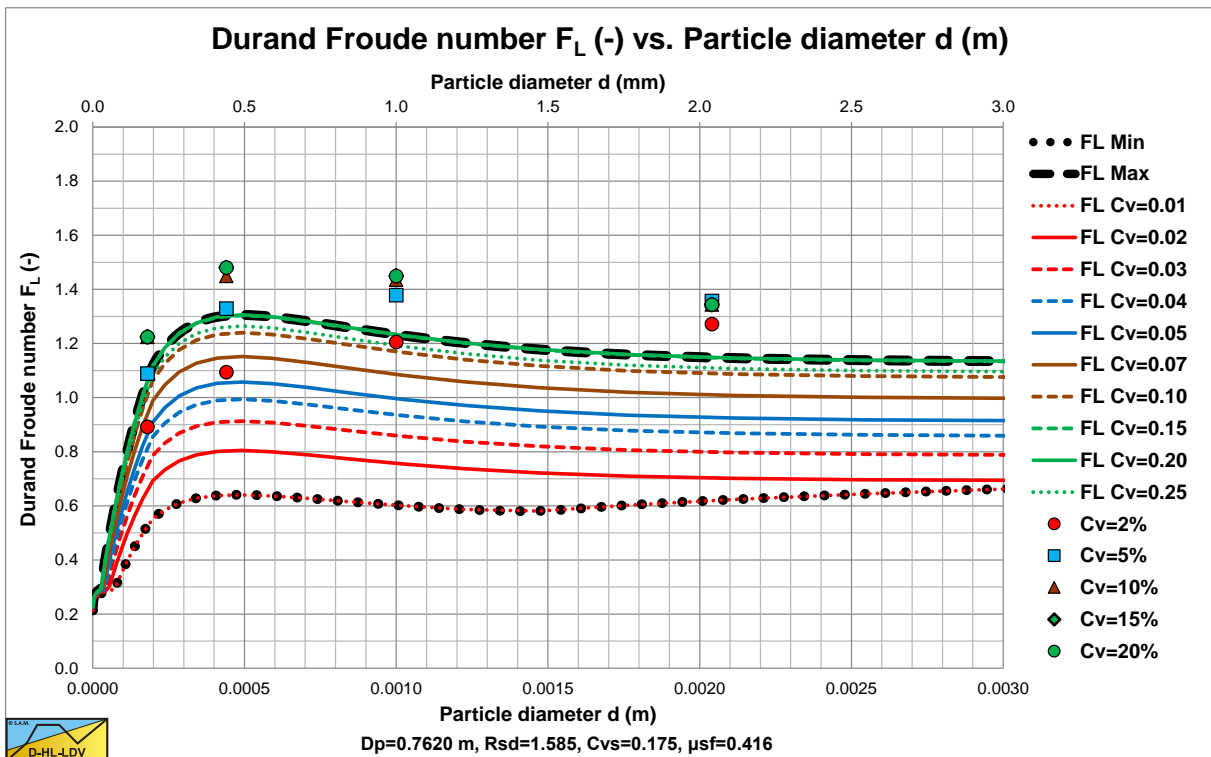
Figure 7.8-12: The resulting LDV curve for different concentrations on a linear axis.
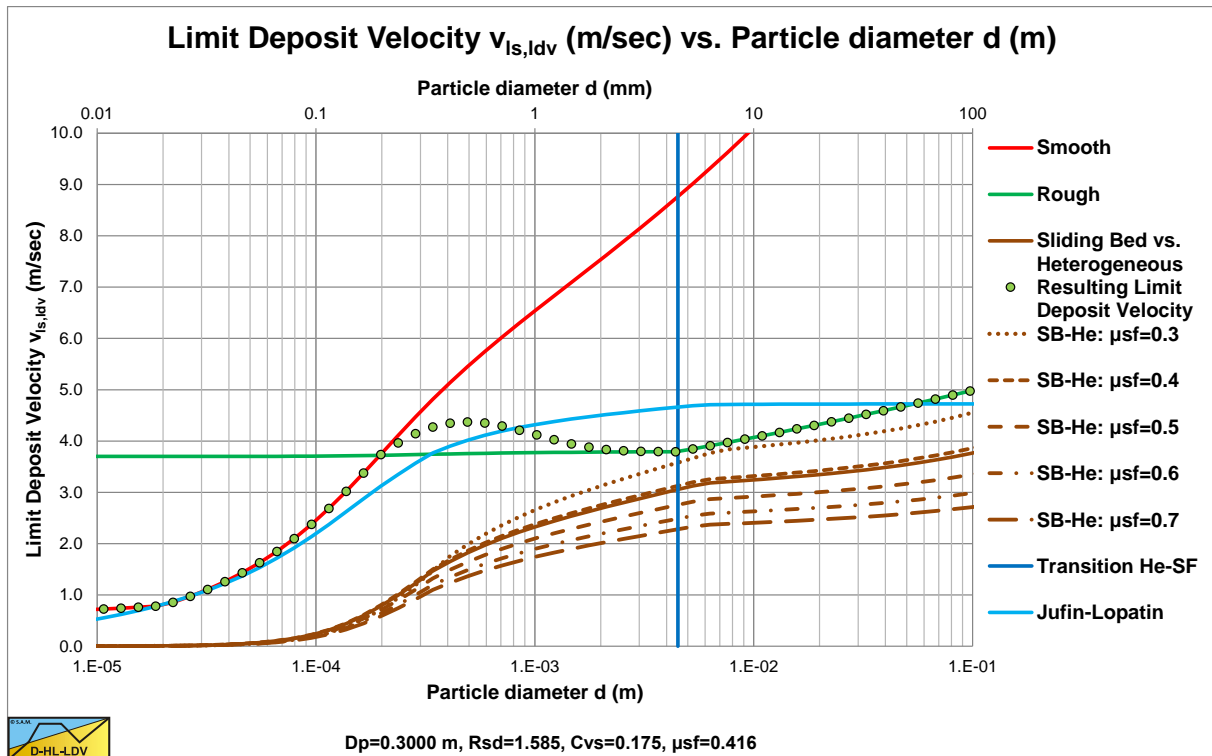
Figure 7.8-13: The construction of the LDV curve for a 30 cm diameter pipe.
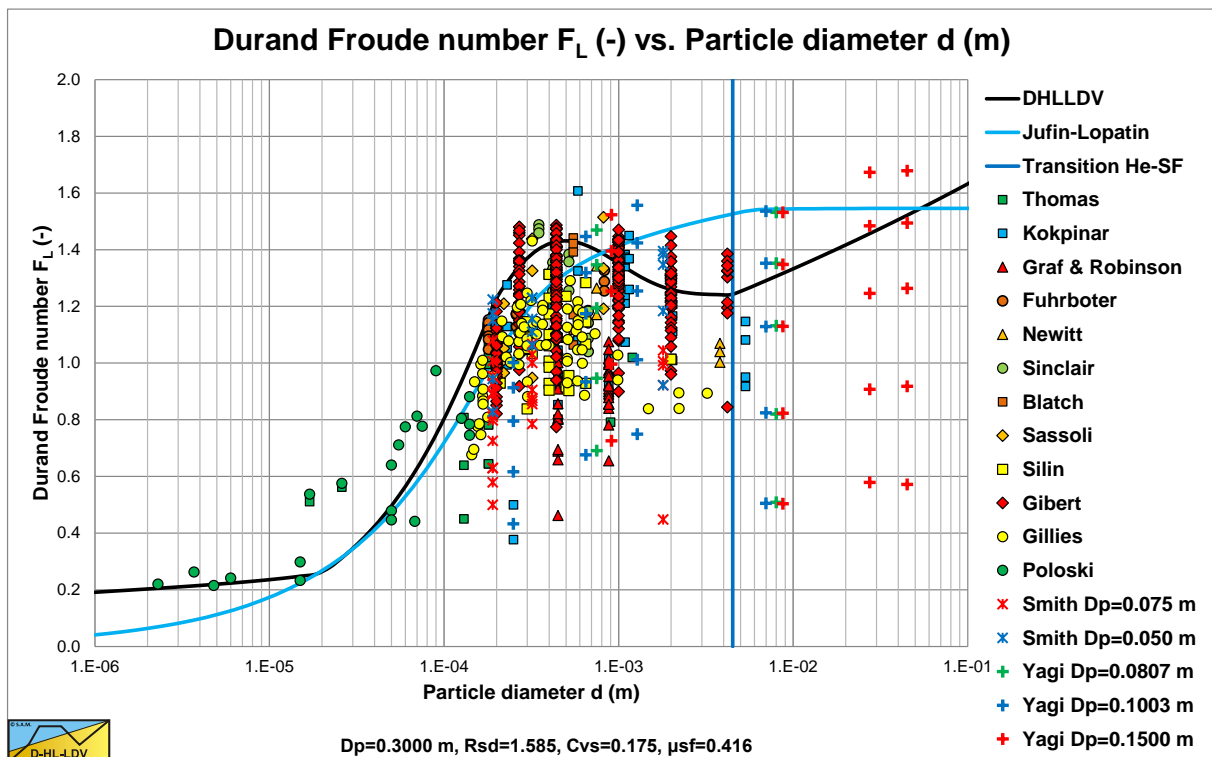
Figure 7.8-14: The 30 cm pipe diameter LDV curve versus experimental data.

Figure 7.8-11 shows the construction of the LDV curve for large diameter pipes. For a volumetric concentration of about 20%, the transition velocity between the sliding bed and the heterogeneous regime does not play a role anymore. However at small concentrations it still does as is shown in Figure 7.8-12. The Jufin & Lopatin equation still matches well, although it underestimates the LDV for medium sands compared with the model developed here. It should be noted that the intersection point between a smooth and a rough bed is at a particle diameter of about 0.14 mm for all pipe diameters with sands and gravels. Figure 7.8-12 also shows that for large diameter

pipes, the curves do not converge for larger particles, but each volumetric concentration has an LDV curve, unless the transition velocity between the sliding bed and the heterogeneous regime takes over.

Figure 7.8-13 and Figure 7.8-14 show the LDV curve for a 30 cm pipe and 20% volumetric concentration. The data points of Fuhrboter (1961) match the LDV curve closely.

It should be mentioned that not all researchers use the same methodology to determine the LDV. Yagi et al. (1972) determined the minimum hydraulic gradient velocity instead of the LDV. For high concentrations these are almost equal, but for low concentrations the minimum hydraulic gradient velocity is much smaller than the LDV, explaining the location of the data points at low concentrations.
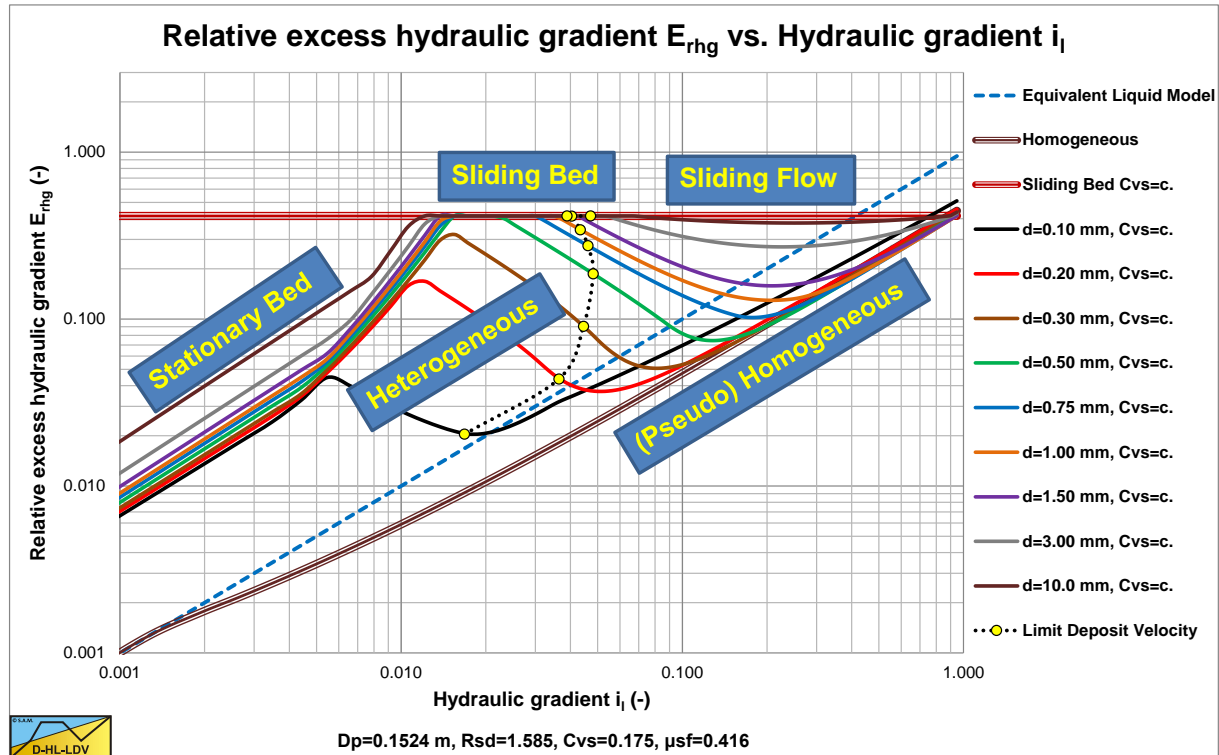
Figure 7.8-15: The path of the LDV curve in a E_{rhg} graph for a 6 inch (0.1524 m) pipe.

Figure 7.8-15 shows the path of the LDV curve in a E_{rhg} graph. The points are calculated for particle diameters of 0.1, 0.2, 0.3, 0.5, 0.75, 1, 1.5, 3 and 10 mm. It is shown that for very small particles the LDV follows the homogeneous curve closely. From 0.2 to 3 mm the curve transits from the homogeneous curve to the sliding bed curve. Above 3mm the LDV will follow the sliding bed curve. For smaller pipe diameters (Figure 7.8-16) the LDV curve moves to the right, meaning that the distance between the homogeneous curve and the sliding bed curve decreases. Particles smaller than 3 mm will already reach the sliding bed curve. For larger pipe diameters (Figure 7.8-17) the LDV curve moves to the left, meaning that the distance between the homogeneous curve and the sliding bed curve increases. Particles smaller than 3 mm will not even reach the sliding bed curve.

Figure 7.8-18 shows the LDV as a function of the pipe diameter for 5 different particle sizes. In the graph also the average powers of the LDV curves with respect to the pipe diameters are shown. Equations (7.8-37) and (7.8-51) give a power of 1/3 based on the presence of the pipe diameter in the equations. However, the equations also contain the Darcy-Weisbach friction factor in the denominator, increasing the powers slightly to a value around 0.4. For small diameter pipes, the limiting transition velocity between the sliding bed and the heterogeneous regime results in a flat part. For particles with **d>0.015·D$_p$,** the adjustment of the LDV according to equation (7.8-52) will reduce the power.

Based on this analysis, it is impossible to model the LDV with a one term equation. There are 5 different regions of the LDV and a limiting transition velocity. Very small particles, a smooth bed, a rough bed, a transition region and the criterion **d>0.015·D$_p$** together with the limiting transition velocity between the sliding bed and the heterogeneous regime. Curve fit techniques on experimental data will always give a result, but this will be a different result based on the particle and pipe diameters used in the experiments.
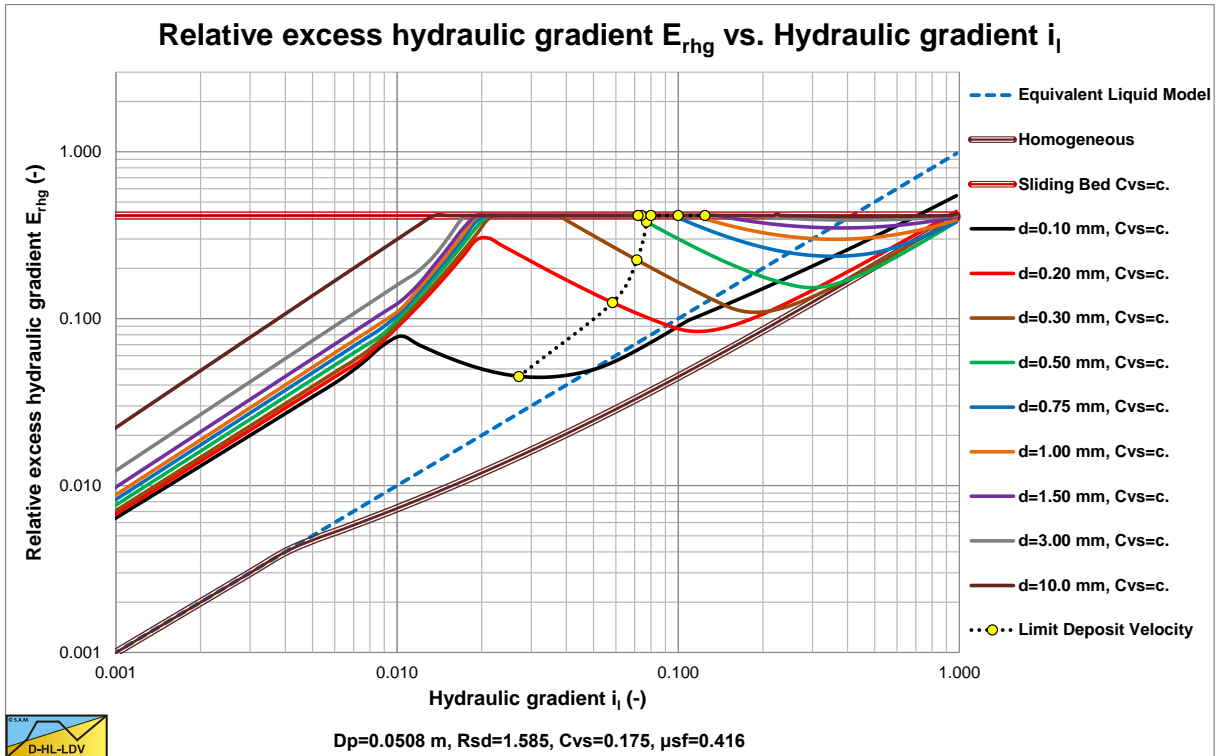
Figure 7.8-16: The path of the LDV curve in a E_{rhg} graph for a 2 inch (0.0508 m) pipe.
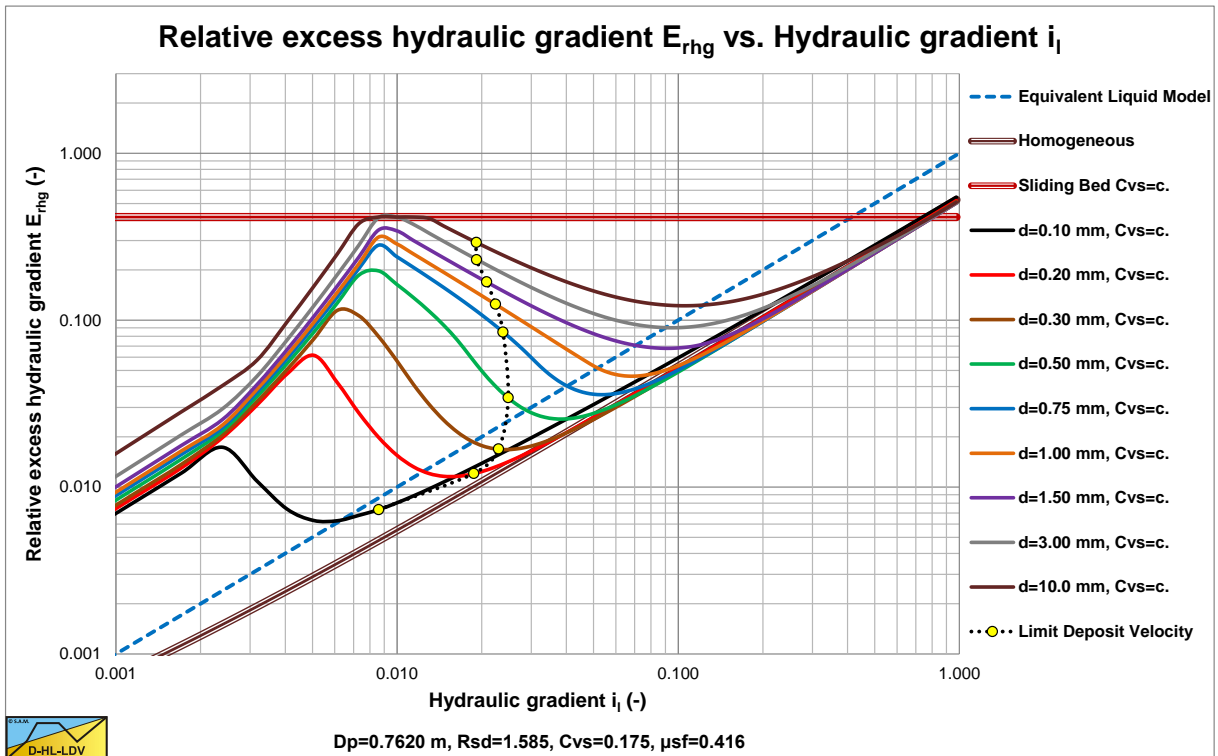
Figure 7.8-17: The path of the LDV curve in a E_{rhg} graph for a 30 inch (0.762 m) pipe.
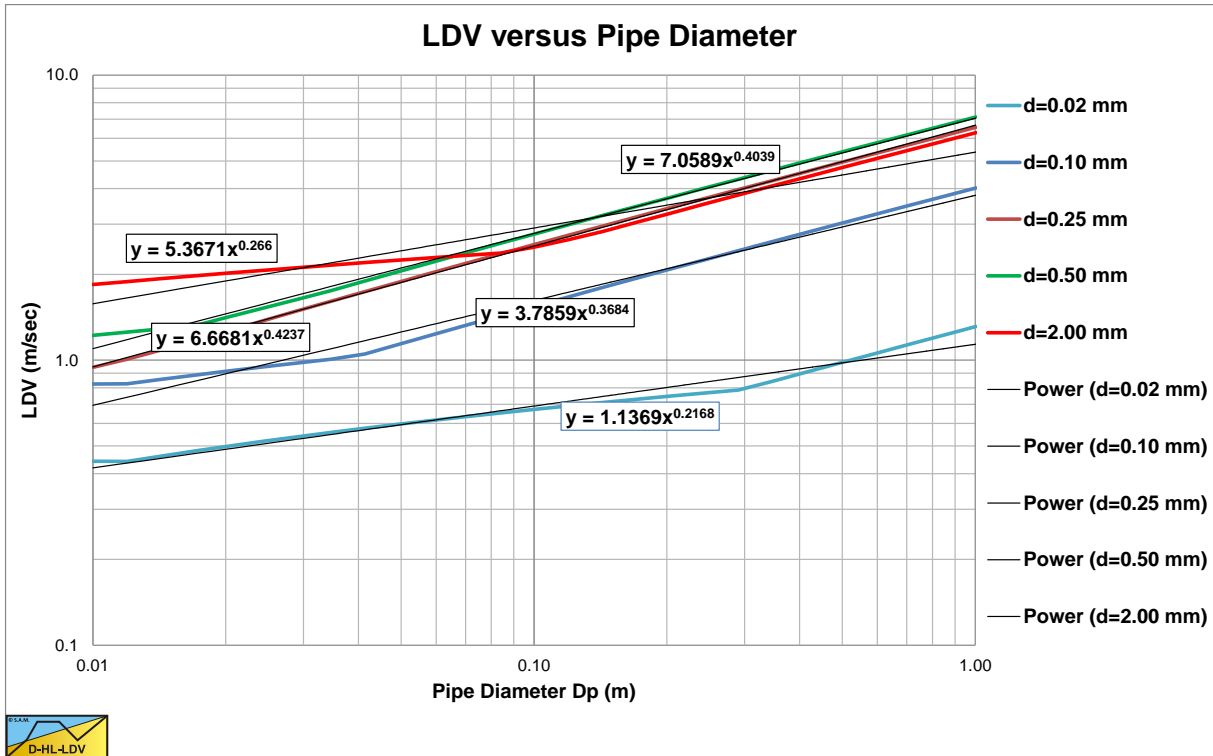
Figure 7.8-18: The LDV as a function of the pipe diameter for 5 particle sizes.
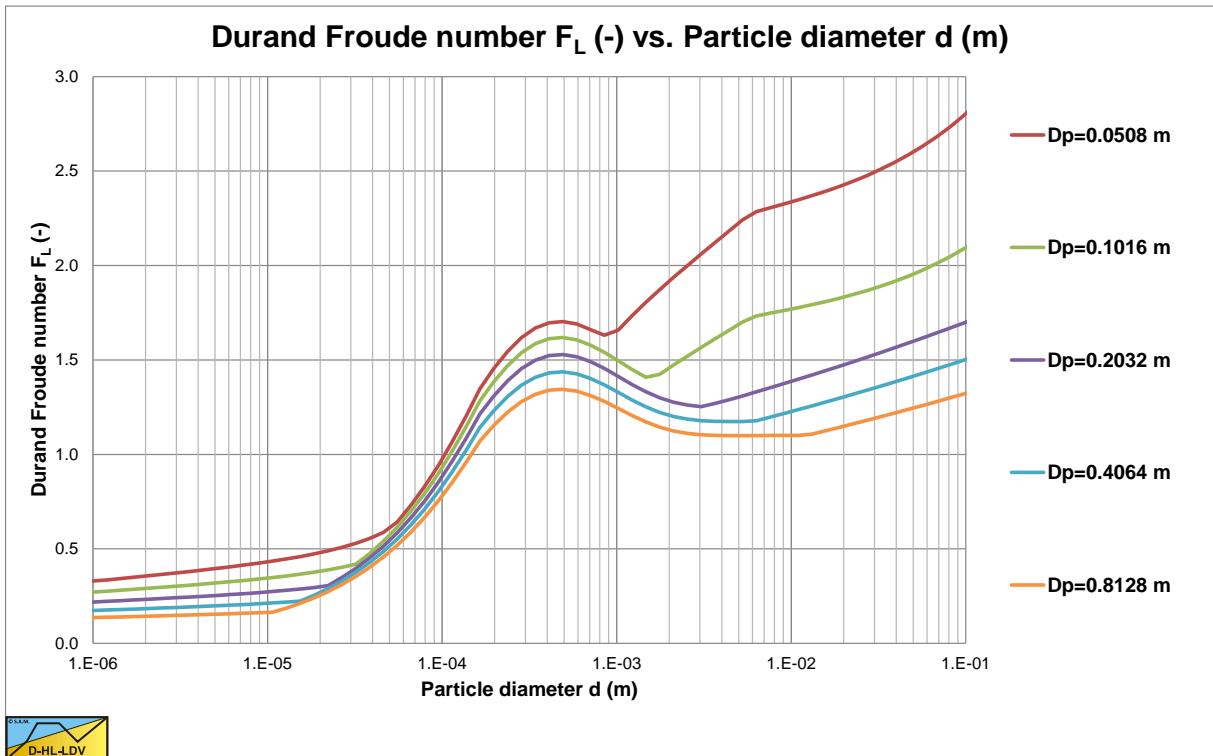
Figure 7.8-19: The LDV as a function of the particle diameter for 5 pipe diameters.

7.8.12 Conclusions & Discussion.

There are many definitions and names for the critical velocity. Here the critical velocity is defined as the Limit Deposit Velocity, the line speed above which there is no stationary bed or sliding bed. Below the LDV there may be either a stationary or fixed bed or a sliding bed, depending on the particle diameter and the pipe diameter and of course the liquid properties.

The DHLLDV Framework divides particles in 5 regions and a lower limit. These regions are for sand and gravel; very small particles up to about δ_v, small particles up to 0.2 mm, a transition region from 0.2 mm to 2 mm, particles larger than 2 mm and particles larger than 0.015 times the pipe diameter. The lower limit is the transition between a sliding bed and heterogeneous transport.

Each region is modelled separately, resulting in dynamic transition particle diameters, depending on the parameters involved. The modelling is independent of head loss models. The modelling is calibrated mainly with sand and gravel experimental data, although limited data is used for other relative submerged densities. The equations found give an upper limit to the LDV and are thus conservative, but safe.

Although the model seems completed, there are still a number of issues that required further investigation. For region 1, very fine particles, the liquid viscosity and density may need adjustment, however it is the question whether this is necessary in the viscous sub-layer. For region 5, very large particles, it is the question whether an LDV exists. At concentrations above a certain threshold (related to sheet flow) the bed concentration may decrease continuously. Still some characteristic LDV value is required to determine the slip velocity in the DHLLDV Framework. For all regions the relative submerged density has not yet been investigated thoroughly, although it is part of the model. For the limited data investigated the model gives good results, but more experimental data could adjust the implementation of the relative submerged density. For dredging purposes however the model is suitable.

In Figure 7.8-7 the flow regime transitions are determined based on the equations of each flow regime. This results in sharp flow regime transitions. In reality these transitions may be smooth. This is the reason why the LDV curve does not coincide exactly with the flow regime transitions.

7.8.13 Nomenclature Limit Deposit Velocity.

A_p	Cross section pipe	m^2
A_H	Cross section of the restricted area above the bed (also named A_1)	m^2
C_{vb}	Bed volumetric concentration	-
C_{vs}	Spatial volumetric concentration	-
$C_{vs,ldv}$	Concentration of bed at LDV	-
$C_{vr,ldv}$	Bed fraction at LDV	-
C_{vt}	Transport or delivered volumetric concentration	-
C_x	Durand & Condolios coefficient	-
d	Particle diameter	m
d_0	Transition particle diameter	m
D_p	Pipe diameter	m
D_H	Hydraulic diameter cross section above the bed	m
E_{rhg}	Relative excess hydraulic gradient	-
F_L	Durand Limit Deposit Velocity Froude number	-
$F_{L,s}$	Durand Limit Deposit Velocity Froude number smooth bed	-
$F_{L,r}$	Durand Limit Deposit Velocity Froude number rough bed	-
F_{sf}	Sliding friction force	kN
F_W	Weight of bed at LDV	kN
g	Gravitational constant (9.81)	m/s^2
h	Thickness of bed layer at LDV	m
i_l	Hydraulic gradient of liquid	-
i_m	Hydraulic gradient of mixture	-
$i_{m,sb}$	Hydraulic gradient sliding bed	-
i_{sf}	Hydraulic gradient solids effect sliding bed	-
$i_{m,fb}$	Hydraulic gradient fixed bed	-
$i_{m,ho}$	Hydraulic gradient homogeneous transport	-
i_s	Hydraulic gradient solids in homogeneous transport	-
k_s	Bed roughness	m
k_s^+	Dimensionless bed roughness	-
ΔL	Length of pipeline	m
n	Porosity of bed	-
R_{sd}	Relative submerged density	-
Re_*	Roughness Reynolds number	-
u	Velocity above the bed	m/s
u_*	Friction velocity	m/s
v_{ls}	Cross-section averaged line speed	m/s
$v_{ls,ldv}$	Line speed at Limit Deposit Velocity	m/s
$v_{ls,r}$	Line speed through restricted area above the bed	m/s
$v_{ls,sb-ho}$	Line speed at intersection sliding bed and homogeneous regimes	m/s
v_t	Particle terminal settling velocity	m/s
y	Distance above the bed	m
$y+$	Dimensionless distance above the bed	-
y_0	Constant in logarithmic velocity profile	m
α_p	Energy fraction coefficient	-
β	Richardson & Zaki hindered settling power	-
δ_v	Thickness of viscous sub layer	m
λ_l	Darcy-Weisbach friction factor between liquid and pipe wall	-
λ_r	Resulting Darcy Weisbach friction factor in restricted area above the bed	-
κ	Von Karman constant (about 0.4)	-
κ_C	Concentration eccentricity constant	-
ρ_l	Density of liquid	ton/m^3
ν_l	Kinematic viscosity liquid	m^2/s
μ_{sf}	Sliding friction coefficient	-
τ_{12}	Bed shear stress	kPa
θ	Shields number	-

7.9 The Slip Velocity.

7.9.1 Introduction.

Miedema &Ramsdell (2013) derived a new model for determining the head losses in heterogeneous slurry transport based on energy considerations. The head losses consist of the viscous losses, potential energy losses and kinetic energy losses. The total pressure required to push the slurry mixture through the pipeline is:

$$
\Delta p_m = \Delta p_l + \Delta p_{s,pot} + \Delta p_{s,kin} = \Delta p_l \cdot \left(1 + \frac{\Delta p_{s,\,pot}}{\Delta p_l} + \frac{\Delta p_{s,\,kin}}{\Delta p_l} \right)
\tag{7.9-1}
$$

This can also be written in terms of the hydraulic gradients according to:

$$
i_m = i_l + i_{s,\,pot} + i_{s,\,kin} = i_l \cdot \left(1 + \frac{i_{s,\,pot}}{i_l} + \frac{i_{s,\,kin}}{i_l} \right)
\tag{7.9-2}
$$

The potential energy contribution to the excess head losses due to the solids effect can be written as:

$$
\Delta p_{s,pot} = \rho_l \cdot \left(\frac{v_t \cdot \left(1 - \dfrac{C_{vs}}{\kappa_C} \right)^\beta}{v_{ls}} \right) \cdot g \cdot R_{sd} \cdot C_{vs} \cdot \Delta L \quad \text{or} \quad i_{s,pot} = \frac{\Delta p_{s,pot}}{\rho_l \cdot g \cdot \Delta L} = \left(\frac{v_t \cdot \left(1 - \dfrac{C_{vs}}{\kappa_C} \right)^\beta}{v_{ls}} \right) \cdot R_{sd} \cdot C_{vs}
\tag{7.9-3}
$$

The kinetic energy contribution to the excess head losses due to the solids effect can be written as:

$$
\Delta p_{s,kin} = \rho_l \cdot \left(\frac{v_{sl}}{v_t} \right)^2 \cdot g \cdot R_{sd} \cdot C_{vs} \cdot \Delta L \quad \text{or} \quad i_{s,kin} = \frac{\Delta p_{s,kin}}{\rho_l \cdot g \cdot \Delta L} = \left(\frac{v_{sl}}{v_t} \right)^2 \cdot R_{sd} \cdot C_{vs}
\tag{7.9-4}
$$

Giving for the total hydraulic gradient for head losses of a mixture in slurry transport:

$$
i_m = i_l \cdot \left(1 + \frac{\left(2 \cdot g \cdot R_{sd} \cdot D_p \right)}{\lambda_l} \cdot C_{vs} \cdot \frac{1}{v_{ls}^2} \cdot \left(v_t \cdot \left(1 - \frac{C_{vs}}{\kappa_C} \right)^\beta \cdot \frac{1}{v_{ls}} + \left(\frac{v_{sl}}{v_t} \right)^2 \right) \right)
\tag{7.9-5}
$$

For determining the viscous losses, the well-known Darcy Weisbach equation will be used:

$$
\Delta p_l = \lambda_l \left(Re_{fl} \right) \cdot \frac{\Delta L}{D_p} \cdot \frac{1}{2} \cdot \rho_l \cdot v_{ls}^2 \quad \text{or} \quad i_l = \frac{\Delta p_l}{\rho_l \cdot g \cdot \Delta L} = \frac{\lambda_l \left(Re_{fl} \right) \cdot v_{ls}^2}{2 \cdot g \cdot D_p}
\tag{7.9-6}
$$

The potential energy contribution, as already derived by Newitt et al. (1955), to the excess head losses depends on the terminal settling velocity v_t and on the hindered settling power β as determined by Richardson and Zaki (1954).

An equation for the transitional region (in m and m/sec) for v_t has been derived by Ruby & Zanke (1977):

$$
v_t = \frac{10 \cdot \nu_l}{d} \cdot \left(\sqrt{1 + \frac{R_{sd} \cdot g \cdot d^3}{100 \cdot \nu_l^2}} - 1 \right)
\tag{7.9-7}
$$

This equation also gives good results for very fine and very large particles and has been used everywhere in this book developing the head loss model. According to Rowe (1987) the power β can be approximated by:

$$\beta = \frac{4.7 + 0.41 \cdot \mathbf{Re}_p^{0.75}}{1 + 0.175 \cdot \mathbf{Re}_p^{0.75}} \tag{7.9-8}$$

The kinetic energy contribution to the excess head losses depends on the ratio of the so called slip velocity $\mathbf{v_{sl}}$ to the line speed $\mathbf{v_{ls}}$. For a derivation of equation (7.9-4), see Miedema &Ramsdell (2013). The slip velocity $\mathbf{v_{sl}}$ is defined as the difference between the average liquid velocity $\mathbf{v_l}$ and the average particle velocity $\mathbf{v_p}$ resulting in a drag force.

$$\mathbf{v_{sl}} = \mathbf{v_l} - \mathbf{v_p} \tag{7.9-9}$$

This slip velocity $\mathbf{v_{sl}}$ however is unknown and not much has been published about this. This slip velocity however is very important for dredging practice and slurry transport in general because it determines the ratio of the so called volumetric transport (delivered) concentration $\mathbf{C_{vt}}$ to the volumetric spatial concentration $\mathbf{C_{vs}}$. The spatial volumetric concentration $\mathbf{C_{vs}}$ is defined as the volume of solids divided by the volume of the mixture containing these solids. So the spatial volumetric concentration is based on a volume ratio, while the delivered volumetric concentration is based on a volume rate ratio. One of the few publications regarding the slip velocity is Yagi et al. (1972) who measured both concentrations in order to determine the slip velocity to line speed ratio.

7.9.2 Slip Ratio in the Heterogeneous Regime.

Based on the analysis, the following coefficients (powers) are determined, not by mathematical regression, but by visual observation of graphs (Miedema (2014W)) of the experimental data. The reason for this is that very often the data points are in a transition region between two regimes and do not exactly follow the formulation of one of the regimes. Mathematical regression would lead to the wrong conclusions. Based on the new dimensionless parameters the following is found (the two formulations are based on the line speed **ls** or the friction velocity **fv**):

$$\mathbf{v_{sl}} = \frac{8.5}{\sqrt{\lambda_l}} \cdot \mathbf{Ct} \cdot \mathbf{Th_{ls}} \cdot \mathbf{v_t} = \frac{8.5}{\sqrt{8}} \cdot \mathbf{Ct} \cdot \mathbf{Th_{fv}} \cdot \mathbf{v_t}$$

$$\tag{7.9-10}$$

$$\left(\frac{\mathbf{v_{sl}}}{\mathbf{v_t}}\right)^2 = \frac{8.5^2}{\lambda_l} \cdot \mathbf{Ct}^2 \cdot \mathbf{Th_{ls}^2} = \frac{8.5^2}{8} \cdot \mathbf{Ct}^2 \cdot \mathbf{Th_{fv}^2}$$

Substituting equation (7.9-10) in equation (7.9-5) gives for the hydraulic gradient:

$$\mathbf{i_m} = \mathbf{i_l} \cdot \left(1 + \frac{\left(2 \cdot \mathbf{g} \cdot \mathbf{R_{sd}} \cdot \mathbf{D_p}\right)}{\lambda_l} \cdot \mathbf{C_{vs}} \cdot \frac{1}{\mathbf{v_{ls}^2}} \cdot \left(\mathbf{La} + \frac{8.5^2}{8} \cdot \mathbf{Ct}^2 \cdot \mathbf{Th_{fv}^2}\right)\right)$$

or $\qquad\qquad\qquad\qquad\qquad\qquad\qquad\qquad\qquad\qquad$ (7.9-11)

$$\mathbf{i_m} = \mathbf{i_l} + \left(\mathbf{La} + \frac{8.5^2}{8} \cdot \mathbf{Ct}^2 \cdot \mathbf{Th_{fv}^2}\right) \cdot \mathbf{R_{sd}} \cdot \mathbf{C_{vs}}$$

The contribution of the kinetic energy losses to the excess head losses is completely determined by the two dimensionless numbers, **Cát** and **Thủy** (collision impact and collision intensity). The contribution of the potential energy losses to the excess head losses is completely determined by the ratio of the hindered terminal settling velocity to the line speed (the capability to form sediment), the dimensionless number **Lắng** (sedimentation capability). It is obvious from this analysis that the excess pressure losses should not be described by two Froude numbers, but by the collision impact number **Ct** (which is a Froude number), the collision intensity number **Th** and the sedimentation capability number **La**. It is also obvious that there is not just one term describing the excess head losses, but there are two terms, the first term describing the potential energy losses (the capability to form sediment) and a second term describing the kinetic energy losses (the collision impact influence times the collision intensity influence).

The time averaged slip ratio will be about 50% of the slip velocity as used to determine the kinetic energy losses. The slip velocity or ratio here is the value determined to explain for the kinetic energy losses, so in fact it is a delta slip velocity. So it is the difference between the maximum and minimum slip velocity. The average slip velocity is undetermined. Now this average will not differ to much from the slip velocity found and it is proposed to take this as the slip velocity. In fact as will be shown later, this part of the slip velocity at high line speeds is not to important for converting spatial to delivered concentration. So the slip ratio is about:

$$\xi = \frac{v_{sl}}{v_{ls}} = \frac{8.5}{\sqrt{\lambda_l}} \cdot Ct \cdot Th_{ls} \cdot \frac{v_t}{v_{ls}} = \frac{8.5}{\sqrt{8}} \cdot Ct \cdot Th_{fv} \cdot \frac{v_t}{v_{ls}}$$

(7.9-12)

7.9.3 Comparison with the Yagi et al. (1972) Data Step 1.

In order to validate the theoretical slip velocities, the data of Yagi et al. (1972) are available. Figure 7.9-1 shows the theoretical curves (equation (7.9-12)) for all the pipe diameter/particle diameter combinations Yagi et al. (1972) applied. It is remarkable that the theoretical curves for gravel (**d=7 mm** up to **d=45 mm**) match the data points pretty well, although they are a bit too low. In fact the theoretical lines are straight and miss the curvature required to match the data points better, however the Limit Deposit Velocities match on the horizontal axis but are too low. The theoretical curves for sand (**d=0.25 mm** up to **d=1.28 mm**) are all too low on the vertical axis. It should be mentioned that in the graph the theoretical curves are divided by 2, since the theoretical slip velocity equation determines the maximum slip velocity and not the time averaged slip velocity. Figure 7.9-1 shows that around the Limit Deposit Velocities the slip ratio should increase rapidly with a decreasing line speed, while at very low line speeds, the slip ratio should approach an asymptotic value, since the slip ratio can never be bigger than 1. Whether this asymptotic value is 1 or a value smaller than 1 is a question. If one considers that at a volumetric delivered concentration equal to the bed concentration, the slip ratio will be zero, since the whole bed is moving, an asymptotic slip ratio depending on the volumetric transport concentration is expected.

A second approach has to be considered for line speeds around and below the Limit Deposit Velocity.
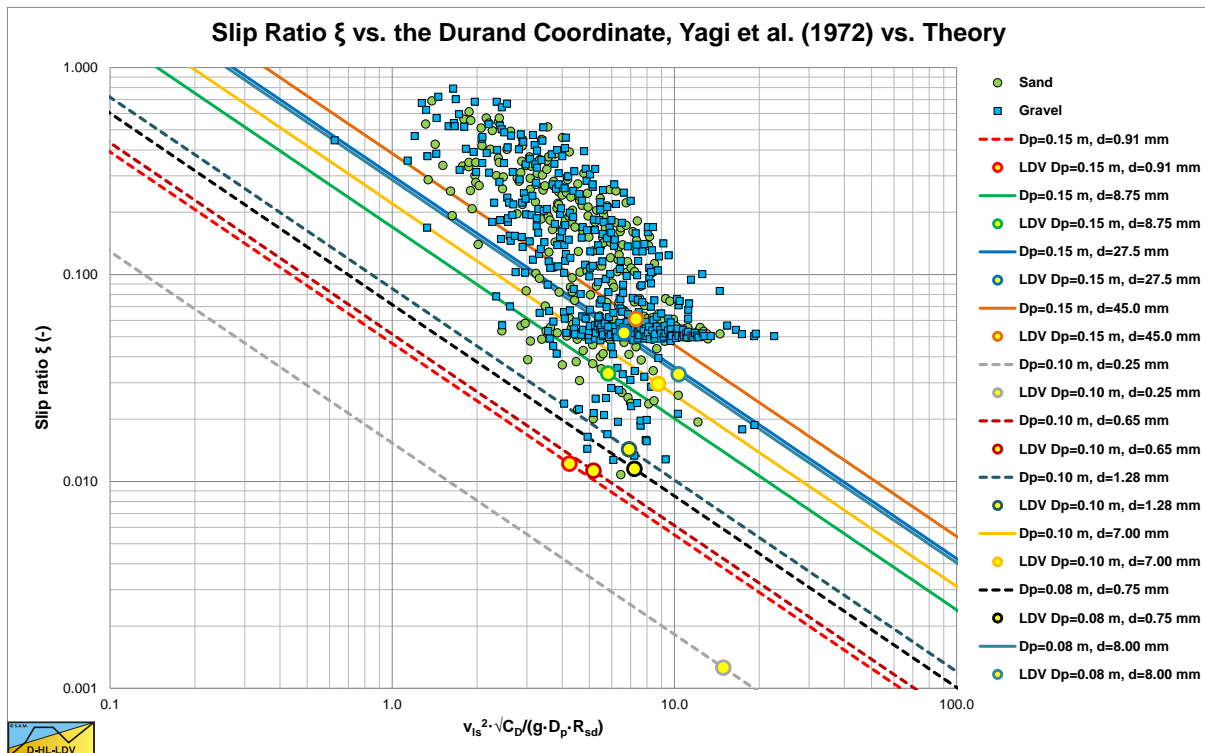
Figure 7.9-1: The data of Yagi et al. (1972) compared with the theoretical slip velocities, step 1.

7.9.4 Derivation of the Slip Ratio at High A_b/A_p Ratios.

When the A_b/A_p ratio is high, the slip ratio ξ might become larger than 1 according to Figure 7.9-1, which is physically impossible, so apparently the above equations are not valid for very low line speeds (around and below the Limit Deposit Velocity). In order to find a better estimate for the slip ratio in this case, the following logic is applied.

A fixed bed is considered, where it is assumed that the velocity above the bed is constant and equal to the line speed at the Limit Deposit Velocity. Further the constant transport concentration case is considered. The volumetric spatial concentration over the full cross section of the pipe can be related to the volumetric transport concentration over the full cross section of the pipe according to:

$$C_{vs} = \frac{A_b \cdot C_{vb} + A_s \cdot C_{vs,s}}{A_p} = \left(\frac{v_{ls}}{v_{ls} - v_{sl}} \right) \cdot C_{vt} \qquad (7.9-13)$$

Suppose the volumetric spatial concentration $C_{vs,s}$ and the volumetric transport concentration $C_{vt,s}$ in the suspension phase are related according to their ratio at the transition velocity between the sliding bed regime or the fixed bed regime and the heterogeneous regime (the Limit Deposit Velocity):

$$C_{vs,s} = \kappa_{ldv} \cdot C_{vt,s} = \left(\frac{v_{ls,ldv}}{v_{ls,ldv} - v_{sl,ldv}} \right) \cdot C_{vt,s} \quad \text{with:} \quad \kappa_{ldv} = \left(\frac{v_{ls,ldv}}{v_{ls,ldv} - v_{sl,ldv}} \right) = \left(\frac{1}{1 - \xi_{ldv}} \right) \qquad (7.9-14)$$

Where κ_{ldv} equals the ratio between the two volumetric concentrations at the line speed $v_{ls,ldv}$ where the sliding or fixed bed regime transits to the heterogeneous regime (LDV). Because there are only particles being transported in the suspension phase, the transport of particles over the full cross section has to be equal to the transport of particles in the suspension phase, thus:

$$A_p \cdot C_{vt} \cdot v_{ls} = A_s \cdot C_{vt,s} \cdot v_s$$
$$\text{With:} \quad A_p \cdot v_{ls} = A_s \cdot v_s \quad \Rightarrow \quad C_{vt} = C_{vt,s} \qquad (7.9-15)$$

This implies that the volumetric transport concentration over the full cross section of the pipe equals the volumetric transport concentration in the suspension phase. The volumetric spatial concentration in the suspension phase is assumed to be constant when there is a fixed bed/sliding bed below the LDV and can be written as:

$$C_{vs,s} = \kappa_{ldv} \cdot C_{vt} \qquad (7.9-16)$$

The volumetric spatial concentration over the full cross section of the pipe can now be written as:

$$C_{vs} = \frac{A_b \cdot C_{vb} + A_s \cdot C_{vs,s}}{A_p} = \frac{A_b \cdot C_{vb} + A_s \cdot \kappa_{ldv} \cdot C_{vt}}{A_p} = \left(\frac{v_{ls}}{v_{ls} - v_{sl}} \right) \cdot C_{vt} \qquad (7.9-17)$$

The line speed and slip velocity in this equation are both related to the full cross section of the pipe. The cross section of the suspension phase equals the full cross section of the pipe minus the cross section of the fixed bed/sliding bed.

$$A_p \cdot C_{vs} = A_b \cdot C_{vb} + \left(A_p - A_b \right) \cdot \kappa_{ldv} \cdot C_{vt} = A_p \cdot \left(\frac{v_{ls}}{v_{ls} - v_{sl}} \right) \cdot C_{vt} \qquad (7.9-18)$$

Separating the terms with the bed cross section and the pipe cross section gives:

$$A_b \cdot \left(C_{vb} - \kappa_{ldv} \cdot C_{vt} \right) + A_p \cdot \kappa_{ldv} \cdot C_{vt} = A_p \cdot \left(\frac{v_{ls}}{v_{ls} - v_{sl}} \right) \cdot C_{vt} \qquad (7.9-19)$$

Or:

$$A_b \cdot \left(C_{vb} - \kappa_{ldv} \cdot C_{vt}\right) \cdot \left(v_{ls} - v_{sl}\right) + A_p \cdot \kappa_{ldv} \cdot C_{vt} \cdot \left(v_{ls} - v_{sl}\right) = A_p \cdot C_{vt} \cdot v_{ls} \tag{7.9-20}$$

To find the slip ratio ξ, all the terms with the slip velocity have to be separated from the terms with the line speed according to:

$$A_b \cdot \left(C_{vb} - \kappa_{ldv} \cdot C_{vt}\right) \cdot v_{ls} - A_b \cdot \left(C_{vb} - \kappa_{ldv} \cdot C_{vt}\right) \cdot v_{sl} + A_p \cdot \kappa_{ldv} \cdot C_{vt} \cdot v_{ls} - A_p \cdot \kappa_{ldv} \cdot C_{vt} \cdot v_{sl}$$
$$= A_p \cdot C_{vt} \cdot v_{ls}$$

$$\left(A_b \cdot \left(C_{vb} - \kappa_{ldv} \cdot C_{vt}\right) + A_p \cdot \kappa_{ldv} \cdot C_{vt}\right) \cdot v_{ls} - \left(A_b \cdot \left(C_{vb} - \kappa_{ldv} \cdot C_{vt}\right) + A_p \cdot \kappa_{ldv} \cdot C_{vt}\right) \cdot v_{sl} = A_p \cdot C_{vt} \cdot v_{ls} \tag{7.9-21}$$

Giving:

$$\xi = \frac{v_{sl}}{v_{ls}} = \frac{A_b \cdot \left(C_{vb} - \kappa_{ldv} \cdot C_{vt}\right) + A_p \cdot \kappa_{ldv} \cdot C_{vt} - A_p \cdot C_{vt}}{A_b \cdot \left(C_{vb} - \kappa_{ldv} \cdot C_{vt}\right) + A_p \cdot \kappa_{ldv} \cdot C_{vt}} \tag{7.9-22}$$

$$\textbf{With}: \quad \hat{A}_b = \frac{A_b}{A_p} \quad \Rightarrow \quad \xi = \frac{v_{sl}}{v_{ls}} = \frac{\hat{A}_b \cdot \left(C_{vb} - \kappa_{ldv} \cdot C_{vt}\right) + \left(\kappa_{ldv} - 1\right) \cdot C_{vt}}{\hat{A}_b \cdot \left(C_{vb} - \kappa_{ldv} \cdot C_{vt}\right) + \kappa_{ldv} \cdot C_{vt}}$$

And for the bed fraction:

$$\hat{A}_b = \frac{A_b}{A_p} = \frac{C_{vt} \cdot \left(v_{ls} \cdot \left(1 - \kappa_{ldv}\right) + \kappa_{ldv} \cdot v_{sl}\right)}{\left(C_{vb} - \kappa_{ldv} \cdot C_{vt}\right) \cdot \left(v_{ls} - v_{sl}\right)} \tag{7.9-23}$$

Based on the line speed of transition between the fixed bed regime and the heterogeneous regime and the mixture velocity in the suspension phase, the following is valid:

$$A_p \cdot v_{ls} = A_s \cdot v_{s,ldv} = \left(A_p - A_b\right) \cdot v_{s,ldv} \tag{7.9-24}$$

$$A_b \cdot v_{s,ldv} = A_p \cdot \left(v_{s,ldv} - v_{ls}\right) \quad \Rightarrow \quad \hat{A}_b = \frac{A_b}{A_p} = \frac{v_{s,ldv} - v_{ls}}{v_{s,ldv}}$$

This gives for the slip ratio ξ:

$$\xi = \frac{v_{sl}}{v_{ls}} = \frac{\left(\dfrac{v_{s,ldv} - v_{ls}}{v_{s,ldv}}\right) \cdot \left(C_{vb} - \kappa_{ldv} \cdot C_{vt}\right) + \left(\kappa_{ldv} - 1\right) \cdot C_{vt}}{\left(\dfrac{v_{s,ldv} - v_{ls}}{v_{s,ldv}}\right) \cdot \left(C_{vb} - \kappa_{ldv} \cdot C_{vt}\right) + \kappa_{ldv} \cdot C_{vt}} \tag{7.9-25}$$

Rewriting this equation gives the following equation for the slip ratio ξ assuming a fixed bed below the LDV:

$$\xi = \frac{v_{sl}}{v_{ls}} = 1 - \frac{C_{vt}}{\left(\dfrac{v_{s,ldv} - v_{ls}}{v_{s,ldv}}\right) \cdot \left(C_{vb} - \kappa_{ldv} \cdot C_{vt}\right) + \kappa_{ldv} \cdot C_{vt}} \tag{7.9-26}$$

Because at the LDV the full cross section is suspension this can be written as:

$$\xi = \frac{v_{sl}}{v_{ls}} = 1 - \frac{C_{vt} \cdot v_{ls,ldv}}{\left(C_{vb} - \kappa_{ldv} \cdot C_{vt}\right) \cdot \left(v_{ls,ldv} - v_{ls}\right) + \kappa_{ldv} \cdot C_{vt} \cdot v_{ls,ldv}} \tag{7.9-27}$$

Case 1: The line speed v_{ls} equals the Limit Deposit Velocity $v_{ls,ldv}=v_{s,ldv}$:

$$\xi_{ldv} = \frac{v_{sl}}{v_{ls}} = 1 - \frac{C_{vt} \cdot v_{ls,ldv}}{\left(C_{vb} - \kappa_{ldv} \cdot C_{vt}\right) \cdot \left(v_{ls,ldv} - v_{ls,ldv}\right) + \kappa_{ldv} \cdot C_{vt} \cdot v_{ls,ldv}} = 1 - \frac{1}{\kappa_{ldv}} = \frac{v_{sl,ldv}}{v_{ls,ldv}} \tag{7.9-28}$$

This is correct, since the factor κ_{ldv} was introduced as the ratio between the volumetric spatial concentration to the volumetric transport concentration at the LDV.

Case 2: the line speed v_{ls} equals zero:

$$\xi_0 = \frac{v_{sl}}{v_{ls}} = 1 - \frac{C_{vt} \cdot v_{ls,ldv}}{\left(C_{vb} - \kappa_{ldv} \cdot C_{vt}\right) \cdot \left(v_{ls,ldv} - 0\right) + \kappa_{ldv} \cdot C_{vt} \cdot v_{ls,ldv}} = 1 - \frac{C_{vt}}{C_{vb}} \tag{7.9-29}$$

The slip ratio now depends on the volumetric transport concentration and is equal to 0 if the volumetric transport concentration is equal to the bed concentration, a bed moving with the line speed.

The assumption of having a fixed bed with a constant speed above the fixed bed is questionable. In reality there will be a sliding bed above a certain line speed, resulting in a different slip ratio at constant transport concentration. The equation as derived here can be considered to give an upper limit of the slip ratio.

7.9.5 Comparison with the Yagi et al. (1972) Data Step 2.

Incorporating the upper limit for the slip velocity according equation (7.9-26) for line speeds below the Limit Deposit Velocity gives the result for very low concentrations (C_{vt}=0.05) as shown in Figure 7.9-2 and for the highest concentrations as used by Yagi et al. (1972) (C_{vt}=0.11-0.34) this is shown in Figure 7.9-3. Both figures also show the Limit Deposit Velocities for the different sands and gravels. The abscissa of the Limit Deposit Velocities is determined with the theory in chapter 7.8, the ordinate with equation (7.9-32).
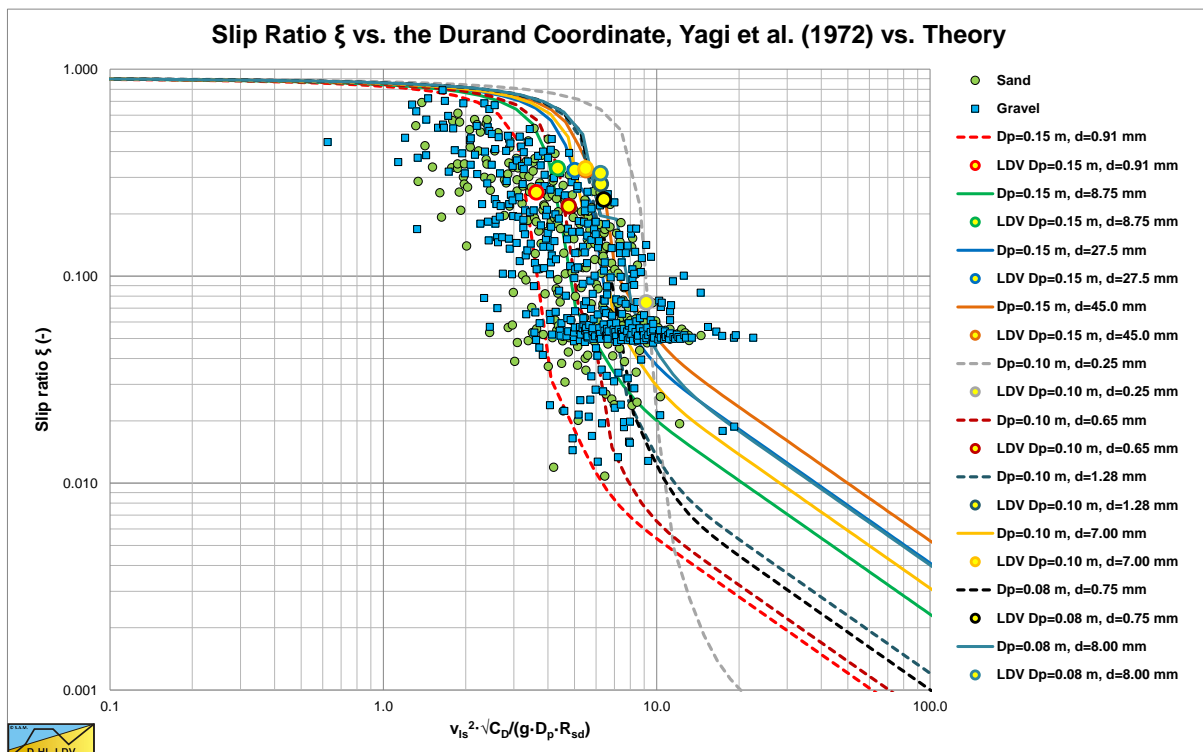
Figure 7.9-2: The data of Yagi et al. (1972) compared with the theoretical slip velocities, step 2, C_{vt}=0.05.

The original data of Yagi et al. (1972) show that the data points of sand and gravel overlap and that for each type of sand and gravel, data points are found on the left, on the right and in the middle of the cloud of points. At a slip ratio of 0.04-0.08 there is a concentration of data points both for sands and gravels. Since Yagi et al. (1972) carried out experiments below and above the Limit Deposit Velocity about 50/50, it is expected that the slip ratio at the Limit Deposit Velocity will be above this concentration of data points. How far above depends on the type of material and on the volumetric concentration of the experiments.
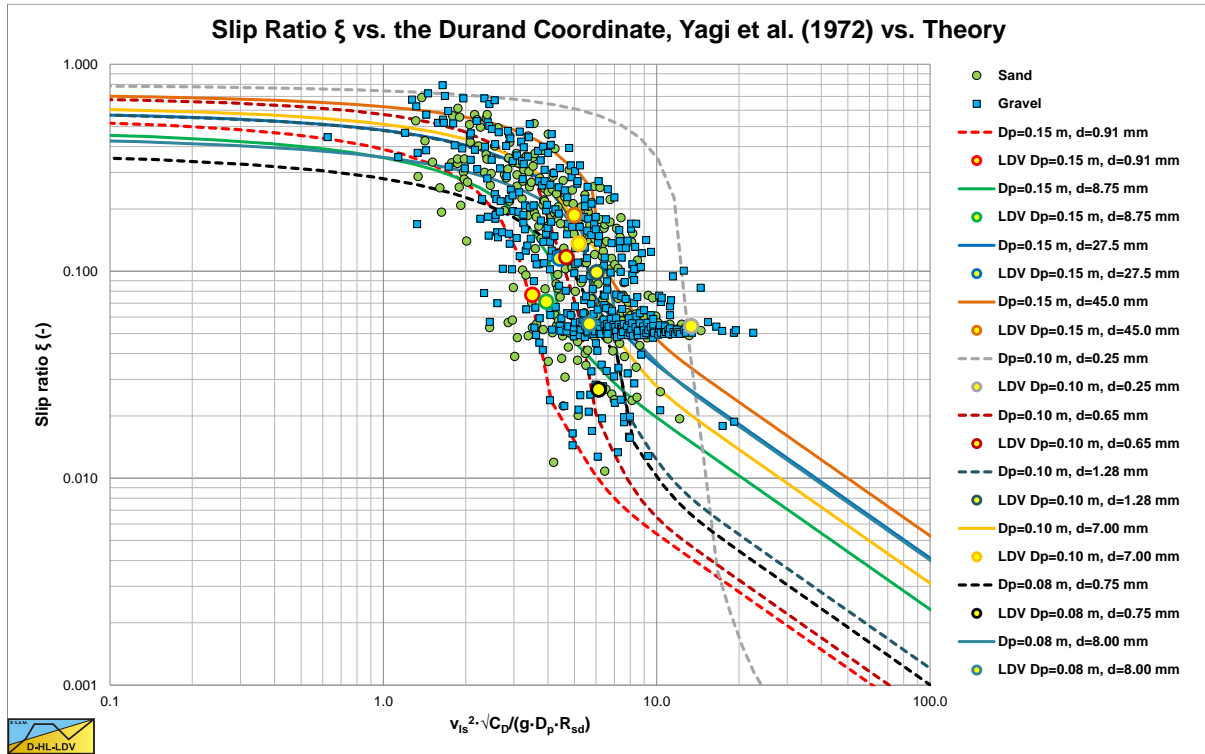
Figure 7.9-3: The data of Yagi et al. (1972) compared with the theoretical slip velocities, step 2, C_{vt}=0.11-0.34.

Figure 7.9-2 and Figure 7.9-3 show a sudden increase of the slip ratio with a decreasing line speed close to the Limit Deposit Velocity. Both graphs also show an asymptotic behavior at very low line speeds, matching the data points. With a minimum volumetric concentration of about 5% (Figure 7.9-2) and a maximum volumetric concentration from 11% to 34% depending on the material (Figure 7.9-3) the curvature of the data points is covered completely. Close to the Limit Deposit Velocity however, the slip ratio is overestimated. This is caused by the fact that equation (7.9-26) is based on a fixed bed and not on a sliding bed. Considering a fixed volumetric delivered concentration, a fixed bed approach will give a much higher slip ratio than a sliding bed approach, since the fact that the bed is sliding always reduces the slip ratio. Apparently there are 3 regions regarding the slip ratio. The region of line speeds much lower than the Limit Deposit Velocity, the region of line speeds around the Limit Deposit Velocity and the region of line speeds higher than the Limit Deposit Velocity. For the region around the Limit Deposit Velocity an approach has to be found.

7.9.6   The Region around the Limit Deposit Velocity.

For very low line speeds, the slip ratio approaches (**1-C_{vt}/C_{vb}**) according to equation (7.9-27). For line speeds above the Limit Deposit Velocity, the slip ratio will behave according to equation (7.9-10) divided by 2, because this equation gives the maximum slip velocity and here the time averaged slip velocity is required. Yagi et al. (1972) found that the slip ratio decreases with the line speed to a power of -2.8, based on their measurements.

However, the experiments of Yagi et al. (1972) contain experiments at relatively low line speeds where the slip ratio tends to curve towards the asymptotic behavior at very low line speeds. In the region around the Limit Deposit Velocity a higher power may be expected. Matousek (1996) carried out experiments in a **D_p=0.15 m** pipe with sand with a **d=0.35 mm**, measuring both the volumetric spatial concentration and the volumetric delivered concentration, resulting in the slip factor (1-slip ratio). Sobota & Kril (1992) proposed an approximation correlation for the slip factor according to (source Matousek (1997)):

$$\frac{v_s}{v_{ls}} = \frac{v_{ls} - v_{sl}}{v_{ls}} = 1 - \frac{v_{sl}}{v_{ls}} = \frac{C_{vt}}{C_{vs}} = 1 - f_t \cdot \left(1 - \frac{C_{vs}}{C_{vb}}\right)^{2.16} \cdot \left(\frac{v_{ls,ldv}}{v_{ls}}\right)^{1.66} \tag{7.9-30}$$

This correlation was based on results of the microscopic model of Kril (1990) for the internal structure of slurry flow. Berman (1994) determined the coefficient f_t to be:

$$f_t = 0.45 \cdot \left(1 + \text{sign}\left(\ln\left(\text{Re}_p\right) - 0.88\right) \cdot \tanh\left(0.967 \cdot \text{abs}\left(\ln\left(\text{Re}_p\right) - 0.88\right)^{0.6}\right)\right) \tag{7.9-31}$$

The 3 terms in these equations make sense. The f_t term gives the relation between the slip ratio and the particle diameter, but in a complicated way. Using the Durand drag coefficient is more transparent. The term $(1-C_{vs}/C_{vb})$ matches the asymptotic behavior of the theoretical slip ratio at very small line speeds with the difference that the constant spatial concentration is used here. Whether this is intentional or a typing error is not clear, but using the constant transport concentration makes more sense. The third term seems logic in the area around the Limit Deposit Velocity. The power of 1.66 seems low, but can be explained from a wide range of line speeds, see Figure 7.9-3. Both the Yagi et al. (1972) and the Matousek (1996) data point to a much higher power like 4.

Based on the Matousek (1996) experiments (see Figure 7.9-4) and the Yagi et al. (1972) experiments, the following equation is derived for the slip ratio in the region around the Limit Deposit Velocity for sand and gravel.

$$\frac{v_{sl}}{v_{ls}} = \frac{v_t^2}{4 \cdot g \cdot d} \cdot \left(1 - \frac{C_{vt}}{C_{vb}}\right)^{2.5} \cdot \left(\frac{v_{ls,ldv}}{v_{ls}}\right)^4 \tag{7.9-32}$$
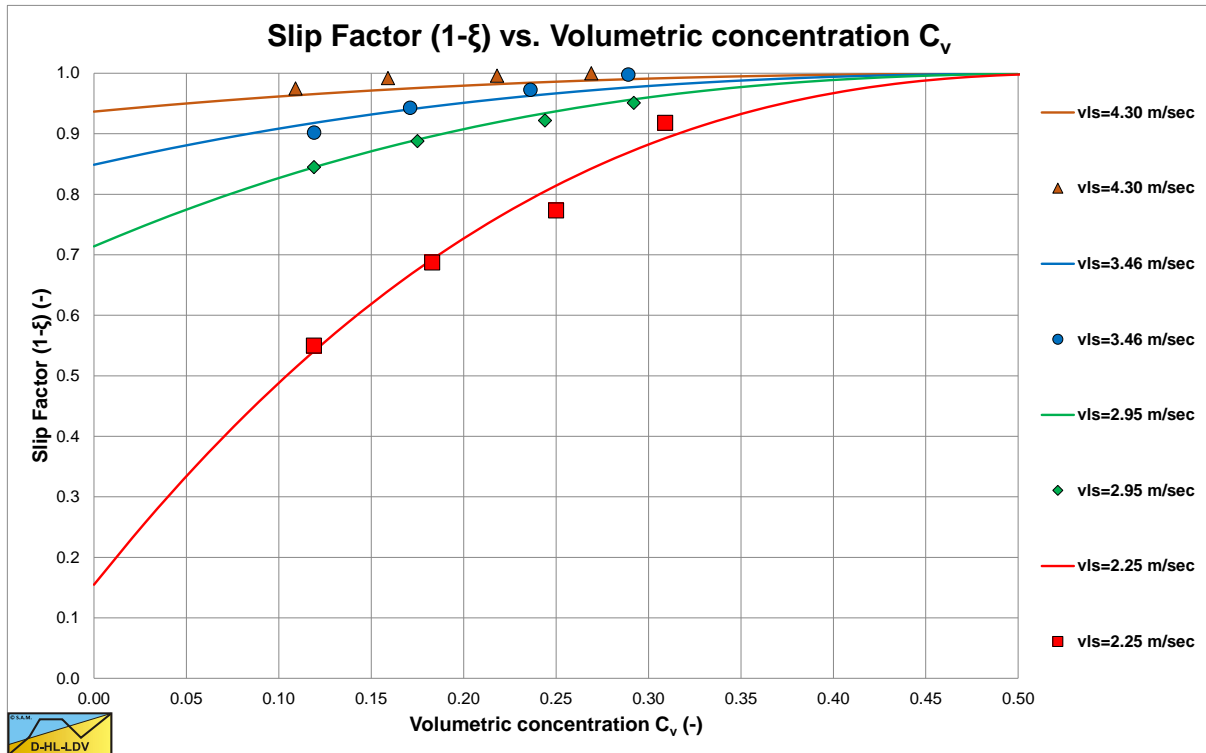
Figure 7.9-4: The slip factor (1-slip ratio) according to Matousek (1996).

Yagi et al. (1972) found an equation of the following form.

$$\xi = \frac{v_{sl}}{v_{ls}} = A \cdot \left(\frac{g \cdot R_{sd} \cdot D_p}{v_{ls}^2 \cdot \sqrt{C_x}}\right)^B \tag{7.9-33}$$

Since the slip ratio at zero line speed equals **(1-C$_{vt}$/C$_{vb}$)** the equation is modified (later another equation is derived). For all materials the following equation is proposed:

$$\xi = \frac{v_{sl}}{v_{ls}} = \frac{R_{sd}}{3} \cdot \frac{3}{4} \cdot \frac{v_t^2}{g \cdot R_{sd} \cdot d} \cdot \left(1 - \frac{C_{vt}}{C_{vb}}\right) \cdot \left(\frac{v_{ls,ldv}}{v_{ls}}\right)^4 = 0.33 \cdot \frac{R_{sd}}{C_D} \cdot \left(1 - \frac{C_{vt}}{C_{vb}}\right) \cdot \left(\frac{v_{ls,ldv}}{v_{ls}}\right)^4 \qquad \textbf{(7.9-34)}$$

7.9.7   Comparison with the Yagi et al. (1972) Data Step 3.

Comparing equation (7.9-34) with the Yagi et al. (1972) (Figure 7.9-5 & Figure 7.9-6) shows that at low concentrations the data points at the upper right are covered, while at the highest concentrations the data points in the middle and at the lower left are covered. Also the steepness of the lines match the steepness of the cloud of data points. Apparently the behavior of the slip ratio around the Limit Deposit Velocity is well described by equation (7.9-34).

Constructing the slip ratio curves according to equation (7.9-26) for the fixed bed regime, equation (7.9-34) around the Limit Deposit Velocity and equation (7.9-12) for the heterogeneous transport result in Figure 7.9-7 for low concentrations and Figure 7.9-8 for the highest concentrations. The curves match well and also show that both the lines of the sands and the gravels cover the whole area of data points which matches the findings of Yagi et al. (1972). The transition however from the fixed bed regime to the regime around the Limit Deposit Velocity is still to abrupt and tends to overestimate the slip ratio measured by Yagi et al. (1972). One more step has to be taken to smoothen this transition.

7.9.8   Construction of the Slip Ratio Curve, Step 4.

Figure 7.9-10 shows how the resulting slip ratio curve is constructed. First the semi-empirical slip ratio curve based on equation (7.9-34) is drawn, which is the LDV Region slip ratio curve in the figure. Secondly the theoretical slip ratio curve for the Fixed Bed according to equation (7.9-26) is drawn. Now one could construct a resulting slip ratio curve by choosing the smallest slip ratio (of the two) at each line speed, but this results in a rather abrupt transition between the LDV Region slip ratio curve and the theoretical Fixed Bed slip ratio curve. So how to make this transition more smooth? Taking the tangent to the LDV Region slip ratio curve, starting at a slip ratio according to equation (7.9-29) could be a solution, but the results are not yet satisfactory comparing it with the experiments of Doron et al. (1987). Taking a weighted average of the LDV Region and the Fixed Bed slip ratio curve and the tangent curve, gives a good correlation as is shown in Figure 7.9-11 and Figure 7.9-12 for a 4.2% and an 18% volumetric transport concentration (Doron et al. (1987)).

Looking at Figure 7.9-7 it is clear that there are not many data points with a slip velocity higher than 50% of the line speed. So this correction does not really influence the outcome of Figure 7.9-7. Grunsven (2012) defined the slip factor as 1 minus the slip ratio as used by Yagi et al. (1972). He carried out experiments in a 40 mm Perspex pipe with sands with a d$_{50}$ of 0.132 mm (GB), 0.325 mm (D9) and 0.570 mm (D8), measuring both the volumetric spatial and the volumetric transport concentration. Based on these measurements he determined the slip factor. Since these experiments are carried out independently from the experiments of Yagi et al. (1972), as used to calibrate the slip efficiency, it is interesting to compare the results of equation (7.9-12), (7.9-26) and (7.9-32) with the data of Grunsven (2012). Figure 7.9-13 shows this comparison. From this figure it can be concluded that the theory matches the experiments closely. Of course there is some scatter, but the theoretical curves of a specific sand, match the data points of that specific sand rather well. For smaller line speeds, the data points of the slip factor seem to deviate based on the concentration, matching the trend of the theoretical curves, although the data points for the lowest line speeds seem to have a smaller slip factor then predicted.

7.9.9   Conclusions & Discussion.

To estimate the slip ratio 3 regions have to be distinguished, the fixed bed region at line speeds much smaller than the Limit Deposit Velocity, the region around the Limit Deposit Velocity and the heterogeneous region at line speeds higher than the Limit Deposit Velocity. For each region an equation has been derived. In order to match the theoretical curves with the data points of Yagi et al. (1972), Doron et al. (1987) and Grunsven (2012), smoothing of the transition between the fixed bed regime and the LDV regime is applied.

The resulting slip ratio curves give a good correlation with the measurements of Yagi et al. (1972), Doron et al. (1987) and Grunsven (2012). Since these experiments are carried out independently in different periods of time and under different conditions, the method described gives promising results.
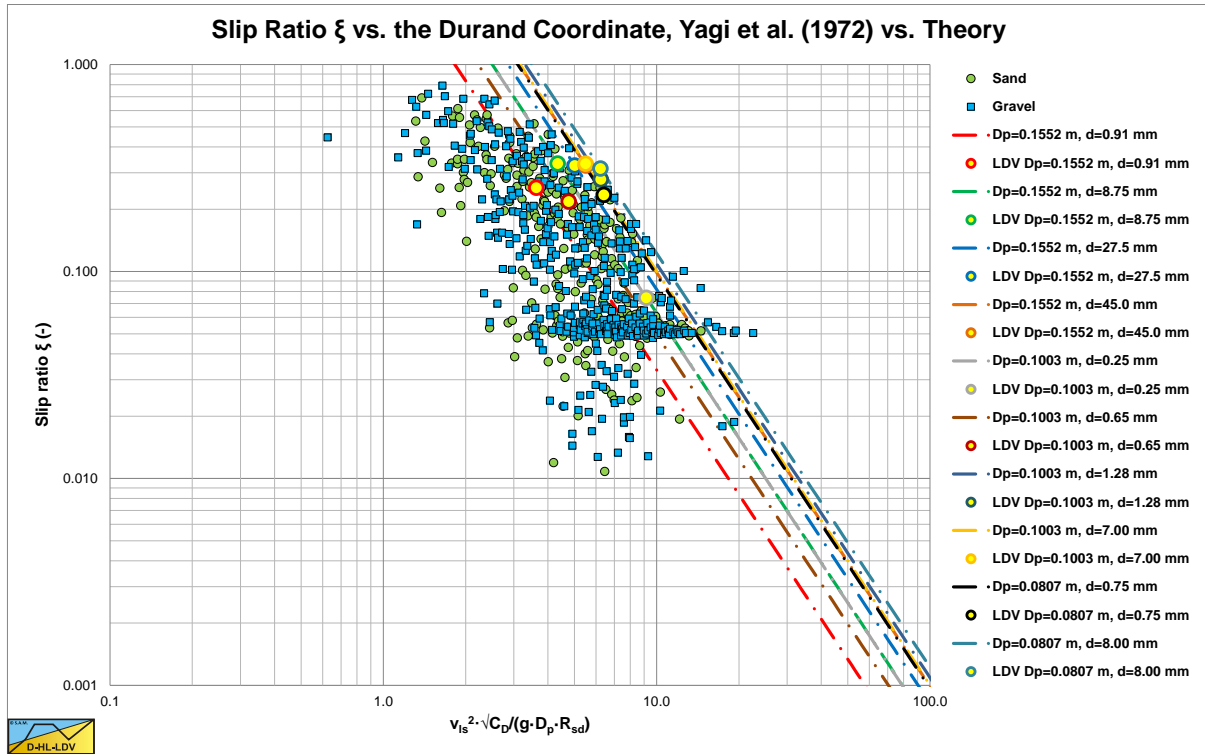
Figure 7.9-5: The data of Yagi et al. (1972) compared with the theoretical slip velocities, step 3, C$_{vt}$=0.05.
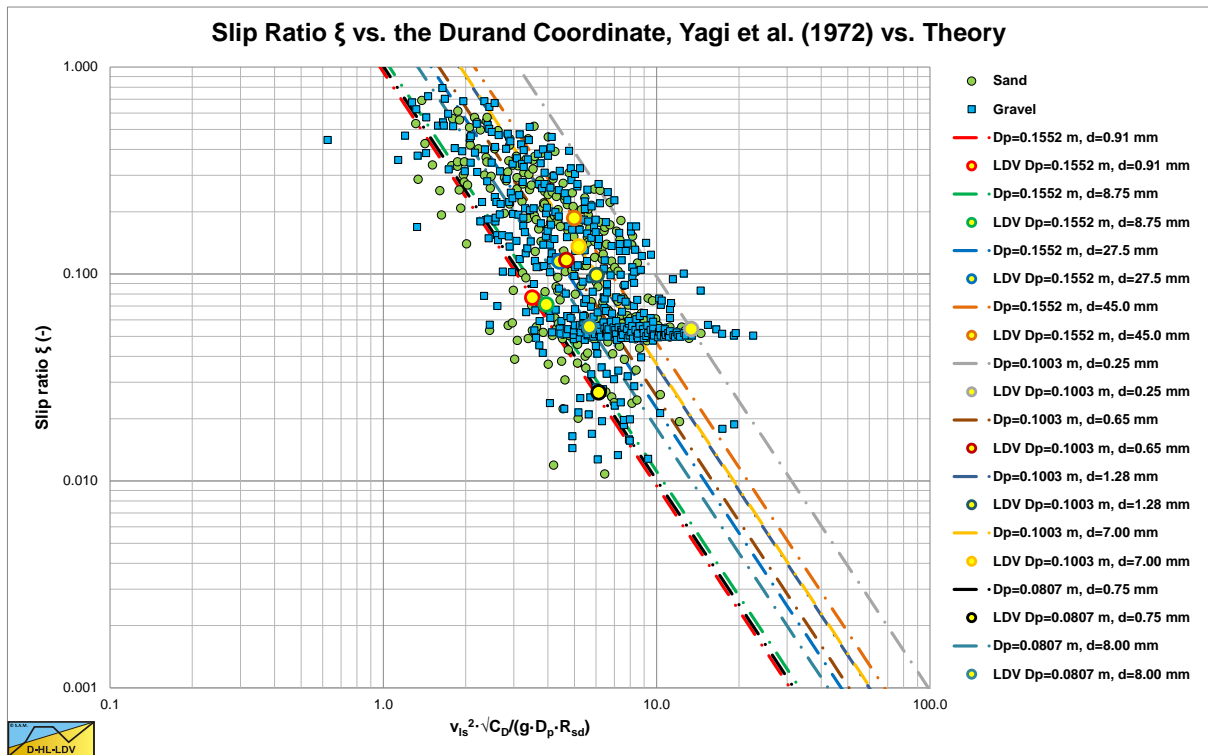
Figure 7.9-6: The data of Yagi et al. (1972) compared with the theoretical slip velocities, step 3, C$_{vt}$=0.11-0.34.
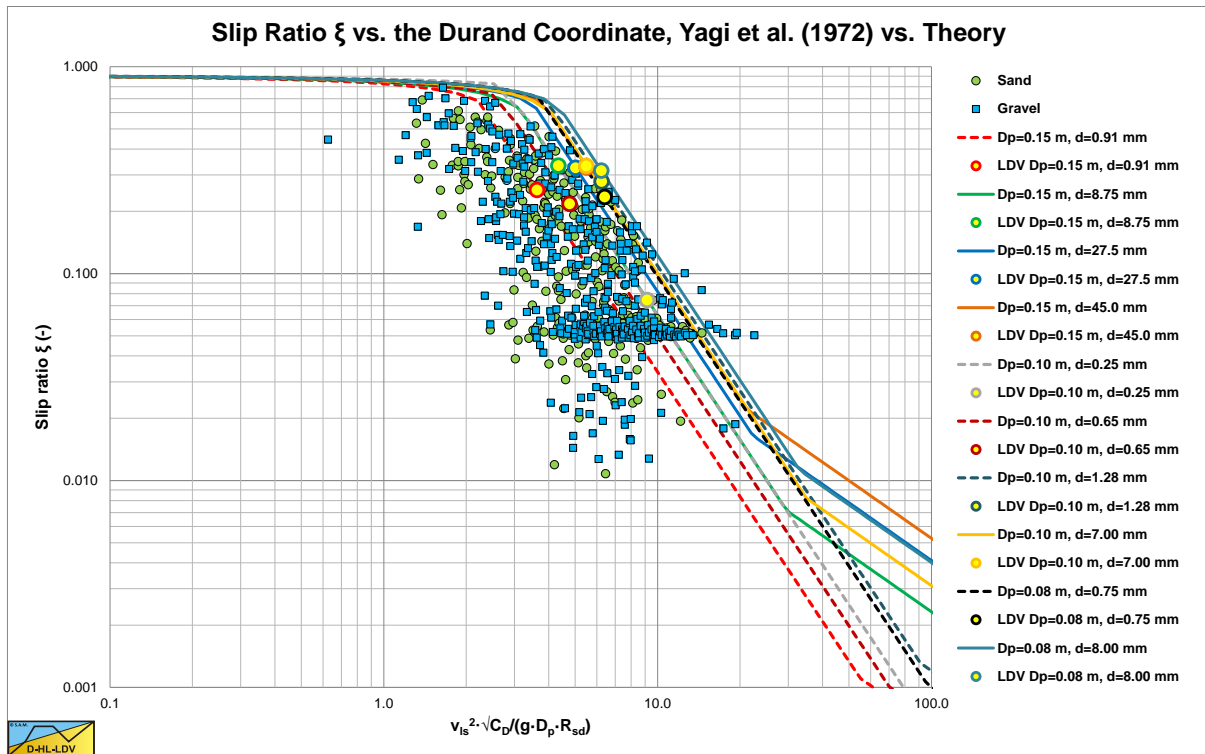
Figure 7.9-7: The data of Yagi et al. (1972) compared with the theoretical slip velocities, step 3, C_{vt}=0.05.
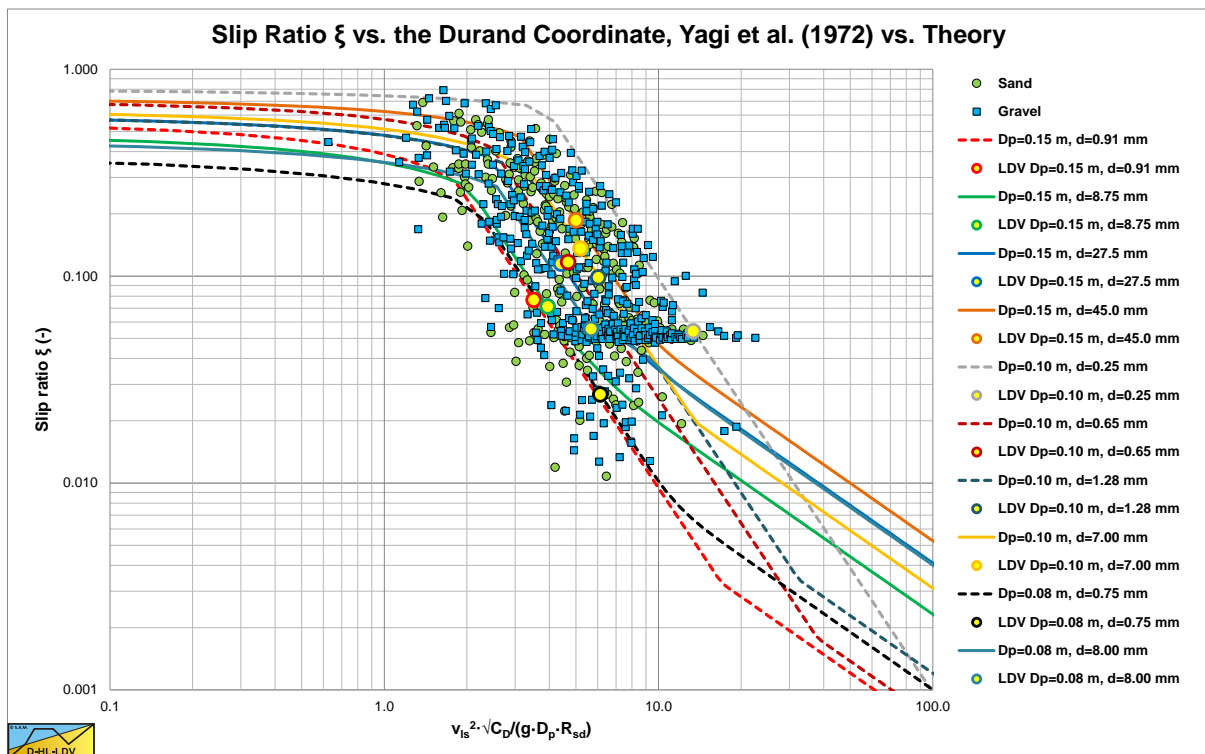
Figure 7.9-8: The data of Yagi et al. (1972) compared with the theoretical slip velocities, step 3, C_{vt}=0.11-0.34.
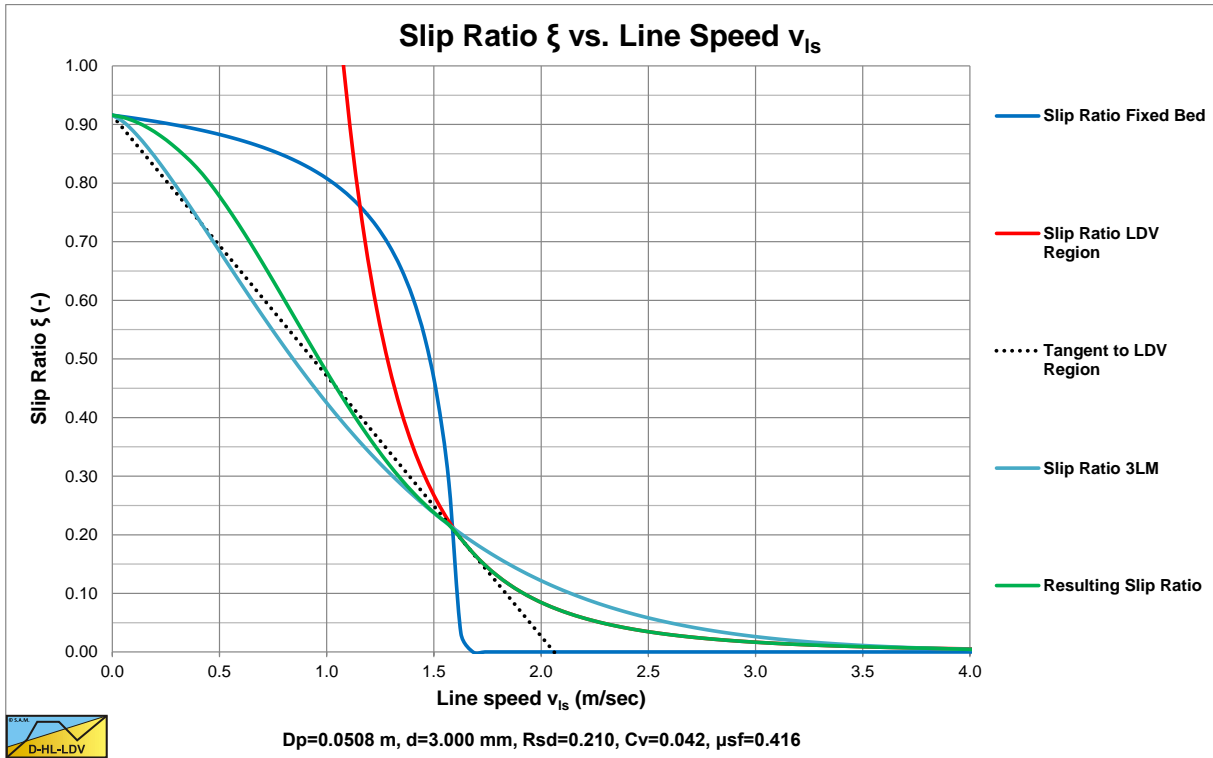
Figure 7.9-9: Construction of the slip ratio curve, step 4 on linear axis.
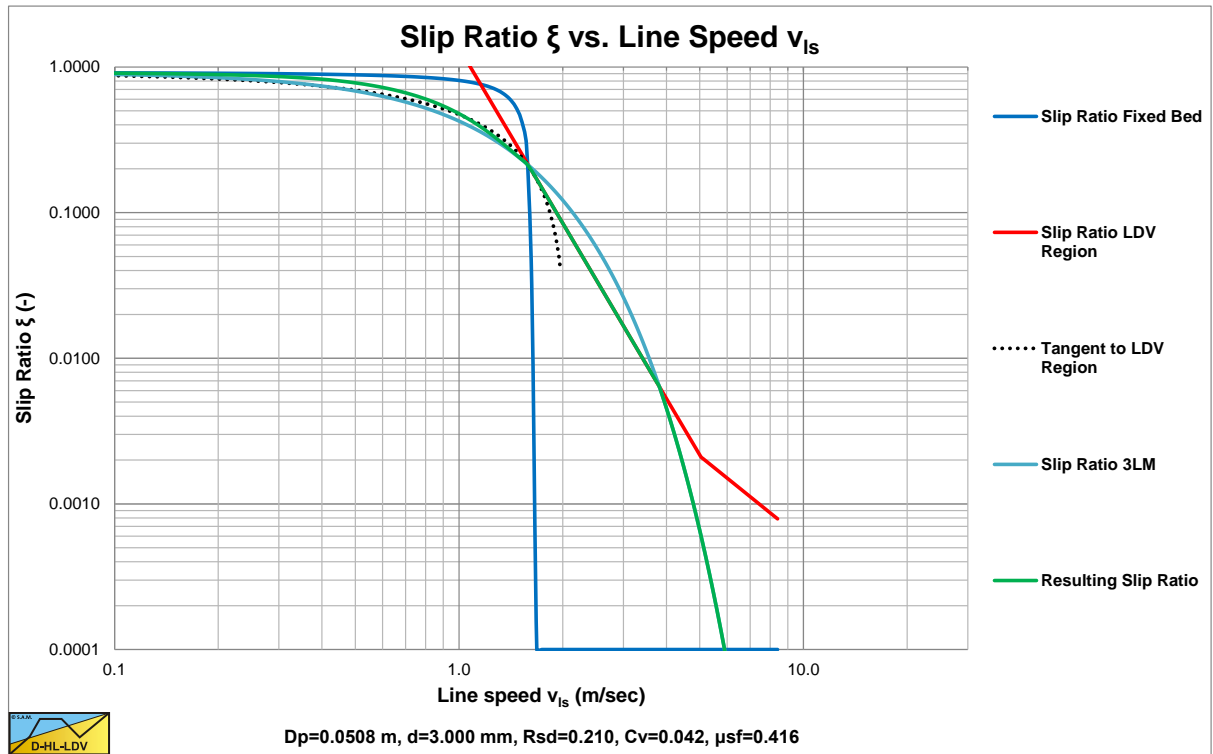
Figure 7.9-10: Construction of the slip ratio curve, step 4 on logarithmic axis.
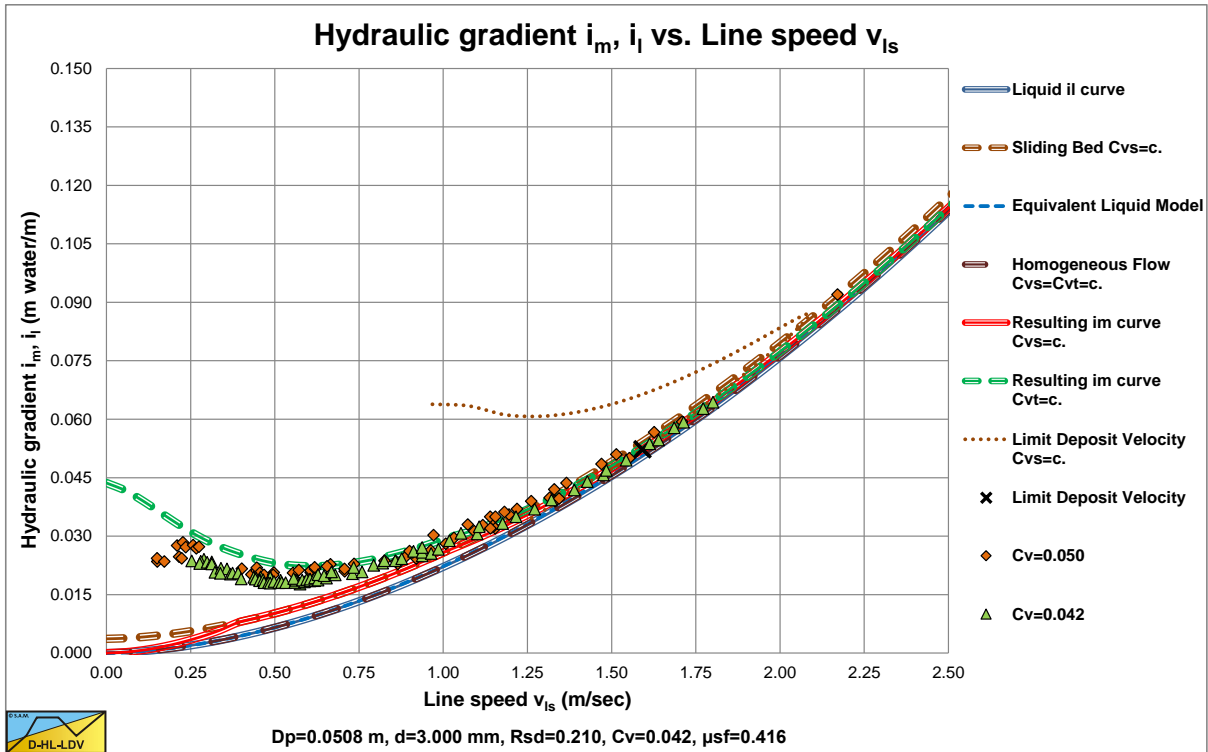
Figure 7.9-11: The resulting slip ratio applied to the experiments of Doron et al. (1987), C_{vt}=0.042-0.050.
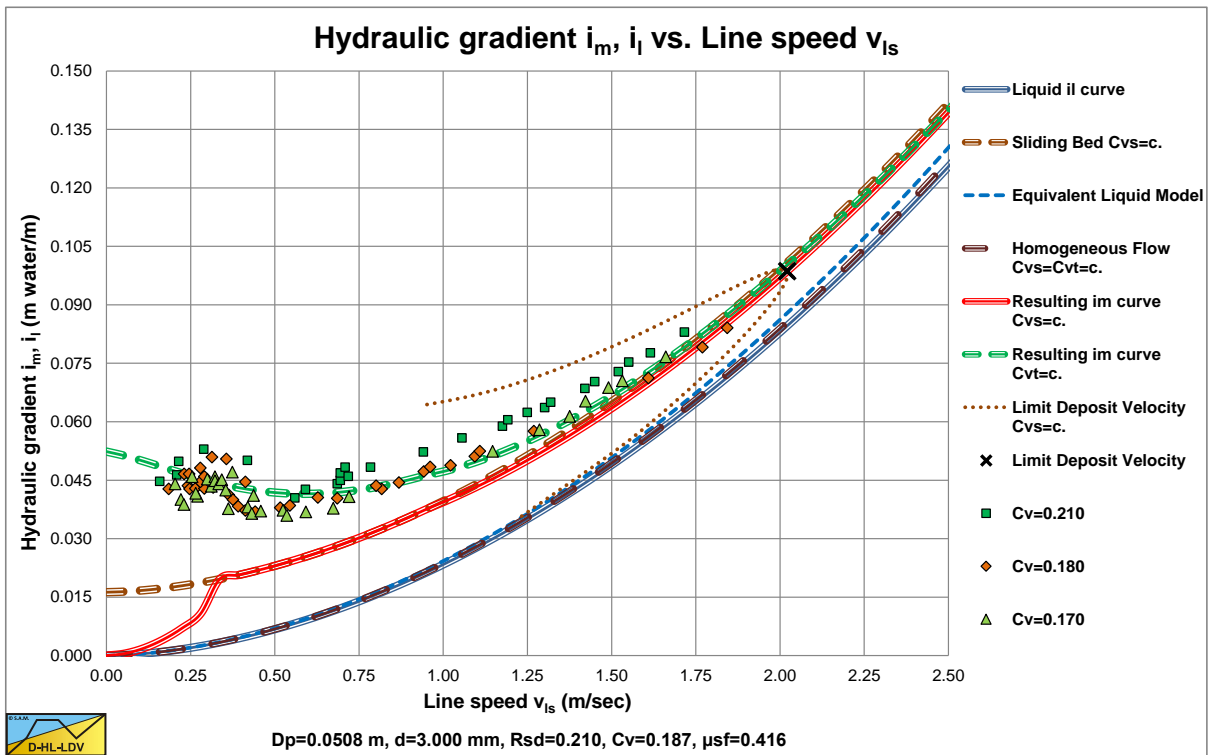
Figure 7.9-12: The resulting slip ratio applied to the experiments of Doron et al. (1987), C_{vt}=0.17-0.21.
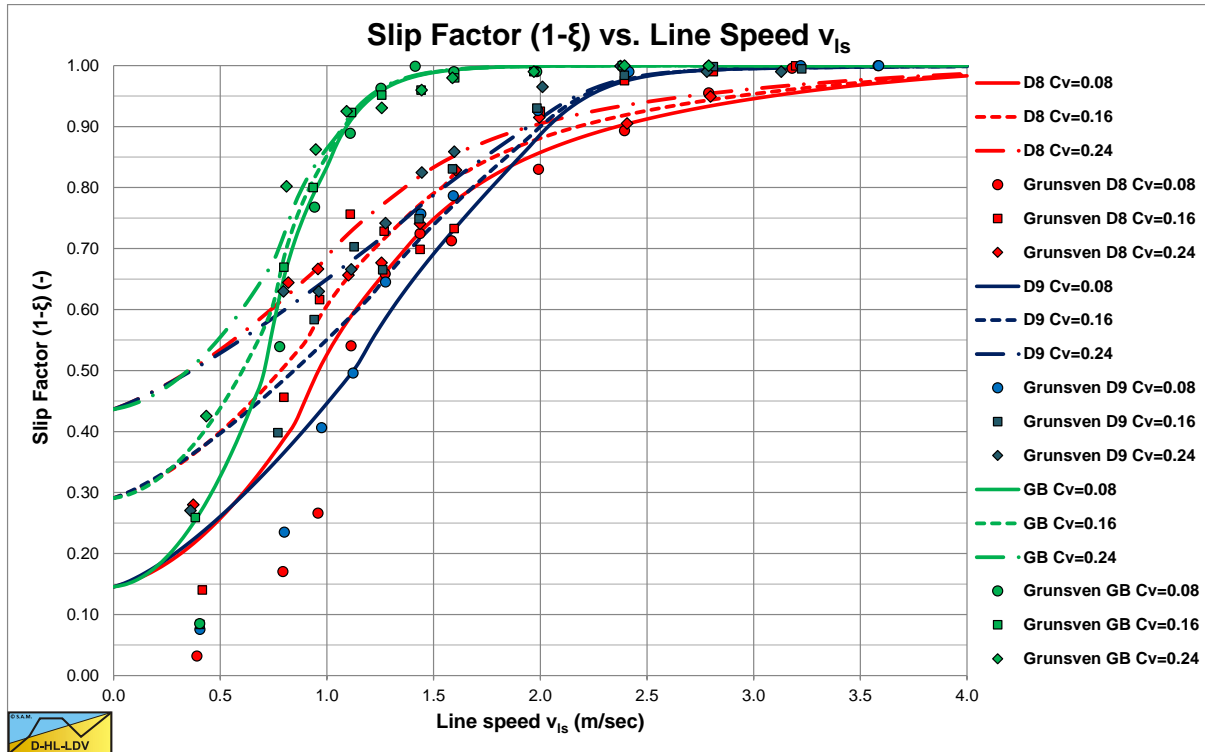
Figure 7.9-13: The slip factor, theory and experiments (data Grunsven (2012)).
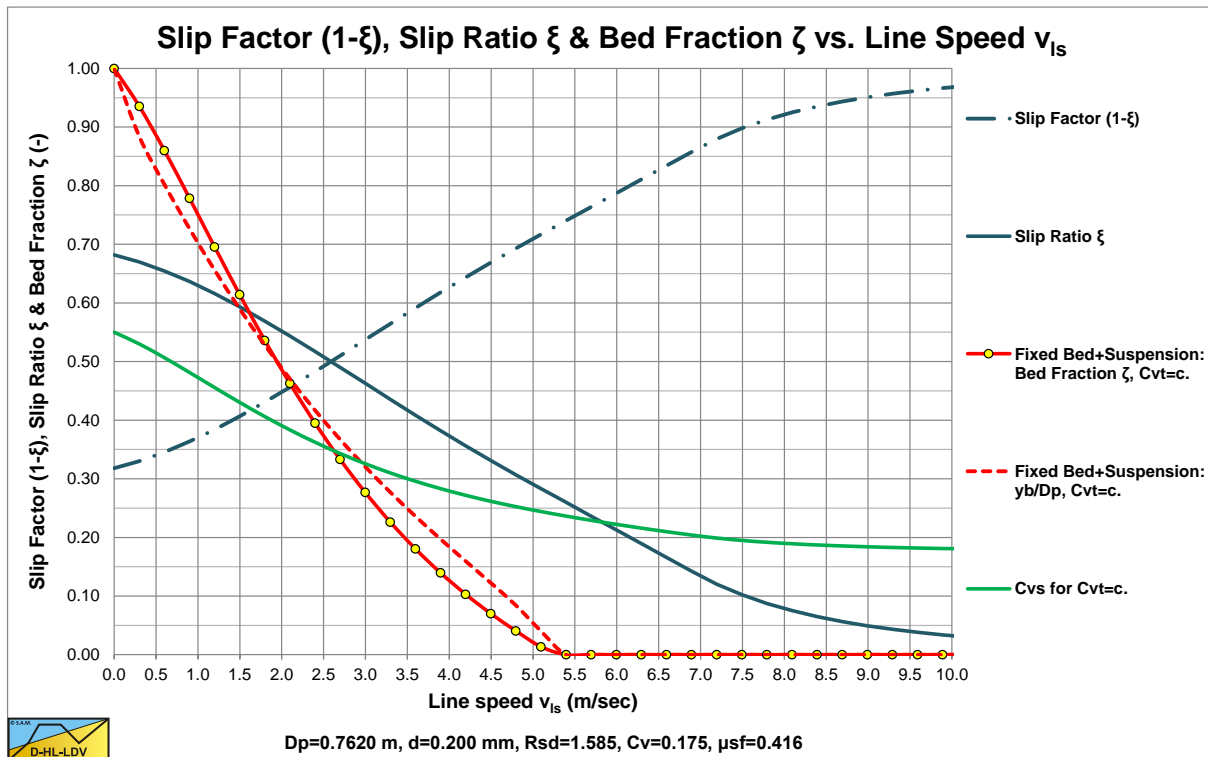
Figure 7.9-14: The slip ratio and factor, the bed fraction and the spatial concentration.

Figure 7.9-14 shows the resulting slip ratio, slip factor, bed fraction, bed height and spatial volumetric concentration in case of constant delivered volumetric concentration. The maximum spatial concentration is the bed concentration, which in the case considered is 55%.

7.9.10 The Slip Velocity, a Pragmatic Solution.

There are 3 theoretical equations derived for the slip ratio, the region of line speeds below the LDV, the region of line speeds around the LDV and the region of line speeds above the LDV.

The slip ratio ξ_{HeHo} in the heterogeneous and homogeneous regime above the LDV is:

$$\xi_{HeHo} = \frac{v_{sl}}{v_{ls}} = 8.5 \cdot \left(\frac{1}{\sqrt{\lambda_l}}\right) \cdot \left(\frac{v_t}{\sqrt{g \cdot d}}\right)^{5/3} \cdot \left(\frac{(v_l \cdot g)^{1/3}}{v_{ls}}\right) \cdot \frac{v_t}{v_{ls}} \tag{7.9-35}$$

The slip ratio ξ_{ldv} without suspension around the LDV can be approximated by (based on the 3LM equation (7.4-93)):

$$\xi_{aldv} = \frac{v_{sl}}{v_{ls}} = \left(1 - C_{vr}\right) \cdot e^{\left(-\left(0.83 + \frac{\mu_{sf}}{4} + \left(C_{vr} - 0.5 - 0.075 \cdot D_p\right)^2 + 0.025 \cdot D_p\right) \cdot D_p^{0.025} \cdot \left(\frac{v_{ls,ldv}}{v_{ls,lsdv}}\right)^{\alpha} \cdot C_{vr}^{0.65} \cdot \left(\frac{R_{sd}}{1.585}\right)^{0.1}\right)} \cdot \left(\frac{v_{ls,ldv}}{v_{ls}}\right)^4$$

With : $\alpha = 0.58 \cdot C_{vr}^{-0.42}$ (7.9-36)

At the LDV:

$$\xi_{ldv} = \frac{v_{sl}}{v_{ls}} = \left(1 - C_{vr}\right) \cdot e^{\left(-\left(0.83 + \frac{\mu_{sf}}{4} + \left(C_{vr} - 0.5 - 0.075 \cdot D_p\right)^2 + 0.025 \cdot D_p\right) \cdot D_p^{0.025} \cdot \left(\frac{v_{ls,ldv}}{v_{ls,lsdv}}\right)^{\alpha} \cdot C_{vr}^{0.65} \cdot \left(\frac{R_{sd}}{1.585}\right)^{0.1}\right)}$$

The slip ratio ξ_{fb} based on a fixed bed below the LDV is, with suspension above the bed:

$$\xi_{fb} = \frac{v_{sl}}{v_{ls}} = 1 - \frac{C_{vt} \cdot v_{ls,ldv}}{\left(C_{vb} - \kappa_{ldv} \cdot C_{vt}\right) \cdot \left(v_{ls,ldv} - v_{ls}\right) + \kappa_{ldv} \cdot C_{vt} \cdot v_{ls,ldv}} \tag{7.9-37}$$

With : $\kappa_{ldv} = \left(\frac{v_{ls,ldv}}{v_{ls,ldv} - v_{sl,ldv}}\right) = \left(\frac{1}{1 - \xi_{ldv}}\right)$

The slip ratio according to the 3LM model is:

$$\xi_{3LM} = \frac{v_{sl}}{v_{ls}} = \left(1 - C_{vr}\right) \cdot e^{\left(-\left(0.83 + \frac{\mu_{sf}}{4} + \left(C_{vr} - 0.5 - 0.075 \cdot D_p\right)^2 + 0.025 \cdot D_p\right) \cdot D_p^{0.025} \cdot \left(\frac{v_{ls}}{v_{ls,lsdv}}\right)^{\alpha} \cdot C_{vr}^{0.65} \cdot \left(\frac{R_{sd}}{1.585}\right)^{0.1}\right)} \tag{7.9-38}$$

The resulting theoretical slip ratio curve is determined by:

$$\xi_{fb} < \xi_{aldv} \quad \Rightarrow \quad \xi_{th} = \xi_{fb}$$

$$\xi_{fb} \geq \xi_{aldv} \quad \Rightarrow \quad \xi_{th} = \xi_{aldv} \tag{7.9-39}$$

$$\xi_{HeHo} > \xi_{aldv} \quad \Rightarrow \quad \xi_{th} = \xi_{HeHo}$$

In reality ξ_{HeHo} may be larger, because the equation only covers the slip ratio required to explain the head losses, which would mean that particles always reach the line speed before being slowed down by collisions. This is not

necessarily the case, resulting in a larger slip ratio. Multiplying with a factor 2 is suggested. On the other hand, the slip ratio resulting from this equation is very small and does not influence the resulting slip ratio curve much.

The resulting theoretical slip ratio curve however is based on a fixed bed for line speeds below the LDV. Maybe this is true at line speed zero, but at higher line speeds there will probably be a sliding bed, resulting in a smaller slip ratio. A method is described here to get a good estimate of the slip ratio in this region.

The tangent line to equation (7.9-36), going through the point on the vertical axis **(1-C$_{vt}$/C$_{vb}$)** is:

$$
\xi_t = \frac{v_{sl}}{v_{ls}} = \left(1 - \frac{C_{vt}}{C_{vb}}\right) - 4 \cdot \left(1 - \frac{C_{vt}}{C_{vb}}\right) \cdot e^{\left(-\left(0.83 + \frac{\mu_{sf}}{4} + \left(C_{vr} - 0.5 - 0.075 \cdot D_p\right)^2 + 0.025 \cdot D_p\right) \cdot D_p^{0.025} \cdot \left(\frac{v_{ls,ldv}}{v_{ls,lsdv}}\right)^{\alpha} \cdot C_{vr}^{0.65} \cdot \left(\frac{R_{sd}}{1.585}\right)^{0.1}\right)}
$$
$$
\cdot \left(\frac{v_{ls,ldv}}{v_{ls,t}}\right)^4 \cdot \left(\frac{v_{ls}}{v_{ls,t}}\right)
$$

$$
\text{With:} \quad v_{ls,t} = \left(5 \cdot e^{\left(-\left(0.83 + \frac{\mu_{sf}}{4} + \left(C_{vr} - 0.5 - 0.075 \cdot D_p\right)^2 + 0.025 \cdot D_p\right) \cdot D_p^{0.025} \cdot \left(\frac{v_{ls,ldv}}{v_{ls,lsdv}}\right)^{\alpha} \cdot C_{vr}^{0.65} \cdot \left(\frac{R_{sd}}{1.585}\right)^{0.1}\right)}\right)^{1/4} \cdot v_{ls,ldv}
$$

(7.9-40)

Giving for the slip ratio of this tangent line:

$$
\xi_t = \frac{v_{sl}}{v_{ls}} = \left(1 - \frac{C_{vt}}{C_{vb}}\right) \cdot \left(1 - \frac{4}{5} \cdot \left(\frac{v_{ls}}{v_{ls,t}}\right)\right)
$$

(7.9-41)

The approximation of the slip ratio ξ up to the tangent point **v$_{ls,t}$** is now a weighed slip ratio according to:

$$
\xi_{SBHeHo} = \xi_{th} \cdot \left(1 - \left(\frac{v_{ls}}{v_{ls,t}}\right)^{\alpha}\right) + \xi_t \cdot \left(\frac{v_{ls}}{v_{ls,t}}\right)^{\alpha} \quad \text{if} \quad v_{ls} < v_{ls,t}
$$

$$
\xi_{SBHeHo} = \xi_{th} \quad \text{if} \quad v_{ls} \geq v_{ls,t}
$$

(7.9-42)

With: α=0-1

$$
\xi_{SBHeHo} > \xi_{3LM} \quad \Rightarrow \quad \xi_{SBHeHo} = \xi_{3LM}
$$

This is shown in Figure 7.9-9 and Figure 7.9-10.

In the case of sliding flow, the slip ratio has to be corrected. A pragmatic approach to determine the relative excess hydraulic gradient in the sliding flow regime is to use a weighted average between the heterogeneous regime and the sliding bed regime. First the factor between particle size and pipe diameter is determined:

$$
f = \frac{4}{3} - \frac{1}{3} \cdot \frac{d}{r_{d/Dp} \cdot D_p} \quad \text{with:} \ 0 \leq f \leq 1
$$

(7.9-43)

Secondly the weighted average slip ratio is determined:

$$\xi_{SF} = \xi_{SBHeHo} \cdot f + \xi_{3LM} \cdot (1-f) \qquad \text{(7.9-44)}$$

The resulting relative excess hydraulic gradient can be determined by multiplying the E_{rhg} curve for $C_{vt}=C_{vs}$ with the factor $1/(1-\xi)$.

$$C_{vs}(\xi) = \left(\frac{1}{1-\xi}\right) \cdot C_{vt} \quad \Rightarrow \quad E_{rhg,Cvt} = \left(\frac{1}{1-\xi}\right) \cdot E_{rhg,Cvs=Cvt} \qquad \text{(7.9-45)}$$

Now there are 2 cases, with constant C_{vs} a sliding bed is found or the fixed bed transits directly to heterogeneous transport.

Case sliding bed:

One should use the sliding bed equation also in the stationary bed range of the constant spatial volumetric concentration curve, so from line speed zero until the sliding bed curve intersects with the heterogeneous curve.

Case no sliding bed:

If the stationary bed regime curve intersects with the heterogeneous regime curve below the sliding bed curve, one should continue the heterogeneous curve with decreasing line speed, up to the intersection with the sliding bed curve and from there with decreasing line speed follow the sliding bed curve.

Applying this pragmatic solution to the Doron et al. (1987) experiments, as shown in Figure 7.9-11 and Figure 7.9-12, gives a good match.

The hydraulic gradient for the constant delivered volumetric concentration curve is now:

$$i_m = i_l + E_{rhg,Cvt} \cdot R_{sd} \cdot C_{vt} = i_l + \left(\frac{1}{1-\xi}\right) \cdot E_{rhg,Cvs=Cvt} \cdot R_{sd} \cdot C_{vt} \qquad \text{(7.9-46)}$$

This gives for the pressure difference:

$$\Delta p_m = \Delta p_l + \rho_l \cdot g \cdot \Delta L \cdot E_{rhg,Cvt} \cdot R_{sd} \cdot C_{vt} = \Delta p_l + \rho_l \cdot g \cdot \Delta L \cdot \left(\frac{1}{1-\xi}\right) \cdot E_{rhg,Cvs=Cvt} \cdot R_{sd} \cdot C_{vt} \qquad \text{(7.9-47)}$$

7.9.11 Nomenclature Slip Velocity.

A_b	Pipe cross section occupied by the bed	m^2
$\hat{A}_b$	Bed cross section divided by pipe cross section	-
A_p	Pipe cross section	m^2
A_s	Pipe cross section restricted area above the bed	m^2
C_D	Particle drag coefficient	-
C_x	Durand particle Froude number	-
C_v	Volumetric concentration	-
C_{vb}	Volumetric bed concentration	-
C_{vs}	Volumetric spatial concentration	-
C_{vt}	Volumetric transport/delivered concentration	-
$C_{vs,s}$	Volumetric spatial concentration in restricted area above the bed	-
$C_{vt,s}$	Volumetric delivered concentration in restricted area above the bed	-
d	Particle diameter	m
d_{50}	Particle diameter at which 50% by weight is smaller	m
D_p	Pipe diameter	m
$E_{rhg,Cvt}$	Relative excess hydraulic gradient delivered concentration	-
$E_{rhg,Cvs=Cvt}$	Relative excess hydraulic gradient spatial concentration	-
f_t	Slip function Berman	-
g	Gravitational constant 9.81 m/s^2	m/s^2
i	Hydraulic gradient	m/m
i_m	Hydraulic gradient mixture	m/m
i_l	Hydraulic gradient water/liquid, based on viscous friction	m/m
$i_{s,pot}$	Hydraulic gradient potential energy losses	m/m
$i_{s,kin}$	Hydraulic gradient kinetic energy losses	m/m
K	Durand constant (85/181)	-
ΔL	Length of the pipeline	-
Δp	Head loss over a pipeline length ΔL	kPa
Δp_m	Head loss of mixture over a pipeline length ΔL	kPa
Δp_l	Head loss of liquid/water over a pipeline length ΔL	kPa
$\Delta p_{s,kin}$	Pressure required to compensate for kinetic energy losses	kPa
$\Delta p_{s,pot}$	Pressure required to compensate for potential energy losses	kPa
R_{sd}	Relative submerged density	-
$R_{sd,q}$	Relative submerged density quarts	-
R_{sdr}	Relative submerged density/Relative submerged density quarts	-
v_l	Liquid velocity in pipe	m/s
v_{ls}	Line speed	m/s
$v_{ls,ldv}$	Limit Deposit Velocity	m/s
v_p, v_s	Particle velocity in direction of average flow	m/s
v_{sl}	Slip velocity	m/s
$v_{sl,ldv}$	Slip velocity at the LDV	m/s
$v_{sl,real}$	Real slip velocity	m/s
$v_{sl,real,c}$	Real slip velocity, corrected	m/s
$v_{ls,t}$	Line speed at tangent point	m/s
v_t	Terminal settling velocity of particles	m/s
$\alpha - \alpha_{13}$	Model coefficients	-
β	Power of Richardson & Zaki equation	-
κ_C	Concentration eccentricity factor	-
κ	Ratio C_{vs} to C_{ts}	-
κ_{ldv}	Ratio C_{vs} to C_{ts} at the LDV	-
ρ_l	Liquid/liquid density	ton/m^3
ρ_w	Density of water	ton/m^3
ρ_s	Density of solids	ton/m^3
ρ_q	Density of quarts (2.65 ton/m^3)	ton/m^3
λ	Darcy-Weisbach friction factor	-
λ_l	Darcy-Weisbach friction factor liquid with pipe wall	-

μ_{sf}	Friction coefficient for sliding bed (see also S_{rs})	-
Φ	Durand relative excess pressure coefficient	-
Ω	Excess pressure factor	$(m/s)^3$
ψ	Durand abscissa	-
ν_w, ν_l	Kinematic viscosity of water/liquid	m^2/s
ξ	Slip ratio v_{sl}/v_{ls}	-
ξ_0	Slip ratio at line speed zero	-
ξ_{ldv}	Slip ratio v_{sl}/v_{ls} at the LDV	-
ξ_{fb}	Slip ratio considering a fixed bed	-
ξ_{HeHo}	Slip ratio at high line speeds	-
ξ_{th}	Theoretical slip ratio	-
ξ_t	Slip ratio tangent line	-
ζ	Fraction of the pipe occupied by the sediment (bed)	-
η_{sl}	Slip efficiency	-
Fr_p	Particle Froude number of the particle settling velocity	-
Re_{fl}	Reynolds number of the slurry flow	-
Re_p	Reynolds number of the particle terminal settling velocity	-
Ct	The **Cát** number (sand grains)	-
Th	The **Thủy** number (water)	-
La	The **Lắng** number (sediment)	-

7.10 The Concentration Distribution.

7.10.1 The Advection Diffusion Equation.

In chapter 5 sediment transport in open channel flow and pipe flow has been discussed. The advection diffusion equation is derived and solved for low concentrations and for high concentrations including the effect of upwards liquid flow. Wasp et al. (1977) and Doron et al. (1987) use the solution for low concentrations, while Karabelas (1977) and Kaushal & Tomita (2002B) use the Hunt (1954) approach with upwards liquid flow. Hindered settling is not yet included in the basic solutions, but added by replacing the terminal settling velocity by the hindered terminal settling velocity. For the diffusivity and the relation between the sediment diffusivity and the turbulent eddy momentum diffusivity different approaches are possible.

If we assume the diffusivity is a constant, the advection diffusion equation can be solved. Giving the differential equation in the equilibrium situation with hindered settling, but without the upwards liquid velocity, since this is assumed to be part of the hindered settling (with **r** the vertical distance from the bottom of the pipe):

$$C_{vs}(r) \cdot v_{th} + \varepsilon_s \cdot \frac{dC_{vs}(r)}{dr} = C_{vs}(r) \cdot v_{th} + \beta_{sm} \cdot \varepsilon_m \cdot \frac{dC_{vs}(r)}{dr} = 0 \tag{7.10-1}$$

The coordinate **r** ranges from **0** to D_p, the pipe diameter. Now the variables have to be separated according to:

$$\frac{dC_{vs}(r)}{C_{vs}(r)} \cdot = -\frac{v_{th}}{\beta_{sm} \cdot \varepsilon_m} \cdot dr \quad \Rightarrow \quad \ln\left(C_{vs}(r)\right) = -\frac{v_{th}}{\beta_{sm} \cdot \varepsilon_m} \cdot r + C \tag{7.10-2}$$

With $C_{vs}(0) = C_{vB}$, the bottom concentration, the integration constant can be determined, giving:

$$C_{vs}(r) = C_{vB} \cdot e^{-\frac{v_{th}}{\beta_{sm} \cdot \varepsilon_m} \cdot r} \tag{7.10-3}$$

This basic solution is still equal to the solution for open channel flow. Although this is just an indicative equation for open channel flow, Doron et al. (1987) and Doron & Barnea (1993) used it in their 2 and 3 layer models. The difference between pipe flow and open channel flow is in the determination of the diffusivity. Assuming the Law of the Wall, one can also determine the average diffusivity by integration (Lane & Kalinske (1941)):

$$\varepsilon_s = \beta_{sm} \cdot \kappa \cdot u_* \cdot r \cdot \left(\frac{R-r}{R}\right) = \beta_{sm} \cdot \kappa \cdot u_* \cdot R \cdot \frac{r}{R} \cdot \left(1 - \frac{r}{R}\right) = \beta_{sm} \cdot \kappa \cdot u_* \cdot R \cdot \tilde{r} \cdot (1 - \tilde{r}) \tag{7.10-4}$$

Integration over the cross section of the pipe gives:

$$\overline{\varepsilon}_s = \frac{1}{\pi \cdot R^2} \cdot \int_0^{2 \cdot \pi} \int_{r=0}^{r=R} \varepsilon_s \cdot dr \cdot r \cdot d\phi = \beta_{sm} \cdot \kappa \cdot u_* \cdot \frac{R^3}{\pi \cdot R^2} \cdot \int_0^{2 \cdot \pi} \int_{\tilde{r}=0}^{\tilde{r}=1} \tilde{r}^2 \cdot (1 - \tilde{r}) \cdot d\tilde{r} \cdot d\phi$$

$$= \beta_{sm} \cdot \kappa \cdot u_* \cdot R \cdot \frac{1}{\pi} \cdot \int_0^{2 \cdot \pi} \int_{\tilde{r}=0}^{\tilde{r}=1} \tilde{r}^2 \cdot (1 - \tilde{r}) \cdot d\tilde{r} \cdot d\phi = \beta_{sm} \cdot \kappa \cdot u_* \cdot R \cdot \frac{1}{\pi} \cdot \int_0^{2 \cdot \pi} \int_{\tilde{r}=0}^{\tilde{r}=1} \left(\tilde{r}^2 - \tilde{r}^3\right) \cdot d\tilde{r} \cdot d\phi \tag{7.10-5}$$

$$= \beta_{sm} \cdot \kappa \cdot u_* \cdot R \cdot \frac{2 \cdot \pi}{\pi} \cdot \left(\frac{1}{3} \cdot \tilde{r}^3 - \frac{1}{4} \cdot \tilde{r}^4\right)_0^1 = \frac{\beta_{sm} \cdot \kappa \cdot u_* \cdot R}{6} = \frac{\beta_{sm} \cdot \kappa \cdot u_* \cdot D_p}{12}$$

This gives for the concentration as a function of the vertical distance from the pipe bottom:

$$C_{vs}(r) = C_{vB} \cdot e^{-12 \cdot \frac{v_{th}}{\beta_{sm} \cdot \kappa \cdot u_*} \cdot \frac{r}{D_p}} \tag{7.10-6}$$

Based on integration, assuming open channel flow and settling in the vehicle, the bottom concentration C_{vB} can be found, at the LDV $C_{vB}=C_{vb}$:

$$C_{vB} = C_{vs} \cdot \frac{\left(\dfrac{12 \cdot v_{tv}}{\beta_{sm} \cdot \kappa \cdot u_*} \right)}{\left(1 - e^{-12 \cdot \frac{v_{tv}}{\beta_{sm} \cdot \kappa \cdot u_*}} \right)} \qquad (7.10\text{-}7)$$

7.10.2 The Diffusivity Based on the LDV.

In order to have a consistent model, the bottom concentration should be equal to the bed concentration at the LDV, since this is the definition of the LDV. Now most concentration profile equations are not related to the LDV, but make use of a modified diffusivity to match experiments. Here an attempt is made to make the concentration profile match the LDV. At the Limit Deposit Velocity the bottom concentration C_{vB} equals the bed concentration C_{vb} giving:

$$C_{vb} = C_{vs} \cdot \frac{\left(\dfrac{12 \cdot v_{tv,ldv}}{\beta_{sm,ldv} \cdot \kappa \cdot u_{*,ldv}} \right)}{\left(1 - e^{-12 \cdot \frac{v_{tv,ldv}}{\beta_{sm} \cdot \kappa \cdot u_{*,ldv}}} \right)} \qquad (7.10\text{-}8)$$

Neglecting the denominator at low concentrations, since it's close to unity (say the denominator equals a factor α_{sm}), the diffusivity can be derived.

$$\beta_{sm,ldv} = 12 \cdot \frac{C_{vs}}{C_{vb}} \cdot \frac{v_{tv,ldv}}{\alpha_{sm} \cdot \kappa \cdot u_{*,ldv}} = 12 \cdot C_{vr} \cdot \frac{v_{tv,ldv}}{\alpha_{sm} \cdot \kappa \cdot u_{*,ldv}} \qquad (7.10\text{-}9)$$

This gives for the concentration distribution in the pipe:

$$C_{vs}(r) = C_{vB} \cdot e^{-12 \cdot \frac{v_{tv}}{\left(12 \cdot C_{vr} \cdot \frac{v_{tv,ldv}}{\alpha_{sm} \cdot \kappa \cdot u_{*,ldv}} \right) \cdot \kappa \cdot u_*} \cdot \frac{r}{D_p}} = C_{vB} \cdot e^{-\frac{\alpha_{sm}}{C_{vr}} \cdot \frac{u_{*,ldv}}{u_*} \cdot \frac{v_{tv}}{v_{tv,ldv}} \cdot \frac{r}{D_p}} \qquad (7.10\text{-}10)$$

The bottom concentration is now, using the fact that the denominator equals the factor α_{sm}:

$$C_{vB} = C_{vs} \cdot \frac{\left(\dfrac{\alpha_{sm}}{C_{vr}} \cdot \dfrac{u_{*,ldv}}{u_*} \cdot \dfrac{v_{tv}}{v_{tv,ldv}} \right)}{\left(1 - e^{-\frac{\alpha_{sm}}{C_{vr}} \frac{u_{*,ldv}}{u_*} \frac{v_{tv}}{v_{tv,ldv}}} \right)} = C_{vb} \cdot \frac{\left(\dfrac{\alpha_{sm}}{C_{vr}} \cdot \dfrac{u_{*,ldv}}{u_*} \cdot \dfrac{v_{tv}}{v_{tv,ldv}} \right)}{\left(1 - e^{-\frac{\alpha_{sm}}{C_{vr}} \frac{u_{*,ldv}}{u_*} \frac{v_{tv}}{v_{tv,ldv}}} \right)} = C_{vb} \cdot \frac{u_{*,ldv}}{u_*} \cdot \frac{v_{tv}}{v_{tv,ldv}} \qquad (7.10\text{-}11)$$

The correction factor has to be determined at the LDV, giving an implicit equation with only the relative volumetric concentration as the parameter:

$$\alpha_{sm} = \left(1 - e^{-\frac{\alpha_{sm}}{C_{vr}}} \right) \qquad (7.10\text{-}12)$$

The correction factor appears to depend only on the relative concentration C_{vr} according to:

$$\alpha_{sm} = 0.9847 + 0.304 \cdot C_{vr} - 1.196 \cdot C_{vr}^2 - 0.5564 \cdot C_{vr}^3 + 0.47 \cdot C_{vr}^4 \tag{7.10-13}$$

At low relative concentrations, $C_{vr} < 0.3$, this factor is about 1. Based on the diffusivity derived, the portion of the solids in the vehicle according to the Wasp criterion can be determined by:

$$\frac{C_{vs,v}}{C_{vs}} = e^{-(0.92-0.5) \cdot \frac{\alpha_{sm}}{C_{vr}} \cdot \frac{u_{*,ldv}}{u_*} \cdot \frac{v_{tv}}{v_{tv,ldv}}} \tag{7.10-14}$$

7.10.3 Simplification of the Equations.

Now in reality, the concentration distribution depends on more than just the advection diffusion processes. At line speeds below the LDV there is a bed with possibly sheet flow and also collisions play a dominant role in the heterogeneous regime. Above the LDV the Darcy Weisbach friction factor is not changing much at higher line speeds. The power of the line speed is about -0.15 for larger pipe diameters. The power of the pipe diameter is about -0.175.

$$\lambda_l = 0.01216 \cdot \left(v_{ls} \right)^{-0.15} \cdot \left(D_p \right)^{-0.175} \tag{7.10-15}$$

Substituting this for the friction velocities gives:

$$C_{vs}(r) = C_{vB} \cdot e^{-\frac{\alpha_{sm}}{C_{vr}} \cdot \frac{\sqrt{\lambda_{l,ldv}/8} \cdot v_{ls,ldv}}{\sqrt{\lambda_l/8} \cdot v_{ls}} \cdot \frac{v_{tv}}{v_{tv,ldv}} \cdot \frac{r}{D_p}}$$

$$= C_{vB} \cdot e^{-\frac{\alpha_{sm}}{C_{vr}} \cdot \frac{\sqrt{0.01216 \cdot (v_{ls,ldv})^{-0.15} \cdot (D_p)^{-0.175} \cdot v_{ls,ldv}}}{\sqrt{0.01216 \cdot (v_{ls})^{-0.15} \cdot (D_p)^{-0.175} \cdot v_{ls}}} \cdot \frac{v_{tv}}{v_{tv,ldv}} \cdot \frac{r}{D_p}} \tag{7.10-16}$$

$$= C_{vB} \cdot e^{-\frac{\alpha_{sm}}{C_{vr}} \cdot \left(\frac{v_{ls,ldv}}{v_{ls}} \right)^{0.925} \cdot \frac{v_{tv}}{v_{tv,ldv}} \cdot \frac{r}{D_p}}$$

The bottom concentration is now for line speeds above the LDV:

$$C_{vB} = C_{vb} \cdot \left(\frac{v_{ls,ldv}}{v_{ls}} \right)^{0.925} \cdot \frac{v_{tv}}{v_{tv,ldv}} \quad \text{or} \quad C_{vB} = C_{vb} \cdot \left(\frac{v_{ls,ldv}}{v_{ls}} \right)^{0.925} \cdot \frac{v_{thv}}{v_{thv,ldv}} \tag{7.10-17}$$

For line speeds below the LDV there is a bed, so the concentration profile has to be adjusted for the presence of the bed. The portion of the solids in the vehicle according to the Wasp criterion can be determined by:

$$\frac{C_{vs,v}}{C_{vs}} = e^{-(0.92-0.5) \cdot \frac{\alpha_{sm}}{C_{vr}} \cdot \left(\frac{v_{ls,ldv}}{v_{ls}} \right)^{0.925} \cdot \frac{v_{tv}}{v_{tv,ldv}}} \quad \text{or} \quad \frac{C_{vs,v}}{C_{vs}} = e^{-(0.92-0.5) \cdot \frac{\alpha_{sm}}{C_{vr}} \cdot \left(\frac{v_{ls,ldv}}{v_{ls}} \right)^{0.925} \cdot \frac{v_{thv}}{v_{thv,ldv}}} \tag{7.10-18}$$

The above equations give the solution for both hindered settling and non-hindered settling. If the hindered settling is based on the total volumetric concentration, it has no influence, since it gives a constant reduction factor. However if the hindered settling is based on the local volumetric concentration at a certain location in the pipe, it will influence the outcome.

In chapter 6, the Wasp model, the behavior of the concentration profile based on the friction velocities is shown, compared with the models of Abulnaga (2002), Lahiri (2009) and Kaushal & Tomita (2002B). All models are based on a vertical concentration profile, without correction for the circular shape of a pipe, similar to the original Wasp et al. (1977) model for uniform sands. The advantage of this approach is that the concentration profiles can be determined analytically. The full Kaushal & Tomita (2002B) approach requires a numerical solution.

Figure 7.10-1, Figure 7.10-3, Figure 7.10-5 and Figure 7.10-7 show the relative excess hydraulic gradient of the Wasp model for 6 different implementations as described in chapter 6. The DHLLDV implementation is based on the simplified equations, including hindered settling. Figure 7.10-2, Figure 7.10-4, Figure 7.10-6 and Figure 7.10-8 show the fractions in suspension of the 6 implementations. The calculations are carried out for uniform sands with particle diameters of d=0.1, 0.2, 0.5 and 1.0 mm in a 0.1524 m diameter pipe. For the 0.1 mm particle, the DHLLDV Framework gives a smaller suspended fraction compared to the other implementations.
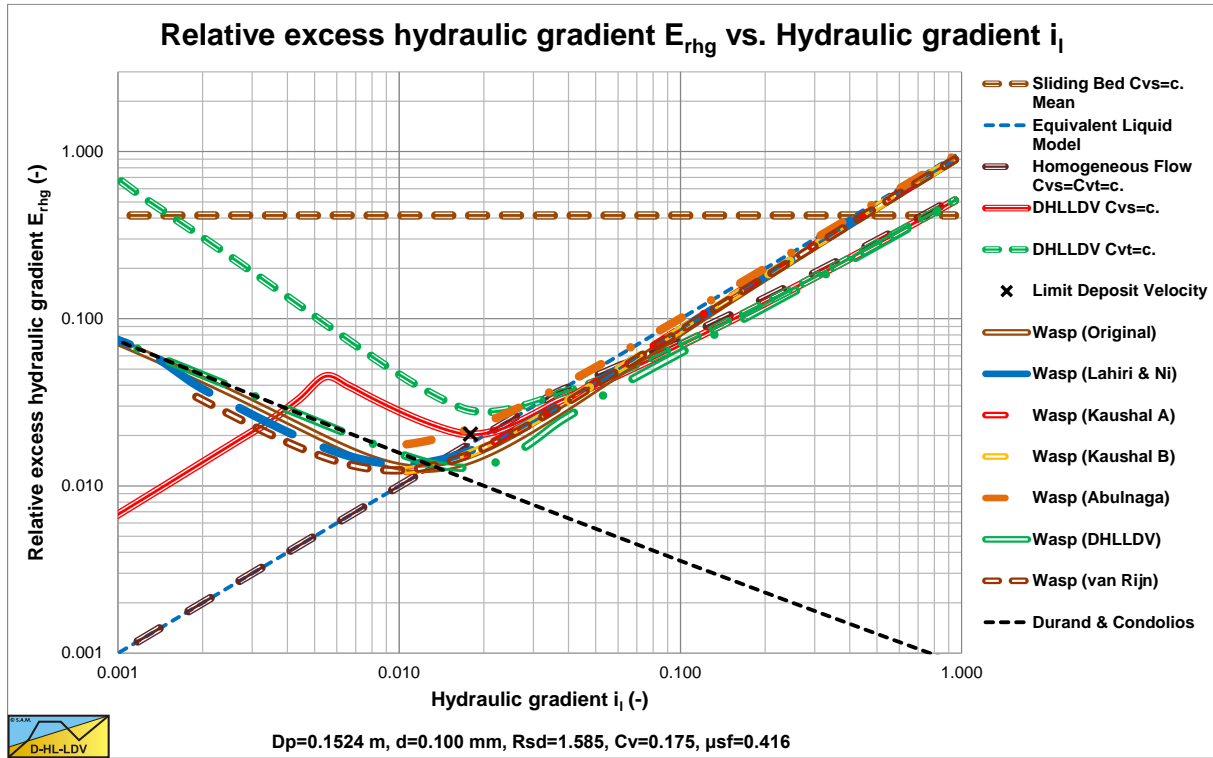
Figure 7.10-1: The Wasp model for a d=0.1 mm sand particle, modified diffusivity and hindered settling.
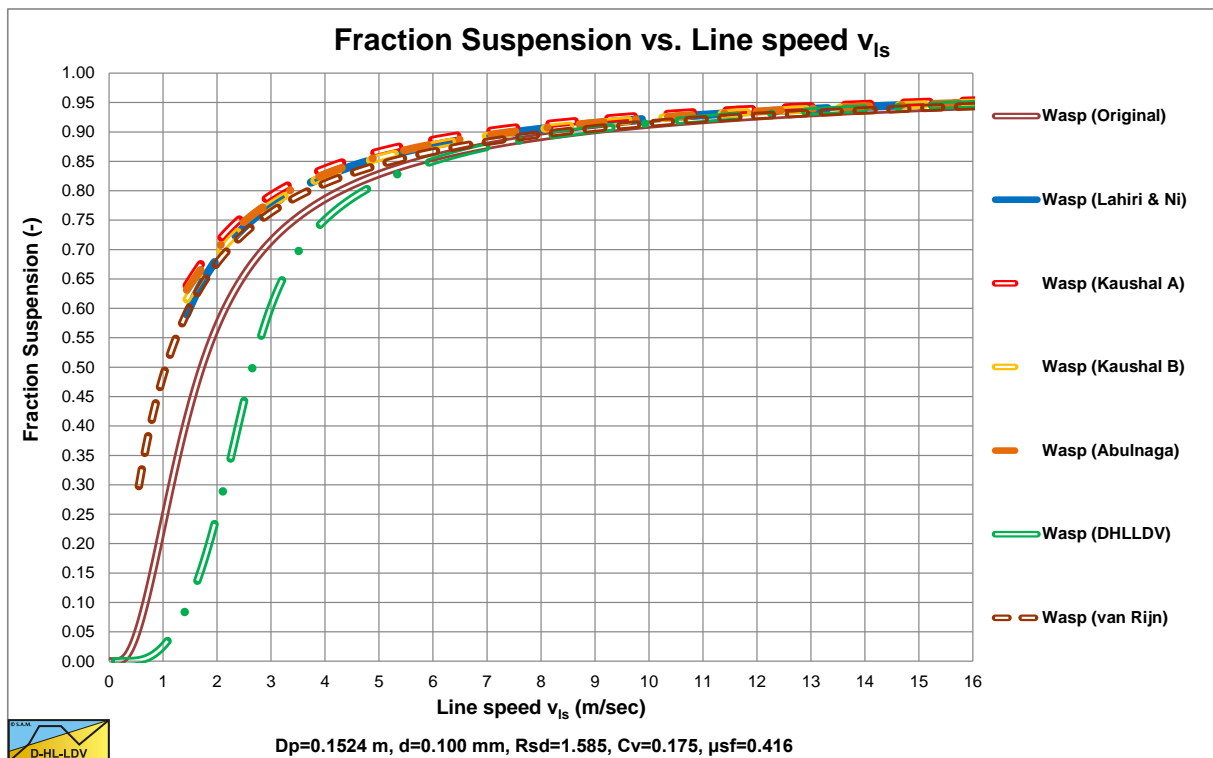
**Figure 7.10-2: The suspended fraction for a d=0.1 mm sand particle,
modified diffusivity and hindered settling.**
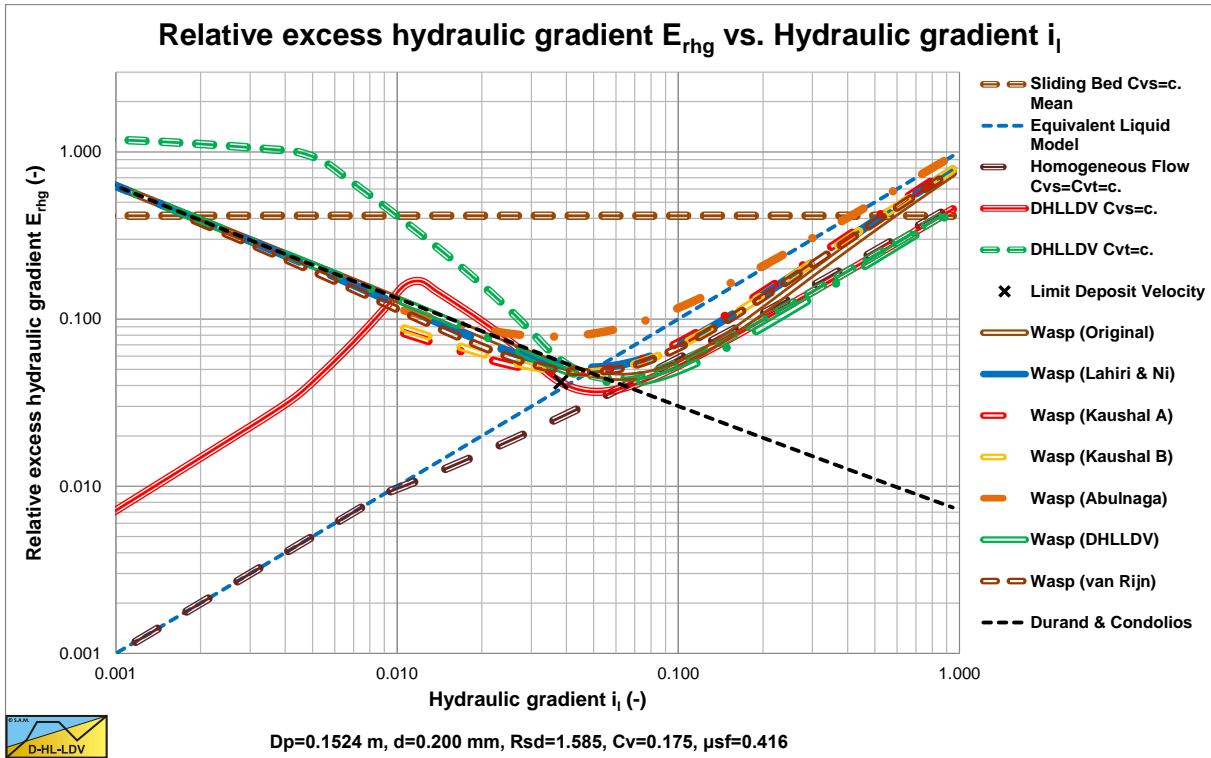
Figure 7.10-3: The Wasp model for a d=0.2 mm sand particle, modified diffusivity and hindered settling.
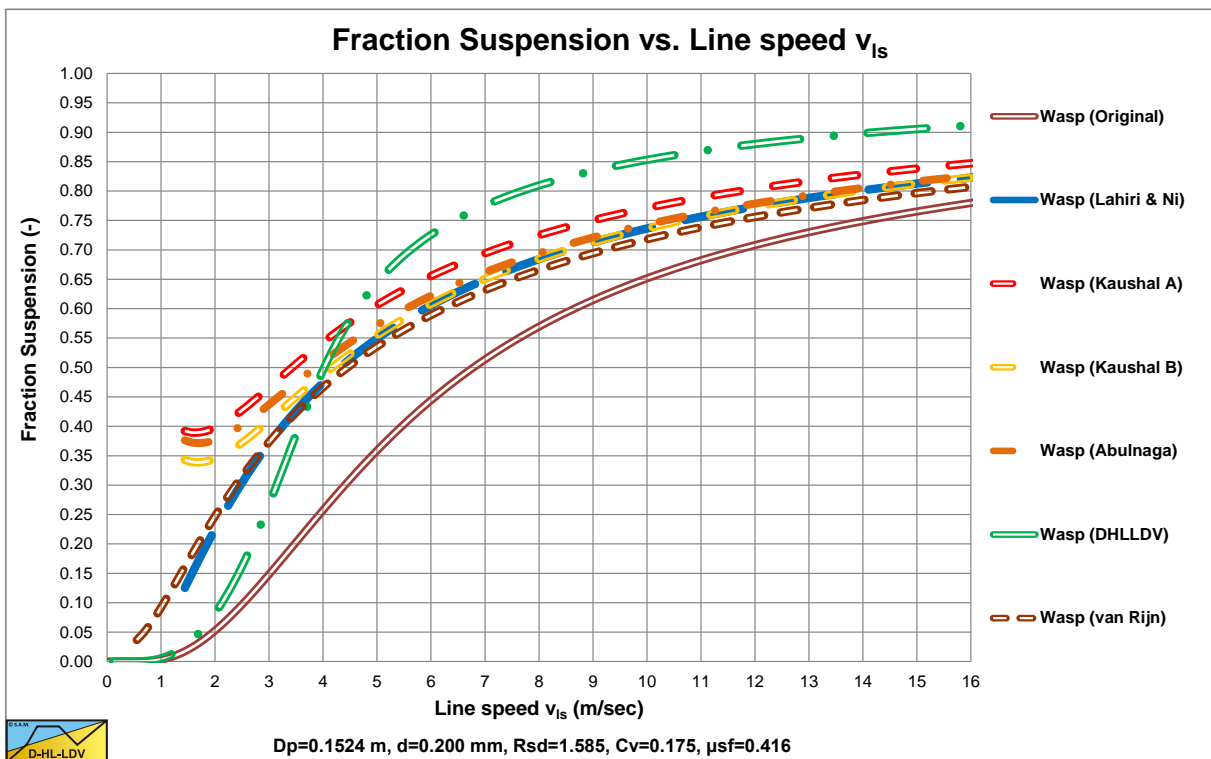
**Figure 7.10-4: The suspended fraction for a d=0.2 mm sand particle,
modified diffusivity and hindered settling.**

For the 0.2 mm particle, the DHLLDV implementation gives a larger suspended fraction compared to the other implementations above a line speed of about 4.5 m/sec. In terms of the E_{rhg} value, the differences are small. In terms of the hydraulic gradient, the differences are very small.
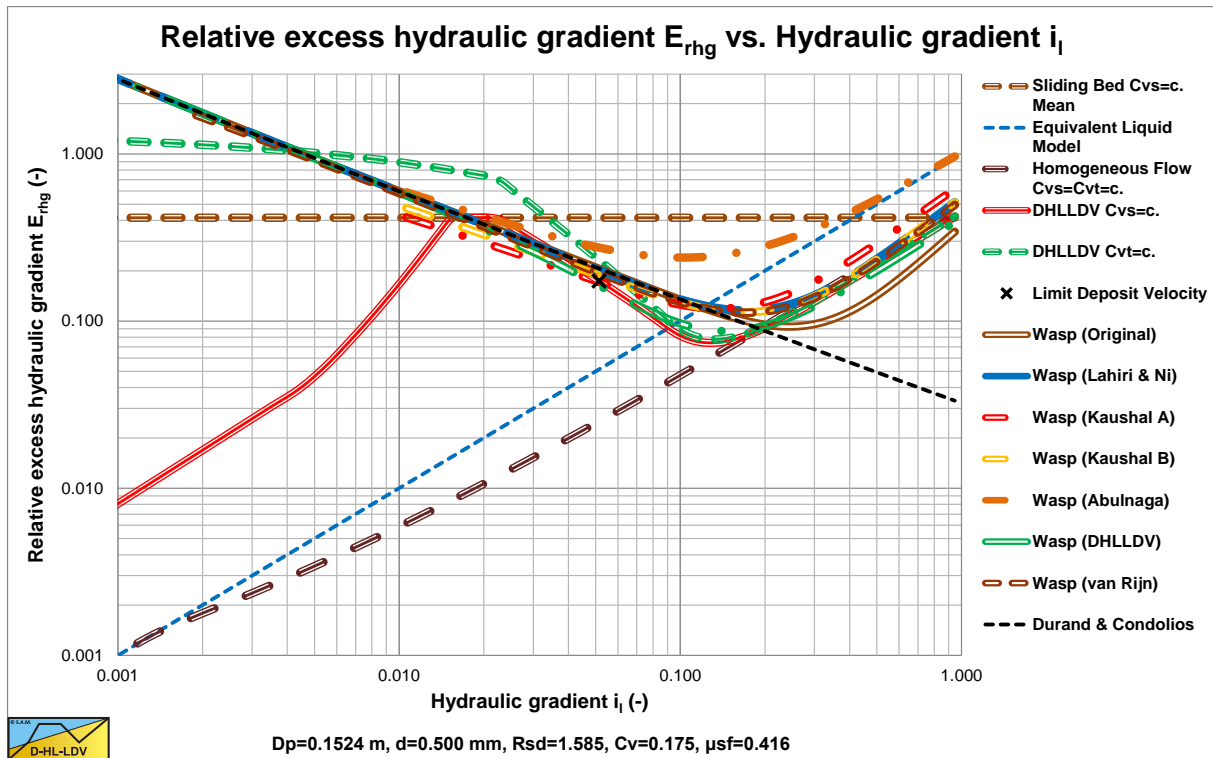
Figure 7.10-5: The Wasp model for a d=0.5 mm sand particle, modified diffusivity and hindered settling.
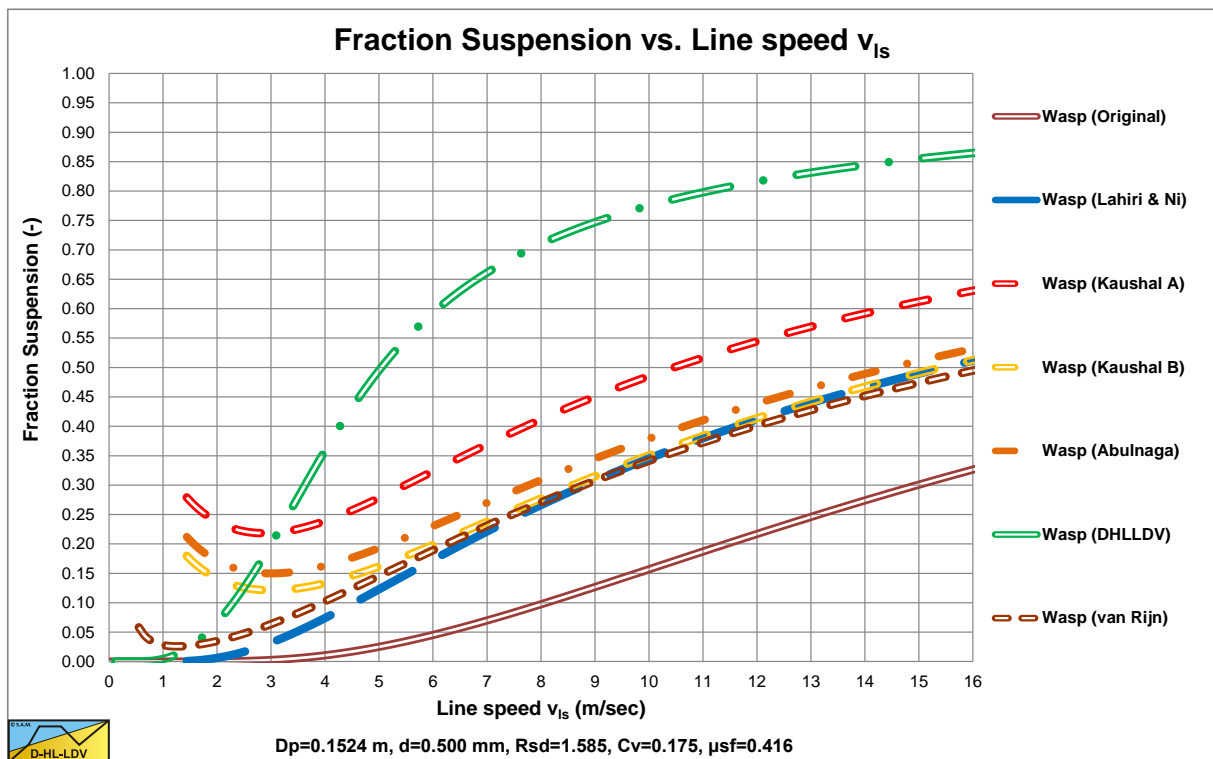
**Figure 7.10-6: The suspended fraction for a d=0.5 mm sand particle,
modified diffusivity and hindered settling.**

For the 0.5 mm particle, the DHLLDV implementation gives a larger suspended fraction compared to the other implementations. In terms of the **E_{rhg}** value, the differences are small. In terms of the hydraulic gradient, the differences are very small.
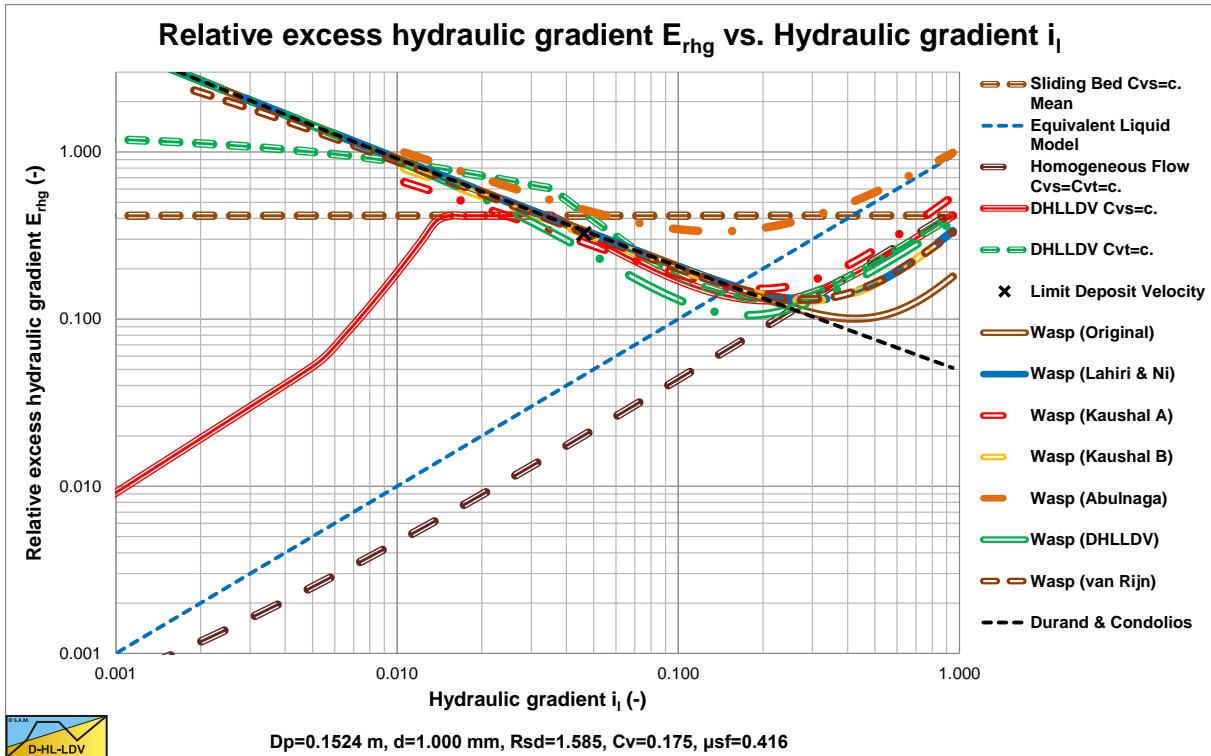
Figure 7.10-7: The Wasp model for a d=1.0 mm sand particle, modified diffusivity and hindered settling.
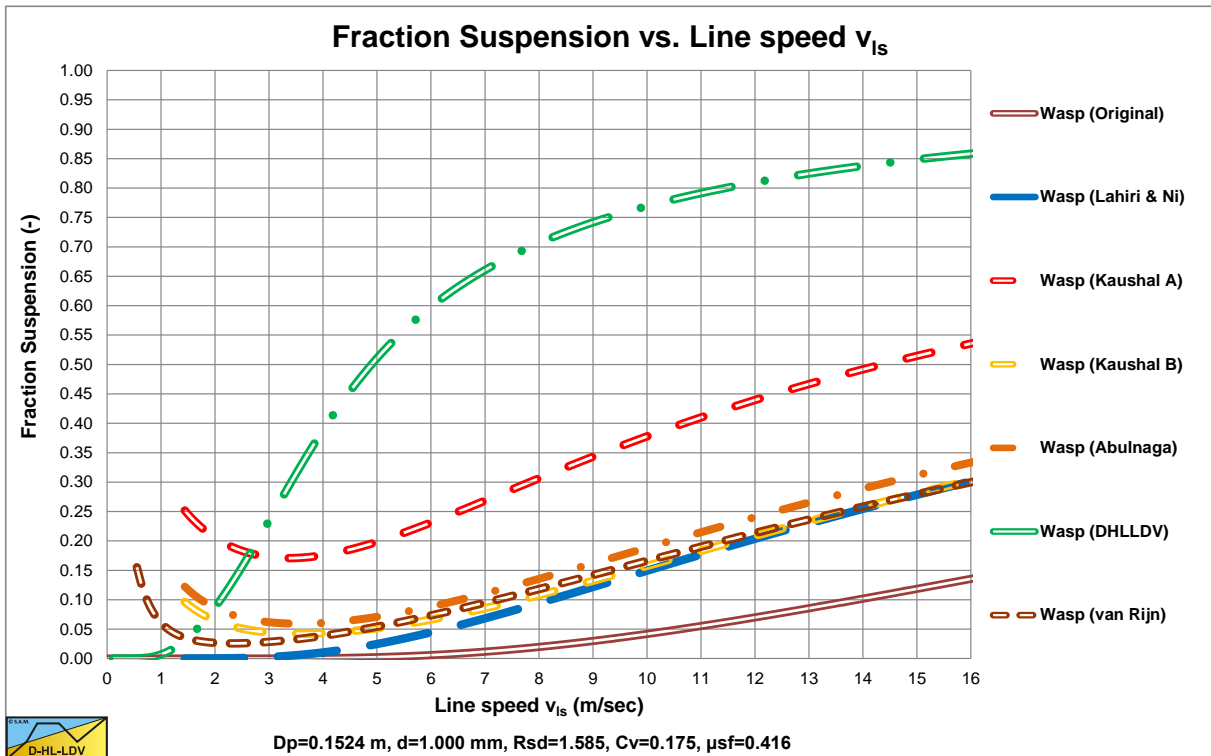
Figure 7.10-8: The suspended fraction for a d=1.0 mm sand particle, modified diffusivity and hindered settling.

For the 1.0 mm particle, the DHLLDV implementation gives a much larger suspended fraction compared to the other implementations. In terms of the E_{rhg} value, the differences are not small anymore. In terms of the hydraulic gradient, the differences are still small.

7.10.4 Numerical Implementation.

The concentration in the pipe can be described according to:

$$
C_{vs}(r) = C_{vB} \cdot e^{-\frac{\alpha_{sm}}{C_{vr}} \left(\frac{v_{ls,ldv}}{v_{ls}} \right)^{0.925} \cdot \frac{v_{tv}}{v_{tv,ldv}} \cdot \frac{r}{D_p}} \quad \text{or} \quad C_{vs}(r) = C_{vB} \cdot e^{-\frac{\alpha_{sm}}{C_{vr}} \left(\frac{v_{ls,ldv}}{v_{ls}} \right)^{0.925} \cdot \frac{v_{thv}}{v_{thv,ldv}} \cdot \frac{r}{D_p}} \tag{7.10-19}
$$

The bottom concentration is now for line speeds above the LDV:

$$
C_{vB} = C_{vb} \cdot \left(\frac{v_{ls,ldv}}{v_{ls}} \right)^{0.925} \cdot \frac{v_{tv}}{v_{tv,ldv}} \quad \text{or} \quad C_{vB} = C_{vb} \cdot \left(\frac{v_{ls,ldv}}{v_{ls}} \right)^{0.925} \cdot \frac{v_{thv}}{v_{thv,ldv}} \tag{7.10-20}
$$

Now assuming that the terminal (hindered) settling velocity in the suspension lightly depends on the line speed, these equations can be written as:

The concentration in the pipe can be described according to:

$$
C_{vs}(r) = C_{vB} \cdot e^{-\frac{\alpha_{sm}}{C_{vr}} \cdot \frac{u_{*,ldv}}{u_*} \cdot \frac{v_{tv}}{v_{tv,ldv}} \cdot \frac{r}{D_p}} \approx C_{vB} \cdot e^{-\frac{\alpha_{sm}}{C_{vr}} \left(\frac{v_{ls,ldv}}{v_{ls}} \right)^{1.15} \cdot \frac{r}{D_p}} \tag{7.10-21}
$$

The bottom concentration is now for line speeds above the LDV:

$$
C_{vB} = C_{vb} \cdot \frac{\left(\alpha_{sm} \cdot \frac{u_{*,ldv}}{u_*} \cdot \frac{v_{tv}}{v_{tv,ldv}} \right)}{\left(1 - e^{-\frac{\alpha_{sm}}{C_{vr}} \frac{u_{*,ldv}}{u_*} \frac{v_{tv}}{v_{tv,ldv}}} \right)} = C_{vb} \cdot \frac{\left(\alpha_{sm} \cdot \left(\frac{v_{ls,ldv}}{v_{ls}} \right)^{1.15} \right)}{\left(1 - e^{-\frac{\alpha_{sm}}{C_{vr}} \left(\frac{v_{ls,ldv}}{v_{ls}} \right)^{1.15}} \right)} \tag{7.10-22}
$$

These equations describe the concentration distribution well for 2D channel flow above the LDV. However for a circular pipe and below the LDV some adjustments have to be made. When the concentration found is integrated over the circular cross section of the pipe, the cross sectional averaged concentration has to be equal to the average concentration that is input to the calculations, which might be the case for a symmetrical concentration distribution, but certainly not for an asymmetrical concentration distribution.

The concentration in the pipe can be described according to:

$$
C_{vs}(r) = C_{vB} \cdot e^{-\frac{\alpha_{sm}}{C_{vr}} \left(\frac{v_{ls,ldv}}{v_{ls}} \right)^{1.15} \cdot \frac{r}{D_p}} \tag{7.10-23}
$$

Now in the case of a circular pipe the vertical coordinate r/D_p should be replaced by the fraction of the cross section f. This gives a much better match with the cross sectional averaged concentration in case there is no bed, so above the LDV. This fraction can be determined by the angle β matching a certain vertical coordinate, similar to the angle β for the stationary and sliding bed.

$$
\beta = a\cos\left(\frac{0.5 - \frac{r}{D_p}}{0.5} \right) \tag{7.10-24}
$$

The fraction **f** is now:

$$f = \frac{\beta - \sin(\beta) \cdot \cos(\beta)}{\pi}$$

(7.10-25)

The concentration at **f** is now:

$$C_{vs}(f) = C_{vB} \cdot e^{-\frac{\alpha_{sm}}{C_{vr}} \cdot \left(\frac{v_{ls,ldv}}{v_{ls}}\right)^{1.15} \cdot f}$$

(7.10-26)

The bottom concentration is now for line speeds above the LDV:

$$C_{vB} = C_{vb} \cdot \frac{\left(\alpha_{sm} \cdot \left(\frac{v_{ls,ldv}}{v_{ls}}\right)^{1.15}\right)}{\left(1 - e^{-\frac{\alpha_{sm}}{C_{vr}} \cdot \left(\frac{v_{ls,ldv}}{v_{ls}}\right)^{1.15}}\right)}$$

(7.10-27)

Because the Limit Deposit Velocity is based on the occurrence of some bed at the bottom of the pipe, this bed does not need to have the maximum bed density. A bed may start to occur with a bottom concentration of about 50%, while the maximum bed concentration will be in the range of 60%-65%. In order to find a bottom concentration of about 50% at the LDV assuming a maximum bed concentration of 60%, an additional velocity ratio **r_LDV** is introduced giving:

$$C_{vB} = C_{vb} \cdot \frac{\left(\alpha_{sm} \cdot \left(r_{LDV} \cdot \frac{v_{ls,ldv}}{v_{ls}}\right)^{1.15}\right)}{\left(1 - e^{-\frac{\alpha_{sm}}{C_{vr}} \cdot \left(r_{LDV} \cdot \frac{v_{ls,ldv}}{v_{ls}}\right)^{1.15}}\right)} \quad \text{and} \quad C_{vs}(f) = C_{vB} \cdot e^{-\frac{\alpha_{sm}}{C_{vr}} \cdot \left(r_{LDV} \cdot \frac{v_{ls,ldv}}{v_{ls}}\right)^{1.15} \cdot f}$$

(7.10-28)

The additional velocity ratio **r_LDV** can be estimated by, considering the maximum LDV occurs at a concentration of 17.5%:

SF = Shape Factor   **SF=0.77 for sand**   **SF=1.0 for spheres**

$$C_{vrMax} = \frac{0.175}{C_{vb}}$$

$$\alpha_\beta = 1.8 - 56 \cdot v_t \quad \text{with:} \quad \alpha_\beta \geq 1.1$$

If $C_{vr} < C_{vrMax}$ then

(7.10-29)

$$r_{LDV} = 0.6 \cdot \frac{e^{(\beta/2.34)^{\alpha_\beta}}}{e} \cdot \left(\frac{0.0005}{d}\right)^{SF^6} \cdot \left(\frac{C_{vrMax}}{C_{vr}}\right)^{1/3} \quad \text{with:} \quad r_{LDV} \geq 1.2 \cdot \left(\frac{C_{vrMax}}{C_{vr}}\right)^{1/3}$$

If $C_{vr} \geq C_{vrMax}$ then

$$r_{LDV} = 0.6 \cdot \frac{e^{(\beta/2.34)^{\alpha_\beta}}}{e} \cdot \left(\frac{0.0005}{d}\right)^{SF^6} \cdot \left(\frac{C_{vr}}{C_{vrMax}}\right)^{1/6} \quad \text{with:} \quad r_{LDV} \geq 1.2 \cdot \left(\frac{C_{vr}}{C_{vrMax}}\right)^{1/6}$$

7.10.5 Examples Numerical Implementation.

In Figure 7.10-9, Figure 7.10-10 and Figure 7.10-11 the bottom concentration is limited to the bed concentration. If equation (7.10-11) gives a higher concentration, the top of the bed is determined at the level where the concentration equals the bed concentration and above the bed a new concentration profile is determined. This is repeated until a concentration profile is found matching the input spatial concentration.

Cvb=0.60, VlsRatio=0.25, β=2.738, α1=2.000, α2=1.250
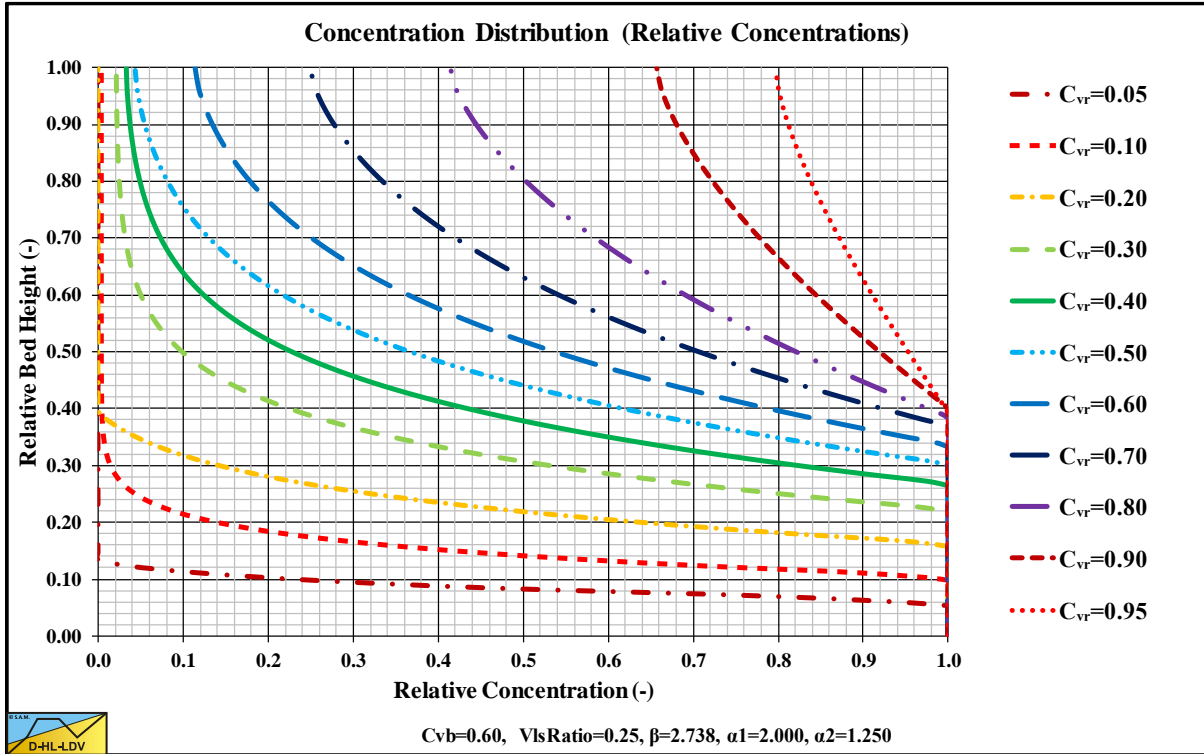
Figure 7.10-9: The concentration profiles at $v_{ls}=0.25 \cdot v_{ls,ldv}$.

Cvb=0.60, VlsRatio=0.50, β=2.738, α1=2.000, α2=1.250
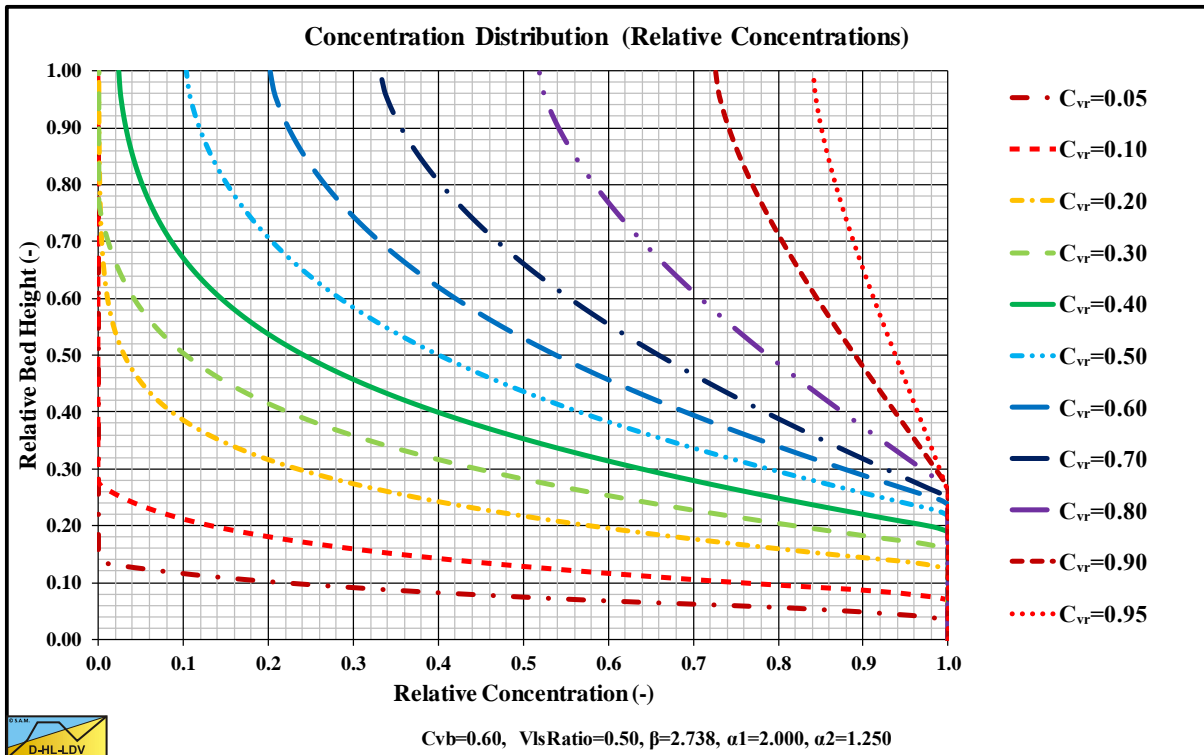
Figure 7.10-10: The concentration profiles at $v_{ls}=0.50 \cdot v_{ls,ldv}$.

The profiles are corrected numerically for the circular shape of a pipe, resulting in the correct cross section averaged spatial concentration. In other words, the cross sectional averaged relative concentration is always equal to the input relative concentration, which it should be. This way the turbulent diffusion equation is not used to determine the concentration in the stationary or sliding bed, which would be inappropriate, since the bed behavior is soil mechanics and not fluid mechanics.

Cvb=0.60, VlsRatio=0.75, β=2.738, α1=2.000, α2=1.250
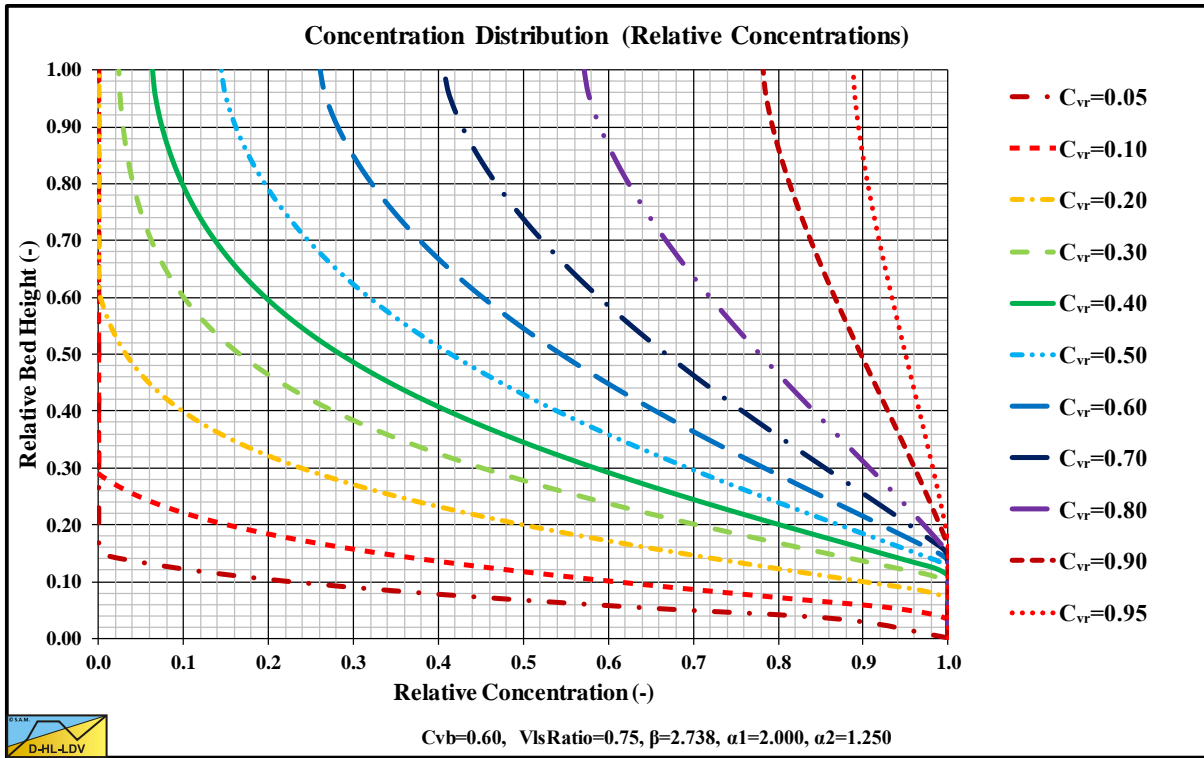
Figure 7.10-11: The concentration profiles at $v_{ls}=0.75 \cdot v_{ls,ldv}$.

Cvb=0.60, VlsRatio=1.00, β=2.738, α1=2.000, α2=1.250
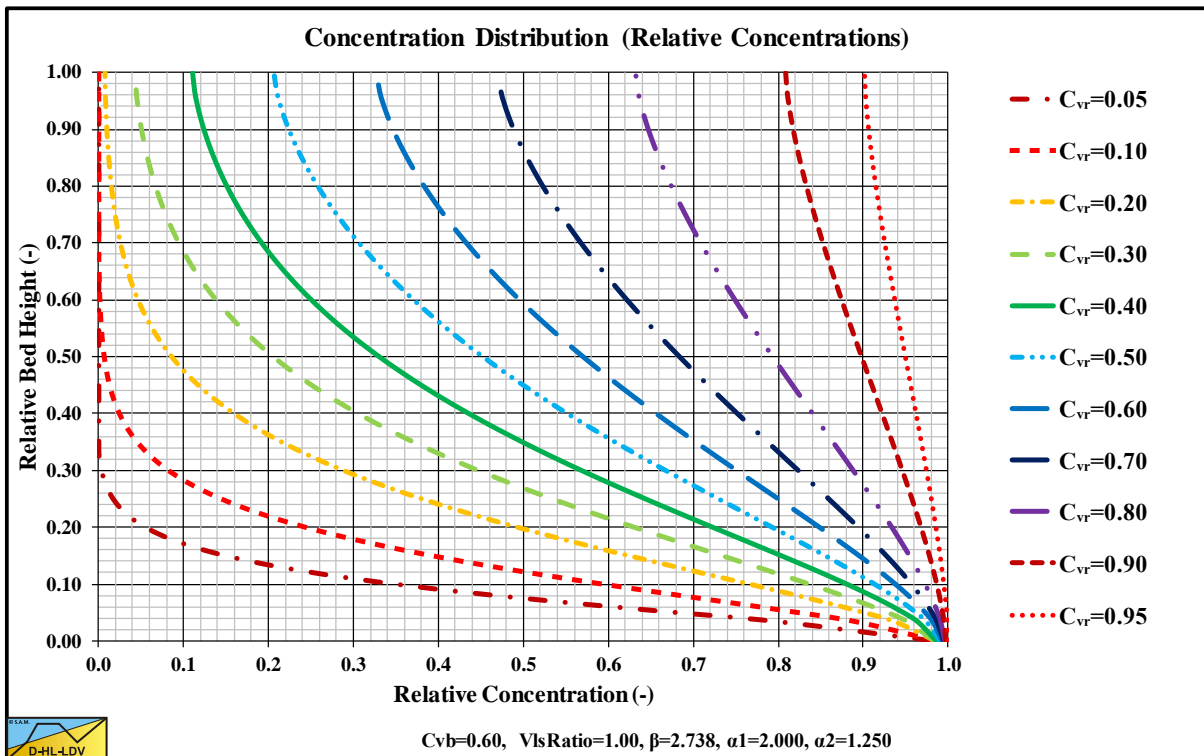
Figure 7.10-12: The concentration profiles at $v_{ls}=1.00 \cdot v_{ls,ldv}$.

Figure 7.10-9, Figure 7.10-10, Figure 7.10-11, Figure 7.10-12, Figure 7.10-13, Figure 7.10-14, Figure 7.10-15 and Figure 7.10-16 show the concentration profiles for relative concentrations, $C_{vr}=C_{vs}/C_{vb}$, ranging from 0.05 to 0.95 and line speeds of 0.25, 0.5, 0.75, 1.0, 1.5, 2.0, 3.0 and 4.0 times the LDV. When the line speed equals the LDV, the concentrations at the bottom of the pipe are equal to the bed concentration. Since the model is using the relative concentration and the relative line speed, the graphs are applicable for each type of material, particle size or solids density.

Cvb=0.60, VlsRatio=1.50, β=2.738, α1=2.000, α2=1.250
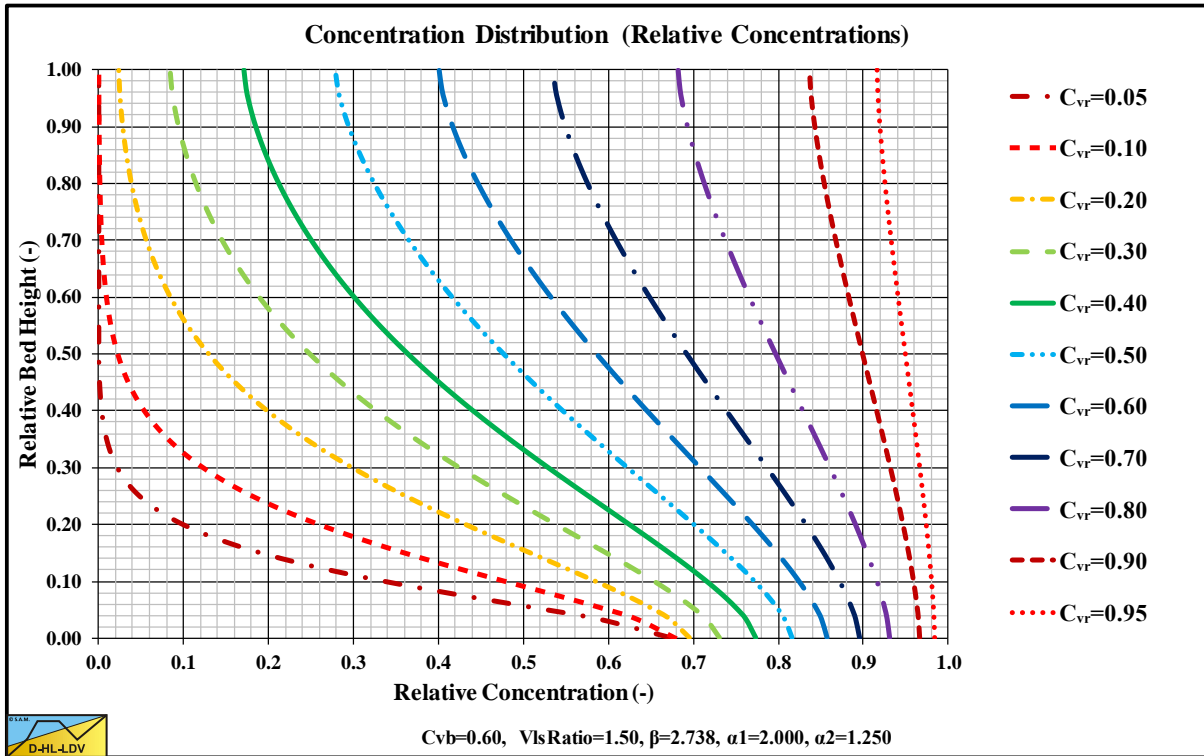
Figure 7.10-13: The concentration profiles at $v_{ls}=1.50 \cdot v_{ls,ldv}$.

Cvb=0.60, VlsRatio=2.00, β=2.738, α1=2.000, α2=1.250
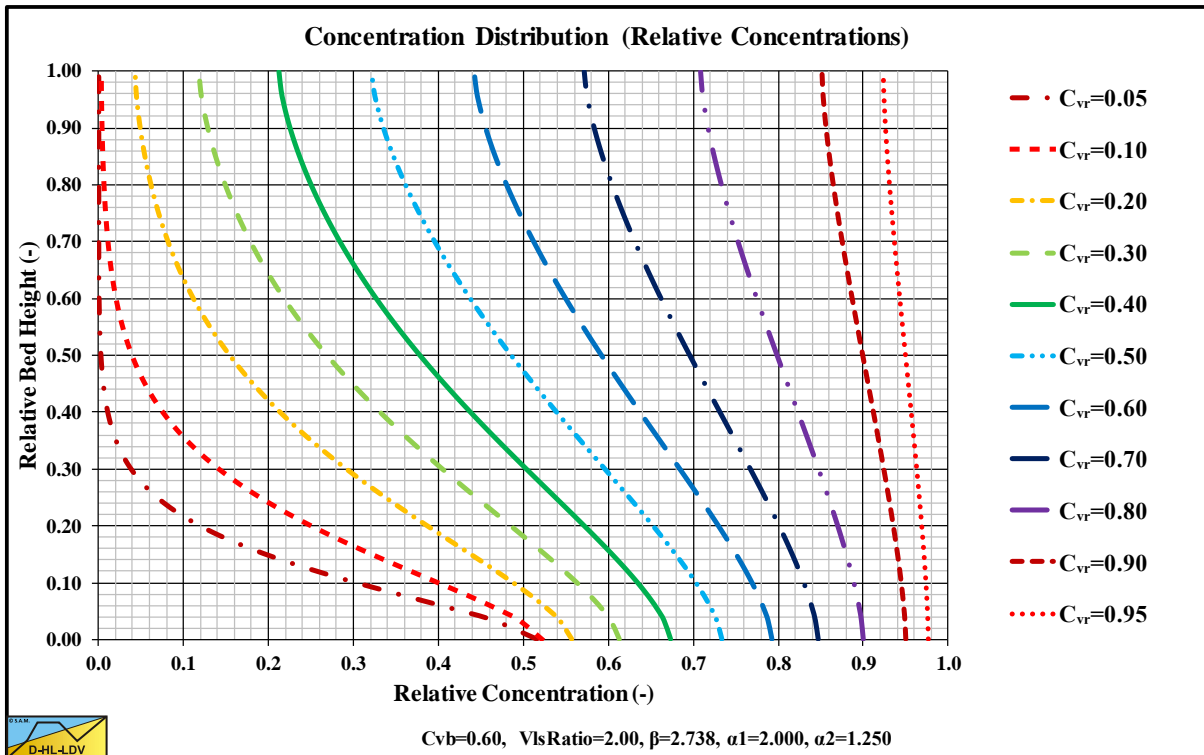
Figure 7.10-14: The concentration profiles at $v_{ls}=2.00 \cdot v_{ls,ldv}$.
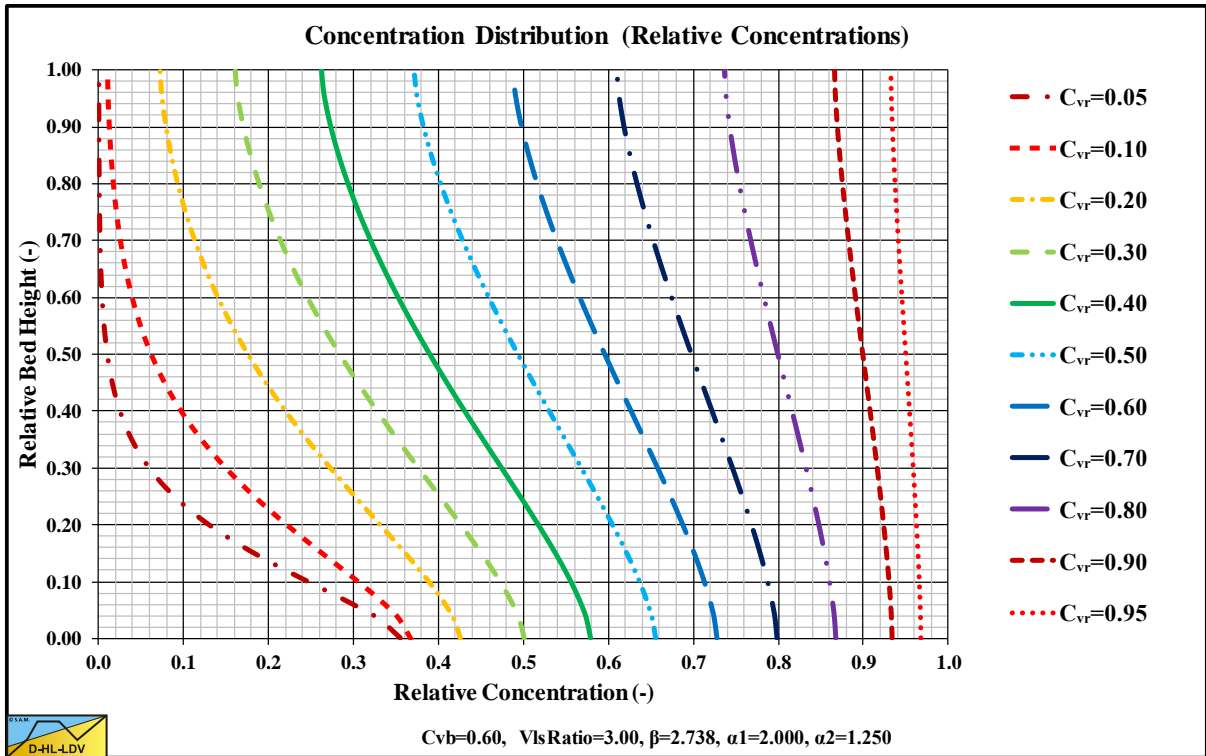
Figure 7.10-15: The concentration profiles at $v_{ls}=3.00 \cdot v_{ls,ldv}$.
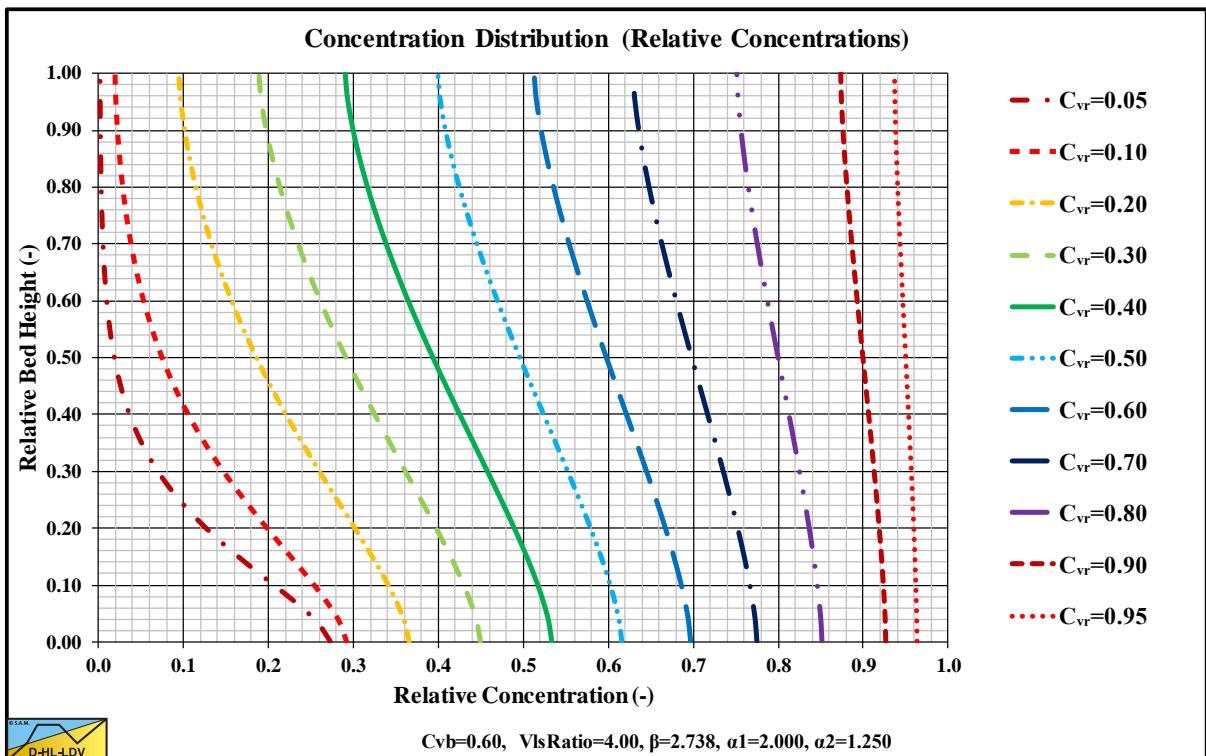
Figure 7.10-16: The concentration profiles at $v_{ls}=4.00 \cdot v_{ls,ldv}$.

The curves are compared with data from Kaushal et al. (2005) with **d=0.44 mm** and **D_p=0.0549 m**. The maximum LDV for this sand and pipe diameter is about 2.5 m/s. The data points are at 3 m/s, so a bit above the LDV depending on the concentration, resulting in smaller concentrations at the bottom of the pipe.
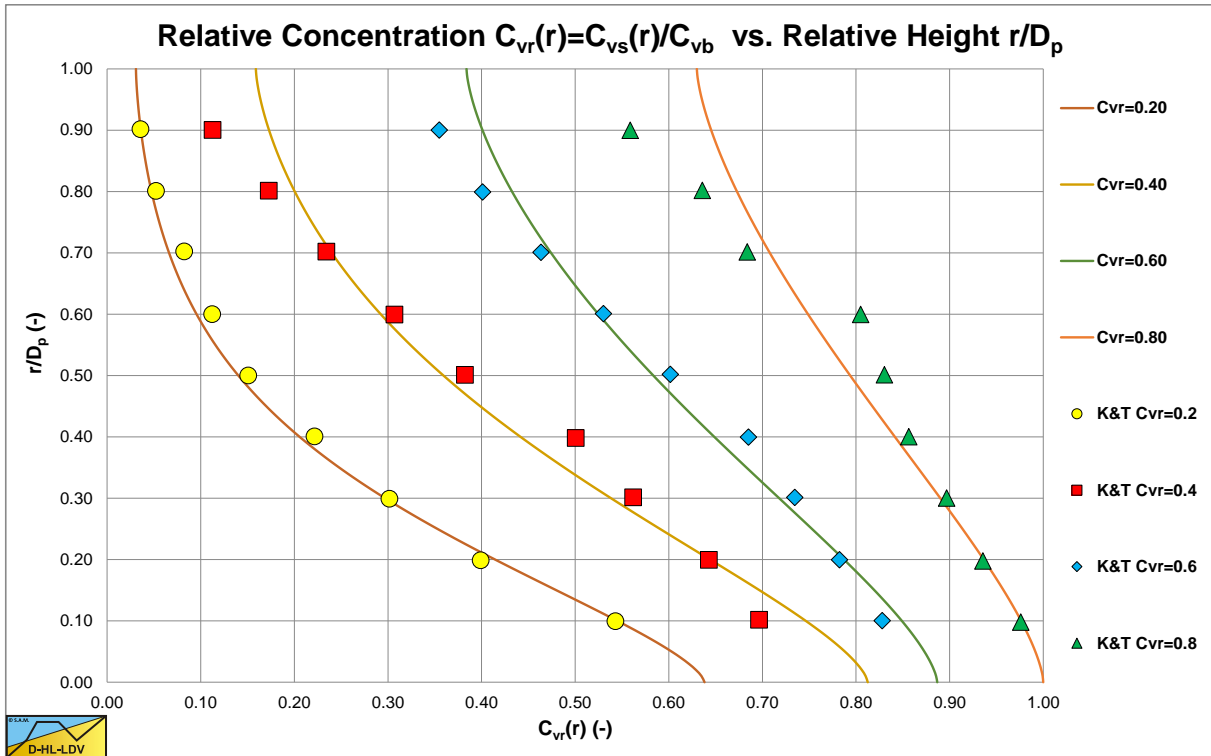
Figure 7.10-17: Data from Kaushal et al. (2005).

The data and the curves match pretty well, although at the top of the pipe the measured concentrations are a bit smaller. This is probably the effect of the local value of the hindered terminal settling velocity, which is higher at lower concentration, resulting in a higher downwards flux of the particles.
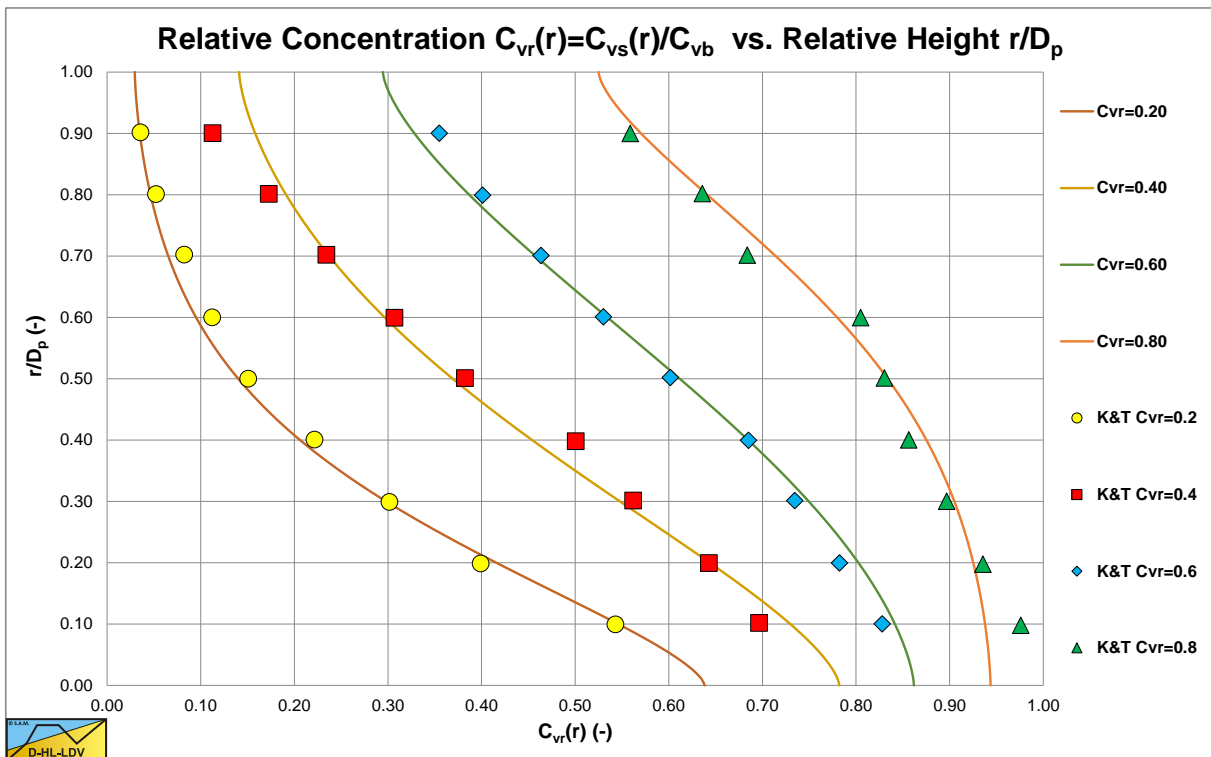
Figure 7.10-18: Data from Kaushal et al. (2005) with local hindered settling.

7.10.6 Hindered Settling Numerical Implementation.

The concentration profiles found match well except for the influence of local hindered settling, which will decrease the concentration at the top of the pipe and increase the concentration at the bottom of the pipe.

The concentration in the pipe without the local hindered settling effect can be described according to:

$$
C_{vB} = C_{vb} \cdot \frac{\left(\alpha_{sm} \cdot \left(r_{LDV} \cdot \frac{v_{ls,ldv}}{v_{ls}} \right)^{1.15} \right)}{\left(1 - e^{-\frac{\alpha_{sm}}{C_{vr}} \cdot \left(r_{LDV} \cdot \frac{v_{ls,ldv}}{v_{ls}} \right)^{1.15}} \right)} \quad \text{and} \quad C_{vs}(f) = C_{vB} \cdot e^{-\frac{\alpha_{sm}}{C_{vr}} \cdot \left(r_{LDV} \cdot \frac{v_{ls,ldv}}{v_{ls}} \right)^{1.15} \cdot f} \tag{7.10-30}
$$

Hindered settling is not explicitly present in this equation. However, the Limit Deposit Velocity depends strongly on the concentration and on hindered settling, so implicitly hindered settling is present. The Limit Deposit Velocity increases with the concentration up to a concentration of 17.5%. For higher concentrations the Limit Deposit Velocity decreases with increasing concentration. This of course influences the concentration distribution.

In the derivation of the concentration distribution it is assumed that the terminal settling velocity or the hindered terminal settling velocity is a constant, determined by the cross sectional average concentration. In reality the concentration is not a constant but decreases from top to bottom. So, the hindered terminal settling velocity at the top of the pipe will be higher than at the bottom, since at the top the concentration is lower. This could be implemented in the basic advection diffusion equation and solved numerically by iteration. However, one can also add a correction to adjust for this hindered settling effect. Such a correction should take the cross sectional averaged concentration into account, since the effect of hindered settling is larger at higher concentrations. After trial and error, the following method is found to take the effect of hindered settling into account:

$$
C_{vs}(f) \cdot v_{th}(f) + \beta_{sm} \cdot \epsilon_m \cdot \frac{dC_{vs}(f)}{df} = 0 \implies
$$

$$
\tag{7.10-31}
$$

$$
\frac{dC_{vs}(f)}{df} = -\frac{C_{vs}(f) \cdot v_{th}(f)}{\beta_{sm} \cdot \epsilon_m} = -\frac{C_{vs}(f) \cdot v_t \cdot \left(1 - C_{vs}(f)\right)^{\beta}}{\beta_{sm} \cdot \epsilon_m}
$$

This is the advection diffusion equation with location dependent hindered settling. To determine the location dependent hindered settling, the local concentration must be known. In the zero step (index 0) the concentration profile is determined without local hindered settling based on equation (7.10-30). The location dependent concentration is already part of the solution and should not be considered in the first iteration (correction) step. Now at each level in the pipe the corrected concentration gradient can be determined according to:

$$
\left(\frac{dC_{vs,1}(f)}{df} \right) = \left(\frac{dC_{vs,0}(f)}{df} \right) \cdot \left(\frac{1 - C_{vs,0}(f)}{1 - C_{vs}} \right)^{\beta} \tag{7.10-32}
$$

The left-hand side is the corrected concentration gradient, the first term on the right-hand side the concentration gradient determined with equation (7.10-30). The second term on the right-hand side gives the correction factor according to the Richardson & Zaki (1954) equation, but with a relative concentration dependent power. The power β is the Richardson & Zaki (1954) power with a value of 4.7 for very small particles and 2.34 for large particles. After determining the corrected concentration gradient at each level in the pipe, the new concentration profile is found by integrating the concentration gradient from bottom to top. It is assumed that the bottom concentration is unchanged. This process can be repeated several times until there is no significant change in the concentration profile. Here 12 iteration steps are used. For the next iteration steps (starting at index 2) also the location dependent concentration ratio is added, because it influences the concentration gradient, giving:

$$\left(\frac{dC_{vs,i}(f)}{df}\right) = \left(\frac{dC_{vs,i-1}(f)}{df}\right) \cdot \left(\frac{C_{vs,i-1}(f)}{C_{vs,i-2}(f)}\right) \cdot \left(\frac{1-C_{vs,i-1}(f)}{1-C_{vs,i-2}(f)}\right)^{\beta} \tag{7.10-33}$$

Although this method gives good results, there are still issues. One of the main issues is that the Richardson & Zaki (1954) hindered settling equation is based on the spatial volumetric concentration C_{vs} and not on the relative spatial volumetric concentration $C_{vr}=C_{vs}/C_{vb}$.

$$\frac{v_{th}}{v_t} = \left(1-C_{vs}\right)^{\beta} \tag{7.10-34}$$

So even when the spatial volumetric concentration reaches a concentration where a bed with maximum porosity occurs, for sand at about $C_{vs}=50\%$, still a hindered settling velocity is determined, while in reality this hindered settling velocity will be close to zero. Normal sands will have a porosity of about 40%, so $C_{vb}=60\%$. A fixed bed may have a porosity of 40%, but a sliding bed will have a higher porosity in between 40% and 50%. The porosities mentioned here depend on the type of sand but are mentioned to give a feeling of the order of magnitude. An equation that may work better is:

$$\frac{v_{th}}{v_t} = \left(1-C_{vr}\right)^{\alpha \cdot \frac{\beta}{2.34}} \tag{7.10-35}$$

For small concentrations this equation gives the same result as the original equation, but for concentrations approaching the bed concentration, this equation approaches a zero-settling velocity. This would describe the bed behavior much better. So, for small concentrations this equation describes hindered settling, while for large relative concentrations approaching 1, the behavior is closer to consolidation behavior. The power β in this equation is equal to the original power β.

To determine the location dependent hindered settling, the local concentration must be known. In the zero step (index 0) the concentration profile is determined without local hindered settling based on equation (7.10-35). The location dependent concentration is already part of the solution and should not be considered in the first iteration (correction) step. Now at each level in the pipe the corrected concentration gradient can be determined according to:

$$\left(\frac{dC_{vs,1}(f)}{df}\right) = \left(\frac{dC_{vs,0}(f)}{df}\right) \cdot \left(\frac{\left(1-C_{vr,0}\right)}{\left(1-C_{vr}\right)}\right)^{\alpha \cdot \frac{\beta}{2.34}} \tag{7.10-36}$$

The left-hand side is the corrected concentration gradient, the first term on the right-hand side the concentration gradient determined with equation (7.10-35). The second term on the right-hand side gives the correction factor according to equation (7.10-35), but with a relative concentration dependent power. The power β is the Richardson & Zaki (1954) power with a value of 4.7 for very small particles and 2.34 for large particles. After determining the corrected concentration gradient at each level in the pipe, the new concentration profile is found by integrating the concentration gradient from bottom to top. It is assumed that the bottom concentration is unchanged. This process can be repeated several times until there is no significant change in the concentration profile. Here 12 iteration steps are used. For the next iteration steps (starting at index 2) also the location dependent relative concentration ratio is added, because it influences the concentration gradient, giving:

$$\left(\frac{dC_{vs,i}(f)}{df}\right) = \left(\frac{dC_{vs,i-1}(f)}{df}\right) \cdot \left(\frac{C_{vr,i-1}(f)}{C_{vr,i-2}(f)}\right) \cdot \left(\frac{\left(1-C_{vr,i-1}\right)}{\left(1-C_{vr,i-2}\right)}\right)^{\alpha \cdot \frac{\beta}{2.34}} \tag{7.10-37}$$

Using this new equation gives significant different concentration profiles. The concentration profile of a sliding bed with sheet flow is simulated well with this equation. The power **α** is determined with the following equations:

<div style="border: 2px solid green; padding: 10px;">

SF = Shape Factor   SF=0.77 for sand   SF=1.0 for spheres

$$C_{vrMax} = \frac{0.175}{C_{vb}}$$

$$\alpha = 0.275 \cdot \left(\frac{SF}{0.77}\right)^{1.5} \cdot \left(\frac{C_{vr}}{C_{vrMax}}\right)^{3} \cdot \left(\frac{v_{ls,LDV}}{v_{ls}}\right)^{0.15} \qquad \text{for } C_{vr} < C_{vrMax}$$

$$\alpha = 0.275 \cdot \left(\frac{SF}{0.77}\right)^{1.5} \cdot \left(\frac{C_{vr}}{C_{vrMax}}\right)^{2/3} \cdot \left(\frac{v_{ls,LDV}}{v_{ls}}\right)^{0.15} \qquad \text{for } C_{vr} \geq C_{vrMax}$$

(7.10-38)

</div>

Cvb=0.60, Cvs=0.300, VlsRatio=1.00, β=2.738, α1=2.000, α2=1.250
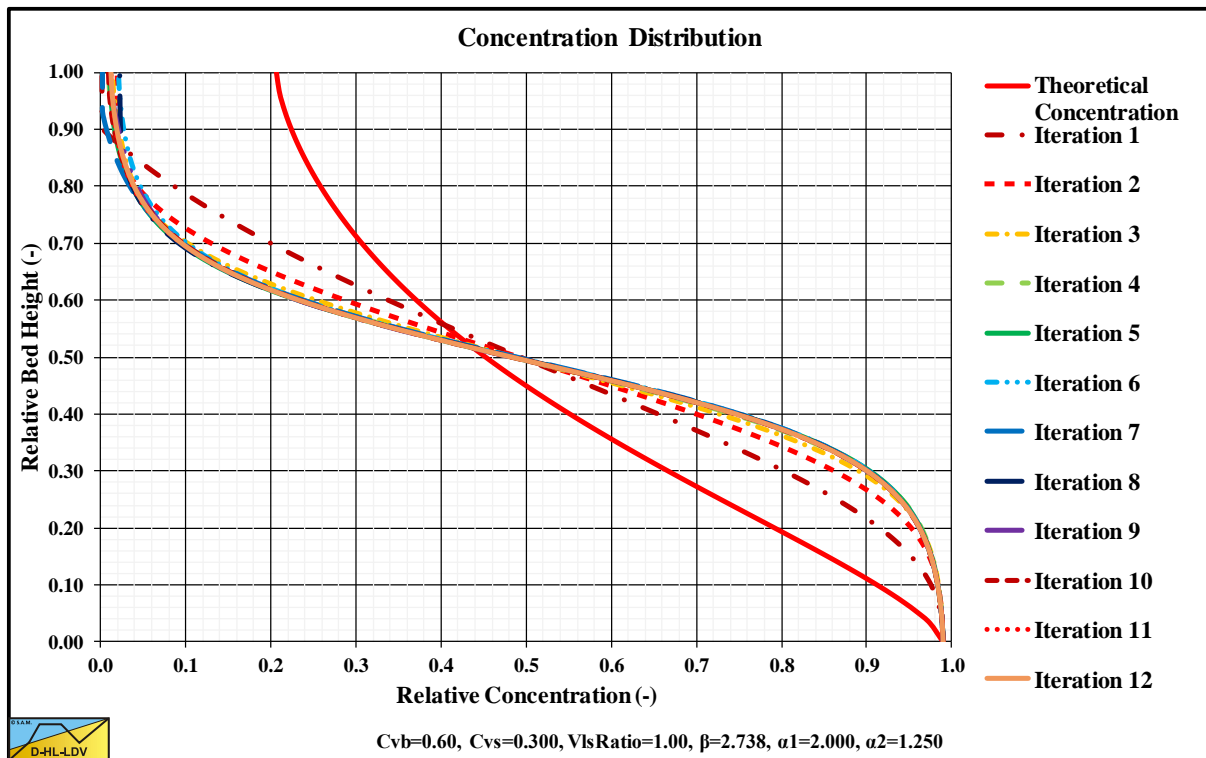
Figure 7.10-19: Concentration profiles with and without local hindered setting.

Figure 7.10-19 shows a concentration profile for a line speed of 1 times the LDV and a relative concentration of 50% of the bed concentration. The red line shows the concentration profile as determined with equation (7.10-35). This results in the 12 iteration steps, where above the bottom the concentration is increased, while at the top the concentration has decreased. It is clear from this figure that 12 iteration steps give enough convergence.

Figure 7.10-20, Figure 7.10-21, Figure 7.10-22, Figure 7.10-23, Figure 7.10-24, Figure 7.10-25, Figure 7.10-26 and Figure 7.10-27 show the concentration profiles with the effect of local hindered settling after applying the local hindered settling influence. Of course, this is a pragmatic solution, but it does give a closer fit to the data in Figure 7.10-18 compared to Figure 7.10-17. At high concentrations the concentration profile at the top of the pipe may not be accurate, especially at small line speeds. This is caused by the high concentrations at the bottom of the pipe. The standard graphs are determined with an average of **β=2.7** for medium sized particles.

To use these graphs, one should first determine the LDV at different concentrations for a specific particle diameter. Based on the LDV, the line speed to LDV ratio can be determined. Once this ratio is known, the graph the closest to the ratio should be chosen.

7.10.7 Examples Hindered Settling Numerical Implementation.
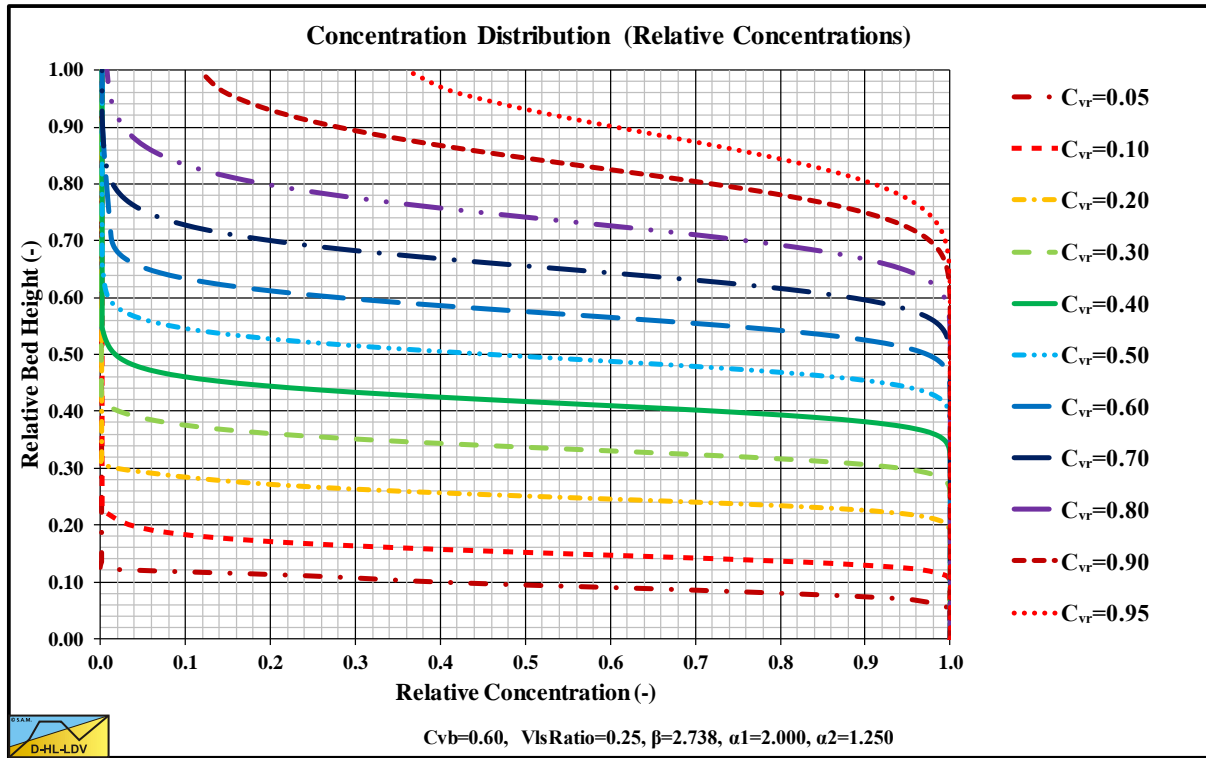
Figure 7.10-20: The concentration profiles at $v_{ls}=0.25 \cdot v_{ls,ldv}$ with hindered settling.
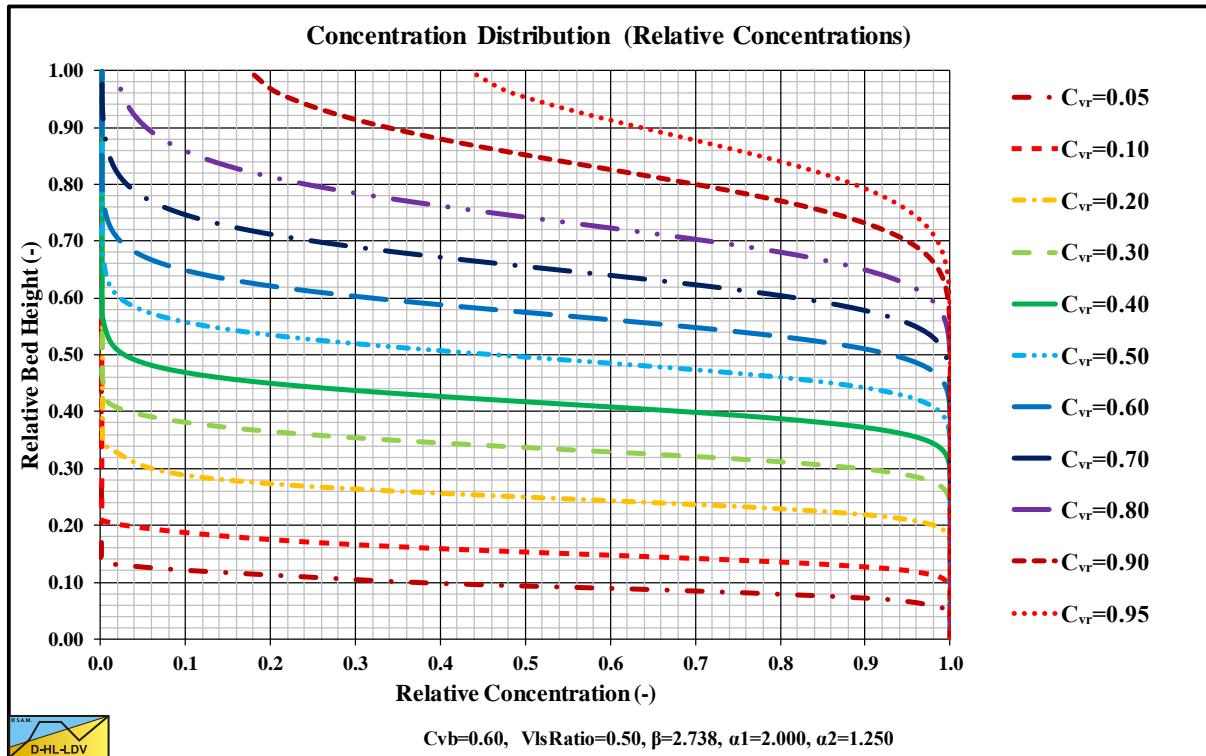
Figure 7.10-21: The concentration profiles at $v_{ls}=0.50 \cdot v_{ls,ldv}$ with hindered settling.

The graphs are determined with a maximum bed concentration of 60%, which is reasonable for dense sand. For line speeds below the LDV sheet flow is observed by many researchers. Sheet flow is a layer of fast moving particles on top of a stationary or sliding bed. The particles closest to the bed move with the speed of the bed, while the particles at the top of the sheet flow layer move with a speed related to the speed of the liquid above the bed. The concentration is assumed to decrease almost linear, starting at the bed with the bed concentration, to almost

zero at the top of the sheet flow layer. The start of the sheet flow layer is not at the maximum bed concentration, but at a concentration where the particles still form a solid bed, which would be at about 50% bed concentration, a relative concentration of about 0.83 or 83%. The graphs show an almost linear concentration profile from a relative concentration of 83% to a relative concentration of 10%, except for the highest overall relative concentrations of 90% and 95%. The steepness of the almost linear part of the concentration profiles increases with increasing overall (cross sectional averaged) relative concentration and decreases with decreasing line speed.

Cvb=0.60, VlsRatio=0.75, β=2.738, α1=2.000, α2=1.250
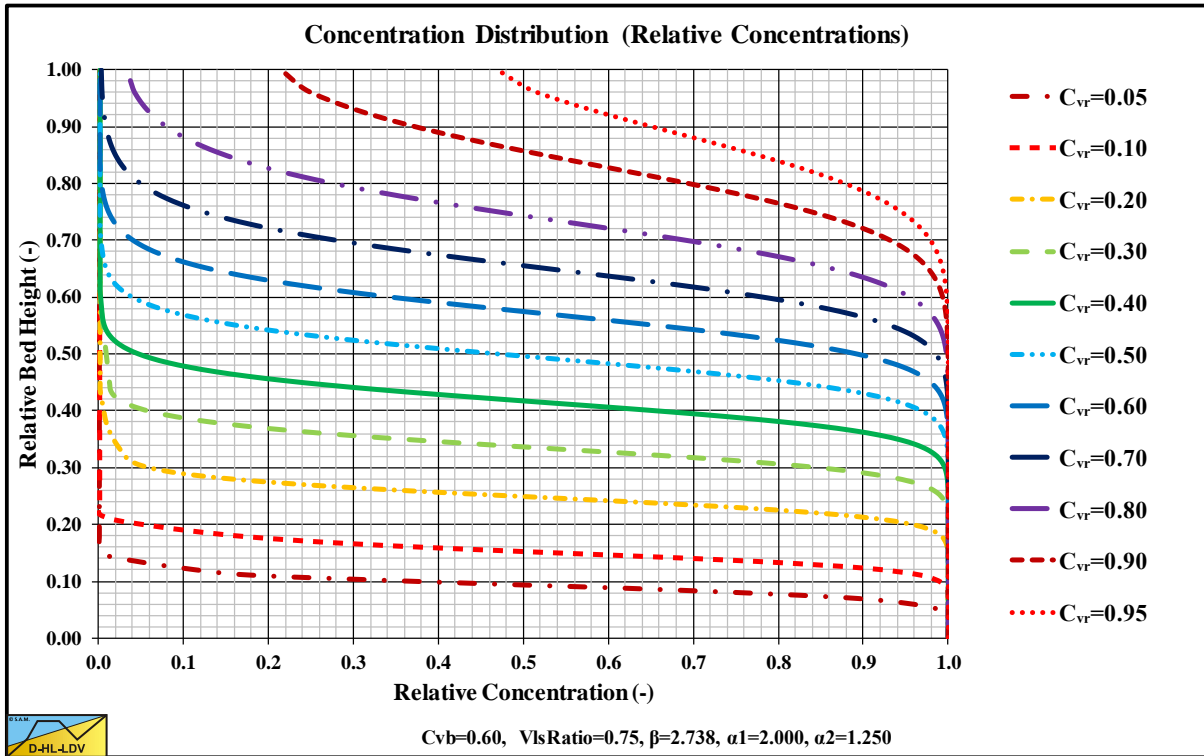
Figure 7.10-22: The concentration profiles at $v_{ls}=0.75 \cdot v_{ls,ldv}$ with hindered settling.

Cvb=0.60, VlsRatio=1.00, β=2.738, α1=2.000, α2=1.250
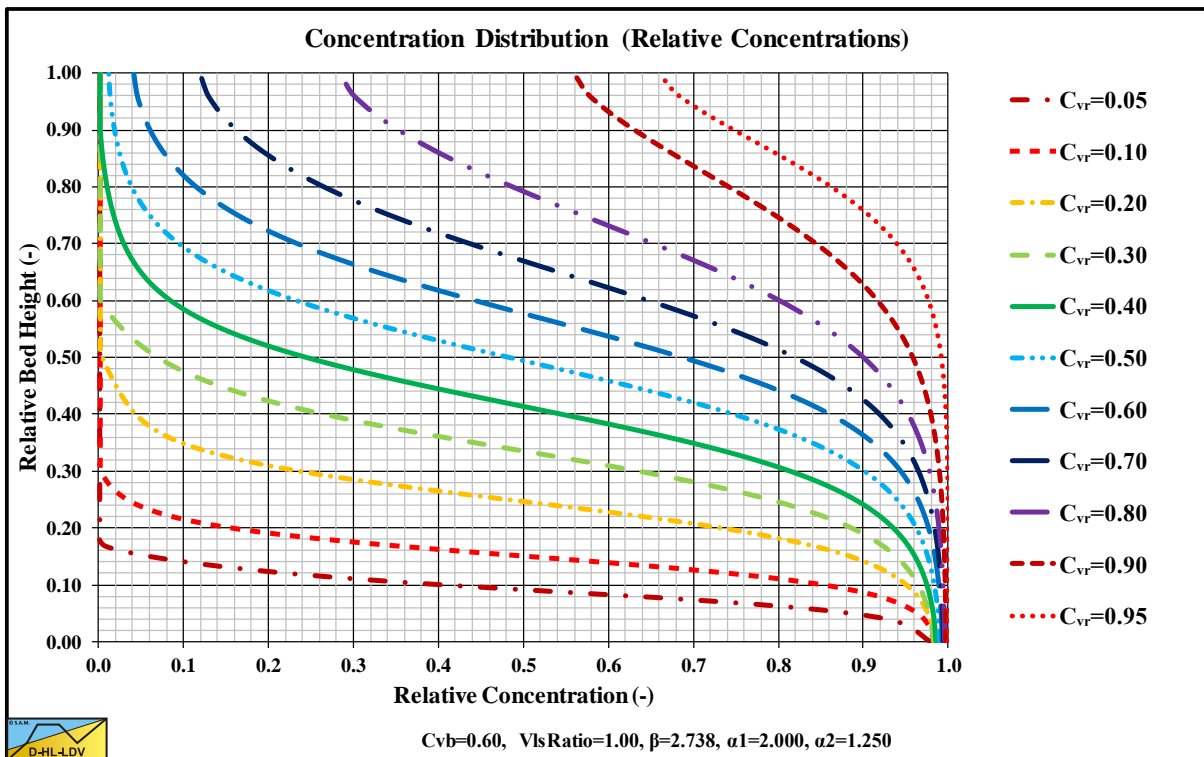
Figure 7.10-23: The concentration profiles at $v_{ls}=1.00 \cdot v_{ls,ldv}$ with hindered settling.
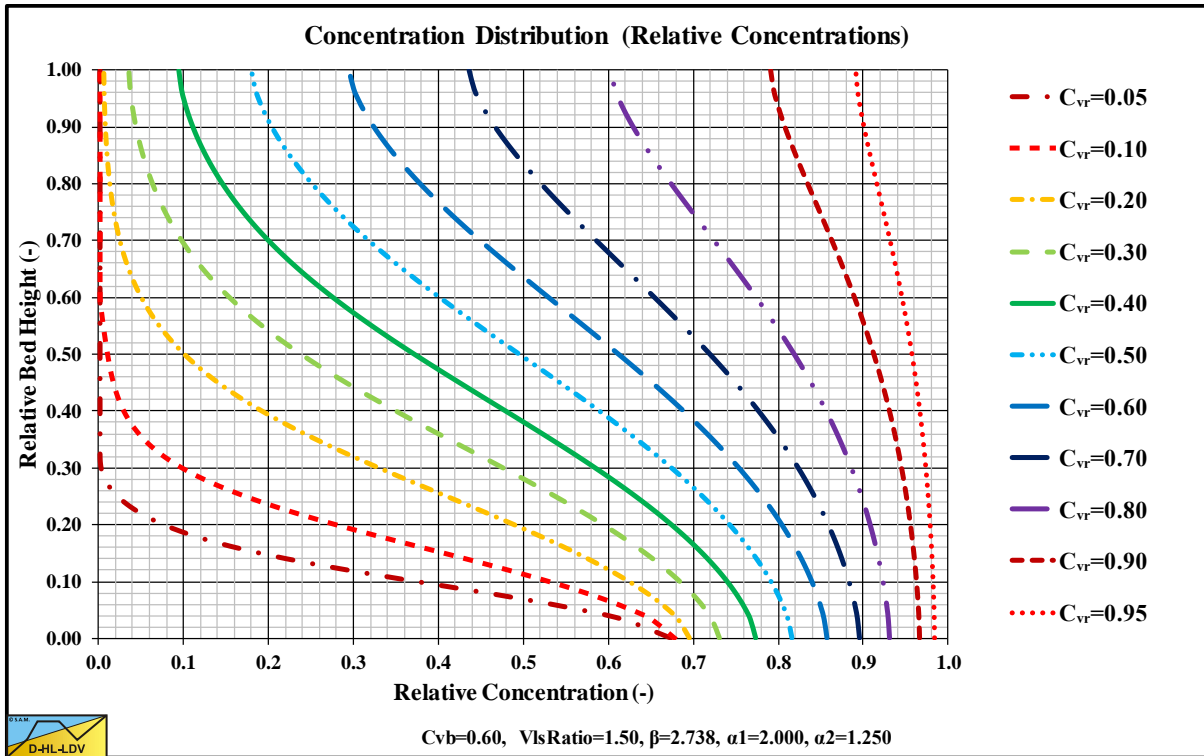
Figure 7.10-24: The concentration profiles at $v_{ls}=1.50 \cdot v_{ls,ldv}$ with hindered settling.
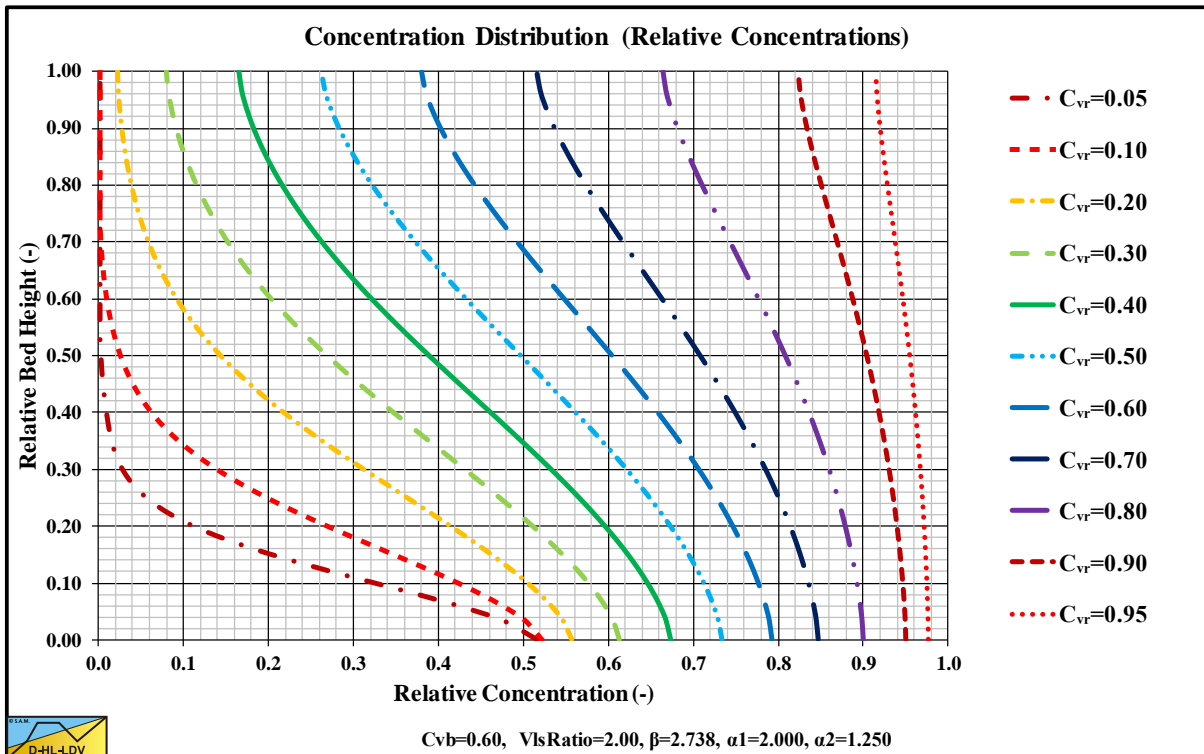
Figure 7.10-25: The concentration profiles at $v_{ls}=2.00 \cdot v_{ls,ldv}$ with hindered settling.

The sheet flow behavior is simulated well with the new hindered settling equation and the method used. Above the LDV the bottom concentration is reduced depending on the line speed to LDV ratio. The concentration profiles become steeper with increasing line speed. In the range of the line speed to LDV ratio of 1-1.5 the concentration profiles change significantly. The sheet flow behavior completely disappears. Also the stationary or sliding bed completely disappears. There is not much difference between the use of the original Richardson & Zaki (1954) equation and equation (7.10-35), since they give the same hindered settling velocity at lower concentrations.

Since the graphs are constructed for a hindered settling power of 3, one should only apply the graphs for medium sands. Fine sands will have a higher power, gravel a lower power. Richardson & Zaki (1954) derived their equation for spheres, so non spherical particles will have a different power. Usually non spherical particles have a higher power than spherical particles. So although the graphs are constructed for medium sands, they do give a good impression of the development of the concentration profiles as a function of the line speed to LDV ratio.
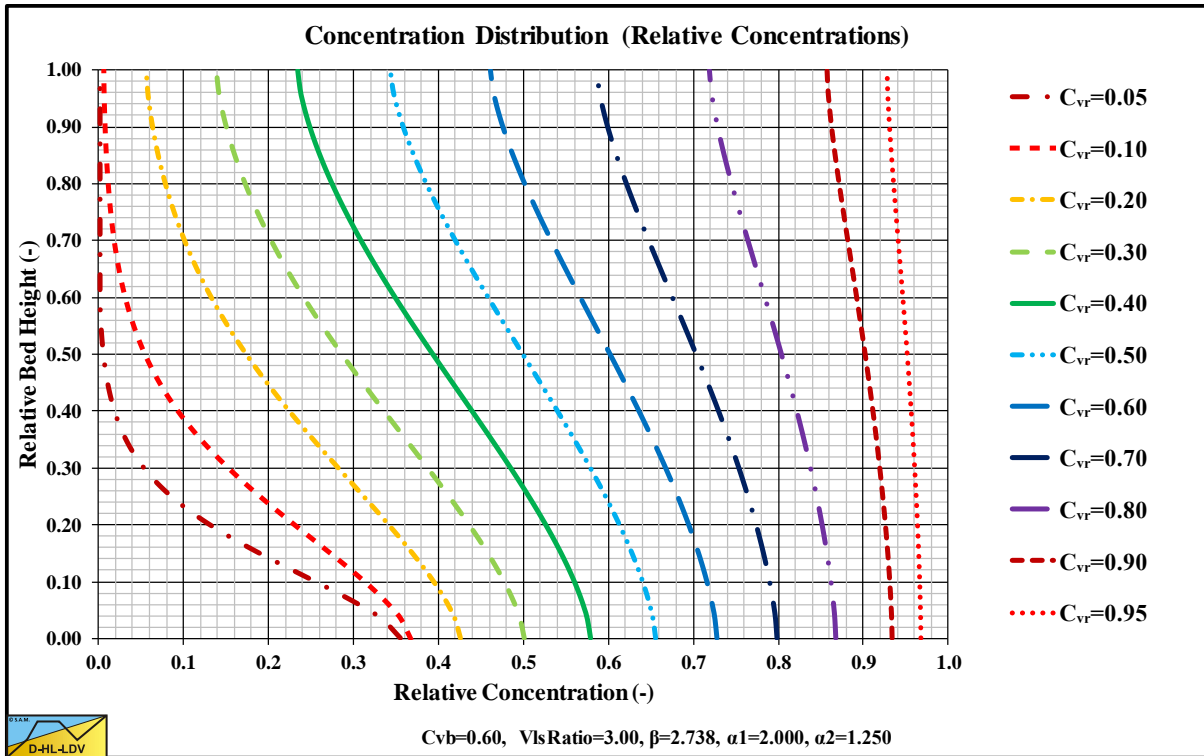
Figure 7.10-26: The concentration profiles at $v_{ls}=3.00 \cdot v_{ls,ldv}$ with hindered settling.
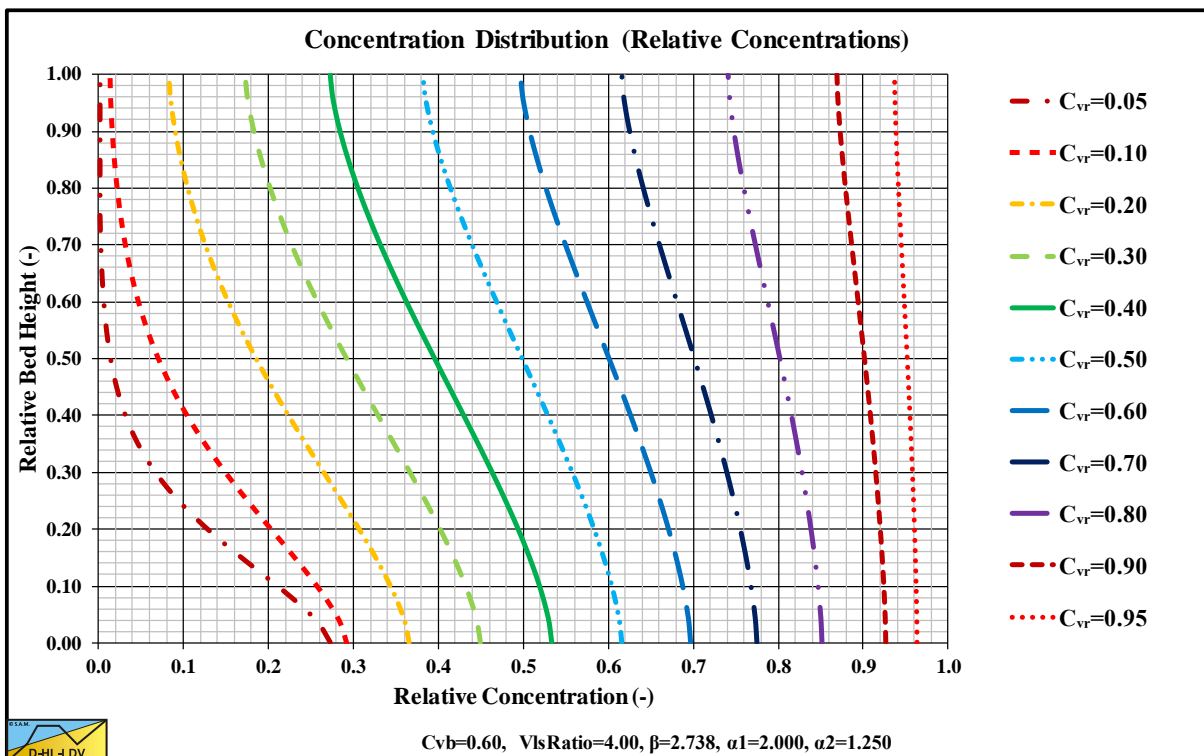
Figure 7.10-27: The concentration profiles at $v_{ls}=4.00 \cdot v_{ls,ldv}$ with hindered settling.

7.10.8 Experiments.
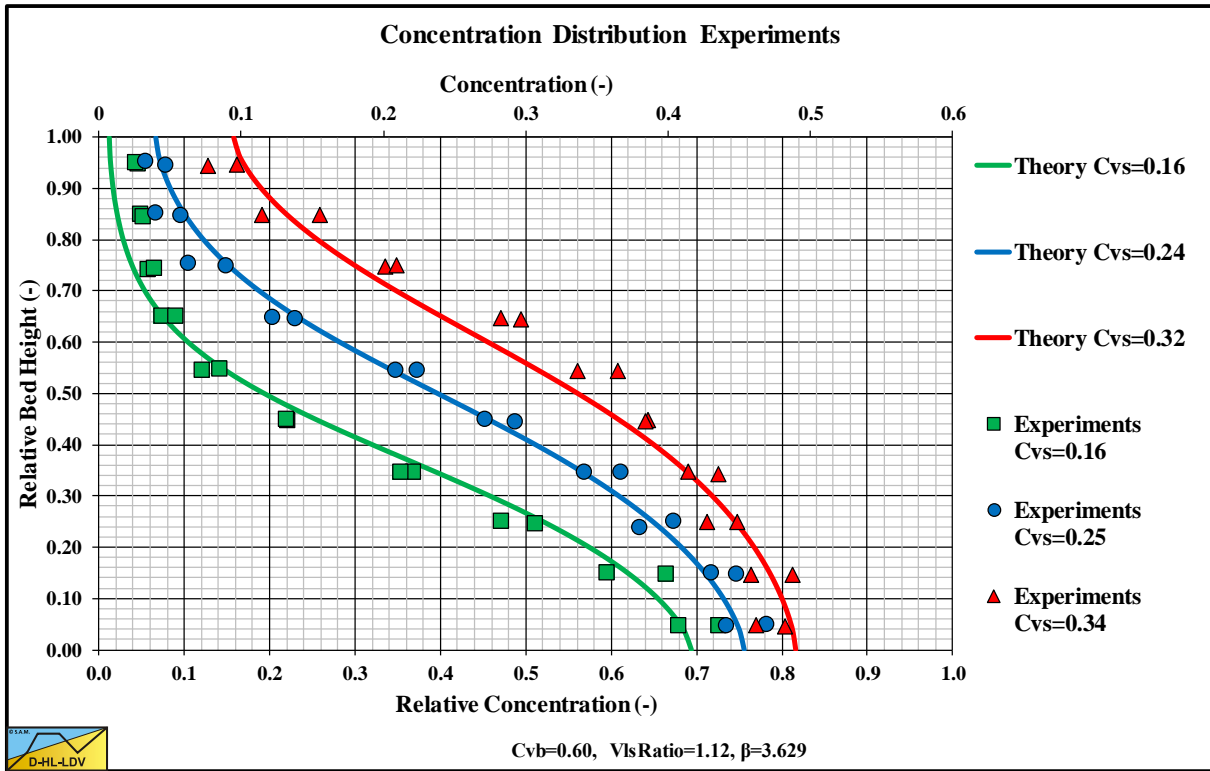
Figure 7.10-28: Gillies (1993) data, d=0.29 mm, D$_p$=0.263 m, vls=4.0-4.7 m/s, β=3.45, LDV=3.43-4.04 m/s.
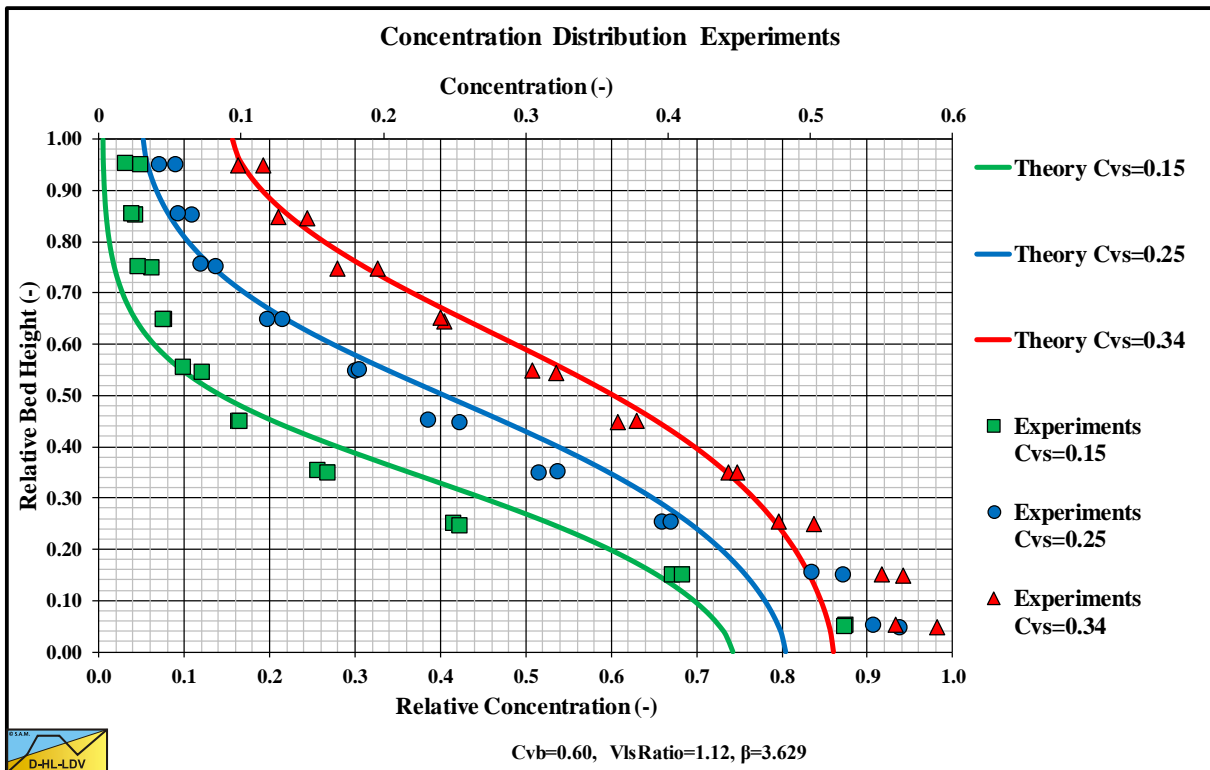
Figure 7.10-29: Gillies (1993) data, d=0.38 mm, D$_p$=0.263 m, vls=4.1-4.8 m/s, β=3.21, LDV=3.55-4.22 m/s.

Figure 7.10-28, Figure 7.10-29, Figure 7.10-30 and Figure 7.10-31 are based on experiments carried out by Gillies (1993). The experiments were carried out at two line speeds for each particle diameter. The bed concentrations are estimated at 0.55-0.60. In general the concentration profiles are similar for the different particle diameters, however the **d=0.55 mm** particle shows a very low concentration at the top of the pipe, which cannot be predicted.
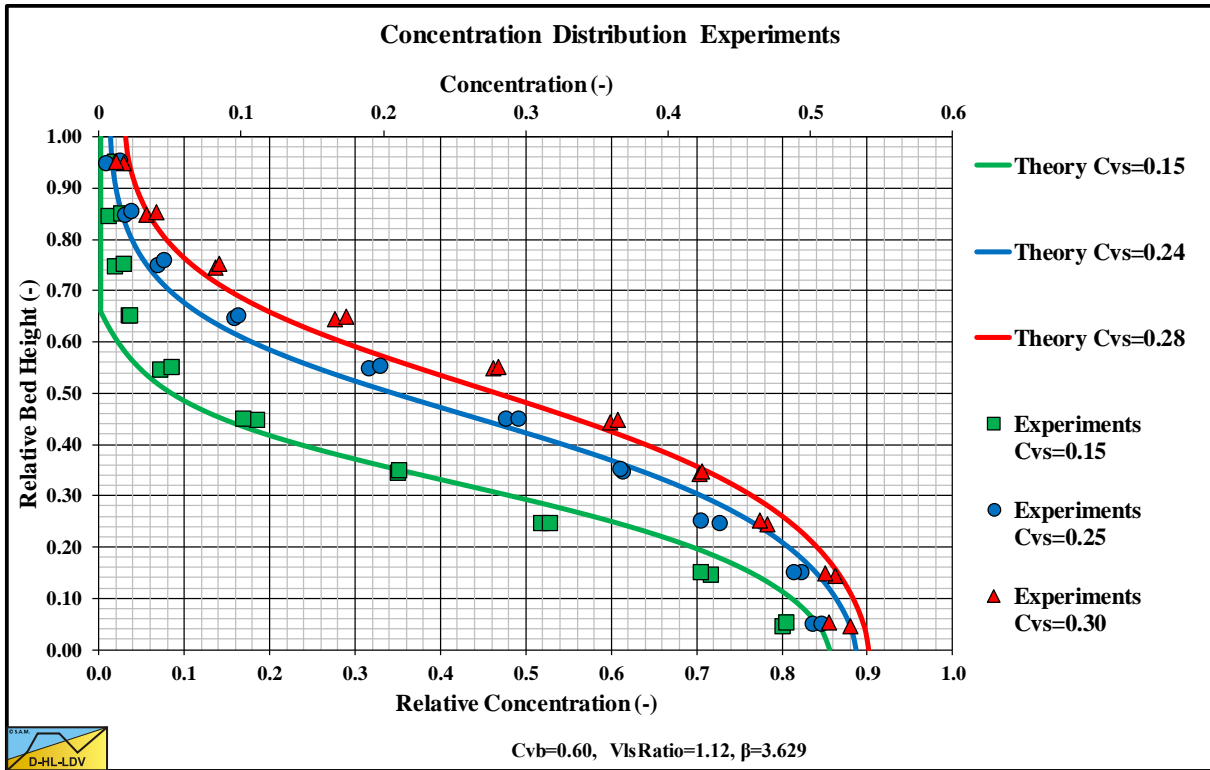
Figure 7.10-30: Gillies (1993) data, d=0.55 mm, D_p=0.263 m, vls=3.9-4.4 m/s, β=2.95, LDV=3.89-4.27 m/s.
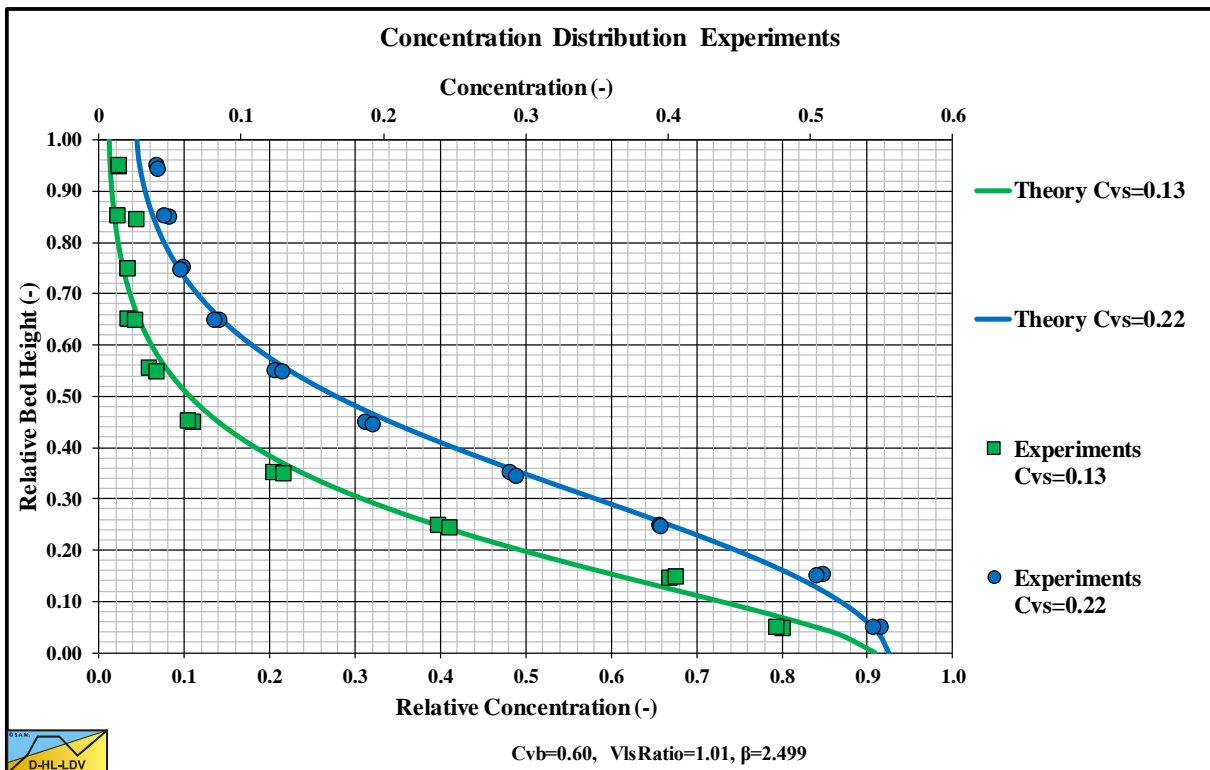
Figure 7.10-31: Gillies (1993) data, d=2.40 mm, D_p=0.263 m, vls=3.3-4.0 m/s, β=2.47, LDV=3.59-3.61 m/s.

It is remarkable that the LDV approach, relating the concentration profile to the LDV instead of some diffusivity, gives such good results for the different particle diameters. The only difference between the particle diameters is the Richardson & Zaki power **β**. The downside of this approach is, that each concentration has a different LDV, so a different line speed to LDV ratio has to be used for each concentration. Here constant ratios are used for convenience.

7.10.9 Concentration Distribution Sliding Flow Regime.

In the case of **Sliding Flow**, the bottom concentration decreases with increasing line speed and with decreasing spatial concentration. The bottom concentration can be determined with the following equation, where the bottom concentration can never be larger than the maximum bed concentration C_{vb} and never smaller than the spatial concentration C_{vs}. The Limit of Stationary Deposit Velocity (LSDV) has to be determined at a concentration of 17.5%, because the equation is calibrated for $C_{vs}=0.175$.

$$C_{vB} = 3.1 \cdot C_{vb} \cdot \left(\frac{v_{ls,lsdv}}{v_{ls}} \right)^{0.4} \cdot \left(\frac{C_{vs}}{C_{vb}} \right)^{0.5} \cdot v_t^{1/6} \cdot e^{D_p} \quad \text{with: } 1.1 \cdot C_{vs} \leq C_{vB} \leq C_{vb} \qquad (7.10\text{-}39)$$

To determine the concentration distribution, the procedure outlined in chapter 7.10 should be followed with a line speed to Limit Deposit Velocity ratio of 1 and a bottom/bed concentration as determined with the above equation. Physically this means that a sliding bed will transit to sliding flow by increasing the porosity between the particles with increasing line speed. The Limit Deposit Velocity has no physical meaning in the Sliding Flow Regime.

The concentration distribution is now:

$$C_{vs}(f) = C_{vB} \cdot e^{-\frac{\alpha_{sm}}{C_{vr}} \cdot f} \quad \text{with: } C_{vr} = \frac{C_{vs}}{C_{vB}}$$

$$\alpha_{sm} = 0.9847 + 0.304 \cdot C_{vr} - 1.196 \cdot C_{vr}^2 - 0.5564 \cdot C_{vr}^3 + 0.47 \cdot C_{vr}^4$$

$(7.10\text{-}40)$

Figure 7.10-32 shows an example of the concentration distribution in the **Sliding Flow Regime**.
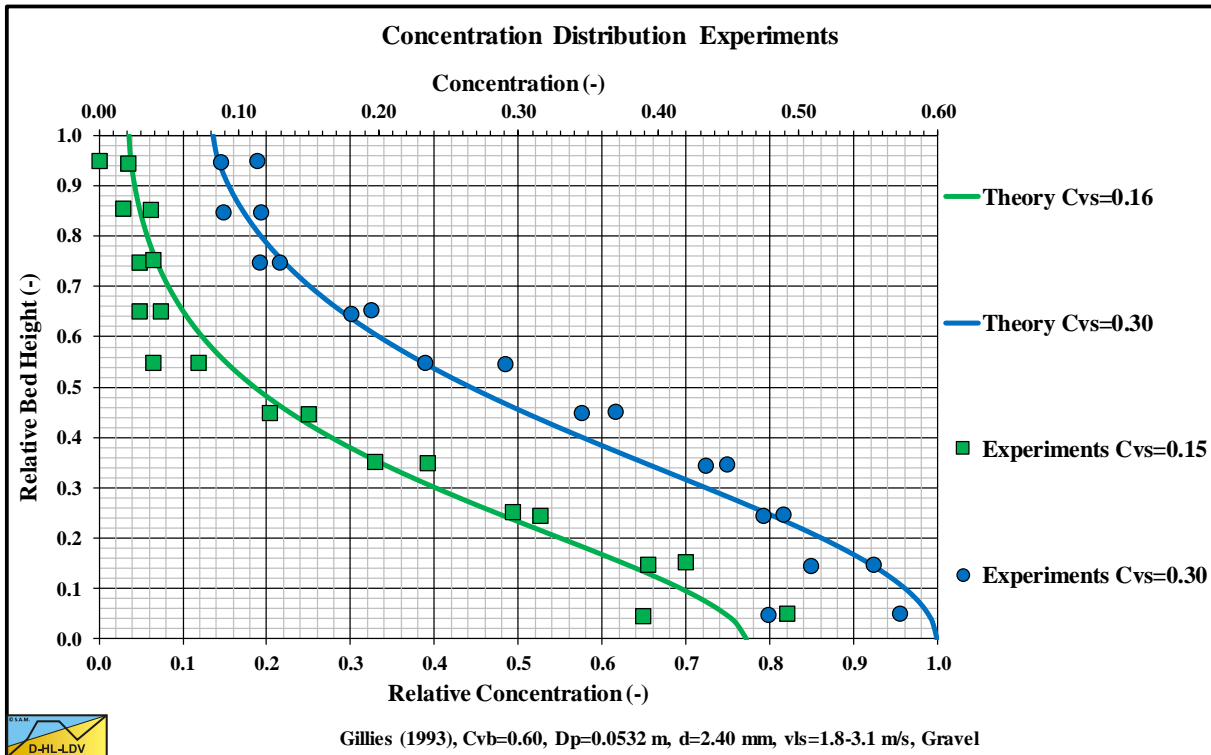
Figure 7.10-32: Gillies (1993) data, d=2.40 mm, D_p=0.0532 m, vls=1.8-3.1 m/s.

7.10.10 Conclusions & Discussion.

The concentration profiles are based on an exponential power, containing the hindered terminal settling velocity. This hindered settling velocity is implemented as a constant over the vertical coordinate. Since in reality and also following from the above graphs, the concentration decreases with an increasing vertical coordinate, one may expect that the hindered settling velocity increases with the vertical coordinate. So in the top part the hindered settling velocity is higher than in the bottom part. This will result in slightly lower concentrations at the top and higher concentrations at the bottom, compared with the graphs without the local hindered settling velocity. The graphs with local hindered settling velocity have a correction for this effect. Also the repulsive effects near the pipe wall will influence the concentration profiles, which is not taken into account here.

It is also assumed that the concentration profile is 1 dimensional with constant concentration in the transverse direction of the pipe. This is also questionable, since the repulsive effect near the pipe wall is effective at the whole pipe circumference and the local velocities are also influenced by the pipe wall. Recent CFD simulations have shown both effects (Ofei & Ismail (August 2016)).

Since the model assumes a constant concentration in the transverse direction and is not corrected for the repulsive effect at the pipe wall, experimental data will never match exactly with the model. since usually the experimental data only show the measured concentrations on the vertical axis.

Figure 7.10-28, Figure 7.10-29, Figure 7.10-30 and Figure 7.10-31 show the calculated curves, including the local hindered settling effect with data of Gillies (1993) in a D_p=0.263 m pipe. The experiments were carried out with particles of d=0.29 mm, d=0.38 mm, d=0.55 mm and d=2.4 mm. The line speeds varied from line speeds just below the LDV to line speeds just above the LDV. Since the LDV differs based on the particle diameter and the volumetric concentrations, these are given in the caption of each figure. In general the correlation is good, especially in the center of the pipe. At the top and bottom of the pipe the model may deviate from the experimental data. Figure 6.22-23, Figure 6.22-24, Figure 6.22-25, Figure 6.22-26, Figure 6.22-27, Figure 6.22-28, Figure 6.22-29 and Figure 6.22-30 show the data of Gillies (1993) in a D_p=0.0532 m pipe. These experiments were carried out with particles of d=0.18 mm, d=0.29 mm, d=0.55 mm and d=2.4 mm. The line speeds varied from 1.8 m/s to 3.1 m/s. The line speed of 1.8 m/s is close to the LDV depending on the particle diameter and the concentration.

The current model gives a good estimate of the concentration distribution and is corrected for the cross sectional averaged concentration and the local hindered settling velocity, which is not the case for most models from literature.

The choice of using the fraction of the cross sectional area of the pipe instead of the vertical coordinate seems to be a good choice. Even with the constant hindered settling velocity the concentration profiles match the experimental data much better. Using the adjustment of local hindered settling gives an even better correlation with the experimental data. The choice of an LDV based diffusivity gives good results. Of course this depends on the correctness of the determination of the LDV, but based on the comparison with experimental data, the model is close.

It should be mentioned that the concentration profiles are determined with 100 steps, so a stepsize of $0.01 \cdot r/D_p$. It should also be mentioned that the LDV values used are an average based on the DHLLDV Framework, while the LDV is concentration dependent. The DHLLDV Framework is a bit conservative giving high values for the LDV.

To validate the model, two issues have to be addressed. The first issue is the value of the LDV. If the value of the LDV is not correct, the wrong line speed to LDV ratio will be used. The second issue is the shape of the concentration profile. Using the correct LDV, the shape of the concentration profile should match the experimental data. In general the shapes of the concentration profiles match well given the LDV values used. The LDV values from chapter 7.8 are a bit conservative, giving slightly to high values in order to have safe operations. Especially for the smallest particles of d=0.18 mm in a D_p=0.0532 m pipe, and LDV of 1.2 m/s is applied, while the theoretical LDV varies from 1.2 m/s to 1.8 m/s.
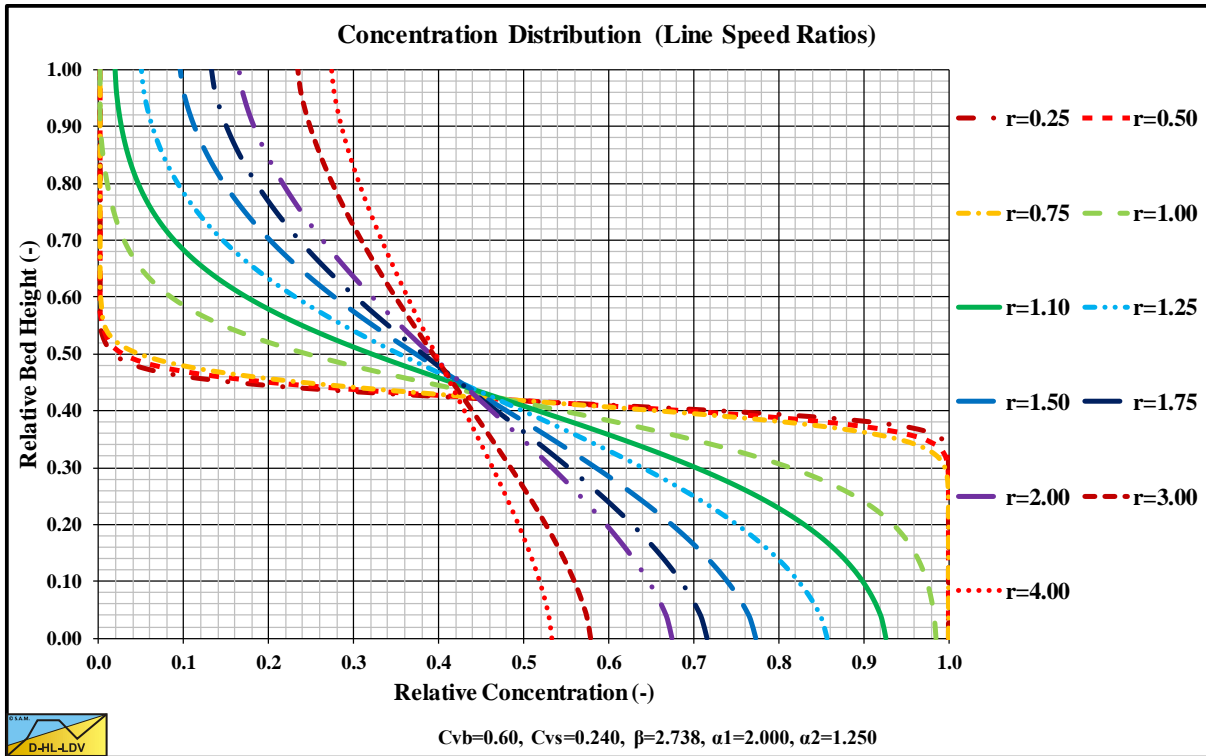
Figure 7.10-33: The concentration profiles as a function of the line speed for C$_{vr}$=0.4.
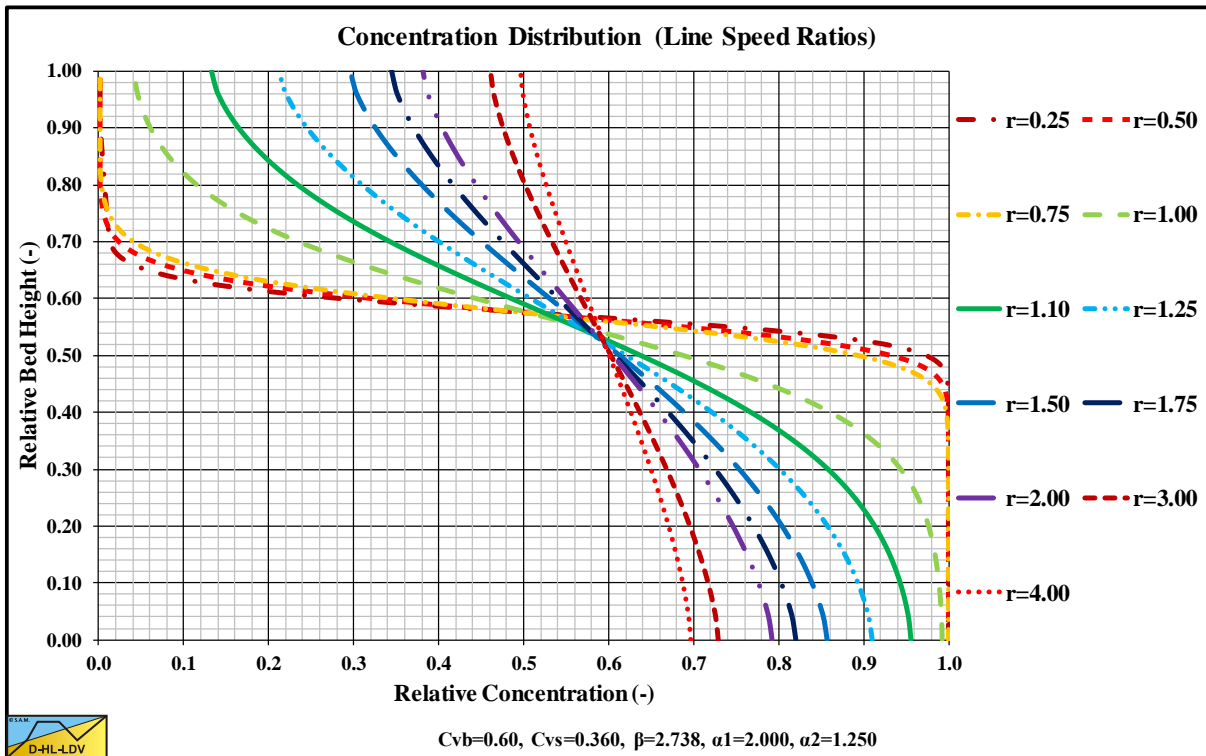
Figure 7.10-34: The concentration profiles as a function of the line speed for C$_{vr}$=0.6.

Figure 7.10-33 and Figure 7.10-34 show the concentration profiles as a function of the line speed. A new term is introduced, the Maximum Limit Deposit Velocity. The reason for this is, that the observed LDV is based on the line speed where the bed completely disappeared. This will occur for a bed concentration close to 50%. In reality however, bed concentrations up to 60% are possible at lower line speeds. The line speed where this maximum bed concentration (60%) occurs is named the MLDV and the line speed where the 50% bed concentration occurs is named the LDV (the observed LDV). The LDV always occurs at a line speed higher than the MLDV. For a relative cross sectional averaged concentration of 0.4 (Figure 7.10-33) the LDV will occur at about 1.4 times the MLDV. For a relative cross sectional averaged concentration of 0.6 (Figure 7.10-34) the LDV will occur at about 1.9 times the MLDV. The higher the relative cross sectional averaged concentration, the larger this factor. The minimum value of this factor is about 1.25 for very low concentrations.

Relating the concentration profile to the LDV is possible, but should be corrected for the fact that there is not just one bed concentration. A bed will start with the lowest possible bed concentration of about 50% or even a few percent lower and increases with decreasing line speed up to about 60% or even a few percent higher, depending on the type of sand, the PSD and the angularity.

7.10.11 Nomenclature Concentration Distribution.

vehicle	Pseudo liquid formed by carrier liquid and suspended particles	**-**
C	Integration constant	**-**
$C_{vs}(r)$	Volumetric concentration as a function of vertical coordinate in pipe	**-**
$C_{vs,v}$	Volumetric concentration in vehicle	**-**
C_{vb}	Volumetric concentration bed	**-**
C_{vB}	Volumetric concentration bottom of channel or pipe	**-**
C_{vr}	Relative volumetric concentration	**-**
d	Particle diameter	**m**
D_p	Pipe diameter	**m**
g	Gravitational constant (9.81 m/s^2)	**m/s^2**
r	Vertical coordinate in pipe	**m**
$\tilde{r}$	Dimensionless vertical coordinate in pipe	**-**
R	Radius of pipe	**m**
R_{sd}	Relative submerged density (about 1.65 for sand)	**-**
u_*	Friction velocity	**m/s**
$u_{*,ldv}$	Friction velocity at LDV	**m/s**
v_{ls}	Line speed	**m/s**
$v_{ls,ldv}$	Limit Deposit Velocity	**m/s**
v_t	Terminal settling velocity	**m/s**
v_{tv}	Terminal settling velocity in vehicle	**m/s**
$v_{tv,ldv}$	Terminal settling velocity in vehicle at LDV	**m/s**
v_{th}	Terminal settling velocity hindered	**m/s**
$v_{th,ldv}$	Terminal settling velocity hindered at LDV	**m/s**
v_{thv}	Terminal settling velocity hindered in vehicle	**m/s**
$v_{thv,ldv}$	Terminal settling velocity hindered in vehicle at LDV	**m/s**
α_{sm}	Correction factor	**-**
α_{c1}	Correction factor	**-**
α_{c2}	Correction factor	**-**
β	Richardson & Zaki power hindered settling	**-**
β_{sm}	Relation sediment mass diffusivity to eddy momentum diffusivity.	**-**
$\beta_{sm,ldv}$	Relation sediment mass diffusivity to eddy momentum diffusivity at LDV	**-**
ε_m	Eddy momentum diffusivity	**m/s**
ε_s	Sediment diffusivity	**m/s**
$\overline{\varepsilon_s}$	Average sediment diffusivity	**m/s**
λ_1	Darcy Weisbach friction factor	**-**
$\lambda_{1,ldv}$	Darcy Weisbach friction factor at LDV	**-**
κ	von Karman constant	**-**
φ	Pipe angle	**o**

7.11 The Transition Heterogeneous vs. Homogeneous in Detail.

7.11.1 The Transition Heterogeneous-Homogeneous.

In the previous paragraphs the heterogeneous regime and the homogeneous regime are discussed. The question is now, is there a sharp transition between the two flow regimes, or is this more complicated. Figure 7.11-2, Figure 7.11-3, Figure 7.11-4, Figure 7.11-5, Figure 7.11-6 and Figure 7.11-7 show experiments of Clift et al. (1982) in pipes with 0.2032 m and 0.44 m diameters. The particle diameters in these experiments were 0.29 mm, 0.42 mm and 0.68 mm. The graphs show that the behavior near the ELM curve depends on the pipe diameter. The experiments in the 0.2 m diameter pipe show a rather smooth transition, while the experiments in the 0.44 diameter pipe show a collapse of the relative excess hydraulic gradient near the intersection point of the two flow regimes. Wilson et al. (1992) explain this phenomena with near wall lift, based on the ratio of the submerged weight of a particle to the lift force. There may, however be other phenomena influencing this behavior.

7.11.2 The Lift Ratio.

When the particle diameter approaches the thickness of the viscous sub-layer at the transition velocity heterogeneous-homogeneous a peculiar phenomenon occurs. On one hand the kinetic losses collapse due to the lift forces available just above the viscous sub-layer, assuming there are no lift forces in the viscous sub-layer, on the other hand the eddies in the turbulent layer are not yet strong enough to integrate the particles with the main flow. When the line speed increases, the lift forces are strong to counteract the submerged weight and kinetic energy of the particles, but not enough to integrate the particles in the eddy behavior. This results in a sort of delay between the collapse of the kinetic losses and the mobilization of the RELM (Reduced ELM).

Wilson et al. (2010) introduced the lift force on a particle as:

$$\mathbf{F_L} = \mathbf{C_L} \cdot \frac{\mathbf{1}}{\mathbf{2}} \cdot \rho_l \cdot \mathbf{u}_*^2 \cdot \frac{\pi}{\mathbf{4}} \cdot \mathbf{d}^2 \tag{7.11-1}$$

And for the submerged weight of the particle (including the shape factor):

$$\mathbf{F_G} = \left(\rho_s - \rho_l\right) \cdot \mathbf{g} \cdot \frac{\pi}{\mathbf{6}} \cdot \mathbf{d}^3 \cdot \psi \tag{7.11-2}$$

Giving, assuming a shape factor of about 0.75:

$$\mathbf{L_R} = \frac{\mathbf{F_L}}{\mathbf{F_G}} = \frac{\mathbf{C_L} \cdot \frac{\mathbf{1}}{\mathbf{2}} \cdot \rho_l \cdot \mathbf{u}_*^2 \cdot \frac{\pi}{\mathbf{4}} \cdot \mathbf{d}^2}{\left(\rho_s - \rho_l\right) \cdot \mathbf{g} \cdot \frac{\pi}{\mathbf{6}} \cdot \mathbf{d}^3 \cdot \psi} = \mathbf{C_L} \cdot \frac{\mathbf{3}}{\mathbf{4}} \cdot \frac{\mathbf{u}_*^2}{\mathbf{R_{sd}} \cdot \mathbf{g} \cdot \mathbf{d} \cdot \psi} = \mathbf{C_L} \cdot \frac{\mathbf{3}}{\mathbf{32}} \cdot \frac{\lambda_l \cdot \mathbf{v}_{ls}^2}{\mathbf{R_{sd}} \cdot \mathbf{g} \cdot \mathbf{d} \cdot \psi} = \mathbf{C_L} \cdot \theta \tag{7.11-3}$$

The difference in kinetic energy of a particle with a horizontal and a vertical velocity component (the hindered settling velocity) compared with the kinetic energy of a particle with only the horizontal velocity component is:

$$\mathbf{E_K} = \frac{\mathbf{1}}{\mathbf{2}} \cdot \mathbf{m_p} \cdot \mathbf{v}_{th}^2 = \frac{\mathbf{1}}{\mathbf{2}} \cdot \rho_s \cdot \frac{\pi}{\mathbf{6}} \cdot \mathbf{d}^3 \cdot \psi \cdot \mathbf{v}_{th}^2 \tag{7.11-4}$$

The force to reduce the vertical component of a particle to zero over a certain distance **x** equals:

$$\mathbf{F_K} = \frac{\mathbf{1}}{\mathbf{2}} \cdot \mathbf{m_p} \cdot \frac{\mathbf{v}_{th}^2}{\mathbf{x}} = \frac{\mathbf{1}}{\mathbf{2}} \cdot \rho_s \cdot \frac{\pi}{\mathbf{6}} \cdot \mathbf{d}^3 \cdot \psi \cdot \frac{\mathbf{v}_{th}^2}{\mathbf{x}} = \frac{\mathbf{E_K}}{\mathbf{x}} \tag{7.11-5}$$

Which is the kinetic energy divided by the distance **x**, so it also matches the principle that the work carried out equals the force times the distance is equal to the destroyed kinetic energy.

To prevent a particle from having a collision with the pipe wall, the lift force has to counteract both the submerged weight of the particle and the kinetic energy force, giving for the lift ratio:

$$L_R = \frac{F_L}{F_G + F_K} = \frac{C_L \cdot \frac{1}{2} \cdot \rho_l \cdot u_*^2 \cdot \frac{\pi}{4} \cdot d^2}{(\rho_s - \rho_l) \cdot g \cdot \frac{\pi}{6} \cdot d^3 \cdot \psi + \frac{1}{2} \cdot \rho_s \cdot \frac{\pi}{6} \cdot d^3 \cdot \psi \cdot \frac{v_{th}^2}{x}} \approx \frac{C_L \cdot u_*^2}{d \cdot \left(R_{sd} \cdot g + \frac{1}{2} \cdot \frac{\rho_s}{\rho_l} \cdot \frac{v_{th}^2}{x} \right)} \tag{7.11-6}$$

Now suppose the distance to stop the particle equals a number of times the thickness of the viscous sub layer, this gives:

$$L_R = \frac{C_L \cdot u_*^2}{d \cdot \left(R_{sd} \cdot g + \frac{1}{2} \cdot \frac{\rho_s}{\rho_l} \cdot \frac{v_{th}^2 \cdot u_*}{\alpha \cdot 11.6 \cdot \nu_l} \right)} \cdot \left(1 - \frac{C_{vs}}{C_{vb}} \right) \tag{7.11-7}$$

The concentration term is added, because the higher the concentration, the smaller the capacity of the turbulent flow to generate lift forces. When the spatial concentration C_{vs} equals the bed concentration C_{vb}, there will not be any lift forces anymore. For now a linear relation is chosen.
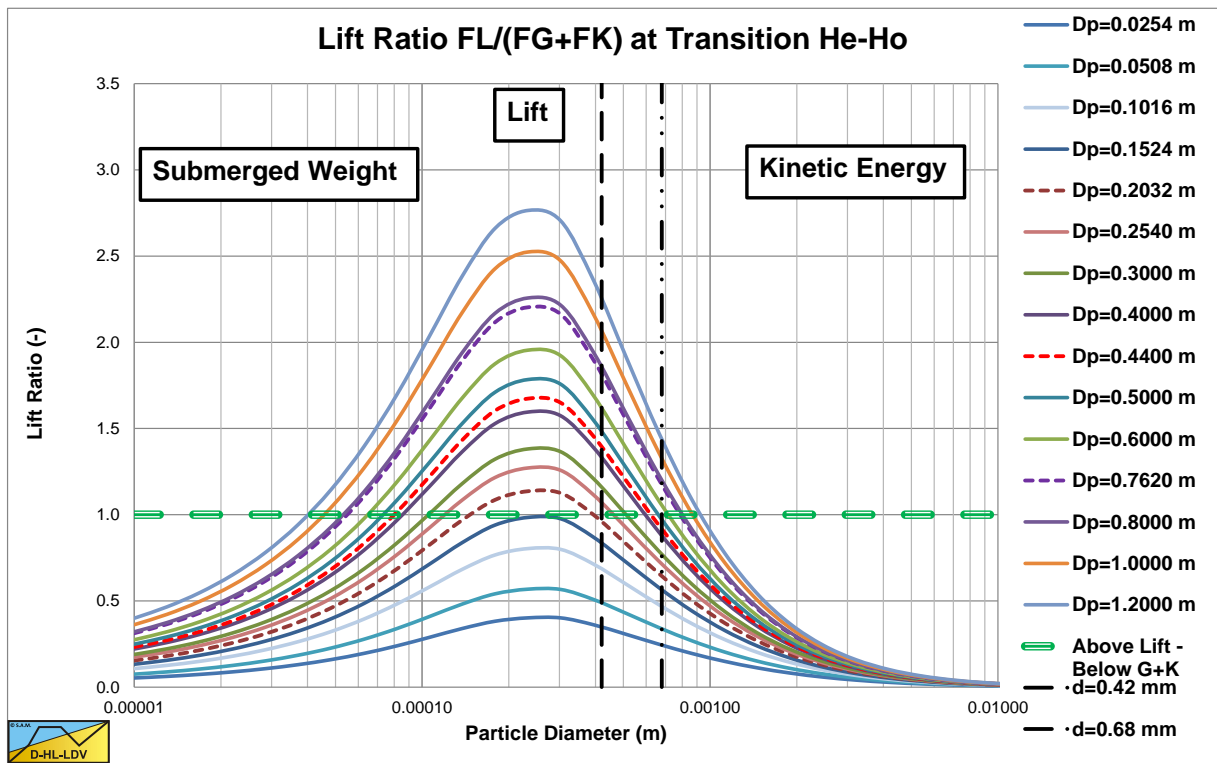
Figure 7.11-1: The lift ratio at the transition line speed heterogeneous-homogeneous.

Figure 7.11-1 shows this lift ratio at the intersection line speed between the heterogeneous and homogeneous flow regimes for **α=10, C_{vs}=0.175** and **C_{vb}=0.55** (which is also used in the graphs), where the intersection line speed can be computed with:

$$\frac{v_t \cdot \left(1 - \frac{C_{vs}}{0.175 \cdot (1 + \beta)} \right)^\beta}{v_{ls}} + 8.5^2 \cdot \left(\frac{1}{\lambda_l} \right) \cdot \left(\frac{v_t}{\sqrt{g \cdot d}} \right)^{10/3} \cdot \left(\frac{(\nu_l \cdot g)^{1/3}}{v_{ls}} \right)^2 = \frac{\lambda_l \cdot v_{ls}^2}{2 \cdot g \cdot D_p} \tag{7.11-8}$$

In reality the intersection line speed will be a bit higher, due to the reduced ELM because of the particle poor viscous sub layer (reduction ELM 50%-60%). From the figure it is shown that for very small particles the submerged weight dominates and the lift ratio hardly reaches a value of 1. For medium sized particles the near wall lift dominates giving a lift ratio above 1. It must be mentioned that for small diameter pipes the lift ratio never reaches 1, while the lift ratio increases with increasing pipe diameter. For large particles both submerged weight

and kinetic energy dominate, resulting in a lift ratio never reaching 1. So the conclusion can be drawn that very small and very large particles do not show a collapse of the heterogeneous E_{rhg}, but medium sized particles do, where the collapse is stronger in larger diameter pipes.

So how to model this collapse? The kinetic energy contribution in the heterogeneous flow regime equation is subject to the influence of the near wall lift force, so only this term is reduced. Based on the experiments considered, the reduction is not linear with the lift ratio, but quadratic, resulting in:

$$E_{rhg} = \frac{v_t \cdot \left(1 - \dfrac{C_{vs}}{0.175 \cdot (1+\beta)}\right)^{\beta}}{v_{ls}} + 8.5^2 \cdot \left(\frac{1}{\lambda_l}\right) \cdot \left(\frac{v_t}{\sqrt{g \cdot d}}\right)^{10/3} \cdot \left(\frac{(v_l \cdot g)^{1/3}}{v_{ls}}\right)^2 \cdot \left(1 - L_R^2\right) \qquad (7.11\text{-}9)$$

When the lift ratio has a value close to 1, theoretically there are no more collisions with the wall. However not all particles will have exactly the same kinetic energy, so even when the lift ratio is larger than 1, still some particles will have collisions. Therefore a smoothing function is proposed for lift ratio's larger than 70% (ζ=0.5), giving:

$$E_{rhg} = \frac{v_t \cdot \left(1 - \dfrac{C_{vs}}{0.175 \cdot (1+\beta)}\right)^{\beta}}{v_{ls}} + 8.5^2 \cdot \left(\frac{1}{\lambda_l}\right) \cdot \left(\frac{v_t}{\sqrt{g \cdot d}}\right)^{10/3} \cdot \left(\frac{(v_l \cdot g)^{1/3}}{v_{ls}}\right)^2 \cdot (1 - \zeta) \cdot \frac{\zeta}{L_R^2} \qquad (7.11\text{-}10)$$

Figure 7.11-2, Figure 7.11-3, Figure 7.11-4, Figure 7.11-5, Figure 7.11-6 and Figure 7.11-7 show the decrease of the heterogeneous relative excess hydraulic gradient (heterogeneous flow with near wall lift), based on the lift ratio reduction. It is clear that a larger pipe diameter results in a larger decrease. The reason the E_{rhg} does not go to zero, is that the potential energy losses are not affected by the lift ratio.

7.11.3 Limit Deposit Velocity & Concentration Distribution.

Now that the collapse of the heterogeneous E_{rhg} has been modelled, the question is, how does the homogeneous E_{rhg} behave? The background of the ELM is that small particles rotate with turbulent eddies. This implies that the kinetic rotational energy of an eddy increases if the mass of the eddy increases. Since the mass of an eddy increases with the mixture density, the rotational energy also increases with the mixture density. So at high line speeds, where turbulence has fully developed, head losses will be proportional with the mixture density. Because of the particle poor viscous sub layer there is a lubrication effect, resulting in a smaller increase, as has been described with equation (7.6-40). This equation however assumes that turbulence has fully developed and particles follow the eddies. This may be true at high line speeds, but certainly not at low line speeds. It is also the question whether larger particles will follow this principle. At lower line speeds, the RELM effect will not be fully mobilized. The question is, how much of the RELM effect is mobilized as a function of the line speed?

To answer this question, first the Limit Deposit Velocity (LDV) is considered. The Limit Deposit Velocity is defined as the line speed above which there is no stationary or sliding bed. The definition of Wilson et al. (1992) is the line speed where a bed starts sliding, the Limit of Stationary Deposit Velocity (LSDV). The latter will only occur if the particle diameter to pipe diameter ratio exceeds a certain value. For small particles, the bed will never start sliding, because it already dissolves into heterogeneous transport, before the shear stress on the bed is large enough to initiate a sliding bed. The two different definitions also give different results. The LDV found by Durand & Condolios (1952) gives higher values than the LSDV found by Wilson et al. (1992). Goedde (1978) investigated the LDV by measuring the bed height at different line speeds below the LDV and found the LDV by drawing a straight line through the data points in order to obtain the line speed where the bed height is zero. He carried out experiments on plastic, coal, sand and iron ore. He concluded that the LDV found matched the findings of Durand & Condolios (1952) very well. Durand & Condolios (1952) in their publications only mention that their LDV is the line speed above which there is no deposit, but with the findings of Goedde (1978) this definition can be made more explicit, no deposit means, nor a stationary deposit, nor a sliding bed.

Miedema & Ramsdell (2015A) developed a model for the LDV based on the definition of Goedde (1978) and Durand & Condolios (1952). This definition implies that at the LDV, the spatial concentration at the pipe bottom equals the bed concentration.

The advection diffusion equation when in equilibrium shows the balance between the upwards flow of particles due to diffusion and the downwards flow of particles due to gravity (the terminal settling velocity). Wasp et al. (1977) and Doron et al. (1987) use the solution of the advection diffusion equation for low concentrations, while Karabelas (1977) and Kaushal & Tomita (2002) use the Hunt (1954) approach with upwards liquid flow. Hindered settling is not yet included in the basic solutions, but added by replacing the terminal settling velocity v_t by the hindered terminal settling velocity v_{th}.

Dp=0.2032 m, d=0.290 mm, Rsd=1.585, Cv=0.230, μsf=0.416
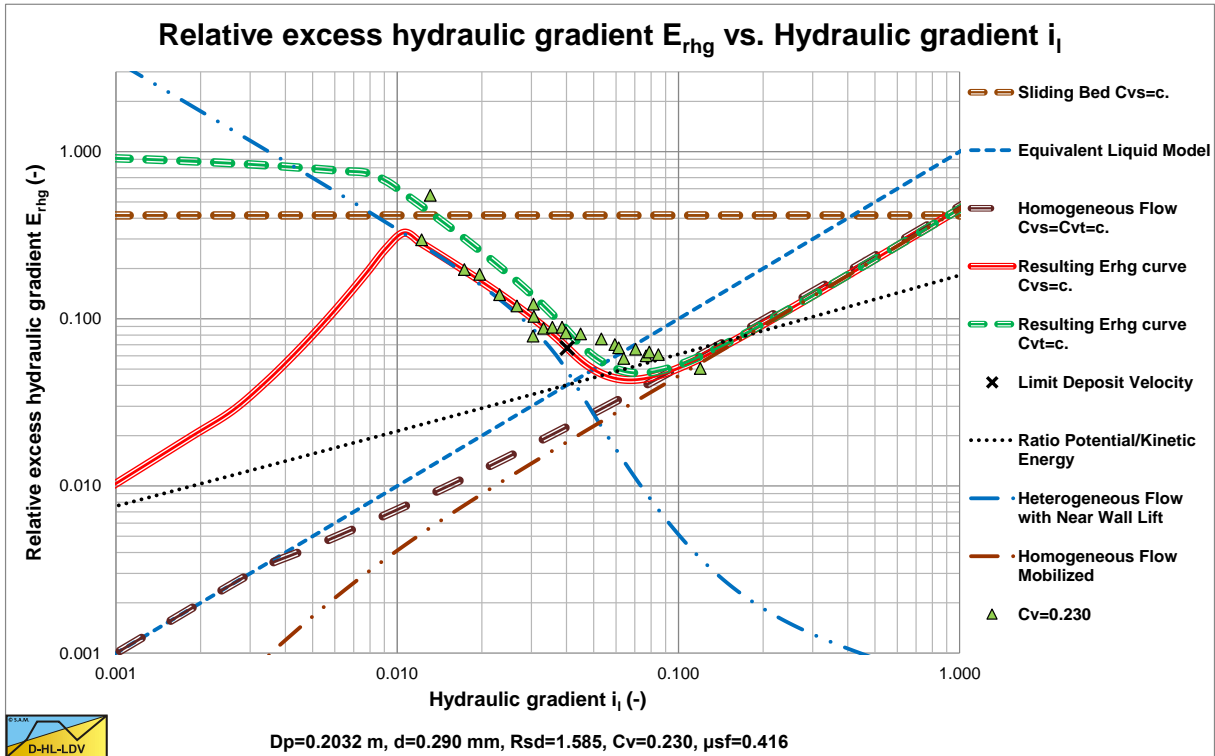
Figure 7.11-2: Experiments of Clift et al. (1982) in a 0.2082 m diameter pipe and a 0.29 mm particle.

Dp=0.4400 m, d=0.290 mm, Rsd=1.585, Cv=0.230, μsf=0.416
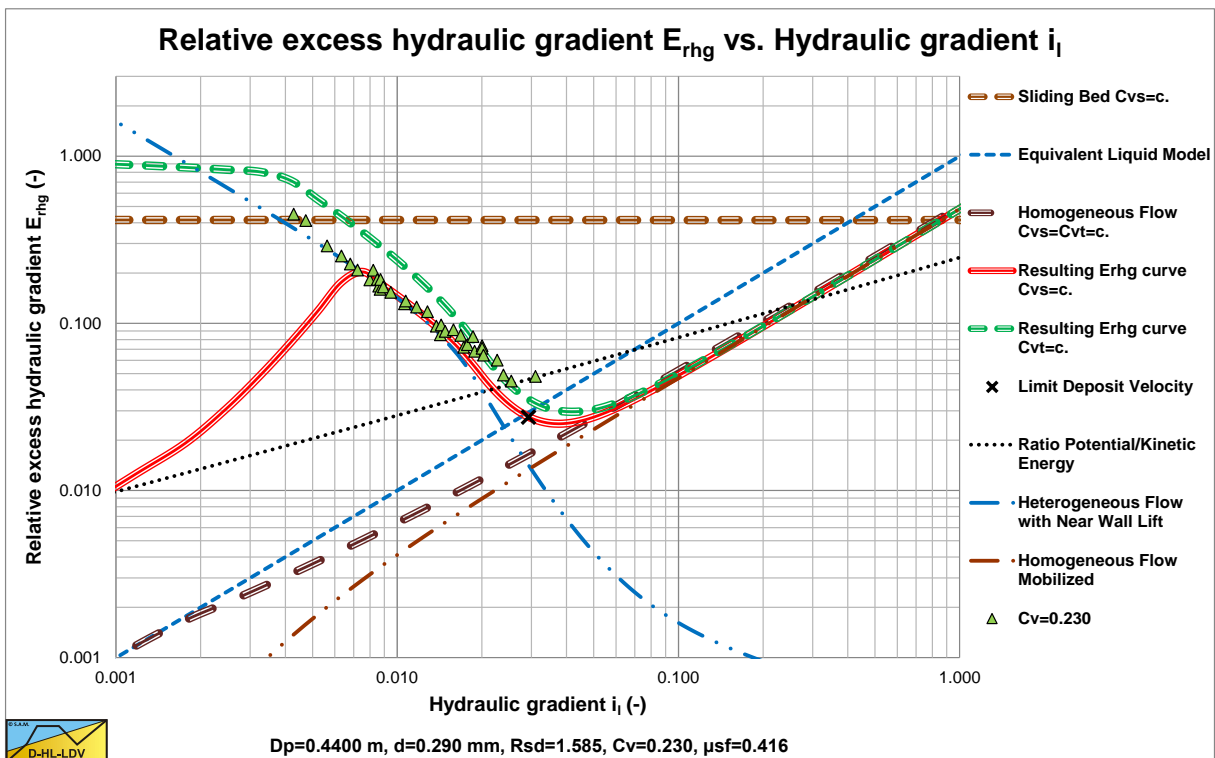
Figure 7.11-3: Experiments of Clift at al. (1982) in a 0.4400 m diameter pipe and a 0.29 mm particle.
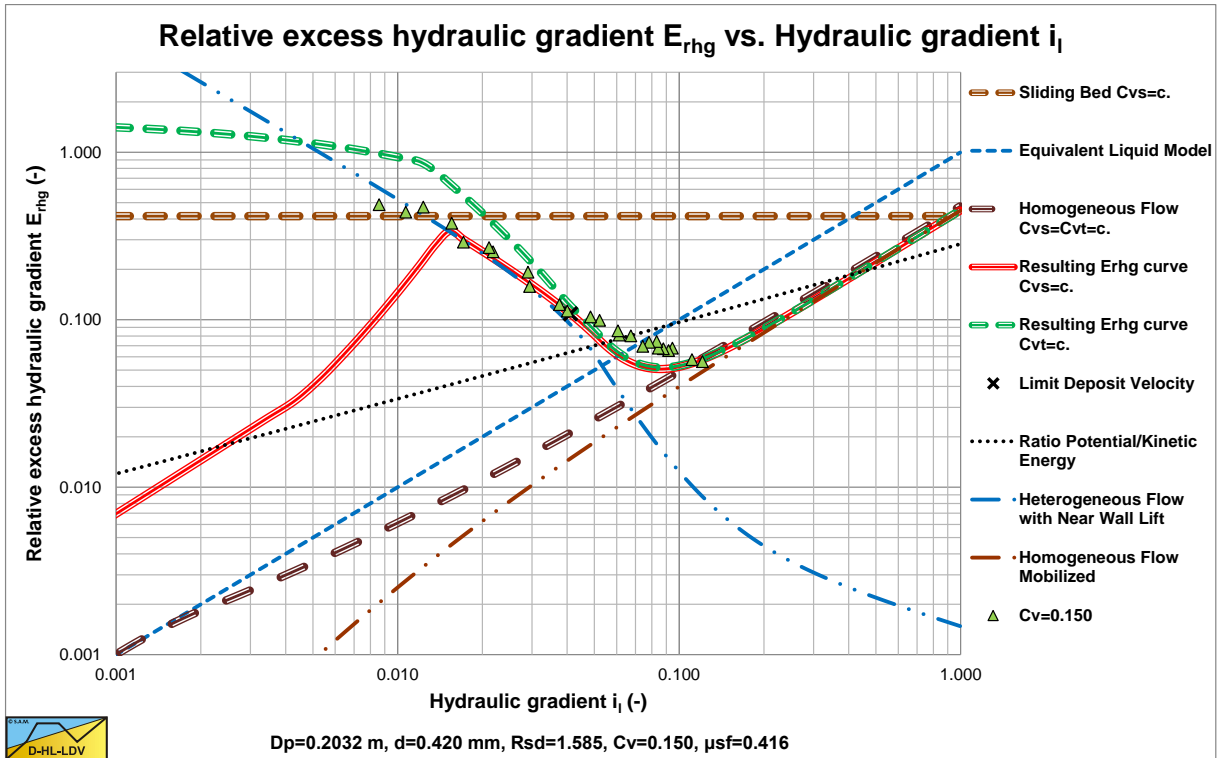
Figure 7.11-4: Experiments of Clift et al. (1982) in a 0.2082 m diameter pipe and a 0.42 mm particle.
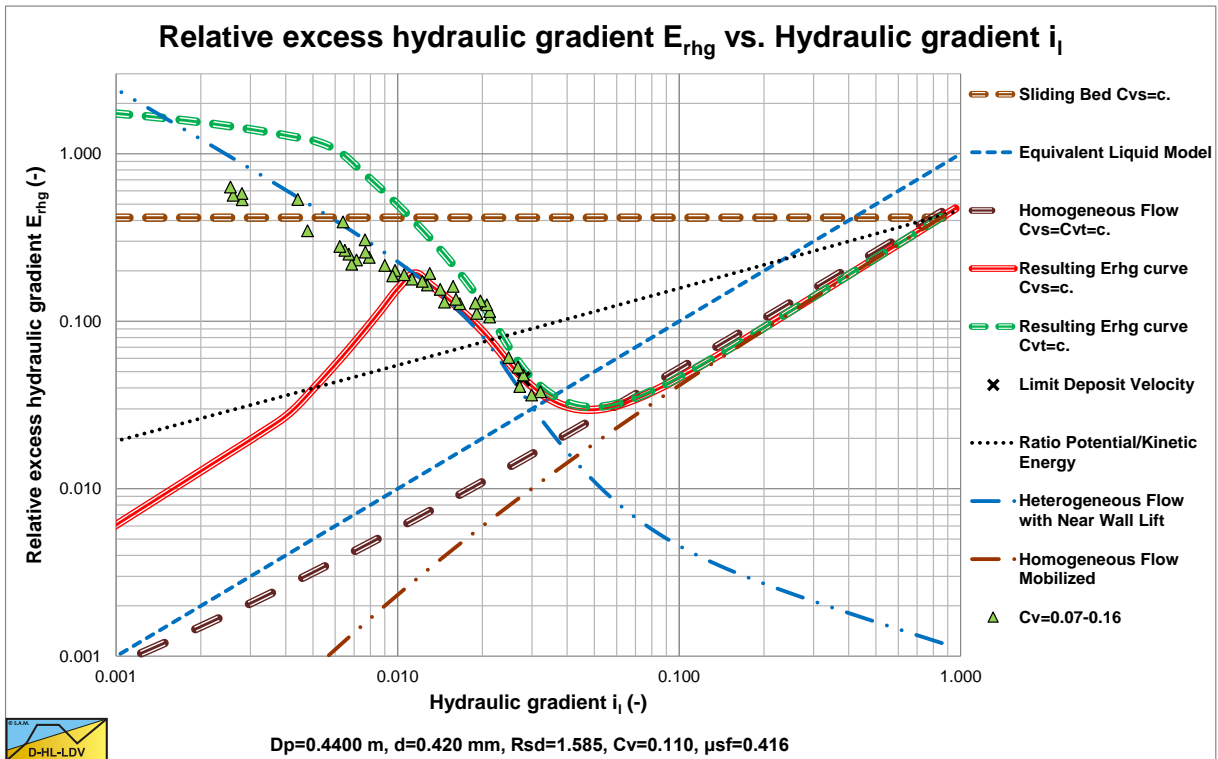
Figure 7.11-5: Experiments of Clift at al. (1982) in a 0.4400 m diameter pipe and a 0.42 mm particle.
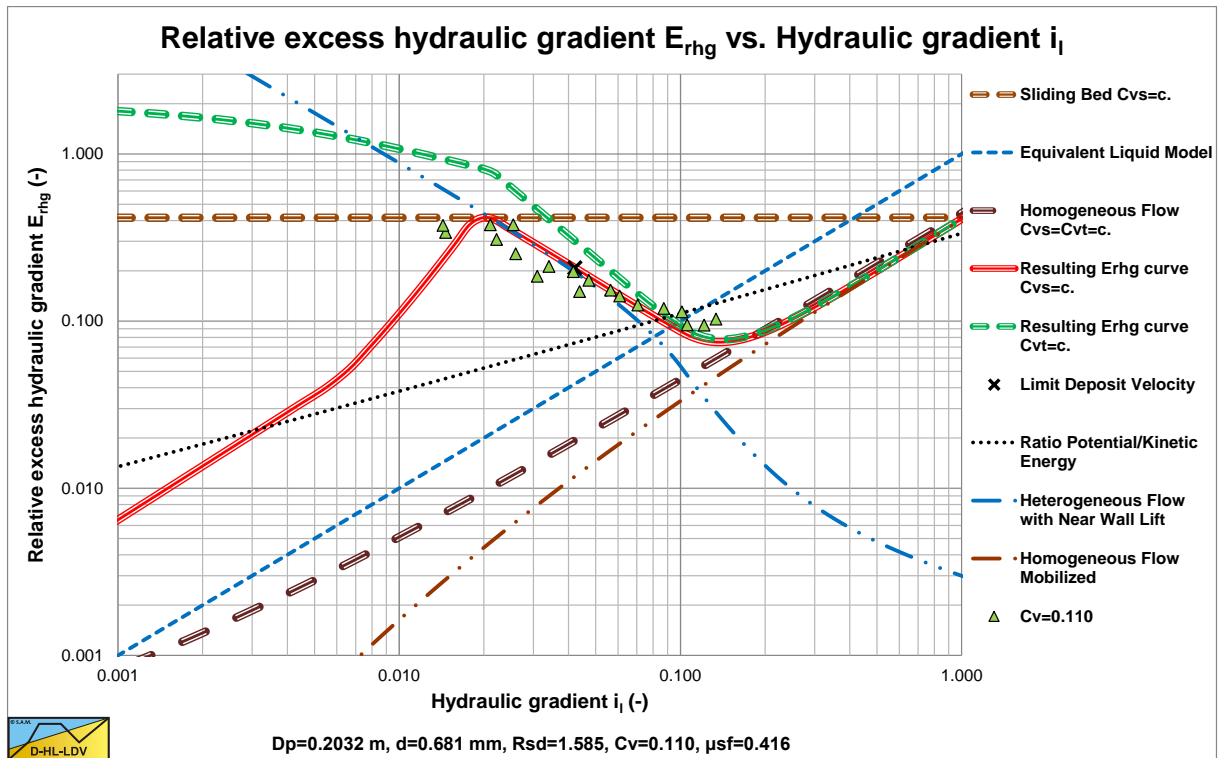
Figure 7.11-6: Experiments of Clift et al. (1982) in a 0.2082 m diameter pipe and a 0.68 mm particle.
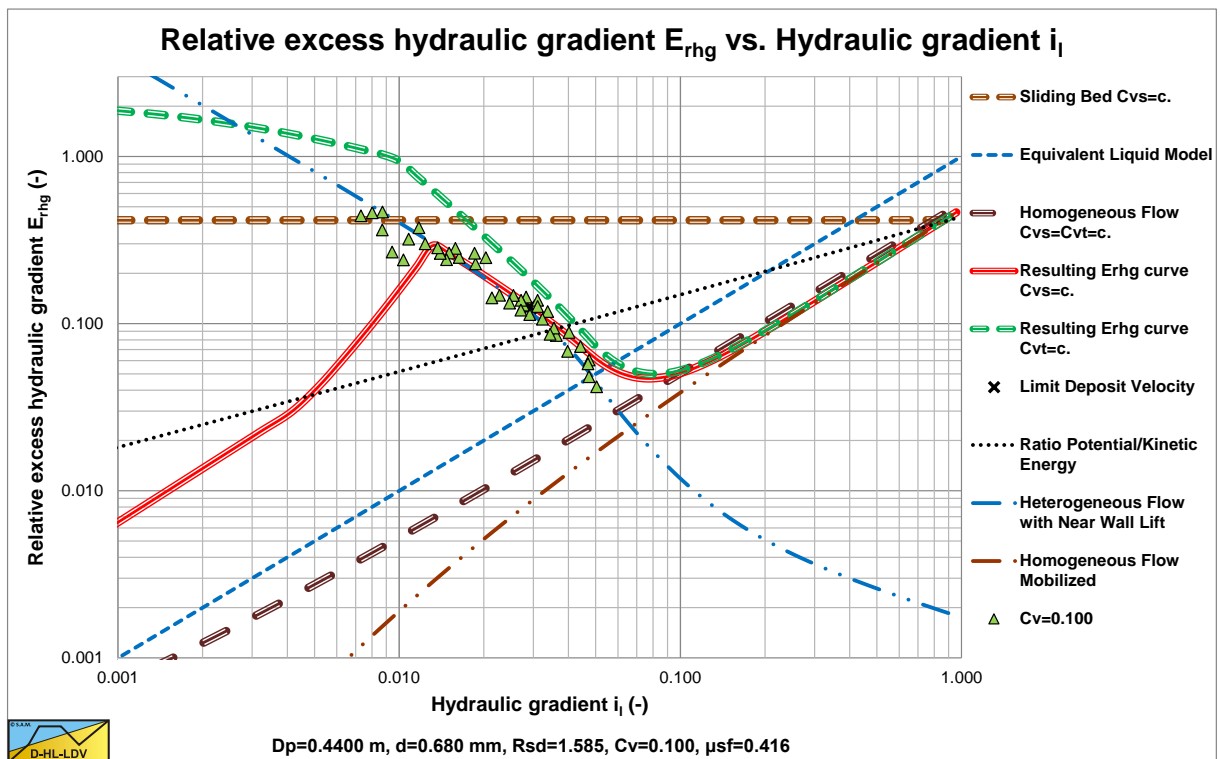
Figure 7.11-7 Experiments of Clift at al. (1982) in a 0.4400 m diameter pipe and a 0.68 mm particle.
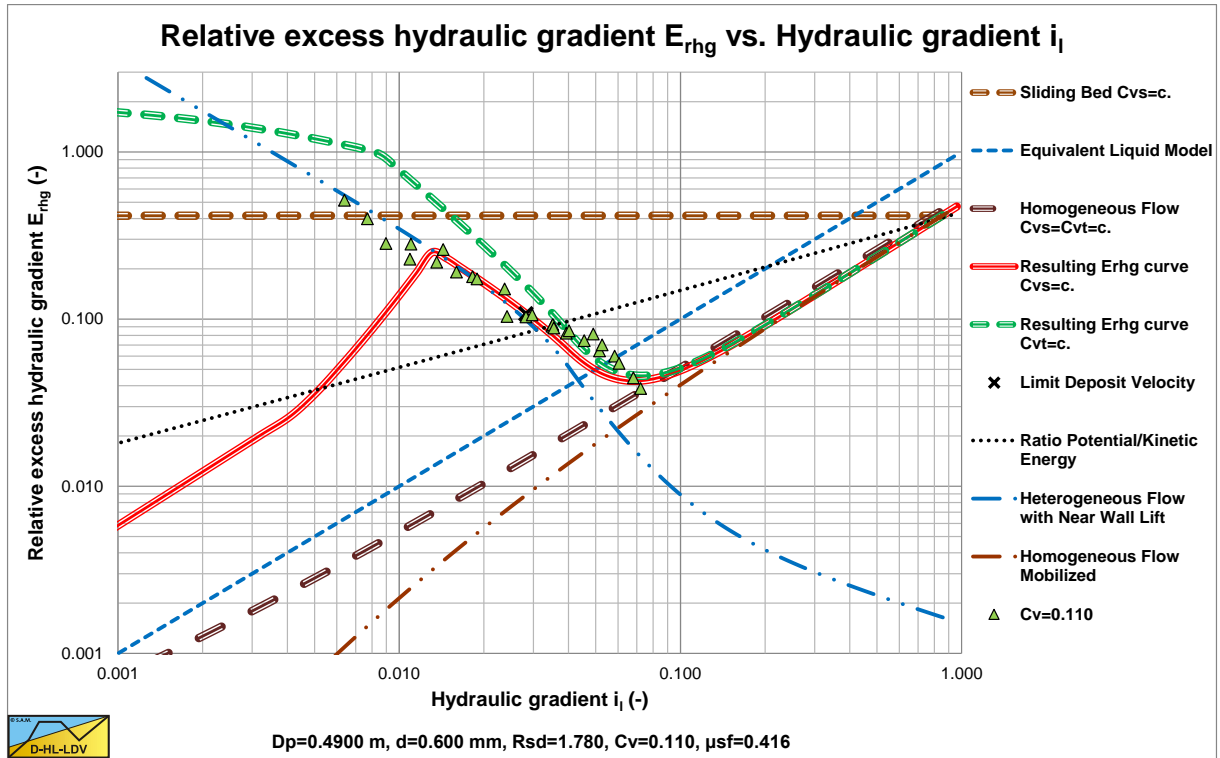
Figure 7.11-8 Experiments of Clift at al. (1982) in a 0.4900 m diameter pipe and a 0.60 mm particle.

For the diffusivity and the relation between the sediment diffusivity and the turbulent eddy momentum diffusivity different approaches are possible. Using the Lane & Kalinske (1941) approach, the following equation can be derived for pipe flow:

$$
C_{vs}(r) = C_{vB} \cdot e^{-12 \cdot \frac{v_{th}}{\beta_{sm} \cdot \kappa \cdot u_*} \cdot \frac{r}{D_p}} \tag{7.11-11}
$$

Now based on the assumption that the diffusivity has to have a value such that at the LDV the concentration at the bottom of the pipe equals the bed concentration (the definition of the LDV), the following equation is derived by Miedema & Ramsdell (2015B):

$$
C_{vs}(r) = C_{vB} \cdot e^{-\frac{\alpha_{sm}}{C_{vr}} \cdot \frac{u_{*,ldv}}{u_*} \cdot \frac{v_{th}}{v_{th,ldv}} \cdot \frac{r}{D_p}} \quad \text{with:} \quad \alpha_{sm} = 1.0046 + 0.1727 \cdot C_{vr} - 1.1905 \cdot C_{vr}^2 \tag{7.11-12}
$$

The settling velocity v_{th} is the hindered settling velocity of the particle, based on the properties of the liquid, adjusted for the homogeneous fraction, resulting in the vehicle liquid according to Wasp et al. (1977). The correction factor α_{sm} appears to depend only on the relative concentration C_{vr}. The bottom concentration C_{vB} is now for line speeds above the LDV:

$$
C_{vB} = C_{vb} \cdot \frac{u_{*,ldv}}{u_*} \cdot \frac{v_{th}}{v_{th,ldv}} \tag{7.11-13}
$$

Figure 7.11-9 shows the concentration profiles for different relative concentrations, adjusted for the circular shape of the pipe at the LDV, compared with data from Kaushal et al. (2005) for a 0.44 mm particle, giving a reasonable match. Since hindered settling is applied for the average vehicle concentration, applying the local concentration may alter the profiles slightly. Especially at higher concentrations, the hindered settling in the upper half of the pipe will be less than in the bottom half of the pipe, resulting in lower concentrations in the upper half of the pipe and higher concentrations in the lower half of the pipe, as shown in Figure 7.11-9.
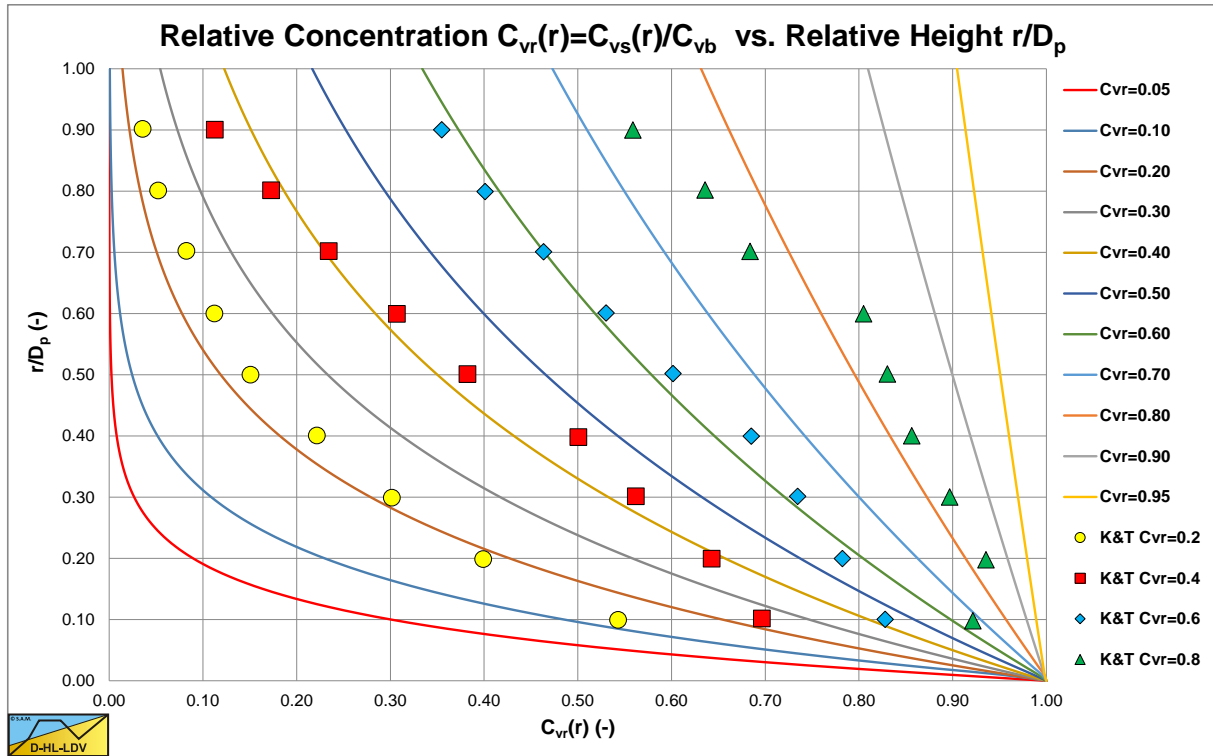
Figure 7.11-9: The concentration distribution at the LDV as a function of the relative concentration.

Now how does this contribute to the mobilization of the RELM? Assume this mobilization **m** depends on the ratio of the concentration at two levels r_1 and r_2 in the pipe, this gives:

$$m = \frac{C_{vs}(r_2)}{C_{vs}(r_1)} = \frac{e^{-\frac{\alpha_{sm}}{C_{vr}} \cdot \frac{u_{*,ldv}}{u_*} \cdot \frac{v_{th}}{v_{th,ldv}} \cdot \frac{r_2}{D_p}}}{e^{-\frac{\alpha_{sm}}{C_{vr}} \cdot \frac{u_{*,ldv}}{u_*} \cdot \frac{v_{th}}{v_{th,ldv}} \cdot \frac{r_1}{D_p}}} = e^{-\left(\frac{r_2}{D_p} - \frac{r_1}{D_p}\right) \cdot \frac{\alpha_{sm}}{C_{vr}} \cdot \frac{u_{*,ldv}}{u_*} \cdot \frac{v_{th}}{v_{th,ldv}}} \tag{7.11-14}$$

Wasp et al. (1977) use $r_1=0.5 \cdot D_p$ and $r_2=0.92 \cdot D_p$ to determine the vehicle fraction, which is not the same as the mobilization factor of the RELM. Different values are tested and the best outcome was found choosing $r_1=0.45 \cdot D_p$ and $r_2=0.55 \cdot D_p$, giving:

$$m = \frac{C_{vs}(r_2)}{C_{vs}(r_1)} = \frac{e^{-\frac{\alpha_{sm}}{C_{vr}} \cdot \frac{u_{*,ldv}}{u_*} \cdot \frac{v_{th}}{v_{th,ldv}} \cdot 0.55}}{e^{-\frac{\alpha_{sm}}{C_{vr}} \cdot \frac{u_{*,ldv}}{u_*} \cdot \frac{v_{th}}{v_{th,ldv}} \cdot 0.45}} = e^{-0.1 \cdot \frac{\alpha_{sm}}{C_{vr}} \cdot \frac{u_{*,ldv}}{u_*} \cdot \frac{v_{th}}{v_{th,ldv}}} \tag{7.11-15}$$

Basically this shows the concentration gradient at the center of the pipe. Figure 7.11-4 and Figure 7.11-5 show the mobilized homogeneous flow E_{rhg} according to:

$$E_{rhg} = \frac{i_m - i_l}{R_{sd} \cdot C_{vs}} = m \cdot i_l \cdot \left(1 - \left(1 - \frac{\left(1 + R_{sd} \cdot C_{vs} - \left(\frac{A_{C_v}}{\kappa} \cdot \ln\left(\frac{\rho_m}{\rho_l}\right) \cdot \sqrt{\frac{\lambda_l}{8}} + 1\right)\right)^2}{R_{sd} \cdot C_{vs} \cdot \left(\frac{A_{C_v}}{\kappa} \cdot \ln\left(\frac{\rho_m}{\rho_l}\right) \cdot \sqrt{\frac{\lambda_l}{8}} + 1\right)^2} \right) \left(1 - \left(\frac{\delta_v}{d}\right)\right) \right) \tag{7.11-16}$$

7.11.4 Resulting Relative Excess Hydraulic Gradient Curves.

Figure 7.11-10 gives an example of the resulting relative excess hydraulic gradient curves for a 0.2032 m diameter pipe and particles ranging from 0.1 mm to 10 mm, showing the different flow regimes for the transport (delivered) concentration case. Figure 7.11-11 shows the resulting relative excess hydraulic gradient curves for a 0.44 m diameter pipe for the transport (delivered) concentration case. From these two figures it is clear that the larger pipe diameter shows a steeper decrease of the **E$_{rhg}$** in the heterogeneous regime for particles of 0.2 mm, 0.3 mm and 0.5 mm, so medium sands. Very small particles are dominated by the submerged weight, while larger particles are dominated by their kinetic energy.

7.11.5 Conclusions & Discussion.

The transition of different flow regimes is important, but the transition of the heterogeneous flow regime with the homogeneous flow regime is very important, due to the fact that this coincides often with operational line speeds. To model this transition it is necessary to have appropriate models for the heterogeneous and the homogeneous flow regimes. The homogeneous flow regime is modelled as a reduced equivalent liquid model (RELM) with mobilization of the reduction based on the ratio between the thicknesses of the viscous sub layer to the particle diameter. For very small particles there is no reduction at low line speeds. The reduction is in effect at higher line speeds. Medium and large particles encounter this reduction however also at lower line speeds. The heterogeneous flow regime is modelled based on potential and kinetic energy losses, where the potential energy losses are reversely proportional to the line speed and the kinetic energy losses (based on collisions) are reversely proportional to the line speed squared.

At the transition (intersection line speed) of the two flow regimes, the heterogeneous head losses collapse in larger pipe diameters for medium sized particles. It appears that these particles encounter the highest lift forces, compared to their submerged weight and kinetic energy. For very small particles the submerged weight dominates, due to the fact that transition line speed is very small and there is hardly lift. For very large particles the kinetic energy dominates and the lift is not capable to decelerate the particles. But for medium sized particles, the lift is stronger than the combined effect of submerged weight and kinetic energy. In a 0.2032 m diameter pipe the collapse of the collisions is still weak, but in a 0.44 m diameter pipe this is already strong. Larger pipe diameter will most probably show a stronger effect, explaining also why dredging companies state that medium sized particles in large diameter pipes have head losses close to the head losses of pure water.

The RELM is not yet fully mobilized at low line speeds, due to the fact that turbulent eddies are not yet capable of integrating particles in the rotation of the eddies. The higher the line speed, the more the particles become an integrated part of the turbulence (if they are not too large). Based on the definition of the LDV and the concentration distribution equation from the advection diffusion equation, a mobilization factor has been defined for the mobilization of the RELM. The concentration distribution is such that at the LDV the concentration at the bottom of the pipe equals the bed concentration.

Resuming it can be stated that the new model explains for the homogeneous behavior of very small particles, regarding the mobilization of the lubrication effect of the particle poor viscous sub layer. It can also be stated that an explanation is found for the collapse of the heterogeneous head losses of medium sized particles in larger pipes, based on near wall lift and the mobilization of the RELM.
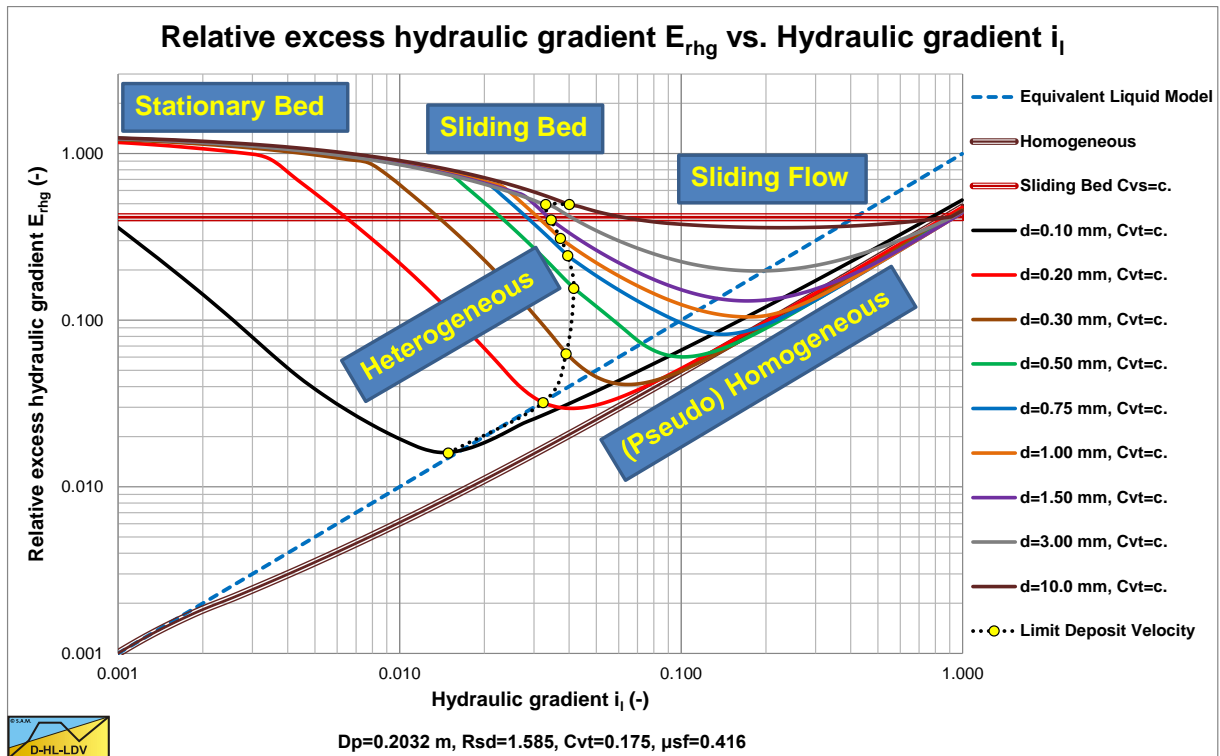
Figure 7.11-10: The main flow regimes for constant delivered/transport concentration, pipe diameter D_p=0.2032 m.
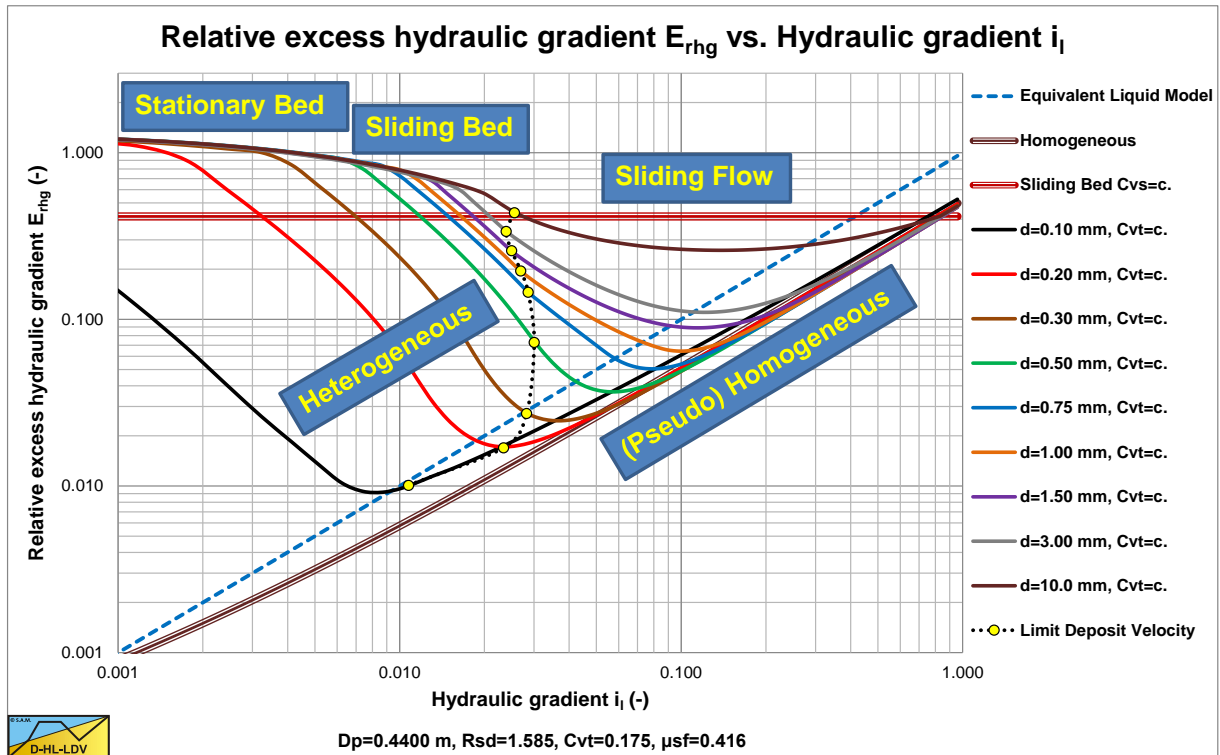
Figure 7.11-11: The main flow regimes for constant delivered/transport concentration, pipe diameter D_p=0.44 m.

7.11.6 Nomenclature.

A_{cv}	Coefficient RELM (default 3)	-
C_D	Particle drag coefficient	-
C_L	Lift coefficient	-
C_{vt}	Delivered (transport) volumetric concentration	-
C_{vs}	Spatial volumetric concentration	-
C_{vb}	Spatial volumetric concentration bed (1-n)	-
C_{vB}	Spatial concentration at the bottom of the pipe	-
C_{vr}	Relative spatial concentration	-
d	Particle diameter	m
D_p	Pipe diameter	m
ELM	Equivalent liquid model	-
E_{rhg}	Relative excess hydraulic gradient	-
E_k	Kinetic energy in vertical direction	N·m
F_L	Lift force on particle	N
F_G	Submerged weight of particle	N
F_K	Kinetic energy deceleration force	N
g	Gravitational constant 9.81 m/s^2	m/s^2
i_l	Pure liquid hydraulic gradient	m/m
i_m	Mixture hydraulic gradient	m/m
LDV	Limit Deposit Velocity	m/s
LSDV	Limit of Stationary Deposit Velocity	m/s
L_R	Lift ratio	-
m	Mobilized RELM factor	-
m_p	Mass particle	kg
n	Porosity	-
RELM	Reduced equivalent liquid model	-
r, r_1, r_2	Vertical distance in pipe	m
R	Stratification ratio Wilson	-
R_{sd}	Relative submerged density	-
S_{hr}	Settling velocity Hindered Relative	-
S_{rs}	Slip velocity Relative Squared	-
u_*	Friction velocity	m/s
$u_{*,ldv}$	Friction velocity at LDV	m/s
v_{ls}	Line speed	m/s
v_{sl}	Slip velocity	m/s
v_t	Terminal settling velocity particle	m/s
v_{th}	Hindered terminal settling velocity particle	m/s
$v_{th,ldv}$	Hindered terminal settling velocity particle at LDV	m/s
$v_{\delta v}$	Velocity at viscous sub layer thickness	m/s
x	Distance to decelerate particle	m
α	Number of times thickness viscous sub layer	-
α_{sm}	Coefficient concentration distribution	-
β	Richardson & Zaki hindered settling power	-
β_{sm}	Diffusivity factor	-
δ_v	Viscous sub layer thickness	m
ε	Pipe wall roughness	-
κ	Von Karman constant (about 0.4)	-
κ_C	Concentration eccentricity factor	-
λ_l	Darcy Weisbach friction factor liquid	-
μ_{sf}	Sliding friction factor	-
ρ_l	Density liquid	ton/m^3
ρ_m	Density mixture	ton/m^3
ρ_s	Density solid	ton/m^3
ν_l	Kinematic viscosity liquid	m^2/s
ψ	Shape factor	-

| ζ | Smoothing parameter lift ratio | - |

7.12 The Bed Height.

7.12.1 Concentration Transformation Equations.

For a certain control volume the volumetric transport concentration can be determined if the volumetric spatial concentration and the slip velocity are known, given a certain line speed.

$$
\mathbf{C_{vt}} = \left(1 - \frac{\mathbf{v_{sl}}}{\mathbf{v_{ls}}}\right) \cdot \mathbf{C_{vs}} = (1 - \xi) \cdot \mathbf{C_{vs}}
\tag{7.12-1}
$$

With the slip ratio:

$$
\xi = \frac{\mathbf{v_{sl}}}{\mathbf{v_{ls}}}
\tag{7.12-2}
$$

Likewise, for a certain control volume, the volumetric spatial concentration can be determined if the volumetric transport concentration and the slip velocity are known, given a certain line speed.

$$
\mathbf{C_{vs}} = \left(\frac{\mathbf{v_{ls}}}{\mathbf{v_{ls}} - \mathbf{v_{sl}}}\right) \cdot \mathbf{C_{vt}} = \left(\frac{1}{1 - \xi}\right) \cdot \mathbf{C_{vt}}
\tag{7.12-3}
$$

These two equations will be used a lot in the following derivations and are considered to be well known.

7.12.2 Fixed Bed.

Continuum Equations.

Considering a fixed bed, two phases are present, the fixed bed phase and the suspension phase. All the particles that transfer the head losses by inter-particle interactions are considered to be part of the fixed bed phase. All the particles that transfer their head loss contribution through turbulent dispersion are considered to be in the suspension phase. The flow of sediment can be expressed in terms of the pipe cross section times the volumetric spatial concentration times the line speed minus the slip velocity, where the slip velocity is considered to be the average over the whole pipe cross section. Since a fixed bed is considered, this has to be equal to the amount of solids transported in the suspension phase, which is the cross section of the suspension phase times the volumetric transport concentration of this suspension phase times the line speed.

The volume flow of solids is (with a fixed bed the bed velocity is zero):

$$
\mathbf{Q_s} = \mathbf{A_p} \cdot \mathbf{C_{vt}} \cdot \mathbf{v_{ls}} = \mathbf{A_p} \cdot \mathbf{C_{vs}} \cdot (\mathbf{v_{ls}} - \mathbf{v_{sl}}) = \mathbf{A_b} \cdot \mathbf{C_{vb}} \cdot \mathbf{v_b} + \mathbf{A_s} \cdot \mathbf{C_{vt,s}} \cdot \mathbf{v_s}
\tag{7.12-4}
$$

The total volume flow, liquid plus solids, is:

$$
\mathbf{Q_v} = \mathbf{A_p} \cdot \mathbf{v_{ls}} = \mathbf{A_b} \cdot \mathbf{v_b} + \mathbf{A_s} \cdot \mathbf{v_s}
\tag{7.12-5}
$$

The volume of solids in a pipe section with length $\mathbf{\Delta L}$ is:

$$
\mathbf{V_s} = \mathbf{A_p} \cdot \mathbf{C_{vs}} \cdot \mathbf{\Delta L} = \mathbf{A_b} \cdot \mathbf{C_{vb}} \cdot \mathbf{\Delta L} + \mathbf{A_s} \cdot \mathbf{C_{vs,s}} \cdot \mathbf{\Delta L}
\tag{7.12-6}
$$

The total pipe cross section is the sum of the suspension cross section and the bed cross section:

$$
\mathbf{A_s} + \mathbf{A_b} = \mathbf{A_p}
\tag{7.12-7}
$$

Derivation.

The fraction of the pipe cross section occupied by solids is the sum of the fraction in the bed and the fraction in suspension:

$$A_p \cdot C_{vs} = A_b \cdot C_{vb} + \left(A_p - A_b\right) \cdot C_{vs,s} = A_p \cdot C_{vt} \cdot \left(\frac{v_{ls}}{v_{ls} - v_{sl}}\right) = A_p \cdot \left(\frac{1}{1-\xi}\right) \cdot C_{vt} \tag{7.12-8}$$

Now suppose that: $C_{vs,s} = \kappa_{ldv} \cdot C_{vt}$ with: $\kappa_{ldv} = \left(\dfrac{v_{ls,ldv}}{v_{ls,ldv} - v_{sl,ldv}}\right) = \left(\dfrac{1}{1-\xi_{ldv}}\right)$, based on the slip ratio at the

Limit Deposit Velocity, this gives:

$$A_b \cdot C_{vb} + \left(A_p - A_b\right) \cdot \kappa_{ldv} \cdot C_{vt} = A_p \cdot C_{vt} \cdot \left(\frac{v_{ls}}{v_{ls} - v_{sl}}\right) = A_p \cdot \left(\frac{1}{1-\xi}\right) \cdot C_{vt} \tag{7.12-9}$$

This can be written as:

$$A_b \cdot C_{vb} \cdot \left(v_{ls} - v_{sl}\right) + \left(A_p - A_b\right) \cdot \kappa_{ldv} \cdot C_{vt} \cdot \left(v_{ls} - v_{sl}\right) = A_p \cdot C_{vt} \cdot v_{ls} \tag{7.12-10}$$

Combining the terms with the bed cross section gives:

$$A_b \cdot \left(C_{vb} - \kappa_{ldv} \cdot C_{vt}\right) \cdot \left(v_{ls} - v_{sl}\right) + A_p \cdot \kappa_{ldv} \cdot C_{vt} \cdot \left(v_{ls} - v_{sl}\right) = A_p \cdot C_{vt} \cdot v_{ls} \tag{7.12-11}$$

Moving the terms with the full pipe cross section to the right hand side gives:

$$A_b \cdot \left(C_{vb} - \kappa_{ldv} \cdot C_{vt}\right) \cdot \left(v_{ls} - v_{sl}\right) = A_p \cdot \left(1 - \kappa_{ldv}\right) \cdot C_{vt} \cdot v_{ls} + A_p \cdot \kappa_{ldv} \cdot C_{vt} \cdot v_{sl} \tag{7.12-12}$$

This results in an equation for the bed fraction:

$$\zeta = \hat{A}_b = \frac{A_b}{A_p} = \frac{\left(1 - \kappa_{ldv}\right) \cdot C_{vt} \cdot v_{ls} + \kappa_{ldv} \cdot C_{vt} \cdot v_{sl}}{\left(C_{vb} - \kappa_{ldv} \cdot C_{vt}\right) \cdot \left(v_{ls} - v_{sl}\right)} \tag{7.12-13}$$

This can be written as:

$$\boxed{\zeta = \hat{A}_b = \frac{A_b}{A_p} = \frac{\left(1 - \kappa_{ldv}\right) \cdot C_{vt} + \kappa_{ldv} \cdot C_{vt} \cdot \xi}{\left(C_{vb} - \kappa_{ldv} \cdot C_{vt}\right) \cdot \left(1-\xi\right)} = \frac{\left(1 - \kappa_{ldv} \cdot \left(1-\xi\right)\right) \cdot C_{vt}}{\left(C_{vb} - \kappa_{ldv} \cdot C_{vt}\right) \cdot \left(1-\xi\right)}} \tag{7.12-14}$$

Because of the choice of κ_{ldv}, the relative bed fraction is zero at a line speed equal to the Limit Deposit Velocity.

At the LDV this gives a bed fraction:

$$\zeta_{ldv} = \hat{A}_b = \frac{A_b}{A_p} = \frac{\left(1 - \kappa_{ldv} \cdot \left(1-\xi_{ldv}\right)\right) \cdot C_{vt}}{\left(C_{vb} - \kappa_{ldv} \cdot C_{vt}\right) \cdot \left(1-\xi_{ldv}\right)} = \frac{0}{\left(C_{vb} - \kappa_{ldv} \cdot C_{vt}\right) \cdot \left(1-\xi_{ldv}\right)} = 0 \tag{7.12-15}$$

With : $\kappa_{ldv} = \dfrac{1}{\left(1-\xi_{ldv}\right)}$

This makes sense, since the definition of the LDV is that there is no stationary or sliding bed.

7.12.3 Sliding Bed.

Continuum Equations.

The volume flow of solids is (with a sliding bed the bed velocity is non-zero):

$$Q_s = A_p \cdot C_{vt} \cdot v_{ls} = A_b \cdot C_{vb} \cdot v_b + A_s \cdot C_{vt,s} \cdot v_s \tag{7.12-16}$$

The total volume flow, liquid plus solids, is:

$$Q_v = A_p \cdot v_{ls} = A_b \cdot v_b + A_s \cdot v_s \tag{7.12-17}$$

The volume of solids in a pipe section per unit of length is:

$$V_s = A_p \cdot C_{vs} \cdot \Delta L = A_b \cdot C_{vb} \cdot \Delta L + A_s \cdot C_{vs,s} \cdot \Delta L \tag{7.12-18}$$

The total pipe cross section is the sum of the suspension cross section and the bed cross section:

$$A_s + A_b = A_p \tag{7.12-19}$$

Derivation.

The volume of solids in a pipe section per unit of length can be expressed in terms of the delivered volumetric concentrations, assuming the delivered volumetric concentration in the suspension phase is equal to this concentration at the LDV times a factor **α**, by:

$$V_s = A_p \cdot C_{vs} \cdot \Delta L = A_p \cdot \left(\frac{1}{1-\xi}\right) \cdot C_{vt} \cdot \Delta L = A_b \cdot C_{vb} \cdot \Delta L + A_s \left(\frac{\alpha}{1-\xi_{ldv}}\right) \cdot C_{vt} \cdot \Delta L \tag{7.12-20}$$

Replacing the suspension cross section by the pipe cross section minus the bed cross section gives:

$$V_s = A_p \cdot C_{vs} \cdot \Delta L = A_p \cdot \left(\frac{1}{1-\xi}\right) \cdot C_{vt} \cdot \Delta L = A_b \cdot C_{vb} \cdot \Delta L + \left(A_p - A_b\right) \cdot \left(\frac{\alpha}{1-\xi_{ldv}}\right) \cdot C_{vt} \cdot \Delta L \tag{7.12-21}$$

Moving all terms with the pipe cross section to the left hand side and all terms with the bed cross section to the right hand side, gives:

$$A_p \cdot \left(\frac{1}{1-\xi} - \frac{\alpha}{1-\xi_{ldv}}\right) \cdot C_{vt} = A_b \cdot \left(C_{vb} - \frac{\alpha \cdot C_{vt}}{1-\xi_{ldv}}\right) \tag{7.12-22}$$

This gives for the bed fraction:

$$\zeta = \hat{A}_b = \frac{A_b}{A_p} = \frac{\left(1 - \alpha \cdot \kappa_{ldv} \cdot (1-\xi)\right) \cdot C_{vt}}{\left(C_{vb} - \frac{\alpha \cdot C_{vt}}{1-\xi_{ldv}}\right)} = \frac{\left(1 - \alpha \cdot \kappa_{ldv} \cdot (1-\xi)\right) \cdot C_{vt}}{\left(C_{vb} - \alpha \cdot \kappa_{ldv} \cdot C_{vt}\right) \cdot (1-\xi)} \tag{7.12-23}$$

When **α=1** this gives the same result as the fixed bed approach. At the LDV this only gives a bed height of zero and a bed height of 100% if **α=1**. A value of **α>1** will give a higher bed fraction, A value of **α<1** will give a lower bed fraction. So **α** could be a function of the line speed with a value of 1 at both zero line speed and at the LDV.

The examples in this book are made with **α=1**, so with a fixed bed approach.
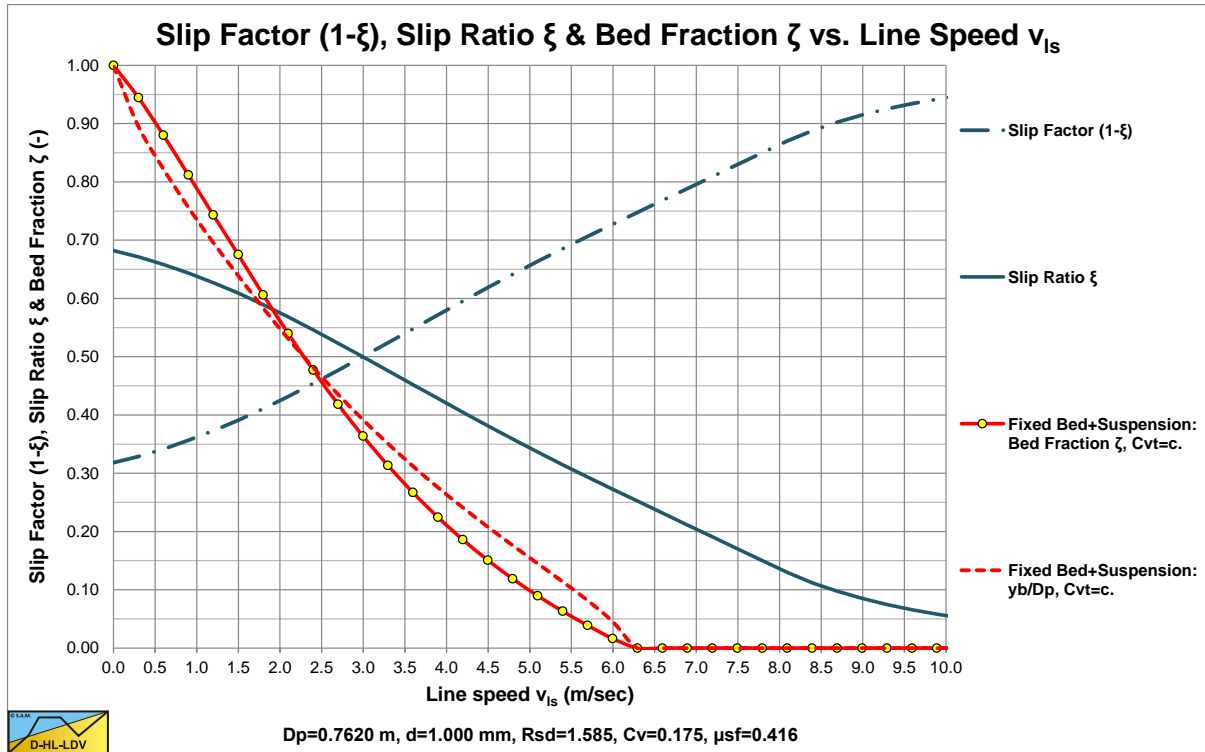
Figure 7.12-1: The bed fraction and height of the bed.
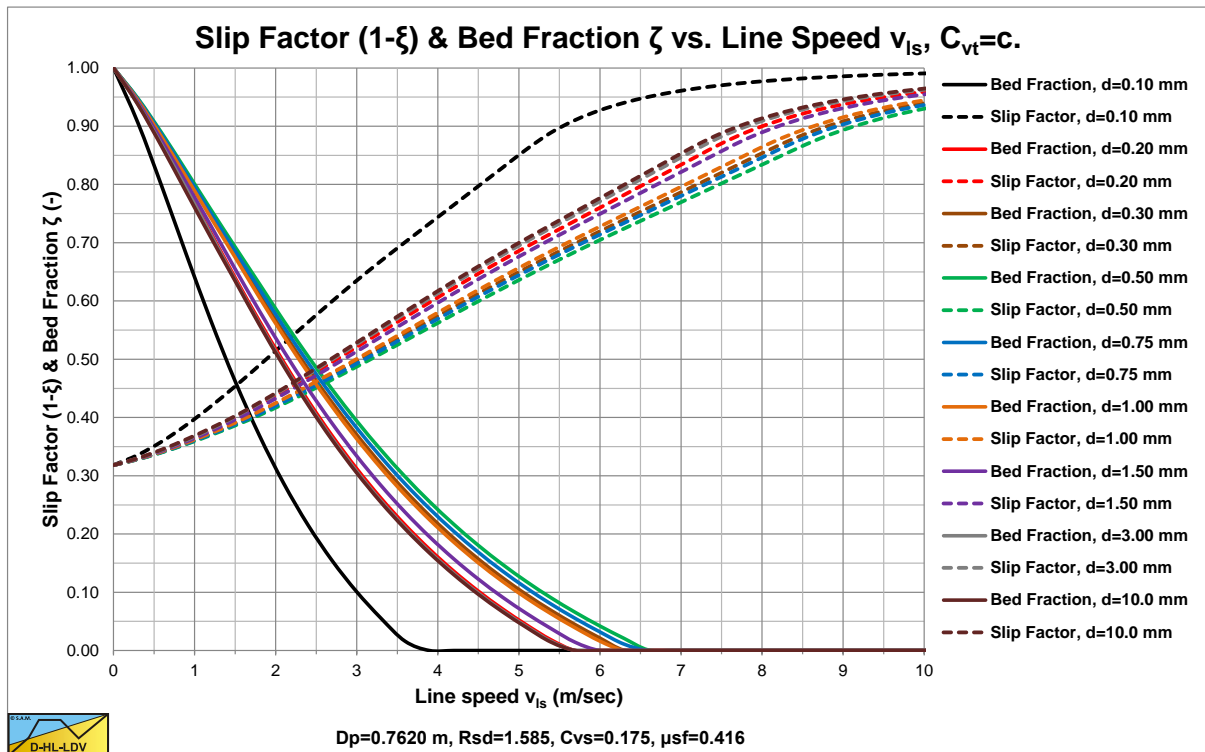
Figure 7.12-2: The bed fraction and height of the bed for different particle diameters.

7.12.4 Some Results.

Based on the real slip velocity, the spatial concentration and the transport concentration can be converted into each other, giving the possibility to determine the spatial concentration eat each line speed, given a certain constant transport concentration. This also makes it possible to determine the fraction of the bed occupying the pipe cross section assuming a fixed bed, which is very valuable for dredging companies. Below the Limit Deposit Velocity, the bed fraction increases slowly with decreasing line speed. At a certain line speed however, the bed fraction will increase more rapidly with further decreasing line speed. Maybe the definition of the Limit Deposit Velocity should be reconsidered. Now the definition is the line speed at which a bed disappears completely with increasing line speed or appears with decreasing line speed. A definition based on an acceptable fraction of the bed occupying the pipe cross section would be more appropriate. Accepting a bed fraction of 10% would reduce the Limit Deposit Velocity from, in the example in Figure 7.12-1 and Figure 7.12-2, 6.25 m/sec to about 5 m/sec for the **d=1 mm** particles.

The graphs shown are based on the fixed bed equation, so the bed height curves may differ slightly for a sliding bed.

7.12.5 Nomenclature Bed Height.

A_b	Bed cross section	m^2
A_p	Pipe cross section	m^2
A_s	Suspension cross section (cross section above the bed)	m^2
$\tilde{A}_b$	Bed fraction	-
C_{vt}	Delivered (transport) volumetric concentration	-
$C_{vt,s}$	Delivered (transport) volumetric concentration in suspended layer	-
C_{vs}	Spatial volumetric concentration	-
$C_{vs,s}$	Spatial volumetric concentration in suspended layer	-
C_{vb}	Spatial volumetric concentration bed (1-n)	-
d	Particle diameter	m
D_p	Pipe diameter	m
ΔL	Pipe length	m
n	Porosity	-
Q_s	Total solids flow	m^3/s
Q_v	Total flow, liquid + solids	m^3/s
R_{sd}	Relative submerged density	-
v_{ls}	Line speed	m/s
v_b	Bed velocity	m/s
v_s	Suspension velocity	m/s
$v_{ls,ldv}$	Limit Deposit Velocity	m/s
v_{sl}	Slip velocity	m/s
$v_{sl,ldv}$	Slip velocity at the LDV	m/s
V_s	Volume of solids in a pipe section	m^3
α	Slip ratio factor	-
κ_{ldv}	Reversed slip ratio at LDV	-
μ_{sf}	Sliding friction factor	-
ξ	Slip ratio	-
ξ_{ldv}	Slip ratio at LDV	-
ζ	Bed fraction	-
ζ_{ldv}	Bed fraction at the LDV	-

7.13 Influence of the Particle Size Distribution

7.13.1 Introduction.

The i_m curve for graded sands and gravels can be determined by:
1. Determine the fraction fines **X**. The limiting particle diameter for the fines can be determined with equation (7.13-2).
2. Determine the PSD and split the PSD in **n** fractions. Correct the PSD so the fines are not part of the PSD anymore. Adjust the volumetric concentration by deducting the fines fraction **X**.
3. Adjust the pseudo liquid dynamic viscosity μ_x, density ρ_x and relative submerged density $R_{sd,x}$ for the presence of fines and determine the resulting hydraulic gradient curve for the pseudo liquid, $i_{l,x}$.
4. Determine curves related to the pseudo liquid.
   a. Determine the $i_{m,x,i}$ curve for each ith fraction individually for both the spatial volumetric concentration and the delivered volumetric concentration, using the adjusted pseudo liquid properties.
   b. Sum the $i_{m,x,i}$ curves for the **n** fractions multiplied by the fraction f_i to determine the total hydraulic gradient $i_{m,x}$, for both the spatial volumetric concentration and the delivered volumetric concentration, in the pseudo liquid.
   c. Determine the resulting $E_{rhg,x}$ curve, for both the spatial volumetric concentration and the delivered volumetric concentration.
5. Determine curves related to the carrier liquid.
   a. Determine the $i_{m,i}$ curves for the **n** fractions by multiplying the $i_{m,x,i}$ curves by the ratio of the pseudo liquid density to the carrier liquid density ρ_x/ρ_l.
   b. Sum the $i_{m,i}$ curves for the **n** fractions multiplied by the fraction f_i to determine the total hydraulic gradient i_m, for both the spatial volumetric concentration and the delivered volumetric concentration, in the carrier liquid.
   c. Determine the resulting E_{rhg} curve, for both the spatial volumetric concentration and the delivered volumetric concentration.
6. Determine the bed fraction curves for each fraction multiplied by the fraction f_i.
7. Sum the bed fraction curves for the **n** fractions multiplied by the fraction f_i to obtain the total bed fraction curve.
8. Determine the slip ratio curves for each fraction multiplied by the fraction f_i.
9. Sum the slip ratio curves for the **n** fractions multiplied by the fraction f_i to obtain the total slip ratio curve.

Step 2 needs some clarification. Suppose we have a sand with 3 fractions, each 1/3 by weight. The first fraction consists of fines, the second fraction of particles with a **d=0.5 mm** and the third fraction of particles with **d=1 mm**. The spatial volumetric concentration of the sand in the carrier liquid is 30%.

Now the fines form a pseudo homogeneous liquid together with the carrier liquid. So in terms of solids effect they do not take part in the solids effect and have to be removed from the PSD. What is left is a PSD with 50% particles with a **d=0.5 mm** and 50% particles with **d=1 mm**. The spatial volumetric concentration of this sand is now 20%. So the hydraulic gradients have to be determined for this remaining sand and not for the original sand.

If a sand does not contain fines, the liquid properties and the PSD do not have to be adjusted.

7.13.2 The Adjusted Pseudo Liquid Properties.

First the limiting particle diameter is determined, based on a Stokes number of 0.03. The value of 0.03 is found based on many experiments from literature. Since the Stokes number depends on the line speed, here the Limit Deposit Velocity is used as an estimate of the operational line speed.

The LDV is approximated by:

$$v_{ls,ldv} = 7.5 \cdot D_p^{0.4} \tag{7.13-1}$$

Giving for the limiting particle diameter:

$$d_{lim} = \sqrt{\frac{Stk \cdot 9 \cdot \rho_l \cdot \nu_l \cdot D_p}{\rho_s \cdot v_{ls,ldv}}} \approx \sqrt{\frac{Stk \cdot 9 \cdot \rho_l \cdot \nu_l \cdot D_p}{\rho_s \cdot 7.5 \cdot D_p^{0.4}}} \tag{7.13-2}$$

The fraction of the sand in suspension, resulting in a homogeneous pseudo fluid is named **X**. This gives for the density of the homogeneous pseudo fluid:

$$\rho_x = \rho_l + \rho_l \cdot \frac{X \cdot C_{vs} \cdot R_{sd}}{\left(1 - C_{vs} + C_{vs} \cdot X\right)} \quad \text{if } X = 1 \quad \Rightarrow \quad \rho_x = \rho_m = \rho_l + \rho_l \cdot C_{vs} \cdot R_{sd} \tag{7.13-3}$$

So the concentration of the homogeneous pseudo fluid is not $C_{vs,x} = X \cdot C_{vs}$, but:

$$C_{vs,x} = \frac{X \cdot C_{vs}}{\left(1 - C_{vs} + C_{vs} \cdot X\right)} \tag{7.13-4}$$

This is because part of the total volume is occupied by the particles that are not in suspension. The remaining spatial concentration of solids to be used to determine the individual hydraulic gradients curves of the fractions is now:

$$C_{vs,r} = (1 - X) \cdot C_{vs} \tag{7.13-5}$$

The dynamic viscosity can now be determined according to Thomas (1965):

$$\mu_x = \mu_l \cdot \left(1 + 2.5 \cdot C_{vs,x} + 10.05 \cdot C_{vs,x}^2 + 0.00273 \cdot e^{16.6 \cdot C_{vs,x}}\right) \tag{7.13-6}$$

The kinematic viscosity of the homogeneous pseudo fluid is now:

$$\nu_x = \frac{\mu_x}{\rho_x} \tag{7.13-7}$$

One should realize however that the relative submerged density has also changed to:

$$R_{sd,x} = \frac{\rho_s - \rho_x}{\rho_x} \tag{7.13-8}$$

With the new homogeneous pseudo liquid density, kinematic viscosity, relative submerged density and volumetric concentration the hydraulic gradient can be determined for each fraction of the adjusted PSD.

7.13.3 A Method To Generate a PSD.

The original fractions of the PSD can be determined manually by sieve analysis, or generated based on for example the d_{50}/d_{15} and d_{85}/d_{50} ratios. A mathematical function describing the shape of a PSD up to the d_{50} is:

$$
f_y = \frac{1}{1+e^{A_x \cdot \left(\frac{\log 10(d_y)}{\log 10(d_{50})}-1\right)}} \quad \text{with:} \quad A_x = \frac{1}{\left(\frac{\log 10(d_x)}{\log 10(d_{50})}-1\right)} \cdot \ln\left(\frac{1-f_x}{f_x}\right) \tag{7.13-9}
$$

Now suppose:

$$
\alpha_{15} = \frac{d_{50}}{d_{15}} \quad \text{and} \quad \alpha_{85} = \frac{d_{85}}{d_{50}} \tag{7.13-10}
$$

This gives:

$$
A_{15} = \frac{1}{\left(\frac{\log 10(d_{15})}{\log 10(d_{50})}-1\right)} \cdot \ln\left(\frac{1-0.15}{0.15}\right) = \frac{1}{\left(\frac{\log 10\left(\frac{d_{50}}{\alpha_{15}}\right)}{\log 10(d_{50})}-1\right)} \cdot \ln\left(\frac{0.85}{0.15}\right) \tag{7.13-11}
$$

$$
= -\frac{\log 10(d_{50})}{\log 10(\alpha_{15})} \cdot \ln\left(\frac{0.85}{0.15}\right) = -1.7346 \cdot \frac{\ln(d_{50})}{\ln(\alpha_{15})}
$$

$$
A_{85} = \frac{1}{\left(\frac{\log 10(d_{85})}{\log 10(d_{50})}-1\right)} \cdot \ln\left(\frac{1-0.85}{0.85}\right) = \frac{1}{\left(\frac{\log 10(\alpha_{85} \cdot d_{50})}{\log 10(d_{50})}-1\right)} \cdot \ln\left(\frac{0.85}{0.15}\right) \tag{7.13-12}
$$

$$
= -\frac{\log 10(d_{50})}{\log 10(\alpha_{85})} \cdot \ln\left(\frac{0.85}{0.15}\right) = -1.7346 \cdot \frac{\ln(d_{50})}{\ln(\alpha_{85})}
$$

Now suppose for the ratios d_{50}/d_{15} and d_{85}/d_{50}:

$$
\alpha_{15} = \frac{d_{50}}{d_{15}} = e^1 = 2.7183 \quad \text{and} \quad \alpha_{85} = \frac{d_{85}}{d_{50}} = e^1 = 2.7183 \tag{7.13-13}
$$

This gives for A_{15} and A_{85} positive values as long as the $d_{50} < 1$ m:

$$
A_{15} = -1.7346 \cdot \ln(d_{50}) \tag{7.13-14}
$$

$$
A_{85} = -1.7346 \cdot \ln(d_{50})
$$

So the fraction passing in the PSD is in this particular symmetrical case:

$$
f_y = \frac{1}{1+e^{A_{15} \cdot \left(\frac{\log 10(d_y)}{\log 10(d_{50})}-1\right)}} = \frac{1}{1+e^{A_{85} \cdot \left(\frac{\log 10(d_y)}{\log 10(d_{50})}-1\right)}} = \frac{1}{1+e^{-1.7346 \cdot \left(\ln(d_y)-\ln(d_{50})\right)}} \tag{7.13-15}
$$

Of course there are other ways to generate PSD's, but this way works well and gives the possibility to create an asymmetrical PSD if α_{15} and α_{85} are chosen differently.

7.13.4 Determination of the Hydraulic Gradient.

After adjusting for the new homogeneous pseudo liquid density ρ_x, kinematic viscosity ν_x and relative submerged density $R_{sd,x}$ the hydraulic gradient can be determined for each fraction of the adjusted PSD using the volumetric concentration of the remaing solids. It is important to determine the hydraulic gradient curve for the full velocity range for both spatial and delivered concentrations and not the relative excess hydraulic gradient curves. The reason is, that the hydraulic gradient curves include the liquid curve for the adjusted homogeneous pseudo fluid properties, while the relative excess hydraulic gradient curves don't. Later the relative excess hydraulic gradient curves can be determined using the hydraulic gradient of the pure carrier liquid and the relative submerged density of the solids in the pure carrier liquid.

The resulting hydraulic gradient i_m based on the pseudo liquid and relative excess hydraulic gradient E_{rhg} are:

$$
i_{m,x} = \sum_{i=1}^{n} f_i \cdot i_{m,x,i} \cdot w_i \quad \text{with:} \quad \sum_{i=1}^{n} f_i = 1 \quad \text{and} \quad \frac{1}{n} \cdot \sum_{i=1}^{n} w_i = 1
$$

$$
E_{rhg,x} = \frac{i_{m,x} - i_{l,x}}{R_{sd,x} \cdot C_{vs}} \quad \text{or} \quad E_{rhg,x} = \frac{i_{m,x} - i_{l,x}}{R_{sd,x} \cdot C_{vt}}
$$

(7.13-16)

These are shown in Figure 7.13-1, Figure 7.13-2, Figure 7.13-3 and Figure 7.13-4 for 9 fractions. The thick blue lines show the curves for the d_{50} (uniform sand), while the black dashed lines show the resulting curves by adding up the curves of each fraction, giving the curve for graded sand. From Figure 7.13-2 and Figure 7.13-4 it is clear that the curve for graded sand is less steep than the curve for uniform sand. In Figure 7.13-4 there is an intersection point between the two curves which in fact is the v_{50} point of the Wilson et al. (1992) theory. The graded curve will sort of pivot around this point and be less steep the more graded the sand. Uniform sand will, of course follow the blue d_{50} curve, which is the steepest. It must be noted that the method described here follows the same trend as the Wilson et al. (1992) theory, but not exactly the same steepness is found. The shape of the graded curve also strongly depends on the particle and pipe diameter.

The resulting hydraulic gradient $i_{m,x}$ based on the original carrier liquid and relative excess hydraulic gradient $E_{rhg,x}$ are:

$$
i_m = \frac{\rho_x}{\rho_l} \cdot i_{m,x} = \frac{\rho_x}{\rho_l} \cdot \sum_{i=1}^{n} f_i \cdot i_{m,x,i} \cdot w_i \quad \text{with:} \quad \sum_{i=1}^{n} f_i = 1 \quad \text{and} \quad \frac{1}{n} \cdot \sum_{i=1}^{n} w_i = 1
$$

$$
E_{rhg} = \frac{i_m - i_l}{R_{sd} \cdot C_{vs}} \quad \text{or} \quad E_{rhg} = \frac{i_m - i_l}{R_{sd} \cdot C_{vt}}
$$

(7.13-17)

The variable w_i is a weighing factor, enabling to give certain particle diameters more weight in the total hydraulic gradient. Here the weighing factors are set to 1.

The resulting bed fraction is:

$$
\zeta = \tilde{A}_b = \sum_{i=1}^{n} f_i \cdot \tilde{A}_{b,i} = \sum_{i=1}^{n} f_i \cdot \zeta_i \quad \text{with:} \quad \sum_{i=1}^{n} f_i = 1
$$

(7.13-18)

In the next sub-chapters examples are given for 4 particle diameters, d_{50}, and 1 grading in a $D_p=0.1524$ m (6 inch) pipe and a $D_p=0.762$ m (30 inch) pipe. The choice of the particle diameters is such that the particle diameter of 0.2 mm will have a fines fraction influencing the liquid properties. First the 4 PSD's are shown for $d_{50}=0.2$ mm, $d_{50}=0.5$ mm, $d_{50}=1.0$ mm and $d_{50}=3.0$ mm. The ratios d_{50}/d_{15} and d_{85}/d_{50} are set to 2.7183 as in the above equations. So the grading of each of the 4 sands is the same. For each sand the resulting relative excess hydraulic

gradient curve, and the slip ratio/bed height curves are shown for both pipe diameters. The interpretation and conclusion are given below the graphs.
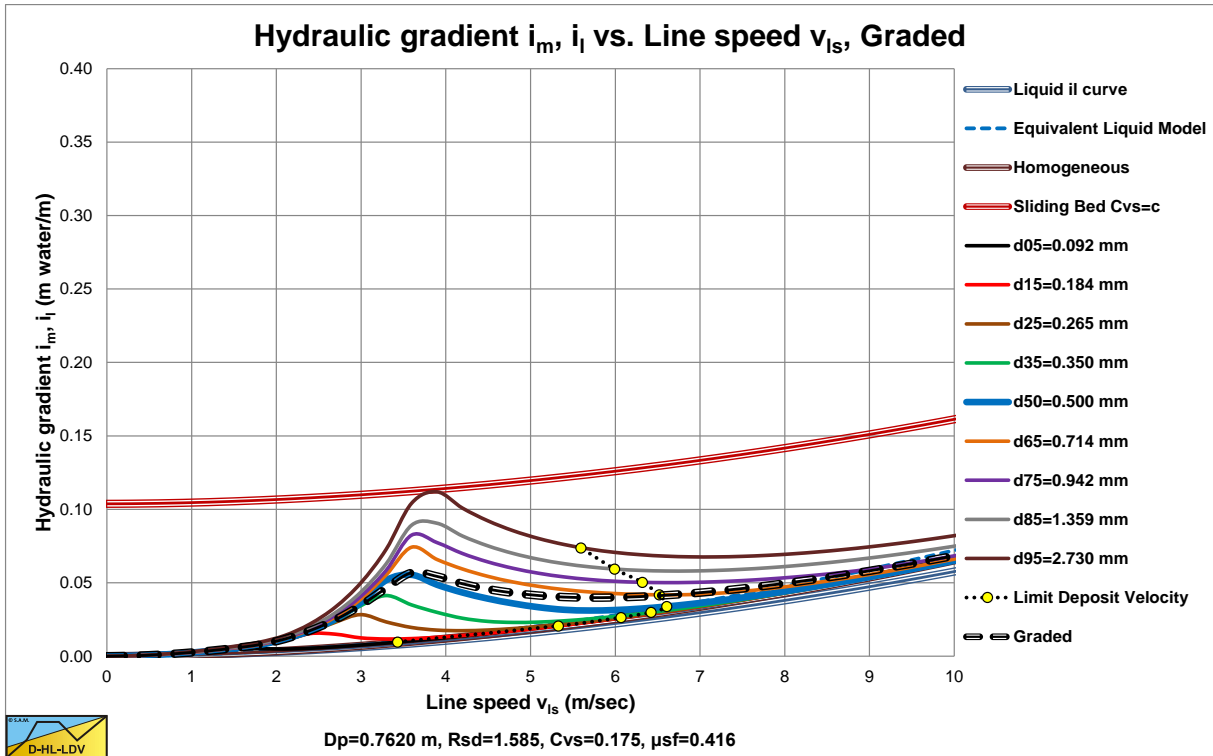
Figure 7.13-1: The hydraulic gradient based on the pseudo liquid properties in a large pipe, C$_{vs}$.
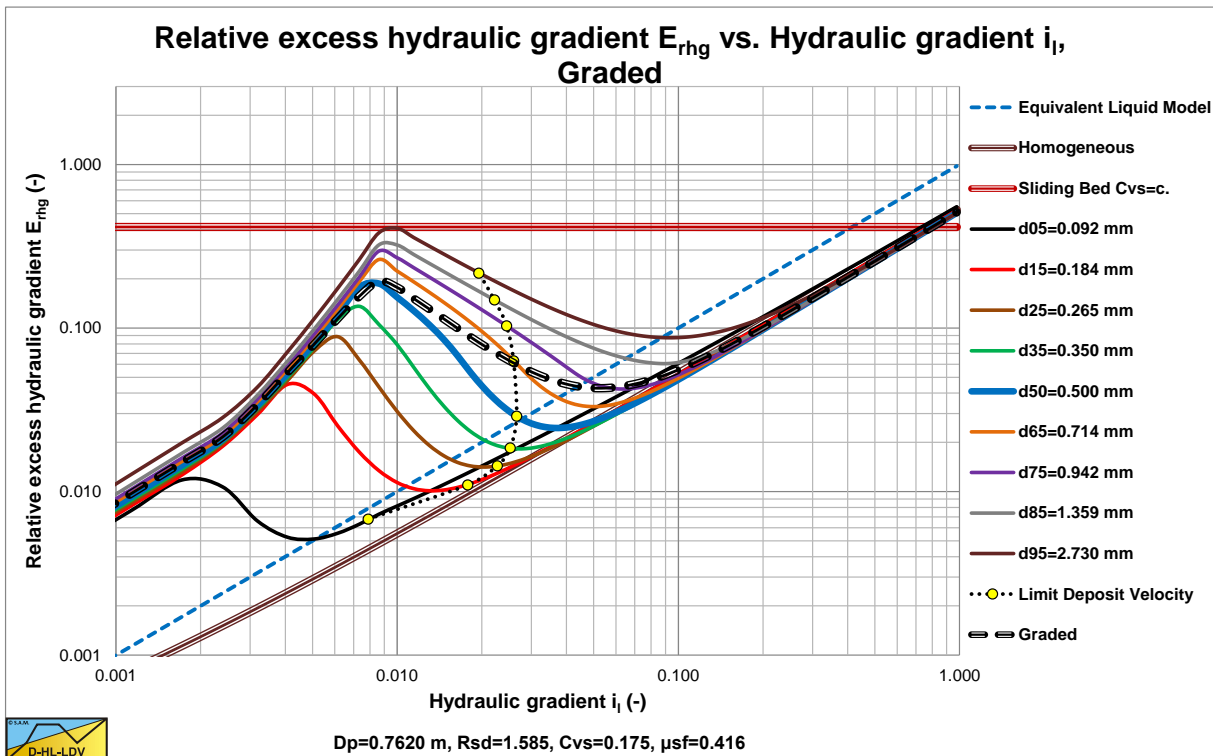
Figure 7.13-2: The corresponding relative excess hydraulic gradient in a large pipe, C$_{vs}$.
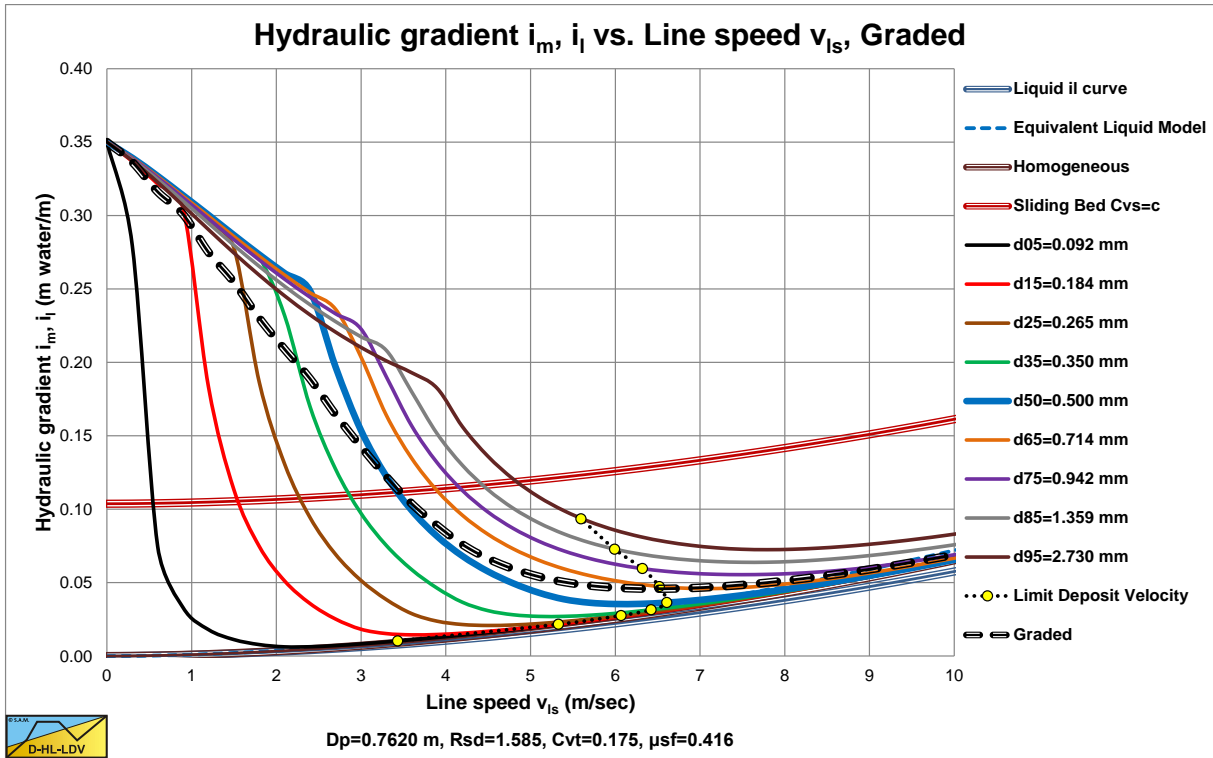
Figure 7.13-3: The hydraulic gradient based on the pseudo liquid properties in a large pipe, C_vt.
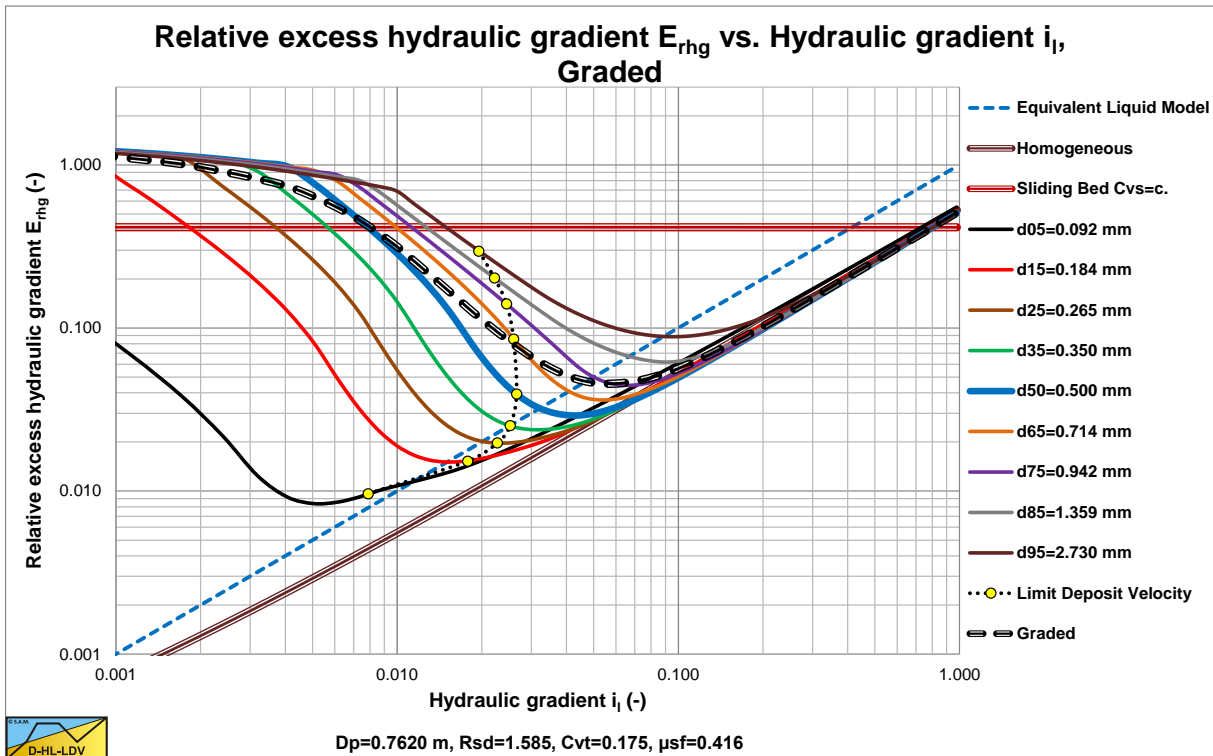
Figure 7.13-4: The corresponding relative excess hydraulic gradient in a large pipe, C_vt.

7.13.5 The Particle Size Distributions.
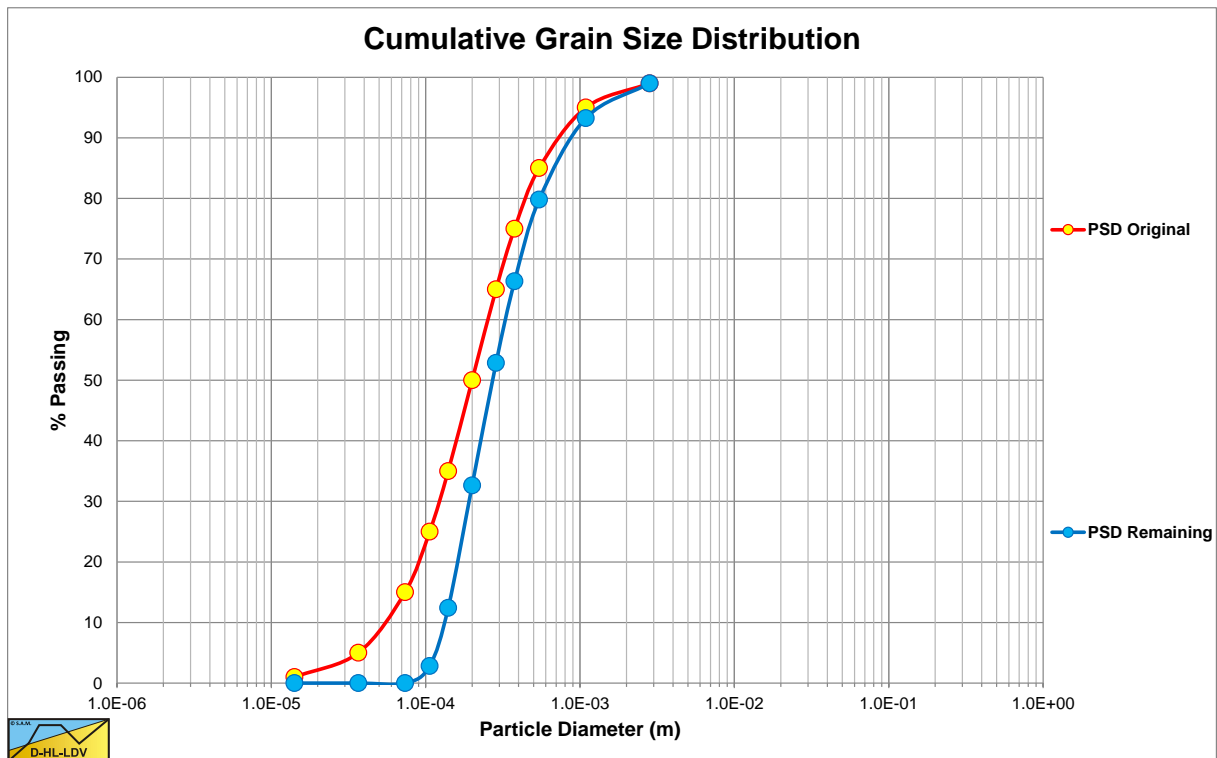
Figure 7.13-5: Cumulative grain size distribution, d₅₀=0.2 mm.
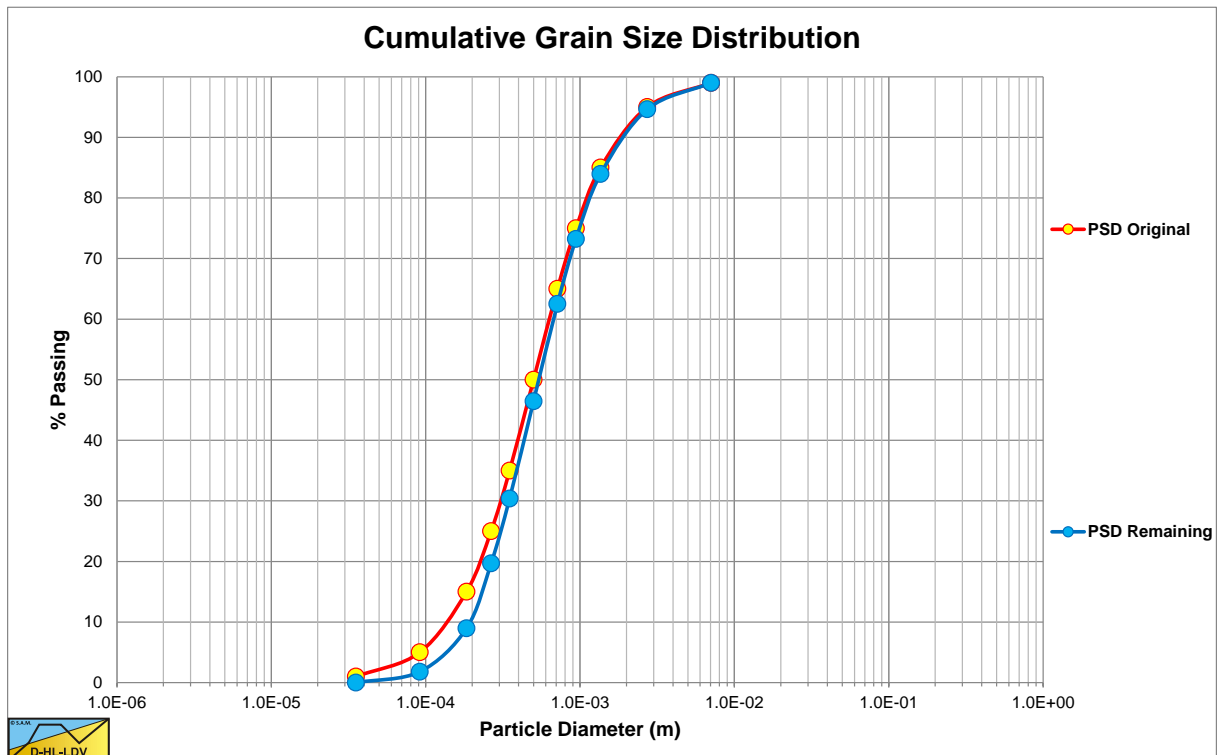
Figure 7.13-6: Cumulative grain size distribution, d₅₀=0.5 mm.
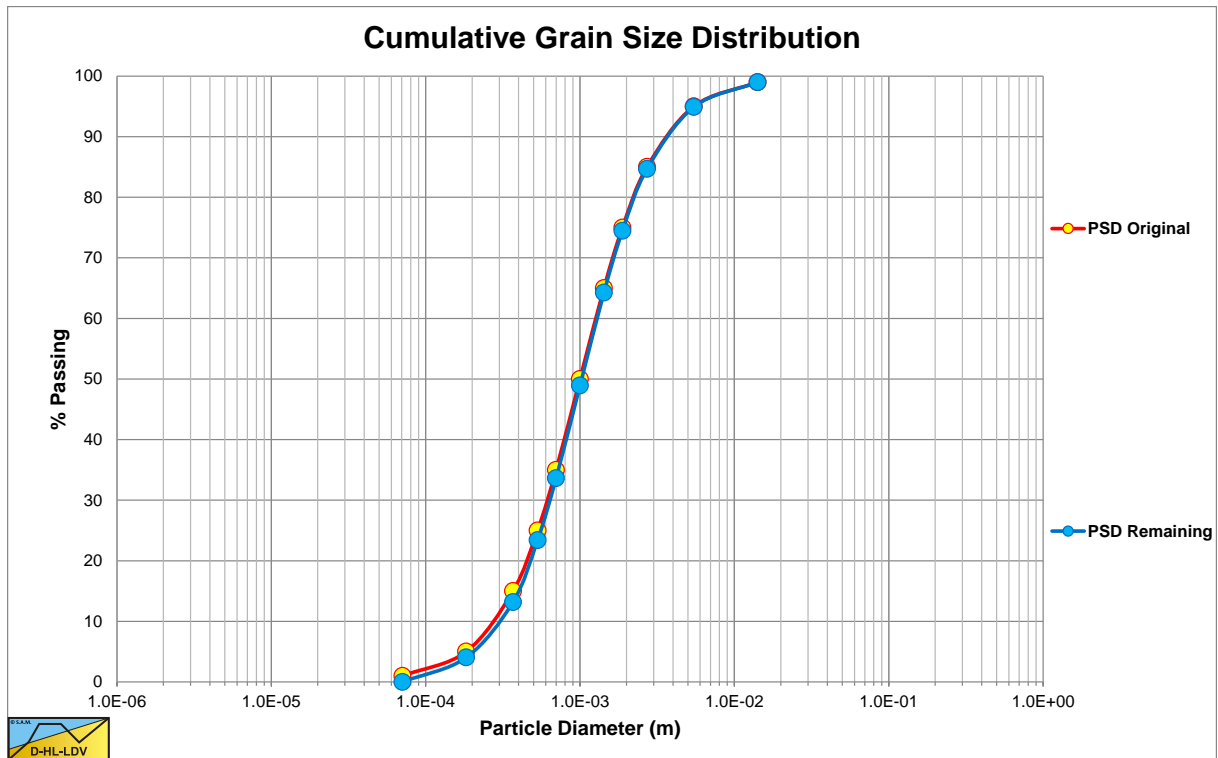
Figure 7.13-7: Cumulative grain size distribution, d_{50}=1.0 mm.
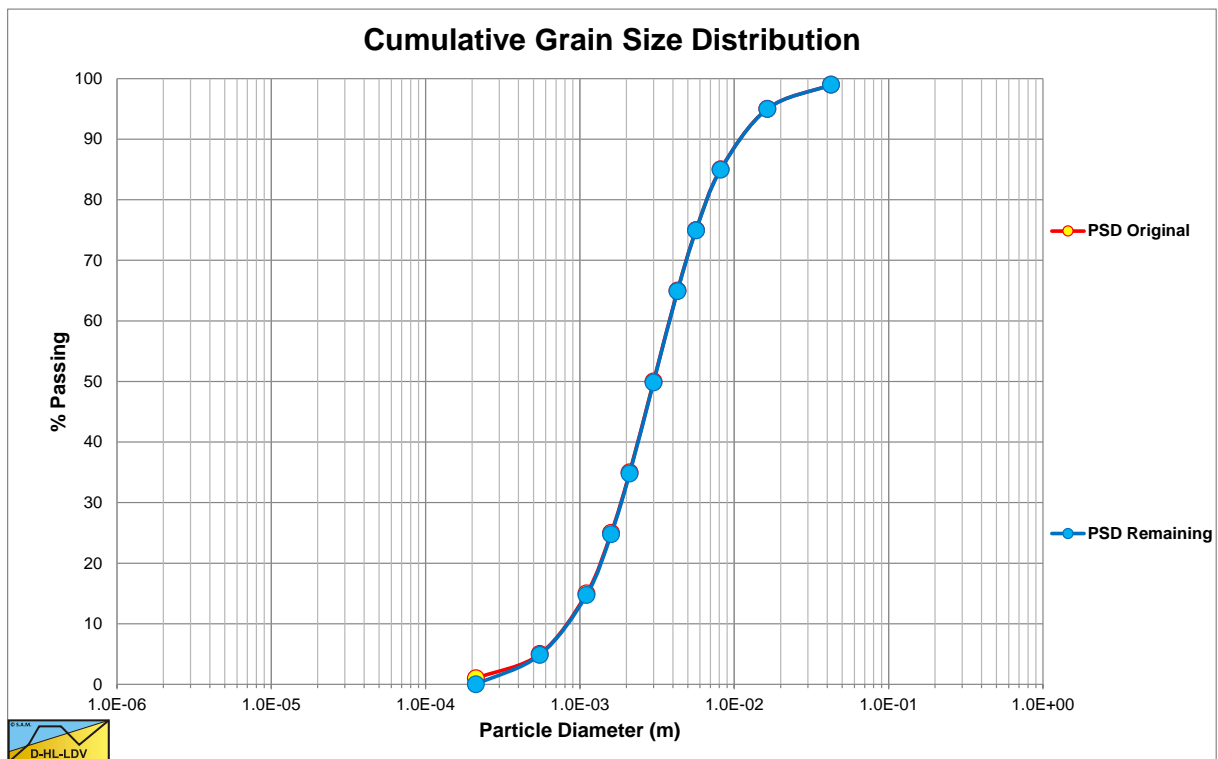
Figure 7.13-8: Cumulative grain size distribution, d_{50}=3.0 mm.

7.13.6 Particle Diameter d_{50}=0.2 mm.
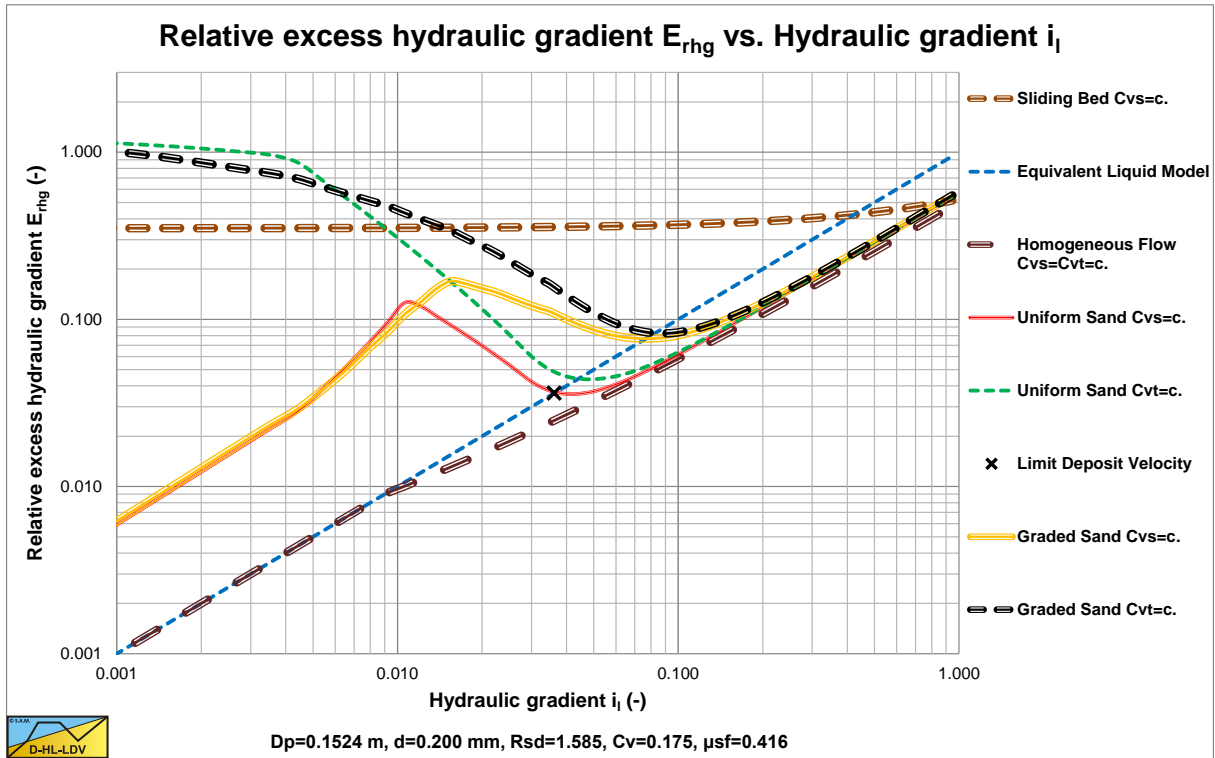
Figure 7.13-9: Relative excess hydraulic gradient for d_{50}=0.2 mm and D_p=0.1524 m.
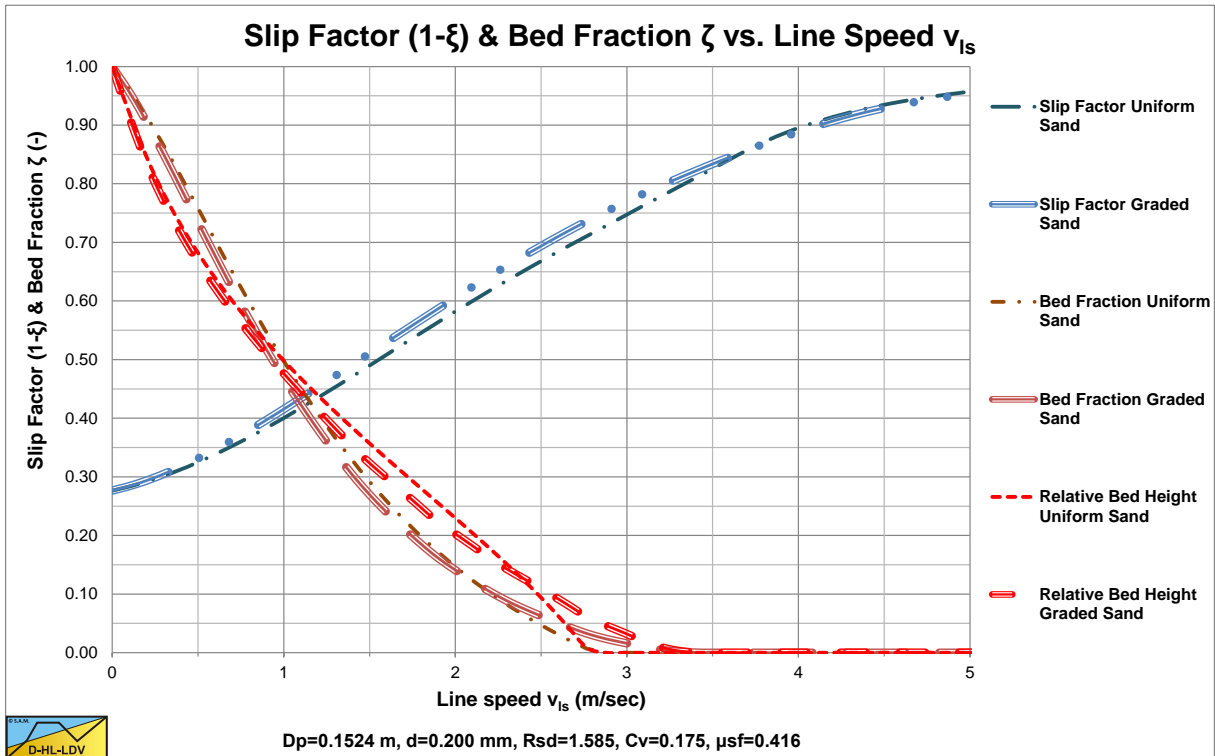
Figure 7.13-10: Slip factor, bed fraction and bed height for d_{50}=0.2 mm and D_p=0.1524 m.

The values for A_{15} and A_{85} are 14.78. The graded relative excess hydraulic gradient curves are higher than the uniform curves in the operational range of hydraulic gradients (0.01-0.1). In the homogeneous region, the curves are higher than the theoretical homogeneous curve, because of the adjusted pseudo fluid properties. The fines diameter is **d=0.067 mm** and the percentage fines is **13.07%** of the solids. The bed of the graded sand is lower than the bed of the uniform sand.
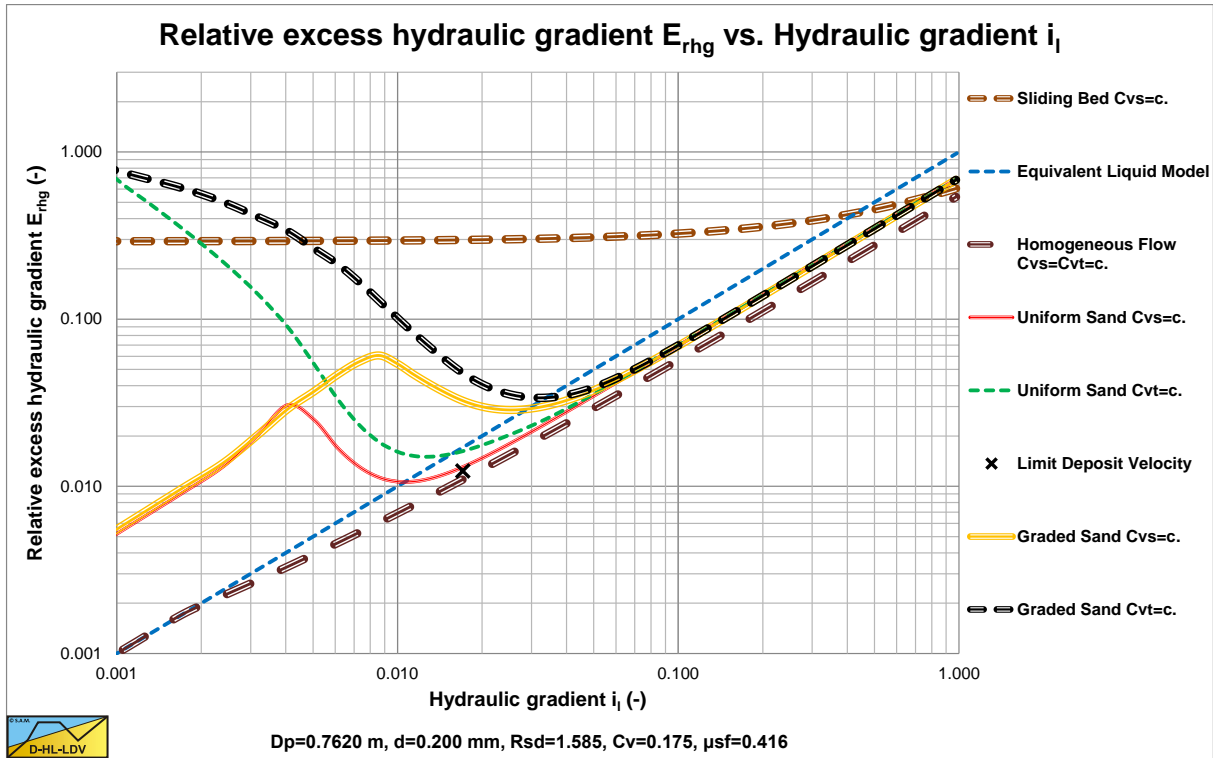
Figure 7.13-11: Relative excess hydraulic gradient for d₅₀=0.2 mm and Dₚ=0.762 m.
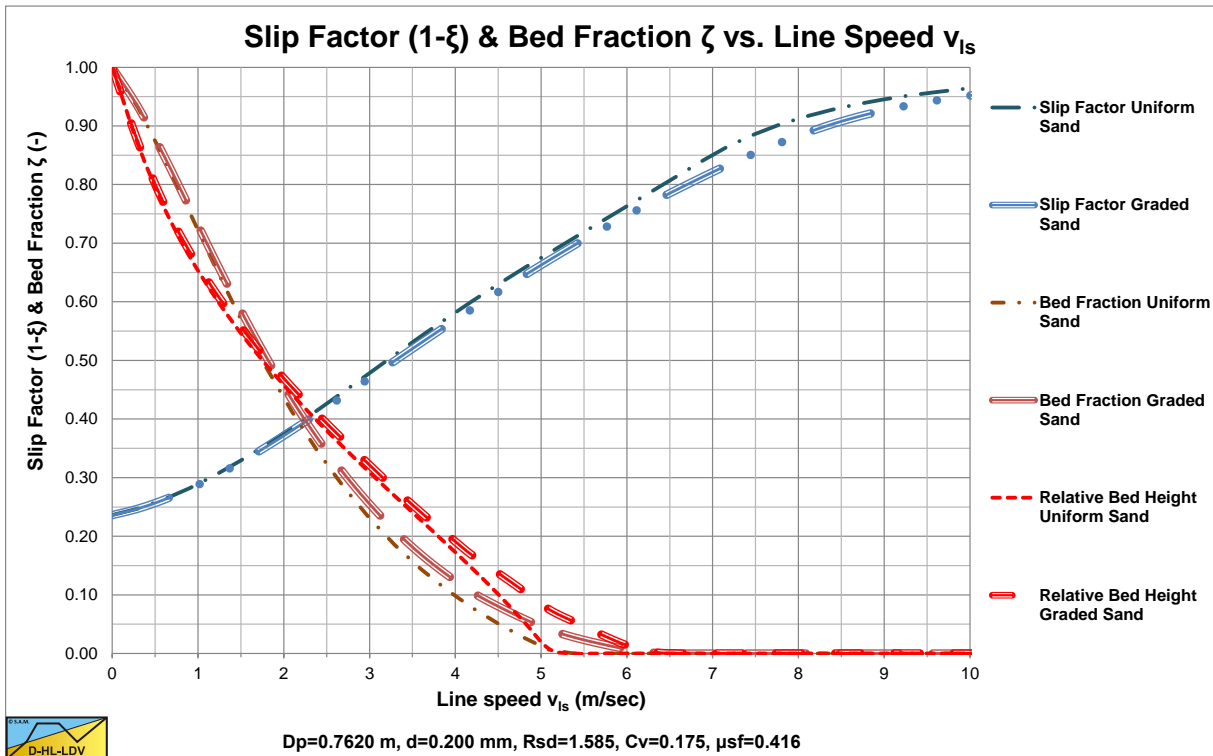
Figure 7.13-12: Slip factor, bed fraction and bed height for d₅₀=0.2 mm and Dₚ=0.762 m.

The values for **A₁₅** and **A₈₅** are 14.78. The graded relative excess hydraulic gradient curves are higher than the uniform curves in the operational range of hydraulic gradients (0.01-0.1). In the homogeneous region, the curves are higher than the theoretical homogeneous curve, because of the adjusted pseudo fluid properties. The fines diameter is **d=0.109 mm** and the percentage fines is **25.79%** of the solids. The bed of the graded sand is lower than the bed of the uniform sand. A larger pipe gives a larger fines diameter and a larger fines fraction.

7.13.7 Particle Diameter d₅₀=0.5 mm.
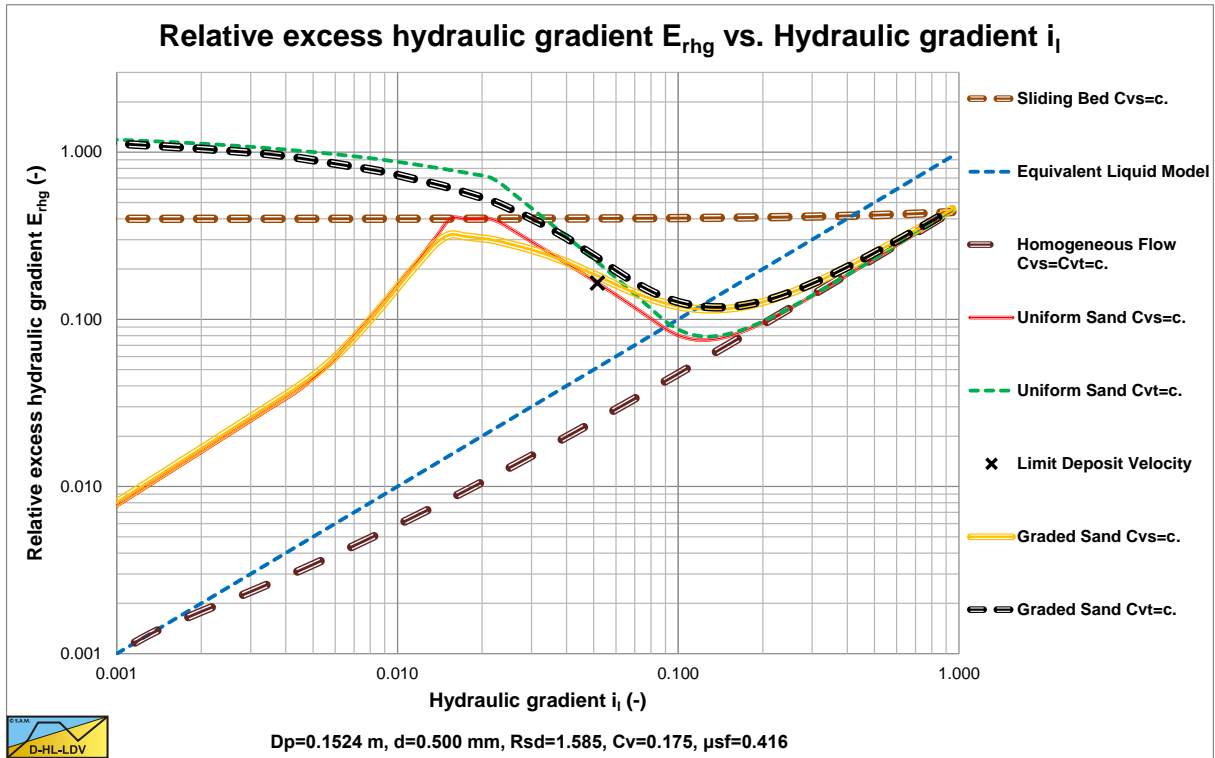
Figure 7.13-13: Relative excess hydraulic gradient for d₅₀=0.5 mm and Dₚ=0.1524 m.
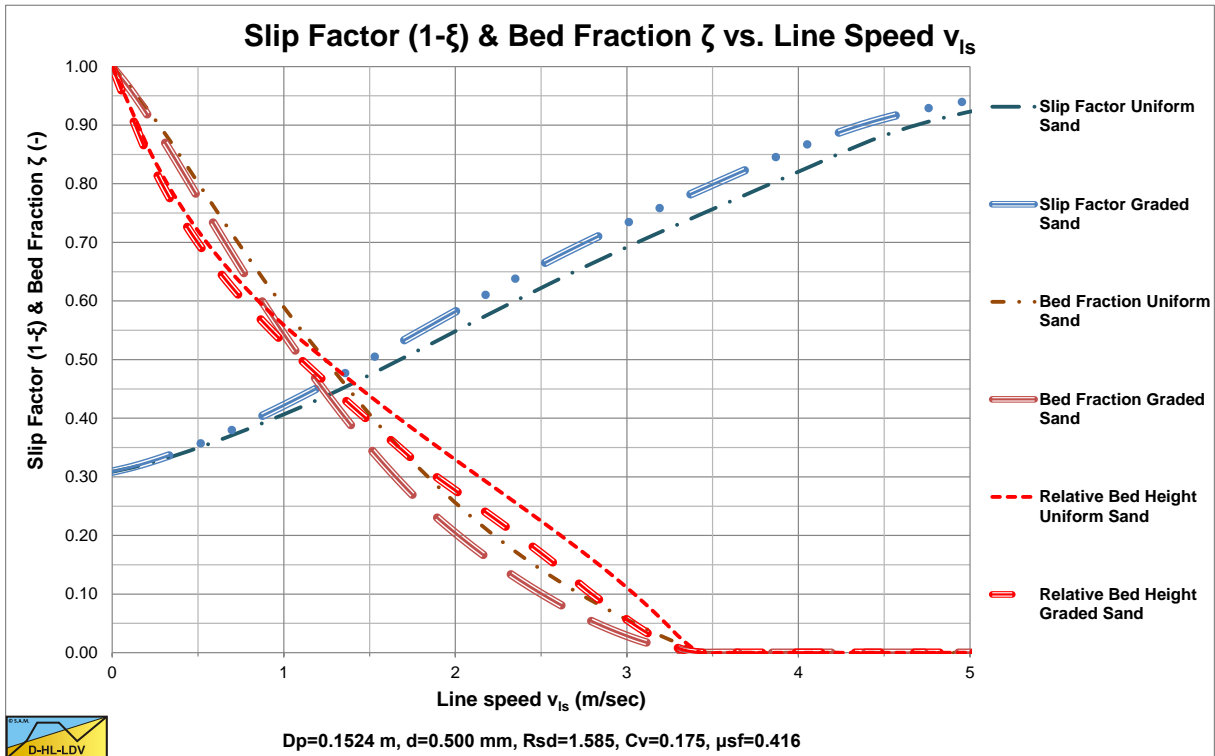
Figure 7.13-14: Slip factor, bed fraction and bed height for d₅₀=0.5 mm and Dₚ=0.1524 m.

The values for **A₁₅** and **A₈₅** are 13.19. The graded relative excess hydraulic gradient curves are higher than the uniform curves in the operational range of hydraulic gradients (0.01-0.1). In the homogeneous region, the curves are slightly higher than the theoretical homogeneous curve, because of the adjusted pseudo fluid properties. The fines diameter is **d=0.067 mm** and the percentage fines is **2.98%** of the solids. The bed of the graded sand is lower than the bed of the uniform sand.
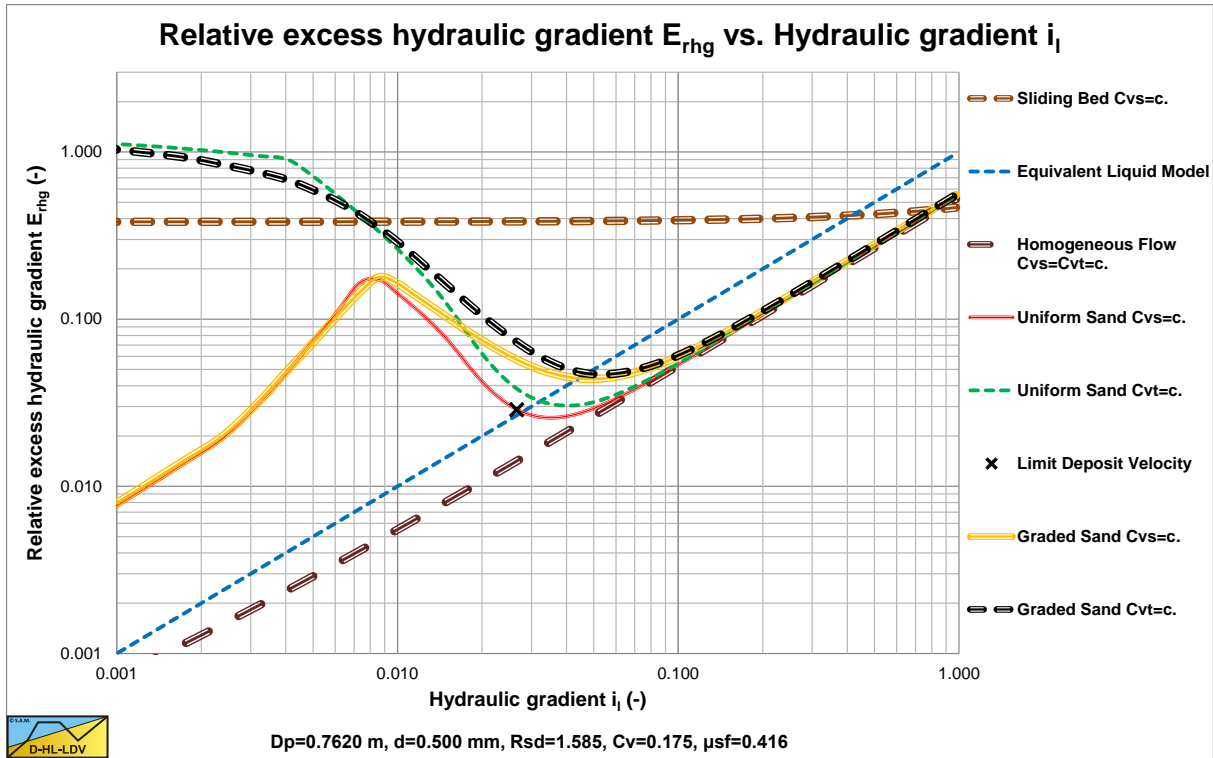
Figure 7.13-15: Relative excess hydraulic gradient for d_{50}=0.5 mm and D_p=0.762 m.
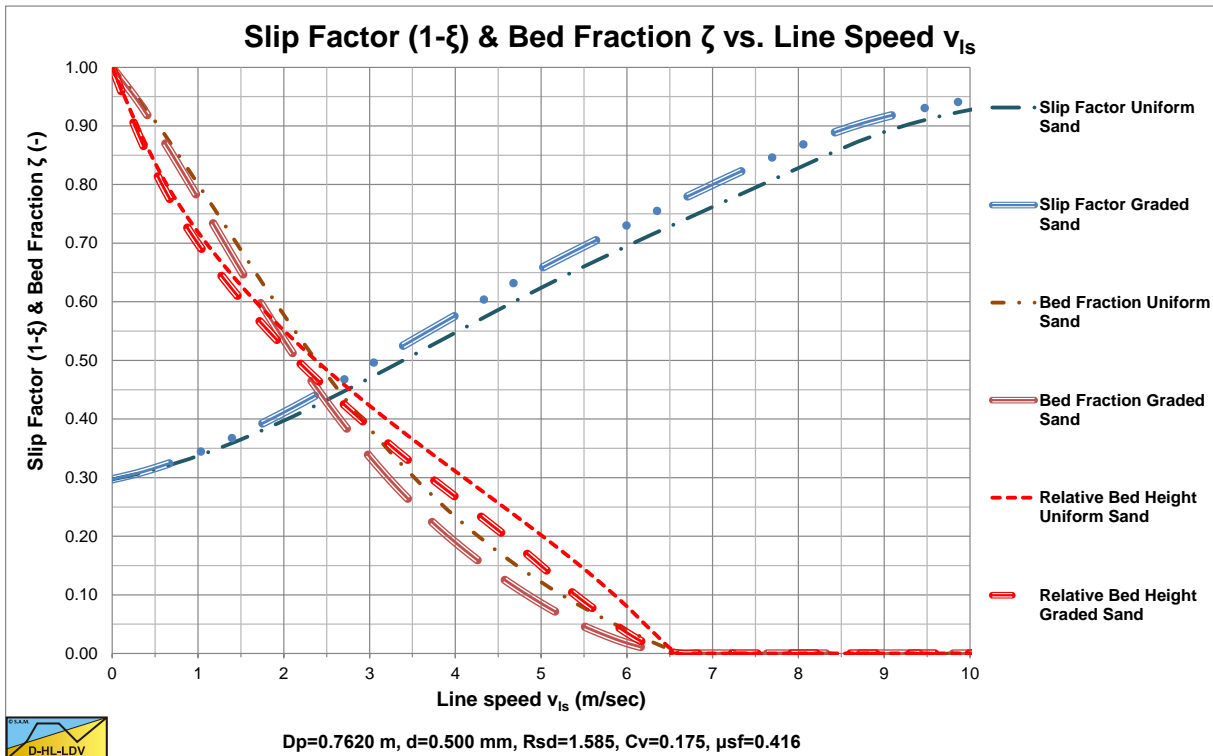
Figure 7.13-16: Slip factor, bed fraction and bed height for d_{50}=0.5 mm and D_p=0.762 m.

The values for A_{15} and A_{85} are 13.19. The graded relative excess hydraulic gradient curves are higher than the uniform curves in the operational range of hydraulic gradients (0.01-0.1). In the homogeneous region, the curves are slightly higher than the theoretical homogeneous curve, because of the adjusted pseudo fluid properties. The fines diameter is **d=0.109 mm** and the percentage fines is **6.62%** of the solids. The bed of the graded sand is lower than the bed of the uniform sand. A larger pipe gives a larger fines diameter and a larger fines fraction.

7.13.8 Particle Diameter d₅₀=1.0 mm.
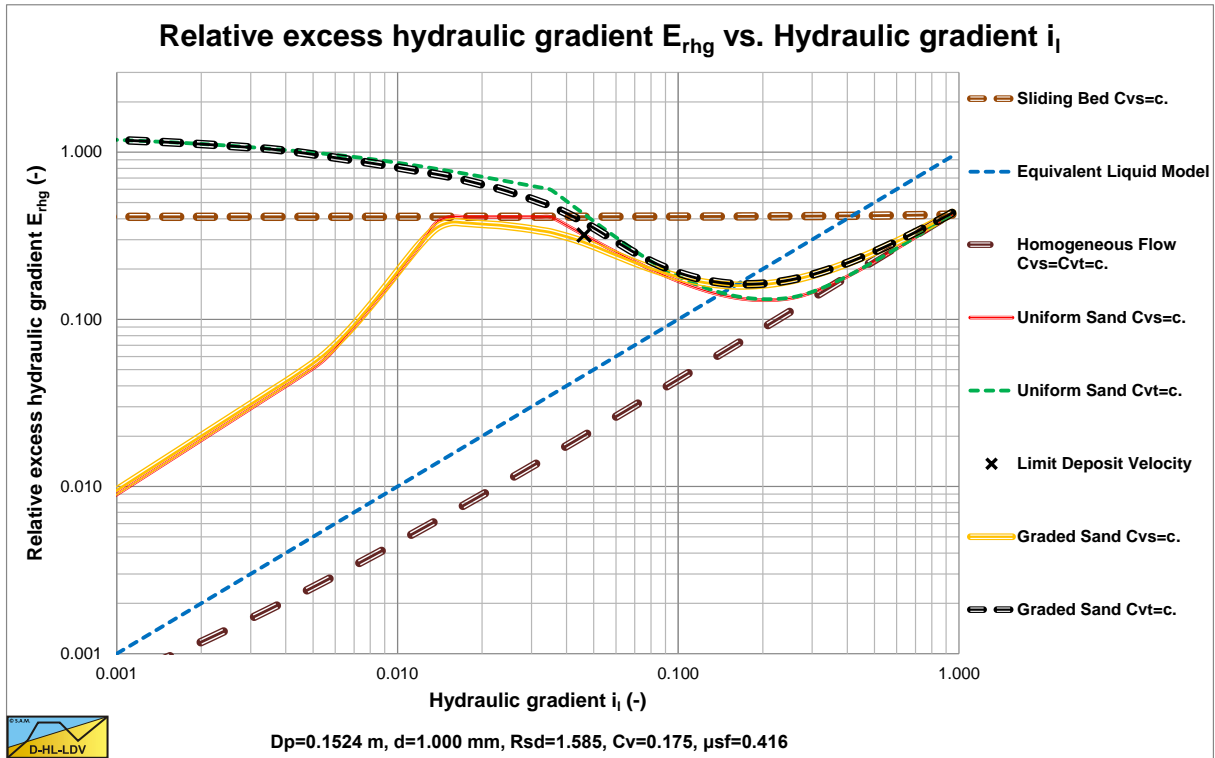
Figure 7.13-17: Relative excess hydraulic gradient for d₅₀=1.0 mm and Dₚ=0.1524 m.
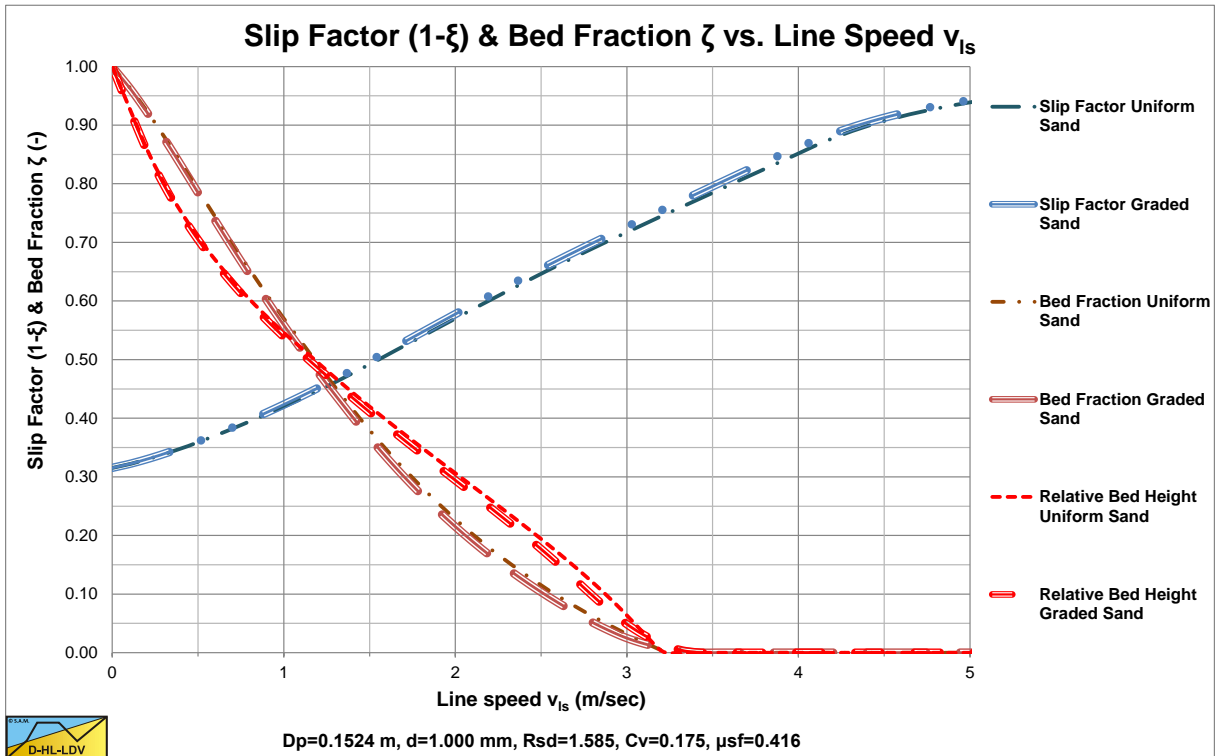
Figure 7.13-18: Slip factor, bed fraction and bed height for d₅₀=1.0 mm and Dₚ=0.1524 m.

The values for A_{15} and A_{85} are 11.98. The graded relative excess hydraulic gradient curves are slightly higher than the uniform curves in the operational range of hydraulic gradients (0.01-0.1). In the homogeneous region, the curves are hardly higher than the theoretical homogeneous curve, because of the adjusted pseudo fluid properties. The fines diameter is **d=0.067 mm** and the percentage fines is **0.91%** of the solids. The bed of the graded sand is hardly lower than the bed of the uniform sand.
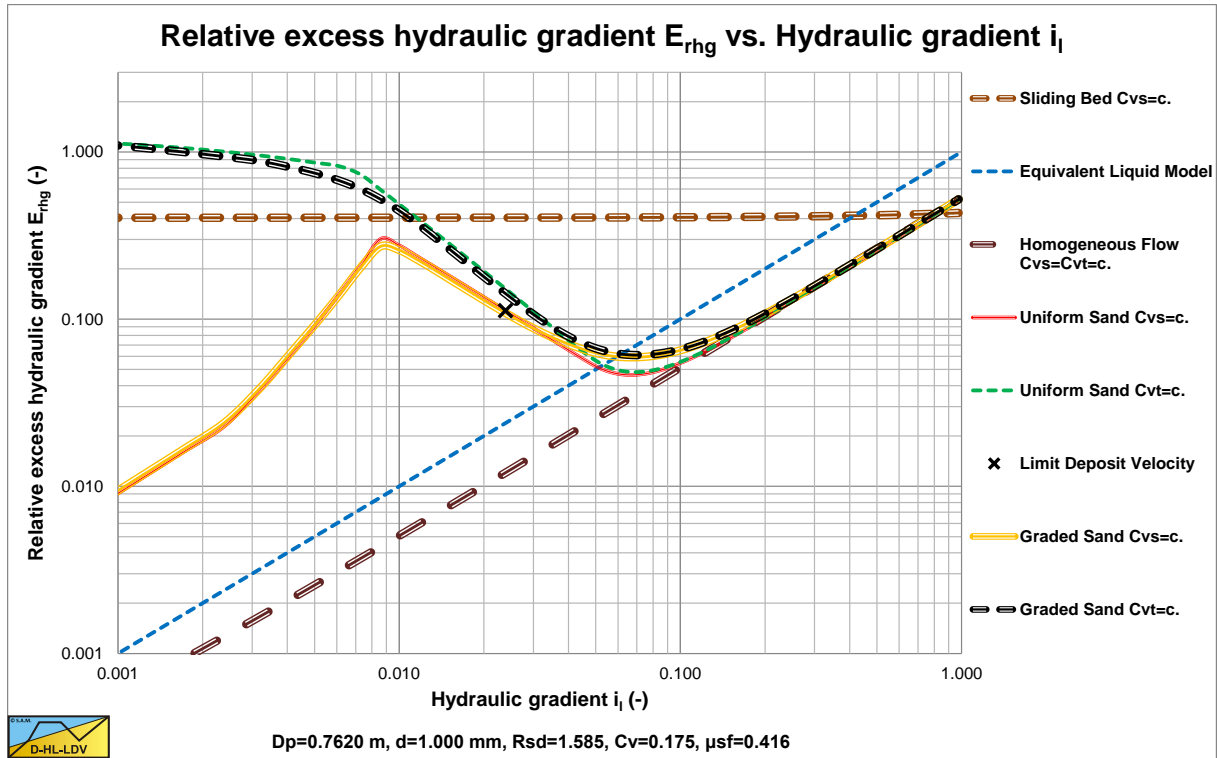
Figure 7.13-19: Relative excess hydraulic gradient for d₅₀=1.0 mm and Dₚ=0.762 m.
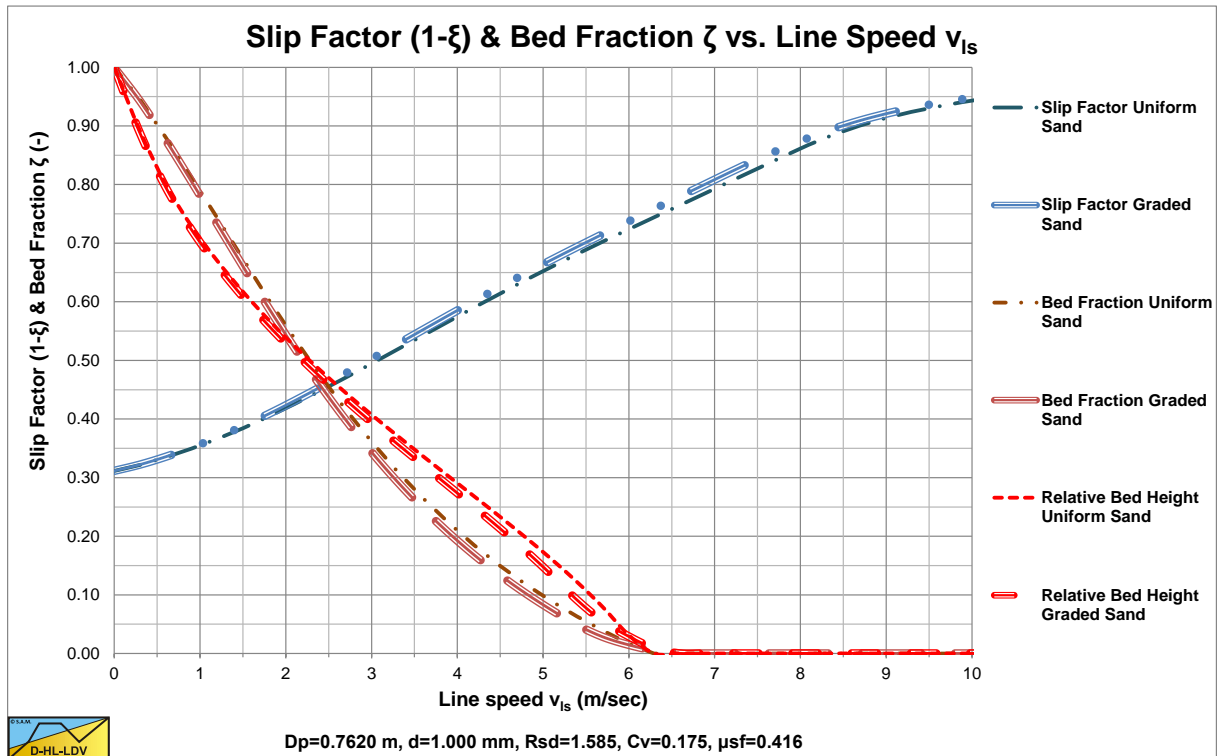
Figure 7.13-20: Slip factor, bed fraction and bed height for d₅₀=1.0 mm and Dₚ=0.762 m.

The values for **A₁₅** and **A₈₅** are 11.98. The graded relative excess hydraulic gradient curves are slightly higher than the uniform curves in the operational range of hydraulic gradients (0.01-0.1). In the homogeneous region, the curves are hardly higher than the theoretical homogeneous curve, because of the adjusted pseudo fluid properties. The fines diameter is **d=0.109 mm** and the percentage fines is **2.09%** of the solids. The bed of the graded sand is hardly lower than the bed of the uniform sand. A larger pipe gives a larger fines diameter and a larger fines fraction.

7.13.9 Particle Diameter d₅₀=3.0 mm.
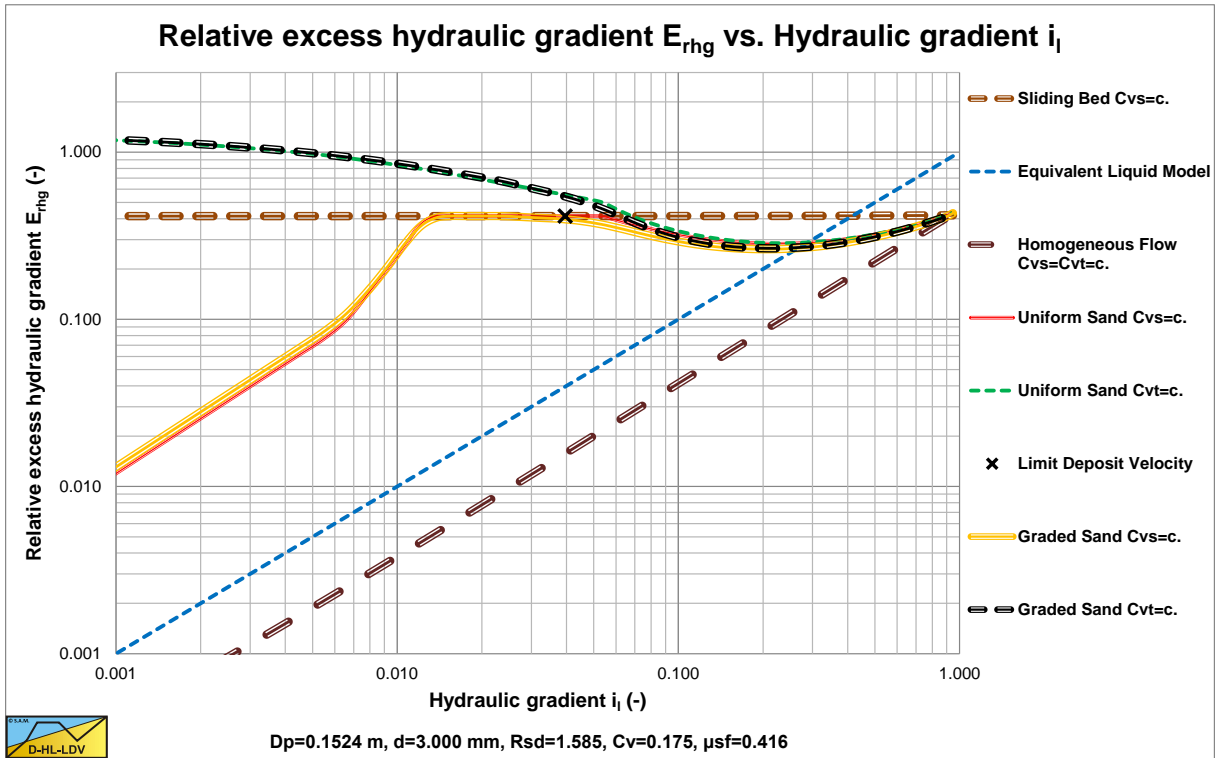
Figure 7.13-21: Relative excess hydraulic gradient for d₅₀=3.0 mm and Dₚ=0.1524 m.
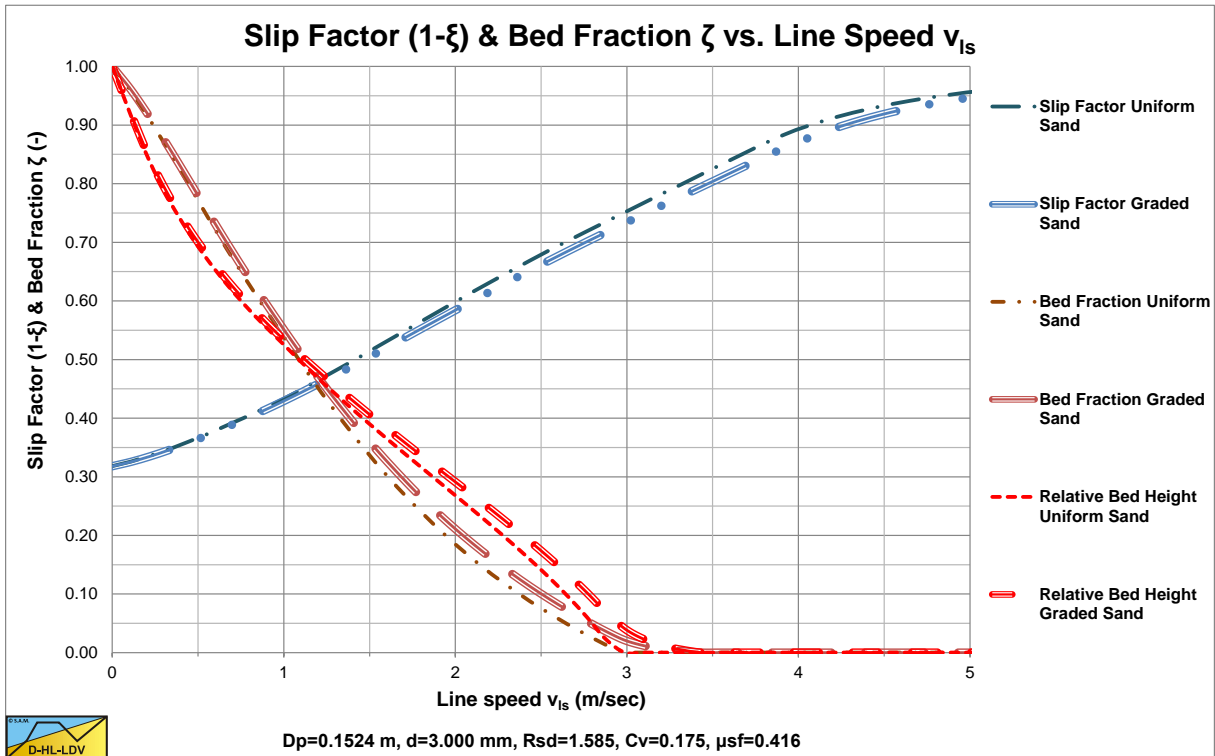
Figure 7.13-22: Slip factor, bed fraction and bed height for d₅₀=3.0 mm and Dₚ=0.1524 m.

The values for A_{15} and A_{85} are 10.08. The graded relative excess hydraulic gradient curves are hardly higher than the uniform curves in the operational range of hydraulic gradients (0.01-0.1). In the homogeneous region, the curves are hardly higher than the theoretical homogeneous curve, because of the adjusted pseudo fluid properties. The fines diameter is **d=0.067 mm** and the percentage fines is **0.14%** of the solids. The bed of the graded sand is slightly higher than the bed of the uniform sand.
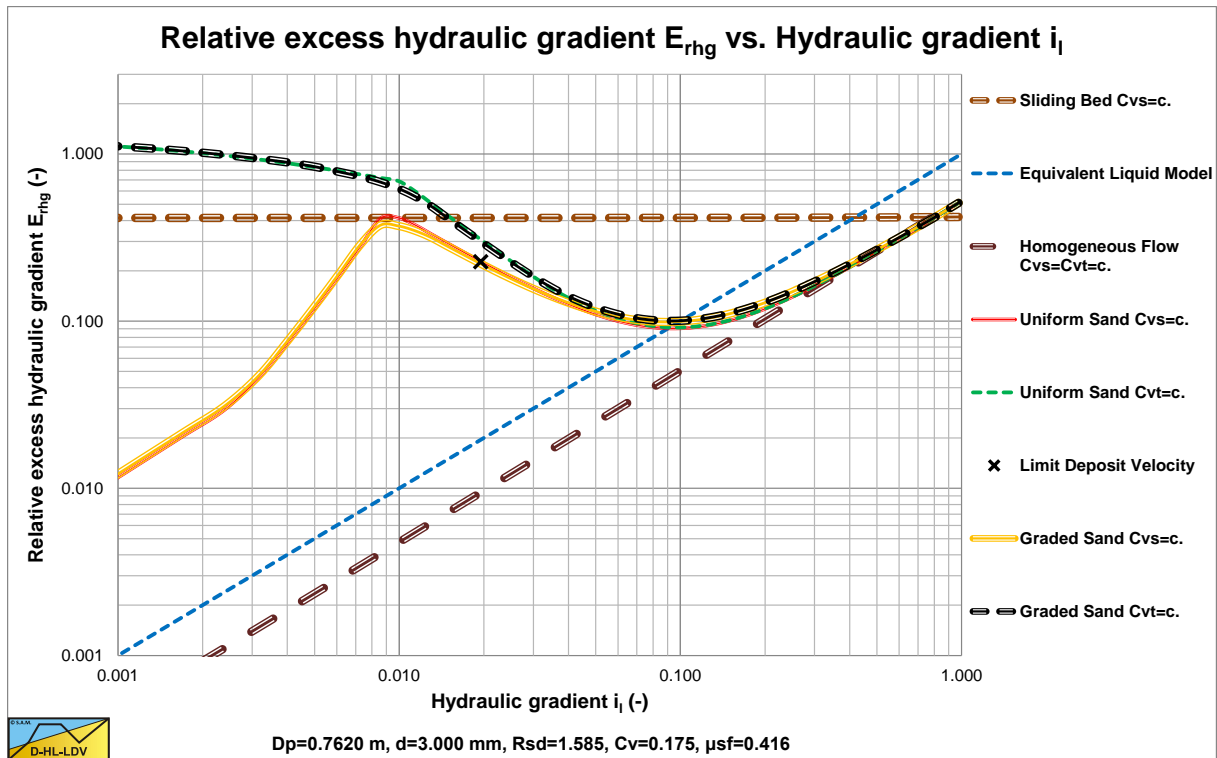
Figure 7.13-23: Relative excess hydraulic gradient for d₅₀=3.0 mm and Dₚ=0.762 m.
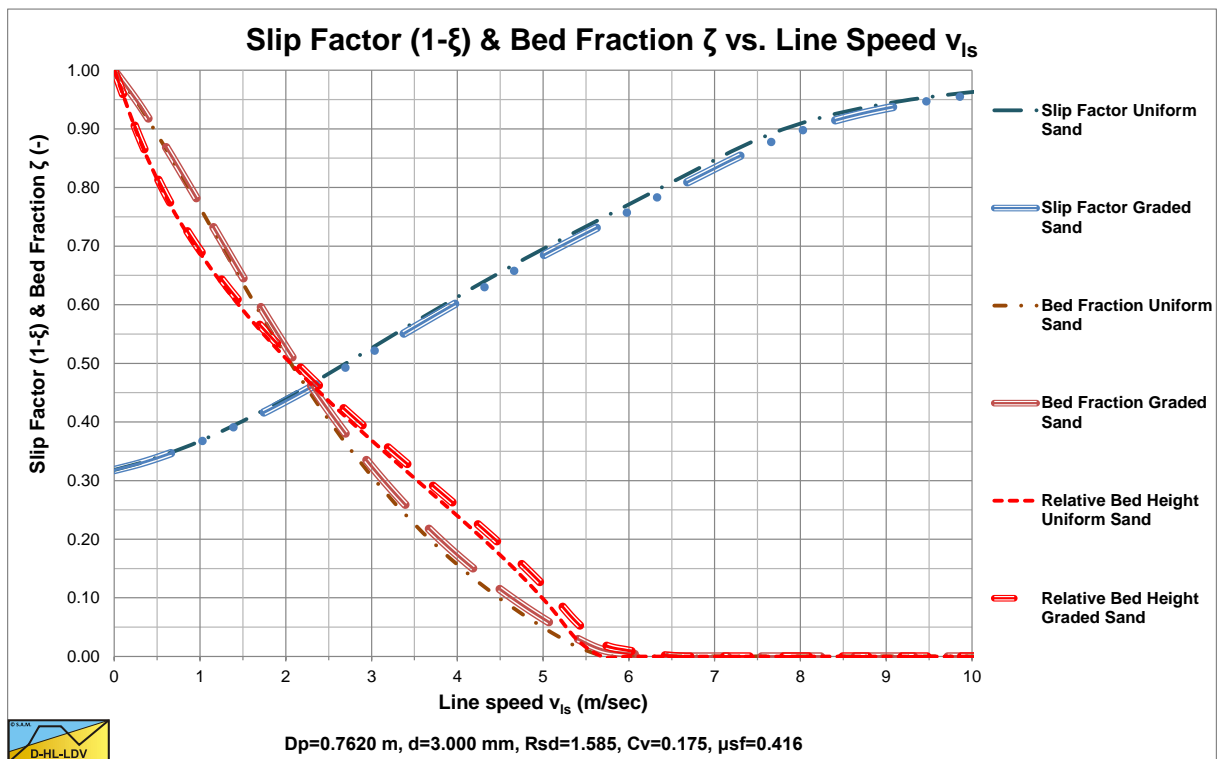
Figure 7.13-24: Slip factor, bed fraction and bed height for d₅₀=3.0 mm and Dₚ=0.762 m.

The values for **A₁₅** and **A₈₅** are 10.08. The graded relative excess hydraulic gradient curves are hardly higher than the uniform curves in the operational range of hydraulic gradients (0.01-0.1). In the homogeneous region, the curves are hardly higher than the theoretical homogeneous curve, because of the adjusted pseudo fluid properties. The fines diameter is **d=0.109 mm** and the percentage fines is **0.32%** of the solids. The bed of the graded sand is slightly higher than the bed of the Funiform sand. A larger pipe gives a larger fines diameter and a larger fines fraction.

7.13.10 Nomenclature PSD Influence.

$\tilde{A}_b$	Bed fraction	-
$\tilde{A}_{b,i}$	Bed fraction fraction i	-
A_x	Constant in PSD function	-
A_{15}	Constant in PSD function below d_{50}	-
A_{85}	Constant in PSD function above d_{50}	-
C_{vt}	Delivered (transport) volumetric concentration	-
C_{vs}	Spatial volumetric concentration	-
$C_{vs,x}$	Solids spatial concentration in pseudo liquid (fines)	-
$C_{vs,r}$	Solids spatial concentration remaining after removing the fines from the PSD	-
C_{vb}	Spatial volumetric concentration bed (1-n)	-
d	Particle diameter	m
d_{15}	Particle diameter with 15% passing	m
d_{50}	Particle diameter with 50% passing	m
d_{85}	Particle diameter with 85% passing	m
d_{lim}	Limiting particle diameter	m
d_x	Particle diameter	m
d_y	Particle diameter	m
D_p	Pipe diameter	m
E_{rhg}	Relative excess hydraulic gradient in carrier liquid	-
$E_{rhg,x}$	Relative excess hydraulic gradient in pseudo liquid	-
f_i	Fraction i	-
f_x	PSD function	-
f_y	PSD function	-
g	Gravitational constant 9.81 m/s^2	m/s^2
i_l	Pure liquid hydraulic gradient	m/m
$i_{l,x}$	Hydraulic gradient pseudo liquid	m/m
i_m	Mixture hydraulic gradient	m/m
$i_{m,x}$	Total mixture hydraulic gradient in pseudo liquid	m/m
$i_{m,x,i}$	Mixture hydraulic gradient fraction i in pseudo liquid	m/m
n	Number of fractions	-
p	Probability distribution	-
Δp_i	Fraction i	-
R_{sd}	Relative submerged density in carrier liquid	-
$R_{sd,x}$	Relative submerged density in pseudo liquid	-
Stk	Stokes number	-
X	Fraction of sand in pseudo liquid	-
v_{ls}	Line speed	m/s
$v_{ls,ldv}$	Limit Deposit Velocity	m/s
v_{sl}	Slip velocity	m/s
v_t	Terminal settling velocity particle	m/s
w_i	Weigh factor fraction i	-
α_{15}	d_{50} to d_{15} ratio	-
α_{85}	d_{85} to d_{50} ratio	-
ρ_l	Density liquid	ton/m^3
ρ_s	Density solids	ton/m^3
ρ_x	Density pseudo liquid	ton/m^3
ξ	Slip ratio	-
ζ	Bed fraction	-
ζ_i	Bed fraction i	-
μ_{sf}	Sliding friction coefficient	-
μ_l	Dynamic viscosity carrier liquid	Pa·s
μ_x	Dynamic viscosity pseudo liquid	Pa·s
ν_l	Kinematic viscosity carrier liquid	m^2/s
ν_x	Kinematic viscosity pseudo liquid	m^2/s

7.14 Inclined Pipes.

In dredging and other industries often parts of a pump/pipeline system are inclined or vertical. So it is interesting to see what the implications of an inclined pipe on the pressure losses are. This chapter gives an analytical solution to this problem. Figure 7.14-1 shows the definitions of perimeters and cross sections of the pipe.
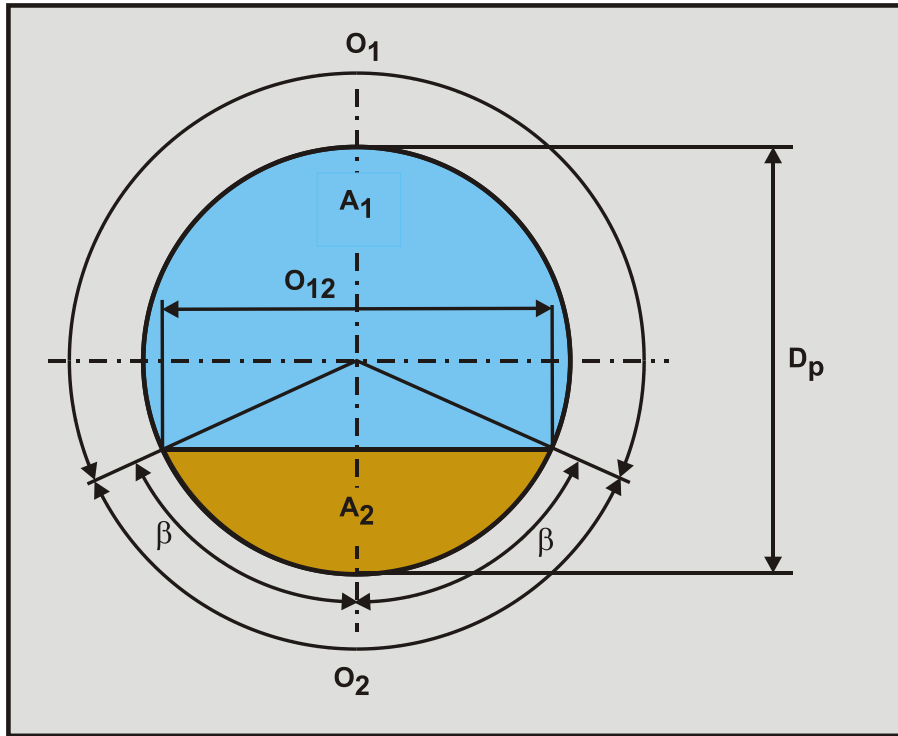
Figure 7.14-1: Definitions.

7.14.1 Pure Carrier Liquid.

First of all, the flow of pure carrier liquid. The perimeter $O=O_1$ for $\beta=0$ in the case of zero concentration. The equilibrium of forces on the liquid in a pipe with inclination angle θ is:

$$-\frac{dp}{dx} \cdot A \cdot L = \tau_l \cdot O \cdot L + \rho_l \cdot A \cdot L \cdot g \cdot \sin(\theta) \qquad (7.14-1)$$

The shear stress τ_l can be determined with the well known Darcy-Weisbach equation.
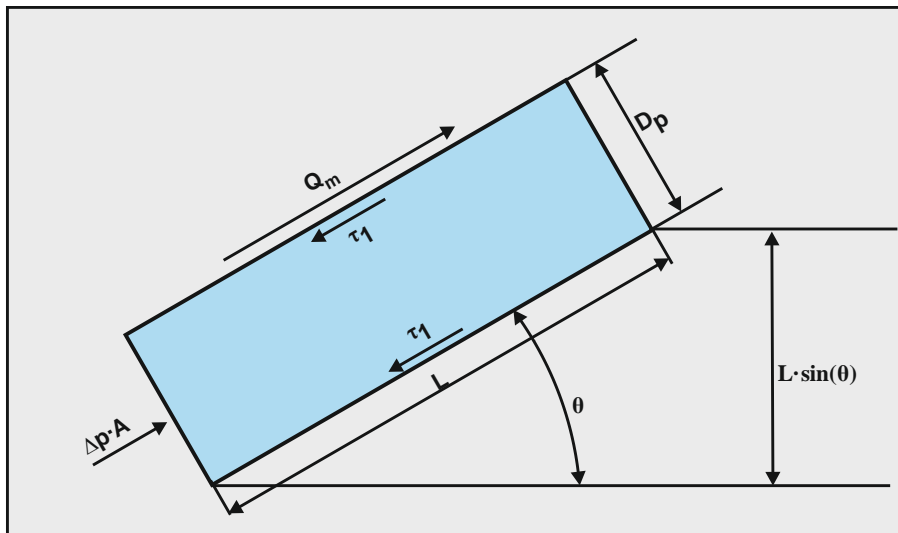
Figure 7.14-2: Pure carrier liquid in an inclined pipe.

Figure 7.14-2 shows the driving force and resisting shear stresses in the pipe. The shear stress, in general, is defined by, based on the Darcy Weisbach equation:

$$\tau = \frac{\lambda_l}{8} \cdot \rho_l \cdot v_{ls}^2 \tag{7.14-2}$$

The hydraulic gradient can now be determined with:

$$i_{l,\theta} = -\frac{dp}{dx} \cdot \frac{A \cdot L}{\rho_l \cdot A \cdot L \cdot g} = \frac{\tau_l \cdot O \cdot L}{\rho_l \cdot A \cdot L \cdot g} + \frac{\rho_l \cdot A \cdot L \cdot g \cdot \sin(\theta)}{\rho_l \cdot A \cdot L \cdot g} = i_l + \sin(\theta) \tag{7.14-3}$$

So apparently the hydraulic gradient increases with the sine of the inclination angle. Which also means that a downwards slope with a negative inclination angle gives a negative sine and thus a reduction of the hydraulic gradient. In this case the total hydraulic gradient may even become negative.

7.14.2 Stationary Bed Regime.

The equilibrium of forces on the layer of liquid above the bed is, where Figure 7.14-3 shows the driving force and the resisting shear stresses on the liquid above the bed:

$$-\frac{dp}{dx} \cdot A_1 \cdot L = \tau_1 \cdot O_1 \cdot L + \tau_{12} \cdot O_{12} \cdot L + \rho_l \cdot A_1 \cdot L \cdot g \cdot \sin(\theta) \tag{7.14-4}$$

Since the bed is not moving, the friction between the bed and the pipe wall compensates for the weight component of the bed. The hydraulic gradient can now be determined with:

$$i_{m,\theta} = -\frac{dp}{dx} \cdot \frac{A_1 \cdot L}{\rho_l \cdot A_1 \cdot L \cdot g} = \frac{\tau_1 \cdot O_1 \cdot L + \tau_{12} \cdot O_{12} \cdot L}{\rho_l \cdot A_1 \cdot L \cdot g} + \sin(\theta) = i_m + \sin(\theta) \tag{7.14-5}$$

Which is the hydraulic gradient of a stationary bed in a horizontal pipe plus the sine of the inclination angle. The weight of the solids do not give a contribution to the hydraulic gradient.
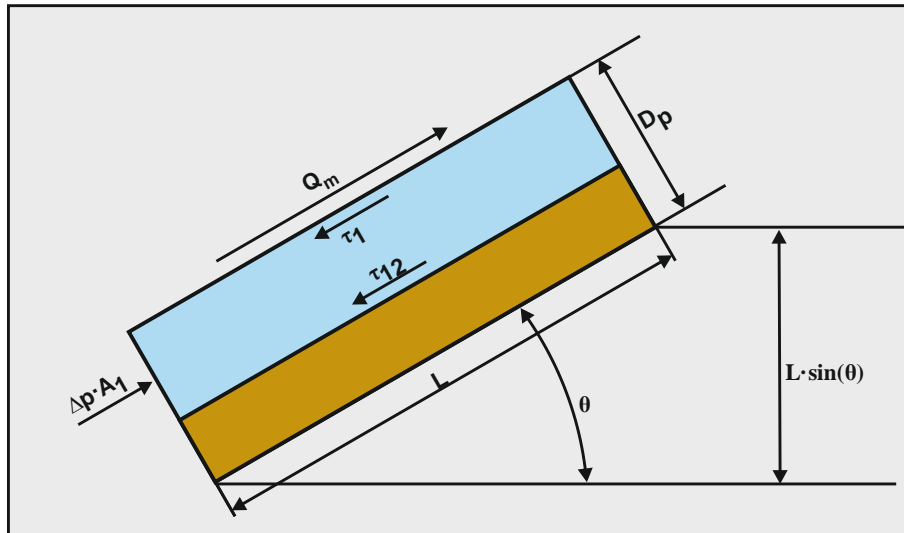
Figure 7.14-3: The stationary bed regime in an inclined pipe.

7.14.3 Sliding Bed Regime.

The equilibrium of forces on the layer of liquid above the bed is:

$$-\frac{dp}{dx} \cdot A_1 \cdot L = \tau_1 \cdot O_1 \cdot L + \tau_{12} \cdot O_{12} \cdot L + \rho_l \cdot A_1 \cdot L \cdot g \cdot \sin(\theta) \tag{7.14-6}$$

Figure 7.14-4 shows how the submerged weight of the bed results in a resisting force, a normal force on the pipe wall and a sliding friction force between the bed and the pipe wall. Figure 7.14-5 shows the driving forces and resisting forces and shear stresses, both on the liquid above the bed and on the bed.

The cross-section of the bed can be determined with:

$$A_2 = \frac{C_{vs}}{C_{vb}} \cdot A \tag{7.14-7}$$

The weight of the bed, including pore water is:

$$
\begin{aligned}
W_b &= \rho_b \cdot A_2 \cdot L \cdot g = \left(\rho_s \cdot C_{vb} + \rho_l \cdot \left(1 - C_{vb}\right)\right) \cdot A_2 \cdot L \cdot g \\
&= \left(\left(\rho_s - \rho_l\right) \cdot C_{vb} + \rho_l\right) \cdot A_2 \cdot L \cdot g = \rho_l \cdot R_{sd} \cdot C_{vs} \cdot A \cdot L \cdot g + \rho_l \cdot A_2 \cdot L \cdot g
\end{aligned}
\tag{7.14-8}
$$

The submerged weight of the bed can be determined with:

$$W_{b,s} = \left(\rho_s - \rho_l\right) \cdot C_{vb} \cdot A_2 \cdot L \cdot g = \rho_l \cdot R_{sd} \cdot C_{vs} \cdot A \cdot L \cdot g \tag{7.14-9}$$

This gives for the equilibrium of forces on the bed:

$$-\frac{dp}{dx} \cdot A_2 \cdot L = \tau_2 \cdot O_2 \cdot L - \tau_{12} \cdot O_{12} \cdot L + W_b \cdot \sin(\theta) + \mu_{sf} \cdot W_{b,s} \cdot \cos(\theta) \tag{7.14-10}$$

$$-\frac{dp}{dx} \cdot A_2 \cdot L = \tau_2 \cdot O_2 \cdot L - \tau_{12} \cdot O_{12} \cdot L + W_{b,s} \cdot \sin(\theta) + \mu_{sf} \cdot W_{b,s} \cdot \cos(\theta) + \rho_l \cdot A_2 \cdot L \cdot g \cdot \sin(\theta)$$

For the whole pipe cross section the two contributions can be added, giving:

$$-\frac{dp}{dx} \cdot A \cdot L = \tau_1 \cdot O_1 \cdot L + \tau_2 \cdot O_2 \cdot L + \rho_l \cdot A \cdot L \cdot g \cdot \sin(\theta) \tag{7.14-11}$$

$$+ \rho_l \cdot R_{sd} \cdot C_{vs} \cdot A \cdot L \cdot g \cdot \sin(\theta) + \mu_{sf} \cdot \rho_l \cdot R_{sd} \cdot C_{vs} \cdot A \cdot L \cdot g \cdot \cos(\theta)$$

This can also be written as:

$$-\frac{dp}{dx} \cdot A \cdot L = \tau_1 \cdot O_1 \cdot L + \tau_2 \cdot O_2 \cdot L + \rho_m \cdot A \cdot L \cdot g \cdot \sin(\theta) \tag{7.14-12}$$

$$+ \mu_{sf} \cdot \rho_l \cdot R_{sd} \cdot C_{vs} \cdot A \cdot L \cdot g \cdot \cos(\theta)$$

In terms of the hydraulic gradient this gives:

$$i_{m,\theta} = -\frac{dp}{dx} \cdot \frac{A \cdot L}{\rho_l \cdot g \cdot L \cdot A} = \frac{\tau_1 \cdot O_1 \cdot L + \tau_2 \cdot O_2 \cdot L}{\rho_l \cdot g \cdot L \cdot A} + \left(1 + R_{sd} \cdot C_{vs}\right) \cdot \sin(\theta) \tag{7.14-13}$$

$$+ \mu_{sf} \cdot R_{sd} \cdot C_{vs} \cdot \cos(\theta)$$

In chapter 7.4 it has been proven that the first term on the right hand side almost equals the pure liquid hydraulic gradient i_l, without pipe inclination, so:

$$
\begin{aligned}
i_{m,\theta} &= i_l + \left(1 + R_{sd} \cdot C_{vs}\right) \cdot \sin(\theta) + \mu_{sf} \cdot R_{sd} \cdot C_{vs} \cdot \cos(\theta) \\
i_{m,\theta} &= \left(i_l + \sin(\theta)\right) + R_{sd} \cdot C_{vs} \cdot \left(\mu_{sf} \cdot \cos(\theta) + \sin(\theta)\right)
\end{aligned}
\tag{7.14-14}
$$

The hydraulic gradient for pure liquid with pipe inclination can now be expressed as:

$$i_{l,\theta} = i_l + \sin(\theta)$$

(7.14-15)
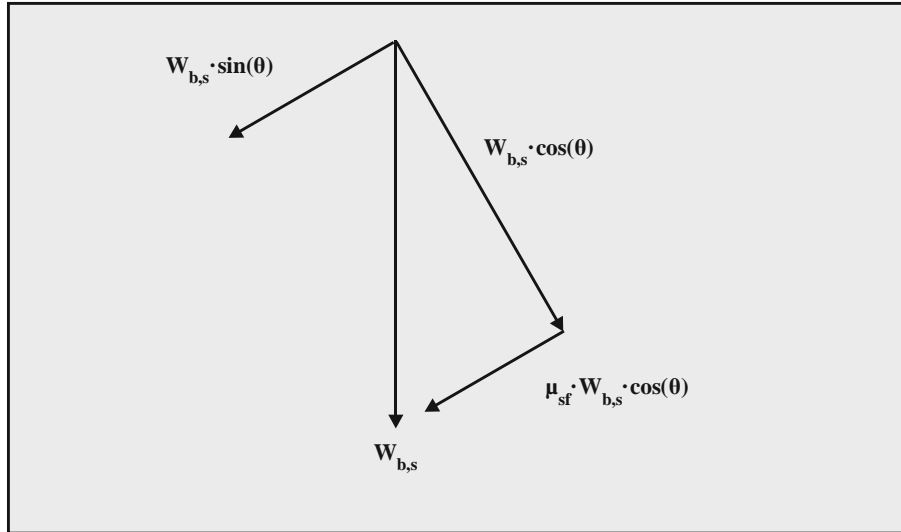
Figure 7.14-4: The submerged weight components and the sliding friction force.

Giving for the mixture hydraulic gradient with pipe inclination:

$$i_{m,\theta} = i_{l,\theta} + R_{sd} \cdot C_{vs} \cdot \left(\mu_{sf} \cdot \cos(\theta) + \sin(\theta)\right)$$

(7.14-16)

The relative excess hydraulic gradient $E_{rhg,\theta}$ is now:

$$E_{rhg,\theta} = \frac{i_{m,\theta} - i_{l,\theta}}{R_{sd} \cdot C_{vs}} = \mu_{sf} \cdot \cos(\theta) + \sin(\theta)$$

(7.14-17)
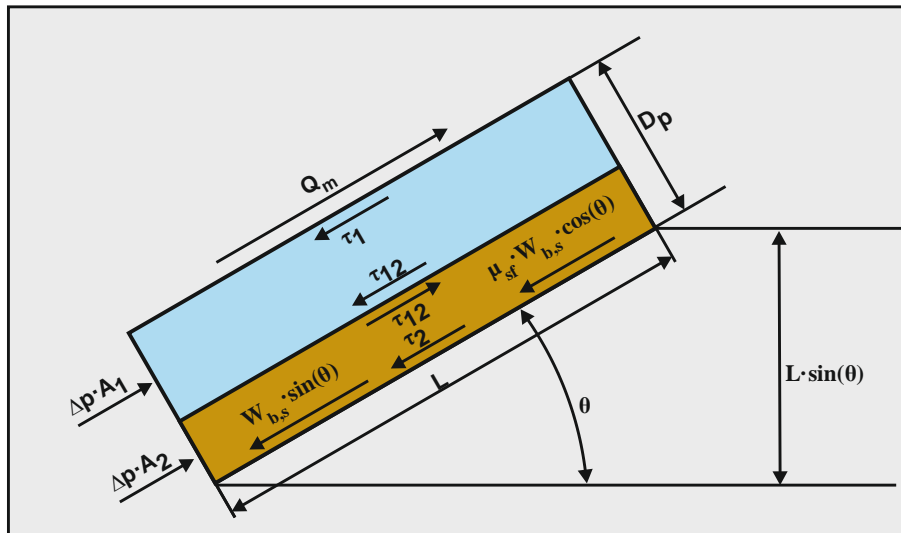
Figure 7.14-5: A sliding bed in an inclined pipe.

Apparently the mixture hydraulic gradient in a sliding bed flow regime does not depend on the velocity of the sliding bed. As soon as the bed starts sliding, the above equations are valid. The above equations match the assumption that the solids effect has to be multiplied by the cosine of the inclination angle to a power of 1. This is in accordance with the Worster & Denny (1955) assumptions. The powers of 1.5 by Durand & Condolios (1952) and 1-1.7 by Wilson et al. (1992) seem to be to high.

7.14.4 Heterogeneous Regime.

In the heterogeneous flow regime, the energy losses consist of the potential energy losses and the kinetic energy losses. Figure 7.14-6 shows the change of the angle of attack resulting from an inclination angle. The equation for the total head loss in a horizontal pipe is:

$$E_{rhg} = S_{hr} + S_{rs}$$

$$i_m = i_l + (S_{hr} + S_{rs}) \cdot R_{sd} \cdot C_{vs}$$

(7.14-18)

The potential energy contribution of the DHLLDV Framework in a horizontal pipe is:

$$S_{hr} = \frac{v_t \cdot \left(1 - \dfrac{C_{vs}}{\kappa_C}\right)^\beta}{v_{ls}}$$

(7.14-19)

The kinetic energy contribution of the DHLLDV Framework in a horizontal pipe is:

$$S_{rs} = \left(\frac{v_{sl}}{v_t}\right)^2 = c \cdot \left(\frac{\delta_v}{d}\right)^{2/3} \cdot \left(\frac{v_t}{11.6 \cdot u_*}\right)^{4/3} \cdot \left(\frac{v_t}{\sqrt{g \cdot d}}\right)^2$$

(7.14-20)

In an inclined pipe the effective terminal settling velocity perpendicular to the pipe wall, the terminal settling velocity times the cosine of the inclination angle, gives a potential energy term of:

$$S_{hr,\theta} = S_{hr} \cdot \cos(\theta) = \frac{v_t \cdot \cos(\theta) \cdot \left(1 - \dfrac{C_{vs}}{\kappa_C}\right)^\beta}{v_{ls}}$$

(7.14-21)

For the kinetic energy losses, the angle of attack has to be adjusted in an inclined pipe. The angle of attack is defined as the ratio between the terminal settling velocity component perpendicular to the pipe wall and the resulting velocity at the thickness of the viscous sub layer, giving:

$$S_{rs,\theta} = c \cdot \left(\frac{\delta_v}{d}\right)^{2/3} \cdot \left(\frac{v_t \cdot \cos(\theta)}{11.6 \cdot u_* - v_t \cdot \sin(\theta)}\right)^{4/3} \cdot \left(\frac{v_t}{\sqrt{g \cdot d}}\right)^2$$

(7.14-22)
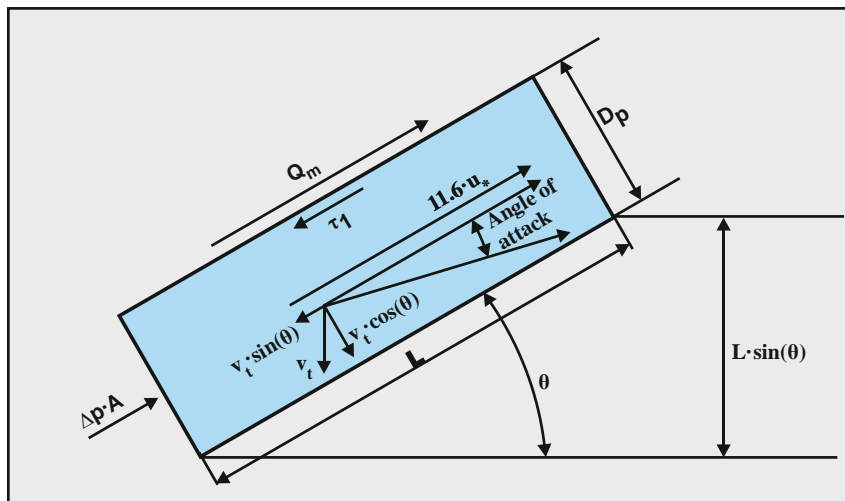
Figure 7.14-6: Heterogeneous flow in an inclined pipe, the angle of attack.

So for very small particles with $v_t << 11.6 \cdot u_*$, the kinetic energy losses are proportional to the cosine of the inclination angle to a power of 4/3. For larger particles, the term in the denominator becomes significant resulting in different behavior of a positive versus a negative inclination angle. Apart from this, also the lifting of the mixture has to be added, giving:

$$E_{rhg,\theta} = S_{hr,\theta} + S_{rs,\theta} + \sin(\theta)$$

$$i_{m,\theta} = i_{l,\theta} + \left(S_{hr,\theta} + S_{rs,\theta} + \sin(\theta) \right) \cdot R_{sd} \cdot C_{vs}$$

(7.14-23)

Literature (see chapter 6) shows a power of the cosine between 1 and 1.7. Here a more complicated formulation is found. Considering that the potential energy losses are much smaller than the kinetic energy losses, a power of about 4/3 is found for small particles, while larger particles will show a smaller power depending on the terminal settling velocity (see equation (7.14-22)). The higher the terminal settling velocity, the smaller the power. Theoretically this power may even become zero when nominator and denominator decrease in the same way with increasing inclination angle.

7.14.5 Homogeneous Regime.

In the homogeneous flow regime the relative excess hydraulic gradient is, including the lubrication effect:

$$E_{rhg} = \alpha_E \cdot i_l$$

$$i_m = i_l + i_l \cdot \alpha_E \cdot R_{sd} \cdot C_{vs} = i_l \cdot \left(1 + \alpha_E \cdot R_{sd} \cdot C_{vs} \right)$$

(7.14-24)

For an inclined pipe only the lifting of the mixture has to be added, giving:

$$E_{rhg,\theta} = \alpha_E \cdot i_l + \sin(\theta)$$

$$i_{m,\theta} = i_{l,\theta} + \left(\alpha_E \cdot i_l + \sin(\theta) \right) \cdot R_{sd} \cdot C_{vs}$$

$$= i_l \cdot \left(1 + \alpha_E \cdot R_{sd} \cdot C_{vs} \right) + \sin(\theta) \cdot \left(1 + R_{sd} \cdot C_{vs} \right)$$

(7.14-25)

7.14.6 Sliding Flow Regime.

The method for determining the Sliding Flow Regime is not affected by pipe inclination. Of course the equations for a pipe with inclination for the sliding bed regime and the heterogeneous regime have to be applied. However in the Sliding Flow Regime the particles are so large that they do not follow the eddies anymore. The particles will have a slip velocity with respect to the liquid velocity related to the hindered settling velocity and the inclination angle. As a result, the liquid velocity is a bit higher than the cross sectional averaged line speed. The result is a higher hydraulic gradient for the carrier liquid. This gives:

$$i_{m,\theta} = i_l + \sin(\theta) + i_l \cdot \frac{2 \cdot v_{th} \cdot \sin(\theta) \cdot C_{vs}}{v_{ls}} + \sin(\theta) \cdot R_{sd} \cdot C_{vs}$$

$$i_{m,\theta} = i_{l,\theta} + + i_l \cdot \frac{2 \cdot v_{th} \cdot \sin(\theta) \cdot C_{vs}}{v_{ls}} + \sin(\theta) \cdot R_{sd} \cdot C_{vs}$$

$$E_{rhg,\theta} = i_l \cdot \frac{2 \cdot v_{th} \cdot \sin(\theta)}{v_{ls} \cdot R_{sd}} + \sin(\theta)$$

(7.14-26)

7.14.7 The Limit Deposit Velocity.

The Limit of Stationary Deposit Velocity is affected by the pipe inclination. In an ascending pipe, the cross sectional averaged line speed has to be higher compared to a horizontal pipe in order to make a bed start sliding. In a descending pipe this line speed is lower. It is even possible that in a descending pipe the bed will always slide because of gravity.

The Limit Deposit Velocity is defined as the line speed above which there is no stationary of sliding bed, is determined by either the potential energy losses or a limiting sliding bed. In both cases this is affected by the cosine of the inclination angle, the component of gravity perpendicular to the pipe wall. Since in both cases the Limit Deposit Velocity depends on the cube root of this cosine, the Limit Deposit Velocity will decrease according to:

$$v_{ls,ldv,\theta} = v_{ls,ldv} \cdot \cos(\theta)^{1/3} \tag{7.14-27}$$

Because of the cube root of this cosine, this means that for angles up to 45º the reduction is less than 10%.

7.14.8 Conclusions & Discussion.

For the stationary bed regime, only the potential energy term of the pure liquid has to be added to the hydraulic gradient of the mixture. For all other flow regimes the potential energy term of the mixture has to be added, together with a correction of the so called solids effect. The result of this is a higher line speed for the intersection point of the stationary bed curve and the sliding bed curve. So in general an increase of the Limit of Stationary Deposit Velocity. This may however also result in omission of the occurrence of a sliding bed for an inclined pipe, where a sliding bed would occur in a horizontal pipe. This makes sense, since a higher line speed is required to make a bed start sliding, there is the possibility that the bed is already fully suspended before it could start sliding.

In the sliding bed regime and the heterogeneous regime, the hydraulic gradient is lower for an inclined pipe compared with a horizontal pipe, if the potential energy term of the mixture (static head) is not taken into account, especially for small particles in the heterogeneous regime. For the heterogeneous regime there is a difference between ascending and descending pipes, due to the term with the angle of attack in the kinetic energy losses. The decrease in an ascending pipe is smaller than in a descending pipe and could even be a small increase in an ascending pipe at low line speeds. The transition line speed of the heterogeneous flow regime to the homogeneous flow regime will also decrease with increasing inclination angle.

In case of a sliding bed one may expect more stratification in an ascending pipe compared to a descending pipe, due to the higher line speed in an ascending pipe to make the bed start sliding. In other words, a higher shear stress on the bed is required in an ascending pipe, resulting in a thicker sheet flow layer at the top of the bed.

Figure 7.14-7 and Figure 7.14-8 show the hydraulic gradient in a horizontal pipe with **D_p=0.1524 m** and **d=0.5 mm**, an ascending pipe with slope 30º and a descending pipe with slope -30º. In a horizontal pipe, for constant spatial concentration, a sliding bed will occur. The ascending pipe does not show a sliding bed, in fact the resulting curve just touches the sliding bed curve at a higher line speed than the start of a sliding bed in a horizontal pipeline. The descending pipe show a sliding bed from zero line speed up to the line speed where the heterogeneous flow regime starts, which happens at a lower line speed than for the horizontal pipe.

Figure 7.14-9 and Figure 7.14-10 show the same phenomena in a pipe with **D_p=0.762 m**. Here a **d=3 mm** particle is required to have a sliding bed. The figures also show a slight decrease of the Limit Deposit Velocity for the pipes with a slope.

Figure 7.14-11 and Figure 7.14-12 show the same for a **d=5 mm** particle. Now the ascending pipeline also has a sliding bed, but it starts at a higher line speed and stops at a lower line speed, compared to the horizontal pipe. A sliding bed in an ascending pipe will encounter a higher bed shear stress and have a lower bed velocity, compared to a horizontal pipeline.

In order to find the correct hydraulic gradient curves for an inclined pipe, one first has to determine the hydraulic gradient curves for each flow regime individually. The resulting curve can be found by comparing flow regime curves.

1. If the sliding bed hydraulic gradient (SB) is smaller than the stationary (fixed) bed hydraulic gradient (FB), the sliding bed hydraulic gradient (SB) is chosen, otherwise the stationary bed hydraulic gradient. The resulting curve is named the FB-SB curve.
2. If the heterogeneous flow regime hydraulic gradient (He) is smaller than the FB-SB hydraulic gradient, the heterogeneous hydraulic gradient (He) is chosen, otherwise the FB-SB hydraulic gradient. The resulting curve is named the FB-SB-He curve. Depending on the parameters (particle and pipe diameter), it is possible that this curve does not contain a sliding bed regime.
3. If the homogeneous flow regime hydraulic gradient (Ho) is larger than the FB-SB-HE hydraulic gradient. The homogeneous hydraulic gradient (Ho) is chosen, otherwise the FB-SB-He hydraulic gradient. The resulting curve is named the FB-SB-He-Ho curve.

The hydraulic gradients of the inclined pipes are determined per meter of inclined pipe and not per meter of horizontal pipe.
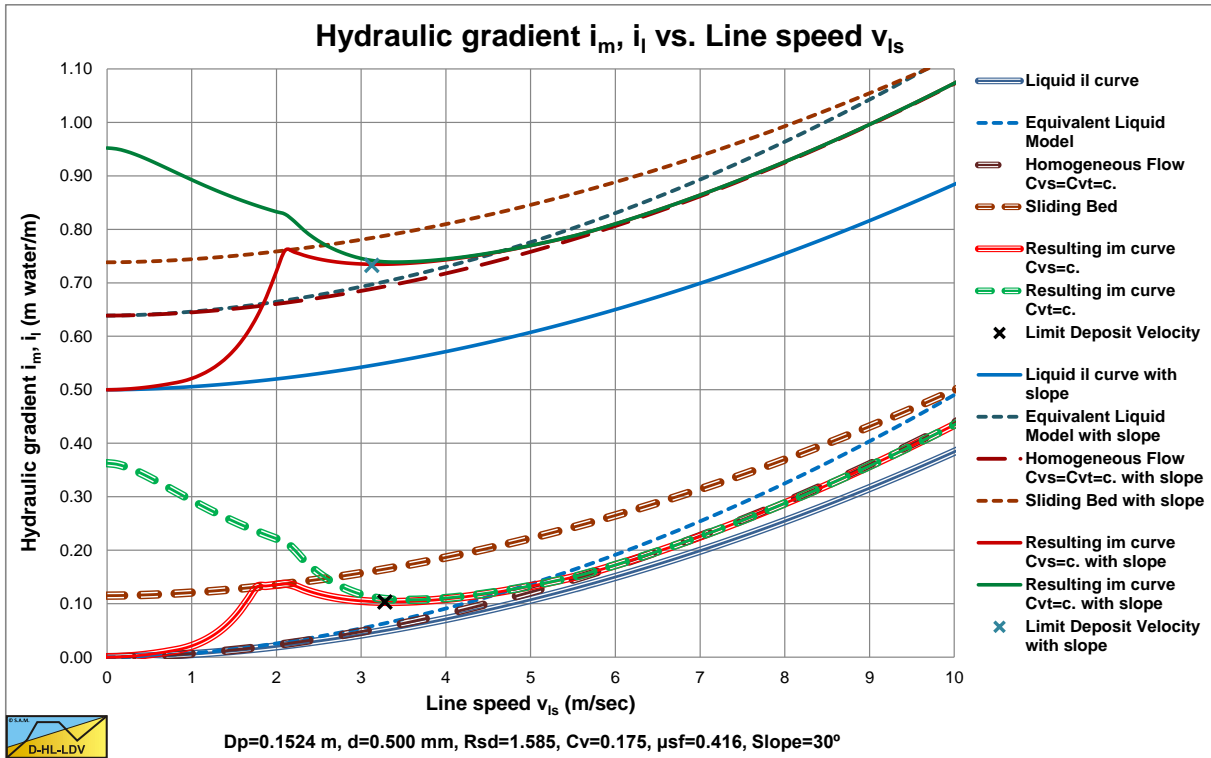
Figure 7.14-7: The hydraulic gradient in an ascending pipeline, d=0.5 mm, D_p=0.1524 m.
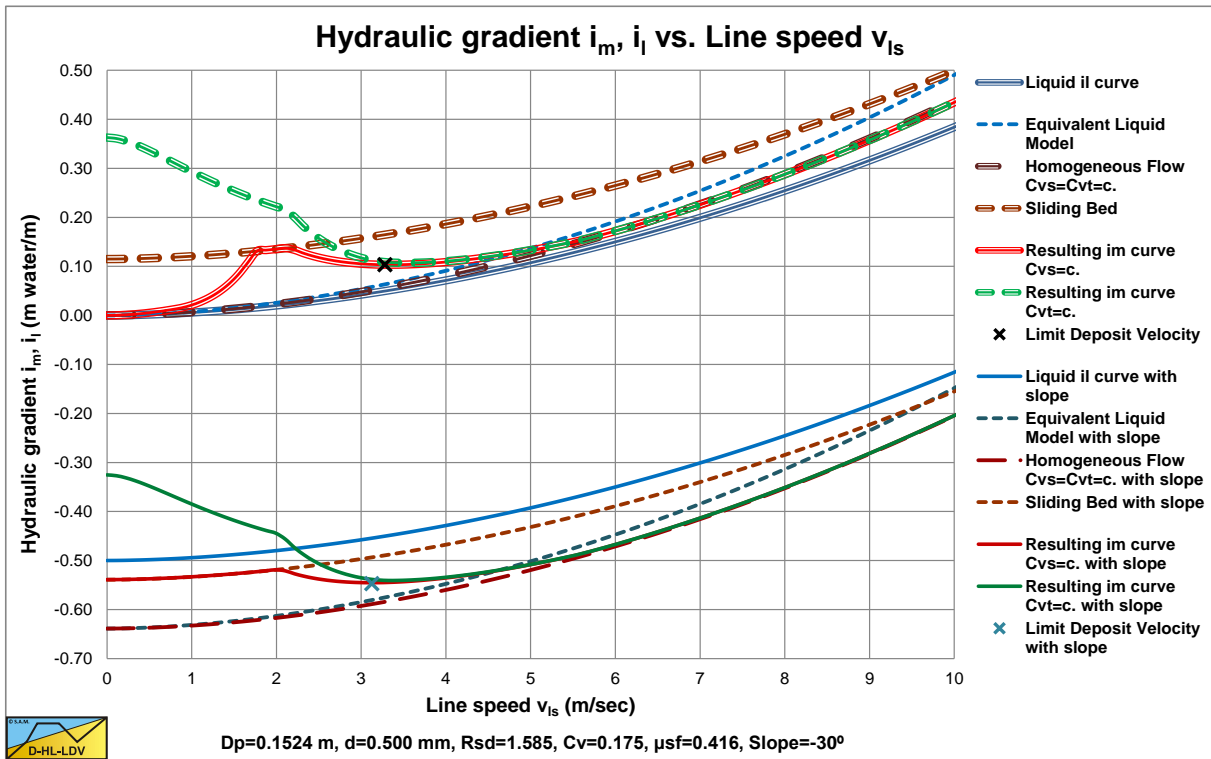
Figure 7.14-8: The hydraulic gradient in a descending pipeline, d=0.5 mm, D_p=0.1524 m.
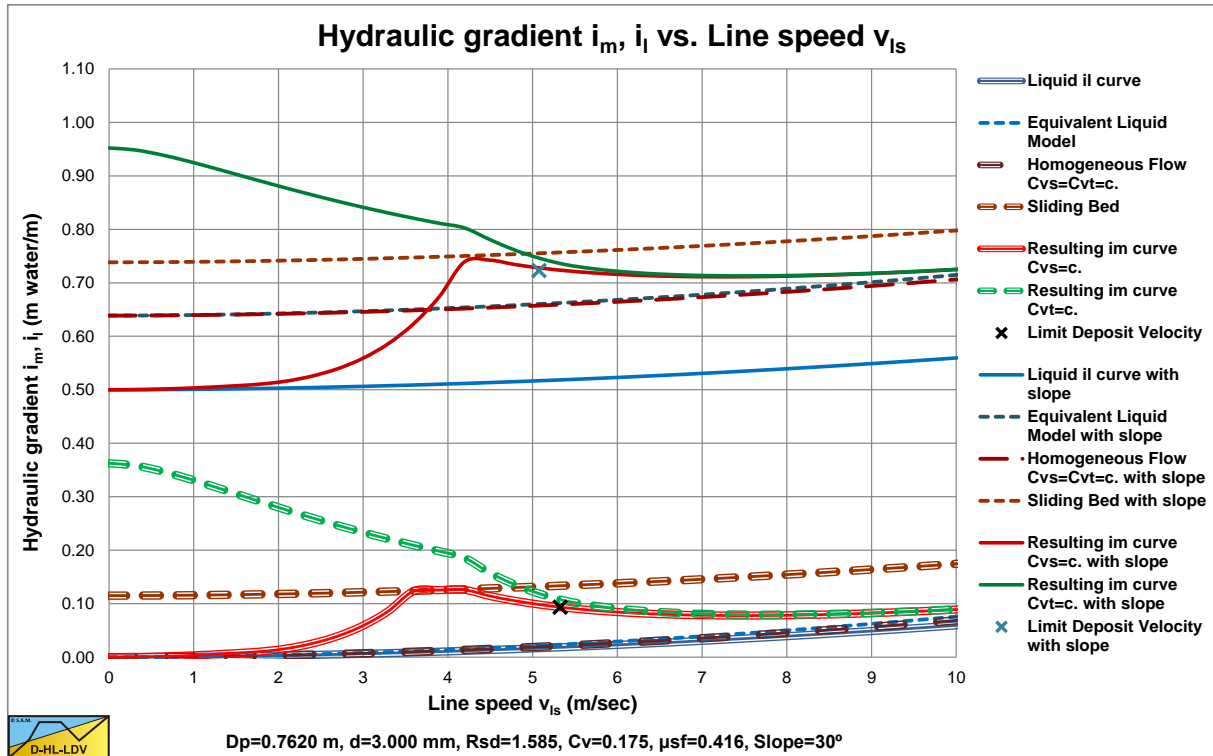
Figure 7.14-9: The hydraulic gradient in an ascending pipeline, d=3 mm, D$_p$=0.762 m.
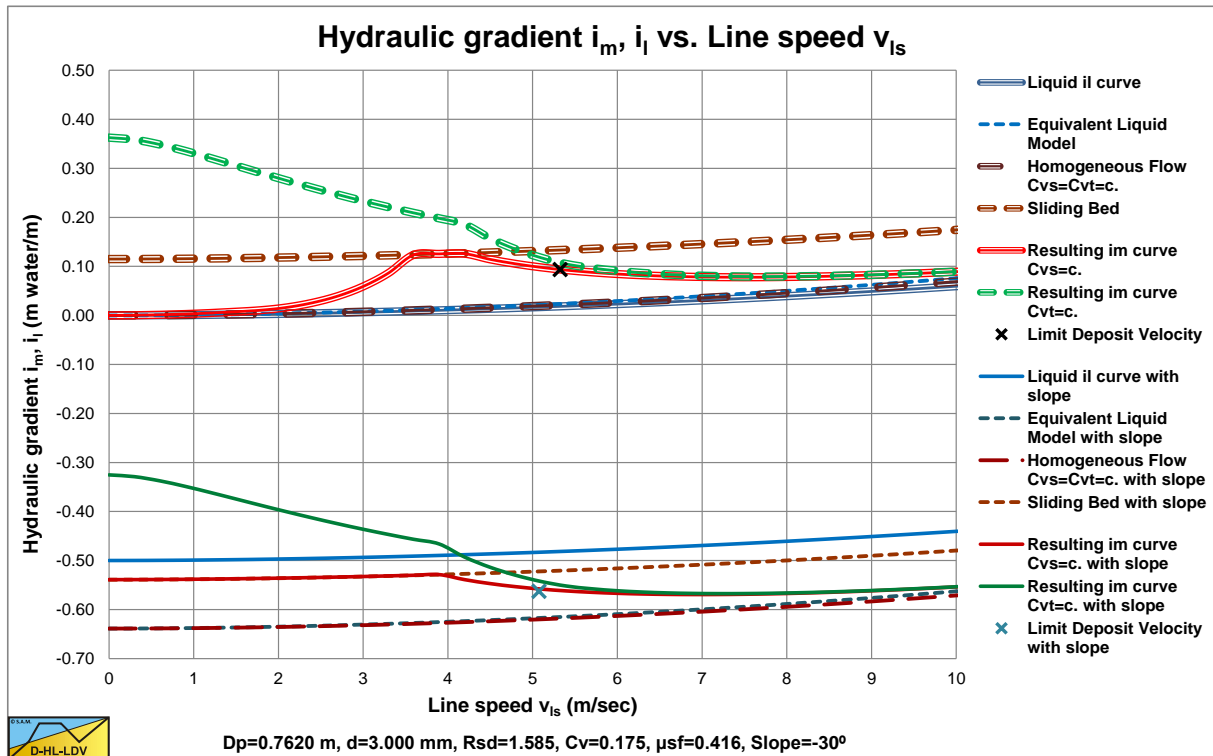
Figure 7.14-10: The hydraulic gradient in a descending pipeline, d=3 mm, D$_p$=0.762 m.
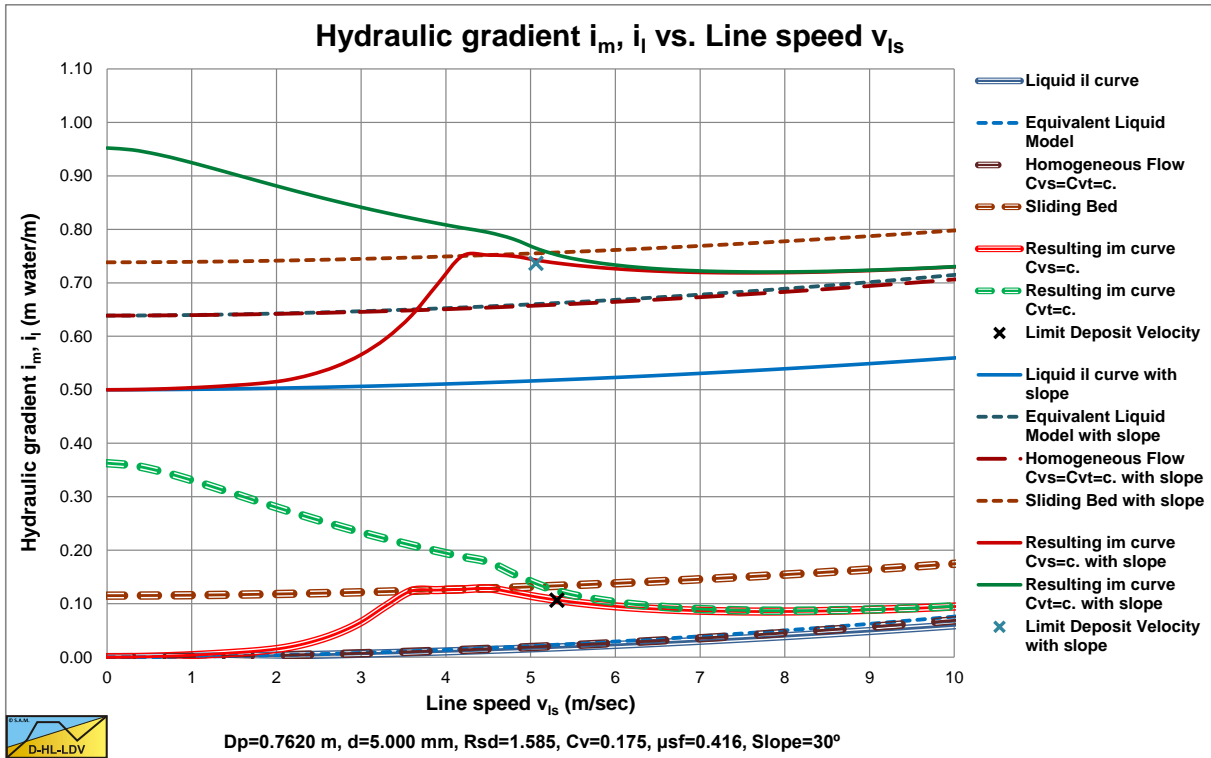
Figure 7.14-11: The hydraulic gradient in an ascending pipeline, d=5 mm, D_p=0.762 m.
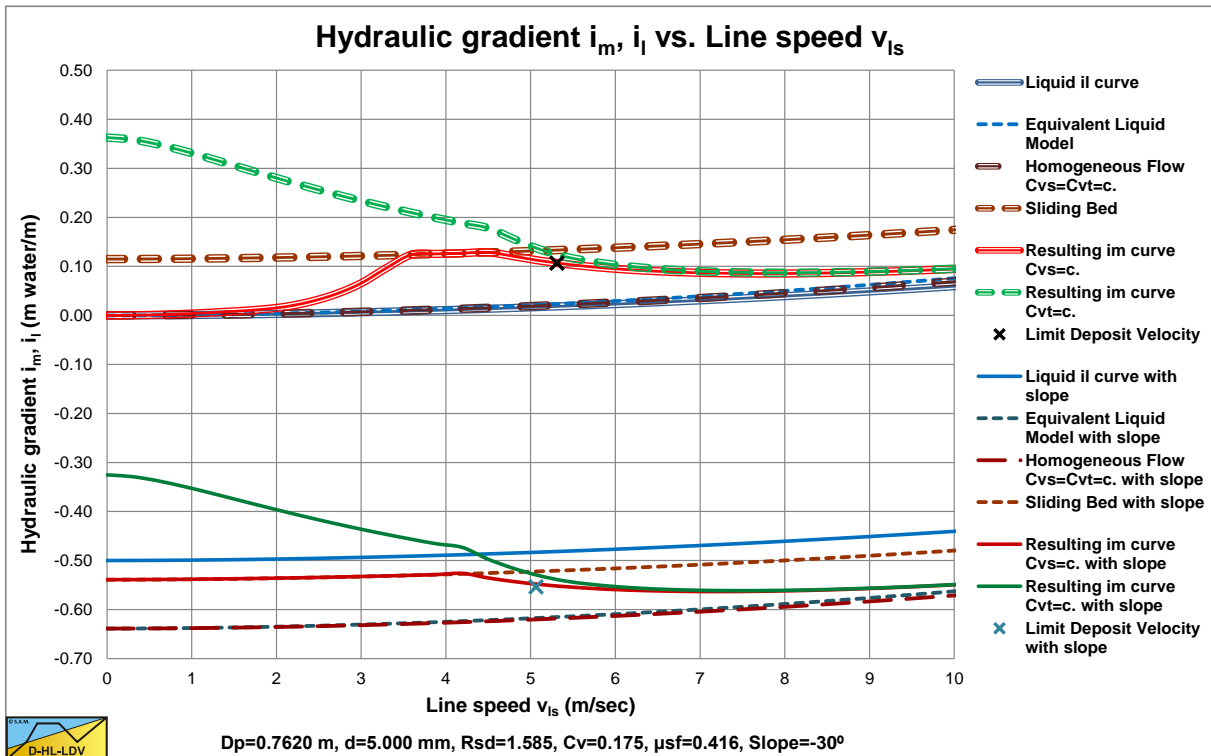
Figure 7.14-12: The hydraulic gradient in a descending pipeline, d=5 mm, D_p=0.762 m.

7.14.9 Nomenclature Inclined Pipes.

A,A$_p$	Cross section pipe	**m^2**
A$_1$	Cross section restricted area above the bed	**m^2**
A$_2$	Cross section bed	**m^2**
c	Proportionality constant	**-**
C$_{vb}$	Bed volumetric concentration	**-**
C$_{vs}$	Spatial volumetric concentration	**-**
d	Particle diameter	**m**
E$_{rhg}$	Relative excess hydraulic gradient without pipe inclination	**-**
E$_{rhg,\theta}$	Relative excess hydraulic gradient with pipe inclination	**-**
g	Gravitational constant (9.81)	**m/s^2**
i$_l$	Hydraulic gradient liquid without pipe inclination	**-**
i$_{l,\theta}$	Hydraulic gradient liquid with pipe inclination	**-**
i$_m$	Hydraulic gradient mixture without pipe inclination	**-**
i$_{m,\theta}$	Hydraulic gradient mixture with pipe inclination	**-**
L	Length of pipe	**m**
O$_1$	Circumference restricted area above the bed in contact with pipe wall	**m**
O$_2$	Circumference of bed with pipe wall	**m**
O$_{12}$	Width of the top of the bed	**m**
p	Pressure in pipe	**kPa**
R$_{sd}$	Relative submerged density of solids	**-**
S$_{hr}$	Settling velocity Hindered Relative without pipe inclination	**-**
S$_{hr,\theta}$	Settling velocity Hindered Relative with pipe inclination	**-**
S$_{rs}$	Slip Ratio Squared without pipe inclination	**-**
S$_{rs,\theta}$	Slip Ratio Squared with pipe inclination	**-**
u$_*$	Friction velocity	**m/s**
v$_{ls}$	Line speed	**m/s**
v$_t$	Terminal settling velocity	**m/s**
v$_{sl}$	Slip velocity solids	**m/s**
v$_{ls,ldv}$	Limit Deposity Velocity without pipe inclination	**m/s**
v$_{ls,ldv,\theta}$	Limit Deposity Velocity with pipe inclination	**m/s**
W$_b$	Weight of the bed	**ton**
W$_{b,s}$	Submerged weight of the bed	**ton**
x	Distance in pipe length direction	**m**
α_E	Homogeneous lubrication factor	**-**
β	Richardson & Zaki hindered settling power	**-**
δ_v	Thickness viscous sub-layer	**m**
ρ_b	Density of the bed including pore water	**ton/m^3**
ρ_s	Density of the solids	**ton/m^3**
ρ_l	Density of the liquid	**ton/m^3**
ρ_m	Mixture density	**ton/m^3**
τ_1	Shear stress between liquid and pipe wall	**kPa**
τ_{12}	Shear stress on top of the bed	**kPa**
θ	Inclination angle (positive upwards, negative downwards)	**^{o}**
μ_{sf}	Sliding friction coefficient	**-**
κ_C	Concentration eccentricity factor	**-**

Chapter 8:   Usage of the DHLLDV Framework.

8.1   Introduction.

The DHLLDV Framework is based on the philosophy that pressure/hydraulic gradients and Limit Deposit Velocities can only be determined based on the spatial volumetric concentration for uniform PSD's, in contrary to most models from literature. For heterogeneous and homogeneous transport the spatial and transport volumetric concentrations are almost identical, but for the fixed and the sliding bed regimes the difference is substantial. To use the model the following steps have to be carried out:

1. The hydraulic gradient curves and the relative excess hydraulic gradient curves for the fixed or stationary bed regime (FB), for the sliding bed regime (SB), for the heterogeneous flow regime (He) and for the homogeneous flow regime (Ho) have to be determined.
2. The resulting curve, based on the algorithm according to Figure 8.1-1 has to be constructed.
3. The Limit Deposit Velocity has to be determined. There are 3 possible Limit Deposit Velocities, the transition heterogeneous-homogeneous (HH) for very small particles, the transition fixed bed-heterogeneous (FH) for medium sized particles and the transition sliding bed-heterogeneous (SH) for coarse particles. Which one to apply depends on the algorithm according to Figure 8.11-1.
4. The transport or delivered concentration curves are determined based on a holdup or slip factor function, where the Limit Deposit Velocity plays a very important role.
5. The bed height and bed fraction are determined based on the Limit Deposit Velocity and the slip factor.
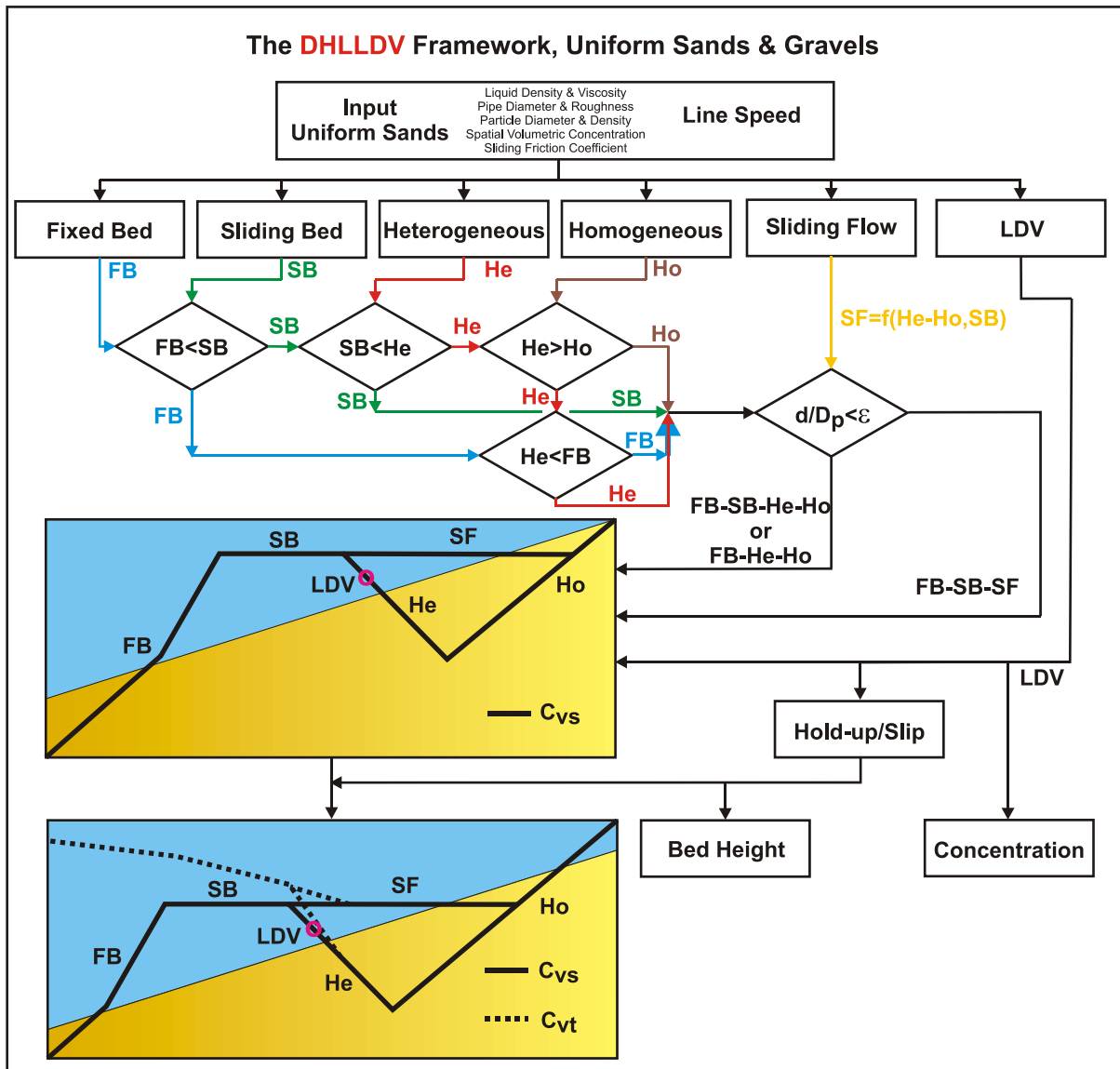
Figure 8.1-1: The algorithm to determine the constant C_{vs} and C_{vt} curve for uniform sands and gravels.

In the following chapters the different steps are explained. All equation have two numbers, the first number refers to the location where the equation is derived or first used, and the second number is the equation number in this chapter.

The book is accompanied with an Excel Workbook showing the DHLLDV Framework, and also many other models. This Excel Workbook can be downloaded from ResearchGate or send an email to s.a.miedema@tudelft.nl.

8.2   Default Equations Used In This Book.

The relative submerged density $\mathbf{R_{sd}}$ is defined as:

$$\mathbf{R_{sd}} = \frac{\rho_s - \rho_l}{\rho_l}$$

<div align="right">(2.4-10)
(8.2-1)</div>

The equation for the terminal settling velocity (in m and m/sec) has been derived by Ruby & Zanke (1977):

$$\mathbf{v_t} = \frac{10 \cdot \nu_l}{d} \cdot \left(\sqrt{1 + \frac{R_{sd} \cdot g \cdot d^3}{100 \cdot \nu_l^2}} - 1 \right)$$

<div align="right">(4.4-5)
(8.2-2)</div>

The general equation for the hindered terminal settling velocity according to Richardson & Zaki (1954) yields:

$$\mathbf{v_{th}} = \mathbf{v_t} \cdot \left(1 - C_{vs} \right)^{\beta}$$

<div align="right">(4.6-1)
(8.2-3)</div>

According to Rowe (1987) the power can be approximated by:

$$\beta = \frac{4.7 + 0.41 \cdot Re_p^{0.75}}{1 + 0.175 \cdot Re_p^{0.75}} \quad \text{with:} \quad Re_p = \frac{v_t \cdot d}{\nu_l}$$

<div align="right">(4.6-4)
(8.2-4)</div>

When clear water flows through the pipeline, the pressure loss can be determined with the well-known Darcy-Weisbach equation:

$$\Delta p_l = \lambda_l \cdot \frac{\Delta L}{D_p} \cdot \frac{1}{2} \cdot \rho_l \cdot v_{ls}^2$$

<div align="right">(3.1-6)
(8.2-5)</div>

The hydraulic gradient $\mathbf{i_w}$ (for pure water) or $\mathbf{i_l}$ (for a liquid in general) is meters of liquid per meter of pipeline:

$$\mathbf{i_w} = \frac{\Delta p_l}{\rho_w \cdot g \cdot \Delta L} = \frac{\lambda_l \cdot v_{ls}^2}{2 \cdot g \cdot D_p} \quad \text{or} \quad \mathbf{i_l} = \frac{\Delta p_l}{\rho_l \cdot g \cdot \Delta L} = \frac{\lambda_l \cdot v_{ls}^2}{2 \cdot g \cdot D_p}$$

<div align="right">(3.1-8)
(8.2-6)</div>

Over the whole range of Reynolds numbers above 2320 the Swamee Jain (1976) equation gives a good approximation for the Darcy Weisbach friction factor:

$$\lambda_l = \frac{1.325}{\left(\ln\left(\frac{\varepsilon}{3.7 \cdot D_p} + \frac{5.75}{Re^{0.9}} \right) \right)^2} = \frac{0.25}{\left(\log_{10}\left(\frac{\varepsilon}{3.7 \cdot D_p} + \frac{5.75}{Re^{0.9}} \right) \right)^2}$$

<div align="right">(3.2-8)
(8.2-7)</div>

With the Reynolds number:

$$\mathbf{Re} = \frac{v_{ls} \cdot D_p}{\nu_l}$$

<div align="right">(8.2-8)</div>

The relative excess hydraulic gradient as defined and used in this book:

$$E_{rhg} = \frac{i_m - i_l}{R_{sd} \cdot C_{vs}} \quad \text{or} \quad E_{rhg} = \frac{i_m - i_l}{R_{sd} \cdot C_{vt}}$$

(7.1-5)
(8.2-9)

When mixture flows through the pipeline, the pressure loss can be determined with the well-known Darcy-Weisbach equation for the ELM:

$$\Delta p_m = \lambda_l \cdot \frac{\Delta L}{D_p} \cdot \frac{1}{2} \cdot \rho_m \cdot v_{ls}^2$$

(3.3-1)
(8.2-10)

For the Equivalent Liquid Model (ELM) this gives for the hydraulic gradient:

$$i_m = \frac{\Delta p_m}{\rho_l \cdot g \cdot \Delta L} = \frac{\rho_m}{\rho_l} \cdot \frac{\lambda_l \cdot v_{ls}^2}{2 \cdot g \cdot D_p}$$

(3.3-2)
(8.2-11)

The relative excess hydraulic gradient is for the ELM:

$$E_{rhg} = \frac{i_m - i_l}{R_{sd} \cdot C_{vs}} = i_l$$

(7.6-3)
(8.2-12)

The DHLLDV Framework is calibrated, based on these equations. Other equations, especially for the terminal settling velocity, may give slightly different results.

8.3 The Influence of Fines.

The fraction of the sand in suspension, the fines, resulting in a homogeneous pseudo liquid is named **X**. This gives for the density of the homogeneous pseudo liquid:

$$\rho_{pl} = \rho_l + \rho_l \cdot \frac{X \cdot C_{vs} \cdot R_{sd}}{\left(1 - C_{vs} + C_{vs} \cdot X\right)}$$

(7.13-3)
(8.3-1)

So the concentration of the fines in the homogeneous pseudo liquid is not $C_{vs,pl} = X \cdot C_{vs}$, but:

$$C_{vs,pl} = \frac{X \cdot C_{vs}}{\left(1 - C_{vs} + C_{vs} \cdot X\right)}$$

(7.13-4)
(8.3-2)

This is because part of the total volume is occupied by the particles that are not in suspension. The remaining spatial concentration of solids to be used to determine the hydraulic gradients curve of the solids is now:

$$C_{vs,r} = \left(1 - X\right) \cdot C_{vs}$$

(7.13-5)
(8.3-3)

The dynamic viscosity can now be determined according to Thomas (1965):

$$\mu_{pl} = \mu_l \cdot \left(1 + 2.5 \cdot C_{vs,pl} + 10.05 \cdot C_{vs,pl}^2 + 0.00273 \cdot \left(e^{16.6 \cdot C_{vs,pl}} - 1\right)\right)$$

(7.13-6)
(8.3-4)

The kinematic viscosity of the homogeneous pseudo liquid is now:

$$\nu_{pl} = \frac{\mu_{pl}}{\rho_{pl}}$$

(7.13-7)
(8.3-5)

One should realize however that the relative submerged density has also changed to:

$$R_{sd,pl} = \frac{\rho_s - \rho_{pl}}{\rho_{pl}}$$

(7.13-8)
(8.3-6)

Over the whole range of Reynolds numbers above 2320 the Swamee Jain (1976) equation gives a good approximation for the Darcy Weisbach friction factor:

$$\lambda_{pl} = \frac{1.325}{\left(\ln\left(\dfrac{\epsilon}{3.7 \cdot D_p} + \dfrac{5.75}{Re_{pl}^{0.9}} \right) \right)^2} = \frac{0.25}{\left(\log_{10}\left(\dfrac{\epsilon}{3.7 \cdot D_p} + \dfrac{5.75}{Re_{pl}^{0.9}} \right) \right)^2}$$

(3.2-8)
(8.3-7)

With the Reynolds number for the pseudo liquid:

$$Re_{pl} = \frac{v_{ls} \cdot D_p}{\nu_{pl}}$$

(8.3-8)

The equation for the terminal settling velocity in pseudo liquid (in m and m/sec) has been derived by Ruby & Zanke (1977):

$$v_{t,pl} = \frac{10 \cdot \nu_{pl}}{d} \cdot \left(\sqrt{1 + \frac{R_{sd,pl} \cdot g \cdot d^3}{100 \cdot \nu_{pl}^2}} - 1 \right)$$

(8.3-9)

The general equation for the hindered terminal settling velocity in pseudo liquid according to Richardson & Zaki (1954) yields:

$$v_{th,pl} = v_{t,pl} \cdot \left(1 - C_{vs,r}\right)^{\beta}$$

(8.3-10)

According to Rowe (1987) the power in pseudo liquid can be approximated by:

$$\beta = \frac{4.7 + 0.41 \cdot Re_{p,pl}^{0.75}}{1 + 0.175 \cdot Re_{p,pl}^{0.75}} \quad \text{with:} \quad Re_{p,pl} = \frac{v_{t,pl} \cdot d}{\nu_{pl}}$$

(8.3-11)

With the new homogeneous pseudo liquid density, kinematic viscosity, relative submerged density and volumetric concentration the hydraulic gradient can be determined for the remaining solids, with the adjusted volumetric concentration.

8.3.1 Based on the Pseudo Liquid (A).

When pseudo liquid flows through the pipeline, the pressure loss can be determined with the well-known Darcy-Weisbach equation, this pressure loss is in kPa:

$$\Delta p_{pl,A} = \lambda_{pl} \cdot \frac{\Delta L}{D_p} \cdot \frac{1}{2} \cdot \rho_{pl} \cdot v_{ls}^2 = \frac{\lambda_{pl}}{\lambda_l} \cdot \frac{\rho_{pl}}{\rho_l} \cdot \lambda_l \cdot \frac{\Delta L}{D_p} \cdot \frac{1}{2} \cdot \rho_l \cdot v_{ls}^2 = \Delta p_{pl,B} = \frac{\lambda_{pl}}{\lambda_l} \cdot \frac{\rho_{pl}}{\rho_l} \cdot \Delta p_l$$

(8.3-12)

The hydraulic gradient i_{pl} based on the pseudo liquid is in meters of liquid per meter of pipeline:

$$i_{pl,A} = \frac{\Delta p_{pl,A}}{\rho_{pl} \cdot g \cdot \Delta L} = \frac{\lambda_{pl} \cdot v_{ls}^2}{2 \cdot g \cdot D_p} = \frac{\lambda_{pl}}{\lambda_l} \cdot \frac{\lambda_l \cdot v_{ls}^2}{2 \cdot g \cdot D_p} = \frac{\lambda_{pl}}{\lambda_l} \cdot i_l$$

(8.3-13)

The relative excess hydraulic gradient related to the pseudo liquid as defined and used in this book is (which is zero for only the pseudo liquid):

$$E_{rhg,pl,A} = \frac{i_{m,pl,A} - i_{pl,A}}{R_{sd,pl} \cdot C_{vs,r}} \quad \text{or} \quad E_{rhg,pl,A} = \frac{i_{m,pl,A} - i_{pl,A}}{R_{sd,pl} \cdot C_{vt,r}} \qquad (8.3-14)$$

When mixture flows through the pipeline, the pressure loss can be determined with the well-known Darcy-Weisbach equation for the ELM, based on the pseudo liquid:

$$\Delta p_{m,pl,A} = \lambda_{pl} \cdot \frac{\Delta L}{D_p} \cdot \frac{1}{2} \cdot \rho_m \cdot v_{ls}^2 = \frac{\rho_m}{\rho_{pl}} \cdot \lambda_{pl} \cdot \frac{\Delta L}{D_p} \cdot \frac{1}{2} \cdot \rho_{pl} \cdot v_{ls}^2 = \frac{\rho_m}{\rho_{pl}} \cdot \Delta p_{pl,A} \qquad (8.3-15)$$

For the Equivalent Liquid Model (ELM) this gives for the hydraulic gradient based on the pseudo liquid:

$$i_{m,pl,A} = \frac{\Delta p_{m,pl,A}}{\rho_{pl} \cdot g \cdot \Delta L} = \frac{\rho_m}{\rho_{pl}} \cdot \frac{\lambda_{pl} \cdot v_{ls}^2}{2 \cdot g \cdot D_p} = \frac{\rho_m}{\rho_{pl}} \cdot i_{pl,A} \qquad (8.3-16)$$

The relative excess hydraulic gradient is for the ELM, based on the pseudo liquid:

$$E_{rhg,pl,A} = \frac{i_{m,pl,A} - i_{pl,A}}{R_{sd,pl} \cdot C_{vs,r}} = \frac{\dfrac{\rho_m}{\rho_{pl}} \cdot i_{pl,A} - i_{pl,A}}{R_{sd,pl} \cdot C_{vs,r}} = i_{pl,A} \qquad (8.3-17)$$

8.3.2 Based on the Carrier Liquid (B).

Since here the hydraulic gradient and the relative excess hydraulic gradient are based on the pseudo liquid density, these parameters have to be corrected in order to express them in terms of the carrier liquid density and the carrier liquid Darcy Weisbach friction factor according to, this pressure loss is in kPa:

$$\Delta p_{pl,B} = \lambda_{pl} \cdot \frac{\Delta L}{D_p} \cdot \frac{1}{2} \cdot \rho_{pl} \cdot v_{ls}^2 = \frac{\lambda_{pl}}{\lambda_l} \cdot \frac{\rho_{pl}}{\rho_l} \cdot \lambda_l \cdot \frac{\Delta L}{D_p} \cdot \frac{1}{2} \cdot \rho_l \cdot v_{ls}^2 = \Delta p_{pl,A} = \frac{\lambda_{pl}}{\lambda_l} \cdot \frac{\rho_{pl}}{\rho_l} \cdot \Delta p_l \qquad (8.3-18)$$

This gives for the hydraulic gradient, carrier liquid based:

$$i_{pl,B} = \frac{\Delta p_{pl,B}}{\rho_l \cdot g \cdot \Delta L} = \frac{\lambda_{pl}}{\lambda_l} \cdot \frac{\rho_{pl}}{\rho_l} \cdot \frac{\lambda_l \cdot v_{ls}^2}{2 \cdot g \cdot D_p} = \frac{\lambda_{pl}}{\lambda_l} \cdot \frac{\rho_{pl}}{\rho_l} \cdot i_l = \frac{\rho_{pl}}{\rho_l} \cdot i_{pl,A} \qquad (8.3-19)$$

The relative excess hydraulic gradient related to the carrier liquid as defined and used in this book (which is non-zero for the pure pseudo liquid):

$$E_{rhg,pl,B} = \frac{\dfrac{\rho_{pl}}{\rho_l} \cdot i_{m,pl,A} - i_l}{R_{sd} \cdot C_{vs}} \quad \text{or} \quad E_{rhg,pl,B} = \frac{\dfrac{\rho_{pl}}{\rho_l} \cdot i_{m,pl,A} - i_l}{R_{sd} \cdot C_{vt}} \qquad (8.3-20)$$

When mixture flows through the pipeline, the pressure loss can be determined with the well-known Darcy-Weisbach equation for the ELM, based on the pseudo liquid:

$$\Delta p_{m,pl,B} = \lambda_{pl} \cdot \frac{\Delta L}{D_p} \cdot \frac{1}{2} \cdot \rho_m \cdot v_{ls}^2 = \frac{\rho_m}{\rho_{pl}} \cdot \lambda_{pl} \cdot \frac{\Delta L}{D_p} \cdot \frac{1}{2} \cdot \rho_{pl} \cdot v_{ls}^2 = \Delta p_{m,pl,A} \qquad (8.3-21)$$

For the Equivalent Liquid Model (ELM) this gives for the hydraulic gradient based on the carrier liquid:

$$i_{m,pl,B} = \frac{\Delta p_{m,pl,B}}{\rho_l \cdot g \cdot \Delta L} = \frac{\rho_m}{\rho_l} \cdot \frac{\lambda_{pl} \cdot v_{ls}^2}{2 \cdot g \cdot D_p} = \frac{\rho_{pl}}{\rho_l} \cdot i_{m,pl,A} = \frac{\rho_{pl}}{\rho_l} \cdot \frac{\rho_m}{\rho_{pl}} \cdot i_{pl,A} = \frac{\rho_m}{\rho_l} \cdot i_{pl,A} == \frac{\lambda_{pl}}{\lambda_l} \cdot \frac{\rho_m}{\rho_l} \cdot i_l \qquad (8.3-22)$$

The relative excess hydraulic gradient is for the ELM, based on the carrier liquid:

$$
E_{rhg,pl,B} = \frac{i_{m,pl,B} - i_l}{R_{sd} \cdot C_{vs}} = \frac{\dfrac{\rho_m}{\rho_l} \cdot i_{pl,A} - i_l}{R_{sd} \cdot C_{vs}} = \frac{\left(\dfrac{\rho_m}{\rho_l} \cdot \dfrac{\lambda_{pl}}{\lambda_l} - 1\right) \cdot i_l}{R_{sd} \cdot C_{vs}}
\tag{8.3-23}
$$

8.3.3   The Different Flow Regimes.

For the different flow regimes, the pressure losses should be determined with the adjusted kinematic viscosity, relative submerged density and terminal settling velocity with the equations that are also used without fines. Based on the pressure losses found, first the hydraulic gradient and the relative solids effect are determined based on the pseudo liquid properties.

This gives for the hydraulic gradient based on the pseudo liquid properties:

$$
i_{m,pl,A} = \frac{\Delta p_{m,pl,A}}{\rho_{pl} \cdot g \cdot \Delta L} = \frac{\Delta p_{m,pl,B}}{\rho_{pl} \cdot g \cdot \Delta L} \quad \text{with:} \quad \Delta p_{m,pl,A} = \Delta p_{m,pl,B}
\tag{8.3-24}
$$

The relative excess hydraulic gradient is, based on the pseudo liquid properties:

$$
E_{rhg,pl,A} = \frac{i_{m,pl,A} - i_{pl,A}}{R_{sd,pl} \cdot C_{vs,r}}
\tag{8.3-25}
$$

The above two equations assume the pseudo liquid is the carrier liquid. In processing experimental data, it is assumed that the real carrier liquid is the carrier liquid (often water). The fraction of fines is often unknown. So to compare model results with experimental results, the hydraulic gradient of the mixture and the relative solids effect have to be related to the real carrier liquid properties and to the hydraulic gradient of the real carrier liquid.

This gives for the hydraulic gradient based on the carrier liquid properties (division by the real carrier liquid density):

$$
i_{m,pl,B} = \frac{\Delta p_{m,pl,B}}{\rho_l \cdot g \cdot \Delta L} = \frac{\rho_{pl}}{\rho_l} \cdot i_{m,pl,A}
\tag{8.3-26}
$$

The relative excess hydraulic gradient or relative solids effect is, based on the carrier liquid properties (deducting the hydraulic gradient of the real carrier liquid in the nominator):

$$
E_{rhg,pl,B} = \frac{i_{m,pl,B} - i_l}{R_{sd} \cdot C_{vs}}
\tag{8.3-27}
$$

8.4 The Fixed or Stationary Bed Regime.

The fixed bed or stationary bed model is only required for determining the constant spatial volumetric concentration curves. For the constant delivered volumetric concentration curves, the sliding bed model forms the basis. The cross section of the pipe with a particle bed as defined in the Wilson et al. (1992) two layer model has been illustrated by Figure 8.4-1.
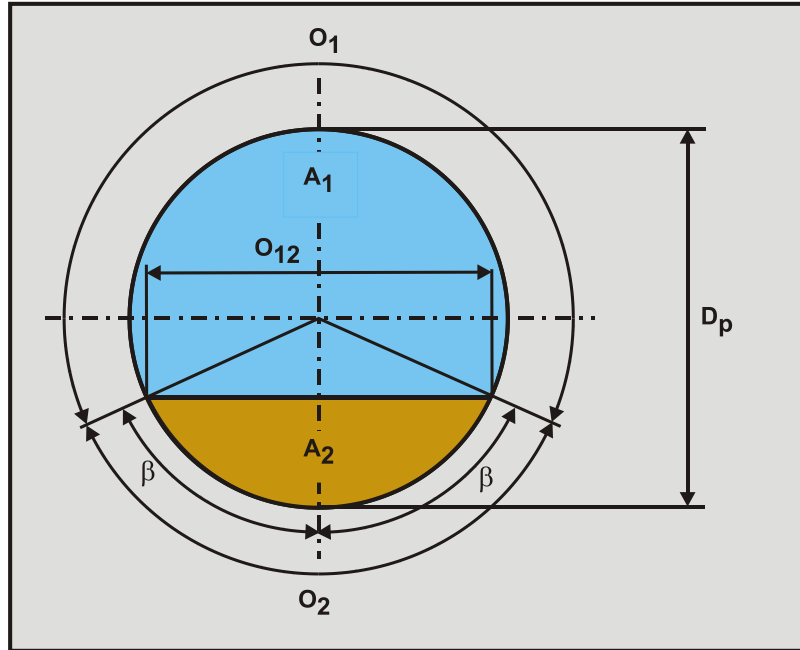
Figure 8.4-1: The definitions for fully stratified and heterogeneous flow.

The geometry is defined by the following equations. The length of the liquid in contact with the whole pipe wall, in a cross-section, if there is no bed is:

$$O_p = \pi \cdot D_p$$

(7.3-1)
(8.4-1)

The length of the liquid or the suspension in contact, in a cross-section, with the pipe wall:

$$O_1 = D_p \cdot (\pi - \beta)$$

(7.3-2)
(8.4-2)

The length of the fixed or sliding bed in contact with the wall, in a cross-section:

$$O_2 = D_p \cdot \beta$$

(7.3-3)
(8.4-3)

The top surface length of the fixed or sliding bed, in a cross-section:

$$O_{12} = D_p \cdot \sin(\beta)$$

(7.3-4)
(8.4-4)

The cross sectional area A_p of the pipe is:

$$A_p = \frac{\pi}{4} \cdot D_p^2$$

(7.3-5)
(8.4-5)

The cross sectional area A_2 of the fixed or sliding bed is:

$$A_2 = A_p \cdot \frac{C_{vs}}{C_{vb}} = \frac{\pi}{4} \cdot D_p^2 \cdot \frac{(\beta - \sin(\beta) \cdot \cos(\beta))}{\pi}$$

(7.3-6)
(8.4-6)

The cross sectional area A_1 above the bed, where the liquid or the suspension is flowing, also named the restricted area, is:

$$A_1 = A_p - A_2$$

(7.3-7)
(8.4-7)

The hydraulic diameter $D_{H,1}$ as function of the bed height, is equal to four times the cross sectional area divided by the wetted perimeter:

$$D_{H,1} = \frac{4 \cdot A_1}{O_1 + O_{12}} \quad \text{or simplified:} \quad D_{H,1} = \sqrt{\frac{4 \cdot A_1}{\pi}}$$

(7.3-8)
(8.4-8)

The volume balance gives a relation between the line speed v_{ls}, the velocity in the restricted area above the bed v_1 and the velocity of the bed v_2.

$$v_{ls} \cdot A_p = v_1 \cdot A_1 + v_2 \cdot A_2$$

(7.3-9)
(8.4-9)

Thus the velocity in the restricted area above the bed is:

$$v_1 = \frac{v_{ls} \cdot A_p - v_2 \cdot A_2}{A_1}$$

(7.3-10)
(8.4-10)

And the velocity of the bed is (in the case of a fixed bed this is zero):

$$v_2 = \frac{v_{ls} \cdot A_p - v_1 \cdot A_1}{A_2}$$

(7.3-11)
(8.4-11)

8.4.1 The Shear Stresses Involved.

In order to determine the forces involved, first the shear stresses involved have to be determined. Over the whole range of Reynolds numbers above 2320 the Swamee Jain equation gives a good approximation for the Darcy-Weisbach friction coefficient. For the flow in the restricted area above the bed, the shear stress between the liquid and the pipe wall is:

$$\tau_{1,l} = \frac{\lambda_1}{4} \cdot \frac{1}{2} \cdot \rho_l \cdot v_1^2 \quad \text{with:} \quad \lambda_1 = \frac{1.325}{\left(\ln\left(\frac{0.27 \cdot \varepsilon}{D_{H,1}} + \frac{5.75}{Re^{0.9}} \right) \right)^2} \quad \text{and} \quad Re = \frac{v_1 \cdot D_{H,1}}{v_l}$$

(7.3-17)
(8.4-12)

For the flow in the restricted area, the shear stress between the liquid and the bed for small values of v_1, when sheet flow is not occurring, is:

$$\tau_{12,l} = \frac{\lambda_{12}}{4} \cdot \frac{1}{2} \cdot \rho_l \cdot v_1^2 \quad \text{with:} \quad \lambda_{12} = \frac{\alpha \cdot 1.325}{\left(\ln\left(\frac{0.27 \cdot d}{D_{H,1}} + \frac{5.75}{Re^{0.9}} \right) \right)^2} \quad \text{and} \quad Re = \frac{v_1 \cdot D_{H,1}}{v_l}$$

(7.3-18)(8.4-13)

For larger values of values of v_1, when sheet flow does occur, the following equation has to be applied:

$$\tau_{12,l} = \frac{\lambda_{12}}{4} \cdot \frac{1}{2} \cdot \rho_l \cdot v_1^2 \quad \text{with:}$$

$$\lambda_{12} = 0.83 \cdot \lambda_1 + 0.37 \cdot \left(\frac{v_1}{\sqrt{2 \cdot g \cdot D_{H,1} \cdot R_{sd}}} \right)^{2.73} \cdot \left(\frac{\rho_s \cdot \frac{\pi}{6} \cdot d^3}{\rho_l \cdot 1^3} \right)^{0.094}$$

(7.3-57)(8.4-14)

$$= 0.83 \cdot \lambda_1 + 0.37 \cdot Fr_{DC}^{2.73} \cdot \left(\frac{m_p}{\rho_l} \right)^{0.094}$$

Miedema & Matousek (2014) derived the above equation, except for the particle mass term, which is added by Miedema & Ramsdell (2014). This last term increases the correlation coefficient of the curve fit of experimental data from 0.86 (without this term) to 0.91 (including this term). Reason for adding this last term is, that in sheet flow energy losses are not only determined by the submerged weight of the particles, but also by the mass of the particles. The use of equations (7.3-18)(8.4-13) and (7.3-57)(8.4-14) is simple, if equation (7.3-57)(8.4-14)>(7.3-18)(8.4-13), equation (7.3-57)(8.4-14) is used and sheet flow is assumed, otherwise equation (7.3-18)(8.4-13) is used and a flat bed with maybe individual particles moving is assumed.

8.4.2 The Forces Involved.

First the equilibrium of the forces on the liquid above the bed is determined. This is necessary to find the correct hydraulic gradient.

The resisting shear force on the pipe wall O_1 above the bed is:

$$F_{1,l} = \tau_{1,l} \cdot O_1 \cdot \Delta L$$

(7.3-22)
(8.4-15)

The resisting shear force on the bed surface O_{12} is:

$$F_{12,l} = \tau_{12,l} \cdot O_{12} \cdot \Delta L$$

(7.3-23)
(8.4-16)

The pressure Δp on the liquid above the bed is:

$$\Delta p = \Delta p_2 = \Delta p_1 = \frac{\tau_{1,l} \cdot O_1 \cdot \Delta L + \tau_{12,l} \cdot O_{12} \cdot \Delta L}{A_1} = \frac{F_{1,l} + F_{12,l}}{A_1}$$

(7.3-24)(8.4-17)
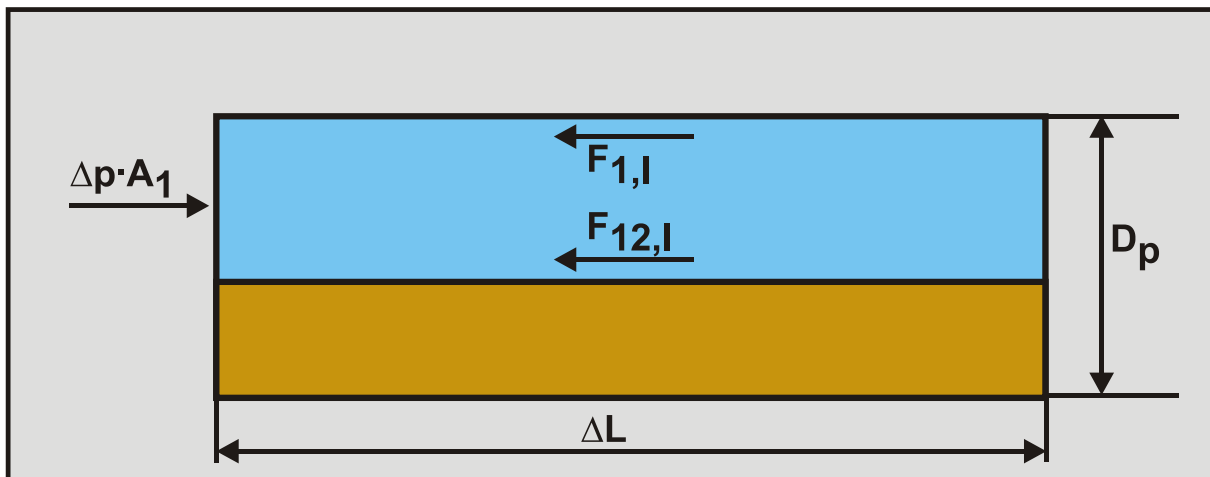
Figure 8.4-2: The forces on the liquid above the bed.

The force equilibrium on the liquid above the bed is shown in Figure 8.4-2. Secondly the equilibrium of forces on the bed is determined as is shown in Figure 8.4-3.
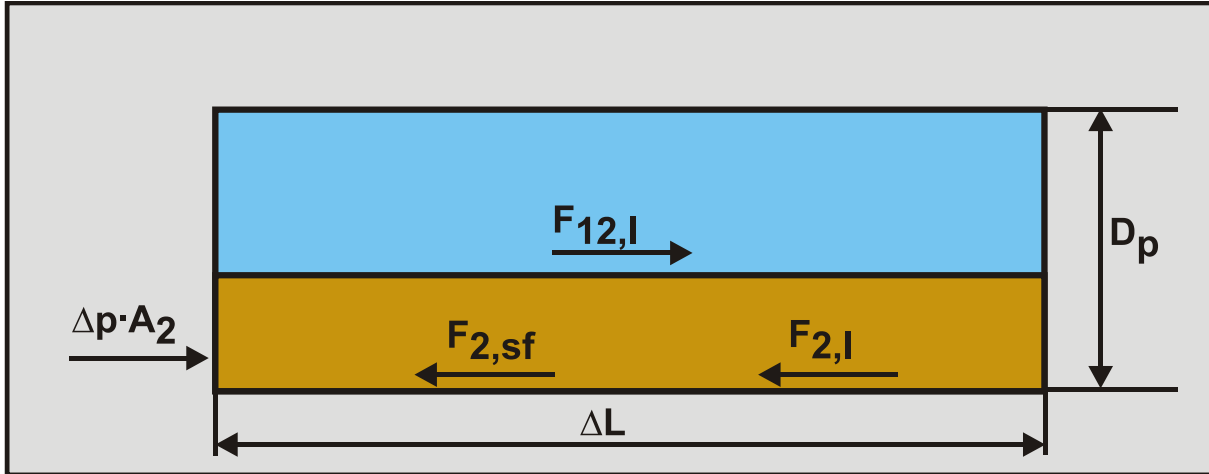
Figure 8.4-3: The forces on the bed.

The driving shear force on the bed surface is:

$$F_{12,l} = \tau_{12,l} \cdot O_{12} \cdot \Delta L$$

(7.3-25)
(8.4-18)

The driving force resulting from the pressure Δp on the bed is:

$$F_{2,pr} = \Delta p \cdot A_2$$

(7.3-26)
(8.4-19)

The resisting force between the bed and the pipe wall due to sliding friction is:

$$F_{2,sf} = \tau_{2,sf} \cdot O_2 \cdot \Delta L$$

(7.3-27)
(8.4-20)

The resisting shear force between the liquid in the bed and the pipe wall is:

$$F_{2,l} = \tau_{2,l} \cdot O_2 \cdot n \cdot \Delta L$$

(7.3-28)
(8.4-21)

This shear force is multiplied by the porosity **n**, in order to correct for the fact that the bed consists of a combination of particles and water. There is an equilibrium of forces when:

$$F_{12,l} + F_{2,pr} = F_{2,sf} + F_{2,l}$$

(7.3-29)
(8.4-22)

Below the Limit of Stationary Deposit Velocity, the bed is not sliding and the force $F_{2,l}$ equals zero. Equation (7.3-24)(8.4-17) is used to determine the pressure losses with a stationary bed. Since the problem is implicit with respect to the velocities v_1 and v_2, it has to be solved with an iteration process.

The mixture pressure is now:

$$\Delta p_m = \frac{\lambda_1 \cdot O_1 + \lambda_{12} \cdot O_{12}}{4 \cdot (1 - C_{vr}) \cdot A_p} \cdot \frac{1}{2} \cdot \rho_l \cdot v_1^2 \cdot \Delta L \quad \text{with:} \quad C_{vr} = \frac{C_{vs}}{C_{vb}}$$

(7.3-30)
(8.4-23)

8.4.3 Pressure, Hydraulic Gradient & Relative Solids Effect.

The excess pressure and excess hydraulic gradient can be written as:

$$\Delta p_m - \Delta p_l = \left(\left(\lambda_1 \cdot O_1 + \lambda_{12} \cdot O_{12} \right) \cdot \left(\frac{1}{1 - C_{vr}} \right)^3 - \lambda_1 \cdot O_p \right) \cdot \frac{1}{2} \cdot \rho_l \cdot v_{ls}^2 \cdot \frac{\Delta L}{4 \cdot A_p}$$

and

$$i_m - i_l = \left(\left(\lambda_1 \cdot O_1 + \lambda_{12} \cdot O_{12} \right) \cdot \left(\frac{1}{1 - C_{vr}} \right)^3 - \lambda_1 \cdot O_p \right) \cdot \frac{v_{ls}^2}{8 \cdot g \cdot A_p}$$

(7.3-31)
(8.4-24)

In terms of the relative excess hydraulic gradient or relative solids effect this can be written as:

$$E_{rhg} = \frac{i_m - i_l}{R_{sd} \cdot C_{vs}} = \left(\left(\lambda_1 \cdot O_1 + \lambda_{12} \cdot O_{12} \right) \cdot \left(\frac{1}{1 - C_{vr}} \right)^3 - \lambda_1 \cdot O_p \right) \cdot \frac{v_{ls}^2}{8 \cdot g \cdot A_p \cdot R_{sd} \cdot C_{vs}}$$

(7.3-32)
(8.4-25)

For practical purposes, the stationary/fixed bed regime is not very usefull and can be replaced by the sliding bed regime, also for very low line speeds. In all the DHLLDV Framework graphs however it has been taken into account for the constant spatial volumetric concentration curves, showing the LSDV as the intersection of the fixed bed curve and the sliding bed curve.

8.5 The Sliding Bed Regime.

Figure 8.5-1 shows the E_{rhg} parameter as a function of the relative volumetric concentration ($C_{vr}=C_{vs}/C_b$) and the relative line speed ($v_{ls}/v_{ls,ldv,max}$) for the weight approach sliding bed friction (Miedema & Ramsdell (2014)) and a sliding bed friction factor $\mu_{sf}=0.4$. The E_{rhg} parameter is very close to the sliding friction coefficient μ_{sf}, especially for relative line speeds up to 1.5, the region where most probably the sliding bed will occur. So for the sliding bed regime the E_{rhg} parameter is defined to be equal to the sliding friction coefficient μ_{sf}. Apparently the force equilibrium on the bed is not required to determine the hydraulic gradient. For determining the bed velocity and the slip, it still is.

$$E_{rhg} = \frac{i_m - i_l}{R_{sd} \cdot C_{vs}} = \mu_{sf}$$

(7.4-72)
(8.5-1)

The hydraulic gradient is now:

$$i_m = i_l + R_{sd} \cdot C_{vs} \cdot \mu_{sf}$$

(8.5-2)

This gives for the pressure difference:

$$\Delta p_m = \Delta p_l + \rho_l \cdot g \cdot \Delta L \cdot R_{sd} \cdot C_{vs} \cdot \mu_{sf}$$

(8.5-3)

The sliding friction coefficient μ_{sf} is the tangent of the external friction angle δ between the sand or gravel and the steel pipe wall. From soil mechanics it is known that the external friction angle δ is about 2/3 of the internal friction angle φ. This internal friction angle has a minimum of about 30° for loose packed sand, giving 20° for the external friction angle. The tangent of 20° is 0.364. Miedema & Ramsdell (2014) also analyzed the hydrostatic approach of Wilson et al. (1992) and the normal stress carrying the weight approach. These two approaches are similar up to a relative concentration of 0.5, giving an increase of the E_{rhg} parameter with a factor 1.3 compared to the weight approach as used here. In practice the relative concentration will be between 0 and 0.5 giving a multiplication factor between 1 and 1.3 depending on the relative concentration. Taking an average gives a sliding friction factor of about 0.415. Resuming it can be stated that the E_{rhg} parameter should have a value of about 0.364 if the weight approach is applied, or a value of about 0.415 if the hydrostatic or normal stress carrying the weight approach are applied. In the current model a constant value of 0.415 is used to be on the safe side, resulting in hydraulic gradient curves parallel to the liquid curve as already observed by Newitt et al. (1955) and others.
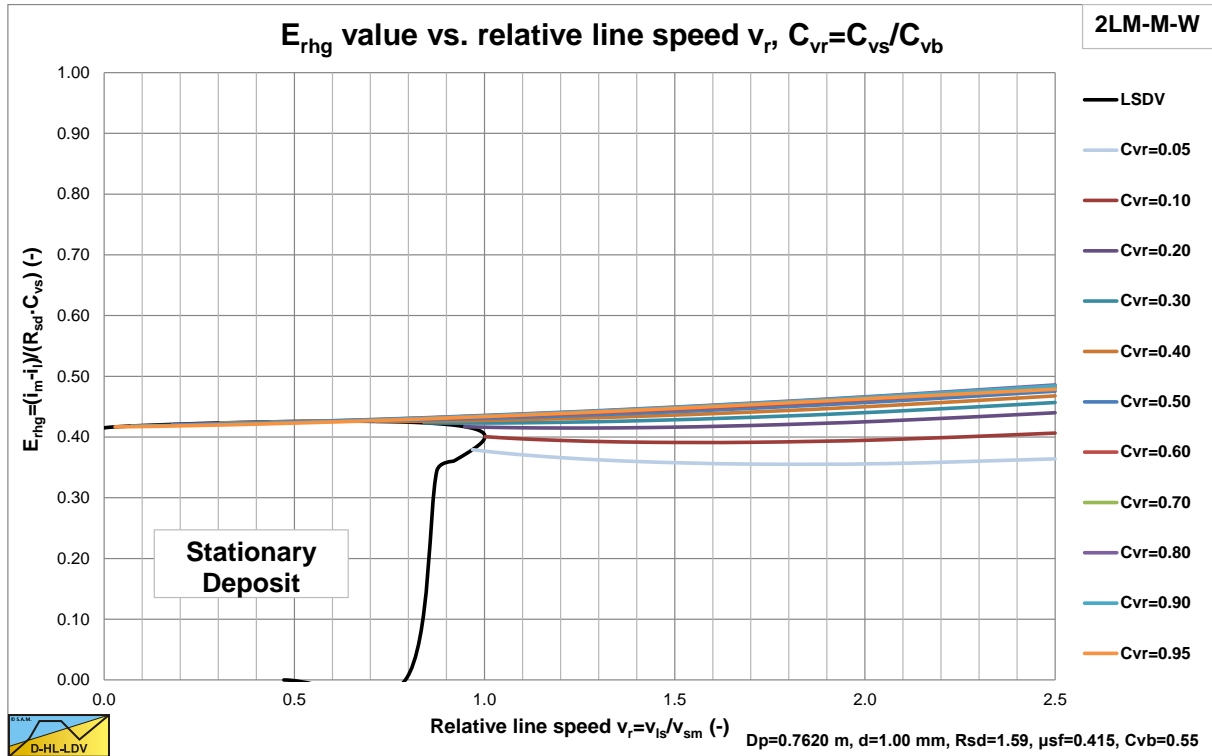
Figure 8.5-1: The E_{rhg} parameter versus the relative line speed.

8.6 The Heterogeneous Transport Regime.

Miedema & Ramsdell (2013) derived an equation for the **Relative Excess Hydraulic Gradient** for heterogeneous transport based on energy considerations. This equation consists of two parts. A first part for the contribution due to potential energy losses and a second part for the kinetic energy losses. The equation is based on uniform sands or gravels, but Miedema (2014) also derived a modified equation for graded sands and gravels. In its basic form the equation looks like:

$$E_{rhg} = \frac{i_m - i_l}{R_{sd} \cdot C_{vs}} = \frac{v_t \cdot \left(1 - \dfrac{C_{vs}}{\kappa_C}\right)^{\beta}}{v_{ls}} + \left(\frac{v_{sl}}{v_t}\right)^2 = S_{hr} + S_{rs} \qquad \begin{array}{l}(7.5\text{-}42)\\(8.6\text{-}1)\end{array}$$

The **Settling** Velocity **Hindered Relative**, S_{hr}, is the **Hindered Settling Velocity** of a particle $v_t \cdot (1-C_{vs}/\kappa_C)^{\beta}$ divided by the line speed v_{ls}. The S_{hr} value gives the contribution of the potential energy losses to the **Relative Excess Hydraulic Gradient**. The S_{hr} is derived for and can be applied to the heterogeneous regime. The **Slip Relative Squared** S_{rs} is the **Slip Velocity** of a particle v_{sl} divided by the **Terminal Settling Velocity** of a particle v_t squared and this S_{rs} value is a good indication of the **Relative Excess Hydraulic Gradient** due to the solids, since its contribution to the total is 90%-100%. The S_{rs} value gives the contribution of the kinetic energy losses to the **Relative Excess Hydraulic Gradient**. The S_{rs} is derived for and can be applied to the heterogeneous regime.

The potential energy term is explicit and all the variables involved are known, so this term can be solved. The kinetic energy term however contains the slip velocity, which is not known. The kinetic energy term has been derived by Miedema & Ramsdell (2013) based on kinetic energy losses due to collisions or interactions with the pipe wall or the viscous sub layer. This means that the slip velocity used in the above equation is not necessarily the average slip velocity, but it is the slip velocity necessary to explain the kinetic energy losses. The average slip velocity of the particles will probably be larger, but of the same magnitude. The derivation of the slip velocity equation for uniform sands or gravels will be subject of another paper, but the resulting equation for the E_{rhg} parameter is given here. Giving for the relative excess hydraulic gradient, the E_{rhg} parameter:

$$Fr_p = \frac{v_t}{\sqrt{g \cdot d}}$$

$$E_{rhg} = \frac{i_m - i_l}{R_{sd} \cdot C_{vs}} = S_{hr} + S_{rs} = \frac{v_t \cdot \left(1 - \dfrac{C_{vs}}{\kappa_C}\right)^{\beta}}{v_{ls}} + 8.5^2 \cdot \left(\frac{1}{\lambda_l}\right) \cdot \left(\frac{v_t}{\sqrt{g \cdot d}}\right)^{10/3} \cdot \left(\frac{(\nu_l \cdot g)^{1/3}}{v_{ls}}\right)^2 \qquad \begin{matrix}(7.5\text{-}63)\\(8.6\text{-}2)\end{matrix}$$

$$\kappa_C = 0.175 \cdot (1 + \beta)$$

The equation has been modified slightly since the original article of Miedema & Ramsdell (2013). The derivation is published in Miedema (2015). The hydraulic gradient for the mixture is now:

$$i_m = i_l + \left(\frac{v_t \cdot \left(1 - \dfrac{C_{vs}}{\kappa_C}\right)^{\beta}}{v_{ls}} + 8.5^2 \cdot \left(\frac{1}{\lambda_l}\right) \cdot \left(\frac{v_t}{\sqrt{g \cdot d}}\right)^{10/3} \cdot \left(\frac{(\nu_l \cdot g)^{1/3}}{v_{ls}}\right)^2\right) \cdot R_{sd} \cdot C_{vs} \qquad (8.6\text{-}3)$$

This gives for the pressure difference of the mixture:

$$\Delta p_m = \Delta p_l + \rho_l \cdot g \cdot \Delta L \cdot \left(\frac{v_t \cdot \left(1 - \dfrac{C_{vs}}{\kappa_C}\right)^{\beta}}{v_{ls}} + 8.5^2 \cdot \left(\frac{1}{\lambda_l}\right) \cdot \left(\frac{v_t}{\sqrt{g \cdot d}}\right)^{10/3} \cdot \left(\frac{(\nu_l \cdot g)^{1/3}}{v_{ls}}\right)^2\right) \cdot R_{sd} \cdot C_{vs} \qquad (8.6\text{-}4)$$

8.7 The Homogeneous Transport Regime.

The basis of the homogeneous transport regime model is the equivalent liquid model (ELM). In terms of the relative excess hydraulic gradient, E_{rhg}, this can be written as:

$$E_{rhg} = \frac{i_m - i_l}{R_{sd} \cdot C_{vs}} = \frac{\lambda_l \cdot v_{ls}^2}{2 \cdot g \cdot D_p} = i_l \qquad \begin{matrix}(7.6\text{-}3)\\(8.7\text{-}1)\end{matrix}$$

Talmon (2013) derived an equation to correct the homogeneous equation (the ELM model) for the slurry density, based on the hypothesis that the viscous sub-layer hardly contains solids at very high line speeds in the homogeneous regime. This theory results in a reduction of the resistance compared with the ELM, but the resistance is still higher than the resistance of clear water. Talmon (2013) used the Prandl approach for the mixing length, which is a 2D approach for open channel flow with a free surface. The Prandl approach was extended with damping near the wall to take into account the viscous effects near the wall, according to von Driest (Schlichting, 1968). Miedema (2015) extended the model with pipe flow and a concentration distribution, resulting in the following equations.

The value of the Darcy Weisbach wall friction factor λ_l depends on the Reynolds number:

$$Re = \frac{v_{ls} \cdot D_p}{\nu_l} \qquad \begin{matrix}(3.2\text{-}1)\\(8.7\text{-}2)\end{matrix}$$

Over the whole range of Reynolds numbers above 2320 the Swamee Jain (1976) equation gives a good approximation:

$$\lambda_l = \frac{1.325}{\left(\ln\left(\dfrac{\varepsilon}{3.7 \cdot D_p} + \dfrac{5.75}{Re^{0.9}}\right)\right)^2} = \frac{0.25}{\left(\log_{10}\left(\dfrac{\varepsilon}{3.7 \cdot D_p} + \dfrac{5.75}{Re^{0.9}}\right)\right)^2}$$

(3.2-8)
(8.7-3)

For the resulting Darcy-Weisbach friction factor ratio this can be approximated by:

$$\frac{\lambda_m}{\lambda_l} = \frac{1}{\left(\dfrac{A_{C_v}}{\kappa} \cdot \ln\left(\dfrac{\rho_m}{\rho_l}\right) \cdot \sqrt{\dfrac{\lambda_l}{8}} + 1\right)^2}$$

(7.6-36)
(8.7-4)

The hydraulic gradient i_l (for a liquid including the fine solids effect in general) is:

$$i_l = \frac{\Delta p_l}{\rho_l \cdot g \cdot \Delta L} = \frac{\lambda_l \cdot v_{ls}^2}{2 \cdot g \cdot D_p}$$

(3.1-8)
(8.7-5)

The relative excess hydraulic gradient E_{rhg} is now:

$$E_{rhg} = \frac{i_m - i_l}{R_{sd} \cdot C_{vs}} = i_l \cdot \frac{1 + R_{sd} \cdot C_v - \left(\dfrac{A_{C_v}}{\kappa} \cdot \ln\left(\dfrac{\rho_m}{\rho_l}\right) \cdot \sqrt{\dfrac{\lambda_l}{8}} + 1\right)^2}{R_{sd} \cdot C_v \cdot \left(\dfrac{A_{C_v}}{\kappa} \cdot \ln\left(\dfrac{\rho_m}{\rho_l}\right) \cdot \sqrt{\dfrac{\lambda_l}{8}} + 1\right)^2} = \alpha_E \cdot i_l$$

(7.6-37)
(8.7-6)

The relative excess hydraulic gradient E_{rhg} is mobilized at larger line speeds depending on the ratio between the thickness of the viscous sub-layer and the particle diameter:

$$\frac{\delta_v}{d} = \frac{11.6 \cdot \nu_l}{u_* \cdot d} = \frac{11.6 \cdot \nu_l}{\sqrt{\dfrac{\lambda_l}{8}} \cdot v_{ls} \cdot d}$$

(8.7-7)

Where this ratio can never be larger than 1! This gives for the relative excess hydraulic gradient E_{rhg}:

$$E_{rhg} = \frac{i_m - i_l}{R_{sd} \cdot C_{vs}} = i_l \cdot \left(1 - \left(1 - \frac{1 + R_{sd} \cdot C_{vs} - \left(\dfrac{A_{C_v}}{\kappa} \cdot \ln\left(\dfrac{\rho_m}{\rho_l}\right) \cdot \sqrt{\dfrac{\lambda_l}{8}} + 1\right)^2}{R_{sd} \cdot C_{vs} \cdot \left(\dfrac{A_{C_v}}{\kappa} \cdot \ln\left(\dfrac{\rho_m}{\rho_l}\right) \cdot \sqrt{\dfrac{\lambda_l}{8}} + 1\right)^2}\right)\left(1 - \left(\dfrac{\delta_v}{d}\right)\right)\right)$$

(7.6-40)
(8.7-8)

A value of $A_{Cv}=3$ is advised. The hydraulic gradient of the mixture is now:

$$i_m = i_l + i_l \cdot \left(1 - \left(1 - \frac{1 + R_{sd} \cdot C_{vs} - \left(\dfrac{A_{C_v}}{\kappa} \cdot \ln\left(\dfrac{\rho_m}{\rho_l}\right) \cdot \sqrt{\dfrac{\lambda_l}{8}} + 1\right)^2}{R_{sd} \cdot C_{vs} \cdot \left(\dfrac{A_{C_v}}{\kappa} \cdot \ln\left(\dfrac{\rho_m}{\rho_l}\right) \cdot \sqrt{\dfrac{\lambda_l}{8}} + 1\right)^2}\right)\left(1 - \left(\dfrac{\delta_v}{d}\right)\right)\right) \cdot R_{sd} \cdot C_{vs}$$

(8.7-9)

The pressure difference of the mixture gives:

$$\Delta p_m = \Delta p_l + \Delta p_l \cdot \left(1 - \left(1 - \frac{1 + R_{sd} \cdot C_{vs} - \left(\frac{A_{C_v}}{\kappa} \cdot \ln\left(\frac{\rho_m}{\rho_l}\right) \cdot \sqrt{\frac{\lambda_l}{8}} + 1 \right)^2}{R_{sd} \cdot C_{vs} \cdot \left(\frac{A_{C_v}}{\kappa} \cdot \ln\left(\frac{\rho_m}{\rho_l}\right) \cdot \sqrt{\frac{\lambda_l}{8}} + 1 \right)^2} \right) \left(1 - \left(\frac{\delta_v}{d}\right) \right) \right) \cdot R_{sd} \cdot C_{vs} \qquad (8.7\text{-}10)$$

8.8 The Transition Heterogeneous Regime - Homogeneous Regime.

8.8.1 Introduction.

Some general equations that are required:

The Reynolds number in general is:

$$Re = \frac{v_{ls} \cdot D_p}{\nu_l} \qquad \begin{array}{c}(2.2\text{-}1)\\(8.8\text{-}1)\end{array}$$

The Darcy Weisbach friction factor can now be determined with:

$$\lambda_l = \frac{1.325}{\left(\ln\left(\frac{\varepsilon}{3.7 \cdot D_p} + \frac{5.75}{Re^{0.9}} \right) \right)^2} = \frac{0.25}{\left(\log_{10}\left(\frac{\varepsilon}{3.7 \cdot D_p} + \frac{5.75}{Re^{0.9}} \right) \right)^2} \qquad \begin{array}{c}(3.2\text{-}8)\\(8.8\text{-}2)\end{array}$$

The friction velocity is:

$$u_* = \sqrt{\frac{\lambda_l}{8}} \cdot v_{ls} \qquad \begin{array}{c}(2.1\text{-}1)\\(8.8\text{-}3)\end{array}$$

8.8.2 The Lift Ratio.

The near wall lift pushes particles away from the pipe wall. The ratio of the lift force to the sum of submerged weight and momentum of a particle is named the Lift Ratio.

$$L_R = \frac{C_L \cdot u_*^2}{d \cdot \left(R_{sd} \cdot g + \frac{1}{2} \cdot \frac{\rho_s}{\rho_l} \cdot \frac{v_{th}^2 \cdot u_*}{\alpha \cdot 11.6 \cdot \nu_l} \right)} \cdot \left(1 - \frac{C_{vs}}{C_{vb}} \right) \qquad \begin{array}{c}(7.11\text{-}7)\\(8.8\text{-}4)\end{array}$$

8.8.3 The Heterogeneous Equation.

The heterogeneous losses reduce (collapse) if the near wall lift pushes harder than the sum of the submerged weight and the momentum of a particle, resulting in:

For $L_R < 0.7$ the heterogeneous equation becomes:

$$E_{rhg,He} = \frac{v_t \cdot \left(1 - \frac{C_{vs}}{0.175 \cdot (1+\beta)} \right)^\beta}{v_{ls}} + 8.5^2 \cdot \left(\frac{1}{\lambda_l} \right) \cdot \left(\frac{v_t}{\sqrt{g \cdot d}} \right)^{10/3} \cdot \left(\frac{(\nu_l \cdot g)^{1/3}}{v_{ls}} \right)^2 \cdot \left(1 - L_R^2 \right) \qquad \begin{array}{c}(7.11\text{-}9)\\(8.8\text{-}5)\end{array}$$

When the lift ratio has a value close to 1, theoretically there are no more collisions with the wall. However not all particles will have exactly the same kinetic energy, so even when the lift ratio is larger than 1, still some particles will have collisions. Therefore a smoothing function is proposed for lift ratio's larger than 70% (ζ=0.5), giving:

$$
E_{rhg,He} = \frac{v_t \cdot \left(1 - \frac{C_{vs}}{0.175 \cdot (1+\beta)}\right)^{\beta}}{v_{ls}} + 8.5^2 \cdot \left(\frac{1}{\lambda_l}\right) \cdot \left(\frac{v_t}{\sqrt{g \cdot d}}\right)^{10/3} \cdot \left(\frac{(v_l \cdot g)^{1/3}}{v_{ls}}\right)^2 \cdot (1-\zeta) \cdot \frac{\zeta}{L_R^2}
\qquad \begin{matrix}(7.11\text{-}10)\\(8.8\text{-}6)\end{matrix}
$$

8.8.4   The Homogeneous Equation.

The mobilization factor of the homogeneous equation is:

$$
m = e^{-0.1 \cdot \frac{\alpha_{sm}}{C_{vr}} \cdot \frac{u_{*,ldv}}{u_*} \cdot \frac{v_{th}}{v_{th,ldv}}}
\qquad \begin{matrix}(7.11\text{-}15)\\(8.8\text{-}7)\end{matrix}
$$

Basically this shows the concentration gradient at the center of the pipe. The mobilized homogeneous flow E_{rhg} is now:

$$
E_{rhg,Ho} = m \cdot i_l \cdot \left(1 - \left(1 - \frac{1 + R_{sd} \cdot C_{vs} - \left(\frac{A_{C_v}}{\kappa} \cdot \ln\left(\frac{\rho_m}{\rho_l}\right) \cdot \sqrt{\frac{\lambda_l}{8}} + 1\right)^2}{R_{sd} \cdot C_{vs} \cdot \left(\frac{A_{C_v}}{\kappa} \cdot \ln\left(\frac{\rho_m}{\rho_l}\right) \cdot \sqrt{\frac{\lambda_l}{8}} + 1\right)^2} \right) \left(1 - \left(\frac{\delta_v}{d}\right)\right) \right)
\qquad \begin{matrix}(7.11\text{-}16)\\(8.8\text{-}8)\end{matrix}
$$

8.8.5   The Resulting Relative Excess Hydraulic Gradient.

The resulting relative excess hydraulic gradient near the transition area can now be determined by:

$$
E_{rhg,HeHo} = E_{rhg,He} + E_{rhg,Ho}
\qquad (8.8\text{-}9)
$$

The hydraulic gradient resulting from this relative excess hydraulic gradient is now:

$$
i_{m,HeHo} = i_l + E_{rhg,HeHo} \cdot R_{sd} \cdot C_{vs}
\qquad (8.8\text{-}10)
$$

This hydraulic gradient is now valid for the combination of the heterogeneous flow regime and the homogeneous flow regime, but still has to be combined with the stationary bed regime and the sliding bed regime. In the case of **d/D$_p$>0.015** the sliding flow regime will occur and the above equation is not used.

The pressure difference in the transition zone can now be determined with:

$$
\Delta p_{m,HeHo} = \Delta p_l + \rho_l \cdot g \cdot \Delta L \cdot E_{rhg,HeHo} \cdot R_{sd} \cdot C_{vs}
\qquad (8.8\text{-}11)
$$

8.9   The Sliding Flow Regime.

For large particles the turbulence is not capable of lifting the particles enough resulting in a sort of sliding bed behavior above this transition line speed. One reason for this is that the largest eddies are not large enough with respect to the size of the particles. Sellgren & Wilson (2007) use the criterion **d/D$_p$>0.015** for this to occur. Zandi & Govatos (1967) use a factor **N<40** as a criterion, with:

$$
N = \frac{v_{ls}^2 \cdot \sqrt{C_D}}{g \cdot R_{sd} \cdot D_p \cdot C_{vt}}
\qquad \begin{matrix}(7.7\text{-}1)\\(8.9\text{-}1)\end{matrix}
$$

At the Limit Deposit Velocity $v_{ls,ldv}$ this equation can be simplified by using:

$$F_L = \frac{v_{ls,ldv}}{\sqrt{2 \cdot g \cdot D_p \cdot R_{sd}}} \approx 1.34 \quad \text{and} \quad \sqrt{C_D} \approx 0.6 \text{ for coarse sand}$$

<div align="right">(7.7-2)
(8.9-2)</div>

Giving:

$$N = \frac{v_{ls,ldv}^2 \cdot \sqrt{C_D}}{g \cdot R_{sd} \cdot D_p \cdot C_{vt}} = \frac{v_{ls,ldv}^2}{2 \cdot g \cdot R_{sd} \cdot D_p} \cdot \frac{2 \cdot \sqrt{C_D}}{C_{vt}} = 1.34^2 \cdot \frac{2 \cdot 0.6}{C_{vt}} = \frac{2.37}{C_{vt}}$$

<div align="right">(7.7-3)
(8.9-3)</div>

This gives **$N=2.37/C_{vt}<40$** or **$C_{vt}>0.059$** for sliding flow to occur. This criterion apparently is based on the thickness of sheet flow. If the bed is so thin that the whole bed becomes sheet flow, there will not be sliding flow, but more heterogeneous behavior. The values used in both criteria are a first estimate based on literature and may be changed in the future. A pragmatic approach to determine the relative excess hydraulic gradient in the sliding flow regime is to use a weighted average between the heterogeneous regime and the sliding bed regime. First the factor between particle size and pipe diameter is determined:

$$f = \frac{4}{3} - \frac{1}{3} \cdot \frac{d}{r_{d/Dp} \cdot D_p}$$

<div align="right">(7.7-4)
(8.9-4)</div>

With:

$$r_{d/Dp} = \frac{1}{2} \cdot \frac{d}{D_p} = \frac{1}{2} \cdot \frac{3 \cdot \pi}{16} \cdot \frac{C_D}{\psi} \cdot \frac{\mu_{sf} \cdot C_{vb} \cdot C_{vr} \cdot (1 - C_{vr})}{(\sin(\beta) + \alpha_\tau \cdot (\pi - \beta) \cdot C_{vr})}$$

<div align="right">(7.7-21)
(8.9-5)</div>

Secondly the weighted average hydraulic gradient or relative excess hydraulic gradient is determined:

$$\Delta p_{m,SF} = \Delta p_{m,HeHo} \cdot f + \Delta p_{m,SB} \cdot (1-f)$$
$$= \Delta p_l + \rho_l \cdot g \cdot \Delta L \cdot R_{sd} \cdot C_{vs} \cdot \left(E_{rhg,HeHo} \cdot f + \mu_{sf} \cdot (1-f) \right)$$

or

$$i_{m,SF} = i_{m,HeHo} \cdot f + i_{m,SB} \cdot (1-f) = i_l + R_{sd} \cdot C_{vs} \cdot \left(E_{rhg,HeHo} \cdot f + \mu_{sf} \cdot (1-f) \right)$$

<div align="right">(7.7-5)
(8.9-6)</div>

or

$$E_{rhg,SF} = \frac{i_{m,SF} - i_l}{R_{sd} \cdot C_{vs}} = E_{rhg,HeHo} \cdot f + \mu_{sf} \cdot (1-f)$$

The concentration at the bottom of the pipe, a bed concentration, decreases with the line speed according to:

$$C_{vB} = 3.1 \cdot C_{vb} \cdot \left(\frac{v_{ls,lsdv}}{v_{ls}} \right)^{0.4} \cdot \left(\frac{C_{vs}}{C_{vb}} \right)^{0.5} \cdot v_t^{1/6} \cdot e^{D_p} \quad \text{with: } 1.1 \cdot C_{vs} \le C_{vB} \le C_{vb}$$

<div align="right">(7.7-6)
(8.9-7)</div>

In the case of **Sliding Flow**, the bottom concentration decreases with increasing line speed and with decreasing spatial concentration. The bottom concentration can be determined with the following equation, where the bottom concentration can never be larger than the maximum bed concentration **C_{vb}** and never smaller than the spatial concentration **C_{vs}**. The Limit of Stationary Deposit Velocity (LSDV) has to be determined at a concentration of 17.5%, because the equation is calibrated for **$C_{vs}=0.175$**.

8.10 The Resulting E_{rhg} Constant Spatial Volumetric Concentration Curve.

The constant spatial volumetric concentration E_{rhg} curve for a single diameter particle forms the basis of the DHLLDV Framework. A short rehearsal of the steps to be taken to construct this curve.

1. Determine the fines fraction.
2. Adjust the pseudo liquid density, kinematic viscosity and relative submerged density, based on the fines content. Adjust the spatial volumetric concentration based on the fines content (see chapter 8.3).
3. If there are fines the following steps are carried out with the pseudo liquid properties, if there are no fines the following steps are carried out with the carrier liquid properties.
4. Determine the terminal settling velocity and the hindered settling velocity (see chapter 8.3).
5. Determine the stationary/fixed bed curve (**FB**) with the bed shear stress based on a bed roughness equal to the particle diameter and a bed shear stress based on sheet flow. The largest of the two at a certain line speed is the required bed shear stress. This results in a curve with bed shear stress based on a bed roughness equal to the particle diameter for line speeds starting at zero and bed shear stress based on sheet flow above a certain line speed. Usually the transition is at a Shields number around 1. The result is the **FB** curve (see chapter 8.4).
6. Determine the sliding bed (**SB**) curve, a horizontal line with value μ_{sf} in the E_{rhg} graph (see chapter 8.5).
7. Determine the heterogeneous flow regime (**He**) curve including the lift ratio influence (near wall lift effect) (see chapter 8.6 and 8.8).
8. Determine the homogeneous flow regime (**Ho**) curve including the mobilization factor (see chapter 8.7 and 8.8).
9. Add up the heterogeneous curve and the homogeneous curve. The result is the **He-Ho** curve (see chapter 8.8).
10. If a sliding bed exists (intersection **FB-SB** at lower line speed than the intersection **FB-He**):
    a. If the fixed bed curve is smaller than the sliding bed curve, take the fixed bed curve. Otherwise take the sliding bed curve. The result is the **FB-SB** curve.
    b. The intersection line speed of the fixed bed curve and the sliding bed curve is the Limit of Stationary Deposit Velocity (**LSDV**).
    c. Add up the heterogeneous curve and the homogeneous curve. The result is the **He-Ho** curve.
    d. The particle diameter to pipe diameter ratio $d/D_p < r_{d/Dp}/2$, equation (8.9-5): At line speeds above the intersection line speed of the sliding bed regime (**SB**) and the heterogeneous regime (**He**), the **He-Ho** curve is valid otherwise the **FB-SB** curve is valid.
    e. The particle diameter to pipe diameter ratio $d/D_p > r_{d/Dp}/2$, equation (8.9-5): For line speeds above the intersection line speed between sliding bed transport (**SB**) and heterogeneous transport (**He**), a weighted average of the sliding bed curve **SB** and the **He-Ho** curve has to be determined, equation (8.9-6). The result is the sliding flow (**SF**) curve. For ratios above $d/D_p = 2 \cdot r_{d/Dp}$ this results in the **SB** curve (see chapter 8.9).
11. If a sliding bed does not exist (intersection **FB-SB** at higher line speed than intersection **FB-He**):
    a. At line speeds above the intersection line speed of the fixed bed regime (**FB**) and the heterogeneous regime (**He**), the **He-Ho** curve is valid otherwise the **FB** curve is valid.
    b. The Limit of Stationary Deposit Velocity (**LSDV**) does not exist in this case.
    c. Both the sliding bed (**SB**) regime and the sliding flow (**SF**) regime do not exist in this case.

The resulting E_{rhg} curve follows from the flow chart Figure 8.1-1 and the steps described above. The hydraulic gradient and the pressure difference for the mixture can be determined with, once the E_{rhg} curve is determined:

$$i_m = i_l + E_{rhg} \cdot R_{sd} \cdot C_{vs} \quad \text{and} \quad \Delta p_m = \Delta p_l + \rho_l \cdot g \cdot \Delta L \cdot E_{rhg} \cdot R_{sd} \cdot C_{vs} \tag{8.10-1}$$

8.11 Determining the Limit Deposit Velocity.

8.11.1 Introduction.
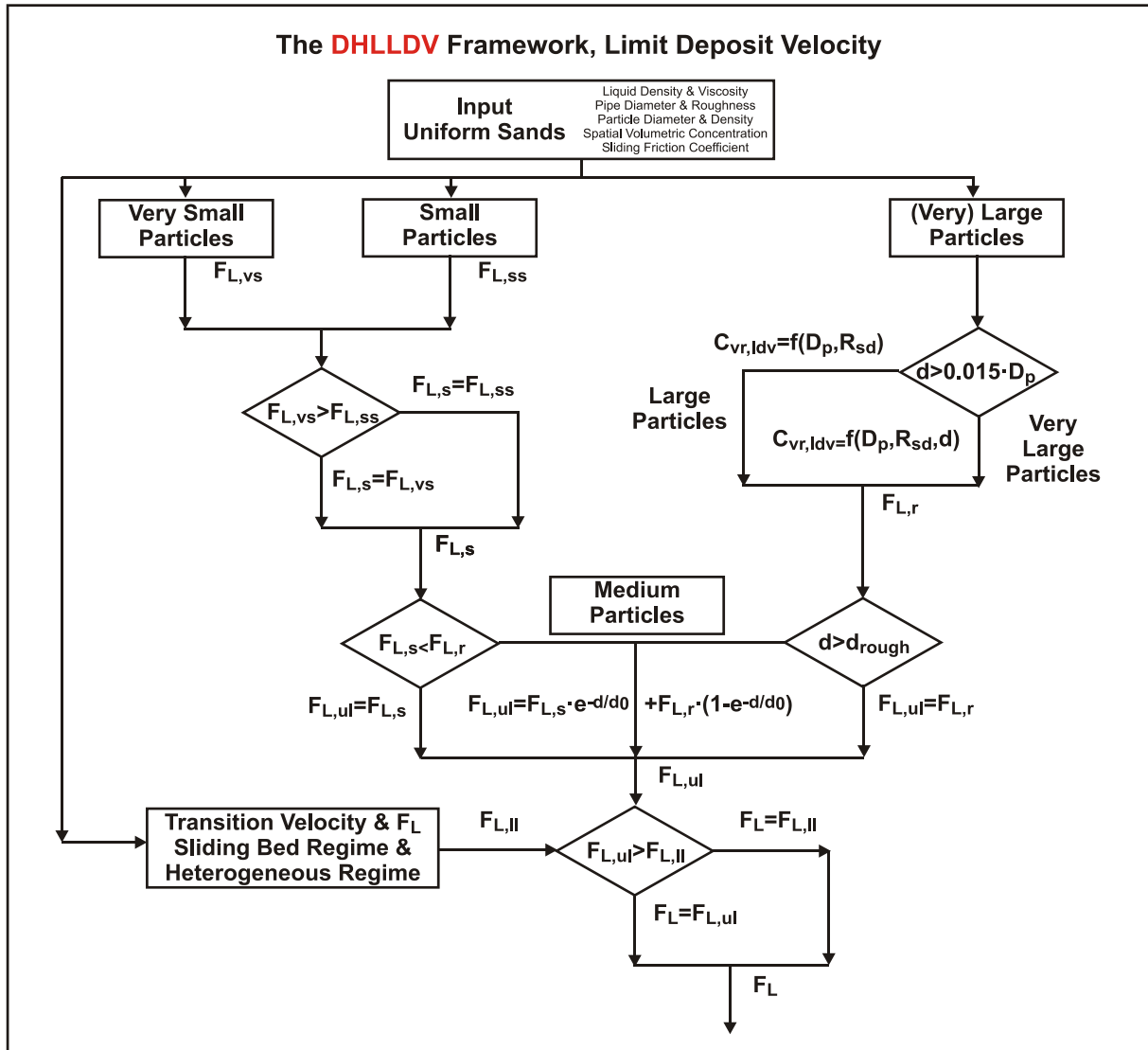
Figure 8.11-1: The algorithm to determine the Limit Deposit Velocity.

Figure 8.11-1 shows the algorithm to determine the Limit Deposit Velocity. The different steps are discussed in the next chapters.

8.11.2 Very Small & Small Particles.

For very small particles, smaller than about 50% of the thickness of the viscous sub layer, the LDV and the Froude number F_L are:

$$v_{ls,ldv} = 1.4 \cdot \left(v_l \cdot R_{sd} \cdot g \right)^{1/3} \cdot \sqrt{\frac{8}{\lambda_l}}$$

$$F_{L,vs} = \frac{v_{ls,ldv}}{\left(2 \cdot g \cdot R_{sd} \cdot D_p \right)^{1/2}} = \frac{1.4 \cdot \left(v_l \cdot R_{sd} \cdot g \right)^{1/3} \cdot \sqrt{\frac{8}{\lambda_l}}}{\left(2 \cdot g \cdot R_{sd} \cdot D_p \right)^{1/2}}$$

(7.8-34)
(8.11-1)

For small particles and a smooth bed, in the case of sand particles smaller than about **d=0.15 mm**, this gives for the Limit Deposit Velocity:

$$
v_{ls,ldv}^3 = \alpha_p^3 \cdot \frac{v_t \cdot \left(1 - \dfrac{C_{vs}}{\kappa_C}\right)^\beta \cdot C_{vs} \cdot \left(2 \cdot g \cdot R_{sd} \cdot D_p\right)}{\lambda_l}
$$

(7.8-37)
(8.11-2)

In terms of the Durand & Condolios LDV Froude number $\mathbf{F_L}$ factor this can be written as:

$$
F_{L,ss} = \frac{v_{ls,ldv}}{\left(2 \cdot g \cdot R_{sd} \cdot D_p\right)^{1/2}} = \alpha_p \cdot \left(\frac{v_t \cdot \left(1 - \dfrac{C_{vs}}{\kappa_C}\right)^\beta \cdot C_{vs}}{\lambda_l \cdot \left(2 \cdot g \cdot R_{sd} \cdot D_p\right)^{1/2}} \right)^{1/3}
$$

(7.8-38)
(8.11-3)

$$
\text{with:} \quad \alpha_p = 3.4 \cdot \left(\frac{1.65}{R_{sd}}\right)^{2/9}, \quad \kappa_C = 0.175 \cdot (1 + \beta)
$$

The coefficient $\mathbf{\alpha_p=3.4}$ is an upper limit. The minimum found is about 3.0, the average 3.2. To be on the safe side, the value of 3.4 should be used. To find the highest correlation with experimental data, the value of 3.2 should be used. With the following conditions the Froude number $\mathbf{F_L}$ for very small and small particles can be determined:

$$
\begin{aligned}
\text{If} \quad & F_{L,vs} > F_{L,ss} \quad \Rightarrow \quad F_{L,s} = F_{L,vs} \\
\text{If} \quad & F_{L,vs} \leq F_{L,ss} \quad \Rightarrow \quad F_{L,s} = F_{L,ss}
\end{aligned}
$$

(8.11-4)

8.11.3 Large & Very Large Particles.

The Limit Deposit Velocity LDV is for medium and large particles and a rough bed:

$$
v_{ls,ldv}^3 = \alpha_p^3 \cdot \frac{\left(1 - \dfrac{C_{vs}}{\kappa_C}\right)^\beta \cdot C_{vs} \cdot \left(\mu_{sf} \cdot C_{vb} \cdot \dfrac{\pi}{8}\right)^{1/2} \cdot C_{vr,ldv}^{1/2}}{\lambda_l} \cdot \left(2 \cdot g \cdot R_{sd} \cdot D_p\right)^{3/2}
$$

(7.8-50)
(8.11-5)

And the Durand & Condolios LDV Froude number:

$$
F_{L,r} = \frac{v_{ls,ldv}}{\left(2 \cdot g \cdot R_{sd} \cdot D_p\right)^{1/2}} = \alpha_p \cdot \left(\frac{\left(1 - \dfrac{C_{vs}}{\kappa_C}\right)^\beta \cdot C_{vs} \cdot \left(\mu_{sf} \cdot C_{vb} \cdot \dfrac{\pi}{8}\right)^{1/2} \cdot C_{vr,ldv}^{1/2}}{\lambda_l} \right)^{1/3}
$$

(7.8-51)
(8.11-6)

The bed fraction at the Limit Deposit Velocity is, depending on the particle diameter to pipe diameter ratio:

$$
d \leq 0.015 \cdot D_p \quad C_{vr,ldv} = 0.0002 \cdot D_p^{-1} \cdot \left(\frac{R_{sd}}{1.65}\right)^{-1} = \frac{0.0065}{2 \cdot g \cdot R_{sd} \cdot D_p}
$$

(7.8-52)
(8.11-7)

$$
d > 0.015 \cdot D_p \quad C_{vr,ldv} = 0.0002 \cdot D_p^{-1} \cdot \left(\frac{R_{sd}}{1.65}\right)^{-1} \cdot \left(\frac{d}{0.015 \cdot D_p}\right)^{1/2} = \frac{0.053}{2 \cdot g \cdot R_{sd} \cdot D_p} \cdot \left(\frac{d}{D_p}\right)^{1/2}
$$

8.11.4 The Resulting Upper Limit Froude Number.

The resulting upper limit of the Froude number $\mathbf{F_{L,ul}}$ value can now be determined according to (for sand):

$$\mathbf{F_{L,s} \leq F_{L,r} \quad \Rightarrow \quad F_{L,ul} = F_{L,s}}$$

$$\mathbf{F_{L,s} > F_{L,r} \quad \Rightarrow \quad F_{L,ul} = F_{L,s} \cdot e^{-d/d_0} + F_{L,r} \cdot \left(1 - e^{-d/d_0}\right)}$$

$$\mathbf{d > d_{rough} \quad \Rightarrow \quad F_{L,ul} = F_{L,r}}$$

$$\text{(7.8-53)}$$
$$\text{(8.11-8)}$$

$$\mathbf{with: \quad d_0 = 0.0005 \cdot \left(\frac{1.65}{R_{sd}}\right)}$$

8.11.5 The Lower Limit.

The lower limit of the LDV is the transition velocity between the sliding bed regime and the heterogeneous regime, resulting in the transition velocity at:

$$\mathbf{v_{ls,ldv}^2 = \frac{v_t \cdot \left(1 - \dfrac{C_{vs}}{\kappa_C}\right)^{\beta} \cdot v_{ls,ldv} + \dfrac{8.5^2}{\lambda_l} \cdot \left(\dfrac{1}{\sqrt{C_x}}\right)^{10/3} \cdot \left(v_l \cdot g\right)^{2/3}}{\mu_{sf}}}$$

$$\text{(7.8-14)}$$
$$\text{(8.11-9)}$$

This equation shows that the transition between the sliding bed regime and the heterogeneous regime depends on the sliding friction coefficient. The equation derived is a second degree function and can be written as:

$$\mathbf{-v_{ls,ldv}^2 + \frac{v_t \cdot \left(1 - \dfrac{C_{vs}}{\kappa_C}\right)^{\beta}}{\mu_{sf}} \cdot v_{ls,ldv} + \frac{\dfrac{8.5^2}{\lambda_l} \cdot \left(\dfrac{1}{\sqrt{C_x}}\right)^{10/3} \cdot \left(v_l \cdot g\right)^{2/3}}{\mu_{sf}} = 0}$$

$$\text{(7.8-15)}$$
$$\text{(8.11-10)}$$

With:

$$\mathbf{A = -1}$$

$$\mathbf{B = \frac{v_t \cdot \left(1 - \dfrac{C_{vs}}{\kappa_C}\right)^{\beta}}{\mu_{sf}}}$$

$$\text{(7.8-16)}$$
$$\text{(8.11-11)}$$

$$\mathbf{C = \frac{\dfrac{8.5^2}{\lambda_l} \cdot \left(\dfrac{1}{\sqrt{C_x}}\right)^{10/3} \cdot \left(v_l \cdot g\right)^{2/3}}{\mu_{sf}}}$$

$$\mathbf{v_{ls,ldv} = \frac{-B - \sqrt{B^2 - 4 \cdot A \cdot C}}{2 \cdot A}}$$

In terms of the Durand & Condolios LDV Froude number F_L factor this can be written as:

$$F_{L,ll} = \frac{v_{ls,ldv}}{\left(2 \cdot g \cdot R_{sd} \cdot D_p\right)^{1/2}}$$

(8.11-12)

8.11.6 The Resulting Froude Number.

The resulting Froude F_L value can now be determined according to:

$$F_{L,ul} \geq F_{L,ll} \quad \Rightarrow \quad F_L = F_{L,ul}$$

(8.11-13)

$$F_{L,ll} > F_{L,ul} \quad \Rightarrow \quad F_L = F_{L,ll}$$

For small particles and/or concentrations near 20% and/or large pipe diameters, usually the upper limit Froude number will be valid. For large particles and/or low concentrations and/or very small to small pipe diameters, usually the lower limit Froude number will be valid.
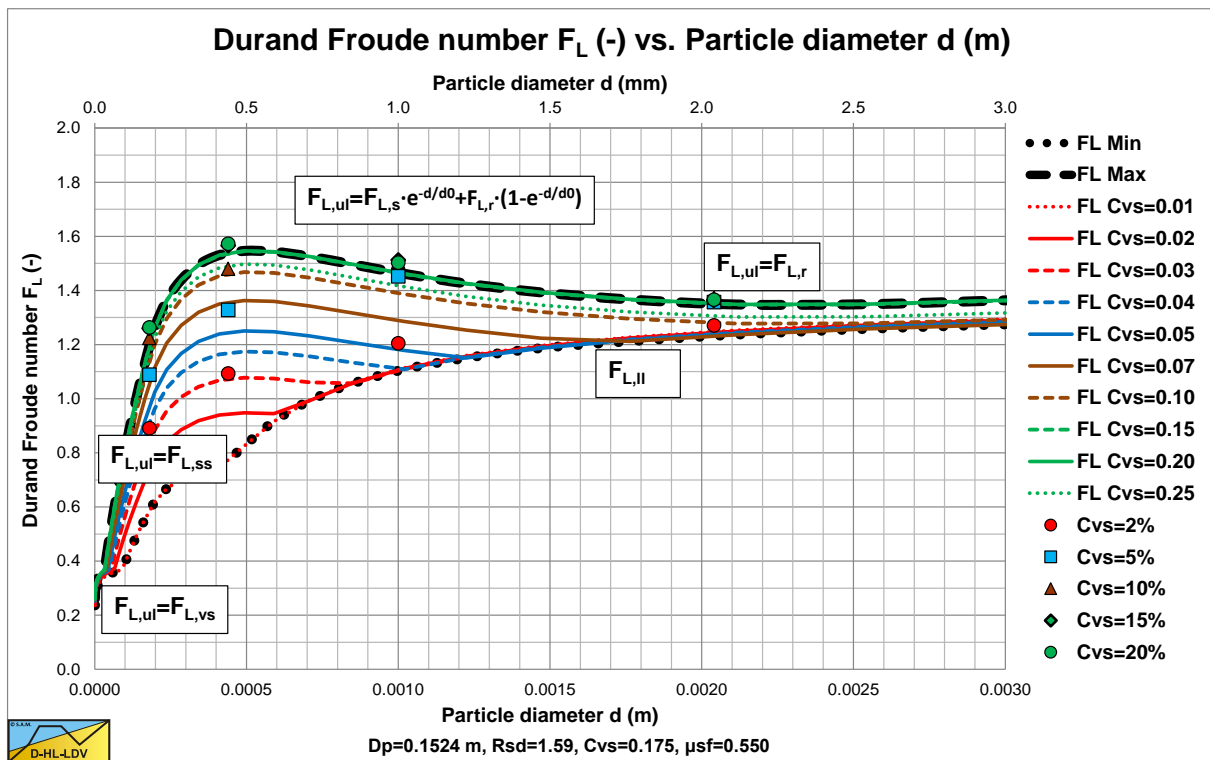
Figure 8.11-2: The resulting $F_L$curves.

Figure 8.11-2 shows the resulting LDV curves for a number of volumetric concentrations, including the Durand & Condolios (1952) data. The graph matches the graph as published by Durand (1953) very well. The use of the lower limit based on the transition sliding bed regime to heterogeneous regime is not exact, since this transition velocity will not be exact. It is possible that this lower limit should be set to 90% or 95% of this transition velocity. Here the theoretical transition velocity is used.

8.11.7 The Transition Fixed Bed – Sliding Bed (LSDV).

The transition fixed bed – sliding bed is not considered to be a real Limit Deposit Velocity, but it is a regime change and thus will be discussed here. This transition is named the Limit of Stationary Deposit Velocity (LSDV) resulting from 2LM or 3LM analysis like the Wilson et al. (1992) model. This transition will only occur above a certain particle diameter to pipe diameter ratio. Very small particles will never have a sliding bed. But medium sized particles that will have a sliding bed in small pipe diameters, may not have a sliding bed in large pipe diameters. Mathematically however, the transition line speed can always be determined, even though the transition will not occur in reality. In such a case the bed is already completely suspended before it could start sliding.

The total hydraulic gradient of a sliding bed $\mathbf{i_{m,sb}}$ is considered to be equal to the hydraulic gradient required to move clear liquid through the pipe $\mathbf{i_l}$ and the sliding friction hydraulic gradient resulting from the friction force between the solids and the pipe $\mathbf{i_{sf}}$, is:

$$
\mathbf{i_{m,sb}} = \mathbf{i_l} + \mathbf{i_{sf}} = \lambda_l \cdot \frac{v_{ls}^2}{2 \cdot g \cdot D_p} + \mu_{sf} \cdot C_{vs} \cdot R_{sd}
$$

(7.8-8)
(8.11-14)

The hydraulic gradient $\mathbf{i_{m,fb}}$ due to the flow through the restricted area $\mathbf{A_H}$ above the bed is:

$$
\mathbf{i_{m,fb}} = \lambda_r \cdot \frac{v_{ls,r}^2}{2 \cdot g \cdot D_H} = \lambda_r \cdot \frac{v_{ls}^2}{2 \cdot g \cdot D_H} \cdot \left(\frac{A_p}{A_H}\right)^2
$$

(7.8-9)
(8.11-15)

This gives for the transition line speed:

$$
v_{ls,FBSB}^2 = \frac{2 \cdot \mu_{sf} \cdot g \cdot C_{vs} \cdot R_{sd}}{\dfrac{\lambda_r}{D_H} \cdot \left(\dfrac{A_p}{A_H}\right)^2 - \dfrac{\lambda_l}{D_p}}
$$

(7.8-10)
(8.11-16)

8.11.8 The Transition Heterogeneous – Homogeneous (LDV Very Fine Particles).

For very fine particles, the Limit Deposit Velocity is close to the transition line speed between the heterogeneous regime and the homogeneous regime. Values found in literature (Thomas (1976)) are between 80% and 100% of this transition velocity. This transition velocity can be determined by making the relative excess pressure contributions of both regimes equal, according to:

$$
R_{sd} \cdot C_{vs} = \frac{\left(2 \cdot g \cdot R_{sd} \cdot D_p\right)}{\lambda_l} \cdot C_{vs} \cdot \frac{1}{v_{ls}^2} \cdot \left(\frac{v_t}{v_{ls}} \cdot \left(1 - \frac{C_{vs}}{\kappa_C}\right)^\beta + \frac{8.5^2}{\lambda_l} \cdot \left(\frac{v_t}{\sqrt{g \cdot d}}\right)^{10/3} \cdot \left(\frac{(\nu_l \cdot g)^{1/3}}{v_{ls}}\right)^2 \right)
$$

(7.8-11)
(8.11-17)

This gives for the transition velocity between the heterogeneous regime and the homogeneous regime:

$$
v_{ls,HeHo}^4 = \frac{2 \cdot g \cdot D_p}{\lambda_l} \cdot \left(v_t \cdot \left(1 - \frac{C_{vs}}{\kappa_C}\right)^\beta \cdot v_{ls,HeHo} + \frac{8.5^2}{\lambda_l} \cdot \left(\frac{v_t}{\sqrt{g \cdot d}}\right)^{10/3} \cdot (\nu_l \cdot g)^{2/3} \right)
$$

(7.8-12)
(8.11-18)

This equation implies that the transition line speed depends reversely on the Darcy Weisbach viscous friction coefficient $\mathbf{\lambda_l}$. Since the viscous friction coefficient $\mathbf{\lambda_l}$ depends reversely on the pipe diameter $\mathbf{D_p}$ with a power of about **0.2**, the transition line speed will depend on the pipe diameter with a power of about **(1.2/4) =0.3**. It is advised to use the Thomas (1965) viscosity correction for this transition line speed, otherwise to high transition velocities may be found. The equation derived is implicit and has to be solved iteratively.

8.11.9 The Transition Sliding Bed – Heterogeneous (LDV Coarse Particles).

When a sliding bed is present, particles will be in suspension above the sliding bed. The higher the line speed, the more particles will be in suspension. The interaction between the particles in suspension and the particles in the bed will still be by inter particle interactions, reason that the sliding bed is still carrying the weight of all the particles in suspension. Apparently the weight of all the particles is resulting in sliding friction. At a certain line speed all the particles will be in suspension and the sliding bed regime transits to heterogeneous flow. The particles now interact with the pipe wall by collisions and not by sliding friction anymore.

At the transition line speed the excess pressure losses of both regimes should be equal, giving

$$\mu_{sf} = \frac{v_t}{v_{ls}} \cdot \left(1 - \frac{C_{vs}}{\kappa_C}\right)^\beta + \frac{8.5^2}{\lambda_l} \cdot \left(\frac{v_t}{\sqrt{g \cdot d}}\right)^{10/3} \cdot \left(\frac{(v \cdot g)^{1/3}}{v_{ls}}\right)^2 \qquad \begin{array}{c}(7.8\text{-}13)\\(8.11\text{-}19)\end{array}$$

Resulting in the transition velocity at:

$$v_{ls,SBHe}^2 = \frac{v_t \cdot \left(1 - \frac{C_{vs}}{\kappa_C}\right)^\beta \cdot v_{ls,SBHe} + \frac{8.5^2}{\lambda_l} \cdot \left(\frac{v_t}{\sqrt{g \cdot d}}\right)^{10/3} \cdot (v_l \cdot g)^{2/3}}{\mu_{sf}} \qquad \begin{array}{c}(7.8\text{-}14)\\(8.11\text{-}20)\end{array}$$

This equation shows that the transition between the sliding bed regime and the heterogeneous regime depends on the sliding friction coefficient. Implicitly Newitt et al. (1955) already found this, but didn't explicitly mention this, because they assumed that potential energy is responsible for all the excess head losses in heterogeneous flow. The equation derived is a second degree function and can be written as:

$$-v_{ls,SBHe}^2 + \frac{v_t \cdot \left(1 - \frac{C_{vs}}{\kappa_C}\right)^\beta}{\mu_{sf}} \cdot v_{ls,SBHe} + \frac{\frac{8.5^2}{\lambda_l} \cdot \left(\frac{v_t}{\sqrt{g \cdot d}}\right)^{10/3} \cdot (v_l \cdot g)^{2/3}}{\mu_{sf}} = 0 \qquad \begin{array}{c}(7.8\text{-}15)\\(8.11\text{-}21)\end{array}$$

With:

$$A = -1$$

$$B = \frac{v_t \cdot \left(1 - \frac{C_{vs}}{\kappa_C}\right)^\beta}{\mu_{sf}}$$

$$\begin{array}{c}(7.8\text{-}16)\\(8.11\text{-}22)\end{array}$$

$$C = \frac{\frac{8.5^2}{\lambda_l} \cdot \left(\frac{v_t}{\sqrt{g \cdot d}}\right)^{10/3} \cdot (v_l \cdot g)^{2/3}}{\mu_{sf}}$$

$$V_{ls,SBHe} = \frac{-B - \sqrt{B^2 - 4 \cdot A \cdot C}}{2 \cdot A}$$

The lower limit of the LDV is found to be about 80% of this transition line speed. This also implies that the transition of a sliding bed to heterogeneous transport is not sharp, an intersection point, but it's a gradual process starting at about 80% of the transition line speed.

8.12 Constructing the Transport Concentration Curves.

There are 4 theoretical equations derived for the slip ratio, the region of line speeds below the LDV, the region of line speeds around the LDV and the region of line speeds above the LDV.

The slip ratio ξ_{HeHo} in the heterogeneous and homogeneous regime above the LDV is:

$$\xi_{HeHo} = \frac{v_{sl}}{v_{ls}} = 8.5 \cdot \left(\frac{1}{\sqrt{\lambda_l}}\right) \cdot \left(\frac{v_t}{\sqrt{g \cdot d}}\right)^{5/3} \cdot \left(\frac{(v_l \cdot g)^{1/3}}{v_{ls}}\right) \cdot \frac{v_t}{v_{ls}}$$

(7.9-35)
(8.12-1)

The slip ratio ξ_{ldv} around the LDV can be approximated by, based on the 3LM model for a sliding bed with sheet flow:

$$\xi_{aldv} = \frac{v_{sl}}{v_{ls}} = \left(1 - C_{vr}\right) \cdot e^{\left(-\left(0.83 + \frac{\mu_{sf}}{4} + \left(C_{vr} - 0.5 - 0.075 \cdot D_p\right)^2 + 0.025 \cdot D_p\right) \cdot D_p^{0.025} \cdot \left(\frac{v_{ls,ldv}}{v_{ls,lsdv}}\right)^\alpha \cdot C_{vr}^{0.65} \cdot \left(\frac{R_{sd}}{1.585}\right)^{0.1}\right)} \cdot \left(\frac{v_{ls,ldv}}{v_{ls}}\right)^4$$

With : $\quad \alpha = 0.58 \cdot C_{vr}^{-0.42}$

(7.9-36)
(8.12-2)

At the LDV:

$$\xi_{ldv} = \left(1 - C_{vr}\right) \cdot e^{\left(-\left(0.83 + \frac{\mu_{sf}}{4} + \left(C_{vr} - 0.5 - 0.075 \cdot D_p\right)^2 + 0.025 \cdot D_p\right) \cdot D_p^{0.025} \cdot \left(\frac{v_{ls,ldv}}{v_{ls,lsdv}}\right)^\alpha \cdot C_{vr}^{0.65} \cdot \left(\frac{R_{sd}}{1.585}\right)^{0.1}\right)}$$

The slip ratio ξ_{fb} based on a fixed bed with suspension above the bed is:

$$\xi_{fb} = \frac{v_{sl}}{v_{ls}} = 1 - \frac{C_{vt} \cdot v_{ls,ldv}}{\left(C_{vb} - \kappa_{ldv} \cdot C_{vt}\right) \cdot \left(v_{ls,ldv} - v_{ls}\right) + \kappa_{ldv} \cdot C_{vt} \cdot v_{ls,ldv}}$$

(7.9-37)
(8.12-3)

With : $\quad \kappa_{ldv} = \left(\frac{v_{ls,ldv}}{v_{ls,ldv} - v_{sl,ldv}}\right) = \left(\frac{1}{1 - \xi_{ldv}}\right)$

The slip ratio according to the 3LM model is:

$$\xi_{3LM} = \frac{v_{sl}}{v_{ls}} = \left(1 - C_{vr}\right) \cdot e^{\left(-\left(0.83 + \frac{\mu_{sf}}{4} + \left(C_{vr} - 0.5 - 0.075 \cdot D_p\right)^2 + 0.025 \cdot D_p\right) \cdot D_p^{0.025} \cdot \left(\frac{v_{ls}}{v_{ls,lsdv}}\right)^\alpha \cdot C_{vr}^{0.65} \cdot \left(\frac{R_{sd}}{1.585}\right)^{0.1}\right)}$$

(7.9-36)
(8.12-4)

With : $\quad \alpha = 0.58 \cdot C_{vr}^{-0.42}$

The resulting theoretical slip ratio curve is determined by:

$$\xi_{fb} < \xi_{aldv} \quad \Rightarrow \quad \xi_{th} = \xi_{fb}$$

$$\xi_{fb} \geq \xi_{aldv} \quad \Rightarrow \quad \xi_{th} = \xi_{aldv}$$

(7.9-39)
(8.12-5)

$$\xi_{HeHo} > \xi_{aldv} \quad \Rightarrow \quad \xi_{th} = \xi_{HeHo}$$

The tangent line equation ξ_t is, tangent to the slip ratio around the LDV:

$$\xi_t = \frac{v_{sl}}{v_{ls}} = \left(1 - \frac{C_{vt}}{C_{vb}}\right) - 4 \cdot \left(1 - \frac{C_{vt}}{C_{vb}}\right) \cdot e^{\left(-\left(0.83 + \frac{\mu_{sf}}{4} + \left(C_{vr} - 0.5 - 0.075 \cdot D_p\right)^2 + 0.025 \cdot D_p\right) \cdot D_p^{0.025} \cdot \left(\frac{v_{ls,ldv}}{v_{ls,lsdv}}\right)^\alpha \cdot C_{vr}^{0.65} \cdot \left(\frac{R_{sd}}{1.585}\right)^{0.1}\right)}$$

$$\cdot \left(\frac{v_{ls,ldv}}{v_{ls,t}}\right)^4 \cdot \left(\frac{v_{ls}}{v_{ls,t}}\right)$$

(7.9-40)
(8.12-6)

The tangent point $v_{ls,t}$ is now:

$$v_{ls,t} = \left(5 \cdot e^{\left(-\left(0.83 + \frac{\mu_{sf}}{4} + \left(C_{vr} - 0.5 - 0.075 \cdot D_p\right)^2 + 0.025 \cdot D_p\right) \cdot D_p^{0.025} \cdot \left(\frac{v_{ls,ldv}}{v_{ls,lsdv}}\right)^\alpha \cdot C_{vr}^{0.65} \cdot \left(\frac{R_{sd}}{1.585}\right)^{0.1}\right)}\right)^{1/4} \cdot v_{ls,ldv}$$

(7.9-40)
(8.12-7)

Giving for the tangent line:

$$\xi_t = \frac{v_{sl}}{v_{ls}} = \left(1 - \frac{C_{vt}}{C_{vb}}\right) \cdot \left(1 - \frac{4}{5} \cdot \left(\frac{v_{ls}}{v_{ls,t}}\right)\right)$$

(7.9-41)
(8.12-8)

The approximation of the slip ratio is now a weighed slip ratio according to:

$$\xi_{SBHeHo} = \xi_{th} \cdot \left(1 - \left(\frac{v_{ls}}{v_{ls,t}}\right)^\alpha\right) + \xi_t \cdot \left(\frac{v_{ls}}{v_{ls,t}}\right)^\alpha \qquad \text{if} \qquad v_{ls} < v_{ls,t}$$

$$\xi_{SBHeHo} = \xi_{th} \qquad\qquad\qquad\qquad\qquad \text{if} \qquad v_{ls} \geq v_{ls,t}$$

(7.9-42)
(8.12-9)

With : $\alpha = 0\text{-}1$

$$\xi_{SBHeHo} > \xi_{3LM} \qquad \Rightarrow \qquad \xi_{SBHeHo} = \xi_{3LM}$$

In the case of sliding flow, the slip ratio has to be corrected. A pragmatic approach to determine the relative excess hydraulic gradient in the sliding flow regime is to use a weighted average between the heterogeneous regime and the sliding bed regime. First the factor between particle size and pipe diameter is determined:

$$f = \frac{4}{3} - \frac{1}{3} \cdot \frac{d}{r_{d/Dp} \cdot D_p} \qquad \text{with: } 0 \leq f \leq 1$$

(7.7-4)
(8.12-10)

Secondly the weighted average slip ratio is determined:

$$\xi_{SF} = \xi_{SBHeHo} \cdot f + \xi_{3LM} \cdot \left(1 - f\right)$$

(7.7-5)
(8.12-11)

The resulting curve can be adjusted by changing the power α, however a value of 0.5 gives good results. The resulting slip ratio can never be larger than the slip ratio from the 3LM model. The resulting relative excess hydraulic gradient can be determined by multiplying the E_{rhg} curve for constant C_{vs} with the factor $\kappa = 1/(1-\xi)$. The volumetric spatial concentration on a constant delivered volumetric concentration curve equals:

$$C_{vs}(\xi) = \left(\frac{1}{1-\xi}\right) \cdot C_{vt} \quad \Rightarrow \quad E_{rhg,Cvt} = \left(\frac{1}{1-\xi}\right) \cdot E_{rhg,Cvs=Cvt} \qquad \begin{array}{c} \textbf{(7.9-45)} \\ \textbf{(8.12-12)} \end{array}$$

Doing so, one should use the sliding bed equation also in the stationary bed range of the constant spatial volumetric concentration curve. If the stationary bed regime curve intersects with the heterogeneous regime curve below the sliding bed curve, one should continue the heterogeneous curve up to the intersection with the sliding bed curve and from there with decreasing line speed follow the sliding bed curve. The hydraulic gradient for the constant delivered volumetric concentration curve is now:

$$i_m = i_l + E_{rhg,Cvt} \cdot R_{sd} \cdot C_{vt} = i_l + \left(\frac{1}{1-\xi}\right) \cdot E_{rhg,Cvs=Cvt} \cdot R_{sd} \cdot C_{vt} \qquad \textbf{(8.12-13)}$$

This gives for the pressure difference:

$$\Delta p_m = \Delta p_l + \rho_l \cdot g \cdot \Delta L \cdot E_{rhg,Cvt} \cdot R_{sd} \cdot C_{vt} = \Delta p_l + \rho_l \cdot g \cdot \Delta L \cdot \left(\frac{1}{1-\xi}\right) \cdot E_{rhg,Cvs=Cvt} \cdot R_{sd} \cdot C_{vt} \qquad \textbf{(8.12-14)}$$

8.13 The Bed Height.

The bed fraction can be determined with the following equation:

$$\zeta = \hat{A}_b = \frac{A_b}{A_p} = \frac{\left(1-\kappa_{ldv}\right)\cdot C_{vt} + \kappa_{ldv}\cdot C_{vt}\cdot \xi}{\left(C_{vb} - \kappa_{ldv}\cdot C_{vt}\right)\cdot\left(1-\xi\right)} = \frac{\left(1-\kappa_{ldv}\cdot\left(1-\xi\right)\right)\cdot C_{vt}}{\left(C_{vb} - \kappa_{ldv}\cdot C_{vt}\right)\cdot\left(1-\xi\right)}$$

<div align="right">(7.12-23)
(8.13-1)</div>

The bed fraction **f** is related to the bed angle according to:

$$\zeta = \frac{\beta - \sin\left(\beta\right)\cdot\cos\left(\beta\right)}{\pi}$$

<div align="right">(7.10-25)
(8.13-2)</div>

Since this is an implicit equation, the bed angle has to be determined by iteration. Once the bed angle is determined, the bed height can be determined with:

$$\beta = a\cos\left(\frac{0.5 - \dfrac{r}{D_p}}{0.5}\right) \quad \Leftrightarrow \quad \frac{r}{D_p} = \frac{1-\cos\left(\beta\right)}{2}$$

<div align="right">(7.10-24)
(8.13-3)</div>

Very often in literature the bed height is used in graphs.

8.14 The Concentration Distribution.

The fraction can be determined by the angle **β** matching a certain vertical coordinate, similar to the angle **β** for the stationary and sliding bed.

$$\beta = a\cos\left(\frac{0.5 - \dfrac{r}{D_p}}{0.5}\right) \quad \Leftrightarrow \quad \frac{r}{D_p} = \frac{1 - \cos(\beta)}{2}$$

(7.10-24)
(8.14-1)

The fraction **f** is now:

$$f = \frac{\beta - \sin(\beta) \cdot \cos(\beta)}{\pi}$$

(7.10-25)
(8.14-2)

The concentration distribution is (without or with hindered settling):

$$C_{vs}(f) = C_{vB} \cdot e^{-\frac{\alpha_{sm}}{C_{vr}}\left(\frac{v_{ls,ldv}}{v_{ls}}\right)^{0.925} \cdot \frac{v_{tv}}{v_{tv,ldv}} \cdot f} \quad or \quad C_{vs}(f) = C_{vB} \cdot e^{-\frac{\alpha_{sm}}{C_{vr}}\left(\frac{v_{ls,ldv}}{v_{ls}}\right)^{0.925} \cdot \frac{v_{thv}}{v_{thv,ldv}} \cdot f}$$

(7.10-16)
(8.14-3)

The correction factor appears to depend only on the relative concentration **C_vr** according to:

$$\alpha_{sm} = 0.9847 + 0.304 \cdot C_{vr} - 1.196 \cdot C_{vr}^2 - 0.5564 \cdot C_{vr}^3 + 0.47 \cdot C_{vr}^4$$

(7.10-13)
(8.14-4)

The bottom concentration is now (without or with hindered settling):

$$C_{vB} = C_{vb} \cdot \frac{\left(\alpha_{sm} \cdot \left(\dfrac{v_{ls,ldv}}{v_{ls}}\right)^{0.925} \cdot \dfrac{v_{tv}}{v_{tv,ldv}}\right)}{\left(1 - e^{-\frac{\alpha_{sm}}{C_{vr}}\left(\frac{v_{ls,ldv}}{v_{ls}}\right)^{0.925} \cdot \frac{v_{tv}}{v_{tv,ldv}}}\right)} \quad or \quad C_{vB} = C_{vb} \cdot \frac{\left(\alpha_{sm} \cdot \left(\dfrac{v_{ls,ldv}}{v_{ls}}\right)^{0.925} \cdot \dfrac{v_{thv}}{v_{thv,ldv}}\right)}{\left(1 - e^{-\frac{\alpha_{sm}}{C_{vr}}\left(\frac{v_{ls,ldv}}{v_{ls}}\right)^{0.925} \cdot \frac{v_{thv}}{v_{thv,ldv}}}\right)}$$

(7.10-17)
(8.14-5)

If the bottom concentration is higher than the bed concentration, the concentration profile has to be adjusted. If it is assumed that the settling velocity in the suspension hardly changes as a function of the line speed, the equation for the concentration distribution becomes:

$$C_{vs,0}(f) = C_{vB} \cdot e^{-\frac{\alpha_{sm}}{C_{vr}}\left(\frac{v_{ls,ldv}}{v_{ls}}\right)^{1.15} \cdot f}$$

(7.10-16)
(8.14-6)

The bottom concentration is now:

$$C_{vB} = C_{vb} \cdot \frac{\left(\alpha_{sm} \cdot \left(\dfrac{v_{ls,ldv}}{v_{ls}}\right)^{1.15}\right)}{\left(1 - e^{-\frac{\alpha_{sm}}{C_{vr}}\left(\frac{v_{ls,ldv}}{v_{ls}}\right)^{1.15}}\right)}$$

(7.10-17)
(8.14-7)

At each level in the pipe the corrected concentration gradient can be determined for the first iteration step according to:

$$\left(\frac{dC_{vs,1}(f)}{dr}\right) = \left(\frac{dC_{vs,0}(f)}{dr}\right) \cdot \left(\frac{\left(1-C_{vr,0}\right)}{\left(1-C_{vr}\right)}\right)^{\alpha \cdot \frac{\beta}{2.34}}$$

<div align="right">(7.10-36)
(8.14-8)</div>

For the following iteration steps the concentration gradient has to be adjusted according to:

$$\left(\frac{dC_{vs,i}(f)}{dr}\right) = \left(\frac{dC_{vs,i-1}(f)}{dr}\right) \cdot \left(\frac{C_{vr,i-1}(f)}{C_{vr,i-2}(f)}\right) \cdot \left(\frac{\left(1-C_{vr,i-1}\right)}{\left(1-C_{vr,i-2}\right)}\right)^{\alpha \cdot \frac{\beta}{2.34}}$$

<div align="right">(7.10-37)
(8.14-9)</div>

Integrating the concentration profile again, starting at the bottom with either the bottom concentration (above the LDV) or the bed concentration (below the LDV), gives a concentration profile adjusted for local hindered settling. The power α is determined with the following equations:

SF = Shape Factor   SF=0.77 for sand   SF=1.0 for spheres

$$C_{vrMax} = \frac{0.175}{C_{vb}}$$

$$\alpha = 0.275 \cdot \left(\frac{SF}{0.77}\right)^{1.5} \cdot \left(\frac{C_{vr}}{C_{vrMax}}\right)^{3} \cdot \left(\frac{v_{ls,LDV}}{v_{ls}}\right)^{0.15} \qquad C_{vr} < C_{vrMax}$$

<div align="right">(7.10-38)
(8.14-10)</div>

$$\alpha = 0.275 \cdot \left(\frac{SF}{0.77}\right)^{1.5} \cdot \left(\frac{C_{vr}}{C_{vrMax}}\right)^{2/3} \cdot \left(\frac{v_{ls,LDV}}{v_{ls}}\right)^{0.15} \qquad C_{vr} \geq C_{vrMax}$$
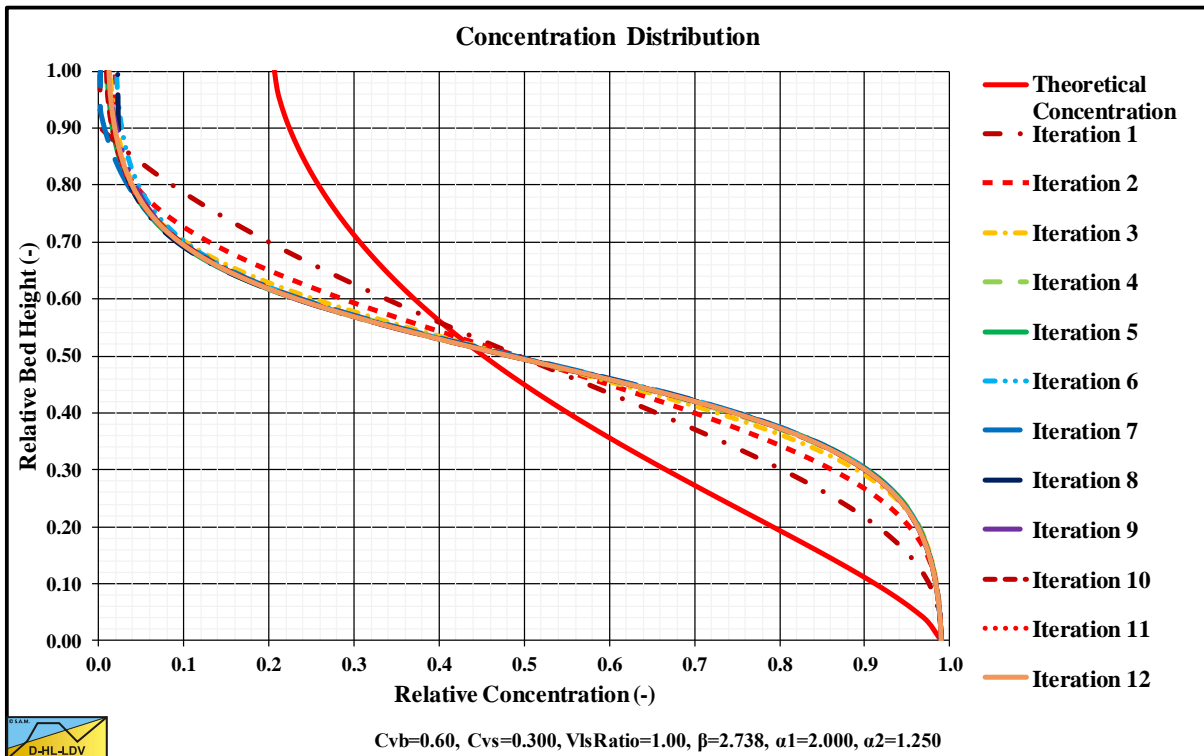
Figure 8.14-1: The concentration profile without local hindered settling (red line) and with local hindered settling (iteration 1-12).

Because the Limit Deposit Velocity is based on the occurrence of some bed at the bottom of the pipe, this bed does not need to have the maximum bed density. A bed may start to occur with a bottom concentration of about 50%, while the maximum bed concentration will be in the range of 60%-65%. In order to find a bottom concentration of about 50% at the LDV, an additional velocity ratio $\mathbf{r_{LDV}}$ is introduced giving:

$$C_{vB} = C_{vb} \cdot \frac{\left(\alpha_{sm} \cdot \left(r_{LDV} \cdot \frac{v_{ls,ldv}}{v_{ls}} \right)^{1.15} \right)}{\left(1 - e^{-\frac{\alpha_{sm}}{C_{vr}} \cdot \left(r_{LDV} \cdot \frac{v_{ls,ldv}}{v_{ls}} \right)^{1.15}} \right)} \quad \text{and} \quad C_{vs}(f) = C_{vB} \cdot e^{-\frac{\alpha_{sm}}{C_{vr}} \cdot \left(r_{LDV} \cdot \frac{v_{ls,ldv}}{v_{ls}} \right)^{1.15} \cdot f}$$

(7.10-28)
(8.14-11)

The additional velocity ratio $\mathbf{r_{LDV}}$ can be estimated by:

SF = Shape Factor   SF=0.77 for sand   SF=1.0 for spheres

$$C_{vrMax} = \frac{0.175}{C_{vb}}$$

$$\alpha_\beta = 1.8\text{-}56 \cdot v_t \quad \text{with:} \quad \alpha_\beta \geq 1.1$$

If $C_{vr} < C_{vrMax}$ then

(7.10-29)
(8.14-12)

$$r_{LDV} = 0.6 \cdot \frac{e^{(\beta/2.34)^{\alpha_\beta}}}{e} \cdot \left(\frac{0.0005}{d} \right)^{SF^6} \cdot \left(\frac{C_{vrMax}}{C_{vr}} \right)^{1/3} \quad \text{with:} \quad r_{LDV} \geq 1.2 \cdot \left(\frac{C_{vrMax}}{C_{vr}} \right)^{1/3}$$

If $C_{vr} \geq C_{vrMax}$ then

$$r_{LDV} = 0.6 \cdot \frac{e^{(\beta/2.34)^{\alpha_\beta}}}{e} \cdot \left(\frac{0.0005}{d} \right)^{SF^6} \cdot \left(\frac{C_{vr}}{C_{vrMax}} \right)^{1/6} \quad \text{with:} \quad r_{LDV} \geq 1.2 \cdot \left(\frac{C_{vr}}{C_{vrMax}} \right)^{1/6}$$

The factor 1.2 is based on the ratio 60% to 50%, the maximum bed concentration to the minimum bed concentration. For most of the experimental data analysed, a maximum bed concentration of 60% gives very good results. The LDV has a maximum at a concentration of 17.5%.

8.15 Graded Sands & Gravels.
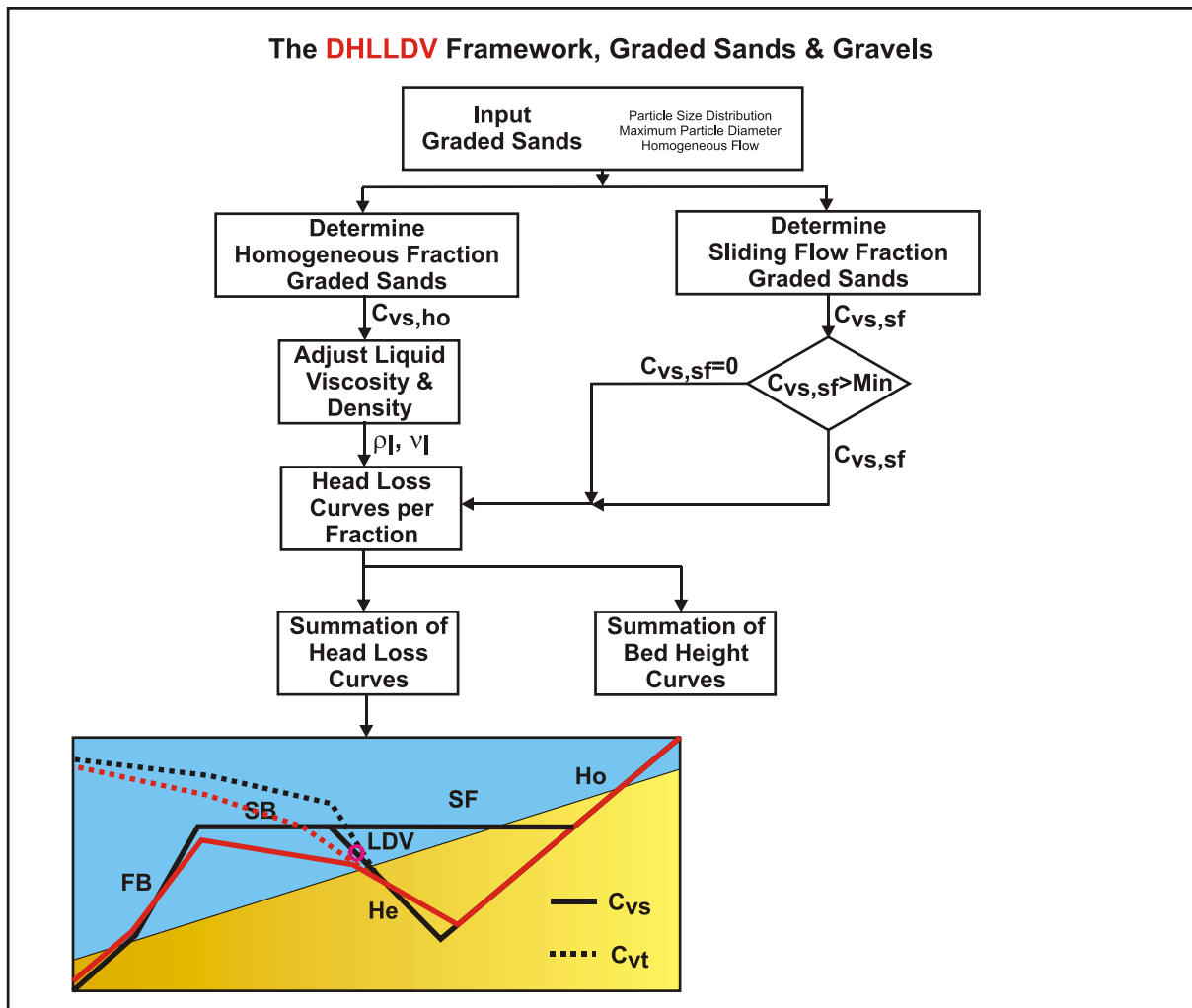
Figure 8.15-1: The algorithm to determine the constant C_{vs} and C_{ts} curve for graded sands and gravels.

8.15.1 Introduction.

The i_m curve for graded sands and gravels can be determined by:

1. Determine the fraction fines **X**. The limiting particle diameter for the fines can be determined with equation (7.13-2).
2. Determine the PSD and split the PSD in **n** fractions. Correct the PSD so the fines are not part of the PSD anymore. Adjust the volumetric concentration by deducting the fines fraction **X**.
3. Adjust the pseudo liquid dynamic viscosity μ_x, density ρ_x and relative submerged density $R_{sd,x}$ for the presence of fines and determine the resulting hydraulic gradient curve for the pseudo liquid, $i_{l,x}$.
4. Determine curves related to the pseudo liquid.
   a. Determine the $i_{m,x,i}$ curve for each ith fraction individually for both the spatial volumetric concentration and the delivered volumetric concentration, using the adjusted pseudo liquid properties.
   b. Sum the $i_{m,x,i}$ curves for the **n** fractions multiplied by the fraction f_i to determine the total hydraulic gradient $i_{m,x}$, for both the spatial volumetric concentration and the delivered volumetric concentration, in the pseudo liquid.
   c. Determine the resulting $E_{rhg,x}$ curve, for both the spatial volumetric concentration and the delivered volumetric concentration.
5. Determine curves related to the carrier liquid.
   a. Determine the $i_{m,i}$ curves for the **n** fractions by multiplying the $i_{m,x,i}$ curves by the ratio of the pseudo liquid density to the carrier liquid density ρ_x/ρ_l.
   b. Sum the $i_{m,i}$ curves for the **n** fractions multiplied by the fraction f_i to determine the total hydraulic gradient i_m, for both the spatial volumetric concentration and the delivered volumetric concentration, in the carrier liquid.
   c. Determine the resulting E_{rhg} curve, for both the spatial volumetric concentration and the delivered volumetric concentration.
6. Determine the bed fraction curves for each fraction multiplied by the fraction f_i.
7. Sum the bed fraction curves for the **n** fractions multiplied by the fraction f_i to obtain the total bed fraction curve.
8. Determine the slip ratio curves for each fraction multiplied by the fraction f_i.
9. Sum the slip ratio curves for the **n** fractions multiplied by the fraction f_i to obtain the total slip ratio curve.

Step 2 needs some clarification. Suppose we have a sand with 3 fractions, each 1/3 by weight. The first fraction consists of fines, the second fraction of particles with a **d=0.5 mm** and the third fraction of particles with **d=1 mm**. The spatial volumetric concentration of the sand in the carrier liquid is 30%.

Now the fines form a pseudo homogeneous liquid together with the carrier liquid. So in terms of solids effect they do not take part in the solids effect and have to be removed from the PSD. What is left is a PSD with 50% particles with a **d=0.5 mm** and 50% particles with **d=1 mm**. The spatial volumetric concentration of this sand is now 20%. So the hydraulic gradients have to be determined for this remaining sand and not for the original sand.

If a sand does not contain fines, the liquid properties and the PSD do not have to be adjusted.

8.15.2 The Adjusted Pseudo Liquid Properties.

First the limiting particle diameter is determined, based on a Stokes number of 0.03. The value of 0.03 is found based on many experiments from literature. Since the Stokes number depends on the line speed, here the Limit Deposit Velocity is used as an estimate of the operational line speed.

The LDV is approximated by:

$$v_{ls,ldv} = 7.5 \cdot D_p^{0.4}$$

(7.13-1)
(8.15-1)

Giving for the limiting particle diameter:

$$d_{lim} = \sqrt{\frac{Stk \cdot 9 \cdot \rho_l \cdot \nu_l \cdot D_p}{\rho_s \cdot v_{ls,ldv}}} \approx \sqrt{\frac{Stk \cdot 9 \cdot \rho_l \cdot \nu_l \cdot D_p}{\rho_s \cdot 7.5 \cdot D_p^{0.4}}}$$

(7.13-2)
(8.15-2)

The fraction of the sand in suspension, resulting in a homogeneous pseudo fluid is named **X**. This gives for the density of the homogeneous pseudo fluid:

$$\rho_x = \rho_l + \rho_l \cdot \frac{X \cdot C_{vs} \cdot R_{sd}}{\left(1 - C_{vs} + C_{vs} \cdot X\right)} \quad \text{if } X = 1 \quad \Rightarrow \quad \rho_x = \rho_m = \rho_l + \rho_l \cdot C_{vs} \cdot R_{sd}$$

(7.13-3)
(8.15-3)

So the concentration of the homogeneous pseudo fluid is not $C_{vs,x} = X \cdot C_{vs}$, but:

$$C_{vs,x} = \frac{X \cdot C_{vs}}{\left(1 - C_{vs} + C_{vs} \cdot X\right)}$$

(7.13-4)
(8.15-4)

This is because part of the total volume is occupied by the particles that are not in suspension. The remaining spatial concentration of solids to be used to determine the individual hydraulic gradients curves of the fractions is now:

$$C_{vs,r} = \left(1 - X\right) \cdot C_{vs}$$

(7.13-5)
(8.15-5)

The dynamic viscosity can now be determined according to Thomas (1965):

$$\mu_x = \mu_l \cdot \left(1 + 2.5 \cdot C_{vs,x} + 10.05 \cdot C_{vs,x}^2 + 0.00273 \cdot e^{16.6 \cdot C_{vs,x}}\right)$$

(7.13-6)
(8.15-6)

The kinematic viscosity of the homogeneous pseudo fluid is now:

$$\nu_x = \frac{\mu_x}{\rho_x}$$

(7.13-7)
(8.15-7)

One should realize however that the relative submerged density has also changed to:

$$R_{sd,x} = \frac{\rho_s - \rho_x}{\rho_x}$$

(7.13-8)
(8.15-8)

With the new homogeneous pseudo liquid density, kinematic viscosity, relative submerged density and volumetric concentration the hydraulic gradient can be determined for each fraction of the adjusted PSD.

8.15.3 Determination of the Hydraulic Gradient.

After adjusting for the new homogeneous pseudo liquid density ρ_x, kinematic viscosity v_x and relative submerged density $R_{sd,x}$ the hydraulic gradient can be determined for each fraction of the adjusted PSD using the volumetric concentration of the remaing solids. It is important to determine the hydraulic gradient curve for the full velocity range for both spatial and delivered concentrations and not the relative excess hydraulic gradient curves. The reason is, that the hydraulic gradient curves include the liquid curve for the adjusted homogeneous pseudo fluid properties, while the relative excess hydraulic gradient curves don't. Later the relative excess hydraulic gradient curves can be determined using the hydraulic gradient of the pure carrier liquid and the relative submerged density of the solids in the pure carrier liquid.

The resulting hydraulic gradient $i_{m,x}$ based on the pseudo liquid and relative excess hydraulic gradient $E_{rhg,x}$ are:

$$i_{m,x} = \sum_{i=1}^{n} f_i \cdot i_{m,x,i} \cdot w_i \quad \text{with:} \quad \sum_{i=1}^{n} f_i = 1 \quad \text{and} \quad \frac{1}{n} \cdot \sum_{i=1}^{n} w_i = 1$$

$$\text{(7.13-16)}$$
$$\text{(8.15-9)}$$

$$E_{rhg,x} = \frac{i_{m,x} - i_{l,x}}{R_{sd,x} \cdot C_{vs}} \quad \text{or} \quad E_{rhg,x} = \frac{i_{m,x} - i_{l,x}}{R_{sd,x} \cdot C_{vt}}$$

The resulting hydraulic gradient i_m based on the original carrier liquid and relative excess hydraulic gradient E_{rhg} are:

$$i_m = \frac{\rho_x}{\rho_l} \cdot i_{m,x} = \frac{\rho_x}{\rho_l} \cdot \sum_{i=1}^{n} f_i \cdot i_{m,x,i} \cdot w_i \quad \text{with:} \quad \sum_{i=1}^{n} f_i = 1 \quad \text{and} \quad \frac{1}{n} \cdot \sum_{i=1}^{n} w_i = 1$$

$$\text{(7.13-17)}$$
$$\text{(8.15-10)}$$

$$E_{rhg} = \frac{i_m - i_l}{R_{sd} \cdot C_{vs}} \quad \text{or} \quad E_{rhg} = \frac{i_m - i_l}{R_{sd} \cdot C_{vt}}$$

The variable w_i is a weighing factor, enabling to give certain particle diameters more weight in the total hydraulic gradient. Here the weighing factors are set to 1.

The resulting bed fraction is:

$$\zeta = \tilde{A}_b = \sum_{i=1}^{n} f_i \cdot \tilde{A}_{b,i} = \sum_{i=1}^{n} f_i \cdot \zeta_i \quad \text{with:} \quad \sum_{i=1}^{n} f_i = 1$$

$$\text{(7.13-18)}$$
$$\text{(8.15-11)}$$

8.16 Inclined Pipes.

8.16.1 Pure Liquid.

The hydraulic gradient can be determined with:

$$
i_{l,\theta} = -\frac{dp}{dx} \cdot \frac{A \cdot L}{\rho_l \cdot A \cdot L \cdot g} = \frac{\tau_l \cdot O \cdot L}{\rho_l \cdot A \cdot L \cdot g} + \frac{\rho_l \cdot A \cdot L \cdot g \cdot \sin(\theta)}{\rho_l \cdot A \cdot L \cdot g} = i_l + \sin(\theta)
$$

(7.14-3)
(8.16-1)

8.16.2 Sliding Bed Regime.

The hydraulic gradient can be determined with:

$$
i_{m,\theta} = i_{l,\theta} + R_{sd} \cdot C_{vs} \cdot \left(\mu_{sf} \cdot \cos(\theta) + \sin(\theta) \right)
$$

(7.14-16)
(8.16-2)

The relative excess hydraulic gradient $E_{rhg,\theta}$ is now:

$$
E_{rhg,\theta} = \frac{i_{m,\theta} - i_{l,\theta}}{R_{sd} \cdot C_{vs}} = \mu_{sf} \cdot \cos(\theta) + \sin(\theta)
$$

(7.14-17)
(8.16-3)

8.16.3 Heterogeneous Regime.

In an inclined pipe the effective terminal settling velocity perpendicular to the pipe wall gives a potential energy term of:

$$
S_{hr,\theta} = S_{hr} \cdot \cos(\theta) = \frac{v_t \cdot \cos(\theta) \cdot \left(1 - \dfrac{C_{vs}}{\kappa_C} \right)^{\beta}}{v_{ls}}
$$

(7.14-21)
(8.16-4)

For the kinetic energy losses, the angle of attack has to be adjusted in an inclined pipe. The angle of attack is defined as the ratio between the terminal settling velocity and the velocity at the thickness of the viscous sub layer, giving:

$$
S_{rs,\theta} = c \cdot \left(\frac{\delta_v}{d} \right)^{2/3} \cdot \left(\frac{v_t \cdot \cos(\theta)}{11.6 \cdot u_* - v_t \cdot \sin(\theta)} \right)^{4/3} \cdot \left(\frac{v_t}{\sqrt{g \cdot d}} \right)^2
$$

(7.14-22)
(8.16-5)

The relative excess hydraulic gradient and the hydraulic gradient are now:

$$
E_{rhg,\theta} = S_{hr,\theta} + S_{rs,\theta} + \sin(\theta)
$$

$$
i_{m,\theta} = i_{l,\theta} + \left(S_{hr,\theta} + S_{rs,\theta} + \sin(\theta) \right) \cdot R_{sd} \cdot C_{vs}
$$

(7.14-23)
(8.16-6)

8.16.4 Homogeneous Regime.

For an inclined pipe only the lifting of the mixture has to be added, giving:

$$\mathbf{E}_{\mathbf{rhg},\theta} = \boldsymbol{\alpha}_{\mathbf{E}} \cdot \mathbf{i}_{\mathbf{l}} + \sin(\theta)$$

$$\mathbf{i}_{\mathbf{m},\theta} = \mathbf{i}_{\mathbf{l},\theta} + \left(\boldsymbol{\alpha}_{\mathbf{E}} \cdot \mathbf{i}_{\mathbf{l}} + \sin(\theta)\right) \cdot \mathbf{R}_{\mathbf{sd}} \cdot \mathbf{C}_{\mathbf{vs}} \qquad \begin{matrix} \textbf{(7.14-25)} \\ \textbf{(8.16-7)} \end{matrix}$$

$$= \mathbf{i}_{\mathbf{l}} \cdot \left(1 + \boldsymbol{\alpha}_{\mathbf{E}} \cdot \mathbf{R}_{\mathbf{sd}} \cdot \mathbf{C}_{\mathbf{vs}}\right) + \sin(\theta) \cdot \left(1 + \mathbf{R}_{\mathbf{sd}} \cdot \mathbf{C}_{\mathbf{vs}}\right)$$

8.16.5 Sliding Flow Regime.

The method for determining the Sliding Flow Regime is not affected by pipe inclination. Of course the equations for a pipe with inclination for the sliding bed regime and the heterogeneous regime have to be applied.

8.16.6 The Limit Deposit Velocity.

The Limit of Stationary Deposit Velocity is affected by the pipe inclination. In an ascending pipe, the cross sectional averaged line speed has to be higher compared to a horizontal pipe in order to make a bed start sliding. In a descending pipe this line speed is lower. It is even possible that in a descending pipe the bed will always slide because of gravity. The Limit Deposit Velocity as defined as the line speed above which there is no stationary of sliding bed is determined by either the potential energy losses or a limiting sliding bed. In both cases this is affected by the cosine of the inclination angle. Since in both cases the Limit Deposit Velocity depends on the cube root, the Limit Deposit Velocity will decrease according to:

$$\mathbf{v}_{\mathbf{ls},\mathbf{ldv},\theta} = \mathbf{v}_{\mathbf{ls},\mathbf{ldv}} \cdot \cos(\theta)^{1/3} \qquad \begin{matrix} \textbf{(7.14-27)} \\ \textbf{(8.16-8)} \end{matrix}$$

Because of the cube root, this means that for angles up to 45° the reduction is less than 10%.

8.17 Conclusions & Discussion.

The DHLLDV Framework is explained for determining head losses and the Limit Deposit Velocity based on uniform sands and gravels and a spatial volumetric concentration. Using a holdup function, the delivered concentration head loss curve(s) can be determined and from there the bed height. By means of superposition, after some adjustments of the liquid properties, the head loss curve(s) for graded sands and gravels can also be determined. The full DHLLDV Framework is more complicated and detailed as described here and would require a multiple of pages. On the website www.dhlldv.com many additional graphs can be found and the latest developments will be shown after being published, including a list of papers about this subject.

The choice of basing the model on spatial volumetric concentration and uniform sands or gravels enables an explicit formulation for the different sub-models.

The criteria determining heterogeneous flow or sliding flow still require more investigation, although they match the Doron & Barnea (1993) experiments and the SCR model. Concentrations of 4.2% and 5% of their experiments clearly show heterogeneous behavior, while all higher concentrations show sliding flow behavior.

The method for graded sands is promising, but may need some fine tuning. Unfortunately there is not much experimental data available, while only Wasp (1963), Kaushal & Tomita (2002C) and Sellgren & Wilson (2007) developed models for graded PSD's.

The DHLLDV Framework has been compared with the Wasp (1963), the Wilson et al. (1992), the Kaushal & Tomita (2002C) and the SCR model, as well as many more from literature, with good results. In addition the model compares well to a wide range of experimental data from literature. These comparisons are also available on the website.

The DHLLDV Framework enables the user to implement user defined sub models for the different flow regimes, for the holdup function, for the bed height function and for the concentration distribution function.

The DHLLDV Framework gives a reference Framework for slurry flow in horizontal pipes and inclined pipes.

8.18 Nomenclature DHLLDV Framework.

A_{Cv}	Coefficient homogeneous regime (1.3 by default)	-
A_p	Cross section of the pipe	m^2
A_b	Bed cross section	m^2
A_1	Cross section restricted area above the bed	m^2
A_2	Cross section of the bed	m^2
C_{vb}	Bed volumetric concentration	-
$C_{vb,max}$	Maximum bed volumetric concentration	-
C_{vB}	Concentration at the bottom of the pipe	-
C_D	Particle drag coefficient	-
C_{vs}	Spatial volumetric concentration	-
$C_{vs,x}$	Spatial volumetric concentration fines	-
$C_{vs,r}$	Spatial volumetric concentration without fines	-
C_{vr}	Relative concentration C_{vs}/C_{vb}	-
$C_{vr,ldv}$	Relative concentration in bed at LDV	-
C_{vt}	Transport or delivered volumetric concentration	-
C_x	Durand & Condolios coefficient	-
C_L	Lift coefficient	-
d	Particle diameter	m
d_0	Particle diameter LDV transition region	m
d_{lim}	Limiting particle diameter pseudo liquid	m
D_H	Hydraulic diameter	m
$D_{H,1}$	Hydraulic diameter restricted area above the bed	m
D_p	Pipe diameter	m
E_{rhg}	Relative excess hydraulic gradient	-
$E_{rhg,SB}$	Relative excess hydraulic gradient in the sliding bed regime	-
$E_{rhg,SF}$	Relative excess hydraulic gradient in the sliding flow regime	-
$E_{rhg,He}$	Relative excess hydraulic gradient in the heterogeneous regime	-
$E_{rhg,Ho}$	Relative excess hydraulic gradient in the homogeneous regime	-
$E_{rhg,HeHo}$	Relative excess hydraulic gradient in the heterogeneous/ homogeneous flow regimes	-
$E_{rhg,Cvt}$	Relative excess hydraulic gradient with constant transport concentration	-
$E_{rhg,Cvs=Cvt}$	Relative excess hydraulic gradient with constant spatial concentration	-
f	Factor determining sliding flow	-
f_i	Fraction of the ith fraction in PSD	-
$F_{1,l}$	Force due to shear stress between liquid and wall	kN
$F_{12,l}$	Force due to shear stress between liquid and bed	kN
$F_{2,pr}$	Force due to pressure gradient on the bed	kN
$F_{2,sf}$	Force due to sliding friction between bed and pipe wall	kN
$F_{2,l}$	Force due to shear stress of liquid in the pores with the pipe wall	kN
F_L	Durand limit deposit velocity Froude number	-
$F_{L,s}$	Durand limit deposit velocity Froude number, smooth bed	-
$F_{L,ss}$	Durand limit deposit velocity Froude number, small particles smooth bed	-
$F_{L,vs}$	Durand limit deposit velocity Froude number, smooth bed, very small particles	-
$F_{L,r}$	Durand limit deposit velocity Froude number, rough bed, large particles	-
$F_{L,ul}$	Durand limit deposit velocity Froude number, upper limit	-
$F_{L,ll}$	Durand limit deposit velocity Froude number, lower limit	-
Fr_{DC}	Durand & Condolios Froude number	-
Fr_p	Particle Froude number	-
g	Gravitational constant (9.81)	m/s^2
h	Thickness of bed at LDV	m
i_l, i_w	Hydraulic gradient of liquid (water)	-
i_m	Hydraulic gradient of mixture	-
$i_{m,i}$	Hydraulic gradient of ith fraction of PSD	-
$i_{m,ldv}$	Hydraulic gradient mixture at LDV	-
$i_{m,SF}$	Hydraulic gradient sliding flow	-
K	Durand & Condolios constant (85)	-
ΔL	Length of pipe segment considered	m

L_R	Lift ratio	-
m	Mobilization factor homogeneous equation	-
m_p	Mass particle	kg
N	Zandi & Govatos deposit criterion	-
O_p	Circumference pipe	m
O_1	Circumference pipe in contact with liquid	m
O_2	Circumference pipe in contact with bed	m
O_{12}	Width of the bed	m
Δp_l	Pressure loss over pipeline length ΔL	kPa
Δp_m	Pressure loss mixture over pipeline length ΔL	kPa
r	Position in pipe starting at the bottom	-
Re	Reynolds number based on velocity difference liquid flow - bed	-
Re_p	Particle Reynolds number	-
R_{sd}	Relative submerged density solids in carrier liquid	-
$R_{sd,x}$	Relative submerged density solids in pseudo liquid	-
S_{hr}	**Settling** Velocity **Hindered Relative**	-
S_{rs}	**Slip** Velocity **Relative Squared**	-
Stk	Stokes number	-
u_*	Friction velocity	m/s
$u_{*,ldv}$	Friction velocity at the LDV	m/s
v_1	Average velocity above the bed	m/s
v_2	Velocity of the bed	m/s
v_{12}	Velocity difference bed interface (v_1-v_2)	m/s
v_{ls}	Cross-section averaged line speed	m/s
$v_{ls,ldv}$	Limit Deposit Velocity (LDV)	m/s
$v_{ls,t}$	Line speed at tangent point slip ratio	m/s
v_r	Relative line speed $v_{ls}/v_{ls,ldv,max}$ or v_{ls}/v_{sm}	m/s
v_{sl}	Slip velocity (velocity difference between particle and liquid)	m/s
v_{sm}	Maximum LSDV according to Wilson	m/s
v_t	Particle terminal settling velocity	m/s
v_{th}	Hindered settling velocity	m/s
v_{thv}	Hindered settling velocity vehicle (Wasp model)	
v_{tv}	(Hindered) settling velocity in the vehicle (Wasp model)	m/s
$v_{tv,ldv}$	(Hindered) settling velocity in the vehicle (Wasp model) at LDV	m/s
X	Fraction of fines	-
α	Factor in lift ratio	-
α	Factor in concentration distribution	-
$α_E$	Coefficient homogeneous equation	-
$α_p$	LDV factor	-
$α_{sm}$	Factor concentration distribution	-
β	Angle of bed with vertical	rad
β	Power of Richardson & Zaki hindered settling factor	-
$β_{sm}$	Relation sediment diffusivity eddy momentum diffusivity	-
ε	Critical particle diameter to pipe diameter ratio	-
ε	Pipe wall roughness	m
φ	Internal friction angle	rad
δ	External friction angle	rad
$δ_v$	Thickness viscous sub layer	m
$λ_1$	Darcy Weisbach friction factor liquid to pipe wall	-
$λ_{12}$	Darcy Weisbach friction factor bed interface	-
κ	Von Karman constant (about 0.4)	-
$κ_{ldv}$	Slip ratio factor at the LDV	-
$κ_C$	Concentration distribution constant	-
$ρ_l, ρ_w$	Density of liquid (water)	ton/m^3
$ρ_x$	Density of liquid including fines (pseudo liquid)	ton/m^3
$ρ_m$	Mixture density	ton/m^3
$ρ_s$	Density of solids	ton/m^3

ν_l	Kinematic viscosity carrier liquid	m^2/s
ν_x	Kinematic viscosity pseudo liquid	m^2/s
μ_l	Dynamic viscosity liquid	$Pa \cdot s$
μ_x	Dynamic viscously liquid including fines (pseudo liquid)	$Pa \cdot s$
μ_{sf}	Sliding friction coefficient	-
$\tau_{1,l}$	Shear stress liquid-pipe wall	kPa
$\tau_{2,sf}$	Shear stress bed – pipe wall due to sliding friction	kPa
$\tau_{12,l}$	Bed shear stress	kPa
ξ	Slip ratio	-
ξ_0	Slip ratio asymptotically for line speed zero	-
ξ_{fb}	Slip ratio with fixed bed	-
ξ_{ldv}	Slip ratio at the LDV	-
ξ_{HeHo}	Slip ratio in heterogeneous and homogeneous flow regimes	-
ξ_{th}	Resulting slip ratio	-
ξ_t	Tangent line slip ratio	-
ζ	Bed fraction	-
ζ	Smoothing factor lift ratio	-
FB	Fixed bed regime	-
He	Heterogeneous flow regime	-
Ho	Homogeneous flow regime	-
LDV	Limit Deposit Velocity	-
SB	Sliding bed regime	-
SF	Sliding flow regime	-

9.1 Introduction.

In order to compare the different models discussed, criteria have to be defined. Models may be considered as black boxes, only considering the input and the output, which is possible for all models. Models can be distinguished in fully empirical, semi empirical and mechanistic/fundamental. Models can be compared based on their origin, the range of the parameters used in the experiments.

The main parameters of influence on the head losses are the pipe diameter D_p, the particle diameter d or the whole PSD, the relative submerged density of the solids R_{sd}, the spatial or delivered volumetric concentration C_{vs} or C_{vt} and the range of operational line speeds (related to the pipe diameter). The sliding friction coefficient μ_{sf} also plays a role, but only for large particles with a sliding bed in the range of operational parameters.

So basically there are 4 main parameters, the pipe diameter, the particle diameter, the relative submerged density and the volumetric concentration. If for each of these parameters 10 values are used, D_p from 0.0254 m to 1 m, d from 0.1 mm to 10 mm, R_{sd} from 0.1 to 10 and C_{vs} or C_{vt} from 0.01 to 0.5, 10,000 possibilities are found for the comparison. Figure 9.1-1 and Figure 9.1-3 show such a comparison of 22 models in a hydraulic gradient i_m versus line speed v_{ls} graph. There would be 10,000 graphs required to give a good overview of all possible combinations. Figure 9.1-2 and Figure 9.1-4 show the relative excess hydraulic gradient E_{rhg} versus the pure liquid hydraulic gradient i_l. Since the relative excess hydraulic gradient equals the mixture hydraulic gradient minus the pure liquid hydraulic gradient, which is the solids effect, divided by the relative submerged density and the volumetric concentration, an almost dimensionless graph is created. Almost dimensionless because most models are proportional to the volumetric concentration and more or less proportional to the relative submerged density. Using a concentration of about 20% and the relative submerged density of sand and gravel already limits the number of graphs to 100. However this is still to many.

The remaining parameters are the pipe diameter and the particle diameter. With the knowledge that the ELM often used for the homogeneous regime and most models for the heterogeneous regime are proportional or close to proportional to both the volumetric concentration and the relative submerged density, the conclusion can be drawn that the intersection point of these two regimes (the transition velocity) is almost independent of the volumetric concentration and the relative submerged density. With the knowledge that this transition velocity is often in the range of operational line speeds for medium sands, this transition velocity seems to be a good indicator for a model. For each particles diameter and each model a transition velocity is found, resulting in a graph with the transition velocity versus the particle diameter. The only parameter left is thus the pipe diameter. The following graphs (Figure 9.2-5, Figure 9.2-6, Figure 9.2-7, Figure 9.2-8 Figure 9.2-9, Figure 9.2-10, Figure 9.2-11, Figure 9.2-12, Figure 9.2-13, Figure 9.2-14, Figure 9.2-15, Figure 9.2-16, Figure 9.2-17 and Figure 9.2-18) have a dimensionless vertical axis by dividing the transition line speed by the maximum transition line speed occurring in one of the 11 models. Although most models are proportional with the volumetric concentration, a few are not. This is why the graphs are given for volumetric concentrations of 5% and 30%, limiting the number of graphs to 14 for sands and gravels.

In order to understand the graphs the following variables are given:

The hydraulic gradient of the pure liquid i_l is:

$$i_l = \frac{\lambda_l \cdot v_{ls}^2}{2 \cdot g \cdot D_p} \tag{9.1-1}$$

The relative excess hydraulic gradient E_{rhg} is, for spatial and delivered concentrations:

$$E_{rhg} = \frac{i_m - i_l}{R_{sd} \cdot C_{vs}} \quad \text{or} \quad E_{rhg} = \frac{i_m - i_l}{R_{sd} \cdot C_{vt}} \tag{9.1-2}$$

The hydraulic gradient in the homogeneous regime, according to ELM i_m so without corrections, is:

$$i_m = i_l \cdot \left(1 + R_{sd} \cdot C_{vs}\right) \quad \text{and} \quad E_{rhg} = \frac{i_m - i_l}{R_{sd} \cdot C_{vs}} = i_l \tag{9.1-3}$$
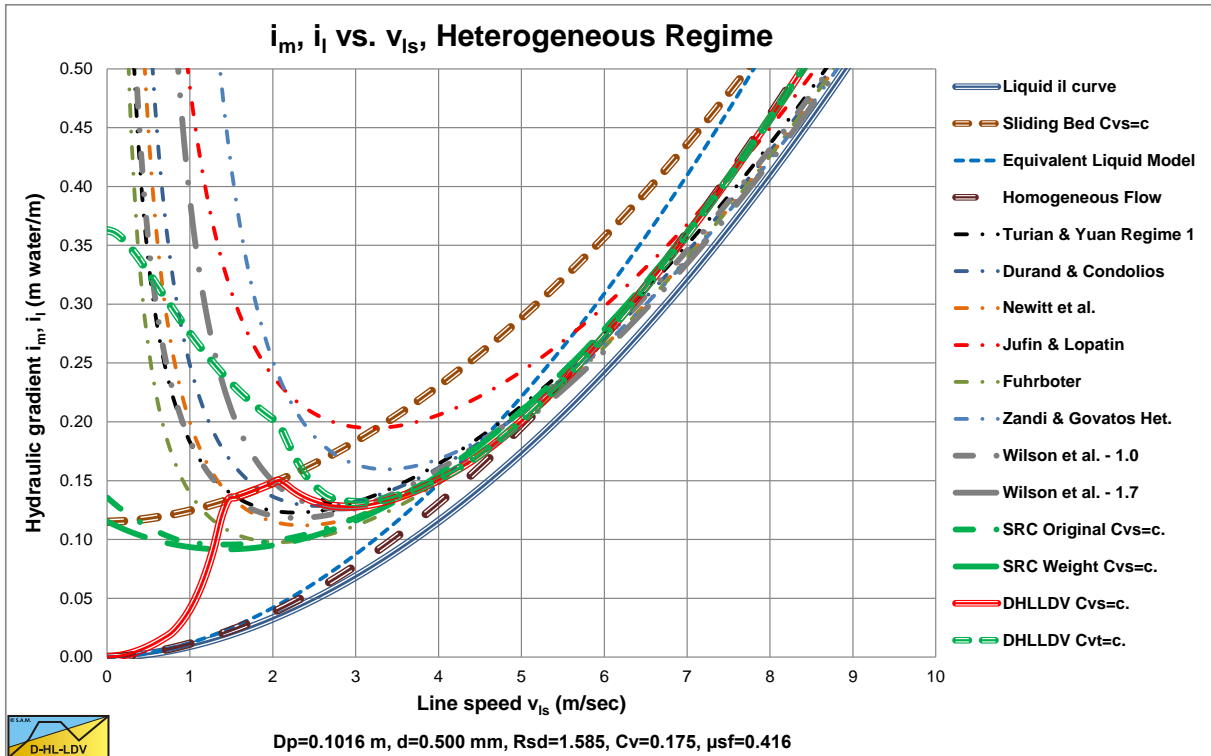
Figure 9.1-1: Comparison of 22 models in a i_m-v_{ls} graph in a D_P=0.1016 m (4 inch) pipe.
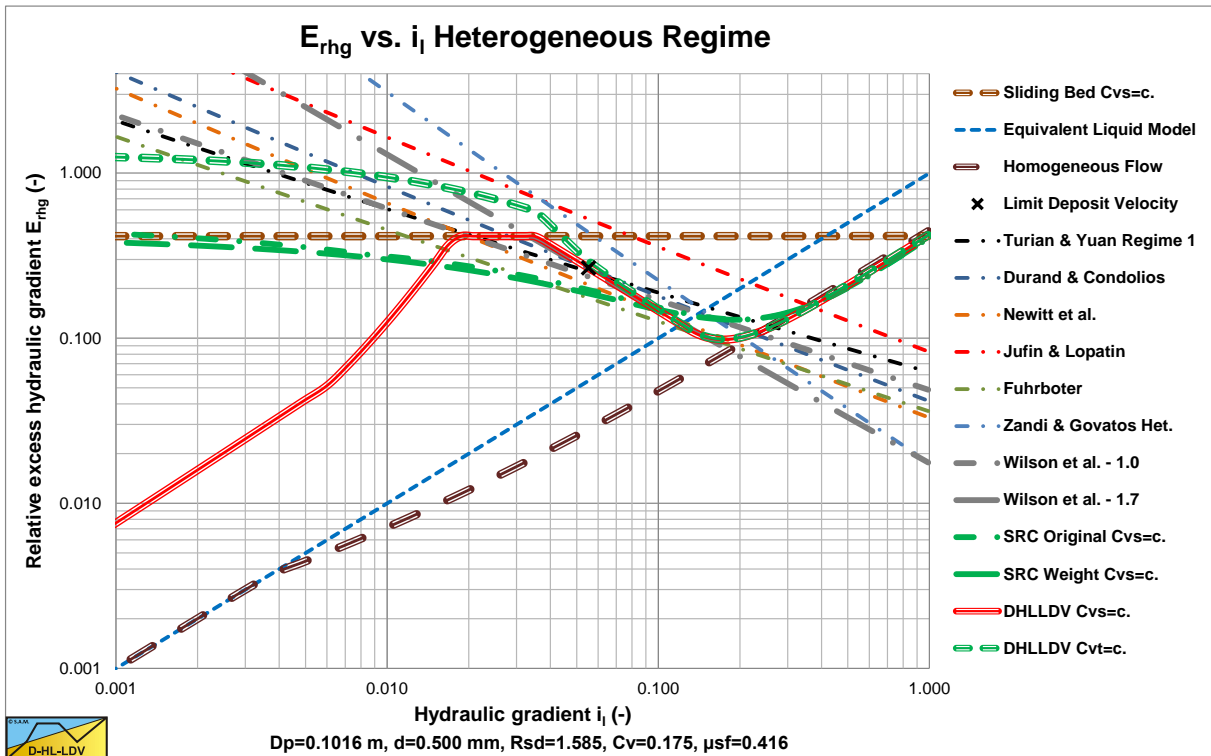
Figure 9.1-2: Comparison of 22 models in a E_{rhg}-i_l graph in a D_P=0.1016 m (4 inch) pipe.

Comparison of the DHLLDV Framework with Other Models.
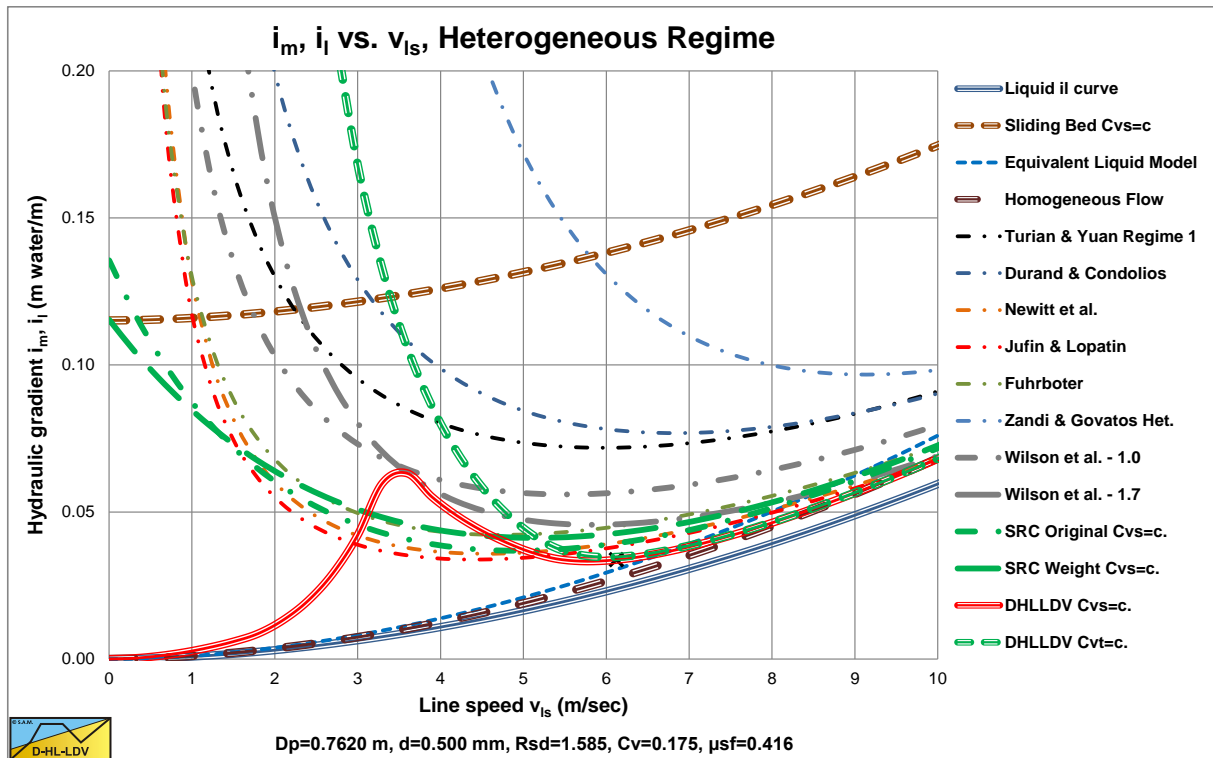
Figure 9.1-3: Comparison of 22 models in a i_m-v_{ls} graph in a D_p=0.762 m (30 inch) pipe.
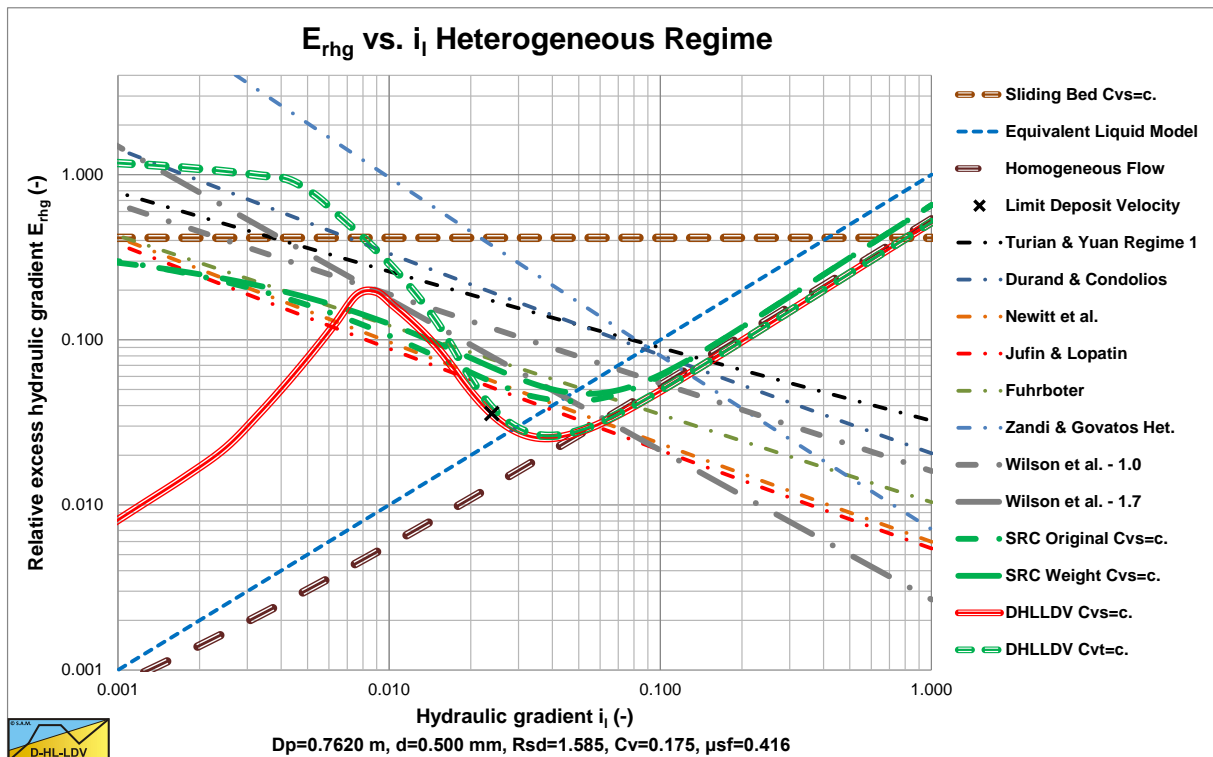
Figure 9.1-4: Comparison of 22 models in a E_{rhg}-i_l graph in a D_p=0.762 m (30 inch) pipe.

9.2   The Transition Velocity Heterogeneous-Homogeneous.

9.2.1   Considerations.

The theoretical transition velocity between the heterogeneous regime and the homogeneous regime gives a good indication of the excess pressure losses due to the solids. For normal dredging applications with large diameter pipes and rather high line speeds, this transition velocity will be at a line speed higher than the Limit Deposit Velocity and will often be near the operating range of the dredging operations. The excess head losses are in some way proportional to this transition velocity. For a **D_p=0.15 m** diameter pipe most models match pretty well, due to the fact that most experiments are carried out in small diameter pipes and the models are fitted to the experiments. Although the different models may have a different approach, the resulting equations go through the same cloud of data points. Since there are numerous fit lines of numerous researchers it is impossible to cover them all, so a choice is made to compare Durand & Condolios (1952), Newitt et al. (1955), Fuhrboter (1961), Jufin & Lopatin (1966), Zandi & Govatos (1967), Turian & Yuan (1977), the SRC model and Wilson et al. (1992) with the DHLLDV Framework as developed here, Miedema & Ramsdell (2013).

9.2.2   The DHLLDV Framework.

This theoretical transition velocity can be determined by making the relative excess pressure contributions of the heterogeneous regime and the homogeneous regime equal. This is possible if transition effects are omitted and the basic equations are applied.

The hydraulic gradient in the homogeneous regime, according to ELM so without corrections, is:

$$i_m = i_l \cdot \left(1 + R_{sd} \cdot C_{vs} \right) \tag{9.2-1}$$

The hydraulic gradient in the heterogeneous regime is, Miedema (2015):

$$i_m = i_l \cdot \left(1 + R_{sd} \cdot C_{vs} \cdot \frac{\left(2 \cdot g \cdot D_p \right)}{\lambda_l \cdot v_{ls}^2} \cdot \left(La + \frac{8.5^2}{8} \cdot Ct^2 \cdot Th_{fv}^2 \right) \right) \tag{9.2-2}$$

So the resulting equation, making equations (9.2-1) and (9.2-2) equal gives:

$$R_{sd} \cdot C_{vs} = R_{sd} \cdot C_{vs} \cdot \frac{\left(2 \cdot g \cdot D_p \right)}{\lambda_l \cdot v_{ls,hh}^2} \cdot \left(La + \frac{8.5^2}{8} \cdot Ct^2 \cdot Th_{fv}^2 \right) \tag{9.2-3}$$

Because we want to derive the transition velocity, the intersection point, the dimensionless numbers La (sedimentation capability), Ct (collision impact) and Th (collision intensity) have to be expanded to full equations.

$$1 = \frac{\left(2 \cdot g \cdot D_p \right)}{\lambda_l \cdot v_{ls,hh}^2} \cdot \left(\frac{v_t}{v_{ls,hh}} \cdot \left(1 - \frac{C_{vs}}{0.175 \cdot (1+\beta)} \right)^{\beta} + \frac{8.5^2}{8} \cdot \left(\left(\frac{v_t}{\sqrt{g \cdot d}} \right)^{5/3} \right)^2 \cdot \left(\frac{\left(\nu_l \cdot g \right)^{1/3}}{\sqrt{\lambda_l / 8} \cdot v_{ls,hh}} \right)^2 \right) \tag{9.2-4}$$

This gives for the transition velocity between the heterogeneous regime and the homogeneous regime:

$$v_{ls,hh}^4 = \frac{2 \cdot g \cdot D_p}{\lambda_l} \cdot \left(v_t \cdot \left(1 - \frac{C_{vs}}{0.175 \cdot (1+\beta)} \right)^{\beta} \cdot v_{ls,hh} + \frac{8.5^2}{\lambda_l} \cdot \left(\frac{v_t}{\sqrt{g \cdot d}} \right)^{10/3} \cdot \left(\nu_l \cdot g \right)^{2/3} \right) \tag{9.2-5}$$

This equation implies that the transition velocity depends reversely on the viscous friction coefficient λ_l. Since the viscous friction coefficient λ_l depends reversely on the pipe diameter D_p with a power of about **0.2**, the transition velocity will depend on the pipe diameter with a power of about **(1.2/4) =0.35.** The equation derived is implicit and has to be solved iteratively.
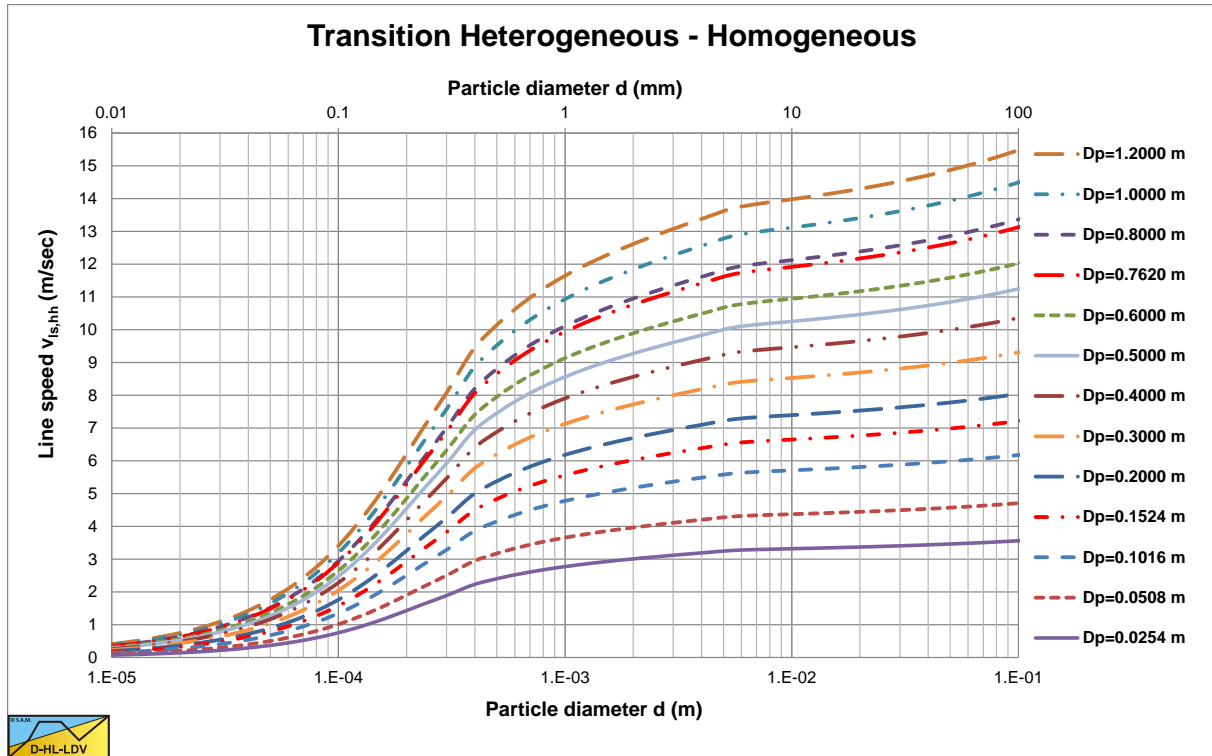
Figure 9.2-1: The transition line speed as a function of the particle diameter and the pipe diameter.

Figure 9.2-1 shows the transition line speed of the Miedema & Ramsdell (2013) DHLLDV Framework as a function of the particle diameter and the pipe diameter.

9.2.3 Durand & Condolios (1952) & Gibert (1960).

The equation for heterogeneous transport of Durand & Condolios (1952) and later Gibert (1960) is:

$$\Delta p_m = \Delta p_l \cdot \left(1 + \Phi \cdot C_{vt}\right) \quad \text{or} \quad i_m = i_l \cdot \left(1 + \Phi \cdot C_{vt}\right) \tag{9.2-6}$$

With:

$$\Phi = \frac{i_m - i_l}{i_l \cdot C_{vt}} = \frac{\Delta p_m - \Delta p_l}{\Delta p_l \cdot C_{vt}} = K \cdot \psi^{-3/2} = K \cdot \left(\frac{v_{ls}^2}{g \cdot D_p \cdot R_{sd}} \cdot \sqrt{C_x}\right)^{-3/2} \tag{9.2-7}$$

$$K \approx 85$$

The hydraulic gradient in the homogeneous regime, according to ELM so without corrections, is:

$$i_m = i_l \cdot \left(1 + R_{sd} \cdot C_{vs}\right) \quad \Rightarrow \quad \frac{i_m - i_l}{i_l \cdot C_{vs}} = \frac{\Delta p_m - \Delta p_l}{\Delta p_l \cdot C_{vs}} = R_{sd} \tag{9.2-8}$$

Rewriting this equation into a form that shows the line speed where the heterogeneous transport equation and the homogeneous transport equation are equal, with $C_{vs} = C_{vt}$, gives:

$$K \cdot \left(\frac{v_{ls}^2}{g \cdot D_p \cdot R_{sd}} \cdot \sqrt{C_x}\right)^{-3/2} = \frac{1}{v_{ls}^3} \cdot K \cdot \left(\frac{1}{g \cdot D_p \cdot R_{sd}} \cdot \sqrt{C_x}\right)^{-3/2} = R_{sd} \tag{9.2-9}$$

This gives for the transition velocity between the heterogeneous regime and the homogeneous regime:

$$v_{ls,hh}^3 = \frac{K}{R_{sd}} \cdot \left(\frac{g \cdot D_p \cdot R_{sd}}{\sqrt{C_x}} \right)^{3/2} \tag{9.2-10}$$

This is an explicit equation, which can be solved directly. The Wasp et al. (1977) related models also follow this equation.

9.2.4 Newitt et al. (1955).

The equation for heterogeneous transport of Newitt et al. (1955) is:

$$\frac{i_m - i_l}{i_l \cdot C_{vt}} = \frac{\Delta p_m - \Delta p_l}{\Delta p_l \cdot C_{vt}} = K_1 \cdot \left(g \cdot D_p \cdot R_{sd} \right) \cdot v_t \cdot \left(\frac{1}{v_{ls}} \right)^3 \tag{9.2-11}$$

$$K_1 = 1100$$

The hydraulic gradient in the homogeneous regime, according to ELM so without corrections, is:

$$i_m = i_l \cdot \left(1 + R_{sd} \cdot C_{vs} \right) \quad \Rightarrow \quad \frac{i_m - i_l}{i_l \cdot C_{vs}} = \frac{\Delta p_m - \Delta p_l}{\Delta p_l \cdot C_{vs}} = R_{sd} \tag{9.2-12}$$

Rewriting this equation into a form that shows the line speed where the heterogeneous transport equation and the homogeneous transport equation are equal, with $C_{vs}=C_{vt}$, gives:

$$K_1 \cdot \left(g \cdot D_p \cdot R_{sd} \right) \cdot v_t \cdot \left(\frac{1}{v_{ls}} \right)^3 = R_{sd} \tag{9.2-13}$$

This gives for the transition velocity between the heterogeneous regime and the homogeneous regime:

$$v_{ls,hh}^3 = K_1 \cdot \left(g \cdot D_p \right) \cdot v_t \tag{9.2-14}$$

This is an explicit equation, which can be solved directly.

9.2.5 Fuhrboter (1961).

The equation for heterogeneous transport of Fuhrboter (1961) is, using an approximation for the S_k value:

$$i_m = i_l + \frac{S_k}{v_{ls}} \cdot C_{vt} \quad \text{with:} \quad C_{vt} = C_{vs}$$

$$\frac{i_m - i_l}{i_l \cdot C_{vs}} = \frac{\Delta p_m - \Delta p_l}{\Delta p_l \cdot C_{vs}} = R_{sd} \cdot \frac{2 \cdot g \cdot D_p}{\lambda_l \cdot v_{ls}^2} \cdot \left(\frac{43.5 \cdot R_{sd} \cdot \sqrt{C_x}^{-1} \cdot \zeta(d_m) \cdot (v_l \cdot g)^{1/3}}{R_{sd} \cdot v_{ls}} \right) \tag{9.2-15}$$

$$\text{With:} \quad \zeta(d_m) = \left(1 - e^{-\frac{d_m}{0.0007}} \right) \cdot \left(1 + 10 \cdot e^{-\frac{d_m}{0.00005}} \right)$$

The hydraulic gradient in the homogeneous regime, according to ELM so without corrections, is:

$$i_m = i_l \cdot \left(1 + R_{sd} \cdot C_{vs}\right) \quad \Rightarrow \quad \frac{i_m - i_l}{i_l \cdot C_{vs}} = \frac{\Delta p_m - \Delta p_l}{\Delta p_l \cdot C_{vs}} = R_{sd} \tag{9.2-16}$$

Rewriting this equation into a form that shows the line speed where the heterogeneous transport equation and the homogeneous transport equation are equal, gives:

$$R_{sd} \cdot \frac{2 \cdot g \cdot D_p}{\lambda_l} \cdot \left(\frac{43.5 \cdot R_{sd} \cdot \sqrt{C_x}^{-1} \cdot \zeta(d_m) \cdot (\nu_l \cdot g)^{1/3}}{R_{sd}}\right) \cdot \left(\frac{1}{v_{ls}}\right)^3 = R_{sd} \tag{9.2-17}$$

This gives for the transition velocity between the heterogeneous regime and the homogeneous regime:

$$v_{ls,hh}^3 = \frac{2 \cdot g \cdot D_p}{\lambda_l \cdot R_{sd}} \cdot \left(43.5 \cdot \sqrt{C_x}^{-1} \cdot R_{sd} \cdot \zeta(d_m) \cdot (\nu_l \cdot g)^{1/3}\right) = \frac{2 \cdot g \cdot D_p}{\lambda_l \cdot R_{sd}} \cdot S_k \tag{9.2-18}$$

This is an explicit equation, which can be solved directly.

9.2.6 Jufin & Lopatin (1966).

The equation for heterogeneous transport of Jufin & Lopatin (1966) is, with added terms to make the dimensions correct:

$$\Delta p_m = \Delta p_l \cdot \left(1 + 2 \cdot \left(\frac{v_{min}}{v_{ls}}\right)^3\right) \quad \text{or} \quad i_m = i_l \cdot \left(1 + 2 \cdot \left(\frac{v_{min}}{v_{ls}}\right)^3\right)$$

$$v_{min} = 5.5 \cdot \left(C_{vt} \cdot \psi^* \cdot D_p\right)^{1/6} \quad \text{with:} \quad \psi^* = \left(\frac{v_t}{\sqrt{g \cdot d}}\right)^{3/2} \tag{9.2-19}$$

$$\frac{i_m - i_l}{i_l \cdot C_{vt}} = 2 \cdot \frac{\left(5.5 \cdot \left(C_{vt} \cdot \left(\frac{v_t}{\sqrt{g \cdot d}}\right)^{3/2} \cdot D_p\right)^{1/6} \cdot 7.92 \cdot (g \cdot R_{sd})^{1/6} \cdot (\nu_l \cdot g)^{2/9}\right)^3}{C_{vt}} \cdot \left(\frac{1}{v_{ls}}\right)^3$$

The hydraulic gradient in the homogeneous regime, according to ELM so without corrections, is:

$$i_m = i_l \cdot \left(1 + R_{sd} \cdot C_{vs}\right) \quad \Rightarrow \quad \frac{i_m - i_l}{i_l \cdot C_{vs}} = \frac{\Delta p_m - \Delta p_l}{\Delta p_l \cdot C_{vs}} = R_{sd} \tag{9.2-20}$$

Rewriting this equation into a form that shows the line speed where the heterogeneous transport equation and the homogeneous transport equation are equal, gives:

$$2 \cdot 82654 \cdot \left(\frac{v_t}{\sqrt{g \cdot d}}\right)^{3/4} \cdot \left(g \cdot D_p \cdot R_{sd}\right)^{1/2} \cdot (\nu_l \cdot g)^{2/3} \cdot \left(C_{vt}\right)^{-1/2} \left(\frac{1}{v_{ls}}\right)^3 = R_{sd} \tag{9.2-21}$$

This gives for the transition velocity between the heterogeneous regime and the homogeneous regime:

$$v_{ls,hh}^3 = 2 \cdot 82654 \cdot \left(\frac{v_t}{\sqrt{g \cdot d}}\right)^{3/4} \cdot \left(\frac{g \cdot D_p}{R_{sd}}\right)^{1/2} \cdot (\nu_l \cdot g)^{2/3} \cdot \left(C_{vt}\right)^{-1/2} \tag{9.2-22}$$

This is an explicit equation, which can be solved directly.

9.2.7 Zandi & Govatos (1967).

The final equation for heterogeneous transport of Zandi & Govatos (1967) is:

$$\Delta p_m = \Delta p_l \cdot \left(1 + 280 \cdot \psi^{-1.93} \cdot C_{vt}\right) \tag{9.2-23}$$

$$\psi = \left(\frac{v_{ls}^2}{g \cdot D_p \cdot R_{sd}}\right) \cdot \sqrt{C_x} \tag{9.2-24}$$

The hydraulic gradient in the homogeneous regime, according to ELM so without corrections, is:

$$i_m = i_l \cdot \left(1 + R_{sd} \cdot C_{vs}\right) \quad \Rightarrow \quad \frac{i_m - i_l}{i_l \cdot C_{vs}} = \frac{\Delta p_m - \Delta p_l}{\Delta p_l \cdot C_{vs}} = R_{sd} \tag{9.2-25}$$

Rewriting this equation into a form that shows the line speed where the heterogeneous transport equation and the homogeneous transport equation are equal, gives:

$$280 \cdot \left(\left(\frac{v_{ls}^2}{g \cdot D_p \cdot R_{sd}}\right) \cdot \sqrt{C_x}\right)^{-1.93} = 280 \cdot \left(\frac{g \cdot D_p \cdot R_{sd}}{\sqrt{C_x}}\right)^{1.93} \cdot \left(\frac{1}{v_{ls}}\right)^{3.86} = R_{sd} \tag{9.2-26}$$

This gives for the transition velocity between the heterogeneous regime and the homogeneous regime:

$$v_{ls,hh}^{3.86} = 280 \cdot \left(\frac{g \cdot D_p \cdot R_{sd}}{\sqrt{C_x}}\right)^{1.93} \cdot \frac{1}{R_{sd}} \tag{9.2-27}$$

This is an explicit equation, which can be solved directly.

9.2.8 Turian & Yuan (1977) 1: Saltation Regime.

According to Turian & Yuan (1977), the pressure losses with saltating transport can be described by:

$$f_m - f_l = \frac{\lambda_m}{4} - \frac{\lambda_l}{4} = 107.1 \cdot C_{vt}^{1.018} \cdot \left(\frac{\lambda_l}{4}\right)^{1.046} \cdot C_D^{*-0.4213} \cdot Fr^{-1.354} = R_{sd} \cdot C_{vt} \cdot \frac{\lambda_l}{4} \tag{9.2-28}$$

This equation can be made equal to the equation for homogeneous transport giving:

$$Fr^{1.354} = 107.1 \cdot C_{vt}^{1.018} \cdot \left(\frac{\lambda_l}{4}\right)^{0.046} \cdot C_D^{*-0.4213} \cdot \left(R_{sd} \cdot C_{vt}\right)^{-1} \tag{9.2-29}$$

Rewriting this equation into a form that shows the line speed where the saltating transport equation and the homogeneous transport equation are equal, gives:

$$v_{ls,hh} = \left(g \cdot R_{sd} \cdot D_p \left(107.1 \cdot C_{vt}^{1.018} \cdot \left(\frac{\lambda_l}{4}\right)^{0.046} \cdot C_D^{*-0.4213} \cdot \left(R_{sd} \cdot C_{vt}\right)^{-1}\right)^{1/1.354}\right)^{0.5} \tag{9.2-30}$$

The equation of Turian & Yuan (1977) for homogeneous transport is not used here, because we want to compare the intersection point of saltating and homogeneous transport, using the same equation for homogeneous transport for all models.

9.2.9 Turian & Yuan (1977) 2: Heterogeneous Regime.

According to Turian & Yuan (1977), the pressure losses with heterogeneous transport can be described by:

$$\mathbf{f_m - f_l = \frac{\lambda_m}{4} - \frac{\lambda_l}{4} = 30.11 \cdot C_{vt}^{0.868} \cdot \left(\frac{\lambda_l}{4}\right)^{1.200} \cdot C_D^{*-0.1677} \cdot Fr^{-0.6938} = R_{sd} \cdot C_{vt} \cdot \frac{\lambda_l}{4}}$$

(9.2-31)

This equation can be made equal to the equation for homogeneous transport giving:

$$\mathbf{Fr^{0.6938} = 30.11 \cdot C_{vt}^{0.868} \cdot \left(\frac{\lambda_l}{4}\right)^{0.200} \cdot C_D^{*-0.1677} \cdot \left(R_{sd} \cdot C_{vt}\right)^{-1}}$$

(9.2-32)

Rewriting this equation into a form that shows the line speed where the heterogeneous transport equation and the homogeneous transport equation are equal, gives:

$$\mathbf{v_{ls,hh} = \left(g \cdot R_{sd} \cdot D_p \left(30.11 \cdot C_{vt}^{0.868} \cdot \left(\frac{\lambda_l}{4}\right)^{0.200} \cdot C_D^{*-0.1677} \cdot \left(R_{sd} \cdot C_{vt}\right)^{-1}\right)^{1/0.6938}\right)^{0.5}}$$

(9.2-33)

The equation of Turian & Yuan (1977) for homogeneous transport is not used here, because we want to compare the intersection point of heterogeneous and homogeneous transport, using the same equation for homogeneous transport for all models.

9.2.10 Wilson et al. (1992) (Power 1.0, Non-Uniform Particles).

The final simplified equation for heterogeneous transport of Wilson et al. (1992) is:

$$\mathbf{\frac{i_m - i_l}{i_l \cdot C_{vt}} = \frac{\Delta p_m - \Delta p_l}{\Delta p_l \cdot C_{vs}} = 44.1^M \cdot \frac{\mu_{sf} \cdot g \cdot R_{sd} \cdot D_p}{\lambda_l} \cdot \left(d_{50}\right)^{0.35 \cdot M} \cdot \left(\frac{1}{v_{ls}}\right)^{2+M}}$$

(9.2-34)

The hydraulic gradient in the homogeneous regime, according to ELM so without corrections, is:

$$\mathbf{i_m = i_l \cdot \left(1 + R_{sd} \cdot C_{vs}\right) \quad \Rightarrow \quad \frac{i_m - i_l}{i_l \cdot C_{vs}} = \frac{\Delta p_m - \Delta p_l}{\Delta p_l \cdot C_{vs}} = R_{sd}}$$

(9.2-35)

Rewriting this equation into a form that shows the line speed where the heterogeneous transport equation and the homogeneous transport equation are equal, gives:

$$\mathbf{44.1^M \cdot \frac{\mu_{sf} \cdot g \cdot R_{sd} \cdot D_p}{\lambda_l} \cdot \left(d_{50}\right)^{0.35 \cdot M} \cdot \left(\frac{1}{v_{ls}}\right)^{2+M} = R_{sd}}$$

(9.2-36)

This gives for the transition velocity between the heterogeneous regime and the homogeneous regime for **M=1**:

$$\mathbf{v_{ls,hh}^3 = 44.1 \cdot \frac{\mu_{sf} \cdot g \cdot D_p}{\lambda_l} \cdot \left(d_{50}\right)^{0.35}}$$

(9.2-37)

It should be mentioned that this is based on the simplified model of Wilson et al. (1992) for heterogeneous transport. The full model may give slightly different results.

9.2.11 Wilson et al. (1992) (Power 1.7, Uniform Particles).

The final simplified equation for heterogeneous transport of Wilson et al. (1992) is:

$$\frac{i_m - i_l}{i_l \cdot C_{vt}} = \frac{\Delta p_m - \Delta p_l}{\Delta p_l \cdot C_{vs}} = 44.1^M \cdot \frac{\mu_{sf} \cdot g \cdot R_{sd} \cdot D_p}{\lambda_l} \cdot \left(d_{50}\right)^{0.35 \cdot M} \cdot \left(\frac{1}{v_{ls}}\right)^{2+M} \tag{9.2-38}$$

The hydraulic gradient in the homogeneous regime, according to ELM so without corrections, is:

$$i_m = i_l \cdot \left(1 + R_{sd} \cdot C_{vs}\right) \quad \Rightarrow \quad \frac{i_m - i_l}{i_l \cdot C_{vs}} = \frac{\Delta p_m - \Delta p_l}{\Delta p_l \cdot C_{vs}} = R_{sd} \tag{9.2-39}$$

Rewriting this equation into a form that shows the line speed where the heterogeneous transport equation and the homogeneous transport equation are equal, gives:

$$44.1^M \cdot \frac{\mu_{sf} \cdot g \cdot R_{sd} \cdot D_p}{\lambda_l} \cdot \left(d_{50}\right)^{0.35 \cdot M} \cdot \left(\frac{1}{v_{ls}}\right)^{2+M} = R_{sd} \tag{9.2-40}$$

This gives for the transition velocity between the heterogeneous regime and the homogeneous regime:

$$v_{ls,hh}^{3.7} = 44.1^{1.7} \cdot \frac{\mu_{sf} \cdot g \cdot D_p}{\lambda_l} \cdot \left(d_{50}\right)^{0.35 \cdot 1.7} \tag{9.2-41}$$

It should be mentioned that this is based on the simplified model of Wilson et al. (1992) for heterogeneous transport. The full model may give slightly different results.

9.2.12 Wilson & Sellgren (2012) Near Wall Lift Model.

The relative excess hydraulic gradient of the near wall lift model is:

$$E_{rhg} = R = \frac{10 \cdot \left(R_{sd} \cdot g \cdot d\right)^{1/2} \cdot \left(R_{sd} \cdot g \cdot v_l\right)^{1/3}}{\lambda_l \cdot v_{ls}^2} \tag{9.2-42}$$

The near wall lift based equation gives for sand and water:

$$E_{rhg} = R = \frac{d^{1/2}}{\lambda_l \cdot v_{ls}^2} \tag{9.2-43}$$

The relative excess hydraulic gradient in the homogeneous regime, according to ELM so without corrections, is:

$$E_{rhg} = \frac{i_m - i_l}{R_{sd} \cdot C_{vs}} = i_l = \frac{\lambda_l \cdot v_{ls}^2}{2 \cdot g \cdot D_p} \tag{9.2-44}$$

This gives for the transition velocity between the heterogeneous regime and the homogeneous regime:

$$v_{ls,hh}^4 = \frac{2 \cdot g \cdot D_p}{\lambda_l^2} \cdot d^{1/2} \tag{9.2-45}$$

9.2.13 The Saskatchewan Research Council Model.

The SRC model consists of two terms regarding the excess hydraulic gradient. A term for the contact load and a term for the suspended load. Here only the term for the contact load is considered, assuming the contact load results in a small bed and there is no buoyancy from the suspended load.

Comparison of the DHLLDV Framework with Other Models.

The hydraulic gradients of the heterogeneous (contact load) model should be equal to the homogeneous model giving:

$$\mu_{sf} \cdot e^{-0.0212 \cdot \frac{v_{ls,hh}}{v_t}} \cdot R_{sd} \cdot C_{vs} = \frac{\lambda_l \cdot v_{ls,hh}^2}{2 \cdot g \cdot D_p} \cdot R_{sd} \cdot C_{vs} \tag{9.2-46}$$

The SRC model results in an implicit relation if only the contact load is considered, this gives:

$$v_{ls,hh}^2 = \mu_{sf} \cdot e^{-0.0212 \cdot \frac{v_{ls,hh}}{v_t}} \cdot \frac{2 \cdot g \cdot D_p}{\lambda_l} \quad \text{or} \quad v_{ls,hh}^2 \cdot e^{0.0212 \cdot \frac{v_{ls,hh}}{v_t}} = \mu_{sf} \cdot \frac{2 \cdot g \cdot D_p}{\lambda_l} \tag{9.2-47}$$

9.2.14 Examples Heterogeneous versus Homogeneous.

The comparison is based on models for saltating or heterogeneous transport. As mentioned before, the transition line speed from heterogeneous to homogeneous transport is a good indicator for the excess pressure losses. A higher transition line speed indicates higher excess pressure losses. For a pipe diameter of 0.1016 m (4 inch) and medium sized particles (0.1 mm to 2 mm) all models are close for high concentrations (around 30%), shown in Figure 9.2-10. This is caused by the fact that most experiments are carried out in small diameter pipes, resulting in a cloud of data points because of scatter. Many curves will fit through this cloud of data points.

The following graphs (Figure 9.2-5, Figure 9.2-6, Figure 9.2-7, Figure 9.2-8 Figure 9.2-9, Figure 9.2-10, Figure 9.2-11, Figure 9.2-12, Figure 9.2-13, Figure 9.2-14, Figure 9.2-15, Figure 9.2-16, Figure 9.2-17 and Figure 9.2-18) have a dimensionless vertical axis by dividing the transition line speed by the maximum transition line speed occurring in one of the 11 models. This maximum transition line speed is shown in the lower right corner of each graph. For normal dredging operations, particles diameters from 0.1 mm up to 10 mm are of interests. The different models are compared with the DHLLDV Framework of Miedema & Ramsdell (2013). For very small pipe diameters (<0.1 m) the Newitt et al. (1955) model is representative, for medium pipe diameters (0.1-0.3 m) the Fuhrboter (1961) model and the Durand & Condolios (1952) model are representative and for large pipe diameters (>0.3 m) the Jufin & Lopatin (1966) model is representative, although this model tends to underestimate the pressure losses slightly for large pipe diameters and high concentrations. The Wilson et al. (1992) and the SRC models have developed over the years and are based on many experimental data and can thus be considered to be representative in all cases for medium sized particles.

In the following paragraphs the influence of 6 parameters on the transition velocity between the heterogeneous and the homogeneous regimes is discussed. When the word model is used, it refers to the model or equation of this transition velocity.

9.2.14.1 The Influence of the Particle Diameter & Terminal Settling Velocity.

Two groups of models can be distinguished.
The first group: models based on the terminal settling velocity, Newitt et al. (1955) and the SRC model, or a directly related parameter, Wilson et al. (1992). The small DHLLDV Framework potential energy term also depends on the hindered settling velocity.
The second group: models based on the particle Froude number, Durand & Condolios (1952), Jufin & Lopatin (1966) (values from a table) and the large DHLLDV Framework kinetic energy term, or based on the particle drag coefficient, Fuhrboter (1961) (values from a graph), Zandi & Govatos (1967) and Turian & Yuan (1977). The difference between the particle Froude number and the particle drag coefficient is mainly the relative submerged density and a constant. In other words, the particle drag coefficient is independent of the relative submerged density, while the particle Froude number is dependent. As long as sand and gravel are considered, the two are related by a fixed factor, but for other solids this factor changes.

The difference between the two groups is, that the terminal settling velocity continuously increases with the particle diameter, while the particle Froude number and the particle drag coefficient have a constant asymptotic value for large particle diameters.
So models from the first group tend to overestimate the transition line speed for large particles. This is however not surprising, since both Newitt et al. (1955), SRC and Wilson et al. (1992) use a 2LM or sliding bed model for this case, so the large particle part of the curves is not relevant.

9.2.14.2 The Influence of the Pipe Diameter.

Some models give a direct relation between the transition velocity and the pipe diameter, other models include the Darcy Weisbach friction factor which decreases with the pipe diameter with a power of about 0.2. For these models the powers mentioned are an estimate.
The Durand & Condolios (1952) and Zandi & Govatos (1967) models show a proportionality of the transition line speed with the pipe diameter with a power of 0.5. The two Turian & Yuan (1977) models also. The Newitt et al. (1955) model shows a proportionality with a power of 1/3. Fuhrboter (1961) also a power of 1/3. Jufin & Lopatin (1966) a power of 1/6. The two Wilson et al. (1992) models 0.3-0.4. The SRC model about 0.2 for small particles (**d=0.1 mm**), 0.3 for medium particles (**d=0.4 mm**), 0.4 for medium/coarse particles (**d=1 mm**) and 0.5 for large particles (**d=10 mm**), due to the exponential function in the equation. This results in a proportionality power related to the terminal settling velocity. Finally the DHLLDV Framework with a power of about 0.35.

In general one can say that the transition line speed is proportional to the pipe diameter with a power of 0.3 to 0.4, based on the Wilson et al. (1992) models, the SRC model and the DHLLDV Framework.

9.2.14.3 The Influence of the Concentration.

The model of Jufin & Lopatin (1966) strongly depends on the volumetric concentration, the DHLLDV Framework of Miedema & Ramsdell (2013) weakly as well as the models of Turian & Yuan (1977). Turian & Yuan (1977) saltating has a small positive power (+0.13), while the heterogeneous equation shows a small negative power (-0.22). Jufin & Lopatin (1966) give a power of -1/6. These small negative powers match the DHLLDV Framework for homogeneous flow based on a particle free viscous sub-layer. The DHLLDV Framework heterogeneous model consists of a potential energy term and a kinetic energy term. The small potential energy term depends on the concentration due to the hindered settling effect.
The models of Durand & Condolios (1952) & Gibert (1960), Newitt et al. (1955), Fuhrboter (1961), Zandi & Govatos (1967), Wilson et al. (1992) and the SRC model do not depend on the volumetric concentration.
In general one can say that the transition line speed depends weakly on the spatial concentration.

9.2.14.4 The Influence of the Sliding Friction Coefficient.

The Wilson et al. (1992) and the SRC models are based on a sliding bed and a stratification ratio. It is assumed that the heterogeneous regime consists of a sliding bed of which the thickness decreases with increasing line speed according to a certain relation. Since the excess head losses of a sliding bed are proportional to the sliding friction factor, so is the transition velocity. The power of this proportionality is between 1/3 and 1/4. However, since the sliding friction coefficient does not vary much, this parameter is not very important. Wilson et al. (1992) uses values of 0.4 and 0.44, while SRC advises 0.5. All other models do not use the sliding friction coefficient.

In general one can say that there is no influence of the sliding friction coefficient on the transition velocity of the heterogeneous and the homogeneous regimes.

9.2.14.5 The Influence of the Relative Submerged Density.

In the DHLLDV Framework there is no direct influence of the relative submerged density, only an indirect influence through the particle Froude number. The Durand & Condolios (1952) model shows a weak influence with a power of 1/6 and an indirect influence through the particle Froude number. The Newitt et al. (1955) model is independent of the relative submerged density, for the transition velocity. Apparently the influence of the relative submerged density on the heterogeneous and the homogeneous (ELM) regimes is the same. The Fuhrboter (1961) model gives the same conclusion with the approximation equation for the S_k value. The original Jufin & Lopatin (1966) model only depends indirectly through the particle Froude number on the relative submerged density. The Zandi & Govatos (1967) model depends both directly and indirectly on the relative submerged density. Directly with a power of about 0.25. The Turian & Yuan (1977) models depend weakly on the relative submerged density with powers of +0.15 and -0.2. The Wilson et al. (1992) models and the SRC model do not depend on the relative submerged density.

In general one can say that there is a weak or no direct dependency of the transition velocity of the heterogeneous and the homogeneous regimes on the relative submerged density. Some models give a weak indirect dependency on the particle Froude number.

9.2.14.6 The Influence of the Line Speed.

In the models of Durand & Condolios (1952), Newitt et al. (1955), Fuhrboter (1961), Jufin & Lopatin (1966) and Wilson et al. (1992) (the -1 power model) the pressure losses or hydraulic gradient decreases reversely with the line speed.
The Zandi & Govatos (1967), Wilson et al. (1992) (the -1.7 power model) and the DHLLDV Framework with a power between -1.7 and -2.0.
The Turian & Yuan (1977) saltating regime has a power of about -0.7, while the Turian & Yuan (1977) heterogeneous equation has a positive power of about +0.6. These powers are probably the result of curve fitting of experimental data in the sliding bed + the heterogeneous regimes (powers of 0 and -1 to -2), resulting in the power of -0.7 and data in the heterogeneous + the (pseudo) homogeneous regimes (powers of -1 to -2 and +2), resulting in the power of +0.6.

In general one can say that the more negative the power of the line speed in the heterogeneous hydraulic gradient equation, the smaller the transition velocity between the regimes. One has to take this into account interpreting the graphs.

9.2.14.7 Summary.

The standard deviation of the 12 models for $C_{vs}=0.175$ is shown in Figure 9.2-2. For pipe diameters close to 0.1016 m (4 inch) and particle diameters in the range of 0.3 to 4 mm, the standard deviation is less than 10%. This is also the particle diameter region of heterogeneous transport. Smaller pipes and larger pipes show a larger standard deviation. This means that for pipe diameters close to 0.1016 m and particles in the range of 0.3 to 4 mm, all models give about the same result in terms of the solids effect in the hydraulic gradient. The smaller the pipe or the larger the pipe the more the models deviate. Figure 9.2-3 shows the standard deviation omitting the 3 Wilson et al. models, since these give very high transition velocities for very small particles. The same trends are observed here.
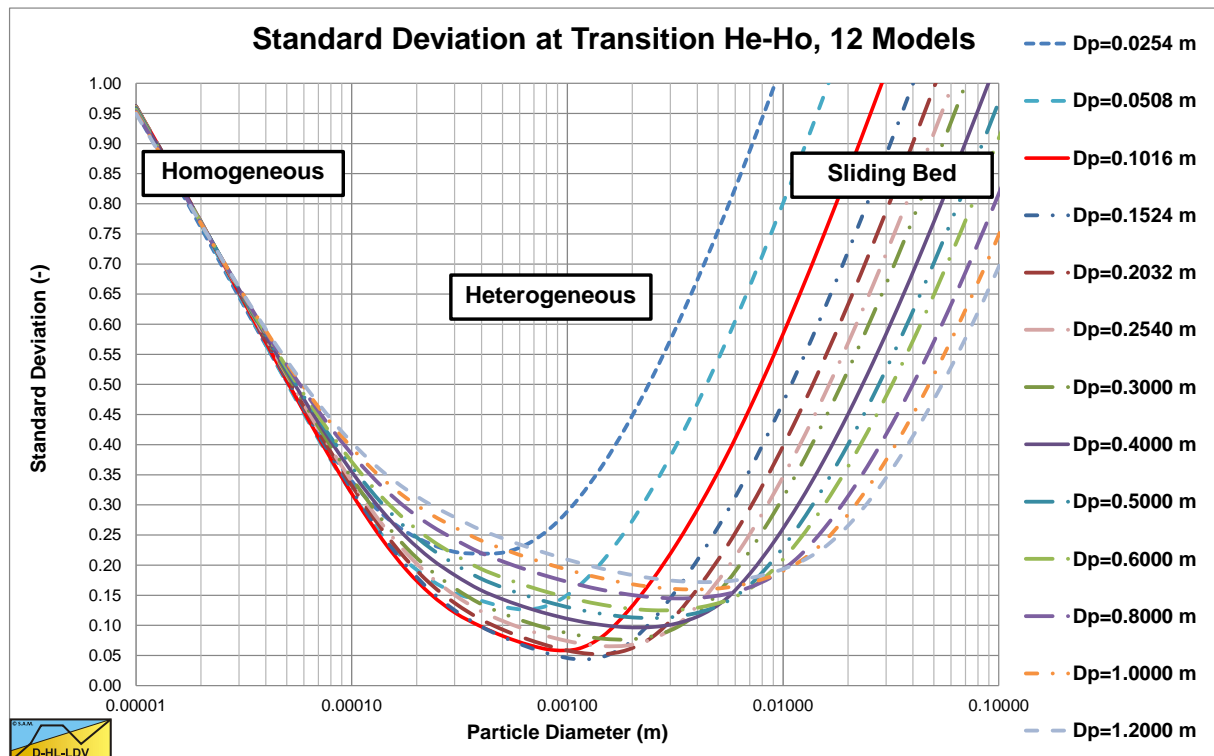
Figure 9.2-2: The standard deviation of 12 models.

Figure 9.2-4 shows the standard deviation of the DHLLDV Framework, the SRC model and the Wilson et al. models with a power of 1.7 and the near wall lift method (NWL). In the range of particle diameters from 0.25 mm to 1-3 mm the standard deviation is less than 10% and does not really depend on the pipe diameter. Very small particles show a high standard deviation, but the heterogeneous models are not applicable there. At normal operational line speeds, which are much higher than the transition line speeds found, the transport will be according

to the homogeneous flow regime (ELM related). Very large particles show an increasing standard deviation, resulting from the fact that here the sliding bed or sliding flow regimes are applicable and not the heterogeneous flow regime.

Although the physics behind the 4 models considered, the DHLLDV Framework, the SRC model and the 2 Wilson et al. models, are different, the 4 models give about the same result for medium sands in terms of the solids effect, irrespective of the pipe diameter.
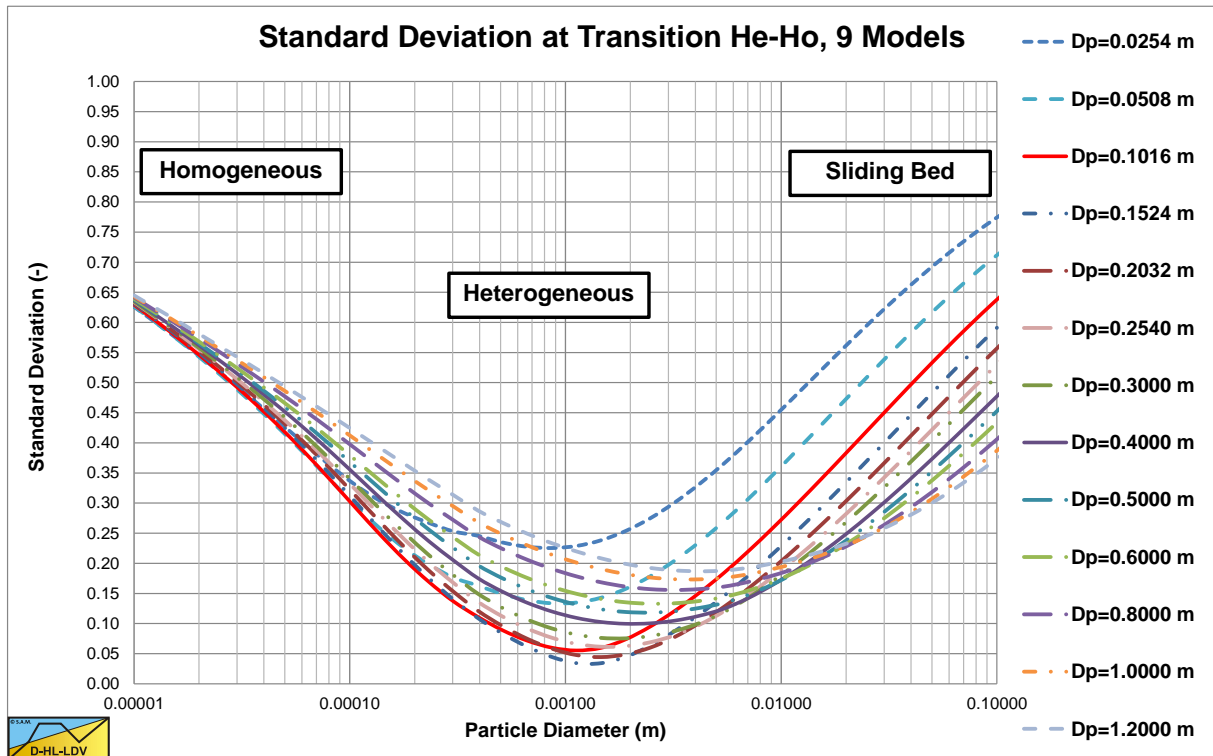
Figure 9.2-3: The standard deviation of 9 models.
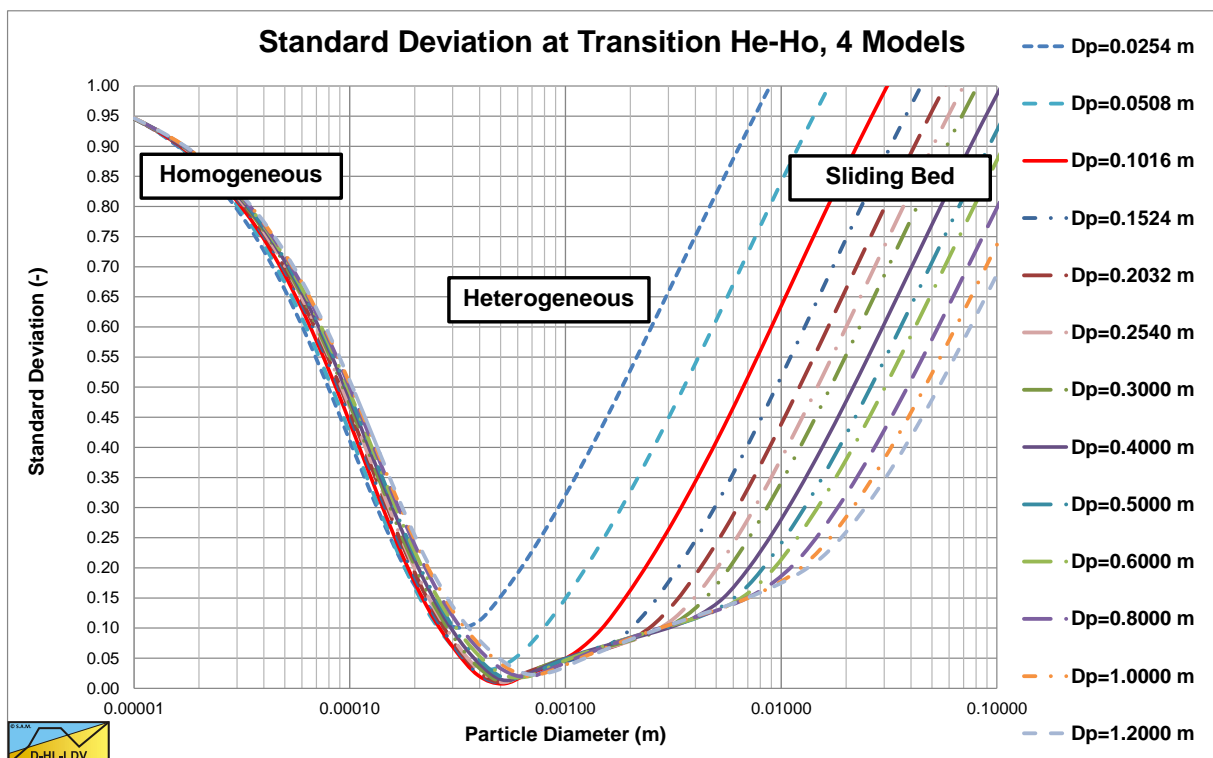
Figure 9.2-4: The standard deviation of 4 models.

9.2.14.8 A 0.0254 m Diameter Pipe (1 inch).
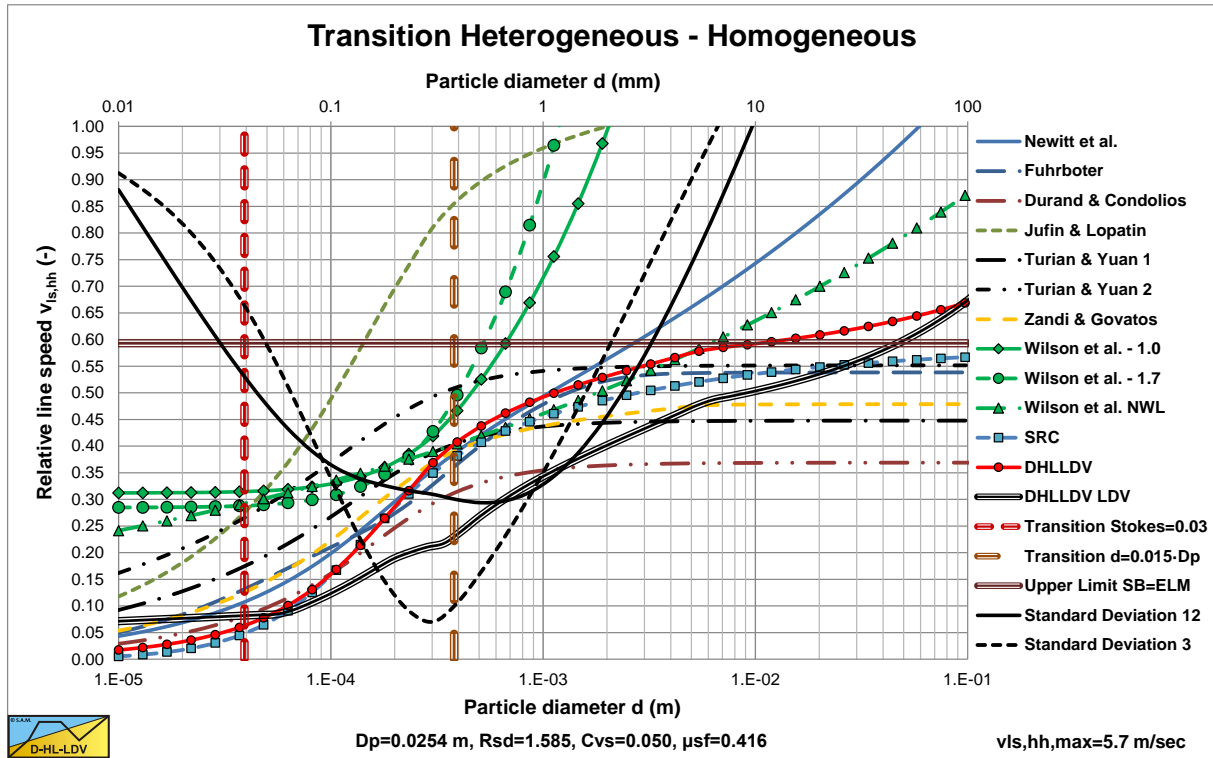
Figure 9.2-5: The transition line speed He-Ho for D_p=0.0254 m and C_v=0.05.
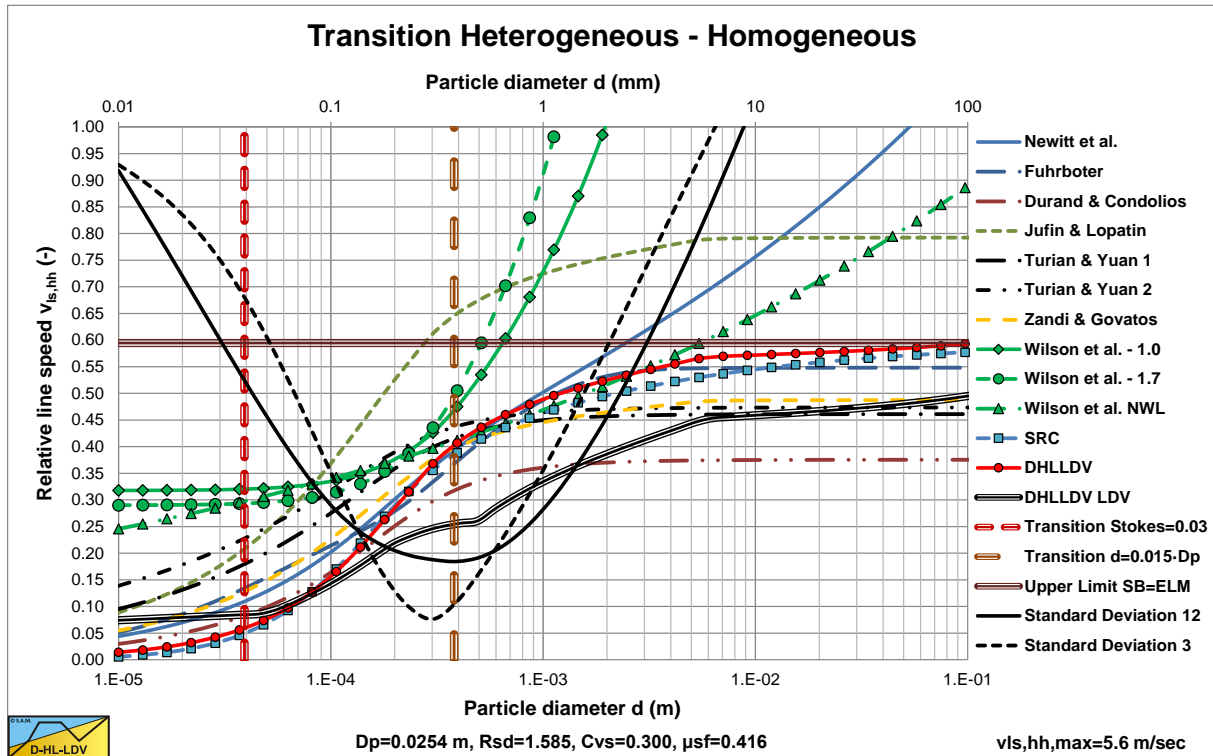
Figure 9.2-6: The transition line speed He-Ho for D_p=0.0254 m and C_v=0.30.

In the range of medium sized particles most models are very close. The Durand & Condolios model however seems to underestimate the transition velocity, while the Jufin & Lopatin and the Turian & Yuan 2 models overestimate the transition velocity. The SRC and the DHLLDV Framework are very close up to a particle size of about 10 mm.

9.2.14.9 A 0.0508 m Diameter Pipe (2 inch).
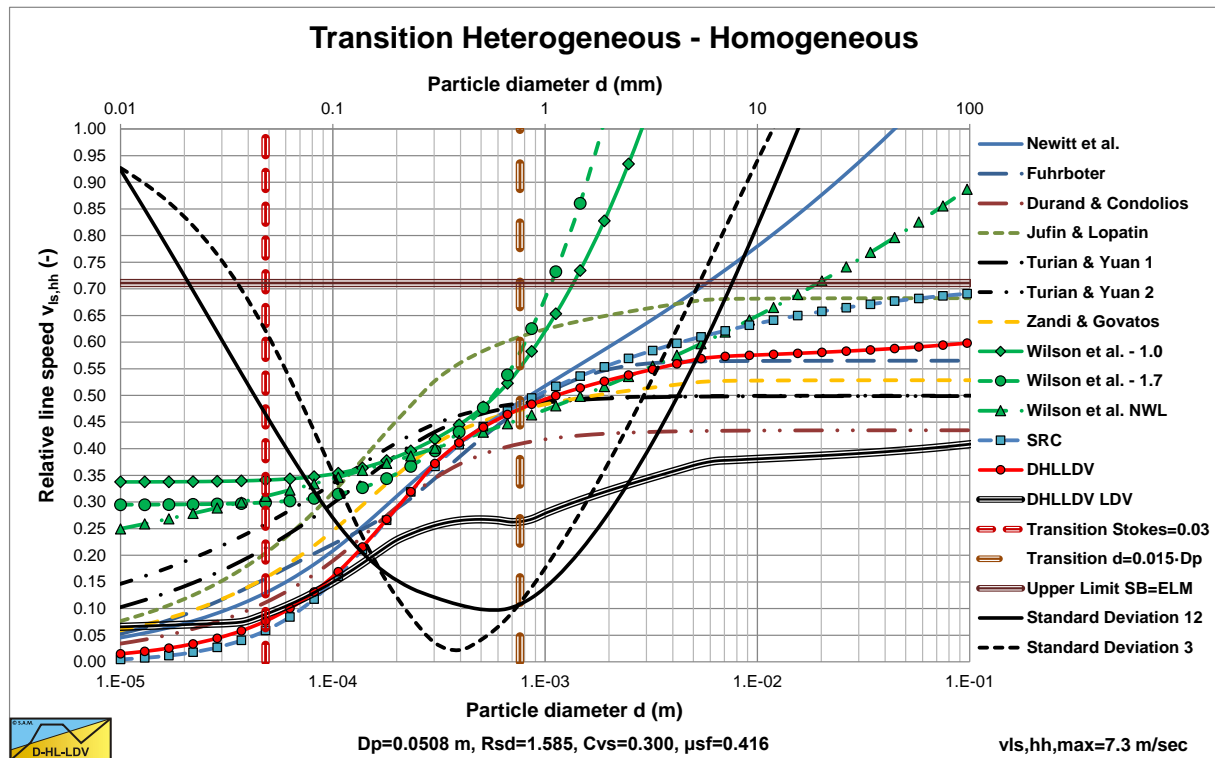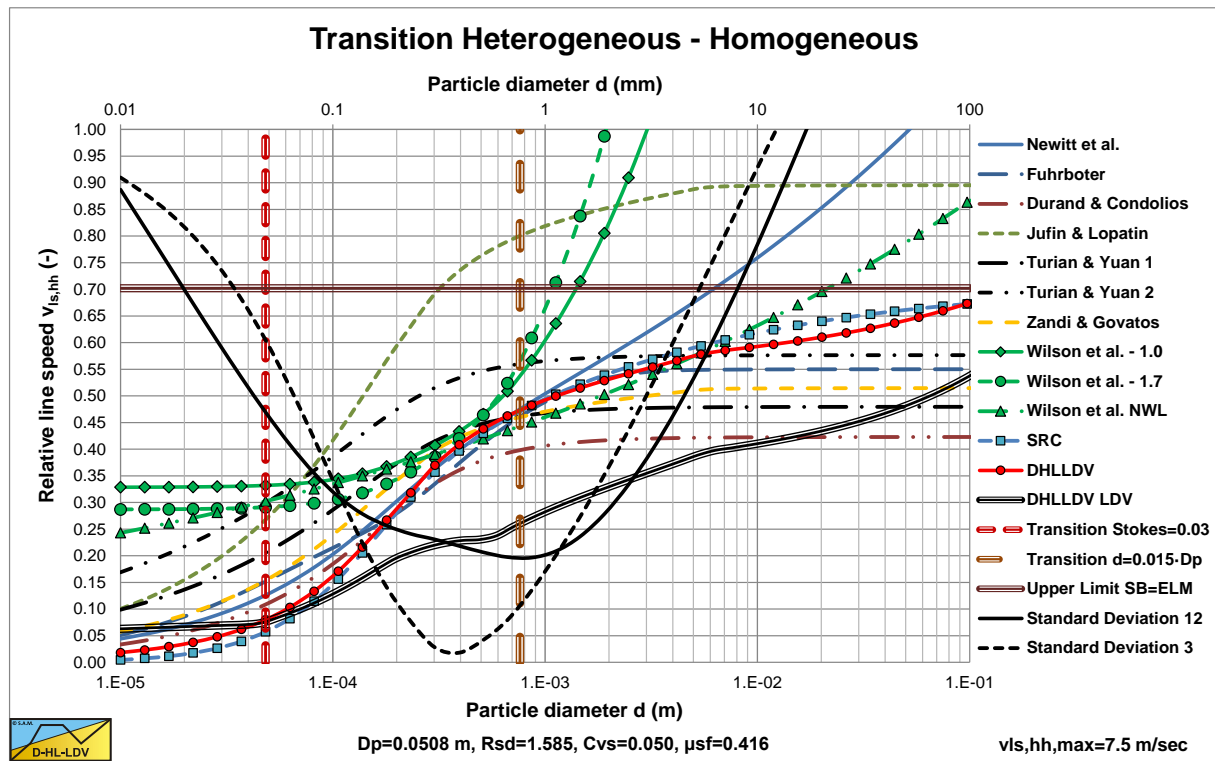
Figure 9.2-7: The transition line speed He-Ho for D_p=0.0508 m and C_v=0.05.

Figure 9.2-8: The transition line speed He-Ho for D_p=0.0508 m and C_v=0.30.

In the range of medium sized particles most models are very close. The Durand & Condolios model however seems to underestimate the transition velocity, while the Jufin & Lopatin and the Turian & Yuan 2 models overestimate the transition velocity. The SRC and the DHLLDV Framework are very close up to a particle size of about 2 mm.

9.2.14.10 A 0.1016 m Diameter Pipe (4 inch).
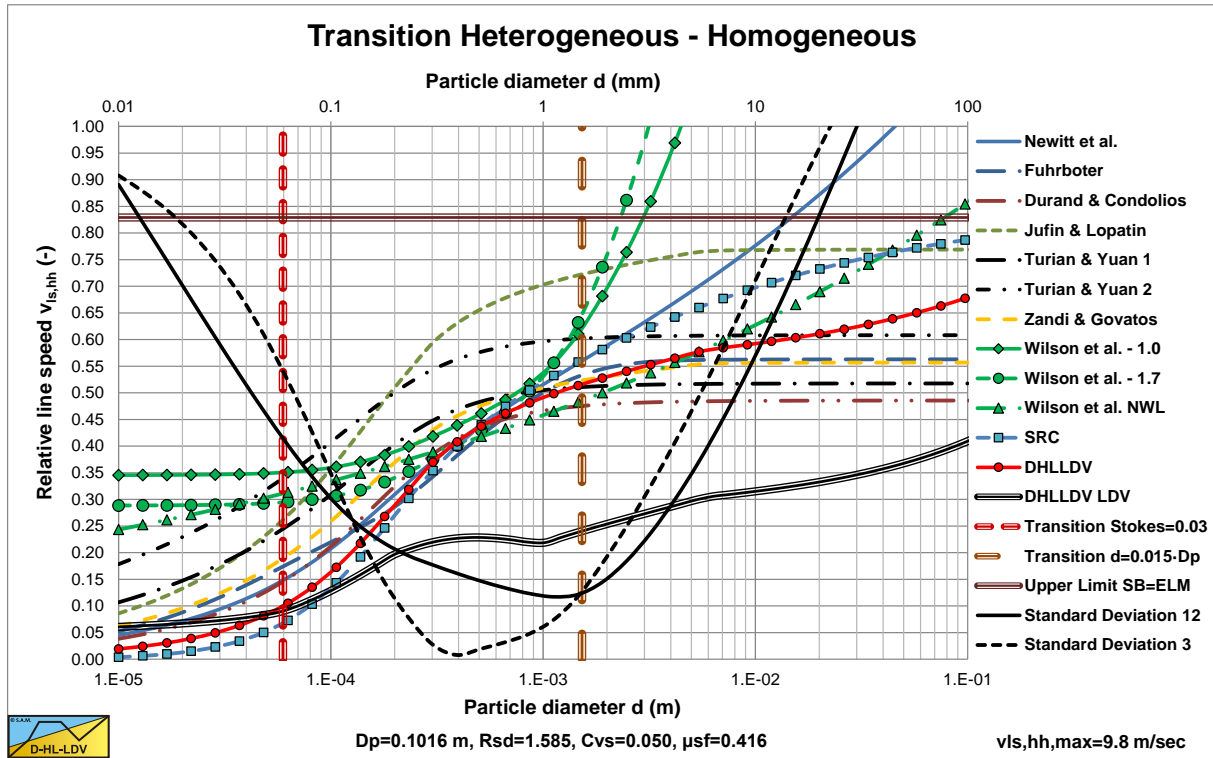
Figure 9.2-9: The transition line speed He-Ho for D_p=0.1016 m and C_v=0.05.
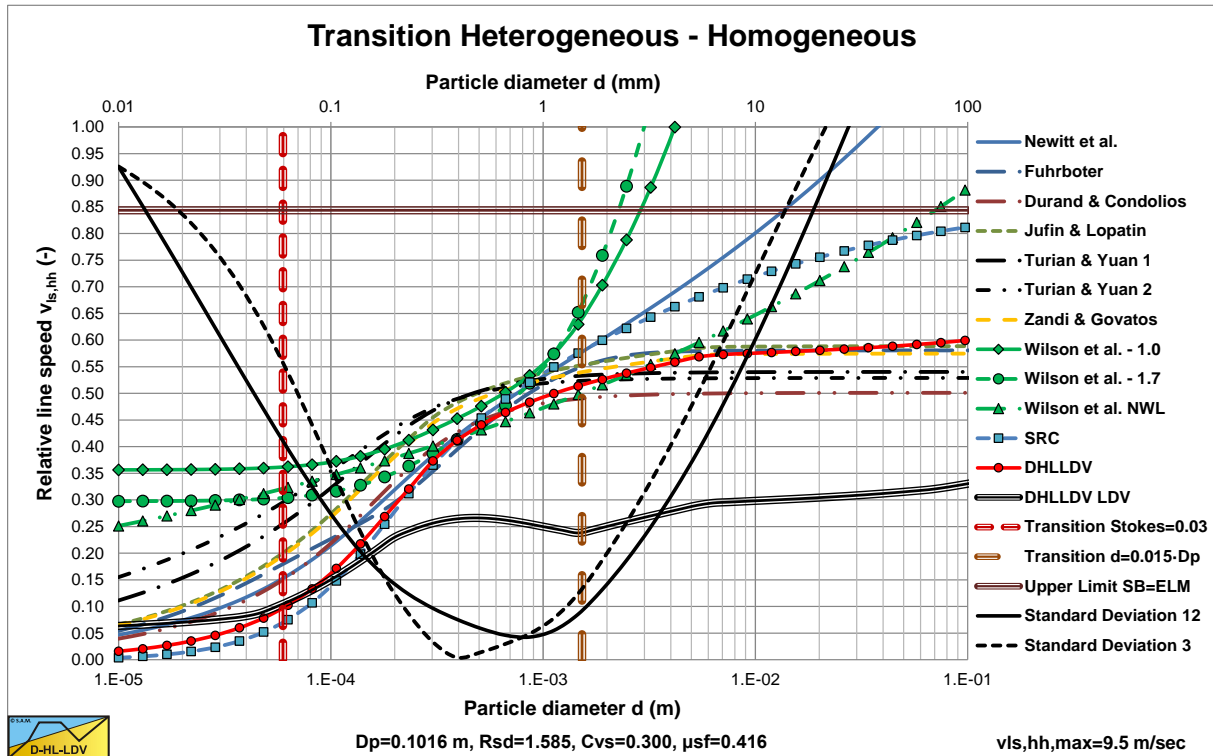
Figure 9.2-10: The transition line speed He-Ho for D_p=0.1016 m and C_v=0.30.

Most models are close for medium sized particles for higher concentrations. The Turian & Yuan 2 and the Jufin & Lopatin models depend on the concentration as can be seen clearly in the figures. The SRC and DHLLDV Framework match closely up to a particle diameter of about 1 mm. The Wilson et al. models matches both models for particle diameters close to 1 mm.

9.2.14.11 A 0.2032 m Diameter Pipe (8 inch).
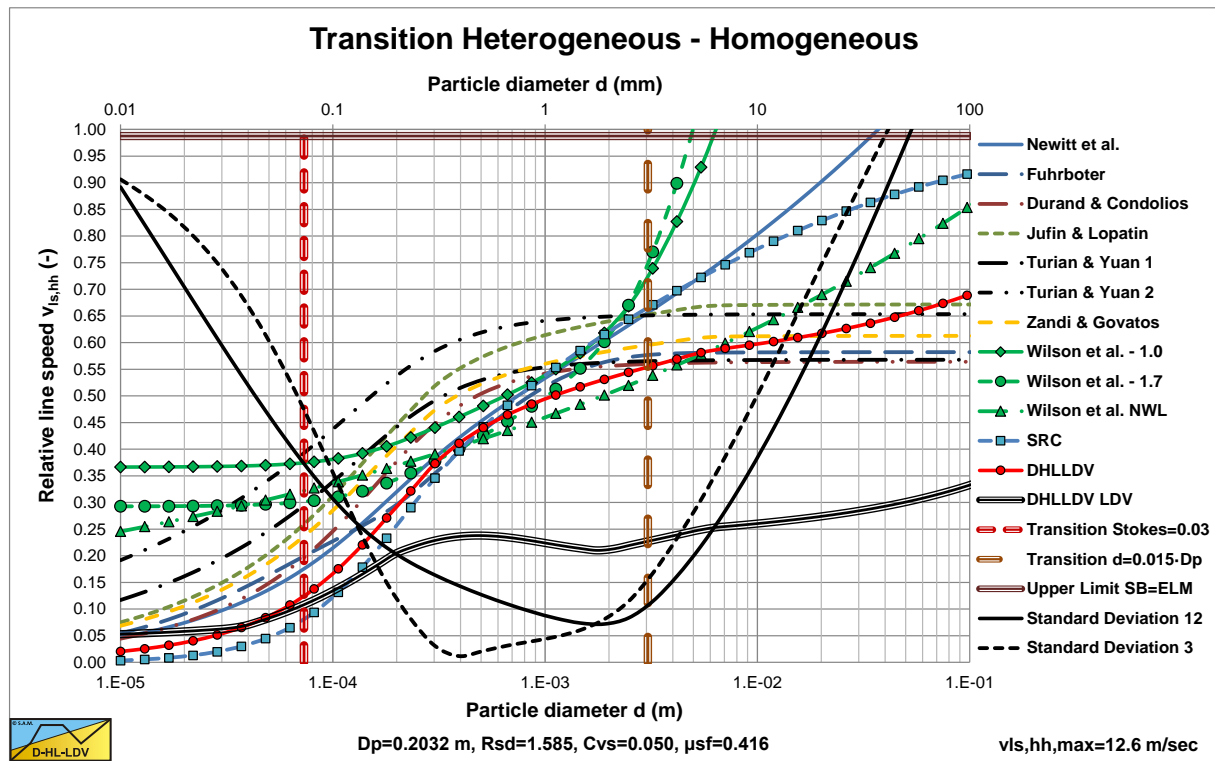
Figure 9.2-11: The transition line speed He-Ho for D_p=0.2032 m and C_v=0.05.
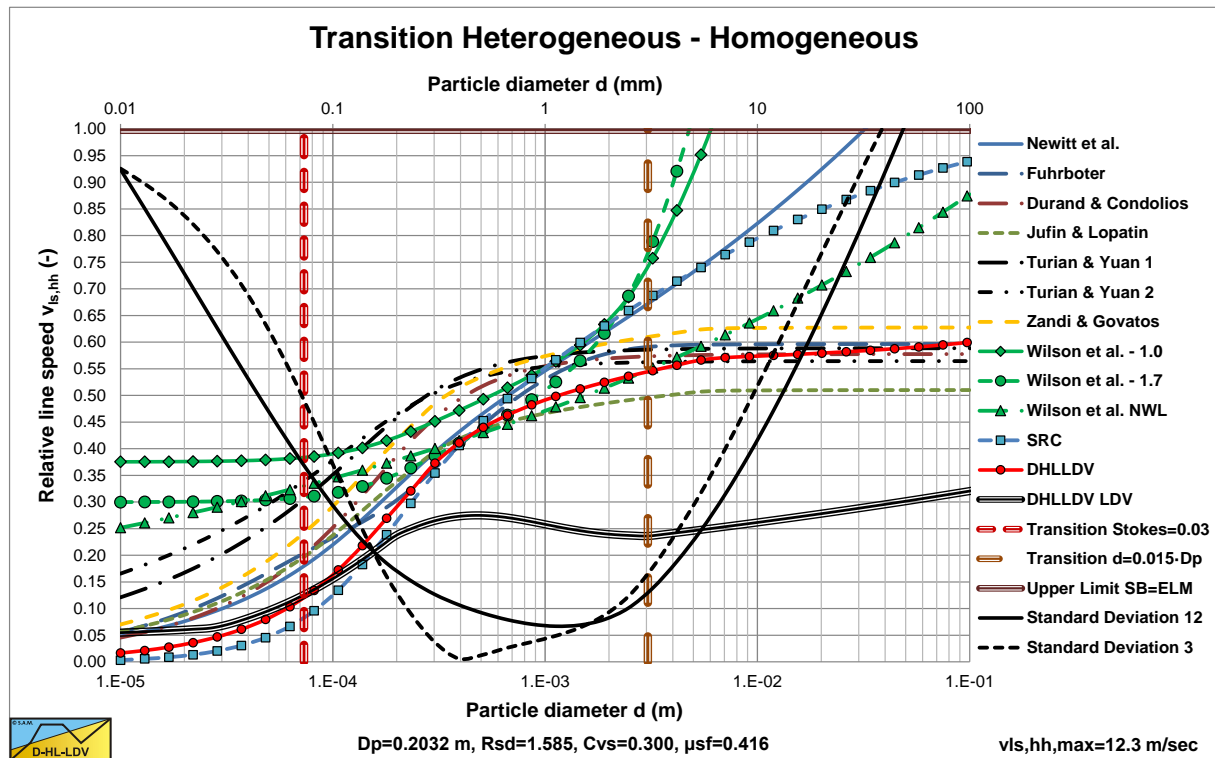
Figure 9.2-12: The transition line speed He-Ho for D_p=0.2032 m and C_v=0.30.

Most models are close for medium sized particles for higher concentrations. The Turian & Yuan 2 and the Jufin & Lopatin models depend on the concentration as can be seen clearly in the figures. The SRC and DHLLDV Framework match closely up to a particle diameter of about 0.6 mm. The Wilson et al. models matches both models for particle diameters close to 1 mm.

9.2.14.12 A 0.4064 m Diameter Pipe (16 inch).
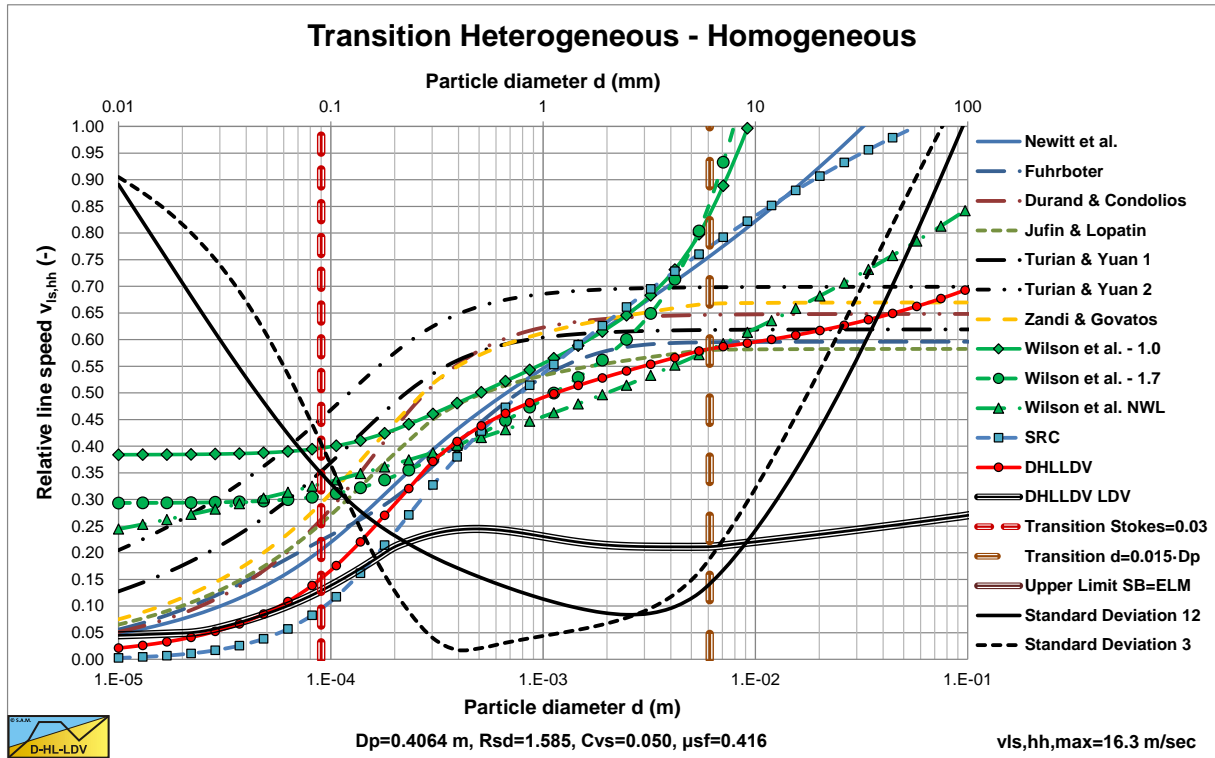
Figure 9.2-13: The transition line speed He-Ho for D_p=0.4064 m and C_v=0.05.
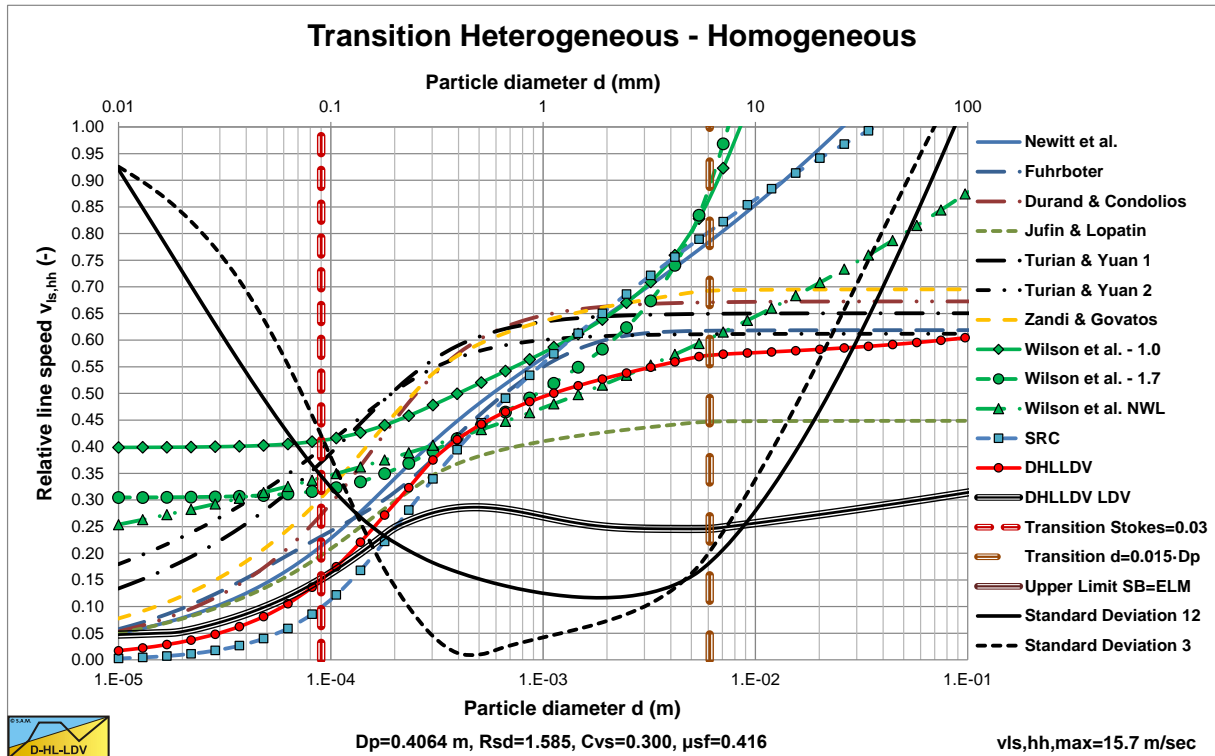
Figure 9.2-14: The transition line speed He-Ho for D_p=0.4064 m and C_v=0.30.

The models start to deviate strongly. Durand & Condolios, Zandi & Govatos and Turian & Yuan 1 and 2 give high transition velocities. Fuhrboter, Newitt et al. and Wilson et al. -1.0 medium transition velocities, while DHLLDV, SRC (small particles), Wilson et al. -1.7 and Jufin & Lopatin (medium concentrations) give low transition velocities.

9.2.14.13 A 0.762 m Diameter Pipe (30 inch).
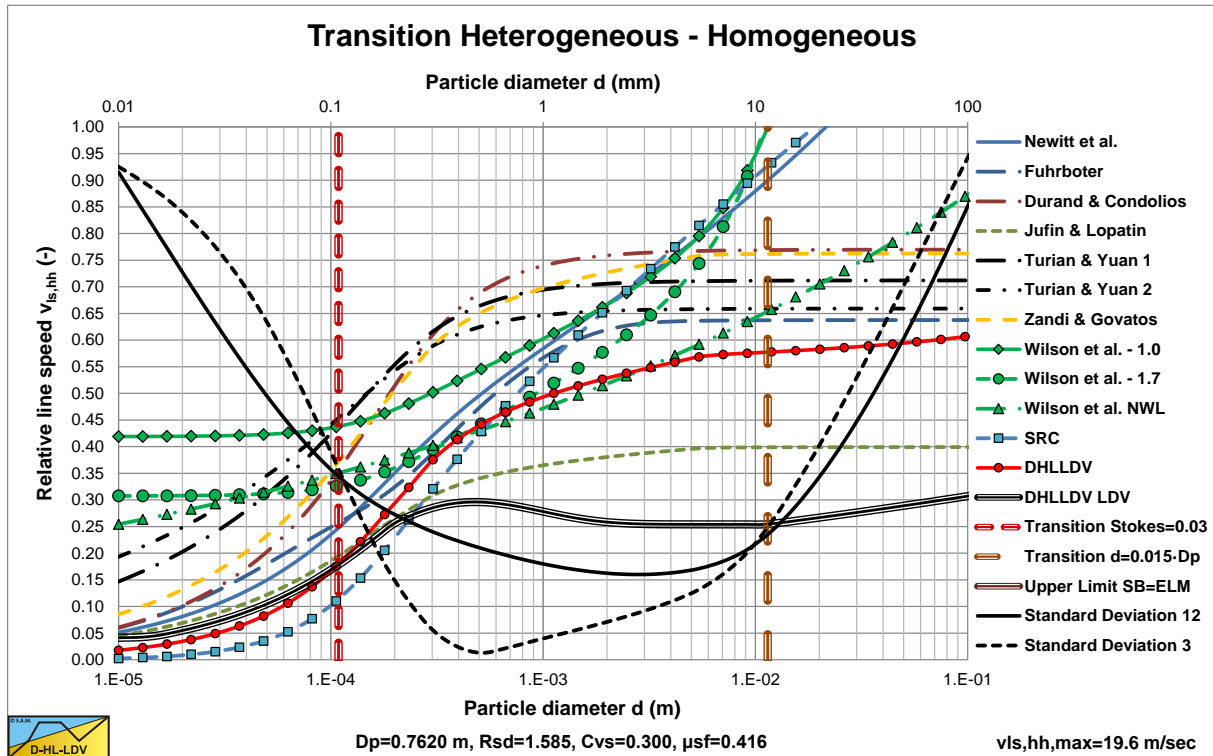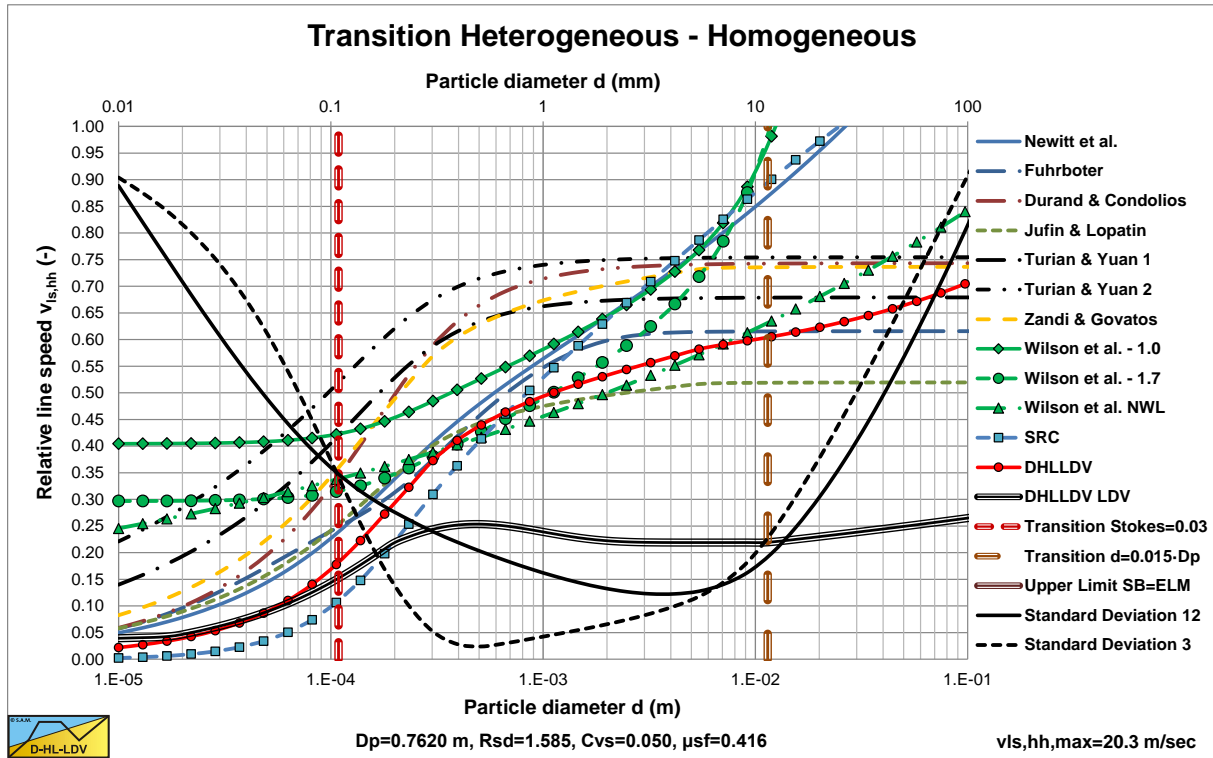
Figure 9.2-15: The transition line speed He-Ho for D_p=0.762 m and C_v=0.05.

Figure 9.2-16: The transition line speed He-Ho for D_p=0.762 m and C_v=0.30.

The models deviate strongly. Durand & Condolios, Zandi & Govatos and Turian & Yuan 1 and 2 give high transition velocities. Fuhrboter, Newitt et al. and Wilson et al. -1.0 medium transition velocities, while DHLLDV, SRC (small particles), Wilson et al. -1.7 and Jufin & Lopatin (medium concentrations) give low transition velocities.

9.2.14.14 A 1.2 m Diameter Pipe.
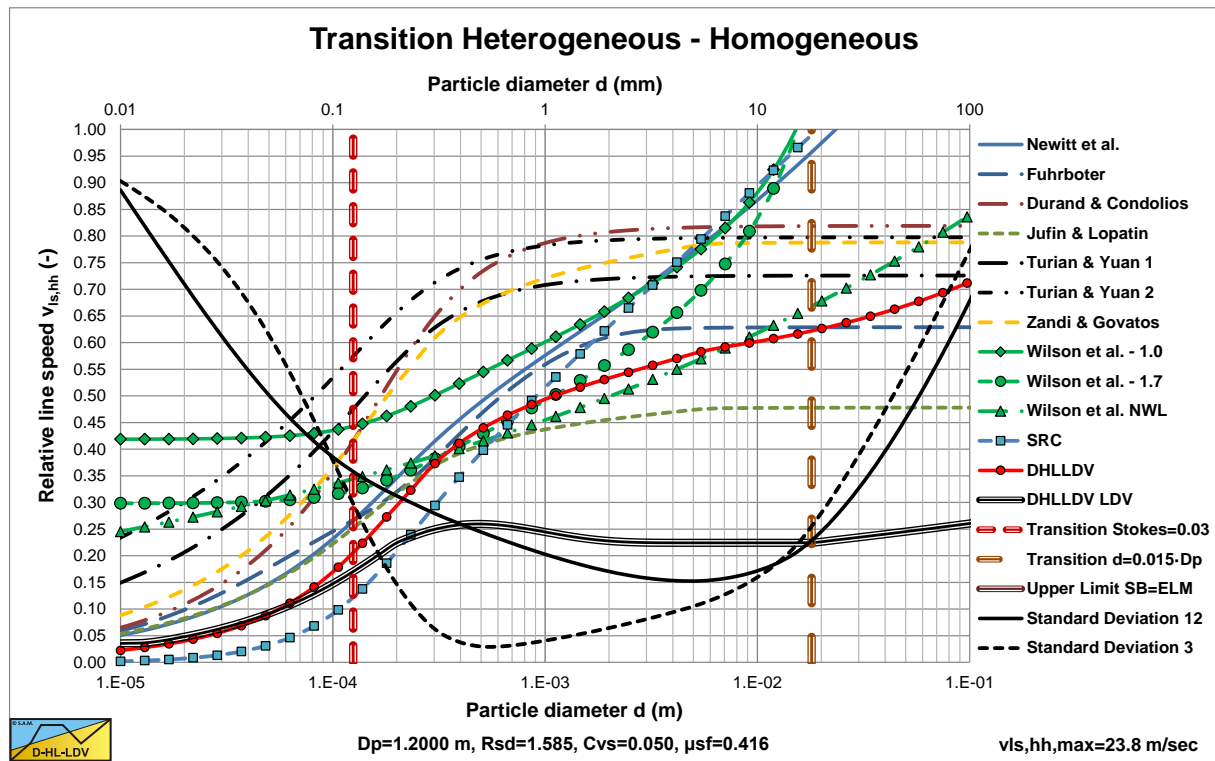
Figure 9.2-17: The transition line speed He-Ho for D_p=1.2 m and C_v=0.05.
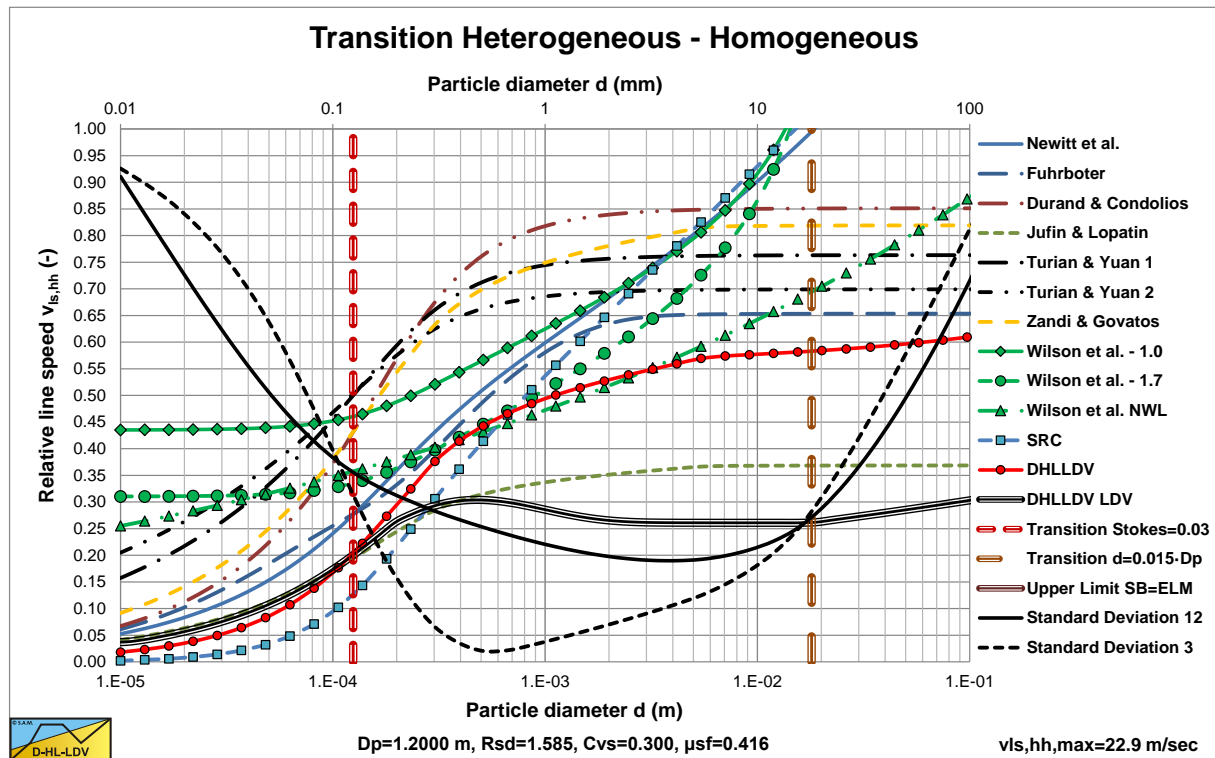
Figure 9.2-18: The transition line speed He-Ho for D_p=1.2 m and C_v=0.30.

The models deviate strongly. Durand & Condolios, Zandi & Govatos and Turian & Yuan 1 and 2 give high transition velocities. Fuhrboter, Newitt et al. and Wilson et al. -1.0 medium transition velocities, while DHLLDV, SRC (small particles), Wilson et al. -1.7 and Jufin & Lopatin (medium concentrations) give low transition velocities.

9.2.15 Conclusions & Discussion Heterogeneous-Homogeneous Transition.

The transition velocity of the heterogeneous regime equation with the ELM equation seems to be a good indicator for comparing the different models. A requirement is of course that the heterogeneous component can be isolated. The hydraulic gradient or head losses can be easily determined at the transition velocity, since the ELM is valid in this intersection point. The solids effect of the hydraulic gradient or head losses is proportional to the transition velocity squared.

When interpreting the graphs, one has to consider the operational line speeds for the pipe diameter considered. For example in Figure 9.2-17 and Figure 9.2-18 the maximum line speeds are 26.3 m/s and 24.6 m/s (the full vertical scale). With a maximum Limit Deposit Velocity of 6-7 m/s and a maximum line speed of about 9 m/s, the operational line speed will be in the range of 0.25 to 0.4 on the vertical axis. If the relative transition velocity is below 0.25 the slurry transport will be in the homogeneous regime, following the ELM or related model. If the relative transition velocity is above 0.4 the slurry transport will probably be a fixed or sliding bed. In between there will be heterogeneous or pseudo homogeneous transport.

Models are based on the terminal settling velocity or models are based on the particle Froude number. The difference between the two groups is, that the terminal settling velocity continuously increases with the particle diameter, while the particle Froude number and the particle drag coefficient have a constant asymptotic value for large particle diameters. So models from the first group tend to overestimate the transition line speed for large particles. This is however not surprising, since both Newitt et al. (1955), SRC and Wilson et al. (1992) use a 2LM or sliding bed model for this case, so the large particle part of the curves is not relevant.

In general one can say that the transition line speed is proportional to the pipe diameter with a power of 0.3 to 0.4, based on the Wilson et al. (1992) models, the SRC model and the DHLLDV Framework.

In general one can say that the transition line speed depends weakly on the spatial concentration.

In general one can say that there is no or hardly no influence of the sliding friction coefficient on the transition velocity of the heterogeneous and the homogeneous regimes.

In general one can say that there is a weak or no direct dependency of the transition velocity of the heterogeneous and the homogeneous regimes on the relative submerged density. Some models give a weak indirect dependency on the particle Froude number.

In general one can say that the more negative the power of the line speed in the heterogeneous hydraulic gradient equation, the smaller the transition velocity between the regimes. One has to take this into account interpreting the graphs.

Based on the amount of experimental data, the SRC model and the Wilson et al. model seem to be the most reliable. The DHLLDV Framework is close to these models for medium sized particles, although DHLLDV is based on potential and kinetic energy losses, while both SRC and Wilson et al. are based on a diminishing bed with increasing line speed.
For the range of operational line speeds, particles smaller than 0.2 mm will usually behave according to ELM or related models, while large particles will behave according to a fixed or sliding bed or according to the sliding flow regime.

9.3 The Limit Deposit Velocity.

9.3.1 Analysis.

The Limit Deposit Velocity is defined here as the line speed above which is no stationary bed or sliding bed, Thomas (1962). Below the LDV there may be either a stationary or fixed bed or a sliding bed.

For the critical velocity often the Minimum Hydraulic Gradient Velocity (MHGV) is used, Wilson (1942). For higher concentrations this MHGV may be close to the LDV, but for lower concentrations this is certainly not the case. Yagi et al. (1972) reported using the MHGV, making the data points for the lower concentrations too low, which is clear from Figure 9.3-1. Another weak point of the MHGV is, that it depends strongly on the model used for the heterogeneous flow regime. Durand and Condolios (1952), Fuhrboter (1961), Jufin and Lopatin (1966) and others will each give a different MHGV. In dredging the process is instationary, meaning a constantly changing PSD and concentration in long pipelines, making it almost impossible to determine the MHGV.

Wilson (1979) derived a method for determining the transition velocity between the stationary bed and the sliding bed, which is named here the Limit of Stationary Deposit Velocity (LSDV). Since the transition stationary bed versus sliding bed, the LSDV, will always give a smaller velocity value than the moment of full suspension or saltation, the LDV, one should use the LDV, to be sure there is no deposit at all. For small particles it is also possible that the bed is already completely suspended before the bed could ever start sliding (theoretically). In that case an LSDV does not even exist.

This is the reason for choosing the LDV as the critical velocity, independent of the head loss model and always existing Miedema & Ramsdell (2015A).

The Froude number F_L is often used for the LDV, because it allows comparison of the LDV for different pipe diameters D_p and relative submerged densities R_{sd} without having to change the scale of the graph, this is defined as:

$$F_L = \frac{v_{ls,ldv}}{\sqrt{2 \cdot g \cdot R_{sd} \cdot D_p}} \tag{9.3-1}$$

It should be noted that sometimes the 2 and sometimes the relative submerged density R_{sd} are omitted.

Because there are numerous data and equations for the critical velocity (LSDV, LDV or MHGV), some equations based on physics, but most based on curve fitting, a selection is made of the equations and methods from literature. The literature analyzed are from Wilson (1942), Durand and Condolios (1952), Newitt et al. (1955), Jufin and Lopatin (1966), Zandi and Govatos (1967), Charles (1970), Graf et al. (1970), Wilson and Judge (1976), Wasp et al. (1977), Wilson and Judge (1977), Thomas (1979), Oroskar and Turian (1980), Parzonka et al. (1981), Turian et al. (1987), Davies (1987), Schiller and Herbich (1991), Gogus and Kokpinar (1993), Gillies (1993), Berg (1998), Kokpinar and Gogus (2001), Shook et al. (2002), Wasp and Slatter (2004), Sanders et al. (2004), Lahiri (2009), Poloski et al. (2010) and Souza Pinto et al. (2014).

The research consisted of two parts, analyzing the experimental data and analyzing the resulting models based on these data. First the experimental data will be discussed.

Figure 9.3-1 shows many data points of various authors for sand and gravel in water. Each column of data points shows the results of experiments with different volumetric concentrations, where the highest points were at volumetric concentrations of about 15%–20%, higher concentrations gave lower points. The experimental data also shows that smaller pipe diameters, in general, give higher Durand and Condolios (1952) Froude F_L numbers. The two curves in the graph are for the Jufin and Lopatin (1966) equation, which is only valid for sand and gravel, and the DHLLDV Framework which is described by Miedema & Ramsdell (2015A).

Both models give a sort of upper limit to the LDV. The data points of the very small particle diameters, Thomas (1979) and Poloski (2010), were carried out in very small to medium diameter pipes, while the two curves are constructed for a 0.1524 (6 inch) pipe, resulting in slightly lower curves. Data points above the DHLLDV curve are in general for pipe diameters smaller than 0.1524 m. Some special attention is given to the relation between the Durand Froude F_L number and the pipe diameter D_p. Both Thomas (1979) and Wasp et al. (1977) carried out research with a **d = 0.18 mm** particle in 6 pipe diameters. These experiments show a slight decrease of the F_L value with increasing pipe diameter with a power close to –0.1, meaning the LDV increases with the pipe diameter to a power close to 0.4 and not to 0.5 as assumed by Durand and Condolios (1952).

Figure 9.3-2 to Figure 9.3-11 show the Limit Deposit Velocities of DHLLDV, Durand and Condolios (1952), Jufin and Lopatin (1966), Wasp et al. (1970), Wasp and Slatter (2004), Souza Pinto et al. (2014), Hepy et al. (2008), Gogus and Kokpinar (1993), Kokpinar and Gogus (2001), Berg (1998), Turian et al. (1987) and Gillies (1993) for

10 pipe diameters. The figures also show the LSDV and the transition sliding bed to heterogeneous transport. The intersection between these two curves gives the smallest particle diameter where a sliding bed can exist.

The curves of Hepy et al. (2008), Gogus and Kokpinar (1993) and Kokpinar and Gogus (2001) show a maximum F_L value for particles with a diameter near $d = 0.5$ mm. However these models show an increasing F_L value with the pipe diameter, which contradicts the numerous experimental data, showing a slight decrease. The models of Turian et al. (1987) , Wasp et al. (1970), Wasp and Slatter (2004) and Souza Pinto et al. (2014) show an increasing F_L value with increasing particle diameter and a slight decrease with the pipe diameter.

Jufin and Lopatin (1966) show an increase with the particle diameter and a slight decrease with the pipe diameter (power –1/6). The model of van den Berg (1998) shows an increasing F_L with the particle diameter, but no dependency on the pipe diameter. Durand and Condolios (1952) did not give an equation but a graph. The data points as derived from the original publication in (1952) and from Durand (1953) are shown in the graphs. The data points show a maximum for $d = 0.5$ mm. They did not report any dependency on the pipe diameter. The model of Gillies (1993) tries to quantify the Durand and Condolios (1952) data points, but does not show any dependency on the pipe diameter for the F_L Froude number. The increase of the F_L value with the pipe diameter of the Hepy et al. (2008), Gogus and Kokpinar (1993) and Kokpinar and Gogus (2001) models is probably caused by the forced d/D_p relation. With a strong relation with the particle diameter and a weak relation for the pipe diameter, the pipe diameter will follow the particle diameter. Another reason may be the fact that they used pipe diameters up to 0.1524 m (6 inch) and the smaller the pipe diameter the more probable the occurrence of a sliding bed and other limiting conditions, due to the larger hydraulic gradient helping the bed to start sliding.

The figures show that for medium pipe diameters all models are close. The reason is probably that most experiments are carried out with medium pipe diameters. Only Jufin and Lopatin (1966) covered a range from 0.02 m to 0.9 m pipe diameters. Recently Thomas (2014) gave an overview and analysis of the LDV (or sometimes the LSDV). He repeated the findings that the LDV depends on the pipe diameter with a power smaller than 0.5 but larger than 0.1. The value of 0.1 is for very small particles, while for normal sand and gravels a power is expected between 1/3 according to Jufin and Lopatin (1966) and 1/2 according to Durand and Condolios (1952). Most equations are one term equations, making it impossible to cover all aspects of the LDV behavior. Only Gillies (1993) managed to construct an equation that gets close to the original Durand and Condolios (1952) graph.

Figure 9.3-1: The Durand & Condolios Froude number F_L, experimental data.

The models analyzed result in a number of dominating parameters. These are the particle diameter d, the pipe diameter D_p, the liquid density ρ_l and kinematic viscosity ν_l, the solids density ρ_s, the sliding friction coefficient μ_{sf}, the bed concentration C_{vb} and the spatial volumetric concentration C_{vs}. Derived parameters are the relative submerged density R_{sd}, the Darcy Weisbach friction factor for pure liquid flow λ_l and the thickness of the viscous sub-layer δ_v. Dimensionless numbers are not considered at first, since they may lead to wrong interpretations. Lately Lahiri (2009) performed an analysis using artificial neural network and support vector regression.

Azamathulla and Ahmad (2013) performed an analysis using adaptive neuro-fuzzy interference system and gene-expression programming. Although these methodologies may give good correlations, they do not explain the physics. Lahiri (2009) however did give statistical relations for the dependency on the volumetric concentration, the particle diameter, the pipe diameter and the relative submerged density. Resuming, the following conclusions can be drawn for sand and gravel:

The pipe diameter D_p: The LDV is proportional to the pipe diameter D_p to a power between 1/3 and 1/2 (about 0.4) for small to large particles (Thomas (1979), Wasp et al. (1977), Lahiri (2009) and Jufin and Lopatin (1966)) and a power of about 0.1 for very small particles (Thomas (1979), Wilson and Judge (1976), Sanders et al. (2004) and Poloski et al. (2010)).

The particle diameter d: The LDV has a lower limit for very small particles, after which it increases to a maximum at a particle diameter of about $d = 0.5$ mm (Thomas (1979), Thomas (2014), Durand and Condolios (1952), Gillies (1993) and Poloski et al. (2010)). For medium sized particles with a particle size $d > 0.5$ mm, the F_L value decreases to a minimum for a particle size of about $d = 2$ mm (Durand and Condolios, 1952; Gillies, 1993; Poloski et al., 2010). Above 2 mm, the F_L value will remain constant according to Durand and Condolios (1952) and Gillies (1993). For particles with $d/D_p > 0.015$, the Wilson et al. (1992) criterion for real suspension/saltation, the F_L value increases again. This criterion is based on the ratio particle diameter to pipe diameter and will start at a large particle diameter with increasing pipe diameter. Yagi et al. (1972) reported many data points in this region showing an increasing F_L value.

The relative submerged density R_{sd}: The relation between the LDV and the relative submerged density is not very clear, however the data shown by Kokpinar and Gogus (2001) and the conclusions of Lahiri (2009) show that the F_L value decreases with increasing solids density and thus relative submerged density R_{sd} to a power of –0.1 to –0.2.

The spatial volumetric concentration C_{vs}: The volumetric concentration leading to the maximum LDV is somewhere between 15% and 20% according to Durand and Condolios (1952). Lahiri (2009) reported a maximum at about 17.5%, while Poloski et al. (2010) derived 15%. This maximum LDV results from on one hand a linear increase of the sedimentation with the concentration and on the other hand a reduced sedimentation due to the hindered setting. These two counteracting phenomena result in a maximum, which is also present in the equation of the potential energy of the DHLLDV Framework. For small concentrations a minimum LDV is observed by Durand and Condolios (1952). This minimum LDV increases with the particle diameter and reaches the LDV of 20% at a particle diameter of 2 mm with a pipe diameter of 0.1524 m (6 inch).

For the dredging industry the Jufin and Lopatin (1966) equation gives a good approximation for sand and gravel, although a bit conservative. The model of van den Berg (1998) is suitable for large diameter pipes as used in dredging for sand and/or gravel, but underestimates the LDV for pipe diameters below 0.8 m. Both models tend to underestimate the LDV for particle diameters below 1 mm.

9.3.2 Conclusions Limit Deposit Velocity.

The Limit Deposit Velocity (LDV) and the Limit of Stationary Deposit Velocity (LSDV) are distinguished. Wilson et al. (1992) use the LSDV, while Durand & Condolios (1952) and the DHLLDV Framework use the LDV. The LDV will always give higher F_L values than the LSDV. Not because of scatter or because of a safety factor, but because of a different definition. The LDV (the line speed above which there is no stationary of sliding bed) always exists, the LSDV only at the lower boundary of a sliding bed region.

It should be noted that for small particles, the LDV and the transition of the heterogeneous regime to the ELM are very close. For very small particles however viscous effects may play a role, which is not taken into consideration here.

The graphs in Figure 9.3-2 to Figure 9.3-11 show a number of LDV models and also the LSDV of Wilson (1979), the LSDV of the DHLLDV Framework and the transition of the sliding bed to the heterogeneous regime according to the DHLLDV Framework. It should be noted that the LSDV of the Wilson model shows the maximum curve. It should further be noted that for the DHLLDV Framework a sliding bed can only exist if the transition velocity of the sliding bed regime to the heterogeneous regime is higher than the LSDV. If this is lower, a sliding bed will never exist. The bed will be completely suspended before the bed could ever start sliding.

The data points in the graphs are all for a $D_p = 0.1524$ m (6 inch) pipe. Durand and Condolios (1952) assumed that their Froude number is independent of the pipe diameter. From all the experiments it appeared that the Froude number decreases slightly with the pipe diameter.

9.3.3 Graphs.
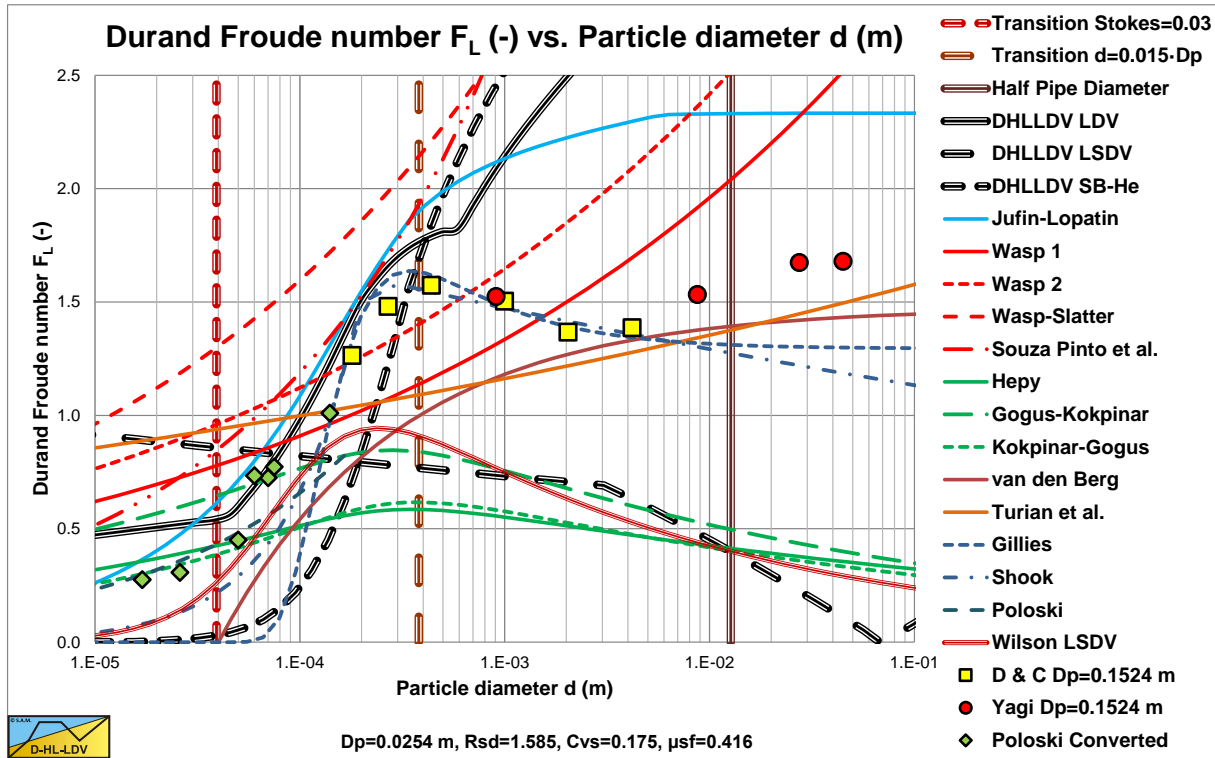
Figure 9.3-2: The LDV Froude number for a D_p=0.0254 m (1 inch) pipe.
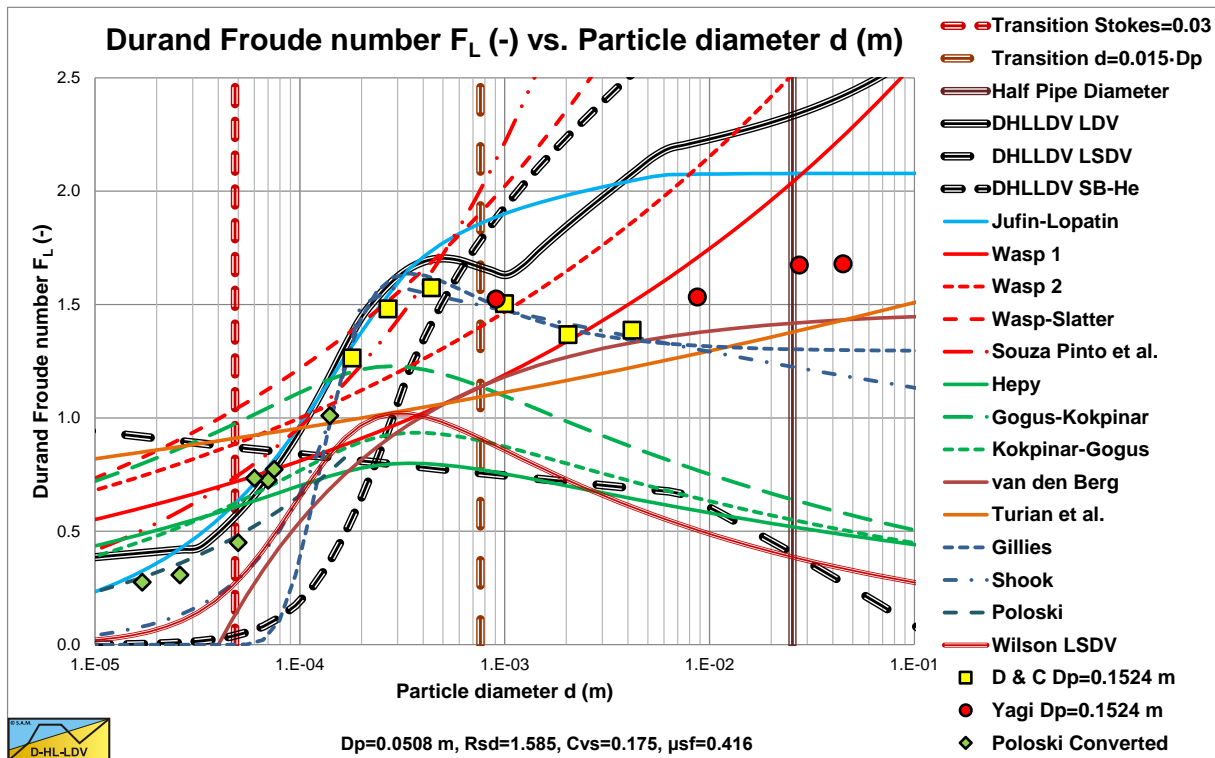
Figure 9.3-3: The LDV Froude number for a D_p=0.0508 m (2 inch) pipe.
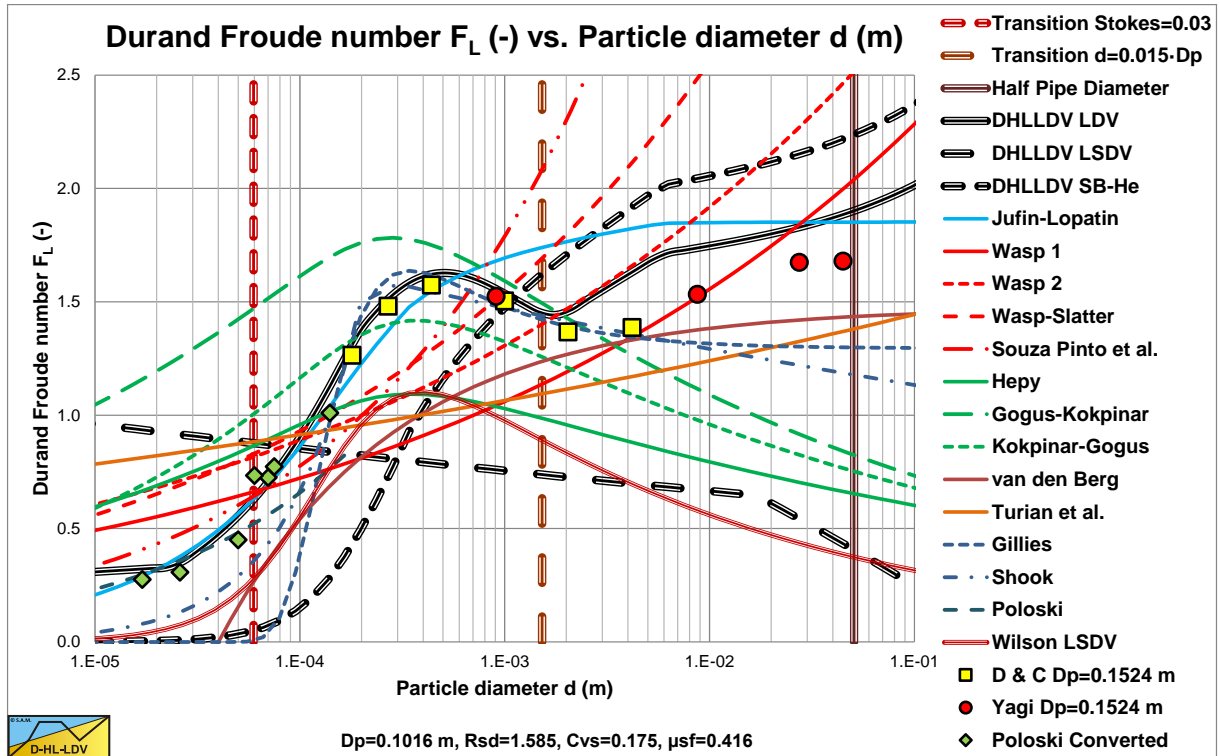
Figure 9.3-4: The LDV Froude number for a D_p=0.1016 m (4 inch) pipe.
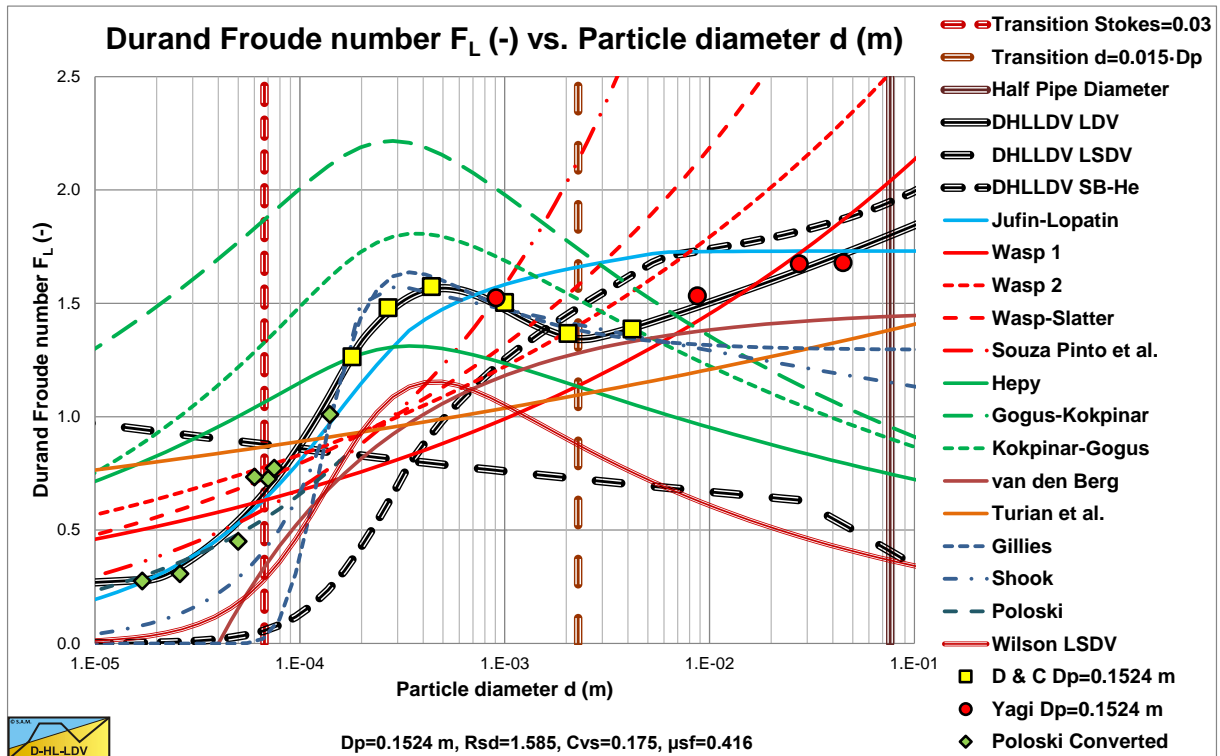
Figure 9.3-5: The LDV Froude number for a D_p=0.1524 m (6 inch) pipe.
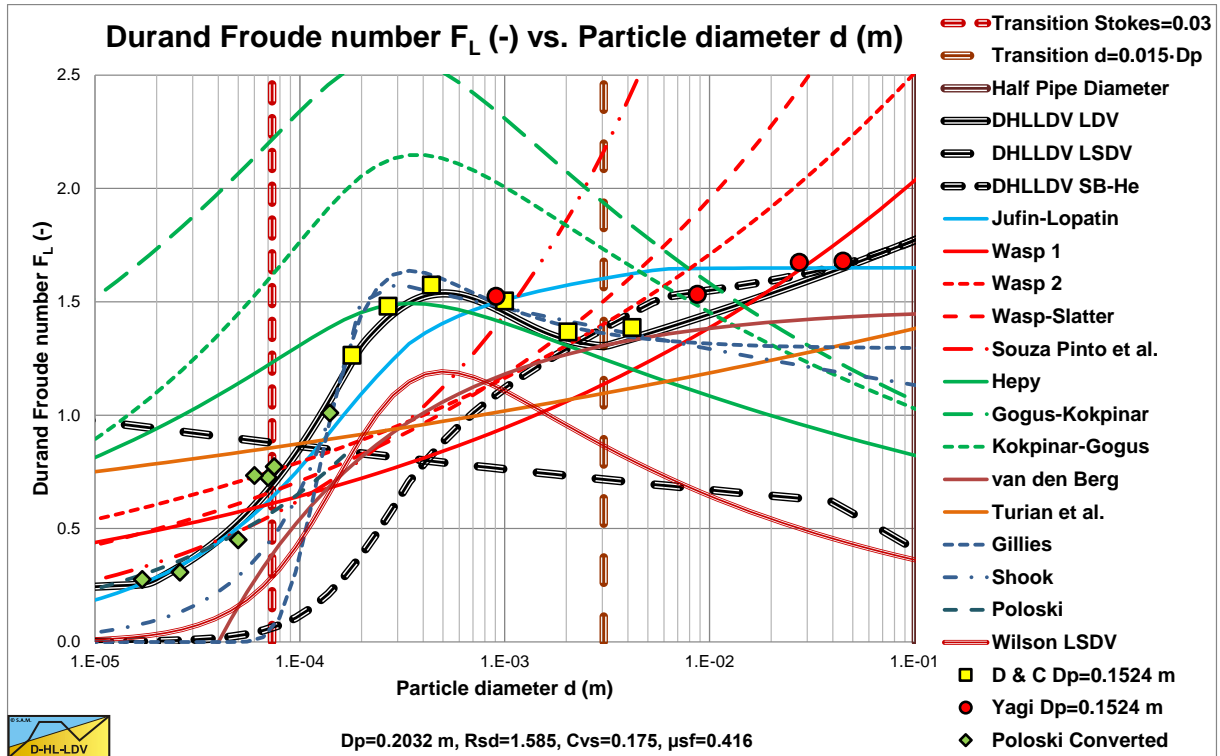
Figure 9.3-6: The LDV Froude number for a D_p=0.2032 m (8 inch) pipe.
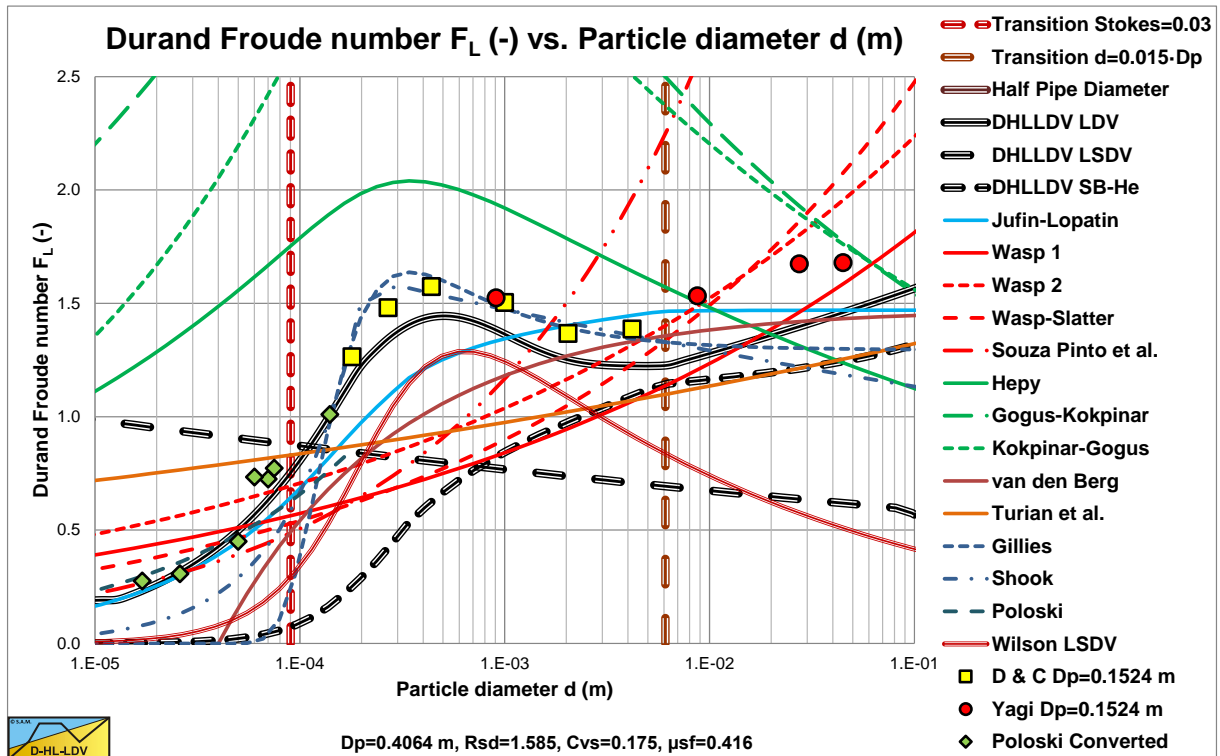
Figure 9.3-7: The LDV Froude number for a D_p=0.4064 m (16 inch) pipe.
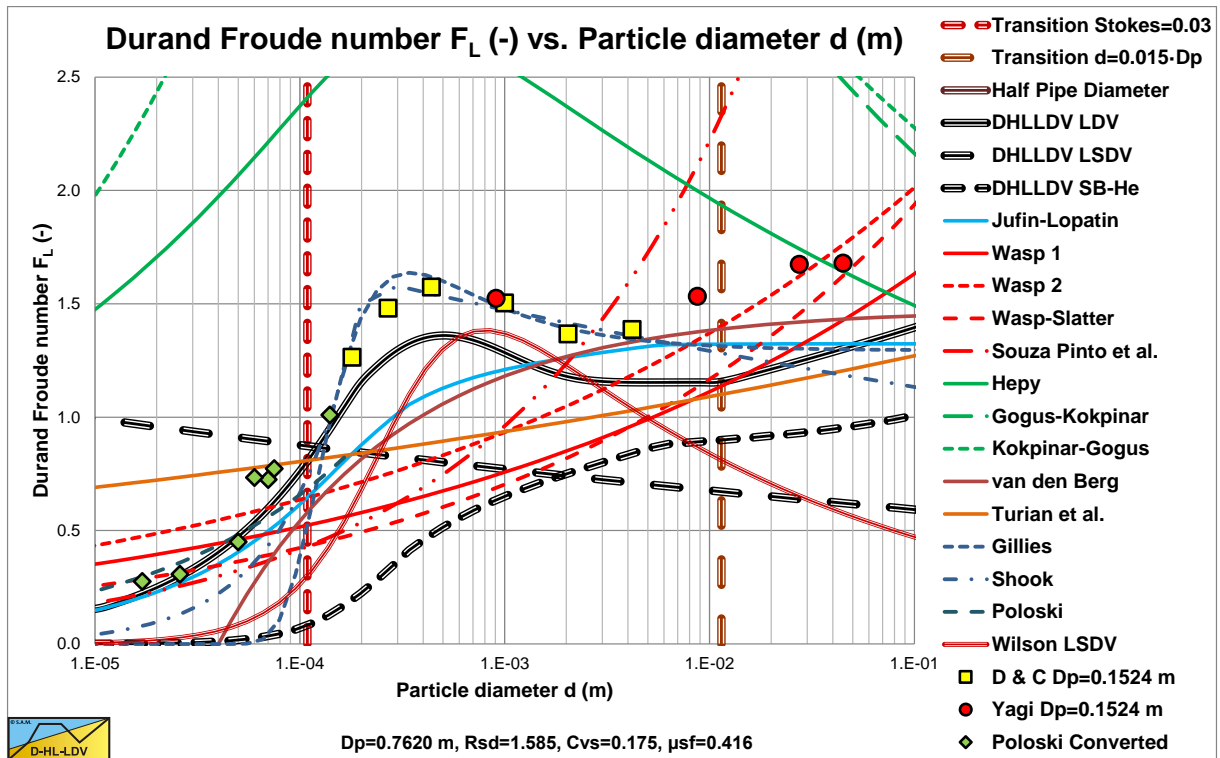
Figure 9.3-8: The LDV Froude number for a D_p=0.7620 m (30 inch) pipe.
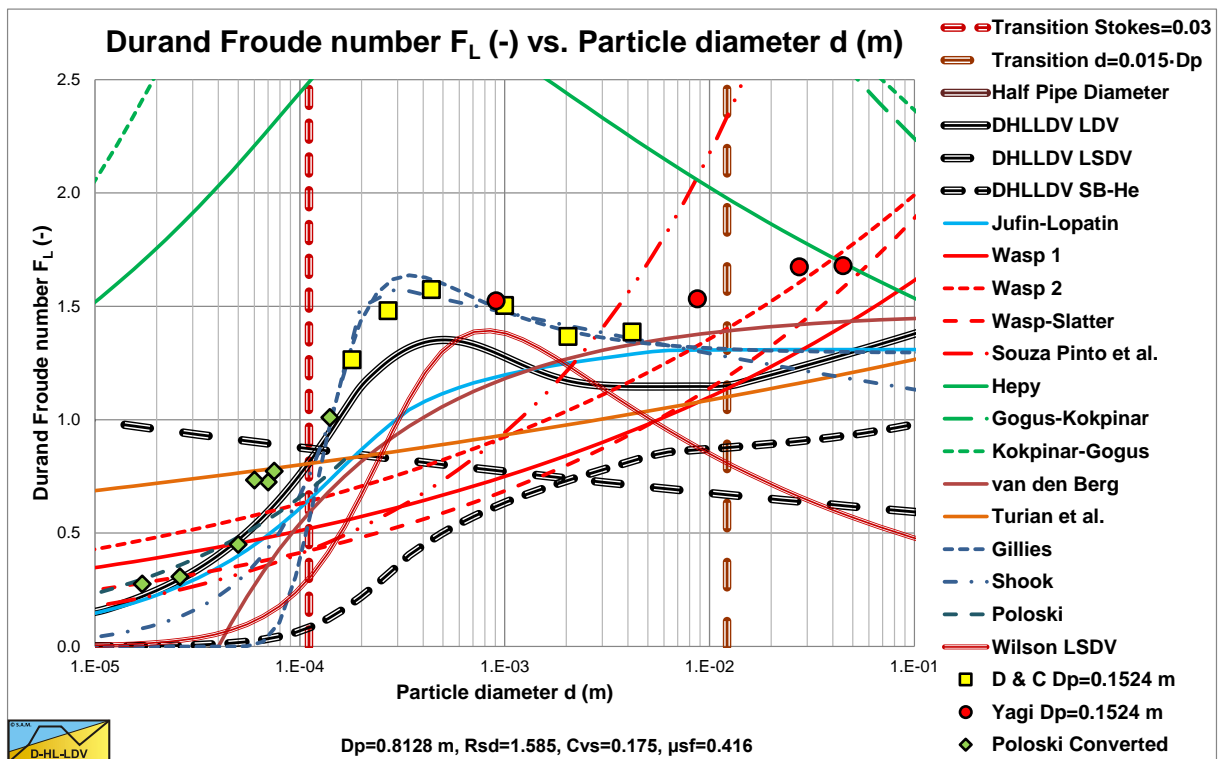
Figure 9.3-9: The LDV Froude number for a D_p=0.8128 m (32 inch) pipe.
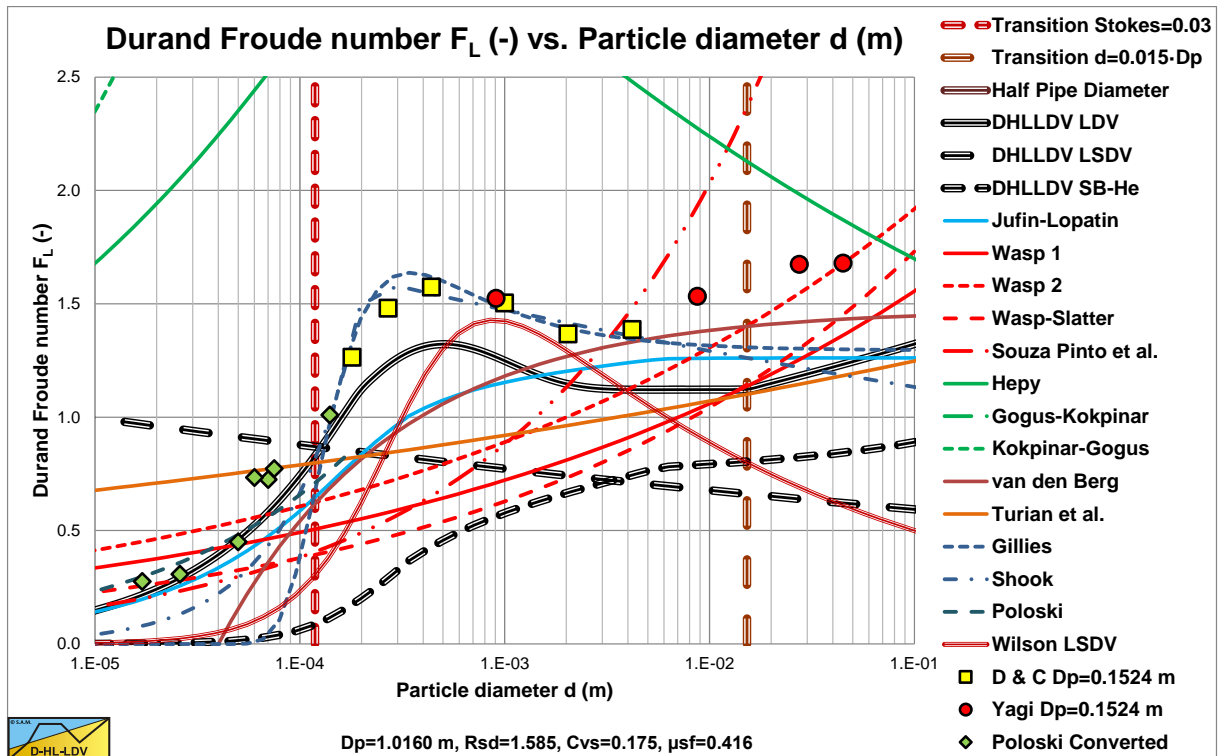
Figure 9.3-10: The LDV Froude number for a D_p=1.0160 m (40 inch) pipe.
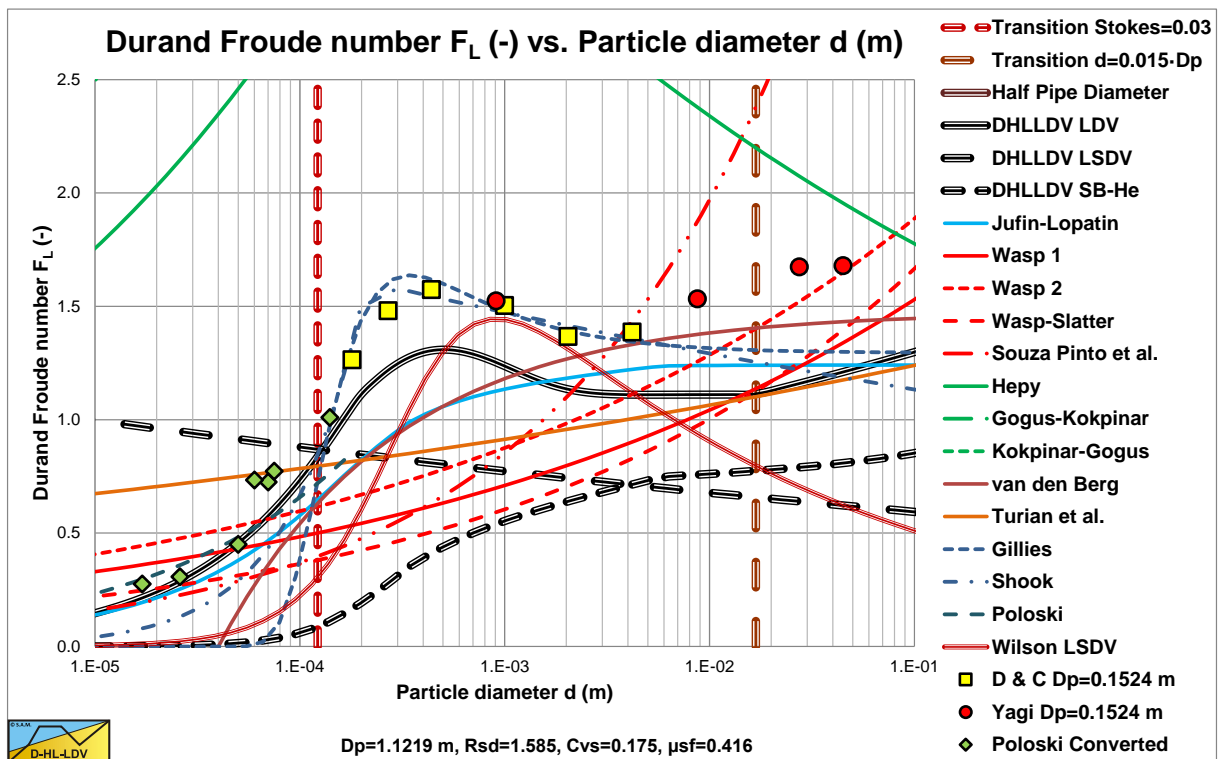
Figure 9.3-11: The LDV Froude number for a D_p=1.1218 m (48 inch) pipe.

9.4 Nomenclature Comparisons.

C_D	Particle drag coefficient	-
C_L	Lift coefficient	-
C_{vt}	Delivered (transport) volumetric concentration	-
C_{vs}	Spatial volumetric concentration	-
C_{vb}	Spatial volumetric concentration bed (1-n)	-
C_x	Durand & Condolios reversed particle Froude number	-
d	Particle diameter	m
d_m	Mean particle diameter Fuhrboter	m
d_{50}	Particle diameter with 50% passing	m
D_p	Pipe diameter	m
E_{rhg}	Relative excess hydraulic gradient	-
f_l	Fanning friction factor liquid	-
f_m	Fanning friction factor mixture	-
F_L	Lift force on particle	N
F_L	Durand & Condolios LDV Froude number	-
F_W	Submerged weight of particle	N
Fr	Froude number	-
g	Gravitational constant 9.81 m/s^2	m/s^2
i_l	Pure liquid hydraulic gradient	m/m
i_m	Mixture hydraulic gradient	m/m
K	Durand & Condolios constant	-
K_1	Newitt constant	-
ΔL	Pipe length	m
L_R	Lift force to submerged weight ratio	-
M	Power Wilson heterogeneous model	-
n	Porosity	-
Δp_l	Pressure loss liquid	kPa
Δp_m	Pressure loss mixture	kPa
R	Stratification ratio	-
Re	Reynolds number	-
R_{sd}	Relative submerged density	-
S_k	Fuhrboter particle coefficient	m/s
u_*	Friction velocity	-
v_{ls}	Line speed	m/s
$v_{ls,hh}$	Intersection velocity heterogeneous-homogeneous regimes	m/s
$v_{ls,ldv}$	Limit Deposit Velocity	m/s
v_{min}	Minimum hydraulic gradient line speed Jufin-Lopatin	m/s
v_{sl}	Slip velocity	m/s
v_t	Terminal settling velocity particle	m/s
$\alpha_{\delta v=d}$	Influence factor thickness viscous sub layer	-
α_{1a}	Proportionality factor thickness viscous sub layer	-
α_{1b}	Offset factor thickness viscous sub layer	-
$\alpha_{He=Ho}$	Influence factor intersection heterogeneous – homogeneous regimes	-
α_{2a}	Proportionality factor intersection heterogeneous – homogeneous regimes	-
α_{2b}	Offset factor intersection heterogeneous – homogeneous regimes	-
$\alpha_{LR=1}$	Influence factor lift ratio equals 1	-
α_{3a}	Proportionality factor lift ratio equals 1	-
α_{3b}	Offset factor lift ratio equals 1	-
β	Richardson & Zaki hindered settling power	-
δ_v	Viscous sub layer thickness	m
$\delta_{v,hh}$	Viscous sub layer thickness at intersection heterogeneous-homogeneous regimes	m
ε	Pipe wall roughness	-
κ_C	Concentration eccentricity factor	-
λ_l	Darcy Weisbach friction factor liquid	-
λ_m	Darcy Weisbach friction factor mixture	-

μ_{sf}	Sliding friction factor	-
ρ_l	Density liquid	ton/m^3
ρ_s	Density solid	ton/m^3
ν_l	Kinematic viscosity liquid	m^2/s
Φ	Durand & Condolios parameter	-
ψ	Durand & Condolios parameter	-
ψ^*	Jufin-Lopatin particle Froude number	-
ζ	Fit function Fuhrboter	-
Ct	The **Cát** number (sand grains)	-
Th$_{fv}$	The **Thủy** number (water) based on friction velocity	-
La	The **Lắng** number (sediment)	-

9.5 Comparison Graded Sands & Gravels.

9.5.1 Introduction.

Most slurry transport models in literature are based on a uniform Particle Size Diagram (PSD). So, all the particles have the same size. The experiments on which these models are based were carried out with either a narrow graded PSD or a uniform PSD. Most empirical models are also based on the delivered volumetric concentration, since that is what was measured. The more fundamental 2LM and 3LM models are based on a uniform PSD and a spatial volumetric concentration. Delivered concentration curves are achieved by interpolation of delivered concentrations derived from slip ratios. For non-uniform graded or broad graded PSD's the problem is, that the interaction between the different fractions is not known. So, one can assume there is no interaction, all fractions behave independently, or one can assume a certain interaction between the fractions. The models considered here have some interaction.

The models of Durand & Condolios (1952) and Wilson et al. (1992) are both based on an adjustment of the equation for the heterogeneous flow regime, but in different ways. Durand & Condolios (1952) assume the particle Froude number has to be weighted based on a parallel resistor method, leaving the power of the line speed in the equation -1. So, the pressure losses and the hydraulic gradient are reversely proportional to the line speed. This model always gives a reduction of the solids effect. For the Durand & Condolios (1952) model one can also define a v_{50}, if the sliding friction coefficient μ_{sf} is known. However, this v_{50} will change with the grading.

Wilson et al. (1992) assume that the v_{50}, the line speed where 50% stratification occurs, does not change because of the grading. However, the proportionality of the pressure losses and the hydraulic gradient changes. Uniform PSD's are reversely proportional to the line speed with a power of 1.7 (the maximum power), medium graded PSD's are reversely proportional to the line speed to a power around 1 and very broad graded PSD's are reversely proportional to the line speed with a power of 0.25 (the minimum power).

Comparing the two models one can say that in the Durand & Condolios (1952) model the v_{50} decreases with increasing grading of the PSD, with a constant proportionality of the pressure losses and the hydraulic gradient with the line speed, while the Wilson et al. (1992) model keeps the v_{50} constant, but changes the proportionality of the pressure losses and the hydraulic gradient with the line speed.

Where the previous two models are based on heterogeneous transport only, the other three models are based on a combination of different flow regimes.

The Sellgren & Wilson (2007) 4 component model divides the PSD in 4 components based on particle size boundaries. These components are:
Homogeneous flow (the fines **d<0.04 mm**).
Pseudo homogeneous flow (**0.04 mm<d<0.2·v_r mm**).
Heterogeneous flow (**0.2·v_r mm<d<0.015·D_p**).
Fully stratified flow (**d>0.015·D_p**).
The first boundary from homogeneous to pseudo homogeneous flow is fixed. The second boundary from pseudo homogeneous to heterogeneous flow only depends on the relative viscosity of the carrier liquid, so for clear water it is also fixed. The third boundary from heterogeneous to fully stratified flow depends on the pipe diameter. By splitting up the PSD in the 4 fractions, determining the hydraulic gradient as a function of the line speed for each fraction and adding up the weighed hydraulic gradient curves found, the hydraulic gradient curve of the entire PSD is found. In this method, some adjustments are made for concentrations and relative submerged densities, based on the assumed properties of the carrier liquid. Any dependency of the line speed on the boundaries between the different components is not present in this model. The interactions between the fractions are based on the viscosity and density of the homogeneous carrier liquid and the resulting relative submerged density of the coarser components.

As an alternative to the 4CM the author combined the different Wilson flow regime models into a Wilson 4 regime model (4RM). The flow regimes are the homogeneous flow regime where very small particles influence the viscosity and the density of the carrier liquid creating a pseudo liquid, the stratified flow regime, the heterogeneous flow regime and the homogeneous flow regime at very high line speeds. The last 3 flow regimes use the adjusted properties of the carrier liquid. The PSD is also adjusted, since the fines now are part of the carrier liquid. If the stratified flow regime gives a smaller hydraulic gradient than the heterogeneous flow regime, the stratified flow regime is chosen, otherwise the heterogeneous flow regime. The transition of the heterogeneous flow regime to the homogeneous flow regime is determined based on the so-called stratification ration. If a certain percentage of the particles is stratified, then 1 minus this percentage is in suspension.

The DHLLDV Framework of Miedema (June 2016) includes all flow regimes depending on the particle size of a fraction. First the homogeneous fraction is determined, based on a Stokes number. The carrier liquid properties are adjusted based on the homogeneous fraction, both the viscosity and the density. For all other particles, it is assumed they are transported by this new homogeneous pseudo liquid. Until here the model is similar to the 4-component model, except for the value of the boundary. When the homogeneous fraction is known, the PSD of the remaining particles can be constructed. This PSD is divided into a number of fractions. This number can be any number; however, 9 fractions is sufficient in most cases. For each fraction the hydraulic gradient curve is determined, including all flow regimes that may occur, from line speed zero to some maximum, for example 10 m/s, depending on the pipe diameter. Both hydraulic gradient curves for spatial and delivered volumetric concentration are determined. The hydraulic gradient curves are summed based on the percentage of each fraction in the modified PSD, resulting in a constant spatial volumetric concentration curve and a constant delivered volumetric concentration curve. By multiplying the resulting curves with the ratio of the pseudo liquid density to the water density, the hydraulic gradient curves with respect to water are found. Here the boundaries between the flow regimes are not fixed, but depend on the line speed, the particle diameter and the pipe diameter.

Good methods should match the following requirements:
- The resulting hydraulic gradient curve has to match experimental data.
- The PSD should be based on the spatial situation; the delivered PSD follows.
- The method should give continuous results with respect to particle diameter and line speed.
- The method should converge to the uniform model for narrow graded PSD's.

Before discussing the 5 models in detail, a method is given to determine a PSD and how to determine the pseudo liquid properties.

9.5.2 A Method to Generate a PSD.

In order to compare the different models a Particle Size Diagram (PSD) has to be generated. The original fractions of the PSD can be determined manually by sieve analysis, or generated based on for example the d_{50}/d_{15} and d_{85}/d_{50} ratios. A mathematical function describing the shape of a PSD up to the d_{50} is:

$$f_y = \frac{1}{1 + e^{A_x \cdot \left(\frac{\log 10(d_y)}{\log 10(d_{50})} - 1 \right)}}$$

(9.5-1)

$$\text{with:} \quad A_x = \frac{1}{\left(\frac{\log 10(d_x)}{\log 10(d_{50})} - 1 \right)} \cdot \ln\left(\frac{1 - f_x}{f_x} \right)$$

Now suppose a symmetrical PSD:

$$\alpha_{15} = \frac{d_{50}}{d_{15}} \quad \text{and} \quad \alpha_{85} = \frac{d_{85}}{d_{50}}$$

(9.5-2)

This gives for the factors A_{15} and A_{85} and the d_{50} in m:

$$A_{15} = \frac{1}{\left(\frac{\log 10(d_{15})}{\log 10(d_{50})} - 1 \right)} \cdot \ln\left(\frac{1 - 0.15}{0.15} \right) = -1.7346 \cdot \frac{\ln(d_{50})}{\ln(\alpha_{15})}$$

(9.5-3)

$$A_{85} = \frac{1}{\left(\frac{\log 10(d_{85})}{\log 10(d_{50})} - 1 \right)} \cdot \ln\left(\frac{1 - 0.85}{0.85} \right) = -1.7346 \cdot \frac{\ln(d_{50})}{\ln(\alpha_{85})}$$

(9.5-4)

Now suppose for the ratios d_{50}/d_{15} and d_{85}/d_{50}:

$$\alpha_{15} = \frac{d_{50}}{d_{15}} = e^1 = 2.7183 \quad \textbf{and} \quad \alpha_{85} = \frac{d_{85}}{d_{50}} = e^1 = 2.7183 \tag{9.5-5}$$

This gives for A_{15} and A_{85} positive values as long as the $d_{50} < 1$ m:

$$A_{15} = -1.7346 \cdot \ln(d_{50})$$

$$A_{85} = -1.7346 \cdot \ln(d_{50}) \tag{9.5-6}$$

So the fraction passing in the PSD is in this particular symmetrical case:

$$f_y = \frac{1}{1+e^{\left(A_{15} \cdot \left(\frac{\log 10(d_y)}{\log 10(d_{50})} - 1\right)\right)}} = \frac{1}{1+e^{\left(A_{85} \cdot \left(\frac{\log 10(d_y)}{\log 10(d_{50})} - 1\right)\right)}} = \frac{1}{1+e^{-1.7346 \cdot \left(\ln(d_y) - \ln(d_{50})\right)}} \tag{9.5-7}$$

Of course there are other ways to generate PSD's, but this way works well and gives the possibility to create an asymmetrical PSD if α_{15} and α_{85} are chosen differently.

9.5.3 The adjusted liquid properties.

The boundary between the homogeneous and the pseudo homogeneous flow regimes is named the limiting particle diameter. The limiting particle diameter is determined, based on a Stokes number of 0.03 for the DHLLDV Framework and 0.04 mm for the 4CM. The value of 0.03 is found based on many experiments from literature. Since the Stokes number depends on the line speed, here the Limit Deposit Velocity is used as an estimate of the operational line speed.

The LDV is approximated by:

$$v_{ls,ldv} = 7.5 \cdot D_p^{0.4} \tag{9.5-8}$$

Giving for the limiting particle diameter:

$$d_{lim} = \sqrt{\frac{Stk \cdot 9 \cdot \rho_l \cdot v_l \cdot D_p}{\rho_s \cdot v_{ls,ldv}}} \approx \sqrt{\frac{Stk \cdot 9 \cdot \rho_l \cdot v_l \cdot D_p}{\rho_s \cdot 7.5 \cdot D_p^{0.4}}} \tag{9.5-9}$$

The fraction of the sand in suspension, resulting in a homogeneous pseudo fluid is named X. So, this is the fraction of particles smaller than d_{lim}. This gives for the density of the homogeneous pseudo fluid:

$$\rho_x = \rho_l + \rho_l \cdot \frac{X \cdot C_{vs} \cdot R_{sd}}{(1 - C_{vs} + C_{vs} \cdot X)} \tag{9.5-10}$$

$$\textbf{if } X = 1 \quad \Rightarrow \quad \rho_x = \rho_m = \rho_l + \rho_l \cdot C_{vs} \cdot R_{sd}$$

So, the concentration of the homogeneous pseudo fluid is not $C_{vs,x} = X \cdot C_{vs}$, but:

$$C_{vs,x} = \frac{X \cdot C_{vs}}{(1 - C_{vs} + C_{vs} \cdot X)} \tag{9.5-11}$$

This is because part of the total volume is occupied by the particles that are not in suspension, so the percentage of carrier liquid is reduced. The remaining spatial concentration of solids to be used to determine the individual hydraulic gradients curves of the fractions is now:

$$C_{vs,r} = (1-X) \cdot C_{vs}$$ (9.5-12)

The dynamic viscosity can now be determined according to Thomas (1965):

$$\mu_x = \mu_l \cdot \left(1 + 2.5 \cdot C_{vs,x} + 10.05 \cdot C_{vs,x}^2 + 0.00273 \cdot e^{16.6 \cdot C_{vs,x}}\right)$$ (9.5-13)

The kinematic viscosity of the homogeneous pseudo fluid is now:

$$\nu_x = \frac{\mu_x}{\rho_x}$$ (9.5-14)

One should realize however that the relative submerged density has also changed to:

$$R_{sd,x} = \frac{\rho_s - \rho_x}{\rho_x}$$ (9.5-15)

With the new homogeneous pseudo liquid density, kinematic viscosity, relative submerged density and volumetric concentration the hydraulic gradient can be determined for each fraction of the adjusted PSD in both the 4-component model and the DHLLDV Framework. However, one can also combine this with the Durand & Condolios (1952) and Wilson et al. (1992) models, although not mentioned by the authors. In this paper this is not applied.

In general, a higher pseudo liquid density and viscosity will increase the water based hydraulic gradient of homogeneous flow according to Darcy Weisbach, but will decrease the water based hydraulic gradient in fully stratified flow (the sliding bed regime) and in the heterogeneous flow regime, both due to the reduced relative submerged density of the particles and in the heterogeneous flow regime also because of the reduced terminal settling velocity due to the higher viscosity.

9.5.4 Models.

A brief description is given here of the 4 models/methods considered. For a detailed description of all models one can consult the appropriate chapters in Miedema (June 2016).

9.5.4.1 Durand & Condolios.

In normal sands, there is not only one grain diameter, but a grain size distribution has to be considered. The Froude number for a grain size distribution can be determined by integrating the Froude number as a function of the probability according to:

$$Fr_p = \frac{v_t}{\sqrt{g \cdot d}} = \frac{1}{\sqrt{C_x}} = \frac{1}{\int_0^1 \frac{\sqrt{g \cdot d}}{v_t} dp} = \frac{1}{\sum_{i=1}^n \left(\sqrt{C_x}\right)_i \cdot \Delta p_i}$$ (9.5-16)

It is also possible to split the particle size distribution into **n** fraction and determine the weighted average particle Froude number. Gibert (1960) published a graph with values for the particle Froude number that matches the findings of Durand & Condolios (1952). Figure 6.4-20 shows these published values. If one uses the values of Gibert (1960), the whole discussion about whether the C_D or the C_x value should be used can be omitted. Analyzing this figure however, shows that a very good approximation of the table values can be achieved by using the particle Froude number to the power 20/9 instead of the power 1, assuming that the terminal settling velocity v_t is determined correctly for the solids considered (Stokes, Budryck, Rittinger or Zanke).

Figure 6.4-20 shows the original data points, the theoretical reciprocal particle Froude numbers using the Zanke (1952) equation for the terminal settling velocity of sand particles and the curve using a power of 20/9. Only for large particles there may be a small difference between the original data and the theoretical curve applying the power of 20/9.

The final equation of Durand & Condolios (1952) and later Gibert (1960) for the pressure losses now becomes:

$$\Delta p_m = \Delta p_l \cdot \left(1 + \Phi \cdot C_{vt}\right) \tag{9.5-17}$$

With the use of the PSD modified particle Froude number:

$$\Phi = \frac{i_m - i_l}{i_l \cdot C_{vt}} = \frac{\Delta p_m - \Delta p_l}{\Delta p_l \cdot C_{vt}} = K \cdot \psi^{-3/2} = 83 \cdot \left(\frac{v_{ls}^2}{g \cdot D_p \cdot R_{sd}} \cdot \sqrt{C_x}\right)^{-3/2} \tag{9.5-18}$$

Based on the current research and Figure 6.4-20 this can be written as:

$$\Phi = 83 \cdot \left(\frac{v_{ls}^2}{g \cdot D_p \cdot R_{sd}} \cdot \frac{1}{Fr_p^{20/9}}\right)^{-3/2} \tag{9.5-19}$$
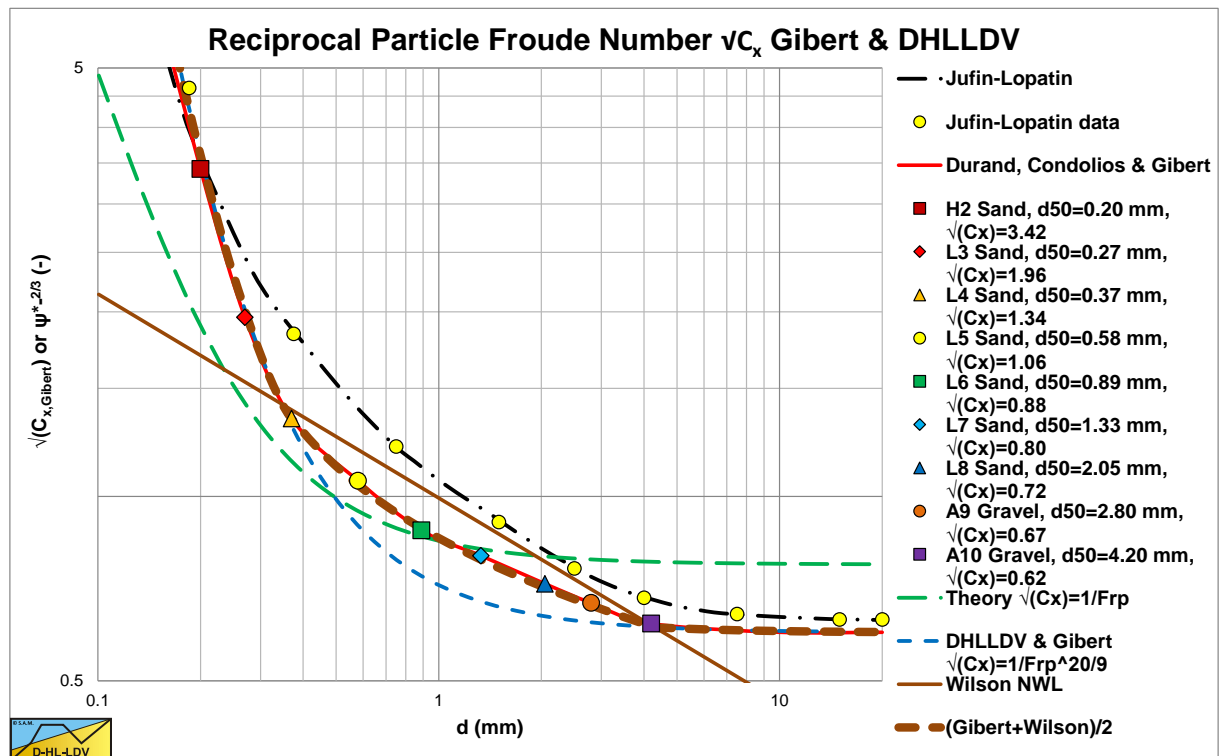
Figure 9.5-1: Modified reciprocal particle Froude number, determined experimentally for various sorts of sand and gravel by Durand & Condolios (1952) and Gibert (1960).

9.5.4.2 Wilson et al. Heterogeneous.

Wilson (1997) has defined a stratification ratio or relative solids effect, which tells which fraction of the particles is in suspension and which part is in the fixed or moving bed, supported by granular contact. Wilson (1997) gives the following general equation for the head losses in hydraulic transport, where μ_{sf} equals the friction factor of a sliding bed, which he has determined to be $\mu_{sf}=0.44$. For the 50% case at line speed v_{50} this gives:

$$E_{rhg} = R = \frac{i_m - i_l}{R_{sd} \cdot C_{vt}} = \frac{\Delta p_m - \Delta p_l}{\rho_l \cdot g \cdot \Delta L \cdot R_{sd} \cdot C_{vt}} = \frac{\mu_{sf}}{2} \cdot \left(\frac{v_{50}}{v_{ls}}\right)^M \tag{9.5-20}$$

When the line speed v_{ls} equals the v_{50}, the stratification ratio is 0.22 or half the sliding friction coefficient μ_{sf}. This can be written in terms of pressures instead of hydraulic gradient as:

$$\Delta p_m = \Delta p_l + \frac{\mu_{sf}}{2} \cdot \rho_l \cdot g \cdot \Delta L \cdot \left(\frac{v_{50}}{v_{ls}}\right)^M \cdot R_{sd} \cdot C_{vt} \tag{9.5-21}$$

Notice that here the solids effect does not depend on the carrier liquid pressure or hydraulic gradient as it does in equation (6.4-9). This equation can be written in the more generic form, matching the notations of the other theories:

$$\Delta p_m = \Delta p_l \cdot \left(1 + \frac{\mu_{sf} \cdot g \cdot R_{sd} \cdot D_p}{\lambda_l} \cdot \left(v_{50} \right)^M \cdot \left(\frac{1}{v_{ls}} \right)^{2+M} \cdot C_{vt} \right)$$

(9.5-22)

For the line speed, where 50% of the particles are in granular contact, v_{50}, Wilson gives the following equation:

$$v_{50} = w_{50} \cdot \sqrt{\frac{8}{\lambda_l}} \cdot \cosh\left(\frac{60 \cdot d_{50}}{D_p} \right)$$

(9.5-23)

When the power **M** equals 1, equation (6.20-53) has the same form as the equation of Durand & Condolios (1952), Gibert (1960), Fuhrboter (1961), Jufin Lopatin (1966) and Newitt et al. (1955). The power **M** depends on the grading of the sand and can be determined by:

$$M = \left(0.25 + 13 \cdot \sigma^2 \right)^{-1/2}$$

(9.5-24)

The variance **σ** of the PSD (Particle Size Distribution), can be determined by some ratio between the v_{50} and the v_{85}:

$$\sigma = \log\left(\frac{v_{85}}{v_{50}} \right) = \log\left(\frac{w_{85} \cdot \sqrt{\frac{8}{\lambda_l}} \cdot \cosh\left(\frac{60 \cdot d_{85}}{D_p} \right)}{w_{50} \cdot \sqrt{\frac{8}{\lambda_l}} \cdot \cosh\left(\frac{60 \cdot d_{50}}{D_p} \right)} \right)$$

(9.5-25)

The terminal settling velocity related parameter **w**, the particle associated velocity, can be determined by:

$$w = 0.9 \cdot v_t + 2.7 \cdot \left(R_{sd} \cdot g \cdot \nu_l \right)^{1/3}$$

(9.5-26)

It seems this equation mixes the homogeneous and heterogeneous regimes. For very small particles the second term gives a constant particle associated velocity, which matches homogeneous behavior at operational line speeds. Since the homogeneous behavior does not depend on the particle size, this gives a constant or asymptotic particle associated velocity. The model of Wilson can be simplified with some fit functions, according to:

$$v_{50} \approx 3.93 \cdot \left(\frac{d_{50}}{0.001} \right)^{0.35} \cdot \left(\frac{R_{sd}}{1.65} \right)^{0.45} \cdot \left(\frac{\nu_{l,actual}}{\nu_{w,20}} \right)^{-0.25}$$

(9.5-27)

In which the particle diameter d_{50} is in m and the resulting v_{50} in m/s. The third term on the right had side is the relative viscosity, the actual liquid viscosity divided by the viscosity of water at 20 degrees Centigrade. In normal dredging practice this term is about unity and can be neglected. The factor 1.65 is based on sand in clear water.

The simplified exponent **M** is given by the approximation:

$$M \approx \left(\ln\left(\frac{d_{85}}{d_{50}} \right) \right)^{-1}$$

(9.5-28)

Later the simplified equation for the v_{50} has been adjusted for particles with diameters from 0.2 mm to 0.5 mm with a factor, Sellgren et al. (2016) and Miedema (June 2016):

$$f = \frac{d_h - 0.0002}{0.0005 - 0.0002} \quad \text{or} \quad f = \frac{d_h - 0.0001}{0.0004 - 0.0001} \tag{9.5-29}$$

The second equation however gives a more reasonable fit for particles between 0.1 mm and 0.4 mm. An even better simplification of the v_{50} is achieved with the following equation (DHLLDV simplified, the dash-dot green line):

$$v_{50} \approx 3 \cdot \left(\frac{d_{50}}{0.0005}\right)^{0.45} \cdot \left(\frac{R_{sd}}{1.65}\right)^{0.45} \cdot \left(\frac{\nu_{l,actual}}{\nu_{w,20}}\right)^{-0.25} \cdot \left(\frac{D_p}{0.1524}\right)^{0.092} \tag{9.5-30}$$

A better approach of the v_{50} however is the following equation, based on the DHLLDV Framework:

$$v_{50} \approx 3.4 \cdot \left(\frac{v_t}{\sqrt{g \cdot d}}\right)^{1.96} \cdot \left(\frac{D_p}{0.1524}\right)^{0.092} \cdot \left(\frac{R_{sd}}{1.65}\right)^{-0.092} \cdot \left(\frac{\nu_{l,actual}}{\nu_{w,20}}\right)^{0.27} \tag{9.5-31}$$
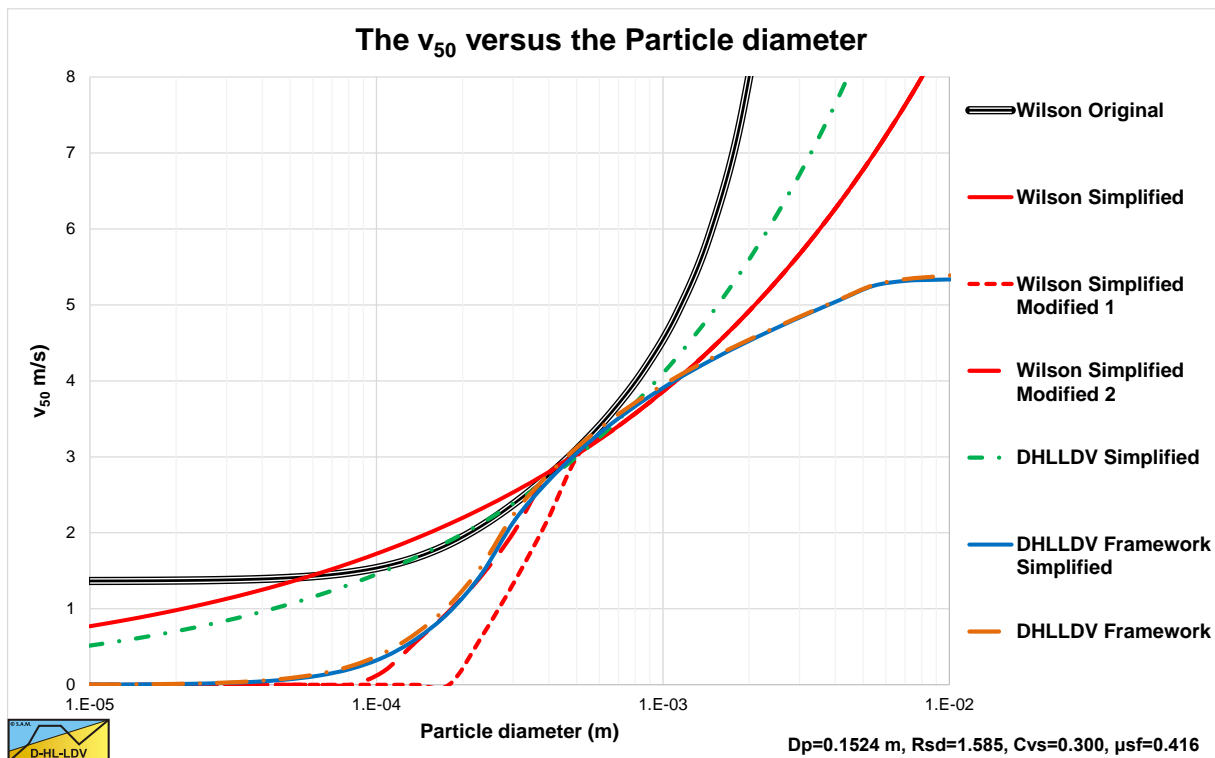
Figure 9.5-2: The different v_{50} methods.

Figure 9.5-2 shows the different v_{50} methods. The thick black solid line shows the original v_{50} method of Wilson et al. (1992). For very small particles and very large particles this method overestimates the v_{50}. For very small particles because of homogeneous transport under operational conditions, for very large particles because of the occurrence of a sliding bed. For particles in the range of d=0.3 mm to d=0.8 mm the estimated v_{50} values seem to be reasonable. The thin red solid line shows the simplified equation, which is close to the original in the range of d=0.1 mm to d=1 mm, although the fit could be much better. The dash-dot green line shows the result of the DHLLDV simplified equation, giving a much closer fit to the original Wilson et al. (1992) method. Later the simplified equation (6.20-58) was adjusted with a factor to get rid of the overestimation for small particles with equation (6.20-75). Both possibilities are drawn in Figure 9.5-2. The first equation is the red dashed line and the second equation the dash-dot red line. Still the equations include the influence of the homogeneous regime for very small particles and the sliding bed regime for very large particles. Using a factor to compensate for the homogeneous overestimation is understandable, but not based on physics. Based on the DHLLDV Framework the v_{50} can also be determined. Although this Framework is more complicated, the line speed where the heterogeneous hydraulic gradient matches the hydraulic gradient of a sliding bed with 50% of the sliding friction coefficient is possible. This is the light brown dash-dot line in the graph. For medium sands this line matches both the original Wilson et al. (1992) method and the simplified equations. It also matches the use of the factor (2nd) to get rid of

the overestimation for very small particles. For very large particles this gives much smaller v_{50} values, since the formulation of the heterogeneous regime of the DHLLDV Framework is not influenced by the sliding bed regime. Equation (9.5-31) is a simplification of the DHLLDV Framework (the solid blue line), matching the full Framework very accurate. For the Wilson et al. (1992) model for graded sands equation (9.5-31) will be used for the determination of the v_{50}.

It should be mentioned that the original Wilson et al. (1992) method and the simplified equation are not consistent with regard to the viscosity. With an increasing viscosity, the original method will give an increasing v_{50}, while the simplified equation gives a decreasing v_{50}. This is caused by the second term in equation (9.5-26) for the particle associated velocity, which increases with increasing viscosity, while the settling velocity will decrease. The correct behavior is a decreasing v_{50} with increasing viscosity, due to the decrease of the settling velocity. In equation (9.5-31) the term containing the settling velocity decreases much faster than the increase of the term with the viscosity, giving a decrease of the v_{50} with increasing viscosity, similar to the simplified equations.

9.5.4.3 The Modified 4 Component Model.

The original 4 component model (4CM) (Sellgren & Wilson (2007)) assumes that each coarser fraction is moving in a carrier liquid containing all finer fractions. So, the coarsest stratified fraction is moving in a carrier liquid containing the homogeneous, pseudo homogeneous and heterogeneous fractions, increasing the carrier liquid density and thus decreasing the relative submerged density and the settling velocity. Only the homogeneous fraction influences the viscosity of the carrier liquid. The original 4CM model up to Sellgren et al. (2014) contains some errors regarding the determination of the different carrier liquid densities, which have been corrected, after Miedema & Ramsdell (2015) discovered this, in Sellgren et al. (2016) as also mentioned in Miedema (June 2016). Still in Sellgren et al. (2016) there is an error in equation 13 for the fully stratified flow. The factor 0.55 should be to the power 0.25. In the original article, Sellgren et al. (2014) this was still correct. The original model for fully stratified flow is, using the sliding friction factor of 0.44:

$$
i_m = i_l + B' \cdot R_{sd} \cdot C_{vt} \cdot \left(\frac{0.55 \cdot v_{sm}}{v_{ls}} \right)^{0.25}
$$

$$
i_m = i_l + B' \cdot R_{sd} \cdot C_{vt} \cdot 2 \cdot \mu_{sf} \cdot \left(\frac{v_{sm}}{v_{ls}} \right)^{0.25}
$$

(9.5-32)

Wilson et al. (1992) used a sliding friction factor of 0.44 in the derivation of the 2-layer model. Based on his hydrostatic approach the factor 2 is valid for plug flow if the spatial volumetric concentration equals the bed concentration. A more general notation can be given by, based on the spatial concentration (note the factor 2 is omitted):

$$
i_m = i_l + B \cdot R_{sd} \cdot C_{vs} \cdot \mu_{sf} \cdot \left(\frac{v_{sm}}{v_{ls}} \right)^{0.25}
$$

(9.5-33)

With the factor **B** in the hydrostatic normal stress approach equals (with **β** the bed angle with the vertical):

$$
B = \frac{2 \cdot \left(\sin(\beta) - \beta \cdot \cos(\beta) \right)}{\left(\beta - \sin(\beta) \cdot \cos(\beta) \right)}
$$

(9.5-34)

The factor **B** is included, because with **β=π** the term describes plug flow, **B=2**. For **β<π** the factor **B** decreases with **β**, **β=π/2** gives **B=1.3** and **β=0** gives **B=1.** So, for low concentrations and small fully stratified fractions a value of **B=1** should be chosen, which matches the later choice of Wilson for a **B'=0.5** (originally he mentioned **B'** is close to unity). Sellgren et al. (2014) use **B'=0.25 (B=0.5)**, while in the reprint of the article Sellgren et al. (2016) they use **B'=0.35 (B=0.7)**. The weight approach of Miedema & Ramsdell (2014) also uses **B=1**. To convert the equation from spatial volumetric concentration to delivered volumetric concentration, the slip ratio ξ_{vsm} at the line speed v_{sm} should be known, giving:

$$i_m = i_l + B \cdot R_{sd} \cdot \frac{C_{vt}}{1-\xi_{vsm}} \cdot \mu_{sf} \cdot \left(\frac{v_{sm}}{v_{ls}}\right)^{0.25} \qquad (9.5-35)$$

The effect of the decreasing slip ratio with increasing line speed is taken into account with the term $(v_{sm}/v_{ls})^{0.25}$. The slip ratio can be estimated by the following empirical equation, based on the 2-layer model with sheet flow added (so 3LM), Miedema (June 2016):

$$C_{vr} = \frac{C_{vt}}{C_{vb}} \quad \text{and} \quad \alpha = 0.58 \cdot C_{vr}^{-0.42} \quad \text{and} \quad \frac{B}{1-\xi_{vsm}} = C_{vr}^{-0.5}$$

$$\xi = (1-C_{vr}) \cdot e^{\left(-\left(0.83 + \frac{\mu_{sf}}{4} + \left(C_{vr}-0.5-0.075\cdot D_p\right)^2 + 0.025\cdot D_p\right)\cdot D_p^{0.025} \cdot \left(\frac{v_{ls}}{v_{sm}}\right)^{\alpha} \cdot C_{vr}^{0.65}\right)} \qquad (9.5-36)$$

This way the slip ratio is incorporated in the model and **B'** depends on this slip ratio. A better approximation of the hydraulic gradient is, using the line speed dependent slip ratio (**B=1** weight approach, **B=equation (9.5-34)** hydrostatic approach):

$$i_m = i_l + B \cdot R_{sd} \cdot \frac{C_{vt}}{1-\xi} \cdot \mu_{sf} \qquad (9.5-37)$$

The maximum of course is plug flow, so if plug flow is reached, the hydrostatic Wilson approach gives as an upper limit:

$$i_m = i_l + 2 \cdot R_{sd} \cdot C_{vb} \cdot \mu_{sf} \qquad (9.5-38)$$

The weight approach of Miedema & Ramsdell (2014) gives for the plug flow upper limit (this follows from substituting equation (7.4-93) in equation (9.5-37) at $v_{ls}=0$):

$$i_m = i_l + R_{sd} \cdot C_{vb} \cdot \mu_{sf} \qquad (9.5-39)$$

In the 4CM each coarser fraction floats in all finer fractions. So, the buoyancy of coarser fractions increases with increasing finer fractions. This seems strange since a bed is a bed, including all fractions in the bed. The small fractions in the bed do not make the coarse fractions lighter. So, in the modified 4CM, only the homogeneous fraction is assumed to influence the density and the viscosity of the carrier liquid (see the adjusted liquid properties). This gives for the relative density S_f of the homogeneous mixture of particles with **d<0.000040 m**:

$$S_f = \frac{\rho_f}{\rho_l} = 1 + \frac{X_f \cdot C_{vs} \cdot R_{sd}}{1-C_{vs}\cdot(1-X_f)} \qquad (9.5-40)$$

The hydraulic gradient of the homogeneous flow regime i_f is now:

$$i_f = \frac{\rho_f}{\rho_l} \cdot \frac{\lambda_f \cdot v_{ls}^2}{2\cdot g \cdot D_p} = S_f \cdot \frac{\lambda_f \cdot v_{ls}^2}{2\cdot g \cdot D_p} = \frac{\rho_f}{\rho_l} \cdot i_l = S_f \cdot i_l \qquad (9.5-41)$$

The difference with pure carrier liquid is the Darcy Weisbach friction factor and the relative density S_f of the resulting homogeneous fluid. For small homogeneous fractions, the Darcy Weisbach friction factor will not differ much from the factor determined for the carrier liquid. So, the main difference is the use of the relative density $S_f>1$ instead of 1. The resulting hydraulic gradient of the modified 4 component model is now:

$$i_m = \frac{\rho_f}{\rho_l} \cdot i_f + \frac{\rho_f}{\rho_l} \cdot C_{vt} \cdot R_{sd,f} \cdot \left(A \cdot X_{ph} \cdot i_f + X_h \cdot \frac{\mu_{sf}}{2} \cdot \left(\frac{v_{50,f}}{v_{ls}}\right)^M + B \cdot \frac{X_s}{1-\xi_{vsm}} \cdot \mu_{sf} \cdot \left(\frac{v_{sm,f}}{v_{ls}}\right)^{0.25}\right) \qquad (9.5-42)$$

The factor **A<1** is included because often the excess hydraulic gradient is smaller than the ELM would give, because of near wall lift. A value of **A=0.5-0.6** is found to be reasonable. For the factor **B** a value of 1 is applied. Sellgren et al. (2016) give a smaller value of about 0.7, which is difficult to compare, since they do not use the slip ratio. The power **M** in the 4CM model is assumed to be 1. The $v_{50,f}$ and $v_{sm,f}$ values are determined based on the adjusted carrier liquid. Physically this is a 3-layer model, with the homogeneous fraction forming an adjusted carrier liquid, the fully stratified fraction forming a sliding bed, the heterogeneous fraction on top of the sliding bed and the pseudo homogeneous fraction at the top of the pipe. For small concentrations, however, there is not much difference with the original 4CM model, but for large concentrations there may be a difference depending on the PSD. The d_{50} of the heterogeneous fraction of the 4CM should be determined according to:

$$d_{50,4CM} = \sqrt{0.0002 \cdot 0.015 \cdot D_p}$$

(9.5-43)

Or by constructing the PSD of the heterogeneous fraction and reading the d_{50} from the resulting graph. Both methods give about the same d_{50}.

9.5.4.4 Wilson 4 Regime Model.

The adjustment of the properties of the carrier liquid is similar to the other models as described in this chapter. The determination of the stratified flow regime is similar tot he fully stratified flow in the 4CM, but now with 100% of the particles in the stratified flow regime. The determination of the heterogeneous flow regime is similar to the original Wilson heterogeneous flow regime. The new element in this model is the transition of the Wilson heterogeneous flow regime tot he high speed homogeneous flow regime. Wilson defined a stratification ratio determining the fraction of the solids being in the stratified flow. This stratification ratio is:

$$R = \frac{1}{2} \cdot \left(\frac{v_{50}}{v_{ls}}\right)^M$$

(9.5-44)

So if the line speed v_{ls} equals the v_{50} of Wilson, 50% of the solids is stratified. This also implies that the other 50% is in suspension. The total solids effect is thus the stratification ratio **R** times the hydraulic gradient of a sliding bed plus **(1-R)** times the hydraulic gradient of homogeneous flow. This gives a smooth transition of the heterogeneous flow regime to the homogeneous flow regime, giving:

$$i_m - i_l = C_{vt} \cdot R_{sd} \cdot \left(\mu_{sf} \cdot \frac{1}{2} \cdot \left(\frac{v_{50}}{v_{ls}}\right)^M + A \cdot i_l \cdot \left(1 - \frac{1}{2} \cdot \left(\frac{v_{50}}{v_{ls}}\right)^M\right) \right)$$

(9.5-45)

The factor A is introduced, because from experiments it is known that the hydraulic gradient in the homogeneous flow regime is smaller than the ELM, with a reduction of **A=0.5-0.6**. In the above reasoning it is assumed that the two flow regimes are independent and can be summed in a linear way. In reality there will be a certain interaction, influencing the transition.

9.5.4.5 The DHLLDV Framework.

The DHLLDV Framework is extensively described in Miedema (June 2016) and will not be described in detail here. The Framework combines the 5 main flow regimes, the stationary bed regime, the sliding bed regime, the heterogeneous flow regime or sliding flow regime and the homogeneous flow regime, for uniform sands and gravels and constant spatial volumetric concentrations. The result is a hydraulic gradient curve where all flow regimes may be present depending on pipe and particle diameter, concentration and line speed. Based on a Limit Deposit Velocity model of Miedema (June 2016) the slip ratio curve is constructed and based on the slip ratio curve the constant delivered concentration curve is determined. For graded sands or gravels, the PSD is divided into a number of fractions. First the liquid properties are adjusted as described in this paper. Secondly the PSD is adjusted, not containing the fines anymore. For each resulting fraction the hydraulic gradient curve is determined based on the spatial/delivered concentration of the whole PSD in order to take hindered settling into account in a correct way. The resulting hydraulic gradient curves are multiplied with the corresponding fraction and added up. The result is a hydraulic gradient curve for the whole PSD.

9.5.5 Example of a Graded Sand.

As an example of the comparison of the 5 methods a pipe diameter of **D$_p$=0.1524 m** and a **d$_{50}$=0.5 mm** are chosen, because the models for uniform sands give very similar hydraulic gradients under operational conditions (line speeds). The different **v$_{50}$** equations also give about the same **v$_{50}$**. This way only the grading of the PSD may be the reason of differences.
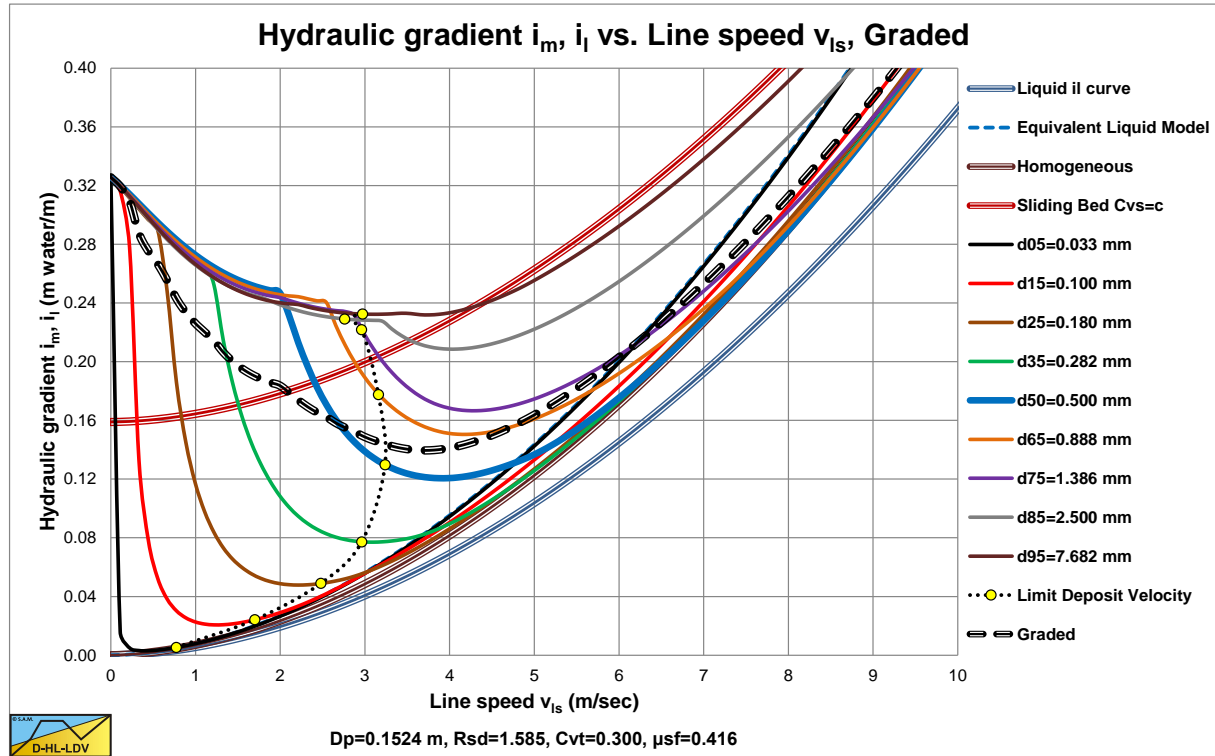
Figure 9.5-3: The hydraulic gradient curves of the fractions and the resulting hydraulic gradient curve.
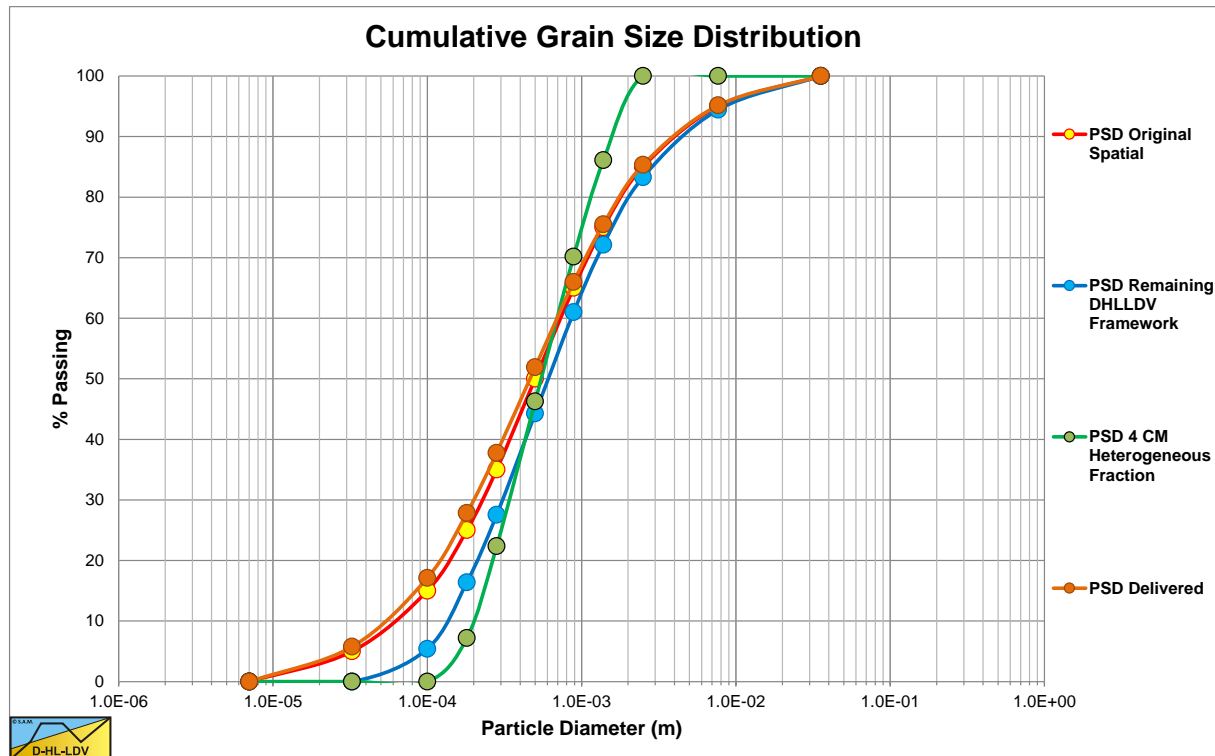
Figure 9.5-4: The PSD of the sand considered, D$_p$=0.1524 m.

Dp=0.1524 m, d=0.500 mm, Rsd=1.585, Cv=0.300, µsf=0.416
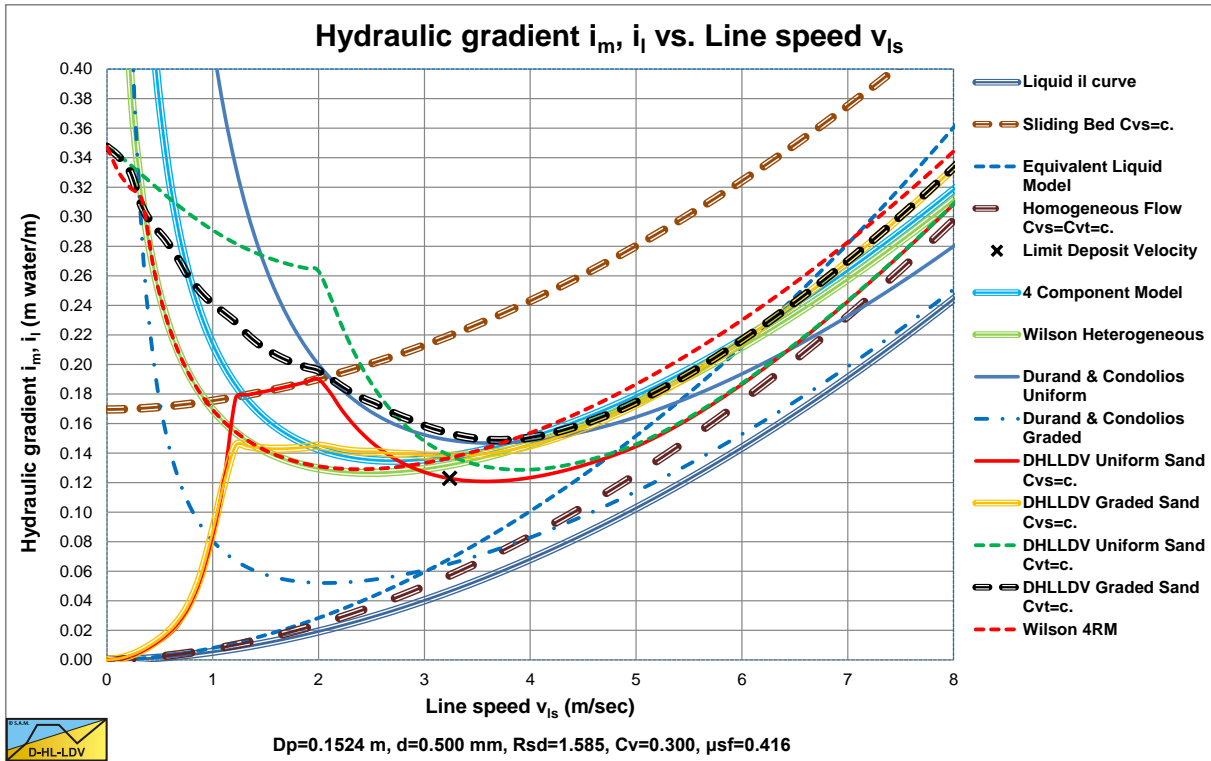
Figure 9.5-5: The resulting hydraulic gradient curves, D_p=0.1524 m.

Figure 9.5-3 shows the hydraulic gradient curves of 9 fractions and the resulting hydraulic gradient curve for the DHLLDV Framework. The PSD given in Figure 9.5-4 is a very broad graded PSD in order to emphasize the effect of grading. This figure also shows the PSD corrected for the fines of the DHLLDV Framework and the heterogeneous PSD as used in the 4CM model. The graph also shows the delivered PSD which is slightly finer than the spatial PSD.

Dp=0.1524 m, d=0.500 mm, Rsd=1.585, Cv=0.300, µsf=0.416
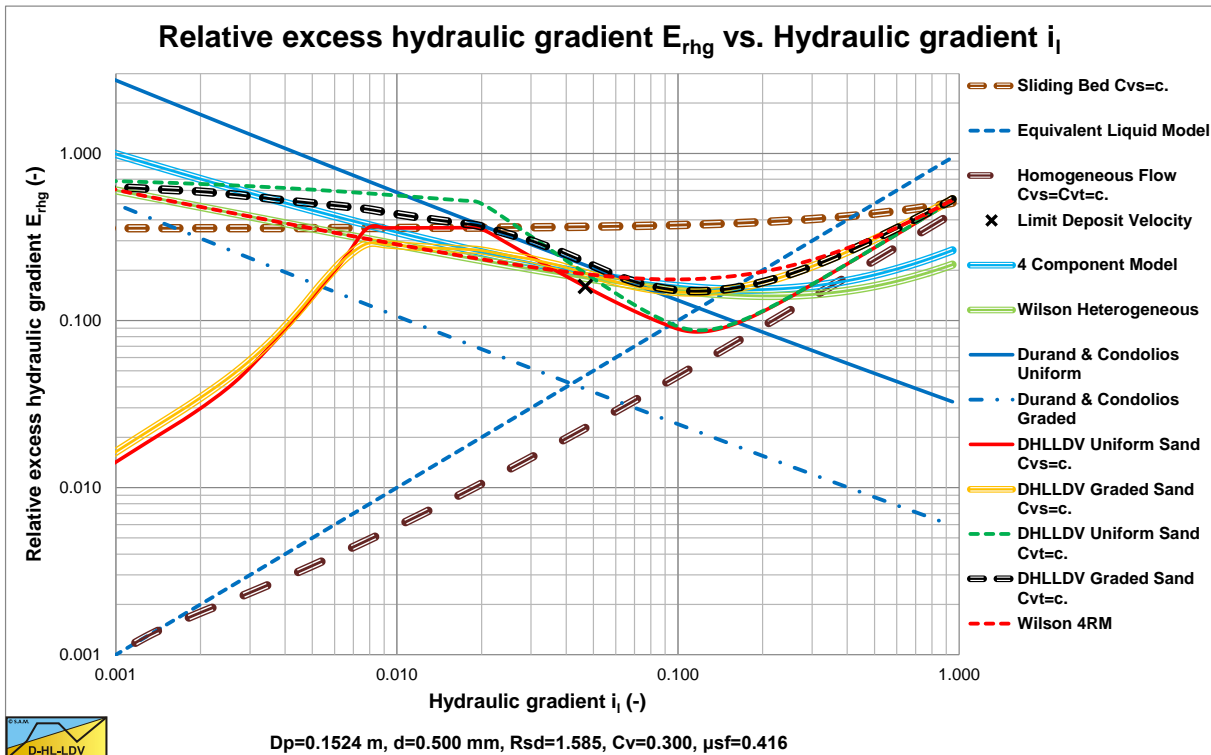
Figure 9.5-6: The resulting relative excess hydraulic gradient curves, also named the stratification ratio, D_p=0.1524 m.

Figure 9.5-3 shows that for small line speeds the resulting hydraulic gradient (the thick dashed black line) is smaller than the corresponding hydraulic gradient of the uniform sand (the thick solid blue line). For larger line speeds (above about 2.6 m/s) however, the resulting hydraulic gradient is larger. This is similar to the effect of a reduced power **M** in the Wilson heterogeneous **v₅₀** method, with a **v₅₀** of about 3 m/s for all equations. Figure 9.5-5 and Figure 9.5-6 show a comparison of the 5 different methods. In Figure 9.5-6 the relative excess hydraulic gradient or stratification ratio as Wilson named it is shown, which is defined as:

$$\mathbf{E_{rhg}} = \frac{\mathbf{i_m} - \mathbf{i_l}}{\mathbf{R_{sd}} \cdot \mathbf{C_{vt}}} \quad \text{or} \quad \mathbf{E_{rhg}} = \frac{\mathbf{i_m} - \mathbf{i_l}}{\mathbf{R_{sd}} \cdot \mathbf{C_{vs}}} \qquad \text{(9.5-46)}$$

Figure 9.5-5 and Figure 9.5-6 also show the uniform curves for the Durand & Condolios (1952) model and the DHLLDV Framework (June 2016).
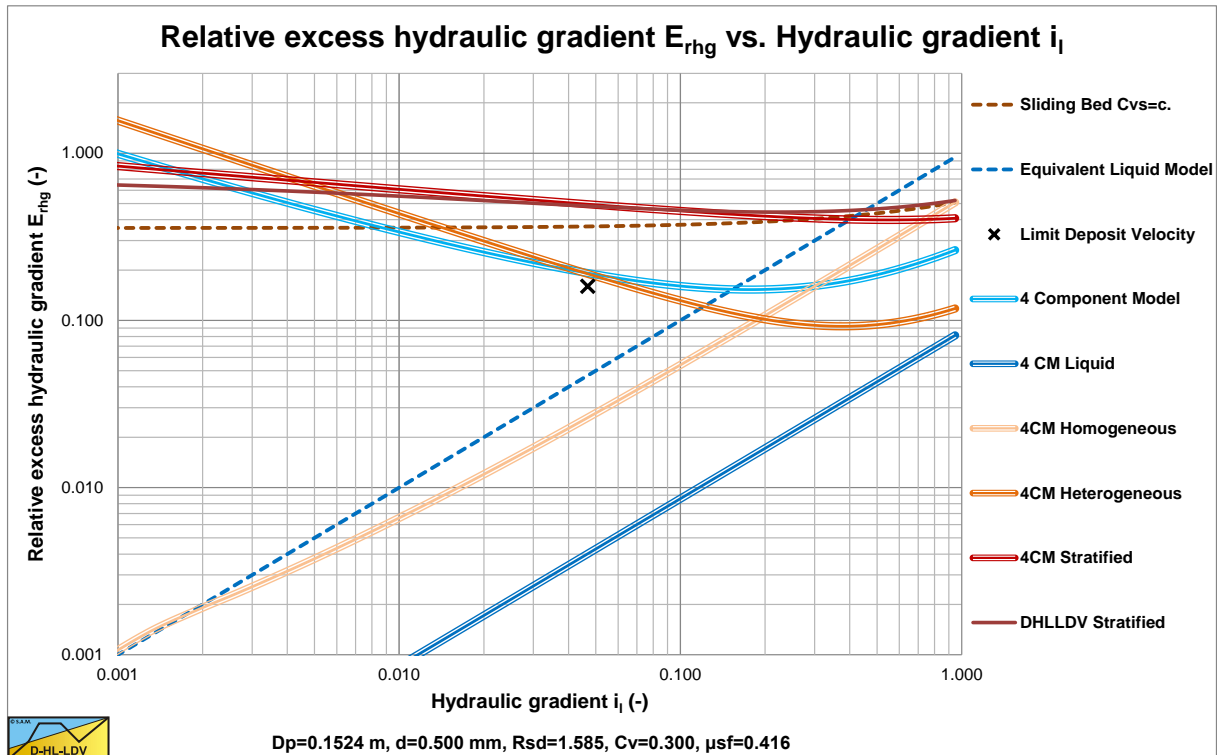
Figure 9.5-7: The behavior of the 4 components, D$_p$=0.1524 m.

Figure 9.5-7 shows the behavior of the 4 components and the resulting 4CM curve. The graph also shows the stratified curve based on slip velocity (DHLLDV stratified). The latter is less steep as the original stratified curve with a power of 0.25. The steepness of the DHLLDV stratified curve however depends strongly on the volumetric concentration. An increasing concentration gives a decreasing steepness.

Figure 9.5-8 and Figure 9.5-9 give a close up of the hydraulic gradient and the solids effect in the operational region of line speeds. Above the LDV the hydraulic gradients are very close and within the margin of experimental scatter. The solids effect seems to give more difference, but this is because of the double logarithmic graph. The curvature of the 4CM and Wilson heterogeneous models at high hydraulic gradients is due to the adjustment of the carrier liquid properties. The Durand & Condolios model is omitted here because it is rejected. The 4CM curve location is influenced by the volumetric concentration. This curve will be higher if the concentration decreases. The other 3 models are hardly influenced by the concentration in the solids effect graph.
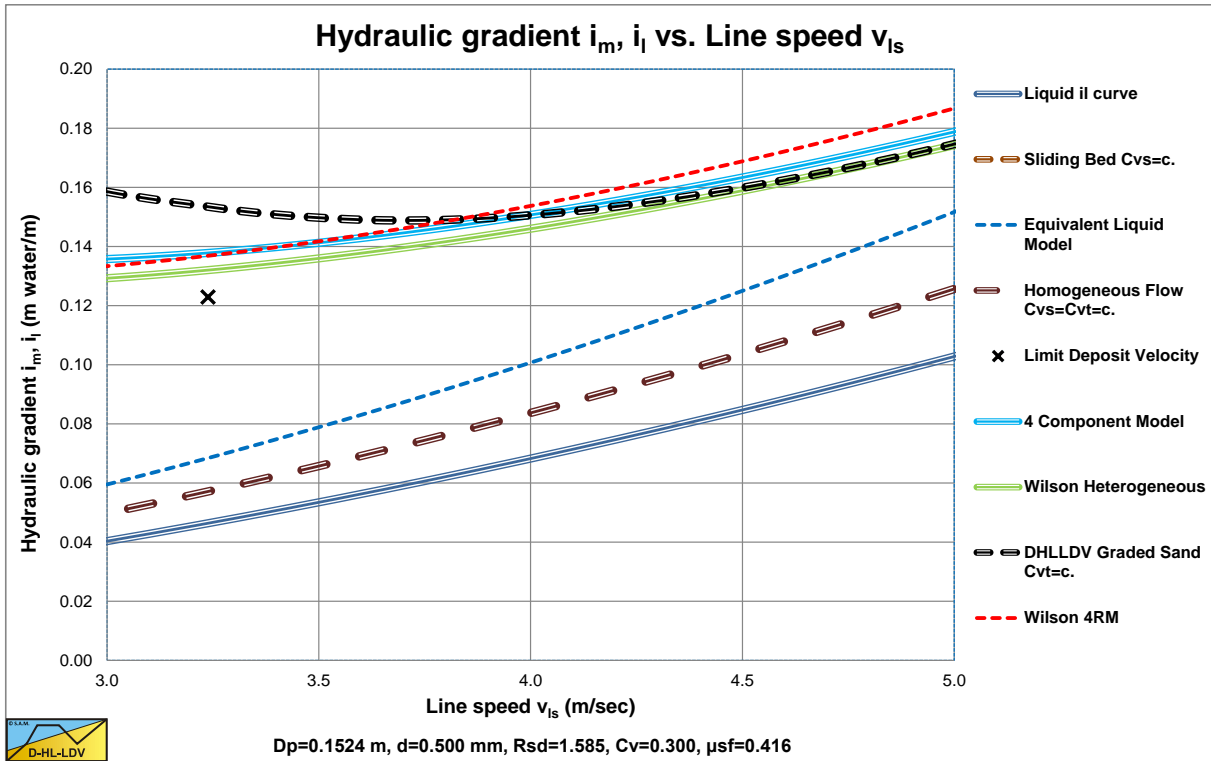
Figure 9.5-8: Close up of the hydraulic gradient, D_p=0.1524 m.
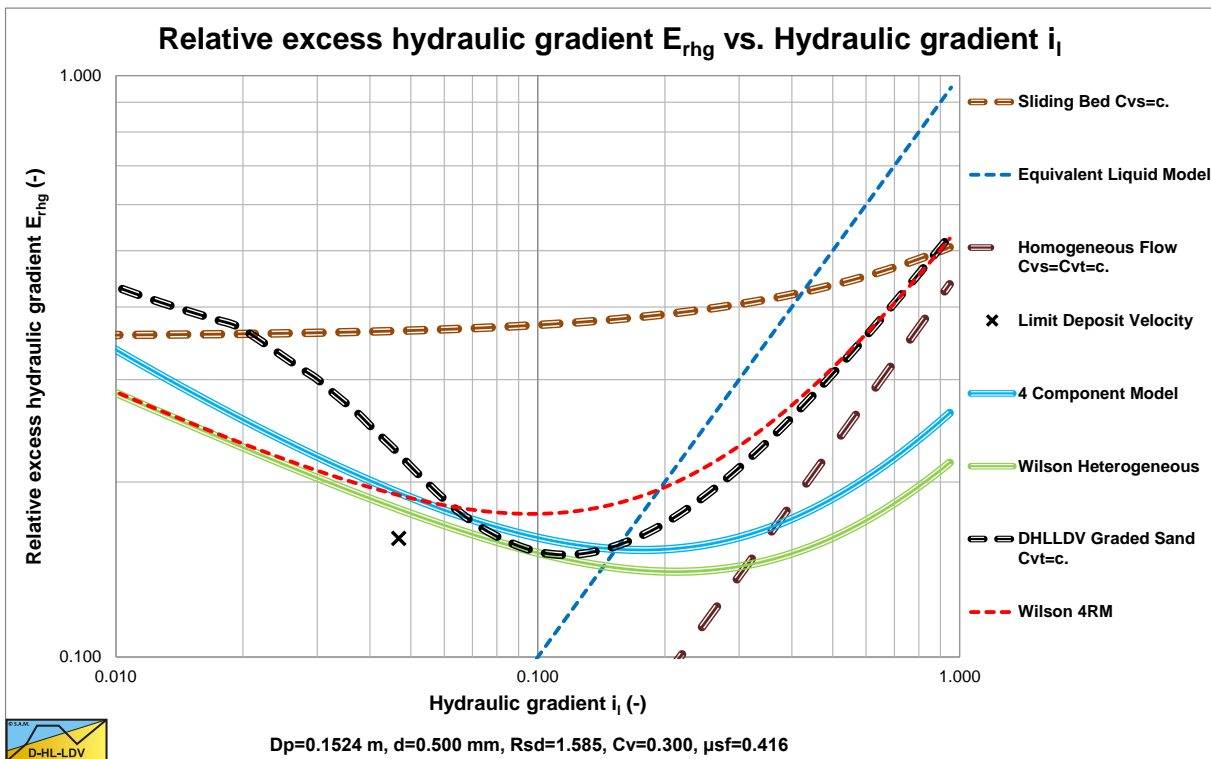
Figure 9.5-9: Close up of the solids effect, D_p=0.1524 m.
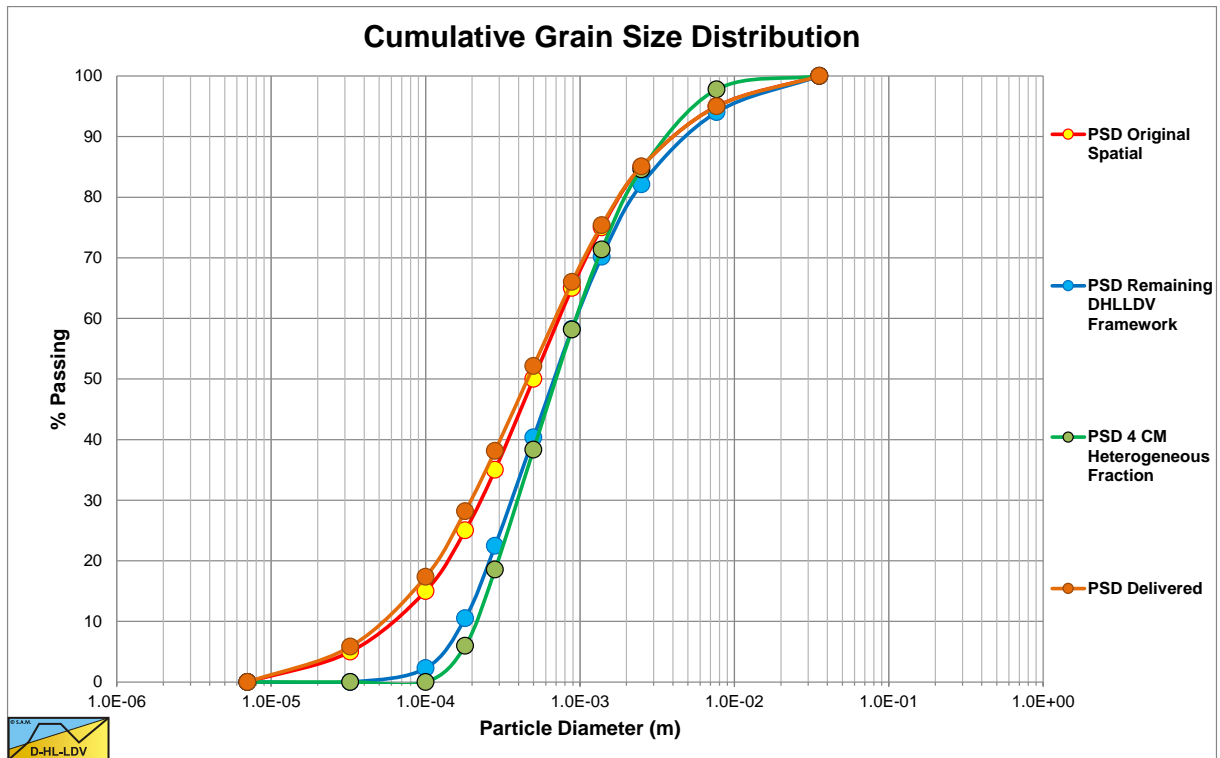
Figure 9.5-10: The PSD of the sand considered, D_p=0.762 m.

Dp=0.7620 m, d=0.500 mm, Rsd=1.585, Cv=0.300, μsf=0.416
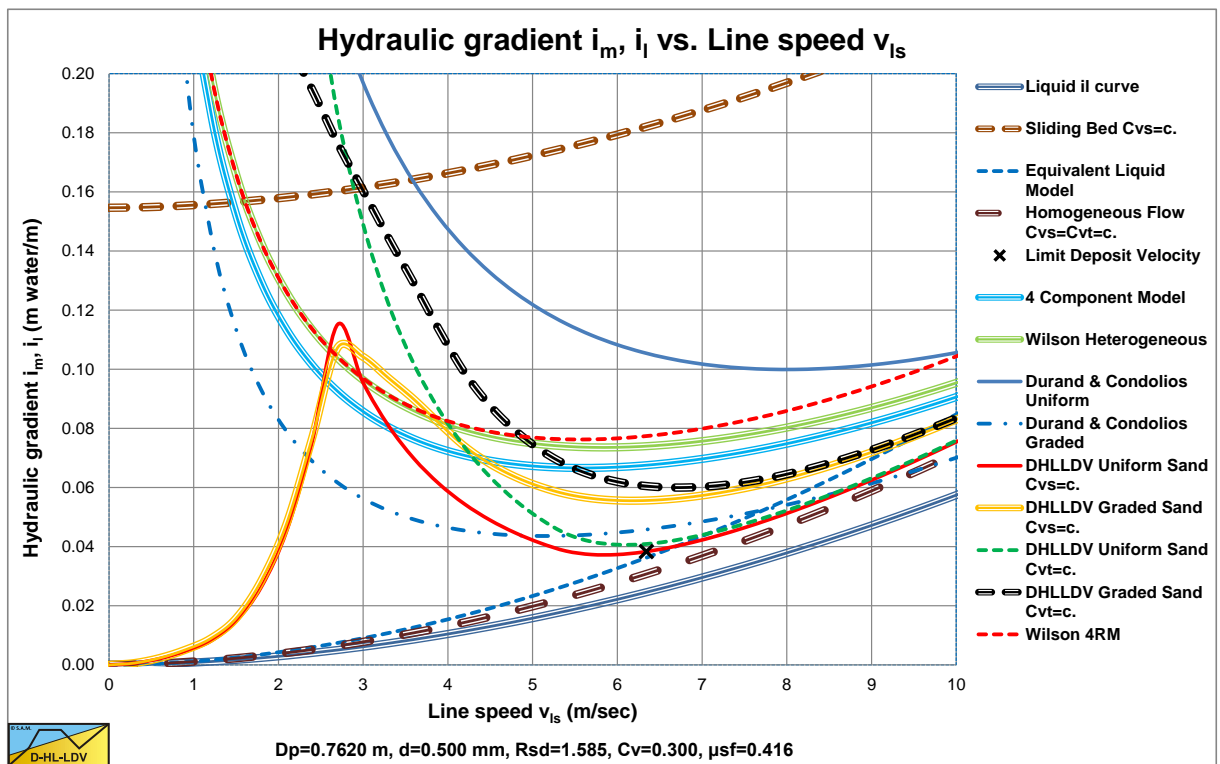
Figure 9.5-11: The resulting hydraulic gradient curves, D_p=0.762 m.

Figure 9.5-10 shows the PSD's of the original sand, the PSD of the heterogeneous fraction of the 4CM, the corrected PSD of the DHLLDV Framework (without the fines) and the delivered PSD. The delivered PSD has a slightly smaller d_{50}, due to the slip velocity of the particles. Very small particles have a smaller slip velocity than larger particles.

Figure 9.5-11 and Figure 9.5-12 show the hydraulic gradient curves and the solids effect curves. In this larger pipe the Wilson and 4CM curves are higher than the DHLLDV Framework curve. The main reason is the

implementation of near wall lift in the DHLLDV Framework and the absence of the sliding flow regime, resulting in a sharper decrease of the hydraulic gradient and solids effect near the transition heterogeneous flow regime and homogeneous flow regime. The Wilson models and 4CM do not incorporate these effects, resulting in an almost pipe diameter independent shape of the curves.
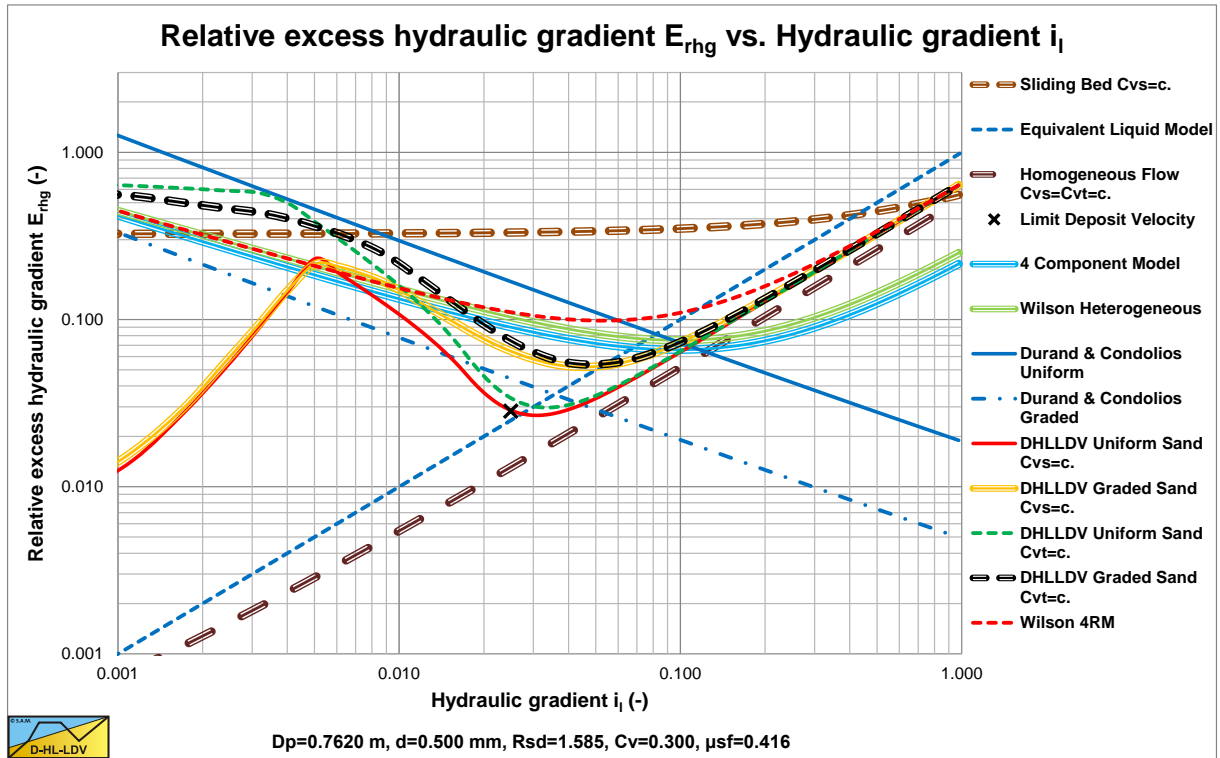
Figure 9.5-12: The resulting relative excess hydraulic gradient curves, also named the stratification ratio, D_p=0.762 m.

9.5.6 Conclusions & Discussion.

The Durand & Condolios (1952) model always gives a lower hydraulic gradient curve for graded sands or gravels, compared with uniform sand or gravel, which contradicts with the 3 other methods. This is caused by the shape of the $\sqrt{C_x}$ number graph in Figure 6.4-20. In the example considered the value increases from 1.13 for uniform sand (the thin solid blue line) to 3.54 for graded sand (the thin dash dot blue line). The effect of this is a reduction to 20% of the solids effect in the hydraulic gradient for the graded sand. This does not seem to be reasonable and also contradicts measurements of Clift et al. (1982) with broad graded crushed granite, which matches the other 3 methods.

For the **D_p=0.1524 m** pipe diameter, the Limit Deposit Velocity, the line speed above which there is no stationary or sliding bed, is estimated by the DHLLDV Framework to be about 3.1 m/s. Under operational conditions, line speeds in the range of 3-5 m/s in the pipe diameter considered, the Wilson heterogeneous model (thick green solid line), the 4CM model (thick light blue solid line) and the DHLLDV Framework (thick dashed black line) give very similar hydraulic gradients and E_{rhg} curves, of which the 4CM gives a slightly higher hydraulic gradient.

The DHLLDV Framework has 10.3% of the particles to adjust the carrier liquid properties, which is a 3% concentration in the case considered (30% solids). About 16.3% of the particles are in the sliding flow regime, which is an integral part of the Framework. The original Wilson heterogeneous model gives a power **M=0.587**, the simplified model **M=0.621**. For the 4CM model a power of **M=1** is applied, according to Sellgren et al. (2016). The 4CM has about 6% of the particles in the homogeneous component (1.8% concentration), 21% in the pseudo homogeneous component, 57% in the heterogeneous component and 16% in the fully stratified component. For both the DHLLDV Framework and the 4CM, the carrier liquid properties were adjusted, but only slightly.

The differences between the 3 models occur outside the operational line speed range. The solids effect of the Wilson heterogeneous model and the 4 CM go to infinity for very small line speeds, due to the formulation of the heterogeneous component, see equation (9.5-21) and equation (9.5-33) for the stratified component in the 4CM.

The solids effect of the Wilson heterogeneous model goes to zero at very high line speeds, see also equation (9.5-21). The solids effect of the 4CM will increase at very high line speeds due to the effects of the homogeneous and pseudo homogeneous fractions. The 4CM curve would be a bit lower if the reduced relative submerged density was used as in the original model.

The D_p=0.762 m pipe simulations show a difference between the models. Here the LDV is about 6.3 m/s and the operational range from 6 m/s to 9 m/s. The DHLLDV Framework curve is much lower than Wilson 4RM (highest), the Wilson heterogeneousand the Wilson & Sellgren 4CM.

The Durand & Condolios model contradicts with these 4 models and is rejected.

The main difference between the 4CM and the DHLLDV Framework is, the 4CM uses fixed boundaries based on particle diameters to divide the PSD into 4 components. These boundaries do not depend on the line speed. The DHLLDV Framework determines the hydraulic gradient curves for each fraction separately. The result is a changing flow regime division depending on the line speed and the particle diameter. Particles that may be in a sliding bed at low line speeds, behave heterogeneous at a higher line speed and homogeneous at a very high line speed. Here the PSD is divided into 9 fractions, which seems to be enough, however the number of fractions can be unlimited.

The concept of the v_{50} pivot point of Wilson, the heterogeneous line of Wilson in the E_{rhg} graph pivots around the v_{50} when the power M is changed, matched the results of the DHLLDV Framework. At line speeds higher than the v_{50} the solids effect increases while at lower line speeds it decreases with increased grading, although the line speed of this pivot point is not exactly the same in both models, but it is close.

Under operational conditions all 4 models, the Wilson heterogeneous model, the Wilson 4RM, the Sellgren & Wilson 4CM and the DHLLDV Framework, can be used for small pipe diameters. Outside the operational conditions, low and high line speeds, the DHLLDV Framework takes the behavior of a possible sliding bed and homogeneous flow better into account. For large pipe diameters the 4 models differ. However there are no experimental data proving which model is the best.

Only the Wilson 4RM and the DHLLDV Framework match all criteria from the beginning of this chapter.

As final remarks it should be stated that the interaction between fractions and/or components is not taken into account and could influence the outcome. The use of the delivered volumetric concentration for a graded sand or gravel is not very convenient since the delivered PSD does not have to be the same as the spatial PSD.

9.5.7 Nomenclature Graded Sands & Gravels.

A_x, A_{15}, A_{85}	Factor PSD	-
A	Correction factor pseudo homogeneous flow	-
B	Correction factor stratified flow	-
C_{vs}	Spatial volumetric concentration	-
C_{vt}	Delivered/transport volumetric concentration	-
C_{vb}	Volumetric bed concentration	-
C_{vr}	Relative volumetric concentration C_{vr}=C_{vt}/C_{vb}	-
$C_{vs,r}$	Remaining spatial volumetric concentration	-
$C_{vs,x}$	Volumetric concentration of fraction x	-
C_x	Durand & Condolios particle drag coefficient	-
C_D	Particle drag coefficient	-
d	Particle diameter	m
d_x, d_y	Particle diameter	m
d_{50}	Particle diameter 50% passing by weight	m
d_{15}, d_{85}	Particle diameter 15%/85% passing by weight	m
d_{lim}	Limiting particle diameter homogeneous fraction	m
D_p	Pipe diameter	m
E_{rhg}	Relative excess hydraulic gradient (stratification ratio)	-
f	Correction factor determination v_{50}	-
f_y, f_x	Fraction passing	-
Fr	Froude number	-

g	Gravitational constant	m/s²
i_l	Hydraulic gradient liquid	-
i_m	Hydraulic gradient mixture	-
i_f	Hydraulic gradient adjusted carrier liquid	-
K	Durand & Condolios constant	-
ΔL	Length of pipeline	m
M	Power Wilson heterogeneous equation (0.25-1.7)	-
n	Porosity	-
NWL	Near Wall Lift	-
dp, p_i	Probability	-
Δp_l	Liquid pressure	kPa
Δp_m	Mixture pressure	kPa
R	Stratification ratio (E_{rhg})	-
R_{sd}	Relative submerged density	-
$R_{sd,f}$	Relative submerged density in adjusted carrier liquid	-
S_f	Relative density adjusted carrier liquid	-
Stk	Stokes number	-
v_{ls}	Line speed	m/s
$v_{ls,ldv}$	Limit Deposit Velocity	m/s
v_{50}	50% stratification ratio line speed for d_{50}	m/s
$v_{50,f}$	50% stratification ratio line speed for d_{50} in adjusted carrier liquid	m/s
v_t	Terminal settling velocity particle	m/s
v_{sm}	Maximum Limit of Stationary Deposit Velocity	m/s
$v_{sm,f}$	Maximum Limit of Stationary Deposit Velocity in adjusted carrier liquid	m/s
w_{50}	Particle associated velocity Wilson for d_{50}	m/s
w_{85}	Particle associated velocity Wilson for d_{85}	m/s
X	Fraction	-
X_f	Fraction of PSD in homogeneous component	-
X_{ph}	Fraction of PSD in pseudo homogeneous component	-
X_h	Fraction of PSD in heterogeneous component	-
X_s	Fraction of PSD in fully stratified component	-
α_{15}, α_{85}	Ratio	-
β	Bed angle with vertical	rad
λ_l	Darcy Weisbach friction coefficient liquid	-
λ_f	Darcy Weisbach friction coefficient adjusted carrier liquid	-
ρ_l	Liquid density	ton/m³
ρ_s	Solids density	ton/m³
ρ_x	Pseudo liquid density	ton/m³
ρ_m	Mixture density	ton/m³
σ	Variance PSD	-
ν_l, ν_w	Kinematic viscosity liquid/water	m²/s
ν_x	Kinematic viscosity pseudo liquid	m²/s
μ_l	Dynamic viscosity liquid	Pa·s
μ_x	Dynamic viscosity pseudo liquid	Pa·s
μ_{sf}	Sliding friction factor	-
Φ	Durand & Condolios solids effect	-
ψ	Durand & Condolios solids effect	-
ξ	Slip ratio	-
ξ_{vsm}	Slip ratio at v_{sm}	-

Chapter 10:   Application of the Theory on a Cutter Suction Dredge.

10.1 Head Loss Equation.

In dredging and other industries it is important to be able to predict the required pressure and power to transport solid-liquid mixtures over a short to very long distance, with or without pipe inclination and/or elevation in a system with one or more pumps (usually centrifugal pumps). The pipeline resistance, pressure difference between entrance (suction mouth) and discharge, is an ascending curve, ascending with increasing flow. The pump pressure curve is usually a second degree descending curve, descending with increasing flow. The two curves will intersect at a certain flow rate, meaning that the pressure required to transport the mixture through the pipeline equals the available pump pressure. This is called the working point. At lower flows the available pump pressure is higher than the pressure required to transport the mixture through the pipeline, meaning that the mixture in the pipe will accelerate until the working point is reached. At higher flows the available pump pressure is lower than the pressure required to transport the mixture through the pipeline, meaning that the mixture in the pipe will decelerate until the working point is reached. The second degree pump curve, second degree with the flow rate Q_m, also depends on the mixture density ρ_m, usually a linear relation, and depends on the particle diameter d. The latter is because large particles influence the efficiency of the pump. Figure 10.1-1 shows a pump/pipeline system with multiple centrifugal pumps. The question is now, how can the theory developed in this book, the DHLLDV Framework, be applied to such a pump/pipeline system?
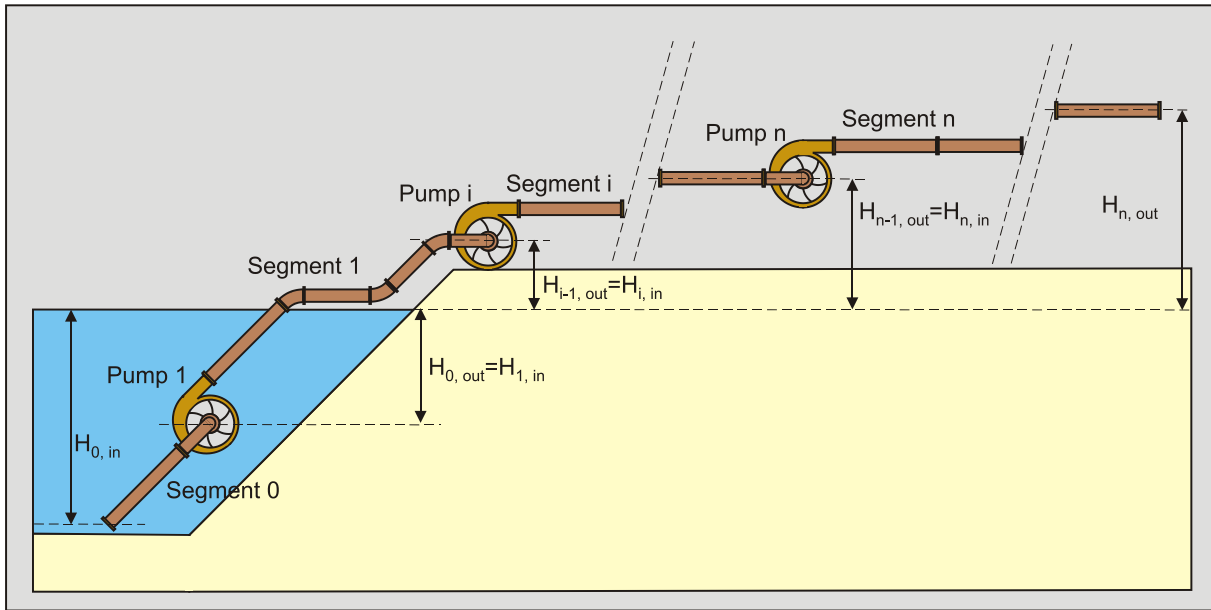
Figure 10.1-1: A pump pipeline system with boosters.

To answer this question, first the total pipeline resistance is analyzed. The pressure losses from the suction mouth (the entrance) to the end of the pipeline (the discharge), assuming many fittings in the pipeline, are, assuming one pipe diameter for all **n** pipe segments, one mixture density in the whole pipeline and a stationary process (not time or position dependent):

$$\Delta p_m = \frac{1}{2} \cdot \rho_m \cdot v_{ls}^2 + \lambda_l \cdot \frac{L_{tot}}{D_p} \cdot \frac{1}{2} \cdot \rho_l \cdot v_{ls}^2 + \rho_l \cdot g \cdot L_{tot} \cdot R_{sd} \cdot C_{vt} \cdot E_{rhg} + \frac{1}{2} \cdot \rho_m \cdot v_{ls}^2 \cdot \sum_{i=1}^{n}\left(\sum_{l=1}^{m_i}\left(\xi_{l,i}\right)\right)$$

$$+ \rho_m \cdot g \cdot \left(H_{n,out} - H_{0,in}\right)$$

(10.1-1)

In this example it is assumed that the suction pipe and the discharge pipe have the same diameter. In reality this is often not the case. The suction pipe is usually a bit larger than the discharge pipe. However for this example it does not make a lot of difference.

The pressure loss equation consists of 5 terms:

1. The **1st** term represents the acceleration losses. Outside the pipe the mixture is assumed not to have a velocity, but inside the pipe it has the line speed. So the mixture has to be accelerated from zero velocity to the line speed, resulting in some pressure loss. Basically this can be determined from the Bernouilli equation. For the total pressure loss this is negligible, but for the calculation of possible cavitation at the inlet of the first pump it is.
2. The **2nd** term is the so called Darcy-Weisbach term for straight pipeline resistance of pure liquid (water in this case). The Darcy-Weisbach friction factor can be determined from the Moody diagram. For large diameter pipes and high line speeds the Darcy Weisbach friction factor is close to λ_l=**0.01**.
3. The **3rd** term is the solids effect based on the DHLLDV Framework.
4. The **4th** term represents the pressure losses due to many fittings, telescopes and so on.
5. The **5th** term represents the total elevation pressure loss, from suction mouth to discharge.
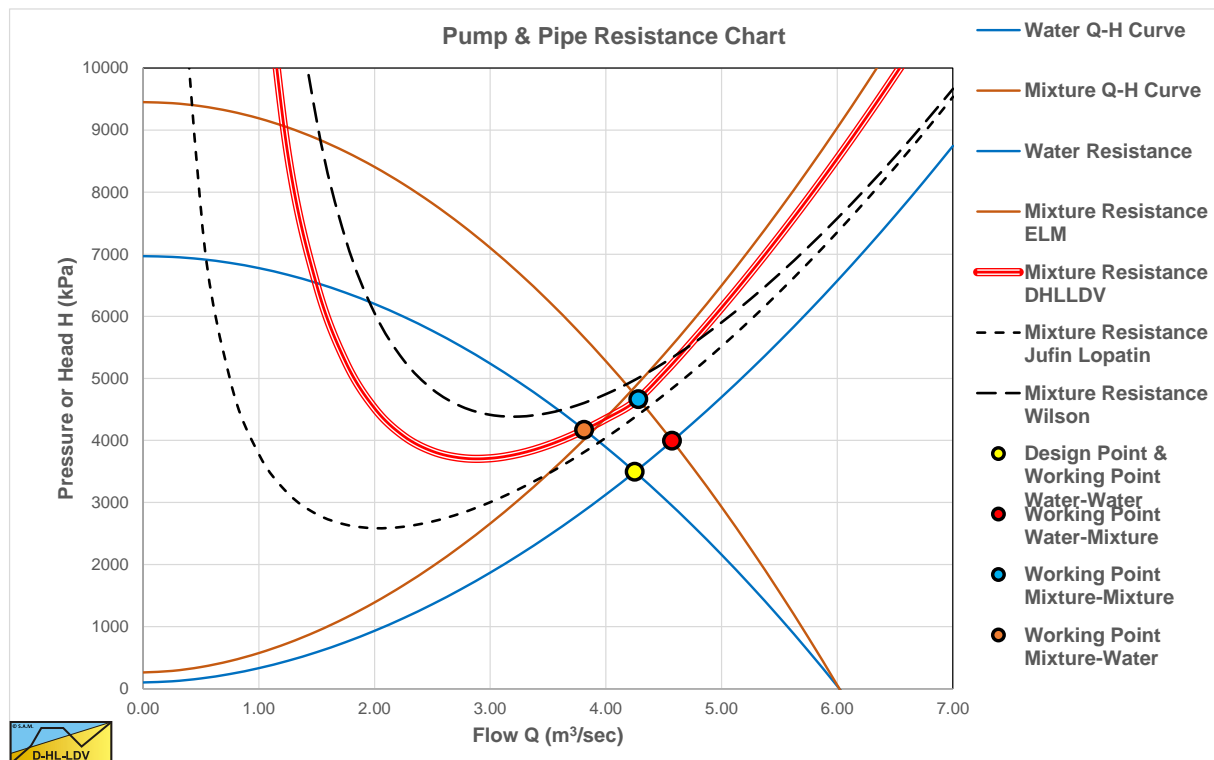
Figure 10.1-2: A pump pressure and pipeline resistance graph, D_p=0.85 m, d=0.3 mm, L=10 km.

Figure 10.1-2 shows two pump curves, one for pure liquid (water, the blue descending line) and one for a mixture density ρ_m of about 1.4 tons/m³ (the brown descending line). The pipeline resistance curve for pure liquid (water, the blue ascending line) and the ELM curve (the brown ascending line). For the ELM curve it is assumed that the water density can be replaced by the mixture density and there is no further solids effect. The thick red line gives the result of equation (10.1-1) using the DHLLDV Framework for heterogeneous and homogeneous transport. The two dashed lines give the result of equation (10.1-1) using the Jufin-Lopatin (1966) model and the Wilson et al. (1992) heterogeneous model. The 4 colored circles give the 4 possible working points.
1. Yellow, the pipeline is 100% full of water and the pump is full of water.
2. Red, the pipeline is close to 100% full of water, but the pump is full of mixture.
3. Blue, the pipeline is 100% full of mixture and the pump is full of mixture.
4. Brown, the pipeline is close to 100% full of mixture, but the pump is full of water.
The Jufin-Lopatin (1966) model and the Wilson et al. (1992) heterogeneous model are also shown here to illustrate that different models may give different working (intersection) points. In real life there is not just one working point, but there is a working area, formed by the 4 points in Figure 10.1-2 under the assumption that the graph is made for the maximum achievable mixture density.

The mixture resistance of the DHLLDV Framework (the thick red line) has a verticle distance compared with the water resistance curve. This distance depends on the mixture flow. This distance is the result of the so called solids effect which is the third term in equation (10.1-1). This solids effect is modeled in this book. On very short pipelines this solids effect is not to important. The first, fourth and fifth terms in equation (10.1-1) dominate the

pressure losses. The second and third terms contain the length of the pipeline and will thus be small compared to the other terms. In long pipelines however, the second and third terms will dominate. The influence of the pipe elevation completely depends on the value of the pipe elevation.
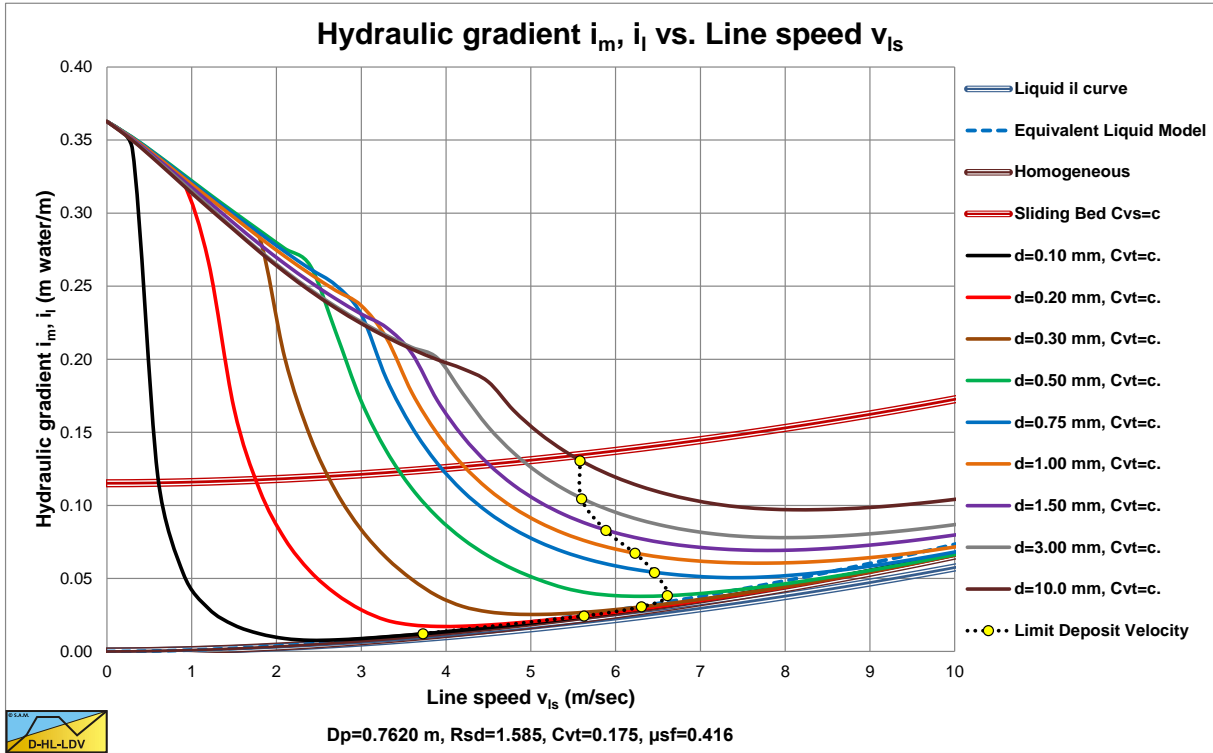
Figure 10.1-3: The hydraulic gradient for a 0.762 m (30 inch) pipe and 9 particle diameters for a constant delivered volumetric concentration of 17.5%.
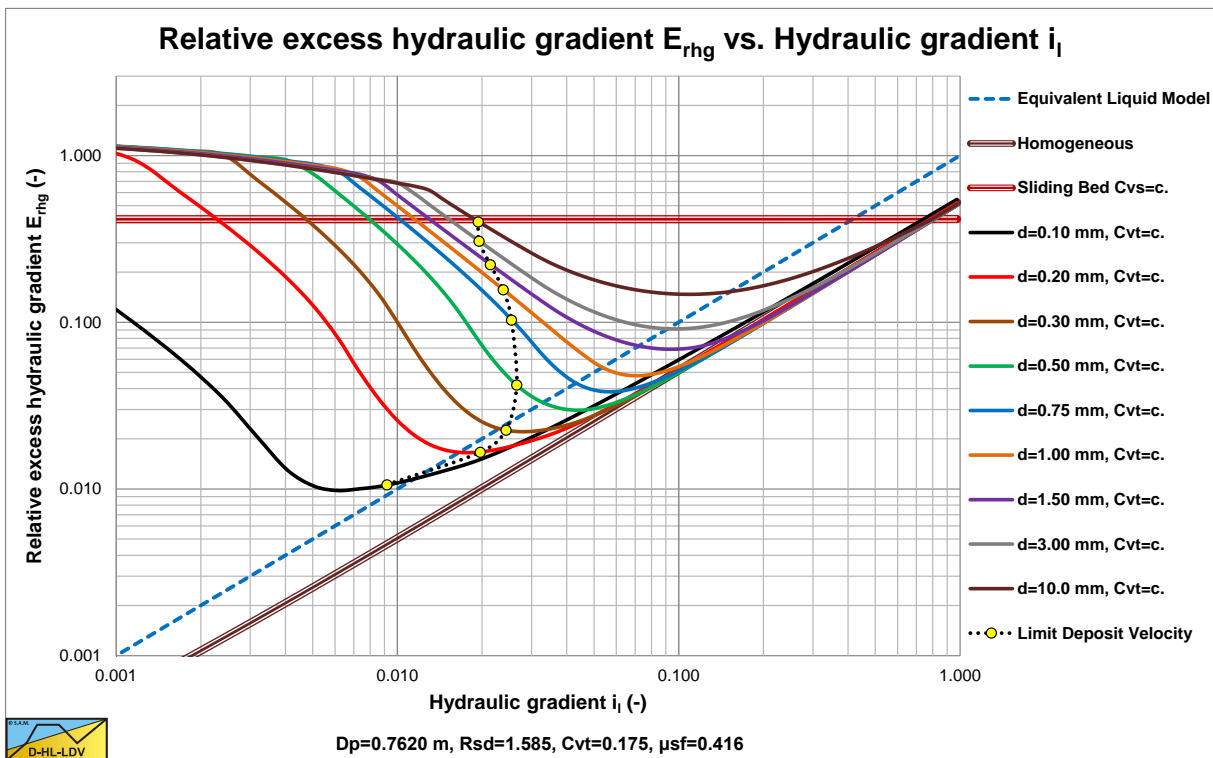
Figure 10.1-4: The relative excess hydraulic gradient for a 0.762 m (30 inch) pipe and 9 particle diameters for a constant delivered volumetric concentration of 17.5%.

Often the pressure losses are expressed in terms of the hydraulic gradient. The hydraulic gradient is the pressure loss divided by the density of the liquid (water, 1-1.025 ton/m³), the gravitational constant (9.81 m/s²) and the length of the pipeline. Figure 10.1-3 shows the hydraulic gradient in a **Dp=0.762 m** (30 inch) pipe and a delivered volumetric concentration of 17.5% for 9 particle diameters. It is clear from this figure that the hydraulic gradient depends strongly on the particle diameter.

Figure 10.1-4 shows the relative excess hydraulic gradient **E_rhg** for different particle diameters in a **Dp=0.762 m** (30 inch) pipe as a function of the hydraulic gradient **i_l**. The graph is also constructed for a 17.5% constant delivered volumetric concentration. For other concentrations the graph can also be used for the heterogeneous (downwards) and the homogeneous (upwards) regimes (so if the slip can be neglected), but not for the sliding bed regime (almost horizontal left top).

10.2 The Limit Deposit Velocity.

The Limit Deposit Velocity is defined in this book as the line speed above which there is no stationary or sliding bed. So below this line speed there is either a stationary (small particles) or a sliding (large particles) bed.

The Limit Deposit Velocity can be determined with:

$$v_{ls,ldv} = F_L \cdot \left(2 \cdot g \cdot R_{sd} \cdot D_p \right)^{1/2}$$

(10.2-1)

The value of the LDV can be found in Figure 10.2-1 for a **Dp=0.762 m** (30 inch) pipe..
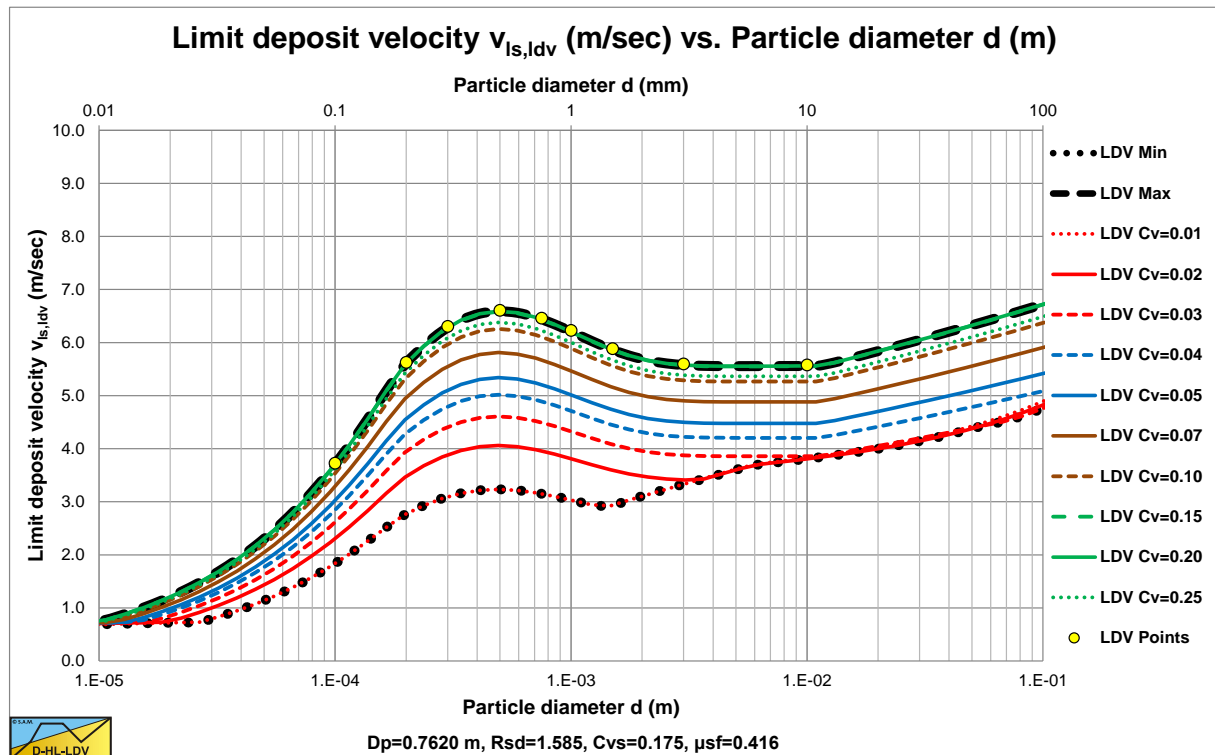
Figure 10.2-1: The limit deposit velocity for a Dp=0.762 m (30 inch) pipe.

10.3 The Resulting Head Loss versus Mixture Flow Graph.

For a **Dp=0.762 m** (30 inch) pipe, a particle diameter of **d=0.5 mm**, a pipe length of 4000 m, a water depth of 20 m and an elevation of 10 m, the pressure losses are given in Figure 10.3-1. The graph shows the water resistance curve (blue), the homogeneous curve (light brown), the DHLLDV Framework curve for constant spatial volumetric concentration (red),), the DHLLDV Framework curve for constant delivered volumetric concentration (dashed green) and the resulting pump curves for water (dark blue) and the mixture (dark brown). The graph also shows the LDV and the concentration dependent LDV curves. The LDV is 6.35 m/s or 10417 m³/hour. The working point (intersection of pump and resistance curves) is above 11000 m³/hour. The pressure losses at this

working point are about 1500 kPa or 15 bar. It should be mentioned that in this example one should not stop pumping and later try to restart, since at low flow rates the pipe resistance is higher than the available pump pressure (the green dashed line).
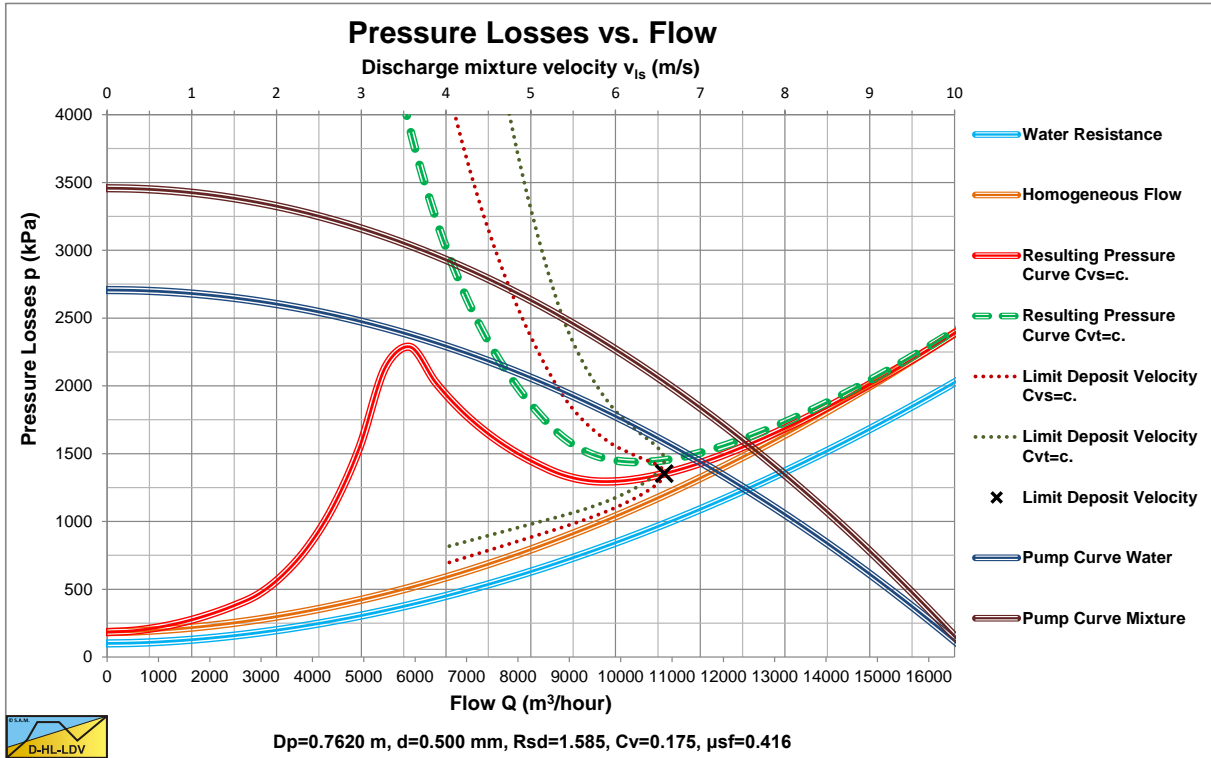
Figure 10.3-1: Pressure losses versus flow for d=0.5 mm particles.

10.4 The Relative Excess Hydraulic Gradient of Pump and Pipeline.
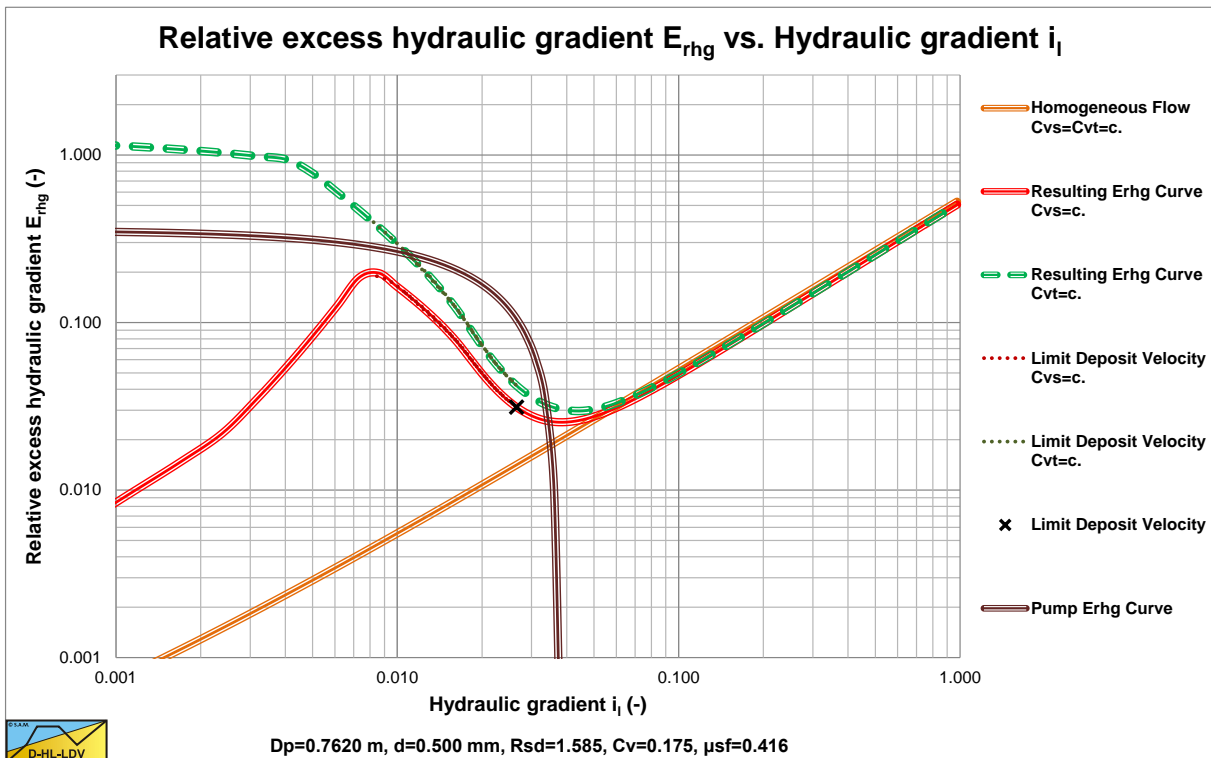
Figure 10.4-1: The relative excess hydraulic gradient for d=0.5 mm particles.

For a D_p=0.762 m (30 inch) pipe, a particle diameter of d=0.5 mm, a pipe length of 4000 m, a water depth of 20 m and an elevation of 10 m, the relative excess hydraulic gradient curves are given in Figure 10.4-1. The graph shows the homogeneous curve (light brown), the DHLLDV Framework curve for constant spatial volumetric concentration (red), the DHLLDV Framework curve for constant delivered volumetric concentration (dashed green) and the resulting pump curve for the mixture (dark brown). The graph also shows the LDV.

10.5 A Segmented Pipeline System.

Splitting the pressure losses over **n** pipe segments gives a more detailed impression of the pressure losses in a system with more than 1 pump. The pumps are numbered from number 1 to number **n**. The pipe segments are numbered from number 0 (the suction pipe) to number **n**. One could consider the hydrostatic pressure $p_{0,in}$ at the suction mouth as the result of a virtual pump number 0, the result of the layer of water above the suction mouth plus the atmospheric pressure above the waterline. First the pressure losses in the suction pipe, resulting in the absolute pressure at the entrance of the first real pump (pump 1) and showing whether there will be cavitation, will be determined. Next equations are derived for all other pipe segments. The mixture flow Q_m is either a constant in the whole system, or increases slightly because of the gland water in each pump. The latter may result in a decreasing mixture density after each pump. The pipe diameter D_p and thus the line speed v_{ls} may differ for each pipe segment.

Absolute pressure start with the symbol **p**, while pressure difference start with **Δp**. So pump head and pipeline resistance are pressure differences.

10.5.1 The Suction Pipe.

The cross section of the suction pipe (segment 0) is:

$$A_{p,0} = \frac{\pi}{4} \cdot D_{p,0}^2 \qquad (10.5\text{-}1)$$

The line speed in the suction pipe, assuming a mixture flow $Q_{m,0}$, is:

$$v_{ls,0} = \frac{Q_{m,0}}{A_{p,0}} \qquad (10.5\text{-}2)$$

The pressure losses from the suction mouth to the entrance of the first pump (segment 0) are:

$$\Delta p_{m,0} = \frac{1}{2} \cdot \rho_{m,0} \cdot v_{ls,0}^2 \qquad \text{(Acceleration losses)}$$

$$+ \lambda_{l,0} \cdot \frac{L_0}{D_{p,0}} \cdot \frac{1}{2} \cdot \rho_l \cdot v_{ls,0}^2 \qquad \text{(Darcy Weisbach friction losses)}$$

$$+ \frac{1}{2} \cdot \rho_{m,0} \cdot v_{ls,0}^2 \cdot \sum_{l=1}^{m_0} \xi_{l,0} \qquad \text{(Losses due to } m_0 \text{ fittings)} \qquad (10.5\text{-}3)$$

$$+ \rho_{m,0} \cdot g \cdot L_0 \cdot \sin(\theta_0) \qquad \text{(Losses due to pipe inclination or elevation)}$$

$$+ \rho_l \cdot g \cdot L_0 \cdot R_{sd} \cdot C_{vt} \cdot E_{rhg,0} \qquad \text{(Losses due to the solids effect)}$$

With: $\quad H_{0,out} - H_{0,in} = L_0 \cdot \sin(\theta_0)$

The mixture density is based on the delivered/transport volumetric concentration.

The absolute hydrostatic pressure at the inlet of the suction mouth of the cutter head or in the drag head $p_{0,in}$ is the elevation at the waterline H_{wl} (which is defined as zero) minus the elevation of the suction mouth $H_{0,in}$ (which is a negative elevation) times the liquid (water) density and the gravitational constant plus the atmospheric pressure:

$$p_{0,in} = \rho_l \cdot g \cdot \left(H_{wl} - H_{0,in}\right) + p_{atm} \qquad (10.5\text{-}4)$$

This gives for the absolute pressure at the inlet of the first pump, the absolute pressure at the inlet of the suction pipe $p_{0,in}$ minus the pressure losses in the suction pipe $\Delta p_{m,0}$ (segment 0):

$$P_{0,out} = P_{0,in} - \Delta p_{m,0} \tag{10.5-5}$$

The absolute pressure at the inlet of the first pump is $p_{0,out}$ and should be above a certain minimum p_{cav} to avoid cavitation. Although theoretically the cavitation pressure is almost absolute 0, in reality locally cavitation may appear at higher absolute mean pressures, because locally velocities may differ from the mean velocity.

$$P_{0,out} > P_{cav} \tag{10.5-6}$$

In a stationary situation, the mixture density $\rho_{m,0}$ has to be smaller than a certain limit to avoid cavitation in the first pump. So the condition is:

$$p_{0,in} - \Delta p_{m,0} > p_{cav} \quad \text{or} \quad p_{0,in} - p_{cav} - \Delta p_{m,0} > 0$$

$$\rho_l \cdot g \cdot \left(H_{wl} - H_{0,in} \right) + p_{atm} - p_{cav} - \Delta p_{m,0} > 0 \tag{10.5-7}$$

Substituting the pressure losses in the suction pipe gives:

$$\rho_l \cdot g \cdot \left(H_{wl} - H_{0,in} \right) + p_{atm} - p_{cav} - \lambda_{l,0} \cdot \frac{L_0}{D_{p,0}} \cdot \tfrac{1}{2} \cdot \rho_l \cdot v_{ls,0}^2 - \rho_l \cdot g \cdot L_0 \cdot R_{sd} \cdot C_{vt} \cdot E_{rhg,0}$$

$$- \tfrac{1}{2} \cdot \rho_{m,0} \cdot v_{ls,0}^2 - \tfrac{1}{2} \cdot \rho_{m,0} \cdot v_{ls,0}^2 \cdot \sum_{l=1}^{m_0} \xi_{l,0} - \rho_{m,0} \cdot g \cdot L_0 \cdot \sin(\theta_0) > 0 \tag{10.5-8}$$

This gives for the maximum mixture density not having cavitation:

$$\rho_{m,0} < \frac{\rho_l \cdot g \cdot \left(H_{wl} - H_{0,in} \right) + p_{atm} - p_{cav} - \lambda_{l,0} \cdot \dfrac{L_0}{D_{p,0}} \cdot \tfrac{1}{2} \cdot \rho_l \cdot v_{ls,0}^2 - \rho_l \cdot g \cdot L_0 \cdot R_{sd} \cdot C_{vt} \cdot E_{rhg,0}}{\tfrac{1}{2} \cdot v_{ls,0}^2 + \tfrac{1}{2} \cdot v_{ls,0}^2 \cdot \displaystyle\sum_{l=1}^{m_0} \xi_{l,0} + g \cdot L_0 \cdot \sin(\theta_0)} \tag{10.5-9}$$

10.5.2 Other Pipe Segments.

All other pipe segments start after a pump with index **i** and also have the index **i** (so segment **i**). Since each pipe segment may have a different pipe diameter, first the pipe cross section and the line speed in the pipe segment have to be determined. The flow $Q_{m,i}$ of course is the same in each pipe segment, because of continuity considerations. However if gland water flow is taken into consideration, after each pump the flow may increase slightly. That's the reason why in the equations the flow also has an indez **i**. In most cases the gland water flow is neglected and the flow in each pipe segment is the same.

The cross section of a pipe segment (segment i) is:

$$A_{p,i} = \frac{\pi}{4} \cdot D_{p,i}^2 \tag{10.5-10}$$

The flow in pipe section **i**, corrected for gland water flow is:

$$Q_{m,i} = Q_{m,i-1} + Q_{gw,i} \tag{10.5-11}$$

The line speed in the pipe segment, assuming a mixture flow $Q_{m,i}$, is:

$$v_{ls,i} = \frac{Q_{m,i}}{A_{p,i}}$$

(10.5-12)

The pressure losses of pipe segment **i** with an inclined pipe are:

$$\Delta p_{m,i} = \tfrac{1}{2} \cdot \rho_{m,i} \cdot \left(v_{ls,i}^2 - v_{ls,i-1}^2 \right) + \lambda_{l,i} \cdot \frac{L_i}{D_{p,i}} \cdot \tfrac{1}{2} \cdot \rho_l \cdot v_{ls,i}^2 + \tfrac{1}{2} \cdot \rho_{m,i} \cdot v_{ls,i}^2 \cdot \sum_{l=1}^{m_i} \xi_{l,i}$$

$$+ \rho_{m,i} \cdot g \cdot L_i \cdot \sin\left(\theta_i \right) + \rho_l \cdot g \cdot L_i \cdot R_{sd} \cdot C_{vt} \cdot E_{rhg,i}$$

(10.5-13)

With: $\quad H_{i,out} - H_{i,in} = L_i \cdot \sin\left(\theta_i \right)$

In case there is no pipe inclination, but a vertical part in the pipe section, the 4th term can be replaced by:

$$\Delta p_{m,i} = \tfrac{1}{2} \cdot \rho_{m,i} \cdot \left(v_{ls,i}^2 - v_{ls,i-1}^2 \right) + \lambda_{l,i} \cdot \frac{L_i}{D_{p,i}} \cdot \tfrac{1}{2} \cdot \rho_l \cdot v_{ls,i}^2 + \cdot \tfrac{1}{2} \cdot \rho_{m,i} \cdot v_{ls,i}^2 \cdot \sum_{l=1}^{m_i} \xi_{l,i}$$

$$+ \rho_{m,i} \cdot g \cdot \left(H_{i,out} - H_{i,in} \right) + \rho_l \cdot g \cdot L_i \cdot R_{sd} \cdot C_{vt} \cdot E_{rhg,i}$$

(10.5-14)

10.5.3 Adding Pump Head to the Equations.

Now suppose each pump has a pump head, depending on the flow through the pump, the mixture density and the particle diameter. The latter influences the efficiency of the pump. Small particles have hardly any influence, but large particles, like gravel, do. The pump head is named $\Delta p_{p,i}(Q_{m,i-1}, \rho_m, d)$. The absolute pressure at the entrance of pump **k+1, $p_{e,k+1}$,** so at the end of segment **k**, can now be determined with:

$$p_{e,k+1} = \rho_l \cdot g \cdot \left(H_{wl} - H_{0,in} \right) + p_{atm} - \Delta p_{m,0} - \sum_{i=1}^{k} \left(\tfrac{1}{2} \cdot \rho_{m,i} \cdot \left(v_{ls,i}^2 - v_{ls,i-1}^2 \right) \right)$$

$$- \sum_{i=1}^{k} \left(\lambda_{l,i} \cdot \frac{L_i}{D_{p,i}} \cdot \tfrac{1}{2} \cdot \rho_l \cdot v_{ls,i}^2 \right) - \sum_{i=1}^{k} \left(\tfrac{1}{2} \cdot \rho_{m,i} \cdot v_{ls,i}^2 \cdot \sum_{l=1}^{m_i} \xi_{l,i} \right)$$

(10.5-15)

$$- \sum_{i=1}^{k} \left(\rho_{m,i} \cdot g \cdot L_i \cdot \sin\left(\theta_i \right) \right) - \rho_l \cdot g \cdot R_{sd} \cdot C_{vt} \cdot \sum_{i=1}^{k} \left(L_i \cdot E_{rhg,i} \right) + \sum_{i=1}^{k} \left(\Delta p_{p,i} \right)$$

The absolute pressure at the discharge of pump **k+1, $p_{d,k+1}$,** can now be determined with:

$$p_{d,k+1} = \rho_l \cdot g \cdot \left(H_{wl} - H_{0,in} \right) + p_{atm} - \Delta p_{m,0} - \sum_{i=1}^{k} \left(\tfrac{1}{2} \cdot \rho_{m,i} \cdot \left(v_{ls,i}^2 - v_{ls,i-1}^2 \right) \right)$$

$$- \sum_{i=1}^{k} \left(\lambda_{l,i} \cdot \frac{L_i}{D_{p,i}} \cdot \tfrac{1}{2} \cdot \rho_l \cdot v_{ls,i}^2 \right) - \sum_{i=1}^{k} \left(\tfrac{1}{2} \cdot \rho_{m,i} \cdot v_{ls,i}^2 \cdot \sum_{l=1}^{m_i} \xi_{l,i} \right)$$

(10.5-16)

$$- \sum_{i=1}^{k} \left(\rho_{m,i} \cdot g \cdot L_i \cdot \sin\left(\theta_i \right) \right) - \rho_l \cdot g \cdot R_{sd} \cdot C_{vt} \cdot \sum_{i=1}^{k} \left(L_i \cdot E_{rhg,i} \right) + \sum_{i=1}^{k+1} \left(\Delta p_{p,i} \right)$$

At the end (the discharge) of the pump/pipeline system the pressure is atmospheric again in a stationary situation. This give the following equation:

$$p_{atm} = \rho_l \cdot g \cdot \left(H_{wl} - H_{0,in}\right) + p_{atm} - \Delta p_{m,0} - \tfrac{1}{2} \cdot \sum_{i=1}^{n} \left(\rho_{m,i} \cdot \left(v_{ls,i}^2 - v_{ls,i-1}^2\right)\right)$$

$$-\sum_{i=1}^{n} \left(\lambda_{l,i} \cdot \frac{L_i}{D_{p,i}} \cdot \tfrac{1}{2} \cdot \rho_l \cdot v_{ls,i}^2\right) - \sum_{i=1}^{n} \left(\tfrac{1}{2} \cdot \rho_{m,i} \cdot v_{ls,i}^2 \cdot \sum_{l=1}^{m_i} \xi_{l,i}\right) \qquad \textbf{(10.5-17)}$$

$$-\sum_{i=1}^{n} \left(\rho_{m,i} \cdot g \cdot L_i \cdot \sin\left(\theta_i\right)\right) - \rho_l \cdot g \cdot R_{sd} \cdot C_{vt} \cdot \sum_{i=1}^{n} \left(L_i \cdot E_{rhg,i}\right) + \sum_{i=1}^{n} \left(\Delta p_{p,i}\right)$$

One could even make the equations more detailed by dividing pipe segments into pipe sections. At the point where a pipe segment is split into sections, a virtual pump with zero head could be added. This way the above equations are also valid for a system where the segment boundaries do not have to be a pump, the entrance or the discharge of the pipeline, but can also be a zero head virtual pump. This enables to create a detailed graph of the pressure in the pipeline as a function of the distance from the entrance.

Now assuming a constant pipe diameter in the whole system, no gland water, and a constant mixture density in the whole system. Equation (10.5-17) can be reduced to:

$$\rho_l \cdot g \cdot \left(H_{wl} - H_{0,in}\right) + \sum_{i=1}^{n} \left(\Delta p_{p,i}\right) - \tfrac{1}{2} \cdot \rho_m \cdot v_{ls}^2 - \lambda_l \cdot \frac{L_{tot}}{D_p} \cdot \tfrac{1}{2} \cdot \rho_l \cdot v_{ls}^2 - \tfrac{1}{2} \cdot \rho_m \cdot v_{ls}^2 \cdot \sum_{i=0}^{n} \left(\sum_{l=1}^{m_i} \xi_{l,i}\right)$$

$$-\rho_m \cdot g \cdot \left(H_{n,out} - H_{0,in}\right) - \rho_l \cdot g \cdot L_{tot} \cdot R_{sd} \cdot C_{vt} \cdot E_{rhg} = 0 \qquad \textbf{(10.5-18)}$$

$$\textbf{With:} \quad L_{tot} = \sum_{i=0}^{n} \left(L_i\right)$$

Or using the pipeline resistance pressure Δp_m from equation (10.1-1):

$$\rho_l \cdot g \cdot \left(H_{wl} - H_{0,in}\right) + \sum_{i=1}^{n} \left(\Delta p_{p,i}\right) - \Delta p_m = 0 \qquad \textbf{(10.5-19)}$$

So in the working point there is an equilibrium between the sum of the hydrostatic pressure in the suction mouth and the added heads of all the pumps on one hand and the total pipeline resistance on the other hand. If there is no equilibrium, the mixture is either accelerating or decelerating in order to reach an equilibrium, which is described with the following equation:

$$\rho_l \cdot g \cdot \left(H_{wl} - H_{0,in}\right) + \sum_{i=1}^{n} \left(\Delta p_{p,i}\right) - \Delta p_m = \rho_m \cdot L_{tot} \cdot \dot{v}_{ls} \qquad \textbf{(10.5-20)}$$

If the left hand side is positive there is acceleration, if it's negative there is deceleration.

With the derived equations one can construct a detailed graph of the pressure in the pipeline versus the length of the pipeline and check whether cavitation occurs at the entrance of one of the pumps.

Figure 10.5-1 shows an example of a pump/pipeline system with a ladder pump, a main pump and a booster pump.
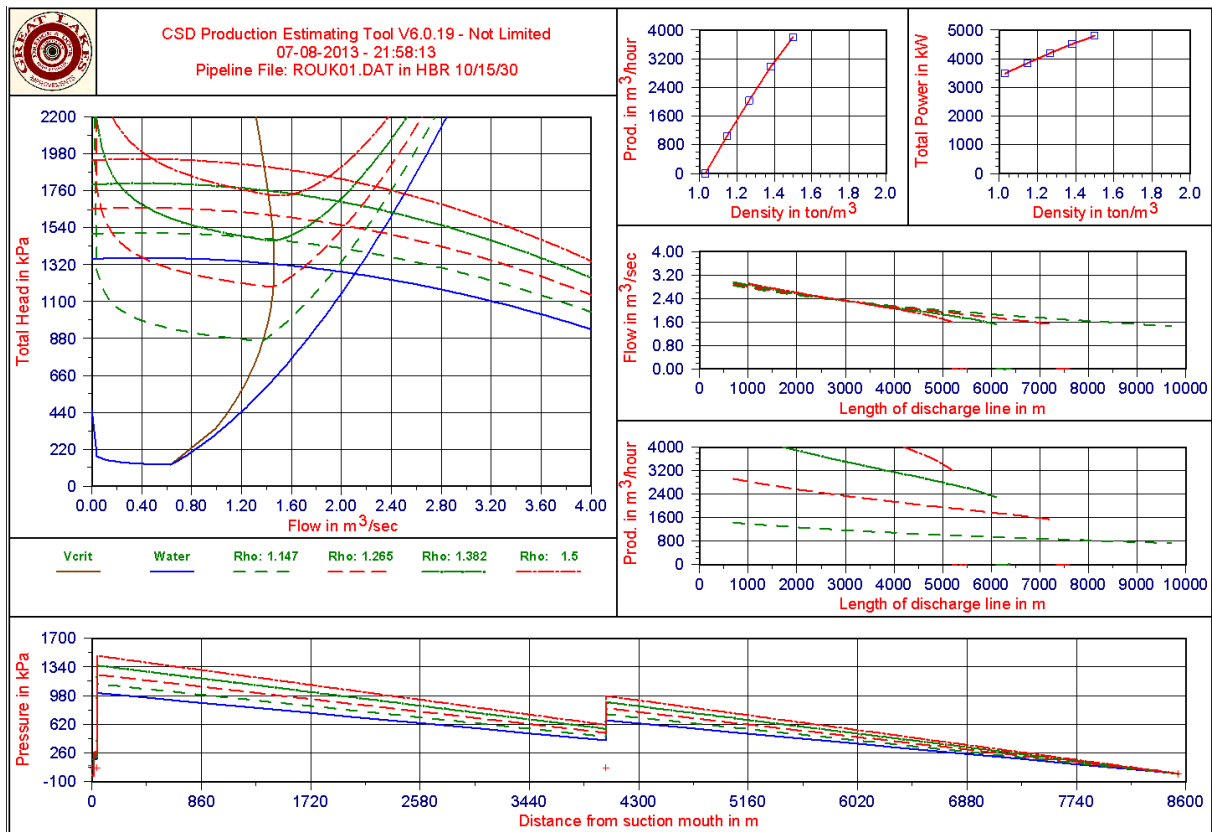
Figure 10.5-1: An example of a system with ladder pump, main pump and booster pump.

10.5.4 The Inertial Effects in the Pipeline.

A steady state process requires a constant mixture density and solids properties in the system and thus at the suction mouth. In practice it is known, that the solids properties and the mixture density change with respect to time. As a result, the pump discharge pressure and vacuum will change with respect to time and the pipeline resistance will change with respect to time and place. A change of the discharge pressure of a pump will result in a change of the torque on the axis of the pump drive on one hand and in a change of the flow velocity on the other hand. The mixture in the pipeline has to accelerate or decelerate. Since centrifugal pumps respond to a change in density and solids properties at the moment the mixture passes the pump, while the pipeline resistance is determined by the contents of the pipeline as a whole, this forms a complex dynamic system with different time constants.

The inertial pressure of the mixture has to be added to the resistance of the mixture (see equation). In fact, the inertial pressure is always equal to the difference between the total pressure generated by the pumps plus the absolute pressure at the suction mouth on one hand and the total resistance of the mixture in the pipeline system on the other hand. If this difference is positive (for example the pump pressure has increased due to an increase of the mixture density), the mixture will accelerate. If negative, the mixture will decelerate. As a result of the acceleration and deceleration, the mixture velocity (line speed) will vary as a function of time.

To realize a stable dredging process, it is required to have a line speed that will not vary too much. The line speed can be controlled by varying the revolutions of one of the dredge pumps, where the last pump is preferred.

From the above one can distinguish the different effects by the time they require to change/occur:

1. Very fast (within a second), the change in discharge pressure of a centrifugal pump due to a sudden change of the mixture density in the pump.
2. Fast (seconds), the change in revolutions of the pump drive and the change in line speed (acceleration and deceleration).
3. Slow (minutes), filling up the pipeline with mixture or a change in mixture content. In large diameter pipelines this may take 2-2.5 minutes per kilometer of pipeline length.
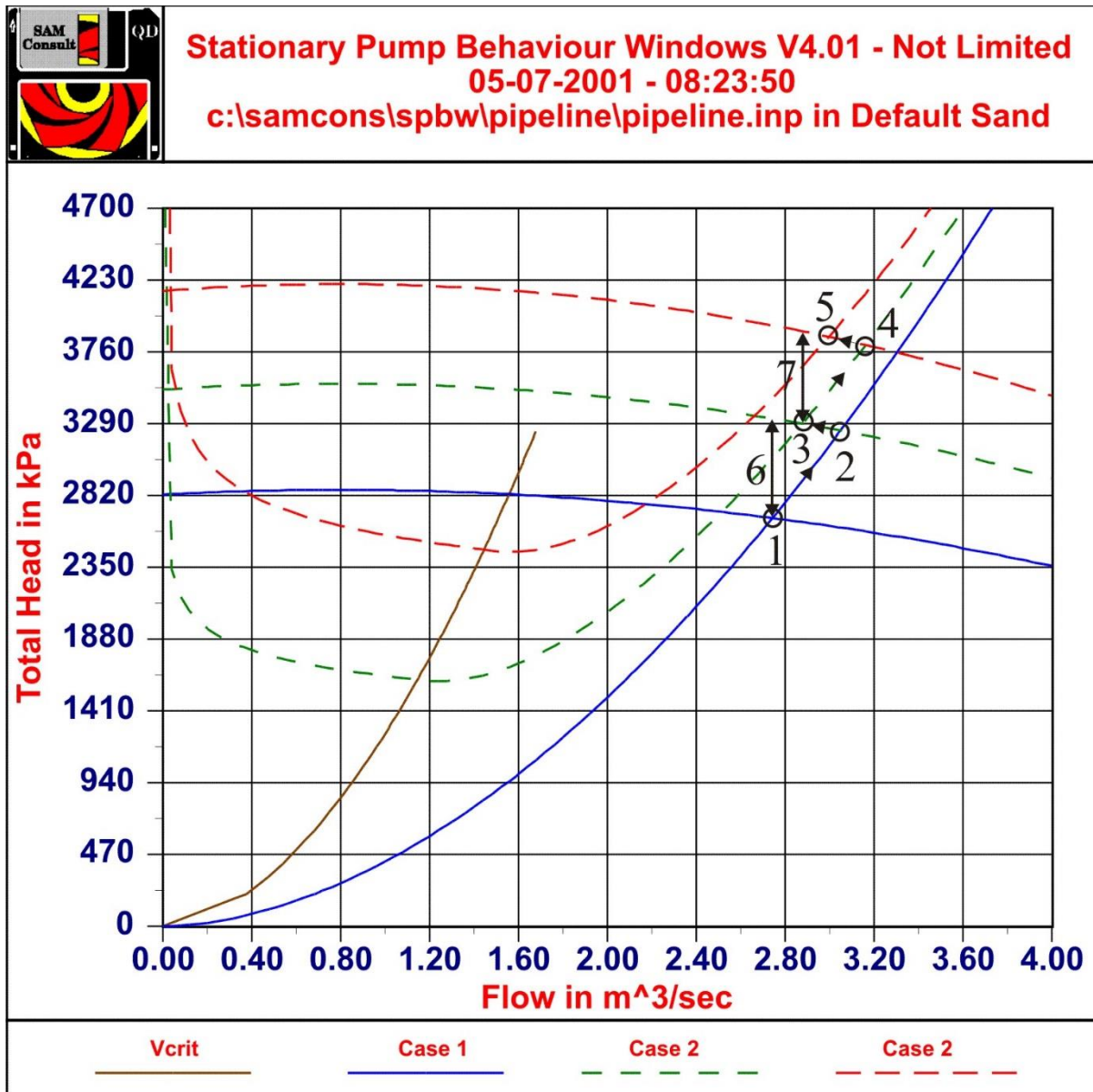
Figure 10.5-2: The system curves for 3 cases, accelerating.

Figure 10.5-2 is a representation of a number of phenomena that occur subsequently when the system (Figure 10.1-1) filled with water, is filled with mixture with a density of 1.6 ton/m^3. In this figure case 1 represents the system and the pump curve for the system filled with water. Case 2 represents the system with the pipeline filled with mixture up to a point just before the 3rd pump (the booster pump). Case 3 represents the system filled entirely with the mixture.

Now, what happens if a system filled with water is continuously filled with the mixture?

First the working point is point 1 in Figure 10.5-2. This is the intersection point of the pump and system curves for water. When mixture enters the system, within a few (about 8) seconds the mixture has reached the ladder and main pump, since the distance is only about 44 m and the line speed about 5 m/sec. At that moment, the discharge pressure of the ladder pump and main pump increase proportionally to the pressure matching the mixture density, resulting in a pump curve according to case 2 and a working point 2. The flow and thus the line speed will not change instantly because of the inertia of the fluid and solids mass in the pipeline. Number 6 shows the excess pressure caused by the sudden increase of the discharge pressure of the first two pumps. This excess pressure has to take care of the acceleration of the pipeline contents. This acceleration will take in the order of 10-20 seconds.

The filling of the system continues and the resistance of the mixture slowly increases, so the working point moves from point 2 to point 3. With the line speed of 5 m/s, this will take about 400 seconds or almost 7 minutes. When

the mixture reaches the booster pump, at once the discharge pressure increases, resulting in the pump curve according to case 3, the top pump curve. The working point will move to point 4, while 7 represents the excess pressure causing the acceleration of the pipeline contents. Moving from 3 to 4 will take 10-20 seconds. When the pipeline continues to be filled with mixture, the resistance increases, resulting in the working point moving from 4 to 5 in about 400 seconds.
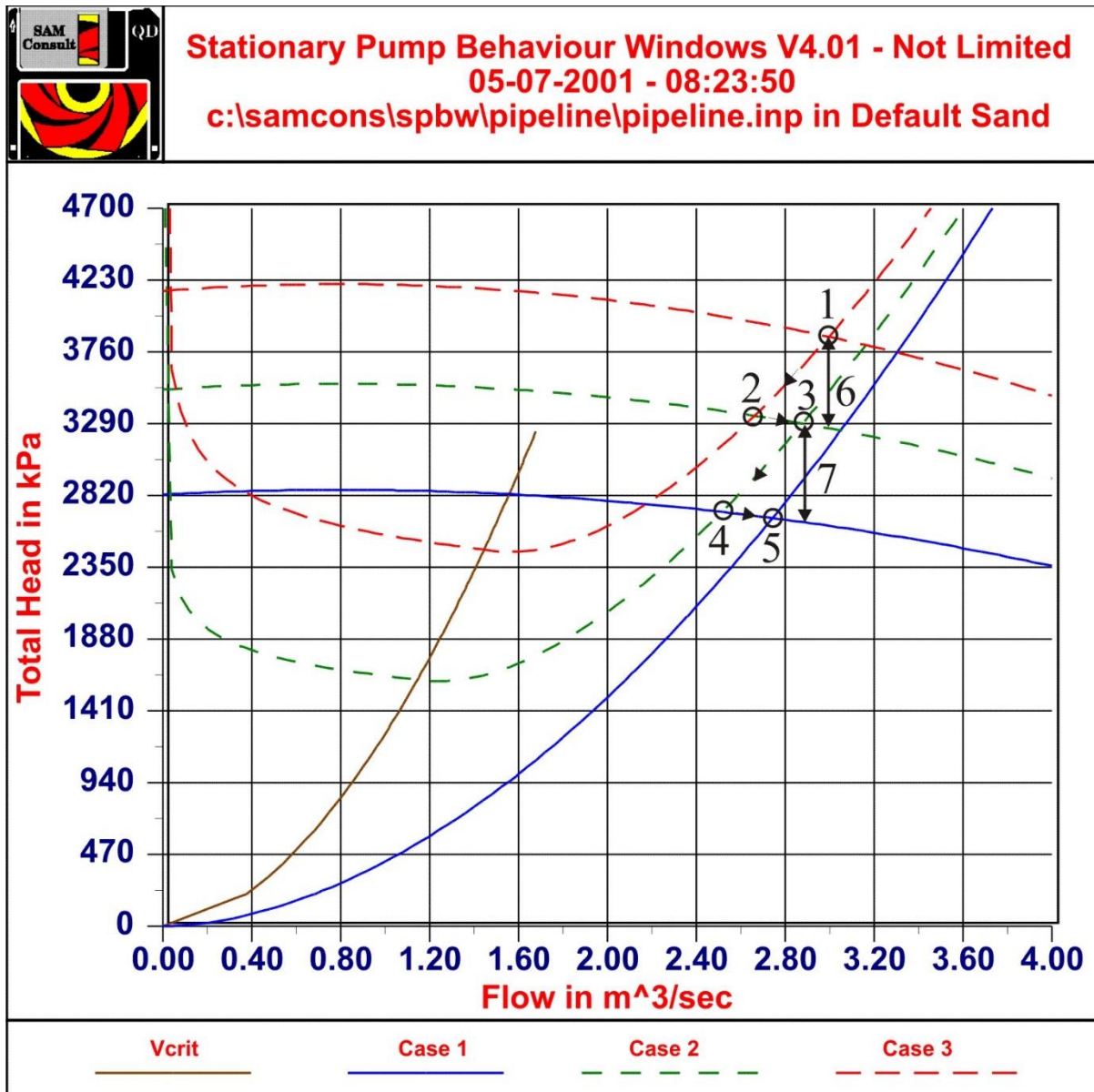
Figure 10.5-3: The system curves for 3 cases, decelerating.

Figure 10.5-3 shows the same procedure for a pipeline filled with a mixture of density 1.6 ton/m^3. In this case the pipeline, containing mixture of 1.6 ton/m^3, is filled with water, resulting in decreasing discharge pressures and pipeline resistance. The procedure is almost the inverse, but Figure 10.5-3 shows that the path followed is different. In working point 1, all the pumps and the pipeline are filled with the mixture. When the water reaches the ladder and main pump, the pump head is decreased to case 2 and the new working point is point 2. Number 6 gives the deceleration pressure, so the contents of the pipeline will decelerate from 1 to 2 in about 10-20 seconds. From 2-3 the pipeline is filled with water up to the booster pump, resulting in a decrease of the pipeline resistance, taking about 400 seconds. When the water reaches the booster pump, the pump head curve decreases again to case 1, resulting in working point 4. Again it takes 10-20 seconds to move from point 3 to point 4. At last the pipeline behind the booster pump is filled with water, resulting in a decrease of the pipeline resistance, taking about 400 seconds. The final working point is point 5. Both Figure 10.5-2 and Figure 10.5-3 give an example of the non-stationary effects in a multi-pump/pipeline system.

10.6 Conclusions & Discussion.

The theory described in this book can be applied to a real life pump/pipeline system with the equations derived in this chapter. In these equations the relative excess hydraulic gradient E_{rhg} has to be determined with the DHLLDV Framework. This can be both for a constant spatial volumetric concentration and/or a constant delivered volumetric concentration.

By defining 5 different flow regimes and using these flow regimes to construct the relative excess hydraulic gradient curve, a good representation of the physics of two pase flow is achieved. Most other models only consider one flow regime.

The behaviour of a multi pump/pipeline system is hard to understand. An infinite number of system configurations and soil conditions exist. Systems are usually configured, based on steady state calculations, while the dynamic behaviour is ignored. Combining the steady state approach for pipeline resistance with the dynamic behaviour of pumps, pump drives and the second law of Newton, the dynamic behaviour can be simulated.

Multi pump/pipeline systems can be configured in an infinite number of configurations. Phenomena that occur in one configuration do not have to occur in other configurations. So the configuration to carry out simulations to examine certain phenomena has to be chosen carefully. The examples show, that moving from one working point to the next working point, does not occur instantaneously, but with a time delay, where the time delay depends on the phenomena.

The simulation model used is very well suitable for fully suspended load, but has a deficiency for two phase flow. The main shortcoming is the fact that suspended load and bed load move through the system at two different velocities, not being equal to the average line speed.

A second shortcoming is the lack of availability of a good model for the vertical diffusion between the suspended load and the bed load. This will be subject for further research.

10.7 Nomenclature Application of the Theory on a Cutter Suction Dredge.

$A_{p,o}$	Cross section suction pipe (pipe segment 0)	m^2
$A_{p,i}$	Cross section pipe segment i	m^2
C_{vs}	Spatial volumetric concentration	-
C_{vt}	Transport/delivered volumetric concentration	-
d	Particle diameter	m
D_p	Pipe diameter	m
$D_{p,0}$	Pipe diameter suction pipe (pipe segment 0)	m
$D_{p,i}$	Pipe diameter pipe segment i	m
E_{rhg}	Relative excess hydraulic gradient	-
$E_{rhg,0}$	Relative excess hydraulic gradient suction pipe (pipe segment 0)	-
$E_{rhg,i}$	Relative excess hydraulic gradient pipe section i	-
F_L	Limit Deposit Velocity Froude number	-
g	Gravitational constant (9.81)	m/s^2
$H_{0,in}$	Elevation of suction mouth (negative)	m
$H_{0,out}$	Elevation entrance of first pump/end of suction pipe (may be negative)	m
$H_{i,in}$	Elevation start of pipe segment i	m
$H_{i,out}$	Elevation end of pipe segment i	m
$H_{n,out}$	Elevation end of the pipeline system (discharge)	m
H_{wl}	Elevation waterline (defined as zero)	m
i	Index pipe segment	-
i_l	Hydraulic gradient liquid	-
l	Index fitting	-
L_{tot}	Total pipeline length	m
L_0	Length suction pipe (pipe segment 0)	m
L_i	Length of pipe section i	m
m_0	Number of fittings in suction pipe (pipe segment 0)	-
m_i	Number of fittings in pipe segment i	-

n	Number of pipe segments	**-**
p	Absolute pressure	**kPa**
p_{cav}	Absolute pressure to avoid cavitation	**kPa**
p_{atm}	Atmospheric pressure (normally 100 kPa)	**kPa**
$p_{0,in}$	Absolute pressure at suction mouth (pipe segment 0)	**kPa**
$p_{0,out}$	Absolute pressure at the end of the suction pipe (pipe segment 0)	**kPa**
$p_{e,k+1}$	Absolute pressure at entrance pump k+1	**kPa**
$p_{d,k+1}$	Absolute pressure at discharge pump k+1	**kPa**
Δp	Pressure difference	**kPa**
Δp_m	Pressure loss in pipeline	**kPa**
$\Delta p_{m,0}$	Pressure loss in suction pipe (pipe segment 0)	**kPa**
$\Delta p_{m,i}$	Pressure loss in pipe segment i	**kPa**
$\Delta p_{p,i}$	Pump head pump i	**kPa**
$Q_{gw,i}$	Additional glad water flow in pump i	**m³/s**
Q_m	Mixture flow	**m³/s**
$Q_{m,0}$	Mixture flow in suction pipe (pipe segment 0)	**m³/s**
$Q_{m,i}$	Mixture flow in pipe segment i	
R_{sd}	Relative submerged density solids	**-**
v_{ls}	Line speed	**m/s**
$v_{ls,ldv}$	Limit Deposit Velocity (LDV)	**m/s**
$v_{ls,0}$	Line speed in suction pipe (pipe segment 0)	**m/s**
$v_{ls,i}$	Line speed in pipe segment i	**m/s**
ρ_l	Liquid density	**ton/m³**
ρ_m	Mixture density	**ton/m³**
$\rho_{m,0}$	Mixture density in suction pipe (pipe segment 0)	**ton/m³**
$\rho_{m,i}$	Mixture density in pipe segment i	**ton/m³**
λ_l	Darcy Weisbach friction factor	**-**
$\lambda_{l,0}$	Darcy Weisbach friction factor in suction pipe (pipe segment 0)	**-**
$\lambda_{l,i}$	Darcy Weisbach friction factor in pipe section i	**-**
θ_0	Pipe inclination angle suction pipe (pipe segment 0)	**º**
θ_i	Pipe inclination pipe segment i	**º**
$\xi_{l,0}$	Fittings factor of fitting l in suction pipe (pipe segment 0)	**-**
$\xi_{l,i}$	Fittings factor of fitting **l** in pipe segment **i**	**-**
μ_{sf}	Sliding friction factor (0.3-0.5)	**-**

Chapter 11:   Publications.

This book is based on the following publications of the authors (green conference paper, blue journal paper):

1. Riet, E. van, Matousek, V. & Miedema, S.A., "A Reconstruction of and Sensitivity Analysis on the Wilson Model for Hydraulic Particle Transport". Proc. 8th Int. Conf. on Transport and Sedimentation of Solid Particles, 24-26 January 1995, Prague, Czech Republic.
2. Riet, E.J. van, Matousek, V. & Miedema, S.A., "A Theoretical Description and Numerical Sensitivity Analysis on Wilson's Model for Hydraulic Transport in Pipelines". Journal of Hydrology & Hydromechanics, Slovak Ac. of Science, Bratislava. Spring 1996.
3. Miedema, S.A., "Modeling and Simulation of the Dynamic Behavior of a Pump/Pipeline System". 17th Annual Meeting & Technical Conference of the Western Dredging Association. New Orleans, June 1996.
4. Miedema, S.A., "A Numerical Method of Calculating the Dynamic Behaviour of Hydraulic Transport". 21st Annual Meeting & Technical Conference of the Western Dredging Association, June 2001, Houston, USA 2001.
5. Miedema, S.A., & Riet, E.J. van, & Matousek, V., "Theoretical Description And Numerical Sensitivity Analysis On Wilson Model For Hydraulic Transport Of Solids In Pipelines ". WEDA Journal of Dredging Engineering, March 2002.
6. Ma, Y., Vlasblom, W.J., Miedema, S.A., Matousek, V., "Measurement of Density and Velocity in Hydraulic Transport using Tomography". Dredging Days 2002, Dredging without boundaries, Casablanca, Morocco, V64-V73, 22-24 October 2002.
7. Ma, Y., Miedema, S.A., Vlasblom, W.J., "Theoretical Simulation of the Measurements Process of Electrical Impedance Tomography". Asian Simulation Conference/5th International Conference on System Simulation and Scientific Computing, Shanghai, 3-6 November 2002, p. 261-265, ISBN 7-5062-5571-5/TP.75.
8. Ma, Y., Miedema, S.A., Matousek, V., Vlasblom, W.J., "Tomography as a Measurement Method for Density and Velocity Distributions". 23rd WEDA Technical Conference & 35th TAMU Dredging Seminar, Chicago, USA, June 2003.
9. Miedema, S.A., Lu, Z., Matousek, V., "Numerical Simulation of a Development of a Density Wave in a Long Slurry Pipeline". 23rd WEDA Technical Conference & 35th TAMU Dredging Seminar, Chicago, USA, June 2003.
10. Miedema, S.A., Lu, Z., Matousek, V., "Numerical simulation of the development of density waves in a long pipeline and the dynamic system behavior". Terra et Aqua, No. 93, p. 11-23. December 2003.
11. Miedema, S.A., "An Analytical Method To Determine Scour". WEDA XXVIII & Texas A&M 39. St. Louis, USA, June 8-11, 2008.
12. Ramsdell, R.C., Miedema, S.A., "Hydraulic transport of sand/shell mixtures". WODCON XIX, Beijing China, September 2010.
13. Miedema, S.A., "Constructing the Shields curve, a new theoretical approach and its applications". WODCON XIX, Beijing China, September 2010.
14. Miedema, S.A., "The effect of the bed rise velocity on the sedimentation process in hopper dredges". WODCON XIX, Beijing China, September 2010.
15. Miedema, S.A. & R.C. Ramsdell, "Hydraulic transport of sand/shell mixtures in relation with the critical velocity". Terra et Aqua 122, March 2011, IADC, The Hague, The Netherlands.
16. Ramsdell, R.C. & Miedema, S.A., "Hydraulic transport of sand/shell mixtures". OMAE 2011 ASME, June 19-24, Rotterdam, The Netherlands.
17. Miedema, S.A., "Constructing the Shields curve". OMAE 2011 ASME, June 19-24, Rotterdam, The Netherlands.
18. Miedema, S.A., "Constructing the Shields Curve Part A: Fundamentals of the Sliding, Rolling and Lifting Mechanisms for the Entrainment of Particles". Journal Of Dredging Engineering, Vol. 12, No. 1., 2012, www.westerndredging.org.
19. Miedema, S.A., "Constructing the Shields Curve Part B: Sensitivity Analysis, Exposure and Protrusion Levels, Settling Velocity, Shear Stress and Friction Velocity, Erosion Flux and Laminar Main Flow". Journal of Dredging Engineering, Vol. 12, No. 1., 2012, www.westerndredging.org.
20. Ramsdell, R.C. & Miedema, S.A., "An Overview of Flow Regimes Describing Slurry Transport". WODCON XX, Brussels, Belgium, June 2013.
21. Miedema, S.A. & Ramsdell, R.C., "A Head Loss Model for Slurry Transport Based on Energy Considerations". WODCON XX, Brussels, Belgium, June 2013.
22. Miedema, S.A., "Constructing the Shields Curve, Part C: Cohesion by Silt". WODCON XX, Brussels, Belgium, June 2013.
23. Miedema S.A., "An Overview of Theories Describing Head Losses in Slurry Transport, A Tribute to Some of the Early Researchers". OMAE 2013, Nantes, France, June 2013.

24. Miedema, S.A., "Constructing the Shields Curve, Part C: Cohesion by Silt, Hjulstrom, Sundborg". OMAE 2013, Nantes, France, June 2013.

25. Miedema, S.A., "An Overview of Theories Describing Head Losses in Slurry Transport, A Tribute to Some of the Early Researchers". Journal of Dredging Engineering, Vol. 14, No. 1, 2014.

26. Miedema, S.A., "An Analysis of Slurry Transport at Low Line Speeds". ASME-OMAE 2014, San Francisco, USA, June 2014.

27. Miedema, S.A., Ramsdell, R.C., "An Analysis of the Hydrostatic Approach of Wilson for the Friction of a Sliding Bed". WEDA 34/TAMU 45, Toronto, Canada, June 2014.

28. Miedema, S.A. & Matousek V., "An explicit formulation for the Darcy-Weisbach friction factor of sheet flow". 15th International Freight Pipeline Society Symposium 2014. 24-26 June 2014, Prague, Czech Republic.

29. Miedema, S.A., & Ramsdell, R.C., "The Delft Head Loss & Limit Deposit Velocity Model". 19th International Conference on HydroTransport. Denver, Colorado, USA, 24-26 September 2014.

30. Miedema, S.A., "Slurry Transport, an Analytical Approach to Explain the Fuhrboter Equation". Maritime Engineering Journal, Vol. 167, Issue 2, 2014, Special Dredging Issue.

31. Miedema, S.A., "A Head Loss Model for Homogeneous Slurry Transport". Journal of Hydrology & Hydromechanics, Vol. 63(1), 2015.

32. Miedema, S.A., " Head Loss Model for Slurry Transport in the Heterogeneous Regime". Ocean Engineering Vol. 106, pp. 360-370, September 2015.

33. Miedema, S.A. & Ramsdell, R.C., "The Limit Deposit Velocity, a New Approach". Journal of Hydrology & Hydromechanics, Vol. 63(4), 2015.

34. Miedema, S.A., "The Slip Ratio or Holdup Function in Slurry Transport". Dredging Summit & Expo, Houston, USA, June 2015. WEDA/TAMU.

35. Ramsdell, R.C., & Miedema, S.A., "The Delft Head Loss & Limit Deposit Velocity Model". Dredging 2015, SavannaH, Georgia, USA. Pianc USA, Copri ASCE.

36. Miedema, S.A. "A Method to compare slurry transport models". 17th International Conference: Transport & Sedimentation of Solid Particles. September 22-25, 2015, Delft, The Netherlands.

37. Miedema, S.A. & Ramsdell, R.C., "The Delft Head Loss & Limit Deposit Velocity Framework". Journal of Dredging Engineering. Volume 15, Issue 2 (June 2016).

38. Miedema, S.A. & Ramsdell, R.C., "A comparison of different slurry transport models". WODCON XXI, Miami, USA, June 2016.

39. Ramsdell, R.C. & Miedema, S.A., "DHLLDV – Open Source Software for Slurry Transport". WODCON XXI, Miami, USA, June 2016.

40. Miedema, S.A., "The heterogeneous to homogeneous transition for slurry flow in pipes". Ocean Engineering, Vol. 123, pp. 422-431. September 2016.

41. Miedema, S.A., "A comparison of graded PSD methods in slurry transport". 20th International Conference on Hydrotransport. Melbourne, Australia. May 2017.

42. Miedema, S.A., "Slurry transport of very large particles at high line speeds". 20th International Conference on Hydrotransport. Melbourne, Australia. May 2017.

43. Miedema, S.A. & Ramsdell, R.C., "A head loss & limit deposit velocity framework". Journal of Marine & Environmental EngineeringVol. 10(1), pp. 45-69, June 2017.

44. Miedema, S.A., "A new approach to determine the concentration distribution in slurry transport". Dredging Summit & Expo, Vancouver, Canada, June 2017.

45. Miedema, S.A., "Slurry transport in inclined pipes". Dredging Summit & Expo, Vancouver, Canada, June 2017.

46. Miedema, S.A., "The influence of local hindered settling on the concentration distribution in slurry transport". 18th International Conference: Transport & Sedimentation of Solid Particles. September 22-25, 2017, Prague, Czech Republic.

47.

Chapter 12: Bibliography.

Abulnaga, B. E. (2002). *Slurry Systems Handbook.* USA: McGraw Hill.

Azamathulla, H. M., & Ahmad, Z. (2013). Estimation of critical velocity for slurry transport through pipeline using adaptive neuro-fuzzy interference system and gene-expression programming. *Journal of Pipeline Systems Engineering and Practice.*, 131-137.

Babcock, H. A. (1970). The sliding bed flow regime. *Hydrotransport 1* (pp. H1-1 - H1-16). Bedford, England: BHRA.

Bagnold, R. A. (1954). Experiments on a gravity free dispersion of large solid spheres in a Newtonian fluid under shear. *Proceedings Royal Society, Vol. A225.*, 49-63.

Bagnold, R. A. (1957). The flow of cohesionless grains in fluids. *Phil. Trans. Royal Society, Vol. A249*, 235-297.

Bain, A. G., & Bonnington, S. T. (1970). *The hydraulic transport of solids by pipeline.* Pergamon Press.

Berg, C. H. (1998). *Pipelines as Transportation Systems.* Kinderdijk, the Netherlands: European Mining Course Proceedings, IHC-MTI.

Berg, C. v. (2013). *IHC Merwede Handbook for Centrifugal Pumps & Slurry Transportation.* Kinderdijk, Netherlands: IHC Merwede.

Berman, V. P. (1994). *Gidro i aerodinamiceskie osnovy rascota truboprovodnych sistem gidrokontejnernogo i vysokonapornogo pnevmaticeskogo transporta.* Lugansk: East Ukrainian State University.

Bisschop, F., Miedema, S. A., Rhee, C. v., & Visser, P. J. (2014). Erosion experiments on sand at high velocities. *To be submitted to the Journal of Hydraulic Engineering*, 28.

Blatch, N. S. (1906). Discussion of Works for the purification of the water supply of Washington D.C. *Transactions ASCE 57.*, 400-409.

Blythe, C., & Czarnotta, Z. (1995). Determination of hydraulic gradient for sand slurries. *8th International Freight Pipeline Society Symposium*, (pp. 125-130). Pittsburg, USA.

Bonneville, R. (1963). *essais de synthese des lois debut d'entrainment des sediment sous l'action d'un courant en regime uniform.* Chatou: Bulletin Du CREC, No. 5.

Bonnington, S. T. (1961). *Estimation of Pipe Friction Involved in Pumping Solid Material.* BHRA, TN 708 (December 1961).

Boothroyde, J., Jacobs, B. E., & Jenkins, P. (1979). Coarse particle hydraulic transport. *Hydrotransport 6: 6th International Conference on the Hydraulic Transport of Solids in Pipes.* (p. Paper E1). BHRA.

Brauer, H. (1971). *Grundlagen der einphasen- und mehrphasenstromungen.* Verslag Sauerlander.

Brooks, F. A., & Berggren, W. (1944). Remarks on turbulent transfer across planes of zero momentum exchange. *Transactions of the American Geophysics Union, Pt. VI.*, 889-896.

Brownlie, W. (1981). *Compilation of alluvial channel data: laboratory and field, Technical Report KH-R-43B.* Pasadena, California, USA: California Institute of Technology.

Buffington, J. M. (1999). The legend of A.F. Shields. *Journal of Hydraulic Engineering, 125*, 376–387.

Buffington, J. M., & Montgomery, D. R. (1997). A systematic analysis of eight decades of incipient motion studies, with special reference to gravel-bedded rivers. *Water Resources Research, 33*, 1993-2029.

Camenen, B., & Larson, M. (2013). Accuracy of Equivalent Roughness Height Formulas in Practical Applications. *Journal of Hydraulic Engineering.*, 331-335.

Camenen, B., Bayram, A. M., & Larson, M. (2006). Equivalent roughness height for plane bed under steady flow. *Journal of Hydraulic Engineering*, 1146-1158.

Charles, M. E. (1970). Transport of solids by pipeline. *Hydrotransport 1.* Cranfield: BHRA.

Chaskelberg, K., & Karlin. (1976). *Rascot gidrotransporta pesanych materialov.* Moskov: Gidromechanizacija.

Chepil, W. (1958). The use of evenly spaced hemispheres to evaluate aerodynamic force on a soil failure. *Transaction of the American Geophysics Union, Vol. 39(3)*, 397-404.

Chin, C. O., & Chiew, Y. M. (1993). Effect of bed surface structure on spherical particle stability. *Journal of Waterway, Port, Coastal and Ocean Engineering, 119(3)*, 231–242.

Clift, R., Wilson, K. C., Addie, G. R., & Carstens, M. R. (1982). A mechanistically based method for scaling pipeline tests for settling slurries. *Hydrotransport 8* (pp. 91-101). Cranfield, UK.: BHRA Fluid Engineering.

Clift, R., Wilson, K., Addie, G., & Carstens, M. (1982). A mechanistically based method for scaling pipeline tests for settling slurries. *Hydrotransport 8* (pp. 91-101). Cranfield, UK.: BHRA.

Colebrook, C. F., & White, C. M. (1937). Experiments with Fluid Friction in Roughened Pipes. *Proceedings of the Royal Society of London. Series A, Mathematical and Physical Sciences 161 (906).* (pp. 367-381). London: Royal Society of London.

Coleman, N. L. (1967). A theoretical and experimental study of drag and lift forces acting on a sphere resting on a hypothetical stream bed. *International Association for Hydraulic Research,12th Congress*, *3*, pp. 185-192.

Condolios, E., & Chapus, E. E. (1963A). Transporting Solid Materials in Pipelines, Part I. *Journal of Chemical Engineering, Vol. 70(13).*, 93-98.

Condolios, E., & Chapus, E. E. (1963B). Designing Solids Handling Pipelines Part II. *Journal of Chemical Engineering, Vol. 70(14).*, 131-138.

Condolios, E., & Chapus, E. E. (1963C). Operating solids pipelines, Part III. *Journal of Chemical Engineering, Vol. 70(15).*, 145-150.

Crowe, C. T. (2006). *MultiPhase Flow Handbook.* Boca Raton, Florida, USA: Taylor & Francis Group.

Davies, J. T. (1987). Calculation of critical velocities to maintain solids in suspension in horizontal pipes. *Chemical Engineering Science, Vol. 42(7).*, 1667-1670.

Dey, S. (1999). Sediment threshold. *Applied Mathematical Modelling*, 399-417.

Dey, S. (2003). Incipient motion of bivalve shells on sand beds under flowing water. *Journal of Hydraulic Engineering*, 232-240.

Dey, S. (2014). *Fluvial Hydrodynamics.* Kharagpur, India: Springer, GeoPlanet: Earth and Planetary Sciences.

DHL. (1972). *Systematic Investigation of Two Dimensional and Three Dimensional Scour, Report M648/M863.* Delft, Netherlands: Delft Hydraulics Laboratory.

Di Filice, R. (1999). The sedimentation velocity of dilute suspensions of nearly monosized spheres. *International Journal of Multiphase Flows 25*, 559-574.

Dittrich, A., Nestmann, F., & Ergenzinger, P. (1996). Ratio of lift and shear forces over rough surfaces. *Coherent flow structures in open channels.*, 126-146.

Doron, P., & Barnea, D. (1993). A three layer model for solid liquid flow in horizontal pipes. *International Journal of Multiphase Flow, Vol. 19, No.6.*, 1029-1043.

Doron, P., & Barnea, D. (1995). Pressure drop and limit deposit velocity for solid liquid flow in pipes. *Chemical Engineering Science, Vol. 50, No. 10.*, 1595-1604.

Doron, P., & Barnea, D. (1996). Flow pattern maps for solid liquid flow in pipes. *International Journal of Multiphase Flow, Vol. 22, No. 2.*, 273-283.

Doron, P., Granica, D., & Barnea, D. (1987). Slurry flow in horizontal pipes, experimental and modeling. *International Journal of Multiphase Flow, Vol. 13, No. 4.*, 535-547.

Doron, P., Simkhis, M., & Barnea, D. (1997). Flow of solid liquid mixtures in inclined pipes. *International Journal of Multiphase Flow, Vol. 23, No. 2.*, 313-323.

Duckworth, & Argyros. (1972). Influence of density ratio on the pressure gradient in pipes conveying suspensions of solids in liquids. *Hydrotransport 2.* Coventry: BHRA.

Durand, R. (1953). Basic Relationships of the Transportation of Solids in Pipes - Experimental Research. *Proceedings of the International Association of Hydraulic Research.* Minneapolis.

Durand, R., & Condolios, E. (1952). Etude experimentale du refoulement des materieaux en conduites en particulier des produits de dragage et des schlamms. *Deuxiemes Journees de l'Hydraulique.*, 27-55.

Durand, R., & Condolios, E. (1952). Etude experimentale du refoulement des materieaux en conduites en particulier des produits de dragage et des schlamms. (Experimental study of the discharge pipes materieaux especially products of dredging and slurries). *Deuxiemes Journees de l'Hydraulique.*, 27-55.

Durand, R., & Condolios, E. (1956). Donnees techniques sur le refoulement des mixture en conduites. *Revue de lÍndustriele Minerale, no. 22F*, 460-481.

Durand, R., & Condolios, E. (1956). *Technical data on hydraulic transport of solid materials in conduits.* Revue de L'Industrie Minerale, Numero Special 1F.

Durepaire, M. P. (1939). Contribution a létude du dragage et du refoulement des deblais a état de mixtures. *Annales des ponts et chaussees, Memoires I.*, 165-254.

Egiazarof, I. (1965). Calculation of non-uniform sediment concentrations. *Journal of the Hydraulic Division, ASCE, 91(HY4)*, 225-247.

Einstein, A. (1905). On the motion of small particles suspended in liquids at rest required by the molecular kinetic theory of heat. *Annalen der Physik Vol.17.*, 549-560.

Ellis, H. S., & Round, G. F. (1963). Laboratory studies on the flow of Nickel-Water suspensions. *Canadian Journal on Minerals & Mettalurgy, Bull. 56.*

Engelund, F., & Hansen, E. (1967). A monograph on sediment transport to alluvial streams. *Copenhagen: Technik Vorlag*.

Fenton, J. D., & Abbott, J. E. (1977). Initial movement of grains on a stream bed: The effect of relative protrusion. *Proceedings of Royal Society*, *352(A)*, pp. 523–537. London.

Fisher, J., Sill, B., & Clark, D. (1983). Organic Detritus Particles: Initiation of Motion Criteria on Sand and Gravel Beds. *Water Resources Research, Vol. 19, No. 6.*, 1627-1631.

Fitton, T. G. (2015). A deposit velocity equation for open channels and pipes. *17th International Conference on Transport & Sedimentatin of Solid Particles.* (pp. 69-77). Delft, The Netherlands: Delft University of Technology.

Bibliography.

Fowkes, R. S., & Wancheck, G. A. (1969). *Materials handling research: Hydraulic transportation of coarse solids.* U.S. Department of the interior, Bureau of Mines, Report 7283.

Franzi, G. (1941). *Sul moto dei liquidi con materie solide in suspensione.* Milano, Italy: Instituto di idraulica e costrusioni idrauliche dei politechnico di Milano, No. 47.

Fuhrboter, A. (1961). *Über die Förderung von Sand-Wasser-Gemischen in Rohrleitungen.* Mitteilungen des Franzius-Instituts, H. 19.

Fuhrboter, A. (1961). *Über die Förderung von Sand-Wasser-Gemischen in Rohrleitungen. (On the advances of sand -water mixtures in pipelines).* Mitteilungen des Franzius-Instituts, H. 19.

Gandhi, R. (2015, February). Personal communication.

Garcia, M. H. (2008). *Sedimentation Engineering* (Vol. 110). ASCE Manuals & Reports on Engineering Practise No. 110.

Garside, J., & Al-Dibouni, M. (1977). Velocity-Voidage Relationships for Fluidization and Sedimentation in Solid-Liquid Systems. *2nd Eng. Chem. Process Des. Dev., 16, 206.*

Gibert, R. (1960). Transport hydraulique et refoulement des mixtures en conduites. *Annales des Ponts et Chausees.*, 130(3), 307-74, 130(4), 437-94.

Gillies, D. P. (2013). *Particle contributions to kinematic friction in slurry pipeline flow, MSc Thesis.* University of Alberta, Department of Chemical Engineering.

Gillies, R. G. (1993). *Pipeline flow of coarse particles, PhD Thesis.* Saskatoon: University of Saskatchewan.

Gillies, R. G. (2015). Personal communication.

Gillies, R. G., & Shook, C. A. (1994). Concentration distributions of sand slurries in horizontal pipe flow. *Particulate Science and Technology, Vol. 12.*, 45-69.

Gillies, R. G., & Shook, C. A. (2000A). Modeling high concentration settling slurry flows. *Canadian Journal of Chemical Engineering, Vol. 78.*, 709-716.

Gillies, R. G., Schaan, J., Sumner, R. J., McKibben, M. J., & Shook, C. A. (2000B). Deposition velocities for Newtonian slurries in turbulent flow. *Canadian Journal of Chemical Engineering, Vol. 78.*, 704-708.

Gillies, R. G., Shook, C. A., & Wilson, K. C. (1991). An improved two layer model for horizontal slurry pipeline flow. *Canadian Journal of Chemical Engineering, Vol. 69.*, 173-178.

Gillies, R. G., Shook, C. A., & Xu, J. (2004). Modelling heterogeneous slurry flows at high velocities. *The Canadian Journal of Chemical Engineering, Vol. 82.*, 1060-1065.

Gogus, M., & Kokpinar, M. A. (1993). Determination of critical flow velocity in slurry transporting pipeline systems. *Proceeding of the 12th International Conference on Slurry Handling and Pipeline Transport.* (pp. 743-757). Bedfordshire, UK.: British Hydraulic Research Group.

Govier, G. W., & Aziz, K. (1972). *The Flow of Complex Mixtures in Pipes.* New York: University of Calgary, Alberta, Canada.

Grace, J. (1986). Contacting modes and behaviour classification of gas-solid and other two-phase suspensions. *Canadian Journal of Chemical Engineering, vol. 64.*, 353-363.

Graf, W. H., & Pazis, G. C. (1977). Les phenomenes de deposition et d'erosion dans un canal alluvionnaire. *Journal of Hydraulic Research, 15*, 151-165.

Graf, W. H., Robinson, M. P., & Yucel, O. (1970). *Critical velocity for solid liquid mixtures.* Bethlehem, Pensylvania, USA.: Fritz Laboratory Reports, Paper 386. Lehigh University.

Graf, W. H., Robinson, M., & Yucel, O. (1970). The critical deposit velocity for solid-liquid mixtures. *Hydrotransport 1* (pp. H5-77-H5-88). Cranfield, UK: BHRA.

Grant, W. D., & Madsen, O. S. (1982). Movable bed roughness in unsteady oscillatory flow. *Journal Geophysics Resources*, 469-481.

Grunsven, F. v. (2012). *Measuring the slip factor for various slurry flows using temperature calibrated Electrical Resistance Tomography.* Delft, The Netherlands.: Delft University of Technology.

Guo, J., & Julien, P. (2007). Buffer law and transitional roughness effects in turbulent open-channel flows. *5th International Symposium on Environmental Hydraulics, 4-7 December 2007.* Tempe, Arizona, USA: ISEH.

Harada, E., Kuriyama, M., & Konno, H. (1989). Heat transfer with a solid liquid suspension flowing through a horizontal rectangular duct. *Heat Transfer Jap. Res. Vol. 18.*, 79-94.

Hepy, F. M., Ahmad, Z., & Kansal, M. L. (2008). Critical velocity for slurry transport through pipeline. *Dam Engineering, Vol. XIX(3).*, 169-184.

Hinze, J. (1975). *Turbulence.* McGraw Hill Book company.

Hjulstrøm, F. (1935). Studies of the morphological activity of rivers as illustrated by the River Fyris. *Bulletin of the Geological Institute, 25*, 221–527. University of Uppsala.

Hjulstrøm, F. (1939). Transportation of debris by moving water, in Trask, P.D., ed., Recent Marine Sediments. *A Symposium: Tulsa, Oklahoma, American Association of Petroleum Geologists*, (pp. 5-31). Tulsa, Oklahoma.

Hofland, B. (2005). *Rock & Roll.* Delft, The Netherlands: PhD Thesis, Delft University of Technology.

Howard, G. W. (1938). Transportation of Sand and Gravel in a 4 Inch Pipe. *Transactions ASCE Vol. 104., No. 2039.*, 1334-1348.

Howard, G. W. (1939). Discussion on: Transportation of sand and gravel in a four inch pipe. *Transactions ASCE Vol. 104.*, 157, 316, 460, 1011.

Hsu. (1986). *Flow of non-colloidal slurries in pipeline.* PhD Thesis, University of Illinois.

Huisman, L. (1973-1995). *Sedimentation & Flotation 1973-1995.* Delft, Netherlands: Delft University of Technology.

Hunt, J. N. (1954). The turbulent transport of suspended sediment in open channels. *Royal Society of London, Proc. Series A, Vol. 224(1158).*, 322-335.

Ikeda, S. (1982). Incipient motion of sand particles on side slopes. *Journal of the Hydraulic division, ASCE, 108*(No. HY1).

Ismail, H. M. (1952). Turbulent transfer mechanism and suspended sediment in closed channels. *Transactions of ASCE, Vol. 117.*, 409-446.

Iwagaki, Y. (1956). Fundamental study on critical tractive force. *Transactions of the Japanese Society of Civil Engineers, Vol. 41*, 1-21.

Jufin, A. P. (1965). *Gidromechanizacija.* Moskau.

Jufin, A. P., & Lopatin, N. A. (1966). O projekte TUiN na gidrotransport zernistych materialov po stalnym truboprovodam. *Gidrotechniceskoe Strojitelstvo, 9.*, 49-52.

Julien, P. (1995). Erosion and sedimentation. *Cambridge University Press*.

Karabelas, A. J. (1977). Vertical Distribution of Dilute Suspensins in Turbulent Pipe Flow. *AIChE Journal, Vol. 23(4).*, 426-434.

Karasik, U. A. (1973). Hydraulische Forderung von feinkorniqen Suspensionen (in russisch). *Gidromechanika, S.BO ff, Vol. 25. Kiew.*

Kaushal, D. R. (1995). *Prediction of particle distribution in the flow of multisized particulate slurries through closed ducts and open channels.* Delhi, India: I.I.T.. Department of Applied Mechanics, PhD Thesis.

Kaushal, D. R., & Tomita, Y. (2002B). Solids concentration profiles and pressure drop in pipeline flow of multisized particulate slurries. *International Journal of Multiphase Flow, Vol. 28.*, 1697-1717.

Kaushal, D. R., & Tomita, Y. (2002C). An improved method for predicting pressure drop along slurry pipeline. *Particulate Science and Technology: An International Journal, Vol. 20(4).*, 305-324.

Kaushal, D. R., & Tomita, Y. (2003B). Comparative study of pressure drop in multisized particulate slurry flow through pipe and rectangular duct. *International Journal of Multiphase Flow, Vol. 29.*, 1473-1487.

Kaushal, D. R., & Tomita, Y. (2013). Prediction of concentration distribution in pipeline flow of highly concentrated slurry. *Particulate Science and Technology: An International Journal, Vol. 31(1).*, 28-34.

Kaushal, D. R., Sato, K., Toyota, T., Funatsu, K., & Tomita, Y. (2005). Effect of particle size distribution on pressure drop and concentration profile in pipeline flow of highly concentrated slurry. *International Journal of Multiphase Flow, Vol. 31.*, 809-823.

Kaushal, D. R., Seshadri, V., & Singh, S. N. (2002D). Prediction of concentration and particle size distribution in the flow of multi-sized particulate slurry through rectangular duct. *Applied Mathematical Modelling, Vol. 26.*, 941-952.

Kaushal, D. R., Seshadri, V., & Singh, S. N. (2003A). Concentration and particle size distribution in the flow of multi-sized particulate slurry through rectangular duct. *Journal of Hydrology & Hydromechanics*, 114-121.

Kaushal, D. R., Tomita, Y., & Dighade, R. R. (2002A). Concentration at the pipe bottom at deposition velocity for transportation of commercial slurries through pipeline. *Powder Technology Vol. 125.*, 89-101.

Kazanskij, I. (1967). *Vyzkum proudeni hydrosmesi voda-pisek (untersuchung uber sans-wasser stromungen).* Mitteilungen des Franzius Instituts, Heft 33.

Kazanskij, I. (1972). *Berechnungsverfahren fur die Forderung von Sand-Wasser Gemischen in Rohrleitungen.* Hannover: Franzius Institut, Heft 33.

Kazanskij, I. (1978). Scale-up effects in hydraulic transport theory and practice. *Hydrotransport 5* (pp. B3: 47-74). Cranfield, UK: BHRA Fluid Engineering.

Kazanskij, I. (1980). Vergleich verschiedener Rohrmaterialen in Bezug auf Verschleiss und Energieverbrauch beim Hydrotransport in Rohrleitungen. *VDI Berichte Nr. 371*, pp. 51-58.

Kim, J., Moin, P., & Moser, R. (1987). Turbulence statistics in fully developed channel flow at low Reynolds number. *Journal of Fluid Mechanics, 177*, 133-166.

King, R. P. (2002). *Introduction to Practical Fluid Flow.* University of Utah.: Butterworth Heineman.

Kokpinar, M. A., & Gogus, M. (2001). Critical velocity in slurry transport in horizontal pipelines. *Journal of Hydraulic Engineering, Vol. 127(9).*, 763-771.

Korzajev, M. (1964). Metod rascota parametrov gidrotransporta gruntov. *Gidromechanizacija, Moskau.*

Kril, S. I. (1990). *Nopernye vzvesenesuscie potoki (pressurised slurry flows).* Kiev: Naukova Dumka.

Bibliography.

Krivenko. (1970). Energieverlust in zwei phasen stromungen in hochkonzentrierten grobdispersionen. *Gidromechanica, Kiev.*

Kumar, U., Mishra, R., Singh, S. N., & Seshadri, V. (2003). Effect of particle gradation on flow characteristics of ash disposal pipelines. *Powder Technology Vol. 132.*, 39-51.

Kumar, U., Singh, S. N., & Seshadri, V. (2008). Prediction of flow characteristics of bimodal slurry in horizontal pipe flow. *Particulate Science and Technology, Vol. 26.*, 361-379.

Kurihara, M. (1948). On the critical tractive force. *Research Institute for Hydraulic Engineering*, Report No. 3, Vol. 4.

Lahiri, S. K. (2009). *Study on slurry flow modelling in pipeline.* Durgapur, India: National Institute of Technology, Durgapur, India.

Lane, E. W., & Kalinske, A. A. (1941). Engineering calculations of suspended sediment. *Trans. Am. Geophysics Union, Vol. 20(3).*, 603-607.

Liu, Z. (2001). Sediment Transport. *Lecture notes*. Aalborg University.

Longwell, P. A. (1977). *Mechanics of Fluid Flow.* New York: McGraw Hill.

Luckner, T. (2002). Zum Bewegungsbeginn von Sedimenten. *Dissertation.* Darmstadt, Germany: Technische Universitat Darmstadt.

Madsen, O. S., Wright, L. D., Boon, J. D., & Chrisholm, T. A. (1993). *Wind stress, bed roughness and sediment suspension on the inner shelf during an extreme storm event.* Continental Shelf Research 13, 1303-1324.

Madsen, O., & Grant, W. (1976). *Sediment transport in the coastal environment.* Cambridge, Massachusetts, USA: Technical report 209, M.I.T.

Mantz, P. A. (1977). Incipient transport of fine grains and flakes by fluids—Extended Shields diagram. *Journal of Hydraulic Division, ASCE, 103(6)*, 601-615.

Marsh, N. A., Western, A. W., & Grayson, R. B. (2004, July 1). Comparison of Methods for Predicting Incipient Motion for Sand Beds. *Journal of Hydraulic Engineering, 130*(No. 7, July 1, 2004)).

Matousek, V. (1996). Solids Transportation in a Long Pipeline Connected with a Dredge. *Terra et Aqua 62.*, 3-11.

Matousek, V. (1997). *Flow Mechanism of Sand/Water Mixtures in Pipelines, PhD Thesis.* Delft, Netherlands: Delft University of Technology.

Matousek, V. (2004). *Dredge Pumps & Slurry Transport, Lecture Notes.* Delft: Delft University of Technology.

Matousek, V. (2007). Interaction of slurry pipe flow with a stationary bed. *Journal of the South African Institute of Mining and Metallurgy, 107(6).*, 367-374.

Matousek, V. (2009). Predictive model for frictional pressure drop in settling-slurry pipe with stationar deposit. *Powder Technology*, 367-374.

Matousek, V. (2011). Solids Transport Formula in Predictive Model for Pipe Flow of Slurry above Deposit. *Particulate Science and Technology, Vol. 29(1).*, 89-106.

Matousek, V., & Krupicka, J. (2009). On equivalent roughness of mobile bed at high shear stress. *Journal of Hydrology & Hydromechanics, Vol. 57-3.*, 191-199.

Matousek, V., & Krupicka, J. (2010). Modeling of settling slurry flow around deposition limit velocity. *Hydrotransport 18* (p. 12). Rio de Janeiro, Brazil: BHR Group.

Matousek, V., & Krupicka, J. (2010). Semi empirical formulae for upper plane bed friction. *Hydrotransport 18* (pp. 95-103). BHRA.

Matousek, V., & Krupicka, J. (2011). Unified model for coarse slurry flow with stationary and sliding bed. *15th International Conference on Transport & Sedimentation of Solid Particles.*, (p. 8). Wroclaw, Poland.

Matousek, V., & Krupicka, J. (2014). Interfacial friction and transport in stratified flows. *Maritime Engineering, Vol. 167(MA3)*, 125-134.

Matousek, V., & Krupicka, J. (2014). One dimensional modelling of concentration distribution in pipe flow of combined load slurry. *Powder Technology, Vol. 260.*, 42-51.

Matousek, V., Krupicka, J., & Penik, V. (2014). Distribution of medium to coarse glass beads in slurry pipe flow: Evaluation of measured concentration profiles. *Particulate Science and Technology, Vol. 32*, 186-196.

Meyer-Peter, E., & Muller, R. (1948). Formulas for bed load transport. *2nd Meeting of the International Association for Hydraulic Structures Research.*, (pp. 39-64).

Miedema, S. (2010). Constructing the Shields curve, a new theoretical approach and its applications. *WODCON XIX* (p. 22 pages). Beijing, September 2010: WODA.

Miedema, S. A. (1995). Dynamic Pump/Pipeline Behavior Windows. *Software*. Delft, The Netherlands: SAM-Consult.

Miedema, S. A. (2012). *Dredging Processes Hydraulic Transport.* Delft, Netherlands: Delft University of Technology.

Miedema, S. A. (2012A). Constructing the Shields Curve: Part A Fundamentals of the Sliding, Rolling and Lifting Mechanisms for the Entrainment of Particles. *Journal of Dredging Engineering.*

Miedema, S. A. (2012B). Constructing the Shields Curve: Part B Sensitivity Analysis, Exposure & Protrusion Levels, Settling Velocity, Shear Stress & Friction Velocity, Erosion Flux and Laminar Main Flow. *Journal of Dredging Engineering.*

Miedema, S. A. (2013). An overview of theories describing head losses in slurry transport. A tribute to some of the early researchers. *OMAE 2013, 32nd International Conference on Ocean, Offshore and Arctic Engineering.* (p. 18). Nantes, France: ASME.

Miedema, S. A. (2013). Constructing the Shields Curve: Part C Cohesion by Silt, Hjulstrom, Sundborg. *OMAE* (p. 22). Nantes: ASME.

Miedema, S. A. (2013S). *Software MS Excel 2LM & 3LM.* Retrieved from The Delft Head Loss & Limit Deposit Velocity Model: www.dhlldv.com

Miedema, S. A. (2014). An analysis of slurry transport at low line speeds. *ASME 2014 33rd International Conference on Ocean, Offshore and Arctic Engineering, OMAE.* (p. 11). San Francisco, USA.: ASME.

Miedema, S. A. (2014). An analytical approach to explain the Fuhrboter equation. *Maritime Engineering, Vol. 167, Issue 2.*, 68-81.

Miedema, S. A. (2014). An Overview of Theories Describing Head Losses in Slurry Transport, A Tribute to Some of the Early Researchers. *WEDA Journal of Dredging Engineering, Vol. 14, No. 1.*

Miedema, S. A. (2014W). *DHLLDV/Experiments.* Retrieved from The Delft Head Loss & Limit Deposit Velocity Model.: www.dhlldv.com

Miedema, S. A. (2015). A head loss model for homogeneous slurry transport. *Journal of Hydrology & Hydrodynamics, Vol. 63(1).*, 1-12.

Miedema, S. A. (2015). Head Loss Model for Slurry Transport in the Heterogeneous Regime. *Ocean Engineering, Vol. 106.*, 360-370.

Miedema, S. A. (2015A). A head loss model for homogeneous slurry transport for medium sized particles. *Journal of Hydrology & Hydrodynamics, Vol. 63(1).*, 1-12.

Miedema, S. A. (2016). The heterogeneous to homogeneous transition for slurry flow in pipes. *Ocean Engineering, Vol. 123.*, 422-431.

Miedema, S. A. (June 2016). *Slurry Transport: Fundamentals, A Historical Overview & The Delft Head Loss & Limit Deposit Velocity Framework.* (1st Edition ed.). (R. C. Ramsdell, Ed.) Miami, Florida, USA: Delft University of Technology.

Miedema, S. A. (September 2015). *OE4607 Introduction Dredging Engineering* (1st Edition ed.). Delft, The Netherlands: Delft University of Technology.

Miedema, S. A. (September 2016). *OE4607 Introduction Dredging Engineering* (2nd Edition ed.). Delft, The Netherlands: Delft University of Technology.

Miedema, S. A., & Matousek, V. (2014). An explicit formulation of bed friction factor for sheet flow. *International Freight Pipeline Society Symposium, 15th.* (p. 17 pages). Prague, Czech Republic: IFPS.

Miedema, S. A., & Ramsdell, R. C. (2011). Hydraulic transport of sand/shell mixtures in relation with the critical velocity. *Terra et Aqua, Vol. 122.*

Miedema, S. A., & Ramsdell, R. C. (2013). A head loss model for slurry transport based on energy considerations. *World Dredging Conference XX* (p. 14). Brussels, Belgium: WODA.

Miedema, S. A., & Ramsdell, R. C. (2014). An Analysis of the Hydrostatic Approach of Wilson for the Friction of a Sliding Bed. *WEDA/TAMU* (p. 21). Toronto, Canada: WEDA.

Miedema, S. A., & Ramsdell, R. C. (2014). The Delft Head Loss & Limit Deposit Velocity Model. *Hydrotransport* (p. 15). Denver, USA.: BHR Group.

Miedema, S. A., & Ramsdell, R. C. (2015, May). *Pages from The Delft Head Loss & Limit Deposit Velocity Framework: Wilson.* Retrieved from ResearchGate: https://www.researchgate.net/publication/277340666_Pages_from_The_Delft_Head_Loss_Limit_Deposit_Velocity_Framework_Wilson

Miedema, S. A., & Ramsdell, R. C. (2015). The Limit Deposit Velocity Model, a New Approach. *Journal of Hydrology & Hydromechanics, Vol. 63(4).*, 15.

Miedema, S. A., & Ramsdell, R. C. (2016). The Delft Head Loss & Limit Deposit Velocity Framework. *Journal of Dredging Engineering, Vol. 15(2).*, 3-33.

Miedema, S. A., Riet, E. J., & Matousek, V. (2002). Theoretical Description And Numerical Sensitivity Analysis On Wilson Model For Hydraulic Transport Of Solids In Pipelines. *WEDA Journal of Dredging Engineering.*

Miller, R., & Byrne, R. (1966). The angle of repose for a single grain on a fixed rough bed. *Sedimentology 6*, 303-314.

Ming, G., Ruixiang, L., Ni, F., & Liqun, X. (2007). Hydraulic transport of coarse gravel. *WODCON XVIII.* Orlando, Florida, USA: WODA.

Moody, L. F. (1944). Friction Factors for Pipe Flow. *Transactions of the ASME 66 (8).*, 671-684.

Bibliography.

Morsi, S., & Alexander, A. (1972). An investigation of particle trajectories in two-phase flow systems. *Journal of Fluid Mechanics, Vol. 55*, 193-208.

Mukhtar, A. (1991). *Investigations of the flow of multisized heterogeneous slurries in straight pipe and pipe bends.* Delhi, India: PhD Thesis, IIT.

Nakagawa, H., & Nezu, I. (1977). Prediction of the contribution to the Reynolds stress from the bursting events in open-channel flows. *Journal of Fluid Mechanics, 80*, 99–128.

Newitt, D. M., Richardson, J. F., & Gliddon, B. J. (1961). Hydraulic conveying of solids in vertical pipes. *Transactions Institute of Chemical Engineers, Vol. 39.*, 93-100.

Newitt, D. M., Richardson, J. F., Abbott, M., & Turtle, R. B. (1955). Hydraulic conveying of solids in horizontal pipes. *Transactions of the Institution of Chemical Engineers Vo.l 33.*, 93-110.

Nezu, I., & Nakagawa, H. (1993). *Turbulence in Open Channel Flows.* A. A. Balkema.

Nezu, I., & Rodi, W. (1986). Open-channel flow measurements with a laser Doppler anemometer. *Journal of Hydraulic Engineering . ASCE, 112*, 335–355.

Ni, F., Zhao, L., Matousek, V., Vlasblom, W. J., & Zwartbol, A. (2004). Two phase flow of highly concentrated slurry in a pipeline. *Journal of Hydrodynamics, Series B, Vol. 16, No. 3.*, 325-331.

Ni, F., Zhao, L., Xu, L., & Vlasblom, W. J. (2008). A model calculation for flow resistance in the hydraulic transport of sand. *WODCON 18* (pp. 1377-1384). Orlando, Florida, USA: WODA.

Nielsen, P. (1981). Dynamics and geometry of wave generated ripples. *Journal of Geophysics Research, Vol. 86.*, 6467-6472.

Nikuradse, J. (1933, July/August). Stromungsgesetze in rauen Rohren. *VDI Forschungsheft 361, Beilage zo "Forschung auf dem Gebiete des Ingenieurwesens", Ausgabe B, Band 4.*

Nnadi, F. N., & Wilson, K. C. (1992). Motion of contact load particles at high shear stress. *Journal of Hydraulic Engineering, Vol. 118.*, 1670-1684.

Nnadi, F. N., & Wilson, K. C. (1995). Bed Load Motion at High Shear Stress: Dune Washout and Plane Bed Flow. *Journal of Hydraulic Engineering, Vol. 121.*, 267-273.

O'Brien, M. P. (1933). Review of the theory of turbulent flow and its relations to sediment transportation. *Transactions of the American Geophysics Union, Vol. 14.*, 487-491.

O'Brien, M. P., & Folsom, R. G. (1939). The transportation of sand in pipelines. *Vol. 3,No. 7 of University of California publications in engineering.*

Ofei, T. N., & Ismail, A. Y. (August 2016). Eulerian-Eulerian simulation of particle liquid slurry flow in horizontal pipe. *Journal of Petroleum Engineering.*, 18.

Oroskar, A. R., & Turian, R. M. (1980). The hold up in pipeline flow of slurries. *AIChE, Vol. 26.*, 550-558.

Paphitis, D. (2001). Sediment movement under unidirectional flows: an assesment of empirical threshold curves. *Coastal Engineering*, 227-245.

Parzonka, W., Kenchington, J. M., & Charles, M. E. (1981). Hydrotransport of solids in horizontal pipes: Effects of solids concentration and particle size on the deposit velocity. *Canadian Journal of Chemical Engineering, Vol. 59.*, 291-296.

Peker, S. M., & Helvaci, S. S. (2008). *Solid-Liquid Two Phase Flow.* Amsterdam, The Netherlands: Elsevier.

Pilotti, M., & Menduni, G. (2001). Beginning of sediment transport of incoherent grains in shallow shear flows. *Journal of Hydraulic Research, Vol. 39, No. 2.*, 115-124.

Poloski, A. P., Etchells, A. W., Chun, J., Adkins, H. E., Casella, A. M., Minette, M. J., & Yokuda, S. (2010). A pipeline transport correlation for slurries with small but dense particles. *Canadian Journal of Chemical Engineering, Vol. 88.*, 182-189.

Postma, H. (1967). Sediment transport and sedimentation in the estuarine environment. *Estuaries, AAAS, Washington D.C. Publ. 83.*, 158-179.

Prandl, L. (1925). Z. angew. *Math. Mech. 5 (1)*, 136-139.

Pugh, F. J., & Wilson, K. C. (1999). Role of the interface in stratified slurry flow. *Powder Technology, Vol. 104.*, 221-226.

Pugh, F. J., & Wilson, K. C. (1999). Velocity and concentration distribution in sheet flow above plane beds. *Journal of Hydraulic Engineering*, 117-125.

Ramsdell, R. C., & Miedema, S. A. (2010). Hydraulic transport of sand/shell mixtures. *WODCON XIX*. Beijing, China.: WODA.

Ramsdell, R. C., & Miedema, S. A. (2013). An overview of flow regimes describing slurry transport. *WODCON XX* (p. 15). Brussels, Belgium.: WODA.

Ramsdell, R. C., Miedema, S. A., & Talmon, A. (2011). Hydraulic transport of sand/shell mixtures. *OMAE 2011*. Rotterdam, Netherlands.: ASME.

Raudviki, A. J. (1990). *Loose Boundary Hydraulics.* University of Auckland: Pergamon Press.

Ravelet, F., Bakir, F., Khelladi, S., & Rey, R. (2012). Experimental study of hydraulic transport of large particles in horizontal pipes. *Experimental Thermal and Fluid Science*, 13.

Reichardt, H. (1951). Vollstandige Darstellung der Turbulenten Geswindigkeitsverteilung in Glatten Leitungen. *Zum Angew. Math. Mech., 3(7)*, 208-219.

Richardson, J. F., & Zaki, W. N. (1954). Sedimentation & Fluidization: Part I. *Transactions of the Institution of Chemical Engineering 32*, 35-53.

Riet, E. J., Matousek, V., & Miedema, S. A. (1995). A Reconstruction of and Sensitivity Analysis on the Wilson Model for Hydraulic Particle Transport. *Proc. 8th Int. Conf. on Transport and Sedimentation of Solid Particles.* Prague, Czech Republic.

Riet, E. J., Matousek, V., & Miedema, S. A. (1996). A Theoretical Description and Numerical Sensitivity Analysis on Wilson's Model for Hydraulic Transport in Pipelines. *Journal of Hydrology & Hydromechanics*.

Rijn, L. v. (1984). Sediment transport: Part I: Bed load transport. *Journal of Hydraulic Engineering, Vol. 110(10)*, 1431-1456.

Rijn, L. v. (1993). *Principles of Sediment Transport, Part 1. .* Blokzijl: Aqua Publications.

Rijn, L. v. (2006). *Principles of sediment transport in rivers, estuaries and coastal areas, Part II: Supplement 2006.* Utrecht & Delft: Aqua Publications, The Netherlands.

Roberts, J., Jepsen, R., Gotthard, D., & Lick, W. (1998). Effects of particle size and bulk density on erosion of quartz particles. *Journal of Hydraulic Engineering*, 1261-1267.

Robinson, M. P. (1971). *Critical deposit velocities for low concentration solid-liquid mixtures. MSc Thesis.* Lehigh University, Fritz Laboratory.

Robinson, M. P., & Graf, W. H. (1972). *Critical deposit velocities for low concentration sand water mixtures. ASCE National Water Resources EnVg Meeting Preprint 1637, January 1972. Paper 1982.* Atlanta, Georgia, USA.: Lehigh University, Fritz Laboratory.

Roco, M. C., & Shook, C. A. (1983). Modeling of Slurry Flow: The effect of particle size. *The Canadian Journal of Chemical Engineering, Vol. 61.*, 494-503.

Rouse, H. (1937). Modern conceptions of the mechanics of fluid turbulence. *Transactions of the American Society of Cicil Engineers, Vol. 102*, 463-505, Discussion 506-543.

Rowe, P. (1987). A convinient empirical equation for estimation of the Richardson-Zaki exponent. *Chemical Engineering Science Vol. 42, no. 11*, 2795-2796.

Rowe, P. N. (1987). A convinient empirical equation for estimation of the Richardson-Zaki exponent. *Chemical Engineering Science Vol. 42, no. 11*, 2795-2796.

Saffman, P. G. (1965). The lift on small sphere in a slow shear low. *Journal of Fluid Mechanics, 22*, 385-400.

Sanders, R. S., Sun, R., Gillies, R. G., McKibben, M., Litzenberger, C., & Shook, C. A. (2004). Deposition Velocities for Particles of Intermediate Size in Turbulent Flows. *Hydrotransport 16* (pp. 429-442). Santiago, Chile.: BHR Group.

Schaan, J., & Shook, C. A. (2000). Anomalous friction in slurry flows. *Canadian Journal of Chemical Engineering, Vol. 78.*, 726-730.

Scheurel, H. G. (1985). *Rohrverschleiss beim hydraulischen feststoffentransport.* Karlsruhe: Universitat Karlsruhe.

Schiller, R. E., & Herbich, J. B. (1991). *Sediment transport in pipes. Handbook of dredging.* New York: McGraw-Hill.

Schlichting, H. (1968). *Boundary layer theory.* 6th ed. New York: McGraw-Hill.

Sellgren, A., & Wilson, K. (2007). Validation of a four-component pipeline friction-loss model. *Hydrotransport 17* (pp. 193-204). BHR Group.

Sellgren, A., Visintainer, R., Furlan, J., & Matousek, V. (2014). Pump and pipeline performance when pumping slurries with different particle gradings. *Hydrotransport 19* (pp. 131-143). Denver, Colorado, USA.: BHR Group.

Sellgren, A., Visintainer, R., Furlan, J., & Matousek, V. (2016). Pump and pipeline performance when pumping slurries with different particle gradings. *The Canadian Journal of Chemical Engineering, Vol. 94(6)*, 1025-1031.

Seshadri, V., Singh, S. N., & Kaushal, D. R. (2006). A model for the prediction of concentration and particle size distribution for the flow of multisized particulate suspensions through closed ducts and open channels. *Particulate Science and Technology: An International Journal.*, 239-258.

Shields, A. (1936). Anwendung der Aehnlichkeitsmechanik und der Turbulenzforschung auf die Geschiebebewegung. *Mitteilung der Preussischen Versuchsanstalt fur Wasserbau und Schiffbau, Heft 26, Berlin.* Belin.

Shook, C. A., Geller, L., Gillies, R. G., Husband, W. H., & Small, M. (1986). Experiments with coarse particles in a 250 mm pipeline. *10th International Conference on the Hydraulic Transport of Solids in Pipelines (Hydrotransport 10).* (pp. 219-227). Cranfield, UK.: BHRA Fluid Eng.

Shook, C. A., Gillies, R. G., & Sanders, R. S. (2002). *Pipeline Hydrotransport with Application in the Oil Sand Industry.* Saskatoon, Canada: Saskatchewan Research Council, SRC Publication 11508-1E02.

Shook, C., & Roco, M. (1991). *Slurry Flow, Principles & Practice.* Boston: Butterworth Heineman.

Bibliography.

Silin, M. O., Kobernik, S. G., & Asaulenko, I. A. (1958). *Druckhohenverluste von Wasser und Wasser-Boden-Gemischen in Rohrleitungen grossen Durchmessers.* Ukrain: Dopovidi Akad. Nauk. Ukrain RSR.

Silin, N. A., & Kobernik, S. G. (1962). Rezimy raboty zemljesosnych snarjadov, Kijev.

Simons, D. (1957). *Theory and design of stable channels in alluvial material.* PhD thesis: Colorado State University.

Sinclair, C. G. (1962). The limit deposit velocity of heterogeneous suspensions. *Proceedings Symposium on the Interaction Btween Fluids and Particles.* Institute of Chemical Engineers.

Smoldyrev. (1970). *Truboprowodnyi transport(rohrleitungstransport).* Moskau.

Sobota, J., & Kril, S. I. (1992). Liquid and solid velocity during mixture flow. *Proceedings 10th International Colloquium Massenguttransport durch Rohrleitungen.*, (p. K). Meschede, Germany.

Soleil, G., & Ballade, P. (1952). Le transport hydraulique des materiaux dans les travaux publics, observations des resultats d'essais en grandeur nature. *Deuxiemes Journees de l'Hydraulique*, 9-26.

Soulsby, R., & Whitehouse, R. (1997). Threshold of sediment motion in coastal environment. *Proceedings Pacific Coasts and Ports.* (pp. 149-154). Christchurch, New Zealand: University of Canterbury.

Souza Pinto, T. C., Moraes Junior, D., Slatter, P. T., & Leal Filho, L. S. (2014). Modelling the critical velocity for heterogeneous flow of mineral slurries. *International Journal of Multiphase Flow.*, 31-37.

Spelay, R., Hashemi, S. A., Gillies, R. G., Hegde, R., Sanders, R. S., & Gillies, D. G. (2013). Governing friction loss mechanisms and the importance of offline characterization tests in the pipeline transport of dense coarse particle slurries. *Proceedings of the ASME 2013 Fluids Engineering Division Summer Meeting.* (pp. 1-7). Incline Village, Nevada, USA.: FEDSM2013.

Stevenson, P., Cabrejos, F. J., & Thorpe, R. B. (2002). Incipient motion of particles on a bed of like particles in hydraulic and pneumatic conveying. *Fourth World Congress of Particle Technology, Sydney, 21st–25th July (paper 400).* Sydney.

Stevenson, P., Thorpe, R. B., & Davidson, J. F. (2002). Incipient motion of a small particle in the viscous boundary-layer at a pipe wall. *Chemical Engineering Science, 57*, 4505–4520.

Sundborg, A. (1956). The River Klarålven: Chapter 2. The morphological activity of flowing water erosion of the stream bed. *Geografiska Annaler, 38*, 165-221.

Swamee, P. K. (1993). Critical depth equations for irrigation canals. *Journal of Irrigation and Drainage Engineering, ASCE.*, 400-409.

Swamee, S. E., & Jain, K. A. (1976). Explicit equations for pipe-flow problems. *Journal of the Hydraulics Division (ASCE) 102 (5).*, 657-664.

Talmon, A. (2011). Hydraulic Resistance of Sand-Water Mixture Flow in Vertical Pipes. *T&S, Transport and Sedimentation of Solid Particles* (pp. 137-147). Wroclaw, Poland: T&S.

Talmon, A. (2013). Analytical model for pipe wall friction of pseudo homogeneous sand slurries. *Particulate Science & technology: An International Journal*, 264-270.

Televantos, Y., Shook, C. A., Carleton, A., & Street, M. (1979). Flow of slurries of coarse particles at high solids concentrations. *Canadian Journal of Chemical Engineering, Vol. 57.*, 255-262.

Thomas, A. (1976). SCALE-UP METHODS FOR PIPELINE TRANSPORT OF SLURRIES. *International Journal of Mineral Processing, Vol. 3.*, 51-69.

Thomas, A. D. (1979). Predicting the deposit velocity for horizontal turbulent pipe flow of slurries. *International Journal of Multiphase Flow, Vol. 5.*, 113-129.

Thomas, A. D. (2014). Slurries of most interest to the mining industry flow homogeneously and the deposit velocity is the key parameter. *HydroTransport 19.* (pp. 239-252). Denver, Colorado, USA.: BHR Group.

Thomas, A. D. (2015). A modification of the Wilson & Judge deposit velocity, extending its application to finer particles and larger pipe sizes. *17th International Conference on Transport & Sedimentation of Solid Particles.* (pp. 335-344). Delft, The Netherlands: Delft Univesity of Technology.

Thomas, D. G. (1962). Transport Characteristics of Suspensions: Part VI. Minimum velocity for large particle size suspensions in round horizontal pipes. *A.I.Ch.E. Journal, Vol.8(3).*, 373-378.

Thomas, D. G. (1965). Transport characteristics of suspensions: VIII. A note on the viscosity of Newtonian suspensions of uniform spherical particles. *Journal Of Colloidal Sciences, Vol. 20.*, 267-277.

Turian, R. M., & Yuan, T. F. (1977). Flow of slurries in pipelines. *AIChE Journal, Vol. 23.*, 232-243.

Turian, R. M., Hsu, F. L., & Ma, T. W. (1987). Estimation of the critical velocity in pipeline flow of slurries. *Powder Technology, Vol. 51.*, 35-47.

Turner, T. (1996). *Fundamentals of Hydraulic Dredging.* New York: ASCE.

Turton, R., & Levenspiel, O. (1986). A short note on the drag correlation for spheres. *Powder technology Vol. 47*, 83-85.

Vanoni, V. A. (1975). *Sedimentation Engineering: American Society of Civil Engineers, Manuals and Reports on Engineering Practice. No. 54. P.745.*

Vlasak, P. (2008). *Laminar, transitional and turbulent flow of fine grained slurries in pipelines.* Prague.: Czech Technical University in Prague, Fakulty of Civil Engineering.

Vlasak, P., Chara, Z., Krupicka, J., & Konfrst, J. (2014). Experimental investigation of coarse particles water mixture flow in horizontal and inclined pipes. *Journal of Hydrology & Hydromechanics, Vol. 62(3).*, 241-247.

Vlasak, P., Kysela, B., & Chara, Z. (2012). FLOW STRUCTURE OF COARSE-GRAINED SLURRY IN A HORIZONTAL PIPE. *Journal of Hydrology & Hydromechanics, Vol. 60.*, 115-124.

Vocadlo, J. J. (1972). Prediction of pressure gradient for the horizontal turbulent flow of slurries. *Hydrotransport 2.* Coventry: BHRA.

Vocadlo, J. J., & E., C. M. (1972). Prediction of pressure gradient for the horizontal turbulent flow of slurries. *Conference on the Hydraulic Transport of Solids in Pipes.* Warwick, England: British Hydromechanics Research Association.

Wallis, G. (1969). *One Dimensional Two Phase Flow.* McGraw Hill.

Wasp, E. J. (1963). Cross country coal pipeline hydraulics. *Pipeline News.*, 20-28.

Wasp, E. J., & Slatter, P. T. (2004). Deposition velocities for small particles in large pipes. *12th International Conference on Transport & Sedimentation of Solid Particles*, (pp. 20-24). Prague, Czech Republic.

Wasp, E. J., Kenny, J. P., & Gandhi, R. L. (1977). Solid liquid flow slurry pipeline transportation. *Transactions Technical Publications.*

Wasp, E. J., Kenny, J. P., Aude, T. C., Seiter, R. H., & Jacques, R. B. (1970). Deposition velocities transition velocities and spatial distribution of solids in slurry pipelines. *Hydro Transport 1, paper H42.* (pp. 53-76). Coventry: BHRA Fluid Engineering.

Welte, A. (1971). Grundlagen der Berechnung der Rohrleitungsdruckverluste. *Konstruction 23, Heft 5 & 6.*

Westendorp, J. H. (1948). *Verslag literatuurstudie over persen van zand M.276.* Delft, Netherlands: Delft Hydraulics Laboratory.

White, C. M. (1940). The equilibrium of grains on the bed of a stream. *Proceedings Royal Society of London*, *A174*, pp. 322-338.

Whitlock, L., Wilson, K. C., & Sellgren, A. (2004). Effect of near-wall lift on frictional characteristics of sand slurries. *Hydrotransport 16* (pp. 443-454). Cranfield, UK.: BHR Group.

Wiberg, P. L., & Smith, J. D. (1987A). Calculations of the critical shear stress for motion of uniform and heterogeneous sediments. *Water Resources Research, 23*(8), 1471–1480.

Wiberg, P., & Smith, J. (1987B). Initial motion of coarse sediment in streams of high gradient. *Proceedings of the Corvallis Symposium.* IAHS Publication No. 165.

Wiedenroth, W. (1967). *Untersuchungen uber die forderung von sand wasser gemischen durch rohrleitungen und kreiselpumpen.* Hannover: PhD Thesis, Technische Hochschule Hannover.

Wikramanayake, P. N., & Madsen, O. S. (1991). *Calculation of movable bed friction factors.* Vicksburg, Mississippi.: Tech. Rep. DACW-39-88-K-0047, 105 pp., Coastal Eng. Res. Cent.,.

Wilcock, P. (1993). Critical shear stress of natural sediments. *Journal of Hydraulic Engineering Vol. 119, No. 4.*, 491-505.

Wilson, K. C. (1965). *Application of the minimum entropy production principle to problems in two-phase flow, PhD Thesis.* Kingston, Ontario, Canada.: Queens University.

Wilson, K. C. (1966). Bed Load Transport at High Shear Stress. *Journal of the Hydraulics Division*, 49-59.

Wilson, K. C. (1970). Slip point of beds in solid liquid pipeline flow. *Journal of Hydraulic Division, Vol 96(HY1)*, 1-12.

Wilson, K. C. (1970). Slip point of beds in solid-liquid pipeline flow. *Proceedings American Society of Civil Engineers, Vol. 96, HY1.*

Wilson, K. C. (1972). A Formula for the Velocity Required to Initiate Particle Suspension in Pipeline Flow. *Hydrotransport 2* (pp. E2 23-36). Warwick, UK.: BHRA Fluid Engineering.

Wilson, K. C. (1974). Coordinates for the Limit of Deposition in Pipeline Flow. *Hydrotransport 3* (pp. E1 1-13). Colorado School of Mines, Colorado, USA.: BHRA Fluid Engineering.

Wilson, K. C. (1975). Stationary Deposits and Sliding Beds in Pipes Transporting Solids. *Dredging Technology* (pp. C3 29-40). College Station, Texas, USA.: BHRA Fluid Engineering.

Wilson, K. C. (1976). A Unified Physically based Analysis of Solid-Liquid Pipeline Flow. *Hydrotransport 4* (pp. A1 1-16). Banff, Alberta, Canada: BHRA Fluid Engineering.

Wilson, K. C. (1979). Deposition limit nomograms for particles of various densities in pipeline flow. *Hydrotransport 6* (p. 12). Canterbury, UK: BHRA Fluid Engineering.

Wilson, K. C. (1979). Deposition limit nomograms for particles of various densities in pipeline flow. *Hydrotransport 6* (p. 12). Canterbury, UK: BHRA.

Wilson, K. C. (1980). Analysis of Slurry Flows with a Free Surface. *Hydrotransport 7* (pp. 123-132). Sendai, Japan: BHRA Fluid Engineering.

Wilson, K. C. (1984). Analysis of Contact Load Distribution and Application to Deposition Limit in Horizontal Pipes. *Journal of Pipelines, Vol. 4.*, 171-176.

Wilson, K. C. (1986). Effect of Solids Concentration on Deposit Velocity. *Journal of Pipelines, Vol. 5.*, 251-257.

Wilson, K. C. (1987). Analysis of Bed Load Motion at High Shear Stress. *Journal of Hydraulic Engineering, Vol. 113.*, 97-103.

Wilson, K. C. (1988). Evaluation of interfacial friction for pipeline transport models. *Hydrotransport 11* (p. B4). BHRA Fluid Engineering.

Wilson, K. C. (1989). Mobile Bed Friction at High Shear Stress. *Journal of Hydraulic Engineering, Vol. 115.*, 825-830.

Wilson, K. C., & Addie, G. R. (1997). Coarse particle pipeline transport: effect of particle degradation on friction. *Powder Technology, Vol. 94.*, 235-238.

Wilson, K. C., & Brown, N. P. (1982). Analysis of Fluid Friction in dense Phase Pipeline Flow. *The Canadian Journal of Chemical Engineering, Vol. 60.*, 83-86.

Wilson, K. C., & Judge, D. G. (1976). New Techniques for the Scale-Up of Pilot Plant Results to Coal Slurry Pipelines. *Proceedings International Symposium on Freight Pipelines.* (pp. 1-29). Washington DC, USA: University of Pensylvania.

Wilson, K. C., & Judge, D. G. (1977). Application of Analytical Model to Stationary Deposit Limit in Sand Water Slurries. *Dredging Technology* (pp. J1 1-12). College Station, Texas, USA.: BHRA Fluid Engineering.

Wilson, K. C., & Judge, D. G. (1978). Analytically based Nomographic Charts for Sand-Water Flow. *Hydrotransport 5* (pp. A1 1-12). Hannover, Germany: BHRA Fluid Engineering.

Wilson, K. C., & Judge, D. G. (1980). New Techniques for the Scale-up of Pilot Plant Results to Coal Slurry Pipelines. *Journal of Powder & Bulk Solids Technology.*, 15-22.

Wilson, K. C., & Nnadi, F. N. (1990). Behavior of Mobile Beds at High Shear Stress. *Proceedings Coastal Engineering 22.*, (pp. 2536-2541). Delft.

Wilson, K. C., & Pugh, F. J. (1988). Dispersive Force Basis for Concentration Profiles. *Journal of Hydraulic Engineering, Vol. 114, No. 7.*, 806-810.

Wilson, K. C., & Pugh, F. J. (1988). Dispersive Force Modelling of Turbulent Suspension in Heterogeneous Slurry Flow. *The Canadian Journal of Chemical Engineering, Vol. 66.*, 721-727.

Wilson, K. C., & Sellgren, A. (2001). *Hydraulic transport of solids, Pump Handbook, pp. 9.321-9.349.* McGraw-Hill.

Wilson, K. C., & Sellgren, A. (2003). Interaction of Particles and Near-Wall Lift in Slurry Pipelines. *Journal of Hydraulic Engineering, Vol. 129.*, 73-76.

Wilson, K. C., & Sellgren, A. (2010). Behavior of intermediate particle slurries in pipelines. *Hydrotransport 18* (pp. 117-128). Rio de Janeiro: BHR Group.

Wilson, K. C., & Sellgren, A. (2012). Revised Method for Calculating Stratification Ratios for Heterogeneous Flows. *14th International Conference on Transport & Sedimentation of Solid Particles.*, (pp. 334-340).

Wilson, K. C., & Watt, W. E. (1974). Influence of Particle Diameter on the Turbulent Support of Solids in Pipeline Flow. *Hydrotransport 3* (pp. D1 1-9). Colorado School of Mines, Colorado, USA.: BHRA Fluid Engineering.

Wilson, K. C., Addie, G. R., & Clift, R. (1992). *Slurry Transport using Centrifugal Pumps.* New York: Elsevier Applied Sciences.

Wilson, K. C., Addie, G. R., Clift, R., & Sellgren, A. (1997). *Slurry Transport using Centrifugal Pumps.* Glasgow, UK.: Chapman & Hall, Blackie Academic & Professional.

Wilson, K. C., Addie, G. R., Sellgren, A., & Clift, R. (2006). *Slurry transport using centrifugal pumps.* New York: Springer Science+Business Media Inc.

Wilson, K. C., Clift, R., & Sellgren, A. (2002). Operating points for pipelines carrying concentrated heterogeneous slurries. *Powder Technology, Vol. 123.*, 19-24.

Wilson, K. C., Clift, R., Addie, G. R., & Maffet, J. (1990). Effect of Broad Particle Grading on Slurry Stratification Ratio and Scale-up. *Powder Technology, 61.*, 165 - 172.

Wilson, K. C., Sanders, R. S., Gillies, R. G., & Shook, C. A. (2010). Verification of the near wall model for slurry flow. *Powder Technology, Vol. 197.*, 247-253.

Wilson, K. C., Sellgren, A., & Addie, G. R. (2000). Near-wall fluid lift of particles in slurry pipelines. *10th Conference on Transport and Sedimentation of Solid Particles.* Wroclav, Poland: T&S10.

Wilson, K. C., Streat, M., & Bantin, R. A. (1972). Slip model correlation of dense two phase flow. *Hydrotransport 2* (pp. B1 1-10). Warwick, UK: BHRA Fluid Engineering.

Wilson, W. E. (1942). Mechanics of flow with non colloidal inert solids. *Transactions ASCE Vol. 107.*, 1576-1594.

Wood, D. J. (1966). An explicit friction factor relationship. *Civil Engineering, Vol. 36, ASCE.*, 60-61.

Worster, R. C., & Denny, D. F. (1955). Hydraulic transport of solid materials in pipelines. *Institution of Mechanical Engineers (London)*, 563-586.

Wu, W., & Wang, S. (2006). Formulas for sediment porosity and settling velocity. *Journal of Hydraulic Engineering, 132(8)*, 858-862.

Yagi, T., Okude, T., Miyazaki, S., & Koreishi, A. (1972). *An Analysis of the Hydraulic Transport of Solids in Horizontal Pipes.* Nagase, Yokosuka, Japan.: Report of the Port & Harbour Research Institute, Vol. 11, No. 3.

Yalin, M. S., & Karahan, E. (1979). Inception of sediment transport. *ASCE Journal of the Hydraulic Division, 105*, 1433–1443.

Zandi, I. (1971). Hydraulic transport of bulky materials. In I. Zandi, *Advances in Solid–Liquid Flow in Pipes and its Applications.* (pp. 1-38). Oxford: Pergamon Pres.

Zandi, I., & Govatos, G. (1967). Heterogeneous flow of solids in pipelines. *Proc. ACSE, J. Hydraul. Div.,, 93(HY3).*, 145-159.

Zanke, U. C. (1977). *Berechnung der Sinkgeschwindigkeiten von Sedimenten.* Hannover, Germany: Mitteilungen Des Francius Instituts for Wasserbau, Heft 46, seite 243, Technical University Hannover.

Zanke, U. C. (2001). *Zum Einfluss der Turbulenz auf den Beginn der Sedimentbewegung.* Darmstadt, Germany: Mitteilungen des Instituts fur Wasserbau und Wasserwirtschaft der TU Darmstadt, Heft 120.

Zanke, U. C. (2003). On the influence of turbulence on the initiation of sediment motion. *International Journal of Sediment Research, 18*(1), 17–31.

List of Figures.

Chapter 13:   List of Figures.

List of Figures.

List of Figures.

List of Figures.

Chapter 14: List of Tables.

Appendices.

15.1 Appendix A: List of Solids Densities.

Source: www.EngineeringToolbox.com.

Table 15.1-1: Specific Gravities of many solids.

Product	Specific Gravity	Product	Specific Gravity
ABS, extrusion grade	1.05	Manganese	7.21 - 7.44
ABS, high impact	1.03	Manganese ore, pyrolusite	3.7 - 4.6
Acetal, 20% glass	1.55	Magnesium	1.738
Acetal, copolymer	1.41	Marble min.	2.6
Acetyl, homopolymer	1.41	Marble max.	2.86
Acrylic	1.19	Masonry	2.4
Alumina	3.4 - 3.6	Mercury	13.534
Aluminum min.	2.55	Mica	2.7
Aluminum max.	2.8	Mineral wool blanket	0.1
Aluminum Bronze	7.8	Molybdenum	10.22
Andesite, solid	2.8	Monel metal, rolled	8.97
Antimony	6.69	Mortar	1.5
Asbestos, cement board	1.4	Mullite beads	2.8
Asbestos, mill board	1	Neodymium	7
Asbestos, shredded	0.3 - 0.4	Nickel	8.9
Asbestos, rock	1.6	Niobium (Columbium)	8.57
Asphalt	1.1	Nylon 6 Cast	1.16
Asphaltum	1.4	Nylon 6/6, Cast	1.3
Azdel	1.19	Nylon 6/6, Extruded	1.14
Bakelite, solid	1.4	Nylon 60L, Cast	1.16
Bark	0.25	Oak, red	0.7
Barite	4.5	Osmium	22.57
Barium	3.62	Paper	0.9
Barium sulfate	4.5	Palladium	12.02
Basalt, broken	1.95	Paraffin wax	0.9
Basalt solid	3	PET, unfilled	1.36
Beeswax	0.95	Phenolics	1.38
Bentonite	2.4	Phosphorus	1.8
Beryllium	1.848	Plaster, light	0.7
Bismuth	9.79	Plaster, sand	1.8
Borax min.	1.7	Plaster of Paris	1.8
Borax min.	1.8	Plastics, foamed	0.2

Boron	2.32	Plastics, solid	1.2
Brass, cast rolled	8.4 - 8.7	Platinum	21.45
Brick, common red	1.75	Plutonium	19.84
Brick, fire clay (firebrick)	2.4	Polycarbonate	1.19
Brick, hard	2	Polyethylene, HD	0.97
Brickwork, in cement	1.8	Polyethylene, UHMW	0.94
Brickwork, in mortar	1.6	Polyethermide	1.27
Brickwood, in cement	1.8	Polyphenylene Sulfide	1.3
Brickwood, in mortar	1.6	Polymethylpentene	0.83
Bronze aluminum	7.7	Polymid, unfilled	1.41
Bronze phosphor	8.88	Polypropylene	0.91
Bronze, 7.9 - 14% Sn	7.4 - 8.9	Polysulfone	1.25
Cadmium	8.65	Polyurethane	1.05
Calcium	4.58	Porcelain	2.5
Calcium carbonate	2.7	Potassium	0.86
Carbon, solid	2.1	Praseodymium	6.77
Carbon, powdered	0.08	PTFE (teflon)	2.19
Cement	1.2 - 1.5	PVC	1.39
Cement, Portland (set)	3.1	PVDF	1.77
Cerium	6.77	Quartz min.	2.5
Cesium	1.873	Quartz max.	2.8
Chalk	2.3	Rhenium	21.02
Charcoal, wood	0.4	Rhodium	12.41
Chromium	7.19	Rubidium	1.532
Chromium dioxide (Cr203)	5.22	Ruthenium	12.45
Clay min.	1.8	Salt	2.2
Clay max.	2.6	Samarium	7.52
Coal, anthracite	1.5	Sand, silica	2.6
Coal, bitumious	1.2	Sand, Quartz	7
Coal, slag	2.7	Sandstone min.	2
Cobalt	8.71	Sandstone max.	2.6
Concrete, ligth	1.4	Sawdust	0.15
Concrete, stone	2.2	Selenium	4.28
Corkboard	0.2	Scandium	2.989
Copper	8.89	Serpentine min.	2.7
CPVC	1.55	Selenium	4.8
Diamond	3.51	Serpentine max.	2.8
Dolomite rock	2.9	Sialon	3.26

Appendices.

Dysprosium	8.55	Silica aerogel	0.11
Earth, dry	1.4	Silicon	2.33
Emery	4	Silicon carbide	3.1
Epoxy	1.8	Silicon nitride	3.2
Erbium	9.066	Silver	10.5
Europium	5.244	Silver, German	8.58
Ferrosilicon - 15%	6.7 - 7.1	Slate	2.8
Fiberboard, ligth	0.24	Soapstone	2.7
Fiber hardboard	1.1	Sodium	0.968
Fiber glass sheet	1.87	Steatite beads	2.6 - 2.7
Flint stones / pebbles	2.4 - 2.6	Steel, 440C stainless	7.7
Gadolinium	7.9	Steel, carbon	7.8
Gallium	5.91	Steel, chrome	7.8
Germanium	5.32	Steel, cold-drawn	7.83
German silver	8.58	Steel, machine	7.8
Glass min.	2.4	Steel, tool	7.70 - 7.73
Glass max.	2.8	Strontium	2.64
Glass beads	2.5	Sulfur	2
Glass crystal min.	2.9	Talc min.	2.6
Glass crystal max.	3	Talc max.	2.8
Glass plate min.	2.45	Tantalium	16.69
Glass plate max.	2.72	Tar, bituminous	1.2
Gold, 22 carat fine1)	17.5	Tellurium min.	6
Gold, pure	19.32	Tellurium max.	6.24
Gold, US coin1)	17.18 - 17.2	Thallium	11.85
Granite min.	2.4	Thorium	11.7
Graphite	2.07	Thulium	9.32
Gypsum, solid	2.8	Tile	1.8
Gypsum, board	0.8	Tin	7.31
Hafnium	13.31	Tin ore, cassiterite	6.4 - 7.0
Hairfelt	0.1	63 Sn & 37 Pb	8.42
Hematite	5.2	10 Sn & 90 Pb	10.5
Holmium	8.795	Titanium	4.506
Hornblende	3	Titanium dioxide, Anatase	3.77
Ice (0ºC, 32ºF)	0.92	Trap rock	3
Ilmenite	4.5- 5.0	Tungsten	19.22
Indium	7.31	Tungsten carbide	14.29
Iodine	4.93	Uranium	18.8

Iridium min.	21.78	Vanadium	5.96
Iridium max.	22.42	Vermiculite	0.13
Iron cast min.	7.03	Vinyl ester	1.8
Iron cast max.	7.13	Water	1
Iron carbonate	3.9 +	White metal	7.3
Iron slag	2.7	Wood, balsa	0.16
Iron wrought min.	7.6	Wood, oak	0.7
Iron wrought max.	7.9	Wood, white pine	0.5
Lanthanum	6.17	Wood, felt	0.3
Leather, dry	0.9	Wood, loose	0.1
Limestone min.	2.1	Wool	1.32
Limestone max.	2.86	Ytterbium	6.97
Lead	11.35	Yttrium	4.47
Lead ore, galena	7.3 - 7.6	Zinc, cast-rolled	6.9 - 7.2
Lead oxide (yellow)	9.5 - 9.9	Zinc blend min	3.9
Leather	0.95	Zinc blend max	4.2
Limestone	2.6	Zinc min.	6.9
Lithium	0.53	Zinc max.	7.2
Lutetium	9.84	Zirconium	6.506
Magnesite	3	Zirconium silicate	3.85
Magnetite	3.2		

Appendices.

15.2 Appendix B: List of Liquid Densities.

Source: www.EngineeringToolbox.com.

Table 15.2-1: List of liquid densities.

Liquid	Temperature T (°C)	Density ρ_l (kg/m³)	Liquid	Temperature T (°C)	Density ρ_l (kg/m³)
Acetic Acid	25	1049	Heptane	25	679.5
Acetone	25	784.6	Hexane	25	654.8
Acetonitrile	20	782	Hexanol	25	811
Alcohol, ethyl (ethanol)	25	785.1	Hexene	25	671
Alcohol, methyl (methanol)	25	786.5	Hydrazine	25	795
Alcohol, propyl	25	800	Ionene	25	932
Ammonia (aqua)	25	823.5	Isobutyl Alcohol	20	802
Aniline	25	1019	Iso-Octane	20	692
Automobile oils	15	880 - 940	Isopropyl Alcohol	20	785
Beer (varies)	10	1010	Isopropyl Myristate	20	853
Benzene	25	873.8	Kerosene	60°F	820.1
Benzil	15	1230	Linolenic Acid	25	897
Brine	15	1230	Linseed oil	25	929.1
Bromine	25	3120	Machine oil	20	910
Butyric Acid	20	959	Mercury		13590
Butane	25	599	Methane	-164	465
n-Butyl Acetate	20	880	Methanol	20	791
n-Butyl Alcohol	20	810	Methyl Isoamyl Ketone	20	888
n-Butylhloride	20	886	Methyl Isobutyl Ketone	20	801
Caproic acid	25	921	Methyl n-Propyl Ketone	20	808
Carbolic acid	15	956	Methyl t-Butyl Ether	20	741
Carbon disulfide	25	1261	N-Methylpyrrolidone	20	1030
Carbon tetrachloride	25	1584	Methyl Ethyl Ketone	20	805
Carene	25	857	Milk	15	1020 - 1050
Castor oil	25	956.1	Naphtha	15	665
Chloride	25	1560	Naphtha, wood	25	960
Chlorobenzene	20	1106	Napthalene	25	820
Chloroform	20	1489	Nitric acid	0	1560

Chloroform	25	1465	Ocimene	25	798
Citric acid, 50% aqueous solution	15	1220	Octane	15	698.6
Coconut oil	15	924	Oil of resin	20	940
Cotton seed oil	15	926	Oil of turpentine	20	870
Cresol	25	1024	Oil, lubricating	20	900
Creosote	15	1067	Olive oil	20	800 - 920
Crude oil, 48o API	60ºF	790	Oxygen (liquid)	-183	1140
Crude oil, 40o API	60ºF	825	Paraffin		800
Crude oil, 35.6o API	60ºF	847	Palmitic Acid	25	851
Crude oil, 32.6o API	60ºF	862	Pentane	20	626
Crude oil,alifornia	60ºF	915	Pentane	25	625
Crude oil, Mexican	60ºF	973	Perchlor ethylene	20	1620
Crude oil, Texas	60ºF	873	Petroleum Ether	20	640
Cumene	25	860	Petrol, natural	60ºF	711
Cyclohexane	20	779	Petrol, Vehicle	60ºF	737
Cyclopentane	20	745	Phenol	25	1072
Decane	25	726.3	Phosgene	0	1378
Diesel fuel oil 20 to 60	15	820 - 950	Phytadiene	25	823
Diethyl ether	20	714	Pinene	25	857
o-Dichlorobenzene	20	1306	Propane	-40	493.5
Dichloromethane	20	1326	Propane, R-290	25	494
Diethylene glycol	15	1120	Propanol	25	804
Dichloromethane	20	1326	Propylenearbonate	20	1201
Dimethyl Acetamide	20	942	Propylene	25	514.4
N,N-Dimethylformamide	20	949	Propylene glycol	25	965.3
Dimethyl Sulfoxide	20	1100	Pyridine	25	979
Dodecane	25	754.6	Pyrrole	25	966
Ethane	-89	570	Rape seed oil	20	920
Ether	25	713.5	Resorcinol	25	1269
Ethylamine	16	681	Rosin oil	15	980
Ethyl Acetate	20	901	Sea water	25	1025
Ethyl Alcohol (Ethanol, pure alcohol, grain alcohol or drinking alcohol)	20	789	Silane	25	718
Ethyl Ether	20	713	Silicone oil	25	965 - 980

Ethylene Dichloride	20	1253	Sodium Hydroxide (caustic soda)	15	1250
Ethylene glycol	25	1097	Sorbaldehyde	25	895
Freon (Fluorine) refrigerant R-11	25	1476	Soya bean oil	15	924 - 928
Fluorine refrigerant R-12	25	1311	Stearic Acid	25	891
Fluorine refrigerant R-22	25	1194	Sulfuric Acid 95% onc.	20	1839
Formaldehyde	45	812	Sulfurus acid	-20	1490
Formic acid 10%oncentration	20	1025	Sugar solution 68 brix	15	1338
Formic acid 80%oncentration	20	1221	Sunflower oil	20	920
Freon - 11	21	1490	Styrene	25	903
Freon - 21	21	1370	Terpinene	25	847
Fuel oil	60ºF	890	Tetrahydrofuran	20	888
Furan	25	1416	Toluene	20	867
Furforol	25	1155	Trichlor ethylene	20	1470
Gasoline, natural	60ºF	711	Triethylamine	20	728
Gasoline, Vehicle	60ºF	737	Trifluoroacetic Acid	20	1489
Gas oils	60ºF	890	Turpentine	25	868.2
Glucose	60ºF	1350 - 1440	Water, heavy	11.6	1105
Glycerine	25	1259	Water - pure	4	1000
Glycerol	25	1126	Water - sea	77ºF	1022
Heating oil	20	920	Whale oil	15	925
			o-Xylene	20	880

Appendices.

15.3 Appendix C: List of Mesh Sizes.

Source: www.WikiPedia.com.

Table 15.3-1: Commercial sieve mesh dimensions.

Sieve size	Opening		Standard Mesh	
(mm)	(in)	(μm)	US	Tyler
5.6	0.22	5600	3.5	-
4.75	0.187	4750	4	-
4	0.157	4000	5	-
3.35	0.132	3350	6	-
2.8	0.11	2800	7	-
2.36	0.093	2360	8	-
2	0.079	2000	10	-
1.7	0.0661	1700	12	10
1.4	0.0555	-	14	12
1.18	0.0469	-	16	14
1	0.0394	-	18	16
0.85	0.0331	850	20	20
0.71	0.0278	710	25	24
0.6	0.0232	600	30	28
0.5	0.0197	500	35	32
0.47	-	-	-	-
0.465	-	-	-	-
0.437	-	-	-	-
0.425	0.0165	425	40	35
0.389	-	-	-	-
0.368	-	-	-	-
0.355	0.0139	355	45	42
0.31	-	-	-	-
0.3	0.0117	300	50	48
0.282	-	-	-	-
0.27	-	-	-	-
0.26	-	-	-	-
0.25	0.0098	250	60	60
0.241	-	-	-	-
0.231	-	-	-	-
0.212	0.0083	212	70	65
0.193	-	-	-	-
0.18	0.007	180	80	80

0.165	-	-	-	-
0.15	0.0059	150	100	100
0.125	0.0049	125	120	115
0.105	0.0041	105	140	150
0.09	0.0035	90	170	170
0.074	0.0029	74	200	200
0.063	0.0024	63	230	250
0.053	0.0021	53	270	270
0.044	0.0017	44	325	325
0.037	0.0015	37	400	400
0.025	0.001	25	500	-

15.4 Appendix D: Flow Regime Diagrams.

15.4.1 D_p=0.0254 m (1 inch).
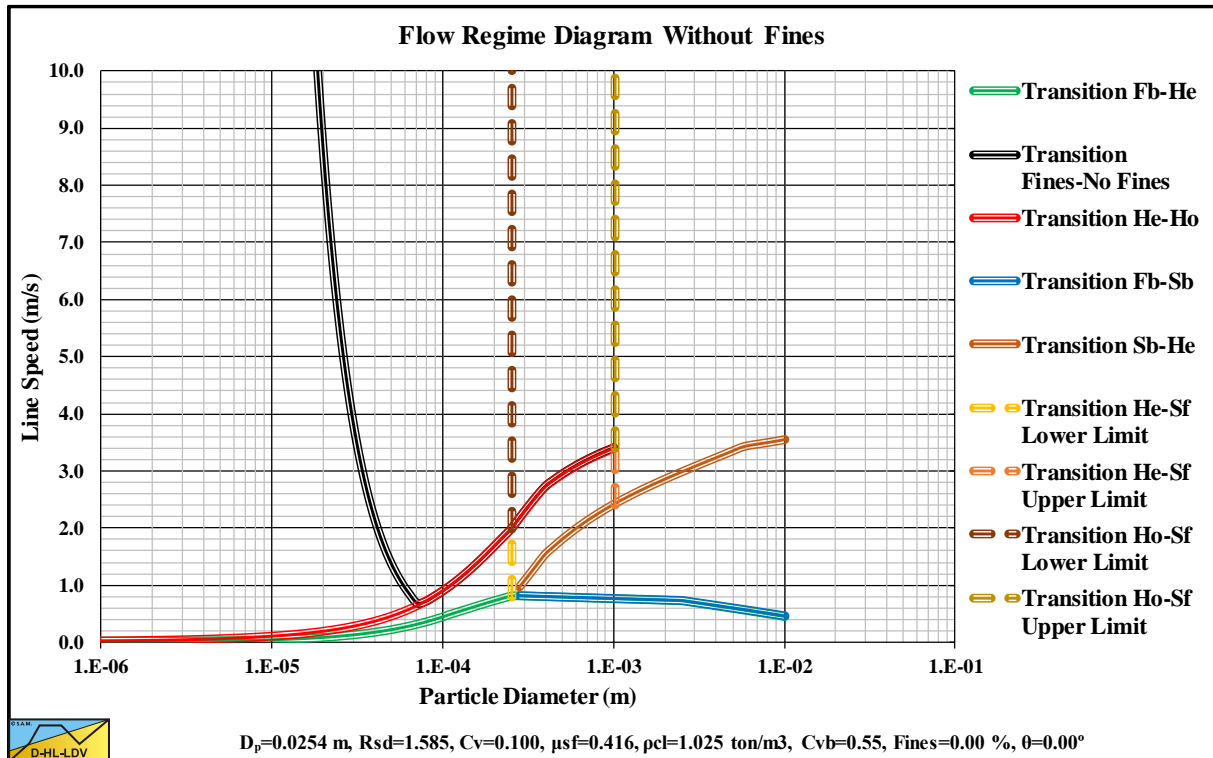
Figure 15.4-1: Flow regime diagram D_p=0.0254 m (1 inch) and C_{vs}=0.100.
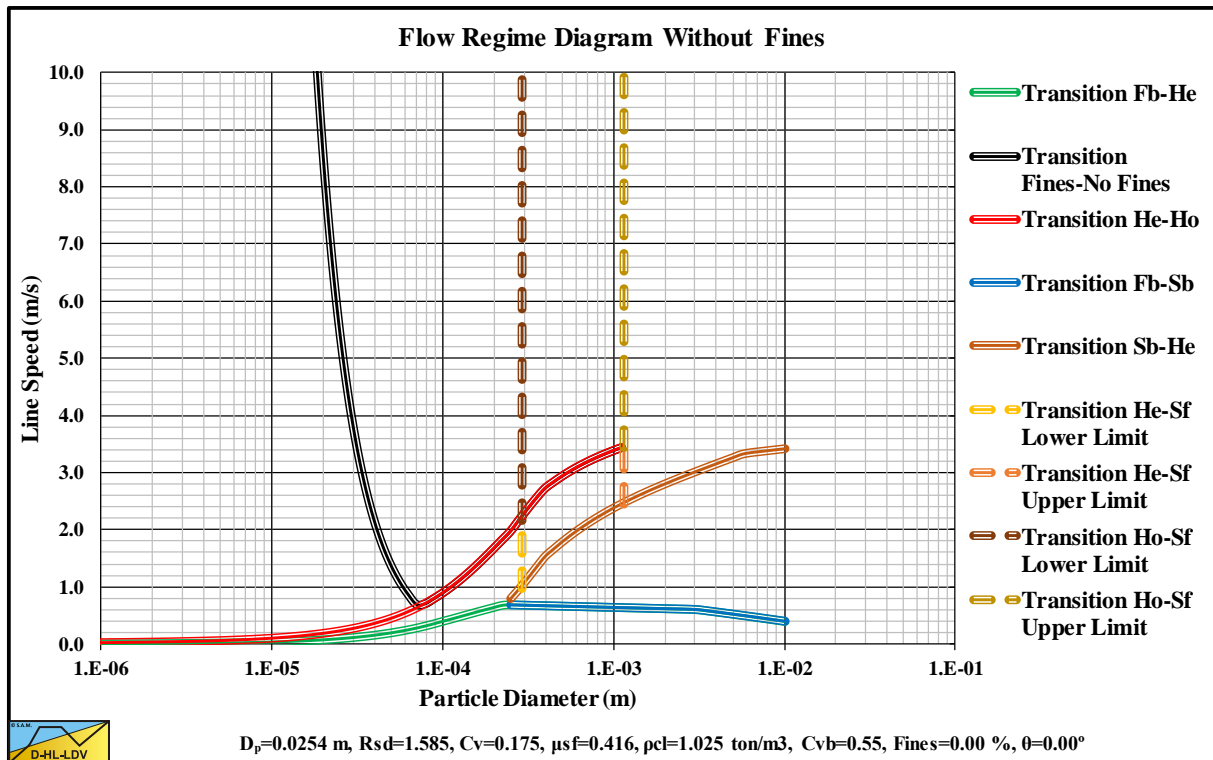
Figure 15.4-2: Flow regime diagram D_p=0.0254 m (1 inch) and C_{vs}=0.175.
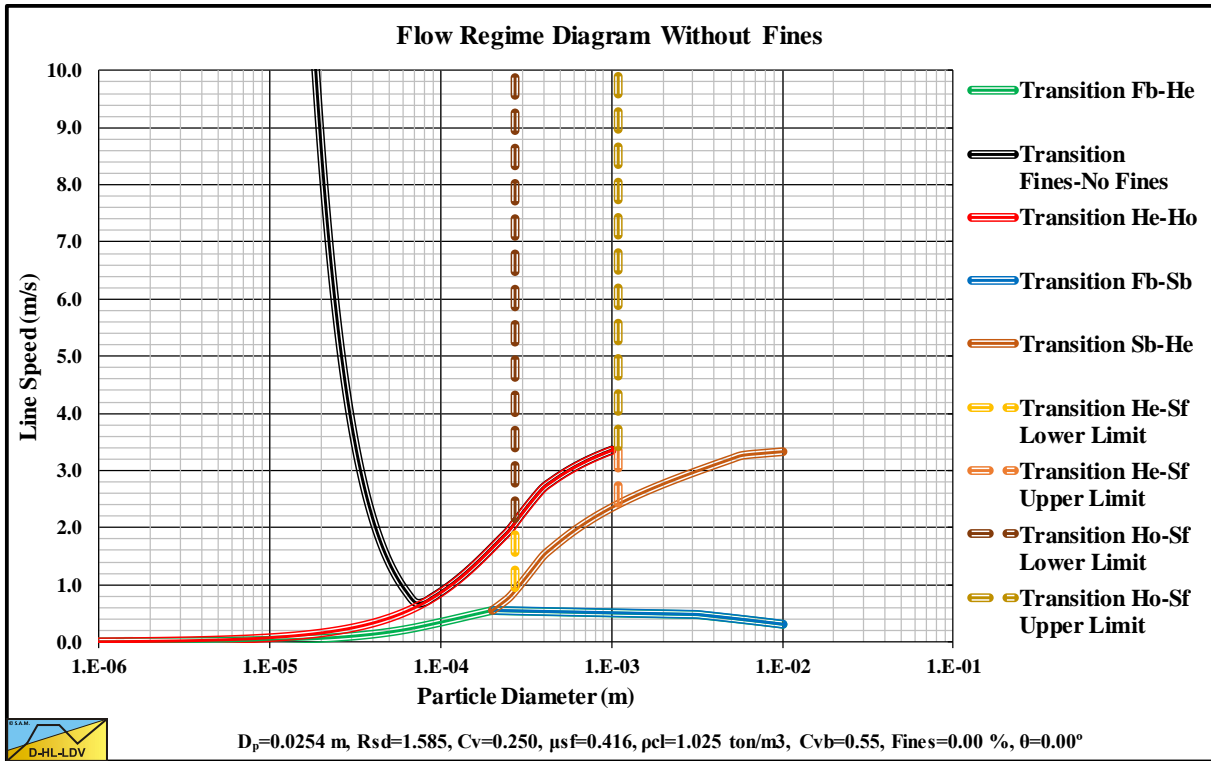
Figure 15.4-3: Flow regime diagram D_p=0.0254 m (1 inch) and C_vs=0.250.
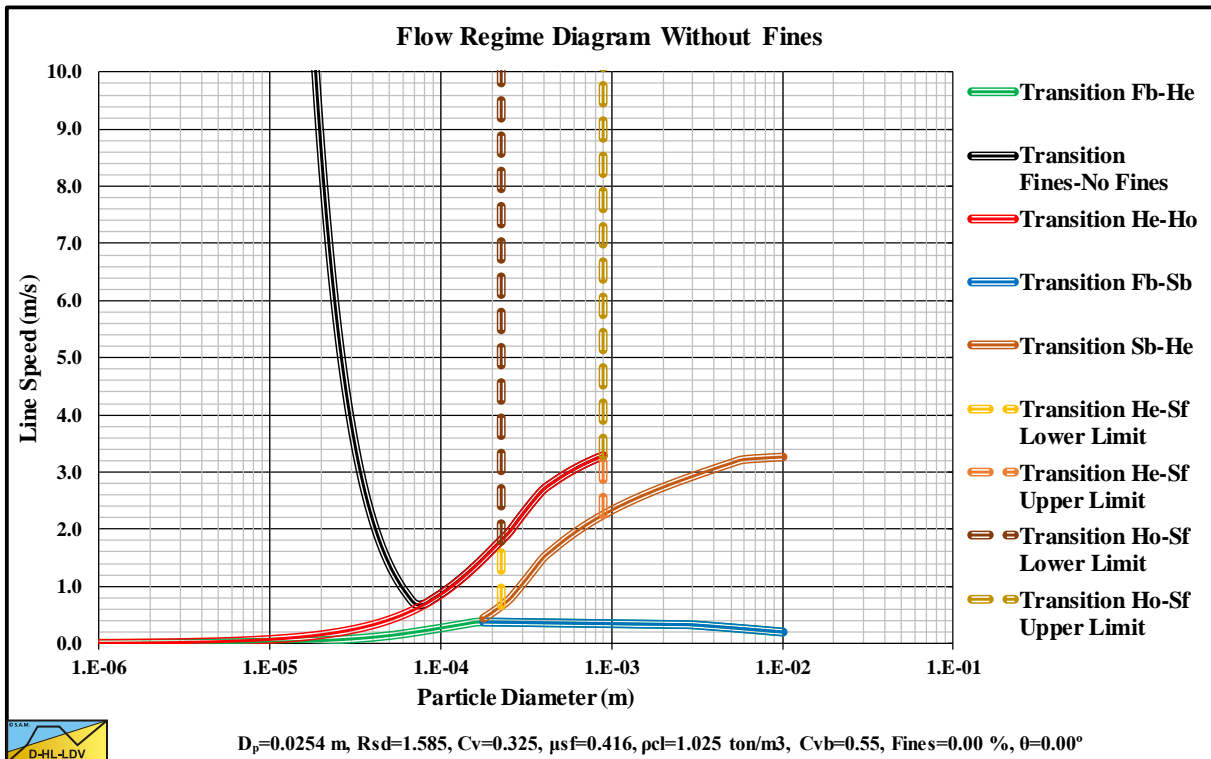
Figure 15.4-4: Flow regime diagram D_p=0.0254 m (1 inch) and C_vs=0.325.

Appendices.
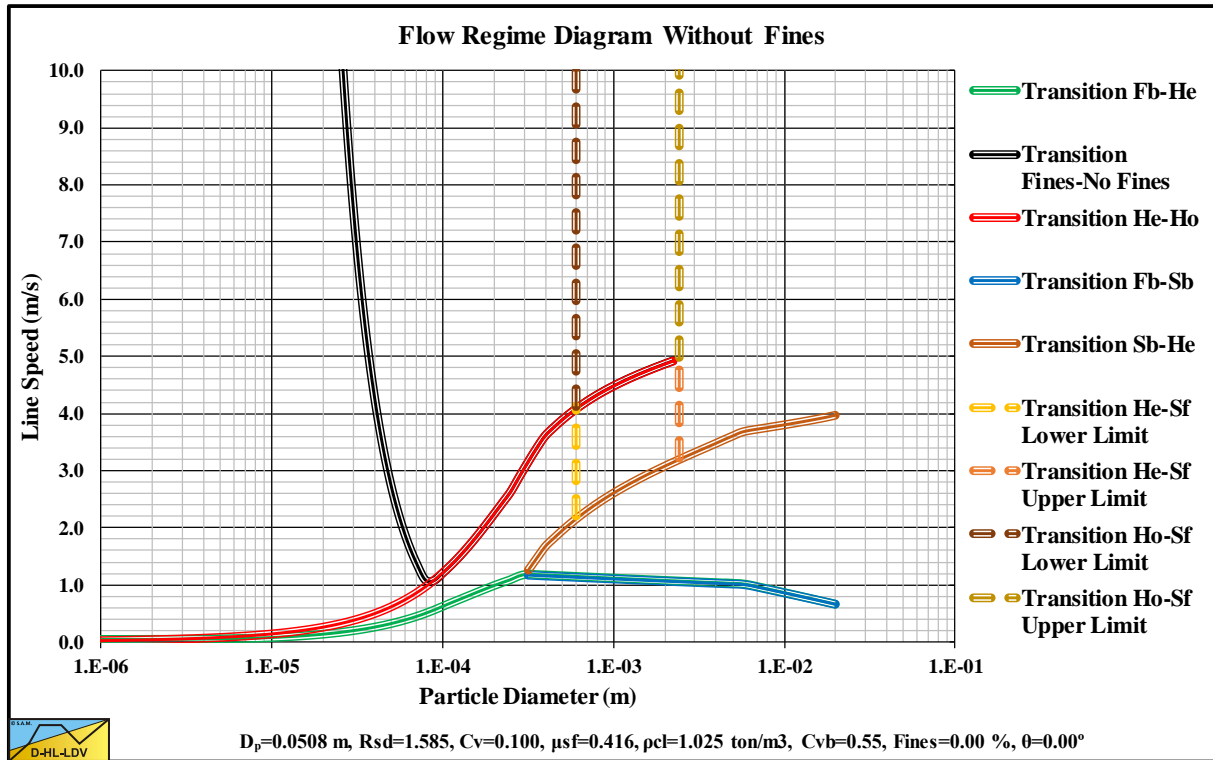
Figure 15.4-5: Flow regime diagram D_p=0.0508 m (2 inch) and C_{vs}=0.100.

D_p=0.0508 m, Rsd=1.585, Cv=0.100, μsf=0.416, ρcl=1.025 ton/m3, Cvb=0.55, Fines=0.00 %, θ=0.00°
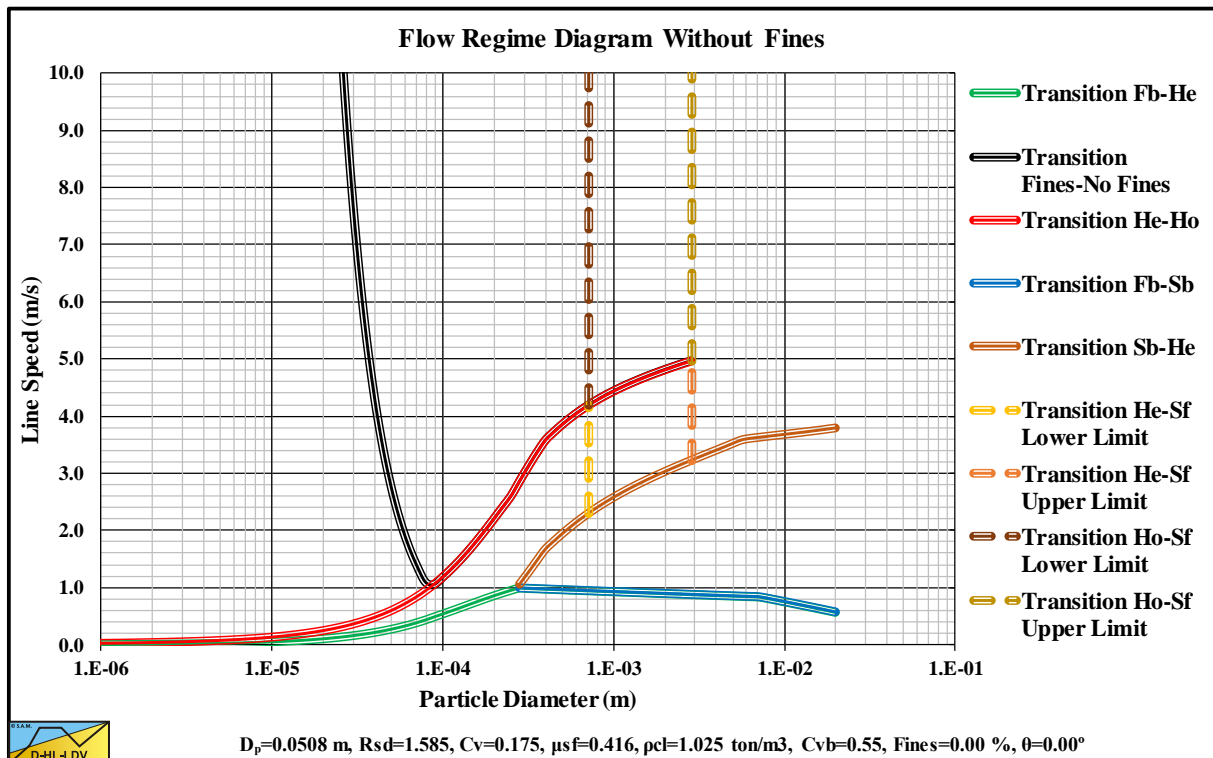
Figure 15.4-6: Flow regime diagram D_p=0.0508 m (2 inch) and C_{vs}=0.175.

D_p=0.0508 m, Rsd=1.585, Cv=0.175, μsf=0.416, ρcl=1.025 ton/m3, Cvb=0.55, Fines=0.00 %, θ=0.00°
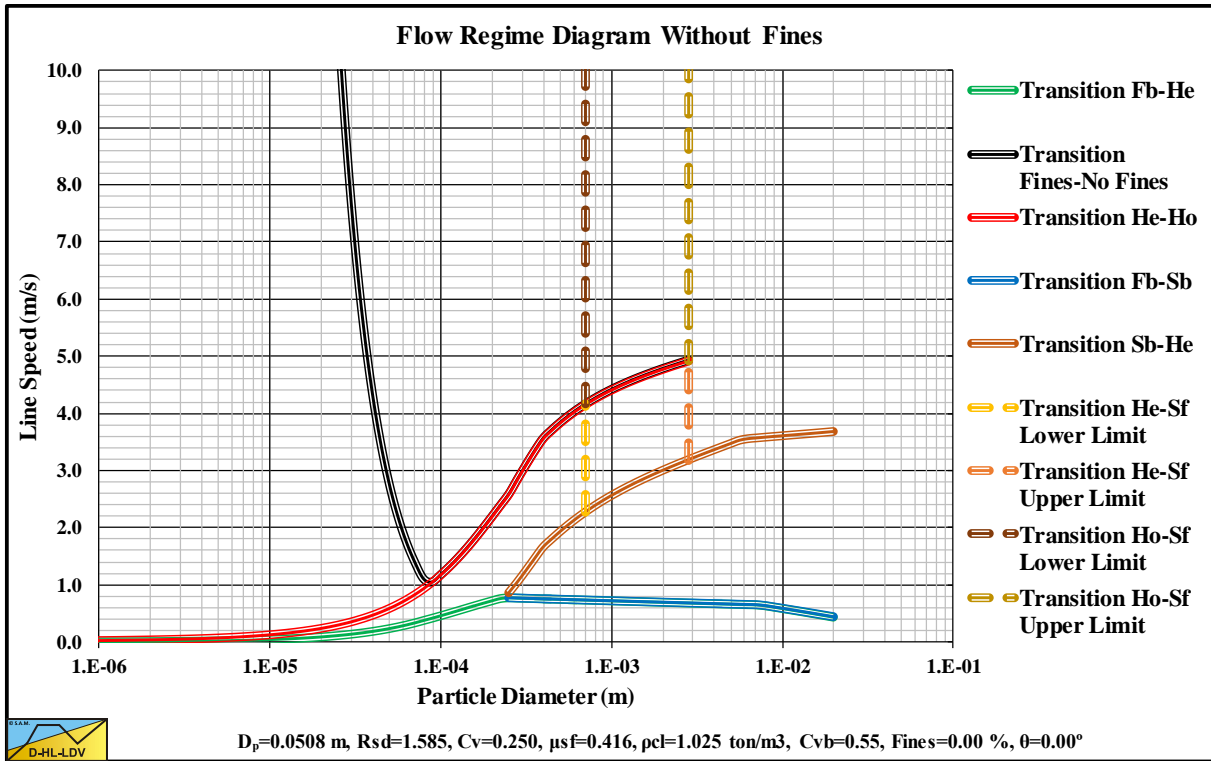
Figure 15.4-7: Flow regime diagram D_p=0.0508 m (2 inch) and C_{vs}=0.250.
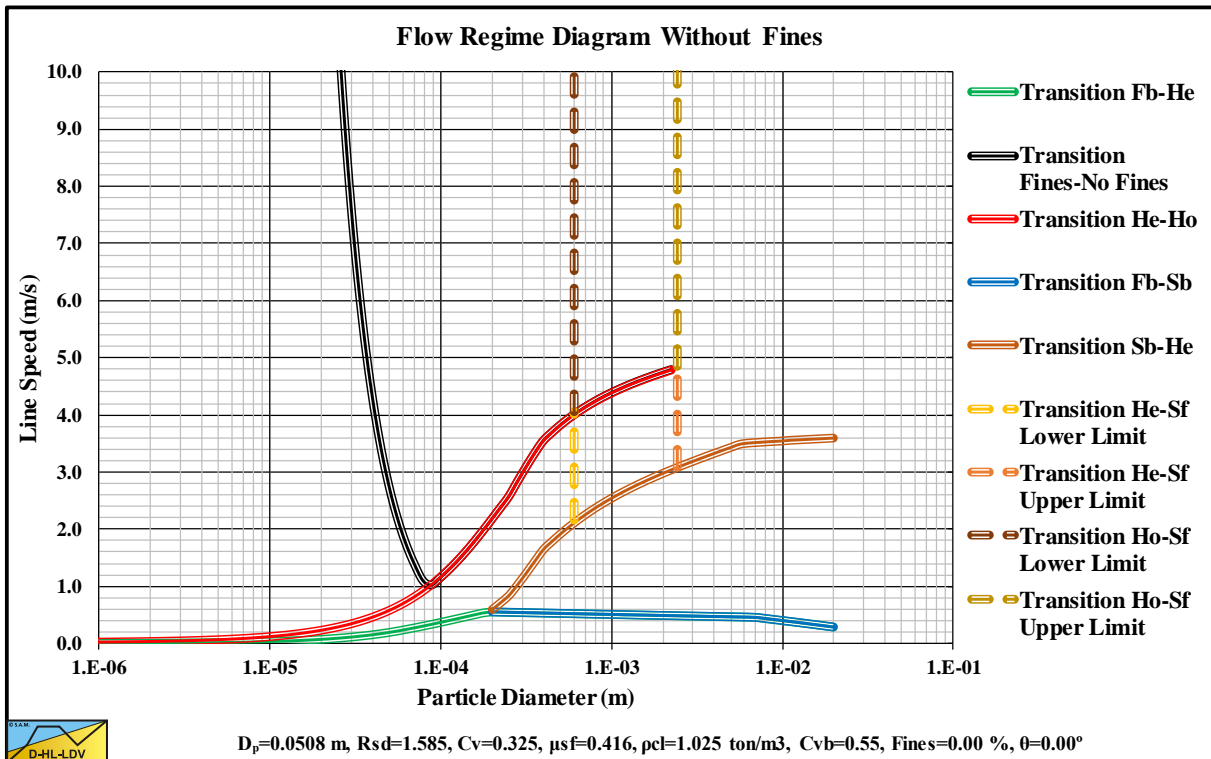
Figure 15.4-8: Flow regime diagram D_p=0.0508 m (2 inch) and C_{vs}=0.325.

15.4.3 D_p=0.1016 m (4 inch).
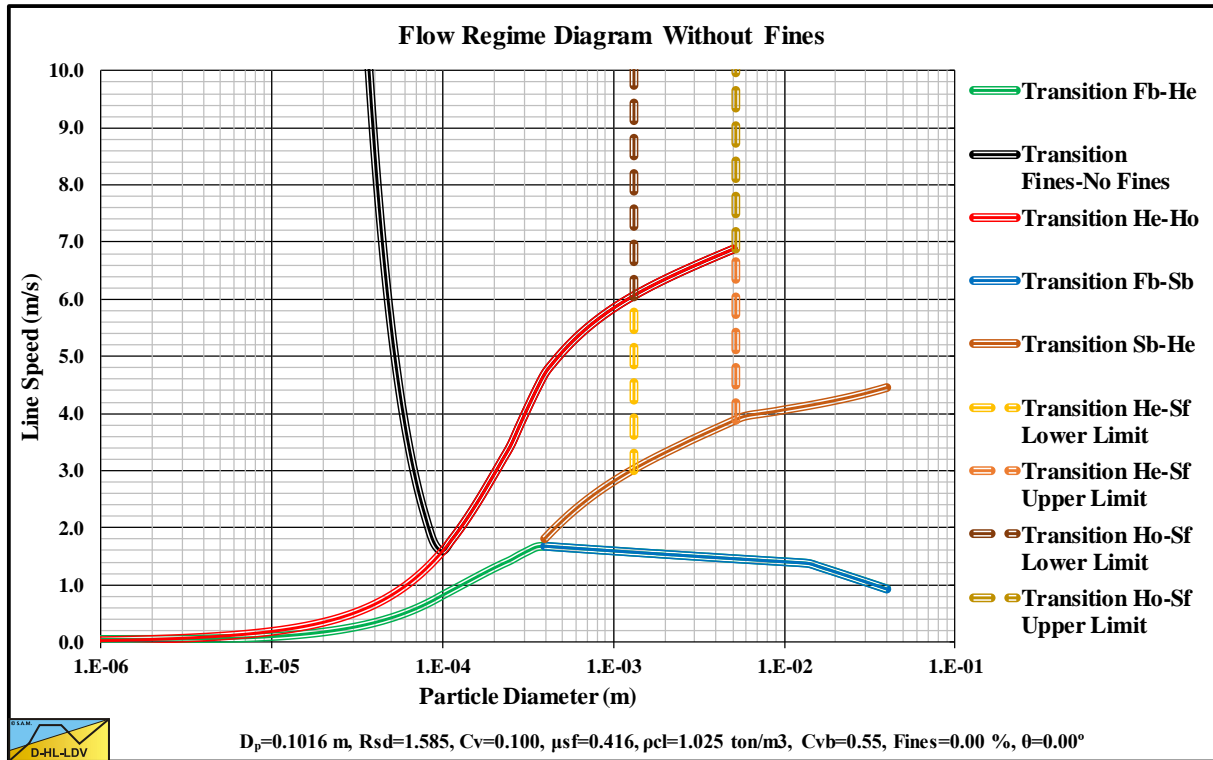
Figure 15.4-9: Flow regime diagram D_p=0.1016 m (4 inch) and C_{vs}=0.100.
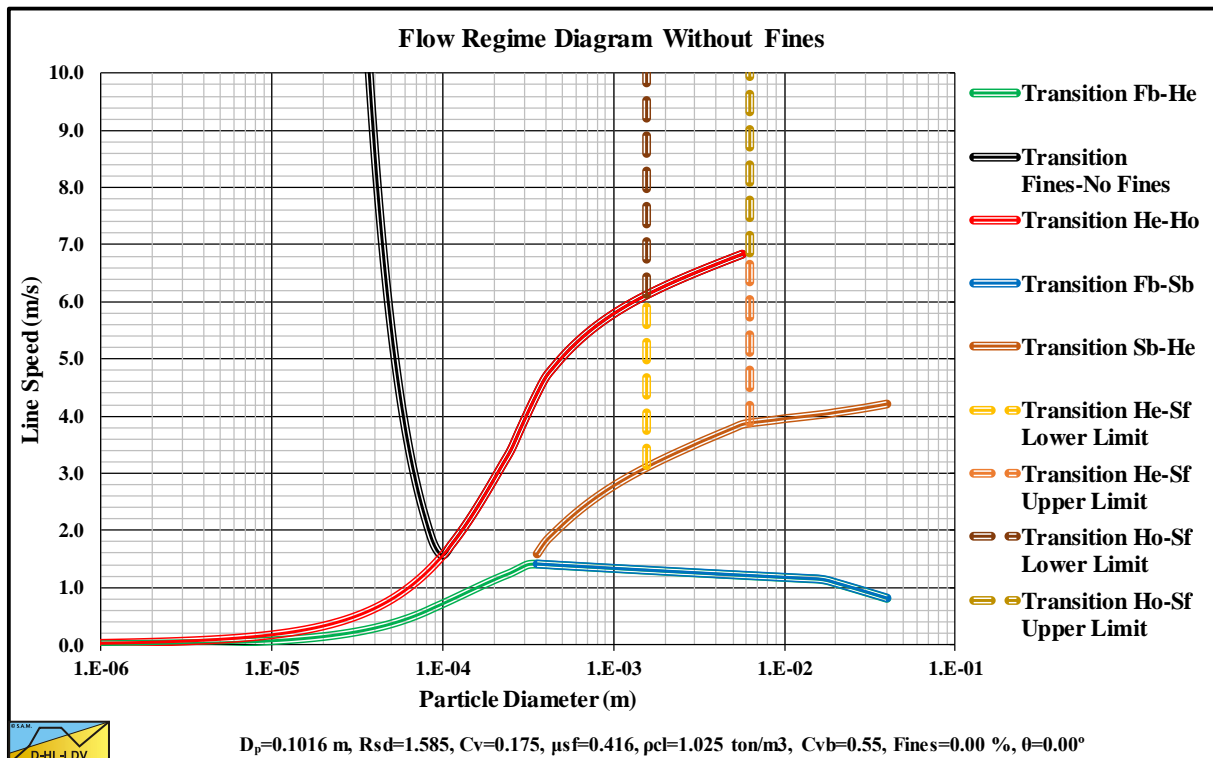
Figure 15.4-10: Flow regime diagram D_p=0.1016 m (4 inch) and C_{vs}=0.175.
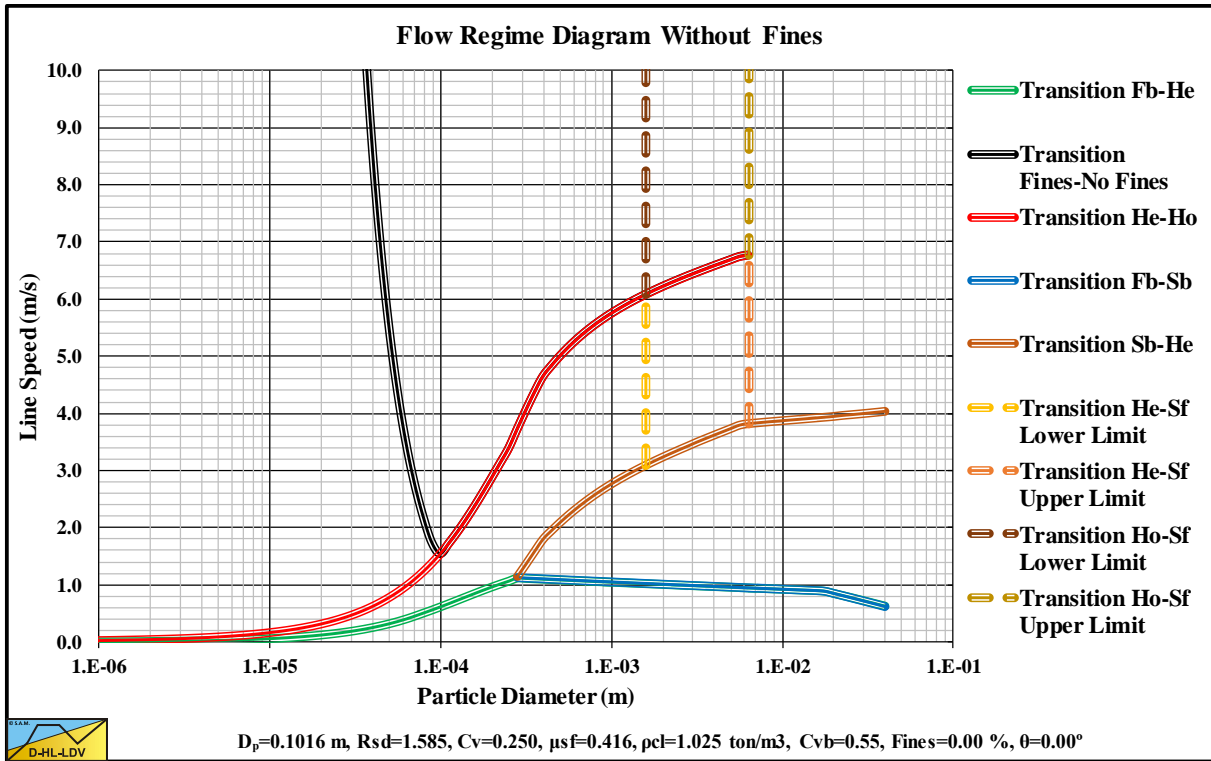
Figure 15.4-11: Flow regime diagram D$_p$=0.1016 m (4 inch) and C$_{vs}$=0.250.
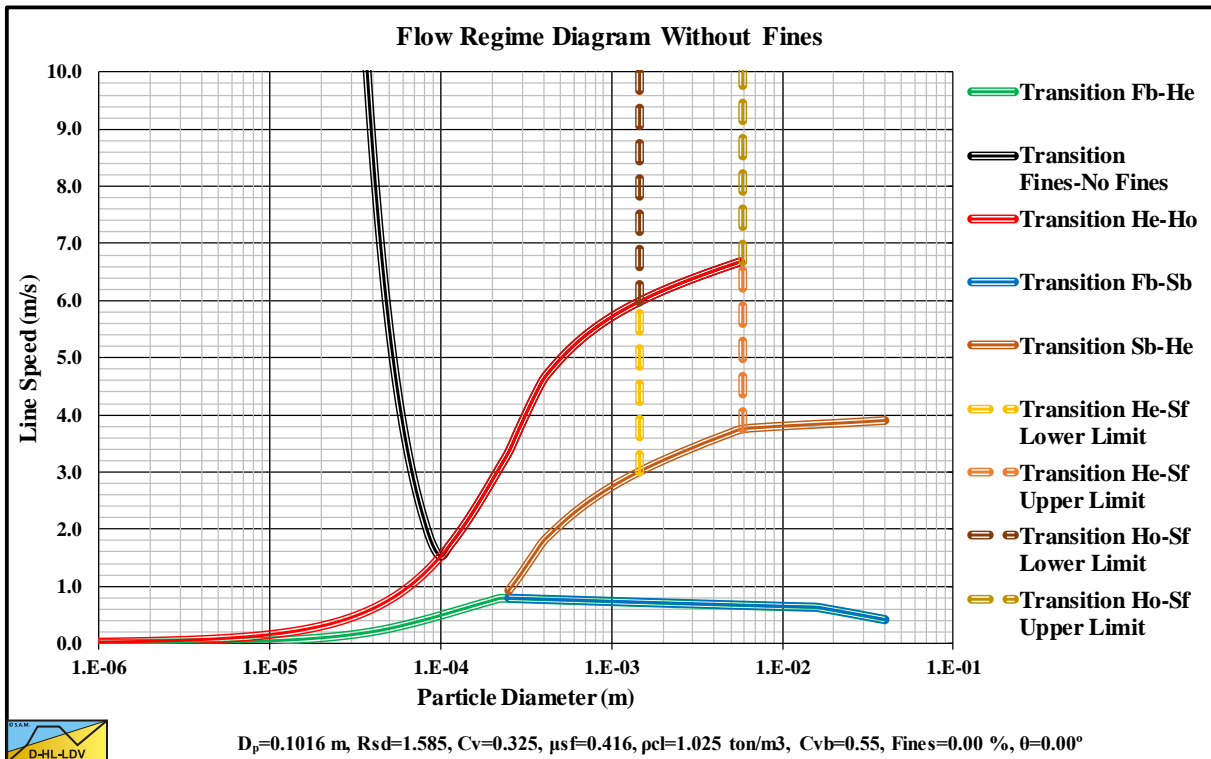
Figure 15.4-12: Flow regime diagram D$_p$=0.1016 m (4 inch) and C$_{vs}$=0.325.

15.4.4 D_p=0.1524 m (6 inch).
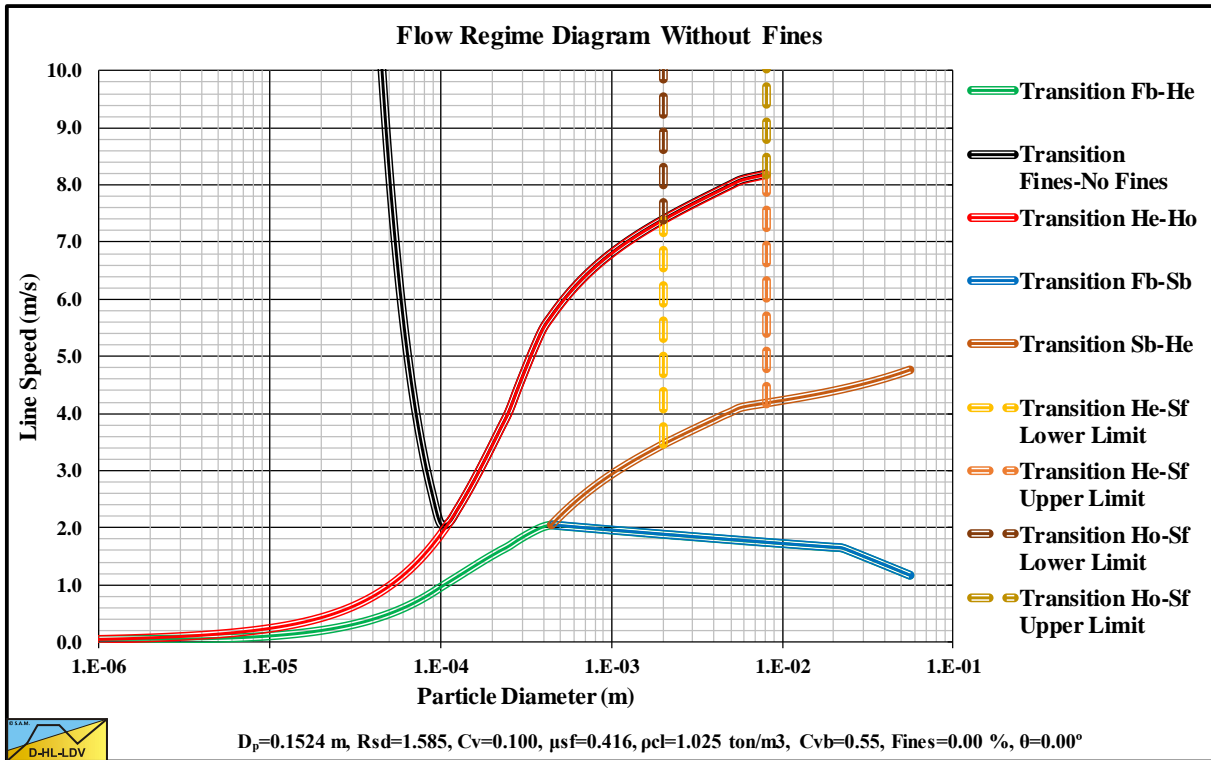
Figure 15.4-13: Flow regime diagram D_p=0.1524 m (6 inch) and C_{vs}=0.100.
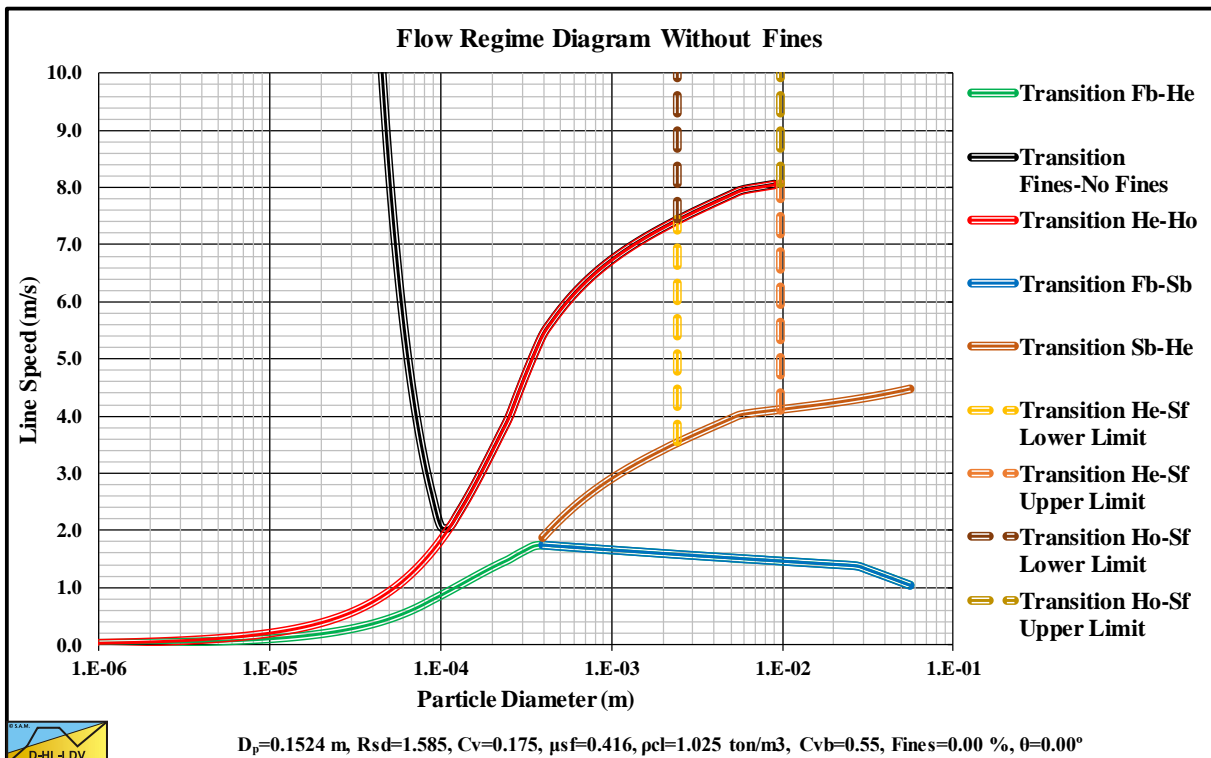
Figure 15.4-14: Flow regime diagram D_p=0.1524 m (6 inch) and C_{vs}=0.175.
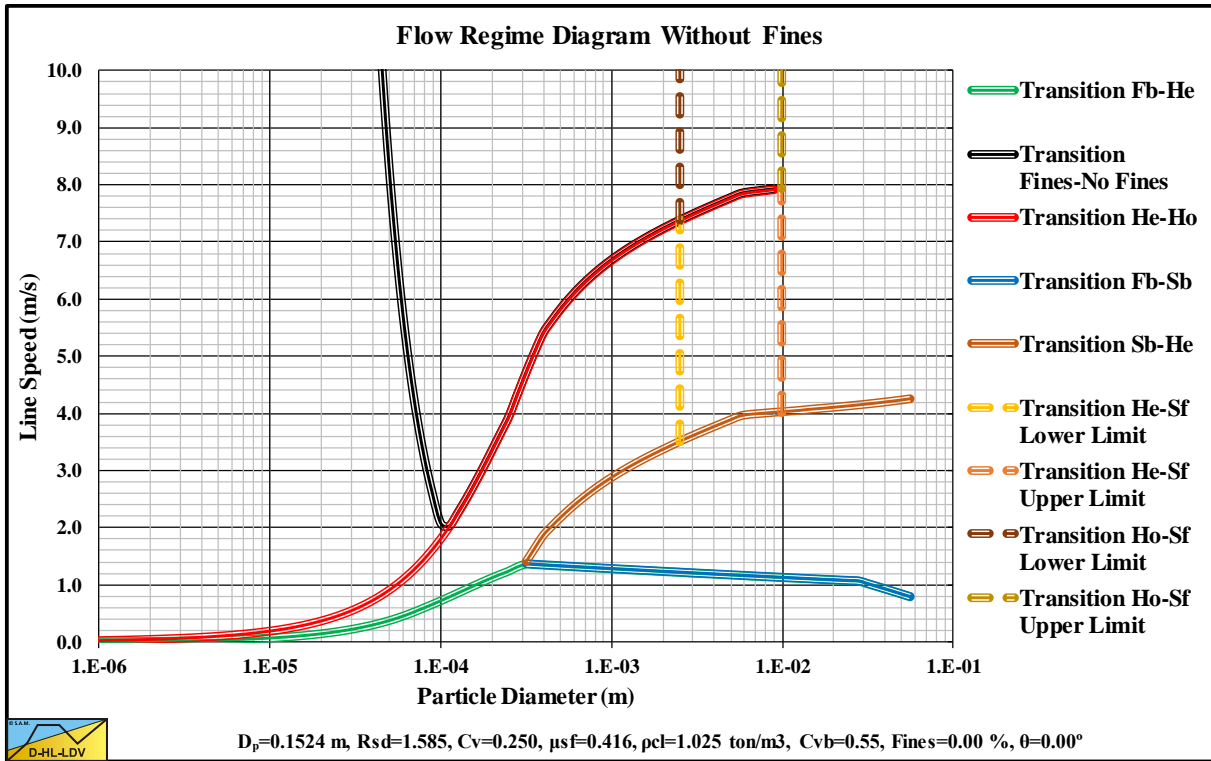
Figure 15.4-15: Flow regime diagram D_p=0.1524 m (6 inch) and C_{vs}=0.250.
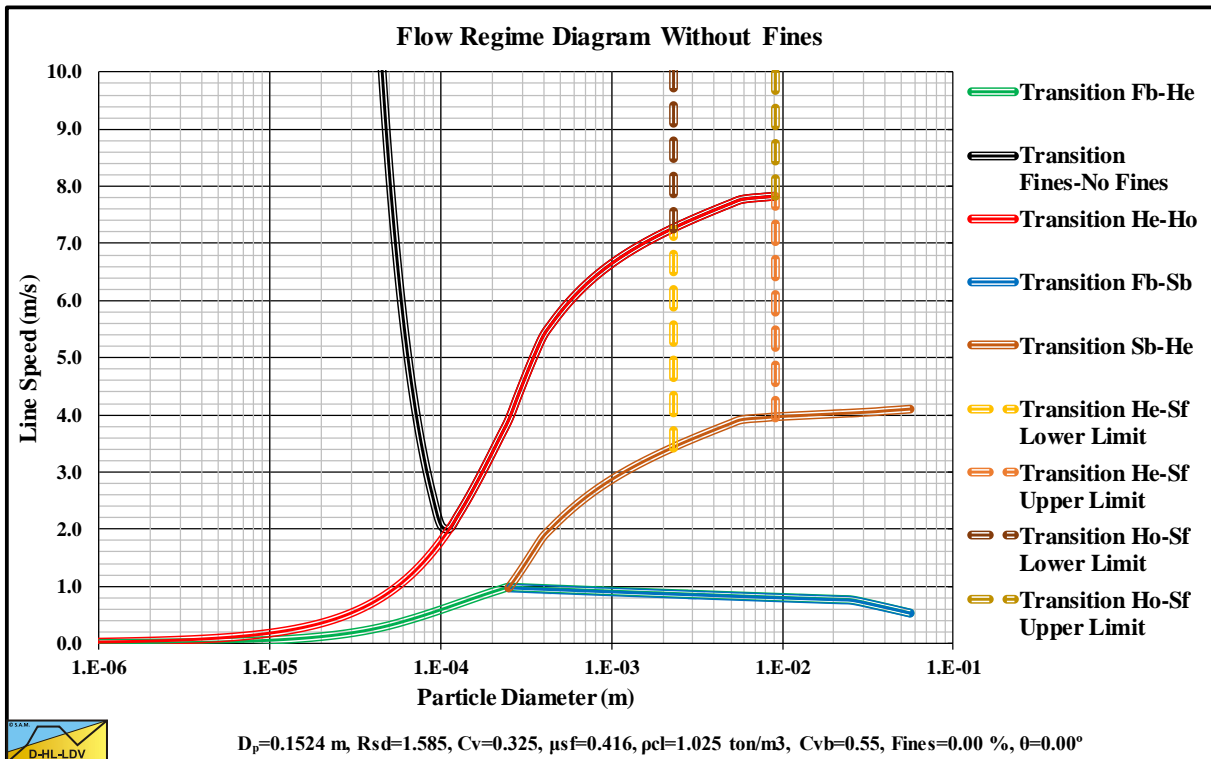
Figure 15.4-16: Flow regime diagram D_p=0.1524 m (6 inch) and C_{vs}=0.325.

15.4.5 D$_p$=0.2032 m (8 inch).
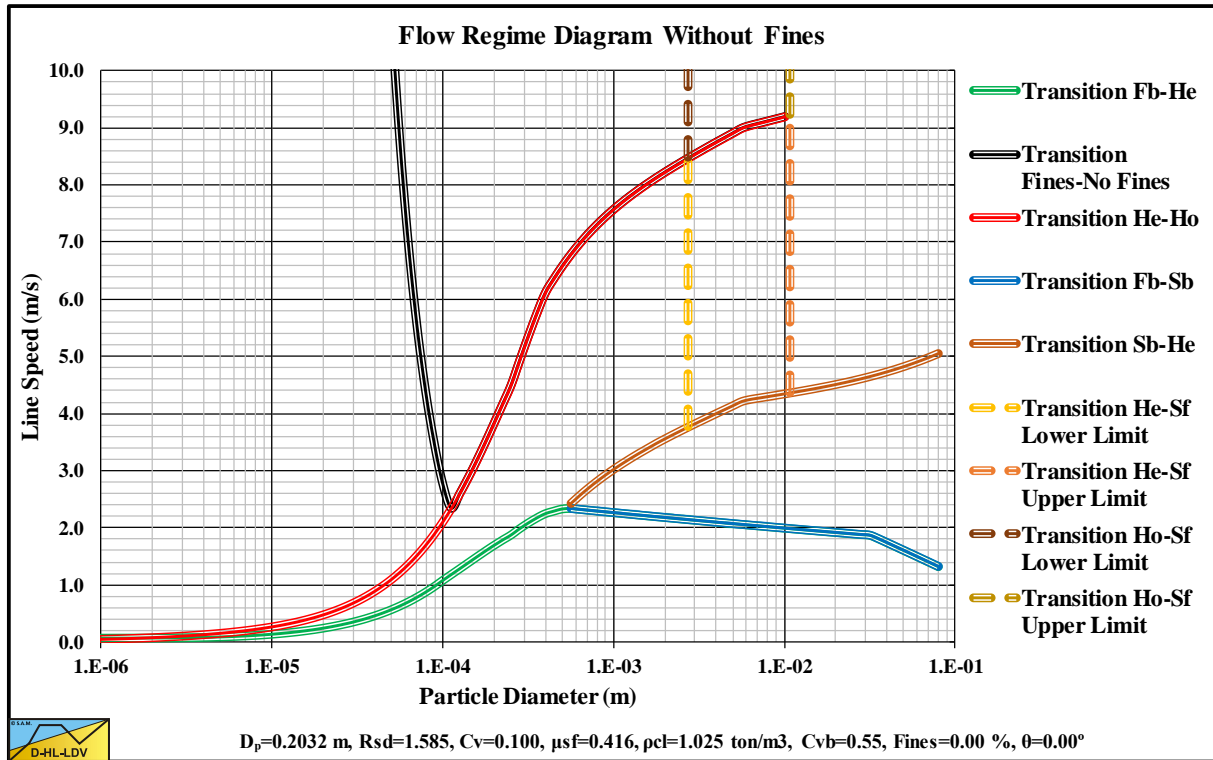
Figure 15.4-17: Flow regime diagram D$_p$=0.2032 m (8 inch) and C$_{vs}$=0.100.
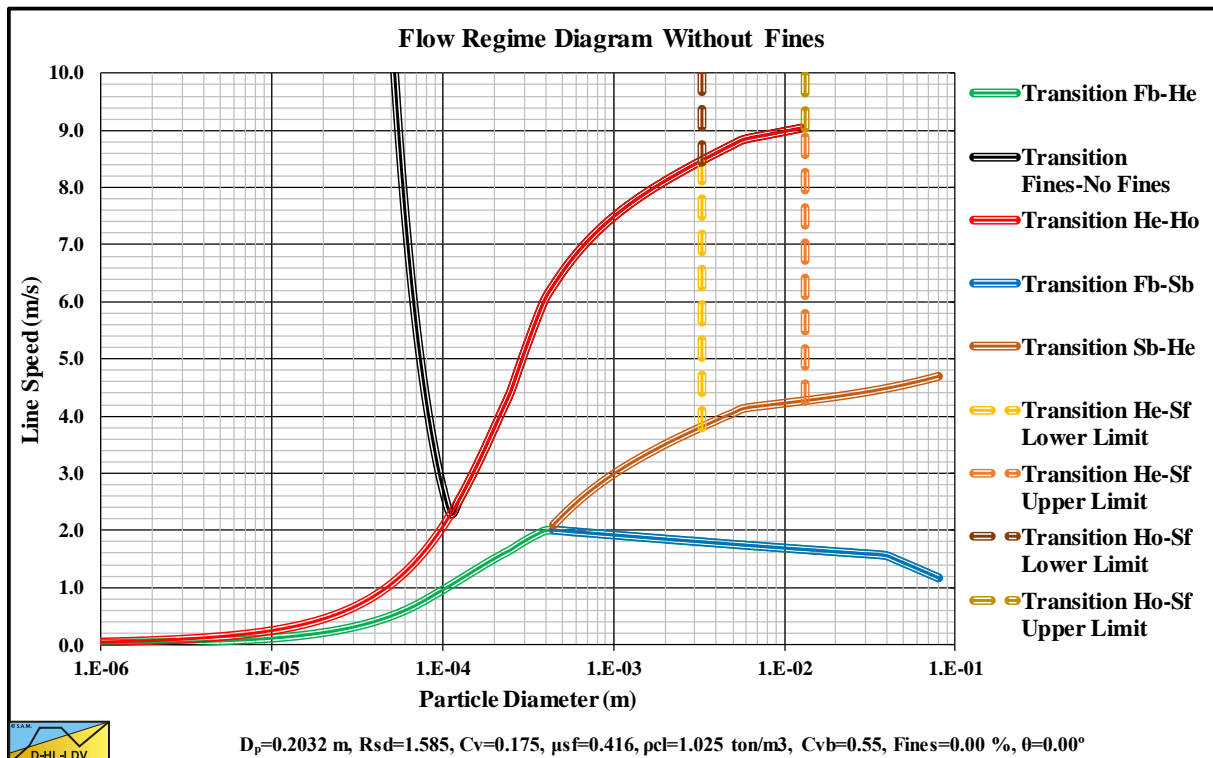
Figure 15.4-18: Flow regime diagram D$_p$=0.2032 m (8 inch) and C$_{vs}$=0.175.
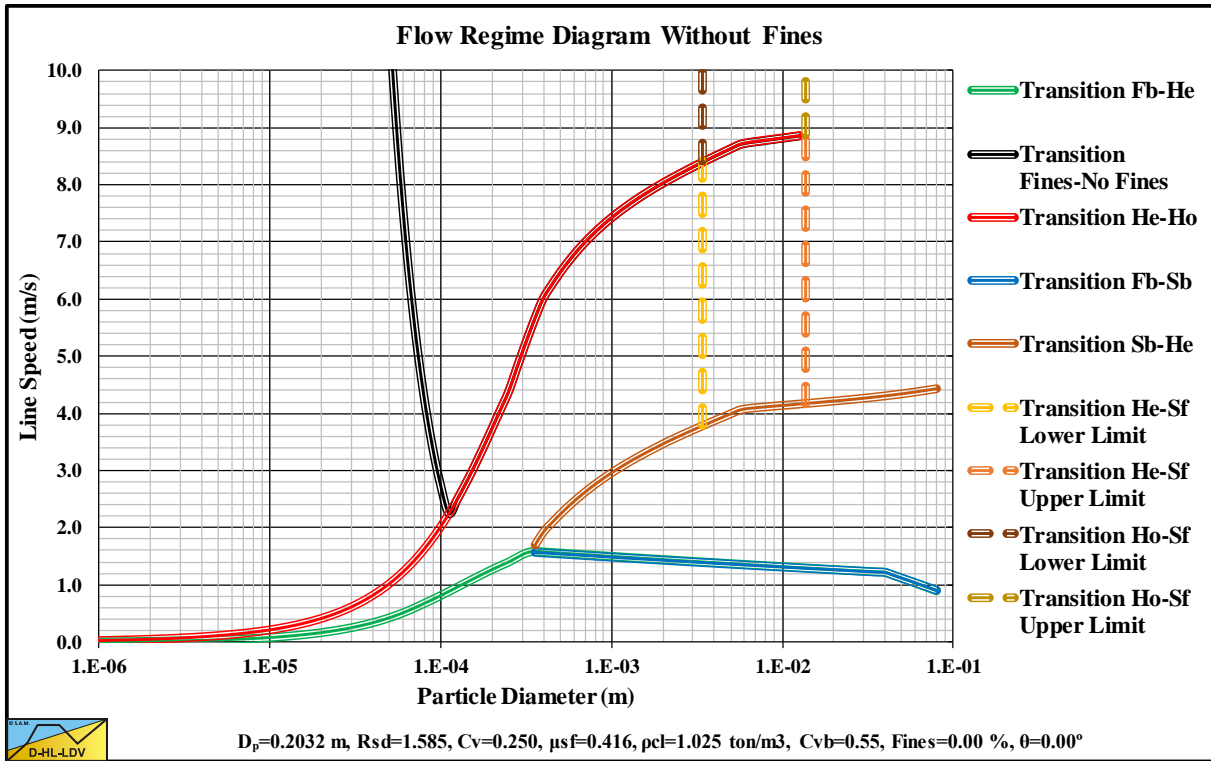
Figure 15.4-19: Flow regime diagram D$_p$=0.2032 m (8 inch) and C$_{vs}$=0.250.
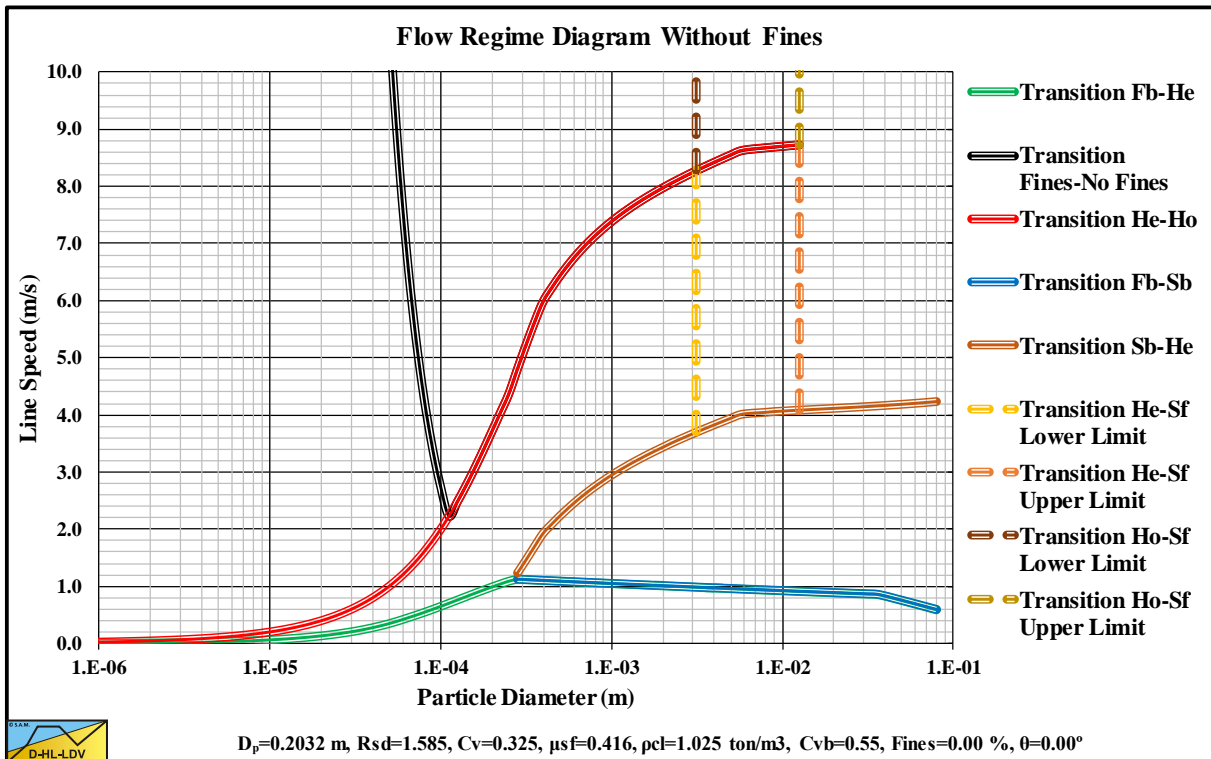
Figure 15.4-20: Flow regime diagram D$_p$=0.2032 m (8 inch) and C$_{vs}$=0.325.

15.4.6 D_p=0.2540 m (10 inch).
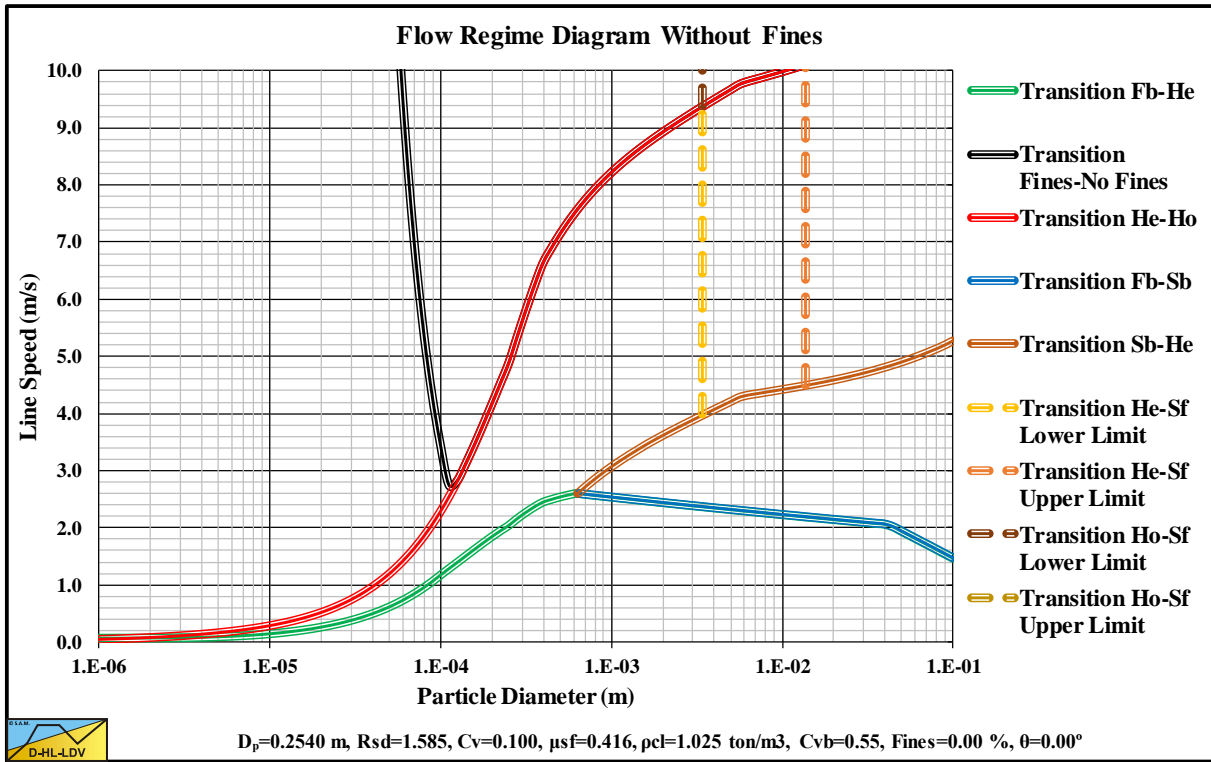
Figure 15.4-21: Flow regime diagram D_p=0.2540 m (10 inch) and C_vs=0.100.
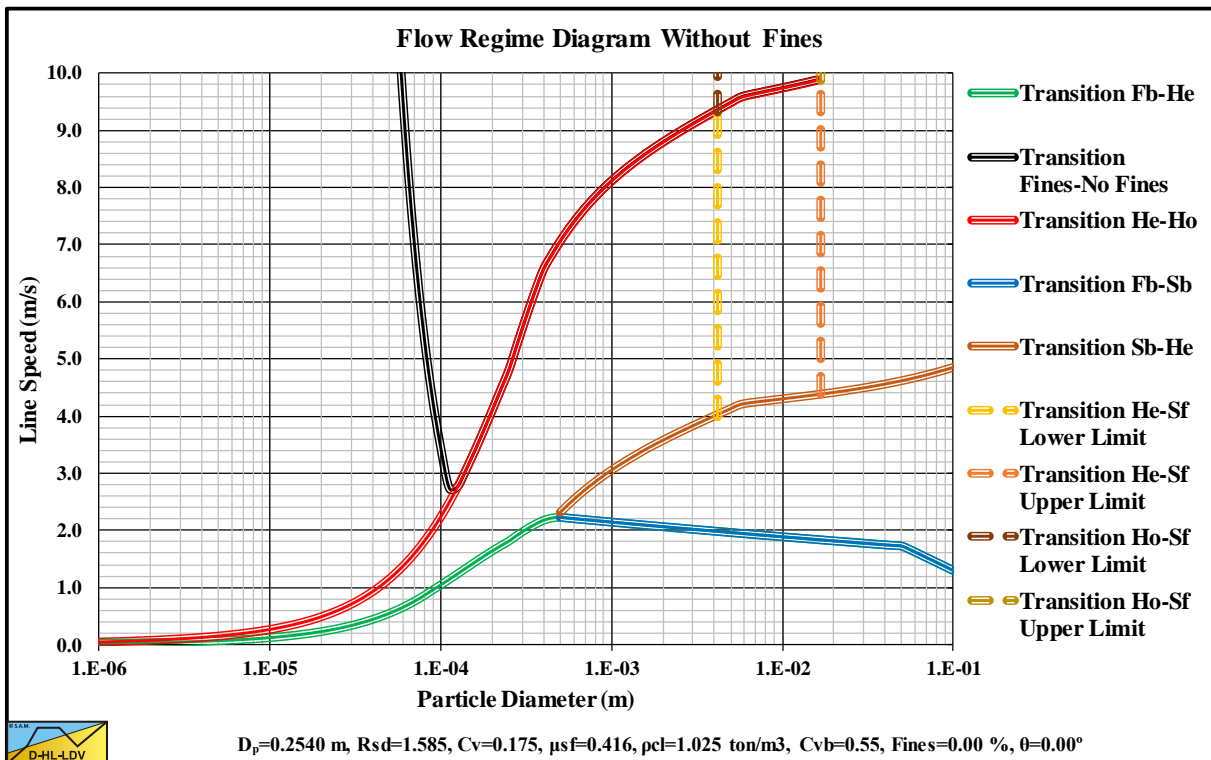
Figure 15.4-22: Flow regime diagram D_p=0.2540 m (10 inch) and C_vs=0.175.
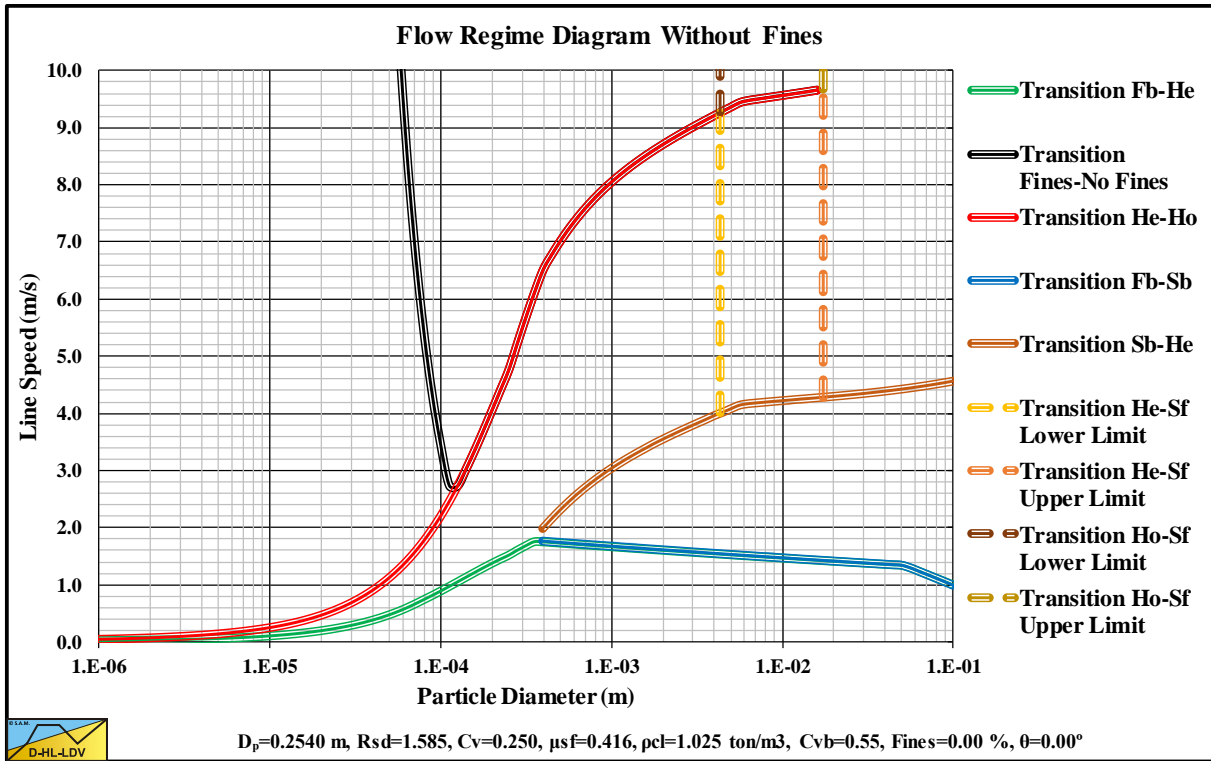
Figure 15.4-23: Flow regime diagram D_p=0.2540 m (10 inch) and C_{vs}=0.250.
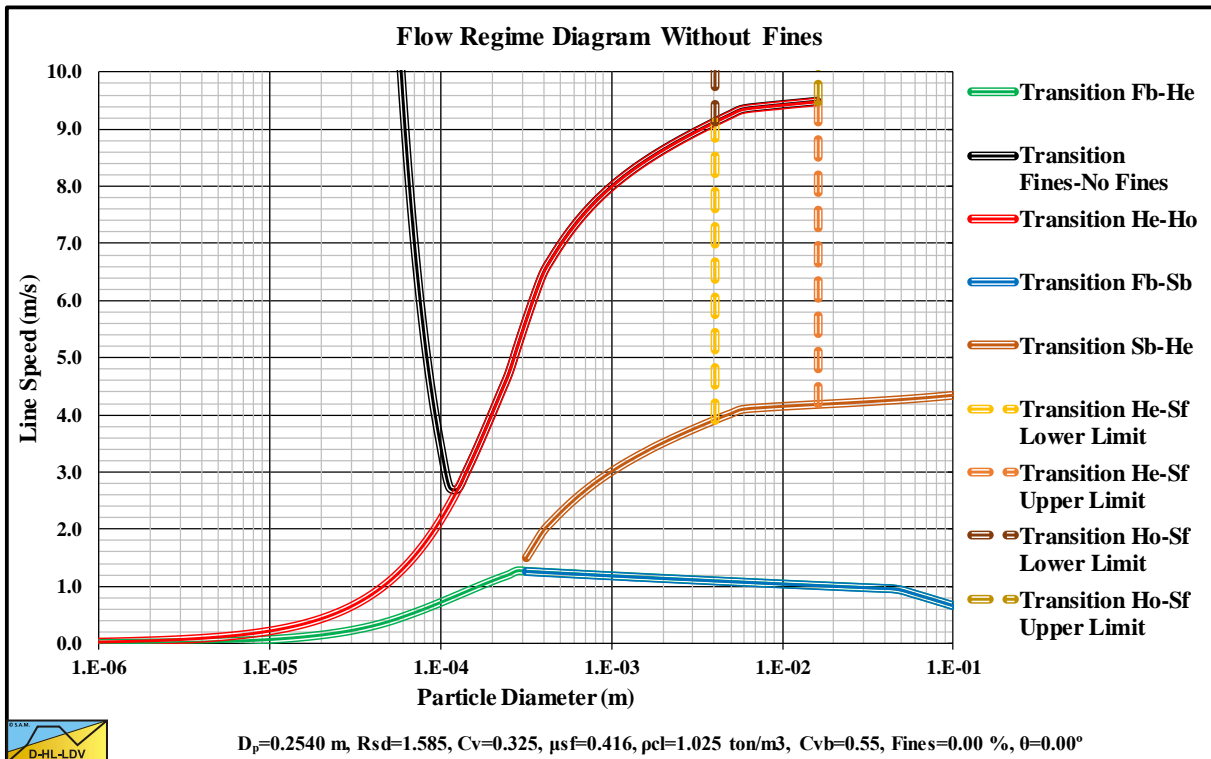
Figure 15.4-24: Flow regime diagram D_p=0.2540 m (10 inch) and C_{vs}=0.325.

15.4.7 D$_p$=0.3048 m (12 inch).
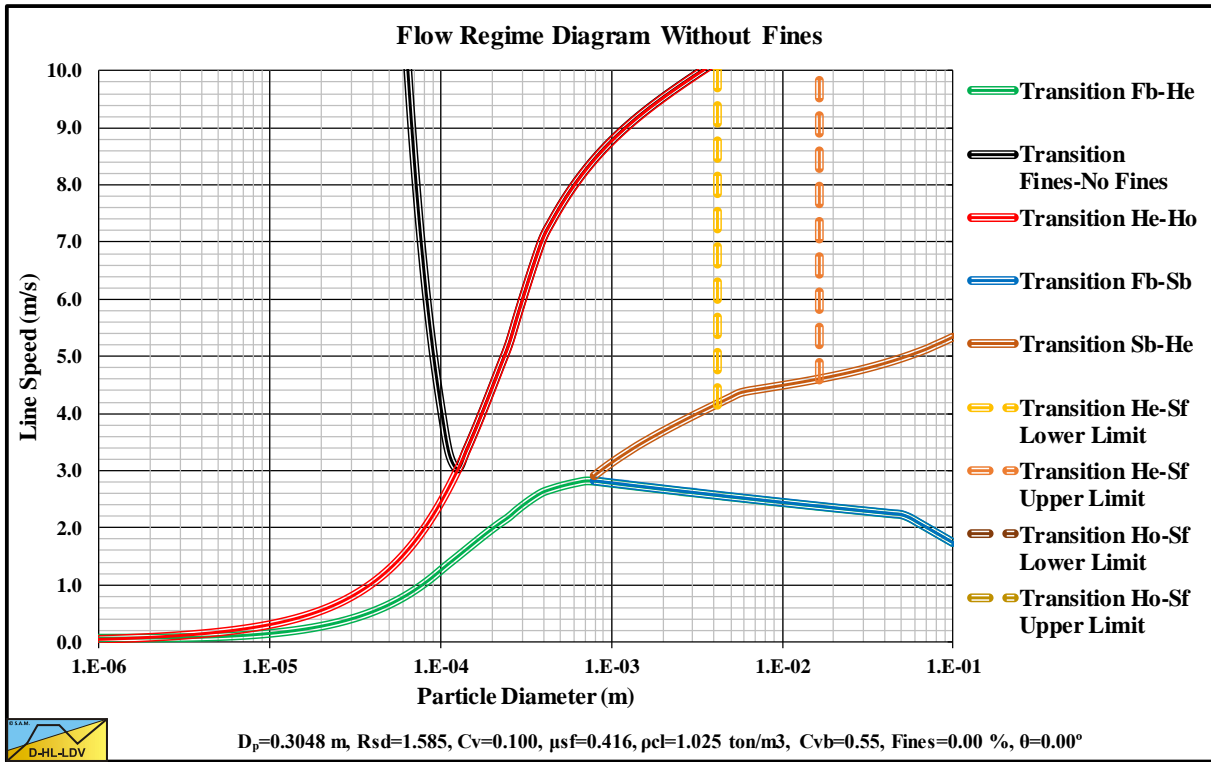
Figure 15.4-25: Flow regime diagram D$_p$=0.3048 m (12 inch) and C$_{vs}$=0.100.
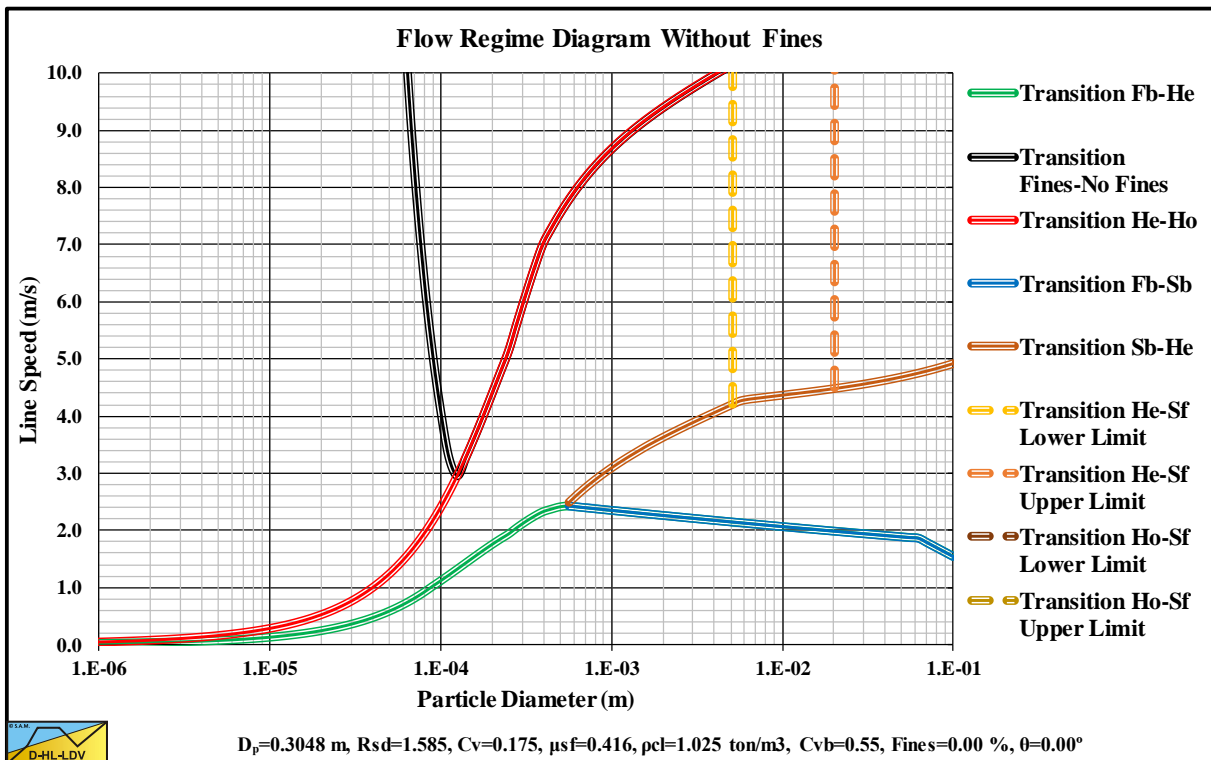
Figure 15.4-26: Flow regime diagram D$_p$=0.3048 m (12 inch) and C$_{vs}$=0.175.
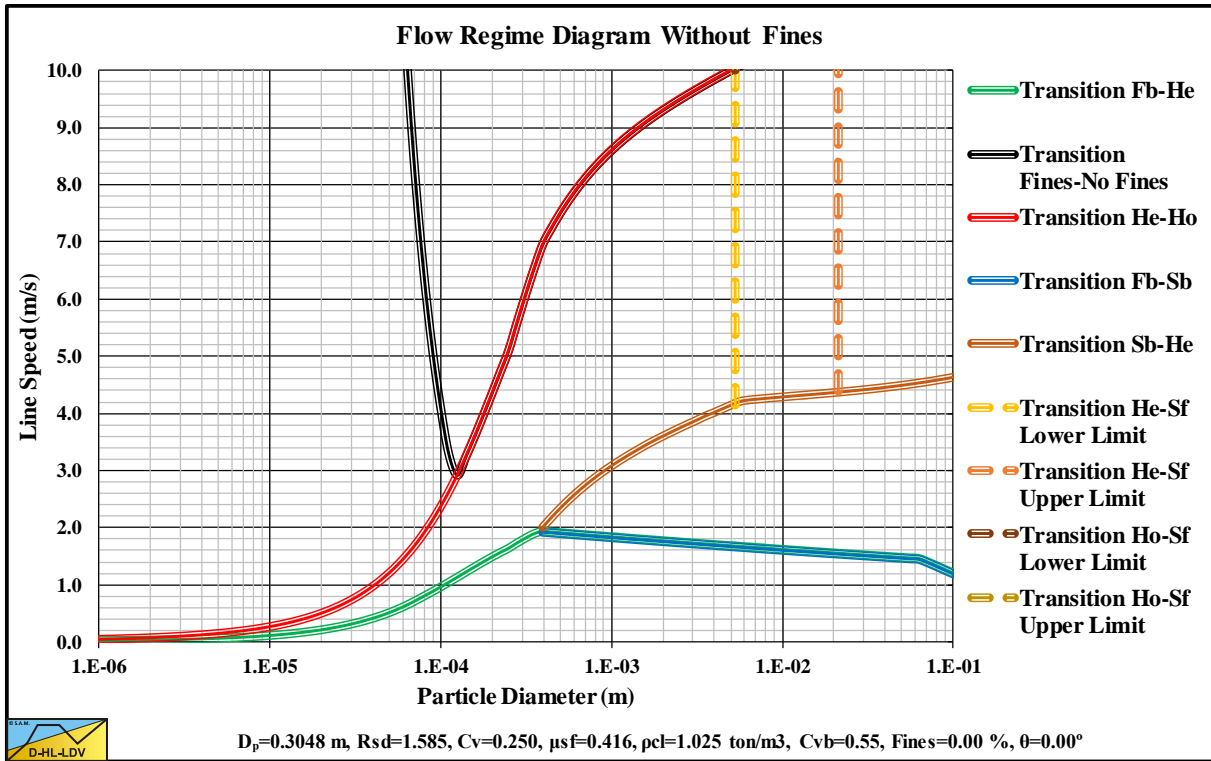
Figure 15.4-27: Flow regime diagram D_P=0.3048 m (12 inch) and C_{vs}=0.250.
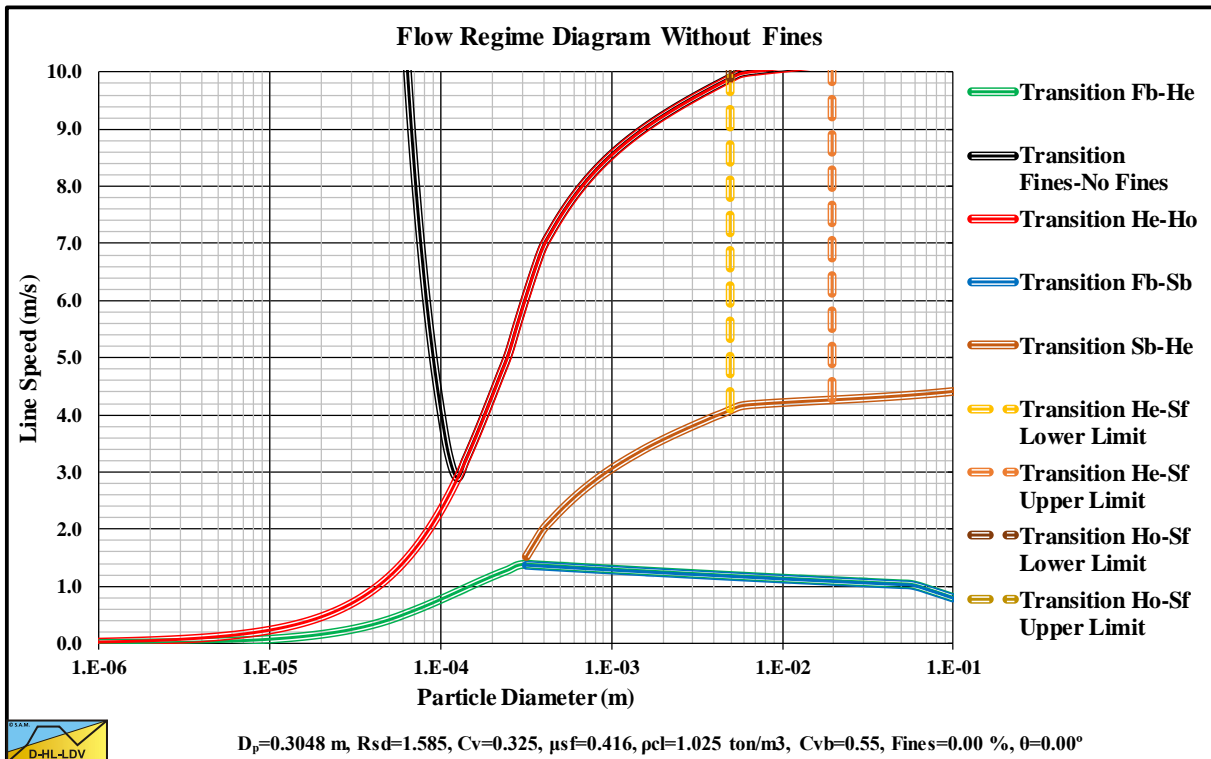
Figure 15.4-28: Flow regime diagram D_P=0.3048 m (12 inch) and C_{vs}=0.325.

15.4.8 D_p=0.4064 m (16 inch).
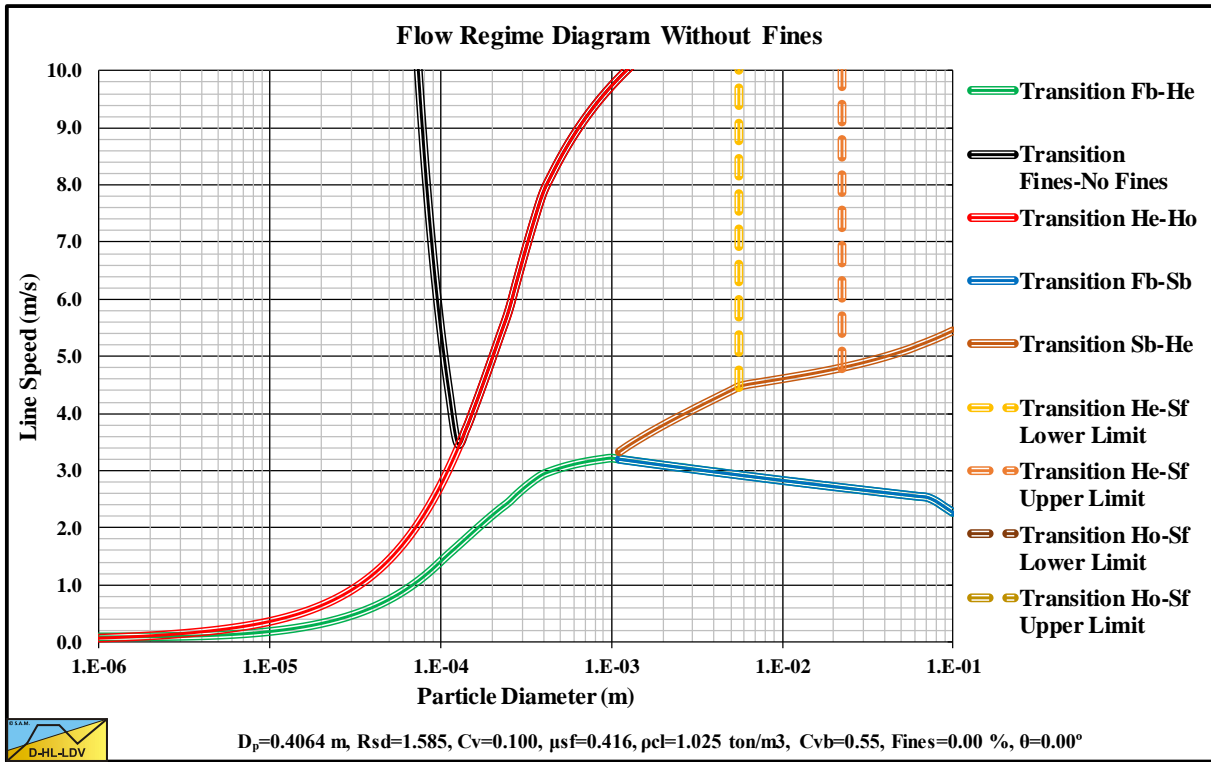
Figure 15.4-29: Flow regime diagram D_p=0.4064 m (16 inch) and C_{vs}=0.100.
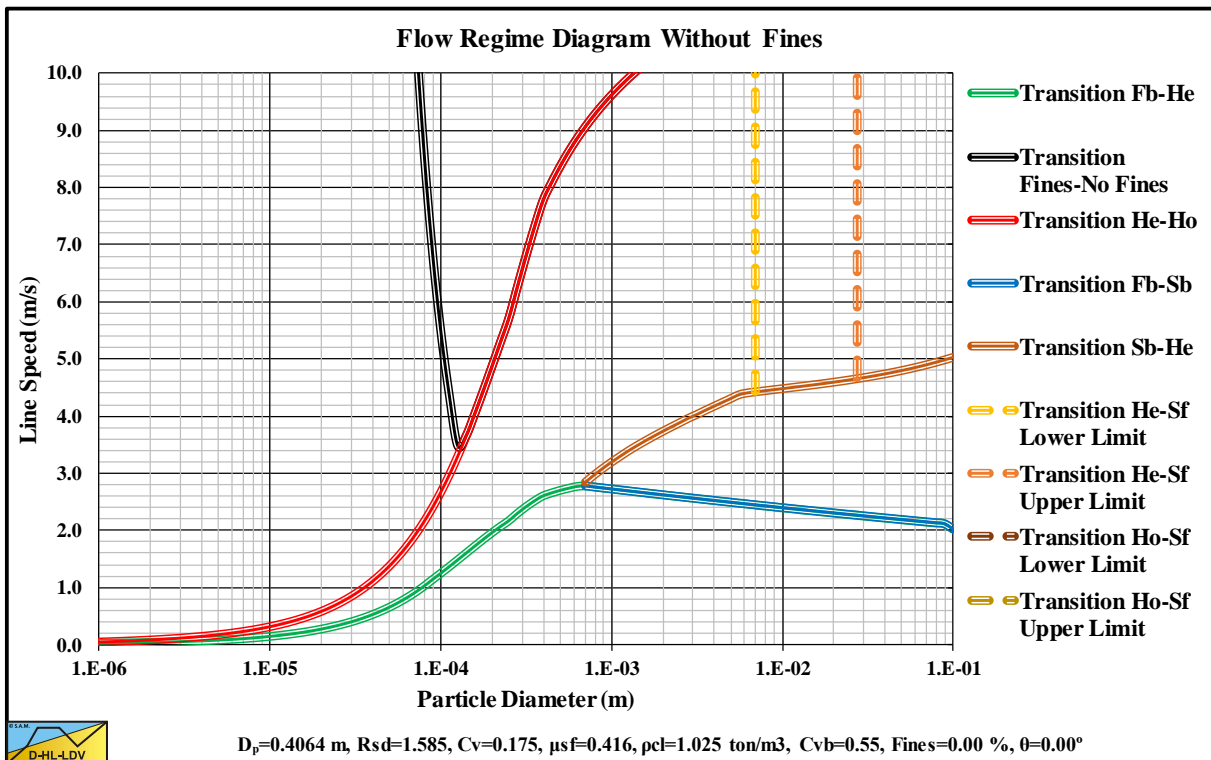
Figure 15.4-30: Flow regime diagram D_p=0.4064 m (16 inch) and C_{vs}=0.175.
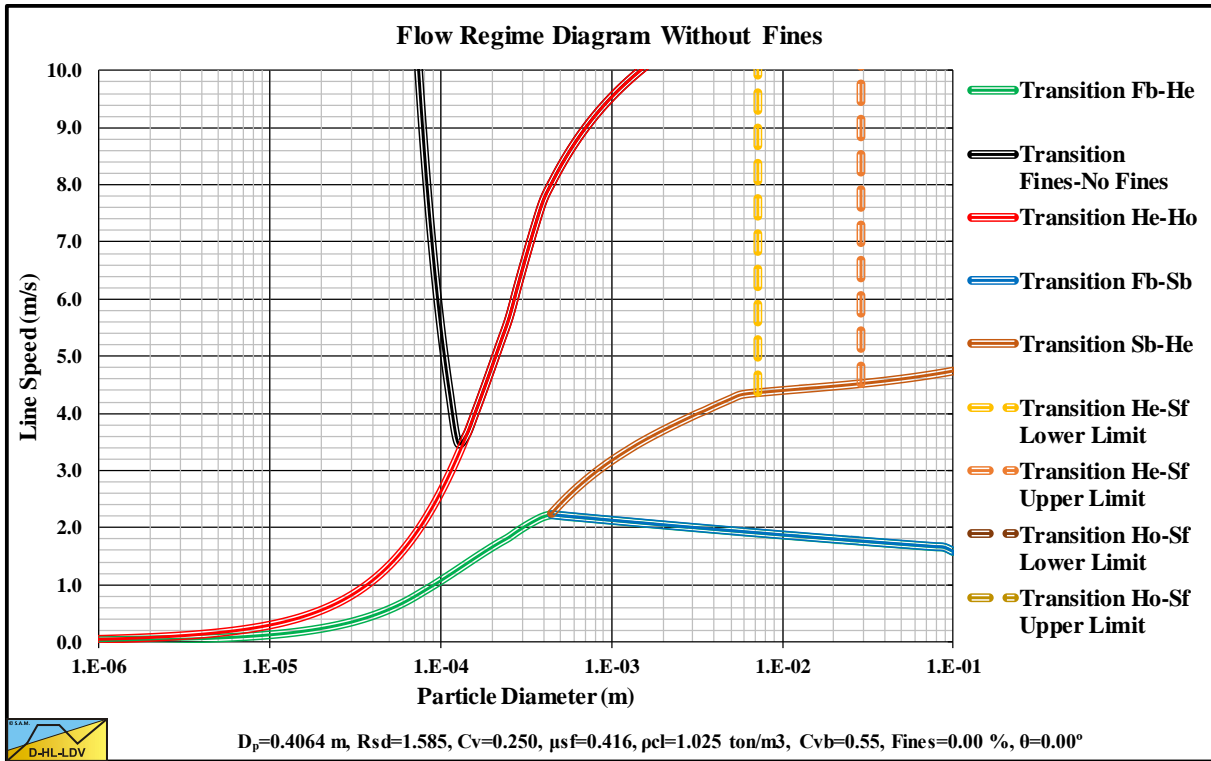
Figure 15.4-31: Flow regime diagram D_p=0.4064 m (16 inch) and C_vs=0.250.
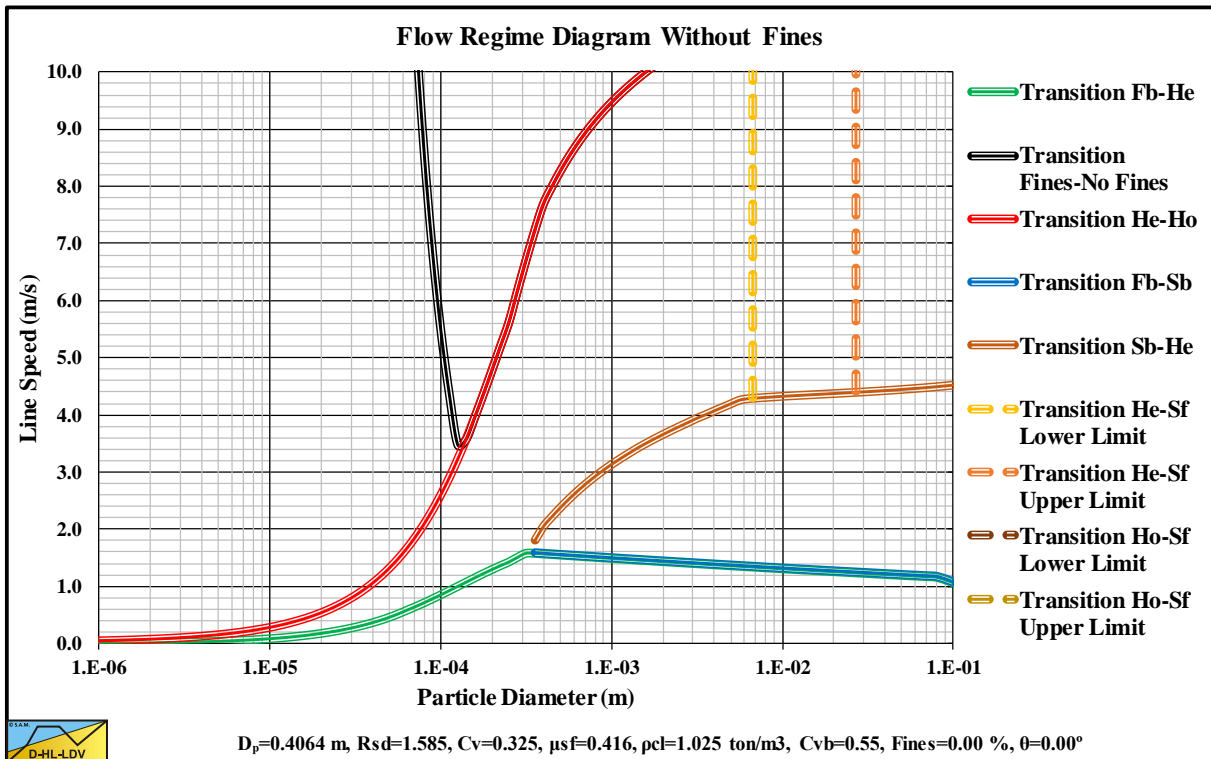
Figure 15.4-32: Flow regime diagram D_p=0.4064 m (16 inch) and C_vs=0.325.

Appendices.

15.4.9 D_p=0.5080 m (20 inch).
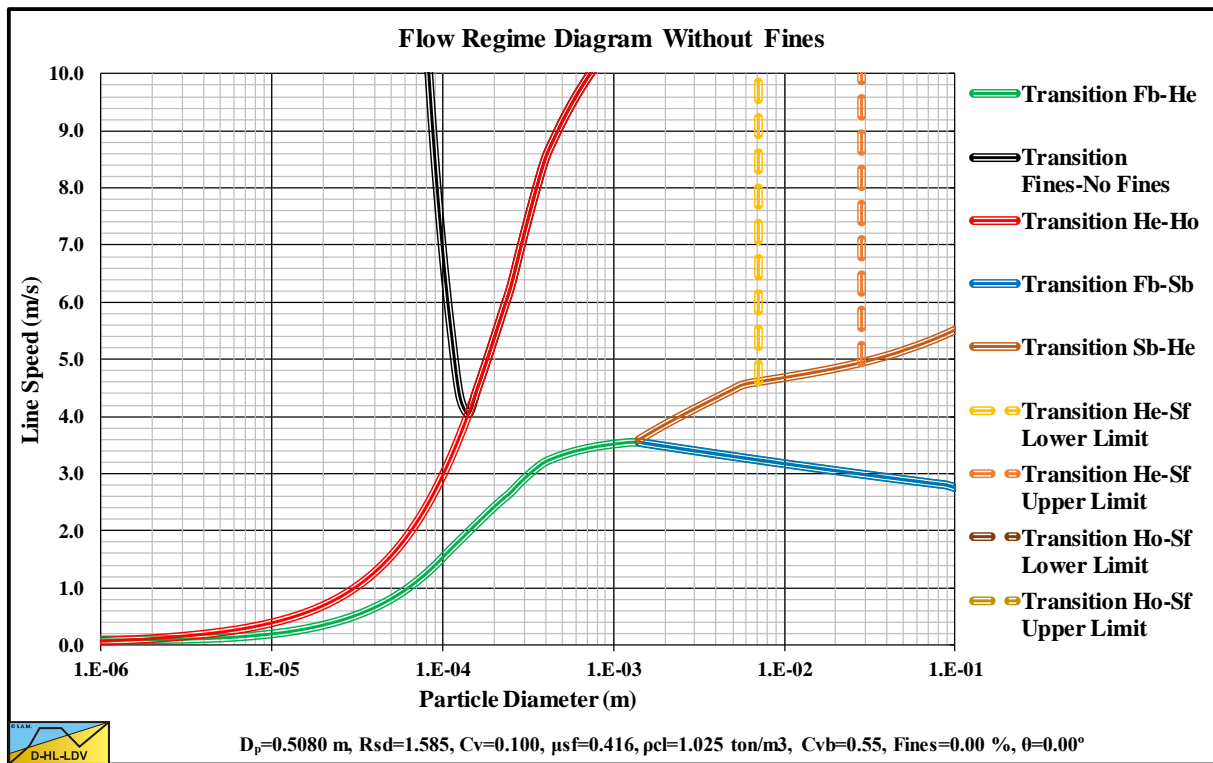
Figure 15.4-33: Flow regime diagram D_p=0.5080 m (20 inch) and C_{vs}=0.100.
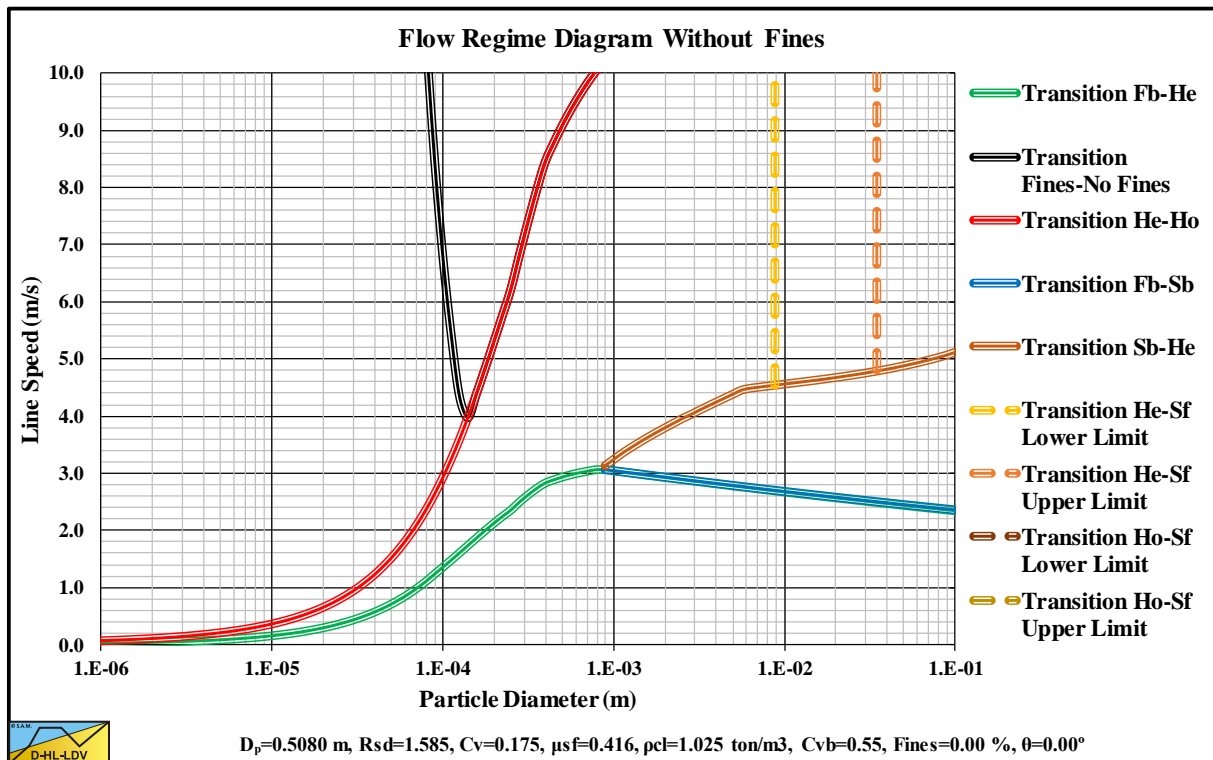
Figure 15.4-34: Flow regime diagram D_p=0.5080 m (20 inch) and C_{vs}=0.175.

D_P=0.5080 m, Rsd=1.585, Cv=0.250, μsf=0.416, ρcl=1.025 ton/m3, Cvb=0.55, Fines=0.00 %, θ=0.00º
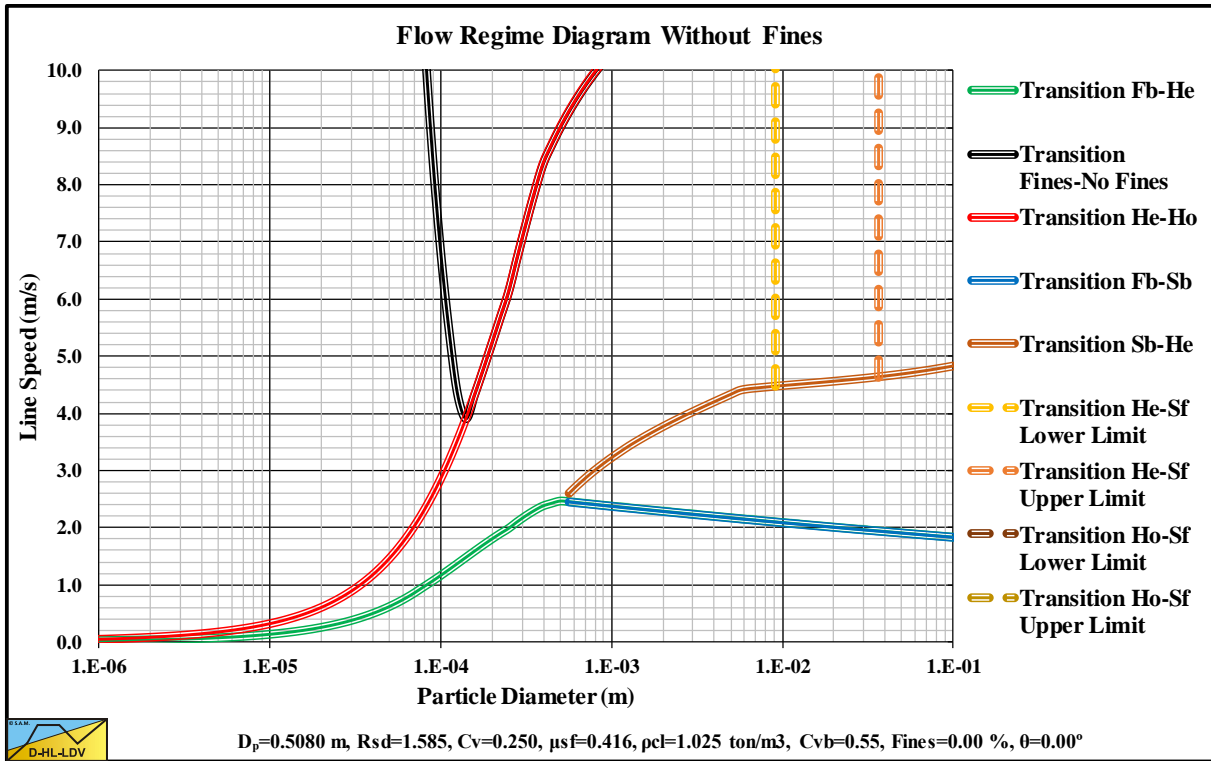
Figure 15.4-35: Flow regime diagram D_p=0.5080 m (20 inch) and C_{vs}=0.250.

D_P=0.5080 m, Rsd=1.585, Cv=0.325, μsf=0.416, ρcl=1.025 ton/m3, Cvb=0.55, Fines=0.00 %, θ=0.00º
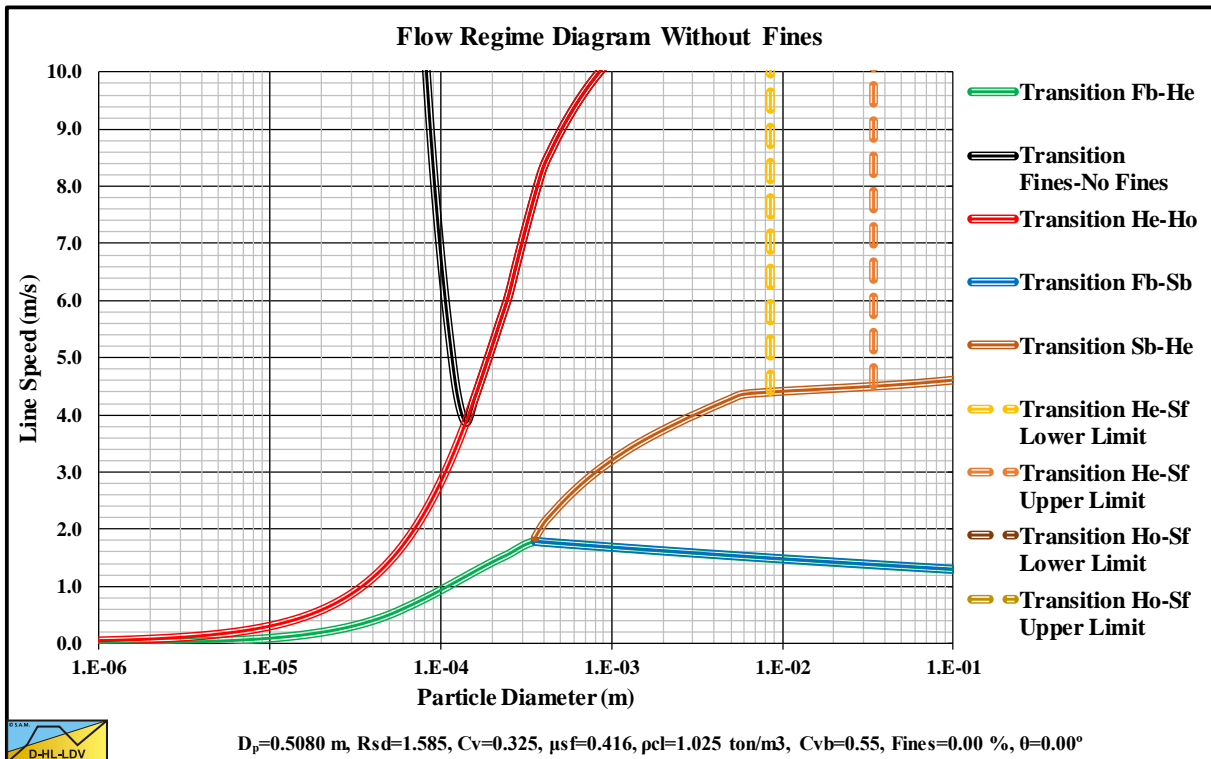
Figure 15.4-36: Flow regime diagram D_p=0.5080 m (20 inch) and C_{vs}=0.325.

Appendices.
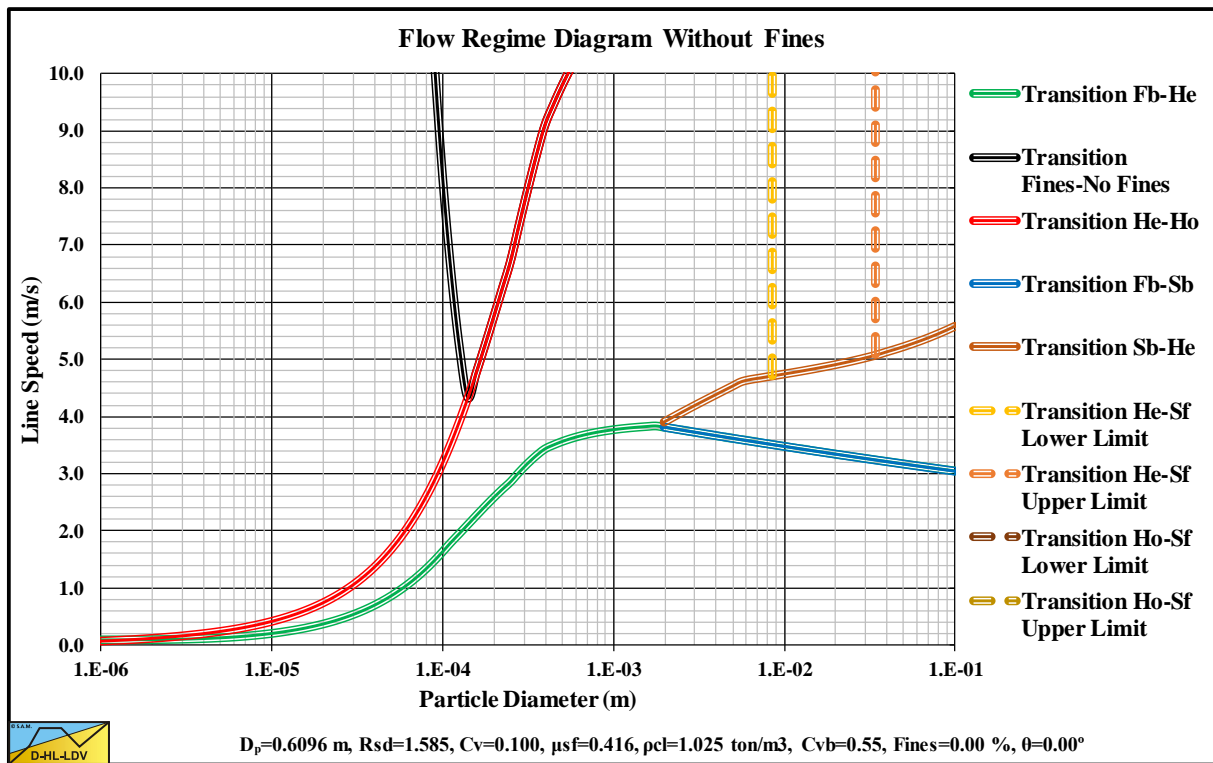
Figure 15.4-37: Flow regime diagram D_p=0.6096 m (24 inch) and C_{vs}=0.100.
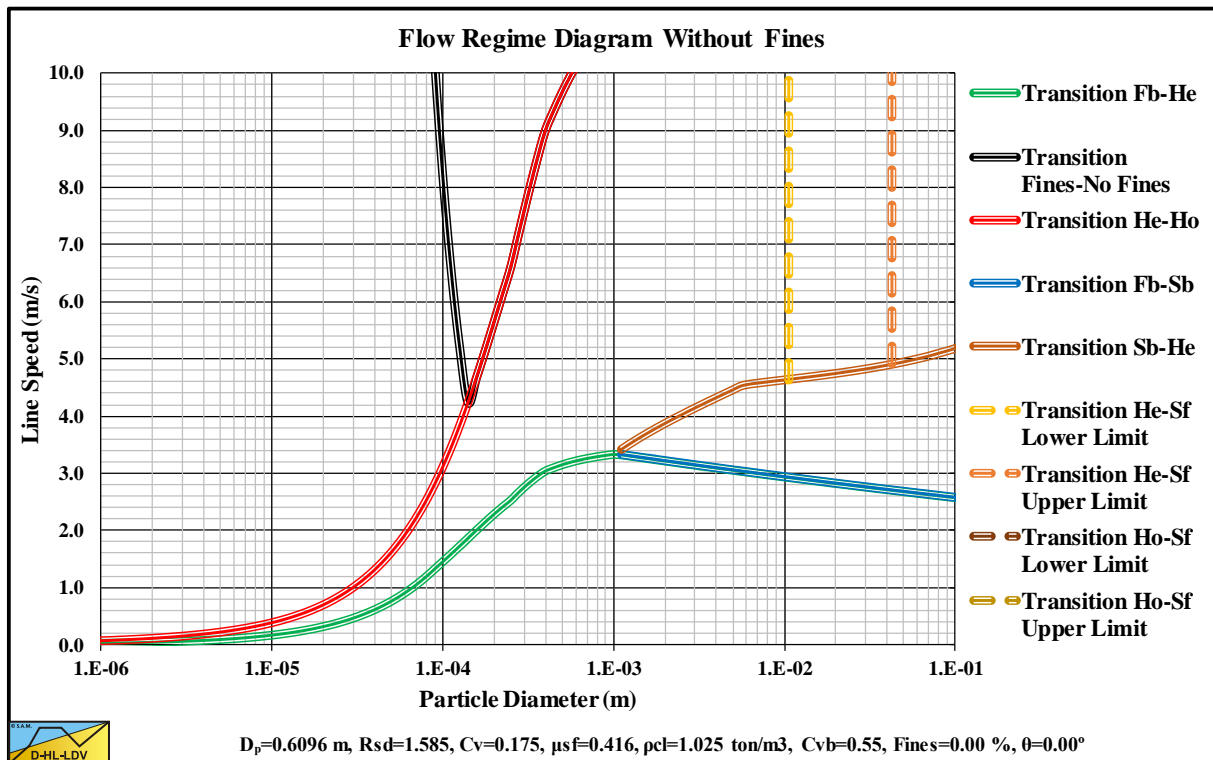
Figure 15.4-38: Flow regime diagram D_p=0.6096 m (24 inch) and C_{vs}=0.175.
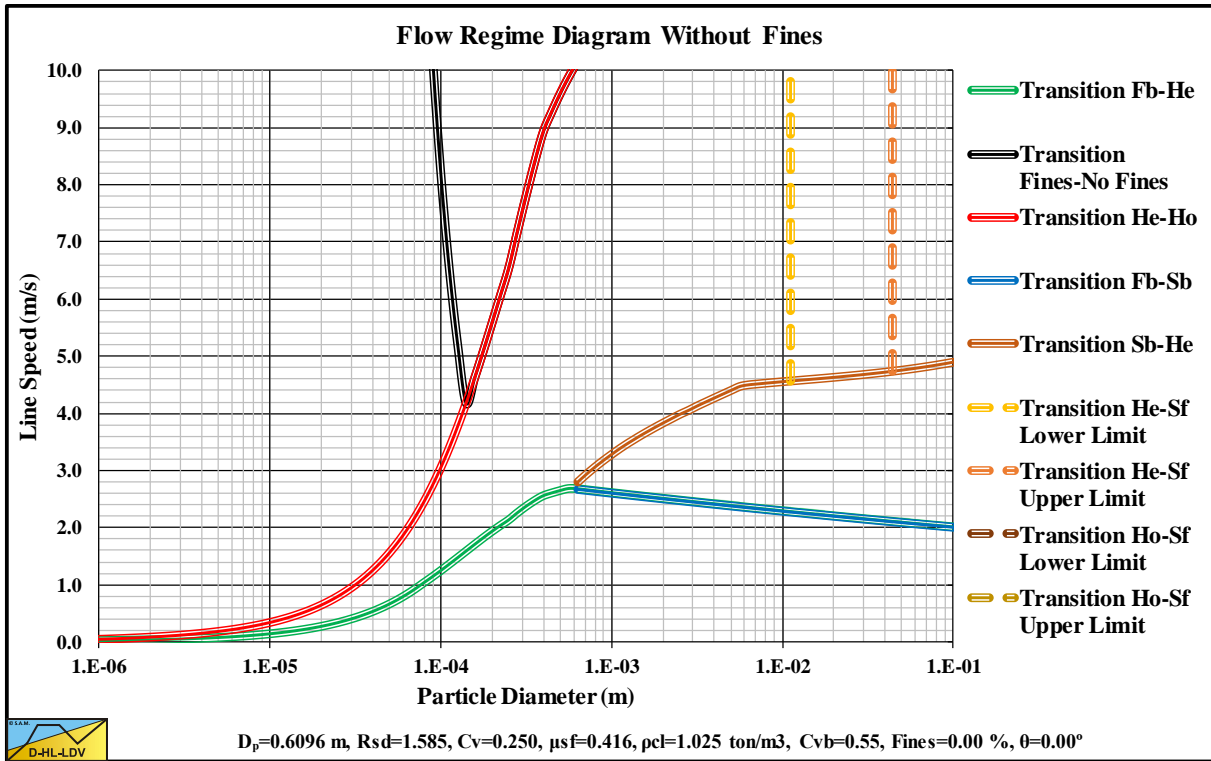
Figure 15.4-39: Flow regime diagram D$_p$=0.6096 m (24 inch) and C$_{vs}$=0.250.
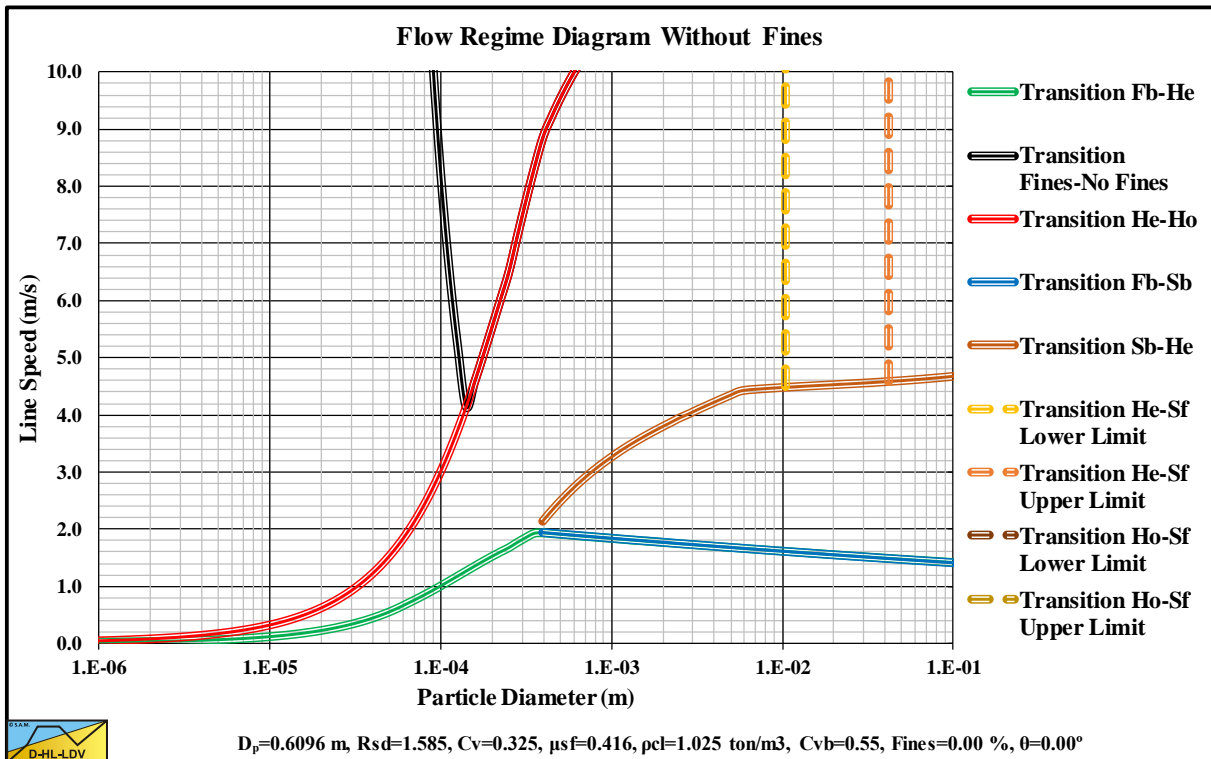
Figure 15.4-40: Flow regime diagram D$_p$=0.6096 m (24 inch) and C$_{vs}$=0.325.

Appendices.

15.4.11 D_p=0.7112 m (28 inch).
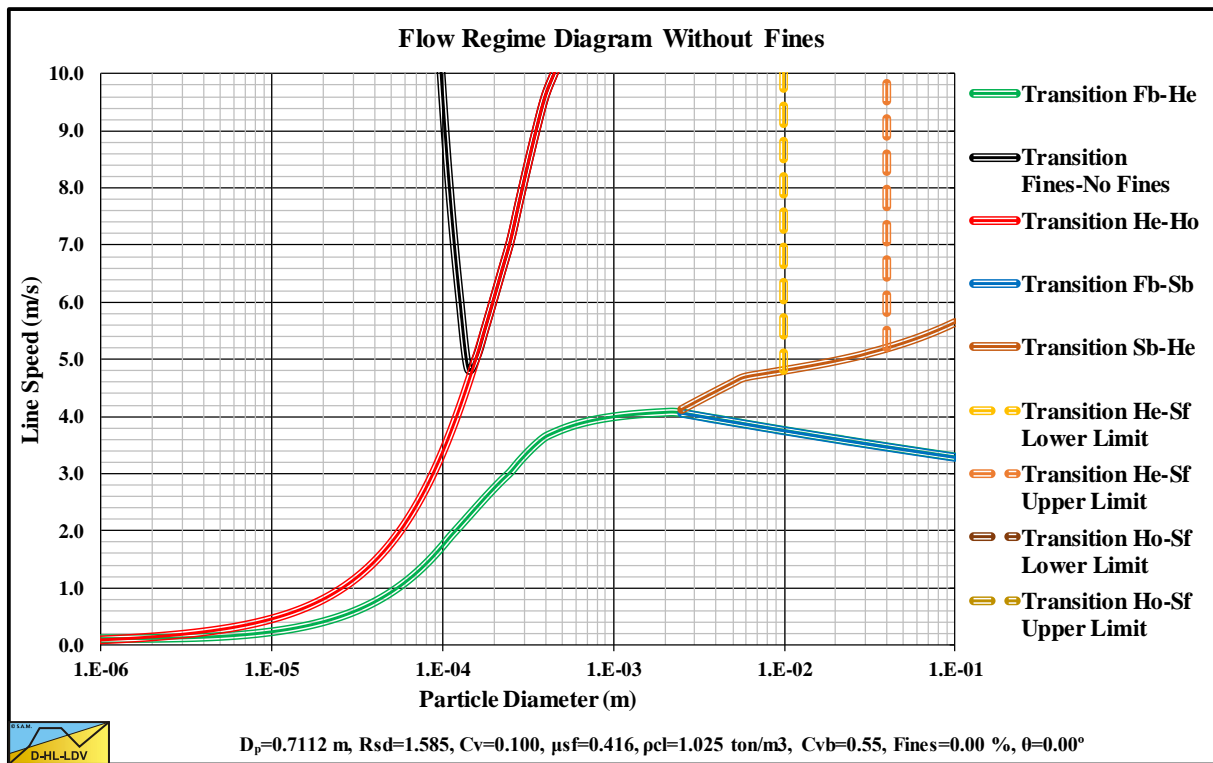
Figure 15.4-41: Flow regime diagram D_p=0.7112 m (28 inch) and C_{vs}=0.100.
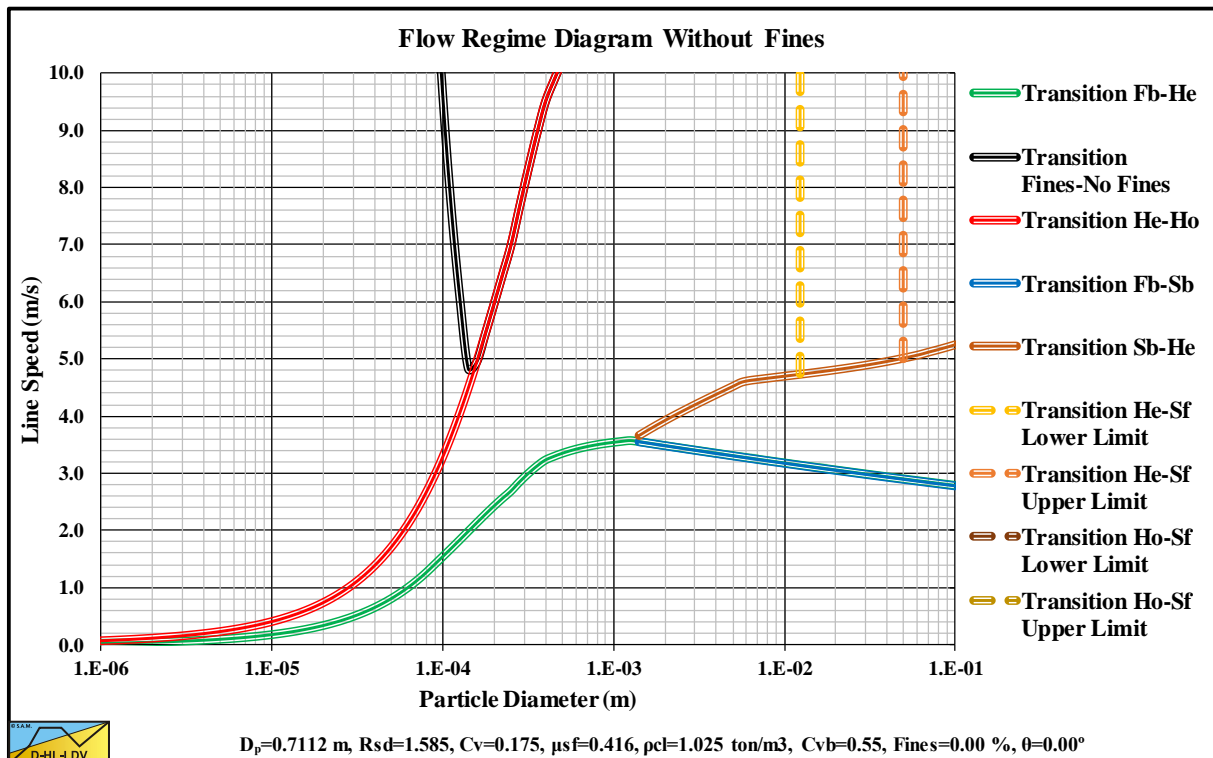
Figure 15.4-42: Flow regime diagram D_p=0.7112 m (28 inch) and C_{vs}=0.175.
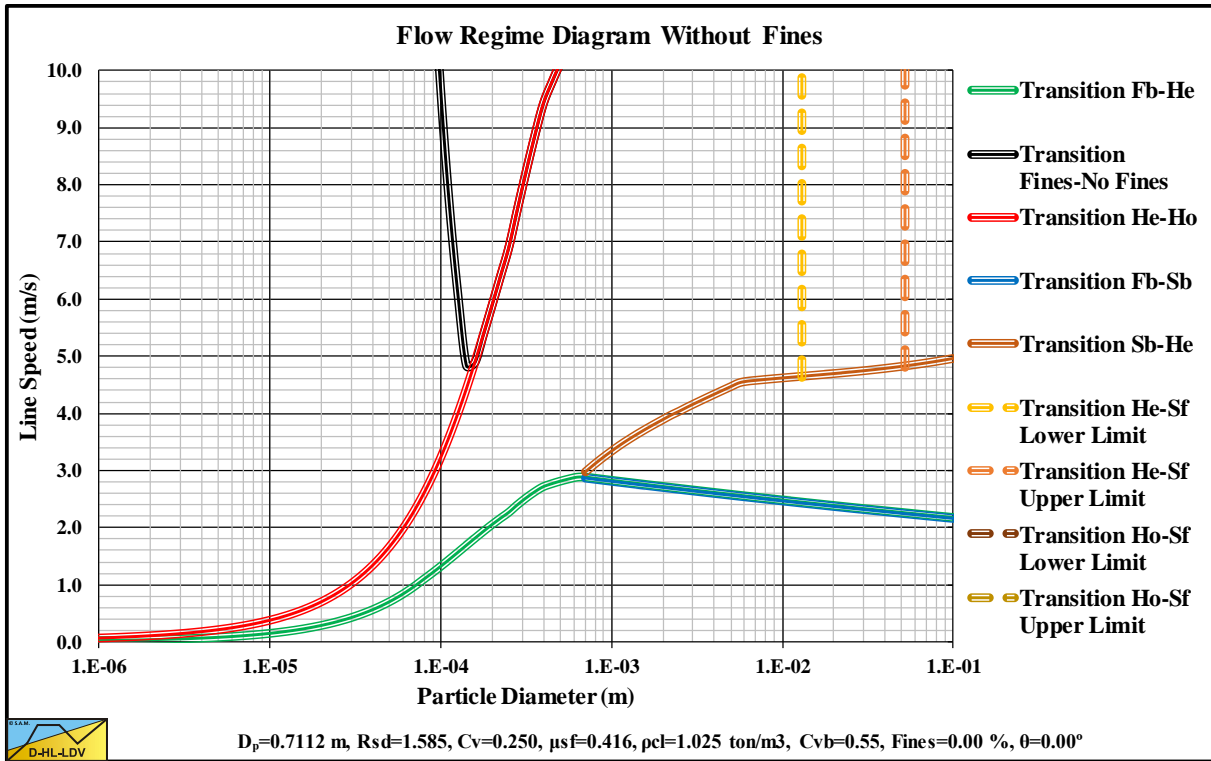
Figure 15.4-43: Flow regime diagram D_p=0.7112 m (28 inch) and C_{vs}=0.250.
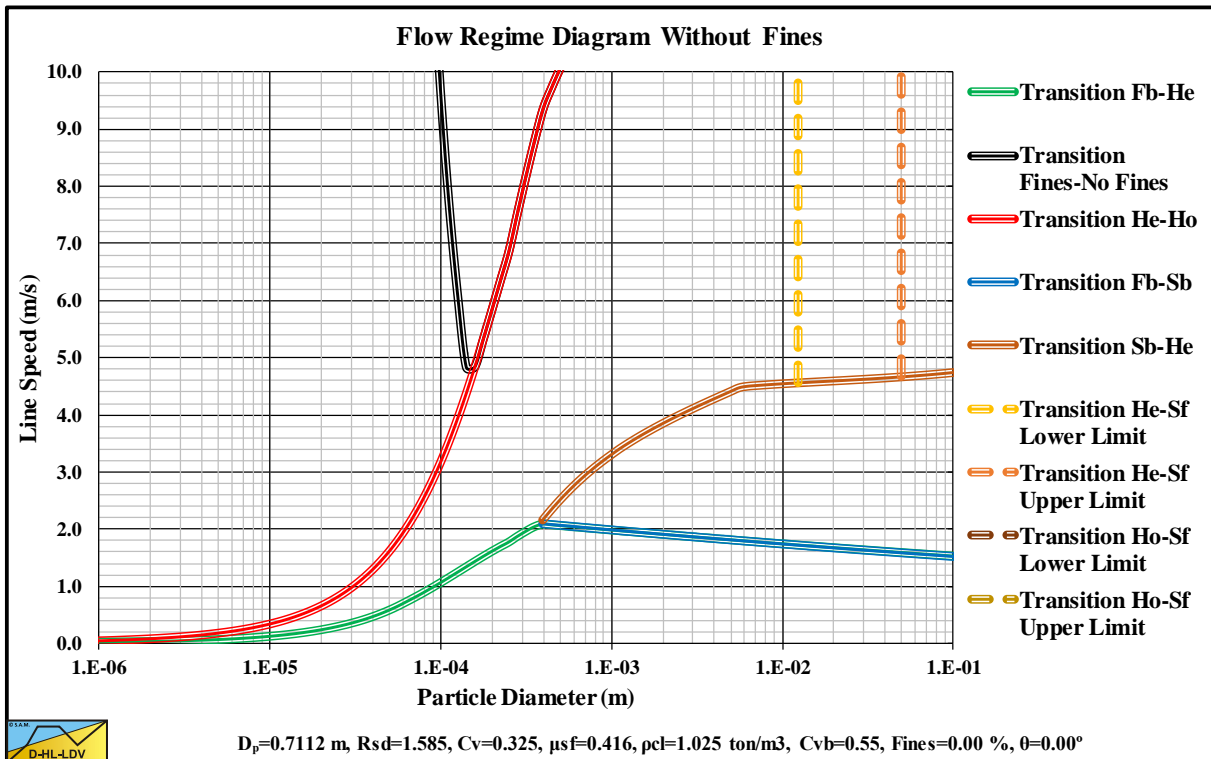
Figure 15.4-44: Flow regime diagram D_p=0.7112 m (28 inch) and C_{vs}=0.325.

Appendices.

15.4.12 D_p=0.7620 m (30 inch).

D_p=0.7620 m, Rsd=1.585, Cv=0.100, μsf=0.416, ρcl=1.025 ton/m3, Cvb=0.55, Fines=0.00 %, θ=0.00°
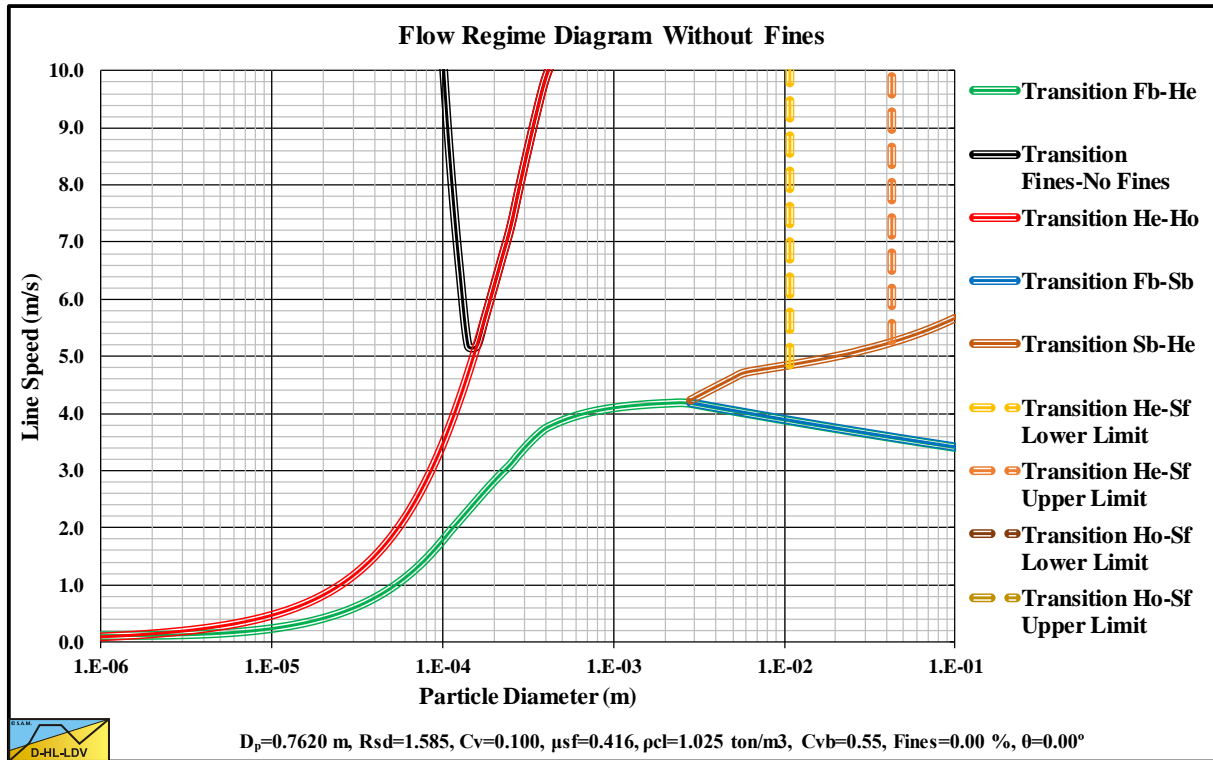
Figure 15.4-45: Flow regime diagram D_p=0.7620 m (30 inch) and C_{vs}=0.100.

D_p=0.7620 m, Rsd=1.585, Cv=0.175, μsf=0.416, ρcl=1.025 ton/m3, Cvb=0.55, Fines=0.00 %, θ=0.00°
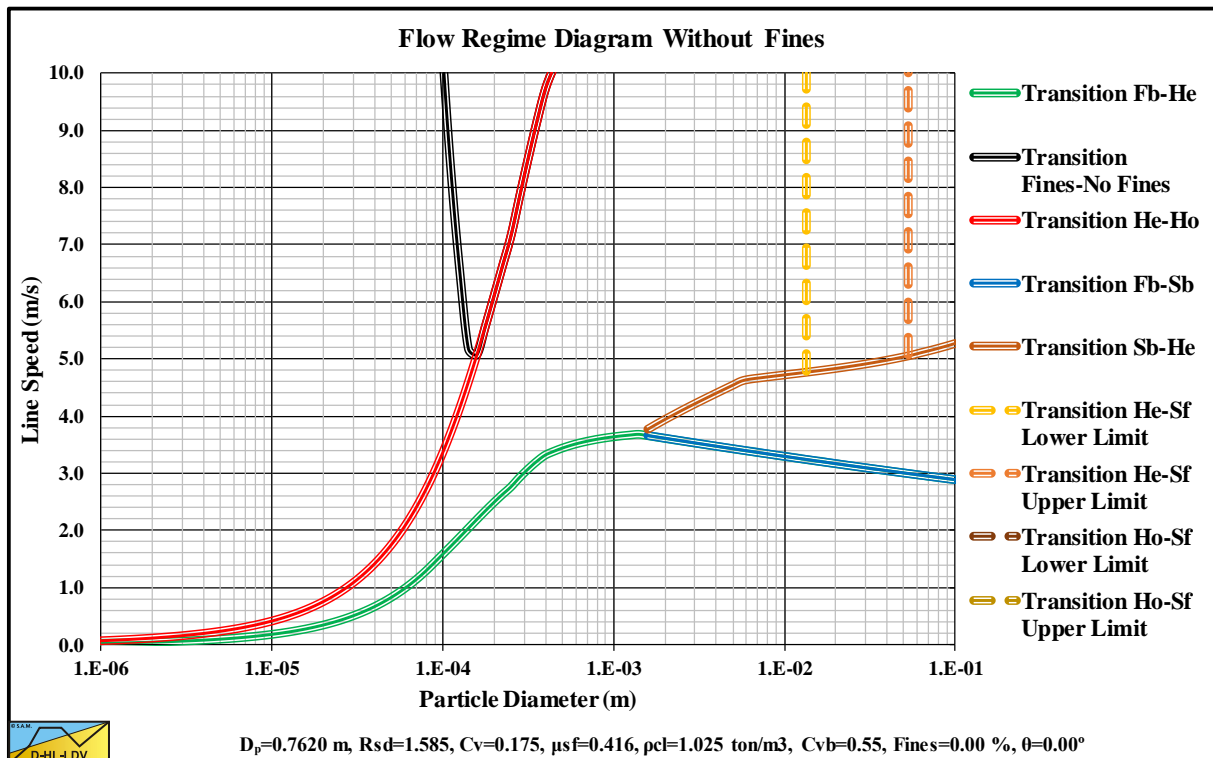
Figure 15.4-46: Flow regime diagram D_p=0.7620 m (30 inch) and C_{vs}=0.175.
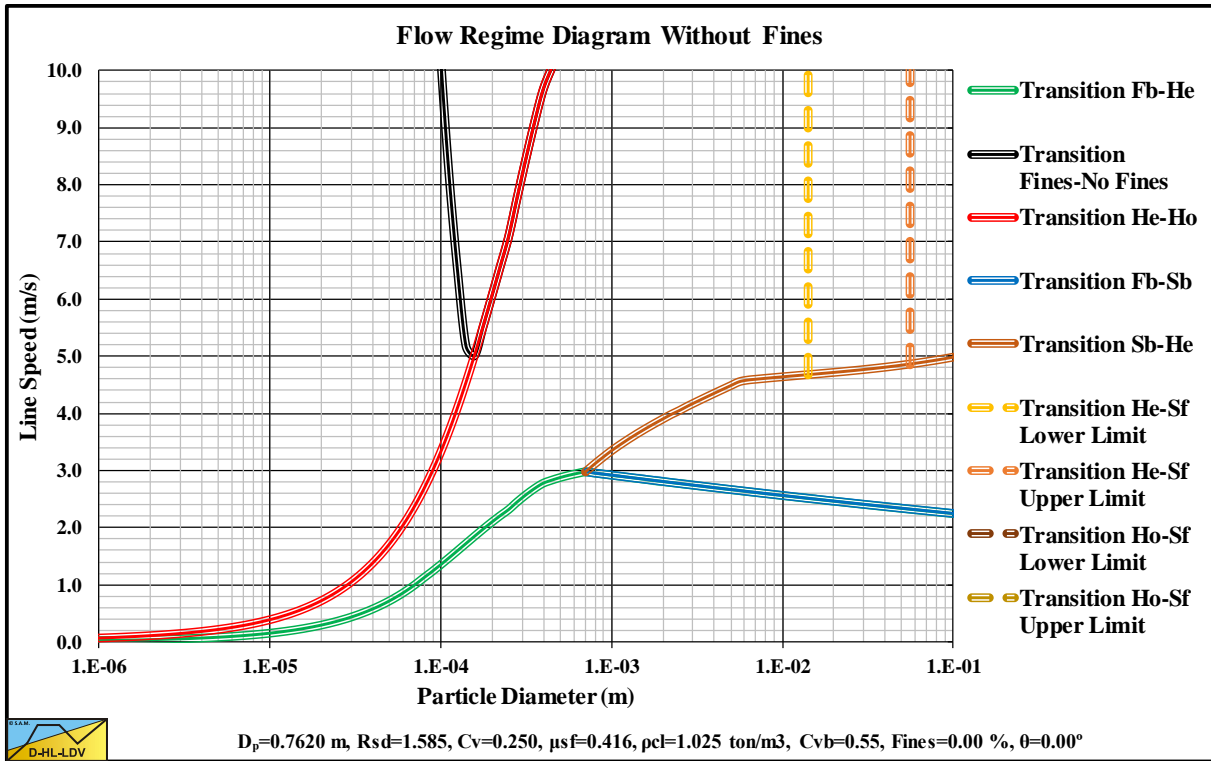
Figure 15.4-47: Flow regime diagram D_p=0.7620 m (30 inch) and C_{vs}=0.250.
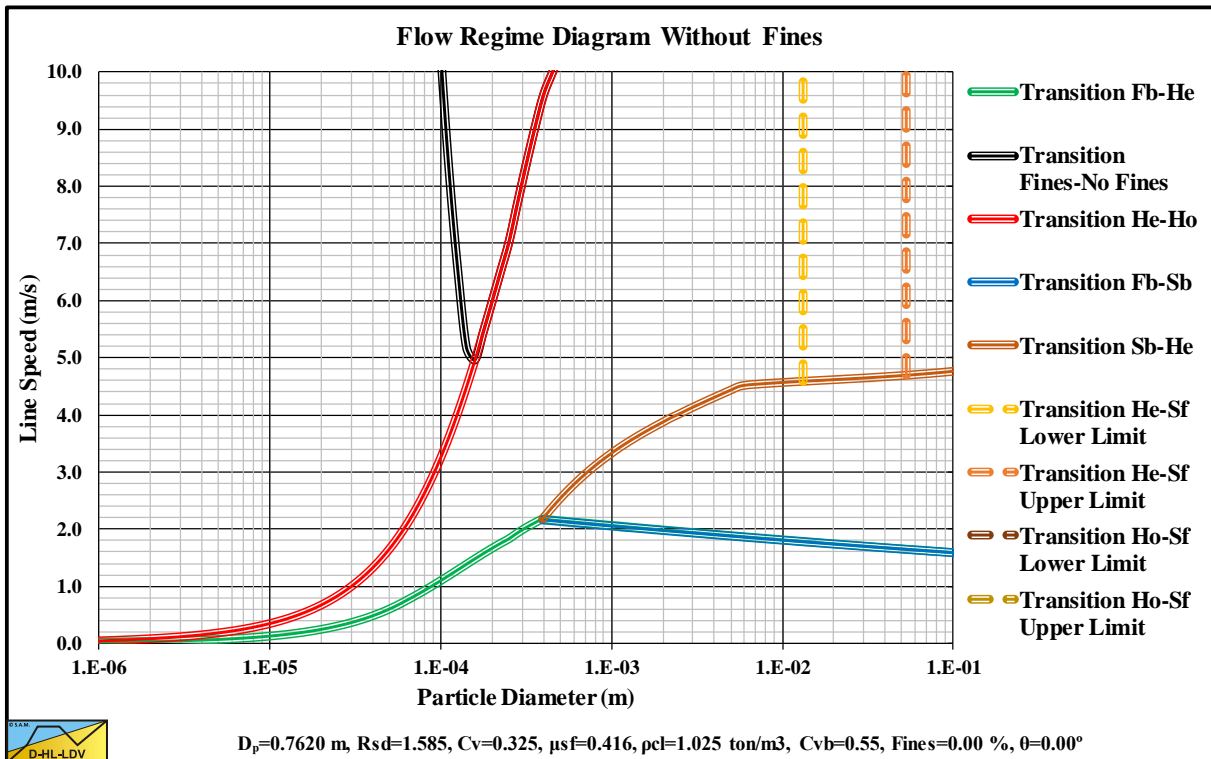
Figure 15.4-48: Flow regime diagram D_p=0.7620 m (30 inch) and C_{vs}=0.325.

Appendices.

15.4.13 D_p=0.8128 m (32 inch).
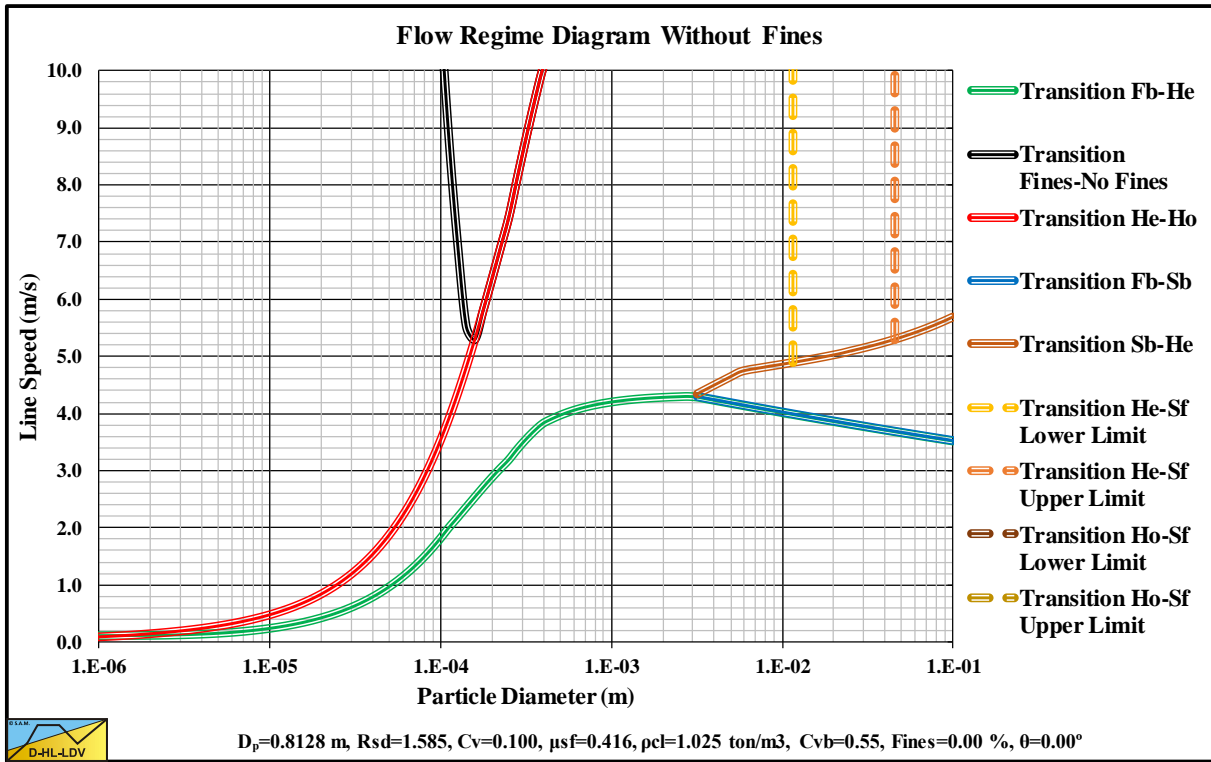
Figure 15.4-49: Flow regime diagram D_p=0.8128 m (32 inch) and C_{vs}=0.100.
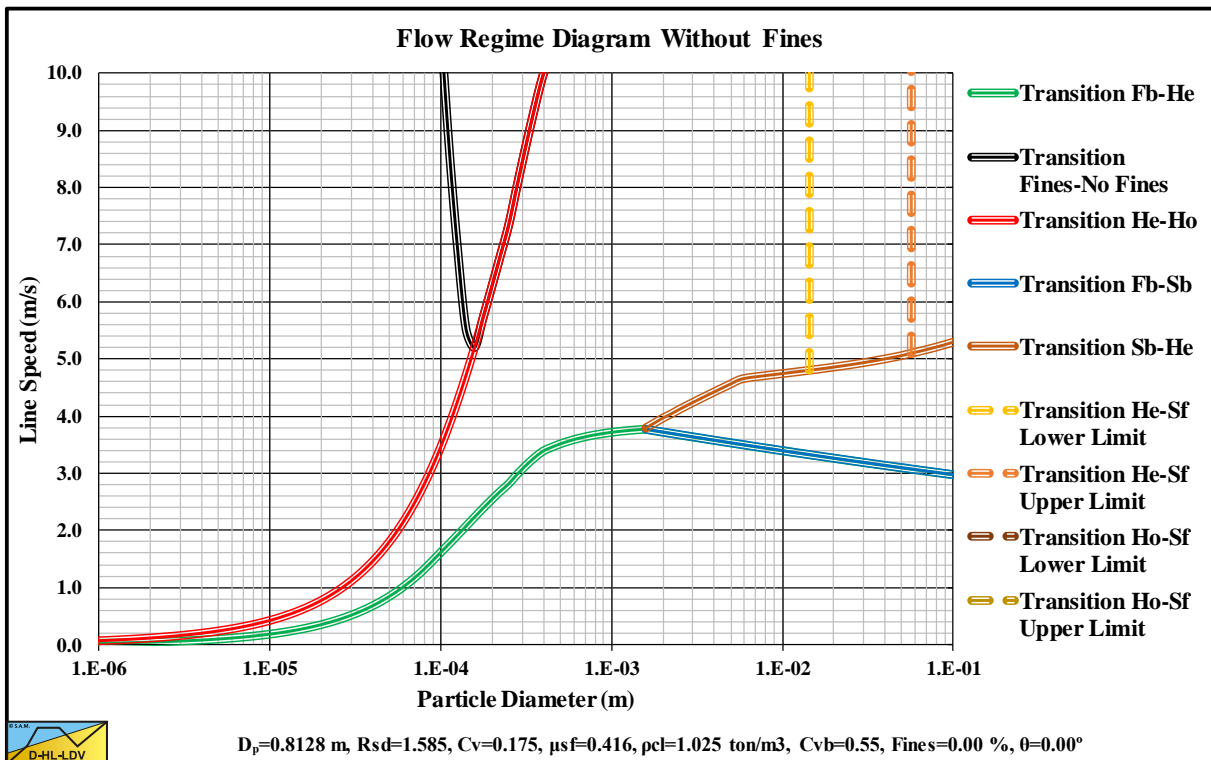
Figure 15.4-50: Flow regime diagram D_p=0.8128 m (32 inch) and C_{vs}=0.175.

D$_p$=0.8128 m, Rsd=1.585, Cv=0.250, μsf=0.416, ρcl=1.025 ton/m3, Cvb=0.55, Fines=0.00 %, θ=0.00º
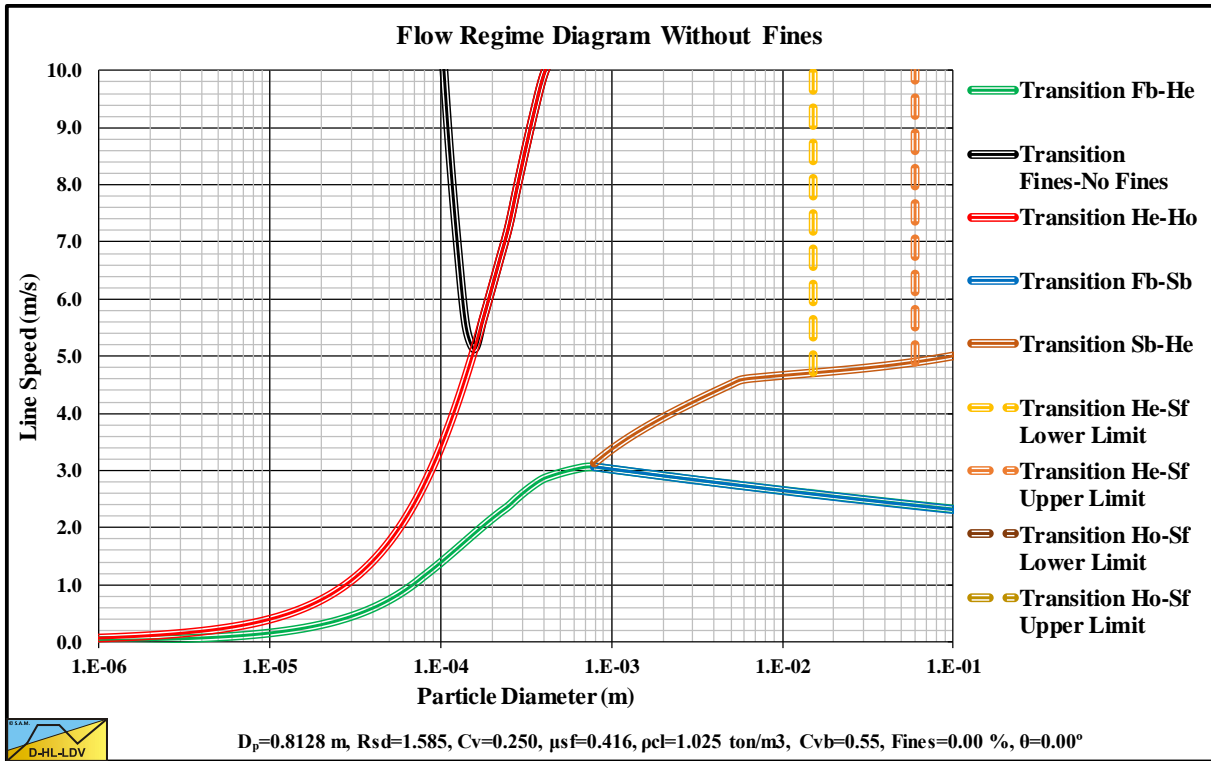
Figure 15.4-51: Flow regime diagram D$_p$=0.8128 m (32 inch) and C$_{vs}$=0.250.

D$_p$=0.8128 m, Rsd=1.585, Cv=0.325, μsf=0.416, ρcl=1.025 ton/m3, Cvb=0.55, Fines=0.00 %, θ=0.00º
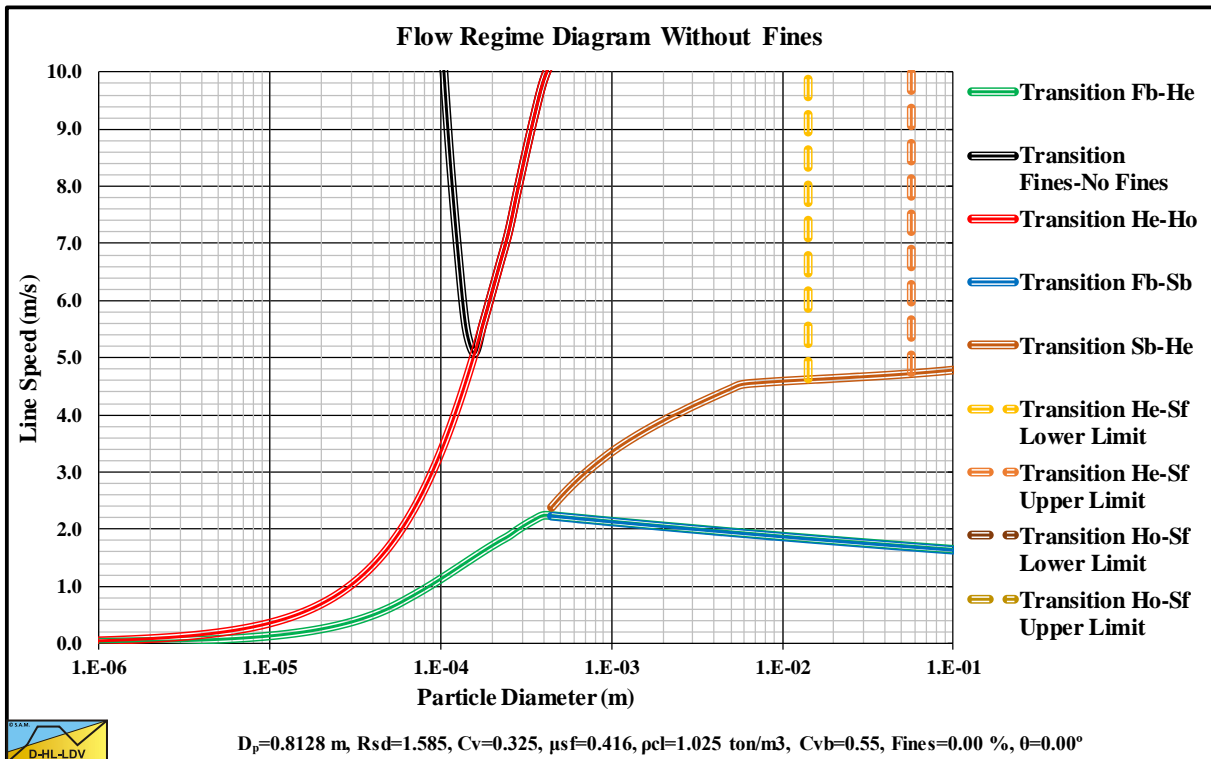
Figure 15.4-52: Flow regime diagram D$_p$=0.8128 m (32 inch) and C$_{vs}$=0.325.

Appendices.

15.4.14 D_p=0.9144 m (36 inch).
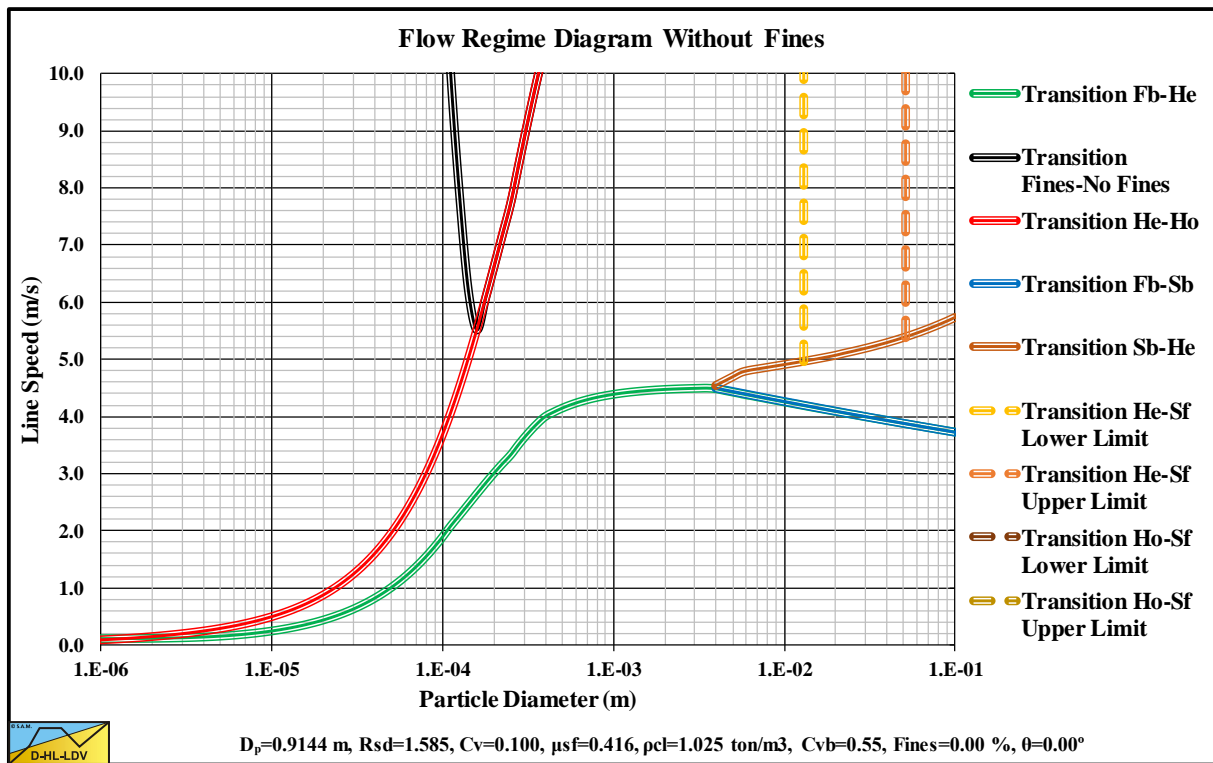
Figure 15.4-53: Flow regime diagram D_p=0.9144 m (36 inch) and C_{vs}=0.100.
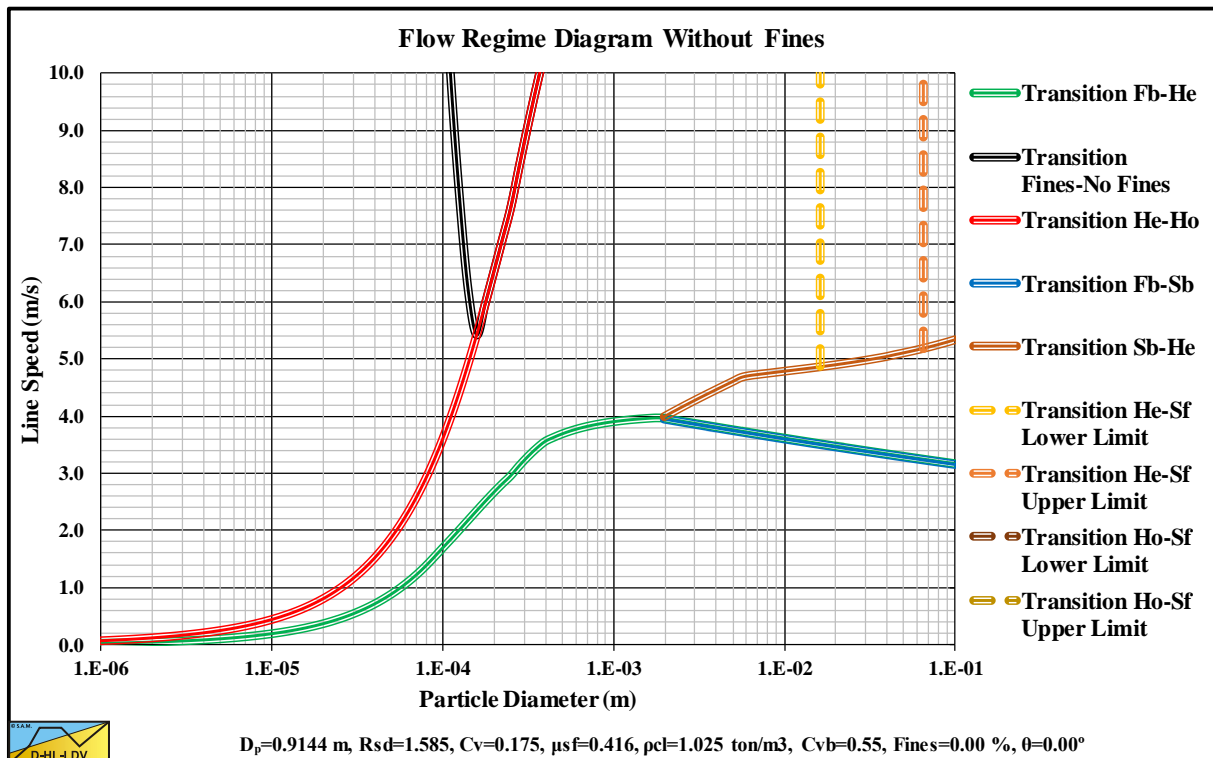
Figure 15.4-54: Flow regime diagram D_p=0.9144 m (36 inch) and C_{vs}=0.175.
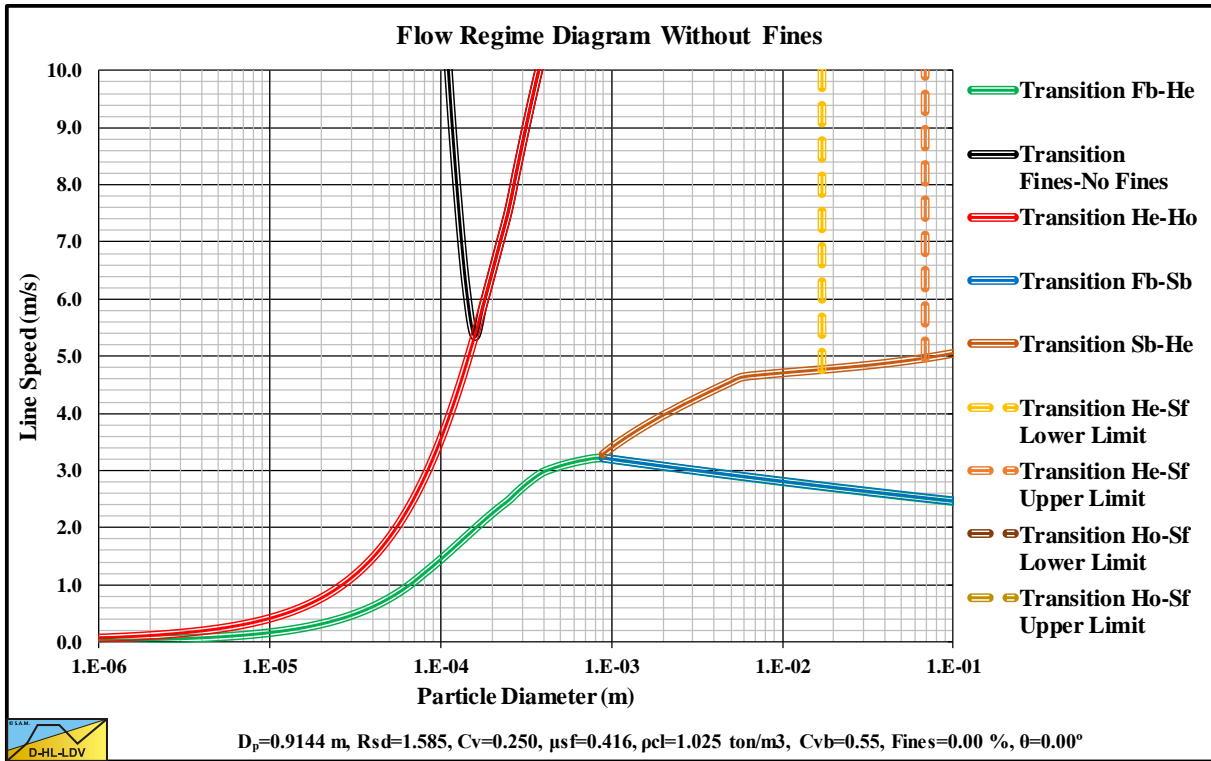
Figure 15.4-55: Flow regime diagram D_p=0.9144 m (36 inch) and C_{vs}=0.250.
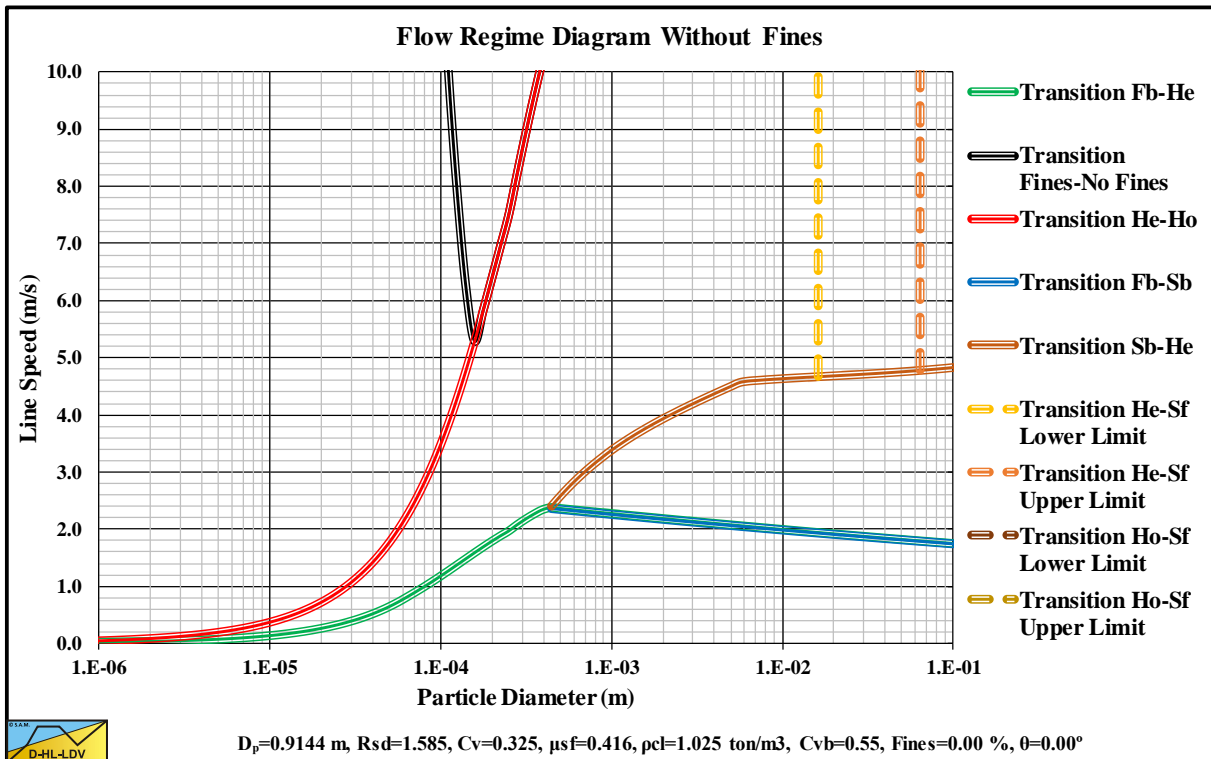
Figure 15.4-56: Flow regime diagram D_p=0.9144 m (36 inch) and C_{vs}=0.325.

Appendices.

15.4.15 D_p=1.0160 m (40 inch).
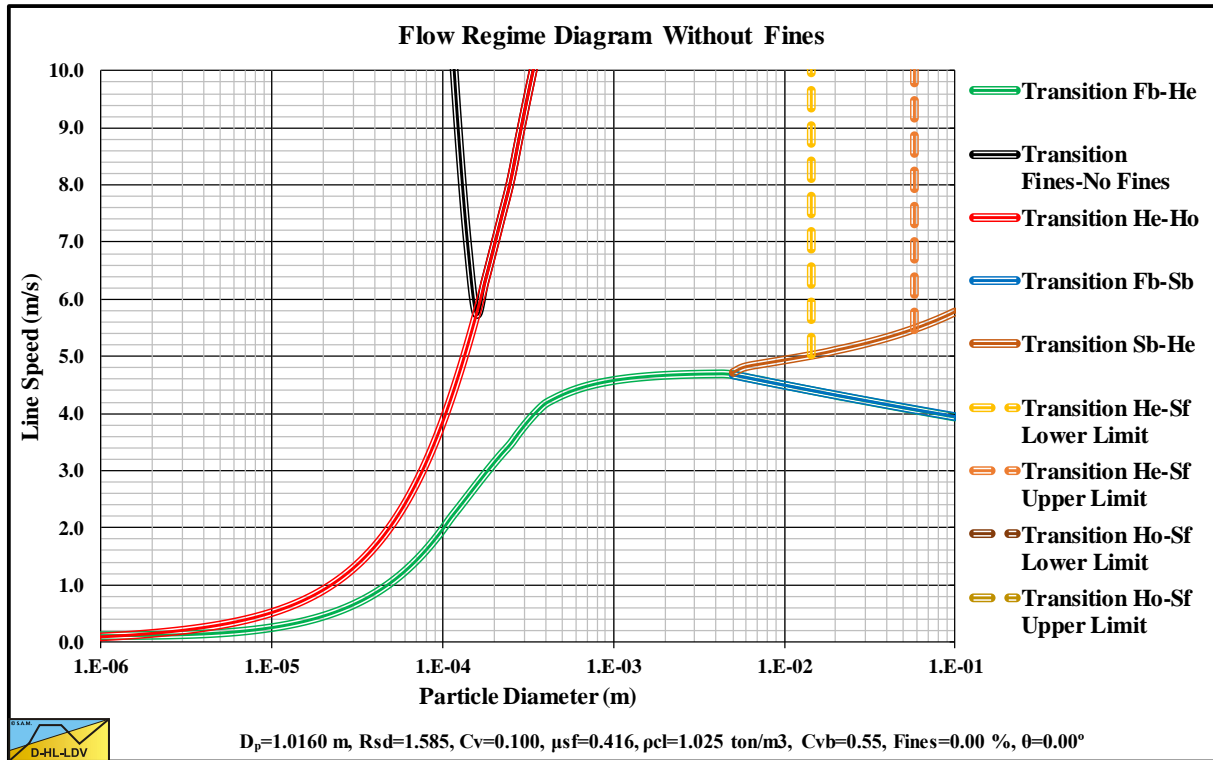
Figure 15.4-57: Flow regime diagram D_p=1.0160 m (40 inch) and C_{vs}=0.100.
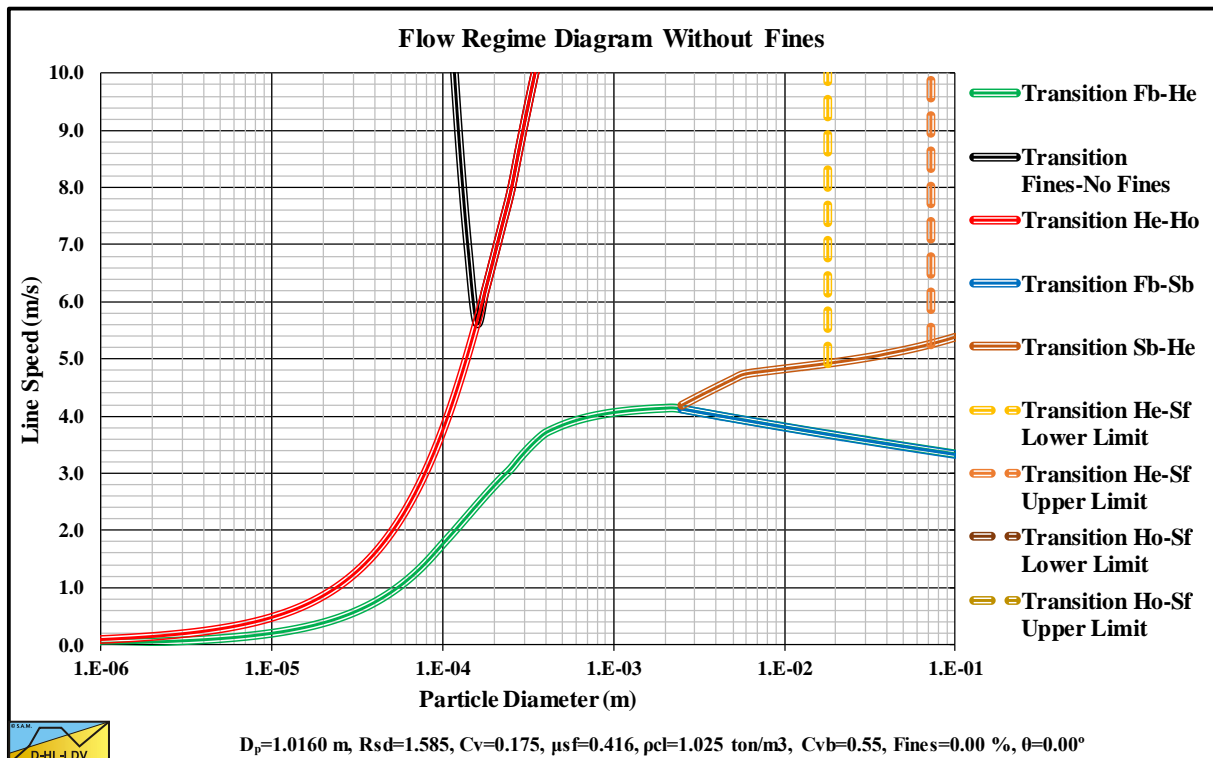
Figure 15.4-58: Flow regime diagram D_p=1.0160 m (40 inch) and C_{vs}=0.175.
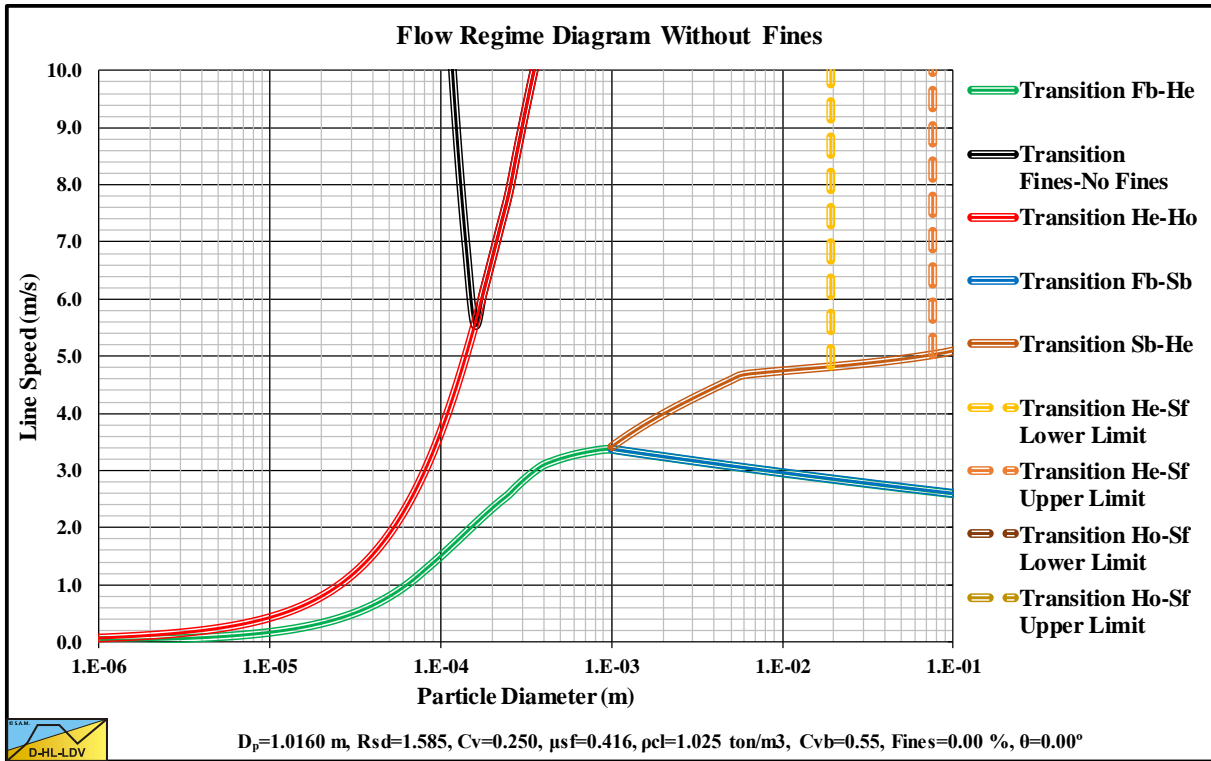
Figure 15.4-59: Flow regime diagram D$_p$=1.0160 m (40 inch) and C$_{vs}$=0.250.
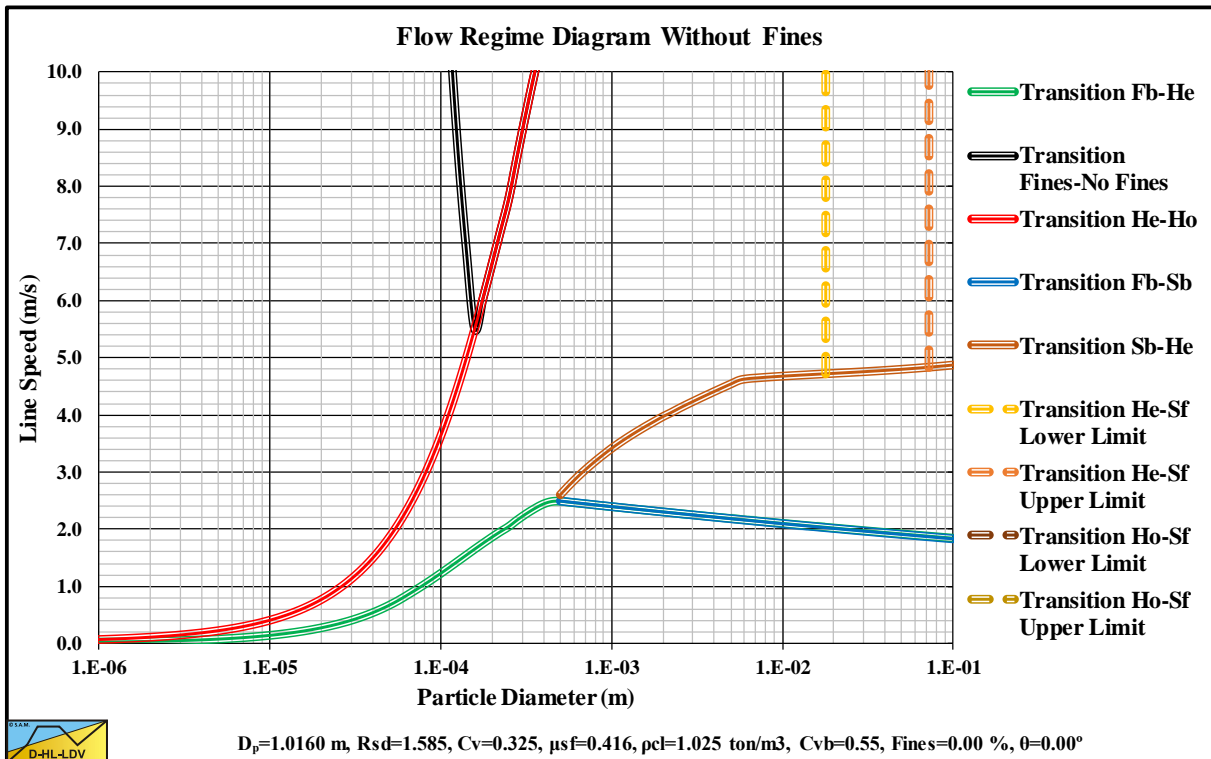
Figure 15.4-60: Flow regime diagram D$_p$=1.0160 m (40 inch) and C$_{vs}$=0.325.

Appendices.

15.4.16 D_p=1.1176 m (44 inch).
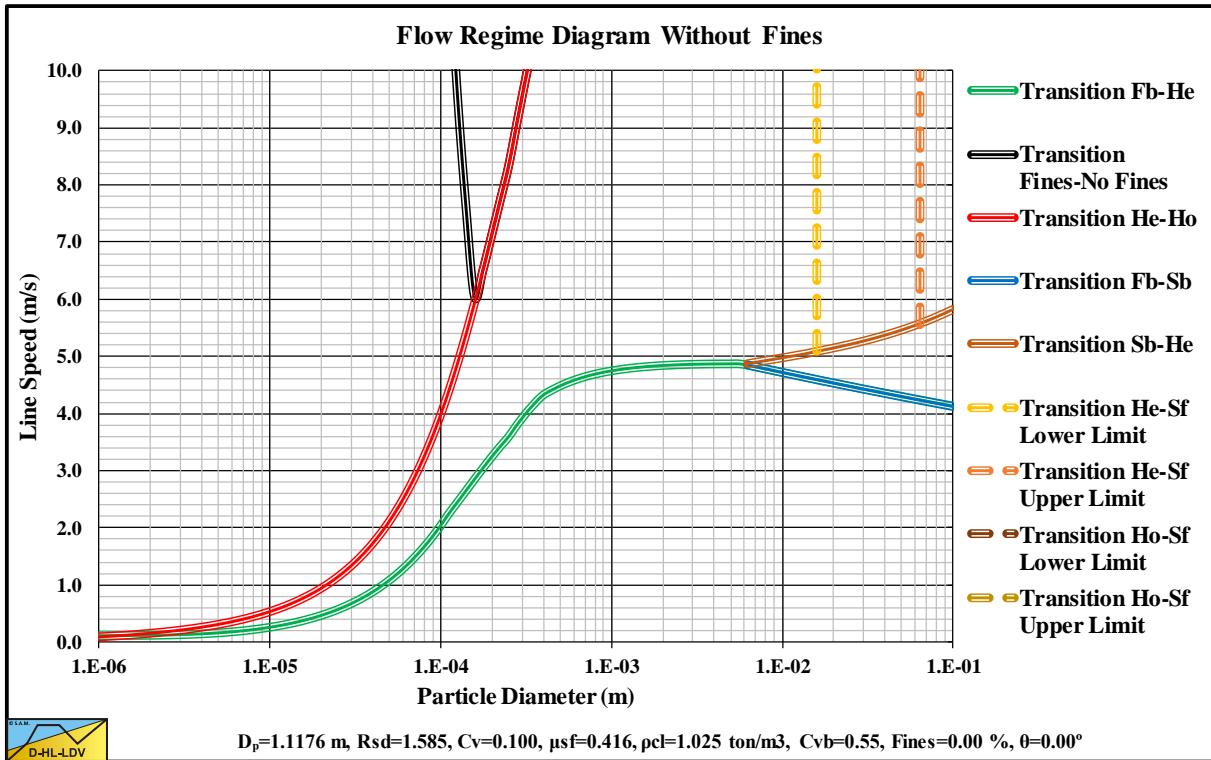
Figure 15.4-61: Flow regime diagram D_p=1.1176 m (44 inch) and C_{vs}=0.100.
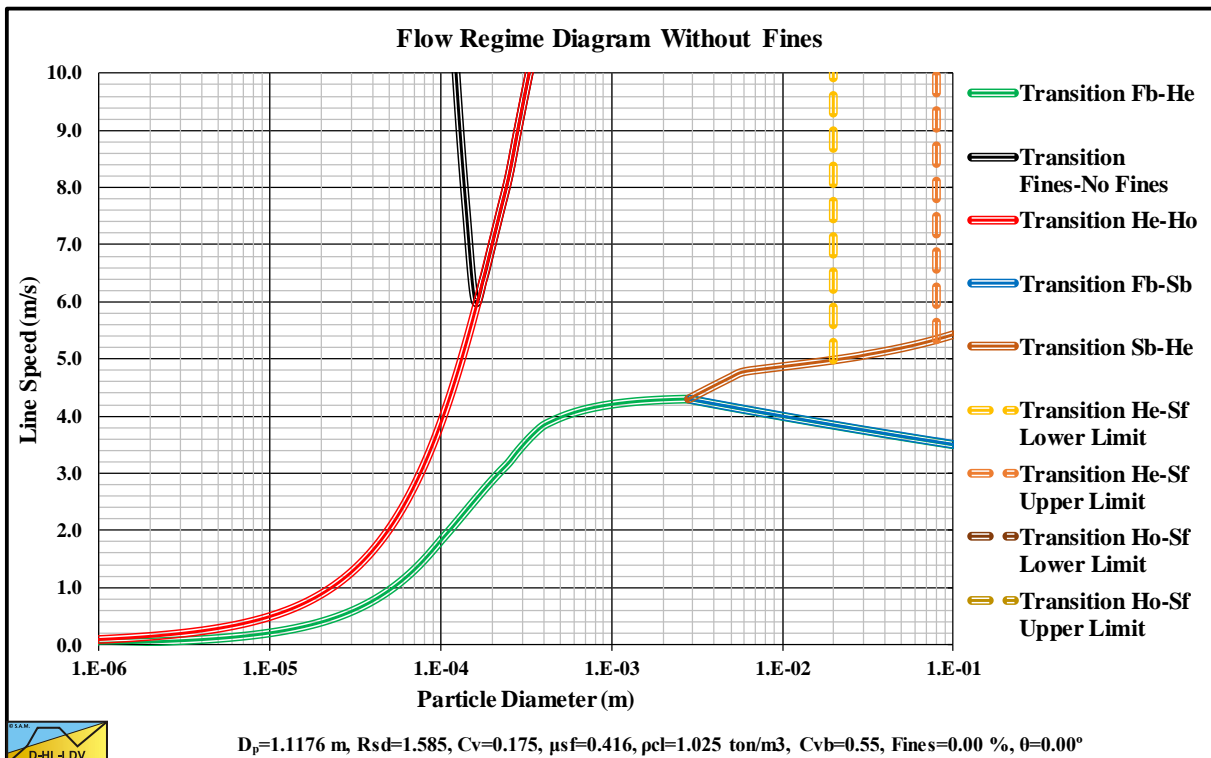
Figure 15.4-62: Flow regime diagram D_p=1.1176 m (44 inch) and C_{vs}=0.175.
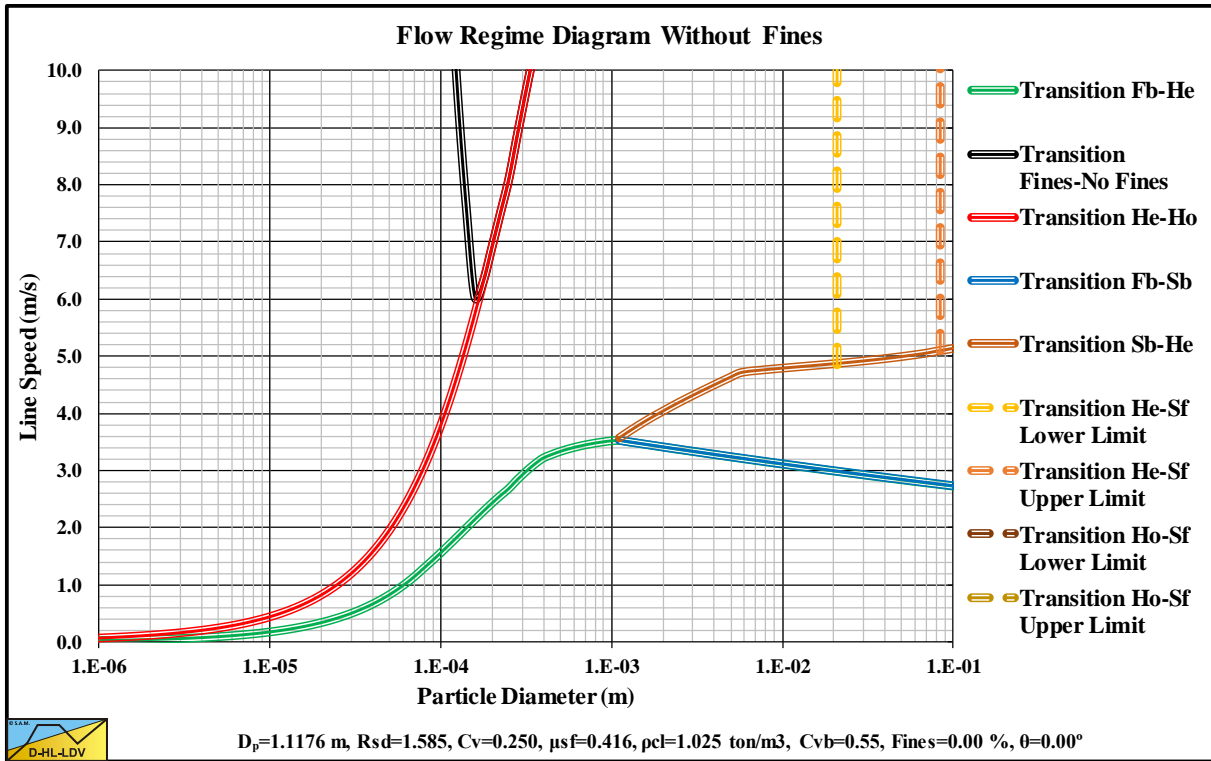
Figure 15.4-63: Flow regime diagram D_p=1.1176 m (44 inch) and C_vs=0.250.
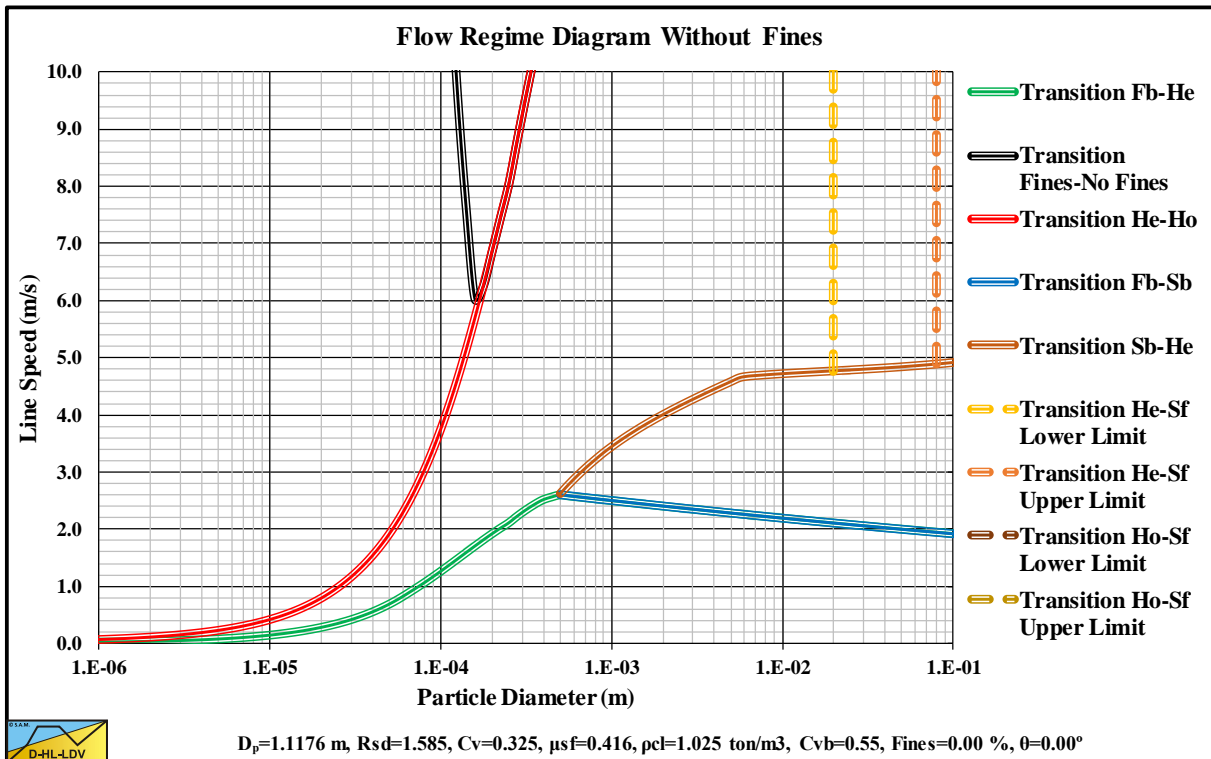
Figure 15.4-64: Flow regime diagram D_p=1.1176 m (44 inch) and C_vs=0.325.

Appendices.

15.4.17 D_p=1.2192 m (48 inch).
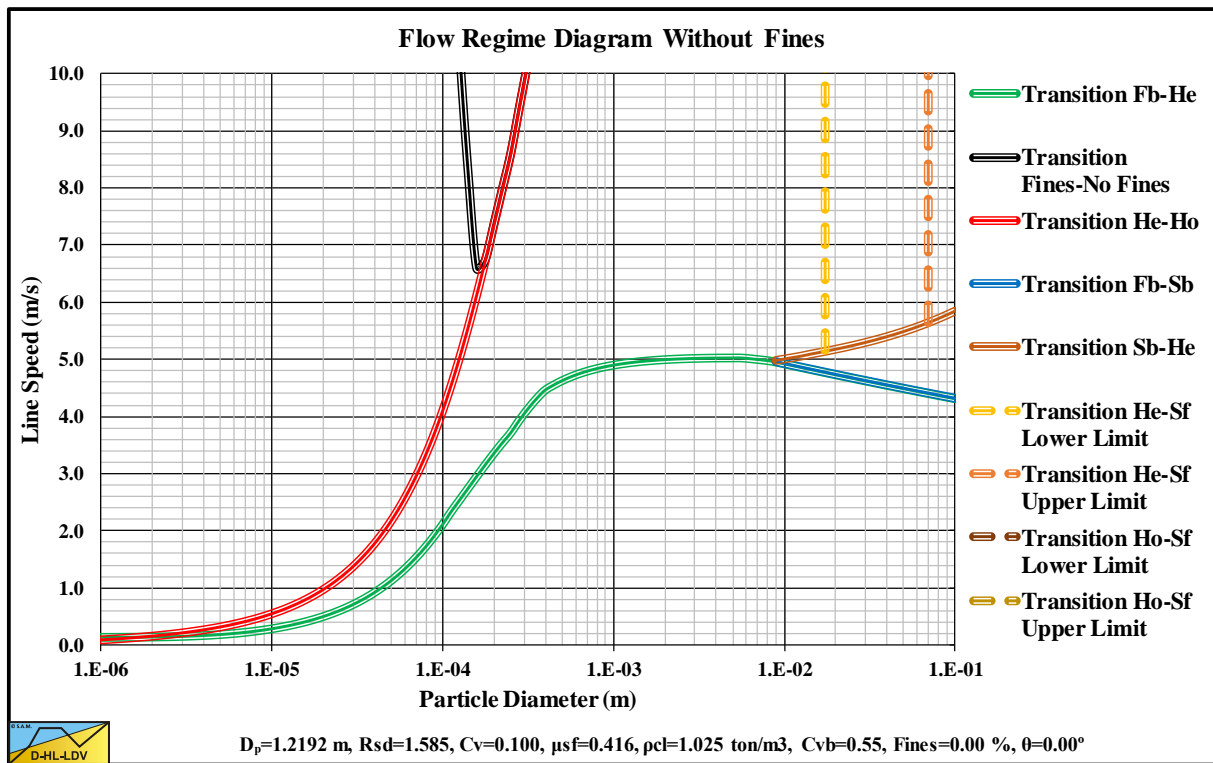
Figure 15.4-65: Flow regime diagram D_p=1.2192 m (48 inch) and C_{vs}=0.100.
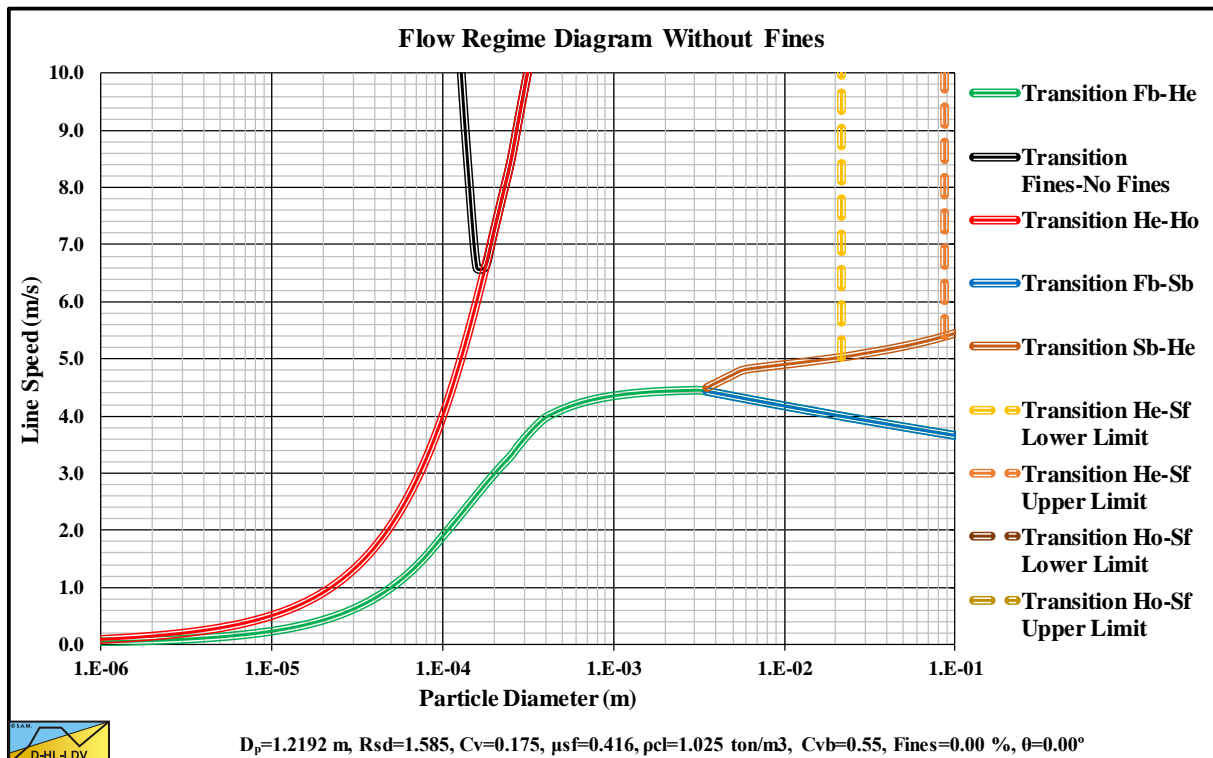
Figure 15.4-66: Flow regime diagram D_p=1.2192 m (48 inch) and C_{vs}=0.175.
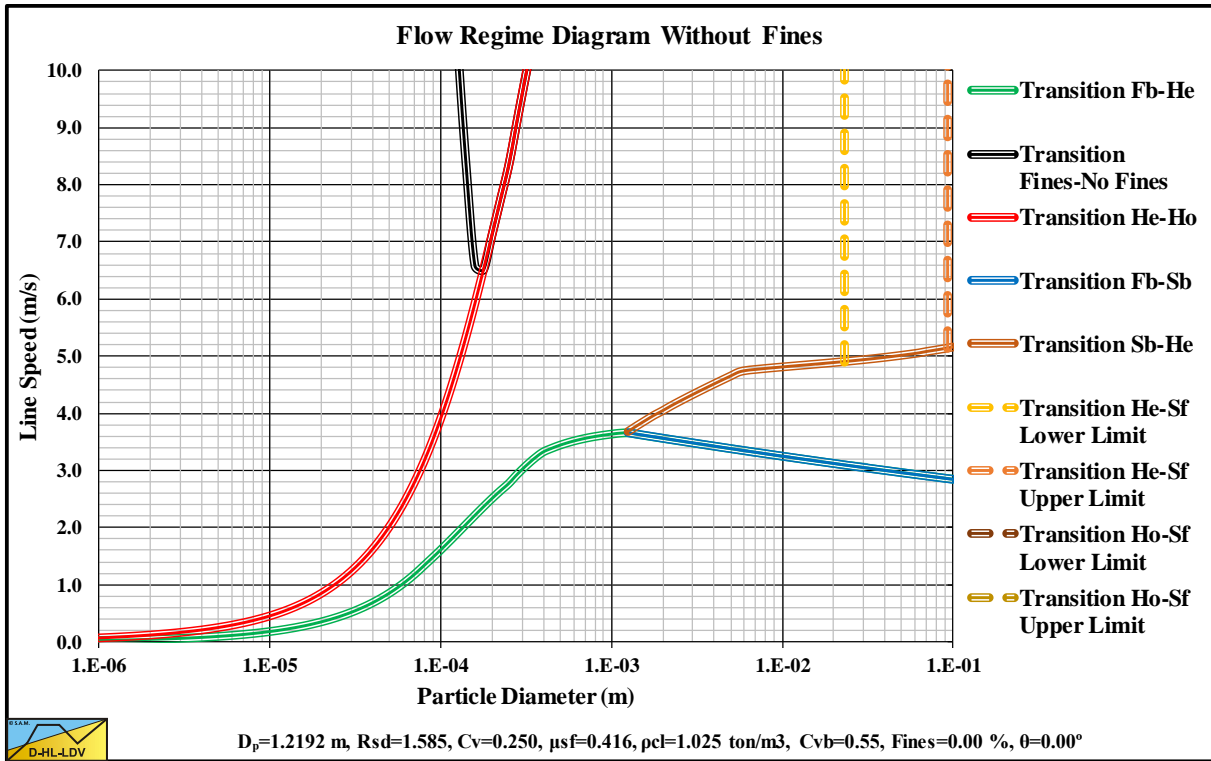
Figure 15.4-67: Flow regime diagram D$_p$=1.2192 m (48 inch) and C$_{vs}$=0.250.
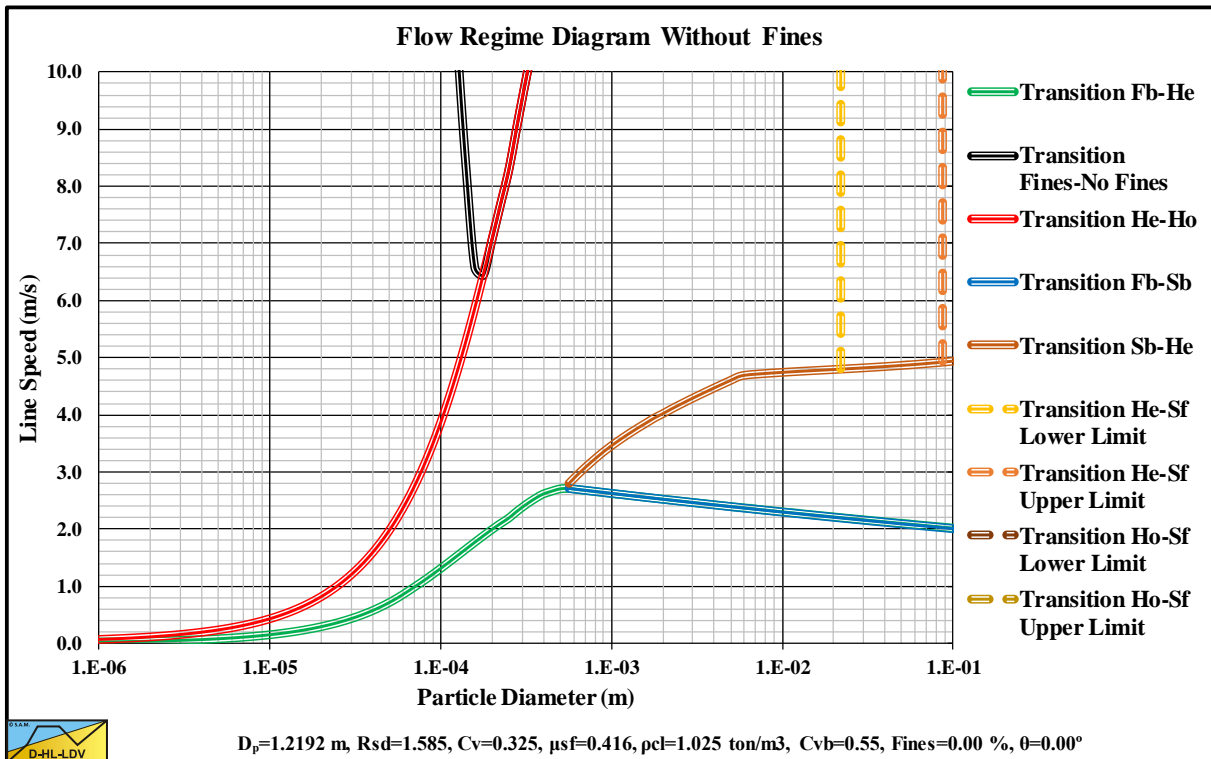
Figure 15.4-68: Flow regime diagram D$_p$=1.2192 m (48 inch) and C$_{vs}$=0.325.

Appendices.

15.5 A Set of Resulting Graphs.

15.5.1 Single Particle.
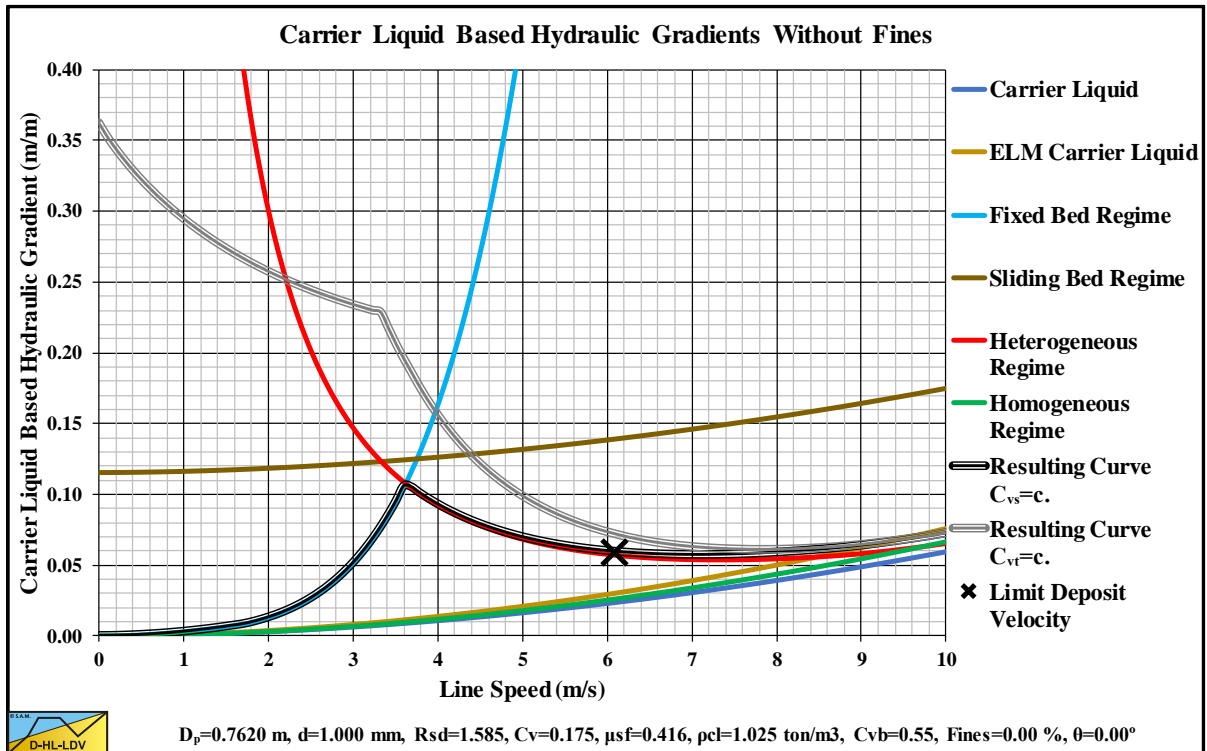
Figure 15.5-1: The hydraulic gradient versus the line speed.
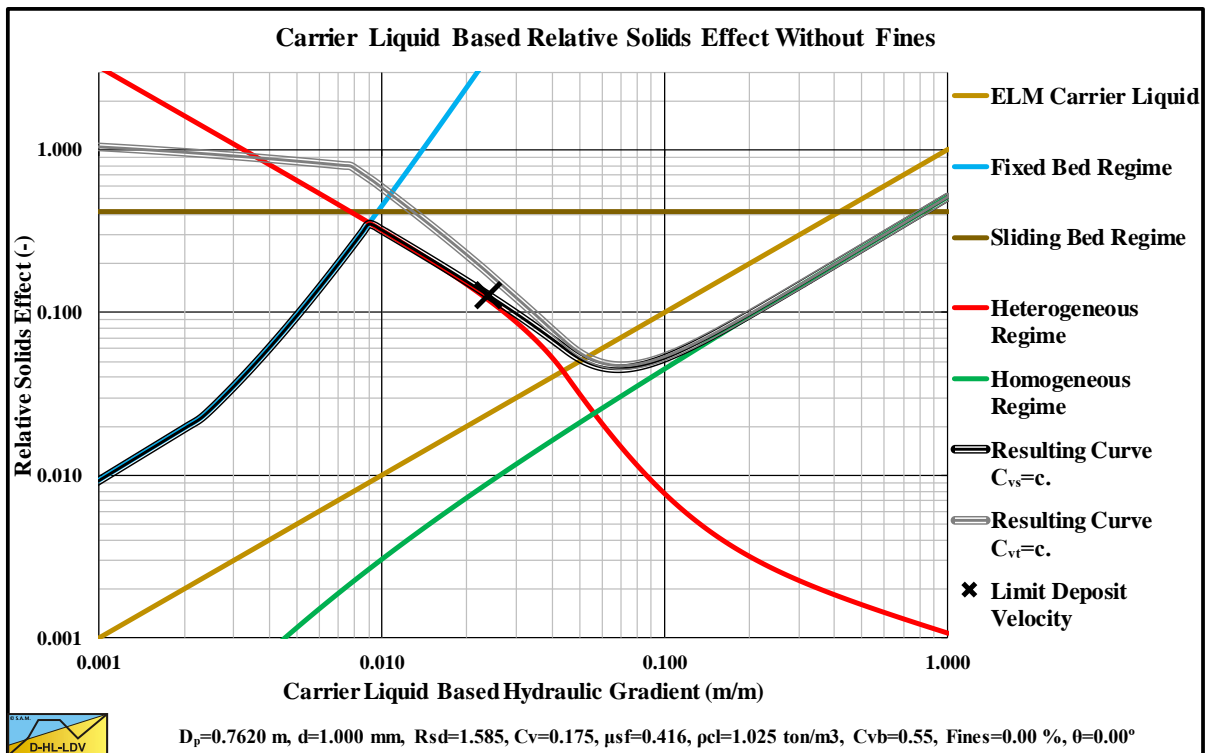
Figure 15.5-2: The relative excess hydraulic gradient versus the liquid hydraulic gradient.
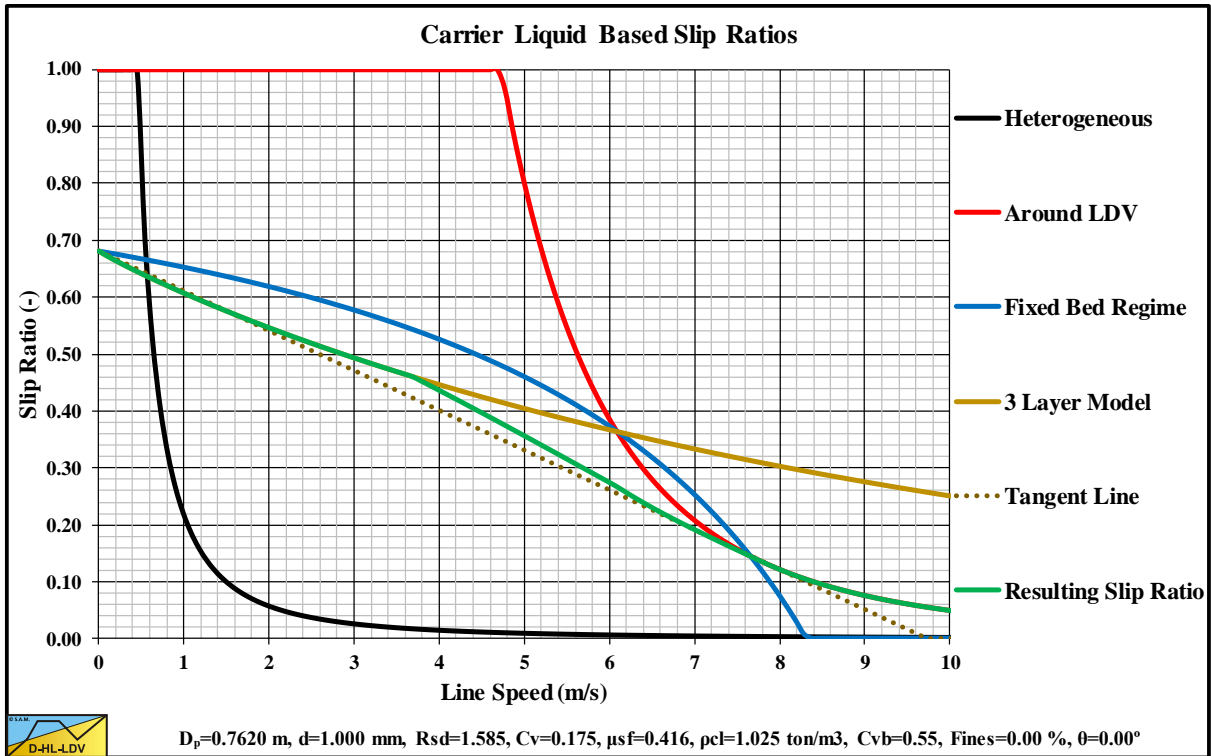
Figure 15.5-3: The slip ratio versus the line speed.
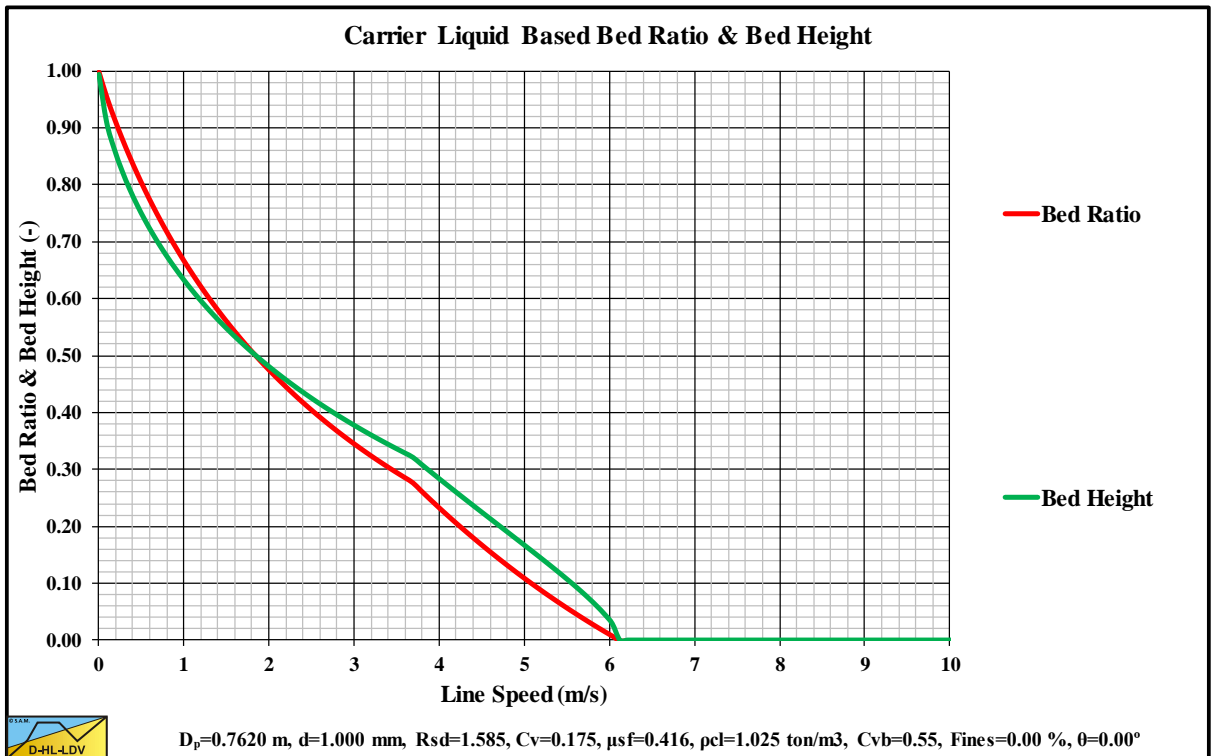
Figure 15.5-4: The bed fraction and bed height versus the line speed.

Appendices.
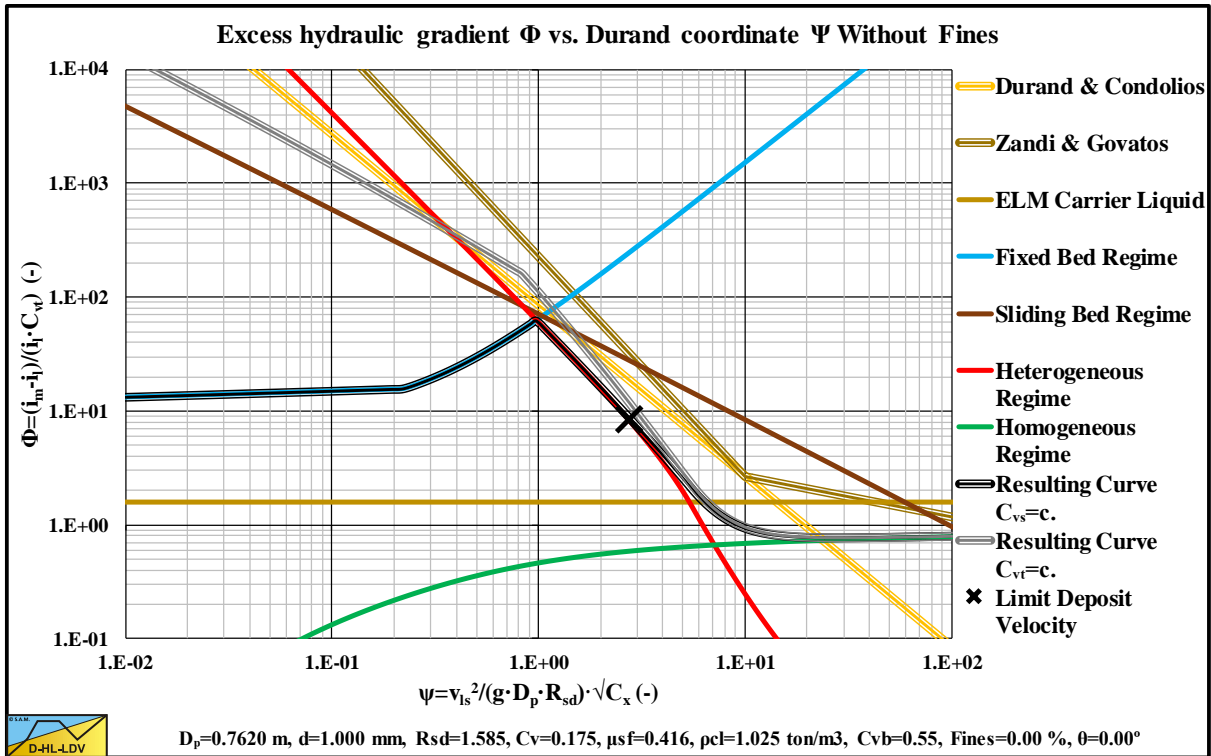
Figure 15.5-5: The hydraulic gradient on Durand coordinates.
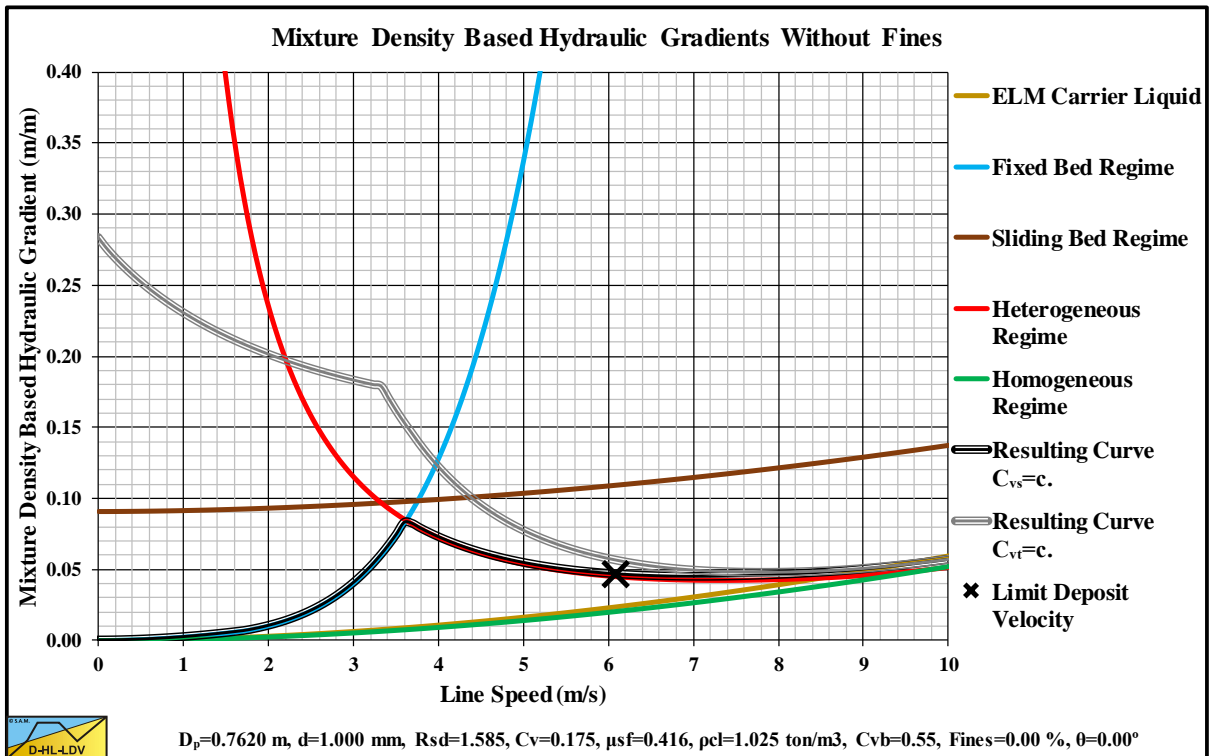
Figure 15.5-6: The hydraulic gradient versus the line speed, mixture density based.

Figure 15.5-7: The Limit Deposit Velocity.

Figure 15.5-8: The Limit Deposit Velocity versus the pipe diameter for 5 sands.
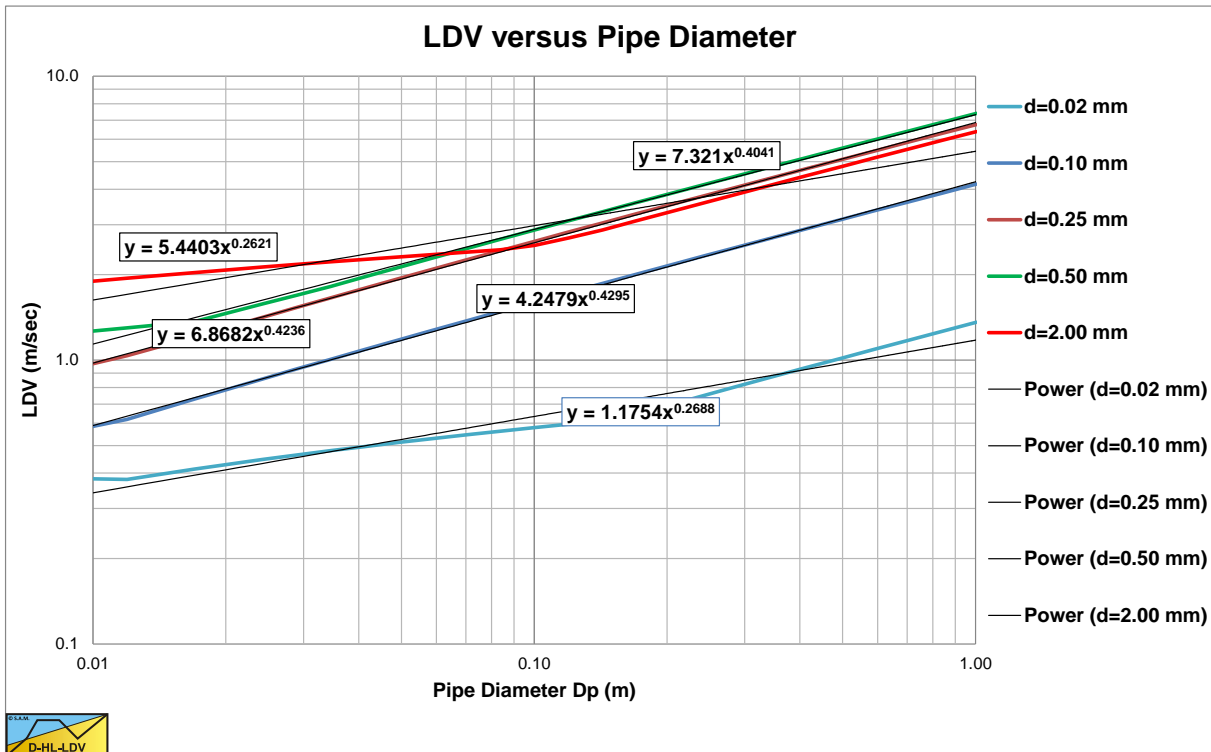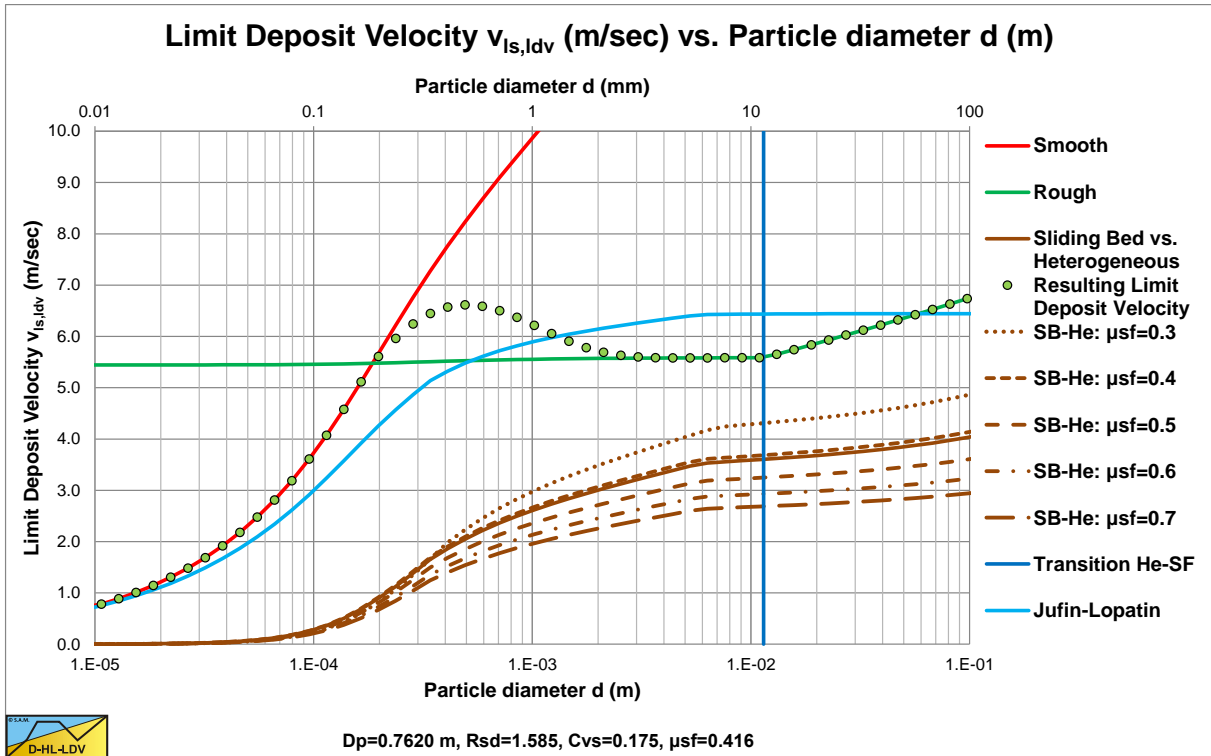
Appendices.

15.5.2 9 Particle Diameters.
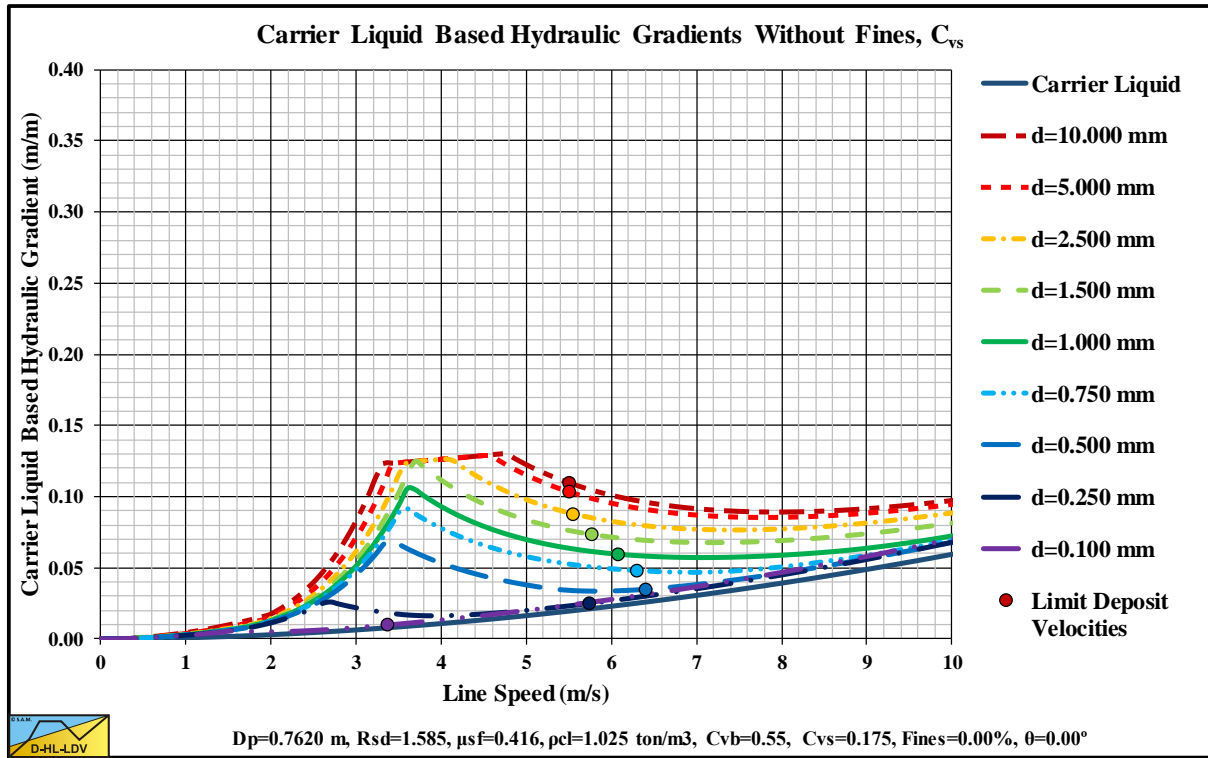
Figure 15.5-9: The hydraulic gradient versus the line speed for 9 particle diameters, C$_{vs}$.
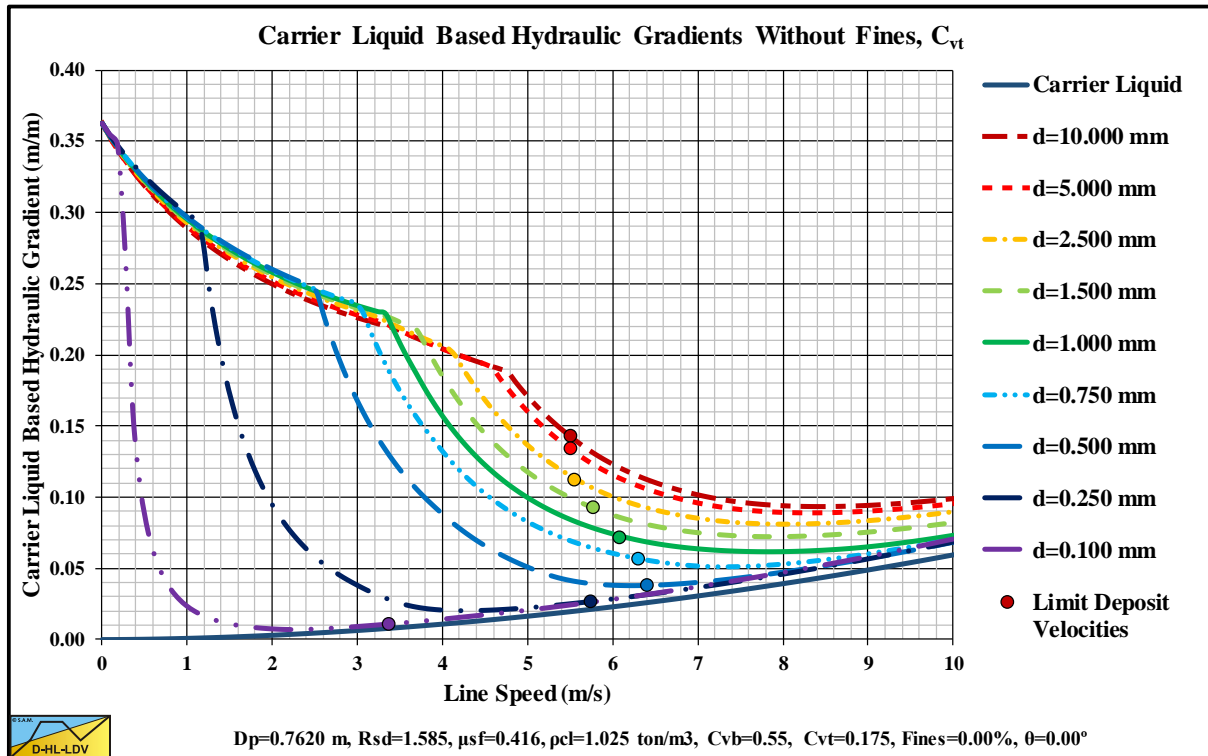
Figure 15.5-10: The hydraulic gradient versus the line speed for 9 particle diameters, C$_{vt}$.
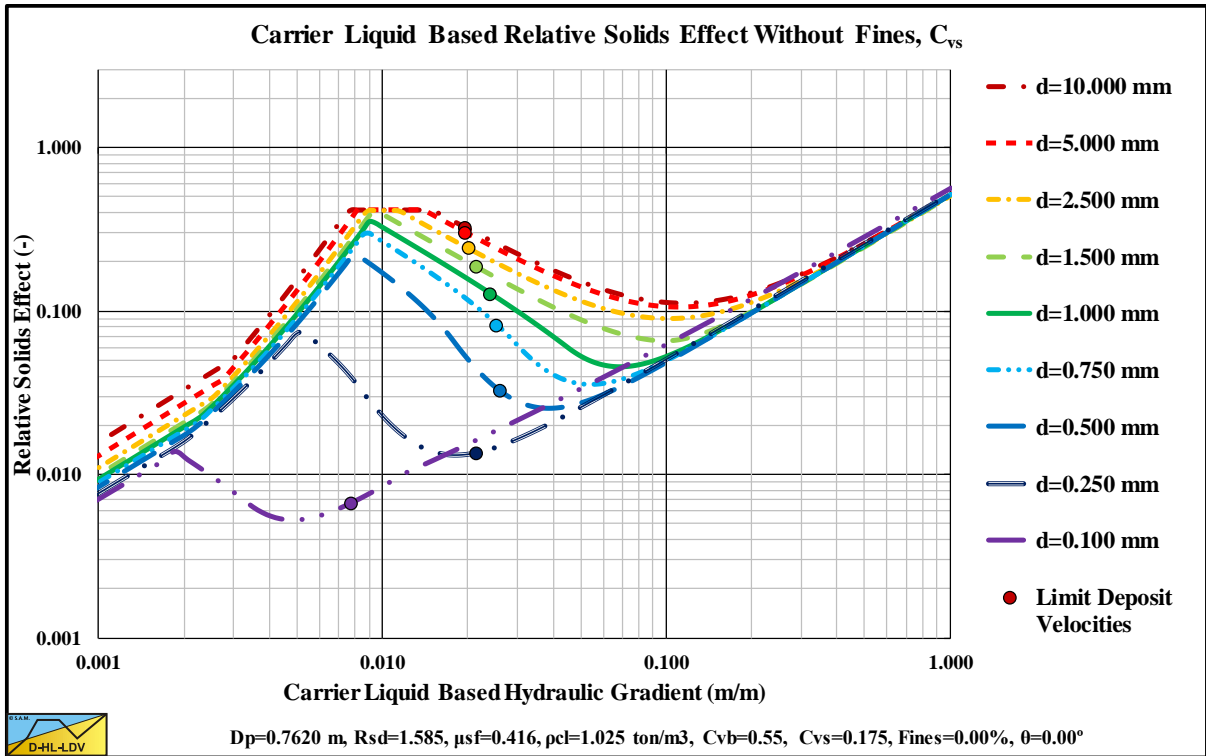
Figure 15.5-11: The relative excess hydraulic gradient versus the liquid hydraulic gradient for 9 particle diameters, C_{vs}.
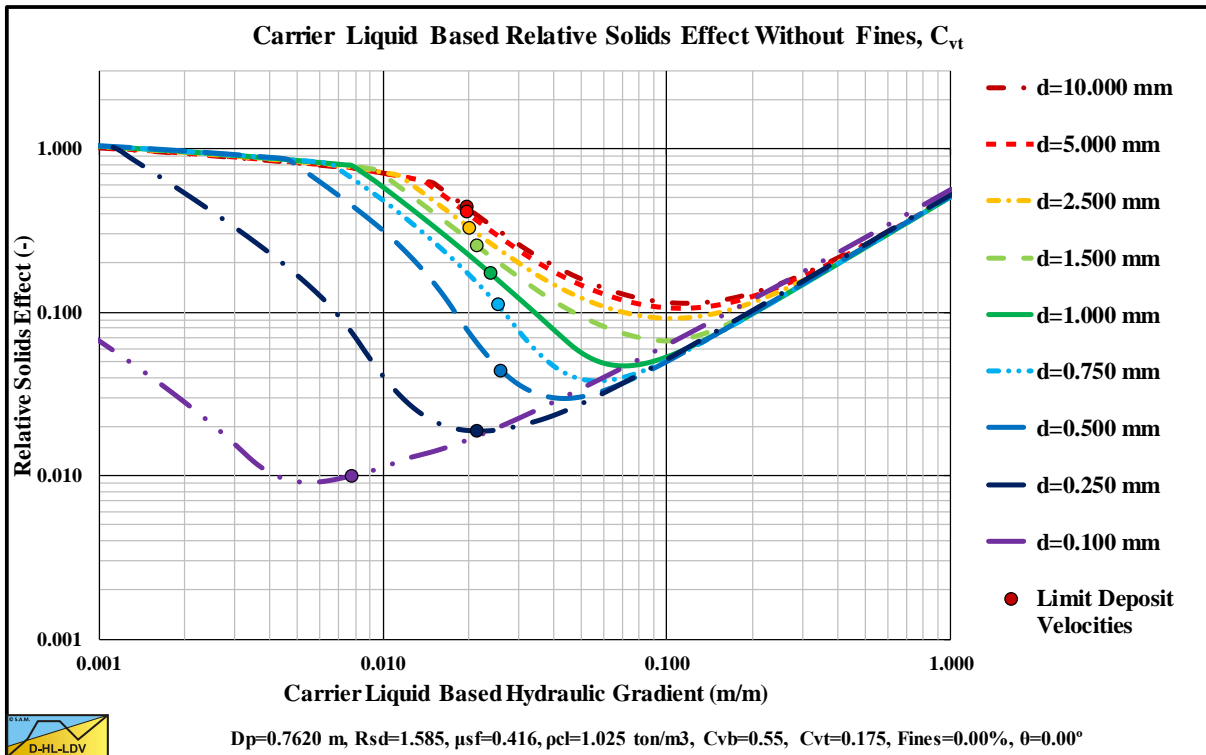
Figure 15.5-12: The relative excess hydraulic gradient versus the liquid hydraulic gradient for 9 particle diameters, C_{vt}.

Figure 15.5-13: The hydraulic gradient on Durand coordinates for 9 particle diameters, C_{vs}.
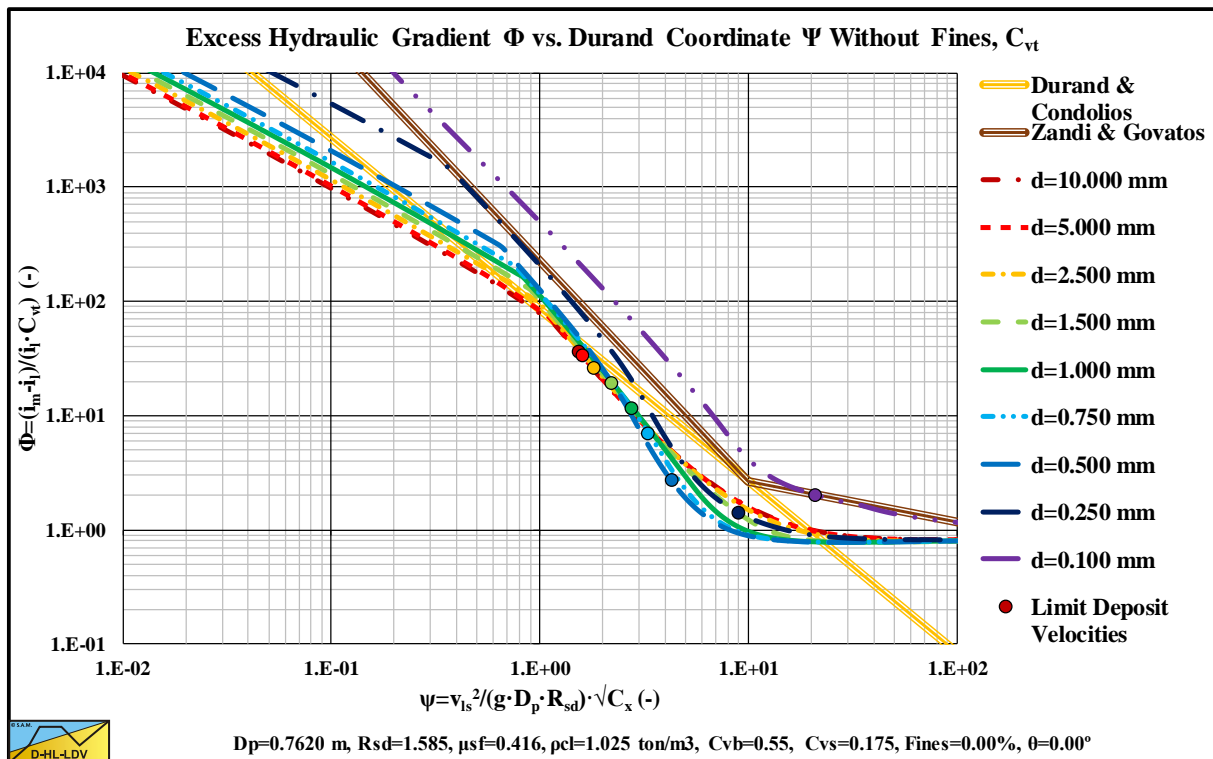
Figure 15.5-14: The hydraulic gradient on Durand coordinates for 9 particle diameters, C_{vt}.

Dp=0.7620 m, Rsd=1.585, μsf=0.416, ρcl=1.025 ton/m3, Cvb=0.55, Cvt=0.175, Fines=0.00%, θ=0.00°
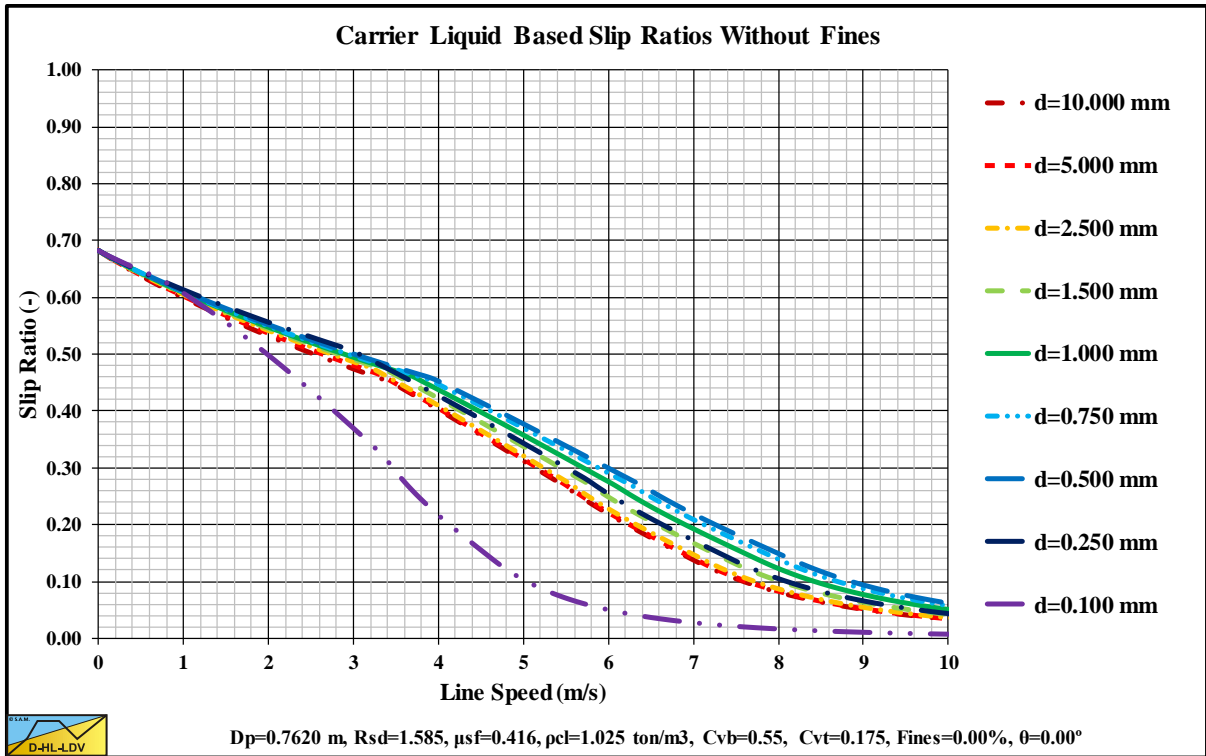
Figure 15.5-15: The slip ratio for 9 particle diameters.

Dp=0.7620 m, Rsd=1.585, μsf=0.416, ρcl=1.025 ton/m3, Cvb=0.55, Cvt=0.175, Fines=0.00%, θ=0.00°
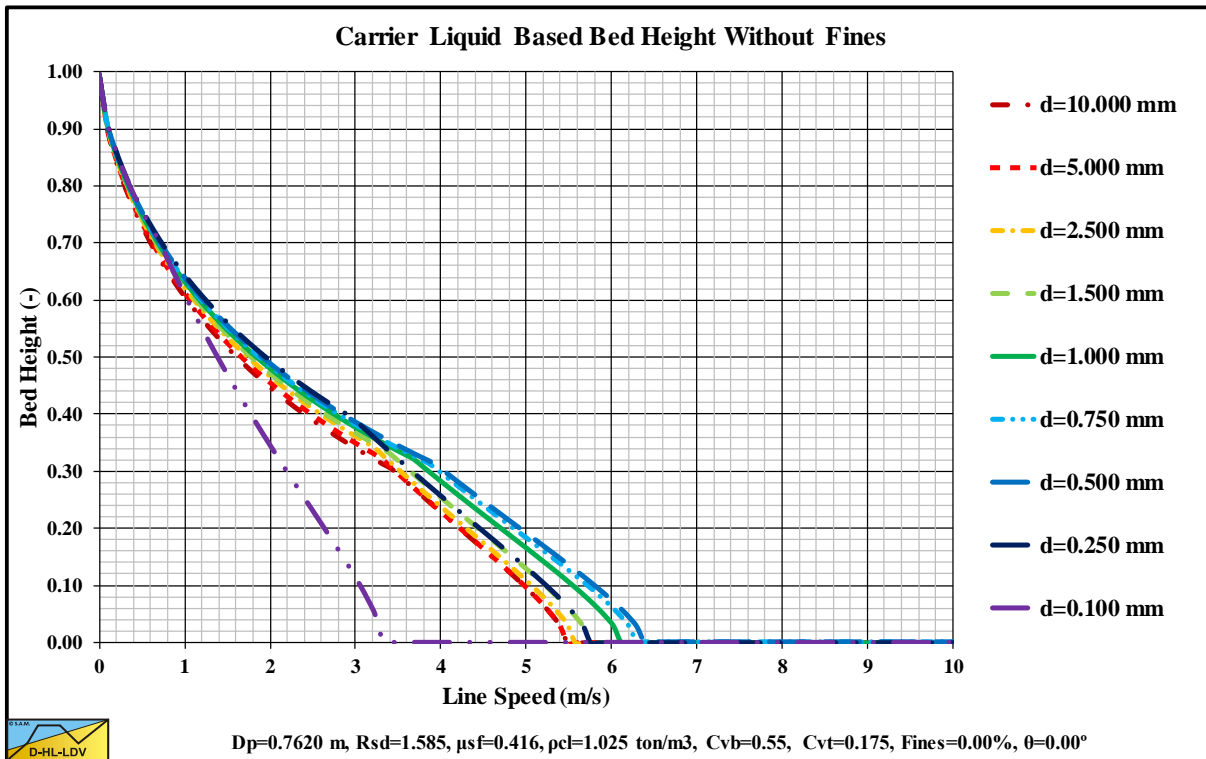
Figure 15.5-16: The bed height for 9 particle diameters.

15.5.3 9 Concentrations.
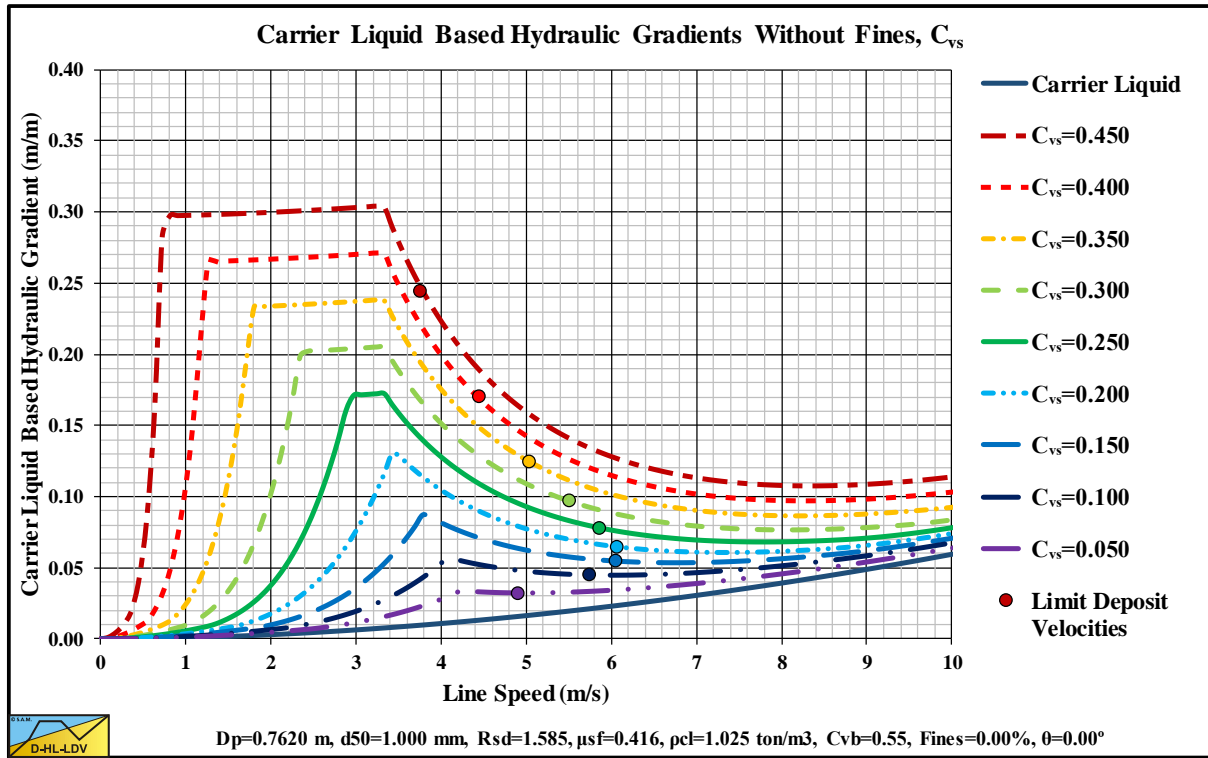
Figure 15.5-17: The hydraulic gradient versus the line speed for 9 concentrations, C$_{vs}$.
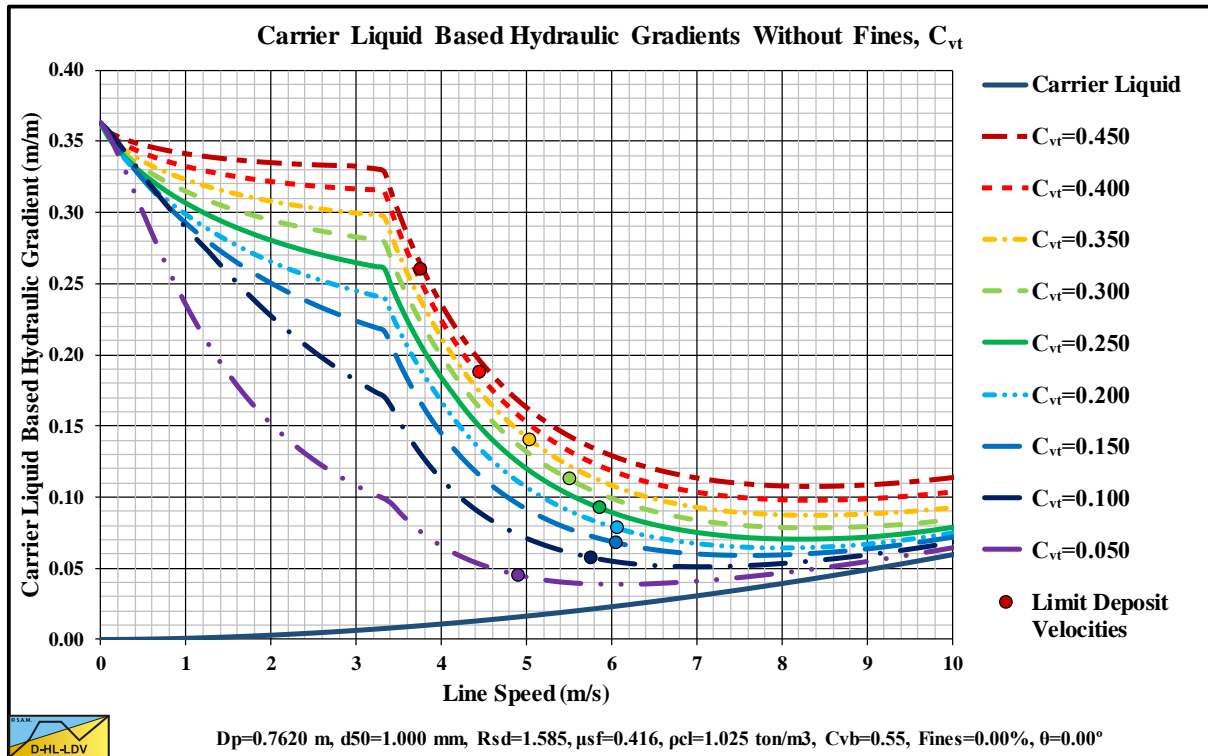
Figure 15.5-18: The hydraulic gradient versus the line speed for 9 concentrations, C$_{vt}$.
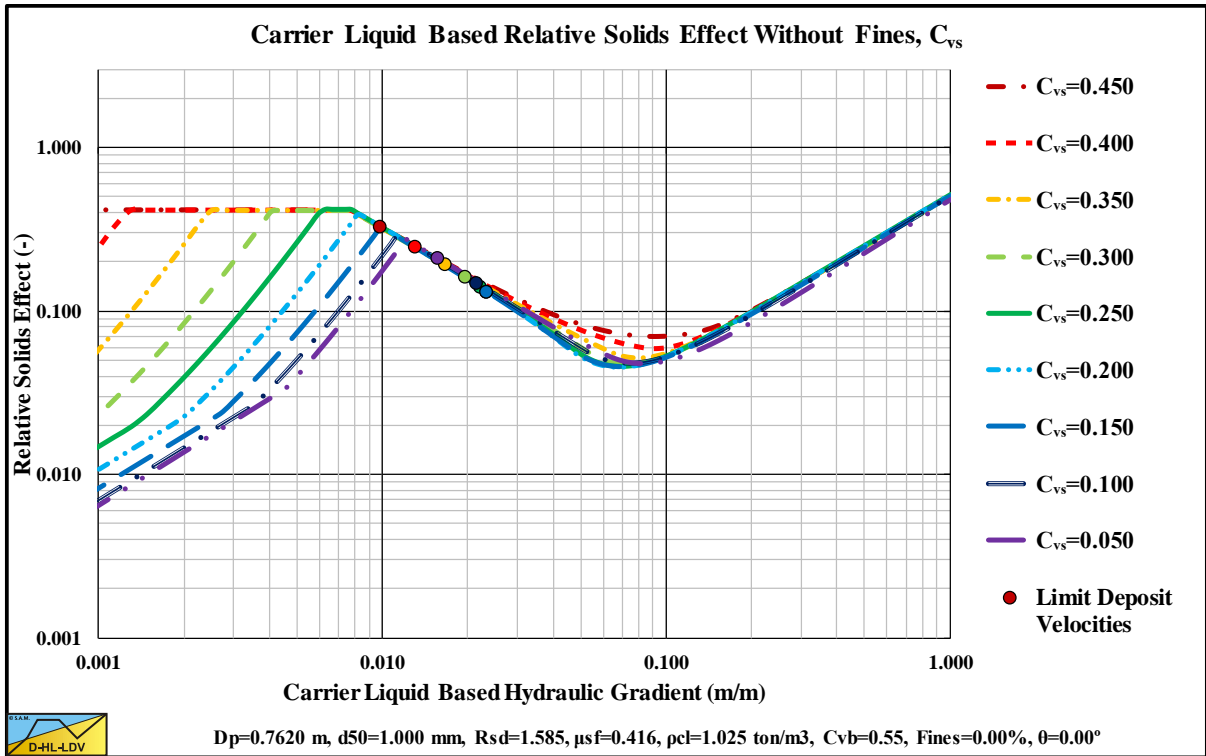
Figure 15.5-19: The relative excess hydraulic gradient versus the liquid hydraulic gradient for 9 concentrations, C$_{vs}$.
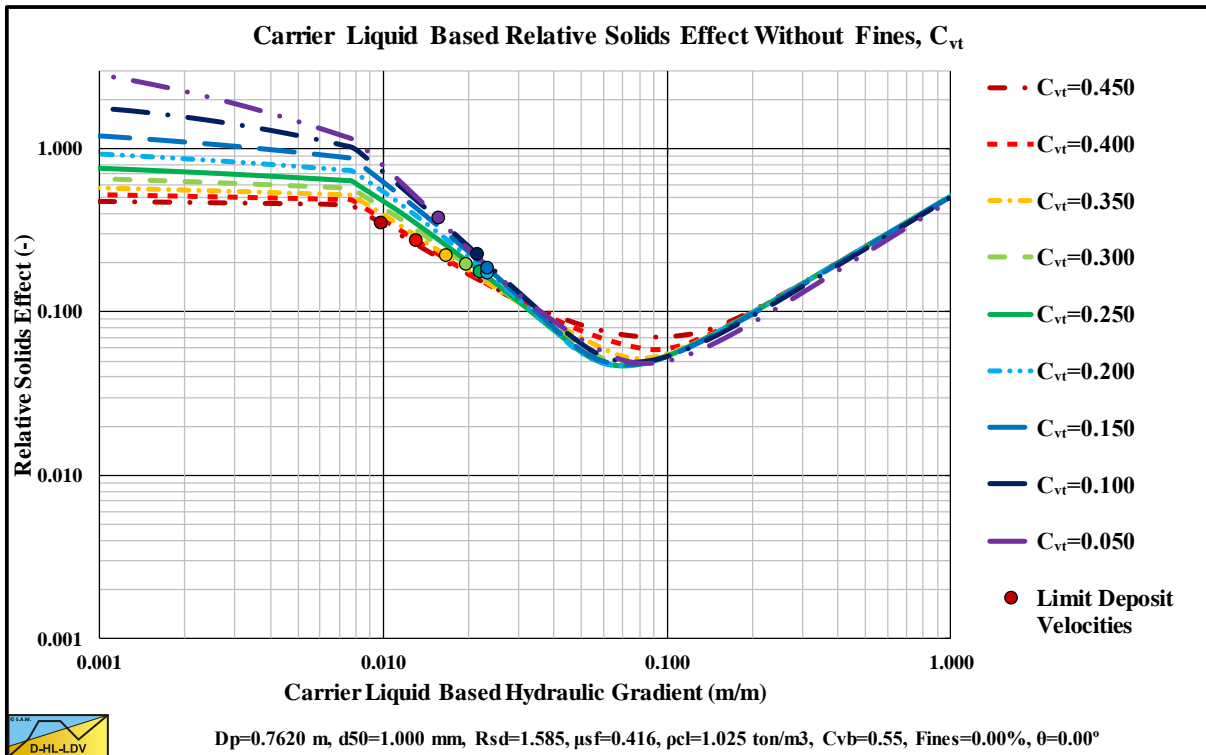
Figure 15.5-20: The relative excess hydraulic gradient versus the liquid hydraulic gradient for 9 concentrations, C$_{vt}$.
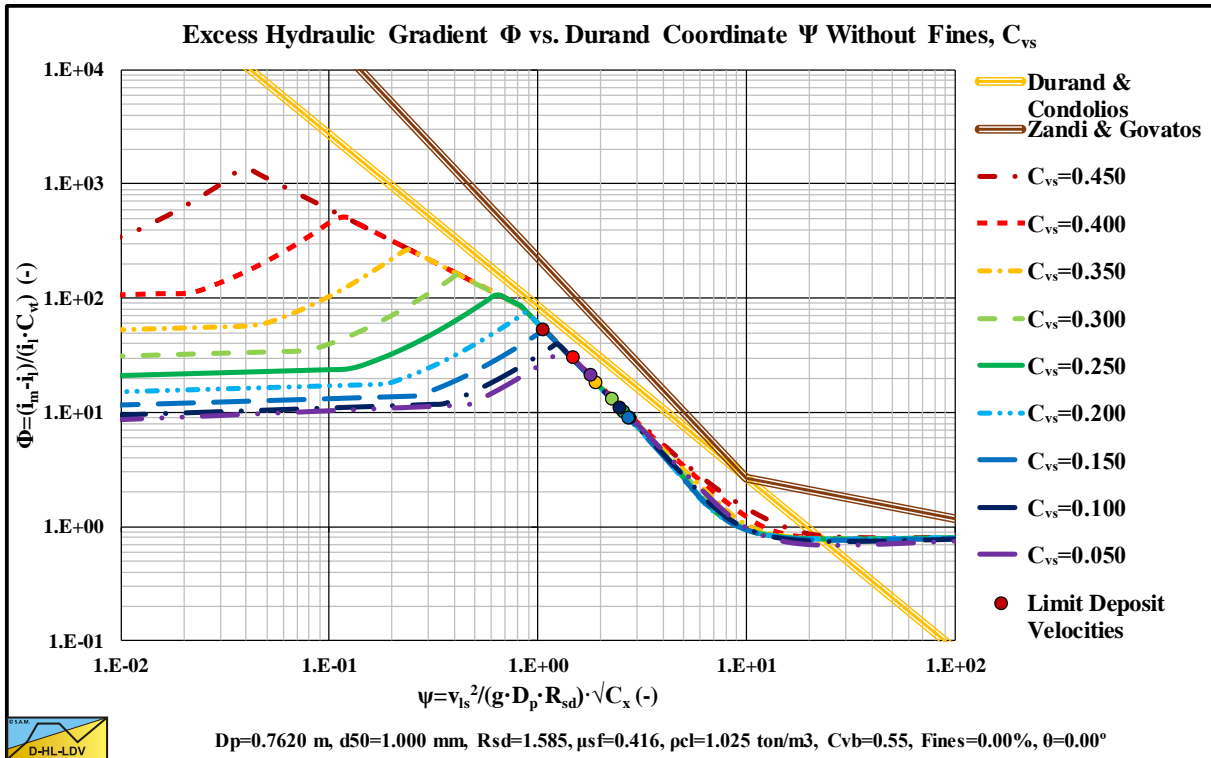
Figure 15.5-21: The hydraulic gradient on Durand coordinates for 9 concentrations, C_{vs}.
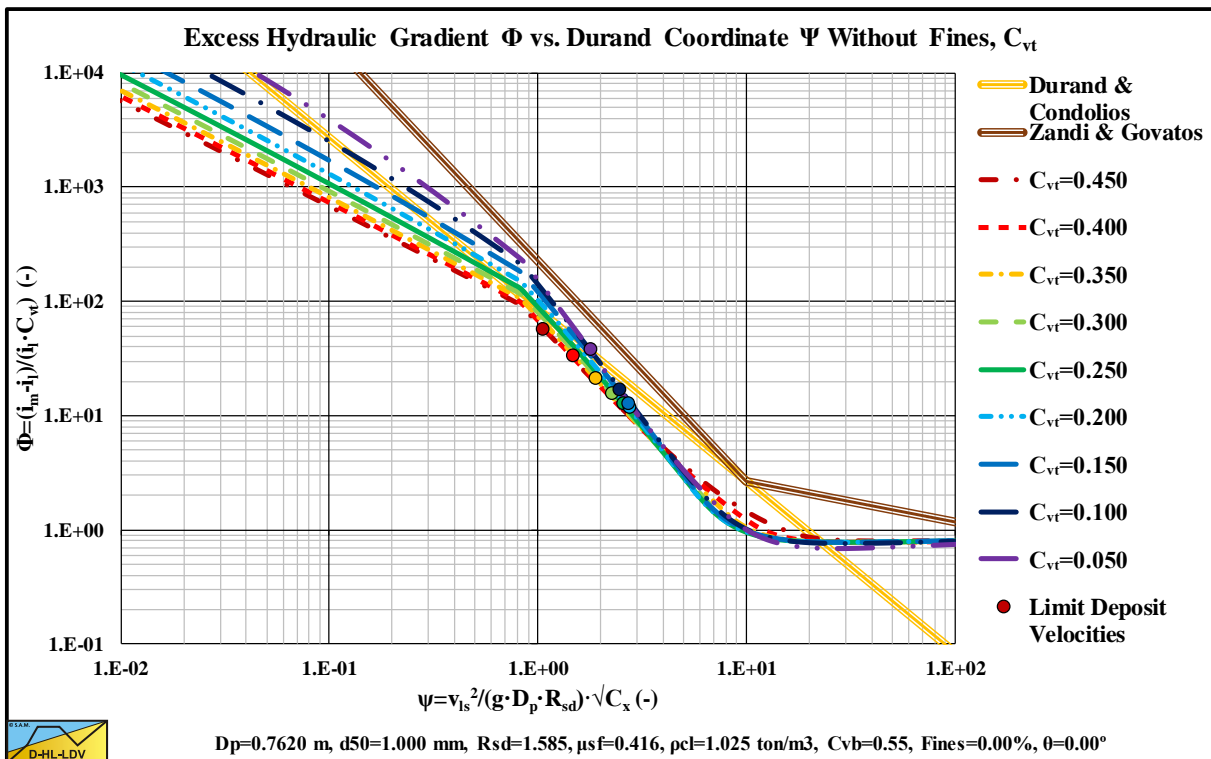
Figure 15.5-22: The hydraulic gradient on Durand coordinates for 9 concentrations, C_{vt}.
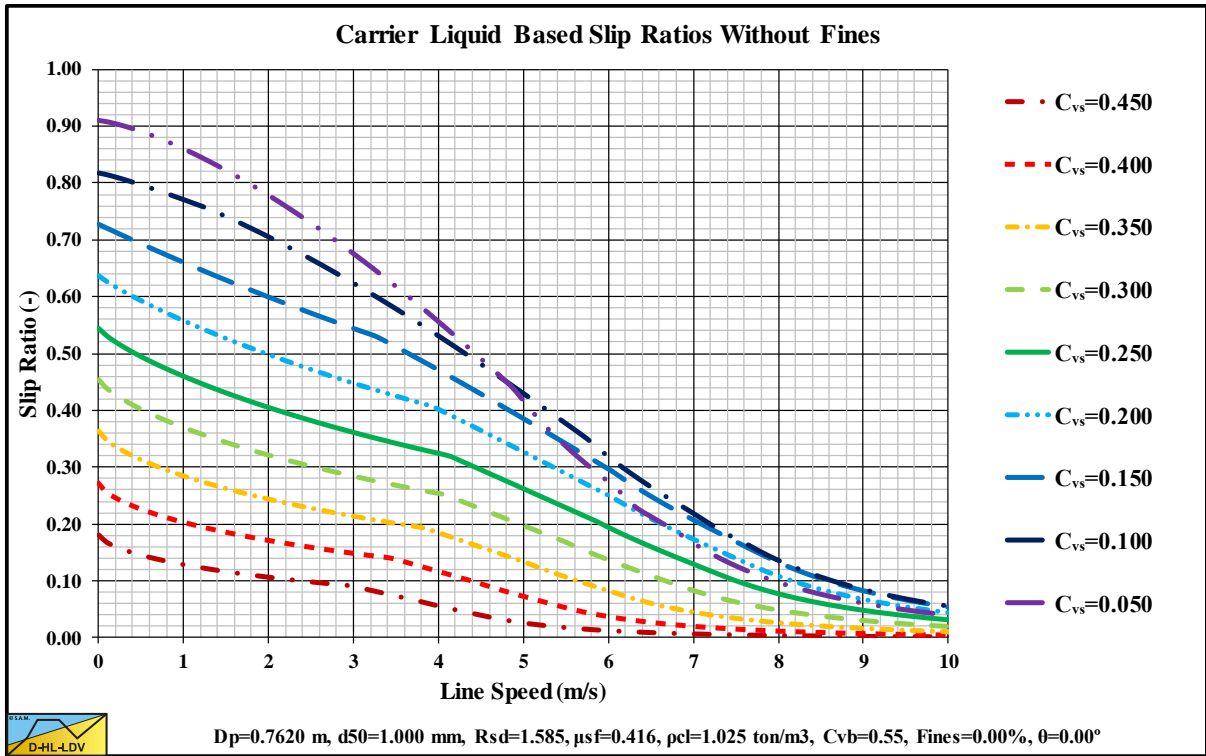
Figure 15.5-23: The slip ratio for 9 concentrations.
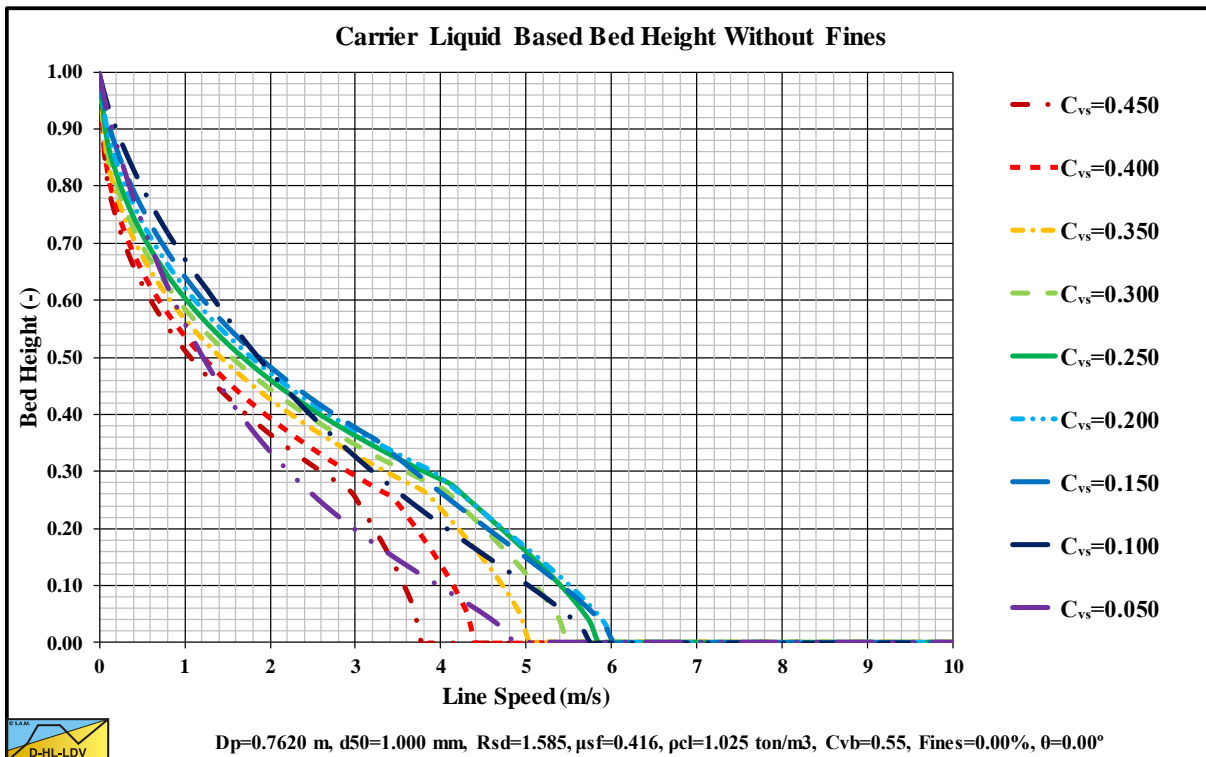
Figure 15.5-24: The bed height for 9 concentrations.
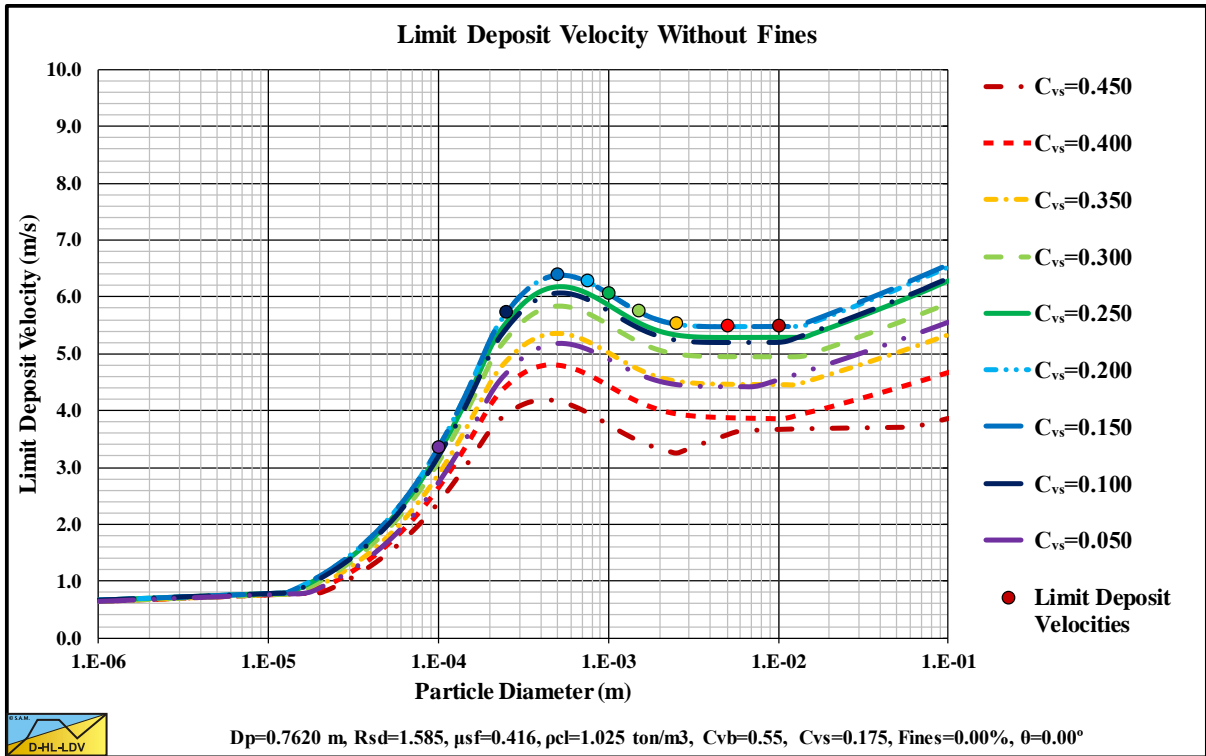
Figure 15.5-25: The Limit Deposit Velocity versus the particle diameter for 9 concentrations.

15.5.4 9 Pipe Diameters.
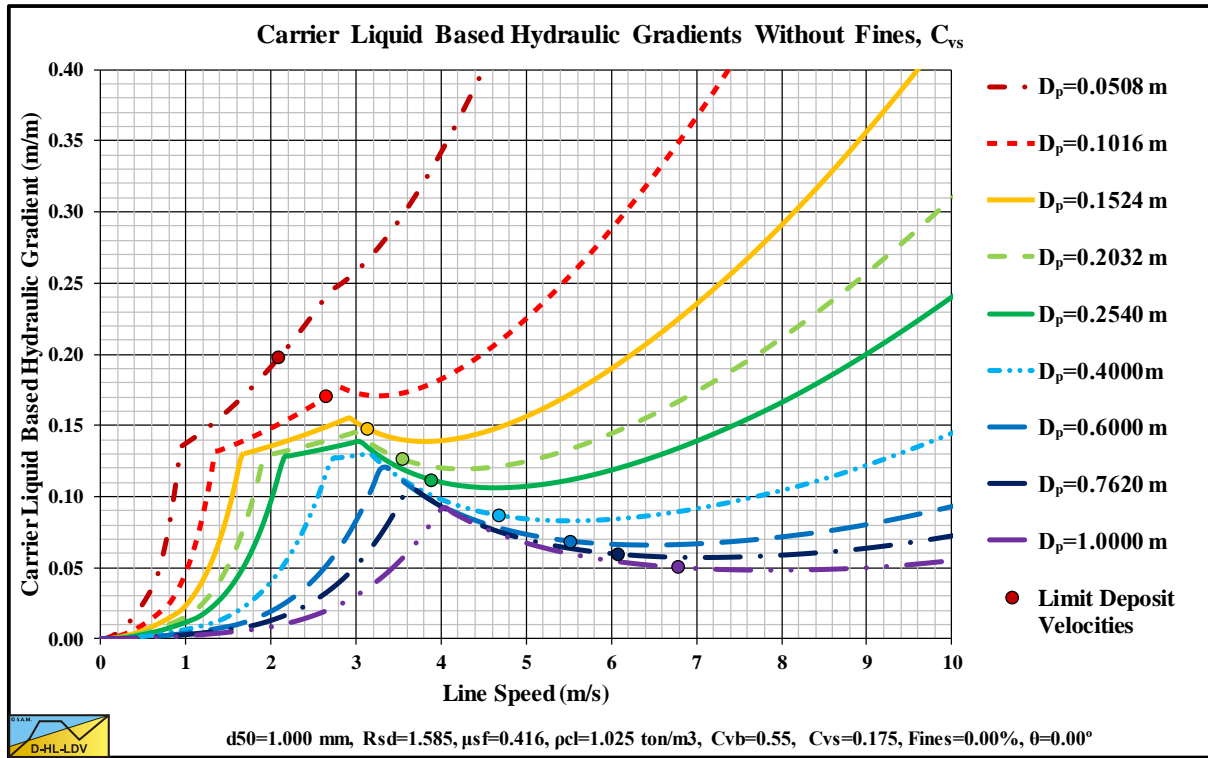
Figure 15.5-26: The hydraulic gradient versus the line speed for 9 pipe diameters, C$_{vs}$.
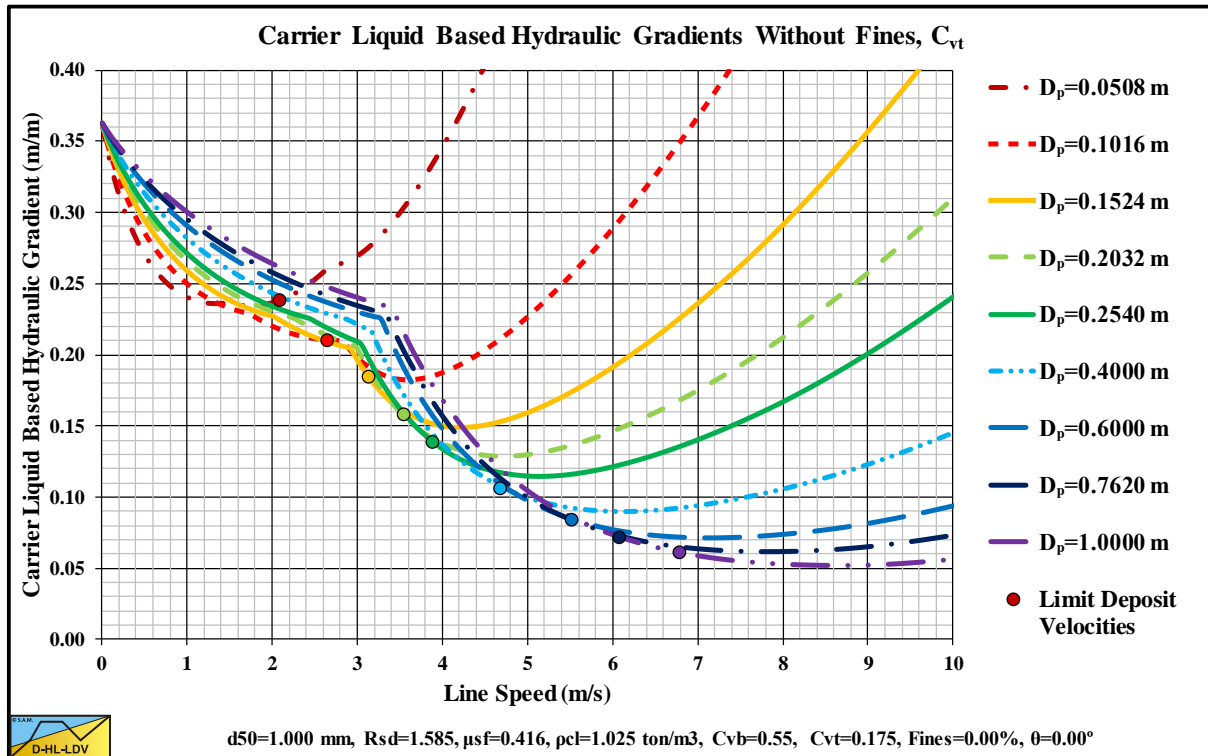
Figure 15.5-27: The hydraulic gradient versus the line speed for 9 pipe diameters, C$_{vt}$.
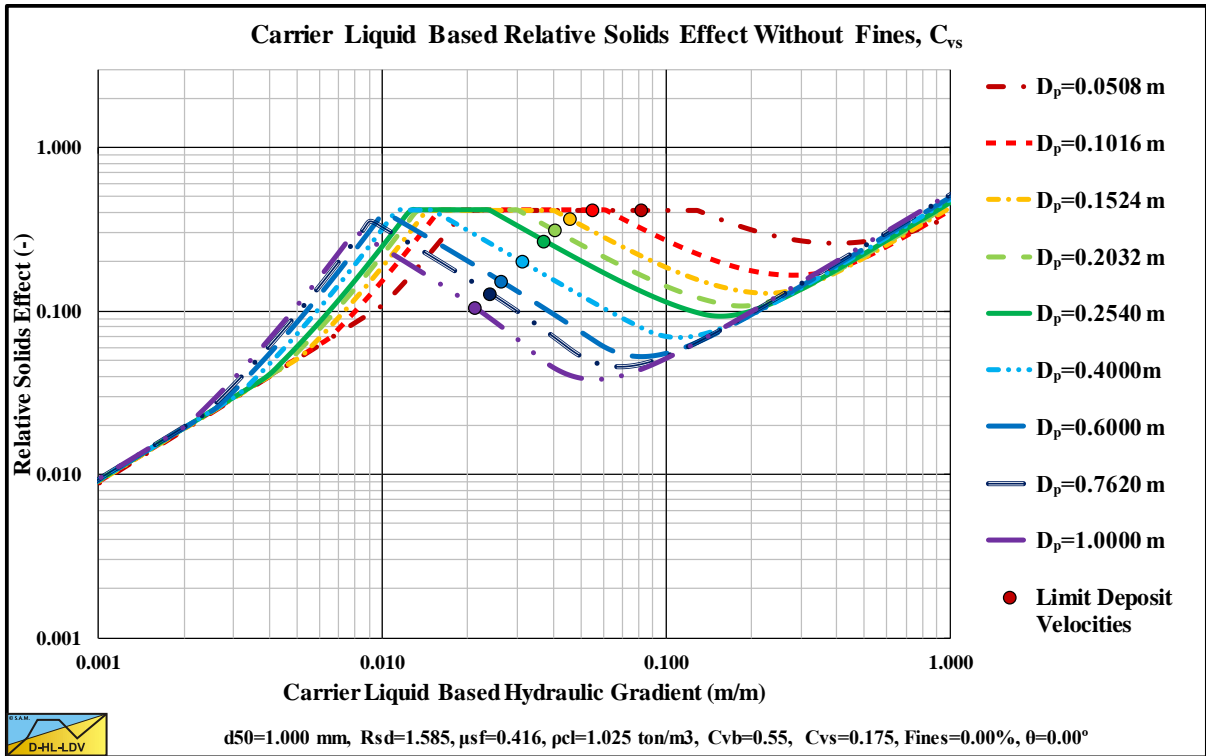
Figure 15.5-28: The relative excess hydraulic gradient versus the liquid hydraulic gradient for 9 pipe diameters, C$_{vs}$.
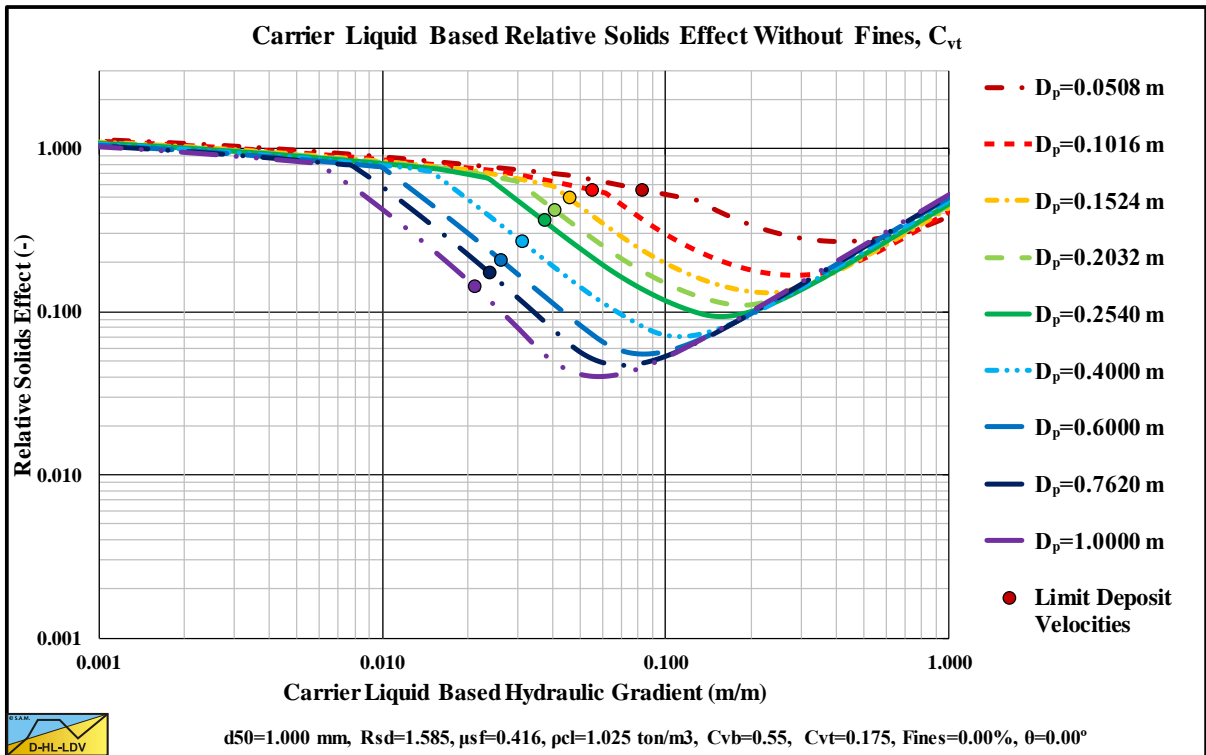
Figure 15.5-29: The relative excess hydraulic gradient versus the liquid hydraulic gradient for 9 pipe diameters, C$_{vt}$.

Appendices.
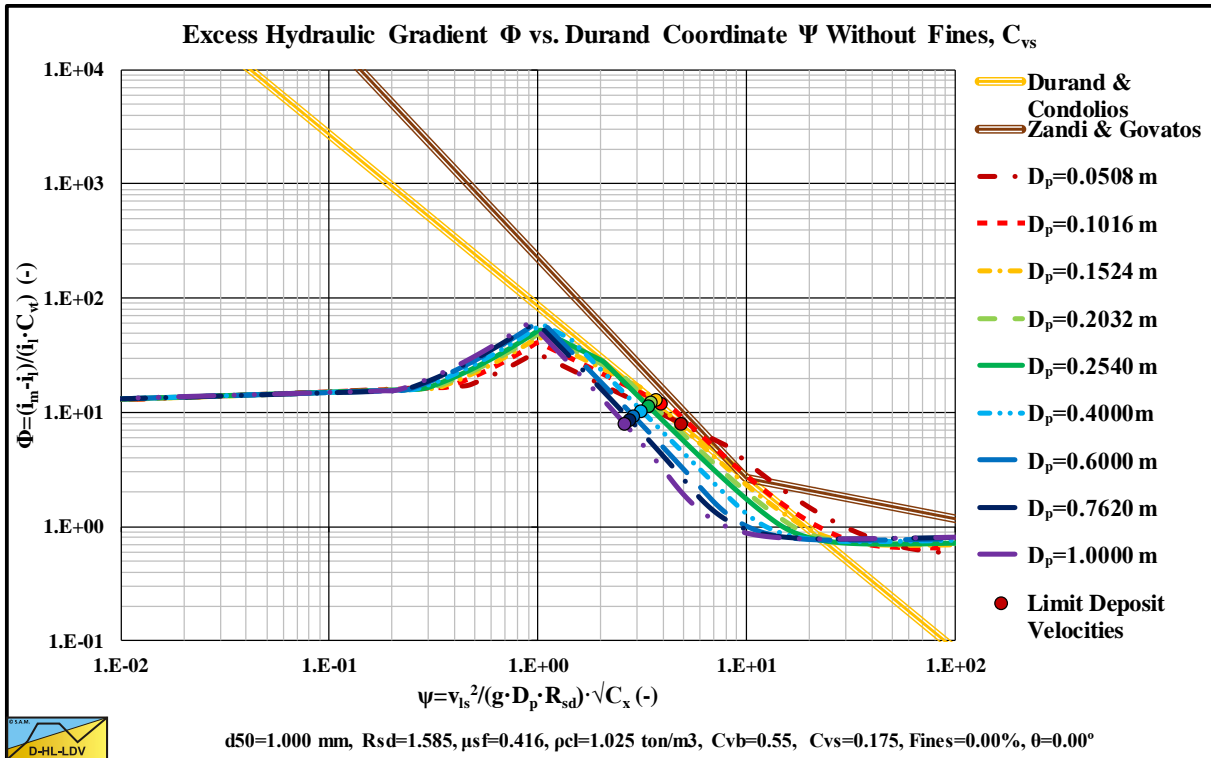
Figure 15.5-30: The hydraulic gradient on Durand coordinates for 9 pipe diameters, C_{vs}.
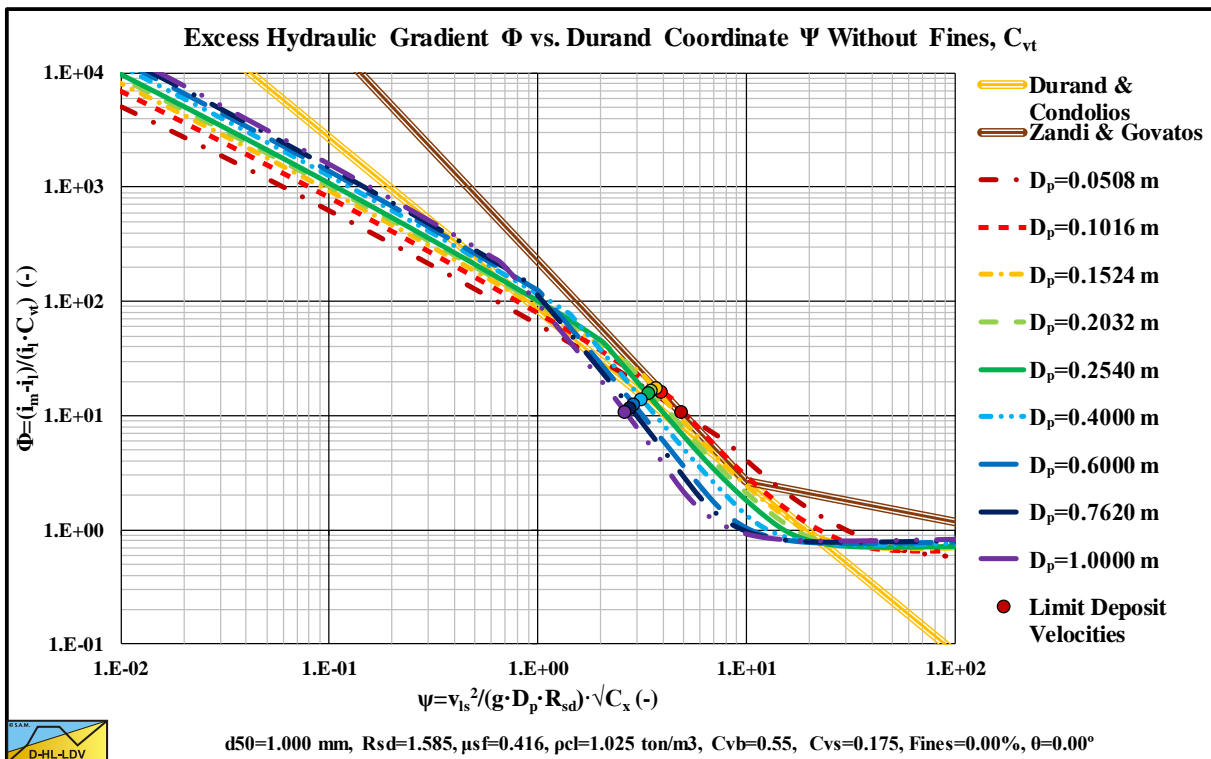
Figure 15.5-31: The hydraulic gradient on Durand coordinates for 9 pipe diameters, C_{vt}.

d50=1.000 mm, Rsd=1.585, µsf=0.416, ρcl=1.025 ton/m3, Cvb=0.55, Cvt=0.175, Fines=0.00%, θ=0.00º
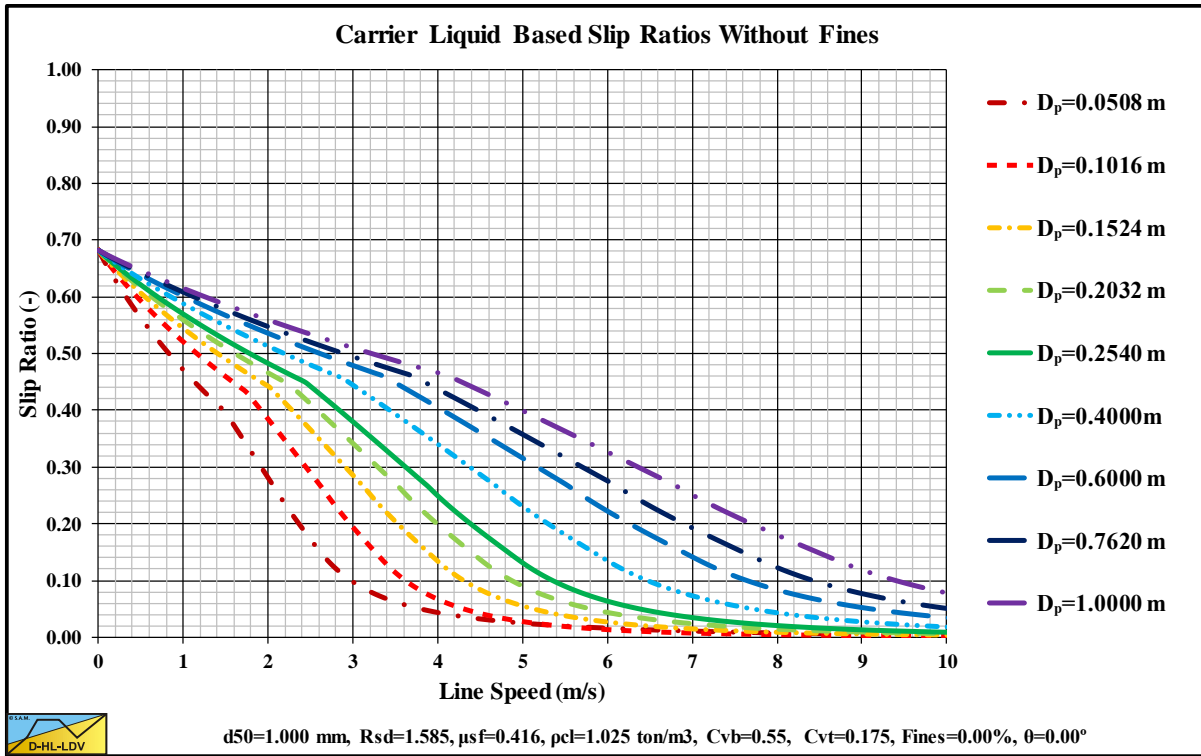
Figure 15.5-32: The slip ratio for 9 pipe diameters.

d50=1.000 mm, Rsd=1.585, µsf=0.416, ρcl=1.025 ton/m3, Cvb=0.55, Cvt=0.175, Fines=0.00%, θ=0.00º
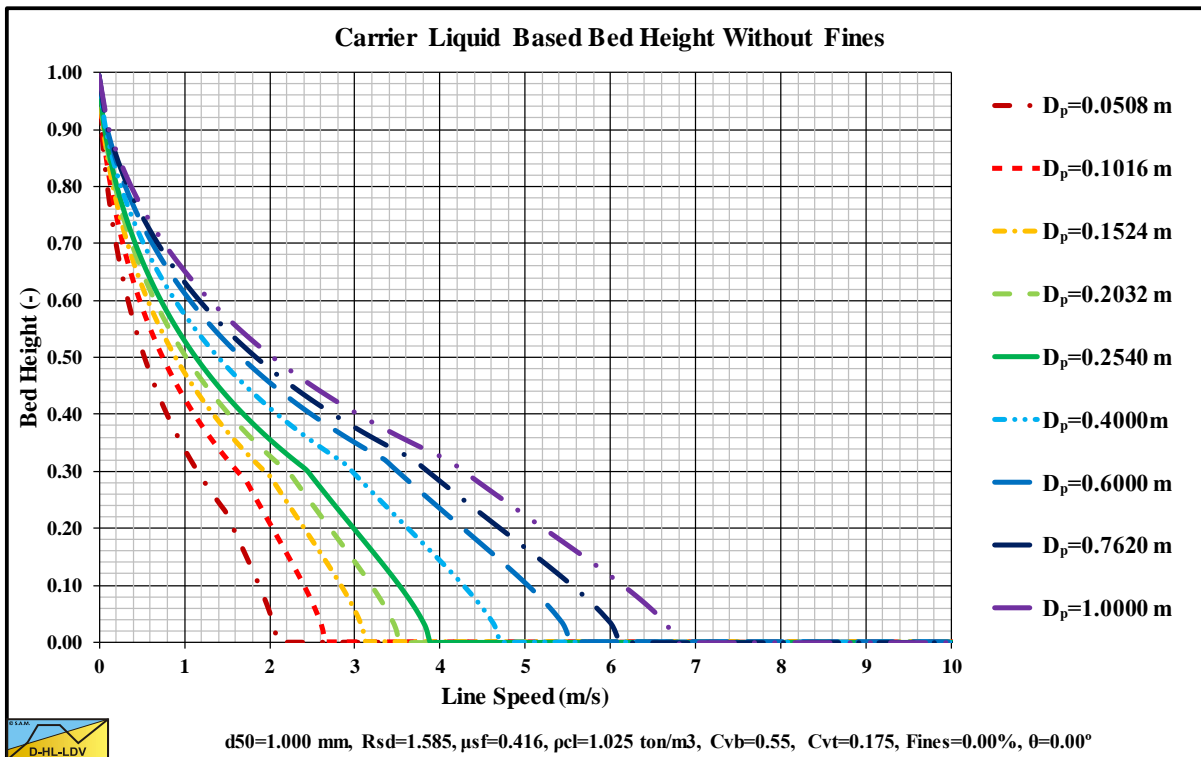
Figure 15.5-33: The bed height for 9 pipe diameters.
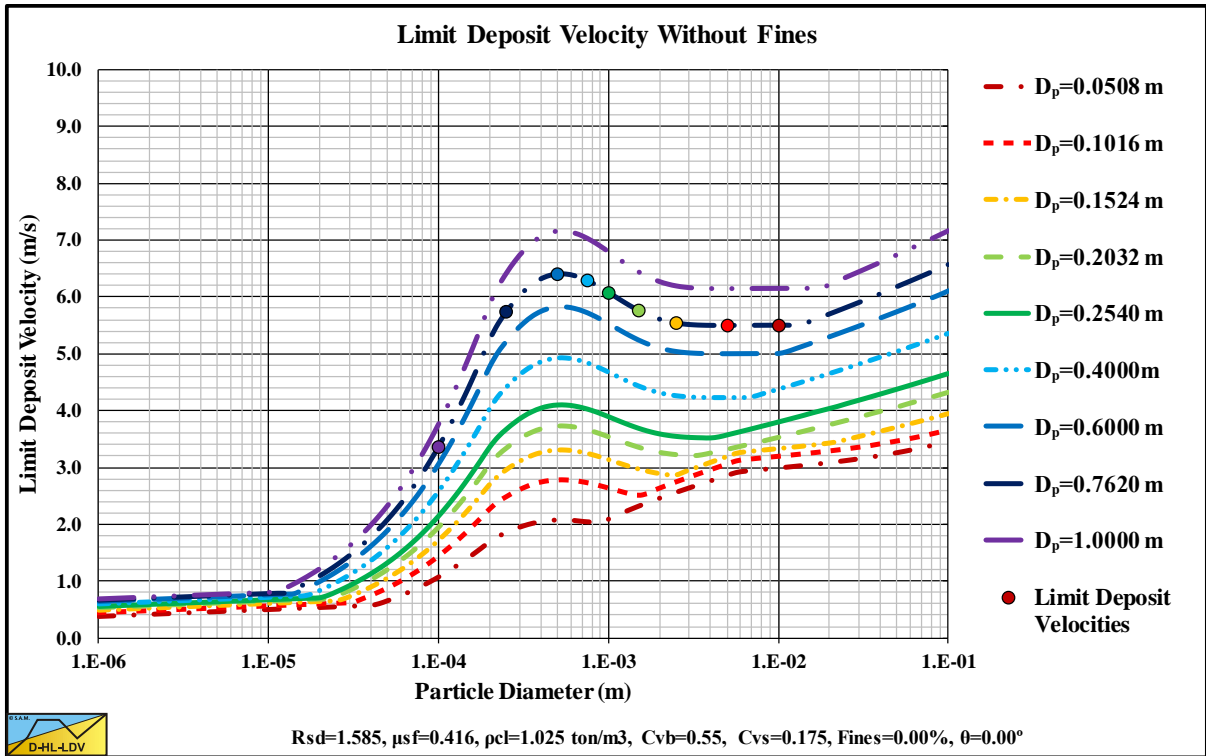
Figure 15.5-34: The Limit Deposit Velocity versus the particle diameter for 9 pipe diameters.

Appendices.

15.5.5 9 Inclination Angles.
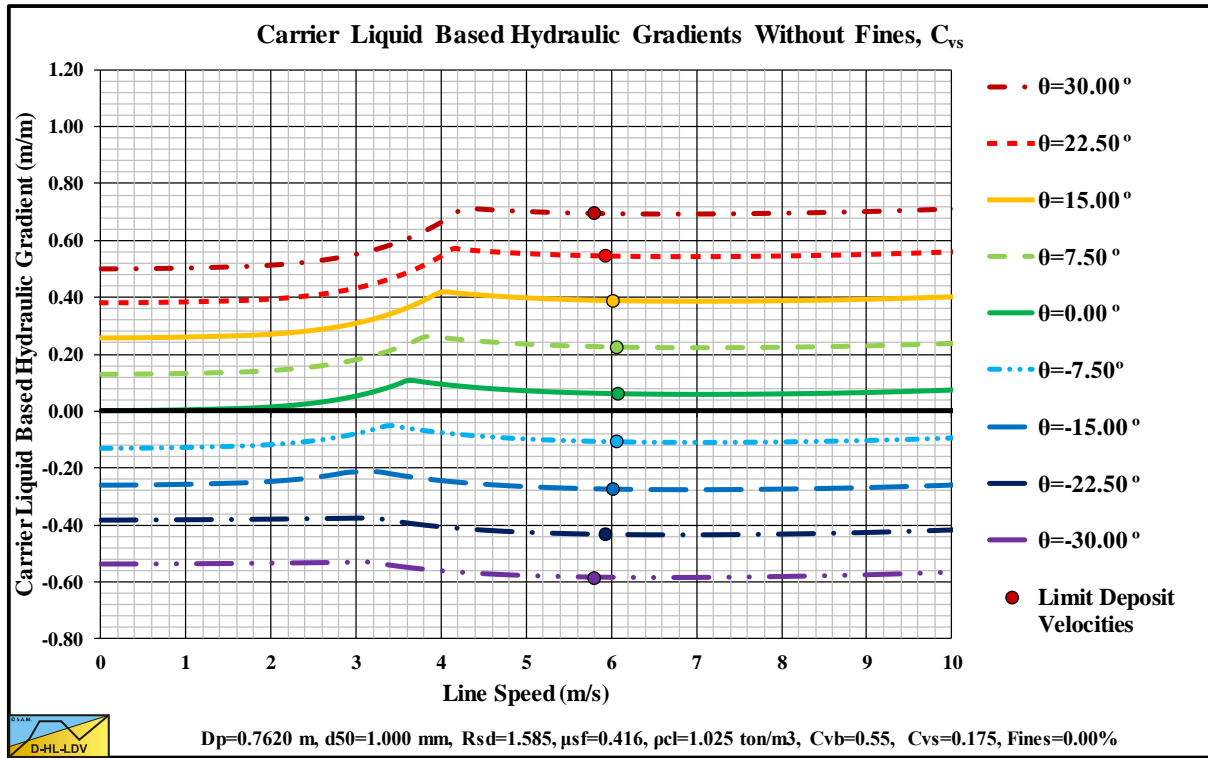
Figure 15.5-35: The hydraulic gradient versus the line speed for 9 inclination angles, C$_{vs}$.
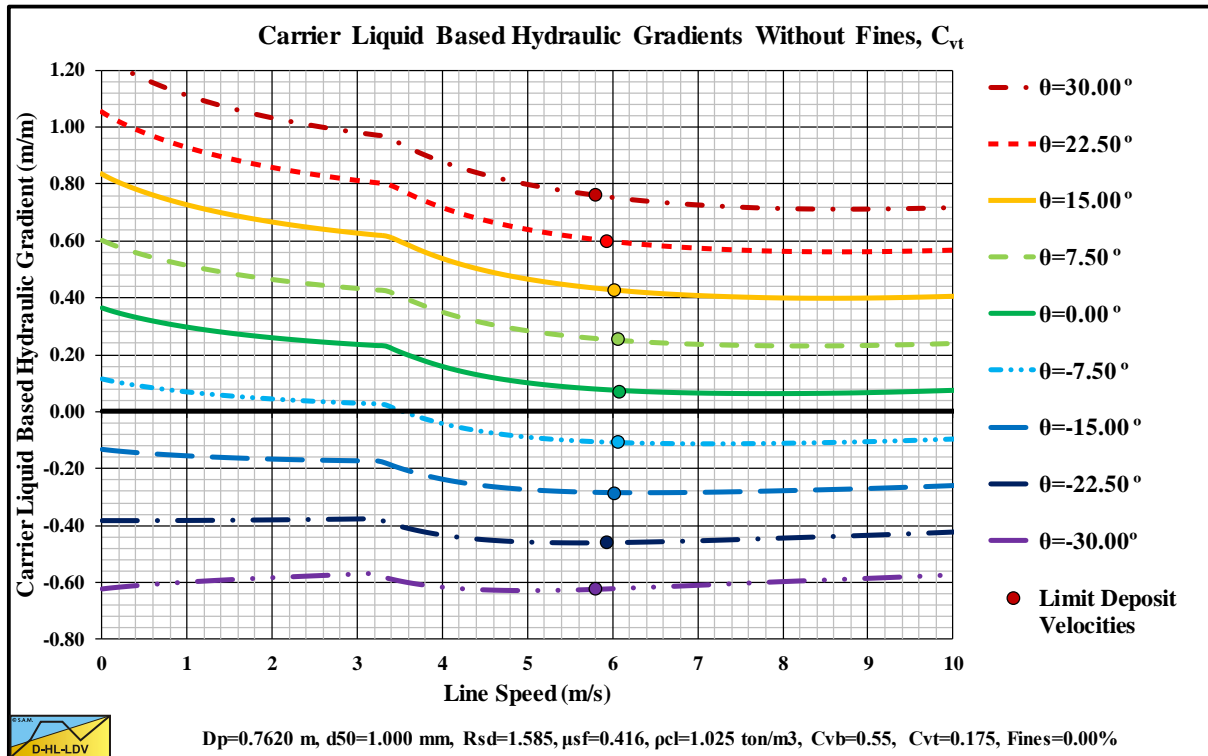
Figure 15.5-36: The hydraulic gradient versus the line speed for 9 inclination angles, C$_{vt}$.
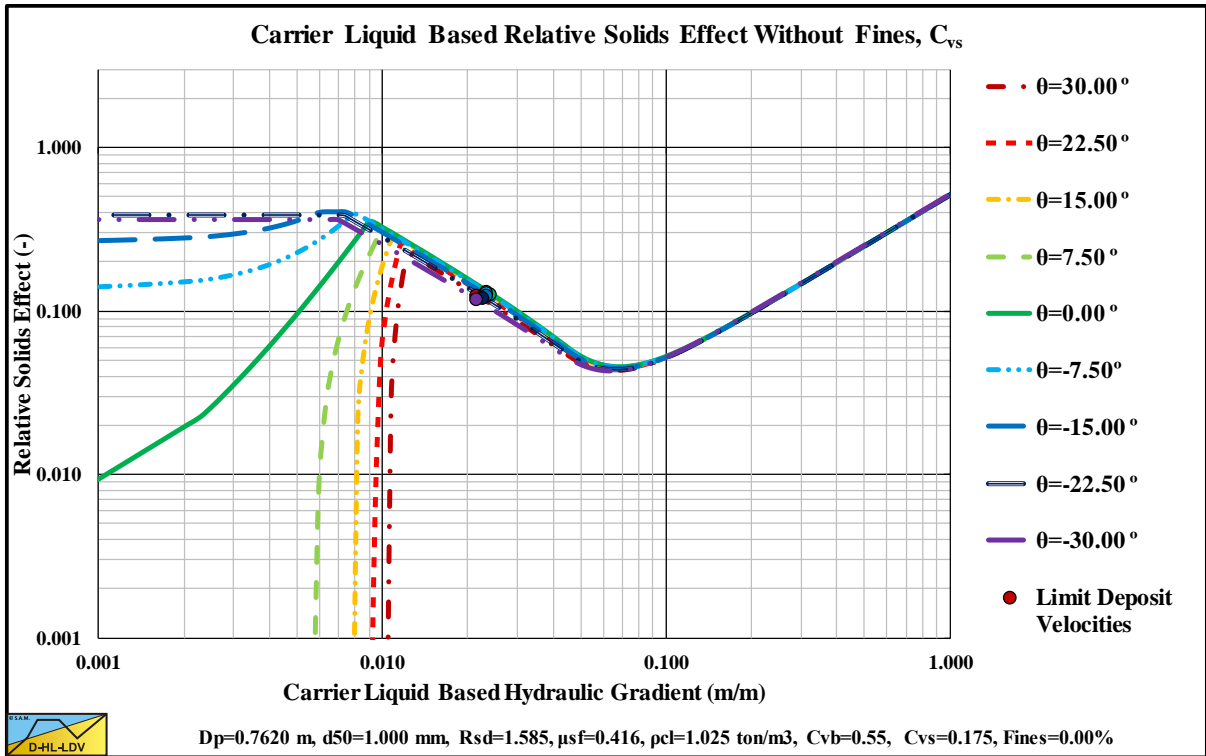
Figure 15.5-37: The relative excess hydraulic gradient versus the liquid hydraulic gradient for 9 inclination angles, C_{vs}.
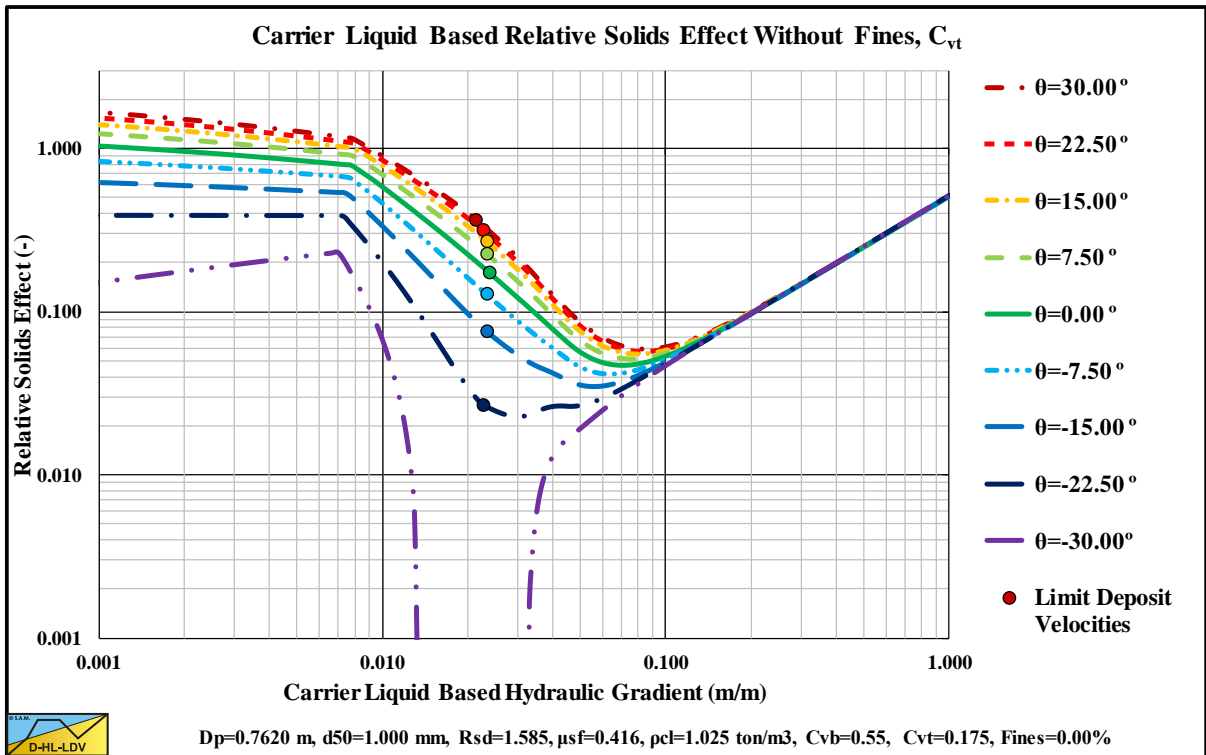
Figure 15.5-38: The relative excess hydraulic gradient versus the liquid hydraulic gradient for 9 inclination angles, C_{vt}.
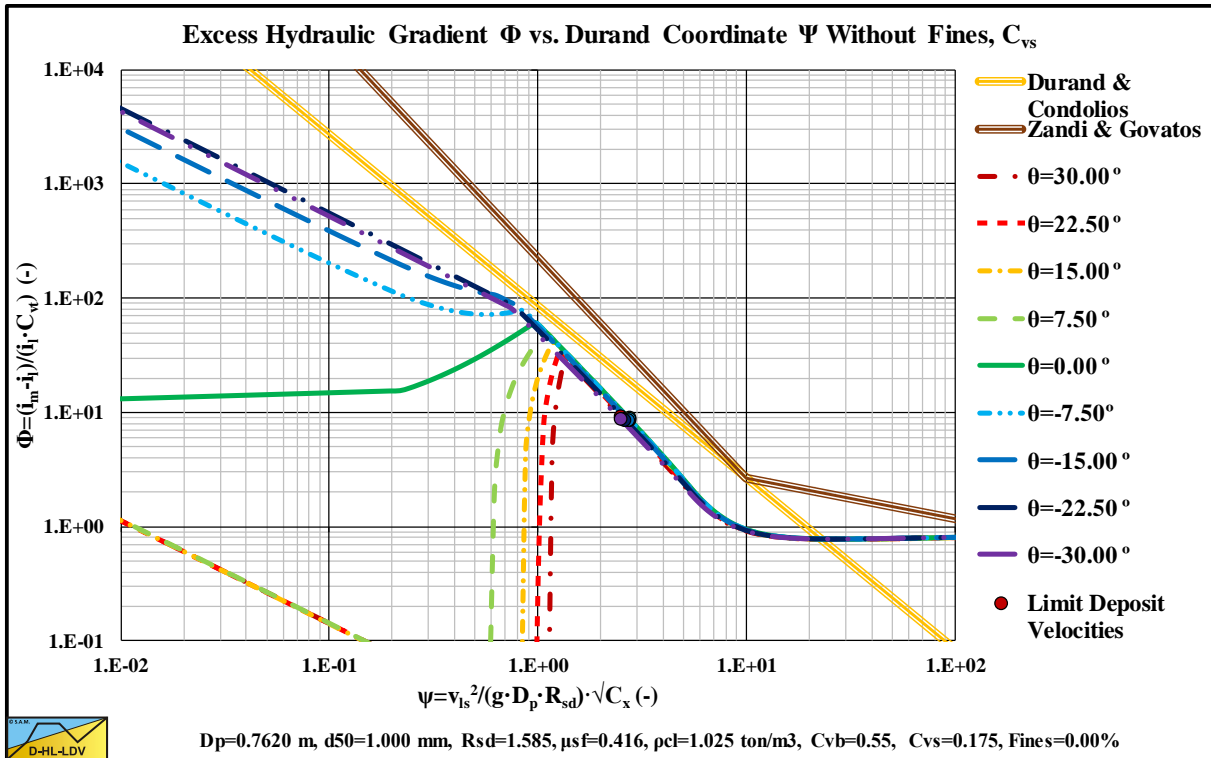
Figure 15.5-39: The hydraulic gradient on Durand coordinates for 9 inclination angles, C$_{vs}$.
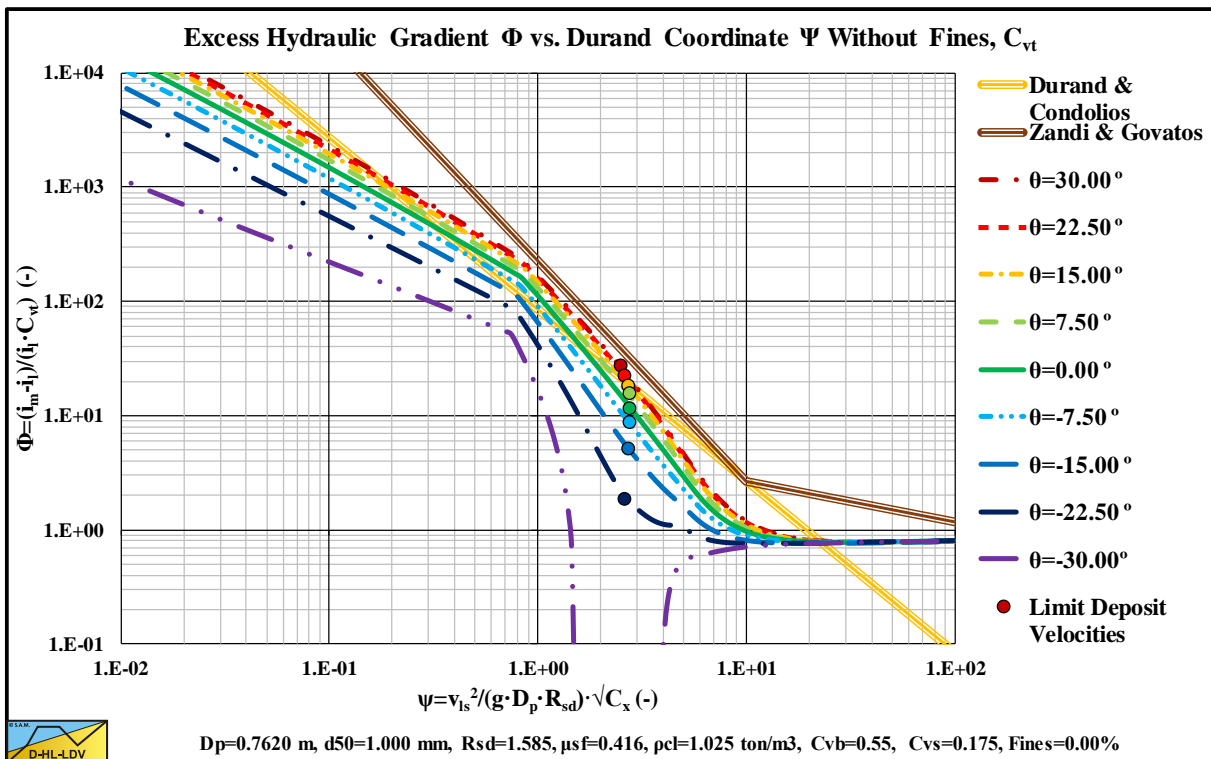
Figure 15.5-40: The hydraulic gradient on Durand coordinates for 9 inclination angles, C$_{vt}$.
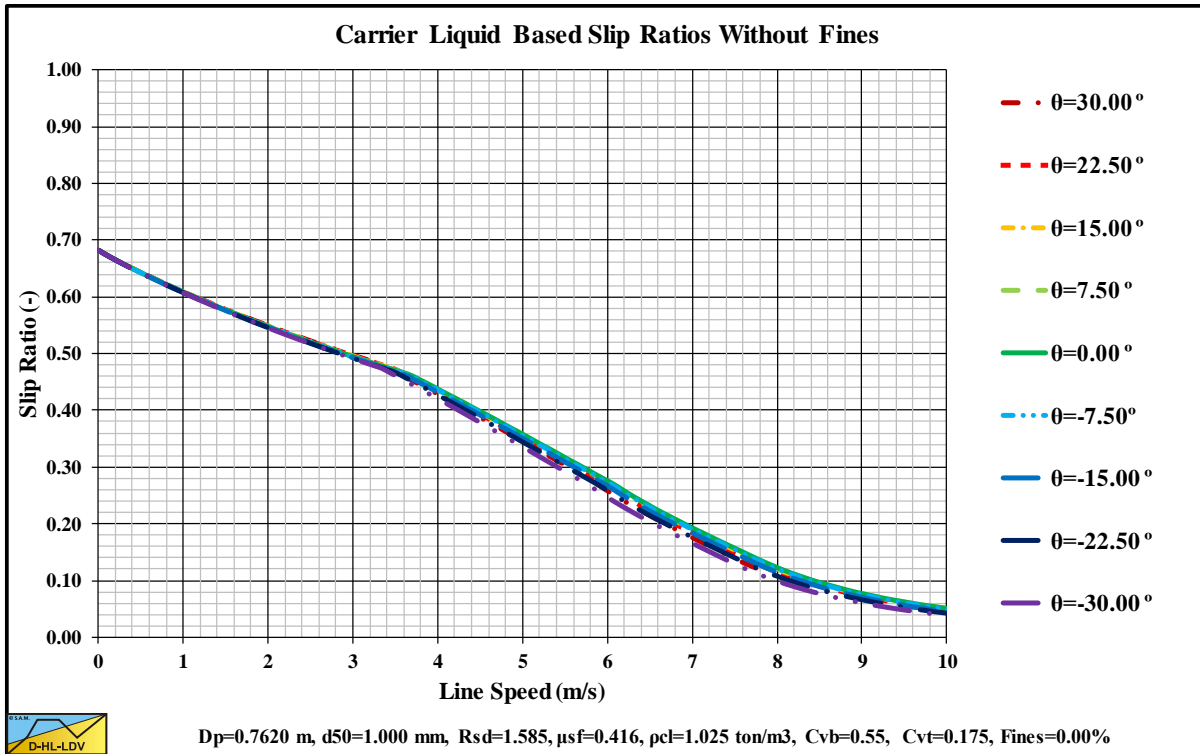
Figure 15.5-41: The slip ratio for 9 inclination angles.
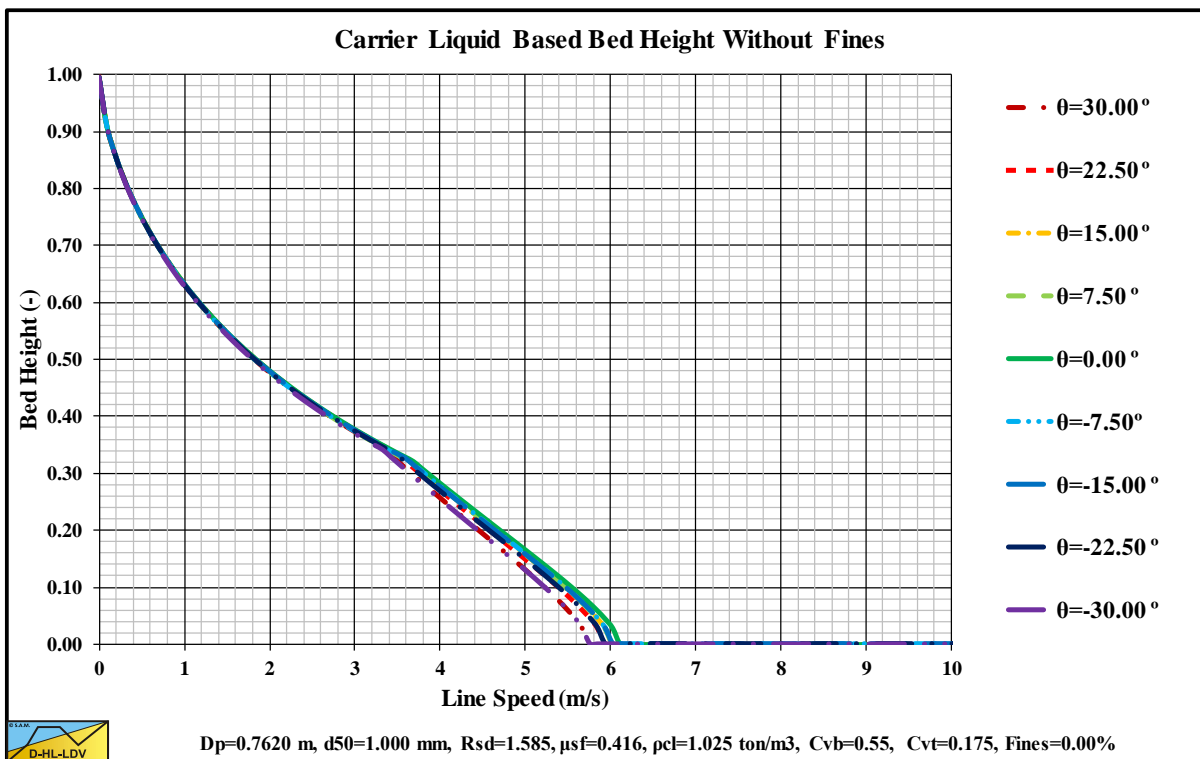
Figure 15.5-42: The bed height for 9 inclination angles.
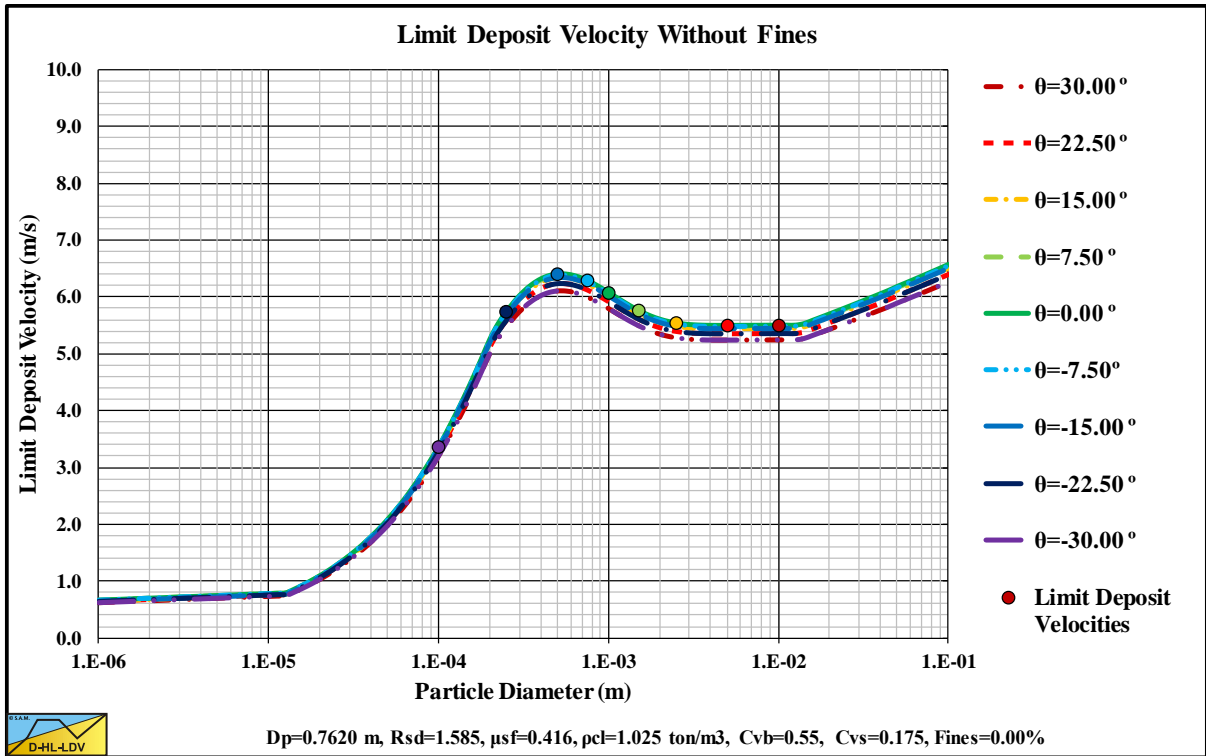
Figure 15.5-43: The Limit Deposit Velocity versus the particle diameter for 9 inclination angles.

15.5.6 9 Solids Densities.
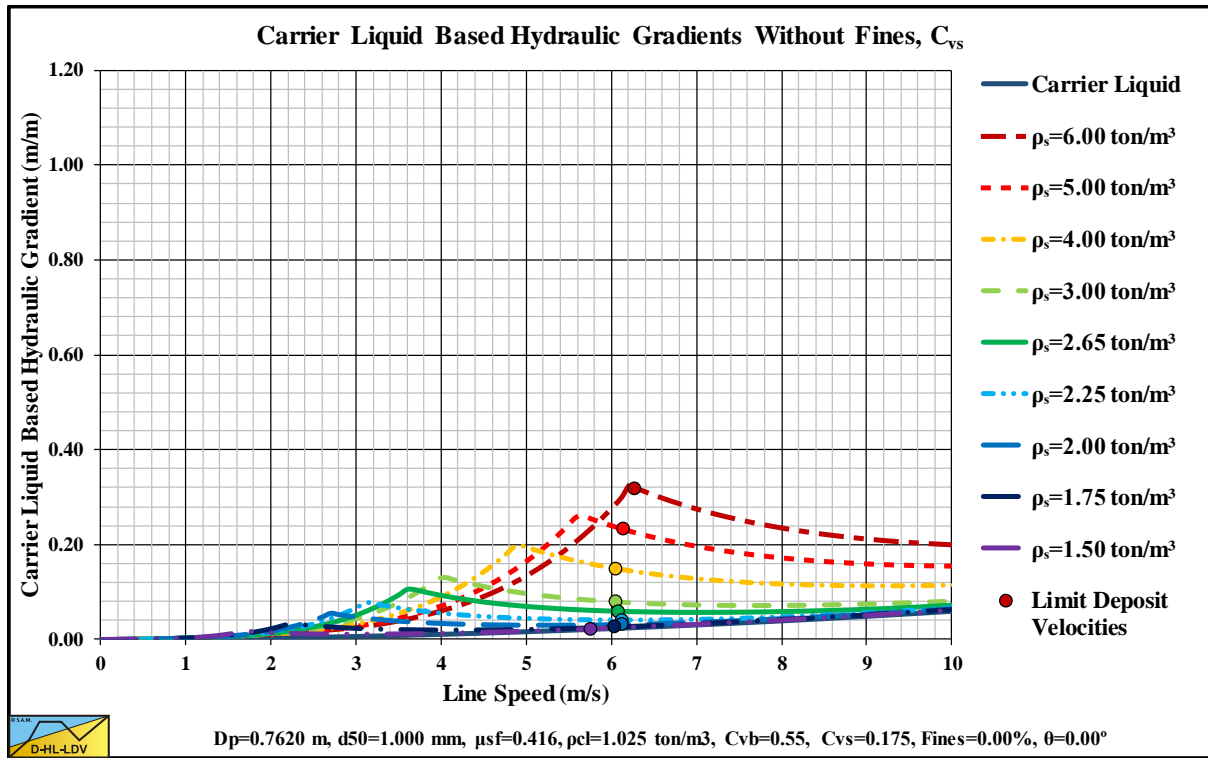
Figure 15.5-44: The hydraulic gradient versus the line speed for 9 solids densities, C$_{vs}$.
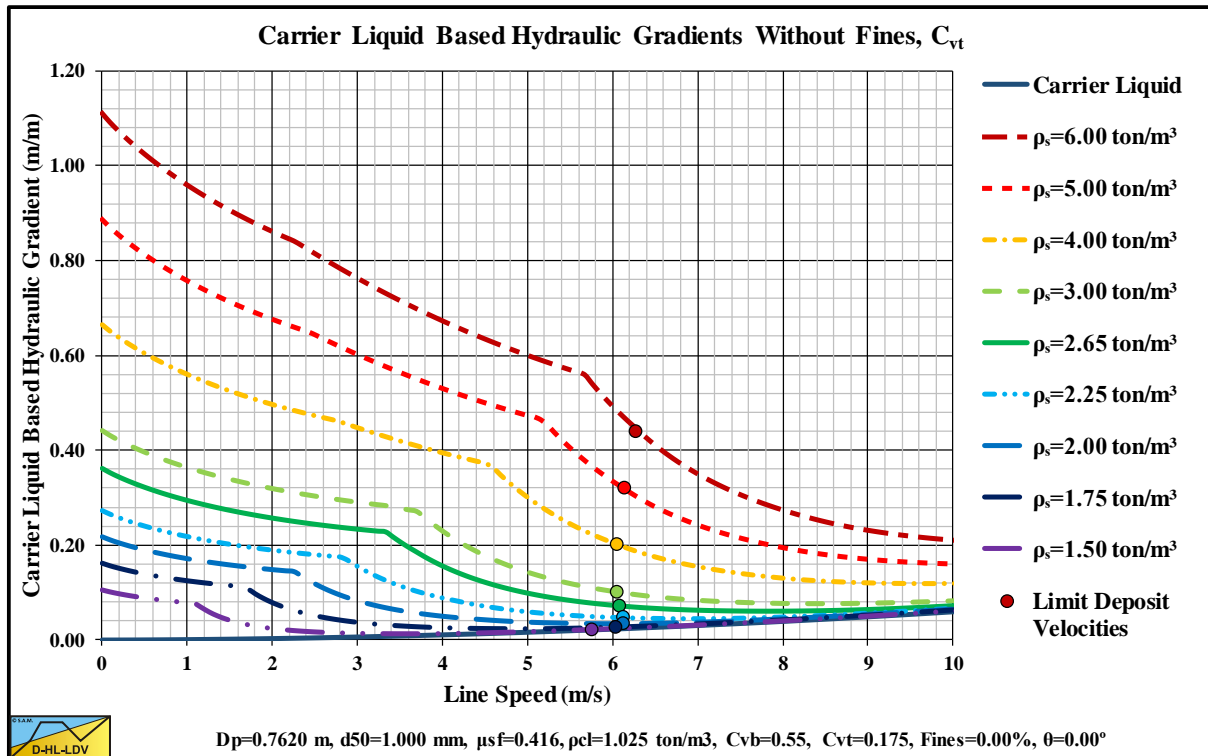
Figure 15.5-45: The hydraulic gradient versus the line speed for 9 solids densities, C$_{vt}$.
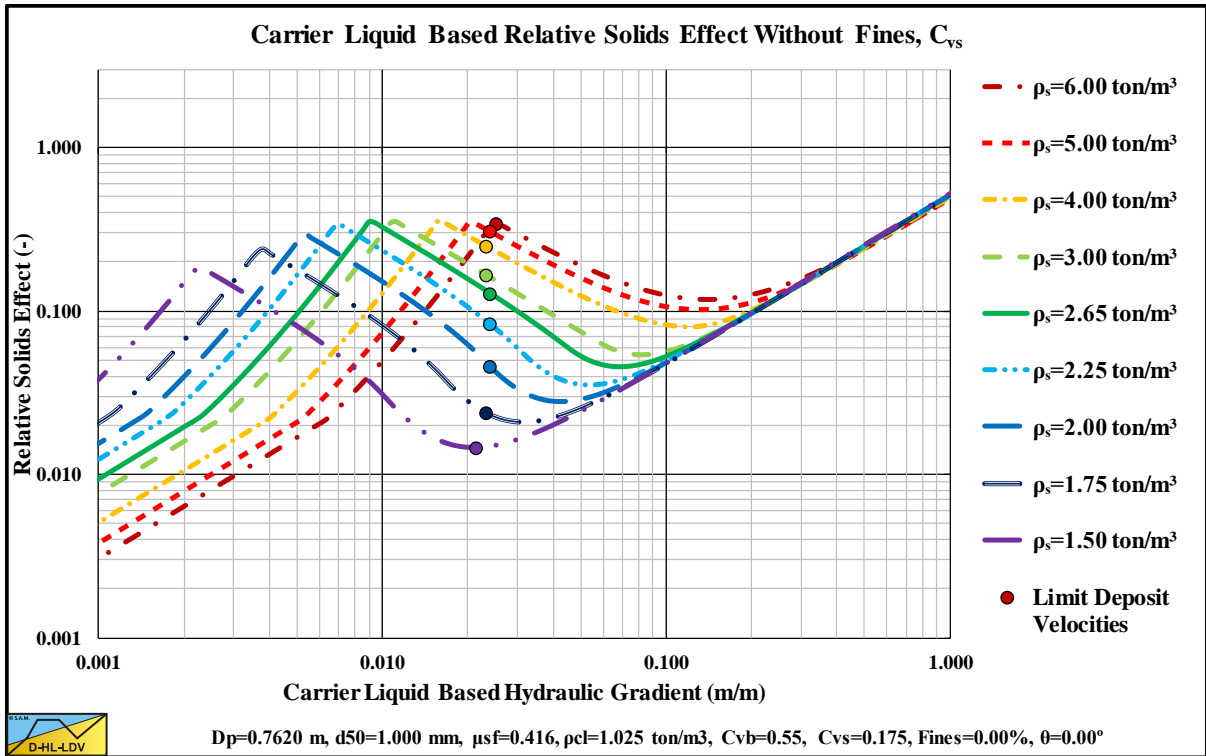
Figure 15.5-46: The relative excess hydraulic gradient versus the liquid hydraulic gradient for 9 solids densities, C_{vs}.
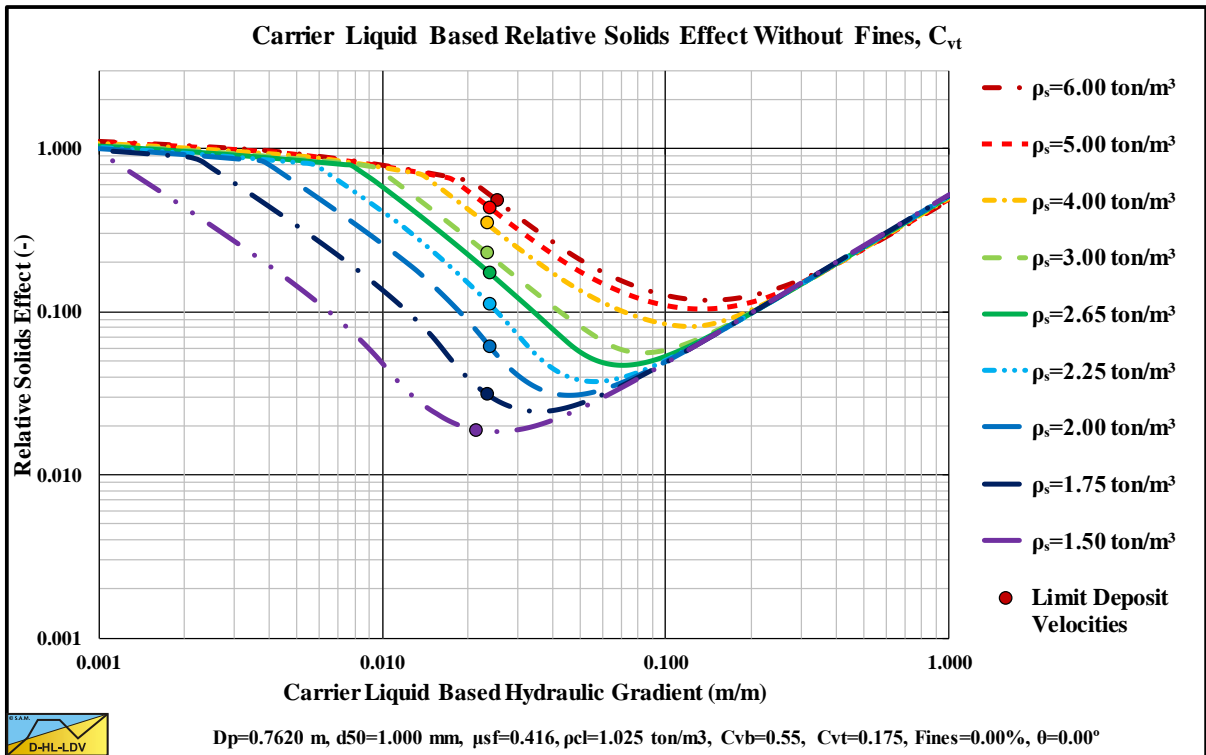
Figure 15.5-47: The relative excess hydraulic gradient versus the liquid hydraulic gradient for 9 solids densities, C_{vt}.
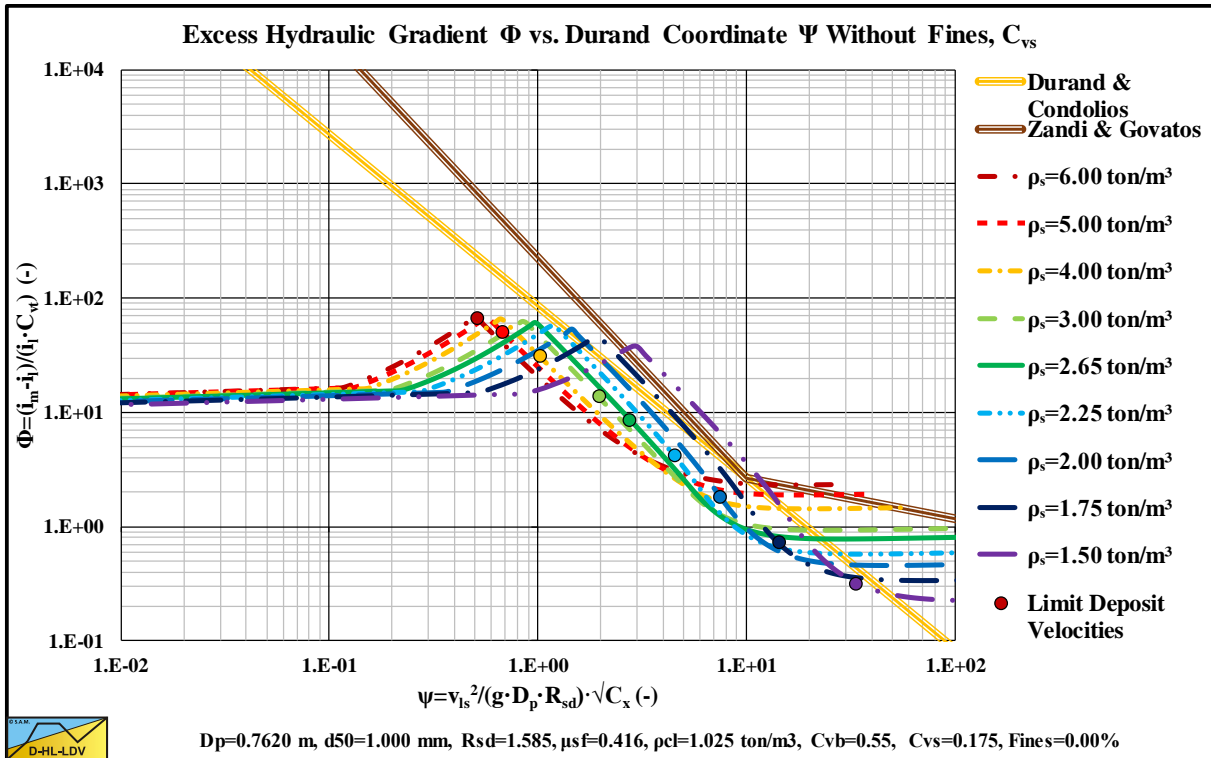
Figure 15.5-48: The hydraulic gradient on Durand coordinates for 9 solids densities, C_{vs}.
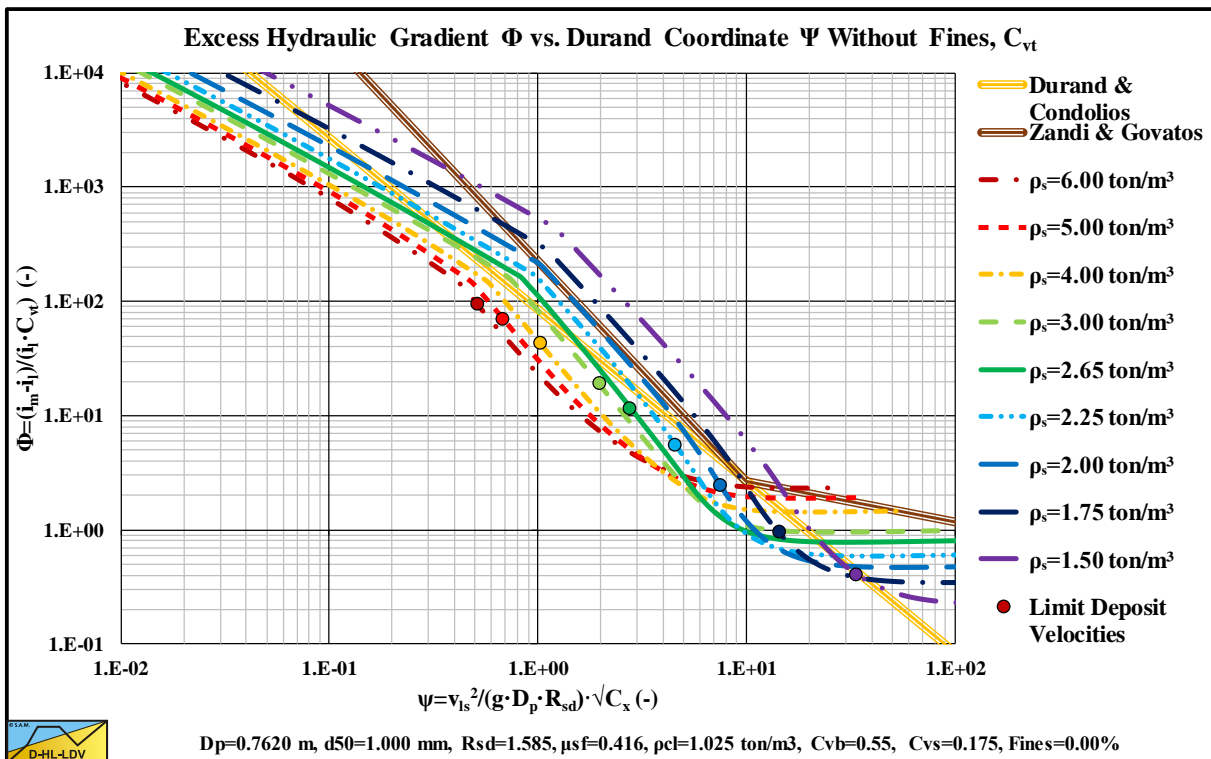
Figure 15.5-49: The hydraulic gradient on Durand coordinates for 9 solids densities, C_{vt}.
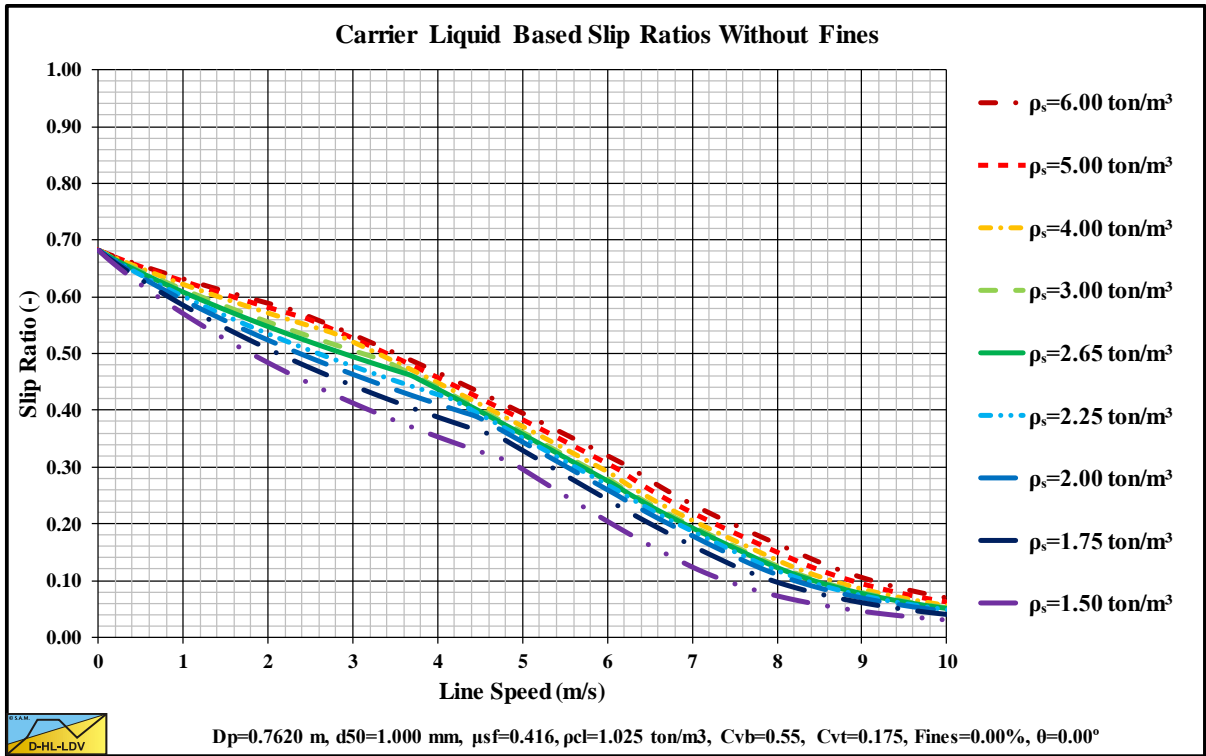
Figure 15.5-50: The slip ratio for 9 solids densities.
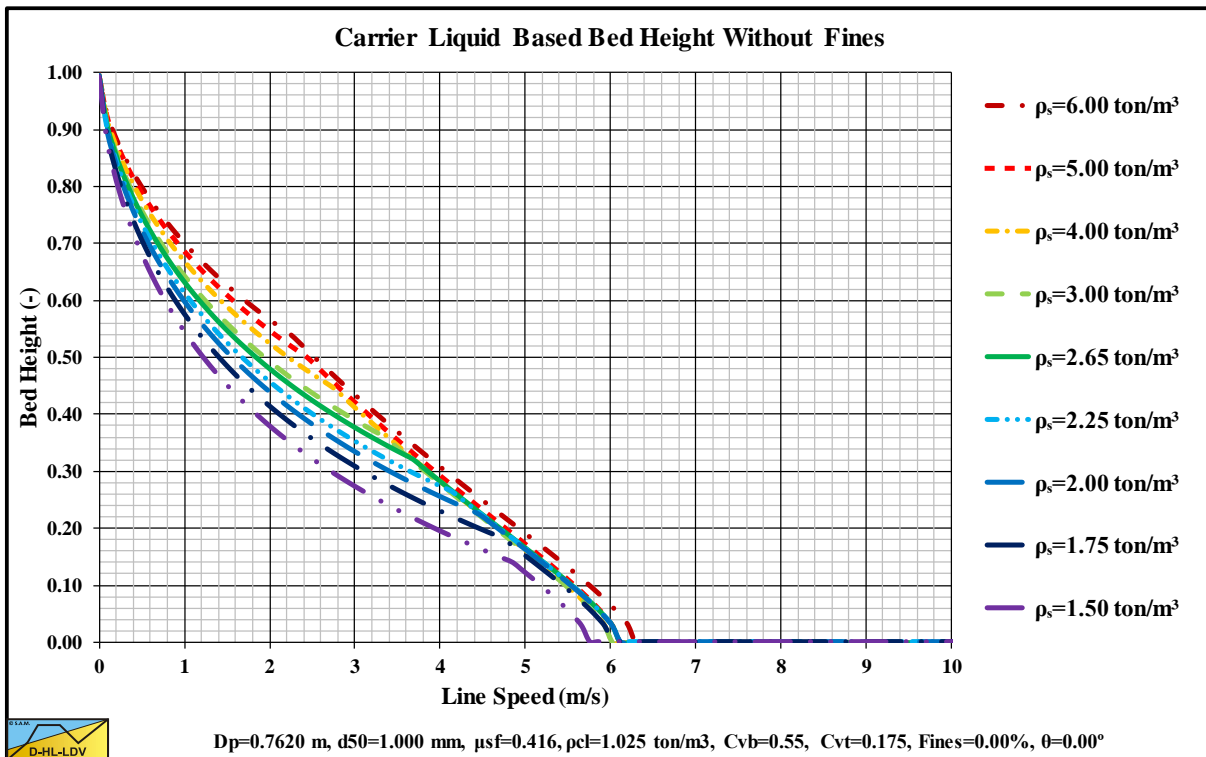
Figure 15.5-51: The bed height for 9 solids densities.
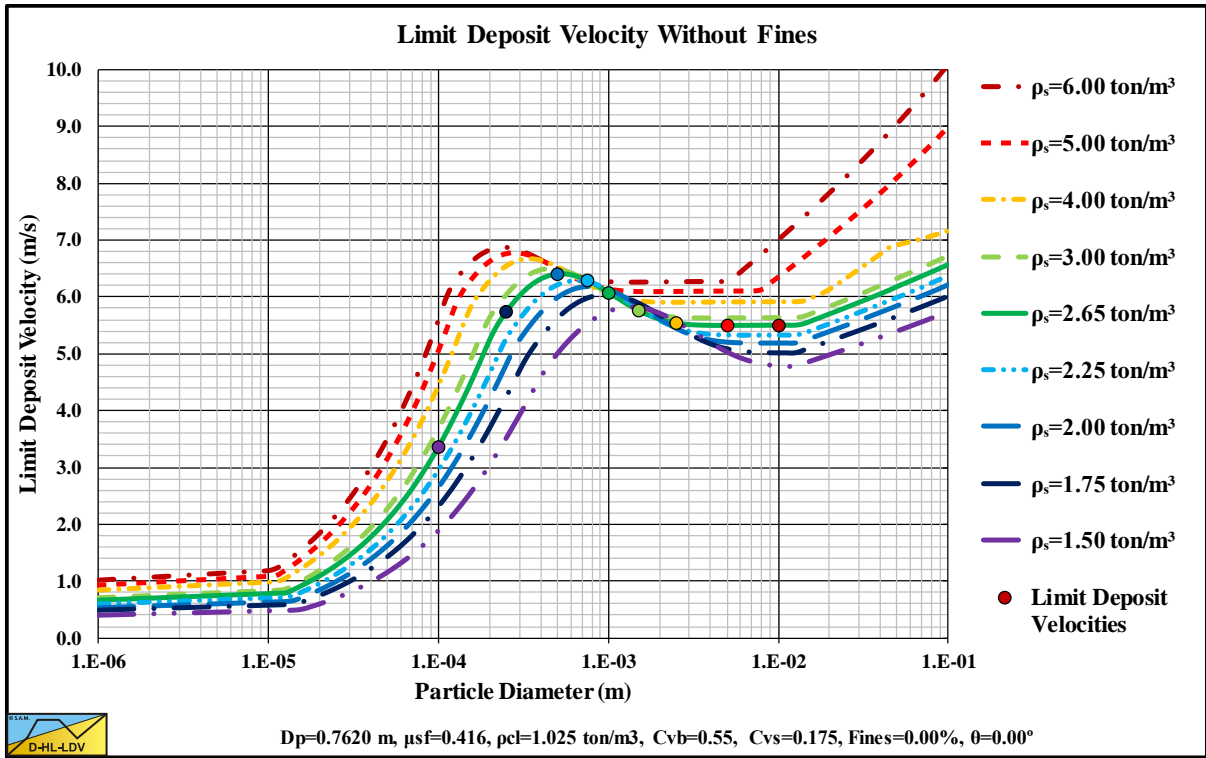
Figure 15.5-52: The Limit Deposit Velocity versus the particle diameter for 9 solids densities.

15.5.7 Graded Solids.
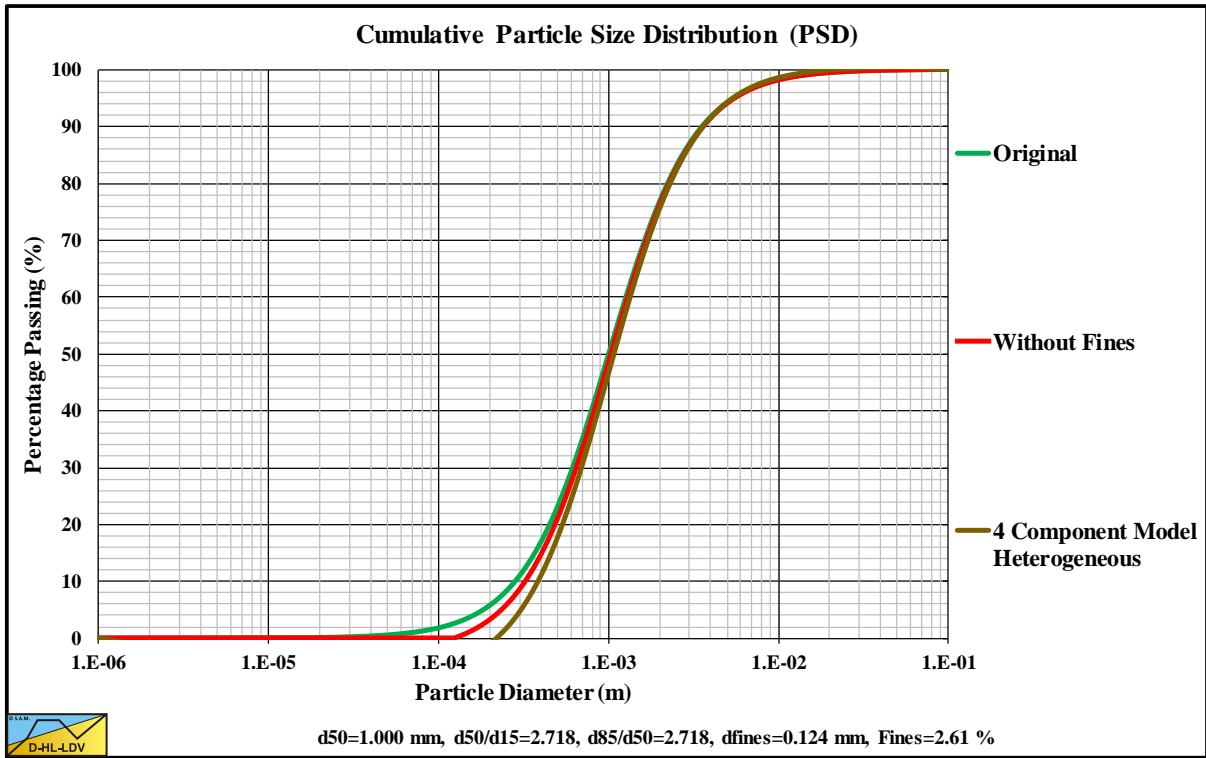
Figure 15.5-53: The Particle Size Distribution of a graded sand.
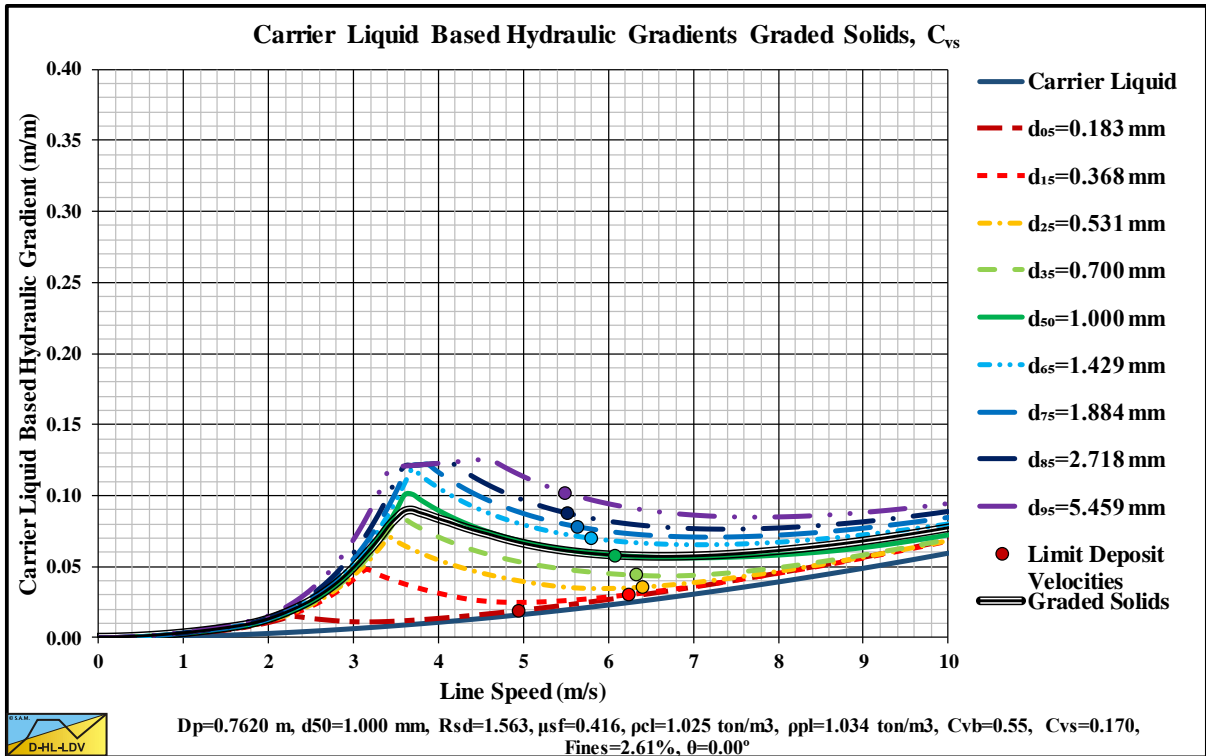
Figure 15.5-54: The hydraulic gradient versus the line speed for a graded sand, C$_{vs}$.
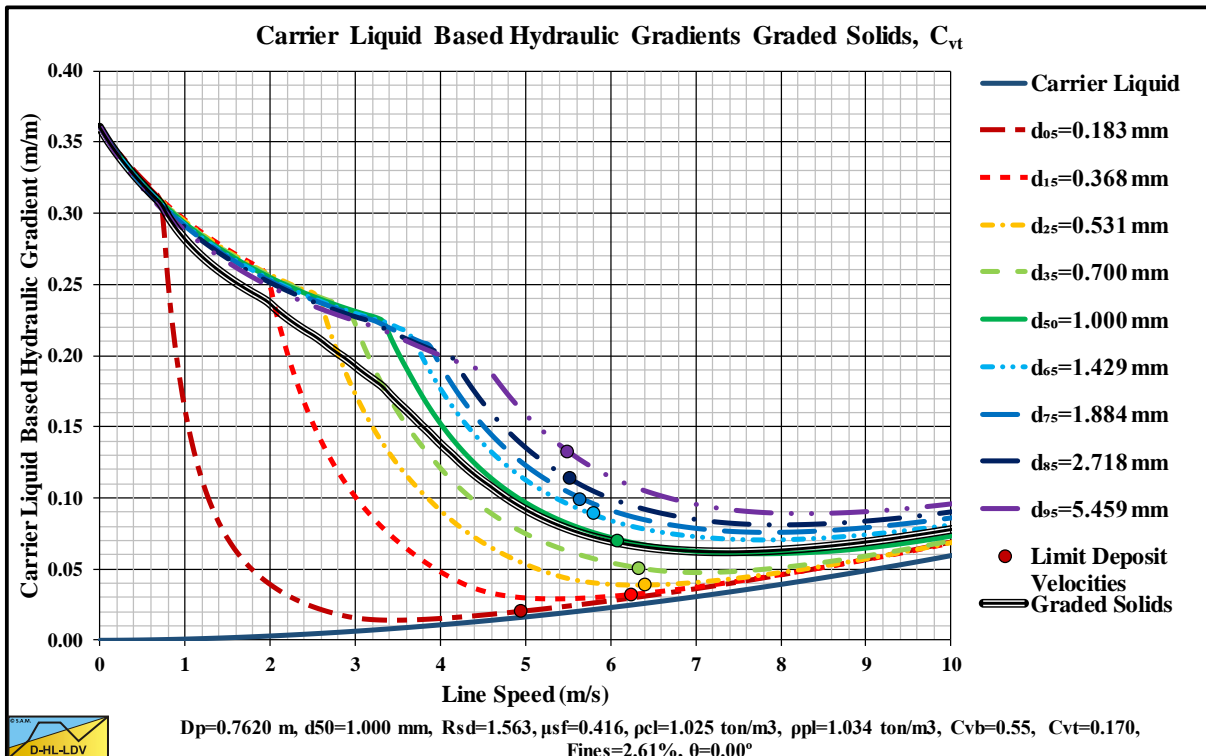
Figure 15.5-55: The hydraulic gradient versus the line speed for a graded sand, C$_{vt}$.
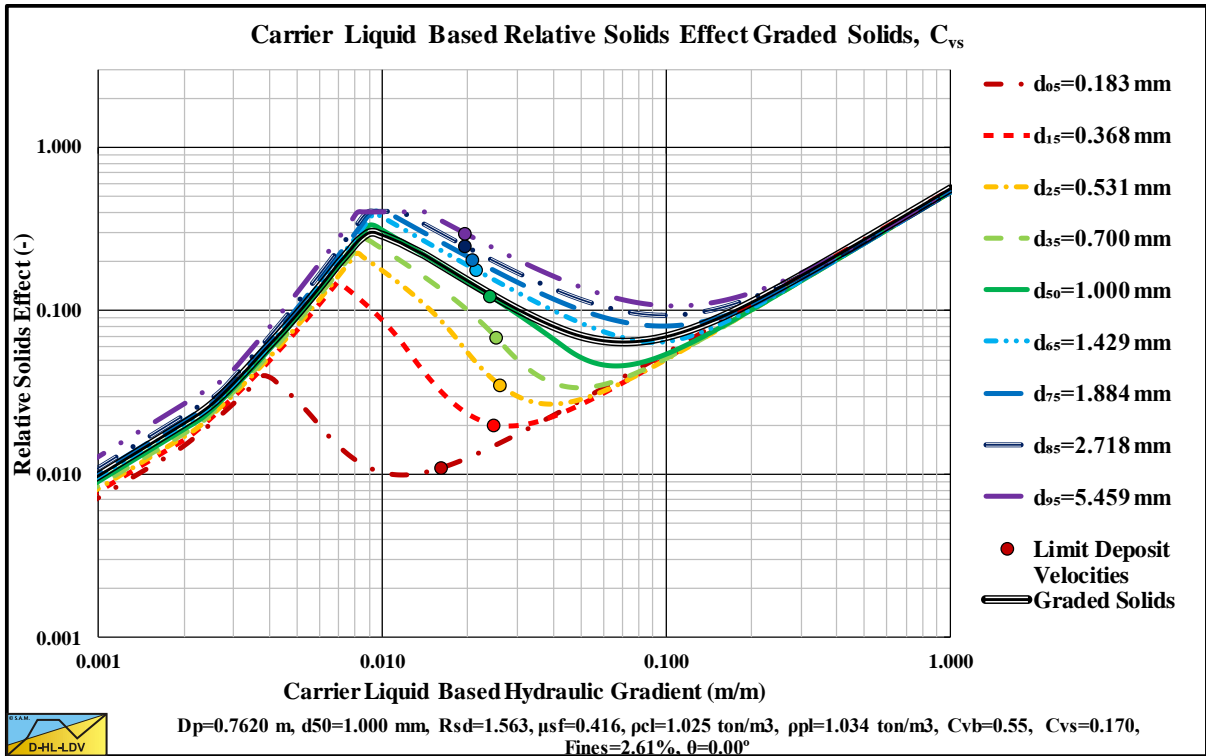
Figure 15.5-56: The relative excess hydraulic gradient versus the liquid hydraulic gradient for a graded sand, C_{vs}.
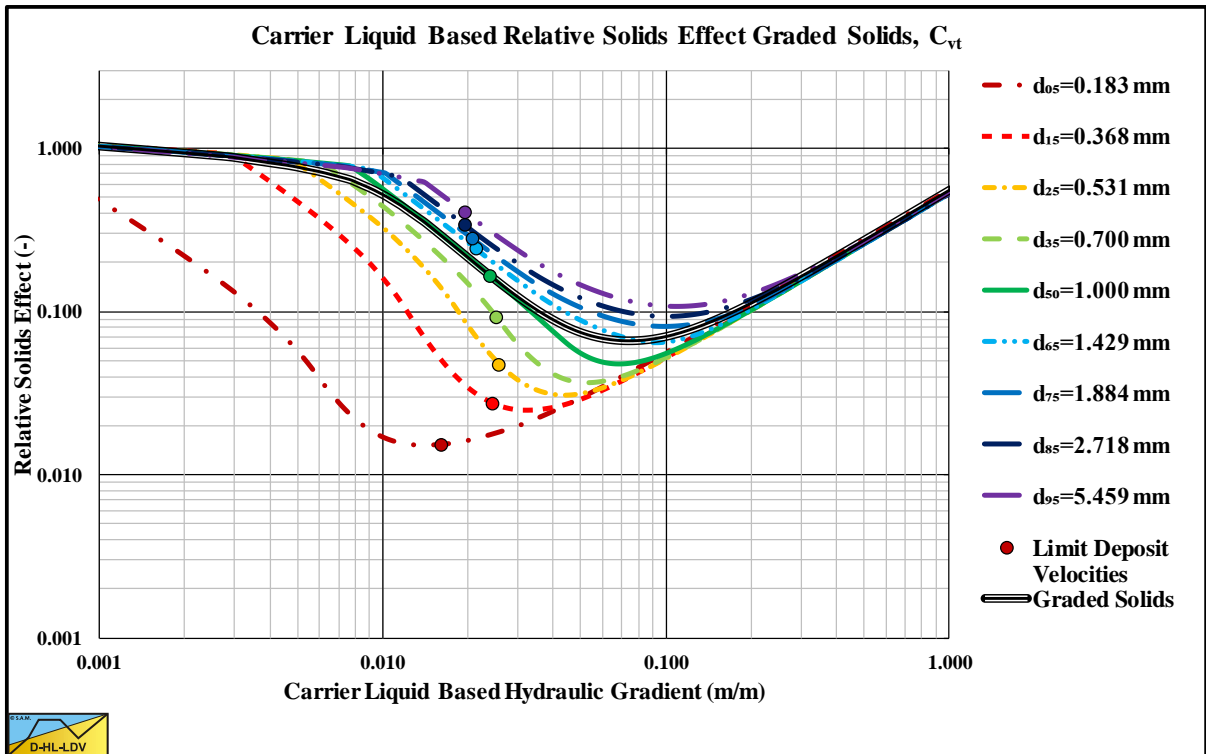
Figure 15.5-57: The relative excess hydraulic gradient versus the liquid hydraulic gradient for a graded sand, C_{vt}.
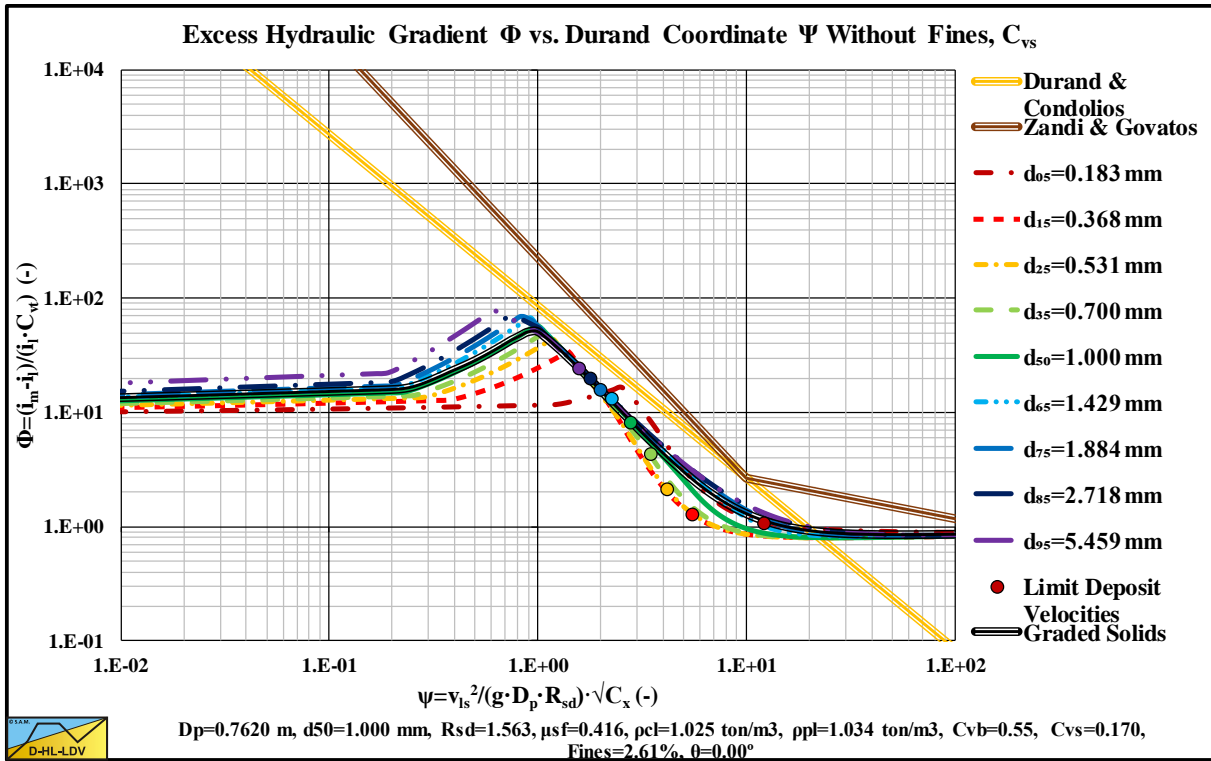
Figure 15.5-58: The hydraulic gradient on Durand coordinates for a graded sand, C_{vs}.
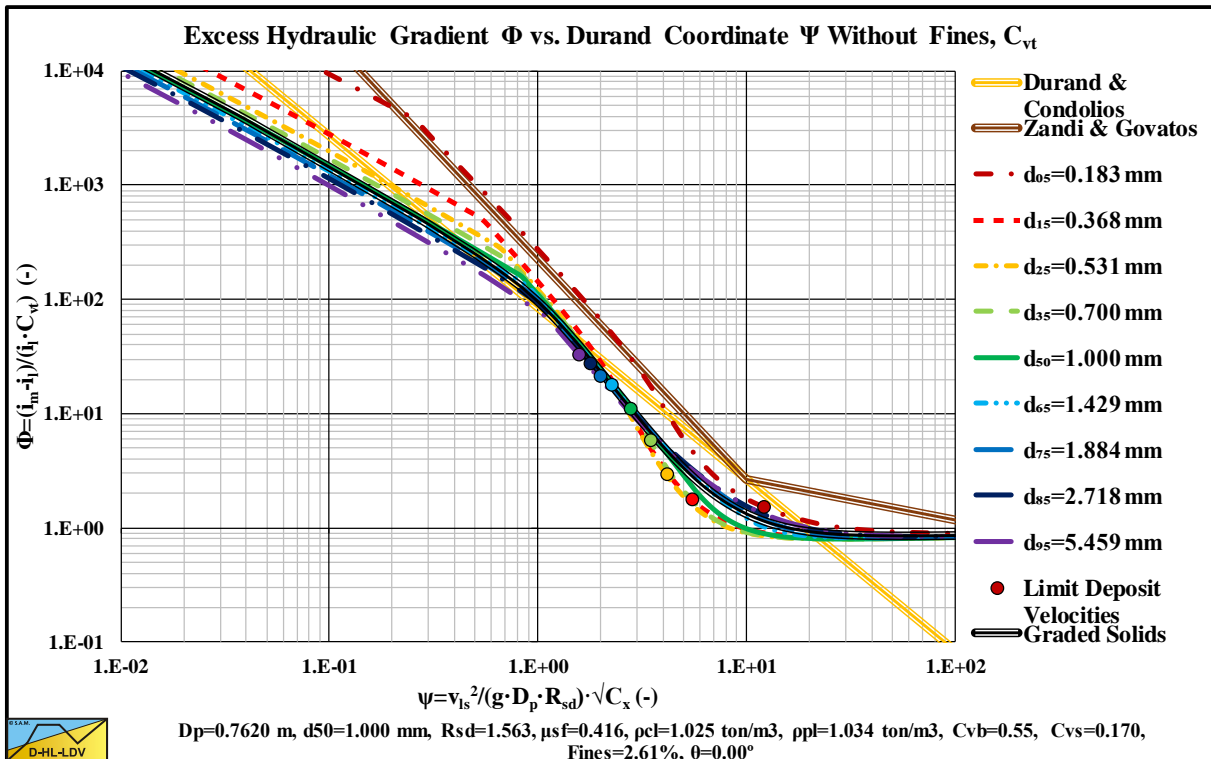
Figure 15.5-59: The hydraulic gradient on Durand coordinates for a graded sand, C_{vt}.
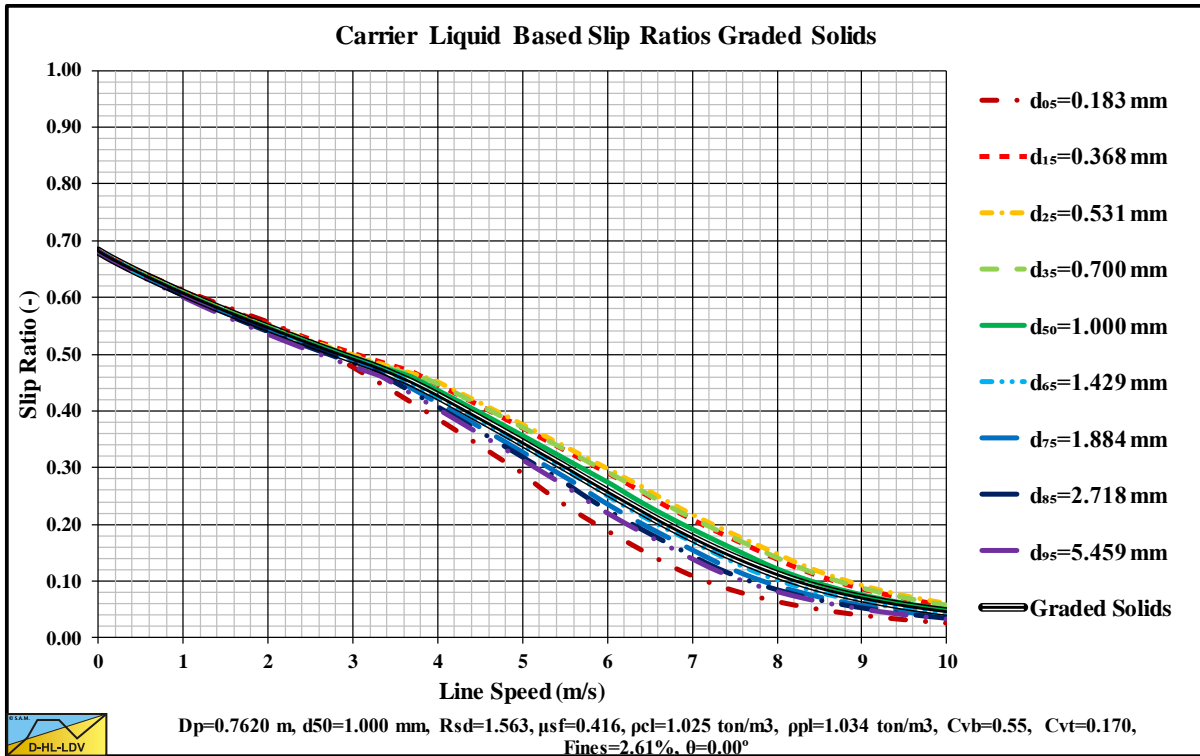
Figure 15.5-60: The slip ratio for a graded sand.
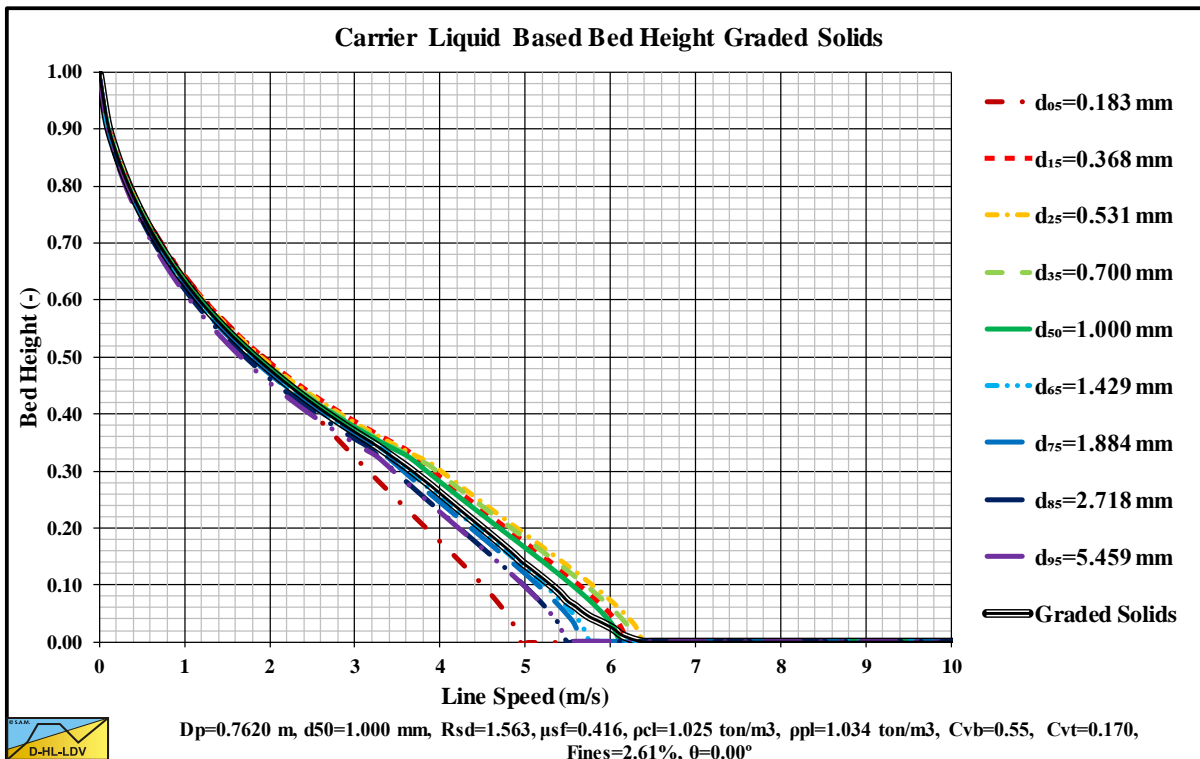
Figure 15.5-61: The bed height for a graded sand.

15.5.8 Flow Regime Transitions 9 Concentrations.
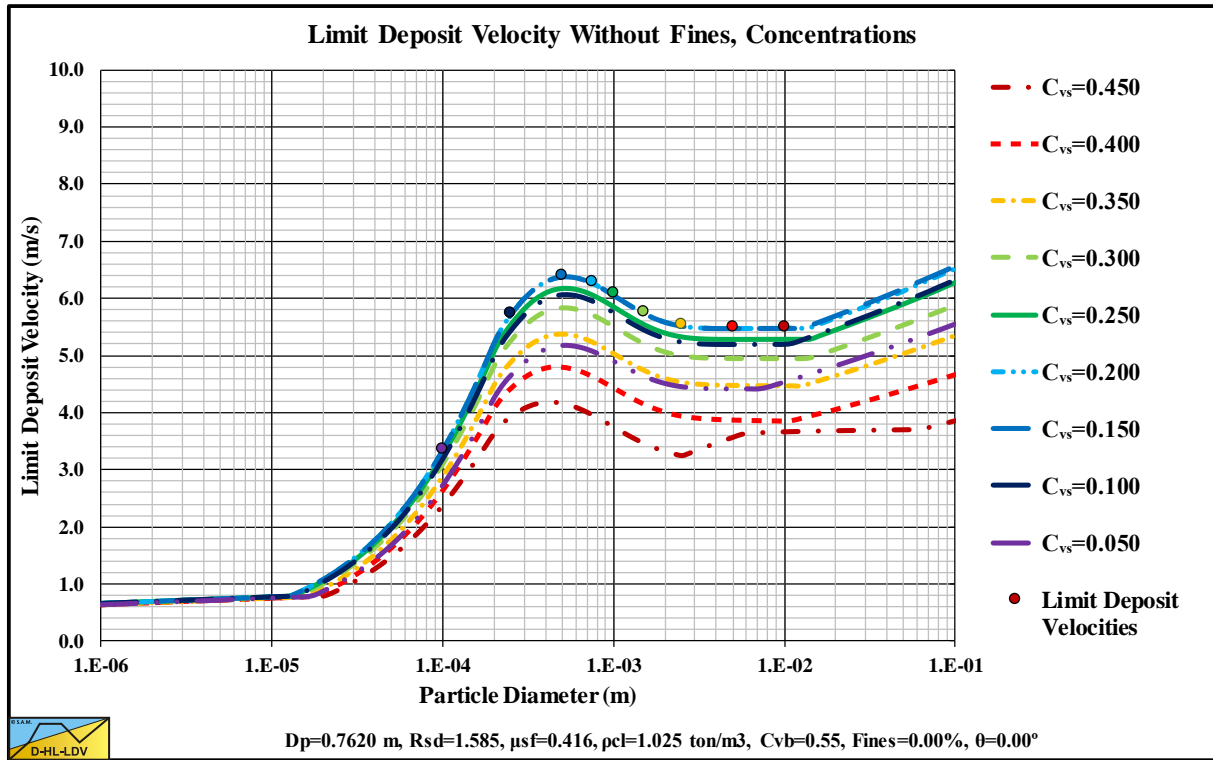
Figure 15.5-62: The Limit Deposit Velocity at 9 volumetric concentrations.
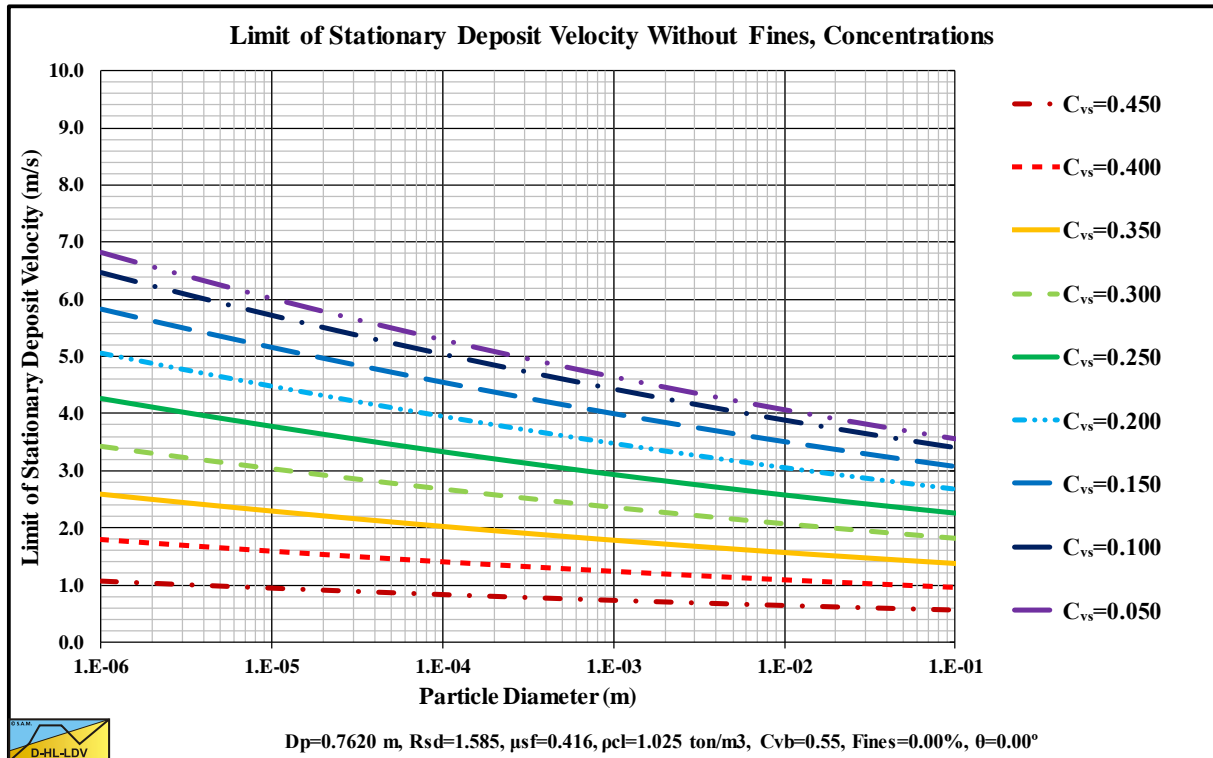
Figure 15.5-63: The transition Fixed Bed-Sliding Bed (LSDV) at 9 volumetric concentrations.
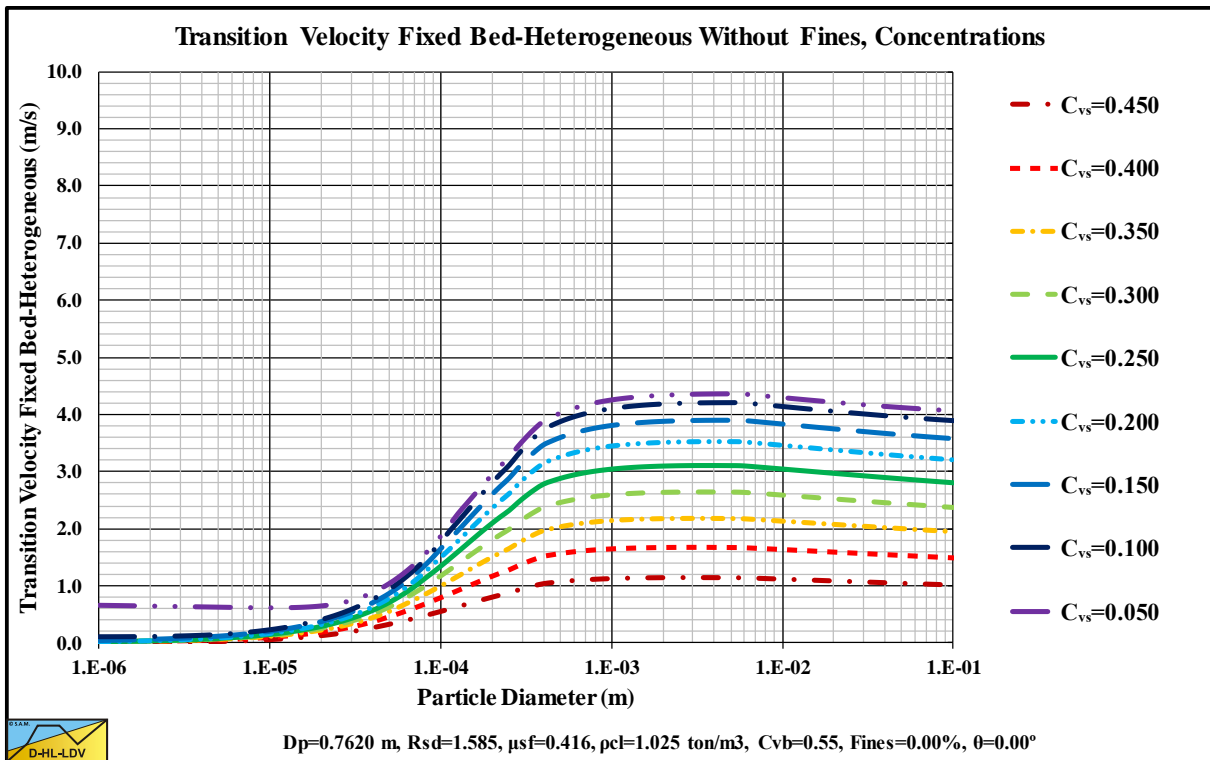
Figure 15.5-64: The transition Fixed Bed-Heterogeneous Regime at 9 volumetric concentrations.
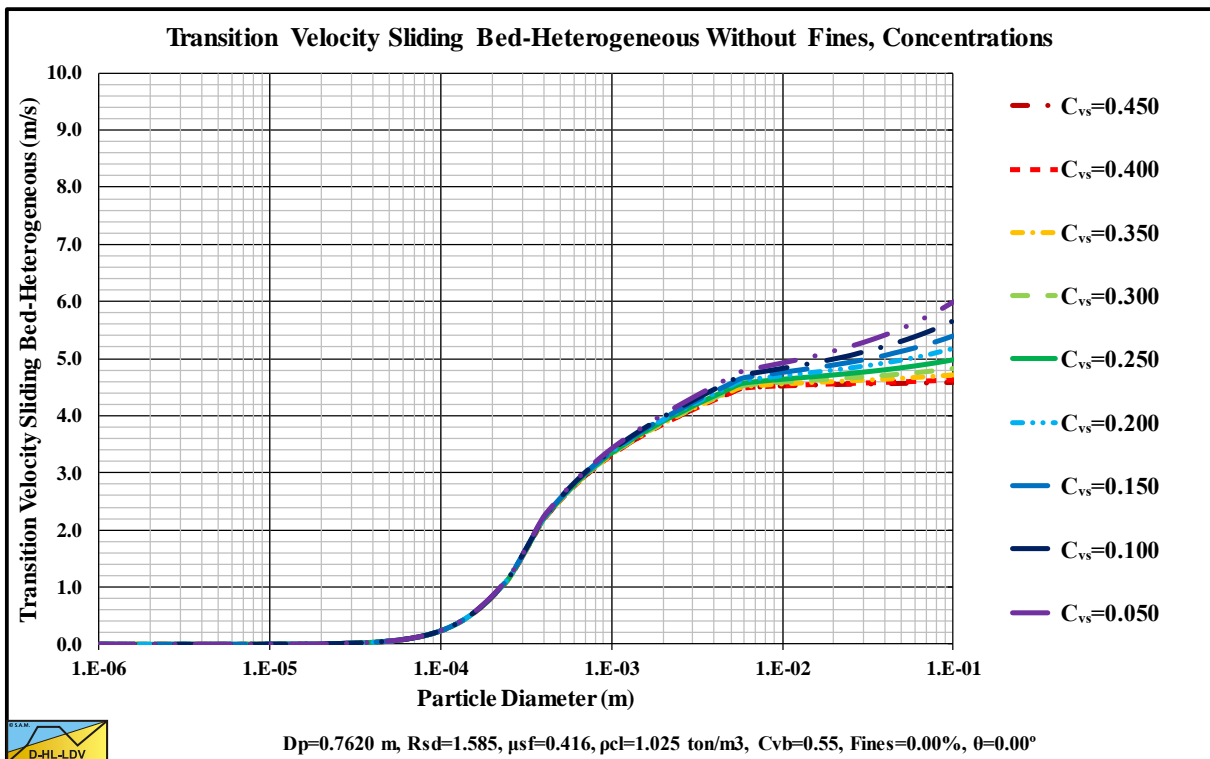
Figure 15.5-65: The transition Sliding Bed-Heterogeneous Regime at 9 volumetric concentrations.
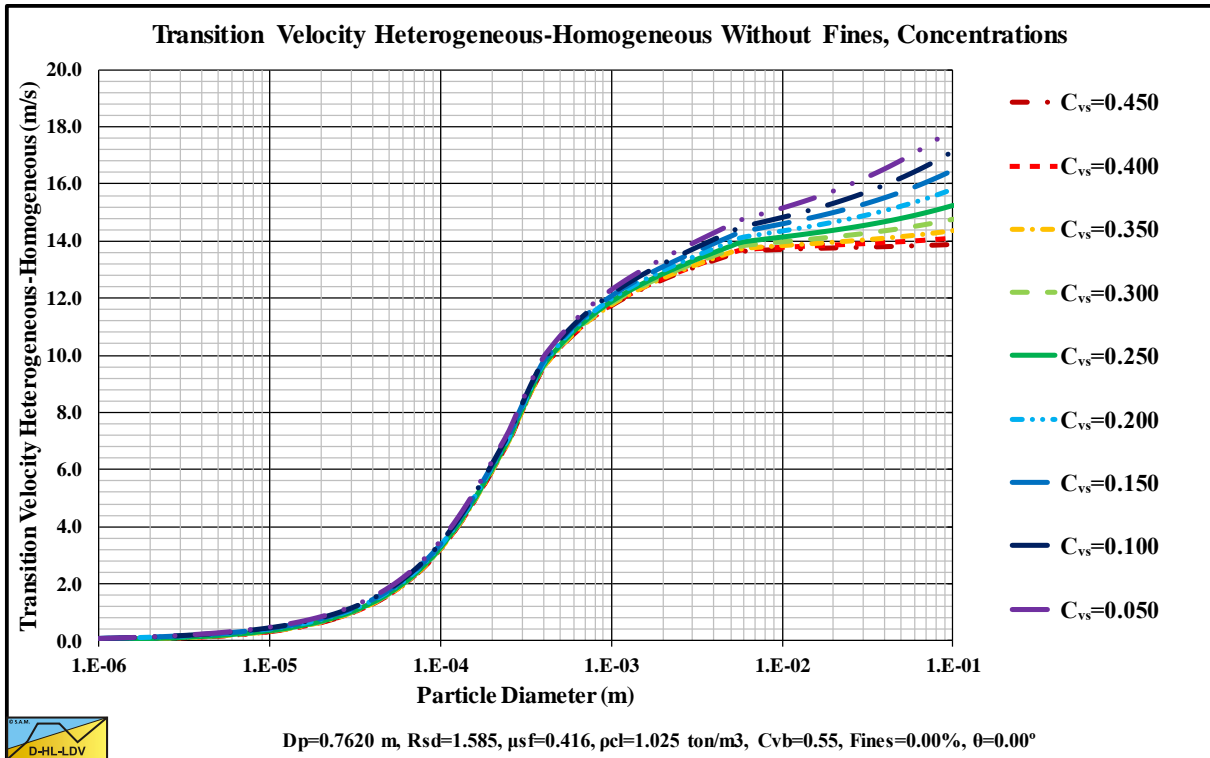
Figure 15.5-66: The transition Heterogeneous-Homogeneous at 9 volumetric concentrations.
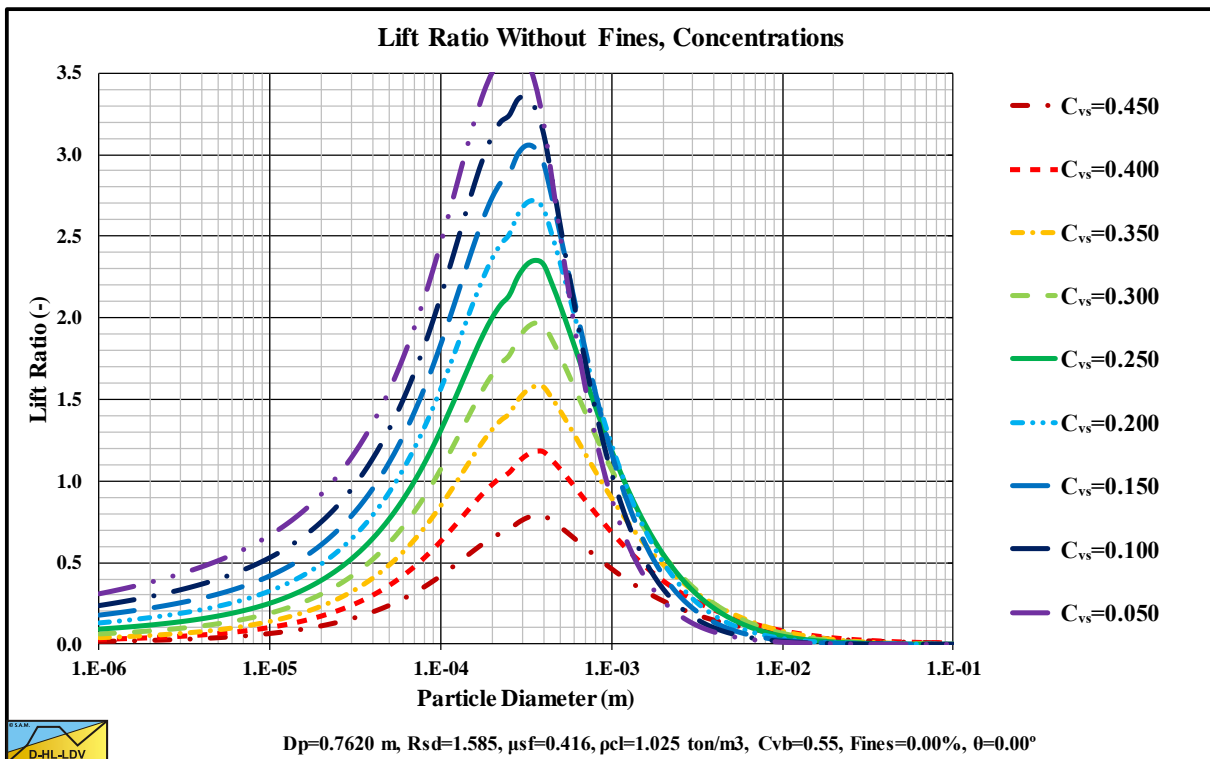
Figure 15.5-67: The lift ratio (near wall lift to gravity ratio) at 9 volumetric concentrations.

15.5.9 Flow Regime Transitions 9 Pipe Diameters.
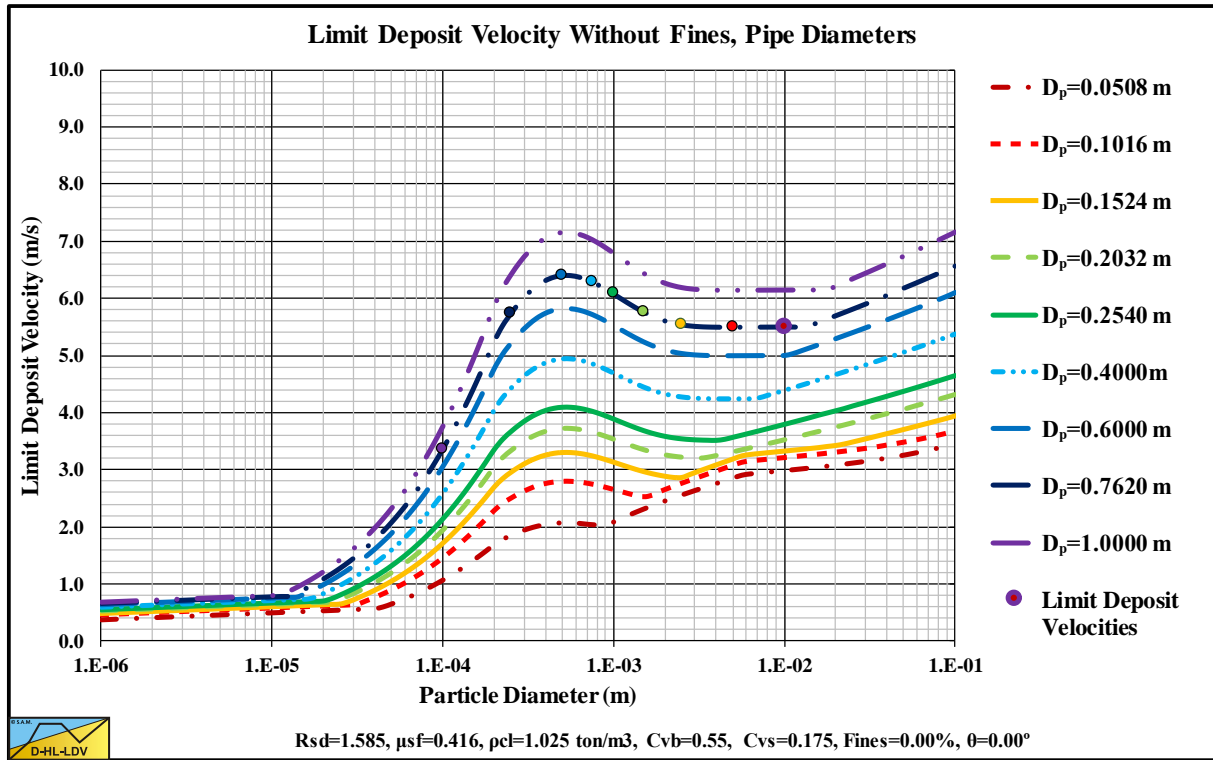
Figure 15.5-68: The Limit Deposit Velocity at 9 pipe diameters.
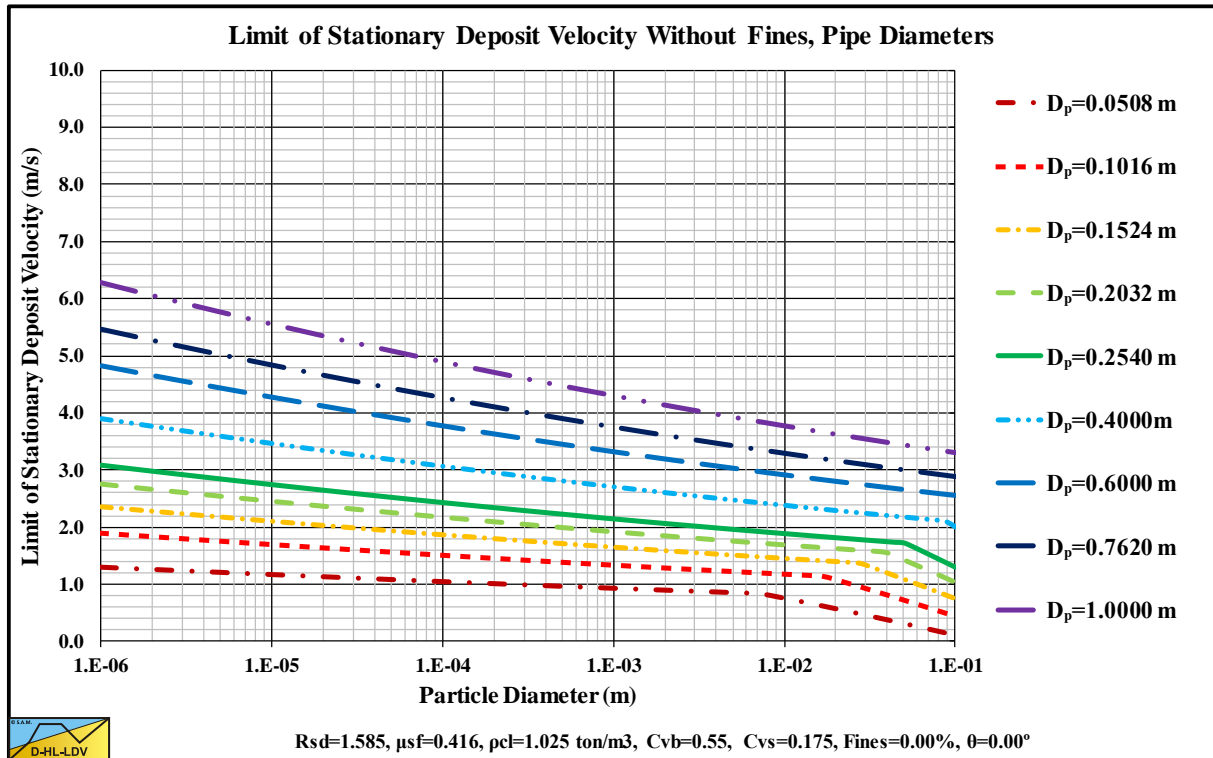
Figure 15.5-69: The transition Fixed Bed-Sliding Bed (LSDV) at 9 pipe diameters.
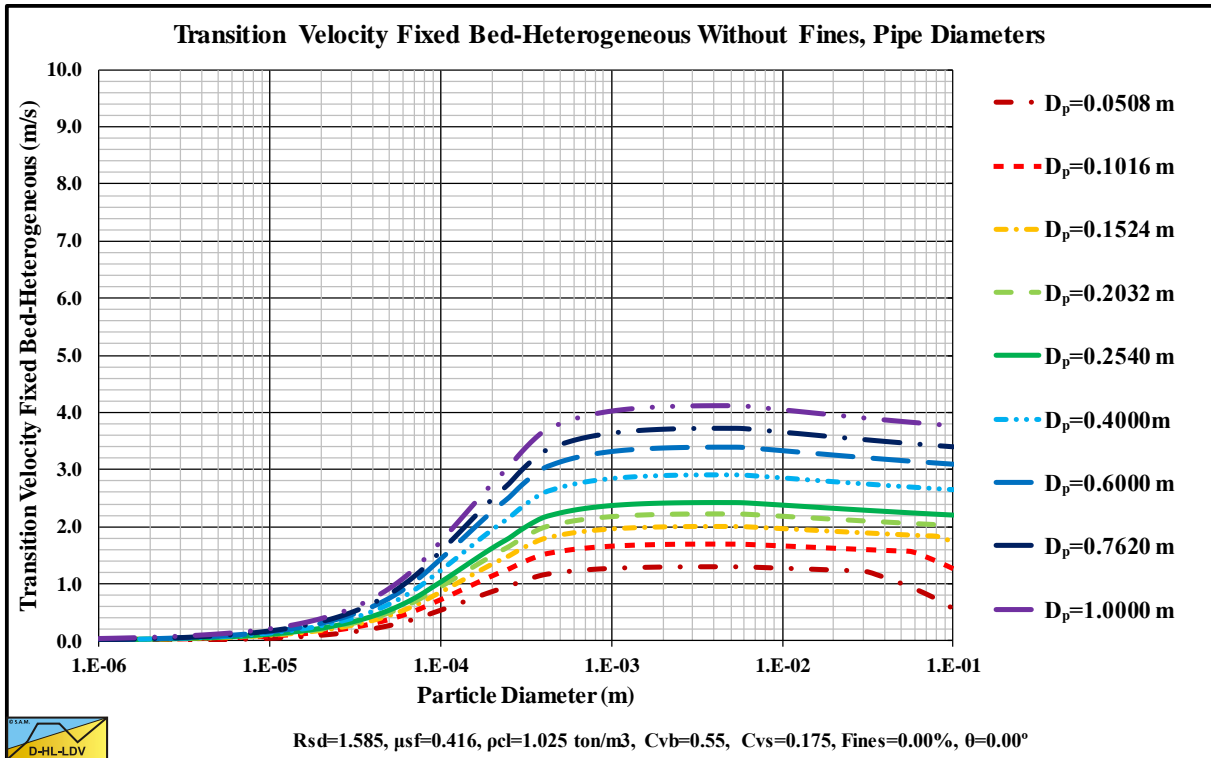
Figure 15.5-70: The transition Fixed Bed-Heterogeneous Regime at 9 pipe diameters.
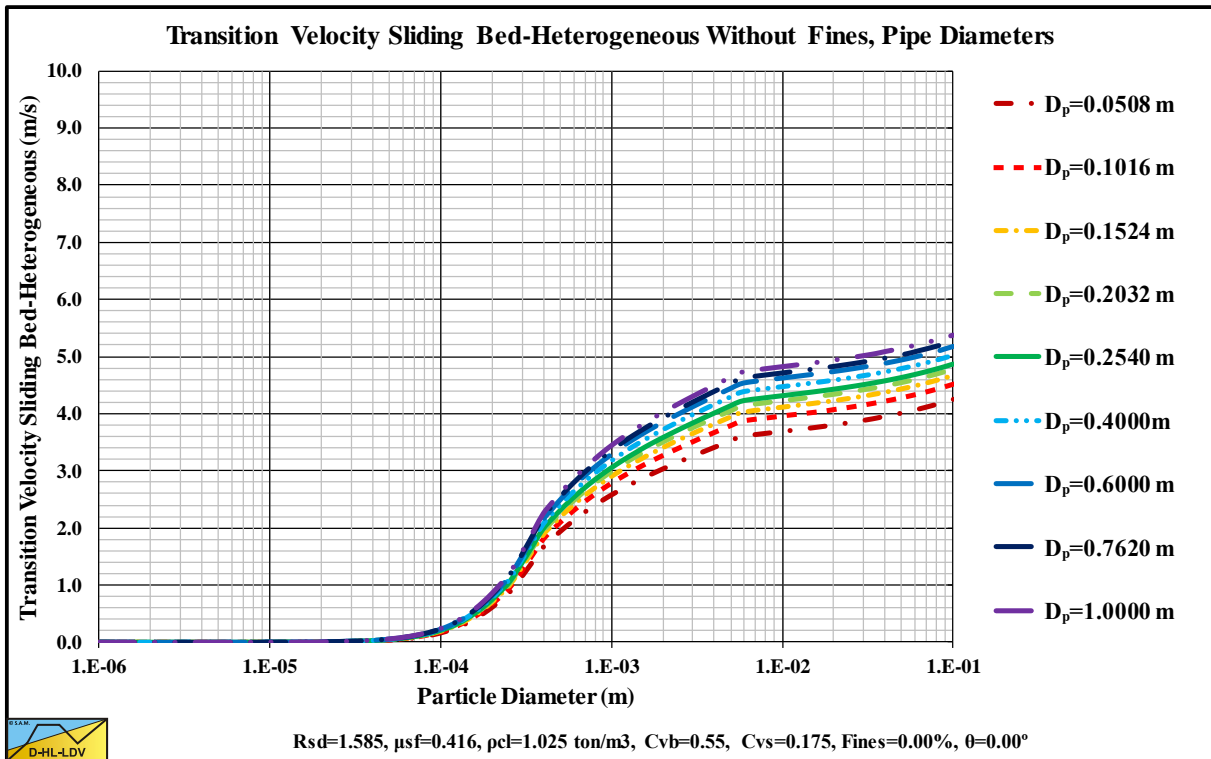
Figure 15.5-71: The transition Sliding Bed-Heterogeneous Regime at 9 pipe diameters.
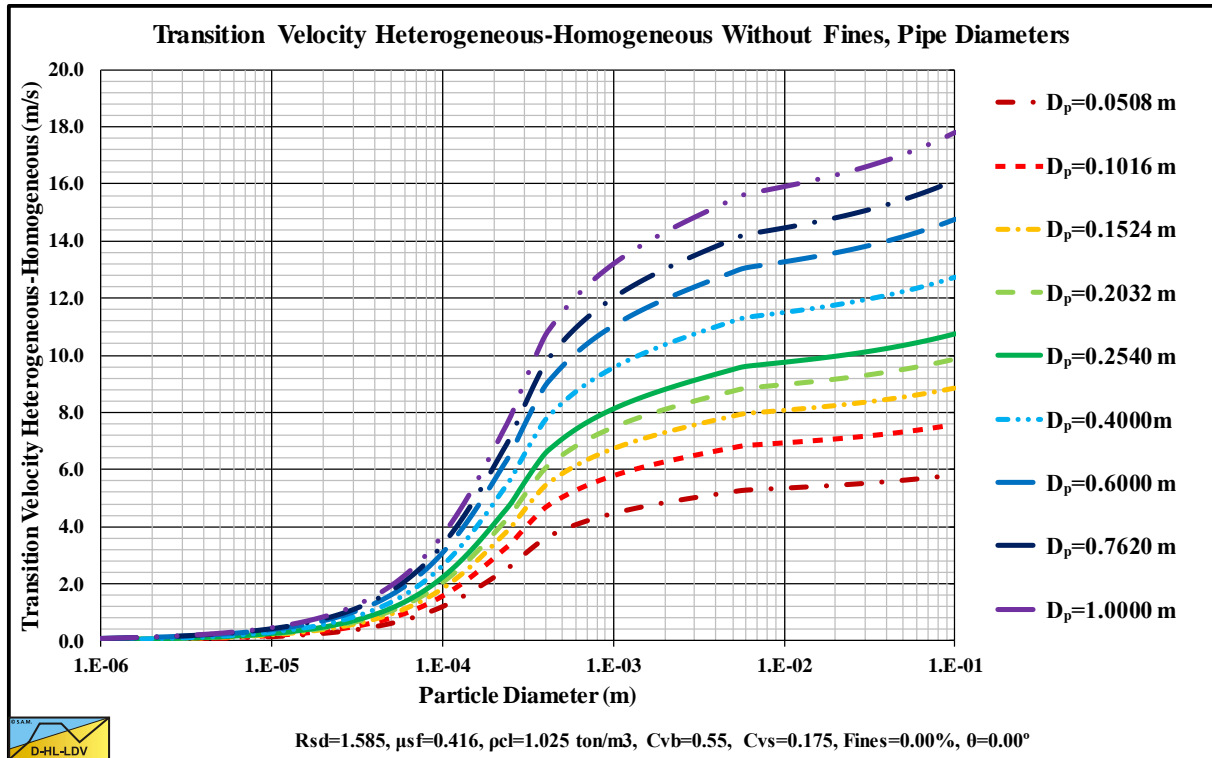
Figure 15.5-72: The transition Heterogeneous-Homogeneous at 9 pipe diameters.
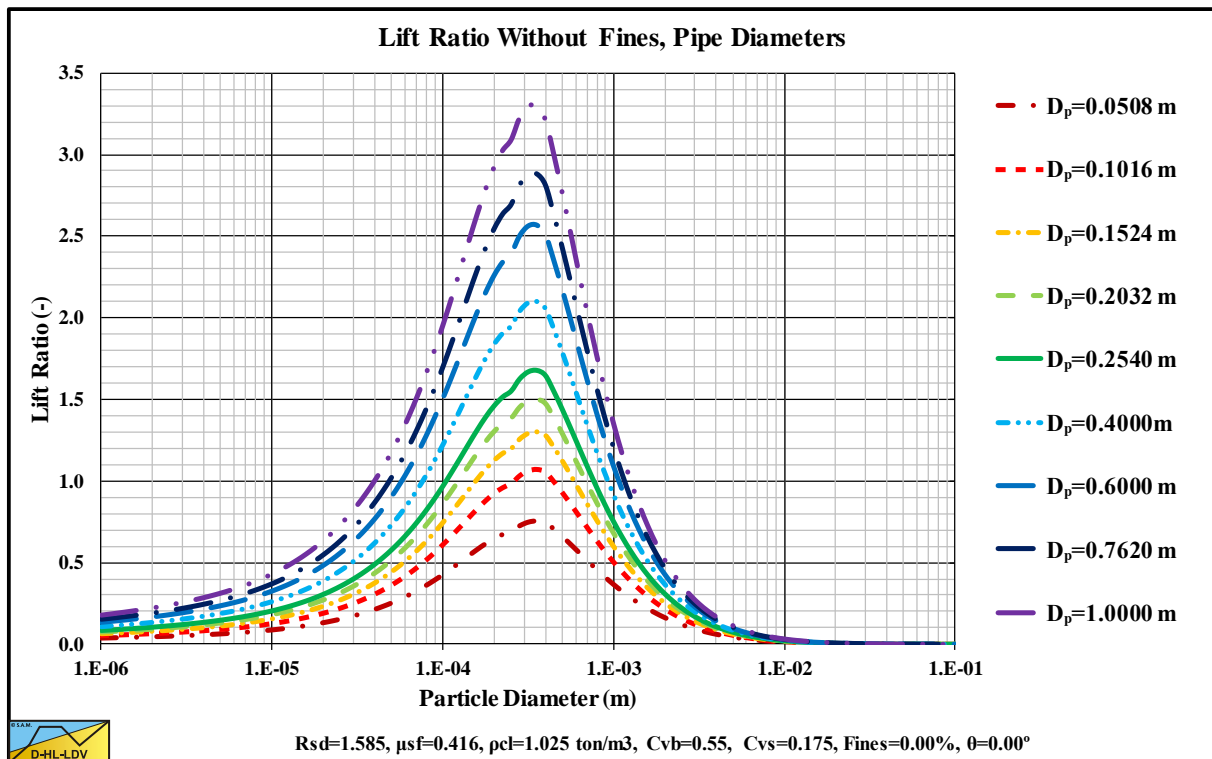
Figure 15.5-73: The lift ratio (near wall lift to gravity ratio) at 9 pipe diameters.

Appendices.

15.5.10 Flow Regime Transitions 9 Solids Densities.
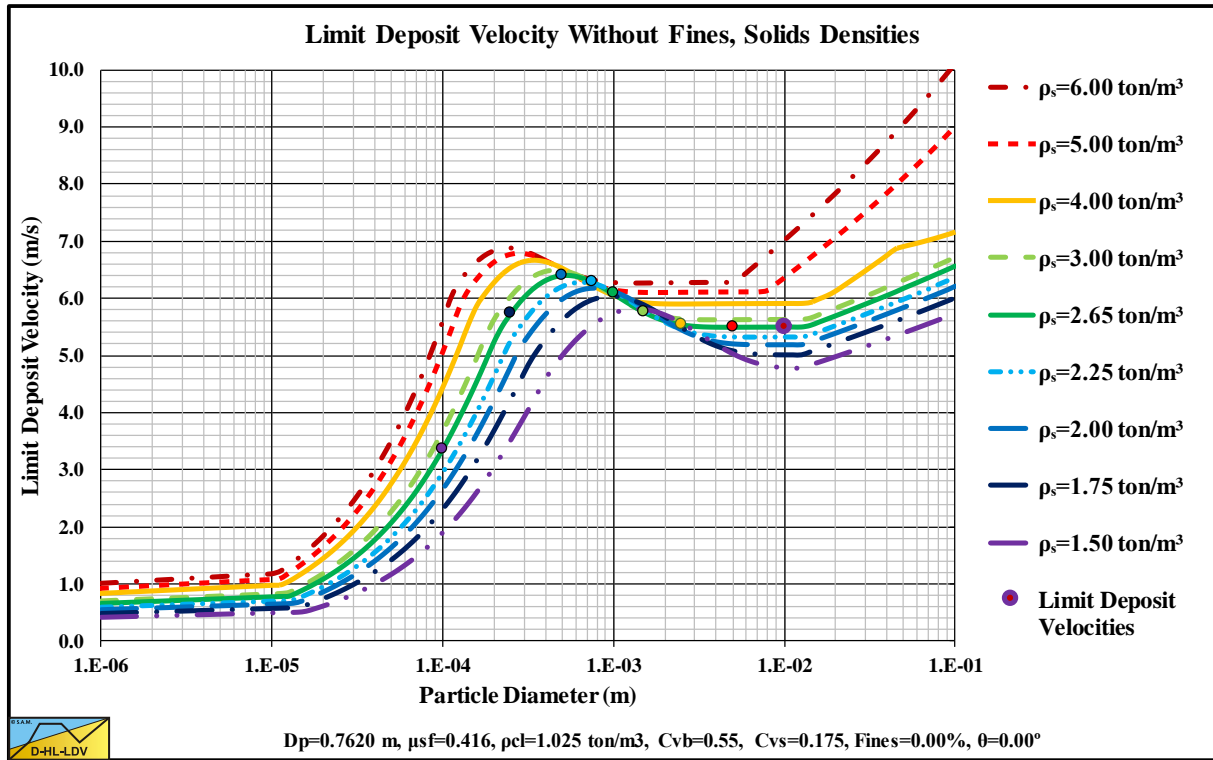
Figure 15.5-74: The Limit Deposit Velocity at 9 solids densities.
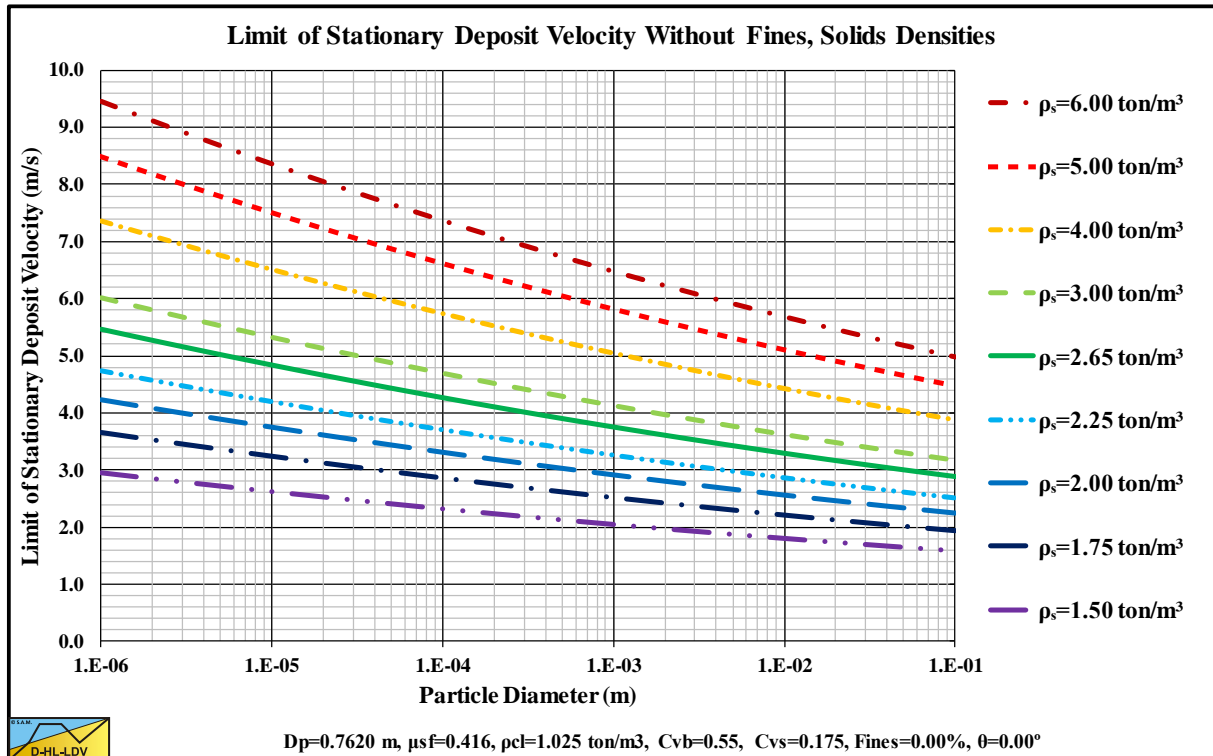
Figure 15.5-75: The transition Fixed Bed-Sliding Bed (LSDV) at 9 solids densities.
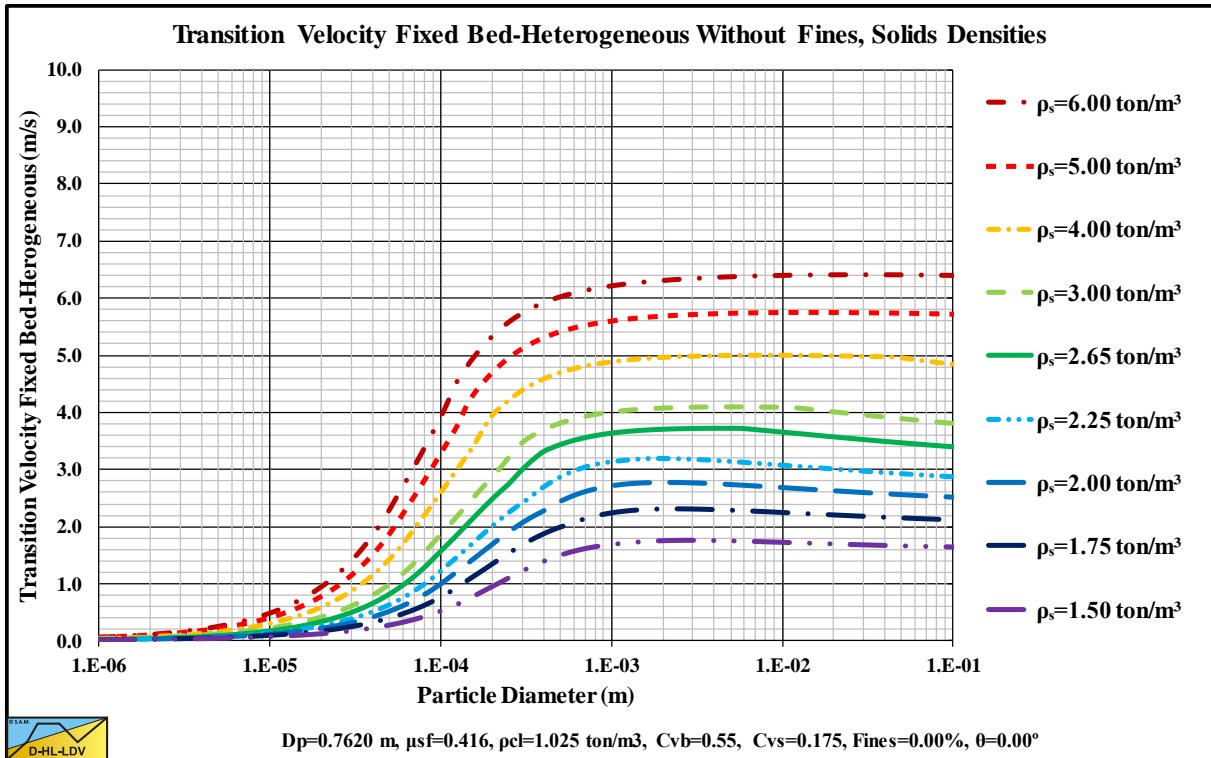
Figure 15.5-76: The transition Fixed Bed-Heterogeneous Regime at 9 solids densities.
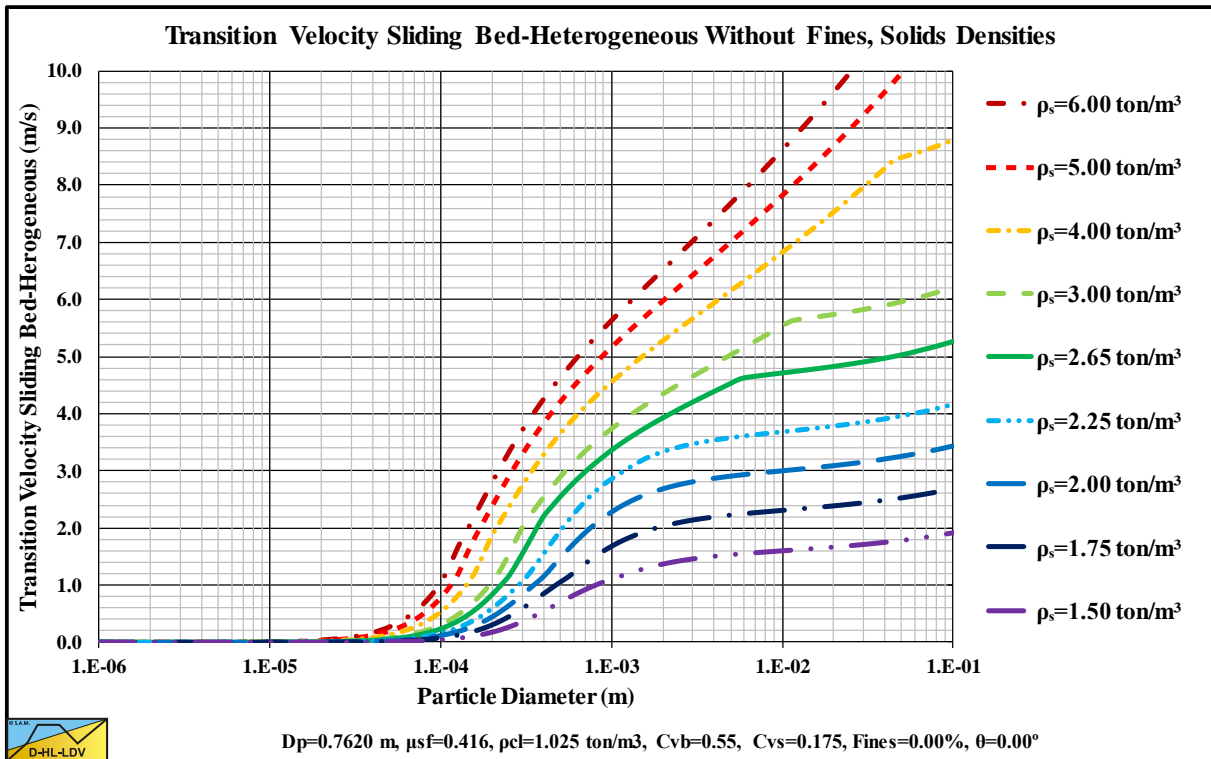
Figure 15.5-77: The transition Sliding Bed-Heterogeneous Regime at 9 solids densities.

Appendices.
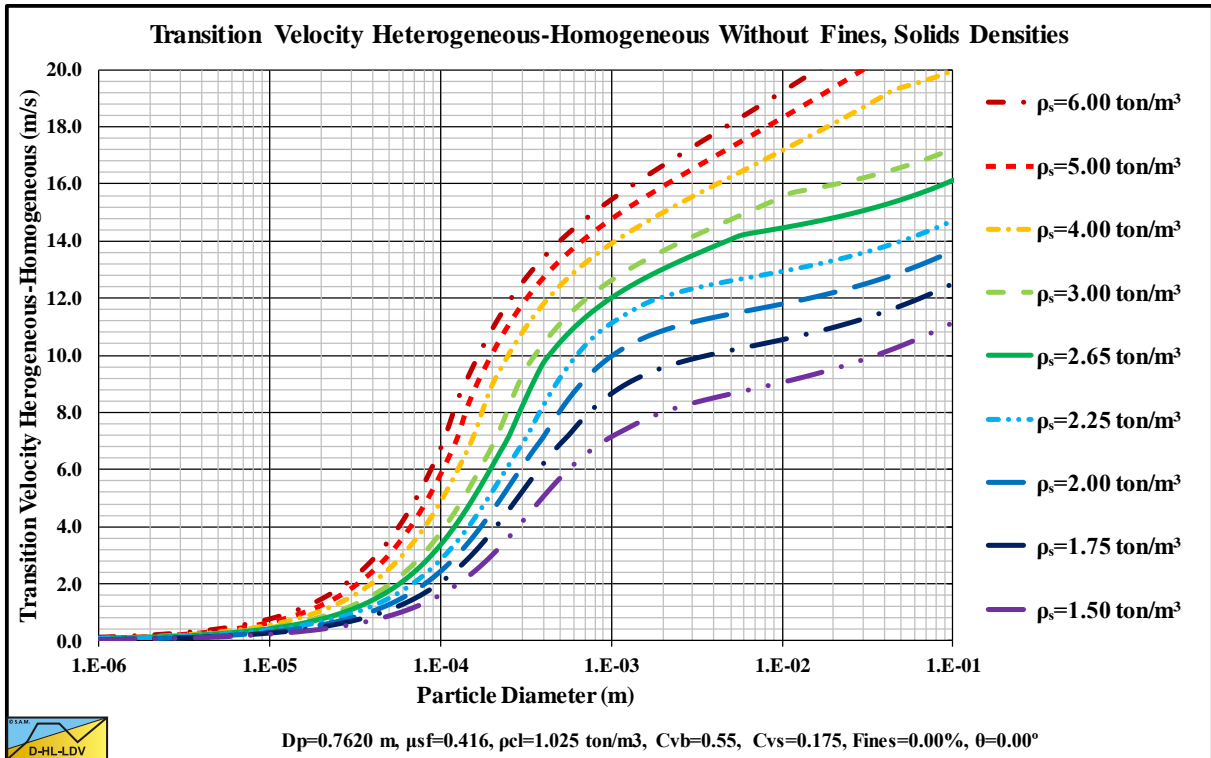
Figure 15.5-78: The transition Heterogeneous-Homogeneous at 9 solids densities.
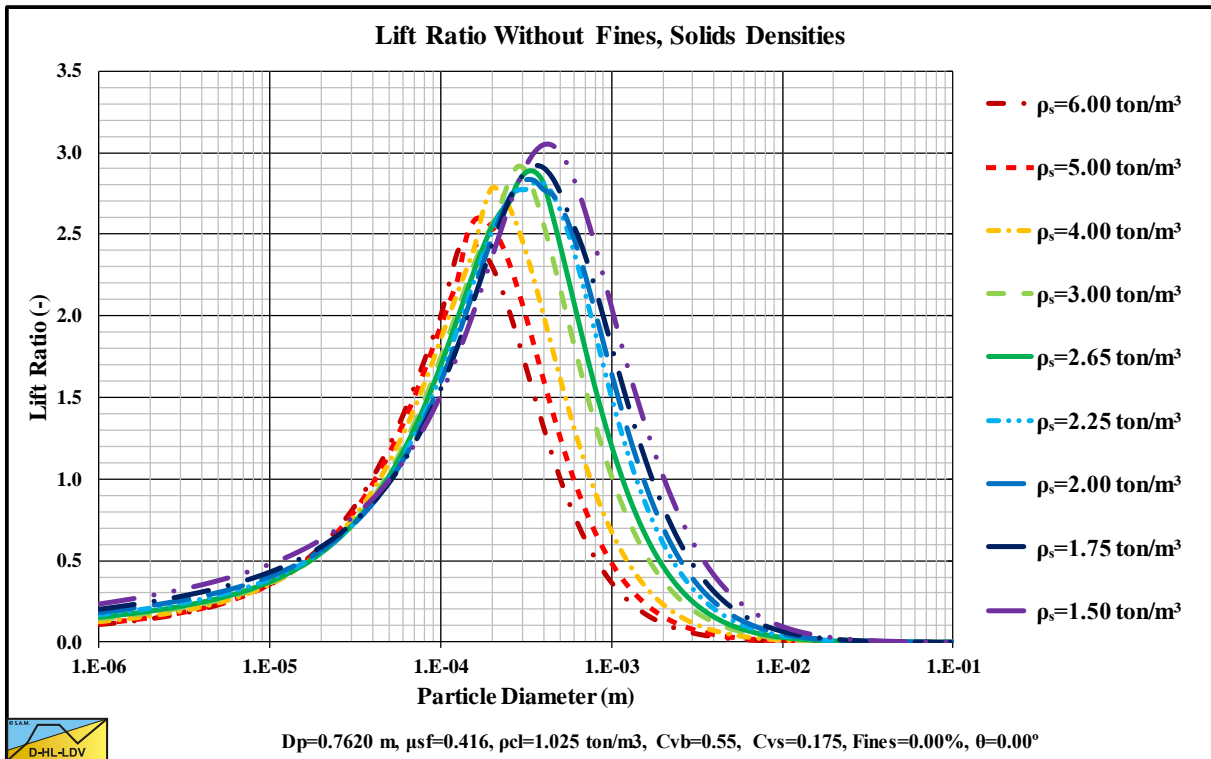
Figure 15.5-79: The lift ratio (near wall lift to gravity ratio) at 9 solids densities.

15.6 3 Layer Model Graphs (Sliding Bed & Sliding Flow).
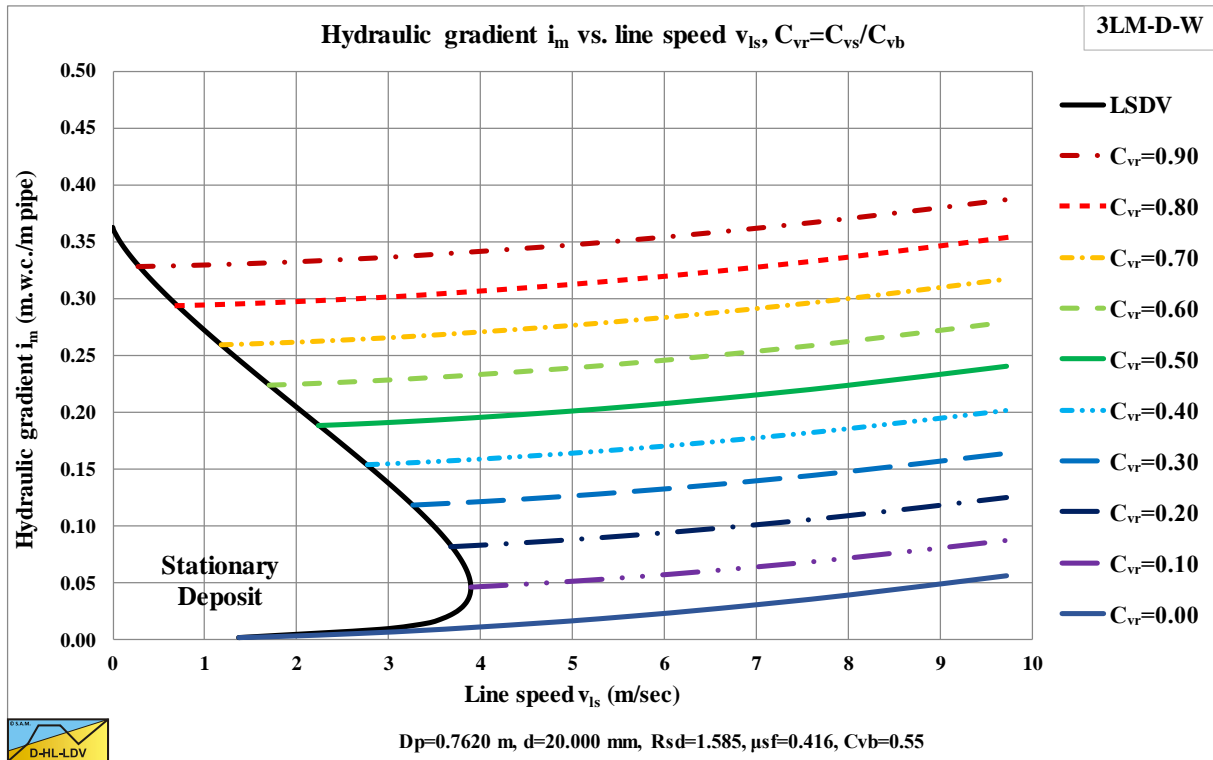
Figure 15.6-1: The hydraulic gradient versus the line speed, Cvs.
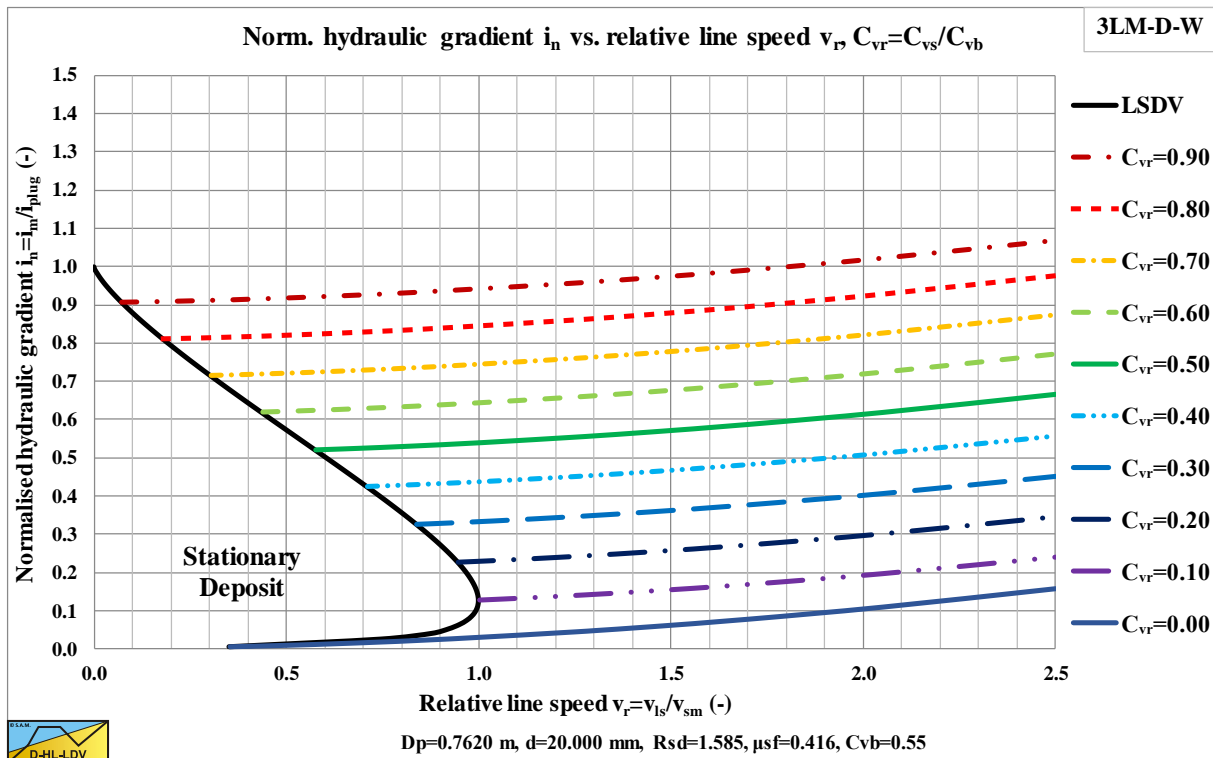
Figure 15.6-2: The normalized hydraulic gradient versus the relative line speed, Cvs.
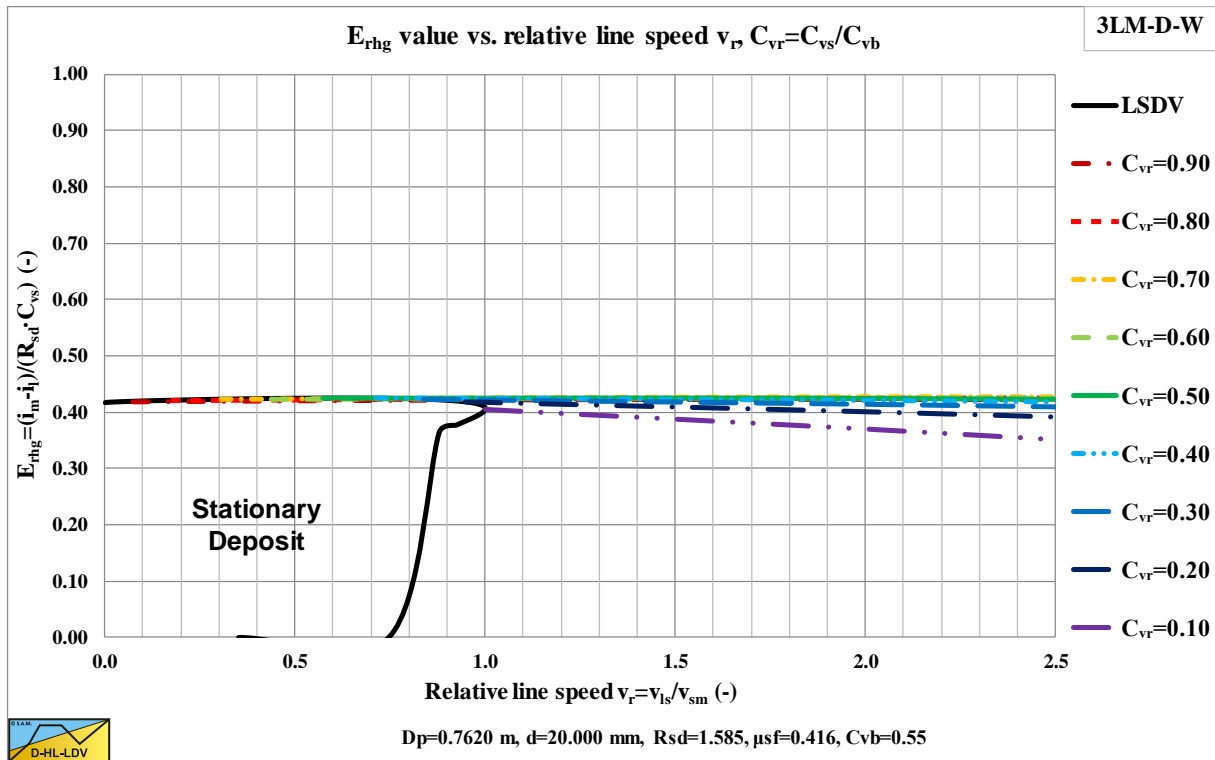
Figure 15.6-3: The relative solids effect versus the relative line speed, Cvs.
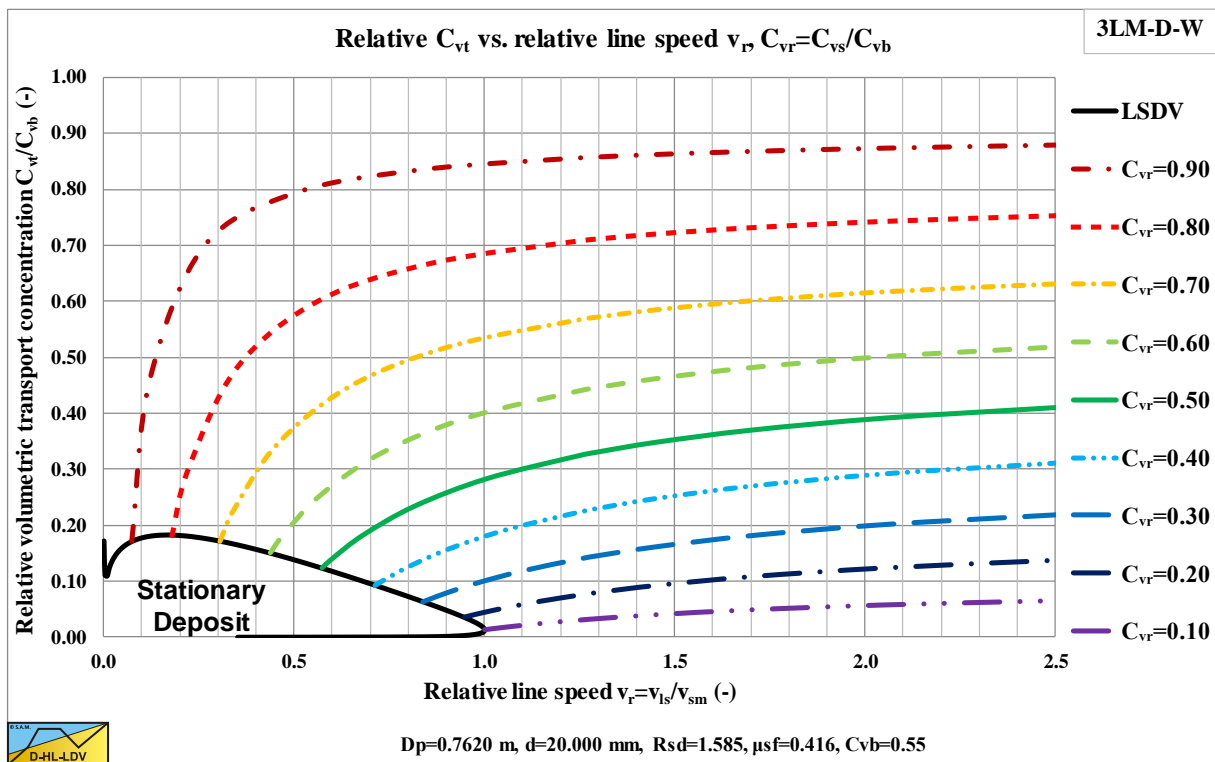
Figure 15.6-4: The delivered concentration versus the relative line speed, Cvs.
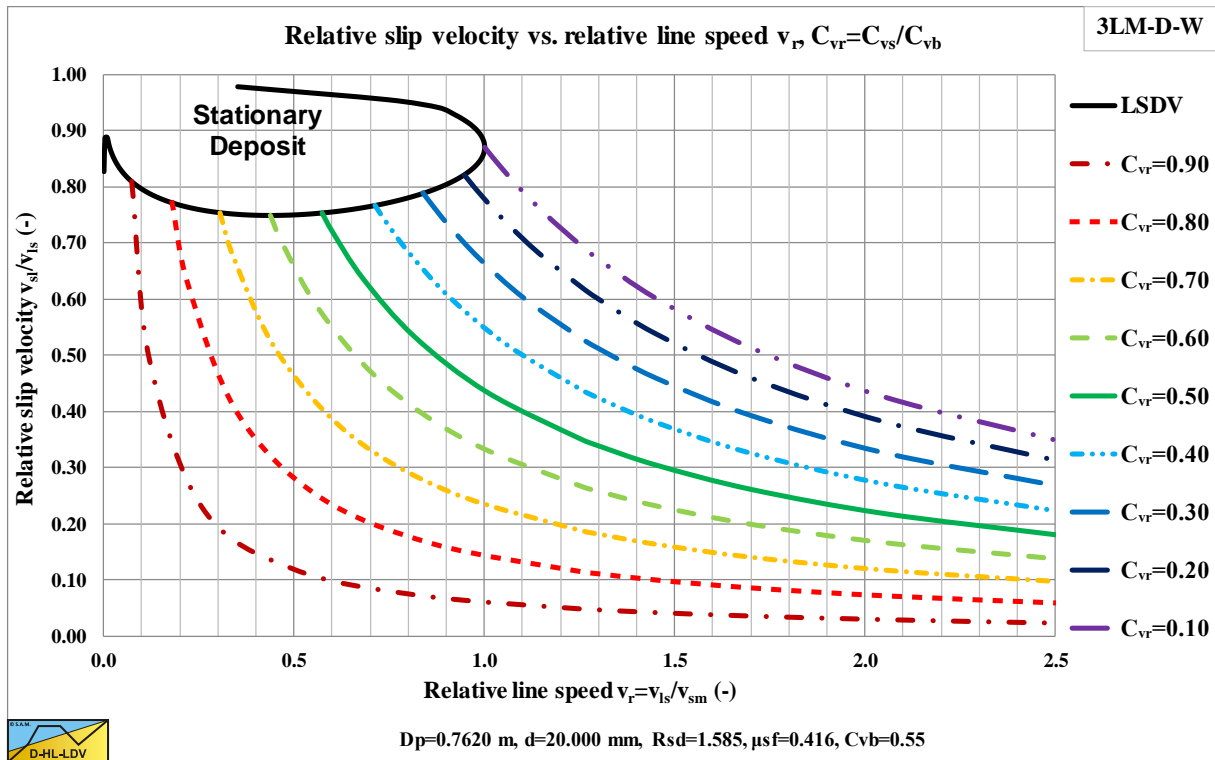
Figure 15.6-5: The relative slip velocity versus the relative line speed, C_vs.
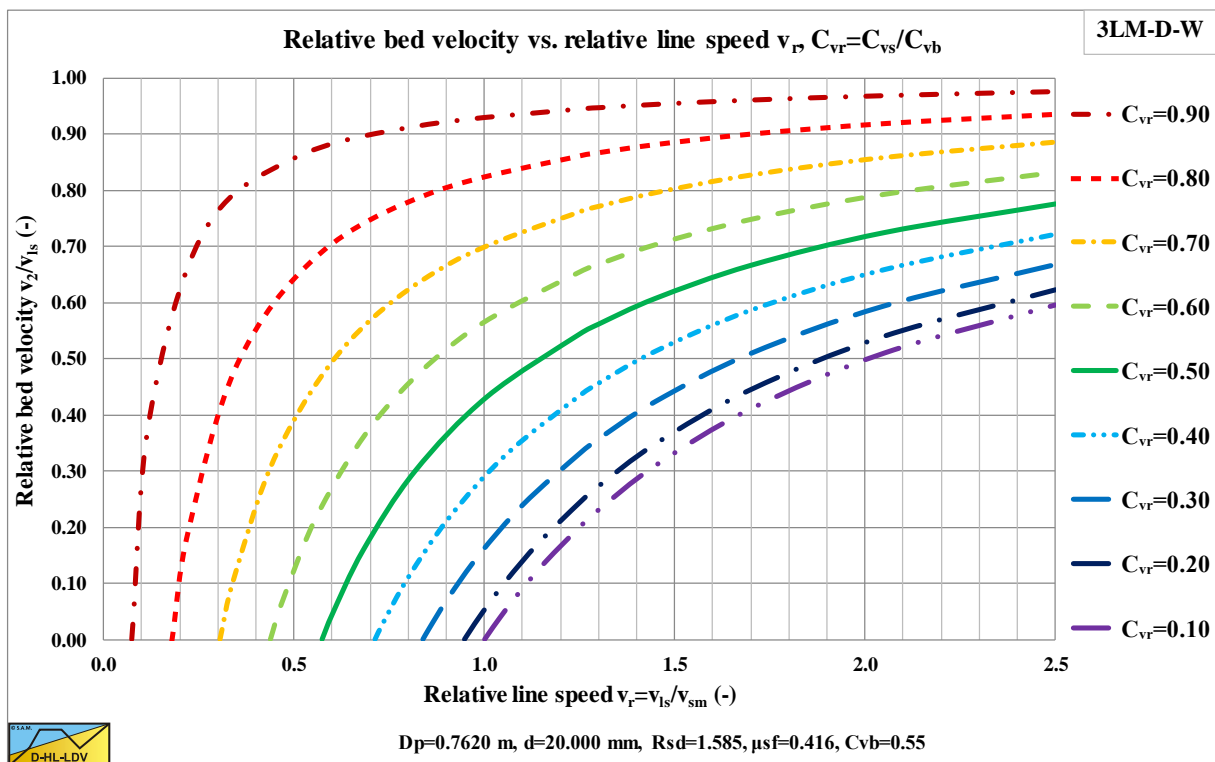
Figure 15.6-6: The relative bed velocity versus the relative line speed, C_vs.
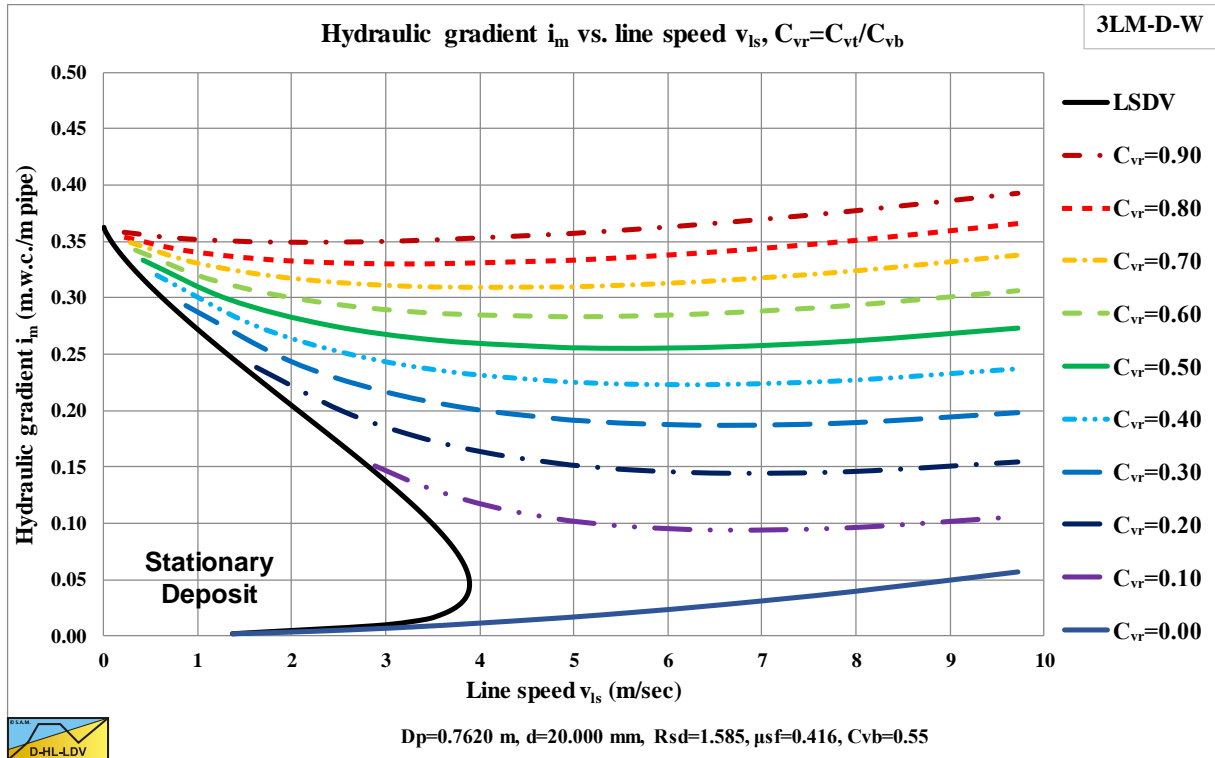
Figure 15.6-7: The hydraulic gradient versus the line speed, C_{vt}.
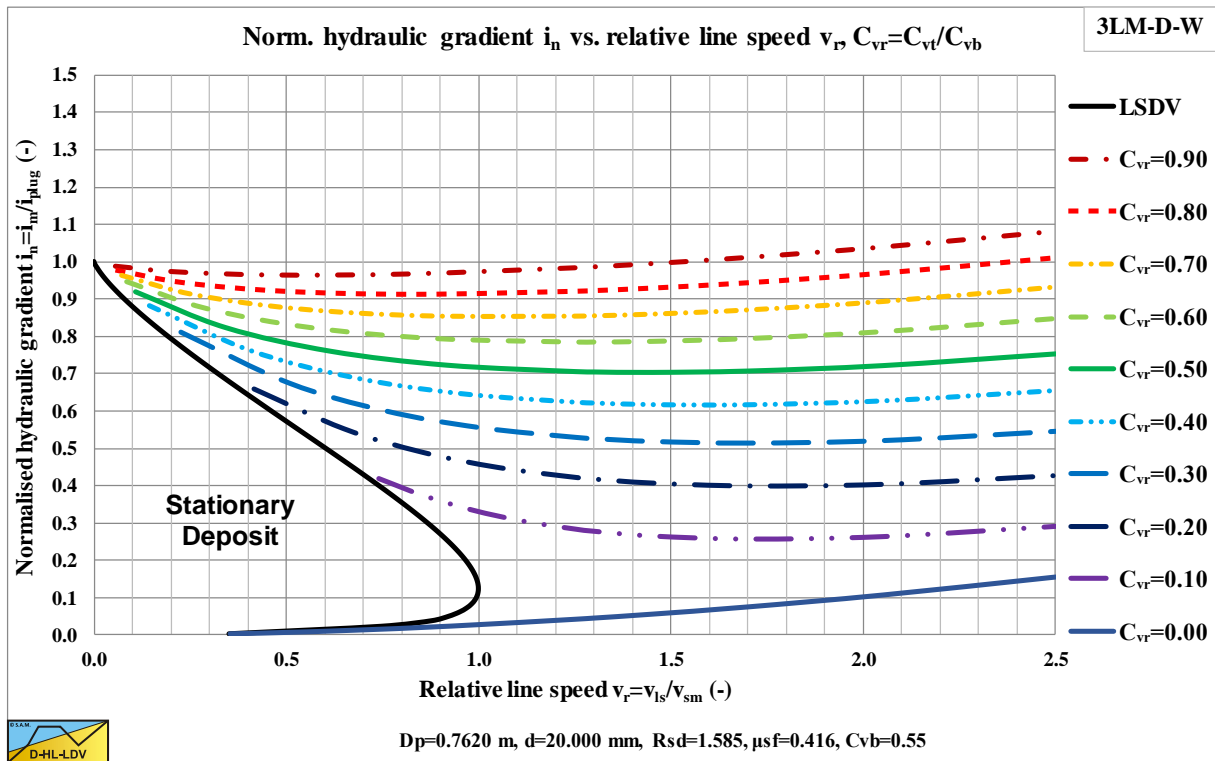
Figure 15.6-8: The normalized hydraulic gradient versus the relative line speed, C_{vt}.
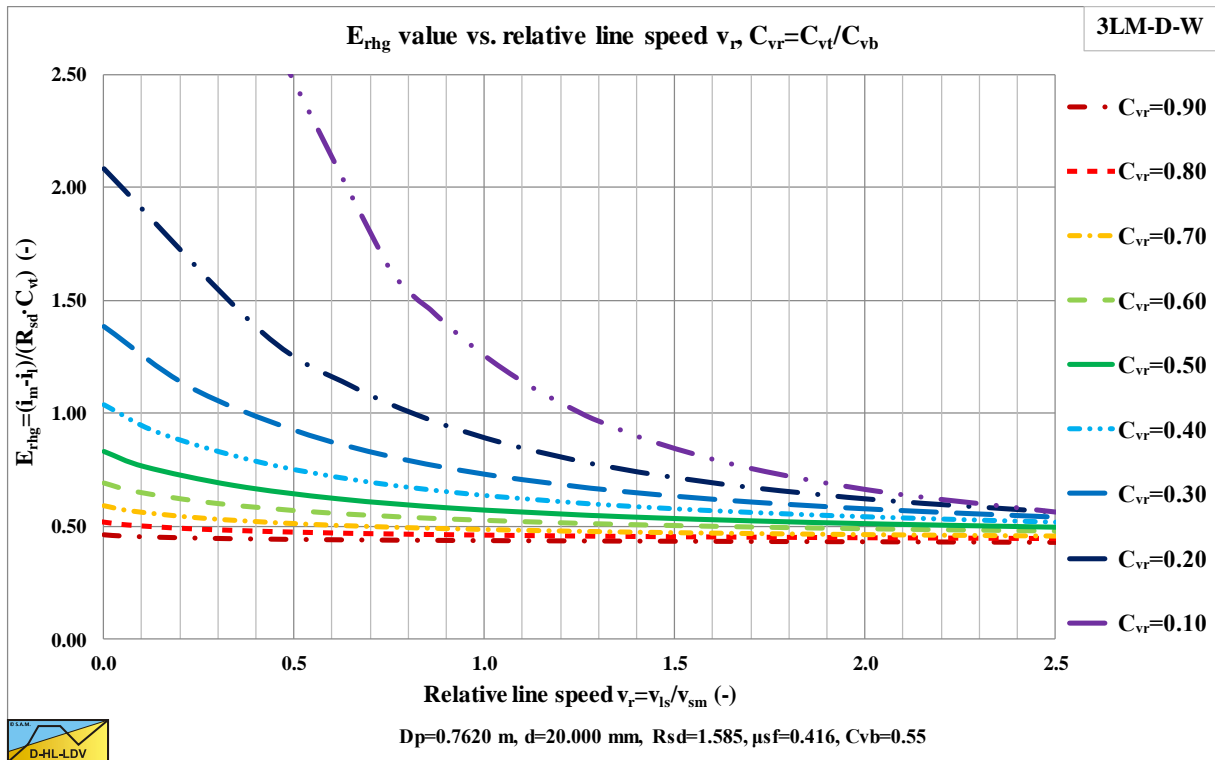
Figure 15.6-9: The relative solids effect versus the relative line speed, C$_{vt}$.
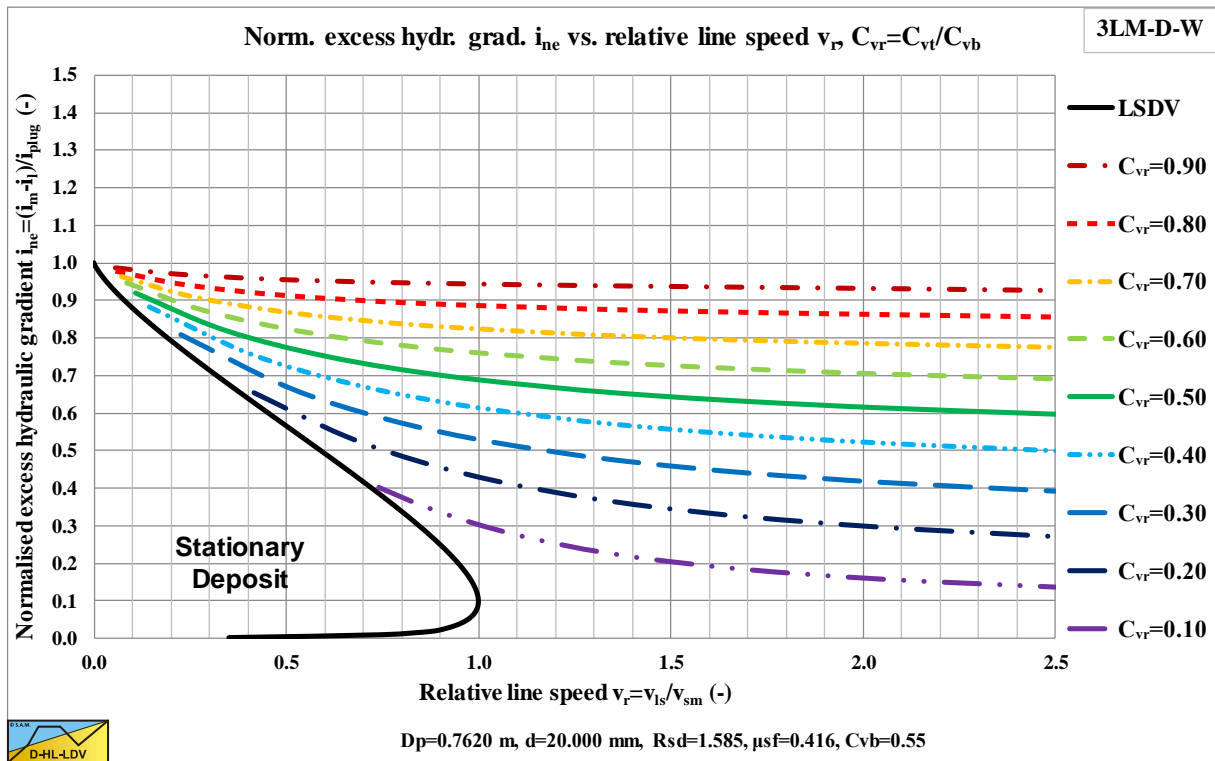
Figure 15.6-10: The normalized excess hydraulic gradient versus the relative line speed, C$_{vt}$.
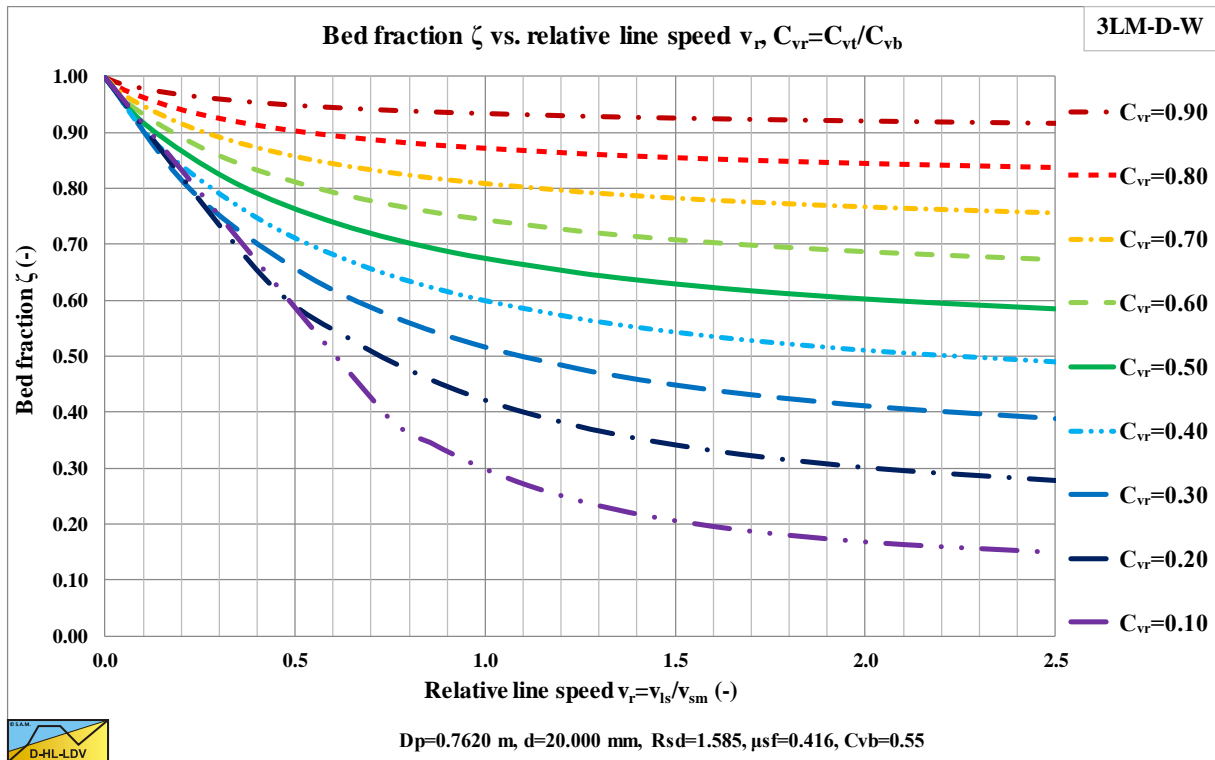
Figure 15.6-11: The bed fraction versus the relative line speed, C$_{vt}$.
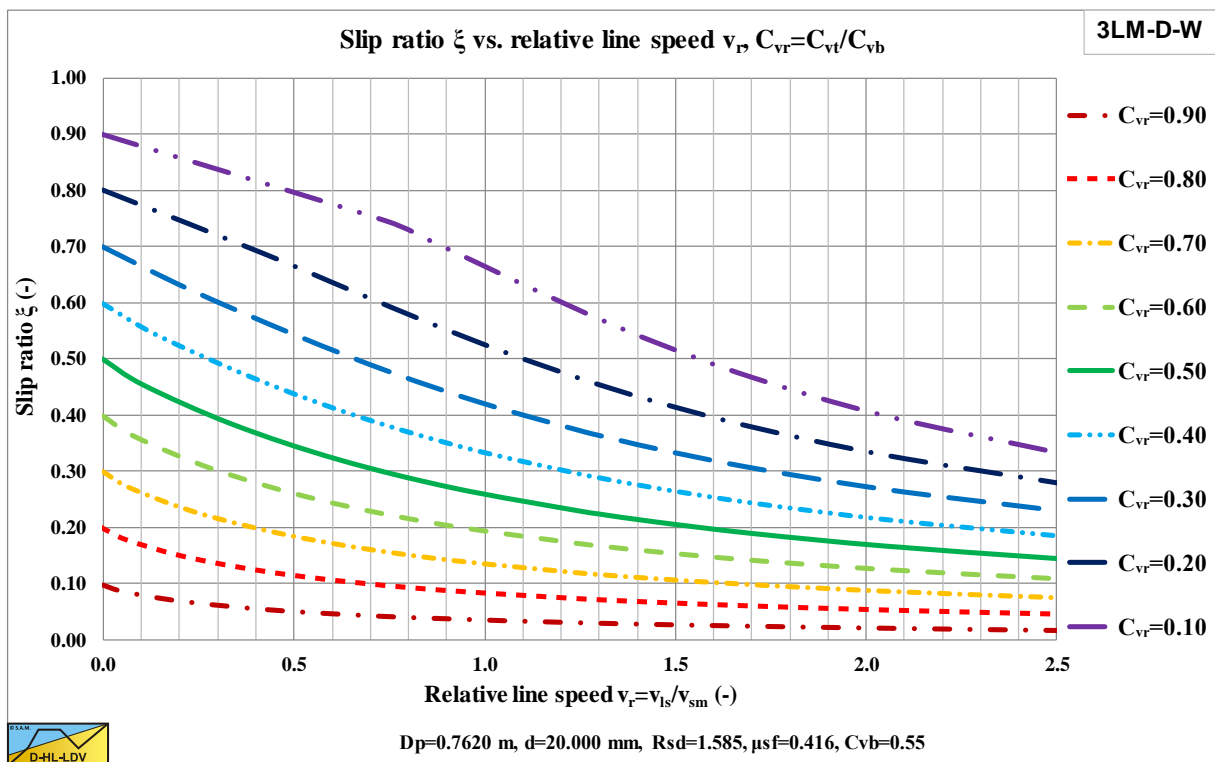
Figure 15.6-12: The slip ratio versus the relative line speed, C$_{vt}$.
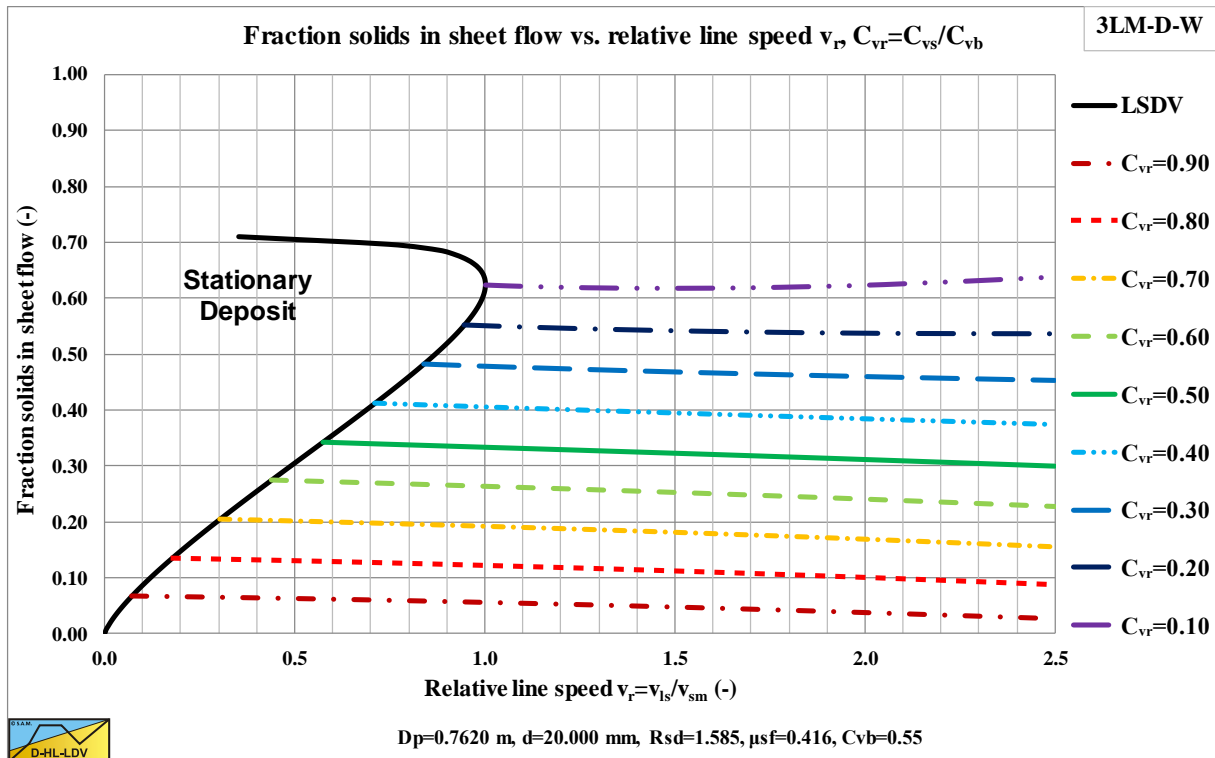
Figure 15.6-13: The solids fraction in sheet flow versus the relative line speed, C_{vs}.
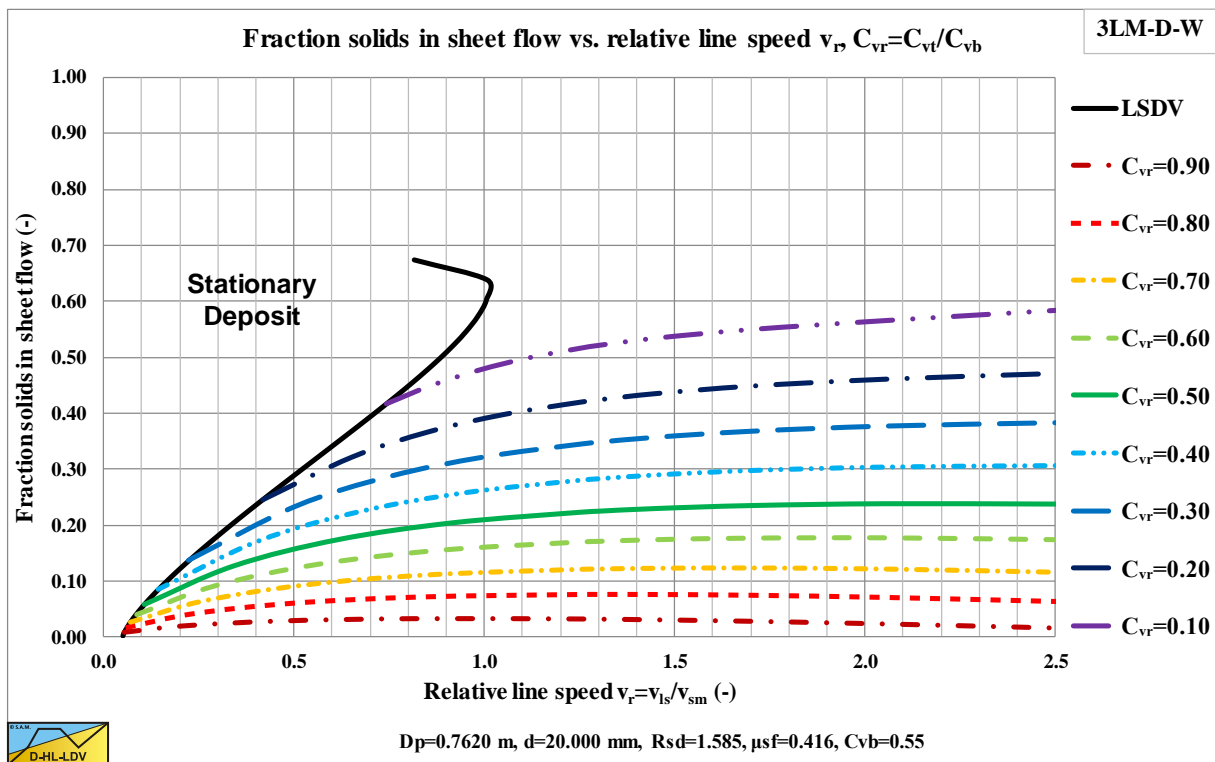
Figure 15.6-14: The solids fraction in sheet flow versus the relative line speed, C_{vt}.
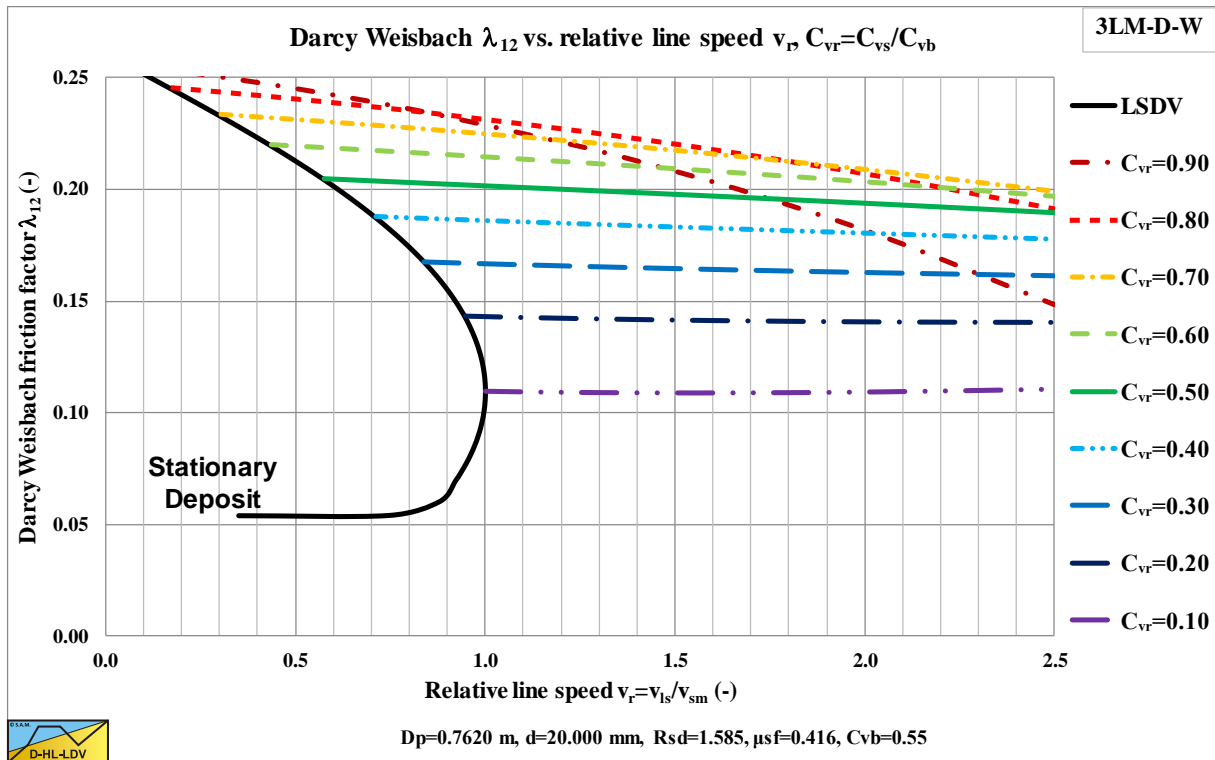
Figure 15.6-15: The bed friction factor versus the relative line speed, C_{vs}.
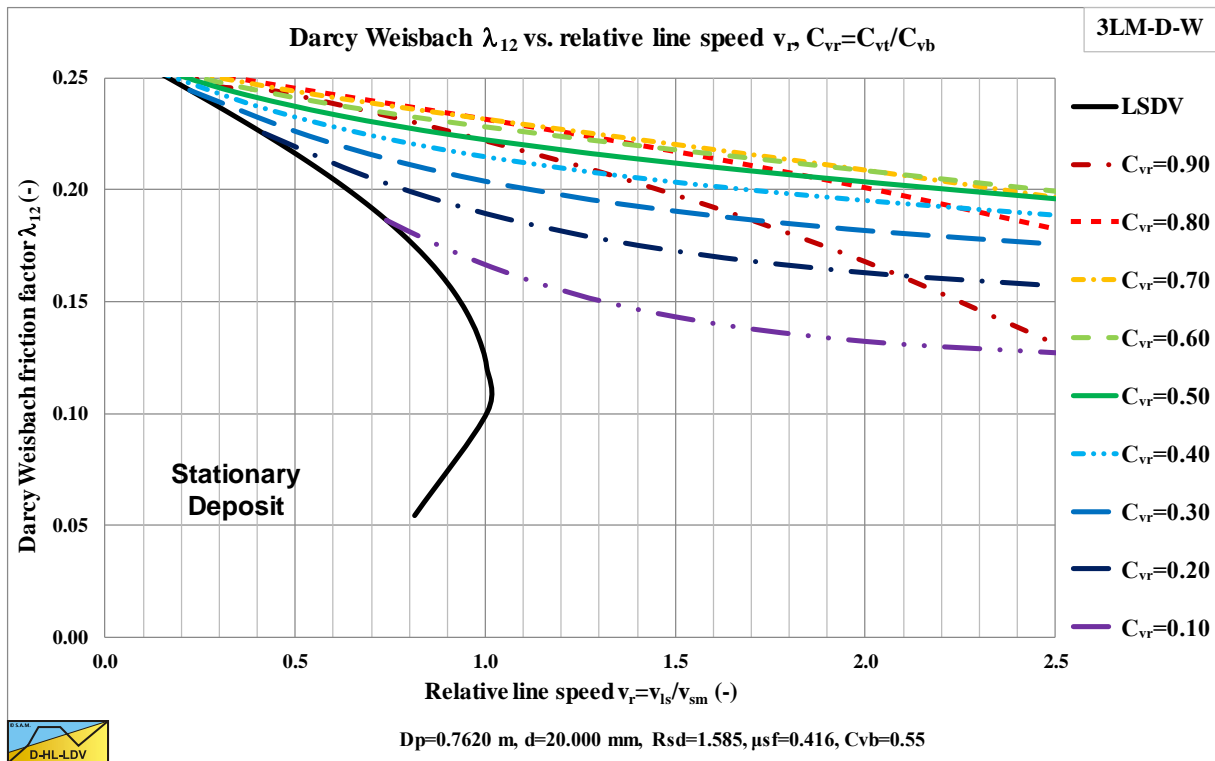
Figure 15.6-16: The bed friction factor versus the relative line speed, C_{vt}.

Appendices.
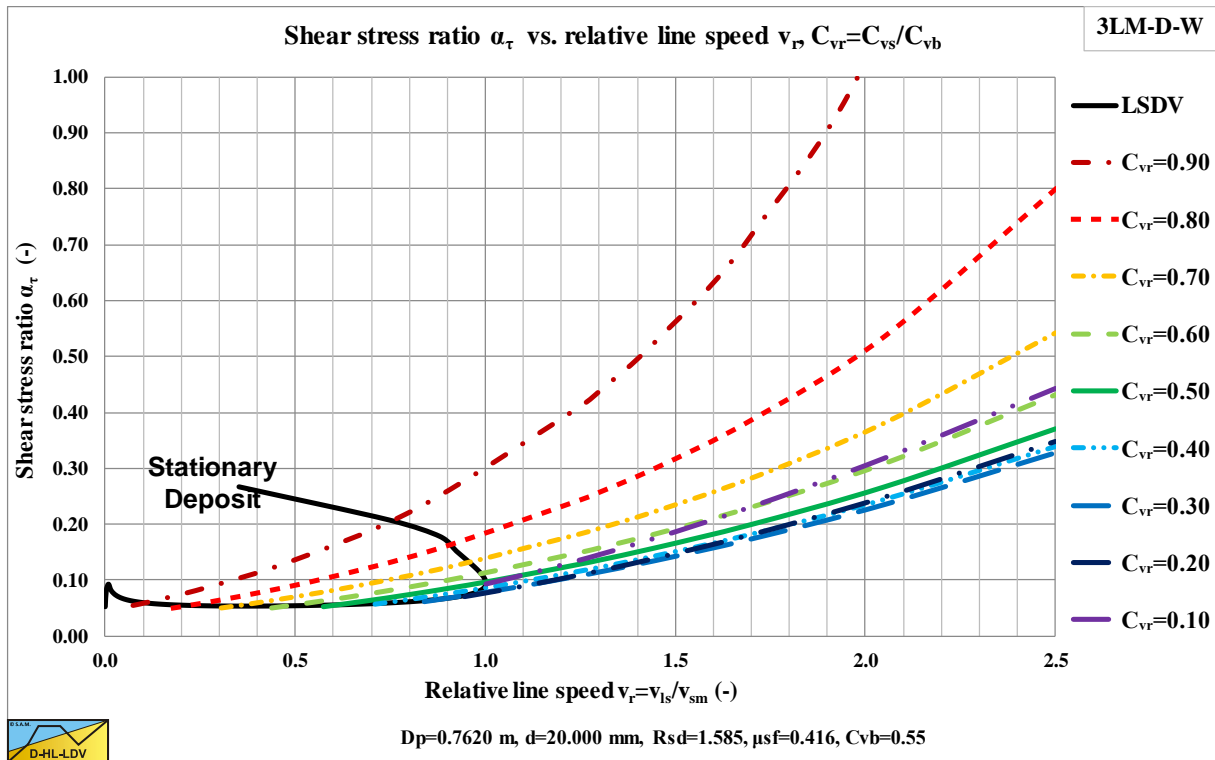
Figure 15.6-17: The shear stress ratio versus the relative line speed, C_{vs}.
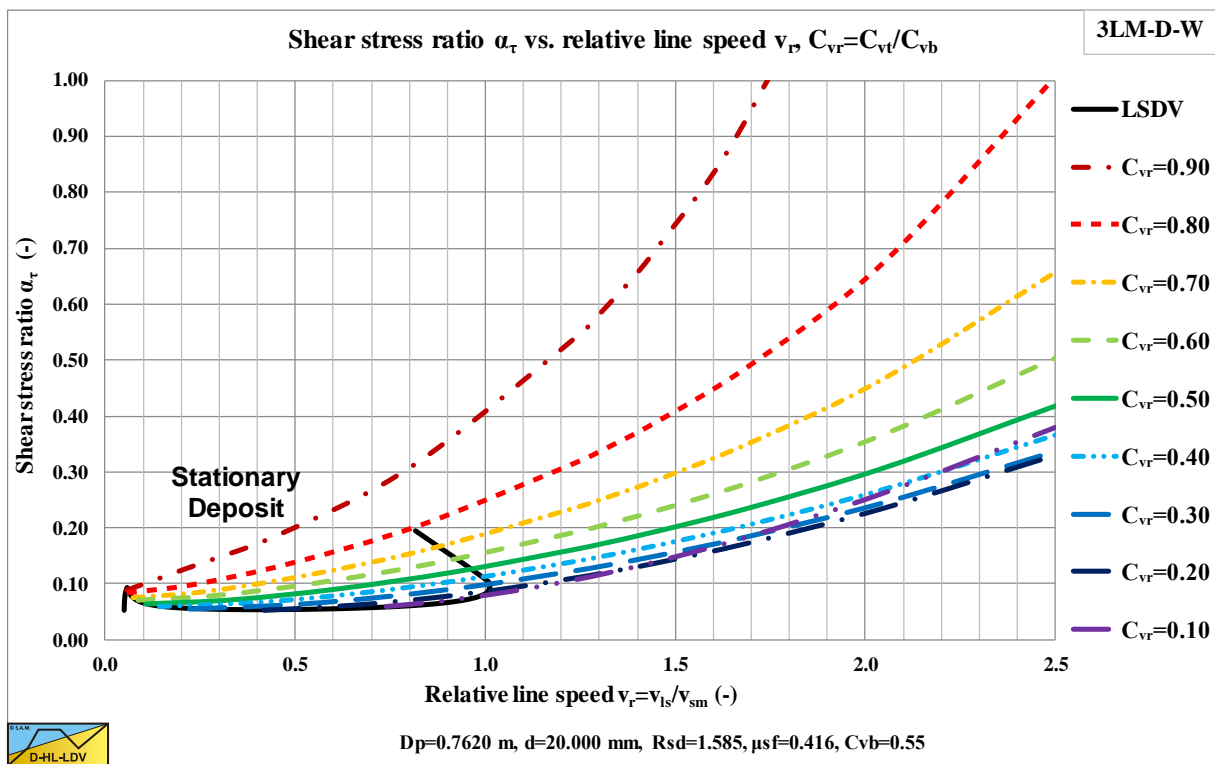
Figure 15.6-18: The shear stress ratio versus the relative line speed, C_{vt}.

Appendices.

15.7 Concentration Distributions.

15.7.1 Roco & Shook (1983).

Roco & Shook (1983), Cvb=0.60, Dp=0.0515 m, d=0.165 mm, vls=3.78-4.33 m/s, Sand
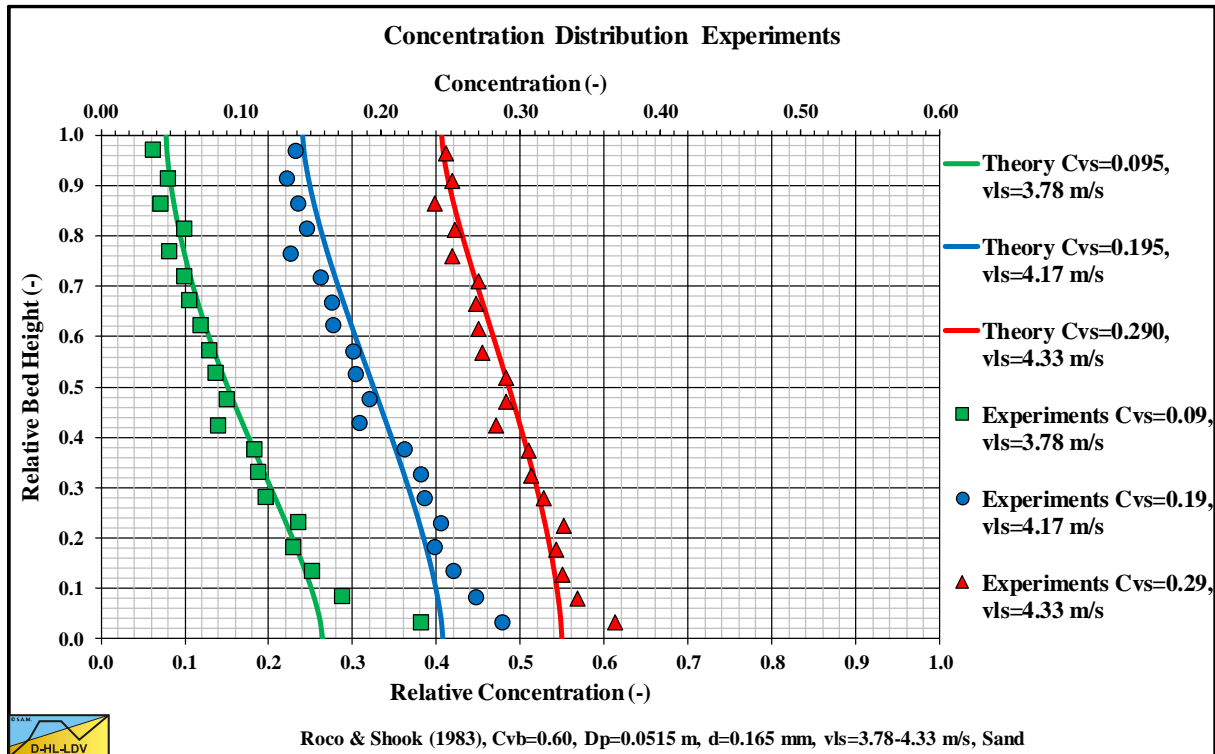
Figure 15.7-1: Roco & Shook (1983) d=0.165 mm, D$_P$=0.0515 m.

Roco & Shook (1983), Cvb=0.60, Dp=0.263 m, d=0.165 mm, vls=3.5 m/s, Sand
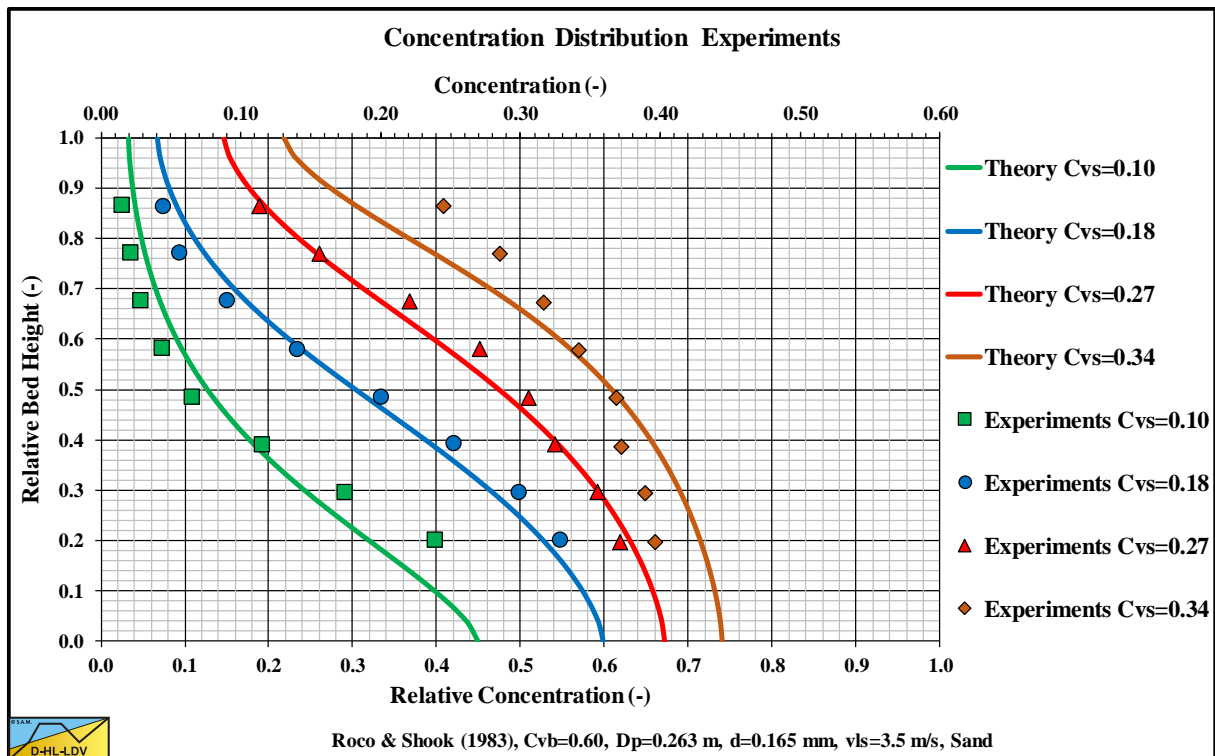
Figure 15.7-2: Roco & Shook (1983) d=0.165 mm, D$_P$=0.2630 m.
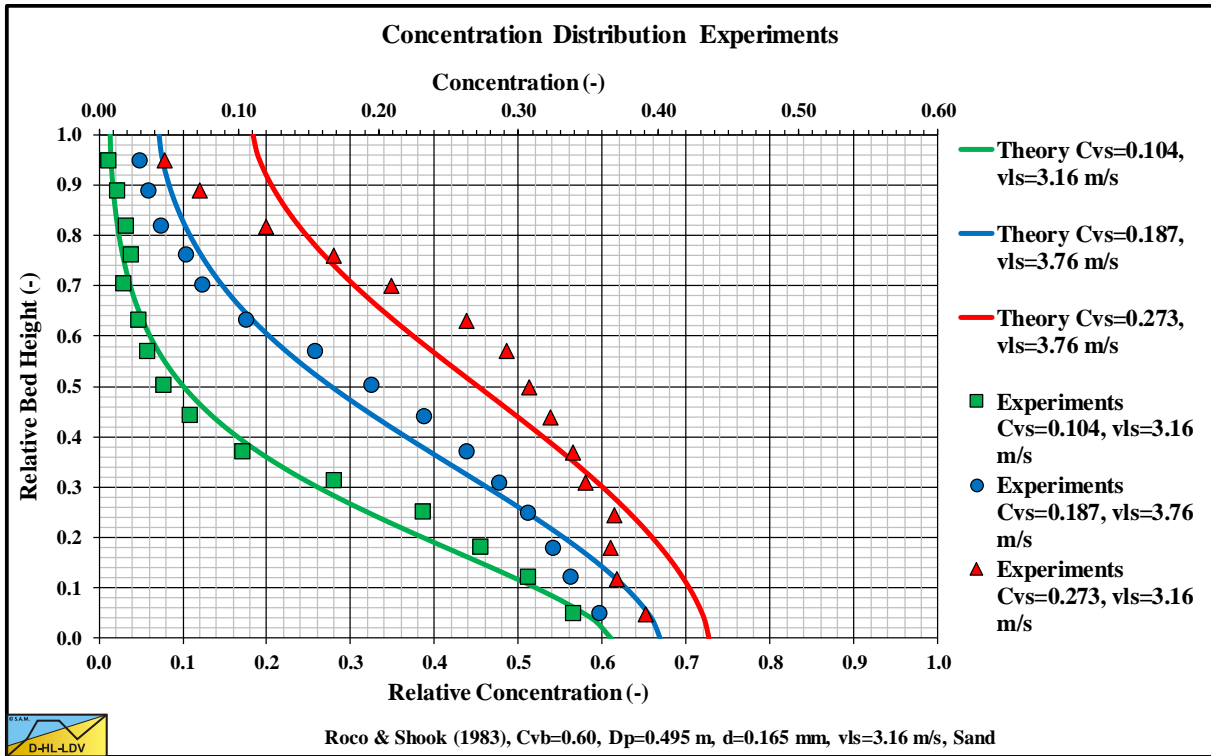
Figure 15.7-3: Roco & Shook (1983) d=0.165 mm, D_p=0.4950 m.
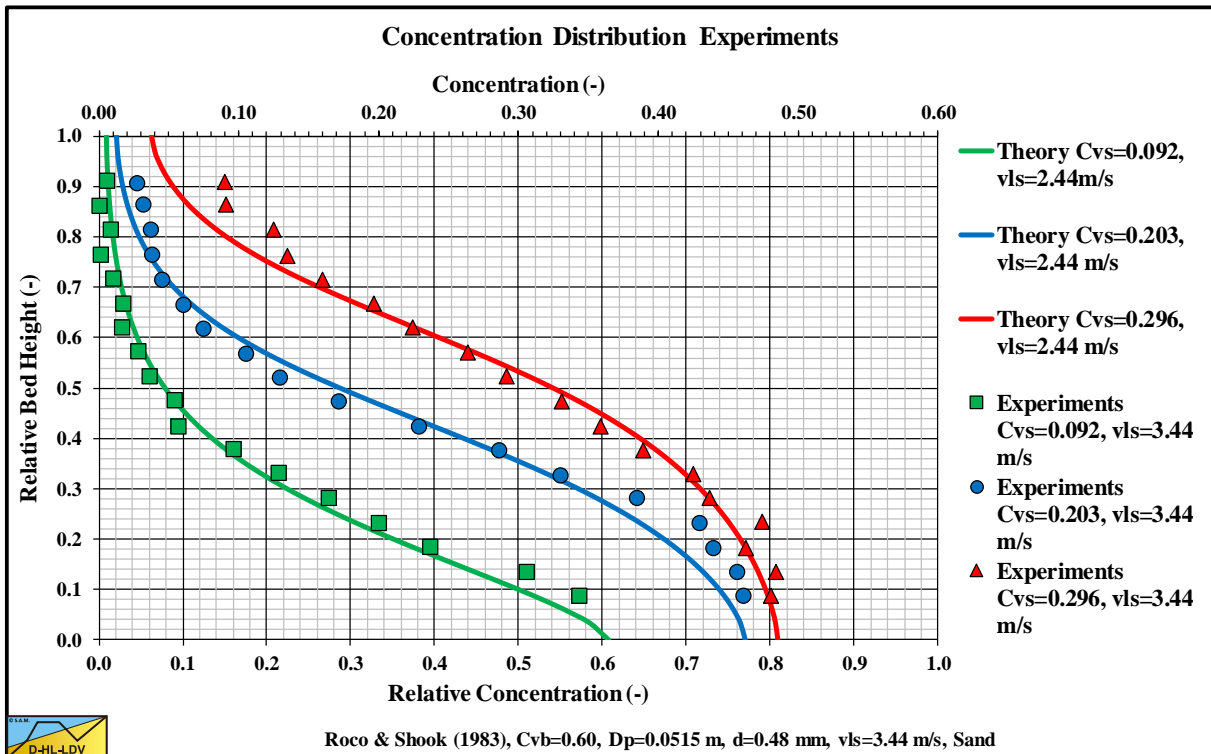
Figure 15.7-4: Roco & Shook (1983) d=0.480 mm, D_p=0.0515 m.
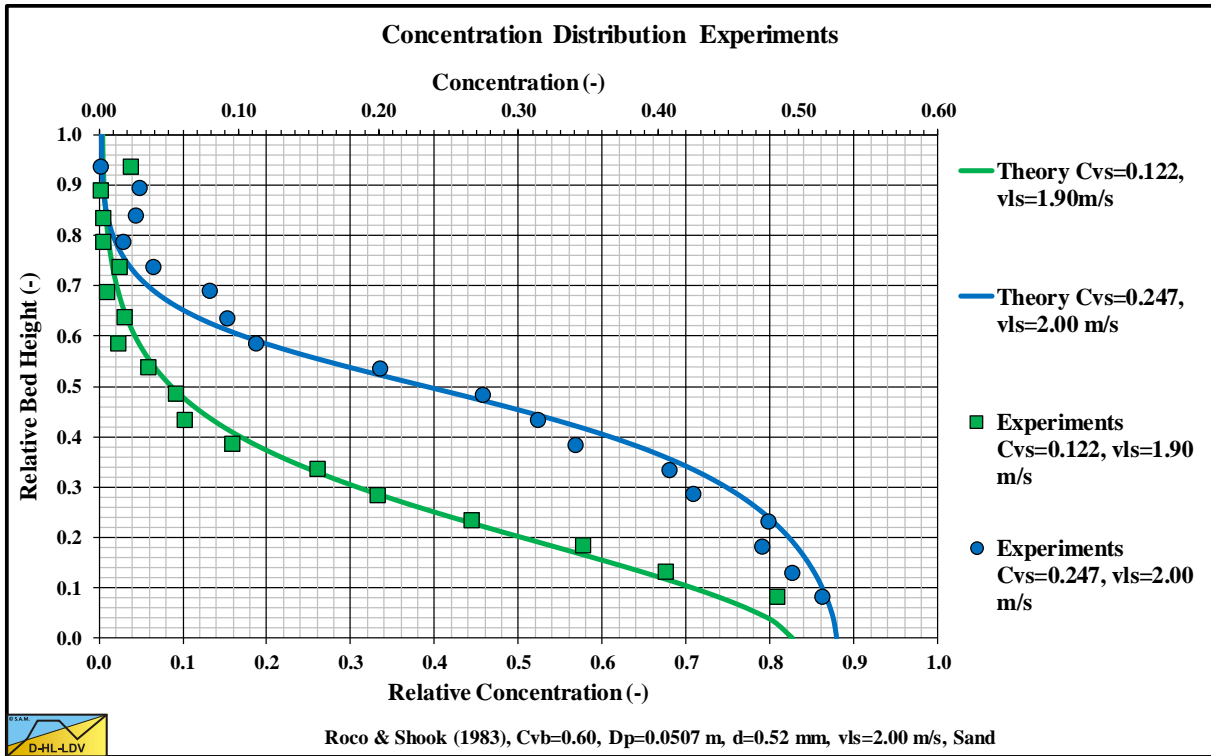
Figure 15.7-5: Roco & Shook (1983) d=0.520 mm, D$_p$=0.0507 m.
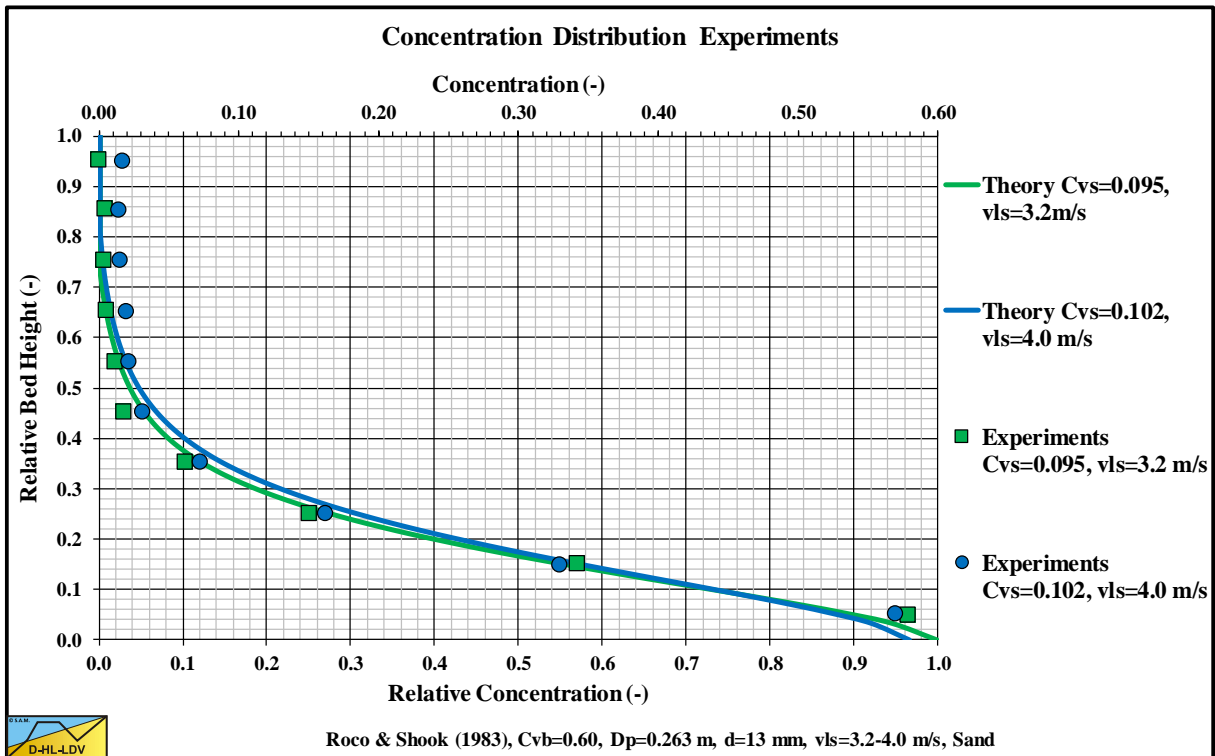
Figure 15.7-6: Roco & Shook (1983) d=13.0 mm, D$_p$=0.2630 m.

Appendices.

15.7.2 Gillies (1993).
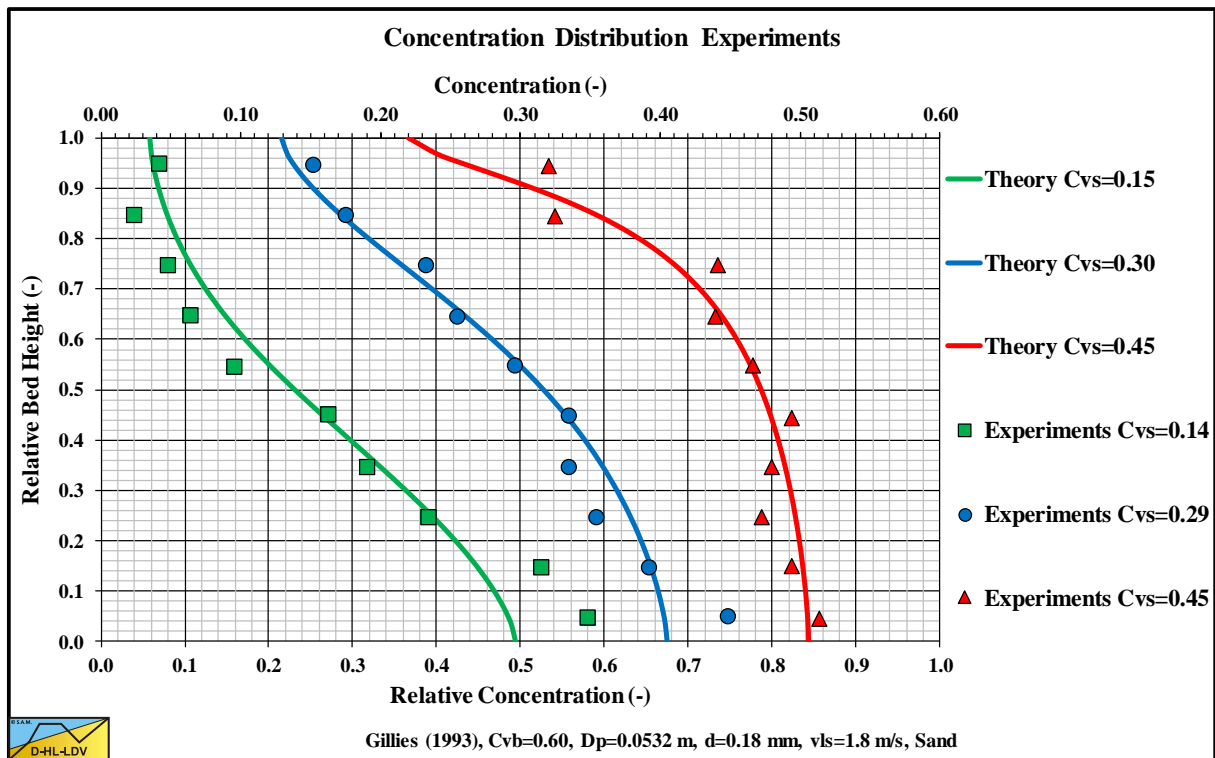
Figure 15.7-7: Gillies (1993) d=0.180 mm, D_p=0.0532 m, v_ls=1.8 m/s.
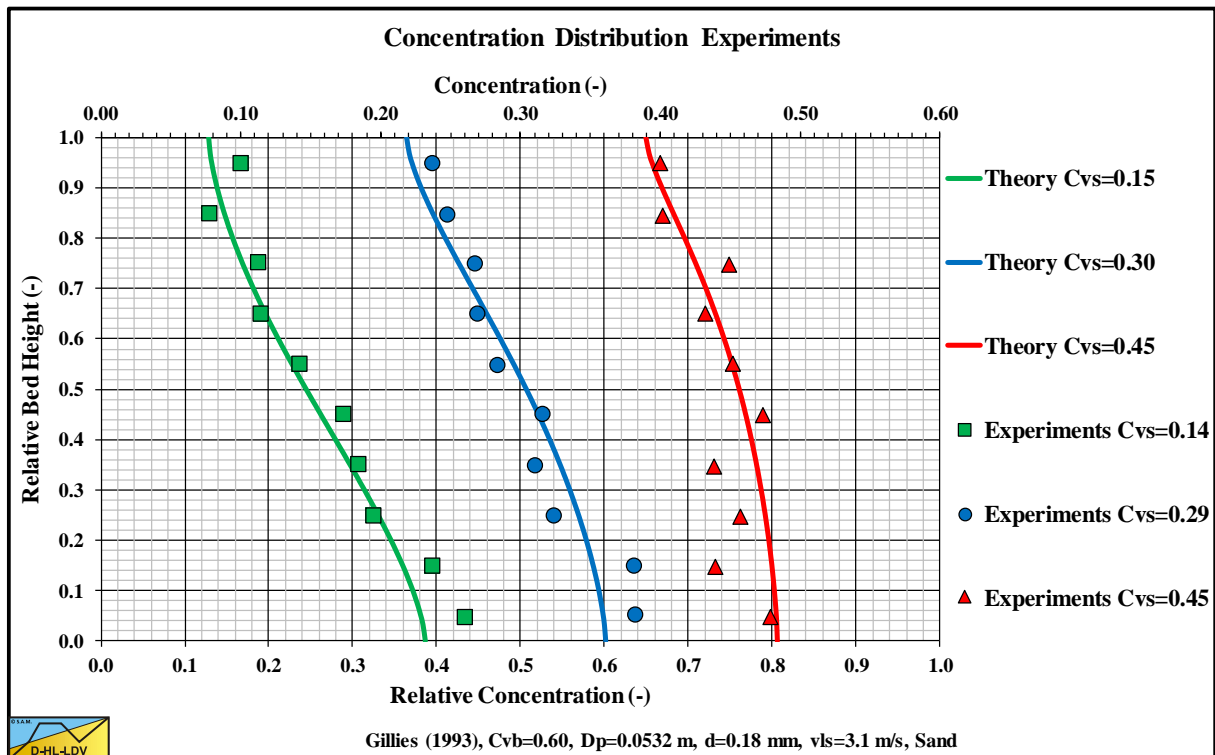
Figure 15.7-8: Gillies (1993) d=0.180 mm, D_p=0.0532 m, v_ls=3.1 m/s.
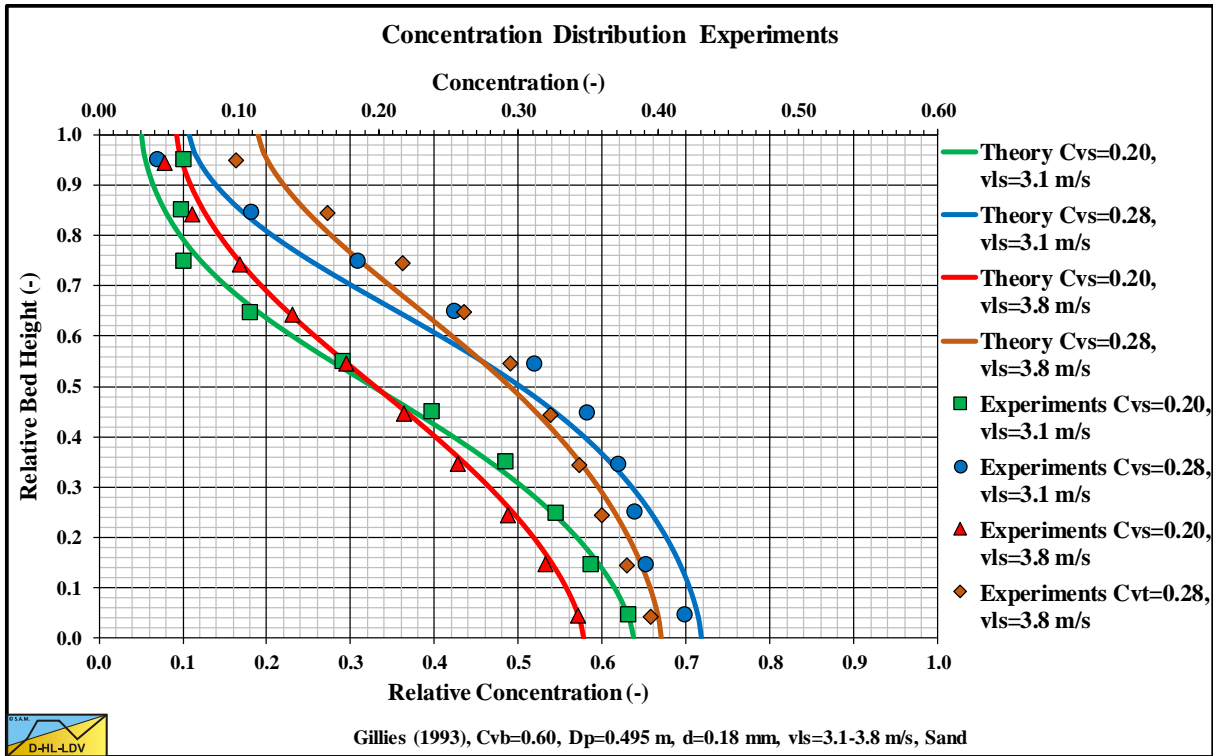
Figure 15.7-9: Gillies (1993) d=0.180 mm, D_p=0.4950 m, v_{ls}=3.1-3.8 m/s.
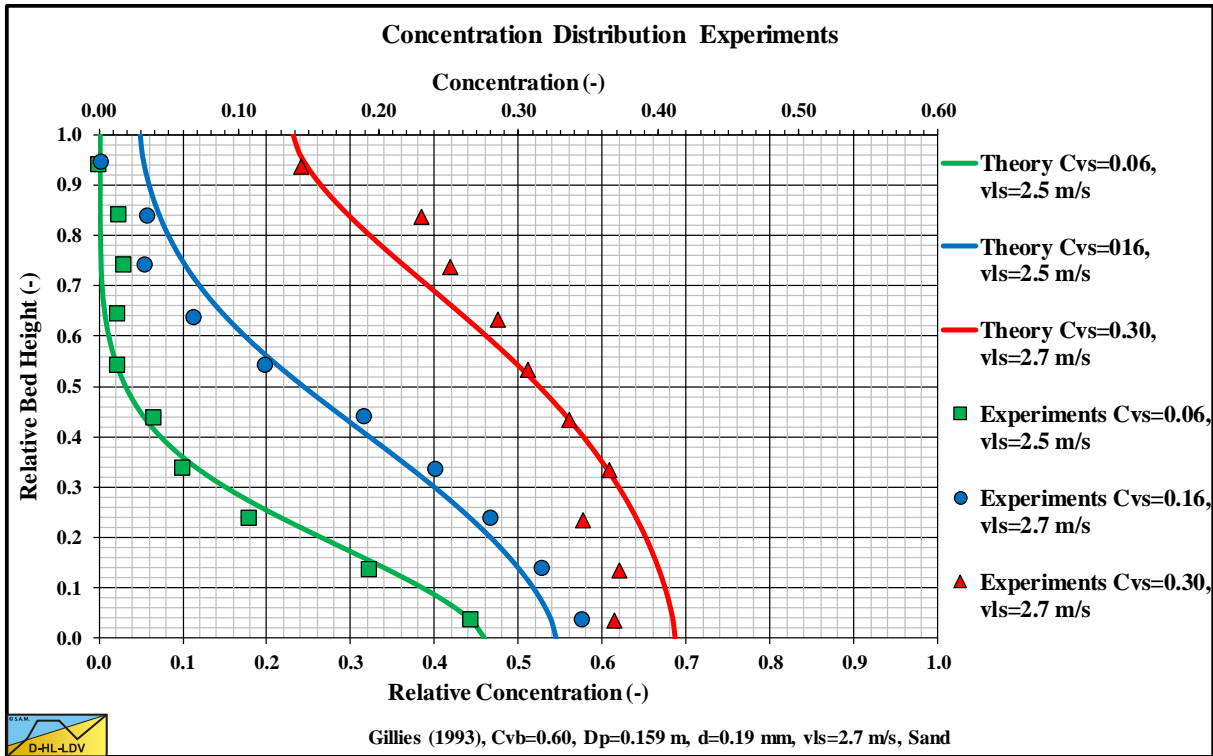
Figure 15.7-10: Gillies (1993) d=0.190 mm, D_P=0.1590 m, v_{ls}=2.5-2.7 m/s.
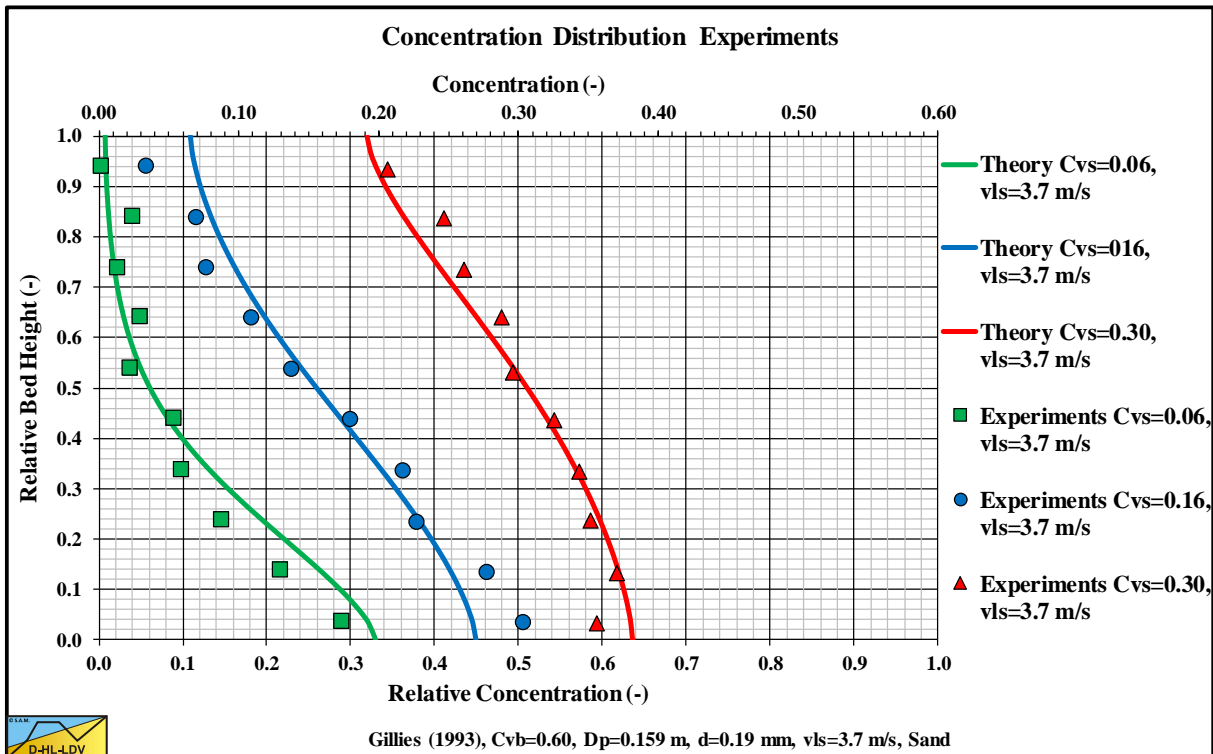
Figure 15.7-11: Gillies (1993) d=0.190 mm, D_P=0.1590 m, v_{ls}=3.7 m/s.
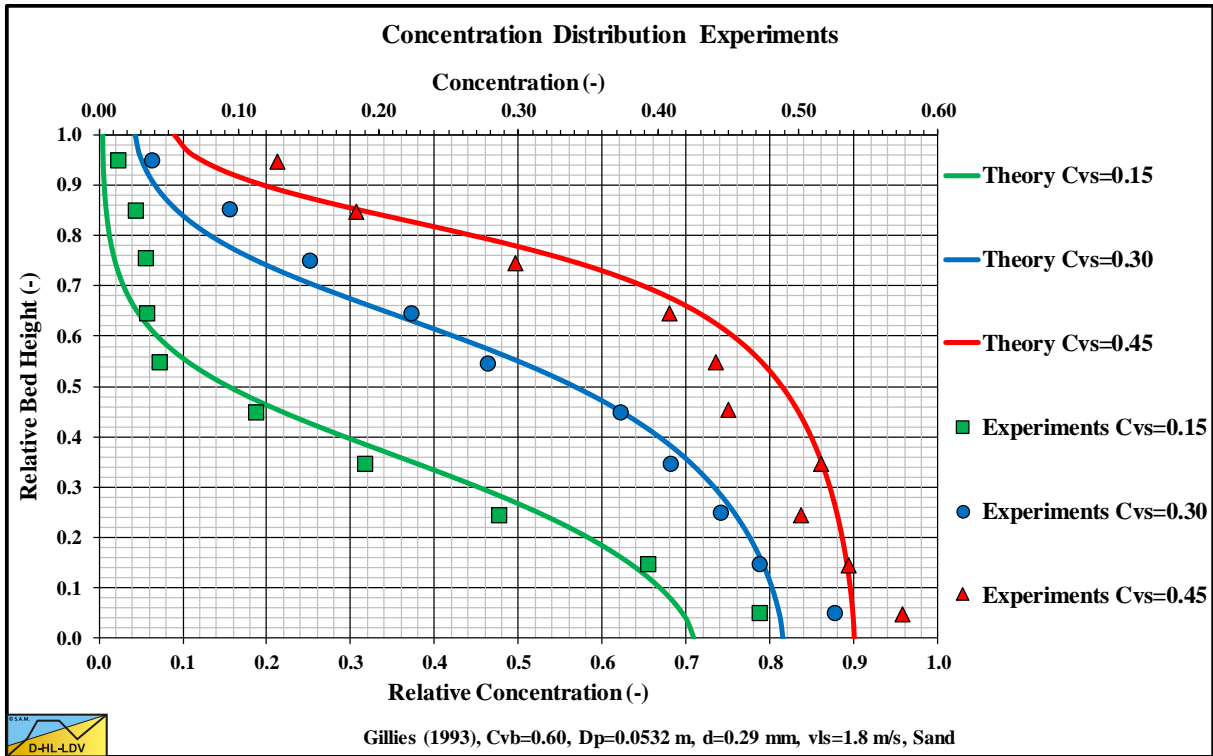
Figure 15.7-12: Gillies (1993) d=0.290 mm, D$_P$=0.0532 m, v$_{ls}$=1.8 m/s.
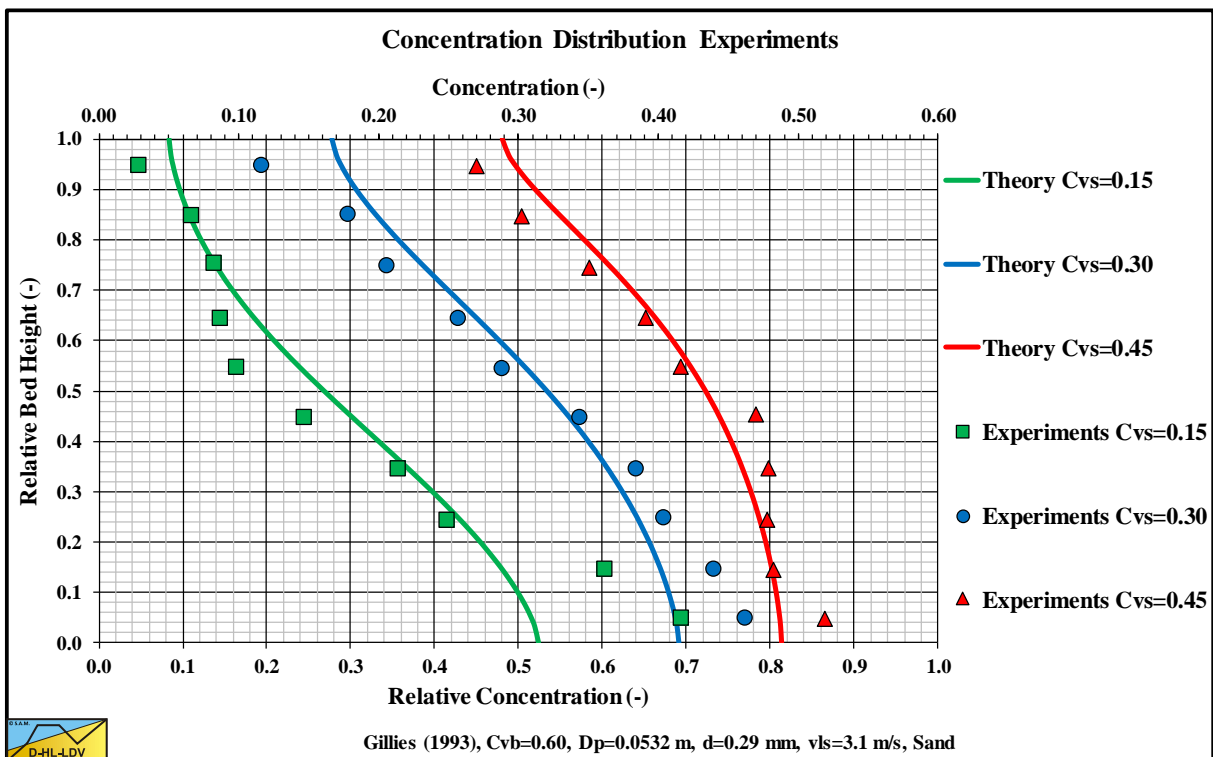
Figure 15.7-13: Gillies (1993) d=0.290 mm, D$_P$=0.0532 m, v$_{ls}$=3.1 m/s.

Appendices.
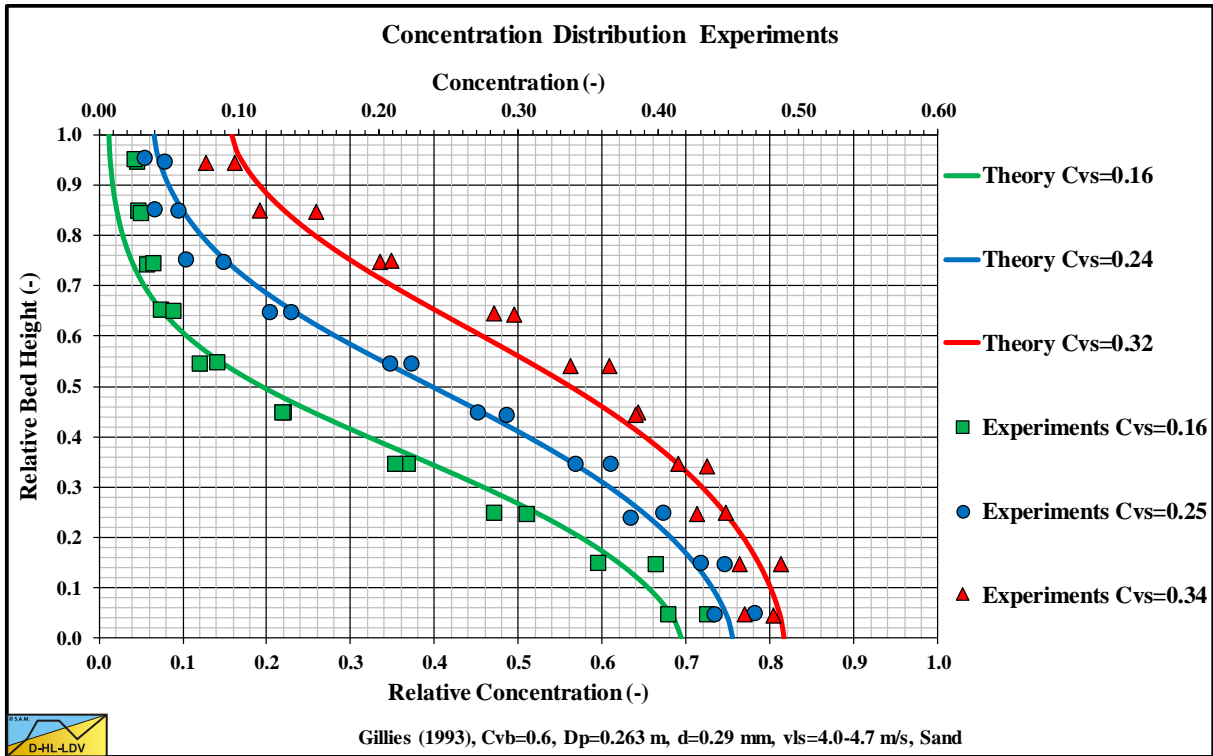
Figure 15.7-14: Gillies (1993) d=0.290 mm, D$_p$=0.2630 m, v$_{ls}$=4.0-4.7 m/s.
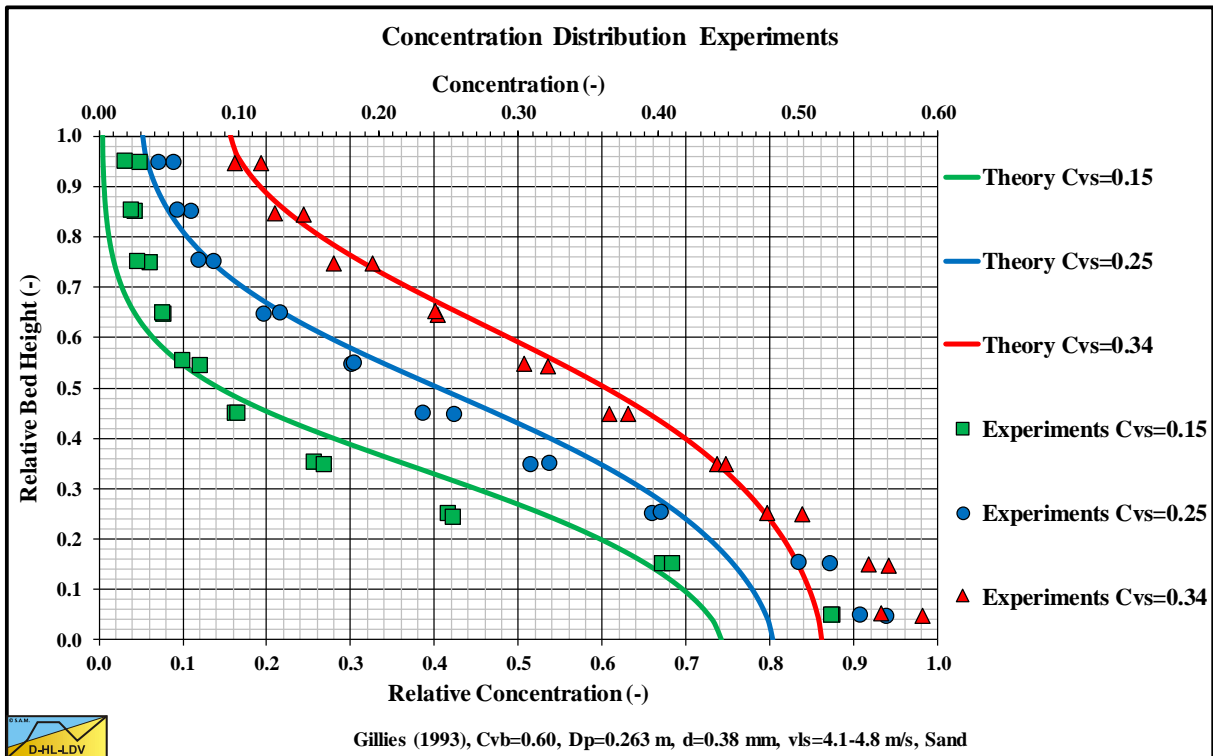
Figure 15.7-15: Gillies (1993) d=0.380 mm, D$_p$=0.2630 m, v$_{ls}$=4.1-4.8 m/s.
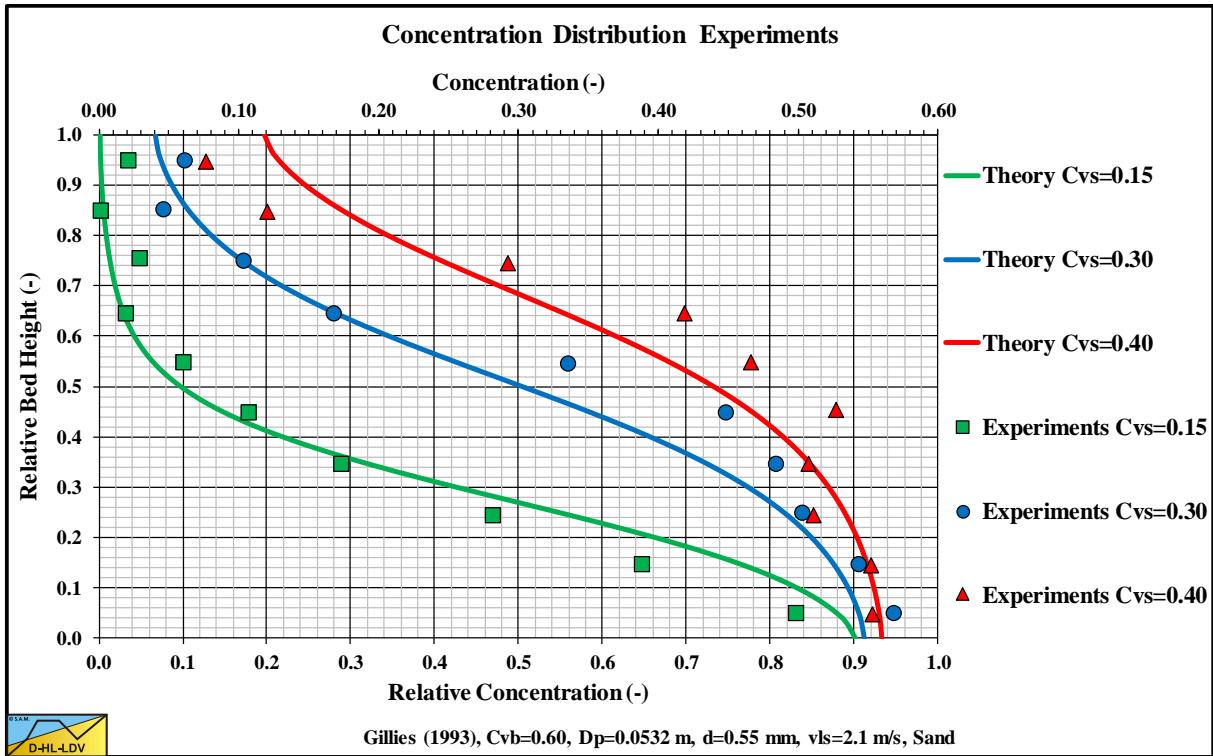
Figure 15.7-16: Gillies (1993) d=0.550 mm, D$_P$=0.0532 m, v$_{ls}$=2.1 m/s.
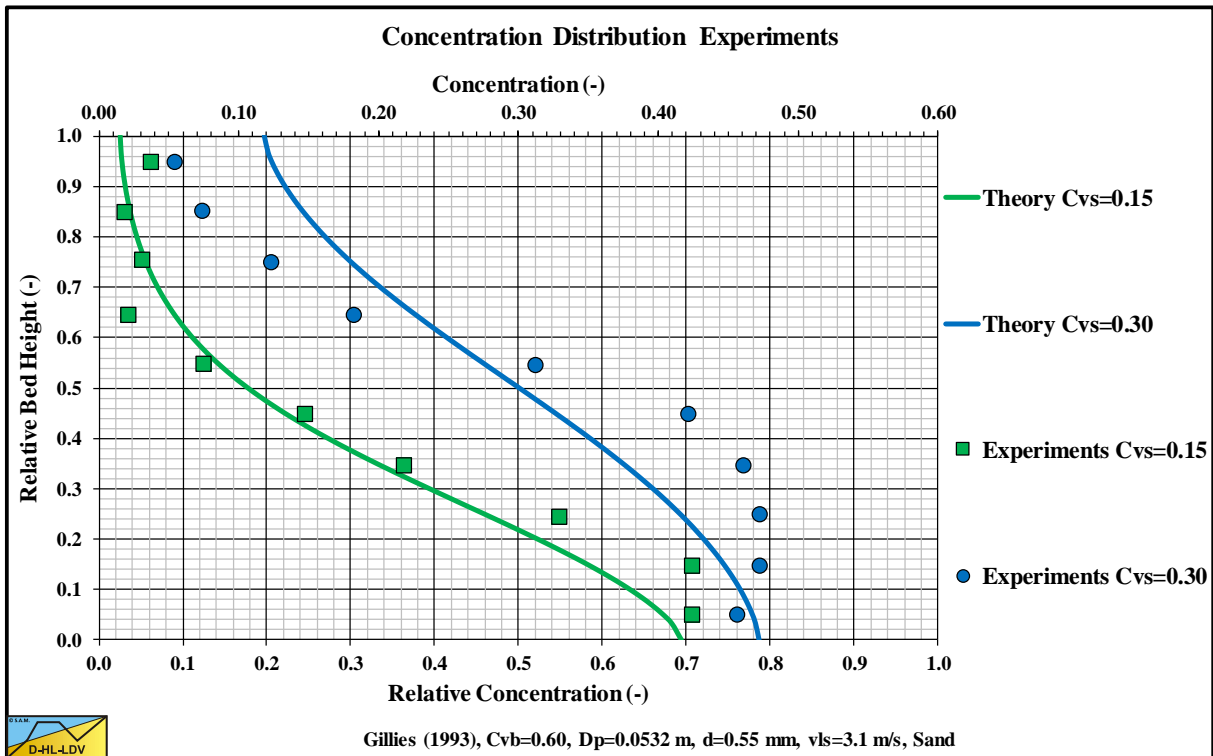
Figure 15.7-17: Gillies (1993) d=0.550 mm, D$_P$=0.0532 m, v$_{ls}$=3.1 m/s.
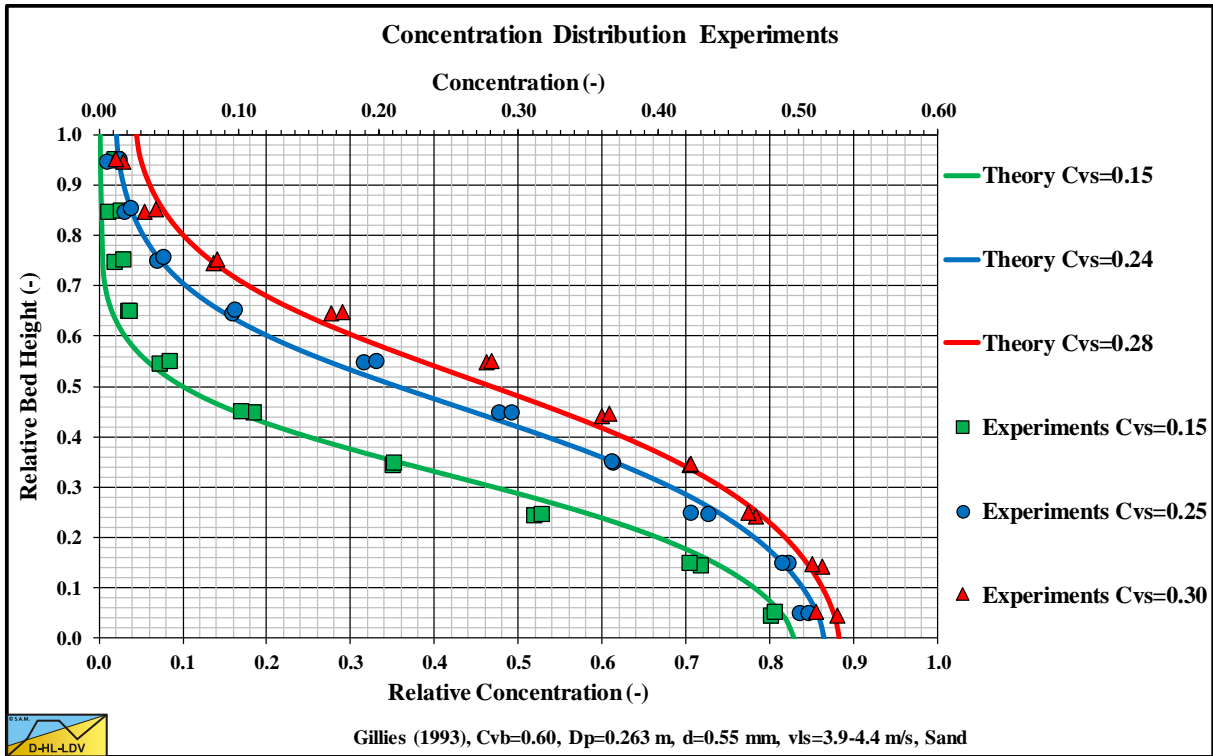
Figure 15.7-18: Gillies (1993) d=0.550 mm, D_P=0.2630 m, v_ls=3.9-4.4 m/s.
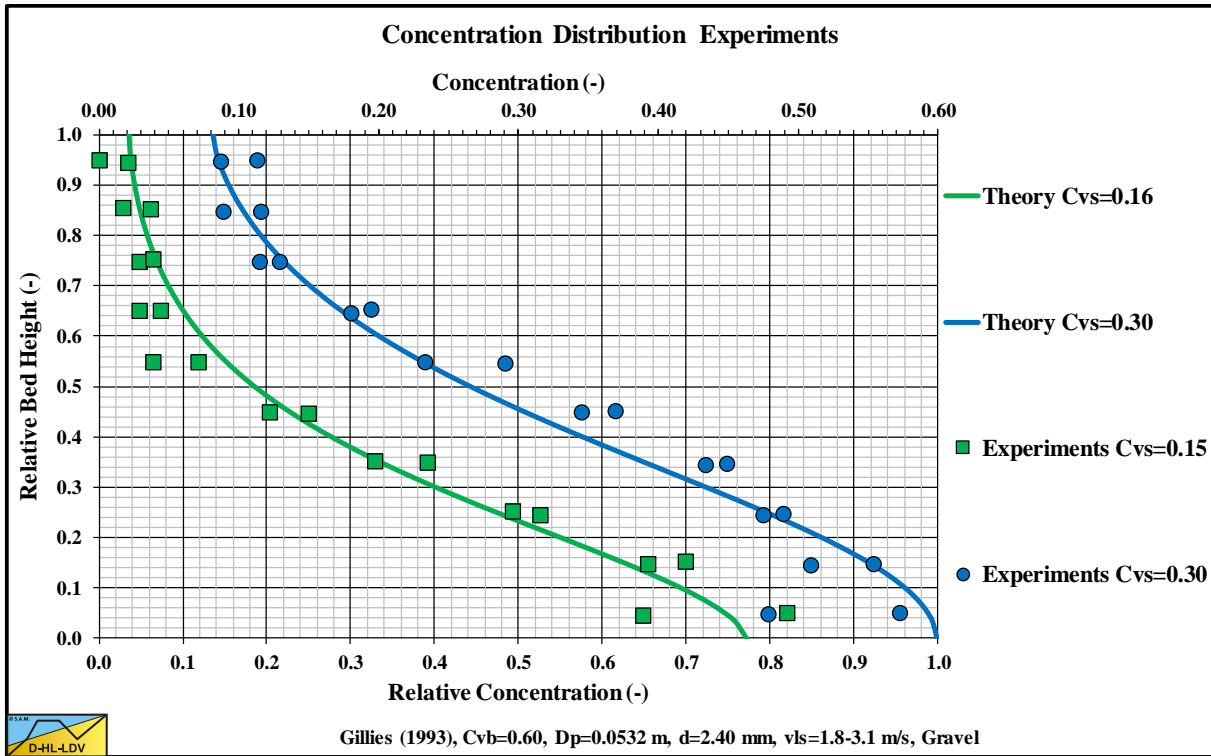
Figure 15.7-19: Gillies (1993) d=2.4 mm, D_p=0.0532 m, v_{ls}=1.8-3.1 m/s.
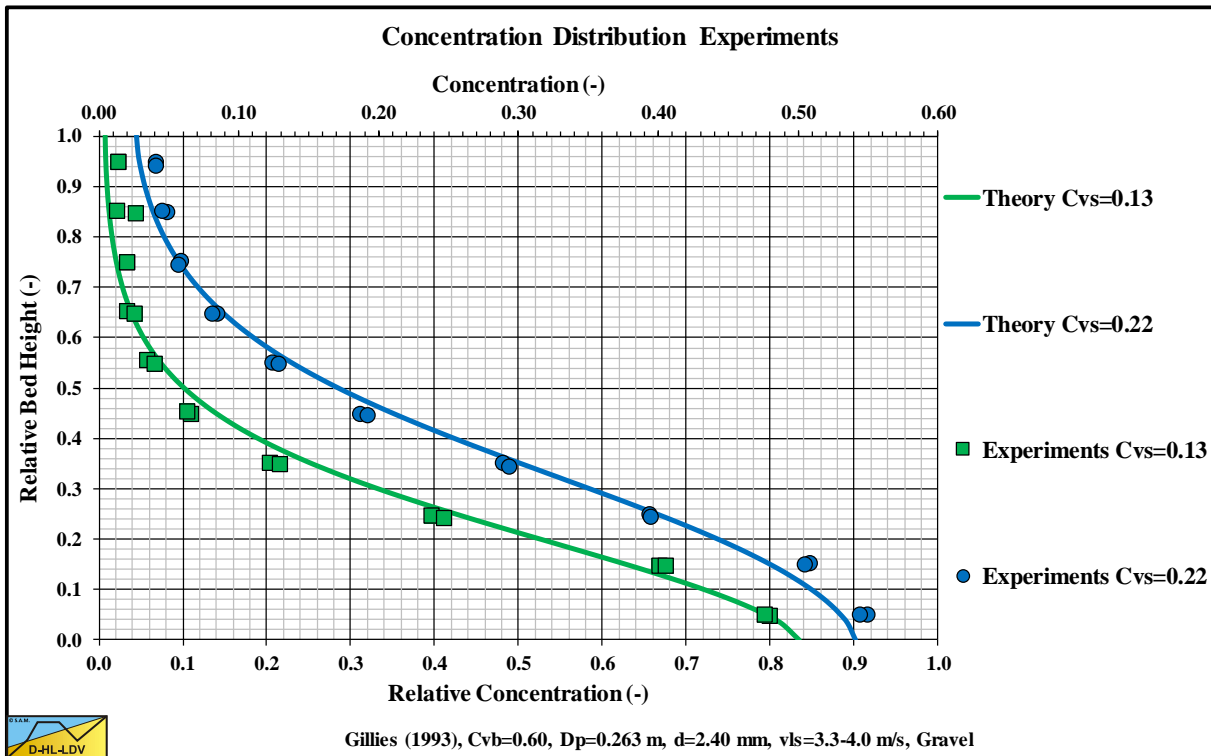
Figure 15.7-20: Gillies (1993) d=2.4 mm, D_p=0.2630 m, v_{ls}=3.3-4.0 m/s.

Appendices.

15.7.3 Gillies (2004).
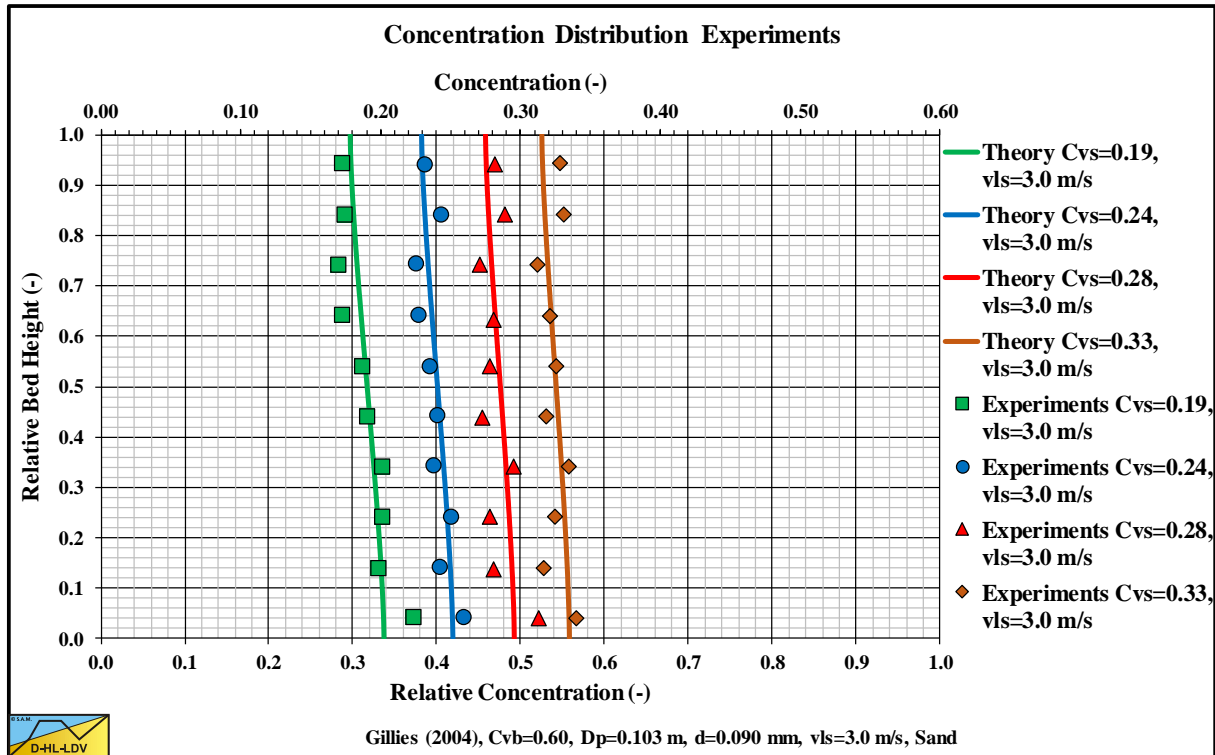
Figure 15.7-21: Gillies (2004) d=0.090 mm, D_p=0.1030 m, v_{ls}=3.0 m/s.
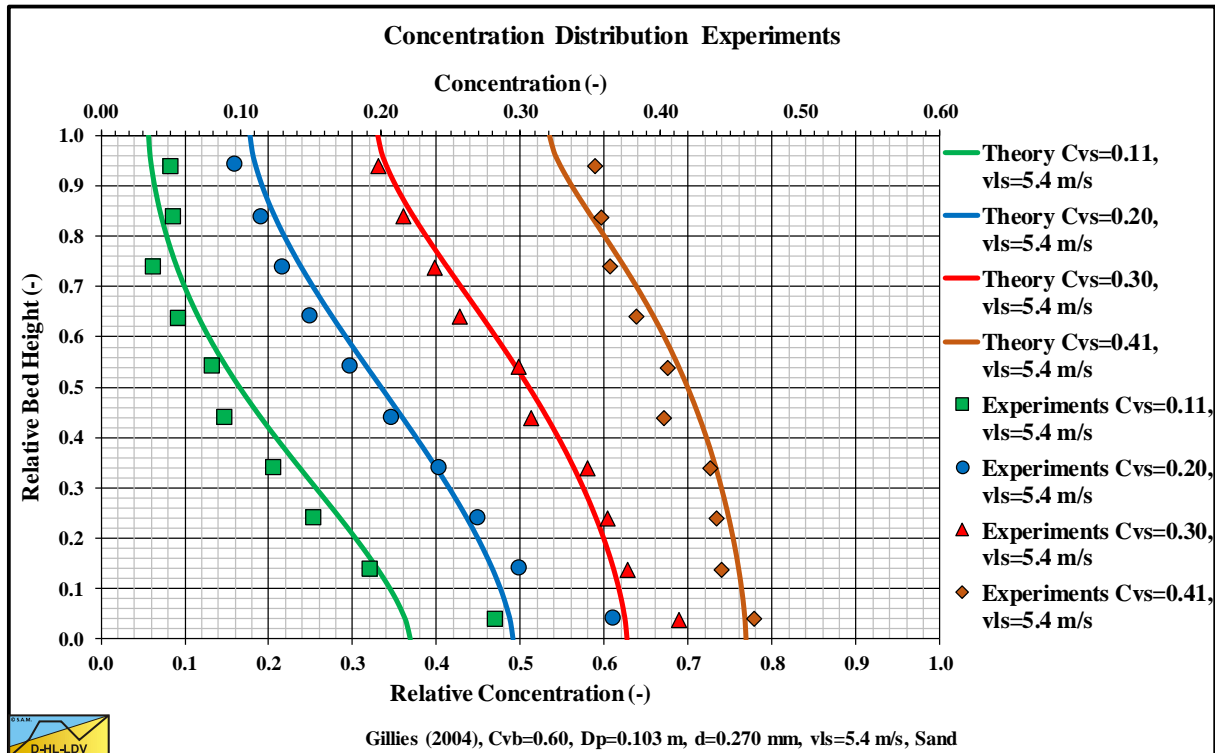
Figure 15.7-22: Gillies (2004) d=0.270 mm, D_p=0.1030 m, v_{ls}=5.4 m/s.

Appendices.

15.7.4 Kaushal & Tomita (2005).
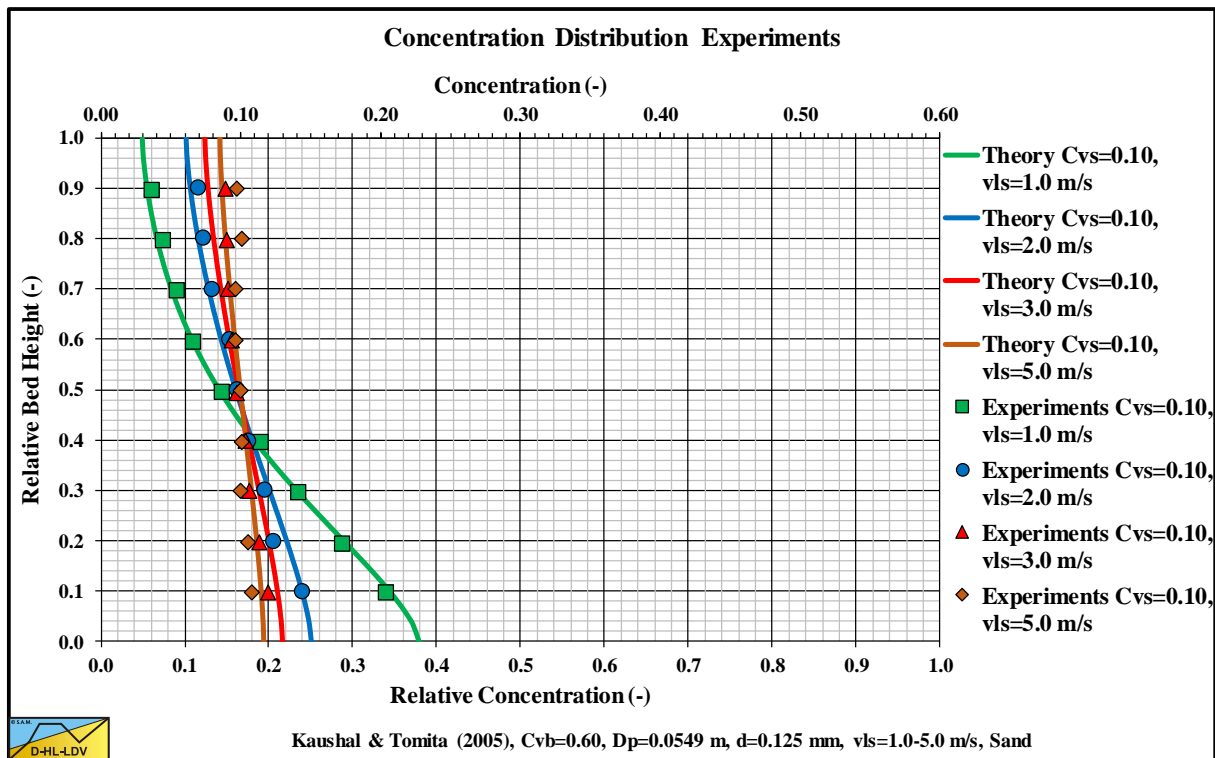
Figure 15.7-23: Kaushal & Tomita (2005) d=0.125 mm, D$_p$=0.0549 m, C$_{vs}$=0.10.
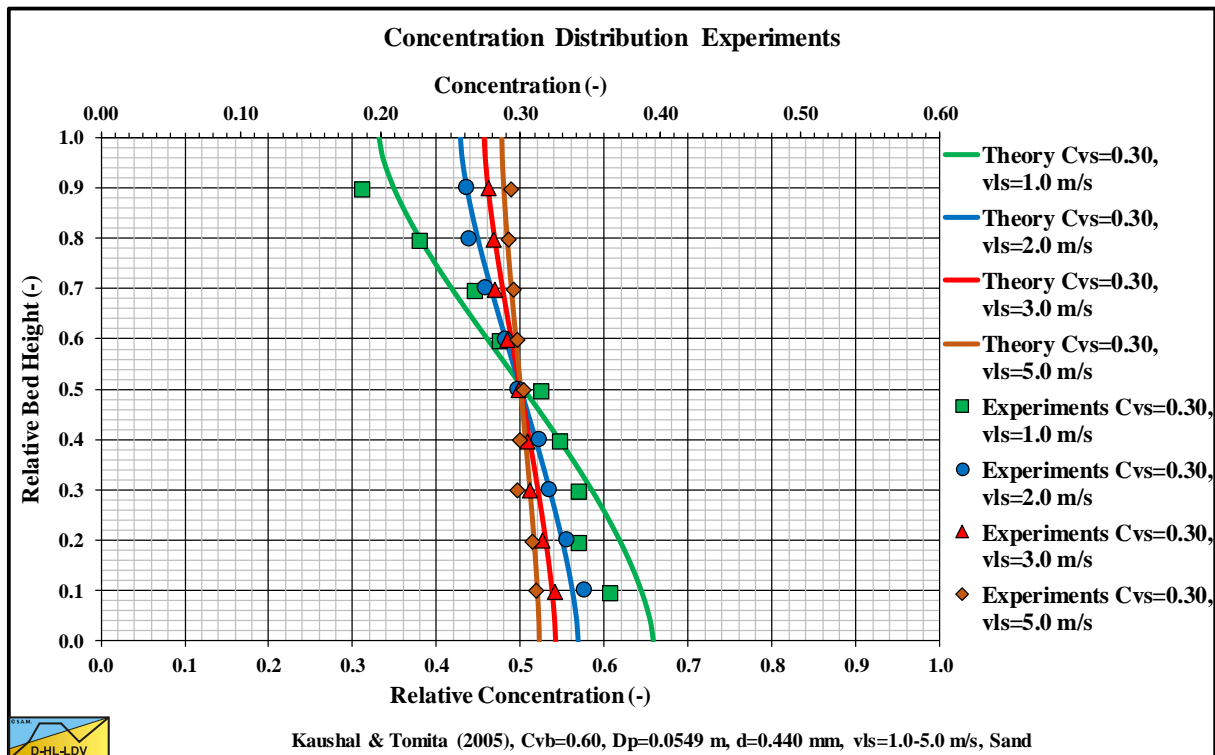
Figure 15.7-24: Kaushal & Tomita (2005) d=0.125 mm, D$_p$=0.0549 m, C$_{vs}$=0.30.
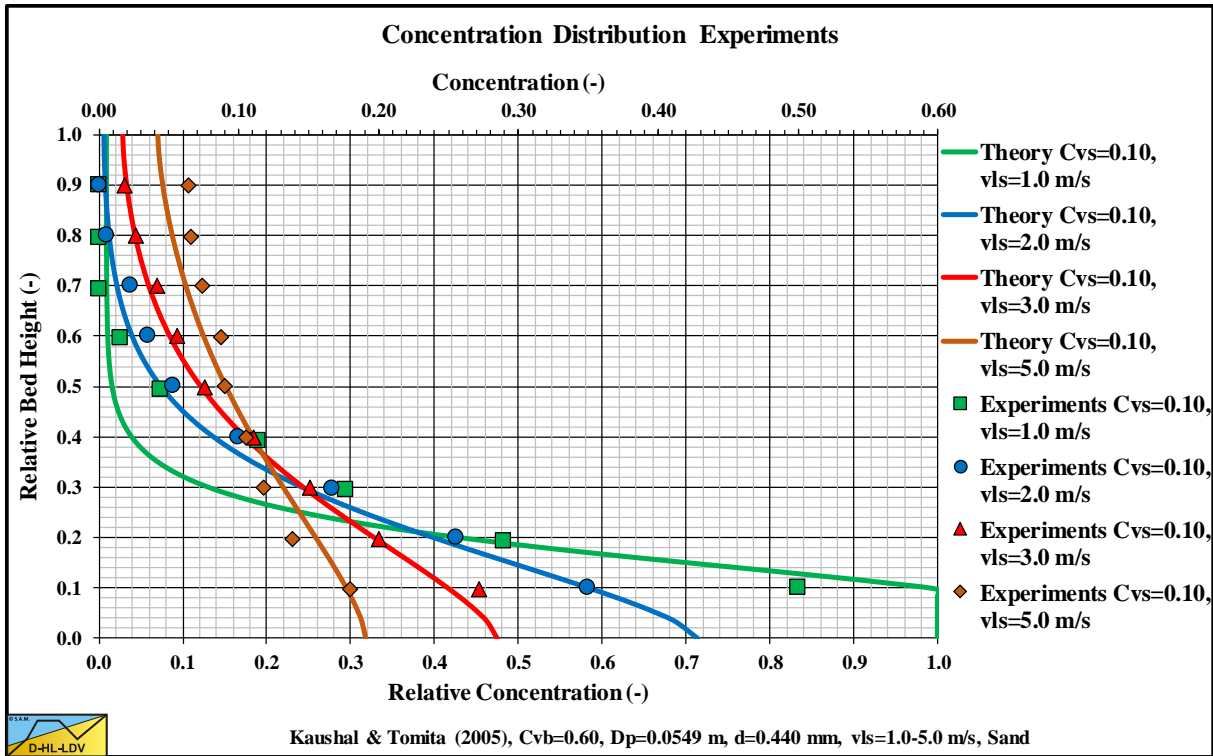
Figure 15.7-25: Kaushal & Tomita (2005) d=0.440 mm, D_p=0.0549 m, C_vs=0.10.
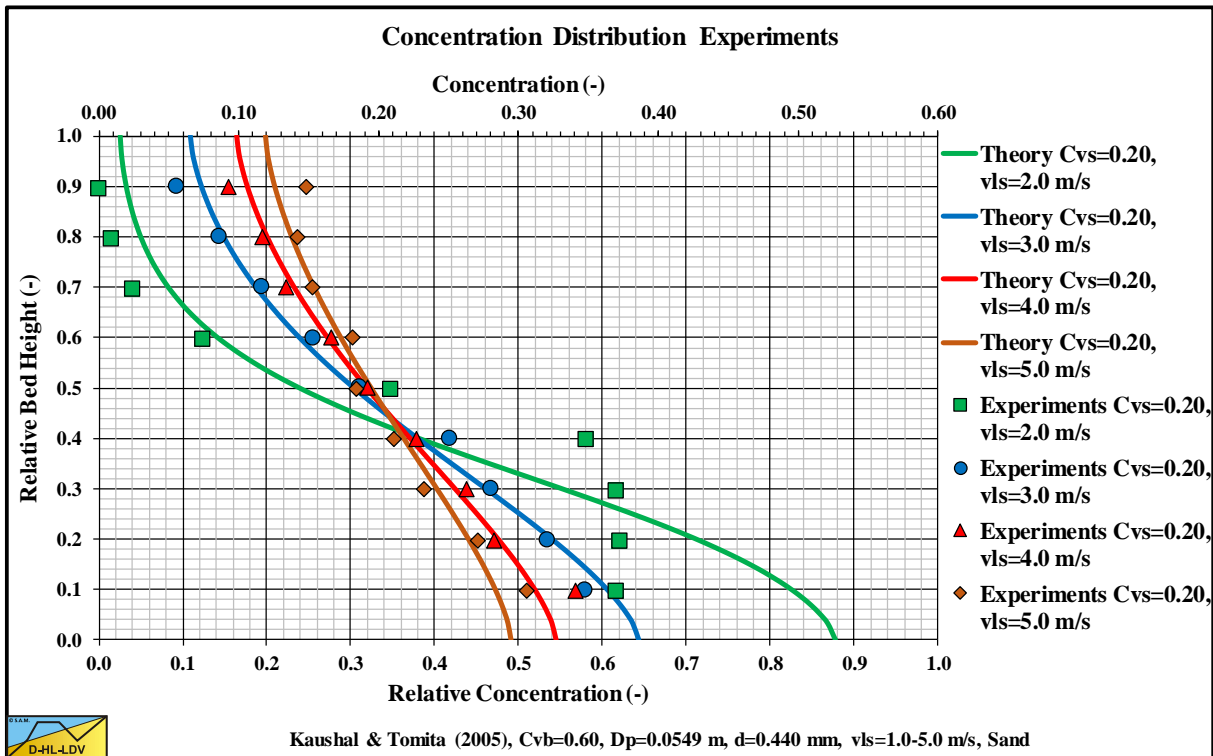
Figure 15.7-26: Kaushal & Tomita (2005) d=0.440 mm, D_p=0.0549 m, C_vs=0.20.
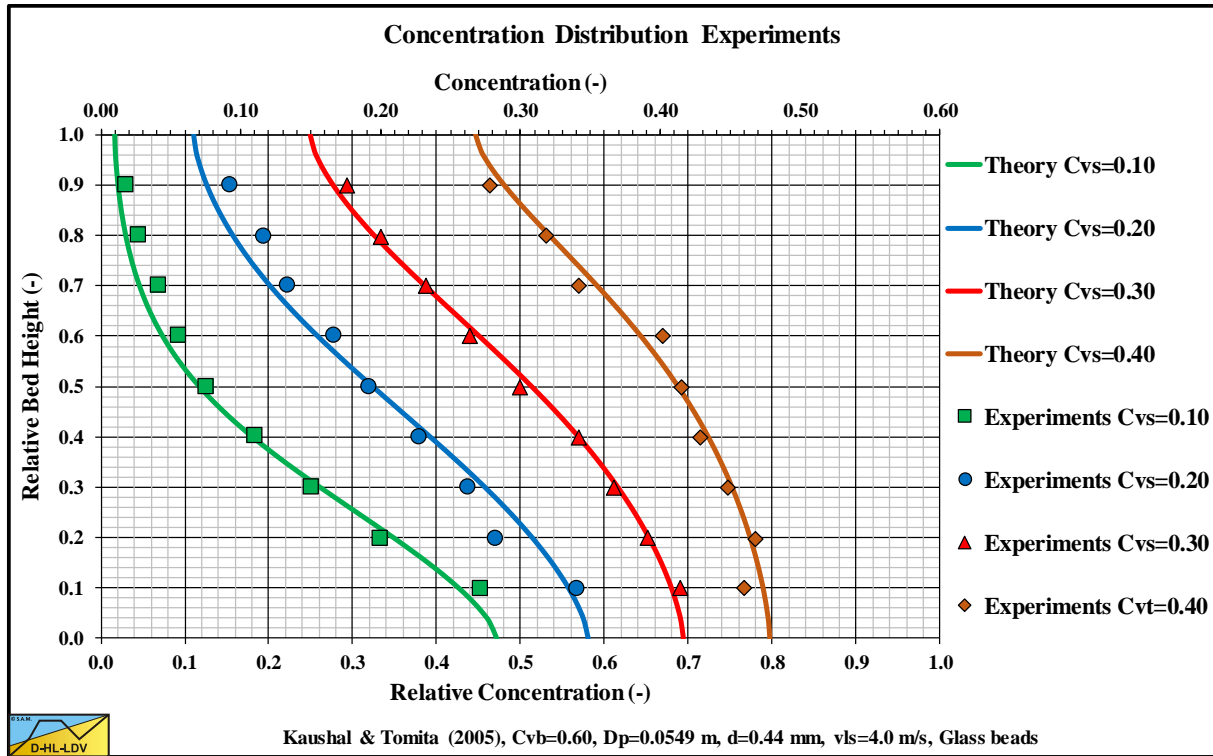
Figure 15.7-27: Kaushal & Tomita (2005) d=0.440 mm, D$_p$=0.0549 m, v$_{ls}$=4.0 m/s.

# Appendices.

15.7.5 Matousek et al. (2009) & (2014).
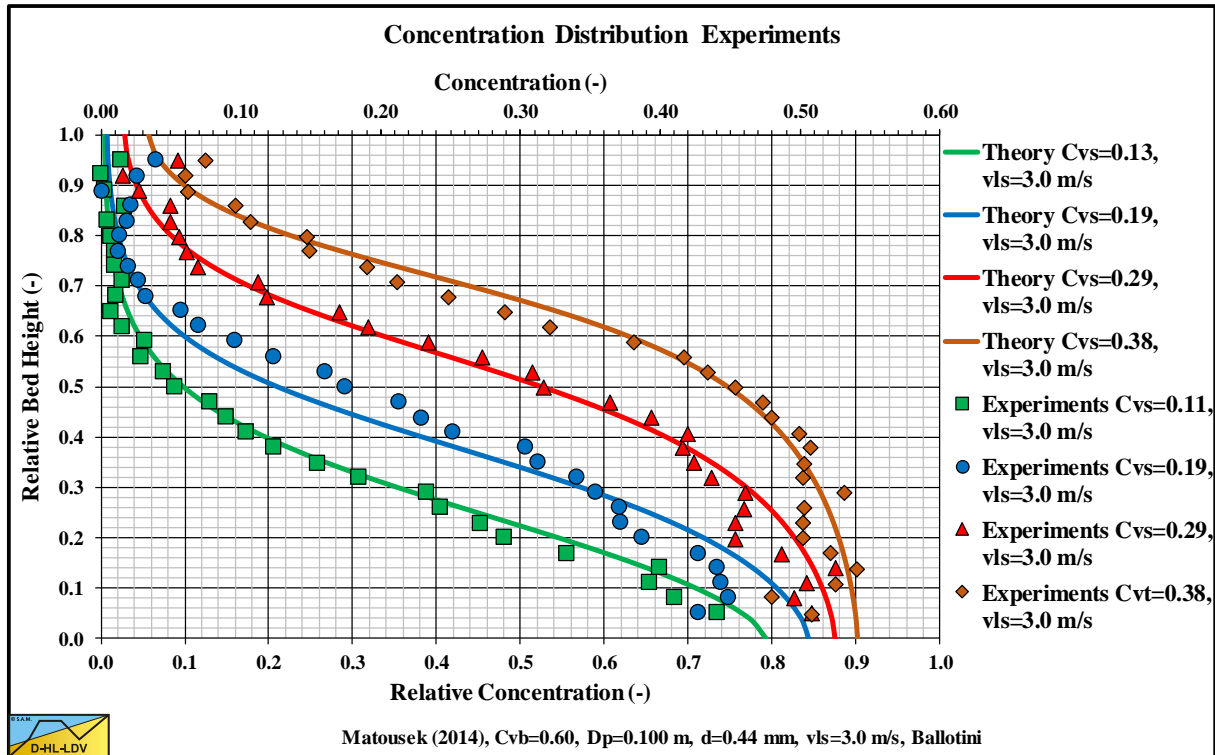
Figure 15.7-28: Matousek et al. (2014) d=0.440 mm, D$_p$=0.1000 m, v$_{ls}$=3.0 m/s.
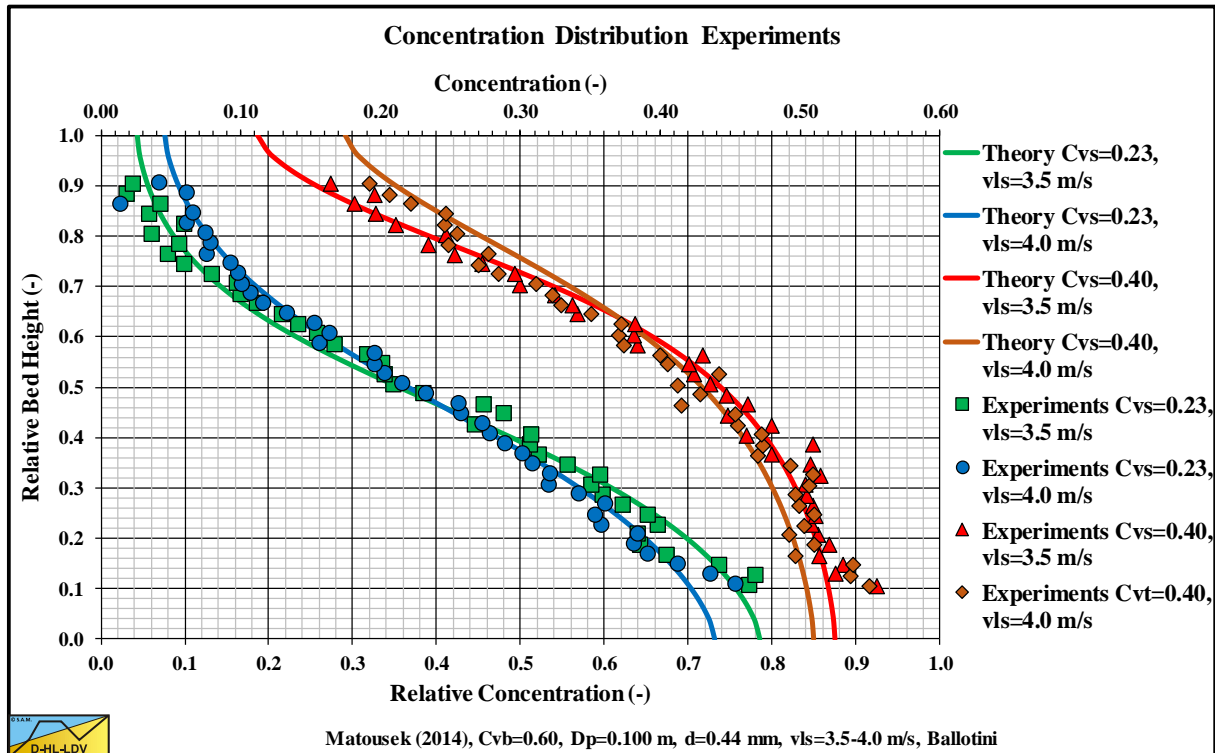
Figure 15.7-29: Matousek et al. (2014) d=0.440 mm, D$_p$=0.1000 m, v$_{ls}$=3.5-4.0 m/s.
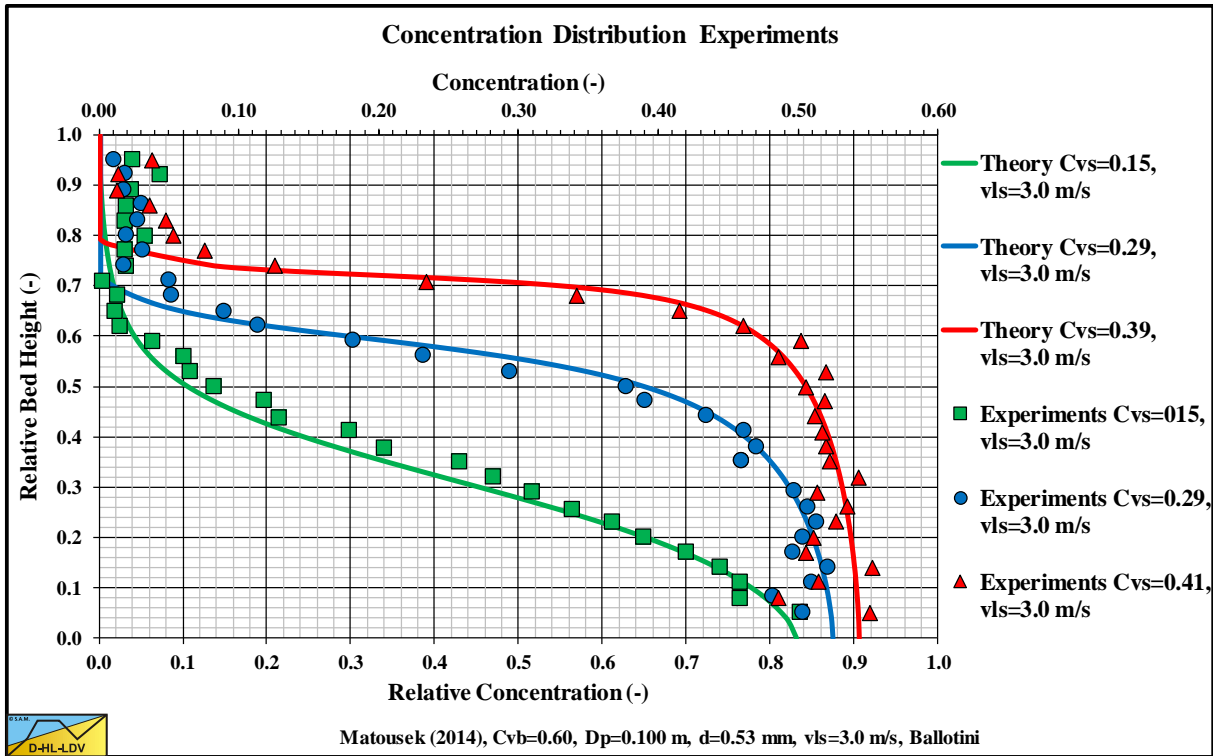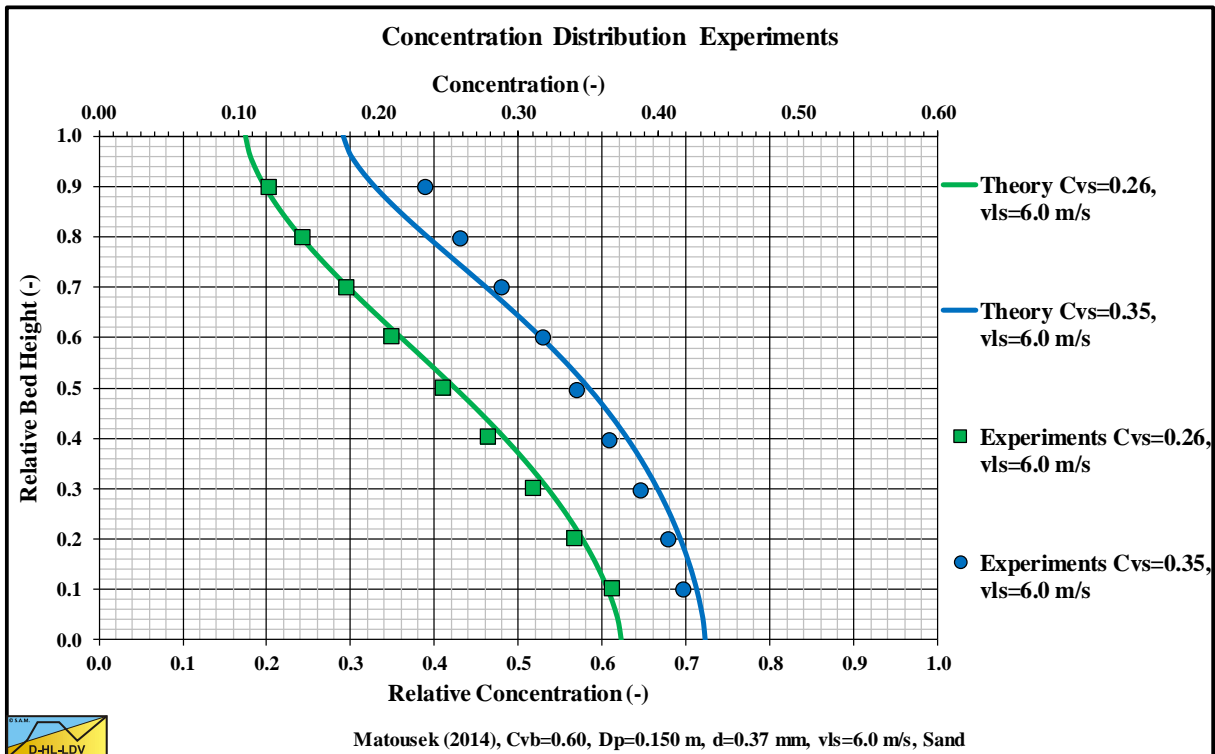
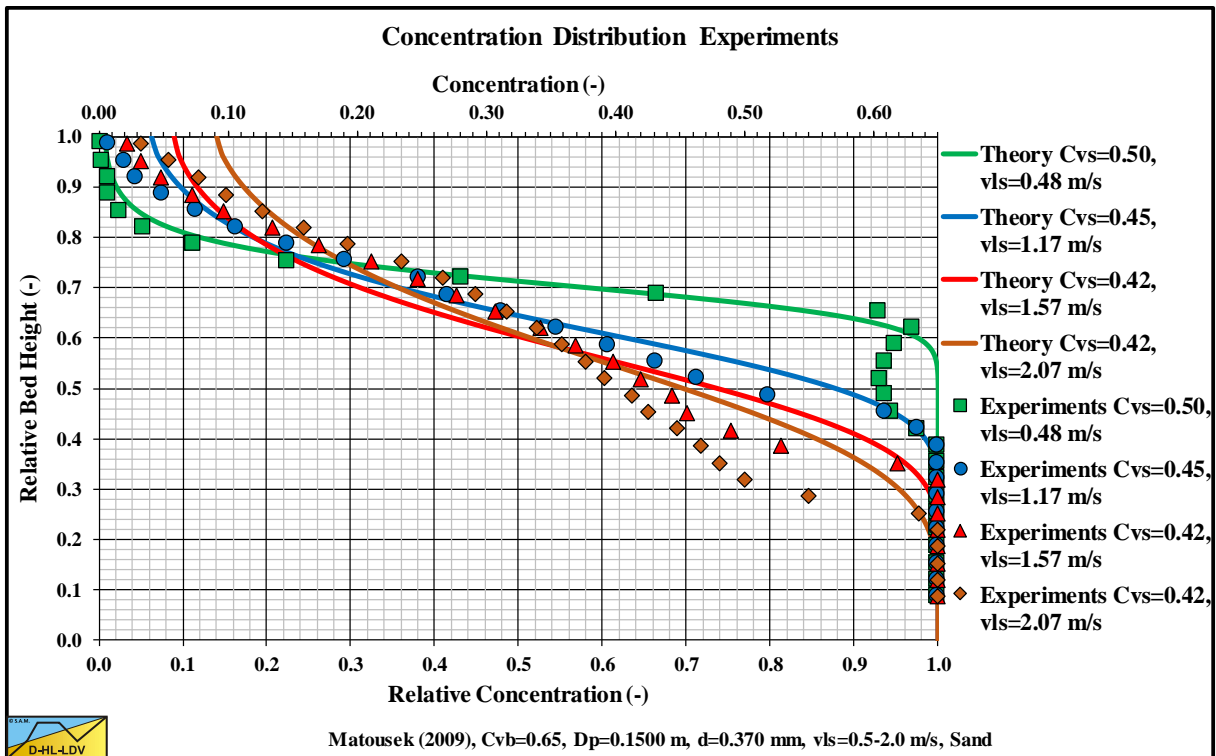**Figure 15.7-30: Matousek et al. (2014) d=0.530 mm, D_p=0.1000 m, v_{ls}=3.0 m/s.**
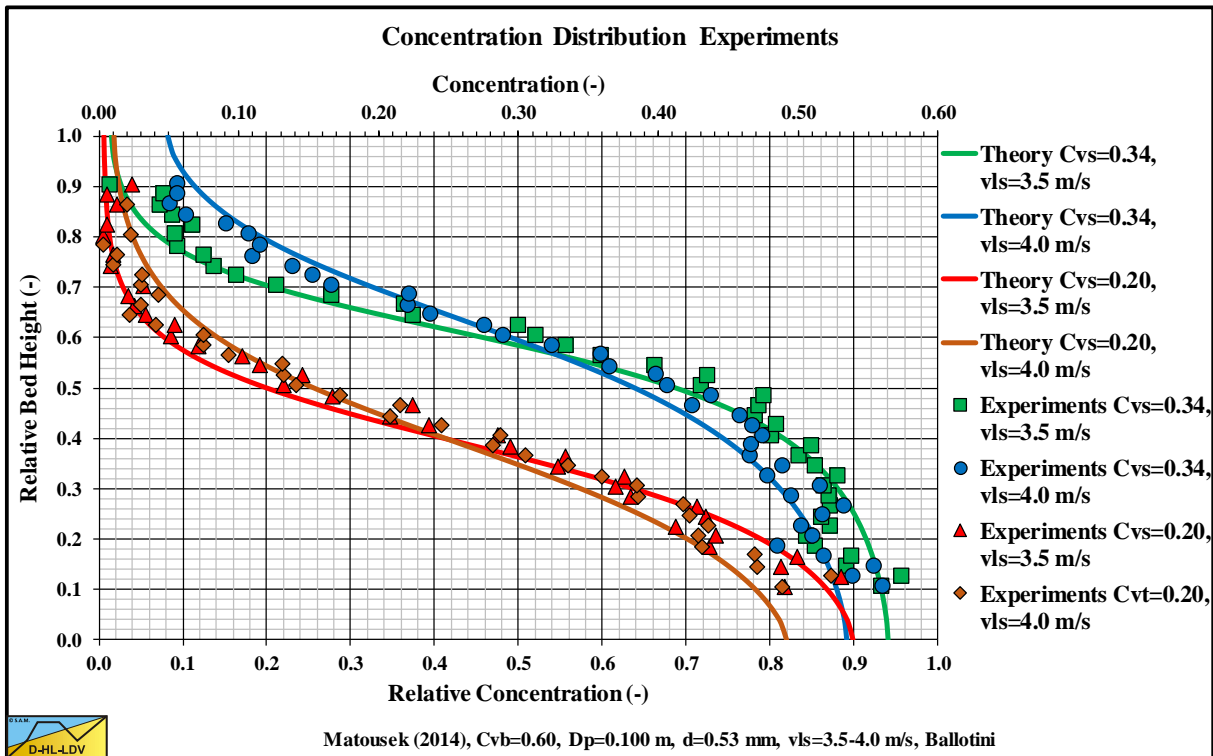
Figure 15.7-31: Matousek et al. (2014) d=0.530 mm, D_p=0.1000 m, v_{ls}=3.5-4.0 m/s.
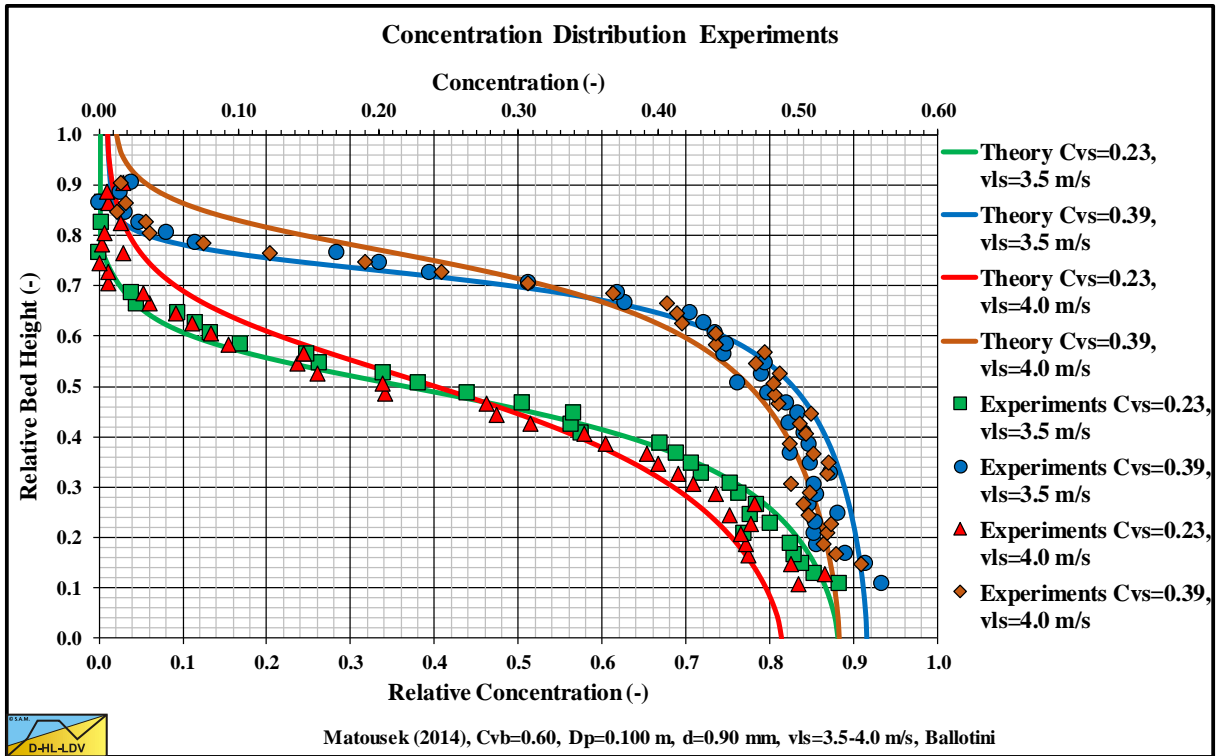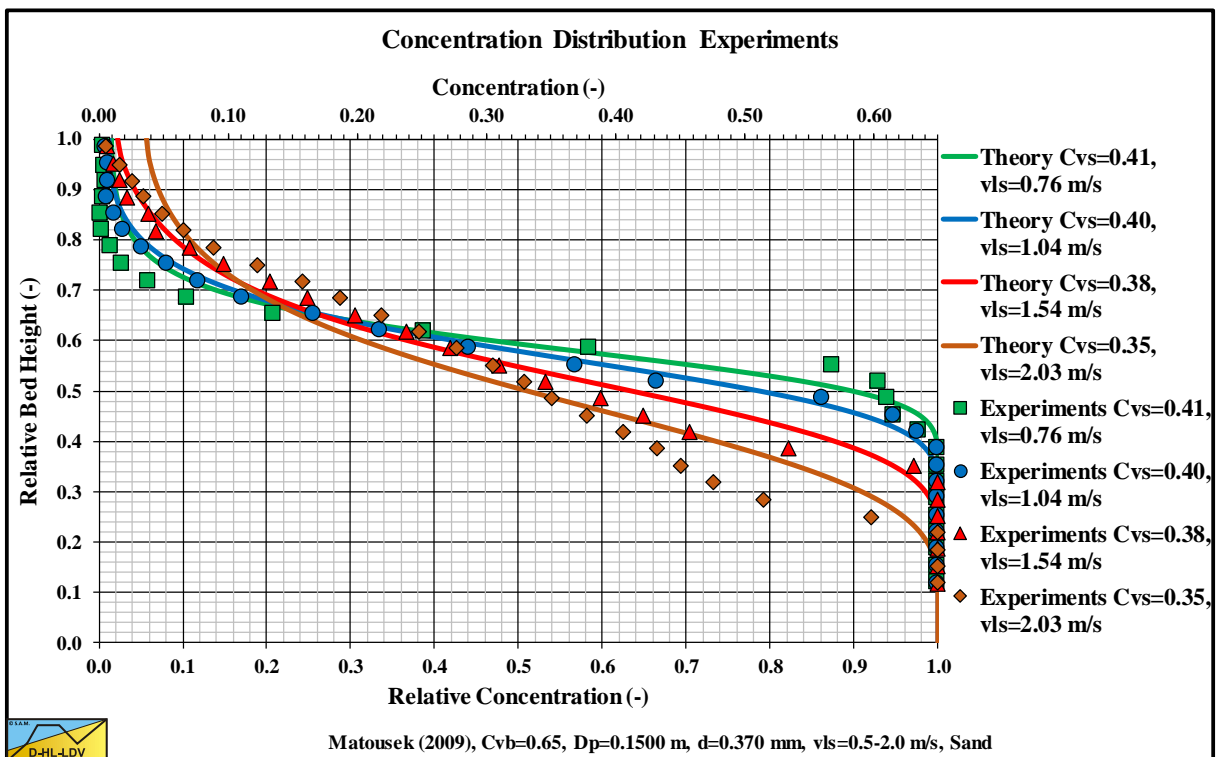
Figure 15.7-32: Matousek et al. (2014) d=0.900 mm, D_p=0.1000 m, v_ls=3.5-4.0 m/s A.
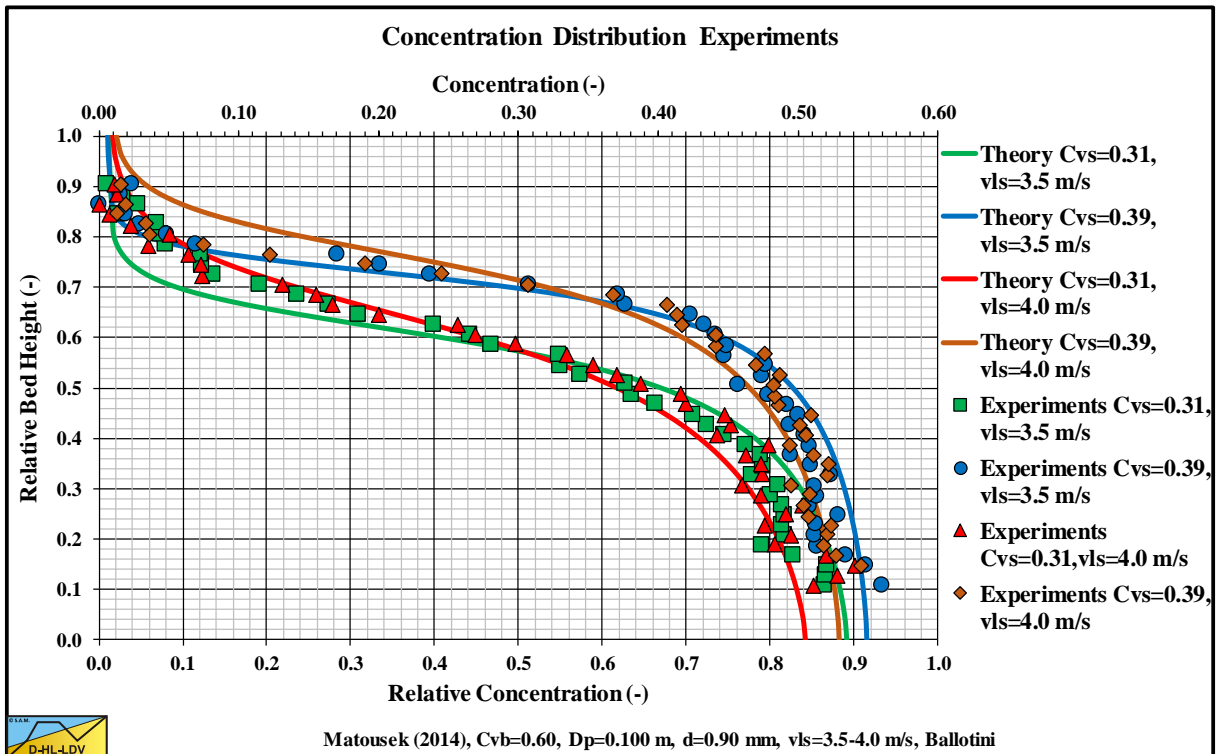
Figure 15.7-33: Matousek et al. (2014) d=0.900 mm, D_p=0.1000 m, v_ls=3.5-4.0 m/s B.
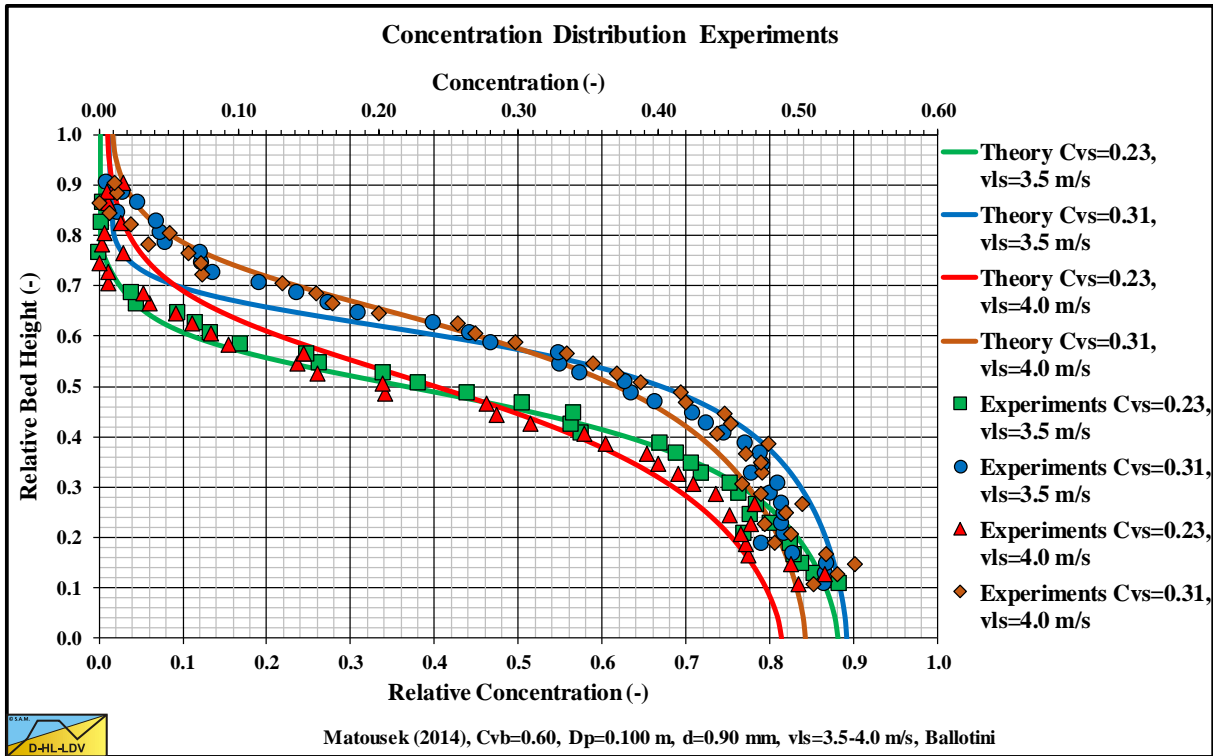
Figure 15.7-34: Matousek et al. (2014) d=0.900 mm, D_P=0.1000 m, v_{ls}=3.5-4.0 m/s C.
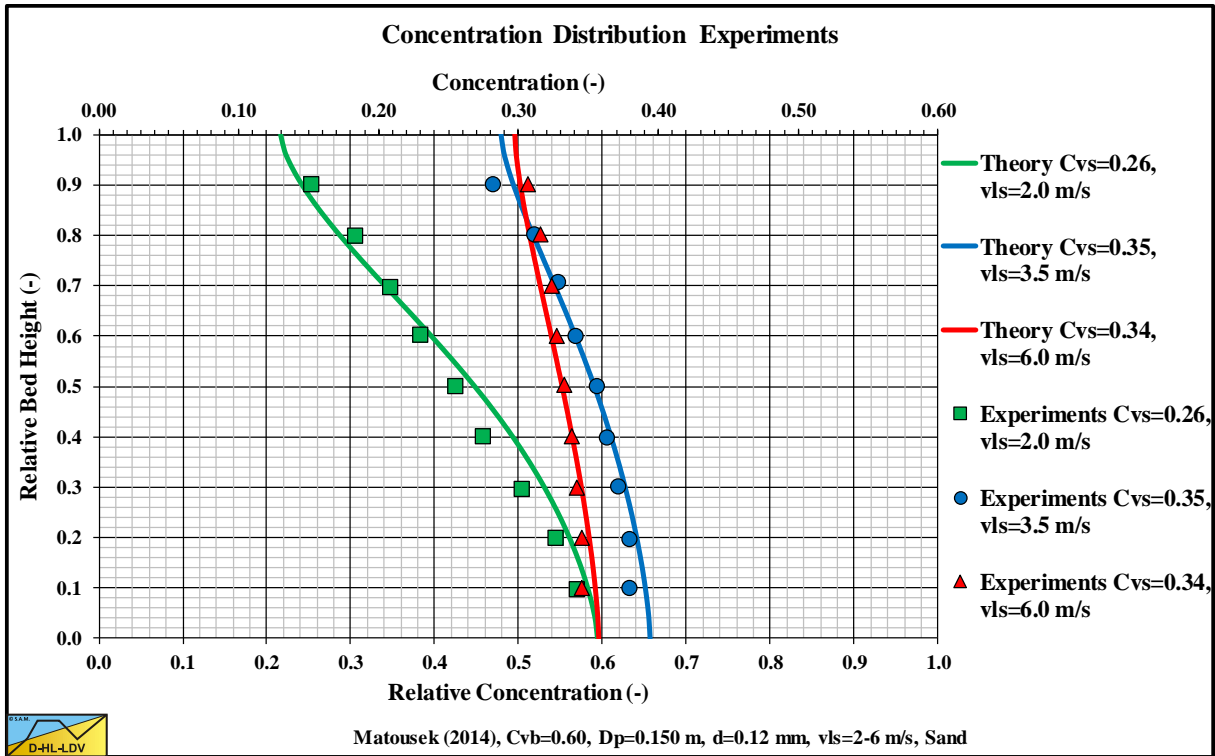
Figure 15.7-35: Matousek et al. (2014) d=0.120 mm, D_p=0.1500 m, v_{ls}=2.0-6.0 m/s.

Figure 15.7-36: Matousek et al. (2014) d=0.370 mm, D_p=0.1500 m, v_{ls}=6.0 m/s.

Figure 15.7-37: Matousek et al. (2009) d=0.370 mm, D_P=0.1500 m, v_{ls}=0.5-2.0 m/s.

Figure 15.7-38: Matousek et al. (2009) d=0.370 mm, D_P=0.1500 m, v_{ls}=0.5-2.0 m/s.

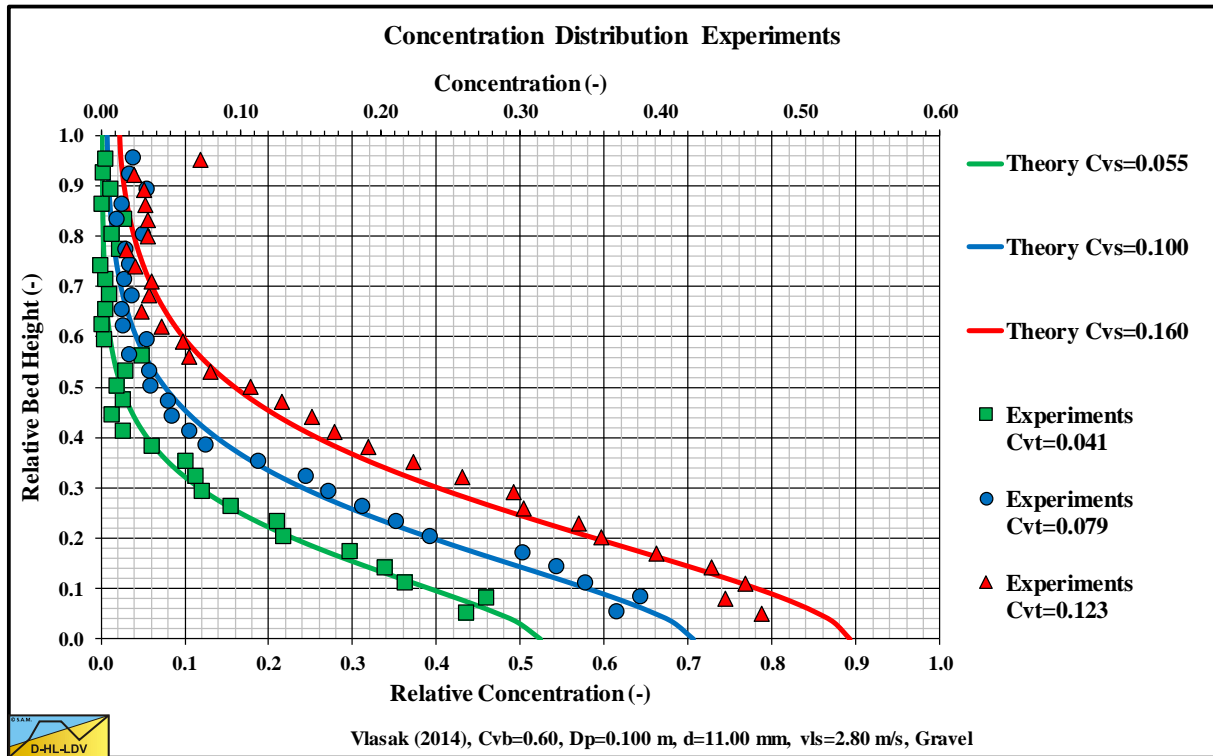# Appendices.

15.7.6 Vlasak et al. (2014).
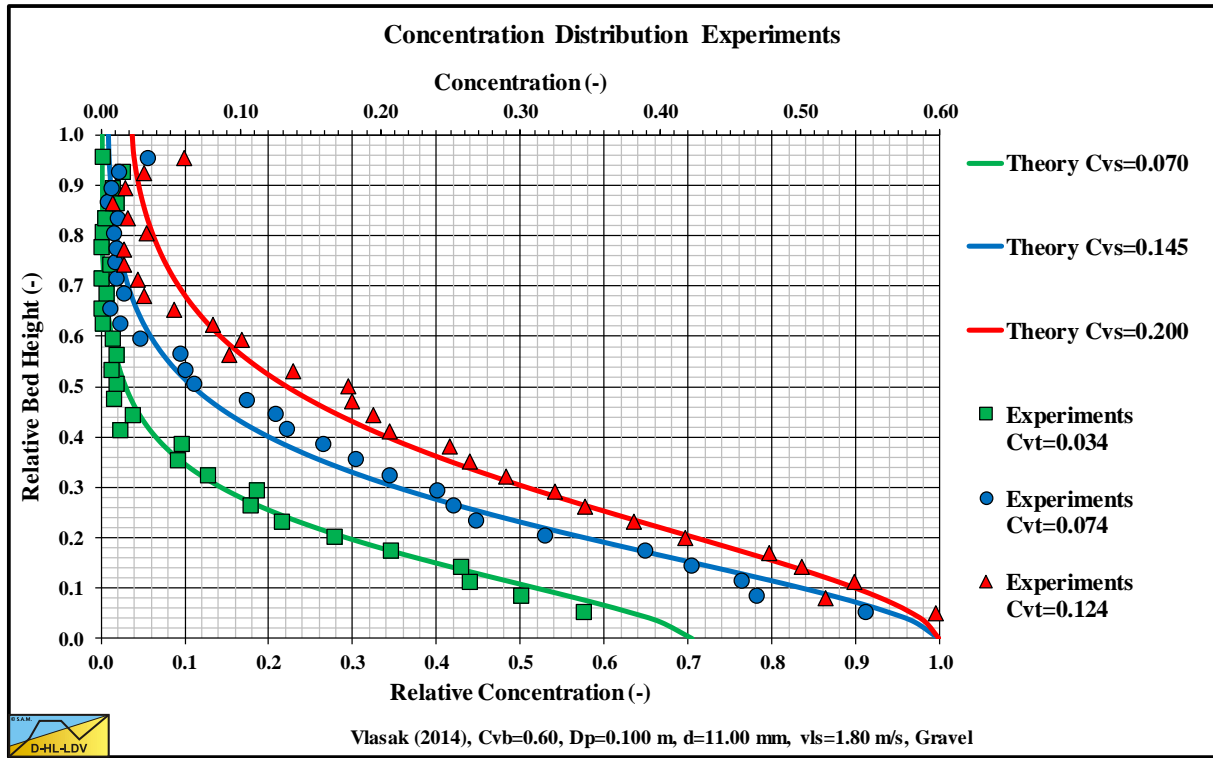
Figure 15.7-39: Vlasak et al. (2014) d=11.0 mm, D_P=0.1000 m, v_{ls}=1.8 m/s.

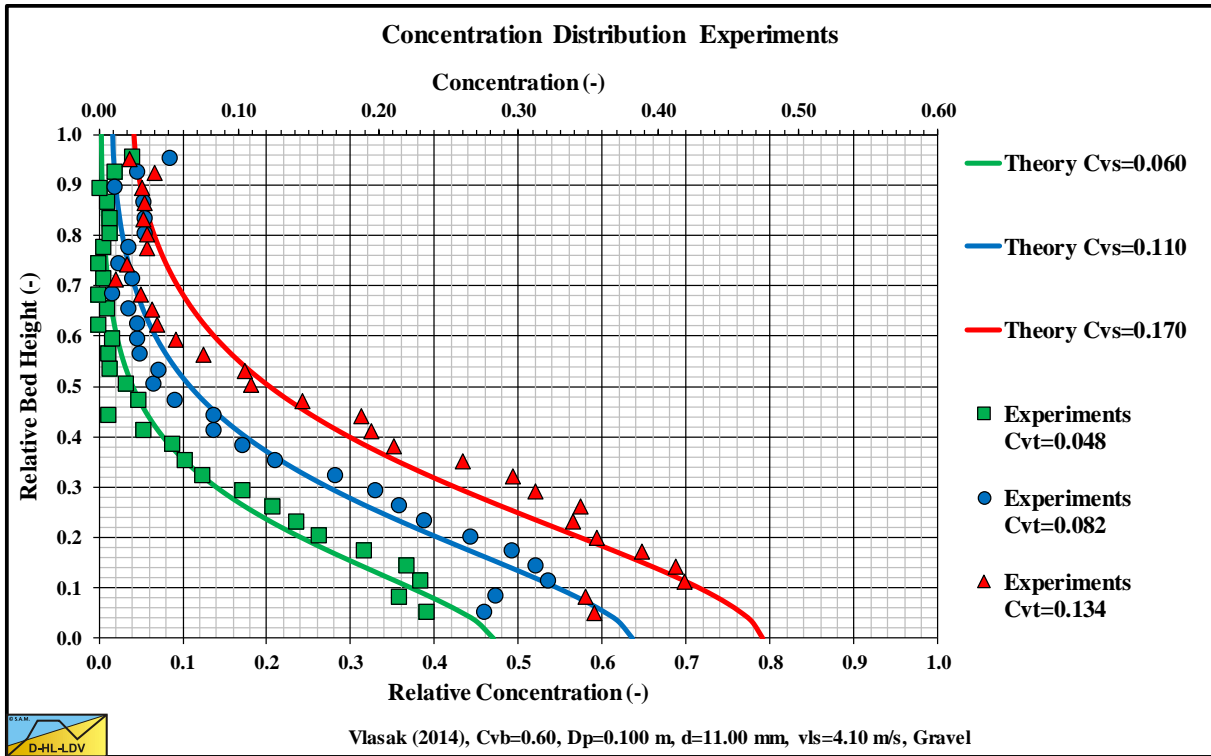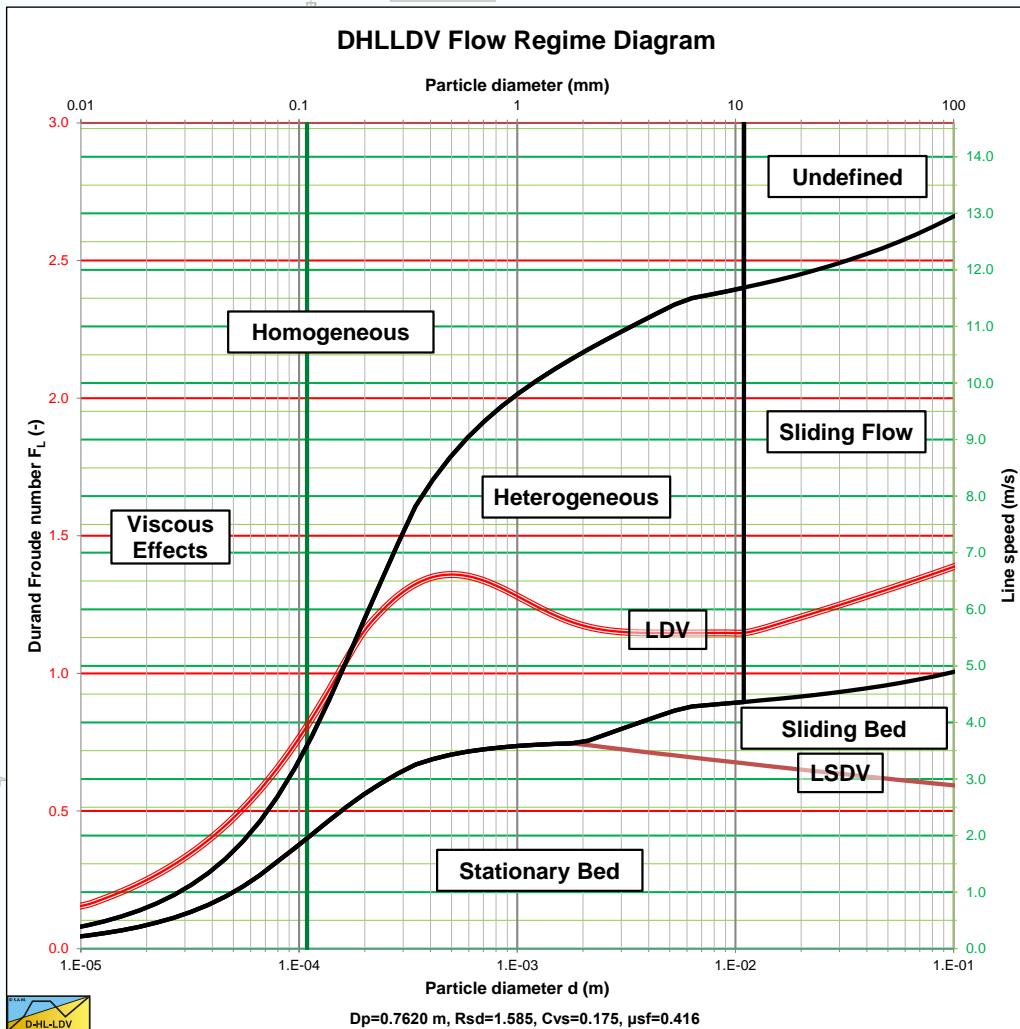**Figure 15.7-40: Vlasak et al. (2014) d=11.0 mm, D_P=0.1000 m, v_{ls}=2.8 m/s.**

Figure 15.7-41: Vlasak et al. (2014) d=11.0 mm, D$_P$=0.1000 m, v$_{ls}$=4.1 m/s.

Slurry Transport

Fundamentals, A Historical Overview & The Delft Head Loss & Limit Deposit Velocity Framework

2nd Edition

DHLLDV Flow Regime Diagram

Dp=0.7620 m, Rsd=1.585, Cvs=0.175, µsf=0.416

By

Sape A. Miedema

Edited by

Robert C. Ramsdell

Slurry Transport: Fundamentals, A Historical Overview & The Delft Head Loss & Limit Deposit Velocity Framework

Sape A. Miedema

In dredging, trenching, (deep sea) mining, drilling, tunnel boring and many other applications, sand, clay or rock has to be excavated. The book covers horizontal transport of settling slurries (Newtonian slurries). Non-settling (non-Newtonian) slurries are not covered.

Dr.ir. Sape A. Miedema
TU Delft | Applied Sciences

Dr.ir. S.A. Miedema teaches (or has taught) courses on soil mechanics and soil cutting, pumps and slurry transport, hopper sedimentation and erosion, mechatronics, applied thermodynamics related to energy, drive system design principles, mooring systems, hydromechanics and mathematics. He is (or has been) also teaching at Hohai University, Changzhou, China, at Cantho University, Cantho Vietnam, at Petrovietnam University, Baria, Vietnam and different dredging companies in the Netherlands and the USA. His research focuses on the mathematical modeling of dredging systems like, cutter suction dredges, hopper dredges, clamshell dredges, backhoe dredges and trenchers. The fundamental part of the research focuses on the cutting processes of sand, clay and rock, sedimentation processes in Trailing Suction Hopper Dredges and the associated erosion processes. Lately the research focuses on hyperbaric rock cutting in relation with deep sea mining and on hydraulic transport of solids/liquid settling slurries.